

# **Advances in Organometallic Chemistry and Catalysis**

The Silver/Gold Jubilee  
International Conference on  
Organometallic Chemistry  
Celebratory Book



Edited by  
**Armando J. L. Pombeiro**



**WILEY**



**ADVANCES IN ORGANOMETALLIC  
CHEMISTRY AND CATALYSIS**



# **ADVANCES IN ORGANOMETALLIC CHEMISTRY AND CATALYSIS**

---

**The Silver/Gold Jubilee International Conference on  
Organometallic Chemistry Celebratory Book**

Edited by

**ARMANDO J. L. POMBEIRO**

**WILEY**

Copyright © 2014 by John Wiley & Sons, Inc. All rights reserved

Published by John Wiley & Sons, Inc., Hoboken, New Jersey  
Published simultaneously in Canada

No part of this publication may be reproduced, stored in a retrieval system, or transmitted in any form or by any means, electronic, mechanical, photocopying, recording, scanning, or otherwise, except as permitted under Section 107 or 108 of the 1976 United States Copyright Act, without either the prior written permission of the Publisher, or authorization through payment of the appropriate per-copy fee to the Copyright Clearance Center, Inc., 222 Rosewood Drive, Danvers, MA 01923, (978) 750-8400, fax (978) 750-4470, or on the web at [www.copyright.com](http://www.copyright.com). Requests to the Publisher for permission should be addressed to the Permissions Department, John Wiley & Sons, Inc., 111 River Street, Hoboken, NJ 07030, (201) 748-6011, fax (201) 748-6008, or online at <http://www.wiley.com/go/permission>.

**Limit of Liability/Disclaimer of Warranty:** While the publisher and author have used their best efforts in preparing this book, they make no representations or warranties with respect to the accuracy or completeness of the contents of this book and specifically disclaim any implied warranties of merchantability or fitness for a particular purpose. No warranty may be created or extended by sales representatives or written sales materials. The advice and strategies contained herein may not be suitable for your situation. You should consult with a professional where appropriate. Neither the publisher nor author shall be liable for any loss of profit or any other commercial damages, including but not limited to special, incidental, consequential, or other damages.

For general information on our other products and services or for technical support, please contact our Customer Care Department within the United States at (800) 762-2974, outside the United States at (317) 572-3993 or fax (317) 572-4002.

Wiley also publishes its books in a variety of electronic formats. Some content that appears in print may not be available in electronic formats. For more information about Wiley products, visit our web site at [www.wiley.com](http://www.wiley.com).

***Library of Congress Cataloging-in-Publication Data:***

Advances in organometallic chemistry and Catalysis : the silver/gold jubilee International Conference on Organometallic Chemistry celebratory book / edited by Armando J. L. Pombeiro.

pages cm

“A John Wiley & Sons, Inc. publication.”

“Published simultaneously in Canada”—Title page verso.

Includes bibliographical references and index.

ISBN 978-1-118-51014-8 (cloth)

1. Organometallic chemistry—Research—Congresses. 2. International Conference on Organometallic Chemistry—Anniversaries, etc. I. Pombeiro, A. J. L. (Armando J. L.) II. International Conference on Organometallic Chemistry.

QD410.A39 2013

547'.05—dc23

2013026531

Printed in the United States of America

10 9 8 7 6 5 4 3 2 1

# CONTENTS

PREFACE	xi
CONTRIBUTORS	xv
<b>PART I ACTIVATION AND FUNCTIONALIZATION OF CARBON SINGLE BONDS AND OF SMALL MOLECULES</b>	1
1    Organometallic Complexes as Catalysts in Oxidation of C—H Compounds <i>Georgiy B. Shul'pin</i>	3
2    Toward Functionalization of Alkanes Under Environmentally Benign Conditions <i>Armando J. L. Pombeiro</i>	15
3    Self-assembled Multicopper Complexes and Coordination Polymers for Oxidation and Hydrocarboxylation of Alkanes <i>Alexander M. Kirillov, Marina V. Kirillova, and Armando J. L. Pombeiro</i>	27
4    Activation of C—O and C—F Bonds by Pincer-iridium Complexes <i>Jason Hackenberg, Karsten Krogh-Jespersen, and Alan S. Goldman</i>	39
5    Functionalization of $sp^2$ and $sp^3$ Carbon Centers Catalysed by Polyoxometalates and Metalloporphyrins <i>Mário M. Q. Simões, Isabel C. M. S. Santos, Maria Graça P. M. S. Neves, Ana M. V. Cavaleiro, and José A. S. Cavaleiro</i>	59
6    Quasi-borinium Cation Based on Cobalt Bis(dicarbollide): Its Lewis Acidity and C—H and C—X Bond Activation <i>V. I. Bregadze, I. B. Sivaev, I. D. Kosenko, I. A. Lobanova, Z. A. Starikova, and I. A. Godovikov</i>	73
7    Transition-metal-promoted Functionalization of Carboranes <i>Zaozao Qiu and Zuowei Xie</i>	81
8    Weak Interactions and M—H Bond Activation <i>Elena Shubina, Natalia Belkova, Oleg Filippov, and Lina Epstein</i>	97

<b>PART II ORGANOMETALLIC SYNTHESIS AND CATALYSIS</b>	<b>111</b>
<b>9 Complexes with Protic N-Heterocyclic Carbene (NR,NH-NHC) Ligands</b>	<b>113</b>
<i>F. Ekkehardt Hahn</i>	
<b>10 Cyclopentadienyl-functionalized N-Heterocyclic Carbene Complexes of Iron and Nickel: Catalysts for Reductions</b>	<b>133</b>
<i>Beatriz Royo</i>	
<b>11 Palladium-(acyclic diaminocarbene) Species as Alternative to Palladium-(nitrogen heterocyclic carbenes) in Cross-coupling Catalysis</b>	<b>145</b>
<i>Vadim P. Boyarskiy, Konstantin V. Luzyanin, and Vadim Yu. Kukushkin</i>	
<b>12 Synthesis of Metallocenes Via Metathesis in Metal Coordination Spheres</b>	<b>157</b>
<i>Antoni Pietrzykowski and Włodzimierz Buchowicz</i>	
<b>13 Metal-mediated [2 + 3] Dipolar Cycloaddition to Substrates with CN Triple Bond: Recent Advances</b>	<b>171</b>
<i>Konstantin V. Luzyanin and Maxim L. Kznetsov</i>	
<b>14 Coordination Chemistry of Oxazoline/Thiazoline-based P,N Ligands</b>	<b>185</b>
<i>Shuanming Zhang, Roberto Pappacini, and Pierre Braunstein</i>	
<b>15 “Click” Copper Catalyzed Azide-alkyne Cycloaddition (CuAAC) in Aqueous Medium</b>	<b>199</b>
<i>Joaquín García-Álvarez and José Gimeno</i>	
<b>16 Organogold Catalysis: Homogeneous Gold-catalyzed Transformations for a Golden Jubilee</b>	<b>207</b>
<i>Fabien Gagosz</i>	
<b>17 Vanadium(IV) Complexes Derived from Aromatic o-Hydroxyaldehydes and Tyrosine Derivatives: Catalytic Evaluation in Sulfoxidations</b>	<b>227</b>
<i>João Costa Pessoa, Isabel Correia, and Pedro Adão</i>	
<b>18 Microwave-assisted Catalytic Oxidation of Alcohols to Carbonyl Compounds</b>	<b>233</b>
<i>Yauhen Yu. Karabach, Maximilian N. Kopylovich, Kamran T. Mahmudov, and Armando J. L. Pombeiro</i>	
<b>19 Oxidation of Glycerol with Hydrogen Peroxide Catalyzed by Metal Complexes</b>	<b>247</b>
<i>Dalmo Mandelli, Wagner A. Carvalho, Lidia S. Shul’pina, Alexander M. Kirillov, Marina V. Kirillova, Armando J. L. Pombeiro, and Georgiy B. Shul’pin</i>	
<b>20 Involvement of an Acetato Ligand in the Reductive Elimination Step of the Rhodium-catalyzed Methanol Carbonylation</b>	<b>259</b>
<i>Duc Hanh Nguyen, Nicolas Lassauque, Thomas Davin, Laurent Maron, Carole Le Berre, Philippe Serp, and Philippe Kalck</i>	
<b>21 Half-sandwich Rhodium(III), Iridium(III), and Ruthenium(II) Complexes with Ancillary Pyrazole-based Ligands</b>	<b>269</b>
<i>Claudio Pettinari, Riccardo Pettinari, Corrado Di Nicola, and Fabio Marchetti</i>	
<b>22 Carbon-scorpionate Complexes in Oxidation Catalysis</b>	<b>285</b>
<i>Luísa M. D. R. S. Martins and Armando J. L. Pombeiro</i>	
<b>23 Toward Chemoselective Bioconjugative Desulfurative Catalysis</b>	<b>295</b>
<i>Lanny S. Liebeskind and Ethel C. Garnier-Amblard</i>	

<b>24 Sulfoxide Redox Chemistry with Molybdenum Catalysts</b>	<b>305</b>
<i>Maria José Calhorda and Luis F. Veiro</i>	
<b>25 A New Family of Zirconium Complexes Anchored by Dianionic Cyclam-based Ligands: Syntheses, Structures, and Catalytic Applications</b>	<b>315</b>
<i>Ana M. Martins, Rui F. Munhá, Luis G. Alves, and Shanmuga Bharathi</i>	
<b>26 Metal-organo Multicatalysis: An Emerging Concept</b>	<b>325</b>
<i>Alexandre F. Trindade, João N. Rosa, Fábio M. F. Santos, and Pedro M. P. Gois</i>	
<b>PART III ORGANOMETALLIC POLYMERIZATION CATALYSIS</b>	<b>343</b>
<b>27 Coordinative Chain Transfer Polymerisations and Copolymerisations by Means of Rare Earths Organometallic Catalysts for the Synthesis of Tailor-made Polymers</b>	<b>345</b>
<i>Marc Visseaux, Thomas Chenal, and Philippe Zinck</i>	
<b>28 Charge-neutral and Cationic Complexes of Large Alkaline Earths for Ring-opening Polymerization and Fine Chemicals Catalysis</b>	<b>359</b>
<i>Jean-François Carpentier, Bo Liu, and Yann Sarazin</i>	
<b>PART IV ORGANOMETALLIC POLYMERS AND MATERIALS</b>	<b>379</b>
<b>29 Organometallic Polymers</b>	<b>381</b>
<i>Manuel Serrano-Ruiz, Franco Scalambra, and Antonio Romerosa</i>	
<b>30 From Serendipity to Porosity: Synthesis and Reactivity of Coordination Polymers Based on Copper Trinuclear Triangular Motifs</b>	<b>407</b>
<i>Luciano Pandolfo</i>	
<b>31 Organometallic Nanoparticles</b>	<b>421</b>
<i>Patricia Lara, Karine Philippot, Lise-Marie Lacroix, Sébastien Lachaize, Nikos Liakakos, Katerina Soulantica, and Bruno Chaudret</i>	
<b>32 Organometallic Compounds in the Synthesis of New Materials: Old Ligands, New Tricks</b>	<b>437</b>
<i>Piotr Sobota and Łukasz John</i>	
<b>33 The Role of Organometallic Complexes in the Synthesis of Shaped Carbon Materials</b>	<b>445</b>
<i>Neil J. Coville and Edward N. Nxumalo</i>	
<b>34 Metal Catalysis in Fullerene Chemistry</b>	<b>459</b>
<i>Salvatore Filippone, Enrique E. Maroto, Ángel Martín-Domenech, and Nazario Martín</i>	
<b>35 Organometallic Complexes of Sumanene</b>	<b>473</b>
<i>Toru Amaya and Toshikazu Hirao</i>	
<b>36 Advances in Luminescent Tetracoordinate Organoboron Compounds</b>	<b>485</b>
<i>D. Suresh and Pedro T. Gomes</i>	
<b>37 Mechanochemistry: A Tool in the Synthesis of Catalysts, Metallocdrugs, and Metallopharmaceuticals</b>	<b>493</b>
<i>Vânia André, Clara S. B. Gomes, and M. Teresa Duarte</i>	

<b>PART V ORGANOMETALLIC CHEMISTRY AND SUSTAINABLE ENERGY</b>	<b>501</b>
<b>38 Organometallic Complexes for Dye-sensitized Solar Cells (DSSC)</b>	<b>503</b>
<i>Delele W. Ayele, Wei-Nein Su, John Rick, Hung-Ming Chen, Chun-Jern Pan, Nibret G. Akalework, and Bing-Joe Hwang</i>	
<b>39 Synthetic Photosynthesis for the Conversion of Large Volumes of Carbon Dioxide into Energy-Rich Molecules: Saving Fossil Fuels by Recycling Carbon</b>	<b>513</b>
<i>Michele Aresta and Angela Dibenedetto</i>	
<b>40 Ionic Liquids for Hydrogen Storage: Opportunities for Organometallic Chemistry</b>	<b>529</b>
<i>Martin H. G. Prechtl and Sebastian Sahler</i>	
<b>PART VI BIOORGANOMETALLIC CHEMISTRY</b>	<b>543</b>
<b>41 Metal Carbonyls for CO-based Therapies: Challenges and Successes</b>	<b>545</b>
<i>Carlos C. Romão and Helena L. A. Vieira</i>	
<b>42 The Ferrocifen Family as Potent and Selective Antitumor Compounds: Mechanisms of Action</b>	<b>563</b>
<i>Gérard Jaouen and Siden Top</i>	
<b>43 On the Track to Cancer Therapy: Paving New Ways With Ruthenium Organometallics</b>	<b>581</b>
<i>Tânia S. Morais and M. Helena Garcia</i>	
<b>44 Organometallic Chemistry of Rhenium and Technetium Fueled by Biomedical Applications</b>	<b>589</b>
<i>António Paulo, Goreti Ribeiro Morais, and Isabel Santos</i>	
<b>45 Metal-based Indolobenzazepines and Indoloquinolines: From Moderate cdk Inhibitors to Potential Antitumor Drugs</b>	<b>605</b>
<i>Michael F. Primik, Lukas K. Filak, and Vladimir B. Arion</i>	
<b>46 Metal-based Chelates and Nanosystems as MRI Contrast Agents</b>	<b>619</b>
<i>Sara Figueiredo and Carlos F. G. C. Geraldes</i>	
<b>PART VII ORGANOMETALLIC ELECTROCHEMISTRY</b>	<b>631</b>
<b>47 Electrochemistry and Supramolecular Interactions of “Ferrocifen” Anticancer Drugs with Cyclodextrins and Lipid Bilayers: An Electrochemical Overview</b>	<b>633</b>
<i>Olivier Buriez, Eric Labbé, and Christian Amatore</i>	
<b>48 Electrochemistry of Fischer Aminocarbene Complexes: Effects of Structure on Redox Properties, Electron Distribution, and Reaction Mechanisms</b>	<b>653</b>
<i>Jiří Ludvík and Irena Hoskovcová</i>	
<b>49 Electron Transfer-induced Coordination Changes in Organometallic Complexes with Non-innocent Hemilabile Ligands</b>	<b>667</b>
<i>Wolfgang Kaim, Martina Bubrin, and Ralph Hübner</i>	
<b>50 Redox Potential–Structure Relationships and Parameterization in Characterization and Identification of Organometallic Compounds</b>	<b>677</b>
<i>M. Fátima C. Guedes da Silva and Armando J. L. Pombeiro</i>	

<b>51 Endohedral Metallofullerenes Today: More and More Versatile Ships in Multiform Bottles—Electrochemistry of X-Ray Characterized Monometallofullerenes</b>	<b>691</b>
<i>Fabrizia Fabrizi de Biani and Piero Zanotto</i>	
<b>POSTSCRIPT: A SHORT HISTORY OF THE ICOMC CONFERENCES</b>	<b>703</b>
<i>Ekkehardt Hahn</i>	
<b>INDEX</b>	<b>707</b>



# PREFACE

## 1.1 ORGANOMETALLIC CHEMISTRY, THE SCIENCE AND APPLICATIONS

*Organometallic chemistry* concerns the compounds with *carbon–metal bonds*, but, in a *broader sense*, deals with (i) transformations of organic compounds with the assistance of metals or (ii) even organometallic-type compounds that bear a metalloid or a nonmetal instead of a metal. This wide meaning is followed in this book.

Although Prussian blue, nowadays known to concern cyano-iron complexes, is present in colored pigments that had already been used in the antiquity, the first organometallic synthesis appears to have been achieved (in 1760) at a military pharmacy in Paris by Cadet, who, when studying inks based on cobalt salts (containing As), obtained a malodorous fuming liquid containing cacodyl oxide  $[(\text{Me}_2\text{As})_2\text{O}]$  and tetramethyldiarsine, compounds of organo-arsenium that were identified only later. However, the Zeise's salt  $\text{Na}[\text{PtCl}_3(\eta^2\text{-C}_2\text{H}_4)]$ , a  $\pi$ -complex of ethylene and Pt, prepared in 1827, is usually considered to be the first organometallic compound to be reported. The chemistry of the metal–carbon bond compounds has developed in a systematic manner since the middle of the nineteenth century, with works, for example, by Bunsen (who prepared and tasted (!)  $[\text{Me}_2\text{AsCN}]$ , in 1840) and his disciple Frankland (since 1849) who appears to have introduced the term “*organometallic*.” During the same century, a diversity of organometallic compounds were prepared by him and/or others (namely, Löwig, Schweizer, Hallwachs, Schafarik, Friedel, Crafts, Wanklyn, Schützenberger, Mond, and Berthelot), including organo-Zn, organo-Hg, organo-B, organo-Pb, organo-Al, organo-Si compounds and the first metal-carbonyls. The end of that century and beginning of the next one (the twentieth century) witnessed the development of organomagnesium compounds (by Barbier and his disciple Grignard) and the emergence of catalysis, in which organometallic chemistry played a fundamental role (e.g., Sabatier, Fischer, Tropsch, Roelen).

The growth of organometallic chemistry during the twentieth century was impressive (it is not possible in this short preface even to list the main achievements) and it became one of the fields of chemistry that has expanded mostly in the past decades, as attested, for example, by the good number of relevant international *journals*, huge number of *papers*, and prominent international *conferences* dealing with it, as well as by the many *Nobel prizes* awarded to scientists on account of their contributions within that overall field, namely, Grignard and Sabatier (1912); Ziegler and Natta (1963); Crowfoot-Hodgkin (1964); Fisher and Wilkinson (1973); Lipscomb (1976); Brown and Wittig (1979); Hoffmann and Fukui (1981); Taube (1983); Knowles, Noyori, and Sharpless (2001); Chauvin, Grubbs, and Schrock (2005); Heck, Negishi, and Suzuki (2010) (adding up already to nine prize winners in the current century!).

The influence of organometallic chemistry on the development of other fields of chemistry and other sciences has been growing in such an *interdisciplinary* way that nowadays organometallic chemistry interfaces with *most of branches of chemistry* and also with *materials science, biology, pharmacology*, etc.; so, naturally it should be viewed in a much broader sense than the strict requirement of M–C bonds, as mentioned above.

Catalysis conceivably provides the current highest contribution of chemistry toward *sustainable development*, and *organometallic catalysis*, in particular, promotes the use of carbon compounds and feedstocks for synthetic applications under milder conditions (*energy saving*) and superior selectivities (*waste reduction*), with resulting *cost savings*.

Development of systems operating under *environmentally benign conditions* toward the establishment of *sustainable energy processes* (e.g., artificial photosynthesis for conversion of carbon dioxide, dye-sensitized solar cells) is a scientific challenge that has been pursued by organometallic chemistry and catalysis.

Therefore, *Organometallic Chemistry* and *Catalysis* have grown in synergy and often indissoluble links can be disclosed. Organometallic compounds, under different perspectives, are involved in very important *applications*, such as

- *Activation* of small molecules with industrial, environmental, biological, or pharmacological significance, for example, alkanes (including natural gas and oil), olefins, carbon monoxide and carbon dioxide, and dihydrogen.

Hence, the *petrochemical industry* and *carbon dioxide fixation* (e.g., to prevent global warming) illustrate relevant fields of application of organometallic chemistry.

- *Synthesis* of important added value organic compounds, in both *commodity and fine chemistries* (large- and low-scale productions, respectively), namely, via catalytic processes where reactions are accelerated by organometallic catalysts. Examples of the former are polymers, carboxylic acids, aldehydes, alcohols, and ketones. Examples of the latter are compounds with biological/pharmacological activity.
- *New carbon materials* with a diversity of potential applications.

Apart from being widely used in industry, organometallic chemistry is also connected to *biology*, as there are enzymes that present organometallic active centers and catalyze organometallic reactions, which constitute inspiring biological motifs for development. Accordingly, *bioorganometallic chemistry* is a promising field with *pharmacological and biomedical applications*.

## 1.2 THIS BOOK AND THE INTERNATIONAL CONFERENCES ON ORGANOMETALLIC CHEMISTRY (ICOMC)

An important indicator of the strength and health of organometallic chemistry is the organization of a large number of important international conferences dealing with this science, the most representative ones being the prestigious series of *International Conferences on Organometallic Chemistry (ICOMC)*, which was launched in 1963 when the first conference was held in Cincinnati. This book follows the XXV ICOMC, which was held in Lisbon (2012) and gathered over 1200 delegates (circa 1100 being foreigners) from 54 countries, in spite of the world economic crisis and the competition with other relevant congresses in chemistry in the same year. It intends to celebrate the *Silver edition* (twenty-fifth edition) and the *Gold year* (fiftieth year since the first conference) of the series, constituting the major *Silver/Gold Jubilee celebratory initiative* of the ICOMCs.

The coinage of a *medal* (Fig. 1) on the occasion of the XXV ICOMC was another celebratory initiative, honoring the places where all these conferences have been held, and relevant landmarks in the history of this science: the ferrocene molecule (the conference logo) and the Chatt–Dewar–Duncanson model of ethylene coordination.

Further details on the XXV ICOMC, including the distributions of participants from countries and particulars of their contributions by scientific areas, as well as a review on representative works presented therein and concerning the platinum group metals are found in [1].



Figure 1 ICOMC Silver/Gold Jubilee medal.

Although the invited authors of this book have been Speakers at the XXV ICOMC, the book is *neither the Proceedings of the Conference nor a conventional book* with comprehensive and long chapters, but instead is *aimed* (i) to present *recent advances and hot topics of current interest* (with the concepts behind them, illustrative relevant cases, and their prospects), (ii) to highlight the *synergy between Organometallic Chemistry and Catalysis*, and (iii) to show the versatility, richness, and potential of *Organometallic Chemistry (in the broad sense) and Catalysis*, including their relations with other sciences, that is, their boosting *interdisciplinarity*.

It provides an updated account of the scientific and applied interest and prospect of major fields of chemistry with high relevance in modern perspectives of science.

It can also be an inspiration for research topics for PhD and MSc theses, projects, and research lines. It is addressed to both expert and nonexpert readers, allowing the latter to get the sensitivity and encouragement for the field.

The main topics of the book follow the general *areas* of the XXV ICOMC itself. *Catalysis* was the most represented area (circa 22% of the total contributions), followed by *Fundamental Organometallic Chemistry* (circa 13%). Other areas (which, nevertheless can include the ones already mentioned or significantly overlap with them) can be ordered as follows: *Activation of Small Molecules, C–H and C–C Bond Activation and Functionalization, Metal-Mediated Synthesis* (each with circa 7%); *Organometallic and Green Chemistry, Bioorganometallic and Bioinorganic Chemistry, Organometallics-Related Chemistry* (each with circa 6%); *Organometallics for Materials* (circa 5%); *Polynuclear and Supramolecular Assemblies, Polymers, and Reaction Mechanisms* (circa 4% each); *Theoretical and Physical Methods, Electrochemistry*, and others.

These areas are assembled in the following main *sections of the Book*:

- Activation and Functionalization of Carbon Single Bonds and of Small Molecules;
- Organometallic Synthesis and Catalysis;
- Organometallic Polymerization Catalysis;
- Organometallic Polymers and Materials;
- Organometallic Chemistry and Sustainable Energy;
- Bioorganometallic Chemistry;
- Organometallic Electrochemistry.

*Catalysis* is the driving force within most of these sections (areas), thus being the most represented overall area of the book, also in accord with what turned out to be the main interest of the conference attendees, reflecting the current organometallic scientific community in general. However, the other areas are not neglected and some of them, with particularly promising prospects, are even emphasized herein relative to their quota at the conference.

The book ends with a postscript providing a brief historical summary of the ICOMCs.

As a recognition of the innovative character of Organometallic Chemistry and Catalysis, providing novel routes to the discoveries of science, the cover picture of this book is inspired on the *Monument of the Discoveries*, at the mouth of the river Tejo (Tagus), Belém, Lisboa, which, with its rising boat prow shape, celebrates the (Portuguese) discoveries of new lands and sea routes during the fifteenth and sixteenth centuries.

As editor of this book and Chairman of the XXV ICOMC, I acknowledge the authors of the various chapters for their valuable contributions (an asterisk has been assigned to the correspondence authors' names who have requested so), and the members of the International Advisory Board (IAB) of the ICOMC for having accepted my proposals for this and the other celebratory initiatives. The support of the Portuguese Electrochemical Society is also acknowledged. Special thanks are due to Dr. Fatima Guedes da Silva and Dr. Manas Sutradhar for their inestimable and generous editorial assistance. The support of the Portuguese Electrochemical Society is also acknowledged.

ARMANDO J. L. POMBEIRO

Centro de Química Estrutural, Instituto Superior Técnico,  
Universidade de Lisboa, Lisboa, Portugal

## REFERENCE

1. Guedes da Silva, M. F. C.; Pombeiro, A. J. L. XXV International Conference on Organometallic Chemistry. Vital role of platinum group metals at Jubilee conference. *Platinum Metals Rev.* **2013**, *57*, 17–31, DOI: <http://dx.doi.org/10.1595/147106713X659127>.



## CONTRIBUTORS

**Pedro Adão**, Centro de Química Estrutural, Instituto Superior Técnico, Universidade de Lisboa, Lisboa, Portugal

**Christian Amatore**, Département de Chimie, Ecole Normale Supérieure, Paris, France

**Toru Amaya**, Department of Applied Chemistry, Graduate School of Engineering, Osaka University, Osaka, Japan

**Vânia André**, Departamento de Engenharia Química, Instituto Superior Técnico, Universidade de Lisboa, Lisboa, Portugal

**Nibret G. Akalework**, Department of Chemical Engineering, National Taiwan University of Science and Technology, Taipei, Taiwan, Republic of China

**Luis G. Alves**, Centro de Química Estrutural, Instituto Superior Técnico, Universidade de Lisboa, Lisboa, Portugal

**Michele Aresta**, Department of Chemistry, University of Bari, Bari, Italy

**Vladimir B. Arion**, Institute of Inorganic Chemistry, University of Vienna, Vienna, Austria

**Delele Worku Ayele**, Department of Chemical Engineering, National Taiwan University of Science and Technology, Taipei, Taiwan, Republic of China

**Fabrizia Fabrizi de Biani**, Dipartimento di Chimica dell'Università di Siena, Siena, Italy

**Shanmuga Bharathi**, Centro de Química Estrutural, Instituto Superior Técnico, Universidade de Lisboa, Lisboa, Portugal

**Natalia Belkova**, A. N. Nesmeyanov Institute of Organoelement Compounds (INEOS), Russian Academy of Sciences, Moscow, Russia

**Vadim Boyarskiy**, Department of Chemistry, St. Petersburg State University, St. Petersburg, Russia

**Pierre Braunstein**, Laboratoire de Chimie de Coordination, Institut de Chimie, Université de Strasbourg, Strasbourg, France

**V. I. Bregadze**, A. N. Nesmeyanov Institute of Organoelement Compounds (INEOS), Russian Academy of Sciences, Moscow, Russia

**Martina Bubrin**, Institut für Anorganische Chemie, Universität Stuttgart, Stuttgart, Germany

**Włodzimierz Buchowicz**, Faculty of Chemistry, Warsaw University of Technology, Warsaw, Poland

**Olivier Buriez**, Département de Chimie, Ecole Normale Supérieure, Paris, France

**Maria José Calhorda**, Departamento de Química e Bioquímica, Centro de Química e Bioquímica, Faculdade de Ciências, Universidade de Lisboa, Lisboa, Portugal

**Jean-François Carpentier**, Organometallics, Materials and Catalysis Department, Institut des Sciences Chimiques de Rennes, Université de Rennes, Rennes, France

**Wagner A. Carvalho**, Center for Natural and Human Science, Federal University of ABC, Santo André, Brazil

**Ana M. V. Cavaleiro**, Department of Chemistry, University of Aveiro, Aveiro, Portugal

**José A.S. Cavaleiro**, Department of Chemistry, University of Aveiro, Aveiro, Portugal

**Bruno Chaudret**, Laboratoire de physique et Chimie des Nano-Objets, Institut National des Sciences Appliquées-CNRS-Université Paul Sabatier, Université de Toulouse, Toulouse, France

**Hung-Ming Chen**, Department of Chemical Engineering, National Taiwan University of Science and Technology, Taipei, Taiwan, Republic of China

**Thomas Chenal**, ENSCL, Univ Lille Nord de France, Lille, France; USTL, Univ Lille Nord de France, Lille, France; CNRS, Univ Lille Nord de France, Lille, France

**Isabel Correia**, Centro de Química Estrutural, Instituto Superior Técnico, Universidade de Lisboa, Lisboa, Portugal

**Neil J. Coville**, DST/NRF Centre of Excellence in Strong Materials and Molecular Sciences Institute, School of Chemistry, University of the Witwatersrand, Johannesburg, South Africa

**Thomas Davin**, University of Toulouse, UPS, INSA, INPT, LCC, ENSIACET, Toulouse, France

**Angela Dibenedetto**, CIRCC, University of Bari, Bari, Italy; Department of Chemistry, University of Bari, Bari, Italy

**Corrado Di Nicola**, School of Pharmacy, Chemistry Section, S. Agostino 1, University of Camerino, Camerino, Italy

**F. Ekkehardt Hahn**, Institut für Anorganische und Analytische Chemie Westfälische Wilhelms-Universität Münster, Münster, Germany

**Lina Epstein**, A. N. Nesmeyanov Institute of Organoelement Compounds (INEOS), Russian Academy of Sciences, Moscow, Russia

**Sara Figueiredo**, Department of Life Sciences, University of Coimbra, Coimbra, Portugal

**Lukas K. Filak**, Institute of Inorganic Chemistry, University of Vienna, Vienna, Austria

**Salvatore Filippone**, Departamento de Química Orgánica I, Universidad Complutense, Madrid, Spain

**Oleg Filippov**, A. N. Nesmeyanov Institute of Organoelement Compounds (INEOS), Russian Academy of Sciences, Moscow, Russia

**I. A. Godovikov**, A. N. Nesmeyanov Institute of Organoelement Compounds (INEOS), Russian Academy of Sciences, Moscow, Russia

**Fabian Gagasz**, Ecole Polytechnique, Laboratoire de Synthèse Organique (DCSO), Palaiseau, France

**Joaquín García-Álvarez**, Laboratorio de Compuestos Organometálicos y Catálisis (Unidad Asociada al CSIC), Departamento de Química Orgánica e Inorgánica, IUQOEM, Facultad de Química, Universidad de Oviedo, Oviedo, Spain

**Ethel C. Garnier-Amblard**, Department of Chemistry, Emory University, Atlanta, Georgia

**Carlos F. G. C. Geraldes**, Department of Life Sciences, University of Coimbra, Coimbra, Portugal; Center of Neurosciences and Cell Biology, University of Coimbra, Coimbra, Portugal; Coimbra Chemistry Center, University of Coimbra, Coimbra, Portugal

**José Gimeno**, Laboratorio de Compuestos Organometálicos y Catálisis (Unidad Asociada al CSIC), Departamento de Química Orgánica e Inorgánica, IUQOEM, Facultad de Química, Universidad de Oviedo, Oviedo, Spain

**Pedro M. P. Gois**, Research Institute for Medicines and Pharmaceutical Sciences (iMed.UL), Universidade de Lisboa, Lisboa, Portugal

**Alan S. Goldman**, Department of Chemistry and Chemical Biology, Rutgers, The State University of New Jersey, New Brunswick, NJ, USA

**Clara S. B. Gomes**, Departamento de Engenharia Química, Instituto Superior Técnico, Universidade de Lisboa, Lisboa, Portugal

**Pedro T. Gomes**, Centro de Química Estrutural, Instituto Superior Técnico, Universidade de Lisboa, Lisboa, Portugal

**M. Fátima C. Guedes da Silva**, Centro de Química Estrutural, Instituto Superior Técnico, Universidade de Lisboa; Universidade Lusófona de Humanidades Tecnologias (ULHT) Lisboa, Portugal

**Jason Hackenberg**, Department of Chemistry and Chemical Biology, Rutgers, The State University of New Jersey, New Brunswick, NJ, USA

**M. Helena Garcia**, Centro de Ciências Moleculares e Materiais, Faculdade de Ciências da Universidade de Lisboa, Lisboa, Portugal

**Toshikazu Hirao**, Department of Applied Chemistry, Graduate School of Engineering, Osaka University, Osaka, Japan

**Irena Hoskova**, Department of Inorganic Chemistry, Institute of Chemical Technology Prague, Prague, Czech Republic

**Ralph Hübler**, Institut für Anorganische Chemie, Universität Stuttgart, Stuttgart, Germany

**Bing-Joe Hwang**, Department of Chemical Engineering, National Taiwan University of Science and Technology, Taipei, Taiwan; National Synchrotron Radiation Research Center, Hsinchu Taiwan, Republic of China

**Gérard Jaouen**, Chimie ParisTech (Ecole Nationale Supérieure de Chimie de Paris), Laboratoire Charles Friedel, Paris, France

**Lukasz John**, Faculty of Chemistry, University of Wrocław, Wrocław, Poland

**Wolfgang Kaim**, Institut für Anorganische Chemie, Universität Stuttgart, Stuttgart, Germany

**Yauhen Yu. Karabach**, Centro de Química Estrutural, Instituto Superior Técnico, Universidade de Lisboa, Lisboa, Portugal

**Alexander M. Kirillov**, Centro de Química Estrutural, Instituto Superior Técnico, Universidade de Lisboa, Lisboa, Portugal

**Marina V. Kirillova**, Centro de Química Estrutural, Instituto Superior Técnico, Universidade de Lisboa, Lisboa, Portugal

**Maximilian N. Kopylovich**, Centro de Química Estrutural, Instituto Superior Técnico, Universidade de Lisboa, Lisboa, Portugal

**I.D. Kosenko**, A. N. Nesmeyanov Institute of Organoelement Compounds (INEOS), Russian Academy of Sciences, Moscow, Russia

**Karsten Krogh-Jespersen**, Department of Chemistry and Chemical Biology, Rutgers, The State University of New Jersey, New Brunswick, NJ, USA

**Philippe Kalck**, University of Toulouse, UPS, INSA, INPT, LCC, ENSIACET, Toulouse, France

**Vadim Yu. Kukushkin**, Department of Chemistry, St. Petersburg State University, St. Petersburg, Russia

**Maxim L. Kuznetsov**, Centro de Química Estrutural, Instituto Superior Técnico, Universidade de Lisboa, Lisboa, Portugal; Department of Chemistry, St. Petersburg State University, St. Petersburg, Russia

**Eric Labb  **, D  partement de Chimie, Ecole Normale Sup  rieure, Paris, France

**S  bastien Lachaize**, Laboratoire de physique et Chimie des Nano-Objets, Institut National des Sciences Appliqu  es-CNRS-Universit   Paul Sabatier, Universit   de Toulouse, Toulouse, France

**Lise-Marie Lacroix**, Laboratoire de physique et Chimie des Nano-Objets, Institut National des Sciences Appliqu  es-CNRS-Universit   Paul Sabatier, Universit   de Toulouse, Toulouse, France

**Patricia Lara**, CNRS, LCC (Laboratoire de Chimie de Coordination), Toulouse, France; UPS, INPT, LCC, Universit   de Toulouse, Toulouse, France

**Nicolas Lassauque**, University of Toulouse, UPS, INSA, INPT, LCC, ENSIACET, Toulouse, France

**Carole Le Berre**, University of Toulouse, UPS, INSA, INPT, LCC, ENSIACET, Toulouse, France

**Nikos Liakakos**, Laboratoire de physique et Chimie des Nano-Objets, Institut National des Sciences-Appliquées-CNRS-Université Paul Sabatier, Université de Toulouse, Toulouse, France

**Lanny S. Liebeskind**, Department of Chemistry, Emory University, Atlanta, GA, USA

**Bo Liu**, Organometallics, Materials and Catalysis department, Institut des Sciences Chimiques de Rennes, Université de Rennes, Rennes, France

**I. A. Lobanova**, A. N. Nesmeyanov Institute of Organoelement Compounds (INEOS), Russian Academy of Sciences, Moscow, Russia

**Jiří Ludvík**, J. Heyrovský Institute of Physical Chemistry, Academy of Sciences of the Czech Republic, Prague, Czech Republic

**Konstantin Luzyanin**, Centro de Química Estrutural, Instituto Superior Técnico, Universidade de Lisboa, Lisboa, Portugal; Department of Chemistry, St. Petersburg State University, St. Petersburg, Russia

**Kamran T. Mahmudov**, Centro de Química Estrutural, Instituto Superior Técnico, Universidade de Lisboa, Lisboa, Portugal

**Dalmo Mandelli**, Center for Natural and Human Science, Federal University of ABC, Santo André, Brazil

**Fabio Marchetti**, School of Science and Technology, Chemistry Section, S. Agostino 1, University of Camerino, Camerino, Italy

**Laurent Maron**, UPS, INPT, INSA, LCC, ENSIACET, University of Toulouse, Toulouse, France

**Enrique E. Maroto**, Departamento de Química Orgánica I, Universidad Complutense, Madrid, Spain

**Ana M. Martins**, Centro de Química Estrutural, Instituto Superior Técnico, Universidade de Lisboa, Lisboa, Portugal

**Luísa M. D. R. S. Martins**, Chemical Engineering Department, ISEL; Centro de Química Estrutural, Instituto Superior Técnico, Universidade de Lisboa, Lisboa, Portugal

**Nazario Martín**, Departamento de Química Orgánica I, Universidad Complutense; IMDEA Nanoscience, Madrid, Spain

**Ángel Martín-Domenech**, Departamento de Química Orgánica I, Universidad Complutense, Madrid, Spain

**Goreti Ribeiro Morais**, Unidade de Ciências Químicas e Radiofarmacêuticas, Campus Tecnológico e Nuclear, Instituto Superior Técnico, Universidade de Lisboa, Portugal

**Tânia S. Morais**, Centro de Ciências Moleculares e Materiais, Faculdade de Ciências da Universidade de Lisboa, Lisboa, Portugal

**Rui F. Munhá**, Centro de Química Estrutural, Instituto Superior Técnico, Universidade de Lisboa, Lisboa, Portugal

**Maria Graça P. M. S. Neves**, Department of Chemistry, University of Aveiro, Aveiro, Portugal

**Duc Hanh Nguyen**, University of Toulouse, UPS, INSA, INPT, LCC, ENSIACET, Toulouse, France

**Edward N. Nxumalo**, Department of Applied Chemistry, University of Johannesburg, Johannesburg, Doornfontein, South Africa

**Chun-Jern Pan**, Department of Chemical Engineering, National Taiwan University of Science and Technology, Taipei, Taiwan, Republic of China

**Luciano Pandolfo**, Department of Chemical Sciences, University of Padova, Padova, Italy

**Roberto Pattacini**, Laboratoire de Chimie de Coordination, Institut de Chimie, Université de Strasbourg, Strasbourg, France

**António Paulo**, Unidade de Ciências Químicas e Radiofarmacêuticas, Campus Tecnológico e Nuclear, Instituto Superior Técnico, Universidade de Lisboa, Portugal

**João Costa Pessoa**, Centro de Química Estrutural, Instituto Superior Técnico, Universidade de Lisboa, Lisboa, Portugal

**Claudio Pettinari**, School of Pharmacy, Chemistry Section, S. Agostino 1, University of Camerino, Camerino, Italy

**Riccardo Pettinari**, Schools of Pharmacy, Chemistry Section, S. Agostino 1, University of Camerino, Camerino, Italy

**Antoni Pietrzykowski**, Faculty of Chemistry, Warsaw University of Technology, Warsaw, Poland

**Karine Philippot**, CNRS, LCC (Laboratoire de Chimie de Coordination), Toulouse, France; UPS, INPT, LCC, Université de Toulouse, Toulouse, France

**Armando J. L. Pombeiro**, Centro de Química Estrutural, Instituto Superior Técnico, Universidade de Lisboa, Lisboa, Portugal

**Martin H. G. Prechtl**, Institute of Inorganic Chemistry, Department of Chemistry, University of Cologne, Cologne, Germany

**Michael F. Primik**, Institute of Inorganic Chemistry, University of Vienna, Vienna, Austria

**Zaozao Qiu**, Shanghai-Hong Kong Joint Laboratory in Chemical Synthesis, Shanghai Institute of Organic Chemistry, The Chinese Academy of Sciences, Shanghai, China; Department of Chemistry, The Chinese University of Hong Kong, Shatin, New Territories, Hong Kong, China

**John Rick**, Department of Chemical Engineering, National Taiwan University of Science and Technology, Taipei, Taiwan, Republic of China

**Carlos C. Romão**, Instituto de Tecnologia Química e Biológica António Xavier (ITQB), Universidade Nova de Lisboa, Oeiras, Portugal; Alfama Lda, Instituto de Biologia Experimental e Tecnológica (IBET), Oeiras, Portugal

**Antonio Romerosa**, Área de Química Inorgánica-CIESOL, University of Almeria, Almería, Spain

**João N. Rosa**, Research Institute for Medicines and Pharmaceutical Sciences (iMed.UL), Universidade de Lisboa, Lisboa, Portugal

**Beatriz Royo**, Instituto de Tecnologia Química e Biológica, Universidade Nova de Lisboa, Oeiras, Portugal

**Fábio M. F. Santos**, Research Institute for Medicines and Pharmaceutical Sciences (iMed.UL), Universidade de Lisboa, Lisboa, Portugal

**Isabel C. M. S. Santos**, Department of Chemistry, University of Aveiro, Aveiro, Portugal

**Isabel Santos**, Unidade de Ciências Químicas e Radiofarmacêuticas, Campus Tecnológico e Nuclear, Instituto Superior Técnico, Universidade de Lisboa, Lisboa, Portugal

**Sebastian Sahler**, Institute of Inorganic Chemistry, Department of Chemistry, University of Cologne, Cologne, Germany

**Yann Sarazin**, Organometallics, Materials and Catalysis department, Institut des Sciences Chimiques de Rennes, Université de Rennes, Rennes, France

**Franco Scalambra**, Área de Química Inorgánica-CIESOL, University of Almeria, Almería, Spain

**Philippe Serp**, University of Toulouse, UPS, INSA, INPT, LCC, ENSIACET, Toulouse, France

**Manuel Serrano-Ruiz**, Área de Química Inorgánica-CIESOL, University of Almeria, Almería, Spain

**Elena Shubina**, A. N. Nesmeyanov Institute of Organoelement Compounds (INEOS), Russian Academy of Sciences, Moscow, Russia

**Georgiy B. Shul'pin**, Semenov Institute of Chemical Physics, Russian Academy of Sciences, Moscow, Russia

**Lidia S. Shul'pina**, Nesmeyanov Institute of Organoelement Compounds, Russian Academy of Sciences, Moscow, Russia

**Mário M. Q. Simões**, Department of Chemistry, University of Aveiro, Aveiro, Portugal

**I. B. Sivaev**, A. N. Nesmeyanov Institute of Organoelement Compounds (INEOS), Russian Academy of Sciences, Moscow, Russia

**Piotr Sobota**, Faculty of Chemistry, University of Wrocław, Wrocław, Poland

**Katerina Soulantica**, Laboratoire de physique et Chimie des Nano-Objets, Institut National des Sciences Appliquées-CNRS-Université Paul Sabatier, Université de Toulouse, Toulouse, France

**Z. A. Starikova**, A. N. Nesmeyanov Institute of Organoelement Compounds (INEOS), Russian Academy of Sciences, Moscow, Russia

**We-Nein Su**, Graduate Institute of Applied Science and Technology, National Taiwan University of Science and Technology, Taiwan, Republic of China

**D. Suresh**, Centro de Química Estrutural, Instituto Superior Técnico, Universidade de Lisboa, Lisboa, Portugal

**M. Teresa Duarte**, Departamento de Engenharia Química, Instituto Superior Técnico, Universidade de Lisboa, Lisboa, Portugal

**Siden Top**, Chimie ParisTech (Ecole Nationale Supérieure de Chimie de Paris), Laboratoire Charles Friedel, Paris, France

**Alexandre F. Trindade**, Research Institute for Medicines and Pharmaceutical Sciences (iMed.UL), Universidade de Lisboa, Lisboa, Portugal

**Luis F. Veiros**, Centro de Química Estrutural, Instituto Superior Técnico, Universidade de Lisboa, Lisboa, Portugal

**Helena. L. A. Vieira**, Instituto de Biologia Experimental e Tecnológica (IBET), Oeiras, Portugal; Chronic Diseases Research Center (CEDOC), Faculdade de Ciências Médicas, Universidade Nova de Lisboa, Lisboa, Portugal

**Marc Visseaux**, ENSCL, Univ Lille Nord de France, Lille, France; USTL, Univ Lille Nord de France, Lille, France; CNRS, Univ Lille Nord de France, Lille, France

**Zuowei Xie**, Shanghai-Hong Kong Joint Laboratory in Chemical Synthesis, Shanghai Institute of Organic Chemistry, The Chinese Academy of Sciences, Shanghai, China; Department of Chemistry, The Chinese University of Hong Kong, Shatin, New Territories, Hong Kong, China

**Shuanming Zhang**, Laboratoire de Chimie de Coordination, Institut de Chimie, Université de Strasbourg, Strasbourg, France

**Piero Zanello**, Dipartimento di Chimica dell'Università di Siena, Siena, Italy

**Philippe Zinck**, ENSCL, Univ Lille Nord de France, Lille, France; USTL, Univ Lille Nord de France, Lille, France; CNRS, Univ Lille Nord de France, Lille, France

## **PART I**

---

### **ACTIVATION AND FUNCTIONALIZATION OF CARBON SINGLE BONDS AND OF SMALL MOLECULES**



---

# 1

---

## ORGANOMETALLIC COMPLEXES AS CATALYSTS IN OXIDATION OF C–H COMPOUNDS

GEORGIY B. SHUL'PIN

*Department of Kinetics and Catalysis, Semenov Institute of Chemical Physics, Russian Academy of Sciences, Moscow, Russia*

### 1.1 INTRODUCTION

Organometallic (i.e., containing  $\pi$  or  $\sigma$  metal–carbon bonds) derivatives of transition metals are known as *excellent catalysts* in reactions that do not involve the insertion of oxygen atoms [1]. They are used in (selected examples of recent publications are given) hydrogen/deuterium (H/D) exchange [2a], dehydrogenation [2b–e], homogeneous syngas conversion [2f], hydrosilylation [2g], carbonylation [2h], and homogeneous water gas shift reaction [2i]. In other recent works, complex  $[(Cp^*)Ru(IPr^*)Cl]$ , where  $Cp^* = \eta^5\text{-}C_5\text{Me}_5$  and  $IPr^* = 1,3\text{-bis}(2,6\text{-bis(diphenylmethyl)}\text{-}4\text{-methylphenyl})\text{imidazol-2-ylidene}$ , was used as a catalyst in the racemization of chiral alcohols [2j], neutral  $\eta^6$ -arene ruthenium complexes with monodentate P-donor ligands found to catalyze the transfer hydrogenation reaction [2k].

Organometallic catalysts were employed in oxidation reactions of some organic compounds. Thus, complex  $[CpMo(CO)_3CF_3]$  is a precatalyst for olefin epoxidation [3a], heterodinuclear ruthenium–iron complexes showed high activity for the catalytic oxidation of secondary alcohols with *tert*-butyl hydroperoxide to give ketones in aqueous media [3b]. In contrast, organometallic complexes were very rarely used as (pre)catalysts in oxygenation reactions of aromatic and saturated hydrocarbons [4a–e] (the latter can be called *noble gases of organic chemistry* because of their known inertness).

In various C–H oxygenation reactions, organometallic complexes can play the role of precatalyst. Compounds bearing carbon–metal bonds can also be some of intermediate compounds in the catalytic cycles. In this chapter, we discuss reactions in which an organometallic complex catalyzes the insertion of oxygen atoms into C–H bonds of hydrocarbons or other organic compounds. The focus will be made on the author's own works.

### 1.2 OXYGENATION REACTIONS WITH OXIDANTS OTHER THAN PEROXIDES

The first example of a metal-catalyzed oxygen atom insertion into the C–H bond was the reaction found by Shilov and Shtainman and their coworkers in 1972 (for reviews, see References 1h and 5). These authors demonstrated that  $Pt^{II}Cl_4^{2-}$  ion could catalyze H/D exchange in methane in a  $D_2O/CD_3COOD$  solution and, if  $Pt^{IV}Cl_6^{2-}$  is added, the latter oxidizes methane to methanol (Shilov chemistry). The catalytic cycle in which  $\sigma$ -methyl complexes of platinum(II) and platinum(IV) are involved is shown in Fig. 1.1.

Later, Periana and coworkers proposed (2,2'-bipyrimidyl)platinum(II)dichloride as a catalyst ("Periana system"; see a recent review [4d]). Fuming sulfuric acid is the oxidant in this case. A simplified scheme of the catalytic cycle is shown in Fig. 1.2. It can be seen that some intermediates contain  $\sigma$ -methyl-platinum bonds.

Complexes containing the fragment  $Cp^*Ir$  ( $Cp^*$  is pentamethylcyclopentadienyl) are active precatalysts in the C–H oxidation of *cis*-decalin and cyclooctane. Ceric ammonium nitrate was a sacrificial oxidant and water was the oxygen source

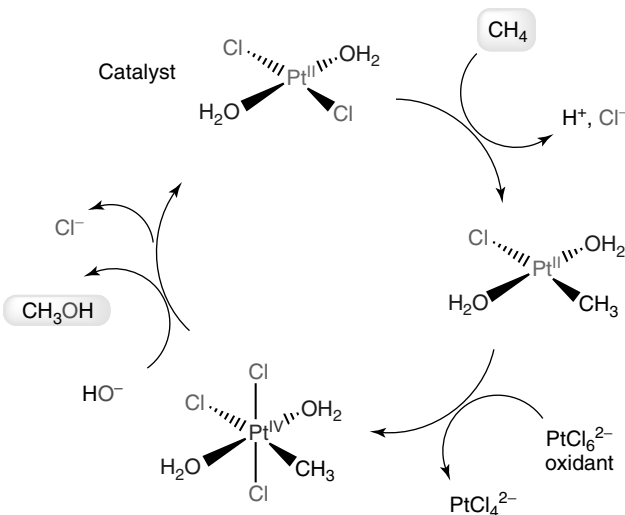


**Figure 1.1** The catalytic cycle proposed for the methane oxidation to methanol by  $\text{Pt}^{\text{IV}}\text{Cl}_6^{2-}$  catalyzed by  $\text{Pt}^{\text{II}}\text{Cl}_4^{2-}$ .

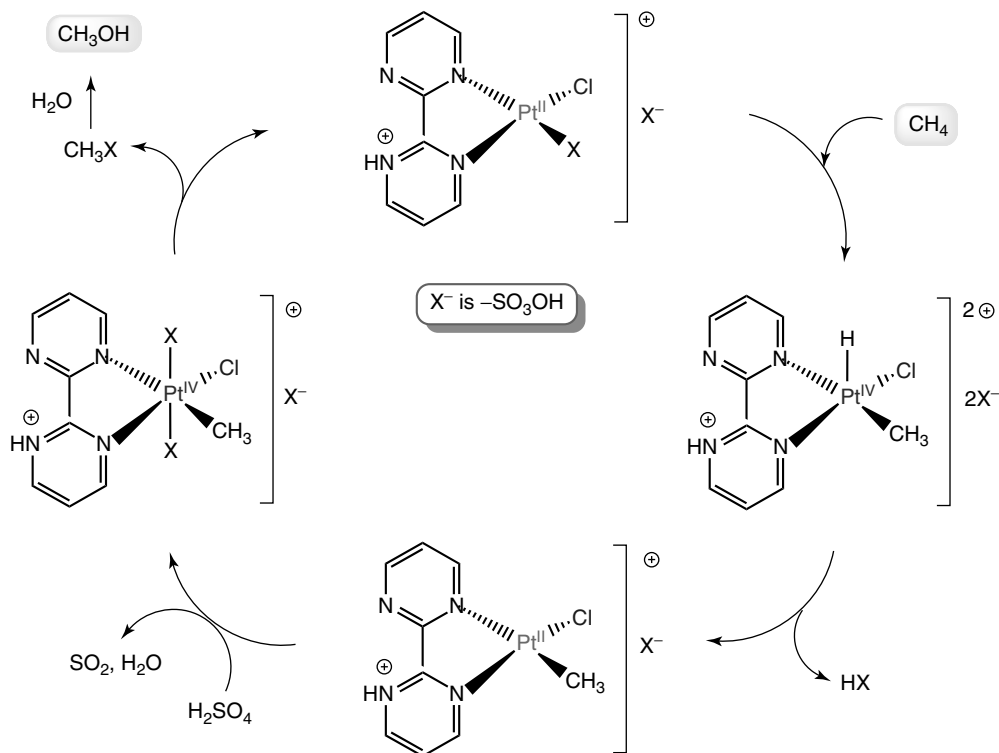


**Figure 1.2** The simplified catalytic cycle for the methane oxidation by the Periana system. Adapted from Reference 4d.

(Fig. 1.3). Calculations using the Density functional theory (DFT) method showed that the C–H oxidation of *cis*-decalin by  $\text{Cp}^*\text{Ir}(\text{ppy})(\text{Cl})$  (ppy = *o*-phenylpyridine) follows a direct oxygen insertion mechanism on the singlet potential energy surface [6]. The authors proposed that some of intermediate species contain the  $\text{Cp}^*$  ring coordinated to the iridium ion. The authors also made a general conclusion: oxidation catalysis by organometallic species can be hard to interpret because of the possibility that the real catalyst is an oxidation product of the precursor.

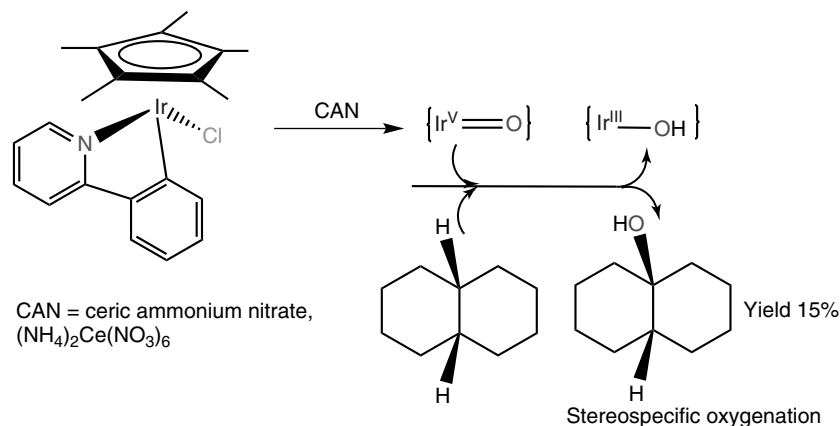


**Figure 1.3** Stereospecific oxygenation of *cis*-decalin catalyzed by the Ir organometallic derivative [6].

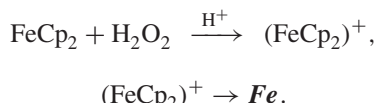
Indeed, organometallic precatalysts can be transformed during an induction period into catalytically active species that do not contain metal–carbon bonds. For example, molybdenum [7a] and tungsten [7b] carbonyls catalyze aerobic photooxygenation of cyclohexane to cyclohexyl hydroperoxide (primary product) and cyclohexanol and cyclohexanone (Fig. 1.4). The proposed mechanism is shown in Fig. 1.5. It includes the formation during the induction period of an oxo derivative. Complexes  $\text{CpFe}(\pi\text{-PhH})\text{BF}_4$  and  $(\pi\text{-durene})_2\text{Fe}(\text{BF}_4)_2$  also catalyzed the aerobic alkane photooxygenation [7c]. The mechanism has not been studied.

### 1.3 OXYGENATION OF C–H BONDS WITH PEROXIDES

In the course of our systematic studies of hydrocarbon oxidation with peroxides, we have found a few organometallic catalysts and systems based on organometallic compounds. In some cases, these systems turned out to be extremely efficient, much more efficient than systems containing “simple” salts of transition metals.

Recently, we have discovered [8], for the first time, that ferrocene (catalyst **1.1**) is an efficient (pre)catalyst for several types of oxidative transformations, namely, the oxidation of alkanes and benzene by  $\text{H}_2\text{O}_2$  or *tert*-butyl hydroperoxide. The oxidation of gaseous and liquid alkanes to alkyl hydroperoxides by  $\text{H}_2\text{O}_2$  proceeds in MeCN at 50 °C. An obligatory cocatalyst is pyrazine-2-carboxylic acid (PCA, or H<sub>pca</sub>, where H is a proton and pca is the anion of PCA). In the cyclohexane oxidation, the yield and TON after 1.5 h attained 32% and 1200, respectively. In the ethane oxidation, TON reached 970. Maximum yield (58% based on the alkane) was obtained for the *n*-butane oxidation after 4 h.

The simplest kinetic scheme of the alkane oxygenation based on the kinetic data was proposed. In the first stage, ferrocene  $\text{FeCp}_2$  is oxidized to ferricinium cation ( $\text{FeCp}_2^+$ ), which is in turn transformed into species **Fe** that is a fragment containing one iron ion.



These are the fast stages of the generation from  $\text{FeCp}_2$  and  $\text{H}_2\text{O}_2$  the main species, which is active in the catalytic process. Produced fragment **Fe** interacts with a PCA molecule to form the complex **Fe**(PCA):



Here (PCA) is a PCA fragment (possibly pyrazinecarboxylate, pca). The formed complex can react with the second PCA molecule yielding in this case an adduct containing two PCA fragments per one Fe ion:



Two adducts **Fe**(PCA) can dimerize to afford the dinuclear complex  $\mathbf{Fe}_2(\text{PCA})_2$ :



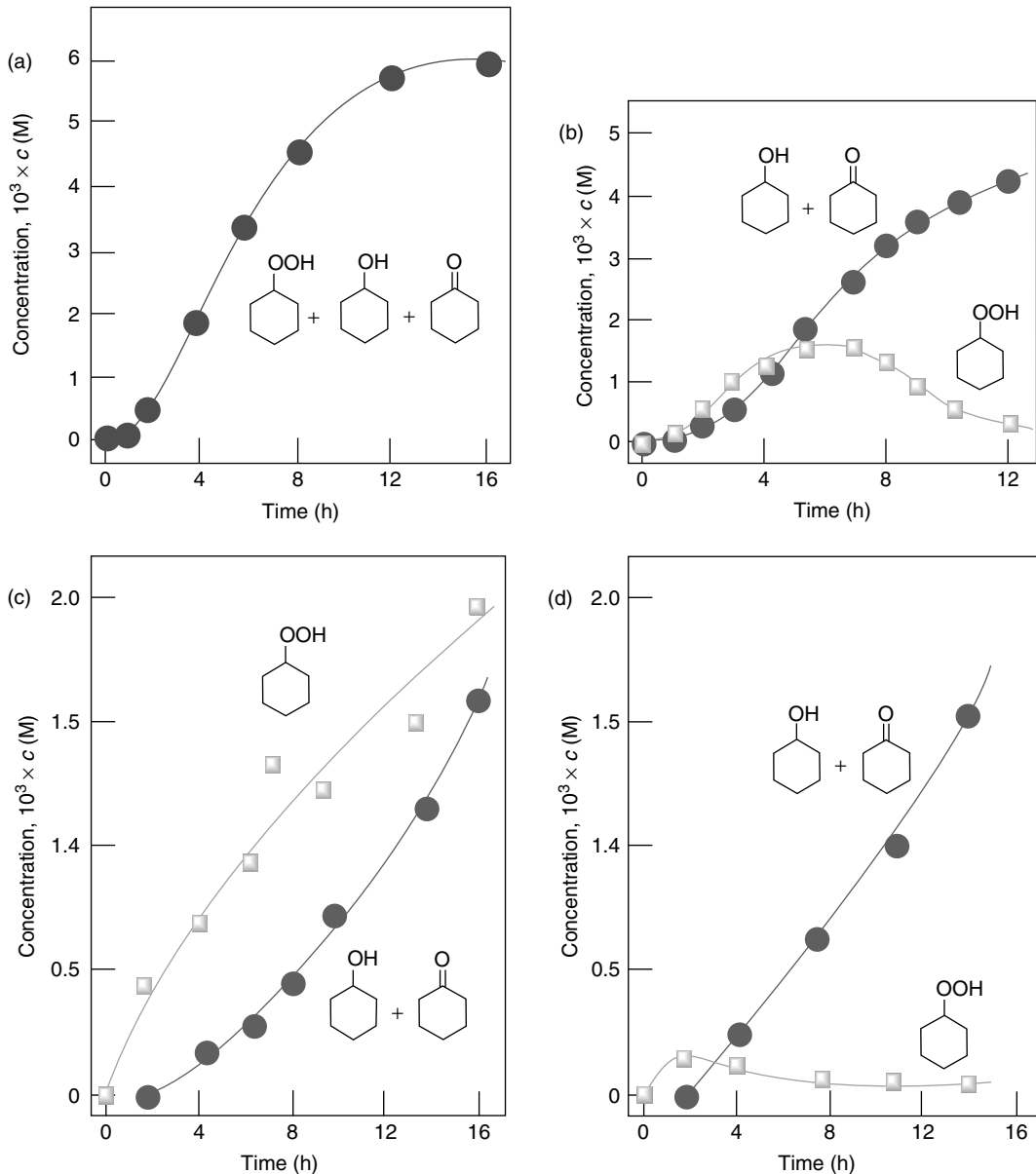


**Figure 1.4** Oxidation of cyclohexane (CyH, 0.46 M) to cyclohexyl hydroperoxide, cyclohexanol, and cyclohexanone with air under irradiation with full light of high pressure Hg arc (1000 W) in MeCN (15 °C). Photocatalysts ( $5 \times 10^{-4}$  M) : M(CO)<sub>6</sub> (where M = Mo, graph a [7a] and W, graph b [7b]) and complexes CpFe( $\pi$ -PhH)BF<sub>4</sub> (graph c) and ( $\pi$ -durene)<sub>2</sub>Fe(BF<sub>4</sub>)<sub>2</sub> (graph d) [7c] are shown.

Complex  $\text{Fe}_2(\text{PCA})_2$  is a catalytically active species that produces hydroxyl radicals from  $\text{H}_2\text{O}_2$ :



Hydroxyl radicals react in parallel routes with solvent (acetonitrile) and substrate (cyclohexane, RH):



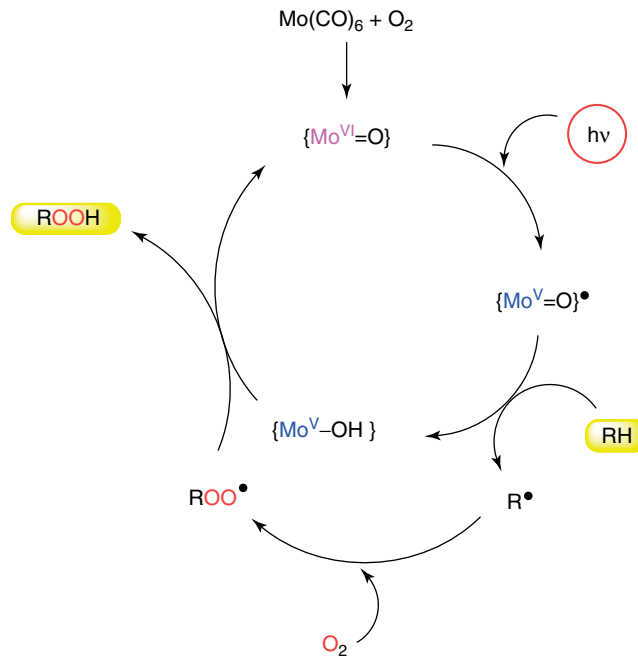


**Figure 1.5** Mechanism proposed for the photooxygenation of alkanes,  $\text{RH}$ , in the presence of Mo or W carbonyls. (See insert for color representation of the figure.)

The last reaction is the rate-limiting step in the sequence of alkane transformations into cyclohexyl hydroperoxide. If we assume that the concentration of  $\text{HO}^\bullet$  is quasi-stationary and concentrations of all iron complexes are in quasi-equilibrium and take into account conditions  $[\text{Fe}(\text{PCA})] \ll [\text{FeCp}_2]_0$  and  $[\text{Fe}_2(\text{PCA})_2] \ll [\text{FeCp}_2]_0$ , we obtain the equation for the initial reaction rate as follows:

$$W_0 = \frac{k_4[\text{Fe}_2(\text{PCA})_2][\text{H}_2\text{O}_2]_0}{1 + k_5[\text{MeCN}]/k_6[\text{RH}]_0},$$

where

$$[\text{Fe}_2(\text{PCA})_2] = K_3[\text{Fe}(\text{PCA})]^2,$$

and

$$[\text{Fe}(\text{PCA})] = \frac{K_1[\text{FeCp}_2]_0[\text{PCA}]_0}{1 + K_1 K_2 [\text{PCA}]_0^2}.$$

We can rewrite the equation for the initial reaction rate in the following form:

$$W_0 = \frac{\alpha[\text{PCA}]_0^2}{(1 + \beta [\text{PCA}]_0^2)^2},$$

where

$$\alpha = \frac{k_4[\text{H}_2\text{O}_2]_0(K_1[\text{FeCp}_2]_0)^2}{1 + k_5[\text{MeCN}]/k_6[\text{RH}]_0},$$

and

$$\beta = K_1 K_2.$$

The following values  $\alpha = 30 \text{ M}^{-1} \text{s}^{-1}$  and  $\beta = 1.1 \times 10^5 \text{ M}^{-2}$  have been calculated for the conditions of our experiments. Using these values for parameters  $\alpha$  and  $\beta$ , the initial reaction rates (presented by a dotted curve) have been calculated at different concentrations of PCA under conditions described in the caption of Fig. 1.6b.

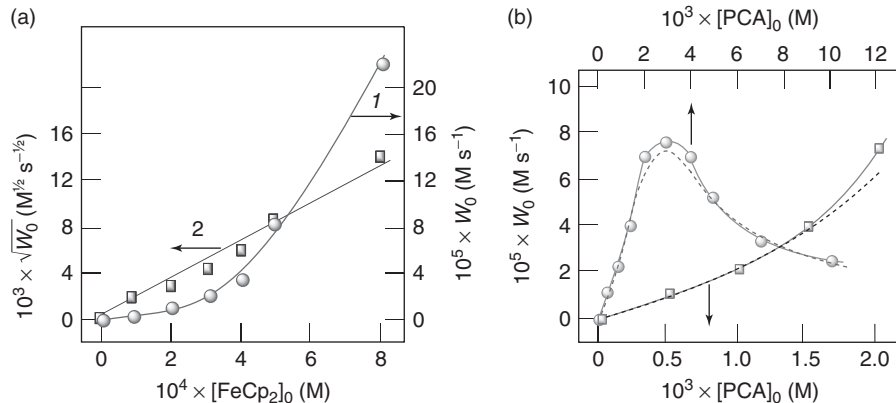


**Figure 1.6** (a) Dependence of the initial rate  $W_0$  of oxygenate accumulation in the cyclohexane oxidation with  $H_2O_2$  catalyzed by ferrocene **1.1** in MeCN on the initial concentration of ferrocene (curve 1). Conditions:  $[PCA]_0 = 3 \times 10^{-3} M$ ,  $[H_2O_2]_0 = 0.32 M$ ,  $[cyclohexane]_0 = 0.37 M$ ,  $50^\circ C$ . Curve 2: linearization of curve 1 in coordinates  $[FeCp_2]_0 - W_0^{1/2}$ . (b) Dependence of the initial rate  $W_0$  of oxygenate accumulation in the cyclohexane oxidation with  $H_2O_2$  catalyzed by **1.1** in MeCN on the initial concentration of PCA (in the intervals  $0 - 10 \times 10^{-3} M$  and  $0 - 2 \times 10^{-3} M$ ). Conditions:  $[FeCp_2]_0 = 5.0 \times 10^{-4} M$ ,  $[H_2O_2]_0 = 0.32 M$ ,  $[cyclohexane]_0 = 0.37 M$ ,  $50^\circ C$ . Dotted curves present the simulated dependences.

*tert*-Butyl hydroperoxide (0.58 M; 70% aqueous) oxidizes cyclohexane (0.92 M) in MeCN at  $50^\circ C$  in the presence of **1.1** ( $1 \times 10^{-3} M$ ) and PCA ( $25 \times 10^{-3} M$ ), affording (after reduction with  $PPPh_3$ ) cyclohexanol (0.02 M) and cyclohexanone (0.001 M) after 4.5 h. Heating a solution of benzene (0.58 M) with  $H_2O_2$  (1.28 M) in MeCN at  $50^\circ C$  in the presence of **1.1** ( $5 \times 10^{-4} M$ ) and PCA ( $1 \times 10^{-2} M$ ) gave phenol (0.038 M after 1 h). In the presence of 2,2'-bipyridine ( $4 \times 10^{-3} M$ ) instead of PCA, **1.1** ( $5 \times 10^{-4} M$ ) catalyzes the oxygenation with  $H_2O_2$  (1.28 M) of benzene (0.58 M) to phenol (0.05 M after 3 h) with a long induction period.

We also found recently [8] the first example of alkane hydrocarboxylation in aqueous acetonitrile with the  $CO/S_2O_8^{2-}/H_2O$  system catalyzed by an iron complex, that is, ferrocene (Table 1.1). For example, the reaction of propane (1 atm) with CO (10 atm) at  $60^\circ C$  during 4 h gave isomeric butyric acids in 60% total yield.

Another metallocene, namely, decamethylosmocene,  $(Me_5C_5)_2Os$  (catalyst **1.2**), turned out to be a good precatalyst in a very efficient oxidation of alkanes with hydrogen peroxide in acetonitrile at  $20 - 60^\circ C$  [9]. The reaction proceeds with a substantial lag period that can be reduced by the addition of pyridine in a small concentration. Alkanes, RH, are oxidized primarily to the corresponding alkyl hydroperoxides, ROOH. TONs attain 51,000 in the case of cyclohexane (maximum turnover frequency was  $6000 h^{-1}$ ) and 3600 in the case of ethane. The oxidation of benzene and styrene afforded phenol and benzaldehyde, respectively. A kinetic study of cyclohexane oxidation catalyzed by **1.2** and selectivity parameters (measured in the oxidation of *n*-heptane, methylcyclohexane, isoctane, *cis*-dimethylcyclohexane, and *trans*-dimethylcyclohexane) indicated that the oxidation of saturated, olefinic, and aromatic hydrocarbons proceeds with the participation of hydroxyl radicals.

We discovered [10] that triosmium dodecacarbonyl (compound **1.3**, Fig. 1.7) catalyzes a very efficient oxidation of alkanes by  $H_2O_2$  in MeCN to afford alkyl hydroperoxides (primary products) as well as alcohols and ketones (aldehydes) at  $60^\circ C$  if pyridine is added in a low concentration. TONs attained 60,000 (Fig. 1.8a) and turnover frequencies were up to  $24,000 h^{-1}$ . A plateau in the dependence of  $W_0$  on initial concentration of cyclooctane,  $[RH]$  (Fig. 1.8b), indicates that there is a competition between RH and another component of the reaction mixture for a transient oxidizing species. Indeed, at high concentration of the hydrocarbon, all oxidizing species are accepted by RH and the maximum possible oxidation rate is attained. This concurrence can be described by the following kinetic scheme:



**TABLE 1.1** Hydrocarboxylation of Alkanes by the 1.1/CO/K<sub>2</sub>S<sub>2</sub>O<sub>8</sub> System<sup>a</sup>

Alkane <sup>b</sup> , atm; mmol	CO, atm	Products	Yield, %	Total Yield, %
<i>Cyclohexane</i> <sup>c</sup>				
1.0	20	<i>c</i> -C <sub>6</sub> H <sub>11</sub> COOH	18.3	19.4
		<i>c</i> -C <sub>6</sub> H <sub>11</sub> OH	0.8	
		<i>c</i> -C <sub>6</sub> H <sub>10</sub> O	0.3	
<i>n</i> -Heptane <sup>d</sup>				
1.0	20	Me(CH <sub>2</sub> ) <sub>6</sub> COOH	0.3	9.2
		MeCH(COOH)(CH <sub>2</sub> ) <sub>4</sub> Me	3.6	
		EtCH(COOH)(CH <sub>2</sub> ) <sub>3</sub> Me	3.5	
		Me(CH <sub>2</sub> ) <sub>2</sub> CH(COOH)(CH <sub>2</sub> ) <sub>2</sub> Me	1.8	
<i>n</i> -Hexane <sup>d</sup>				
1.0	20	Me(CH <sub>2</sub> ) <sub>5</sub> COOH	0.4	8.3
		MeCH(COOH)(CH <sub>2</sub> ) <sub>3</sub> Me	4.0	
		EtCH(COOH)(CH <sub>2</sub> ) <sub>2</sub> Me	3.9	
<i>n</i> -Pentane <sup>d</sup>				
1.0	20	Me(CH <sub>2</sub> ) <sub>4</sub> COOH	0.8	12.6
		MeCH(COOH)(CH <sub>2</sub> ) <sub>2</sub> Me	8.2	
		EtCH(COOH)Et	3.6	
<i>n</i> -Butane				
0.75 <sup>e</sup>	10	EtCH(Me)COOH	19	21
		Me(CH <sub>2</sub> ) <sub>3</sub> COOH	2	
Propane				
6	20	Me <sub>2</sub> CHCOOH	17	19
		Me(CH <sub>2</sub> ) <sub>2</sub> COOH	2	
1 <sup>e</sup>	10	Me <sub>2</sub> CHCOOH	51	60
		Me(CH <sub>2</sub> ) <sub>2</sub> COOH	9	
Ethane				
10	20	EtCOOH	9	9
1 <sup>e</sup>	10	EtCOOH	15	15

Adapted from Reference 8.

<sup>a</sup>Conditions. Amounts: ferrocene **1.1**, 4 × 10<sup>-3</sup> mmol; K<sub>2</sub>S<sub>2</sub>O<sub>8</sub>, 1.5 mmol; MeCN, 4 ml; H<sub>2</sub>O, 2 ml; 60 °C, 4 h. Volume of the autoclave was 13 ml. Yield is based on the alkane.

<sup>b</sup>Amounts as pressure for gaseous ethane, propane, and *n*-butane and as mmol for other alkanes are given.

<sup>c</sup>At 50 °C; CH<sub>3</sub>CN, 3 ml; H<sub>2</sub>O, 3 ml.

<sup>d</sup>Regioselectivity parameters C(1):C(2):C(3):C(4) for pentane, hexane, and heptane are 1:15:14, 1:15:15, and 1:18:18:18, respectively.

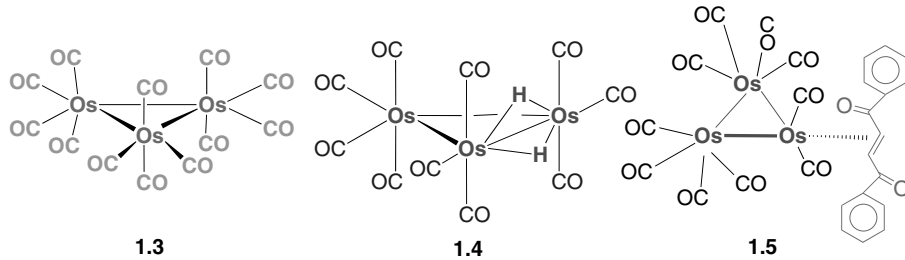
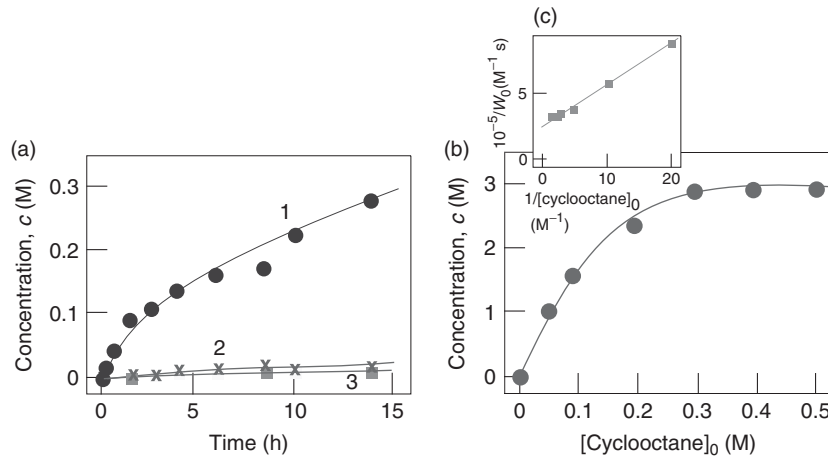
<sup>e</sup>K<sub>2</sub>S<sub>2</sub>O<sub>8</sub>, 1.0 mmol.



where  $W_i$  is the rate of generation of oxidizing species X. The analysis of this scheme in a quasi-stationary approximation relative to species X leads to the following equation:

$$W_0 = \frac{d[\text{ROOH}]}{dt} = \frac{W_i}{1 + \frac{k_2[\text{py}] + k_3[H_2O_2] + k_4[\text{MeCN}]}{k_1[\text{RH}]}}.$$

In accord with the last equation, we can see the linear dependence of the experimentally measured reciprocal parameter  $1/W_0$  on reciprocal concentration  $1/[\text{RH}]_0$  (Fig. 1.8c). The tangent of this straight line slope angle corresponds to the value

**Figure 1.7** Efficient oxidation catalysts based on osmium carbonyls.**Figure 1.8** (a) Kinetic curves of accumulation of cyclooctyl hydroperoxide (curve 1), cyclooctanone (curve 2), and cyclooctanol (curve 3) in the cyclooctane (0.5 M) oxidation with H<sub>2</sub>O<sub>2</sub> catalyzed by Os<sub>3</sub>(CO)<sub>12</sub> (**1.3**) in MeCN at 60 °C. Concentrations of the three products were measured using a simple method, previously developed by us [10–12] with the reduction of samples with PPh<sub>3</sub>. (b) Dependence of  $W_0$  on the initial concentration of cyclooctane ([**1.3**]<sub>0</sub> = 5 × 10<sup>-5</sup> M). (c) Linearization of dependence shown in (b) using coordinates  $1/W_0 - 1/[cyclooctane]_0$ . Adapted from Reference 10(a).

$(k_2[\text{py}] + k_3[\text{H}_2\text{O}_2] + k_4[\text{MeCN}])/k_1 W_i$ . The segment that is cut off by the line on  $Y$ -axis is equal to  $1/W_i$ . Thus, we can calculate the following value:

$$\frac{k_2[\text{py}] + k_3[\text{H}_2\text{O}_2] + k_4[\text{MeCN}]}{k_1} = 0.14.$$

At our conditions [py] = 0.1 M, [H<sub>2</sub>O<sub>2</sub>] = 2 M, and [MeCN] ≈ 18 M, we can calculate the following parameters (s<sup>-1</sup>) for different data found in the literature:  $k_2[\text{py}] = 2.3 \times 10^8$  or  $4.5 \times 10^8$ ,  $k_3[\text{H}_2\text{O}_2] = (9 \pm 2.8) \times 10^7$ , and  $k_4[\text{MeCN}] = 6.4 \times 10^7$  or  $3.9 \times 10^8$ . It follows from this estimation that the most probable competitors of cyclooctane for hydroxyl radicals are pyridine and acetonitrile. Rate constants (M<sup>-1</sup> s<sup>-1</sup>) can be calculated as follows:  $k_1 = 1.6 \times 10^9$  or  $3.2 \times 10^9$  in the case of pyridine and  $k_1 = 4.5 \times 10^8$  or  $2.8 \times 10^9$  in the case of acetonitrile. These values are typical for the reactions of hydroxyl radicals with alkanes:  $k_1 = 1.2 \times 10^9$  for cyclopentane,  $k_1 = 1.3 \times 10^9$  for cyclohexane, and  $k_1 = 1.6 \times 10^9$  for cycloheptane in aqueous solution. It can be seen that the experimentally found competition is in good agreement with the assumption that the oxidizing species in our system is hydroxyl radical. Radical HO<sup>•</sup> attacks the hydrocarbon RH to generate alkyl radical R<sup>•</sup>, which very rapidly reacts with molecular oxygen.

Similar trinuclear carbonyl hydride cluster, Os<sub>3</sub>(CO)<sub>10</sub> ( $\mu$ -H)<sub>2</sub> (compound **1.4**), catalyzes the oxidation of cyclooctane to cyclooctyl hydroperoxide by hydrogen peroxide in acetonitrile solution [12]. Selectivity parameters obtained in oxidations of various linear and branched alkanes as well as kinetic features of the reaction indicated that the alkane oxidation occurs with the participation of hydroxyl radicals. A similar mechanism operates in the transformation of benzene into phenol and styrene into benzaldehyde. The system also oxidizes 1-phenylethanol to acetophenone. The kinetic study

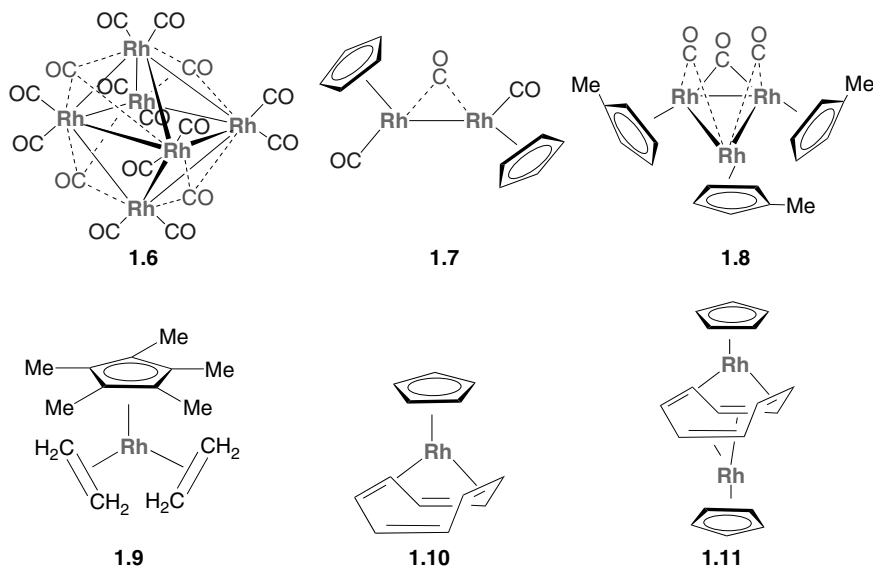


**Figure 1.9** Compound **1.6** is an efficient catalyst for the benzene oxidation, compounds **1.7** and **1.8** are less efficient, and compounds **1.9**, **1.10**, and **1.11** are inactive.

led to a conclusion that the oxidation of alcohols does not involve hydroxyl radicals as the main oxidizing species and apparently proceeds with the participation of osmyl species, “Os = O.” Finally, a carbonyl osmium(0) complex with  $\pi$ -coordinated olefin, (2, 3- $\eta$ -1,4-diphenylbut-2-en-1,4-dione)undecacarbonyl triangulotriosmium (**1.5**, Fig. 1.7), catalyzes the oxygenation of alkanes (cyclohexane, cyclooctane, *n*-heptane, isoctane, etc.) with hydrogen peroxide, as well as with *tert*-butyl hydroperoxide and *meta*-chloroperoxybenzoic acid in acetonitrile solution [13]. “Simple” osmium salts ( $\text{OsCl}_3$ ,  $\text{Na}_2\text{OsCl}_6$ ) also catalyze (especially in the presence of pyridine or other N-bases) alkane hydroperoxidation with  $\text{H}_2\text{O}_2$  in acetonitrile [14a] or water [14b], but these reactions are less efficient in comparison with processes catalyzed by organoosmium compounds.

Hexanuclear rhodium carbonyl cluster,  $\text{Rh}_6(\text{CO})_{16}$  (compound **1.6**, Fig. 1.9), catalyzes benzene hydroxylation with hydrogen peroxide in acetonitrile solution [15a]. Phenol and quinone (in less concentration) are formed with the maximum attained total yield and TON of 17% and 683, respectively. It is noteworthy that certain other rhodium carbonyl complexes, containing cyclopentadienyl ligands,  $\text{Rh}_2\text{Cp}_2(\text{CO})_3$  (**1.7**) and  $\text{Rh}_3(\text{CpMe})_3(\text{CO})_3$  (**1.8**), are less efficient catalysts, whereas cyclopentadienyl derivatives of rhodium, which do not contain the carbonyl ligands,  $\text{Rh}(\text{CpMe}_5)(\text{CH}_2 = \text{CH}_2)_2$  (**1.9**),  $\text{RhCp}(\text{cyclooctatetraene})$  (**1.10**) and  $\text{Rh}_2\text{Cp}_2(\text{cyclooctatetraene})$  (**1.11**), turned out to be absolutely inactive in the benzene hydroxylation. In the presence of compound **1.6**, styrene is transformed into benzaldehyde and (in less concentration) acetophenone and 1-phenylethanol. Addition of acids is known to accelerate some metal-catalyzed oxidation reactions. In our case, when trifluoroacetic acid was added to the reaction solution catalyzed by cluster **1.6**, the initial reaction rate was approximately three times higher. It should be emphasized that no oxygenated products have been detected when alkanes were used as substrates in the **1.6**-catalyzed oxidation. Ethyl groups in ethylbenzene were also not oxygenated. It has been tentatively assumed that the interaction of cluster **1.6** with hydrogen peroxide leads to splitting Rh–Rh and Rh–CO bonds to form vacant sites that coordinate benzene molecules. Possibly, the **Rh**–CO fragment is oxidized in the initial period of the reaction to afford **Rh**–C(O)OH and **Rh**–C(O)OOH species. The catalytic cycle presented in Fig. 1.10 was proposed for the oxidation reaction. In the initial period, a rhodium complex under the action of hydrogen peroxide and water is transformed into a hydroxy derivative A. The interaction of species A with hydrogen peroxide affords a hydroperoxo derivative B. The latter forms a  $\pi$ -arene complex C. Species C can be converted into rhodadioxolane D, which decomposes further to produce phenol and initial catalytically active species A.

Cyclopentadienylbenzeneiridium(III) tetrafluoroborate [ $\pi\text{-C}_5\text{H}_5\text{Ir}(\pi\text{-C}_6\text{H}_6)\text{](BF}_4)_2$ ] (complex **1.12**) was completely inactive in oxidation with hydrogen peroxide and *tert*-butyl hydroperoxide but exhibited a moderate activity in oxidation with *m*-chloroperoxybenzoic acid at room temperature [15b]. The  $\text{H}_2\text{O}_2$ –**1.12** system showed a moderate activity in the oxidation of secondary alcohols. For example, cyclohexanol was oxidized at room temperature to cyclohexanone (30% yield for 6 h) when a fourfold excess of PCA as a cocatalyst was added to the reaction solution.

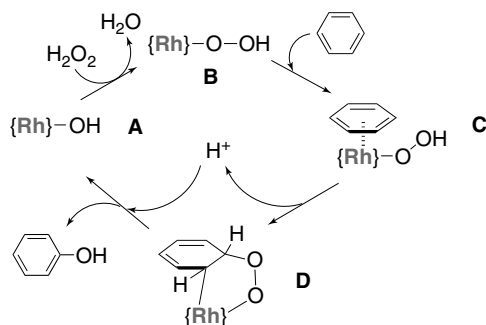


**Figure 1.10** A catalytic cycle proposed for the benzene hydroxylation catalyzed by a rhodium complex ( $\{\text{Rh}\}$  is a Rh-containing fragment). Adapted from Reference 15a.

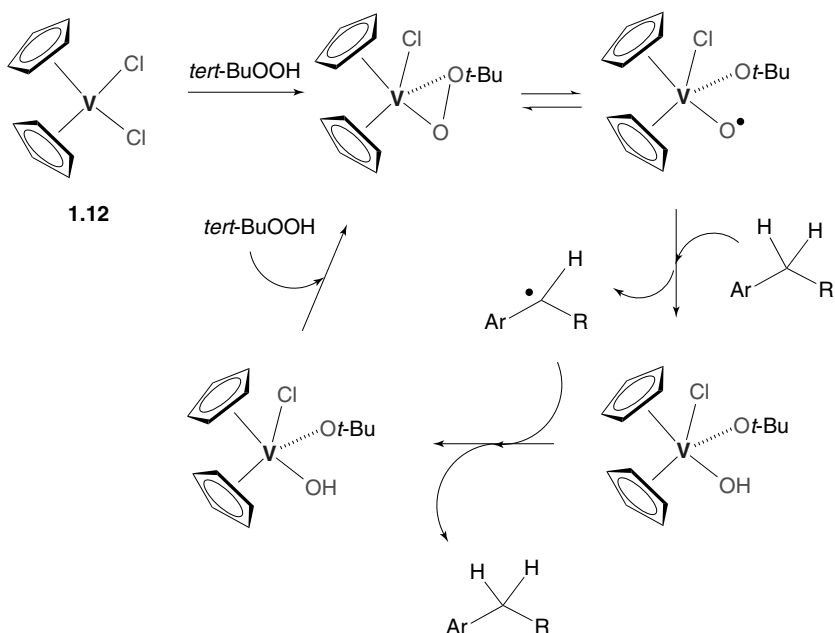


**Figure 1.11** A catalytic cycle proposed for the benzyl hydroxylation catalyzed by vanadium complex **1.12**. Adapted from Reference 16.

It has been shown recently that cyclopentadienyl vanadium complexes catalyze the oxidation of benzylic groups by *tert*-BuOOH [16]. Compound  $\text{Cp}_2\text{VCl}_2$  (**1.12**) catalyzes benzylic C–H oxidation selectively and effectively, giving no aromatic oxidation products. The authors assume that intermediate catalytically active species contain Cp rings (Fig. 1.11).

#### 1.4 CONCLUSIONS AND OUTLOOK

It is clearly seen from this chapter that organometallic complexes are not leading catalysts for various reactions that afford valuable oxygenates from hydrocarbons and other C–H compounds. Such complexes are usually expensive and their synthesis is often not simple. However, in some cases, organometallics outrival commercially available inorganic salts in activity and selectivity. One can expect that the research on the application of organometallic catalysts in oxidation reactions will continue in the future.

#### ACKNOWLEDGMENT

This work was supported by the Russian Foundation for Basic Research (Grant 12-03-00084-a).

## REFERENCES

1. (a) Steinborn, D. *Fundamentals of Organometallic Catalysis*; Wiley-VCH: Weinheim, **2012**; (b) Pignataro, B., Ed.; *New Strategies in Chemical Synthesis and Catalysis*, Wiley-VCH, Weinheim, **2012**; (c) Basset, J. -M.; Psaro, R.; Roberto, D.; Ugo, R., Eds.; *Modern Surface Organometallic Chemistry*; Wiley-VCH: Weinheim, **2009**; (d) Bolm, C.; Hahn, F. E., Eds.; *Activating Unreactive Substrates*, Wiley-VCH: Weinheim, **2009**; (e) Togni, A.; Hayashi, T., Eds.; *Ferrocenes: Homogeneous Catalysis, Organic Synthesis, Materials Science*, John Wiley & Sons, Inc.: Chichester, E-book, **2008**; (f) Beller, M.; Bolm C., Eds.; *Transition Metals for Organic Synthesis*, Wiley-VCH: Weinheim, **2004**; (g) Cornils, B.; Herrmann, W. A., Eds.; *Aqueous-Phase Organometallic Catalysis*, Wiley-VCH: Weinheim, **2004**; (h) Cornils, B.; Herrmann, W. A., Eds.; *Applied Homogeneous Catalysis with Organometallic Compounds*, Wiley-VCH: Weinheim, **2002**; (i) Shilov, A. E.; Shul'pin, G. B. *Activation and Catalytic Reactions of Saturated Hydrocarbons in the Presence of Metal Complexes*, Kluwer Academic Publishers: Dordrecht/Boston/London, **2000**; (j) Crabtree, R. H. *Organometallics* **2011**, *30*, 17; (k) Hillard, E. A.; Jaouen, G. *Organometallics* **2011**, *30*, 20.
2. (a) Iluc, V. M.; Fedorov, A.; Grubbs, R. H. *Organometallics* **2012**, *31*, 39; (b) Choi, J.; MacArthur, A. H. R.; Brookhart, M.; Goldman, A. S. *Chem. Rev.* **2011**, *111*, 1761; (c) Haibach, M. C.; Kundu, S.; Brookhart, M.; Goldman, A. S. *Acc. Chem. Res.* **2012**, *45*, 947; (d) Grellier, M.; Sabo-Etienne, S. *Chem. Commun.* **2012**, *48*, 34; (e) Barrata, W.; Bossi, G.; Putignano, E. *Chimica Oggi* **2012**, *30*, 48; (f) West, N. M.; Miller, A. J. M.; Labinger, J. A.; Bercaw, J. E. *Coord. Chem. Rev.* **2011**, *255*, 881; (g) Castro, L. C. M.; Sortais, J. -B.; Darcel, C. *Chem. Commun.* **2012**, *48*, 151; (h) Lassauque, N.; Davin, T.; Nguyen, D. H.; Adcock, R. J.; Coppel, Y.; Le Berre, C.; Serp, P.; Maron, L.; Kalck, P. *Inorg. Chem.* **2012**, *51*, 4; (i) Kuriakose, N.; Kadam, S.; Vanka, K. *Inorg. Chem.* **2012**, *51*, 377; (j) Balogh, J.; Slawin, A. M. Z.; Nolan, S. P. *Organometallics* **2012**, *31*, 3259; (k) Grabulosa, A.; Mannu, A.; Alberico, E.; Denurra, S.; Gladiali, S.; Muller, G. *J. Mol. Catal. A: Chem.* **2012**, *363–364*, 49–57.
3. (a) Hauser, S. A.; Cokoja, M.; Drees, M.; Kühn, F. E. *J. Mol. Catal. A: Chem.* **2012**, *363–364*, 237–244; (b) Tauchman, J.; Therrien, B.; Süss-Fink, G.; Štěpnička, P. *Organometallics* **2012**, *31*, 3985.
4. (a) Campbell, A. N.; Stahl, S. S. *Acc. Chem. Res.* **2012**, *45*, 851; (b) Vedernikov, A. N. *Acc. Chem. Res.* **2012**, *45*, 803; (c) Sigman, M. S.; Werner, E. W. *Acc. Chem. Res.* **2012**, *45*, 874; (d) Hashiguchi, B. G.; Bischof, S. M.; Konnick, M. M.; Periana, R. A. *Acc. Chem. Res.* **2012**, *45*, 885; (e) Cavaliere, V. N.; Mindiola, D. J. *Chem. Sci.* **2012**, *3*, 3356–3365.
5. Shilov, A. E.; Shul'pin, G. B. *Chem. Rev.* **1997**, *97*, 2879.
6. Zhou, M.; Balcells, D.; Parent, A. R.; Crabtree, R. H.; Eisenstein, O. *ACS Catal.* **2012**, *2*, 208.
7. (a) Shul'pin, G. B.; Druzhinina, A. N. *React. Kinet. Catal. Lett.* **1991**, *44*, 387; (b) Shul'pin, G. B.; Druzhinina, A. N. *Petrol. Chem.* **1993**, *33*, 247; (c) Shul'pin, G. B.; Druzhinina, A. N.; Shul'pina, L. S. *Petrol. Chem.* **1993**, *33*, 321.
8. Abstracts of XXV Int. Conf. Organometal. Chem., Lisbon, Portugal, 2012: (a) Shul'pin, G. B. Lecture K-1; (b) Shul'pina, L. S.; Kirillova, M. V.; Pombeiro, A. J. L.; Shul'pin, G. B.; Karslyan, E. E.; Kozlov, Y. N. Poster PB-43; (c) Shul'pin, G. B.; Kirillova, M. V.; Shul'pina, L. S.; Pombeiro, A. J. L.; Karslyan, E. E.; Kozlov, Y. N. *Catal. Commun.* **2013**, *31*, 32–36; (d) Shul'pina, L. S.; Durova, E. L.; Kozlov, Y. N.; Kudinov, A. R.; Strelkova, T. V.; Shul'pin, G. B. *Russ. J. Phys. Chem. A* **2013**, *87*, No. 12.
9. Shul'pin, G. B.; Kirillova, M. V.; Kozlov, Y. N.; Shul'pina, L. S.; Kudinov, A. R.; Pombeiro, A. J. L. *J. Catal.* **2011**, *277*, 164.
10. (a) Shul'pin, G. B.; Kozlov, Y. N.; Shul'pina, L. S.; Kudinov, A. R.; Mandelli, D. *Inorg. Chem.* **2009**, *48*, 10480; (b) Shul'pin, G. B.; Kozlov, Y. N.; Shul'pina, L. S.; Carvalho, W.; Mandelli, D. *RSC Adv.* **2013**, *3*, 15065.
11. (a) Shul'pin, G. B. *J. Mol. Catal. A: Chem.* **2002**, *189*, 39; (b) Shul'pin, G. B. *Comptes Rendus, Chimie* **2003**, *6*, 163; (c) Shul'pin, G. B. *Mini-Rev. Org. Chem.* **2009**, *6*, 95; (d) Shul'pin, G. B.; Kozlov, Y. N.; Shul'pina, L. S.; Petrovskiy, P. V. *Appl. Organometal. Chem.* **2010**, *24*, 464.
12. Shul'pin, G. B.; Kozlov, Y. N.; Shul'pina, L. S.; Petrovskiy, P. V. *Appl. Organometal. Chem.* **2010**, *24*, 464.
13. (a) Shul'pin, G. B. ; Kudinov, A. R. ; Shul'pina, L. S.; Petrovskaya, E. A. *J. Organometal. Chem.* **2006**, *691*, 837; (b) Shul'pina, L. S.; Kudinov, A. R.; Petrovskaya, E. A.; Strelkova, T. V.; Shul'pin, G. B. *Petrol. Chem.* **2006**, *46*, 164.
14. (a) Shul'pin, G. B.; Süss-Fink, G.; Shul'pina, L. S. *Chem. Commun.* **2000**, 1131; (b) Yuan, Q.; Deng, W.; Zhang, Q.; Wang, Y. *Adv. Synth. Catal.* **2007**, *349*, 1199.
15. (a) Shul'pin, G. B.; Muratov, D. V.; Shul'pina, L. S.; Kudinov, A. R.; Strelkova, T. V.; Petrovskiy, P. V. *Appl. Organometal. Chem.* **2008**, *22*, 684; (b) Shul'pina, L. S.; Kudinov, A. R.; Süss-Fink, G.; Loginov, D. A.; Shul'pin, G. B. *Petrol. Chem.* **2005**, *45*, 309.
16. Xia, J.-B.; Cormier, K. W.; Chen, C. *Chem. Sci.* **2012**, *3*, 2240.



---

# 2

---

## TOWARD FUNCTIONALIZATION OF ALKANES UNDER ENVIRONMENTALLY BENIGN CONDITIONS

ARMANDO J. L. POMBEIRO

*Centro de Química Estrutural, Instituto Superior Técnico, Universidade de Lisboa, Lisboa, Portugal*

### 2.1 INTRODUCTION

Alkanes are very rich carbon compounds but their use as raw materials for organic synthesis has been hampered by their high inertness. Their conversion into organic products with an added value (for reviews, see e.g., [1–15]), is a challenge in modern chemistry, and alkanes are used generally as fuels (full oxidation to CO<sub>2</sub>), with complete loss of carbon to the atmosphere and resulting noxious environmental effects associated with carbon dioxide accumulation therein.

The development of mild and green processes for their partial oxidation and functionalization would promote the potential of their application toward alternative raw materials for organic synthesis. Single-pot methods to achieve functionalized products, such as carboxylic acids, would be highly advantageous also in terms of simplicity, in comparison with the current multistage and energy-demanding processes used in industry.

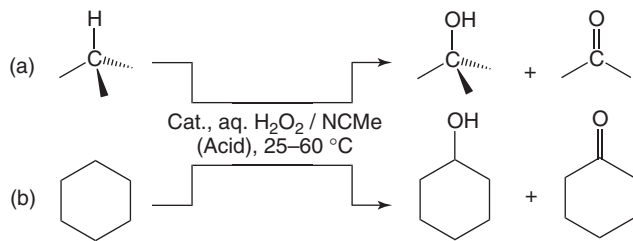
Of particular significance to achieve environmentally benign systems would be the use of water as a solvent, but this is also challenging in view of the lack of solubility of the alkanes and, commonly, also of the metal catalysts. The approach followed in the author's group often involves the use of hydrosoluble ligands at appropriate metal centers, which can lead to the formation of water-soluble catalyst precursors. Examples are indicated in the following sections.

### 2.2 PEROXIDATIVE OXIDATIONS OF ALKANES TO ALCOHOLS AND KETONES, CATALYZED BY TRANSITION METAL COMPLEXES

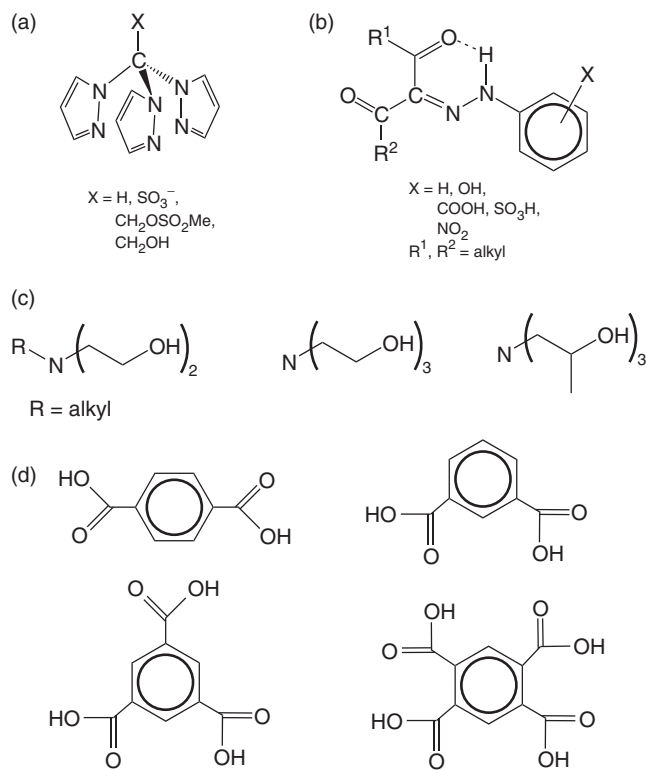
Both cyclic and acyclic alkanes undergo partial oxidation to alcohols and ketones, with hydrogen peroxide and under mild conditions (Scheme 2.1a) in the catalytic systems discussed herein, but the oxidation of cyclohexane to cyclohexanol and cyclohexanone (Scheme 2.1b) has been typically used as the model reaction, in view, for example, of its simplicity (cyclohexane bears only one type of carbon atoms) and its industrial significance (the mixture of cyclohexanol and cyclohexanone obtained by such a reaction is used for the preparation of adipic acid, a key intermediate for the production of nylon-6,6).

#### 2.2.1 Scorpionate Complexes as Catalyst Precursors

In contrast to boron-based scorpionates, such as *tris*(pyrazolyl)borate and derivatives, those based on carbon, namely *tris*(pyrazolyl)methane, HC(pz)<sub>3</sub>, and hydrosoluble-derived ones (Scheme 2.2a), are still underexplored, in spite of their potential, when suitably functionalized, to form *water-soluble complexes*. A good example is the sulfonate derivative, that is, *tris*(pyrazolyl)methane sulfonate (Tpms), which is hydrolytically stable over a wide pH range and leads to sandwich



**Scheme 2.1** Peroxidative oxidation of an alkane (a) and, in particular, of cyclohexane (b) to the corresponding alcohol and ketone, with aqueous  $\text{H}_2\text{O}_2$ , catalyzed by a transition metal catalyst (Cat.), under typical mild reaction conditions of this work.

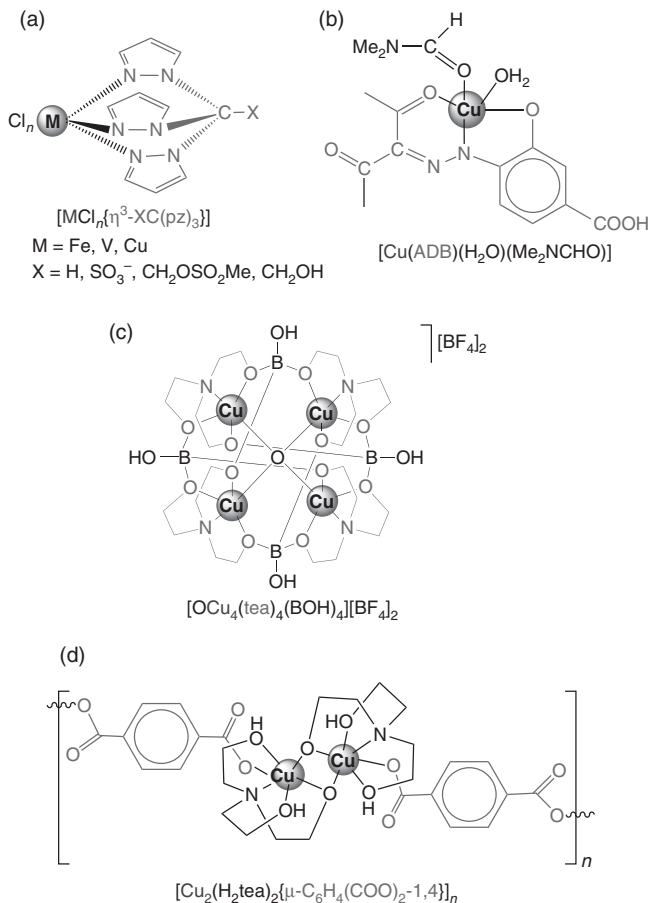


**Scheme 2.2** Examples of types of ligands (or their precursors) in metal catalysts for the peroxidative oxidation of alkanes: (a) C-based scorpiononates, (b) azoderivatives or arylhydrazones of  $\beta$ -diketones, (c) aminopolyalcohols, and (d) benzene polycarboxylic acids.

and/or half-sandwich complexes with various transition metals. The *half-sandwich compounds of iron, vanadium, and copper*, bearing this or a related scorpionate ligand (Scheme 2.3a) [16–20], act as good catalyst precursors for the partial oxidation of alkanes to the corresponding alcohols and ketones, in acetonitrile, with aqueous hydrogen peroxide as an oxidant, under mild conditions (e.g., 20–40 °C), typically in acidic medium.

This is illustrated for the peroxidative oxidation of cyclohexane to a mixture of cyclohexanol and cyclohexanone (Scheme 2.1b), a reaction with industrial application (see above). The conditions required in the industrial process (quite higher temperatures) are much harsher than ours, and the conversions are rather low in order to achieve a good selectivity. In our systems based on a half-sandwich complex, turnover numbers (TONs, moles of product per mole of catalyst precursor) up to 690 and yields up to 25% have been achieved with the Fe precatalyst  $[\text{Fe}(\text{C1})_2(\text{Tpms})]$  [20].

In a few cases (with Fe or Cu hydrosoluble precatalysts), the system can operate in the absence of any added organic solvent (even acetonitrile) [20], a feature that is noteworthy toward the development of a green catalytic system. However, our catalysts are not effective when using air (or dioxygen) instead of hydrogen peroxide as the oxidant, a disadvantage relative to the industrial process.



**Scheme 2.3** Examples of transition metal catalyst precursors for the peroxidative oxidation of alkanes, bearing (a) a C-scorpionate [16–20], (b) an azoderivative of a  $\beta$ -diketone [21], (c) an aminopolyalcohol derivative ( $\text{tea}^{3-}$  = deprotonated form of triethanolamine,  $\text{H}_3\text{tea}$ ) [33, 34], and (d) a benzene dicarboxylate [33, 34] ligand.

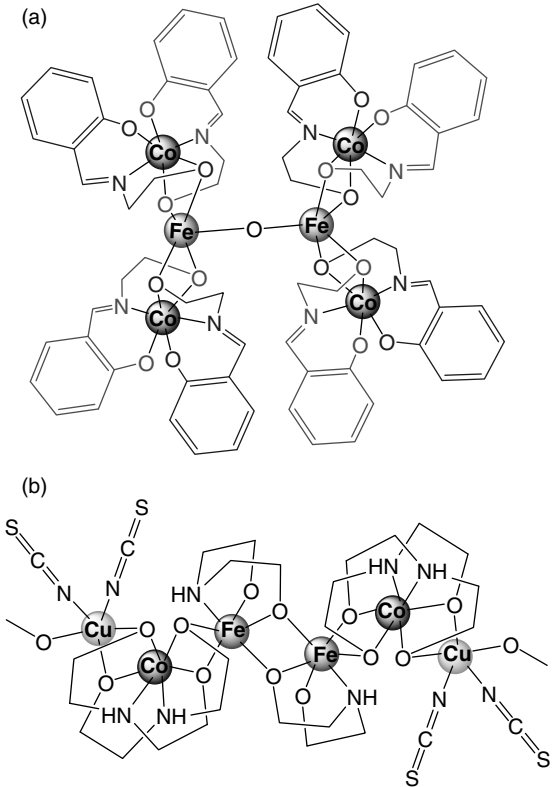
A broader discussion on the use of scorpionate complexes in catalysis is given in Chapter 22.

### 2.2.2 Azoderivatives of $\beta$ -Diketone Complexes as Catalyst Precursors

Suitably functionalized azoderivatives of  $\beta$ -diketones (ADB or arylhydrazone of  $\beta$ -diketones, AHBD) (Scheme 2.2b) are also convenient hydrosoluble species toward water-soluble catalyst precursors in this field and of particular interest are those bearing an acid substituent (carboxylic or sulfonic group) [21], which can operate without requiring the common presence of an added acid promoter. The acidic moiety conceivably has two main roles: provides water solubility and acts as the acid promoter. Hence, the complexes  $[\text{Cu}(\text{ADB})(\text{H}_2\text{O})(\text{Me}_2\text{NCHO})]$  (Scheme 2.3b) and  $[\{\text{Cu}(\mu\text{-ADB})(\text{MeOH})\}_2]\text{[ADB} = p\text{-COOH substituted (2-hydroxy-phenylhydrazone)pentane-2,4-dione]}$  appear to behave as *dual-role* catalyst precursors, in *acid-free* medium, combining, in each molecule, an active copper center and an acid site (TONs and yields up to 163 and 14%, respectively, are achieved for the model oxidation of cyclohexane, in  $\text{NCMe}/\text{aqueous H}_2\text{O}_2$ , at  $50^\circ\text{C}$ ) [21].

### 2.2.3 Multinuclear Complexes as Catalyst Precursors

Although the mononuclear Cu half-sandwich scorpionate complexes (see above) are commonly less active than the Fe ones, copper complexes can be more effective in *multinuclear assemblies* (including coordination polymers) and our approach for these species concerns their *self-assembly synthesis* by using a suitable combination of a metal source, a main chelating ligand, a spacer or linker, apart from a pH regulator. A wide discussion on the types of self-assembled multicopper complexes and their use for alkane functionlization is presented in Chapter 3, and only a very brief overall view is outlined here.



**Scheme 2.4** Direct self-assembled *heterometallic* catalyst precursors for the peroxidative oxidation of alkanes: (a)  $[\text{Co}_4\text{Fe}_2\text{O}(\text{Sae})_8]$  ( $\text{H}_2\text{Sae}$  = salicylidene-2-ethanolamine) [35] and (b)  $[\text{FeCuCo}(\mu\text{-L})_3(\text{NCS})_2(\text{MeOH})]_2$  ( $\text{H}_2\text{L}$  = diethanolamine) [36].

Typical examples of chelating ligands and spacers applied for self-assembly of multicopper coordination compounds and polymers include (see above) AHBD [21–24], aminopolyalcohols, and benzenopolycarboxylic acids [25–34] (Scheme 2.2b–d).

A diversity of 1D, 2D, or 3D copper assemblies can be obtained, including coordination polymers, as well as multi- or mononuclear species with discrete molecules. Among the latter, the tetranuclear  $\mu$ -oxo complex derived from triethanolamine  $[\text{OCu}_4(\text{tea})_4(\text{BOH})_4]\text{[BF}_4\text{]}_2$  (Scheme 2.3c) is particularly active (TONs or yields up to 380 or 39%, respectively, for the conversion of cyclohexane to cyclohexanol and cyclohexanone) [33, 34]. It is also active (although less effectively, by one order of magnitude) for the oxidation of methane and ethane to methanol and ethanol, respectively [34].

*Heterometallic* species can be conveniently obtained, in particular by *direct self-assembly*, from a metal powder, and they can exhibit a metal synergic effect with a remarkable catalytic activity. Hence, the hexanuclear heterodimetallic  $\text{Co}^{\text{III}}_4\text{Fe}^{\text{III}}_2$  Schiff base complex  $[\text{Co}_4\text{Fe}_2\text{O}(\text{Sae})_8]$  ( $\text{H}_2\text{Sae}$  = salicylidene-2-ethanolamine) (Scheme 2.4), without copper, self-assembled from Co powder,  $\text{FeCl}_2$ ,  $\text{H}_2\text{Sae}$ , and  $\text{Et}_3\text{N}$  under air, exhibits an outstanding TON of  $3.6 \times 10^3$  (corresponding to a turnover frequency of  $1.1 \times 10^4 \text{ h}^{-1}$ ), for the oxidation of cyclohexane in  $\text{NCMe}/\text{aqueous H}_2\text{O}_2$ , at room temperature [35].

A good activity with a synergic effect is also achieved (TON and yield up to 100 and 25%, respectively) by the heterotrimetallic  $\text{Fe}/\text{Cu}/\text{Co}$  complex  $[\text{FeCuCo}(\mu\text{-L})_3(\text{NCS})_2(\text{MeOH})]_2$  ( $\text{H}_2\text{L}$  = diethanolamine) [36].

#### 2.2.4 Role of Water

The use of water as a solvent, even when mixed with an organic one, is a positive feature of a catalytic system, which aims to be of environmental significance.

However, the role of water can lie beyond that of a mere solvent, as suggested by the observation, in some cases, that water promotes the catalytic activity, and attested by theoretical density functional theory (DFT) calculations [37–40]. This was studied in detail for the aqueous  $\text{H}_2\text{O}_2-\text{NCMe}$  systems based on the oxo–Re complex  $[\text{MeReO}_3]$  (methyl trioxo-rhenium, MTO) [37] and on the vanadate ( $\text{VO}_3^-$ ) or vanadatrane ( $[\text{VO}\{\text{N}(\text{CH}_2\text{CH}_2\text{O})_3\}]$ ) [38] catalyst precursors, which are effective



**Scheme 2.5** Overall reactions involved in a vanadium(V/IV)-assisted generation of hydroxyl radical ( $\text{HO}^{\bullet}$ ) from hydrogen peroxide. The  $\text{V}^{\text{V}} + \text{OH}^-$  products can stand for  $\text{V}^{\text{V}}=\text{O} + \text{H}^+$ .

for the peroxidative oxidation of alkanes to the corresponding alcohols and ketones. The vanadate system was initially established by Shul'pin et al. [41] and included pyrazinecarboxylic acid (PCAH) as a promoter.

As indicated by radical trap experiments, various types of selectivity (regio-, bond-, and stereo-selectivity), and kinetic and theoretical studies [18–24, 27, 29, 33–40], these peroxidative oxidations of alkanes occur via radical mechanisms. They are believed to proceed via free hydroxyl radical ( $\text{HO}^{\bullet}$ ) that acts as an H-abstractor from the alkane RH to yield the corresponding alkyl radical  $\text{R}^{\bullet}$ . Fast reaction of  $\text{R}^{\bullet}$  with  $\text{O}_2$  generates the alkylperoxy radical  $\text{ROO}^{\bullet}$ , which, following known pathways [38, 39, and references therein], lead to the formation of the final alcohol (ROH) and the corresponding ketone via the alkylperoxide ROOH.

The hydroxyl radical is generated on metal-assisted reduction of  $\text{H}_2\text{O}_2$  (see Scheme 2.5, for a  $\text{V}^{\text{V}/\text{IV}}$  catalytic system) [38, 40–42].

The concerned overall  $\text{H}_2\text{O}_2$  reactions involve proton-transfer steps, for example, from ligated  $\text{H}_2\text{O}_2$  to an oxo ligand, which are promoted by water on bridging both ligands with the formation of six-membered transition states (TSs) that are thus stabilized [37–40]. This is exemplified by  $[\text{VO}_3(\text{HOOH}\cdots\text{OH}_2\cdots)(\text{PCA})]^{\pm}$ , the TS involved in such a proton transfer in the  $\text{VO}_3^-$ –pyrazinecarboxylate (PCA) system (Scheme 2.6) [38]. The assistance of water, which acts as a *catalyst*, lowers (Scheme 2.6a) the activation barrier by 7–11 kcal/mol, in comparison with the four- or five-membered TSs that would form if the proton transfer would occur [41–43] with the assistance of the PCA ligand (Shul'pin “robot-type mechanism,” Scheme 2.6b) or directly from the  $\text{H}_2\text{O}_2$  ligand to an oxo ligand. Hence, water, in a controlled amount, can be more effective for this purpose than the more complex PCA ligand.

A similar effect of water has been proposed for other types of reactions without involving alkanes, for example, olefin epoxidations catalyzed by cyclopentadienyl–Mo systems [44], and thus it can be of a considerable generality.

It is noteworthy to mention that the involvement of a second metal center can also promote the proton transfer, as believed to occur in di- or oligovanadate catalysts, which exhibit a higher activity than monovanadate [40]. In such systems, six-membered oxo–divanadium TSs (Scheme 2.6c) can be formed, lowering the energy barrier by circa 4.2 kcal/mol relatively to the proton transfer at a monovanadate center [40].

Furthermore, water can have an even deeper role in alkane functionalizaton, as a hydroxylating reagent, which will be discussed in Section 4.

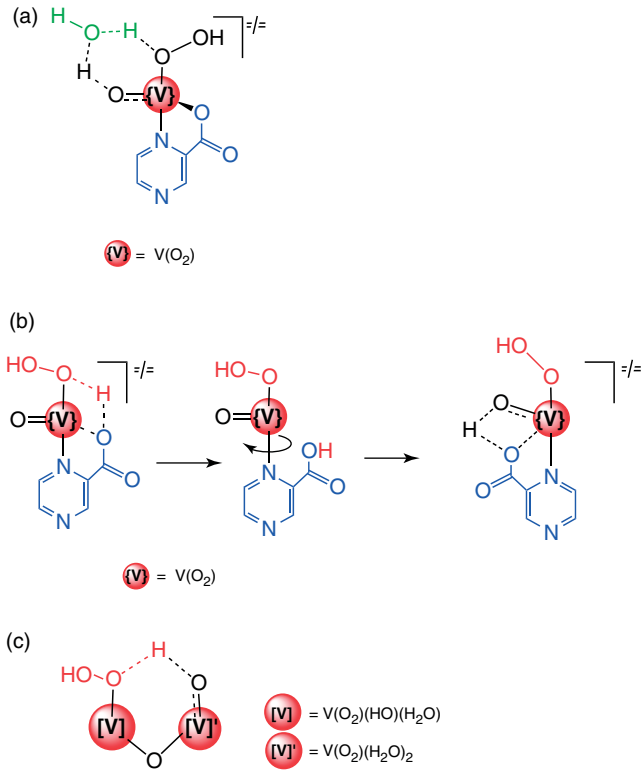
## 2.2.5 Nontransition Metal Catalyzed Alkane Oxidation

When thinking on green catalysis, one is encouraged to try to avoid the use of any transition metal catalyst that commonly has an environmentally nonbenign character (although, in some cases, namely with Fe, Cu, or V catalysts, they can be tolerated). Of significance toward this aim is the recognition by Mandelli and Shul'pin [45] that aluminum, a nontransition metal, can replace a transition metal catalyst, as shown by the  $\text{Al}(\text{NO}_3)_3-\text{H}_2\text{O}_2-\text{NCMe}-\text{H}_2\text{O}$  system, which catalyzes the oxidation of octane and heptane to the corresponding alcohols and ketones.

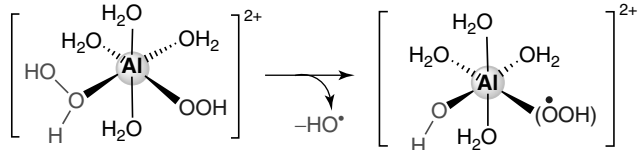
This is particularly interesting in the view that a redox-inactive metal is replacing a redox-active metal, in oxidation catalysis, and was investigated by DFT calculations [46].

These theoretical studies indicate the crucial role played by the intermediate  $[\text{Al}(\text{OOH})(\text{HOOH})(\text{H}_2\text{O})_4]^{2+}$ , bearing (i) a highly activated hydrogen peroxide ligand with a dramatically decreased HO–OH bond energy (6.1 kcal/mol) in comparison with free  $\text{H}_2\text{O}_2$  (39.4 kcal/mol), and (ii) a ligated monodeprotonated form ( $\text{HOO}^-$ ). At this intermediate, this latter ligand reduces (intramolecular redox process) hydrogen peroxide to hydroxide ( $\text{HO}^-$ ) and hydroxyl ( $\text{HO}^{\bullet}$ ), being itself oxidized to the hydroperoxyl radical ( $\text{HOO}^{\bullet}$ ), a labile ligand that liberates from the metal (Scheme 2.7) [46].

Therefore, the transition metal is avoided in this  $\text{H}_2\text{O}_2$ –Al catalytic system on account of a suitable redox-active co-ligand ( $\text{HOO}^-$ ) that can play the redox role of the transition metal, by acting as a reducing agent of  $\text{H}_2\text{O}_2$  toward the generation of the hydroxyl radical. The generality of such an interesting behavior is worth to be investigated.



**Scheme 2.6** Examples of transition states (TSs) involved in a proton-transfer step from a ligated  $H_2O_2$  to an oxo ligand on the way to generate the hydroxyl radical: (a) six-membered TS (water-assisted  $H^+$ -transfer) at a PCA-V catalyst (PCA=pyrazine carboxylate) [38]; (b) five- or four-membered TSs (PCA-assisted  $H^+$ -transfer, “robot’s arm” mechanism) at a PCA-V catalyst [41–43]; and (c) six-membered oxo-divanadium TS at a divanadate-type model [40]. (See insert for color representation of the figure.)



**Scheme 2.7** Key hydrogen peroxide intermediate  $[Al(OOH)(HOOH)(H_2O)_4]^{2+}$  in the hydroxyl radical formation, at the  $Al^{3+}$ -catalyzed peroxidative oxidation of alkanes [46].

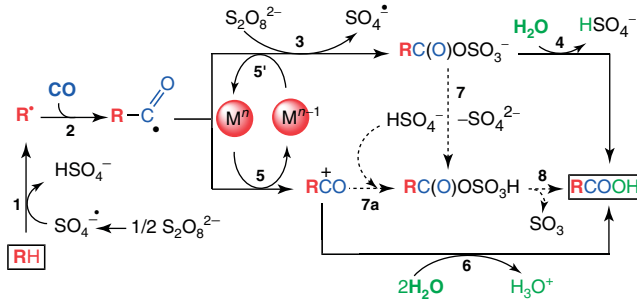
### 2.3 METAL-FREE ALKANE HYDROCARBOXYLATION AND RELATED CARBOXYLATION

Because, as shown above, in the oxidation catalysis of alkanes, one can replace a transition metal catalyst by a redox-inactive nontransition metal catalyst, the question arises whether it would be possible to go even further and eliminate completely the use of any metal catalyst, thus establishing a metal-free system capable of oxidizing alkanes under mild conditions.

This has been achieved in the hydrocarboxylation of alkanes in water-acetonitrile (2 : 1–1 : 2 volume ratio range) medium, with CO and peroxydisulfate ( $S_2O_8^{2-}$ ) (Eq. 2.1). [25, 26, 28, 47–51].



The conditions are rather mild (30–60 °C), they do not require any acid addition, and yields up to 72% are obtained. Water behaves as a hydroxylating agent as demonstrated by using  $H_2^{18}O$ , which leads to the  $^{18}O$ -labeled acid  $R-CO^{18}OH$  as the major product.



**Scheme 2.8** Main radical mechanism of the hydrocarboxylation of alkanes with peroxydisulfate, CO, and water, in aqueous ( $\text{H}_2\text{O}/\text{MeCN}$ ) medium [51]. The minor 7 (or 7a) to 8 alternative pathway does not concern water as the hydroxylating agent. (See insert for color representation of the figure.)

The system is active for both liquid and gaseous alkanes, but with a rather low activity for methane. Although operating under metal-free conditions, it is also metal-promoted namely by some copper complexes that act as catalyst precursors for the oxidation of alkanes with hydrogen peroxide, typically the abovementioned tetranuclear  $\mu$ -oxo triethanolamine complex  $[\text{OCu}_4(\text{tea})_4(\text{BOH})_4][\text{BF}_4]_2$

The mechanism is also radical, as indicated by the suppression of acid ( $\text{RCOOH}$ ) formation by a radical trap and the preferable carbonylation at a secondary carbon relative to a primary one. According to DFT calculations [51], it proceeds mainly as shown in Scheme 2.8.

Peroxydisulfate acts as a radical source and as an oxidant (a third minor role as a hydroxylating agent is mentioned below). The first role concerns its homolysis that leads to the sulfate radical  $\text{SO}_4^{\cdot-}$ , which abstracts hydrogen from the alkane (RH) forming the alkyl radical  $\text{R}^{\bullet}$  (step 1, Scheme 2.8). This is carbonylated by CO to give the acyl radical  $\text{RC}^{\bullet}\text{O}$  (step 2), which is oxidized either by peroxydisulfate (its second role) with coupling to sulfate to give the acyl sulfate  $\text{RC(O)OSO}_3^-$  (step 3, metal-free pathway) or by the metal promoter to form the acyl cation  $\text{RCO}^+$  (step 5, metal-promoted route) [51].

Nucleophilic attack of water, either at the acyl sulfate or at the acyl cation (step 4 or 6, respectively), leads to the formation of the carboxylic acid  $\text{RCOOH}$ , as the final product [51]. Hence, apart from being a solvent, water also plays a fundamental role as a stoichiometric nucleophilic reagent toward alkane-derived acyl species.

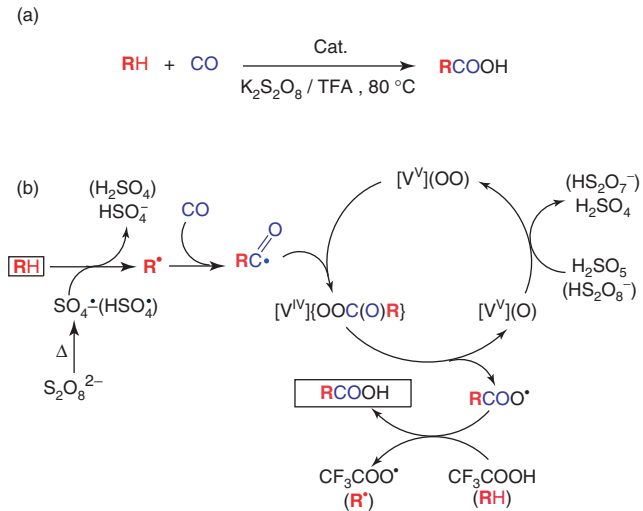
When using  $\text{H}_2^{18}\text{O}$ , a minor amount of nonlabeled  $\text{RCOOH}$  is also obtained, which can be accounted for by steps 7 (or 7a) and 8, where  $\text{HSO}_4^-$  (derived from peroxydisulfate), instead of water, acts as the hydroxylating agent [51].

This alkane-hydrocarboxylating system can be considered as a development toward the “green” direction of a previous carboxylation system based on the use of peroxydisulfate in trifluoroacetic acid (TFA) at  $80^\circ\text{C}$  (Scheme 2.9a), which was pioneered by Fujwara [12, 15], and further improved by the author’s group [52–60] by finding more active and convenient metal catalysts, and establishing the mechanism of the catalysis. In fact, the water–acetonitrile mixture, in the above alkane-hydrocarboxylating system (Eq. 2.1, Scheme 2.8), has replaced successfully the noxious TFA as a solvent in the latter carboxylation system, the operating conditions became much milder and environmentally tolerable, and a role of water as a reagent was found. However, peroxydisulfate could not be replaced by a greener oxidant, such as  $\text{H}_2\text{O}_2$ .

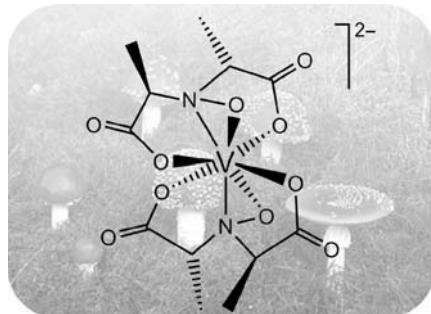
In the  $\text{S}_2\text{O}_8^{2-}$ /TFA system, vanadium catalysts were found to be the most active, in particular amavadin (also spelled amavadine) and its models [52–54, 57, 59, 61]. Amavadin is the nonoxo–vanadium complex  $[\text{V}(\text{HIDPA})_2]^{2-}$  [ $\text{HIDPA}$  = deprotonated basic form of  $N$ -(hydroxyimino)dipropionic acid] (Scheme 2.10) that is present in some toadstools (*amanita muscaria*), but its biological role still remains undiscovered [61]. Its catalytic activity, and those of its models, such as  $[\text{V}(\text{HIDA})_2]^{2-}$  [ $\text{HIDA}$  = deprotonated basic form of  $N$ -(hydroxyimino)diacetic acid] and related vanadatrane  $[\text{VO}(\text{N}(\text{CH}_2\text{CH}_2\text{O})_3)]$ , are so high (TONs up to over  $10^4$  or carboxylic acids yields up to over 90%, for the most inert alkanes, methane, or ethane) [52, 53] that amavadin and the toadstools where it is found have been considered by this author as a *kind of magic* (inspired on a well-known Queen band song) and the latter were called elsewhere [62] as “magic mushrooms, new catalysts from Nature.”

The initial steps of the mechanism of the alkane (RH) carboxylation (Scheme 2.9b) [52, 53] are identical to those of the hydrocarboxylation, discussed above, with  $\text{S}_2\text{O}_8^{2-}$  as the source of the sulfate radical, which acts as H-abstractor from the alkane to give the alkyl radical  $\text{R}^{\bullet}$ , and CO as the carbonylating agent of this radical to yield the acyl radical  $\text{RC}^{\bullet}\text{O}$ .

However, peroxydisulfate, instead of water, provides the source of the hydroxyl oxygen as substantiated by DFT calculations [52, 53], which indicate the plausible addition of the acyl radical to a peroxy-V intermediate to form a



**Scheme 2.9** Alkane carboxylation with CO and  $\text{K}_2\text{S}_2\text{O}_8$ , in TFA: (a) General reaction [12, 15, 52–60] and (b) proposed mechanism for an oxo-vanadium catalyst [52, 53]. (See insert for color representation of the figure.)



**Scheme 2.10** Amavadin complex  $[\text{V}(\text{HIDPA})_2]^{2-}$  [HIDPA = deprotonated basic form of *N*-(hydroxyimino)dipropionic acid] with its natural source, *amanita muscaria*.

percarboxylate ligand,  $\text{RC(O)OO}$ , which, on O–O bond homolysis, generates the carboxyl radical  $\text{RCOO}^\bullet$  that, via H-abstraction from the alkane or from TFA, yields the acid  $\text{RCOOH}$ .

It is noteworthy to mention that both the hydrocarboxylation and the carboxylation of alkanes processes discussed herein provide single-pot routes to carboxylic acids that are much simpler and operate under much milder conditions in comparison with the industrial processes. This is well illustrated for the case of the industrial production of acetic acid [63, 64], which involves three distinct stages under energy-demanding and environmentally nontolerable conditions: high temperature catalytic steam reforming of methane or coal to CO and dihydrogen, high temperature catalytic conversion of synthesis gas into methanol, and carbonylation of methanol with expensive Rh or Ir catalysts (Monsanto or Cativa process, respectively), still at a considerably elevated temperature.

Moreover, amavadin also catalyses the abovementioned peroxidative oxidation of alkanes, as well as their peroxidative halogenations [65], although with a much lower activity.

## 2.4 FINAL REMARKS

Steps have been taken toward eco-friendly catalytic systems active in alkane functionalization under mild conditions, preferably in aqueous media, by using *hydrosoluble catalysts* obtained from ligands that are water soluble. Systems can operate usually with a *green oxidant* (aqueous hydrogen peroxide) and in partially *aqueous media*.

Moreover, *water* can play a fundamental role beyond that of a mere solvent, acting as a *promoter* of the catalytic activity (by favoring proton-transfer steps) or even as a *reagent*, that is, the hydroxylating reagent in the alkane functionalization.

A transition metal can be avoided, by using a *nontransition metal* catalyst, provided a suitable redox-active co-ligand is present.

A *metal-free* system was already established for the carboxylation of alkanes with CO and water, operating in water–acetonitrile and under *acid-free* conditions. The latter feature (no added acid) is common to a few other catalytic systems active for alkane hydroxylation, namely by taking advantage of a ligand bearing an acid group (“dual-role catalyst”).

The alkane functionalization reactions proceed via *radical mechanisms*, with a *high chemoselectivity*, although with low regio-, bond-, and stereo-selectivities as expected for the involvement of the hydroxyl radical, features that were not discussed in this chapter.

*Theoretical DFT studies* allow to disclose conceivable reaction mechanisms.

The systems exhibit a *high simplicity* and provide the oxidized and carboxylated (carboxylic acids) products in a *single-pot* process, thus contrasting with the higher complexity of the industrial synthetic processes for the same products.

In addition, a number of the developed catalysts are also active, under different experimental conditions, in *oxidations of other substrates*, in particular some of the copper catalysts for alcohol aerobic (TEMPO-mediated) or peroxidative oxidations [21, 22]. The reactions may be microwave-assisted (details are given in Chapter 18).

It is also worth mentioning the *biological significance* of these studies and the inspiration of biology on their development. In fact, pMMO (particulate methane monooxygenase), a main enzyme in the metabolic pathway of methanotrophs, is a membrane multicopper enzyme that catalyzes the oxidation of alkanes to the corresponding alcohols [66–68], which is mimicked by the multinuclear copper systems.

Moreover, *amavadin*, a water-soluble natural vanadium complex, still with an undisclosed biological role in the mushrooms where it is accumulated, has been successfully applied as a remarkably effective catalyst precursor in the field of alkane carboxylation, although under conditions that are not found in biological systems. Concerning the peroxydisulfate/TFA system for alkane carboxylation, this acid solvent has already been replaced by a mixture of water/acetonitrile, operating under milder conditions, but a cheaper and less noxious oxidant (hydrogen peroxide or dioxygen) conceivably has yet to be found before the process gains a widespread use.

## ACKNOWLEDGMENTS

The co-authors of the cited references are gratefully acknowledged. Dr. M. F. C. Guedes da Silva is further acknowledged for the assistance in the preparation of the schemes. The work has been supported by the Fundação para a Ciência e a Tecnologia (FCT), Portugal (projects PTDC/QUI-QUI/102150/2008 and PEst-OE/QUI/UI0100/2013).

## REFERENCES

1. Kirillov A. M.; Kirillova, M. V.; Pombeiro, A. J. L. *Adv. Inorg. Chem.* **2013**, *65*, 1.
2. Kirillov A. M.; Kirillova, M. V.; Pombeiro, A. J. L. *Coord. Chem. Rev.* **2012**, *256*, 2741.
3. Hashiguchi, B. G.; Bischof, S. M.; Konnick, M. M.; Periana, R. A. *Acc. Chem. Res.* **2012**, *45*, 885 (other reviews in the same journal topical issue also include alkane reactions).
4. Chepaikin, E. G. *Russ. Chem. Rev.* **2011**, *80*, 363.
5. da Silva, J. A. L.; Fraústo da Silva, J. R., Pombeiro, A. J. L. *Coord. Chem. Rev.* **2011**, *255*, 2232.
6. Shul'pin, G. B. *Mini-rev. Org. Chem.* **2009**, *6*, 95.
7. Diaz-Requejo, M. M.; Perez, P. J. *Chem. Rev.* **2008**, *108*, 3379.
8. Que, L., Jr.; Tolman, W. B. *Nature* **2008**, *455*, 333.
9. Pombeiro, A. J. L. In *Vanadium, the Versatile Metal*; Kustin, K., Pessoa, J. C., Crans, D. C., Eds.; American Chemical Society Symposium Series 974; American Chemical Society, Washington DC, **2007**; Chapter 4, pp 51–60.
10. Pombeiro, A. J. L. in *Perspectives of Coordination Chemistry*; Trzeciak, A., Ed.; Education in Advanced Chemistry Series 9; Poznan-Wroclaw, **2005**; pp 93–113.
11. (a) Lersch, M.; Tilset, M. *Chem. Rev.* **2005**, *105*, 2471; (b) Crabtree, R. H. *J. Organomet. Chem.* **2004**, *689*, 4083.
12. (a) Labinger, J. A.; Bercaw, J. E. *Nature* **2002**, *417*, 507; (b) Fokin, A. A.; Schreiner, P. R. *Chem. Rev.* **2002**, *102*, 1551.

13. Jia, C.; Kitamura, T.; Fujiwara, Y. *Acc. Chem. Res.* **2001**, *34*, 633.
14. Costas, M.; Chen, K.; Que, L., Jr. *Coord. Chem. Rev.* **2000**, *200–202*, 517.
15. Sen, A. *Acc. Chem. Res.* **1998**, *31*, 550.
16. Shilov, A. E.; Shul'pin, G. B. *Chem. Rev.* **1997**, *97*, 2879.
17. Fujiwara, Y.; Takaki, K.; Taniguchi, Y. *Synlett* **1996**, 591.
18. Silva, T. F. S.; Mac Leod, T. C. O.; Martins, L. M. D. R. S.; Guedes da Silva, M. F. C.; Schiavon, M. A.; Pombeiro, A. J. L. *J. Mol. Catal. A: Chem.* **2013**, *367*, 52.
19. Silva, T. F. S.; Guedes da Silva, M. F. C.; Mishra, G. S.; Martins, L. M. D. R. S.; Pombeiro, A. J. L. *J. Organomet. Chem.* **2011**, *696*, 1310.
20. Silva T. F. S.; Luzyanin, K. V.; Kirillova, M. V.; Guedes da Silva, M. F. C.; Martins, L. M. D.R.S.; Pombeiro, A. J. L. *Adv. Synth. Catal.*, **2010**, *352*, 171.
21. Silva, T. F. S.; Mishra, G. S.; Guedes da Silva, M. F. C.; Wanke, R.; Martins, L. M. D. R. S.; Pombeiro, A. J. L. *Dalton Trans.* **2009**, *9207*.
22. Silva, T. S. F.; Alegria, E. C. B. A.; Martins, L. M. D. R. S.; Pombeiro, A. J. L.. *Adv. Synth. Catal.* **2008**, *350*, 706.
23. Kopylovich, M. N.; Gajewska, M. J.; Mahmudov, K. T.; Kirillova, M. V.; Figiel, P. J.; Guedes da Silva, M. F. C.; Gil-Hernández, B.; Sanchiz, J.; Pombeiro, A. J. L. *New J. Chem.* **2012**, *36*, 1646.
24. Kopylovich, M. N.; Mahmudov, K. T.; Guedes da Silva, M. F. C.; Figiel, P. J.; Karabach, Y. Y.; Kuznetsov, M. L.; Luzyanin, K. V.; Pombeir, A. J. L. *Inorg. Chem.* **2011**, *50*, 918.
25. Kopylovich, M. N.; Nunes, A. C. C.; Mahmudov, K. T.; Haukka, M.; Mac Leod, T. C. O.; Martins, L. M. D. R. S.; Kuznetsov, M. L.; Pombeiro A. J. L. *Dalton Trans.* **2011**, *40*, 2822.
26. Mahmudov, K. T.; Kopylovich, M. N.; Guedes da Silva, M. F. C.; Figiel, P. J.; Karabach, Y. Y.; Pombeiro, A. J. L. *J. Mol. Catal. A:Chem.* **2010**, *318*, 44.
27. Kirillov, A. M.; Karabach, Y. Y.; Kirillova, M. V.; Haukka, M.; Pombeiro, A. J. L. *Cryst. Growth Des.* **2012**, *12*, 1069.
28. Kirillova, M. V.; Kirillov, A. M.; Martins, A. N. C.; Graiff, C.; Tiripicchio, A.; Pombeiro, A. J. L. *Inorg. Chem.* **2012**, *51*, 5224.
29. Kirillov, A. M.; Kirillova, M. V.; Shul'pina, L. S.; Figiel, P. J.; Gruenwald, K.; Guedes da Silva, M. F. C.; Haukka, M.; Pombeiro, A. J. L. *J. Mol. Catal. A: Chem.* **2011**, *350*, 26.
30. Kirillov, A. M.; Karabach, Y. Y.; Kirillova, M. V.; Haukka, M.; Pombeiro, A. J. L. *Dalton Trans.* **2011**, *40*, 637.
31. Gruenwald, K. R.; Kirillov, A. M.; Haukka, M.; Sanchiz, J.; Pombeiro, A. J. L. *Dalton Trans.* **2009**, 2109.
32. Karabach, Y. Y.; Kirillov, A. M.; Haukka, M.; Sanchiz, J.; Kopylovich, M. N.; Pombeiro, A. J. L. *Cryst. Growth Des.* **2008**, *8*, 4100.
33. Kirillov, A. M.; Karabach, Y. Y.; Haukka, M.; Guedes da Silva, M. F. C.; Sanchiz, J.; Kopylovich, M. N.; Pombeiro, A. J. L. *Inorg. Chem.* **2008**, *47*, 162.
34. Karabach, Y. Y.; Kirillov, A. M.; Guedes da Silva, M. F. C.; Kopylovich, M. N.; Pombeiro, A. J. L. *Cryst. Growth Des.* **2006**, *6*, 2200.
35. Kirillov, A. M.; Kopylovich, M. N.; Kirillova, M. V.; Karabach, Y. Y.; Haukka, M.; Guedes da Silva, M. F. C.; Pombeiro, A. J. L. *Adv. Synth. Catal.* **2006**, *348*, 159.
36. Kirillov, A. M.; Kopylovich, M. N.; Kirillova, M. V.; Haukka, M.; Guedes da Silva, M. F. C.; Pombeiro, A. J. L. *Angew. Chem. Int. Ed.* **2005**, *44*, 4345.
37. Nesterov, D. S.; Chygorin, E. N.; Kokozay, V. N.; Bon, V. V.; Boča, R.; Kozlov, Y. N.; Shul'pina, L. S.; Jezierska, J.; Ozarowski, A.; Pombeiro, A. J. L.; Shul'pin, G. B. *Inorg.Chem.* **2012**, *51*, 9110.
38. Nesterov, D. S.; Kokozay, V. N.; Dyakonenko, V. V.; Shishkin, O. V.; Jezierska, J.; Ozarowski, A.; Kirillov, A. M.; Kopylovich, M. N.; Pombeiro, A. J. L. *Chem. Commun.* **2006**, 4605.
39. Kuznetsov, M. L.; Pombeiro, A. J. L. *Inorg. Chem.* **2009**, *48*, 307.
40. Kirillova, M. V.; Kuznetsov, M. L.; Romakh, V. B.; Shul'pina, L. S.; Fraústo da Silva, J. J. R.; Pombeiro, A. J. L.; Shul'pin, G. B. *J. Catal.* **2009**, *267*, 140.
41. Kirillova, M. V.; Kozlov, Y. N.; Shul'pina, L. S.; Lyakin, O. Y.; Kirillov, A. M.; Talsi, E. P.; Pombeiro, A. J. L.; Shul'pin, G. B. *J. Catal.* **2009**, *268*, 26.
42. Kirillova, M. V.; Kuznetsov, M. L.; Kozlov, Y. N.; Shul'pina, L. S.; Kitaygorodskiy, A.; Pombeiro, A. J. L.; Shul'pin, G. B. *ACS Catal.* **2011**, *1*, 1511.
43. Shul'pin, G. B.; Kozlov, Y. N.; Nizova, G. V.; Suss-Fink, G.; Stanisla, S.; Kitaygorodskiy, A.; Kulikova, V. S.. *J. Chem. Soc., Perkin Trans.* **2001**, *2*, 1351.
44. Kozlov, Y. N.; Romakh, V. B.; Kitaygorodskiy, A.; Buglyó, P.; Suss-Fink, G.; Shul'pin, G. B. *J. Phys. Chem. A* **2007**, *111*, 7736.
45. Khaliullin, R. Z.; Bell, A. T.; Head-Gordon, M. *J. Phys. Chem. B* **2005**, *109*, 17984.

46. Jee, J. -E.; Comas-Vives, A.; Dinoi, C.; Ujaque, G.; van Eldik, R.; Lledós, A.; Poli, R. *Inorg. Chem.* **2007**, *46*, 4103.
47. Mandelli, D.; Chiacchio, K. C.; Kozlov, Y. N.; Shul'pin, G. B. *Tetrahedron Lett.* **2008**, *49*, 6693.
48. Kuznetsov, M. L.; Kozlov, Y. N.; Mandelli, D.; Pombeiro, A. J. L.; Shul'pin, G. B. *Inorg. Chem.* **2011**, *50*, 3996.
49. Kirillova, M. V.; Kirillov, A. M.; Pombeiro, A. J. L. *Appl. Catal. A: Gen.* **2011**, *401*, 106.
50. Kirillov, A. M.; Coelho, J. A. S.; Kirillova, M. V.; Guedes da Silva, M. F. C.; Nesterov, D. S.; Gruenwald, K. R.; Haukka, M.; Pombeiro, A. J. L. *Inorg. Chem.* **2010**, *49*, 6390.
51. Kirillova, M. V.; Kirillov, A. M.; Pombeiro, A. J. L. *Chem. Eur. J.* **2010**, *16*, 9485.
52. Kirillova, M.V.; Kirillov, A.M.; Pombeiro, A.J.L. *Adv. Synth.Catal.* **2009**, *351*, 2936.
53. Kirillova, M. V.; Kirillov, A. M.; Kuznetsov, M. L.; Silva, J. A. L.; Fraústo da Silva, J. J. R.; Pombeiro, A. J. L. *Chem. Commun.* **2009**, *1999*, 2353.
54. Kirillova, M. V.; Kuznetsov, M. L.; Reis, P. M.; Silva, J. A. L.; Fraústo da Silva, J. J. R.; Pombeiro, A. J. L. *J. Am. Chem. Soc.* **2007**, *129*, 10531.
55. Kirillova, M. V.; Kuznetsov, M. L.; Silva, J. A. L.; Guedes da Silva, M. F. C.; Fraústo da Silva, J. J. R.; Pombeiro, A. J. L. *Chem. Eur. J.* **2008**, *14*, 1828.
56. Reis, P. M.; Silva, J. A. L.; Palavra, A. F.; Fraústo da Silva, J. J. R.; Kitamura, T.; Fujiwara, Y.; Pombeiro, A. J. L. *Angew. Chem.* **2003**, *115*, 845.
57. Silva, T. F. S.; Alegria, E. C. B. A.; Martins, L. M. D. R. S.; Pombeiro, A. J. L. *Adv. Synth. Catal.* **2008**, *350*, 706.
58. Kirillova, M. V.; Kirillov, A. M.; Reis, P. M.; Silva, J. A. L.; Fraústo da Silva, J. J. R.; Pombeiro, A. J. L. *J. Catal.* **2007**, *248*, 130.
59. Kirillova, M. V.; Silva, J. A. L.; Fraústo da Silva, J. J. R.; Palavra, A. F.; Pombeiro, A. J. L. *Adv. Synth. Catal.* **2007**, *349*, 1765.
60. Kirillova, M. V.; Silva, J. A. L.; Fraústo da Silva, J. J. R.; Pombeiro, A. J. L. *Appl. Catal. A: Gen.* **2007**, *332*, 159.
61. Reis, P. M.; Silva, J. A. L.; Palavra, A. F.; Fraústo da Silva, J. J. R.; Pombeiro, A. J. L. *J. Catal.* **2005**, *235*, 333.
62. Kirillov, A. M.; Haukka, M.; Kirillova, M. V.; Pombeiro, A. J. L. *Adv. Synth. Catal.* **2005**, *347*, 1435.
63. Silva, J. A. L.; Fraústo da Silva, J. J. R.; Pombeiro, A. J. L. In: *Vanadium, Biochemical and Molecular Biological Approaches*; Michibata, M., Ed.; Springer, **2012**, Chapter 2; pp 35–49.
64. Dux, E. *Chem. Rev.* (The University of York) **2008**, *18*, 22.
65. Ullmann's Encyclopedia of Industrial Chemistry, 6th ed., Wiley-VCH; Weinheim; 2002.
66. Encyclopedia of Chemical Technology, 5th ed., Kirk-Othmer; Wiley; 2004.
67. Reis, P. M.; Silva, J. A. L.; Fraústo da Silva, J. J. R.; Pombeiro, A. J. L. *J. Chem. Soc., Chem. Commun.* **2000**, 1845.
68. Himes, R. A.; Karlin, K. D. *Curr. Opin. Chem. Biol.* **2009**, *13*, 119.
69. Chan, S. I.; Yu, S. S. F. *Acc. Chem. Res.* **2008**, *41*, 969.
70. Lieberman, R. L.; Rosenzweig, A. C. *Nature* **2005**, *434*, 177.



---

# 3

---

## SELF-ASSEMBLED MULTICOPPER COMPLEXES AND COORDINATION POLYMERS FOR OXIDATION AND HYDROCARBOXYLATION OF ALKANES

ALEXANDER M. KIRILLOV\*, MARINA V. KIRILLOVA\*, AND ARMANDO J. L. POMBEIRO\*

*Centro de Química Estrutural, Instituto Superior Técnico, Universidade de Lisboa, Lisboa, Portugal*

### 3.1 INTRODUCTION

The selective and atom-efficient oxidative functionalization of alkanes under mild conditions, toward the synthesis of various added-value organic products (alcohols, ketones, aldehydes, and carboxylic acids), constitutes a challenge to modern chemistry because of the exceptionally high inertness of these hydrocarbons [1, 2]. An important research direction is toward the search for new bioinspired catalytic systems [1a–3] that are capable of converting alkanes into different oxidation products. Given the recognized biological function of copper and its presence in the active sites of many oxidation enzymes [3, 4], including the multicopper particulate methane monooxygenase (pMMO) [5], the development of new bioinspired multicopper catalysts and efficient alkane functionalization protocols thereof constitutes a subject of high importance.

Recently, we have developed a versatile aqueous medium self-assembly method for the generation of diverse multicopper(II) complexes and coordination polymers derived from cheap and commercially available ligands such as aminoalcohols and benzenecarboxylates [6–15]. The obtained compounds were applied as highly efficient and versatile catalysts or catalyst precursors in two different alkane functionalization reactions. These include the mild oxidation of alkanes (typically cyclohexane as a model substrate) by hydrogen peroxide into alkyl hydroperoxides, alcohols, and ketones [6–9, 11, 16, 17], as well as the hydrocarboxylation of gaseous and liquid  $C_n$  ( $n = 2 – 9$ ) alkanes, by carbon monoxide, water, and potassium peroxodisulfate into the corresponding  $C_{n+1}$  carboxylic acids [12–15, 18–22].

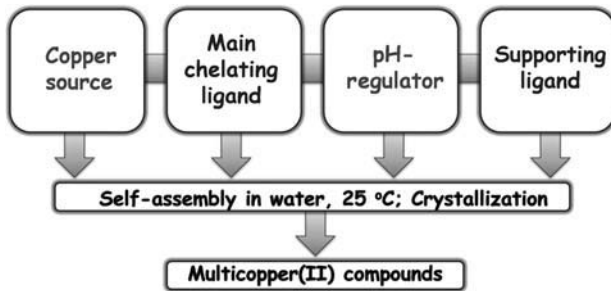
Hence, in this chapter, we describe the principle of aqueous medium self-assembly synthesis, the selected self-assembled aminoalcoholate multicopper(II) complexes and coordination polymers, and their catalytic application in homogeneous oxidative functionalization of alkanes.

### 3.2 SELF-ASSEMBLY SYNTHESIS IN AQUEOUS MEDIUM

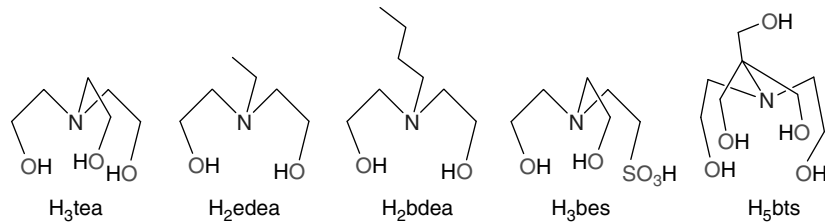
From the environmental and economical viewpoints, water is the ideal green solvent for both the synthesis of coordination compounds and the catalytic transformations of organic molecules including the oxidative functionalization of alkanes [23]. However, the performance of catalytic reactions in aqueous medium typically requires the use of hydrosoluble catalysts that often mimic the functions of enzymes. Although various bioinspired multicopper complexes were synthesized as models of pMMO and related copper-based enzymes [3–5a], those catalysts were often not soluble in water, exhibited modest activities, or were almost not tested in oxidative transformations wherein alkanes are used as substrates.

*Advances in Organometallic Chemistry and Catalysis: The Silver/Gold Jubilee International Conference on Organometallic Chemistry Celebratory Book*, First Edition. Edited by Armando J. L. Pombeiro.

© 2014 John Wiley & Sons, Inc. Published 2014 by John Wiley & Sons, Inc.



**Scheme 3.1** General scheme of self-assembly synthesis. Adapted from Reference 10.



**Scheme 3.2** Aminoalcohols applied in self-assembly synthesis of multicopper(II) compounds.

Bearing the above-mentioned points in mind, we have developed a simple and versatile self-assembly protocol for the synthesis of diverse multicopper(II) complexes and coordination polymers in aqueous medium, under ambient conditions, and using simple and commercially available chemicals (Scheme 3.1). This self-assembly method is based on a combination with water, at room temperature (rt) and in air, of copper source, main chelating ligand, pH-regulator, and supporting ligand or spacer, followed by crystallization [10–15]. As a metal source, simple copper salts such as copper(II) nitrate or acetate were used, whereas triethanolamine ( $H_3\text{tea}$ ) and closely related aminoalcohols [ $N$ -ethyl- and  $N$ -butyldiethanolamine ( $H_2\text{edea}$ ,  $H_2\text{bdea}$ ),  $N,N$ -bis(2-hydroxyethyl)-2-aminoethanesulfonic acid ( $H_3\text{bes}$ ), or bis(2-hydroxyethyl)amino-tris(hydroxymethyl)methane ( $H_5\text{bts}$ )] were applied as main chelating ligands (Scheme 3.2). Alkali or alkaline earth metal hydroxides [ $\text{NaOH}$ ,  $\text{LiOH}$ , or  $\text{Mg}(\text{OH})_2$ ] were utilized as pH-regulators, while the supporting ligands were selected from benzenecarboxylates (e.g., benzoic, terephthalic, or pyromellitic acids), simple inorganic anions (azide, thiocyanate, or tetrafluoroborate), or cyanometallates (e.g.,  $[\text{Fe}(\text{CN})_6]^{3-/4-}$ ) [6, 8–15, 24].

By modifying the type of main chelating ligand, pH-regulator or supporting ligand, we have synthesized a considerable number of aminoalcoholate multicopper compounds, ranging from discrete di-, tri-, and tetracopper(II) complexes, to 1D, 2D, and 3D coordination polymers [6–15, 24]. Many of the obtained compounds are water soluble and have also been tested as catalysts or catalyst precursors in the oxidative functionalization of alkanes. Although some parent compounds are not soluble in water, they can also act as catalyst precursors of active hydrosoluble species on treatment with an acid promoter and/or oxidant [7, 9, 15, 24]. The representative examples of highly active di-, tri-, tetra-, and polynuclear copper catalysts or catalyst precursors are summarized in Table 3.1 and their structures and catalytic behavior are briefly described in the following sections.

### 3.3 AMINOALCOHOLATE MULTICOPPER COMPLEXES AND COORDINATION POLYMERS

The dicopper(II) complexes  $[\text{Cu}_2(\mu-\text{H}_2\text{tea})_2(\text{ba})_2] \cdot 2\text{H}_2\text{O}$  (**1**),  $[\text{Cu}_2(\mu-\text{Hede})_2(\text{NCS})_2]$  (**2**), and  $[\text{Cu}_2(\mu-\text{Hbdea})_2(\text{N}_3)_2]$  (**3**) composed of related dicopper cores were easily self-assembled by the treatment of  $\text{Cu}(\text{NO}_3)_2$  and respective aminoalcohols ( $H_3\text{tea}$ ,  $H_2\text{edea}$ , or  $H_2\text{bdea}$ ) with benzoic acid (for **1**), sodium thiocyanate (**2**), or sodium azide (**3**) in alkaline aqueous solution (Table 3.1) [6, 9, 11]. As a representative example, the structure of **3** is given in Fig. 3.1. It bears two five-coordinate copper atoms that adopt distorted square-pyramidal geometries, being filled by  $N, O_2$ -tridentate  $\mu$ -Hbdea ligands and azide moieties [11].

The discrete tricopper(II) complexes  $[\text{Cu}_3(\mu-\text{H}_2\text{tea})_2(\mu-\text{poba})_2(\text{H}_2\text{O})] \cdot 4\text{H}_2\text{O}$  (**4**) and  $[\text{Cu}_3(\mu_3-\text{BO})(\mu-\text{H}_3\text{bts})_3][\text{BF}_4] \cdot 2\text{H}_2\text{O}$  (**5**) self-assembled from triethanolamine ( $H_3\text{tea}$ ) or Bis-Tris ( $H_5\text{bts}$ ) aminoalcohols are particularly interesting

**TABLE 3.1** Selected Self-Assembled Multicopper(II) Compounds as Catalysts or Catalyst Precursors in Oxidation and Hydrocarboxylation of Alkanes

Compound Number	Formula	Alkane Substrates <sup>a</sup>	References
1	[Cu <sub>2</sub> (μ-H <sub>2</sub> tea) <sub>2</sub> (ba) <sub>2</sub> ] · 2H <sub>2</sub> O	C <sub>6</sub> H <sub>12</sub>	6, 7
2	[Cu <sub>2</sub> (μ-Hdeea) <sub>2</sub> (NCS) <sub>2</sub> ]	Cyclic and linear C <sub>5</sub> –C <sub>8</sub> <sup>b</sup>	9
3	[Cu <sub>2</sub> (μ-Hbdea) <sub>2</sub> (N <sub>3</sub> ) <sub>2</sub> ]	C <sub>6</sub> H <sub>12</sub>	11
4	[Cu <sub>3</sub> (μ-H <sub>2</sub> tea) <sub>2</sub> (μ-poba) <sub>2</sub> (H <sub>2</sub> O)] · 4H <sub>2</sub> O	C <sub>6</sub> H <sub>12</sub> , CH <sub>4</sub> , C <sub>2</sub> H <sub>6</sub>	6, 7
5	[Cu <sub>3</sub> (μ <sub>3</sub> -BO)(μ-H <sub>3</sub> bts) <sub>3</sub> ][BF <sub>4</sub> ] <sup>-</sup> · 2H <sub>2</sub> O	Linear C <sub>2</sub> –C <sub>8</sub> <sup>b</sup> , cyclic C <sub>5</sub> –C <sub>8</sub> <sup>b</sup>	13
6	[Cu <sub>4</sub> (μ <sub>4</sub> -O)(μ <sub>3</sub> -tea) <sub>4</sub> (μ <sub>3</sub> -BOH) <sub>4</sub> ][BF <sub>4</sub> ] <sub>2</sub>	C <sub>6</sub> H <sub>12</sub> , CH <sub>4</sub> , C <sub>2</sub> H <sub>6</sub> , MCH, DMCH, n-C <sub>7</sub> H <sub>16</sub> , n-C <sub>8</sub> H <sub>20</sub> ; linear C <sub>2</sub> –C <sub>8</sub> <sup>b</sup> , cyclic C <sub>5</sub> –C <sub>8</sub> <sup>b</sup>	6, 7, 16–21
7	[Li(H <sub>2</sub> O) <sub>4</sub> ][Cu <sub>4</sub> (μ-Hbes) <sub>4</sub> (μ-ba)] · H <sub>2</sub> O	Linear C <sub>2</sub> –C <sub>9</sub> , <sup>b</sup> cyclic C <sub>5</sub> –C <sub>8</sub> <sup>b</sup>	14
8	[Cu <sub>2</sub> (μ-H <sub>2</sub> tea) <sub>2</sub> (μ <sub>2</sub> -tpa)] <sub>n</sub> · 2nH <sub>2</sub> O	C <sub>6</sub> H <sub>12</sub>	6, 7
9	[Cu <sub>2</sub> (μ <sub>3</sub> -H <sub>2</sub> tea) <sub>2</sub> (μ <sub>4</sub> -pma){Na <sub>2</sub> (H <sub>2</sub> O) <sub>4</sub> }] <sub>n</sub> · 10nH <sub>2</sub> O	C <sub>6</sub> H <sub>12</sub>	8, 9
10	[Cu <sub>6</sub> (μ-H <sub>2</sub> tea) <sub>6</sub> {Fe(μ-CN) <sub>6</sub> }] <sub>n</sub> (NO <sub>3</sub> ) <sub>2n</sub> · 6nH <sub>2</sub> O	C <sub>6</sub> H <sub>12</sub>	24
11	[Cu <sub>4</sub> (μ <sub>3</sub> -Hbes) <sub>2</sub> (μ-Hbes) <sub>2</sub> (μ-phba){Na(H <sub>2</sub> O) <sub>4</sub> }] <sub>n</sub>	C <sub>3</sub> H <sub>8</sub> , n-C <sub>4</sub> H <sub>10</sub> <sup>b</sup>	12
12	[Cu <sub>4</sub> (μ <sub>3</sub> -Hbes) <sub>4</sub> (μ-ba)(Na)] <sub>n</sub>	C <sub>3</sub> H <sub>8</sub> , n-C <sub>4</sub> H <sub>10</sub> <sup>b</sup>	12
13	[Cu <sub>4</sub> (μ <sub>3</sub> -Hbes) <sub>4</sub> (μ-mhba){Li(H <sub>2</sub> O) <sub>2</sub> }] <sub>n</sub> · 3nH <sub>2</sub> O	Linear C <sub>2</sub> –C <sub>9</sub> , <sup>b</sup> cyclic C <sub>5</sub> –C <sub>8</sub> <sup>b</sup>	14
14	[{Cu(H <sub>3</sub> tea)} <sub>2</sub> (μ <sub>4</sub> -pma)] <sub>n</sub>	C <sub>6</sub> H <sub>12</sub>	9
15	[Cu <sub>2</sub> Mg <sub>2</sub> (μ-Htea) <sub>2</sub> (μ <sub>6</sub> -pma)(H <sub>2</sub> O) <sub>6</sub> ] <sub>n</sub> · 6nH <sub>2</sub> O	Linear C <sub>5</sub> –C <sub>9</sub> , <sup>b</sup> cyclic C <sub>5</sub> –C <sub>8</sub> <sup>b</sup>	15

<sup>a</sup>Unless stated otherwise, the substrates were used in oxidation reactions.

<sup>b</sup>Substrates were used in hydrocarboxylation reactions.

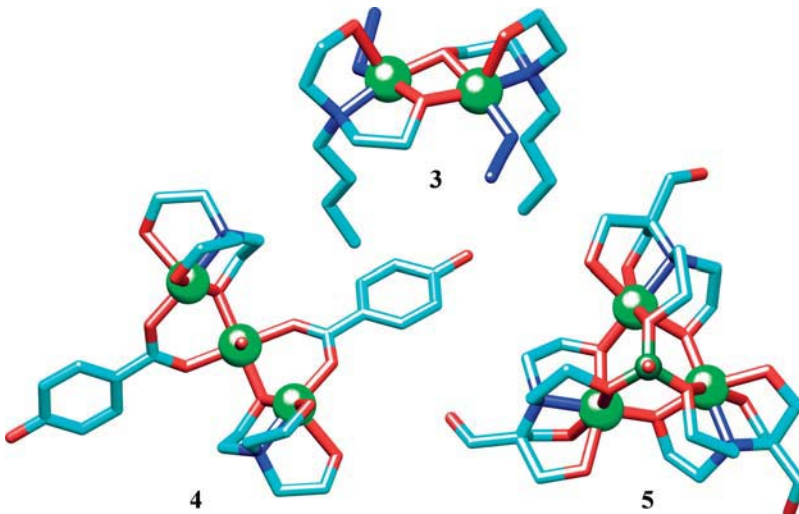


**Figure 3.1** X-ray crystal structures of complexes [Cu<sub>2</sub>(μ-Hbdea)<sub>2</sub>(N<sub>3</sub>)<sub>2</sub>] (**3**), [Cu<sub>3</sub>(μ-H<sub>2</sub>tea)<sub>2</sub>(μ-poba)<sub>2</sub>(H<sub>2</sub>O)] · 4H<sub>2</sub>O (**4**), and [Cu<sub>3</sub>(μ<sub>3</sub>-BO)(μ-H<sub>3</sub>bts)<sub>3</sub>][BF<sub>4</sub>]<sup>-</sup> · 2H<sub>2</sub>O (**5**). All H atoms, [BF<sub>4</sub>]<sup>-</sup> anion (in **5**), and crystallization H<sub>2</sub>O molecules (in **4**, **5**) are omitted for clarity. Color codes: Cu, green balls; O, red; N, blue; C, cyan; B, dark green ball. Adapted from References 6, 11, and 13. (See insert for color representation of the figure.)

examples because of their solubility in water, unusual structural features, and good substrate versatility in the oxidative functionalization of alkanes [6, 7, 13]. The structure of **4** (Fig. 3.1) possesses three five-coordinate Cu(II) atoms that are clustered by two μ-O atoms of H<sub>2</sub>tea and two μ-COO groups of 4-oxybenzoate(2-) into a nonplanar {Cu<sub>3</sub>(μ-O)<sub>2</sub>(μ-COO)<sub>2</sub>} core, wherein the “central” Cu atom has a labile H<sub>2</sub>O ligand [6]. The structure of **5** (Fig. 3.1) possesses a [Cu<sub>3</sub>(μ<sub>3</sub>-BO)(H<sub>3</sub>L)<sub>3</sub>]<sup>+</sup> cluster cation, wherein the six-coordinate Cu centers are interconnected by the μ-O atoms from three pentadentate H<sub>3</sub>bts ligands acting in a *N,O*<sub>4</sub>-coordination mode [13]. An additional stabilization of the structure is achieved by a μ<sub>3</sub>-BO moiety that simultaneously binds to other μ-O atoms from H<sub>3</sub>bts [13].

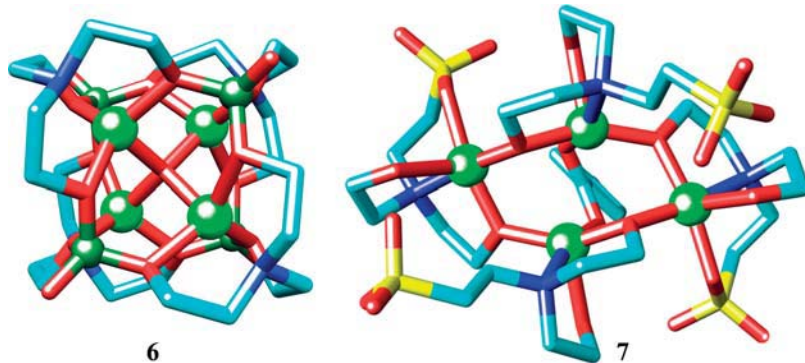


**Figure 3.2** X-ray crystal structures of complexes  $[\text{Cu}_4(\mu_4\text{-O})(\mu_3\text{-tea})_4(\mu_3\text{-BOH})_4][\text{BF}_4]_2$  (**6**) and  $[\text{Li}(\text{H}_2\text{O})_4][\text{Cu}_4(\mu\text{-Hbes})_4(\mu\text{-ba})]\cdot\text{H}_2\text{O}$  (**7**). All H atoms,  $[\text{BF}_4]^-$  anions (in **6**),  $[\text{Li}(\text{H}_2\text{O})_4]^+$  cations, and crystallization  $\text{H}_2\text{O}$  molecules (in **7**) are omitted for clarity. Color codes: Cu, green balls; O, red; N, blue; C, cyan; B, dark green balls. Adapted from References 6 and 14. (See insert for color representation of the figure.)

There are also two different aminoalcoholate tetracopper(II) cores in the discrete tetracopper(II) complexes,  $[\text{Cu}_4(\mu_4\text{-O})(\mu_3\text{-tea})_4(\mu_3\text{-BOH})_4][\text{BF}_4]_2$  (**6**) and  $[\text{Li}(\text{H}_2\text{O})_4][\text{Cu}_4(\mu\text{-Hbes})_4(\mu\text{-ba})]\cdot\text{H}_2\text{O}$  (**7**) [6, 14]. The triethanolamine Cu(II) complex **6** is the most remarkable multicopper catalyst, in view of its high solubility and stability in aqueous medium, facile self-assembly synthesis from simple and cheap chemicals [6], recyclability [7], high efficiency, and substrate versatility for the oxidation [6, 7, 16, 17] and hydrocarboxylation [18–21] of various alkanes [17, 18]. The intricate cage-like structure of **6** (Fig. 3.2) features four Cu(II) atoms that are clustered via the triethanolamine  $\mu_3\text{-O}$  atoms and  $\mu_3\text{-BOH}$  groups, being further stabilized by the “central”  $\mu_4\text{-O}$  oxo atom [6]. The hydrosoluble tetracopper(II) compound **7** [14] derived from a well-known biobuffer H<sub>3</sub>bes (Scheme 3.2) bears the  $[\text{Cu}_4(\mu\text{-Hbes})_4(\mu\text{-ba})]^-$  anion, which is constructed from two pairs of Cu atoms, four  $\mu\text{-O}$  bridging Hbes ligands, and one  $\mu\text{-COO}$  benzoate ligand (Fig. 3.2). All four Cu atoms act as square pyramids fused via common vertexes into the  $\{\text{Cu}_4(\mu\text{-O})_4(\mu\text{-COO})\}$  cluster cores, wherein the copper centers are almost coplanar [14].

A number of aminoalcoholate copper(II) coordination polymers were applied as catalyst precursors in oxidative functionalization of alkanes [6–9, 14, 15, 22, 24]. Although coordination polymers are typically used in heterogeneous catalysis [25], compounds that are soluble in aqueous and/or organic medium can also act as catalyst precursors in homogeneous catalysis. Selected examples of coordination polymers obtained by aqueous medium self-assembly protocol concern the compounds **8–15** (Table 3.1), several types of which can be identified on the basis of the nature of ligands and nuclearity of the Cu-containing building blocks. The first type includes the polymers  $[\text{Cu}_2(\mu\text{-H}_2\text{tea})_2(\mu_2\text{-tpa})]_n\cdot 2n\text{H}_2\text{O}$  (**8**) [6],  $[\text{Cu}_2(\mu_3\text{-H}_2\text{tea})_2(\mu_4\text{-pma})\{\text{Na}_2(\text{H}_2\text{O})_4\}]_n\cdot 10n\text{H}_2\text{O}$  (**9**) [8], and  $[\text{Cu}_6(\mu\text{-H}_2\text{tea})_6\{\text{Fe}(\mu\text{-CN})_6\}]_n(\text{NO}_3)_2n\cdot 6n\text{H}_2\text{O}$  (**10**) [24]. These bear dimeric  $[\text{Cu}_2(\mu\text{-aminoalcoholate})_2]^{2+}$  units (similar to those in **1–3**), which are assembled into 1D (**8**), 2D (**9**), and 3D (**10**) coordination networks through different linkers (Fig. 3.3) based on aromatic carboxylates or  $[\text{Fe}(\text{CN})_6]^{4-}$  moieties [6, 8, 24]. A particularly interesting example concerns the highly water-soluble compound **9** assembled from dicopper(II) triethanolamate and aqua-sodium building blocks, and  $\mu_4^-$  pyromellitate linkers (Fig. 3.3) [8].

The coordination polymers **11–13** represent another type of compounds that contain tetracopper(II)  $[\text{Cu}_4(\mu\text{-Hbes})_4(\mu\text{-benzenecarboxylate})]^-$  building blocks similar to that of the discrete complex **7**, but assembled into 1D (**11**) or 3D (**12,13**) coordination networks through bridging and charge-balancing  $\{\text{Na}\}^+$ ,  $\{\text{Na}(\text{H}_2\text{O})_4\}^+$ , or  $\{\text{Li}(\text{H}_2\text{O})_2\}^+$  moieties [12, 14]. Other coordination polymers also include the 1D network  $[\{\text{Cu}(\text{H}_3\text{tea})\}_2(\mu_4\text{-pma})]_n$  (**14**) built from the cationic monocupper  $\{\text{Cu}(\text{H}_3\text{tea})\}^{2+}$  units and  $\mu_4\text{-pma}(4-)$  linkers [9]. In the related compound  $[\text{Cu}_2\text{Mg}_2(\mu\text{-Htea})_2(\mu_6\text{-pma})(\text{H}_2\text{O})_6]_n\cdot 6n\text{H}_2\text{O}$  (**15**), two  $\{\text{Cu}(\mu\text{-Htea})\}^+$  fragments are clustered with a  $\{\text{Mg}(\text{H}_2\text{O})_2\}^{2+}$  moiety and  $\mu_6\text{-pma}(4-)$  spacer, forming an unusual heterometallic  $\{\text{Cu}_2\text{Mg}(\mu\text{-O})_2(\mu\text{-COO})_2\}^-$  core [15]. Such cores are further assembled by  $\{\text{Mg}(\text{H}_2\text{O})_4\}^{2+}$  linkers and  $\mu_6\text{-pma}$  ligands into 2D metal–organic sheets [15].

### 3.4 APPLICATION IN ALKANE OXIDATION

The multicopper(II) complexes and coordination polymers **1, 3, 4, 6, 8–10**, and **14** (Table 3.1) act as efficient catalyst or catalyst precursors toward the mild oxidation of cyclohexane by hydrogen peroxide. This cycloalkane is typically used as a

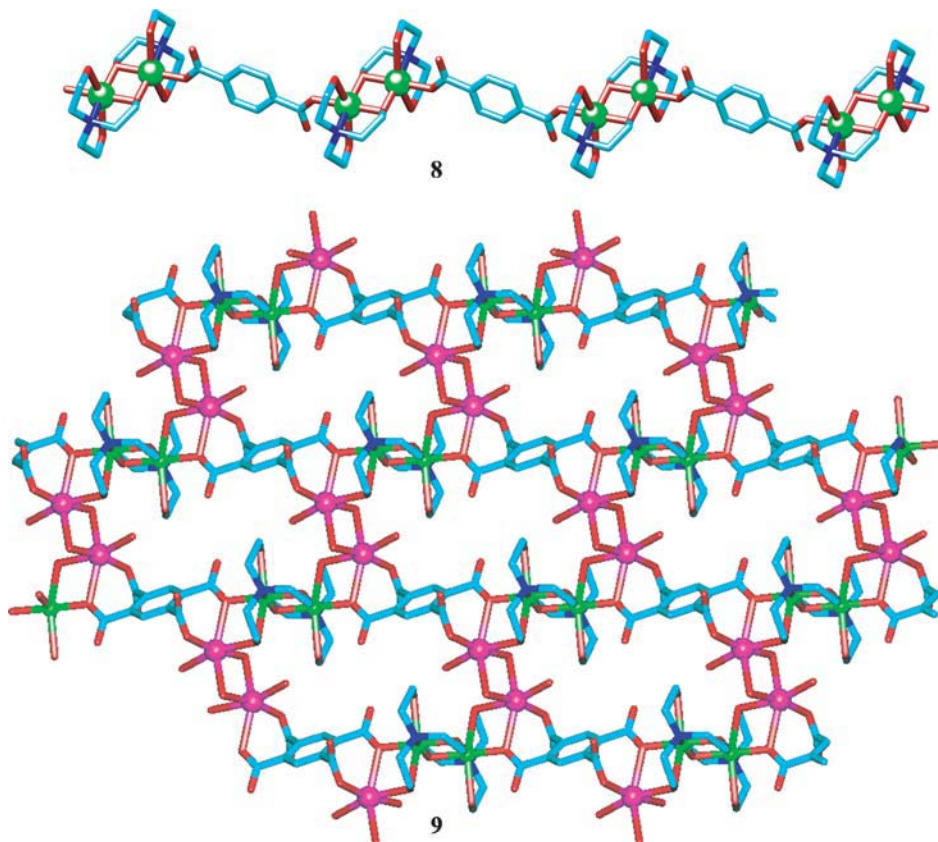
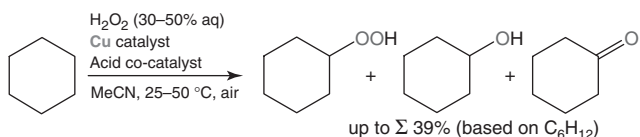


**Figure 3.3** X-ray crystal structures of 1D and 2D polymers  $[\text{Cu}_2(\mu\text{-H}_2\text{tea})_2(\mu_2\text{-tpa})]_n \cdot 2n\text{H}_2\text{O}$  (**8**) and  $[\text{Cu}_2(\mu_3\text{-H}_2\text{tea})_2(\mu_4\text{-pma})\{\text{Na}_2(\text{H}_2\text{O})_4\}]_n 10n\text{H}_2\text{O}$  (**9**), respectively. All H atoms and crystallization  $\text{H}_2\text{O}$  molecules are omitted for clarity. Color codes: Cu, green balls; O, red; N, blue; C, cyan; Na, magenta. Adapted from References 6 and 8. (See insert for color representation of the figure.)



**Scheme 3.3** Mild oxidation of cyclohexane to cyclohexyl hydroperoxide (primary product), and cyclohexanol and cyclohexanone (final products). Adapted from Reference 11.

recognized model substrate, in view of the importance of its oxidation products. In fact, cyclohexanol and cyclohexanone are intermediates in nylon-6,6' and polyamide-6 production [26, 27]. Although the industrial Dupont process undergoes at approximately 150 °C using air as oxidant (~12 atm) and cobalt(III) naphthenate as a homogeneous catalyst, its main limitation consists in achieving only 4% cyclohexane conversion with 85% selectivity to the main products [7, 27]. Therefore, the search for new, more efficient, and selective protocols of cyclohexane oxidation continues to be an important research direction.

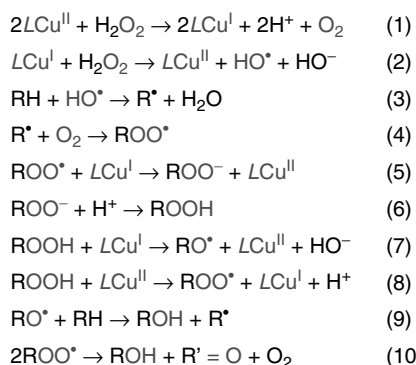
Hence, in the presence of various multicopper catalytic systems [6, 7, 9, 11, 16, 24],  $\text{C}_6\text{H}_{12}$  is oxidized by aq.  $\text{H}_2\text{O}_2$  into a mixture of cyclohexyl hydroperoxide (CyOOH, main primary product), cyclohexanol and cyclohexanone that are the major final products after the autodecomposition of CyOOH or its reduction with  $\text{PPh}_3$  [28]. This mild oxidation of cyclohexane (Scheme 3.3) proceeds in aqueous MeCN, under atmospheric pressure, at rt or with a slight heating (50 °C), and in the presence of an acid cocatalyst (typically  $\text{HNO}_3$ ). Among the tested multicopper(II) compounds, the activity in terms of total yields (moles of oxidation products per 100 moles of substrate) follows the trend: **6** (39%) > **4** (37%) > **3** (31%) > **9** (29%) > **10** (17%) > **8** (16%) > **1** (15%).

As indicated earlier, the multicopper(II) catalytic systems require the presence of an acid cocatalyst (promoter). Nitric acid was used (typically 10 equiv relative to Cu compound) as a reference cocatalyst and the activity of Cu compounds depends significantly on the amount of this acid [7, 9, 11, 24]. For the compounds **3** [11], **6** [16], and **10** [24], the effects of other acid cocatalysts were studied. In the case of the dicopper complex  $[\text{Cu}_2(\mu\text{-Hbdea})_2(\text{N}_3)_2]$  (**3**), the promoting effect of various acid cocatalysts in the  $\text{C}_6\text{H}_{12}$  oxidation by  $\text{H}_2\text{O}_2$  follows the trend  $\text{CF}_3\text{COOH} > \text{HNO}_3 \geq \text{HCl} > \text{H}_2\text{SO}_4 >> \text{CH}_3\text{COOH}$  [11]. The type of acid cocatalyst is also a relevant factor that affects the reaction rate [16] in the cyclohexane oxidation catalyzed by  $[\text{Cu}_4(\mu_4\text{-O})(\mu_3\text{-tea})_4(\mu_3\text{-BOH})_4]\text{[BF}_4\text{]}_2$  (**6**), wherein all strong acids exhibit a noticeable promoting effect. However, the reaction is very fast only in the presence of HCl, being one order faster than those promoted by the other acids ( $\text{HNO}_3$ ,  $\text{CF}_3\text{COOH}$ , and  $\text{H}_2\text{SO}_4$ ), resulting thus in the high turnover frequencies (TOFs) of circa  $600 \text{ h}^{-1}$  [16]. Another remarkable promoting behavior of HCl over  $\text{HNO}_3$  was observed in the  $\text{C}_6\text{H}_{12}$  oxidation catalyzed by  $[\text{Cu}_6(\mu\text{-H}_2\text{tea})_6\{\text{Fe}(\mu\text{-CN})_6\}]_n(\text{NO}_3)_2n \cdot 6n\text{H}_2\text{O}$  (**10**) [24]. The role of the acid cocatalyst presumably consists in (i) promoting proton transfer steps, (ii) activation of catalyst by unsaturation of the Cu(II) centers on ligand protonation, (iii) enhancement of oxidative properties of the catalyst and  $\text{H}_2\text{O}_2$ , (iv) facilitation of the formation of peroxy complexes, and (v) preventing the decomposition of  $\text{H}_2\text{O}_2$  to water and oxygen [7, 11, 16].

Besides the type and the amount of cocatalyst, the efficiency of Cu-catalyzed oxidations significantly depends on other factors, such as the amounts of oxidant (typically two- to fivefold molar excess relatively to substrate), catalyst (typically 1–3 mol% vs  $\text{C}_6\text{H}_{12}$ ), and solvent (MeCN/ $\text{H}_2\text{O}$ ), reaction temperature, and time. To optimize the cyclohexane oxidation, the effects of these parameters were studied in detail for compounds **1** [7], **3** [11], **4** [7], **6** [7, 16], **8** [7], and **9** [9]. The mild oxidation of  $\text{C}_6\text{H}_{12}$  undergoes in aqueous acetonitrile medium, where water usually appears with aq.  $\text{H}_2\text{O}_2$  and/or the catalyst solution. The use of the mixed MeCN/ $\text{H}_2\text{O}$  solvent is essential to solubilize both substrate and catalyst, as the oxidation of cyclohexane does not occur to a considerable extent only in water as a sole solvent [7]. Another feature of the catalysts  $[\text{Cu}_4(\mu_4\text{-O})(\mu_3\text{-tea})_4(\mu_3\text{-BOH})_4]\text{[BF}_4\text{]}_2$  (**6**) and  $[\text{Cu}_2(\mu_3\text{-H}_2\text{tea})_2(\mu_4\text{-pma})\{\text{Na}_2(\text{H}_2\text{O})_4\}]_n \cdot 10n\text{H}_2\text{O}$  (**9**) consists in the possibility of their recycling [7, 9], because they can maintain almost full activity even after five (**6**) or three (**9**) reaction cycles in the cyclohexane oxidation.

The complexes **4** and **6** can also be applied for the oxidation of inert gaseous alkanes, methane, and ethane, although less effectively than in the case of cyclohexane [6]. Thus, methanol (TON = 47, 2.2% yield) and ethanol (TON = 23, 2.1% yield) are obtained in the oxidation of  $\text{CH}_4$  and  $\text{C}_2\text{H}_6$ , respectively, using the **6**/ $\text{HNO}_3/\text{H}_2\text{O}_2$  system [6]. Besides, bond-, regio-, and stereoselectivity studies were carried out [16, 17] with the most versatile catalyst **6** in the oxidation by  $\text{H}_2\text{O}_2$  of methylcyclohexane (MCH), *cis*- and *trans*-1,2-dimethylcyclohexanes (*cis*- and *trans*-DMCH), *n*-heptane, and *n*-octane. The observed selectivity parameters suggest the involvement of hydroxyl radicals as active oxidizing species [16]. The radical type of mechanism was also supported by studying the effects of various C- and O-centered radical traps [CBrCl<sub>3</sub>, 2,2,6,6-tetramethylpiperidine-1-oxyl (TEMPO), and diphenylamine], which strongly decrease the yields of main products in cyclohexane oxidation [7].

A simplified mechanistic pathway (Scheme 3.4) in Cu-catalyzed alkane oxidations by  $\text{H}_2\text{O}_2$  involves the H-abstraction from alkane (RH) presumably by the hydroxyl radical  $\text{HO}^\bullet$ , generated through the Cu-assisted decomposition of  $\text{H}_2\text{O}_2$  (reactions 1, 2), furnishing the alkyl radical  $\text{R}^\bullet$  (reaction 3) [1a, 16, 28, 29]. Then  $\text{R}^\bullet$  rapidly reacts with  $\text{O}_2$  to form



**Scheme 3.4** Simplified mechanism for the Cu-catalyzed oxidation of alkanes (RH) by  $\text{H}_2\text{O}_2$  to alkyl hydroperoxides (ROOH), alcohols (ROH), and ketones ( $\text{R}'=\text{O}$ ). Multicopper catalyst precursor and derived species are schematically depicted as  $\text{LCu}^{\text{II}}$  and  $\text{LCu}^{\text{I}}$ . Adapted from Reference 16.

the organoperoxy radical  $\text{ROO}^\bullet$  (reaction 4). The  $\text{ROO}^\bullet$  can be reduced by a  $\text{LCu(I)}$  species to the corresponding anion that is further converted into the main primary alkyl hydroperoxide product,  $\text{ROOH}$  (reactions 5, 6). This undergoes the Cu-assisted homolytic decomposition giving the alkoxyl  $\text{RO}^\bullet$  and alkylperoxy  $\text{ROO}^\bullet$  radicals (reactions 7, 8). The  $\text{RO}^\bullet$  radicals are converted to the alcohol ( $\text{ROH}$ ) by H-abstraction from the alkane (reaction 9), whereas the peroxy radicals dismutate (reaction 10) to yield both the alcohol and the ketone ( $\text{R}' = \text{O}$ ) [2a, 16, 28, 30].

### 3.5 APPLICATION IN ALKANE HYDROCARBOXYLATION

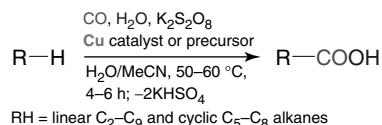
The direct carboxylation of alkanes by CO to give carboxylic acids is a very attractive transformation [12–15, 18–22], as aliphatic carboxylic acids are important commodity chemicals [27]. However, their industrial synthetic methods still represent a number of limitations [20, 27], such as the use of relatively expensive olefins and aldehydes as starting materials, the requirement of harsh reaction conditions, multistage transformations, and expensive metal catalysts.

We have recently developed a new and cleaner method for the direct and highly efficient hydrocarboxylation of various  $C_n$  alkanes into the corresponding  $C_{n+1}$  carboxylic acids [18, 31]. It consists in reacting an alkane with CO,  $\text{H}_2\text{O}$ , and  $\text{K}_2\text{S}_2\text{O}_8$ , and in the presence of Cu-catalyst (Scheme 3.5). In contrast to prior alkane carboxylation methods [32, 33], this protocol does not require absolute trifluoroacetic acid as a solvent, and undergoes efficiently at mild temperatures ( $50\text{--}60^\circ\text{C}$ ) and in aqueous acid-solvent-free medium ( $\text{H}_2\text{O}/\text{MeCN}$  mixed solvent), wherein water also plays a main role as a reagent, apart from being a component of the solvent system [18].

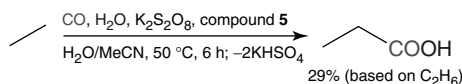
Interestingly, these hydrocarboxylation reactions also occur to some extent in metal-free systems, but the reaction efficiency can be improved significantly by the use of metal catalysts or promoters [18]. Among the variety of different transition metal catalysts, multicopper(II) compounds were usually the most active ones [18, 20], leading to product yields that are circa two to five times superior to those in the metal-free systems. The water-soluble tetracopper(II) complex  $[\text{Cu}_4(\mu_4\text{-O})(\mu_3\text{-tea})_4(\mu_3\text{-BOH})_4][\text{BF}_4]_2$  (**6**) was formerly used as a model catalyst in the hydrocarboxylations of  $\text{C}_2\text{--}\text{C}_6$  alkanes [18, 31]. Since then, the reactions have been optimized further [19–21] and extended to other alkanes and multicopper catalysts, namely including the dimer **2** [22], the trimer **5** [13], the tetramer **7** [14], and the polymers **11** [12], **12** [12], **13** [14], and **15** [15] (Table 3.1). Interestingly, in contrast to alkane oxidation, the hydrocarboxylation reactions do not require an acid cocatalyst.

Although the hydrocarboxylation of methane to acetic acid has so far been unsuccessful [18, 19], other quite inert gaseous  $\text{C}_2\text{--}\text{C}_4$  alkanes can be transformed into the corresponding  $C_{n+1}$  carboxylic acids, when using the compounds **5**, **6**, **7**, and **11–13** as catalysts or catalyst precursors. Owing to the presence of only primary carbon atoms,  $\text{C}_2\text{H}_6$  is the least reactive alkane, the selective transformation of which to propanoic acid occurs with reasonable efficiency (up to 29% yield based on substrate) in the presence of **5** [13] (Scheme 3.6).

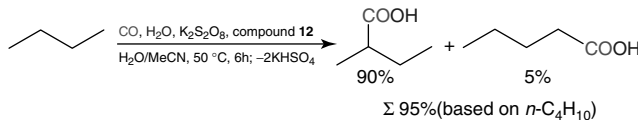
Similarly, propane can be transformed into a mixture of 2-methylpropanoic and butanoic acids, whereas *n*-butane gives 2-methylbutanoic and pentanoic acids [12, 18, 19]. Although the yields of linear carboxylic acids typically do not exceed 5–9%, the presence of significantly more reactive secondary carbon atoms in these alkanes facilitates their efficient conversion into the branched acids (main products). In these hydrocarboxylation reactions, the hydrosoluble compounds **7** and **11–13** are highly active, exhibiting comparable product yields because of the presence of resembling tetracopper(II)  $\{\text{Cu}_4(\mu\text{-Hbes})(\mu\text{-COO})\}^-$  cores [12, 14]. The maximum total yields of carboxylic acids attain values of 78% and 95% (Scheme 3.7) when using catalyst precursor **12** in the reactions of  $\text{C}_3\text{H}_8$  and *n*- $\text{C}_4\text{H}_{10}$ , respectively [12].



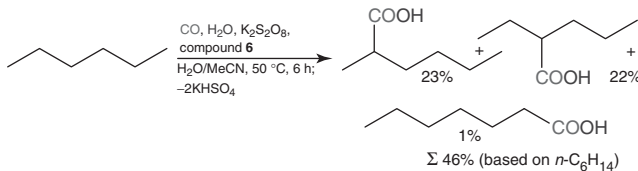
**Scheme 3.5** General scheme for the hydrocarboxylation of  $\text{C}_n$  alkanes to  $\text{C}_{n+1}$  carboxylic acids. Adapted from Reference 18.



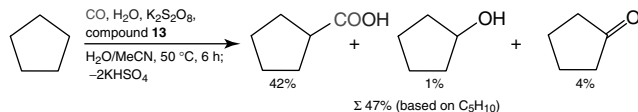
**Scheme 3.6** Hydrocarboxylation of ethane to propanoic acid.



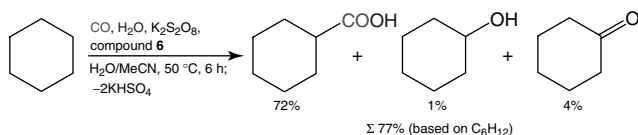
**Scheme 3.7** Hydrocarboxylation of *n*-butane to 2-methylbutanoic and propanoic acids.



**Scheme 3.8** Hydrocarboxylation of *n*-hexane to 2-methylhexanoic, 2-ethylpentanoic, and heptanoic acids.



**Scheme 3.9** Hydrocarboxylation of cyclopentane to cyclopentanecarboxylic acid (major product). Cyclopentanol and cyclopentanone are formed as by-products of oxidation.

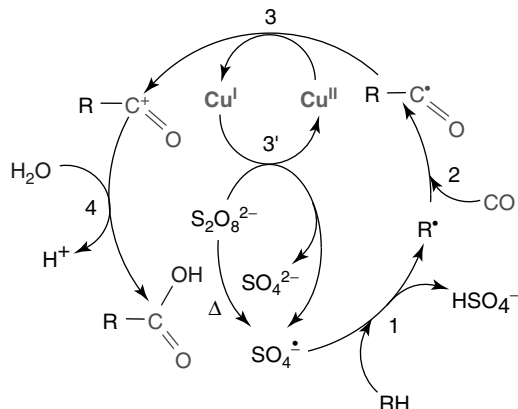


**Scheme 3.10** Hydrocarboxylation of cyclohexane to cyclohexanecarboxylic acid (major product). Cyclohexanol and cyclohexanone are formed as by-products of oxidation.

Multicopper(II) catalytic systems are also efficient in the hydrocarboxylation of linear  $\text{C}_5\text{--C}_9$  alkanes [14, 15, 18, 21, 22], generating a mixture of isomeric monocarboxylic acids. Branched acids are the major products derived from the hydrocarboxylation at different secondary C(2), C(3), C(4), or C(5) carbon atoms of the alkane chain, while the corresponding fatty acids are formed in minor amounts (<2% yield). *n*-Pentane and *n*-hexane (Scheme 3.8) are more reactive substrates, giving 39% and 46% total product yields when using catalysts **2** and **6**, respectively [14, 21]. The hydrocarboxylation reactions of higher alkanes are less efficient [14, 21, 22], leading to the maximum total product yields of 26% (*n*- $\text{C}_7\text{H}_{16}$ ), 22% (*n*- $\text{C}_8\text{H}_{18}$ ), and 18% (*n*- $\text{C}_9\text{H}_{20}$ ), when using catalyst precursors **13**, **2**, and **6**, respectively.

Cyclic  $\text{C}_5\text{--C}_8$  alkanes also undergo hydrocarboxylation to give the corresponding cycloalkanecarboxylic acids [13–15, 18, 20, 22]. The formation of only one carboxylic acid product is observed because of the presence of a single type of carbon atoms in these cycloalkanes. Cyclopentane and cyclohexane were the most reactive cycloalkane substrates [13, 14, 20]. Their transformations (Schemes 3.9 and 3.10) result in cyclopentanecarboxylic and cyclohexanecarboxylic acids in up to 42% (with **13**) and 72% (with **6**) yields, respectively [14, 18]. The hydrocarboxylation reactions of cycloheptane and cyclooctane are less efficient [14, 15], with the highest yields of cycloheptanecarboxylic (29%) and cyclooctanecarboxylic (14%) acids achieved in the presence of **7** and **15**, respectively. In contrast to linear alkanes, the reactions involving cycloalkanes as substrates [13–15, 18, 20, 22] also generate the oxidation products (cyclic ketones and alcohols).

Given the high activity of the tetracopper(II) complex **6**, the hydrocarboxylations of ethane, propane, *n*-butane, *n*-pentane, cyclopentane, *n*-hexane, and cyclohexane were optimized to a variety of reaction parameters, including solvent composition, temperature, time, CO pressure, and relative amounts of substrate, oxidant, and catalyst [18–21]. The solvent composition is a reaction parameter of crucial importance [18, 19], as the hydrocarboxylation reactions practically do not occur in either only  $\text{H}_2\text{O}$  or only  $\text{MeCN}$ , or in the absence of both of them. Acetonitrile solubilizes the organic species, while water



**Scheme 3.11** Simplified mechanism for the Cu-catalyzed hydrocarboxylation of alkanes (RH) to carboxylic acids (RCOOH). Adapted from Reference 14.

dissolves the catalyst and peroxodisulfate oxidant, also providing the main source of the hydroxyl group for the carboxylic acid. The optimal solvent compositions for linear and cyclic alkanes typically consist of 1 : 2 or 1 : 1  $\text{H}_2\text{O}/\text{MeCN}$  volumetric ratios, respectively [18–21]. The use of  $\text{K}_2\text{S}_2\text{O}_8$  is also indispensable, as it acts as both a radical initiator and an oxidant, and the hydrocarboxylation reactions do not occur in its absence or on its substitution for  $\text{O}_2$ ,  $\text{H}_2\text{O}_2$ , or  $t\text{-BuOOH}$  [14, 18, 19]. An important feature consists in the fact that  $\text{K}_2\text{S}_2\text{O}_8$  is almost quantitatively transformed during the reaction to give  $\text{KHSO}_4$  [18, 20], which can be easily crystallized, separated by filtration, and potentially reconverted to peroxodisulfate via established electrochemical processes [18–20].

A simplified mechanistic pathway (Scheme 3.11) was proposed [14, 15, 18] for the Cu-catalyzed hydrocarboxylation of various alkanes (RH) on the basis of experimental data, including the analysis of various selectivity parameters [14, 18–21], tests with radical traps [18–20] and  $^{18}\text{O}$ -labeled  $\text{H}_2\text{O}$  [18], DFT calculations, and other studies [18, 33]. It includes the following steps [12–15, 18–22]: (1) generation of the alkyl radicals  $\text{R}^{\bullet}$  from an alkane [formed via H-abstraction by sulfate radical  $\text{SO}_4^{\cdot-}$  derived from  $\text{K}_2\text{S}_2\text{O}_8$ ], (2) carbonylation of  $\text{R}^{\bullet}$  by CO to form the acyl radicals  $\text{RCO}^{\bullet}$ , (3) oxidation of  $\text{RCO}^{\bullet}$  by copper(II) species to the acyl cations  $\text{RCO}^+$  (with concomitant formation of  $\text{Cu}(\text{I})$  species), (3') the regeneration of the Cu(II) species on oxidation of Cu(I) by  $\text{K}_2\text{S}_2\text{O}_8$ , and (4) the hydrolysis of  $\text{RCO}^+$  to furnish the carboxylic acid products. The step (4) was also confirmed [18] on the basis of experiments with  $^{18}\text{O}$ -labeled  $\text{H}_2\text{O}$  in the hydrocarboxylation of  $\text{C}_6\text{H}_{12}$ , and theoretical calculations on ethane hydrocarboxylation. The active role of sulfate radical  $\text{SO}_4^{\cdot-}$  was supported by various selectivity tests, while the involvement of alkyl radicals was also proved by performing carboxylation reactions in the presence of the carbon-centered radical trap  $\text{CBrCl}_3$  [18–20].

The described alkane hydrocarboxylations show a number of important features. In particular, very high product yields (up to 95% based on alkane) can be attained [12–15, 18–22], especially considering the exceptional inertness of saturated hydrocarbons and the fact that such reactions involve C–H bond cleavage, C–C bond formation, and proceed in an acid-solvent-free  $\text{H}_2\text{O}/\text{MeCN}$  medium and at very mild temperatures (50–60 °C). Besides, these hydrocarboxylation reactions contrast with most of the state-of-the-art processes [1, 2] for the relatively mild transformations of alkanes that require the use of strongly acidic reaction media, such as concentrated trifluoroacetic or sulfuric acid, or a superacid.

### 3.6 CONCLUDING REMARKS

This chapter showed that various multicopper(II) complexes and coordination polymers bearing different di-, tri-, and tetracopper aminoalcoholate cores can be easily generated by aqueous medium self-assembly method, using simple and commercially available chemicals. Apart from representing a number of important features (e.g., solubility in water and structural diversity), these multicopper(II) compounds act as highly efficient catalysts or catalyst precursors for the oxidation and hydrocarboxylation of various alkanes, under mild conditions. Although the described single-pot protocols for the Cu-catalyzed transformation of alkanes to alcohols, ketones, or carboxylic acids are characterized by a variety of advantages (i.e., high yields, mild reaction conditions, use of aqueous medium, and good substrate versatility and selectivity), further exploration and optimization of both alkane oxidation and hydrocarboxylation reactions to overcome some limitations

of the current systems should be continued. These consist of searching for other cheaper and cleaner oxidants and solvents, carbonylating agents, recyclable catalysts, and more favorable reaction conditions.

Although a rational design of highly efficient and versatile metal complex catalysts still remains a difficult task, the analysis of multicopper compounds that have already shown recognized applications in the oxidation and hydrocarboxylation of alkanes helps to identify some favorable requirements for a desirable homogeneous copper catalyst. These include (i) the presence of *N,O*-ligands or environment, (ii) low coordination numbers (i.e., 4 and/or 5) of Cu centers that preferably possess labile ligands, (iii) high stability of the multicopper cores with relatively close separations of Cu atoms, (iv) solubility and stability of catalysts in water and/or aqueous acetonitrile medium, and (v) their easy preparation from simple, cheap, and commercially available chemicals. We believe that future research in the field of Cu-catalyzed oxidative functionalization of alkanes should envisage the development of both synthetic and catalytic directions, by widening the type of multicopper(II) catalysts, alkane substrates, and the respective catalytic transformations.

## ABBREVIATIONS

aq.	Aqueous
Bis-Tris	See H <sub>5</sub> bts
cis-DMCH	cis-1,2-Dimethylcyclohexane
CyOOH	Cyclohexyl hydroperoxide
DFT	Density functional theory
equiv	Equivalents
GC	Gas chromatography
H <sub>2</sub> bdea	<i>N</i> -Butyldiethanolamine
H <sub>2</sub> edea	<i>N</i> -Ethyldiethanolamine
H <sub>2</sub> tpa	Terephthalic acid
H <sub>3</sub> bes	<i>N,N</i> -Bis(2-hydroxyethyl)-2-aminoethanesulfonic acid
H <sub>3</sub> tea	Triethanolamine
H <sub>4</sub> pma	Pyromellitic acid
H <sub>5</sub> bts	Bis-Tris (bis(2-hydroxyethyl)amino-tris(hydroxymethyl)methane)
Hba	Benzoic acid
Hmhba	3-Hydroxybenzoic acid
Hphba	4-Hydroxybenzoic acid
MCH	Methylcyclohexane
pMMO	Particulate methane monooxygenase
poba	4-Oxybenzoate(2-)
rt	Room temperature (20–25 °C)
TEMPO	2,2,6,6-Tetramethylpiperidine-1-oxyl
TOF	Catalyst turnover frequency (moles of products per mol of catalyst per hour)
TON	Catalyst turnover number (moles of products per mol of catalyst)
trans-DMCH	trans-1,2-Dimethylcyclohexane.

## ACKNOWLEDGMENTS

This work was supported by the Foundation for Science and Technology (FCT) (projects PTDC/QUI-QUI/102150/2008, PTDC/QUI-QUI/121526/2010, and PEst-OE/QUI/UI0100/2013), Portugal. Thanks are also due to all the coauthors of joint publications, namely Dr. M. F. C. Guedes da Silva and Prof. M. Haukka for the X-ray structural analyses.

## REFERENCES

1. (a) Shilov, A. E.; Shul'pin, G. B. *Activation and Catalytic Reactions of Saturated Hydrocarbons in the Presence of Metal Complexes*; Kluwer Academic Publishers: Dordrecht, **2000**; (b) Olah, G. A.; Molnár, Á. *Hydrocarbon Chemistry*; John Wiley & Sons, Inc.: Hoboken, NJ, **2003**.

2. (a) Shul'pin, G. B. *Mini-Rev. Org. Chem.* **2009**, *6*, 95; (b) Díaz-Requejo, M. M.; Pérez, P. J. *Chem. Rev.* **2008**, *108*, 3379. (c) Labinger, J. A.; Bercaw, J. E. *Nature* **2002**, *417*, 507; (d) Fokin, A. A.; Schreiner, P. R. *Chem. Rev.* **2002**, *102*, 1551; (e) Sen, A. *Acc. Chem. Res.* **1998**, *31*, 550; (f) Shilov, A. E.; Shul'pin, G. B. *Chem. Rev.* **1997**, *97*, 2879.
3. (a) Brissos, R. S.; Garcia, S.; Presa, A.; Gamez, P. *Comment. Inorg. Chem.* **2011**, *32*, 219; (b) Gamez, P.; Aubel, P. G.; Driessens, W. L.; Reedijk, J. *Chem. Soc. Rev.* **2001**, *30*, 376; (c) Mirica, L. M.; Ottenwaelder, X.; Stack, T. D. P.; *Chem. Rev.* **2004**, *104*, 1013; (d) Lewis, E. A.; Tolman, W. B. *Chem. Rev.* **2004**, *104*, 1047.
4. (a) Itoh, S. In *Comprehensive Coordination Chemistry*, 2nd ed.; McCleverty, J. A., Meyer, T. J., Que, L., Tolman, W. B., Eds.; Elsevier: Dordrecht, **2003**; Vol. 8, pp 369–393, Chapter 8.15; (b) Lee, D. H. In *Comprehensive Coordination Chemistry*, 2nd ed.; McCleverty, J. A.; Meyer, T. J.; Que, L.; Tolman, W. B., Eds.; Elsevier: Dordrecht, **2003**; Vol. 8, pp 437–457, Chapter 8.17; (c) Fraústo da Silva, J. J. R.; Williams, R. J. P. *The Biological Chemistry of the Elements*; Oxford University Press: Oxford, **2001**.
5. (a) Himes, R. A.; Karlin, K. D. *Curr. Opin. Chem. Biol.* **2009**, *13*, 119; (b) Lieberman, R. L.; Rosenzweig, A. C. *Nature* **2005**, *434*, 177; (c) Chan, S. I.; Wang, V. C.-C.; Lai, J. C.-H.; Yu, S. S.-F.; Chen, P. P.-Y.; Chen, K. H.-C.; Chen, C.-L.; Chan, M. K. *Angew. Chem., Int. Ed.* **2007**, *46*, 1992; (d) Elliot, S. J.; Zhu, M.; Tso, L.; Nguyen, H.-H. T.; Yip, J. H.-K.; Chan, S. I. *J. Am. Chem. Soc.* **1997**, *119*, 9949.
6. Kirillov, A. M.; Kopylovich, M. N.; Kirillova, M. V.; Haukka, M.; da Silva, M. F. C. G.; Pombeiro, A. J. L. *Angew. Chem., Int. Ed.* **2005**, *44*, 4345.
7. Kirillov, A. M.; Kopylovich, M. N.; Kirillova, M. V.; Karabach, E. Y.; Haukka, M.; da Silva, M. F. C. G.; Pombeiro, A. J. L. *Adv. Synth. Catal.* **2006**, *348*, 159.
8. Karabach, Y. Y.; Kirillov, A. M.; da Silva, M. F. C. G.; Kopylovich, M. N.; Pombeiro, A. J. L. *Cryst. Growth Des.* **2006**, *6*, 2200.
9. Karabach, Y. Y.; Kirillov, A. M.; Haukka, M.; Kopylovich, M. N.; Pombeiro, A. J. L. *J. Inorg. Biochem.* **2008**, *102*, 1190.
10. Kirillov, A. M.; Karabach, Y. Y.; Haukka, M.; Guedes da Silva, M. F. C.; Sanchiz, J.; Kopylovich, M. N.; Pombeiro, A. J. L. *Inorg. Chem.* **2008**, *47*, 162.
11. Gruenwald, K. R.; Kirillov, A. M.; Haukka, M.; Sanchiz, J.; Pombeiro, A. J. L. *Dalton Trans.* **2009**, 2109.
12. Kirillov, A. M.; Coelho, J. A. S.; Kirillova, M. V.; Guedes da Silva, M. F. C.; Nesterov, D. S.; Gruenwald, K. R.; Haukka, M.; Pombeiro, A. J. L. *Inorg. Chem.* **2010**, *49*, 6390.
13. Kirillov, A. M.; Karabach, Y. Y.; Kirillova, M. V.; Haukka, M.; Pombeiro, A. J. L. *Dalton Trans.* **2011**, *40*, 6378.
14. Kirillova, M. V.; Kirillov, A. M.; Martins, A. N. C.; Graiff, C.; Tiripicchio, A.; Pombeiro, A. J. L. *Inorg. Chem.* **2012**, *51*, 5224.
15. Kirillov, A. M.; Karabach, Y. Y.; Kirillova, M. V.; Haukka, M.; Pombeiro, A. J. L. *Cryst. Growth Des.* **2012**, *12*, 1069.
16. Kirillova, M. V.; Kozlov, Y. N.; Shul'pina, L. S.; Lyakin, O. Y.; Kirillov, A. M.; Talsi, E. P.; Pombeiro, A. J. L.; Shul'pin, G. B. *J. Catal.* **2009**, *268*, 26.
17. Kirillova, M. V.; Kirillov, A. M.; Mandelli, D.; Carvalho, W. A.; Pombeiro, A. J. L.; Shul'pin, G. B. *J. Catal.* **2010**, *272*, 9.
18. Kirillova, M. V.; Kirillov, A. M.; Kuznetsov, M. L.; Silva, J. A. L.; Fraústo da Silva, J. J. R.; Pombeiro, A. J. L. *Chem. Commun.* **2009**, 2353.
19. Kirillova, M. V.; Kirillov, A. M.; Pombeiro, A. J. L. *Chem. Eur. J.* **2010**, *16*, 9485.
20. Kirillova, M. V.; Kirillov, A. M.; Pombeiro, A. J. L. *Adv. Synth. Catal.* **2009**, *351*, 2936.
21. Kirillova, M. V.; Kirillov, A. M.; Pombeiro, A. J. L. *Appl. Catal. A: Gen.* **2011**, *401*, 106.
22. Kirillov, A. M.; Kirillova, M. V.; Shul'pina, L. S.; Figiel, P. J.; Gruenwald, K. R.; Guedes da Silva, M. F. C.; Haukka, M.; Pombeiro, A. J. L.; Shul'pin, G. B. *J. Mol. Catal. A: Chem.* **2011**, *350*, 26.
23. (a) Figiel, P. J.; Kirillov, A. M.; Karabach, Y. Y.; Kopylovich, M. N.; Pombeiro, A. J. L. *J. Mol. Catal. A: Chem.* **2009**, *305*, 178; (b) Sheldon, R. A. *Green Chem.* **2005**, *7*, 267; (c) Lindström, U. M. *Chem. Rev.* **2002**, *102*, 2751; (d) *Aqueous-Phase Organometallic Catalysis: Concepts and Applications*; Herrmann, W. A., Cornils B., Eds.; Wiley-VCH: Weinheim, **2004**. (e) Sheldon, R. A. *Chem. Commun.* **2008**, 3352.
24. Karabach, Y. Y.; Guedes da Silva, M. F. C.; Kopylovich, M. N.; Gil-Hernández, B.; Sanchiz, J.; Kirillov, A. M.; Pombeiro, A. J. L. *Inorg. Chem.* **2010**, *49*, 11096.
25. (a) Farrusseng, D.; Aguado, S.; Pinel, C. *Angew. Chem., Int. Ed.* **2009**, *48*, 7502; (b) Corma, A.; Garcia, H.; Xamena, F. X. L. *Chem. Rev.* **2010**, *110*, 4606; (c) Ranocchiari, M.; van Bokhoven, J. A. *Phys. Chem. Chem. Phys.* **2011**, *13*, 6388.
26. Schuchardt, U.; Cardoso, D.; Sercheli, R.; Pereira, R.; da Cruz, R. S.; Guerreiro, M. C.; Mandelli, D.; Spinace, E. V.; Pires, E. L. *Appl. Catal. A: Gen.* **2001**, *211*, 1.
27. (a) Ullmann's Encyclopedia of Industrial Chemistry; 6th ed.; Wiley-VCH: Weinheim, **2002**; (b) *Encyclopedia of Chemical Technology*; 5th ed.; Wiley: New York, **2004**; (c) Wittcoff, H.; Reuben, B. G.; Plotkin, J. S. *Industrial Organic Chemicals*, 2nd ed.; John Wiley & Sons, Inc, New York, **2004**.
28. (a) Shul'pin, G. B. *J. Mol. Catal. A: Chem.* **2002**, *189*, 39; (b) Shul'pin, G. B. *C.R. Chim.* **2003**, *6*, 163.
29. Kirillova, M. V.; Kirillov, A. M.; Guedes da Silva, M. F. C.; Pombeiro, A. J. L. *Eur. J. Inorg. Chem.* **2008**, 3423.

30. (a) Costas, M.; Mehn, M. P.; Jensen, M. P.; Que, L., Jr., *Chem. Rev.* **2004**, *104*, 939; (b) Costas, M.; Chen, K.; Que, L., Jr. *Coord. Chem. Rev.* **2000**, *200*–202, 517.
31. Pombeiro, A. J. L.; Kirillova, M. V.; Kirillov, A. M.; Silva, J. A. L.; Fraústo da Silva J. J. R. *Int. Patent Appl.* WO/2008/088234, **2008**.
32. (a) Jia, C.; Kitamura, T.; Fujiwara, Y. *Acc. Chem. Res.* **2001**, *34*, 633; (b) Fujiwara, Y.; Takaki, K.; Taniguchi, Y. *Synlett* **1996**, 591.
33. (a) Reis, P. M.; Silva, J. A. L.; Palavra, A. F.; Fraústo da Silva, J. J. R.; Kitamura, T.; Fujiwara, Y.; Pombeiro, A. J. L. *Angew. Chem., Int. Ed.* **2003**, *42*, 821; (b) Kirillova, M. V.; Kuznetsov, M. L.; Reis, P. M.; da Silva, J. A. L.; Fraústo da Silva, J. J. R.; Pombeiro, A. J. L. *J. Am. Chem. Soc.* **2007**, *129*, 10531; (c) Kirillova, M. V.; da Silva, J. A. L.; Fraústo da Silva, J. J. R.; Pombeiro, A. J. L. *Appl. Catal. A: Gen.* **2007**, *332*, 159; (d) Kirillova, M. V.; da Silva, J. A. L.; Fraústo da Silva, J. J. R.; Palavra, A. F.; Pombeiro, A. J. L. *Adv. Synth. Catal.* **2007**, *349*, 1765; (e) Kirillova, M. V.; Kuznetsov, M. L.; da Silva, J. A. L.; Guedes da Silva, M. F. C.; Fraústo da Silva, J. J. R.; Pombeiro, A. J. L. *Chem. Eur. J.* **2008**, *14*, 1828.

---

# 4

---

## ACTIVATION OF C–O AND C–F BONDS BY PINCER–IRIDIUM COMPLEXES

JASON HACKENBERG, KARSTEN KROGH-JESPERSEN, AND ALAN S. GOLDMAN\*

*Department of Chemistry and Chemical Biology, Rutgers, The State University of New Jersey, New Brunswick, NJ, USA*

### 4.1 INTRODUCTION

Pincer-ligated metal complexes have displayed extraordinarily rich chemistry and have found widespread use in catalysis. Pincer complexes of numerous transition metals have been synthesized, but the most well-studied probably involve Ru, Rh, Ir, and Pd [1–7]. Our group has largely focused on pincer–iridium complexes, which have shown a strong tendency toward the activation of C–H bonds. These complexes have been found to effect the oxidative addition of a variety of C–H bonds including those with  $sp^2$ - and  $sp$ -hybridized carbon [8–10]. Most notable, however, has been the activation of  $C(sp^3)$ –H bonds, leading to alkane dehydrogenation [6, 7].

The first pincer–iridium-based alkane dehydrogenation catalyst,  $(PCP)IrH_2$  ( $PCP = \kappa^3\text{-}C_6H_3\text{-}2,6\text{-}[CH_2P(t\text{-}Bu)_2]_2$ ) (**1**– $H_2$ ), was reported by Kaska and Jensen [11] in the mid-1990s, and is active for the transfer dehydrogenation of *n*-alkanes and cycloalkanes, a reaction that we have developed and studied mechanistically [12–17]. The initial success of  $(PCP)Ir$  in transfer dehydrogenation was followed by the development of a series of (pincer)Ir catalysts with varied steric and electronic properties [18–20]. We subsequently combined the high activity for C–H bond activation of (pincer)Ir complexes with Schrock-type olefin metathesis catalysts to afford a novel tandem process for alkane metathesis, relying on (pincer)Ir to dehydrogenate *n*-alkanes to olefins, followed by olefin metathesis to generate two new olefins, and then subsequent hydrogenation of these olefins by (pincer)IrH<sub>2</sub> to yield two new alkanes [21–23]. We have also found that certain pincer–iridium complexes are capable of taking *n*-alkanes to arenes through multiple dehydrogenations and subsequent electrocyclization (dehydroaromatization) [20]. Taken together, these three processes (dehydrogenation, alkane metathesis, and dehydroaromatization) hold great potential for converting low value *n*-alkanes into valuable fuels, feedstock, and commodity chemicals; these reports have been reviewed [6, 24].

This ability of  $(PCP)Ir$  to oxidatively add covalent bonds has been found to extend to O–H [25, 26], N–H [27–29], and C–I [30] bonds. We have also found that the Ir–H bond resulting from alkynyl C–H addition could add across an acetylene triple bond to give a vinyl–alkynyl iridium complex that undergoes C–C elimination to give the corresponding enyne [10]. This led us to study C–C elimination from a range of complexes  $(PCP)IrRR'$  [30]. Some of this chemistry is illustrated in Fig. 4.1. We were interested in extending this work to the elimination of other C–X bonds, including X = O. Density functional theory (DFT) calculations suggested, however, that such reactions might be thermodynamically favorable in the direction of oxidative addition; this made such studies all the more intriguing. Herein, we describe our efforts toward oxidative addition of C–O [31, 32] bonds by  $(PCP)Ir$ , subsequently extended to C–F [33] bonds, and in both cases extended to 1,2-H–X elimination. Quite surprisingly, these transformations all occur via the addition of  $C(sp^3)$ –H bonds.

*Advances in Organometallic Chemistry and Catalysis: The Silver/Gold Jubilee International Conference on Organometallic Chemistry Celebratory Book*, First Edition. Edited by Armando J. L. Pombeiro.

© 2014 John Wiley & Sons, Inc. Published 2014 by John Wiley & Sons, Inc.

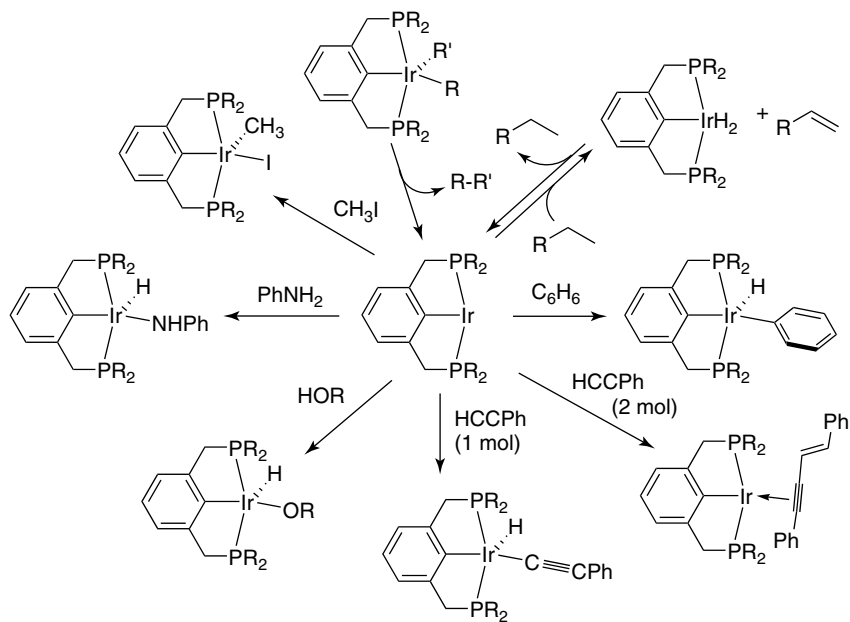
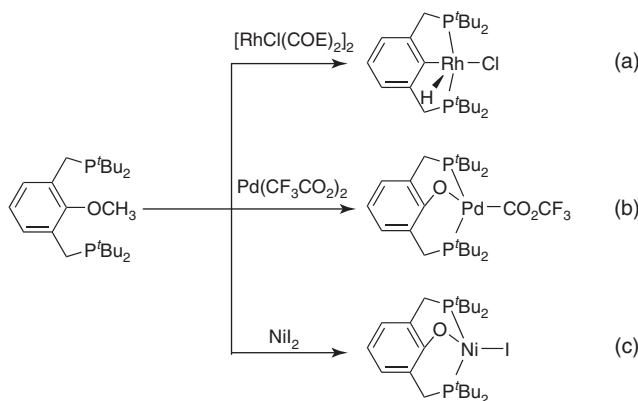


Figure 4.1 Some reactions of (PCP)Ir complexes.

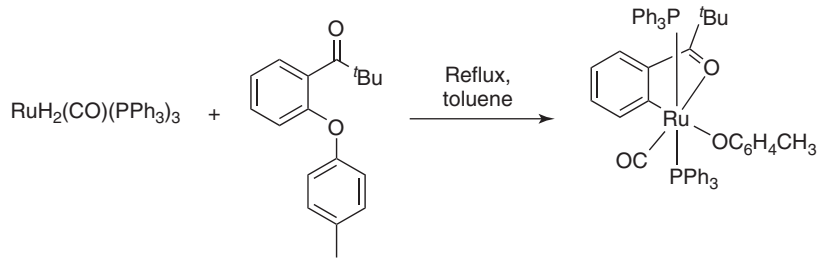


Scheme 4.1

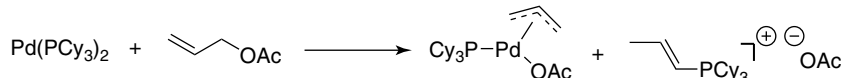
## 4.2 CLEAVAGE AND OXIDATIVE ADDITION OF C–O BONDS

### 4.2.1 Introduction

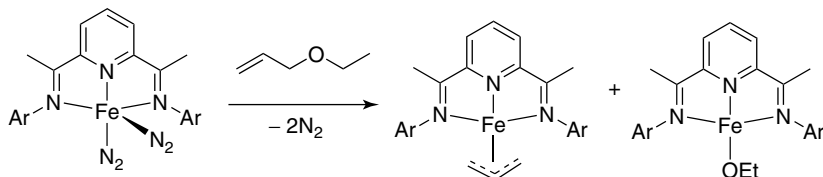
The oxidative addition to metal centers of unactivated C–O bonds, and particularly C(sp<sup>3</sup>)–O bonds, is not common. Before this work, there was only one well-characterized example of intermolecular oxidative addition of a C(sp<sup>3</sup>)–O bond (discussed below) [34, 35]. In the late 1990s, Milstein and coworkers [36, 37] reported several examples of intramolecular cleavage of C(sp<sup>3</sup>)–O and C(sp<sup>2</sup>)–O bonds of an analogous (PCP) ligand, where the phosphine moieties coordinate to the metal complex and serve to direct activation of the C–O bond on the aryl ring of the ligand. Interestingly, the authors found that they could control the selectivity of C(sp<sup>3</sup>)–O versus C(sp<sup>2</sup>)–O cleavage based on the metal complex employed; nucleophilic Rh(I) complexes yielded aryl C–O bond cleavage to afford (PCP)Rh complexes (Scheme 4.1a), while electrophilic Pd(II) or Ni(II) complexes afforded alkyl C–O bond cleavage giving rise to phenoxy-ligated metal complexes (Scheme 4.1b and c) [38]. Further, Kakuichi [39] later observed direct aryl C–O oxidative addition to Ru directed by a pendant ketone (Scheme 4.2).



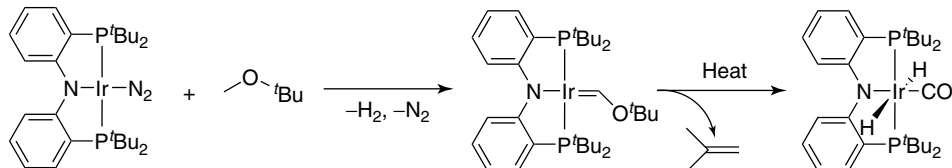
Scheme 4.2



Scheme 4.3



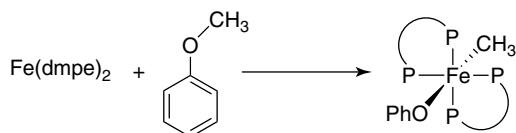
Scheme 4.4



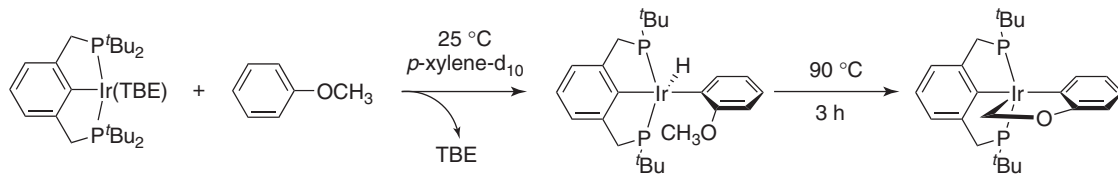
Scheme 4.5

Examples of intermolecular cleavage of “activated” C–O bonds are well precedented, for example, involving allylic C–O bonds. Early work by Yamamoto [40, 41] revealed cleavage of allylic C–O bonds in acetates and ethers, likely proceeding via a  $\pi$ -allyl mechanism (Scheme 4.3). More recently, Chirik [42] reported the activation and cleavage of allylic ethers and acyl/ester C–O bonds by bis(imido)pyridine iron complexes (Scheme 4.4). Carmona and Panque [43–45] have reported the extraordinary rearrangement reactions of methyl aryl ethers by a tris(pyrazolyl)borate iridium complex involving cleavage of the methyl–oxygen bond. Grubbs and Ozerov [46] have investigated the reactions of (PNP)Ir and anthraphos-based (PCP)Ir complexes with methyl t-butyl and methyl benzyl ether, resulting in methoxy C–H activation and the formation of alkoxycarbene complexes (Scheme 4.5) found to be active for multiple-bond metatheses with various electrophilic heterocumulenes (e.g., CO<sub>2</sub>, CS<sub>2</sub>, and AdN<sub>3</sub>). Remarkably, the formation of a carbonyl ligand results from the cleavage of every bond to the original ether methoxy carbon *except* the C–O bond [47, 48]. To our knowledge, however, the only example before this work of “simple” intermolecular oxidative addition of an unactivated C(sp<sup>3</sup>)–O bond was reported by Ittel and Tolman [34, 35] who observed cleavage of the C–O bond of anisole by the highly nucleophilic Fe(dmpe)<sub>2</sub> (Scheme 4.6).

During the course of this work, Ozerov et al. and Jones et al. [48, 49] reported C(sp<sup>3</sup>)–O bond addition in the reactions of benzyl methyl ether with an Ir complex and methyl benzoate with a Pt complex, respectively.



Scheme 4.6



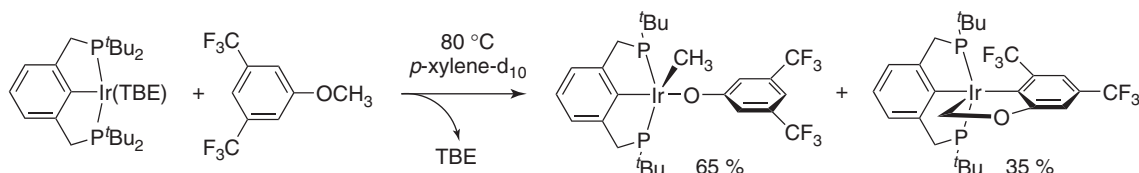
Scheme 4.7

#### 4.2.2 Cleavage and Oxidative Addition of Aryl Alkyl Ether C(sp<sup>3</sup>)–O Bonds

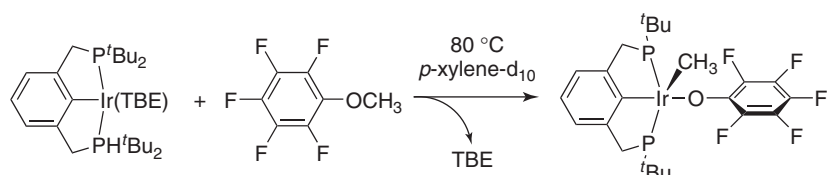
Our exploration of the reactivity of (PCP)Ir toward C–O bonds began with anisole. At room temperature, we observed immediate formation of product resulting from oxidative addition of the aryl C–H bond *ortho* to the methoxy substituent, which was spectroscopically analogous to (but significantly more thermodynamically stable than) the previously reported (PCP)Ir(Ph)(H) complex [8]. In an effort to effect subsequent C–O bond activation, (PCP)Ir(H)(*o*-C<sub>6</sub>H<sub>4</sub>OCH<sub>3</sub>) was heated for 3 h at 90 °C, but this yielded exclusively the cyclometalated product arising from activation of the methoxy C(sp<sup>3</sup>)–H bond (Scheme 4.7).

In order to disfavor aryl C–H addition, and hopefully thereby allow C–O addition to proceed, we investigated anisole derivatives in which the *ortho*-C–H bonds were either replaced with *ortho*-methyl groups or sterically blocked by *meta*-methyl groups. Unfortunately, reactions with either 2,6-dimethylanisole or 3,5-dimethylanisole resulted in complex mixtures that showed no indication of the desired C–O activation products.

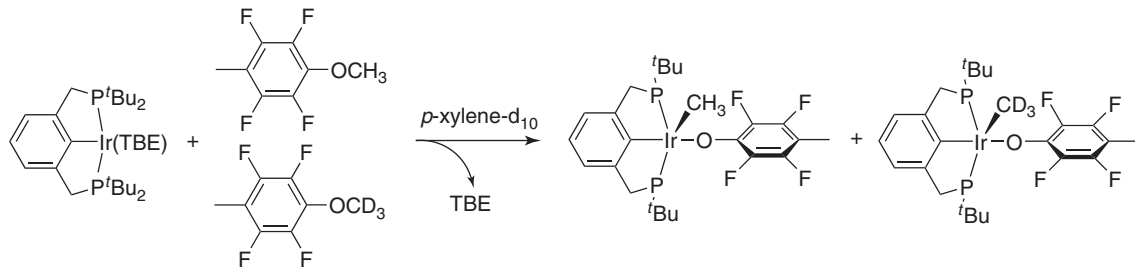
We considered that electron-withdrawing groups could be used to favor C–O addition as well as blocking C–H addition. Indeed, addition of 3,5-bis(trifluoromethyl)anisole to a solution of (PCP)Ir(TBE) resulted in formation of the C–O cleavage product, (PCP)Ir(CH<sub>3</sub>)[O-3, 5-C<sub>6</sub>H<sub>3</sub>(CF<sub>3</sub>)<sub>2</sub>] (65%) as well as *ortho*-cyclometalated product (35%) (Scheme 4.8). Pentafluoroanisole gave quantitative conversion at room temperature to the C–O addition product, (PCP)Ir(CH<sub>3</sub>)(OC<sub>6</sub>F<sub>5</sub>) (Scheme 4.9) [31]. These results were only the second example of *intermolecular* oxidative addition of an unactivated ether C(sp<sup>3</sup>)–O bond (three decades after the first such report, noted earlier, by Ittel and Tolman [34, 35]).



Scheme 4.8



Scheme 4.9



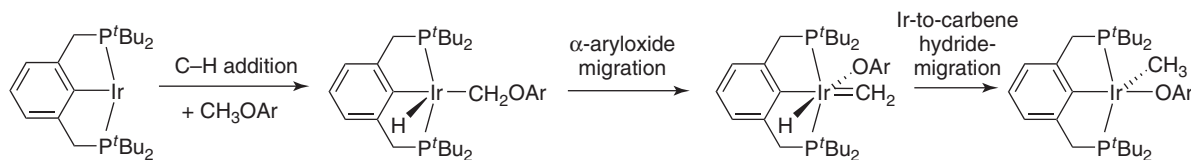
Scheme 4.10

Studies by Goldberg and Williams [50–52] have demonstrated that reductive elimination of C–O bonds (the reverse of oxidative addition) from Pt(IV) metal centers proceeds by dissociation of a hydroxide or phenoxide anion, which subsequently attacks the alkyl group to form an alcohol or ether. In view of the high nucleophilicity of Fe(dmpe)<sub>2</sub>, and the trans disposition of the added methyl and phenoxy groups, it seems quite likely that the mechanism proposed by Goldberg and Williams applies to the Ittel and Tolman system as well, with the metal complex attacking the anisole methyl group in an S<sub>N</sub>2 manner. Such a mechanism would seem unlikely in the case of (PCP)Ir, however, as its chemistry is dominated by the addition of nucleophiles or covalent bonds, rather than by any nucleophilicity of the complex. Accordingly, a kinetic isotope effect (KIE) competition experiment was conducted comparing the relative reactivity of 4-methoxy-2,3,5,6-tetrafluorotoluene and its CD<sub>3</sub>-deuterated analog (Scheme 4.10). A significant primary, normal KIE,  $k_{\text{OCH}_3}/k_{\text{OCD}_3} = 4.3(3)$ , was found at 25 °C. This KIE is inconsistent with either a direct C–O oxidative addition mechanism or a nucleophilic attack on the methyl group, but instead indicates that cleavage of a C–H bond is involved in, or occurs before, the rate-determining step.

DFT calculations indicate that direct oxidative addition of the C–O bond of MeO(*p*-C<sub>6</sub>F<sub>4</sub>Me), via a three-centered transition state (TS), would have a prohibitively high activation barrier, with a computed TS free energy of 33.4 kcal/mol relative to free ether and (PCP)Ir, using M06 functionals [32]. Relative to the precursor (PCP)Ir(TBV)(H), or a calculated resting state of (PCP)Ir(MeOAr), the overall barriers would be circa 5 kcal/mol greater.

An alternative mechanism, proceeding through the initial addition of a methoxy C–H bond, shown in Fig. 4.2, is calculated to have an activation barrier that is nearly 18 kcal/mol lower than direct C–O oxidative addition ( $\Delta G^\ddagger = 33.4$  kcal/mol). Addition of the C(sp<sup>3</sup>)–H bond adjacent to oxygen forms a five-coordinate Ir(III) intermediate, which undergoes  $\alpha$ -aryloxy elimination to afford a methylidene complex. 1,2-Migration of the hydride from Ir to the methylidene ligand affords the observed C–O oxidative addition product. Figure 4.3 shows the Gibbs free energy profile for this mechanism.

The  $\alpha$ -aryloxide migration is calculated to have a slightly lower barrier than the hydride-to-methylidene migration, but the difference is probably too small to be significant when comparing such different species. The calculations, however, predict a significant difference in the KIE depending on which of these steps is rate-determining. If the rate-determining step is hydride transfer (as suggested by the slightly higher barrier for this step than for  $\alpha$ -aryloxide migration), the overall KIE is calculated to be 7.2, which is significantly greater than the experimental value. If  $\alpha$ -aryloxide migration is rate-determining, however, the calculated KIE is 4.16, in excellent agreement with experiment. This value may be decomposed as the product of (i) the equilibrium isotope effect (EIE) for the pre-equilibrium of free ether plus (PCP)Ir precursor (e.g., (PCP)Ir(TBV)H) with the aryloxymethyl hydride/deuteride, calculated to be 3.13; and (ii) the secondary KIE for  $\alpha$ -aryloxide migration, calculated as 1.33. The EIE of 3.13 is slightly higher than typical C–H(D) addition EIEs [53, 54]; this may be attributable to low Ir–H(D) bending frequencies in the addition product resulting from the shallow energy surface for deformation of the ligand arrangement in the equatorial plane of the five-coordinate d<sup>6</sup> complex [55]. The value of 1.33 (1.15 per C–H/D

Figure 4.2 Mechanism for the net oxidative addition of methyl aryl ether C(sp<sup>3</sup>)-O bonds via initial C–H activation.

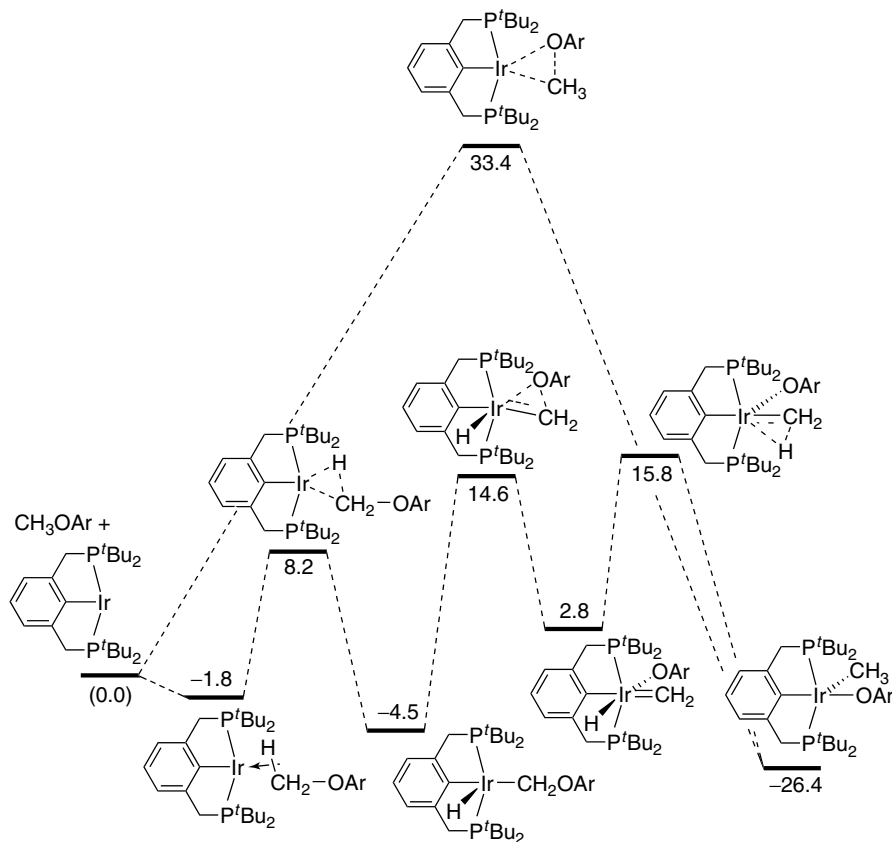
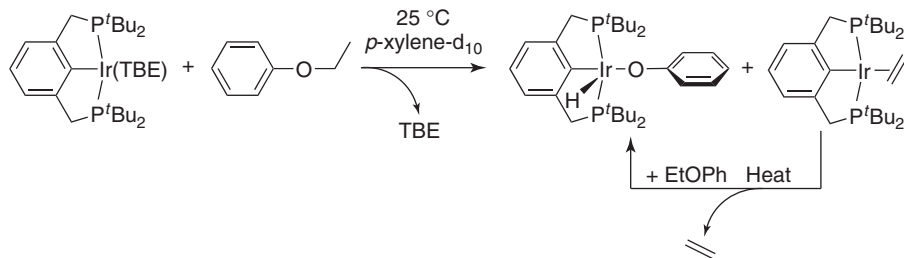


**Figure 4.3** Calculated Gibbs free energies (in kcal/mol; relative to free (PCP)Ir and ether) for the reaction of (PCP)Ir with  $\text{CH}_3\text{OAr}$ ,  $\text{Ar} = p\text{-C}_6\text{F}_4\text{Me}$ .

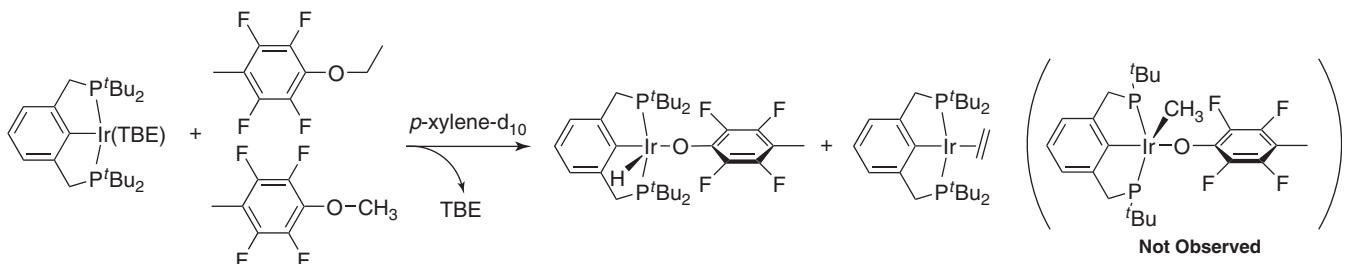
bond) may seem high for a secondary KIE, but it is fully consistent with the KIE reported for related  $\text{S}_{\text{N}}1$  reactions of organic species with oxygenate-leaving groups, for which values above 1.2 per H/D atom are common [56–63].

#### 4.2.3 1,2-H–OAr Eliminations of Ethers with Higher Alkyl Groups

Alkyl aryl ethers with a  $\beta$ -C(sp<sup>3</sup>)–H bond were also found to undergo C–O bond cleavage on reaction with (PCP)Ir, but of a distinctly different type than observed for methyl aryl ethers. Thus, ethoxybenzene reacts with (PCP)Ir at room temperature to give a 1 : 1 mixture of (PCP)Ir(H)(OPh) and (PCP)Ir(ethylene), which on heating at 125 °C eventually gives pure (PCP)Ir(H)(OPh) and free ethylene (Scheme 4.11). The net reaction is thus a 1,2-dehydroaryloxylation. As was found with methyl aryl ethers, enhanced reactivity is observed when the fluorinated analog, 4-ethoxy-2,3,5,6-tetrafluorotoluene,



**Scheme 4.11**



Scheme 4.12

was employed, giving the analogous aryloxy hydride and ethylene products at room temperature, followed by full conversion to give exclusively the aryloxy hydride at 80 °C.

The observation that the C–O cleavage reaction of ethyl aryl ethers occurs without the need to block *ortho* C–H activation suggests that the 1,2-dehydroaryloxylation is a more facile reaction than the ether C–O oxidative addition. Accordingly a competition experiment, in which a mixture of 4-methoxy-2,3,5,6-tetrafluorotoluene and 4-ethoxy-2,3,5,6-tetrafluorotoluene was added to (PCP)Ir(TBE), resulted in exclusive formation of (PCP)Ir(H)(OAr) and (PCP)Ir(ethylene) (the products obtained from C–O cleavage of the ethyl ether), and no evidence of any reaction of the methyl ether (Scheme 4.12).

DFT calculations were employed to gain insight into the mechanism of the 1,2-dehydroaryloxylation. One possible pathway could involve initial direct C–O oxidative addition followed by  $\beta$ -hydride elimination; however, the earlier observations that direct C–O oxidative addition does not occur for methyl aryl ethers along with the observation that 4-ethoxy-2,3,5,6-tetrafluorotoluene reacts faster than 4-methoxy-2,3,5,6-tetrafluorotoluene (i.e., the substrate with the  $\beta$ -C–H bond reacts faster than the substrate with the  $\alpha$ -C–H bond) would argue against such a mechanism. Accordingly, the barriers to direct C–O addition for 4-ethoxy-2,3,5,6-tetrafluorotoluene and ethoxybenzene were calculated to be prohibitively high, 35.0 and 40.8 kcal/mol, respectively. In contrast, the barriers for addition of the  $\beta$ -C–H bond followed by  $\beta$ -aryloxy elimination and loss of ethylene (Fig. 4.4) were found to be considerably lower (Fig. 4.5).

#### 4.2.4 Oxidative Addition of Ester C(sp<sup>3</sup>)–O Bonds

The C(sp<sup>3</sup>)–O cleavage reactions observed for ethers were found to extend to other alkyl oxygenates, specifically esters and tosylates. In contrast with the methyl ether reaction, however, the reaction of methyl acetate proved more forthcoming with respect to mechanistic clues in the form of reaction intermediates. Methyl acetate (8.3 mmol) was observed to rapidly react with *in situ*-generated (PCP)Ir(TBV)(H) (8.3 mmol) at room temperature to yield (PCP)Ir(H)( $\kappa^2$ -CH<sub>2</sub>OAc), the product of carbomethoxy C(sp<sup>3</sup>)–H bond oxidative addition and coordination of the carbonyl oxygen (Scheme 4.13). Heating this species at 80 °C for 5 h affords a very surprising product, characterized spectroscopically and crystallographically (Fig. 4.6a), which apparently results from insertion of the iridium-bound methylidene group into the PCP *ipso*-C–Ir bond. Further heating to 125 °C for 6 h yields a mixture of the net product of oxidative addition of the methyl acetate methoxy C–O bond, (PCP)Ir(CH<sub>3</sub>)( $\kappa^2$ -OAc), and the cyclometalated-pincer product, ( $\kappa^4$ -PCP)Ir( $\kappa^2$ -OAc) (Fig. 4.6b), which appears to result from decomposition of (PCP)Ir(CH<sub>3</sub>)( $\kappa^2$ -OAc) with the loss of methane.

DFT calculations were employed to study the mechanism of methyl ester C–O addition. A low barrier [8.4 kcal/mol relative to free (PCP)Ir and methyl acetate] was calculated for C–H addition to give (PCP)Ir(H)( $\kappa^2$ -CH<sub>2</sub>OAc), the species that was observed to form at room temperature. This intermediate has two potential coordination isomers: one where

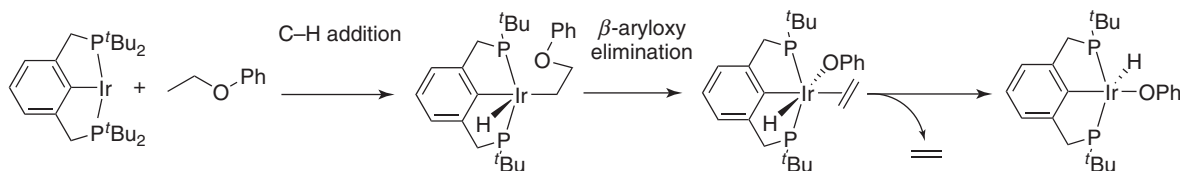
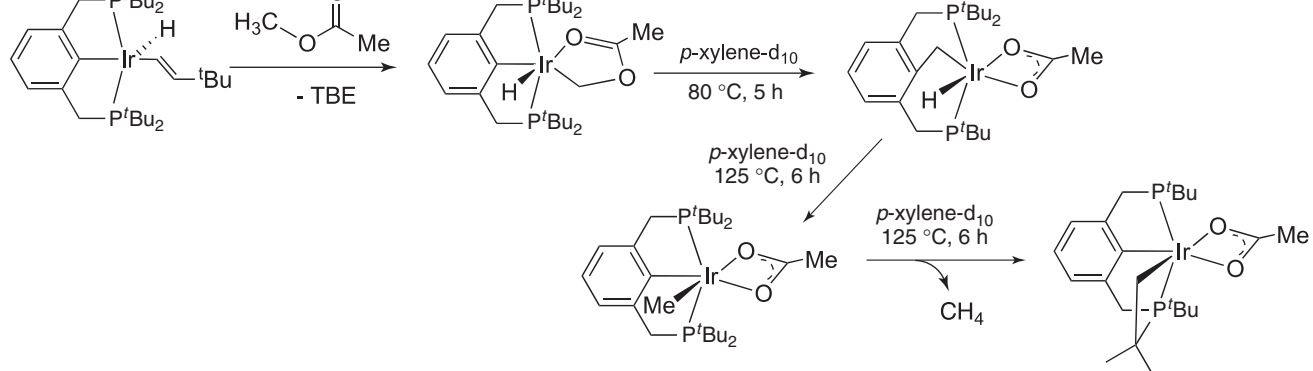
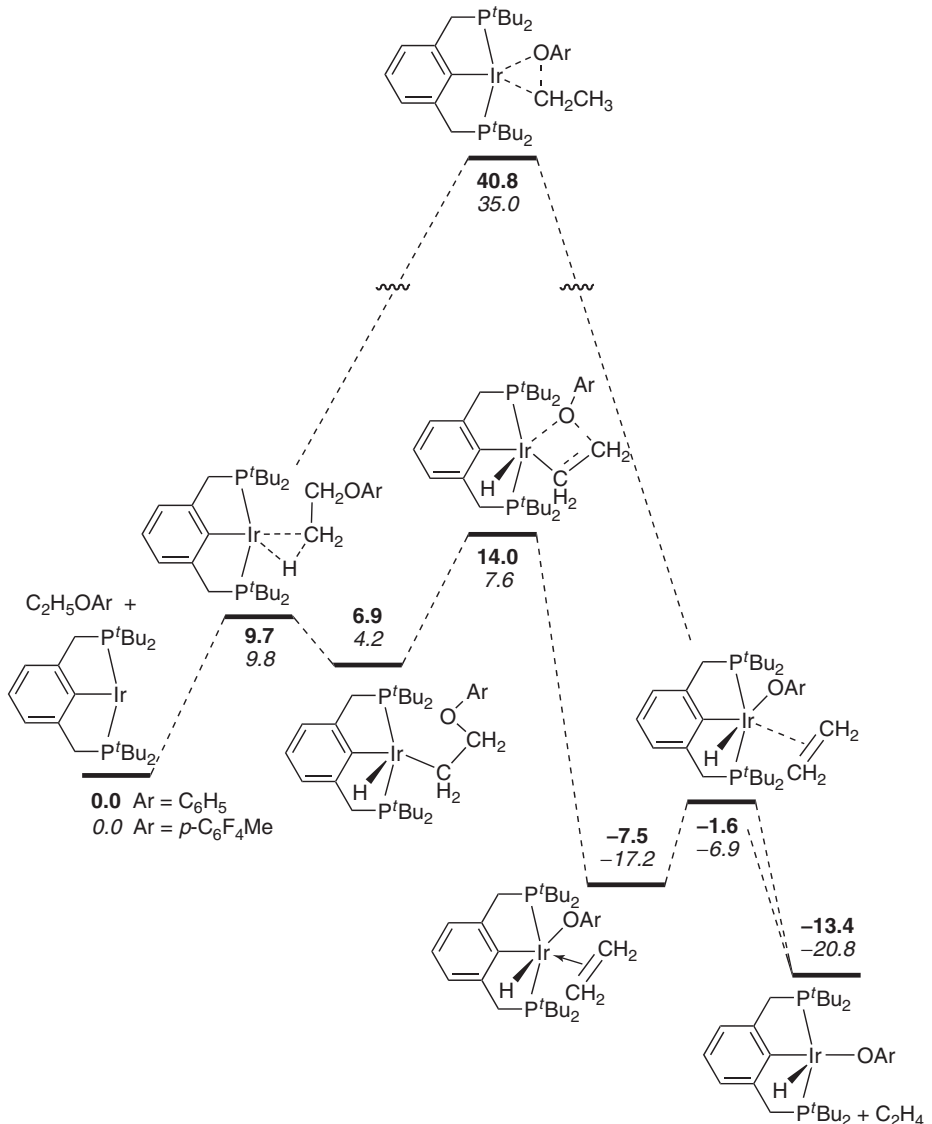
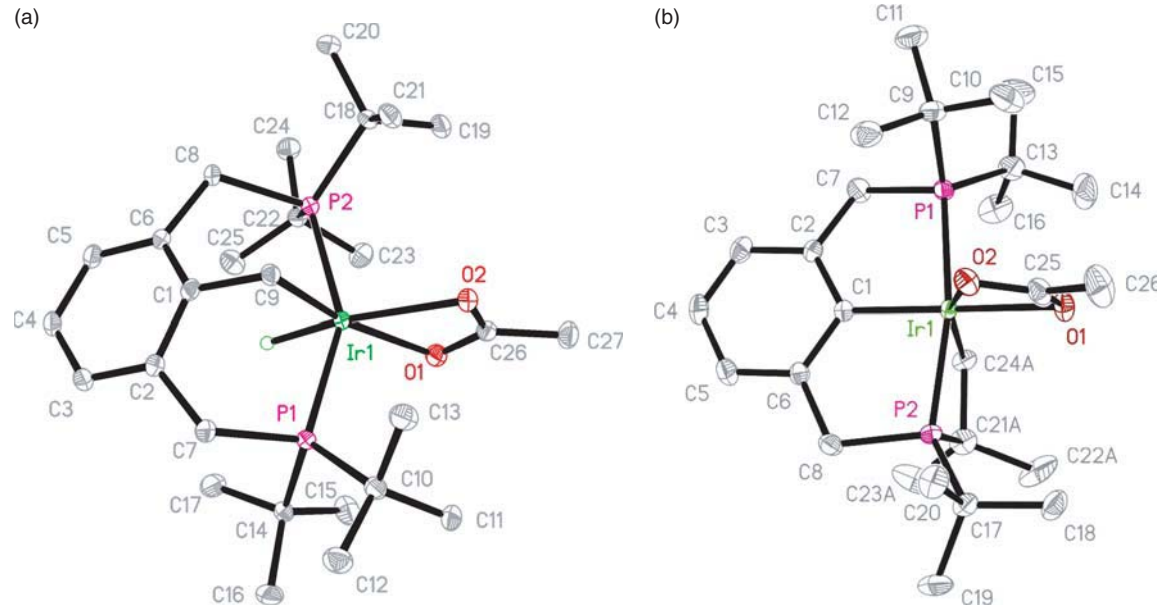
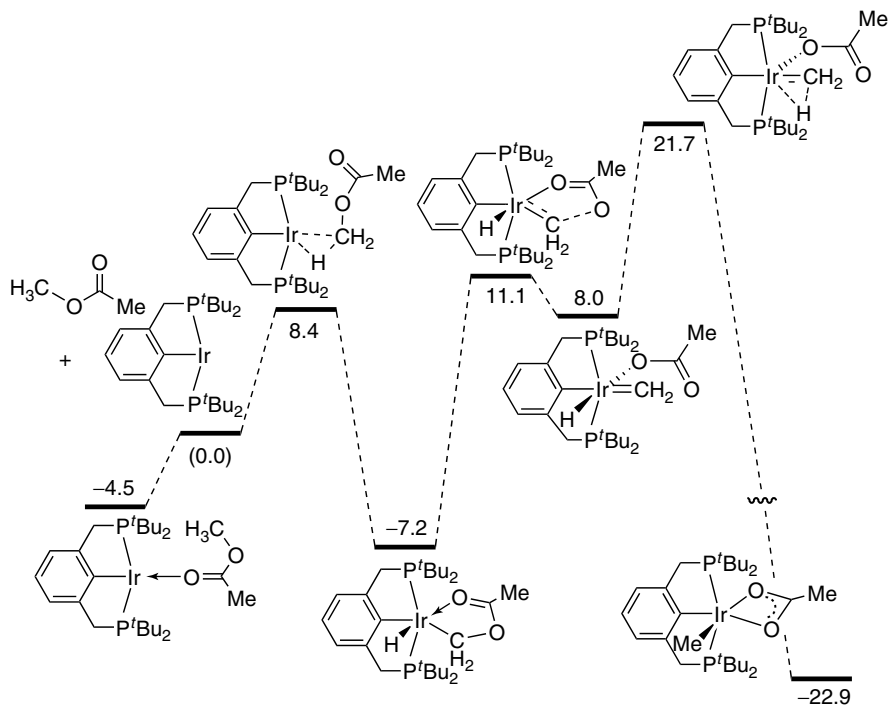


Figure 4.4 Mechanism of 1,2-dehydroaryloxylation of ethyl aryl ethers.





**Figure 4.6** X-ray structures of (a)  $(\text{PCP} - \text{CH}_2)\text{Ir}(\text{H})(\kappa^2\text{-O}_2\text{CMe})$  and (b) cyclometalated  $(\text{PCP})\text{Ir}(\text{acetate})$ ,  $[\kappa^4\text{-C}_6\text{H}_3\text{-2-(CH}_2\text{P}^t\text{Bu}_2\text{-6-(CH}_2\text{P}^t\text{Bu}(\text{CMe}_2\text{CH}_2))]\text{Ir}(\kappa^2\text{-O}_2\text{CMe})$ . (See insert for color representation of the figure.)



**Figure 4.7** Calculated Gibbs free energies (in kcal/mol; relative to free  $(\text{PCP})\text{Ir}$  and ester) for the reaction of  $(\text{PCP})\text{Ir}$  with methyl acetate occurring via a *cis* methylene hydride intermediate (a hypothetical pathway, *not* proposed).

the iridium-bound methylene group is *cis* to the hydride (isolated experimentally) (Fig. 4.7), and one of slightly higher energy (by ca. 5 kcal/mol) with the methylene unit *trans* to the hydride (Fig. 4.8). For the experimentally observed C–H-*cis* isomer, a relatively low barrier (18.3 kcal/mol) was calculated for  $\alpha$ -acetate migration, in analogy with the pathway proposed for C–O addition of the methyl aryl ether methoxy group. This migration is calculated to proceed via a

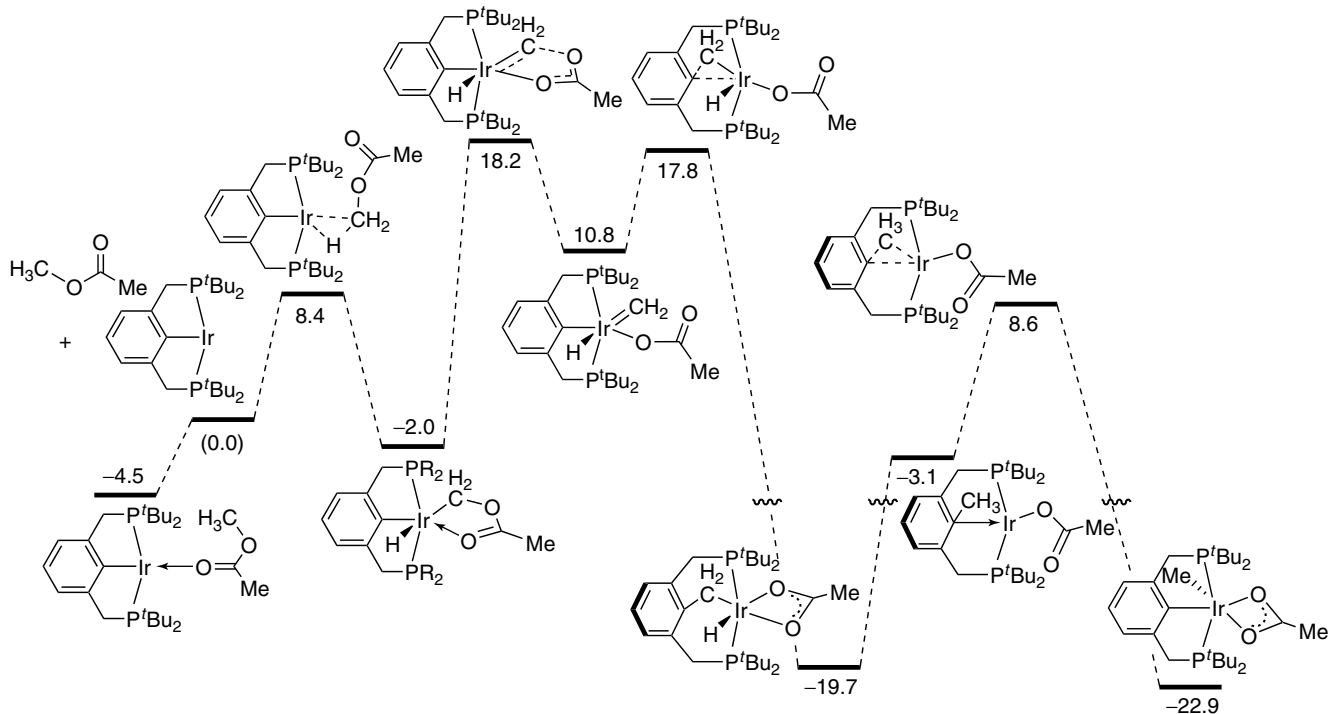
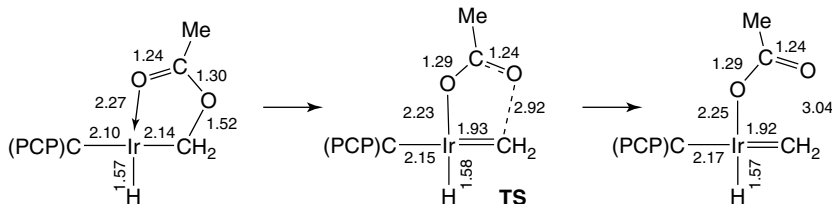


**Figure 4.8** Calculated Gibbs free energies (in kcal/mol; relative to free (PCP)Ir and ester) for the reaction of (PCP)Ir with methyl acetate occurring via a *trans* methylene hydride intermediate (proposed pathway).



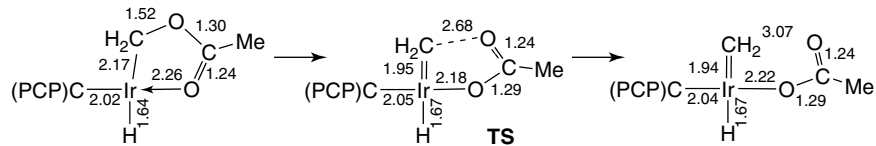
**Scheme 4.14** Acetate migration by *cis*-(PCP)Ir(H)( $\kappa^2$ - $\text{CH}_2\text{OAc}$ ).

five-membered TS in which the dative bond with the carbonyl oxygen gives rise to a covalent iridium–acetate bond (Scheme 4.14). The resulting species *cis*-(PCP)Ir(H)( $\text{CH}_2$ )(OAc) can then undergo iridium-to-methylidene hydride migration, which would give the observed C–O oxidative addition product. However, the barrier for this reaction, 28.9 kcal/mol (relative to  $\text{C–H–cis}(\text{PCP})\text{Ir}(\text{H})(\kappa^2\text{-CH}_2\text{OAc})$ ) is fairly high; moreover, this pathway does not account for the experimental observation and isolation of  $(\text{PCP}\text{-CH}_2)\text{Ir}(\text{H})(\text{OAc})$ .

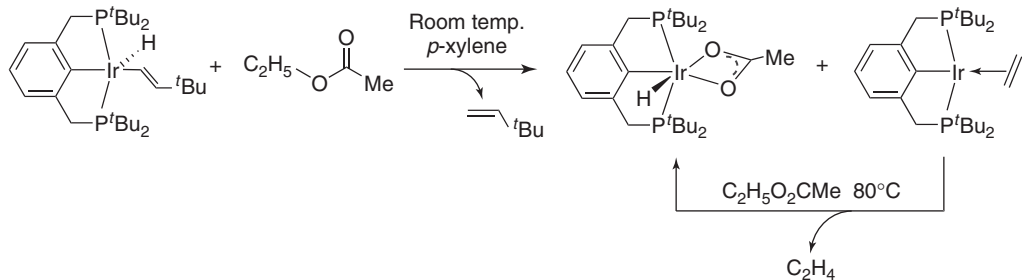
A low barrier is calculated for the conversion of *cis*-(PCP)Ir(H)( $\text{CH}_2$ )(OAc) to the coordination isomer *trans*-(PCP)Ir(H)( $\text{CH}_2$ )(OAc), which is circa 5 kcal/mol higher than the *cis* isomer. The *trans* isomer can then undergo  $\alpha$ -acetate migration, as in the case of the *cis* isomer, with an analogous five-membered TS (Scheme 4.15).

The product of this migration, in which the methylidene and hydride are in a mutually *trans* disposition, is geometrically incapable of undergoing iridium-to-methylidene hydride migration. However, it can very readily (7.0 kcal/mol barrier) undergo an aryl *ipso*-carbon-to methylidene migration (Fig. 4.8); this gives the isolated  $(\text{PCP}\text{-CH}_2)\text{Ir}(\text{H})(\text{OAc})$  intermediate. As is well preceded in the work by Milstein et al. [64, 65], such species may undergo C(PPC-CH<sub>2</sub>)-H elimination followed by C–C cleavage; this results, in this case, in the formation of  $(\text{PCP})\text{Ir}(\text{CH}_3)(\kappa^2\text{-OAc})$ , the C–O oxidative addition product.

As with aryl ether substrates, we also investigated alkyl esters with alkyl groups higher than methyl. As with the higher alkyl ethers, such species undergo 1,2-H–O elimination instead of C–O oxidative addition. Ethyl acetate, for example,



Scheme 4.15 Acetate migration by *trans*-(PCP)Ir(H)( $\kappa^2$ -CH<sub>2</sub>OAc).



Scheme 4.16 Transition state for  $\beta$ -acetate migration in the reaction of ethyl acetate.

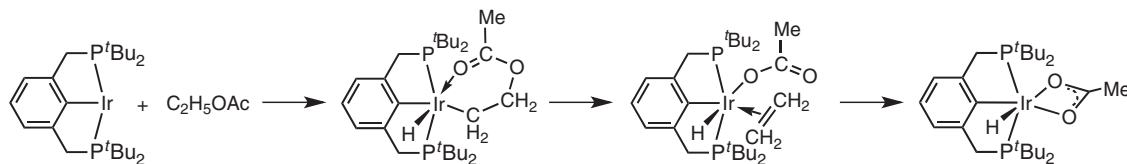
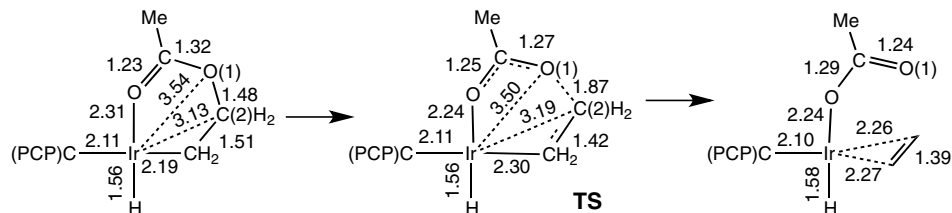


Figure 4.9 Mechanism for 1,2-H–OAc elimination from ethyl acetate.



Scheme 4.17 Transition state for  $\beta$ -acetate migration in the reaction of ethyl acetate.

readily reacts with (PCP)Ir(TBV)(H) at room temperature to afford a mixture of (PCP)Ir(H)(OAc) and (PCP)Ir(ethylene) [subsequent heating results in the loss of ethylene and quantitative conversion to (PCP)Ir(H)(OAc)] (Scheme 4.16), while isopropylacetate rapidly reacts to give (PCP)Ir(H)(OAc) and free propylene.

DFT calculations are consistent with a pathway for the H–OAc eliminations initiated by addition of the  $\beta$ -C–H bond, proceeding by the mechanism shown in Fig. 4.9. In the case of ethyl acetate, this yields the cyclometalated intermediate (PCP)Ir( $\kappa^2$ -CH<sub>2</sub>CH<sub>2</sub>OAc). This complex then undergoes  $\beta$ -acetate migration, cleaving the C–O bond to form the resulting ethylene-bound intermediate, (PCP)Ir(H)(OAc)(ethylene). The TS structure for the  $\beta$ -acetate migration (Scheme 4.17) is unusual, containing a six-membered ring in which the C–O bond is cleaved without any direct participation from the iridium center.

This TS has a free energy of 12 kcal/mol relative to free reactants, slightly higher in energy than the preceding TS for C–H activation (Fig. 4.10). The resulting ethylene complex can then lose ethylene to yield the product, (PCP)Ir(H)( $\kappa^2$ -OAc), while the free ethylene then reacts with (PCP)Ir(TBV)(H) to form the observed byproduct, (PCP)Ir(ethylene). A TS corresponding to the loss of ethylene from (PCP)Ir(H)(OAc)(ethylene) was not found, but olefin loss is calculated to be 4.5 kcal/mol

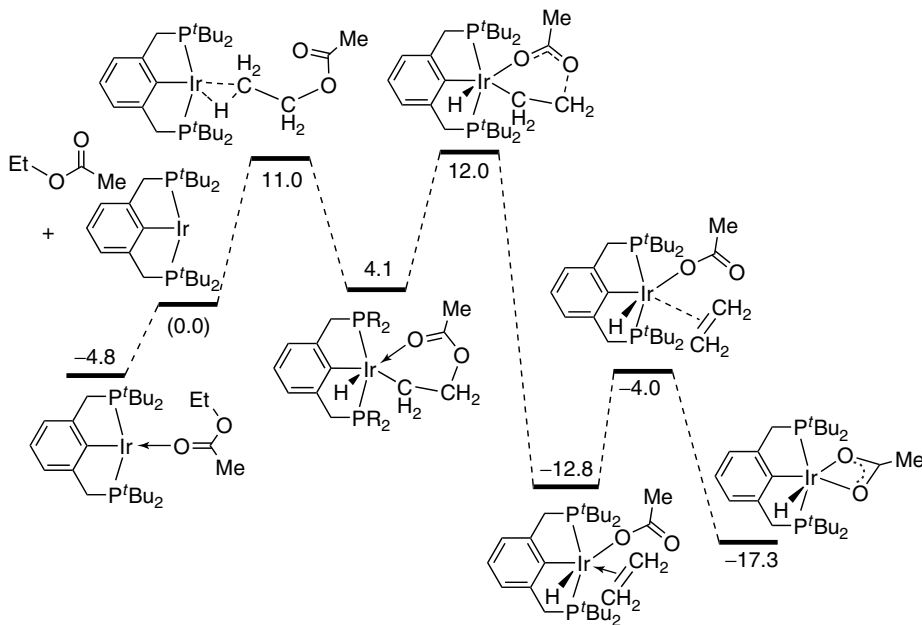


**Figure 4.10** Calculated Gibbs free energies (in kcal/mol; relative to free (PCP)Ir and ethyl acetate) for the cleavage of the C–O bond of ethyl acetate by (PCP)Ir.

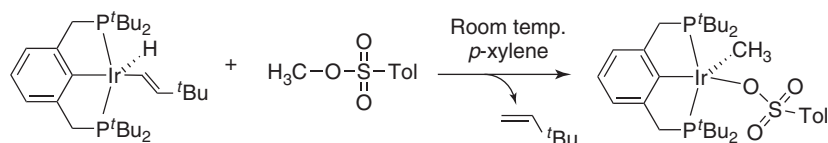
exergonic (entropically favored), and certainly the barrier to an exergonic ligand loss is expected to be much less than the circa 25 kcal/mol barrier to the acetate-migration back reaction.

#### 4.2.5 Cleavage and Oxidative Addition of Tosylate C–O Bonds

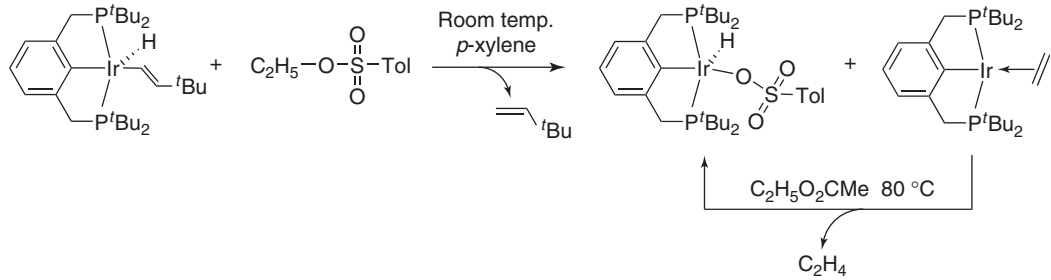
Methyl tosylate has also been found to react with (PCP)Ir to undergo C(sp<sup>3</sup>)–O oxidative addition. (PCP)Ir(TBV)(H) reacts rapidly at room temperature with methyl tosylate (1.1 equiv) to give the C–O oxidative addition product, (PCP)Ir(Me)(OTs), in quantitative yield (Scheme 4.18). KIE experiments involving competition between a 10-fold excess each of CH<sub>3</sub>OTs and CD<sub>3</sub>OTs yielded a KIE,  $k_{\text{CH}_3}/k_{\text{CD}_3} = 2.4(2)$ , that again indicates that C–H activation is involved during or before the rate-determining step.

Also in analogy with the ether and ester chemistry, ethyl tosylate reacts with (PCP)Ir(TBV)(H) at room temperature to quickly yield an equimolar mixture of (PCP)Ir(H)(OTs) and (PCP)Ir(ethylene), which on heating to 80 °C for several hours results in the loss of ethylene and full conversion to (PCP)Ir(H)(OTs) (Scheme 4.19).

DFT calculations indicate that the C–OTs addition proceeds analogously to the ether C–O additions (Fig. 4.11). Initial oxidative addition of the MeOTs methoxy C–H bond, calculated to be exergonic by 5.8 kcal/mol, is followed by  $\alpha$ -migration of the OTs group with a barrier of 21.5 kcal/mol and a TS that is 15.7 kcal/mol above the free reactants. The TS for the subsequent Ir-to-methylidene hydride migration, to yield the observed C–O oxidative addition product, was calculated to have an essentially identical free energy (15.8 kcal/mol). Thus, the DFT calculations alone cannot reliably predict the identity of the rate-determining TS. However, these two TSs would each give rise to a very different overall OCH<sub>3</sub> / OCD<sub>3</sub> KIE for the C–O addition, depending on which is rate-determining. If  $\alpha$ -OTs migration is rate-determining, the KIE is calculated to be



Scheme 4.18



Scheme 4.19

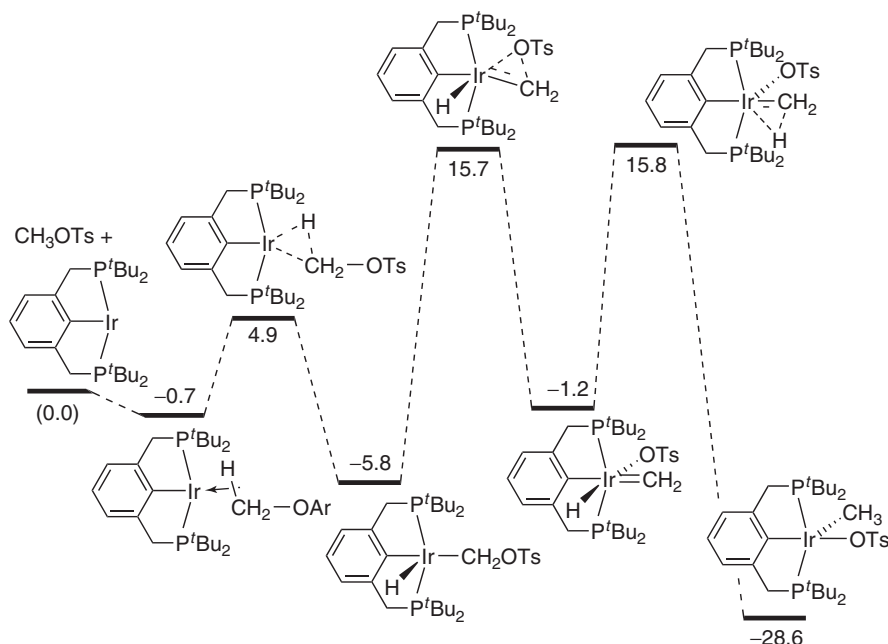


**Figure 4.11** Calculated Gibbs free energies (in kcal/mol; relative to free (PCP)Ir and methyl tosylate) for the reaction of (PCP)Ir with methyl tosylate.

2.9, whereas a rate-determining step involving H-migration is predicted to yield a significantly greater KIE of 6.7. Comparing these values to our experimentally determined KIE of 2.4, we clearly see much better agreement with rate-determining  $\alpha$ -OTs migration.

#### 4.3 CLEAVAGE AND OXIDATIVE ADDITION OF C–F BONDS

Having made headway into facile C–O bond cleavage via initial C–H bond activation, we next sought to extend the same strategy to the activation of C–F bonds. Although oxidative addition of C–Cl, C–Br, and C–I bonds to metal centers is well studied [66], there is no precedent for oxidative addition of unactivated C(sp<sup>3</sup>)–F bonds. Thus, C(sp<sup>3</sup>)–F oxidative addition is even less well preceded than C(sp<sup>3</sup>)–O oxidative addition; perhaps, this is not surprising in the light of the greater bond dissociation energies of C(sp<sup>3</sup>)–F bonds (e.g., the C–F BDE of fluoromethane is 110 kcal/mol while the anisole C(sp<sup>3</sup>)–O BDE is only 65 kcal/mol) [67]. Note, however, there are numerous reported examples of C–F oxidative addition (and reductive elimination), generally involving fluorine bound to sp<sup>2</sup>-hybridized vinyl or aryl carbon atoms (Fig. 4.12) [68–81].

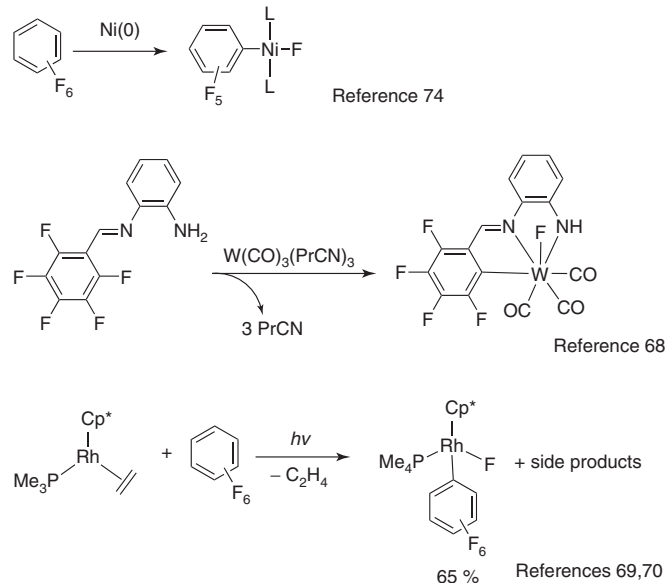
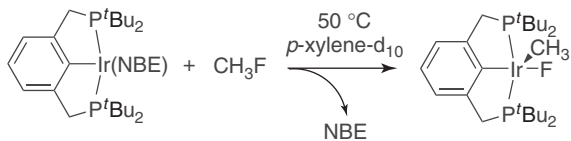
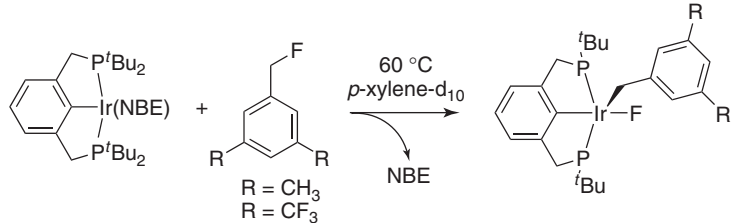


**Figure 4.12** Some notable examples of oxidative addition of  $C_{sp}^2$ -F bonds to transition metal centers.



**Scheme 4.20**



**Scheme 4.21**

Nevertheless, the  $\text{C}(\text{sp}^3)$ –OR cleavage chemistry indicated that the tendency toward oxidative addition correlated with the electron-withdrawing ability of the R group. This suggested that  $\text{C}(\text{sp}^3)$ –F addition would be even more favorable than any of the  $\text{C}(\text{sp}^3)$ –OR additions. Indeed,  $(\text{PCP})\text{Ir}(\text{NBE})$  was found to react readily with fluoromethane at  $50^\circ\text{C}$  to yield a single major species, the oxidative addition product  $(\text{PCP})\text{Ir}(\text{CH}_3)\text{F}$  (Scheme 4.20) [33]. Likewise, benzyl fluoride derivatives [containing either methyl or trifluoromethyl substituents *meta* to the  $-\text{CH}_2\text{F}$  group to prevent  $\text{C}(\text{sp}^2)$ –H activation] also react readily at  $60^\circ\text{C}$  to afford  $(\text{PCP})\text{Ir}(\text{F})(\text{CH}_2\text{Ar})$  complexes (Scheme 4.21). In the case of the trifluoromethyl-substituted substrate, a clean conversion to the product in 95% yield is observed, while the methyl substituted substrate exhibits a lower yield (70%) with significant amounts of unidentified side products.

As in the case of the C–O addition reactions, a KIE was measured to probe the reaction pathway.  $(\text{PCP})\text{Ir}$  was reacted with a fivefold excess of 3,5-bis(trifluoromethyl)benzylfluoride and its deuterated ( $\text{CD}_2\text{F}$ ) analog at  $60^\circ\text{C}$  (Fig. 4.13). The KIE ( $k_{\text{CH}_2\text{F}}/k_{\text{CD}_2\text{F}}$ ) was determined to be 2.7, indicating that the C–F addition proceeds via C–H addition. Analogously to the C–O additions, we propose that the reaction proceeds via the initial C–H activation to yield the five-coordinate

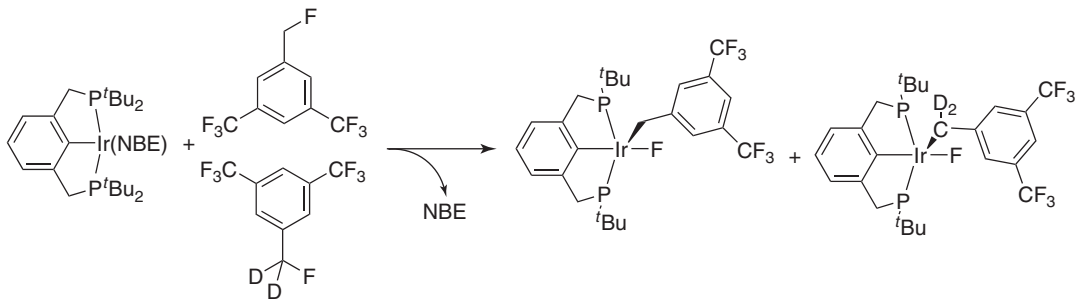


**Figure 4.13** Competition kinetic isotope effect experiment for the addition of 3,5-bis(trifluoromethyl)benzylfluoride and its deuterated analog to (PCP)Ir(NBE).

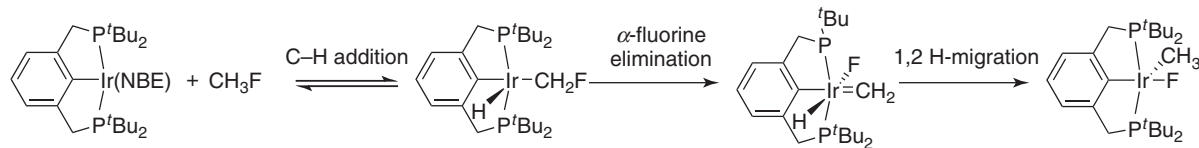


**Figure 4.14** Mechanism for the net oxidative addition of CH<sub>3</sub>-F to (PCP)Ir.

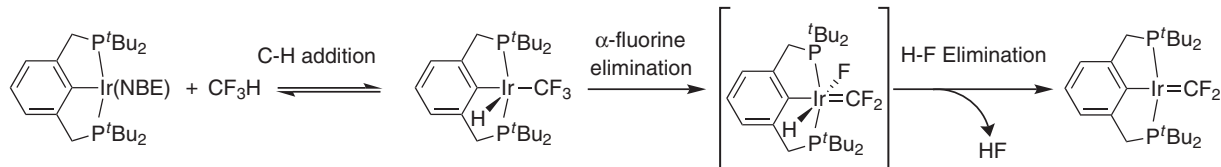


**Figure 4.15** Mechanism for the reaction of (PCP)Ir(NBE) and CHF<sub>3</sub> to yield the difluorocarbene complex, (PCP)IrCF<sub>2</sub>.

Ir(III) intermediate, (PCP)Ir(H)(CH<sub>2</sub>F), followed by  $\alpha$ -F elimination to yield a methylidene intermediate, and then hydride migration from iridium to the carbene to afford the overall oxidative addition product (Fig. 4.14).

In an effort to observe the proposed intermediates (or analogs thereof), we investigated the reaction of trifluoromethane [33] with the hope that additional fluoro groups might stabilize either of the two intermediates shown in Fig. 4.14 [82–84]. Indeed, at moderately low temperature ( $-10^{\circ}\text{C}$ ), an intermediate species was observed that is apparently the C–H addition intermediate (Fig. 4.15), most characteristically evidenced by a broad hydride triplet at  $-45.5\text{ ppm}$  (this high upfield shift is consistent with a square pyramidal complex where the hydride is *trans* to a vacant coordination site). On warming to room temperature, conversion of this intermediate to a major new product characterized as the four-coordinate square planar difluorocarbene, (PCP)Ir(CF<sub>2</sub>), occurred, along with a minor product corresponding to (PCP)Ir(CO) and an additional unidentified product. The four-coordinate carbene product would result from HF elimination from the putative six-coordinate (PCP)Ir(CF<sub>2</sub>)(H)(F) complexes (Fig. 4.15). The reaction of four-coordinate metal difluorocarbene complexes with adventitious water has been previously shown to yield corresponding metal carbonyls [83–85]. The unidentified product revealed spectroscopic features strongly indicative of metal bifluoride complexes presumably resulting from reaction with free H–F [86].

The pathway leading to net C–F oxidative addition via initial C–H activation is supported by DFT calculations (Fig. 4.16). Direct oxidative addition of the C–F bond of fluoromethane was calculated to have an activation barrier of 31.1 kcal/mol relative to free fluoromethane and (PCP)Ir [or 37.5 kcal/mol relative to (PCP)Ir(NBE)], corresponding to the three-centered TS for C–F cleavage. In contrast, the pathway leading to net C–F oxidative addition through C–H activation has a calculated barrier of 16.5 kcal/mol relative to free fluoromethane and (PCP)Ir, or 22.9 kcal/mol relative to (PCP)Ir(NBE), with  $\alpha$ -elimination of fluorine being the rate-determining step. This calculated value of  $\Delta G^{\ddagger}$  is fully consistent with the experimentally determined (approximate) reaction rate.

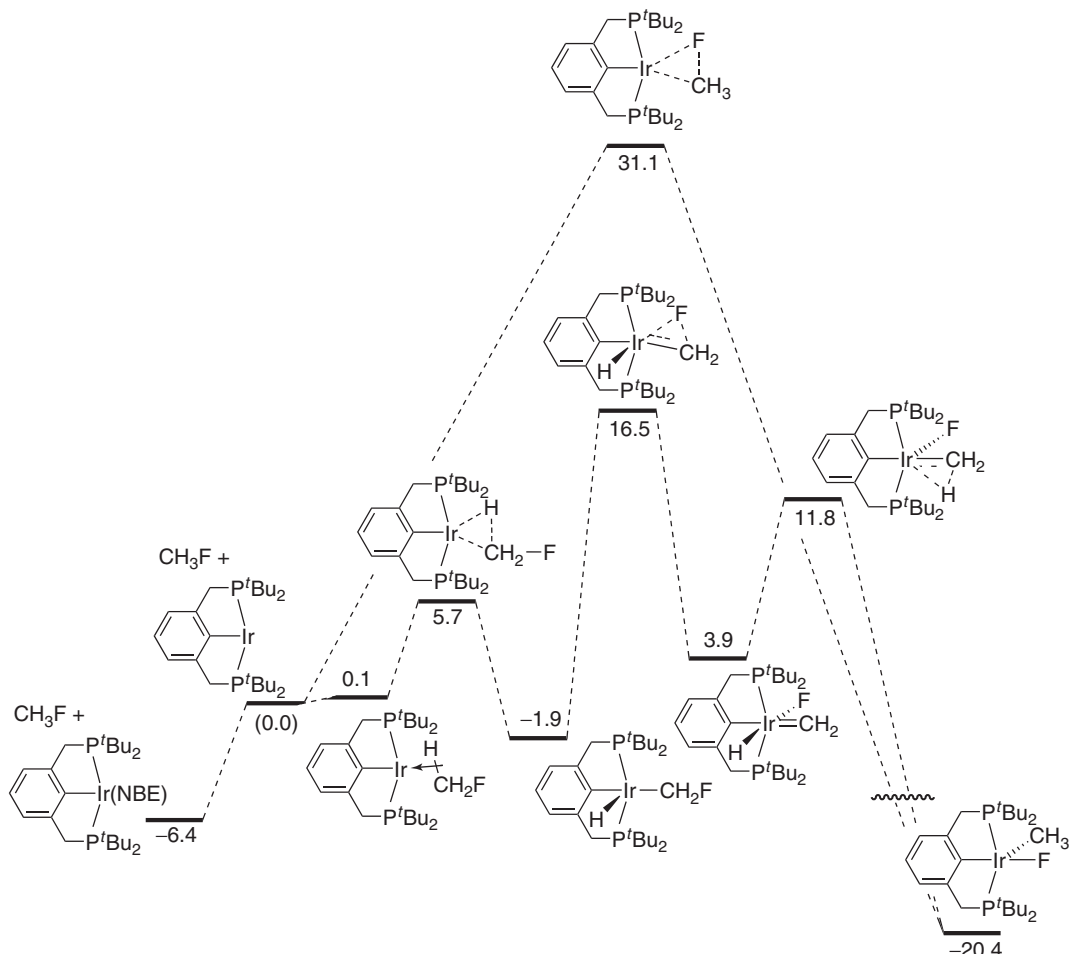
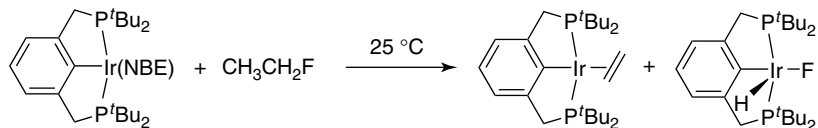
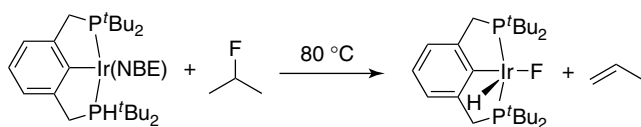


**Figure 4.16** Calculated Gibbs free energies (in kcal/mol; relative to free (PCP)Ir and  $\text{CH}_3\text{F}$ ) for the reaction of (PCP)Ir and  $\text{CH}_3\text{F}$ .



**Scheme 4.22**



**Scheme 4.23**

As discussed earlier, alkyl oxygenates with  $\beta$ -C–H bonds undergo 1,2-H–O elimination as opposed to C–O addition. The analogous behavior is observed with alkyl fluorides. Thus, the reaction of (PCP)Ir(NBE) with fluoroethane results in rapid formation of an equimolar mixture of (PCP)Ir(H)(F) and (PCP)Ir(ethylene) (Scheme 4.22). Reaction of (PCP)Ir(NBE) with 2-fluoropropane, followed by heating to  $80^\circ\text{C}$ , resulted in quantitative conversion to (PCP)Ir(H)(F) (Scheme 4.23).

The mechanism for the reaction of alkyl fluorides bearing a  $\beta$ -hydrogen atom, in analogy with the oxygenates, likely proceeds via initial C–H oxidative addition to give (PCP)Ir(H)(fluoroalkyl), which then undergoes  $\beta$ -F elimination to yield

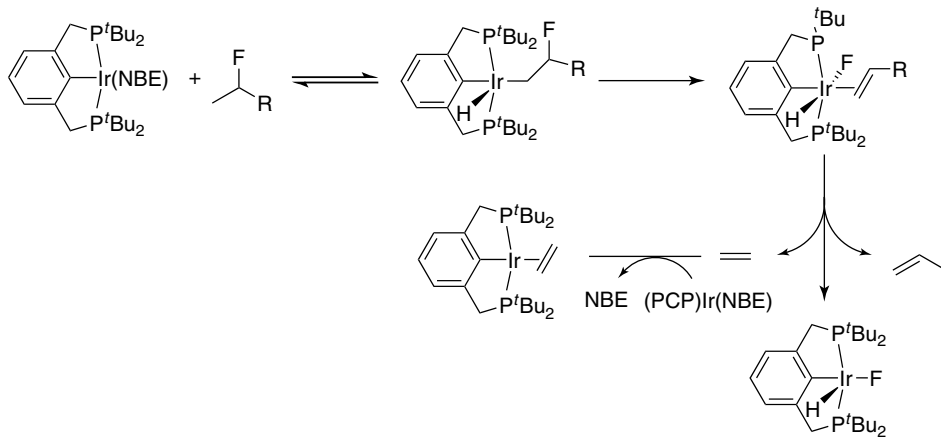


**Figure 4.17** Mechanism for the reaction of (PCP)Ir(NBE) with fluoroethane and 2-fluoropropane.

(PCP)Ir(H)(F)(olefin) (Fig. 4.17). Presumably, ethylene is lost from this six-coordinate species to afford the hydrido fluoride product; the free ethylene then displaces NBE from (PCP)Ir(NBE) to form the (PCP)Ir(ethylene). For 2-fluoropropane, the same general mechanism applies, but the propylene formed from  $\beta$ -fluorine elimination binds less strongly than ethylene to (PCP)Ir, thus eventually allowing quantitative conversion to (PCP)Ir(H)(F).

#### 4.4 SUMMARY

We have found that typically unreactive C(sp<sup>3</sup>)–O and C(sp<sup>3</sup>)–F bonds, including those of methyl aryl ethers (with electron-poor aryl groups), methyl esters, methyl tosylate, and methyl or benzyl fluoride, can undergo relatively unprecedented oxidative additions of the C(sp<sup>3</sup>)–X bond to the 14-electron fragment (PCP)Ir (X = OR, including OAr, OAc, or OTs, or X = F). Perhaps even more surprisingly, the reactions are found to proceed not via direct oxidative addition of the C–X bond (which is computationally predicted to have a prohibitively high energy barrier), but rather through the initial activation of a C–H bond positioned  $\alpha$  to the O or F atom. In the case of alkyl oxygenates or fluorides in which the alkyl groups have H atoms in the  $\beta$ -position, reaction with (PCP)Ir also results in C–X bond cleavage, but of a very different type, namely, 1,2-dehydro-oxygenation or 1,2-dehydrofluorination. In this case, the reaction appears to proceed via oxidative addition of a  $\beta$ -C–H bond, followed by  $\beta$ -C–X migration, to give (PCP)IrHX and olefin.

While C–H addition has been an intensively studied field of chemistry for several decades now, this has almost invariably been with an eye toward “functionalizing the C–H bond” in some manner. This work indicates that C–H addition can represent a route toward activating a different bond in the molecule, in this case a C–X bond located either  $\alpha$  or  $\beta$  to the C–H bond that undergoes addition.

By the principle of microscopic reversibility, these reaction mechanisms suggest new routes for the formation of C(sp<sup>3</sup>)–X bonds. Perhaps most intriguing, the mechanism elucidated for C–X oxidative addition implies that its microscopic reverse, C–X reductive elimination, must occur, for these systems, via an initial  $\alpha$ -H migration from alkyl group to the metal center to generate the key alkylidene intermediate. The generality of this with respect to systems beyond (PCP)Ir(alkyl)X remains to be determined, but given that reductive elimination from late metal systems often proceeds via five-coordinate d<sup>6</sup> complexes, this mechanism may well be more broadly applicable. Likewise, the mechanism of the 1,2-H–X elimination reactions may offer insight applicable to the design of potential catalysts for 1,2-H–X addition reactions.

#### ACKNOWLEDGMENTS

The studies that are the focus of this chapter were conducted, with great thought, skill, and dedication, by Jongwook Choi, Sabuj Kundu, Yuriy Choliy, David Y. Wang, Xiawei Zhang, and Thomas J. Emge. This material is based on work supported by the National Science Foundation under Grant CHE #1112456 to A.S.G and K.K.-J. J.H. thanks the NSF IGERT program (Renewable and Sustainable Fuel Solutions for the 21st Century) for a Graduate Training Fellowship.

## REFERENCES

- Albrecht, M.; van Koten, G. *Angew. Chem., Int'l. Ed.* **2001**, *40*, 3750.
- The Chemistry of Pincer Compounds*; Morales-Morales, D., Jensen, C., Eds.; Elsevier: Amsterdam, **2007**.
- van der Boom, M. E.; Milstein, D. *Chem. Rev.* **2003**, *103*, 1759.
- Leis, W.; Mayer, H. A.; Kaska, W. C. *Coord. Chem. Rev.* **2008**, *252*, 1787.
- Benito-Garagorri, D.; Kirchner, K. *Acc. Chem. Res.* **2008**, *41*, 201.
- Choi, J.; MacArthur, A. H. R.; Brookhart, M.; Goldman, A. S. *Chem. Rev.* **2011**, *111*, 1761.
- Haibach, M. C.; Kundu, S.; Brookhart, M.; Goldman, A. S. *Acc. Chem. Res.* **2012**, *45*, 947.
- Kanzelberger, M.; Singh, B.; Czerw, M.; Krogh-Jespersen, K.; Goldman, A. S. *J. Am. Chem. Soc.* **2000**, *122*, 11017.
- Zhang, X.; Kanzelberger, M.; Emge, T. J.; Goldman, A. S. *J. Am. Chem. Soc.* **2004**, *126*, 13192.
- Ghosh, R.; Zhang, X.; Achord, P.; Emge, T. J.; Krogh-Jespersen, K.; Goldman, A. S. *J. Am. Chem. Soc.* **2007**, *129*, 853.
- Gupta, M.; Hagen, C.; Flesher, R. J.; Kaska, W. C.; Jensen, C. M. *Chem. Commun.* **1996**, *2083*.
- Liu, F.; Pak, E. B.; Singh, B.; Jensen, C. M.; Goldman, A. S. *J. Am. Chem. Soc.* **1999**, *121*, 4086.
- Krogh-Jespersen, K.; Czerw, M.; Summa, N.; Renkema, K. B.; Achord, P. D.; Goldman, A. S. *J. Am. Chem. Soc.* **2002**, *124*, 11404.
- Krogh-Jespersen, K.; Czerw, M.; Kanzelberger, M.; Goldman, A. S. *J. Chem. Inf. Comput. Sci.* **2001**, *41*, 56.
- Renkema, K. B.; Kissin, Y. V.; Goldman, A. S. *J. Am. Chem. Soc.* **2003**, *125*, 7770.
- Goldman, A. S.; Renkema, K. B.; Czerw, M.; Krogh-Jespersen, K. In *Activation and Functionalization of C–H Bonds*; Goldberg, K. I., Goldman, A. S., Eds.; ACS Symposium Series, Vol. 885; American Chemical Society: Washington, DC, **2004**; p 198.
- Zhu, K.; Achord, P. D.; Zhang, X.; Krogh-Jespersen, K.; Goldman, A. S. *J. Am. Chem. Soc.* **2004**, *126*, 13044.
- Göttker-Schnetmann, I.; White, P.; Brookhart, M. *J. Am. Chem. Soc.* **2004**, *126*, 1804.
- Kundu, S.; Choliy, Y.; Zhuo, G.; Ahuja, R.; Emge, T. J.; Warmuth, R.; Brookhart, M.; Krogh-Jespersen, K.; Goldman, A. S. *Organometallics* **2009**, *28*, 5432.
- Ahuja, R.; Punji, B.; Findlater, M.; Supplee, C.; Schinski, W.; Brookhart, M.; Goldman, A. S. *Nature Chem.* **2011**, *3*, 167.
- Goldman, A. S.; Roy, A. H.; Huang, Z.; Ahuja, R.; Schinski, W.; Brookhart, M. *Science* **2006**, *312*, 257.
- Huang, Z.; Rolfe, E.; Carson, E. C.; Brookhart, M.; Goldman, A. S.; El-Khalafy, S. H.; MacArthur, A. H. R. *Adv. Synth. Catal.* **2010**, *352*, 125.
- Bailey, B. C.; Schrock, R. R.; Kundu, S.; Goldman, A. S.; Huang, Z.; Brookhart, M. *Organometallics* **2009**, *28*, 355.
- Santana, R. C.; Do, P. T.; Santikunaporn, M.; Alvarez, W. E.; Taylor, J. D.; Sughrue, E. L.; Resasco, D. E. *Fuel* **2006**, *85*, 643.
- Morales-Morales, D.; Lee, D. W.; Wang, Z.; Jensen, C. M. *Organometallics* **2001**, *20*, 1144.
- Morales-Morales, D.; Redon, R.; Wang, Z.; Lee, D. W.; Yung, C.; Magnuson, K.; Jensen, C. M. *Can. J. Chem.* **2001**, *79*, 823.
- Kanzelberger, M.; Zhang, X.; Emge, T. J.; Goldman, A. S.; Zhao, J.; Incarvito, C.; Hartwig, J. F. *J. Am. Chem. Soc.* **2003**, *125*, 13644.
- Zhao, J.; Goldman, A. S.; Hartwig, J. F. *Science* **2005**, *307*, 1080.
- Morgan, E.; MacLean, D. F.; McDonald, R.; Turculet, L. *J. Am. Chem. Soc.* **2009**, *131*, 14234.
- Ghosh, R.; Emge, T. J.; Krogh-Jespersen, K.; Goldman, A. S. *J. Am. Chem. Soc.* **2008**, *130*, 11317.
- Choi, J.; Choliy, Y.; Zhang, X.; Emge, T. J.; Krogh-Jespersen, K.; Goldman, A. S. *J. Am. Chem. Soc.* **2009**, *131*, 15627.
- Kundu, S.; Choi, J.; Wang, D. Y.; Choliy, Y.; Emge, T. J.; Krogh-Jespersen, K.; Goldman, A. S. *J. Am. Chem. Soc.*, **2013**, *135*, 5127.
- Choi, J.; Wang, D. Y.; Kundu, S.; Choliy, Y.; Emge, T. J.; Krogh-Jespersen, K.; Goldman, A. S. *Science* **2011**, *332*, 1545.
- Ittel, S. D.; Tolman, C. A.; English, A. D.; Jesson, J. P. *J. Am. Chem. Soc.* **1978**, *100*, 7577.
- Tolman, C. A.; Ittel, S. D.; English, A. D.; Jesson, J. P. *J. Am. Chem. Soc.* **1979**, *101*, 1742.
- van der Boom, M. E.; Liou, S.-Y.; Ben-David, Y.; Vigalok, A.; Milstein, D. *Angew. Chem., Int'l.* **1997**, *36*, 625.
- van der Boom, M. E.; Liou, S.-Y.; Ben-David, Y.; Shimon, L. J. W.; Milstein, D. *J. Am. Chem. Soc.* **1998**, *120*, 6531.
- For an example of catalytic cleavage of C(sp<sup>2</sup>)-O bonds, and a lead reference for such chemistry, see: Sergeev, A. G.; Hartwig, J. F. *Science* **2011**, *332*, 439.
- Ueno, S.; Mizushima, E.; Chatani, N.; Kakiuchi, F. *J. Am. Chem. Soc.* **2006**, *128*, 16516.
- Yamamoto, T.; Akimoto, M.; Yamamoto, A. *Chem. Lett.* **1983**, 1725.
- Yamamoto, T.; Akimoto, M.; Saito, O.; Yamamoto, A. *Organometallics* **1986**, *5*, 1559.
- Trovitch, R. J.; Lobkovsky, E.; Bouwkamp, M. W.; Chirik, P. J. *Organometallics* **2008**, *27*, 6264.
- Lara, P.; Paneque, M.; Poveda, M. L.; Salazar, V.; Santos, L. L.; Carmona, E. *J. Am. Chem. Soc.* **2006**, *128*, 3512.
- Conejero, S.; Paneque, M.; Poveda, M. L.; Santos, L. L.; Carmona, E. *Acc. Chem. Res.* **2010**, *43*, 572.

45. Santos, L. L.; Mereiter, K.; Paneque, M. *Organometallics* **2013**, *32*, 565.
46. Ozerov, O. V.; Guo, C.; Papkov, V. A.; Foxman, B. M. *J. Am. Chem. Soc.* **2004**, *126*, 4792.
47. Whited, M. T.; Grubbs, R. H. *Acc. Chem. Res.* **2009**, *42*, 1607.
48. Whited, M. T.; Zhu, Y.; Timpa, S. D.; Chen, C.-H.; Foxman, B. M.; Ozerov, O. V.; Grubbs, R. H. *Organometallics* **2009**, *28*, 4560.
49. Manbeck, K. A.; Kundu, S.; Walsh, A. P.; Brennessel, W. W.; Jones, W. D. *Organometallics* **2012**, *31*, 5018.
50. Williams, B. S.; Holland, A. W.; Goldberg, K. I. *J. Am. Chem. Soc.* **1999**, *121*, 252.
51. Williams, B. S.; Goldberg, K. I. *J. Am. Chem. Soc.* **2001**, *123*, 2576.
52. Smythe, N. A.; Grice, K. A.; Williams, B. S.; Goldberg, K. I. *Organometallics* **2009**, *28*, 277.
53. Northcutt, T. O.; Wick, D. D.; Vetter, A. J.; Jones, W. D. *J. Am. Chem. Soc.* **2001**, *123*, 7257.
54. Parkin, G. *Acc. Chem. Res.* **2009**, *42*, 315.
55. (a) Rachidi, I. E.-I.; Eisenstein, O.; Jean, Y. *New J. Chem.* **1990**, *14*, 671–677; (b) Riehl, J.-F.; Jean, Y.; Eisenstein, O.; Pélissier, M. *Organometallics* **1992**, *11*, 729.
56. Chan, J.; Tang, A.; Bennet, A. J. *J. Am. Chem. Soc.* **2012**, *134*, 1212.
57. Singh, V.; Schramm, V. L. *J. Am. Chem. Soc.* **2007**, *129*, 2783.
58. Adcock, W.; Trout, N. A.; Vercoe, D.; Taylor, D. K.; Shiner, V. J.; Sorensen, T. S. *J. Org. Chem.* **2003**, *68*, 5399.
59. Asperger, S.; Kukric, Z.; Saunders, W. H.; Sutic, D. *J. Chem. Soc., Perkin Trans. 1* **1992**, *2*, 275.
60. Asperger, S.; Pavlovic, D.; Kukric, Z.; Sutic, D. *Inorg. Chim. Acta* **1990**, *171*, 5.
61. Sutic, D.; Asperger, S.; Borcic, S. *J. Org. Chem.* **1982**, *47*, 5120.
62. Streitwieser, A.; Dafforn, G. A. *Tetrahedron Lett.* **1969**, *10*, 1263.
63. Shiner, V. J.; Rapp, M. W.; Halevi, E. A.; Wolfsberg, M. *J. Am. Chem. Soc.* **1968**, *90*, 7171.
64. Rybtchinski, B.; Vigalok, A.; Ben-David, Y.; Milstein, D. *J. Am. Chem. Soc.* **1996**, *118*, 12406.
65. For examples of the (PCP-CH<sub>2</sub>) ligand motifs in Rh and Ni complexes, see: (a) Vigalok, A.; Rybtchinski, B.; Shimon, L. J. W.; Ben-David, Y.; Milstein, D. *Organometallics* **1999**, *18*, 895; (b) van der Boom, M. E.; Liou, S.-Y.; Shimon, L. J. W.; Ben-David, Y.; Milstein, D. *Inorg. Chim. Acta* **2004**, *357*, 4015.
66. Hartwig, J. F. In *Organotransition Metal Chemistry*; University Science Books: Sausalito, CA, **2010**, p 301.
67. McMillen, D. F.; Golden, D. M. *Annu. Rev. Phys. Chem.* **1982**, *33*, 493.
68. Richmond, T. G.; Osterberg, C. E.; Arif, A. M. *J. Am. Chem. Soc.* **1987**, *109*, 8091.
69. Jones, W. D.; Partridge, M. G.; Perutz, R. N., Jr. *Chem. Soc. Chem. Commun.* **1991**, 264.
70. Belt, S. T.; Hellwell, M.; Jones, W. D.; Partridge, M. G.; Perutz, R. N. *J. Am. Chem. Soc.* **1993**, *115*, 1429.
71. Kiplinger, J. L.; Richmond, T. G.; Osterberg, C. E. *Chem. Rev.* **1994**, *94*, 373.
72. Richmond, T. G. *Top. Organomet. Chem.* **1999**, *3*, 243.
73. Jones, W. D. *Dalton Trans.* **2003**, 3991.
74. Reinhold, M.; McGrady, J. E.; Perutz, R. N. *J. Am. Chem. Soc.* **2004**, *126*, 5268.
75. Torrens, H. *Coord. Chem. Rev.* **2005**, *249*, 1957.
76. Hull, K. L.; Anani, W. Q.; Sanford, M. S. *J. Am. Chem. Soc.* **2006**, *128*, 7134.
77. Muller, K.; Faeh, C.; Diederich, F. *Science* **2007**, *317*, 1881.
78. Perutz, R. N. *Science* **2008**, *321*, 1168.
79. Amii, H.; Uneyama, K. *Chem. Rev.* **2009**, *109*, 2119.
80. Grushin, V. V. *Acc. Chem. Res.* **2010**, *43*, 160.
81. Johnson, S. A.; Hatnean, J. A.; Doster, M. E. *Prog. Inorg. Chem.* **2012**, *57*, 255.
82. Vetter, A. J.; Rieth, R. D.; Brennessel, W. W.; Jones, W. D. *J. Am. Chem. Soc.* **2009**, *131*, 10742.
83. Brothers, P. J.; Roper, W. R. *Chem. Rev.* **1988**, *88*, 1293.
84. Hughes, R. P.; Laritchev, R. B.; Yuan, J.; Golen, J. A.; Rucker, A. N.; Rheingold, A. L. *J. Am. Chem. Soc.* **2005**, *127*, 15020.
85. Hughes, R. P. *Eur. J. Inorg. Chem.* **2009**, 4591.
86. Jasim, N. A.; Perutz, R. N. *J. Am. Chem. Soc.* **2000**, *122*, 8685.



## FUNCTIONALIZATION OF $sp^2$ AND $sp^3$ CARBON CENTERS CATALYZED BY POLYOXOMETALATES AND METALLOPORPHYRINS

MÁRIO M. Q. SIMÕES\*, ISABEL C. M. S. SANTOS, MARIA GRAÇA P. M. S. NEVES, ANA M. V. CAVALEIRO, AND JOSÉ A. S. CAVALEIRO

*Department of Chemistry, University of Aveiro, Aveiro, Portugal*

### 5.1 INTRODUCTION

The increasing concern with sustainability and the critical need for cleaner technologies have definitively contributed to the development and spreading of catalytic processes, including those related with oxidative transformations. In fact, the conversion of organic compounds into oxygenated derivatives has been widely investigated over the last decades since such products are valuable intermediates for organic synthesis both in the laboratory and in industry [1–7]. One of the main challenges in studying metal complex catalysis is to find novel, efficient systems able to oxidize organic compounds with high selectivity, preferably with cheap, environmentally friendly oxidants such as air or hydrogen peroxide. The latter has a high (47%) active oxygen content and is widely available, and its only by-product is water. Therefore, its chemistry is considered to be environmentally safe. Unfortunately, as with oxygen itself, hydrogen peroxide generally exhibits one of the most complex and minimally controllable oxidation chemistry of all the potentially attractive oxidants [8–10].

In this context, metalloporphyrins, perhaps the best understood and well-studied bio-inspired catalysts, have emerged because of their ability to mimic the catalytic activity of cytochrome P450 enzymes in the presence of numerous oxygen donors [11–15]. The first system capable of mimicking the cytochrome P450 reactions, namely the epoxidation of olefins and the hydroxylation of alkanes, was reported by Groves and collaborators in 1979. That system was based on the Fe(III) complex of the *meso*-tetraphenylporphyrin [Fe(TPP)Cl] as catalyst and PhIO as the oxygen donor [16]. The use of metalloporphyrins as catalysts in oxidation reactions, such as epoxidation of olefins and hydroxylation of saturated hydrocarbons, has been largely documented during the last decades [17–22]. Many studies were focused on the relation between the porphyrin structure and the corresponding catalytic efficiency. In the past years, the emphasis has been on the promising applications of metalloporphyrins, both under homogeneous and heterogeneous catalytic conditions [23–27]. The oxygenation mechanism operating in cytochrome P450 enzymes and in synthetic metalloporphyrin models has been the aim of numerous studies in the last decades [13, 28, 29].

The oxidation of organic compounds catalyzed by polyoxometalates (POMs) is also a very promising way to obtain value-added products from comparatively cheap starting materials [30–32]. POMs are oxoanions comprising groups 5 and 6 transition metals. Transition-metal-substituted polyoxometalates (TMSPs), that is, POMs of certain families incorporating other d-metals in their structures, have been much studied as oxidative catalysts, frequently with hydrogen peroxide or molecular oxygen as the oxidants [32–35]. Some of these TMSPs have many similarities with metal complexes of macrocyclic ligands as, for example, with metalloporphyrins and related species, since they possess rigid coordination

*Advances in Organometallic Chemistry and Catalysis: The Silver/Gold Jubilee International Conference on Organometallic Chemistry Celebratory Book*, First Edition. Edited by Armando J. L. Pombeiro.

© 2014 John Wiley & Sons, Inc. Published 2014 by John Wiley & Sons, Inc.

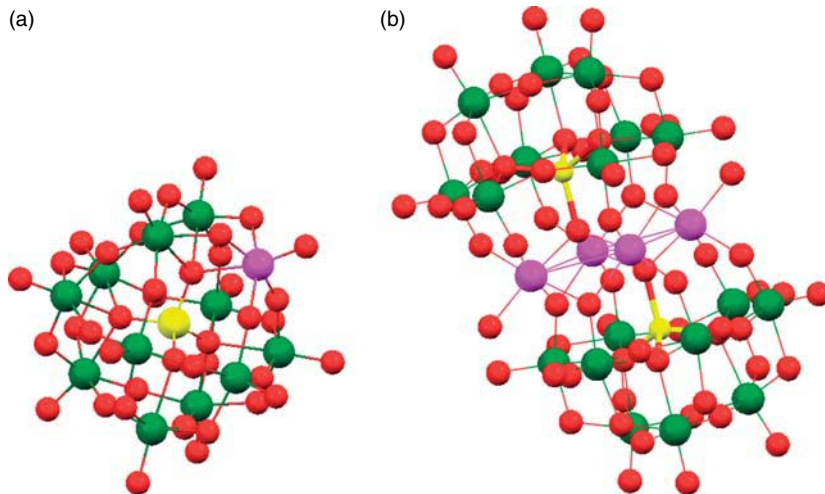


**Figure 5.1** General structure of the Keggin-type (a) and sandwich-type (b) transition metal substituted polyoxometalates (TMSPs) used in catalysis; W (green); O (red); heteroatom X (yellow); transition metal M (pink). (See insert for color representation of the figure.)

sites surrounding a metal center [34, 36]. Keggin-type TMSPs were even considered as inorganic analogs of metalloporphyrins, an arguable designation, concerning their reactivity, despite some similarities observed in oxidative catalysis [37–39].

In the past years, our group has been able to build up a promising line of research in the field of catalytic oxidation of organic compounds using almost exclusively hydrogen peroxide as oxidant, both using Keggin-type or sandwich-type TMSPs (Fig. 5.1) [40–52] and Mn(III) or Fe(III) porphyrins (Fig. 5.2) [53–72] in homogeneous or heterogeneous conditions. A brief account of this research is presented here. Unless otherwise stated, all studies were performed with hydrogen peroxide as oxidant and acetonitrile as solvent.

## 5.2 FUNCTIONALIZATION OF SP<sup>3</sup> CARBON CENTERS UNDER HOMOGENEOUS CONDITIONS

The functionalization studies of sp<sup>3</sup> carbon centers in cycloalkanes and alkylbenzenes (Fig. 5.3) with hydrogen peroxide were carried out in acetonitrile, under homogeneous conditions, using various POMs, namely the tetrabutylammonium (TBA) salts of the heteropolyanions  $[XW_{11}M(H_2O)O_{39}]^{P-}$  ( $XW_{11}M$ ), where X = P, Si, or B and M = Fe<sup>III</sup> or Mn<sup>III</sup> and  $[M_4(H_2O)_2(PW_9O_{34})_2]^{q-}$ , where M = Co<sup>II</sup>, Mn<sup>II</sup>, and Fe<sup>III</sup> ( $M_4(PW_9)_2$ ). The influence of the substrate/catalyst (S/C) molar ratio, the amount of oxidant added, or the reaction time was investigated.

The results obtained for cyclohexane (**1**), cyclooctane (**2**), and cyclododecane (**3**) are summarized in Table 5.1 and the major products observed are presented in Fig. 5.4. For cyclohexane (**1**), the main product obtained was cyclohexanone (**1.1**) (with **1.1/1.2** molar ratio between 1.4 and 2.6) with all catalysts, except with  $Fe_4(PW_9)_2$ , which gave cyclohexyl hydroperoxide (**1.3**) as the main product [42, 45]. Turnover numbers (TONs) higher than 1300 were obtained when higher S/C molar ratios were tested.

The results obtained for the oxidation of cyclooctane (**2**) with hydrogen peroxide in the presence of POMs resemble those obtained for **1** (Table 5.1). However, in this case, all the iron catalysts tested gave higher selectivity for cyclooctyl hydroperoxide (**2.3**) [42, 43, 45]. Moreover, with the sandwich iron complex, TONs higher than 1900 were reached after 12 h of reaction under the appropriate conditions, without significant alterations on selectivity. When a very high excess of  $H_2O_2$  was used ( $H_2O_2/\text{sub} = 9.8$ ), the rate of oxidation increased and 100% conversion was reached before 12 h of reaction for almost all the POMs. Besides that, high selectivity for **2.3** was observed for  $H_2O_2/\text{sub} = 9.8$ . Nevertheless, the oxidation of **2** into cyclooctanone (**2.1**) could be obtained with high selectivity (83%) and conversion (92%) using  $Co_4(PW_9)_2$  and  $H_2O_2/\text{sub} = 9.8$  [42, 43, 45].

The homogeneous catalytic oxidation of cyclododecane (**3**) was performed using iron-substituted Keggin-type POMs as catalysts, cyclododecanone (**3.1**) and cyclododecanol (**3.2**) being the main products obtained [44, 46]. However, cyclododecyl hydroperoxide (**3.3**) and dodecanal may also be obtained, depending on the reaction conditions. The best results were found for a molar ratio  $S/C = 667$  and  $H_2O_2/\text{sub} = 6$  (Table 5.1). All the catalysts studied in the oxidation of **3** had identical

(a)

(b)

Ar, Ar' =	Fe(TPP)Cl	M = Fe	R = H
Ar, Ar' =	Mn(TDCPP)Cl	M = Mn	R = H
	Mn( $\beta$ -NO <sub>2</sub> TDCPP)Cl	M = Mn	R = NO <sub>2</sub>
Ar, Ar' =	Mn(TF <sub>5</sub> PP)Cl	M = Mn	R = H
	Mn( $\beta$ -NO <sub>2</sub> TF <sub>5</sub> PP)Cl	M = Mn	R = NO <sub>2</sub>
	Mn(TDMImP)Cl	M = Mn	R = H
	Mn(TPyP)Cl	M = Mn	R = H
	Mn(TMePyP)Cl	M = Mn	R = H
	Mn(TrisDCPPyP)Cl	M = Mn	R = H
	Mn(TrisDCPMePyP)Cl	M = Mn	R = H

**Figure 5.2** (a) Structures and (b) abbreviations of Mn(III) or Fe(III) porphyrin complexes.

behavior, affording **3.1** as the major product after 12 h of reaction. Nevertheless, the hydroperoxide **3.3** can be obtained as the main product if the reaction is ended after 3 h. This system was the first one to afford cyclododecyl hydroperoxide and dodecanal in the catalytic oxidation of cyclododecane [44, 46]. Dodecanal, obtained with identical selectivity with all the three iron catalysts, may be formed via  $\beta$ -cleavage of the intermediate cycloalkyloxy radical, which may be formed via metal-catalyzed decomposition of the corresponding hydroperoxide [73, 74].

Another example of oxidative functionalization of sp<sup>3</sup> carbon centers is the homogeneous liquid phase oxidation of indane (**4**) and tetralin (**5**) with hydrogen peroxide catalyzed both by TBA salts of iron(III)-substituted POMs XW<sub>11</sub>Fe, where X = P, Si, or B [48], and by manganese(III) porphyrin complexes [60]. The TMSp systems yield, after 24 h of reaction, the corresponding ketones **4.1** and **5.1** as the major products, accompanied by the benzylic monooxygenation (**4.2** and **5.2**) and the dioxygenation (**4.3** and **5.3**) products. The indane oxidation reactions produce also dehydrogenation and hydroperoxidation products, such as 1*H*-indene (**16**) and indane hydroperoxide (**4.4**), respectively. Interestingly, in the oxidation of **5**, the important carbon–carbon bond oxidative cleavage of tetralin hydroperoxide (**5.4**), affording 4-(2-hydroxyphenyl)butanal (**5.5**), is also observed. These studies demonstrated that iron(III)-substituted Keggin-type POMs are efficient catalysts for indane (**4**) and tetralin (**5**) oxidation, with conversion up to 59% for indane and 34% for tetralin, using the environmentally safe hydrogen peroxide as oxidant. The best catalyst was BW<sub>11</sub>Fe, since the conversions obtained after 3 h of reaction were significantly higher, for both substrates, than those registered using the other catalysts. To the best

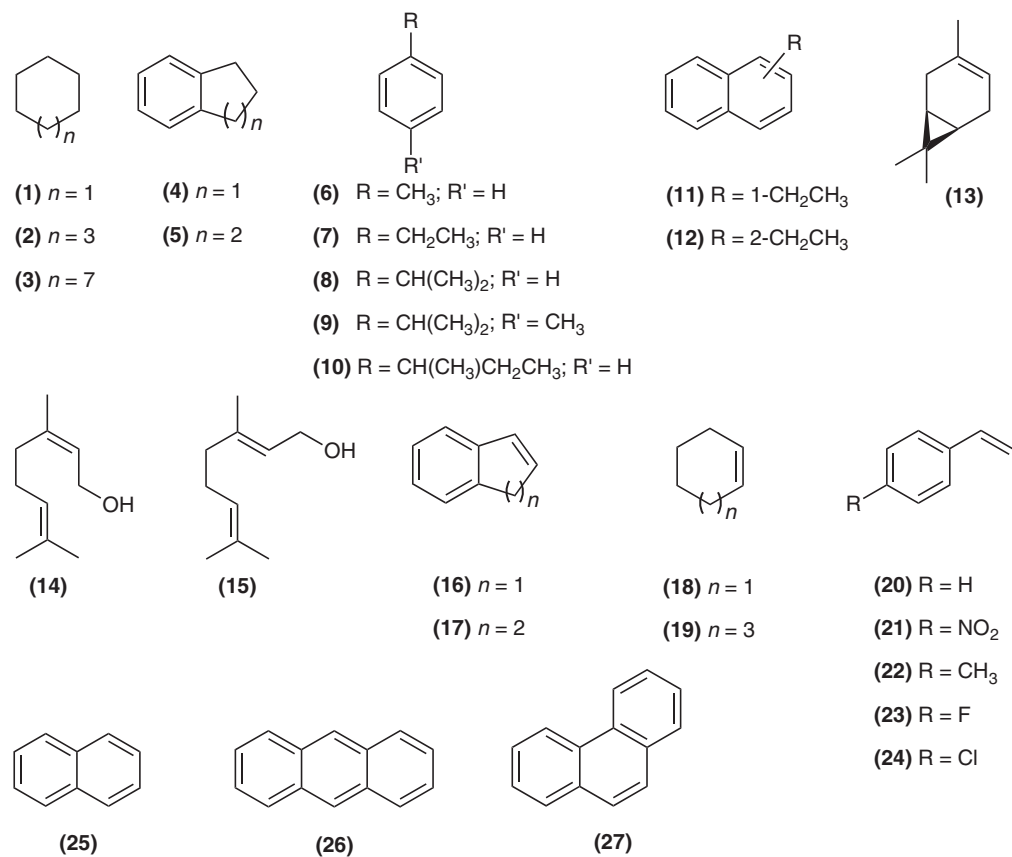


**Figure 5.3** Substrates considered in the catalytic oxidation studies.

of our knowledge, this is the first study on the use of iron(III)-substituted POMs in the oxidation of these arenes [48]. In the metalloporphyrin system, the oxidation of **4** and **5**, catalyzed by Mn(TDCPP)Cl and Mn( $\beta$ -NO<sub>2</sub>TDCPP)Cl (Fig. 5.2), gave rise mainly to benzylic monooxygenation products, namely the corresponding ketones **4.1** and **5.1** and alcohols **4.2** and **5.2** with high substrate conversions, that is 96% or 95% (both after 2 h) for **4** and 97% (after 3 h) or 96% (after 3.5 h) for **5**. The reactions catalyzed by Mn(TF<sub>5</sub>PP)Cl and Mn( $\beta$ -NO<sub>2</sub>TF<sub>5</sub>PP)Cl (Fig. 5.2) showed higher capability to generate dehydrogenated products such as 1*H*-indene (**16**) and naphthalene (**25**) [60].

The oxidation of some alkylbenzenes, namely ethylbenzene (**7**), cumene (**8**), *p*-cymene (**9**), and *s*-butylbenzene (**10**), with aqueous H<sub>2</sub>O<sub>2</sub> in the presence of iron-substituted POMs was also evaluated [49]. With these systems, the corresponding acetophenones **7.1** and **9.1** and hydroperoxides **7.2**, **8.1**, **9.2**, and **10.1** were the main products obtained. The oxidation of **7** and **8** occurred with maximum conversion of 26% and 37%, respectively, in the presence of PW<sub>11</sub>Fe, both after 24 h of reaction, whereas the maximum conversion of **9** (35%) was found when BW<sub>11</sub>Fe was used. The higher hydroperoxide selectivity was obtained with PW<sub>11</sub>Fe. In the presence of BW<sub>11</sub>Fe, the oxidation of **7** and **8** yielded acetophenone (**7.1**) in moderate selectivity, while in general *p*-methylacetophenone (**9.1**) was the major product obtained in the oxidation of **9**. This system based on POMs showed good catalytic efficiency associated with a different product distribution when compared with other systems using hydrogen peroxide and POMs [75–77]. Actually, the conversions obtained with these conditions are higher than those often observed for this kind of substrates, accompanied by an unusual formation of high amounts of the corresponding hydroperoxides, which were detected for the first time in catalysis with POMs [49].

The oxidation of toluene (**6**), ethylbenzene (**7**), and cumene (**8**) with hydrogen peroxide in the presence of Mn(III) porphyrins having electron-withdrawing substituents was also studied [56]. In general, 2-methyl-1,4-benzoquinone (**6.1**) was the main toluene oxidation product for catalysts Mn(TF<sub>5</sub>PP)Cl and Mn( $\beta$ -NO<sub>2</sub>TF<sub>5</sub>PP)Cl. On the other hand, benzoic acid (**6.2**) was the main toluene oxidation product for Mn(TDCPP)Cl and Mn( $\beta$ -NO<sub>2</sub>TDCPP)Cl. Thus, depending on the catalyst, the oxidative attack took place at sp<sup>2</sup> or sp<sup>3</sup> centers, respectively. In the oxidation of **7**, acetophenone (**7.1**) was the major product for all the catalysts tested. The higher conversions for these two substrates **6** and **7** were observed with

**TABLE 5.1** Oxidation of Cycloalkanes (**1–3**) with H<sub>2</sub>O<sub>2</sub> Catalyzed by Polyoxometalates (POMs)<sup>a</sup>

POM	Substrate	Conversion, %	TON	Selectivity, %			References
				-one	-ol	-OOH	
BW <sub>11</sub> Fe	( <b>1</b> )	87	580	49	19	32	42
Co <sub>4</sub> (PW <sub>9</sub> ) <sub>2</sub>		83	549	62	38	0	45
Mn <sub>4</sub> (PW <sub>9</sub> ) <sub>2</sub>		68	453	59	41	0	45
Fe <sub>4</sub> (PW <sub>9</sub> ) <sub>2</sub>		94 <sup>b</sup>	628	41	6	53	45
BW <sub>11</sub> Fe	( <b>2</b> )	99 <sup>c</sup>	660	28	7	65	42
BW <sub>11</sub> Mn		88	587	71	10	19	42
PW <sub>11</sub> Fe		96	640	37	6	57	43
PW <sub>11</sub> Mn		89	594	53	10	37	43
SiW <sub>11</sub> Fe		79	527	39	9	52	43
SiW <sub>11</sub> Mn		89	594	60	14	26	43
Co <sub>4</sub> (PW <sub>9</sub> ) <sub>2</sub>		85	567	63	32	5	45
Mn <sub>4</sub> (PW <sub>9</sub> ) <sub>2</sub>		68	452	49	16	5	45
Fe <sub>4</sub> (PW <sub>9</sub> ) <sub>2</sub>		96	645	41	2	57	45
BW <sub>11</sub> Fe	( <b>3</b> ) <sup>d</sup>	61	407	58	32	3	46
BW <sub>11</sub> Fe		70 <sup>e</sup>	467	52	22	17	46
PW <sub>11</sub> Fe		57	380	42	38	10	46
PW <sub>11</sub> Fe		73 <sup>e</sup>	487	44	18	25	46
SiW <sub>11</sub> Fe		25	167	50	23	10	46
SiW <sub>11</sub> Fe		41 <sup>e</sup>	273	52	25	18	46

<sup>a</sup>Reaction conditions: 1 mmol of substrate, 1.5 μmol of catalyst, 2 mmol of H<sub>2</sub>O<sub>2</sub>, 1.5 ml of CH<sub>3</sub>CN; after 12 h at reflux.

<sup>b</sup>After 6 h of reaction.

<sup>c</sup>After 9 h of reaction.

<sup>d</sup>3 ml of CH<sub>3</sub>CN.

<sup>e</sup>6 mmol of H<sub>2</sub>O<sub>2</sub>.

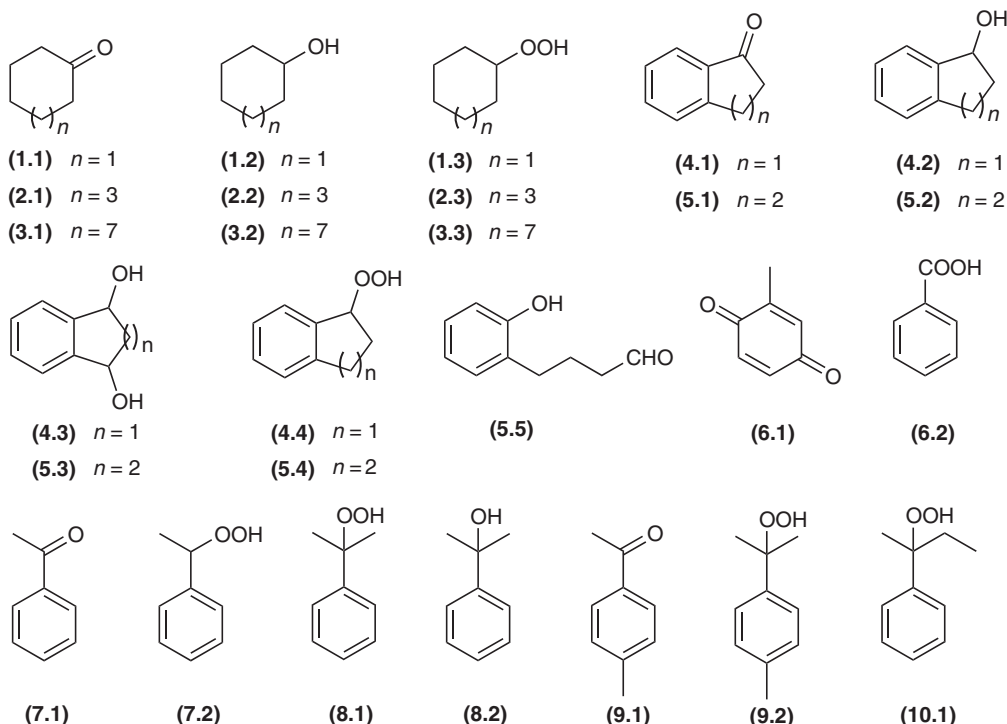


**Figure 5.4** Oxidation products obtained in the catalytic oxidation studies of compounds **1** to **10**.

the *meso*-tetra-2,6-dichlorophenylporphyrin manganese complex containing an electron-withdrawing group at the  $\beta$ -pyrrolic position, Mn( $\beta$ -NO<sub>2</sub>TDCPP)Cl. In the case of cumene (**8**), the higher conversion was obtained with Mn(TF<sub>5</sub>PP)Cl, and 2-phenyl-2-propanol (**8.2**) was always the main product obtained, independent of the catalyst used [56].

The oxidation of 1-ethylnaphthalene (**11**) and 2-ethylnaphthalene (**12**), which are known polycyclic aromatic hydrocarbons (PAHs), was studied in the presence of TBA salts of Mn<sup>III</sup> or Fe<sup>III</sup> POMs [51]. Only the iron-substituted POMs were able to catalyze the oxidation of these two substrates, in moderate conversions. The oxidation of **11** and **12** occurs mainly at the alkyl substituent, along with the formation of phthalic anhydrides resulting from the aromatic ring oxidation. The higher conversions of **11** and **12** were obtained in the presence of BW<sub>11</sub>Fe or PW<sub>11</sub>Fe and when a molar ratio of H<sub>2</sub>O<sub>2</sub>/sub = 9.8 was used [51].

### 5.3 FUNCTIONALIZATION OF SP<sup>2</sup> CARBON CENTERS UNDER HOMOGENEOUS CONDITIONS

Studies on the functionalization of sp<sup>2</sup> carbon centers (Fig. 5.3) carried out in the presence of either TMSPs or metalloporphyrins, using hydrogen peroxide as oxidant, gave rise to the products exemplified in Fig. 5.5.

The oxidation of some monoterpenes, such as (+)-3-carene (**13**), nerol (**14**), and geraniol (**15**), were studied in the presence of Mn(III) porphyrins [55] and Mn(III)-substituted POMs [41]. The oxidation of **13** showed high conversions with all Mn(III) porphyrins tested, and four major products were identified, namely  $\alpha$ -3,4-epoxycarane (**13.1**),  $\beta$ -3,4-epoxycarane (**13.2**), 3-carene-5-one (**13.3**), and 3-carene-2,5-dione (**13.4**) [55]. However, in the presence of BW<sub>11</sub>Mn at moderate conversions and under appropriate reaction conditions, (+)-3-carene (**13**) afforded only the  $\alpha$ -epoxide **13.1** and no allylic oxidation was observed. Higher conversions of **13** were accompanied by a decrease in selectivity [41]. Nerol (**14**) and geraniol (**15**) oxidations gave rise to 2,3-epoxides (**14.1**, **15.1**), 6,7-epoxides (**14.2**, **15.2**), and 2,3,6,7-diepoxides (**14.3**, **15.3**). Allylic oxidation was never found with the systems studied. Using Mn(III) porphyrins, the terminal 6,7-double bond of nerol and

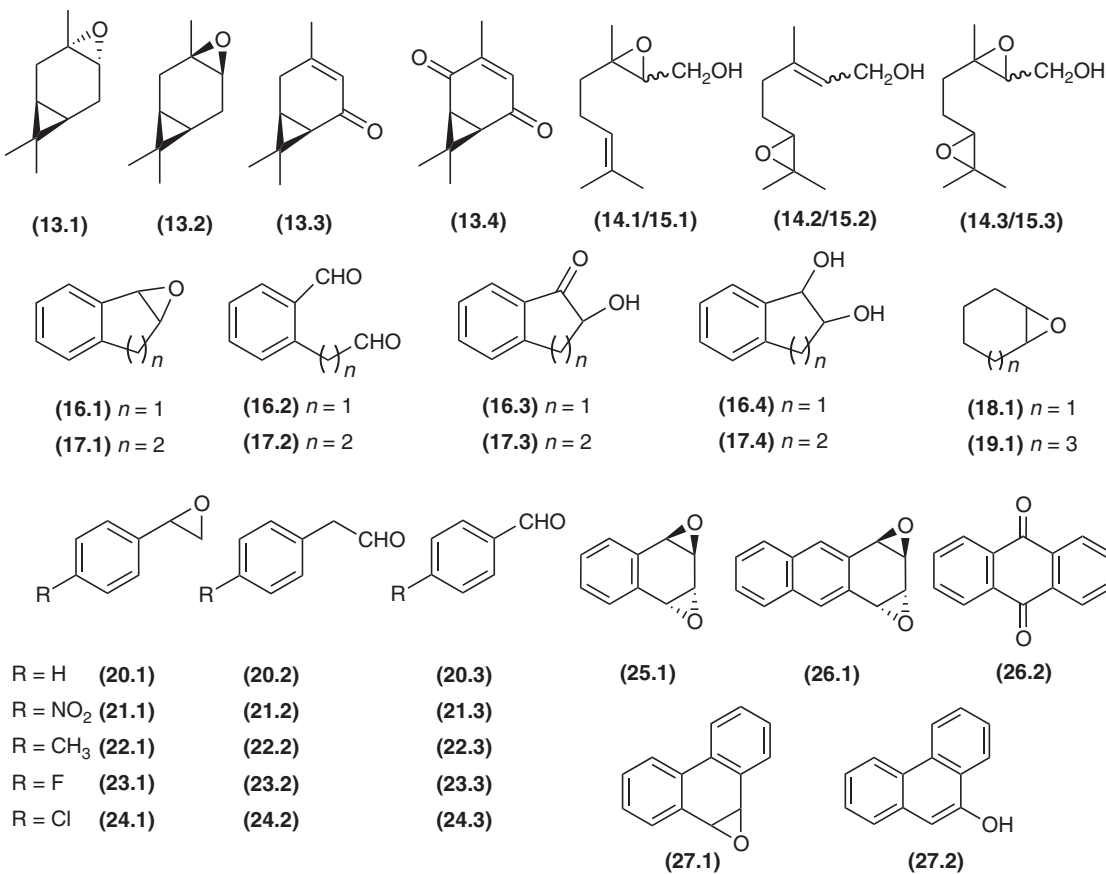


Figure 5.5 Oxidation products obtained in the catalytic oxidation studies of compounds **13** to **27**.

geraniol was preferentially epoxidized [55]. On the other hand, in the presence of the TBA salts of BW<sub>11</sub>Mn, **14** and **15** were preferentially epoxidized at the C<sub>2</sub> – C<sub>3</sub> double bond with conversions that can reach 96% with 86% selectivity, depending on reaction conditions, representing a possible hydroxyl-directed epoxidation of olefins [41]. Other studies on the oxidation of monoterpenes using PW<sub>11</sub>Fe and M<sub>4</sub>(PW<sub>9</sub>)<sub>2</sub>, M = Fe<sup>III</sup>, Co<sup>II</sup> were also published [52, 78].

The oxidation of 1*H*-indene (**16**) and 1,2-dihydronaphthalene (**17**) usually do not proceed much further than the formation of the corresponding epoxides **16.1** and **17.1**, respectively [79, 80]. However, in the presence of the TBA salts of XW<sub>11</sub>M, where X = P, Si, B and M = Mn, Fe, these reactions lead to the formation of several oxygenated products, including those obtained through C – C or C=C bond cleavage [47]. The conversion and selectivity for these two substrates were found to be dependent on the POM used, the amount of oxidant added, and the reaction time. For instance, the oxidation of **16** and **17** after 5–7 h of reaction, and when using a fivefold excess of H<sub>2</sub>O<sub>2</sub>, yielded two or three main products, namely the hydroxyketones **16.3** and **17.3** and the dialdehydes **16.2** and **17.2**. Under these conditions, naphthalene (**25**) was also obtained by oxidative dehydrogenation of **17** [47]. The formation of **16.2** and **17.2**, through the oxidative cleavage of carbon–carbon bonds of 1,2-diols and/or C = C bonds, was achieved under mild and environmentally friendly conditions, using hydrogen peroxide as oxidant. In synthetic organic chemistry, this important type of ring-opening cleavage usually requires stronger oxidants such as potassium permanganate, periodic acid, sodium or potassium periodate, and lead tetraacetate [2, 81].

The catalytic behavior of Mn(TDMImP)Cl was described, for the first time, in 2008 for the homogeneous epoxidation of alkenes, such as 1*H*-indene (**16**), cyclohexene (**18**), *cis*-cyclooctene (**19**), and styrene (**20**) [64]. It is known that allylic oxidation and epoxidation are two competing processes both *in vivo* and *in vitro*. With this catalyst, only the epoxides from *cis*-cyclooctene, cyclohexene, and 1*H*-indene were obtained. For styrene, the corresponding epoxide **20.1** was obtained as the main product (95%), together with phenylacetaldehyde (**20.2**) (5%) [64]. These studies were extended to the oxidation of other styrene derivatives (**21–24**) with H<sub>2</sub>O<sub>2</sub>, catalyzed by Mn(TDMImP)Cl and other cationic Mn(III) imidazolium-based porphyrins, and the results were compared with those obtained for the robust and well-studied Mn(TDCPP)Cl. It is known that the conversion of styrene (**20**) into the epoxide **20.1** is not always a clean reaction since undesired side products, such as phenylacetaldehyde (**20.2**), can be formed. In some cases, benzaldehyde (**20.3**) is also observed as a by-product and its formation is usually associated with radical processes taking place [82, 83]. The tested catalysts have shown to be efficient in the oxidation of styrene and its derivatives with hydrogen peroxide. For *p*-nitrostyrene (**21**) oxidation, only the epoxide **21.1** was produced, whereas for *p*-methylstyrene (**22**) a considerable yield of the corresponding phenylacetaldehyde (**22.1**) was obtained. *p*-Fluorostyrene (**23**) and *p*-chlorostyrene (**24**) showed similar epoxide/phenylacetaldehyde ratio when compared to the unsubstituted styrene [68].

An efficient system for the epoxidation of aromatic hydrocarbons with hydrogen peroxide in the presence of Mn(TDCPP)Cl, Mn( $\beta$ -NO<sub>2</sub>TDCPP)Cl, and Mn(TPFPP)Cl as catalysts was also described [57]. In particular, if using Mn(TDCPP)Cl and Mn( $\beta$ -NO<sub>2</sub>TDCPP)Cl, naphthalene (**25**) and anthracene (**26**) afforded the *anti*-1,2 : 3,4-arene diepoxides with very good conversion and selectivity. For example, **25** and **26** were oxidized in the presence of Mn(TDCPP)Cl with high selectivity to the corresponding *anti*-1,2 : 3,4-arene diepoxides (**25.1**, 81%) and (**26.1**, 74%) at 91% and 100% of conversion, respectively. These results demonstrate the development of a very useful procedure for the synthesis of epoxides **25.1** and **26.1**, in just one step, under mild conditions. Mn( $\beta$ -NO<sub>2</sub>TDCPP)Cl gave rise to similar results on the oxidation of **25** and **26**. The oxidation of phenanthrene (**27**) by Mn(TDCPP)Cl showed high selectivity for the epoxidation of the 9,10-bond affording **27.1**. With both catalysts Mn(TDCPP)Cl and Mn( $\beta$ -NO<sub>2</sub>TDCPP)Cl, complete phenanthrene conversions were obtained. Mn( $\beta$ -NO<sub>2</sub>TDCPP)Cl afforded compound **27.2** as the major product. With Mn(TPFPP)Cl, the aromatic hydroxylation of substrates (**25–27**) and the transformation of the phenols to the corresponding quinones were always the main transformations observed [57]. TMSPs had a completely different behavior in the oxidation of aromatic hydrocarbons. Anthracene (**26**) was selectively oxidized to 9,10-anthraquinone (**26.2**) in the presence of XW<sub>11</sub>M, X = P, or B and M = Mn<sup>III</sup> or Fe<sup>III</sup>. In particular, BW<sub>11</sub>Mn gave rise to 100% of conversion. Contrarily, naphthalene (**25**) could not be oxidized under the conditions tested [51].

Novel bifunctional catalysts, specifically salts with a porphyrin/POM (Porph/POM) stoichiometric ratio of 0.75 or 1, were prepared by the reaction of Keggin-type POMs with Mn(III) porphyrins bearing appropriate positively charged substituents at the meso positions, namely Mn(TPyP)Cl, Mn(TMePyP)Cl, Mn(TrisDCPPyP)Cl, and Mn(TrisDCPMePyP)Cl [62]. The oxidation of (+)-3-carene (**13**), geraniol (**15**), and *cis*-cyclooctene (**19**) with hydrogen peroxide was examined in the presence of these new Porph/POM compounds. In the conditions studied, the Porph/POM associations, POM = (PW<sub>12</sub>O<sub>40</sub>)<sup>3-</sup>, afforded conversions significantly higher than those obtained with the corresponding Mn(III) porphyrin alone, without significant change in the regio, chemo, and stereoselectivity of the reactions: **19** afforded selectively epoxycyclooctane (**19.1**), **15** gave rise to 6,7-epoxygeraniol (**15.2**) as the major product, and **13** was preferentially oxidized to the  $\alpha$ -3,4-epoxycarane (**13.1**). The POMs seemed to contribute to the stabilization of the metalloporphyrins (used as counter cations) against deactivation during the catalytic cycles, but their effect as catalysts was not clearly observed, with the exception of the oxidation of

geraniol, in which conversions trebled in the presence of the POM. In this work, the Porph/POM compounds could be used at higher temperatures than those usually described, and the Porph/POM combinations were more efficient catalysts than the corresponding metalloporphyrins alone [62].

#### 5.4 FUNCTIONALIZATION OF SP<sup>2</sup> AND SP<sup>3</sup> CARBON CENTERS UNDER HETEROGENEOUS CONDITIONS

A common undesirable feature associated with homogeneous systems is the problematic catalyst/products separation and the poor or nonexistent catalyst reusability. To overcome these problems, many approaches have been adopted to immobilize known active homogeneous catalysts onto appropriate supports without loss of their intrinsic activity and selectivity. The TMSPs,  $XW_{11}M$ , where  $X = P$ , Si, or B and  $M^{III} = Fe$  or  $Mn$ , were successfully immobilized on triethylpropylammonium-functionalized silica (silicaNEt<sub>3</sub>) by an electrostatic methodology (Fig. 5.6). Through different techniques, such as Fourier transform (FT) Raman and infrared (IR) spectroscopy, as well as elemental analysis, it was possible to provide enough evidence of the presence of the TMSPs supported on the modified silica. [50]. The heterogeneous oxidation of cyclooctane (**2**) gave conversions as high as 71–74%, with moderate selectivity for cyclooctanone (**2.1**), cyclooctanol (**2.2**), and cyclooctyl hydroperoxide (**2.3**), together with minor amounts of 1,2-epoxycyclooctane (**19.1**). Considering the recovery and reuse of the catalysts, the best performance was observed for silicaNEt<sub>3</sub>/PW<sub>11</sub>Fe, with conversions still around 65% in the third cycle. The advantages of the new materials (recovery and reuse) can compensate the lower conversion values obtained, when compared to those under homogeneous conditions. The product selectivity is not affected by the reuse of the catalyst, giving **2.1** and **2.3** as the main products for silicaNEt<sub>3</sub>/PW<sub>11</sub>Fe or silicaNEt<sub>3</sub>/SiW<sub>11</sub>Fe and **2.1** for silicaNEt<sub>3</sub>/BW<sub>11</sub>Fe. However, the selectivity obtained under heterogeneous conditions is different from that achieved under homogeneous conditions. Actually, in the heterogeneous system, higher amounts of **2.2** are observed, and in addition minor amounts of 1,2-epoxycyclooctane (**19.1**) are also detected. This different selectivity may be a consequence of cyclooctyl hydroperoxide (**2.3**) decomposition due to silica acidity [50].

The epoxidation reaction of *cis*-cyclooctene (**19**) was also studied in the presence of the immobilized POM silicaNEt<sub>3</sub>/PW<sub>11</sub>Mn [50]. Under heterogeneous conditions, **19** was epoxidized with an appreciably higher conversion (65%) than that obtained in the homogeneous system (22%), always with 100% selectivity for the epoxide **19.1**. The unproductive dismutation of hydrogen peroxide is faster under homogeneous conditions, when compared to the reactions using the heterogeneous silicaNEt<sub>3</sub>/PW<sub>11</sub>Mn, which can justify this remarkable behavior. In fact, the efficiency of utilization of H<sub>2</sub>O<sub>2</sub> is higher in the heterogeneous system. It was possible to maintain good performance under heterogeneous conditions during four cycles; the fifth run gave still 26% of conversion after 6 h of reaction. Moreover, the heterogeneous catalysis results suggest that PW<sub>11</sub>Mn does not leach into the reaction mixture, thus proving the heterogeneous nature of this catalytic system [50].

Heterogeneous Mn(III) porphyrin [63] and Mn(III) chlorin [65] covalently immobilized on silica (Fig. 5.6) were used in the oxidation of *cis*-cyclooctene (**19**). The efficiency of the immobilized Mn( $\beta$ -NO<sub>2</sub>TDCPP)Cl was evaluated under several conditions, and the best performance was achieved when a lower volume of solvent and a lower rate of oxidant addition were used. In this case, 89% of conversion was obtained after 21 h at 20 °C. The recovered catalyst was reused, but affording only 5% of substrate conversion. Nevertheless, by increasing the catalyst amount to a ratio *S/C* of 100 instead of 600, the

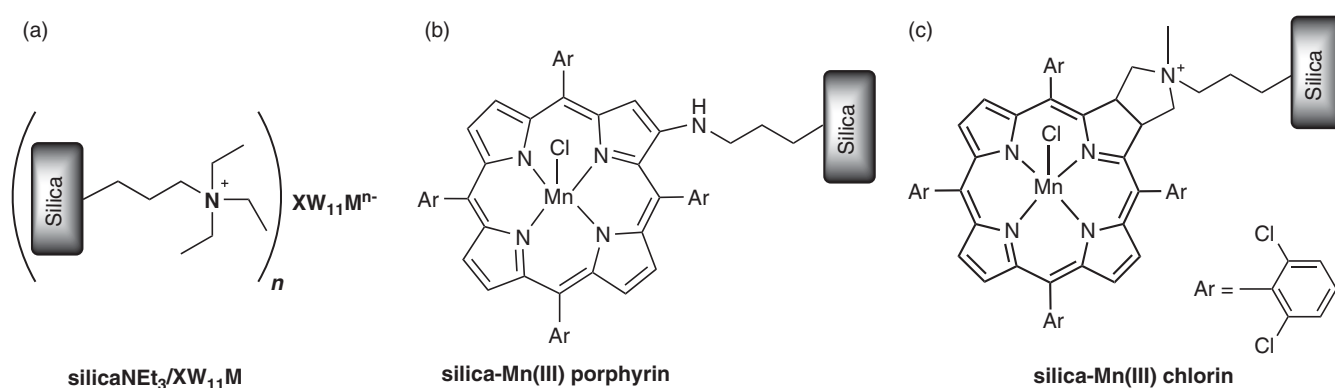


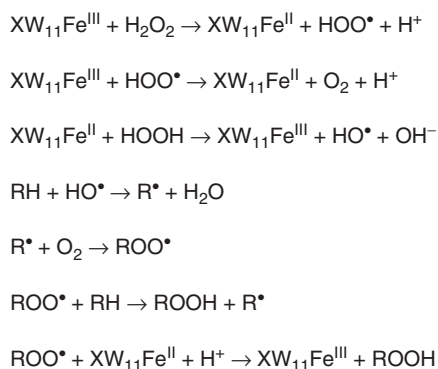
Figure 5.6 Heterogeneous catalysts. (a) Silicanet<sub>3</sub>/XW<sub>11</sub>M. (b) Silica–Mn(III) porphyrin. (c) Silica–Mn(III) chlorin.

second and third catalyst reuse afforded good conversions of **19** (88% and 51%, respectively). No Mn(III) porphyrin was observed by UV-vis analyses of the reaction supernatant, and the analyses of the silica recovered after reaction showed that only minor leaching had occurred [63]. The catalytic activity evaluation of the supported Mn(III) chlorin (a macrocycle related to porphyrins) showed that this heterogeneous catalyst is efficient, selective, and, under appropriate conditions, can also be reused in the epoxidation of **19**. One factor that seems to influence the catalyst activity is the frequency of addition of H<sub>2</sub>O<sub>2</sub>. For example, when this addition is made every 60 min, the first and second runs give 100% and 88% of conversion, respectively, but this was inactive at the third cycle. Better results were obtained using *t*-butyl hydroperoxide (TBHP) as oxidant, which allowed a good recyclability of the immobilized chlorin with no significant loss of activity. Depending on the conditions used, it is possible to reach a fifth cycle with good conversion of **19** using TBHP as an oxidant [65].

Recently, the preparation and characterization of silica nanoparticles supporting TMSPs, particularly iron(III) containing POMs, were reported [52]. These new POM/SiO<sub>2</sub> composites, enclosing Keggin-type POMs (PW<sub>11</sub>Fe/SiO<sub>2</sub>) and sandwich-type POMs Fe<sub>4</sub>(PW<sub>9</sub>)<sub>2</sub>/SiO<sub>2</sub>, were synthesized by a reverse micelle system, giving rise to nanoscale spherical particles with diameters between 25 and 35 nm. It was found that core/shell structures could be formed, with the POM being encapsulated by the silica, while in other cases the POM was dispersed on the nanoparticles surface. The nanocomposites prepared were tested as heterogeneous catalysts in the oxidation of geraniol (**15**) with H<sub>2</sub>O<sub>2</sub>. The best catalytic activity for this oxidation reaction was achieved with the PW<sub>11</sub>Fe/SiO<sub>2</sub> composite, reaching 96% of conversion of **15** after 3 h of reaction, with 88%–91% of selectivity for 2,3-epoxygeraniol. Globally, the new POM-nanostructured catalysts seem to be more selective than the corresponding TBA salts used under homogeneous conditions, adding the advantage of possible separation and catalyst reuse [52].

## 5.5 FINAL REMARKS

Some mechanistic considerations on the functionalization studies of the sp<sup>3</sup> carbon centers by hydrogen peroxide in the presence of POMs were proposed. In all these studies, no substrate oxidation took place in the presence of a radical scavenger, which suggests that these oxidations are processes involving radicals. However, taking into account all the results obtained, it is clear that even if the reaction mechanisms are radical in nature, some details must vary, depending on the catalyst and reaction conditions. This is due to the existence of several possible concurrent phenomena, namely the hydroperoxidation and the hydroxylation reactions, the decomposition of the hydroperoxide formed, and the dismutation of H<sub>2</sub>O<sub>2</sub>, all putatively catalyzed by the transition metals [43, 46, 48, 49]. Hydroperoxidation was observed with several substrates, mainly when an excess of H<sub>2</sub>O<sub>2</sub> was used. In the presence of the iron catalysts, it was assumed that the formation of the alkyl hydroperoxides occurred by an iron(III)-initiated generation of HO<sup>•</sup> [84]. The first step should be a reduction of iron(III) in acetonitrile (Scheme 5.1) [85], which does not occur in aqueous solution [86], and this was confirmed by cyclic voltammetry [43]. The molecular oxygen to obtain ROO<sup>•</sup> is probably originated *in situ* from H<sub>2</sub>O<sub>2</sub>, since some systems involving iron complexes, with excess H<sub>2</sub>O<sub>2</sub>, can produce their own O<sub>2</sub> atmosphere (Scheme 5.1) [87, 88]. This may explain the higher hydroperoxide yields when an excess of H<sub>2</sub>O<sub>2</sub> was used (H<sub>2</sub>O<sub>2</sub>/sub molar ratio = 9.8), and would be in good agreement with the catalytic results obtained when similar reactions were performed under a nitrogen atmosphere. The formation of the other products, such as ketones and alcohols, may be explained by considering also the Fenton reactions [87, 89]. Furthermore, as some



Scheme 5.1

results obtained with the Keggin-type XW<sub>12</sub> and the lacunary-type XW<sub>11</sub> anions are similar to those obtained with the transition-metal-substituted anions (XW<sub>11</sub>M), it is likely that in the presence of XW<sub>11</sub>M anions the activation of H<sub>2</sub>O<sub>2</sub> may occur simultaneously at the W and the transition metal (M) [43].

In the case of sp<sup>2</sup> carbon center oxyfunctionalization with hydrogen peroxide in the presence of POMs, the possibility of autoxidation seems to be ruled out, since similar results were obtained under an argon atmosphere, in comparison with those achieved in the presence of air. Moreover, radical processes can be ruled out, as the presence of a radical scavenger in the reaction media did not inhibit the formation of any reaction products [52].

Studies dedicated to oxidation reactions catalyzed by synthetic metalloporphyrins showed that iron and manganese porphyrin complexes are exceptional catalytic models of biologically important iron- and manganese-containing enzymes [5, 11–14, 17, 18]. In fact, metalloporphyrins are known to work as biomimetic monooxygenase or as superoxide dismutase enzymes, each pathway being attained by the correct choice of the fifth ligand [90, 91]. This ligand is known to be crucial to the stabilization of the oxo–metal complex formed during the reactions and to facilitate the substrate hydrogen abstraction [91–96] and the heterocyclic cleavage in hydroperoxy-type oxidants [59, 90], similar to the cysteinate residue function in cytochrome P450 monooxygenase enzymes [92, 97, 98]. It is usually recognized that the reactions occur with the contribution of a high valent oxo–metal species that can be produced by the interaction of the metalloporphyrin with oxygen donors such as hydrogen peroxide, alkyl hydroperoxides, iodosylarenes, sodium hypochlorite, potassium monopersulfate, amine N-oxides, and peracids, among others [11, 13, 14, 17]. Hydrogen peroxide has the advantage of being a green, clean, and cheap oxidant. Hydrogen peroxide's main problems, as an oxidant, are connected with metalloporphyrin stability under the reaction conditions and its own unproductive dismutation (catalase pathway) [90, 91, 99]. Mechanistic studies have suggested that the reactions occur in steps or involve a stepwise branch with an intermediate that generates the by-products. Two types of intermediates, namely radicals and carbocations, are usually invoked to account for the side-product formation, while the stereospecific epoxidation is thought to occur by a concerted oxygen transfer mechanism [68]. Density functional theory (DFT) studies using compound I ( $\text{[Fe}^{\text{IV}} = \text{O}(\text{protoporphyrin IX})^{\bullet+}$ ) coordinated to a thiolate residue) suggested that a multiscenario can be found for sp<sup>2</sup> carbon center oxygenation and that, depending on the catalyst, the substrate, and the reaction conditions, a cationic and/or a radical species can be generated thereby giving rise to the final products [82].

In conclusion, POMs and metalloporphyrins have been shown to be excellent catalysts for the *in vitro* biomimetic oxidative transformation of organic compounds, namely their sp<sup>2</sup> and sp<sup>3</sup> carbon centers, when hydrogen peroxide is used as the oxygen donor and acetonitrile as solvent.

## ACKNOWLEDGMENTS

The authors wish to thank FCT/FEDER for funding the Organic Chemistry Research Unit (Project PEst-C/QUI/UI0062/2011) and CICECO (Pest-C/CTM/LA0011/2011). Thanks are also due to their colleagues and students involved in the work cited here.

## REFERENCES

1. Activation and Functionalization of Alkanes; Hill, C. L., Ed.; John Wiley & Sons, Inc: New York, **1989**.
2. Hudlicky, M. *Oxidations in Organic Chemistry*; American Chemical Society: Washington, DC, **1990**.
3. *Catalytic Selective Oxidation*; Oyama, S. T.; Hightower, J. W., Eds.; American Chemical Society: Washington, DC, **1993**.
4. *Advances in Catalytic Activation of Dioxygen by Metal Complexes*; Simádi, L. I., Ed.; Kluwer Academic Publishers: Dordrecht, **2003**.
5. *Modern Oxidation Methods*; Backvall, J. E., Ed.; Wiley-VCH: Weinheim, **2004**.
6. *Organometallic Oxidation Catalysis*; Meyer, F.; Limberg, C., Eds.; Springer-Verlag: Berlin, Heidelberg, **2007**.
7. Sheldon, R. A.; Arends, I. W. C. E.; Hanefeld, U. *Green Chemistry and Catalysis*; Wiley-VCH: Weinheim, **2007**.
8. *Catalytic Oxidations with Hydrogen Peroxide as Oxidant*; Strukul, G., Ed.; Kluwer Academic Publishers: Dordrecht, **1992**.
9. Sanderson, W. R. *Pure Appl. Chem.* **2000**, 72, 1289.
10. Noyori, R.; Aoki, M.; Sato, K. *Chem. Commun.* 2003, **1977**.
11. Meunier, B.; Robert, A.; Pratviel, G.; Bernadou, J. In *The Porphyrin Handbook*; Kadish, K. M., Smith, K. M., Guilard, R., Eds.; Academic Press: San Diego, CA, **2000**; Vol. 4, p 119.
12. Bernadou, J.; Meunier, B. *Adv. Synth. Catal.* **2004**, 346, 171.

13. Groves, J. T. In *Cytochrome P-450: Structure, Mechanism, and Biochemistry*; 3rd ed.; Ortiz de Montellano, P. R., Ed.; Kluwer Academic/Plenum Publishers: New York, **2005**, p 1.
14. Mansuy, D. *C. R. Chim.* **2007**, *10*, 392.
15. Lohmann, W.; Karst, U. *Anal. Bioanal. Chem.* **2008**, *391*, 79.
16. Groves, J. T.; Nemo, T. E.; Myers, R. S. *J. Am. Chem. Soc.* **1979**, *101*, 1032.
17. *Metalloporphyrins in Catalytic Oxidations*; Sheldon, R. A., Ed.; Marcel Dekker: New York, **1994**.
18. *Metalloporphyrins Catalyzed Oxidations*; Montanari, F.; Casella, L., Eds.; Kluwer Academic Publishers: Dordrecht, **1994**.
19. Meunier, B. *Chem. Rev.* **1992**, *92*, 1411.
20. Quici, S.; Banfi, S.; Pozzi, G. *Gazz. Chim. Ital.* **1993**, *123*, 597.
21. Mansuy, D. *Pure Appl. Chem.* **1994**, *66*, 737.
22. Dolphin, D.; Traylor, T. G.; Xie, L. Y. *Acc. Chem. Res.* **1997**, *30*, 251.
23. Saladino, R.; Bernini, R.; Mincione, E.; Tagliatesta, P.; Boschi, T. *Tetrahedron Lett.* **1996**, *37*, 2647.
24. Tagliatesta, P.; Bernini, R.; Crestini, C.; Monti, D.; Boschi, T.; Mincione, E.; Saladino, R. *J. Org. Chem.* **1999**, *64*, 5361.
25. Saladino, R.; Carlucci, P.; Crestini, C.; Tagliatesta, P.; Monti, D.; Boschi, T. *Nucleosides Nucleotides* **1999**, *18*, 1123.
26. Thellend, A.; Battioni, P.; Sanderson, W.; Mansuy, D. *Synthesis* **1997**, 1387.
27. Ito, N.; Etoh, T.; Hagiwara, H.; Kato, M. *Synthesis* **1997**, 153.
28. McLain, J. L.; Lee, J.; Groves, J. T. In *Biomimetic Oxidations Catalysed by Transition Metal Complexes*; Meunier, B., Ed.; Imperial College Press: London, **2000**, p 91.
29. Ortiz de Montellano, P. R.; De Voss, J. J. In *Cytochrome P450: Structure, Mechanism, and Biochemistry*; 3rd ed.; Ortiz de Montellano, P. R., Ed.; Kluwer Academic/Plenum Publishers: New York, **2005**, p 183.
30. Neumann, R. *Prog. Inorg. Chem.* **1998**, *47*, 317.
31. Kozhevnikov, I. V. *Chem. Rev.* **1998**, *98*, 171.
32. Hill, C. L. *J. Mol. Catal. A: Chem.* **2007**, *262*, 2.
33. Hill, C. L.; Prosser-McCartha, C. M. *Coord. Chem. Rev.* **1995**, *143*, 407.
34. Hill, C. L.; Kim, G. S.; Prosser-McCartha, C. M.; Judd, D. In *Polyoxometallates: From Platonic Solids to Anti-retroviral Activity*; Pope, M. T., Müller, A., Eds.; Kluwer Academic Publishers: Dordrecht, **1994**, p 359.
35. *Polyoxometalate Chemistry: From Topology via Self-Assembly to Applications*; Pope, M. T.; Müller, A., Eds.; Kluwer Academic Publishers: Dordrecht, **2001**.
36. Katsoulis, D. E.; Pope, M. T. *J. Chem. Soc., Chem. Commun.* **1986**, 1186.
37. Hill, C. L.; Brown, R. B. *J. Am. Chem. Soc.* **1986**, *108*, 536.
38. Mansuy, D.; Bartoli, J. F.; Battioni, P.; Lyon, D. K.; Finke, R. G. *J. Am. Chem. Soc.* **1991**, *113*, 7222.
39. Khenkin, A. M.; Hill, C. L. *J. Am. Chem. Soc.* **1993**, *115*, 8178.
40. Simões, M. M. Q.; Conceição, C. M. M.; Gamelas, J. A. F.; Domingues, P. M. D. N.; Cavaleiro, A. M. V.; Cavaleiro, J. A. S.; Ferrer-Correia, A. J. V.; Johnstone, R. A. W. *J. Mol. Catal. A: Chem.* **1999**, *144*, 461.
41. Santos, I. C. M. S.; Simões, M. M. Q.; Pereira, M. M. M. S.; Martins, R. R. L.; Neves, M. G. P. M. S.; Cavaleiro, J. A. S.; Cavaleiro, A. M. V. *J. Mol. Catal. A: Chem.* **2003**, *195*, 253.
42. Santos, I. C. M. S.; Balula, M. S. S.; Simões, M. M. Q.; Neves, M. G. P. M. S.; Cavaleiro, J. A. S.; Cavaleiro, A. M. V. *Synlett* **2003**, 1643.
43. Balula, M. S. S.; Santos, I. C. M. S.; Simões, M. M. Q.; Neves, M. G. P. M. S.; Cavaleiro, J. A. S.; Cavaleiro, A. M. V. *J. Mol. Catal. A: Chem.* **2004**, *222*, 159.
44. Simões, M. M. Q.; Santos, I. C. M. S.; Balula, M. S. S.; Gamelas, J. A. F.; Cavaleiro, A. M. V.; Neves, M. G. P. M. S.; Cavaleiro, J. A. S. *Catal. Today* **2004**, *91–92*, 211.
45. Santos, I. C. M. S.; Gamelas, J. A. F.; Balula, M. S. S.; Simões, M. M. Q.; Neves, M. G. P. M. S.; Cavaleiro, J. A. S.; Cavaleiro, A. M. V. *J. Mol. Catal. A: Chem.* **2007**, *262*, 41.
46. Santos, I. C. M. S.; Simões, M. M. Q.; Balula, M. S. S.; Neves, M. G. P. M. S.; Cavaleiro, J. A. S.; Cavaleiro, A. M. V. *Synlett* **2008**, 1623.
47. Estrada, A. C.; Simões, M. M. Q.; Santos, I. C. M. S.; Neves, M. G. P. M. S.; Silva, A. M. S.; Cavaleiro, J. A. S.; Cavaleiro, A. M. V. *Catal. Lett.* **2009**, *128*, 281.
48. Estrada, A. C.; Simões, M. M. Q.; Santos, I. C. M. S.; Neves, M. G. P. M. S.; Silva, A. M. S.; Cavaleiro, J. A. S.; Cavaleiro, A. M. V. *Appl. Catal. A: General* **2009**, *366*, 275.
49. Estrada, A. C.; Simões, M. M. Q.; Santos, I. C. M. S.; Neves, M. G. P. M. S.; Cavaleiro, J. A. S.; Cavaleiro, A. M. V. *Monatsh. Chem.* **2010**, *141*, 1223.

50. Estrada, A. C.; Santos, I. C. M. S.; Simões, M. M. Q.; Neves, M. G. P. M. S.; Cavaleiro, J. A. S.; Cavaleiro, A. M. V. *Appl. Catal. A: General* **2011**, *392*, 28.
51. Estrada, A. C.; Simões, M. M. Q.; Santos, I. C. M. S.; Neves, M. G. P. M. S.; Cavaleiro, J. A. S.; Cavaleiro, A. M. V. *ChemCatChem* **2011**, *3*, 771.
52. Sousa, J. L. C.; Santos, I. C. M. S.; Simões, M. M. Q.; Cavaleiro, J. A. S.; Nogueira, H. I. S.; Cavaleiro, A. M. V. *Catal. Commun.* **2011**, *12*, 459.
53. Cavaleiro, J. A. S.; Nascimento, G. M. S. F. C.; Neves, M. G. P. M. S.; Pinto, M. T.; Silvestre, A. J. D.; Vicente, M. G. H. *Tetrahedron Lett.* **1996**, *37*, 1893.
54. Martins, R. R. L.; Neves, M. G. P. M. S.; Silvestre, A. J. D.; Silva, A. M. S.; Cavaleiro, J. A. S. *J. Mol. Catal. A: Chem.* **1999**, *137*, 41.
55. Martins, R. R. L.; Neves, M. G. P. M. S.; Silvestre, A. J. D.; Simões, M. M. Q.; Silva, A. M. S.; Tomé, A. C.; Cavaleiro, J. A. S.; Tagliatesta, P.; Crestini, C. *J. Mol. Catal. A: Chem.* **2001**, *172*, 33.
56. Rebelo, S. L. H.; Simões, M. M. Q.; Neves, M. G. P. M. S.; Cavaleiro, J. A. S. *J. Mol. Catal. A: Chem.* **2003**, *201*, 9.
57. Rebelo, S. L. H.; Simões, M. M. Q.; Neves, M. G. P. M. S.; Silva, A. M. S.; Cavaleiro, J. A. S. *Chem. Commun.* **2004**, *10*, 608.
58. Rebelo, S. L. H.; Simões, M. M. Q.; Neves, M. G. P. M. S.; Silva, A. M. S.; Cavaleiro, J. A. S.; Peixoto, A. F.; Pereira, M. M.; Silva, M. R.; Paixão, J. A.; Beja, A. M. *Eur. J. Org. Chem.* **2004**, 4778.
59. Rebelo, S. L. H.; Pereira, M. M.; Simões, M. M. Q.; Neves, M. G. P. M. S.; Cavaleiro, J. A. S. *J. Catal.* **2005**, *234*, 76.
60. Rebelo, S. L. H.; Simões, M. M. Q.; Neves, M. G. P. M. S.; Silva, A. M. S.; Tagliatesta, P.; Cavaleiro, J. A. S. *J. Mol. Catal. A: Chem.* **2005**, *232*, 135.
61. Vinhado, F. S.; Gandini, M. E. F.; Iamamoto, Y.; Silva, A. M. G.; Simões, M. M. Q.; Neves, M. G. P. M. S.; Tomé, A. C.; Rebelo, S. L. H.; Pereira, A. M. V. M.; Cavaleiro, J. A. S. *J. Mol. Catal. A: Chem.* **2005**, *239*, 138.
62. Santos, I. C. M. S.; Rebelo, S. L. H.; Balula, M. S. S.; Martins, R. R. L.; Pereira, M. M. M. S.; Simões, M. M. Q.; Neves, M. G. P. M. S.; Cavaleiro, J. A. S.; Cavaleiro, A. M. V. *J. Mol. Catal. A: Chem.* **2005**, *231*, 35.
63. Rebelo, S. L. H.; Gonçalves, A. R.; Pereira, M. M.; Simões, M. M. Q.; Neves, M. G. P. M. S.; Cavaleiro, J. A. S. *J. Mol. Catal. A: Chem.* **2006**, *256*, 321.
64. De Paula, R.; Simões, M. M. Q.; Neves, M. G. P. M. S.; Cavaleiro, J. A. S. *Catal. Commun.* **2008**, *10*, 57.
65. Pires, S. M. G.; Paula, R. D.; Simões, M. M. Q.; Neves, M. G. P. M. S.; Santos, I. C. M. S.; Tomé, A. C.; Cavaleiro, J. A. S. *Catal. Commun.* **2009**, *11*, 24.
66. Simões, M. M. Q.; De Paula, R.; Neves, M. G. P. M. S.; Cavaleiro, J. A. S. *J. Porphyrins Phthalocyanines* **2009**, *13*, 589.
67. Neves, C. M. B.; Simões, M. M. Q.; Santos, I. C. M. S.; Domingues, F. M. J.; Neves, M. G. P. M. S.; Almeida Paz, F. A.; Silva, A. M. S.; Cavaleiro, J. A. S. *Tetrahedron Lett.* **2011**, *52*, 2898.
68. De Paula, R.; Simões, M. M. Q.; Neves, M. G. P. M. S.; Cavaleiro, J. A. S. *J. Mol. Catal. A: Chem.* **2011**, *345*, 1.
69. Pires, S. M. G.; Paula, R. D.; Simões, M. M. Q.; Silva, A. M. S.; Domingues, M. R. M.; Santos, I. C. M. S.; Vargas, M. D.; Ferreira, V. F.; Neves, M. G. P. M. S.; Cavaleiro, J. A. S. *RSC Adv.* **2011**, *1*, 1195.
70. Neves, C. M. B.; Simões, M. M. Q.; Domíngues, M. R. M.; Santos, I. C. M. S.; Neves, M. G. P. M. S.; Paz, F. A. A.; Silva, A. M. S.; Cavaleiro, J. A. S. *RSC Adv.* **2012**, *2*, 7427.
71. Neves, C. M. B.; Simões, M. M. Q.; Domingues, F. M. J.; Neves, M. G. P. M. S.; Cavaleiro, J. A. S. *Quim. Nova* **2012**, *35*, 1477.
72. Pires, S. M. G.; Simões, M. M. Q.; Santos, I. C. M. S.; Rebelo, S. L. H.; Pereira, M. M.; Neves, M. G. P. M. S. Cavaleiro, J. A. S. *Appl. Catal. A: General* **2012**, *439–440*, 51.
73. Baucherel, X.; Gonsalvi, L.; Arends, I. W. C. E.; Ellwood, S.; Sheldon, R. A. *Adv. Synth. Catal.* **2004**, *346*, 286.
74. Pires, E. L.; Wallau, M.; Schuchardt, U. *J. Mol. Catal. A: Chem.* **1998**, *136*, 69.
75. Tangestaninejad, S.; Mirkhani, V.; Moghadam, M.; Mohammadpoor-Baltork, I.; Shams, E.; Salavati, H. *Ultrason. Sonochem.* **2008**, *15*, 438.
76. Attanasio, D.; Orru, D.; Suber, L. *J. Mol. Catal.* **1989**, *57*, L1.
77. Neumann, R.; De la Vega, M. *J. Mol. Catal.* **1993**, *84*, 93.
78. Balula, S. S.; Santos, I. C. M. S.; Cunha-Silva, L.; Carvalho, A. P.; Pires, J.; Freire, C.; Cavaleiro, J. A. S.; Castro, B.; Cavaleiro, A. M. V. *Catal. Today* **2012**, doi:10.1016/j.cattod.2012.02.020.
79. Canali, L.; Cowan, E.; Deleuze, H.; Gibson, C. L.; Sherrington, D. C. *J. Chem. Soc., Perkin Trans. I*, **2000**, 2055.
80. Kureshy, R. I.; Ahmad, I.; Khan, N. H.; Abdi, S. H. R.; Pathak, K.; Jasra, R. V. *V. J. Catal.* **2006**, *238*, 134.
81. Haines, A. H. *Methods for the Oxidation of Organic Compounds*; Academic Press: New York, 1988.
82. Kumar, D.; de Visser, S. P.; Shaik, S. *Chem. Eur. J.* **2005**, *11*, 2825.
83. Liu, Y.; Zhang, H. J.; Lu, Y.; Cai, Y. Q.; Liu, X. L. *Green Chem.* **2007**, *9*, 1114.
84. Shul'pin, G. B.; Nizova, G. V.; Kozlov, Y. N.; Cuervo, L. G.; Suss-Fink, G. *Adv. Synth. Catal.* **2004**, *346*, 317.

85. Kuznetsova, L. I.; Detusheva, L. G.; Kuznetsova, N. I.; Fedotov, M. A.; Likholobov, V. A. *J. Mol. Catal. A: Chem.* **1997**, *117*, 389.
86. Toth, J. E.; Melton, J. D.; Cabelli, D.; Bielski, B. H. J.; Anson, F. C. *Inorg. Chem.* **1990**, *29*, 1952.
87. Gozzo, F. *J. Mol. Catal. A: Chem.* **2001**, *171*, 1.
88. Sawyer, D. T. *Coord. Chem. Rev.* **1997**, *165*, 297.
89. Jones, C. W. *Applications of Hydrogen Peroxide and Derivatives*; The Royal Society of Chemistry: Cambridge, **1999**.
90. Wang, R.; de Visser, S. P. *J. Inorg. Biochem.* **2007**, *101*, 1464.
91. Takahashi, A.; Kurahashi, T.; Fujii, H. *Inorg. Chem.* **2009**, *48*, 2614.
92. Jin, S.; Makris, T. M.; Bryson, T. A.; Sligar, S. G.; Dawson, J. H. *J. Am. Chem. Soc.* **2003**, *125*, 3406.
93. Kamachi, T.; Kouno, T.; Nam, W.; Yoshizawa, K. *J. Inorg. Biochem.* **2006**, *100*, 751.
94. de Visser, S. P. *J. Biol. Inorg. Chem.* **2006**, *11*, 168.
95. Crestoni, M. E.; Fornarini, S.; Lanucara, F. *Chem. Eur. J.* **2009**, *15*, 7863.
96. Sun, Y.; Hu, X. B.; Li, H. R.; Jalbout, A. F. *Comput. Theor. Chem.* **2011**, *966*, 62.
97. Woggon, W. D. *Acc. Chem. Res.* **2005**, *38*, 127.
98. Luthra, A.; Denisov, I. G.; Sligar, S. G. *Arch. Biochem. Biophys.* **2011**, *507*, 26.
99. Belal, R.; Momenteau, M.; Meunier, B. *J. Chem. Soc., Chem. Commun.* **1989**, 412.



---

# 6

---

## QUASI-BORINIUM CATION BASED ON COBALT BIS(DICARBOLLIDE): ITS LEWIS ACIDITY AND C–H AND C–X BOND ACTIVATION

V. I. BREGADZE\*, I. B. SIVAEV, I. D. KOSENKO, I. A. LOBANOVA, Z. A. STARIKOVA, AND I. A. GODOVIKOV

*A. N. Nesmeyanov Institute of Organoelement Compounds (INEOS), Russian Academy of Sciences, Moscow, Russia*

### 6.1 INTRODUCTION

Acidity and basicity belong to the most important concepts in chemistry. There are several different definitions of acids and bases available, but in Lewis theory they are specified in the most general terms as the electron-pair acceptors and electron-pair donors, respectively [1]. The importance of Lewis's conceptual approach is rooted in the fact that it can be applied to compounds such as  $\text{BF}_3$  and  $\text{CO}$ , which do not contain protons. An important family of compounds is given by borane derivatives, which, because of the electron deficiency of the central boron atom having vacant p orbital, represent Lewis acids par excellence. Highly Lewis-acidic borane derivatives play key roles as catalysts in organic synthesis [2, 3], as activators for olefin polymerization organometallic precatalysts [4, 5], as sensors for detection of fluoride and cyanide anions [6, 7], and as a component in frustrated Lewis pairs that promote activation of dihydrogen and other small molecules [8, 9]. Much effort has been devoted to enhancing the Lewis acidity of boranes and thereby to improving their performance for such applications.

An intriguing strategy for increasing the Lewis acidity is an enlargement of the cationic character of the boron atom by removing the halide or its replacement by a stabilizing  $\text{R}_3\text{N}$  group that enhances the reactivity of boron as electrophile [10]. The boron cations can be classified into three structural classes based on the coordination number at boron. Borinium cations  $\text{R}_2\text{B}^+$  are 2-coordinate and typically are ligated by bulky and strongly  $\pi$ -donating substituents that effectively shield the boron cation from the solvent and anion. Borenium cations  $\text{LR}_2\text{B}^+$  are 3-coordinate species that comprise two  $\sigma$ -bound substituents (R) and one dative interaction with a ligand (L) that serves to occupy a third coordination site as well as to reduce some of the electron deficiency at boron. The third, and the most common, class of boron cations is that of the tetrahedral, 4-coordinate boronium cations  $\text{L}_2\text{R}_2\text{B}^+$ , with two coordination sites occupied by  $\sigma$ -bound substituents and the other two populated by neutral donor ligands.

The coordinative saturation at the boron center in boronium cations renders these species particularly stable and some of them were proposed as novel electrolytes for rechargeable lithium batteries [11]. On the contrary, borenium cations with weakly stabilizing substituents can be classified as superelectrophiles, combining a monocationic charge with an unoccupied p orbital [12]. The unfilled p orbitals of the boron atom in borinium cations can become partially occupied as a result of  $\pi$ -donation from covalently bound substituents, analogous to the isoelectronic allenes. Bidentate ligation of boron generates a "chelate-restrained" borinium cation in which electrophilicity is enhanced by the nonlinear geometry at boron, resulting in an empty boron p orbital that cannot be stabilized by ligand  $\pi$ -donation. As result, such chelate-restrained borinium cations are able to activate C–H bonds of arenes with the formation of arylboron derivatives [13].

*Advances in Organometallic Chemistry and Catalysis: The Silver/Gold Jubilee International Conference on Organometallic Chemistry Celebratory Book*, First Edition. Edited by Armando J. L. Pombeiro.

© 2014 John Wiley & Sons, Inc. Published 2014 by John Wiley & Sons, Inc.

## 6.2 QUASI-BORINIUM CATIONS: FORMATION AND REACTIVITY

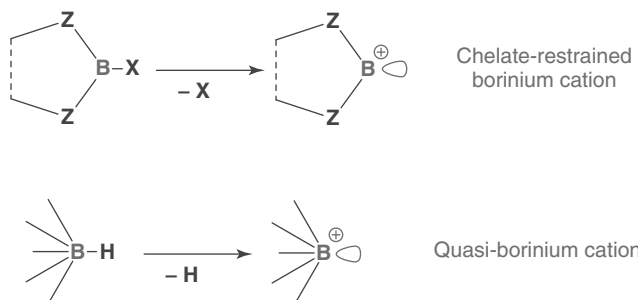
In the chemistry of polyhedral boron hydrides, boron-centered cations were postulated to be key intermediates of an electrophile-induced nucleophilic substitution mechanism that is responsible for the formation of a variety of boron-substituted derivatives [14]. Such boron-centered cations can be easily generated by abstraction of a hydride by the treatment of polyhedral boron hydrides with Lewis or Brønsted acids [15]. Similar to the “classical” chelate-restrained borinium cations based on 3-coordinate boron, these species, which we called *quasi-borinium cations*, have an unstabilized p orbital and are strong electrophiles (Scheme 6.1). Such quasi-borinium cations are highly reactive and react with even weak nucleophiles, such as ether or nitrile solvent molecules giving the corresponding oxonium and nitrilium derivatives whose properties are close to those of similar complexes of transition metals [15–17].

Generation of quasi-borinium cations from polyhedral boron hydrides usually requires the presence of an excess of Lewis (L) or Brønsted (HA) acids, which, taking into account the high reactivity of these species, results in the formation of side reaction products of the general formula BL and  $[BA]^-$  derived from the attack of quasi-borinium cation with nucleophilic bases. To study the reactivity of quasi-borinium cations derived from polyhedral boron hydrides, the iodonium derivative of the cobalt bis(dicarbollide) anion  $[\mu\text{-}8,8'\text{-I}\text{-}3,3'\text{-Co}(1,2\text{-C}_2\text{B}_9\text{H}_{10})_2]$  was chosen as a mild generator of quasi-borinium cation formed on the breakage of the highly strained iodonium bridge (Scheme 6.2). The iodonium derivative is easily accessible by reaction of the monoiodo derivative  $[8\text{-I}\text{-}3,3'\text{-Co}(1,2\text{-C}_2\text{B}_9\text{H}_{10})(1,2\text{-C}_2\text{B}_9\text{H}_{11})]^-$  with  $\text{AlCl}_3$  in benzene [18].

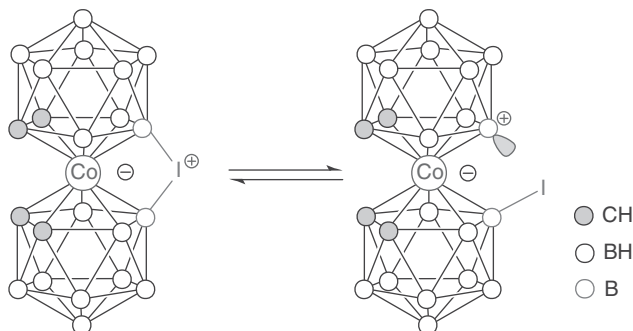
Earlier it was shown that reactions of  $[\mu\text{-}8,8'\text{-I}\text{-}3,3'\text{-Co}(1,2\text{-C}_2\text{B}_9\text{H}_{10})_2]$  with Lewis bases proceed through the iodonium bridge opening followed by attack of the formed quasi-borinium cation with Lewis base resulting in charge-compensated bifunctional derivatives  $[8\text{-L}\text{-}8'\text{-I}\text{-}3,3'\text{-Co}(1,2\text{-C}_2\text{B}_9\text{H}_{10})_2]$  ( $L = \text{NH}_3, \text{NEt}_3, \text{Py}, \text{N}\equiv\text{CR}$  ( $R = \text{Me}, \text{Ph}, \text{CH}=\text{CH}_2$ ),  $\text{SMe}_2, \text{O}(\text{CH}_2\text{CH}_2)_2\text{O}$ ) [18–20].

## 6.3 C–H ACTIVATION OF ARENES

Here we describe the reactions of C–H activation of arenes and C–X activation of halogen alkanes with a quasi-borinium cation generated from the iodonium derivative of cobalt bis(dicarbollide)  $[\mu\text{-}8,8'\text{-I}\text{-}3,3'\text{-Co}(1,2\text{-C}_2\text{B}_9\text{H}_{10})_2]$ , as well as an assessment of the Lewis acidity of this highly reactive intermediate.



Scheme 6.1

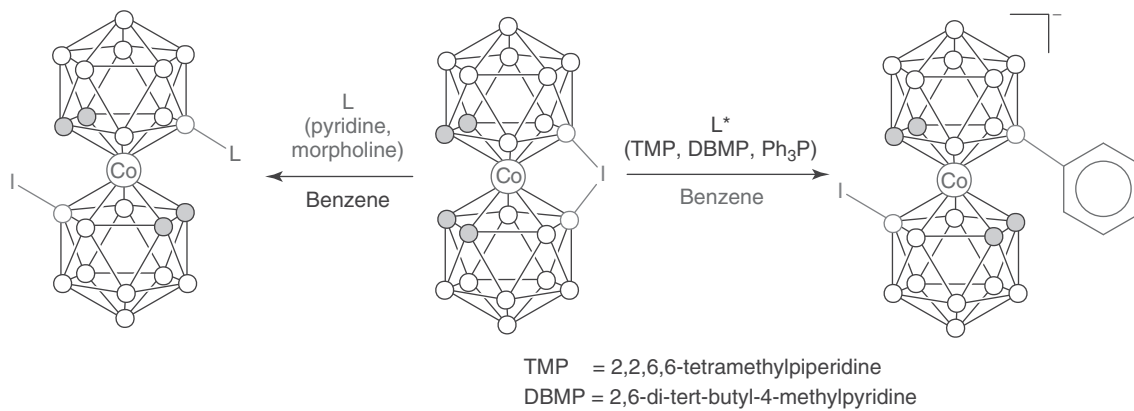


Scheme 6.2

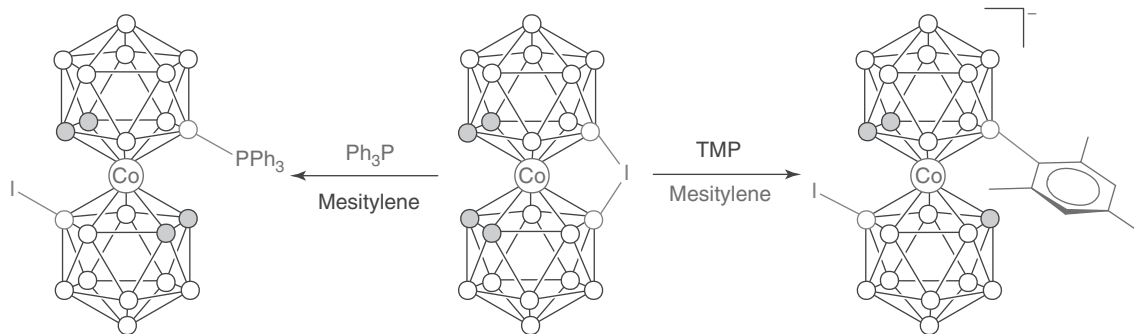
So far as the iodonium derivative was synthesized by the reaction in benzene solution, benzene can be considered to be rather stable toward the quasi-borinium cation formed, and reactions with unhindered Lewis bases such as pyridine and morpholine in benzene result smoothly in the corresponding charge-compensated ammonium derivatives [ $8\text{-C}_5\text{H}_5\text{N}\text{-}8'\text{-I-3,3}'\text{-Co(1,2-C}_2\text{B}_9\text{H}_{10}\text{)}_2$ ] and [ $8\text{-O(CH}_2\text{CH}_2)_2\text{NH}\text{-}8'\text{-I-3,3}'\text{-Co(1,2-C}_2\text{B}_9\text{H}_{10}\text{)}_2$ ] (Scheme 6.3) [18, 21]. In the case of sterically hindered Lewis bases, such as triphenylphosphine, 2,2,6,6-tetramethylpiperidine, or 2,6-di-*tert*-butyl-4-methylpyridine, no reaction was found at room temperature; however, short-term heating resulted in the benzene C–H activation with the formation of the corresponding phenyl derivative [ $8\text{-Ph-8'\text{-I-3,3}'-Co(1,2-C}_2\text{B}_9\text{H}_{10}\text{)}_2$ ] (Scheme 6.3) [21].

The C–H activation of more active aromatics, such as toluene, does not require the presence of a Lewis base and proceeds simply on heating the iodonium derivative in toluene at 70 °C to give a mixture of isomeric tolyl derivatives [ $8\text{-Tol-8'\text{-I-3,3}'-Co(1,2-C}_2\text{B}_9\text{H}_{10}\text{)}_2$ ]<sup>–</sup>. In the case of strongly sterically hindered mesitylene as solvent, no reaction was observed in the absence of a Lewis base, while in the presence of Lewis bases the reaction route depended both on the steric accessibility of the Lewis base center and on its basicity. In the presence of triphenylphosphine, the reaction results in the formation of the triphenylphosphonium derivative [ $8\text{-Ph}_3\text{P-8'\text{-I-3,3}'-Co(1,2-C}_2\text{B}_9\text{H}_{10}\text{)}_2$ ]<sup>–</sup>, whereas the reaction in the presence of 2,2,6,6-tetramethylpiperidine gives the arene C–H activation product [ $8\text{-(2,4,6-Me}_3\text{C}_6\text{H}_2\text{)-8'\text{-I-3,3}'-Co(1,2-C}_2\text{B}_9\text{H}_{10}\text{)}_2$ ]<sup>–</sup> (Scheme 6.4) [21].

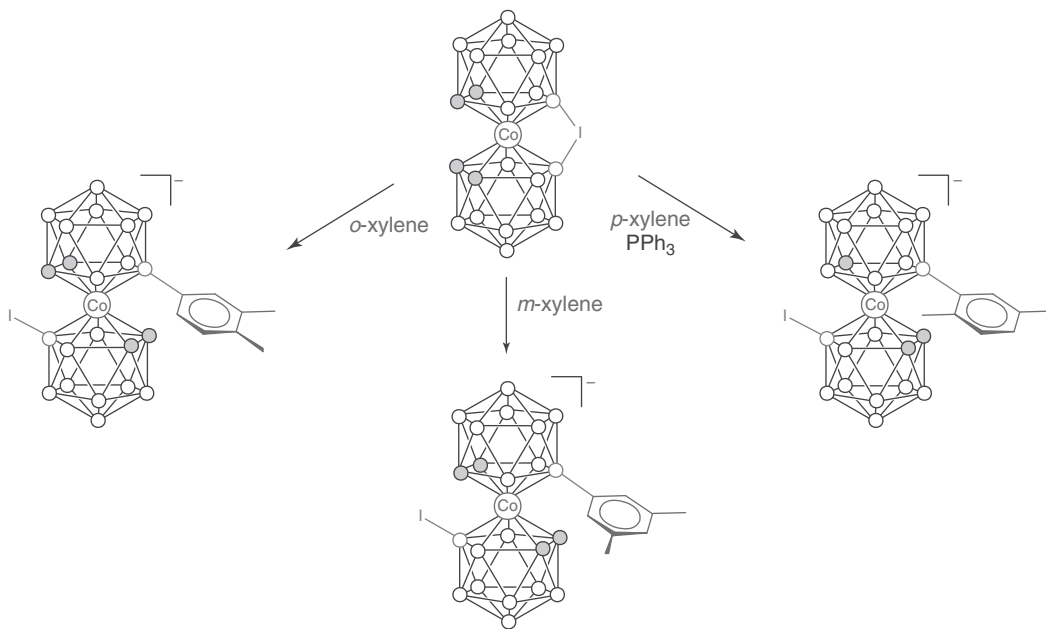
It would be expected that xylenes that are more electron-rich than toluene and less sterically hindered than mesitylene will react easily with [ $\mu\text{-8,8'-I-3,3}'\text{-Co(1,2-C}_2\text{B}_9\text{H}_{10}\text{)}_2$ ] in the absence of the Lewis base. Indeed, *ortho*- and *meta*-xylenes react slowly (5–6 days) with the iodonium derivative without the Lewis base even at room temperature, whereas on heating to 80 °C the conversion completes during less than 1 h. In both cases, the xylene borylation proceeds at positions that are the most distant from the methyl groups and, as a result, only one isomer is formed in each case, [ $8\text{-I-8'\text{-(3,4-Me}_2\text{C}_6\text{H}_3\text{)-3,3}'\text{-Co(1,2-C}_2\text{B}_9\text{H}_{10}\text{)}_2$ ]<sup>–</sup> and [ $8\text{-I-8'\text{-(3,5-Me}_2\text{C}_6\text{H}_3\text{)-3,3}'\text{-Co(1,2-C}_2\text{B}_9\text{H}_{10}\text{)}_2$ ]<sup>–</sup> in the cases of *ortho*- and *meta*-xylenes, respectively. In contrast to the *ortho*- and *meta*-isomers, *para*-xylene has no aromatic CH groups that are not adjacent to CMe groups, therefore the borylation reaction without the Lewis base does not proceed. However, the addition of PPh<sub>3</sub> as a Lewis base



Scheme 6.3



Scheme 6.4



Scheme 6.5

results in smooth C–H activation of xylene even at room temperature giving  $[8\text{-I-8}'\text{-(2,5-Me}_2\text{C}_6\text{H}_3\text{)}\text{-3,3}'\text{-Co(1,2-C}_2\text{B}_9\text{H}_{10}\text{)}_2]^-$  (Scheme 6.5) [22].

The  $^{11}\text{B}$  NMR spectra of the aryl derivatives of cobalt bis(dicarbollide) demonstrate characteristic singlets of boron atoms substituted with the aryl group and iodine atom at 12 and –6 ppm, respectively. The  $^1\text{H}$  NMR spectra contain signals of the corresponding aryl group as well as two broad carborane  $\text{C}_{\text{carb}}\text{-H}$  signals from different carborane ligands. The rather high difference in chemical shifts of these signals (>0.7 ppm) was interpreted in terms of aromatic  $\text{CH}_{\text{carb}}\cdots\pi$  interactions between the dicarbollide ligands. The  $^1\text{H}$  NMR spectrum of the *p*-xylene derivative exhibits four carborane  $\text{C}_{\text{carb}}\text{-H}$  signals at 4.48, 4.44, 3.88, and 3.78 ppm, indicating the nonequivalence of all carborane CH groups in solution. It can be explained by a combination of two factors: frozen rotation of the aryl group and mutual rotation of ligands due to  $\text{CH}_{\text{carb}}\cdots\pi$  interactions between the carborane ligands, and asymmetry of the aryl group containing different substituents (H and Me) at the positions involved in the  $\text{CH}_{\text{carb}}\cdots\pi$  aromatic interactions. The  $^1\text{H}$ – $^1\text{H}$  NOESY correlation demonstrates the evident cross-peak of the  $\text{CH}_{\text{carb}}$  signal at 3.88 ppm with the C(6)H aromatic singlet at 7.23 ppm, indicating their spatial proximity and providing clear proof of the  $\text{CH}_{\text{carb}}\cdots\pi$  interaction in solution (Fig. 6.1a).

Similar to the  $^1\text{H}$  NMR spectrum, the  $^{13}\text{C}$  NMR spectrum of the *p*-xylene derivative contains four signals from nonequivalent  $\text{C}_{\text{carb}}$  atoms at 61.0, 57.8, 53.9, and 51.1 ppm. The  $^1\text{H}$ – $^{13}\text{C}$  inverse HSQC correlation (Fig. 6.1b) was used to assign signals of the carborane atoms in the  $^{13}\text{C}$  NMR spectrum. Good correlation between the  $^1\text{H}$  and  $^{13}\text{C}$  signals at 3.88 and 53.9 ppm and 3.77 and 51.1 ppm, respectively, confirms that their upfield shifts were caused by the  $\text{CH}_{\text{carb}}\cdots\pi$  interaction.

Single-crystal X-ray diffraction study of  $(\text{Me}_3\text{NH})[8\text{-I-8}'\text{-Ph-3,3}'\text{-Co(1,2-C}_2\text{B}_9\text{H}_{10}\text{)}_2]$  and  $(\text{Me}_4\text{N})[8\text{-I-8}'\text{-(2,5-Me}_2\text{C}_6\text{H}_3\text{)}\text{-3,3}'\text{-Co(1,2-C}_2\text{B}_9\text{H}_{10}\text{)}_2]$  revealed that in the both structures the dicarbollide ligands are mutually rotated by  $178^\circ$ , producing the transoid conformation of the anions (Fig. 6.2).

The transoid conformations are stabilized by the formation of intramolecular hydrogen  $\text{CH}_{\text{carb}}\cdots\text{IB}$  bonds (2.88–3.05 Å) as well as by short aromatic  $\text{CH}_{\text{carb}}\cdots\pi$  interactions (2.61/2.65 Å) between the dicarbollide ligands.

#### 6.4 C–X ACTIVATION OF HALOGEN ALKANES

Besides aromatic C–H activation, the high reactivity of  $[\mu\text{-8,8'-I-3,3'-Co(1,2-C}_2\text{B}_9\text{H}_{10}\text{)}_2]$  results in mild room-temperature C–X activation of halogen alkanes with the formation of the corresponding halogen derivatives  $[8\text{-X-8}'\text{-I-3,3}'\text{-Co(1,2-C}_2\text{B}_9\text{H}_{10}\text{)}_2]^-$  (X = Cl, Br) (Scheme 6.6) [23].

It should be noted that all reactions are very sensitive to traces of moisture, and the use of nonanhydrous solvents results in formation of hydroxy derivative  $[8\text{-HO-8}'\text{-I-3,3}'\text{-Co(1,2-C}_2\text{B}_9\text{H}_{10}\text{)}_2]^-$  as the side product [23].

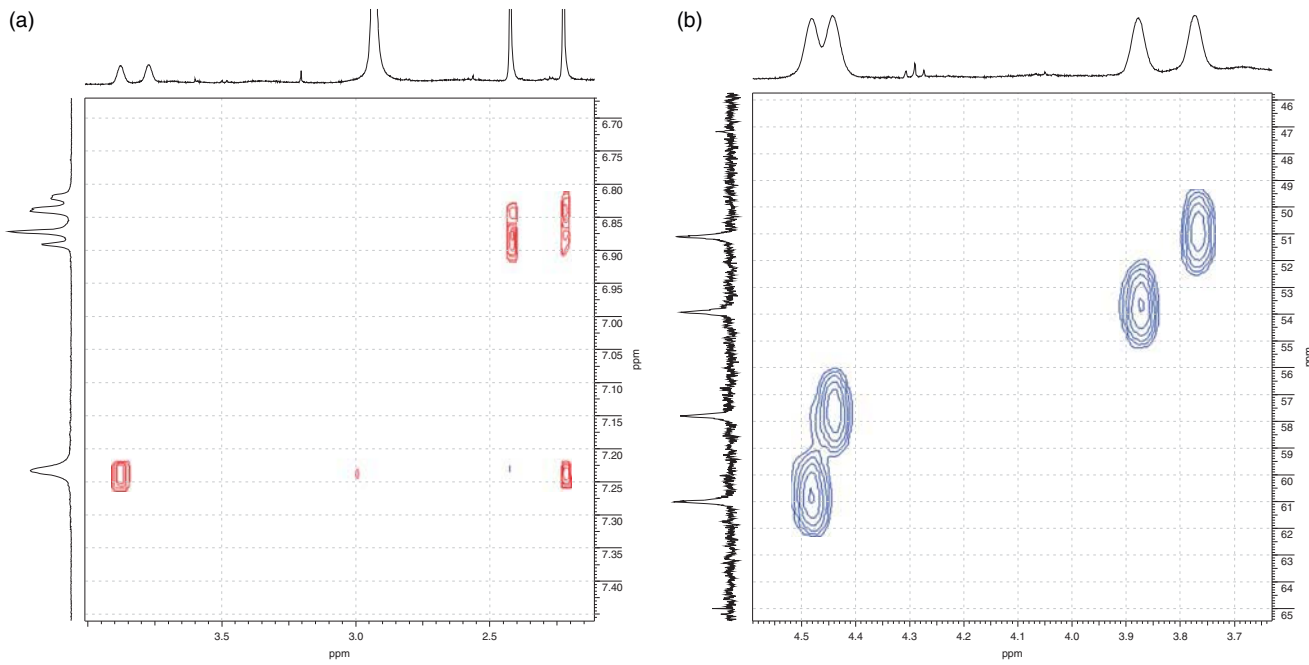


**Figure 6.1**  $^1\text{H}$ - $^1\text{H}$  NOESY (a) and  $^1\text{H}$ - $^{13}\text{C}$  HSQC (b) spectra of  $[8\text{-I-}8'\text{-(2,5-}\text{Me}_2\text{C}_6\text{H}_3\text{)-}3,3'\text{-Co(1,2-}\text{C}_2\text{B}_9\text{H}_{10}\text{)}_2]^-$ . (See insert for color representation of the figure.)

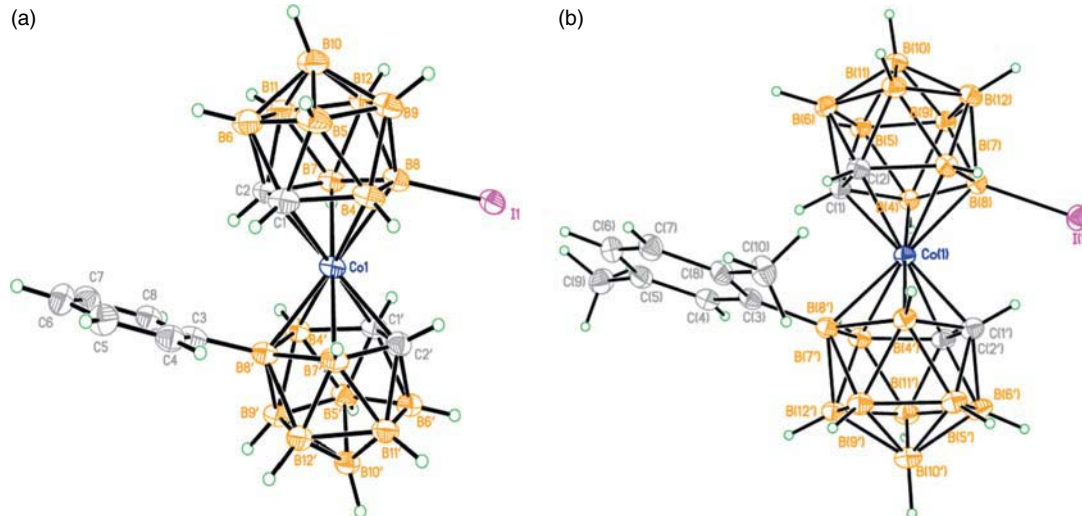
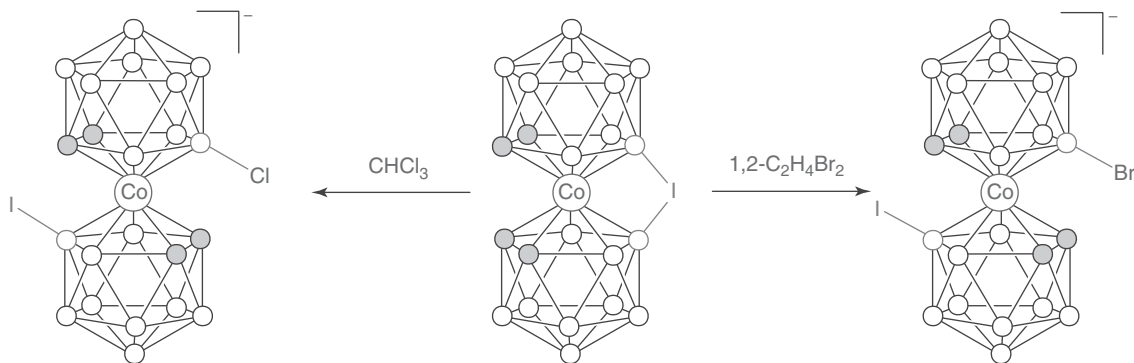


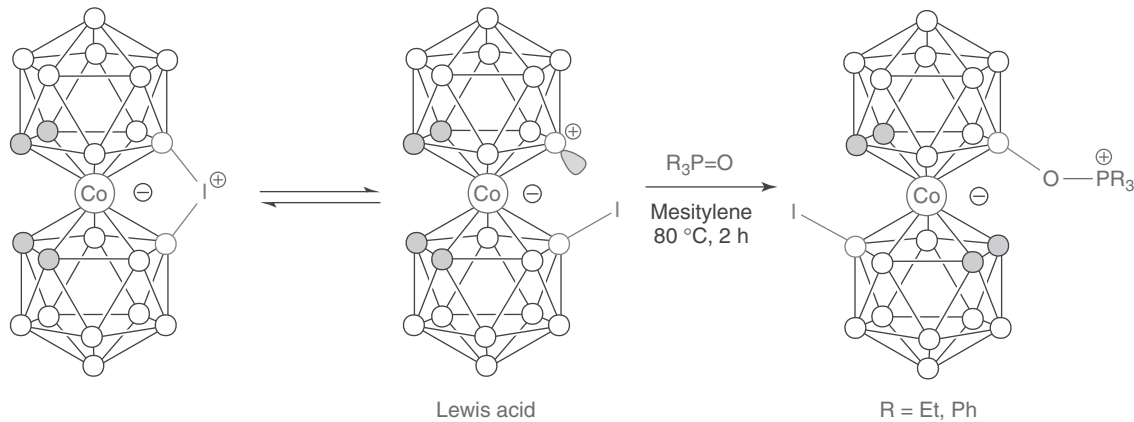
**Figure 6.2** Molecular structures of  $[8\text{-I-}8'\text{-Ph-}3,3'\text{-Co(1,2-}\text{C}_2\text{B}_9\text{H}_{10}\text{)}_2]^-$  (a) and  $[8\text{-I-}8'\text{-(2,5-}\text{Me}_2\text{C}_6\text{H}_3\text{)-}3,3'\text{-Co(1,2-}\text{C}_2\text{B}_9\text{H}_{10}\text{)}_2]^-$  (b) anions. Adapted with permission from Reference 21. Copyright (2010) American Chemical Society. (See insert for color representation of the figure.)

## 6.5 LEWIS ACIDITY OF QUASI-BORINIUM CATION

To evaluate the Lewis acidity of the quasi-borinium cation formed on the iodonium bridge breakage in  $[\mu\text{-}8,8'\text{-I-}3,3'\text{-Co(1,2-}\text{C}_2\text{B}_9\text{H}_{10}\text{)}_2]$ , the Beckett–Gutmann method based on the change in the  $^{31}\text{P}$  NMR chemical shift of Et<sub>3</sub>PO on coordination to Lewis acids [24, 25] was used. We found that reactions of  $[\mu\text{-}8,8'\text{-I-}3,3'\text{-Co(1,2-}\text{C}_2\text{B}_9\text{H}_{10}\text{)}_2]$  with triethylphosphine and triphenylphosphine oxides in mesitylene resulted in the corresponding phosphonium derivatives  $[8\text{-I-}8'\text{-R}_3\text{PO-}3,3'\text{-Co(1,2-}\text{C}_2\text{B}_9\text{H}_{10}\text{)}_2]$  ( $\text{R} = \text{Et, Ph}$ ) (Scheme 6.7) [22].



Scheme 6.6



Scheme 6.7

The  $^{31}\text{P}$  NMR chemical shift of  $[\mu\text{-}8,8'\text{-I-3,3'}\text{-Co}(1,2\text{-C}_2\text{B}_9\text{H}_{10})_2]$  in  $\text{CD}_2\text{Cl}_2$  was found to be 91.9 ppm (94.1 ppm in acetone- $d_6$ ), which corresponds to Gutmann's acceptor number  $\text{AN} = 112$  (117). According to this parameter, the Lewis acidity of the quasi-borinium cation considered is more toward  $\text{Et}_3\text{P=O}$  than  $\text{Et}_3\text{Si}^+$  [13] and it belongs to the strongest boron Lewis acids. In accordance with known Olah's definition [26] that Lewis acids that are stronger than anhydrous  $\text{AlCl}_3$  ( $\text{AN} = 86$  [25]) should be categorized as Lewis superacids, the quasi-borinium cation derived from  $[\mu\text{-}8,8'\text{-I-3,3'}\text{-Co}(1,2\text{-C}_2\text{B}_9\text{H}_{10})_2]$  can be considered as a Lewis superacid.

## REFERENCES

- Lewis, J. N. *Valence and the Structure of Atoms and Molecules*; Chemical Catalog Co.: New York, 1923.
- Ishihara, K. In *Lewis Acids in Organic Synthesis*, Yamamoto H., Ed.; Wiley-VCH, New York, 2000, p 89.
- Ishihara, K.; Yamamoto, H. *Eur. J. Org. Chem.* **1999**, 527.
- Chen, E. Y.-X.; Marks, T. J. *Chem. Rev.* **2000**, *100*, 1391.
- Erker, G. *Chem. Commun.* **2003**, 1469.
- Wade, C. R.; Brooms Grove, A. E. J.; Aldridge, S.; Gabbaï, F. P. *Chem. Rev.* **2010**, *110*, 3958.
- Galbraith, E.; James, T. D. *Chem. Soc. Rev.* **2010**, *39*, 3831.
- Stephan, D. W. *Dalton Trans.* **2009**, 3129.
- Jiang, C.; Blacque, O.; Fox, T.; Berke, H. *Organometallics* **2011**, *30*, 2117.
- Piers, W.; Bourke, S. C.; Conroy, K. D. *Angew. Chem., Int. Ed.* **2005**, *44*, 5016.
- Rüther, T.; Huynh, T. D.; Huang, J.; Hollenkamp, A. F.; Salter, E. A.; Wierzbicki, A.; Mattson, K.; Lewis, A.; Davis, J. H. *Chem. Mater.* **2010**, *22*, 1038.

12. De Vries, T. S.; Prokofjevs, A.; Harvey, J. N.; Vedejs, E. *J. Am. Chem. Soc.* **2009**, *131*, 14679.
13. Del Grosso, A.; Pritchard, R. G.; Muryn, C. A.; Ingleson, M. J. *Organometallics* **2010**, *29*, 241.
14. Bregadze, V. I.; Timofeev, S. V.; Sivaev, I. B.; Lobanova, I. A. *Russ. Chem. Rev.* **2004**, *73*, 433.
15. Semioshkin, A. A.; Sivaev, I. B.; Bregadze, V. I. *Dalton Trans.* **2008**, 977.
16. Sivaev, I. B.; Bregadze, V. I. In *Boron Science: New Technologies and Applications*; Hosmane, N. S., Ed.; Taylor & Francis Books/CRC Press, Boca Raton, **2011**; p 623.
17. Mindich, A. L.; Bokach, N. A.; Dolgushin, F. M.; Haukka, M.; Lisitsyn, L. A.; Zhdanov, A. P.; Zhizhin, K. Y.; Miltsov, S. A.; Kuznetsov, N. T.; Kukushkin, V. Y. *Organometallics* **2012**, *31*, 1716.
18. Plešek, J.; Štibr, B.; Hefmánek, S. *Collect. Czech. Chem. Commun.* **1984**, *49*, 1492.
19. Knyazev, S. P.; Kirin, V. N.; Chernyshev, E. A. *Dokl. Chem.* **1996**, *350*, 252.
20. Selucky, P.; Plešek, J.; Rais, J.; Kyrš, M.; Kadlekova, L. J. *Radioanal. Nucl. Chem.* **1991**, *149*, 131.
21. Bregadze, V. I.; Kosenko, I. D.; Lobanova, I. A.; Starikova, Z. A.; Godovikov, I. A.; Sivaev, I. B. *Organometallics* **2010**, *29*, 5366.
22. Kosenko, I. D.; Lobanova, I. A.; Godovikov, I. A.; Starikova, Z. A.; Sivaev, I. B.; Bregadze, V. I. *J. Organomet. Chem.* **2012**, *721–722*, 70.
23. Kosenko, I. D.; Lobanova, I. A.; Sivaev, I. B.; Petrovskii, P. V.; Bregadze, V. I. *Russ. Chem. Bull.* **2011**, *60*, 2354.
24. Gutmann, V. *Coord. Chem. Rev.* **1976**, *18*, 225.
25. Beckett, M. A.; Brassington, D. S.; Coles, S. J.; Hursthouse, M. B. *Inorg. Chem. Commun.* **2000**, *3*, 530.
26. Olah, G. A.; Prakash, G. K. S.; Molnar, A.; Sommer, J. *Superacid Chemistry*, John Wiley & Sons, Inc., Hoboken, NJ: **2009**.



# TRANSITION-METAL-PROMOTED FUNCTIONALIZATION OF CARBORANES

ZAOZAO QIU AND ZUOWEI XIE\*

*Shanghai-Hong Kong Joint Laboratory in Chemical Synthesis, Shanghai Institute of Organic Chemistry, The Chinese Academy of Sciences, Shanghai, China; Department of Chemistry, The Chinese University of Hong Kong, Shatin, N. T., Hong Kong, China*

## 7.1 INTRODUCTION

Carboranes are a class of boron hydride clusters in which one or more BH vertices are replaced by CH units (Fig. 7.1). They have many characteristics such as spherical geometry, remarkable thermal and chemical stability, and a hydrophobic molecular surface, leading to many applications in medicine as boron neutron capture therapy (BNCT) agents [1], in supramolecular design as building blocks [2], and in transition-metal chemistry as ligands [3]. To broaden the application scope, functionalization of carboranes is necessary. In general, there are two conventional synthetic methods leading to the cage carbon substituted carboranes: reaction of alkynes with decaborane [4] and  $\text{Li}_2\text{C}_2\text{B}_{10}\text{H}_{10}$  with electrophiles [5].

On the other hand, carboryne, 1,2-dehydro-*o*-carborane, is a three-dimensional relative of benzyne (Fig. 7.1) [6]. It can react with alkenes, dienes, and alkynes in [2+2], [4+2] cycloaddition and ene-reaction patterns [7], similar to those of benzyne [8]. Although these reactions show the potential for the preparation of functionalized carboranes in a single operation, they are complex and do not proceed in a controlled manner. In view of the spectacular role of transition metals in synthetic chemistry, we envisage that the aforementioned reactions may work efficiently and in a controlled way with the help of transition metals. In this connection, we initiated a research program to develop transition-metal-mediated/catalyzed synthetic methodologies for the functionalization of carboranes. This chapter summarizes the recent progress in this research area.

## 7.2 [2 + 2 + 2] CYCLOADDITION OF Ni-CARBORYNE WITH ALKYNES

The M–C<sub>cage</sub> (C<sub>cage</sub>: hypervalent carbon)  $\sigma$  bonds in metal–carboranyl complexes (Fig. 7.1) are generally inert toward various electrophiles for steric reasons, as evidenced in our previous work [9]. It indicates that the chemistry of M–C<sub>cage</sub>  $\sigma$  bonds is significantly different, in terms of reactivities, from that of traditional M–C  $\sigma$  bonds. To overcome this problem, we thought that the construction of a metallacyclop propane (metal–carboryne, Fig. 7.1) would reduce the steric hindrance around the M–C<sub>cage</sub> bond and create the ring strains, thus facilitating the reactivity of the M–C<sub>cage</sub> bonds.

Like benzyne, carboryne can be trapped and stabilized by transition metals. Salt metathesis between  $\text{Li}_2\text{C}_2\text{B}_{10}\text{H}_{10}$  and metal halides is a useful method for the preparation of metal–carboryne complexes [10]. Density functional theory (DFT) calculations suggest that such bonding interactions between the metal atom and carboryne ligand are best described as a resonance hybrid of both the M–C  $\sigma$  and M–C  $\pi$  bonding forms (Fig. 7.2) [11], similar to those described for metal–benzyne complexes [12].

In view of the analogy between nickel–benzyne and nickel–carboryne complexes, we envisage that they may share chemical properties in reaction with unsaturated substrates. In fact, *in situ* generated ( $\eta^2\text{-C}_2\text{B}_{10}\text{H}_{10}$ )Ni(PPh<sub>3</sub>)<sub>2</sub> (**1**)

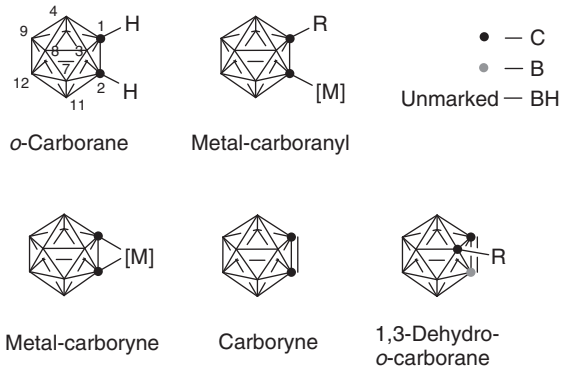


Figure 7.1 Carborane derivatives.

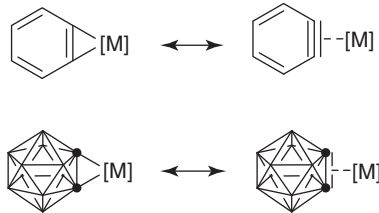


Figure 7.2 Bonding description.

[10, 13] can react with 2 equiv of internal alkynes  $R^1C\equiv CR^2$  to give highly substituted 1,2-benzo-*o*-carboranes  $1,2-[C(R^1)=C(R^2)C(R^1)=C(R^2)]-1,2-C_2B_{10}H_{10}$  (**2**) via a [2 + 2 + 2] cycloaddition (Scheme 7.1) [14]. The localized double bonds in the X-ray structures of products suggest that there is no substantial  $\pi$ -delocalization in the six-membered ring. Steric factors play an important role in the reactions. Sterically less demanding linear dialkylalkynes offer the best results in comparison to the phenyl- and *tert*-butyl-substituted ones. Compared to the reactions of Ni benzyne with alkynes, those of Ni carboryne have a limited substrate scope but higher regioselectivity. Terminal alkynes do not insert into Ni carboryne since they can protonate the Ni–carboryne complex to give *o*-carborane.

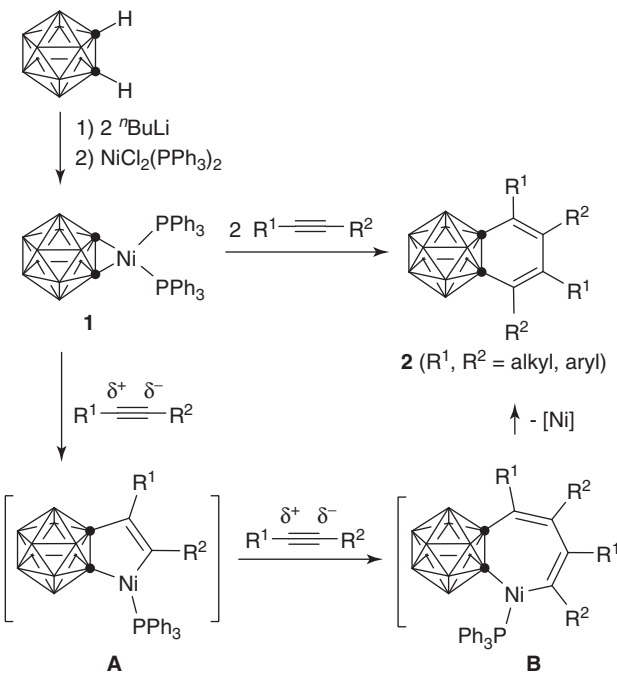
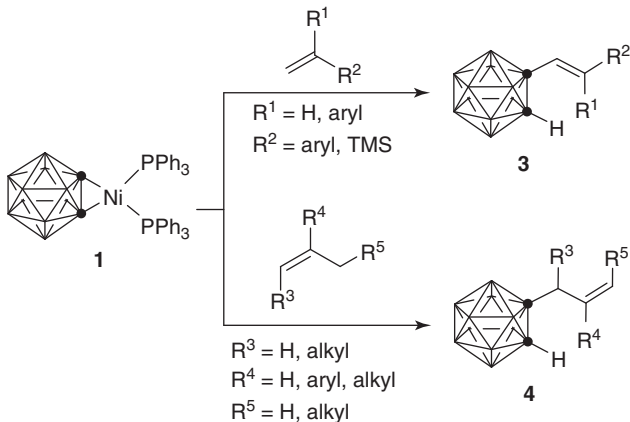
The exclusive formation of the head-to-tail product in the reaction with unsymmetrical aryl alkynes suggests that the insertion regioselectivity is determined by the polarity of alkynes [15]. The formation of **2** can be rationalized by the sequential insertion of alkynes into the Ni–C bonds, followed by reductive elimination (Scheme 7.1). The first regioselective alkyne insertion into the Ni–C<sub>cage</sub> bond in **1** gives a nickelacyclopentene intermediate **A**. The head-to-tail insertion products suggest that the Ni–C<sub>vinyl</sub> bond is highly preferred over the Ni–C<sub>cage</sub> bond in the second alkyne insertion.

### 7.3 COUPLING REACTION OF Ni–CARBORYNE WITH ALKENES

In the reaction of **1** with alkenes, the C–C coupling products alkenylcarboranes **3** or **4** are formed in moderate to very good yields with excellent regio- and stereoselectivity (Scheme 7.2) [16]. For styrenes, the “Heck-type” of products **3** are obtained as single regioisomers. The nature of the substituents on the phenyl ring has no obvious effect on the reaction results. On the other hand, the “ene-reaction-type” of products **4** are obtained for aliphatic alkenes and  $\alpha$ -methylstyrene. It is noted that in the reaction of **1** with cyclohexene, the “ene-reaction-type” of product is isolated in 67% yield, which is much higher than the 10–20% yield from the direct reaction of carboryne (generated *in situ*) with the same substrate [7]. Bulkyl alkenes such as *cis*- and *trans*-stillbene are not compatible with this reaction.

Furthermore, **1** does not react with anthracene, furan, or thiophene, whereas these 4 $\pi$  systems react readily with *in situ* generated carboryne to give [4+2] cycloaddition products [7]. This result suggests that carboryne and Ni–carboryne should undergo different reaction pathways.

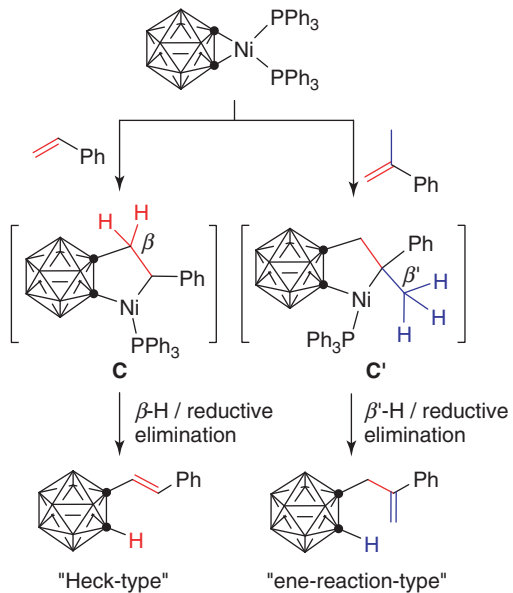
In the plausible mechanism, coordination followed by insertion of the alkene gives a nickelacyclopentane intermediate C/C'. The regioselectivity observed in the reaction can be ascribed to the large steric effect of the carborane moiety and

**Scheme 7.1** [2 + 2 + 2] Cycloaddition of Ni–carbonyne with alkynes.**Scheme 7.2** Coupling reaction of Ni–carbonyne with alkenes.

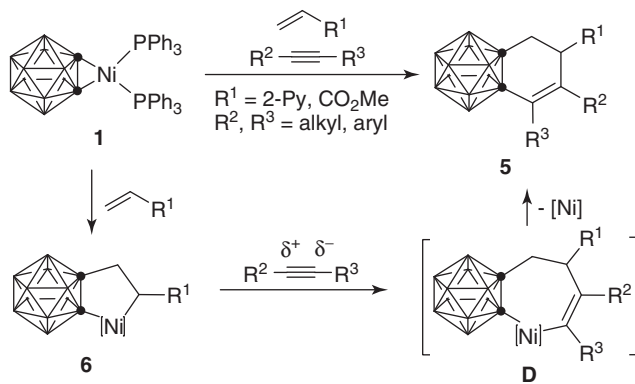
polarity of the C=C bond.  $\beta$ -H/ $\beta'$ -H elimination prior to the insertion of the second molecule of alkene followed by reductive elimination affords alkenylcarboranes 1-[HC=CH(Ph)]-1,2-C<sub>2</sub>B<sub>10</sub>H<sub>11</sub> (“Heck-type” product) or 1-[CH<sub>2</sub>C(Ph)=CH<sub>2</sub>]-1,2-C<sub>2</sub>B<sub>10</sub>H<sub>11</sub> (“ene-reaction-type” product) (Scheme 7.3). The  $\beta$ -H elimination is more difficult than  $\beta'$ -H elimination because of the ring strain of the metallacycle [17]. Labeling experiments support the proposed reaction mechanism: treatment of **1** with styrene-d<sub>3</sub> affords 1-[DC=CD(Ph)]-2-D-1,2-C<sub>2</sub>B<sub>10</sub>H<sub>10</sub>.

#### 7.4 [2 + 2 + 2] CYCLOADDITION OF NI-CARBORYNE WITH ACTIVATED ALKENES AND ALKYNES

The  $\beta$ -H elimination reaction of the nickelacyclopentane may be suppressed by intramolecular coordination of the heteroatom, which would lead to the formation of stable nickelacyclopentanes. In the reaction of **1** with activated alkenes such as methyl



**Scheme 7.3** Proposed mechanism for reaction of Ni–carboryne with alkenes. (See insert for color representation of the figure.)

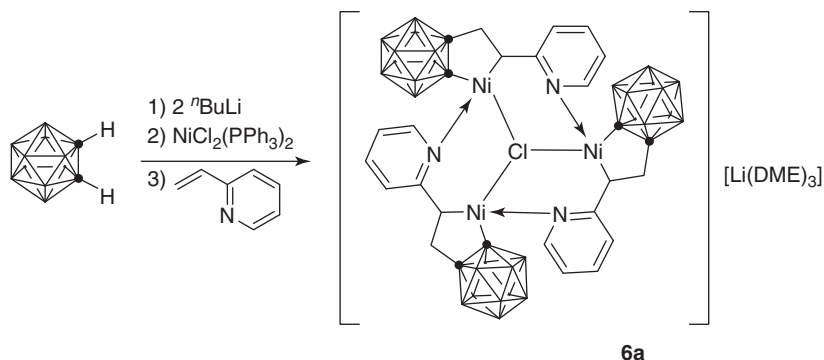


**Scheme 7.4** Cycloaddition of Ni–carboryne with activated alkenes and alkynes.

acrylate or 2-vinylpyridine, the product  $1-[CH_2CH_2(CO_2Me)]-1,2-C_2B_{10}H_{11}$  or  $1-[CH_2CH_2(o-C_5H_4N)]-1,2-C_2B_{10}H_{11}$  is obtained upon hydrolysis.

The stabilized five-membered nickelacyclopentane intermediates can react readily with alkynes to give three-component [2 + 2 + 2] cycloaddition products dihydrobenzocarboranes **5** (Scheme 7.4). As activated alkenes are much more reactive than alkynes toward Ni–carboryne, the reaction can be carried out in one pot to achieve an assembling process that is capable of excellent control over the chemo- and regioselectivity of the dihydrobenzocarborane products [18]. A variety of alkynes are compatible with this nickel-mediated three-component cyclization. Both steric and electric factors play important roles in the reaction. Sterically less demanding 3-hexyne offers the highest yield; and no reaction proceeds for the bulky diphenylacetylene and bis(trimethylsilyl)acetylene. Unsymmetrical aryl alkynes give only one isomer of the products because of the electronic effects [15]. Only  $C\equiv C$  insertion product is observed in the reaction of  $CH_2=CHCH_2C\equiv CC_6H_5$ , and nitriles, isonitriles, or carbodiimides do not yield any insertion products.

The reaction mechanism is proposed after the isolation and structural confirmation of the activated alkene insertion species nickelacyclopentanes **6a** from the reaction of nickel–carboryne with 2-vinylpyridine (Scheme 7.5). The sequential insertion of alkene and alkyne with excellent regioselectivity control by electronic effect results in the formation of **5**. Alkyne inserts regioselectively into the  $Ni-C_{alkyl}$  bond of the nickelacyclopentane, whereas the  $Ni-C_{cage}$  bond remains intact. Reductive elimination yields the final products **5**. In fact, treatment of **6a** with 3-hexyne affords the expected dihydrobenzocarborane



**Scheme 7.5** Preparation of nickelacyclopentane intermediate.

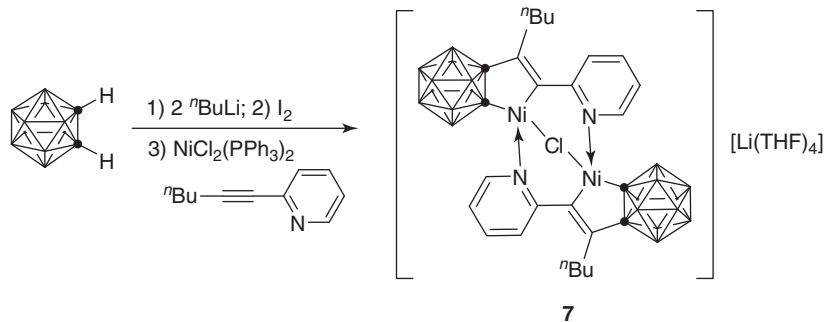
in greater than 90% yield. This work offers a direct route to the synthesis of dihydrobenzocarborane derivatives from simple molecules.

### 7.5 NI-CATALYZED [2 + 2 + 2] CYCLOADDITION OF CARBORYNE WITH ALKYNES

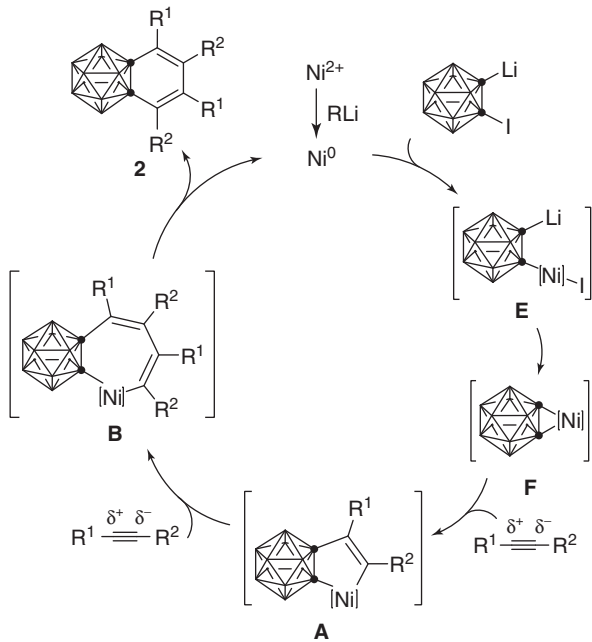
The above reactions of carbonyne with alkenes and alkynes are mediated by a stoichiometric amount of the Ni reagent. In view of the fact that benzene can undergo Ni-catalyzed reactions with alkenes and/or alkynes [19], carbonyne is expected to produce a catalytic cycle by making use of the Ni(0) species generated from the reductive elimination step of the above process. 1-Iodo-2-lithiocarborane is chosen as the carbonyne precursor, as it can be conveniently prepared *in situ* from the reaction of dilithiocarborane with 1 equiv of iodine at room temperature and is much more thermally stable than 1-bromo-2-lithiocarborane. Furthermore, it is a more efficient precursor than the bromo one [7]. We anticipate that 1-iodo-2-lithiocarborane might undergo oxidative addition on Ni(0) followed by an elimination of LiI to afford the Ni–carbonyne complex required for a catalytic cycle [20].

Screening experiments suggest that  $\text{NiCl}_2(\text{PPh}_3)_2$  is the best catalyst among a variety of metal complexes, although Ni(0) complexes show some catalytic activities in the reactions [20]. In sharp contrast, palladium, iron, and cobalt complexes such as  $\text{PdCl}_2(\text{PPh}_3)_2$ ,  $\text{Pd}(\text{PPh}_3)_4$ ,  $\text{FeCl}_2/2\text{PPh}_3$ , and  $\text{CoCl}_2(\text{PPh}_3)_2$  are inactive. The activities of the nickel catalysts also depend largely on the ligands. In the presence of 20 mol% of  $\text{NiCl}_2(\text{PPh}_3)_2$ , interaction of 1-I-2-Li-1,2- $\text{C}_2\text{B}_{10}\text{H}_{10}$  with 2 equiv of alkynes in hot toluene gives [2 + 2 + 2] cycloaddition products 1,2-benzo-*o*-carboranes in very comparable yields with those of stoichiometric reactions.

The NMR experiment indicates the formation of  $(\eta^2\text{-C}_2\text{B}_{10}\text{H}_{10})\text{Ni}(\text{PPh}_3)_2$  from the reaction of 1-I-2-Li-1,2- $\text{C}_2\text{B}_{10}\text{H}_{10}$  with 1 equiv of  $\text{Ni}(\text{cod})_2/2\text{PPh}_3$  at room temperature, suggesting that an oxidative addition of I–C<sub>cage</sub> bond to Ni(0) proceeds. In addition, mixing *n*-butyl-2-pyridinylacetylene, 1-I-2-Li-1,2- $\text{C}_2\text{B}_{10}\text{H}_{10}$ , and  $\text{NiCl}_2(\text{PPh}_3)_2$  results in the isolation of an alkyne insertion product **7**  $[(2\text{-C}(^n\text{Bu})=\text{C}(o\text{-C}_5\text{H}_4\text{N})-1,2\text{-C}_2\text{B}_{10}\text{H}_{10})\text{Ni}]_2(\mu\text{-Cl})[\text{Li}(\text{THF})_4]$  (Scheme 7.6). Its structure was



**Scheme 7.6** Preparation of nickelacyclopentene intermediate.



**Scheme 7.7** Ni-catalyzed  $[2 + 2 + 2]$  cycloaddition of carboryne with alkynes.

determined by single-crystal X-ray analyses. It is believed that the coordination of the pyridinyl to the Ni atom can stabilize complex **7** and prevent the further insertion of the second equivalent of *n*-butylpyridinylacetylene.

It is very likely that the catalysis is initiated by a  $\text{Ni}(0)$  species which is generated from the reduction of  $\text{Ni}(\text{II})$  by the lithiocarbaborane salt [21]. Oxidative addition of the  $\text{C}_{\text{cage}}-\text{I}$  bond on  $\text{Ni}(0)$ , followed by the elimination of  $\text{LiI}$ , affords the  $\text{Ni}$ –carboryne intermediate **F**. Sequential insertion of alkynes into  $\text{Ni}-\text{C}_{\text{cage}}$  and  $\text{Ni}-\text{C}_{\text{vinyl}}$  bonds produces the seven-membered nickelacycle **B**. Reductive elimination yields the cycloaddition product **2** and regenerates the  $\text{Ni}(0)$  species (Scheme 7.7). This work represents the first example of metal-catalyzed reaction of carboryne with unsaturated molecules.

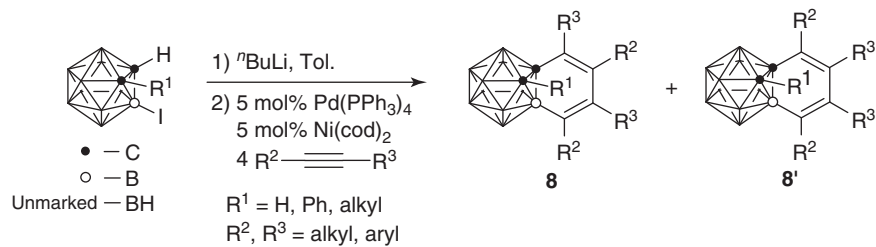
## 7.6 Pd/Ni-COCATALYZED $[2 + 2 + 2]$ CYCLOADDITION OF 1,3-DEHYDRO-*o*-CARBORANE WITH ALKYNES

As *o*-carboryne can be generated *in situ* by heating  $1\text{-Li-2-X-1,2-C}_2\text{B}_{10}\text{H}_{10}$  ( $\text{X} = \text{Br, I}$ ) via the elimination of  $\text{LiX}$  [7], it is rational to speculate that 1,3-dehydro-*o*-carborane (Fig. 7.1) might be produced in a similar manner using  $1\text{-Li-3-X-1,2-C}_2\text{B}_{10}\text{H}_{10}$  as precursors. Unfortunately,  $1\text{-Li-3-I-1,2-C}_2\text{B}_{10}\text{H}_{10}$  is thermally very stable, and no decomposition is observed in refluxing toluene. We then anticipated that an oxidative addition of the cage  $\text{B}-\text{I}$  in  $1\text{-Li-3-I-1,2-C}_2\text{B}_{10}\text{H}_{10}$  on  $\text{Pd}(0)$  [22], followed by a subsequent elimination of  $\text{LiI}$ , would afford the target complex  $\text{Pd-1,3-dehydro-}o\text{-carborane}$ .

In an initial attempt, the  $^{11}\text{B}$  NMR spectrum showed almost quantitative formation of 1-methyl-*o*-carborane upon heating a toluene solution of  $1\text{-Li-2-Me-3-I-1,2-C}_2\text{B}_{10}\text{H}_9$  in the presence of 10 mol % of  $\text{Pd}(\text{PPh}_3)_4$ . This catalytic deiodination process may be due to the thermal decomposition of  $\text{Pd-2-methyl-1,3-dehydro-}o\text{-carborane}$  presumably via a radical process under thermal conditions [14], in which the solvent acts as the hydrogen source.

Attempts to isolate pure  $(\eta^2\text{-1,3-}o\text{-C}_2\text{B}_{10}\text{H}_9\text{Me})\text{Pd(L)}$ , an analog of  $(\eta^2\text{-1,2-}o\text{-C}_2\text{B}_{10}\text{H}_{10})\text{Ni(L)}$ , from a stoichiometric reaction in the presence of  $\text{PPh}_3$  or dppe (dppe = 1,2-bis(diphenylphosphino)ethane) fail, as the reaction does not occur at  $T < 70^\circ\text{C}$  and the resulting metal complex slowly decomposes at higher temperatures. However, this reactive intermediate can be trapped by unsaturated molecules, such as alkynes, leading to the formation of the  $[2 + 2 + 2]$  cycloaddition products **8/8'** (Scheme 7.8) [23]. Although  $\text{Pd}(\text{PPh}_3)_4$  can catalyze the  $[2 + 2 + 2]$  cycloaddition reaction of  $1\text{-Li-2-Me-3-I-1,2-C}_2\text{B}_{10}\text{H}_9$  with alkynes, affording 1,3-benzo-*o*-carboranes, addition of  $\text{Ni}(\text{cod})_2$  can significantly accelerate the above reactions.

Both aliphatic and aromatic alkynes as well as diynes can undergo such  $[2 + 2 + 2]$  cycloaddition reactions, and steric factors of alkynes play a crucial role. In case of sterically demanding alkynes bearing a trimethylsilyl (TMS) or *o*-tolyl group, only deiodination carborane is observed. Alkynes bearing carbonyl groups are incompatible with this reaction because they

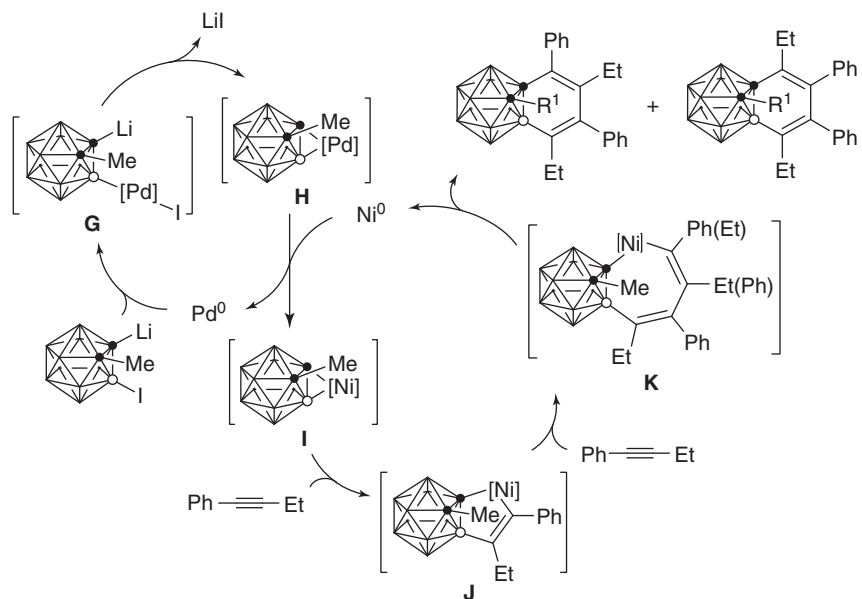


Scheme 7.8 Pd/Ni co-catalyzed [2 + 2 + 2] cycloaddition of 1,3-dehydro-*o*-carborane with alkynes.

react with the carboryne precursor 1-Li-2-Me-3-I-1,2-C<sub>2</sub>B<sub>10</sub>H<sub>9</sub>. Substituents at the cage C(2) position also affect the yields of [2 + 2 + 2] cycloaddition products. Results show that steric effects of substituents are much less significant than electronic effects; for example, an electron-withdrawing group such as phenyl leads to a big drop in the yield. X-ray structures indicate that the six-membered C<sub>5</sub>B rings in the C,B-substituted benzocarboranes are planar with alternative short and long bonds, similar to those observed in 1,2-benzocarboranes [14, 20], suggesting that there is no substantial  $\pi$ -delocalization in such rings and that the C<sub>4</sub> unit may be described as a butadiene moiety.

A possible reaction mechanism for such a cooperative catalysis is proposed in Scheme 7.9. Since Ni(0) can hardly insert into the cage B–I bond, the Pd-1,3-dehydro-*o*-carborane **H** is formed via oxidative addition of B–I on Pd(0) followed by subsequent LiI elimination. Indicated by the aforementioned experiments that a two-component catalyst system is much more effective than Pd species alone in catalyzing the reaction of 1,3-dehydro-*o*-carborane with alkynes, a transmetalation process between Pd and Ni may occur, affording a more reactive nickel-1,3-dehydro-*o*-carborane intermediate **I** [24]. Such a transmetalation process can be evidenced by the following reactions: ( $\eta^2$ -*o*-C<sub>2</sub>B<sub>10</sub>H<sub>10</sub>)Ni(PPh<sub>3</sub>)<sub>2</sub> can be observed by treatment of ( $\eta^2$ -*o*-C<sub>2</sub>B<sub>10</sub>H<sub>10</sub>)Pd(PPh<sub>3</sub>)<sub>2</sub> with 1 equiv of Ni(cod)<sub>2</sub> in toluene at room temperature as indicated by <sup>31</sup>P NMR; and the addition of 20 mol% of Ni(cod)<sub>2</sub> to the mixture of ( $\eta^2$ -*o*-C<sub>2</sub>B<sub>10</sub>H<sub>10</sub>)Pd(PPh<sub>3</sub>)<sub>2</sub> and 3-hexyne leads to the isolation of benzocarborane in 18% yield, while ( $\eta^2$ -*o*-C<sub>2</sub>B<sub>10</sub>H<sub>10</sub>)Pd(PPh<sub>3</sub>)<sub>2</sub> alone does not show any activity toward alkyne. The relatively high activity of the Ni species may probably be ascribed to the weaker Ni–B bond over the Pd–B one or the Ni–B bonding pair being more nucleophilic [25].

In the reaction with unsymmetrical alkyne PhC≡CEt, the electronically controlled regioselective insertion into the Ni–B bond gives the nickelacyclopentene intermediate **J**. The alkyne insertion can be viewed as a nucleophilic attack of the M–C/B  $\sigma$ -bond on one of the two alkyne carbons. The exclusive insertion of the first equivalent of alkyne into the Ni–B bond with



Scheme 7.9 Proposed mechanism for Pd/Ni co-catalyzed formation of 1,3-benzocarboranes.

electronically controlled regioselectivity is well supported by the absence of 2-Me-1,3-[EtC=C(C<sub>6</sub>H<sub>5</sub>)-C(Et)=C(C<sub>6</sub>H<sub>5</sub>)]-1,2-C<sub>2</sub>B<sub>10</sub>H<sub>10</sub> in the products, as an M–B bond is much more nucleophilic than an M–C one [25]. The nucleophilic attack in nature also explains the regioselectivity observed in the insertion of unsymmetrical alkynes, in which the boron is bonded to the carbon having the electron-donating ethyl substituent. Subsequent insertion of the second molecule of PhC≡CEt into the Ni–C<sub>vinyl</sub> bond in both head-to-tail (major) and head-to-head (minor) manners followed by reductive elimination affords the final products (Scheme 7.9). It is noted that the insertion of alkynes into the M–C<sub>cage</sub> bond in **J** is prohibited for steric reasons. This work offers a new methodology for cage B-functionalization of carboranes and demonstrates that metal-1,3-*o*-carboryne can be viewed as a new kind of boron nucleophile.

## 7.7 REACTION OF ZIRCONOCENE–CARBORYNE WITH POLAR UNSATURATED MOLECULES

X-ray structures of metal–carborynes show that electronic configurations of a metal center can have large effects on the bonding interactions between the metal atom and carboryne unit, which may in turn influence their chemical properties [26]. Structural analyses also indicate that the interactions between the Ni atom and carboryne have more  $\pi$  character than that in Zr–carboryne complexes [27], which may facilitate the reactivity studies on these metal complexes. As a result, the Ni–carboryne complexes can react well with alkynes and alkenes, but they are inert toward polar unsaturated molecules such as nitriles and carbodiimides. On the other hand, the Zr–carboryne can react with a variety of polar unsaturated molecules, affording insertion products.

The first zirconium–carboryne complex  $\{[\eta^5:\sigma\text{-Me}_2\text{C}(\text{C}_9\text{H}_6)(\text{C}_2\text{B}_{10}\text{H}_{10})]\text{ZrCl}(\eta^3\text{-C}_2\text{B}_{10}\text{H}_{10})\}[\text{Li}(\text{THF})_4]$  was prepared from the reaction of *in situ* generated  $[\eta^5:\sigma\text{-Me}_2\text{C}(\text{C}_9\text{H}_6)(\text{C}_2\text{B}_{10}\text{H}_{10})]\text{ZrCl}_2$  with 1 equiv of Li<sub>2</sub>C<sub>2</sub>B<sub>10</sub>H<sub>10</sub> [11]. The anionic nature of this molecule results in inertness toward unsaturated molecules. On the other hand, treatment of Cp<sub>2</sub>ZrCl<sub>2</sub> with 1 equiv of Li<sub>2</sub>C<sub>2</sub>B<sub>10</sub>H<sub>10</sub> in ether gives the ate-complex Cp<sub>2</sub>Zr( $\mu$ -Cl)( $\mu$ -C<sub>2</sub>B<sub>10</sub>H<sub>10</sub>)Li(OEt<sub>2</sub>)<sub>2</sub> (**9**) in 70% isolated yield [28]. It can be viewed as a precursor of zirconocene–carboryne Cp<sub>2</sub>Zr( $\eta^2\text{-C}_2\text{B}_{10}\text{H}_{10}$ ). In addition, a series of neutral group 4 metal–carboryne complexes bearing amidinato ligands L, ( $\eta^2\text{-C}_2\text{B}_{10}\text{H}_{10}$ )M(L)<sub>2</sub>, were synthesized by salt metathesis reactions between Li<sub>2</sub>C<sub>2</sub>B<sub>10</sub>H<sub>10</sub> and diamidinato group 4 metal dichloride complexes MCl<sub>2</sub>(L)<sub>2</sub> (L = [ $\eta^2\text{-R}^2\text{C}(\text{NR}^1)_2$ ]) [29].

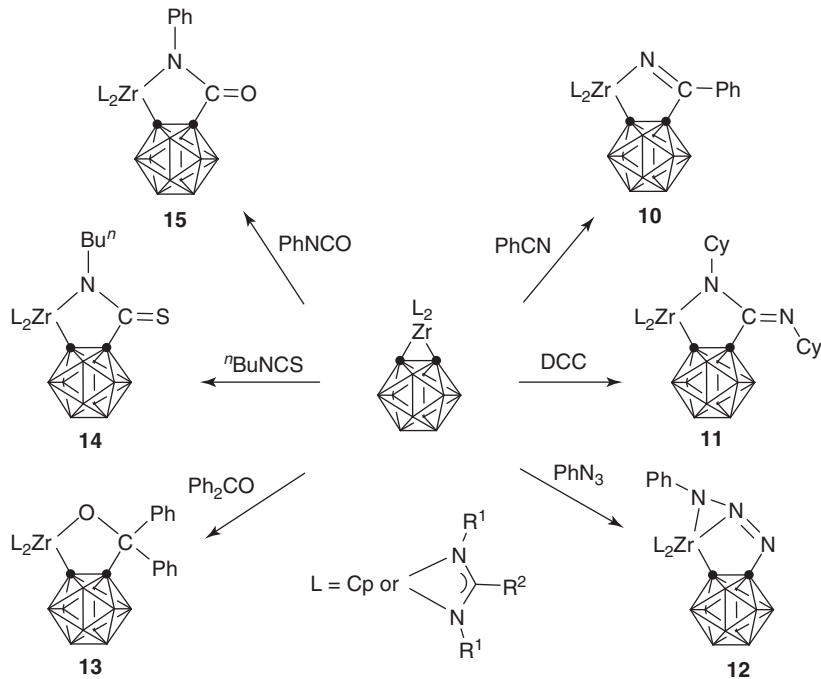
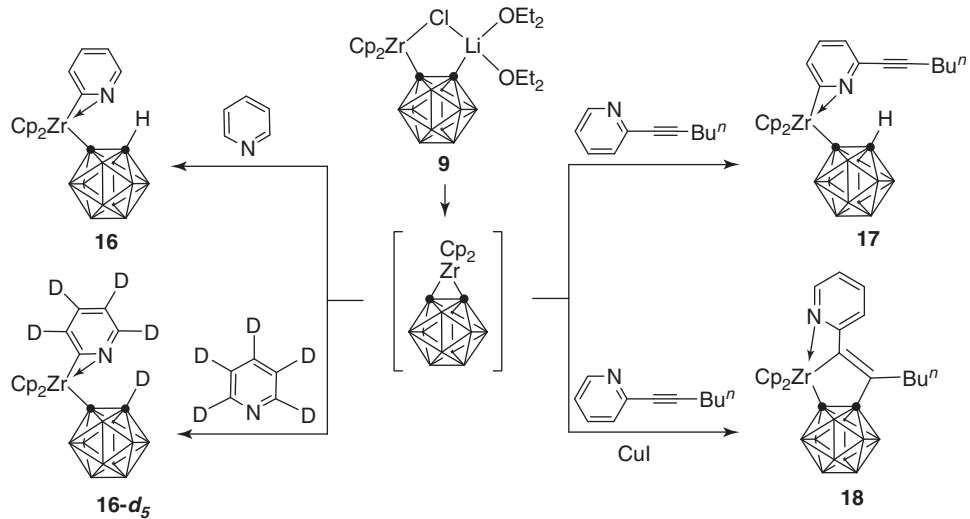
Treatment of ( $\eta^2\text{-C}_2\text{B}_{10}\text{H}_{10}$ )M(L)<sub>2</sub> (L = Cp, [ $\eta^2\text{-R}^2\text{C}(\text{NR}^1)_2$ ]) with PhCN, CyN=C=NCy, PhN<sub>3</sub>, Ph<sub>2</sub>C=O, "BuN=C=S, and PhN=C=O affords the corresponding monoinsertion products L<sub>2</sub>Zr[ $\sigma$ : $\sigma$ -N=C(Ph)(C<sub>2</sub>B<sub>10</sub>H<sub>10</sub>)] (**10**), L<sub>2</sub>Zr[ $\sigma$ : $\sigma$ -CyNC(=NCy)(C<sub>2</sub>B<sub>10</sub>H<sub>10</sub>)] (**11**), L<sub>2</sub>Zr[ $\eta^2$ : $\sigma$ -(PhNN=N)(C<sub>2</sub>B<sub>10</sub>H<sub>10</sub>)] (**12**), L<sub>2</sub>Zr[ $\sigma$ : $\sigma$ -OC(Ph)<sub>2</sub>(C<sub>2</sub>B<sub>10</sub>H<sub>10</sub>)] (**13**), L<sub>2</sub>Zr[ $\sigma$ : $\sigma$ -"BuNC(=S)(C<sub>2</sub>B<sub>10</sub>H<sub>10</sub>)] (**14**), and L<sub>2</sub>Zr[ $\sigma$ : $\sigma$ -PhNC(=O)(C<sub>2</sub>B<sub>10</sub>H<sub>10</sub>)] (**15**), respectively, in moderate to high yields (Scheme 7.10) [28, 29]. In these reactions, unsaturated molecules insert into only one Zr–C<sub>cage</sub> bond, and the other Zr–C<sub>cage</sub> bond remains inert. No double insertion products are observed even under forced reaction conditions in the presence of an excess amount of substrates. This reaction offers an efficient route to zirconaheterocycles incorporating a carboranyl unit.

## 7.8 REACTION OF ZIRCONOCENE–CARBORYNE WITH PYRIDINES

In attempts to isolate Cp<sub>2</sub>Zr( $\eta^2\text{-C}_2\text{B}_{10}\text{H}_{10}$ )L, when pyridine is added to Cp<sub>2</sub>Zr( $\mu$ -Cl)( $\mu$ -C<sub>2</sub>B<sub>10</sub>H<sub>10</sub>)Li(OEt<sub>2</sub>)<sub>2</sub> (**9**), an unexpected C–H activation product, Cp<sub>2</sub>Zr[ $\eta^2$ (C,N)-pyridine]( $\sigma$ -C<sub>2</sub>B<sub>10</sub>H<sub>11</sub>) (**16**), is isolated in 90% yield. If deuterated pyridine C<sub>5</sub>D<sub>5</sub>N is used, the  $\alpha$ -deuteron of pyridine is transferred to *o*-carborane, leading to the formation of Cp<sub>2</sub>Zr[ $\eta^2$ (C,N)-pyridine-*d*<sub>4</sub>]( $\sigma$ -C<sub>2</sub>B<sub>10</sub>H<sub>10</sub>D) (**16-d<sub>5</sub>**) in 87% isolated yield (Scheme 7.11) [30].

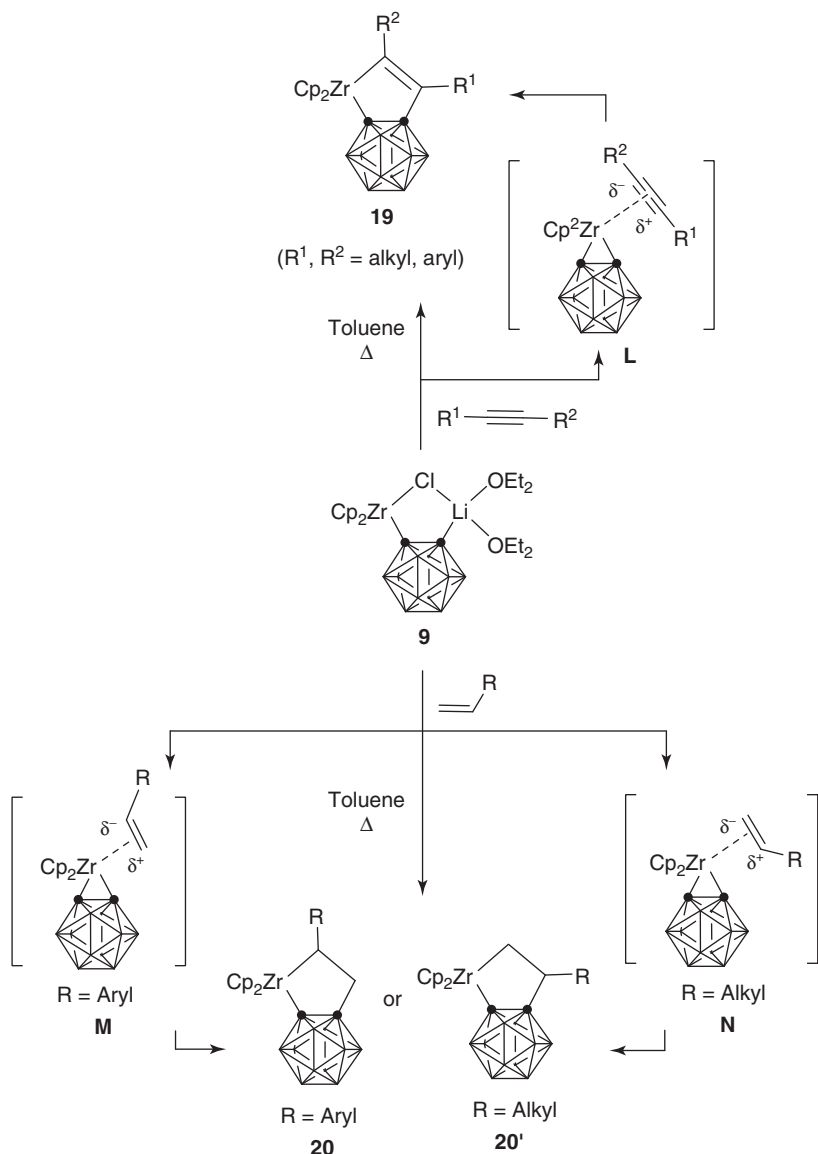
Other pyridine derivatives such as 2-bromo-pyridine, 2,4-lutidine, and quinolinecan can all react with **9** to afford the corresponding  $\alpha$ -C–H activation products Cp<sub>2</sub>Zr[ $\eta^2$ (C,N)-(2-bromopyridine)]( $\sigma$ -C<sub>2</sub>B<sub>10</sub>H<sub>11</sub>), Cp<sub>2</sub>Zr[ $\eta^2$ (C,N)-(2,4-lutidine)]( $\sigma$ -C<sub>2</sub>B<sub>10</sub>H<sub>11</sub>), and Cp<sub>2</sub>Zr( $\eta^2$ (C,N)-quinoline)( $\sigma$ -C<sub>2</sub>B<sub>10</sub>H<sub>11</sub>), respectively. These results are similar to those observed in the interaction of Cp<sub>2</sub>Zr(CH<sub>3</sub>)(THF)<sup>+</sup> with pyridines [31]. It is noted that the interaction of **9** with acridine generates an insertion product Cp<sub>2</sub>Zr{2-[9-( $\sigma$ -10(N)-dihydroacridine)]}( $\sigma$ -1-C<sub>2</sub>B<sub>10</sub>H<sub>10</sub>).

Treatment of **9** with 1 equiv of 2-(1-hexynyl)pyridine in toluene at room temperature affords the  $\alpha$ -C–H activation product Cp<sub>2</sub>Zr{ $\eta^2$ (C,N)-[2-(1-<sup>n</sup>BuC≡C)pyridine]}( $\sigma$ -C<sub>2</sub>B<sub>10</sub>H<sub>11</sub>) (**17**) in 56% isolated yield. However, if 2 equiv of CuI is added to the above reaction, the  $\alpha$ -C–H activation ( $\sigma$ -bond metathesis) reaction is completely blocked, and, instead, the alkyne insertion product 1,2-[Cp<sub>2</sub>ZrC(2-pyridinyl)=CBu<sup>n</sup>]-1,2-C<sub>2</sub>B<sub>10</sub>H<sub>10</sub> (**18**) is generated (Scheme 7.11) [30]. These results suggest that the coordination of pyridine to the Zr atom activates the  $\alpha$ -C–H bond, leading to the formation of  $\alpha$ -C–H activation ( $\sigma$ -bond metathesis) products, and the Cu atom can compete for Zr's binding site of pyridine to block the  $\alpha$ -C–H activation path and facilitate the alkyne insertion.

**Scheme 7.10** Reaction of zirconocene–carboryne with polar unsaturated molecules.**Scheme 7.11** Reaction of zirconocene–carboryne with pyridines.

## 7.9 REACTION OF ZIRCONOCENE–CARBORYNE WITH ALKYNES AND ALKENES

Zirconacycles are in general much more stable than their nickel analogs and often serve as very important and versatile intermediates for the construction of the carbon–carbon bond [32]. The carborane version of zirconacyclopentenes 1,2-[ $Cp_2ZrC(R)=C(R)]-1,2-C_2B_{10}H_{10}$  (**19**) can be obtained by the treatment of complex **9** with various kinds of alkynes (Scheme 7.12) in refluxing toluene [33]. This reaction cannot proceed in donor solvents such as  $Et_2O$  and THF, suggesting that the coordination of alkyne to the Zr atom is essential for the subsequent insertion.

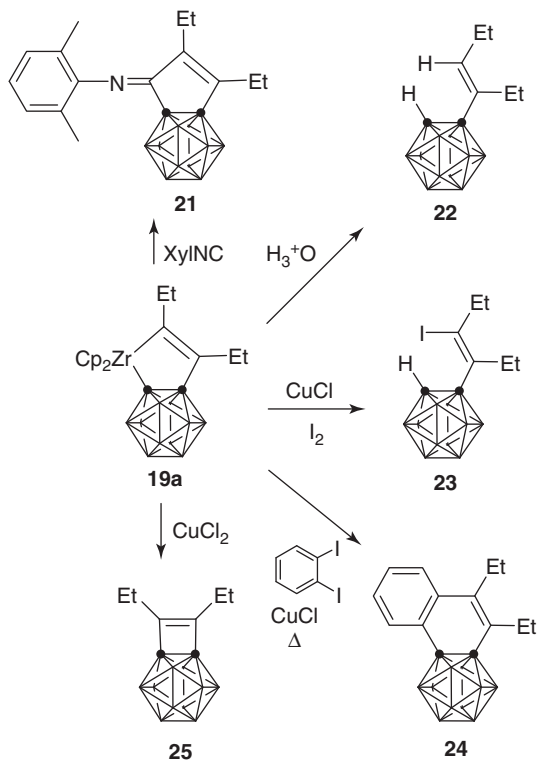


Scheme 7.12 Reaction of zirconocene–carboryne with alkynes and alkenes.

Both symmetrical and unsymmetrical alkynes bearing alkyl or aryl substituents are compatible with this reaction, in which steric factors play an important role.  $\text{Me}_3\text{SiC}\equiv\text{CSiMe}_3$  is inert toward **9**, and  $\text{PhC}\equiv\text{CPh}$  offers a much lower yield than linear alkynes. In case of unsymmetrical alkynes, the excellent regioselectivity of the insertion is generally determined by the polarity of alkynes. This reaction can tolerate many functional groups such as vinyl, chloro, amido, alkoxy, and tetrahydro-2-pyranyl. X-ray structures show that the sum of the five interior angles of the zirconacyclopentene ring is very close to  $540^\circ$ , suggestive of a planar geometry. These structural features resemble those of zirconacyclopentadienes. In contrast to Ni–carborynes, no double insertion products are formed even under forced reaction conditions in the presence of an excess amount of alkynes.

On the other hand, reaction of complex **9** with terminal alkenes  $\text{RCH}=\text{CH}_2$  in refluxing toluene gives zirconacyclopentanes  $1,2\text{-}[\text{Cp}_2\text{ZrCH}(\text{R})\text{CH}_2]\text{-}1,2\text{-C}_2\text{B}_{10}\text{H}_{10}$  (**20**,  $\text{R} = \text{aryl}$ ) or  $1,2\text{-}[\text{Cp}_2\text{ZrCH}_2\text{CH}(\text{R})]\text{-}1,2\text{-C}_2\text{B}_{10}\text{H}_{10}$  (**20'**,  $\text{R} = \text{alkyl}$ ) in good to high isolated yields with high regioselectivity (Scheme 7.12) [34]. Disubstituted alkenes such as  $\alpha$ -methylstyrene and cyclohexene cannot react with **9** probably because of steric reasons.

A reaction pathway for the formation of zirconacycles, involving the Zr–carboryne  $\text{Cp}_2\text{Zr}(\eta^2\text{-C}_2\text{B}_{10}\text{H}_{10})$ , has been proposed (Scheme 7.12). In general, electron-withdrawing aryl substituents go to the  $\alpha$  position (via intermediate **M**),



**Scheme 7.13** Reactivity study of zirconacyclopentene incorporating a carboranyl unit.

whereas the electron-donating alkyl substituents prefer the  $\beta$  position (via intermediate N). High temperatures are required for the reactions, which can not only promote the dissociation of LiCl from **9** forming the zirconocene–carboryne intermediate but also facilitate the insertion reactions between carboryne and the coordinated alkyne or alkene via the intermediates L, M, or N.

Zirconacyclopentene **19** can be converted to a variety of functionalized carboranes. Scheme 7.13 outlines their representative reactivity patterns in the example of 1,2-[ $\text{Cp}_2\text{ZrC(Et)=C(Et)}$ ]-1,2- $\text{C}_2\text{B}_{10}\text{H}_{10}$  (**19a**) [35]. It can react readily with 2,6-( $\text{CH}_3$ ) $_2\text{C}_6\text{H}_3\text{NC}$  to give a Zr–C<sub>vinyl</sub> bond insertion product 1,2-[ $(2',6'\text{-Me}_2\text{C}_6\text{H}_3\text{N=})\text{CC(Et)=C(Et)}$ ]-1,2- $\text{C}_2\text{B}_{10}\text{H}_{10}$  (**21**) in refluxing toluene. Hydrolysis of **19a** under acidic media affords alkenylcarborane 1-[ $\text{HC(Et)=C(Et)}$ ]-1,2- $\text{C}_2\text{B}_{10}\text{H}_{11}$  (**22**). Interaction of **19a** with  $\text{I}_2$  in the presence of CuCl generates a monoiodosubstituted product 1-[ $\text{CI(Et)=C(Et)}$ ]-1,2- $\text{C}_2\text{B}_{10}\text{H}_{11}$  (**23**) but not the disubstituted species 1-I-2-[ $\text{CI(Et)=C(Et)}$ ]-1,2- $\text{C}_2\text{B}_{10}\text{H}_{10}$ . It is suggested that, after transmetalation to Cu(I), only the Cu–C<sub>vinyl</sub> bond is reactive toward  $\text{I}_2$  whereas the Cu–C<sub>cage</sub> bond is inert probably because of steric reasons [9, 36]. This is very different from zirconacyclopentadienes, in which the diido-substituted compound is the major product in the presence of CuCl [37]. Reaction of **19a** with *o*-diiodobenzene in the presence of CuCl produces naphthalocarborane 1,2-[ $\text{o-C}_6\text{H}_4\text{C(Et)=C(Et)}$ ]-1,2- $\text{C}_2\text{B}_{10}\text{H}_{10}$  (**24**). Treatment of **19a** with CuCl<sub>2</sub> in toluene at  $80^\circ\text{C}$  gives the C–C coupling product 1,2-[ $\text{C(Et)=C(Et)}$ ]-1,2- $\text{C}_2\text{B}_{10}\text{H}_{10}$  (**25**). It is suggested that the intermediate 1,2-[ $\text{CuC(Et)=C(Et)}$ ]-1,2- $\text{C}_2\text{B}_{10}\text{H}_{10}$  is formed by the transmetalation of **19a** to Cu(II). Subsequent reductive elimination affords the four-membered ring product and Cu mirror. These results indicate that zirconacyclopentenes incorporating a carboranyl unit resemble their analogous zirconacyclopentadienes  $\text{Cp}_2\text{Zr}[\text{C(R)=C(R)-C(R)=C(R)}]$  in some reactions [38], while they have some unique properties of their own due to the presence of highly sterically demanding carboranyl unit.

## 7.10 Zr/Ni CO-MEDIATED [2 + 2 + 2] CYCLOADDITION OF CARBORYNE WITH TWO DIFFERENT ALKYNES

Previous work shows that nickel–carboryne reacts with 2 equiv of alkynes to afford 1,2-benzo-*o*-caboranes, and no selectivity is observed if two different kinds of alkynes are used in the reaction system. It is noted that in the intermolecular

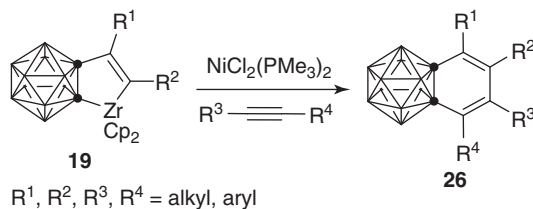
[2 + 2 + 2] cycloaddition of alkynes, selectivity among three different alkynes can be achieved by using unsymmetrical zirconacyclopentadienes, prepared from oxidative coupling of two different alkynes with  $\text{Cp}_2\text{Zr}(\text{II})$ , as intermediates to react with the third alkyne in the presence of  $\text{NiBr}_2(\text{PPh}_3)_2$  [39].

Zirconacyclopentenes incorporating a carboranyl unit are thermally very stable and chemically inert toward unsaturated organic molecules such as alkenes, alkynes, nitriles, CO, and  $\text{CO}_2$ , which is significantly different from zirconacyclopentenes without the carboranyl group [40]. However, the corresponding nickelacyclopentenes incorporating the carboranyl unit are very reactive toward alkynes. These results clearly indicate that the nature of transition metals dominates the reactivity of the corresponding metallacycles. Transmetalation from zirconacycles to nickel should allow the insertion of the second alkyne, making chemoselective [2 + 2 + 2] cycloaddition of *o*-carbonyne with two different alkynes possible.

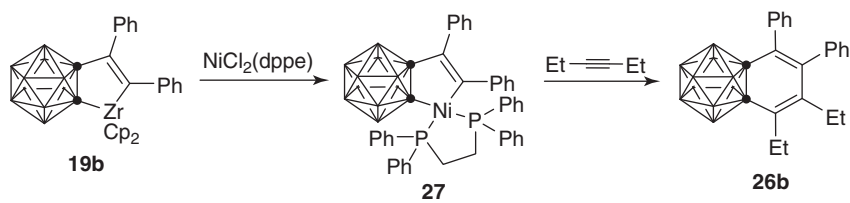
Reaction of zirconacyclopentenes with alkynes in the presence of a stoichiometric amount of  $\text{NiCl}_2(\text{PMe}_3)_2$  in hot toluene affords the expected 1,2-benzo-*o*-caborane **26** (Scheme 7.14) [41]. Both alkyl and aryl alkynes are compatible with this reaction except for those containing ester, amino, and very bulky TMS groups. A very reactive alkyne such as  $\text{MeO}_2\text{CC}\equiv\text{CCO}_2\text{Me}$  (DMAD) is homo-cyclotrimerized in the presence of Ni(0) prior to the insertion. Unsymmetrical alkynes produce two regioisomers and their ratios are affected by both steric and electronic factors. Only one isomer is generated for highly polar alkynes [15]. It is noted that these benzocarboranes can be also prepared in similar yields from one-pot reaction of  $\text{Cp}_2\text{Zr}(\mu\text{-Cl})(\mu\text{-C}_2\text{B}_{10}\text{H}_{10})\text{Li}(\text{OEt}_2)_2$  with alkyne, followed by treatment with another type of alkyne in the presence of  $\text{NiCl}_2(\text{PMe}_3)_2$ . This approach represents an equivalent of a three-component [2 + 2 + 2] cycloaddition of carbonyne with two different alkynes.

On the other hand, using a catalytic amount of nickel in the presence of 3 equiv of  $\text{FeCl}_3$  in the above reaction system can dramatically reduce the formation of homo-trimerization products of alkynes, allowing the insertion of activated alkynes such as DMAD. This catalytic reaction represents an important advance in the development of zirconacycle-based synthetic methodologies.

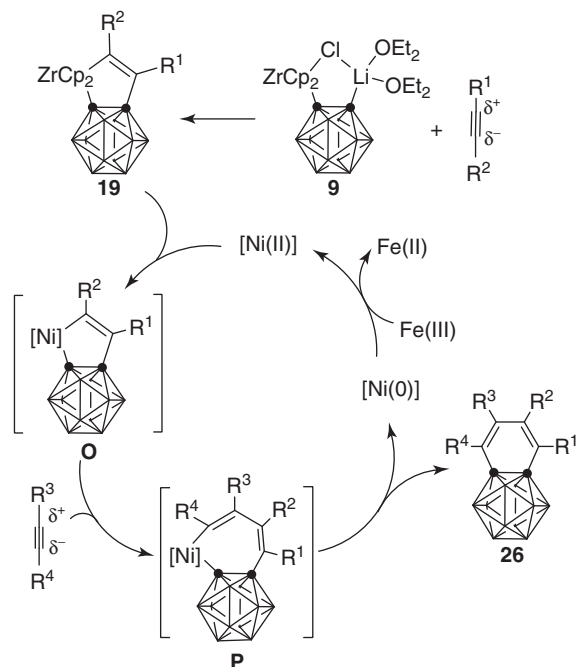
Transmetalation of zirconacycle to nickel is supported by the isolation and structural characterization of the nickelacyclopentene 1,2-[ $(\text{dppe})\text{NiC}(\text{Ph})=\text{C}(\text{Ph})$ ]-1,2- $\text{C}_2\text{B}_{10}\text{H}_{10}$  (**27**) from the reaction of 1,2-[ $\text{Cp}_2\text{ZrC}(\text{Ph})=\text{C}(\text{Ph})$ ]-1,2- $\text{C}_2\text{B}_{10}\text{H}_{10}$  (**19b**) with 1 equiv of  $\text{NiCl}_2(\text{dppe})$  (Scheme 7.15). The use of diphenylacetylene can avoid the  $\beta$ -H elimination of the resultant nickelacycle. Furthermore, the presence of the dppe ligand makes complex **27** thermodynamically stable. Treatment of **27** with 3-hexyne yields 1,2-benzo-*o*-carborane 1,2-[ $\text{C}(\text{Ph})=\text{C}(\text{Ph})-\text{C}(\text{Et})=\text{C}(\text{Et})$ ]-1,2- $\text{C}_2\text{B}_{10}\text{H}_{10}$  (**26b**). With the full characterization of this key intermediate, a proposed reaction mechanism is shown in Scheme 7.16. This reaction serves as an efficient protocol for the preparation of a new class of highly substituted benzocarboranes in a one-pot or a two-step manner via transmetalation of zirconacyclopentenes incorporating a carboranyl unit to nickel.



**Scheme 7.14** Reaction of zirconacycle with alkyne in the presence of  $\text{NiCl}_2(\text{PMe}_3)_2$ .



**Scheme 7.15** Isolation and reaction of nickelacyclopentene intermediate.



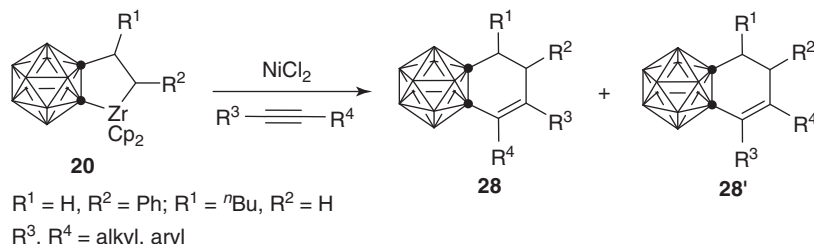
**Scheme 7.16** Proposed reaction mechanism for Ni-catalyzed cycloaddition.

### 7.11 Zr/Ni CO-MEDIATED [2 + 2 + 2] CYCLOADDITION OF CARBORYNE WITH UNACTIVATED ALKENES AND ALKYNES

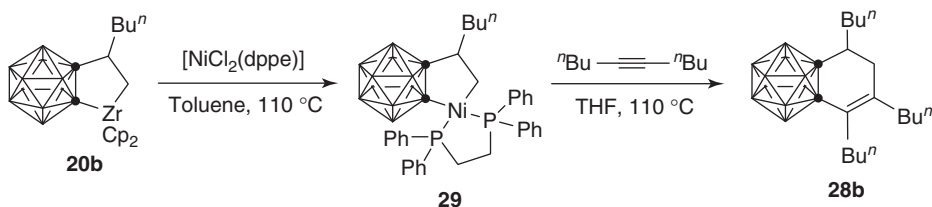
Transition-metal-mediated cycloaddition of alkenes and alkynes meets a major challenge to achieve both high reactivity and predictable selectivity between different unsaturated substrates in the formation of complex molecules. The employment of zirconacyclopentanes incorporating a carboranyl unit to reaction with alkynes after transmetalation to nickel can realize the three-component [2 + 2 + 2] cycloaddition of carbonyne, unactivated alkenes, and alkynes.

Zirconacyclopentanes **20**, prepared by the treatment of  $\text{Cp}_2\text{Zr}(\mu\text{-Cl})(\mu\text{-C}_2\text{B}_{10}\text{H}_{10})\text{Li(OEt}_2)_2$  with 1 equiv of 1-hexene or styrene, are used to react with a variety of alkynes in the presence of 1 equiv of  $\text{NiCl}_2$ , affording dihydrobenzocarboranes **28** and **28'** (Scheme 7.17) [42]. Symmetrical alkynes give the single products in very good isolated yields. The regioselectivity in the reaction of unsymmetrical alkynes is dependent on both the polarity of the alkynes and relative bulkiness of two substituents.

Similar to zirconacyclopentenes incorporating a carboranyl unit, the transmetalation species nickelacyclopentane 1,2-[ $\text{Ni}(\text{dppe})\text{CH}_2\text{CH}(\text{Bu}^{\prime\prime})$ ]-1,2- $\text{C}_2\text{B}_{10}\text{H}_{10}$  (**29**) can also be isolated from the reaction of 1,2- $\text{Cp}_2\text{Zr}[\text{CH}_2\text{CH}(\text{Bu}^{\prime\prime})]$ -1,2- $\text{C}_2\text{B}_{10}\text{H}_{10}$  with 1 equiv of  $\text{NiCl}_2(\text{dppe})$ . Its reaction with 5-decyne in THF at 110 °C gives the corresponding dihydrobenzocarborane **28b** in greater than 90% yield (Scheme 7.18). Accordingly, the formation of the products can be rationalized by the steps of transmetalation of Zr to Ni, insertion of alkyne into the nickel-C<sub>alkyl</sub> bond, and reductive elimination reaction. This



**Scheme 7.17** Reaction of zirconacycle with alkyne in the presence of  $\text{NiCl}_2$ .



**Scheme 7.18** Isolation and reaction of nickelacyclopentane intermediate.

offers an example to control the chemoselectivity among different alkenes and alkynes for assembling complex molecular architectures.

## 7.12 CONCLUSIONS AND PERSPECTIVES

The above results demonstrate that the metal–carbon bonds in metal–carbonyl complexes are reactive toward electrophiles, whereas those in metal–carboranyl complexes are inert, which leads to very high chemoselectivity in the respective reactions. The chemical properties of metal–carbonyl complexes are dependent on the electronic configurations of the metal center, and they show a diverse array of reactions toward unsaturated molecules. Ni–carbonyl can react with 2 equiv of alkynes to afford benzo-*o*-carboranes, and with 1 equiv of alkenes to generate alkenylcarborane coupling products. However, it does not show any activity toward polar unsaturated molecules. In contrast, the Zr–carbonyl can undergo monoinsertion reaction with alkynes, alkenes, and polar unsaturated molecules to afford zirconacycles. Such zirconacycles are very useful intermediates for the synthesis of various kinds of functionalized carboranes, while transmetalation to other metals creates further synthetic opportunities. In fact, after transmetalation of zirconacyclopentanes or zirconacyclopentenes incorporating a carboranyl unit to nickel, the resultant nickelacycles can react further with another kind of alkyne to give cycloaddition products. This represents an equivalent of a three-component [2 + 2 + 2] cycloaddition of carbonyl with two different alkynes or with an alkene and an alkyne in one single operation. These techniques offer new methodologies for the functionalization of carboranes that cannot be achieved by other means.

Compared to the very rich literature concerning the chemistry of metal–benzyne complexes, studies of metal–carbonyl complexes remain a very young research area. It is anticipated that their reaction scope would be further explored. The synthesis of carborane heterocycles would be expected via metal–carbonyles intermediates.

## ACKNOWLEDGMENT

The authors are grateful to all coworkers involved in the studies described in this paper for their valuable contributions. Financial supports from The Research Grants Council of The Hong Kong Special Administration Region and The Chinese University of Hong Kong are also gratefully acknowledged.

## REFERENCES

- (a) Hawthorne, M. F. *Angew. Chem. Int. Ed Engl.* **1993**, *32*, 950; (b) Soloway, A. H.; Tjarks, W.; Barnum, J. G. *Chem. Rev.* **1998**, *98*, 1515; (c) Valliant, J. F.; Guenther, K. J.; King, A. S.; Morel, P.; Schaffer, P.; Sogbein, O. O.; Stephenson, K. A. *Coord. Chem. Rev.* **2002**, *232*, 173; (d) Armstrong, A. F.; Valliant, J. F. *Dalton Trans.* **2007**, 4240; (e) Issa, F.; Kassiou, M.; Rendina, L. M. *Chem. Rev.* **2011**, *111*, 5701.
- (a) Yang, X.; Jiang, W.; Knobler, C. B., M. F. Hawthorne *J. Am. Chem. Soc.* **1992**, *114*, 9719; (b) Colquhoun, H. M.; Herbertson, P. L.; Wade, K.; Baxter, I.; Williams, D. J. A. *Macromolecules* **1998**, *31*, 1694; (c) Jude, H.; Disteldorf, H.; Fischer, S.; Wedge, T.; Hawkridge, A. M.; Arif, A. M.; Hawthorne, M. F.; Muddiman, D. C.; Stang, P. J. *J. Am. Chem. Soc.* **2005**, *127*, 12131; (d) Dash, B. P.; Satapathy, R.; Gaillard, E. R.; Maguire, J. A.; Hosmane; N. S. *J. Am. Chem. Soc.* **2010**, *132*, 6578.

3. (a) Hosmane, N. S.; Maguire, J. A. *Comprehensive Organometallic Chemistry III*, 1st Edition; Crabtree R. H.; Mingos, D. M. P. Eds; Elsevier: Oxford, **2007**; Vol. 3, Chapter 5; (b) Xie Z. *Coord. Chem. Rev.* **2002**, *231*, 23; (c) Xie, Z. *Acc. Chem. Res.* **2003**, *36*, 1; (d) Deng, L.; Xie, Z. *Coord. Chem. Rev.* **2007**, *251*, 2452; (e) Zhang, J.; Xie, Z. *Chem. Asian J.* **2010**, *5*, 1742.
4. (a) Heying, T. L.; Ager, J. W.; Jr.; Clark, S. L.; Mangold, D. J.; Goldstein, H. L.; Hillman, M.; Polak, R. J.; Szymanski, J. W. *Inorg. Chem.* **1963**, *2*, 1089; (b) Kusari, U.; Li, Y.; Bradley, M. G.; Sneddon, L. G. *J. Am. Chem. Soc.* **2004**, *126*, 8662.
5. (a) Heying, T. L.; Ager, J. W.; Clark, S. L.; Alexander, R. P.; Papetti, S.; Reid, J. A.; Trotz, S. I. *Inorg. Chem.* **1963**, *2*, 1097; (b) Gomez, F. A.; Johnson, S. E.; Hawthorne, M. F. *J. Am. Chem. Soc.* **1991**, *111*, 5915.
6. Kiran, B.; Anoop, A.; Jemmis, E. D. *J. Am. Chem. Soc.* **2002**, *124*, 4402.
7. (a) Gingrich, H. L.; Ghosh, T.; Huang, Q.; Jones, M., Jr. *J. Am. Chem. Soc.* **1990**, *112*, 4082; (b) Ghosh, T.; Gingrich, H. L.; Kam, C. K.; Mobraaten, E. C. M.; Jones, M. Jr. *J. Am. Chem. Soc.* **1991**, *113*, 1313; (c) Cunningham, R. J.; Bian, N.; Jones, M. Jr. *Inorg. Chem.* **1994**, *33*, 4811; (d) Jeon, J.; Kitamura, T.; Yoo, B.-W.; Kang, S. O.; Ko, J. *Chem. Commun.* **2001**, 2110; (e) Lee, T.; Jeon, J.; Song, K. H.; Jung, I.; Baik, C.; Park, K.-M.; Lee, S. S.; Kang, S. O.; Ko, J. *Dalton Trans.* **2004**, 933; (f) Wang, S. R.; Qiu, Z.; Xie, Z. *J. Am. Chem. Soc.* **2010**, *132*, 9988; (g) Wang, S. R.; Qiu, Z.; Xie, Z. *J. Am. Chem. Soc.* **2011**, *133*, 5760.
8. (a) Franzen, V.; Joschek, H. I. *Ann.* **1967**, *703*, 90–95; (b) Jones, M. Jr.; Levin, R. H. *J. Am. Chem. Soc.* **1969**, *91*, 6411.
9. (a) Xie, Z. *Coord. Chem. Rev.* **2006**, *250*, 259; (b) Shen, H.; Xie, Z. *Chem. Commun.* **2009**, 2431; (c) Qiu, Z.; Xie Z. *Sci. China Ser. B-Chem.* **2009**, *52*, 1544; (d) Qiu, Z.; Ren, S.; Xie, Z. *Acc. Chem. Res.* **2011**, *44*, 299.
10. Sayler, A. A.; Beall, H.; Sieckhaus, J. F. *J. Am. Chem. Soc.* **1973**, *95*, 5790.
11. Wang, H.; Li, H.-W.; Huang, X.; Lin, Z.; Xie, Z. *Angew. Chem. Int. Ed.* **2003**, *42*, 4347.
12. Buchwald, S. L.; Watson, B. T. *J. Am. Chem. Soc.* **1986**, *108*, 7411.
13. Qiu, Z.; Deng, L.; Chan, H.-S.; Xie, Z. *Organometallics* **2010**, *29*, 4541.
14. Deng, L.; Chan, H.-S.; Xie, Z. *J. Am. Chem. Soc.* **2006**, *128*, 7728.
15. (a) Bennett, M. A.; Wenger, E. *Organometallics* **1995**, *14*, 1267; (b) Retbøll, M.; Edwards, A. J.; Rae, A. D.; Willis, A. C.; Bennett, M. A.; Wenger, E. *J. Am. Chem. Soc.* **2002**, *124*, 8348; (c) Bennett, M. A.; Macgregor, S. A.; Wenger, E. *Helv. Chim. Acta* **2001**, *84*, 3084.
16. Qiu, Z.; Xie Z. *Angew. Chem. Int. Ed.* **2008**, *47*, 6572.
17. Huang, X.; Zhu, J.; Lin, Z. *Organometallics* **2004**, *23*, 4154.
18. Qiu, Z.; Xie, Z. *J. Am. Chem. Soc.* **2009**, *131*, 2084.
19. (a) Hsieh, J.-C.; Cheng, C.-H. *Chem. Commun.* **2005**, 2459; (b) Qiu, Z.; Xie, Z. *Angew. Chem. Int. Ed.* **2009**, *48*, 5729.
20. Qiu, Z.; Wang, S. R.; Xie, Z. *Angew. Chem. Int. Ed.* **2010**, *49*, 4649.
21. Terao, J.; Tomita, M.; Singh, S. P.; Kambe, N. *Angew. Chem. Int. Ed.* **2010**, *49*, 144.
22. Zheng, Z.; Jiang, W.; Zinn, A. A.; Knobler, C. B.; Hawthorne, M. F. *Inorg. Chem.* **1995**, *34*, 2095.
23. Qiu, Z. Xie, Z. *J. Am. Chem. Soc.* **2010**, *132*, 16085.
24. Cho, C. S.; Lee, J. W.; Lee, D. Y.; Shim, S. C.; Kim, T. J. *Chem. Commun.* **1996**, 2115.
25. Dang, L.; Lin, Z.; Marder, T. B. *Chem. Commun.* **2009**, 3987.
26. Elschenbroich, C.; Salzer, A. *Organometallics. A Concise Introduction*, VCH: New York, **1992**, p 256.
27. Crabtree, R. H. *The Organometallic Chemistry of the Transition Metals*, John Wiley & Sons, Inc: Hoboken, NJ, **2005**, p 47.
28. Deng, L.; Chan, H.-S.; Xie, Z. *J. Am. Chem. Soc.* **2005**, *127*, 13774.
29. Ren, S.; Deng, L.; Chan, H.-S.; Xie, Z. *Organometallics* **2009**, *28*, 5749.
30. Ren, S.; Xie, Z. *Organometallics* **2011**, *30*, 5953.
31. (a) Jordan, R. F.; Taylor, D. F.; Baenziger, N. C. *Organometallics* **1990**, *9*, 1546; (b) Jordan, R. F.; Guram, A. S. *Organometallics* **1990**, *9*, 2116; (c) Thompson, M. E.; Baxter, S. M.; Bulls, A. R.; Burger, B. J.; Nolan, M. C.; Santarsiero, B. D.; Schaefer, W. P.; Bercaw, J. E. *J. Am. Chem. Soc.* **1987**, *109*, 203; (d) Scollard, J. D.; McConville, D. H.; Vittal, J. J. *Organometallics* **1995**, *14*, 5478;
32. (a) Takahashi, T.; Tsai, F.-Y.; Li, Y.; Nakajima, K.; Kotora, M. *J. Am. Chem. Soc.* **1999**, *121*, 11093; (b) Takahashi, T.; Tsai, F.-Y.; Kotora, M. *J. Am. Chem. Soc.* **2000**, *122*, 4994; (c) Takahashi, T.; Tsai, F.-Y.; Li, Y.; Nakajima, K. *Organometallics* **2001**, *20*, 4122.
33. Ren, S.; Chan, H.-S.; Xie, Z. *Organometallics* **2009**, *28*, 4106.
34. Ren, S.; Qiu, Z.; Xie, Z. *Organometallics* **2012**, *31*, 4435.
35. Ren, S.; Chan, H.-S.; Xie, Z. *J. Am. Chem. Soc.* **2009**, *131*, 3862.
36. (a) Ren, S. K.; Xie, Z. *Organometallics* **2008**, *27*, 5167; (b) Sun, Y.; Chan, H.-S.; Zhao, H.; Lin, Z.; Xie, Z. *Angew. Chem. Int. Ed.* **2006**, *45*, 5533.
37. (a) Xi, C.; Huo, S.; Afifi, T. H.; Hara, R.; Takahashi, T. *Tetrahedron Lett.* **1997**, *38*, 4099; (b) Ashe, III, A. J.; Kampf, J. W.; Pilote, S.; Rousseau, R. *Organometallics* **1994**, *13*, 4067; (c) Freeman, W. P.; Tilley, T. D.; Liable-Sands, L. M.; Rheingold, A. L. *J. Am. Chem. Soc.* **1996**, *118*, 10457.

38. Marek, I. *Titanium and Zirconium in Organic Synthesis*, Wiley-VCH: Weinheim, Germany, 2002.
39. (a) Dufková, L.; Kotorax, M.; Císařová, I. *Eur. J. Org. Chem.* **2005**, 2491; (b) Takahashi, T.; Tsai, F.-Y.; Li, Y.; Nakajima, K.; Kotora, M. *J. Am. Chem. Soc.* **1999**, *121*, 11093; (c) Takahashi, T.; Xi, Z.; Yamazaki, A.; Liu, Y.; Nakajima, K.; Kotora, M. *J. Am. Chem. Soc.* **1998**, *120*, 1672.
40. (a) Xi, Z.; Fischer, R.; Hara, R.; Sun, W.-H.; Obora, Y.; Suzuki, N.; Nakajima, K.; Takahashi, T. *J. Am. Chem. Soc.* **1997**, *119*, 12842; (b) Liu, Y.; Shen, B.; Kotora, M.; Takahashi, T. *Angew. Chem. Int. Ed.* **1999**, *38*, 949; (c) Sun, H.; Burlakov, V. V.; Spannenberg, A.; Baumann, W.; Arndt, P.; Rosenthal, U. *Organometallics* **2001**, *20*, 5472.
41. Ren, S.; Qiu, Z.; Xie, Z. *J. Am. Chem. Soc.* **2012**, *134*, 3242.
42. Ren, S.; Qiu, Z.; Xie, Z. *Angew. Chem. Int. Ed.* **2012**, *51*, 1010.

---

# 8

---

## WEAK INTERACTIONS AND M–H BOND ACTIVATION

ELENA SHUBINA\*, NATALIA BELKOVA, OLEG FILIPPOV, AND LINA EPSTEIN

A. N. Nesmeyanov Institute of Organoelement Compounds (INEOS), Russian Academy of Sciences, Moscow, Russia

### 8.1 INTRODUCTION

The term “Y–Z bond activation” is traditionally understood as a reaction that cleaves the bond [1]. Often, the term is restricted to reactions involving organometallic complexes and proceeding by Y–Z coordination to the inner sphere of metal, either via an intermediate state or as a transition state. We are inclined to use the term “activation” for weaker (noncovalent) binding that results in the altered reactivity of a molecule through associated changes in the relative energies of its orbitals or in verified polarity.

The ability of transition-metal hydrides to be a source of H<sup>+</sup> or H<sup>−</sup> is a well-known phenomenon. It serves as a basis for the use of hydride complexes in various catalytic processes as, for example, hydrogenation or reduction of H<sup>+</sup> to H<sub>2</sub> [2]. Transition-metal hydrides exhibit the same two modes of reactivity in proton transfer reactions, behaving as either acid or base. In spite of being a seemingly simple reaction, the proton transfer is a multistep process occurring via hydrogen-bonded intermediates of molecular and ionic types. The position of equilibrium depends on the relative acidity and basicity of interacting molecules as well as on the media properties and temperature. With a small interaction enthalpy, hydrogen bonding usually results only in a small perturbation of the electronic structure of the participating molecules. Nevertheless, it modifies their properties, giving the opportunity to fine-tune the properties of an organometallic complex [3–5] and to influence the reactions they are involved in [6, 7]. Data have begun to appear confirming the importance of this phenomenon in catalytic reduction [8–10] and hydrogen activation [11].

One major recent achievement in this area is the discovery of nonclassical hydrogen bonds between transition-metal hydrides and proton donors, M–H<sup>δ−</sup>···H<sup>δ+</sup>–X, now widely called a *dihydrogen bond* [12–14]. These bonds precede the proton transfer to hydrides, yielding in most cases nonclassical η<sup>2</sup>-H<sub>2</sub> complexes. More recently, we have shown that neutral hydrides can behave as proton donors in the hydrogen bond M–H<sup>δ+</sup>···Y and such hydrogen bonds precede the proton transfer from a transition-metal hydride to a base Y [15, 16]. The structural parameters and spectral properties of hydrogen bonds involving hydride ligands are similar to those of classical hydrogen bonds [13, 17, 18]. Also, hydrogen bonding activates the participating M–H bonds and induces them to take part in proton transfer reactions.

### 8.2 METAL HYDRIDES IN HYDROGEN BONDING

#### 8.2.1 Hydrides as Proton Acceptors

In full accord with the hydrogen-bond definition [18], dihydrogen bonds feature short contacts H<sup>δ−</sup>···H<sup>δ+</sup> (less than the sum of the van der Waals radii, 2.4 Å) and close to the linear H<sup>δ−</sup>···H<sup>δ+</sup>–X arrangement of atoms [13, 19]. As a result of the interacting bonds, both M–H and H–X are slightly elongated (by 0.003–0.030 Å). The deviations of proton from

*Advances in Organometallic Chemistry and Catalysis: The Silver/Gold Jubilee International Conference on Organometallic Chemistry Celebratory Book*, First Edition. Edited by Armando J. L. Pombeiro.

© 2014 John Wiley & Sons, Inc. Published 2014 by John Wiley & Sons, Inc.

the hydrogen bond axis (line between the heavy atom in X–H and the hydridic H in a transition-metal hydride complex) are usually within the 10–12° range, which is regular for classical intermolecular hydrogen bonds [20]. According to our recent computational analysis [21], those stronger than 10–12° are caused by simultaneous interaction with a core metal atom. The  $M \cdots H^{\delta+} - X$  interaction becomes stronger for 5d transition metals and this increase can be evoked to explain the difference in the spectroscopic and chemical behavior of 5d and 3d/4d metal hydrides [22–24].

The hydrogen-bond formation involves the transfer of electron density from the highest occupied molecular orbital (HOMO) of the base to an empty  $\sigma_{M-H}^*$  orbital of the acid that has its main coefficient on the “protic” hydrogen. In the case of dihydrogen bonds, the donor orbital is of  $\sigma_{M-H}$  nature, mainly centered on the hydridic hydrogen (Fig. 8.1) [21, 25]. In “hydridic” hydrides bearing electron-donating ligands, the metal-bound hydrogen has a small negative charge and more than 45% share in the total electron density on  $\sigma_{M-H}$  orbital (Table 8.1). The presence of electron-accepting ligands obviously diminishes the electron density on the “hydride” ligand (see below, Table 8.2) and makes such a hydride complex prone to be a proton donor. Interestingly, in none of the hydrides studied the  $\sigma_{M-H}$  orbital is HOMO, but nevertheless this orbital is involved in dihydrogen bonding. The electron density redistribution caused by dihydrogen bond formation leads to an increase of the negative charge on the “hydride” hydrogen (Table 8.1). Accordingly the M–H bond polarization,  $\text{pol}(M-H)$ , determined here as the electron density at the metal-bound hydrogen relative to the total electron density on  $\sigma_{M-H}$ , changes to higher values. The corresponding value for the O–H bond changes to lower numbers, reflecting an increase of positive charge on the “protic” hydrogen (Table 8.1).

### 8.2.2 Hydrides as Proton Donors

When neutral hydrides act as proton donors in hydrogen bonds, the changes of M–H bond properties are similar to those of H–X bond of “regular” proton donors (O–H, N–H, C–H donors), as mentioned above. For neutral transition-metal hydrides, we have shown the formation of such hydrogen bonds on the example of  $CpMH(CO)_3$  complexes (2, M = Mo (a), W (b)) interacting with organic bases (amines,  $R_3PO$ ; Fig. 8.2a) [15, 16]. The formation energy of these  $M-H^{\delta+} \cdots Y$  bonds is very low and, accordingly, the changes induced by the hydrogen bonding are quite small (Table 8.2).

The formation of the  $M-H^{\delta+} \cdots Y$  hydrogen bond involves the transfer of electron density from the HOMO orbital of the base to an empty  $\sigma_{M-H}^*$  orbital of the hydride complex as in the case of any classical hydrogen bond. The induced change of the M–H bond polarization ( $\Delta\text{pol}(M-H)$ , Table 8.2) is similar to that observed for C–H  $\cdots$  Y bonds of halomethanes with nitrogen bases [26] but occurs at notably lower energies of  $n_Y$  to  $\sigma_{M-H}^*$  donation [16]. This easier polarization facilitates

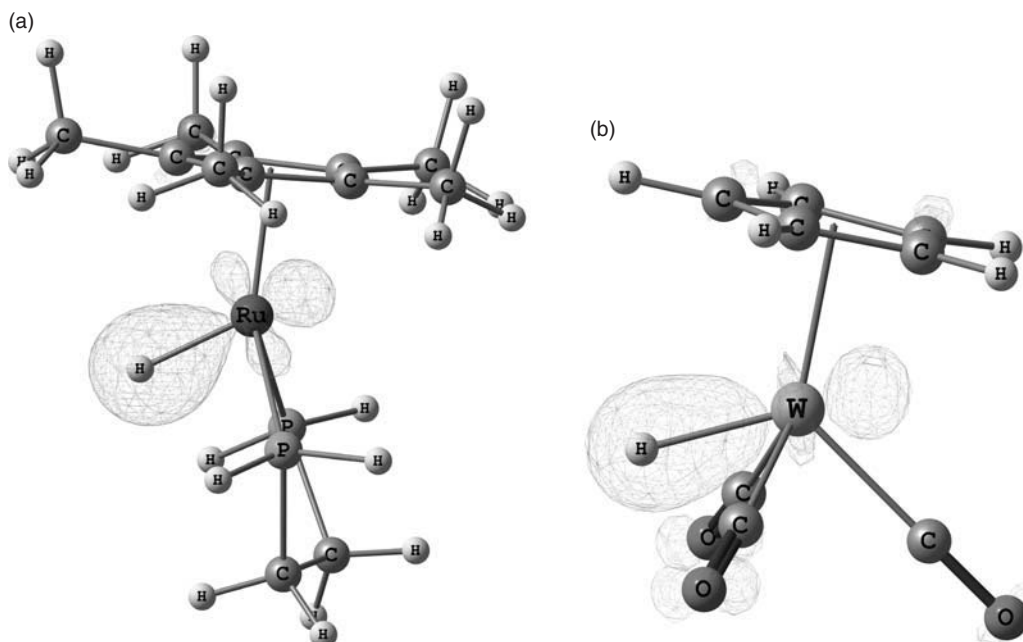


**Figure 8.1** Typical  $\sigma(M-H)$  molecular orbitals on the example of (a)  $Cp^*MH(\text{dppe})$  (HOMO-5) and (b)  $CpMH(CO)_3$  (HOMO-4) complexes (as isosurface at 0.08958).

**TABLE 8.1 Selected Structural and Electronic Parameters Calculated (DFT/B3PW91) for Dihydrogen-Bonded Complexes of  $\text{Cp}^*\text{MH(dppe)}$  Hydrides with  $\text{CF}_3\text{CH}_2\text{OH}$  (1, M = Fe (a), Ru (b), Os (c))**

	1a	1b	1c
$\Delta E_{\text{ZPVE}}$ , kcal/mol	-9.1	-9.2	-9.5
$\Delta r(\text{M}-\text{H})$ , Å	0.011	0.011	0.006
$\Delta r(\text{O}-\text{H})$ , Å	0.022	0.021	0.022
$r(\text{H}\cdots\text{H}_\text{O})$ , Å	1.612	1.735	1.795
$r(\text{M}\cdots\text{H}_\text{O})$ , Å	2.561	2.573	2.571
$\angle \text{H}_\text{M}\cdots\text{H}-\text{O}$ , deg	156.8	147.6	144.7
$\angle \text{M}\cdots\text{H}-\text{O}$ , deg	168.5	171.4	171.6
$\Delta q(\text{H}_\text{M})^a$	-0.067	-0.060	-0.044
$\Delta q(\text{M})^a$	0.027	0.003	-0.014
$\Delta q(\text{H}_\text{O})^a$	0.008	0.012	0.013
$\Delta \text{pol}(\text{M}-\text{H})$ , % <sup>b,c</sup>	9.1	3.4	2.6
$\Delta \text{pol}(\text{O}-\text{H})$ , % <sup>b,d</sup>	-2.8	-2.6	-2.7

<sup>a</sup>Change of the NBO charge at the given atom.

<sup>b</sup>The bond polarization (pol(Z-H), in percentage on H) determined as electron density at the heavy atom bound hydrogen relative to the total electron density on  $\sigma_{\text{Z}-\text{H}}$ , Z = M or O;  $\Delta \text{pol}(\text{Z}-\text{H}) = \text{pol}(\text{Z}-\text{H})^{\text{complex}} - \text{pol}(\text{Z}-\text{H})^{\text{initial}}$ .

<sup>c</sup>pol(M-H) is 47.1 for FeH, 47.6 for RuH, and 48.7 for OsH in free  $\text{Cp}^*\text{MH(dppe)}$  complexes.

<sup>d</sup>pol(O-H) = 24.9 for free  $\text{CF}_3\text{CH}_2\text{OH}$ .

**TABLE 8.2 Selected Structural and Electronic Parameters Calculated (DFT/M05) for Complexes of  $\text{CpMH(CO)}_3$  Hydrides (2, M = Mo (a), W (b)) with  $\text{Me}_3\text{N}$  and  $\text{BH}_3$ <sup>a</sup>**

	2a/ $\text{Me}_3\text{N}$	2a/ $\text{BH}_3$	2b/ $\text{Me}_3\text{N}$	2b/ $\text{BH}_3$
$\Delta E_{\text{ZPVE}}$ , kcal/mol	-4.8	-5.65	-4.6	-6.16
$\Delta r(\text{M}-\text{H})$ , Å	0.012	0.081	0.005	0.072
$r(\text{H}\cdots\text{Y})$ , Å	2.329	1.500	2.431	1.498
$\angle \text{MH}\cdots\text{Y}$ , deg	177.7	142.6	170.2	139.6
$\Delta q(\text{M})$	+0.051	+0.137	+0.036	+0.160
$\Delta q(\text{H})$	+0.053	-0.122	+0.058	-0.114
$\Delta q(\text{Y})$	-0.006		-0.008	
$\Delta \text{pol}(\text{M}-\text{H})$ , % <sup>c</sup>	-4.4	7.2	-2.8	9.4

<sup>a</sup>See footnote to Table 8.1.

<sup>b</sup>Y = N or B.

<sup>c</sup>pol(M-H) is 40.5 for MoH and 42.1 for WH in free  $\text{CpMH(CO)}_3$  complexes.

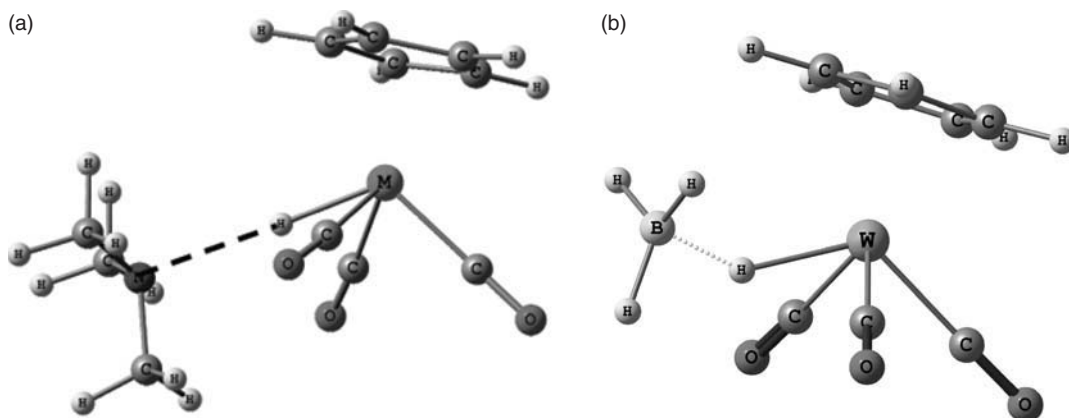


**Figure 8.2** Optimized (DFT/M05) structures of complexes formed by  $\text{CpMH(CO)}_3$  and  $\text{Me}_3\text{N}$  (a) and  $\text{BH}_3$  (b).

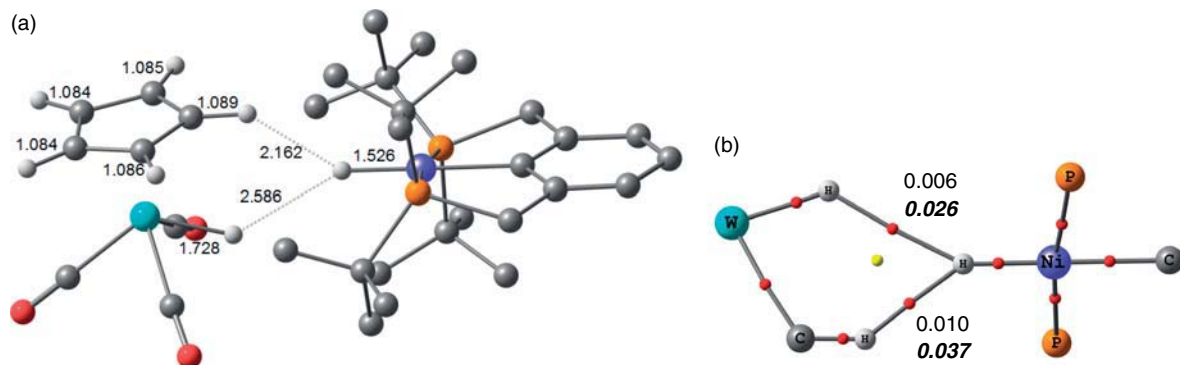


**Figure 8.3** (a) Optimized structure of dihydrogen-bonded adduct between (<sup>t</sup>BuPCP)Ni(H) and CpWH(CO)<sub>3</sub> with selected bond lengths (Å). Hydrogen atoms of the <sup>t</sup>BuPCP ligand are omitted for clarity. (b) Fragment of molecular graph of the system. Electron density at the (3,−1) bond critical point and bond order (as a delocalization index [21], in bold italic) are reported for W–H···H–Ni and C–H···H–Ni contacts. Color codes: •-bond critical points, •-ring critical points. (See insert for color representation of the figure.)

the M<sup>δ−</sup>–H<sup>δ+</sup> heterolytic splitting. The deprotonation of these hydrides occurs readily, placing the CpMH(CO)<sub>3</sub> complexes between medium-strength OH proton donors on the pK<sub>a</sub>(CH<sub>3</sub>CN) scale (compare pK<sub>a</sub>(CH<sub>3</sub>CN) of 13.9 and 16.1 in CH<sub>3</sub>CN for CpMoH(CO)<sub>3</sub> and CpWH(CO)<sub>3</sub>, respectively, to, for example, 20.55 of (CF<sub>3</sub>)<sub>3</sub>COH, 16.66 of 2,4-dinitrophenol, or 11.00 of 2,4,6-trinitrophenol [27]).

The easy polarization of the M–H bond and rather low electron density possessed by hydride ligand in free CpMH(CO)<sub>3</sub> complexes allow these compounds to exhibit three types of reactivity depending on the partner reagent. These complexes are classical examples of one compound being a source of H<sup>+</sup>, H<sup>−</sup>, and H<sup>•</sup>[28–30]. We computed the adducts of CpMH(CO)<sub>3</sub> hydrides with BH<sub>3</sub> as a mild Lewis acid (Fig. 8.2, Table 8.2). This interaction is based on the σ<sub>M–H</sub> to LP<sub>B</sub>\* donation and thus leads to the increase of electron density on the metal-bound hydrogen making it more “hydridic.” In a sense, it is similar to dihydrogen bonding and shows that the change of M–H bond polarization occurs at the stage of formation of the intermolecular adduct. Despite the rather low energy of these interactions (hydrogen bonding or Lewis acid–base interaction), they activate the participating M–H (and O–H) bonds and induce them to take part in a subsequent reaction.

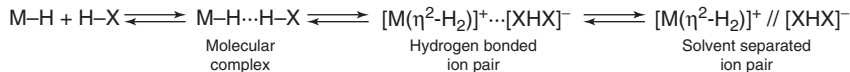
The most challenging task in this area of research was to detect a hydrogen bond between the two hydride complexes, one of which would be a proton donor and the other a proton acceptor. The experimental evidence for the formation of such dihydrogen-bonded adduct came only recently, provided by the spectroscopic study of the interaction between the nickel(II) pincer hydride (<sup>t</sup>BuPCP)Ni(H) [<sup>t</sup>BuPCP = 2,6-C<sub>6</sub>H<sub>3</sub>(CH<sub>2</sub>PtBu<sub>2</sub>)<sub>2</sub>] and the already-mentioned tungsten complex CpWH(CO)<sub>3</sub> (**2b**) [31]. The computational (density functional theory (DFT)/M06) analysis revealed interesting peculiarities of this complex. Two H<sup>δ−</sup>···H<sup>δ+</sup> contacts were found between NiH, both WH and CH of the Cp ring (Fig. 8.3). AIM (atom-in-molecule) analysis gave two (3,−1) critical points. The interaction energies calculated for each H···H contact were −0.7 and −1.5 kcal/mol, respectively, in agreement with the shorter distance to C–H than to W–H found.

### 8.3 HYDROGEN BONDING AND PROTON TRANSFER

Hydrogen bonds of different types not only accompany the proton transfer reactions but also influence the kinetics and thermodynamics of different reaction steps. In the following paragraphs, we illustrate this idea by highlighting the peculiarities of M–H bond behavior.

#### 8.3.1 Hydrides as Proton Acceptors

When a transition metal bears electron-rich ligands, the metal-bound hydrogen has a partial negative charge and acts as a proton-accepting site in dihydrogen bonding. The reaction with acids does not stop at this stage and proton transfer yields usually the nonclassical η<sup>2</sup>-H<sub>2</sub> complexes (Scheme 8.1). Numerous experimental data support the participation of a second proton-donor molecule in the proton transfer step [22, 32, 33].



Scheme 8.1

The observation of an equilibrium between molecular and ionic hydrogen-bonded complexes evidences the two minima on the potential energy surface [34]. We have not only observed such equilibria spectroscopically but have also been able to obtain the thermodynamic parameters of each step. These data show that the stronger the hydrogen bond, the more favorable the proton transfer (Fig. 8.4) [33].

The proton-accepting ability in hydrogen bonding,  $E_j$ , [13, 35, 36] determined for transition-metal hydrides varies in the same range as that of classical oxygen- or nitrogen-containing bases [34]. Also, the proton affinity PA (taken as  $-\Delta H_{298.15\text{K}}$  for the reaction  $\text{B} + \text{H}^+ \rightarrow \text{BH}^+$ ) of hydrides studied so far (243–267 kcal/mol) is larger than that of the reference organic compounds (198–230 kcal/mol) [34]. Probably for this reason, the proton transfer is easier for hydride systems than for classical organic bases. This could be due to the better delocalization of the acquired positive charge in the presence of the transition metal in comparison to traditional organic bases. And this is true not only for the gas phase, as suggested by quantum chemical calculations, but in solution as well. For example, no proton transfer is observed from *p*-nitrophenol to Et<sub>3</sub>N in *i*-octane ( $\Delta H_{\text{HB}} = -9.3$  kcal/mol) [37] or from CF<sub>3</sub>CH<sub>2</sub>OH to pyridine in CCl<sub>4</sub> ( $\Delta H_{\text{HB}} = -9.3$  kcal/mol), whereas it does occur in case of transition-metal hydrides even at weaker hydrogen bond formation enthalpy [33] as, for example, for the CpRuH(CO)(PCy<sub>3</sub>)/(CF<sub>3</sub>)<sub>3</sub>COH pair in hexane with  $\Delta H_{\text{DHB}} = -7.3$  kcal/mol [38].

There is also a relationship between the dihydrogen bond strength and the activation free energy of proton transfer. The latter decreases with the increase of  $-\Delta H_{\text{DHB}}$  (Fig. 8.5). This experimental trend is also predicted by theoretical calculations, which show the ultimate disappearance of the dihydrogen bond minimum and a spontaneous proton transfer with the increase of dihydrogen bond strength [38–40].

The calculations show also that the proton transfer transition state features the already formed H–H bond (H–H distance ca. 0.9 Å), with the H<sub>2</sub> unit being simultaneously bonded to both the [M]<sup>+</sup> unit and the anion (M–H and H–O distances are ca. 1.6–1.9 and 1.3–1.5 Å, respectively) [23, 32, 41]. Such a highly ordered transition state explains the substantial negative activation entropy ( $\Delta S_{\text{PT}}^\ddagger$  from -15 to -40 cal/mol/K) determined experimentally for the proton transfer, yielding  $\eta^2\text{-H}_2$  complexes [33, 42, 38].

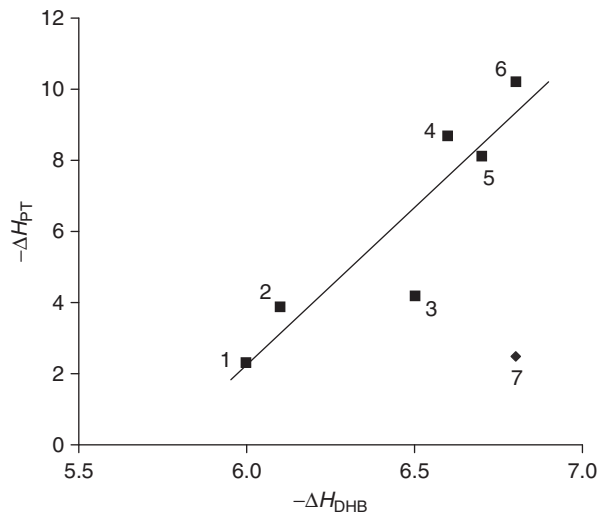


**Figure 8.4** Correlation between the enthalpies ( $-\Delta H$ , kcal/mol) of dihydrogen bond formation (DHB) and proton transfer (PT). Data obtained in CH<sub>2</sub>Cl<sub>2</sub> for the reaction of (CF<sub>3</sub>)<sub>3</sub>COH with (triphos)Re(CO)<sub>2</sub>H (1) [52], (CF<sub>3</sub>)<sub>2</sub>CHOH with Cp\*FeH(dppe) (3) [42], (triphos)Ru(CO)H<sub>2</sub> (4) [53], Cp\*RuH(dppe) (5) [44], RuH<sub>2</sub>(dpmm)<sub>2</sub> (6) [54], and CF<sub>3</sub>CH<sub>2</sub>OH with Cp\*MoH<sub>3</sub>(dppe) (2) [23], (PP<sub>3</sub>)OsH<sub>2</sub> (7) [47]. Reproduced from Reference 33 by permission of the John Wiley and Sons.

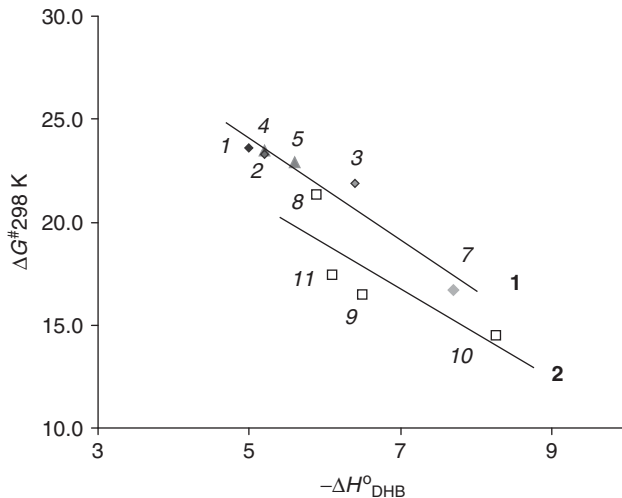


**Figure 8.5** Correlation between the dihydrogen bond formation enthalpies ( $-\Delta H^{\circ}_{\text{DHB}}$ , kcal/mol) and the activation free energies ( $\Delta G^{\ddagger}_{298}$ , kcal/mol) in hexane (1, rhombi and triangles 1–7), dichloromethane (2, open squares 8–11). Data for the reaction of  $\text{WH}(\text{CO})_2(\text{NO})(\text{PEt}_3)_2$  with PhOH (1),  $(\text{CF}_3)_2\text{CHOH}$  (2),  $(\text{CF}_3)_3\text{COH}$  (3),  $\text{WH}(\text{CO})_2(\text{NO})(\text{PMe}_3)_2$  with PhOH (4),  $(\text{CF}_3)_2\text{CHOH}$  (5) [55];  $\text{CpRuH}(\text{CO})(\text{PCy}_3)$  with  $(\text{CF}_3)_3\text{COH}$  (7) [38];  $\text{Cp}^*\text{FeH}(\text{dppe})$  with  $\text{CF}_3\text{CH}_2\text{OH}$  (8),  $(\text{CF}_3)_2\text{CHOH}$  (9),  $(\text{CF}_3)_3\text{COH}$  (10) [32, 42];  $\text{Cp}^*\text{MoH}_3(\text{dppe})$  with  $\text{CF}_3\text{CH}_2\text{OH}$  (11) [23]. Reproduced from Reference 33 by permission of the John Wiley and Sons.

### 8.3.2 Hydrides as Proton Acceptors: Cooperative Effect

The hydrides reactivity depends, of course, on the metal atom and the ligand environment. But additional weak interactions are similarly important and can be used to fine-tune the M–H bond properties. Thus, in an excess of acid, the coordination of a second molecule of the proton donor yields  $\text{M}-\text{H}^{\delta+}\cdots\text{H}^{\delta+}-\text{X}\cdots\text{H}^{\delta+}-\text{X}$  associates. That entails strengthening of dihydrogen bond because of the cooperative effect and further M–H bond activation. According to our DFT calculations for  $\text{Cp}^*\text{MoH}(\text{CO})(\text{PMe}_3)_2$  interacting with trifluoroacetic acid (Fig. 8.6), a cooperativity effect was found for the formation of dihydrogen-bonded complex with  $(\text{CF}_3\text{COOH})_2$ ,  $\Delta E_{\text{coop}} = \Delta E(\mathbf{1}\cdot\text{2HOR}) - \Delta E(\mathbf{1}\cdot\text{HOR}) - \Delta E((\text{HOR})_2)$  is  $-2.2$  kcal/mol [43]. The formation of the dihydrogen bond with the first  $\text{CF}_3\text{COOH}$  molecule lengthens the Mo–H bond by  $0.037$  Å. The binding of second  $\text{CF}_3\text{COOH}$  molecule entails the additional stretching by  $0.020$  Å, whereas the dihydrogen bond itself becomes shorter ( $1.244$  vs  $1.365$  Å) (Fig. 8.6). The cooperative enhancement of the dihydrogen bond strength in the complex of  $\text{Cp}^*\text{MoH}(\text{CO})(\text{PMe}_3)_2$  with two  $\text{CF}_3\text{COOH}$  molecules also reduces the proton transfer barrier from  $8.5$  to only  $1.9$  kcal/mol (Fig. 8.6) [43]. Similar effects have been calculated, for example, for  $(\text{PP}_3)\text{RuH}_2$  interacting with alcohols (see below) [25].

In low-polarity solvents, the products of proton transfer exist as contact ion pairs stabilized by the hydrogen bond between the  $\eta^2\text{-H}_2$  cation and the anion. Experimental data show that the anion is in its homoconjugated form,  $[\text{ROHOR}]^-$  [23, 42, 44]. This is because the basicity of  $[\text{ROHOR}]^-$  is reduced relative to that of simple  $\text{RO}^-$ , which prevents pulling out a proton from the cationic dihydrogen complex and allows it to be a stable species. In agreement with the experimental data, the DFT calculations often fail to optimize the  $[\text{M}(\eta^2\text{-H}_2)][\text{OR}]$  ion pair [23, 42, 38, 39, 45]. And even when they are successful, as in the case of  $[\text{Cp}^*(\text{CO})(\text{PMe}_3)_2\text{Mo}(\eta^2\text{-H}_2)]^+[\text{OCOCF}_3]^-$ , they show clearly the thermodynamic preference of  $[\text{M}(\eta^2\text{-H}_2)]^+[\text{ROHOR}]^-$  ion pairs (Fig. 8.6) [43].

### 8.3.3 Hydrides as Proton Donors

Deprotonation of  $\text{CpMH}(\text{CO})_3$  hydrides occurs readily even in nonpolar media (hexane) [16]. This is due to the low proton transfer barrier, which is related to the easy M–H bond activation and the thermodynamic favorability of the ion pair (Fig. 8.7), which is backed up by good localization of negative charge in  $[\text{CpM}(\text{CO})_3]^-$ . According to DFT calculations, the proton transfer barrier height is less than  $8$  kcal/mol [16] and decreases from tungsten to molybdenum and from pyridine to trimethylamine, in agreement with the increase of their acid/base strength and M–H $\cdots$ Y bond energy. Hydrogen-bond and ion-pair formation become more favorable in the same row (Fig. 8.7). The spectroscopic study shows that the reaction is immediate at the timescale of conventional infrared (IR) measurements even at low temperatures [15, 16]. This is in

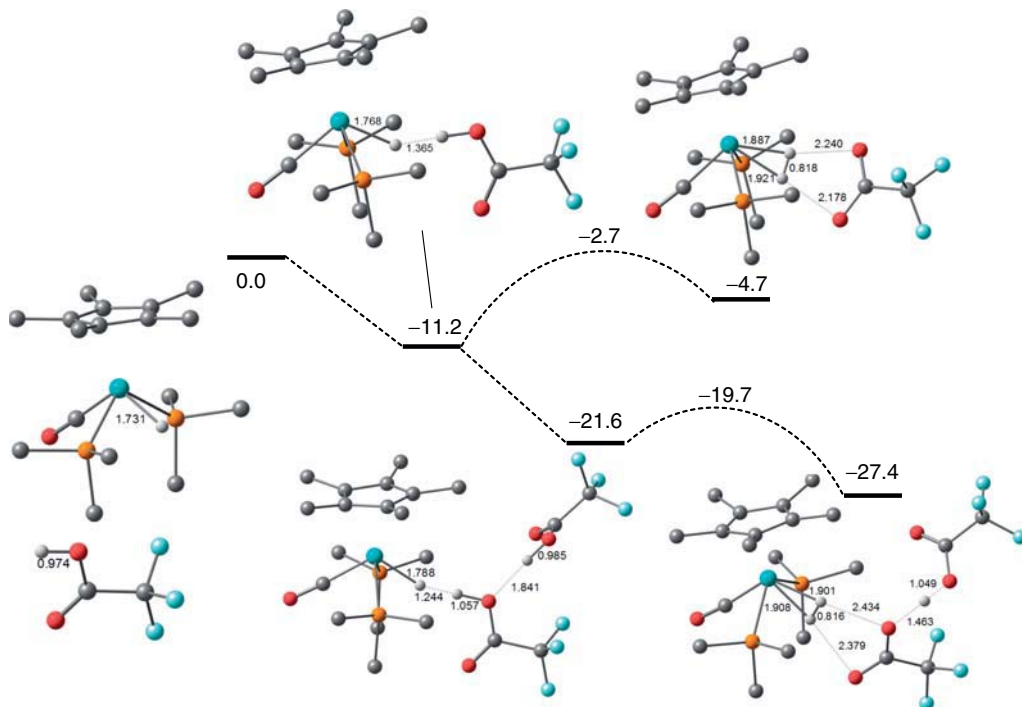


**Figure 8.6** Optimized (DFT M05) geometries and energy profile ( $\Delta E$ , kcal/mol) calculated for protonation of  $\text{Cp}^*\text{MoH}(\text{CO})(\text{PMe}_3)_2$  by  $\text{CF}_3\text{COOH}$  (one and two molecules) in gas phase. Selected bond lengths are reported ( $\text{\AA}$ ). Hydrogen atoms of  $\text{CH}_3$  groups are removed for transparency. Data from Reference 43. (See insert for color representation of the figure.)

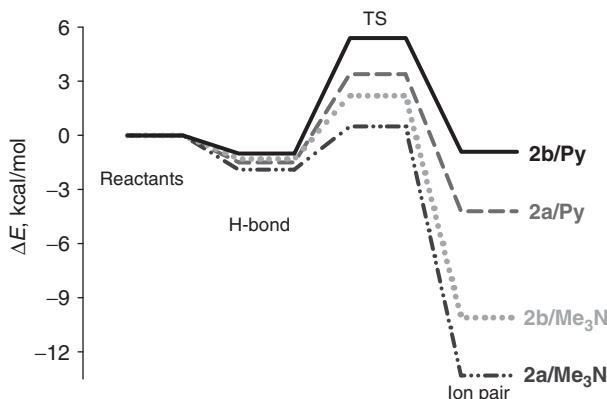
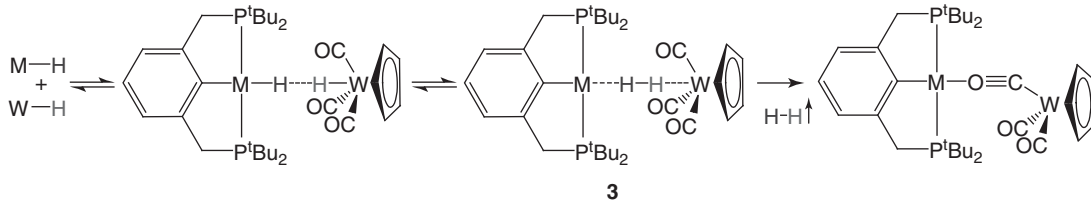


**Figure 8.7** Energy profile for  $\text{CpMH}(\text{CO})_3$  (M = Mo (**2a**), W (**2b**)) deprotonation by nitrogen bases computed in acetonitrile (DFT/M05, CPCM). The energies in solvent have been obtained by adding the contribution of the free energy of solvation to the gas-phase potential energy. According to the data from Reference 16.

agreement with the activation parameters reported for the proton transfer from the hydrides **2** to various anilines ( $\Delta H^\ddagger$  5–7 kcal/mol,  $\Delta S^\ddagger$  ca. –30 cal/mol/K) [46].

As the result of an easier polarization and heterolytic splitting of M–H bonds in comparison to C–H, the proton transfer from W–H of **2b** to (<sup>18</sup>uCPCP)NiH occurs despite the stronger Ni–H interaction with the C–H proton. The reaction between these two hydrides yields ionic species, which were detected experimentally (Scheme 8.2) [31]. Similar reactivity was determined for the (<sup>18</sup>uCPCP)PdH/**2b** pair. According to the DFT calculations, the reaction intermediate **3** has a very unusual structure, in which the elongated  $\text{H}_2$  molecule connects the two metal centers in a  $\mu,\eta^{1:1}$  end-on mode (Fig. 8.8).



Scheme 8.2

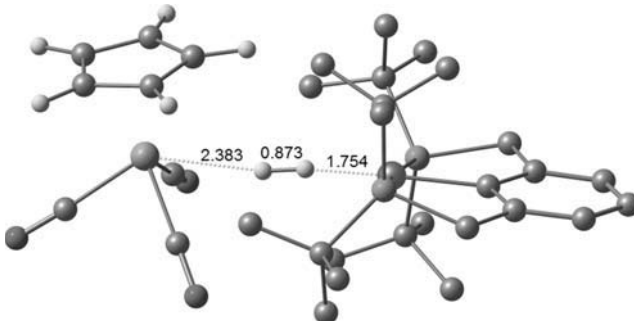


**Figure 8.8** Optimized structure of the kinetic product of proton transfer from  $\text{CpWH}(\text{CO})_3$  to  $(^{\text{t}\text{Bu}}\text{PCP})\text{NiH}$ . Selected bond lengths are reported ( $\text{\AA}$ ). Hydrogen atoms of the  ${}^{\text{t}\text{Bu}}\text{PCP}$  ligand are omitted for clarity.

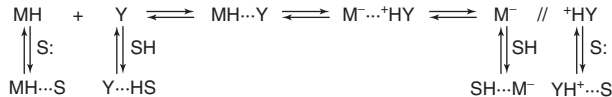
**TABLE 8.3 Experimentally Determined Activation Parameters for the Reaction of  $(^{\text{t}\text{Bu}}\text{PCP})\text{MH}$  ( $\text{M} = \text{Ni, Pd}$ ) with  $\text{CpWH}(\text{CO})_3$  in THF**

	Ni	Pd
$\Delta G^\ddagger(298 \text{ K}), \text{kcal/mol}$	21.0	17.0
$\Delta H^\ddagger, \text{kcal/mol}$	10.6	7.2
$\Delta S^\ddagger, \text{cal/mol/K}$	-34	-32

Complex **3** is stable only at low temperatures and evolves  $\text{H}_2$  above 230 K yielding  $[\text{CpW}(\text{CO})_2(\mu-\kappa,\text{C}: \kappa,\text{O}-\text{CO})\cdots\text{M}(^{\text{t}\text{Bu}}\text{PCP})]$  as a thermodynamic reaction product [31]. The proton transfer is the rate-determining step of the reaction, which is faster for the more basic Pd analog. The activation parameters determined (Table 8.3) indicate a highly ordered transition state and are similar to those found for the formation of  $\eta^2\text{-H}_2$  complexes (Fig. 8.5) [33] despite the difference in the transition state structure.

### 8.3.4 Solvent Effect

The peculiarity of  $\text{CpMH}(\text{CO})_3$  hydrides as proton donors is a lack of possibility to form conjugated systems  $\text{XH}\cdots\text{MH}\cdots\text{Base}$  (analogous to those in Scheme 8.1), which would strengthen hydrogen-bonded complex and promote proton transfer. This is because of high d-electron lone-pair delocalization (according to the natural bond orbital (NBO) analysis) [16]. Thus, the position of the tautomeric equilibrium  $\text{M}-\text{H}\cdots\text{Y}\cdots\text{M}^- \cdots ^+\text{HY}$  (central part on Scheme 8.3) could be affected only by media polarity. Indeed, the experimental data show that the substantial polarity increase on going from hexane to acetonitrile shifts overall equilibrium to the right, toward the proton transfer product [16]. However, the proton transfer equilibrium constants and the reaction free energies are lower in solvents of medium polarity ( $\text{CH}_2\text{Cl}_2$ , tetrahydrofuran (THF)) than in hexane. The key to understanding this phenomenon lies in specific solute–solvent interactions. The  $\text{CH}\cdots\text{OC}$  bonds between  $\text{CpMH}(\text{CO})_3$  and the solvent molecules (denoted as SH in Scheme 8.3) are evidently present even in those solvents that are traditionally considered as proton acceptors (THF,  $\text{CH}_3\text{CN}$ ). In turn, the hydrogen-bond-donating  $\text{CH}_2\text{Cl}_2$  interacts not only with the carbonyl ligands of  $\text{CpMH}(\text{CO})_3$  but also with bases. According to our



Scheme 8.3

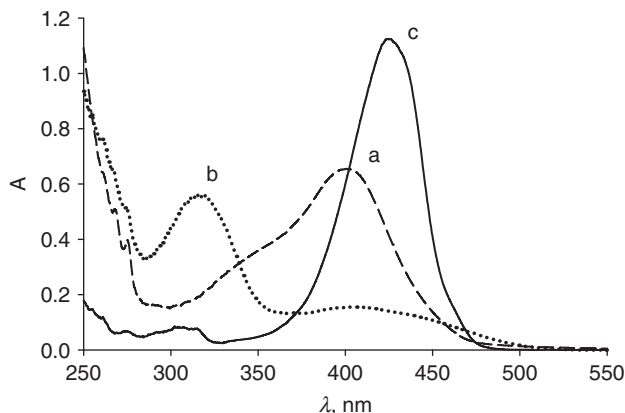


**Figure 8.9** UV-visible spectra of  $[\text{Cp}^*\text{WH}_4(\text{dppe})]^+\text{BF}_4^-$  ( $c = 0.001$  M) interacting with equimolar amount of  $[\text{Bu}_4\text{N}]^+[\text{4-NO}_2\text{-C}_6\text{H}_4\text{-O}]^-$  in  $\text{CH}_2\text{Cl}_2$  (a) and THF (b) at 200 K. Spectrum of  $[\text{Bu}_4\text{N}]^+[\text{4-NO}_2\text{-C}_6\text{H}_4\text{-O}]^-$  (c) in THF is given for comparison. Path length 0.4 mm.

experimental and computational results, both  $\text{CH}\cdots\text{Base}$  and  $\text{M}-\text{H}\cdots\text{S}$  interactions ( $\text{S} = \text{N}$  of acetonitrile or  $\text{O}$  of THF) have energy comparable to that of the  $\text{M}-\text{H}\cdots\text{Base}$  hydrogen bond. Thus, these competitive interactions lower the hydride or base activity in proton transfer reaction and in this way affect the position of the proton transfer equilibrium (Scheme 8.3).

The pronounced specific solvent effects are observed for proton transfer to “basic” transition-metal hydrides as well. In this case, the effect originates mainly from the different specific solvation of the proton donor. Thus, the interaction of proton donors with aprotic (proton accepting) solvents hampers the proton transfer, shifting the equilibrium (Scheme 8.1) to the left [22, 25, 47, 48]. For example, mixing the  $[\text{Cp}^*\text{WH}_4(\text{dppe})]^+\text{BF}_4^-$  salt with *p*-nitrophenolate yields the predominant formation of the hydrogen-bonded ion pair  $[\text{Cp}^*\text{WH}_4(\text{dppe})]^+[\text{OAr}]^-$  in  $\text{CH}_2\text{Cl}_2$  with the band at 400 nm in UV-visible spectra (Fig. 8.9a), whereas the equilibrium appears to be completely shifted to the left in THF where the envelop of the overlapping bands of “free” *p*-nitrophenol (317 nm) and  $[\text{Cp}^*\text{WH}_3(\text{dppe})]$  (ca. 410 nm) was observed (Fig. 8.9b) because of the highly favored specific solvation of the *p*-nitrophenol (hydrogen-bonding *p*-nitrophenol THF) [22].

At comparable polarity, protic solvents are not innocent as well; they shift the proton transfer equilibrium to the right. According to our model experiment, the addition of just 8 vol% of  $\text{CH}_3\text{OH}$  instead of  $\text{CH}_3\text{CN}$  to THF causes a substantial change in the amount hydrogen-bonded ion pairs  $[(\text{PP}_3)\text{RuH}(\eta^2\text{-H}_2)]^+\cdots[\text{AroHOAr}]^-$  formed as the result of proton transfer from *p*-nitrophenyl-aza-phenol with  $[(\text{PP}_3)\text{RuH}_2]$  (compare the intensities of the ion-pair band at 525–540 nm, Fig. 8.10) [25]. These solvents have similar polarity ( $\epsilon_{\text{CH}_3\text{CN}} = 35.94$ ;  $\epsilon_{\text{CH}_3\text{OH}} = 32.66$  at 298 K [49]), and thus their addition produces similar increase of the media polarity. This increase alone cannot account for the spectral changes observed and has to be considered together with the bonding properties of the two solvents. Indeed, the computational study [25] has shown that the molecule of protic solvent,  $\text{CH}_3\text{OH}$  or even  $\text{CH}_2\text{Cl}_2$ , can take part in the formation of  $\text{M}-\text{H}^{\delta-}\cdots\text{H}^{\delta+}-\text{X}\cdots\text{H}^{\delta+}-\text{X}'$  associates. The cooperative effect in such hydrogen-bonded complexes ( $\Delta E_{\text{coop}}$ ) follows the order of proton donor abilities:  $\text{H}_2\text{O} > \text{CH}_3\text{OH} > \text{CH}_2\text{Cl}_2$  (Fig. 8.11). This cooperative enhancement of the dihydrogen bond promotes the proton transfer, which becomes more favorable in the same order.

#### 8.4 ACTIVATION OF H<sub>2</sub> IN THE METAL COORDINATION SPHERE

Nonclassical  $\eta^2\text{-H}_2$  complexes can be obtained not only by proton transfer to a transition-metal hydride but also by  $\text{H}_2$  addition to an unsaturated metal complex [50]. Though less commonly used for the preparation of  $\eta^2\text{-H}_2$  complexes, this

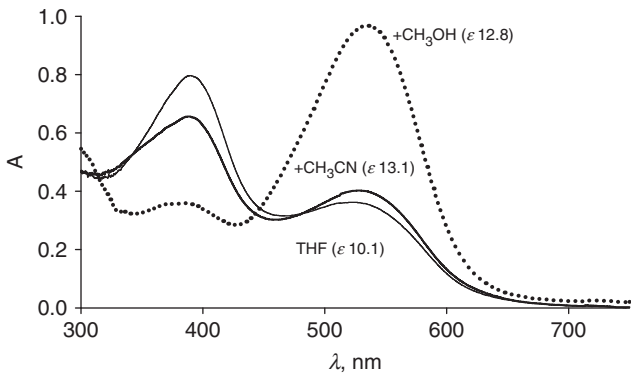


**Figure 8.10** UV–visible spectra of the equimolar mixture of *p*-nitrophenyl-aza-phenol with  $[(\text{PP}_3)\text{RuH}_2]$  in the presence of 8 vol% of  $\text{CH}_3\text{CN}$  and  $\text{CH}_3\text{CN}$  in THF.  $c = 0.001 \text{ M}$ , 230 K. The spectrum in pure THF is given for reference. The resulting media polarity (in parenthesis) was calculated according to the formula  $\epsilon = (c_{\text{THF}}\epsilon_{\text{THF}} + c_i\epsilon_i)/100$ , where  $c_i$  is the relative concentration of the  $i$ th component ( $c_{\text{THF}} + c_i = 100\%$  v/v), and  $\epsilon_i$  is its dielectric permittivity at 230 K [25].

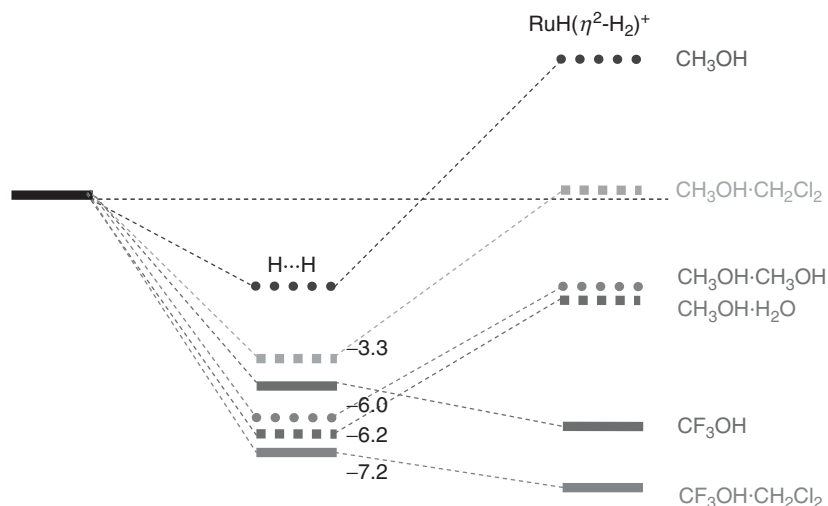
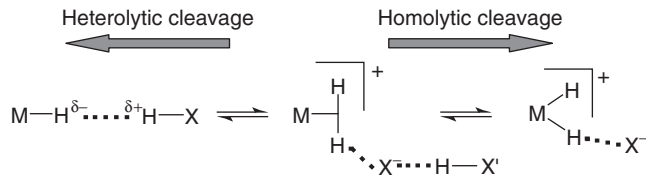


**Figure 8.11** Schematic energy profiles calculated (DFT/B3LYP) for proton transfer to  $(\text{PP}_3)\text{RuH}_2$ . Numbers indicate cooperative effect (in kcal/mol) in dihydrogen bonding with HOR-HX associates relative to dihydrogen bond with HOR. From the data in Reference 25.

process is an important step in many catalytic reactions involving  $\text{H}_2$ . The metal-bound  $\text{H}_2$  molecule is stretched relative to the free one and thus activated for further transitions. It can undergo homolytic cleavage to yield a classical dihydride or to give a proton to the anion or an external base (substrate) and thus undergo heterolytic cleavage yielding the metal hydride (Scheme 8.4). The balance between these two ways of reactivity is determined not only by the properties of the metal and its ligands but also by the strength of the cation–anion interaction. When it is too strong, deprotonation takes place, the  $\eta^2\text{-H}_2$  complex being converted into dihydrogen-bonded one.

When the cation–anion interaction is not strong enough, it allows  $[\text{M}(\eta^2\text{-H}_2)] \rightarrow [\text{M}(\text{H})_2]$  transformation. Our calculations [23] on  $[\text{CpMoH}_4(\text{dpe})]^+[\text{ROHOR}]^-$  as models of  $[\text{Cp}^*\text{MoH}_4(\text{dppe})]^+[\text{ROHOR}]^-$  have shown that this process does not require significant movement of the anion when the  $[\text{M}(\eta^2\text{-H}_2)] \cdots \text{OR}$  contact is already loose as proved by the evolution of the  $\text{H} \cdots \text{O}$  distance (from 2.106 Å in the dihydrogen structure to 2.493 Å in the tetrahydride) (Fig. 8.12). In these ion pairs, the dihydrogen–dihydride  $\rightarrow$  tetrahydride rearrangement takes place easily and is reversible. The energy barrier is only 1.8 kcal/mol in the gas phase and 1.3 kcal/mol in  $\text{CH}_2\text{Cl}_2$ , with the tetrahydride ion pair being only 1.5 kcal/mol more stable than the dihydrogen–dihydride complex in the gas phase ( $-1.7$  kcal/mol in  $\text{CH}_2\text{Cl}_2$ ).

The most striking example on how the cation–anion interaction determines the structure of cationic dihydride and how it can be fine-tuned by additional weak interactions is provided by  $[\text{Cp}^*\text{MoH}_2(\text{CO})(\text{PMe}_3)_2]^+$  [51]. When obtained by



Scheme 8.4

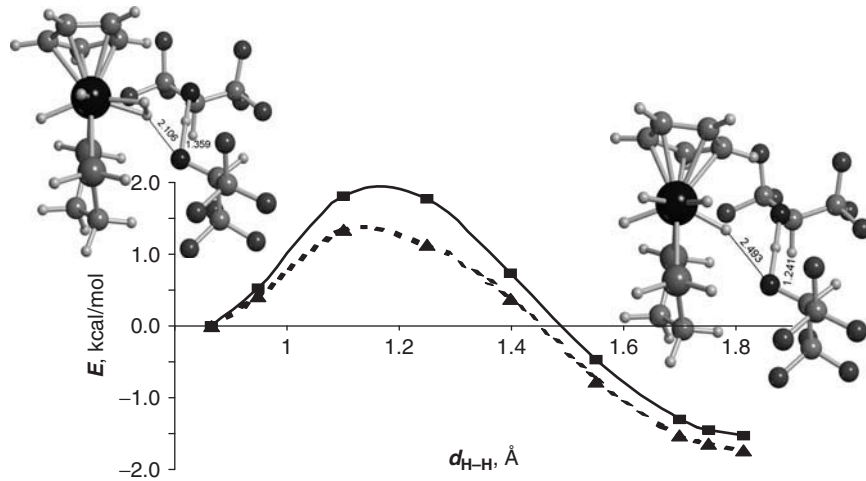


**Figure 8.12** Optimized (DFT/B3LYP) geometries of the  $[\text{CpMo}(\eta^2\text{-H}_2)\text{H}_2(\text{dpe})]^+[\text{ROHOR}]^-$  and  $[\text{CpMo}(\text{H})_4(\text{dpe})]^+[\text{ROHOR}]^-$  ion pairs ( $\text{RO} = (\text{CF}_3)_2\text{CHO}$ ) and potential energy curve for their interconversion. Plain curves and squares: in the gas phase; dashed lines and triangles: in dichloromethane solution. The H–H length of the coordinated dihydrogen has been taken as the reaction coordinate.

low-temperature protonation of  $\text{Cp}^*\text{MoH}(\text{CO})(\text{PMe}_3)_2$  by  $\text{HBF}_4 \cdot \text{Et}_2\text{O}$  in THF, this cation exists as the  $\eta^2\text{-H}_2$  complex, whereas in  $\text{CH}_2\text{Cl}_2$  the formation of classical dihydride is observed. DFT calculations show that it is the specific solvation of  $\text{BF}_4^-$  anion that affects the strength of the cation–anion interaction and ultimately the possibility of  $\text{H}_2$  homolytic cleavage. Interestingly, both solvents (THF and  $\text{CH}_2\text{Cl}_2$ ) act as CH-proton donors in binding with  $\text{BF}_4^-$  (Fig. 8.13). The stronger proton donor  $\text{CH}_2\text{Cl}_2$  gives stronger adducts with  $\text{BF}_4^-$ , which in turn weakens the  $\text{MoH}_2 \cdots \text{FBF}_3$  interaction and allows  $\text{H}_2$  cleavage in this solvent.

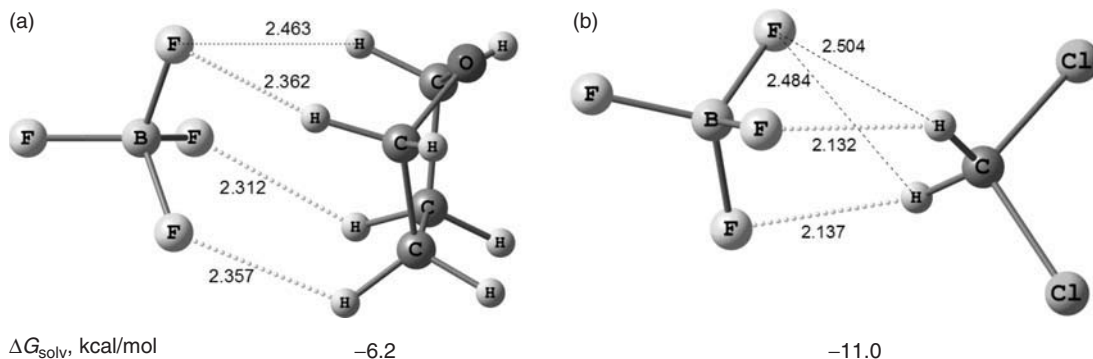


**Figure 8.13** Optimized (DFT/M05) geometries of the  $\text{BF}_4^-$  adducts with (a) THF and (b)  $\text{CH}_2\text{Cl}_2$  and their formation energies in the corresponding solvent.

## 8.5 CONCLUSIONS

Hydrogen bonds formed by transition-metal hydrides,  $M-H^{\delta-}\dots^{\delta+}HX$  or  $M-H^{\delta+}\dots Y$ , entail the lengthening of the participating bonds and their additional polarization (repolarization) due to the electron density redistribution. It leads to the increase of positive charge on “protic” hydrogen and of negative charge on the “hydridic” one. Thus, the dihydrogen bond formation allows activation of two Z–H bonds in one step. These changes (and thus the degree of the M–H bond activation) can be induced through the formation of  $M-H^{\delta-}\dots^{\delta+}HX\dots^{\delta+}HX'$  associates, in which H–X' could be even a solvent molecule. Such cooperative enhancement of the dihydrogen bond promotes the proton transfer, decreasing the energy barrier of  $\eta^2\text{-H}_2$  formation and making it more favorable thermodynamically. Activation of  $H_2$  molecule in the metal coordination sphere depends mostly on the properties of the organometallic fragment but can be further governed by weak solute–solvent interactions. Finally, the hydrogen-bonded complex  $M-H^{\delta-}\dots^{\delta+}H-M'$  formed by two hydride complexes of opposite polarity precedes the proton transfer but leads to the unusual product featuring the  $\mu,\eta^{1:1}$  end-on coordination of the  $H_2$  molecule between the two metal centers. Overall, this knowledge opens the possibility for tuning the properties of hydride and dihydrogen complexes and for governing their reactivity pattern.

## ACKNOWLEDGMENT

This work was supported by the Russian Foundation for Basic Research (projects 11-03-01210, 12-03-33018) and by the Division of Chemistry and Material Sciences of RAS.

## REFERENCES

- (a) Murakami, M., Ito, Y. In *Activation of Unreactive Bonds and Organic Synthesis*; Murai, S., Alper, H., Gossage, R. A., Grushin, V. V., Hidai, M., Ito, Y., Jones, W. D., Kakiuchi, F., Koten, G., Lin, Y. S., Mizobe, Y., Murai, S., Murakami, M., Richmond, T. G., Sen, A., Sugimoto, M., Yamamoto, A., Eds.; Springer: Berlin, Heidelberg, **1999**; Vol. 3; p 97; (b) Clot, E., Eisenstein, O., Jasim, N., Macgregor, S. A., McGrady, J. E., Perutz, R. N. *Acc. Chem. Res.* **2011**, *44*, 333; (c) J.-Q. Yu, Z. Shi, *C-H Activation*; Springer-Verlag: Berlin, Heidelberg, **2010**; p 400; (d) Labinger, J. A., Bercaw, J. E. *Nature* **2002**, *417*, 507 and preceding chapters in this book.
- Recent Advances in Hydride Chemistry*; Peruzzini, M., Poli, R., Eds.; Elsevier: Amsterdam, **2001**; p 580.
- Yandulov, D. V., Caulton, K. G., Belkova, N. V., Shubina, E. S., Epstein, L. M., Khoroshun, D. V., Musaev, D. G., Morokuma, K. *J. Am. Chem. Soc.* **1998**, *120*, 12553.
- Ayllon, J. A., Sabo-Etienne, S., Chaudret, B., Ulrich, S., Limbach, H.-H. *Inorg. Chim. Acta* **1997**, *259*, 1.
- Thiyagarajan, B., Michalczyk, L., Bollinger, J. C., Huffman, J. C., Bruno, J. W. *Organometallics* **1996**, *15*, 1989.
- Wiedner, E. S., Yang, J. Y., Chen, S., Raugei, S., Dougherty, W. G., Kassel, W. S., Helm, M. L., Bullock, R. M., Rakowski DuBois, M., DuBois, D. L. *Organometallics* **2012**, *31*, 144.
- Guari, Y., Ayllon, J. A., Sabo-Etienne, S., Chaudret, B., Hessen, B. *Inorg. Chem.* **1998**, *37*, 640.
- Fung, W. K., Huang, X., Man, M. L., Ng, S. M., Hung, M. Y., Lin, Z., Lau, C. P. *J. Am. Chem. Soc.* **2003**, *125*, 11539.
- Handgraaf, J.-W., Meijer, E. J. *J. Am. Chem. Soc.* **2007**, *129*, 3099.
- Urakawa, A., Jutz, F., Laurenczy, G., Baiker, A. *Chem. Eur. J.* **2007**, *13*, 3886.
- Yang, X., Hall, M. B. *J. Am. Chem. Soc.* **2009**, *131*, 10901.
- Crabtree, R. H. *Encyclopedia of Inorganic Chemistry*; John Wiley & Sons, Ltd: Chichester, **2006**.
- Belkova, N. V., Shubina, E. S., Epstein, L. M. *Acc. Chem. Res.* **2005**, *38*, 624.
- Besora, M., Lledós, A., Maseras, F. *Chem. Soc. Rev.* **2009**, *38*, 957.
- Belkova, N. V., Gutsul, E. I., Filippov, O. A., Levina, V. A., Valyaev, D. A., Epstein, L. M., Lledós, A., Shubina, E. S. *J. Am. Chem. Soc.* **2006**, *128*, 3486.
- Levina, V. A., Filippov, O. A., Gutsul, E. I., Belkova, N. V., Epstein, L. M., Lledós, A., Shubina, E. S. *J. Am. Chem. Soc.* **2010**, *132*, 11234.
- Jeffrey, G. A. *An Introduction to Hydrogen Bonding*; Oxford University Press: New York, **1997**.
- Arunan, E., Desiraju, G. R., Klein, R. A., Sadlej, J., Scheiner, S., Alkorta, I., Clary, D. C., Crabtree, R. H., Dannenberg, J. J., Hobza, P., Kjaergaard, H. G., Legon, A. C., Mennucci, B., Nesbitt, D. J. *Pure Appl. Chem.* **2011**, *83*, 1637.
- Epstein, L. M., Shubina, E. S. *Coord. Chem. Rev.* **2002**, *231*, 165.
- Scheiner, S. *Hydrogen Bonding. A Theoretical Perspective*; Oxford University Press: New York, **1997**; p 375.

21. Filippov, O. A., Belkova, N. V., Epstein, L. M., Lledós, A., Shubina, E. S. *ChemPhysChem* **2012**, *13*, 2677.
22. Belkova, N. V., Besora, M., Baya, M., Dub, P. A., Epstein, L. M., Lledós, A., Poli, R., Revin, P. O., Shubina, E. *Chem. Eur. J.* **2008**, *14*, 9921.
23. Belkova, N. V., Revin, P. O., Besora, M., Baya, M., Epstein, L. M., Lledós, A., Poli, R., Shubina, E. S., Vorontsov, E. V. *Eur. J. Inorg. Chem.* **2006**, 2192.
24. Andrieu, J., Belkova, N. V., Besora, M., Collange, E., Epstein, L. M., Lledós, A., Poli, R., Revin, P. O., Shubina, E. S., Vorontsov, E. V. *Russ. Chem. Bull.* **2003**, *52*, 2679.
25. Belkova, N. V., Gribanova, T. N., Gutsul, E. I., Minyaev, R. M., Bianchini, C., Peruzzini, M., Zanobini, F., Shubina, E. S., Epstein, L. M. *J. Mol. Struct.* **2007**, *844*, 115.
26. Alabugin, I. V., Manoharan, M., Peabody, S., Weinhold, F. *J. Am. Chem. Soc.* **2003**, *125*, 5973.
27. Kuejtt, A., Leito, I., Kaljurand, I., Soovaeli, L., Vlasov, V. M., Yagupolskii, L. M., Koppel, I. A. *J. Org. Chem.* **2006**, *71*, 2829.
28. Jordan, R. F., Norton, J. R. *J. Am. Chem. Soc.* **1982**, *104*, 1255.
29. Cheng, T.-Y., Brunschwig, B. S., Bullock, R. M. *J. Am. Chem. Soc.* **1998**, *120*, 13121.
30. Jacobsen, E. N., Bergman, R. G. *J. Am. Chem. Soc.* **1985**, *107*, 2023.
31. Levina, V. A., Rossin, A., Belkova, N. V., Chierotti, M. R., Epstein, L. M., Filippov, O. A., Gobetto, R., Gonsalvi, L., Lledós, A., Shubina, E. S., Zanobini, F., Peruzzini, M. *Angew. Chem. Int. Ed.* **2011**, *50*, 1367.
32. Belkova, N. V., Revin, P. O., Epstein, L. M., Vorontsov, E. V., Bakhmutov, V. I., Shubina, E. S., Collange, E., Poli, R. *J. Am. Chem. Soc.* **2003**, *125*, 11106.
33. Belkova, N. V., Epstein, L. M., Shubina, E. S. *Eur. J. Inorg. Chem.* **2010**, *2010*, 3555.
34. Belkova, N. V., Epstein, L. M., Shubina, E. S. *Arkivoc* **2008**, *iv*, 120.
35. Epstein, L. M., Belkova, N. V., Shubina, E. S. In *Recent Advances in Hydride Chemistry*; Peruzzini, M., Poli, R., Eds.; Elsevier: Amsterdam, **2001**, p 391.
36. Iogansen, A. V. *Theor. Experim. Khim.* **1971**, *7*, 312.
37. Baba, H., Matsuyama, A., Kokubun, H. *Spectrochim. Acta Part A: Mol. Spectr.* **1969**, *25*, 1709.
38. Belkova, N. V., Besora, M., Epstein, L. M., Lledós, A., Maseras, F., Shubina, E. S. *J. Am. Chem. Soc.* **2003**, *125*, 7715.
39. Bakhmutova, E. V., Bakhmutov, V. I., Belkova, N. V., Besora, M., Epstein, L. M., Lledós, A., Nikonov, G. I., Shubina, E. S., Tomas, J., Vorontsov, E. V. *Chem. Eur. J.* **2004**, *10*, 661.
40. Orlova, G., Scheiner, S. *J. Phys. Chem. A* **1998**, *102*, 4813.
41. Belkova, N. V., Ionidis, A. V., Epstein, L. M., Shubina, E. S., Gruendemann, S., Golubev, N. S., Limbach, H. H. *Eur. J. Inorg. Chem.* **2001**, 1753.
42. Belkova, N. V., Collange, E., Dub, P., Epstein, L. M., Lemenovskii, D. A., Lledós, A., Maresca, O., Maseras, F., Poli, R., Revin, P. O., Shubina, E. S., Vorontsov, E. V. *Chem. Eur. J.* **2005**, *11*, 873.
43. Dub, P. A., Filippov, O. A., Belkova, N. V., Daran, J.-C., Epstein, L. M., Shubina, E. S., Poli, R. *Dalton Trans.* **2010**, *39*, 2008.
44. Belkova, N. V., Dub, P. A., Baya, M., Houghton, J. *Inorg. Chim. Acta* **2007**, *360*, 149.
45. Rossin, A., Gutsul, E. I., Belkova, N. V., Epstein, L. M., Gonsalvi, L., Lledós, A., Lyssenko, K. A., Peruzzini, M., Shubina, E. S., Zanobini, F. *Inorg. Chem.* **2010**, *49*, 4343.
46. Edidin, R. T., Sullivan, J. M., Norton, J. R. *J. Am. Chem. Soc.* **1987**, *109*, 3945.
47. Gutsul, E. I., Belkova, N. V., Sverdlov, M. S., Epstein, L. M., Shubina, E. S., Bakhmutov, V. I., Gribanova, T. N., Minyaev, R. M., Bianchini, C., Peruzzini, M., Zanobini, F. *Chem. Eur. J.* **2003**, *9*, 2219.
48. Dub, P. A., Baya, M., Houghton, J., Belkova, N. V., Daran, J. C., Poli, R., Epstein, L. M., Shubina, E. S. *Eur. J. Inorg. Chem.* **2007**, 2813.
49. Reichardt, C. *Solvents and Solvent Effects in Organic Chemistry*; 3rd ed.; Wiley-VCH: Weinheim, **2003**, p 653.
50. Kubas, G. J. *Chem. Rev.* **2007**, *107*, 4152.
51. Dub, P. A., Belkova, N. V., Filippov, O. A., Daran, J.-C., Epstein, L. M., Lledós, A., Shubina, E. S., Poli, R. *Chem. Eur. J.* **2010**, *16*, 189.
52. Belkova, N. V., Bakhmutova, E. V., Shubina, E. S., Bianchini, C., Peruzzini, M., Bakhmutov, V. I., Epstein, L. M. *Eur. J. Inorg. Chem.* **2000**, 2163.
53. Bakhmutov, V. I., Bakhmutova, E. V., Belkova, N. V., Bianchini, C., Epstein, L. M., Masi, D., Peruzzini, M., Shubina, E. S., Vorontsov, E. V., Zanobini, F. *Can. J. Chem.* **2001**, *79*, 479.
54. Aylon, J. A., Gervaux, C., Sabo-Etienne, S., Chaudret, B. *Organometallics* **1997**, *16*, 2000.
55. Belkova, N. V., Epstein, L. M., Krylova, A. I., Faerstein, E. G., Shubina, E. S. *Russ. Chem. Bull.* **2007**, *56*, 870.



## **PART II**

---

### **ORGANOMETALLIC SYNTHESIS AND CATALYSIS**



---

# 9

---

## COMPLEXES WITH PROTIC N-HETEROCYCLIC CARBENE (NR,NH-NHC) LIGANDS

F. EKKEHARDT HAHN

*Institut für Anorganische und Analytische Chemie, Westfälische Wilhelms-Universität Münster, Münster, Germany*

### 9.1 INTRODUCTION

Enzymatic reactions are often based on the combination of molecular recognition and catalysis. Multiple noncovalent interactions between the substrate and the active site of the enzyme lead to a high degree of substrate selectivity, and regio- or stereoselective catalytic reactions can be achieved this way [1]. Adaption of these principles to homogeneous catalysis with transition metal complexes has led to the emerging field of supramolecular catalysis, in which the recognition, selection, and/or orientation of a given substrate by the catalyst is based on supramolecular interactions [2]. Although different research groups have tried to combine classical transition metal catalysis with noncovalent substrate recognition and binding, only few approaches combining high substrate selectivity and rate enhancement in the catalytic transformation have been reported to date [3]. Among the early examples is the rhodium-catalyzed asymmetric hydrogenation of trisubstituted acrylic acids in the presence of a chiral (aminoalkyl)ferrocenylphosphine where the stereoselectivity of the reaction is believed to result from an interaction of the amino group of the ferrocenylphosphine with the carboxyl group of the substrate [4]. Later, manganese-porphyrins with attached cyclodextrin groups have been shown to catalyze the regioselective hydroxylation of steroid derivatives via an interaction of the substituents at the steroid with the cyclodextrin groups, thereby causing the proper orientation of the substrate [5]. In addition, the hydrogen bonding between the carboxylic acid groups of a  $Mn(\mu-O_2)Mn$ -coordinated ligand and the carboxyl group of ibuprofen led to a specific substrate orientation, thereby enabling the regioselective functionalization of  $sp^3$  C–H bonds in ibuprofen remote from the –COOH recognition unit [6]. Finally, Breit et al. [7] introduced the concept of a temporary substrate-bound reagent-directing group for catalytic hydroformylations. Here, the substrate is covalently linked to a phosphine. Simultaneous coordination of the phosphine and the functional group of the substrate to rhodium(I) allowed for highly regio- and stereoselective transformations. A major drawback of this approach is the required covalent linkage of the substrate to the phosphine.

More recently, efforts have been directed toward the design of catalytically active complexes bearing ligands that can interact and arrange substrates via noncovalent interactions. Such an orientation can, for example, be achieved via the formation of hydrogen bonds between a ligand coordinated to the catalytically active metal center and a suitable functional group of the substrate [8]. In selected cases, hydrogen bonding between coordinated ligands and substrate molecules enforced a substrate orientation that enabled highly selective rhodium-catalyzed hydrogenation [9] or hydroformylation [10] reactions. The potential of catalytically active complexes bearing protonated pyrazole [11], oxime [12], amine [13], or protic *N*-heterocyclic carbene (NHC) ligands [14] capable of forming hydrogen bonds to selected substrate molecules has also been recognized.

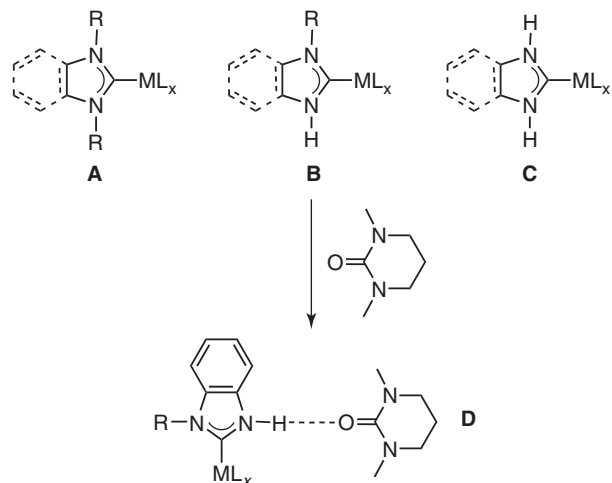


**Figure 9.1** Complexes bearing NR,NR- (**A**), NR,NH- (**B**), and NH,NH-substituted (**C**) *N*-heterocyclic carbenes (NHC)s and hydrogen bonding between a coordinated NR,NH-NHC and DMPU (**D**).

We became interested in supramolecular catalysis using complexes bearing the currently ubiquitous NHC ligands [15]. Different NHC ligands have been employed as spectator ligands for the preparation of various catalytically active metal complexes [16]. In most of these complexes, the NHC ligand is responsible for imparting the desired steric and electronic properties to the metal center. Consequently, in complexes bearing the commonly used *N,N'*-dialkylated NR,NR-NHC ligands (Fig. 9.1A), the catalytic transformations take place at the NHC-coordinated metal center. As an expansion of this concept, we have studied the coordination chemistry of complexes bearing protic NHC ligands, that is, NHC ligands featuring an NR,NH (**B**) or NH,NH (**C**) substitution pattern (Fig. 9.1) [15c,d]. The N–H groups in complexes of types **B** and **C** are potent hydrogen bond donors that might function as molecular recognition units. Contrary to many related compounds [6, 9, 10], the N–H moiety/recognition unit in complexes of types **B** and **C** is located in proximity to the metal center. For example, complexes of type **C** have been shown by  $^1\text{H}$  NMR spectroscopy to engage in hydrogen bonds between the N–H group of the NHC ligand and the hydrogen bond acceptor DMPU in solution (Fig. 9.1D) [17].

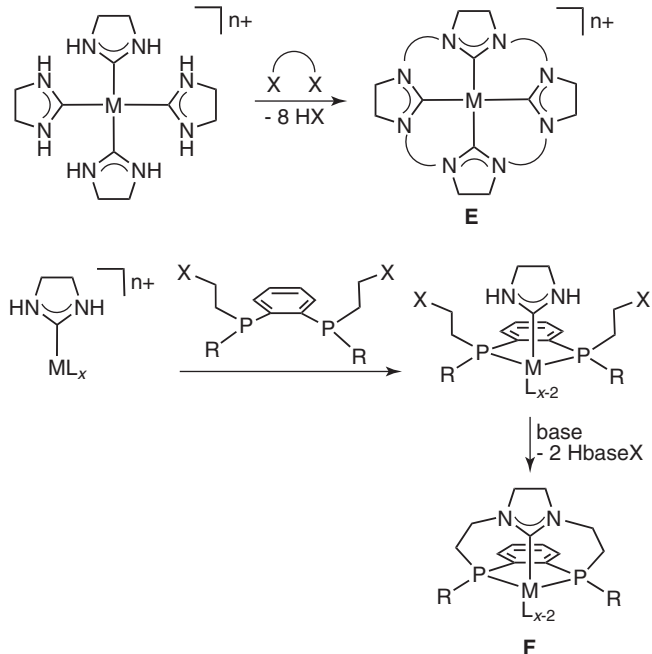
Complex  $[\text{Rh}(\text{Cl})(\text{PPh}_3)_2(\text{NR},\text{NH}-\text{NHC})]$  bearing a protic NR,NH-NHC ligand provided proof of concept for a catalytic reaction that is preceded by a recognition equilibrium [17]. In competitive hydrogenation experiments with 1-dodecene and 3-butenoic acid ester using  $[\text{Rh}(\text{Cl})(\text{PPh}_3)_2(\text{NR},\text{NH}-\text{NHC})]$  as the catalyst, the substrate with the carbonyl function was clearly preferred. This preference is most likely based on simultaneous olefin coordination to the metal center and a precatalytic interaction of the carbonyl group of the substrate with the N–H group of the NR,NH-NHC ligand leading to a two-point interaction between the substrate and the catalyst. Hydrogenation of the C=C double bond leads to a one-point interaction (N–H · · O-substrate) that facilitates the substitution of the hydrogenated substrate for another molecule of 3-butenoic acid ester, thereby preventing the deactivation of the catalyst [17].

Apart from providing hydrogen bond donors, coordinated protic NHC ligands can be deprotonated at the ring-nitrogen atom followed by reaction with an electrophile. Thus, complexes of types **B** and **C** are easily mono- or dialkylated. Such alkylation reactions can be utilized for the template-controlled synthesis of linear or macrocyclic homodonor (**E**) or heterodonor (**F**) ligands (Scheme 9.1) [15d].

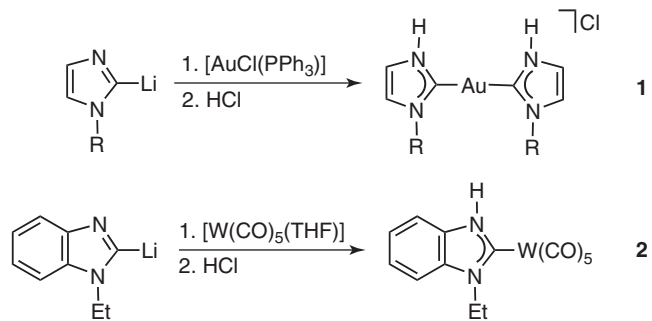
In this contribution, a review on methods for the preparation of complexes bearing protic NR,NH- and NH,NH-NHCs is presented. In addition, potential applications for these complexes are discussed.

## 9.2 COMPLEXES WITH NR,NH- AND NH,NH-NHCS FROM CYCLIC LIGAND PRECURSORS

Compared to their analogs bearing the ubiquitous NR,NR-NHCs complexes featuring protic NR,NH- and NH,NH-NHC ligands have received much less attention. This can be attributed to the more challenging synthetic protocols required for the preparation of complexes with protic NHC ligands. Unlike NR,NR-substituted azolium cations that are easily deprotonated at the C2-position to yield the free NHCs, neutral NR- or NH-substituted azoles are not this easily deprotonated at the C2 atom and the NHC complexes obtained after such a deprotonation are prone to tautomerization leading to complexes



**Scheme 9.1** Template-controlled synthesis of homodonor (**E**) or heterodonor (**F**) ligands.



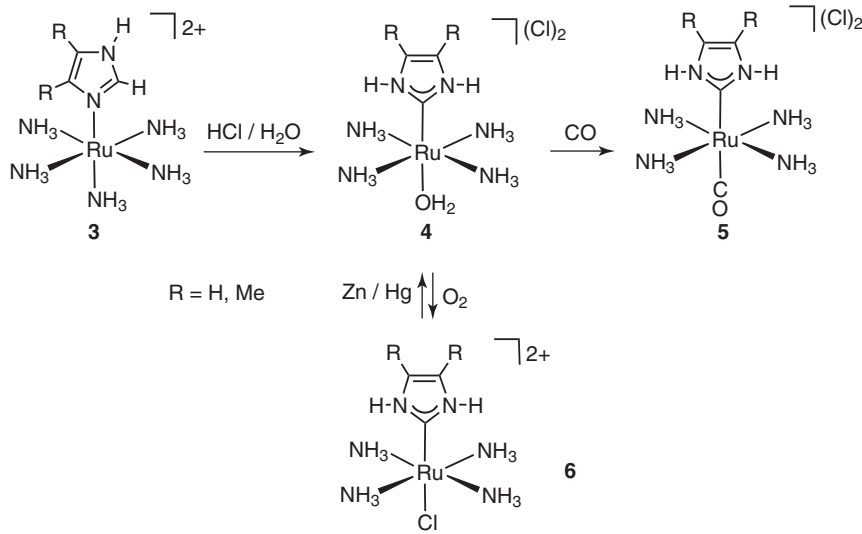
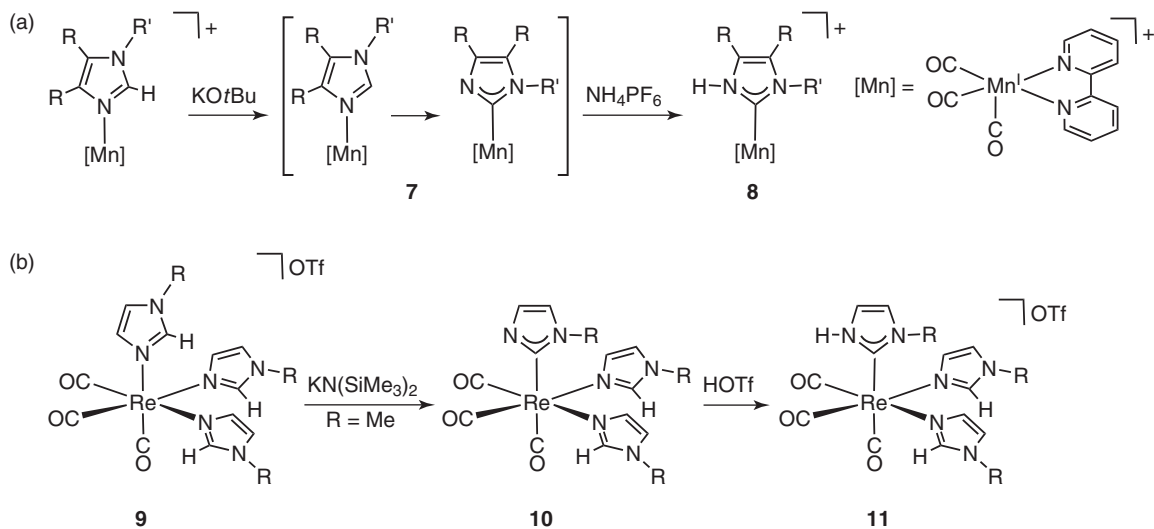
**Scheme 9.2** Synthesis of complexes bearing protic NHCs from C2-lithiated azoles.

with N-coordinated azoles [17, 18]. While it has been calculated that the free imidazolin-2-ylidene is less stable than its isomer imidazole, these calculations also predict that protic NHC ligands could be stabilized by  $\pi$ -basic metal centers or by hydrogen bonding involving the  $\beta$ -NH group of the NHC ligand [19].

Complexes with protic NHC ligands have been prepared from neutral azole precursors. In spite of the problems often encountered during the deprotonation of neutral *N*-alkylimidazoles, some complexes bearing protic NHC ligands have been generated from C2-lithiated azoles followed by N-protonation as depicted in Scheme 9.2. Complex **1** is stable [20a], but complexes of type **2** have been shown to tautomerize to the complexes bearing N-bound azoles [17]. The C2-deprotonation of various thiiazoles and the use of the resulting salts for the preparation of NHC complexes have been demonstrated by Raubenheimer [20b].

Tautomerization of N-bound azoles can be utilized for the generation of complexes bearing protic NHC ligands. For example, Taube and coworkers [21] reported as early as 1974 the acid-promoted tautomerization of the N-coordinated imidazole in **3** to yield complexes **4–6** bearing protic NHC ligands (Scheme 9.3).

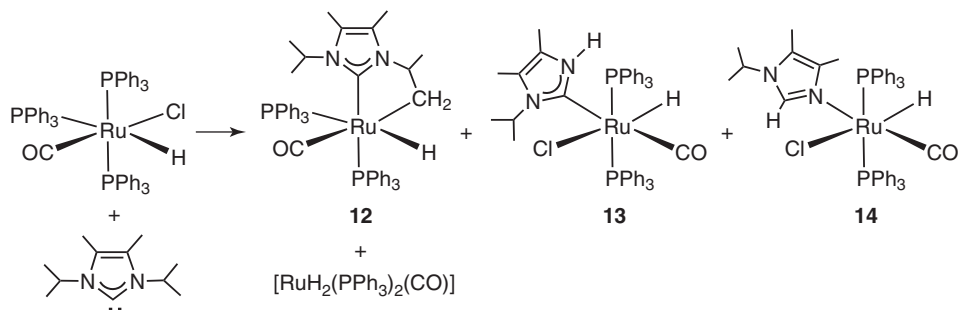
The C2-deprotonation of N-coordinated imidazoles followed by partial N $\rightarrow$ C metal transfer gave a mixture of isomeric complexes **7**. Complex **8** bearing a protic NHC ligand **8** was obtained from **7** after addition of a proton source (Scheme 9.4a) [18a]. A similar reactivity was observed for the Re<sup>I</sup> complex **9** bearing three N-coordinated imidazole ligands. On C2-deprotonation, one of these reacted under N $\rightarrow$ C metal shift to give **10** that on protonation yielded the complex **11** bearing

**Scheme 9.3** Acid-promoted tautomerization of N-coordinated azoles to yield complexes with protic NHC ligands.**Scheme 9.4** Tautomerization of N-coordinated azoles by (a) C2-deprotonation followed by (b) metal shift and N-protonation.

a protic NHC ligand (Scheme 9.4b) [18b]. *N*-Alkylation of the anionic NHC ligand in **10** to give a classical NR,NR-NHC ligand is also possible.

The tautomerization reactions of N-coordinated azoles described earlier is limited to selected metal centers. A different reaction leading to complexes with protic NHC ligands starts the ubiquitous *N,N'*-dialkylated azolium salts. Such salts can be deprotonated to yield the free NHCs that on reaction with suitable metal precursors yield NHC complexes. Alternatively, azolium salts react directly with suitable metal precursors in the presence of internal or external bases to yield NHC complexes [15]. If the azolium salt and subsequently the coordinated NHC are functionalized with removable N-substituents, protic NHC ligand can be generated at the metal template by the removal of an N-substituent from the coordinated NHC.

Such a reaction was discovered in 2006 for complex **12**, which was obtained by coordination of a free NHC to Ru<sup>II</sup> with concurrent C–H activation at one of the methyl groups of an N-substituent (Scheme 9.5). Heating of **12** leads to cleavage of an exocyclic N–C bond and, among other reaction products, to the formation of the NHC complex **13** bearing a protic NHC and its tautomer **14** (Scheme 9.5) [22].



**Scheme 9.5** Cleavage of an exocyclic N–C bond in **12** to give the complex with a protic NHC ligand.

The accidental removal of an *N*-acetyl substituent during silica gel chromatography has been observed for complex **15** giving complex **16** with a protic NHC ligand (Scheme 9.6a) [23a]. This type of accidental removal of an *N*-wingtip substituent has also been described for complexes bearing *N*-silyl-substituted NHCs [23b].

Crabtree and coworkers described an acyl *N*-protection strategy for the directed synthesis of complexes bearing protic NHCs (Scheme 9.6b). The *N*-benzoyl-substituted benzimidazolium salt **17** reacts on deprotonation with [IrCl(COD)]<sub>2</sub> to yield the NHC complex **18**. Exchange of the chloro ligand in **18** for PPh<sub>3</sub> gave the salt **19** that undergoes *N*-deprotection with methanol to yield complex **20** with a protic NHC ligand [24]. A similar deprotection strategy leading to NH,NH-NHC complexes of gold(I) has recently been described. Reaction of imidazole with triethyl orthoformate gave the *N*-substituted imidazole **21** that on C-lithiation and reaction with [AuCl(THT)] yields salt **22** (see also Scheme 9.2a). The subsequent reaction of **22** with CF<sub>3</sub>SO<sub>3</sub>H and HCl proceeded under stepwise protonation of the free nitrogen atom followed by the removal of the *N*-protection groups with the formation of complexes **23** and finally **24** bearing two NH,NH-NHC ligands (Scheme 9.6c) [25].

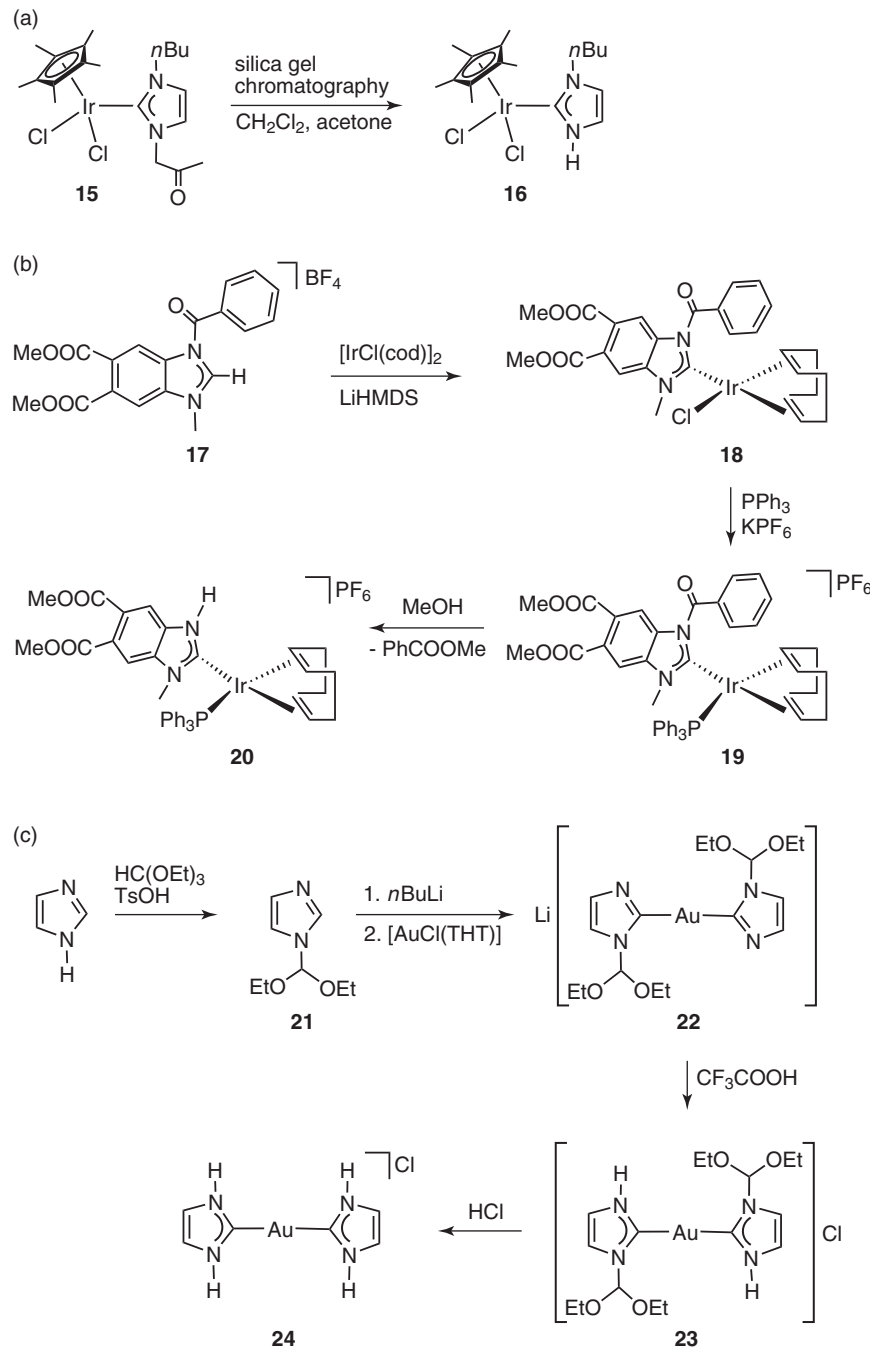
### 9.3 COMPLEXES WITH NR,NH- AND NH,NH-NHCS BY TEMPLATE-CONTROLLED CYCLIZATION REACTIONS

The majority of NHCs and their metal complexes, including those bearing protic NHC ligands described earlier, have been obtained from cyclic azole or azolium derivatives. Alternatively, NHC ligands can be generated at a suitable metal template from coordinated isocyanide ligands. For example, Ugi four-component cyclization [26a] (cyano complexes, isocyanides, aldehydes, and amine hydrochlorides) and the Ugi three-component cyclization reactions [26b] (cyano complexes, isocyanides, and carbonyl compounds) have been used successfully for the template synthesis of complexes bearing protic NHC ligands.

Generally, isocyanides can be attacked by proton bases HX (X = OR, RNH) in a nucleophilic reaction that leads to acyclic heterocarbene complexes [27, 28]. The use of functionalized isocyanides containing both the isocyanide group and the nucleophile in the same molecule gives access to complexes with heterocyclic carbene ligands via an 1,2-addition across the C≡N triple bond [29]. A number of research groups have been active in the development of nucleophile-functionalized isocyanides, which could subsequently be cyclized in metal template-controlled reactions.

Initially, the functionalized isocyanides were prepared in template syntheses at metal centers. Beck et al. [30], Fehlhammer et al. [31], and Michelin et al. [32] describe the reactions of complexes bearing isocyanic acid or isocyanide ligands with epoxides or aziridine. These reactions led to  $\beta$ -functionalized ethyl isocyanides that subsequently cyclized at the metal template to yield cyclic heterocarbenes (Scheme 9.7, method a). Complexes bearing  $\beta$ -nucleophile substituted isocyanide ligands can also be obtained by the reaction of ethylenediamine or ethanolamine with coordinated trichloromethyl isocyanide [33] or dichlorocarbene ligands [34] followed by cyclization of the intermediately formed  $\beta$ -functionalized isocyanide ligand (Scheme 9.7, method b).

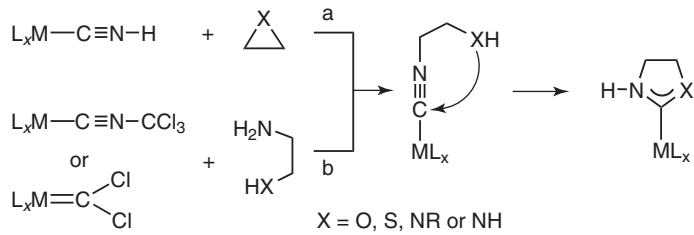
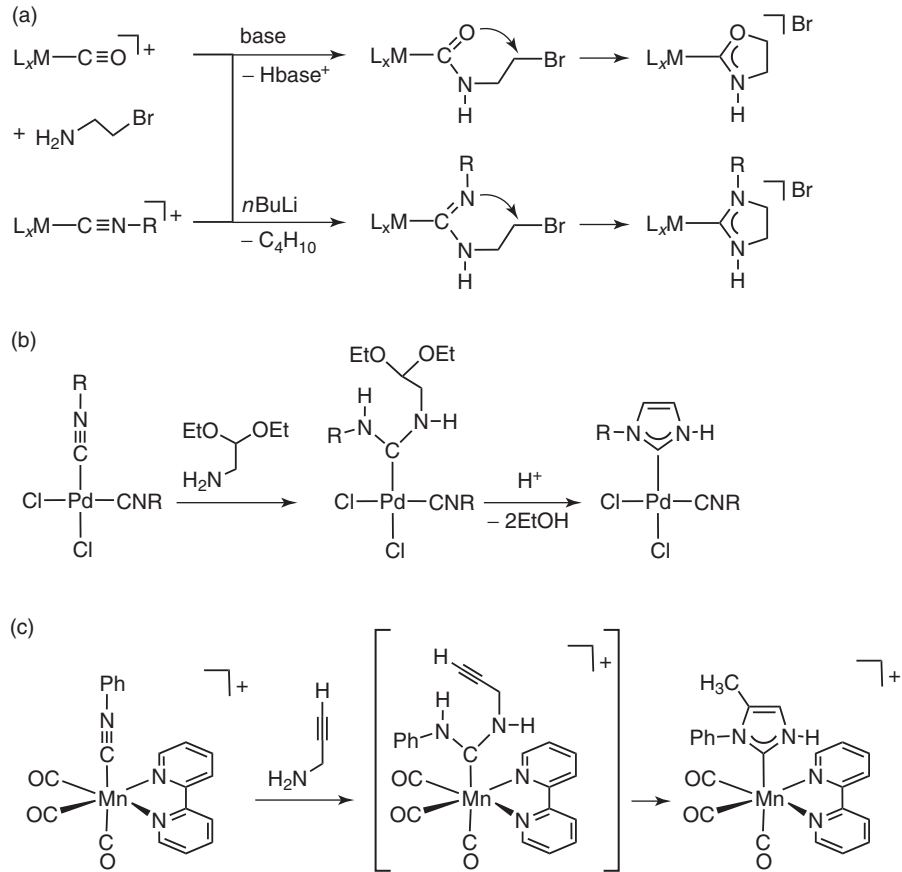
Some additional templates syntheses of complexes containing protic cyclic heterocarbene ligands using isocyanide or carbonyl complexes as the starting material have been described. Special attention deserve the reactions of carbonyl [35] or isocyanide complexes [36] with 2-bromoethyl amine leading to complexes with protic oxazolidin-2-ylidene or imidazolidin-2-ylidene ligands, respectively (Scheme 9.8a). The nucleophilic attack of the diacetal-protected amino acetaldehyde at a diisocyanide palladium complex followed by an acid-catalyzed cyclization reaction resulted in the formation of the complex bearing an NH,NR-substituted imidazolin-2-ylidene ligand (Scheme 9.8b) [37a]. The synthesis of tetracarbene complexes



**Scheme 9.6** (a–c) Syntheses of complexes bearing protic NHC ligands by the removal of N-substituents from the coordinated NHC ligand.

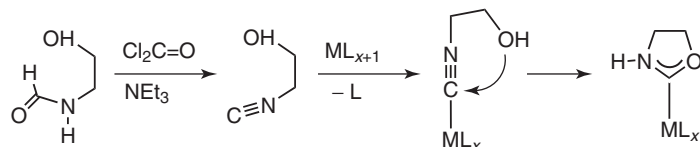
using this methodology has also been demonstrated [37b]. Even the metal template-controlled reaction of propargyl amine with phenyl isocyanide followed by cyclization to yield the complex with an unsaturated protic NHC ligand has been described (Scheme 9.8c) [38]. In addition, the  $\alpha$ -metallation of coordinated isocyanides followed by reaction with 1,2-dipolar substrates with subsequent cyclization is also known to lead complexes bearing protic heterocarbene ligands [39].

Much simpler than the template-controlled generation of  $\beta$ -functionalized isocyanides is their direct use in the synthesis of NHC complexes. Hydroxyalkylisocyanides such as 2-hydroxyethyl isocyanide are stable molecules but they are also known to become activated on contact with selected metal ions where they isomerizes to *N,O*-heterocycles. Fehlhammer et al. [40]

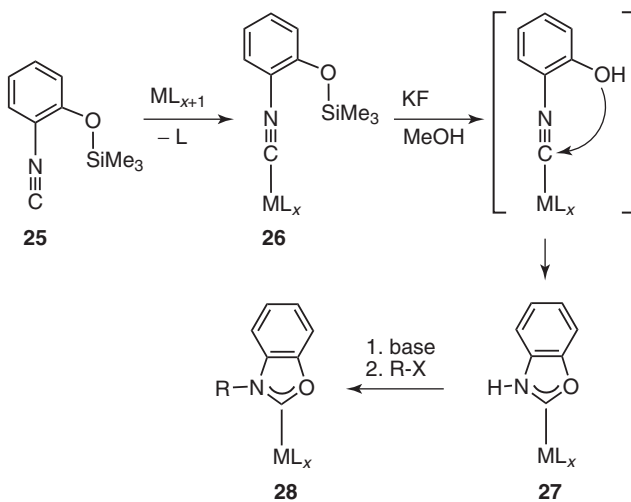
**Scheme 9.7** Syntheses of  $\beta$ -functionalized isocyanides followed by cyclization at a metal template.**Scheme 9.8** (a–c) Metal template-controlled syntheses of complexes with protic NHC ligands.

used this type of cyclization for the metal template-controlled generation of  $NH_2O$ -heterocarbene ligands. On coordination and activation of 2-hydroxyphenyl isocyanide at an electron-poor metal center, spontaneous cyclization to an oxazolidin-2-ylidene ligand was observed (Scheme 9.9). Homoleptic tetra- [41] and hexa-NHC complexes [42] have been obtained through this route. The cyclization of the 2-hydroxyethyl isocyanide ligand is prevented when the ligand coordinates to an electron-rich metal center as enhanced  $M\rightarrow CNR$   $\pi$ -backbonding deactivates the isocyanide for the intramolecular nucleophilic attack by the hydroxyl group [40c].

We have studied the metal template-controlled cyclization of 2-hydroxyphenyl isocyanide [43]. This ligand contains the isocyanide and the nucleophile within the same molecule and both groups are already arranged in one plane. This arrangement together with the aromaticity of the five-membered ring obtained after cyclization to the benzoxazolin-2-ylidene particularly favors the intramolecular nucleophilic attack and the formation of cyclic heterocarbene ligands. In contrast to 2-hydroxyethyl isocyanide, free 2-hydroxyphenyl isocyanide is unstable and cyclizes spontaneously to benzoxazole [44]. The heterocycle



Scheme 9.9 Cyclization of coordinated 2-hydroxyethyl isocyanide.

Scheme 9.10 Template-controlled cyclization of 2-hydroxyphenyl isocyanide followed by *N*-alkylation.

of benzoxazole, however, opens up on treatment with *n*BuLi, and the isocyanide obtained this way can be stabilized as 2-trimethylsiloxyphenyl isocyanide by reaction with trimethylsilyl chloride [45].

2-Trimethylsiloxyphenyl isocyanide **25** (Scheme 9.10) coordinates to various electrophilic metal centers with the formation of isocyanide complexes of type **26**. Subsequent cleavage of the O–SiMe<sub>3</sub> bond leads to spontaneous cyclization and the formation of heterocarbene complexes of type **27** with the cyclic benzoxazolin-2-ylidene ligand. The *N*-alkylation of the carbene heterocycle in **27** to give complexes of type **28** proceeds readily (Scheme 9.10). A large number of complexes with NH,O- and NR,O-substituted benzoxazolin-2-ylidene ligands coordinated to different template metals have been prepared [46], and this synthetic procedure has also been reviewed [29].

As in the case of the 2-hydroxyethyl isocyanide, the intramolecular nucleophilic attack of the hydroxyl group at the isocyanide carbon atom in 2-hydroxyphenyl isocyanide complexes is controlled by the strength of the M→C≡NR backbonding. Deactivation of the isocyanide ligand for a nucleophilic attack has been observed in the case of strong backbonding. In such cases, the O–SiMe<sub>3</sub> bond cleavage leads to complexes with the 2-hydroxyphenyl isocyanide, a ligand that is unstable in the free state, but can be stabilized by coordination and backbonding from the metal center.

Force constants for the C≡NR bonds calculated from IR data for various 2-trimethylsiloxyphenyl isocyanide complexes have allowed to predict the behavior of the coordinated ligand in complexes of type **26** after cleavage of the O–SiMe<sub>3</sub> bond [47]. The 2-hydroxyphenyl isocyanide coordinated to electron-poor Re<sup>V</sup> cyclizes immediately after O–SiMe<sub>3</sub> bond cleavage to give complex **29**, whereas the same isocyanide ligand is stable toward cyclization when coordinated to the more electron-rich Re<sup>III</sup> in **30** (Fig. 9.2) [48]. Cleavage of the O–SiMe<sub>3</sub> bonds in the iron(II) complex bearing three ligands **25** yields complex **31** (Fig. 9.2) with only two benzoxazolin-2-ylidene ligands. The heterocarbene ligands are stronger σ-donors and weaker π-acceptors than the phenyl isocyanide ligands from which they were formed. Consequently, the electron density at the iron(II) atom is increased with each cyclization and so is the backbonding to the remaining 2-hydroxyphenyl isocyanide ligand. This situation ultimately prevents the cyclization of the third isocyanide ligand, which is stabilized in complex **31** [49]. Cyclization of the remaining isocyanide ligand in **31** can be initiated by a reduction of the Fe<sup>II</sup>→C≡NR backbonding, which is best achieved by oxidation of the metal ion with elemental iodine from iron(II) to iron(III). The equilibrium between complexes with the 2-hydroxyphenyl isocyanide and the benzoxazolin-2-ylidene ligands can also be influenced by the addition of selected bases that engage in hydrogen bonds to the hydroxyl group [50].

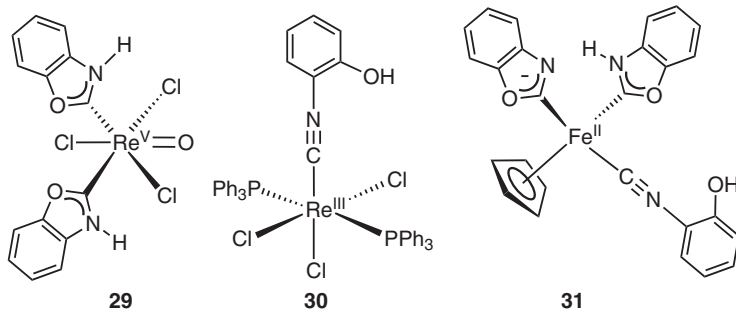
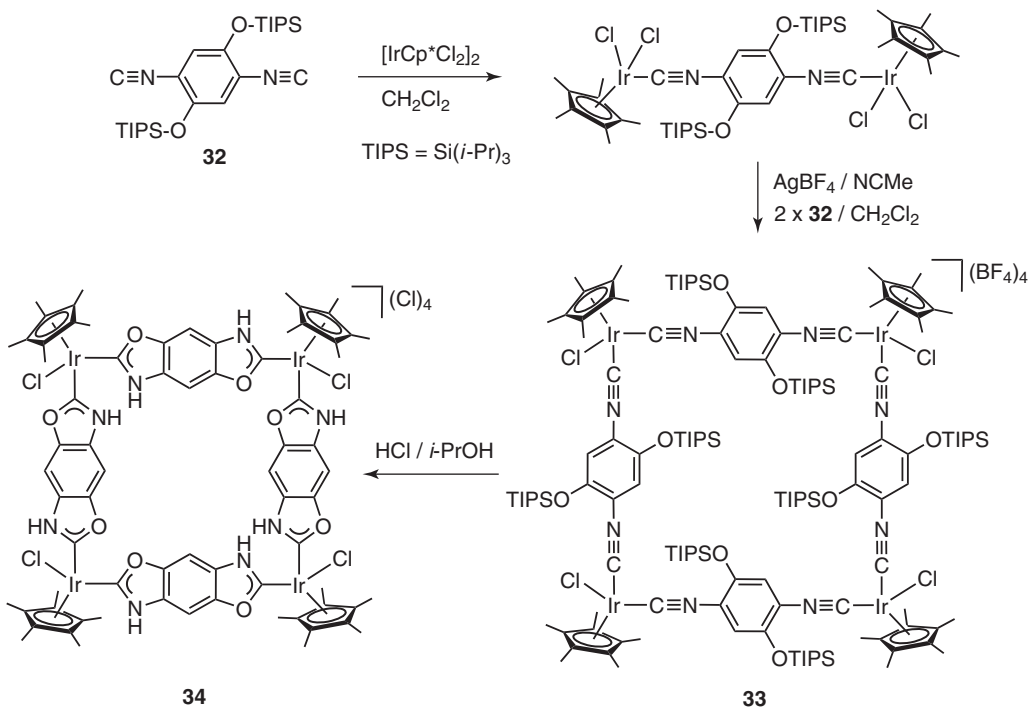


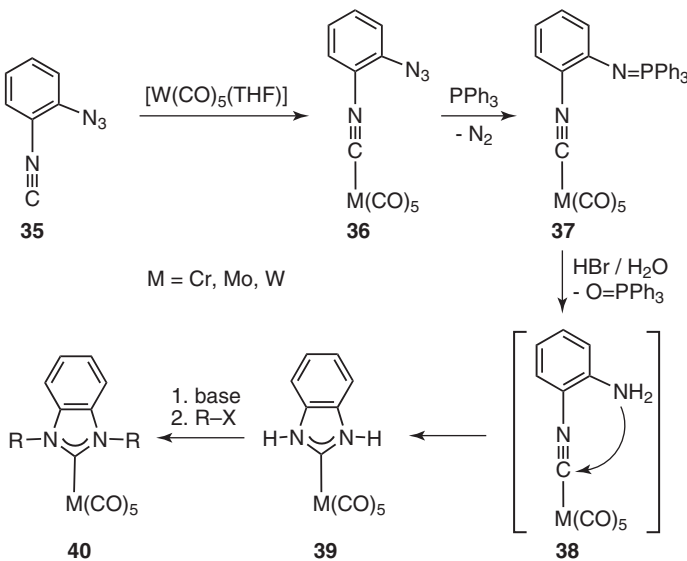
**Figure 9.2** Complexes with benzoxazolin-2-ylidene and 2-hydroxyphenyl isocyanide ligands.



**Scheme 9.11** Synthesis of the molecular square **34** from the tetrakis(diisocyanide)-bridged complex **33**.

The template-controlled synthesis of  $\text{NH}_2\text{O}-\text{NHC}$  ligands from coordinated  $\beta$ -hydroxyphenyl isocyanides has recently been shown to be useful for the preparation of organometallic molecular squares and rectangles where four metal centers are bridged by benzobiscarbene ligands [51]. A properly  $\beta,\beta'$ -functionalized phenyl-1,4-diisocyanide such as **32** can act as a bridging ligand in the synthesis of tetranuclear organometallic molecular squares in **33** that on hydrolysis of the eight  $\beta,\beta'$ -trialkylsiloxy groups converts into the tetrakis(dicarbene) bridged molecular square **34** (Scheme 9.11) [52].

The metal template-controlled cyclization of  $\beta$ -functionalized isocyanides can be extended to the synthesis of cyclic  $\text{NH}_2\text{NH}-\text{NHC}$  ligands. The required 2-aminophenyl isocyanide, however, is not stable. It rapidly cyclizes to give benzimidazole. Therefore, 2-azidophenyl isocyanide **35** (Scheme 9.12) was used as a synthon for 2-aminophenyl isocyanide. Isocyanide **35** can be coordinated to transition metals to give isocyanide complex **36**. A subsequent Staudinger reaction with  $\text{PR}_3$  at the azido function followed by hydrolysis of the resulting phosphinimine in **37** generates the required primary amine group in **38**. Complex **38** could not be isolated as it rapidly reacts under intramolecular nucleophilic attack of the amino group at the isocyanide carbon atom with the formation of the  $\text{NH}_2\text{NH}-\text{NHC}$  complex **39**. The alkylation of both NH functions to yield complex **40** proceeds readily [53]. A related reaction sequence starting from 2-(azidomethyl)phenyl isocyanide and leading to a six-membered  $\text{NH}_2\text{NH}-\text{NHC}$  has been reported by Michelin et al. [54]. Alternatively, the azido function of



**Scheme 9.12** Template-controlled reduction and cyclization of 2-azidophenyl isocyanide.

ruthenium(II) coordinated 2-azidophenyl isocyanide **35** has been reduced with Zn/NH<sub>4</sub>Cl followed by cyclization to the NH,NH-NHC ligand [55]. The template-controlled generation of NH,NH-NHC ligands is also possible by reduction of the nitro group in coordinated 2-nitrophenyl isocyanide with Sn/HCl. In this reaction, it proved essential that the 2-nitrophenyl isocyanide is coordinated to a redox-inert metal center like the one found in the pentacarbonyl chromium, molybdenum, and tungsten complex fragments [56].

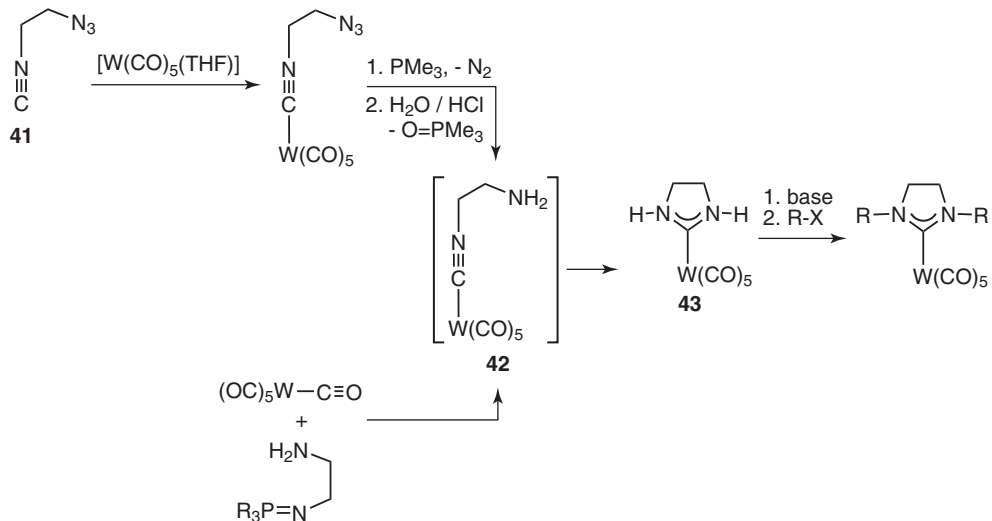
The option to alkylate the coordinated NH,NH-NHC ligand offers the possibility to generate macrocyclic poly-NHC ligands in a template-controlled approach. For example, four NH,NH-NHC ligands coordinated to Pt<sup>II</sup> in a square-planar complex have been linked to a macrocyclic tetra-NHC ligand with crown-ether topology [57].

Contrary to the difficulty to synthesize 2-azidophenyl isocyanide **35** [53], the aliphatic ligand 2-azidoethyl isocyanide **41** is readily available. This ligand, when coordinated to a suitable transition metal and after reduction of the azido group to an amino group (complex **42**), also spontaneously cyclizes to give, for example, complex **43** with a saturated NH,NH-NHC ligand (Scheme 9.13, top) [58]. Again, the *N,N'*-dialkylation of the NHC ligand in **43** proceeds readily and stepwise. Complex **43** has been obtained previously by Liu et al. from the reaction of an amine-phosphinimine with [W(CO)<sub>6</sub>] that most likely proceeds via initial deoxygenation of one carbonyl ligand by the iminophosphine to give an isocyanide ligand (complex **42**), which subsequently undergoes an intramolecular attack by the amino group at the isocyanide carbon atom to give the NH,NH-NHC ligand (Scheme 9.13, bottom) [59].

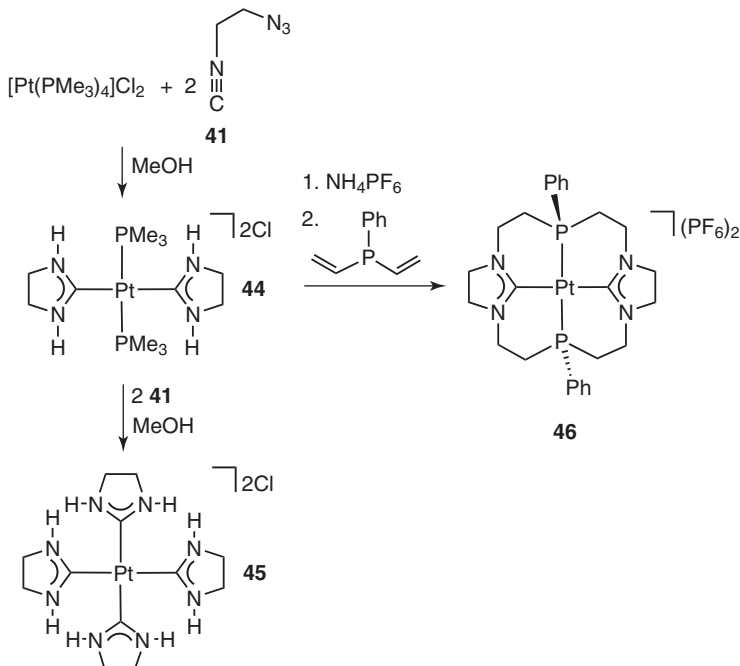
As described for the complexes of 2-azidophenyl isocyanide, the azido function of coordinated 2-azidoethyl isocyanide **41** can be reduced with different reducing agents. Next to the Staudinger reaction depicted in Scheme 9.13, Zn/NH<sub>4</sub>Cl, In/NH<sub>4</sub>Cl and [Sn(bdt)<sub>2</sub>]/NaBH<sub>4</sub> have been used as reducing agents [55] in addition to FeCl<sub>3</sub>/NaI [60]. The cyclization reactions of 2-aminophenyl or 2-aminoethyl isocyanide followed by *N,N'*-dialkylation constitute a complementary methodology for the preparation of complexes bearing cyclic diaminocarbenes relative to the classic method starting from azolium cations [15]. In addition, the coordinated NH,NH-NHC ligands are useful building blocks for the synthesis of complexes bearing macrocyclic ligands with NHC donor functions.

For example, three saturated NH,NH-NHC ligands like those found in complex **43** have been generated at a rhenium(I) template [55]. At the platinum(II) template, both the *trans*-dicarbene complex **44** [61] and the tetracarbene complex **45** [62] have been prepared (Scheme 9.14). Exchange of the PMe<sub>3</sub> ligands in **44** for phenyldivinylphosphine ligands allows for a hydroamination reaction with the formation of a neutral [16]ane-P<sub>2</sub>C<sup>NHC</sup><sub>2</sub> macrocycle [61]. Tridentate [11]ane-P<sub>2</sub>C<sup>NHC</sup> macrocycles have been obtained from complexes bearing one saturated NH,NH-NHC ligand and functionalized diphosphines [63].

Attempts to generate three NH,NH-NHC ligands at the {CpFe}<sup>+</sup>-template demonstrated again the important role of the electronic situation at the metal center. Reduction and cyclization of the 2-azidoethyl isocyanide ligands in complex **47** creates NH,NH-NHC ligands that are much better  $\sigma$ -donors than their  $\sigma$ -donor/ $\pi$ -acceptor predecessor isocyanide ligands **41**. Thus, every cyclization of an isocyanide ligand to an NH,NH-NHC leads to a more electron-rich metal center. After the



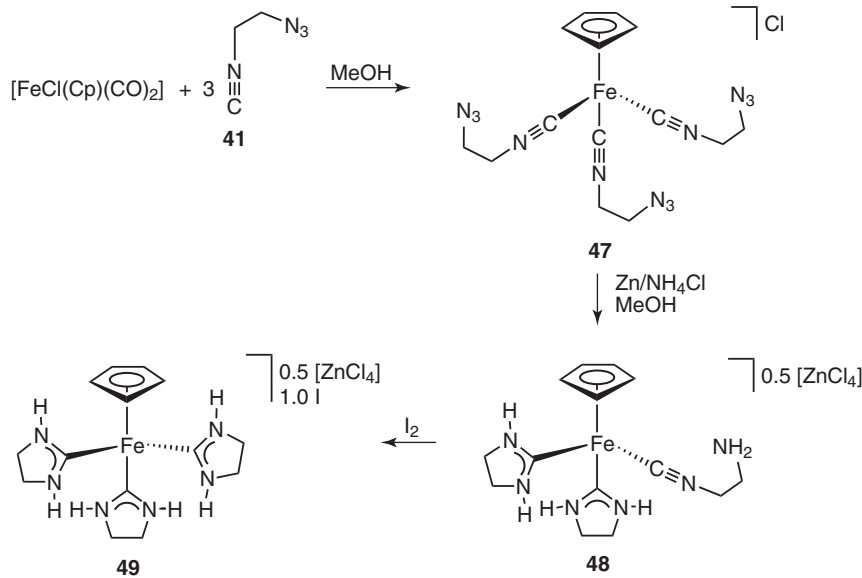
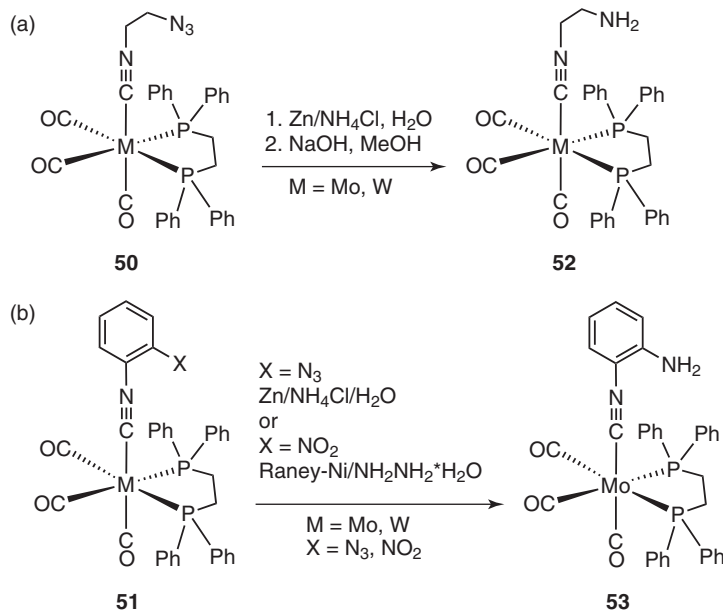
**Scheme 9.13** Template syntheses of a complex bearing a saturated NH,NH-NHC ligand.



**Scheme 9.14** Cyclization of 2-azidoethyl isocyanides at the Pt<sup>II</sup> template and follow-up reactions.

formation of two NHCs in **48**, the backbonding from the iron atom to the remaining isocyanide ligand apparently becomes strong enough to prevent another intramolecular nucleophilic attack. Thus, even after complete reduction of all three azido groups, complex **48** did not react further (Scheme 9.15). Cyclization of the remaining 2-aminoethyl isocyanide in **48** is possible if the Fe $\rightarrow$ C $\equiv$ NR backbonding is reduced. This was achieved by addition of elemental iodine to a methanolic solution of **48** leading to the oxidation of the metal center to Fe<sup>III</sup> with concurrent formation of **49** [62].

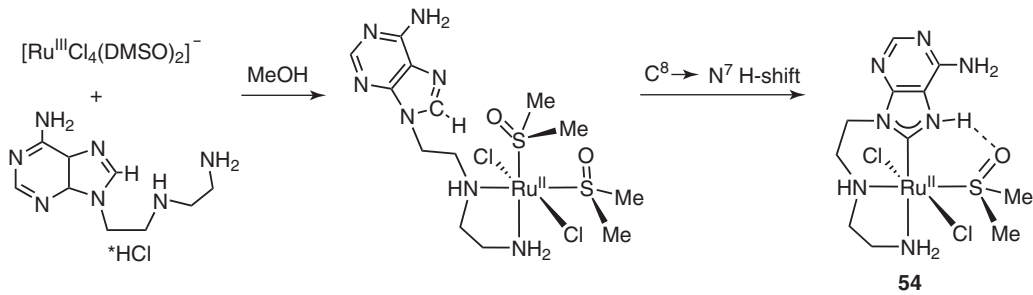
While the template-stabilized 2-aminoethyl isocyanide ligand in **48** was observed more or less by accident, the directed stabilization of  $\beta$ -amino functionalized isocyanides is possible at electron-rich metal templates. Isocyanides **35**, **41** and 2-nitrophenyl isocyanide form the electron-rich complexes of types **50** and **51**. Reduction of the 2-azido or 2-nitro functions leads to the 2-amino-substituted isocyanides in complexes **52** and **53** that are stabilized by M $\rightarrow$ C $\equiv$ NR backbonding and thus undergo no cyclization to the NH,NH-NHC ligands (Scheme 9.16) [64].

Scheme 9.15 Cyclization of 2-azidoethyl isocyanide at the  $\{\text{CpFe}\}^+$  template.

Scheme 9.16 (a, b) Stabilization of 2-aminoethyl isocyanide and 2-aminophenyl isocyanide at metal templates.

#### 9.4 COMPLEXES WITH NR,NH-NHCS BY OXIDATIVE ADDITION OF AZOLES

In 1997, the reaction of an ethylenediamine-tethered adenine with complex anion  $[\text{Ru}^{\text{III}}\text{Cl}_4(\text{DMSO})_2]^-$  was described to proceed under C8-metallation of the adenine moiety and formation of a tether-substituted protic NHC ligand. The resulting complex **54** featured a neutral tridentate NR,NH-NHC/diamine ligand Scheme 9.17 [65]. Formally, this reaction can be considered to be a tautomerization of the purine moiety ( $\text{C8-H} \rightarrow \text{N7-H}$ ) generating a neutral NR,NH-NHC. The metal center did not change its oxidation state. This unusual reactivity was attributed to the tethered chelating diamine group. In the absence of the tether, the more typical metal coordination at N7 of the nucleobase was observed [66]. As the oxidation state of the metal center did not change, an oxidative addition of the C8-H bond does appear unlikely but the



**Scheme 9.17** Metallation at C8 of a diamine-tethered adenine to give **54**.

simple C8–H→N7–H tautomerization generating the NR,NH-NHC is also very unlikely. No mechanistic proposal for the formation of **55** has been put forward.

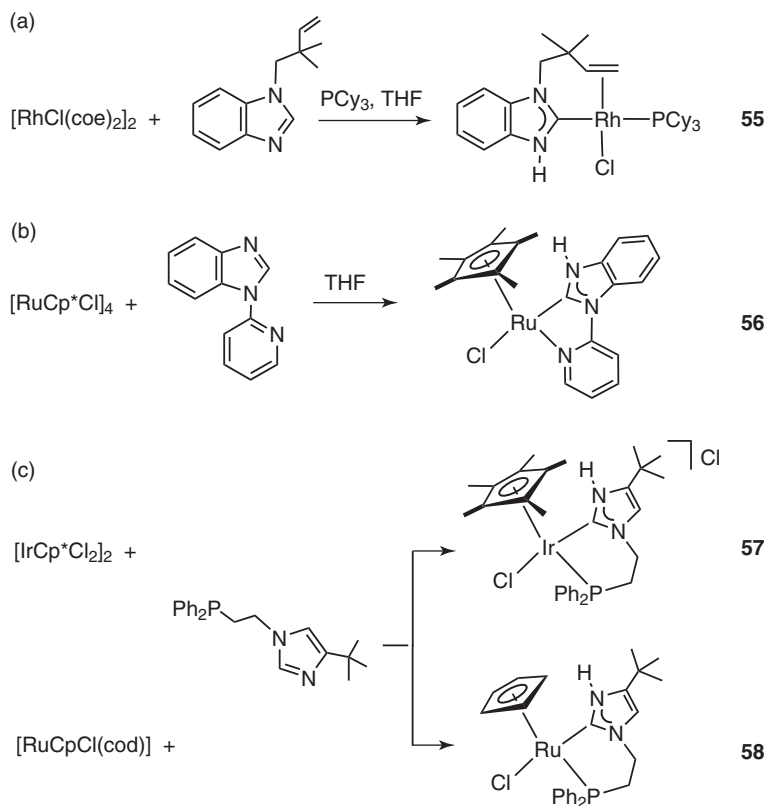
Related chelate-assisted formal tautomerization reactions of neutral C2–H-substituted azoles have been described. Bergman and coworkers [67] showed that an *N*-olefin substituted benzimidazole reacts with [RhCl(coc)<sub>2</sub>]<sub>2</sub> to yield the NR,NH-NHC/olefin chelate complex **55** (Scheme 9.18a). Ikariya and Kuwata [68] used *N*1-(2-pyridyl)benzimidazole for the synthesis of the C2<sup>+</sup>(pyridyl) chelate complex **56** featuring also a protic NHC ligand (Scheme 9.18b). Grothjahn and coworkers reacted an *N*-ethylenephosphine-substituted imidazole with Ru<sup>II</sup> or Ir<sup>III</sup> to prepare the C<sup>+</sup>P chelate complexes **57** [69a] and **58** (Scheme 9.18c) [69b]. Apart from their unusual mode of formation, complexes **56–58** show an interesting follow-up chemistry. For example, the deprotonation of the NR,NH-NHC moiety in these complexes is possible leading to anionic NHC ligands with an unsubstituted ring-nitrogen atom. The formation of complexes **55–58** has been attributed to a “tautomerization” reaction of the azoles, possibly aided by the tethered donor function. While this description represents the reaction products correctly, a simple tautomerization of an azole to an NR,NH-NHC is altogether not very likely. The exact mechanism for the formation of these complexes has not been established at the time of publication.

We became interested in the reaction of N-donor-functionalized benzimidazoles with transition metals and prepared the precursors for bidentate C(NHC)<sup>+</sup>P(phosphine) ligands **59–62**. The benzimidazoles **59** and **60** react with [RuCp<sup>\*</sup>Cl]<sub>4</sub> to give complexes **63** and **64**, respectively (Scheme 9.16a) [70]. The N-donor-substituted benzimidazoles **61** and **62** react with [RhCl(coc)<sub>2</sub>]<sub>2</sub> in the presence of different tertiary phosphines (Scheme 9.16b) to give complexes *cis/trans*-**65** and **66** bearing protic NHC ligands [71]. Here, the length of the linker between the NHC-nitrogen atom and the phosphine as well as the steric demand of the used monodentate phosphines determine the geometry of the resulting complexes. In the presence of the sterically demanding tricyclohexyl phosphine, ligand precursor **61** yields a mixture of the *cis*-P,P (*cis*-**65**, major 77%) and the *trans*-P,P complexes (*trans*-**65**, minor 23%). The P'C ligand precursor **62** with an ethylene spacer between the ring-nitrogen atom and the di(*t*Bu)phosphine donor yields in the presence of PCy<sub>3</sub> exclusively the *trans*-P,P complex **66**. The introduction of a longer space with the concurrent expansion of the C(NHC)–Rh–P(*t*Bu) angle and the use of the sterically demanding PCy<sub>3</sub> apparently prevent the *cis*-coordination of the phosphine donors.

The mechanism for the formation of complexes **63–66** has not been established unambiguously yet. As mentioned before, related complexes bearing bidentate imidazolin-2-ylidene/donor or benzimidazolin-2-ylidene/donor ligands (Scheme 9.18) have been described as formed by tautomerization of the azole to the NR,NH-substituted NHC that then together with the tethered donor coordinates to the metal center. This rather simple type of reaction mechanism is not very likely to be operative.

Although the oxidation state of the metal center does not change in the reactions depicted in Scheme 9.19, we still assumed that a C2–H oxidative addition step, among others, is involved in the formation of complexes **63–66**. To test this hypothesis, we have prepared C2–X (X = Cl, I) substituted neutral benzimidazoles that are thought to be more reactive in oxidative addition reactions than their C2–H-substituted analogs. The oxidative addition of NR,NR-substituted benzimidazolium cations to transition metals is a well-established reaction [72]. Much less is known about the C2–X oxidative addition of neutral azoles. An early study indicated that 2-chloroazoles do indeed oxidatively add to transition metals and that the resulting negatively charged NHC ligand can be N-protonated to yield complexes with protic NHC ligands [73].

In the presence of NH<sub>4</sub>BF<sub>4</sub>, neutral 2-chloro-*N*-methylbenzimidazole oxidatively adds to Pd<sup>0</sup> and Pt<sup>0</sup> leading to complexes of type **69** [74a]. A similar one-pot oxidative addition was observed between 2-halogenato-*N*-methylbenzimidazoles and Ni<sup>0</sup> complexes in the presence of NH<sub>4</sub>BF<sub>4</sub> as a proton source [74b]. It was proposed that these reactions proceed by an initial oxidative addition of the C2–X bond to the transition metal to give the intermediate **67** (Scheme 9.20 for M = Pd, pathway a).



**Scheme 9.18** (a–c) Reactions of donor-functionalized C2-H azoles with selected transition metals.

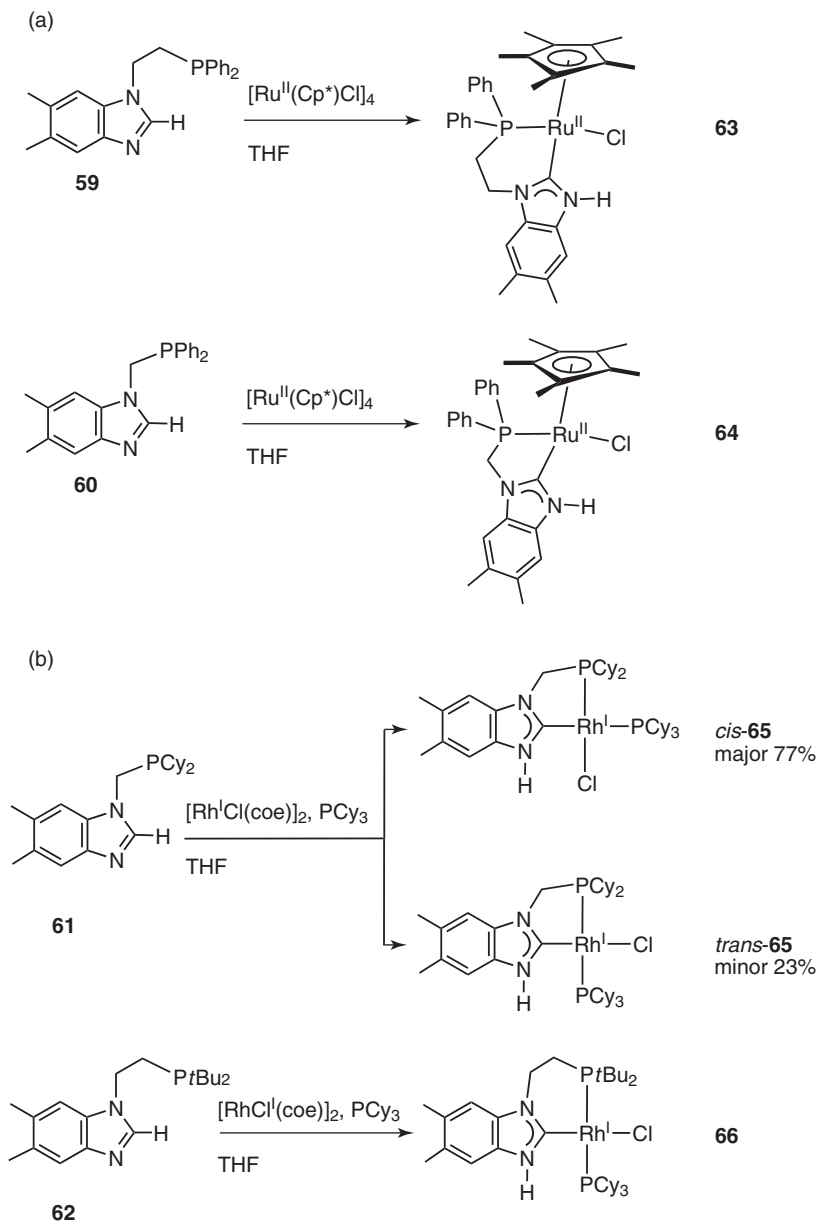
This intermediate would feature an unusual anionic NHC ligand with an unsubstituted ring-nitrogen atom. Subsequent N-protonation leads to complex **69**. Alternatively, but not very likely, the 2-chloro-*N*-methylbenzimidazolium cation **68** that then oxidatively adds as described [72] to the transition metal (Scheme 9.20, pathway b).

While the protonation of benzimidazoles by  $\text{NH}_4\text{BF}_4$  is not very likely (pathway b in Scheme 9.20), the formation of **69** does not provide any information on which pathway is operative. Such information can be obtained if the oxidative addition is performed in the absence of a proton source. The reaction of 2-chloro-*N*-methylbenzimidazole with  $[\text{Pt}^0(\text{PPh}_3)_4]$  in toluene yields a mixture of complexes **70** and **71** (Scheme 9.21). Complex **71** is formed by dimerization of the reaction product of the initial oxidative addition clearly demonstrating that the oxidative addition precedes the protonation step (pathway a in Scheme 9.20). Related dinuclear complexes have been obtained by N-deprotonation and dimerization of complexes bearing protic NHC ligands [32, 75].

Even more interesting is complex **70** that constitutes the initial product of the oxidative addition of the 2-chloro-*N*-methylbenzimidazole. This complex, which has been characterized by X-ray diffraction [76], bears an anionic NHC ligand with a naked, unsubstituted nitrogen atom. Density functional theory (DFT) calculations show that the negative charge is located at the unsubstituted ring-nitrogen atom.

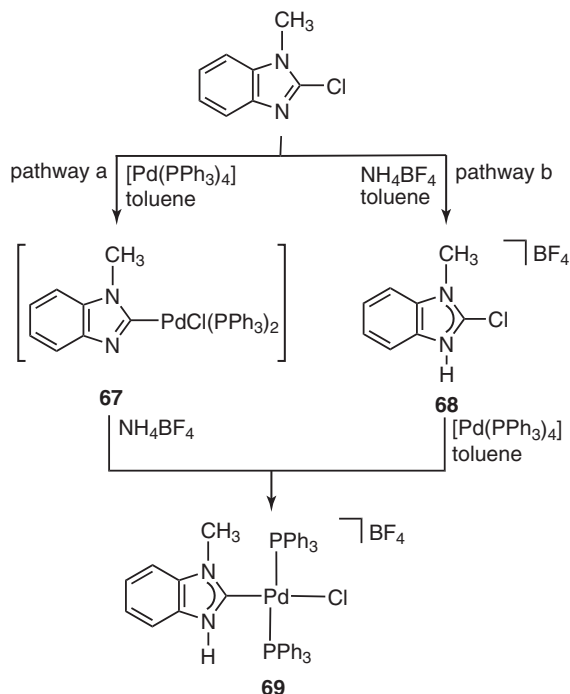
The electronic situation within the heterocycle of **70** explains its reactivity as a strong Lewis base. Preparation of complexes of type **70** in the presence of a proton source leads to the complex with the protonated NR,NH-NHC ligand (Scheme 9.20). In the absence of a proton source, complex **70** can react to give the dinuclear species **71** via interaction of the anionic nitrogen atom with the metal center of a neighboring molecule. The nucleophilic ring-nitrogen atom in **70** can also react with haloalkanes to yield complexes with classical NR,NR-NHC ligands. This type of reactivity was first observed when a dichloromethane solution of **70** was allowed to stand for a few weeks. The observed *N*-alkylation reaction could be reproduced and accelerated by dissolving **70** in a small amount of dichloromethane and heating the solution to 100 °C in a pressure tube for 16 h. After purification, **72** was obtained as a colorless solid in 67% yield (Scheme 9.21) [76].

It should be noted that the oxidative addition of the C2–X bond (X = H, halogen) of neutral *N*-alkylazoles yields different reaction products depending on the substituent X. It was proposed that the reaction of C2–H azoles (Scheme

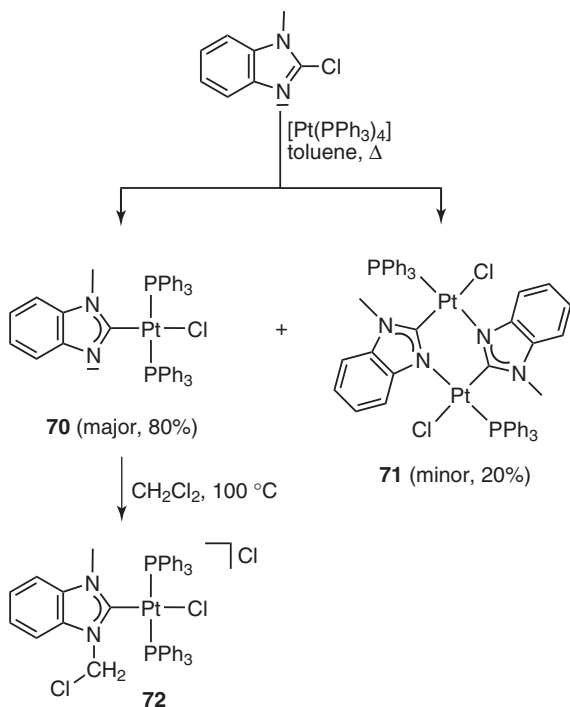


**Scheme 9.19** (a, b) Reactions of *N*-alkylphosphine functionalized benzimidazoles with  $\text{Ru}^{\text{II}}$  and  $\text{Rh}^{\text{I}}$ .

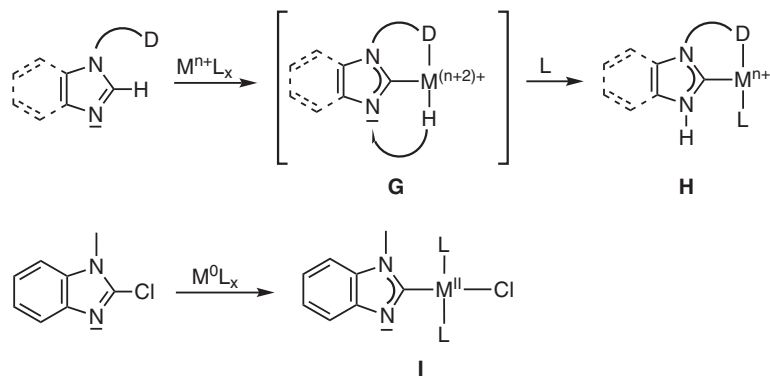
9.18 and Scheme 9.19) most likely proceeds under initial C2–H oxidative addition [76]. The initial reaction product, metal hydride complex **G** (Scheme 9.22), is not stable in the presence of the strongly basic anionic  $\text{NR,NH-NHC}$  ligand and reacts further via reductive elimination of a proton that subsequently protonates the anionic ring-nitrogen atom of the NHC. The result is complex **H** featuring the metal center in the initial oxidation state. It is not clear yet if the proton shift proceeds in an intra- or intermolecular manner. The reductive elimination of a proton from metal hydride complexes after the oxidative addition of a C2–H bond is a well-established reaction, at least for azolium salts [77]. Quantum chemical calculations have shown that this reaction sequence is also feasible for the C2–H oxidative addition of neutral *N*-alkyl substituted azoles [78]. Thus, the “formal tautomerization” [67–69] observed in the reaction of neutral C2–H azoles with transition metals is best described as a “redox-tautomerization” [71, 76] involving an oxidative addition/reductive elimination reaction sequence. This type of ligand shift from the metal to the coordinated NHC ligand is not observed after the oxidative addition of the C2–Cl bond of 2-chloro-*N*-methylbenzimidazole to  $\text{Pt}^0$  or  $\text{Ni}^0$ , which (in the absence of a proton source) leads to isolable complexes of type **I** featuring an NHC ligand with an anionic unsubstituted ring-nitrogen atom (Scheme 9.22).



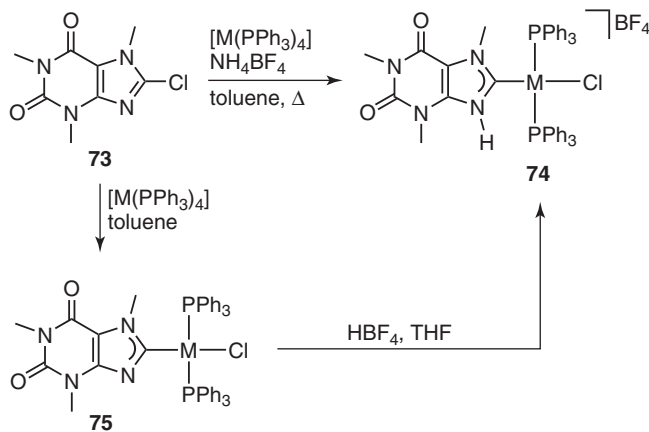
**Scheme 9.20** Alternative pathways for the oxidative addition of 2-chloro-*N*-methylbenzimidazole to  $\text{Pd}^0$ .



**Scheme 9.21** Oxidative addition of 2-chloro-*N*-methylbenzimidazole to  $\text{Pt}^0$  in the absence of a proton source.



**Scheme 9.22** Proposed mechanism for the oxidative addition of C2–H and C2–X bonds of azoles to transition metals.



**Scheme 9.23** Synthesis of complexes bearing C8-metallated caffeine.

Complexes of type **G** are rather rare and have so far only been obtained by deprotonation of coordinated NR,NH-NHCs [67, 68]. The direct access to complexes featuring NR,N-NHC ligands by the oxidative addition of the C2–Cl bond of a 2-halogenato-*N*-alkylbenzimidazole is much more facile and allows a rich follow-up chemistry like the N-protonation or *N*-alkylation of the NR,N-NHC ligand. Particularly, complexes bearing “protic” NHC ligands can be obtained easily by this way.

The oxidative addition of neutral azoles can be utilized for the synthesis of C-metallated biomolecules such as caffeine or adenine. For example, 8-chlorocaffeine **73** reacts with Pd<sup>0</sup> or Pt<sup>0</sup> complexes to yield the complexes bearing a C8-metallated caffeine “carbene” ligand. Depending on the reaction conditions, both the N-protonated derivatives **74** and the complexes bearing a caffeine ligand with an unsubstituted nitrogen atom adjacent to the carbene carbon atom **75** have been isolated and crystallographically characterized (Scheme 9.23) [79].

## 9.5 CONCLUSION

Complexes bearing protic NHC ligands are accessible by various synthetic routes such as the deprotonation of azoles followed by reaction with a transition metal complex, the template-controlled cyclization of functionalized isocyanides, and the oxidative addition of different azoles to transition metal complexes. The complexes with simple monodentate NR,NH-NHCs often tend to tautomerize to give the N-bound azoles. This type of tautomerization is prevented in complexes with donor-functionalized NR,NH-NHCs. Recent studies demonstrate that complexes with protic NHCs obtained from C2–H azoles are formed by an oxidative addition/reductive elimination reaction sequence. The N–H group in complexes with protic NR,NH-NHCs can serve as a hydrogen bond donor and thus as a molecular recognition unit and may enable various types of bifunctional catalysis. Recent studies indicate that even biomolecules such as caffeine can be C8-metallated. It

should be possible to extend this chemistry to other biomolecules such as DNA building blocks (such as adenine), which would lead to new bioorganometallic chemistry.

## ACKNOWLEDGMENT

The author thanks the Deutsche Forschungsgemeinschaft (SFB 858) for financial support.

## REFERENCES

- Bruice, T. C.; Lightstone, F. C. *Acc. Chem. Res.* **1999**, *32*, 127.
- (a) Coolen, H. K. A. C.; van Leeuwen, P. W. N. M.; Nolte, R. J. M. *Angew. Chem. Int. Ed Engl.* **1992**, *31*, 905. (b) Reetz, M. T.; Waldvogel, S. R. *Angew. Chem. Int. Ed Engl.* **1997**, *36*, 865. (c) Reetz, M. T. *Top. Catal.* **1997**, *4*, 187. (d) Rowlands, G. J. *Tetrahedron* **2001**, *57*, 1865. (e) Wilkinson, M. J.; van Leeuwen, P. W. N. M.; Reek, J. N. H. *Org. Biomol. Chem.* **2005**, *3*, 2371.
- (a) Larsen, J.; Rasmussen, B. S.; Hazell, R. G.; Skrydstrup, T. *Chem. Commun.* **2004**, 202. (b) Takacs, J. M.; Reddy, D. S.; Moteki, S. A.; Wu, D.; Palencia, H. *J. Am. Chem. Soc.* **2004**, *126*, 4494. (c) Duckmanton, P. A.; Blake, A. J.; Love, J. B. *Inorg. Chem.* **2005**, *44*, 7708. (d) Jiang, X.-B.; Lefort, L.; Goudriaan, P. E.; de Vries, A. H. M.; van Leeuwen, P. W. N. M.; de Vries, J. G.; Reek, J. N. H. *Angew. Chem. Int. Ed.* **2006**, *45*, 1223. (e) Goettmann, F.; Le Floch, P.; Sanchez, C. *Chem. Commun.* **2006**, 2036. (f) Jónsson, S.; Odille, F. G. J.; Norrby, P.-O.; Wärnmark, K. *Org. Biomol. Chem.* **2006**, *4*, 1927. (g) Šmejkal, T.; Breit, B. *Organometallics* **2007**, *26*, 2461. (h) Jiang, X.-B.; van Leeuwen, P. W. N. M.; Reek, J. N. H. *Chem. Commun.* **2007**, 2287. (i) Sandee, A. J.; van der Burg, A. M.; Reek, J. N. H. *Chem. Commun.* **2007**, 864. (j) Waloch, C.; Wieland, J.; Keller, M.; Breit, B. *Angew. Chem. Int. Ed.* **2007**, *46*, 3037. (k) Weis, M.; Waloch, C.; Seiche, W.; Breit, B. *J. Am. Chem. Soc.* **2006**, *128*, 4188. (l) Clarke, M. L.; Fuentes, J. A. *Angew. Chem. Int. Ed.* **2007**, *46*, 930.
- Hayashi, T.; Kawamura, N.; Ito, Y. *J. Am. Chem. Soc.* **1987**, *109*, 7876.
- Yang, J.; Gabriele, B.; Belvedere, S.; Huang, Y.; Breslow, R. *J. Org. Chem.* **2002**, *67*, 5057.
- Das, S.; Incarvito, C. D.; Crabtree, R. H.; Brudvig, G. W. *Science* **2006**, *312*, 1941.
- (a) Breit, B. *Chem. Eur. J.* **2000**, *6*, 1519. (b) Breit, B. *Acc. Chem. Res.* **2003**, *36*, 264.
- Grothjahn, D. B. *Chem. Eur. J.* **2005**, *11*, 7146.
- Breuil, P.-A. R.; Patureau, F. W.; Reek, J. N. H. *Angew. Chem. Int. Ed.* **2009**, *48*, 2162.
- Šmejkal, T.; Breit, B. *Angew. Chem. Int. Ed.* **2008**, *47*, 311.
- Yoshinari, A.; Tazawa, A.; Kuwata, S.; Ikariya, T. *Chem. Asian J.* **2012**, *7*, 1417.
- Watanabe, M.; Kashiwame, Y.; Kuwata, S.; Ikariya, T. *Eur. J. Inorg. Chem.* **2012**, 504.
- Touge, T.; Hakamata, T.; Nara, H.; Kobayashi, T.; Sayo, N.; Saito, T.; Kayaki, Y.; Ikariya, T. *J. Am. Chem. Soc.* **2011**, *133*, 14960.
- Kuwata, S.; Ikariya, T. *Chem. Eur. J.* **2011**, *17*, 3542.
- (a) Melaimi, M.; Soleilhavoup, M.; Bertrand, G. *Angew. Chem. Int. Ed.* **2010**, *49*, 8810. (b) de Frémont, P.; Marion, N.; Nolan, S. P. *Coord. Chem. Rev.* **2009**, *293*, 862. (c) Hahn, F. E.; Jahnke, M. C. *Angew. Chem. Int. Ed.* **2008**, *47*, 3122. (d) Edwards, P. G.; Hahn, F. E. *Dalton Trans.* **2011**, *40*, 10278.
- (a) Herrmann, W. A. *Angew. Chem. Int. Ed.* **2002**, *41*, 1290. (b) Díez-González, S.; Marion, N.; Nolan, S. P. *Chem. Rev.* **2009**, *109*, 3612. (c) Poyatos, M.; Mata, J. A.; Peris, E. *Chem. Rev.* **2009**, *109*, 3677.
- Meier, N.; Hahn, F. E.; Pape, T.; Siering, C.; Waldvogel, S. R. *Eur. J. Inorg. Chem.* **2007**, 1210.
- (a) Ruiz, J.; Perandones, B. F. *J. Am. Chem. Soc.* **2007**, *129*, 9298. (b) Huertos, M. A.; Pérez, J.; Riera, L.; Díaz, J.; López, R. *Angew. Chem. Int. Ed.* **2010**, *49*, 6409.
- (a) Sini, G.; Eisenstein, O.; Crabtree, R. H. *Inorg. Chem.* **2002**, *41*, 602. (b) Häller, L. J. L.; Macgregor, S. A. *Eur. J. Inorg. Chem.* **2009**, 2000.
- (a) Bonati, F.; Burini, A.; Pietroni, B. R.; Bovio, B. *J. Organomet. Chem.* **1989**, *375*, 147. (b) Raubenheimer, H. G.; Cronje, S. J. *Organomet. Chem.* **2001**, *617–618*, 170.
- Sundberg, R. J.; Bryan, R. F.; Taylor, I. F. Jr.; Taube, H. *J. Am. Chem. Soc.* **1974**, *96*, 381.
- Burling, S.; Mahon, M. F.; Powell, R. E.; Whittlesey, M. K.; Williams, J. M. J. *J. Am. Chem. Soc.* **2006**, *128*, 13702.
- (a) Wang, X.; Chen, H.; Li, X. *Organometallics* **2007**, *26*, 4684–4687. (b) Brendler, E.; Hill, A. F.; Wagler, J. *Chem. Eur. J.* **2008**, *14*, 11300.
- Dobereiner, G. E.; Chamberlin, C. A.; Schley, N. D.; Crabtree, R. H. *Organometallics* **2010**, *29*, 5728.
- Kunz, P. C.; Wetzel, C.; Kögel, S.; Kassack, M. U.; Spingler, B. *Dalton Trans.* **2011**, *40*, 35.

26. (a) Rieger, D.; Lotz, S. D.; Kernbach, U.; Schröder, S.; André, C.; Fehlhammer, W. P. *Inorg. Chim. Acta* **1994**, *222*, 275. (b) Rieger, D.; Lotz, S. D.; Kernbach, U.; André, C.; Bertran-Nadal, J.; Fehlhammer, W. P. *J. Organomet. Chem.* **1995**, *491*, 135.
27. Tschugajeff, L.; Skanawy-Grigorjewa, M.; Posnjak, A. *Z. Anorg. Allg. Chem.* **1925**, *148*, 37.
28. (a) Rouschias, G.; Shaw, B. L. *Chem. Commun.* **1970**, 183. (b) Burke, A.; Balch, A. L.; Enemark, J. H. *J. Am. Chem. Soc.* **1970**, *92*, 2555. (c) Butler, W. M.; Enemark, J. H.; Parks, J.; Balch, A. L. *Inorg. Chem.* **1973**, *12*, 451. (d) Slaughter, L. M. *Comments Inorg. Chem.* **2008**, *29*, 46. (e) Vignolle, J.; Cattoën, X.; Bourissou, D. *Chem. Rev.* **2009**, *109*, 3333.
29. (a) Tamm, M.; Hahn, F. E. *Coord. Chem. Rev.* **1999**, *182*, 175. (b) Michelin, R. A.; Pombeiro, A. J. L.; Guedes da Silva, M. F. C. *Coord. Chem. Rev.* **2001**, *218*, 75.
30. Beck, W.; Weigand, W.; Nagel, U.; Schaal, M. *Angew. Chem. Int. Ed Engl.* **1984**, *23*, 377.
31. (a) Bär, E.; Völkl, A.; Beck, F.; Fehlhammer, W. P.; Robert, A. *J. Chem. Soc. Dalton Trans.* **1986**, 863. (b) Kunz, R.; Le Grel, P.; Fehlhammer, W. P. *J. Chem. Soc. Dalton Trans.* **1996**, 3231.
32. (a) Bertani, R.; Mozzon, M.; Michelin, R. A. *Inorg. Chem.* **1988**, *27*, 2809. (b) Bertani, R.; Mozzon, M.; Michelin, R. A.; Benetollo, F.; Bombieri, G.; Castilho, T. J.; Pombeiro, A. J. L. *Inorg. Chim. Acta* **1991**, *189*, 175.
33. (a) Beck, G.; Fehlhammer, W. P. *Angew. Chem. Int. Ed Engl.* **1988**, *27*, 1344. (b) Fehlhammer, W. P.; Beck, G. *J. Organomet. Chem.* **1989**, *369*, 105.
34. Brothers, P. J.; Roper, W. R. *Chem. Rev.* **1988**, *88*, 1293.
35. Motschi, H.; Angelici, R. J. *Organometallics* **1982**, *1*, 343.
36. Michelin, R. A.; Zanotto, L.; Braga, D.; Sabatino, P.; Angelici, R. J. *Inorg. Chem.* **1988**, *27*, 93.
37. (a) Ito, Y.; Hirao, T.; Tsubata, K.; Saegusa, T. *Tetrahedron Lett.* **1978**, *19*, 1535. (b) Fehlhammer, W. P.; Bliß, T.; Fuchs, J.; Holzmann, G. Z. *Naturforsch.* **1992**, *47b*, 79.
38. (a) Ruiz, J.; García, G.; Mosquera, M. E. G.; Perandones, B. F.; Gonzalo, M. P.; Vivanco, M. *J. Am. Chem. Soc.* **2005**, *127*, 8584. (b) Ruiz, J.; Perandones, B. F.; García, G.; Mosquera, M. E. G. *Organometallics* **2007**, *26*, 5687.
39. (a) Grundy, K. R.; Roper, W. R. *J. Organomet. Chem.* **1975**, *91*, C61. (b) Fehlhammer, W. P.; Bartel, K.; Petri, W. *J. Organomet. Chem.* **1975**, *87*, C34. (c) Fehlhammer, W. P.; Völkl, A.; Plaia, U.; Beck, G. *Chem. Ber.* **1987**, *120*, 2031. (d) Fehlhammer, W. P.; Zinner, G.; Beck, G.; Fuchs, J. *J. Organomet. Chem.* **1989**, *379*, 277.
40. (a) Bartel, K.; Fehlhammer, W. P. *Angew. Chem. Int. Ed.* **1974**, *13*, 599. (b) Kernbach, U.; Fehlhammer, W. P. *Inorg. Chim. Acta* **1995**, *235*, 299. (c) Fehlhammer, W. P.; Bartel, K.; Weinberger, P.; Plaia, U. *Chem. Ber.* **1985**, *118*, 2220.
41. Fehlhammer, W. P.; Bartel, K.; Plaia, U.; Völkl, A.; Liu, A. T. *Chem. Ber.* **1985**, *118*, 2235.
42. Plaia, U.; Stolzenberg, H.; Fehlhammer, W. P. *J. Am. Chem. Soc.* **1985**, *107*, 2171.
43. Hahn, F. E. *Angew. Chem. Int. Ed Engl.* **1993**, *32*, 650.
44. Ferris, J. P.; Antonucci, F. R.; Trimmer, R. W. *J. Am. Chem. Soc.* **1973**, *95*, 919.
45. Jutzi, P.; Gilge, U. *J. Organomet. Chem.* **1983**, *246*, 159.
46. (a) Hahn, F. E.; Tamm, M. *J. Organomet. Chem.* **1993**, *456*, C11. (b) Hahn, F. E.; Tamm, M. *J. Chem. Soc. Chem. Commun.* **1993**, 842. (c) Tamm, M.; Lügger, T.; Hahn, F. E. *Organometallics* **1996**, *15*, 1251. (d) Kernbach, U.; Lügger, T.; Hahn, F. E. Fehlhammer, W. P. *J. Organomet. Chem.* **1997**, *541*, 51. (e) Tamm, M.; Hahn, F. E. *Inorg. Chim. Acta* **1999**, *288*, 47. (f) Hahn, F. E.; Hein, P.; Lügger, T. *Z. Anorg. Allg. Chem.* **2003**, *629*, 1316. (g) Hahn, F. E.; Klusmann, D.; Pape, T. *Eur. J. Inorg. Chem.* **2008**, 4420.
47. Hahn, F. E.; Tamm, M. *Organometallics* **1995**, *14*, 2597.
48. Hahn, F. E.; Imhof, L. *Organometallics* **1997**, *16*, 763.
49. Hahn, F. E.; Tamm, M. *J. Chem. Soc. Chem. Commun.* **1995**, 569.
50. Hahn, F. E.; Tamm, M.; Lügger, T. *Angew. Chem. Int. Ed Engl.* **1994**, *33*, 1356.
51. (a) Hahn, F. E.; Radloff, C.; Pape, T.; Hepp, A. *Organometallics* **2008**, *27*, 6408. (b) Radloff, C.; Hahn, F. E.; Pape, T.; Fröhlich, R. *Dalton Trans.* **2009**, 7215.
52. (a) Conrady, F. M.; Fröhlich, R.; Schulte to Brinke, C.; Pape, T.; Hahn, F. E. *J. Am. Chem. Soc.* **2011**, *133*, 11496. (b) Schmidtendorf, M.; Pape, T.; Hahn, F. E. *Angew. Chem. Int. Ed.* **2012**, *51*, 2195.
53. Hahn, F. E.; Langenhahn, V.; Meier, N.; Lügger, T.; Fehlhammer, W. P. *Chem. Eur. J.* **2003**, *9*, 704.
54. Basato, M.; Michelin, R. A.; Mozzon, M.; Sgarbossa, P.; Tassan, A. *J. Organomet. Chem.* **2005**, *690*, 5414.
55. Flores-Figueroa, A.; Kaufhold, O.; Feldmann, K.-O.; Hahn, F. E. *Dalton Trans.* **2009**, 9334.
56. Hahn, F. E.; García Plumed, C.; Münder, M.; Lügger, T. *Chem. Eur. J.* **2004**, *10*, 6285.
57. Hahn, F. E.; Langenhahn, V.; Lügger, T.; Pape, T.; Le Van, D. *Angew. Chem. Int. Ed.* **2005**, *44*, 3759.
58. Hahn, F. E.; Langenhahn, V.; Pape, T. *Chem. Commun.* **2005**, 5390.
59. (a) Liu, C.-Y.; Chen, D.-Y.; Lee, G.-H.; Peng, S.-M.; Liu, S.-T. *Organometallics* **1996**, *15*, 1055. (b) Ku, R.-Z.; Chen, D.-Y.; Lee, G.-H.; Peng, S.-M.; Liu, S.-T. *Angew. Chem. Int. Ed Engl.* **1997**, *36*, 2631.
60. Kaufhold, O.; Flores-Figueroa, A.; Pape, T.; Hahn, F. E. *Organometallics* **2009**, *28*, 896.

61. Flores-Figueroa, A.; Pape, T.; Feldmann, K.-O.; Hahn, F. E. *Chem. Commun.* **2010**, *46*, 324.
62. Flores-Figueroa, A.; Blase, V.; Hahn, F. E., to be published.
63. (a) Kaufhold, O.; Stasch, A.; Edwards, P. G.; Hahn, F. E. *Chem. Commun.* **2007**, 1822. (b) Kaufhold, O.; Stasch, A.; Pape, T.; Hepp, A.; Edwards, P. G.; Newman, P. D.; Hahn, F. E. *J. Am. Chem. Soc.* **2009**, *131*, 306. (c) Flores-Figueroa, A.; Kaufhold, O.; Hepp, A.; Fröhlich, R.; Hahn, F. E. *Organometallics* **2009**, *28*, 6362. (d) Flores-Figueroa, A.; Pape, T.; Weigand, J. J.; Hahn, F. E. *Eur. J. Inorg. Chem.* **2010**, 2907. (e) Blasé, V.; Pape, T.; Hahn, F. E. *J. Organomet. Chem.* **2011**, *696*, 3337.
64. Dumke, A. C.; Pape, T.; Kösters, J.; Feldmann, K.-O.; Schulte to Brinke, C.; Hahn, F. E. *Organometallics* **2013**, *32*, 289.
65. Price, C.; Elsegood, M. R.; Clegg, W.; Rees, N. H.; Houlton, A. *Angew. Chem. Int. Ed Engl.* **1997**, *36*, 1762.
66. (a) Price, C.; Shipman, M. A.; Gummerson, S. L.; Houlton, A.; Clegg, W.; Elsegood, M. R. J. *J. Chem. Soc. Dalton Trans.* **2001**, 353. (b) Price, C.; Shipman, M. A.; Rees, N. H.; Elsegood, M. R. J.; Edwards, A. J.; Clegg, W.; Houlton, A. *Chem. Eur. J.* **2001**, *7*, 1194.
67. Tan, K. L.; Bergman, R. G.; Ellman, J. A. *J. Am. Chem. Soc.* **2002**, *124*, 3202.
68. Araki, K.; Kuwata, S.; Ikariya, T. *Organometallics* **2008**, *27*, 2176.
69. (a) Miranda-Soto, V.; Grotjahn, D. B.; DiPasquale, A. G.; Rheingold, A. L. *J. Am. Chem. Soc.* **2008**, *130*, 13200. (b) Miranda-Soto, V.; Grotjahn, D. B.; Cooksy, A. L.; Golen, J. A.; Moore, C. E.; Rheingold, A. L. *Angew. Chem. Int. Ed.* **2011**, *50*, 631.
70. Hahn, F. E.; Naziruddin, A. R.; Hepp, A.; Pape, T. *Organometallics* **2010**, *29*, 5283.
71. Naziruddin, A. R.; Hepp, A.; Pape, T.; Hahn, F. E. *Organometallics* **2011**, *30*, 5859.
72. Cavell, K. J.; McGuinness, D. S. *Coord. Chem. Rev.* **2004**, *248*, 671.
73. (a) Fraser, P. J.; Roper, W. R.; Stone, F. G. A. *J. Organomet. Chem.* **1973**, *50*, C54. (b) Fraser, P. J.; Roper, W. R.; Stone, F. G. A. *J. Chem. Soc. Dalton Trans.* **1974**, 102.
74. (a) Kösterke, T.; Pape, T.; Hahn, F. E. *J. Am. Chem. Soc.* **2011**, *133*, 2112. (b) Kösterke, T.; Pape, T.; Hahn, F. E. *Chem. Commun.* **2011**, *47*, 10773.
75. Zanotto, L.; Bertani, R.; Michelin, R. A. *Inorg. Chem.* **1990**, *29*, 3265.
76. Kösterke, T.; Kösters, J.; Würthwein, E.-U.; Mück-Lichtenfeld, C.; Schulte to Brinke, C.; Lahoz, F.; Hahn, F. E. *Chem. Eur. J.* **2012**, *18*, 14594.
77. (a) Viciana, M.; Poyatos, M.; Sanaú, M.; Peris, E.; Rossin, A.; Ujaque, G.; Lledós, A. *Organometallics* **2006**, *25*, 1120. (b) Viciana, M.; Mas-Marzá, E.; Poyatos, M.; Sanaú, M.; Crabtree, R. H.; Peris, E. *Angew. Chem. Int. Ed.* **2005**, *44*, 444.
78. Hawkes, K. J.; Cavell, K. J.; Yates, B. F. *Organometallics* **2008**, *27*, 4758.
79. Jahnke, M. C.; Herve, A.; Pape, T.; Schulte to Brinke, C.; Hahn, F. E. *Chem. Commun.*, to be published.

## CYCLOPENTADIENYL-FUNCTIONALIZED *N*-HETEROCYCLIC CARBENE COMPLEXES OF IRON AND NICKEL: CATALYSTS FOR REDUCTIONS

BEATRIZ ROYO

*Instituto de Tecnologia Química e Biológica, Universidade Nova de Lisboa, Oeiras, Portugal*

### 10.1 INTRODUCTION

*N*-heterocyclic carbenes (NHCs), singlet carbenes with the carbene being incorporated in a nitrogen-containing heterocyclic, have emerged as a new class of versatile ancillary ligands in organometallic chemistry [1–4]. Their powerful electron-donating properties, strong binding energies, and specific topology are key features that make NHCs very attractive ligands. The easy access to NHCs and their potential application in a large number of homogeneously catalyzed processes has led to a rapid development in the design of new NHC-containing ligands with different topologies [5–8]. Now, we can find in the literature a large number of examples in which NHCs are incorporated into chelating [9], pincer [10, 11], and chiral [12, 13] architectures. Polydentate NHC ligands in which the carbene is bound to a neutral or an anionic donor by an organic linker are under constant development, because they can offer stability and fine-tuning of the stereoelectronic properties of their metal complexes [14]. It has been demonstrated that NHC ligands are compatible with a large set of functionalities including pyridines, phosphines, oxazolines, amino, ethers, alkoxo, amides, and other donor groups [14–17]. Recently, cyclopentadienyls tethered to NHC ligands (Cp-NHCs) have attracted the interest of some research groups [18–35]. The cyclopentadienyl ( $\text{Cp} = \text{C}_5\text{R}_5$ ) ligand is probably the most popular spectator ligand in organometallic chemistry. The Cp, an electron donor ligand of five electrons, binds very strongly to transition metal centers, predominantly in a  $\eta^5$  manner and its steric and electronic properties can be easily modified by introducing appropriate substituents on the five-membered ring [36, 37]. Cyclopentadienyl ligands with pendant donors such as phosphines and amino groups have been the subject of intensive research [38–41].

Cp-functionalized *N*-heterocyclic ligands remained elusive until the work reported by Danopoulos and coworkers in 2006, in which two indenyl- and fluorenyl-NHC-functionalized ligands were reported [18]. Two years later, our group described the synthesis of the first tetramethylcyclopentadienyl tethered to an NHC ( $\text{Cp}^*\text{-NHC}$ ) ( $\text{Cp}^* = \eta^5\text{-C}_5\text{Me}_4$ ) [27]. The introduction of chelating Cp-NHC ligands in the coordination sphere of metal complexes has some interesting consequences because they can increase the thermal stability of their metal complexes and favor the rigidity required for the preparation of effective catalysts. The possibility to independently vary their structural components, the cyclopentadienyl ring, the spacer, and the azole unit offers an enormous synthetic flexibility and allows the fine-tuning of the steric and electronic properties of the metal center. In addition, the indirect tuning of metal-NHC bonding by the adjustment of the length of the tether may have important consequences in catalyst design.

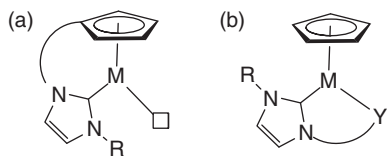


**Figure 10.1** Chelation introduced through the Cp-NHC unit (a) or through a bidentate NHC-Y ligand (b).

An important advantage of the Cp tethered to NHC ligands compared to the nonlinked systems is that chelation does not consume an “extra” coordination site, leaving the metal complexes with an additional site for catalysis (Fig. 10.1). As we have already pointed out, the tethered NHC unit could not only increase the stability of the half-sandwich metal–NHC complexes by chelation, but also could enhance the catalytic activity of their metal complexes by the stabilization of intermediate active species. In addition, the hemilabile dynamic behavior of the Cp-NHC ligand may allow to efficiently control the reactivity and stability of the catalytically active center.

An interesting feature of these bidentate ligands is that the introduction of chirality in the linker between the Cp and the NHC units can help to control the stereochemistry of reactions taking place at the metal center and eventually can increase the stereoselection in asymmetric processes. In this line, half-sandwich complexes bearing chiral Cp-NHC ligands may offer a good opportunity to design organometallic chiral-at-metal complexes, as the linked Cp-NHC system could assist in controlling the metal configuration. This approach has already afforded some degrees of success in metal half-sandwich complexes bearing cyclopentadienyls tethered to chiral phosphines [42]. In addition, the different strength of the metal–NHC bond across the periodic table may lead to versatile coordination chemistry.

## 10.2 PREPARATION OF CYCLOPENTADIENYL-FUNCTIONALIZED N-HETEROCYCLIC CARBENE LIGANDS

Several synthetic pathways are used for the synthesis of NHCs tethered to cyclopentadienyl ligands. Each of the available procedures presents both advantages and limitations. A convenient and flexible entry to tetramethylcyclopentadienyl-functionalized NHC ligands is by deprotonation at the methylene group of benzylimidazole with *n*-BuLi, followed by the reaction with 1,2,3,4-tetramethylfulvene, and treatment with methanol. Subsequent reaction with iodomethane affords the corresponding tetramethylcyclopentadienyl-functionalized imidazolium salts as a mixture of three isomers resulting from the different position of the double bonds in the cyclopentadienyl ring (Fig. 10.2). However, this fact does not interfere with the coordination to a metal center [27].

An advantage of this pathway is that it permits the introduction of different substituents on the cyclopentadienyl ring and at the carbon adjacent to the Cp unit by choosing the appropriate fulvenes. Following this synthetic procedure, differently substituted cyclopentadienyl-functionalized NHCs, Cp<sup>x</sup>-NHCs [ $\text{Cp}^x = \text{Cp}(\eta^5\text{-C}_5\text{H}_4)$ ;  $\text{Cp}^*(\eta^5\text{-C}_5\text{Me}_4)$ ;  $\text{Cp}^{\text{Bz}}(\eta^5\text{-C}_5(\text{CH}_2\text{Ph})_4)$ ] can be prepared (Fig. 10.3) [29]. In addition, this synthetic approach introduces a stereogenic center at the linker between the Cp and the NHC units, affording a chiral ligand, although racemic mixtures of the two possible enantiomers of the final pro-ligands are isolated. However, it does not allow preparing pure chiral ligands. Starting from enantiomerically pure *S*-1-(phenylethyl)imidazole and following the synthetic procedure previously described, the final imidazolium pro-ligand is obtained as a racemate, probably deprotonation of *S*-1-(phenylethyl)imidazole with *n*-BuLi produces racemization of the imidazolyl intermediate [28].

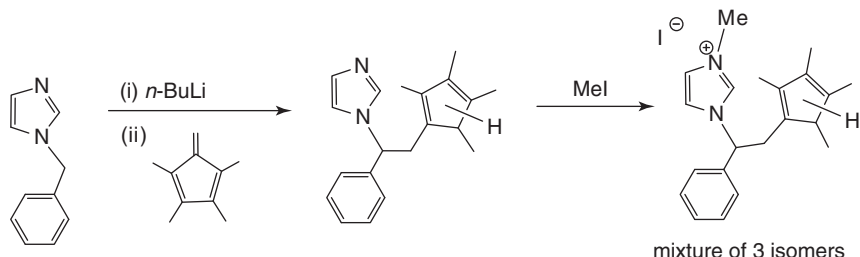


**Figure 10.2** Synthesis of tetramethylcyclopentadienyl-functionalized imidazolium salts.

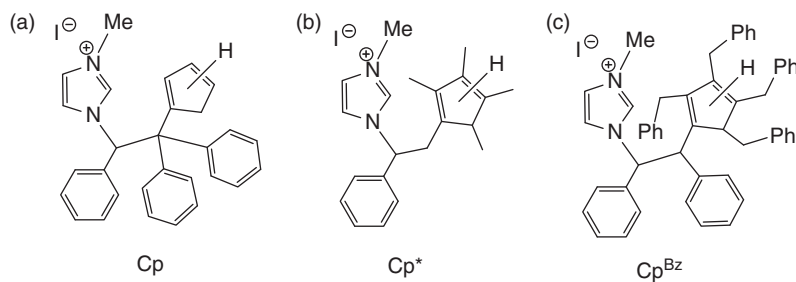


**Figure 10.3** Unsubstituted and substituted cyclopentadienyl-functionalized imidazolium pro-ligands.

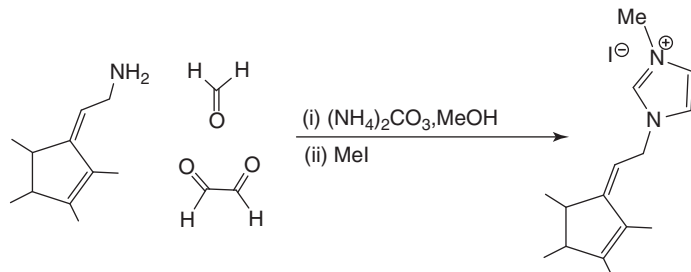


**Figure 10.4** One pot synthesis of tetramethylcyclopentadienyl-functionalized imidazolium iodide.

An alternative method for the preparation of tetramethylcyclopentadiene imidazolium pro-ligand is the one pot synthesis route, starting from the easily accessible 2-(2,3,4-tetramethylcyclopentadienyl)-ethylamine [43] by condensation with glyoxal and formaldehyde. Further quaternization with iodomethane yields the corresponding imidazolium iodide (Fig. 10.4) [28]. Isomerization of the exocyclic double bond of the linker chain to give the endocyclic double bond isomers has to be addressed before coordination to a metal center. However, it has been noticed that late transition metals mediate isomerization of the exocyclic bond forming the  $\eta^5$ -cyclopentadienyl fragment in the presence of acetic acid [28]. The advantage of this protocol as compared to the synthetic approach described earlier is that the one pot reaction can be performed in large scale, and the final product is purified by a simple crystallization without further need of column chromatography, which is required in the purification of the 1-alkylimidazoles described earlier. This synthesis is restricted to the preparation of tetramethylcyclopentadienyl-functionalized imidazolium salts.

The previously described procedures are limited to the introduction of a primary alkyl on the nitrogen atom of the imidazole ring. When substituents other than primary alkyls are required on the nitrogen atom, the appropriate secondary and tertiary 1-alkylimidazoles have to be reacted with the Cp ligand carrying an alkyl halide linker group. This synthetic approach has been used to synthesize indenyl- and fluorenyl-functionalized NHCs (Fig. 10.5) [18]. The length of the linker can be easily modified using this synthetic approach, and in fact the corresponding three carbon side chain was introduced by the reaction of 3-bromo-propylindene with the corresponding 1-alkyl imidazole [19, 22]. However, this synthetic method cannot be applied for the synthesis of substituted cyclopentadienyl-functionalized imidazolium salts. Direct alkylation of 1,2,3,4-tetraalkylcyclopentadienides with alkyl halides or alkyl toluenesulfonates has no use in the preparation of 5-alkyl-1,2,3,4-tetraalkylcyclopentadienides because of problems with regioselectivity [44]. An inseparable mixture of nongeminal (Fig. 10.6a) and geminal-substituted cyclopentadienides (Fig. 10.6b and c) is often obtained.

Enantiomerically pure Cp-functionalized NHC ligands are synthesized starting from readily available, enantiomerically pure amino acids, such as L-valinol. The corresponding imidazole carrying a pendant alcohol is generated following

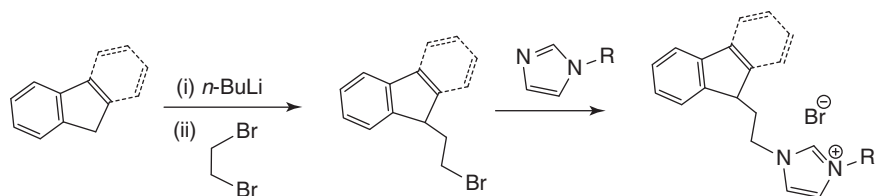


**Figure 10.5** Synthesis of indenyl- and fluorenyl-functionalized imidazolium pro-ligands.

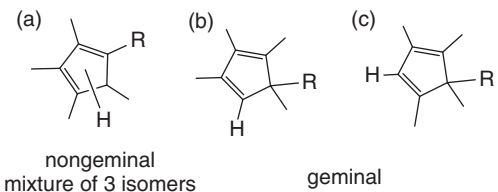


**Figure 10.6** (a–c) Regio-isomers of substituted tetraalkylcyclopentadienyl ligands.

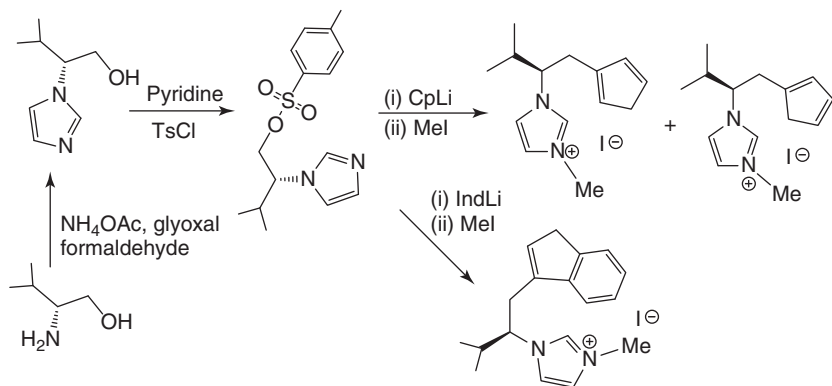


**Figure 10.7** Synthesis of chiral cyclopentadienyl- and indenyl-imidazolium pro-ligands.

the procedure introduced by Saigo by the condensation reaction of the amino alcohol with ammonium acetate, glyoxal, and formaldehyde [45]. The alcohol is then converted to the corresponding tosylate, which is a better leaving group [46]. Subsequent reaction of the imidazole tosylate with cyclopentadienyl lithium salt, followed by treatment with iodomethane, affords the corresponding chiral cyclopentadienyl-functionalized imidazolium pro-ligand [32] (Fig. 10.7). This method is limited to preparing unsubstituted cyclopentadienyls because of the lack of regioselectivity in the reaction with alkylsubstituted cyclopentadienides previously discussed, but it can be extended to the synthesis of indenyl-functionalized NHCs.

### 10.3 CYCLOPENTADIENYL-FUNCTIONALIZED N-HETEROCYCLIC CARBENE COMPLEXES OF IRON AND NICKEL

Iron and other first-row transition metal–NHC complexes are generally prepared either via free carbenes, generated by deprotonation of imidazolium salts with a strong base ( $\text{NaH}$ ,  $n\text{-BuLi}$ ,  $t\text{-BuOK}$ ) [47–51], or by the reaction of a metal amide with an imidazolium salt [52–55]. Transmetallation from silver NHC adducts has rarely been used in iron chemistry [56, 57]. Piano-stool iron complexes bearing cyclopentadienyl-functionalized NHCs are prepared by treating the bifunctional  $\text{Cp}^x\text{-NHC}$  pro-ligands with two equivalents of  $n\text{-BuLi}$  to provide the corresponding lithium salts ( $\text{Cp}^x\text{-NHC}\text{Li}(\text{THF})_n$ ), which are used *in situ* to form the half-sandwich Fe–NHC complexes, after addition of the appropriate iron precursor (Fig. 10.8). The lithium salts ( $\text{Cp}^x\text{-NHC}\text{Li}(\text{THF})_n$ ) are stable enough to be isolated and characterized by nuclear magnetic resonance (NMR) spectroscopy. Following this synthetic pathway, the iron(II) carbonyl complexes of general type ( $\text{Cp}^x\text{-NHC}\text{Fe}(\text{CO})\text{I}$ ) (Fig. 10.9a–c), and the coordinatively and electronically unsaturated iron(II) species ( $\text{Cp}^*\text{-NHC}\text{FeCl}$ ) (Fig. 10.9d), are prepared [31].

Remarkably, the iron complexes of the general type ( $\text{Cp}^x\text{-NHC}\text{Fe}(\text{CO})\text{I}$ ) can also be obtained by direct reaction of the corresponding imidazolium pro-ligands with commercially available triiron dodecacarbonyl,  $\text{Fe}_3(\text{CO})_{12}$ , in refluxing toluene (Fig. 10.10). This reaction gives the iron carbonyl complexes with high yield and purity, providing an easy access to these organometallic half-sandwich Fe–NHC complexes [34]. Moreover, the reaction can be performed in large scale (up to 2 g). The main advantage of this one-step synthesis is that it avoids the generation of free carbenes, which requires harsh conditions such as strong base ( $n\text{-BuLi}$ ), and in addition, it does not require the preparation of the iron precursor  $\text{FeI}_2(\text{CO})_4$ . The formation of the chelating iron complexes ( $\text{Cp}^x\text{-NHC}\text{Fe}(\text{CO})\text{I}$ ) probably implies the oxidative addition of the

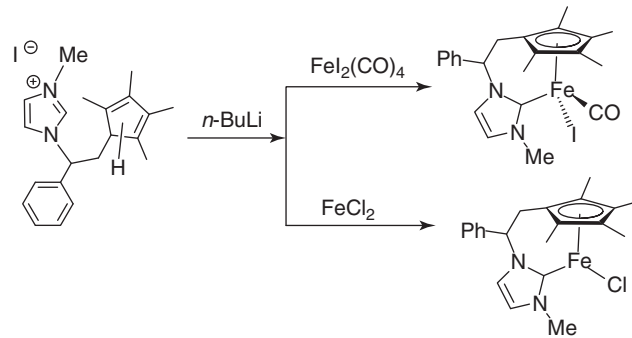


**Figure 10.8** Synthesis of iron(II) complexes bearing tetramethylcyclopentadienyl-functionalized NHC ligands.

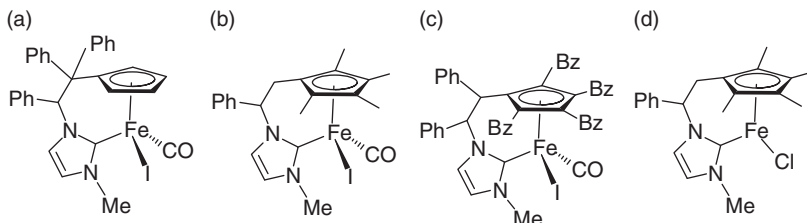


**Figure 10.9** (a–d) Iron(II) complexes with Cp-tethered NHC ligands.

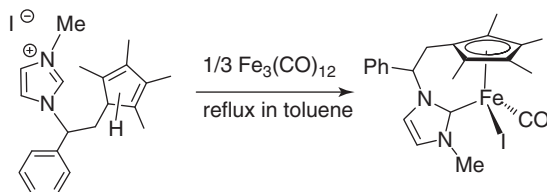


**Figure 10.10** Direct reaction of Cp\*-functionalized imidazolium pro-ligands with  $\text{Fe}_3(\text{CO})_{12}$ .

imidazolium salt to  $\text{Fe}(0)$ , followed by the elimination of the  $\text{Fe}-\text{H}$  intermediate and the cyclopentadienyl proton. A similar reaction pathway was reported for the synthesis of related ruthenium complexes [23, 30]. However, C–H activation of an imidazolium salt mediated by an iron(0) species has no precedent in Fe–NHC chemistry. Remarkably, the presence of base is not required in this reaction.

Following this synthetic method, substituted and unsubstituted cyclopentadienyl-functionalized NHCs of Fe(II) can be prepared. These iron complexes, isolated as green crystalline solids, are very stable in the solid state and can be handled in air.

Infrared spectroscopy provides valuable information on the donor strength of the Cp–NHC ligands. The lower frequency of the CO-stretching band in the tetramethylcyclopentadienyl complex ( $\text{Cp}^*-\text{NHC}\text{Fe}(\text{CO})\text{I}$ ) [ $\nu(\text{CO})$   $1906\text{ cm}^{-1}$ ] indicates the stronger electron donation of  $\text{Cp}^*$  compared to  $\text{Cp}$  and  $\text{Cp}^{\text{Bz}}$  in  $(\text{Cp}-\text{NHC})\text{Fe}(\text{CO})\text{I}$  [ $\nu(\text{CO})$   $1949\text{ cm}^{-1}$ ] and  $(\text{Cp}^{\text{Bz}}-\text{NHC})\text{Fe}(\text{CO})\text{I}$  [ $\nu(\text{CO})$   $1920\text{ cm}^{-1}$ ] complexes, respectively. The presence of the NHC fragment also has a clear influence on the frequency of the band, as we can see if we compare the bands shown for the  $(\text{Cp}-\text{NHC})\text{Fe}(\text{CO})\text{I}$  complex with the bands displayed by  $\text{Cp}\text{Fe}(\text{CO})_2\text{I}$  [ $\nu(\text{CO})$   $2035, 2000\text{ cm}^{-1}$ ] [58]. Interestingly, the linker between the Cp and the NHC fragment seems to have an effect on the electronic situation of the metal center; the  $\nu(\text{CO})$  of the tethered complex ( $\text{Cp}-\text{NHC})\text{Fe}(\text{CO})\text{I}$  appears at higher wave numbers ( $1949\text{ cm}^{-1}$ ) than those for the related nonlinked Cp, NHC systems, which display a CO-stretching band at circa  $1936\text{ cm}^{-1}$  [49, 59]. This shift suggests lower electron density on the metal center in the tethered ( $\text{Cp}-\text{NHC})\text{Fe}(\text{CO})\text{I}$  complex compared to the nonlinked systems (Fig. 10.11).

The presence of the sterogenic centers at the aliphatic linker between the NHC and the cyclopentadienyl ring, and at the metal center, implies that a mixture of diastereomeric complexes is expected. NMR experiments (variable temperature

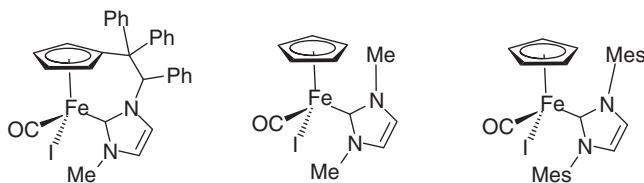


**Figure 10.11** Tethered and untethered Fe(II) complexes bearing Cp and NHC ligands.

NMR studies and NMR carried out in different solvents) suggest that only one distereomer is formed in the reaction [60]. The  $^{13}\text{C}$  NMR spectra display the characteristic  $\text{Fe}-\text{C}_{\text{carbene}}$  signals at 188 (for a, 10.9a), 195 (for b, 10.9b), and 193 (for c, 10.9c) as expected because of the stronger electron donor capability of the  $\text{Cp}^*$  ligand in complex **B** compared to Cp and  $\text{Cp}^{\text{Bz}}$  (Fig. 10.9a–c).

The known crystal structures of the cyclopentadienyl-functionalized NHC iron carbonyl complexes show distorted four-legged piano-stool geometry [31]. The cyclopentadienyl-NHC ligand adopts a bidentate coordination mode, chelating through the five-membered ring of the cyclopentadienyl and the NHC groups (Fig. 10.12). The small difference (ca.  $3^\circ$ ) in the exocyclic and endocyclic  $\text{N}-\text{C}_{\text{NHC}}-\text{Fe}$  angles indicates low strain in the chelate. The  $\text{Fe}-\text{carbene}$  bond distance of 1.942(4) Å is slightly shorter than in the nonlinked monocarbene complex  $\text{CpFe}(\text{IMes})(\text{CO})\text{I}$  1.980(5) Å [59], probably as a consequence of both steric constrains of the chelate and the steric effect of the bulkier mesityl substituent of the imidazole ring compared to the methyl group in the tethered ( $\text{Cp-NHC}\text{Fe}(\text{CO})\text{I}$ ) complex. The chelating configuration can also explain the slightly longer distance of the  $\text{Fe}-\text{I}$  bond in ( $\text{Cp-NHC}\text{Fe}(\text{CO})\text{I}$ ) (2.6452 Å) compared to that distance in the related nonlinked system  $\text{CpFe}(\text{IMes})(\text{CO})\text{I}$  (2.6311 Å).

The nickel complex bearing the tetramethylcyclopentadienyl-functionalized NHC ( $\text{Cp}^*\text{-NHC}\text{NiCl}$ ) is prepared by the reaction of  $\text{NiCl}_2(\text{DME})$  (DME, dimethoxyethane) with the corresponding lithium salt ( $\text{Cp}^*\text{-NHC}\text{Li}(\text{THF})_n$ ) [35] (Fig. 10.13). This complex is thermally stable; its toluene solutions are heated up to 120 °C without notice of any decomposition. However, it is rather sensitive to air and moisture and it has to be manipulated under nitrogen atmosphere.

The  $^{13}\text{C}$  NMR spectrum of ( $\text{Cp}^*\text{-NHC}\text{NiCl}$ ) displays the characteristic signal for the  $\text{Ni}-\text{C}_{\text{carbene}}$  at 176 ppm, which appears in the region of previously reported Ni–NHC complexes (170–180 ppm) [61–67]. The related nonlinked  $\text{Cp}^*\text{Ni}(\text{IMe})\text{I}$  (IMe, 1,3-dimethylimidazol-2-ylidene) complex exhibits similar resonance for its  $\text{Ni}-\text{C}_{\text{carbene}}$  at 175 ppm [61]. The only other known example of a Ni complex bearing a cyclopentadienyl-functionalized NHC ligand was reported in 2009 by Shen et al. [22]. Reaction of  $\text{NiCl}_2(\text{DME})$  with the *in situ* generated lithium salt of the indenyl-functionalized NHC

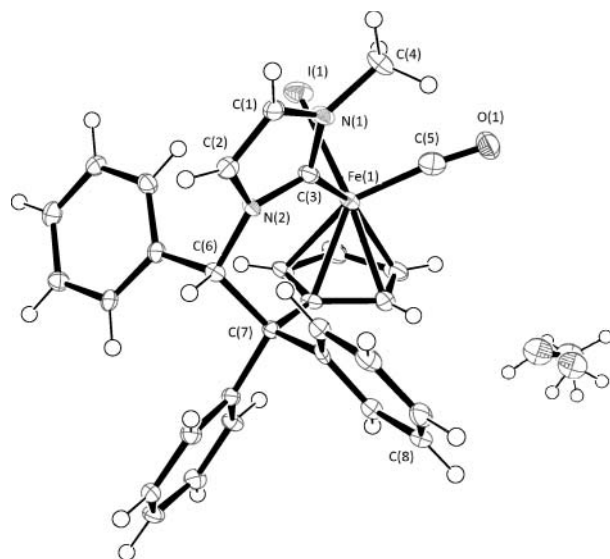


**Figure 10.12** Molecular diagram of ( $\text{Cp-NHC}\text{Fe}(\text{CO})\text{I}$ ). Selected bond distances (Å) and angles (deg):  $\text{Fe}(1)\text{-C}(3)$  1.942(4),  $\text{Fe}(1)\text{-I}(1)$  2.6452(6),  $\text{Fe}(1)\text{-C}(5)$  1.759(5),  $\text{C}(5)\text{-O}(1)$  1.134(5),  $\text{Fe}(1)\text{-Cpccentroid}$  2.0972,  $\text{C}(3)\text{-Fe}(1)\text{-I}(1)$  90.69(11),  $\text{C}(3)\text{-Fe}(1)\text{-C}(5)$  97.46(18),  $\text{C}(5)\text{-Fe}(1)\text{-I}(1)$  94.06(14),  $\text{Cpccentroid-Fe}(1)\text{-C}(3)$  120.538,  $\text{Cpccentroid-Fe}(1)\text{-I}(1)$  118.462,  $\text{Cpccentroid-Fe}(1)\text{-C}(5)$  117.06.

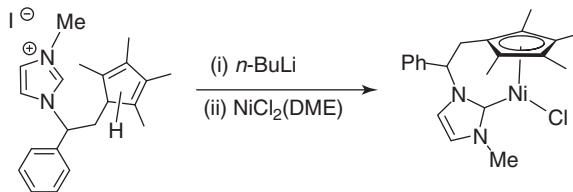


**Figure 10.13** Synthesis of a nickel tetramethylcyclopentadienyl-functionalized NHC complex.

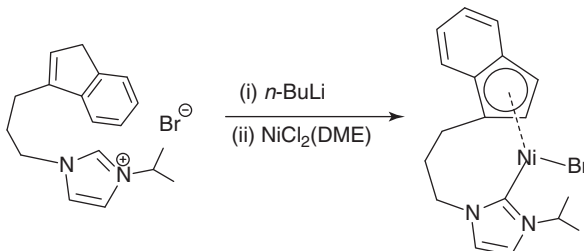


**Figure 10.14** Synthesis of a nickel Ind-functionalized NHC complex.

ligand afforded the half-sandwich (*Ind*-NHC) $\text{NiBr}$  complex (Fig. 10.14). The  $\text{Ni}-\text{C}_{\text{carbene}}$  signal in its  $^{13}\text{C}$  NMR spectrum (170 ppm) reflects the weaker donation of the indenyl ligand compared to the tetramethylcyclopentadienyl ligand.

#### 10.4 HALF-SANDWICH IRON AND NICKEL NHC COMPLEXES AS CATALYSTS FOR REDUCTIONS

In recent years, there has been significant interest in developing catalytic processes based on first-row transition metals. Global efforts in sustainability, coupled with increasing prices and concerns over long term supplies of precious metals, have pressured researchers to look for cheaper alternatives. The use of iron- and nickel-based catalysts is highly attractive, not only because of their low price and high abundance, but also because these metals are typically used in enzymes for numerous transformations of natural products. Among catalytic applications being developed, the reduction of carbonyl groups mediated by first-row transition metals is emerging as an exciting area of research [68–70]. The reduction of carbonyl groups is a fundamental process in organic synthesis. The catalytic reduction of aldehydes and ketones to the corresponding alcohols can be carried out either by hydrosilylation followed by hydrolysis or by transfer hydrogenation usually in the presence of an alcohol as a hydrogen donor and a base, or else by hydrogenation, which uses hydrogen as a reducing agent [71]. So far, the majority of the homogeneously catalyzed processes for the reduction of carbonyl groups are based on precious metals such as palladium, platinum, ruthenium, and rhodium. Replacement of these rare and expensive metals by first-row transition metals is highly desirable.

Recent developments on iron catalysis have shown the enormous potential of this metal in the reduction of carbonyl groups with hydrogen or using transfer hydrogen and silanes as reducing agents [69]. However, the use of well-defined iron–NHC complexes as catalysts for these reduction processes is rather undeveloped [72].

Cyclopentadienyl-functionalized NHCs of iron have shown to be active catalysts in the reduction of organic functionalities. Catalytic studies showed the potential of  $(\text{Cp}^{\text{x}}\text{-NHC})\text{Fe}(\text{CO})\text{I}$  and  $(\text{Cp-NHC})\text{FeCl}$  complexes (Fig. 10.9a–d) catalyzing the reduction of aldehydes and ketones through hydrogen transfer and hydrosilylation reactions [31]. A series of  $(\text{Cp}^{\text{x}}\text{-NHC})\text{Fe}(\text{CO})\text{I}$  complexes catalyzes the hydrogenation of  $\text{C}=\text{O}$  via hydrogen transfer from 2-propanol in the presence of a strong base (KOH) at  $80\text{ }^{\circ}\text{C}$ , achieving quantitative conversion to the corresponding alcohol in 6 h of reaction. Catalytic studies showed that different substitution on the cyclopentadienyl ring does not affect the catalytic performance in the hydrogen transfer of acetophenone. Comparable reactivity is displayed by the coordinatively unsaturated iron  $(\text{Cp}^*\text{-NHC})\text{FeCl}$  complex, which exhibited also good catalytic efficiency in the hydrosilylation of aldehydes [31].

In 2011, Sortais and Darcel described the activity of the related nonlinked half-sandwich iron complex  $[\text{CpFe}(\text{IMes})(\text{CO})_2]\text{I}$  [ $\text{IMes} = 1,3\text{-bis}(2,4,6\text{-trimethylphenyl})\text{imidazol-2-ylidene}$ ] (Fig. 10.15c) in the hydrosilylation of aldehydes and ketones [73], and more recently, they extended these studies to the reduction of amides [74], nitriles [74], imines

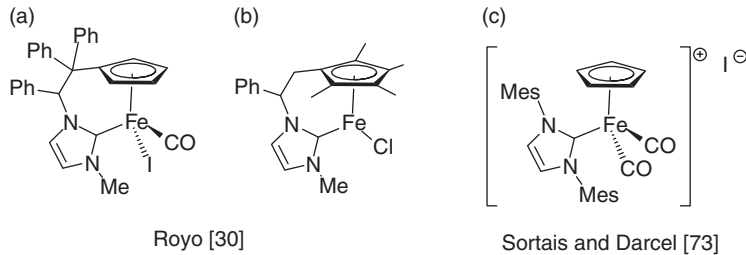


**Figure 10.15** (a, b)Tethered and (c) untethered Fe(II) catalysts for the reduction of organic functionalities.

[75], and esters [76]. The cationic  $[CpFe(IMes)(CO)_2]I$  species catalyzes the reaction under solvent-free conditions with light irradiation. The role of light and the nature of the active catalytic species are undisclosed. The formation of the neutral species  $CpFe(IMes)(CO)I$  by light irradiation of  $[CpFe(IMes)(CO)_2]I$  complexes is known [44], but the effect of light irradiation in the catalytic reaction remains unclear. Despite the mechanism of the hydrosilylation reactions catalyzed by the nonlinked  $[CpFe(IMes)(CO)_2]I$  and the tethered  $(Cp\text{-NHC})Fe(CO)I$  and  $(Cp\text{-NHC})FeCl$  complexes is currently unknown, the ability of the NHC ligand to stabilize coordinatively unsaturated iron complexes seems to play a crucial role. The implications that the presence of the linker between the Cp and the NHC units may have in the stability and reactivity of the catalytically active species is an interesting issue that undoubtedly will be explored in the future.

More recently, a novel catalytic system based on the iron complex  $(Cp\text{-NHC})Fe(CO)I$  (Fig. 10.15a) combined with  $AgBF_4/PhSiH_3$  resulted to be an efficient and selective method for the reduction of sulfoxides to sulfides [34]. The catalytic reaction is suitable for a variety of sulfoxides including aromatic and aliphatic. Radical scavenger experiments indicate the presence of free radicals in the catalytic reaction, suggesting a radical-base mechanism. The addition of both carbon- and oxygen-centered spin traps such as TEMPO (2,2,6,6-tetramethyl-piperidinyloxy) and BHT (2,6-di-*tert*-butyl-4-methylphenol) has a clear effect on the efficiency of the catalytic reaction. So far, the nature of the radical species is unknown.

Regarding the use of well-defined nickel complexes as catalysts for reduction of carbonyl groups, only three examples are described in the literature. In 2009, Guan and coworkers [77] described the efficiency of a nickel PCP-pincer complex performing the hydrosilylation of aldehydes. In the same year, the catalytic hydrosilylation of ketones via a transient Ni–H complex supported by a monoanionic bidentate amidophosphine ligand was reported by Mindiola [78]. Later, Jones investigated well-defined PNP nickel pincer complexes, which catalyzed the hydrosilylation of aldehydes [79] (Fig. 10.16).

Half-sandwich tetramethylcyclopentadienyl-functionalized NHC nickel complexes have proved to be very effective catalysts in the reduction of aldehydes and ketones. The nickel alkoxide  $(Cp^*\text{-NHC})Ni(OBu')_2$ , prepared by treatment of  $(Cp^*\text{-NHC})NiCl$  with  $KOBu'$  (Fig. 10.17), was isolated as a rather stable crystalline solid, which could be stored for weeks without noticeable decomposition. The tethered  $(Cp^*\text{-NHC})Ni(OBu')$  compound displays remarkable catalytic activity in the hydrosilylation of aldehydes using phenylsilane as a reducing agent. The catalytic reactions afford quantitative conversion to the corresponding alcohol in 5 min of reaction, at  $25^\circ C$ . Ketones are also reduced, although longer reaction times and higher temperatures are required to achieve good conversions of the corresponding alcohols.

Mechanistic studies, based on stoichiometric reactions, revealed that the transient nickel hydride  $(Cp^*\text{-NHC})NiH$  complex, generated by reaction of  $(Cp^*\text{-NHC})Ni(OBu')$  with phenylsilane, is the active species in the hydrosilylation of aldehydes. The identity of  $(Cp^*\text{-NHC})NiH$  was demonstrated by NMR spectroscopy (the characteristic hydride resonance appeared at  $-18$  ppm). Surprisingly, the Ni–H is fairly stable in solution; no decomposition is observed after being kept in solution for

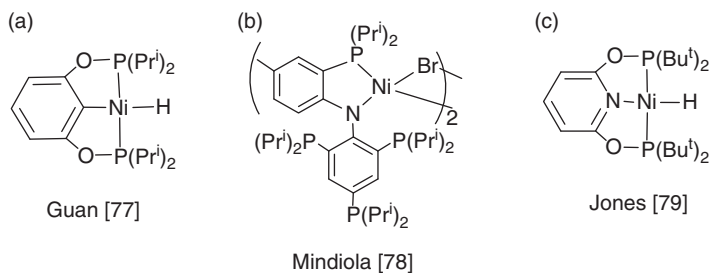


**Figure 10.16** (a–c) Well-defined Ni(II) complexes catalyzing the hydrosilylation of carbonyl groups.

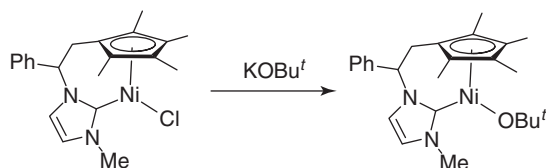


**Figure 10.17** Synthesis of a nickel alkoxo complex bearing a Cp\*-functionalized NHC ligand.

several days. This Ni hydride complex readily reacts with benzaldehyde to give the corresponding nickel benzyloxide. The fast C=O insertion of PhCHO into the nickel hydride suggests that the catalytic reaction may occur through the classical *hydride mechanism*, already proposed for other Cu- and Ni-alkoxo catalysts [78, 80–82]. This mechanistic proposal is based on the formation of a metal hydride intermediate on the addition of silane to the corresponding nickel alkoxo compound, followed by carbonyl insertion into the M–H bond to give an alkoxide (the *hydride mechanism*) [68]. However, isotopic labeling experiments carried out with deuterated silanes show that the hydride ligand does not directly participate in the reduction product, ruling out the classical hydride mechanism [35, 83]. Similar mechanistic details have been found in the hydrosilylation reaction catalyzed by a Fe–H complex recently reported by Guan [84]. Further mechanistic studies are needed to clarify the true role of the hydride ligand in the reduction of carbonyl groups mediated by the tethered half-sandwich nickel (Cp\*-NHC)Ni(OBu<sup>t</sup>) complexes. Related nonlinked half-sandwich nickel NHC hydride complex has been described by Darcel and Sortais [85].

The use of these relatively new tethered Cp-NHC ligands in iron and nickel chemistry reveals an interesting potential in catalysis that certainly will be further exploited in the near future.

## REFERENCES

1. Hahn, F. E.; Jahnke, M. C. *Angew. Chem. Int. Ed.* **2008**, *47*, 3122.
2. Sommer, W. J.; Weck M. *Coord. Chem. Rev.* **2007**, *251*, 860.
3. Arnold, P. L.; Pearson, S. *Coord. Chem. Rev.* **2007**, *251*, 596.
4. Herrmann, W. A. *Angew. Chem. Int. Ed.* **2002**, *41*, 1290.
5. Herrmann, W. A.; Kocher, C. *Angew. Chem. Int. Ed.* **1997**, *36*, 2163.
6. Herrmann, W. A.; Weskamp, T.; Bohm, V. P. W. *Adv. Organomet. Chem.* **2001**, *48*, 1.
7. Arduengo, A. J. *Acc. Chem. Res.* **1999**, *32*, 913.
8. Bourissou, D.; Guerret, O.; Gabbaï, F. P.; Bertrand, G. *Chem. Rev.* **2000**, *100*, 39.
9. Mata, J. A.; Poyatos, M.; Peris, E. *Coord. Chem. Rev.* **2007**, *251*, 841.
10. Peris, E.; Crabtree, R. H. *Coord. Chem. Rev.* **2004**, *248*, 2239.
11. Pugh, D.; Danopoulos, A. A. *Coord. Chem. Rev.* **2007**, *251*, 610.
12. César, V.; Bellemín-Lapponaz, S.; Gade, L. H. *Chem. Soc. Rev.* **2004**, *33*, 619.
13. Gade, L. H.; Bellemín-Lapponaz, S. *Coord. Chem. Rev.* **2007**, *251*, 718.
14. Kühl, O. *Functionalised N-Heterocyclic Carbene Complexes*; John Wiley & Sons, Inc: New York, **2010**.
15. Normand, A. T.; Cavell, K. J. *Eur. J. Inorg. Chem.* **2008**, 2781.
16. Liddle, S. T.; Edworthy, I. S.; Arnold, P. L. *Chem. Soc. Rev.* **2007**, *36*, 1732.
17. Kühl, O. *Chem. Soc. Rev.* **2007**, *36*, 592.
18. Downing, S. P.; Danopoulos, A. A. *Organometallics* **2006**, *25*, 1337.
19. Downing, S. P.; Guadaño, S. C.; Pugh, D.; Danopoulos, A. A.; Bellabarba, R. M.; Hanton, M.; Smith, D.; Tooze, R. P. *Organometallics* **2007**, *26*, 3762.
20. Downing, S.P.; Pogorzelec, P. J.; Danopoulos, A. A.; Cole-Hamilton, D. J. *Eur. J. Inorg. Chem.* **2009**, *1816*.
21. Guadaño, S. C.; Danopoulos, A. A.; Pattacini, R.; Hanton, M.; Tooze, R. P. *Organometallics* **2012**, *31*, 1643.
22. Sun, H.- M.; Hu, D.-M.; Wang, Y.-S.; Shen, Q.; Zhang, Y. *J. Organomet. Chem.* **2007**, *692*, 903.
23. Zhang, C.; Luo, F.; Cheng, B.; Li, B.; Song, H.; Xu, S.; Wang, B. *Dalton Trans.* **2009**, 7230.
24. Takaki, D.; Okayama, T.; Shuto, H.; Matsumoto, S.; Yamaguchi, Y.; Matsumoto, S. *Dalton Trans.* **2011**, *40*, 1445.
25. Wang, B.; Wang, D.; Cui, D.; Gao, W.; Tang, T.; Chen, X.; Jing, X. *Organometallics* **2007**, *26*, 3167.

26. Wang, B.; Tang, T.; Li, Y.; Cui, D. *Dalton Trans.* **2009**, 8963.
27. da Costa, A. P.; Viciano, M.; Sanaú, M.; Merino, S.; Tejeda, J.; Peris, E.; Royo B. *Organometallics* **2008**, 27, 1305.
28. da Costa, A. P.; Sanaú, M.; Peris, E.; Royo B. *Dalton Trans.* **2009**, 6960.
29. Kandepi, V. V. K. M.; da Costa, A. P.; Peris, E.; Royo B. *Organometallics* **2009**, 28, 4544.
30. da Costa, A. P.; Mata, J. A.; Royo B.; Peris, E. *Organometallics* **2010**, 29, 1832.
31. Kandepi, V. V. K. M.; Cardoso, J. M. S.; Peris, E.; Royo B. *Organometallics* **2010**, 29, 2777.
32. da Costa, A. P.; Lopes, R.; Cardoso, J. M. S.; Mata, J. A.; Peris, E.; Royo B. *Organometallics* **2011**, 30, 4437.
33. Royo B.; Peris, E. *Eur. J. Inorg. Chem.* **2012**, 1309.
34. Cardoso, J. M. S.; Royo B. *Chem. Commun.* **2012**, 48, 4944.
35. Postigo, L.; Royo, B. *Adv. Syn. Catal.* **2012**, 354, 2613.
36. Crabtree, R. H. *The Organometallic Chemistry of the Transition Metals*; John Wiley & Sons, Inc: New York, **2005**.
37. Okuda, J. *Top. Curr. Chem.* **1992**, 160, 97.
38. Siemeling, U. *Chem. Rev.* **2000**, 100, 1495.
39. Jutzi, P.; Siemeling, U. *J. Organomet. Chem.* **1995**, 500, 175.
40. Butenschön, H. *Chem. Rev.* **2000**, 100, 1527.
41. Jutzi, P.; Redeker, T. *Eur. J. Inorg. Chem.* **1998**, 663.
42. Ganter, C. *Chem. Soc. Rev.* **2003**, 32, 130.
43. van Leusen, D.; Beetstra, D. J.; Hessen, B.; Teuben, J. H. *Organometallics* **2000**, 19, 4084.
44. Krut'ko, D. P.; Borzov, M. V.; Veksler, E. N.; Kirsanov, R. S.; Churakov, A. V. *Eur. J. Inorg. Chem.* **1999**, 1973.
45. Matsuoka, Y.; Ishida, Y.; Sasaki, D.; Saigo, K. *Tetrahedron* **2006**, 62, 8199.
46. Nagel, U.; Diez, C. *Eur. J. Inorg. Chem.* **2009**, 1248.
47. Przyojski, J. A.; Arman, H. D.; Tonzetich, Z. J. *Organometallics* **2012**, 31, 3264.
48. Xiang, L.; Deng, L. *Organometallics* **2011**, 30, 2018.
49. Mercs, L.; Labat, G.; Neels, A.; Ehlers, A.; Albrecht, M. *Organometallics* **2006**, 25, 5648.
50. Hatanaka, T.; Ohki, Y.; Tatsumi, K. *Chem. Asian J.* **2010**, 5, 1657.
51. Ohki, Y.; Hatanaka, T.; Tatsumi, K. *J. Am. Chem. Soc.* **2008**, 130, 17174.
52. Danopoulos, A. A.; Braunstein, P.; Stylianides, N.; Wesolek, M. *Organometallics* **2011**, 30, 6514.
53. Zlatogorsky, S.; Muryn, C. A.; Tuna, F.; Evans, D. J.; Ingleson, M. J. *Organometallics* **2011**, 30, 4974.
54. Layfield, R. A.; McDouall, J. J. W.; Scheer, M.; Schwarzmaier, C.; Tuna, F. *Chem. Commun.* **2011**, 47, 10623.
55. Meyer, S.; Orben, C. M.; Demeshko, S.; Dechert, S.; Meyer, F. *Organometallics* **2011**, 30, 6691.
56. Smith, J. M.; Long, J. R. *Inorg. Chem.* **2010**, 49, 11223.
57. Liu, B.; Xia, Q.; Chen, W. *Angew. Chem. Int. Ed.* **2009**, 121, 5621.
58. King, R. B. *Organometallic Synthesis*; Academic Press: New York, **1965**.
59. Buchgraber, P.; Toupet, L.; Guerchais, V. *Organometallics* **2003**, 22, 5144.
60. Faller, J. W.; Parr, J.; Lavoie, A.R. *New J. Chem.* **2003**, 27, 899.
61. Ritleng, V.; Barth, C.; Brenner, E.; Milosevic, S.; Chetcuti, M. J. *Organometallics* **2008**, 27, 4223.
62. Ritleng, V.; Oertel, A. M.; Chetcuti, M. J. *Dalton Trans.* **2010**, 39, 8153.
63. Oertel, A. M.; Ritleng, V.; Chetcuti M. J.; Veiros, L. F. *J. Am. Chem. Soc.* **2010**, 132, 13588.
64. Oertel, A. M.; Freudenreich, J.; Gein, J.; Ritleng, V.; Veiros, L. F.; Chetcuti, M. *Organometallics* **2011**, 30, 3400.
65. Oertel, A. M.; Ritleng, V.; Busiah, A.; Veiros, L. F.; Chetcuti, M. J. *Organometallics* **2011**, 30, 6495.
66. Oertel, A. M.; Ritleng, V.; Burr, L.; Chetcuti, M. J. *Organometallics* **2011**, 30, 6685.
67. Oertel, A. M.; Ritleng, V.; Chetcuti, M. J. *Organometallics* **2012**, 31, 2829.
68. Chakraborty, S.; Guan, H. *Dalton Trans.* **2010**, 39, 7427.
69. Junge, K.; Schröder, K.; Beller, M. *Chem. Commun.* **2011**, 47, 4849.
70. Le Bailly, B. A. F.; Thomas, S. P. *RSC Adv.* **2011**, 1, 1435.
71. Yamamoto, K.; Hayashi, T. In *Transition Metals for Organic Synthesis*; Beller, M., Bolm, C., Eds.; Wiley-VCH: Weinheim, **2005**.
72. Ingleson, M. J.; Layfield, R. A. *Chem. Commun.* **2012**, 48, 3579.
73. Jiang, F.; Bézier, D.; Sortais, J.-B.; Darcel, C. *Adv. Synth. Catal.* **2011**, 353, 239.
74. Bézier, D.; Venkanna, G. T.; Sortais, J.-B.; Darcel, C. *ChemCatChem.* **2011**, 3, 1747.
75. Castro, L. C. M.; Sortais, J.-B.; Darcel, C. *Chem. Commun.* **2012**, 48, 151.

76. Bézier, D.; Venkanna, G. T.; Castro, L. C. M.; Zheng, J.; Roisnel, T.; Sortais, J.-B.; Darcel, C. *Adv. Synth. Catal.* **2012**, *354*, 1879.
77. Chakraborty, S.; Krause, J. A.; Guan, H. *Organometallics* **2009**, *28*, 582.
78. Tran, B. L.; Pink, M.; Mindiola, D. J. *Organometallics* **2009**, *28*, 2234.
79. Kundu, S.; Brennessel, W. W.; Jones, W. D. *Inorg. Chem.* **2011**, *50*, 9443.
80. Kaur, H.; Zinn, F. K.; Stevens, E. D.; Nolan, S. P. *Organometallics* **2004**, *23*, 1157.
81. Díez-González, S.; Scott, N. M.; Nolan, S. P. *Organometallics* **2006**, *25*, 2355.
82. Díez-González, S.; Nolan, S. P. *Acc. Chem. Res.* **2008**, *41*, 349.
83. Shirobokov, O. G.; Kuzmina, L. G.; Nikonov, G. I. *J. Am. Chem. Soc.* **2011**, *133*, 6487.
84. Bhattacharya, P.; Krause, J. A.; Guan, H. *Organometallics* **2011**, *30*, 4720.
85. Bheeter, L. P.; Henrion, M.; Brelo, L.; Darcel, C.; Chetcuti, M. J.; Sortais, J. -B.; Ritleng, V. *Adv. Synth. Catal.* **2012**, *354*, 2619.



---

# 11

---

## PALLADIUM-(ACYCLIC DIAMINOCARBENE) SPECIES AS ALTERNATIVE TO PALLADIUM-(NITROGEN HETEROCYCLIC CARBENES) IN CROSS-COUPING CATALYSIS

VADIM P. BOYARSKIY\*

*Department of Chemistry, St. Petersburg State University, St. Petersburg, Russian Federation*

KONSTANTIN V. LUZYANIN\*

*Department of Chemistry, Centro de Química Estrutural, Instituto Superior Técnico, Universidade de Lisboa, Lisboa, Portugal;  
Department of Chemistry, St. Petersburg State University, St. Petersburg, Russia*

VADIM YU. KUKUSHKIN\*

*Department of Chemistry, St. Petersburg State University, St. Petersburg, Russian Federation*

### 11.1 INTRODUCTION

Palladium complexes featuring *N*-heterocyclic carbene ligands (NHCs, Fig. 11.1) are a class of compounds of supreme importance in modern chemistry, which are extensively applied, in particular, in catalysis of cross-coupling reactions [1–4]. Complexes with these species have challenged the dominance of the commonly used tertiary phosphine-based catalysts in a wide range of palladium-catalyzed organic processes [3, 4].

In spite of the broad field of successful applications of (NHC)Pd complexes, these species have some disadvantages. In particular, the preparation of many of the NHCs (and/or their precursors) for further coordination to metal centers is not an easy synthetic task and it limits the possibilities for the tuning of the steric properties of the NHC ligands [5–7]. In addition, precise tuning of prepared metal carbenes toward selected catalytic applications requires a continuous search for novel carbene-based species and optimization of their properties [2, 3, 8, 9].

In this stream, acyclic diaminocarbene (ADCs, Fig. 11.1) represent an alternative class of ligands able to overcome certain disadvantages of both phosphines and NHCs [2, 4, 10]. Indeed, first, ADCs exhibit electronic stabilization similar to those of the structurally related nonaromatic NHCs [11–17]. Second, acyclic diaminocarbene ligands possess wider N–C–N bond angles [18] than the structurally relevant NHCs [19, 20] and occupy more space at a metal center. The higher steric hindrance of ADCs favors reductive elimination, which represents the final stage of the cross-coupling catalytic cycle. Finally, the rotational freedom of the ADC ligands makes them capable of adopting multiple conformations [21–24] and this, as believed, can lead to the easier catalyst adaptation to different steric requirements of various stages of the cross-coupling catalytic cycle.

In this chapter, we attempt to provide a brief overview of the most developed synthetic methods to (ADC)Pd complexes and to systematize reports published until now on cross-coupling reactions catalyzed by (ADC)Pd systems. We also attempt to compare, whenever possible, the catalytic properties of (ADC)Pd versus (NHC)Pd species, and, eventually, to draw attention to the potential of ADCs and to the advantages that application of ADCs gives to the cross-coupling chemistry.

*Advances in Organometallic Chemistry and Catalysis: The Silver/Gold Jubilee International Conference on Organometallic Chemistry Celebratory Book*, First Edition. Edited by Armando J. L. Pombeiro.

© 2014 John Wiley & Sons, Inc. Published 2014 by John Wiley & Sons, Inc.

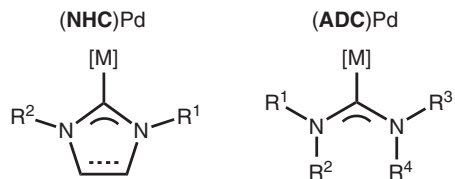


**Figure 11.1** Palladium complexes with *N*-heterocyclic carbenes (NHCs) and acyclic diaminocarbenes (ADCs).

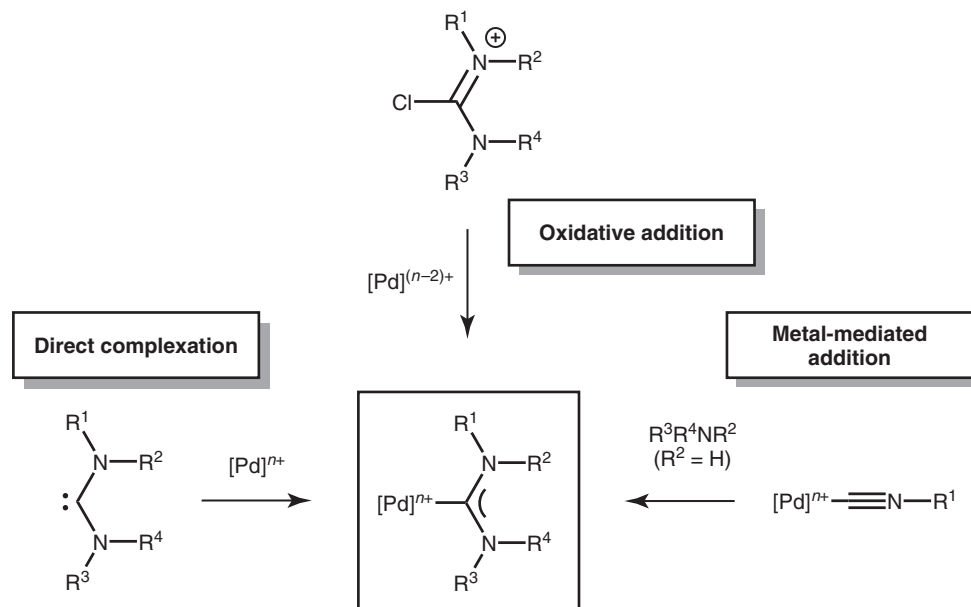
## 11.2 SYNTHETIC APPROACHES TO PALLADIUM COMPLEXES BEARING ADC LIGANDS

Palladium complexes with ADC ligands are easily accessible and several synthetic methods have been satisfactorily developed for their generation [2, 10]. Three of those (Scheme 11.1) are currently the most explored and allowed the generation of all (ADC)Pd complexes discussed in this chapter.

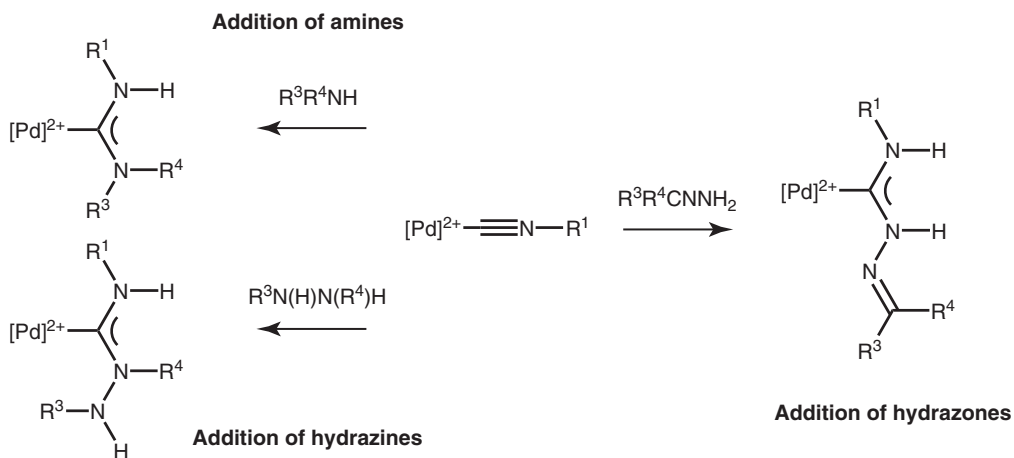
The conventional synthetic approach based on *direct complexation* involves the preparation of the carbene precursors, for example, *N,N,N',N'*-tetraalkylformamidinium salts [25, 26]. These species are further deprotonated generating free carbenes that, upon reaction with an appropriate metal source, furnish the target metal–ADC species. This route is generally restricted to the species bearing bulky lipophilic substituents at the N atoms owing to the insufficient stability of the free carbenes [25, 26]. The main advantage of this approach refers to its versatility in terms of electronic properties of a metal (both electron-rich and electron-poor metal centers could be employed) and absence of prerequisites on secondary ligands (no phosphines are necessary as in the case of an *oxidative addition* route). The principal limitation of this method concerns the *N,N,N',N'*-tetraalkylformamidinium salts that are in many instances difficult to prepare [18, 25–27]. Furthermore, the *in situ* deprotonation of the carbene precursors followed by coordination to a metal center typically implicates the purification of the target carbene complexes [11, 13, 15, 21], and, in case when an excess of the carbene precursor is used, this route becomes economically and environmentally unfavorable [28].

The approach closely related to the previous one is based on an oxidative addition of metals into C-chloro iminium and -formamidinium salts (*oxidative addition*, Scheme 11.1). This method is limited to electron-rich metal centers (e.g., Pd<sup>0</sup>) [2, 29] that should be additionally stabilized by the  $\pi$ -acceptor ligands such as phosphines.

An alternative to the previous two is the approach based on a metal-mediated nucleophilic addition to isocyanides (*metal-mediated addition*). This reaction does not proceed via the generation of a free carbene, thus, allowing the synthesis



**Scheme 11.1** Common synthetic methodologies for the preparation of palladium-(ADC) species.



**Scheme 11.2** Examples of (ADC)Pd complexes generated via *metal-mediated approach*.

of complexes with both hindered and unhindered ADCs [2, 10]. The stoichiometric addition to a metal-bound isocyanide ensures the preparation of well-defined ADC complexes. With regard to nucleophilic species, the addition of nucleophiles bearing  $sp^3$ -*N*- (amines, hydrazines) [2, 10],  $sp^2$ -*N*- (imines) [30–32], or mixed  $sp^3$ / $sp^2$ -*N*- (hydrazones, amidines) [33, 34] nucleophilic centers is reported (Scheme 11.2).

One of the principal drawbacks of this approach is the requirement for an electron-poor late transition metal center (e.g., Pt<sup>II</sup>, Pd<sup>II</sup>, and Au<sup>III</sup>) that should guarantee a sufficient electrophilic activation of ligated isocyanides. Furthermore, *N,N,N',N'*-tetrasubstituted aminocarbenes cannot be assembled via this route [2, 10].

Another less-common method to achieve (ADC)Pd complexes is based on transmetallation of the previously prepared silver or lithium-ADC species [14].

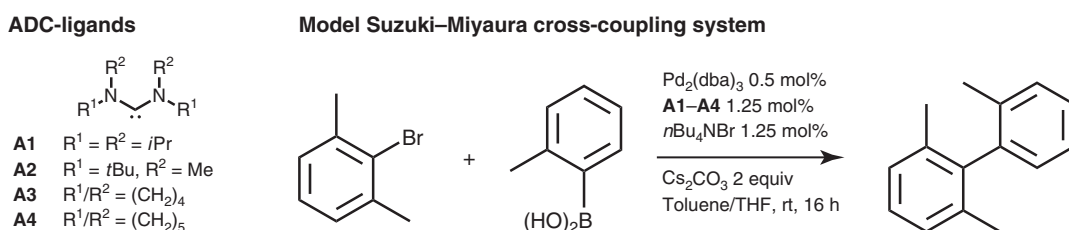
### 11.3 CATALYTIC APPLICATIONS OF PALLADIUM-(ADC)S

#### 11.3.1 Suzuki–Miyaura Cross-Coupling

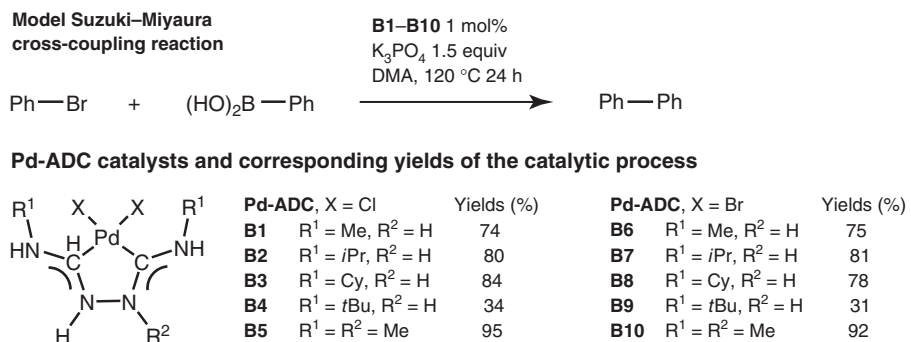
(ADC)Pd complexes were prepared *in situ* from  $Pd_2(dbu)_3$  and carbenes **A1–A4** (Scheme 11.3) [28]. Although their structures were not elucidated, they were further evaluated as catalysts in the model Suzuki–Miyaura cross-coupling (for recent reviews on this reaction and its applications, see References 35–40).

The authors found that palladium complexes with ADC ligands **A1** and **A2** exhibit superior catalytic activities as compared to those with **A3** and **A4**, and preferred the palladium complexes with **A1** for further studies on the scope of the coupling. Using the latter species as catalysts, the coupling of several aryl- and alkenylbromides (85–95% yields, RT), and chlorides (80–92% yields, 45 °C), was accomplished. Comparison of these results [28] with those reported for some of the most efficient M-NHC systems [41, 42] indicates that palladium complexes with **A1** exhibit lower activities, namely, require at least 10 times higher catalyst loading.

Slaughter and coworkers employed a series of the Chugaev-type palladium complexes (Scheme 11.4) as catalysts for the Suzuki–Miyaura reaction [17, 43, 44].



**Scheme 11.3** Palladium-ADC species employed and the model Suzuki–Miyaura cross-coupling [28].



**Scheme 11.4** Chugaev-type (ADC)Pd complexes and their catalytic activity [17, 43, 44].

The authors screened these (ADC)Pd complexes for the model coupling of bromobenzene with phenylboronic acid (Scheme 11.3). It was found that the catalysts bearing secondary alkyl substituents (*i*Pr; **B2**, **B7**; Cy; **B3**, **B8**) displayed higher activity than those with methyl (**B1**, **B6**) or tertiary alkyl (*t*Bu; **B4**, **B9**) groups. In addition, methylhydrazine-derived complexes **B5** and **B10** demonstrated the highest activity among the catalysts studied. No significant difference in activity was observed between catalysts containing chloride versus bromide ligands.

For the most promising species (**B5**), the functional group tolerance (scope) as well as its efficiency in the presence of moisture and air, were estimated. Conducting these reactions open to air and in undried dimethylacetamide led to identical or slightly lower yields (in comparison with the conventional inert conditions) in the coupling of electron-deficient or electron-neutral aryl bromides. However, substrates with Me or OMe substituents showed significant drop in the yield under aerobic conditions. The cross-coupling of 4-chloronitrobenzene and 4-chlorobenzonitrile with phenylboronic acid provided good yields of the target products, but the catalyst demonstrated poor performance in the coupling of less electron-poor aryl chlorides as compared to that reported for the well-defined (NHC)Pd's [41, 42].

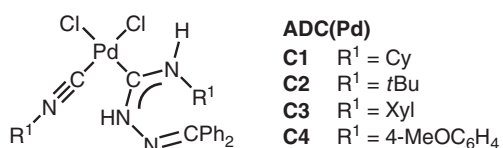
The chelates depicted in Scheme 11.4 do not exhibit conformational freedom, which is one of the advantages specific for nonchelated ADCs. In this context, the addition of hydrazine-type nucleophiles (e.g., *N,N*-disubstituted hydrazones) to isocyanide ligands leading to the monodentate carbene ligands is of potential interest. These nucleophilic species are easily accessible and generally exhibit higher nucleophilicity as compared to structurally related imines. Thus, in the other study, a reported metal-mediated addition of benzophenone hydrazone, H<sub>2</sub>N—N=CPh<sub>2</sub>, to one isocyanide ligand in *cis*-[PdCl<sub>2</sub>(CNR)<sub>2</sub>] leads to complexes **C1–C4** featuring monodentate ADCs (Fig. 11.2) [33].

These complexes were found to be excellent air/moisture insensitive catalysts for the Suzuki–Miyaura cross-coupling (Scheme 11.5). In solvent and base optimization studies conducted for the model system, EtOH and K<sub>2</sub>CO<sub>3</sub> are the most adequate for further operation.

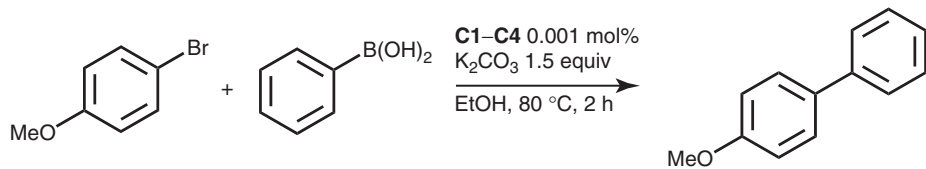
Palladium complexes **C1**, **C3**, and **C4** (Scheme 11.5) demonstrated the highest efficiencies furnishing the coupling product in 94–97% yield, while **C2**, derived from [PdCl<sub>2</sub>(CN*t*Bu)<sub>2</sub>], exhibits a moderate activity (64% yield). Both 4-R<sup>1</sup>C<sub>6</sub>H<sub>4</sub>Br bearing either electron-donor (R<sup>1</sup> = H, Me, OMe) or electron-withdrawing (NO<sub>2</sub>) groups react with phenylboronic acid to give excellent yields of the biphenyl species. Maximum TON reached in the model reaction (with catalyst **C1**) was 1.4 × 10<sup>6</sup> that is at least 100 times higher than reported for some of the most efficient well-defined Pd-NHC systems [41, 42].

Hong et al. [24] reported the preparation of palladium catalysts **D1–D4** containing the chiral ADC ligands (Fig. 11.3) via the oxidative addition of several chloroamidinium salts to a palladium source.

The catalytic activity of **D1–D4** in the nonasymmetric and asymmetric Suzuki–Miyaura cross-coupling was evaluated (Scheme 11.6). Moderate yields (25–50%) for the coupling of simple substrates employing the (ADC)Pd complexes (1 mol%) as the catalyst, were achieved. Changing the base from K<sub>2</sub>CO<sub>3</sub> to CsF and increasing the amount of catalyst to 3 mol%

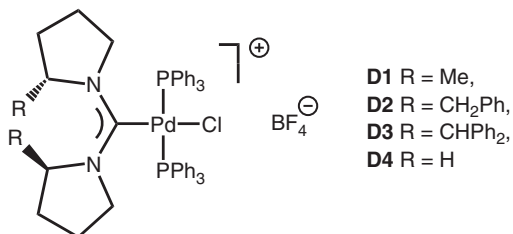


**Figure 11.2** Complexes generated by the nucleophilic addition to (R<sup>1</sup>NC)Pd species [33].

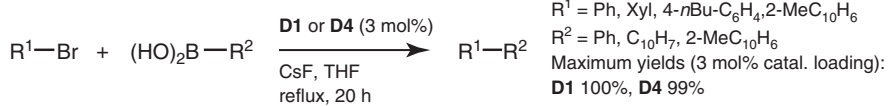
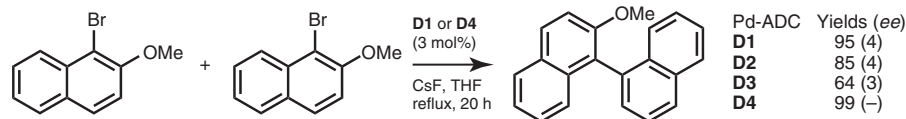
**Model Suzuki–Miyaura cross-coupling system**

Yields of the cross-coupling reaction with Pd-ADC: **C1** 97%, **C2** 64%, **C3** 96%, **C4** 94%

**Scheme 11.5** Catalytic activity of **C1–C4** in the model Suzuki–Miyaura coupling [33].



**Figure 11.3** Palladium-ADC complexes **D1–D4** [24].

**Non asymmetric Suzuki–Miyaura cross-coupling****Asymmetric Suzuki–Miyaura cross-coupling**

**Scheme 11.6** Catalytic systems studied by Hong et al. [24].

led to an improved yield up to 100%. Hindered tri-*ortho*-substituted biaryls were produced in excellent yields (93–99%) and the catalysts allowed the tolerance of both methoxy and nitro functionalities. However, preparation of the challenging tetra-*ortho*-substituted biaryls was not successful and no reaction was observed. The catalyst was varied when producing binaphthyl species, indicating that the carbenes with the highest steric hindrance provided the lowest yields in this coupling. The authors believe that this might be attributed to the increasing steric repulsion making the ligands more labile. Catalyst **D3**, generated *in situ* from chloroamidinium and [Pd(PPh<sub>3</sub>)<sub>4</sub>], was tested in the catalysis, giving 64% yield of the target product. Unfortunately, the observed *ee*'s (3–4%) in the abovementioned asymmetric Suzuki–Miyaura coupling reaction were low with any of **D1–D4**.

Recently an attempt was made [45] to use palladium(II) cationic complexes bearing ADCs, further stabilized by pyridine or other N-donor ligands (**E1–E7** Fig. 11.4), as catalysts for the cross-coupling.

Unfortunately, these interesting compounds were not effective catalysts for the Suzuki–Miyaura reaction of bromobenzene requiring a significant amount of Pd (up to 2 mol%) and inferior complexes with NHCs. The surprising and promising fact is that chlorobenzene in the presence of these catalysts proved to be as reactive as bromobenzene.

Another feature of the Suzuki–Miyaura cross-coupling catalyzed by (ADC)Pd complexes is a very high reaction rate, as shown recently by the two groups [46, 47] who determined TOF for such catalysts. Thus, Hashmi and colleagues [47] synthesized a series of (ADC)Pd complexes via the addition of amines to coordinated isocyanides (Scheme 11.7). They found

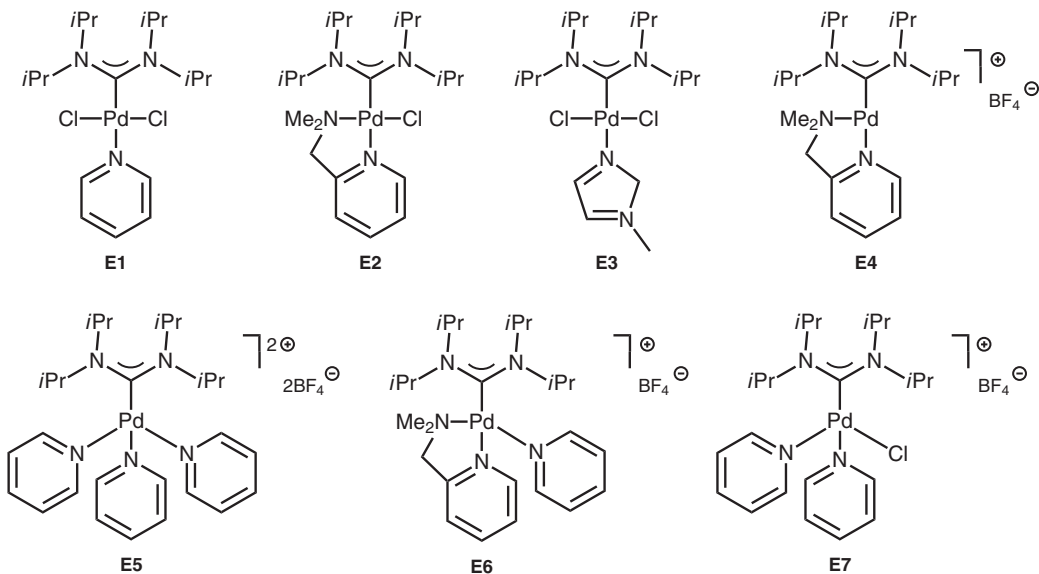
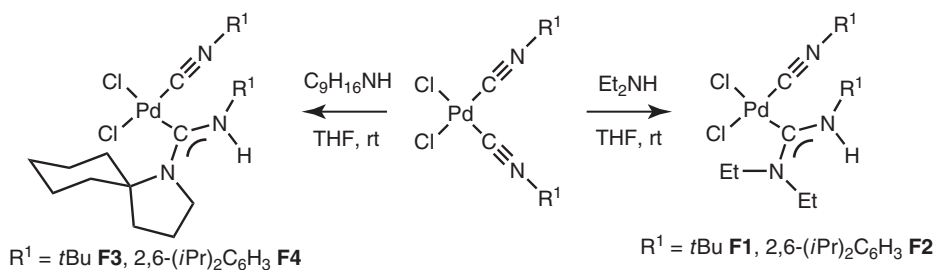


**Figure 11.4** Neutral (E1–E3) and cationic (E4–E7) (ADC)Pd complexes [45].



**Scheme 11.7** Systems studied by Hashmi and colleagues [47].

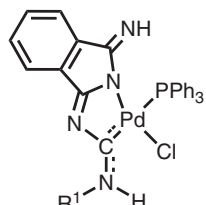
that the Suzuki–Miyaura cross-coupling of 4-bromobenzaldehyde and 2-methoxyphenylboronic acid catalyzed by **F1–F4** provided the target biaryls with 83–96% yields and with the TOFs up to 18,050 h<sup>-1</sup>.

In other reports [32, 46], the authors investigated novel (ADC)Pd-chelated species derived from metal-mediated coupling of isocyanides and heterocyclic imines, for example, 3-iminoisoindolin-1-ones [31, 32] or 1,3-diiminoisoindoline [46]. Among the latter species, complexes containing one aminocarbene and one phosphine ligand (Fig. 11.5, **G1–G3**) demonstrated highest efficiency in the coupling of aryl bromides with arylboronic acids (yields 77–99%) with the TOFs up to 37,000 h<sup>-1</sup>.

### 11.3.2 Heck Reaction

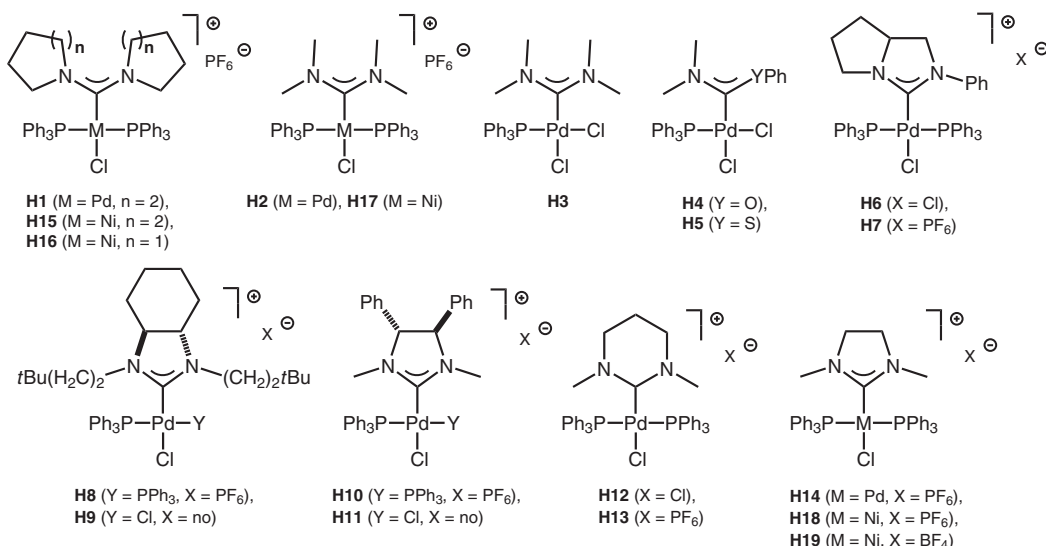
Furstner and colleagues [29] reported on application of (ADC)Pd complexes as catalysts for the Heck reaction (for recent surveys on the Heck reaction and its applications, see References [48–52]). They have prepared a series of (ADC)Pd complexes (Fig. 11.6, **H1–H5**) via an oxidative insertion of [Pd(PPh<sub>3</sub>)<sub>4</sub>] into the C–Cl bond of various acyclic 2-chloroamidinium salts and related compounds. The generated species were engaged as catalysts for the Heck coupling of bromo- or iodobenzene with butyl acrylate (Scheme 11.8). The catalytic system operated at 120 °C for 18 h using *N*-methyl-2-pyrrolidone (NMP) as a solvent and Cs<sub>2</sub>CO<sub>3</sub> as a base. The target disubstituted olefins were prepared in 56–92% yields in the systems based on **H1–H3**. Activities exhibited by the ADC systems are comparable to those demonstrated by the related complexes bearing NHCs (Fig. 11.6, **H6–H13**).

Dhudshia and Thadani [28] used (ADC)Pd complexes with **A1** (Scheme 11.3) in an intermolecular Heck reaction of aryl bromides with an electron-deficient alkene. The target species were isolated in 78–85% yields under optimized catalytic

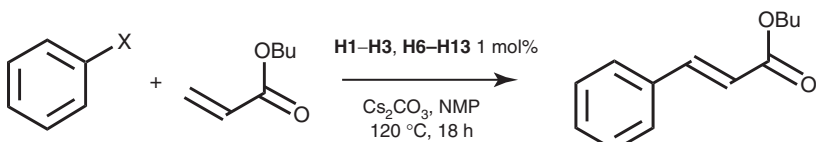
**Catalysts G1–G3**

$R^1 = Cy$  (**G1**),  $tBu$  (**G2**),  
 $CMe_2CH_2CMe_3$  (**G3**)

**Figure 11.5** Chelated ADC-Pd complexes as catalysts of the Suzuki–Miyaura reaction [46].



**Figure 11.6** Series of (ADC)Pd complexes with additional phosphine ligands [29].

**Model Heck cross-coupling system**

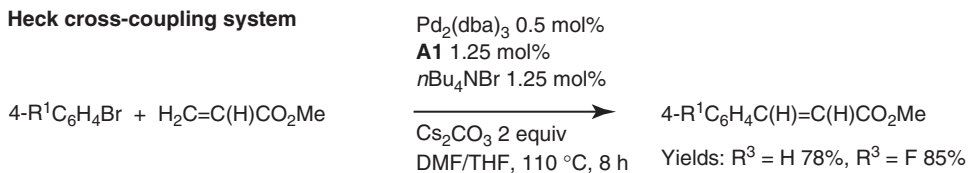
$X = I$ : Yields up to 80–92% for **H1–H3** (87–100% for **H6–H13**)

$X = Br$ : Yields up to 56–77% for **H1–H3** (51–98% for **H6–H13**)

**Scheme 11.8** Comparison of the catalytic properties for **H1–H3** (ADCs) and **H6–H13** (NHCs) in the Heck reaction [29].

conditions (Scheme 11.9). The corresponding aryl chlorides, however, were poorer substrates for the Heck reaction (35% and 29% isolated yields of the target species) under the conditions shown in Scheme 11.9.

For comparison, the previously described [29] system employing (NHC)Pd's **H6–H13** (note that butyl acrylate was employed as the substrate instead of methyl acrylate) was used. Inspection of these results clearly indicates that (ADC)Pd catalyst containing **A1** ligands and NHC catalysts **H6–H13** exhibit comparable catalytic properties. Moreover, the reaction catalyzed by Pd-**A1** requires shorter reaction time (8 h vs 18 h for **H6–H13**) and lower catalyst loadings (0.5 mol% of Pd-**A1** vs 1.0 mol% of **H6–H13**).



**Scheme 11.9** Heck reaction catalyzed by palladium-diaminocarbene complexes with **A1** [28].

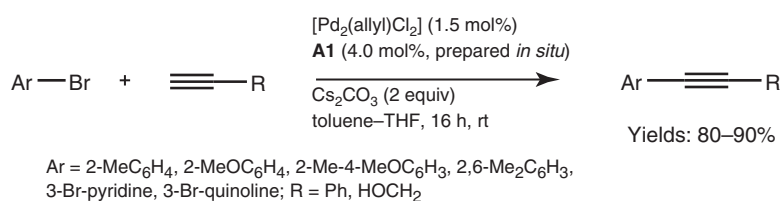
Thus, both the described (ADC)Pd complexes systems demonstrated comparable or higher activity than those based on (NHC)Pd's, furnishing products in similar yields under comparable reaction conditions, and employing lower or similar catalyst loadings [29].

### 11.3.3 Sonogashira Coupling

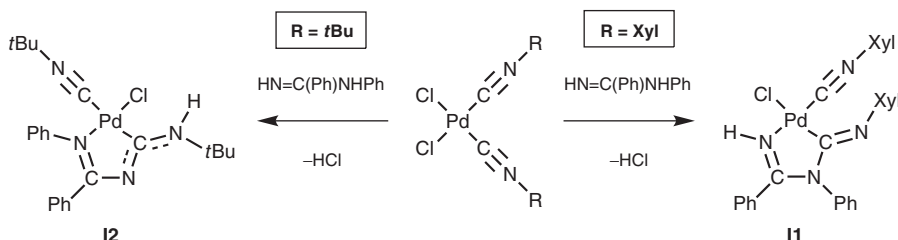
One example for both copper cocatalyzed and copper-free protocols for the (ADC)Pd-catalyzed Sonogashira coupling was reported (for recent surveys on the Sonogashira coupling and its applications, see References [53, 54]). The (ADC)Pd with **A1** (Scheme 11.3) was studied in the Sonogashira reaction of several aryl bromides and both aromatic (phenyl acetylene) and aliphatic alkynes (prop-2-yn-1-ol) [28]. The optimized Cu-free protocol acts at RT, furnishing target species in 80–91% yields (Scheme 11.10). In conclusion, this reported system demonstrated at least comparable efficiency (similar catalyst loading, reaction time, and temperature) to some of the most efficient (NHC)Pd's [55–59].

A series of (ADC)Pd complexes was generated via the metal-mediated coupling between one or two isocyanide ligands in *cis*-[PdCl<sub>2</sub>(CNR)<sub>2</sub>] (R = Xyl, *t*Bu, Cy) and *N*-phenylbenzimidine, HN=C(Ph)NHPh. This coupling proceeds with different regioselectivity upon varying the substituent R of an isocyanide (Scheme 11.11) [34].

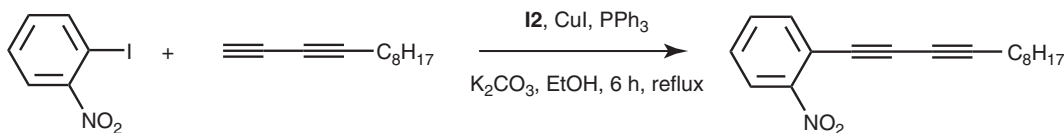
The catalytic activity of two representative species, that is, **I1** and **I2** in the Sonogashira cross-coupling of 4-NO<sub>2</sub>C<sub>6</sub>H<sub>4</sub>I with oct-1-yne (EtOH, K<sub>2</sub>CO<sub>3</sub>, 60 °C) yielding 1-nitro-2-(oct-1-ynyl)benzene, was evaluated. The system involving **I2** exhibits slightly higher catalytic efficiency (yields up to 99%, TONs up to 2000; TOFs up to 280 h<sup>-1</sup>) than that constructed on **I1** (yields up to 99%, TONs up to 1400; TOFs up to 120 h<sup>-1</sup>). Moreover, catalytic activities of both systems are substantially higher than that of the conventional system based on [PdCl<sub>2</sub>(PPh<sub>3</sub>)<sub>2</sub>] (yield 40%, TON 400; TOF 22 h<sup>-1</sup>) [60]. In addition, **I2** was also used for the synthesis of 1-(dodeca-1,3-diyn-1-yl)-2-nitrobenzene (Scheme 11.12) from 1-iodo-2-nitrobenzene and dodeca-1,3-diyne (EtOH, K<sub>2</sub>CO<sub>3</sub>, 50 °C). The authors found that this acyclic carbene is a significantly more efficient catalyst for the Sonogashira reaction with diynes (as compared to the previously used Pd(OAc)<sub>2</sub>) [61], providing 1-(dodeca-1,3-diyn-1-yl)-2-nitrobenzene in 97% yield with TON up to 1400. However, it is difficult to compare



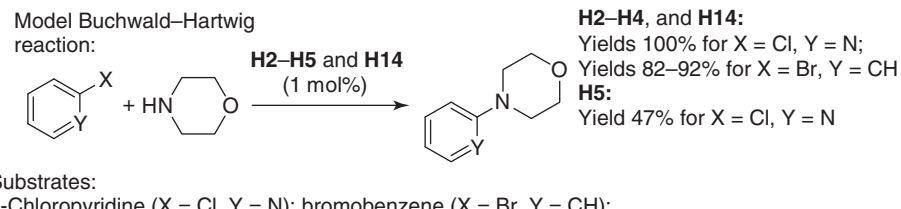
**Scheme 11.10** Catalytic properties of palladium complex with **A1** in the Sonogashira reaction [28].



**Scheme 11.11** Preparation of aminocarbene complexes **I1** and **I2** [34].



**Scheme 11.12** Synthesis of 1-(dodeca-1,3-diyn-1-yl)-2-nitrobenzene catalyzed by **I2** [34].



**Scheme 11.13** Amination reaction catalyzed by ADCs (**H2**, **H4**, **H5**), and NHC (**H14**) [29].

the efficiency of the system based on **I1** or **I2** with the related (NHC)M's, because in the former case, very specific substrates were employed.

#### 11.3.4 Buchwald–Hartwig Amination

Preprepared (ADC)Pd complexes **H2** (Fig. 11.6) was employed [29] as catalyst for the Buchwald–Hartwig amination of aryl halides (for the recent surveys on the Buchwald–Hartwig cross-coupling, see References [62–65]). The obtained results (Scheme 11.13) were compared with those for the structurally related oxyamino- (**H4**), thioaminocarbene (**H5**), and the related NHC complex, **H14**. Catalysts **H2**, **H4**, and **H5** were efficient in the amination of bromobenzene (yields range from 82% to 92%), demonstrating activities similar to those of the NHC complex **H14** (yield 84%). With 2-chloropyridine as the substrate, **H2**, **H4**, and **H14**, allowed the preparation of the target product in a quantitative yield. Catalyst **H5** demonstrated a moderate efficiency (yield 47%).

### 11.4 FINAL REMARKS

In this chapter, we examined the accumulated data on application of (ADC)Pd complexes as catalysts for various cross-coupling reactions. Although all reports discussed here indicate that (ADC)Pd complexes exhibit comparable or even higher activities than the corresponding (NHC)Pd's, in our opinion, it is rather premature to make any conclusions based on a limited number of reports on catalytic applications of (ADC)Pd complexes. Another consequence of the latter fact is that no clear relationship between the structure of (ADC)Pd complexes and their catalytic properties could be currently arrived at. More experimental data as well as mechanistic studies on (ADC)Pd-catalyzed cross-coupling processes are required to open up a possibility for an intelligent (e.g., "in silica") design of the catalyst instead of those based on an empirical variation of functional groups.

We believe that the principal advantage of (ADC)Pd-based catalysts as compared to Pd-NHCs, verified at the current stage of the studies, is the more modular character of the former species. Among routes leading to (ADC)Pd complexes, metal-mediated reactions of isocyanides with various nucleophiles permit a straightforward assembly of a wide range of well-defined metal carbene catalysts, including unsymmetrically substituted and chiral compounds.

Finally, taking into account the current trends in transition metal-catalyzed organic transformations, it is anticipated that further applications of (ADC)Pd complexes should include, among others, (i) development of mild and efficient systems acting in alternative solvents (e.g., ionic liquids) or under heterogeneous catalytic conditions and (ii) usage of chiral (ADC)Pd complexes for asymmetric catalytic transformations. All these expected fields of applications resemble those where (NHC)Pd catalysts have already demonstrated great benefits.

## ACKNOWLEDGMENTS

The authors thank Saint Petersburg State University for a research grant, the Federal Targeted Program “Scientific and Scientific-Pedagogical Personnel of the Innovative Russia in 2009–2013” (contract P676 from 20/05/2010), Russian Fund for Basic Research (grants 11-03-00048-a, 12-03-00076-a, 12-03-33071, 13-03-12411-ofim), and RAS Presidium Subprogram coordinated by acad. N. T. Kuznetsov. In addition, this work has been partially supported by the Fundação para a Ciência e a Tecnologia (FCT), Portugal, its PPCDT program (FEDER funded), and through the research projects PTDC/QUI-QUI/098760/2008 and PTDC/QUI-QUI/109846/2009.

## REFERENCES

- Díez-González, S.; Marion, N.; Nolan, S. P. *Chem. Rev.* **2009**, *109*, 3612.
- Vignolle, J.; Catton, X.; Bourissou, D. *Chem. Rev.* **2009**, *109*, 3333.
- Fortman, G. C.; Nolan, S. P. *Chem. Soc. Rev.* **2011**, *40*, 5151.
- Boyarskiy, V. P.; Luzyanin, K. V.; Kukushkin, V. Yu. *Coord. Chem. Rev.* **2012**, *256*, 2029.
- Hahn, F. E.; Jahnke, M. C. *Angew. Chem. Int. Ed. Engl.* **2008**, *47*, 3122.
- Glorius, F. *Top. Organomet. Chem.* **2007**, *21*, 1.
- Peris, E. *Top. Organomet. Chem.* **2007**, *21*, 83.
- Liddle, S. T.; Edworthy, I. S.; Arnold, P. L. *Chem. Soc. Rev.* **2007**, *36*, 1732.
- Schuster, O.; Yang, L.; Raubenheimer, H. G.; Albrecht, M. *Chem. Rev.* **2009**, *109*, 3445.
- Michelin, R. A.; Pombeiro, A. J. L.; Guedes da Silva, M. F. C. *Coord. Chem. Rev.* **2001**, *218*, 75.
- Herrmann, W. A.; Öfele, K.; Preysing, D. V.; Herdtweck, E. *J. Organomet. Chem.* **2003**, *684*, 235.
- Frey, G. D.; Herrmann, W. A. *J. Organomet. Chem.* **2005**, *690*, 5876.
- Frey, G. D.; Herdtweck, E.; Herrmann, W. A. *J. Organomet. Chem.* **2006**, *691*, 2465.
- Snead, D. R.; Chiviriga, I.; Abboud, K. A.; Hong, S. *Org. Lett.* **2009**, *11*, 3274.
- Denk, K.; Sirsch, P.; Herrmann, W. A. *J. Organomet. Chem.* **2002**, *649*, 219.
- Lee, M.-T.; Hu, C.-H. *Organometallics* **2004**, *23*, 976.
- Slaughter, L. M. *Comm. Inorg. Chem.* **2008**, *29*, 46.
- Alder, R. W.; Allen, P. R.; Murray, M.; Orpen, A. G. *Angew. Chem. Int. Ed. Engl.* **1996**, *35*, 1121.
- Arduengo III, A. J.; Goerlich, J. R.; Marshall, W. J. *J. Am. Chem. Soc.* **1995**, *117*, 11027.
- Arduengo III, A. J.; Harlow, R. L.; Kline, M. *J. Am. Chem. Soc.* **1991**, *113*, 361.
- Rosen, E. L.; Sanderson, M. D.; Saravanakumar, S.; Bielawski, C. W. *Organometallics* **2007**, *26*, 5774.
- Rosen, E. L.; Sung, D. H.; Chen, Z.; Lynch, V.; Bielawski, C. W. *Organometallics* **2010**, *29*, 250.
- Collins, M. S.; Rosen, E. L.; Lynch, V.; Bielawski, C. W. *Organometallics* **2010**, *29*, 3047.
- Snead, D. R.; Inagaki, S.; Abboud, K. A.; Hong, S. *Organometallics* **2010**, *29*, 1729.
- Alder, R. W.; Blake, M. E.; Bufali, S.; Butts, C. P.; Orpen, A. G.; Schütz, J.; Williams, S. J. *J. Chem. Soc. Perkin Trans. I* **2001**, *14*, 1586.
- Alder, R. W.; Chaker, L.; Paolini, F. P. V. *Chem. Commun.* **2004**, 2172.
- Wicherink, S. C.; Scheeren, J. W.; Nivard, R. J. F. *Synthesis* **1977**, 273.
- Dhudshia, B.; Thadani, A. N. *Chem. Commun.* **2006**, 668.
- Kremzow, D.; Seidel, G.; Lehmann, C. W.; Furstner, A. *Chem. Eur. J.* **2005**, *11*, 1833.
- Luzyanin, K. V.; Guedes da Silva, M. F. C.; Kukushkin, V. Yu.; Pombeiro, A. J. L. *Inorg. Chim. Acta* **2009**, *362*, 833.
- Luzyanin, K. V.; Pombeiro, A. J. L.; Haukka, M.; Kukushkin, V. Yu. *Organometallics* **2008**, *27*, 5379.
- Chay, R. S.; Luzyanin, K. V. *Inorg. Chim. Acta* **2012**, *380*, 322.
- Luzyanin, K. V.; Tskhovrebov, A. G.; Carias, M. C.; Guedes da Silva, M. F. C.; Pombeiro, A. J. L.; Kukushkin, V. Yu. *Organometallics* **2009**, *28*, 6559.
- Tskhovrebov, A. G.; Luzyanin, K. V.; Kuznetsov, M. L.; Sorokoumov, V. N.; Balova, I. A.; Haukka, M.; Kukushkin, V. Yu. *Organometallics* **2011**, *30*, 863.
- Alonso, F.; Beletskaya, I. P.; Yus, M. *Tetrahedron* **2008**, *64*, 3047.
- Nicolaou, K. C.; Bulger, P. G.; Sarlah, D. *Angew. Chem. Int. Ed.* **2005**, *44*, 4442.

37. Miyaura, N. *Top. Curr. Chem.* **2002**, *219*, 11.
38. Suzuki, A. *Proc. Jpn. Acad. Ser. B* **2004**, *80*, 359.
39. Kotha, S.; Lahiri, K.; Kashinath, D. *Tetrahedron* **2002**, *58*, 9633.
40. Martin, R.; Buchwald, S. L. *Acc. Chem. Res.* **2008**, *41*, 1461.
41. Navarro, O.; Kaur, H.; Mahjoor, P.; Nolan, S. P. *J. Org. Chem.* **2004**, *69*, 3173.
42. Marion, N.; Navarro, O.; Mei, J.; Stevens, E. D.; Scott, N. M.; Nolan, S. P. *J. Am. Chem. Soc.* **2006**, *128*, 4101.
43. Moncada, A. I.; Manne, S.; Tanski, J. M.; Slaughter, L. M. *Organometallics* **2006**, *25*, 491.
44. Moncada, A. I.; Khanb, M. A.; Slaughter, L. M. *Tetrahedron Lett.* **2005**, *46*, 1399.
45. Abdur-Rashid, K.; Amoroso, D.; Tsang, C.-W.; Jia, W. WO 2011127579 A1 20111020.
46. Chay, R. S.; Luzyanin, K. V.; Kukushkin, V. Y.; Guedes da Silva, M. F. C.; Pombeiro, A. J. L. *Organometallics* **2012**, *31*, 2379.
47. Hashmi, A. S. K.; Lothschutz, C.; Boohling, C.; Rominger, F. *Organometallics* **2011**, *30*, 2411.
48. Belestskaya, I. P.; Cheprakov, A. V. *Chem. Rev.* **2000**, *100*, 3009.
49. Crisp, G. T. *Chem. Soc. Rev.* **1998**, *27*, 427.
50. Shibasaki, M.; Boden, C. D. J.; Kojima, A. *Tetrahedron* **1997**, *53*, 7371.
51. Franzén, R. *Can. J. Chem.* **2000**, *78*, 957.
52. Fu, G. C. *Acc. Chem. Res.* **2008**, *41*, 1555.
53. Sonogashira, K. In *Metal-Catalyzed Cross-Coupling Reactions*; Stang, P. J.; Diederich, F., Eds.; John Wiley & Sons, Ltd: Weinheim, **1998**, pp. 203–229.
54. Negishi, E. -I.; Anastasia, L. *Chem. Rev.* **2003**, *103*, 1979.
55. Batey, R. A.; Shen, M.; Lough, A. J. *Org. Lett.* **2002**, *4*, 1411.
56. Altenhoff, G.; Würtz, S.; Glorius, F. *Tetrahedron Lett.* **2006**, *47*, 2925.
57. John, A.; Shaikh, M. M.; Ghosh, P. *Dalton Trans.* **2009**, 10581.
58. Ray, L.; Barman, S.; Shaikh, M. M.; Ghosh, P. *Chem. Eur. J.* **2008**, *14*, 6646.
59. Samantaray, M. K.; Shaikh, M. M.; Ghosh, P. *J. Organomet. Chem.* **2009**, *694*, 3477.
60. Bailar Jr, J. C.; Itatani, H. *Inorg. Chem.* **1965**, *4*, 1618.
61. Balova, I. A.; Morozkina, S. N.; Sorokoumov, V. N.; Vinogradova, O. V.; Knight, D. W.; Vasilevsky, S. F. *Eur. J. Org. Chem.* **2005**, 882.
62. Surry, D. S.; Buchwald, S. L. *Chem. Sci.* **2011**, *2*, 27.
63. Hartwig, J. F. *Acc. Chem. Res.* **2008**, *41*, 1534.
64. Muci, A. R.; Buchwald, S. L. *Top. Curr. Chem.* **2002**, *219*, 131.
65. Surry, D. S.; Buchwald, S. L. *Angew. Chem. Int. Ed.* **2008**, *47*, 6338.



# 12

## SYNTHESIS OF METALLOCENES VIA METATHESIS IN METAL COORDINATION SPHERES

ANTONI PIETRZYKOWSKI\* AND WŁODZIMIERZ BUCHOWICZ

Faculty of Chemistry, Warsaw University of Technology, Warsaw, Poland

### 12.1 INTRODUCTION

Olefin metathesis is a transition-metal-catalyzed reaction commonly applied in organic and polymer chemistry [1]. Therefore, application of olefin metathesis in coordination and organometallic chemistry as a synthetic tool might initially appear as something unusual, however providing that (i) the metal-containing substrate is sufficiently stable to withstand the presence of the catalyst and (ii) the ligand(s) feature at least one olefinic moiety, this approach proved to be successful.

The development and commercial availability of Grubbs' catalysts rendered the former condition relatively easy to fulfill, while the latter is limited only by our imagination. The examples of metathesis in metal coordination spheres present in the literature until 2003 were described in the book by Bauer and Gładysz [2] and are discussed briefly in this review.

This chapter is arranged by the well-recognized types of olefin metathesis reactions, that is, ring-opening metathesis polymerization (ROMP), acyclic diene metathesis (ADMET) polymerization, ring-closing metathesis (RCM), and cross-metathesis (CM) (Fig. 12.1). Examples of alkyne metathesis are also included.

Catalysts applied in reactions described in this chapter are depicted in Fig. 12.2. Symbols of catalysts shown in this figure are used in the text.

### 12.2 POLYMERS BEARING METALLOCENE MOIETIES BY RING-OPENING METATHESIS POLYMERIZATION OR ACYCLIC DIENE METATHESIS POLYMERIZATION

Ferrocene is a very robust organometallic complex that has been incorporated into an impressive number of molecules with various applications and properties. Therefore, ferrocene-containing polymers have been pursued for many possible applications by different routes. Three metathesis-based approaches toward metallocene-containing polymers (mainly ferrocenes) have been reported so far: (i) homo-ROP or co-ROP of olefins bearing a metallocenyl substituent, (ii) ROP of strained *ansa*-metallocenes, and (iii) ADMET polymerization of bis(alkenyl)metallocenes, including ADMET copolymerization with  $\alpha,\omega$ -dienes.

The first examples involving homo- or copolymerization of olefins (e.g., norbornene) bearing a ferrocenyl substituent were performed using Mo-based initiators by Schrock and coworkers [3] (Scheme 12.1a). Depending on the reaction conditions and monomer(s) ratio, redox-active polymers or block copolymers were obtained with narrow polydispersities. Solution measurements showed that the redox centers in homo- and copolymers were electrochemically independent.

*Advances in Organometallic Chemistry and Catalysis: The Silver/Gold Jubilee International Conference on Organometallic Chemistry Celebratory Book*, First Edition. Edited by Armando J. L. Pombeiro.

© 2014 John Wiley & Sons, Inc. Published 2014 by John Wiley & Sons, Inc.

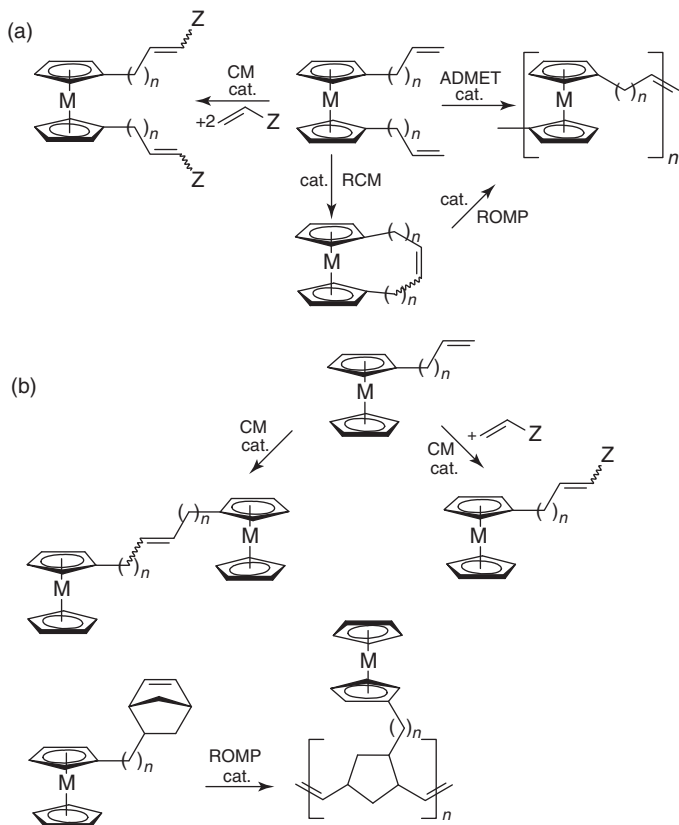


**Figure 12.1** Schematic representation of reported metathesis reactions for metallocene derivatives: (a) 1,1'-bis(alkenyl), (b) monoalkenyl. cat., suitable metathesis catalyst.

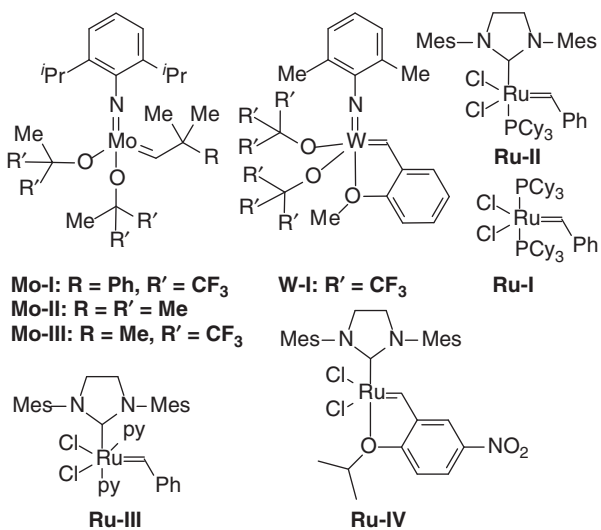
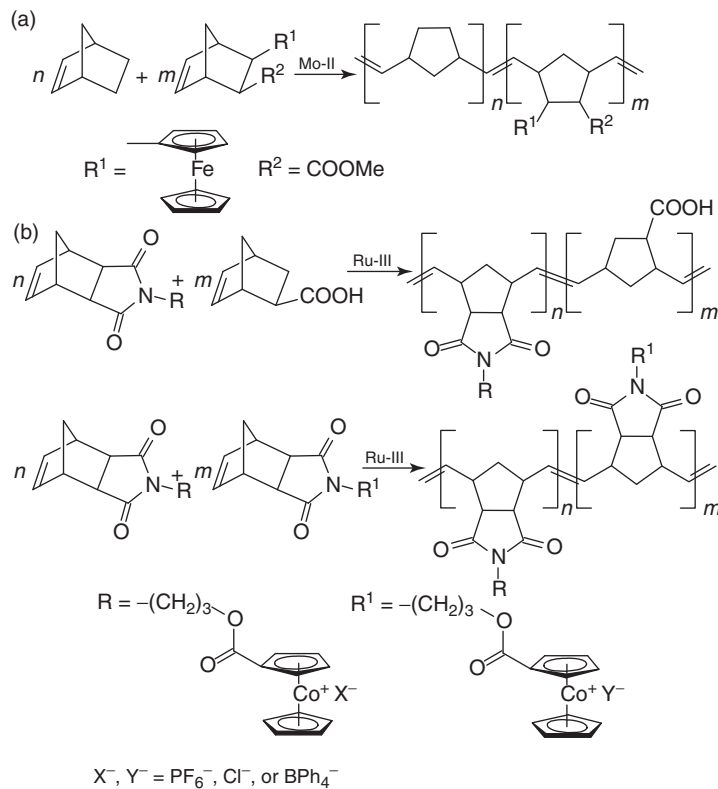


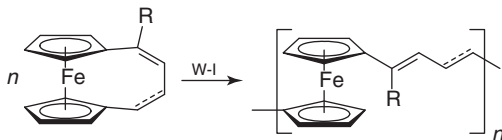
**Figure 12.2** Structures of catalysts applied in reactions described in this review.

In another report, by means of suitably functionalized norbornene monomers and Ru-I catalyst, ferrocene units were incorporated into hybrid gold nanoparticles with shell structures [4].

More recently, by using a similar approach and derivatives of norbornene-*exo*-2,3-dicarboximide, cobaltocenium-containing copolymers were obtained [5]. Two classes of copolymers were studied: (i) a cobaltocenium-containing block



Scheme 12.1

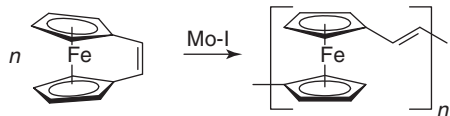
Scheme 12.2  $R = \text{H, } ^1\text{Bu}$ .

followed with the second metal-free block and (ii) a cobaltocenium-containing block followed with the second cobaltocenium-containing block with a different counterion (Scheme 12.1b). These copolymers self-assembled into spherical core/shell micelles in solutions. Treatment of these micelles under UV/ozoneolysis and pyrolysis conditions gave Co(II) or Co(III) containing nanoparticles.

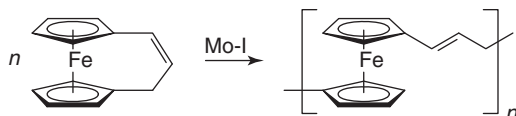
Grubbs and coworkers [6] studied ROMP of strained [4]ferrocenophanes as a plausible route to poly(ferrocenylene-divinylene) and related poly(ferrocenylenebutenylene) (Scheme 12.2,  $R = \text{H}$ ) employing a W-based catalyst. The obtained polymers ( $R = \text{H}$ ) with  $n > 10$  displayed somewhat limited solubility in common organic solvents. Gel permeation chromatography (GPC) analyses of the  $\text{CH}_2\text{Cl}_2$ -soluble fractions showed oligomeric structure of these products with chain lengths of circa 10.

Introduction of an aliphatic substituent (Scheme 12.2,  $R = ^1\text{Bu}$ ) solved the solubility problem. Deep red, stable to the atmosphere polymers soluble in benzene,  $\text{CH}_2\text{Cl}_2$ , and tetrahydrofuran (THF) were obtained with a W-based catalyst. The molecular weight of the product increased qualitatively with the monomer/catalyst ratio, and polymers with  $M_n \geq 300,000$  were obtained and characterized by thermogravimetric analysis, GPC, and UV/vis spectroscopy. The results were consistent with a moderate degree of conjugation in the polymer [7].

Similarly, the highly strained [2]ferrocenophane underwent slow polymerization in benzene at room temperature to yield the poly(ferrocenylenevinylene) as an insoluble (toluene, THF,  $\text{CH}_2\text{Cl}_2$ , dimethylformamide (DMF), dimethylsulfoxide (DMSO)) orange solid (Scheme 12.3) [8].



Scheme 12.3



Scheme 12.4

Partially soluble diblock copolymers resulted from copolymerization of the [2]ferrocenophane with norbornene in a benzene solution [8].

ROMP of [3] ferrocenophane was reported as moderately successful (Scheme 12.4) [9].

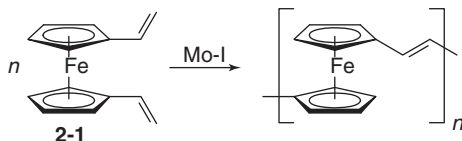
Polymerization with Ru-I in benzene was not complete even after 7 days at 60 °C. When a Mo-I initiator was used, the monomer was consumed after 3 days at 40 °C. The GPC analysis of the THF-soluble fraction of the product showed low molecular weight ( $M_n = 350$ ). The authors discussed some possible structures of linear and cyclic oligomers.

The cross-metathesis of vinylferrocene was apparently studied as a model reaction of ADMET of 1,1'-divinylferrocene (**2-1**) (see 12.4 section) [10]. Using a Mo-I initiator and 1,1'-divinylferrocene **2-1**, oligomers corresponding to the products resulting from the ROMP of [2]ferrocenophane (Scheme 12.3) with an average of  $n = 4$  were obtained (Scheme 12.5).

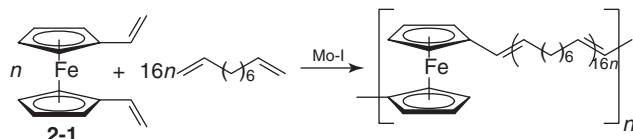
The conjugated oligomers displayed low solubility in toluene. In order to overcome this limitation, ADMET copolymerization of 1,1'-divinylferrocene **2-1** with 1,9-decadiene was studied (Scheme 12.6) at 1 : 16 molar ratio. Random copolymers with  $M_n$  circa 3000 were obtained with the same monomer ratio as in the feed.

ADMET polymerization of 1,1'-di-*t*-butyl-3,3'-divinylferrocene was also examined in order to increase the solubility. Unfortunately, its homopolymerization failed under the same conditions as for **2-1**; copolymerization with 1,9-decadiene gave a random copolymer with  $M_n = 11,000$  [10].

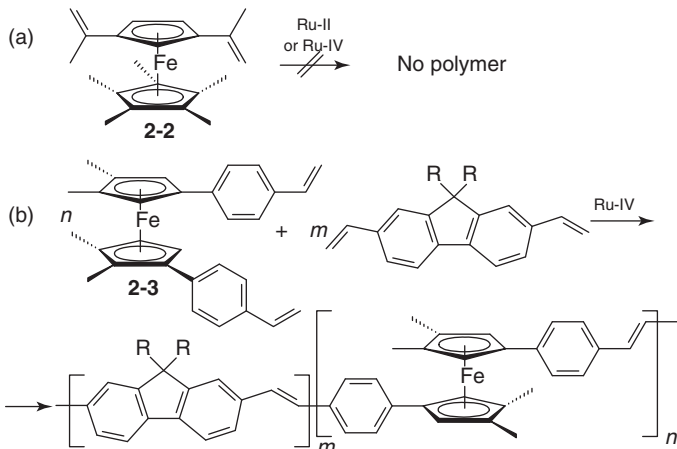
1,3-(Diisopropenyl)-1',2',3',4',5'-pentamethylferrocene (**2-2**) could not be polymerized under the optimized ADMET conditions with Ru-II-type catalysts (Scheme 12.7a) even under forcing conditions (75 °C, only the starting material was recovered by chromatography). Ferrocene-containing polymers were, however, obtained from another monomer, namely, a 1,1'-divinylphenyl derivative **2-3** (Scheme 12.7b). ADMET copolymerization of the latter compound with a divinylfluorene ( $R = 2$ -ethylhexyl) was accomplished with Ru-IV catalyst (3 days, 55 °C) [11]. The resulting copolymer ( $M_n = 25,100$ , PDI = 1.6) displayed considerably higher solubility than the corresponding homo-poly(fluorene). However, incorporation of the ferrocene unit into the polymer backbone resulted in a significant decrease of the fluorescence intensity compared to the homo-poly(fluorene).



Scheme 12.5



Scheme 12.6



**Scheme 12.7** R = 2-ethylhexyl.

### 12.3 SYNTHESIS OF METALLOCENES BY RING-CLOSING METATHESIS

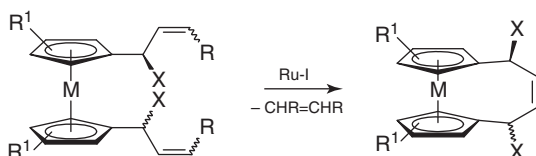
The discovery and commercialization of Grubbs' catalysts allowed for routine application of olefin metathesis in organic synthesis. A ferrocenemethyl moiety might serve as a protecting group on a nitrogen atom; two research groups have shown its inertness toward the Ru-catalyzed RCM. Thus, complex organic molecules bearing ferrocenylmethyl protecting groups were successfully transformed via RCM, however, without any significant changes in the Fe coordination spheres [12, 13].

The original idea that RCM of 1,1'-diallylferrocenes could be employed to synthesize [4]ferrocenophanes via RCM was discovered by Richards and coworkers [14] and further explored by Ogasawara and coworkers [15] (Scheme 12.8).

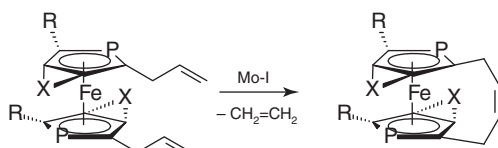
Several *ansa*-ferrocenes and *ansa*-ruthenocenes (M = Fe or Ru; R = H or Me; R<sup>1</sup> = H or Me) were synthesized via the RCM route in high yields employing the commercial Ru-I catalysts. Significant diastereoselectivity of these reactions was observed when mixtures of *meso* and *rac* complexes (X = Me or Ph) were used as substrates. Thus, the *meso*-diastereoisomer was cyclized to give the *meso-ansa* product whereas the *rac*-diastereoisomer did not react in the presence of Ru-I catalyst. The less reactive *rac*-isomer was recovered by chromatography and reacted with Ru-II to give the *rac-ansa* complex in high yield.

In the following report from the same research group, diphosphaferroceneces were tested as plausible substrates for the Ru-catalyzed RCM (Scheme 12.9) [16].

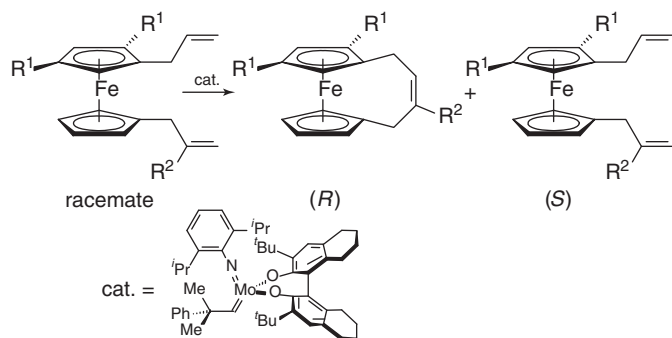
However, both Ru-I and Ru-II catalysts were not effective with these substrates (the starting material was recovered). The authors supposed that the P-containing substrates coordinated to the Ru-center and deactivated it in accordance with the generally accepted catalytic cycle. Fortunately, the Schrock Mo-I catalyst transformed the phosphaferroceneces into the



**Scheme 12.8** M = Fe or Ru; R = H or Me; R<sup>1</sup> = H or Me; X = H, Me, or Ph.



**Scheme 12.9** R = Me, <sup>t</sup>Bu, Ph, allyl; X = -(CH<sub>2</sub>)<sub>4</sub>-.

Scheme 12.10  $R^1 = {^t\text{Bu}}$ , Cy, or  $\text{SiMe}_3$ ,  $R^2 = \text{H}$  or Me.

expected *ansa* products in reasonable yields, albeit rather high catalyst loadings (10–20%) and prolonged reaction time under reflux conditions were required.

Enantioselective RCM of planar-chiral ferrocenes was accomplished with a Mo-chiral catalyst (Scheme 12.10) [17].

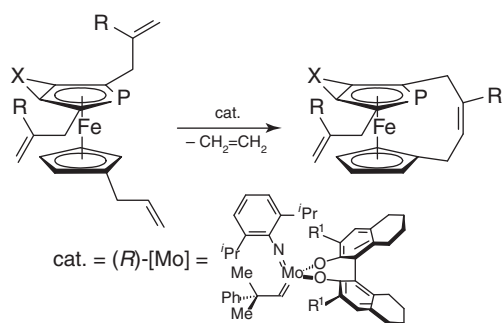
The racemic substrates were kinetically resolved to yield (*R*)-*ansa* products and the recovered (*S*)-substrates with *ee* up to >99.5% and 95%, respectively. However, the presence of a methylallyl substituent in the monosubstituted Cp ligand ( $R^2 = \text{Me}$ ) was essential for the metathesis to proceed with high enantioselectivity. The authors suggested that the initial metathesis reaction of chiral (*R*)-[Mo] catalyst should occur preferably with the olefinic group in the planar-chiral trisubstituted Cp in order to provide significant stereoselectivity. Accordingly, the olefinic group that was remote from the planar-chiral moiety in the substrate should be less reactive than the other group (i.e., methylallyl vs allyl) to render the reaction stereoselective.

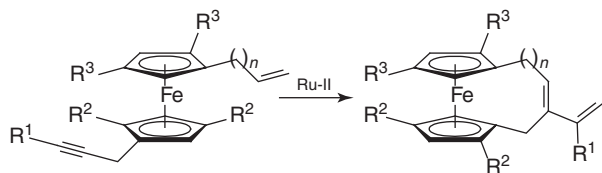
Enantioselective synthesis of planar-chiral phosphaferrocenes was recently achieved by asymmetric ring-closing synthesis using an appropriate chiral Mo catalyst (Scheme 12.11) [18].

The reactions proceeded with high yields (up to 95%) and *ee* (up to 99%) in the presence of the chiral (*R*)-[Mo] catalyst that was efficient in the kinetic resolution of the racemic planar-chiral substrates [17]. The stereochemical outcome of the reaction strongly depended on the structure of the allylic group in the phospholyl ligand: for  $R = \text{H}$ ,  $R^1 = {^t\text{Bu}}$  (Scheme 12.11), the bridged product was obtained in 65% yield but with only marginal *ee* (1%). Fortunately, for  $R = \text{Me}$ , the *ansa*-ferrocenophane was isolated in 72% yield with excellent enantioselectivity (99%).

Interligand ring-closing ene–yne metathesis of 1-alkenyl-1'-propargyl ferrocenes provided the expected [4]- or [5]ferrocenophanes in yields up to 84% (Scheme 12.12) [19].

These reactions could be performed with Ru-I or Ru-II catalysts in benzene or  $\text{CH}_2\text{Cl}_2$  at moderate temperature (40–60 °C); however, Ru-II was much more effective than the first-generation catalyst. In the presence of Schrock-Mo catalyst, the substrate ( $R^1 = \text{Me}$ ,  $R^2 = R^3 = \text{H}$ ,  $n = 1$ ) was completely consumed into an undefined mixture of oligomeric products. A reaction of the substrate with a terminal alkyne moiety ( $R^1 = \text{H}$ ) was moderately successful only under an ethylene atmosphere (15% yield). In this case, products of intermolecular metathesis with ethylene were also formed (17% yield). The complex with  $R^1 = \text{SiMe}_3$  did not react under these conditions. In the case of the complex with a butenyl substituent ( $n = 2$ ), because of the competition between intra- and intermolecular metathesis, high dilution conditions (0.01 mol/l) and higher temperature (60 °C) were needed to facilitate 81% yield of the cyclic product. The ring-closing reaction was also

Scheme 12.11  $R = \text{H}, \text{Me}$ ;  $X = -(CH_2)_4-$ ,  $-(CH_2)_5-$ ,  $-\text{CH}_2\text{OCH}_2-$ ;  $R^1 = {^t\text{Bu}}$ ,  $-\text{C}_6\text{H}_3\text{-}3,5\text{-(CF}_3)_2$ ,  $-\text{C}_6\text{H}_3\text{-}2,5\text{-(CF}_3)_2$ .



**Scheme 12.12**  $R^1 = \text{Me}$ ,  $R^2$ ,  $R^3 = \text{H}$ ,  $\text{Me}$ , or  ${}^t\text{Bu}$ ,  $n = 1$  or 2.

accomplished with two complexes bearing trisubstituted Cp ligands ( $R^2$  or  $R^3 = {}^t\text{Bu}$ ). The molecular structure of the cyclic product ( $R^1 = \text{Me}$ ,  $R^2 = R^3 = \text{H}$ ,  $n = 1$ ) was determined by X-ray diffraction. The two Cp ligands are nearly eclipsed and slightly tilted (the dihedral angle =  $5.04^\circ$ ), which is comparable to other [4]ferrocenophanes [15].

Nickelocene is a unique, moderately stable metallocene with 20 valence electrons (VE). Cyclopentadienyl ligands of nickelocene are labile and at least one of them is easily substituted in majority of its reactions [20]. Therefore, its stability in the presence of the Ru-metathesis catalysts was questionable; however, RCM of 1,1'-bis(alkenyl)nickelocenes proved to be successful (Schemes 12.13 and 12.14) [21].

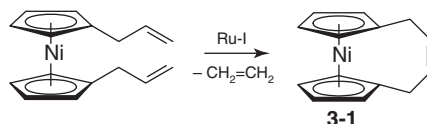
Compound **3-1** is the first example of *ansa*-nickelocene. It is a dark-green, paramagnetic solid ( $\text{mp} = 95\text{--}97^\circ\text{C}$ ), stable under an inert atmosphere, and soluble in common organic solvents. The molecular structure of **3-1** reveals that both cyclopentadienyl rings are flat and not parallel (Fig. 12.3). They are slightly inclined toward the bridge with the angle between the two Cp planes of  $8.1(2)^\circ$ . The average Ni–C (2.179 Å) and cyclopentadienyl C–C (1.424 Å) bond distances in **3-1** are close to those determined for nickelocene at 101 K (2.185 Å and 1.423 Å, respectively [22]). Cyclopentadienyl rings in the compound **3-1** are in an eclipsed conformation (unlike in nickelocene), which is caused by the rigid bridge. The stereochemistry of the double bond in crystalline **3-1** is Z.

When butenyl-substituted nickelocene was used, a mixture of the expected *ansa*-nickelocene (**3-2**) and a dinickelocene (**3-3**) resulting from homocoupling of two molecules of the substrate were produced (Scheme 12.14) [21].

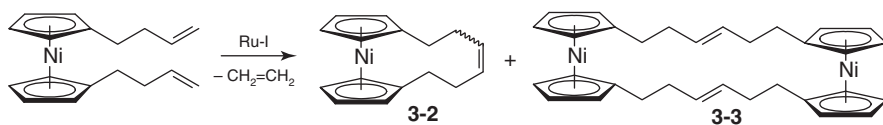
X-ray studies reveal that the molecule of **3-3** is centrosymmetric consisting of two nickelocenes coupled by two 3-hexenylene bridges with E stereochemistry of the double bonds. The Cp ligands and the bridges are in an eclipsed conformation (Fig. 12.4). The rings are flat and slightly inclined (in an opposite direction than in **3-1**) with a dihedral angle of  $5.4(2)^\circ$ . The authors attributed this bending to the steric repulsion of the bridging hydrocarbon chains. Average Ni–C (2.183 Å) and C–C cyclopentadienyl (1.423 Å) bond distances are the same as in nickelocene.

Consequently, metallocene derivatives featuring four alkenyl substituents with 1,3,1',3'-pattern (**3-4**, **3-5**) [23] seemed as challenging substrates for any metathesis catalyst. Ring-closing reactions of **3-4** and **3-5** might provide a considerable number of regio- and stereoisomers with an unprecedented connectivity between the cyclopentadienyl ligands. Indeed, while the Ru-I was effective for the closure of only one bridge, employment of the more reactive Ru-II provided the first *diansa*-nickelocene **3-6** as a single isomer in good yield (Scheme 12.15) [24].

A single-crystal X-ray structure analysis revealed that the cyclopentadienyl rings in complex **3-6** were linked with 1,2',3,4'-connectivity by two E-hex-3-enylene chains (Fig. 12.5). Consequently, the molecule exhibits screw-shape geometry (i.e., axial chirality). The cyclopentadienyl rings are in an eclipsed conformation and are not parallel (dihedral angle  $9.3^\circ$ ). Surprisingly, the corresponding ferrocene derivative yielded the *diansa*-ferrocene as a mixture of geometric isomers that formed mixed crystals (Scheme 12.16).



**Scheme 12.13**



**Scheme 12.14**

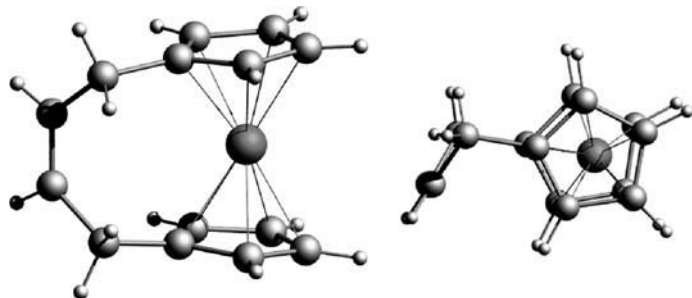


**Figure 12.3** The molecular structure of **3-1** showing its eclipsed conformation.

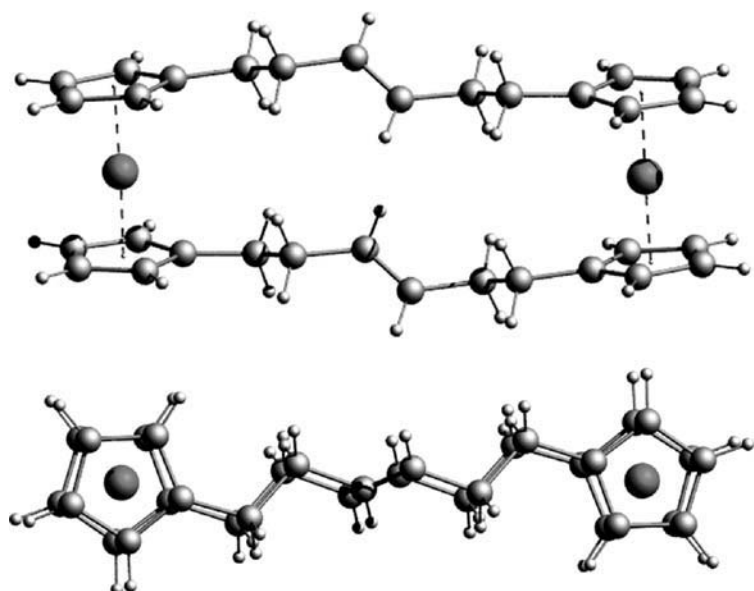
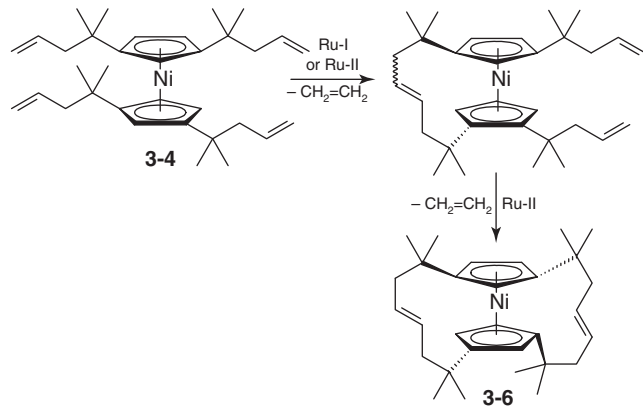


**Figure 12.4** The molecular structure of **3-3**.



**Scheme 12.15**

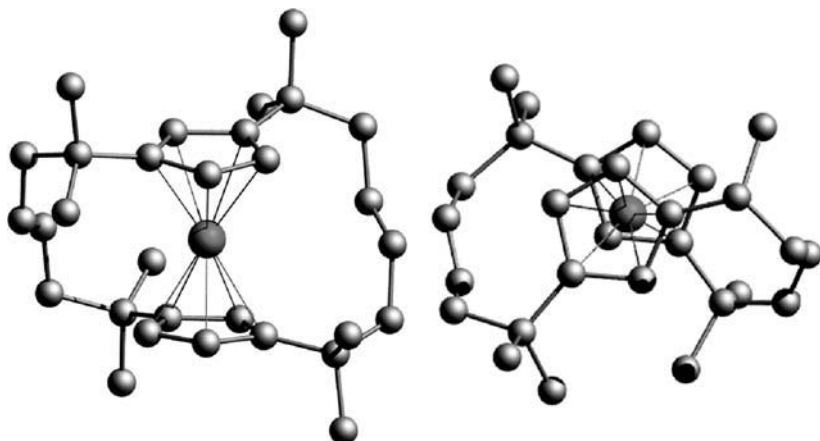
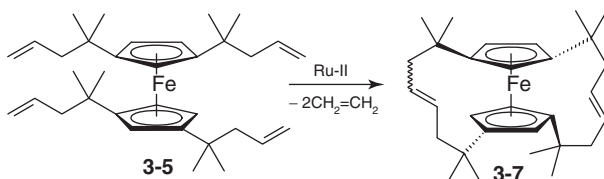
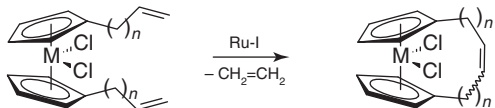


**Figure 12.5** The molecular structure of **3-6**. Hydrogen atoms were omitted for clarity.



**Scheme 12.16**



**Scheme 12.17**  $M = \text{Zr}$  or  $\text{Hf}$ ,  $n = 1$  or 4.

GC/MS analyses of the reaction mixture confirmed the presence of three isomers of the *diansa*-ferrocene, presumably *E,E*, *E,Z*, and *Z,Z* isomers. The structural data of the *E,E*-**3-7** and *E,Z*-**3-7** isomers were extracted from the X-ray data of the mixed crystals. Unexpectedly, the structure of the metallocene core of **3-7** compounds was not affected by the geometry of the double bonds in the bridges [24].

RCM was also efficiently performed for 16-electron, early transition metal metallocene dichlorides. Two research groups concurrently [15, 25] reported the intramolecular Ru-catalyzed reactions of bis(cyclopentadienylalkenyl) group IV bent metallocene derivatives shown on Scheme 12.17.

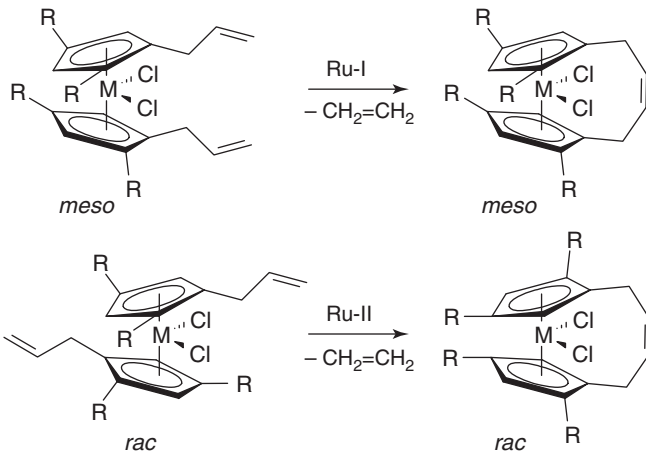
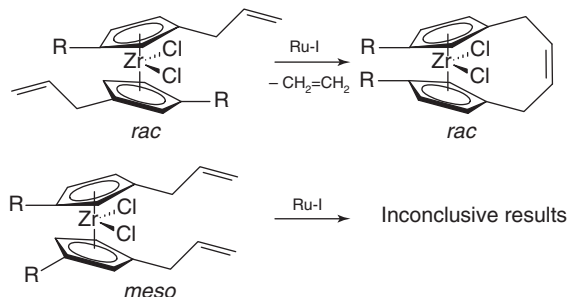
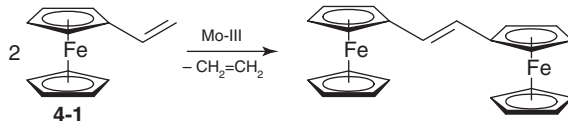
Products with *Z*-double bonds were obtained for allyl-substituted complexes ( $n = 1$ ), while the longer chain ( $n = 4$ ) produced the cyclic product with the *E*-configured double bond. Similarly to the substituted ferrocene derivatives, significant diastereoselectivity was observed for the substrates bearing additional substituents in the Cp ligands (Scheme 12.18).

When a mixture of *meso* and *rac* complexes was treated with Ru-I catalyst, the *meso*-diastereoisomer reacted faster than the *rac*-diastereoisomer. The *rac*-diastereoisomer underwent RCM reaction with the Ru-II catalyst.

In another report, *rac*- and *meso*-metallocene dichlorides were separated by recrystallization. The metathesis of *meso*-isomer with Ru-I was inconclusive and no product was identified. However, the *rac*-isomer produced cleanly the expected *rac*-*ansa* complex in 87% yield (Scheme 12.19) [26].

## 12.4 SYNTHESIS OF METALLOCENES BY CROSS-METATHESIS

The first example of self-metathesis of a metallocene derivative, namely, vinylferrocene **4-1**, to yield the *E*-homodimer, appeared in 1993 (Scheme 12.20) [10]. This reaction was considered as a model for ADMET polymerization of

Scheme 12.18  $M = \text{Zr}$ ,  $R = t\text{-Bu}$ .Scheme 12.19  $R = t\text{-Bu}$ .

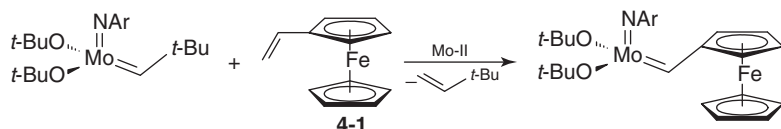
Scheme 12.20

divinylferrocenes and, owing to the isolation of the expected product in 54% yield, prompted further studies in this field (Schemes 12.5 and 12.6).

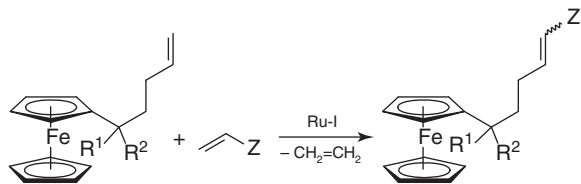
Cross-metathesis was recognized as a convenient route to introduce various functionalities into organometallic frameworks, initially including ferrocenes. For example, catalyst with a methyleneferrocenyl ligand was prepared by a stoichiometric reaction of vinylferrocene (**4-1**) with the Schrock catalyst (Scheme 12.21) [3]. Polymers with one ferrocenyl redox-active end group were obtained with this unique initiator.

Suitably substituted ferrocenyl alcohols and ketones were elaborated into more complex molecules using Ru-I catalyst under reflux conditions in  $\text{CH}_2\text{Cl}_2$  (Scheme 12.22) [27].

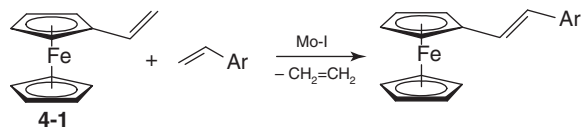
Predominantly *E* products were isolated in good yields together with small amounts of the self-metathesis products.



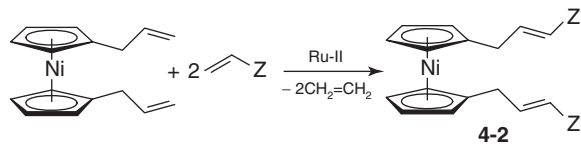
Scheme 12.21



**Scheme 12.22**  $R^1 = H$ ,  $R^2 = OH$ , or  $R^1 = R^2 = O$ ;  $Z = Ph$ ,  $CH_2SiMe_3$ ,  $CH_2OAc$ ,  $CO_2CH_3$ .



**Scheme 12.23**  $Ar = Ph$ ,  $4\text{-Me-C}_6H_4$ , 2-thiophene, 2-furane, 2-naphthalene, 4-biphenyl.



**Scheme 12.24**  $Z = CO_2Me$ ,  $COMe$ ,  $CO_2C(Me)_3$ .

The chemoselective cross-metathesis was further investigated for vinylferrocene **4-1** and a series of vinylarenes with the Mo-Schrock catalyst to yield  $\pi$ -conjugated molecules (Scheme 12.23) [28].

The desired heterodimers were obtained in good yields together with small amounts of homodimers. Only *E* products were reported in this system.

Following these successful reports, olefin cross-metathesis of suitably substituted ferrocene derivatives was used in the synthesis of complex molecules, including dinuclear Zr/Fe polymerization catalysts (see Scheme 12.26) [29], rotaxanes [30], dendrimers [31].

In this context, taking into account that the Cp ligands in nickelocene are labile [20], we decided to develop novel nickelocene derivatives with polar functional groups by means of selective cross-metathesis. Thus, reactions of 1,1'-diallylnickelocene with  $\alpha,\beta$ -unsaturated carbonyl compounds catalyzed with Ru-II were performed, using an excess of the organic olefin (Scheme 12.24) [32a].

Compound **4-2** ( $Z = COMe$ ) crystallized in the monoclinic space group  $P2_1/c$  with the Ni atom at the inversion center. The molecule adopts a staggered *anti* conformation. The average Ni–C (2.170 Å) and C–C(cyclopentadienyl ring) (1.417 Å) bond lengths are slightly shorter than those in nickelocene. The molecule of complex **4-2** ( $Z = CO_2Me$ ) in the solid state also adopts a staggered conformation; however, unlike in **4-2** ( $Z = COMe$ ), the substituents are slightly inclined toward the Ni center [32b]. In both complexes, the substituents are approximately flat with *E* double bonds (Fig. 12.6).

Cross-metathesis of the allyl-Cp substituted titanocene dichloride leads to the formation of dinuclear titanium complexes (Scheme 12.25,  $M = Ti$ ,  $n = 1$ ) [33]. The composition of the reaction mixture depends on the catalyst used. Treatment of the substrate with Ru-I (3 mol%) in benzene, toluene, or dichloromethane gave a mixture of *Z* and *E* isomers in a 1 : 1 ratio, while application of the Ru-II catalyst resulted with the formation of the pure *E* isomer.

Similar reactions of the allyl-, 3-butetyl-, and 4-pentenyl-Cp substituted zirconocene dichloride have been described by Kuwabara et al. [29] (Scheme 12.25,  $M = Zr$ ,  $n = 1 \div 3$ ). Metathesis of the allyl-substituted zirconocene dichloride with Ru-II (5 mol%, room temperature) gave a mixture of *E* and *Z* isomers at 99 : 1 ratio. When Ru-I was used at 40 °C, the ratio of isomers has changed to 6 : 1, still in favor of the *E* isomer.

Heterodinuclear Zr/Fe complex has been prepared by cross-metathesis of 3-butenyl-Cp-substituted zirconocene dichloride with ferrocenylmethyl acrylate (Scheme 12.26) [29]. This Zr/Fe complex exhibited catalytic activity in ethylene and propylene polymerization similar to those of the starting Zr complex.

Selective cross-metathesis of allyl-substituted *ansa*-zirconocene dichloride with Pd, Co, and Ni complexes having the acrylate pendant resulted in the synthesis of heterobimetallic complexes Zr/Pd, Zr/Co, and Zr/Ni (Scheme 12.27) [34].

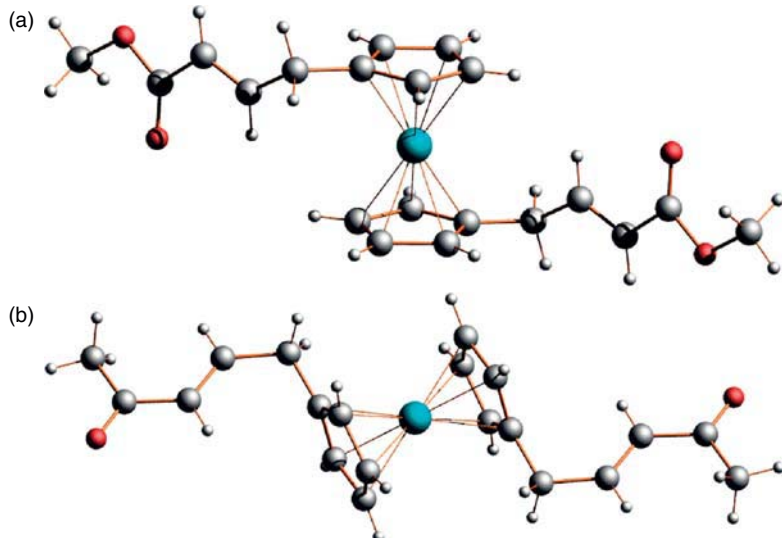
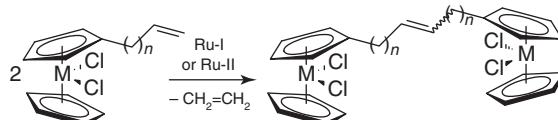
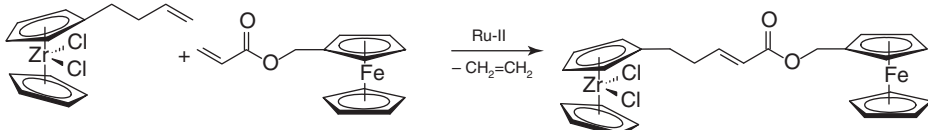


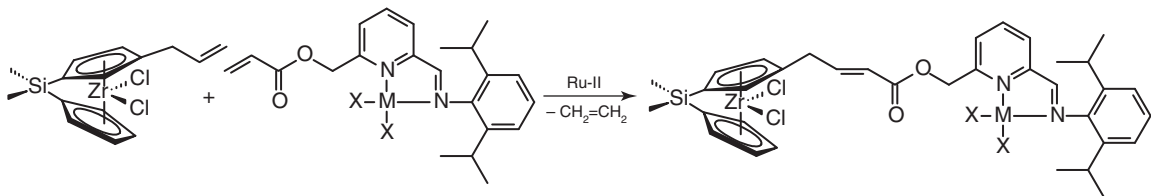
**Figure 12.6** The molecular structures of **4-2**; (a)  $Z = \text{CO}_2\text{Me}$  and (b)  $Z = \text{COMe}$ . (See insert for color representation of the figure.)



**Scheme 12.25**  $M = \text{Ti}$  [33],  $\text{Zr}$  [29];  $n = 1 \div 3$ .



**Scheme 12.26**

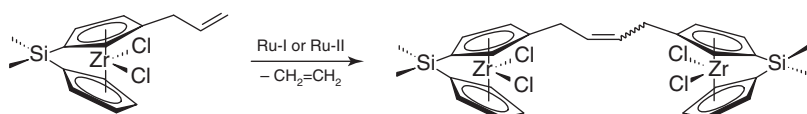


**Scheme 12.27**  $\text{MX}_2 = \text{PdCl}_2; \text{CoCl}_2; \text{NiBr}_2(\text{H}_2\text{O})$ .

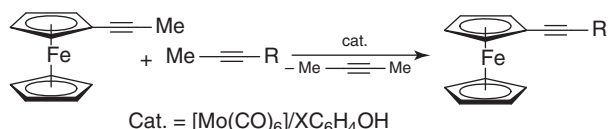
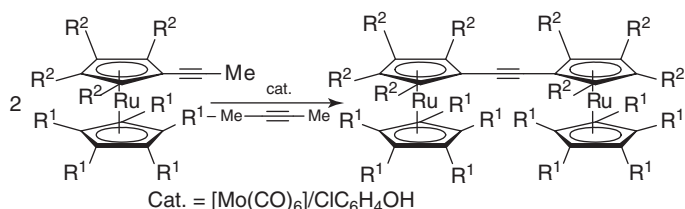
These complexes have been tested as initiators for ethylene polymerization in order to afford branched polyethylene. Catalytic activity of complexes, properties, and branched structures of polymers depended on the type of the late transition metal.

Allyl-Cp-substituted *ansa*-zirconocene dichloride also undergoes self-metathesis (Scheme 12.28) [33]. Owing to the planar chirality of the substrate and the possibility of the formation of *Z* and *E* isomers, coupling of two such molecules should lead to four possible stereoisomeric products. Reactions with Ru-I or Ru-II catalysts in various solvents (dichloromethane, benzene, or toluene) gave mixtures of products, in which a single isomer predominates (from circa 80% to 95%). The authors assumed that it was one of the two *E* isomers, but it was not clear whether *rac*- or *meso*isomer was formed.

A few examples of Mo-catalyzed alkyne cross-metathesis have been reported for ferrocenes and ruthenocenes. These reactions are summarized on Schemes 12.29 [35] and 12.30 [36].



Scheme 12.28

Scheme 12.29 R = Fc, Ph, n-C<sub>6</sub>H<sub>13</sub>, CH<sub>2</sub>CH<sub>2</sub>OAc, 4-R'-C<sub>6</sub>H<sub>4</sub> (R' = Me, MeO, Ph, Ac, CF<sub>3</sub>, CN); X = F, Cl.Scheme 12.30 R<sup>1</sup>, R<sup>2</sup> = H, Me.

## 12.5 CONCLUSIONS AND OUTLOOK

Olefin metathesis reaction catalyzed by well-defined metal (mainly ruthenium and molybdenum) carbene complexes is increasingly being applied in organic and organometallic synthesis [37]. Ruthenium, molybdenum, and tungsten carbene complexes appeared to be widely compatible with functional groups present in metallocenes. The application of these complexes as catalysts for olefin metathesis in metal coordination spheres resulted in the synthesis of a considerable number of novel metallocene derivatives. This methodology appeared to be compatible even with the very sensitive metallocenes functional groups such as nickelocene or the group 4 bent metallocenes. In this review, we have shown that olefin metathesis has been successfully used to synthesize derivatives of 18 VE ferrocenes, ruthenocenes, 20 VE nickelocenes, and 16 VE group 4 bent metallocene dichlorides. This method has also been used for the preparation of polymers bearing metallocenes as parts of the polymer chain or side groups. We consider this method as a major advantage in synthetic organometallic chemistry that will probably open up a variety of entries to novel metallocene derivatives. Further development in this field depends on possibilities of practical applications of these products, for example, as components of active catalytic systems or ligands.

## REFERENCES

- Ivin, K. J.; Mol, J. C. *Olefin Metathesis and Metathesis Polymerization*; Academic Press: San Diego, **1997**.
- Bauer, E. B.; Gladysz, J. A. In *Handbook of Metathesis*; Grubbs, R. H., Ed.; Wiley-VCH Verlag GmbH: Weinheim, Germany, **2003**; Vol. 2; Chapter 2.11.
- Albagli, D.; Bazan, G.; Wrighton, M. S.; Schrock, R. R. *J. Am. Chem. Soc.* **1992**, *114*, 4150.
- Watson, K. J.; Zhu, J.; Nguyen, S. T.; Mirkin, C. A.. *J. Am. Chem. Soc.* **1999**, *121*, 462.
- Ren, L.; Zhang, J.; Hardy, C. G.; Ma, S.; Tang, C. *Macromol. Rapid Commun.* **2012**, *33*, 510.
- Stanton, C. E.; Lee, T. R.; Grubbs, R. H.; Lewis, N. S.; Pudelski, J. K.; Callstrom, M. R.; Erickson, M. S.; McLaughlin, M. L. *Macromolecules* **1995**, *28*, 8712.
- Heo, R. W.; Somoza, F. B.; Lee, T. R. *J. Am. Chem. Soc.* **1998**, *120*, 1621.
- Burete, M. A.; Tilley, T. D. *Organometallics* **1997**, *16*, 1507.
- Arisandy, C.; Cowley, A. R.; Barlow, S. *J. Organomet. Chem.* **2004**, *689*, 775.
- Gamble, A. S.; Patton, J. T.; Boncella, J. M. *Macromol. Chem. Rapid Commun.* **1993**, *13*, 109.
- Weychardt, H.; Plenio, H. *Organometallics* **2008**, *27*, 1479.

12. Garro-Hélion, F.; Guibé, F. *Chem. Commun.* **1996**, 641.
13. Rutjes, F. P. J. T.; Schoemaker, H. E. *Tetrahedron Lett.* **1997**, 38, 677.
14. Locke, A. J.; Jones, C.; Richards, C. J. *J. Organomet. Chem.* **2001**, 637–639, 669.
15. Ogasawara, M.; Nagano, T.; Hayashi, T. *J. Am. Chem. Soc.* **2002**, 124, 9068.
16. Ogasawara, M.; Nagano, T.; Hayashi, T. *Organometallics* **2003**, 22, 1174.
17. (a) Ogasawara, M.; Watanabe, S.; Fan, L.; Nakajima, K.; Takahashi, T. *Organometallics* **2006**, 25, 5201; (b) Ogasawara, M.; Watanabe, S.; Nakajima, K.; Takahashi, T. *Pure Appl. Chem.* **2008**, 80, 1109.
18. Ogasawara, M.; Watanabe, S.; Nakajima K.; Takahashi, T. *J. Am. Chem. Soc.* **2010**, 132, 2136.
19. Ogasawara, M.; Watanabe, S.; Nakajima, K.; Takahashi, T. *Organometallics* **2008**, 27, 6565.
20. Jolly, P. W. *Comprehensive Organometallic Chemistry*, Vol. 6, Chapter 37.8; Pergamon Press: Oxford, **1982**.
21. Buchowicz, W.; Jerzykiewicz, L. B.; Krasinska, A.; Losi, S.; Pietrzykowski, A.; Zanello, P. *Organometallics* **2006**, 25, 5076.
22. Seiler, P.; Dunitz, J. D. *Acta Crystallogr., Sect. B* **1980**, 36, 2255.
23. Vos, D.; Salmon, A.; Sammler, H. -G.; Neumann, B.; Jutzi, P. *Organometallics* **2000**, 19, 3874.
24. Buchowicz, W.; Furmańczyk, A.; Zachara, J.; Majchrzak, M. *Dalton Trans.* **2012**, 41, 9269.
25. Hüerländer, D.; Kleigrewe, N.; Kehr, G.; Erker, G.; Fröhlich, R. *Eur. J. Inorg. Chem.* **2002**, 2633.
26. Tumay, T. A.; Kehr, G.; Frohlich, R.; Erker, G. *Dalton Trans.* **2009**, 8923.
27. Seshadri, H.; Lovely, C. J. *Org. Lett.* **2000**, 2, 327.
28. (a) Yasuda, T.; Abe, J.; Iyoda, T.; Kawai, T. *Chem. Lett.* **2001**, 30, 812; (b) Yasuda, T.; Abe, J.; Yoshida, H.; Iyoda, T.; Kawai, T. *Adv. Synth. Catal.* **2002**, 344, 705.
29. Kuwabara, J.; Takeuchi, D.; Osakada, K. *Organometallics* **2005**, 24, 2705.
30. (a) Suzuki, Y.; Osakada, K. *Chem. Lett.* **2006**, 374–375; (b) Suzuki, Y.; Osakada, K. *Dalton Trans.* **2007**, 2376.
31. Ornelas, C.; Méry, D.; Cloutet, E.; Aranzaes, J. R.; Astruc, D. *J. Am. Chem. Soc.* **2008**, 130, 1495.
32. (a) Buchowicz, W.; Szmajda, M. *Organometallics* **2009**, 28, 6838; (b) Buchowicz, W.; Kamiński, R.; Woźniak, K. unpublished results.
33. Sierra, J. C.; Hüerländer, D.; Hill, M.; Kehr, G.; Erker, G.; Fröhlich, R. *Chem. Eur. J.* **2003**, 9, 3618.
34. Kuwabara, J.; Takeuchi, D.; Osakada, K. *Chem. Commun.* **2006**, 3815.
35. (a) Kotora, M.; Nečas, D.; Štěpnička, P. *Collect. Czech. Chem. Commun.* **2003**, 68, 1897; (b) Bobula, T.; Hudlický, J.; Novák, P.; Gyepes, R.; Cisařová, I.; Štěpnička, P.; Kotora, M. *Eur. J. Inorg. Chem.* **2008**, 1, 3911.
36. (a) Sato, M.; Watanabe, M. *Chem. Commun.* **2002**, 1574; (b) Sato, M.; Kubota, Y.; Kawata, Y.; Fujihara, T.; Unoura, K.; Oyama, A. *Chem. Eur. J.* **2006**, 12, 2282.
37. Grubbs, R. H., Ed. *Handbook of Metathesis*; Wiley-VCH: Weinheim, Germany, **2003**.

# METAL-MEDIATED [2 + 3] DIPOLAR CYCLOADDITION TO SUBSTRATES WITH CN TRIPLE BOND: RECENT ADVANCES

KONSTANTIN V. LUZYANIN\* AND MAXIM L. KUZNETSOV\*

*Centro de Química Estrutural, Instituto Superior Técnico, Universidade de Lisboa, Lisboa, Portugal; Department of Chemistry, St. Petersburg State University, St. Petersburg, Russia*

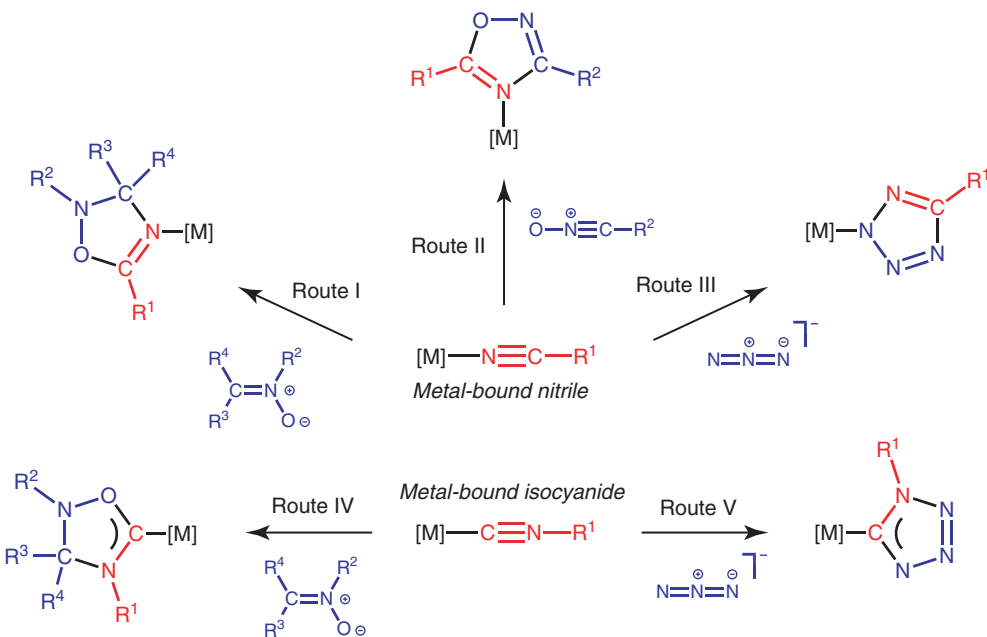
## 13.1 INTRODUCTION

Nitriles and isocyanides are among the most versatile organic substrates and are widely employed as starting materials in both industry and laboratory (e.g., for production of amides via hydrolysis of nitriles [1] or application of isocyanides in multicomponent reactions [2–4]). The transformation of these synthons offers an attractive route for the creation of novel C–X (X = C, N, O, and S) bonds, in particular, through reactions of nucleophilic addition or a dipolar cycloaddition (DCA) [1, 3, 5, 6].

The main drawback associated with the reactions of nitriles and isocyanides is their insufficient electrophilic activation (toward nucleophilic addition) or a very moderate dipolarophilicity (toward a DCA). This problem can be successfully overcome by coordination of the substrate to a metal center (Scheme 13.1) [1, 5, 7–9]. Under these conditions, the integration between nitriles (or isocyanides) proceeds at metal centers, giving new species, which, in contrast to metal-catalyzed processes, persist in the coordination state after coupling. In many instances, these metal-mediated processes allow the performance of certain reactions that are not feasible without the involvement of metal, and provide the stabilization of organic species that do not exist in a free state [1, 5–10].

Several types of reactivity for metal-bound nitriles and isocyanides should be recognized [1, 7, 8]. For instance, the nucleophilic addition to metal-bound nitriles allows the generation of imine complexes [1], electrophilic addition produces metal-bound azavinylidenes [1], and the DCA results in coordinated heterocyclic imines (Route I, Scheme 13.1) [5, 6, 10]. With respect to the metal-ligated isocyanides, the addition of nucleophiles furnishes complexes with acyclic aminocarbenes [7, 9, 11], electrophilic addition gives aminocarbynes [8, 12], while the DCA brings about the formation of *N*-heterocyclic carbene derivatives (Route II, Scheme 13.1) [6, 10].

Among the depicted reactivity modes, we are particularly interested in the reactions of DCA that is accounted as an alternative route for the generation of heterocyclic imines (Route I) and *N*-heterocyclic carbenes (Route II). While the reactions of the metal-mediated DCA to nitriles have been extensively reviewed circa 10 years ago [1], over the past decade, many new reactions illustrating this approach have appeared. In addition, previously unknown examples for [2 + 3] DCA to isocyanides have emerged. In this survey, we describe the recent trends in metal-mediated transformation of CN substrates via the reactions of [2 + 3] DCA exemplified by the most representative papers. The mechanistic features and driving forces of these processes as well as the reasons of activation effect upon coordination of substrate to the metal center are also discussed.



**Scheme 13.1** Metal-mediated dipolar cycloaddition to nitriles and isocyanides and dipoles employed. (See insert for color representation of the figure.)

## 13.2 METAL-MEDIATED [2 + 3] DIPOLE CYCLOADDITION TO NITRILES AND ISOCYANIDES: SYNTHETIC STUDIES

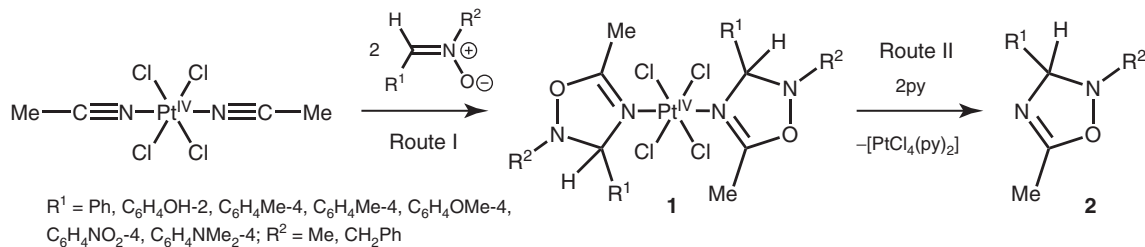
### 13.2.1 Addition of Nitrones and *N*-Oxides to Nitriles

Reported [2 + 3] cycloaddition between acetonitrile ligands in the platinum(IV) complex  $[PtCl_4(MeCN)_2]$  and the aldonitrones  $R^1CH=N^+(R^2)O^-$  proceeds at 20–25°C for 4 h affording  $\Delta^4$ -1,2,4-oxadiazoline complexes  $[PtCl_4\{N^a=C(Me)ON(R^2)C^bH(R^2)\}_2(N^a-C^b)]$  (**1**) (Route I, Scheme 13.2) as a 1 : 1 mixture of two diastereoisomers [13]. Free  $\Delta^4$ -1,2,4-oxadiazolines (**2**) were liberated almost quantitatively by reaction of the complexes with a slight excess of pyridine (Route II, Scheme 13.2) [13].

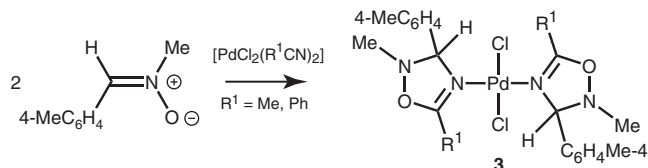
In the related studies [14–18], the ligated benzonitriles in the platinum(II) complex  $[PtCl_2(PhCN)_2]$  or *cis*- $[PtCl_2(R^3MeSO)(PhCN)]$  underwent metal-mediated [2 + 3] cycloaddition with nitrones  $R^1CH=N^+(R^2)O^-$  to give  $\Delta^4$ -1,2,4-oxadiazoline species,  $[PtCl_2\{N^a=C(Ph)N(R^1)C^bH(R^2)\}_2(N^a-C^b)]$  [14, 16] or  $[PtCl_2(R_3MeSO)\{N^a=C(Ph)N(R^1)C^bH(R^2)\}_2(N^a-C^b)]$  [15], correspondingly. Under similar conditions, platinum(II) complex  $[PtCl_2(MeCN)_2]$  was reported inactive. Liberation of the free  $\Delta^4$ -1,2,4-oxadiazolines was accomplished upon reaction of corresponding complexes with ethane-1,2-diamine (en) [15].

The [2 + 3] DCA of an acyclic aldonitronite  $4\text{-MeC}_6\text{H}_4\text{CH=N}^+(\text{Me})\text{O}^-$  to nitriles in palladium(II) complex *trans*- $[\text{PdCl}_2(\text{RCN})_2]$  ( $\text{R} = \text{Ph}, \text{Me}$ ) proceeds at 45°C ( $\text{R} = \text{Ph}$ ) or reflux ( $\text{R} = \text{Me}$ ) for 1 day leading to  $\Delta^4$ -1,2,4-oxadiazoline complexes  $[\text{PdCl}_2\{N^a=C(\text{R})\text{ON}(\text{Me})\text{C}^b\text{H}(\text{C}_6\text{H}_4\text{Me}-4)\}_2(N^a-C^b)]$  (**3**, Scheme 13.3) [19, 20]. The authors found that use of focused microwave irradiation in the place of conventional heating drastically reduces the reaction time. A similar reactivity pattern was demonstrated for platinum(II) and palladium(II) complexes with (*E*)-cinnamonnitrile [21].

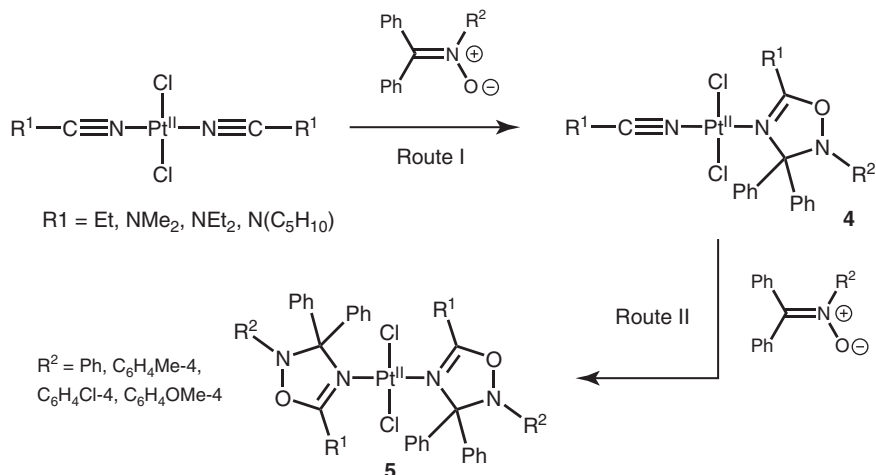
Platinum(II)-bound dialkylcyanamides  $\text{NCNR}^1_2$  reacted smoothly with the acyclic aldonitronites  $R^2\text{CH=N}^+(\text{O}^-)\text{R}^3$  in the Z-form giving corresponding cycloadducts [22]. By performing a competitive reactivity study of DCA between *trans*- $[\text{PtCl}_2(\text{R}^4\text{CN})_2]$  ( $\text{R}^4 = \text{Ph}$  and  $\text{NR}^1_2$ ) species and the acyclic nitronite  $4\text{-MeC}_6\text{H}_4\text{CH=N}^+(\text{O}^-)\text{Me}$ , the authors revealed that both coordinated PhCN and  $\text{R}^1_2\text{NCN}$  exhibit comparable reactivity. Under similar conditions, alkynitrile ligands did not react with this dipole. Metal-free 5- $\text{NR}^1_2$ -2,3-dihydro-1,2,4-oxadiazoles were liberated from the corresponding platinum(II) complexes by treatment with excess NaCN [22]. In the related study, the Z-configured nitronites  $4\text{-R}^2\text{C}_6\text{H}_4\text{CH=N}^+(\text{O}^-)\text{Me}$  reacted with the nitrile functionality of the *clos*-dodecaborate clusters  $[\text{nBu}_4\text{N}][\text{B}_{10}\text{H}_9(\text{NCR}^1)]$  to afford borylated 2,3-dihydro-1,2,4-oxadiazoles  $[\text{nBu}_4\text{N}][\text{B}_{10}\text{H}_9\{N^a=\text{CR}^1\text{ON}(\text{Me})\text{C}^b\text{H}(\text{C}_6\text{H}_4\text{R}^2-4)\}(N^a-C^b)]$ . This reaction represents the first example of boron-mediated 1,3-DCA of allyl anion type dipoles, that is, nitronites, to the nitrile group.



Scheme 13.2 [2 + 3] cycloaddition between MeCN in  $[\text{PtCl}_4(\text{MeCN})_2]$  and  $\text{R}^1\text{CH}=\text{N}^+(\text{R}^2)\text{O}^-$  [13].



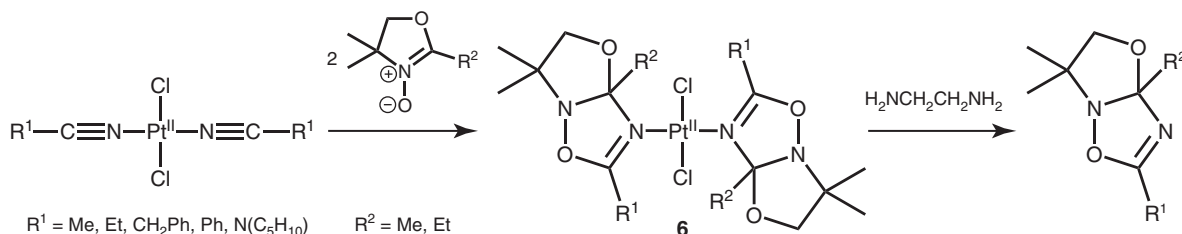
Scheme 13.3 Palladium(II)-mediated dipolar cycloaddition of nitrones to nitriles [19].



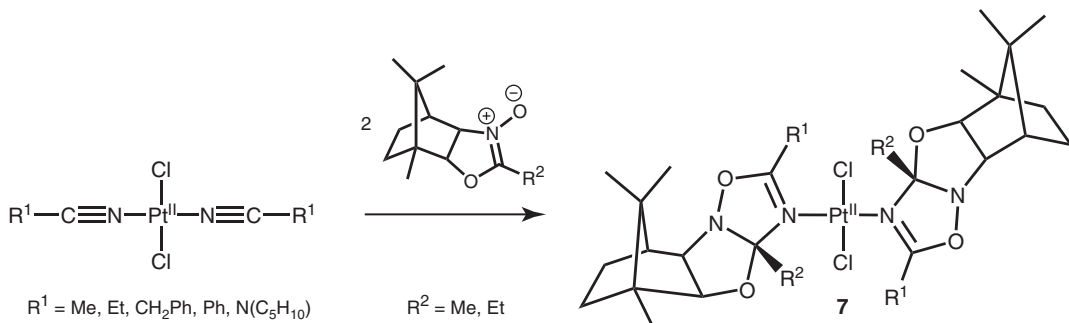
Scheme 13.4 Dipolar cycloaddition of  $\text{Ph}_2\text{C}=\text{N}^+(\text{R}^2)\text{O}^-$  to nitriles in  $\text{trans-}[\text{PtCl}_2(\text{R}^1\text{CN})_2]$  [23].

The described [23] reaction between  $\text{trans-}[\text{PtCl}_2(\text{R}^1\text{CN})_2]$  and the acyclic triaryl ketonitrones  $\text{Ph}_2\text{C}=\text{N}^-(\text{R}^2)\text{O}^+$  proceeded as a consecutive two-step intermolecular cycloaddition to give the monocycloaddition products  $\text{trans-}[\text{PtCl}_2(\text{N}^a=\text{C}(\text{R}^1)\text{ON}(\text{R}^2)\text{C}^b\text{Ph}_2)\{\text{N}^a-\text{C}^b\}]$  (**4**, Scheme 13.4) and then the bis-2,3-dihydro-1,2,4-oxadiazole complexes  $\text{trans-}[\text{PtCl}_2\{\text{N}^a=\text{C}(\text{R}^1)\text{ON}(\text{R}^2)\text{C}^b\text{Ph}_2\}_2\{\text{N}^a-\text{C}^b\}]$  (**5**) [23]. Ketonitrones  $\text{Ph}_2\text{C}=\text{N}^-(\text{R}^2)\text{O}^+$  were found to be unexpectedly more reactive toward the platinum(II)-bound nitriles if compared to the related aldonitrones  $\text{R}^3\text{CH}=\text{N}^+(\text{R}^2)\text{O}^-$ . The difference in the reactivity in 1,3-DCA of the keto- and aldonitrones was interpreted by theoretical calculations (see below) [23].

In the other study [24], complexes containing heterocycles of a new type, namely, 2,3a-disubstituted 5,6-dihydro-3a*H*-[1,3]oxazolo[3,2-*b*][1,2,4]oxadiazoles (**6**, Scheme 13.5), were prepared via the intermolecular platinum(II)-mediated DCA between coordinated nitriles in  $\text{trans/cis-}[\text{PtCl}_2(\text{R}^1\text{CN})_2]$  and the oxazoline *N*-oxide  $\text{C}^a(\text{Me})_2\text{CH}_2\text{OC}(\text{R}^2)=\text{N}^{b+}(\text{O}^-)(\text{C}^a-\text{N}^b)$ . With the exception of benzonitrile species, cycloaddition of oxazoline *N*-oxides to the platinum(II)-ligated nitriles proceeds diastereoselectively giving mixtures of enantiomers. The heterocyclic ligands in **6** were liberated by treatment with excess ethane-1,2-diamine [24].



**Scheme 13.5** Platinum(II)-mediated dipolar cycloaddition of oxazoline *N*-oxides to nitriles and liberation of free 2,3a-disubstituted 5,6-dihydro-3aH-[1,3]oxazolo[3,2-b][1,2,4]oxadiazoles [24].



**Scheme 13.6** Preparation of the diastereomerically pure platinum(II) complexes bearing tetrahydro-5,8-methanocyclohexa-[3',2':4,5][1,3]oxazolo[3,2-b][1,2,4]oxadiazole [26].

In the related study [25], (tetrahydroimidazo[1,2-*b*][1,2,4]-oxadiazole)Pt<sup>II</sup> complexes were assembled via an intermolecular platinum(II)-mediated 1,3-DCA between the imidazoline *N*-oxides and the coordinated nitriles in *cis*- and *trans*-[PtCl<sub>2</sub>(R<sup>1</sup>CN)<sub>2</sub>]. Tetrahydroimidazo[1,2-*b*][1,2,4]-oxadiazoles exist only in the coordinated state, and an attempt to liberate the heterocyclic ligands from the complexes by treatment with 1,2-bis(diphenylphosphino)ethane (dppe) led to formation of the free parent imidazoline *N*-oxides and the nitriles [25].

Preparation of the diastereomerically pure platinum(II) complexes bearing tetrahydro-5,8-methanocyclohexa-[3', 2': 4, 5][1,3]oxazolo[3,2-*b*][1,2,4]oxadiazole ligands (**7**, Scheme 13.6) was accomplished via the intermolecular 1,3-DCA between enantiomerically pure camphor-derived oxazoline-*N*-oxides and the coordinated nitriles in *trans*-[PtCl<sub>2</sub>(R<sup>1</sup>CN)<sub>2</sub>] [26]. The reaction proceeds at 20–25 °C. Free heterocyclic species were liberated as single stereoisomers from the respective platinum(II) complexes by treatment with excess NaCN [26].

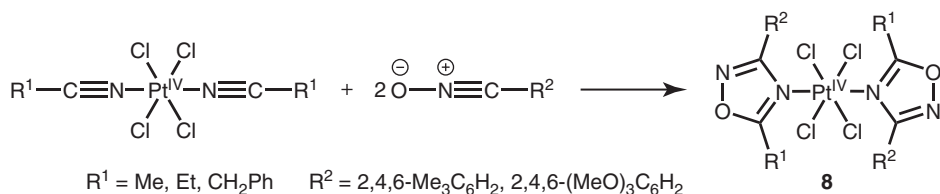
### 13.2.2 Addition of Nitrile Oxides to Nitriles

The coupling of [PtCl<sub>4</sub>(R<sup>1</sup>CN)<sub>2</sub>] with the nitrile oxides R<sup>2</sup>CNO at 20–25 °C afforded the (1,2,4-oxadiazole)platinum(IV) complexes [PtCl<sub>4</sub>{N<sup>a</sup>=C(R<sup>1</sup>)ON=C<sup>b</sup>R<sub>2</sub>}<sub>2</sub>(N<sup>a</sup>-C<sup>b</sup>)] (**8**, Scheme 13.7) [27]. The reduction of **8** with Ph<sub>3</sub>P=CHCO<sub>2</sub>Me led to the appropriate platinum(II) complexes that cannot be obtained via a direct synthesis starting from the corresponding platinum(II)-nitrile species. Furthermore, the reaction of **8** with an excess of pyridine in chloroform allowed to obtain free 1,2,4-oxadiazoles, that were isolated in nearly quantitative yields [27].

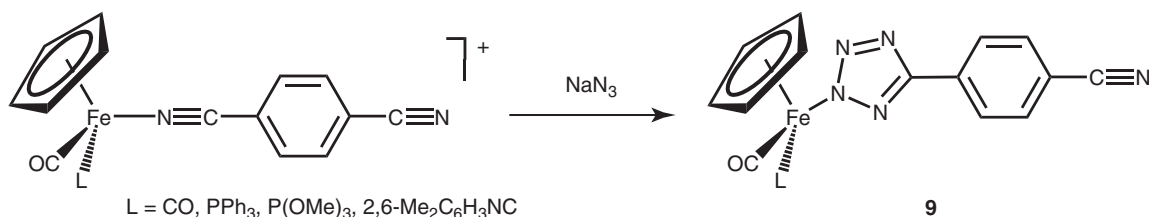
In a related study [28], the coupling between palladium(II)-bound nitriles in [PdCl<sub>2</sub>(R<sup>1</sup>CN)<sub>2</sub>] and the nitrile oxides R<sup>2</sup>CNO in neat nitrile at 40 °C for 12–18 h furnished 1,2,4-oxadiazole complexes *trans*-[PdCl<sub>2</sub>{N<sup>a</sup>=C(R<sup>1</sup>)ON=C<sup>b</sup>R<sub>2</sub>}<sub>2</sub>(N<sup>a</sup>-C<sup>b</sup>)] in 40–85 % yields. Liberation of the free 1,2,4-oxadiazole species was accomplished by the action of 2 equiv of dppe in chloroform or excess Na<sub>2</sub>S•7H<sub>2</sub>O in methanol [28].

### 13.2.3 Addition of Azides to Nitriles

Iron(II) 5-aryl tetrazolate complexes [CpFe(CO)(L)(N<sub>4</sub>CC<sub>6</sub>H<sub>4</sub>CN)] (**9**, Cp =  $\eta$ -C<sub>5</sub>H<sub>5</sub>) were prepared by the room-temperature cycloaddition of sodium azide to parent 1,4-dicyanobenzene complexes [CpFe(CO)(L)(NCC<sub>6</sub>H<sub>4</sub>CN)][O<sub>3</sub>SCF<sub>3</sub>] (Scheme 13.8) [29].



**Scheme 13.7** Platinum(IV)-mediated dipolar cycloaddition of nitrile oxides to nitriles [27].

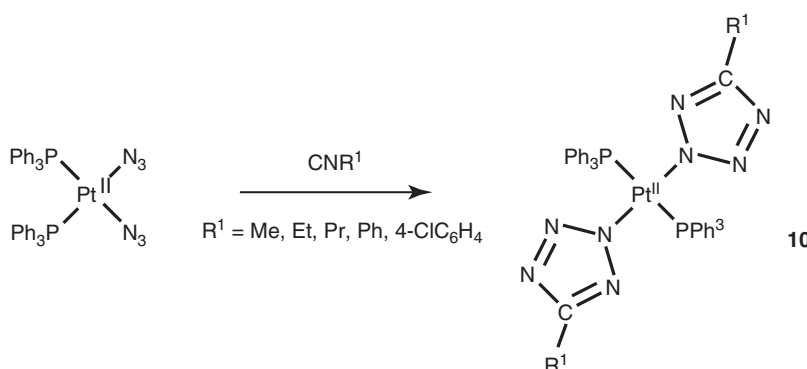


**Scheme 13.8** Reaction between  $[\text{CpFe}(\text{CO})(\text{L})(\text{N}_4\text{CC}_6\text{H}_4\text{CN})]$  and sodium azide [29].

Manganese(II) complexes with 5-(2-pyridyl) tetrazole, 5-(3-cyano-4-pyridyl) tetrazole, or 5-(4-pyridyl) tetrazole ligands were generated by reaction of the corresponding cyanopyridines with sodium azide in the presence of manganese(II) salts [30]. Acidification of the complexes produces the corresponding free 5-(pyridyl)-1H-tetrazole [30]. In another study [31], the [2 + 3] cycloaddition reaction of molybdenum(II) azide complexes with nitriles afforded tetrazolate complexes  $\text{Mo}(\eta^3\text{-C}_3\text{H}_5)(\text{CO})_2(\text{en})(\text{R}^1\text{CN}_4)$ . They are the first examples of a complex with a heterocyclic ligand prepared via the reaction of a group VIB metal azide with an unsaturated dipolarophile.

Solvothermal reactions of  $\text{AgNO}_3$ ,  $\text{NaN}_3$  with  $\text{MeCN}$  and  $\text{EtCN}$  in methanol yield two noninterpenetrated supramolecular networks,  $[\text{Ag}(\text{mtta})]_n$  and  $[\text{Ag}(\text{etta})]_n$  (mtta, 5-methyl tetrazolate; etta 5-ethyl tetrazolate), respectively, involving ligand *in situ* formation by cycloaddition of nitriles and azides [32]. Furthermore, two new d<sup>10</sup> coordination polymers of zinc and cadmium containing tetrazolate ligands have been synthesized by the *in situ* [3 + 2] cycloaddition reaction of 5-benzylacetonitrile, sodium azide, and  $\text{MCl}_2$  ( $\text{M} = \text{Zn, Cd}$ ) under hydrothermal conditions [33, 34].

The [2 + 3] cycloaddition reactions of the diazidoplatinum(II) complexes *cis*- $[\text{Pt}(\text{N}_3)_2(\text{PPh}_3)_2]$  and *cis*- $[\text{Pt}(\text{N}_3)_2(2,2\text{-bipy})]$  with nitriles  $\text{R}^1\text{CN}$  (Scheme 13.9) furnished the bis(tetrazolato) complexes *trans*- $[\text{Pt}(\text{R}^1\text{CN}_4)_2(\text{PPh}_3)_2]$  (**10**) or *cis*- $[\text{Pt}(\text{R}^1\text{CN}_4)_2(2,2\text{-bipy})]$  (bipy, bipyridine), correspondingly. Both reactions are greatly accelerated by microwave irradiation [35]. In a related study [36], the [2 + 3] cycloaddition reaction of the *cis*- $[\text{Pt}(\text{N}_3)_2(\text{PPh}_3)_2]$  with 4-cyanobenzaldehyde furnished the  $N^2N^2$ -bonded isomer of bis[5-(4-formylphenyl)tetrazol-2-ate] platinum(II) *trans*- $[\text{Pt}(\text{N}_4\text{CC}_6\text{H}_4(4\text{-CH=O}))_2(\text{PPh}_3)_2]$  as the major product, along with the  $N^1N^2$ -bonded isomer. In another study by the



**Scheme 13.9** Reactions of the diazidoplatinum(II) complexes *cis*- $[\text{Pt}(\text{N}_3)_2(\text{PPh}_3)_2]$  with platinum(II)-bound nitriles [35].

same authors [37], microwave synthesis of bis(tetrazolato)-palladium(II) complexes with  $\text{PPh}_3$  and water-soluble 1,3,5-triaza-7-phosphaadamantane was accomplished using a similar strategy.

Preparation of new tetrazolate complexes  $\text{trans}\text{-}[\text{PtCl}_2(\text{R}^1\text{CN}_4)_2]^{2-}$  and  $\text{trans}\text{-}[\text{PtCl}_4(\text{R}^1\text{CN}_4)_2]^{2-}$  with  $\text{Ph}_3\text{PCH}_2\text{Ph}^+$  and  $(\text{CH}_3)_2\text{NH}_2^+$  counterions was accomplished via the direct azidation of nitriles in  $\text{trans}\text{-}[\text{PtCl}_2(\text{R}^1\text{CN})_2]$  and  $\text{trans}\text{-}[\text{PtCl}_4(\text{R}^1\text{CN})_2]$  [38]. The authors indicated that the coordination of nitriles to Pt(II) and Pt(IV) significantly activated the azidation: the reaction proceeded with a higher rate and at relatively low temperature compared with the classical 1,3-dipolar addition of azides to nitriles.

### 13.2.4 Addition of Nitrones to Isocyanides

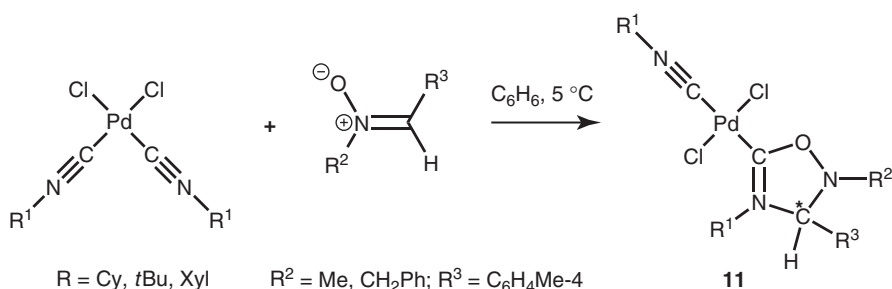
The first example for the metal-mediated [2 + 3] cycloaddition of a nitrone to an isonitrile was reported [39]. Thus, the reaction between equimolar amounts of  $\text{cis}\text{-}[\text{PdCl}_2(\text{R}^1\text{NC})_2]$  and the acyclic nitrones  $\text{O}^+\text{N}^-(\text{R}^2)=\text{C}(\text{H})\text{R}^3$  performed in  $\text{C}_6\text{H}_6$  at 5 °C provided the carbene complexes  $[\text{PdCl}_2\{\text{C}(\text{ONR}_2\text{C}^a\text{HR}^3)=\text{N}^b\text{R}^1\}(\text{CNR}^1)(\text{C}^a-\text{N}^b)]$  (**11**) in good (70–54%) yields (Scheme 13.10).

The interplay between equimolar amounts of  $\text{cis}\text{-}[\text{PdCl}_2(\text{R}^1\text{NC})_2]$  and the nonaromatic cyclic nitrone  $-\text{O}^+\text{N}=\text{CHCH}_2\text{CH}_2\text{C}^d\text{Me}_2(\text{N}^c-\text{C}^d)$  in  $\text{CHCl}_3$  at 5 °C led to the corresponding carbene species  $[\text{PdCl}_2\{\text{C}(\text{ON}^c\text{CMe}_2\text{CH}_2\text{CH}_2\text{C}^d\text{H})=\text{N}^e\text{R}^1\}(\text{R}^1\text{NC})(\text{N}^c-\text{C}^d)(\text{C}^d-\text{N}^e)]$ , isolated in 92–78% yields [39].

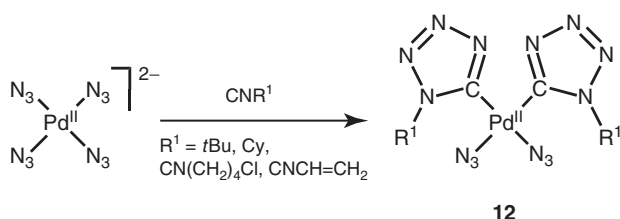
### 13.2.5 Addition of Azides to Isocyanides

Metal-mediated DCA between azides and isocyanides typically starts from metal–azide complexes and free isocyanides. Thus, the azido complexes  $[\text{RhCp}^*(\mu\text{-N}_3)(\text{N}_3)]_2$  ( $\text{Cp}^* = \eta\text{-C}_5\text{Me}_5$ ),  $\text{trans}\text{-}\text{Rh}(\text{N}_3)(\text{CO})(\text{PPh}_3)_2$ ,  $\text{Na}_2[\text{Pd}(\text{N}_3)_4]$ ,  $\text{Na}_2[\text{Pd}_2(\mu\text{-N}_3)_2(\text{N}_3)_4]$ , and  $\text{Na}[\text{Au}(\text{N}_3)_4]$ , reacted with aliphatic isocyanides to give a series of new metal–carbon bonded tetrazolato complexes [40]. All azide ligands in the coordination sphere undergo this cycloaddition with isocyanides except on palladium(II), where only two tetrazol-5-ato groups are formed (**12**, Scheme 13.11).

In the other study [41], Pd-bis(azido) compounds  $[\text{Pd}(\text{dpnn})(\text{N}_3)_2]$ ,  $[\text{Pd}(\text{dppf})(\text{N}_3)_2]$ , and  $[\text{Pt}(1\text{-dpn})(\text{SMe}_2)(\text{N}_3)_2]$  [ $\text{dpnn}$ , 1,8-bis(diphenylphosphino)naphthalene;  $\text{dppf}$ , 1,10-bis(diphenylphosphino)ferrocene; 1-dpn 1-diphenylphosphinonaphthalene] underwent [2 + 3] cycloaddition with isocyanides  $\text{R}^1\text{NC}$  ( $\text{R}^1 = \text{cyclohexyl}$ ,  $t\text{Bu}$ , 2,6-dimethylphenyl) to convert azido ligands to five-membered, C-coordinated tetrazolate rings. In a related study [42], alkynyl palladium(II)-azido species of the type  $[\text{Pd}(\text{N}_3)(\text{C}\equiv\text{CR})\text{PM}_3]$  reacted with  $t\text{BuNC}$  to give corresponding complexes with C-bound tetrazolates.



Scheme 13.10 Reaction between  $\text{cis}\text{-}[\text{PdCl}_2(\text{R}^1\text{NC})_2]$  and acyclic nitrones [39].



Scheme 13.11 Palladium(II)-mediated cycloaddition of azides to isocyanides [40].

### 13.3 METAL-MEDIATED [2 + 3] CYCLOADDITION TO NITRILES AND ISOCYANIDES: THEORETICAL STUDIES

#### 13.3.1 Cycloaddition of Nitrones to Nitriles

A vast majority of theoretical works on this topic published during past decade deals with the CAs of nitrones ( $\text{R}^1\text{CH}=\text{N}(\text{R}^2)\text{O}$ ) to nitriles ( $\text{N}\equiv\text{CR}$ ) affording  $\Delta^4$ -1,2,4-oxadiazoline species (Route I, Scheme 13.1).

**13.3.1.1 Nature of the Activation Effect** One of the principal questions that may be interpreted with the help of theoretical methods is the reasons for the activation of nitriles toward DCA upon their coordination to a metal center. Traditionally, the reactivity of dipoles and dipolarophiles in the DCA reactions is explained in terms of the frontier molecular orbital (FMO) theory and depends on the predominant type of the FMO interaction. The coupling of nitrones with nitriles is usually controlled by the interaction of the highest occupied molecular orbital (HOMO) of nitrone and the lowest unoccupied molecular orbital (LUMO) of nitrile centered on the  $\text{C}\equiv\text{N}$  bond (so-called normal electron demand reactions). For such processes, the coordination of  $\text{N}\equiv\text{CR}$  to a Lewis acid (e.g., to a metal) decreases the  $\text{LUMO}_{\text{NCR}}$  energy, providing a smaller  $\text{HOMO}_{\text{nitrone}} - \text{LUMO}_{\text{NCR}}$  gap and, hence, facilitates the DCA reaction (Fig. 13.1a).

Another factor determining the reactivity of nitriles is the charge factor, which becomes increasingly important in the case of asynchronous DCAs when one of the new bonds forms earlier than another one (Fig. 13.1b). Such reactions may be considered in part as nucleophilic addition processes that are controlled by the atomic charge on the interacting atoms (mostly on the nitrile C atom of  $\text{N}\equiv\text{CR}$ ). The ligation of  $\text{N}\equiv\text{CR}$  to a metal shifts the electron density from the  $\text{C}\equiv\text{N}$  group providing the higher charge on the nitrile C atom and, therefore, favors the DCA process (taking into account that the C atom is an electrophilic center).

**13.3.1.2 Effect of the Nature of the Metal** Considering both orbital and charge arguments, two main criteria for the selection of the metal—the most efficient activator of  $\text{N}\equiv\text{CR}$ —may be formulated. First, such a metal should form a strong coordination bond with nitriles (to be sufficiently “nitrilophilic”); otherwise, the substitution of the coordinated nitrile for the nitronate molecule can be quite competitive with the DCA [43]. Second, the metal should be in a relatively high oxidation state. This provides the most effective shift of the electron density from the nitrile functionality and, hence, the most significant lowering of the  $\text{LUMO}_{\text{NCR}}$  energy and the decrease of the positive charge on the nitrile C atom. Additionally, the selective coordination of nitrile (but not of nitronate) to the metal is important because the joint ligation of nitronate and nitrile results in a concurrent decrease of FMO energies of both reactants and in a lower activation or even inhibition of the reaction. The exclusive coordination of  $\text{N}\equiv\text{CR}$  may be achieved if the metal is a “soft” acid that preferably interacts with the “softer” nitrile N atom rather than with the “harder” O atom of nitronate.

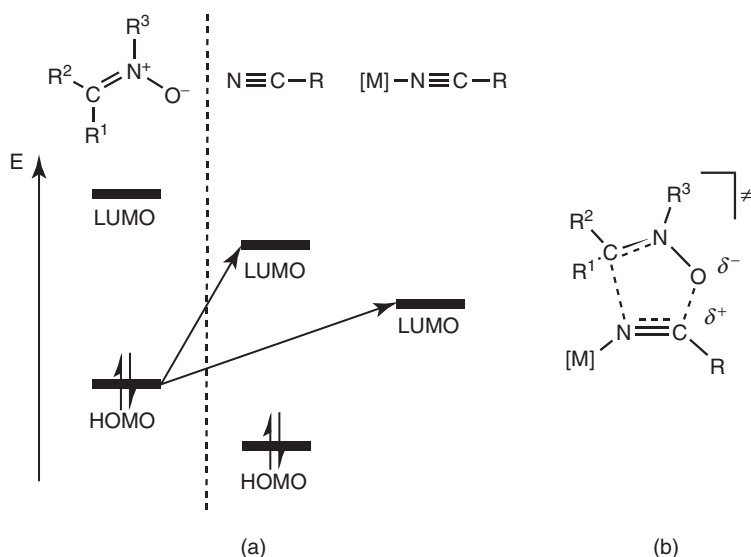


**Figure 13.1** Frontier molecular orbitals of nitronate and free or coordinated nitrile (a) and transition state of the concerted asynchronous mechanism of the nitronate-to-nitrile cycloaddition (b).

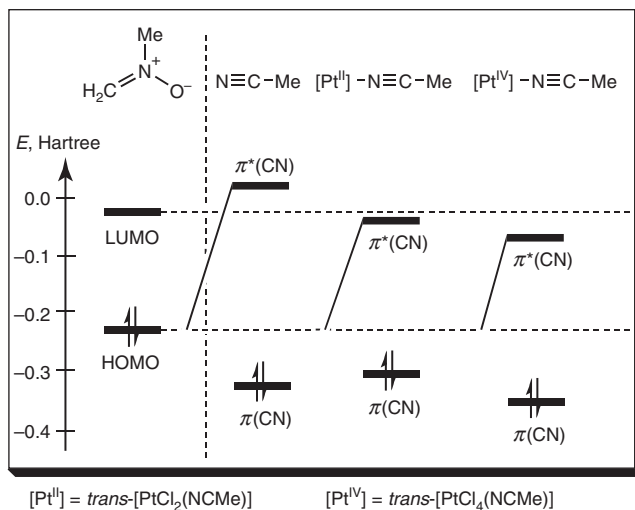


**Figure 13.2** Energies of frontier molecular orbitals of nitrone  $CH_2=N(Me)O$  and free and coordinated acetonitrile.

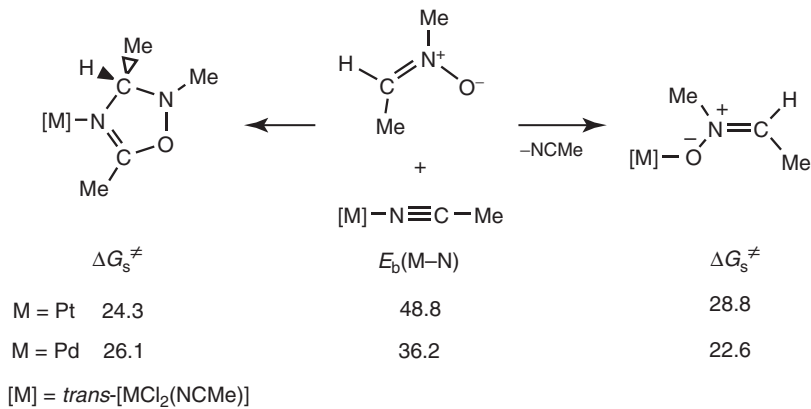
Among various metals, platinum and palladium perfectly fulfill these criteria, being the most efficient activators of nitriles [1]. Theoretical calculations using the density functional theory (DFT) indicate that the coordination of  $N \equiv CMe$  to Pt(II), Pt(IV), or Pd(II) in complexes  $trans\text{-}[MCl_n(N \equiv CMe)_2]$  ( $M = Pt(\mathbf{1T}), Pd(\mathbf{2T}), n = 2; M = Pt(\mathbf{3T}), n = 4$ ) results in a significant decrease of the  $LUMO_{NCMe}$  energy (by 1.95–2.13 eV, Fig. 13.2) and in an increase of the atomic charge on the nitrile C atom from 0.29 e in free  $N \equiv CMe$  to 0.47–0.53 e in the complexes [43–46]. As a result, the calculated activation energy of the DCA of nitrone  $RCH=N(Me)O$  ( $R = H, Me$ ) decreases from 27.65–30.30 kcal/mol (to free  $N \equiv CMe$ ) to 8.04–20.70 kcal/mol (to **1T**–**3T**) that corresponds to the enhancement of the reaction rate by a factor of  $8.3 \times 10^5$ – $2.4 \times 10^{14}$ .

The coordination also affects the thermodynamic characteristics of the process, providing more exothermic and exergonic DCA. The Gibbs free energy of the reaction becomes more negative, changing from (−4.73)–(−7.60) kcal/mol for DCAs to free NCMe to (−13.90)–(−22.17) kcal/mol for the reactions with complexes **1T**–**3T**. Such thermodynamic stabilization of the DCA products explains the experimental isolation of unstable  $\Delta^4$ -1,2,4-oxadiazoline heterocycles (e.g., tetrahydroimidazo[1,2-*b*][1,2,4]oxadiazoles [25]) which cannot survive being uncoordinated to a metal. Thus, the activation of nitriles upon their coordination can be interpreted in terms of both kinetic and thermodynamic arguments.

At the same time, chemical behavior of the Pt and Pd nitrile complexes toward nitrones is rather different, at least under certain experimental conditions. The only isolated product of DCA to the Pt species is a cycloadduct, while, in the case of the Pd complexes  $[PdCl_2(N \equiv CR)_2]$ , the substitution of  $N \equiv CR$  for the nitrone was also observed [19]. Such different behavior is explained by the more labile nature of the Pd nitrile complexes compared to the Pt complexes. The calculated metal–NCMe bond energy in **1T** and **2T** are 48.8 and 36.2 kcal/mol, respectively. Correspondingly, the estimated activation energy of the substitution in **1T** is higher than that of the DCA, whereas a clearly opposite situation was found for complex **2T** (Scheme 13.12) [43].

Ligation of nitriles to a metal center changes features of the reaction mechanism. In the case of metal-free reactions, the mechanism is concerted and highly synchronous, that is, the reaction occurs in one step via formation of one cyclic five-membered transition state (TS), and the changes of chemical bonds directly involved in the process take place simultaneously. The estimated degree of asynchronicity of the reactions between nitrones and uncomplexed nitriles is only 5–15% [43, 45–48]. In contrast, the coordination of nitriles to the metal (Pt or Pd) results in a dramatic increase of the reaction asynchronicity to 19–49%, and, in some cases, the TS of the reaction may become acyclic [47]. At the same time, the global mechanism of the DCA usually remains concerted.

**13.3.1.3 Effect of the Metal Oxidation State** The oxidation state of the metal-activator may significantly change the reactivity of nitriles toward the DCA with nitrones. A higher oxidation state provides a higher activation. This effect is accounted for by the fact that the metal in a high oxidation state shifts the electron density from the  $C \equiv N$  group more efficiently and, hence, lowers the  $LUMO_{NCR}$  energy and enhances the positive charge on the nitrile C atom more significantly, compared to the metal in a lower oxidation state. Indeed, the  $LUMO_{NCMe}$  energy drops from −0.95 eV in **1T**



**Scheme 13.12** Cycloaddition and substitution paths of the reaction between nitrone MeCH=N(Me)O and coordinated acetonitrile. Gibbs free energies of activation and metal–NCMe bond energies are indicated in kilocalories per mole.

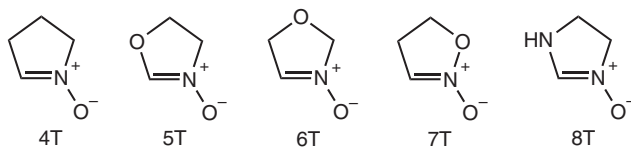
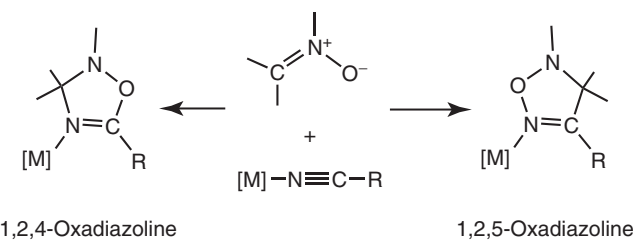
to  $-1.12$  eV in **2T** and the atomic charge increases from  $0.47$  e in **1T** to  $0.53$  e in **2T** [45, 46]. The activation energy of the nitrone coupling with the Pt(IV) complexes *trans*-[PtCl<sub>4</sub>(N≡CR)<sub>2</sub>] ( $R = \text{Me}, \text{C}\equiv\text{CH}, \text{CH}=\text{CH}_2$ ) was calculated to be  $7.95$ – $11.54$  kcal/mol lower than the activation barrier of the reaction with corresponding Pt(II) species, *trans*-[PtCl<sub>2</sub>(N≡CR)<sub>2</sub>] [45–48].

**13.3.1.4 Effect of Substituents in Nitrile** Introduction of a strong electron-acceptor group  $R$  ( $\text{Ph}, \text{CH}_2\text{Cl}, \text{CHCl}_2, \text{CF}_3$ ) into the nitrile molecule  $\text{N}\equiv\text{CR}$  provides a similar effect on the reactivity of nitriles as their coordination to a metal, that is, it activates  $\text{N}\equiv\text{CR}$  toward DCA. Such an effect has the same driving force, that is, the lowering of the  $\text{LUMO}_{\text{NCR}}$  energy upon introduction of this substituent. However, the ligation of  $\text{N}\equiv\text{CR}$  to the metal appears to be more efficient way of the nitrile activation than the variation of substituents. For instance, the activation barrier of the reaction  $\text{CH}_2=\text{N}(\text{Me})\text{O} + \text{N}\equiv\text{CR}$  decreases by  $7.52$  kcal/mol ongoing from  $R = \text{Me}$  to  $\text{CF}_3$  (activation by a factor of  $3.2 \times 10^5$ ) while the drop of the barrier upon the coordination of  $\text{N}\equiv\text{CMe}$  to Pt(IV) reaches  $20.40$  kcal/mol (activation by a factor of  $9.1 \times 10^{14}$ ) [45, 46, 48, 49]. The replacement of the Me with Ph group in  $\text{N}\equiv\text{CR}$  provides even lower activation: only  $0.9$  kcal/mol (by a factor of  $4.6$ ) [45].

Meanwhile, the greatest effect on the reactivity of  $\text{N}\equiv\text{CR}$  may be achieved when the nitrile is doubly activated (by metal and electron-acceptor substituent). The calculated activation energy of the reaction  $\text{CH}_2=\text{N}(\text{Me})\text{O} + \text{trans}-[\text{PtCl}_2(\text{NCMe})(\text{N}\equiv\text{CCF}_3)]$  is  $4.34$  kcal/mol (the  $\text{N}\equiv\text{CCF}_3$  ligand participates in the DCA) versus  $27.65$  kcal/mol for the reaction  $\text{CH}_2=\text{N}(\text{Me})\text{O} + \text{N}\equiv\text{CMe}$  [45, 49].

**13.3.1.5 Effect of the Nature of the Nitrone** The nature of the nitrone plays an important role in the DCA reactions with nitriles. First, theoretical DFT calculations predicted that acyclic C-alkyl nitrones (e.g.,  $\text{MeCH}=\text{N}(\text{Me})\text{O}$ ) are more reactive toward  $\text{N}\equiv\text{CMe}$  than C-aryl nitrones ( $4-\text{RC}_6\text{H}_4\text{CH}=\text{N}(\text{Me})\text{O}$  ( $R = \text{Me}, \text{OMe}$ )) by  $2.9$ – $3.2$  kcal/mol (a factor of  $134$ – $222$ ) [45]. Second, the acyclic nitrone  $\text{MeCH}=\text{N}(\text{Me})\text{O}$  in the usual *Z*-configuration is more inert than the cyclic nitrone with a purely hydrocarbon ring **4T** (Fig. 13.3) by  $2.68$  kcal/mol (by a factor of circa  $100$ ) [25, 46]. This effect is accounted for by the fixation of cyclic nitrones in the more strained and, therefore, more reactive, *E*-configuration. Third, among various cyclic nitrones (**4T**–**8T**), those with a heteroatom (O or N) at the position 1 of the cycle (**5T** and **8T**) are the most reactive, whereas the cyclic nitronate **7T** is the most inert. The reactivity of **4T** and **6T** is similar because the oxygen heteroatom in **6T** is far from the reacting center of nitrone and does not affect its reactivity significantly. It is interesting that nitronate **7T** appears to be less reactive than even acyclic nitrones. Moreover, the nitronate is comparatively little sensitive to the activation by a metal. For example, the activation of **7T** by Pt(IV) is  $14.65$  kcal/mol, while **5T** is activated by  $20.40$  kcal/mol. Nevertheless, the activation energy of the reaction of **7T** bound to Pt(IV) ( $17.0$  kcal/mol) is still sufficiently low for the realization of DCA. This theoretical prediction was fully confirmed later by experiment (see Reference 50).

**13.3.1.6 Effect of the Solvent** In accord with the quantum-chemical calculations [45–48], solvent effects inhibit the DCAs of nitrones to nitriles and decrease the thermodynamic stability of the cycloadduct owing to a higher stabilization of the reactants' level compared to the levels of TS and product. As a consequence, lower-polar solvents are predicted to

**Figure 13.3** Cyclic nitrones used in theoretical calculations.**Scheme 13.13** Two regioisomeric pathways of the cycloaddition of nitrones to nitriles.

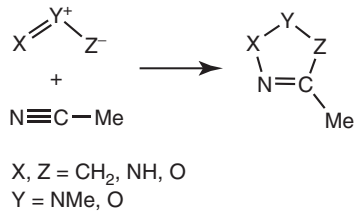
be preferable for these reactions over higher-polar solvents, although other factors, for example, solubility, should be taken into account.

**13.3.1.7 Reaction Selectivity** Cycloaddition of nitrones to nitriles is completely regioselective, affording 1,2,4-oxadiazolines (Scheme 13.13) exclusively. Theoretical calculations indicate that the activation barrier of formation of the 1,2,5-regioisomers is 25–26 kcal/mol higher compared to that of the 1,2,4-isomers [48]. At the same time, if the nitrile molecule bears another functionality (e.g., C=C or C≡C bonds), the reaction may occur via different chemoisomeric pathways (cycloaddition at the CN or C=C/C≡C group).

Two main factors affect the chemoselectivity: (i) coordination of N≡CR to a metal and (ii) nature of the substituents. In the case of metal-free reactions, the DFT calculations predict that the DCA of nitrones to N≡CCH=CH<sub>2</sub> or N≡CC≡CH should occur exclusively at the C=C or C≡C bond [47]. Coordination of these nitriles to Pt(II) and, in particular, to Pt(IV), dramatically facilitates the DCA at the C≡N bond relative to that at the C=C/C≡C bond. However, the reaction at the CC bond still remains more preferable. At the same time, the DCA to phenyl-substituted nitrile in the model complexes *trans*-[PtCl<sub>2</sub>(L)(N≡CCH=CHPh)] (L = NCCHCH<sub>2</sub>, NCMe) takes place already at the C≡N bond [47, 51]. Such a switch of the chemoselectivity is accounted for by (i) the steric repulsion between the bulky Ph groups and (ii) the loss of conjugation in phenylnitrene and phenylcyanoalkene upon formation of the TS. Both these effects are more important for the CC than for CN additions and disfavor the reaction along the former channel.

### 13.3.2 Cycloaddition of Other Dipoles to Nitriles

**13.3.2.1 Other dipoles of allyl-anion type** Besides nitrones, the DCA of 11 other dipoles of allyl-anion type to free and Pt-bound nitriles has been theoretically studied (Scheme 13.14) [48]. The calculations at the B3LYP level demonstrated that three types of these dipoles, that is, azimines (NHN(Me)NH), azoxy compounds (NHN(Me)O), and nitro compounds (ON(Me)O) are inert toward either free or complexed nitriles owing to high activation energies and strongly positive  $\Delta G$  of reactions. Nitroso oxides (NHOO), nitrosimines (NHONH), azomethine imines (CH<sub>2</sub>N(Me)NH), and ozone (OOO) are slightly more reactive with N≡CMe than nitrones, while carbonyl oxides (CH<sub>2</sub>OO), carbonyl imines (CH<sub>2</sub>ONH), and carbonyl and azomethine ylides (CH<sub>2</sub>OCH<sub>2</sub> and CH<sub>2</sub>N(Me)CH<sub>2</sub>) are the most reactive dipoles. Coordination of N≡CMe to Pt(II) and Pt(IV) significantly activates nitriles toward CH<sub>2</sub>N(Me)NH (by a factor of  $1.7 \times 10^6$ – $3.4 \times 10^9$ ). The activation is moderate in the reactions with CH<sub>2</sub>N(Me)CH<sub>2</sub> and CH<sub>2</sub>ONH (by a factor of  $3 \times 10^3$ ) and it is low in the reactions with CH<sub>2</sub>OCH<sub>2</sub>, CH<sub>2</sub>OO, and NHONH (by a factor of 7–230). However, such rather low reaction acceleration is not crucial because of the high reactivity of all these dipoles toward free nitriles. Finally, the DCAs of NHOO and OOO are inhibited by the ligation of N≡CMe due to inverse electron demand character of these processes.



**Scheme 13.14** Cycloaddition of 1,3-dipoles of allyl-anion type to nitriles.

**13.3.2.2 Nitrile Oxides** The reaction between nitrile oxides (RC≡NO)—1,3-dipoles of the propargyl/allenyl-anion type—and nitriles (Route II, Scheme 13.1) belongs to the normal electron demand processes controlled by the HOMO<sub>dipole</sub>–LUMO<sub>nitrile</sub> interaction and the coordination of N≡CR to a metal center should accelerate this reaction. Indeed, the Gibbs free energy of activation for the DCA of MeC≡NO decreases from 26.07 kcal/mol to 22.50 kcal/mol on going from free N≡CMe to the Pt(IV) complex **3T** [52]. However, such an activation (by a factor of 415) is incomparable with the acceleration of the nitronate DCA (by a factor of  $2.4 \times 10^{14}$  [45, 46]). The effect of nitrile coordination to the Pt(II) or Pd(II) centers is even more unexpected. In fact, free acetonitrile and the Pt(II) or Pd(II) complexes **1T** and **2T** have very similar reactivities toward MeC≡NO, while the ligation of N≡CC≡CH and N≡CCH=CH<sub>2</sub> to Pt(II) even inhibits the reaction at the CN bond. In contrast to kinetic behavior, the oxadiazole products of the nitrile oxide DCA are much more thermodynamically stable than the oxadiazoline products of the nitronate DCA ( $\Delta G$  of reaction being  $(-36)$ – $(-40)$  kcal/mol versus  $(-5)$ – $(-22)$  kcal/mol) and the aromatic character of oxadiazoles (but not oxadiazolines) is responsible for this effect.

**13.3.2.3 Azides** Despite the practical importance of this reaction leading to tetrazoles (Route III, Scheme 13.1), the number of recent theoretical studies of the metal-assisted DCAs of azides (RN<sub>3</sub>, N<sub>3</sub><sup>-</sup>) to nitriles is limited. This reaction usually controlled by both types of the FMO interaction (HOMO<sub>dipole</sub>–LUMO<sub>nitrile</sub> and HOMO<sub>nitrile</sub>–LUMO<sub>dipole</sub>) [53]. At the same time, the coordination of the azide ion to Zn(II) in complexes [Zn(H<sub>2</sub>O)<sub>n</sub>N<sub>3</sub>]<sup>+</sup> either has no effect on the activation barrier (when  $n = 3$ ) or inhibits the reaction by 1.8 kcal/mol (when  $n = 5$ ). However, when nitrile or both reactants are coordinated to a metal (e.g., Zn(II) or Sn(IV)), the activation barrier decreases by 2–10 kcal/mol compared to the metal-free reactions [54, 55].

### 13.3.3 Cycloaddition of Nitrones to Isocyanides

There are only few theoretical publications on the DCA of nitrones to isocyanides (C≡NR)—species isomeric and isoelectronic to nitriles (Scheme 13.1) [56–58]. The calculations at the DFT (B3LYP) level predict that the coordination of C≡NMe to Pt(II), Pt(II), Pt(IV), and Re(IV) centers in complexes *trans*-[MCl<sub>n</sub>(C≡NMe)<sub>2</sub>] (M = Pd (**9T**), Pt (**10T**),  $n = 2$ ; M = Pt (**11T**), Re (**12T**),  $n = 4$ ) results in an activation of isocyanide by 9.5–14.2 kcal/mol (by a factor of  $9.3 \times 10^6$ – $2.6 \times 10^{10}$ ), Pt(IV) being the best metal center. Moreover, the coordination enhances the thermodynamic stability of the derived *N,N*-disubstituted oxadiazoline heterocycles by 6.1–10.9 kcal/mol. At the same time, the DCA of another nitrone molecule at the second C≡NMe ligand in complexes **9T**–**12T** requires a higher activation barrier and, hence, is less favorable compared to the first DCA. All these results explain why free isocyanides are completely inert toward DCA with nitrones, while Pd-isocyanide complex yielded corresponding mono-DCA product (Scheme 13.10).

The DCA of nitrones to isocyanides belongs to normal electron demand processes, and the activation of C≡NR by metal centers has the same nature as in the case of nitriles, that is, there is a lowering of the LUMO<sub>CNR</sub> energy and an increase of the charge on the C atom of the C≡N group. The mechanism of this reaction is concerted, highly synchronous for free C≡NR, and asynchronous for metal-bound isocyanides.

## 13.4 FINAL REMARKS

In this chapter, we examined the recent data on DCA to metal-bound nitriles and isocyanides that allow the generation of new heterocyclic structures. In case of cycloaddition to metal-bound nitriles [1, 5, 6, 10], the obtained heterocyclic ligands can be often isolated as free species, and this approach represents an alternative (to a pure organic) route for their preparation. At

the same time, transformation of metal-bound isocyanides [7, 9] furnishes new types of *N*-heterocyclic carbenes, including chiral derivatives, that are not accessible via other synthetic protocols [39].

We also demonstrated that theoretical methods provide a powerful tool for the investigation of 1,3-DCAs to substrates bearing the C≡N bond. The quantum chemical calculations are indispensable for the study of the reaction mechanism and they were successfully applied for the analysis of the reactivity, selectivity, and driving forces of these processes, for the understanding of reasons of the activation effect upon coordination of the substrate to the metal center, and for the interpretation and explanation of such important factors controlling these reactions as the nature of the metal center, dipolarophile, and dipole molecules.

## ACKNOWLEDGMENTS

This work has been partially supported by the Fundação para a Ciência e a Tecnologia (FCT), Portugal, its PPCDT program (FEDER funded), and through the research projects PTDC/QUI-QUI/098760/2008 and PTDC/QUI-QUI/109846/2009. MLK and KVL thank FCT and IST for the research contract within the Ciência 2007 and 2008 programs, respectively.

## REFERENCES

1. Kukushkin, V. Yu.; Pombeiro, A. J. L. *Chem. Rev.* **2002**, *102*, 1771 and references therein.
2. Dömling, A. *Chem. Rev.* **2006**, *106*, 17.
3. Dömling, A.; Ugi, I. *Angew. Chem. Int. Ed.* **2005**, *39*, 3168.
4. Dömling, A.; Wang, W.; Wang, K. *Chem. Rev.* **2012**, *112*, 3083.
5. Bokach, N. A.; Kuznetsov, M. L.; Kukushkin, V. Yu. *Coord. Chem. Rev.* **2011**, *255*, 2946.
6. Bokach, N. A.; Kukushkin, V. Yu. *Russ. Chem. Bull.* **2006**, *55*, 1869.
7. Michelin, R. A.; Pombeiro, A. J. L.; Guedes da Silva, M. F. C., *Coord. Chem. Rev.* **2001**, *218*, 75.
8. Pombeiro, A. J. L.; Guedes da Silva, M. F. C.; Michelin, R. A. *Coord. Chem. Rev.* **2001**, *218*, 43.
9. Luzyanin, K. V.; Pombeiro, A. J. L. In *Carbene Complexes Derived from Metal-Bound Isocyanides*; Nenajdenko, V., Ed.; *Isocyanide Chemistry*; Wiley-VCH Verlag GmbH: Weinheim, **2012**; Chapter 15, p 531.
10. Bokach, N. A. *Russ. Chem. Rev.* **2010**, *79*, 89.
11. Boyarskiy, V. P.; Luzyanin, K. V.; Kukushkin, V. Yu. *Coord. Chem. Rev.* **2012**, *256*, 2029.
12. Pombeiro, A. J. L.; Guedes da Silva, M. F. C. *J. Organomet. Chem.* **2001**, *617–618*, 65.
13. Wagner, G.; Pombeiro, A. J. L.; Kukushkin, V. Yu. *J. Am. Chem. Soc.* **2000**, *122*, 3106.
14. Wagner, G.; Haukka, M.; da Silva, J. J. R. F.; Pombeiro, A. J. L.; Kukushkin, V. Yu. *Inorg. Chem.* **2001**, *40*, 264.
15. Wagner, G.; Haukka, M. *J. Chem. Soc., Dalton Trans.* **2001**, 2690.
16. Desai, B.; Danks, T. N.; Wagner, G. *Dalton Trans.* **2004**, 166.
17. Sarju, J.; Arbour, J.; Sayer, J.; Rohrmoser, B.; Scherer, W.; Wagner, G. *Dalton Trans.* **2008**, *5302*.
18. Wagner, G.; Marchant, A.; Sayer, J. *Dalton Trans.* **2010**, 7747.
19. Bokach, N. A.; Krokhin, A. A.; Nazarov, A. A.; Kukushkin, V. Yu.; Haukka, M.; da Silva, J. J. R. F.; Pombeiro, A. J. L. *Eur. J. Inorg. Chem.* **2005**, 3042.
20. Wagner, G. *Inorg. Chim. Acta* **2004**, *357*, 1320.
21. Desai, B.; Danks, T. N.; Wagner, G. *Dalton Trans.* **2003**, 2544.
22. Kritchakov, A. S.; Bokach, N. A.; Haukka, M.; Kukushkin, V. Yu. *Dalton Trans.* **2011**, 4175.
23. Kritchakov, A. S.; Bokach, N. A.; Kuznetsov, M. L.; Dolgushin, F. M.; Tung, T. Q.; Molchanov, A. P.; Kukushkin, V. Yu. *Organometallics* **2012**, *31*, 687.
24. Makarycheva-Mikhailova, A. V.; Golenetskaya, J. A.; Bokach, N. A.; Balova, I. A.; Haukka, M.; Kukushkin, V. Yu. *Inorg. Chem.* **2007**, *46*, 8323.
25. Bokach, N. A.; Kuznetsov, M. L.; Haukka, M.; Ovcharenko, V. I.; Tretyakov, E. V.; Kukushkin, V. Yu. *Organometallics* **2009**, *28*, 1406.
26. Bokach, N. A.; Balova, I. A.; Haukka, M.; Kukushkin, V. Yu. *Organometallics* **2011**, *30*, 595.
27. Bokach, N. A.; Khripoun, A. V.; Kukushkin, V. Yu.; Haukka, M.; Pombeiro, A. J. L. *Inorg. Chem.* **2003**, *42*, 896.
28. Bokach, N. A.; Kukushkin, V. Y.; Haukka, M.; Pombeiro, A. J. L. *Eur. J. Inorg. Chem.* **2005**, 845.

29. Palazzi, A.; Stagni, S.; Bordoni, S.; Monari, M., Selva, S. *Organometallics* **2002**, *21*, 3774.
30. Lin, P.; Clegg, W.; Harrington, R. W.; Henderson, R. A. *Dalton Trans.* **2005**, 2388.
31. Liu, F. C.; Lin, Y. L.; Yang, P. S.; Lee, G. H.; Peng, S. M. *Organometallics* **2010**, *29*, 4282.
32. Wu, T.; Zhou, R.; Li, D. *Inorg. Chem. Commun.* **2006**, *9*, 341.
33. Liu, B.; Qiu, Y. C.; Peng, G.; Ma, L.; Jin, L. M.; Cai, J. B.; Deng, H. *Inorg. Chem. Commun.* **2009**, *12*, 1200.
34. Chen, F.; Wu, M. F.; Liu, G. N.; Wang, M. S.; Zheng, F. K.; Yang, C.; Xu, Z. N.; Liu, Z. F.; Guo, G. C.; Huang, J. S. *Eur. J. Inorg. Chem.* **2010**, 4982.
35. Mukhopadhyay, S.; Lasri, J.; Charmier, M. A. J.; Guedes da Silva, M. F. C.; Pombeiro, A. J. L. *Dalton Trans.* **2007**, 5297.
36. Lasri, J.; Guedes da Silva, M. F. C.; Kopylovich, M. N.; Mukhopadhyay, B. G.; Pombeiro, A. J. L. *Eur. J. Inorg. Chem.* **2009**, 5541.
37. Lasri, J.; Rodriiguez, M. J. F.; Guedes da Silva, M. F. C.; Smolenski, P.; Kopylovich, M. N.; da Silva, J. J. R. F.; Pombeiro, A. J. L. *J. Organomet. Chem.* **2011**, 696, 3513.
38. Popova, E. A.; Bokach, N. A.; Haukka, M.; Trifonov, R. E.; Ostrovskii, V. A. *Inorg. Chim. Acta* **2011**, 375, 242.
39. Luzyanin, K. V.; Tskhovrebov, A. G.; Guedes da Silva, M. F. C.; Haukka, M.; Pombeiro, A. J. L.; Kukushkin, V. Yu. *Chem. Eur. J.* **2009**, *15*, 5969.
40. Wehlan, M.; Thiel, R.; Fuchs, J.; Beck, W.; Fehlhammer, W. P. *J. Organomet. Chem.* **2000**, *613*, 159.
41. Huh, H. S.; Lee, Y. K.; Lee, S. W. *J. Mol. Struct.* **2006**, 789, 209.
42. Kim, Y.-J.; Lee, S.-H.; Lee, S.-H.; Jeon, S. I.; Lim, M. S.; Lee, S. W. *Inorg. Chim. Acta* **2005**, 358, 650.
43. Kuznetsov, M. L.; Kukushkin, V. Yu., Pombeiro, A. J. L. *Dalton Trans.* **2008**, 1312.
44. Kuznetsov, M. L. *J. Mol. Struct. THEOCHEM* **2004**, 674, 33.
45. Kuznetsov, M. L.; Kukushkin, V. Yu., Dement'ev, A. I.; Pombeiro, A. J. L. *J. Phys. Chem. A* **2003**, *107*, 6108.
46. Kuznetsov, M. L.; Kukushkin, V. Yu. *J. Org. Chem.* **2006**, *71*, 582.
47. Kuznetsov, M. L.; Nazarov, A. A.; Kozlova, L. V.; Kukushkin, V. Yu. *J. Org. Chem.* **2007**, *72*, 4475.
48. Kuznetsov, M. L.; Kukushkin, V. Yu., Pombeiro, A. J. L. *J. Org. Chem.* **2010**, *75*, 1474.
49. Kuznetsov, M. L.; Kozlova, L. V.; Dement'ev, A. I. *Russ. J. Inorg. Chem.* **2006**, *51*, 1602.
50. Bokach, N. A.; Ioffe, S. L.; Dolgushin, F. M.; Antipin, M. Y.; Tartakovskii, V. A.; Kukushkin, V. Yu. *Inorg. Chem. Commun.* **2009**, *12*, 173.
51. Wagner, G.; Danks, T. N.; Desai, B. *Tetrahedron* **2008**, *64*, 477.
52. Kuznetsov, M. L.; Kukushkin, V. Yu.; Haukka, M.; Pombeiro, A. J. L. *Inorg. Chim. Acta* **2003**, 356, 85.
53. Kuznetsov, M. L. *Russ. Chem. Rev. (Uspekhi Khimii)* **2006**, *75*, 935.
54. Himo, F.; Demko, Z. P.; Noddleman, L.; Sharpless, K. B. *J. Am. Chem. Soc.*, **2003**, *125*, 9983.
55. Cantillo, D.; Gutmann, B.; Kappe, C. O. *J. Am. Chem. Soc.*, **2011**, *133*, 4465.
56. Menezes, F. M. C.; Kuznetsov, M. L.; Pombeiro, A. J. L. *Organometallics* **2009**, *28*, 6593.
57. Novikov, A. S.; Kuznetsov, M. L. *Inorg. Chim. Acta* **2012**, 380, 78.
58. Novikov, A. S.; Kuznetsov, M. L.; Pombeiro, A. J. L. *Chem. Eur. J.* **2013**, *19*, 2874.



## COORDINATION CHEMISTRY OF OXAZOLINE/THIAZOLINE-BASED P,N LIGANDS

SHUANMING ZHANG, ROBERTO PATTACINI, AND PIERRE BRAUNSTEIN\*

*Laboratoire de Chimie de Coordination, Institut de Chimie (UMR 7177 CNRS), Université de Strasbourg, Strasbourg, France*

### 14.1 DEFINITION OF POLYFUNCTIONAL LIGANDS

Over the last decades, organometallic chemistry has enjoyed intensive developments in both academic and industrial fields. Among the different facets contributing to such developments, ligand design has become an important part of synthetic chemistry. This is due to the subtle control exerted by the ligands on the geometry and properties of the coordinated metal centers. In particular, ligands possessing significantly different chemical functionalities, such as hard and soft donors (called *hybrid ligands*, Scheme 14.1) have found increasing use in molecular chemistry, as different and contrasting characteristics can be combined in the same molecule and therefore lead to unprecedented properties for the resulting metal complexes [1].

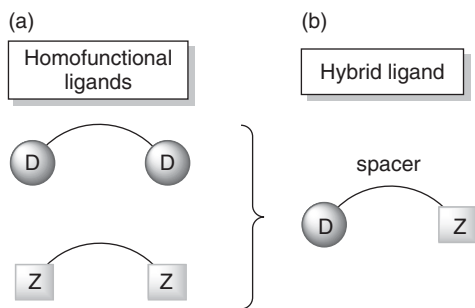
When the donor ability of these groups is chosen to be very different from each other, an increased discrimination between their interactions with the metal center(s) is anticipated (Scheme 14.2). These functionalities will in turn influence the bonding properties and reactivity of the other ligand(s) bonded to the same metal center, especially for those in *trans* position. The useful concept hemilability emerged from the study, usually by variable-temperature nuclear magnetic resonance (NMR) spectroscopy, of the dynamic properties resulting from the reversible coordination of one of the donor groups of hybrid ligands to the metal center [2].

In this chapter, we focus on P,N-chelating ligands and some of their transition metal complexes because their intrinsic properties, immense structural diversity, and broad range of applications attract increasing attention [3]. Such heterofunctional ligands associate hard nitrogen donor(s) with soft phosphorus donor(s) and offer considerable chemical and structural diversity. They may also generate hemilabile systems endowed with enhanced reactivity.

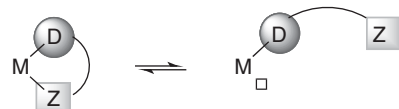
### 14.2 P,N-CHELATING LIGANDS BASED ON OXAZOLINE/THIAZOLINE SYSTEM

Among the diverse N-functional moieties associated with P,N-chelating ligands, the heterocycles oxazoline and thiazoline as well as their substituted derivatives have enjoyed special attention. The P-donor group can be connected through a spacer to the 2-position of the oxazoline ring or to the 4-position, as in the basic subunits shown in Scheme 14.3.

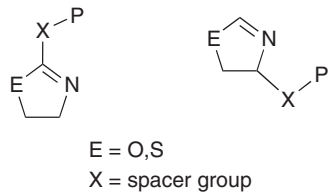
By varying the nature of the spacer X, coordination complexes bearing P,N-chelating rings of different size have been synthesized, and some of them exhibit high activities in diverse catalytic processes. In this account, selected examples of such complexes will be presented, with a focus on our own work, and classified according to the size of the chelate ring, with an emphasis on ligands that can form five- or six-membered rings.



**Scheme 14.1** Homofunctional bidentate ligands (a) and mixed donor or hybrid ligands (b).



**Scheme 14.2** Hemilabile behavior of a hybrid ligand.



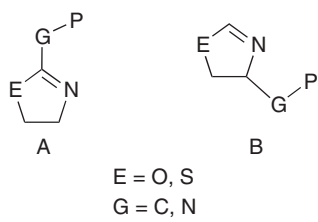
**Scheme 14.3**

#### 14.2.1 Five-Membered Chelating Ring Systems

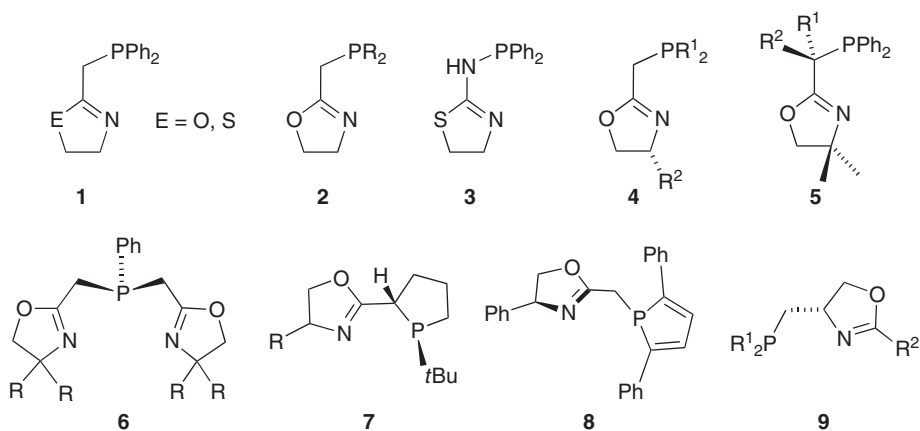
Basic subunits present in the ligands that can form five-membered chelates on metal coordination are shown in Scheme 14.4. We will focus on the coordination behavior of structurally characterized metal complexes and briefly mention their applications in catalysis.

Ligands containing a type A subunit are common in the literature, and significant examples are shown in Scheme 14.5. They include the ligands **1** [4], **2** and **3** [5], with a nonsubstituted heterocycle, and ligands **4** [6], **5** [7], **6** [8], and **7–9** [10], in which the heterocycle carries at least one substituent. Only few ligands containing a type B subunit have been reported, as illustrated with **9** (Scheme 14.5) [11].

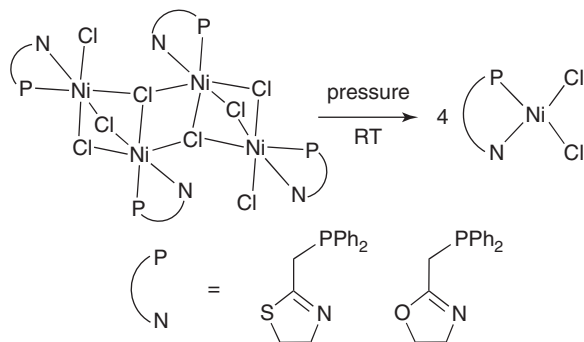
Ligands **1**, **3**, **4**, and **5** are used here as representative candidates to explore the chelating behavior of the ligands in complexes containing a five-membered chelate ring. In the course of attempts to prepare  $[\text{NiCl}_2(\mathbf{1})]$ , the unexpected, green tetranuclear complex  $[\text{NiCl}_2(\mathbf{1})]_4$  was isolated and structurally characterized. Its  $\text{Ni}_4\text{Cl}_8$  core is unprecedented and its geometry is new for any combination of transition metals with halogens. No other complex with a  $M_4X_8$  ( $X = \text{halogen}$ ) stoichiometry appears to have been reported for group 10 metals. This complex in the solid state undergoes an irreversible



**Scheme 14.4**



Scheme 14.5

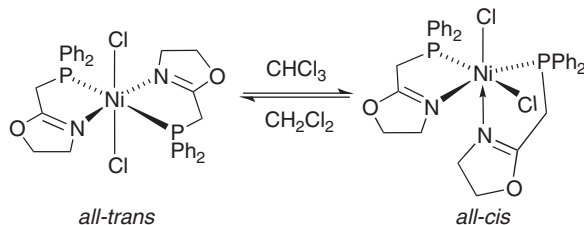


Scheme 14.6

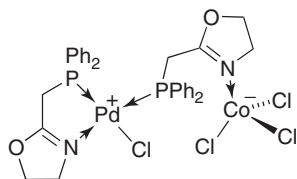
pressure-induced fragmentation into the corresponding monochelated red Ni(II) complexes  $[\text{NiCl}_2(\mathbf{1})]$  (Scheme 14.6) [4c]. Redissolution of the latter restores the equilibrium between the mono- and tetranuclear species. The latter can be obtained again on slow crystallization from  $\text{CH}_2\text{Cl}_2$ . It was also found that the tetranuclear form was more stabilized in the case of  $\text{PN}_{\text{th}}$  than  $\text{PN}_{\text{oxal}}$ .

Bis-chelate complexes have also been obtained with ligand **1**, as illustrated with  $[\text{RuCl}_2(\mathbf{1})_2]$  [41]. In the octahedral complexes of formula  $[\text{NiCl}_2(\mathbf{1})_2]$ , two isomers were structurally characterized (Scheme 14.7): the *all-trans* (left) and the *all-cis* products (right) that were obtained from  $\text{CH}_2\text{Cl}_2$  and  $\text{CHCl}_3$ , respectively. They can interconvert into each other on dissolution in the appropriate solvent and evaporation [4a].

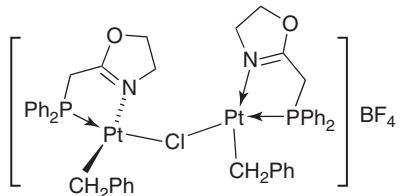
Although ligand **1** ( $E = \text{O}$ ) generally behaves as a P,N-chelate, rare examples of bridging behavior have been structurally characterized in the homo- and heteronuclear complexes  $[\text{CoCl}_2(\mu\text{-}\mathbf{1})]_2$  [4e],  $[(\text{OC})_4\text{Fe}(\mu\text{-}\mathbf{1})_2\text{CoCl}_2]$  [4h], and  $[(\text{OC})_3\text{Fe}(\mu\text{-}\mathbf{1})_2\text{Cu}] \text{BF}_4$  [8d], respectively. Very recently, a heterodinuclear Pd/Co complex was prepared by reaction of  $[\text{CoCl}_2(\mu\text{-}\mathbf{1})]_2$  with  $[\text{PdCl}_2(\mathbf{1})]$  (Scheme 14.8) [4a].



Scheme 14.7



Scheme 14.8

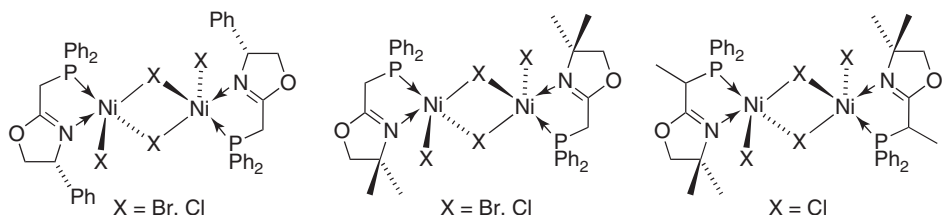


Scheme 14.9

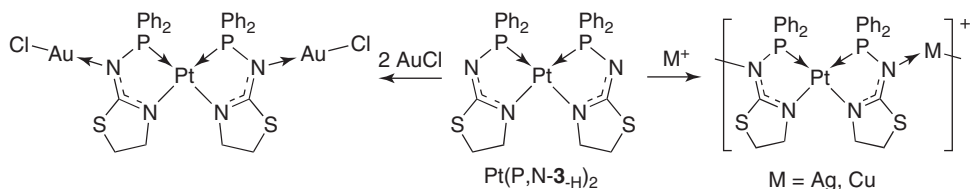
A single chloride-bridged dinuclear Pt(II) complex bearing a benzyl ligand and a chelating ligand **1** on each platinum was structurally characterized (Scheme 14.9) [4g], and several dinuclear Ni(II) complexes based on ligand **4** ( $R^1 = Ph$ ,  $R^2 = Ph$ ) and **5** ( $R^1 = H$ ,  $R^2 = H$  and  $R^1 = H$ ,  $R^2 = Me$ , respectively) containing two chloride bridges were obtained (Scheme 14.10) [7b].

The NH function in **3** facilitates ligand deprotonation when compared to the related P-CH<sub>2</sub> systems, and reaction of the corresponding anionic ligand with a Pt(II) precursor afforded the bis-chelated complex  $[Pt(P,N\text{-}3\text{-H})_2]$  [5], which could be used as a metalloligand for further coordination with coinage metal ions. The reaction of  $[Pt(P,N\text{-}3\text{-H})_2]$  with  $Ag^+$  or  $Cu^+$  in a 1 : 1 ratio gave rise to bimetallic coordination polymers [5b, 5d], while the reaction with AuCl in a 1 : 2 ratio led to a stable heterotrinuclear complex (Scheme 14.11) [5c]. The nucleophilicity of this electron-rich nitrogen atom was also investigated by the reaction of  $[Pt(P,N\text{-}3\text{-H})_2]$  with organic electrophiles such as a isothiocyanate, EtN=C=S. The incorporation of one molecule of EtN=C=S and decoordination of the nitrogen atom of one anionic chelate led to a P,S-chelating ligand, resulting in a five-membered chelate containing five different chemical elements: Pt, P, N, C, and S (Scheme 14.12) [5b].

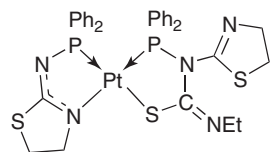
Both the P,N-chelating ligand **3** and a six-membered ring were found in a Ni(II) complex (Scheme 14.13). The new P,P-chelating ligand is formed during the reaction of ligand **3** with  $NiBr_2 \cdot xH_2O$  as a result of rearrangement of two ligands **3**. It is noteworthy that water plays a key role as a reaction promoter.



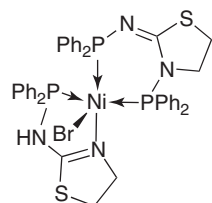
Scheme 14.10



Scheme 14.11



Scheme 14.12



Scheme 14.13

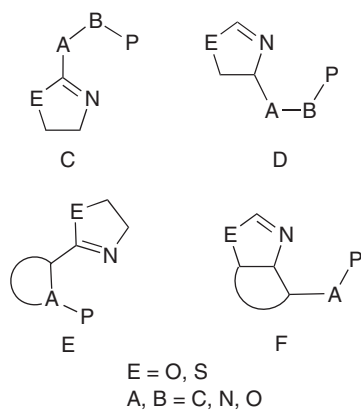
Among the complexes with a five-membered chelate ring, some were applied in catalytic processes, such as asymmetric hydrogenation [6d, 9, 11c], asymmetric isomerization of primary allylic alcohols [9a, 11a], transfer hydrogenation [1, 4i, 7c, 8e], copolymerization of ethylene/CO [4j], ethylene oligomerization [4e, 7a, 7b, 8d], and asymmetric allylation [6e, 11d, 11e].

#### 14.2.2 Six-Membered Chelating Ring Systems

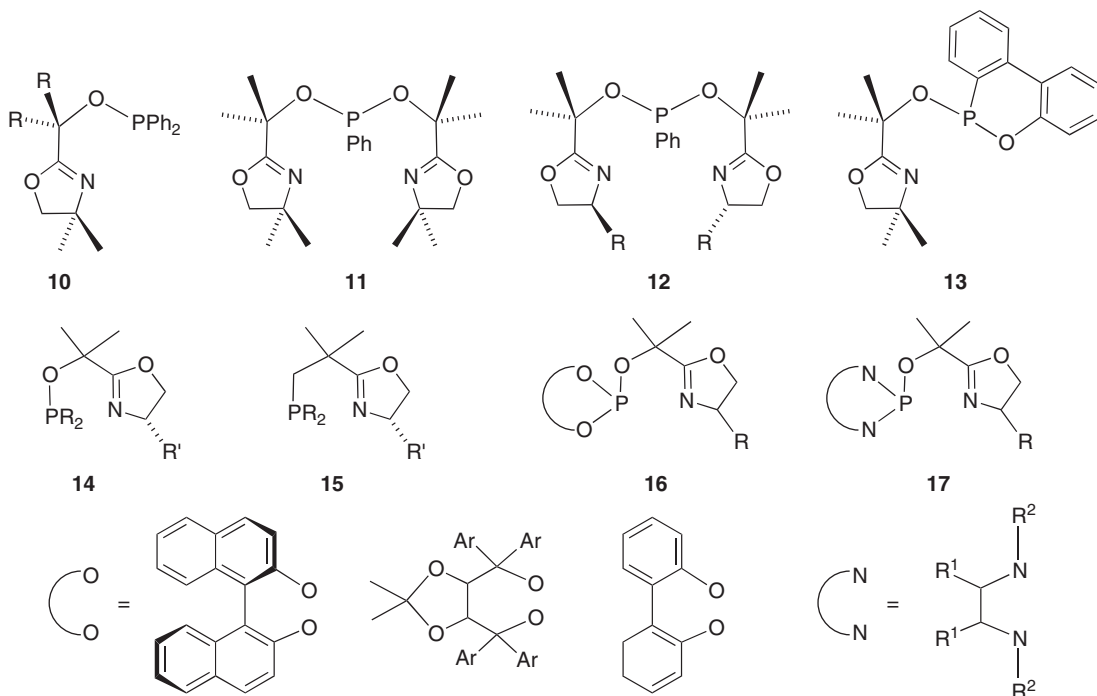
Numerous complexes possess P,N-chelating ligands that form six-membered ring systems. Depending on the relative position of the phosphorus (including phosphines, phosphinites, and aminophosphines) and oxazoline/thiazoline donor groups, four types of subunits can be considered (Scheme 14.14).

Ligands containing a type C subunit are shown in Scheme 14.15 and include **10** [12], and **11** [13], and **12** [14], **13** [15], **14** [16], **15** [17], **16** [18], and **17** [19] that contain an element of chirality. With the N,P,N ligands **11** and **12**, mono- and bis-chelated structures have been characterized.

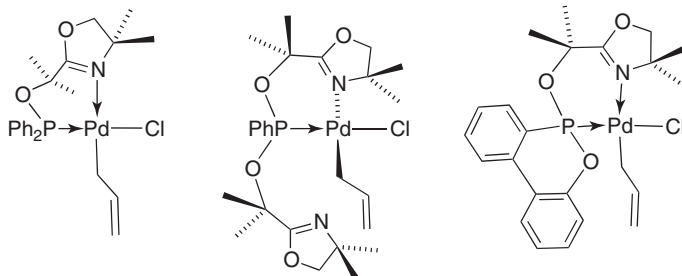
It is noteworthy that ligands **10**, **11**, and **13** have allowed full characterization of Pd(II) complexes containing a  $\eta^1$ -allyl ligand (Scheme 14.16) [13c, 13d, 15]. This still rare bonding mode for the allyl ligand in palladium chemistry facilitates, for example, CO insertion into the Pd–C bond  $\sigma$ -bond, compared to the common  $\eta^3$ -allyl Pd(II) complexes. In the three corresponding crystal structures (Scheme 14.16), the  $\eta^1$ -allyl ligand occupies a *trans* position with respect to the nitrogen donor of the oxazoline ring.



Scheme 14.14

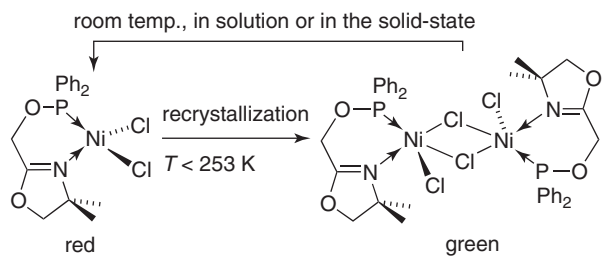


Scheme 14.15



Scheme 14.16

With ligands **10** ( $R = H$ ), Ni(II) complexes of formula  $[\text{NiCl}_2(\mathbf{10})]$  were prepared and investigated for ethylene and propylene oligomerization catalysis and revealed interesting structural transformations [21]. The mononuclear complex was found in equilibrium with the dinuclear, chloride-bridged structure and could be isolated on crystallization below 253 K. Conversely, the latter regenerates the mononuclear form at room temperature, either in solution or in the solid state (Scheme 14.17).



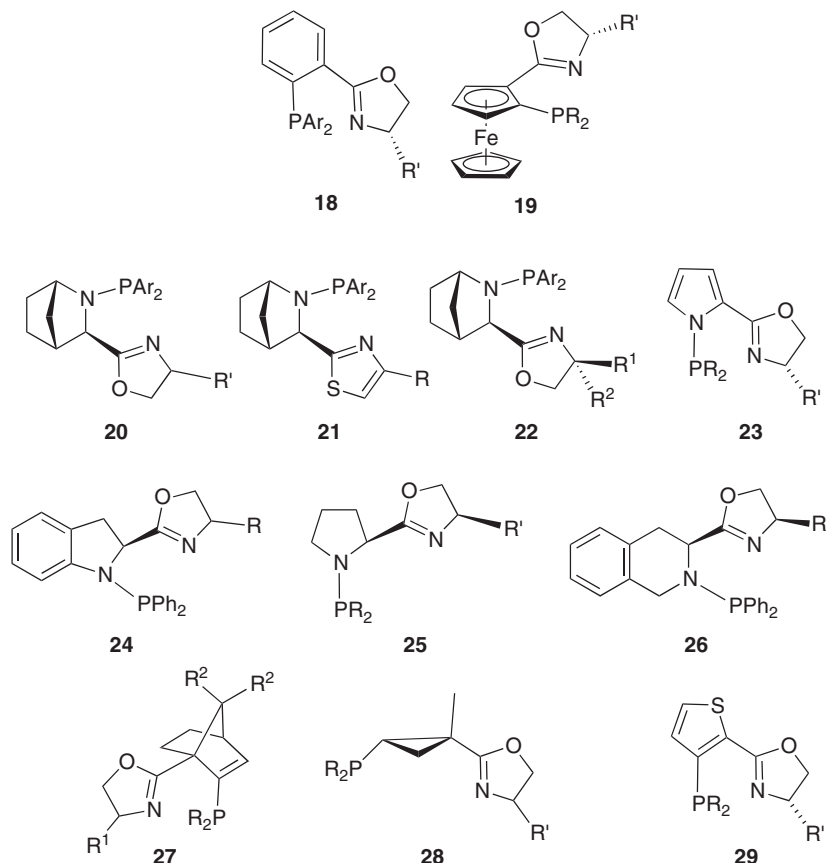
Scheme 14.17

Some of the chiral ligands shown in Scheme 14.15 were successfully employed in diverse asymmetric syntheses [15–20], in particular the air-stable ligands of type **17**, which have been prepared in high yield using simple purification techniques suitable for large-scale preparation. Their iridium complexes show excellent activities and enantioselectivities in the hydrogenation of olefins, including functionalized olefins, and the results obtained in the synthesis of (*R*)-(+)-7-demethyl-2-methoxycalamenene are superior with regard to the number of steps, overall yield, and purification of the intermediates [18].

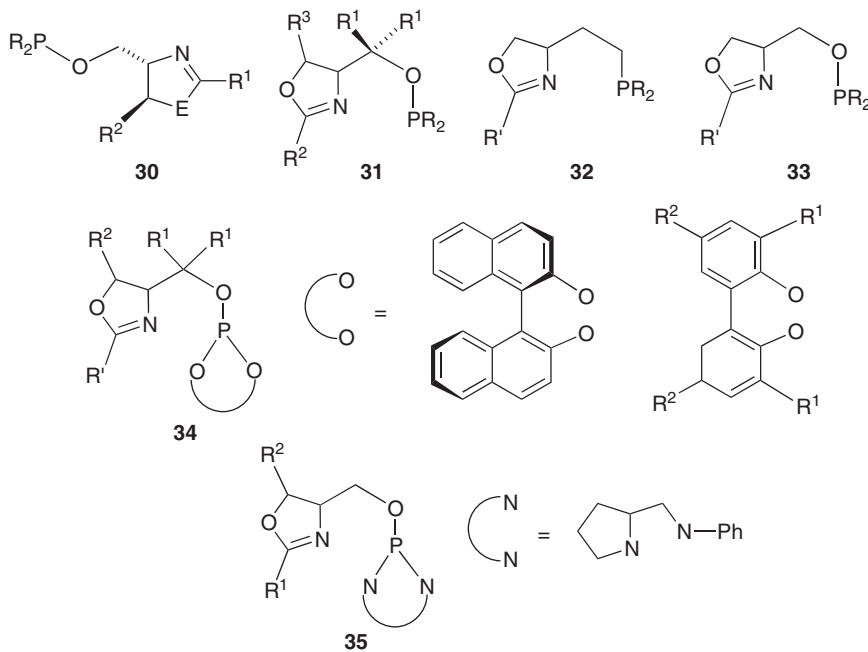
Ligands containing a type **D** subunit have been intensively developed. In particular, the phosphinooxazolines **18** (Scheme 14.18) form iridium complexes that are excellent catalysts for enantioselective hydrogenation [3]. The first-generation PHOX ligands bearing a flat *ortho*-phenylene tether were introduced by Pfaltz, Helmchen, and Williams [22]. There are three crucial features of Pfaltz's catalyst [23]: (i) simple synthetic procedure, purification, and high stability; (ii) easy formation of suitable crystals for X-ray diffraction analysis, which allows full characterization and helps in mechanistic studies [24]; and (iii) the high reactivity and enantioselectivity observed in the hydrogenation of imines and nonfunctionalized olefins [3].

On the basis of the results with systems of type **18**, the introduction of additional elements of chirality into the ligand backbone allowed remarkable improvements of the enantioselective properties of the corresponding catalysts for a number of transformations. Such ligands contain ferrocenyl **19** (Scheme 14.18) [25], 2-aza-norbornanyl **20–22** [26], pyrrolyl **23** [27], indolinyl **24** [28], prolinyl **25** [29], tetrahydroisoquinolinyl **26** [30], apobornenyl **27** [31], cyclopropyl **28** [32], and thiophene **29** [33] fragments (Scheme 14.18). Among them, the most successful planar chiral ferrocenylloxazolinylphosphines **19** (Fc-PHOX) are versatile ligands that have been applied to a wide range of asymmetric catalytic reactions, such as hydrogenation [34], transfer hydrogenation [35], and  $\alpha$ -alkylation of ketones [36], the oxidative kinetic resolution of racemic alcohols [37], allylic substitutions [38], Heck reactions [39], and 1,3-dipolar cycloadditions [40].

One should note that systems **19–29** (except **23**) not only have a stereogenic center in the oxazoline ring, but also possess planar chirality, and these readily form with metals rigid six-membered chelates, which is believed to favor further



Scheme 14.18



Scheme 14.19

chirality transfer. Ligands of types **20–24** have recently led to highly enantioselective iridium catalysts for the hydrogenation of  $\alpha,\beta$ -unsaturated esters [26].

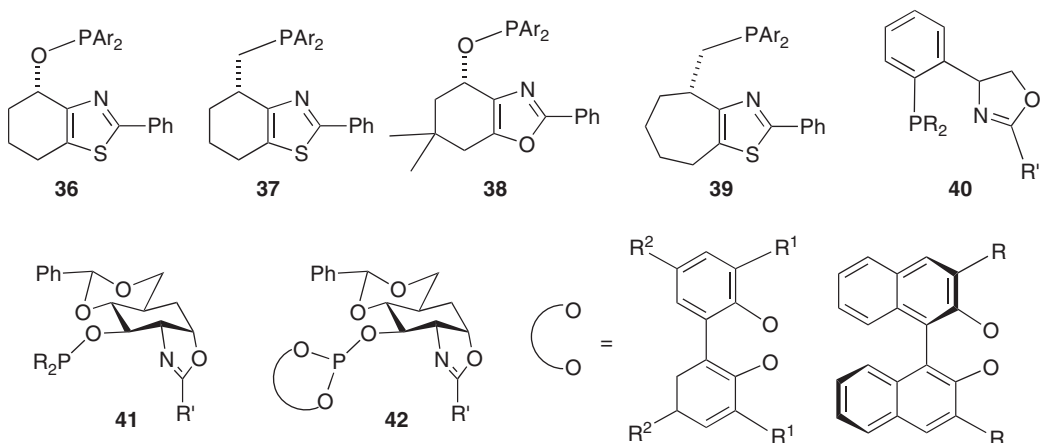
The P-donor can also be introduced at the 4-position of the oxazoline/thiazoline ring, which effectively enhances the scope of such chiral systems, and the corresponding ligand subunits **D** and **F** are shown in Scheme 14.19. Usually, ligands containing subunit **D** possess only chiral center(s) in the N-containing moiety, as in **30** [41], **31** [11], **32** [42], and **33** [43] (Scheme 14.19), and such ligands exhibit high selectivity in asymmetric catalysis. The results obtained with rhodium(I) complexes of ligand **31** in the asymmetric hydrogenation of functionalized olefins using propylene carbonate as a solvent were similar to or better than those obtained in standard solvents, illustrating its potential as a solvent for asymmetric hydrogenation reactions. The asymmetric hydrogenation of nonfunctionalized olefins appears particularly interesting, as nonpolar products are formed, which can be removed by extraction, and the catalyst can be readily recycled [11].

In **34** and **35**, there is one more element of chirality in the phosphite or phosphinite moiety, such as the binaphthyl system [44]. These modifications could potentially influence the origin of the stereochemistry in the asymmetric catalysis process, and sometimes excellent results have been obtained (quantitative conversions and enantiomeric excess values higher than 99%) in the case of **34** ( $R^1 = Ph$ ,  $R^2 = H$ ,  $R' = Ph$ ) that is better than other known catalyst systems for the asymmetric hydrogenation of unfunctionalized 1,1-disubstituted terminal alkenes [44].

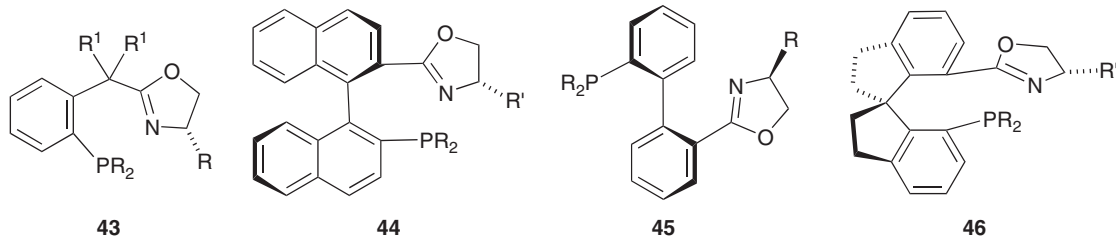
In view of the improvements generally observed in homogeneous catalysis when going from subunit **C** to **E** (Scheme 14.14), it was felt interesting to introduce similar structural modifications from subunit **D** to **F**, which feature a cyclic backbone. Ligands **E** and **F** chelate metal centers to form a six-membered ring, with the imine double bond included in the chelate ring in **E**, in contrast to **F** [45]. Corresponding structural studies on such systems are still rare. Ligands containing a subunit **F** are shown in Scheme 14.20, and most of them exhibit high enantioselectivity in diverse asymmetric syntheses [46].

#### 14.2.3 Seven-, Eight-, and Nine-Membered Chelating Ring Systems

Research on ligand design based on modifications of the spacer group between the P-donor and the oxazoline/thiazoline was extended further, generally to investigate the steric influence of the spacer on stereochemistry. Several ligands that can form seven-, eight-, or nine-membered metal chelates have been prepared and the resulting complexes sometimes display high catalytic activity. Selected ligands such as **43**, **44**, **45**, and **46** are shown in Scheme 14.21, in which **43** was successfully applied in the hydrogenation of  $\alpha,\beta$ -unsaturated ketones [47] and Heck reactions [48], **44** in asymmetric Mannich reactions [49], **45** in hydrogenation of exocyclic  $\alpha,\beta$ -unsaturated carbonyl compounds [50], and **46** in the hydrogenation of imines



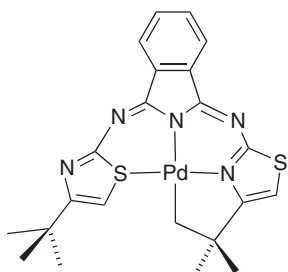
Scheme 14.20



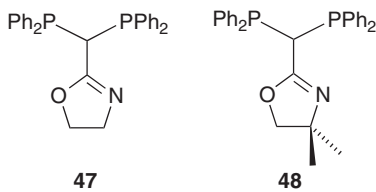
Scheme 14.21

[23] and of  $\alpha,\beta$ -unsaturated carboxylic acids [51]. It is noteworthy that the Ir(I) complexes of ligand **46** ( $R = 3,5-tBu_2C_6H_3$ ,  $R' = \text{Bn, } i\text{Pr, Me, H}$ ) exhibit very high activity and selectivity in asymmetric hydrogenation of (R)-methylcinnamic acid (quantitative conversion, almost quantitative yields, and enantiomeric excess (*ee*) values higher than 99%). This was the first application of such kind of ligands (spiro phosphino-oxazoline) to the highly enantioselective Ir-catalyzed hydrogenation of  $\alpha,\beta$ -unsaturated carboxylic acids.

Although the oxygen or sulfur atom of the heterocycle part of the P,N ligand was never observed to participate in direct coordination to the metal, it may influence the donor properties of the nitrogen of the oxazoline or thiazoline rings. Only few examples in which the oxygen/sulfur atom of an oxazoline/thiazoline ring coordinated to a metal center have been structurally characterized [52], and a recent example is shown in Scheme 14.22 [52].



Scheme 14.22



Scheme 14.23

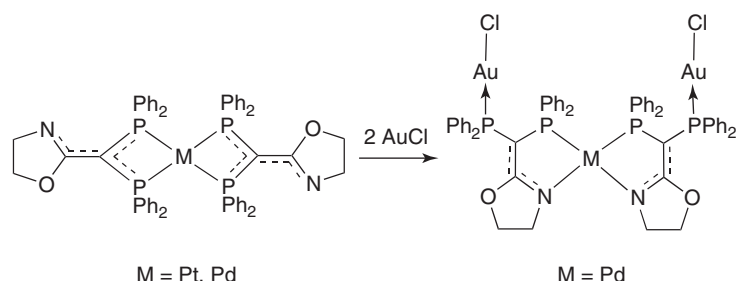
#### 14.2.4 Dppm-Type Ligands Containing an Oxazoline Moiety

In view of the rich chemistry of the dppm [bis(diphenylphosphino)methane], and related short-bite ligands [53], the introduction of additional functionalities at the PCP carbon is anticipated to bring about further structurally diversity and possibilities in coordination chemistry. Among the C-substituted dppm-type ligands, only few examples in which the substituents are N-containing heterocycles, such as imidazole [54], quinoline [55], terpyridine [56], indole [57], and, in particular, 2-pyridine have been reported [58]. In order to extend this chemistry, we have chosen oxazoline and its derivatives as substituents at the PCP carbon. The diphosphine ligands **47** [4, 59] and **48** [4] were found to behave not only as C-substituted dppm but also as P,N ligands and their coordination behavior has only recently begun to be investigated (Scheme 14.23).

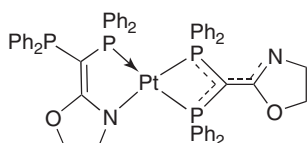
The P,P-chelating mode, which is a typical coordination mode for dppm, was also found for anionic ligand **47** in the P,P bis-chelated Pt(II) [4] and Pd(II) [59] complexes. In view of the presence of free nitrogen donors, further reaction with two equivalents of [AuCl(tht)] led to a trinuclear, bimetallic complex in which both anionic ligands **47** displayed a P,N-chelating/P,P bridging mode as a result of ligand rearrangement (Scheme 14.24). We also characterized a platinum complex in which the anionic ligands **47** exhibit a P,N-chelating and a P,P-chelating mode, the metal center being involved in a five-membered and a four-membered chelating ring, respectively (Scheme 14.25).

As a result of an unexpected metal-induced phosphoryl migration reaction from carbon to nitrogen, ligand **47** can display different isomeric forms that lead to the formation of a cationic bis-chelated platinum complex containing a rearranged and an intact ligand **47** as part of a six-membered and a four-membered chelate (Scheme 14.26).

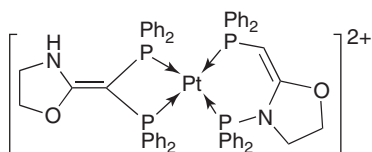
The versatility in bonding mode of functional dppm-type ligands bearing an oxazoline substituent on the PCP carbon atom was thus clearly demonstrated in Pd(II) and Pt(II) complexes with the neutral or the monoanionic forms of the P,N ligand. The chelating, *gem*-diphosphine form resulted from migration of one of the PPh<sub>2</sub> groups from a phosphino-oxazoline nitrogen atom to carbon, whereas metal coordination triggers the reverse migration. The tautomeric/isomeric forms of ligand **47** are shown in Scheme 14.27 [59].



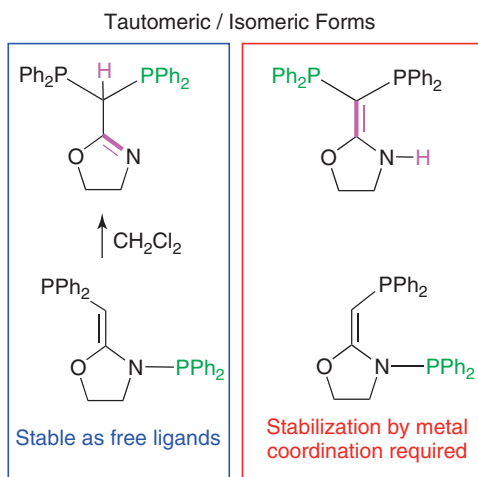
Scheme 14.24



Scheme 14.25



Scheme 14.26



Scheme 14.27 (See insert for color representation of the figure.)

## SUMMARY

The chemistry of P,N-chelating ligands based on oxazoline/thiazoline heterocycles has recently experienced major developments. In this chapter, we wished to provide a selection of recent examples illustrating the bonding and structural diversity encountered as a function of the size of the chelate ring they form on coordination. These features are expected to significantly influence, for example, the catalytic and photophysical properties of their metal complexes. While some of these systems have been known for almost 20 years, research continues to be active, especially toward catalytic applications [60]. Furthermore, oxazoline-substituted dppm ligands such as **47** have been studied and revealed unexpected coordination behavior (Scheme 14.24–14.26). The P,P bis-chelated platinum and palladium complexes shown in Scheme 14.24 are luminescent, probably owing to the electronic delocalization over the anionic ligand. This delocalization can be tuned by linking different functionalities to the PCP carbon, which should allow promising developments toward new C-substituted dppm ligands.

## ACKNOWLEDGMENTS

This work was supported by the CNRS, the Ministère de l'Enseignement Supérieur et de la Recherche, the Institut Français du Pétrole, Energies Nouvelles (IFPEN), and the International Centre for Frontier Research in Chemistry, Strasbourg (icFRC, www.icfrc.fr).

## REFERENCES

- Braunstein, P. *J. Organomet. Chem.* **2004**, *689*, 3953.
- For a review, see: Braunstein, P.; Naud, F. *Angew. Chem. Int. Ed.* **2001**, *40*, 680.
- For example, see: (a) Maggini, S. *Coord. Chem. Rev.* **2009**, *253*, 1793; (b) Mata, Y.; Pamies, O.; Dieguez, M. *Adv. Syn. Catal.* **2009**, *351*, 3217; (c) Willms, H.; Frank, W.; Ganter, C. *Organometallics* **2009**, *28*, 3049; (d) Benito-Garagorri, D.; Kirchner, K. *Acc.*

- Chem. Res.* **2008**, *41*, 201; (e) Roseblade, S. J.; Pfaltz, A. *Acc. Chem. Res.* **2007**, *40*, 1402; (f) Braunstein, P.; *Chem. Rev.* **2006**, *106*, 134; (g) Guiry, P. J.; Saunders, C. P. *Adv. Syn. Catal.* **2004**, *346*, 497; (h) Chelucci, G.; Orru, G.; Pinna, G. A. *Tetrahedron* **2003**, *59*, 9471; (i) Pfaltz, A.; Blankenstein, J.; Hilgraf, R.; Hormann, E.; McIntyre, S.; Menges, F.; Schonleber, M.; Smidt, S. P.; Wustenberg, B.; Zimmermann, N. *Adv. Syn. Catal.* **2003**, *345*, 33; (j) Helmchen, G.; Pfaltz, A. *Acc. Chem. Res.* **2000**, *33*, 336; (k) Slone, C. S.; Weinberger, D. A.; Mirkin, C. A. *Prog. Inorg. Chem.* **1999**, *48*, 233; (l) Espinet, P.; Soulantica, K. *Coord. Chem. Rev.* **1999**, *193–195*, 499.
4. For recent examples, see: (a) Zhang, S.; Pattacini, R.; Jie, S.-Y.; Braunstein, P. *Dalton Trans.* **2012**, *41*, 379; (b) Pattacini, R.; Margraf, G.; Messaoudi, A.; Oberbeckmann-Winter, N.; Braunstein, P. *Inorg. Chem.* **2008**, *47*, 9886; (c) Kermagoret, A.; Pattacini, R.; Chavez, V. P.; Rogez, G.; Welter, R.; Braunstein, P. *Angew. Chem. Int. Ed.* **2007**, *46*, 6438; (d) Agostinho, M.; Braunstein, P. *Chem. Commun.* **2007**, 58; (e) Jie, S.; Agostinho, M.; Kermagoret, A.; Cazin, C. S. J.; Braunstein, P. *Dalton Trans.* **2007**, 4472; (f) Agostinho, M.; Braunstein, P. *C.R. Chim.* **2007**, *10*, 666; (g) Oberbeckmann-Winter, N.; Braunstein, P.; Welter, R. *Organometallics* **2004**, *23*, 6311; (h) Braunstein, P.; Clerc, G.; Morise, X.; Welter, R.; Mantovani, G. *Dalton Trans.* **2003**, *1601*; (i) Braunstein, P.; Naud, F.; Rettig, S. J. *New J. Chem.* **2001**, *25*, 32; (j) Braunstein, P.; Fryzuk, M. D.; Le Dall, M.; Naud, F.; Rettig, S. J.; Speiser, F. *J. Chem. Soc. Dalton Trans.* **2000**, *1067*; (k) Camus, J. M.; Morales, D.; Andrieu, J.; Richard, P.; Poli, R.; Braunstein, P.; Naud, F. *J. Chem. Soc. Dalton Trans.* **2000**, *2577*; (l) Braunstein, P.; Graiff, C.; Naud, F.; Pfaltz, A.; Tiripicchio, A. *Inorg. Chem.* **2000**, *39*, 4468.
  5. (a) Voss, C.; Pattacini, R.; Braunstein, P. *C.R. Chim.* **2012**, *15*, 229; (b) Zhang, S.; Pattacini, R.; Braunstein, P. *Organometallics* **2010**, *29*, 6660; (c) Pattacini, R.; Giansante, C.; Ceroni, P.; Maestri, M.; Braunstein, P. *Chem.-Eur. J.* **2007**, *13*, 10117; (d) Margraf, G.; Pattacini, R.; Messaoudi, A.; Braunstein, P. *Chem. Commun.* **2006**, 3098.
  6. For recent examples, see: (a) Mantilli, L.; Gerard, D.; Torche, S.; Besnard, C.; Mazet, C. *Chem.-Eur. J.* **2010**, *16*, 12736; (b) Mantilli, L.; Gerard, D.; Torche, S.; Besnard, C.; Mazet, C. *Angew. Chem. Int. Ed.* **2009**, *48*, 5143; (c) Bianco, G. G.; Ferraz, H. M. C.; Costa, A. M.; Costa-Lotufo, L. V.; Pessoa, C.; deMoreas, M. O.; Schrems, M. G.; Pfaltz, A.; Silva, L. F. Jr. *J. Org. Chem.* **2009**, *74*, 2561; (d) Schrems, M. G.; Neumann, E.; Pfaltz, A. *Angew. Chem. Int. Ed.* **2007**, *46*, 8274; (e) Danjo, H.; Higuchi, M.; Yada, M.; Imamoto, T. *Tetrahedron Lett.* **2004**, *45*, 603; (f) Apfelbacher, A.; Braunstein, P.; Brissieux, L.; Welter, R. *Dalton Trans.* **2003**, 1669.
  7. (a) Speiser, F.; Braunstein, P.; Saussine, L. *Organometallics* **2004**, *23*, 2633; (b) Speiser, F.; Braunstein, P.; Saussine, L.; Welter, R. *Organometallics* **2004**, *23*, 2613; (c) Braunstein, P.; Naud, F.; Graiff, C.; Tiripicchio, A. *Chem. Commun.* **2000**, 897.
  8. (a) Zhang, J.; Pattacini, R.; Braunstein, P. *Inorg. Chem.* **2009**, *48*, 11954; (b) Kermagoret, A.; Tomicki, F.; Braunstein, P. *Dalton Trans.* **2008**, 2945; (c) Kermagoret, A.; Braunstein, P. *Dalton Trans.* **2008**, 585; (d) Braunstein, P.; Clerc, G.; Morise, X. *New J. Chem.* **2003**, *27*, 68; (e) Braunstein, P.; Fryzuk, M. D.; Naud, F.; Rettig, S. J. *J. Chem. Soc. Dalton Trans.* **1999**, 589.
  9. Thoumazet, C.; Melaimi, M.; Ricard, L.; Le Floch, P. *C.R. Chim.* **2004**, *7*, 823.
  10. (a) Mantilli, L.; Mazet, C. *Chem. Commun.* **2010**, *46*, 445; (b) Jones, G.; Richards, C. J. *Tetrahedron: Asymmetry* **2004**, *15*, 653; (c) Ezhova, M. B.; Patrick, B. O.; James, B. R.; Waller, F. J.; Ford, M. E. *J. Mol. Catal. A: Chem.* **2004**, *224*, 71; (d) Porte, A. M.; Reibenspies, J.; Burgess, K. *J. Am. Chem. Soc.* **1998**, *120*, 9180; (e) Burgess, K.; Porte, A. M. *Tetrahedron: Asymmetry* **1998**, *9*, 2465.
  11. (a) Zhu, Y.; Fan, Y.; Burgess, K. *J. Am. Chem. Soc.* **2010**, *132*, 6249; (b) Baeza, A.; Pfaltz, A. *Chem.-Eur. J.* **2010**, *16*, 2036; (c) Valla, C.; Baeza, A.; Menges, F.; Pfaltz, A. *Synlett* **2008**, 3167; (d) Bayardon, J.; Holz, J.; Schaeffner, B.; Andrushko, V.; Verevkin, S.; Preetz, A.; Boerner, A. *Angew. Chem. Int. Ed.* **2007**, *46*, 5971; (e) Nanchen, S.; Pfaltz, A. *Chem.-Eur. J.* **2006**, *12*, 4550; (f) McIntyre, S.; Hoermann, E.; Menges, F.; Smidt, S. P.; Pfaltz, A. *Adv. Syn. Catal.* **2005**, *347*, 282; (g) Smidt, S. P.; Menges, F.; Pfaltz, A. *Org. Lett.* **2004**, *6*, 2023; (h) Rosen, T. C.; Haufe, G. *Tetrahedron: Asymmetry* **2003**, *13*, 1397; (i) Menges, F.; Pfaltz, A. *Adv. Syn. Catal.* **2002**, *344*, 40; (j) Blankenstein, J.; Pfaltz, A. *Angew. Chem. Int. Ed.* **2001**, *40*, 4445.
  12. Tang, W.; Wang, W.; Zhang, X. *Angew. Chem. Int. Ed.* **2003**, *42*, 943.
  13. (a) Agostinho, M.; Braunstein, P.; Welter, R. *Dalton Trans.* **2007**, 759; (b) Speiser, F.; Braunstein, P.; Saussine, L.; Welter, R. *Inorg. Chem.* **2004**, *43*, 1649.
  14. (a) Peloso, R.; Pattacini, R.; Cazin, C. S. J.; Braunstein, P. *Inorg. Chem.* **2009**, *48*, 11415; (b) Speiser, F.; Braunstein, P.; Saussine, L. *Dalton Trans.* **2004**, *1539*; (c) Braunstein, P.; Zhang, J.; Welter, R. *Dalton Trans.* **2003**, *507*; (d) Braunstein, P.; Naud, F.; Dedieu, A.; Rohmer, M.-M.; DeCian, A.; Rettig, S. J. *Organometallics* **2001**, *20*, 2966.
  15. Braunstein, P.; Naud, F.; Pfaltz, A.; Rettig, S. J. *Organometallics* **2000**, *19*, 2676.
  16. Zhang, J.; Braunstein, P.; Welter, R. *Inorg. Chem.* **2004**, *43*, 4172.
  17. (a) Baeza, A.; Pfaltz, A. *Chem.-Eur. J.* **2010**, *16*, 4003; (b) Baeza, A.; Pfaltz, A. *Chem.-Eur. J.* **2009**, *15*, 2266; (c) Harmata, M.; Hong, X. *Org. Lett.* **2005**, *7*, 3581.
  18. Schrems, M. G.; Pfaltz, A. *Chem. Commun.* **2009**, 6210.
  19. (a) Hilgraf, R.; Pfaltz, A. *Adv. Syn. Catal.* **2005**, *347*, 61; (b) Heldmann, D. K.; Seebach, D. *Helv. Chim. Acta* **1999**, *82*, 1096; (c) Pretot, R.; Lloyd-Jones, G. C.; Pfaltz, A. *Pure Appl. Chem.* **1998**, *70*, 1035.
  20. (a) Schonleber, M.; Hilgraf, R.; Pfaltz, A. *Adv. Syn. Catal.* **2008**, *350*, 2033–2038; (b) Markert, C.; Pfaltz, A. *Angew. Chem. Int. Ed.* **2004**, *43*, 2498.

21. (a) Chavez, P.; Guerrero Rios, I.; Kermagoret, A.; Pattacini, R.; Meli, A.; Bianchini, C.; Giambastiani, G.; Braunstein, P. *Organometallics*, **2009**, *28*, 1776–1784; (b) Flapper, J.; Kooijman, H.; Lutz, M.; Spek, A. L.; van Leeuwen, P. W. N. M.; Elsevier, C. J.; Kamer, P. C. J. *Organometallics*, **2009**, *28*, 3272.
22. (a) von Matt, P.; Pfaltz, A. *Angew. Chem. Int. Ed.* **1993**, *32*, 566; (b) Dawson, G. J.; Frost, C. G.; Williams, J. M. J.; Coote, S. J. *Tetrahedron Lett.* **1993**, *34*, 3149; (c) Sprinz, J.; Helmchen, G. *Tetrahedron Lett.* **1993**, *34*, 1769.
23. Zhu, S.-F.; Xie, J.-B.; Zhang, Y.-Z.; Li, S.; Zhou, Q.-L. *J. Am. Chem. Soc.* **2006**, *128*, 12886.
24. Schrock, R. R.; Hoveyda, A. H. *Angew. Chem. Int. Ed.* **2003**, *42*, 4592.
25. For a review, see: Dai, L.-X.; Tu, T.; You, S.-L.; Deng, W.-P.; Hou, X.-L. *Acc. Chem. Res.* **2003**, *36*, 659.
26. (a) Li, J.-Q.; Quan, X.; Andersson, P. G. *Chem. Eur. J.* **2012**, *18*, 10609; (b) Li, J.-Q.; Papchikhine, A.; Govender, T.; Andersson, P. G. *Tetrahedron: Asymmetry* **2010**, *21*, 1328; (c) Papchikhine, A.; Cheruku, P.; Engman, M.; Andersson, P. G. *Chem. Commun.* **2009**, 5996; (d) Trifonova, A.; Diesen, J. S.; Andersson, P. G. *Chem. Eur. J.* **2006**, *12*, 2318.
27. (a) Burrows, A. D.; Mahon, M. F.; Varrone, M. *Inorg. Chim. Acta* **2003**, *350*, 152; (b) Cozzi, P. G.; Zimmermann, N.; Hilgraf, R.; Schaffner, S.; Pfaltz, A. *Adv. Syn. Catal.* **2001**, *343*, 450.
28. See e.g.: Blanc, C.; Agbossou-Niedercorn, F.; Nowogrocki, G. *Tetrahedron: Asymmetry* **2004**, *15*, 2159.
29. See e.g.: Xu, G.; Gilbertson, S. R. *Tetrahedron Lett.* **2003**, *44*, 953.
30. See e.g.: Chakka, S. K.; Peters, B. K.; Andersson, P. G.; Maguire, G. E. M.; Kruger, H. G.; Govender, T. *Tetrahedron: Asymmetry* **2010**, *21*, 2295.
31. Gilbertson, S. R.; Fu, Z. *Org. Lett.* **2001**, *3*, 161.
32. Rubina, M.; Sherrill, W. M.; Rubin, M. *Organometallics* **2008**, *27*, 6393.
33. Cozzi, P. G.; Menges, F.; Kaiser, S. *Synlett* **2003**, 833.
34. See e.g.: Lu, S.-M.; Han, X.-W.; Zhou, Y.-G. *Adv. Syn. Catal.* **2004**, *346*, 909.
35. For a review, see: Clapham, S. E.; Hadzovic, A.; Morris, R. H. *Coord. Chem. Rev.* **2004**, *248*, 2201.
36. See e.g.: Onodera, G.; Nishibayashi, Y.; Uemura, S. *Angew. Chem. Int. Ed.* **2006**, *45*, 3819.
37. Nishibayashi, Y.; Yamauchi, A.; Onodera, G.; Uemura, S. *J. Org. Chem.* **2003**, *68*, 5875.
38. See e.g.: Geisler, F. M.; Helmchen, G. *J. Org. Chem.* **2006**, *71*, 2486.
39. See e.g.: Tu, T.; Deng, W.-P.; Hou, X.-L.; Dai, L.-X.; Dong, X.-C. *Chem.-Eur. J.* **2003**, *9*, 3073.
40. See e.g.: Yan, X.-X.; Peng, Q.; Zhang, Y.; Zhang, K.; Hong, W.; Hou, X.-L.; Wu, Y.-D. *Angew. Chem. Int. Ed.* **2006**, *45*, 1979.
41. (a) Gavrilov, K. N.; Tsarev, V. N.; Konkin, S. I.; Lyubimov, S. E.; Korlyukov, A. A.; Antipin, M. Y.; Davankov, V. A. *Eur. J. Inorg. Chem.* **2005**, 3311; (b) Polosukhin, A. I.; Bondarev, O. G.; Lyubimov, S. E.; Korostylev, A. V.; Lyssenko, K. A.; Davankov, V. A.; Gavrilov, K. N. *Tetrahedron: Asymmetry* **2001**, *12*, 2197.
42. (a) Perry, M. C.; Cui, X.; Powell, M. T.; Hou, D.-R.; Reibenspies, J. H.; Burgess, K. *J. Am. Chem. Soc.* **2003**, *125*, 113; (b) Hou, D.-R.; Reibenspies, J.; Colacot, T. J.; Burgess, K. *Chem.-Eur. J.* **2001**, *7*, 5391; (c) Hou, D.-R.; Reibenspies, J. H.; Burgess, K. *J. Org. Chem.* **2001**, *66*, 206.
43. Liu, D.; Tang, W.; Zhang, X. *Org. Lett.* **2004**, *6*, 513.
44. (a) Mazuela, J.; Verendel, J. J.; Coll, M.; Schaffner, B.; Borner, A.; Andersson, P. G.; Pamies, O.; Dieguez, M. *J. Am. Chem. Soc.* **2009**, *131*, 12344; (b) Dieguez, M.; Mazuela, J.; Pamies, O.; Verendel, J. J.; Andersson, P. G. *Chem. Commun.* **2008**, 3888; (c) Dieguez, M.; Pamies, O. *Chem.-Eur. J.* **2008**, *14*, 3653; (d) Gavrilov, K. N.; Bondarev, O. G.; Tsarev, V. N.; Shiryaev, A. A.; Lyubimov, S. E.; Kucherenko, A. S.; Davankov, V. A. *Russ. Chem. Bull.* **2003**, *52*, 122.
45. Franco, D.; Gomez, M.; Jimenez, F.; Muller, G.; Rocamora, M.; Maestro, M. A.; Mahia, J. *Organometallics* **2004**, *23*, 3197.
46. Selected references: (a) Mazuela, J.; Papchikhine, A.; Pamies, O.; Andersson, P. G.; Dieguez, M. *Chem.-Eur. J.* **2010**, *16*, 4567; (b) Mazuela, J.; Papchikhine, A.; Tolstoy, P.; Pamies, O.; Dieguez, M.; Andersson, P. G. *Chem.-Eur. J.* **2010**, *16*, 620; (c) Dieguez, M.; Mazuela, J.; Pamies, O.; Verendel, J. J.; Andersson, P. G. *J. Am. Chem. Soc.* **2008**, *130*, 7208; (d) Cheruku, P.; Gohil, S.; Andersson, P. G. *Org. Lett.* **2007**, *9*, 1659; (e) Hedberg, C.; Kaellstroem, K.; Brandt, P.; Hansen, L. K.; Andersson, P. G. *J. Am. Chem. Soc.* **2006**, *128*, 2995; (f) Liu, D.; Dai, Q.; Zhang, X. *Tetrahedron* **2005**, *61*, 6460; (g) Hashizume, T.; Yonehara, K.; Ohe, K.; Uemura, S. *J. Org. Chem.* **2000**, *65*, 5197. (h) Yonehara, K.; Mori, K.; Hashizume, T.; Chung, K. G.; Ohe, K.; Uemura, S. *J. Organomet. Chem.* **2000**, *603*, 40.
47. See e.g.: Lu, W.-J.; Chen, Y.-W.; Hou, X.-L. *Angew. Chem. Int. Ed.* **2008**, *47*, 10133.
48. See e.g.: Wu, W.-Q.; Peng, Q.; Dong, D.-X.; Hou, X.-L.; Wu, Y.-D. *J. Am. Chem. Soc.* **2008**, *130*, 9717.
49. Deng, H.-P.; Wei, Y.; Shi, M. *Adv. Syn. Catal.* **2009**, *351*, 2897.
50. See e.g.: Tian, F.; Yao, D.; Liu, Y.; Xie, F.; Zhang, W. *Adv. Syn. Catal.* **2010**, *352*, 1841.
51. (a) Li, S.; Zhu, S.-F.; Xie, J.-H.; Song, S.; Zhang, C.-M.; Zhou, Q.-L. *J. Am. Chem. Soc.* **2010**, *132*, 1172; (b) Li, S.; Zhu, S.-F.; Zhang, C.-M.; Song, S.; Zhou, Q.-L. *J. Am. Chem. Soc.* **2008**, *130*, 8584.

52. (a) Broring, M.; Kleeberg, C. *Chem. Commun.* **2008**, 2777; (b) Gao, L.-H.; Guan, M.; Wang, K.-Z.; Jin, L.-P.; Huang, C.-H. *Eur. J. Inorg. Chem.* **2006**, 3731; (c) Lopez, C. A.; Fackler, Jr. J. P.; Staples, R. J.; Wang, S.; Winpenny, R. E. P. *Croat. Chem. Acta* **1995**, 68, 793; (d) Fackler, Jr., J. P.; Lopez, C. A.; Staples, R. J.; Wang, S.; Winpenny, R. E. P.; Lattimer, R. P. *J. Chem. Soc., Chem. Commun.* **1992**, 146; (e) Drew, M.G. B.; Pearson, T. R.; Murphy, B. P.; Nelson, S. M. *Polyhedron* **1983**, 2, 269.
53. (a) Mague, J. T. *J. Cluster Sci.* **1995**, 6, 217; (b) Puddephatt, R. J. *Chem. Soc. Rev.* **1983**, 12, 99.
54. Ruiz, J.; Mosquera, M. E. G.; Garcia, G.; Marquinez, F.; Riera, V. *Angew. Chem. Int. Ed.* **2005**, 44, 102.
55. Mosquera, M. E. G.; Ruiz, J.; Garcia, G.; Marquinez, F. *Chem.-Eur. J.* **2006**, 12, 7706.
56. Pickaert, G.; Douce, L.; Ziessel, R.; Cesario, M. *Chem. Commun.* **2000**, 1125.
57. Ruiz, J.; Riera, V.; Vivanco, M.; Lanfranchi, M.; Tiripicchio, A. *Organometallics* **1998**, 17, 3835.
58. (a) Mague, J. T.; Krinsky, J. L. *Inorg. Chem.* **2001**, 40, 1962; (b) Mague, J. T.; Hawbaker, S. W. *J. Chem. Crystallogr.* **1997**, 27, 603; (c) Mague, J. T.; Johnson, M. P. *Organometallics* **1990**, 9, 1254; (d) Mattson, B. M.; Ito, L. N. *Organometallics* **1989**, 8, 391; (e) McNair, R. J.; Pignolet, L. H. *Inorg. Chem.* **1986**, 25, 4717; (f) McNair, R. J.; Nilsson, P. V.; Pignolet, L. H. *Inorg. Chem.* **1985**, 24, 1935; (g) Anderson, M. P.; Tso, C. C.; Mattson, B. M.; Pignolet, L. H. *Inorg. Chem.* **1983**, 22, 3267; (h) Anderson, M. P.; Mattson, B. M.; Pignolet, L. H. *Inorg. Chem.* **1983**, 22, 2644; (i) Anderson, M. P.; Pignolet, L. H. *Organometallics* **1983**, 2, 1246; (j) Nelson, S. M.; Perks, M.; Walker, B. J. *J. Chem. Soc., Perkin Trans. 1* **1976**, 1, 1205; (k) Dahlhoff, W. V.; Dick, T. R.; Ford, G. H.; Kelly, W. S. J.; Nelson, S. M. *J. Chem. Soc. A* **1971**, 3495.
59. Zhang, S.; Pattacini, R.; Braunstein, P. *Inorg. Chem.* **2011**, 50, 3511.
60. For recent examples, see: (a) Zhou, T.; Peters, B.; Maldonado, M. F.; Govender, T.; Andersson, P. G. *J. Am. Chem. Soc.* **2012**, 134, 13592; (b) Cao, T.; Deitch, J.; Linton, E. C.; Kozlowski, M. C. *Angew. Chem. Int. Ed.* **2012**, 51, 2448; (c) Gazic, S. I.; Casas-Arce, E.; Roseblade, S. J.; Nettekoven, U.; Zanotti-Gerosa, A.; Kovacevic, M.; Casar, Z. *Angew. Chem. Int. Ed.* **2012**, 51, 1014; (d) Weise, C. F.; Pischl, M. C.; Pfaltz, A.; Schneider, C. *J. Org. Chem.* **2012**, 77, 1477; (e) Maurer, F.; Huch, V.; Ullrich, A.; Kazmaier, U. *J. Org. Chem.* **2012**, 77, 5139; (f) Belanger, E.; Pouliot, M.-F.; Courtemanche, M.-A.; Paquin, J.-F. *J. Org. Chem.* **2012**, 77, 317; (g) Newton, S.; Ley, S. V.; Arce, E. C.; Grainger, D. M. *Adv. Syn. Catal.* **2012**, 354, 1805; (h) Verevkin, S. P.; Emel'yanenko, V. N.; Bayardon, J.; Schaeffner, B.; Baumann, W.; Boerner, A. *Ind. Eng. Chem. Res.* **2012**, 51, 126; (i) Shang, J.; Han, Z.; Li, Y.; Wang, Z.; Ding, K. *Chem. Commun.* **2012**, 48, 5172; (j) Wang, X.; Han, Z.; Wang, Z.; Ding, K. *Angew. Chem. Int. Ed.* **2012**, 51, 936.

## “CLICK” COPPER CATALYZED AZIDE–ALKYNE CYCLOADDITION (CuAAC) IN AQUEOUS MEDIUM

JOAQUÍN GARCÍA-ÁLVAREZ AND JOSÉ GIMENO\*

*Laboratorio de Compuestos Organometálicos y Catálisis (Unidad Asociada al CSIC), Departamento de Química Orgánica e Inorgánica (IUQOEM), Facultad de Química, Universidad de Oviedo, Oviedo, Spain*

### 15.1 INTRODUCTION

Since the independent discovery by Meldal, Sharpless, and coworkers [1] of the regioselective copper(I) catalyzed 1,3-dipolar cycloaddition of organic azides and terminal alkynes (CuAAC) rendering 1,2,3-triazoles, the applications of this process have grown tremendously. In contrast to the classical Huisgen cycloadditions, which proceed slowly under thermal conditions to give a mixture of regiosomers **A** + **B** (see Scheme 15.1) [2], CuAAC dramatically accelerates the reaction rate to give exclusively disubstituted 1,4-triazoles **A** that are formed rapidly even at room temperature [3]. Because of its efficiency, atom economy, and wide chemical applications in many fields [4], CuAAC is considered one of the most genuine examples of “Click Chemistry” [5]. Although, in fact, a copper-free methodology has also been reported [6], to date only copper catalysis has disclosed an efficient and selective synthetic approach fulfilling the “Click” philosophy [7].

Classical catalysts are often generated *in situ* from a copper(II) salt in the presence of a reducing agent (usually sodium ascorbate). To avoid the intrinsic instability of the resulting copper(I) species, the addition of ligands is often used, which not only stabilizes the metal ion but also improves the catalytic efficiency. In particular, significant developments have been achieved by using *N*-polydentate ligands, which allow smooth reaction conditions and extensive applicability [8]. Nevertheless, several drawbacks are associated with these catalytic systems mainly arising from the oxidation in the presence of air, the use of an excess of the ligand, and, occasionally, metal leaching. Although still scarcely used, preformed catalysts may overcome these limitations and a series of very active copper(I) complexes containing nitrogen [8, 9], sulfur [10], Phosphorous [11, 12], *N*-heterocyclic carbene (NHC) [13], and oxygen [14] donor ligands have been shown to be active catalysts in CuAAC transformations [15].

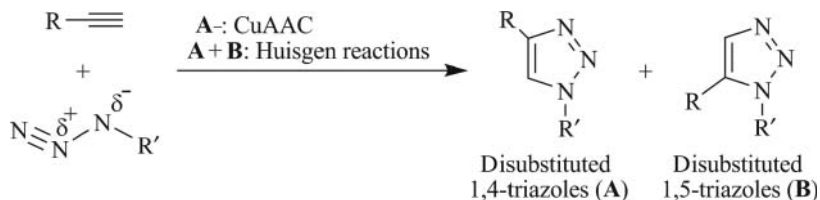
Despite the enhanced reactivity and regioselectivity of many organic reactions in aqueous media, surprisingly, only a few CuAAC reactions have been performed in this reaction media. This chapter provides an overview of these type of catalytic systems, and, particularly, addressing attention to those using well-defined copper(I) catalysts [16].

### 15.2 CuAAC: ORGANIC SOLVENTS VERSUS AQUEOUS MEDIA

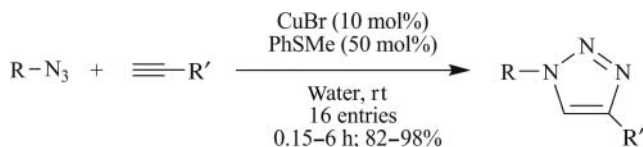
The use of organic solvents as reaction media dominate in CuAAC reactions. However, several examples have been described that proceed in mixtures of organic solvents and water (i.e., *t*BuOH/water [9a, 17], MeOH/water [18], dimethyl sulfoxide (DMSO)/water [8c, 19], MeCN/water [20], or tetrahydrofuran (THF)/water [13g,i]). In addition, several catalytic systems,

*Advances in Organometallic Chemistry and Catalysis: The Silver/Gold Jubilee International Conference on Organometallic Chemistry Celebratory Book*, First Edition. Edited by Armando J. L. Pombeiro.

© 2014 John Wiley & Sons, Inc. Published 2014 by John Wiley & Sons, Inc.



**Scheme 15.1** 1,3-Dipolar cycloaddition of azides and terminal alkynes through Huisgen or CuAAC reactions.



**Scheme 15.2** CuBr/PhSMe-catalyzed cycloaddition of aliphatic, acrylic, or sulfonyl azides with terminal alkynes in water.

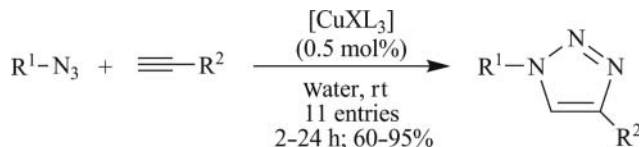
that is, CuI/NET<sub>3</sub> [21], CuI/N-alkylimidazole [22], and CuBr/sulfur ligands [23], have been reported to be active in pure water. As an example, excellent yields are achieved in short reaction times at room temperature with the system CuBr/PhSMe, although a high catalyst loading is required (see Scheme 15.2).

More recently, there has been a growing interest in the use of well-defined copper(I) catalysts as precursors of catalytic active species in water. An updated account of these developments is presented in this chapter, including transformations with terminal and internal alkynes that lead to the preparation of 1,4-disubstituted and 1,4,5-trisubstituted triazoles, respectively.

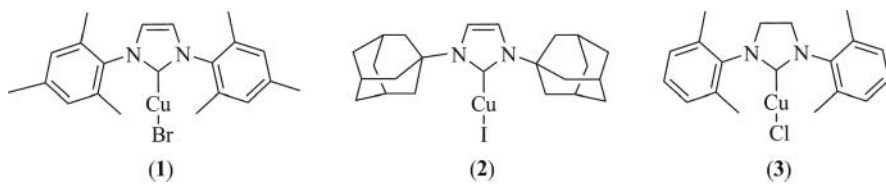
### 15.2.1 Cycloadditions With Terminal Alkynes

Despite [CuBr(PPh<sub>3</sub>)<sub>3</sub>] and [CuI{P(OEt)<sub>3</sub>}] being seminal catalysts in CuAAC [11a], it was only when Díez-González and coworkers reported [24] that phosphine complexes [CuXL<sub>3</sub>] (X = Cl, Br; L = PPh<sub>3</sub>, P(OR)Ph<sub>2</sub>, P(OR)<sub>2</sub>Ph) are efficient and selective catalysts for this transformation in pure water. By using 0.5 mol% of catalyst loading (see Scheme 15.3), the reactions proceed at room temperature and in the absence of any other cocatalyst. The corresponding triazoles were recovered in pure form after simple filtration or extraction in moderated-to-good yields (60–95%).

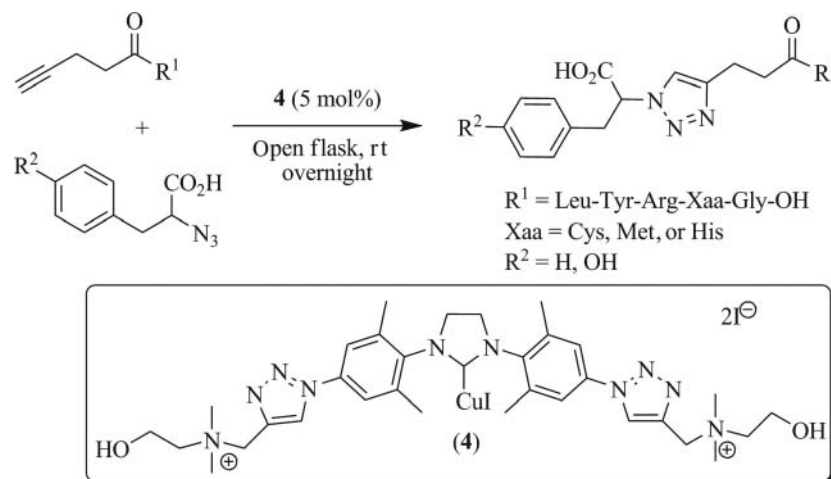
On the basis of the wide catalytic applications of NHC transition metal complexes [25], Nolan and coworkers have thoroughly studied the catalytic activity in CuAAC reactions of well-defined copper(I) complexes with general formula [CuX(NHC)]. Organic solvents, mixtures of EtOH/water, and pure water have been used as reaction media. In particular, it has been reported that complexes [CuBr(SIMes)] (**1** in Fig. 15.1, SIMes = *N,N*-bis(2,4,6-trimethylphenyl)imidazol-2-ylidene) and [CuI(IAd)] (**2** in Fig. 15.1, IAd = *N,N*-adamantyl imidazol-2-ylidene) show a remarkable activity for the synthesis of a



**Scheme 15.3** CuAAC reactions catalyzed by the copper-phosphine or copper-phospho(o)nate complexes [CuXL<sub>3</sub>] in water.



**Figure 15.1** [CuX(NHC)] complexes active in CuAAC reactions in water.

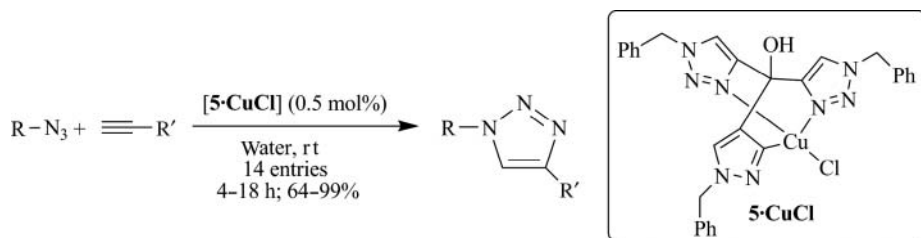
**Scheme 15.4** CuAAC-peptide synthesis mediated by complex **4**.

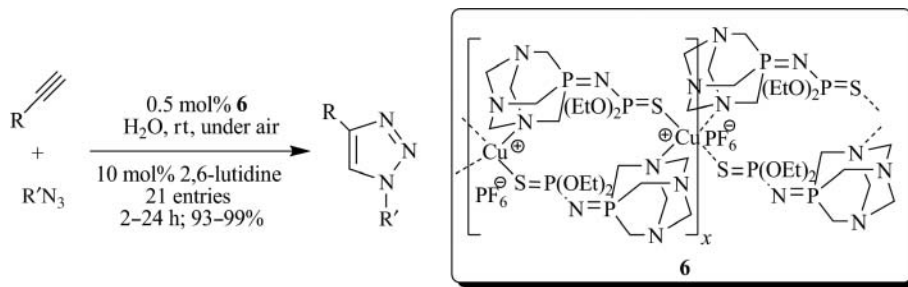
variety of triazoles in aqueous media [13a]. After screening the catalytic activity for a series of  $[\text{CuX}(\text{NHC})]$  complexes in water [13d], it was found that complex  $[\text{CuCl}(\text{SIPr})]$  (**3** in Fig. 15.1, SIPr = *N,N*-bis(2,6-diisopropylphenyl)imidazolidin-2-ylidene) was the least reactive catalyst for this transformation [13e], as no reaction was observed under ambient conditions and gentle heating was required for the efficient preparation of the corresponding triazoles.

A significant improvement of the methodology in the CuAAC reaction in water has been reported recently by Gautier and coworkers [26], based on the synthesis of a hydrosoluble NHC ligand containing two hydrophilic triazolyl-choline arms as a modification (see Scheme 15.4) and the corresponding complex  $[\text{CuI}(\text{NHC})]$ . This new, readily accessible, hydrophilic, and highly stable complex (**4** in Scheme 15.4) allowed performing CuAAC reactions involving clean ligations of unprotected peptides bearing sensitive side chains under challenging conditions such as common aqueous buffer (pH 7.6) solutions under air and low catalyst loading.

Surprisingly, and despite a strong acceleration effect having been observed when using *N*-donor ligands in “Click” CuAAC reactions in organic media, only a few well-defined copper(I) catalysts have been used in water. As mentioned above, several *N*-ligands have been used as protecting ligands of copper(I) in aqueous media including mono-, bi-, and polydentate amines [21, 22, 27]. The first example of an isolated catalyst that is active in water was reported by Pericàs and coworkers [28] (see Scheme 15.5). The air-stable and water-soluble copper(I) complex contains a tripodal tris(1-benzyl-1*H*-1,2,3-triazol-4-yl)methanol ligand (**5**), which is proposed to be coordinated in a  $\kappa^3$ -mode on the basis of the characterization data of the corresponding copper(II) analog. Triazoles are formed in good yields from the corresponding azides in water or in neat conditions at room temperature. Recently, ligand **5** was immobilized onto Merrifield resins. The corresponding S<sub>N</sub>2-supported Cu complex is also active at low catalyst loadings and at low concentration in aqueous media [18].

Iminophosphorane base ligands (also known in the literature as *phosphazenes* or *phosphinimes*,  $R_3P=NR'$ ) have been scarcely used in metal-catalyzed reactions in water. We have recently reported a highly active novel catalyst for the Huisgen 1,3-dipolar cycloadditions in pure water, based on a 1,3,5-triaza-7-phosphaadamantane (PTA)-iminophosphorane Cu(I) complex (**6**) [29]. This complex represents one of the few examples of an isolated and crystallographically characterized

**Scheme 15.5** CuAAC reaction in water catalyzed by complex **5·CuCl**.



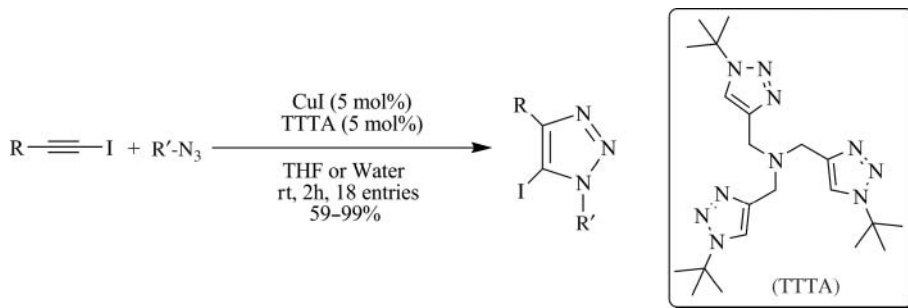
**Scheme 15.6** Synthesis of 1,4-disubstituted triazoles catalyzed by complex **6** in water.

copper(I) catalyst active in water. Its high stability, which allows performing the reactions in air and in aqueous media, precludes either oxidation or disproportionation, which are generally associated with most copper(I) catalysts in CuAAC reactions (see Scheme 15.6).

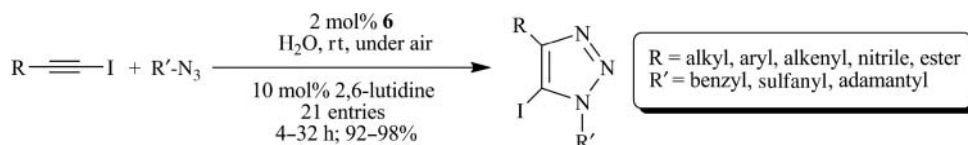
### 15.2.2 Internal 1-Iodoalkynes

The formation of intermediates based on copper(I) alkynyl species is postulated as the first step in CuAAC reactions [16, 30]. In accordance with this proposed mechanistic insight, internal alkynes are not able to undergo the required cycloaddition, a limitation generally observed with conventional copper catalysts [31, 32]. In order to overcome this limitation, several routes for the synthesis of triazoles, starting from internal alkynes, have been devised as alternative synthetic approaches to CuAAC (all of them using organic solvents) [33, 34]. In a seminal work, Sharpless, Fokin, and coworkers [33e] have reported that the readily accessible internal 1-iodoalkynes have revealed an exceptional reactivity in copper(I)-catalyzed processes with organic azides, using an equimolar mixture of CuI and the polyamine ligands tris((1-benzyl-1*H*-1,2,3-triazolyl)-methyl)amine (TBTA) and tris((1-*tert*-butyl-1*H*-1,2,3-triazolyl)methyl)amine (TTTA). In particular, the system containing the ligand TTTA is active in aqueous media (see Scheme 15.7).

We have recently reported that the air-stable and hydrosoluble iminophosphorane copper(I) complex **6** is also active in CuAAC of 1-iodoalkynes in aqueous media, under mild and aerobic conditions according to "click laws" and displaying a broad substrate scope and functional compatibility [29] (see Scheme 15.8). It is important to note the following catalytic features: (i) catalyst **6** was the first example of an isolated and crystallographically characterized copper(I) catalyst active for cycloaddition of 1-iodoalkynes with azides, to give 5-iodo-1,2,3-triazoles exclusively. (ii) The presence of a free thio moiety in the substrate does not deactivate the catalyst, a fact generally observed in CuAAC for functionalized substrates



**Scheme 15.7** Synthesis of 5-iodo-1,4-trisubstituted triazoles catalyzed by CuI-TTTA.



**Scheme 15.8** Synthesis of 5-iodo-1,4-disubstituted triazoles catalyzed by the iminophosphorane-Cu(I) complex **6** in water.

with donor atom groups. Since the reaction is also amenable to low catalyst loadings and is accessible on a multigram scale, the practical application of this methodology provides a valuable synthetic approach to 5-iodo-1,2,3-triazoles, which are versatile intermediates useful for further functionalizations.

Most recently, Buckley et al. [35], have shown that the polymeric alkynylcopper(I) ladder complex  $[\text{PhC}\equiv\text{C}-\text{Cu}]_n$ , can be used as heterogeneous precatalyst in the “on water” click reaction for the synthesis of 5-iodo-1,2,3-triazoles. However, important drawbacks were reported for this catalytic system when compared with complex **6**: (i) high copper loadings were required (10 mol%), (ii) the cycloaddition reaction is restricted to iodophenylacetylene and benzylic azides, and (iii) significant level of protolysis was observed.

### 15.2.3 Three-Component “Click” Reaction

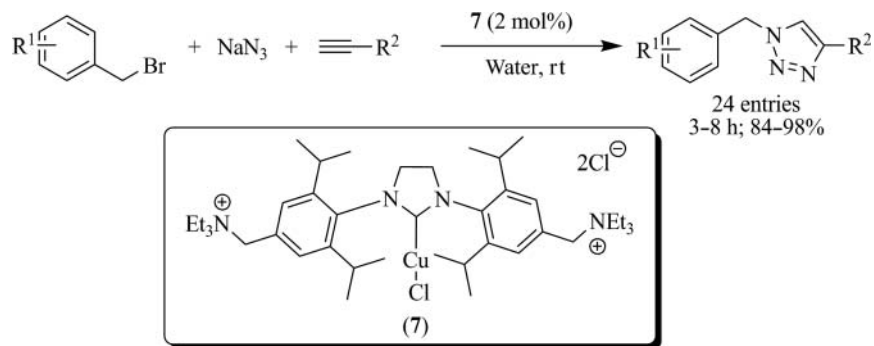
Owing to the danger, difficulty in handling, and isolation problems of low molecular weight organic azides [36], a number of methodologies have been developed for the synthesis of 1,4-disubstituted triazoles via [3 + 2] cycloadditions, avoiding the use of preisolated azides. To this end, a series of three-component synthetic methodologies have been used through the one-pot reaction of the terminal alkyne with organic azides generated *in situ* from sodium azide and an organic bromide [37]. These three-component reactions performed in water are much scarcer. NHC copper(I) complexes  $[\text{CuBr}(\text{SIMes})]$  (**1** in Fig. 15.1) [13a] and  $[\text{CuCl}(\text{SIPr})]$  ( $\text{SIPr} = N,N\text{-bis}(2,6\text{-diisopropylphenyl})\text{imidazolidin-2-ylidene}$ , **7** in Scheme 15.9) [38] show high catalytic activity toward the three-component reactions in aqueous media, the latter improving the catalytic performance as a lower catalyst loading is used (2 mol% vs 5 mol%). This reusable ammonium salt-tagged complex turned out to be a highly efficient catalyst involving a wide range of benzyl bromides and terminal alkynes (Scheme 15.9).

Analogously, the water-soluble complex containing the tripodal ligand **5** tris(1-benzyl-1*H*-1,2,3-triazol-4-yl)methanol **5·CuCl** (see Scheme 15.5), is also able to catalyze the three-component reaction in water but heating and chromatographic purification were required to achieve catalytic efficiency. To date, the most active catalyst for the three-component transformation in water with terminal alkynes is the complex  $[\text{CuBr}(\text{PPh}_3)_3]$ , which proceeds under very mild reaction conditions and with the lowest reported catalyst loading (as low as 50 ppm). Good-to-high yields were observed for the corresponding triazoles (no purification step required) after 24 h of reaction [39].

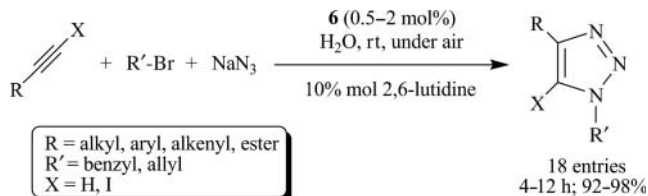
The most versatile catalyst in this three-component transformation is the iminophosphorane copper(I) complex **6**, which is also active under very mild reaction conditions (pure water as solvent, at room temperature, and under air conditions) with both terminal and internal 1-iodoalkynes [40]. The latter, is an unprecedented catalytic reaction that is also efficient for a wide array of 1-iodoalkynes and organic bromides (Scheme 15.10). Both electron-withdrawing and electron-donating substituent groups are tolerated, although a longer reaction time is required for the internal iodoalkynes when compared with their terminal counterparts.

## 15.3 FINAL REMARKS

Since the very beginning of the discovery of CuAAC, synthetic applications have been extensively used, determining its great popularity among different chemical disciplines. These reactions disclose a type of transformations that are experimentally simple, highly efficient, and reliable, becoming the most genuine examples of Click Chemistry. Although remarkable



**Scheme 15.9** Ammonium salt-tagged  $[\text{CuCl}(\text{SIPr})]$ -catalyzed three-component synthesis of triazoles in water.



**Scheme 15.10** Copper catalyzed 1,3-dipolar cycloaddition of *in situ* generated azides (organic bromide and  $\text{NaN}_3$ ) with both terminal and internal 1-iodoalkynes in water.

progress has taken place, including new stabilizing ligands and applications of well-defined catalysts, there is still a gap in designing new experimental methodologies and reaction conditions fulfilling strict “Click” criteria. This chapter clarified these features, emphasizing the state of the art of CuAAC in aqueous media known to date, which can allow for a higher number of applications, thus increasing the economic and environmental benefits.

## ACKNOWLEDGMENTS

Financial support from the Spanish MICINN (Projects CTQ2010-14796/BQU, CTQ2009-08746/BQU, CTQ2008-00506/BQU, and CSD2007-00006) is acknowledged. J. G.-A. also thanks MICINN and the European Social Fund for the award of “Juan de la Cierva” and “Ramón y Cajal” contracts.

## REFERENCES

- (a) Rostovtsev, V. V.; Green, L. G.; Fokin, V. V.; Sharpless, K. B. *Angew. Chem. Int. Ed.* **2002**, *41*, 2596; (b) Tornøe, C. W.; Christensen, C.; Meldal, M. *J. Org. Chem.* **2002**, *67*, 3057.
- (a) Huisgen, R. *Proc. Chem. Soc.* **1961**, 357; (b) Huisgen, R.; Knorr, R.; Moebius, L.; Szeimies, G. *Chem. Ber.* **1965**, *98*, 4014; (c) Huisgen, R.; Szeimies, G.; Moebius, L. *Chem. Ber.* **1967**, *100*, 2494; (d) *1,3-Dipolar Cycloaddition Chemistry*; Huisgen, R.; Pawda, A., Eds; John Wiley & Sons, Ltd: New York, **1984**; Vol. 1; (e) Huisgen, R. *Pure Appl. Chem.* **1989**, *61*, 613.
- 1,5-disubstituted triazoles can be regioselective obtained with ruthenium catalysts. For examples, see: (a) Tam, A.; Arnold, U.; Soellner, M. B.; Raines, R. T. *J. Am. Chem. Soc.* **2007**, *129*, 12670; (b) Boren, B. C.; Narayan, S.; Rasmussen, L. K.; Zhang, L.; Zhao, H.; Lin, Z.; Jia, G.; Fokin, V. V. *J. Am. Chem. Soc.* **2008**, *130*, 8923; (c) Kwok, S. W.; Fotsing, J. R.; Fraser, R. J.; Rodionov, V. O.; Fokin, V. V. *Org. Lett.* **2010**, *12*, 4217; (d) Johansson, J. R.; Lincoln, P.; Nordén, B.; Kann, N. *J. Org. Chem.* **2010**, *76*, 2355.
- “Click Chemistry” has found wide application in pharmaceutical, combinatorial, and material chemistry. For selected reviews see: (a) Wu, P.; Fokin, V. V. *Aldrichim. Acta* **2007**, *40*, 7; (b) Spiteri, A. D.; Moses, J. E. *ChemMedChem* **2008**, *3*, 715; (c) Meldal, M.; Tornøe, C. W. *Chem. Rev.* **2008**, *108*, 2952; (d) Holub, J. M.; Kirshenbaum, K. *Chem. Soc. Rev.* **2010**, *39*, 1325.
- The term “Click chemistry” was coined by K. B. Sharpless et al. in 2001 and describes chemistry tailored to generate substances quickly and reliably by joining small units together. Click chemistry is not a single specific reaction, but was meant to mimic nature, which also generates substances by joining small modular units. Kolb, H. C.; Finn, M. G.; Sharpless, K. B. *Angew. Chem. Int. Ed.* **2001**, *40*, 2004.
- Baskin, J. M.; Bertozzi, C. R. *Aldrichim. Acta* **2010**, *43*, 15.
- For recent AgAAC examples see: McNulty, J.; Keska, K. *Eur. J. Org. Chem.* **2012**, 5462.
- For representative examples see: (a) Rodionov, V. O.; Presolski, S. I.; Gardinier, S.; Lim, Y.-H.; Finn, M. G. *J. Am. Chem. Soc.* **2007**, *129*, 12696; (b) Rodionov, V. O.; Presolski, S. I.; Díaz Díaz, D.; Fokin, V. V.; Finn, M. G. *J. Am. Chem. Soc.* **2007**, *129*, 12705; (c) Presolski, S. I.; Hong, V.; Cho, S. -H.; Finn, M. G. *J. Am. Chem. Soc.* **2010**, *132*, 14570.
- See for example: (a) Chan, T. R.; Hilgraf, R.; Sharpless, K. B.; Fokin, V. V. *Org. Lett.* **2004**, *6*, 2853; (b) Lewis, W. G.; Magallon, F. G.; Fokin, V. V.; Finn, M. G. *J. Am. Chem. Soc.* **2004**, *126*, 9152.
- (a) Liu, Y.; Díaz, D. D.; Accurso, A. A.; Sharpless, K. B.; Fokin, V. V.; Finn, M. G. *J. Polym. Sci., Part A: Polym. Chem.* **2007**, *45*, 5182; (b) Isobe, H.; Fujino, T.; Yamazaki, N.; Guillot-Nieckowski, M.; Nakamura, E. *Org. Lett.* **2008**, *10*, 3729.
- (a) Pérez-Balderas, F.; Ortega-Muñoz, M.; Morales-Sanfrutos, J.; Hernández-Mateo, F.; Calvo-Flores, F. G.; Calvo-Asín, J. A.; Isac-García, J.; Santoyo-González, F. *Org. Lett.* **2003**, *5*, 1951; (b) Moitra, N.; Moreau, J. J. E.; Cattoen, X.; Wong Chi Man, M. *Chem. Commun.* **2010**, *46*, 8416.

12. [CuBr(PPh<sub>3</sub>)<sub>3</sub>] and [CuI{P(OEt)}<sub>3</sub>] complexes have been considered the catalyst of choice for the preparation of glycopolymers, oligomers or more complicated biologically active molecules: (a) Marmuse, L.; Nepogodiev, S. A.; Field, R. A. *Org. Biomol. Chem.* **2005**, *3*, 2225; (b) Ladmíral, V.; Mantovani, G.; Clarkson, G. J.; Cauet, S.; Irwin, J. L.; Haddleton, D. M. *J. Am. Chem. Soc.* **2006**, *128*, 4823; (c) Parrish, B.; Emrick, T. *Bioconjug. Chem.* **2007**, *18*, 263; (d) Shen, J.; Woodward, R.; Kedenburg, J. P.; Liu, X. W.; Chen, M.; Fang, L. Y.; Sun, D. X.; Wang, P. G. *J. Med. Chem.* **2008**, *51*, 7417; (e) Kato, T.; Miyagawa, A.; Kasuya, M. C. Z.; Hatanaka, K. *Open Chem. Biomed. Methods J.* **2009**, *2*, 13; (f) Papin, C.; Doisneau, G.; Beau, J. M. *Chem. Eur. J.* **2009**, *15*, 53; (g) Méndez-Ardoy, A.; Gómez-García, M.; Ortiz-Mellet, C.; Sevillano, N.; Girón, M. D.; Salto, R.; Santoyo-González, F.; García Fernández, J. M. *Org. Biomol. Chem.* **2009**, *7*, 2681.
13. (a) Díez-González, S.; Correa, A.; Cavallo, L.; Nolan, S. P. *Chem. Eur. J.* **2006**, *12*, 7558; (b) Nolte, C.; Mayer, P.; Straub, B. F. *Angew. Chem. Int. Ed.* **2007**, *46*, 2101; (c) Sèverac, M.; Le Pleux, L.; Scarpaci, A.; Blart, E.; Odobel, F. *Tetrahedron Lett.* **2007**, *48*, 6518; (d) Díez-González, S.; Nolan, S. P. *Angew. Chem. Int. Ed.* **2008**, *47*, 8881; (e) Díez-González, S.; Stevens, E. D.; Nolan, S. P. *Chem. Commun.* **2008**, 4747; (f) Broggi, J.; Díez-González, S.; Petersen, J. L.; Berteina-Raboin, S.; Nolan, S. P.; Agrofoglio, L. A. *Synthesis* **2008**, 141; (g) Li, P. H.; Wang, L.; Zhang, Y. C. *Tetrahedron* **2008**, *64*, 10825; (h) Teyssot, M. L.; Chevry, A.; Traïkia, M.; El-Ghozzi, M.; Avignant, D.; Gautier, A. *Chem. Eur. J.* **2009**, *15*, 6322; (i) Pawar, G. M.; Bantu, B.; Weckesser, J.; Blechert, S.; Wurst, K.; Buchmeiser, M. R. *Dalton Trans.* **2009**, 9043; (j) Díez-González, S.; Escudero-Adan, E. C.; Benet-Buchholz, J.; Stevens, E. D.; Slawin, A. M. Z.; Nolan, S. P. *Dalton Trans.* **2010**, *39*, 7595; (k) Teyssot, M. L.; Nauton, L.; Canet, J. -L.; Cisnetti, F.; Chevry, A.; Gautier, A. *Eur. J. Org. Chem.* **2010**, 3507.
14. (a) Shai, C.; Cheng, G.; Su, D.; Xu, J.; Wang, X.; Hu, Y. *Adv. Synth. Catal.* **2010**, *352*, 1587–1592; (b) Gonda, Z.; Novák, Z. *Dalton Trans.* **2010**, *39*, 726.
15. For recent reviews on well-defined copper(I) complexes, see: (a) Díez-González, S. *Catal. Sci. Technol.* **2011**, *1*, 166; (b) Díez-González, S. *Curr. Org. Chem.* **2012**, *15*, 2830.
16. For a review on CuAAC reactions in organic media including mechanistic discussions, see: Hein, J. E.; Fokin, V. V. *Chem. Soc. Rev.* **2010**, *39*, 1302.
17. Cassidy, M. P.; Rauschel, J.; Fokin, V. V. *Angew. Chem. Int. Ed.* **2006**, *45*, 3154.
18. Okzal, E.; Özçubukcu, S.; Jimeno, C.; Pericàs, M. *Catal. Sci. Technol.* **2012**, *2*, 195.
19. Rodionov, V. O.; Fokin, V. V.; Finn, M. G. *Angew. Chem. Int. Ed.* **2005**, *44*, 2210.
20. (a) Bai, S. -Q.; Koh, L.; Hor, T. S. A. *Inorg. Chem.* **2009**, *48*, 1207; (b) Li, F.; Hor, T. S. A. *Chem. Eur. J.* **2009**, *15*, 10585.
21. Cho, S. H.; Chang, S. *Angew. Chem. Int. Ed.* **2007**, *46*, 1897.
22. Asano, K.; Matsubara, S. *Org. Lett.* **2010**, *12*, 4988.
23. (a) Wang, F.; Fu, H.; Jiang, Y. Y.; Zhao, Y. F. *Adv. Synth. Catal.* **2008**, *350*, 1830; (b) Wang, F.; Fu, H.; Jiang, Y. Y.; Zhao, Y. F. *Green Chem.* **2008**, *10*, 452.
24. Lal, S.; McNally, J.; White, A. J. P.; Díez-González, S. *Organometallics* **2011**, *30*, 6225.
25. (a) Díez-González, S.; Marion, N.; Nolan, S. P. *Chem. Rev.* **2009**, *109*, 3612; (b) Samojlowicz, C.; Bieniek, M.; Grela, K. *Chem. Rev.* **2009**, *109*, 3708.
26. Gaulier, C.; Hospital, A.; Legeret, B.; Delmas, A. F.; Aucagne, V.; Cisnetti, F.; Gautier, A. *Chem. Commun.* **2012**, *48*, 4005.
27. (a) Wu, Y. M.; Deng, J.; Fang, X.; Chen, Q. Y. *J. Fluorine Chem.* **2004**, *125*, 1415; (b) Yan, Z. Y.; Zhao, Y. B.; Fan, M. J.; Liu, W. M.; Liang, Y. M. *Tetrahedron* **2005**, *61*, 9331; For other monodentate amines see: (c) Hasegawa, T.; Umeda, M.; Numata, M.; Fujisawa, T.; Haraguchi, S.; Sakurai, K.; Shinkai, S. *Chem. Lett.* **2006**, *35*, 82; (d) Kalesh, K. A.; Liu, K.; Yao, S. Q. *Org. Biomol. Chem.* **2009**, *7*, 5129.
28. Özçubukçu, S.; Ozkal, E.; Jimeno, C.; Pericàs, M. A. *Org. Lett.* **2009**, *11*, 4680.
29. García-Álvarez, J.; Díez, J.; Gimeno, J. *Green Chem.* **2010**, *12*, 2127.
30. (a) Himo, F.; Lovell, T.; Hilgraf, R.; Rostovtsev, V. V.; Noddleman, L.; Sharpless, K. B.; Fokin, V. V. *J. Am. Chem. Soc.* **2005**, *127*, 210; (b) Bock, V. D.; Hiemstra, H.; van Maarseveen, H. *Eur. J. Org. Chem.* **2006**, *51*; (c) Buckley, B. R.; Dann, S. E.; Heaney, H. *Chem. Eur. J.* **2010**, *16*, 6278.
31. Nevertheless, it has been reported that Cu(I) catalyst [CuBr(SIMes)] and **5•CuCl** can mediate the reaction of benzyl azide and 3-hexyne (see Refs 13a and 28, respectively).
32. However, ruthenium mediated cycloaddition reactions of azides and internal alkynes in organic media have been already reported by Fokin and coworkers. In this case, the Ru-catalyzed triazole annulations proceed through the usual alkyne oligomerization sequence which involves (i) the oxidative coupling of an alkyne and an azide on ruthenium, giving rise to a six-membered ruthenacycle, (ii) subsequent rate-determining reductive elimination, releasing the aromatic triazole product. Zhang, L.; Chen, X.; Xue, P.; Sun, H. H. Y.; Williams, I. D.; Sharpless, K. B.; Fokin, V. V.; Jia, G. *J. Am. Chem. Soc.* **2005**, *127*, 15998. See also Ref. 3b.
33. 5-Bromo and 5-iodotriazoles can be accessible through one-pot cycloaddition/halogenations: (a) Wu, Y.-M.; Deng, J.; Li, Y.; Chen, Q.-Y. *Synthesis* **2005**, 1314; (b) Li, L.; Zhang, G.; Zhu, A.; Zhang, L. *J. Org. Chem.* **2008**, *73*, 3630; (c) Smith, N. W.; Polenz, B. P.; Johnson, S. B.; Dzyuba, S. V. *Tetrahedron Lett.* **2010**, *51*, 550; Also, these 5-halogenated-triazoles can be easily synthesized via cycloaddition of halogenated alkynes: (d) Kuijpers, B. H. M.; Dijkmans, G. C. T.; Groothuys, S.; Quaedflieg, P. J. L. M.; Blaauw, R.

- H.; van Delft, F. L.; Rutjes, F. P. J. T. *Synlett* **2005**, 3059; (e) Hein, J. E.; Tripp, J. C.; Krasnova, L. B.; Sharpless, K. B.; Fokin, V. V. *Angew. Chem. Int. Ed.* **2009**, *48*, 8018; (f) Panteleev, J.; Geyer, K.; Aguilar-Aguilar, A.; Wang, L.; Lautens, M. *Org. Lett.* **2010**, *12*, 5092; (g) Juriček, M.; Stout, K.; Kouwer, P. H. J.; Rowan, A. E. *Org. Lett.* **2011**, *13*, 3494; (h) Bogdan, A.; James, K. *Org. Lett.* **2011**, *13*, 4060; (i) Schwartz, E.; Breitenkamp, K.; Fokin, V. V. *Macromolecules* **2011**, *44*, 4735.
34. 1,4-Disubstituted triazoles can be functionalized through the palladium- or copper-catalyzed direct arylation with arylhalides: (a) Chuprakov, S.; Chernyak, N.; Dudnik, A. S.; Gevorgyan, V. *Org. Lett.* **2007**, *9*, 2333; (b) Basolo, L.; Beccalli, E. M.; Borsini, E.; Broggini, G.; Pellegrino, S. *Tetrahedron* **2008**, *64*, 8182; (c) Ackermann, L.; Potukuchi, H. K.; Landsberg, D.; Vicente, R. *Org. Lett.* **2008**, *10*, 3081; (d) Ackermann, L.; Vicente, R. *Org. Lett.* **2009**, *11*, 4922; Alternatively, 1,4,5-trisubstituted triazoles can be easily synthesized via a dehydrogenative intramolecular coupling recently described by the Ackermann group: (e) Ackermann, L.; Jeyachandran, R.; Potukuchi, H. K.; Novák, P.; Büttner, L. *Org. Lett.* **2010**, *12*, 2056.
35. Buckley, B. R.; Dann, S. E.; Heaney, H.; Stubbs, E. C. *Eur. J. Org. Chem.* **2011**, 770.
36. Scriven, E. F. V.; Turnbull, K. *Chem. Rev.* **1988**, 88, 297.
37. For recent examples in the three-component synthetic methodologies in organic solvents see: (a) Kamijo, S.; Jin, T.; Huo, Z.; Yamamoto, Y. *J. Am. Chem. Soc.* **2003**, *125*, 7786; (b) Kamijo, S.; Jin, T.; Yamamoto, Y. *Tetrahedron Lett.* **2004**, *45*, 689; (c) Kamijo, S.; Jin, T.; Huo, Z.; Yamamoto, Y. *J. Org. Chem.* **2004**, *69*, 2386; (d) Appukuttan, P.; Dehaen, W.; Fokin, V. V.; Van der Eycken, E. *Org. Lett.* **2004**, *6*, 4223; (e) Kacpraz, K. *Synlett* **2005**, 943; (f) Miao, T.; Wang, L. *Synthesis* **2008**, 363; (g) Yan, Z. -Y.; Wang, L. *Synthesis* **2010**, 447.
38. Wang, W.; Wu, J.; Xia, C.; Li, F. *Green Chem.* **2011**, *13*, 3440.
39. Lal, S.; Díez-González, S. *J. Org. Chem.* **2011**, *76*, 2367.
40. García-Álvarez, J.; Díez, J.; Gimeno, J.; Suárez, F. J.; Vincent, C. *Eur. J. Inorg. Chem.* **2012**, 5854.

---

## ORGANOGLD CATALYSIS: HOMOGENEOUS GOLD-CATALYZED TRANSFORMATIONS FOR A GOLDEN JUBILEE

FABIEN GAGOSZ

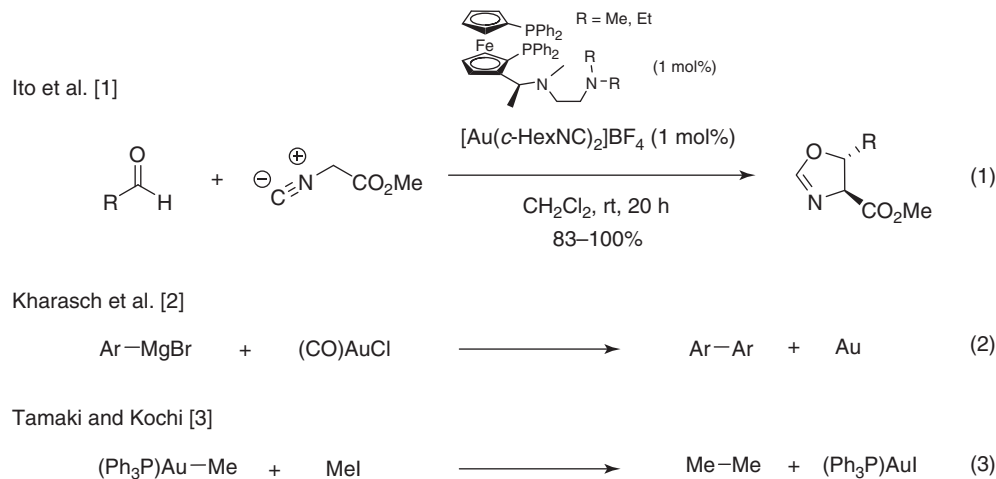
*Ecole Polytechnique, Laboratoire de Synthèse Organique (DCSO), Palaiseau, France*

### 16.1 INTRODUCTION

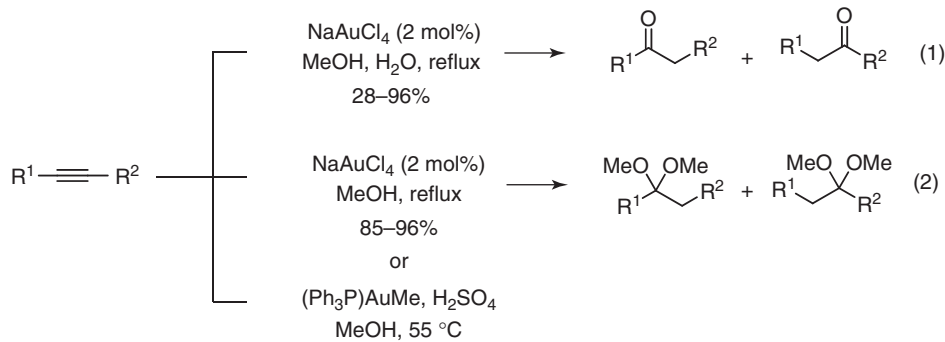
After having been ignored by several generations of synthetic chemists for its supposed scarcity, high price, and chemical inertness, gold has been recently reconsidered as a potentially interesting metal for the design of catalysts that might useful in organic synthesis. The birth of gold catalysis in synthetic organic chemistry is generally associated with the elegant work of Ito et al. [1], who reported in 1986 an efficient procedure for the formation of oxazolines by a gold(I)-catalyzed asymmetric addition of an isocyanoacetate to an aldehyde (Scheme 16.1, Eq. 1). However, it should also be noticed that a series of other less common synthetic transformations involving the use of an organogold compound or a gold complex in a stoichiometric amount had been previously described. The formation of biaryls by reaction of an aromatic Grignard reagent in the presence of  $(CO)AuCl$  reported in 1930 by Kharasch et al. [2] (Scheme 16.1, Eq. 2), or the formation of ethane from  $(Ph_3P)AuMe$  and iodomethane described by Tamaki and Kochi [3] in 1974 (Scheme 16.1, Eq. 3) are examples of such kinds of transformations.

An important breakthrough was made between 1991 and 2000 when Utimoto et al. and Teles et al. first reported that alkynes could be functionalized by an inter- or intramolecular addition of water, alcohols, and amines in the presence of a gold(III) salt or a cationic gold(I) complex (Scheme 16.2, Eqs. 1–3) [4]. This significant advance was followed by the work of Hashmi et al. [5] who demonstrated in 2000 that  $AuCl_3$  could be used as an efficient catalyst for the intramolecular addition of ketones and alcohols to alkynes and for the inter- or intramolecular arylation of alkynes and allenes (Scheme 16.2, Eqs. 4 and 5).

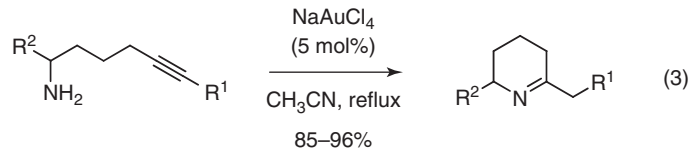
These seminal studies definitely set the foundation for the great majority of the developments that have been made so far in the field of homogeneous gold catalysis. After the use of gold in catalysis had been initially considered as a potential “Eldorado” for synthetic chemists [6], a true “gold rush” [7] took place during the last 10 years. The plethora of studies carried out during this period, mainly on the design of new gold catalysts, the exploration of their reactivity, the development of gold-catalyzed transformations, and their applications in synthesis, have established homogeneous gold catalysis as a viable, efficient, and selective tool for modern synthetic chemistry. One of the most striking and early reported examples of the use of homogeneous gold catalysis, which perfectly highlights its interest in synthesis, can be found in the total synthesis of Azadirachtin by Ley et al. Indeed, the synthetic route employed to access the target molecule features an impressive gold-catalyzed Claisen rearrangement that allows the efficient and selective formation of an allenyl ketone from a propargylic enol ether under mild experimental conditions (Scheme 16.3).

**Scheme 16.1** Early examples in organogold chemistry.

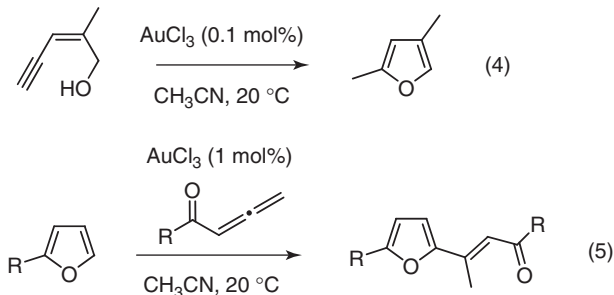
Utimoto et al. (1991) and Teles et al. (1998)

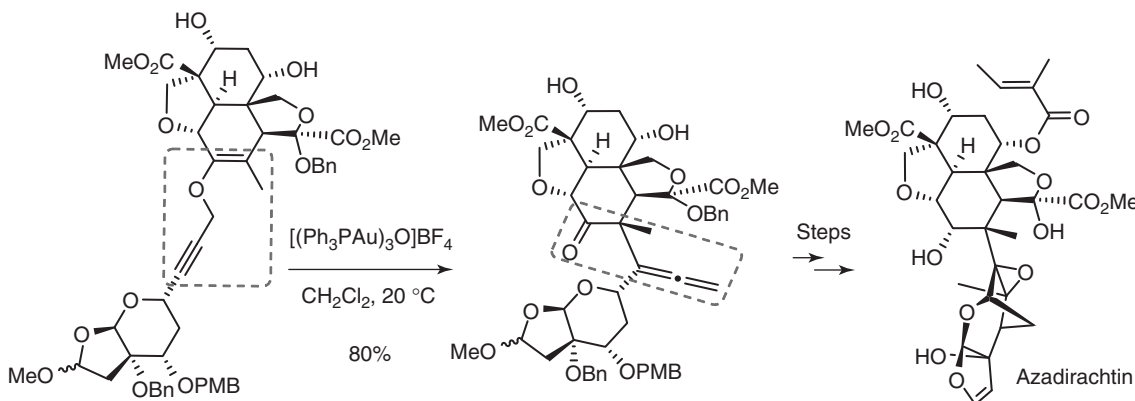


Utimoto et al. (1991)



Hashmi et al. (2000)

**Scheme 16.2** Birth of gold catalysis.



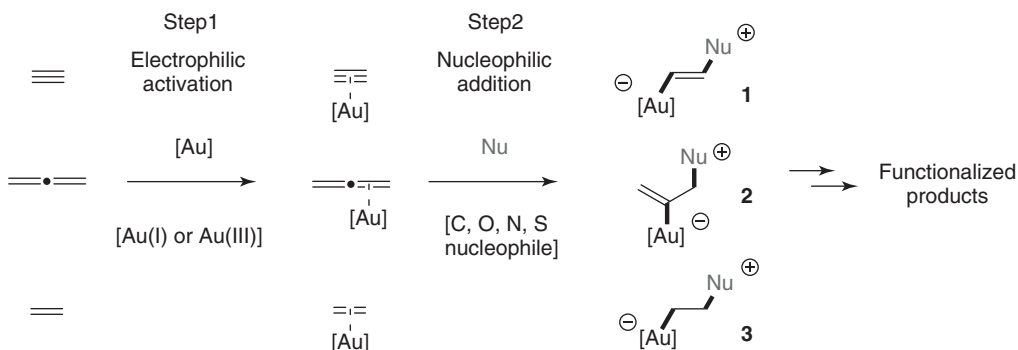
**Scheme 16.3** Total synthesis of Azadirachtin by Ley et al.

The aim of this chapter is not to summarize all the work that has been carried out up to date. Since the field has been largely and continuously reviewed [8], the following sections will preferentially highlight representative aspects of homogeneous gold catalysis that would allow the reader to have a brief overview of its synthetic potential.

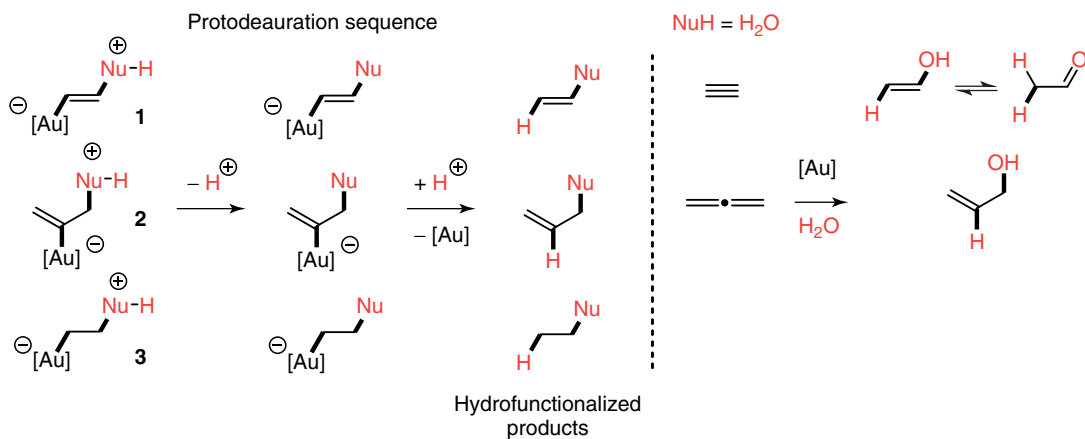
## 16.2 ELECTROPHILIC GOLD SPECIES: PRINCIPLE AND MAIN MODES OF REACTIVITY

The greatest part of the chemistry that has been developed so far in the so-called field of modern gold catalysis is based on the Lewis acid properties of a wide variety of gold(I) and gold(III) species. The pronounced Lewis acidic character of these species originates from the relativistic effects, which are particularly significant in the case of heavy elements such as gold. The lowest unoccupied molecular orbital is indeed relatively low owing to the relativistic contraction of the 6s orbital of gold. From a reactivity point of view, gold(I) and gold(III) species have the aptitude to selectively activate multiple carbon–carbon bonds such as alkynes, allenes, or alkenes (Scheme 16.4, step 1) toward their functionalization by addition of a large variety of nucleophiles comprising oxygen, nitrogen, carbon, or even sulfur species (Scheme 16.4, step 2). The addition step generally operates in an *anti* manner with respect to the activation of the unsaturation by the gold catalyst. It should also be noted that gold(III) species can be less selective than gold(I) ones as the latter are also able to competitively activate carbonyl derivatives such as ketones or aldehydes.

The intermediate aurate species **1–3** can then evolve following different pathways. These can sometimes be extremely complex as cascade reactions, intermolecular trapping, coupling reactions, etc. can occur on the path to the final functionalized products. The simplest mechanistic scenario is found when the nucleophile (Nu) bears a hydrogen atom (Scheme 16.5). The catalytic cycle is terminated in this case by a formal gold to hydrogen exchange (so-called protodeauration sequence) that finally leads to products of hydrofunctionalization. This pathway is exemplified by the gold-catalyzed reaction of alkynes and allenes with water leading respectively to ketones and alcohols.

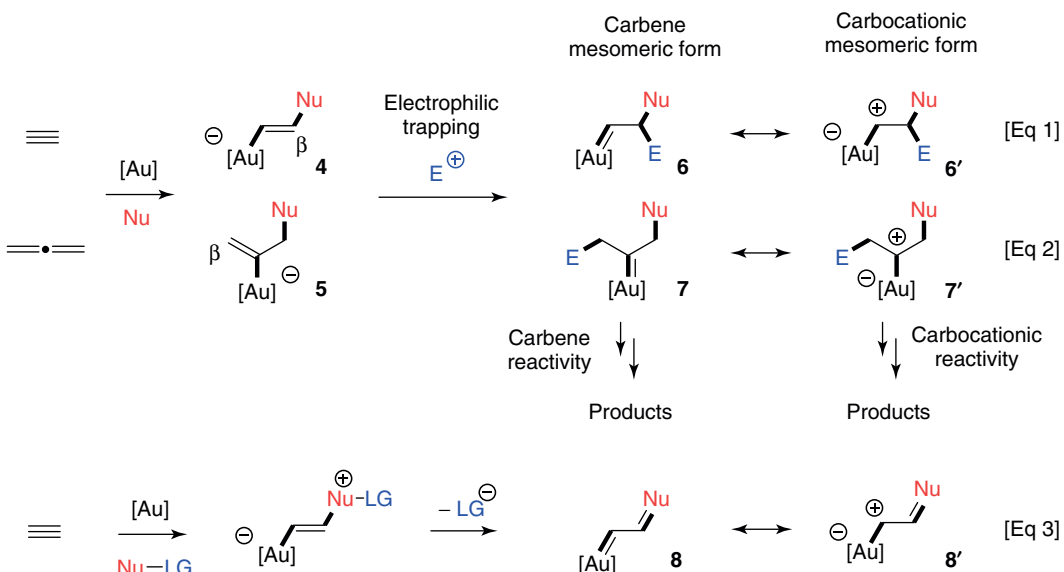


**Scheme 16.4**

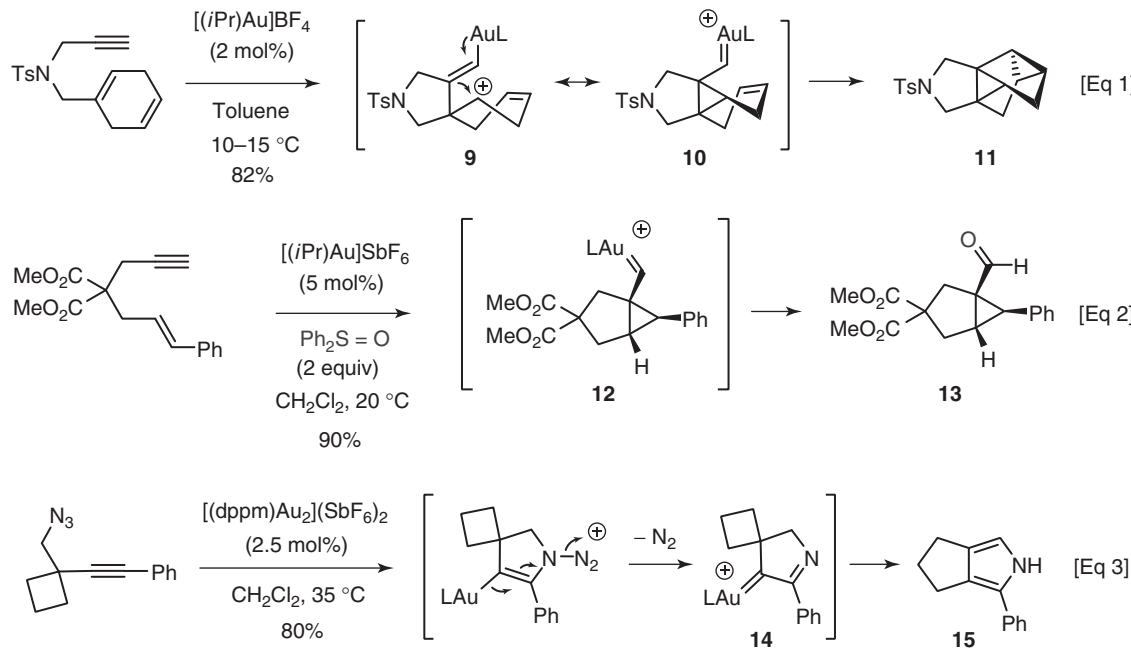


Scheme 16.5 (See insert for color representation of the figure.)

It is important to point out that the reactivity of gold catalysts is not limited to their Lewis acid properties. Complementary to some other electrophilic metallic species that can also activate  $\pi$ -systems toward nucleophilic functionalization, gold has also the capacity to act as an electron donor and help stabilize the cationic intermediates. This singular behavior is an indirect consequence of the relativistic effects [8z]. Since the 6s orbital is contracted, the electrons of the 5d orbital are weakly attracted by the nucleus (due to a shielding effect) and can therefore delocalize. As a result, aurate intermediates of type **4** or **5**, which result from the nucleophilic functionalization of an alkyne or an allene respectively, can undergo an electrophilic trapping at the carbon  $\beta$  to gold to furnish the new “gold carbene” intermediates **6** and **7** (Scheme 16.6, Eqs. 1 and 2). It should however be noted that the terminology “gold carbene” only accounts for the possibility for gold to act as an electron donor stabilizing a carbocationic form and does not imply that intermediates **6** and **7** should have a carbene reactivity. Structures **6** and **6'** (**7** and **7'**) should be seen as extreme mesomeric forms of the same intermediate [9]. The carbene versus carbocationic reactivity is dependent on various parameters, among which are the substrate substitution pattern, the nature of the catalyst and its potential ligand, the nature of the carbene-trapping agent, and the nature of the solvent [10]. The capacity for gold to release some electron density has also been highlighted in a series of transformations involving the use of nucleophiles possessing a leaving group (LG) (Scheme 16.6, Eq. 3). In this case, gold carbenes of type **8** have been proposed as intermediates.



Scheme 16.6 (See insert for color representation of the figure.)



**Scheme 16.7** Examples of transformation taking advantage of the dual Lewis acid/electron donor properties of gold.

A series of representative synthetic transformations taking advantage of this dual Lewis acid/electron donor properties of gold are presented in Scheme 16.7 (further examples are presented in the following sections).

In the first example, reported by the group of Chung [11], one of the unsaturations of the 1,4-cyclohexadiene moiety serves as the nucleophile to produce, in the presence of a gold(I) catalyst, an intermediate homoallylic carbocation **9**. This latter is stabilized by electron donation from gold as the gold carbene mesomeric form **10**, which is then trapped by the second endocyclic alkene to finally produce the structurally complex polycyclic compound **11**. As seen in the second example, the same kind of gold carbene intermediate **12** could be trapped in an intermolecular manner by a sulfoxide to generate the cyclopropylcarboxaldehyde derivative **13** [12]. The last example, reported by the group of Toste [13], involves the use of an azide as the nucleophile, which, after addition to the gold-activated alkyne and extrusion of dinitrogen (favored by electron donation from gold), affords an intermediate  $\alpha$ -imino gold carbene **14**. A sequence of ring expansion and tautomerization produces the bicyclic pyrrole **15**.

### 16.3 GOLD CATALYSTS

A great variety of catalytic systems have proven to be efficient in gold catalysis, even if none can be considered as completely general. The choice of the catalytic system indeed strongly depends on the synthetic transformation that has to be performed. The nature of the catalytic systems can vary according to different criteria: (i) the oxidation level of the metal ( $\text{Au(I)}$ ,  $\text{Au(III)}$ ), (ii) the presence of ligands and their nature, and (iii) the nature of the counteranion. A distinction can also be made regarding the way the catalytically active species is introduced or generated in the reaction medium.

It should also be pointed out that gold catalysts possess a series of interesting properties that render them easy to use and handle: they are generally insensitive to oxygen (and are, by the way, difficult to oxidize) and are compatible with the use of aqueous or alcoholic media. They are also considered to be nontoxic, especially when compared to other  $\pi$ -Lewis acidic species, such as mercury salts, which can be used to accomplish similar transformations.

The main catalytic systems used in gold catalysis are presented in the following sections.

#### 16.3.1 Inorganic Gold Catalysts

Several simple inorganic salts (Scheme 16.8) have been reported as efficient catalysts in a series of synthetic transformations. They are however less commonly used than gold complexes (see Section 16.3.2) and gold(III) salts are more generally

<u>Gold(III) salts:</u>				<u>Gold(I) salts:</u>	
AuCl <sub>3</sub>	AuBr <sub>3</sub>	HAuCl <sub>4</sub>	NaAuCl <sub>4</sub>	KAuCl <sub>4</sub>	AuCl

**Scheme 16.8** Examples of gold salts used as catalysts.

employed than gold(I) salts. It should also be noted that these salts are poorly soluble in noncoordinating solvents and that the great majority are highly hygroscopic. They can also be employed, in the case of gold(III) halides, in combination with a silver salt, such as AgSbF<sub>6</sub> or AgOTf.

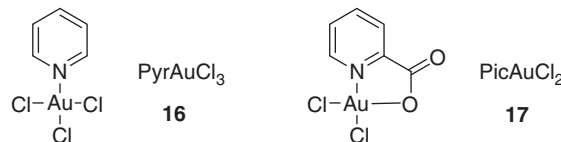
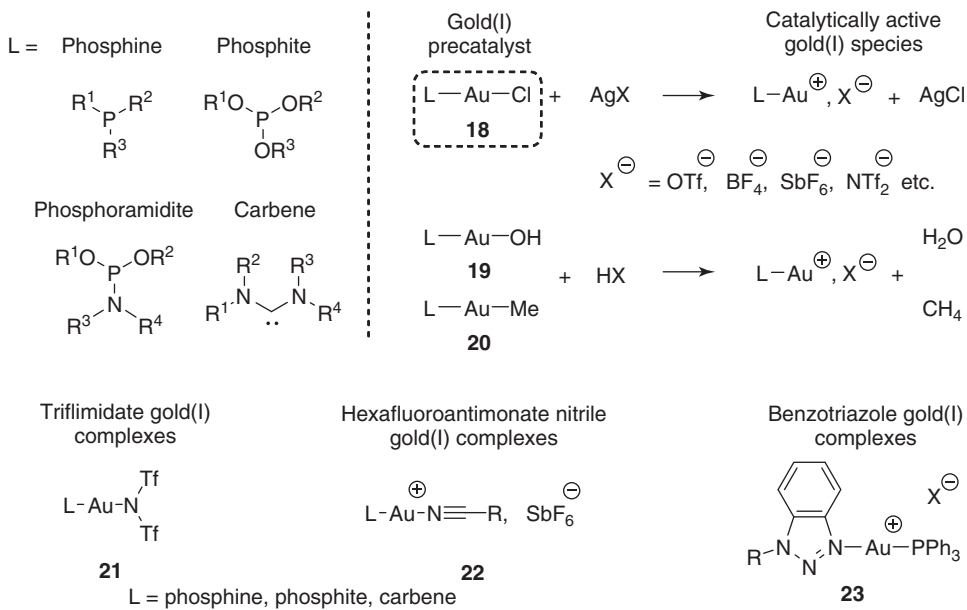
### 16.3.2 Families of Gold(I) and Gold(III) Complexes as Catalysts

Gold complexes, and more especially gold(I) complexes, are by far the most employed catalytic systems. The presence of one or several ligands on the metal center can indeed help to modulate the reactivity of the catalysts (modulation of its Lewis acidic character and/or electron back donation) and optimize its properties for a given transformation [10].

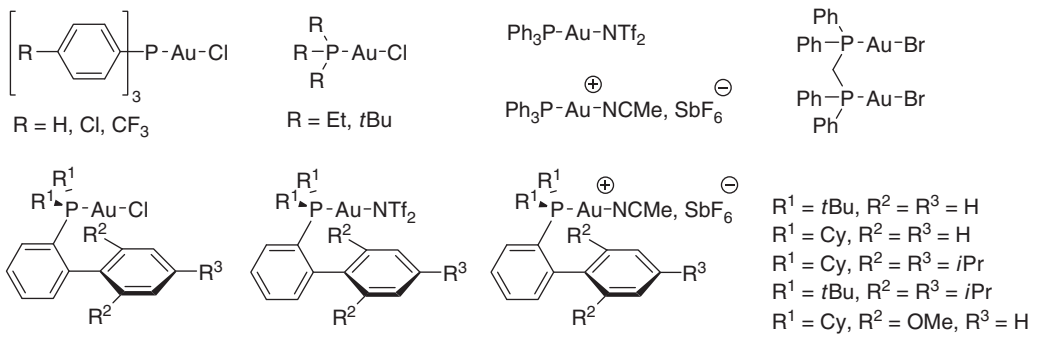
Gold(III) complexes are relatively scarce and the most commonly employed possess a pyridine or a pyridine derivative as ligand, as in PyrAuCl<sub>3</sub> **16** or PicAuCl<sub>2</sub> **17** (Scheme 16.9) [14].

Gold(I) complexes are much more varied, and complexes of type L-Au-Cl **18**, where L represents a ligand, are the most frequently employed (Scheme 16.10). They can be classified depending on the nature of this ligand L, which can be a phosphine, a phosphite, a phosphoramidite, or a carbene.

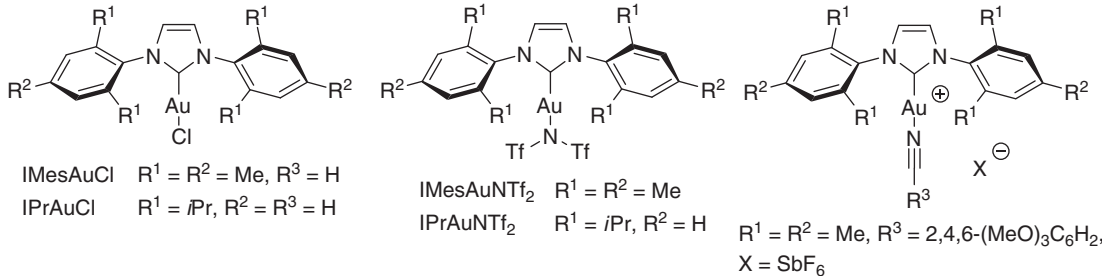
Complexes of type **18** are precatalysts that are generally employed in combination with a silver salt such as AgOTf, AgBF<sub>4</sub>, AgSbF<sub>6</sub>, and AgNTf<sub>2</sub> in order to generate *in situ* a more electrophilic gold species by anion exchange. Besides complexes of type L-Au-Cl **18**, L-Au-OH **19**, or L-Au-Me **20** can also be used as precatalysts. In this case, they are used in

**Scheme 16.9** Examples of gold(III) complexes used as catalysts.**Scheme 16.10** Gold(I) complexes.

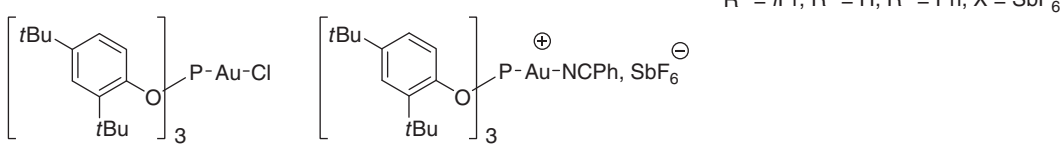
## Phosphine gold(I) complexes:



## NHC gold(I) complexes:



## Phosphite gold(I) complexes:

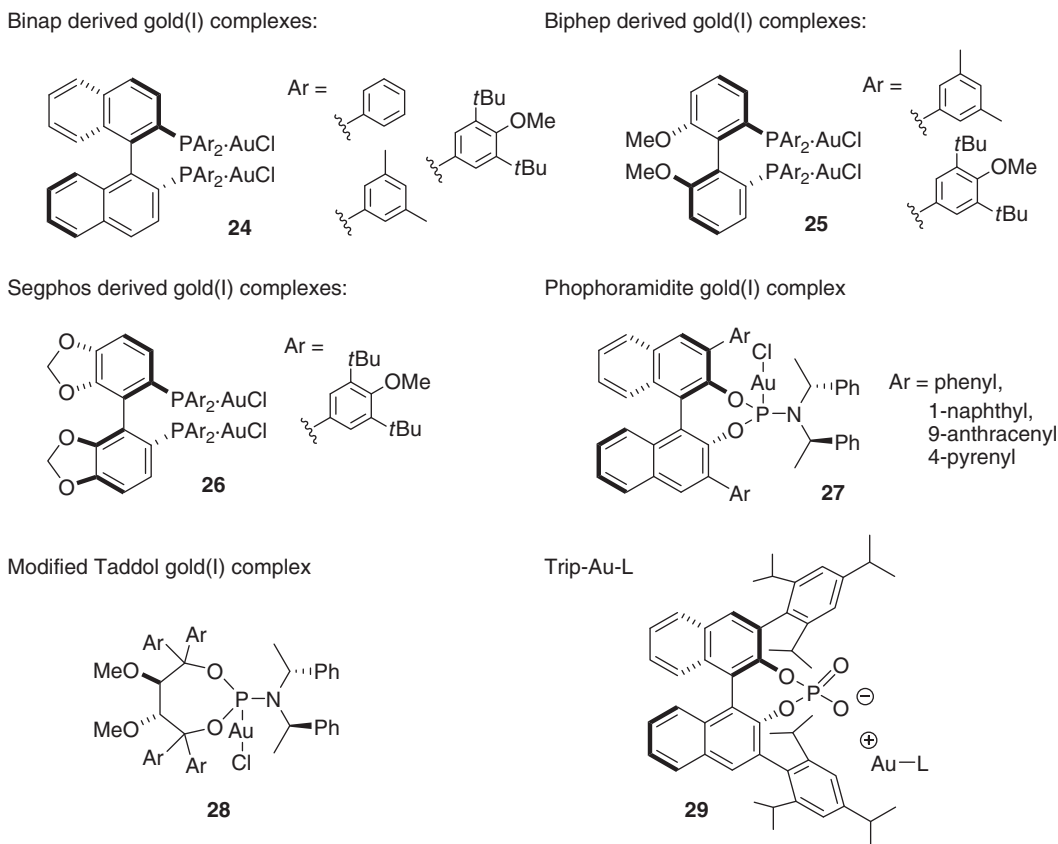


Scheme 16.11 Examples of gold(I) complexes used as catalysts or precatalysts.

combination with a strong Brønsted acid, such as triflic acid to generate the active species. Notably, three different classes of gold catalysts that do not necessitate the use of a cocatalyst (silver salt or Brønsted acid) and are air and moisture stable have been developed: the triflimidate gold(I) complexes **21**, the hexafluoroantimonate nitrile gold(I) complexes **22**, and the benzotriazole gold(I) complexes **23**. A collection of various gold(I) complexes commonly used as precatalysts or catalysts are presented in Scheme 16.11 [15].

## 16.3.3 Chiral Gold Catalysts

Compared to nonasymmetric gold catalysts (Section 16.3.2), chiral gold catalysts are relatively rare even if the last 5 years have seen a growing interest in their development and use [8f,n]. The asymmetric catalytic systems reported so far are nearly all based on the use of a gold(I) metallic center. Their relative scarcity should be linked to the preferential linear arrangement of gold(I) complexes that is not propitious to the transfer of stereochemical information from an asymmetric ligand to the reacting center (gold(I)-coordinated substrate) (see Section 16.9). A series of asymmetric precatalytic systems are presented in Scheme 16.12 [16]. Most dinuclear gold(I) complexes possess a Binap (**24**), a Biphep (**25**), or a Segphos (**26**) backbone. A few others are based on the use of a phosphoramidite ligand whose backbone is derived from Binol (**27**) or Taddol (**28**). Besides employing catalytic systems that possess a bulky asymmetric ligand to efficiently relay the chiral information, another strategy has been developed by the group of Toste in order to circumvent the problems linked to the linear arrangement of gold(I) complexes. In this alternative strategy, a chiral Binol-derived phosphonate (**29**), which can form a close ion pair with the gold–ligand complex, is employed as the counteranion.



**Scheme 16.12** Examples of chiral precatalytic or catalytic systems.

## 16.4 GOLD-CATALYZED ACTIVATION OF MULTIPLE CARBON–CARBON BONDS: FUNCTIONALIZATION BY ADDITION OF OXYGEN, NITROGEN, SULFUR, OR CARBON NUCLEOPHILES

A large array of nucleophiles has been used in electrophilic gold catalysis in order to functionalize  $\pi$ -systems such as alkynes, alenes, and alkenes. The following sections portray some typical synthetic transformations that are classified as a function of the nature of the nucleophile.

### 16.4.1 C–O Bonds Formation

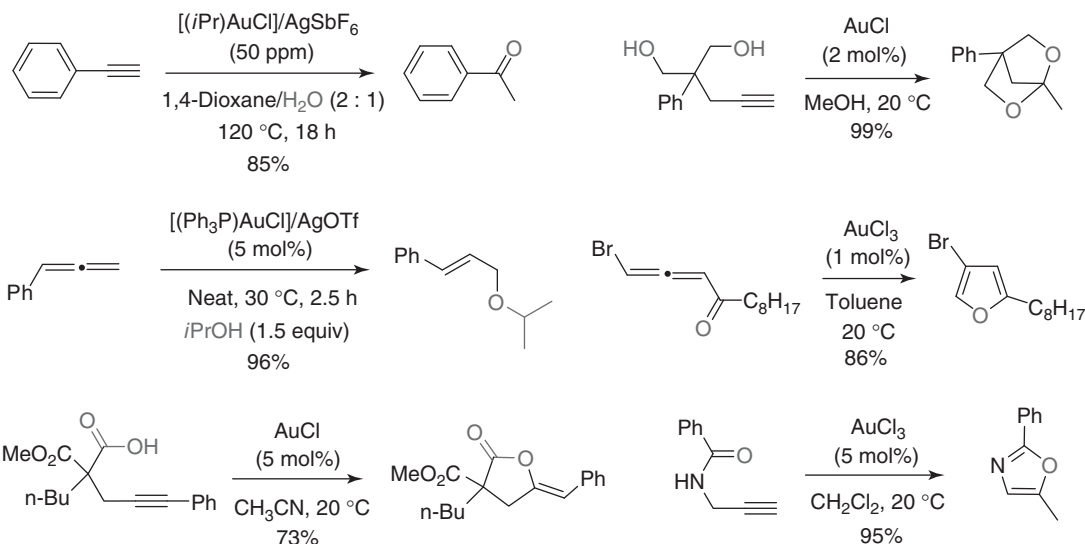
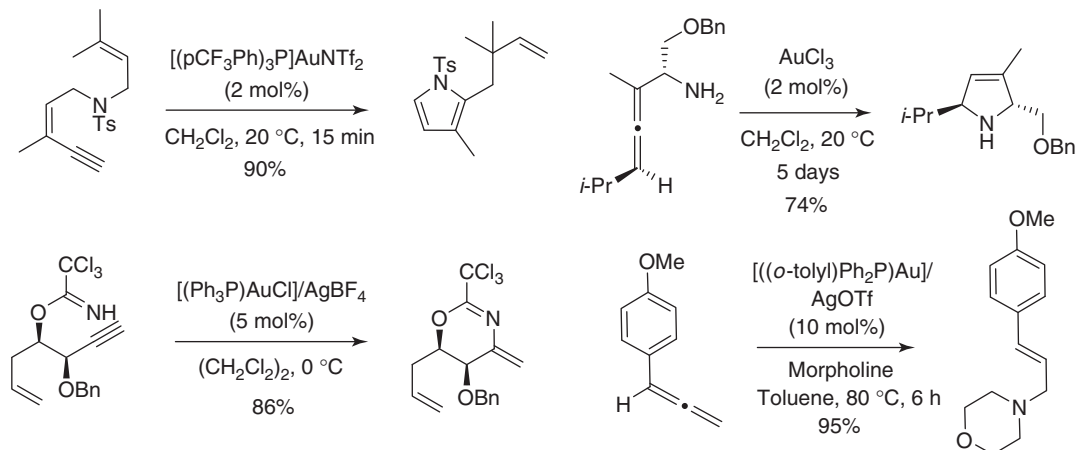
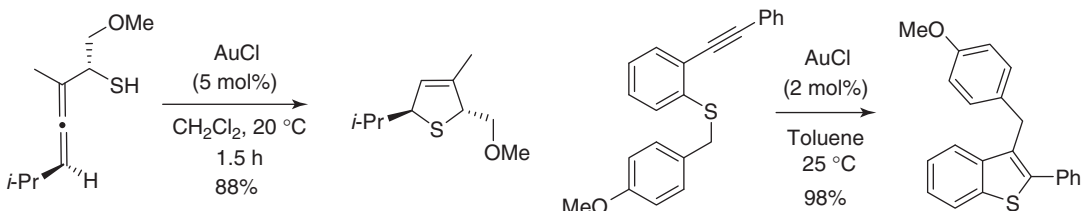
Various oxygen nucleophiles such as water, alcohols, carboxylic acids, ketones, aldehydes, carbonates, amides, have been employed in gold catalysis to functionalize alkynes, alenes, or even alkenes [8]. Their use allows the easy and generally efficient creation of at least one new C–O bond. A short selection of representative examples is shown in Scheme 16.13 [17].

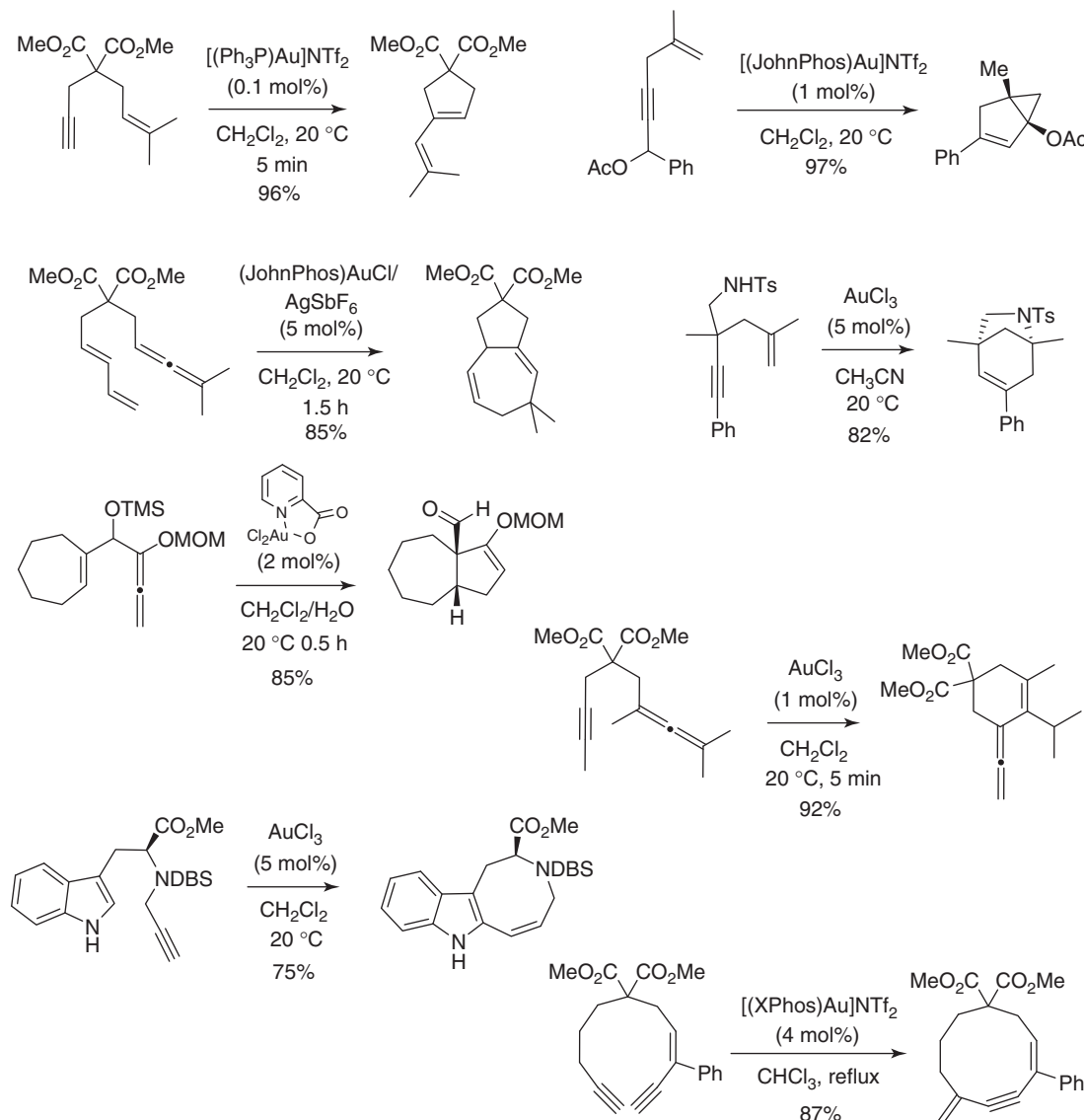
### 16.4.2 C–N Bonds Formation

Nitrogen nucleophiles have also proven to be suitable nucleophiles in a series of gold-catalyzed reactions, as exemplified by the transformations shown below (Scheme 16.14) [18, 17c]. The great majority of the reactions deal with the formation of nitrogen-containing heterocycles.

### 16.4.3 C–S Bonds Formation

While sulfur derivatives are generally considered as being poisonous for gold, they have nevertheless been successfully used in several gold-catalyzed transformations (Scheme 16.15) [19]. Their number remain however very limited when compared to reactions involving oxygen or nitrogen nucleophiles.

**Scheme 16.13** Examples of gold-catalyzed C–O bonds formation.**Scheme 16.14** Examples of gold-catalyzed C–N bonds formation.**Scheme 16.15** Examples of gold-catalyzed C–S bonds formation.

**Scheme 16.16** Examples of gold-catalyzed cycloisomerizations.

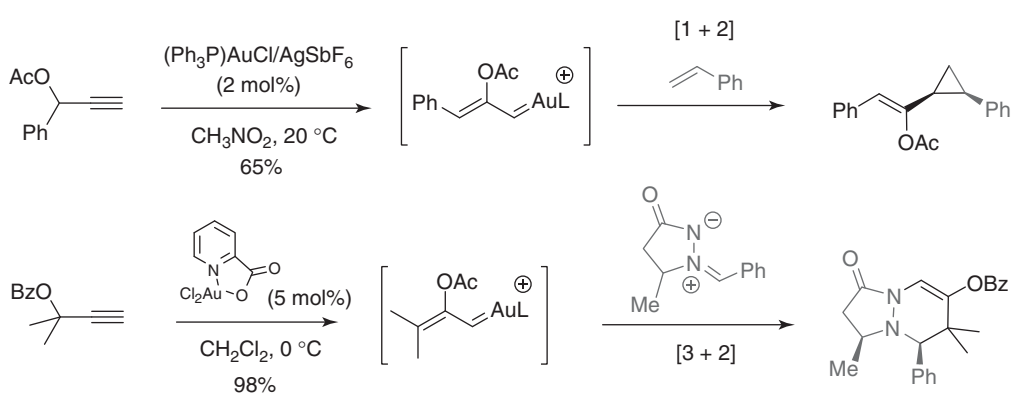
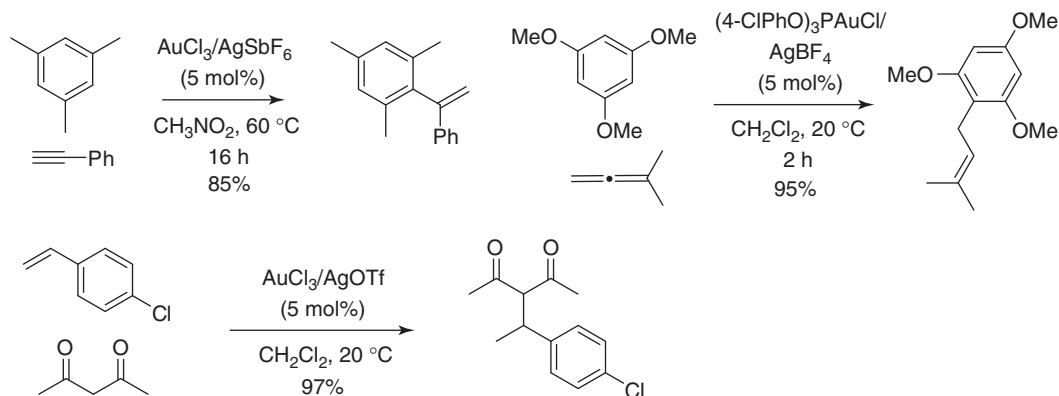
#### 16.4.4 C–C Bonds Formation

The development of new procedures for the creation of C–C bonds is of major importance in organic synthesis. In this respect, gold catalysis has emerged as a very efficient synthetic tool, allowing the generally easy and efficient formation of such bonds by addition of various carbone nucleophiles onto alkynes, allenes, and alkenes. These transformations, which can be performed in an intra- or intermolecular manner, are extremely varied. It should however be noted that the cycloisomerization of ene-ynes, diene-ynes, or ene-allenes remains the most frequently encountered. A very short selection of such transformations is presented in Scheme 16.16 [15g,k, 20].

Besides alkenes, several other carbon nucleophiles, as for instance, diketones and aryl groups, can participate in gold-catalyzed reactions. Selected examples of intermolecular reactions are displayed in Scheme 16.17 [17c, 21].

#### 16.5 INTERMOLECULAR TRAPPING OF REACTIVE ORGANOGOLD INTERMEDIATES

A certain number of aurated intermediates, arising from the initial addition of a nucleophile to a gold-activated  $\pi$ -system, can be trapped in the presence of an external reagent. This is typically the case when propargylic esters are used as the



substrates. In the presence of a gold catalyst, propargylic esters can indeed lead to the formation of reactive gold carbenoid intermediates that can be subsequently intercepted. Two representative examples, in which either an alkene or an azomethine imine is used as the trapping agent, are pictured in Scheme 16.18 [22].

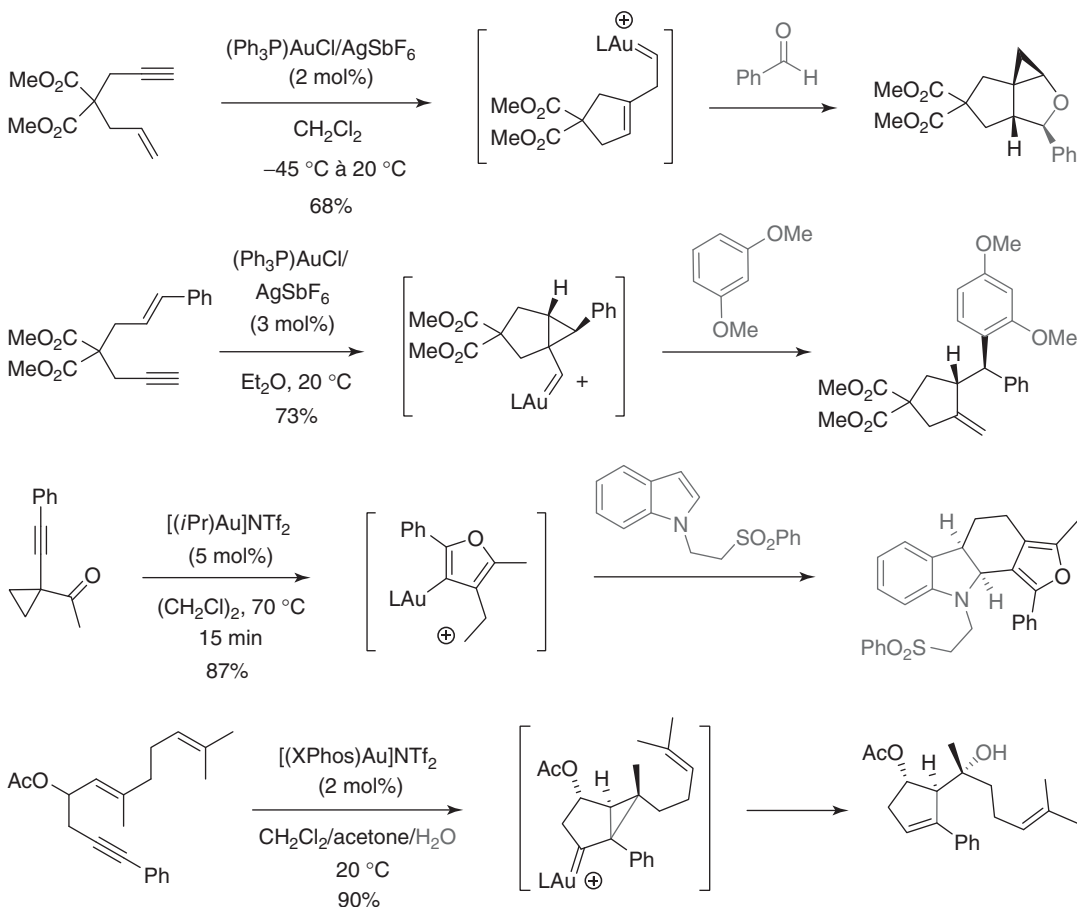
A series of other structurally different cationic intermediates, generated following a gold-catalyzed cyclization step, are also susceptible to be trapped by an oxygen, nitrogen, or even carbon-centered nucleophile (Scheme 16.19) [23].

## 16.6 OXENE AND NITRENE PRECURSORS AS NUCLEOPHILES

As mentioned in Section 16.2, gold-activated alkynes can react with a special family of nucleophiles of type Nu-LG (Nu, nucleophilic moiety; LG, leaving group) in order to generate vinylgold intermediates **30** and gold carbenoid species **31** that can evolve following different pathways in the presence of a nucleophilic trapping agent (Scheme 16.20). These unusual gold intermediates are accessible using oxene or nitrene precursors, such as pyridine oxide, nitrones, sulfoxide, nitro derivatives (for oxenes), or azides (for nitrenes), as the nucleophiles. Reactions involving these species are typical of gold catalysis and can be performed in an inter- or intramolecular manner to produce a broad variety of compounds as demonstrated by the examples depicted in Scheme 16.20 [24].

## 16.7 COUPLING REACTIONS

Even if it is known that gold(I) species are not prone to oxidation, several recent studies have shown that a series of oxidative transformations, such as cross-coupling reactions, can also be performed, thus extending the synthetic possibilities offered



**Scheme 16.19** Examples of transformations involving an intermolecular trapping of a reactive cationic intermediate.

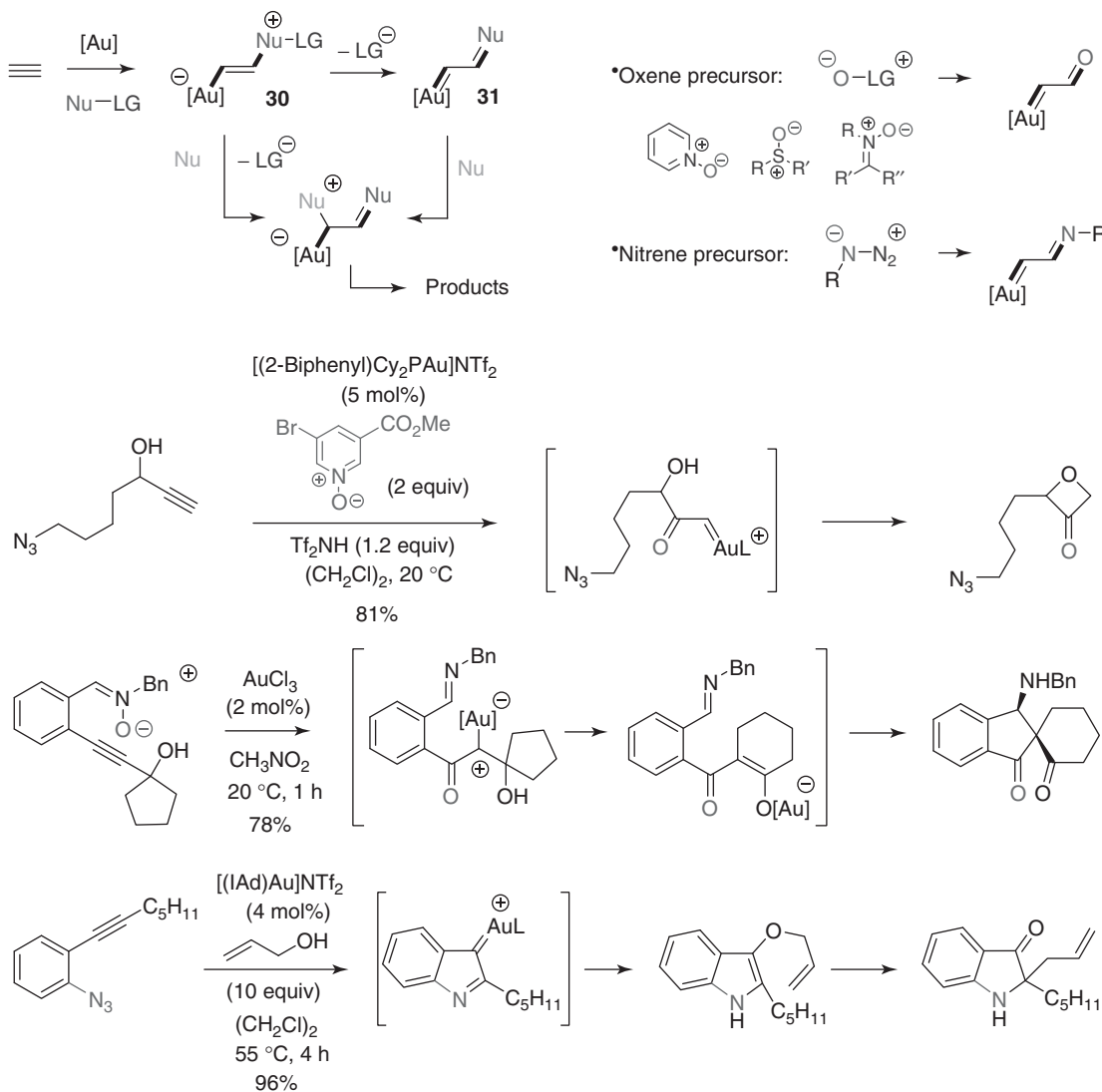
by gold catalysis. These transformations, which can be performed in an inter- or intramolecular manner, generally require the presence of a strong oxidizing agent (Selectfluor® or iodonium species) that may be used in combination with a coupling agent (boronic acids, silyl derivatives). Selected examples are presented in Scheme 16.21 [25]. It should be pointed out that the mechanism has not been clarified for the majority of the reported transformations [26].

## 16.8 GENERATION OF STRUCTURAL COMPLEXITY

As seen from the examples assembled in Scheme 16.22 [27], gold catalysis has proven to be a powerful synthetic tool not only for the generation of molecular diversity but also for the creation of structural complexity [8k]. From easily accessible substrates, especially linear derivatives, it is indeed possible to generate in a rapid, selective, and efficient manner several new cycles and/or asymmetric centers. Notably, the compounds shown in Scheme 16.22 would not be so easily obtained using more traditional synthetic methods.

## 16.9 ASYMMETRIC CATALYSIS

When compared to the plethora of gold-catalyzed synthetic transformations reported so far, the number of asymmetric gold-catalyzed reactions remains relatively low. As noted in Section 16.3.3, this situation is mainly due to the preferential linear structural arrangement of gold(I) complexes, which does not help for efficiently relaying the stereochemical information from the ligand to the gold(I)-activated substrate [8f,n]. Two main strategies have therefore been developed to overcome this

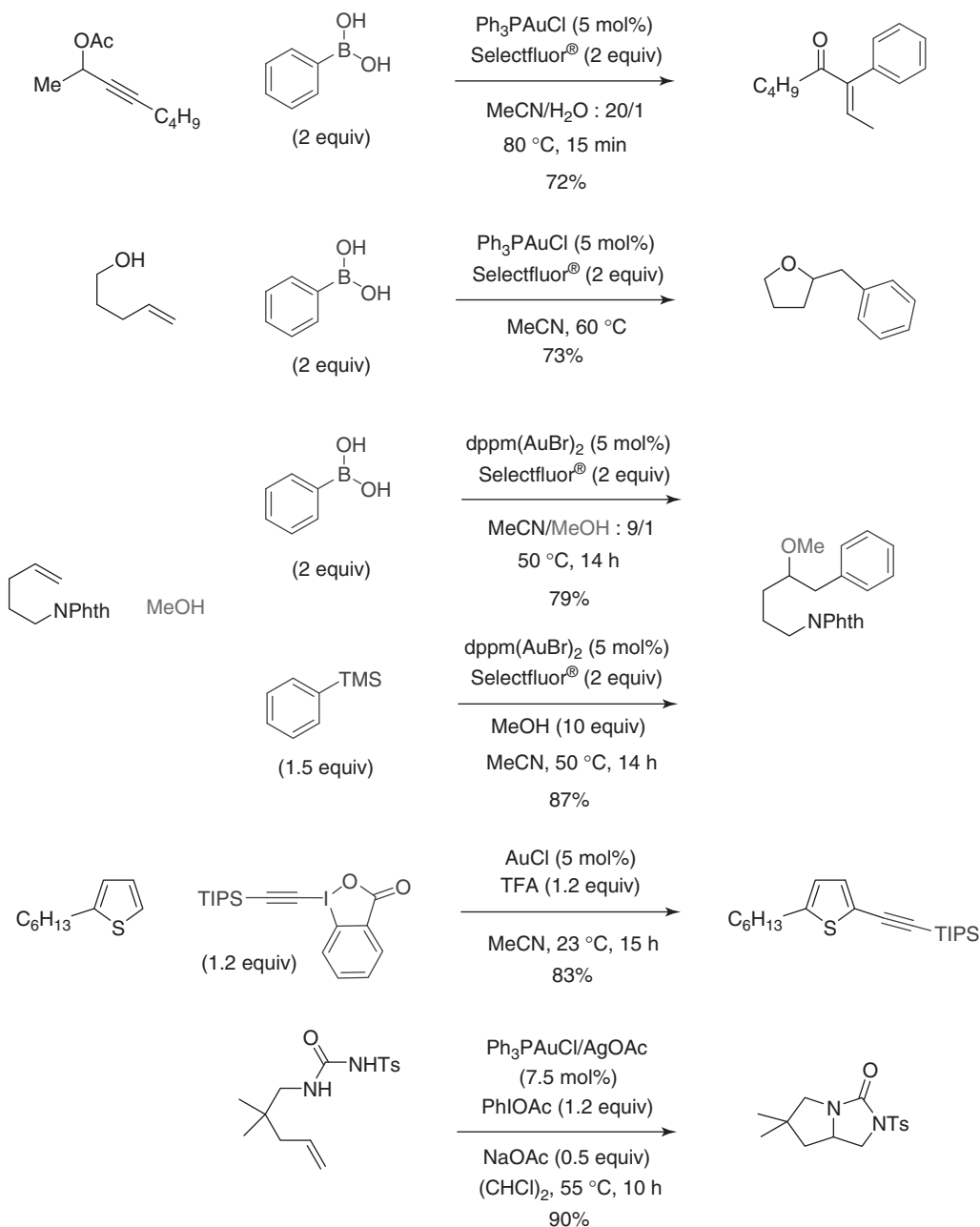


**Scheme 16.20** Examples of transformations involving the use of oxene and nitrene precursors as nucleophiles.

difficulty: the first relies on a control of the enantioselectivity by employing a chiral bulky ligand (a dinuclear gold(I) complex possessing an axially chiral biaryl diphosphine ligand, which is generally used as the catalyst, see Section 16.3.3); the second relies on a control of the enantioselectivity by using a chiral counteranion, which forms a tight ion pair with the cationic gold(I) fragment (which can be itself chiral or not). Several examples of asymmetric gold(I)-catalyzed transformations involving the use of one of these two strategies are depicted in Scheme 16.23 [28]. It should be noted that the control of the enantioselectivity by the ligand is the most commonly employed strategy and that no chiral catalytic system has proven so far to have a wide applicability.

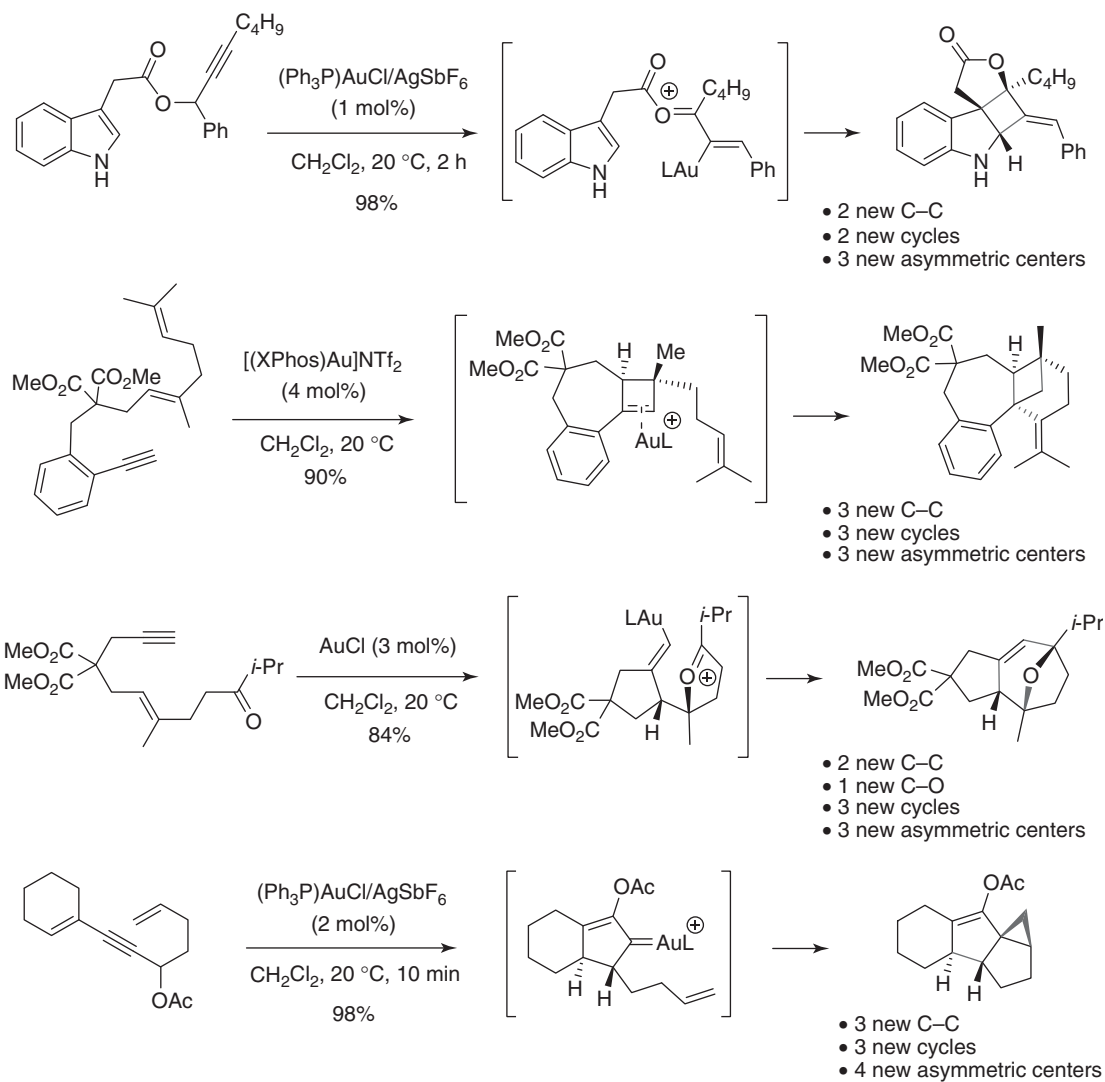
## 16.10 GOLD CATALYSIS AND TOTAL SYNTHESIS

The use of gold-catalyzed reactions in the total synthesis of natural products or biologically active molecules remains so far relatively limited. One can explain such a situation by the fact that the interest in gold catalysis is rather recent, and that most of the efforts carried out in this area have concerned the exploration of the reactivity of gold species and the development of new synthetic methods. The applications of gold catalysis in total synthesis that have been reported so far are however highly characteristic of its synthetic potential, more especially in terms of efficiency, selectivity, and compatibility with various

**Scheme 16.21** Examples of gold-catalyzed coupling reactions.

functional groups. The gold-catalyzed propargyl Claisen rearrangement used in the total synthesis of the Azadirachtine by Ley et al. (see Scheme 16.3) is probably one of the best illustrations of the synthetic potential of gold catalysis. Three other selected examples of total syntheses or synthetic approaches involving the use of a gold-catalyzed transformation are presented below.

During their total synthesis of (–)-rhazinilam, Nelson et al. [29] have employed a gold-catalyzed cycloisomerization of an allene-ene that allows the formation of the tetrahydroindolizidine motif of the targeted molecule (Scheme 16.24). In this transformation, the gold complex ( $\text{Ph}_3\text{P}$ ) $\text{AuOTf}$  catalyzes the efficient and stereoselective 6-*exo* addition of the pyrrole ring to the chiral trisubstituted allene moiety, thus generating the heterobicyclic motif and the adjacent quaternary asymmetric center.



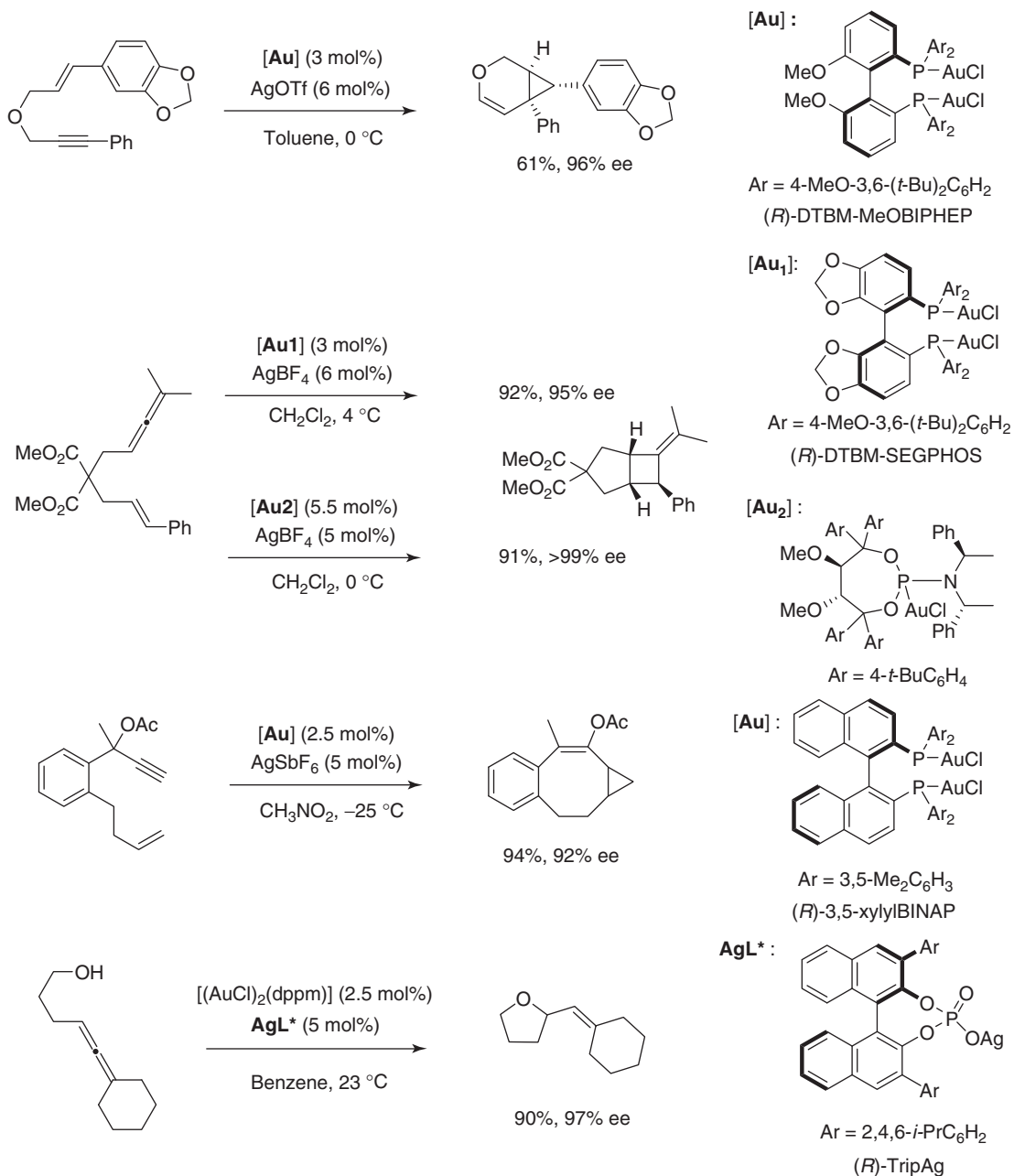
Scheme 16.22 Examples of complex transformations.

In the total synthesis of (+)-lycopladine A by Toste et al. [30], a gold-catalyzed 5-*endo* cyclization of an iodoalkyne with a silyl enol ether has been used (Scheme 16.25). This transformation efficiently produces a  $\beta,\gamma$ -unsaturated bicyclic ketone that possesses the required quaternary asymmetric center at the position  $\alpha$  to the carbonyl group. The vinyl iodide functionality generated during the cyclization was subsequently used in a palladium-catalyzed cross-coupling reaction in order to construct the pyridine ring of (+)-lycopladine A.

The synthetic potential of gold catalysis, more especially for the generation of structural complexity, is particularly well illustrated by the total syntheses of Englerin A and B, reported independently in 2010 by Echavarren et al. and Ma et al. [31] (Scheme 16.26). A very similar approach was used by these two groups to produce, via a gold-catalyzed [2 + 2 + 2] intramolecular cycloaddition between an alkyne, an alkene, and a ketone, the core structure of the Englerins. Notably, this complex gold-catalyzed sequence, which operates with an absolute control of the stereoselectivity, allowed the creation of three new asymmetric centers and three new bonds (2 C-C and 1 C-O bonds).

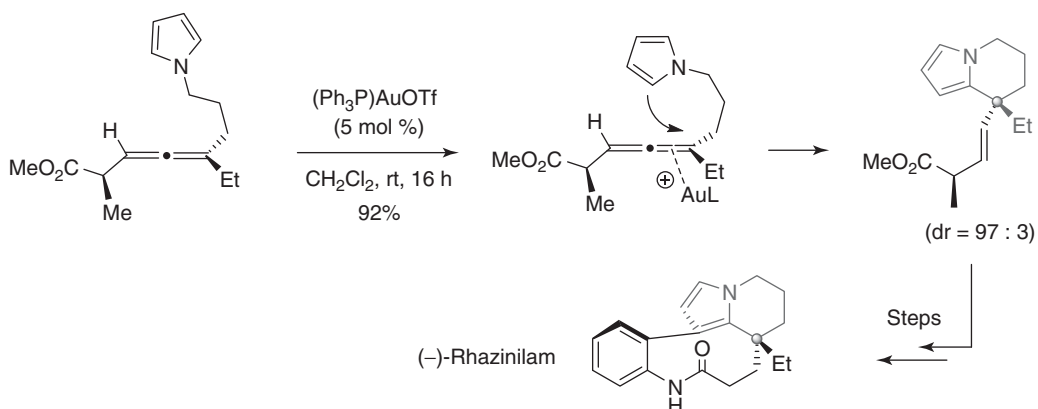
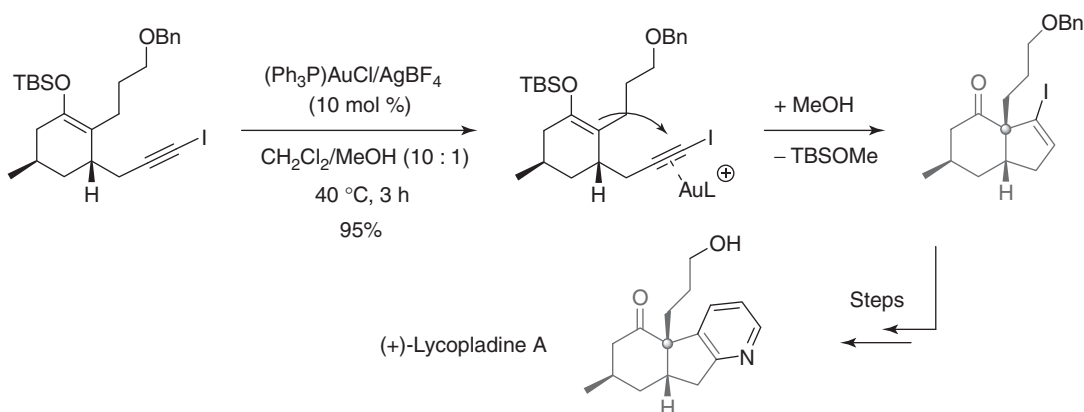
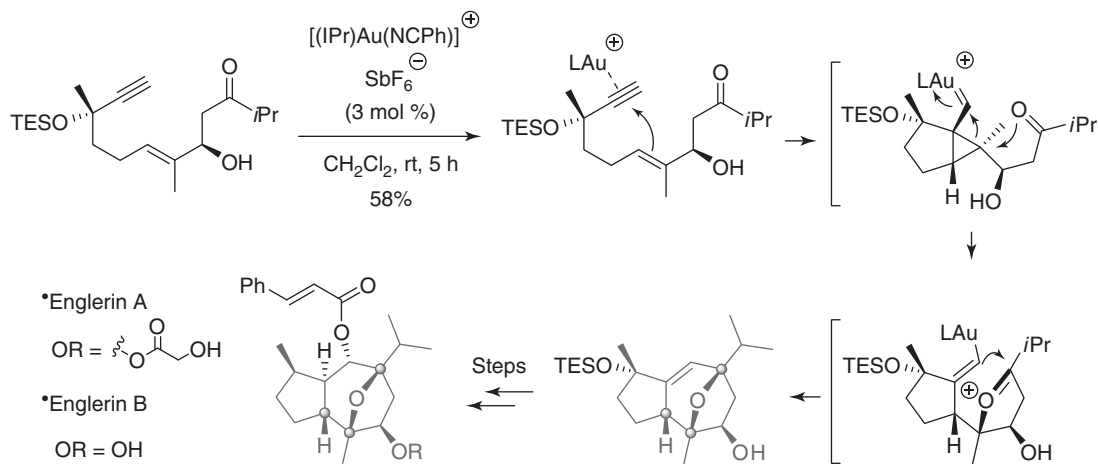
## 16.11 CONCLUSION

As briefly presented in this chapter, modern homogeneous gold catalysis, while being a recent field of research, has already emerged as a powerful tool in the arsenal of synthetic organic chemists. Gold catalysts, some of which are easy to prepare,



Scheme 16.23 Examples of chiral transformations.

store, and handle, possess a rather unique reactivity when compared to other electrophilic metallic species. They allow an efficient access to a large variety of molecules, which could not be so easily synthesized using more traditional methods. Even if many significant advances have been made during the last 10 years, especially in the development of gold-catalyzed transformations and in the understanding of gold catalysts reactivity, several aspects of gold catalysis still require additional studies. Accomplishing efficient and widely applicable gold-catalyzed coupling reactions using the Au(I)/Au(III) couple, and the development of asymmetric catalytic systems, whose scope remains so far rather limited are, for instance, two points of current interest. Given the number of research groups actively engaged in the field of gold catalysis, one can easily imagine that a series of significant discoveries and breakthroughs will be made in the next two decades, thus ushering an even wider use of gold catalysts in synthetic organic chemistry in the future.

**Scheme 16.24** Total synthesis of (*-*)-rhazinilam by Nelson et al.**Scheme 16.25** Total synthesis of (+)-lycopladine A by Toste et al.**Scheme 16.26** Total syntheses of Englerin A and B by Echavarren et al. and Ma et al.

## REFERENCES

- Ito, Y.; Sawamura, M.; Hayashi, T. *J. Am. Chem. Soc.* **1986**, *108*, 6405–6406.
- Kharasch, M. S.; Isbell, H. S. *J. Am. Chem. Soc.* **1930**, *52*, 2919–2927.
- Tamaki, A.; Kochi, J. K. *J. Organomet. Chem.* **1974**, *64*, 411.
- (a) Fukuda, Y.; Utimoto, K. *J. Org. Chem.* **1991**, *56*, 3729–3731; (b) Fukuda, Y.; Utimoto, K. *Synthesis* **1991**, 975–978; (c) Fukuda, Y.; Utimoto, K. *Bull. Chem. Soc. Jpn.* **1991**, *64*, 2013–2015; (d) Teles, J. H.; Brode, S.; Chabanas, M. *Angew. Chem. Int. Ed.* **1998**, *37*, 1415–1418.
- (a) Hashmi, A. S. K.; Schwarz, L.; Choi, J. H.; Frost, T. M. *Angew. Chem. Int. Ed.* **2000**, *39*, 2285–2288; (b) Hashmi, A. S. K.; Frost, T. M.; Bats, J. W. *J. Am. Chem. Soc.* **2000**, *122*, 11553–11554.
- Dyker, G. *Angew. Chem. Int. Ed.* **2000**, *39*, 4237–4239.
- Hashmi, A. S. K. *Angew. Chem. Int. Ed.* **2005**, *44*, 6990–6993.
- Selected reviews: (a) Corma, A.; Leyva-Pérez, A.; Sabater, M. *J. Chem. Rev.* **2011**, *111*, 1657–1712; (b) Krause, N.; Winter, C. *Chem. Rev.* **2011**, *111*, 1994–2009; (c) Aubert, C.; Fensterbank, L.; Garcia, P.; Malacria, M.; Simonneau, A. *Chem. Rev.* **2011**, *111*, 1954–1993; (d) Boorman, T. C.; Larrosa, I. *Chem. Soc. Rev.* **2011**, *40*, 1910–1925; (e) Bandini, M. *Chem. Soc. Rev.* **2011**, *40*, 1358–1367; (f) Pradal, A.; Toullec, P. Y.; Michelet, V. *Synthesis* **2011**, 1501–1514; (g) Rudolph, M.; Hashmi, A. S. K. *Chem. Commun.* **2011**, *47*, 6536–6544; (h) Wang, S.; Zhang, G.; Zhang, L. *Synlett* **2010**, *2010*, 692,706; (i) Shapiro, N. D.; Toste, F. D. *Synlett* **2010**, 675,691; (j) Das, A.; Sohel, S. M. A.; Liu, R.-S. *Org. Biomol. Chem.* **2010**, *8*, 960–979; (k) Fürstner, A. *Chem. Soc. Rev.* **2009**, *38*, 3208–3221; (l) Belmont, P.; Parker, E. *Eur. J. Org. Chem.* **2009**, *2009*, 6075–6089; (m) Abu Sohel, S. M.; Liu, R.-S. *Chem. Soc. Rev.* **2009**, *38*, 2269–2281; (n) Widenhoefer, R. *Chem. Eur. J.* **2008**, *14*, 5382–5391; (o) Skouta, R.; Li, C.-J. *Tetrahedron* **2008**, *64*, 4917–4938; (p) Patil, N. T.; Yamamoto, Y. *Chem. Rev.* **2008**, *108*, 3395–3442; (q) Marion, N.; Nolan, S. P. *Chem. Soc. Rev.* **2008**, *37*, 1776–1782; (r) Li, Z.; Brouwer, C.; He, C. *Chem. Rev.* **2008**, *108*, 3239–3265; (s) Jiménez-Núñez, E.; Echavarren, A. M. *Chem. Rev.* **2008**, *108*, 3326–3350; (t) Hashmi, A. S. K.; Rudolph, M. *Chem. Soc. Rev.* **2008**, *37*, 1766–1775; (u) Gorin, D. J.; Sherry, B. D.; Toste, F. D. *Chem. Rev.* **2008**, *108*, 3351–3378; (v) Arcadi, A. *Chem. Rev.* **2008**, *108*, 3266–3325; (w) Muzart, J. *Tetrahedron* **2008**, *64*, 5815–5849; (x) Jimenez-Nunez, E.; Echavarren, A. M. *Chem. Commun.* **2007**, 333–346; (y) Hashmi, A. S. K. *Chem. Rev.* **2007**, *107*, 3180–3211; (z) Gorin, D. J.; Toste, F. D. *Nature* **2007**, *446*, 395–403; (aa) Fürstner, A.; Davies, P. *Angew. Chem. Int. Ed.* **2007**, *46*, 3410–3449; (ab) Zhang, L.; Sun, J.; Kozmin, S. *Adv. Synth. Catal.* **2006**, *348*, 2271–2296; (ac) Widenhoefer, R. A.; Han, X. *Eur. J. Org. Chem.* **2006**, *2006*, 4555–4563; (ad) Hashmi, A. S. K.; Hutchings, G. J. *Angew. Chem. Int. Ed.* **2006**, *45*, 7896–7936.
- For an highlight, see: (a) Hashmi, A. S. K. *Angew. Chem. Int. Ed.* **2008**, *47*, 6754–6756; For leading references, see: (b) Fürstner, A.; Morency, L. *Angew. Chem. Int. Ed.* **2008**, *47*, 5030–5033; (c) Seidel, G.; Mynott, R.; Fürstner, A. *Angew. Chem. Int. Ed.* **2009**, *48*, 2510–2513; (d) Correa, A.; Marion, N.; Fensterbank, L.; Malacria, M.; Nolan, S.; Cavallo, L. *Angew. Chem. Int. Ed.* **2008**, *47*, 718–721; (e) Fedorov, A.; Moret, M. -E.; Chen, P. *J. Am. Chem. Soc.* **2008**, *130*, 8880–8881.
- Benitez, D.; Shapiro, N. D.; Tkatchouk, E.; Wang, Y.; Goddard III, W. A.; Toste, F. D. *Nat. Chem.* **2009**, *1*, 482–486.
- Kim, S.; Park, J.; Choi, S.; Chung, Y. *Angew. Chem. Int. Ed.* **2007**, *46*, 6172–6175.
- Witham, C. A.; Mauleón, P.; Shapiro, N. D.; Sherry, B. D.; Toste, F. D. *J. Am. Chem. Soc.* **2007**, *129*, 5838–5839.
- Gorin, D. J.; Davis, N. R.; Toste, F. D. *J. Am. Chem. Soc.* **2005**, *127*, 11260–11261.
- Hashmi, A. S. K.; Frost, T. M.; Bats, J. W. *J. Am. Chem. Soc.* **2000**, *122*, 11553–11554.
- (a) Markham, J. P.; Staben, S. T.; Toste, F. D. *J. Am. Chem. Soc.* **2005**, *127*, 9708–9709; (b) Barluenga, J.; Fernández-Rodríguez, M. Á.; García-García, P.; Aguilar, E. *J. Am. Chem. Soc.* **2008**, *130*, 2764–2765; (c) Horino, Y.; Luzung, M. R.; Toste, F. D. *J. Am. Chem. Soc.* **2006**, *128*, 11364–11365; (d) Brenzovich, W. E.; Benitez, D.; Lackner, A. D.; Shunatona, H. P.; Tkatchouk, E.; Goddard, W. A.; Toste, F. D. *Angew. Chem. Int. Ed.* **2010**, *49*, 5519–5522; (e) Nieto-Oberhuber, C.; López, S.; Echavarren, A. M. *J. Am. Chem. Soc.* **2005**, *127*, 6178–6179; (f) Cui, L.; Ye, L.; Zhang, L. *Chem. Commun.* **2010**, *46*, 3351–3353; (g) Buzas, A.; Gagósz, F. *J. Am. Chem. Soc.* **2006**, *128*, 12614–12615; (h) Leyva, A.; Corma, A. *J. Org. Chem.* **2009**, *74*, 2067–2074; (i) López-Carrillo, V.; Echavarren, A. M. *J. Am. Chem. Soc.* **2010**, *132*, 9292–9294; (j) de Frémont, P.; Scott, N. M.; Stevens, E. D.; Nolan, S. P. *Organometallics* **2005**, *24*, 2411–2418; (k) Mézailles, N.; Ricard, L.; Gagósz, F. *Org. Lett.* **2005**, *7*, 4133–4136; (l) Ricard, L.; Gagósz, F. *Organometallics* **2007**, *26*, 4704–4707; (m) Amijs, C. H. M.; López-Carrillo, V.; Raducan, M.; Pérez-Galán, P.; Ferrer, C.; Echavarren, A. M. *J. Org. Chem.* **2008**, *73*, 7721–7730; (n) López, S.; Herrero-Gómez, E.; Pérez-Galán, P.; Nieto-Oberhuber, C.; Echavarren, A. M. *Angew. Chem. Int. Ed.* **2006**, *45*, 6029–6032.
- (a) Bandini, M.; Eichholzer, A. *Angew. Chem. Int. Ed.* **2009**, *48*, 9533–9537; (b) Chao, C. M.; Vitale, M.; Toullec, P.; Genêt, J. P.; Michelet, V. *Chem. Eur. J.* **2009**, *15*, 1319–1323; (c) Chao, C. -M.; Beltrami, D.; Toullec, P. Y.; Michelet, V. *Chem. Commun.* **2009**, 6988–6990; (d) Zhang, Z.; Lee, S. D.; Widenhoefer, R. A. *J. Am. Chem. Soc.* **2009**, *131*, 5372–5373; (e) Martínez, A.; García-García, P.; Fernández-Rodríguez, M.; Rodríguez, F.; Sanz, R. *Angew. Chem. Int. Ed.* **2010**, *49*, 4633–4637; (f) LaLonde, R.; Wang, Z.; Mba, M.; Lackner, A.; Toste, F. *Angew. Chem. Int. Ed.* **2010**, *49*, 598–601; (g) Johansson, M. J.; Gorin, D. J.; Staben, S. T.; Toste, F. D. *J. Am. Chem. Soc.* **2005**, *127*, 18002–18003; (h) Murai, M.; Uenishi, J.; Uemura, M. *Org. Lett.* **2010**, *12*, 4788–4791; (i) Alonso, I.; Trillo, B.; López, F.; Montserrat, S.; Ujaque, G.; Castedo, L.; Lledós, A.; Mascarenas, J. L. *J. Am. Chem. Soc.* **2009**,

- 131, 13020–13030; (j) Teller, H.; Flügge, S.; Goddard, R.; Fürstner, A. *Angew. Chem. Int. Ed.* **2010**, *49*, 1949–1953; (k) Hamilton, G. L.; Kang, E. J.; Mba, M.; Toste, F. D. *Science* **2007**, *317*, 496–499.
17. (a) Marion, N.; Ramón, R. S.; Nolan, S. P. *J. Am. Chem. Soc.* **2009**, *131*, 448–449; (b) Antoniotti, S.; Genin, E.; Michelet, V.; Genêt, J.-P. *J. Am. Chem. Soc.* **2005**, *127*, 9976–9977; (c) Nishina, N.; Yamamoto, Y. *Tetrahedron Lett.* **2009**, *65*, 1799–1808; (d) Sromek, A. W.; Rubina, M.; Gevorgyan, V. *J. Am. Chem. Soc.* **2005**, *127*, 10500–10501; (e) Genin, E.; Toullec, P. Y.; Antoniotti, S.; Brancour, C.; Genêt, J.-P.; Michelet, V. *J. Am. Chem. Soc.* **2006**, *128*, 3112–3113; (f) Hashmi, A. S. K.; Weyrauch, J. P.; Frey, W.; Bats, J. W. *Org. Lett.* **2004**, *6*, 4391–4394.
18. (a) Istrate, F.; Gagosz, F. *Org. Lett.* **2007**, *9*, 3181–3184; (b) Morita, N.; Krause, N. *Org. Lett.* **2004**, *6*, 4121–4123; (c) Kang, J.-E.; Kim, H.-B.; Lee, J.-W.; Shin, S. *Org. Lett.* **2006**, *8*, 3537–3540.
19. (a) Morita, N.; Krause, N. *Angew. Chem. Int. Ed.* **2006**, *45*, 1897–1899; (b) Nakamura, I.; Sato, T.; Yamamoto, Y. *Angew. Chem. Int. Ed.* **2006**, *45*, 4473–4475.
20. (a) Mauleón, P.; Zeldin, R. M.; González, A. Z.; Toste, F. D. *J. Am. Chem. Soc.* **2009**, *131*, 6348–6349; (b) Zhang, L.; Kozmin, S. A. *J. Am. Chem. Soc.* **2005**, *127*, 6962–6963; (c) Huang, X.; Zhang, L. *J. Am. Chem. Soc.* **2007**, *129*, 6398–6399; (d) Lemière, G.; Gandon, V.; Agenet, N.; Goddard, J.-P.; de Kozak, A.; Aubert, C.; Fensterbank, L.; Malacria, M. *Angew. Chem. Int. Ed.* **2006**, *45*, 7596–7599; (e) Ferrer, C.; Echavarren, A. M. *Angew. Chem. Int. Ed.* **2006**, *45*, 1105–1109; (f) Odabachian, Y.; Le Goff, X.-F.; Gagosz, F. *Chem. Eur. J.* **2009**, *15*, 8966–8970.
21. (a) Reetz, M. T.; Sommer, K. *Eur. J. Org. Chem.* **2003**, 3485–3496; (b) Yao, X.-Q.; Li, C.-J. *J. Am. Chem. Soc.* **2004**, *126*, 6884–6885.
22. (a) Johansson, M. J.; Gorin, D. J.; Staben, S. T.; Toste, F. D. *J. Am. Chem. Soc.* **2005**, *127*, 18002–18003; (b) Shapiro, N. D.; Shi, Y.; Toste, F. D. *J. Am. Chem. Soc.* **2009**, *131*, 11654–11655.
23. (a) Schelwies, M.; Dempwolff, A. L.; Rominger, F.; Helmchen, G. *Angew. Chem. Int. Ed.* **2007**, *46*, 5598–5601; (b) Toullec, P. Y.; Genin, E.; Leseurre, L.; Genêt, J.-P.; Michelet, V. *Angew. Chem. Int. Ed.* **2006**, *45*, 7427–7430; (c) Zhang, G.; Huang, X.; Li, G.; Zhang, L. *J. Am. Chem. Soc.* **2008**, *130*, 1814–1815; (d) Buzas, A.; Istrate, F.; Gagosz, F. *Angew. Chem. Int. Ed.* **2007**, *46*, 1141–1144.
24. (a) Ye, L.; He, W.; Zhang, L. *J. Am. Chem. Soc.* **2010**, *132*, 8550–8551; (b) Yeom, H. S.; Lee, Y.; Jeong, J.; So, E.; Hwang, S.; Lee, J. E.; Lee, S.; Shin, S. *Angew. Chem. Int. Ed.* **2010**, *49*, 1611–1614; (c) Wetzel, A.; Gagosz, F. *Angew. Chem. Int. Ed.* **2011**, *50*, 7354–7358.
25. (a) Zhang, G.; Peng, Y.; Cui, L.; Zhang, L. *Angew. Chem. Int. Ed.* **2009**, *48*, 3112–3115; (b) Zhang, G.; Cui, L.; Wang, Y.; Zhang, L. *J. Am. Chem. Soc.* **2010**, *132*, 1474–1475; (c) Melhado, A. D.; Brenzovich, W. E.; Lackner, A. D.; Toste, F. D. *J. Am. Chem. Soc.* **2010**, *132*, 8885–8887; (d) Brenzovich, W. E.; Brazeau, J.-F.; Toste, F. D. *Org. Lett.* **2010**, *12*, 4728–4731; (e) Iglesias, A.; Muñiz, K. *Chem. Eur. J.* **2009**, *15*, 10563–10569; (f) Brand, J. P.; Waser, J. *Angew. Chem. Int. Ed.* **2010**, *49*, 7304–7307.
26. Tkatchouk, E.; Mankad, N. P.; Benitez, D.; Goddard III W. A.; Toste, F. D. *J. Am. Chem. Soc.* **2011**, *133*, 14293–14300.
27. (a) Zhang, L. *J. Am. Chem. Soc.* **2005**, *127*, 16804–16805; (b) Odabachian, Y.; Gagosz, F. *Adv. Synth. Catal.* **2009**, *351*, 379–386; (c) Jiménez-Núñez, E.; Claverie, C. K.; Nieto-Oberhuber, C.; Echavarren, A. M. *Angew. Chem. Int. Ed.* **2006**, *45*, 5452–5455; (d) Lemière, G.; Gandon, V.; Cariou, K.; Hours, A.; Fukuyama, T.; Ghimane, A.-L.; Fensterbank, L.; Malacria, M. *J. Am. Chem. Soc.* **2009**, *131*, 2993–3006.
28. (a) Chao, C.-M.; Beltrami, D.; Toullec, P.-Y.; Michelet, V. *Chem. Commun.* **2009**, 6988–6990; (b) Luzung, M. R.; Mauleón, P.; Toste, F. D. *J. Am. Chem. Soc.* **2007**, *129*, 12402–12403; (c) Teller, H.; Flügge, S.; Goddard, R.; Fürstner, A. *Angew. Chem. Int. Ed.* **2010**, *49*, 1949–1953; (d) Watson, I. D. G.; Ritter, S.; Toste, F. D. *J. Am. Chem. Soc.* **2009**, *131*, 2056–2057; (e) Hamilton, G. L.; Kang, E. J.; Mba, M.; Toste, F. D. *Science* **2007**, *317*, 496–499.
29. Liu, Z.; Wasmuth, A. S.; Nelson, S. G. *J. Am. Chem. Soc.* **2006**, *128*, 10352–10353.
30. Staben, S. T.; Kennedy-Smith, J. J.; Huang, D.; Corkey, B. K.; LaLonde, R. L.; Toste, F. D. *Angew. Chem. Int. Ed.* **2006**, *45*, 5991–5994.
31. (a) Molawi, K.; Delpont, N.; Echavarren, A. *Angew. Chem. Int. Ed.* **2010**, *49*, 3517–3519; (b) Zhou, Q.; Chen, X.; Ma, D. *Angew. Chem. Int. Ed.* **2010**, *49*, 3513–3516.



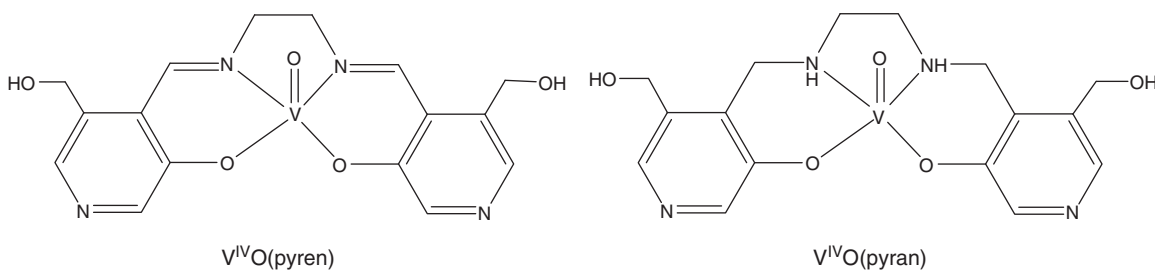
# VANADIUM(IV) COMPLEXES DERIVED FROM AROMATIC *o*-HYDROXYALDEHYDES AND TYROSINE DERIVATIVES: CATALYTIC EVALUATION IN SULFOXIDATIONS

JOÃO COSTA PESSOA\*, ISABEL CORREIA, AND PEDRO ADÃO

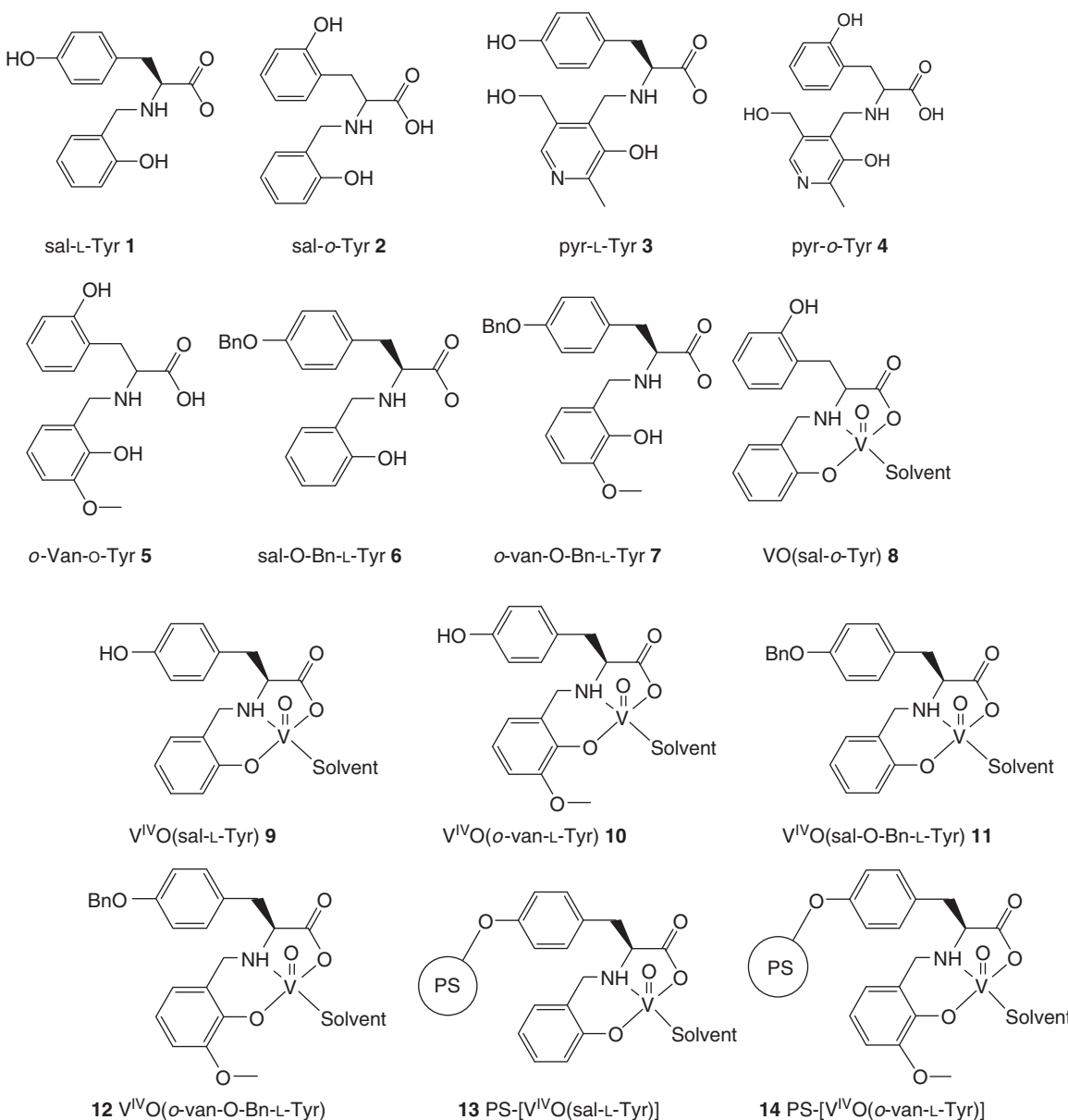
*Centro Química Estrutural, Instituto Superior Técnico, Universidade de Lisboa, Lisboa, Portugal*

## 17.1 INTRODUCTION

The binding of  $\text{V}^{\text{IV}}\text{O}^{2+}$  and vanadate to the tyrosine residues at the Fe-binding sites of transferrin is well documented [1–4], as also the direct binding of vanadate to tyrosine in tyrosyl-DNA-phosphodiesterase [5]. However, the amino acid itself is quite ineffective in the coordination to vanadium. Dipeptides containing Tyr are more effective binders but the main complexes formed exclude Tyr from direct binding [6]. The presence of an anchor group in the ligand may enhance its binding ability and, in this respect, *N*-salicylidene aminoacidato-type complexes have been extensively studied [7–11]; in many cases, they may be easily prepared by the condensation of an aromatic *o*-hydroxyaldehyde and an amino acid in the presence of a metal ion. However, these Schiff bases (SBs) in solution may hydrolyze, and, in many cases, it is not possible to characterize either the ligands or their complexes in the solid state or in solution. This instability can often be overcome by reduction of the SB at the imine function to give an amine [12–16]. For example, the stability constant of the reduced SB  $\text{V}^{\text{IV}}\text{O}$ -complex  $\text{V}^{\text{IV}}\text{O}(\text{pyran})$  is approximately  $10^6$  higher than that of the corresponding  $\text{V}^{\text{IV}}\text{O}(\text{pyren})$ —Scheme 17.1. Moreover, while  $\text{V}^{\text{IV}}\text{O}(\text{pyran})$  is stable in water in the pH range 2–12,  $\text{V}^{\text{IV}}\text{O}(\text{pyren})$  is only stable in the pH range circa 3–6 [12]. Several reduced SB derived from the reactions of salicylaldehyde derivatives and several diamines were prepared and used as catalyst precursors in catalytic oxidations [17]. In our contribution to the advancement of the chemistry of amino acid-based vanadium compounds as well as catalysts, we previously reported the preparation of several aminophenolate-L-tyrosine  $\text{V}^{\text{IV}}\text{O}$ -compounds, specifically: **1–5** and **8** in Scheme 17.2. We now extend this work, preparing a few new ligands and  $\text{V}^{\text{IV}}\text{O}$ -complexes intended for use as catalysts in the enantioselective sulfoxidation of thioanisole. Oxygen donors on the side chain of the L-tyrosine residue allow the preparation of heterogeneous versions, as well as their vanadium complexes by binding them to a polystyrene (PS) Merrifield resin, allowing the preparation of stable metal complexes that will lead to low leaching of the metal ion and possibly increased selectivity. Therefore, the O-benzylated Tyr derivatives **6** and **7**, the polymer anchored sal-L-Tyr compound and the corresponding  $\text{V}^{\text{IV}}\text{O}$ -complexes were obtained, characterized, and studied for their catalytic properties in the enantioselective sulfoxidation of thioanisole. The O-benzylated derivatives **6** and **7** and their  $\text{V}^{\text{IV}}\text{O}$ -complexes **11** and **12** were prepared so that they may be used as models of the PS-supported ligands and  $\text{V}^{\text{IV}}\text{O}$ -complexes.



**Scheme 17.1** Molecular formulae of the water-soluble  $V^{IV}O(\text{pyren})$  and  $V^{IV}O(\text{pyran})$  [12].



**Scheme 17.2** Molecular formulae of the ligand precursor and  $V^{IV}O$ -compounds prepared. Note that Tyr corresponds to L-Tyr and *o*-Tyr to the racemic mixture D,L-*o*-Tyr. The polystyrene polymer is represented by the circle with PS written inside.

## 17.2 RESULTS AND DISCUSSION

### 17.2.1 Synthesis and Characterization

Globally following the method described in [17], the reduced SBs **1–7** depicted in Scheme 17.2 were prepared in alcoholic medium by the condensation of 1 equiv of the appropriate aldehyde with 1 equiv of amino acid in the presence of an equivalent of KOH. Treatment of these condensation products with NaBH<sub>4</sub> resulted in the reduction of the imine bonds, yielding the reduced SBs. Five neat V<sup>IV</sup>O-complexes: **8–12** (Scheme 17.2) were also prepared. The IR spectra of the solid V<sup>IV</sup>O-complexes present the characteristic  $\nu(V=O)$  bands at 950–1000 cm<sup>-1</sup>. The electron paramagnetic resonance (EPR) parameters for the five V<sup>IV</sup>O-compounds are listed in Table 17.1. For **9**, **10**, **11**, and **12**, the parameters are consistent with either a (COO<sup>-</sup>, N<sub>amine</sub>, O<sup>-</sup><sub>phenolato</sub>, O<sub>ROH</sub>)<sub>eq</sub> or a (COO<sup>-</sup>, N<sub>amine</sub>, O<sup>-</sup><sub>phenolato</sub>, O<sub>DMF</sub>)<sub>eq</sub> donor set in methanol and dimethyl formamide (DMF) solutions, respectively. The PS-supported versions of compounds **9** and **10** (PS-[V<sup>IV</sup>O(sal-L-Tyr)] **13** and PS-[V<sup>IV</sup>O(*o*-van-L-Tyr)] **14**, Scheme 17.2) were prepared according to the synthetic procedure shown in Scheme 17.3. The chloromethylated PS is firstly treated with the K<sup>+</sup> salt of L-Tyr to yield a tyrosine-modified PS-resin. The free amine groups therein are then condensed with the appropriate aldehyde and the respective imine is reduced with NaBH<sub>4</sub>. The resulting resin is finally reacted with V<sup>IV</sup>O(acac)<sub>2</sub> to form the desired heterogeneous V<sup>IV</sup>O-compound. The PS-supported compounds were characterized mainly by room temperature EPR. The obtained EPR powder spectra of **13** and **14** are characteristic of magnetically diluted V<sup>IV</sup>O-complexes and the well-resolved EPR pattern indicates that the vanadium centers are well dispersed in the polymer matrix. The spectra were simulated [18] and the spin Hamiltonian parameters obtained (Table 17.1)

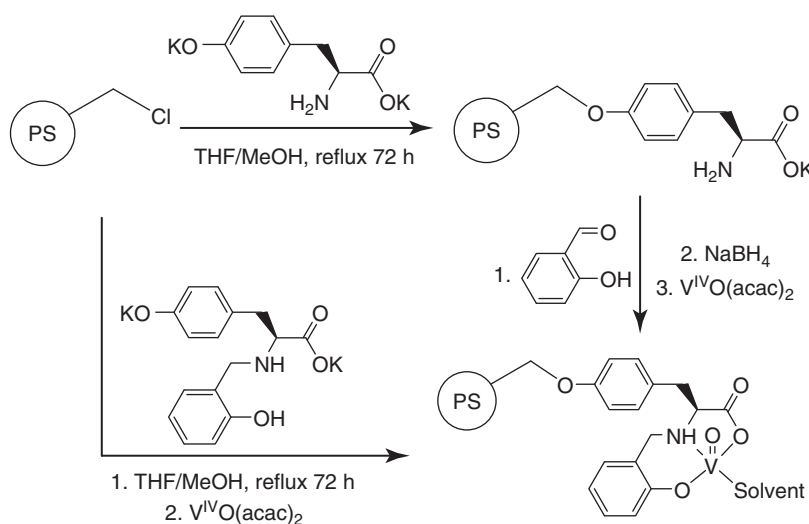
TABLE 17.1 Experimental Spin Hamiltonian Parameters for the Prepared Homogeneous (Measured at 77 K) and Heterogeneous V<sup>IV</sup>O-Compounds at Room Temperature

Compound	$g_x, g_y$	$A_x, A_y, \times 10^4 \text{ cm}^{-1}$	$g_z$	$A_z, \times 10^4 \text{ cm}^{-1}$	Predicted Equatorial Donor Set
<b>9<sup>a</sup></b>	1.978, 1.981	51, 60	1.951	162	O <sub>COO<sup>-</sup></sub> , N <sub>amine</sub> , O <sub>ArO<sup>-</sup></sub> , O <sub>ROH</sub>
<b>10<sup>a</sup></b>	1.980, 1.978	62, 59	1.948	169	O <sub>COO<sup>-</sup></sub> , N <sub>amine</sub> , O <sub>ArO<sup>-</sup></sub> , O <sub>ROH</sub>
<b>11<sup>b</sup></b>	1.979, 1.979	53, 58	1.950	163	N <sub>amine</sub> , O <sub>ArO<sup>-</sup></sub> , O <sub>ROH</sub> , O <sub>ROH</sub>
<b>12<sup>b</sup></b>	1.979, 1.978	58, 56	1.949	164	O <sub>COO<sup>-</sup></sub> , N <sub>amine</sub> , O <sub>ArO<sup>-</sup></sub> , O <sub>DMF</sub>
<b>13<sup>c</sup></b>	1.983, 1.978	66, 60	1.945	170	N <sub>amine</sub> , O <sub>ArO<sup>-</sup></sub> , O <sub>water</sub> , O <sub>water</sub>
<b>14<sup>c</sup></b>	1.983, 1.976	64, 62	1.947	168	O <sub>COO<sup>-</sup></sub> , N <sub>amine</sub> , O <sub>ArO<sup>-</sup></sub> , O <sub>water</sub>

<sup>a</sup>EPR spectrum measured in methanol.

<sup>b</sup>EPR spectrum measured in DMF.

<sup>c</sup>EPR spectrum measured with the neat solid at room temperature.



Scheme 17.3 General synthetic procedures used to obtain polystyrene-anchored compound **13** (and **14**). The circle represents the polystyrene matrix.

were compared with those for **9–12**. The hyperfine coupling constants  $A_z$  for the PS-supported complexes are slightly higher than those found for their homogeneous counterparts. Nevertheless, it is possible to identify the donor set of existing  $\text{V}^{\text{IV}}\text{O}$ -species bound within the polymer resin and, by extension, to confirm the successful immobilization of the tyrosine-based ligand. Additionally thermogravimetric analysis of **13** and **14** gave the amount of V in the resin, the obtained V-loadings being 1.1 mmol V/g for **13**; 0.9 mmol V/g for **14**.

### 17.2.2 Catalytic Studies with the $\text{V}^{\text{IV}}\text{O}$ -Compounds

While the side-chain phenolic moiety of L-Tyr is not in a coordinative position relative to the metal center, deprotonation and coordination of the side-chain phenol to another metal center is possible, especially if the pH is within the range 9–10. The preparation of  $\text{V}^{\text{IV}}\text{O}(\text{sal-O-Bn-L-Tyr})$  **11** gave no problems, but with  $\text{V}^{\text{IV}}\text{O}(o\text{-van-O-Bn-L-Tyr})$  **12**, the final product was unexpectedly water soluble. The solid nature of the PS-supported compounds **13** and **14** does not allow their adequate characterization by the usual spectroscopic methods. Nevertheless, EPR characterization alone provided valuable information regarding the entire preparation procedure. With  $A_z$  values of 170 and  $168 \times 10^{-4} \text{ cm}^{-1}$  for **13** and **14**, respectively, there is strong indication that the sole existing  $\text{V}^{\text{IV}}\text{O}$ -species within the resin are those with the expected ( $\text{O}_{\text{COO}^-}$ ,  $\text{N}_{\text{amine}}$ ,  $\text{O}_{\text{ArO}^-}$ ,  $\text{O}_{\text{water}}^{\text{eq}}$ ) donor group set. In the IR of **13** and **14** the  $\nu(\text{V=O})$  are detected at 955 and  $995 \text{ cm}^{-1}$ , respectively, and medium-to-strong bands are detected at 1625 and  $1610\text{--}1700 \text{ cm}^{-1}$ , assignable to  $\nu(\text{C}-\text{O}_{\text{phenolato}})$  and  $\nu_{\text{as}}(\text{COO})$ , respectively. These compounds were tested as catalysts in the asymmetric sulfoxidation of thioanisole, using  $\text{H}_2\text{O}_2$  as oxidant. The results obtained using both the homogeneous and heterogenized compounds are listed in Tables 17.2 and 17.3. Control reactions made to test the oxidation of thioanisole in the absence of catalyst gave very low conversions to sulfoxide even after a 24 h period at room temperature: 9% in 1,2-dichloroethane (DCE), 3% in acetone, 2% in ethyl acetate, 2% in acetonitrile, 0% of sulfone in all control reactions. In general, the obtained enantiomeric excesses were very low. Nearly complete conversions were obtained with **11** in acetone and ethyl acetate, but no enantioselectivity was observed (entries 1 and 2, Table 17.2).

TABLE 17.2 Sulfoxidation of Thioanisole With the Homogenous  $\text{V}^{\text{IV}}\text{O}$  Catalyst Precursors<sup>a</sup>

Entry	Catalyst	Solvent <sup>b</sup>	<i>t</i> , h	Conversion, %	ee, % <sup>b</sup>	Sulfone, %
1	<b>11</b>	$(\text{CH}_3)_2\text{CO}$	24	99	0	5
2	<b>11</b>	AcOEt	24	>99	0	6
3	<b>12</b>	DCE	24	0	0	0
4	<b>12</b>	$(\text{CH}_3)_2\text{CO}$	24	41	26	2
5	<b>12</b>	$(\text{CH}_3)_2\text{CO}$	48	63	26	4
6	<b>12</b>	EtOH	24	8	0	0
7	<b>12</b>	AcOEt	24	96	3	11

<sup>a</sup>Conditions: 4 ml of solvent; *n*S = 1 mmol; *n* $\text{H}_2\text{O}_2 : n$ S = 1.2; 1 mol% of catalyst; *T* = 0 °C; DCE, 1,2-dichloroethane.

<sup>b</sup>AcOEt, ethyl acetate; DCE, 1,2-dichloroethane; EtOH, ethanol; S, substrate; ee, enantiomeric excess.

TABLE 17.3 Sulfoxidation of Thioanisole With  $\text{V}^{\text{IV}}\text{O}$  Catalyst Precursors **13** and **14**<sup>a</sup>

Entry	Catalyst	Solvent	mol% Catalyst	Cycle	Conversion, %	ee, %	Sulfone, %
1	<b>13</b>	AcOEt	3.6	1	38	0	5
2	<b>13</b>	$(\text{CH}_3)_2\text{CO}$	1.4	1	0	0	0
3	<b>13</b>	DCE	1.4	1	37	0	5
4 <sup>b</sup>	<b>14</b>	$\text{H}_2\text{O}$	3.3	1	37	0	0
5	<b>14</b>	AcOEt	5.5	1	99	0	12
				2	99	0	13
				3	99	0	11
				4	99	0	10
6	<b>14</b>	AcOEt	1.7	1	59	0	8
7	<b>14</b>	$(\text{CH}_3)_2\text{CO}$	3.3	1	91	0	8
8	<b>14</b>	DCE	1.7	1	36	0	5

<sup>a</sup>4 ml of solvent; *n*S = 1 mmol, *n* $\text{H}_2\text{O}_2 : n$ S = 1.2, 4 ml of solvent. Reaction time = 24 h.

<sup>b</sup>Reaction was run at 5 °C.

Only **12** exhibited appreciable enantioselectivity in acetone (entries 4 and 5, Table 17.2), although the reaction was not complete even after a 48 h period. This catalyst showed no activity in DCE (entry 3, Table 17.2), very low activity in ethanol (entry 6, Table 17.2) but demonstrated good activity in ethyl acetate (entry 7, Table 17.2). None of the tested PS-supported V<sup>IV</sup>O-compounds exhibited enantioselectivity. Compound **13** exhibited lower activity in ethyl acetate and acetone when compared to its homogeneous variant **11**, while exhibiting some activity in DCE (entries 1, 2 and 3, Table 17.3). Compound **14** exhibited better catalytic characteristics. For instance, the sulfoxidation could be carried out in water (entry 4, Table 17.3). High conversions and relatively low sulfone percentages were obtained in ethyl acetate and these results were achieved even after five consecutive recycling procedures (entry 5, Table 17.3). Lowering the catalyst loading from 5.5 to 1.7 mol% resulted in lower conversions under the same conditions (entry 6, Table 17.3). Replacing ethyl acetate by acetone and lowering the catalyst loading from 5.5 to 3.3 mol% resulted in a high conversion and a slightly lower sulfone formation (entry 7, Table 17.3). In DCE, **14** performed comparably to **13** although the catalyst loading was slightly higher in the former case (entry 8, Table 17.3). Globally, the performance of the PS-supported V<sup>IV</sup>O-complexes is good and at least equivalent to their homogeneous counterparts, with the advantage of being easily recyclable. However, no enantioselectivity was obtained. The reason for this is not clear. It is known that vanadium may be very active in the racemization of amino acids in the presence of aromatic aldehydes [19 and refs. therein], so it is possible that during the step of addition of V<sup>IV</sup>O(acac)<sub>2</sub> to the PS-supported ligand, which takes place at 50 °C for 24 h, the L-Tyr moiety racemizes, the actual compounds being then better designated as PS-[V<sup>IV</sup>O(sal-D,L-Tyr)] (**13**) and PS-[V<sup>IV</sup>O(*o*-van-D,L-Tyr)] (**14**). Studies will be carried out in the future to evaluate the existence and extent of vanadium-mediated racemization of homogenous analogues, **11** and **12**.

### 17.3 CONCLUSIONS

The PS-supported catalysts are stable, active, and easily recyclable, not losing activity upon use at least after four catalytic cycles. In this respect, they are quite promising products, representing positive steps toward achieving more sustainable sulfoxidation procedures, despite the disappointing enantioselectivities. Globally, the reported catalysts are quite stable and showed better performance in acetone and/or ethyl acetate relative to DCE in all aspects. Water could be used as solvent, moderate conversions being obtained. Complex **12** exhibits better activity and enantioselectivity in sulfoxidation compared to earlier L-alanine- and L-lysine-derived V<sup>IV</sup>O(SB) complexes [20], while requiring less toxic solvents such as acetone and environmentally benign oxidants such as hydrogen peroxide.

### ACKNOWLEDGMENTS

The authors thank Fundação para a Ciência e Tecnologia (FCT), PEst-OE/QUI/UI0100/2013; SFRH/BPD/79778/2013, and the Portuguese NMR and MS Networks (IST-UTL Centers).

### REFERENCES

1. Butler, A.; Eckert, H. *J. Am. Chem. Soc.* **1989**, *111*, 2802.
2. Kiss, T.; Jakusch, T.; Hollender, D.; Dornyei, A.; Enyedy, E. A.; Costa Pessoa, J.; Sakurai, H.; Sanz-Medel, A. *Coord. Chem. Rev.* **2008**, *252*, 1153.
3. Jakusch, T.; Hollender, D.; Enyedy, E. A.; Gonzalez, C. S.; Montes-Bayon, M.; Sanz-Medel, A.; Costa Pessoa, J.; Tomaz, I.; Kiss, T. *Dalton Trans.* **2009**, 2428.
4. Sanna, D.; Micera, G.; Garibba, E. *Inorg. Chem.* **2009**, *48*, 5747.
5. Davies, D. R.; Interthal, H.; Champoux, J. J.; Wim, G. J.; Hol, W. G. J. *Chem. Biol.* **2003**, *10*, 139.
6. Rehder, D.; Hoist, H.; Priebisch, W.; Vute, H. *J. Inorg. Biochem.* **1991**, *41*, 171.
7. Cavaco, I.; Costa Pessoa, J.; Costa, D.; Duarte, M. T.; Gillard, R. D.; Matias, P. M. *J. Chem. Soc., Dalton Trans.* **1994**, 149.
8. Costa Pessoa, J.; Cavaco, I.; Correia, I.; Duarte, M. T.; Gillard, R. D.; Henriques, R. T.; Higes, F. J.; Madeira, C.; Tomaz, I. *Inorg. Chim. Acta* **1999**, *293*, 1.
9. Dutta, S.; Mondal, S.; Chakravorty, A. *Polyhedron* **1995**, *14*, 1163.
10. Cavaco, I.; Costa Pessoa, J.; Duarte, M. T.; Henriques, R. T.; Matias, P. M.; Gillard, R. D. *J. Chem. Soc., Dalton Trans.* **1996**, *1989*.
11. Fulwood, R.; Schmidt, H.; Rehder, D. *J. Chem. Soc., Chem. Commun.* **1995**, 1443.

12. Correia, I.; Costa Pessoa, J.; Duarte, M. T.; Henriques, R. T.; Piedade, M. F. M.; Veiros, L. F.; Jakusch, T.; Dornyei, A.; Kiss, T.; Castro, M. M. C. A.; Geraldes, C. F. G. C.; Avecilla, F. *Chem. -Eur. J.* **2004**, *10*, 2301.
13. Koh, L. P.; Ranford, J. O.; Robinson, W. T.; Svensson, J. O.; Tan, A. L. C.; Wu, D. *Inorg. Chem.* **1996**, *35*, 6466.
14. Maurya, M. R.; Khurana, S.; Rehder, D. *Trans. Met. Chem.* **2003**, *28*, 511.
15. Costa Pessoa, J.; Correia, I.; Kiss, T.; Jakusch, T.; Castro, M. M. C. A.; Geraldes C. F. G. C.; *J. Chem. Soc., Dalton Trans.* **2002**, 4440.
16. Costa Pessoa, J.; Marcão, S.; Correia, I.; Goncalves, G.; Dornyei, A.; Kiss, T.; Jakusch, T.; Tomaz, I.; Castro, M. M. C. A.; Geraldes, C. F. G. C.; Avecilla, F. *Eur. J. Inorg. Chem.* **2006**, 3595.
17. Adão, P.; Costa Pessoa, J.; Henriques, R. T.; Kuznetsov, M. L.; Avecilla, F.; Maurya, M. R.; Kumar, U.; Correia, I. *Inorg. Chem.*, **2009**, *48*, 3542.
18. Rockenbauer, A.; Korecz, L. *Appl. Magn. Reson.* **1996**, *10*, 29.
19. Costa Pessoa, J.; Calhorda, M. J.; Cavaco, I.; Costa, P. J.; Correia, I.; Costa, D.; Vilas-Boas, L. F.; Félix, V.; Gillard, R. D.; Henriques, R. T.; Wiggins, R.; *Dalton Trans.* **2004**, 2855.
20. Nakajima, K.; Kojima, M.; Toriumi, K.; Saito, K.; Fujita, J. *Bull. Chem. Soc. Jpn.* **1989**, *62*, 760.

---

## MICROWAVE-ASSISTED CATALYTIC OXIDATION OF ALCOHOLS TO CARBONYL COMPOUNDS

YAUHEN YU. KARABACH, MAXIMILIAN N. KOPYLOVICH\*, KAMRAN T. MAHMUDOV, AND ARMANDO J. L. POMBEIRO\*

*Centro de Química Estrutural, Complexo I, Instituto Superior Técnico, Universidade de Lisboa, Lisboa, Portugal*

### 18.1 INTRODUCTION

Aldehydes and ketones, which are produced by different methods and starting materials, are important carbonyl compounds that are widely used as such and for further processing [1]. For example, cyclohexanone can be prepared upon cyclohexane oxidation, dehydrogenation of cyclohexanol at high temperature, or via catalytic oxidation of cyclohexanol under milder conditions. Acetophenone can be produced by the Hock process or be obtained via ethylbenzene oxidation with dioxygen, whereas benzaldehyde is produced industrially by toluene oxidation or by hydrolysis of benzal chloride in the presence of different acids and/or metal salts (i.e., tin(II), tin(IV), iron, or zinc chlorides) [1].

Although the methods of production of bulk chemicals often suffer from low selectivity and/or productivity per pass, they continue to be the major methods for the synthesis of carbonyl compounds as the formed by-products are also demanded chemicals. However, such protocols are not economically attractive for the production of specific carbonyl compounds in the fine chemicals industry, where the selective and effective oxidation of valuable starting materials (e.g., alcohols) to the corresponding carbonyl compounds is required. Hence, the development of alcohol oxidation methods in fine chemicals industry directs toward achieving highly selective, efficient, and environmentally friendly catalytic systems [2]. Thus, the oxidation of alcohols with stoichiometric amounts of inorganic oxidants, such as chromium(VI) or manganese compounds, is being substituted for the TEMPO-mediated aerobic (TEMPO-2,2,6,6-tetramethylpiperidin-1-yl)oxidanyl [3], metal-catalyzed oxidations with hydrogen- or organoperoxides [4], or hydrogen-transfer reactions catalyzed by rhodium or ruthenium complexes [5]. Nevertheless, the search for new, environmentally friendly, and efficient alcohol oxidation protocols, as well as the improvement of the known ones, is of current interest. In this respect, leverage points for research concern the application of green oxidants, green solvents, or solvent-free processes, development of new catalytic systems, use of energy efficient heating methods, etc.

Microwave (MW) heating is one of the simplest but effective ways to enhance energy efficiency and productivity in small-scale chemical production [6]. In contrast to conventional heating (CH), MW irradiation interacts directly with the polar molecules (which can be of substrates, intermediates, or catalysts) and, if nonpolar solvents or solvent-free processes are used, it can provide an efficient energy transfer directly to the reactants [7]. Generally, it is assumed that MW irradiation itself can accelerate the reaction rate, on account of (i) thermal and (ii) nonthermal effects, namely, (i) local overheating ("hot spot" effect, etc.); (ii) influence on the preexponential factor  $A$  in the Arrhenius equation  $k = A \exp(-\Delta G^\# / RT)$ , and on the  $-T\Delta S^\#$  part in the  $\Delta G^\# = \Delta H^\# - T\Delta S^\#$  equation for the activation energy [7, 8]. Nevertheless, these effects, especially the nonthermal ones, are still disputed and it has been claimed [9] that there is no direct evidence yet for nonthermal effects. Recent studies of MW-assisted homogeneous reactions have shown that external infrared (IR) temperature controllers that

are mainly used in MW systems do not accurately monitor the sample temperature and usually tend to underestimate its value. Hence, a proper calibration (apart from a fast response) of the IR sensors is required to help overcome this problem. In addition, the sample temperature profile is inhomogeneous within the reaction vessel [9]. Therefore, the interaction of MW irradiation with a reaction mixture is rather complex and the nature of the eventual advantages of the MW irradiation heating method is subject to debate.

However, it is known [10] that the simultaneous application of a catalyst and MW irradiation in some cases has a pronounced synergistic effect in comparison with the catalyst and the MW applied separately, or in comparison with the catalysis under CH. This synergistic effect also deserves particular attention in the important and widely used oxidation of alcohols to the corresponding carbonyl compounds. Thus, the main aim of this chapter is to illustrate recent advances in homogeneous and heterogeneous MW-assisted catalytic oxidation of alcohols. For clarity, the homogeneous and heterogeneous processes are discussed separately.

## 18.2 HOMOGENEOUS CATALYSIS

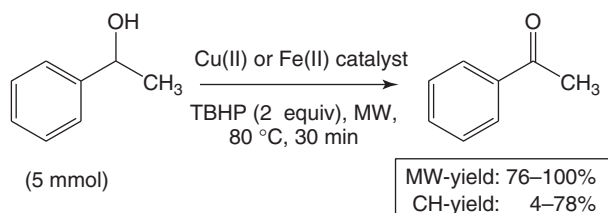
### 18.2.1 Oxidation with *tert*-Butyl Hydroperoxide Catalyzed by Copper(II) and Iron(II) Complexes

Effective solvent-free peroxidative oxidations of 1-phenylethanol (Scheme 18.1) and/or some secondary aliphatic alcohols toward the corresponding ketones with *tert*-butylhydroperoxide (TBHP) under MW irradiation, catalyzed by copper(II)-alkoxy-triazapentadienato ( $\text{Cu}^{\text{II}}\text{-TAP}$ ) [10, 11] complexes **1**, **2**, dicopper(II)-aminopolyalcoholate ( $\text{Cu}^{\text{II}}\text{-APA}$ ) [12] complexes **3**, **4**, arylhydrazone- $\beta$ -diketonate ( $\text{Cu}^{\text{II}}\text{-AHBD}$ ) complex **5** [13], mixed-N,S copper(II) and iron(II) complexes **6–11** [14] and by the tetranuclear copper(II) arylhydrazone of malononitrile complex **12** [15], have been achieved (Scheme 18.2).

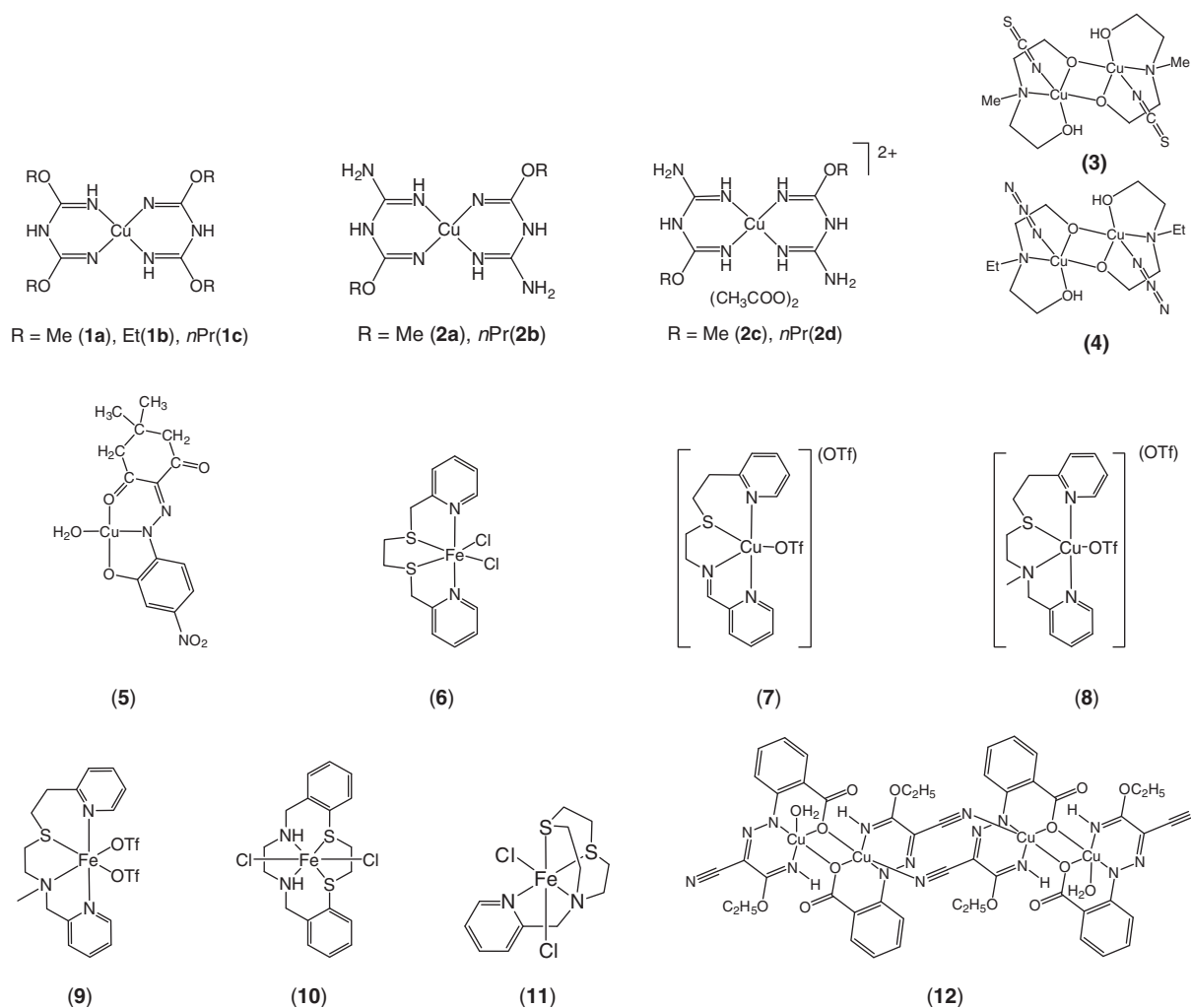
In general, the utilization of MW irradiation instead of CH significantly enhances the conversion of the alcohols, that is, MW-assisted reactions performed in the presence of  $\text{Cu}^{\text{II}}\text{-TAP}$  and  $\text{Cu}^{\text{II}}\text{-APA}$  complexes **1a**, **2a**, **2b**, **2c**, and **4** led to 100%, 90%, 95%, 81%, and 92% yields of acetophenone from 1-phenylethanol in 30 min at 80 °C (Table 18.2, runs 2, 9–11, and 18), while the corresponding yields under CH are 4%, 72%, 78%, 55%, and 51% (Table 18.2, runs 3, 13–15, and 20) [10a, 11, 12]. It is also worth mentioning that under MW irradiation in the presence of **1a** and **4**, yields of circa 58% and 91% were achieved in 15 min (Table 18.2, runs 1 and 17, respectively) [10a, 12]. When hydrogen peroxide was used as oxidant, quite a low yield of acetophenone was obtained in the presence of **1a** at 80 °C (Table 18.2, run 7) [10a] (Scheme 18.3).

The activity of the symmetrical Cu-TAP complexes appear to decrease with the increase in the number of carbon atoms in the alkoxy substituents (Table 18.2, runs 2, 6, and 8) [10a, 11]. The activities of the studied unsymmetrical Cu-TAP complexes mainly depend on their charge, neutral complexes being less active (Table 18.2, runs 9, 10 vs 11, 12) [11]. The  $\text{Cu}^{\text{II}}\text{-AHBD}$  complex **5** and the mixed-N,S copper(II) complexes **7** and **8** are apparently less active and led to circa 31–39% of acetophenone yields in 30 min (Table 18.2, runs 21, 24, and 25) [13, 14b].

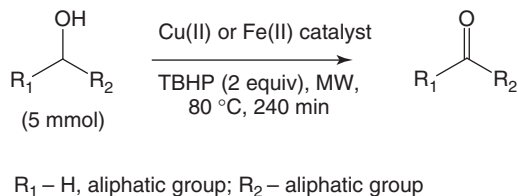
The activity of the iron(II) complexes (**6**, **9–11**) is lower, the overall yields not exceeding 21% (Table 18.2, runs 23, 26–28) [14]. However, the combination of **6–11** with a catalyst promoter, such as, pyrazine-2-carboxylic acid (Hpc), pyridine (py), or pyridazine (pydz), leads to a significant increase of the acetophenone yield, for example, for the systems **6/9/10**-Hpc, **7/8**-py, **7/8**-pydz, yields of circa 92–75% were achieved in 30 min (Table 18.1) [14]. Moreover, for **9**-Hpc, the yield of circa 74% was achieved in 5 min with corresponding turnover frequency (TOF) value of 4440 (Table 18.1, run 9) [14b]. For the systems in Table 18.1, the yields obtained in MW-assisted processes are also superior to those obtained under CH, that is, for the **6**-Hpc system, an acetophenone yield of circa 26 % was achieved in 30 min, while utilization of MW irradiation allowed to obtain a yield of 76% (Table 18.1, run 2 vs 1).



**Scheme 18.1** Oxidation of 1-phenylethanol under MW irradiation or conventional heating (CH) [10a, 11–15].



**Scheme 18.2** Schematic representation of the structures of copper(II) and iron(II) catalysts for the oxidation of alcohols with organoperoxides.



$\text{R}_1 - \text{H}$ , aliphatic group;  $\text{R}_2 - \text{aliphatic group}$

**Scheme 18.3** Catalytic oxidation of primary and secondary aliphatic alcohols [10a, 11, 12, 14a, 15].

It is worthwhile to mention that the performance of the systems strongly depends on the temperature, namely, a temperature decrease from 80 to 50 °C lowers the yields down to circa 10% and 15% with catalyst **1a** (Table 18.2, run 2 vs 5) and **8** (Table 18.1, run 6 vs 7), respectively [10a, 14b]. The range of temperatures that allows obtaining a high alcohol conversion is narrow as shown in Fig. 18.1. Further temperature increase above circa 100 °C leads to TBHP (or H<sub>2</sub>O<sub>2</sub>) decomposition with uncontrollable temperature/pressure increase inside the reactor and to a significant yield drop [14b].

The performance of the catalytic systems toward oxidation of primary and secondary aliphatic alcohols is lower and, in order to achieve reasonable yields of the corresponding ketones, the reaction time was increased up to 4 h (Table 18.3) [10a, 11, 12, 14a].

**TABLE 18.1** Oxidation of 1-Phenylethanol with TBHP Under MW Irradiation Catalyzed by Cu<sup>II</sup> or Fe<sup>II</sup> Complexes<sup>a</sup>

Run	Catalyst, μmol	Heating Method	Time, min	TON (TOF)	Yield, %	References
1	<b>1a</b> (10)	MW	15	290 ( $1.16 \times 10^3$ )	58	[10a]
2	<b>1a</b> (10)	MW	30	500 ( $1.00 \times 10^3$ )	100	
3 <sup>b</sup>	<b>1a</b> (10)	CH	30	20 (40)	4	
4 <sup>b</sup>	<b>1a</b> (10)	CH	300	405 (81)	81	
5 <sup>c</sup>	<b>1a</b> (10)	MW	30	50 (100)	10	
6	<b>1b</b> (10)	MW	30	485 (970)	97	
7 <sup>d</sup>	<b>1a</b> (10)	MW	30	100 (200)	20	
8	<b>1c</b> (10)	MW	30	150 (300)	30	[11]
9	<b>2a</b> (10)	MW	30	450 (900)	90	
10	<b>2b</b> (10)	MW	30	475 (950)	95	
11	<b>2c</b> (10)	MW	30	405 (910)	81	
12	<b>2d</b> (10)	MW	30	360 (720)	72	
13	<b>2a</b> (10)	CH	30	360 (720)	72	
14	<b>2b</b> (10)	CH	30	390 (780)	78	
15	<b>2c</b> (10)	CH	30	275 (550)	55	
16	<b>3</b> (10)	MW	15	105 (420)	21	[12]
17	<b>4</b> (10)	MW	15	455 ( $1.82 \times 10^3$ )	91	
18	<b>4</b> (10)	MW	30	460 (920)	92	
19	<b>3</b> (10)	CH	30	65 (130)	13	
20	<b>4</b> (10)	CH	30	255 (510)	51	
21	<b>5</b> (10)	MW	30	195 (390)	39	[13]
22	<b>5</b> (10)	MW	60	415 (415)	83	
23	<b>6</b> (10)	MW	30	25 (50)	5	[14a]
24	<b>7</b> (10)	MW	30	155 (310)	31	[14b]
25	<b>8</b> (10)	MW	30	165 (330)	33	
26	<b>9</b> (10)	MW	30	85 (170)	17	
27	<b>10</b> (10)	MW	30	75 (155)	15	[14c]
28	<b>11</b> (10)	MW	30	105 (210)	21	

<sup>a</sup>Reaction conditions are those indicated in Scheme 18.1. TON, turnover number (moles of product/moles of catalyst); TOF = TON/h.

<sup>b</sup>Under conventional heating (CH), included for comparative purposes.

<sup>c</sup>50 °C.

<sup>d</sup>Hydrogen peroxide (10 mmol, 2 equiv) used instead of TBHP.

As can be seen from the data in Table 18.3, the activities of the copper(II) catalysts are higher than that of the iron(II) **6**-Hpc system. The highest turnover number (TON) values (up to 910, Table 18.3, run 21) were obtained with the catalyst precursor **12**, but it is worth mentioning that it is tetranuclear (the activity per copper(II) atom is lower than that of the mononuclear complex **1a**) and can dissociate in the reaction mixture to mononuclear and dinuclear species ( $[\text{Cu}(\text{HL}^4)]^+$  and  $[\text{Cu}_2(\text{HL}^4)_2(\text{MeOH})]^+$ , respectively) that, in their turn, can catalyze the oxidation [15].

### 18.2.2 Anaerobic Oxidation Catalyzed by Palladium(II) Complexes

An efficient procedure of anaerobic MW-assisted oxidation of secondary alcohols (Scheme 18.4) in the presence of *N*-heterocyclic carbene palladium (NHC)-Pd catalysts (Scheme 18.5) with 2,4-dichlorotoluene or other aryl halides as oxidants was reported recently [16].

The reactions were performed in the presence of various bases, the best results being achieved with  $\text{NaO}^i\text{Bu}$  (Table 18.4) [16]. The proposed mechanism of the reaction involves addition of the aryl halide and alkoxy anion to the metal center with the elimination of halide anion. The intermediate thus formed undergoes decomposition with the formation of the carbonyl product and regeneration of the initial form of the catalyst (Scheme 18.6) [17]. The formation of an alkoxy anion is promoted by the presence of a base in the reaction mixture.

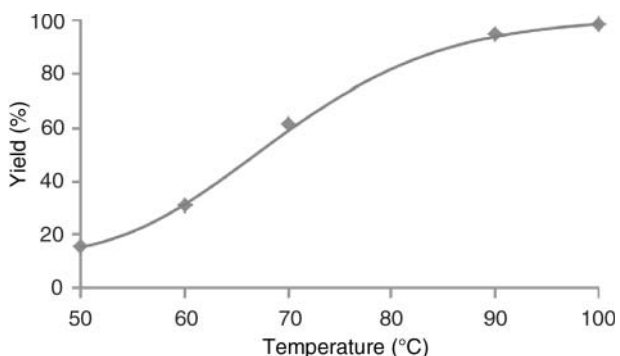


**Figure 18.1** Effect of the temperature variation on the acetophenone yield, in the MW-assisted solvent-free mild peroxidative oxidation of 1-phenylethanol catalyzed by **8**-pydz. Reaction conditions are those indicated in Table 18.1.

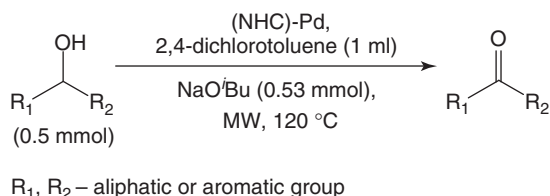
**TABLE 18.2 Oxidation of 1-Phenylethanol with TBHP Under MW Irradiation Catalyzed by Mixed-N,S Cu<sup>II</sup> or Fe<sup>II</sup> Complexes<sup>a</sup>**

Run	Catalyst, $\mu\text{mol}$	Heating Method	Time, min	TON (TOF)	Yield, %	References
1	<b>6</b> -Hpca (10/50)	MW	30	380 (760)	76	
2 <sup>b</sup>	<b>6</b> -Hpca (10/50)	CH	30	130 (260)	26	[14a]
3	<b>7</b> -py (10/200)	MW	30	380 (760)	76	[14b]
4	<b>7</b> -pydz (10/200)	MW	30	405 (810)	81	
5	<b>8</b> -py (10/200)	MW	30	410 (820)	82	
6	<b>8</b> -pydz (10/200)	MW	30	460 (920)	92	
7 <sup>c</sup>	<b>8</b> -pydz (10/200)	MW	30	75 (150)	15	
8	<b>9</b> -Hpca (10/200)	MW	30	385 (770)	77	
9	<b>9</b> -Hpca (10/200)	MW	5	370 ( $4.44 \times 10^3$ )	74	
10	<b>10</b> -Hpca (10/200)	MW	30	375 (750)	75	[14c]
11	<b>11</b> -Hpca (10/200)	MW	30	375 (750)	75	

<sup>a</sup>Reaction conditions are those indicated in Scheme 18.1. TON, turnover number (moles of product/moles of catalyst); TOF = TON/h.

<sup>b</sup>Under conventional heating (CH), included for comparative purposes.

<sup>c</sup>50 °C.



**Scheme 18.4** Catalytic anaerobic oxidation of secondary alcohols [16].

As it can be seen (Table 18.4), the TON values are comparable to those obtained for metal-catalyzed peroxidative oxidation of secondary alcohols discussed above. However, in the case of the anaerobic oxidation, the reaction time is shorter and hence the TOF values (up to  $11.2 \times 10^3$ , Table 18.4, run 1) [16] are superior to those for the peroxidative oxidation (Tables 18.1–18.3) [10a, 11–14].

### 18.2.3 Hydrogen-Transfer Type Oxidations Catalyzed by Rhodium(I) and Ruthenium(II) Complexes

The MW irradiation can also be applied for the hydrogen-transfer-type oxidation [18] of alcohols in the presence of the rhodium(I) or ruthenium(II) complexes with phosphine ligands  $[\text{RhCl}(\text{CO})(\text{PPh}_3)_2]$  (**15**) and  $[\text{RuCl}_2(\text{PPh}_3)_3]$  (**16**).

**TABLE 18.3** Oxidation of Secondary Aliphatic Alcohols with TBHP Under MW Irradiation Catalyzed by Cu<sup>II</sup> or Fe<sup>II</sup> Complexes<sup>a</sup>

Run	Substrate	Catalyst, $\mu\text{mol}$	Product	TON (TOF)	Yield, %	References
1 <sup>b</sup>	1-Hexanol	<b>1a</b> (10)	Hexanoic acid <sup>c</sup>	225 (56)	45	[10a]
2 <sup>d</sup>	2-Hexanol		2-Hexanone	125 (250)	25	
3	2-Hexanol		2-Hexanone	450 (112)	90	
4	3-Hexanol		3-Hexanone	410 (102)	82	
5	Cyclohexanol		Cyclohexanone	485 (121)	97	
6	2-Octanol		2-Octanone	425 (106)	85	
7	1-Hexanol	<b>2a</b> (10)	Hexanoic acid <sup>c</sup>	115 (29)	23	[11]
8	2-Hexanol		2-Hexanone	365 (91)	73	
9	3-Hexanol		3-Hexanone	290 (72)	58	
10	Cyclohexanol		Cyclohexanone	340 (85)	68	
11	1-Hexanol	<b>4</b> (10)	Hexanoic acid <sup>c</sup>	180 (45)	36	[12]
12	2-Hexanol		2-Hexanone	365 (91)	73	
13	3-Hexanol		3-Hexanone	375 (94)	75	
14	Cyclohexanol		Cyclohexanone	320 (80)	64	
15	1-Hexanol	<b>6</b> -Hpca (10/50)	Hexanoic acid	80 (20)	16	[14a]
16	2-Hexanol		2-Hexanone	140 (35)	28	
17	3-Hexanol		3-Hexanone	160 (40)	32	
18	Cyclohexanol		Cyclohexanone	180 (45)	36	
19 <sup>e</sup>	2-Hexanol	<b>12</b> (5)	2-Hexanone	750 (188)	75	[15]
20 <sup>e</sup>	3-Hexanol		3-Hexanone	720 (180)	72	
21 <sup>e</sup>	Cyclohexanol		Cyclohexanone	910 (228)	91	
22 <sup>e</sup>	2-Octanol		2-Octanone	730 (182)	73	

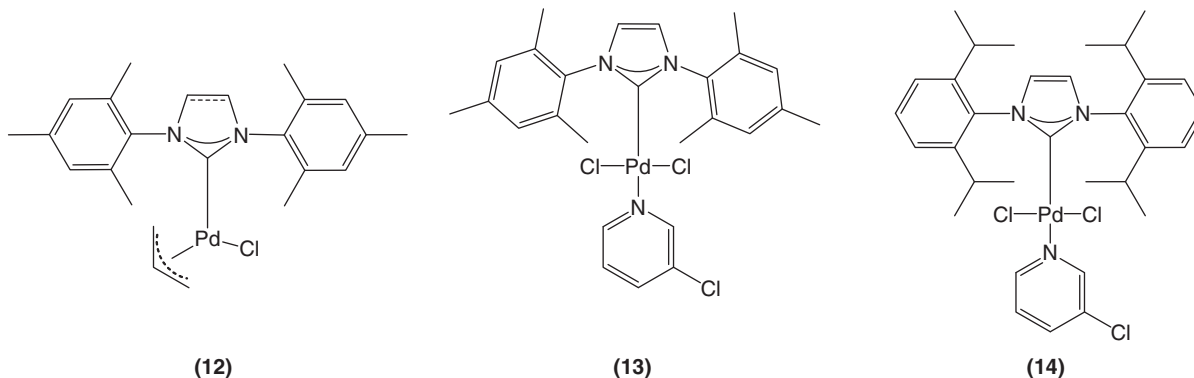
<sup>a</sup>Reaction conditions are those indicated in Scheme 18.3. TON, turnover number (moles of product/moles of catalyst); TOF = TON/h.

<sup>b</sup>20 mmol of TBHP (4 equiv).

<sup>c</sup>Hexanal (<1%) was also detected.

<sup>d</sup>30 min reaction time.

<sup>e</sup>TON and TOF values estimated by us.

**Scheme 18.5** Schematic representation of structures of (NHC)-Pd catalysts.

respectively, as catalyst precursors [19]. The alcohol is a hydrogen donor, while methyl acrylate or methyl vinyl ketone, present in the reaction mixture, plays the role of a hydrogen acceptor (Scheme 18.7).

The reaction can proceed through the formation of metal hydride species. Moreover, it was found that in case of ruthenium catalysts, the reaction rate can be significantly improved by addition of a base to the reaction mixture [20]. The base promotes the formation of ruthenium alkoxide that further undergoes a  $\beta$ -elimination to give, in sequence, a mono- and a dihydride complex (Scheme 18.8) [21], the latter being assumed as an active form of the catalyst [22].

The results on oxidation of the primary and secondary alcohols are combined in Table 18.5.

**TABLE 18.4** Anaerobic Oxidation of Secondary Alcohols Under MW Irradiation Catalyzed by (NHC)-Pd<sup>II</sup><sup>a</sup>

Run	Catalyst, mol%	Time, min	Product	TON (TOF) <sup>b</sup>	Yield, %
1	<b>12</b> (0.025)	2		372 ( $11.2 \times 10^3$ )	93
2	<b>12</b> (0.025)	5		380 ( $4.56 \times 10^3$ )	95
3	<b>13</b> (0.025)	2		336 ( $10.1 \times 10^3$ )	84
4	<b>14</b> (0.025)	2		272 ( $8.16 \times 10^3$ )	68
5	<b>12</b> (0.05)	10		204 ( $1.22 \times 10^3$ )	92
6	<b>12</b> (0.05)	5		215 ( $2.58 \times 10^3$ )	97
7	<b>12</b> (0.05)	5		211 ( $2.53 \times 10^3$ )	95
8	<b>12</b> (0.05)	10		195 ( $1.17 \times 10^3$ )	88
9	<b>12</b> (0.05)	5		189 ( $2.27 \times 10^3$ )	85

<sup>a</sup>Reaction conditions are those indicated in Scheme 18.4 [16]. TON, turnover number (moles of product/moles of catalyst); TOF = TON/h.

<sup>b</sup>Estimated by us.

The rhodium(I) catalyst **15** was found to accelerate the selective oxidation of secondary alcohols (Table 18.5), from their mixture with the primary ones, and the selective conversion of diols into keto alcohols (Scheme 18.9) [19].

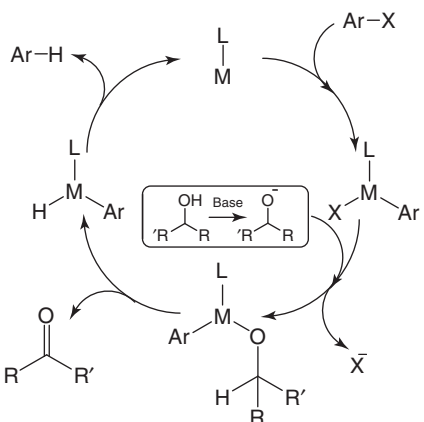
## 18.3 HETEROGENEOUS CATALYSIS

### 18.3.1 Aerobic Oxidation Catalyzed by Metal Oxides

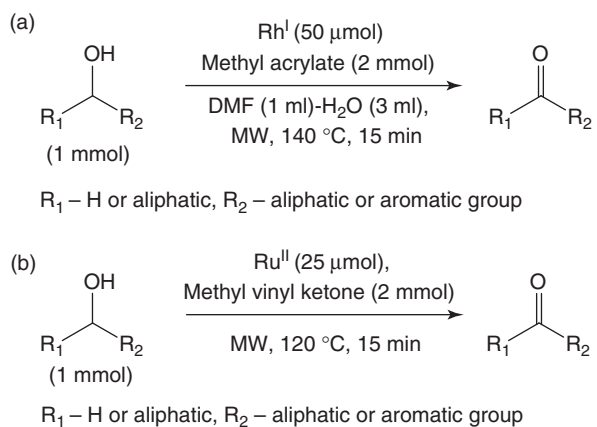
The improvement of the catalytic heterogeneous aerobic oxidation of alcohols is a desired task from environmental and commercial points of view, as air/dioxygen is a cheap and environmentally friendly oxidant.

Catalytic systems based on various metal oxides under MW-assisted, solvent-free, aerobic conditions were compared for benzyl alcohol oxidation (Table 18.6) [23]. The manganese oxides were prepared by solution-based or solid-state reaction procedures [24], while V<sub>2</sub>O<sub>5</sub>, CuO, Fe<sub>2</sub>O<sub>3</sub>, Co<sub>2</sub>O<sub>3</sub>, and NiO were obtained via sol–gel or precipitation methods [25]. The benzyl alcohol oxidation was performed in a glass reactor where the slurry of catalyst with alcohol was stirred under dioxygen pressure and MW irradiation (Scheme 18.10, Table 18.6).

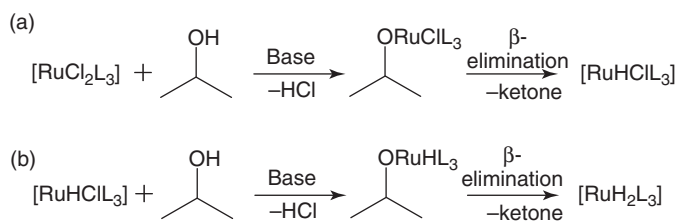
MnO<sub>2</sub> was the most active among the tested metal oxides under the reaction conditions used. Comparison of the activities of the MnO<sub>2</sub>-based catalytic system for the MW-assisted and CH methods in the benzyl alcohol oxidation (with O<sub>2</sub> or air) revealed that MW irradiation significantly increases the reaction rate (by circa two times) with similar selectivities (“hot spot” effect) [23]. The tested MnO<sub>2</sub> catalyst can be recovered and recycled (the activity remains unchanged at least for a few cycles); the catalyst should be washed with deionized water and acetone and then dried at 120 °C [23].



**Scheme 18.6** Proposed mechanism for anaerobic oxidation of secondary alcohols with aryl halides ( $\text{Ar} = \text{aryl}$ ;  $\text{X} = \text{I}, \text{Cl}, \text{Br}$ ) [17].



**Scheme 18.7** Hydrogen-transfer-type oxidation of primary and secondary alcohols [19].



**Scheme 18.8** Formation of ruthenium hydride catalysts in the presence of a base ( $\text{L} = \text{PPh}_3$ ) [21].

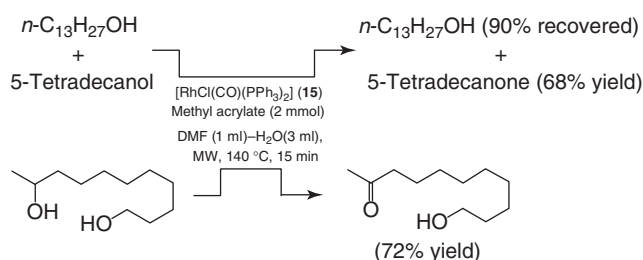
### 18.3.2 Oxidation with Hydrogen Peroxide Catalyzed by Metal Composites

The activity of some heterogeneous catalytic systems based on iron- and titanium-supported catalysts and hydrogen peroxide as oxidant was recently improved by utilization of MW irradiation. Thus, the MW-assisted oxidation of alcohols with hydrogen peroxide in water-acetonitrile media in the presence of various iron-, aluminum-, mixed iron/aluminum-, titanium-, and cobalt-supported (on MCM-41[26] and SBA-15 [27]) catalysts was reported recently [10b, 28]. The supported iron nanoparticles (Fe-NPs) were prepared from a suspension of iron(II) chloride in ethanol under MW [28a]. The preparation of Fe/Al-MCM-41 was similar, but with the use of the Al-derived support. The Ti-<sup>3+</sup>-B-MCM-41 catalyst was prepared from

**TABLE 18.5** Hydrogen-Transfer-Type Oxidation of Alcohols Under MW Irradiation Using the Rhodium(I)  $[\text{RhCl}(\text{CO})(\text{PPh}_3)_2]$  (15) and Ruthenium(II)  $[\text{RuCl}_2(\text{PPh}_3)_3]$  (16) Complexes as Catalyst Precursors<sup>a</sup>

Run	Catalyst	Substrate	Product	Yield, %
1	<b>15</b>	5-Tetradecanol	5-Tetradecanone	86
2		Cyclododecanol	Cyclododecanone	99
3		Cyclooctanol	Cycloocatanone	68
4		Benzyl alcohol	Benzaldehyde	—
5		n-Tridecanol	Tridecanal	—
6	<b>16</b>	n-Heptanol	Heptanal	45
7		n-Tridecanol	Tridecanal	77
8		Benzyl alcohol	Benzaldehyde	54
9		Cyclooctanol	Cycloocatanone	54

<sup>a</sup>Reaction conditions are those indicated in Scheme 18.7 [19].



**Scheme 18.9** Selective hydrogen-transfer-type oxidation of secondary aliphatic alcohols [19].

**TABLE 18.6** Aerobic Oxidation of Benzyl Alcohol Under MW Irradiation Catalyzed by Various Metal Oxides<sup>a</sup>

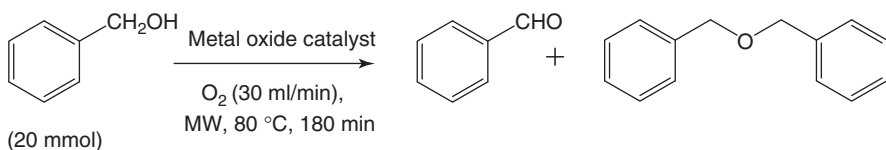
Run	Catalyst (0.5 g)	BET Surface Area, m <sup>2</sup> /g	Conversion, %	Selectivity, %	
				Benzaldehyde	Benzyl Ether
1	MnO <sub>2</sub>	88.6	37.7	98.6	1.4
2	Mn <sub>2</sub> O <sub>3</sub>	47.3	15.4	90.7	9.3
3	Mn <sub>3</sub> O <sub>4</sub>	59.4	17.5	96.1	3.9
4	MnO	41.2	4.0	95.9	4.1
5	V <sub>2</sub> O <sub>5</sub>	35.9	2.5	94.3	5.7
6	CuO	43.1	3.9	95.7	4.3
7	Fe <sub>2</sub> O <sub>3</sub>	66.3	6.7	80.8	19.2
8	Co <sub>2</sub> O <sub>3</sub>	80.1	11.7	87.2	12.8
9	NiO	72.8	13.5	96.5	3.5

<sup>a</sup>Reaction conditions are those indicated in Scheme 18.10 [23].

Ti-MCM-41 composite [29], which was grafted with titanium(IV) *tert*-butoxide. The activities and some properties of these systems are presented in Table 18.7.

Good results were obtained with the Fe/Al-MCM-41 and Fe/Al-SBA-15 catalysts, leading to a maximum of circa 54% conversion of the alcohol with circa 90% selectivity toward benzaldehyde, in 1.5 min (Table 18.7, runs 8, 9) [28b]. The synergistic effect of the Fe/Al supported materials was proposed to result from the possible interaction of Fe<sub>2</sub>O<sub>3</sub> species with the aluminum framework of the support (i.e., formation of Fe–O–Al moieties). Tests also showed that Fe/Al-MCM-41 can be applied as an efficient catalyst for the oxidation of secondary aliphatic alcohols, such as, cyclohexanol, with 37% conversion and 99% selectivity toward the ketone in 3 min [28b].

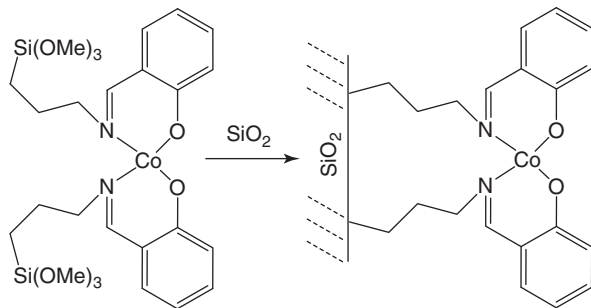
A silica-supported Co(II) salen complex (Co(II)/SBA-15, Scheme 18.11 [27], surface area 450 m<sup>2</sup>/g) was tested as a catalyst for the oxidation of benzyl alcohol and some other primary and secondary alcohols under MW irradiation, at



Scheme 18.10 Aerobic oxidation of benzyl alcohol [23].

TABLE 18.7 Oxidation of Benzyl Alcohol with Hydrogen Peroxide Under MW Irradiation Catalyzed by Iron and Titanium-Supported Catalysts<sup>a</sup>

Run	Catalyst (0.05 g)	Fe Loading, wt%	Surface Area, m <sup>2</sup> /g	Substrate, mmol	H <sub>2</sub> O <sub>2</sub> , mmol	Time, min	Conversion, %	Selectivity <sup>b</sup> , %	References
1 <sup>c</sup>	Fe/MCM-41	0.32	1101	1.85	4.0	60	25	>95	28a
2 <sup>c</sup>	Fe/starch	0.35	—	1.85	4.0	60	30	>95	
3 <sup>c</sup>	Fe/cellulose	0.29	—	1.85	4.0	60	28	>95	
4	Siliceous support	—	879/880	2.0	5.3	60	—	—	28b
5	Fe/Si-MCM-41	0.48	—	2.0	5.3	60	25	>99	
6	Fe/Si-SBA-15	0.42	—	2.0	5.3	60	22	>99	
7	Al-supports	—	937/747	2.0	5.3	60	<15	>99	
8	Fe/Al-MCM-41	0.54	970	2.0	5.3	1.5	53	90	
9	Fe/Al-SBA-15	0.63	688	2.0	5.3	1.5	54	92	
10 <sup>d</sup>	Ti- <sup>1</sup> B-MCM-41	—	926	20.0	15.0	30	40	>99	28c

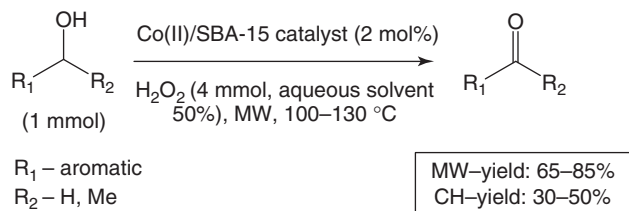
<sup>a</sup>Reaction conditions: acetonitrile (2 ml), MW (300 W).<sup>b</sup>Selectivity concerning benzaldehyde.<sup>c</sup>MW (200 W, 70–90 °C).<sup>d</sup>0.1 g of catalyst, no acetonitrile, MW (300 W, 130–140 °C).

Scheme 18.11 Co(II) salen complex supported on SBA-15 [27].

100–140 °C (Scheme 18.12, Table 18.8) [10b]. It was shown that the performance of the MW-assisted method is superior to that of CH (Table 18.8, runs 1–3 vs 4–6, respectively), in terms of achieving higher yields and selectivities toward benzaldehyde. The catalyst can be recycled, but its activity significantly drops after 5 cycles [10b].

Catalytic systems based on gold clusters confined within mesoporous silica were used for oxidation of primary and secondary alcohols with hydrogen peroxide in aqueous media in the presence of a base under MW irradiation, giving mainly the corresponding ketones and/or aldehydes and/or carboxylic acids (Scheme 18.13, Table 18.9) [30].

Different methods to deposit the gold clusters on silica were used and the activities of the thus obtained Au-SBA-15 composites were compared. [Au-SBA-15(DP)] and [Au-SBA-15(IP)] were obtained by the deposition, precipitation, and impregnation methods, respectively, whereas a multistep procedure was applied for the preparation of [Au-SBA-15(20)], that is,  $\text{Au}_{11}^{3+}$  clusters protected by triphenylphosphine [31] were deposited on SBA-15 in dichloromethane–ethanol, and the obtained  $\text{Au}_{11}:\text{TPP}$ -SBA-15 composite was calcined.



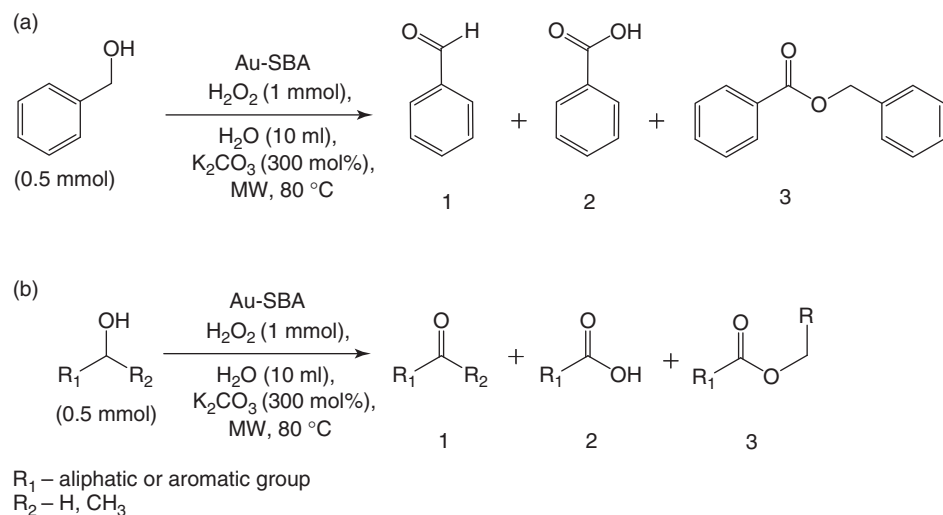
**Scheme 18.12** Oxidation of primary and secondary alcohols catalyzed by Co(II)/SBA-15 [27].

**TABLE 18.8 Oxidation of Primary and Secondary Alcohols with Hydrogen Peroxide Under MW Irradiation Catalyzed by Co(II)/SBA-15 Catalyst<sup>a</sup>**

Run	Substrate	Heating Method	Temperature, °C	Time, h	Conversion, %	Selectivity <sup>b</sup> , %
1	Benzyl alcohol	MW	100	0.75	65	95
2	Benzyl alcohol	MW	120–130	0.75	85	90
3	Benzyl alcohol	MW	120–130	1	85	95
4	Benzyl alcohol	CH	100	48	<30	70
5	Benzyl alcohol	CH	120	48	55	60
6	Benzyl alcohol	CH	140	24	50	80
7	p-Chloro-benzyl alcohol	MW	120–130	0.5	95	>99
8	p-Methyl-benzyl alcohol	MW	120–130	0.75	80	>95
9	1-Phenylethanol	MW	120–130	0.75	90	>99

<sup>a</sup>Reaction conditions are those indicated in Scheme 18.12 [27].

<sup>b</sup>Selectivity concerning corresponding aldehydes and ketones.



**Scheme 18.13** Oxidation of primary and secondary alcohols catalyzed by Au-SBA-15 composites (Au-SBA: 0.25 at%) [30].

A quantitative conversion of benzyl alcohol was achieved in 1 h under MW irradiation, while under CH circa 84% of the alcohol was converted to the carbonyl products in 12 h (Table 18.9, runs 3 and 4). The catalytic system is much less active toward oxidation of aliphatic primary alcohols; only 17% of *n*-pentanol was converted to the corresponding aldehyde in 2 h (Table 18.9, run 9).

**TABLE 18.9 Oxidation of Primary and Secondary Alcohols with Hydrogen Peroxide Under MW Irradiation Catalyzed by Various Au-SBA-15 Composites<sup>a</sup>**

Run	Catalyst	Substrate	Time, min	Conversion, %	Selectivity, %		
					1	2	3
1	Au-SBA-15(DP)	Benzyl alcohol	60	71	20	36	0
2	Au-SBA-15(IP)	Benzyl alcohol	60	76	42	15	2
3	Au-SBA-15(20)	Benzyl alcohol	60	100	6	91	2
4 <sup>b</sup>	Au-SBA-15(20)	Benzyl alcohol	720	84	2	80	0
5	Au-SBA-15(20)	p-Chloro-benzyl alcohol	50	100	4	81	10
6	Au-SBA-15(20)	m-Hydroxy benzyl alcohol	25	100	11	86	0
7	Au-SBA-15(20)	1-Phenylethanol	90	98	96	—	—
8	Au-SBA-15(20)	1-Indanol	30	100	98	—	—
9	Au-SBA-15(20)	n-Pentanol	120	19	17	0	0
10	SBA-15	Benzyl alcohol	60	7	2	0	0

<sup>a</sup>Reaction conditions are those indicated in Scheme 18.13 [30].<sup>b</sup>Conventional heating was used.

## 18.4 CONCLUSIONS

Increase of temperature is the simplest way of reaction rate acceleration, but some drawbacks can be associated with CH, such as, drop of selectivity toward desired products and degradation of the catalyst. Utilization of MW irradiation instead of CH, can present marked advantages relative to the latter method, as described herein for some homogeneous alcohol oxidations, allowing to achieve higher and faster conversions of alcohols with acceptable selectivities. However, the activity of the catalytic systems, even under MW irradiation, is usually still low for the oxidation of aliphatic alcohols, except in a few cases, for example, the anaerobic oxidation catalyzed by some palladium(II) complexes.

Moreover, MW irradiation can enhance the efficiency of various heterogeneous catalytic alcohol oxidation systems (especially those of aromatic alcohols), namely, those concerning aerobic and peroxidative oxidation.

In spite of the disputed MW thermal and nonthermal effects concerning homogeneous reactions, the topic is gaining increased interest.

## REFERENCES

1. *Ulman's Encyclopedia of Industrial Chemistry*, 6th ed.; Wiley-VCH Verlag GmbH: Weinheim, **2002**.
2. *Modern Oxidation Methods*, 2nd ed.; Wiley-VCH Verlag GmbH: Weinheim, Germany, **2010**.
3. Sheldon, R. A.; Arends, I.; Ten Brink, G. J.; Dijksman, A. *Acc. Chem. Res.* **2002**, *35*, 774.
4. Sheldon, R. A.; Arends, I. W. C. E.; Dijksman, A. *Catal. Today* **2000**, *57*, 157.
5. Arends, I. W. C. E.; Sheldon, R. A. In *Modern Oxidation Methods*; Wiley-VCH Verlag GmbH: Weinheim, **2010**; p 147.
6. (a) Larhed, M.; Moberg, C.; Hallberg, A. *Acc. Chem. Res.* **2002**, *35*, 717; (b) Lubinu, M. C.; De Luca, L.; Giacomelli, G.; Porcheddu, A. *Chem.-Eur. J.* **2011**, *17*, 82; (c) Lin, H.-C.; Pan, J.-F.; Chen, Y.-B.; Lin, Z.-P.; Lin, C.-H. *Tetrahedron* **2011**, *67*, 6362; (d) Heropoulos, G. A.; Villalonga-Barber, C. *Tetrahedron Lett.* **2011**, *52*, 5319; (e) Cannon, K. A.; Geuther, M. E.; Kelly, C. K.; Lin, S.; MacArthur, A. H. R. *Organometallics* **2011**, *30*, 4067; (f) Bag, S.; Dasgupta, S.; Toeroek, B. *Curr. Org. Synth.* **2011**, *8*, 237; (g) Bagley, M. C.; Lin, Z.; Phillips, D. J.; Graham, A. E. *Tetrahedron Lett.* **2009**, *50*, 6823; (h) Salvadori, J.; Balducci, E.; Zaza, S.; Petricci, E.; Taddei, M. *J. Org. Chem.* **2010**, *75*, 1841; (i) Young, D. D.; Nichols, J.; Kelly, R. M.; Deiters, A. *J. Am. Chem. Soc.* **2008**, *130*, 10048; (j) Mukhopadhyay, C.; Datta, A. *Catal. Commun.* **2008**, *9*, 2588; (k) Luque, R.; Badamali, S. K.; Clark, J. H.; Fleming, M.; Macquarrie, D. J. *Appl. Catal. A: Gen.* **2008**, *341*, 154.
7. de la Hoz, A.; Diaz-Ortiz, A.; Moreno, A. *Chem. Soc. Rev.* **2005**, *34*, 164.
8. Perreux, L.; Loupy, A. *Tetrahedron* **2001**, *57*, 9199.
9. (a) Herrero, M. A.; Kremsner, J. M.; Kappe, C. O. *J. Org. Chem.* **2007**, *73*, 36; (b) Obermayer, D.; Kappe, C. O. *Org. Biomol. Chem.* **2010**, *8*, 114.
10. (a) Figiel, P. J.; Kopylovich, M. N.; Lasri, J.; Guedes da Silva, M. F. C.; Frausto da Silva, J. J. R.; Pombeiro, A. J. L. *Chem. Commun.* **2010**, *46*, 2766; (b) Rajabi, F.; Balu, A. M.; Toreinia, F.; Luque, R. *Catal. Sci. Technol.* **2011**, *1*, 1051.

11. Kopylovich, M. N.; Karabach, Y. Y.; Guedes da Silva, M. F. C.; Figiel, P. J.; Lasri, J.; Pombeiro, A. J. L. *Chem.-Eur. J.* **2012**, *18*, 899.
12. Figiel, P. J.; Kirillov, A. M.; Guedes da Silva, M. F. C.; Lasri, J.; Pombeiro, A. J. L. *Dalton Trans.* **2010**, *39*, 9879.
13. Kopylovich, M. N.; Mahmudov, K. T.; Guedes da Silva, M. F. C.; Figiel, P. J.; Karabach, Y. Y.; Kuznetsov, M. L.; Luzyanin, K. V.; Pombeiro, A. J. L. *Inorg. Chem.* **2011**, *50*, 918.
14. (a) Fernandes, R. R.; Lasri, J.; Guedes da Silva, M. F. C.; da Silva, J. A. L.; Frausto da Silva, J. J. R.; Pombeiro, A. J. L. *Appl. Catal. A: Gen.* **2011**, *402*, 110; (b) Fernandes, R. R.; Lasri, J.; Guedes da Silva, M. F. C.; da Silva, J. A. L.; Frausto da Silva, J. J. R.; Pombeiro, A. J. L. *J. Mol. Catal. A: Chem.* **2011**, *351*, 100; (c) Fernandes, R. R.; Lasri, J.; Kirillov, A. M.; Guedes da Silva, M. F. C.; da Silva, J. A. L.; Frausto da Silva, J. J. R.; Pombeiro, A. J. L. *Eur. J. Inorg. Chem.* **2011**, *2011*, 3781.
15. Kopylovich, M. N.; Mizar, A.; Guedes da Silva, M. F. C.; Mac Leod, T. C. O.; Mahmudov, K. T.; Pombeiro, A. J. L. *Chem.-Eur. J.* **2013**, *19*, 588.
16. Landers, B.; Berini, C.; Wang, C.; Navarro, O. *J. Org. Chem.* **2011**, *76*, 1390.
17. Berini, C.; Brayton, D. F.; Mocka, C.; Navarro, O. *Org. Lett.* **2009**, *11*, 4244.
18. Brieger, G.; Nestrick, T. *J. Chem. Rev.* **1974**, *74*, 567.
19. Takahashi, M.; Oshima, K.; Matsubara, S. *Tetrahedron Lett.* **2003**, *44*, 9201.
20. Chowdhury, R. L.; Backvall, J. E. *J. Chem. Soc., Chem. Commun.* **1991**, *0*, 1063.
21. Backvall, J. E. *J. Organomet. Chem.* **2002**, *652*, 105.
22. Aranyos, A.; Csjernyik, G.; Szabo, K. J.; Backvall, J. E. *Chem. Commun.* **1999**, 351.
23. Su, Y.; Wang, L.-C.; Liu, Y.-M.; Cao, Y.; He, H.-Y.; Fan, K.-N. *Catal. Commun.* **2007**, *8*, 2181.
24. (a) Wang, X.; Li, Y. D. *J. Am. Chem. Soc.* **2002**, *124*, 2880; (b) Li, X. Q.; Xu, J.; Wang, F.; Gao, J.; Zhou, L. P.; Yang, G. Y. *Catal. Lett.* **2006**, *108*, 137.
25. Kobayashi, S.; Hamasaki, N.; Suzuki, M.; Kimura, M.; Shirai, H.; Hanabusa, K. *J. Am. Chem. Soc.* **2002**, *124*, 6550.
26. Luque, R.; Campelo, J. M.; Luna, D.; Marinas, J. M.; Romero, A. A. *Microporous Mesoporous Mater.* **2005**, *84*, 11.
27. Rajabi, F.; Luque, R.; Clark, J. H.; Karimi, B.; Macquarrie, D. J. *Catal. Commun.* **2011**, *12*, 510.
28. (a) Gonzalez-Arellano, C.; Campelo, J. M.; Macquarrie, D. J.; Marinas, J. M.; Romero, A. A.; Luque, R. *ChemSusChem* **2008**, *1*, 746; (b) Balu, A. M.; Pineda, A.; Yoshida, K.; Manuel Campelo, J.; Gai, P. L.; Luque, R.; Romero, A.A. *Chem. Commun.* **2010**, *46*, 7825; (c) Balu, A. M.; Hidalgo, J. M.; Campelo, J. M.; Luna, D.; Luque, R.; Marinas, J. M.; Romero, A. A. *J. Mol. Catal. A: Chem.* **2008**, *293*, 17.
29. Campelo, J. M.; Hidalgo, J. M.; Luna, D.; Marinas, J. M.; Romero, A. A. In *Molecular Sieves: From Basic Research to Industrial Applications, Pts A and B*; Cejka, J., Zilkova, N., Nachtigall, P., Eds.; Elsevier B.V.: The Netherlands, **2005**; Vol. 158, p 1429.
30. Liu, Y.; Tsunoyama, H.; Akita, T.; Tsukuda, T. *J. Phys. Chem. C* **2009**, *113*, 13457.
31. Shichibu, Y.; Negishi, Y.; Tsukuda, T.; Teranishi, T. *J. Am. Chem. Soc.* **2005**, *127*, 13464.



---

## OXIDATION OF GLYCEROL WITH HYDROGEN PEROXIDE CATALYZED BY METAL COMPLEXES

DALMO MANDELLI\* AND WAGNER A. CARVALHO

*Center for Natural and Human Sciences, Federal University of ABC, Santo André, Brazil*

LIDIA S. SHUL'PINA

*Nesmeyanov Institute of Organoelement Compounds, Russian Academy of Sciences, Moscow, Russia*

ALEXANDER M. KIRILLOV, MARINA V. KIRILLOVA AND ARMANDO J. L. POMBEIRO

*Centro de Química Estrutural, Instituto Superior Técnico, Universidade de Lisboa, Lisboa, Portugal*

GEORGIY B. SHUL'PIN

*Semenov Institute of Chemical Physics, Russian Academy of Sciences, Moscow, Russia*

### 19.1 INTRODUCTION

Glycerol is a by-product from biodiesel manufacturing [1]. It is also a coproduct in the production of fatty acids, alcohols, and soap using fats and oils as a feedstock (for reviews see Ref. [2a–i]). Oxidative transformations of glycerol are especially important from the practical point of view. For example, dihydroxyacetone (DHA) is a valuable and important compound, being the first product in the chain of consecutive glycerol oxidation reactions. DHA does not damage the skin and it is thus widely used in cosmetics as a safe skin coloring agent as well as a nutritional supplement. Besides, DHA is a versatile building block for the synthesis of a variety of fine chemicals [2j–l]. Another primary product of glycerol oxidation, glyceric acid, is used as a biochemical intermediate, being liver stimulant, cholesterolytic, anti-inflammatory and also a base material for functional surfactants [2m]. Glycolic acid that is formed from glycerol via C–C bond cleavage finds applications in skin-care products [2n]. It also reduces hyperpigmentation, wrinkles, and acne scarring [2o]. Finally, tartronic acid generated from glycerol is oxidized to mesoxalic acid, which is known as an antidote to cyanide poisoning [2p] and also has potential use as a complexing agent and as a precursor in organic synthesis [2q].

Different methods of glycerol oxidation employing air or molecular oxygen have been reported, using heterogeneous metal derivatives as catalysts [3]. Gold catalysts are especially active in glycerol oxidation [4]. A limited number of papers deal with heterogeneous metal-catalyzed glycerol oxidation with H<sub>2</sub>O<sub>2</sub> [5]. However, only few publications were devoted to the catalytic glycerol oxidation under homogeneous conditions, most of them using hazardous compounds. Thus, alkaline potassium hexacyanoferrate(III) oxidizes glycerol in an aqueous solution if osmium tetroxide [6a] or ruthenium(VII) oxide [6b] is used as catalyst. Glycerol has been oxidized by acidic solution of *N*-bromoacetamide in the presence of ruthenium(III) chloride as a homogeneous catalyst and mercuric acetate as scavenger [6c]. Qualitative experiments on the oxidation of glycerol catalyzed by iron ions have also been reported [6d].

Since glycerol is a very reactive compound, its oxidation typically gives rise to the formation of several compounds. Owing to the high reactivity of both glycerol and its oxidation products, the oxidation of glycerol usually affords desirable products in low yield and selectivity. Many heterogeneous catalysts lead to the predominant formation of the products of deep oxidation that are not very valuable (formic acid, formaldehyde, and even CO<sub>2</sub>). Unfortunately, DHA was either not produced at all in many aerobic heterogeneous oxidations or its yields were very low [5a]. Bimetallic Pt–Bi catalysts [7] show a high initial selectivity to DHA in acidic media but exhibit a strong deactivation during the reaction, which decreases activity and selectivity to DHA. As a result, only moderate yields may be achieved. In summary, it may be concluded that the selective oxidation of glycerol to DHA is a challenging task of contemporary catalytic chemistry. One of the main problems existing in this field is the over-oxidation of the initially formed reactive products. It is thus very difficult to produce primary oxygenates (e.g., DHA) in appropriate yields.

Therefore, we thought that the quest in finding the selective and atom-efficient oxidation of glycerol may consist in exploring its oxidation under mild conditions and using a homogeneous metal catalyst. Inspired by this idea and the fact that no information on the homogeneously catalyzed oxidation of glycerol with peroxides was reported until 2010, we probed the catalytic application of selected Os, Mn, and Cu complexes in the homogeneous oxidation of glycerol by peroxides. These studies resulted in the development of three different and rather efficient protocols for glycerol oxidation; their main features are summarized in this chapter.

## 19.2 GLYCEROL OXIDATION WITH H<sub>2</sub>O<sub>2</sub> CATALYZED BY THE Os<sub>3</sub>(CO)<sub>12</sub>/PYRIDINE COMBINATION

Earlier some of us discovered [8] an extremely powerful oxidizing system composed of triosmium dodecacarbonyl (**19.1**) and hydrogen peroxide, which was very efficient for the oxidation of alkanes to alkyl hydroperoxides in acetonitrile solution at 60 °C. The addition of pyridine in low concentration sufficiently improves the activity. Turnover number (TON) and turnover frequency (TOF) attained 60,000 and 24,000 h<sup>-1</sup>, respectively. Although the system operates with the formation of free radicals, the product selectivity in the alkane oxidation under certain conditions was very high because an alkyl hydroperoxide is formed as the sole product. We applied this system to the oxidation of alcohols, including easily oxidizable 1-phenylethanol and glycerol. The kinetic curves of the alcohol consumption and ketone accumulation shown in Fig. 19.1 indicate that the ketone is formed in the yield circa 25%.

Glycerol was oxidized to DHA, glycolic acid, and hydroxypyruvic acid (Fig. 19.2). Concentrations (determined by <sup>1</sup>H NMR) and yields of these products are summarized in Table 19.1. The best result was obtained at 60 °C after 13 h. In this experiment (entry 3) glycerol conversion was 32%. The method normally used to quantify the products in the oxidation of glycerol is HPLC. Typically, an ion-exchange column and an acidic mobile phase are used. Two detectors are necessary in this case because, under these conditions, glycerol cannot be separated from DHA. Then, the peak detected by the refractive index (RI) detector corresponds to the mixture of glycerol and DHA. When the UV detector is used the area of the same peak corresponds exclusively to the DHA. By subtraction, it is possible to estimate the concentration of both compounds. In our work in Os- and Mn-catalyzed oxidation reactions, we developed a new protocol to quantify the products of glycerol oxidation using <sup>1</sup>H NMR. An example of the typical spectrum is shown below in Section 19.3 (Fig. 19.3).

## 19.3 OXIDATION OF GLYCEROL WITH H<sub>2</sub>O<sub>2</sub> CATALYZED BY SOLUBLE COMPLEX [LMn(O)<sub>3</sub>MnL](PF<sub>6</sub>)<sub>2</sub> AND ITS HETEROGENIZED FORM [LMn(O)<sub>3</sub>MnL]<sub>2</sub>[SiW<sub>12</sub>O<sub>40</sub>]

Recently, some of us found [9] that glycerol can be easily oxidized with H<sub>2</sub>O<sub>2</sub> (Figs. 19.4) catalyzed by the combination of soluble complex [LMn(μ-O)<sub>3</sub>MnL](PF<sub>6</sub>)<sub>2</sub> (**19.2a**) and its heterogenized form [LMn(μ-O)<sub>3</sub>MnL]<sub>2</sub>[SiW<sub>12</sub>O<sub>40</sub>] (**19.2b**) (L is 1,4,7-trimethyl-1,4,7-triazacyclononane, TMTACN). The data on the homogeneous oxidation catalyzed by soluble catalyst **19.2a** under different conditions are summarized in Tables 19.2 and 19.3. It can be concluded that the main product usually was DHA. However, in some cases, the products of deeper oxidation prevailed (see, e.g., Table 19.2, entries 4, 6, 7, 10, Table 19.3, entries 2–5, 12). Entries 11–14 of Table 19.2 demonstrate that, in the oxidation of glycerol, oxalic acid is

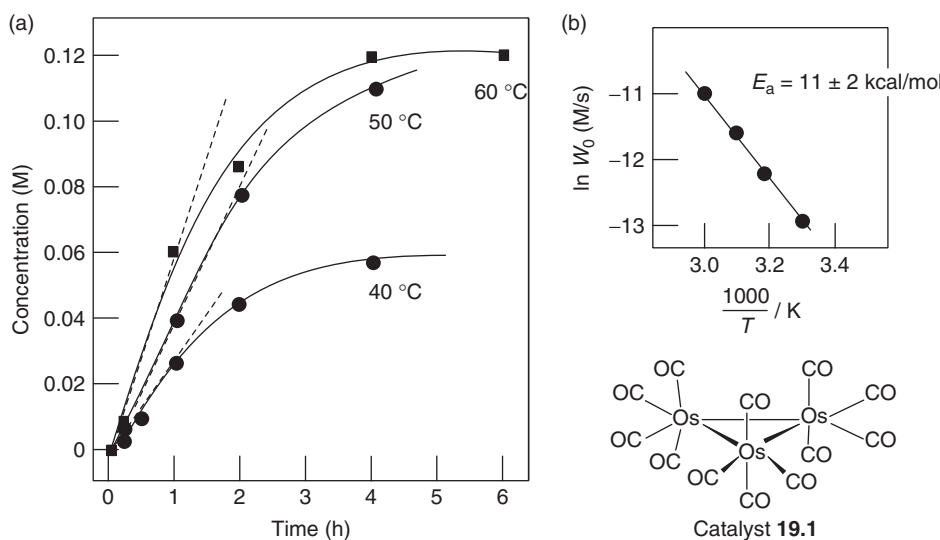


**Figure 19.1** (a) Oxidation of 1-phenylethanol (accumulation of acetophenone) at different temperatures. Conditions: [1-phenylethanol]<sub>0</sub> = 0.5 M, [H<sub>2</sub>O<sub>2</sub>]<sub>0</sub> = 1.0 M, [19.1] = 5 × 10<sup>-5</sup> M, [py] = 0.05 M, total volume of the reaction solution was 2.5 mL. (b) The Arrhenius plot based on the data presented in Graph A.

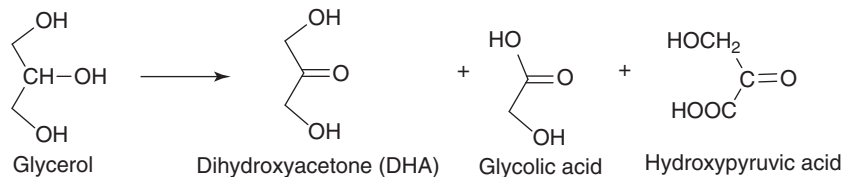


**Figure 19.2** Products obtained in glycerol oxidation catalyzed by the osmium complex (19.1)

**TABLE 19.1** Oxidation of Glycerol with the H<sub>2</sub>O<sub>2</sub>/19.1/Pyridine System<sup>a</sup>

Entry	Temperature, °C	Time, h	Products, Concentration, M (yield, %)		
			DHA	Glycolic Acid	Hydroxypyruvic Acid
1	60	0.5	0.0008 (0.4)	0 (0)	0 (0)
2		5	0.017 (8.3)	0.006 (4.0)	0.005 (2.7)
3		13 <sup>b</sup>	0.015 (7.5)	0.016 (8.0)	0.003 (1.5)
4	17	24	0.007 (4.3)	0 (0)	0 (0)
5		72	0.010 (5.0)	0.005 (2.5)	0.006 (3.0)
6		144	0.011 (5.5)	0.010 (5.0)	0.006 (3.0)

<sup>a</sup>Conditions: Solvent was acetonitrile, [glycerol]<sub>0</sub> = 0.2 M, [H<sub>2</sub>O<sub>2</sub>]<sub>0</sub> = 0.3 M, [Os<sub>3</sub>(CO)<sub>12</sub>] = 5 × 10<sup>-5</sup> M, [py] = 0.05 M, total volume of the reaction solution was 2.5 mL. Yields (%) in parentheses are based on starting glycerol.

<sup>b</sup>Glycerol conversion was 32%.

not an obligatory component of the catalytic system. The maximum yield of all valuable oxidation products attained 45% (Table 19.3, entry 12).

The oxidation of DHA under similar conditions has also been studied (Figs. 19.5 and 19.6). As DHA does not have the secondary hydroxyl groups, it is less reactive than glycerol in the ketonization reaction. The “19.2a/oxalic acid/H<sub>2</sub>O<sub>2</sub>/CH<sub>3</sub>CN”

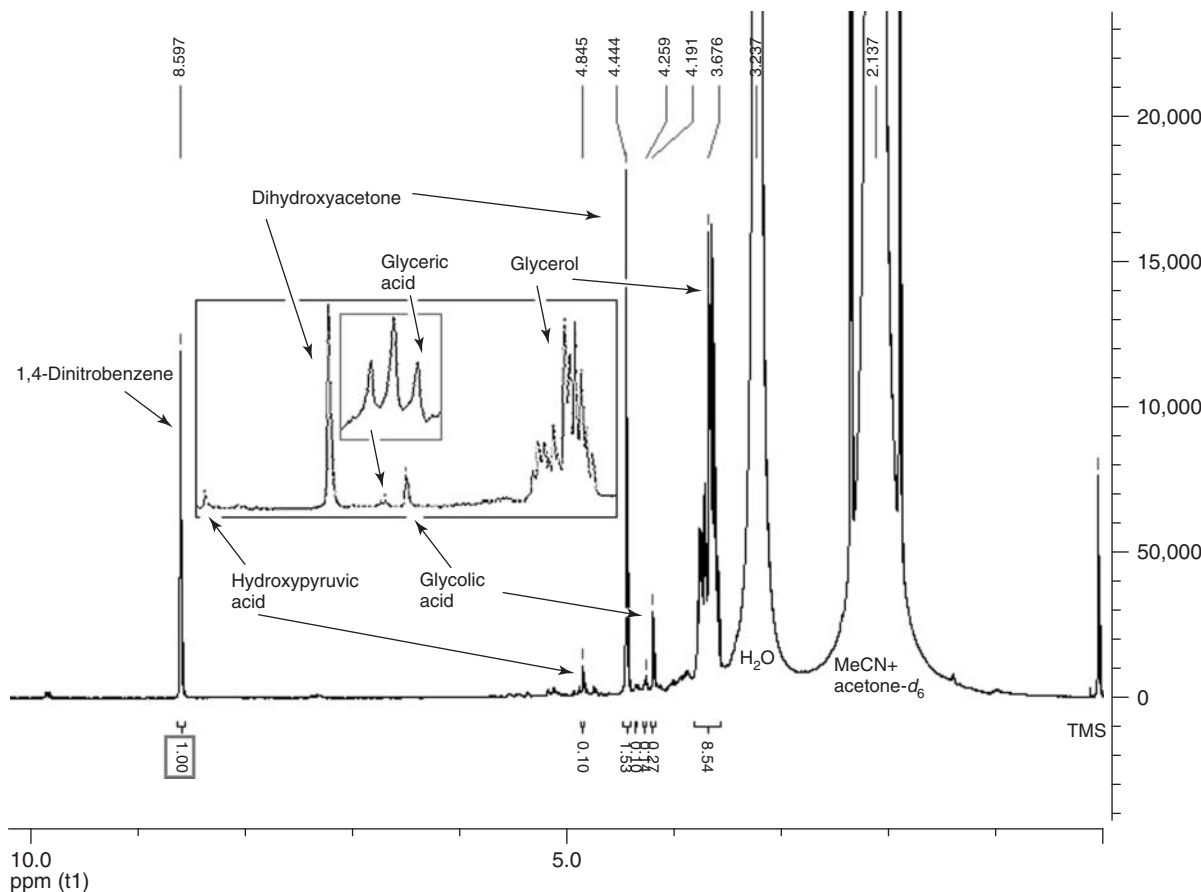


**Figure 19.3** An example of the  $^1\text{H}$  NMR spectrum of the reaction mixture obtained in the glycerol oxidation catalyzed by complex 19.2a.

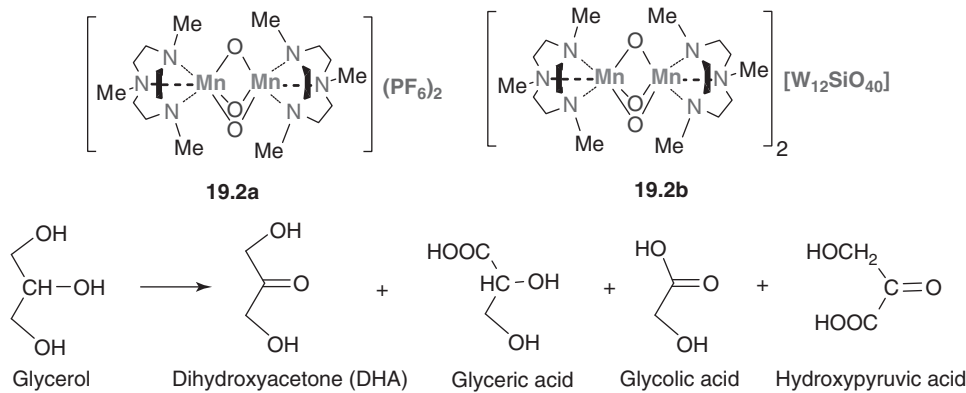


**Figure 19.4** Products obtained in glycerol oxidation catalyzed by the manganese compounds 19.2a and 19.2.

system oxidizes glycerol predominantly and not DHA when the concentration of glycerol is high. In the period of the reaction when the concentration of glycerol is low and some amount of hydrogen peroxide is still present in the solution, DHA is oxidized extensively. If the concentration of  $\text{H}_2\text{O}_2$  after oxidation of all glycerol is very low, obviously, the first product, DHA, will not be oxidized further. Thus, in the absence of glycerol, DHA is oxidized primarily to hydroxypyruvic aldehyde

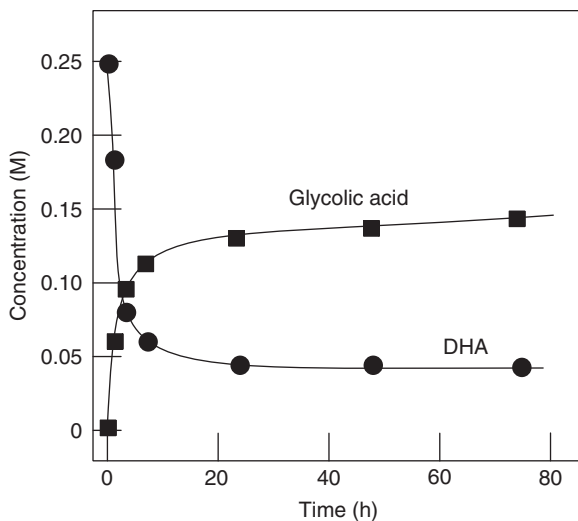


**Figure 19.5** Oxidation of dihydroxyacetone with H<sub>2</sub>O<sub>2</sub> (50% aqueous; initial concentration 0.75 M) catalyzed by complex **19.2a** ( $5 \times 10^{-5}$  M) in the presence of oxalic acid (0.02 M) and added D<sub>2</sub>O (0.2 mL). Solvent was acetonitrile, 22 °C. Adapted from Reference 9.

**TABLE 19.2** Oxidation of Glycerol at its Initial Concentration of 0.5 M<sup>a</sup>

Entry	H <sub>2</sub> O <sub>2</sub> , M	<b>19.2a</b> , M	(COOH) <sub>2</sub> , M	Time	DHA, mM (%)	Glyceric Acid, mM (%)	Glycolic Acid, mM (%)	Hydroxypyruvic Acid, mM (%)
1	1.0	$5.0 \times 10^{-5}$	0.002	10 min	29.0 (5.8)	3.3 (0.7)	6.7 (1.3)	0 (0)
2				30 min	18.5 (4.0)	6.7 (1.3)	4.7 (0.9)	0 (0)
3				4 h	25.9 (5.2)	7.0 (1.2)	10.0 (2.0)	0 (0)
4				24 h <sup>b</sup>	54.0 (10.8)	26.7 (5.3)	97.0 (19.4)	0 (0)
5	1.3	$5.0 \times 10^{-5}$	0.02	4 h	27.9 (5.6)	0 (0)	0 (0)	0 (0)
6				24 h	27.0 (5.5)	0 (0)	54.0 (10.0)	0 (0)
7				48 h	16.7 (3.3)	5.0 (1.0)	10.0 (2.0)	0 (0)
8	0.5	$2.5 \times 10^{-5}$	0.01	10 min	16.7 (3.3)	0 (0)	0 (0)	2.0 (0.4)
9				30 min <sup>c</sup>	20.9 (4.2)	0.5 (0.1)	0.5 (0.1)	3.4 (0.7)
10				1 h	10.0 (2.0)	0.5 (0.1)	6.7 (1.3)	2.0 (0.4)
11	0.3 <sup>d</sup>	$5.0 \times 10^{-5}$	0	10 min	20.0 (6.7)	0.6 (0.2)	3.1 (1.0)	2.0 (0.7)
12				30 min	37.6 (12.5)	40.0 (13.6)	16.7 (5.6)	4.5 (1.5)
13				2 h	33.4 (11.1)	48.0 (15.0)	13.0 (4.0)	4.7 (1.6)
14				24 h	29.0 (9.7)	31.4 (10.5)	13.0 (4.0)	10.0 (3.4)

<sup>a</sup>Conditions: Solvent was acetonitrile, 22 °C. Yields (%) in parentheses are based on starting glycerol.

<sup>b</sup>Glycerol conversion was 40%, mass balance was 89%.

<sup>c</sup>Glycerol conversion was 20%, mass balance was 29%.

<sup>d</sup>Yields were calculated on the basis of hydrogen peroxide. Adapted from Reference 9.

and hydroxypyruvic acid (Fig. 19.6). In both compounds, vicinal carbonyl groups are present, facilitating the decarbonylation to afford glycolic acid.

Heterogenized catalyst **19.2b** is active in the process of glycerol oxidation (Fig. 19.7). Special experiments indicated that the reaction occurs predominantly on the surface of catalyst **19.2b**. Yield of the products after 1 h does not depend on the amount of **19.2b**, which is similar to the behavior found for the oxidation of 1-phenylethanol. It has been assumed that this independence is due to the aggregation of heterogeneous forms of the catalyst, which leads to the contraction of the catalytically active surface. Only negligible leaching of the catalyst was detected. The experiments on recycling showed that some loss of activity upon catalyst recycling occur only for the second run. The third and fourth runs gave the same yields of the products, and the catalyst can be easily isolated from the reaction mixture and reused many times without sufficient

**TABLE 19.3** Oxidation of Glycerol at its Initial Concentration of 0.16–0.08 M<sup>a</sup>

Entry	Glycerol, M	<b>19.2a</b> , M	Time	DHA, mM (%)	Glyceric Acid, mM (%)	Glycolic Acid, mM (%)	Hydroxypyruvic Acid, mM (%)
1	0.16	$5.0 \times 10^{-5}$	5 min	4.5 (2.9)	0 (0)	0 (0)	0 (0)
2			10 min	9.2 (5.9)	13.4 (8.6)	10.0 (6.5)	0 (0)
3			30 min	22.2 (14.2)	14.0 (9.1)	16.7 (10.8)	0 (0)
4			24 h <sup>b</sup>	23.7 (15.3)	16.7 (10.8)	16.7 (10.8)	0.8 (0.5)
5			48 h <sup>c</sup>	16.0 (10.0)	20.0 (12.9)	26.7 (17.2)	0.8 (0.5)
6	0.16	0	24 h	0 (0)	0 (0)	0 (0)	0 (0)
7	0.16	$2.5 \times 10^{-5}$	100 h	6.7 (4.3)	5.0 (3.2)	5.3 (3.4)	0 (0)
8	0.08	$5.0 \times 10^{-5}$	5 min	1.8 (2.4)	0 (0)	0 (0)	0 (0)
9			10 min	3.1 (3.9)	0 (0)	0 (0)	0 (0)
10			30 min	8.0 (10.5)	4.0 (5.0)	4.0 (5.0)	0 (0)
11			1 h	9.6 (12.0)	9.0 (11.3)	9.0 (11.3)	0 (0)
12			24 h	10.0 (12.5)	12.7 (16.0)	12.7 (16.0)	0 (0)

<sup>a</sup>Conditions: Solvent was acetonitrile,  $[H_2O_2]_0 = 0.3$  M,  $[(COOH)_2] = 0$  M, 22 °C. Yields (%) in parentheses are based on starting glycerol.

<sup>b</sup>Glycerol conversion was 40%.

<sup>c</sup>Glycerol conversion was 60%. Adapted from Reference 9.

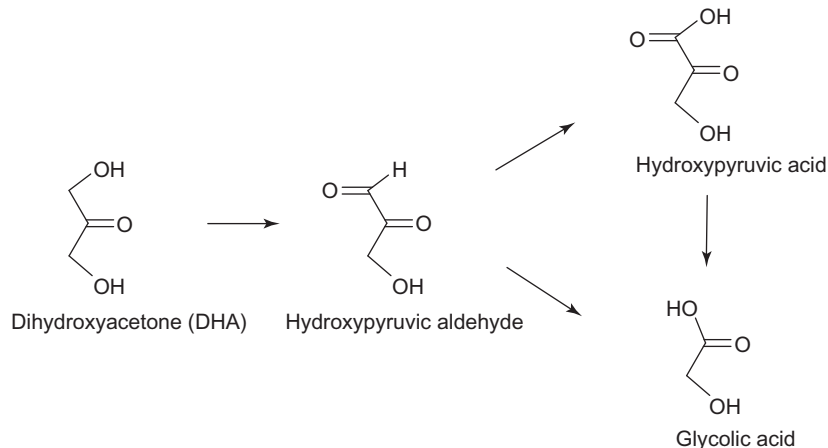


**Figure 19.6** Products of dihydroxyacetone oxidation catalyzed by the manganese complex **19.2a**.

loss of activity. The enhanced stability of the immobilized catalyst may be due to the occurrence of substrate oxidation on the solid surface. Owing to this, TMTACN ligands of the catalyst (which can be relatively easily destroyed in the solution) are protected by the surrounding voluminous polyoxometalate species.

#### 19.4 OXIDATION OF GLYCEROL WITH TBHP OR H<sub>2</sub>O<sub>2</sub> CATALYZED BY WATER-SOLUBLE TETRACOPPER(II) TRIETHANOLAMINATE COPPER COMPLEX

The catalytic systems based on the hydrosoluble tetracopper(II) triethanolamine complex  $[O\subset Cu_4\{N(CH_2CH_2O)_3\}_4(BOH)_4][BF_4]_2$  (**19.3**) [10a] were applied by some of us for the mild oxidation of alcohols [10b]. Given the high performance of this catalyst in alcohol oxidation, we tested the same catalytic system for the homogeneous oxidation of glycerol to DHA [11]. This transformation was undertaken at low temperatures (25–70 °C) in  $H_2O/MeCN$  medium, and the action of various oxidizing agents was screened. The selected results are summarized in Fig. 19.8.

Hydrogen peroxide is considered as a “green” oxidant. Besides having high active oxygen content, the main advantage of  $H_2O_2$  consists in environmental reasons, namely, owing to the generation of water as the only by-product. The application of

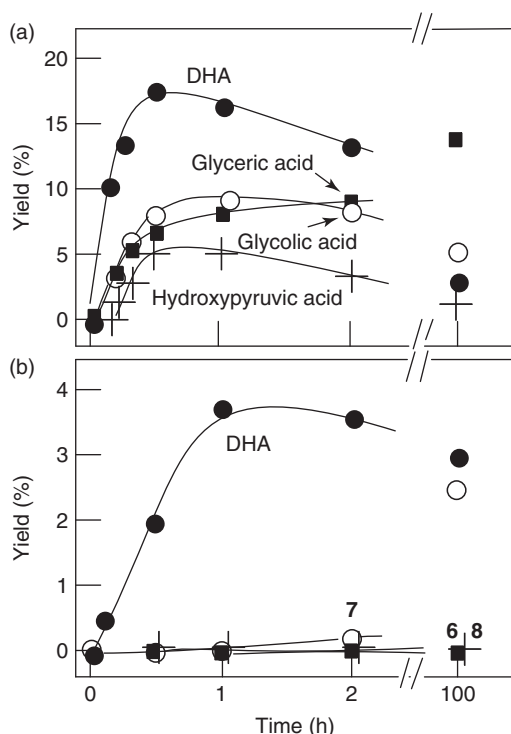


**Figure 19.7** Glycerol oxidation with H<sub>2</sub>O<sub>2</sub> catalyzed by heterogenized complex **19.2b**. Conditions: glycerol, 0.21 M; H<sub>2</sub>O<sub>2</sub> (50% aqueous), 0.3 M; catalyst **19.2b**, 5 mg (which is equivalent to  $4.4 \times 10^{-4}$  M Mn ions); oxalic acid: 0.002 M (a) and 0 M (b). Total volume of the reaction solution was 5 mL; 22 °C. Adapted from Reference 9.

this reagent for the oxidation of glycerol was previously limited almost exclusively to heterogeneous catalytic systems (see above). In the presence of **19.3**, H<sub>2</sub>O<sub>2</sub> taken in a twofold molar excess over glycerol forms an efficient oxidation system that leads to 15% conversion of glycerol, after 1 h at 25 °C (Fig. 19.8). This corresponds to the selectivity to DHA of 51% that is rather low owing to the formation of formic and hydroxyacetic acids as by-products, detected by GS-MS analyses. The extension of the reaction time to 18 h does not have a substantial effect, resulting in a slightly higher glycerol conversion (18%) with the comparable selectivity (49%). With the aim of avoiding the over-oxidation of glycerol and increasing the selectivity toward DHA, we have used a 10-fold reduced amount of hydrogen peroxide, which corresponds to the decrease of the H<sub>2</sub>O<sub>2</sub>/glycerol molar ratio from 2 : 1 to 0.2 : 1. As a result, the reaction is slower and allowed to obtain after 4 h a selectivity to DHA of 96%, with glycerol conversion of 3%. This conversion can be increased up to 8% on prolonging the reaction time to 30 h, showing also a high selectivity to DHA (93%). In the latter case, the DHA yield based on H<sub>2</sub>O<sub>2</sub> is 35%, being rather substantial taking into consideration the mild reaction conditions. Interestingly, if the glycerol oxidation is repeated (under same conditions) with CuCl<sub>2</sub> as a catalyst instead of complex **19.3**, only 11% DHA yield based on H<sub>2</sub>O<sub>2</sub> is obtained. This fact reveals the particular importance of the N,O-ligands and their intricate arrangement in **19.3**.

*tert*-Butyl hydroperoxide (TBHP) was also tested in combination with **19.3** in the oxidation of glycerol (Table 19.4), revealing an inferior activity than that of H<sub>2</sub>O<sub>2</sub>. Thus, at ambient temperature (25 °C) only 2.5% conversion of glycerol is achieved after 3 h of the reaction with TBHP, showing the selectivity and yield to DHA of 88% and 2.2%, respectively (Table 19.4, entry 1). A reaction carried out under the same conditions, but with H<sub>2</sub>O<sub>2</sub> led to 15% conversion and 8% selectivity after only 1 h. However, a higher selectivity to DHA was observed for TBHP, that is, 88% versus 51% for H<sub>2</sub>O<sub>2</sub>. Changing the experimental conditions in the oxidation of glycerol with TBHP, it was observed that an increase of temperature to 50 °C leads to the similar DHA yield of circa 2% (entry 2), which is obtained, however, at a shorter reaction time (0.5 h). At a more prolonged reaction time, increased temperature, and in the presence of catalyst promoter (HCl) and a higher amount of TBHP (4.0 mmol, entry 3), only 6.0% conversion of glycerol is reached with the selectivity to DHA of 90%. The promoting role of a base in glycerol oxidation has been established in various heterogeneous systems. We have also found that the presence of base (Na<sub>2</sub>CO<sub>3</sub>) also accelerates the reaction (entry 4) leading, after 0.5 h, to slightly higher

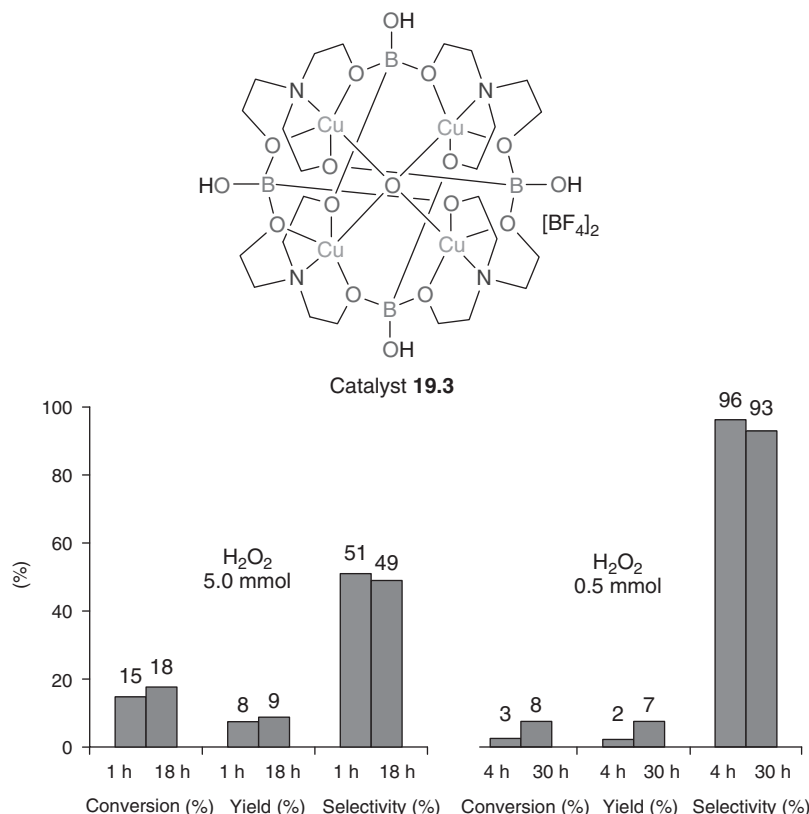


**Figure 19.8** Oxidation of glycerol with  $\text{H}_2\text{O}_2$  catalyzed by the tetracopper(II) triethanolamine complex (**19.3**): effect of the concentration of  $\text{H}_2\text{O}_2$  and reaction time. Conditions: glycerol (2.5 mmol), Cu(II) complex (5.0  $\mu\text{mol}$ ; 0.15 mL aqueous solution), 25 °C, solvent acetonitrile/water; conv, conversion; sel, selectivity to DHA; yield of DHA based on glycerol. Adapted from Reference 11.

**TABLE 19.4** Oxidation of Glycerol with TBHP Catalyzed by the Tetracopper(II) Triethanolamine Complex (**19.3**)<sup>a</sup>

Entry	TBHP, mmol	T, °C	t, h	Conv. GLY, %	Yield DHA, %	Sel. DHA, %
1	5.0 <sup>b</sup>	25	3.0	2.5	2.2	88
2	2.0	50	0.5	2.7	2.3	85
3	4.0 <sup>c</sup>	70	6.0	6.0	5.4	90
4	2.0 <sup>d</sup>	60	0.5	8.5	7.5	88

<sup>a</sup>Conv. GLY, glycerol conversion; sel. DHA, selectivity to dihydroxyacetone; yield DHA, molar yield (%) [moles of DHA/100 moles of glycerol] determined by GC analysis. Conditions ((unless stated otherwise): glycerol (1.0 mmol), Cu(II) complex **19.3** (5.0  $\mu\text{mol}$ ),  $T=25$  °C, solvent acetonitrile/water.

<sup>b</sup>glycerol (2.5 mmol).

<sup>c</sup>In the presence of HCl promoter (40  $\mu\text{mol}$ ; 1 M in  $\text{H}_2\text{O}$ ).

<sup>d</sup>In the presence of  $\text{Na}_2\text{CO}_3$  (3.0 mmol). Adapted from Reference 11.

glycerol conversion (8.5%) and DHA yield (7.5%). Further optimization of oxidations with TBHP did not allow us to obtain substantially better results.

Other oxidants, namely, potassium peroxodisulfate ( $\text{K}_2\text{S}_2\text{O}_8$ ) and air [mediated by 2,2,6,6-tetramethylpiperidine-1-oxyl (TEMPO)] were also tested in the glycerol oxidation (Table 19.5) with **19.3**. Although potassium peroxodisulfate is a very powerful oxidant, the oxidation of glycerol proceeded very slowly and nonselectively, resulting in 12% yield of DHA with selectivity of only 24%. Although some heterogeneous catalytic systems have been reported for the aerobic (or by molecular oxygen) oxidations of glycerol under rather mild conditions, the attempted oxidation of glycerol with air and complex **19.3** herein did not proceed to any extent. However, this reaction can be mediated by the TEMPO radical, which is a recognized mediator in the oxidation of various monoalcohols [10b]. Hence, glycerol could be transformed to DHA (circa

**TABLE 19.5 Oxidation of Glycerol with Different Oxidants Catalyzed by the Tetracopper(II) Triethanolaminate Complex (19.3)<sup>a</sup>**

Oxidant	T, °C	t, h	Conv. GLY, %	Yield DHA, %	Select. DHA, %
K <sub>2</sub> S <sub>2</sub> O <sub>8</sub> <sup>b</sup>	25	120	50.0	12.0	24
Air <sup>c</sup>	60	3.5	0	0	0
Air/TEMPO <sup>d</sup>	60	3.5	10.0	9.6	96

<sup>a</sup>Conv. GLY, glycerol conversion; sel. DHA, selectivity to dihydroxyacetone; yield DHA, molar yield (%) [moles of DHA/100 moles of glycerol] determined by GC analysis. Conditions: solvent acetonitrile/water.

<sup>b</sup>glycerol 2.5 mmol, complex **19.3** (5.0 μmol), K<sub>2</sub>S<sub>2</sub>O<sub>8</sub> 2.5 mmol, in the presence of increased amount of H<sub>2</sub>O (8.0 mL) for dissolving K<sub>2</sub>S<sub>2</sub>O<sub>8</sub>; the total volume of the reaction solution was 11.0 mL.

<sup>c</sup>glycerol 1.0 mmol, complex **19.3** (10.0 μmol; 0.30 mL aqueous solution), air (1 atm) and Na<sub>2</sub>CO<sub>3</sub> (0.5 mmol).

<sup>d</sup>Conditions of footnote *c*, but in the presence of TEMPO (50.0 μmol). Adapted from Reference 11.

10% yield) with a high selectivity (96%) after 3.5 h at 60 °C. Further increase of the reaction time does not lead to somehow better results. Selective TEMPO-mediated oxidation of glycerol to ketomalonic acid [12a] or DHA [12b] has been reported, but requires the use of either of NaOCl/Br<sup>-</sup> oxidant or electrochemical systems, respectively. Although the commercial production of DHA is limited to biological oxidation of glycerol [12c], the formation of DHA in rather good yields, albeit with modest selectivities, can also be achieved in the continuous aerobic oxidation of glycerol on the heterogeneous metallic catalysts.

When using the catalyst **19.3**, the obtained DHA yields are comparable to those achieved in the recently reported (i) H-transfer dehydrogenation of glycerol to DHA, catalyzed by organometallic iridium complexes [12d] and (ii) heterogeneous oxidation of glycerol by the Au/CeO<sub>2</sub>/O<sub>2</sub> system [12e]. However, those processes exhibited significantly lower selectivity of DHA in comparison with our work.

In summary of this section, the complex **19.3** was successfully tested as catalyst in the oxidation of glycerol, resulting in high selectivities to DHA with yields close to 10%. The system is active in the presence of various oxidants, including TBHP, K<sub>2</sub>S<sub>2</sub>O<sub>8</sub>, and air (mediated by TEMPO). Hydrogen peroxide, considered as a green oxidant, led to the best results.

## 19.5 CONCLUSIONS

As an abundant biorenewable feedstock from the manufacture of biodiesel, glycerol is a suitable starting material for the synthesis of a wide variety of value-added organic products. In spite of the recognized difficulties in developing clean and selective transformations of glycerol, the present work showed that the combination of certain types of homogeneous catalysts with hydrogen peroxide or other oxidants (e.g., TBHP) furnishes rather efficient systems (up to 45% yields of valuable products based on glycerol) for the oxidation of glycerol to DHA, glycolic acid, and/or hydroxypyruvic acid. These catalysts include the triosmium carbonyl Os<sub>3</sub>(CO)<sub>12</sub> derivative, the soluble [L<sub>2</sub>MnO<sub>3</sub>](PF<sub>6</sub>)<sub>2</sub> and heterogenized [L<sub>2</sub>MnO<sub>3</sub>]<sub>2</sub>(SiW<sub>12</sub>O<sub>40</sub>) complexes, and the aquasoluble tetracopper(II) triethanolamine compound [OCCu<sub>4</sub>{N(CH<sub>2</sub>CH<sub>2</sub>O)<sub>3</sub>}<sub>4</sub>-(BOH)<sub>4</sub>](BF<sub>4</sub>)<sub>2</sub>. The effects of various reaction parameters have been studied and the preferable reaction conditions have been identified. Apart from representing the first examples of homogeneous systems for the oxidation of glycerol the applied Os, Mn, and Cu catalysts also operate under mild conditions in aqueous acetonitrile medium, showing rather good selectivities and a number of interesting features (e.g., they operate with various oxidants, result in different product distribution patterns, and can be recycled in the case of supported Mn-based catalyst). However, further optimization of all these systems and the search for new catalysts to envisage higher conversions of glycerol and superior selectivities to desirable products should be undertaken.

## ACKNOWLEDGMENTS

This work was supported by the Brazilian National Council on Scientific and Technological Development (CNPq, Brazil; grants Nos. 552774/2007-3, 305014/2007-2, 303828/2010-2), the State of São Paulo Research Foundation (FAPESP, Brazil; grants Nos. 2005/51579-2, 2006/03996-6), the Russian Foundation for Basic Research (grant No. 12-03-00084-a),

and the Foundation for Science and Technology (FCT), Portugal (projects PTDC/QUI-QUI/102150/2008, PTDC/QUI-QUI/121526/2010, and PEst-OE/QUI/UI0100/2011).

## REFERENCES

- (a) Van Gerpen, J. *Fuel Process. Technol.* **2005**, *86*, 1097; (b) de Rezende, S. M.; de Castro Reis, M.; Reid, M. G.; SilvaJr., P. L.; Coutinho, F. M. B.; da Silva San Gil, R. A.; Lachter, E. R. *Appl. Catal. A: Gen.* **2008**, *349*, 198; (c) da Silva, C. R. B.; Gonçalves, V. L. C.; Lachter, E. R.; Mota, C. J. A. *J. Braz. Chem. Soc.* **2009**, *20*, 201.
- (a) Sels, B.; D'Hondt, E.; Jacobs, P. Catalytic Transformation of Glycerol. In Centi, G., van Santen, R. A., Eds; *Catalysis for Renewables*; Wiley-VCH Verlag GmbH: Weinheim, **2007**; p 223; (b) Corma, A.; Iborra, S.; Velty, A. *Chem. Rev.* **2007**, *107*, 2411; (c) Zhou, C.-H.; Beltramini, J. N.; Fan, Y.-X.; Lu, G. Q. *Chem. Soc. Rev.* **2008**, *37*, 527; (d) Zheng, Y.; Chen, X.; Shen, Y. *Chem. Rev.* **2008**, *108*, 5253; (e) Behr, A.; Elting, J.; Irawadi, K.; Leschinski, J.; Lindner, F. *Green Chem.* **2008**, *10*, 13; (f) Pagliaro, M.; Rossi, M. *The Future of Glycerol. New Usages for a Versatile Raw Material*; RSC Publishing: Cambridge, **2008**; p 128; (g) Behr, A. *ChemSusChem* **2008**, *1*, 653; (h) Thanh, L. T.; Okutsu, K.; Boi, L. V.; Maeda, Y. *Catalysts* **2012**, *2*, 191; (i) Bohmer, N.; Roussiere, T.; Kuba, M.; Schunk, S. A. *Comb. Chem. High T. Scr.* **2012**, *15*, 123; (j) Hekmat, D.; Bauer, R.; Fricke, J. *Bioprocess. Biosyst. Eng.* **2003**, *26*, 109; (k) Bauer, R.; Katsikis, N.; Varga, S.; Hekmat, D. *Bioprocess. Biosyst. Eng.* **2005**, *5*, 37; (l) Levy, S. B. *J. Am. Acad. Dermatol.* **1992**, *27*, 989; (m) Habe, H.; Fukuoka, T.; Kitamoto, D.; Sakaki, K. *Appl. Microbiol. Biotechnol.* **2009**, *84*, 445; (n) Wang, C. M.; Huang, C. L.; Hu, C. T.; Chan, H. L. *Dermatol. Surg.* **1997**, *23*, 23; (o) Moy, L. S.; Murad, H.; Moy, R. L. *J. Dermatol. Surg. Oncol.* **1993**, *19*, 243; (p) Moore, S. J. Method for Treatment Cyanide Poisoning. U.S. Patent 5,674,904-A, **1997**; (q) Fordham, P.; Besson, M.; Gallezot, P. *Catal. Lett.* **1997**, *46*, 195.
- (a) Garcia, R.; Besson, M.; Gallezot, P. *Appl. Catal. A: Gen.* **1995**, *127*, 165; (b) Carrettin, S.; McMorn, P.; Johnston, P.; Griffin, K.; Kiely, C. J.; Hutchings, G. J. *Phys. Chem. Chem. Phys.* **2003**, *5*, 1329; (c) Bianchi, C. L.; Canton, P.; Dimitratos, N.; Porta, F.; Prati, L. *Catal. Today* **2005**, *102–103*, 203; (d) Dimitratos, N.; Lopez-Sanchez, J. A.; Lennon, D.; Porta, F.; Prati, L.; Villa, A. *Catal. Lett.* **2006**, *108*, 147; (e) Ketchie, W. C.; Murayama, M.; Davis, R. J. *J. Catal.* **2007**, *250*, 264; (f) Taarning, E.; Madsen, A. T.; Marchetti, J. M.; Egeblad, K.; Christensen, C. H. *Green Chem.* **2008**, *10*, 408; (g) Maurino, V.; Bedini, A.; Minella, M.; Rubertelli, F.; Pelizzetti, E.; Minero, C. *J. Adv. Oxid. Technol.* **2008**, *11*, 184; (h) Pollington, S. D.; Enache, D. I.; Landon, P.; Meenakshisundaram, S.; Dimitratos, N.; Wagland, A.; Hutchings, G. J.; Stitt, E. H. *Catal. Today* **2009**, *145*, 169; (i) Prati, L.; Spontoni, P.; Gaiassi, A. *Top. Catal.* **2009**, *52*, 288; (j) Thomas, J. M.; Hernandez-Garrido, J. C.; Bell, R. G.; *Top. Catal.* **2009**, *52*, 1630; (k) Liang, D.; Gao, J.; Wang, J.; Chen, P.; Hou, Z.; Zheng, X. *Catal. Commun.* **2009**, *10*, 1586; (l) Dimitratos, N.; Villa, A.; Prati, L. *Catal. Lett.* **2009**, *133*, 334; (m) Rennard, D. C.; Kruger, J. S.; Schmidt, L. D. *ChemSusChem* **2009**, *2*, 89.
- (a) Demirel-Gülen, S.; Lucas, M.; Claus, P. *Catal. Today* **2005**, *102–103*, 166; (b) Demirel, S.; Kern, P.; Lucas, M.; Claus, P. *Catal. Today* **2007**, *122*, 292; (c) Demirel, S.; Lucas, M.; Wärnå, J.; Salmi, T.; Murzin, D.; Claus, P. *Top. Catal.* **2007**, *44*, 299; (d) Herzing, A. A.; Kiely, C. J.; Carley, A. F.; Landon, P.; Hutchings, G. J. *Science* **2008**, *321*, 1331; (e) Lopez-Sanchez, J. A.; Dimitratos, N.; Miedziak, P.; Ntainjua, E.; Edwards, J. K.; Morgan, D.; Carley, A. F.; Tiruvalam, R.; Kiely, C. J.; Hutchings, G. J. *Phys. Chem. Chem. Phys.* **2008**, *10*, 1921; (f) Dimitratos, N.; Lopez-Sanchez, J. A.; Anthonykutty, J. M.; Brett, G.; Carley, A. F.; Tiruvalam, R. C.; Herzing, A. A.; Kiely, C. J.; Knight, D. W.; Hutchings, G. J. *Phys. Chem. Chem. Phys.* **2009**, *11*, 4952; (g) Dimitratos, N.; Lopez-Sanchez, J. A.; Anthonykutty, J. M.; Brett, G.; Carley, A. F.; Taylor, S. H.; Knight, D. W.; Hutchings, G. J. *Green Chem.* **2009**, *11*, 1209; (h) Chan-Thaw, C. E.; Villa, A.; Katekomol, P.; Su, D.; Thomas, , Prati, L. *Nano Lett.* **2010**, *10*, 537; (i) Ziolek, M.; Decyk, P.; Sobczak, I.; Trejda, M.; Florek, J.; Golinska, H.; Klimas, W.; Wojtaszek, A. *Appl. Catal. A: Gen.* **2011**, *391*, 194; (j) Zhou, C.-H.; Beltramini, J. N.; Lin, C.-X.; Xu, Z.-P.; Lu, G. Q.; Tanksale, A. *Catal. Sci. Technol.* **2011**, *1*, 111; (k) Painter, R. M.; Pearson, D. M.; Waymouth, R. M. *Angew. Chem. Int. Ed.* **2010**, *49*, 9456; (l) Rodrigues, E. G.; Pereira, M. F. R.; Delgado, J. J.; Chen, X.; Órfão, J. J. M. *Catal. Commun.* **2011**, *16*, 64.
- (a) McMorn, P.; Roberts, G.; Hutchings, G. J. *Catal. Lett.* **1999**, *63*, 193; (b) Luque, R.; Budarin, V.; Clark, J. H.; Macquarrie, D. J. *Appl. Catal. B: Environ.* **2008**, *82*, 157; (c) Sankar, M.; Dimitratos, N.; Knight, D. W.; Carley, A. F.; Tiruvalam, R.; Kiely, C. J.; Thomas, D.; Hutchings, G. J. *ChemSusChem* **2009**, *2*, 1145; (d) Wang, X.; Wu, G.; Wang, F.; Ding, K.; Zhang, F.; Liu, X.; Xue, Y. *Catal. Commun.* **2012**, *28*, 73.
- (a) Srivastava, S. S.; Mathur, P. C. *J. Indian Chem. Soc.* **1976**, *53*, 576; (b) Singh, H. S.; Tandon, P. K.; Singh, K. K. *J. Indian Chem. Soc.* **1994**, *71*, 675; (c) Singh, B.; Singh, D.; Singh, A. K. *Int. J. Chem. Kinet.* **1988**, *20*, 501; (d) Laurie, V. F. A.; Waterhouse, L. J. *Agric. Food Chem.* **2006**, *54*, 4668.
- Wörz, N.; Brandner, A.; Claus, P. *J. Phys. Chem. C* **2010**, *114*, 1164.
- Shul'pin, G. B.; Kozlov, Y. N.; Shul'pina, L. S.; Kudinov, A. R.; Mandelli, D. *Inorg. Chem.* **2009**, *48*, 10480.
- Shul'pin, G. B.; Kozlov, Y. N.; Shul'pina, L. S.; Strelkova, T. V.; Mandelli, D. *Catal. Lett.* **2010**, *138*, 193.
- (a) Kirillov, A. M.; Kopylovich, M. N.; Kirillova, M. V.; Haukka, M.; da Silva, M. F. C. G.; Pombeiro, A. J. L. *Angew. Chem. Int. Ed.* **2005**, *44*, 4345; (b) Figiel, P. J.; Kirillov, A. M.; Karabach, Y. Y.; Kopylovich, M. N.; Pombeiro, A. J. L. *J. Mol. Catal. A: Chem.* **2009**, *305*, 178.

11. Kirillova, M. V.; Kirillov, A. M.; Mandelli, D.; Carvalho, W. A.; Pombeiro, A. J. L.; Shul'pin, G. B. *J. Catal.* **2010**, *272*, 9.
12. (a) Ciriminna R.; Pagliaro, M. *Adv. Synth. Catal.* **2002**, *345*, 383; (b) Ciriminna, R.; Palmisano, G.; Della Pina, C.; Rossi, M.; Pagliaro, M. *Tetrahedron Lett.* **2006**, *47*, 6993; (c) Mishra, R.; Jain, S. R.; Kumar, A. *Biotechnol. Adv.* **2008**, *26*, 293; (d) Farnetti, E.; Kaspar, J.; Crotti, C. *Green Chem.* **2009**, *11*, 704; (e) Demirel, S.; Kern, P.; Lucasm, M.; Claus, P. *Catal. Today* **2007**, *122*, 292.



---

# INVOLVEMENT OF AN ACETATO LIGAND IN THE REDUCTIVE ELIMINATION STEP OF THE RHODIUM-CATALYZED METHANOL CARBONYLATION

DUC HANH NGUYEN\*, NICOLAS LASSAUQUE, THOMAS DAVIN, LAURENT MARON, CAROLE LE BERRE,  
PHILIPPE SERP, AND PHILIPPE KALCK\*

*University of Toulouse, UPS, INSA, INPT, LCC, ENSIACET, Toulouse, France*

## 20.1 INTRODUCTION

Acetic acid is the most important commodity chemical produced by homogeneous catalysis, with world annual production of 9 million tons and a regular growth of approximately 2%. It is used in the manufacture of vinyl acetate for the production of textile fibers, adhesives, and paints or directly employed as solvent in the synthesis of terephthalic acid and its esters as solvents, and finds direct applications in the pharmaceutical and even in the food industry. Another major application concerns the manufacture of acetic anhydride by high temperature dehydration into ketene that is further condensed with acetic acid, whose main application is to synthesize cellulose acetate. Two-thirds of the acetic acid production arises from the carbonylation of methanol, catalyzed by a late transition metal complex. Thus, acetic acid represents the second aliphatic intermediate, after methanol, which is issued from the carbon monoxide/hydrogen chemistry. Since the CO/H<sub>2</sub> couple (syngas) can be generated from various sources, methanol constitutes an abundant raw material for acetic acid, so that a highly selective catalytic process to obtain it by carbonylation (Eq. 20.1) is presumably today the most elegant and convenient synthetic pathway to produce it at low cost [1].

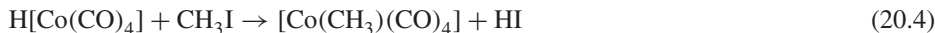


Following the intense work on the carbonylation reaction during the 1920s by BASF and British Celanese [1], Reppe and his research group discovered that cobalt diiodide operating at 680 bar and 250 °C catalyzes this reaction [2, 3]. But it was necessary to solve harsh corrosion problems, until 1950, when highly resistant molybdenum/nickel alloys (whose trademark is Hastelloy©) were discovered and commercialized [1]. The process developed by BASF in 1960 was not selective as the yield in acetic acid was 90% based on methanol and 70% based on CO [4] due to the large amounts of CO<sub>2</sub> coproduced by the water-gas shift (WGS) reaction (Eq. 20.2).



It appeared clearly that an iodo promoter was required to activate methanol and to generate iodomethane (Eq. 20.3), which will further react with the [Co(H)(CO)<sub>4</sub>] species, or more probably the H[Co(CO)<sub>4</sub>] acidic species in the presence of

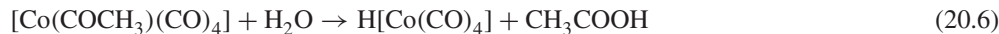
water, to form the methyl-cobalt intermediate  $[\text{Co}(\text{CH}_3)(\text{CO})_4]$  according to Equation 20.4.



Next, the migratory CO insertion, which is considered as the rate-determining step (rds), followed by coordination of a CO ligand gives the acetyl-cobalt complex  $[\text{Co}(\text{COCH}_3)(\text{CO})_4]$  (Eq. 20.5) [5, 6].



Finally, hydrolysis of this latter complex produces acetic acid and regenerates  $\text{H}[\text{Co}(\text{CO})_4]$  (Eq. 20.6). In addition, a nucleophilic attack of a  $\text{I}^-$  ion on the acetyl carbon atom has also been proposed to provide  $\text{CH}_3\text{COI}$ , which is immediately hydrolyzed to acetic acid [7].



In the mid-1960s, Paulik and Roth at Monsanto Co discovered that rhodium and an iodide promoter were more efficient than cobalt, with selectivities of 99% and 85%, with regard to methanol and CO, respectively. Moreover, the reaction is operated under significantly milder conditions such as 40–50 bar pressure and around  $190^\circ\text{C}$  [8]. Even though rhodium was 1000 times more costly than cobalt at this time, Monsanto decided to develop the rhodium-based catalyst system mainly for the selectivity concerns, and thus for the reduction of the process cost induced by the acetic acid purification, even if it was necessary to maintain a 14% w/w level of water in the reactor to keep the stability of the rhodium catalyst. In addition, Paulik et al. [9] demonstrated that iridium can also catalyze the carbonylation of methanol although at a lower rate. However, it is noteworthy that the catalytic system is more stable, especially in the low partial pressure zones of the industrial unit.

The Monsanto rhodium catalyst system has been the subject of numerous reviews [6, 10–17], including a very recent one by Haynes [18]. At high water content, typically more than 8% w/w, the overall rate is first order in both the rhodium complex and the methyl iodide reactant and zero order in both methanol and CO reactants. The catalytic cycle, which is usually adopted is shown in Fig. 20.1. The first step is the  $\text{CH}_3\text{I}$  oxidative addition reaction to the  $[\text{RhI}_2(\text{CO})_2]^-$  active species, which has been determined as rate determining.

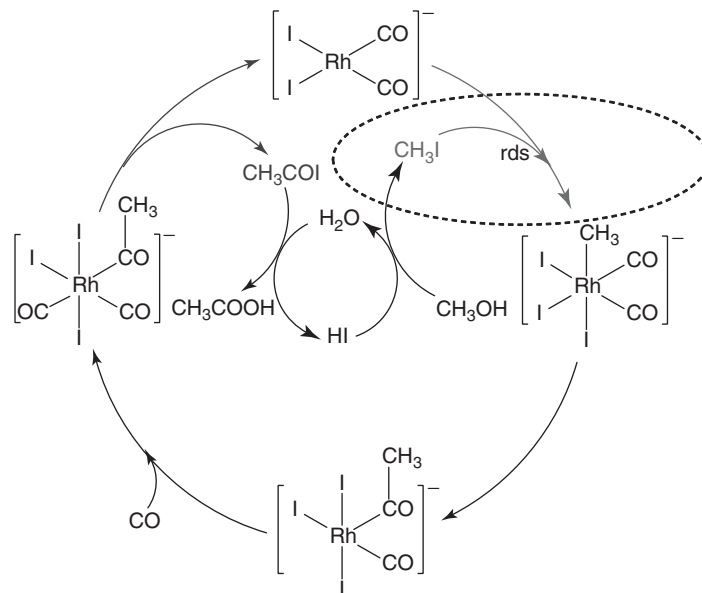


**Figure 20.1** General catalytic cycle for Rh-catalyzed methanol carbonylation reaction.

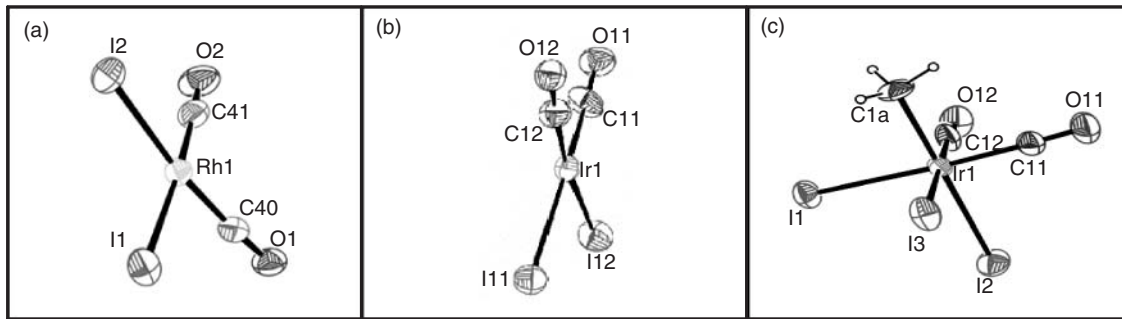


**Figure 20.2** X-Ray crystal structures of (a)  $[\text{RhI}_2(\text{CO})_2]^-$ , (b)  $[\text{IrI}_2(\text{CO})_2]^-$ , and (c)  $[\text{IrI}_3(\text{CH}_3)(\text{CO})_2]^-$ . Part (a) is adapted from Reference 23. Parts (b) and (c) are adapted from Reference 24.

The activation parameters determined by Forster [6] are  $\Delta H^\ddagger = 63.6 \text{ kJ/mol}$  and  $\Delta S^\ddagger = -116 \text{ J/(mol K)}$  and this large negative entropy of activation is consistent with the nucleophilic attack of the rhodium center on the carbon atom of  $\text{CH}_3\text{I}$  to form the  $[\text{RhI}_2(\text{CH}_3)(\text{CO})_2]$  neutral intermediate, which further coordinates the  $\text{I}^-$  ligand. However, below 8% water content, it has been proposed that the rate-determining step becomes the reductive elimination of acetyl iodide [19]. In another context, Cole-Hamilton and coworkers [20] have observed that when using the highly  $\sigma$ -donating  $\text{C}_5\text{Me}_4(\text{CH}_2)_2\text{PET}_2$  ligand, the rhodium center is so electron rich that the reductive elimination becomes the rate-determining step, resulting in accumulation of the acetyl complex in the medium. In comparison with the  $[\text{IrI}_2(\text{CO})_2]^-$  complex, the oxidative addition reaction is 100 times faster than with  $[\text{RhI}_2(\text{CO})_2]^-$  resulting from the higher nucleophilicity of the iridium center [21, 22]. In order to understand the difference in behavior between the iridium and rhodium chemistry, we prepared these two complexes with bis(triphenylphosphoranylidene)ammonium as counterion [23, 24]. The two metal centers are in a square-planar environment (Fig. 20.2a and b) and in  $\text{CH}_2\text{Cl}_2$  solutions, the two  $\nu_{\text{CO}}$  frequencies are 2058 and 1987 for Rh, and 2046 and 1967  $\text{cm}^{-1}$  for Ir, respectively, which reflects a larger retrodonation to the CO ligands of the iridium metal center due to its more diffuse orbitals. Thus, the nucleophilic attack of the iridium center on the methyl carbon atom occurs very easily, followed by iodide coordination, and the methyl-iridium complex  $2[\text{IrI}_3(\text{CH}_3)(\text{CO})_2]^-$  can be isolated as the resting state (Fig. 20.2c).

In order to promote the migratory insertion of the CO ligand, which becomes the rds, it is necessary to remove an iodo ligand, for increasing the electrophilic character of the CO carbon atom subject to the nucleophilic attack of the methyl group. BP Chemicals patented the use of various promoters able to act as the iodo-abstracting reagent. In particular,  $[\text{RuI}_2(\text{CO})_3]$  [25, 26] can efficiently react with  $[\text{IrI}_3(\text{CH}_3)(\text{CO})_2]^-$  under CO to give  $[\text{RuI}_3(\text{CO})_3]^-$  and  $[\text{IrI}_2(\text{CH}_3)(\text{CO})_3]$ . The addition of the ruthenium promoter allows the formation of the neutral acetyl species  $[\text{IrI}_2(\text{COCH}_3)(\text{CO})_3]$  about 700 times much faster than the transformation of  $[\text{IrI}_3(\text{CH}_3)(\text{CO})_2]^-$  into  $[\text{IrI}_3(\text{COCH}_3)(\text{CO})_2]^-$  in the absence of Ru [27]. Although the situation is more complex in the case of iridium as a neutral catalytic pathway can operate in parallel to the anionic one, the CO migratory insertion from the  $[\text{IrI}_3(\text{CH}_3)(\text{CO})_2]^-$  intermediate is about  $10^{-5}$  slower in nonprotic solvents than that observed for rhodium [19, 20]. Operating in methanol has a dramatic accelerating effect, presumably because the dissociation of an iodo ligand is solvent assisted. The promoting role of  $[\text{RuI}_2(\text{CO})_3]$  and  $[\text{PtI}_2(\text{CO})_2]$  [28, 29] has been studied in detail [18]. At present, the Cativa<sup>TM</sup> process developed by BP Chemicals operates with Ir and Ru at 5% w/w water and the high concentrations of the resulting methyl acetate provides high reaction rates [18].

On the other hand, the rhodium catalytic system with LiI stabilizer/promoter, allows operation at around 5% w/w, and the process has been developed by Celanese [15, 30]. Here, the significant amount of methyl acetate reduces the concentration of HI, which is well known to lead to the formation of the  $[\text{RhI}_4(\text{CO})_2]^-$  species. This complex is inactive during carbonylation but responsible for the WGS reaction (Eq. 20.2). The role of LiI is not only to stabilize the  $\text{Li}[\text{RhI}_2(\text{CO})_2]$  catalytic species but also to allow the two reactions in Equations 20.7 and 20.8.



The Celanese researchers [31, 32] have proposed that two dianionic rhodium species can be formed under high concentrations of LiI that accelerate the oxidative addition rate of  $\text{CH}_3\text{I}$ : (i)  $\text{Li}_2[\text{RhI}_3(\text{CO})_2]$ , whose participation has been considered in a theoretical investigation [33] and (ii)  $\text{Li}_2[\text{RhI}_2(\text{OAc})(\text{CO})_2]$ .

We were interested in the coordination involvement of the acetate ligand under reaction conditions of high concentrations of LiI and low water contents. Our spectroscopic data and density functional theory (DFT) calculations lead to the conclusion that this acetate ligand plays a deciding role in the reductive elimination reaction, in which the last step is in fact the formation of acetic anhydride from  $[\text{RhI}_2(\text{CH}_3\text{CO})(\text{OAc})(\text{CO})_2]^-$  with the regeneration of the active  $[\text{RhI}_2(\text{CO})_2]^-$  species.

## 20.2 NMR AND INFRARED HIGH PRESSURE STUDIES AND DFT CALCULATIONS

The complex *cis*-[PPN] $[\text{RhI}_2(\text{CO})_2]$  **1a** has been prepared in high yield by reaction under a CO atmosphere of  $\text{RhI}_3$  with dimethylformamide (DMF) at 160 °C to produce *cis*- $[\text{NH}_2\text{Me}_2]\text{RhI}_2(\text{CO})_2$  and then by metathesis with [bis(triphenylphosphoranylidene)ammonium]chloride ([PPN]Cl). As expected, the infrared (IR) spectra display two  $\nu_{\text{CO}}$  stretching bands of similar intensity, characteristic of two CO ligands in mutual *cis* positions in a square-planar environment. No interaction between the anion  $[\text{RhI}_2(\text{CO})_2]^-$  and its cation counterpart  $[\text{PPN}]^+$  was detected in the solid state. The analogous compounds *cis*-[4-RC<sub>5</sub>H<sub>4</sub>NMe] $[\text{RhI}_2(\text{CO})_2]$  (R=H or Et) have been reported previously by Haynes [34]. Complex **1** reacts under nitrogen with neat  $\text{CH}_3\text{I}$  to provide, presumably through the intermediate [PPN] $[\text{RhI}_3(\text{CH}_3)(\text{CO})_2]$  **2** the  $[\text{PPN}]_2[\text{Rh}(\mu\text{-I})\text{I}_2(\text{COMe})(\text{CO})_2]$  acetyl complex **3**, whose the centrosymmetric isomer has been characterized by an X-ray crystal structure (Fig. 20.3a). Under 1 atm of CO, the two iodo bridges are cleaved to give the *mer,trans*-[PPN] $[\text{RhI}_3(\text{COMe})(\text{CO})_2]$  **4** complex with the two CO ligands being in the apical positions of an octahedron, in which the equatorial plane contains the acetyl ligand and the three iodo atoms (Fig. 20.3b).

In anhydrous dichloromethane and under 15 bar of CO, **4** reacts slowly to yield **1** and  $\text{CH}_3\text{COI}$ , which reacts immediately with water to form acetic acid at 25 °C (Fig. 20.4).

As it has been proposed that the rate-determining step of the reaction may change as a function of the water content in the medium, we performed HP-NMR experiments (Fig. 20.5) under conditions close to the one used for the methanol carbonylation process. In these experiments, we introduced methyl iodide directly as it is the real reactant provided by reaction of HI with methanol.

The <sup>13</sup>C NMR spectra, recorded at 90 °C and 15 bar <sup>13</sup>CO, reveal clearly that at low water content the resting state is indeed the acetyl complex **4**. Between 0% and 5% water, IR monitoring of the reductive elimination reaction to go from **4** to **1** does not show any influence of the water concentration on the kinetics of this reaction. DFT calculations performed for the direct attack of water on the acetyl group of **4** to produce **1**, acetic acid, and HI show a high energy barrier of 44 kcal/mol. Under such conditions, this mechanism appears kinetically unlikely. On the other hand, the classically admitted almost thermoneutral reductive elimination of  $\text{CH}_3\text{COI}$  from **4** corresponds to an energy barrier of 26 kcal/mol (Fig. 20.6).

Thus, below 5% water, it seems reasonable to propose that this latter mechanism operates. However, we have considered the eventual role of water in generating acetate ions in the medium. Conductivity measurements performed on acetic acid–water mixtures (Fig. 20.7) show indeed an increase of the conductivity above 5% water content.

As the generated acetate ions might be involved in the reductive elimination step, we first calculated the direct attack of an acetate anion on the acetyl group of **4** to produce **1** and acetic anhydride (Fig. 20.8). The approach of the acetate to **4** is significantly endergonic (39 kcal/mol) and the energy barrier of 56 kcal/mol is too high to retain such a mechanism.

Furthermore, we explored the substitution on the two different *mer,trans*-**4** and *fac,cis*-**4** isomers of an iodide ligand by an acetate anion to produce  $[\text{RhI}_2(\text{OAc})(\text{CH}_3\text{CO})(\text{CO})_2]^-$  from which reductive elimination gives **1** and acetic anhydride

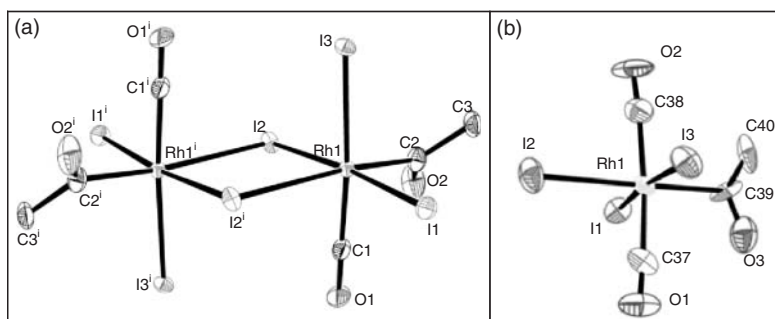


**Figure 20.3** X-Ray crystal structures of (a)  $[\text{PPN}]_2[\text{Rh}(\mu\text{-I})\text{I}_2(\text{COMe})(\text{CO})_2]$  and (b) *mer,trans*-[PPN] $[\text{RhI}_3(\text{COMe})(\text{CO})_2]$ . Adapted from Reference 23.

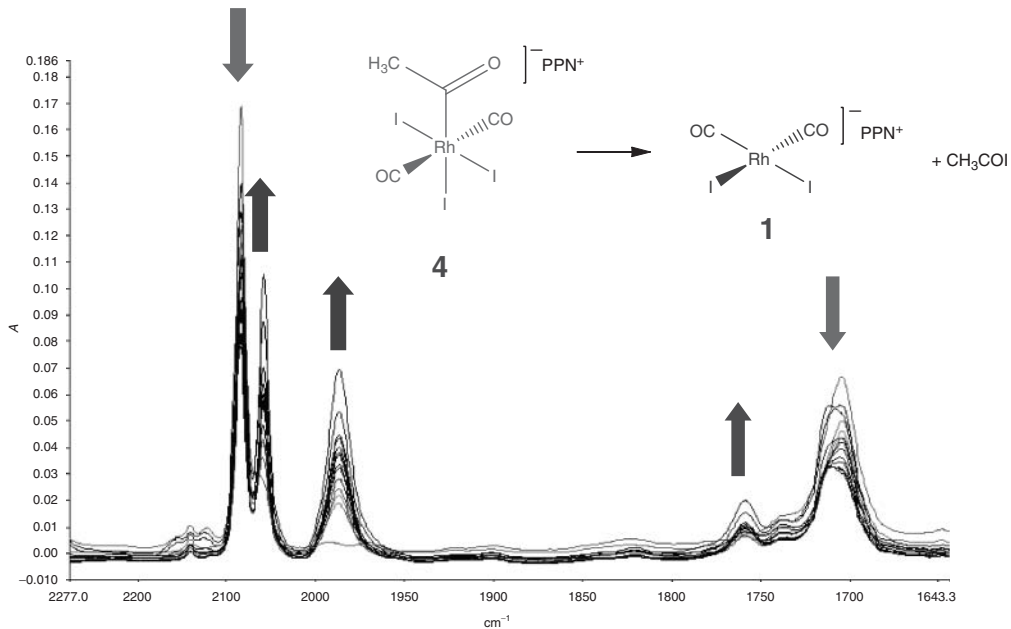


**Figure 20.4** Infrared monitoring of the reaction of **4** under 15 bar CO at 25 °C in dichloromethane.

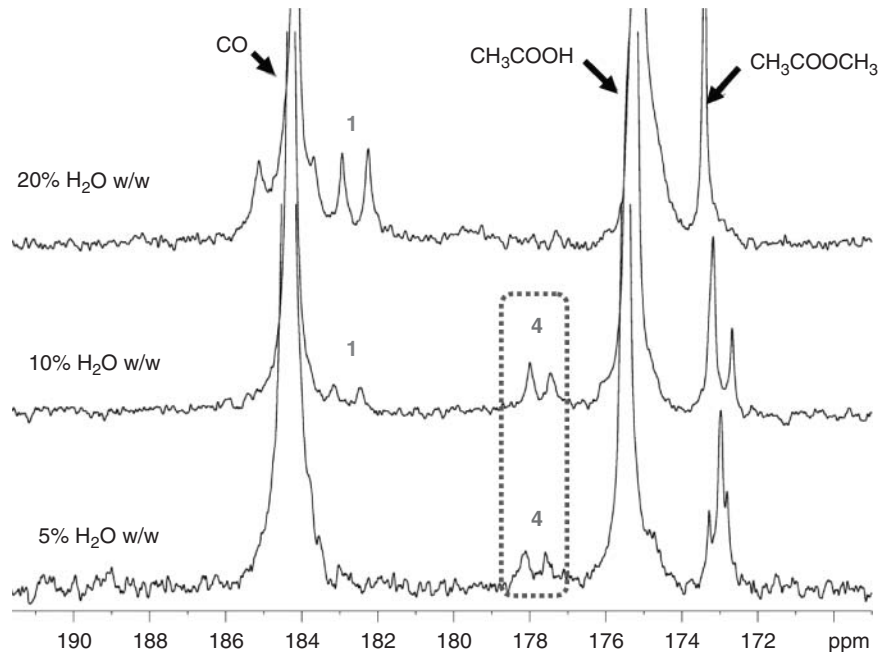


**Figure 20.5** Representative  $^{13}\text{C}$ -HP-NMR spectra recorded under methanol carbonylation conditions (0.1% Rh,  $\text{CD}_3\text{COOD}/\text{MeOAc}/\text{CH}_3\text{I}$ , 15 bar  $^{13}\text{CO}$ , 90 °C) at different water content.

(Figs. 20.9–20.11). Surprisingly, it appears that the obtained energy profiles are dramatically low in energy. First, the intermediate acetate complexes  $[\text{RhI}_2(\text{OAc})(\text{CH}_3\text{CO})(\text{CO})_2]^-$  arising from the two *fac,cis*- or *mer,trans*- species should spontaneously be formed. Second, from the three possible pathways **A**, **B**, and **C**, the energy barrier varies from 14 to 23 kcal/mol (Figs. 20.9–20.11). The first of the two isomers, produced from *mer,trans*-**4**, presents two iodo ligands in trans and the two CO ligands in cis position owing to the moving of one CO in trans of the acetyl ligand (intermediate at –14 kcal/mol, pathway **A**, Fig. 20.9). The second isomer in pathway **B** adopts two CO in trans and the two iodo in cis,

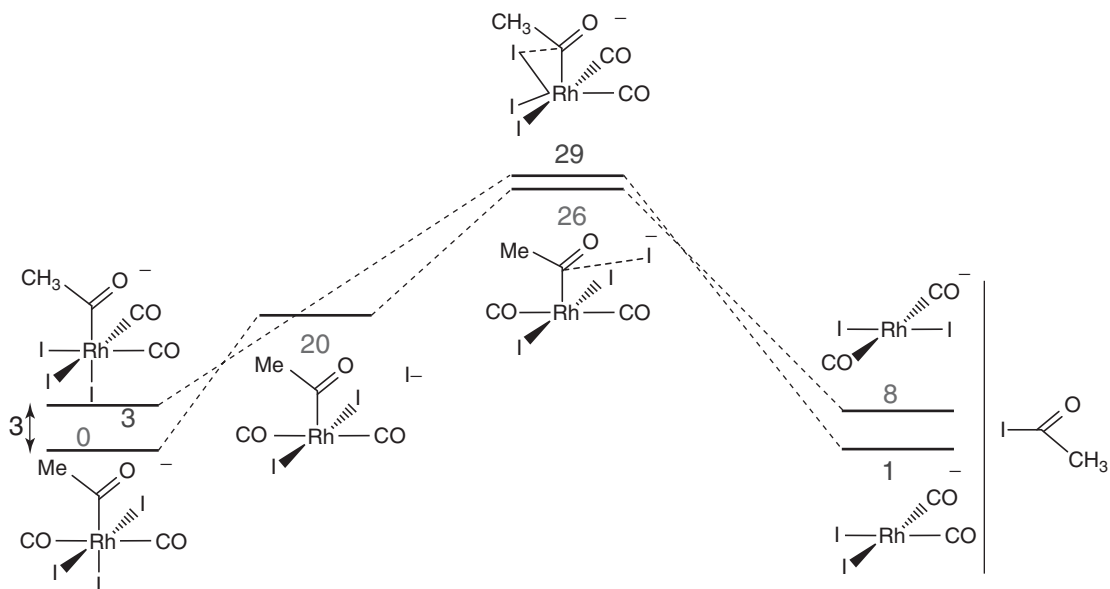


**Figure 20.6** Gibbs free-energy pathway (energies in kcal/mol) computed for the internal rearrangement leading to the reductive elimination of  $\text{CH}_3\text{COI}$  from *mer,trans*- $[\text{RhI}_3(\text{COMe})(\text{CO})_2]^-$  and *fac,cis*- $[\text{RhI}_3(\text{COMe})(\text{CO})_2]^-$ .

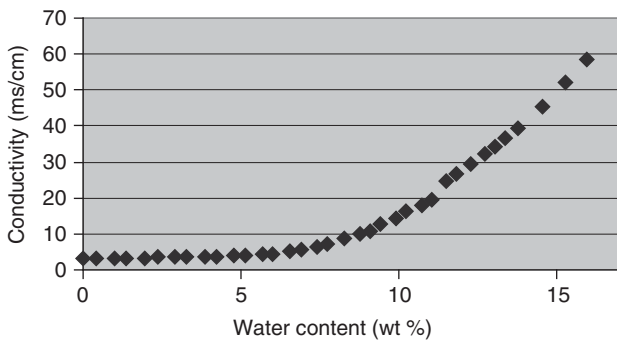


**Figure 20.7** Conductivity measurements of water/acetic acid mixtures.

the acetyl and acetate being trans to the iodo ligands (Fig. 20.10). From *fac,cis*-4, only the isomer in pathway C exists, in which the two iodo and one CO ligand geometry relative to the acetyl ligand remains unchanged (Fig. 20.11). Thus the stabilizations are respectively of  $-14$ ,  $-24$ , and  $-31$  kcal/mol when one iodo ligand is substituted with an acetate ligand.

Correlatively, the transition states to produce 1 equiv of acetic anhydride and regenerate the *cis*- or *trans*- $[\text{RhI}_2(\text{CO})_2]^-$  species display low, although slightly different, energy barriers. If we consider first path A (Fig. 20.9), the transition state, in which the oxygen atom approaches the carbon atom of the acetyl group at a distance of  $1.59 \text{ \AA}$ , the two rhodium–oxygen and rhodium–carbon distances being extended to  $2.15$  and  $2.57 \text{ \AA}$ , has the same energy as the starting *mer,trans*-4 complex. The energy barrier of  $14$  kcal/mol is low, presumably because the back donation of the acetyl group on the CO ligand in *trans* position is important, giving rise to a rather facile C–O bond formation similar to an internal nucleophilic attack of the oxygen atom on the acetyl carbon atom. Then the reductive elimination reaction is largely exergonic ( $-36$  kcal/mol) producing *trans*- $[\text{RhI}_2(\text{CO})_2]^-$  and acetic anhydride.

From the *mer,trans*-4 complex, path B (Fig. 20.10) produces *cis,cis,trans*- $[\text{RhI}_2(\text{OAc})(\text{CH}_3\text{CO})(\text{CO})_2]^-$ , and, because of the polarization of the two Rh–I bonds due to strong  $\sigma$ -effect of the acetyl and acetate ligands, the approach of the two fragments, which can be assimilated to a nucleophilic attack, proceeds less easily than in path A. Thus, the calculated energy

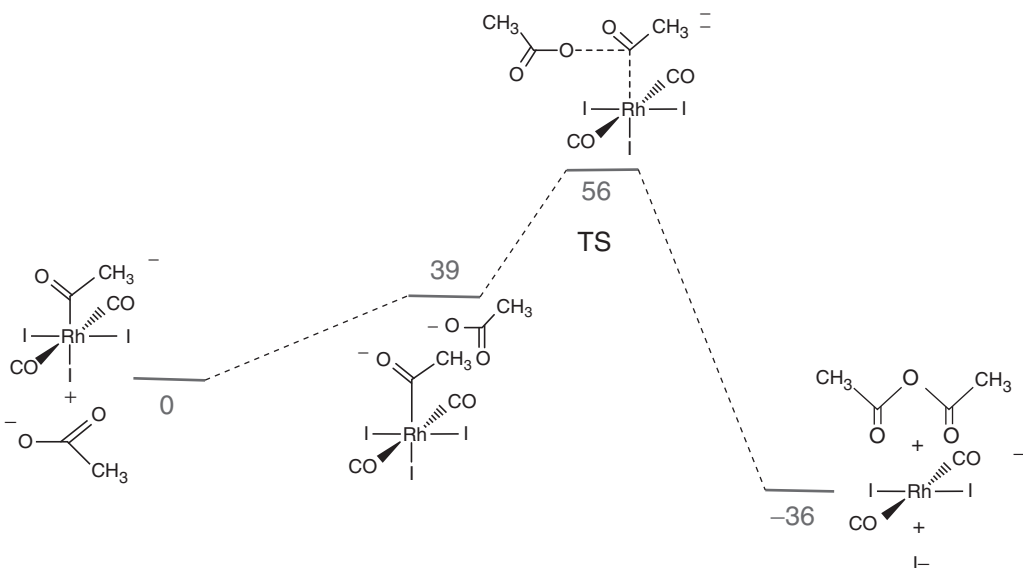


**Figure 20.8** Gibbs free-energy pathway computed for the direct attack of an  $\text{OAc}^-$  ion on the acetyl carbon atom of *mer,trans*- $[\text{RhI}_3(\text{COME})(\text{CO})_2]^-$ .

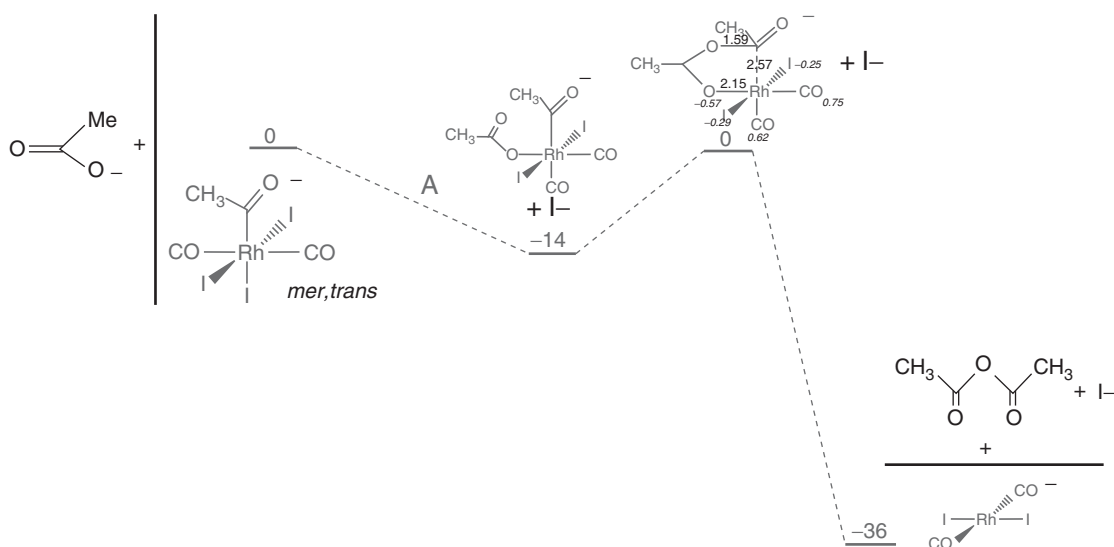


**Figure 20.9** Reaction path A for the substitution of  $\text{I}^-$  with  $\text{OAc}^-$  in *mer,trans*- $[\text{RhI}_3(\text{COMe})(\text{CO})_2]^-$  and reductive elimination of  $\text{CH}_3\text{COOCOCH}_3$  ( $\text{Ac}_2\text{O}$ ).

barrier is 23 kcal/mol, that is, 64% higher than in the first path. Here also, the energy of this intermediate is about the same as that of the starting *mer,trans*-**4** complex. The reductive elimination step liberates 35 kcal/mol.

In path C (Fig. 20.11), the stabilization of *cis,cis,cis*- $[\text{RhI}_2(\text{OAc})(\text{CH}_3\text{CO})(\text{CO})_2]^-$  from *fac,cis*- $[\text{RhI}_3(\text{COMe})(\text{CO})_2]^-$  reaches 31 kcal/mol, the energy barrier is 18 kcal/mol, and the *cis*- $[\text{RhI}_2(\text{CO})_2]^-$  isomer, which is usually found in the catalytic solutions, is at -43 kcal/mol energy level, which is more favorable than the *trans*-isomer by 7 kcal/mol.

Thus the two pathways A and C appear more favorable than the direct reductive elimination of  $\text{CH}_3\text{COI}$  from **4** (energy barrier of 26 kcal/mol) or path B (23 kcal/mol). Indeed, the  $\{[\text{RhI}_2(\text{CO})_2]^- + \text{CH}_3\text{COI}\}$  system is at the same level of energy than the starting acetyl complex **4**, whereas pathways A and C lead to a  $\{[\text{RhI}_2(\text{CO})_2]^- + \text{Ac}_2\text{O}\}$  system characterized by a -36 or -43 kcal/mol energy level. For A and C, the Rh–O and Rh–C(acetate) distances are 2.15 and close to

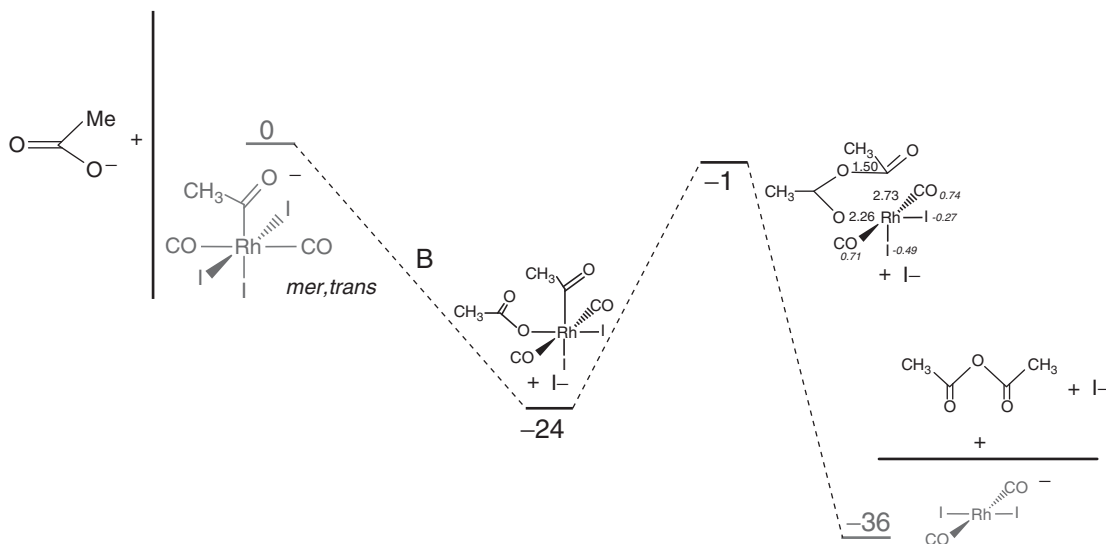


**Figure 20.10** Reaction path **B** for the substitution of  $\text{I}^-$  with  $\text{OAc}^-$  in  $\text{mer,trans}-[\text{RhI}_3(\text{COMe})(\text{CO})_2]^-$  and reductive elimination of  $\text{Ac}_2\text{O}$ .

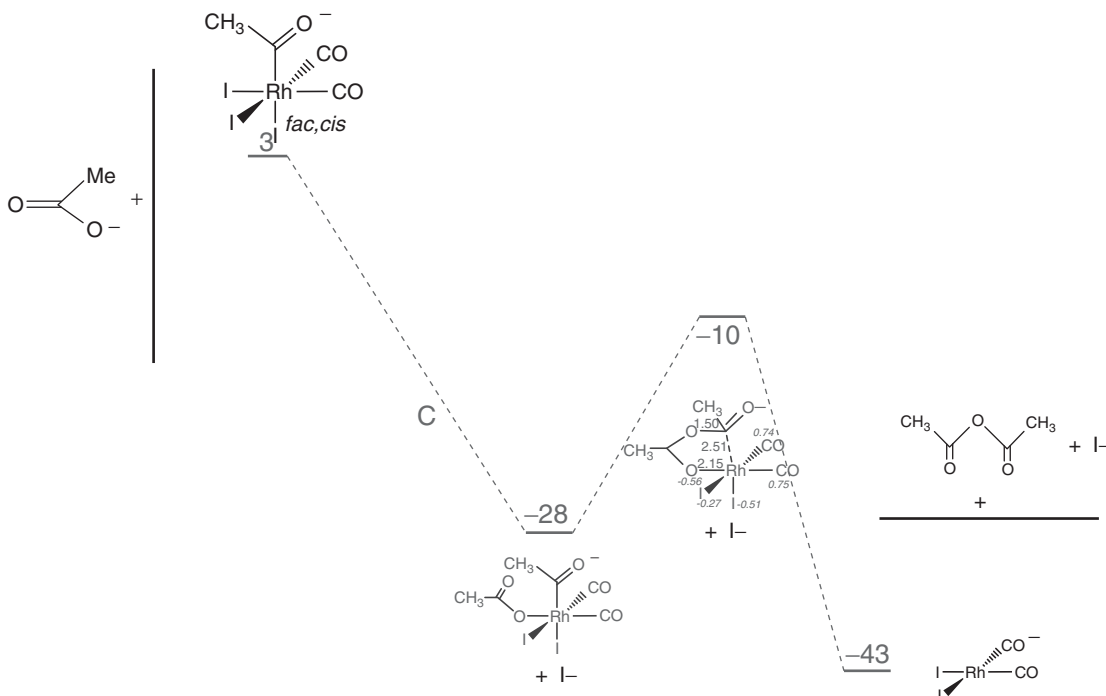


**Figure 20.11** Reaction path **C** for the substitution of  $\text{I}^-$  with  $\text{OAc}^-$  in  $\text{fac,cis}-[\text{RhI}_3(\text{COMe})(\text{CO})_2]^-$  and reductive elimination of  $\text{Ac}_2\text{O}$ .

2.54 Å, respectively, whereas in **B** the Rh–C distance is 2.73 Å, which is consistent with a less electrophilic carbon atom. In addition, path **C** is certainly the most feasible way to produce acetic anhydride and regenerate the active species *cis-1*.

It is interesting to note that a mechanistic study carried out on the palladium-catalyzed biphasic carbonylation of iodobenzene has shown that an indirect route to produce benzoic acid involves benzoic anhydride [35]. For instance, isolation of  $[\text{Pd}(\mu-\text{OH})\text{Ph}(\text{PPh}_3)]_2$  and further reaction with  $\text{PhI}$  under a CO atmosphere leads to  $[\text{Pd}(\mu-\text{I})(\text{COPh})(\text{PPh}_3)]_2$ ,  $(\text{PhCO})_2\text{O}$

and H<sub>2</sub>O in almost quantitative yields. More particularly, the two [Pd(Ph)(COOPh)(PPh<sub>3</sub>)<sub>2</sub>] and [Pd(Ph)(COOPh)(PCy<sub>3</sub>)<sub>2</sub>] complexes, in which the triphenyl- and tricyclohexylphosphine ligands are in trans-position and the benzoate ligand is bonded in a  $\kappa^1$ -mode, undergo a CO insertion in the palladium–phenyl bond to provide the [Pd(COPh)(COOPh)(PPh<sub>3</sub>)<sub>2</sub>] and [Pd(COPh)(COOPh)(PCy<sub>3</sub>)<sub>2</sub>] complexes. Reductive elimination to produce benzoic anhydride occurs very slowly at 70 °C under CO for the latter complex, but rather easily for the PPh<sub>3</sub> containing complex, which leads to the palladium(0) cluster [Pd<sub>3</sub>(CO)<sub>3</sub>(PPh<sub>3</sub>)<sub>3</sub>]. In addition, the carbonylation of an aryl iodide into the corresponding anhydride with yields as high as 98% has been achieved using the {Pd(OAc)<sub>2</sub>/bis(diphenylphosphino)propane/NEt<sub>3</sub>/DMF as solvent/0.5 equiv H<sub>2</sub>O/CO (1 bar)} catalytic system [36]. The authors suppose that the H<sub>2</sub>O molecule attacks the Pd-acyl intermediate to generate a Pd–H species (NEt<sub>3</sub>) reacting to remove [NEt<sub>3</sub>H]I and produce [Pd<sup>(0)</sup>(DPPP)] and the aryl carboxylate which reacts with the Pd-acyl species. Finally, the nucleophilic attack of a palladium-acyl species has been extensively proposed in the alcoholysis step for the termination step of the carbon monoxide/ethylene alternating copolymerization process [37–39]. However, the characterization of the (benzoyl)benzoate)palladium complex shows that this classical reductive elimination step, in which even the two groups are in trans position, can occur in competition with the nucleophilic attack of an acyl group [35].

### 20.3 CONCLUSION

The present experimental and theoretical investigations reveal that in the [RhI<sub>3</sub>(COMe)(CO)<sub>2</sub>]<sup>−</sup> complex, resulting from the successive oxidative addition of CH<sub>3</sub>I on [RhI<sub>2</sub>(CO)<sub>2</sub>]<sup>−</sup>, migratory CO-insertion, and CO coordination, one iodo ligand can be easily substituted with an acetato OAc<sup>−</sup> ligand to provide the [RhI<sub>2</sub>(OAc)(COMe)(CO)<sub>2</sub>]<sup>−</sup> intermediate. From the two *cis,cis,cis*- and *fac,cis*-isomers where the acetyl and acetate groups are in cis-position, a significantly exergonic reductive elimination takes place spontaneously to produce acetic anhydride and regenerate the active [RhI<sub>2</sub>(CO)<sub>2</sub>]<sup>−</sup> species in the methanol carbonylation reaction. The energy barriers can be as low as 14 and 18 kcal/mol and be consistent with this mechanism, which competes with the classically admitted reductive elimination of CH<sub>3</sub>COI, requiring 25–26 kcal/mol but being almost thermoneutral [40].

### REFERENCES

1. Harpe H. J. *Industrial Organic Chemistry*, 5th ed.; Wiley-VCH Verlag: Weinheim, Germany, **2010**; p 175.
2. Reppe, W.; Friederich, H.; von Kutepow, N.; Morsch, W. (BASF). U.S. Patent 2,729,651, 1956.
3. Reppe, W.; Friederich, H. (BASF). U.S. Patent 2,789,137, 1957.
4. Mullen, A. In *New Syntheses with Carbon Monoxide*; Falbe, J., Ed.; Springer-Verlag: Berlin, **1980**; p 243.
5. Forster, D.; Singleton, T. C. *J. Mol. Catal.* **1982**, *17*, 299.
6. Dekleva, T. W.; Forster, D. *Adv. Catal.* **1986**, *34*, 81.
7. Mizoroki, T.; Nakayama, M. *Bull. Chem. Soc. Jap.* **1965**, *38*, 2876; **1968**, *41*, 1628.
8. Paulik, F. E.; Roth, J. F. *J. Chem. Soc. Chem. Commun.* **1968**, 1578.
9. Roth, J. F.; Craddock, J. H.; Hershman, A.; Paulik, F. E. *Chem. Technology* **1971**, 600.
10. Forster, D. *Adv. Organometal. Chem.* **1979**, *17*, 255.
11. Howard, M. J.; Jones, M. D.; Roberts, M. S.; Taylor, S. A. *Catal. Today* **1993**, *18*, 325.
12. Maitlis, P. M.; Haynes, A.; Sunley, G. J.; Howard, M. J. *J. Chem. Soc. Dalton Trans.* **1996**, 2187.
13. Cheung, H.; Tanke, R. S.; Torrence, G. P. *Ullmann's Encyclopedia of Industrial Chemistry*, 6th ed., Wiley-VCH: Weinheim, **2000**.
14. Yoneda, N.; Kusano, S.; Yasui, M.; Pujado, P.; Wilcher, S. *Appl. Catal. A* **2001**, *221*, 253.
15. Gauss, M.; Seidel, A.; Torrence, P.; Heymanns, P. In *Applied Homogeneous Catalysis with Organometallic Compounds*; Cornils, B.; Herrmann, W. A., Eds.; Vol. 1, Wiley-VCH: Weinheim, **1996**; Torrence, P. In *Applied Homogeneous Catalysis with Organometallic Compounds*, 2nd ed.; Cornils, B.; Herrmann, W. A., Eds.; Vol. 1, Wiley-VCH: Weinheim, **2002**; p 104.
16. Thomas, C. M.; Süss-Fink, G. *Coord. Chem. Rev.* **2003**, *243*, 125.
17. Haynes, A. *Top. Organometal. Chem.* **2006**, *18*, 179.
18. Haynes, A. *Adv. Catal.* **2010**, *53*, 1.
19. Jones, J. H. *Platinum Metals Rev.* **2000**, *44*, 94.
20. McConnell, A. C.; Pogorzelec, P. J.; Slawin, M. Z.; Williams, G. L.; Elliott, P. I. P.; Haynes, A.; Marr, A. C.; Cole-Hamilton, D. J. *Dalton Trans.* **2006**, (1), 91.

21. Bassetti, M.; Monti, D.; Haynes, A.; Pearson, J. M.; Stanbridge, I. A.; Maitlis, P. M. *Gazz. Chim. Ital.* **1992**, *122*, 391.
22. Ellis, P. R.; Pearson, J. M.; Haynes, A.; Adams, H.; Bailey, N. A.; Maitlis, P. M. *Organometallics* **1994**, *13*, 3215.
23. Nguyen, D. H.; Lassauque, N.; Vendier, L.; Mallet-Ladeira S.; Le Berre C.; Serp P.; Kalck P. Submitted for publication.
24. Gautron, S.; Giordano, R.; Le Berre, C.; Jaud, J.; Daran, J.-C.; Serp, P.; Kalck, P. *Inorg. Chem.* **2003**, *42*, 5523.
25. Sunley, J.G.; Garland, C.S.; Giles, M. F. (BP Chemicals). European Patent 643 034, **1994**.
26. Garland, C. S.; Giles, M. F.; Poole, A. D.; Sunley, J. G. (BP Chemicals). European Patent 728 726, **1994**.
27. Ghaffar, T.; Adams, H.; Maitlis, P. M.; Sunley, J. G.; Baker, M. J.; Haynes, A. *Chem. Comm.* **1998**, 1023.
28. Le Berre, C.; Serp, P.; Kalck, P.; Layeillon, L.; Thiébaut, D. (Acetex Chimie). French Patent 98.13954, **1998**.
29. Gautron, S.; Lassauque, N.; Le Berre, C.; Azam, L.; Giordano, R.; Serp, P.; Laurenczy, G.; Duhayon, C.; Thiébaut, D.; Kalck, P. *Organometallics*, **2006**, *25*, 5894.
30. Smith, B. L.; Torrence, G. P.; Aguiló, A.; Alder, J. S. (Hoechst Celanese). U.S. Patent 5,001,259, **1991**.
31. Murphy, M. A.; Smith, B. L.; Torrence, G. P.; Aguiló, A. *J. Organometal. Chem.* **1986**, *303*, 257.
32. Smith, B. L.; Torrence, G. P.; Murphy, M. A.; Aguiló, A. *J. Mol. Catal.* **1987**, *39*, 115.
33. Kinnunen, T.; Laasonen, K. *J. Mol. Struct. (Theochem)*, **2001**, *542* (1–3) 273.
34. Haynes, A.; Maitlis, P. M.; Quyoun, R.; Pulling, C.; Adams, H.; Spey, S.E.; Strange, R.W. *J. Chem. Soc. Dalton Trans.*, **2002**, 2565.
35. Grushin, V. V.; Alper H. *J. Am. Chem. Soc.* **1995**, *117*, 4305 and references cited therein.
36. Li, Y.; Xue, D.; Wang, C.; Liu, Z.-T.; Xiao, J. *Chem. Commun.* **2012**, *48*, 1320.
37. van Leeuwen, P. W. N. M.; Zuideveld, M. A.; Swennenhuis, B. H. G.; Freixa, Z.; Kamer, P. C. J.; Goubitz, K.; Fraanje, J.; Lutz, M.; Spek, A. L. *J. Am. Chem. Soc.* **2003**, *125*, 5523.
38. Liu, J.; Heaton, B. T.; Iggo, J. A.; Whyman, R. *Chem. Commun.* **2004**, (11), 1326.
39. Zuidema E., Bo C., van Leeuwen P. W. N. M. *J. Am. Chem. Soc.* **2007**, *129*, 3989.
40. Kinnunen, T.; Laasonen, K. *J. Organomet. Chem.* **2001**, *628*, 222.

---

# 21

---

## HALF-SANDWICH RHODIUM(III), IRIDIUM(III), AND RUTHENIUM(II) COMPLEXES WITH ANCILLARY PYRAZOLE-BASED LIGANDS

Claudio Pettinari\*, Riccardo Pettinari, and Corrado Di Nicola

Schools of Pharmacy, Chemistry Section, S. Agostino 1, University of Camerino, Camerino, Italy

Fabio Marchetti

Schools of Science and Technology, Chemistry Section, S. Agostino 1, University of Camerino, Camerino, Italy

### 21.1 INTRODUCTION

Half-sandwich transition metal complexes are a class of compounds with a three-legged piano-stool pseudo-octahedral geometry at the metal center, where the aromatic five- or six-membered ring occupies three coordinating sites (the seat) with three other ligands (the legs) more or less easily interchangeable. The presence of the aromatic ring stabilizes and protects the metal center, for example, in the case of ruthenium(II), preventing its rapid oxidation to ruthenium(III). Generally, the aromatic ring is relatively inert toward substitution reactions and consequently it is often considered as a spectator ligand. In the three remaining coordination sites opposite the aromatic ligand, it is possible to introduce a wide variety of ligands with C-, N-, O-, S- or P-donor atoms. The resulting derivatives can be neutral, mono- or dicationic, and often these ligands are labile and suitable to be exchanged, a feature in solution that is crucial in self-assemblies, biological, and catalytic processes.

Pyrazole is a five-membered aromatic heterocycle [1], displaying different acid–base features and coordination ability with respect to analogous imidazole. Both imidazole and pyrazole have two nitrogen atoms for which the positive charge can be delocalized upon protonation. However, pyrazoles result in much weaker bases than imidazoles, the difference being due to the fact that the positive charge in pyrazolium ion is less delocalized than in the imidazolium ion. Pyrazole rings are present in a huge number of organic, inorganic and organometallic derivatives for several applications, for example, as building blocks of other compounds, as agrochemicals, in catalysis, and in medicine. Pyrazole and its derivatives are very versatile and a series of analog can be synthesized, thus influencing the steric and electronic features of their metal derivatives. Pyrazole has also been found as a pharmacophore in a number of active biological molecules, with antimicrobial, antiviral, antiglycemic, anti-inflammatory, antiallergic, and anticancer applications [2].

Many classes of pyrazole-based ligands have been developed in the second half of the last century, which have been employed in the coordination chemistry of main group, transition, and lanthanide metal ions and, in the last decade, biological or catalytic applications have been reported [3].

## 21.2 HALF-SANDWICH Ru(II) DERIVATIVES

The first report on half-sandwich derivatives appeared more than thirty years ago, Ferguson et al. describing the reaction of  $[(\eta^6\text{-benzene})\text{RuCl}_2]_2$  or  $[(\eta^5\text{-C}_5\text{Me}_5)\text{RhCl}_2]_2$  with tetrakis(1-pyrazolyl)- and hydrotris(1-pyrazolyl)borate, respectively, which afforded complexes isolated as their  $\text{PF}_6^-$  salts [4]. The crystal structure of the two derivatives confirmed their ionic nature with discrete, well-separated cations containing the scorpionate ligands acting in a tridentate manner and  $\text{PF}_6^-$  anions (Fig. 21.1).

A decade later, attempts to extend the same synthetic procedure in acetonitrile to the more sterically demanding tris(3,5-dimethylpyrazolyl)borate ligand were unsuccessful, leading to the isolation of the amidine cationic complex  $[(\text{C}_6\text{H}_6)\text{Ru}\{\text{NH}=\text{CMe}(\text{Me}_2\text{pz})\}(\text{R}_2\text{Hpz})]^{2+}$ . Reactions of  $[(\text{C}_6\text{H}_6)\text{RuCl}_2]_2$  with pyrazoles, carried out in methanol, afforded  $[(\text{C}_6\text{H}_6)\text{RuCl}(\text{R}_2\text{Hpz})_2]^+$  species ( $\text{R} = \text{H}$  or  $\text{Me}$ ), while in benzene only  $[(\text{C}_6\text{H}_6)\text{RuCl}_2(\text{Me}_2\text{Hpz})]$  was obtained [5].

Several works also appeared on the synthesis of dinuclear cationic (arene)Ru(II) complexes  $\{[(\text{arene})\text{Ru}]_2(\text{L})_3\}^+$  (Fig. 21.2a) (bridged L ligand = pyrazolate (pz), OH, or OMe) from the reaction of  $\{[(\text{arene})\text{Ru}]_2(\text{OH})_3\}^+$  (arene =  $\eta^6\text{-p-cymene}$ ,  $\eta^6\text{-C}_6\text{Me}_6$ ) with pyrazole in refluxing acetone or methanol [6]. Contemporarily, heterobinuclear  $\{[(\text{arene})\text{MCl}_2(\text{pz})\text{M}'(\text{tfb})]\}$  derivatives (Fig. 21.2b) were reported and structurally characterized ( $\text{M} = \text{Ru}$ , arene =  $p$ -cymene,  $\text{M}' = \text{Rh}$ ;  $\text{M} = \text{Ir}$ , arene =  $\text{C}_5\text{Me}_5$ ,  $\text{M}' = \text{Rh}$ ;  $\text{M} = \text{Rh}$ , arene =  $\text{C}_5\text{Me}_5$ ,  $\text{M}' = \text{Ir}$ ) and  $[(\text{C}_5\text{Me}_5)\text{IrCl}(\text{pz})_2\text{Rh}(\text{tfb})]$  (Fig. 21.2c) (tfb = tetrafluorobenzo[5.6]bicyclo[2.2.2]octan-2,5,7-triene) [7].

An extended study on several mixed-ligand derivatives of different composition, as, for example,  $[(p\text{-cymene})\text{Ru}(\text{pz})(\text{acac})]$ ,  $[(p\text{-cymene})\text{Ru}(\text{pzH})(\text{acac})]\text{BF}_4^-$ ,  $[(p\text{-cymene})\text{Ru}(\text{pzH})_2\text{Cl}]\text{BF}_4^-$ , and  $[(p\text{-cymene})\text{Ru}(\text{pzH})_2(\text{pz})]\text{BF}_4^-$  was reported (Fig. 21.3), together with a detailed NMR investigation and X-ray diffraction study on the latter compound [8].

Several studies have been published on neutral and cationic half-sandwich (arene)Ru(II) derivatives containing differently substituted pyrazoles and pyrazolates [9], and also pyrazole–phosphinite ligands, together with preliminary tests on their catalytic activity in transfer hydrogenation of cyclohexanone by propan-2-ol [10].

Different combinations, such as  $[(p\text{-cymene})\text{Ru}(\text{pzH})_3]\text{BF}_4^-$  and  $[(p\text{-cymene})\text{Ru}(\text{pz})_2(\text{pzH})]$ , together with the heterodinuclear complexes  $[(p\text{-cymene})\text{RuCl}(\mu\text{-pz})_2\text{M}(\text{CO})_2]$  ( $\text{M} = \text{Rh}$ ,  $\text{Ir}$ ) (Fig. 21.4a) were also reported. The heterodinuclear complexes  $[(p\text{-cymene})\text{RuCl}(\mu\text{-ClPhpz})_2\text{Ir}(\text{CO})_2]$  and  $[(p\text{-cymene})\text{RuCl}(\mu\text{-MePhpz})_2\text{Ir}(\text{CO})_2]$  exist in

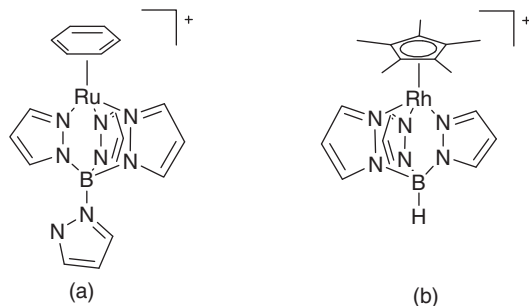


**Figure 21.1** (a)  $[(\text{Benzene})\text{Ru}(\kappa^3\text{-tetrakis(1-pyrazolyl)borate})]^{+}$ ; (b)  $[(\text{C}_5\text{Me}_5)\text{Rh}(\kappa^3\text{-hydrotris(1-pyrazolyl)borate})]^{+}$ .

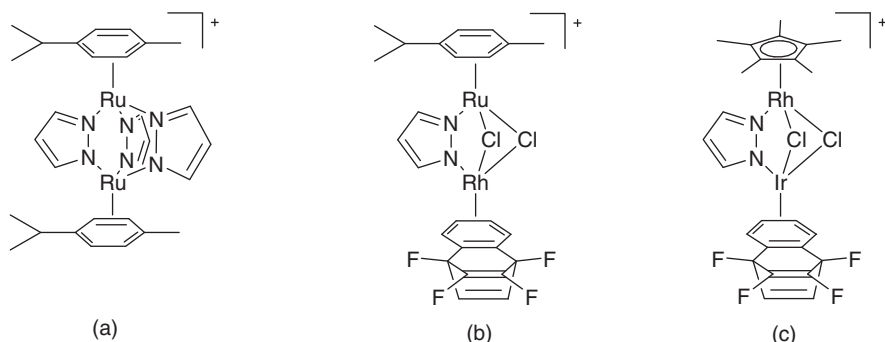


**Figure 21.2** (a)  $\{[(p\text{-Cymene})\text{Ru}]_2(\text{pyrazolate})_3\}^{3+}$ ; (b)  $\{[(p\text{-cymene})\text{Ru}]_2\text{Cl}_2(\text{pz})(\text{tfb})\}^{+}$ ; (c)  $\{[(\text{C}_5\text{M}_5)\text{RhIr}]_2\text{Cl}_2(\text{pz})(\text{tfb})\}^{+}$ .

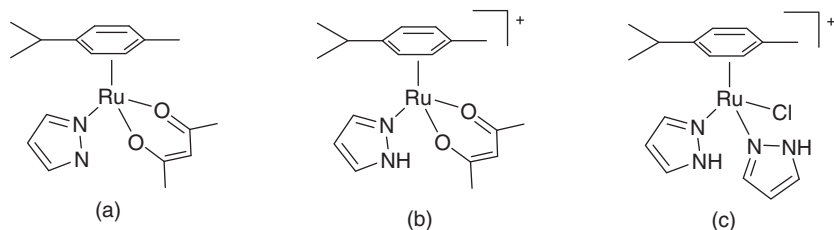


**Figure 21.3** (a)  $[(p\text{-Cymene})\text{Ru}(\text{pz})(\text{acac})]$ ; (b)  $[(p\text{-cymene})\text{Ru}(\text{pzH})(\text{acac})]^+$ ; (c)  $[(p\text{-cymene})\text{Ru}(\text{pzH})_2\text{Cl}]^+$ .

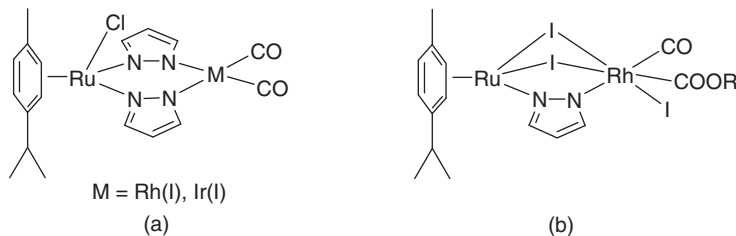


**Figure 21.4** (a)  $[(p\text{-Cymene})\text{RuCl}(\mu\text{-pz})_2\text{M}(\text{CO})_2]$ ; (b)  $[(p\text{-cymene})\text{Ru}(\mu\text{-pz})(\mu\text{-I})_2\text{RhI}(\text{CO})(\text{COOR})]$ .

solution as two isomers in equilibrium with each other that implies a reversible metal–metal bond formation accompanied by halide migration [11]. The same authors described the unusual reactivity of these heterodinuclear complexes containing bridged pyrazolato and terminal carbonyl ligands with alcohols, leading to formation of alcoxycarbonyl derivatives (Fig. 21.4b) [12].

Other heterodinuclear [(*p*-cymene)Ru( $\mu$ -pz)<sub>3</sub>M(PPh<sub>3</sub>)] (M = Cu, Ag, Au), [(*p*-cymene)Ru(pz)( $\mu$ -pz)<sub>2</sub>ML<sub>2</sub>] (M = Rh, L<sub>2</sub> = cod, L = CO, M = Ir, L = CO), and heterotrinuclear cationic complexes [(*p*-cymene)Ru( $\mu$ -pz)<sub>3</sub>{Ag(PPh<sub>3</sub>)<sub>2</sub>}] $\text{BF}_4^-$  (Fig. 21.5) have been synthesized by using bis(pyrazolato)(*p*-cymene)(pyrazole)ruthenium(II) as starting reactant [13]. The carbonyl complexes react with mono- or diphosphines giving [(*p*-cymene)Ru(pz)( $\mu$ -pz)<sub>2</sub>M(CO)(PR<sub>3</sub>)] and [(*p*-cymene)Ru(pz)( $\mu$ -pz)<sub>2</sub>M(diphos)] (PR<sub>3</sub> = PPh<sub>3</sub> or P(OMe)<sub>3</sub>, diphos = bis(diphenylphosphino)methane, 1,2-bis(diphenylphosphino)ethane, *cis*-1,2-bis(diphenylphosphino)ethylene, (*R*)-(+)-1,2-bis(diphenylphosphino)propane, M = Rh, Ir), respectively (Fig. 21.5).

Similar dinuclear bridged pyrazolate Os–Ir and Os–Rh complexes of formula  $[(p\text{-cymene})\text{OsCl}(\mu\text{-pz})_2\text{Ir}(\text{CO})_2]$  were also reported, together with a theoretical study on an isomerization process observed in solution where the chloride moves from one metal center to the other [14]. A different approach was used by Oro [15], in collaboration with Trofimenko, in the reaction of  $[\text{ML}(\text{pz})_2(\text{Hpz})]$  ( $\text{L} = \text{C}_5\text{Me}_5$ ,  $\text{M} = \text{Ir}$  (1);  $\text{L} = \text{mesitylene or } p\text{-cymene}$ ,  $\text{M} = \text{Ru}$ ) with  $[\text{M}'\text{Cl}\{\text{HB}(3\text{-}i\text{-Pr-4-Br-pz})_3\}]$  ( $\text{M}' = \text{Co, Ni}$ ) to yield heterodinuclear complexes of formula  $[\text{LM}(\mu\text{-pz})_2(\mu\text{-Cl})\text{M}'\{\text{HB}(3\text{-}i\text{-Pr-4-Br-pz})_3\}]$  containing a tridentate scorpionate ligand capping one metal, besides bridging the pyrazolates between the two metal centers (Fig. 21.6).

The same starting  $[ML(pz)_2(Hpz)]$  complexes were used to synthesize heterodinuclear Ru–Pt and Ir–Pt complexes of general formula  $[ML(\mu\text{-}pz)_3PtMe_3]$  [16].

Tocher and Bham bri [17] reported the synthesis and characterization, in some cases also by X-ray diffraction techniques, of a number of cationic cyclohexadienyl, (arene)ruthenium(II) poly(pyrazolyl)borate, and poly(pyrazolyl)methane complexes, displaying a similar  $\kappa^3$  coordination on the (arene)ruthenium fragment when the reaction was performed in the presence of  $\text{NH}_4\text{PF}_6$  salt (Fig. 21.7a and b). However, in absence of the former compound, a  $\kappa^2$  coordination of ligands was observed and the (arene)ruthenium fragment holds a chloride, affording neutral derivatives (Fig. 21.7c) [18]. An electrochemical study on  $[(\text{arene})\text{Ru}(\kappa^3-\text{HCp}z_3)]^{2+}$  complexes (arene = *p*-xylene, *p*-cymene, or hexamethylbenzene) has shown that one-electron reduction of the doubly charged cationic complexes does not result in lowering of the hapticity of the scorpionate ligand [19]. An interesting  $\kappa^1$  coordination of  $\text{HBp}z_3$  ligand has been found in the (*p*-cymene) $\text{Ru}(\text{quin})(\kappa^1-\text{HBp}z_3)$  complex (quin = quinolin-8-ate) (Fig. 21.7d), and the same authors reported also the cationic complex  $[(\text{*p*-cymene})\text{Ru}(\text{quin})(\kappa^1-\text{Hp}z)]\text{CF}_3\text{SO}_3$  arising from B–N bond cleavage in the presence of  $\text{AgCF}_3\text{SO}_3$  [20].

A chiral alkyltris(pyrazolyl)borate ligand has been used in the synthesis of  $[(p\text{-cymene})\text{Ru}(\kappa^3\text{-(Ipc)}\text{Bpz}_3)]\text{PF}_6$  (Ipc = isopinocampheyl) (Fig. 21.8a) [21]. The complex  $[(p\text{-cymene})\text{RuCl}(\kappa^2\text{-(dmap)}\text{Bpz}_3)]\text{PF}_6$  has been recently reported

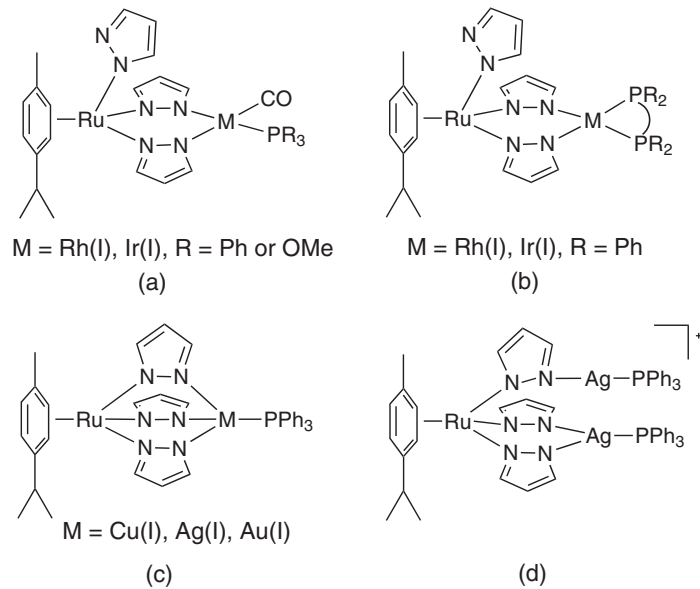


**Figure 21.5** (a)  $[(p\text{-Cymene})\text{Ru}(pz)(\mu\text{-pz})_2\text{M}(\text{CO})(\text{PR}_3)]$ ; (b)  $[(p\text{-cymene})\text{Ru}(pz)(\mu\text{-pz})_2\text{M}(\text{diphos})]$ ; (c)  $[(p\text{-cymene})\text{Ru}(\mu\text{-pz})_3\text{M}(\text{Ph}_3)]$ ; (d)  $[(p\text{-cymene})\text{Ru}(\mu\text{-pz})_3\{\text{Ag}(\text{PPh}_3)_2\}]^+$ .

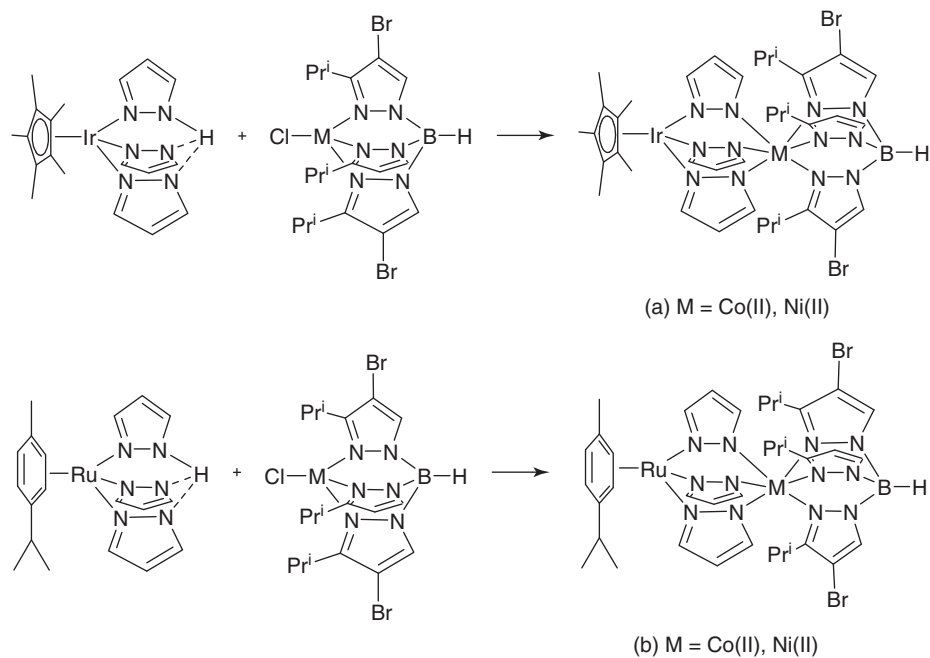


**Figure 21.6** Synthesis of (a)  $[(C_5Me_5)_2Ir(\mu\text{-pz})_3M\{HB(3-i\text{-Pr-4-Br-pz)}_3\}]$  and (b)  $[(p\text{-cymene})Ru(\mu\text{-pz})_3M\{HB(3-i\text{-Pr-4-Br-pz)}_3\}]$ .

(Fig. 21.8b),  $(\text{dmap})\text{Bpz}_3$  ( $\text{dmap} = 4\text{-dimethylaminopyridine}$ ) being a heteroscorpionate ligand that was prepared through a flexible route by interaction of the precursor  $[(\text{HNMe}_2)\text{Bpz}_3]$  (readily available by reaction of  $\text{B}(\text{NMe}_2)_3$  with pyrazole) and dmap in toluene heated at reflux to liberate  $\text{HNMe}_2$  [22].

Dinuclear complexes with tris(pyrazolyl)borates and bridging arenethiolato ligands, of formula  $[(\kappa^3\text{-HBpz}_3)\text{RhCl}(\mu\text{-SR})_2\text{MCp}^*\text{Cl}]$  and  $[(\kappa^3\text{-HBpz}_3)\text{RhCl}(\mu\text{-SR})_2\text{MCp}^*(\text{MeCN})]\text{PF}_6$  ( $\text{M} = \text{Rh, Ir}$ ;  $\text{R} = \text{Ph, Tol}$ ) [23] (Fig. 21.9a and b) and  $[(\kappa^3\text{-HBpz}_3)\text{RhCl}(\mu\text{-EPh})_2\text{RuCp}^*(\text{MeCN})]$  ( $\text{E} = \text{S, Se, Te}$ ) (Fig. 21.9c) have been reported by Mizobe et al. [24]. When

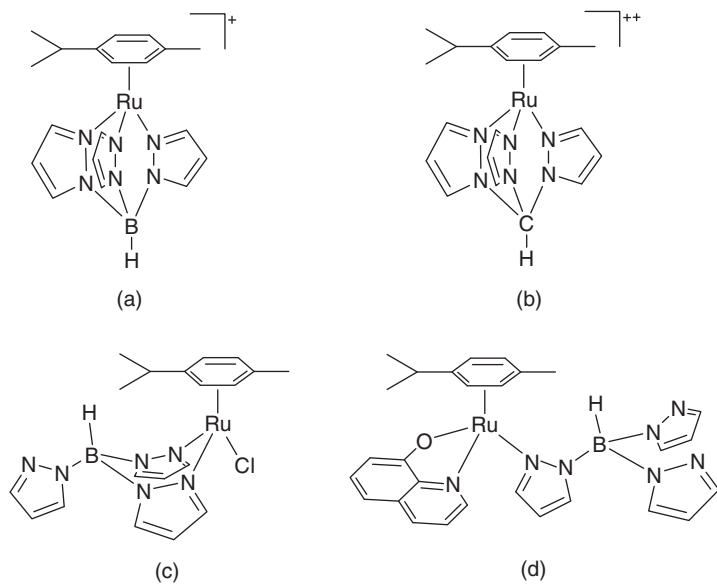


**Figure 21.7** (a)  $[(p\text{-Cymene})\text{Ru}(\kappa^3\text{-HBpz}_3)]^+$ ; (b)  $[(p\text{-cymene})\text{Ru}(\kappa^3\text{-HCpz}_3)]^{2+}$ ; (c)  $[(p\text{-cymene})\text{RuCl}(\kappa^2\text{-HBpz}_3)]$ ; (d)  $[(p\text{-cymene})\text{Ru}(\kappa^1\text{-HBpz}_3)(\text{quin})]$ .

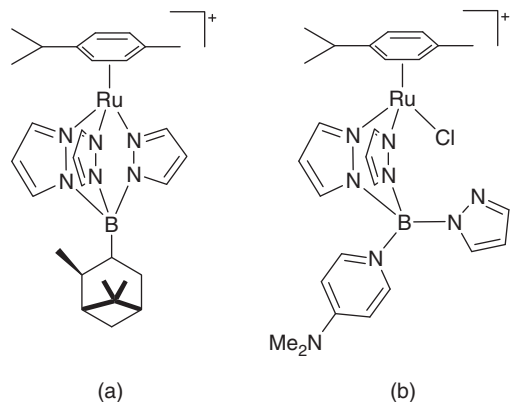


**Figure 21.8** (a)  $[(p\text{-Cymene})\text{Ru}(\kappa^3\text{-(Ipc)}\text{Bpz}_3)]^+$ ; (b)  $[(p\text{-cymene})\text{RuCl}(\kappa^2\text{-(dmap)}\text{Bpz}_3)]^+$ .

the latter dinuclear Rh–Ru complexes was dissolved in tetrahydrofuran (THF) and exposed to air, the MeCN ligand bound to Ru is replaced by dioxygen to give the peroxy complexes  $[(\kappa^3\text{-HBpz}_3)\text{RhCl}(\mu\text{-EPH})_2\text{RuCp}^*(\eta^2\text{-O}_2)]$  (Fig. 21.9d).

A heteroscorpionate tridentate  $N,O,N$ -ligand [ $\text{Li}\cdot(\text{thf})(\text{L})$ ] has been developed by Wagner et al. [25] and used in the synthesis of  $[\text{Cp}^*\text{Ru}(\text{L})]$  and  $[(p\text{-cymene})\text{Ru}(\text{L})]\text{Cl}$  (Fig. 21.10a and b). Other chelating ligands with an *ortho*-hydroquinoline substituent on a bis(3,5-dimethylpyrazolyl)methane moiety have been synthesized and coordinated to  $\text{Cp}^*\text{Ir}(\text{III})$  (Fig. 21.10c) and  $(p\text{-cymene})\text{Ru}(\text{II})$  fragments (Fig. 21.10d) [26].

(Arene)Ru(II) complexes containing third-generation heteroscorpionate ligands, namely, tris(pyrazolyl)methanesulfonates (Fig. 21.11) have been reported by us together with a detailed characterization, also by X-ray techniques and electrochemical studies that allowed to compare the electron-donor character of the scorpionate and arene ligands (arene = *p*-cymene, benzene, hexamethylbenzene) [27].

We have extended our studies also to other polydentate scorpionate ligands, the bis(pyrazolyl)acetates  $\text{L}^-$ , which have been shown to coordinate (arene)Ru(II) fragments (arene = *p*-cymene, benzene, hexamethylbenzene) both in the neutral or anionic forms [28]. While the ligands  $\text{HL}$  in the neutral form coordinate ruthenium in a chelating  $\kappa^2\text{-N,N}$ -bidentate fashion affording 1 : 1 derivatives of formula  $[(\text{arene})\text{Ru}(\kappa^2\text{-N,N-}\text{HL})\text{Cl}]\text{Cl}$ , the anionic  $\text{L}^-$  ligands coordinate in the tripodal  $\kappa^3\text{-N,N,O}$ -tridentate fashion affording  $[(\text{arene})\text{Ru}(\kappa^3\text{-N,N,O-}\text{L})]\text{Cl}$  (Fig. 21.12a and b).

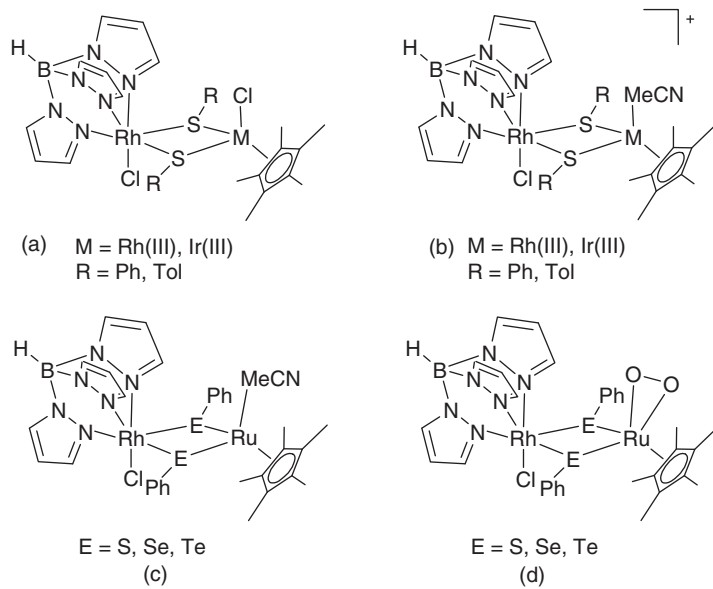


**Figure 21.9** (a)  $[(\kappa^3\text{-HBpz}_3)\text{RhCl}(\mu\text{-SR})_2\text{MCp}^*\text{Cl}]$ ; (b)  $[(\kappa^3\text{-HBpz}_3)\text{RhCl}(\mu\text{-SR})_2\text{MCp}^*(\text{MeCN})]^+$ ; (c)  $[(\kappa^3\text{-HBpz}_3)\text{RhCl}(\mu\text{-EPh})_2\text{RuCp}^*(\text{MeCN})]$ ; (d)  $[(\kappa^3\text{-HBpz}_3)\text{RhCl}(\mu\text{-EPh})_2\text{RuCp}^*(\eta^2\text{-O}_2)]$ .

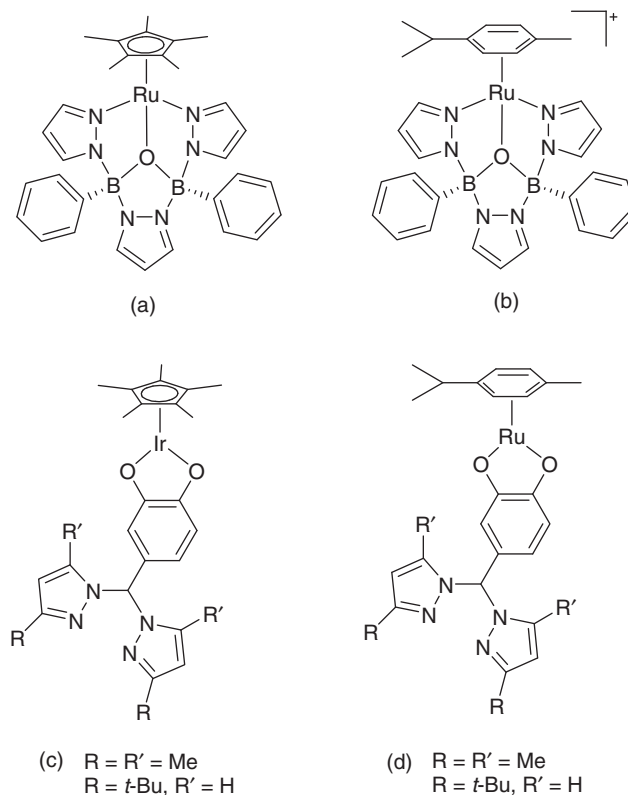


**Figure 21.10** (a)  $[\text{Cp}^*\text{Ru}(\kappa^3\text{-Ph(pz)}\text{B}(\mu\text{-O})(\mu\text{-pz})\text{B(pz)Ph})]$ ; (b)  $[(p\text{-cymene})\text{Ru}(\kappa^3\text{-Ph(pz)}\text{B}(\mu\text{-O})(\mu\text{-pz})\text{B(pz)Ph})]^+$ ; (c)  $[\text{Cp}^*\text{Ir}(\kappa^2\text{-O}_2\text{C}_6\text{H}_3\text{C(H)}(\text{pz}^{R,R'})_2)]$ ; (d)  $[(p\text{-cymene})\text{Ru}(\kappa^2\text{-O}_2\text{C}_6\text{H}_3\text{C(H)}(\text{pz}^{R,R'})_2)]$ .

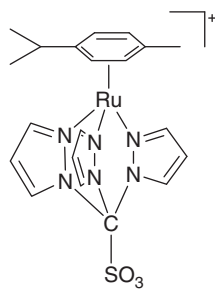


**Figure 21.11**  $[(p\text{-Cymene})\text{Ru}(\kappa^3\text{-(SO}_3\text{)}\text{C(pz}_3\text{)})]^{+}$ .

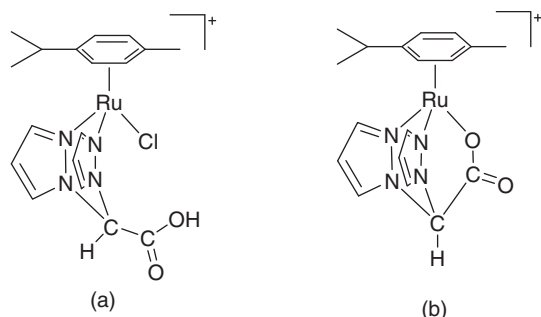


**Figure 21.12** (a)  $[(p\text{-Cymene})\text{Ru}(\kappa^2\text{-N,N-bis(pyrazolyl)acetate})\text{Cl}]^{+}$ ; (b)  $[(p\text{-cymene})\text{Ru}(\kappa^3\text{-N,N,O-bis(pyrazolyl)acetate})]^{+}$ .

Also for this series of complexes, a detailed electrochemical investigation has been performed, which allowed to order the HL and  $\text{L}^-$  ligands according to their electron-donor character. In addition, density functional theory (DFT) calculations showed a relevant contribution of L ligand orbitals to the highest occupied molecular orbitals (HOMOs) when they are coordinated in the monoanionic tridentate form, while for derivatives containing neutral HL ligands, the main contribution to the HOMOs comes from orbitals of the metal and chlorine atoms, the overall contribution from the bidentate HL ligand orbitals being small. All complexes are soluble in water and those with neutral HL ligands show very high conductance values in water, due to the contribution of  $\text{H}_3\text{O}^+$  produced by deprotonation of the  $-\text{COOH}$  fragment in HL ligands and consequent formation of  $[(\text{arene})\text{Ru}(\kappa^3\text{-N,N,O-L})]\text{Cl}$  species. An extensive study on (arene)Ru(II) complexes with bis-, tris-, and tetrakis-pyrazolylborates, containing hindered substituents in the pz rings, has been also reported, together with structural and electrochemical investigations that allowed comparing the electron-donor characters of these and related ligands and estimating the corresponding values of the Lever  $E_L$  ligand parameter [29].

More interestingly, some of these complexes act as catalyst precursors for the diastereoselective nitroaldol reaction of benzaldehyde and nitroethane to the corresponding  $\beta$ -nitroalkanol (up to 82% yield, at room temperature) with diastereoselectivity toward the formation of the threo isomer.

In recent years, catalytic applications of half-sandwich metal complexes have been extensively developed. A series of (*p*-cymene)Ru(II) complexes containing pyrazole-based *N*-heterocyclic carbone (pyrazolin-3-ylidene) ligands (Fig. 21.13a and b) showed excellent catalytic  $\beta$ -alkylation of secondary alcohols with primary alcohols and the dimerization of phenylacetylene [30].

The catalytic activity of ruthenium(II) complexes  $[(\text{arene})\text{RuCl}_2(3,5\text{-Me}_2\text{pz})]$  (arene =  $\text{C}_6\text{H}_6$ , *p*-cymene, or  $\text{C}_6\text{Me}_6$ ) in the redox isomerization of allylic alcohols into carbonyl compounds in water has been reported [31]. Phosphine-pyrazolyl-based tripod ligands L ( $\text{L} = \text{ROCH}_2\text{C}(\text{CH}_2\text{pz})_2(\text{CH}_2\text{PPh}_2)$  where R = H, Me, allyl) afford  $[(p\text{-cymene})\text{RuCl}_2(\text{L})]$  complexes (Fig. 21.13c) that demonstrated poor-to-moderate catalytic activity in the transfer hydrogenation of acetophenone [32].

Arene ruthenium(II) cationic complexes containing bis(pyrazolyl)methane ligands L have been reported, the final products being  $[(\text{arene})\text{Ru}(\text{L})\text{Cl}]\text{Cl}$  or  $[(\text{arene})\text{Ru}(\text{L})\text{Cl}][(\text{arene})\text{RuCl}_3]$  depending to the ratio of reactants employed (Fig. 21.14a and b) [33]. The interionic structure of  $[(p\text{-cymene})\text{Ru}(\text{L})\text{Cl}](\text{O}_3\text{SCF}_3)$  and  $[(p\text{-cymene})\text{Ru}(\text{L})\text{Cl}][(\text{p-cymene})\text{RuCl}_3]$  has been investigated through an integrated approach based on nuclear Overhauser effect (NOE) and pulsed field gradient spin-echo (PGSE) NMR experiments in  $\text{CD}_2\text{Cl}_2$  as a function of the concentration. PGSE NMR measurements indicate the

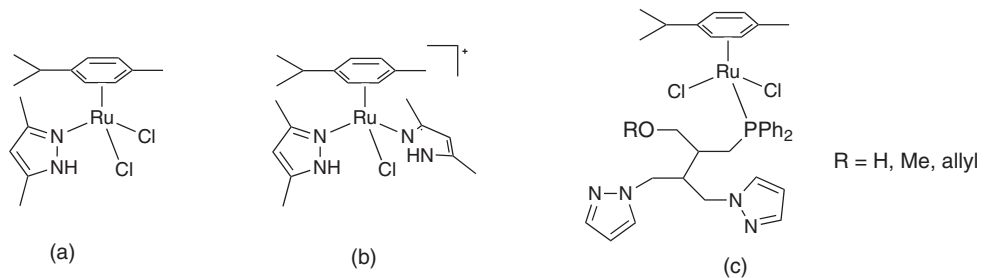


**Figure 21.13** (a)  $[(p\text{-Cymene})\text{RuCl}_2(3,5\text{-Me}_2\text{pz})]$ ; (b)  $[(p\text{-cymene})\text{RuCl}(3,5\text{-Me}_2\text{pz})_2]^+$ ; (c)  $[(p\text{-cymene})\text{RuCl}_2\{\text{ROCH}_2\text{C}(\text{CH}_2\text{pz})_2(\text{CH}_2\text{PPh}_2)\}]$ .

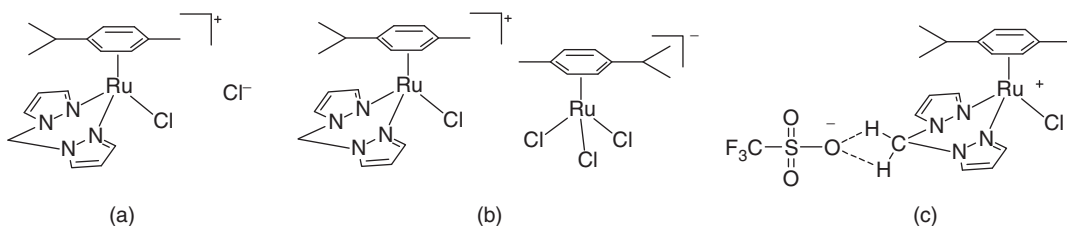


**Figure 21.14** (a)  $[(p\text{-Cymene})\text{Ru}((\kappa^2\text{-H}_2\text{Cpz}_2)\text{Cl})\text{Cl}]$ ; (b)  $[(p\text{-cymene})\text{Ru}((\kappa^2\text{-H}_2\text{Cpz}_2)\text{Cl})][(\text{arene})\text{RuCl}_3]$ ; (c)  $[(p\text{-cymene})\text{Ru}((\kappa^2\text{-H}_2\text{Cpz}_2)\text{Cl})(\text{O}_3\text{SCF}_3)]$ .

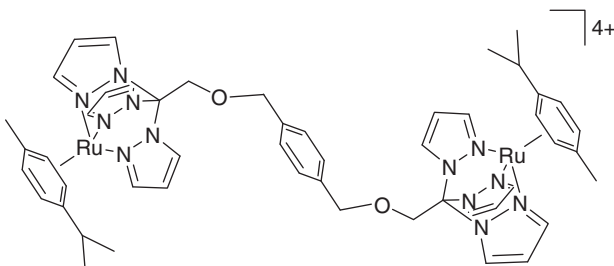


**Figure 21.15**  $\{p\text{-C}_6\text{H}_4[\text{CH}_2\text{OCH}_2\text{Cpz}_3]_2[\text{Ru}(p\text{-cymene})]_2\}^{4+}$ .

predominance of ion pairs in solution. NOE measurements suggest that  $(\text{O}_3\text{SCF}_3)^-$  approaches the cation orienting itself toward the  $\text{CH}_2$  moiety of the  $\text{H}_2\text{Cpz}_2$  ligand as found in the solid state (Fig. 21.14c).

Selected Ru(II) species have been preliminarily investigated as catalysts toward styrene oxidation by dihydrogen peroxide,  $[(p\text{-cymene})\text{Ru}((\kappa^2\text{-H}_2\text{Cpz}_2)(\text{H}_2\text{O})][\text{PF}_6]_2$  being the most active species. In the crystal structures of  $[(p\text{-cymene})\text{Ru}(\text{L})\text{Cl}]\text{Cl}$  complexes, a crystallization water molecule is involved in a weak hydrogen bond with one methylenic hydrogen of the  $\text{H}_2\text{Cpz}_2$  ligand, thus generating infinite helical chains constituted by alternating  $\text{H}_2\text{O}$  and  $\text{Cl}^-$  units running along one crystallographic axis. A similar situation has been found in  $\{p\text{-C}_6\text{H}_4[\text{CH}_2\text{OCH}_2\text{Cpz}_3]_2[\text{Ru}(p\text{-cymene})]_2\}\text{Cl}_4\cdot 14\text{H}_2\text{O}$  (Fig. 21.15), which displays a one-dimensional water chain associated into an inorganic (carbon-free) layer with chloride anions by hydrogen bonds, the layer acting as a “host” supporting the non-self-assembled metal-organic “guests” [34].

Such kind of investigations on small water assemblies represent a significant method to understand the structural variations and mechanisms in the transition from isolated molecules to bulk states and likely to understand their role and behavior at a fundamental level. An analogous situation has been recently found in the crystal structure of  $[(p\text{-cymene})\text{Ru}(\kappa^3\text{-HCpz}_3)]\text{Cl}(\text{OH})\cdot 2\text{H}_2\text{O}$ , isolated from attempted interaction between  $[(p\text{-cymene})\text{RuCl}_2]_2$  and a polytopic nitrogen donor ligand based on the 1,3,5-triazine fragment bearing three  $\{-\text{Cpz}_3\}$  tripodal moieties, which decomposes during the reaction: a supramolecular arrangement has been found, based on hybrid chains involving the anions  $\text{Cl}^-$  and  $\text{OH}^-$  and crystallization water molecules [35].

(Arene)Ru(II) complexes with bis(pyrazolyl)methane ligands in which the central carbon atom bears phenyl rings having different functional substituents such as OMe, OH, NO<sub>2</sub>, or NH<sub>2</sub> (Fig. 21.16a) have been reported: the behavior of these complexes in the transfer hydrogenation of benzophenone in the presence of KOH was studied and, the influence of the arene, the functional group on the phenyl ring, and the substitution on the pyrazole ring evaluated [36]. Kinetic studies confirmed the formation of hydride species after a pretreatment of the precatalyst in 2-propanol, allowing to propose a mechanism of hydrogenation of carbonyl groups under base-free conditions [37].

A number of bis(pyrazolyl)azine ligands have been prepared together with the corresponding mononuclear cationic (arene)Ru(II) complexes (Fig. 21.16b and c), which have been shown active in ketone hydrogenation transfer processes even in the absence of a base [38].

A large number of half-sandwich complexes of Ru(II), Ru(III), Rh(III), and Ir(III) with pyrazole-based ligands with pyridine, pyridazine, and pyrimidine moieties has been recently reported by several authors (Fig. 21.17) [39].

Sadler has focused on the synthesis of novel (arene)Ru(II) complexes with phenylazo-pyrazoles (Fig. 21.18) and on their cytotoxicity toward A2780 human ovarian or A549 human lung cancer cells.

Their aqueous solution chemistry has been deeply investigated by measuring the rate of aquation and the reaction with 9-ethylguanine, to mimic the possible interaction with nucleic acids of DNA, that is thought to be important with respect to their observed cancer cell cytotoxicity [40]. Keppler et al. have contributed in the field of half-sandwich anticancer metal complexes, and in detail on targeted chemotherapy, with a number of works dealing with the synthesis and cytotoxicity evaluation of (arene)Ru(II) derivatives containing pyrazole-based ligands. Ionic derivatives having general formula [(*p*-cymene)Ru(*8*-hydroxyquinoline)(Hazole)]X (Hazole = pyrazole, indazole, imidazole, benzimidazole, or 5,6-dimethylbenzimidazole; X = CF<sub>3</sub>SO<sub>3</sub><sup>-</sup>, PF<sub>6</sub><sup>-</sup>, or Cl<sup>-</sup>) (Fig. 21.19a) have shown water solubility and no evidence of hydrolysis or ligand exchange in aqueous media; moreover, they exhibit excellent cytotoxic effects in the tumor cell lines CH1 and SW480, with IC<sub>50</sub> values ranging from 3.3 to 9.4 μM [41]. Similar ionic complexes [(*p*-cymene)RuCl(L)]Cl, (L = 3-(1*H*-benzimidazol-2-yl)-1*H*-pyrazolo-[3,4-*b*]pyridines) (Fig. 21.19b) have been synthesized, the latter being known as potential cyclin-dependent kinase (Cdk) inhibitors [42]. A study on structure–activity relationships with regard to cytotoxicity and cell cycle effects in human cancer cells, as well as Cdk inhibitory activity, has been also reported. For example, an increased solubility in the biological medium has been observed upon complexation of ligands L, but this lowered the antiproliferative activity in human cancer cell lines.

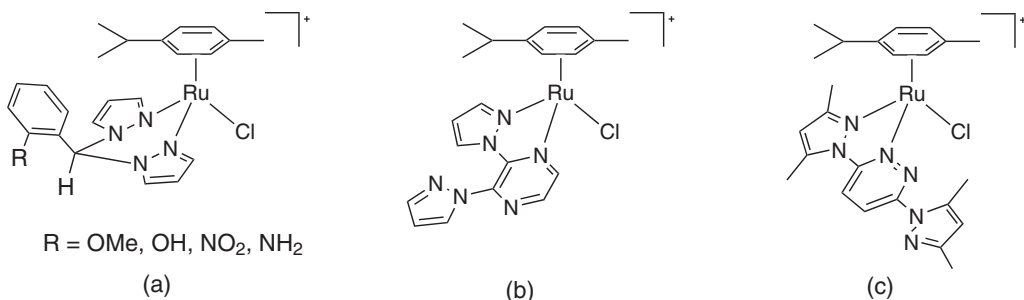


**Figure 21.16** (a) [(*p*-Cymene)Ru( $\kappa^2$ -HC(pz)<sub>2</sub>(C<sub>6</sub>H<sub>4</sub>R)]<sup>+</sup>; (b) [(*p*-cymene)Ru{ $\kappa^2$ -2,3-di(1*H*-pyrazol-1-yl)pyrazine}]<sup>+</sup>; (c) [(*p*-cymene)Ru{ $\kappa^2$ -(3,6-bis(3,5-dimethyl-1*H*-pyrazol-1-yl)pyridazine}]<sup>+</sup>.

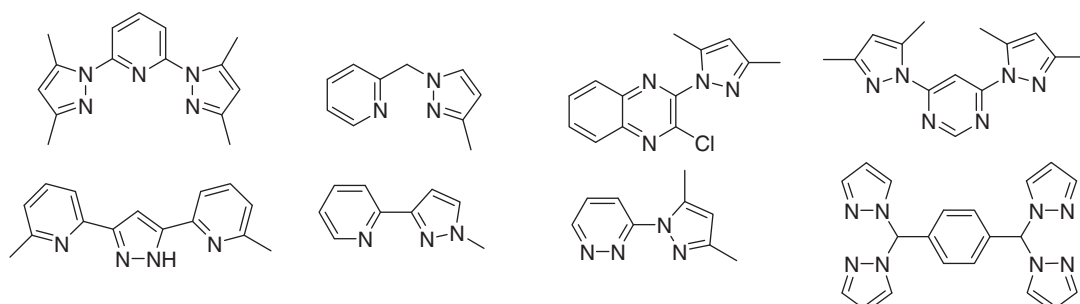


**Figure 21.17** Pyrazole-based ligands with pyridine, pyridazine, and pyrimidine moieties.

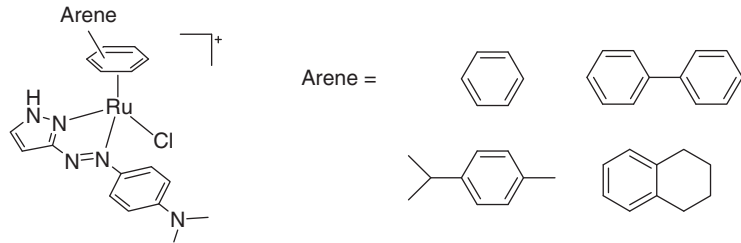


**Figure 21.18**  $(\text{Arene})\text{Ru}(\text{II})$  complexes with phenylazo-pyrazoles.

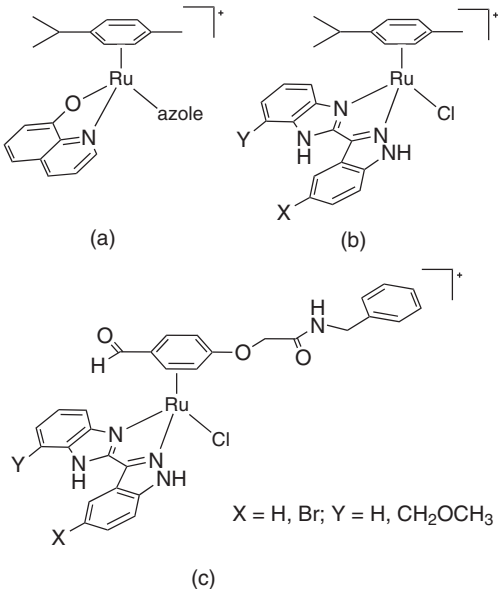


**Figure 21.19** (a)  $[(p\text{-Cymene})\text{Ru}(8\text{-hydroxyquinoline})(\text{Hazole})]^+$ ; (b)  $[(p\text{-cymene})\text{RuCl}(3\text{-1}H\text{-benzimidazol-2-yl})\text{-1}H\text{-pyrazolo[3,4-}b\text{]pyridines}]^+$ ; (c)  $[(4\text{-formylphenoxyacetyl-}\eta^6\text{-benzylamide})\text{RuCl(indolo[3,2-}d\text{]benzazepine)}]^+$ .

$(\text{Arene})\text{RuCl}(\text{L})\text{Cl}$  species where the arene is 4-formylphenoxyacetyl- $\eta^6$ -benzylamide and L is a Cdk inhibitor [3-(1*H*-benzimidazol-2-yl)-1*H*-pyrazolo[3,4-*b*]pyridines or indolo[3,2-*d*]benzazepines] (Fig. 21.19c) have been synthesized and the antiproliferative activities and effects on the cell cycle evaluated, showing moderate cytotoxic to cancer cells (CH1, SW480, A549, A2780, and A2780cisR cell lines) [43]. Moreover, in order to improve their antiproliferative effects, as well as their drug targeting and delivery to cancer cells, the complexes were conjugated to recombinant human serum albumin, and a marked increase in cytotoxicity of the albumin conjugates was observed in all cases.

### 21.3 HALF-SANDWICH Rh(III) AND Ir(III) DERIVATIVES

Since the old reports by Oro et al. [44] and Stobart et al. [45] on the synthesis of half-sandwich Rh(III) and Ir(III) dinuclear complexes of formula  $[\text{CpM}(\mu\text{-pz})_2]_2$ ,  $[\text{Cp}^*\text{M}(\mu\text{-X})(\mu\text{-pz})_2]_2$  (X = Cl, OH, OMe) and  $[\text{Cp}^*\text{M}(\mu\text{-pz})_3]_2$  containing bridged pyrazolato ligands, a number of works have recently appeared on this field showing interesting features and applications.

C–H activation by acetate-assisted cyclometalation of a phenyl group in 1-phenylpyrazole with half-sandwich complexes  $[\text{Cp}^*\text{MCl}_2]_2$  (M = Ir, Rh) and  $[(p\text{-cymene})\text{RuCl}_2]_2$  (Fig. 21.20a) has been recently reported: 1-phenylpyrazole and other phenyl-substituted ligands tested, such as oxazoline, oxime, imidazole, and triazole, cyclometalated at iridium; however, ruthenium and rhodium fail to cause cyclometalation in some cases. Moreover, the reaction with the latter has been shown more sensitive to steric effects [46]. Interestingly, the cyclometalated complexes readily undergo insertion reactions with  $\text{RC}\equiv\text{CR}$  (R = CO<sub>2</sub>Me, Ph) to give mono insertion products; the rhodium complex also reacts with PhC≡CH regiospecifically to give an analogous product [47]. A similar cyclometalated  $[\text{Cp}^*\text{Ir(III)}\text{Cl(L)}]$  complex (Fig. 21.20b) with a C,N-chelating

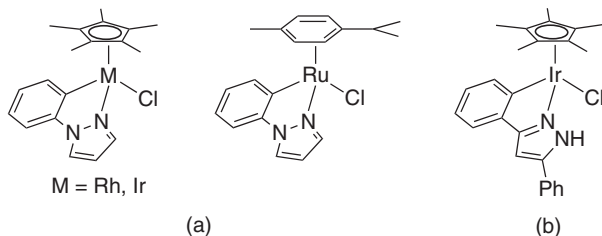


**Figure 21.20** (a)  $[(\text{ring})\text{MCl}(1\text{-phenylpyrazole})]$ ; (b)  $[(\text{Cp}^*)\text{IrCl}(3,5\text{-diphenyl-pyrazole})]$ .

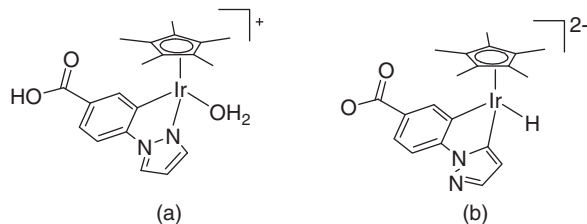


**Figure 21.21** (a)  $[\text{Cp}^*\text{Ir}(4\text{-(1H-pyrazol-1-yl-}\kappa\text{N}^2\text{)benzoic acid-}\kappa\text{C}^3\text{)}(\text{H}_2\text{O})]^+$ ; (b)  $[\text{Cp}^*\text{Ir}(4\text{-(1H-pyrazol-1-yl-}\kappa\text{C}^5\text{)benzoate-}\kappa\text{C}^3\text{)}(\text{H})]^{2-}$ .

3,5-diphenyl-pyrazole has been shown to possess features analogous to those of classic Noyori and Ikariya's transfer-hydrogenation catalysts [48], which have chelate amine ligands to provide a protic NH group at the  $\alpha$ -position to the metal. In fact pyrazole–pyrazolato interconversion let the Ir complex suitable to be applied in catalytic intramolecular hydroamination of aminoalkene [49].

A water-soluble C,N-cyclometalated Ir(III) complex  $[\text{Cp}^*\text{Ir}(4\text{-(1H-pyrazol-1-yl-}\kappa\text{N}^2\text{)benzoic acid-}\kappa\text{C}^3\text{)}(\text{H}_2\text{O})]_2\text{SO}_4$  (Fig. 21.21 a) gives efficient catalytic interconversion between NADH and  $\text{NAD}^+$  accompanied by generation and consumption of  $\text{H}_2$  at ambient pressure and temperature [50]. The Ir complex can be converted to the corresponding hydride by aliphatic alcohols, and the hydride converted in the C,C-cyclometalated Ir-hydride (Fig. 21.21b), which in turn is able to catalyze hydrogen evolution from ethanol in a basic aqueous solution ( $\text{pH} = 11.9$ ) under ambient conditions [51].

Considering the similarities between the cyclopentadienyl and tris(pyrazolyl)borate ligands, the lack of information existing till the end of the last century on the mixed-sandwich derivatives  $[\text{CpM}(\text{HBpz}_3)]$  with  $\text{M} = \text{Rh}$  or  $\text{Ir}$  appeared surprising. Apart from two works of 1986 on Ru(II) with Cp or  $\text{Cp}^*$  aromatic rings and tris(pyrazolyl)borate ligands [52], only  $[\text{Cp}^*\text{Rh}(\text{HBpz}_3)]\text{PF}_6$  was structurally characterized [4]. In 2003, our group decided to explore this field and  $[\text{Cp}^*\text{M}(\text{HBpz}_3)\text{Cl}]$  and  $[\text{Cp}^*\text{M}(\text{HB-3,5-Me}_2\text{pz}_3)\text{Cl}]$  ( $\text{M} = \text{Rh}$  or  $\text{Ir}$ ) complexes were synthesized and fully characterized [53].

In these complexes, the scorpionate ligands are  $\kappa^2$ -coordinated to the metal and in the solid state the complexes can exist as two conformers interconverting to each other in solution (Fig. 21.22a). Metathesis reaction of  $[\text{Cp}^*\text{M}(\text{HBpz}_3)\text{Cl}]$  with  $\text{AgNO}_3$  affords cationic complexes  $[\text{Cp}^*\text{M}(\text{HBpz}_3)]\text{NO}_3$  with tridentate  $\text{HBpz}_3$  ligand (Fig. 21.22b). Reaction of  $[\text{Cp}^*\text{RhCl}_2]_2$  with  $\text{KH}_2\text{Bpz}_2$  produces  $[\text{Cp}^*\text{Rh}(\text{H}_2\text{Bpz}_2)\text{Cl}]$  (Fig. 21.22c), whereas with  $[\text{Cp}^*\text{IrCl}_2]_2$  decomposition of the  $\text{H}_2\text{Bpz}_2$  ligand through B–N cleavage occurs and a binuclear  $[\{\text{Cp}^*\text{IrCl}\}_2(\mu\text{-Cl})(\mu\text{-pz})]$  complex is afforded, which contains bridging chloride and pyrazolate groups.

We have then extended our study to the chemistry of bis(pyrazolyl)methane ligands and a number of Rh and Ir complexes of general formula  $[\text{Cp}^*\text{M}(\text{H}_2\text{Cpz}_2)\text{Cl}]\text{Cl}$  have been prepared (Fig. 21.23a); however, by using an excess  $[\text{Cp}^*\text{MCl}_2]_2$ , the formation of  $[\text{Cp}^*\text{M}(\text{H}_2\text{Cpz}_2)\text{Cl}][\text{Cp}^*\text{MCl}_3]$  species has been observed (Fig. 21.23b) [54]. PGSE NMR measurements indicate the predominance of ion pairs in solution and NOE measurements and X-ray single-crystal studies suggest that the  $[\text{Cp}^*\text{MCl}_3]^-$  approaches the cation, orienting the three Cl-legs of the “piano-stool” toward the  $\text{CH}_2$  moieties of the bis(pyrazolyl)methane ligands. Dicationic complexes  $[\text{Cp}^*\text{M}(\text{H}_2\text{Cpz}_2)(\text{H}_2\text{O})][\text{X}]_2$  have been formed by metathesis with  $\text{AgX}$  ( $\text{X} = \text{ClO}_4^-$  or  $\text{CF}_3\text{SO}_3^-$ ) where single water molecules are directly bonded to the metal atoms. The reaction of  $[\text{Cp}^*\text{M}(\text{H}_2\text{Cpz}_2)(\text{H}_2\text{O})][\text{X}]_2$  with ammonium formate in water or acetone solution allows the generation of the hydride species, the hydride substituting the coordinated water.

Similar complexes have been reported independently in the same year by Messerle [55], who also tested some of the complexes as catalysts in the intramolecular hydroamination of 2-(2-phenylethynyl)aniline to give 2-phenylindole [56].

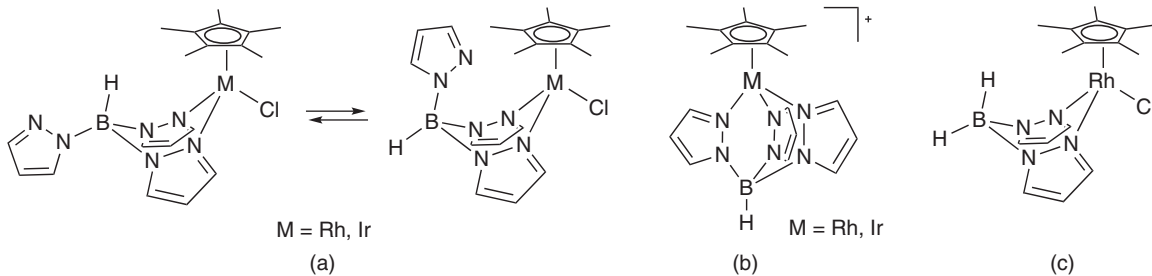


**Figure 21.22** (a) Interconversion between two conformers of  $[\text{Cp}^*\text{M}(\kappa^2\text{-HBpz}_3)\text{Cl}]$ ; (b)  $[\text{Cp}^*\text{M}(\kappa^3\text{-HBpz}_3)]^+$ ; (c)  $[\text{Cp}^*\text{Rh}(\kappa^2\text{-H}_2\text{Bpz}_2)]$ .

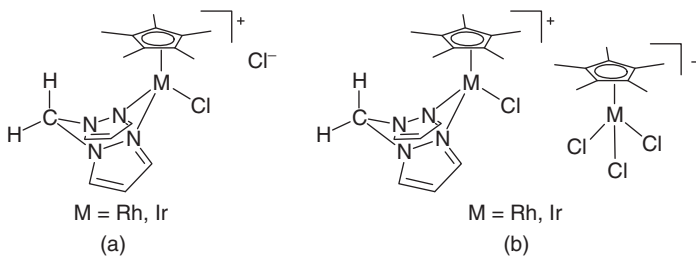


**Figure 21.23** (a)  $[\text{Cp}^*\text{M}(\text{H}_2\text{Cpz}_2)\text{Cl}]^+\text{Cl}^-$ ; (b)  $[\text{Cp}^*\text{M}(\text{H}_2\text{Cpz}_2)\text{Cl}]^+[\text{Cp}^*\text{MCl}_3]^+$ .

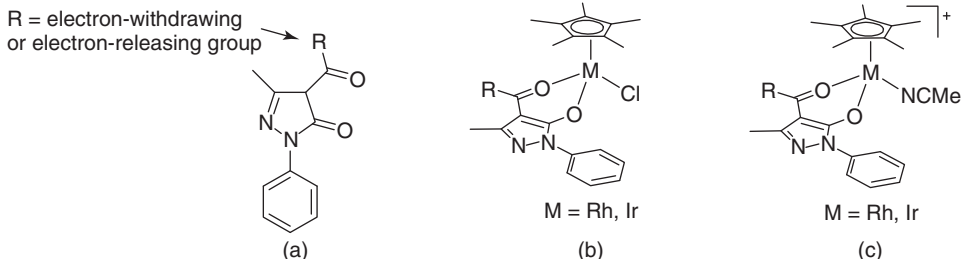


**Figure 21.24** (a) 4-Acyl-5-pyrazolones; (b)  $[\text{Cp}^*\text{M}(4\text{-acetyl}-5\text{-pyrazolone})\text{Cl}]^+$ ; (c)  $[\text{Cp}^*\text{M}(4\text{-acetyl}-5\text{-pyrazolone})(\text{MeCN})]^+$ .

## 21.4 HALF-SANDWICH DERIVATIVES WITH ACYLPYRAZOLONE LIGANDS

In conclusion to this chapter, we have to mention the coordination chemistry of half-sandwich Rh(III), Ir(III), and Ru(II) acceptors with a particular type of pyrazole-based ligands, built on the pyrazolyl fragment by inserting a carbonyl functionality in 5-position of the heterocyclic ring and an acyl moiety in 4-position, named *4-acyl-5-pyrazolones* (HQ) (Fig. 21.24a) [57].

New  $[\text{Cp}^*\text{M}(\text{Q})\text{Cl}]$  complexes ( $\text{M} = \text{Rh}$  or  $\text{Ir}$ ) (Fig. 21.24b) containing several  $\text{Q}^-$  ligands have been synthesized and fully characterized: crystal structure determinations for a number of these compounds show a pseudo-octahedral metal environment, the Q ligand being bonded in the O,O-chelating form [58]. In each case, two enantiomers ( $S_{\text{M}}$ ) and ( $R_{\text{M}}$ ) arise, differing only in the metal chirality. The  $[\text{Cp}^*\text{Rh}(\text{Q})\text{Cl}]$  complexes react with  $\text{PPh}_3$  in dichloromethane yielding the adducts  $\text{Cp}^*\text{Rh}(\text{Q})\text{Cl}/\text{PPh}_3$  (1 : 1), which exist in solution in two different isomeric forms. The interaction of  $[\text{Cp}^*\text{Rh}(\text{Q})\text{Cl}]$  with  $\text{AgX}$  ( $\text{X} = \text{NO}_3^-$ ,  $\text{ClO}_4^-$ ) in MeCN affords ionic complexes  $[\text{Cp}^*\text{Rh}(\text{Q})(\text{MeCN})]\text{X}^-$  (Fig. 21.24c).

More recently, (arene)ruthenium(II) complexes of the formula  $[(\text{arene})\text{Ru}(\text{Q})\text{Cl}]$ , containing diverse 4-acyl-5-pyrazolone ligands Q (arene = *p*-cymene or benzene) have been synthesized and characterized also by X-ray diffraction techniques, showing the Q ligands in the O,O-chelating form (Fig. 21.24) [59]. Their coordination chemistry toward substitution of chloride by  $\text{N}_3^-$  and monodentate donor ligands L ( $\text{L} = \text{triphenylphosphine}$ , 1-methylimidazole, or 1-methyl-2-mercaptopimidazole) and exo-bidentate ditopic donor ligands L-L ( $\text{L-L} = 4,4'$ -bipyridine or bis(diphenylphosphino)propane) in the presence of silver salts  $\text{AgX}$  ( $\text{X} = \text{SO}_3\text{CF}_3^-$  or  $\text{ClO}_4^-$ ) has been explored, neutral azide  $[(\text{arene})\text{Ru}(\text{Q})\text{N}_3]$  complexes and

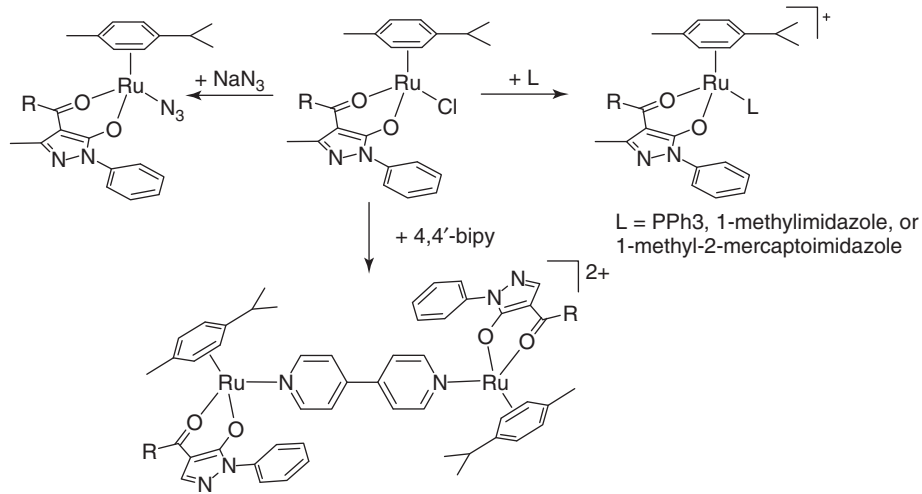


**Figure 21.25** Coordination chemistry of (arene)ruthenium(II) 4-acyl-5-pyrazolonate complexes.

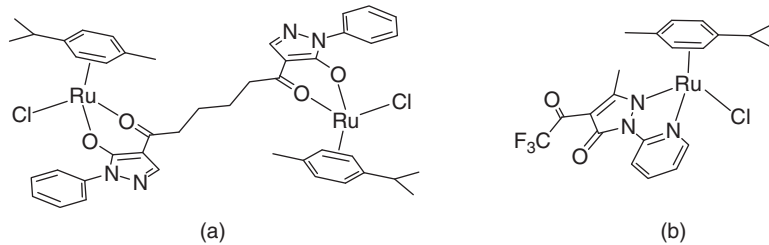


**Figure 21.26** (a)  $\left[\{(p\text{-Cymene})\text{RuCl}\}_2\text{Q}4\text{Q}\right]$ ; (b)  $\left[\{(p\text{-cymene})\text{RuCl(Q)}\}_2\right]$  ( $\text{HQ} = 4\text{-}(2,2,2\text{-trifluoroacetyl})\text{-}1,2\text{-dihydro-}5\text{-methyl-}2\text{-(pyridin-2-yl)pyrazol-3-one}$ ).

ionic mononuclear  $[(p\text{-cymene})\text{Ru(Q)L}]X$  complexes, and ionic dinuclear complexes of the formula  $[(p\text{-cymene})\text{Ru(Q)}_2\text{L-L}]X_2$  being obtained, respectively (Fig. 21.25).

X-ray studies show that all of the crystalline forms are racemates, that is, the complexes exist as two enantiomers ( $S_M$ ) and ( $R_M$ ) differing only in the metal chirality. A dinuclear compound  $\left[\{(p\text{-cymene})\text{RuCl}\}_2\text{Q}4\text{Q}\right]$  ( $\text{H}_2\text{Q}4\text{Q} = \text{bis}(4\text{-(1-phenyl-3-methyl-5-pyrazolone)dioxohexane})$ ), existing in the  $RR\text{RuSRu}$  (meso form), has been prepared similarly (Fig. 21.26a). With a particular Q ligand, containing a pyridine ring bonded to the pyrazole, a completely different coordination mode has been observed, the ligand acting as  $N,N'$ -chelating to ruthenium (Fig. 21.26b).

The redox properties of these complexes have been investigated by cyclic voltammetry and controlled potential electrolysis, which allowed the ordering of the bidentate acylpyrazolonate ligands according to their electron-donor character and are indicative of a small dependence of the HOMO energy upon the change of the monodentate ligand. This was accounted for by DFT calculations, which showed a relevant contribution of acylpyrazolonate ligand orbitals to the HOMOs, whereas that from the monodentate ligand is minor. Rao et al. have expanded this field reporting the [3 + 2] cycloaddition reaction of selective azido complexes  $[(\text{arene})\text{Ru(Q)}\text{N}_3]$  with the activated alkynes dimethyl and diethyl acetylenedicarboxylates, which produced the arene triazolato complexes  $[(\text{arene})\text{Ru(Q)}(\text{triazolato})]$  (Fig. 21.27), where triazolato ligand is always bonded through N(2) [60].

A copper(I) complex  $[\text{Cu(Q)}(\text{PPh}_3)_2]$ , containing the Janus Q ligand coordinated through the  $N,N'$ -chelating moiety, reacts with  $[(p\text{-cymene})\text{RuCl}_2]_2$  in the presence of  $\text{AgPF}_6$  affording the ionic heterobimetallic adduct  $[(p\text{-cymene})\text{Ru(Cl)(}\mu^4\text{-O}_2\text{N}_2\text{-Q)}\text{Cu(PPh}_3)_2]\text{PF}_6\cdot 3\text{H}_2\text{O}$  (Fig. 21.28) [61].

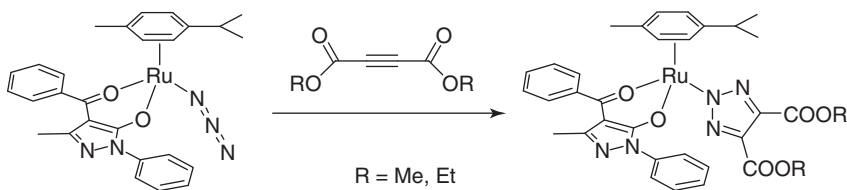


**Figure 21.27** [3 + 2] Cycloaddition reaction between  $[(p\text{-cymene})\text{Ru}(\text{Q})\text{N}_3]$  and acetylenedicarboxylates.

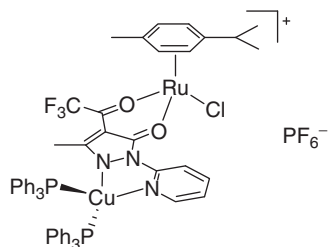


**Figure 21.28**  $[(p\text{-Cymene})\text{Ru}(\text{Cl})(\mu^4\text{-O}_2,\text{N}_2\text{-Q})\text{Cu}(\text{PPh}_3)_2]\text{PF}_6^-$ .

## 21.5 CONCLUSIONS AND PERSPECTIVES

In conclusion, many developments in the last decades on the coordination chemistry of half-sandwich Ru(II), Rh(III), and Ir(III) derivatives with pyrazole-based ligands were proposed, and also interesting applications in catalysis and biochemistry reported. However, there is a vast area of coordination chemistry that is waiting to be further explored and developed, and many of the complexes yet prepared can be further tested to check their catalytic or biological properties.

## REFERENCES

- (a) Trofimenko, S. *Chem. Rev.* **1972**, *72*, 497; (b) Bonati, F. *Gazz. Chim. Ital.* **1989**, *119*, 291.
- Keter, F. K.; Darkwa, J. *Biometals*, **2012**, *25*, 9.
- (a) Mukherjee, R. *Coord. Chem. Rev.* **2000**, *203*, 151; (b) Pettinari, C.; Pettinari, R. *Coord. Chem. Rev.* **2005**, *249*, 525; (c) Pettinari, C.; Pettinari, R. *Coord. Chem. Rev.* **2005**, *249*, 663; (d) Viciana-Chumillas, M.; Tanase, S.; de Jongh, J. L.; Reedijk, J. *Eur. J. Inorg. Chem.* **2010**, 3403.
- (a) O'Sullivan, D. J.; Lalor, F. J. *J. Organomet. Chem.* **1973**, *57*, C58; (b) Restivo, R. J.; Ferguson, G. *J. Chem. Soc. Chem. Commun.* **1973**, 847; (c) Restivo, R. J.; Ferguson, G.; O'Sullivan, D. J.; Lalor, F. J. *Inorg. Chem.* **1975**, *14*, 3046.
- Jones, C. J.; McCleverty, J. A.; Rothin, A. S. *J. Chem. Soc. Dalton Trans.* **1986**, 109.
- Oro, L. A.; Garcia, M. P.; Carmona, D. *Inorg. Chim. Acta* **1985**, *96*, L21.
- Oro, L. A.; Carmona, D.; Garcia, M. P.; Lahoz, F. J.; Reyes, J.; Foces-Foces, C.; Cano, F. H. *J. Organomet. Chem.* **1985**, *296*, C43-C46.
- Carmona, D.; Ferrer, J.; Oro, L. A.; Apreda, M. C.; Foces-Foces, C.; Cano, F. H.; Elguero, J.; Jimeno, M. L. *J. Chem. Soc. Dalton Trans.* **1990**, 1463.
- (a) Govindaswamy, P.; Mozharivskyj, Y. A.; Kollipara, M. R. *J. Organomet. Chem.* **2004**, *689*, 3265; (b) Waheed, A.; Jones, R. A.; Agapiou, K.; Yang, X.; Moore, J. A.; Ekerdt, J. G. *Organometallics* **2007**, *26*, 6778; (c) Albertin, G.; Antoniutti, S.; Castro, J.; García-Fontán, S. *Eur. J. Inorg. Chem.* **2011**, 510.
- (a) Tribó, R.; Pons, J.; Yáñez, R.; Piniella, J. F.; Alvarez-Larena, Á.; Ros, J. *Inorg. Chem. Commun.* **2000**, *3*, 545; (b) Tribó, R.; Muñoz, S.; Pons, J.; Yáñez, R.; Alvarez-Larena, Á.; Piniella, J. F.; Ros, J. *J. Organomet. Chem.* **2005**, *690*, 4072.
- Carmona, D.; Ferrer, J.; Marzal, I. M.; Oro, L. A. *Gazz. Chim. Ital.* **1994**, *124*, 35.
- Carmona, D.; Ferrer, J.; Reyes, J.; Oro, L. A. *Organometallics* **1993**, *12*, 4241.
- Carmona, D.; Ferrer, J.; Atencio, R.; Lahoz, F. J.; Oro, L. A.; Lamata, M. P. *Organometallics* **1995**, *14*, 2057.
- Carmona, D.; Ferrer, J.; Arilla, J. M.; Reyes, J.; Lahoz, F. J.; Elipe, S.; Modrego, F. J.; Oro, L. A. *Organometallics* **2000**, *19*, 798.

15. Carmona, D.; Ferrer, J.; Atencio, R.; Edwards, A. J.; Oro, L. A.; Lamata, M. P.; Esteban, M.; Trofimenko, S. *Inorg. Chem.* **1996**, *35*, 2549.
16. Contreras, R.; Valderrama, M.; Orellana, E. M.; Boys, D.; Carmona, D.; Oro, L. A.; Lamata, M. P.; Ferrer, J. *J. Organomet. Chem.* **2000**, *606*, 197.
17. (a) Bhambri, S.; Tocher, D. A. *J. Organomet. Chem.* **1996**, *507*, 291; (b) Bhambri, S.; Tocher, D. A. *Polyhedron* **1996**, *15*, 2763; (c) Bhambri, S.; Bishop, A.; Kaltsoyannis, N.; Tocher, D. A. *J. Chem. Soc. Dalton Trans.* **1998**, 3379.
18. Bhambri, S.; Tocher, D. A. *J. Chem. Soc. Dalton Trans.* **1997**, 3367.
19. Volcheck, W. M.; Tocher, D. A.; Geiger, W. E. *J. Organomet. Chem.* **2007**, *692*, 3300.
20. Gemel, C.; John, R.; Slugovc, C.; Mereiter, K.; Schmid, R.; Karl, K. *J. Chem. Soc. Dalton Trans.* **2000**, 2607.
21. Bailey, P. J.; Pinho, P.; Parsons, S. *Inorg. Chem.* **2003**, *42*, 8872.
22. Bailey, P. J.; Budd, L.; Cavaco, F. A.; Parsons, S.; Rudolphi, F.; Sanchez-Perucha, A.; White, F. J. *Chem. Eur. J.* **2010**, *16*, 2819.
23. Seino, H.; Yoshikawa, T.; Hidai, M.; Mizobe, Y. *Dalton Trans.* **2004**, 3593.
24. Nagao, S.; Seino, H.; Hidai, M.; Mizobe, Y. *Dalton Trans.* **2005**, 3166.
25. Mutzenbeck, E. V.; Reus, C.; Schödel, F.; Bolte, M.; Lerner, H.-W.; Wagner, M. *Organometallics* **2010**, *29*, 966.
26. Blasberg, F.; Bolte, M.; Lerner, H.-W.; Wagner, M. *Organometallics* **2012**, *31*, 3213.
27. Marchetti, F.; Pettinari, C.; Pettinari, R.; Cerquetella, A.; Martins, L. M. D. R. S.; Guedes da Silva, M. F.; Silva, T. F. S.; Pombeiro, A. J. L. *Organometallics* **2011**, *30*, 6180.
28. Marchetti, F.; Pettinari, C.; Cerquetella, A.; Cingolani, A.; Pettinari, R.; Monari, M.; Wanke, R.; Kuznetsov, M. L.; Pombeiro, A. J. L. *Inorg. Chem.* **2009**, *48*, 6096.
29. Pettinari, C.; Marchetti, F.; Cerquetella, A.; Pettinari, R.; Monari, M.; Mac Leod, T. C. O.; Martins, L. M. D. R. S.; Pombeiro, A. J. L. *Organometallics* **2011**, *30*, 1616.
30. Prades, A.; Viciana, M.; Sanaú, M.; Peris, E. *Organometallics* **2008**, *27*, 4254.
31. Bellarosa, L.; Díez, J.; Gimeno, J.; Lledós, A.; Suárez, F. J.; Ujaque, G.; Vicent, C. *Chem. Eur. J.* **2012**, *18*, 7749.
32. Tan, W.; Zhao, X.; Yu, Z. *J. Organomet. Chem.* **2007**, *692*, 5395.
33. Marchetti, F.; Pettinari, C.; Pettinari, R.; Cerquetella, A.; Di Nicola, C.; Macchioni, A.; Zuccaccia, D.; Monari, M.; Piccinelli, F. *Inorg. Chem.* **2008**, *47*, 11593.
34. Reger, D. L.; Semeniuc, R. F.; Pettinari, C.; Luna-Giles, F.; Smith, M. D. *Cryst. Growth Des.* **2006**, *6*, 1068.
35. Di Nicola, C.; Garau, F.; Marchetti, F.; Monari, M.; Pandolfo, L.; Pettinari, C.; Venzo, A. *Dalton Trans.* **2011**, *40*, 4941.
36. Carrión, M. C.; Jalón, F. A.; Manzano, B. R.; Rodríguez, A. M.; Sepúlveda, F.; Maestro, M. *Eur. J. Inorg. Chem.* **2007**, 3961.
37. Carrión, M. C.; Sepúlveda, F.; Jalón, F. A.; Manzano, B. R. *Organometallics* **2009**, *28*, 3822.
38. Soriano, L.; Jalón, F. A.; Manzano, B. R.; Maestro, M. *Inorg. Chim. Acta* **2009**, *362*, 4486.
39. (a) Catalano, V. J.; Craig, T. J. *Polyhedron* **2000**, *19*, 475; (b) Beach, N. J.; Spivak, G. J. *Inorg. Chim. Acta* **2003**, *343*, 244; (c) Mishra, H.; Mukherjee, R. *J. Organomet. Chem.* **2006**, *691*, 3545; (d) Gupta, G.; Yap, G. P. A.; Therrien, B.; Rao, K. M. *Polyhedron* **2009**, *28*, 844; (e) Gupta, G.; Prasad, K. T.; Das, B.; Yap, G. P. A.; Rao, K. M. *J. Organomet. Chem.* **2009**, *694*, 2618; (f) Prasad, K. T.; Therrien, B.; Geib, S. J.; Rao, K. M. *J. Organomet. Chem.* **2010**, *695*, 495; (g) Prasad, K. T.; Therrien, B.; Rao, K. M. *J. Organomet. Chem.* **2010**, *695*, 1375; (h) Gupta, G.; Prasad, K. T.; Rao, A. V.; Geib, S. J.; Das, B.; Rao, K. M. *Inorg. Chim. Acta* **2010**, *363*, 2287; (i) Gupta, G.; Gloria, S.; Das, B.; Rao, K. M. *J. Mol. Struct.* **2010**, *979*, 205; (j) Gupta, G.; Zheng, C.; Wang, P.; Rao, K. M. *Z. Anorg. Allg. Chem.* **2010**, *636*, 758; (k) Rao, A. V.; Prasad, K. T.; Wang, P.; Rao, K. M. *Z. J. Chem. Sci.* **2012**, *124*, 565.
40. Dougan, S. J.; Melchart, M.; Habtemariam, A.; Parsons, S.; Sadler, P. J. *Inorg. Chem.* **2006**, *45*, 10882.
41. Schuecker, R.; John, R. O.; Jakupc, M. A.; Arion, V. B.; Keppler, B. K. *Organometallics* **2008**, *27*, 6587.
42. Stepanenko, I. N.; Novak, M. S.; Mühlgassner, G.; Roller, A.; Hejl, M.; Arion, V. B.; Jakupc, M. A.; Keppler, B. K. *Inorg. Chem.* **2011**, *50*, 11715.
43. Stepanenko, I. N.; Casini, A.; Edafe, F.; Novak, M. S.; Arion, V. B.; Dyson, P. J.; Jakupc, M. A.; Keppler, B. K. *Inorg. Chem.* **2011**, *50*, 12669.
44. Carmona, D.; Oro, L. A.; Lamata, M. P.; Puebla, M. P.; Ruiz, J.; Maitlis, P. M. *J. Chem. Soc. Dalton Trans.* **1987**, 639.
45. (a) Bailey, J. A.; Grundy, S. L.; Stobart, S. R. *Organometallics* **1990**, *9*, 536; (b) Bailey, J. A.; Grundy, S. L.; Stobart, S. R. *Inorg. Chim. Acta* **1996**, *243*, 47.
46. Boutadla, Y.; Davies, D. L.; Jones, R. C.; Singh, K. *Chem. Eur. J.* **2011**, *17*, 3438.
47. Boutadla, Y.; Davies, D. L.; Al-Duaij, O.; Fawcett, J.; Jones, R. C.; Singh, K. *Dalton. Trans.* **2010**, *39*, 10447.
48. (a) Ikariya, T.; Murata, K.; Noyori, R. *Org. Biomol. Chem.* **2006**, *4*, 393; (b) Ikariya, T.; Blacker, A. J. *Acc. Chem. Res.* **2007**, *40*, 1300.
49. (a) Kashiwame, Y.; Kuwata, S.; Ikariya, T. *Chem. Eur. J.* **2010**, *16*, 766–770; (b) Tobisch, S. *Chem. Eur. J.* **2012**, *18*, 7248.

50. Maenaka, Y.; Suenobu, T.; Fukuzumi, S. *J. Am. Chem. Soc.* **2012**, *134*, 367.
51. Maenaka, Y.; Suenobu, T.; Fukuzumi, S. *J. Am. Chem. Soc.* **2012**, *134*, 9417.
52. (a) Albers, M. O.; Robinson, D. J.; Shaver, A.; Singleton, E. *Organometallics* **1986**, *5*, 2199; (b) McNair, A. M.; Boyd, D. C.; Mann, K. R. *Organometallics* **1986**, *5*, 303.
53. Carmona, E.; Cingolani, A.; Marchetti, F.; Pettinari, C.; Pettinari, R.; Skelton, B. W.; White, A. H. *Organometallics* **2003**, *22*, 2820.
54. Pettinari, C.; Pettinari, R.; Marchetti, F.; Macchioni, A.; Zuccaccia, D.; Skelton, B. W.; White, A. H. *Inorg. Chem.* **2007**, *46*, 896.
55. Kennedy, D. F.; Messerle, B. A.; Smith, M. K. *Eur. J. Inorg. Chem.* **2007**, *80*.
56. Ebrahimi, D.; Kennedy, D. F.; Messerle, B. A.; Hibbert, D. B. *Analyst* **2008**, *133*, 817.
57. Marchetti, F.; Pettinari, C.; Pettinari, R. *Coord. Chem. Rev.* **2005**, *249*, 2909.
58. Pettinari, C.; Pettinari, R.; Fianchini, M.; Marchetti, F.; Skelton, B. W.; White, A. H. *Inorg. Chem.* **2005**, *44*, 7933.
59. Marchetti, F.; Pettinari, C.; Pettinari, R.; Cerquetella, A.; Cingolani, A.; Chan, E. J.; Kozawa, K.; Skelton, B. W.; White, A. H.; Wanke, R.; Kuznetsov, M. L.; Martins, L. M. D. R. S.; Pombeiro, A. J. L. *Inorg. Chem.* **2007**, *46*, 8245.
60. Nongbri, S. L.; Das, B.; Rao, K. M. *J. Organomet. Chem.* **2009**, *694*, 3881.
61. Cingolani, A.; Marchetti, F.; Pettinari, C.; Pettinari, R.; Skelton, B. W.; Somers, N.; White, A. H. *Polyhedron* **2006**, *25*, 124.

## CARBON-SCORPIONATE COMPLEXES IN OXIDATION CATALYSIS

LUÍSA M. D. R. S. MARTINS\*

*Chemical Engineering Department, ISEL, Lisbon, Portugal; Centro de Química Estrutural, Instituto Superior Técnico, Universidade de Lisboa, Lisboa, Portugal*

ARMANDO J. L. POMBEIRO

*Centro de Química Estrutural, Instituto Superior Técnico, Universidade de Lisboa, Lisboa, Portugal*

### 22.1 INTRODUCTION

The development of new transition metal catalysts and single-pot methods for the selective and sustainable oxidative functionalization of alkanes to more valuable products is a topic of high interest in the fields of homogeneous catalysis, organic chemistry, and green chemistry, which remains rather unexplored owing to the high inertness of such species in spite of their constituting huge potential carbon stocks on earth [1].

The present contribution exemplifies a strategy for efficient and highly selective oxidation reactions of industrial interest directed toward organic synthesis, using catalytic systems based on transition metal complexes bearing tris(pyrazol-1-yl)methane-type scorpionates,  $RC(R'pz)_3$  ( $pz$  = pyrazol-1-yl;  $R$  = H or substituent at the methine carbon;  $R'$  = H or substituent at the  $pz$  ring; Fig. 22.1).

The conversion of light hydrocarbons into value-added functionalized products, under mild conditions, is still a serious challenge, but tris(pyrazol-1-yl)methane complexes of V, Fe, Cu, and Re have already been successfully applied as catalysts or catalyst precursors for relevant alkane oxidation reactions, namely, peroxidative oxygenations (to give alcohols and ketones) and carboxylations (to produce carboxylic acids). All these types of alkane reactions are promising toward the eventual exploration of alkanes as unconventional starting materials for synthesis.

The chapter mainly concerns homogeneous catalytic systems, but supported catalysts are also included in view of their advantageous separation and recycling. In fact, the immobilization of a catalyst or a catalyst precursor complex on a support is a common and suitable procedure that combines the advantages of homogeneous and heterogeneous catalyses.

Transition-metal-catalyzed Baeyer–Villiger (BV) oxidations, namely, the transformation of cyclic and acyclic ketones into lactones and esters, respectively, has also become an important research topic in the past years owing to the wide applications of the products [2]. Owing to economic and environmental reasons, a growing attention has been paid to the replacement of organic peroxy acids, traditionally used as stoichiometric oxidants in the BV oxidation, by more atom-efficient and environmentally friendly oxidants such as molecular oxygen [3] or hydrogen peroxide [4].

The catalytic potential of Re complexes bearing tris(pyrazol-1-yl)methane ligands and with the metal in a wide range of oxidation states, for the BV peroxidative oxidation of ketones, is presented as an extension of the above oxidation studies to other substrates and catalytic transformations.

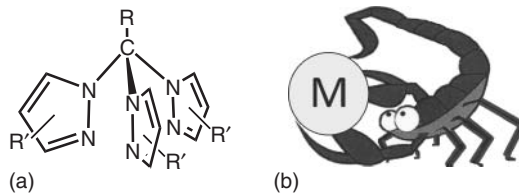


**Figure 22.1** (a) Schematic structure of tris(pyrazol-1-yl)methanes. (b) Comparison between a coordination mode of a tris(pyrazol-1-yl)methane-type scorpionate and a scorpion.

## 22.2 PEROXIDATIVE OXYGENATIONS OF ALKANES

### 22.2.1 In Liquid Systems

Several tris(pyrazol-1-yl)methane complexes of V(III, IV, or V), Fe(II), Cu(II), and Re(III or VII) (Fig. 22.2) have been found to be catalyst precursors for the peroxidative oxidation of cyclohexane (and cyclopentane in the cases tested) to give, in a single pot, the corresponding alcohols and ketones (Scheme 22.1). The reactions are usually carried out in acetonitrile, with aqueous  $H_2O_2$  as the oxidizing agent, in acidic medium, at room temperature. They proceed via radical mechanisms with possible involvement of both C-centered and O-centered radicals as indicated by radical trap experiments.

The C-scorpionate ligands, bearing pyrazolyl moieties, are expected to be able to easily change their denticity during the reaction as they can undergo partial decoordination upon protonation in the used acidic medium (with generation of unsaturated metal centers). They can also assist proton-transfer steps, thus promoting the observed catalytic behavior of their complexes in water/NCMe medium. Moreover, in some cases, they form hydrosoluble complexes, favoring the use of an aqueous reaction medium.

The following compounds reveal considerable catalytic activity for the above single-pot oxidation reaction: dioxygen-vanadium(V) complexes  $[VO_2\{RX(R'pz)_3\}]^n$  ( $X = C$ ,  $R = R' = H$ ,  $n = +1$  (**1**), or  $R = SO_3$ ,  $R' = H$ ,  $n = 0$  (**2**);  $X = B$ ,  $R = H$ ,  $R' = Me$ ,  $n = 0$  (**3**) and  $[VO_2(3,5-Me_2Hpz)_3][BF_4]$  (**4**) [5a], the oxo-vanadium(IV) complexes  $[VOCl_2\{HOCH_2C(pz)_3\}]$  (**5**),  $[VO\{HB(pz)_3\}\{H_2B(pz)_2\}]$  (**6**), and  $[VO(acac)_2(Hpz)] \bullet HC(pz)_3$  ( $acac = acetylacetone$ ) (**7**) [5a,b], bearing scorpionate- or pyrazole-type ligands; hydrotris(pyrazol-1-yl)methane Fe(II), Cu(II), Re(III), or V(III) chlorocomplexes  $[MCl_n\{HC(pz)_3\}]$  ( $M = Fe$  (**8**) or  $Cu$  (**9**),  $n = 2$ ;  $M = V$  (**10**),  $n = 3$ ) or  $[ReCl_2\{HC(pz)_3\}(PPh_3)][BF_4]$  (**12**) [5c,f]; compounds bearing C-functionalized tris(pyrazol-1-yl)methanes such as Fe(II), Cu(II), or V(III) chlorocomplexes  $[MCl_n\{SO_3C(pz)_3\}]^x$  ( $M = Cu$ ,  $n = 1$ ,  $x = 0$  (**13**);  $M = Fe$ ,  $n = 2$ ,  $x = -1$  (**14**);  $M = V$ ,  $n = 3$ ,  $x = 0$  (**15**)) [5c], or the oxo-rhenium compounds  $[ReO_3\{SO_3C(pz)_3\}]$  (**16**),  $[ReOCl\{SO_3C(pz)_3\}(PPh_3)]Cl$  (**17**) [5f], bearing the tris(pyrazol-1-yl)methanesulfonate ligand; 2,2,2-tris(pyrazol-1-yl)ethanol Fe(II) and Cu(II) complexes  $[Fe\{HOCH_2C(pz)_3\}_2][FeCl_4]Cl$  (**18**),  $[Fe\{HOCH_2C(pz)_3\}_2]Cl_2$  (**19**),  $[Fe\{HOCH_2C(pz)_3\}_2][FeCl\{HOCH_2C(pz)_3\}(H_2O)_2]_2(Cl)_4$  (**20**),  $[Fe\{HOCH_2C(pz)_3\}_2]_2[Fe_2OCl_6](Cl)_2 \cdot 4H_2O$  (**21**) [5d], and  $[CuCl_2\{HOCH_2C(pz)_3\}]$  (**22**) [5e]; the 2,2,2-tris(pyrazol-1-yl)ethyl methanesulfonate Cu(II) complex  $[CuCl_2\{CH_3SO_2OCH_2C(pz)_3\}_2]$  (**23**) [5e]; and the related pyrazole complexes of Re(III)  $[ReClX\{N_2C(O)Ph\}(Hpz)_n(PPh_3)_m]$  ( $X = F$ ,  $n = 2$ ,  $m = 1$  (**24**);  $X = Cl$ ,  $n = 1$ ,  $m = 2$  (**25**) or  $n = 2$ ,  $m = 1$  (**26**)) [5f].

Among the V complexes, the dioxygen-vanadium(V) lead to the highest yields (up to 24% for **4**, Table 22.1 [5a]), while  $[VOCl_2\{HOCH_2C(pz)_3\}]$  (**5**) allows to reach turnover numbers (TONs, moles of products per mol of catalyst) up to 405 with hydrogen peroxide or up to  $1.1 \times 10^3$  by using *m*-chloroperoxybenzoic acid (*m*CPBA) as oxidant [5b].

The dichloro-complexes **8** and **14** are the most active iron(II) complexes (Table 22.1) [5c,d]. Their activity is promoted by acid, reaching remarkable TON values up to 690 for **8** or yields (based on the alkane) up to 25% for the complex **14** bearing the tris(pyrazol-1-yl)methanesulfonate ligand. The use of  $H_2O_2$  as oxidant and of acetonitrile–water as the solvent medium leads to the highest catalytic activity, but the hydrosoluble Fe complex  $[FeCl_2\{HC(pz)_3\}]$  (**8**) can operate effectively in water without requiring the presence of any organic solvent. This feature that allows the uncommon use of water as the only solvent is particularly significant in terms of developing a “green” catalytic process for alkane oxidations [5c].

Similar yields, under the same conditions, were obtained for the water-soluble Fe(II) complexes **19–21** bearing the C-functionalized tris(pyrazolyl)methane  $HOCH_2C(pz)_3$  (Table 22.1, [5e]). The hydroxo group of the scorpionate ligand imparts hydrosolubility that allows them to operate also in pure aqueous media (without any organic solvent, although less effectively).

$[CuCl_2\{HOCH_2C(pz)_3\}]$  (**22**) leads to overall yields up to 23% (Table 22.1, [5e]) and to a remarkably high selectivity toward the formation of cyclohexanol, while cyclohexanone is usually obtained in a much lower quantity. The above yields are considerably higher than those presented [5c] by the related half-sandwich complexes  $[CuCl_2\{HC(pz)_3\}]$  (**9**) or

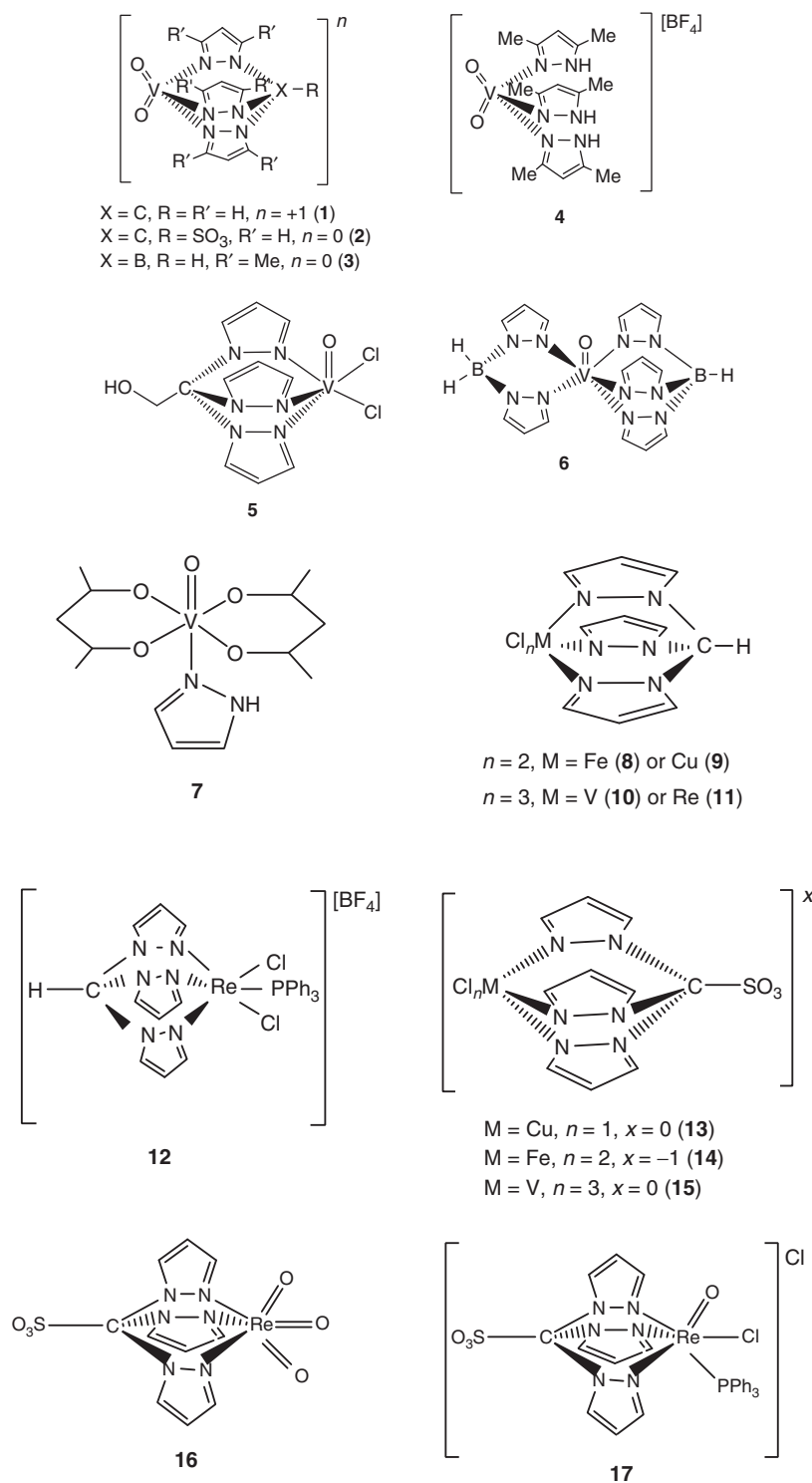


**Figure 22.2** Some scorpionate or pyrazole complexes (catalysts or catalyst precursors) mentioned in the text.

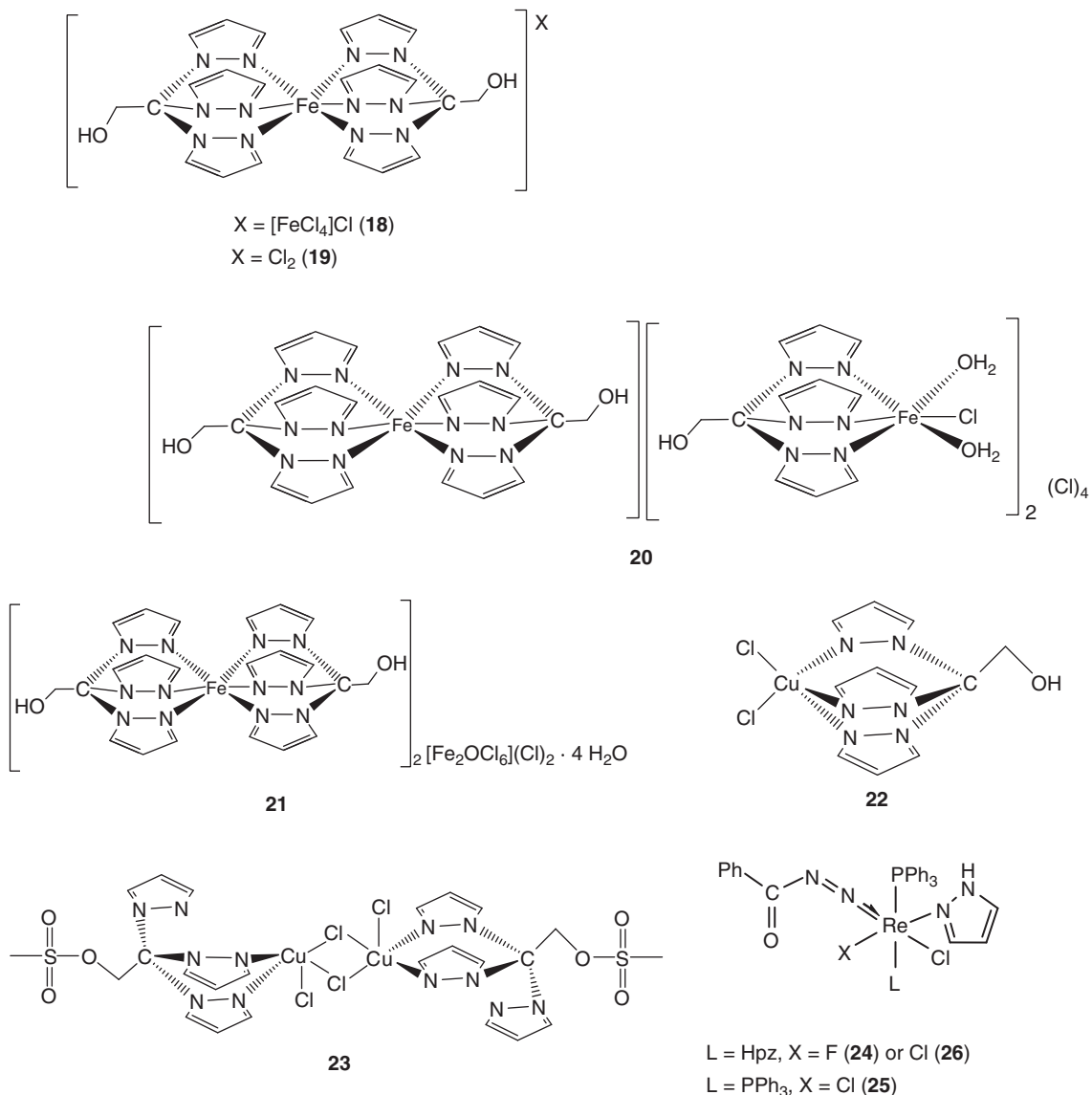
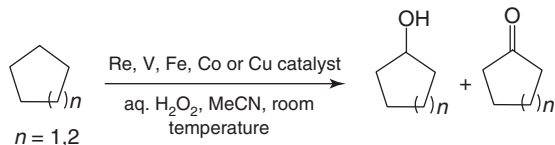


Figure 22.2 (Continued)



**Scheme 22.1** Oxidation of cycloalkane to cycloalkanol and cycloalkanone catalyzed by tris(pyrazol-1-yl)methane Re, V, Fe, or Cu complexes.

$[\text{CuCl}\{\text{SO}_3\text{C}(\text{pz})_3\}]$  (13) (maximum TON of 43 and 32, respectively; maximum yield of circa 4%) or by the full-sandwich hydrotris(pyrazolyl)methane Cu(II) compound  $[\text{Cu}\{\text{HC}(\text{pz})_3\}_2]\text{Cl}_2$  (maximum TON and yield of 18% and 2.5%, respectively), under the same experimental conditions [5c]. Moreover, 22 still exhibits quite a notorious activity in the absence of NCMe, a behavior favored by the good solubility of the catalyst in water.

**TABLE 22.1** Peroxidative Oxidation of Cyclohexane to Cyclohexanol and Cyclohexanone Catalyzed by Scorpionate or Pyrazole V, Fe, or Cu Complexes<sup>a</sup>

Catalyst	Total <sup>b</sup> Yield, %	Total <sup>b</sup> TON <sub>max</sub>	References.
[VO <sub>2</sub> {SO <sub>3</sub> C(pz) <sub>3</sub> }] ( <b>2</b> )	19	117	5a
[VO <sub>2</sub> {HB(3,5-Me <sub>2</sub> pz) <sub>3</sub> }] ( <b>3</b> )	13	86	5a
[VO <sub>2</sub> (3,5-Me <sub>2</sub> Hpz) <sub>3</sub> ][BF <sub>4</sub> ] ( <b>4</b> )	24	113	5a
[VOCl <sub>2</sub> {HOCH <sub>2</sub> C(pz) <sub>3</sub> }] ( <b>5</b> ) <sup>c</sup>	2	1.11 × 10 <sup>3</sup>	5b
[VO{HB(pz) <sub>3</sub> }]{H <sub>2</sub> B(pz) <sub>2</sub> } ( <b>6</b> )	13	75	5a
[VCl <sub>3</sub> {HC(pz) <sub>3</sub> }] ( <b>10</b> )	13	167	5c
[VCl <sub>3</sub> {SO <sub>3</sub> C(pz) <sub>3</sub> }] ( <b>15</b> )	10	121	5c
[FeCl <sub>2</sub> {HC(pz) <sub>3</sub> }] ( <b>8</b> )	13	690	5c
Li[FeCl <sub>2</sub> {SO <sub>3</sub> C(pz) <sub>3</sub> }] ( <b>14</b> )	25	600	5c
[Fe{HOCH <sub>2</sub> C(pz) <sub>3</sub> } <sub>2</sub> ]Cl <sub>2</sub> ( <b>19</b> )	10	385	5d
[Fe{HOCH <sub>2</sub> C(pz) <sub>3</sub> } <sub>2</sub> ][FeCl{HOCH <sub>2</sub> C(pz) <sub>3</sub> }(H <sub>2</sub> O) <sub>2</sub> ] <sub>2</sub> (Cl) <sub>4</sub> ( <b>20</b> )	14	328	5d
[Fe{HOCH <sub>2</sub> C(pz) <sub>3</sub> } <sub>2</sub> ] <sub>2</sub> [Fe <sub>2</sub> OCl <sub>6</sub> ](Cl) <sub>2</sub> ·4H <sub>2</sub> O ( <b>21</b> )	14	317	5d
[CuCl <sub>2</sub> {HOCH <sub>2</sub> C(pz) <sub>3</sub> }] ( <b>22</b> )	23	81	5e

Abbreviation: TON, turnover number.

<sup>a</sup>Selected results: yields (moles of products per 100 mol of cyclohexane); TON (moles of product per moles of catalyst). Typical reaction conditions: oxidant = H<sub>2</sub>O<sub>2</sub>, *n*(catalyst)/*n*(C<sub>6</sub>H<sub>12</sub>) = 5 × 10<sup>-5</sup>, 6 h, room temperature.

<sup>b</sup>Moles of cyclohexanol + cyclohexanone per 100 mol of cyclohexane.

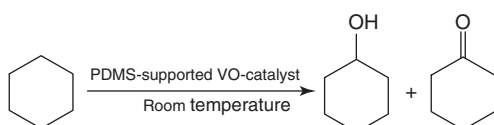
<sup>c</sup>Oxidant = *m*CPBA.

The C-scorpionate Re complexes **11** and **16**, as well as the related pyrazole **24–26** complexes, are the less active of the studied compounds, with TON values up to 285 [5f]. While the tris(pyrazolyl)methanesulfonate compound [ReO<sub>3</sub>{SO<sub>3</sub>C(pz)<sub>3</sub>}] (**16**) is more active for the cyclohexane oxidation if performed in the presence of acid, the fluorodipyrazole complex [ReClF{N<sub>2</sub>C(O)Ph}(Hpz)<sub>2</sub>(PPh<sub>3</sub>)] (**24**) provides the best catalyst, among these rhenium compounds, for the oxidation of cyclohexane in the absence of acid. The fluoride ligand is particularly favorable as the analogous dichlorocomplex [ReCl<sub>2</sub>{N<sub>2</sub>C(O)Ph}(Hpz)<sub>2</sub>(PPh<sub>3</sub>)] (**26**) exhibits circa half of the activity. This feature, which is also displayed by the supported catalysts (see Section 22.2.2), conceivably relates to the stronger electron-donor character of the F<sup>−</sup> ligand compared with Cl<sup>−</sup> [5f], thus promoting the oxidation of the complex to a higher metal oxidation state that is more favorable to the reaction.

## 22.2.2 In Supported Systems

The oxo-vanadium(IV) complexes [VOCl<sub>2</sub>{HOCH<sub>2</sub>C(pz)<sub>3</sub>}] (**5**) and [VO(acac)<sub>2</sub>(Hpz)] (**7**), immobilized on a polydimethylsiloxane (PDMS) membrane, act as supported catalysts for the cyclohexane oxidation (Scheme 22.2) using benzoyl peroxide (BPO), *tert*-butyl hydroperoxide, *m*CPBA, hydrogen peroxide, or the urea-hydrogen peroxide adduct as oxidants (TONs up to 620) [5b]. The best results were obtained with the less polar *m*CPBA or BPO on account of the hydrophobic character of the membrane that favors their sorption.

Although the homogeneous reactions (Section 22.2.1) take place faster than the heterogeneous ones and a higher activity is found in the former case, the use of the PDMS-supported catalysts is promising, as it is based on cheap and easily obtained membrane and vanadium(IV) catalysts, involves a simple way to heterogenize the catalyst without its chemical modification, and allows an easy product separation [5b].



**Scheme 22.2** Cyclohexane oxidation catalyzed by [VOCl<sub>2</sub>{HOCH<sub>2</sub>C(pz)<sub>3</sub>}] or [VO(acac)<sub>2</sub>(Hpz)] encapsulated in a polymeric PDMS-based membrane.

## 22.3 OXIDATION OF ALKANES BY MOLECULAR OXYGEN

The use of molecular oxygen as an oxidant is particularly attractive from ecological and economic perspectives, as it is the best environmentally friendly oxidant and is cheap. It can be used with either liquid or supported systems. This section concerns the use of dioxygen as an oxidant without the assistance of any added peroxide reagent.

The scorpionate vanadium complexes  $[\text{VCl}_3\{\text{HC}(\text{pz})_3\}]$  (**10**) and  $[\text{VCl}_3\{\text{SO}_3\text{C}(\text{pz})_3\}]$  (**15**), which catalyze cyclohexane oxidation with  $\text{H}_2\text{O}_2$  (Section 22.2.1), also operate with dioxygen under solvent-free conditions. Cyclohexane is oxidized to cyclohexanol (the main product) and cyclohexanone (13% conversion), with a high selectivity, typically at the  $\text{O}_2$  pressure of 15 atm, at  $140^\circ\text{C}$ , 18 h reaction time [6]. The reaction is further promoted (to 15% conversion) by pyrazinecarboxylic acid. The reactions proceed via radical mechanisms with possible involvement of both C-centered and O-centered radicals.

The pyrazole complexes  $[\text{ReClF}\{\text{N}_2\text{C}(\text{O})\text{Ph}\}(\text{Hpz})_2(\text{PPh}_3)]$  (**24**),  $[\text{ReCl}_2\{\text{N}_2\text{C}(\text{O})\text{Ph}\}(\text{Hpz})(\text{PPh}_3)_2]$  (**25**) and  $[\text{ReCl}_2\{\text{N}_2\text{C}(\text{O})\text{Ph}\}(\text{Hpz})_2(\text{PPh}_3)]$  (**26**), which act as homogeneous catalysts for cyclohexane peroxidative (by  $\text{H}_2\text{O}_2$ ) oxidation (Section 22.2.1), are inactive with  $\text{O}_2$  [7]. However, when immobilized on 3-aminopropyl functionalized silica, they catalyze the cyclohexane oxidation with dioxygen to cyclohexanol and cyclohexanone (the main product) in the absence of any added solvent and additives and, under relatively mild conditions, up to 16% overall conversion toward the ketone and alcohol, with an overall selectivity of 95% at the  $\text{O}_2$  pressure of 19 atm, at  $150^\circ\text{C}$ , 8 h reaction time (Scheme 22.3) [7].

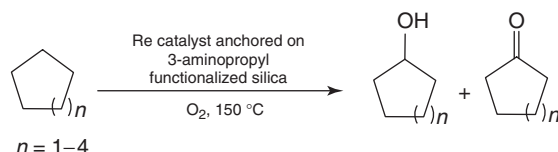
The higher activity of the fluoro-complex  $[\text{ReClF}\{\text{N}_2\text{C}(\text{O})\text{Ph}\}(\text{Hpz})_2(\text{PPh}_3)]$  (**24**), in comparison with the related chlorocomplexes, is in accord with the observed behavior for the homogeneous peroxidative oxidation of cyclohexane (Section 22.2.1), and possibly concerns the overall stronger electron-donor character of the fluoride ligand relative to chloride. Complex **24**, supported on 3-aminopropyl functionalized silica, also catalyzes the oxidation of other cycloalkanes (e.g., cyclopentane, cycloheptane, and cyclooctane) to the corresponding cycloalkanols and cycloalkanones, with conversions and selectivities comparable to those for cyclohexane oxidation [7]. The use of radical traps supports the involvement of a free-radical mechanism via carbon- and oxygen-centered radicals.

## 22.4 CARBOXYLATION OF LIGHT ALKANES

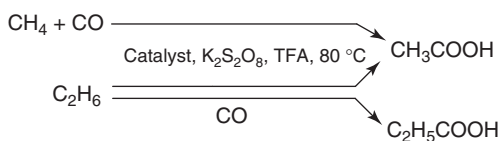
Although carboxylation reactions (which involve C–C bond formation) are not typical oxidation reactions, they are related to those we have discussed above in view of the possible use of common types of catalysts. Moreover, they are also of synthetic relevance, allowing to synthesize carboxylic acids (bearing one more carbon atom than the substrate) and their derivatives, which have several applications in our daily life [8a].

Scorpionate or pyrazole V(V) **1–4**, **6**, **10**, and **15**, and Re(III) **11**, **12**, **16**, **17**, **24–26** complexes have been used as catalysts for the carboxylation of gaseous alkanes via single-pot conversions [5a,f]. These syntheses of carboxylic acids are much simpler than those used in industry. For instance, in the case of the conversion of methane into acetic acid, the current industrial routes commonly involve three distinct stages and use more expensive catalysts and harder experimental conditions (e.g., the Mosanto and BP-Amoco Cativa processes of carbonylation of methanol, at the third stage, are based on Rh and Ir catalysts, respectively) [8b].

The alkane carboxylation reactions are typically undertaken in trifluoroacetic acid (TFA) at  $80^\circ\text{C}$  with a V or Re complex catalyst and peroxydisulfate as the oxidant, under a CO atmosphere, and lead to the corresponding carboxylic acids with one more carbon (Scheme 22.4 for the cases of methane and ethane).



**Scheme 22.3** Oxidation of cycloalkane to cycloalkanol and cycloalkanone catalyzed by a Si-supported pyrazole Re complex.



**Scheme 22.4** Carboxylation of methane and ethane catalyzed by scorpionate V or Re complexes.

**TABLE 22.2** Carboxylation of Alkanes Catalyzed by Scorpionate or Pyrazole V or Re Complexes<sup>a</sup>

Substrate	<i>p</i> CO, atm	CH <sub>4</sub>		C <sub>2</sub> H <sub>6</sub>			Reference
		MeCOOH Yield, %	EtCOOH Yield, %	MeCOOH <sup>b</sup> Yield, %	Total Yield, %		
[VO <sub>2</sub> {SO <sub>3</sub> C(pz) <sub>3</sub> }] ( <b>2</b> )	5	39	13	10	23	5a	
[VO <sub>2</sub> {HB(3,5-Me <sub>2</sub> pz) <sub>3</sub> }] ( <b>3</b> )	5	16	14	11	25	5a	
[VO <sub>2</sub> {HC(pz) <sub>3</sub> }][BF <sub>4</sub> ] ( <b>1</b> )	5	16	12	11	23	5a	
[VO <sub>2</sub> (3,5-Me <sub>2</sub> Hpz) <sub>3</sub> ][BF <sub>4</sub> ] ( <b>4</b> )	5	25	6	11	17	5a	
[VO{HB(pz) <sub>3</sub> }]{H <sub>2</sub> B(pz) <sub>2</sub> } ( <b>6</b> )	5	31	4	3	7	5a	
[VCl <sub>3</sub> {SO <sub>3</sub> C(pz) <sub>3</sub> }] ( <b>10</b> )	5	37	6	2	8	5a	
[VCl <sub>3</sub> {HC(pz) <sub>3</sub> }] ( <b>15</b> )	5	20	2	3	5	5a	
[ReO <sub>3</sub> {SO <sub>3</sub> C(pz) <sub>3</sub> }] <sup>c</sup> ( <b>16</b> )	0		1	28	29	5f	
[ReOCl{SO <sub>3</sub> C(pz) <sub>3</sub> }(PPh <sub>3</sub> )]Cl ( <b>17</b> )	0		0	18	18	5f	
[ReCl <sub>2</sub> {HC(pz) <sub>3</sub> }(PPh <sub>3</sub> )][BF <sub>4</sub> ] ( <b>12</b> )	0		0	16	16	5f	
[ReCl <sub>3</sub> {HC(pz) <sub>3</sub> }] <sup>c</sup> ( <b>11</b> )	0		0	5	5	5f	
[ReClF{N <sub>2</sub> C(O)Ph}(Hpz) <sub>2</sub> (PPh <sub>3</sub> )] ( <b>24</b> )	0		5	41	46	5f	
[ReCl <sub>2</sub> {N <sub>2</sub> C(O)Ph}(Hpz) <sub>2</sub> (PPh <sub>3</sub> ) <sup>c</sup> ( <b>26</b> )	0		1	24	25	5f	
[ReCl <sub>2</sub> {N <sub>2</sub> C(O)Ph}(Hpz)(PPh <sub>3</sub> ) <sub>2</sub> ] <sup>c</sup> ( <b>25</b> )	0		0	4	4	5f	

Abbreviation: TON, turnover number.

<sup>a</sup>Selected results: product yields (moles of product per 100 mol of alkane). Typical reaction conditions for carboxylation: *p*(alkane) = 5 atm (1.02 and 1.53 mmol for CH<sub>4</sub> and C<sub>2</sub>H<sub>6</sub>, respectively), *n*(catalyst) = 0.020 mmol, 80 °C, 20 h, K<sub>2</sub>S<sub>2</sub>O<sub>8</sub> (4.00 mmol), CF<sub>3</sub>COOH (7.5 ml for CH<sub>4</sub> and 5.5 mL for C<sub>2</sub>H<sub>6</sub>).

<sup>b</sup>Formed by oxidation of ethane, rather than carboxylation.

<sup>c</sup>*p*(C<sub>2</sub>H<sub>6</sub>) = 3 atm.

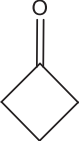
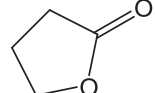
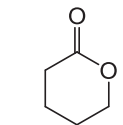
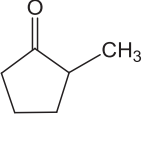
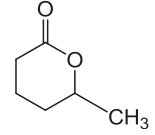
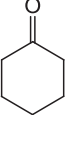
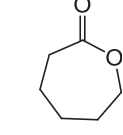
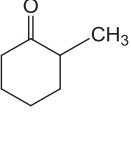
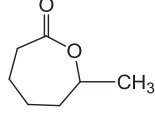
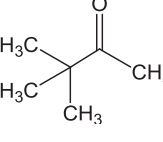
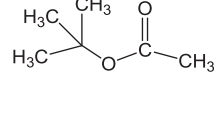
The dioxo-vanadium(V) [VO<sub>2</sub>{HC(pz)<sub>3</sub>}][BF<sub>4</sub>] (**1**), [VO<sub>2</sub>{SO<sub>3</sub>C(pz)<sub>3</sub>}] (**2**), [VO<sub>2</sub>{HB(3,5-Me<sub>2</sub>pz)<sub>3</sub>}] (**3**), and [VO<sub>2</sub>(3,5-Me<sub>2</sub>Hpz)<sub>3</sub>][BF<sub>4</sub>] (**4**); the oxo-vanadium(IV) [VO{HB(pz)<sub>3</sub>}]{H<sub>2</sub>B(pz)<sub>2</sub>} (**6**); and the non-oxo-vanadium(III or IV) [VCl<sub>3</sub>{HC(pz)<sub>3</sub>}] (**10**) and [VCl<sub>3</sub>{SO<sub>3</sub>C(pz)<sub>3</sub>}] (**15**) compounds, bearing scorpionate or pyrazole ligands, exhibit catalytic activity in the single-pot carboxylation of methane and ethane to the corresponding carboxylic acids (yields up to 40%, TONs up to 157, Table 22.2) under mild conditions [5a]. For the alkane carboxylation reaction, the dioxo-scorpionate-V(V) complexes are usually more active than the mono-oxo-discorpionate-V(IV) and the non-oxo catalysts [VCl<sub>3</sub>{HC(pz)<sub>3</sub>}] (**10**) and [VCl<sub>3</sub>{SO<sub>3</sub>C(pz)<sub>3</sub>}] (**15**) [5a]. In addition, the sulfonate derivative is water soluble, which is favorable toward application in a green system. Radical trap experiments suggest the involvement of radical mechanisms for the carboxylations [5a].

The rhenium tris(pyrazolyl)methane compounds [ReCl<sub>3</sub>{HC(pz)<sub>3</sub>}] (**11**), [ReCl<sub>2</sub>{HC(pz)<sub>3</sub>}(PPh<sub>3</sub>)][BF<sub>4</sub>] (**12**), [ReO<sub>3</sub>{SO<sub>3</sub>C(pz)<sub>3</sub>}] (**16**), and [ReOCl{SO<sub>3</sub>C(pz)<sub>3</sub>}(PPh<sub>3</sub>)]Cl (**17**), and the Re pyrazole complexes [ReClF{N<sub>2</sub>C(O)Ph}(Hpz)<sub>2</sub>(PPh<sub>3</sub>)] (**24**), [ReCl<sub>2</sub>{N<sub>2</sub>C(O)Ph}(Hpz)(PPh<sub>3</sub>)<sub>2</sub>] (**25**), and [ReCl<sub>2</sub>{N<sub>2</sub>C(O)Ph}(Hpz)<sub>2</sub>(PPh<sub>3</sub>)] (**26**) also act as selective catalysts (or catalyst precursors) in the K<sub>2</sub>S<sub>2</sub>O<sub>8</sub>/TFA system at 80 °C in the absence of CO, for the single-pot oxidation of ethane to give acetic acid (Scheme 22.4), in a yield up to circa 40% (Table 22.2). Propionic acid can also be formed but normally in a much lower yield [5f]. The formation of propionic acid is, however, promoted by using CO gas which, in addition, hampers the production of acetic acid, thus the selectivity being controlled by adjusting the pressure of this gas. The fluoro-dipyrazole complex [ReClF{N<sub>2</sub>C(O)Ph}(Hpz)<sub>2</sub>(PPh<sub>3</sub>)] (**24**) provides the best catalyst for the oxidation of ethane to acetic acid. The presence of the fluoride ligand, as indicated above for the peroxidative oxidation reactions, is particularly favorable as the analogous dichloro-complex [ReCl<sub>2</sub>{N<sub>2</sub>C(O)Ph}(Hpz)<sub>2</sub>(PPh<sub>3</sub>)] (**26**) exhibits circa half of the activity [5f].

## 22.5 BAEYER–VILLIGER OXIDATION OF KETONES

The BV oxidation by aqueous H<sub>2</sub>O<sub>2</sub> in 1,2-dichloroethane of cyclic and linear ketones to the corresponding lactones and esters (Scheme 22.5) is catalyzed by Re(III or IV) complexes bearing C-scorpionate or pyrazole ligands, which conceivably allow the involvement of coordinative unsaturation at the metal in view of their lability [Hpz,  $\eta^3$ - or  $\eta^2$ -HC(pz)<sub>3</sub> toward lower denticity] and/or proton-transfer steps on account of their basic character—features that are favorable to the occurrence of oxidation catalysis with H<sub>2</sub>O<sub>2</sub> [9].

**TABLE 22.3** Baeyer–Villiger Oxidation of Several Ketones Catalyzed by Tris(pyrazol-1-yl)methane or Pyrazole Re Complexes [9]<sup>a</sup>

Substrate	Catalyst	Yield <sup>b</sup> , %	TON <sup>c</sup>	Conv.	Select.	Product
	[ReCl <sub>2</sub> {N <sub>2</sub> C(O)Ph}(Hpz) <sub>2</sub> (PPh <sub>3</sub> )] ( <b>26</b> )	54	537	99	54	
	[ReClF{N <sub>2</sub> C(O)Ph}(Hpz) <sub>2</sub> (PPh <sub>3</sub> )] ( <b>24</b> )	18	178	65	28	
	[ReCl <sub>3</sub> {HC(pz) <sub>3</sub> }] ( <b>11</b> )	33	329	78	42	
	[ReCl <sub>4</sub> {η <sup>2</sup> -HC(pz) <sub>3</sub> }] ( <b>27</b> )	33	334	100	33	
	[ReCl <sub>2</sub> {N <sub>2</sub> C(O)Ph}(Hpz) <sub>2</sub> (PPh <sub>3</sub> )] ( <b>26</b> )	23	231	63	37	
	[ReClF{N <sub>2</sub> C(O)Ph}(Hpz) <sub>2</sub> (PPh <sub>3</sub> )] ( <b>24</b> )	11	109	58	41	
	[ReCl <sub>2</sub> {N <sub>2</sub> C(O)Ph}(Hpz) <sub>2</sub> (PPh <sub>3</sub> )] ( <b>26</b> )	22	223	28	80	
	[ReClF{N <sub>2</sub> C(O)Ph}(Hpz) <sub>2</sub> (PPh <sub>3</sub> )] ( <b>24</b> )	10	102	40	26	
	[ReCl <sub>3</sub> {HC(pz) <sub>3</sub> }] ( <b>11</b> )	21	209	37	57	
	[ReCl <sub>4</sub> {η <sup>2</sup> -HC(pz) <sub>3</sub> }] ( <b>27</b> )	19	192	37	52	
	[ReCl <sub>2</sub> {N <sub>2</sub> C(O)Ph}(Hpz) <sub>2</sub> (PPh <sub>3</sub> )] ( <b>26</b> )	16	158	24	69	
	[ReClF{N <sub>2</sub> C(O)Ph}(Hpz) <sub>2</sub> (PPh <sub>3</sub> )] ( <b>24</b> )	7	74	47	16	
	[ReCl <sub>3</sub> {HC(pz) <sub>3</sub> }] ( <b>11</b> )	18	180	44	41	
	[ReCl <sub>4</sub> {η <sup>2</sup> -HC(pz) <sub>3</sub> }] ( <b>27</b> )	5	53	46	12	
	[ReCl <sub>2</sub> {N <sub>2</sub> C(O)Ph}(Hpz) <sub>2</sub> (PPh <sub>3</sub> )] ( <b>26</b> )	31	307	77	39	
	[ReClF{N <sub>2</sub> C(O)Ph}(Hpz) <sub>2</sub> (PPh <sub>3</sub> )] ( <b>24</b> )	22	223	79	28	
	[ReCl <sub>3</sub> {HC(pz) <sub>3</sub> }] ( <b>11</b> )	18	177	74	24	
	[ReCl <sub>4</sub> {η <sup>2</sup> -HC(pz) <sub>3</sub> }] ( <b>27</b> )	24	241	65	37	
	[ReCl <sub>2</sub> {N <sub>2</sub> C(O)Ph}(Hpz) <sub>2</sub> (PPh <sub>3</sub> )] ( <b>26</b> )	6	64	8	81	
	[ReClF{N <sub>2</sub> C(O)Ph}(Hpz) <sub>2</sub> (PPh <sub>3</sub> )] ( <b>24</b> )	7	74	11	67	
	[ReCl <sub>3</sub> {HC(pz) <sub>3</sub> }] ( <b>11</b> )	12	118	69	17	

Abbreviation: TON, turnover number.

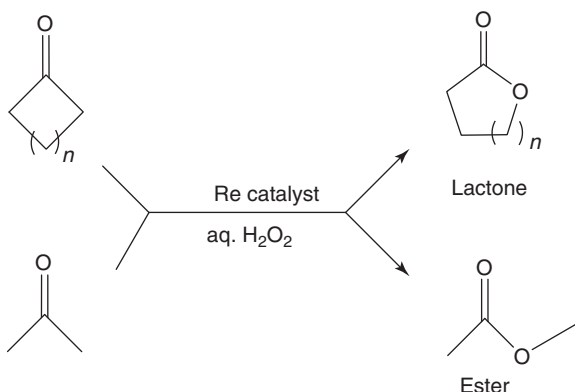
<sup>a</sup>Reaction conditions (unless stated otherwise): rhenium catalyst (1.7 μmol, used as a stock solution in 1,2-dichloroethane), 1.7 mmol of substrate, H<sub>2</sub>O<sub>2</sub> (1.7 mmol, i.e., 1000:1 molar ratio of oxidant to Re catalyst), 1,2-dichloroethane (3.0 mL), 6 h, 70 °C, under dinitrogen. Yield and TON determined by GC analysis.

<sup>b</sup>Molar yield (%) based on the ketone substrate, that is, moles of lactone (or ester) per 100 mol of ketone.

<sup>c</sup>TON (moles of product per mole of Re catalyst).

Hence, [ReCl<sub>3</sub>{HC(pz)<sub>3</sub>}] (**11**), [ReCl<sub>4</sub>{η<sup>2</sup>-HC(pz)<sub>3</sub>}] (**27**), [ReClF{N<sub>2</sub>C(O)Ph}(Hpz)<sub>2</sub>(PPh<sub>3</sub>)] (**24**), and [ReCl<sub>2</sub>{N<sub>2</sub>C(O)Ph}(Hpz)<sub>2</sub>(PPh<sub>3</sub>)] (**26**) catalyze the BV oxidation of 2-methylcyclohexanone, 2-methylcyclopentanone, cyclohexanone, cyclopentanone, cyclobutanone, and 3,3-dimethyl-2-butanone into the corresponding lactones or esters in the presence of aqueous H<sub>2</sub>O<sub>2</sub>, allowing to achieve conversions, for example, up to 79% in the case of 2-methylcyclohexanone or 100% in the case of cyclobutanone [9].

In general, these rhenium compounds are more active for the oxidation of cyclic (four-, five-, and six-membered rings) than acyclic ketones, consistent with the common lower reactivity of the latter ketones. The Re(III) tris(pyrazol-1-yl)methane compound [ReCl<sub>3</sub>{HC(pz)<sub>3</sub>}] (**11**) is the most active one for 2-methylcyclopentanone and cyclohexanone or pinacolone BV oxidations, whereas the most effective oxidations are observed for cyclobutanone with [ReCl<sub>2</sub>{N<sub>2</sub>C(O)Ph}(Hpz)<sub>2</sub>(PPh<sub>3</sub>)] (**26**) (54% yield, 99% conversion, TON of 537) [9].



**Scheme 22.5** Baeyer–Villiger peroxidative oxidation of cyclic and linear ketones to the corresponding lactones or esters.

The use of 1,2-dichloroethane as solvent leads to the highest activity for all ketones, but water can be used as the only solvent, which is particularly important for the development of a green BV system [9].

## 22.6 FINAL REMARKS

The application of tris(pyrazol-1-yl)methane-type scorpionate (or related pyrazole) complexes of several transition metals (V, Fe, Cu, and Re) as catalysts or catalyst precursors for alkane and BV ketone oxidation reactions directed toward single-pot organic synthesis proved to be a promising strategy. Moreover, the hydrosolubility of the scorpionate complexes bearing suitably C-functionalized moieties that allows the uncommon use of water as the only solvent, together with the mild operation conditions, is particularly significant in terms of developing a green catalytic process for alkane and ketone oxidations.

## ACKNOWLEDGMENTS

We gratefully acknowledge the coauthors cited in our publications. This work has been partially supported by the Fundação para a Ciência e a Tecnologia (FCT), Portugal, and projects PTDC/QUI-QUI/102150/2008, PTDC-EQU-EQU-122025-2010, and PEst-OE/QUI/UI0100/2013.

## REFERENCES

- (a) Shul'pin, G. B. *Mini-Rev. Org. Chem.*, **2009**, *6*, 95; (b) Derouane, E. G.; Haber, J.; Lemos, F.; Ramôa Ribeiro, F.; Guinet M. Eds. *Catalytic Activation and Functionalization of Light Alkanes*; NATO ASI Series, Vol. 44; Kluwer Academic Publishers: Dordrecht, The Netherlands, **1998**; (c) Hill, C. L., Ed., *Activation and Functionalization of Alkanes*; John Wiley & Sons, Inc.: New York, **1989**; (d) Wolf, E. E., Ed., *Methane Conversion by Oxidative Processes: Fundamental and Engineering Aspects*; Van Nostrand Reinhold: New York, **1992**; (e) Shilov, A. E.; Shul'pin, G. B. *Activation and Catalytic Reactions of Saturated Hydrocarbons in the Presence of Metal Complexes*; Kluwer Academic Publishers: Dordrecht, The Netherlands, **2000**; (f) Jia, C. G.; Kitamura, T.; Fujiwara, Y. *Acc. Chem. Rev.* **2001**, *34*, 633; (g) Crabtree, R. H. *J. Chem. Soc. Dalton Trans.* **2001**, *17*, 2437; (h) Shul'pin, G. B. *C. R. Chimie*. **2003**, *6*, 163; (i) Shul'pin, G. B. *J. Mol. Catal. A Chem.* **2002**, *189*, 39; (j) Shilov, A. E.; Shul'pin, G. B. *Chem. Rev.* **1997**, *97*, 2879; (k) da Silva, J. A. L.; Fraústo da Silva, J. J. R.; Pombeiro, A. J. L. *Coord. Chem. Rev.* **2011**, *255*, 2232; (l) Pombeiro, A. J. L. In *Vanadium: The Versatile Metal*; Kustin, K.; Pessoa, J. C.; Crans, D. C., Eds.; ACS Symposium Series 974, American Chemical Society: Washington, DC, **2007**, p 51.
- (a) Michelin, R. A.; Sgarbossa, P.; Scarso, A.; Strukul, G. *Coord. Chem. Rev.* **2010**, *254*, 646; (b) ten Brink, G.-J.; Arends, I. W. C. E.; Sheldon, R. A. *Chem. Rev.* **2004**, *104*, 4105; (c) Seiser, T.; Saget, T.; Tran, D. N.; Cramer, N. *Angew. Chem. Int. Ed.* **2011**, *50*, 7740; (d) Jin, P.; Zhu, L.; Wei, D.; Tang, M.; Wang, X. *Comput. Theor. Chem.* **2011**, *966*, 207.
- (a) Kaneda, K.; Ueno, S.; Imanaka, T.; Shimotsuma, E.; Nishiyama, Y.; Ishii, Y. *J. Org. Chem.*, **1994**, *59*, 2915; (b) Li, X.; Wang, F.; Zhang, H.; Wang, C.; Song, G. *Synthetic Commun.* **1996**, *26*, 1613; (c) Chrobok, A. *Tetrahedron* **2010**, *66*, 2940.

4. (a) Greggio, G.; Sgarbossa, P.; Scarso, A.; Michelin, R. A.; Strukul, G. *Inorg. Chim. Acta* **2008**, *361*, 3230; (b) Sgarbossa, P.; Scarso, A.; Pizzo, E.; Sbovata, A.M.; Tassan, A.; Michelin, R.A.; Strukul, G. *J. Mol. Catal. A Chem.* **2007**, *261*, 202; (c) Conte, V.; Floris, B.; Galloni, P.; Mirruzzo, V.; Scarso, A.; Sordi, D.; Strukul, G. *Green Chem.* **2005**, *7*, 262; (d) Uchida, T.; Katsuki, T. *Tetrahedron Lett.* **2001**, *42*, 6911; (e) Bernini, R.; Mincione, E.; Cortese, M.; Aliotta, G.; Oliva, A.; Saladina, R. *Tetrahedron Lett.* **2001**, *42*, 5401; (f) Brunetta, A.; Sgarbossa, P.; Strukul G. *Catal. Today* **2005**, *99*, 227.
5. (a) Silva, T. F. S.; Luzyanin, K. V.; Kirillova, M. V.; Silva, M. F. C. G.; Martins, L. M. D. R. S.; Pombeiro, A. J. L. *Adv. Synth. Catal.* **2010**, *352*, 171; (b) Silva, T. F. S.; Mac Leod, T. C. O.; Martins, L. M. D. R. S.; Guedes da Silva, M. F. C. G.; Pombeiro, A. J. L. *J. Mol. Cat. A Chem.* accepted for publication, **2012**; (c) Silva, T. F. S.; Alegria, E. C. B. A.; Martins, L. M. D. R. S.; Pombeiro, A. J. L. *Adv. Synth. Cat.* **2008**, *350*, 706; (d) Silva, T. F. S.; Silva, M. F. C. G.; Mishra, G. S.; Martins, L. M. D. R. S.; Pombeiro, A. J. L. *J. Organomet. Chem.* **2011**, *696*, 1310; (e) Silva, T. F. S.; Mishra, G. S.; Silva, M. F. G.; Wanke, R.; Martins, L. M. D. R. S.; Pombeiro, A.J.L. *Dalton Trans.* **2009**, *42*, 9207; (f) Alegria, E. C. B. A.; Kirillova, M. V.; Martins, L. M. D. R. S.; Pombeiro, A. J. L. *Appl. Catal. A Gen.* **2007**, *317*, 43.
6. Mishra, G. S.; Silva, T. F. S.; Martins, L. M. D. R. S.; Pombeiro, A. J. L. *Pure Appl. Chem.* **2009**, *81*, 1217.
7. Mishra, G. S.; Alegria, E. C. B. A.; Martins, L. M. D. R. S.; Fraústo da Silva, J. J. R.; Pombeiro, A. J. L. *J. Mol. Catal. A Chem.* **2008**, *285*, 92.
8. (a) *Ullmann's Encyclopedia of Industrial Chemistry*, 6th ed.; Wiley-VCH Verlag GmbH: Weinheim, **2002**; (b) Whyman, R. *Applied Organometallic Chemistry and Catalysis*; Oxford University Press: Oxford, **2001**.
9. Alegria, E. C. B.; Martins, L. M. D. R. S.; Kirillova, M. V.; Pombeiro, A. J. L. *Appl. Catal. A Gen.*, **2012**, *443–444*, 27.

## TOWARD CHEMOSELECTIVE BIOCONJUGATIVE DESULFITATIVE CATALYSIS

LANNY S. LIEBESKIND AND ETHEL C. GARNIER-AMBLARD

*Department of Chemistry, Emory University, Atlanta, Georgia*

### 23.1 INTRODUCTION

Metal-catalyzed desulfitative transformations of sulfur-containing molecules are both challenging and significant. The challenge resides in the fact that many of the catalytic systems that carry out desulfitative transformations require the use of polarizable metal catalysts or precatalysts that can form especially strong bonds to sulfur. Strong metal-to-sulfur bonding, however, inhibits efficient catalytic turnover, particularly when mild reaction conditions are required. The significance rests in the important opportunities, some partly realized, some untapped, for desulfitative transformations. As depicted in Fig. 23.1, these are found in energy-related research with metal-catalyzed desulfurization of carbon-based fuels [1], in the detoxification of chemical warfare agents with metal-catalyzed transformations of phosphonothioate and phosphorothioates [2, 3], as well as in the synthesis of fine chemicals through highly chemoselective desulfitative transformations [4–6].

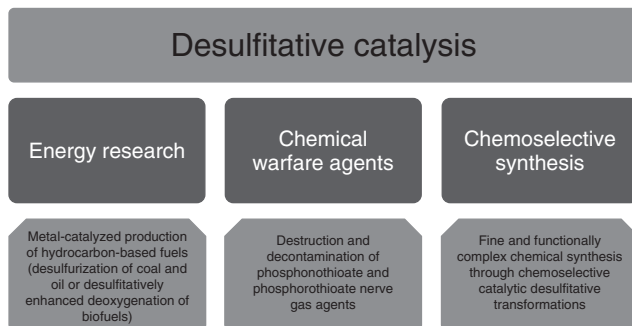
Of the native carbon–heteroatom bonds that are biologically relevant (C–O, C–N, C–S), the C–S bond is particularly polarizable, and it therefore has the potential to engage in highly selective transformations catalyzed by thiophilic metals in the presence of C–O- and C–N-based functional groups. As a consequence, given its inherent chemoselectivity, the desulfitative catalysis could also play an important role in highly selective bioconjugative reactions where a biomolecule is coupled to another biomolecule, to a probe or therapeutic molecule, or to a nanomaterial (dot, tube, particle, etc.) or surface [7].

Nevertheless, developing effective bioconjugative desulfitative catalytic systems will be especially challenging. Not only must a unique C–S bond within a complex biomolecule be targeted for reaction in the presence of numerous O- and N-based moieties and other S-containing groups, but bioconjugative desulfitative catalysis demands the efficient turnover of a strong M–S bond in water at or near neutral pH and at or near ambient temperature, as required by functionally complex, thermally and pH-sensitive biomolecules such as proteins.

This article provides a brief overview of the development of the pH-neutral, desulfitative coupling of thioorganics with boronic acids and describes the evolution of the original process into two new fully catalytic reaction systems that are now poised for bioconjugative desulfitative applications.

### 23.2 THIOORGANIC-BORONIC ACID DESULFITATIVE CROSS-COUPLING

The literature on metal-catalyzed “desulfitative” cross-coupling of thioorganics extends back into the 1970s beginning with the early work of Wenkert [8–10] and Okamura [11] and then Ronzini [12–15] who first showed that thioorganics participate

**Figure 23.1** Desulfidative catalysis overview.

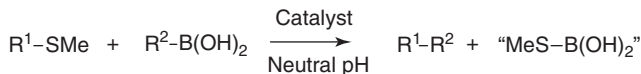
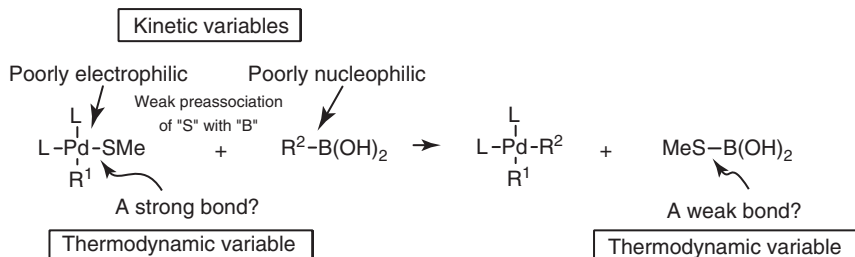
in Ni- and Fe-catalyzed Kumada-like cross-coupling with Grignard reagents. Such desulfidative cross-couplings were then further developed using basic and nucleophilic coupling partners such as Grignard and organozinc reagents by Lu [16], Fukuyama [17–19], Jacobi [20, 21], and others [6]. In contrast to Grignard and organozinc reagents, nonbasic and non-nucleophilic boronic acids offer the unique potential for metal-catalyzed desulfidative cross-coupling with thioorganics at neutral pH potentially in water, an operational condition required in many bioconjugative applications.

The investigation of chemoselective thioorganic–boronic acid couplings began by studying sulfonium salts as participants in a variety of Pd- and Ni-catalyzed coupling protocols, with the sulfonium salts either preformed [22, 23] or generated *in situ* [24]. However, before the year 2000, a straightforward metal-catalyzed cross-coupling of charge-neutral thioorganics with boronic acids was unknown (Scheme 23.1), a situation primarily thwarted by an unfavorable transmetalation from a neutral boronic acid to an organopalladium thiolate intermediate (Scheme 23.2).

The challenge associated with the development of a palladium-catalyzed, pH-neutral desulfidative coupling of a thioorganic and a boronic acid rests with uncovering reaction conditions that would facilitate the unfavorable transmetalation step without perturbing the pH. As a design strategy for accomplishing this goal, we conceived of the incorporation into the reaction system of a pH-neutral, dual thiophilic/borophilic cofactor, M–X, that would simultaneously lower the kinetic barrier and address the thermodynamic deficit implicit in the transmetalation step, all while maintaining pH neutrality (Fig. 23.2).

Using this design strategy, copper(I) carboxylates, such as Cu(I) thiophenecarboxylate (CuTC) and Cu(I) 3-methylsalicylate (CuMeSal) proved to be uniquely effective facilitators of the pH-neutral, palladium-catalyzed desulfidative coupling of thioorganics with boronic acids and their pH-neutral transmetalation partners, organostannanes (Fig. 23.3). The literature is now replete with many examples of this chemistry (Fig. 23.4) [4, 5, 25–42].

All “first-generation” palladium-catalyzed desulfidative couplings of thioorganics and boronic acids highlighted in Fig. 23.4 require the use of stoichiometric quantities of a copper(I) carboxylate cofactor. This requirement is implicit in the mechanism of the transformation (Scheme 23.3).

**Scheme 23.1** Desulfidative coupling of boronic acids and thioorganics.**Scheme 23.2** Unfavorable transmetalation

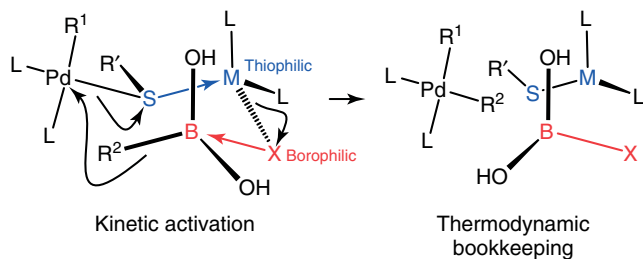


**Figure 23.2** Dual thiophilic–borophilic activation of transmetalation. (See insert for color representation of the figure.)

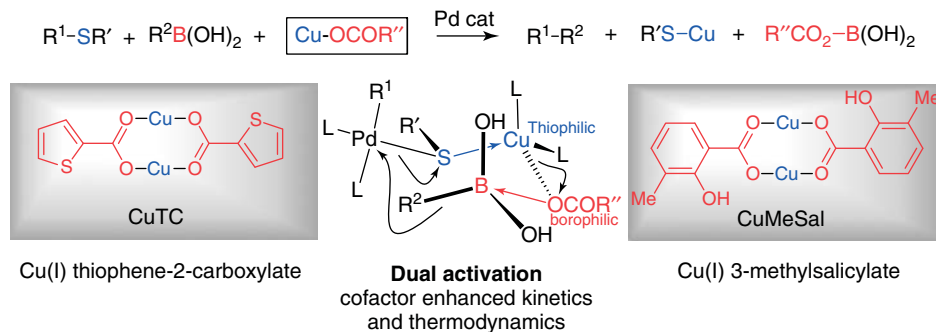


**Figure 23.3** Pd-catalyzed, Cu(I) carboxylate-mediated desulfitative catalysis. (See insert for color representation of the figure.)

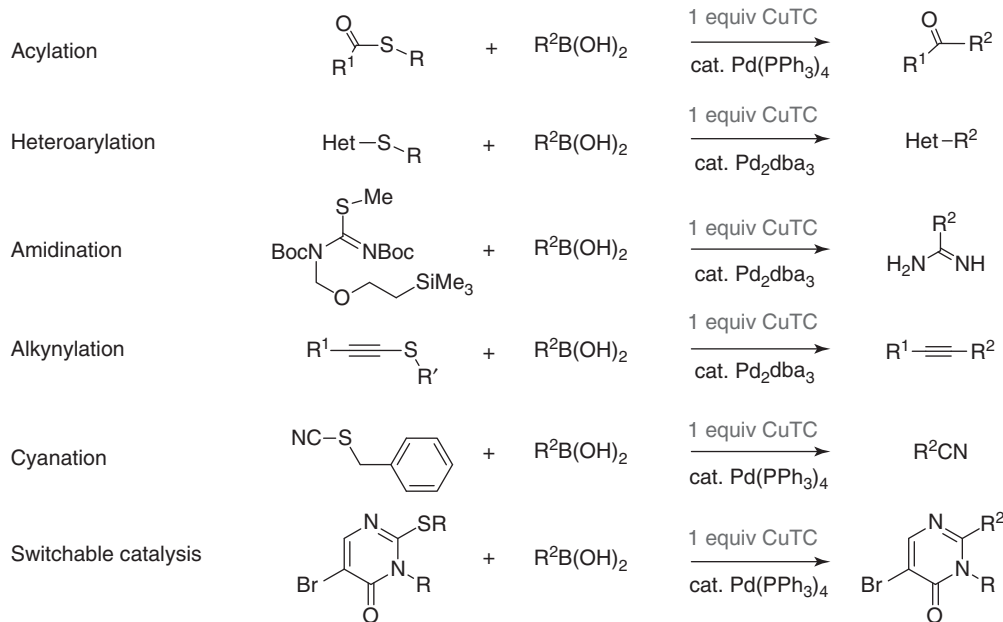
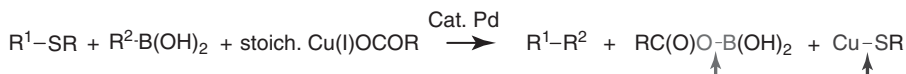


**Figure 23.4** Generalization of Pd-catalyzed, Cu-mediated desulfitative catalysis.

The thiolate residue must be fully scavenged by an equivalent of the Cu(I) and, as dictated by a balanced reaction, the presence of a full equivalent of a strongly bonding third valence for the  $-\text{B}(\text{OH})_2$  fragment is required, in this case, the carboxylate. The mechanistic requirement of a stoichiometric quantity of a Cu(I) carboxylate for pH-neutral desulfitative cross-coupling will be incompatible with any desulfitative bioconjugative transformations of biomolecules, such as proteins, that must be carried out in water.



**Scheme 23.3** Stoichiometry of the Pd-catalyzed, Cu(I) carboxylate-mediated desulfitative coupling.

### 23.3 Cu-CATALYZED DESULFITATIVE COUPLING

Bioconjugative processes require reasonably fast reactions that can take place at ambient temperature, usually in water. Therefore, any anticipated bioconjugative desulfitative cross-coupling with boronic acids will involve reactions that can occur rapidly in water and use only catalytic quantities of palladium and/or copper. The challenge then is clear: in order to transform the first generation of desulfitative cross-couplings, which require stoichiometric amounts of a Cu carboxylate to reach completion, into a reaction system that is catalytic in Cu, *the Cu-SR reaction product must be converted back into a Cu-oxygenate during the catalytic cycle* (Scheme 23.4).

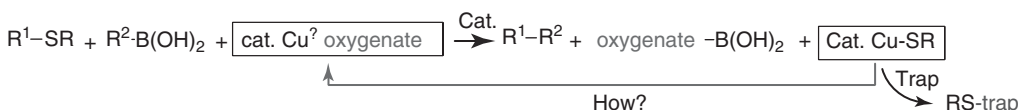
Therefore, a catalytic variant of desulfitative cross-coupling with boronic acids that proceeds through a Cu-thiolate intermediate will necessitate (i) breaking of the strong Cu–S bond, (ii) trapping of the thiolate ligand producing a weakly coordinating derivative, and (iii) regeneration of a Cu-oxygenate in order to continue the catalytic cycle.

#### 23.3.1 Cu-Desulfitative Catalysis under Aerobic Conditions

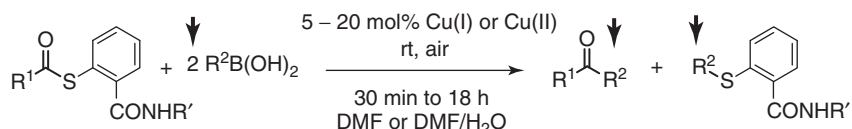
How might a copper thiolate be transformed into a copper oxygenate a neutral pH? Taniguchi [43, 44] disclosed results suggesting that copper thiolates, Cu(I)–SR, react with boronic acids, R'B(OH)<sub>2</sub>, when exposed to air (oxygen) to generate thioethers, R–S–R'. This observation implies that a desulfitative cross-coupling using only catalytic quantities of the Cu source could be achieved if the reaction were carried out open to air, but with a second (sacrificial) equivalent of the boronic acid present to scavenge the thiolate as a thioether. This logical analysis proved fruitful and led to the discovery of a novel aerobic coupling of thiol esters and boronic acids that uses only catalytic quantities of Cu to effect the reaction (Scheme 23.5) [45].

Interesting attributes of this new reaction are (i) the use of only Cu, and not Pd, to catalyze the desulfitative carbon–carbon bond formation, (ii) the strict requirement for a Cu-coordinating functional group on the sulfur-pendant, and (iii) the very mild (room temperature, neutral pH) reaction conditions. S-acylthiosalicylamides proved to be particularly effective substrates for this chemistry. A study of peptidic S-acylthiosalicylamides was used to demonstrate broad functional group compatibility and high stereoretention (Scheme 23.6) [46].

The mechanism of this new aerobic, Cu-catalyzed desulfitative coupling is thought to proceed through a three-stage process (Fig. 23.5) [41] commencing with oxidation of a Cu(I) S-acylthiosalicylamide complex **A** to generate the dimeric species **B**, L'Cu<sup>II/III</sup>-(O<sub>2</sub>)-Cu<sup>II/III</sup>L', for which the side-on  $\mu\text{-}\eta^2\text{:}\eta^2$ -peroxo, bis-( $\mu\text{-O}$ ), and trans end-on  $\mu\text{-}\eta^1\text{:}\eta^1$ -superoxo are known to be dominant bonding motifs [47–50]. A subsequent transmetalation from the boronic acid to the higher oxidation state Cu center generates an intermediate **C** in which a nucleophilic organocopper, R<sup>2</sup>-Cu is positioned in close proximity to the electrophilic thiol ester. An internal transfer produces the anticipated ketone product, R<sup>1</sup>-CO-R<sup>2</sup>, and a



**Scheme 23.4** The catalytic challenge.



**Scheme 23.5** Cu-catalyzed aerobic desulfitative catalysis of S-acylthiosalicylamides.



**Scheme 23.6** Aerobic, room temperature coupling of peptidic *S*-acylthiosalicylamides.

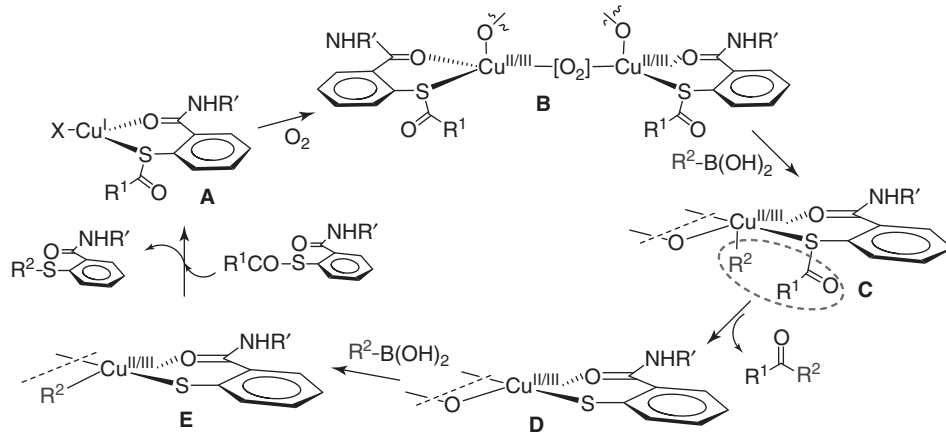


**Figure 23.5** Mechanism of the aerobic, Cu-catalyzed desulfitative coupling.

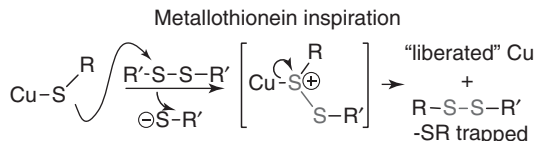
higher oxidation state copper thiolate **D**. The catalytic cycle is completed in stage 3 when the second (sacrificial) equivalent of the boronic acid reacts via transmetalation-reductive elimination with the higher oxidation state copper thiolate **D** to generate **E**, which undergoes reductive elimination to scavenge the thiolate as a thioether and to regenerate a Cu<sup>I</sup>-oxygenate (**A**, X = oxygenate), which continues the cycle.

In contrast to the first generation of Pd-catalyzed, Cu-mediated desulfitative couplings, it should be noted that the aerobic, Cu-catalyzed process does not require the presence of Pd to cleave (and activate) a C–S bond through an oxidative addition. The thiol ester is a native electrophile and possesses sufficient inherent electrophilic reactivity when activated by coordination to copper to capture an *in situ* generated organocupper intermediate. It is therefore likely that the aerobic, Cu-catalyzed desulfitative coupling system will not be broadly extensible to other thioorganics (that require activation by oxidation addition to low valent Pd), although it could prove highly useful for the molecular engineering of complex thiol esters such as those derived from proteins and complex peptides.

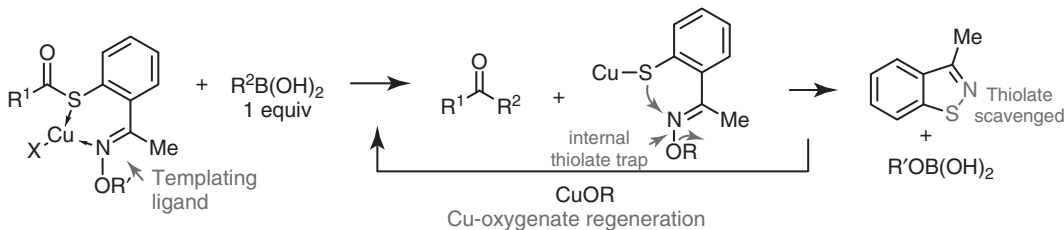
### 23.3.2 Cu-Desulfitative Catalysis under Anaerobic Conditions

The mechanistic requirement of 2 equiv of boronic acid to drive the aerobic, Cu-catalyzed coupling with *S*-acylthiosalicylamides to completion will not be problematic in those cases where the thiol ester partner is far more precious than the boronic acid. However, there are many systems where sacrificing an equivalent of the boronic acid is not appropriate—in those cases where the boronic acid is precious, or where the boronic acid is used as a linker that is structurally integrated to the coupling partner for the thiol esters (i.e., coupling to surfaces via boronic acid linkers or ligations using boronic acid-modified proteins). For these systems, if they are to be used in bioconjugative applications, it is essential to develop mild, pH-neutral Cu (or Pd) catalytic systems that require only 1 equiv of the boronic acid partner. In order to render Cu(I) catalytically viable in a desulfitative chemical transformation without sacrificing a second equivalent of the boronic acid coupling agent, a small molecule analog of the metallothionein (MT) protein system was designed [36]. MTs are small proteins capable of binding up to 7 equiv of mono and divalent metals such as Cu(I) and Zn(II) [51]. Although positioned within a tightly binding thiol/thiolate-rich ligand environment, a thiophilic metal is rapidly released from MT binding when a MT is exposed to an exogenous disulfide (Scheme 23.7) [52, 53].

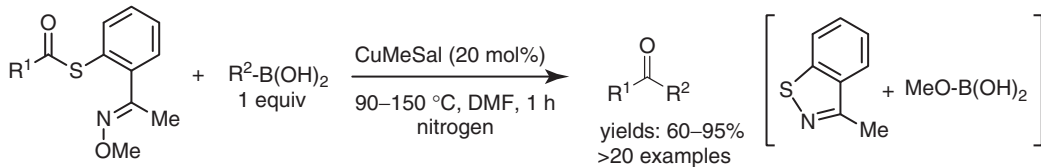
An “MT mimic” was constructed in which the exogenous S–S reactant of the biological system was replaced with an N–O moiety of an oxime integrated into thiolate pendant residue (Scheme 23.8).



Scheme 23.7 Cu-thiolate activation by exogenous disulfide in metallothioneins.



Scheme 23.8 Cu-catalyzed desulfitative catalysis using metallothionein mimics.



Scheme 23.9 Cu-catalyzed anaerobic desulfitative ketone synthesis.

Through its oxime N–O bond the MT mimic internally provides a mild S-centered oxidation of a Cu(I) thiolate thereby converting the strongly bonding thiolate to a weakly bonding disulfide equivalent (in this case the S–N bond of the benzoisothiazole shown). This mild oxidative trapping of thiolate was also intended to continuously regenerate a catalytically viable “oxygenate” form of Cu(I) (and a stoichiometric oxygenate residue to pair with  $-\text{B}(\text{OH})_2$ ) so that a useful Cu(I)-catalyzed desulfitative carbon–carbon bond-forming reaction with boronic acids can ensue. Using only 1 equiv of the boronic acid (or an organostannane) the MT mimic provides an effective vehicle for the production of ketones using only catalytic quantities of Cu (Scheme 23.9).

### 23.4 CONCLUSION: APPROACHING AQUEOUS DESULFITATIVE REACTION CONDITIONS FOR BIOLOGICAL APPLICATIONS

As described above, two new Cu-catalyzed desulfitative transformations have been discovered that can be used for the construction of peptidyl ketones from peptidic thiol esters and boronic acids. Under aerobic reaction conditions, *S*-acylthiosalicylamides are effective and efficient, although 2 equiv of the boronic acid are mechanically required (Scheme 23.6). In comparison, *S*-acyl-2-mercaptoaryloximes function as MT mimics and can produce peptidyl ketones under anaerobic reaction conditions from only a single equivalent of boronic acid. The latter reaction is also efficient and general, but in its current design, it is only catalytically effective at elevated temperatures ( $>90^\circ\text{C}$ ).

Control experiments using stoichiometric quantities of Cu demonstrate that the carbon–carbon bond-forming step of both the aerobic and anaerobic reaction systems proceeds at room temperature (Fig. 23.6).

However, the two systems differ in the Cu-recycle step. The aerobic system recycles Cu for catalysis at room temperature, while Cu-recycle by internal trapping of the Cu-thiolate by the N–O bond of the MT mimic in the current anaerobic reaction system is not effective until the reaction temperature reaches  $90^\circ\text{C}$ . It is this latter step of the anaerobic MT mimic system that will need to be accomplished near room temperature if a biologically relevant variant of the chemistry is to be achieved. To accomplish this task logic suggests that use of a MT mimic substrate with a weaker N–O bond [54].

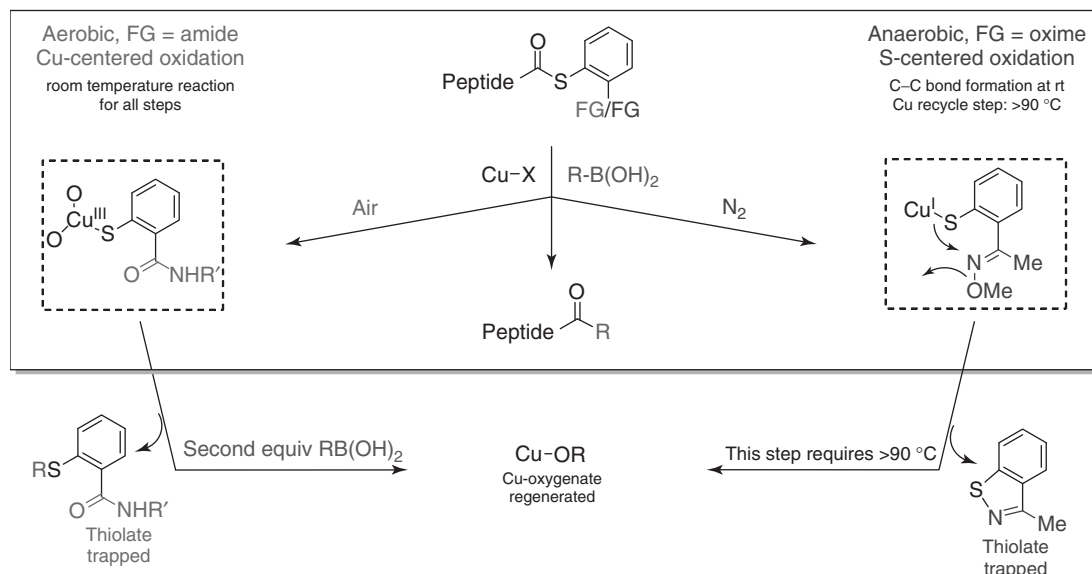
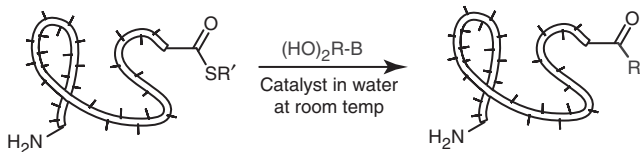


**Figure 23.6** Mechanisms of (a) the aerobic and (b) the anaerobic desulfutative catalysis. Water-solubilizing sites are in gray.



**Scheme 23.10** Proteo-ketones via bioconjugative desulfutative catalysis.

The next phase of development of desulfutative catalysis will focus on its use in the synthetic manipulation of proteins and complex peptides (Scheme 23.10). To achieve this goal, the following hurdles must be overcome: (i) the anaerobic catalysis using MT mimics must be modified for effective catalysis at room temperature and (ii) both the aerobic S-acylthiosalicylamide substrates and the anaerobic MT mimic substrates must be modified for effective reaction in water at room temperature.

For biological applications the metal-catalyzed desulfutative transformations must be made effective in pure water or in aqueous biological buffers as the reaction solvent. This will require the development of substrates that are not only water soluble, but that also retain their effectiveness in desulfutative reactions with boronic acids in both the aerobic and anaerobic reaction systems (Fig. 23.7) [54].

Finally, current efforts in defining water-soluble reactants for both the aerobic and anaerobic reaction systems will guide the use of the new catalytic desulfutative transformations in advanced “ketobioconjugations” as represented in Fig. 23.8 [54].

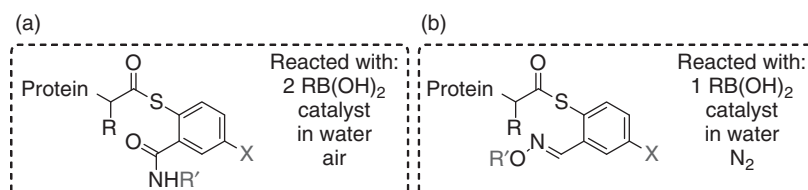


**Figure 23.7** Potential water-soluble substrates for desulfutative catalysis.

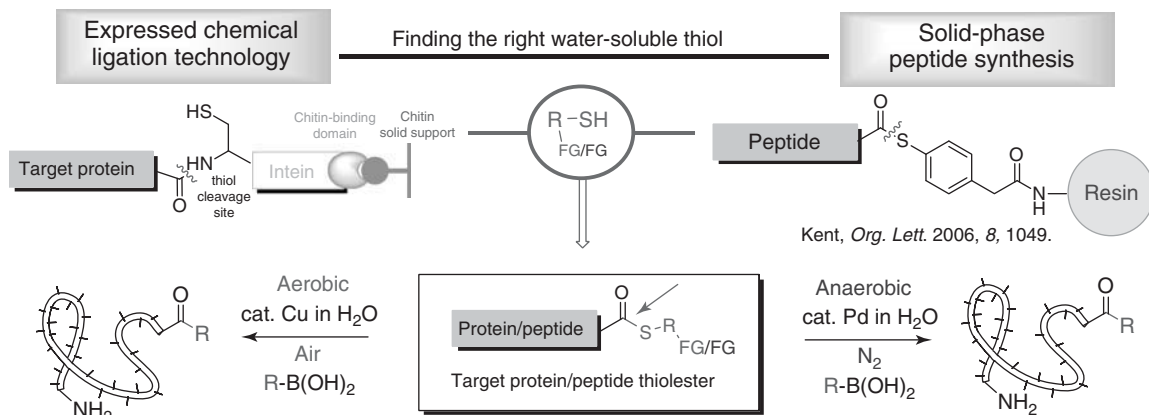


**Figure 23.8** Proposed “ketobioconjugation” of protein and peptide thiol esters.

## REFERENCES

1. Song, C. *Catal. Today* **2003**, *86*, 211.
2. Smith, B. M. *Chem. Soc. Rev.* **2008**, *37*, 470.
3. Melnychuk, S. A.; Neverov, A. A.; Brown, R. S. *Angew. Chem. Int. Ed.* **2006**, *45*, 1767.
4. Garnier-Amblard, E. C.; Liebeskind, L. S. In *Boronic Acids. Preparation and Applications in Organic Synthesis, Medicine and Materials*, 2nd ed.; Hall, D. G., Ed.; Wiley-VCH: Weinheim, Germany, **2011**; Vol. 2, p 363.
5. Prokopcová, H.; Kappe, O. C. *Angew. Chem. Int. Ed.* **2009**, *48*, 2276.
6. Dubbaka, S. R.; Vogel, P. *Angew. Chem. Int. Ed.* **2005**, *44*, 7674.
7. Hermanson, G. T. *Bioconjugate Techniques*, 2nd ed.; Elsevier: Amsterdam, **2008**.
8. Wenkert, E.; Ferreira, T. W.; Michelotti, E. L. *J. Chem. Soc. Chem. Commun.* **1979**, 637.
9. Wenkert, E.; Fernandes, J. B.; Michelotti, E. L.; Sllindel, C. *Synthesis* **1983**, 701.
10. Wenkert, E.; Leftin, M.; Michelotti, E. L. *J. Chem. Soc. Chem. Commun.* **1984**, 617.
11. Okamura, H.; Miura, M.; Takei, H. *Tetrahedron Lett.* **1979**, *20*, 43.
12. Fiandanese, V.; Marchese, G.; Naso, F.; Ronzini, L. *J. Chem. Soc. Chem. Commun.* **1982**, 647.
13. Fiandanese, V.; Miccoli, G.; Naso, F.; Ronzini, L. *J. Organomet. Chem.* **1986**, *312*, 343.
14. Cardelluccio, C.; Fiandanese, V.; Marchese, G.; Ronzini, L. *Tetrahedron Lett.* **1987**, *28*, 2053.
15. Fiandanese, V.; Marchese, G.; Mascolo, G.; Naso, F.; Ronzini, L. *Tetrahedron Lett.* **1988**, *29*, 3705.
16. Luh, T. Y. *Acc. Chem. Res.* **1991**, *24*, 257.
17. Tokuyama, H.; Yokoshima, S.; Yamashita, T.; Fukuyama, T. *Tetrahedron Lett.* **1998**, *39*, 3189.
18. Tokuyama, H.; Yokoshima, S.; Yamashita, T.; Lin, S.-C.; Li, L.; Fukuyama, T. *J. Braz. Chem. Soc.* **1998**, *9*, 381.
19. Fukuyama, T.; Tokuyama, H. *Aldrichimica Acta* **2004**, *37*, 87.
20. Ghosh, I.; Jacobi, P. A. *J. Org. Chem.* **2002**, *67*, 9304.
21. Roberts, W. P.; Ghosh, I.; Jacobi, P. A. *Can. J. Chem.* **2004**, *82*, 279.
22. Srogl, J.; Allred, G. D.; Liebeskind, L. S. *J. Am. Chem. Soc.* **1997**, *119*, 12376.
23. Zhang, S.; Marshall, D.; Liebeskind, L. S. *J. Org. Chem.* **1999**, *64*, 2796.
24. Savarin, C.; Srogl, J.; Liebeskind, L. S. *Org. Lett.* **2000**, *2*, 3229.
25. Dubbaka, S. R.; Vogel, P. *Angew. Chem. Int. Ed.* **2005**, *44*, 7674.
26. Sun, Q.; Suzenet, F.; Guillaumet, G. *J. Org. Chem.* **2010**, *75*, 3473.
27. Movassaghi, M.; Siegel, D. S.; Han, S. *Chem. Sci.* **2010**, *1*, 561.
28. Dandepally, S. R.; Williams, A. L. *Tetrahedron Lett.* **2010**, *51*, 5753.
29. Li, H.; He, A.; Falck, J. R.; Liebeskind, L. S. *Org. Lett.* **2011**, *13*, 3682.
30. Jin, W.; Du, W.; Yang, Q.; Yu, H.; Chen, J.; Yu, Z. *Org. Lett.* **2011**, *13*, 4272.

31. Garnier-Amblard, E. C.; Mays, S. G.; Arrendale, R. F.; Baillie, M. T.; Bushnev, A. S.; Culver, D. G.; Evers, T. J.; Holt, J. J.; Howard, R. B.; Liebeskind, L. S.; Menaldino, D. S.; Natchus, M. G.; Petros, J. A.; Ramaraju, H.; Reddy, G. P.; Liotta, D. C. *Med. Chem. Lett.* **2011**, *2*, 438.
32. Fuwa, H.; Noto, K.; Sasaki, M. *Org. Lett.* **2011**, *13*, 1820.
33. Břehová, P.; Česnek, M.; Dračínský, M.; Holý, A.; Janeba, Z. *Tetrahedron* **2011**, *67*, 7379.
34. Skipsey, M.; Knight, K. M.; Brazier-Hicks, M.; Dixon, D. P.; Steel, P. G.; Edwards, R. *J. Biol. Chem.* **2011**, *286*, 32268.
35. Modha, S. G.; Trivedi, J. C.; Mehta, V. P.; Ermolat'ev, D. S.; Van der Eycken, E. V. *J. Org. Chem.* **2011**, *76*, 846.
36. Zhang, Z.; Lindale, M. G.; Liebeskind, L. S. *J. Am. Chem. Soc.* **2011**, *133*, 6403.
37. Yeyeodu, S.; Gilyazova, N.; Huh, E. Y.; Dandepally, S. R.; Oldham, C.; Williams, A.; Ibeanu, G. *Cell. Mol. Neurobiol.* **2011**, *31*, 145.
38. Tatibouët, A.; Gosling, S.; Rollin, P. *Synthesis* **2011**, *2011*, 3649.
39. Kögler, M.; De Jonghe, S.; Herdewijn, P. *Tetrahedron Lett.* **2012**, *53*, 253.
40. Bouscary-Desforges, G.; Bombrun, A.; Augustine, J. K.; Bernardinelli, G.; Quattropani, A. *J. Org. Chem.* **2012**, *77*, 243.
41. Varela-Álvarez, A.; Liebeskind, L. S.; Musaev, D. G. *Organometallics* **2012**, *31*, 7958.
42. Shook, B. C.; Rassnick, S.; Wallace, N.; Crooke, J.; Ault, M.; Chakravarty, D.; Barbay, J. K.; Wang, A.; Powell, M. T.; Leonard, K.; Alford, V.; Scannevin, R. H.; Carroll, K.; Lampron, L.; Westover, L.; Lim, H. K.; Russell, R.; Branum, S.; Wells, K. M.; Damon, S.; Youells, S.; Li, X.; Beauchamp, D. A.; Rhodes, K.; Jackson, P. F. *J. Med. Chem.* **2012**, *55*, 1402.
43. Taniguchi, N. *Synlett* **2006**, *9*, 1351.
44. Taniguchi, N. *J. Org. Chem.* **2007**, *72*, 1241.
45. Villalobos, J. M.; Srogl, J.; Liebeskind, L. S. *J. Am. Chem. Soc.* **2007**, *129*, 15734.
46. Liebeskind, L. S.; Yang, H.; Li, H. *Angew. Chem. Int. Ed.* **2009**, *48*, 1417.
47. Mirica, L. M.; Ottenwaelder, X.; Stack, T. D. P. *Chem. Rev.* **2004**, *104*, 1013.
48. Chen, P.; Fujisawa, K.; Helton, M. E.; Karlin, K. D.; Solomon, E. I. *J. Am. Chem. Soc.* **2003**, *125*, 6394.
49. Henson, M. J.; Vance, M. A.; Zhang, C. X.; Liang, H.-C.; Karlin, K. D.; Solomon, E. I. *J. Am. Chem. Soc.* **2003**, *125*, 5186.
50. Mirica, L. M.; Rudd, D. J.; Vance, M. A.; Solomon, E. I.; Hodgson, K. O.; Hedman, B.; Stack, T. D. P. *J. Am. Chem. Soc.* **2006**, *128*, 2654.
51. Coyle, P.; Philcoxa, J. C.; Carey, L. C.; Rofea, A. M. *Cell. Mol. Life Sci.* **2002**, *59*, 627.
52. Maret, W. *Proc. Natl. Acad. Sci. U.S.A.* **1994**, *91*, 237.
53. Maret, W. *Neurochem. Int.* **1995**, *27*, 111.
54. Currently under study in the author's laboratory.



## SULFOXIDE REDOX CHEMISTRY WITH MOLYBDENUM CATALYSTS

MARIA JOSÉ CALHORDA\*

*Departamento de Química e Bioquímica, Centro de Química e Bioquímica, Faculdade de Ciências, Universidade de Lisboa, Lisboa, Portugal*

LUIS F. VEIROS

*Centro de Química Estrutural, Instituto Superior Técnico, Universidade de Lisboa, Lisboa, Portugal*

### 24.1 INTRODUCTION

The idea that transition metal complexes with metals in high formal oxidation states could catalyze reactions that are formally reductions was reported for the first time in relation with hydrosilylation of aldehydes or ketones promoted by Re(V) catalysts [1–3]. The traditional mechanism for hydrosilylation reactions started with an oxidative addition reaction of the bond to the metal, increasing its formal oxidation state by two units. Even though Re(V) can be oxidized to Re(VII), both experimental and computational studies proved that the mechanism was a different one, involving a [2+2] addition to a Re=O bond [3–5].

In this context, it was even more challenging to observe that a wide range of Mo(VI) complexes could also very efficiently catalyze the hydrosilylation of aldehydes and ketones [6]. Computational studies helped us to define a pathway that accounts for experimental results and proceeds via a hydride complex, once again formed by a [2+2] addition of a Si–H bond to Mo=O, followed by reaction of the active intermediate with the substrate in a stepwise way [7]. This reaction, based on Si–H activation, looked so promising, that we examined the possibility of using C–H or H–H bonds for analogous purposes. Density functional theory (DFT) calculations showed that the energy requirement for C–H activation was too high to be useful in these systems, but the activation of H–H bonds in cheaply available H<sub>2</sub> seemed feasible. Indeed, alkynes and sulfoxides could be reduced in the lab by Mo(VI) complexes in the presence of dihydrogen [8]. The list of related reactions expanded with the activation of P–H bonds to synthesize hydrophosphonates [9] and reduce imines, esters [10], sulfoxides, pyridine-*N*-oxides [11], and other substrates. As a generalization, one may reach the other extreme, namely, formal oxidation reactions, which involve the activation of the O–H bond of the so-called oxidant, often *t*BuOOH, other times H<sub>2</sub>O<sub>2</sub>, or others. In this view, the catalyst activates an X–H bond of a cocatalyst, promoter, oxidant, etc., which leads to an active species that depends on the electronegativity of X and the stability of [2+2] or [2+3] addition products. In the second step, the substrate reacts with the active species. We have reviewed these reactions occurring with Mo(VI), Re(V), or Re(VII) catalysts [12, 13].

In this work we analyze the role of MoO<sub>2</sub>Cl<sub>2</sub>, a coordinatively unsaturated Mo(VI) complex, which has been proven to oxidize sulfides and sulfoxides to sulfoxides and sulfones [14], respectively, in the presence of H<sub>2</sub>O<sub>2</sub>, while in the presence of boron derivatives, such as HBcat, sulfoxides can be reduced back to sulfides [12]. Other Mo(VI) complexes can catalyze the oxidation of sulfide to sulfone [15–19] but oxidation of sulfoxide to sulfone is less documented [20]. The reduction mechanism differs from the one published recently with Re(V) complexes, where Re(V) is formally oxidized to Re(VII) at some point of the catalytic cycle [21], which cannot happen to the Mo(VI) species.

The mechanisms discussed below were obtained from DFT calculations [22] using Gaussian 03 [23]. The oxidation of sulfides and sulfoxides by  $\text{MoO}_2\text{Cl}_2$  has been described within a study of several molybdenum-derived catalysts [24], while the reduction of sulfoxides and sulfones is reported for the first time in this work.

## 24.2 RESULTS AND DISCUSSION

### 24.2.1 Oxidation of Sulfides and Sulfoxides Promoted by $\text{MoO}_2\text{Cl}_2$

Several Mo(VI) compounds catalyze the epoxidation of olefins. The most famous system is used in the industrial ARCO–Halcon process for propylene epoxidation with *t*-butylhydroperoxide (TBHP) as the source of oxygen [25]. Complexes  $[\text{MoO}_2\text{Cl}_2(\text{N–N})]$ , where N–N are bidentate nitrogen ligands have been widely studied both experimentally [26] and computationally [27] as active catalysts in olefin epoxidation, as the available data suggested that the mechanism taking place, namely, the nature of the active species, was not the same as proposed earlier by Mimoun [28] or Sharpless [29]. A schematic representation of these two mechanisms is given in Fig. 24.1, which emphasizes the idea that the catalyst usually contained coordinated peroxide ligands.

Mo(VI) complexes represented by the family of  $[\text{MoO}_2\text{Cl}_2(\text{N–N})]$  complexes (**A**), however, showed no evidence for the participation of peroxide complexes, a fact that led to a reexamination of the mechanism. It was shown from DFT calculations and confirmed by  $^{17}\text{O}$  isotopic studies that the oxygen atom incorporated in the resulting epoxide originates from the TBHP molecule [27a], the active species being formed according to the O–H activation step ([2+2] addition of O–H to Mo=O) depicted in Fig. 24.2. Intermediate **B** isomerizes to another species containing an intramolecular hydrogen bond between the OH and the  $\beta$  oxygen of OOMe. The substrate adds to the Mo–O bond to form the epoxide and release *t*-butyl alcohol, regenerating the catalyst. The system loses activity as *t*-butyl alcohol in increasing concentration competes with TBHP for the catalyst [27b].

This system gave way to  $\text{CpMoO}_2\text{X}$  ( $\text{X} = \text{Cl}, \text{CH}_3$ ) (**C**), where the cyclopentadienyl Mo fragment is isolobal with  $(\text{N–N})\text{XMo}$  [14]. This complex can be easily prepared *in situ* from  $\text{CpMo}(\text{CO})_3\text{X}$  (**D**) and TBHP [30]. A variety of experimental (kinetic) [31] and DFT [32] studies, also including the  $\text{Cp}^*$  analogues [33], indicated that an important active

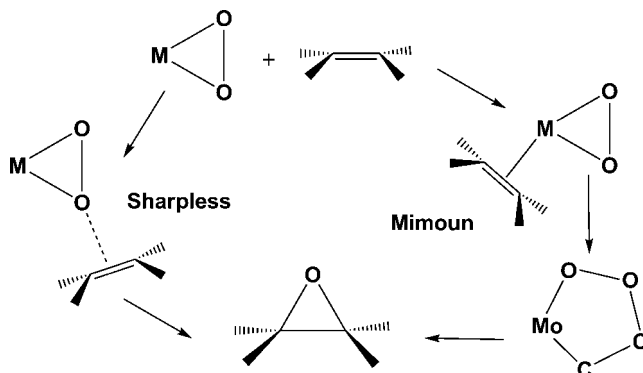


**Figure 24.1** The Mimoun and Sharpless mechanisms for olefin epoxidation.

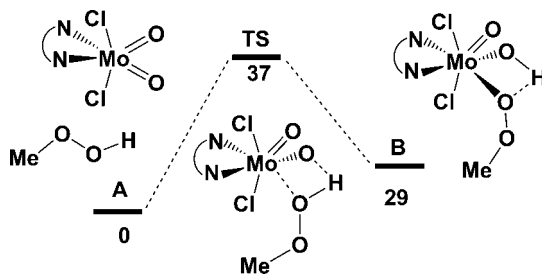


**Figure 24.2** [2+2] O–H addition to the Mo=O bond of  $[\text{MoO}_2\text{Cl}_2(\text{N–N})]$  (free energies in kcal/mol).

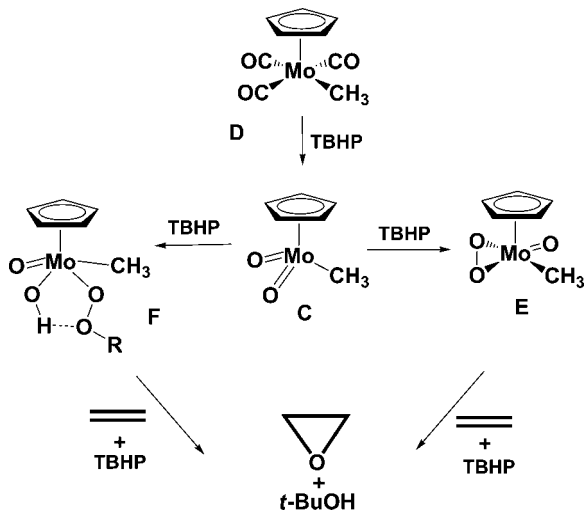


**Figure 24.3** Active intermediates in the olefin epoxidation reaction catalyzed by  $\text{CpMoO}_2(\text{CH}_3)$ .

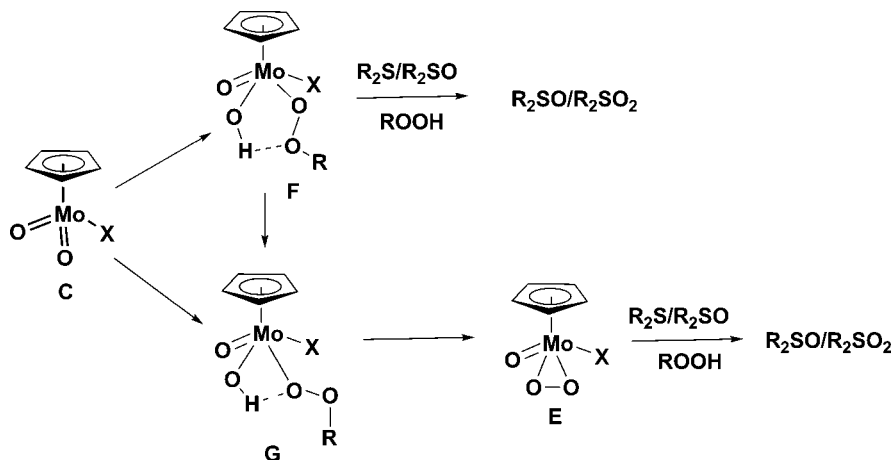


**Figure 24.4** Active intermediates in the oxidation of  $\text{R}_2\text{S}$  and  $\text{R}_2\text{SO}$  reaction catalyzed by  $\text{CpMoO}_2\text{X}$ .

species was **F** (or an isomer with a  $\text{OH}\cdots\text{O}_\alpha$  hydrogen bond, **G**) similar to **B**. The most relevant intermediates are represented in Fig. 24.3, and the most active species proved to be **F**, which derives from the dioxo complex **C**. The peroxy complex **E** is less active in this reaction, although it leads to oxidation when  $\text{X} = \text{CH}_3$  [33]. The situation is less clear when  $\text{X} = \text{Cl}$ .

The same system ( $\text{CpMoO}_2\text{X}$  formed *in situ* from  $\text{CpMo}(\text{CO})_3\text{X}$  (**D**) and TBHP) is active in the oxidation of sulfides and sulfoxides, both with  $\text{H}_2\text{O}_2$  and TBHP, and for  $\text{X} = \text{Cl}$  [15]. The reaction mechanism was investigated with DFT [24] in order to determine whether the same pathways were available for olefin and  $\text{R}_2\text{S}/\text{R}_2\text{SO}$  oxidation. In this study, a lower energy path for the conversion of **G** into the peroxy complex **E** was found by addition of one equivalent of TBHP, which is equivalent to the reaction of **C** with two molecules of TBHP. The same applies to  $\text{H}_2\text{O}_2$  as oxidant. This was not, however, the crucial step that determined the catalytic activity of the peroxy complex in epoxidation (Fig. 24.4).

The lowest energy pathway in these reactions occurs from the peroxy complex **E** rather than from the most active intermediate in epoxidation **F**, at least when  $\text{X} = \text{Cl}$ , with  $\text{R} = \text{H}$ ,  $\text{R}$  in  $\text{HOOR}$ . The oxidation of the substrate consists of the approach to the active species **E** and the removal of the oxygen, forming the product and regenerating the precursor **C** [24].

The two substrates could also undergo the same oxidation reaction when the catalyst was the simpler  $\text{MoO}_2\text{Cl}_2$  (**H**), in water, as reported in 2006. As the complex is electron deficient, a most likely species to exist is  $\text{MoO}_2\text{Cl}_2(\text{H}_2\text{O})_2$ . The reaction was studied by DFT, always keeping one explicit water molecule present in order to assist both hydrogen bond formation

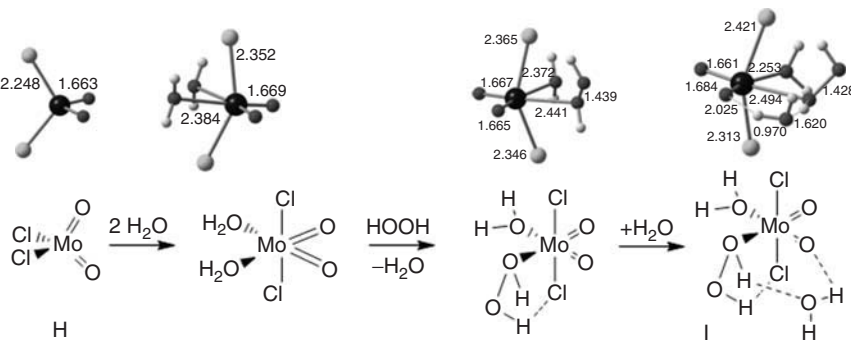


**Figure 24.5** Formation of the active intermediate **I** in the reaction of  $\text{MoO}_2\text{Cl}_2$  (**H**) with  $\text{H}_2\text{O}_2$  (relevant distances in Å).

and hydrogen atom transfer and therefore decrease calculated activation barriers. The formation of  $\text{MoO}_2\text{Cl}_2(\text{H}_2\text{O}_2)(\text{H}_2\text{O})$ , with one extra  $\text{H}_2\text{O}$  molecule (**I**) is depicted in Fig. 24.5 [24].

The only striking difference from the other systems referred to above is that the activation of the OH bond of the oxidant does not proceed all the way to cleavage. One oxygen binds the metal, but the ligand can be described as  $\eta^1\text{-O}(\text{H})\text{OH}$  instead of  $\eta^1\text{-OOH}$  as happened there. Notice that the added water molecule in **I** is hydrogen bonded to this oxygen, contributing to weakening the O–H bond of the peroxide. The activation of the substrate is shown in Fig. 24.6a for  $\text{Me}_2\text{S}$  (**I**, **J**, **K**) and Fig. 24.6b for  $\text{Me}_2\text{SO}$  (**I**<sub>O</sub>, **J**<sub>O</sub>, **K**<sub>O</sub>). The substrate approaches the active species forming a hydrogen bond, either  $\text{S}\cdots\text{HO}$  (**I**) or  $\text{O}\cdots\text{HO}$  (**I**<sub>O</sub>). The activation of the initial OH bond is complete in **J** (or **J**<sub>O</sub>) after the migration of the hydrogen to the  $\text{O}_\beta$ , the hydrogen bond network being modified accordingly. The energy calculated for the corresponding transition states (circa 25 kcal/mol) indicates an accessible process. The oxygen atom can then be captured by the substrate in an outer sphere process. In the transition state, the substrate rotates so that the sulfur atom can approach the accessible  $\text{O}_\alpha$ . The reaction is very similar for the two substrates,  $\text{Me}_2\text{S}$  and  $\text{Me}_2\text{SO}$  [24] and the slightly higher barrier observed for  $\text{Me}_2\text{SO}$  in the second step (**J**<sub>O</sub> to **K**<sub>O</sub>) can be assigned to steric repulsion.

#### 24.2.2 Reduction of Sulfoxides Promoted by $\text{MoO}_2\text{Cl}_2$

The catalytic reduction of a variety of substrates by Mo(VI) catalysts has been described in the introduction and is reviewed in Reference 13. The mechanism of such a reaction cannot involve an oxidative addition, but other options, such as [2+2] or [2+3] additions to the Mo=O bonds, are available (Fig. 24.7) [13].

The preference for a given type of addition depends both on the electronegativity of X and the stability of the products formed. When X =  $\text{SiR}_3$ , the [2+2] addition with formation of a hydride complex (Fig. 24.7, center) is significantly favored and the same is observed for X = H [8]. On the other hand, [3+2] addition is preferred in the activation of the P–H bonds in phosphonates [10].

The reduction of sulfoxides and ketones by  $\text{MoO}_2\text{Cl}_2$  was reported to take place in the presence of catecholborane ( $\text{HBcat}$ ) or  $\text{BH}_3\text{-THF}$ . This reaction occurs with high yields and in mild conditions but, as also happened when the catalyst was a Re(V) complex, it is not very atom efficient. Indeed, two equivalents of HBcat are needed to reduce one substrate and two secondary products,  $\text{H}_2$  and catBOBcat, are formed.

The [2+2] addition of the B–H bond in HBcat to the Mo=O bond of  $\text{MoO}_2\text{Cl}_2(\text{H}_2\text{O})_2$  (**L**) to form the hydride complex [13] can take place with an accessible energy, but the preferred is undoubtedly the [3+2] addition to the two oxide ligands to form OH and OBcat. Experimental studies indicate that the water molecules are substituted by two sulfoxide ligands. Therefore the complex  $\text{MoO}_2\text{Cl}_2(\text{Me}_2\text{SO})_2$  was taken as the initial species in the DFT study. The mechanism for the [3+2] addition of the borane reagent and the reduction of sulfoxide is shown in Fig. 24.8.

The HBcat molecule approaches the complex **L** in such a way that there is a weak interaction between one oxide and the B atom, which will give the new B–O bond in **M**. In the transition state connecting **L** and **M**, this bond is formed and the hydrogen from the B–H bond is transferred to the second oxide. Tridimensional pictures of the intermediates and transition states are given in Fig. 24.9. The S–O bond of the substrate has weakened significantly at this stage (**M**) and it breaks, releasing the reduced molecule,  $\text{Me}_2\text{S}$ . The S–O distance, initially 1.538 Å in **L**, has lengthened to 1.542 Å in **L'**, 1.547 Å in  $\text{TS}_{\text{LM}}$ , 1.587 Å in **M**, and 1.769 Å in the transition state  $\text{TS}_{\text{MN}}$ . The addition of HBcat contributes to weakening the S–O bond of the coordinated  $\text{Me}_2\text{SO}$ . Coordination by itself is not enough to activate it, as shown by the Wiberg indices [34] for the S–O bond going from 1.04 in **L'** to 0.98 in **M**, still indicative of a strong covalent bond.

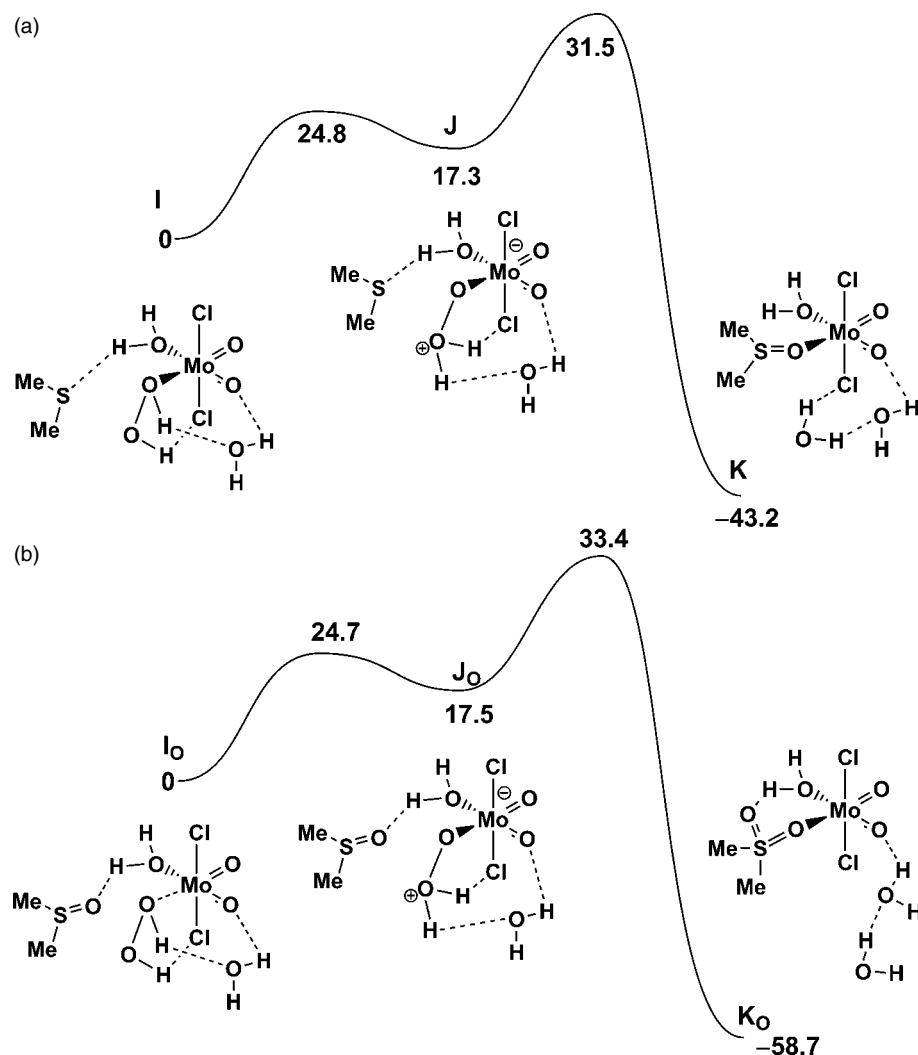


**Figure 24.6** Energy profile for sulfide (a) and sulfoxide (b) oxidation catalyzed by  $\text{MoO}_2\text{Cl}_2$  in the presence of  $\text{H}_2\text{O}_2$  ( $\Delta E$  with solvent effects given by the PCM model, kcal/mol).

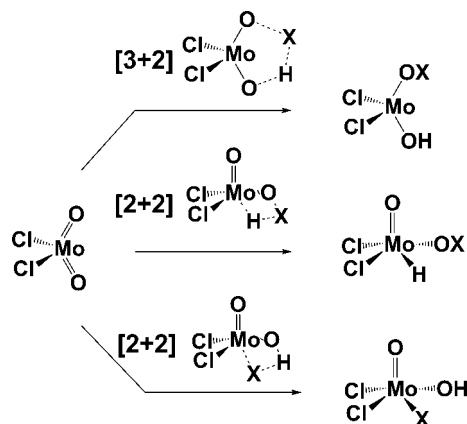


**Figure 24.7** Three pathways for  $\text{X}-\text{H}$  addition to  $\text{MoO}_2\text{Cl}_2$ : [3+2] and [2+2] additions to  $\text{Mo}=\text{O}$ .

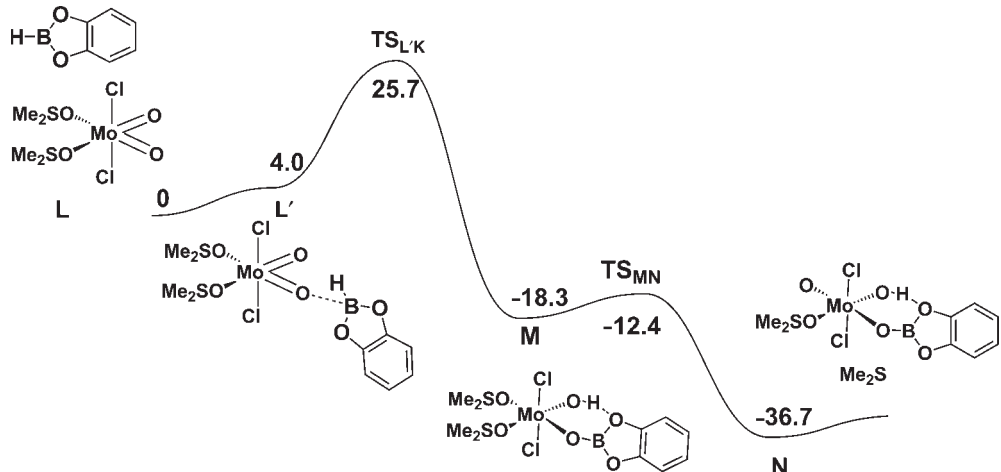


**Figure 24.8** Energy profile for sulfoxide reduction catalyzed by  $\text{MoO}_2\text{Cl}_2(\text{H}_2\text{O})_2$  (**L**) in the presence of HBcat ( $\Delta G$  with solvent effects given by the PCM model, kcal/mol).

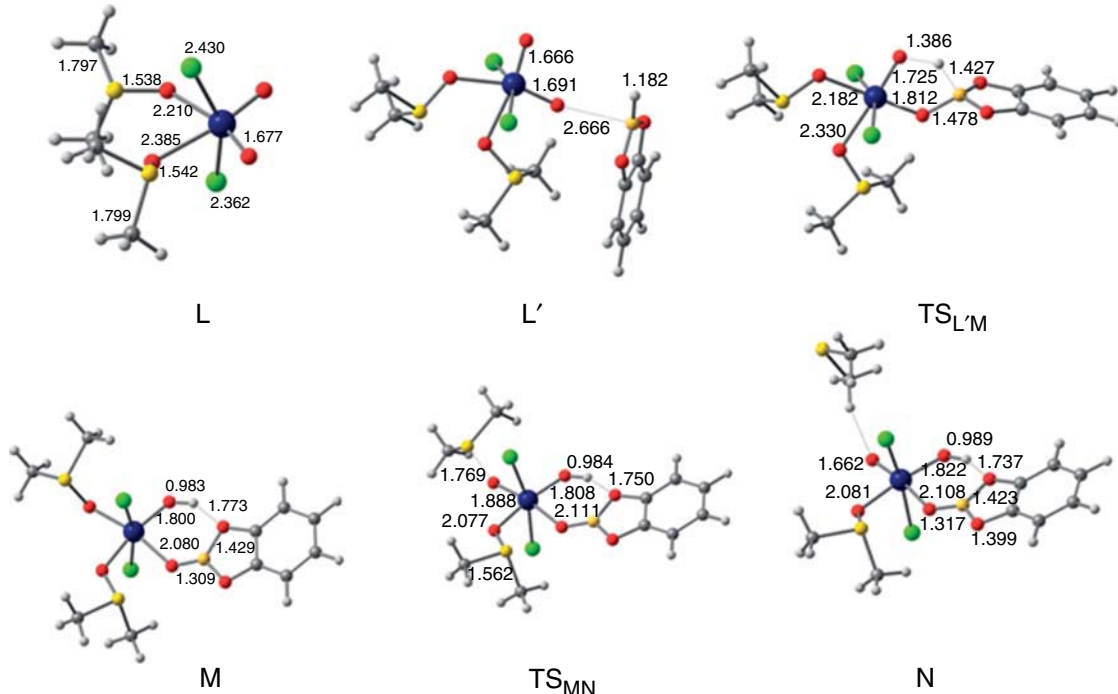


**Figure 24.9** Intermediates and transition states in the sulfoxide reduction catalyzed by  $\text{MoO}_2\text{Cl}_2(\text{H}_2\text{O})_2$  (**L**) with relevant distances (Å). (See insert for color representation of the figure.)

The second part of the reaction involves the recovery of the catalyst, as well as the formation of the secondary products,  $\text{H}_2$  and catBOBcat, and requires the participation of the second HBcat molecule. The formation of another B–O bond is the driving force for the reaction and there are several oxygen atoms in intermediate **N**, after releasing  $\text{Me}_2\text{S}$ . An exhaustive study of such processes has been performed. The most favorable approach is shown in Fig. 24.10, where the boron atom of the second HBcat comes close to the oxygen involved in the B–O bond of **N**. In this way, the catBOBcat is almost immediately formed. More difficult is to twist the new intermediate, so that the two hydrogen atoms come together and give rise to the dihydrogen molecule, also weakly bound in **P**. Release of the two species and addition of a new substrate molecule ( $\text{Me}_2\text{SO}$ ) regenerates the catalyst. The overall barrier is circa 7 kcal/mol and the reaction is exergonic.

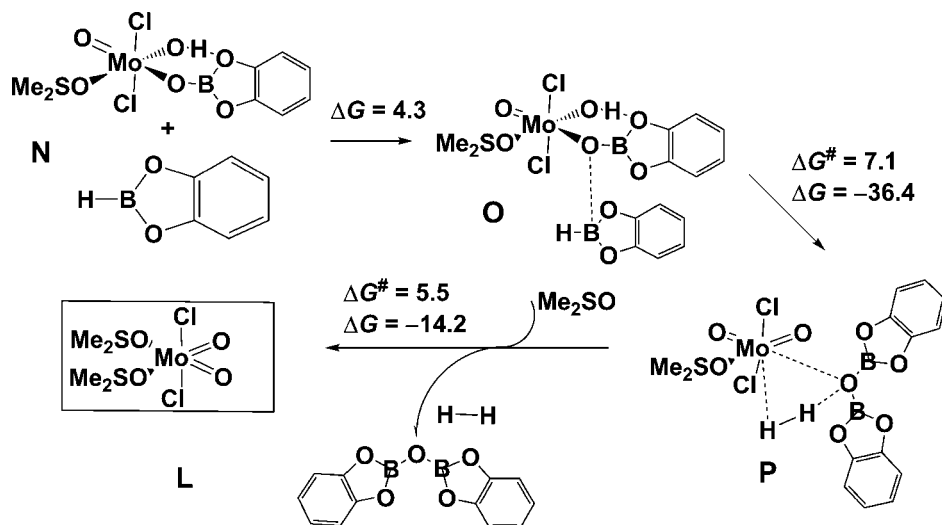


**Figure 24.10** The second step in the reduction of Me<sub>2</sub>SO catalyzed by MoO<sub>2</sub>Cl<sub>2</sub>(H<sub>2</sub>O)<sub>2</sub> (**L**) in the presence of HBcat (ΔG with solvent effects given by the PCM model, kcal/mol).

Several alternatives were checked, namely, the reaction mechanism assuming that HBcat adds to MoO<sub>2</sub>Cl<sub>2</sub>(H<sub>2</sub>O)<sub>2</sub>, the initial reagent, and only then does the sulfoxide substitute water. The barrier increases by 15 kcal/mol compared to the pathway described above, and thus this was discarded. Also, the [2+2] addition of HBcat to MoO<sub>2</sub>Cl<sub>2</sub>(Me<sub>2</sub>SO)<sub>2</sub> to form the hydride complex MoO(OBcat)Cl<sub>2</sub>(Me<sub>2</sub>SO)<sub>2</sub> has a barrier of 30.2 kcal/mol, compared to the [3+2] addition shown in Fig. 24.8 with only 25.7 kcal/mol.

The catalytic cycle for the reduction of Me<sub>2</sub>SO is given in Fig. 24.11 and it emphasizes the need for two molecules of HBcat and the formation of H<sub>2</sub> and catBOBcat in order to reduce one molecule of substrate. This reduction involves two electrons, from S(IV) in sulfoxide to S(II) in the final sulfide, which arise from the formation of H<sub>2</sub>—each hydrogen comes from one HBcat reagent. The addition of the first HBcat formally reduces Mo(VI) to Mo(IV) (intermediate **M**, Fig. 24.8). It is reoxidized back to Mo(VI) when Me<sub>2</sub>S is released, and neutral Me<sub>2</sub>SO is replaced by oxide O<sup>2-</sup>. The second HBcat avoids the metal, only reacting with coordinated ligands. This cycle, involving Mo(VI)/Mo(IV) therefore has similarities with the catalytic cycle driven by Re(V) [21] complexes, which become Re(VII) somewhere in the cycle for analogous reasons.

## 24.3 CONCLUSIONS

MoO<sub>2</sub>Cl<sub>2</sub> is a versatile catalyst, reducing and oxidizing sulfoxides under different conditions. The species in solution is MoO<sub>2</sub>Cl<sub>2</sub>(H<sub>2</sub>O)<sub>2</sub>. In order to oxidize sulfoxides (modeled in the calculations by Me<sub>2</sub>SO), the oxidant H<sub>2</sub>O<sub>2</sub> substitutes one water molecule, which remains close by, providing hydrogen bond assistance to the reaction, leading to a weakening of the O–H bond. The Me<sub>2</sub>SO substrate reacts with this intermediate in an outer sphere mechanism, pulling one oxygen atom from H<sub>2</sub>O<sub>2</sub> and releasing alcohol. The catalyst is simultaneously recovered.

HBcat acts as reductant in the reduction of sulfoxide. The H–B bond adds to the two oxygen atoms of the MoO<sub>2</sub>Cl<sub>2</sub>(Me<sub>2</sub>SO)<sub>2</sub> catalyst, obtained by adding Me<sub>2</sub>SO to MoO<sub>2</sub>Cl<sub>2</sub>(H<sub>2</sub>O)<sub>2</sub>. The S=O bond in the coordinated Me<sub>2</sub>SO is so weakened that Me<sub>2</sub>S is lost. A second molecule of HBcat is needed to recover the catalyst and during that reaction the side products, catBOBcat and H<sub>2</sub>, detected experimentally, are produced.

## 24.4 COMPUTATIONAL DETAILS

The mechanism of the reduction of sulfoxides promoted by MoO<sub>2</sub>Cl<sub>2</sub> was calculated using the Gaussian 03 software package [23], and the PBE0 functional, without symmetry constraints. That functional uses a hybrid, generalized gradient approximation (GGA), including 25% mixture of Hartree–Fock [35] exchange with DFT [22] exchange-correlation, given by the Perdew, Burke, and Ernzerhof functional (PBE) [36]. The optimized geometries were obtained with the LanL2DZ basis

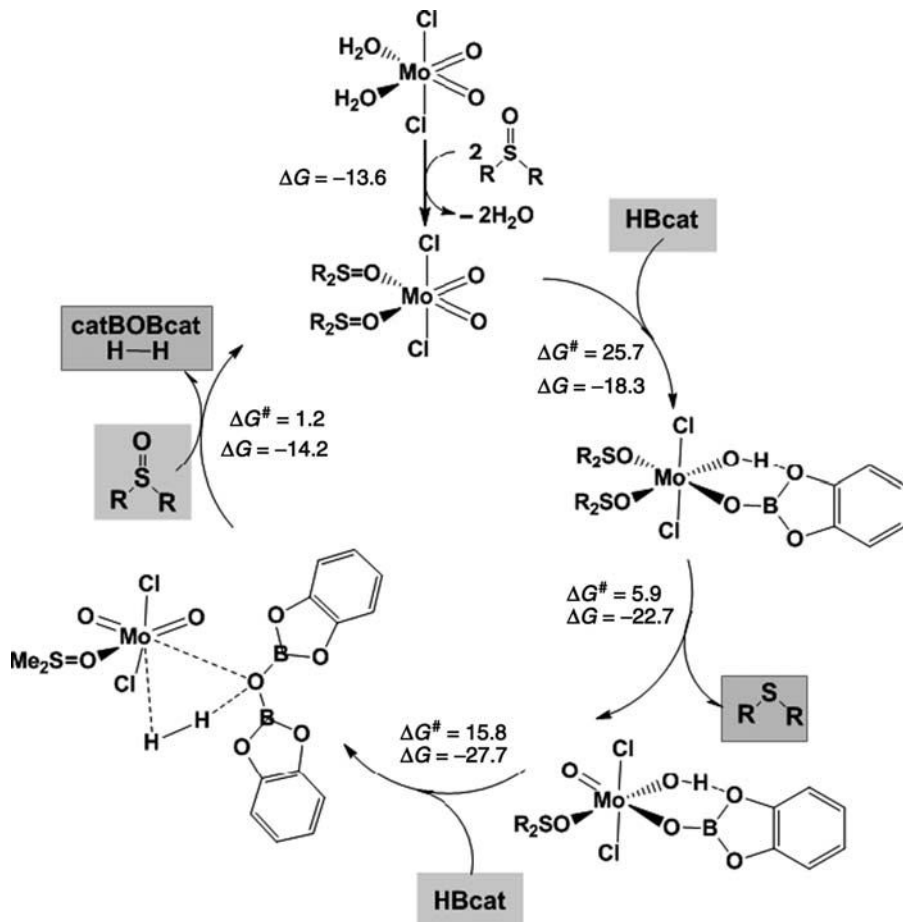


**Figure 24.11** The catalytic cycle for the reduction of  $\text{Me}_2\text{SO}$  catalyzed by  $\text{MoO}_2\text{Cl}_2(\text{H}_2\text{O})_2$  (**L**) in the presence of  $\text{HBcat}$  ( $\Delta G$  with solvent effects given by the PCM model, kcal/mol).

set [37] augmented with an f-polarization function [38] for Mo, and a standard 6-31G(d,p) [39] for the remaining elements (basis b1). Transition state optimizations were performed with the synchronous transit-guided quasi-Newton method (STQN) developed by Schlegel et al. [40], following extensive searches of the potential energy surface. Frequency calculations were performed to confirm the nature of the stationary points, yielding one imaginary frequency for the transition states and none for the minima. Each transition state was further confirmed by following its vibrational mode downhill on both sides and obtaining the minima presented on the energy profile. The electronic energies ( $E_{\text{b}1}$ ) obtained at the PBE0/b1 level of theory were converted to free energy at 298.15 K and 1 atm ( $G_{\text{b}1}$ ) by using zero point energy and thermal energy corrections based on structural and vibration frequency data calculated at the same level. Natural population analysis (NPA) [41] and the resulting Wiberg indices [34] were used to study the electronic structure and bonding of the optimized species.

Single-point energy calculations were performed using an improved basis set (basis b2) and the geometries optimized at the PBE0/b1 level. Basis b2 consisted of the 3-21G set [42] with an extra f-polarization function [38] for Mo, and a standard 6-311++G(d,p) [43] for the remaining elements. Solvent effects (THF) were considered in the PBE0/b2//PBE0/b1 energy calculations using the polarizable continuum model (PCM) initially devised by Tomasi and coworkers [44] as implemented on the Gaussian 03 [45]. The molecular cavity was based on the united atom topological model applied on UAHF radii, optimized for the HF/6-31G(d) level.

The free-energy values presented in the text ( $G_{\text{b}2}^{\text{soln}}$ ) were derived from the electronic energy values obtained at the PBE0/b2//PBE0/b1 level, including solvent effects ( $E_{\text{b}2}^{\text{soln}}$ ), according to the following expression:

$$G_{\text{b}2}^{\text{soln}} = E_{\text{b}2}^{\text{soln}} + G_{\text{b}1} - E_{\text{b}1}$$

Three-dimensional representations were obtained with Chemcraft [46].

## ACKNOWLEDGMENT

We thank Fundação para a Ciência e Tecnologia, Portugal, for financial support (Projects PEst-OE/QUI/UI0612/2011-2012, PEst-OE/QUI/UI0100/2011-2012 and PTDC/QUI-QUI/099389/2008).

## REFERENCES

- Kennedy-Smith, J. J.; Nolin, K. A.; Gunterman, H. P.; Toste, F. D. *J. Am. Chem. Soc.* **2003**, *125*, 4056.
- (a) Du, G.; Abu-Omar, M. M. *Organometallics* **2006**, *25*, 4920; (b) Reis, P. M.; Royo, B. *Catal. Commun.* **2007**, *8*, 1057.
- Nolin, K. A.; Krumper, J. R.; Pluth, M. D.; Bergman, R. G.; Toste, F. D. *J. Am. Chem. Soc.* **2007**, *129*, 14684.
- Chung, L. W.; Lee, H. G.; Lin, Z.; Wu, Y. *J. Org. Chem.* **2006**, *71*, 6000.
- (a) Ison, E. A.; Trivedi, E. R.; Corbin, R. A.; Abu-Omar, M. M. *J. Am. Chem. Soc.* **2005**, *127*, 15374; (b) Du, G.; Fanwick, P. E.; Abu-Omar, M. M. *J. Am. Chem. Soc.* **2007**, *129*, 5180.
- (a) Fernandes, A. C.; Fernandes, R.; Romão, C. C.; Royo, B. *Chem. Commun.* **2005**, 213; (b) Reis, P. M.; Romão, C. C.; Royo, B. *Dalton Trans.* **2006**, 1842.
- Costa P. J.; Romão C. C.; Fernandes A. C.; Reis P. M.; Calhorda M. J. *Chem.-Eur. J.* **2007**, *13*, 3934.
- Reis, P. M.; Costa, P. J.; Romão, C. C.; Fernandes, J. A.; Calhorda, M. J.; Royo, B. *Dalton Trans.* **2008**, 1727.
- Noronha, R. G.; Costa, P. J.; Romão, C. C.; Calhorda, M. J.; Fernandes, A. C. *Organometallics* **2009**, *28*, 6206.
- (a) Fernandes, A. C.; Romão, C. C. *Tetrahedron Lett.* **2005**, *46*, 8881; (b) Fernandes, A. C.; Romão, C. C. *J. Mol. Catal. A-Chem.* **2006**, *253*, 96.
- Fernandes, A. C.; Romão, C. C. *Tetrahedron* **2006**, *62*, 9650.
- Calhorda, M. J.; Costa, P. J. *Dalton Trans.* **2009**, 8155.
- Calhorda, M. J.; Costa, P. J. *Curr. Org. Chem.* **2012**, *16*, 65.
- Jeyakumar, K.; Chand, D. K. *Tetrahedron Lett.* **2006**, *47*, 4573.
- Bonchio, M.; Carofiglio, T.; Di Furia, F.; Fornasier, R. *J. Org. Chem.* **1995**, *60*, 5986.
- Batigalhia, F.; Zaldini-Hernandes, M.; Ferreira, A. G.; Malvestiti, I.; Cass, Q. B. *Tetrahedron* **2001**, *57*, 9669.
- (a) Gharah, N.; Chakraborty, S.; Mukherjee, A. K.; Bhattacharyya, R. *Inorg. Chim. Acta* **2009**, *362*, 1089; (b) Maiti, S. K.; Banerjee, S.; Mukherjee, A. K.; Malik, K. M. A.; Bhattacharyya, R. *New J. Chem.* **2005**, *29*, 554.
- Yang, C.; Jin, Q.; Zhang, H.; Liao, J.; Zhu, J.; Yu, B.; Deng, J. *Green Chem.* **2009**, *11*, 1401.
- Ciclosi, M.; Dinoi, C.; Gonsalvi, L.; Peruzzini, M.; Manoury, E.; Poli, R. *Organometallics* **2008**, *27*, 2281.
- (a) Al-Maksoud, W.; Daniele, S.; Sorokin, A. B. *Green Chem.* **2008**, *10*, 447; (b) Xian-Ying, S.; Jun-Fa, W. *J. Mol. Catal. A: Chem.* **2008**, *280*, 142; (c) Jeyakumar, K.; Chakravarthy, R. D.; Chand, D. K. *Catal. Commun.* **2009**, *10*, 1948.
- Fernandes, A. C.; Fernandes, J. A.; Romão, C. C.; Veiros, L. F.; Calhorda, M. J. *Organometallics* **2010**, *29*, 5517.
- Parr, R. G.; Yang, W. *Density Functional Theory of Atoms and Molecules*; Oxford University Press: New York, **1989**.
- Gaussian 03*, Revision C.02, Frisch, M. J.; Trucks, G. W.; Schlegel, H. B.; Scuseria, G. E.; Robb, M. A.; Cheeseman, J. R.; Montgomery, Jr., J. A.; Vreven, T.; Kudin, K. N.; Burant, J. C.; Millam, J. M.; Iyengar, S. S.; Tomasi, J.; Barone, V.; Mennucci, B.; Cossi, M.; Scalmani, G.; Rega, N.; Petersson, G. A.; Nakatsuji, H.; Hada, M.; Ehara, M.; Toyota, K.; Fukuda, R.; Hasegawa, J.; Ishida, M.; Nakajima, T.; Honda, Y.; Kitao, O.; Nakai, H.; Klene, M.; Li, X.; Knox, J. E.; Hratchian, H. P.; Cross, J. B.; Adamo, C.; Jaramillo, J.; Gomperts, R.; Stratmann, R. E.; Yazayev, O.; Austin, A. J.; Cammi, R.; Pomelli, C.; Ochterski, J. W.; Ayala, P. Y.; Morokuma, K.; Voth, G. A.; Salvador, P.; Dannenberg, J. J.; Zakrzewski, V. G.; Dapprich, S.; Daniels, A. D.; Strain, M. C.; Farkas, O.; Malick, D. K.; Rabuck, A. D.; Raghavachari, K.; Foresman, J. B.; Ortiz, J. V.; Cui, Q.; Baboul, A. G.; Clifford, S.; Cioslowski, J.; Stefanov, B. B.; Liu, G.; Liashenko, A.; Piskorz, P.; Komaromi, I.; Martin, R. L.; Fox, D. J.; Keith, T.; Al-Laham, M. A.; Peng, C. Y.; Nanayakkara, A.; Challacombe, M.; Gill, P. M. W.; Johnson, B.; Chen, W.; Wong, M. W.; Gonzalez, C.; Pople, J. A. Gaussian, Inc., Wallingford CT, **2004**.
- Veiros, L. F.; Gamelas, C. A.; Calhorda, M. J.; Romão, C. C. *Organometallics* **2011**, *30*, 1454.
- (a) Brégeault, J.-M. *Dalton Trans.* **2003**, 3289–3302; (b) Jørgensen, K. A. *Chem. Rev.* **1989**, *89*, 431.
- (a) Groarke, M.; Gonçalves, I. S.; Herrmann, W. A.; Kühn, F. E. *J. Organomet. Chem.* **2002**, *649*, 108; (b) Valente, A. A.; Moreira, J.; Lopes, A. D.; Pillinger, M.; Nunes, C. D.; Romão, C. C.; Kühn, F. E.; Gonçalves, I. S. *New J. Chem.* **2004**, *28*, 308; (c) Valente, A. A.; Petrovski, Z.; Branco, L. C.; Afonso, C. A. M.; Pillinger, M.; Lopes, A. D.; Romão, C. C.; Nunes, C. D.; Gonçalves, I. S. *J. Mol. Catal. A: Chemical* **2004**, *218*, 5; (d) Al-Ajlouni, A. M.; Valente, A. A.; Nunes, C. D.; Pillinger, M.; Santos, T. M.; Zhao, J.; Romão, C. C.; Gonçalves, I. S.; Kühn, F. E. *Eur. J. Inorg. Chem.* **2005**, 1716.

27. (a) Kühn, F. E.; Groarke, M.; Bencze, É.; Herdtweck, E.; Prazeres, A.; Santos, A. M.; Calhorda, M. J.; Romão, C. C.; Gonçalves, I. S.; Lopes, A. D.; Pillinger, M. *Chem.-Eur. J.* **2002**, *8*, 2370; (b) Veiros, L. F.; Prazeres, A.; Costa, P. J.; Romão, C. C.; Kühn, F. E.; Calhorda, M. J. *Dalton Trans.* **2006**, 1383.
28. Mimoun, H.; Chaumette, P.; Mignard, M.; Saussine, L.; Fischer, J.; Weiss, R. *New J. Chem.* **1983**, *7*, 467.
29. Sharpless, K. B.; Townsend, J. M.; Williams D. R. *J. Am. Chem. Soc.* **1972**, *94*, 295.
30. (a) Abrantes, M.; Santos, A. M.; Mink, J.; Kühn, F. E.; Romão, C. C. *Organometallics* **2003**, *22*, 2112; (b) Zhao, J.; Santos, A. M.; Herdtweck, E.; Kühn, F. E. *J. Mol. Catal. A* **2004**, *222*, 265; (c) Valente, A. A.; Seixas, J. D.; Gonçalves, I. S.; Abrantes, M.; Pillinger, M.; Romão, C. C. *Catal. Lett.* **2005**, *101*, 127; (d) Martins, A. M.; Romão, C. C.; Abrantes, M.; Azevedo, M. C.; Cui, J.; Dias, A. R.; Duarte, M. T.; Lemos, M. A.; Lourenço, T.; Poli, R. *Organometallics* **2005**, *24*, 2582; (e) Freund, C.; Abrantes, M. A.; Kühn, F. E. *J. Organomet. Chem.* **2006**, *691*, 3718. (f) Zhao, J.; Herdtweck, E.; Kühn, F. E. *J. Organomet. Chem.* **2006**, *691*, 2199. (g) Abrantes, M. A.; Sakthivel, A.; Romão, C. C.; Kühn, F. E. *J. Organomet. Chem.* **2006**, *691*, 3137. (h) Kühn, F. E.; Santos, A. M.; Abrantes, M. *Chem. Rev.* **2006**, *106*, 2455.
31. Al-Ajlouni, A.; Veljanovski, D.; Capapé, A.; Zhao, J.; Herdtweck, E.; Calhorda, M. J.; Kühn F. E. *Organometallics* **2009**, *28*, 639.
32. Costa, P. J.; Calhorda, M. J.; Kühn, F. E. *Organometallics* **2010**, *29*, 303.
33. (a) Trost, M. K.; Bergman, R. G. *Organometallics* **1991**, *10*, 1172; (b) Pratt, M.; Harper, J. B.; Colbran, S. B. *Dalton Trans.* **2007**, 2746; (c) Comas-Vives, A.; Lledós, A.; Poli, R. *Chem. Eur. J.* **2010**, *16*, 2147.
34. (a) Wiberg, K. B. *Tetrahedron* **1968**, *24*, 1083; (b) Wiberg indices are electronic parameters related to the electron density between atoms. They can be obtained from a Natural Population Analysis and provide an indication of the bond strength.
35. Hehre, W. J.; Radom, L.; Schleyer, P. v. R.; Pople, J. A. *Ab Initio Molecular Orbital Theory*, John Wiley & Sons, NY, **1986**.
36. (a) Perdew, J. P.; Burke, K.; Ernzerhof, M. *Phys. Rev. Lett.* **1997**, *78*, 1396; (b) Perdew, J. P. *Phys. Rev. B* **1986**, *33*, 8822.
37. (a) Dunning Jr., T. H.; Hay, P. J. *Modern Theoretical Chemistry*; Schaefer, H. F. III Ed.; Vol. 3, New York: Plenum, **1976**, p 1; (b) Hay P. J.; Wadt, W. R. *J. Chem. Phys.* **1985**, *82*, 270; (c) Wadt W. R.; Hay, P. J. *J. Chem. Phys.* **1985**, *82*, 284; (d) Hay, P. J.; Wadt, W. R. *J. Chem. Phys.* **1985**, *82*, 2299.
38. Ehlers, A. W.; Böhme, M.; Dapprich, S.; Gobbi, A.; Höllwarth, A.; Jonas, V.; Köhler, K. F.; Stegmann, R.; Veldkamp A.; Frenking, G. *Chem. Phys. Lett.* **1993**, *208*, 111.
39. (a) Ditchfield, R.; Hehre W. J.; Pople, J. A. *J. Chem. Phys.* **1971**, *54*, 724; (b) Hehre, W. J.; Ditchfield, R.; Pople, J. A. *J. Chem. Phys.* **1972**, *56*, 2257; (c) Hariharan, P. C.; Pople, J. A. *Mol. Phys.* **1974**, *27*, 209; (d) Gordon, M. S. *Chem. Phys. Lett.* **1980**, *76*, 163; (e) Hariharan, P. C.; Pople, J. A. *Theor. Chim. Acta* **1973**, *28*, 213.
40. (a) Peng, C.; Ayala, P. Y.; Schlegel, H. B.; Frisch, M. J. *J. Comp. Chem.*, **1996**, *17*, 49; (b) Peng, C.; Schlegel, H. B. *Israel J. Chem.*, **1994**, *33*, 449.
41. (a) Carpenter, J. E.; Weinhold, F. *J. Mol. Struct. (Theochem)* **1988**, *169*, 41; (b) Carpenter, J. E. PhD thesis, University of Wisconsin, Madison, WI, **1987**; (c) Foster, J. P.; Weinhold, F. *J. Am. Chem. Soc.* **1980**, *102*, 7211; (d) Reed, A. E.; Weinhold, F. *J. Chem. Phys.* **1983**, *78*, 4066; (e) Reed, A. E.; Weinhold, F. *J. Chem. Phys.* **1983**, *78*, 1736; (f) Reed, A. E.; Weinstock, R. B.; Weinhold, F. *J. Chem. Phys.* **1985**, *83*, 735; (g) Reed, A. E.; Curtiss, L. A.; Weinhold, F. *Chem. Rev.* **1988**, *88*, 899; (h) Weinhold, F.; Carpenter, J. E. *The Structure of Small Molecules and Ions*, Plenum, NY **1988**, p. 227.
42. (a) Binkley, J. S.; Pople, J. A.; Hehre, W. J. *J. Am. Chem. Soc.* **1980**, *102*, 939; (b) Gordon, M. S.; Binkley, J. S.; Pople, J. A.; Pietro, W. J.; Hehre, W. J. *J. Am. Chem. Soc.* **1982**, *104*, 2797; (c) Pietro, W. J.; Franci, M. M.; Hehre, W. J.; Defrees, D. J.; Pople, J. A.; Binkley, J. S. *J. Am. Chem. Soc.* **1982**, *104*, 5039; (d) Dobbs, K. D.; Hehre, W. J. *J. Comp. Chem.* **1986**, *7*, 359; (e) Dobbs, K. D.; Hehre, W. J. *J. Comp. Chem.* **1987**, *8*, 861; (f) Dobbs, K. D.; Hehre, W. J. *J. Comp. Chem.* **1987**, *8*, 880.
43. (a) McClean, A. D.; Chandler, G. S. *J. Chem. Phys.* **1980**, *72*, 5639; (b) Krishnan, R.; Binkley, J. S.; Seeger, R.; Pople, J. A. *J. Chem. Phys.* **1980**, *72*, 650; (c) Wachters, A. J. H. *J. Chem. Phys.* **1970**, *52*, 1033; (d) Hay, P. J. *J. Chem. Phys.* **1977**, *66*, 4377; (e) Raghavachari, K.; Trucks, G. W. *J. Chem. Phys.* **1989**, *91*, 1062; (f) Binning Jr., R. C.; Curtiss, L. A. *J. Comp. Chem.* **1990**, *11*, 1206; (g) McGrath, M. P.; Radom, L. *J. Chem. Phys.* **1991**, *94*, 511; (h) Clark, T.; Chandrasekhar, J.; Spitznagel, G. W.; Schleyer, P. v. R. *J. Comp. Chem.* **1983**, *4*, 294; (i) Frisch, M. J.; Pople, J. A.; Binkley, J. S. *J. Chem. Phys.* **1984**, *80*, 3265.
44. (a) Cancès, M. T.; Mennucci, B.; Tomasi, J. *J. Chem. Phys.* **1997**, *107*, 3032; (b) Cossi, M.; Barone, V.; Mennucci, B.; Tomasi, J. *Chem. Phys. Lett.* **1998**, *286*, 253; (c) Mennucci, B.; Tomasi, J. *J. Chem. Phys.* **1997**, *106*, 5151.
45. (a) Tomasi, J.; Mennucci, B.; Cammi, R. *Chem. Rev.* **2005**, *105*, 2999; (b) Cossi, M.; Scalmani, G.; Rega, N.; Barone, V. *J. Chem. Phys.* **2002**, *117*, 43.
46. <http://www.chemcraftprog.com/index.html> (accessed May 2013).

# A NEW FAMILY OF ZIRCONIUM COMPLEXES ANCHORED BY DIANIONIC CYCLAM-BASED LIGANDS: SYNTHESSES, STRUCTURES, AND CATALYTIC APPLICATIONS

ANA M. MARTINS\*, RUI F. MUNHÁ, LUIS G. ALVES, AND SHANMUGA BHARATHI

*Centro de Química Estrutural, Instituto Superior Técnico, Universidade de Lisboa, Lisboa, Portugal*

## 25.1 INTRODUCTION

The field of organometallic chemistry was dominated by cyclopentadienyl-based systems until the 1990s. Since then, a growing interest in new ancillary ligand frameworks suitable to disclose new reactivity patterns became an active research topic. Amido ligands were primarily responsible for “the beginning of a postmetallocene era” [1], and have proved successful in taking the chemistry promoted by metallocene systems a step further [1, 2]. The concept of combining different donor atoms in a chelating array has exponentially increased the diversity of metal complexes available, and the resulting new coordination environments has given way to the discovery of well-defined platforms for the study of elementary organometallic reactions and new metal-mediated chemical transformations [3]. Albeit ligand design has reached a high level of sophistication, the chemistry promoted by the corresponding metal complexes remains in many cases incipient, or poorly understood, when compared to their metallocene counterparts.

In the late 1980s, it was anticipated that early transition metal complexes supported by anionic macrocyclic ligands “could establish a chemistry comparable with that of the corresponding bis(cyclopentadienyl) derivatives” [4]. However, it was only recently that macrocyclic ligands have received considerable attention in the context of early transition metal chemistry [4, 5]. The cavity size of the macrocycle can be such that larger metal ions are forced to sit above the plane of the donors, resulting in less sterically hindered reactive sites at the metal center [6]. The out-of-plane coordination mode renders the remaining coordination positions adjacent, which is a prerequisite for many established reaction pathways and catalytic processes. In the case of tetradentate dianionic ancillary ligands, the “ $(L_2X_2)M$ ” fragment can be considered isoelectronic to the “ $Cp_2M$ ” scaffold. However, anionic macrocyclic ligands comprise, in most cases, hard ligands such as amido, alkoxido, or amines, which make the metal–ligand bonds very polar and make these systems more electron releasing than the combination of two cyclopentadienyl units. Consequently, the reactivity of the former complexes is affected by the decreased electrophilicity at the metal center [7].

The work presented here describes the chemistry of Zr(IV) complexes anchored by dissymmetric, disubstituted, dianionic cyclam ligands. In comparison with zirconium complexes supported by unsaturated dianionic tetraazamacrocycles [4,7a,8], the compounds derived from dianionic, trans-disubstituted cyclam ancillary ligands have a more robust skeleton, which is not susceptible to nucleophilic attack and rearrangement, and higher flexibility, suitable to fit to the electronic and steric metal requirements. Part of this work has already been published and the reader will be directed to the original publications for the sake of clarity.

*Advances in Organometallic Chemistry and Catalysis: The Silver/Gold Jubilee International Conference on Organometallic Chemistry Celebratory Book*, First Edition. Edited by Armando J. L. Pombeiro.

© 2014 John Wiley & Sons, Inc. Published 2014 by John Wiley & Sons, Inc.

## 25.2 SYNTHESES AND MOLECULAR STRUCTURES

Trans-disubstituted cyclam-based ligand precursors of the general formulas  $H_2(Bn_2\text{Cyclam})$  and  $H_2(^{3,5-\text{Me}}Bn_2\text{Cyclam})$  ( $Bn = C_6H_5CH_2$ , **1a**,  $^{3,5-\text{Me}}Bn = 3,5\text{-Me}_2C_6H_3CH_2$ , **1b**) were obtained in high yields in a multistep synthetic procedure starting from cyclam. Reactions of  $ZrCl_2(CH_2SiMe_3)_2(Et_2O)_2$  with either **1a** or **1b** resulted in the elimination of tetramethylsilane and formation of  $(Bn_2\text{Cyclam})ZrCl_2$  (**2a**) and  $(^{3,5-\text{Me}}Bn_2\text{Cyclam})ZrCl_2$  (**2b**) in high yields [9]. The latter were used as precursors in the syntheses of alkoxido, thioalkoxido, amido, and alkyl derivatives via chloride metatheses using the appropriate lithium or Grignard reagents (Scheme 25.1) [10].

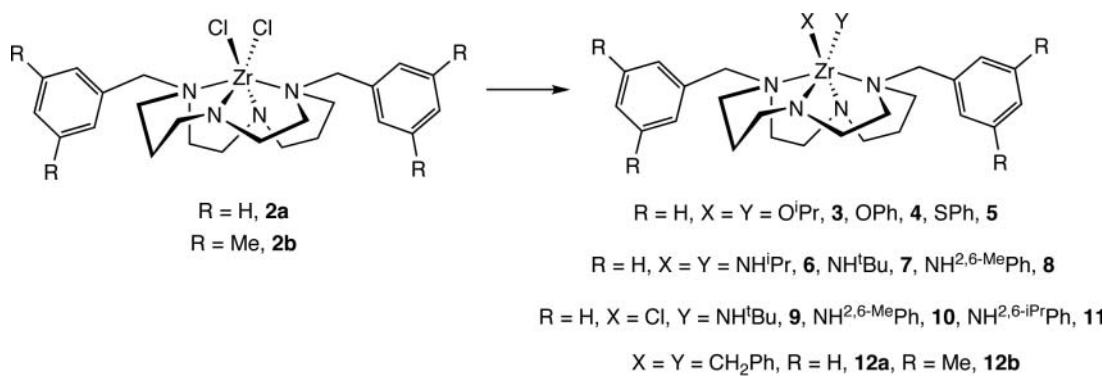
The zirconium complexes shown in Scheme 25.1 fall into three distinct coordination geometries: (i) trigonal prismatic (**P**) where the four nitrogen donors of the macrocyclic ligand are ligated to zirconium and define one rectangular face of the prism, (ii) tetrahedral capped (**T**), for which the distances between zirconium and the two cyclam amine functions fall out of the bonding range observed in zirconium complexes, and (iii) distorted octahedral (**O**), characterized by a conformational twist of the macrocycle such that it is not possible to define an average plane containing the four nitrogen donors of the cyclam ligand.

The molecular structures of all alkoxido and thioalkoxido complexes, as well as those of mono-amido compounds show trigonal prismatic coordination environment around the zirconium. The  $Zr-N_{\text{Cyclam}}$  bond lengths are consistent with values reported for  $Zr-N_{\text{amine}}$  and  $Zr-N_{\text{amido}}$  in other  $Zr(\text{IV})$  complexes and do not vary significantly with the type of the coligands. Figures 25.1 and 25.2 show ORTEP drawings of the molecular structures of  $(Bn_2\text{Cyclam})Zr(OPh)_2$  (**4**) and  $(Bn_2\text{Cyclam})ZrCl(NH'Bu)$  (**9**), as examples of what has been described above. The figure captions include selected bond lengths and angles [10a,c].

The molecular structures of complexes with bulky diamido ligands, such as  $(Bn_2\text{Cyclam})Zr(NH'Bu)_2$  (**7**) and  $(Bn_2\text{Cyclam})Zr(NH^{2,6-\text{Me}}Ph)_2$  (**8**), display two elongated  $Zr-N_{\text{amine}}$  distances triggered by steric constraints. The solid-state structure of **7** and relevant bond distances and angles are depicted in Fig. 25.3.

The bonding of two bulky amido ligands leads to capped tetrahedral zirconium complexes. Taking into account the distances between zirconium and the two cyclam amine units, these complexes may be described as masked tetraamido zirconium derivatives. Density functional theory (DFT) calculations have shown that the change from trigonal prismatic (**P**) to capped tetrahedral (**T**) environments in complexes  $(Bn_2\text{Cyclam})ZrXY$  is associated to the angle between the  $X-Zr-Y$  plane and the  $N_{\text{amide}}-Zr-N_{\text{amide}}$  plane ( $\alpha$ , Fig. 25.4). On going from **P** to **T**, the two  $N_{\text{amine}}$  atoms of the macrocyclic ligand are pushed away from the metal (from 2.51 Å to 2.81 Å) and an increase of the angle  $\alpha$  from 55° to 81° is observed, approaching the value of a perfect tetrahedron (90°) [10a].

The molecular structures of  $(Bn_2\text{Cyclam})Zr(CH_2Ph)_2$  (**12a**) and  $(^{3,5-\text{Me}}Bn_2\text{Cyclam})Zr(CH_2Ph)_2$  (**12b**) disclose the  $\kappa^4-N_2N'_2$  coordination of the macrocycle to the zirconium, complemented by the bonding of two benzyl ligands. The methyl substituents of the pendant benzyl groups in **12b** have no effect on the structural parameters and the molecular structures of both compounds are identical. However, these compounds do differ from all the previously described zirconium complexes, as the geometry around the metal is best described as distorted octahedral. The molecular structure of **12a** reveals that the macrocycle underwent a conformational twist that places one of the cyclam amido nitrogens and one of the benzyl ligands in the octahedron axial positions, defining an angle of 151.29(6)°. The remaining cyclam nitrogens and benzyl ligand occupy a slightly twisted square plane displaying a combined equatorial angle of 364.1° [10b].



Scheme 25.1

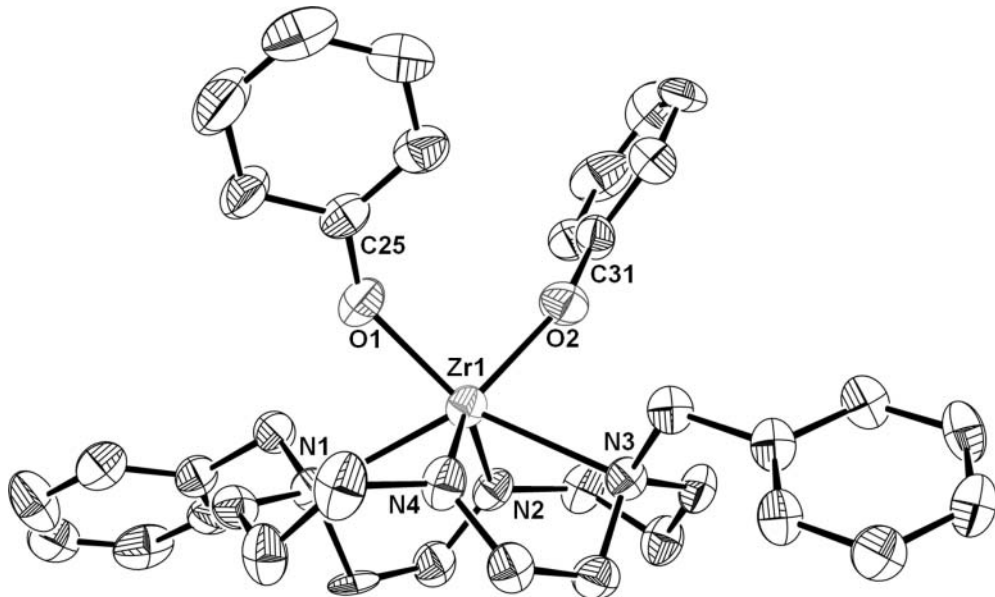


**Figure 25.1** ORTEP view of **4** shown at 40% thermal ellipsoids probability. Selected bond lengths ( $\text{\AA}$ ) and angles ( $^\circ$ ): Zr–O(1) 2.042(6); Zr–O(2) 2.035(6); Zr–N(1) 2.496(7); Zr–N(2) 2.095(7); Zr–N(3) 2.474(7); Zr–N(4) 2.077(7); O(1)–Zr–O(2) 90.7(3).

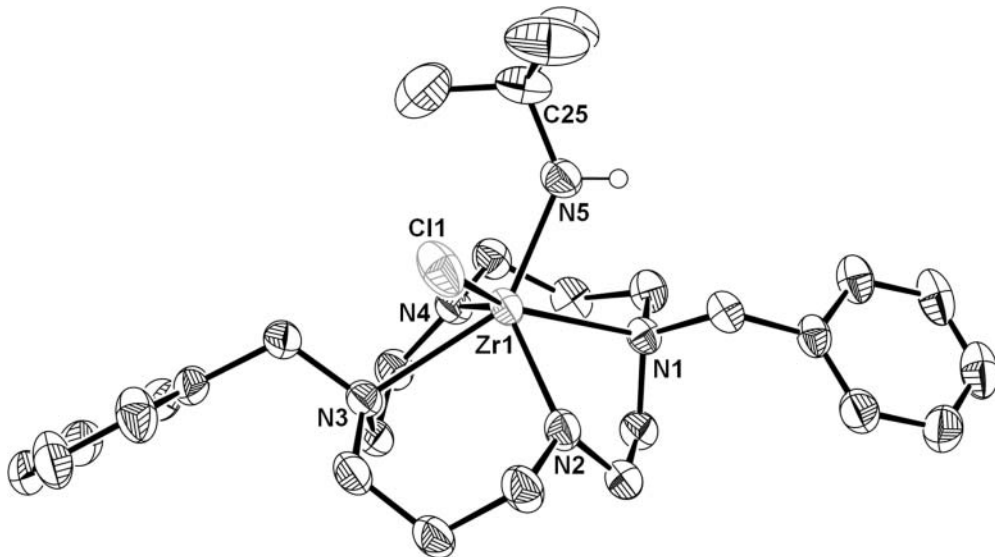


**Figure 25.2** ORTEP view of **9** shown at 50% thermal ellipsoids probability. Selected bond lengths ( $\text{\AA}$ ) and angles ( $^\circ$ ): Zr–Cl 2.5292(13); Zr–N(5) 2.077(3); Zr–N(1) 2.507(3); Zr–N(2) 2.070(3); Zr–N(3) 2.507(3); Zr–N(4) 2.058(3); Cl–Zr–N(5) 87.69(8).

The structural diversity of zirconium complexes supported by ( $\text{Bn}_2\text{Cyclam}$ ) ancillary ligands also includes coordination numbers 7 and 8, as attested by the molecular structures of the chloro-hydrazido complex ( $\text{Bn}_2\text{Cyclam}\text{ZrCl}(\kappa^2:\text{N},\text{N}'\text{-N}(\text{Ph})\text{NPh}(^n\text{Bu}))$  (**13**) [10a] and of ( $\text{Bn}_2\text{Cyclam}\text{Zr}((\kappa^2:\text{O},\text{N-ONMe}_2)_2$ ) (**14**) [11] where both acetoximato ligands exhibit chelating bonding mode (Fig. 25.5).

The hemilabile behavior of trans-disubstituted cyclams and the structural diversity exhibited by zirconium complexes incorporating these ligands are closely related to their properties in intramolecular hydroamination of aminoalkenes and ring-opening polymerization (ROP) of lactide, discussed in the following sections.

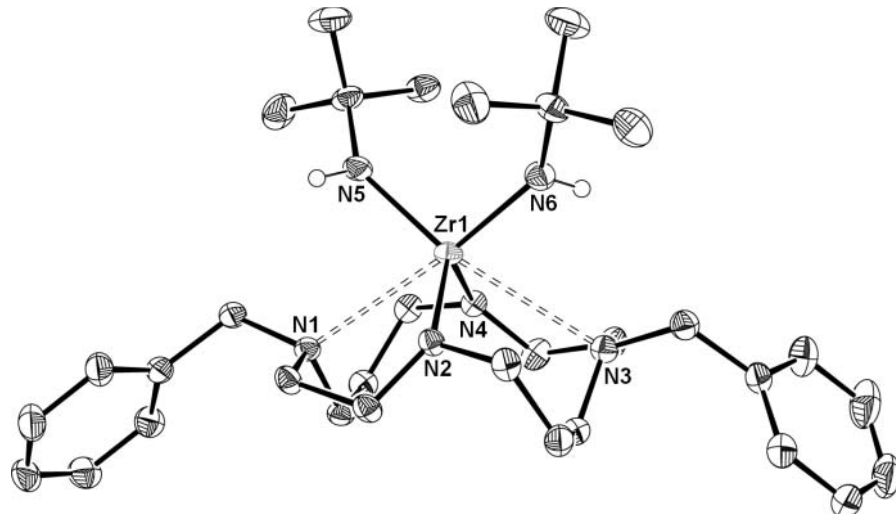


**Figure 25.3** Solid-state molecular structure of **7** shown at 50% thermal ellipsoid probability. Selected bond lengths ( $\text{\AA}$ ) and angles ( $^\circ$ ): Zr–N(5) 2.0616(11); Zr–N(6) 2.0706(11); Zr–N(1) 2.833(1); Zr–N(2) 2.0860(10); Zr–N(3) 2.9768(10); Zr–N(4) 2.0998(10); N(2)–Zr–N(4) 114.35(4); N(5)–Zr–N(6) 99.74(5).

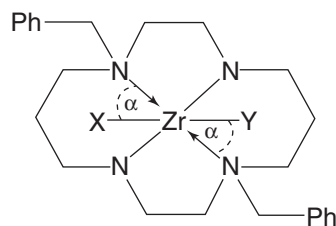


**Figure 25.4** Angle  $\alpha$  defined by the X–Zr–Y plane and the  $\text{N}_{\text{amido}}\text{--Zr--N}_{\text{amido}}$  plane.

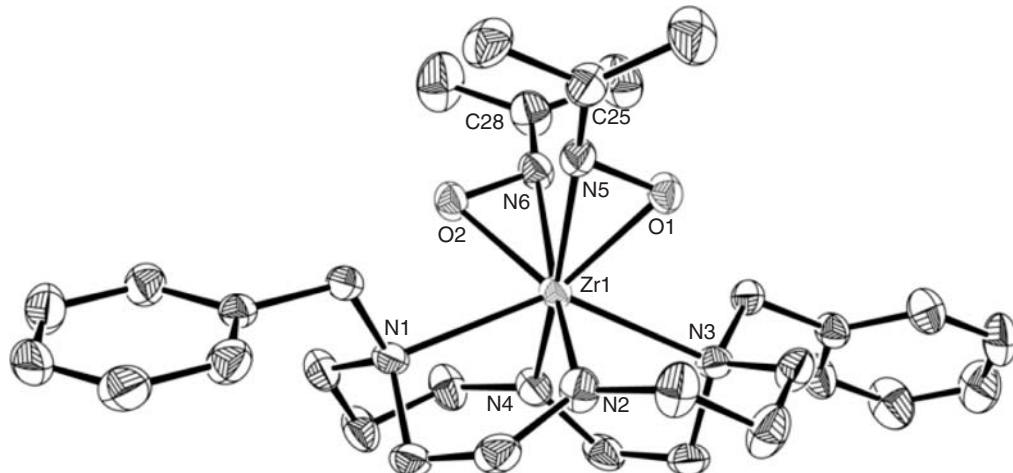


**Figure 25.5** ORTEP view of **14** shown at 40% thermal ellipsoids probability. Selected bond lengths ( $\text{\AA}$ ) and angles ( $^\circ$ ): Zr–O(1) 2.128(2); Zr–O(2) 2.130(2); Zr–N(1) 2.445(2); Zr–N(2) 2.123(2); Zr–N(3) 2.453(2); Zr–N(4) 2.122(2); Zr–N(5) 2.317(2); Zr–N(6) 2.307(2); O(1)–Zr–O(2) 106.12(7).

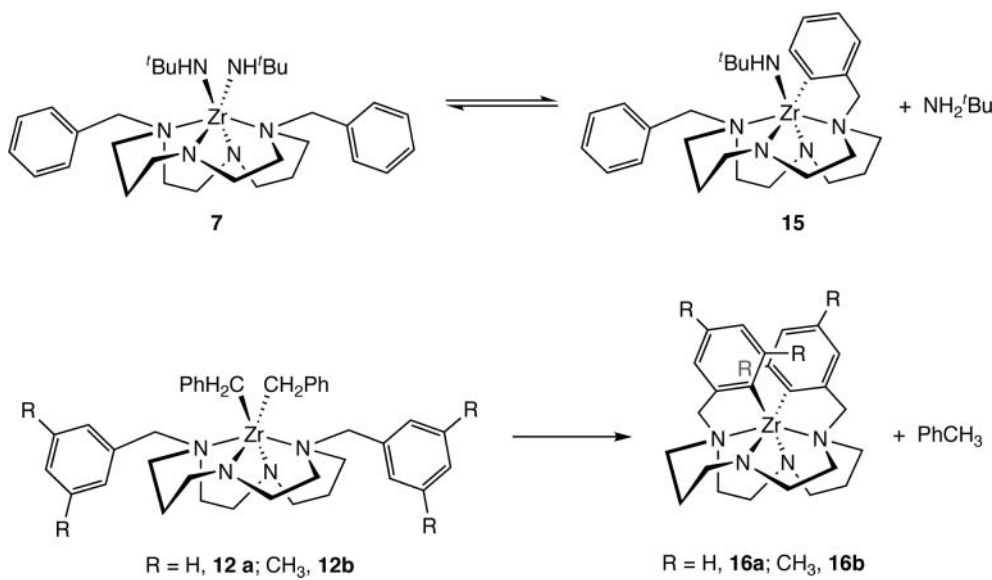
## 25.3 THERMALLY INDUCED ORTHOMETALLATION AND INTRAMOLECULAR HYDROAMINATION OF AMINOALKENES

Early transition metal imido complexes can be prepared by  $\alpha$ -abstraction and extrusion of a good leaving group (e.g., alkane or amine) from a metal amido species. This process depends on how good the leaving group is, and on the acidity of the N–H proton, which is normally dictated by the substituent groups on the amido moiety [12]. In addition, the ancillary ligand plays a crucial role on the reactivity of the amido complexes. For example, the formation of diamido compounds by chloride metathesis, upon addition of two equivalents of a lithium amide to the zirconium dichloro starting material, as described in the previous section, finds a similar reactivity pattern in tetraazaannulene-based systems [7c]. However, in porphyrin or calixarene-based systems the addition of two equivalents of lithium amide generates a monomeric imido complex [13]. Finally, zirconocene imido complexes are readily accessible from amido species through amine or alkane elimination [12a].

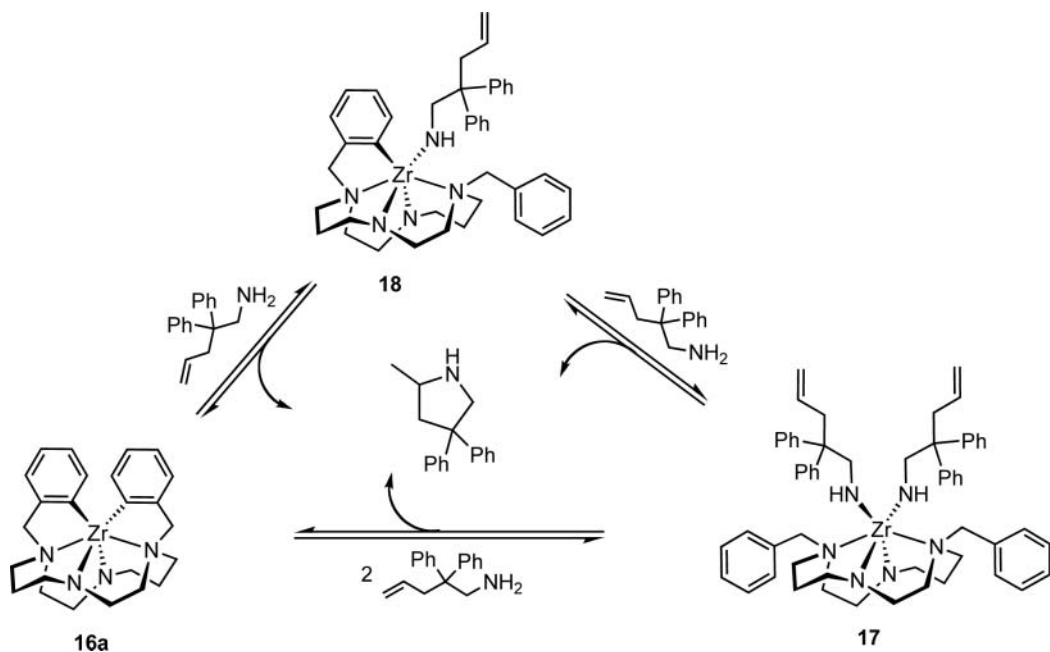
The preparation of imido complexes through intramolecular amine elimination was not possible for trans-disubstituted-cyclam based zirconium compounds. The reaction of  $(Bn_2\text{Cyclam})\text{Zr}(\text{NH}^t\text{Bu})_2$  (**7**) with one equivalent of a more acidic and sterically encumbered amine like  $^{2,6-\text{Me}}\text{PhNH}_2$  generates  $(Bn_2\text{Cyclam})\text{Zr}(\text{NH}^{2,6-\text{Me}}\text{Ph})_2$  (**8**). On the other hand, heating of a benzene solution of  $(Bn_2\text{Cyclam})\text{Zr}(\text{NH}^t\text{Bu})_2$  in an NMR tube at 60 °C led to a mixture of **7**, free  $^t\text{BuNH}_2$ , and the orthometallated-amido complex  $[(C_6\text{H}_4\text{CH}_2)\text{BnCyclam}]\text{Zr}(\text{NH}^t\text{Bu})$  (**15**) (Scheme 25.2).  $\alpha$ -Abstraction of the amine is reversible, and longer reaction times do not affect the relative amounts of these species. The dibenzyl complexes  $(Bn_2\text{Cyclam})\text{Zr}(\text{CH}_2\text{Ph})_2$  (**12a**) and  $(^{3,5-\text{Me}}\text{Bn}_2\text{Cyclam})\text{Zr}(\text{CH}_2\text{Ph})_2$  (**12b**) convert to the di-orthometallated complexes  $[(C_6\text{H}_4\text{CH}_2)_2\text{Cyclam}]\text{Zr}$  (**16a**) and  $[(3,5-\text{Me}_2\text{C}_6\text{H}_2\text{CH}_2)_2\text{Cyclam}]\text{Zr}$  (**16b**) upon thermal activation, although the formation of the latter requires much longer reaction time (7 days vs 24 h at 115 °C).

The ortho-metallation reaction was shown crucial for the catalytic performance of  $(Bn_2Cyclam)ZrX_2$  ( $X = NMe_2, CH_2Ph$ ) in the intramolecular hydroamination of aminoalkenes [14]. Addition of 2 equivalents of 2,2-diphenyl-pent-4-enylamine to the zirconium complex **16a** in benzene- $d_6$  led to quantitative conversion to the diamido  $(Bn_2Cyclam)Zr(N(H)R)_2$  ( $R = CH_2CPh_2CH_2CH=CH_2$ ) (**17**) that, after a few hours at room temperature, converted to the mono-orthometallated  $[(C_6H_4CH_2)BnCyclam]ZrN(H)R$  (**18**) ( $R = CH_2CPh_2CH_2CH=CH_2$ ) and 2-methyl-4,4-diphenylpyrrolidine. Upon heating the solution up to 90 °C, the conversion is quantitative, and further heating produced the di-orthometallated  $[(C_6H_4CH_2)_2Cyclam]Zr$  (**16a**) and the release of a second equivalent of 2-methyl-4,4-diphenylpyrrolidine (see Scheme 25.3).

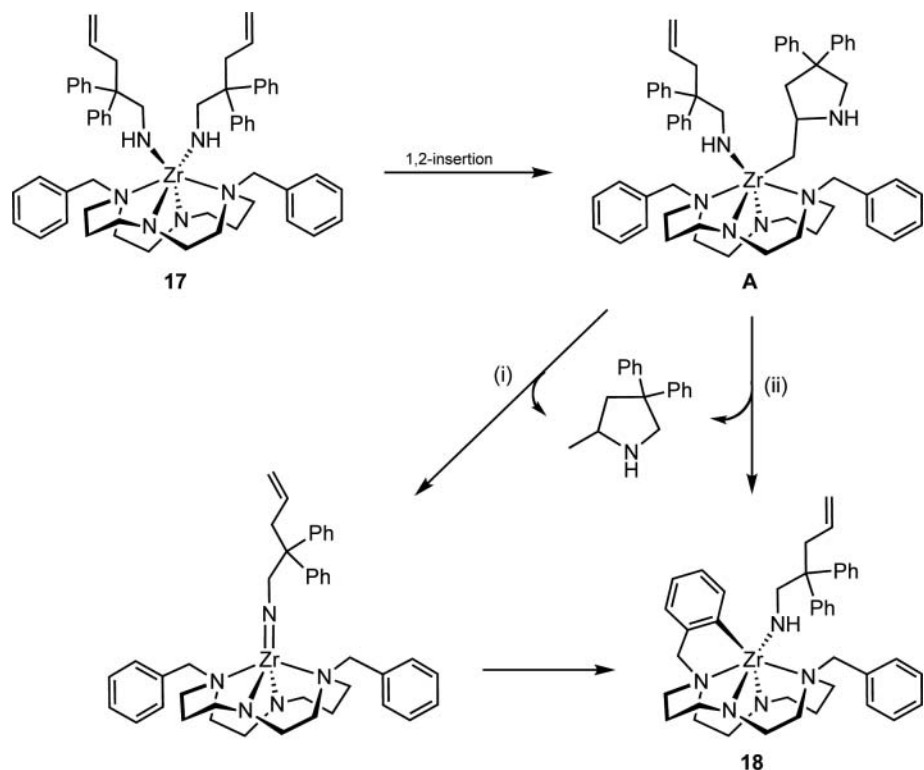
Taking into account that thermal conversion of diamido to imido species is not accessible to  $\text{Bn}_2\text{Cyclam}$  zirconium complexes, the cyclization reaction is likely to occur by 1,2-insertion of the olefin moiety in the  $\text{Zr}-\text{N}$  bond (Scheme 25.4). This pathway was initially proposed by Tobin Marks for lanthanocene and constrained geometry zirconium complexes and was more recently also suggested for other group 4 metal catalysts [15, 16]. The activation of the olefin toward insertion may



## Scheme 25.2



Scheme 25.3



Scheme 25.4

be supported either by the ancillary ligand through the elongation of the Zr–N<sub>amine</sub> bonds or by increasing the coordination number of the metal center.

The cleavage of the Zr–C bond may involve the NH proton of the amido ligand (path i) or the *ortho*-CH bond of the benzyl group (path ii) of species **A** in Scheme 25.4. The product of this step would be, in the first case, the imido complex or, in the second case, the mono-orthometalated species **18**. The pathway disclosed in route (i) is in agreement with the formation of (Bn<sub>2</sub>Cyclam)Zr(NR) (R=2,6-*i*Pr) and CH<sub>4</sub> by reaction of (Bn<sub>2</sub>Cyclam)ZrCl<sub>2</sub> (**2a**) with MeMgCl [10c]. This route cannot be disclosed on the basis of the fact that it was not observed by NMR, as its conversion to **18** may be fast, but the results described below do not fit this hypothesis. Indeed, further insight into this problem was provided by (<sup>3,5-Me</sup>Bn<sub>2</sub>Cyclam)Zr(CH<sub>2</sub>Ph)<sub>2</sub> (**12b**). This complex (i) not only requires much harsh temperature conditions and longer reaction times than (Bn<sub>2</sub>Cyclam)Zr(CH<sub>2</sub>Ph)<sub>2</sub> (**12a**) to give the corresponding orthometallated compound (**16b**) but (ii) revealed inactive in the catalytic hydroamination of 2,2-diphenyl-pent-4-enylamine. If route (i) was a viable pathway to the cyclization reaction, the catalytic activity would not depend on the substitution of the cyclam benzyl rings and **12b** would be expected to catalyze the hydroamination reaction. The lack of catalytic activity of **12b** suggests that the ortho-metallation reaction is a requirement for the catalytic activity and seems to support that the formation of 2-methyl-4,4-diphenylpyrrolidine takes place through path (ii). Further reactivity and DFT studies aiming the definite establishment of the reaction mechanism are in course and will be published soon.

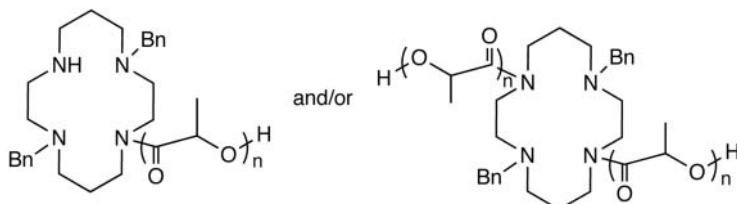
## 25.4 ROP OF LACTIDE AND CYCLAM FUNCTIONALIZATION

Cyclic ester polymers, in particular polylactic acid (PLA) and its copolymers, have noticeable applications that are related to their biocompatible and biodegradable properties [16]. These products may be obtained by ROP using alkoxide derivatives of electrophilic metals as catalysts [17], which provide living and/or stereoregular growing processes that are critical for many polymer applications.

We have found that (Bn<sub>2</sub>Cyclam)Zr(O*i*Pr)<sub>2</sub> (**3**), (Bn<sub>2</sub>Cyclam)Zr(OPh)<sub>2</sub> (**4**), and (Bn<sub>2</sub>Cyclam)Zr(SPh)<sub>2</sub> (**5**) also catalyze the ROP of *rac*-lactide in a well-controlled way as attested by the PDI values and the direct proportionality between monomer conversions and the molecular weights of the polymers [10c]. The polymers obtained using **3** as catalyst have O*i*Pr-end groups in agreement with a polymerization reaction that is initiated by monomer insertion in the Zr–O bonds, as usually observed for metal alkoxido catalysts. Unexpectedly, the polymers obtained with (Bn<sub>2</sub>Cyclam)Zr(OPh)<sub>2</sub> or (Bn<sub>2</sub>Cyclam)Zr(SPh)<sub>2</sub> display Bn<sub>2</sub>Cyclam end-capped PLAs (Scheme 25.5). These results are compatible with an initial insertion of *rac*-lactide in the Zr–N<sub>amide</sub> bonds of the cyclam ligand and subsequent chain propagation through insertion of incoming monomers into the newly formed Zr–O bonds.

The first step of the polymerization reaction was investigated by DFT. It was assumed that the reaction started by the insertion of a carbonyl group in the Zr–N<sub>amide</sub> or the Zr–O bonds of (Bn<sub>2</sub>Cyclam)Zr(OR)<sub>2</sub> (R=*i*Pr, Ph). For each compound, the structures of the intermediates were optimized and the energy of the processes was calculated. In both cases, the coordination of the incoming ligand pushes one of the amine N-atoms of the cyclam ligand away from the metal. For (Bn<sub>2</sub>Cyclam)Zr(OPh)<sub>2</sub> the overall energy balance favors the insertion in Zr–N<sub>amide</sub> bonds by -3.9 kcal/mol, while for (Bn<sub>2</sub>Cyclam)Zr(O*i*Pr)<sub>2</sub> this pathway is essentially thermoneutral (-0.2 kcal/mol). The formation of end-capped Bn<sub>2</sub>Cyclam polymers with complex **4** is thus thermodynamically favored and results from orbital controlled insertion. The global energy variation associated to the insertion in the Zr–O bond of **3** is 2.2 kcal/mol. Albeit this process is slightly disfavored in comparison with the insertion in the Zr–N<sub>amide</sub> bond, the analysis of the charges located on the oxygen atoms of the O*i*Pr ligands suggests that, in the case of **3**, the reaction is likely ruled by charge control [10c].

Although metal–amido bonds have been reported to initiate cyclic esters ROP, (Bn<sub>2</sub>Cyclam)Zr(OPh)<sub>2</sub> and (Bn<sub>2</sub>Cyclam)Zr(SPh)<sub>2</sub> are the unique ROP catalysts reported to date that allow the simultaneous functionalization/polymerization of



Scheme 25.5

lactide. The combination of a biocompatible and biodegradable polymer with a cyclam moiety, which proved useful in biochemical and sensing applications [18], may set the ground for the design of new functional materials, obtained straightforwardly by insertion of adequate substrates in Zr–N bonds of dianionic cyclam-based ligands.

## 25.5 CONCLUDING REMARKS

The results described reveal that dianionic diamido-diamine ligands derived from *trans*-dibenzylcyclams are able to support a variety of zirconium complexes of general formula ( $Bn_2$ Cyclam)ZrXY. These compounds display varied structural motifs, with coordination numbers between 4 and 8, which attest for the hemilabile behavior of the ancillary ligand and revealed critical for the catalytic activity displayed by complexes of this family in intramolecular hydroamination and ROP of lactide. The ability to generate open coordination sites in the 6-coordinated precatalysts by cleavage of Zr–N<sub>amine</sub> bonds of the macrocycle ligand and the possibility to reach higher coordination numbers have proved decisive in the catalytic activity observed.

The intramolecular hydroamination of primary amines, typified in this study by 2,2-diphenyl-pent-4-enylamine, is likely to involve 1,2-insertion of the C=C bond in the Zr–NHR bond followed by  $\sigma$ -bond metathesis of the Zr–C bond and concomitant ortho-metallation of the benzyl groups appended to the cyclam nitrogen atoms.

The ROP of *rac*-lactide with ( $Bn_2$ Cyclam)ZrX<sub>2</sub> catalysts (X = O<sup>i</sup>Pr, OPh, SPh) may be modulated by X. For X = O<sup>i</sup>Pr the polymerization is initiated by substrate insertion in the Zr–O bonds, as usually observed for other metal alkoxidos. A completely different ROP occurs with ( $Bn_2$ Cyclam)Zr(OPh)<sub>2</sub> and ( $Bn_2$ Cyclam)Zr(SPh)<sub>2</sub> catalysts. The insertion of lactide takes place at the Zr–N<sub>amide</sub> bonds of the cyclam, originating the growing of the polymer chain appended to the macrocycle nitrogen atoms. This process, which constitutes a straightforward strategy to the simultaneous ROP of lactide/functionalization of cyclam, will be further extended to other homo- and hetero-biopolymers.

## AKNOWLEDGMENT

Fundaçao para a Ciéncia e Tecnologia is acknowledged for funding (PEst-OE/QUI/UI0100/2011). A. M. Martins thanks Prof. Luis F. Veiros (DFT calculations) and Dr. Samuel Dagorne (ROP catalysis) for their contributions.

## REFERENCES

- Kempe, R. *Angew. Chem., Int. Ed.* **2000**, *39*, 468.
- (a) Sun, J.-F.; Chen, S.-J.; Duan, Y.; Li, Y.-Z.; Chen, X.-T.; Xue, Z.-L. *Organometallics* **2009**, *28*, 3088; (b) Han, H.; Johnson, S. A. *Eur. J. Inorg. Chem.* **2008**, *471*; (c) de Waele, P.; Jazdzewski, B. A.; Klosin, J.; Murray, R. E.; Theriault, C. N.; Vosejpk, P. C.; Petersen, J. L. *Organometallics* **2007**, *26*, 3896; (d) Bai, G.; Wei, P.; Stephan, D. W. *Organometallics* **2006**, *25*, 2649; (e) Irrgang, T.; Kempe, R. *Eur. J. Inorg. Chem.* **2005**, *4382*; (f) Gade, L. H. *Chem. Commun.* **2000**, *173*.
- (a) Werner, H. *Dalton Trans.* **2003**, 3829; (b) Liang, L.-C. *Coord. Chem. Rev.* **2006**, *250*, 1152; (c) Braunstein, P.; Naud, F. *Angew. Chem., Int. Ed.* **2001**, *40*, 680; (d) Lindner, E.; Pautz, S.; Haustein, M. *Coord. Chem. Rev.* **1996**, *155*, 145; (e) Gade, L. H. *Acc. Chem. Res.* **2002**, *35*, 575.
- Floriani, C.; Ciurli, S.; Chiesi-Villa, A.; Guastini, C. *Angew. Chem., Int. Ed.* **1987**, *26*, 70.
- (a) Goedken, V. L.; Ladd, J. A. *J. Chem. Soc., Chem. Commun.* **1982**, 142; (b) Olmstead, M. M.; Power, P. P.; Viggiano, M. *J. Am. Chem. Soc.* **1983**, *105*, 2927; (c) Malinski, T.; Chang, D.; Latour, J. M.; Marchon, J. C.; Gross, M.; Giraudieu, A.; Kadish, K. M. *Inorg. Chem.* **1984**, *23*, 3947; (d) Woo, L. K.; Hays, J. A.; Jacobson, R. A.; Day, C. L. *Organometallics* **1991**, *10*, 2102; (e) Kim, H. J.; Whang, D.; Kim, K.; Do, Y. *Inorg. Chem.* **1993**, *32*, 360; (f) Giannini, L.; Solari, E.; Floriani, C.; Chiesi-Villa, A.; Rizzoli, C. *Angew. Chem., Int. Ed.* **1994**, *33*, 2204; (g) Berreau, L. M.; Young, V. G., Jr.; Woo, L. K. *Inorg. Chem.* **1995**, *34*, 527; (h) Kisko, J. L.; Hascall, T.; Parkin, G. *J. Am. Chem. Soc.* **1997**, *119*, 7609; (i) Cohen, J. D.; Fryzuk, M. D.; Loehr, T. M.; Mylvaganam, M.; Rettig, S. *J. Inorg. Chem.* **1998**, *37*, 112; (j) Floriani, C.; Solari, E.; Solari, G.; Chiesi-Villa, A.; Rizzoli, C. *Angew. Chem., Int. Ed.* **1998**, *37*, 2245; (k) Fryzuk, M. D.; Love, J. B.; Rettig, S. J. *Organometallics* **1998**, *17*, 846; (l) Wang, X.; Gray, S. D.; Chen, J.; Woo, L. K. *Inorg. Chem.* **1998**, *37*, 5; (m) Crescenzi, R.; Solari, E.; Floriani, C.; Re, N.; Chiesi-Villa, A.; Rizzoli, C. *Organometallics* **1999**, *18*, 606; (n) Thorman, J. L.; Young, V. G.; Boyd, P. D. W.; Guzei, I. A.; Woo, L. K. *Inorg. Chem.* **2001**, *40*, 499; (o) Fryzuk, M. D.; Kozak, C. M.; Mehrkhodavandi, P.; Morello, L.; Patrick, B. O.; Rettig, S. J. *J. Am. Chem. Soc.* **2002**, *124*, 516; (p) Dias, A. R.; Martins, A. M.; Ascenso, J. R.; Ferreira, H.; Duarte, M. T.; Henriques, R. T. *Inorg. Chem.* **2003**, *42*, 2675; (q) Monteiro, B.; Roitershtein, D.; Ferreira, H.; Ascenso, J. R.; Martins, A. M.; Domingos, A.; Marques, N. *Inorg. Chem.* **2003**, *42*, 4223; (r) Du, G.;

- Mirafzal, G. A.; Woo, L. K. *Organometallics*, **2004**, *23*, 4230; (s) Morello, L.; Yu, P.; Carmichael, C. D.; Patrick, B. O.; Fryzuk, M. D. *J. Am. Chem. Soc.* **2005**, *127*, 12796; (t) Martins, A. M.; Ascenso, J. R.; Costa, S. M. B.; Dias, A. R.; Ferreira, H.; Ferreira, J. A. B. *Inorg. Chem.* **2005**, *44*, 9017; (u) Martins, A. M.; Ascenso, J. R.; de Azevedo, C. G.; Dias, A. R.; Duarte, M. T.; Ferreira, H.; Ferreira, M. J.; Henriques, R. T.; Lemos, M. A.; Li, L.; Ferreira da Silva, J. *Eur. J. Inorg. Chem.* **2005**, 1689; (v) Barroso, S.; Cui, J.; Dias, A. R.; Duarte, M. T.; Ferreira, H.; Henriques, R. T.; Oliveira, M. C.; Ascenso, J. R.; Martins, A. M. *Inorg. Chem.* **2006**, *45*, 3532; (w) Ohki, Y.; Fryzuk, M. D. *Angew. Chem., Int. Ed.* **2007**, *46*, 3180; (x) Ferreira, H.; Dias, A. R.; Duarte, M. T.; Ascenso, J. R.; Martins, A. M. *Inorg. Chem.* **2007**, *46*, 750; (y) Fryzuk, M. D. *Acc. Chem. Res.* **2009**, *42*, 127; (z) O'Connor, P.; Berg, D. J.; Twamley, B. *Organometallics* **2005**, *24*, 28.
6. Brand, H.; Arnold, J. *Coord. Chem. Rev.* **1995**, *140*, 137.
  7. (a) Giannini, L.; Solari, E.; De Angelis, S.; Ward, T. R.; Floriani, C.; Chiesi-Villa, A.; Rizzoli, C. *J. Am. Chem. Soc.* **1995**, *117*, 5801; (b) Scott, M. J.; Lippard, S. J. *Organometallics* **1998**, *17*, 1769; (c) Mountford, P. *Chem. Soc. Rev.* **1998**, *27*, 105; (d) Martin, A.; Uhrhammer, R.; Gardner, T. G.; Jordan, R. F.; Rogers, R. D. *Organometallics* **1998**, *17*, 382.
  8. (a) Black, D. G.; Swenson, D. C.; Jordan, R. F.; Rogers, R. D. *Organometallics* **1995**, *14*, 3539; (b) Bonomo, L.; Toraman, G.; Solari, E.; Scopelliti, R.; Floriani, C. *Organometallics* **1999**, *18*, 5198.
  9. (a) Munhá, R. F.; Namorado, S.; Barroso, S.; Duarte, M. T.; Ascenso, J. R.; Dias, A. R.; Martins, A. M. *J. Organomet. Chem.* **2006**, *691*, 3853; (b) Alves, L. G.; Antunes, M. A.; Matos, I.; Munhá, R. F.; Duarte, M. T.; Fernandes, A. C.; Marques, M. M.; Martins, A. M. *Inorg. Chim. Acta* **2010**, *363*, 1823.
  10. (a) Munhá, R. F.; Veiros, L. F.; Duarte, M. T.; Fryzuk, M. D.; Martins, A. M. *Dalton Trans.* **2009**, 7494; (b) Munhá, R. F.; Antunes, M. A.; Alves, L. G.; Veiros, L. F.; Fryzuk, M. D.; Martins, A. M. *Organometallics* **2010**, *29*, 3753; (c) Alves, L. G.; Hild, F.; Munhá, R. F.; Veiros, L. F.; Dagorne, S.; Martins, A. M. *Dalton Trans.* **2012**, *41*, 14288.
  11. CIF of **14** may be obtained from CCDC under the deposit number 904587.
  12. (a) Walsh, P. J.; Hollander, F. J.; Bergman, R. G. *Organometallics* **1993**, *12*, 3705; (b) Chiu, M.; Hoyt, H. M.; Michael, F. E.; Bergman, R. G.; van Halbeek, H. *Angew. Chem., Int. Ed.* **2008**, *47*, 6073; (c) Fout, A. R.; Kilgore, U. J.; Mindiola, D. J. *Chem. Eur. J.* **2007**, *13*, 9428; (d) Hazari, N.; Mountford, P. *Acc. Chem. Res.* **2005**, *38*, 839.
  13. (a) Gray, S. D.; Thorman, J. L.; Berreau, L. M.; Woo, L. K. *Inorg. Chem.* **1997**, *36*, 278; (b) Berreau, L. M.; Young, V. G., Jr.; Woo, L. K. *Inorg. Chem.* **1995**, *34*, 527; (c) Dubberley, S. R.; Friedrich, A.; Willman, D. A.; Mountford, P.; Radius, U. *Chem. Eur. J.* **2003**, *9*, 3634.
  14. Antunes, M. A.; Munhá, R. F.; Alves, L. G.; Schafer, L. L.; Martins, A. M. *J. Organomet. Chem.* **2011**, *696*, 2.
  15. (a) Majumder, S.; Odom, A. L. *Organometallics* **2008**, *27*, 1174; (b) Stubbert, B. D.; Marks, T. J. *J. Am. Chem. Soc.* **2007**, *129*, 6149; (c) Straub, B. F.; Bergman, R. G. *Angew. Chem., Int. Ed.* **2001**, *40*, 4632; (d) Leitch, D.; Turner, C.; Schafer, L. *Angew. Chem., Int. Ed.* **2010**, *49*, 6382; (e) Leitch, D. C.; Platel, R. H.; Schafer, L. L. *J. Am. Chem. Soc.* **2011**, *133*, 15453.
  16. (a) Liang X.; Sadler, P. J. *Chem. Soc. Rev.* **2004**, *33*, 246; (b) Méallet-Renault, R.; Pansu, R.; Amigoni, S.; Larpent, C. *Chem. Commun.* **2004**, 2344; (c) Bergamini, G.; Ceroni, P.; Balzani, V.; Cornelissen, L.; Heyst, S.; Lee, K.; Vögtle, F. *J. Mater. Chem.* **2005**, *15*, 2959.
  17. (a) Romain, C.; Heinrich, B.; Bellemín-Lapponnaz, S.; Dagorne, S. *Chem. Commun.* **2012**, *48*, 2213; (b) Poirier, V.; Roisnel, T.; Sinbandhit, S.; Bochmann, M.; Carpentier, J.-F.; Sarazin, Y. *Chem. Eur. J.* **2012**, *18*, 2998; (c) Romain, C.; Rosa, V.; Fliedel, C.; Bier, F.; Hild, F.; Welter, R.; Dagorne, S.; Avilés, T. *Dalton Trans.* **2012**, *41*, 3377; (d) Sun, H.; Ritch, J. S.; Hayes, P. G. *Dalton Trans.* **2012**, *41*, 3701; (e) Sung, C.-Y.; Li, C.-Y.; Su, J.-K.; Chen, T.-Y.; Lin, C.-H.; Ko, B.-T. *Dalton Trans.* **2012**, *41*, 953; (f) Cao, T.-P.A.; Buchard, A.; Le Goff, X. F.; Auffrant, A.; Williams, C. K. *Inorg. Chem.* **2012**, *51*, 2157; (g) Cushion, M. G.; Mountford, P. *Chem. Commun.* **2011**, *47*, 2276; (h) Sanchez-Barba, L. F.; Garces, A.; Fernandez-Baeza, J.; Otero, A.; Alonso-Moreno, C.; Lara-Sanchez, A.; Rodriguez, A. M. *Organometallics* **2011**, *30*, 2775; (i) Buffet, J.-C.; Okuda, J. *Chem. Commun.* **2011**, *47*, 4769; (j) Buffet, J.-C.; Martin, A. N.; Kol, M.; Okuda, J. *Polym. Chem.* **2011**, *2*, 2378; (k) Zhang, Z.; Cui, D. *Chem. Eur. J.* **2011**, *17*, 11520; (l) Bouyahyi, M.; Ajellal, N.; Kirillov, E.; Thomas, C. M.; Carpentier, J.-F. *Chem. Eur. J.* **2011**, *17*, 1872; (m) Platel, R. H.; White, A. J. P.; Williams, C. K. *Inorg. Chem.* **2011**, *50*, 7718; (n) Hild, F.; Haquette, P.; Brelot, L.; Dagorne, S. *Dalton Trans.* **2010**, *39*, 533; (o) Wang, L.; Ma, H. *Macromolecules* **2010**, *43*, 6535; (p) Buffet, J.-C.; Kapelski, A.; Okuda, J. *Macromolecules* **2010**, *43*, 10201; (q) Shen, M.; Huang, W.; Zhang, W.; Hao, X.; Sun, W.-H.; Redshaw, C. *Dalton Trans.* **2010**, *39*, 9912; (r) Nomura, N.; Akita, A.; Ishii, R.; Mizuno, M. *J. Am. Chem. Soc.* **2010**, *132*, 1750.
  18. (a) Lim, M. H.; Lippard, S. J. *Acc. Chem. Res.* **2011**, *40*, 41; (b) Majzoub, A. E.; Cadiou, C.; Déchamps-Olivier, I.; Tinant, B.; Chuburu, F. *Inorg. Chem.* **2011**, *50*, 4029; (c) Bourdolle, A.; Allali, M.; Mulatier, J.-C.; Le Guennic, B.; Zwier, J. M.; Baldeck, P. L.; Bünzli, J.-C. G.; Andraud, C.; Lamarque, L.; Maury, O. *Inorg. Chem.* **2011**, *50*, 4987.



## METAL-ORGANO MULTICATALYSIS: AN EMERGING CONCEPT

ALEXANDRE F. TRINDADE, JOÃO N. ROSA, FÁBIO M. F. SANTOS, AND PEDRO M. P. GOIS\*

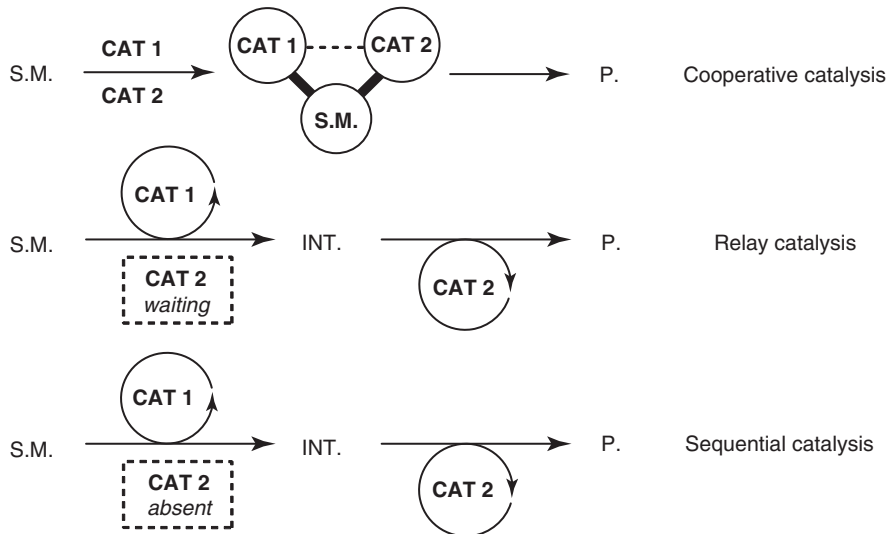
*Research Institute for Medicines and Pharmaceutical Sciences (iMed.UL), Universidade de Lisboa, Lisboa, Portugal*

### 26.1 INTRODUCTION

Over the years, catalysis has proved to be an invaluable tool to prepare myriads of important organic molecules. Metals, namely, transition metals, have a strong foothold in catalysis and synthetic organic chemists learnt to appreciate their high efficiency and reliability when using this unique family of catalysts to promote many key steps in the synthesis of complex molecules [1–4]. Despite the unarguable success of metals, in recent years, the use of small organic molecules as catalysts (organocatalysis), emerged as a very efficient strategy to create new C–C and C–X bonds, often with impressive levels of selectivity [5]. Interestingly, metal catalysis and organocatalysis have independently attained a high level of sophistication, although only recently, the idea of merging these two branches of catalysis resulted in a strategy to unravel unprecedented reactivities [6, 7]. Despite the attractiveness of this multicatalyzed approach, the one-pot combination of metal catalysts and organocatalysts is faced with some significant problems related to catalyst compatibility [8]. Enzymes, which are Nature's chosen catalysts, often exhibit in their active sites metal catalysts and organocatalysts that cooperate in the biotransformation process. Unsurprisingly, the coexistence of these entities benefits from the physical separation imposed by the active site architecture [9–17]. In contrast, the one-pot use of metal catalysts and organocatalysts may rapidly result in both catalysts self-quenching owing to complexation of the Lewis acid and the Lewis base or a redox process [8–17]. Despite these perceived challenges, in recent years, this multicatalyzed approach has developed into a powerful synthetic strategy, whose impact is clearly demonstrated by the number of reviews recently published covering the multiple aspects of this field [8–17].

Multicatalyzed processes are complex systems quite challenging to classify, namely, those involving metal catalysts and organocatalysts, which may engage in different modes of reaction with unknown mechanisms [18]. Moreover, the presence of more than two catalysts in the multicatalyzed process dramatically increases the system's complexity, precluding the implementation of a straightforward classification. Ideally, an informative classification should highlight the individual catalyst mode of action, although given the rich chemistry of metal catalysts and organocatalysts, this would result in an impractical strategy. Therefore, more general methods have been recently proposed on the basis of the relation of each catalytic cycle. Patil et al. [19] proposed a classification for binary metal–organo catalyzed systems that encompasses three main divisions (Scheme 26.1):

*Cooperative (or Synergistic) [9–17] Catalysis.* This is a process, in which two or more catalysts are present from the beginning of the reaction and share the same catalytic cycle. In this case, the desired reaction pathway is favored because of the narrowing of the HOMO–LUMO gap stemming from the individual activation of both intermediates.



**Scheme 26.1** Cooperative (or synergistic), relay, and sequential catalysis (S.M., starting materials; INT., intermediaries; P., products; CAT, catalyst).

**Relay Catalysis.** These are processes in which one or more catalysts are present from the beginning of the reaction but do not share the same catalytic cycle. These processes can be viewed as a set of reactions catalyzed independently in a consecutive manner.

**Sequential Catalysis.** This is a one-pot process in which one of the catalysts is added in the course of the reaction to avoid self-quenching.

Although this sort of classification might be difficult to apply because of a lack of knowledge regarding the exact role of the catalysts involved, it presents a simple and general method to distinguish these multicatalyzed processes, and for that reason will be adopted in this article.

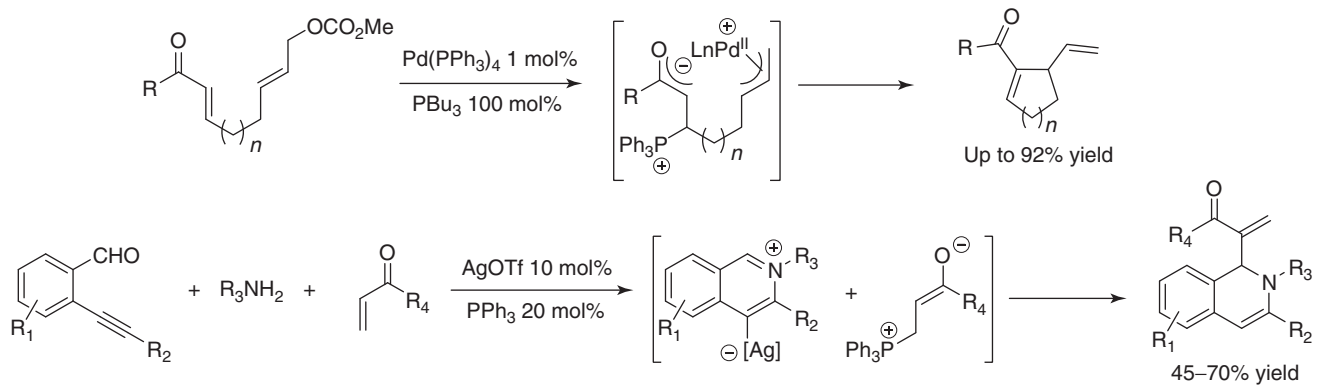
The use of metals as catalysts spans an overwhelming range of transformations in which the substrates are activated via coordination with the metal center; conversely, despite the breathtaking growth of organocatalysis in recent years, it is still possible to consider subareas related with the type of organocatalyst used. Therefore, one can consider the use of [20] (i) Lewis and Brønsted bases as catalysts, (ii) aminocatalysis, (iii) *N*-heterocyclic carbenes (NHCs) as organocatalysts, and (iv) Brønsted acid catalysis. These subareas will be used to organize the recent developments in cooperative, relay, and sequential metal–organo catalysis.

## 26.2 COOPERATIVE CATALYSIS

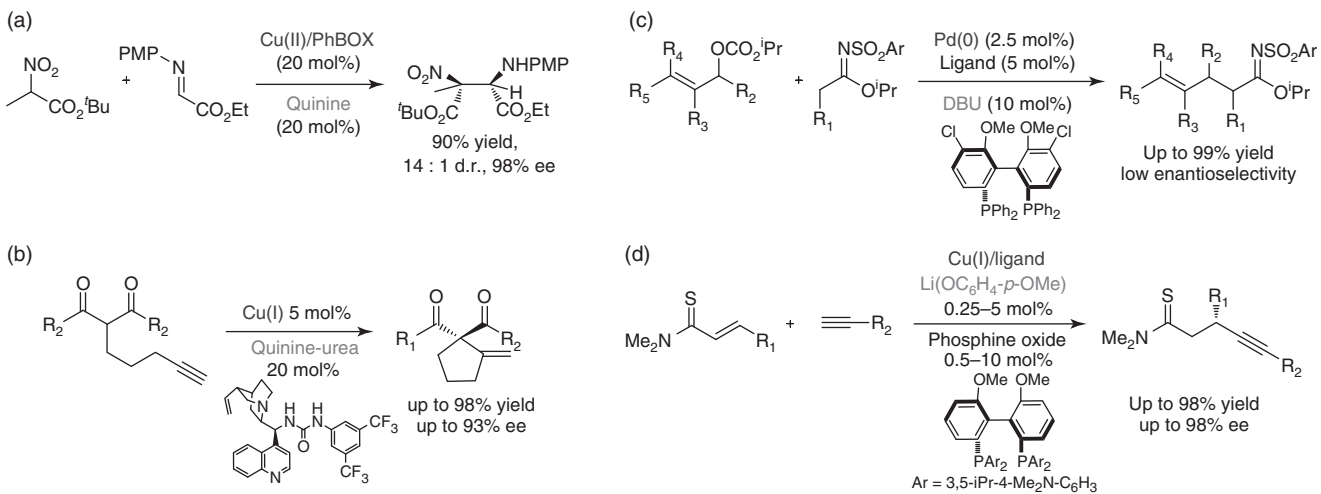
### 26.2.1 Lewis and Brønsted Bases as Catalysts

The concept of merging organocatalysts with metal catalysts to achieve new reaction modes was introduced for the first time by the Kirsche group in their seminal study on intramolecular enolate allylation [7]. The enolate was generated by a conjugate addition of tributylphosphine to an  $\alpha,\beta$ -unsaturated ketone and reacted with a  $\pi$ -allyl palladium complex in an intramolecular manner (Scheme 26.2) [21]. In order to have an efficient cooperative catalysis, the phosphine was not employed in catalytic amounts, highlighting the necessity to have high concentrations of the nucleophilic enolate in solution. A few years later, Wu and collaborators reported a three-component reaction between 2-alkynylbenzaldehydes, amines, and  $\alpha,\beta$ -unsaturated ketones catalyzed by a silver salt and phosphines based on the same Lewis base activation mechanism (Scheme 26.2) [22]. The reduced number of cooperative methodologies using Lewis bases is perhaps due to compatibility issues, as they form stable complexes with many transition metals [7].

Brønsted bases have been explored in cooperative catalysis to deprotonate substrates that subsequently add to metal-activated electrophiles. Regarding the use of these organocatalysts in cooperative catalysis, the combination of quinine and quinidine-derived thiourea organocatalysts with Cu(II)-PhBox and Cu(OTf) has been employed in aza-Henry [23] and



**Scheme 26.2** Selected examples of phosphine catalysis in cooperation with palladium and silver catalysis.



**Scheme 26.3** (a–d) Selected examples of Brønsted basic catalysis in cooperation with copper and palladium catalysts.

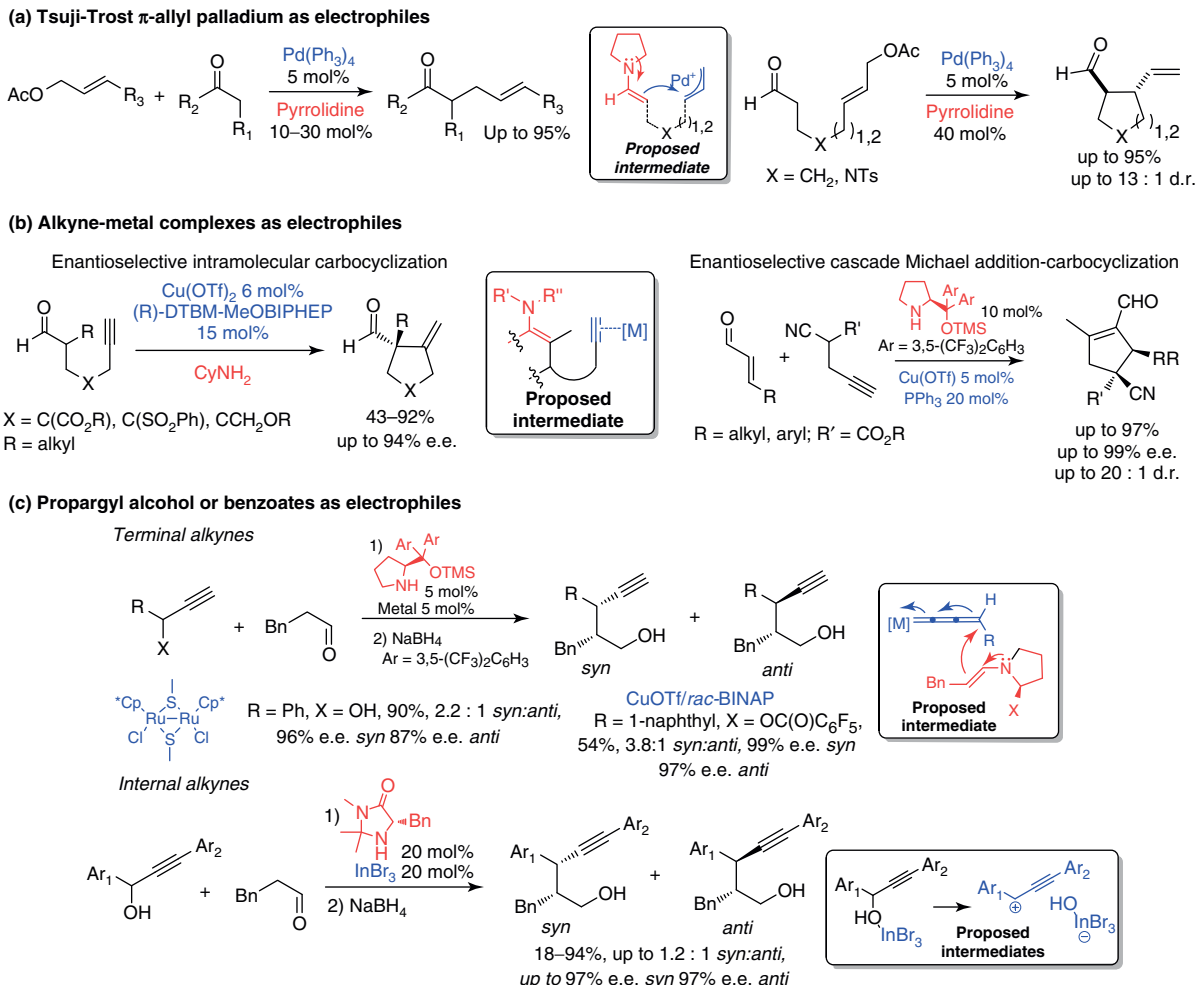
Conia-ene reactions [24], respectively (Scheme 26.3a and b), while DBU has been used to generate enamines for palladium-mediated allylation with allylic carbamates [25] (Scheme 26.3c). More recently, Shibasaki's group studied the cooperation of Cu(CH<sub>3</sub>CN) (soft Lewis acid) and Li(OC<sub>6</sub>H<sub>4</sub>-*p*-OMe) (hard Brønsted base) in the conjugate addition of terminal alkynes to  $\alpha,\beta$ -unsaturated thioamides (Scheme 26.3d) [26, 27].

## 26.3 AMINES AS CATALYSTS

### 26.3.1 Enamine-Based Catalysis

The generation of transient nucleophilic species by the condensation of secondary amines with enolizable aldehydes and ketones is a common mode of activation in organocatalysis. These transient nucleophiles can theoretically react with metal-activated electrophiles, unveiling new reaction pathways that are unachievable using only metal catalysis or organocatalysis. Historically, Tsuji-Trost  $\pi$ -allyl electrophiles were the firsts to be explored in cooperative catalysis with organocatalytically generated enamines. Both intermolecular [28, 29] and intramolecular [30, 31]  $\alpha$ -allylations of aldehydes and ketones could be performed using secondary amines and palladium complexes as catalysts (Scheme 26.4a). While the reaction could be extended to allylic phosphonates [31], bromides [30], and alcohols [32], considerable amounts of organocatalyst (10–50 mol%) are usually required, suggesting the need for a higher concentration of the enamine species in solution or possible interactions between the organocatalyst and palladium complexes.

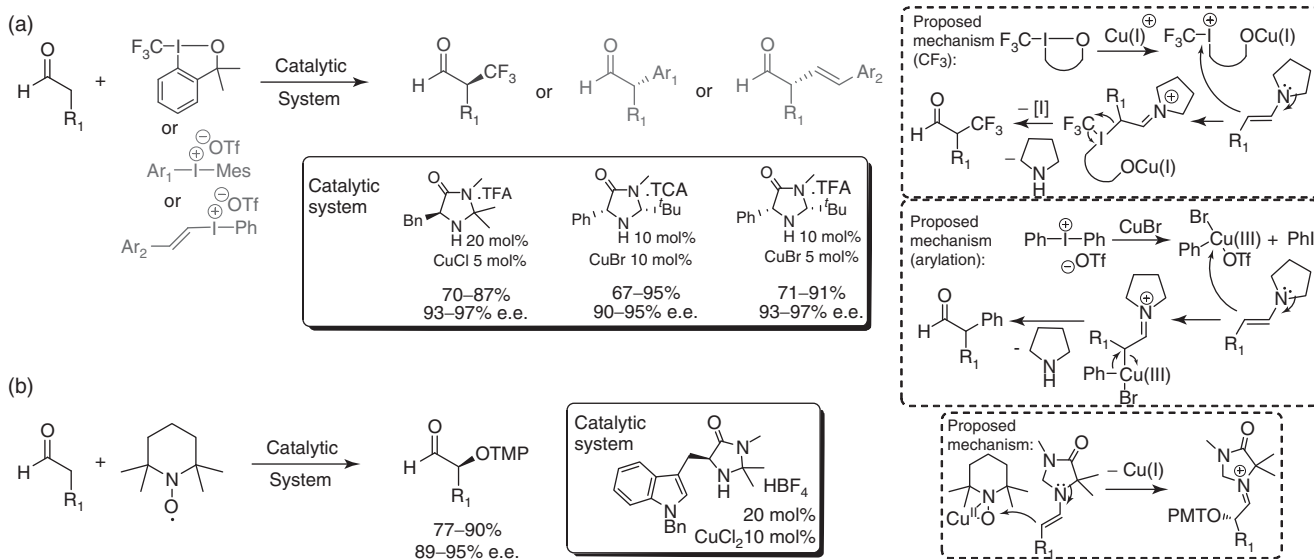
Nowadays, the number of metal-activated electrophiles that can be intercepted by transient enamines has increased considerably. The groups of Córdova, Jørgensen, Michelet, and Ratovelomanana-Vidal independently demonstrated that



**Scheme 26.4** (a–c) Selected examples of cooperative enamine addition into metal-activated electrophiles. (See insert for color representation of the figure.)

enamine nucleophiles add to metal-activated terminal alkynes through *5-exo-dig*-cyclizations. This transformation can be performed intramolecularly using several transition metal sources (such as Ag(I) [33], Cu(II) [34, 35], Cu(I) [36, 37], In(III) [38, 39], and Pd(II) [40–42]) and primary or secondary amines (up to 20 mol%), delivering cyclopentenes [37], dihydrofurans [41], and dihydropyrroles [40] with an internal double bond starting from linear aldehydes, or with an exocyclic double bond with  $\alpha$ -branched aldehydes. The cooperative catalytic system retains its efficiency even if the reaction is performed in a one-pot, two-step manner, through a simple conjugated addition/enamine cooperative cascade (Scheme 26.4b). Mechanistically, it was proposed that the metal coordinates the alkyne and the enamine double bond, followed by the cyclization and consequent protonation of the organometallic intermediate. Unfortunately, in some of the studies cited herein, the necessity of cooperative catalysis was not demonstrated by performing blank tests without the metal or the amine. In parallel, the Nishibayashi group found that enantioselective intermolecular  $\alpha$ -propargylations of aldehydes can be performed using chiral pyrrolidine derivatives and thiolate-bridged diruthenium [43] or copper [44] salts as catalysts (Scheme 26.4c). In this methodology, the metal catalyst activates terminal propargylic alcohols and benzoates to form metal-allenylidene intermediates that are susceptible to attack at the  $\gamma$ -position by the transient enamines [43] or dienamines [45]. In order for internal alkynes to become suitable substrates for this transformation, InBr<sub>3</sub> [46] was employed as catalyst as it is able to generate propargylic cationic intermediates (Scheme 26.4c).

MacMillan et al. studied the reactivity of transient enamines formed with organocatalysts with hypervalent iodine reagents in the presence of metal catalysts (Scheme 26.5a). They found that Cu(I) salts can be used in combination with chiral imidazolidinones to perform  $\alpha$ -electrophilic trifluoromethylation [47], arylation [48], and vinylation [49] of aldehydes. As suggested by the authors, the most likely mechanism involves a copper-mediated I–O bond cleavage furnishing a highly



**Scheme 26.5** (a, b) Examples of cooperative enamine addition into metal-activated electrophiles generated from prevalent iodine reagents.

electrophilic iodonium intermediate that can be attacked by the enamine. The trifluoromethylated aldehyde results from reductive elimination of phenyl iodide. Diaryl- and arylvinyl-iodonium salts were also employed as electrophiles in arylation and vinylation reactions, although the mechanism proposed for these substrates involves oxidative addition of the iodonium salts to Cu(I) catalyst, followed by enamine coordination to copper and consequent enantioselective reductive elimination.

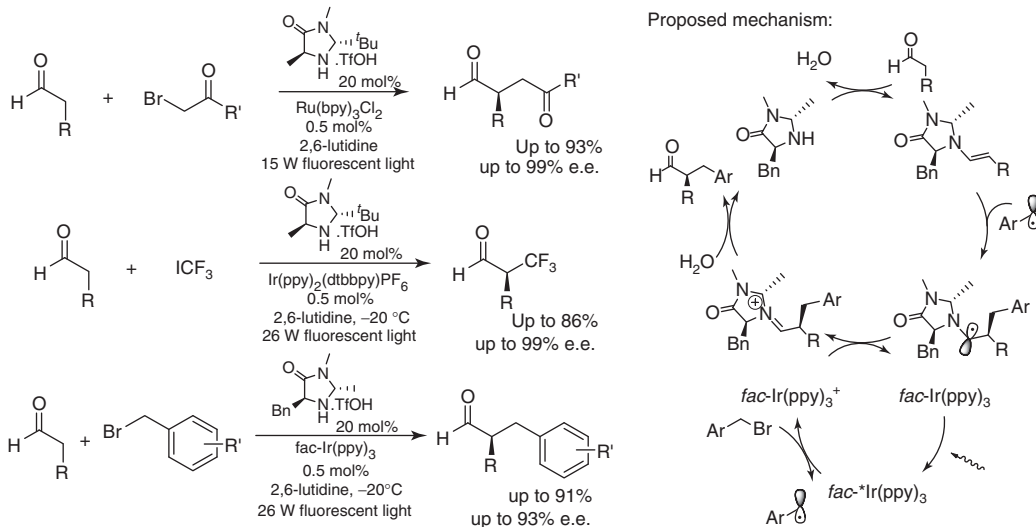
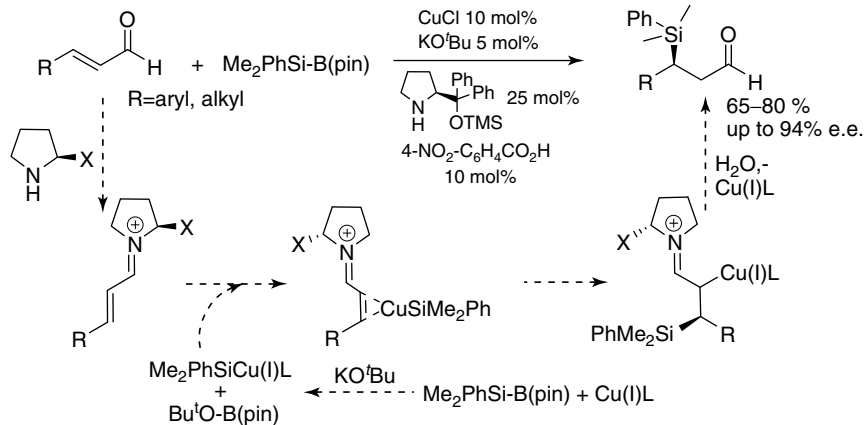
Cooperative catalysis using chiral imidazolidinones and metal catalysts is not restricted to carbon electrophiles. In 2012, the MacMillan group [50] disclosed a general approach to undertake enantioselective  $\alpha$ -oxidation of aldehydes with TEMPO by combining organocatalysis with copper catalysis (Scheme 26.5b).

### 26.3.2 Photocatalysis and Enamine-Based Catalysis

The concept of SOMO catalysis has recently appeared in the literature and is based on the utilization of photocatalysts that can oxidize and reduce organic substrates via the formation of radical intermediates. Some metallic complexes behave like photocatalysts when exposed to weak visible light by accepting a photon that will populate the metal-to-ligand charge transfer excited state. In this state, they become strong reductants and are able to cleave carbon–halide bonds [51]. MacMillan's group took advantage of this chemistry and, by merging it with enamine-based organocatalysis, was able to develop new synthetic methods to perform highly enantioselective  $\alpha$ -alkylation of aldehydes (Scheme 26.6) [52–54]. Enamines, as electron-rich alkenes, couple efficiently with electron-deficient radicals through a one-electron pathway and, for this reason, the alkyl halides explored have electron-withdrawing substituents (acyl groups [53], aryl [54] and perfluorolalkyl [52] chains). As proposed by the authors, the reaction relies on the photocatalyst's ability to reductively cleave the carbon–halide bonds giving a halide anion and a carbon-centered radical. Such radical will attack the transient enamine formed between the organocatalyst and the aldehyde, yielding  $\alpha$ -amino radicals. The latter are then oxidized to the iminium moiety by the photocatalyst and, in the final stage, the iminium is hydrolyzed, freeing the organocatalyst and the alkylated aldehyde (Scheme 26.6). These synthetic methods are unreachable to organocatalysis because most organocatalysts that could be employed are secondary amines that would become alkylated in the presence of alkyl halides.

### 26.3.3 Iminium-Based Organocatalysis

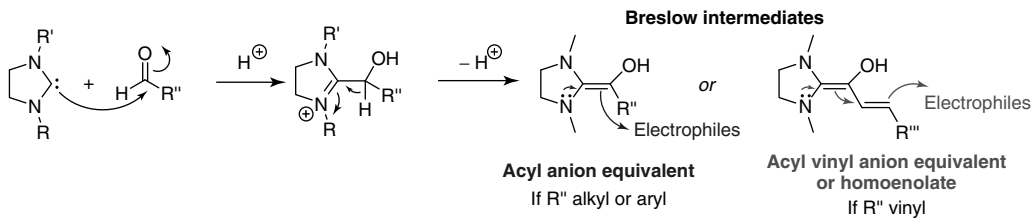
Iminium-based organocatalysis is somewhat less explored than enamine-based organocatalysis and has been mostly used in the activation of  $\alpha,\beta$ -conjugated aldehydes and ketones. Therefore, this type of catalysis has unsurprisingly been the subject of a limited number of studies under the umbrella of the metal–organic cooperative catalysis concept. In 2011, the Córdova group [55] reported the first enantioselective and chemoselective  $\beta$ -silyl addition to  $\alpha,\beta$ -unsaturated aldehydes using copper salts and chiral pyrrolidine derivatives as catalysts. As proposed, the chiral secondary amine forms an iminium salt with

**Scheme 26.6** Alkylation of aldehydes using SOMO catalysis and enamine catalysis.**Scheme 26.7** Enantioselective conjugated addition of silanes into  $\alpha,\beta$ -unsaturated aldehydes catalyzed using copper and chiral iminium catalysts.

the  $\alpha,\beta$ -unsaturated aldehydes, increasing their electrophilicity and providing a chiral environment for the silane-conjugated addition. Protonation of the organocuprate and iminium hydrolysis delivers the free saturated aldehyde (Scheme 26.7).

## 26.4 N-HETEROCYCLIC CARBENES AS ORGANOCATALYSTS

NHCs are probably best known as ligands for metal catalysis, but they are also a class of nucleophilic carbon-centered bases that have been extensively used in organocatalysis [20]. Although NHCs display strong basic properties [56–58], they are rarely used in this role; their classic mode of action involves nucleophilic addition to the carbonyl group of an aldehyde followed by proton migration to what is known as a *Breslow intermediate*; recently, it has also been proposed that the direct NHC/carbonyl adduct may be the main intermediate in some reactions [59]. In Breslow intermediates, the formerly electrophilic carbonyl carbon becomes a strong nucleophile, resulting in polarity reversal (*umpolung*) [60]. If the aldehyde is conjugated to a double bond, the  $\beta$  atom is also rendered nucleophilic, resulting in homoenolate chemistry. Moreover, Breslow intermediates are very electron rich and prone to oxidation, even by atmospheric O<sub>2</sub> [61, 62]. Other nucleophilic catalysts, most notably phosphines [60, 63, 64], share with NHCs the property of stabilizing adjacent negative charges, resulting in *umpolung* type mechanisms; however, the totally different bonding, basicity, and nucleophilicity properties

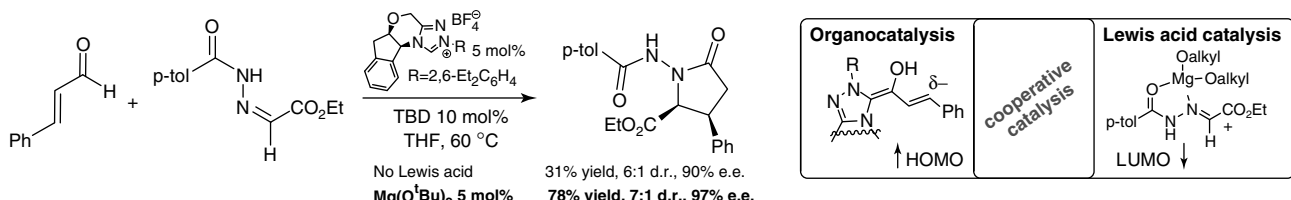


**Scheme 26.8** Reactivity *umpolung* of aldehydes in the presence of *N*-heterocyclic carbenes.

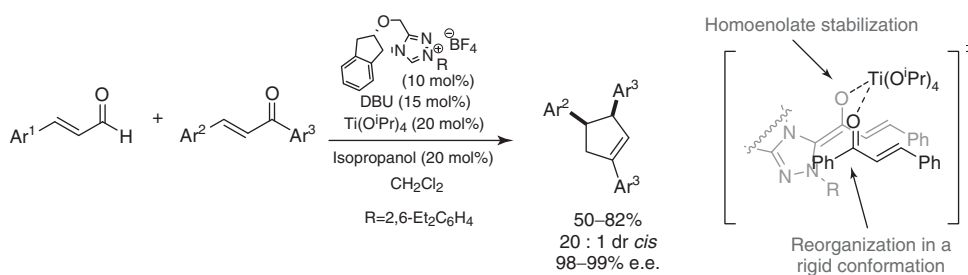
between NHCs and phosphines seldom result in similar organocatalytic activity (Scheme 26.8). The dual role of NHCs as ligands and catalysts motivated their use for cooperative catalysis, aiming to access new structural scaffolds and/or improve the selectivity of known reactions [11, 65].

Scheidt's group demonstrated that NHC-catalyzed homoenolate chemistry of cinnamaldehydes can be improved when using Lewis acids as cocatalysts. In their pioneering work, it was found that the addition of  $Mg(O^tBu)_2$  to the NHC-catalyzed synthesis of  $\gamma$ -lactams from cinnamaldehydes and *N*-benzoyl hydrazones improved the reaction yield and selectivity (Scheme 26.9) [66]. Interestingly, Cu(II), La(III), and Zn(II) triflates or Ti(IV) alkoxides inhibited the catalysis, while Mg(II) halides or triflates appeared to have no impact over this transformation. These observations indicate that the catalysis strongly depends on the Lewis acidity of the cocatalyst, which was tuned by changing the metal and its counterion. Furthermore, mechanistic studies on the role of  $Mg(O^tBu)_2$  unveiled an interesting inverse first-order kinetics that was explained on the basis of negative interactions with the organic base for higher Lewis acid loadings. To rationalize these observations, activation of the hydrazone by double coordination onto the magnesium was hypothesized, lowering the electrophile's LUMO orbital and favoring the attack by the conjugated Breslow intermediate (Scheme 26.9).

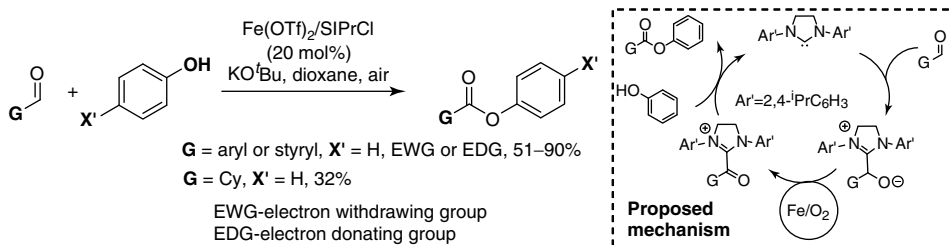
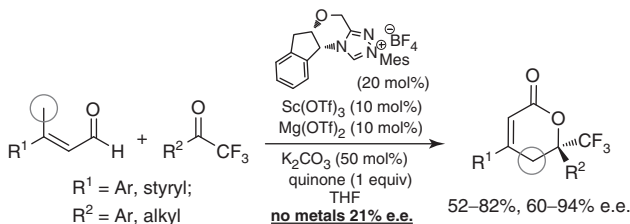
This cooperative strategy was applied to the synthesis of 1,3,4-trisubstituted cyclopentenes using chalcones as electrophiles. The addition of catalytic amounts of  $Ti(O^iPr)_4$  resulted in the exclusive formation of the *cis* diastereomer, which constituted a complete reversion of the selectivity compared to the results obtained in the exclusively organocatalyzed reaction (Scheme 26.10) [67]. To further prove the titanium complex involvement in the catalysis,  $\gamma$ -butyrolactones were synthesized in moderate enantioselectivities using a nonchiral NHC organocatalyst and chiral titanium alkoxides via enantioselective homodimerization of cinnamates. Relatively to the synthesis of 1,3,4-trisubstituted cyclopentenes, the authors at the time suggested that the titanium catalyst played a double role in the organocatalytic cycle by first stabilizing the conjugated Breslow intermediate as homoenolate and then by organizing the two substrates into a rigid transition state that provides exclusively *cis* cyclopentenes upon 1,4-conjugated addition to the chalcone. Domingo's group performed density functional



**Scheme 26.9** Cooperative effect of magnesium alkoxides in the synthesis of  $\gamma$ -lactams catalyzed by NHCs.



**Scheme 26.10** Cooperative effect of titanium alkoxides in the synthesis of cyclopentenes catalyzed by NHCs.

**Scheme 26.11** Esterification of aldehydes based in cooperative NHC and iron catalysis.**Scheme 26.12** Cooperative effect of scandium and magnesium triflates in the synthesis of  $\beta$ -unsaturated lactones catalyzed by NHCs.

theory (DFT) calculations on this system and corroborated the mechanism originally proposed by Scheidt et al. They also shown that stronger Lewis acids such as Zn(OTf)<sub>2</sub> form more stable complexes with the imidazolidene NHCs than Ti(O*i*Pr)<sub>4</sub> [68]. This observation offers a plausible explanation for the negative impact of Zn(OTf)<sub>2</sub> on the catalysis; however, it must be taken with due caution because triazolidene NHCs were employed as organocatalysts.

The Breslow intermediates are quite unstable toward oxidative conditions, providing acyl imidazolinium species that can acylate several nucleophiles or suffer 1,4-conjugated additions. Gois et al. disclosed the oxidative esterification of aldehydes using an iron/NHC catalytic system to prepare benzoic and cinnamic esters using phenols as nucleophiles (Scheme 26.11) [69]. The possibility of cooperative catalysis between the NHC and Fe/oxygen was advanced.

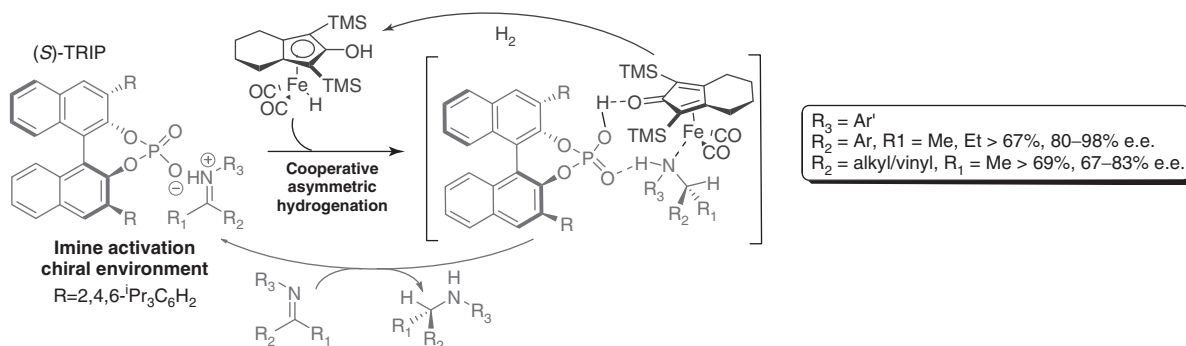
Steric hindrance limits conjugated additions and homoenolate pathways for cinnamaldehydes with two  $\beta$ -carbon substituents, offering the possibility to deprotonate their  $\gamma$ -carbon in oxidized Breslow intermediates. Chi et al. [70] shown that the resulting nucleophiles only undergo highly enantioselective additions to trifluoromethyl ketones, yielding  $\alpha,\beta$ -unsaturated lactones in the presence of a chiral NHC and a mixture of scandium and magnesium triflates (Scheme 26.12). The authors suggested that the Lewis acid organizes the electrophile closer to the nucleophile and the organocatalyst in a way that amplified chiral induction toward the remote  $\gamma$ -carbons.

## 26.5 BRØNSTED ACIDS AS ORGANOCATALYSTS

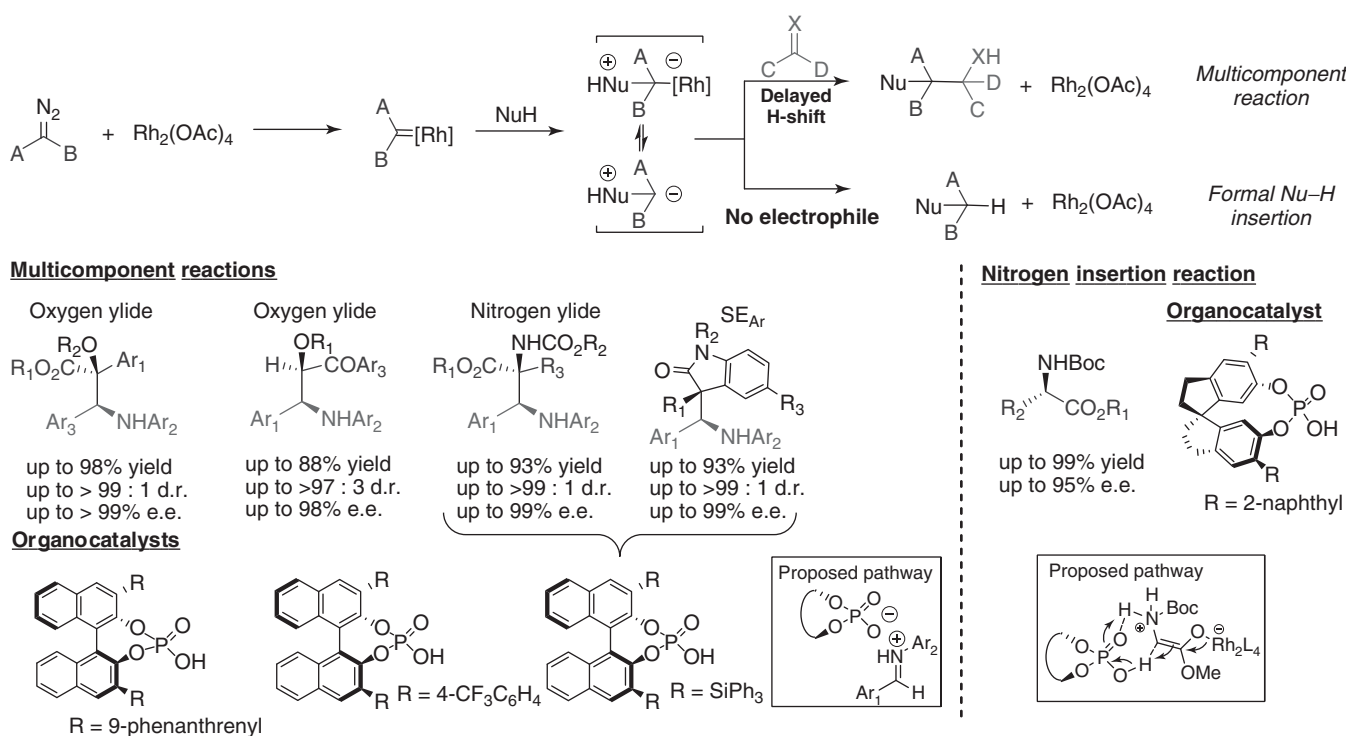
General acid catalysis is surely one of the best known catalytic processes in organic chemistry. Protonation enhances the electrophilic character of a molecule, leading to increased reactivity. Moreover, the formation of tight ion pairs or hydrogen-bonded complexes between a protonated reactant and the conjugate base of chiral acids has been a widely exploited method for enantioselective synthesis [71, 72].

In the context of metal–organo multicatalysis, protic acids offer a definite advantage over other types of organocatalysts because of their reduced tendency to inactivate the metal cocatalyst by coordination. In fact, unlike most other common organocatalysts such as NHCs or proline-like amines, the conjugate bases of these acids are not very strongly coordinating, allowing the metal center to maintain, or even display, enhanced reactivity [73].

Among all Brønsted acids, phosphoric acids derived from BINOL stand out as a class of powerful organocatalysts, activating electrophiles via protonation and providing chiral environments suitable for highly enantioselective addition of nucleophiles [74]. This unique family of organocatalysts became quite useful to activate aldehydes, ketones, and imines toward additions of metal-stabilized nucleophiles. Beller et al. [75] used (*S*)-TRIP to induce excellent levels of enantioselectivities in the hydrogenation of imines using Knölkers complex (a simple achiral iron hydrogenation catalyst). As proposed, the phosphoric acid protonates the imine substrate, which immediately accepts a hydride from the iron complex



Scheme 26.13 Phosphoric acid effect in the activation of imines toward hydrogenation using Knölkers complex.

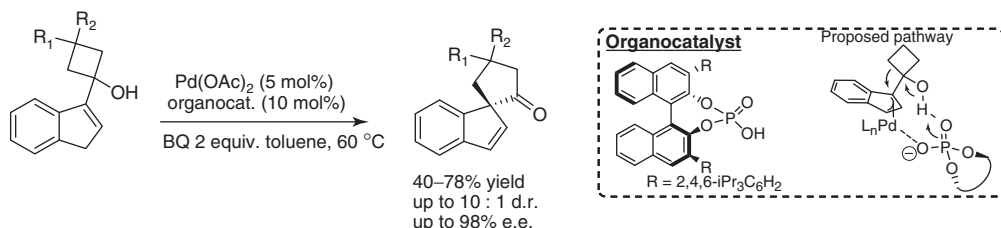


Scheme 26.14 Phosphoric acid effect in the activation of imines toward the addition of oxygen and nitrogen ylides generated in diazo compounds by rhodium(II) catalysis.

(Scheme 26.13). On the basis of this strategy, aryl and alkyl imines were converted to the respective amines with excellent enantioselectivity.

Regarding carbon nucleophiles, phosphoric acids have been applied as organocatalysts in multicomponent reactions between diazo compounds, alcohols, or amines, and aldehydes, imines, or Michael acceptors [76]. Diazo compounds can be converted into the respective metallocarbenes in the presence of dirhodium (II) carboxylates complexes [77]. Such intermediates can suffer a nucleophilic attack from alcohols or amines generating oxygen or nitrogen ylides that may undergo a proton shift, furnishing the respective O–H or N–H insertion products (insertion pathway, Scheme 26.14).

Although it has been documented that such ylides have the ability to attack activated ketones [78], aldehydes [79], or imines [80] due to a delayed hydrogen-shift, initial attempts to induce high levels of asymmetry using chiral dirhodium(II) catalysts failed [78]. High levels of enantioselectivity were only obtained when the groups of Hu, Gong, and Doyle [76, 80–83] introduced chiral phosphoric acids to activate the electrophiles and provide a more pronounced chiral environment for the ylide nucleophilic attack (Scheme 26.14).



**Scheme 26.15** Phosphoric acid effect in the activation of cyclobutanols toward palladium-catalyzed migratory ring expansion.

Phosphoric acids have also been applied as the chiral inductor in combination with palladium (II) catalysts in the migratory ring expansion of cyclobutanols to yield spirocyclic indenes. This transformation is believed to proceed via enantioselective allylic C–H activation followed by semi-pinacol ring expansion to the vicinal  $\pi$ -allylpalladium intermediate (Scheme 26.15) [84].

## 26.6 RELAY AND SEQUENTIAL CATALYSIS

### 26.6.1 Lewis and Brønsted Bases as Catalysts

As aforementioned, amines in general are arguably the most diverse and important class of organocatalysts. They display a range of catalytic mechanisms, including simple general base catalysis [85], nucleophilic catalysis [86–89], and processes involving iminium and enamine intermediates [90–93]. Although hindered (weakly nucleophilic) amines may be used if a simple basic catalyst is required, most catalytically interesting amines also have a strong affinity for metal coordination. This property has to be taken into account when designing metal–organo multicatalytic systems, as it can result in total deactivation of the metallic partner, especially considering the high loadings of amine catalysts that are often used.

In terms of relay and sequential metal–organo multicatalytic systems, these catalysts are most commonly used for 1,2 (aldol type) or 1,4 (Michael type) additions to suitable electrophiles. The most pervasive approach takes advantage of some metal-catalyzed process to generate a substrate for the organocatalyst. The examples illustrated in Scheme 26.16 show how chemical [94] or photochemical [95] metal-catalyzed oxidation of amines generates imine species that then undergo organocatalyzed 1,2 addition.

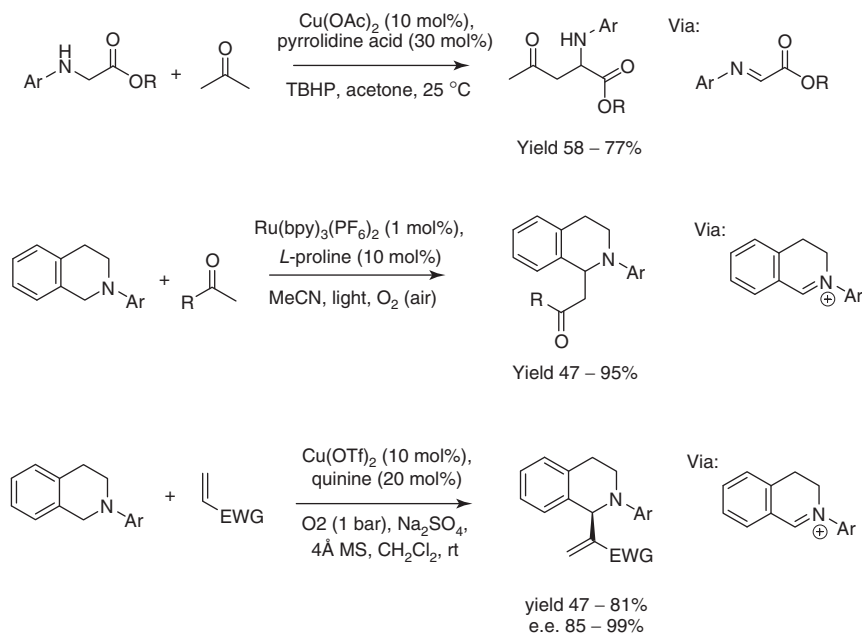
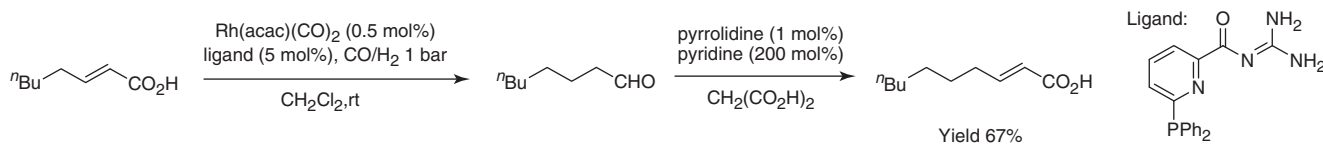
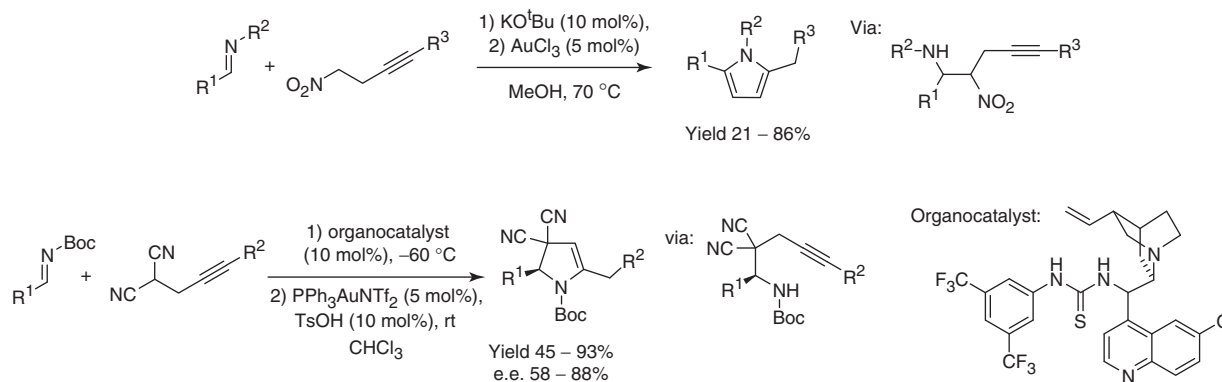
It should be noted that, even though chiral proline was used in the second example, only residual enantioselectivity was observed. The first two examples are typical enamine organocatalysis; the third example [96] probably involves a Baylis–Hillman type mechanism (nucleophilic catalysis).

Rhodium-catalyzed decarboxylative hydroformylation has been used to generate a substrate for a Knoevenagel condensation with malonic acid. This interesting sequence results in two carbon homologation of carboxylic acids (Scheme 26.17) [97].

The 1,2 addition step may also be the first in the reaction sequence, followed by a metal-catalyzed reaction, for example, Au-catalyzed addition to alkynes (Scheme 26.18).

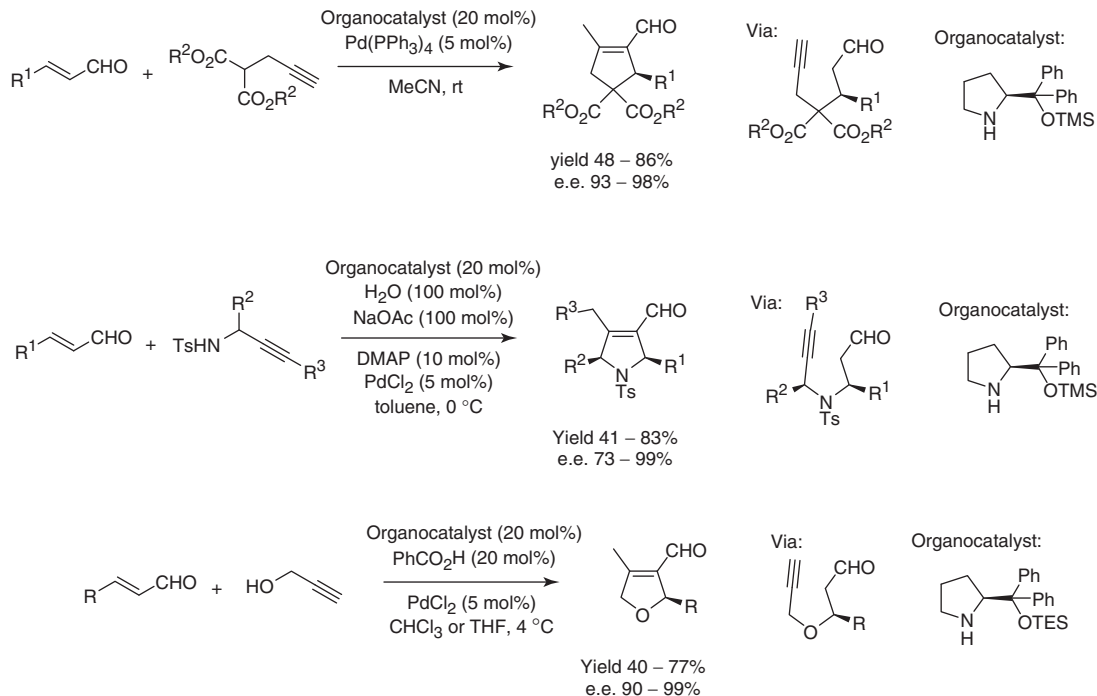
In the first example in Scheme 26.18 above, the authors reported that, despite the compatibility of the catalysts, they had to be added sequentially, to avoid an undesired cooperative process that resulted in the polymerization of the alkyne starting material [98]. In the second case, it was found that both catalysts were deactivated owing to their strong mutual affinity, again requiring sequential addition [99].

Organocatalytic 1,4 additions have also been widely explored as a setup reaction for a metal-catalyzed cyclization with an alkyne. The considerable amount of work in recent literature requires that a selection be made; Scheme 26.19 presents where the first reaction is either a C–C [37, 42, 100, 101] (Michael), N–C [40] (aza-Michael), or O–C [41] (oxa-Michael) 1,4 addition; otherwise, they are quite similar, with good enantioselectivity and moderate to good yields (Scheme 26.19). Particularly noteworthy is that a rather complex catalytic mixture was essential to obtain good results for the aza-Michael example, owing to the difficult balance between the reactivity of the organocatalyst and the metal catalyst. It should be kept in mind that sequential systems where the second step is metal catalyzed are often more challenging in terms of optimization, because the organocatalyst already present may act as a ligand and deactivate the metal center. As already mentioned in the cooperative catalysis section, the organocatalyst also intervenes in the alkyne addition step, activating the aldehyde group via enamine formation.

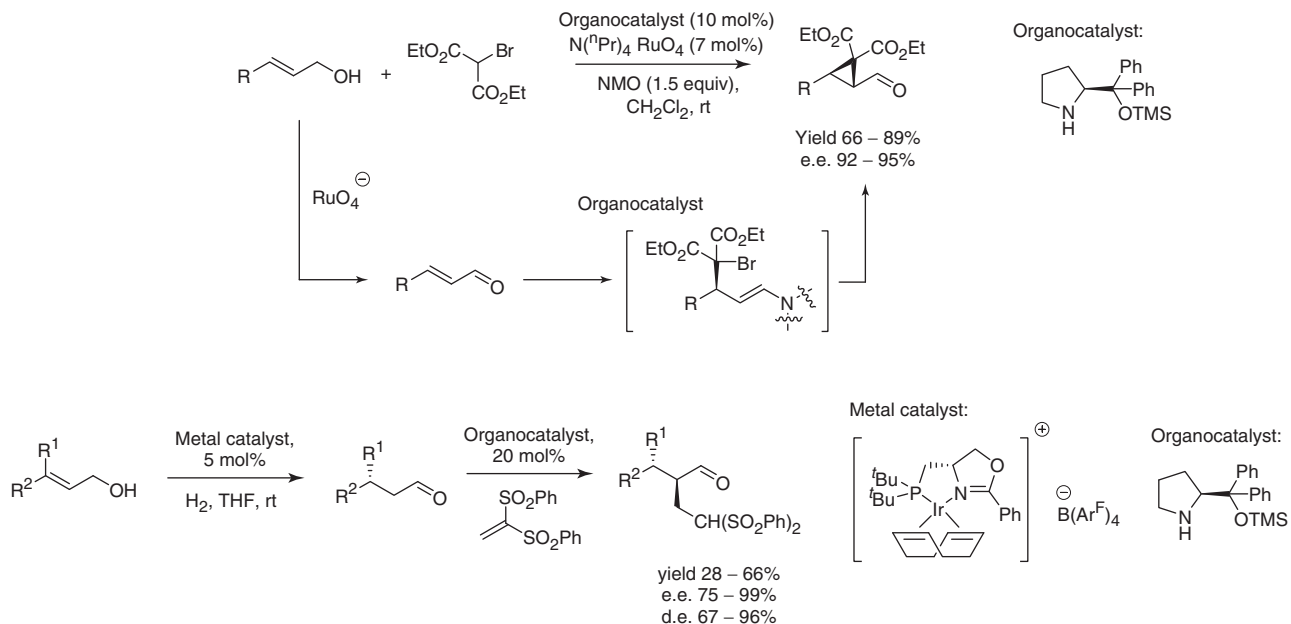
**Scheme 26.16** Metal redox/organocatalytic addition relay processes.**Scheme 26.17** Sequential hydroformylation/Knoevenagel two carbon homologation of 2,3 unsaturated acids.**Scheme 26.18** Sequential 1,2 organocatalytic addition/gold alkyne addition processes.

A wider variety of reactions has been reported if the metal-catalyzed process is the first, followed by the organocatalytic reaction. Recent sequential metal catalysis/organocatalytic 1,4 additions involve allylic oxidation [102] and double bond migration [103] metal-catalyzed processes (Scheme 26.20).

In the second example in Scheme 26.20, although the yields are moderate at best, it is noteworthy that both the metal and the organocatalyst are chiral, and each controls the conformation of a different asymmetric center.



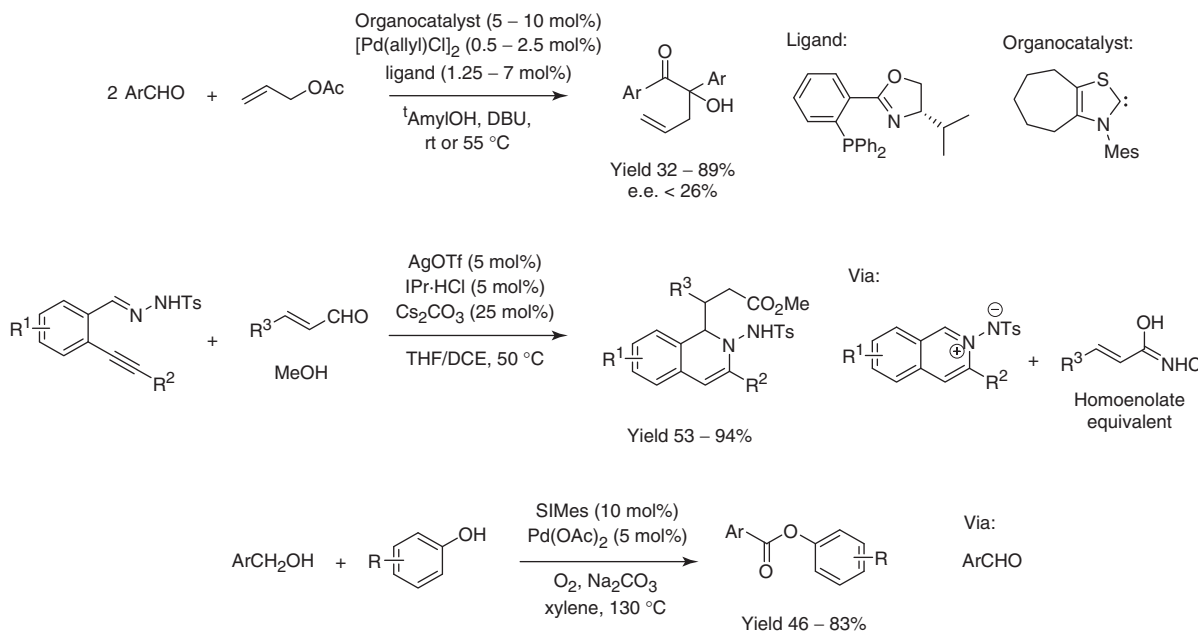
Scheme 26.19 Relay 1,4 organocatalytic addition/palladium alkyne addition processes.



Scheme 26.20 Metal catalysis/organocatalytic 1,4 addition sequences.

## 26.7 N-HETEROCYCLIC CARBENES AS ORGANOCATALYSTS

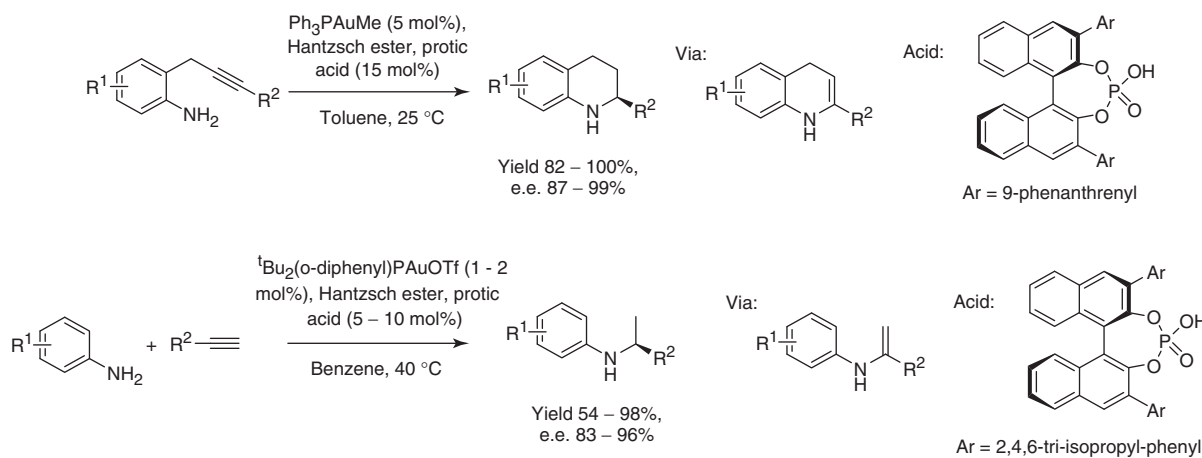
Sequential reactions involving metal and NHC catalysis are quite scarce in the literature; NHCs are powerful ligands that coordinate many metals, resulting in altered activities for both partners, so it may be difficult to create balanced catalytic systems. Fortunately, the few examples available cover several NHC mechanistic pathways, including the benzoin condensation [104], homoenolate addition [105], and NHC-catalyzed oxidation [106, 107] (Scheme 26.21).

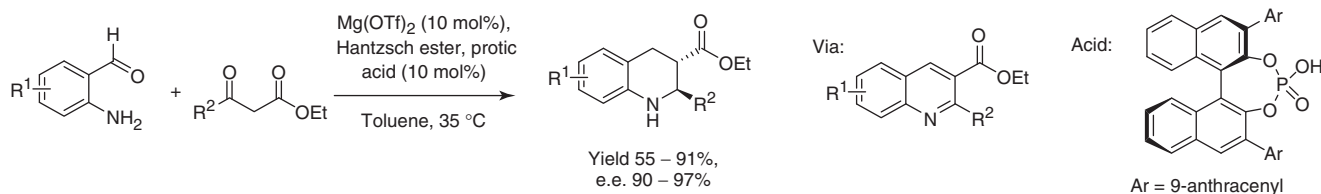
**Scheme 26.21** NHC/metal relay catalytic processes.

The metal processes involved in these reactions are Pd-catalyzed allylation, Ag activation of alkynes, and Pd benzylic oxidation. In the last example, it is interesting to observe that the metal oxidizes the alcohol to aldehyde, while the NHC oxidizes the aldehyde to an activated acyl moiety, resulting in esterification.

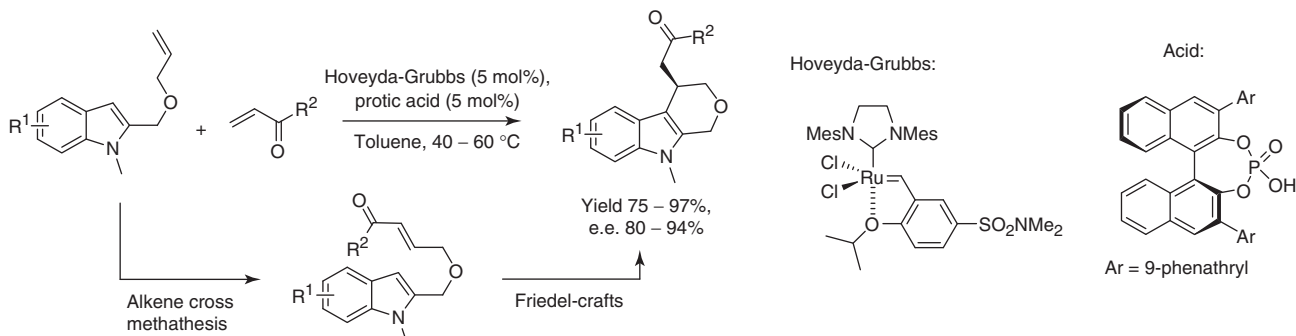
## 26.8 BRØNSTED ACIDS AS ORGANOCATALYSTS

As already stated, the use of protic acids in the context of metal–organo multicatalysis offers a definite advantage over other types of organocatalysts, because of their reduced tendency to inactivate the metal cocatalyst by coordination [73]. Hydride transfer from Hantzsch esters or similar NADH-like molecules is certainly one of the most interesting reactions catalyzed by Brønsted acids [108]. Imines, enamines, or similar substrates are protonated to iminium-reactive intermediates that are then reduced by the hydride donor. Metal-catalyzed processes that can generate these substrates may be combined with the reduction process, yielding a multicatalytic system. For example, intra- [109] or intermolecular [110] gold-catalyzed hydroamination of alkynes generates suitable imines or enamines (Scheme 26.22).

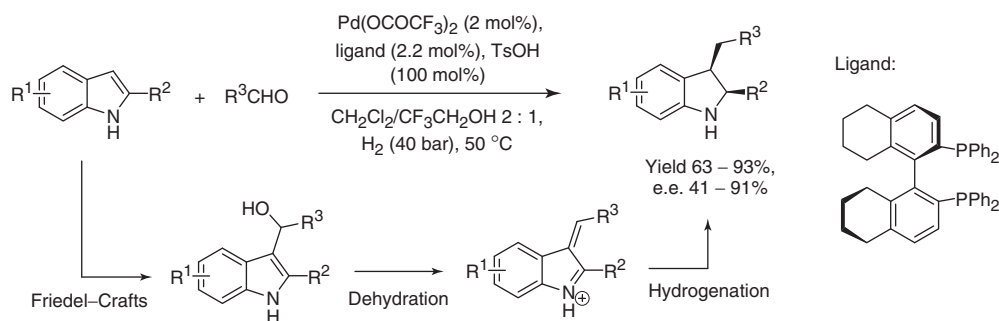
**Scheme 26.22** Gold-catalyzed alkyne addition/acid-catalyzed hydride transfer relay processes.



Scheme 26.23 Cooperatively catalyzed cyclisation/acid-catalyzed hydride transfer relay system.



Scheme 26.24 Cross-methathesis/acid-catalyzed Friedel–Crafts relay system.



Scheme 26.25 Brønsted acid/metal relay system where the enantioselectivity is determined by the metal ligand.

This method allows the reduction of the imine functionality even if included within an aromatic ring. In a recent example [111], a quinoline is formed by a Friedlander reaction, and subsequently reduced by hydride transfer from a Hantzsch ester to a chiral tetrahydroquinoline (Scheme 26.23).

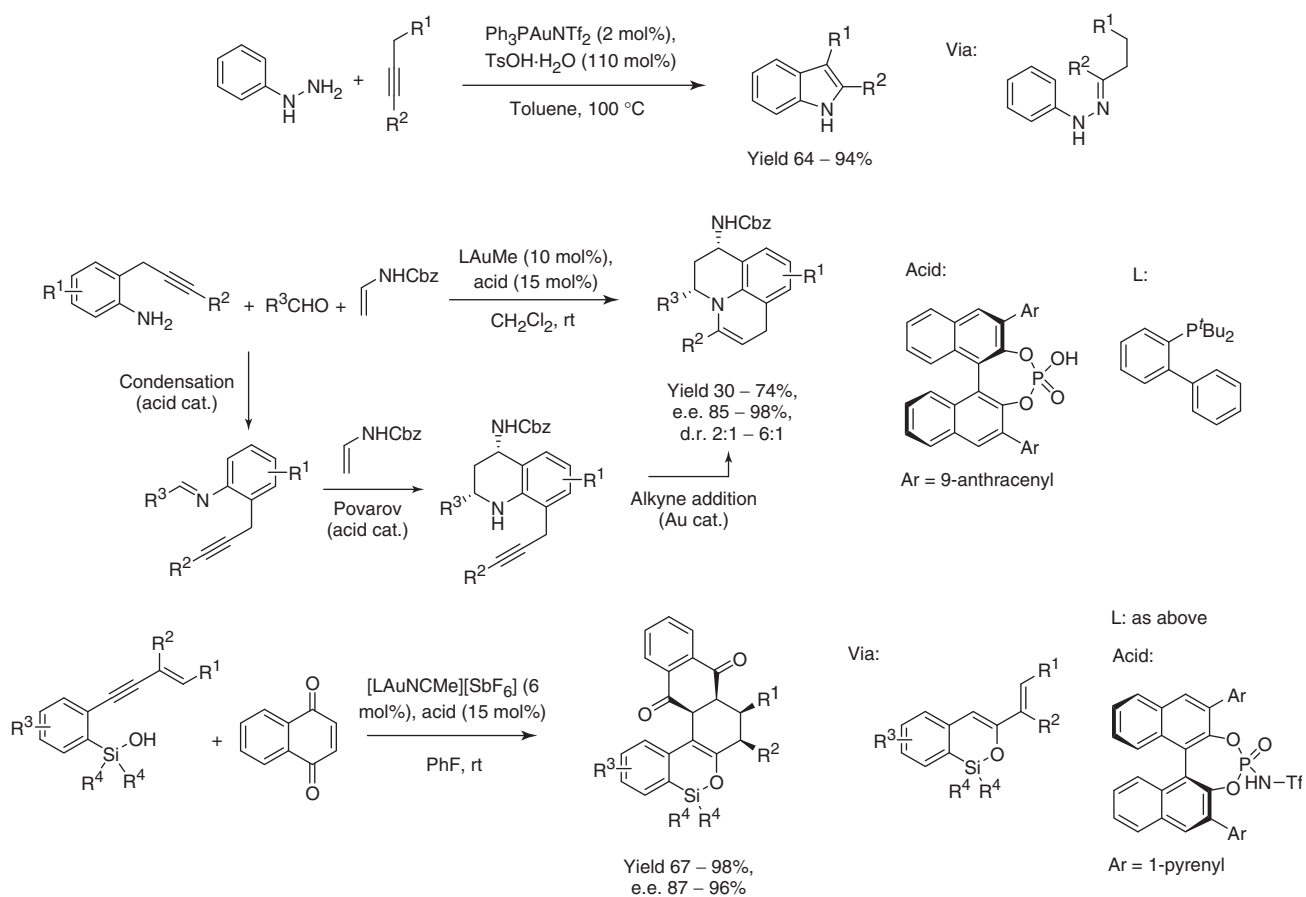
This is an interesting case in which the authors have shown that the first reaction step is cocatalyzed by the Lewis acid and the protic acid, therefore being simultaneously an example of cooperative and relay catalysis.

Brønsted acids can also catalyze a wide range of C–C-forming reactions [72] that can be combined with metal-catalyzed processes in ingenious ways. For example, Ru-catalyzed cross-methathesis [112] has been used to generate substrates for acid-catalyzed Friedel–Crafts reactions (Scheme 26.24).

The Brønsted acid is not always responsible for the chiral induction step; as shown in Scheme 26.25, a Friedel–Crafts product can be the substrate for an enantioselective Pd-catalyzed hydrogenation [113].

Gold-catalyzed addition of N–H and O–H to a triple bond has proven to be a rich source of protic acid-based multicatalytic systems. The setup for hydrogen transfer from Hantzsch esters has already been discussed; other recent examples of Au/protic acid systems include combinations with well-known acid-catalyzed reactions such as the Fischer indole synthesis [114], Povarov reaction [115], and Diels–Alder reaction[116] (Scheme 26.26).

Some of the examples that use TsOH suffer from high catalyst loadings. It is unclear if such high amount of catalyst is actually needed or if the authors were not concerned because of the cheapness of the reagent.



**Scheme 26.26** Relay systems involving alkyne addition and Brønsted acid catalysis other than hydride transfer.

## 26.9 CONCLUSION

As shown herein, the combination of metal catalysts and organocatalysts in a multicatalyzed approach is developing into a powerful strategy to synthesize complex molecules. The coexistence in one pot of a metal catalyst and an organocatalyst offers the possibility to activate both reactants in a synergistic or stepwise manner and this tactic may be explored to improve the reaction efficiency. Considering the current state of the art, and the available metal catalysts and organocatalysts still unstudied, it is clear that this emerging area is still in its infancy and exciting results still await discovery. Future developments will be centered on the discovery of compatible metal–organo catalytic pairs, new multicatalyzed reactions, and in a clearer understanding of the rules that govern the coexistence of these catalytic entities.

## REFERENCES

1. Busacca, C. A.; Fandrick, D. R.; Song, J. J.; Senanayake, C. H. *Adv. Synth. Catal.* **2011**, *353*, 1825.
2. Magano, J.; Dunetz, J. R. *Chem. Rev.* **2011**, *111*, 2177.
3. Torborg, C.; Beller, M. *Adv. Synth. Catal.* **2009**, *351*, 3027.
4. Kotha, S.; Lahiri, K.; Kashinath, D. *Tetrahedron* **2002**, *58*, 9633.
5. Giacalone, F.; Gruttaduria, M.; Agrigento, P.; Noto, R. *Chem. Soc. Rev.* **2012**, *41*, 2406.
6. Shao, Z.; Zhang, H. *Chem. Soc. Rev.* **2009**, *38*, 2745.
7. Zhong, C.; Shi, X. *Eur. J. Org. Chem.* **2010**, *2010*, 2999.
8. Allen, A. E.; MacMillan, D. W. C. *Chem. Sci.* **2012**, *3*, 633.
9. Wende, R. C.; Schreiner, P. R. *Green Chem.* **2012**, *14*, 1821.

10. Stegbauer, L.; Sladojevich, F.; Dixon, D. J. *Chem. Sci.* **2012**, *3*, 942.
11. Cohen, D. T.; Scheidt, K. A. *Chem. Sci.* **2012**, *3*, 53.
12. Rueping, M.; Koenigs, R. M.; Atodiresei, I. *Chem. Eur. J.* **2010**, *16*, 9350.
13. Hashmi, A. S. K.; Hubbert, C. *Angew. Chem. Int. Ed.* **2010**, *49*, 1010.
14. de Armas, P.; Tejedor, D.; García-Tellado, F. *Angew. Chem. Int. Ed.* **2010**, *49*, 1013.
15. Zhou, J. *Chem. Asian J.* **2010**, *5*, 422.
16. Klussmann, M. *Angew. Chem. Int. Ed.* **2009**, *48*, 7124.
17. Park, Y. J.; Park, J.-W.; Jun, C.-H. *Acc. Chem. Res.* **2008**, *41*, 222.
18. Albrecht, L.; Jiang, H.; Jørgensen, K. A. *Angew. Chem. Int. Ed.* **2011**, *50*, 8492.
19. Patil, N. T.; Shinde, V. S.; Gajula, B. *Org. Biomol. Chem.* **2012**, *10*, 211.
20. Grossmann, A.; Enders, D. *Angew. Chem. Int. Ed.* **2012**, *51*, 314.
21. Jellerichs, B. G.; Kong, J.-R.; Krische, M. J. *J. Am. Chem. Soc.* **2003**, *125*, 7758.
22. Ye, S.; Wu, J. *Tetrahedron Lett.* **2009**, *50*, 6273.
23. Knudsen, K. R.; Jorgensen, K. A. *Org. Biomol. Chem.* **2005**, *3*, 1362.
24. Yang, T.; Ferrali, A.; Sladojevich, F.; Campbell, L.; Dixon, D. J. *J. Am. Chem. Soc.* **2009**, *131*, 9140.
25. Kan, S. B. J.; Matsubara, R.; Berthiol, F.; Kobayashi, S. *Chem. Commun.* **2008**, 6354.
26. Yazaki, R.; Kumagai, N.; Shibasaki, M. *J. Am. Chem. Soc.* **2010**, *132*, 10275.
27. Yazaki, R.; Kumagai, N.; Shibasaki, M. *Chem. Asian J.* **2011**, *6*, 1778.
28. Ibrahim, I.; Córdova, A. *Angew. Chem. Int. Ed.* **2006**, *45*, 1952.
29. Afewerki, S.; Ibrahim, I.; Rydfjord, J.; Breistein, P.; Córdova, A. *Chem. Eur. J.* **2012**, *18*, 2972.
30. Bihelovic, F.; Matovic, R.; Vulovic, B.; Saicic, R. N. *Org. Lett.* **2007**, *9*, 5063.
31. Vulovic, B.; Bihelovic, F.; Matovic, R.; Saicic, R. N. *Tetrahedron* **2009**, *65*, 10485.
32. Usui, I.; Schmidt, S.; Breit, B. *Org. Lett.* **2009**, *11*, 1453.
33. Binder, J. T.; Crone, B.; Haug, T. T.; Menz, H.; Kirsch, S. F. *Org. Lett.* **2008**, *10*, 1025.
34. Montaignac, B.; Praveen, C.; Vitale, M. R.; Michelet, V.; Ratovelomanana-Vidal, V. *Chem. Commun.* **2012**, *48*, 6559.
35. Montaignac, B.; Ostlund, V.; Vitale, M. R.; Ratovelomanana-Vidal, V.; Michelet, V. *Org. Biomol. Chem.* **2012**, *10*, 2300.
36. Montaignac, B.; Vitale, M. R.; Ratovelomanana-Vidal, V.; Michelet, V. *Eur. J. Org. Chem.* **2011**, *2011*, 3723.
37. Jensen, K. L.; Franke, P. T.; Arróniz, C.; Kobbelgaard, S.; Jørgensen, K. A. *Chem. Eur. J.* **2010**, *16*, 1750.
38. Montaignac, B.; Vitale, M. R.; Ratovelomanana-Vidal, V.; Michelet, V. *J. Org. Chem.* **2010**, *75*, 8322.
39. Montaignac, B.; Vitale, M. R.; Michelet, V.; Ratovelomanana-Vidal, V. *Org. Lett.* **2010**, *12*, 2582.
40. Sun, W.; Zhu, G.; Hong, L.; Wang, R. *Chem. Eur. J.* **2011**, *17*, 13958.
41. Lin, S.; Zhao, G.-L.; Deiana, L.; Sun, J.; Zhang, Q.; Leijonmarck, H.; Córdova, A. *Chem. Eur. J.* **2010**, *16*, 13930.
42. Zhao, G.-L.; Ullah, F.; Deiana, L.; Lin, S.; Zhang, Q.; Sun, J.; Ibrahim, I.; Dziedzic, P.; Córdova, A. *Chem. Eur. J.* **2010**, *16*, 1585.
43. Ikeda, M.; Miyake, Y.; Nishibayashi, Y. *Angew. Chem. Int. Ed.* **2010**, *49*, 7289.
44. Yoshida, A.; Ikeda, M.; Hattori, G.; Miyake, Y.; Nishibayashi, Y. *Org. Lett.* **2011**, *13*, 592.
45. Ikeda, M.; Miyake, Y.; Nishibayashi, Y. *Organometallics* **2012**, *31*, 3810.
46. Motoyama, K.; Ikeda, M.; Miyake, Y.; Nishibayashi, Y. *Eur. J. Org. Chem.* **2011**, *2011*, 2239.
47. Allen, A. E.; MacMillan, D. W. C. *J. Am. Chem. Soc.* **2010**, *132*, 4986.
48. Allen, A. E.; MacMillan, D. W. C. *J. Am. Chem. Soc.* **2011**, *133*, 4260.
49. Skucas, E.; MacMillan, D. W. C. *J. Am. Chem. Soc.* **2012**, *134*, 9090.
50. Simonovich, S. P.; Van Humbeck, J. F.; MacMillan, D. W. C. *Chem. Sci.* **2012**, *3*, 58.
51. Narayanan, J. M. R.; Stephenson, C. R. J. *Chem. Soc. Rev.* **2011**, *40*, 102.
52. Nagib, D. A.; Scott, M. E.; MacMillan, D. W. C. *J. Am. Chem. Soc.* **2009**, *131*, 10875.
53. Nicewicz, D. A.; MacMillan, D. W. C. *Science* **2008**, *322*, 77.
54. Shih, H.-W.; Vander Wal, M. N.; Grange, R. L.; MacMillan, D. W. C. *J. Am. Chem. Soc.* **2010**, *132*, 13600.
55. Ibrahim, I.; Santoro, S.; Himo, F.; Córdova, A. *Adv. Synth. Catal.* **2011**, *353*, 245.
56. Magill, A. M.; Cavell, K. J.; Yates, B. F. *J. Am. Chem. Soc.* **2004**, *126*, 8717.
57. Higgins, E. M.; Sherwood, J. A.; Lindsay, A. G.; Armstrong, J.; Massey, R. S.; Alder, R. W.; O'Donoghue, A. C. *Chem. Commun.* **2011**, *47*, 1559.
58. Maji, B.; Breugst, M.; Mayr, H. *Angew. Chem. Int. Ed.* **2011**, *50*, 6915.

59. Mahatthananchai, J.; Bode, J. W. *Chem. Sci.* **2012**, *3*, 192.
60. Bugaut, X.; Glorius, F. *Chem. Soc. Rev.* **2012**, *41*, 3511.
61. Chiang, P.-C.; Bode, J. W. *Org. Lett.* **2011**, *13*, 2422.
62. Knappke, C. E. I.; Imami, A.; Jacobi von Wangelin, A. *ChemCatChem* **2012**, *4*, 937.
63. Methot, J. L.; Roush, W. R. *Adv. Synth. Catal.* **2004**, *346*, 1035.
64. Wang, X.-B.; Saga, Y.; Shen, R.; Fujino, H.; Goto, M.; Han, L.-B. *RSC Adv.* **2012**, *2*, 5935.
65. Patil, N. T. *Angew. Chem. Int. Ed.* **2011**, *50*, 1759.
66. Raup, D. E. A.; Cardinal-David, B.; Holte, D.; Scheidt, K. A. *Nat. Chem.* **2010**, *2*, 766.
67. Cardinal-David, B.; Raup, D. E. A.; Scheidt, K. A. *J. Am. Chem. Soc.* **2010**, *132*, 5345.
68. Domingo, L. R.; Zaragoza, R. J.; Arno, M. *Org. Biomol. Chem.* **2011**, *9*, 6616.
69. Reddy, R. S.; Rosa, J. N.; Veiros, L. F.; Caddick, S.; Gois, P. M. P. *Org. Biomol. Chem.* **2011**, *9*, 3126.
70. Mo, J.; Chen, X.; Chi, Y. R. *J. Am. Chem. Soc.* **2012**, *134*, 8810.
71. Rueping, M.; Nachtsheim, B. J.; Ieawsuwan, W.; Atodiresei, I. *Angew. Chem. Int. Ed.* **2011**, *50*, 6706.
72. Terada, M. *Bull. Chem. Soc. Jpn.* **2010**, *83*, 101.
73. Parra, A.; Reboreda, S.; Martin Castro, A. M.; Aleman, J. *Org. Biomol. Chem.* **2012**, *10*, 5001.
74. Rueping, M.; Kuenkel, A.; Atodiresei, I. *Chem. Soc. Rev.* **2011**, *40*, 4539.
75. Zhou, S.; Fleischer, S.; Junge, K.; Beller, M. *Angew. Chem. Int. Ed.* **2011**, *50*, 5120.
76. Qiu, H.; Li, M.; Jiang, L.-Q.; Lv, F.-P.; Zan, L.; Zhai, C.-W.; Doyle, M. P.; Hu, W.-H. *Nat. Chem.* **2012**, *4*, 733.
77. Doyle, M. P.; Duffy, R.; Ratnikov, M.; Zhou, L. *Chem. Rev.* **2009**, *110*, 704.
78. Ji, J.; Zhang, X.; Zhu, Y.; Qian, Y.; Zhou, J.; Yang, L.; Hu, W. *J. Org. Chem.* **2011**, *76*, 5821.
79. Zhang, X.; Huang, H.; Guo, X.; Guan, X.; Yang, L.; Hu, W. *Angew. Chem. Int. Ed.* **2008**, *47*, 6647.
80. Jiang, J.; Xu, H.-D.; Xi, J.-B.; Ren, B.-Y.; Lv, F.-P.; Guo, X.; Jiang, L.-Q.; Zhang, Z.-Y.; Hu, W.-H. *J. Am. Chem. Soc.* **2011**, *133*, 8428.
81. Xu, B.; Zhu, S.-F.; Xie, X.-L.; Shen, J.-J.; Zhou, Q.-L. *Angew. Chem. Int. Ed.* **2011**, *50*, 11483.
82. Xu, X.; Qian, Y.; Yang, L.; Hu, W. *Chem. Commun.* **2011**, *47*, 797.
83. Hu, W.; Xu, X.; Zhou, J.; Liu, W.-J.; Huang, H.; Hu, J.; Yang, L.; Gong, L.-Z. *J. Am. Chem. Soc.* **2008**, *130*, 7782.
84. Chai, Z.; Rainey, T. J. *J. Am. Chem. Soc.* **2012**, *134*, 3615.
85. Palomo, C.; Oiarbide, M.; Lopez, R. *Chem. Soc. Rev.* **2009**, *38*, 632.
86. France, S.; Guerin, D. J.; Miller, S. J.; Lectka, T. *Chem. Rev.* **2003**, *103*, 2985.
87. Wurz, R. P. *Chem. Rev.* **2007**, *107*, 5570.
88. Gaunt, M. J.; Johansson, C. C. C. *Chem. Rev.* **2007**, *107*, 5596.
89. Cowen, B. J.; Miller, S. J. *Chem. Soc. Rev.* **2009**, *38*, 3102.
90. Marigo, M.; Melchiorre, P. *ChemCatChem* **2010**, *2*, 621.
91. Lakhdar, S.; Ofial, A. R.; Mayr, H. *J. Phys. Org. Chem.* **2010**, *23*, 886.
92. Nielsen, M.; Worgull, D.; Zweifel, T.; Gschwend, B.; Bertelsen, S.; Jørgensen, K. A. *Chem. Commun.* **2011**, *47*, 632.
93. Mayr, H.; Lakhdar, S.; Maji, B.; Ofial, A. R.; Beilstein, J. *Org. Chem.* **2012**, *8*, 1458.
94. Xie, J.; Huang, Z.-Z. *Angew. Chem. Int. Ed.* **2010**, *49*, 10181.
95. Rueping, M.; Vila, C.; Koenigs, R. M.; Poscharny, K.; Fabry, D. C. *Chem. Commun.* **2011**, *47*, 2360.
96. Zhang, G.; Ma, Y.; Wang, S.; Zhang, Y.; Wang, R. *J. Am. Chem. Soc.* **2012**, *134*, 12334.
97. Kemme, S. T.; Šmejkal, T.; Breit, B. *Chem. Eur. J.* **2010**, *16*, 3423.
98. Barber, D. M.; Sanganee, H.; Dixon, D. J. *Chem. Commun.* **2011**, *47*, 4379.
99. Monge, D.; Jensen, K. L.; Franke, P. T.; Lykke, L.; Jørgensen, K. A. *Chem. Eur. J.* **2010**, *16*, 9478.
100. Belot, S.; Vogt, K. A.; Besnard, C.; Krause, N.; Alexakis, A. *Angew. Chem. Int. Ed.* **2009**, *48*, 8923.
101. Zweifel, T.; Hollmann, D.; Prüger, B.; Nielsen, M.; Jørgensen, K. A. *Tetrahedron Asymmetry* **2010**, *21*, 1624.
102. Rueping, M.; Sundén, H.; Sugiono, E. *Chem. Eur. J.* **2012**, *18*, 3649.
103. Quintard, A.; Alexakis, A.; Mazet, C. *Angew. Chem. Int. Ed.* **2011**, *50*, 2354.
104. Lebeuf, R. I.; Hirano, K.; Glorius, F. *Org. Lett.* **2008**, *10*, 4243.
105. Chen, Z.; Yu, X.; Wu, J. *Chem. Commun.* **2010**, *46*, 6356.
106. Luo, F.; Pan, C.; Cheng, J.; Chen, F. *Tetrahedron* **2011**, *67*, 5878.
107. Di, Z.; Changduo, P. *Catal. Commun.* **2012**, *20*, 41.

108. de Vries, J. G.; Mrsic, N. *Catal. Sci. Technol.* **2011**, *1*, 727.
109. Han, Z.-Y.; Xiao, H.; Chen, X.-H.; Gong, L.-Z. *J. Am. Chem. Soc.* **2009**, *131*, 9182.
110. Liu, X.-Y.; Che, C.-M. *Org. Lett.* **2009**, *11*, 4204.
111. Ren, L.; Lei, T.; Ye, J.-X.; Gong, L.-Z. *Angew. Chem. Int. Ed.* **2012**, *51*, 771.
112. Cai, Q.; Zhao, Z.-A.; You, S.-L. *Angew. Chem. Int. Ed.* **2009**, *48*, 7428.
113. Duan, Y.; Chen, M.-W.; Ye, Z.-S.; Wang, D.-S.; Chen, Q.-A.; Zhou, Y.-G. *Chem. Eur. J.* **2011**, *17*, 7193.
114. Patil, N. T.; Konala, A. *Eur. J. Org. Chem.* **2010**, *2010*, 6831.
115. Wang, C.; Han, Z.-Y.; Luo, H.-W.; Gong, L.-Z. *Org. Lett.* **2010**, *12*, 2266.
116. Han, Z.-Y.; Chen, D.-F.; Wang, Y.-Y.; Guo, R.; Wang, P.-S.; Wang, C.; Gong, L.-Z. *J. Am. Chem. Soc.* **2012**, *134*, 6532.

## **PART III**

---

### **ORGANOMETALLIC POLYMERIZATION CATALYSIS**



# COORDINATIVE CHAIN TRANSFER POLYMERIZATION AND COPOLYMERIZATION BY MEANS OF RARE EARTH ORGANOMETALLIC CATALYSTS FOR THE SYNTHESIS OF TAILOR-MADE POLYMERS

MARC VISSEAU<sup>\*</sup>, THOMAS CHENAL, AND PHILIPPE ZINCK

*ENSCL, Univ Lille Nord de France, Lille, France; USTL, Univ Lille Nord de France, Lille, France; CNRS, Univ Lille Nord de France, Lille, France*

## 27.1 INTRODUCTION

Polymerization catalysis has seen a huge development with the progress of organometallic chemistry. Metallocenes, post-metallocenes, and constrained geometry complexes (CGC), as single-site catalysts have been used by polymerists to elaborate new polymeric materials with improved properties [1]. Since the beginning of the twenty-first century, in addition to the search for new organometallic architectures that could be exploited as potential catalysts, polymerists have developed new methods and concepts, aiming at better controlling polymerization catalysis. Living (up to immortal) polymerization [2], chain walking [3], and chain shuttling [4] have emerged. Mastering transfer reactions in polymerization catalysis has reappeared recently as a tool that would allow a better control of the whole process, and also open the way to unprecedented macromolecular architectures [5].

The polymerization of olefins using transition metal- and lanthanide-based catalysts often suffers from the occurrence of uncontrolled transfer (and eventually termination) reactions such as, typically,  $\beta$ -hydride abstraction, which limits the range of molecular weight that can be obtained. One of the ways to prevent the latter reaction is to add an organometallic compound in excess which stabilizes the active species. In certain conditions, a reversible transmetalation of the growing polymeric chain can be observed between the two metals, giving rise to the growth of more than one macromolecular chain per catalyst. In addition to catalyst atom economy, polymers of desired molecular weights can be easily prepared. On the other hand, mastering of transfer reactions in polymerization catalysis is also of interest because it allows the preparation of functionalized polymers and/or oligomers.

In the last two decades, the rare earth compounds have importantly contributed to the development of polymerization catalysis [6]. Rare earth derivatives are very versatile catalysts that are able to polymerize with high efficiency a large variety of monomers, from olefinic ones to acrylates, and cyclic polar molecules. Controlled polymerization leading to stereoregular polymers and living processes with polymers yielding well-defined macromolecular characteristics giving rise to the preparation of sequenced copolymers are now quite commonly reachable.

We describe in this chapter our recent results, showing the possibilities offered by controlling transfer reactions in polymerization catalysis involving rare earth derivatives as precatalysts. Borohydrido compounds, which can be used in different catalytic combinations, are emphasized in this frame. We limit our scope to olefinic, nonpolar monomers, which

require a catalytic combination made up of a precatalyst in association with a cocatalyst, although most concepts discussed herein may also be suitable for acrylates and cyclic polar monomers.

## 27.2 BASIC CONCEPTS

Controlled polymerization is basically observed when initiation takes place much faster than propagation, and in the absence of irreversible transfer reactions. Polymerization catalysis involving organometallic combinations (i.e., a precatalyst associated to a cocatalyst) can in the above conditions display a living character. One additional polymerization step may however be considered, which involves a chain transfer agent (CTA). If this CTA is able to exchange reversibly and rapidly the growing polymer chain with the metal catalyst, the living character of the polymerization is in a certain manner preserved (Fig. 27.1).

Coordinative chain transfer polymerization (CCTP, also called *catalytic chain transfer polymerization*) is typically a process that comprises a chain transfer step that must be i) reversible and ii) much faster than propagation. The growing polymer chain is exchanged between a CTA and the catalyst: when attached to the CTA, it is just a dormant chain, whereas propagation takes place on the catalyst (Scheme 27.1). As a consequence, if the CTA is in excess, several macromolecular chains can be produced per catalyst molecule, and ideally (if the transfer rate is not determining), all chains will have the same length.

This concept was first disclosed independently by Samsel [7] and Mortreux [8] in ethylene polymerization, and later extended by the groups of Gibson [9] Kempe [10] and Sita [11]. It is particularly well suited in rare earth-mediated olefin polymerization, where the CTA is a main group alkyl. CCTP is part of the new concepts developed in coordination polymerization catalysis in recent years, also including living degenerative group-transfer coordination polymerization [11], chain-walking polymerization (CWP) [3], and chain-shuttling polymerization (CSP) [4]. Catalyzed chain growth (CCG) is an extension of CCTP and it was introduced by Gibson in 2002 with bis(imino)iron/MAO catalysts combined with ZnEt<sub>2</sub> as CTA and applied to ethylene polymerization. In such a process, all alkyl groups of the CTA metal are involved in the polymer chain transfer, resulting in a Poisson distribution of macromolecules with narrow PDI's [9]. It is worth noting that this was also the case with Mortreux's neodymocene/dialkyl Mg catalysts, the dialkylmagnesium compound being simultaneously used as cocatalyst and CTA. In a CSP process, two different catalysts and one CTA are involved: while each catalyst is growing a polymer chain according to its own catalytic behavior, reversible transfer occurs between them via the CTA, leading finally to the grafting of polymer sequences originating from both catalysts, in a single polymer chain.

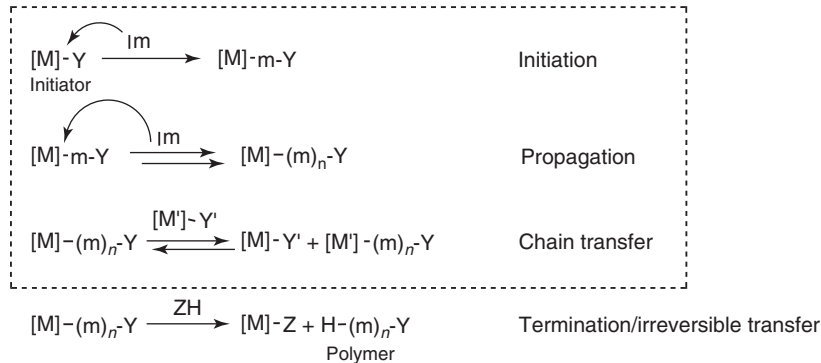
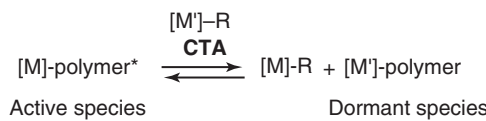


**Figure 27.1** Basic steps of a coordination polymerization process. The dotted line defines a living polymerization.



**Scheme 27.1** Polymer chain transfer in CCTP (CTA = chain transfer agent, polymer\* is a growing polymer chain).

### 27.3 CATALYTIC SYSTEMS AND THEIR APPLICATIONS IN COORDINATIVE CHAIN TRANSFER POLYMERIZATION

We disclosed a few years ago that borohydride derivatives of the rare earths can advantageously be used as precatalysts for the polymerization of nonpolar monomers, in combination with metal-alkyl compounds as cocatalysts [12]. Such catalysts were found to be very versatile as various monomers were successfully tested. Magnesium cocatalysts gave rise to controlled polymerizations, and the results were different depending on the precatalyst/cocatalyst ratio. Aluminum cocatalysts required the addition of a borate activator to afford polymers. Other catalytic combinations starting from phenate and MOF (metal organic framework) derivatives of the rare earths were also assessed and compared with the borohydride-based ones.

#### 27.3.1 Rare Earth Borohydride/Magnesium Dialkyl in Stoichiometric Amount

Figure 27.2 summarizes our results with the (co)polymerization of various nonpolar monomers. The catalysts  $\text{Ln}(\text{BH}_4)_3(\text{THF})_3$ /1 equiv BEM ( $\text{Ln} = \text{Nd}, \text{La}$ ; BEM = *n*-butylethylmagnesium) can efficiently polymerize isoprene with high degree of control, with up to 97% *trans*-1,4 rate [13]. Similar behavior was recently observed with myrcene (7-methyl-3-methylene-octa-1,6-diene,  $\text{C}_{10}\text{H}_{16}$ ), but to our surprise, the selectivity was *cis*-1,4 [14].<sup>1</sup> Toward styrene, the same catalysts afford atactic polystyrene quantitatively and in a living manner [15]. On the other hand, the  $\text{Ln}(\text{BH}_4)_3(\text{THF})_3$ /1 equiv  $\text{MgR}_2$  catalytic combination was found inactive toward the polymerization of ethylene [16]. Under the conditions of a statistical copolymerization, styrene is incorporated into *trans*-polyisoprene backbone in the form of single units. Up to 27% styrene is inserted in the copolymer for a 80:20 (styrene/isoprene) initial feed monomer ratio [17]. In general, replacing the trisborohydride precatalysts by bisborohydride half sandwiches  $\text{Cp}^R\text{Ln}(\text{BH}_4)_2(\text{THF})_2$  ( $\text{Cp}^R$  = substituted cyclopentadienyl ligand) afforded more performing catalysts, in terms of activity and selectivity, with isoprene (>98% *trans*-regular) [18], myrcene (>98% 1,4-regular) [14], styrene (>85% syndiotactic) [19], comonomer incorporation (32% styrene in polyisoprene under the aforementioned conditions [17], and a controlled character allowing the preparation of polystyrene-*b*-poly(*trans*-1,4-isoprene) [20]. In a recent study, we showed that metallocenes ( $\text{Cp}^R\text{Nd}(\text{BH}_4)(\text{THF})_n$ ) and related compounds can be successfully associated to the stoichiometric quantity of magnesium dialkyl to lead to the polymerization of isoprene with quite a fair activity [21]. Although highly *trans*-stereoselective, the heteroleptic  $\text{Cp}^*\text{Nd}\{(\text{p-tol})\text{NN}\}(\text{BH}_4)$

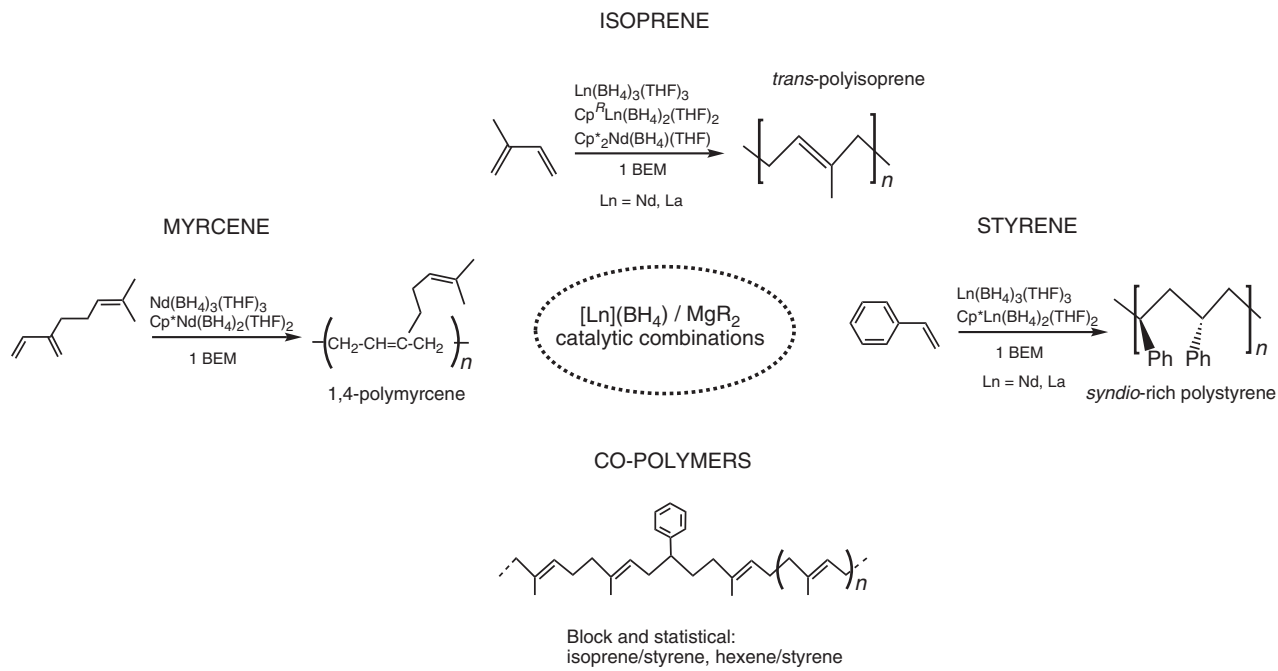


**Figure 27.2** Various olefinic monomers that are polymerized by rare earth borohydride/dialkylmagnesium catalysts.

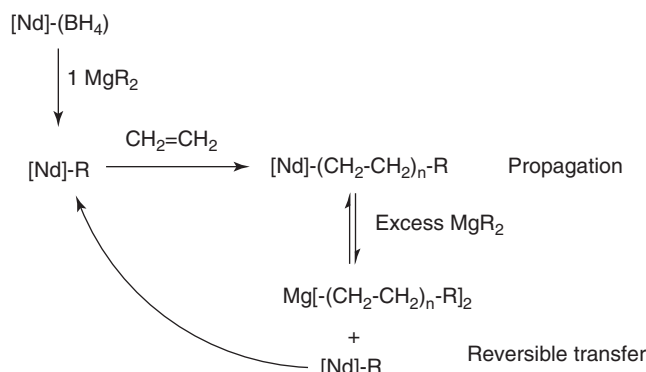
<sup>1</sup>Recent thorough reexamination of the spectra tend to establish a *trans*-selectivity. Manuscript in preparation.

$(Cp^*)' = C_5Me_4(^nPr)$ ,  $(p\text{-tol})NN = (p\text{-tol})\text{NC}(\text{Me})\text{CHC}(\text{Me})\text{N}(p\text{-tol})$ ) was less active than its half-sandwich counterpart  $Cp^*\text{Nd}(\text{BH}_4)_2(\text{THF})_2$  presumably because of lower accessibility to the metal [22]. The neodymocene  $Cp^*_2\text{Nd}(\text{BH}_4)(\text{THF})$  is poorly active and selective when associated to 1 equiv BEM toward isoprene polymerization [23].

### 27.3.2 Rare Earth Borohydride/Magnesium Dialkyl in Excess (Polymer Chain Transfer Conditions)—Homopolymerization

When combined with large excesses of dialkyl magnesium, borohydride rare earth derivatives display a very versatile character, as they afford the chain transfer polymerization of various monomers. By comparison with the stoichiometric addition of  $\text{MgR}_2$  to borohydride precatalysts, significant changes are noticed.

**27.3.2.1 Ethylene** When associated to 20–100 fold excess BEM, borohydrido-neodymocene  $Cp^*_2\text{Nd}(\text{BH}_4)\text{THF}$  affords a highly active catalyst for ethylene polymerization. This combination was the first one devoted to ethylene polymerization that was prepared from a borohydrido organolanthanide precatalyst. The behavior of the system is very similar to the one observed with its chloro analog  $Cp^*_2\text{NdCl}_2\text{Li}(\text{OEt}_2)_2$  [8]: stable activity in a first stage denoting fast and reversible Nd/Mg transfer (Scheme 27.2), and then acceleration of the activity, which corresponds to less transfer efficiency of the  $\text{MgPE}_2$  produced. After a peak of activity where the Nd-alkyl moiety polymerizes alone, a rapid decrease of monomer consumption is observed, associated with catalyst deactivation (Fig. 27.3) [23]. The CTA (in large excess) would thus play several roles,



**Scheme 27.2** Neodymium-catalyzed polyethylene chain growth on magnesium with  $[\text{Nd}](\text{BH}_4)/\text{MgR}_2$  catalyst.

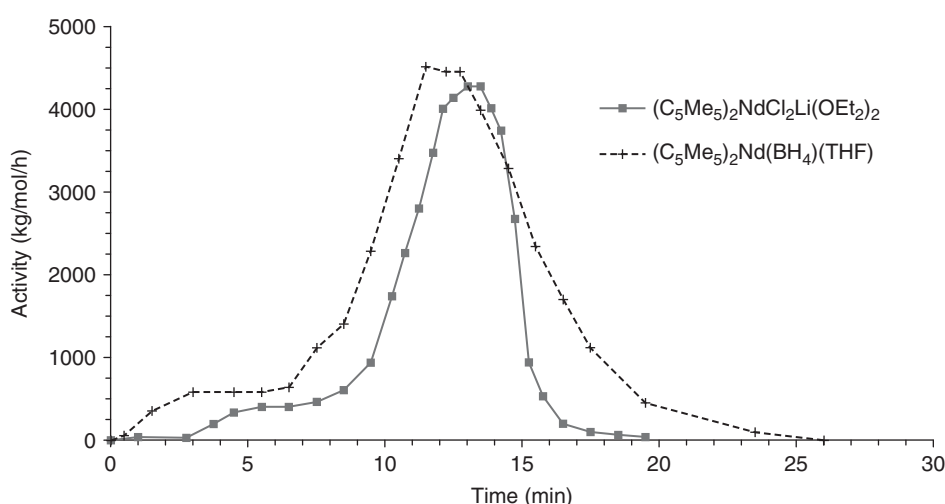


**Figure 27.3** Comparison of the monomer consumption profile in ethylene polymerization with  $Cp^*_2\text{NdCl}_2\text{Li}(\text{OEt}_2)_2/\text{BEM}$  (butylethyl-magnesium) and  $Cp^*_2\text{Nd}(\text{BH}_4)/\text{BEM}$  ( $[\text{Mg}]/[\text{Nd}] = 50$ ,  $P(\text{ethylene}) = 1.05 \text{ atm}$ , toluene (20 ml),  $90^\circ\text{C}$ ,  $[\text{Nd}] = 2 \times 10^{-4} \text{ M}$ ).

by limiting the reactivity of the  $[Ln]$ -R active species, probably through the formation of  $Ln/Mg$  heterometallic species. Consequently, deactivation via  $\beta$ -H abstraction is prevented in the first stage of the process.

One should note that the macromolecular data (Mn, PDI) of the polymer isolated during the first stage, that is, when reversible and fast chain transfer takes place, match well with one initiated polymer chain per alkyl group, which corresponds to a polyethylene CCG. These catalytic properties are comparable to those obtained a little later with *ansa*-lanthanidocene borohydride/ $nBu^nOctMg$  [24]. Interestingly, the  $Cp^*_2Nd(BH_4)_2$ /BEM catalytic system is not deactivated in the presence of large excesses of THF. This accounts for THF coordination to the magnesium atom rather than the neodymium one, as observed in the molecular structure of THF adducts of  $Nd/Mg$  bimetallic borohydrido derivatives [21]. Surprisingly, we also found that after deactivation (see above, and Fig. 27.3), the catalyst can be reactivated several times by addition of subsequent aliquots of BEM CTA. Generally, it is assumed that termination pathways in polymerization reactions involve  $\beta$ -H abstraction, to afford hydride or allyl species. To reactivate the process, displacement by an Mg-R group has been considered. In our case, the catalyst would be under a dormant form after deactivation, possibly of allyl or hydride type, strongly associated. In the presence of a new excess of BEM, regeneration of the active species through a new alkylation initiation takes place (Fig. 27.4) [25; unpublished results]. Another possible deactivation process has been advanced: the catalyst would be embedded in the growing polymer material, but in such situation reactivation by an alkyl main group metal is highly unlikely.

The half-sandwich complex is much less prone to polymerize ethylene when combined with magnesium dialkyl. We observed that  $Cp^*Nd(BH_4)_2(THF)_2/10$  BEM is quite active but 20% vinyl end groups are detected by  $^1H$  NMR, highlighting a substantial occurrence of  $\beta$ -H abstraction [26; unpublished results].

**27.3.2.2 Isoprene** In the presence of 1–10 equiv BEM as CTA combined to  $Cp^*Ln(BH_4)_2(THF)_n$  ( $Ln = La, n = 2.5$ ;  $Ln = Nd, n = 2$ ), the observed molecular weight distributions are monomodal, and the number average molecular weight is close to the calculated one, considering two growing chains per magnesium atom. This, along with reasonable polydispersities (PDI 1.3–1.9), highlights a lanthanide-catalyzed polyisoprene chain growth on magnesium (Scheme 27.3). With  $Ln(BH_4)_3(THF)_3$  ( $Ln = La, Nd$ ) under the same conditions, transfer efficiency is around 50–60%, which accounts for the CCTP process. With all the catalysts, the polymerization is significantly slowed down with BEM excesses versus 1 equiv magnesium dialkyl, as preliminarily observed for neodymium [13b]. The excess of BEM has another consequence to the polymerization process: the transmetalation is accompanied by a modification of the selectivity of the reaction, from 98.5% 1,4-*trans* with

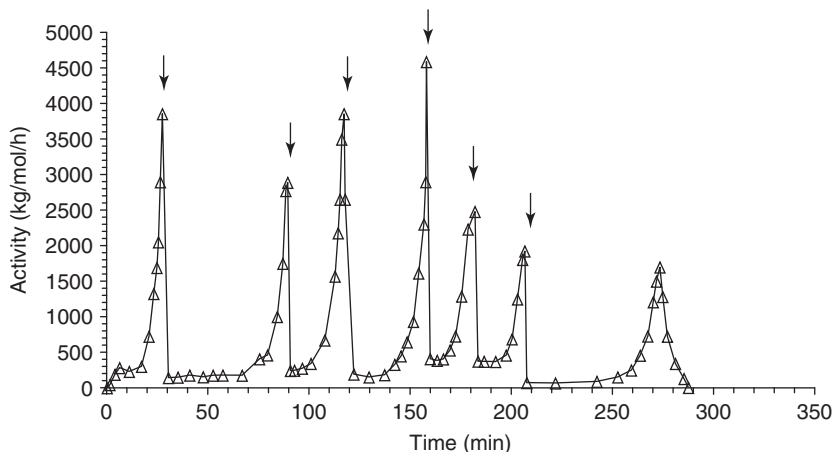
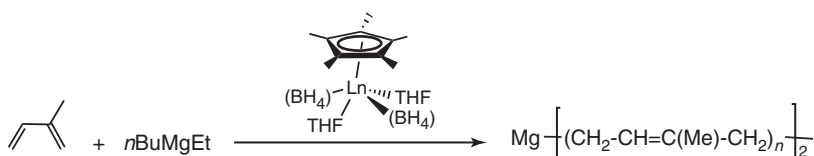


**Figure 27.4** Successive reactivation of  $Cp^*_2Nd(BH_4)_2$ /BEM toward ethylene consumption with addition of new crops of BEM (an arrow corresponds to a new addition of 50 equiv BEM).

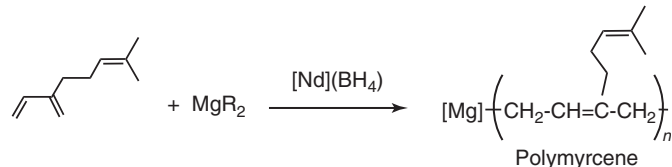


**Scheme 27.3** Rare earth-catalyzed polyisoprene chain growth on magnesium.  $Ln = Nd, La$ .

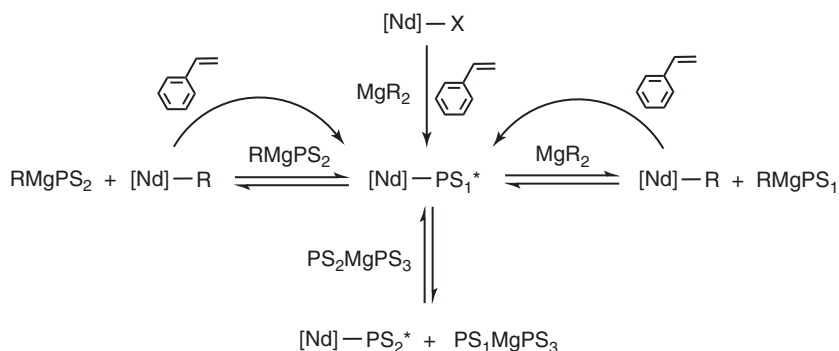
1 BEM to up to 46% 3,4-polyisoprene using 10 equiv CTA. This simply appears as a way to tune the microstructure of the polyisoprene just by adjusting the quantity of CTA [27]. Actually, a gradual decrease of the 1,4-*trans* stereoselectivity of the reaction, leading to a great variety of poly(1,4-*trans*-isoprene)-based materials, is observed at the benefit of 3,4-selectivity with increasing quantities of magnesium dialkyl. This can be at least partially attributed to the growth of 3,4-polyisoprene units on the magnesium atom, which would play a dual role: CTA, but also the propagating species, in a kind of CSP between neodymium and magnesium (see further). Another explanation may be the steric hindrance of a polymetallic Mg/Ln active species that would force the single  $\eta^2$  coordination of the incoming monomer versus a double  $\eta^4$  coordination when only 1 equiv BEM is used (see later in the text). By combining dialkylmagnesium and trialkylaluminum, we disclosed that the *trans*-selectivity can be preserved: a 1,4-*trans* stereospecific reversible CCTP of isoprene leading to the growth of several poly(1,4-*trans*-isoprene) chain per catalyst metal is reached using the half-lanthanocene  $\text{Cp}^*\text{La}(\text{BH}_4)_2(\text{THF})_2$  in combination with a mixture of BEM and  $\text{Al}^t\text{Bu}_3$  in 1/1/9, 1/1/19, or 1/1/39 quantities, respectively [28].

**27.3.2.3 Myrcene** As expected from our previous results with isoprene, polymerization of  $\beta$ -myrcene with neodymium borohydride-based coordination catalysts ( $\text{Cp}^*\text{Nd}(\text{BH}_4)_2(\text{THF})_2$  and  $\text{Nd}(\text{BH}_4)_3(\text{THF})_3$ ) in the presence of gradual excesses of BEM (1–20 equiv) shows high level of transfer reactions efficiency between neodymium and magnesium (Scheme 27.4). For 1–5 Mg cocatalyst equiv, the measured molecular weights (by SEC and end-group integration NMR) match quite well with calculated values for the growth of two chains per magnesium atom. As the BEM quantity increases, polydispersities become more narrow, which accounts for rapid and reversible polymer chain transfer. In addition, the selectivity turns from greater than 98% 1,4 (1 BEM) to 3,4-rich (64%, 20 BEM), thus illustrating the “tuning ability” of the BEM concentration in such processes, as already observed with isoprene. Taking into account the ability of BEM alone to produce low yields of 3,4- polymyrcene 86% regioregular, this switch in selectivity can be regarded as partially resulting, similarly as with isoprene, from a CSP between neodymium and magnesium [14].

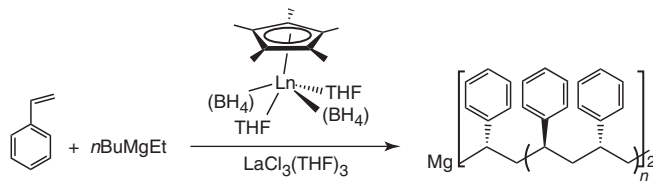
**27.3.2.4 Styrene** Transfer reactions were also evidenced with borohydride precatalysts associated to BEM in styrene polymerization. In a study centered around the structure/reactivity relationships of the precatalyst, it was shown that  $\text{Ln}(\text{BH}_4)_3(\text{THF})_x$  ( $x = 3$ ,  $\text{Ln} = \text{Nd}, \text{La}$ ) as well as the mixed  $\text{La}(\text{BH}_4)_2\text{Cl}(\text{THF})_{2.6}$  led to an efficient transmetalation of the growing polystyrene chain with the Mg-CTA (Scheme 27.5). However,  $^1\text{H}$  NMR and MALDI-TOF studies established the simultaneous occurrence of some  $\beta$ -H abstraction. Such uncontrolled termination reactions were absent with  $\text{LaCl}_3(\text{THF})_3$ ,



**Scheme 27.4** Coordinative chain transfer polymerization (CCTP) of myrcene with neodymium borohydride/dialkyl magnesium catalysts.  $[\text{Nd}](\text{BH}_4) = \text{Nd}(\text{BH}_4)_3(\text{THF})_3$ ,  $\text{Cp}^*\text{Nd}(\text{BH}_4)_2(\text{THF})_2$ ,  $\text{MgR}_2 = \text{BEM}$ .



**Scheme 27.5** Mechanism of the transfer polymerization of styrene in the presence of lanthanide borohydride/dialkylmagnesium systems.  $\text{X} = \text{BH}_4$  group;  $\text{PS}_1^*$  = growing polystyrene chain



**Scheme 27.6** Rare earth-catalyzed polystyrene chain growth on magnesium. 85% syndiotactic polystyrene for  $\text{Cp}^*\text{Ln}(\text{BH}_4)_2(\text{THF})_2$ ,  $\text{Ln} = \text{Nd}, \text{La}$ , and atactic polystyrene for  $\text{LaCl}_3(\text{THF})_3$ .

$\text{Cp}^*\text{Nd}(\text{BH}_4)_2(\text{THF})_2$ , and  $\text{Cp}^*\text{La}(\text{BH}_4)_2(\text{THF})_2$ . The quantitative transfer efficiency observed led us to conclude that there was a CCG on magnesium. Moreover, the reaction remained significantly syndioselective (85%) with the two latter ones, as observed previously when combined with only 1 equiv BEM (Scheme 27.6) [20, 29].

In summary, a CCG process was evidenced for ethylene, isoprene, and styrene, when using Ln/Mg catalytic combinations. In other words, for all these monomers, it was possible to quantitatively produce  $\text{Mg}(\text{polymer})_2$  species.

### 27.3.3 Rare Earth Borohydride/Nonmagnesium Metal Alkyl in Excess Amount

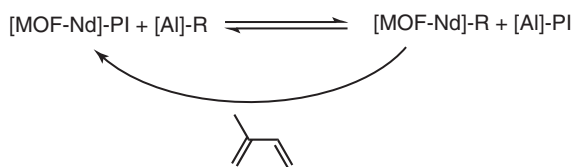
While ethylene was easily polymerized in a controlled CCG manner with a lanthanidocene associated to dialkylmagnesium, it was also observed by the group of Boisson that borohydrido *ansa*-lanthanidocene  $\text{Me}_2\text{Si}(3\text{-Me}_3\text{Si-C}_5\text{H}_3)_2\text{Nd}(\text{BH}_4)(\text{THF})_2$  can be combined with lithium alkylaluminates to yield polyethylene. However, the process is not as controlled as with Mg-cocatalysts regarding molecular weight and polydispersity values that are higher than two [24]. We found that ethylene can be smoothly polymerized by means of catalytic combinations made of a half sandwich of neodymium  $\{\text{Cp}^*\text{Nd}(\text{BH}_4)_2(\text{THF})_2/\text{[TiBA + BuLi]}\}$  (TiBA =  $\text{Al}(i\text{-Bu})_3$ ). From gas chromatography analysis of the resulting oligomers, it was shown that the polymer chain number was related to the alkyl number of the  $\text{MgR}_2$  cocatalyst, indicating that a transfer mechanism had to take place. Second, the polydispersities were rather low (circa 1.4), which denotes a high rate of reversible exchange of alkyl chains between neodymium and the cocatalyst [25; unpublished results].

Chain transfer was reported in *cis*-polymerization of isoprene using  $\text{Nd}(\text{BH}_4)_3(\text{THF})_3/\text{[HNMe}_2\text{Ph][B(C}_6\text{F}_5)_4\text{]/Al}(i\text{-Bu})_3$ . It was assumed, considering the Mn values of isolated polyisoprene, which strongly decreased in the presence of large excesses of Al cocatalyst, that a nonnegligible part of the Al cocatalyst acts as a transfer agent, with a number of growing chains per metal up to circa 10 in certain conditions. Interestingly, the PDI values remained quite narrow, indicating a rapid exchange between Al and Nd, but to the detriment of the *cis*-selectivity [30].

### 27.3.4 Miscellaneous Rare-Earth-Based Catalysts

CCTP was noticed in a study devoted to polymerization of isoprene with Nd phenate  $\text{Nd}(\text{OAr}^*)_3$  (2,6-di-*tert*-butyl-OC<sub>6</sub>H<sub>3</sub>) combined to Al cocatalysts [31]. The transfer efficiency was much lower than previously observed when similar lanthanide phenate compounds were associated to dialkylmagnesium in butadiene polymerization [32].

Keeping in mind the efficiency of aluminum derivatives as cocatalysts and CTA when associated to lanthanide versatate in conjugated diene polymerization, we investigated the behavior of some Nd-carboxylate-based MOF/aluminoxane catalysts versus isoprene polymerization [33]. At elevated temperatures, the value of initiation efficiency (vs neodymium) appeared far higher than 100%, which suggests the probable occurrence of transfer reactions between Nd and Al during the polymerization process. It is worth noting that the *cis*-selectivity remains close to 80% (Scheme 27.7).



**Scheme 27.7** Transfer reactions between Al CTA and MOF-Nd.

## 27.4 CATALYTIC SYSTEMS AND THEIR APPLICATIONS IN COORDINATIVE CHAIN TRANSFER COPOLYMERIZATION (CCTCOP)

Copolymerization presents a one-step, simple, and convenient way of polyolefin functionalization [34]. It implies the use/development of highly versatile catalytic systems able to (co)polymerize a large variety of monomers. In this context, we studied the effect of polymer chain transfer in a coordination copolymerization process.

### 27.4.1 Statistical Chain Transfer Copolymerization

Compared to classical statistical copolymerizations, the occurrence of transfer could have an effect in terms of activity, selectivity, and comonomer contents (modification of reactivity ratios).

Transmetalation between the lanthanide and the magnesium was shown to take place efficiently when monosubstituted bis-borohydrides  $\text{Cp}^*\text{Ln}(\text{BH}_4)_2(\text{THF})_n$  or trisborohydrides  $\text{Ln}(\text{BH}_4)_3(\text{THF})_3$  ( $\text{Ln} = \text{La, Nd}$ ) were combined with magnesium dialkyl in the course of a statistical isoprene/styrene copolymerization: regular decrease of molecular weights (and quite narrow polydispersities) while increasing the CTA amount was noticed. Moreover, and very interestingly, it was found that the transmetalation is accompanied by (i) an increase in the quantity of styrene inserted in the copolymer and (ii) a gradual decrease of the 1,4-*trans* stereoselectivity of the reaction at the benefit of 3,4-selectivity. Indeed, for the same monomer feed (50/50), the amount of styrene inserted in the copolymer (up to 32 mol%, vs 12 mol%) can be increased by a factor of three under CCTP conditions (using 10 equiv dialkylmagnesium) versus conventional conditions (1 equiv  $\text{Mg-CTA}$ ). Such a result in terms of comonomer content could already be obtained with  $\text{Ln/Mg}$  (1 : 1) catalysts but a 80/20 styrene/isoprene feed ratio was necessary [27, 35]. In addition, the content of 3,4-isoprene units increases from 2% to 16%, at the expense of the *trans*-selectivity (Table 27.1).

Such results can be interpreted considering the formation of polymetallic  $\text{Ln/Mg}$  active species (see further), which modify the reactivity ratio of each comonomer, to the benefit of the less active one, styrene. This was also presumably partially attributed to a magnesium-induced co-oligomerization of isoprene and styrene, with a higher reactivity of styrene as compared to neodymium. Finally, we were able to face a challenge: enhance the comonomer content, while maintaining the selectivity, by combining dialkyl magnesium and trialkyl aluminum as cocatalysts/CTA, associated to precatalyst  $\text{Cp}^*\text{La}(\text{BH}_4)_2(\text{THF})_2$ . Under such conditions, a 1,4-*trans* (up to 98%) stereospecific reversible coordinative chain transfer copolymerization (CCTCoP) of isoprene and styrene is observed. The styrene incorporation rate is this time less impressive, around 19%.

Although we did not succeed in the homopolymerization of  $\alpha$ -olefins with our borohydrido lanthanide-based catalysts [36], the  $\text{Cp}^*\text{La}(\text{BH}_4)_2(\text{THF})_2/n$ -butylethylmagnesium catalytic system was nevertheless assessed for the CCTCoP of styrene and 1-hexene. Poly(styrene-*co*-hexene) statistical copolymers were obtained with up to 46% yield, and 23% 1-hexene content (Scheme 27.8). The occurrence of chain transfer reactions in the presence of excess BEM was established in the course of the statistical copolymerization, through significant molecular weights decrease versus 1 equiv BEM, along with narrowing of the polydispersities. It is noteworthy that these transfer reactions do not modify the activity of the catalyst, by contrast with what was observed for isoprene/styrene copolymerizations. Thanks to this transfer process (and as observed in the course of isoprene/styrene copolymerization), the quantity of 1-hexene in the copolymer is increased substantially, from 8.6% to 23.2%, for 80/20 1-hexene/styrene composition in the feed and in the presence of 10 equiv BEM versus 1 equiv. From a run conducted with BEM alone, which gave, although in low yield—15% conversion in 120 h, copolymer containing

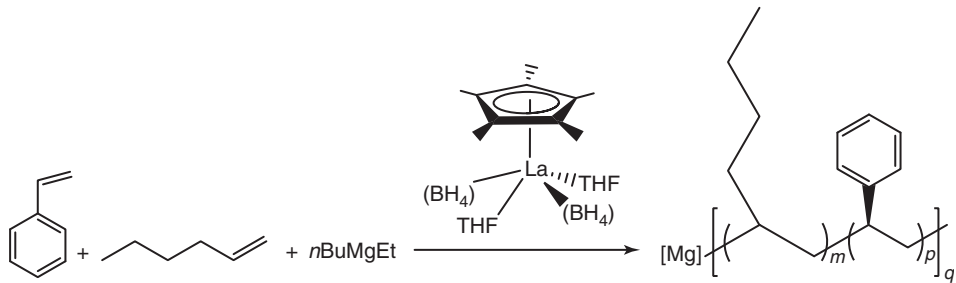
**TABLE 27.1 Isoprene/Styrene Statistical Copolymerization Results under CCTP (Excess CTA) and Conventional (Ln/Mg 1 : 1) Conditions (Precatalyst =  $\text{Cp}^*\text{La}(\text{BH}_4)_2(\text{THF})_2$ , CTA = BEM)**

S/I (feed)	Mg/Ln	Time, h	Yield, %	S, %	1,4- <i>trans</i> %	3,4-%
50/50	1	2	48	12	98	2
50/50	10	40	58	32	84	16
80/20	1 <sup>a</sup>	2	69 <sup>b</sup>	32	96	4
80/20	10	40	35	49	90	10

Monomer/catalyst = 2000 (S = styrene, I = isoprene), 50 °C,  $\text{Ln} = \text{La}$  except line 3.

<sup>a</sup> $\text{Ln} = \text{Nd}$ .

<sup>b</sup>Based on isoprene consumed.



**Scheme 27.8** Half-lanthanocene/BEM-mediated styrene–hexene coordinative chain transfer copolymerization.

37% 1-hexene, it was postulated that a kind of chain shuttling could operate between neodymium and magnesium in the course of the copolymerization [37]. These results extend the range of our concept of a chain transfer-induced control of the composition of statistical copolymers to poly(styrene-*co*-hexene) copolymers.

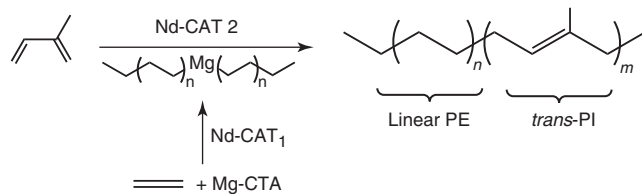
Chain transfer in the course of a metal-catalyzed statistical copolymerization may thus be viewed as a new and innovative way for the control of the composition of a copolymer.

Statistical copolymerization of ethylene and isoprene was achieved by using a borohydrido  $\text{Cp}^*(\text{BH}_4)_2\text{Nd}(\text{THF})_2$ ] ( $\text{Cp}^* = \text{C}_5\text{Me}_5$ ) half-lanthanidocene under polymer chain transfer conditions, and with lithium alkyl aluminum as cocatalyst ( $\text{Al}/\text{Nd} = 5$ ). Polyisoprene-*co*-ethylene was received, with ethylene amount incorporated of circa 25 mol%, and the stereospecificity of isoprene enchainments was found to be around 96% *trans*1,4- [38]. It is noteworthy that, in turn, isoprene/hexene copolymerization did not succeed with the same precatalyst. This was attributed, after theoretical calculations, to a difference of reactivity by comparison with isoprene/ethylene mixtures. It is noteworthy that the absence of chain transfer conditions cannot be advanced to explain this result as we checked that isoprene/hexene copolymerization failed as well with a borohydrido lanthanidocene and excess BEM.

#### 27.4.2 Sequenced Copolymerization

The living character of a CCTP process can be advantageously applied for further functionalization [39]. Considering that some of our catalytic systems could be complementary, we targeted to combine them with the aim to prepare novel macromolecular architectures. Practically, as magnesium dialkyls were found adequate to initiate the growth of polymer chains, the idea was to use a bis(polyethylenyl)magnesium  $[\text{Mg}(\text{PE})_2]$  has been recently used to prepare functionalized polyethylene, similarly to  $[\text{Al}(\text{PE})_3]$  compound as cocatalyst in the *trans*-polymerization of isoprene [16].

For this purpose, as illustrated in Scheme 27.9,  $[\text{Mg}(\text{PE})_2]$  was first prepared by using the already mentioned  $\text{Cp}^*\text{Nd}(\text{BH}_4)(\text{THF})/\text{BEM}$ -based CCTP of ethylene (or the same with the chloro analog  $\text{Cp}^*\text{NdCl}_2\text{Li}(\text{OEt})_2$ , first step, Nd-CAT<sub>1</sub>). Secondly, and without any intermediate polymer isolation, a stoichiometric amount of  $\text{Nd}(\text{BH}_4)_3(\text{THF})_3$  (Nd-CAT<sub>2</sub>) was added to the *in situ* formed  $[\text{Mg}(\text{PE})_2]$  and this mixture was immediately submitted to isoprene polymerization. As expected, the result of this dual process was a sequenced (PE)-*b*-(*trans*-PI), as established by careful analyses for the determination of the junction motives by gas chromatography, MALDI-TOF, and  $^{13}\text{C}$  NMR analysis of oligomers. Differential scanning analysis of the sequenced copolymer formed confirmed the loss of crystallinity of the polyethylene block, in line with the soft-matter character observed (Fig. 27.5).



**Scheme 27.9** Preparation of PE-TPI block copolymer by a controlled dual-catalytic process.

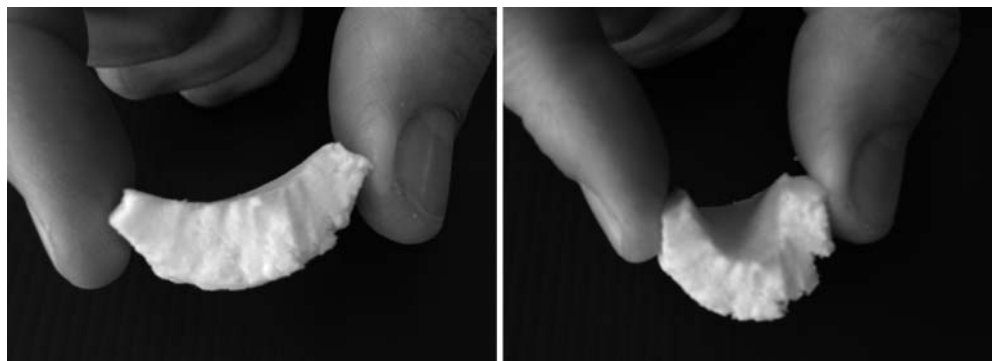


**Figure 27.5** Picture of the PE-TPI block copolymer, showing its soft gummy character.

## 27.5 DISCUSSION

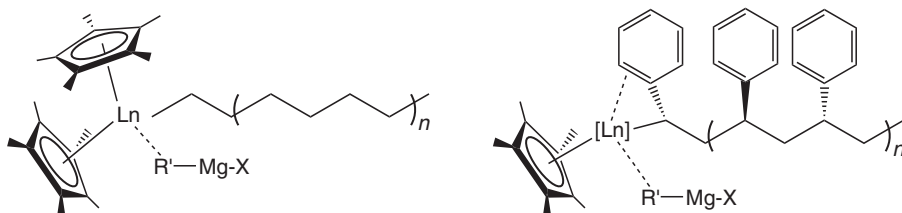
### 27.5.1 Precatalyst/Cocatalyst Adequacy

Reversible and fast chain transfer is a prerequisite in order to control a polymerization process. In this regard, relative amount and synergy between each catalytic partner, that is, precatalyst and cocatalyst/CTA, are of primary importance. This was the case with ethylene, which has been by far the most studied monomer in this frame, as shown by Gibson [9] with Fe/Zn catalysts, after the pioneering studies of Mortreux [8] with Ln/Mg and more recently Kempe with Y/Al systems [40].

Regarding the rare earths, and particularly in the “early” series (the biggest ones, from La to Sm), magnesium dialkyl seems to be the best partner, having at the same time a high transfer efficiency allowing to involve all magnesium in the process, along with very fast ability to transfer a polymer chain, finally resulting in narrow polydispersities, and hence the highest degree in mastering molecular weights. This was established for a variety of monomers: ethylene, isoprene, myrcene, styrene, showing in particular the high versatility of borohydrido lanthanide/alkyl magnesium catalytic combinations. Aluminum CTAs are less prone to transfer reactions than magnesium CTAs when combined to rare earth borohydrides (this is not the case for yttrium alkyls as demonstrated by Kempe), with lower efficiencies and broader polymolecularities. However, aluminum alkyls are mandatory for selective polymerizations that require cationic-like active species, that is, those producing syndiospecific polystyrene and 1,4-*cis* stereoregular polyisoprene.

A judicious combination of several CTAs/cocatalysts may eventually be a solution to fully control a process, like in the *trans*-isoprene CCTP and *trans*-isoprene-*co*-styrene CCTCOP described in this work. Carpentier et al. used yttrium allyl/zinc dialkyl to prepare poly-*trans*-isoprene under CCTP conditions, but the *trans*-rate is limited to circa 90% [41].

On the other hand, the molecular structure of the precatalyst may eventually require an adjustment in the cocatalyst/CTA nature: thus, whereas  $\text{Cp}^*_2\text{Nd}(\text{BH}_4)(\text{THF})$  is fully adapted to dialkyl magnesium for polyethylene CCG, lithium aluminum alkyl seems better suited to half-lanthanidocene  $\text{Cp}^*\text{Nd}(\text{BH}_4)_2(\text{THF})_2$  (see earlier in the text). Regarding the effect of the molecular structure, it was claimed in the case of polyethylene, that CCG should be more favorable for more sterically hindered catalysts [9]. On the basis of steric considerations, we tentatively drew an analogy between lanthanidocene-catalyzed polyethylene chain growth and half-lanthanidocene-catalyzed polystyrene chain growth on magnesium, considering an interaction with the aromatic ring and keeping in mind the secondary insertion of styrene that we observed (Scheme 27.10) [29].



**Scheme 27.10** Analogy between lanthanidocene-mediated polyethylene catalyzed chain growth (CCG) and half-lanthanidocene-mediated polystyrene CCG.

### 27.5.2 Active Species in CCTP

One intriguing feature in CCTP processes is the nature of the active species, as numerous metals—precatalyst, cocatalyst, CTA—are involved. Proposals have been made by several authors to clarify the nature of the active species in the frame of a CCTP, that is, in excess of the second metal [9, 40, 42]. The *in situ* formation of heterobimetallic complexes,  $[M](\mu\text{-R})_2[\text{Mg}]$  and  $[M](\mu\text{-R})_2[\text{Al}]$  ( $M$  precatalyst), depending on the cocatalyst, was advanced, whereas in the presence of a third metal, an equilibrium could take place between bridged bimetallics such as  $[\text{Fe}](\mu\text{-R})_2[\text{Zn}]$  and  $[\text{Fe}](\mu\text{-R})_2[\text{Al}]$  [9]. In turn, the propagating species is supposed to be a monometallic  $[M]\text{-R}$  alkyl derivative. However, it has just been proposed that the propagating active species could also be a singly bridged one, on the basis of calculations [43].

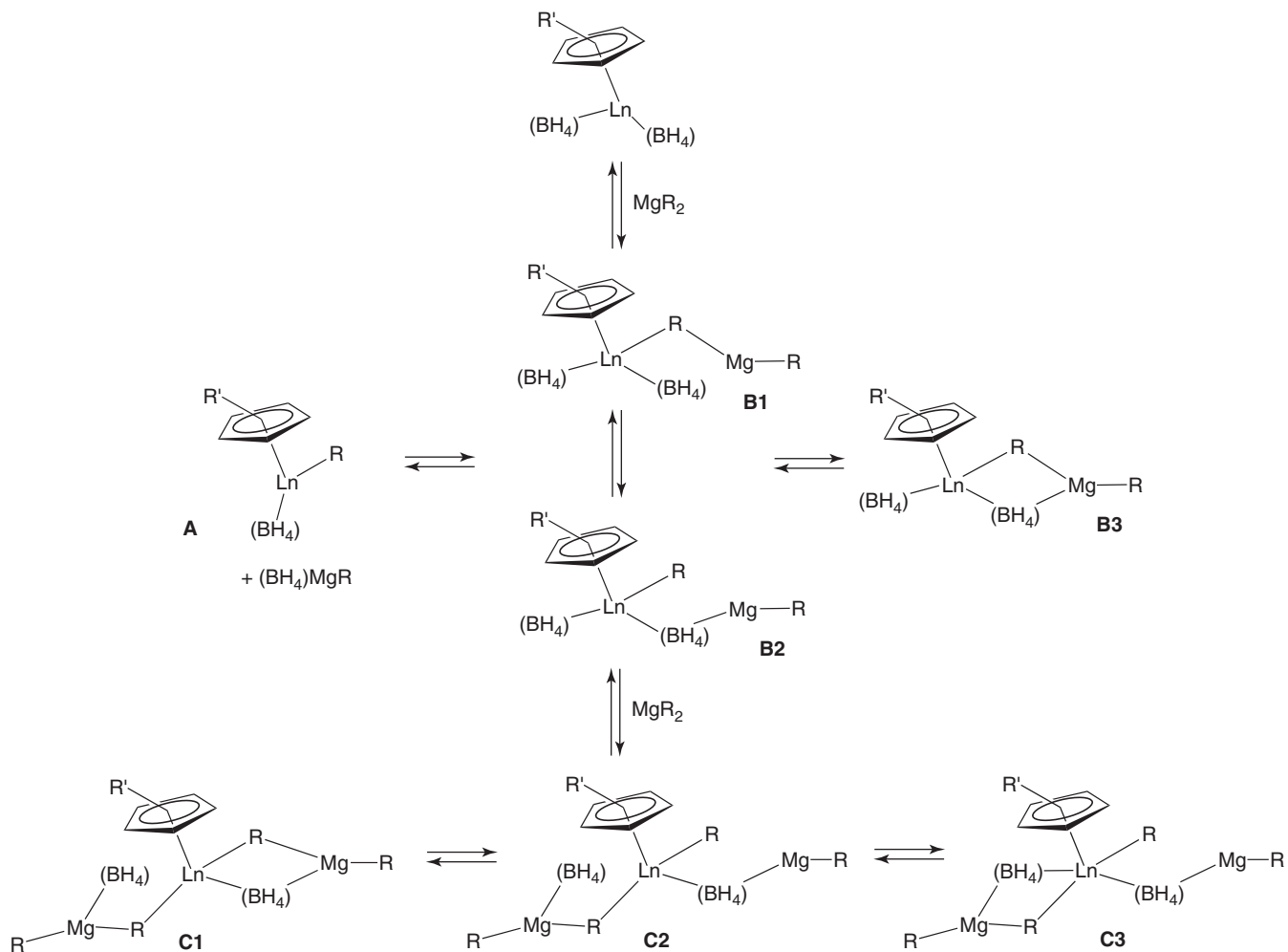
From our results in isoprene polymerization with  $\text{Ln}/\text{Mg}$  catalysts (1,4-*trans* to 3,4- switch) and in copolymerization (increase of comonomer content), it seems obvious that the active species should be different in dual-component catalytic systems, depending on whether the cocatalyst/CTA is in stoichiometric quantity or in excess. Actually, it is accepted that 3,4-polymerization is connected to steric hindrance around the metal catalyst, which will impose a single coordination of the monomer [44]. The 1,4-*trans* selectivity is supposed to result either from single  $\eta^2$  or *s-trans*- $\eta^4$  coordination that affords the *trans*-product, the most thermodynamically stable, whereas the *cis*-product is the kinetic one [45]. Alternatively such selectivity may be connected to limited possibilities of coordination due to the presence of an additional compound in the coordination sphere of the catalyst metal [46]. An *s-trans*- $\eta^4$  coordination mode of butadiene to the active  $\{[\text{Me}_2\text{Si}(\text{C}_5\text{H}_4)(\text{C}_{13}\text{H}_8)]\text{NdR}\}$  species during ethylene–butadiene copolymerization has been proposed to account for the alternate copolymer isolated [47]. Regarding the role of the cocatalyst, magnesium cocatalyst has been known for decades to favor *trans*-polymerization [45]. In our opinion, the very high level ( $>98\%$ ) of *trans*-selectivity encountered with  $\text{Ln}(\text{BH}_4)/\text{Mg}$  catalysts was connected to the existence of heterobimetallic structures (borohydrido bridged  $\text{Ln}/\text{Mg}$  bimetallics were isolated [21]), which association was strengthened by the presence of the borohydride bridge [18a].

As represented in Scheme 27.11, monometallic species A and bimetallics B1, B2 would be prone to propagate the polymerization in a 1,4-*trans* manner, whereas B3 would be a dormant form. C1, C2, and C3 trimetallic species result from the reaction with an additional BEM molecule; among them, C2 and C3 may preferentially lead to 3,4-polyisoprene, while other possible dormant forms are not represented. The more BEM is present in the mixture, the more 3,4-polymer is formed by displacement of equilibria toward polymetallic species. Note that the growth of several polymer chains per catalyst metal is not considered here.

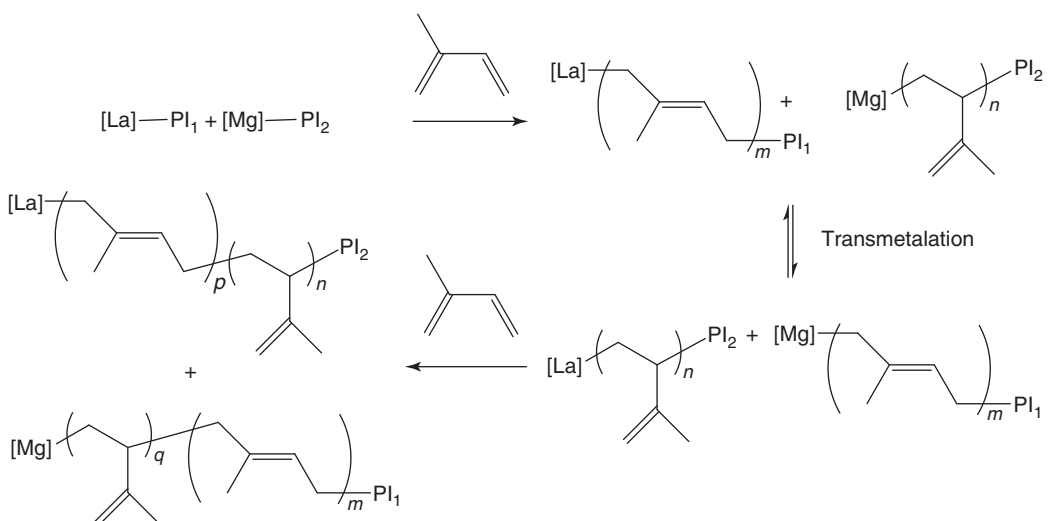
The same reasoning can be considered to account for higher comonomer incorporation in statistical copolymerizations: the higher the steric hindrance due to polymetallic associations, the more the difference of reactivity ratio will decrease in favor of a more bulky comonomer, as the latter is able to compete more efficiently with an  $\eta^2$ -coordinated isoprene molecule than with an  $\eta^4$ -coordinated one [35].

Another possibility to explain both the 3,4- tendency in selectivity (isoprene homopolymerization) and the increase of comonomer incorporation (in copolymerizations) is to consider the propensity of  $\text{MgR}_2$  to propagate a polymer chain by itself. Indeed, we were able to reproduce Yasuda's experiments, showing that magnesium-isoprene “adducts” (actually Mg-isoprenyl compounds) do polymerize isoprene over long reaction times [48], under our experimental conditions, to afford low yields of polyisoprene with 86% 3,4-selectivity [28]. Therefore, we believe that, under isoprene CCTP conditions, the transferred macromolecular chain can grow mainly in a 1,4-*trans* fashion on the lanthanide atom, and it may also be able to grow in a 3,4-fashion on the magnesium atom, leading to the observed modification of the regioselectivity and microstructure. It can thus be considered that at least a part of the 3,4-regioselectivity can be due to the growth of the polyisoprenyl chain on the magnesium atom. A consequence of this process is that isoprenyl magnesium moieties may no longer be considered as dormant species, and the overall polymerization process may result from a highly efficient transmetalation of a growing macromolecular chain between two catalysts exhibiting different catalytic behavior (Scheme 27.12). The fact that BEM too shows a propensity to incorporate rather high amounts in styrene (46%) under isoprene–styrene CCTCoP conditions also supports this hypothesis of a participation of Mg to the polymer growth.

When more than two different metals are associated in a catalytic combination, the nature of the active species will depend on the role played by each metal. In other words, Gibson postulated equilibrium between  $\text{Fe}/\text{Al}$  (alkylation and propagation) and  $\text{Fe}/\text{Zn}$  (transfer) bimetallic species, aluminum and zinc having their own task to accomplish. It is also the case in the chain-shuttling processes, where two metal catalysts interact each on their own side with the same metal-CTA. In the particular situation of our three components  $\text{Ln}/\text{Mg}/\text{Al}$  *trans*-stereospecific isoprene polymerization catalyst, trimetallic active species may be involved in the process. From our experience with all these catalytic systems, it is clear that the selectivity is rather connected to the presence of the magnesium, while the transfer of the growing polymer chains would be a role devoted to aluminum CTA. One can postulate that the “strong”  $[\text{Ln}](\mu\text{-BH}_4)[\text{Mg}]$  association is not perturbed by the polymer chain transfer between  $\text{Ln}$  and  $\text{Al}$ . The driving force of such interactions between metallic species present in the mixture could



**Scheme 27.11** Equilibrium between putative active and dormant species in CCTP conditions. R = alkyl group; R' = alkyl substituent (CpR' features any cyclopentadienyl ligand); Ln = lanthanide.



**Scheme 27.12** Proposed mechanism to account for the increase in 3,4-stereoselectivity of isoprene polymerization under CCTP conditions. PI represents polyisoprene.

be related to hard–soft considerations: the softer early lanthanide would be better “suited” to magnesium, while the late lanthanide, having a more pronounced Lewis acid character, gives more “efficient” combinations with aluminum alkyls. The metal-alkyl strength should be considered, as earlier proposed by Gibson, but in terms of dynamic heterometallic structures.

## 27.6 CONCLUSION—PERSPECTIVES

The high versatility of lanthanide-based catalysts has allowed to extend the concept of CCTP from ethylene and  $\alpha$ -olefins, to monomers such as styrene, and conjugated dienes, including the biosourced myrcene. Borohydrido derivatives are particularly powerfully combined with magnesium dialkyls to afford catalytic systems having up to 100% polymer chain transfer efficiency with these monomers. The CTA, which efficiently plays the role of a protecting agent versus  $\beta$ -H abstraction, also allows catalyst atom economy and high control of molecular weights. In the conditions of a statistical coordinative chain transfer copolymerization, dual borohydrido lanthanide/magnesium alkyl catalysts give access to a range of copolymers, which can be tuned by selectivity and the comonomer content, depending on the precatalyst/cocatalyst (CTA) ratio.

The living macromonomers can subsequently be utilized as building blocks for the elaboration of unprecedented macromolecular block structures such as the PE-*b*-TPI copolymer.

Future challenges in the frame of CCTP will consist of disclosing the most efficient catalytic combinations and by the way particular attention should be paid on the molecular nature of the CTA/cocatalyst. Indeed, the general strategy in polymerization catalysis is based on the search for new organometallic precatalyst architectures, whereas little is done regarding the CTA/cocatalyst itself. One can think about varying its molecular structure as well. In this regard, the *in situ* modification by the simple addition of a molecule that will change the properties of a CTA, in terms of alkylating ability, polymer chain transfer ability, or stereochemical induction, is of primary interest.

In addition, although many polymerization processes have been claimed as living, the subsequent *in situ* functionalization of a growing polymer chain is generally hard to achieve with high yields, and it remains a goal to reach with stereoregular polydienes, for instance. Chain transfer could be more generally seen as a way to render a growing polymer chain active toward functionalization, as the chemistry of a [metal catalyst]-polymer is thus replaced by the chemistry of a [metal-CTA]-polymer.

The degree of intervention of the CTA in selectivity is not clear up to now, and, in this regard, theoretical support would be helpful in getting more mechanistic insights into CCTP. Similarly, in the particular situation where more than two metals are involved in a polymerization process, the specific role of each one—alkylation, chain transfer, stereoregulation assistance—should also be clarified by means of joint theoretical/experimental studies.

The versatility of chain transfer polymerization together with its easiness of use relative to the synthetic effort that would require a “one catalyst, one material” approach or to the difficulties encountered by other routes explored for fine-tuning polymerization selectivities makes this approach undoubtedly an attractive and promising field for the future of coordination polymerization. CCTP renders the emergence of the “one catalyst, several materials” paradigm a reality.

## REFERENCES

- (a) *Stereoselective Polymerization with Single-Site Catalysts*; Baugh, L. S.; Canich, J. M., Eds.; CRC: New York, **2008**; (b) Mitani, M.; Saito, J.; Ishii, S. I.; Nakayama, Y.; Makio, H.; Matsukawa, N.; Matsui, S.; Mohri, J. I.; Furuyama, R.; Terao, H.; Bando, H.; Tanaka, H.; Fujita, T. *Chem. Rec.* **2004**, *4*, 137; (c) Special issue: Gladysz J. A., Ed. *Chem. Rev.* **2000**, *100*, Frontiers of Metal-Catalyzed Polymerization.
- (a) Coates, G. W.; Hustad, P. D.; Reinartz, S. *Angew. Chem. Int. Ed.* **2002**, *41*, 2236; (b) Inoue, S. *J. Polym. Sci., Part A: Polym. Chem.* **2000**, *38*, 2861.
- Guan, Z.; Cotts, P. M.; McCord, E. F.; McLain, S. J. *Science* **1999**, *283*, 2059.
- Arriola, D. J.; Carnahan, E. M.; Hustad, P. D.; Kuhlman, R. L.; Wenzel, T. T. *Science* **2006**, *312*, 714.
- Zhao, Y.; Wang, L.; Xiao, A.; Yu, H. *Prog. Polym. Sci.* **2010**, *35*, 1195.
- (a) Special issue: Roesky, P. W., Ed. *Struct. Bond.* **2010**, *137*, Molecular catalysis of rare earth elements; (b) Hou, Z.; Luo, Y.; Li, X. *J. Organomet. Chem.* **2006**, *691*, 3114.
- (a) Samsel, E. G. U.S. Patent 5,210,338, **1993**; (b) Samsel, E. G.; Eisenberg, D. C. U.S. Patent 5,276,220, **1994**.
- Pelletier, J. F.; Mortreux, A.; Olonde, X.; Bujadoux K. *Angew. Chem. Int. Ed.* **1996**, *35*, 1854.
- (a) Britovsek, G. J. P.; Cohen, S. A.; Gibson, V. C.; Maddox, P. J.; van Meurs, M. *Angew. Chem. Int. Ed.* **2002**, *41*, 489; (b) Britovsek, G. J. P.; Cohen, S. A.; Gibson, V. C.; van Meurs, M. *J. Am. Chem. Soc.* **2004**, *126*, 10701.

10. Kempe, R. *Chem. Eur. J.* **2007**, *13*, 2764.
11. Sita, L. *Angew. Chem. Int. Ed.* **2009**, *48*, 2464.
12. Visseaux, M.; Bonnet, F. *Coord. Chem. Rev.* **2011**, *374*.
13. (a) Bonnet, F.; Visseaux, M.; Pereira, A.; Barbier-Baudry, D. *Macromol. Rapid Commun.* **2004**, *25*, 873; (b) Terrier, M.; Visseaux, M.; Chenal, T.; Mortreux, A. *J. Polym. Sci., Part A: Polym. Chem.* **2007**, *45*, 2400.
14. Loughmari, S.; Hafid, A.; Bouazza, A.; El Bouadili, A.; Zinck, P.; Visseaux, M. *J. Polym. Sci., Part A: Polym. Chem.* **2012**, *50*, 2898.
15. Zinck, P.; Visseaux, M.; Mortreux, A. *Z. Anorg. Allg. Chem.* **2006**, *632*, 1943.
16. Chenal, T.; Visseaux, M. *Macromolecules* **2012**, *45*, 5718.
17. Zinck, P.; Terrier, M.; Valente, A.; Mortreux, A.; Visseaux, M. *Macromol. Chem. Phys.* **2007**, *208*, 973.
18. (a) Bonnet, F.; Visseaux, M.; Pereira, A.; Barbier-Baudry, D. *Macromolecules* **2005**, *38*, 3162. (b) Visseaux, M.; Terrier, M.; Mortreux, A.; Roussel, P. *C.R. Chim.* **2007**, *10*, *12*, 1195; (c) Visseaux, M.; Zinck, P.; Terrier, M.; Mortreux, A.; Roussel, P. *J. Alloy. Compd.* **2008**, *451*, 352.
19. Zinck, P.; Valente, A.; Terrier, M.; Mortreux, A.; Visseaux, M. *C.R. Chim.* **2008**, *11*, 595.
20. Zinck, P.; Valente, A.; Mortreux, A.; Visseaux, M. *Polymer* **2007**, *48*, 4609–4614.
21. Visseaux, M.; Terrier, M.; Mortreux, A.; Roussel, P. *Eur. J. Inorg. Chem.* **2010**, 2867.
22. Bonnet, F.; Visseaux, M.; Barbier-Baudry, D.; Vigier, E.; Kubicki, M. M. *Chem. Eur. J.* **2004**, *10*, 2428.
23. Visseaux, M.; Chenal, T.; Roussel, P.; Mortreux, A. *J. Organomet. Chem.* **2006**, *691*, 86.
24. Thuilliez, J.; Spitz, R.; Boisson, C. *Macromol. Chem. Phys.* **2006**, *207*, 1727.
25. Visseaux, M.; Chenal, T.
26. Average activity = 30 kg/mol Nd/h, ethylene consumption during t > 70 min, DPn ca. 50, Chenal, T.; Visseaux, M.
27. Valente, A.; Zinck, P.; Mortreux, A.; Visseaux, M. *Macromol. Rapid Commun.* **2009**, *30*, 528.
28. Valente, A.; Zinck, P.; Vitorino, M. J.; Mortreux, A.; Visseaux, M. *J. Polym. Sci., Part A: Polym. Chem.* **2010**, *48*, 4640.
29. Zinck, P.; Valente, A.; Bonnet, F.; Violante, A.; Mortreux, A.; Visseaux, M.; Ilinca, S.; Duchateau, R.; Roussel, P. *J. Polym. Sci., Part A: Polym. Chem.* **2010**, *48*, 802.
30. Visseaux, M.; Mainil, M.; Terrier, M.; Mortreux, A.; Roussel, P.; Mathivet, T.; Destarac, M. *Dalton Trans.* **2008**, 4558.
31. Vitorino, M. J.; Zinck, P.; Visseaux, M. *Eur. Polym. J.* **2012**, *48*, 1289.
32. Gromada J.; Le Pichon, L.; Mortreux, A.; Leising, F.; Carpentier J. F. *J. Organomet. Chem.* **2003**, *683*, 44.
33. Vitorino, M. J.; Devic, T.; Tromp, M.; Ferey, G.; Visseaux, M. *Macromol. Chem. Phys.* **2009**, *210*, 1923.
34. Zinck, P.; Bonnet, F.; Mortreux, A.; Visseaux, M. *Prog. Polym. Sci.* **2009**, *34*, 369.
35. Valente, A.; Zinck, P.; Mortreux, A.; Visseaux, M. *J. Polym. Sci., Part A: Polym. Chem.* **2011**, *49*, 1615.
36. Neodymium complexes with bulky *ansa*-bis(cyclopentadienyl) ligands used in combination with magnesium dialkyls were shown to be able to oligomerize 1-octene with the occurrence of chain transfer reactions: Bogaert, S.; Chenal, T.; Mortreux, A.; Nowogrocki, G.; Lehmann, C. W.; Carpentier, J.-F. *Organometallics* **2001**, *20*, 199.
37. Valente, A.; Zinck, P.; Mortreux, A.; Bria, M.; Visseaux, M. *J. Polym. Sci., Part A: Polym. Chem.* **2011**, *49*, 3778.
38. Perrin, L.; Bonnet, F.; Chenal, T.; Visseaux, M.; Maron, L. *Chem. Eur. J.* **2010**, *16*, 11376.
39. Amin S. B.; Marks, T. J. *Angew. Chem. Int. Ed.* **2008**, *47*, 2006.
40. Kretschmer, W. P.; Meetsma, A.; Hessen, B.; Schmalz, T.; Qayyum, S.; Kempe, R. *Chem. Eur. J.* **2006**, *12*, 8969.
41. Annunziata, L.; Duc, M.; Carpentier, J. F. *Macromolecules* **2011**, *44*, 7158.
42. (a) Chenal, T.; Olonde, X.; Pelletier, J. F.; Bujadoux, K.; Mortreux, A. *Polymer* **2007**, *48*, 1844–1856; (b) Boisson, C.; Monteil, V.; Ribour, D.; Spitz, R.; Barbotin, F. *Macromol. Chem. Phys.* **2003**, *204*, 1747.
43. Camara, J. M.; Petros, R. A.; Norton, J. R. *J. Am. Chem. Soc.* **2011**, *133*, 5263.
44. Li, S.; Cui, D.; Li, D.; Hou, Z. *Organometallics* **2009**, *28*, 4814.
45. Friebel, L.; Nuyken, O.; Obrecht W. *Adv. Polym. Sci.* **2006**, *204*, 1.
46. Zhang, Z.; Cui, D.; Wang, B.; Liu, B.; Yang Y. *Struct. Bond.* **2010**, *137*, 49.
47. Thuilliez, J.; Monteil, V.; Spitz, R.; Boisson, C. *Angew. Chem. Int. Ed.* **2005**, *44*, 2593.
48. Yasuda, H.; Nakano, Y.; Natsukawa, K.; Tani, H. *Macromolecules* **1978**, *11*, 586.

# CHARGE-NEUTRAL AND CATIONIC COMPLEXES OF LARGE ALKALINE EARTHS FOR RING-OPENING POLYMERIZATION AND FINE CHEMICALS CATALYSIS

JEAN-FRANÇOIS CARPENTIER\*, BO LIU, AND YANN SARAZIN\*

*Organometallics, Materials and Catalysis Department, Institut des Sciences Chimiques de Rennes, Université de Rennes, Rennes, France*

## 28.1 SYNTHESIS OF CHARGE-NEUTRAL HETEROLEPTIC RING-OPENING POLYMERIZATION CATALYSTS BASED ON LARGE ALKALINE EARTHS

Polyesters derived from bioresourced cyclic monomers such as the ubiquitous L-lactide are enjoying growing attention as green materials, presenting an attractive combination of physical and mechanical properties [1]. Seminal efforts by Coates and Chisholm at the turn of the century triggered the development of many well-defined organometallic initiators for the controlled ring-opening polymerization (ROP) of cyclic esters, and systems based on aluminum, rare-earth metals, and zinc have since played a prominent role [2]; more recently, several breakthroughs have also been achieved with organic catalysts [3].

One of our contributions to the field of ROP catalysis has focused on the development of catalytic systems for the *immortal* ROP of cyclic esters based on the large alkaline earth (Ae) metals: calcium, strontium, and barium. Indeed, these innocuous metals have been largely neglected in the area of ROP catalysis. Such paucity owes much to the synthetic difficulties related to the high reactivity and kinetic lability of heteroleptic complexes of Ca, Sr, and Ba, both of which result from the large ionic radius of these elements (Ca(6): 1.00 Å; Sr(6): 1.18 Å; and Ba(6): 1.35 Å) [4]. With divalent metals ( $M^{II}$ ), typical single-site ROP initiators have the general formula  $\{L_nX\}M^{II}Nu$ , where  $\{L_nX\}^-$  is a (multidentate) monoanionic bulky ancillary ligand and  $Nu^-$  is a reactive nucleophile (typically,  $OR^-$  or  $NR_2^-$ ) that attacks the incoming monomer. Such heteroleptic complexes usually allow for the controlled ROP of cyclic esters according to a coordination-insertion mechanism [2, 5]. With large Ae metals, the stability of  $\{L_nX\}AeNu$  complexes is usually very limited, as they readily decompose during deleterious Schlenk-type equilibria that eventually generate the poorly reactive and ill-defined homoleptic  $\{L_nX\}_2Ae$  and  $\{AeNu_2\}_n$ . The ease of ligand redistribution reactions increases with the ionic radius of the element, and whereas stable  $\{L_nX\}MgNu$  complexes ( $Nu^- = OR^-, NR_2^-, R^-$ ) are available in the plenty (Mg(6): 0.72 Å) [4],  $\{L_nX\}AeNu$  (Ae = Ca, Sr, Ba) analogues are extremely scarce and known essentially for amido derivatives ( $Nu^- = NR_2^-$ ). Early examples of discrete Ca-based ROP heteroleptic initiators include those developed by Chisholm involving sterically encumbered *tris(pyrazolyl)borates* [6] or Daresbourg's complexes stabilized by Schiff-base ligands [7]. Other molecular Ae-based ROP initiators have been reported, but the associated polymerization mechanisms have not been elucidated, and the overall efficiency was rather limited [8].

We chose to develop heteroleptic Ca, Sr, and Ba complexes of the type  $\{LO^x\}AeNu$  supported by multidentate, monoanionic phenolate  $\{LO^x\}^-$  ligands ( $x = 1-5$ , Fig. 28.1), because we anticipated that these ligands would adequately satisfy the electrophilic nature of the Ae elements. Phenolates constitute ubiquitous ligand platforms for the stabilization of

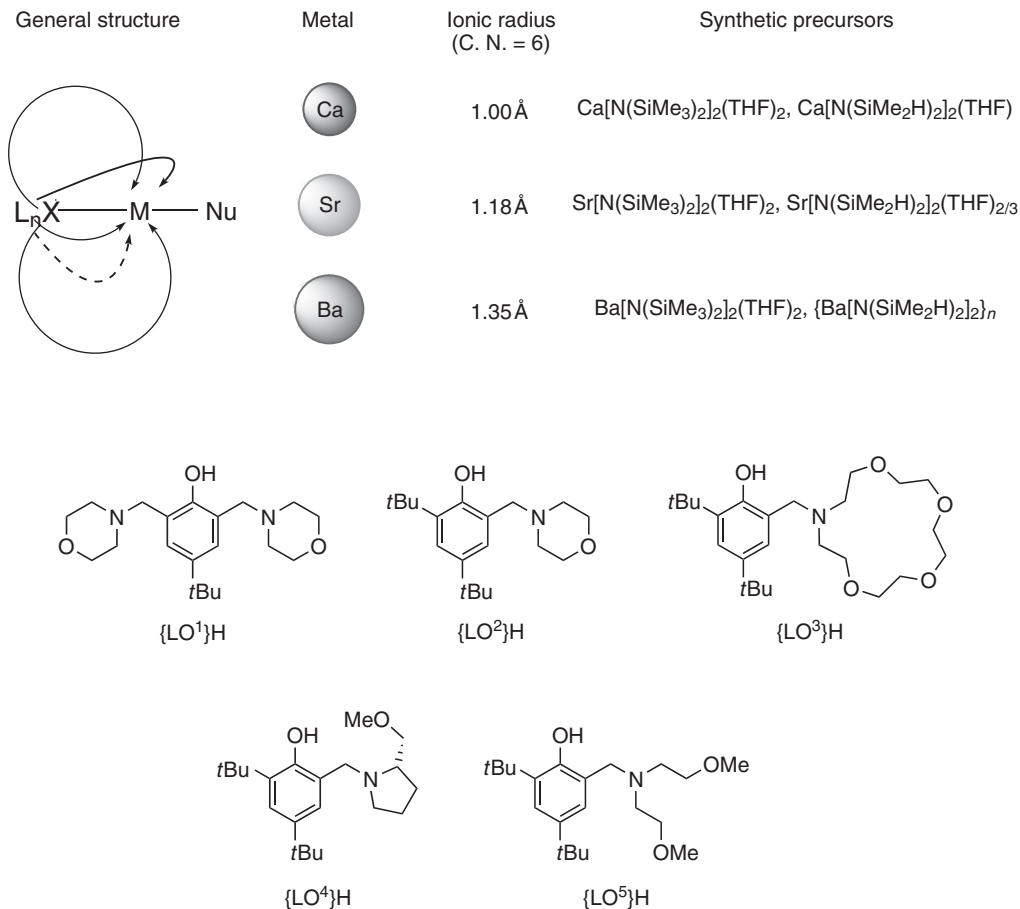
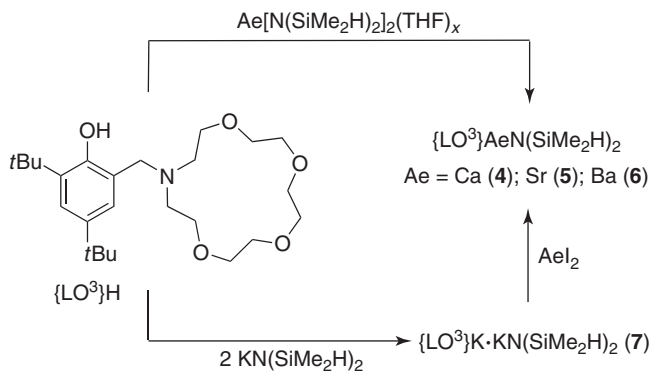


**Figure 28.1** Structures of the targeted heteroleptic complexes and selected phenol pro-ligands.

a large variety of oxophilic metal centers and are readily amenable to the tuning of their steric and electronic properties. Yet, they have barely been used for the preparation of heteroleptic Ae complexes. We employed the pro-ligands  $\{\text{LO}^x\}\text{H}$  depicted in Fig. 28.1, as they offer a broad range of electron-donating and structural features. All are readily prepared on large scales (5–20 g) by Mannich condensation.

The reaction of  $\{\text{LO}^1\}\text{H}$  and  $\text{Ca}[\text{N}(\text{SiMe}_3)_2]_2(\text{THF})_2$  yielded the THF-free heteroleptic  $\{\text{LO}^1\}\text{CaN}(\text{SiMe}_3)_2$  (**1**) [9]. Remarkably, **1** was perfectly stable in solution at room temperature for days. Moreover, the NMR-scale reaction of **1** and 10 equiv of iPrOH in  $\text{C}_6\text{D}_6$  at 60 °C (i.e., under immortal ROP conditions, *vide infra*) indicated the clean and quantitative formation of  $\{\{\text{LO}^1\}\text{CaO}i\text{Pr}\}_n$  with concomitant release of free  $\text{HN}(\text{SiMe}_3)_2$ . However, the analogous reactions between  $\{\text{LO}^1\}\text{H}$  and  $\text{Sr}[\text{N}(\text{SiMe}_3)_2]_2(\text{THF})_2$  or  $\text{Ba}[\text{N}(\text{SiMe}_3)_2]_2(\text{THF})_2$  failed to return the desired heteroleptic complexes, instead yielding intractable mixtures of  $\{\text{LO}^1\}_2\text{Ae}$  and  $\text{Ae}[\text{N}(\text{SiMe}_3)_2]_2$  ( $\text{Ae} = \text{Sr}, \text{Ba}$ ) containing various amounts of THF. Similarly,  $\{\text{LO}^5\}\text{CaN}(\text{SiMe}_3)_2$  (**2**) and  $\{\text{LO}^5\}\text{SrN}(\text{SiMe}_3)_2(\text{THF})$  (**3**) were obtained in good yield (70–75%) using the tetradentate  $\{\text{LO}^5\}^-$ , but the Ba congener could not be synthesized. Ligand redistribution reactions were also most troublesome with  $\{\text{LO}^3\}^-$ , and no heteroleptic complex was cleanly isolated. Hence, it rapidly emerged that owing to the kinetic lability of Ae complexes, procedures involving the archetypical  $\text{Ae}[\text{N}(\text{SiMe}_3)_2]_2(\text{THF})_2$  were often ill-fated, and that other routes to stable heteroleptic complexes had to be devised.

Inspired by Anwander's [10] work with rare-earth elements, we sought to stabilize heteroleptic complexes by the means of intramolecular Ae···H–Si agostic interactions between the large Ae metal and the  $\text{N}(\text{SiMe}_2\text{H})_2$  amido group. Thus, the new precursors  $\text{Ae}[\text{N}(\text{SiMe}_2\text{H})_2]_2(\text{THF})_x$  ( $\text{Ae} = \text{Ca}, x = 1; \text{Sr}, x = \frac{2}{3}; \text{Ba}, x = 0$ ) were synthesized [11]. The heteroleptic complexes  $\{\text{LO}^3\}\text{AeN}(\text{SiMe}_2\text{H})_2$  ( $\text{Ae} = \text{Ca}$ , **4**;  $\text{Sr}$ , **5**;  $\text{Ba}$ , **6**) were subsequently formed in good yields (60–70%) by the addition of  $\{\text{LO}^3\}\text{H}$  to the appropriate precursor (Scheme 28.1). The stability of **4–6** against redistribution reactions was attributed to the presence of  $\beta$ -agostic Si–H···Ae interactions with  $\text{N}(\text{SiMe}_2\text{H})_2$  moieties. Complexes **4–6** could also be



**Scheme 28.1** Synthesis of heteroleptic Ae complexes **4–6** supported by the  $\{LO^3\}^-$  phenolate.

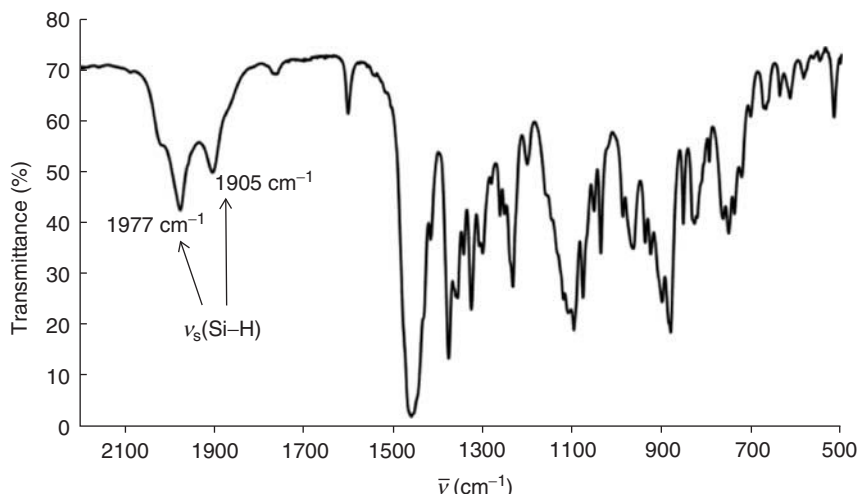


**Figure 28.2** FTIR spectrum of  $\{LO^3\}\text{BaN}(\text{SiMe}_2\text{H})_2$  (**6**) recorded as a nujol mull in KBr plates.

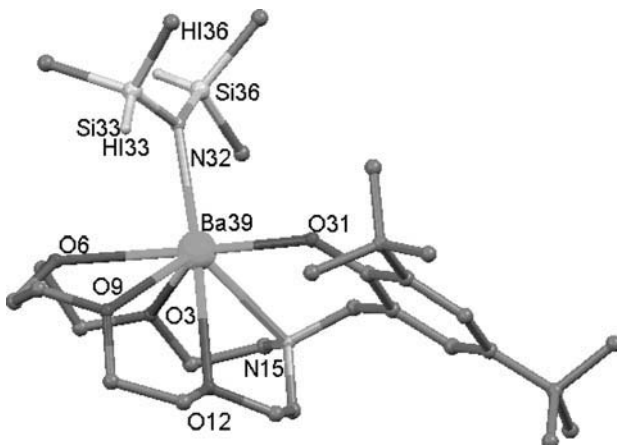
synthesized in a one-pot procedure with improved yields (circa 85%) by salt metathesis upon stoichiometric reaction of  $\{LO^3\}\text{K}\cdot\text{KN}(\text{SiMe}_2\text{H})_2$  (**7**) with  $\text{AeI}_2$ .

The  $^1J_{\text{Si}-\text{H}}$  values observed in the  $^1\text{H}$  or  $^{29}\text{Si}$  NMR spectra of  $\text{Ae}[\text{N}(\text{SiMe}_2\text{H})_2]_2(\text{THF})_x$  fell in the range indicative of mild (140–160 Hz) to weak (160–170 Hz) Si–H…metal agostic interactions. This was corroborated by FTIR spectroscopy, as a small, low energy shoulder (in the area 1900–1980  $\text{cm}^{-1}$ ) diagnostic of agostic interactions with the electrophilic Ae metal center was associated to a comparatively stronger band at higher energy (circa 1960–2030  $\text{cm}^{-1}$ , little or no interaction with the metal).

Comparison was particularly relevant among **4–6**, three complexes with identical ligand environments. In their  $^1\text{H}$  NMR spectra, the Si–H resonances ( $\delta_{1\text{H}} = 5.20\text{--}5.27$  ppm) were deshielded with respect to the free amine ( $\delta_{1\text{H}} = 4.70$  ppm) or the corresponding homoleptic precursors ( $\delta_{1\text{H}} = 4.65\text{--}4.92$  ppm). The  $^1J_{\text{Si}-\text{H}}$  coupling constants (160–165 Hz) were indicative of agostic interactions in solution. In the  $^{29}\text{Si}\{^1\text{H}\}$  NMR spectra, the Si–H resonances shifted significantly toward high fields with increasing size of the metal center ( $\delta_{29\text{Si}}:$  **4**, 25.9; **5**, 27.5; and **6**, 30.5 ppm), which reflected the increasingly ionic character of the Ae–N bond in these complexes. Solid-state IR data provided strong evidence for stabilization by  $\beta$ -Si–H agostic interactions (Table 28.1; Fig. 28.2). The solid-state structure of **6** (Fig. 28.3) represents a unique example of  $\beta$ -Si–H agostic bonding for barium characterized by X-ray diffraction. The Si33–H…Ba agostic interaction is evidenced by the short, nonbonding Ba39–Si33 distance (3.45 Å) and the unusually acute Si33–N32–Ba39 angle of 102.03(8) $^\circ$  (note the large discrepancy with the other Si atom, Si36–N32–Ba39 = 128.79(10) $^\circ$ ). Another feature of interest is the planarity of the Ba39–N32–Si33–Hi33 core.

**TABLE 28.1** Spectroscopic Data for Ae[N(SiMe<sub>2</sub>H)<sub>2</sub>]<sub>2</sub>(THF)<sub>x</sub> and 4–12

Complex	IR <sup>a</sup> $\nu_s$ (Si—H)	<sup>1</sup> H NMR <sup>b</sup> $\delta$ (SiH)	<sup>29</sup> Si NMR <sup>b</sup> $\delta$ (SiH)	<sup>1</sup> J <sub>Si—H</sub> <sup>c</sup>
HN(SiMe <sub>2</sub> H) <sub>2</sub>	2122	4.70	−11.5	194
Ca[N(SiMe <sub>2</sub> H) <sub>2</sub> ] <sub>2</sub> (THF)	2028; 1959	4.92	−20.5	154
Sr[N(SiMe <sub>2</sub> H) <sub>2</sub> ] <sub>2</sub> (THF)(THF) <sub>2/3</sub>	1959; 1925	4.84	−20.7	148
Ba[N(SiMe <sub>2</sub> H) <sub>2</sub> ] <sub>2</sub>	1985; 1935	4.65 <sup>d</sup>	−30.6 <sup>d</sup>	163 <sup>d</sup>
{LO <sup>3</sup> }CaN(SiMe <sub>2</sub> H) <sub>2</sub> ( <b>4</b> )	1989; 1941	5.20	−25.9	165
{LO <sup>3</sup> }SrN(SiMe <sub>2</sub> H) <sub>2</sub> ( <b>5</b> )	2005; 1918	5.27	−27.5	161
{LO <sup>3</sup> }BaN(SiMe <sub>2</sub> H) <sub>2</sub> ( <b>6</b> )	1977; 1905	5.27	−30.5	160
{LO <sup>1</sup> }CaN(SiMe <sub>2</sub> H) <sub>2</sub> ( <b>8</b> )	2015; 1910	4.84	−23.5	167
{LO <sup>4</sup> }CaN(SiMe <sub>2</sub> H) <sub>2</sub> ( <b>9</b> )	2030; 1949	4.71	−24.9	164
{LO <sup>5</sup> }CaN(SiMe <sub>2</sub> H) <sub>2</sub> (THF) ( <b>10</b> )	2043; 1958	5.18	−25.8	167
{LO <sup>5</sup> }SrN(SiMe <sub>2</sub> H) <sub>2</sub> ( <b>11</b> )	1971; 1917	5.18	−27.1	162
{LO <sup>5</sup> }BaN(SiMe <sub>2</sub> H) <sub>2</sub> ( <b>12</b> )	1987; 1910	4.72	−30.4	160

<sup>a</sup> Recorded at room temperature as nujol mulls in KBr plates (cm<sup>−1</sup>).<sup>b</sup> Recorded at 298 K in C<sub>6</sub>D<sub>6</sub> (ppm).<sup>c</sup> Frequencies in hertz.<sup>d</sup> Recorded in THF-d<sub>8</sub>.**Figure 28.3** Solid-state structure of {LO<sup>3</sup>}BaN(SiMe<sub>2</sub>H)<sub>2</sub> (**6**). Selected bond lengths (Å) and angles (°): Ba39—N32 = 2.6885(17), Ba39—Si33 = 3.45, Ba39—Si33 = 3.95; Si33—N32—Ba39 = 102.03(8), Si36—N32—Ba39 = 128.79(10), Si33—N32—Si36 = 129.02(11).

The experimental structure and that calculated by DFT for **6** were remarkably similar. Computations of structures exhibiting a β-Si—H agostic interaction and without agostic interaction were carried out to evaluate the strength of the agostic interaction in **4–6**. For Ba and Sr, the agostically stabilized structure was found to be more stable than nonagostic ones by 3.1 and 3.7 kcal/mol, respectively. In the case of Ca, the two structures were isoenergetic within the accuracy of the method. The computed IR spectrum for Ba displayed two distinct bands (1936 and 2036 cm<sup>−1</sup>); the large difference between the two peaks was a clear indication of agostic bonding.

Such intramolecular agostic interactions were exploited for the preparation of several Ae complexes supported by {LO<sup>x</sup>}—phenolates [12]. The complexes {LO<sup>1</sup>}CaN(SiMe<sub>2</sub>H)<sub>2</sub> (**8**), {LO<sup>4</sup>}CaN(SiMe<sub>2</sub>H)<sub>2</sub> (**9**), and {LO<sup>5</sup>}AeN(SiMe<sub>2</sub>H)<sub>2</sub>(THF)<sub>n</sub> (Ae = Ca, n = 1, **10**; Sr, n = 0, **11**; Ba, n = 0, **12**) were obtained accordingly. The alkoxide complex {LO<sup>5</sup>}CaOCH<sub>2</sub>C≡CH (**13**) was produced by treatment of **10** with propargyl alcohol. Table 28.1 summarizes the relevant spectroscopic data for Ae[N(SiMe<sub>2</sub>H)<sub>2</sub>]<sub>2</sub>(THF)<sub>x</sub> and **4–12**.

In the solid state, the Ca complexes **4** and **10** were monomeric, whereas **8** and **13** formed bridged dimers. The nuclearity of these complexes in solution was assessed by pulse-gradient spin-echo (PGSE) NMR spectroscopy. Comparison of the

**TABLE 28.2 PGSE NMR Measurements and X-Ray Crystallographic Data for 4, 8, 10, and 13<sup>a</sup>**

Complex	$D_t$ , m <sup>2</sup> s <sup>-1</sup> <sup>b</sup>	$r_{H,PGSE}$ , Å	X-Ray	$r_{H,X-ray}$ <sup>c</sup> , Å
			$a$ , Å	$b$ , Å
{LO <sup>3</sup> }CaN(SiMe <sub>2</sub> H) <sub>2</sub> ( <b>4</b> )	(5.59 ± 0.19) × 10 <sup>-10</sup>	6.64	6.72	4.15
{LO <sup>1</sup> }CaN(SiMe <sub>2</sub> H) <sub>2</sub> ( <b>8</b> )	(6.15 ± 0.09) × 10 <sup>-10</sup>	6.54	8.74	6.94
{LO <sup>5</sup> }CaN(SiMe <sub>2</sub> H) <sub>2</sub> (THF) ( <b>10</b> )	(6.86 ± 0.03) × 10 <sup>-10</sup>	5.78	7.18	5.08
{LO <sup>5</sup> }CaOCH <sub>2</sub> C≡CH ( <b>13</b> ) <sup>d</sup>	(9.26 ± 0.08) × 10 <sup>-10</sup>	5.56	10.76	5.35

<sup>a</sup>Data recorded in C<sub>6</sub>D<sub>6</sub> at 298 K unless otherwise mentioned.

<sup>b</sup>Average of the values of  $D_t$  found for at least four clearly separated peaks in the <sup>1</sup>H PGSE NMR spectrum.

<sup>c</sup>Calculated according to  $r_{H,X-ray} = (a^2 \cdot b)^{1/3}$  where  $a$  and  $b$  are, respectively, the major and minor semiaxes of the prolate ellipsoid formed by the complex.

<sup>d</sup>Data recorded in THF-d<sub>8</sub> at 298 K.

hydrodynamic radii determined from their X-ray structures and by PGSE experiments (Table 28.2) demonstrated that the four complexes remained monomeric in solution.

## 28.2 SYNTHESIS OF WELL-DEFINED, SOLVENT-FREE CATIONIC COMPLEXES OF THE LARGE ALKALINE EARTHS

### 28.2.1 Cationic Ae Complexes Supported by Phenolate and Alkoxide Ligands

A better understanding of the reactivity of Ae species entails the study of well-defined cationic complexes. Three factors are crucial to prepare highly reactive well-defined [{L<sub>n</sub>X}Ae]<sup>+</sup>[X]<sup>-</sup> ROP ion pairs ({L<sub>n</sub>X}<sup>-</sup> = monoanionic ancillary ligand): (i) the ligand must provide sufficient steric bulk and electron density for the stabilization of these extremely electrophilic species, (ii) weakly coordinating anions (WCA) X<sup>-</sup> yield cations with enhanced Lewis acidity, and (iii) efficient synthetic protocols devoid of complications due to Schlenk-type equilibria must be devised. The challenge we set upon ourselves was significant in view of the oxophilicity and electropositivity of Ca, Sr, and Ba, and yet it seemed pertinent as the increase of Lewis acidity at the metal center should result in high catalytic efficiency. A first step was achieved in 2001 by Itoh and Kitagawa who characterized cations of Mg, Ca, and Sr stabilized by {LO<sup>3</sup>}<sup>-</sup> and external Lewis bases and studied the physicochemical and redox properties of these aryloxides and aryloxyl radicals [13]. We employed this ligand framework and the related bis(trifluoromethyl)alcohol {RO<sup>3</sup>}<sup>-</sup> and developed original synthetic protocols to prepare the first solvent-free, discrete cationic Ae complexes; later, the less-hindered {LO<sup>5</sup>}<sup>-</sup> was also utilized (Fig. 28.4). Occurrences of alkoxide ligands for the synthesis of *discrete* Ae complexes are scarce [14], because the high  $\pi$ -donating ability of alkoxides readily results in the formation of alkoxy-bridged polynuclear/polymeric species [15], especially when large metals are involved. We explored the capacity of {RO<sup>3</sup>}<sup>-</sup> in relation with its phenolate congener, {LO<sup>3</sup>}<sup>-</sup>. Indeed, fluorinated tertiary alkoxide ligands with bulky, electron-withdrawing CF<sub>3</sub> groups in  $\alpha$  position to the alkoxide are weaker  $\pi$ -donors than conventional alkoxides [16], and they are in many ways similar to phenolate ligands.

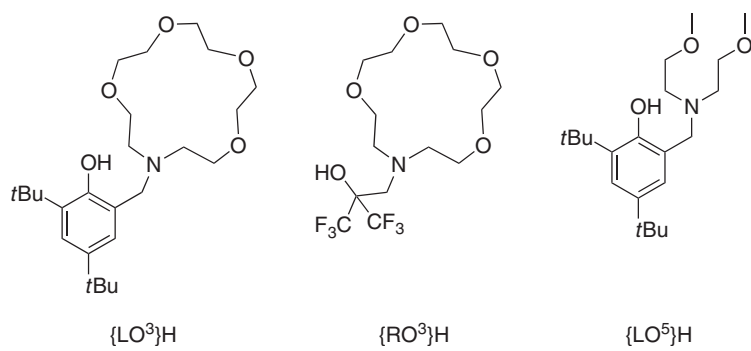
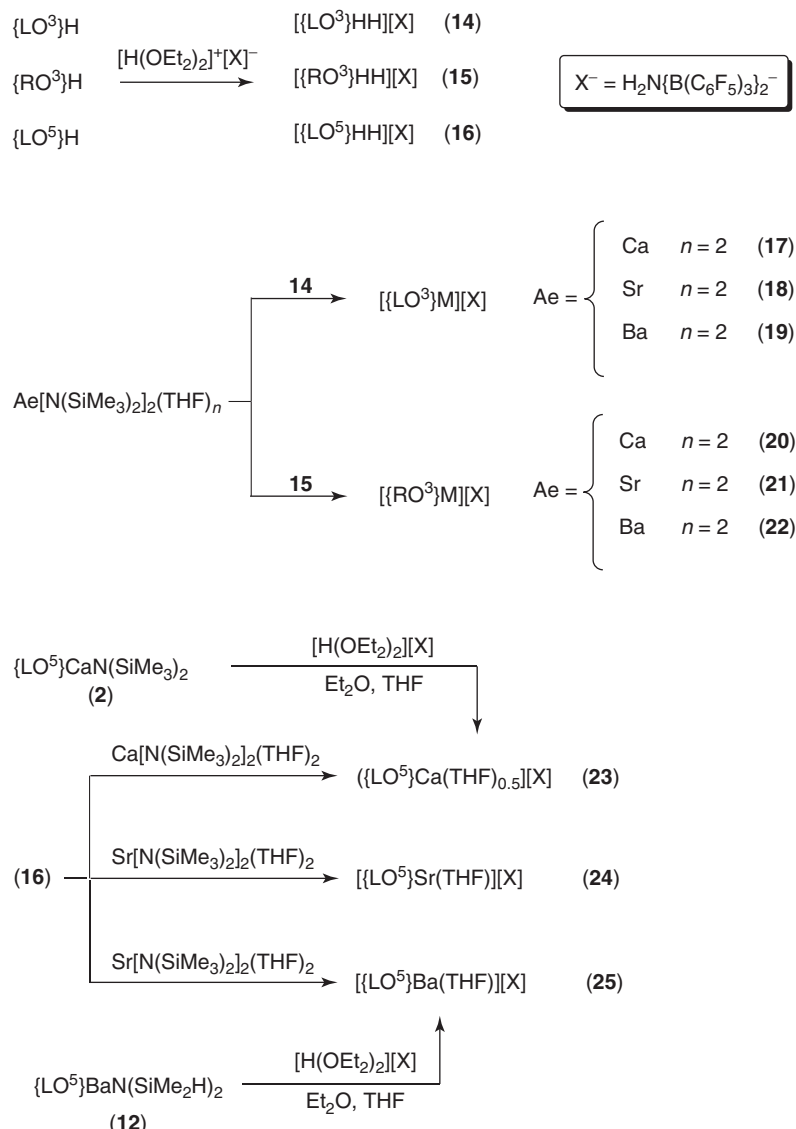


**Figure 28.4** {L<sub>n</sub>X}H pro-ligands used to prepare well-defined cationic Ae complexes.

The syntheses of the ion pairs  $\{[\text{LO}^x]\text{Ae}\}[\text{H}_2\text{N}\{\text{B}(\text{C}_6\text{F}_5)_3\}_2]$  ( $\text{Ae} = \text{Ca, Sr, Ba}$ ) were first targeted [17]. The choice of Bochmann's perfluorinated WCA  $\text{H}_2\text{N}\{\text{B}(\text{C}_6\text{F}_5)_3\}_2^-$  [18] was motivated by two factors. Firstly, it displays better crystallization properties than the traditional  $\text{B}(\text{C}_6\text{F}_5)_4^-$ : while the latter can be considered spherical and often leads to the formation of oily or amorphous materials,  $\text{H}_2\text{N}\{\text{B}(\text{C}_6\text{F}_5)_3\}_2^-$  possesses a dipole moment that induces an orientation toward the cation and facilitates crystallization processes. Secondly,  $\text{H}_2\text{N}\{\text{B}(\text{C}_6\text{F}_5)_3\}_2^-$  is very robust (due to a pattern of internal H...F stabilizing interactions) and the negative charge is delocalized over an extremely large volume (circa  $538 \text{ \AA}^3$ ); as a result, the catalytic performances with this anion are at least equivalent to those displayed by smaller fluorinated WCAs.

The solvent-free ion pairs  $\{[\text{LO}^3]\text{Ae}\}[\text{H}_2\text{N}\{\text{B}(\text{C}_6\text{F}_5)_3\}_2]$  ( $\text{Ae} = \text{Ca, 17; Sr, 18; Ba, 19}$ ) and  $\{[\text{RO}^3]\text{Ae}\}[\text{H}_2\text{N}\{\text{B}(\text{C}_6\text{F}_5)_3\}_2]$  ( $\text{Ae} = \text{Ca, 20; Sr, 21; Ba, 22}$ ) were generated in a one-step protocol by double protonolysis of the suitable homoleptic precursors using the doubly acidic pro-ligands of highest denticity **14** and **15** (Scheme 28.2). Compounds **17–19** could also be obtained by protonolysis of the heteroleptic precursors **4–6** with  $[\text{H}(\text{OEt}_2)_2][\text{H}_2\text{N}\{\text{B}(\text{C}_6\text{F}_5)_3\}_2]$ , but this first required the syntheses of  $\{\text{LO}^3\}\text{AeN}(\text{SiMe}_2\text{H})_2$ . Note that **20–22** represented the first case of a family of solvent-free, well-defined cationic complexes alkaline earth metals supported by an alkoxide ligand. Complexes **17–22** are stable in solution for days. With the less chelating phenolate  $\{\text{LO}^5\}^-$ , the solvated  $\{[\text{LO}^5]\text{Ae}(\text{THF})_n\}[\text{H}_2\text{N}\{\text{B}(\text{C}_6\text{F}_5)_3\}_2]$  complexes ( $\text{Ae} = \text{Ca, } n = 1/2$ ,



**Scheme 28.2** Syntheses of well-defined Ae cations associated to the WCA  $\text{H}_2\text{N}\{\text{B}(\text{C}_6\text{F}_5)_3\}_2^-$ .

**23**; Sr,  $n = 1$ , **24**; Ba,  $n = 1$ , **25**) were obtained. Clearly, the presence of extra donors (THF) was required to stabilize these cations; **23–25** also proved less stable than the more encumbered and more electron-rich **17–22**. NMR spectroscopy showed no evidence for Ae···F interactions with the WCA in any of these cations.

The solid-state structures of **17**, **19–22**, and **(22)<sub>2</sub>·EtOH** were determined by X-ray diffraction crystallography. Complexes **20–22** were found as pairs of bridged bimetallic dication in the solid state, with no Ae···F contacts with the WCA. On the other hand, these dications exhibited stabilizing internal Ae···F secondary interactions between the metal centers and fluorine atoms *on the ligand*. In **20**, the distances between Ca and the internally interacting fluorine atoms on CF<sub>3</sub> groups (2.66–2.68 Å) were considerably shorter than the sum of the van der Waals radii for Ca (2.00 Å) and F (1.47 Å), suggesting strong Ca···F secondary interactions (circa 25 kcal/mol according to DFT calculations) in the solid state. Such secondary interactions have been suggested as a way to stabilize reactive Ae centers [19]. The high coordination number and the participation of fluorine atoms to the coordination in **20** reflected the large metal size and the need for electronic density. The structural features of **21** resembled those of its Ca homolog. The interactions between the strontium atom and fluorine atoms were strong (circa 40 kcal/mol by DFT calculations), with short Sr–F distances (2.74–2.86 Å). The intense Sr···F–C interaction resulted in elongation of the corresponding C–F bond length (1.375 Å) with regard to noninteracting F atoms (C–F = 1.309–1.337 Å). In **22**, each Ba center exhibited one strong (Ba···F–C = 2.92 Å) internal Ba···F–C secondary interaction with a fluorine atom. DFT calculations indicated that the presence of the Ba···F–C resulted in stabilization by circa 25 kcal/mol. The asymmetric unit of **(22)<sub>2</sub>·EtOH** contained two nonequivalent pairs of bridged bimetallic dications and their counterions: one with the expected composition  $\{\text{RO}^3\}\text{Ba}^+$ <sub>2</sub>, which resembled that in **22**, and one corresponding to the adduct  $\{\text{RO}^3\}\text{Ba}^+$ <sub>2</sub>·EtOH. Isolation of crystals of **(22)<sub>2</sub>·EtOH** demonstrated that these cationic species resisted the presence of protic sources typically used as initiator/chain transfer agent in immortal ROP reactions; the coordination onto the metal center of an external protic nucleophilic agent was highly relevant to the study of mechanisms operative in these processes (*vide infra*).

### 28.2.2 Cationic Ae Complexes Supported by a $\beta$ -Diketiminate Ligand

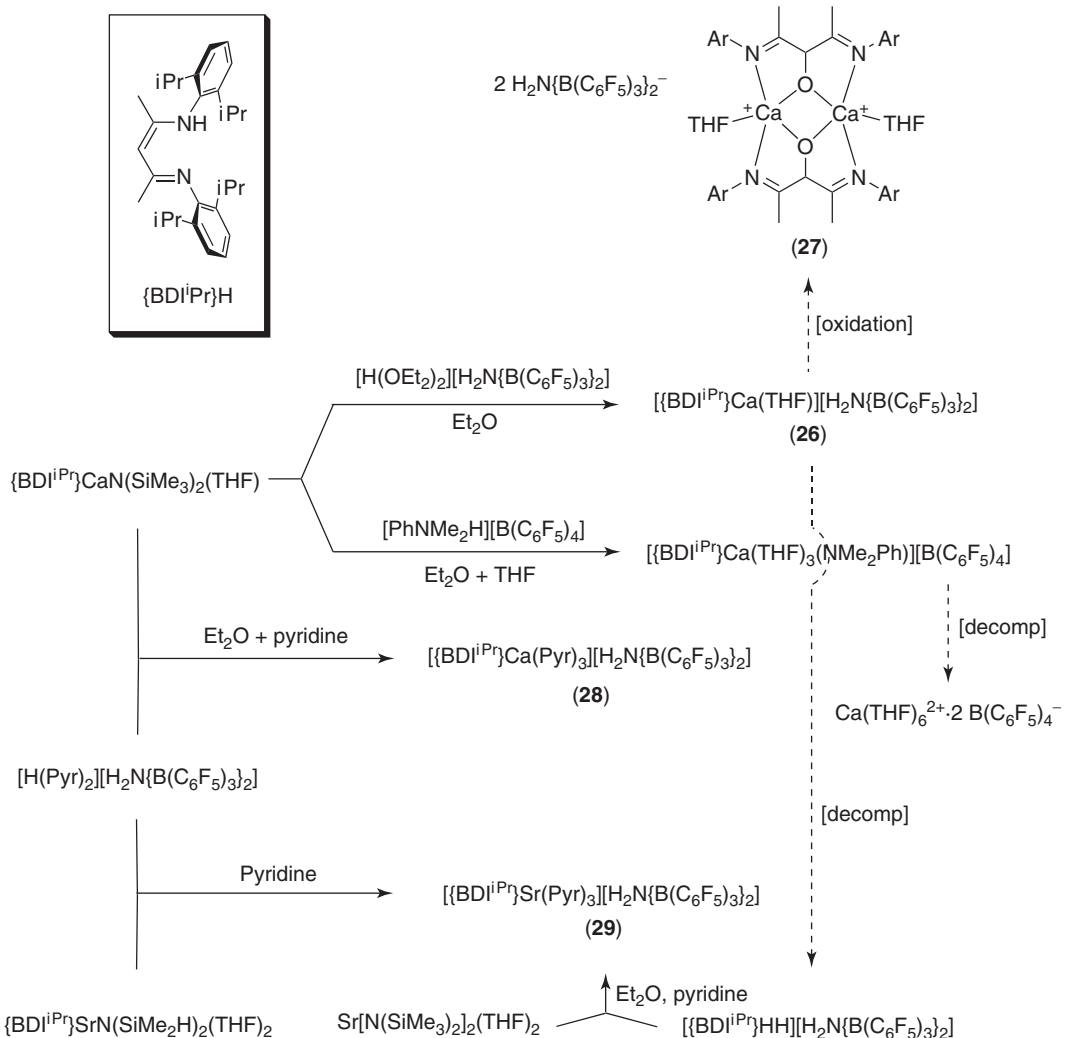
The  $\beta$ -diketiminate complex  $\{\text{BDI}^{i\text{Pr}}\}\text{CaN}(\text{SiMe}_3)_2(\text{THF})$  occupies a prominent place in the range of kinetically stable heteroleptic Ae complexes [20]. However, if  $\{\text{BDI}^{i\text{Pr}}\}\text{CaN}(\text{SiMe}_3)_2(\text{THF})$  is stable in solution even under relatively forcing conditions, its Sr and Ba congeners are prone to ligand scrambling, most likely because of the inability of the bidentate  $\{\text{BDI}^{i\text{Pr}}\}^-$  to kinetically stabilize the very large Sr and Ba elements. The new and stable  $\{\text{BDI}^{i\text{Pr}}\}\text{AeN}(\text{SiMe}_2\text{H})_2(\text{THF})_n$  (Ae = Ca, Sr, Ba) complexes were successfully prepared by reaction of  $\{\text{BDI}^{i\text{Pr}}\}\text{H}$  and  $\text{Ae}[\text{N}(\text{SiMe}_2\text{H})_2]_2(\text{THF})_x$ , thus giving access to the low coordinated cationic species  $[\{\text{BDI}^{i\text{Pr}}\}\text{Ae}(\text{L})_x][\text{H}_2\text{N}\{\text{B}(\text{C}_6\text{F}_5)_3\}_2]$  (Ae = Ca, Sr) (Scheme 28.3) [21].

The complex  $[\{\text{BDI}^{i\text{Pr}}\}\text{Ca}(\text{THF})][\text{H}_2\text{N}\{\text{B}(\text{C}_6\text{F}_5)_3\}_2]$  (**26**), formed upon treatment of  $\{\text{BDI}^{i\text{Pr}}\}\text{CaN}(\text{SiMe}_3)_2(\text{THF})$  with Bochmann's acid, was not stable in solution and spontaneously evolved toward the formation of the doubly protonated pro-ligand  $[\{\text{BDI}^{i\text{Pr}}\}\text{HH}][\text{H}_2\text{N}\{\text{B}(\text{C}_6\text{F}_5)_3\}_2]$  with other unidentified species. Its high but erratic reactivity also showed as crystals of  $[(\text{Ca}\{\text{OCH}(\text{C}(\text{Me})=\text{NC}_6\text{H}_3\text{iPr}_2)_2\})(\text{THF})_2]^{2+} \cdot 2[\text{H}_2\text{N}\{\text{B}(\text{C}_6\text{F}_5)_3\}_2]^-$  (**27**) were isolated serendipitously. Complex **27** represents a unique case of oxidation of the  $\beta$ -diketiminate  $\{\text{BDI}^{i\text{Pr}}\}^-$  ligand framework, which is otherwise known to be extremely robust and well suited to the ligation of electrophilic metal centers. The route leading to the formation of **27** and actual source of oxygen remained unclear.  $[\text{PhNMe}_2\text{H}][\text{B}(\text{C}_6\text{F}_5)_4]$  and  $\{\text{BDI}^{i\text{Pr}}\}\text{CaN}(\text{SiMe}_3)_2(\text{THF})$  reacted in the presence of THF to afford  $[\{\text{BDI}^{i\text{Pr}}\}\text{Ca}(\text{THF})_3(\text{NMe}_2\text{Ph})][\text{B}(\text{C}_6\text{F}_5)_4]$ , which rapidly evolved to give a mixture of unclear composition, from which crystals of  $[\text{Ca}(\text{THF})_6]^{2+} \cdot 2[\text{B}(\text{C}_6\text{F}_5)_4]^-$  were obtained. The reaction of  $\{\text{BDI}^{i\text{Pr}}\}\text{CaN}(\text{SiMe}_3)_2(\text{THF})$  and  $[\text{H}(\text{Pyr})_2][\text{H}_2\text{N}\{\text{B}(\text{C}_6\text{F}_5)_3\}_2]$  afforded the stable  $[\{\text{BDI}^{i\text{Pr}}\}\text{Ca}(\text{Pyr})_3][\text{H}_2\text{N}\{\text{B}(\text{C}_6\text{F}_5)_3\}_2]$  (**28**). The analogous reaction with  $\{\text{BDI}^{i\text{Pr}}\}\text{SrN}(\text{SiMe}_2\text{H})_2(\text{THF})$  yielded  $[\{\text{BDI}^{i\text{Pr}}\}\text{Sr}(\text{Pyr})_3][\text{H}_2\text{N}\{\text{B}(\text{C}_6\text{F}_5)_3\}_2]$  (**29**), which could also be synthesized by addition of  $[\{\text{BDI}^{i\text{Pr}}\}\text{HH}][\text{H}_2\text{N}\{\text{B}(\text{C}_6\text{F}_5)_3\}_2]$  to  $\text{Sr}[\text{N}(\text{SiMe}_3)_2]_2(\text{THF})_2$ . Attempts to produce the Ba derivative according to either of these protocols were unsuccessful, highlighting the greater difficulty in handling these electrophilic cationic complexes where kinetically lability and reactivity increase with the size of the element.

## 28.3 IMMORTAL RING-OPENING POLYMERIZATIONS OF CYCLIC ESTERS CATALYZED BY SINGLE-SITE ALKALINE EARTH CATALYSTS

### 28.3.1 Principles of Immortal Ring-Opening Polymerization Reactions

Metal-based inorganic and organometallic systems belong to the most effective catalyst systems for the ROP of cyclic esters/carbonates, both in terms of reactivity (activity, productivity) and control over the polymerization. In these systems,

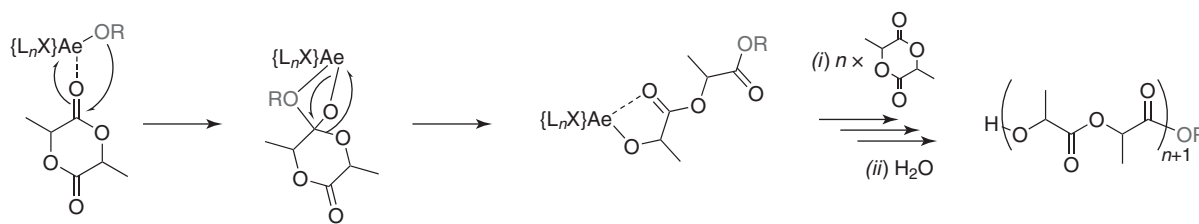


**Scheme 28.3** Synthesis of Ae cations supported by  $\text{[BDI}^{\text{iPr}}\text{]}^-$ .

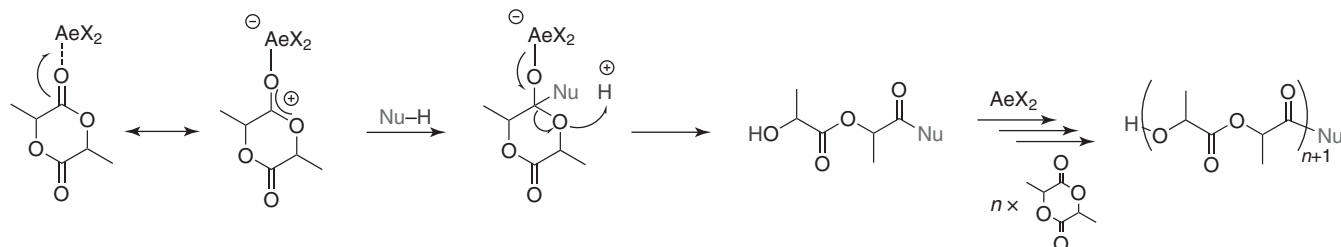
the metal is usually very electrophilic and acts as a Lewis acidic center which activates the cyclic ester via coordination of its carbonyl moiety. Depending on the origin of the nucleophile that will open the monomer, two distinct mechanisms can be envisioned for the metal-mediated ROP of cyclic esters (Scheme 28.4) [2, 5]. Upon coordination of the incoming monomer to the metal center, the electrophilicity at the carbonyl carbon atom enhances greatly. This eventually facilitates attack of either an *internal* nucleophilic moiety—that is, an anionic “active” ligand initially attached to the metal complex that accordingly operates via a so-called “coordination-insertion” mechanism, or an *external* (exogenous) nucleophile—typically a protic compound such as an alcohol or an amine, the global system then operating via a so-called “activated monomer” mechanism.

Note that a distinction is made between *initiator* and *catalyst*. In the “coordination-insertion” mechanism, the nucleophilic group is covalently bound to the metal; its number is definite, and normally ranges from one to the valence of the metal at most. The metal complex is hence branded the name of *initiator* as it determines the number of polymer chains that shall be generated. In the majority of cases, a single reactive nucleophilic group is attached to the metal center, and only one polymer chain can be generated *per* metal center: this grossly corresponds to a “*living*” polymerization. On the other hand, in the “activated monomer” mechanism or in a so-called “*immortal ROP*” (*iROP*) with fast and reversible transfer between growing and dormant macromolecules [5, 22], the number of polymer chains produced is preset by the number of added *exogenous* nucleophiles. The latter can be in much larger excess with respect to the metal complex, which therefore behaves as a true *catalyst* (Scheme 28.5).

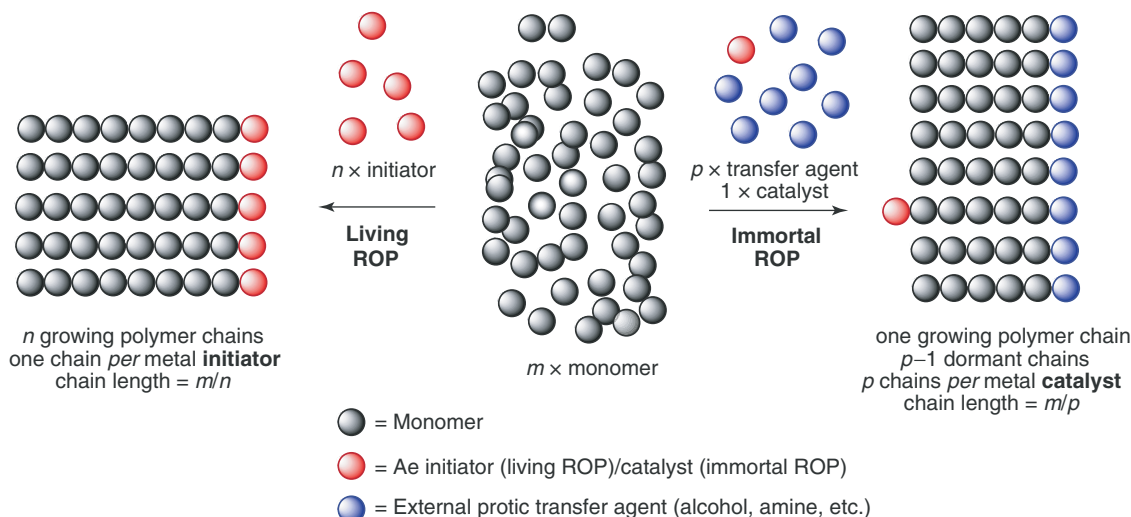
## Coordination - Insertion



## Activated monomer



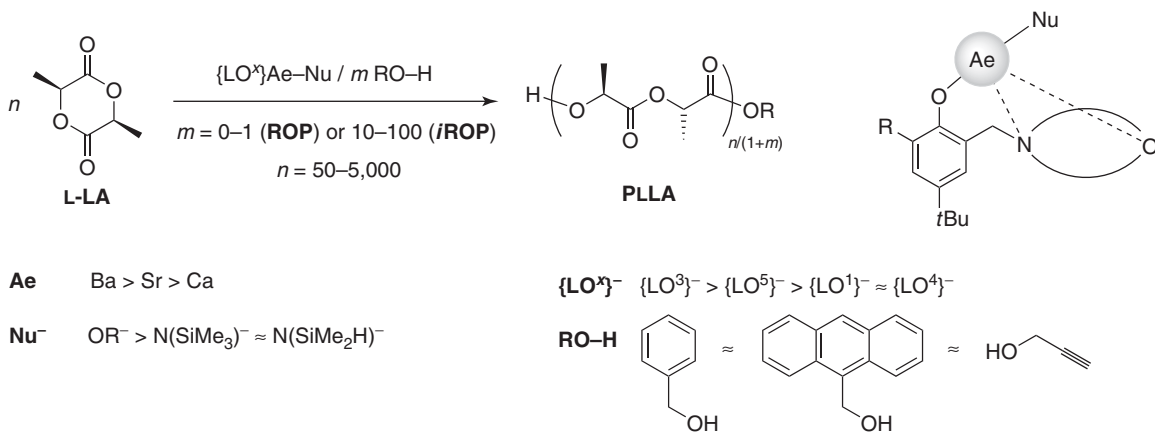
**Scheme 28.4** Accepted mechanisms for the metal-mediated ROP of LA illustrated in the case of an alkaline earth (Ae) metal species.



**Scheme 28.5** Illustrative comparison of the living and immortal ROP processes. (See insert for color representation of the figure.)

In a living *initiating* system, each metal center/reactive nucleophilic group(s) generates a single polymer chain, and all polymer chains are of equal length for a given initiator. Practical indicators for a living system include: (i) a very narrow distribution of molecular weights for the resulting materials ( $M_w/M_n < 1.10$ ), and (ii) a linear dependence of the polymer molecular weight on the monomer-to-metal ratio at a given monomer conversion. However, to fulfill the criteria for a perfectly living ROP, an initiating system must in essence feature: (i) 100% initiation efficiency, that is, all reactive nucleophilic group(s) attached to the metal center initiate the formation of a macromolecule, (ii) an initiation rate constant far greater than the propagation rate constant, and (iii) the absence of termination and transfer reactions.

In an *iROP* performed upon addition of a large excess of an alcohol behaving as an exogenous initiator and a chain transfer agent, the complex acts as a *catalyst*: if the transfer between growing and dormant macromolecules is fast and reversible, the number of polymer chains generated *per* metal center is equal to the [transfer agent]<sub>0</sub>-to-[metal]<sub>0</sub> ratio, while the degree of polymerization is set by the [monomer]<sub>0</sub>-to-[transfer agent]<sub>0</sub> ratio.



Scheme 28.6 (i)ROP of L-LA promoted by Ae metal phenolate complexes.

### 28.3.2 ROP Catalysis with Charge-Neutral Heteroleptic Alkaline Earth Complexes

Complexes **2**, **4–6**, **8–10**, and **13** promoted the *i*ROP of L-LA (Scheme 28.6, Table 28.3). Under the chosen conditions, the activity of complexes **4–6** supported by the {LO<sup>3</sup>}<sup>-</sup> amino-ether phenolate ligand decreased in the order Ca < Sr < Ba. This was linked to the increase of the nucleophilic reactivity of the {L<sub>n</sub>X}Ae-OPLLA(Nu) species on descending from the least (Ca) to the most (Ba) electropositive metal. The catalysts based on **5** and **6** afforded moderate control over the parameters ( $M_w/M_n = 1.36\text{--}1.46$ ) for the *i*ROP of 1000 equiv of L-LA, with turnover frequency (TOF) values of 2080 and 7350 mol<sub>L-LA</sub>/mol<sub>Ae</sub> h, respectively. They converted 5000 equiv of L-LA with up to 100 equiv of HC≡CCH<sub>2</sub>OH, with TOFs in the range 10,500–21,200 mol<sub>L-LA</sub>/mol<sub>Ae</sub> h; good control ( $M_w/M_n = 1.13\text{--}1.20$ ,  $M_{n,calc} \sim M_{n,SEC}$ ) attested to efficient chain transfer between growing and resting (macro)alcohols.

With the most easily controlled system **4** based on Ca, replacing propargyl alcohol for 9-anthracylmethanol or benzyl alcohol did not alter the outcome of the *i*ROP of 1000 equiv of L-LA. In all cases, near-complete conversion of the monomer was observed with suitable control and fully predictable molecular weights. Under nonoptimized reaction conditions, the TOF values reached an impressive 27,300 mol<sub>L-LA</sub>/mol<sub>Ca</sub> h. Sticking with BnOH as the transfer agent, the role of the stabilizing ligand framework in the calcium catalysts **4** and **8–10** was assessed. The activity trend followed the order **4** > **10** > **8** ~ **9**: the more (potentially) chelating the ligand, the more active the catalyst.

The similar *i*ROP activities exhibited by **10** and its alkoxide analogue **13** confirmed that under *immortal* conditions, the nature of the *initial* reactive nucleophile had no impact over the polymerization reaction. The ROP of 200 equiv of L-LA versus the metal *initiator* was performed without exogenous alcohol to assess the role of the nucleophilic moiety in complexes **10**, **13**, and **2**, all supported by the ancillary ligand {LO<sup>5</sup>}<sup>-</sup>. {LO<sup>5</sup>}CaOCH<sub>2</sub>C≡CH (**13**) and its congeners bearing the N(SiMe<sub>2</sub>H)<sub>2</sub> (**10**) or N(SiMe<sub>3</sub>)<sub>2</sub> (**2**) groups polymerized L-LA at comparable rates (TOF = 152–176 mol<sub>L-LA</sub>/mol<sub>Ca</sub> h), but only **13**, with its alkoxide as the reactive nucleophilic group, was capable of efficient control ( $M_w/M_n = 1.24$ ,  $M_{n,SEC} = 18,100$  g/mol,  $M_{n,calc} = 25,400$  g/mol). This highlighted that the Ca–OR (R=CH<sub>2</sub>C≡CH) moiety was a good mimic of the active species in a ROP process, whereas Ca–NR<sub>2</sub> did not replicate adequately the growing Ca–OPLLA species and its greater reactivity (basicity) was not easily tamed.

The question of end-group fidelity is critical to evaluate the efficiency of any *i*ROP catalyst system. All polymer samples were characterized by <sup>1</sup>H NMR spectroscopy (Fig. 28.5), which attested to the presence of the expected *termini*, –C(CH<sub>3</sub>)(H)OH together with HC≡CCH<sub>2</sub>O–C(O)C(H)(CH<sub>3</sub>)–, C<sub>15</sub>H<sub>11</sub>O–C(O)C(H)(CH<sub>3</sub>)–, or BnO–C(O)C(H)(CH<sub>3</sub>)–. MALDI-ToF mass spectrometry corroborated the identity of the polymer end groups and established that intermolecular transesterification reactions occurred at high monomer conversion.

### 28.3.3 iROP Catalysis with Cationic Alkaline Earth Complexes

The catalytic activity of the families of cationic complexes **17–19** and **20–22** toward the *i*ROP of L-LA was evaluated as well (Table 28.4). We reasoned that the weakly coordinating anion H<sub>2</sub>N{B(C<sub>6</sub>F<sub>5</sub>)<sub>3</sub>}<sup>-</sup> and the absence of additional solvent on the metal centers should enhance the Lewis acidity of the cations and produce highly active catalysts. Complexes **23–25**, which contain THF, exhibited good activities but limited control under the chosen conditions.

TABLE 28.3 (i)ROP of L-LA Mediated by 2, 4–6, 8–10, and 13

Complex	[Ae] <sub>0</sub> , mM	ROH	[L-LA] <sub>0</sub> /[Ae] <sub>0</sub> / [ROH] <sub>0</sub>	Solvent	T <sup>re</sup> , °C	Time, min	Yield, % <sup>a</sup>	TOF, mol <sub>L-LA</sub> /mol <sub>Ae</sub> h	M <sub>n,calco</sub> , g/mol <sup>b</sup>	M <sub>n,SEC</sub> , g/mol <sup>c</sup>	M <sub>w</sub> /M <sub>n</sub> <sup>c</sup>
<b>4</b>	0.5	HC≡CCH <sub>2</sub> OH	1000:1:10	Tol.	30	15	52	2,080	7,500	6,600	1.46
<b>5</b>	0.5	HC≡CCH <sub>2</sub> OH	1000:1:10	Tol.	30	15	49	7,350	7,100	6,300	1.36
<b>6</b>	0.5	HC≡CCH <sub>2</sub> OH	1000:1:10	Tol.	30	4	88	21,200	8,500	6,900	1.18
<b>5</b>	1.0	HC≡CCH <sub>2</sub> OH	2,000:1:30	Tol.	30	5	88	10,500	5,100	4,300	1.20
<b>6</b>	0.4	HC≡CCH <sub>2</sub> OH	5,000:1:100	Tol.	30	20	70	10,500	5,100	4,300	1.20
<b>4</b>	2.0	HC≡CCH <sub>2</sub> OH	1000:1:10	Tol.	30	2	91	27,300	13,200	12,000	1.10
<b>4</b>	2.0	C <sub>15</sub> H <sub>11</sub> OH <sup>d</sup>	1000:1:10	Tol.	30	2	88	26,400	12,900	10,200	1.14
<b>4</b>	2.0	BnOH	1000:1:10	Tol.	30	2	87	26,100	12,500	10,800	1.17
<b>8</b>	2.0	BnOH	1000:1:10	Tol.	30	7	17	1,457	2,600	2,700	1.17
<b>9</b>	2.0	BnOH	1000:1:10	Tol.	30	7	20	1,714	3,000	3,400	1.12
<b>10</b>	2.0	BnOH	1000:1:10	Tol.	30	7	53	4,543	7,600	8,000	1.11
<b>13</b>	2.0	BnOH	1000:1:10	Tol.	30	15	83	3,320	10,900 <sup>e</sup>	8,200	1.20
<b>13</b>	5.0	—	200:1:—	THF	30	40	80	240	23,100 <sup>f</sup>	16,600	1.21
<b>13</b>	5.0	—	200:1:—	THF	0	60	88	176	25,400 <sup>f</sup>	18,100	1.24
<b>10</b>	5.0	—	200:1:—	THF	0	60	76	152	21,900 <sup>f</sup>	6,800	1.55
<b>2</b>	5.0	—	200:1:—	THF	0	60	86	172	24,800 <sup>f</sup>	12,000	1.66

<sup>a</sup> Isolated yield after precipitation.<sup>b</sup> Calculated from M<sub>n,theo</sub> = [L-LA]<sub>0</sub>/[ROH]<sub>0</sub> × yield × 144.13 + M<sub>ROH</sub> unless otherwise specified.<sup>c</sup> Determined by size-exclusion chromatography calibrated versus polystyrene standards, and corrected by a factor of 0.58.<sup>d</sup> 9-Anthraenylmethanol.<sup>e</sup> Calculated from M<sub>n,theo</sub> = [L-LA]<sub>0</sub>/([HC≡CCH<sub>2</sub>OH]<sub>0</sub>+[Ae]<sub>0</sub>) × yield × 144.13 + M<sub>HC≡CCH<sub>2</sub>OH</sub>.<sup>f</sup> Calculated from M<sub>n,theo</sub> = [L-LA]<sub>0</sub>/[Ae]<sub>0</sub> × yield × 144.13.

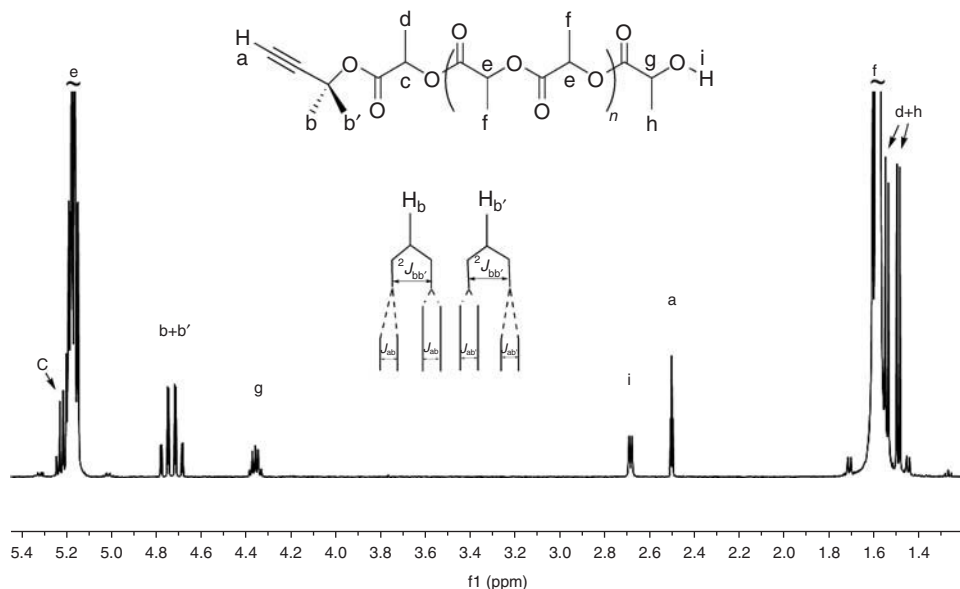


**Figure 28.5**  $^1\text{H}$  NMR spectrum (500.13 MHz,  $\text{CDCl}_3$ , 298 K) of a low molecular weight poly(lactic acid) (PLLA) sample prepared with **4**/ $\text{HC}\equiv\text{CCH}_2\text{OH}$  ( $[\text{L-LA}]_0/[\text{4}]_0/[\text{HC}\equiv\text{CCH}_2\text{OH}]_0 = 5000 : 1 : 100$ ;  $M_{n,\text{SEC}} = 4700 \text{ g/mol}$ ,  $M_w/M_n = 1.13$ ). Note the ABX spin system corresponding to  $\text{H}_a$ ,  $\text{H}_b$ , and  $\text{H}_{b'}$  ( $^2J_{\text{HbHb}'} = 18.0 \text{ Hz}$ ,  $^4J_{\text{HaHb}} = 2.5 \text{ Hz}$ ).

**TABLE 28.4** Immortal ROP of L-LA with 17–22/ROH Systems<sup>a</sup>

$\text{M}^+$	ROH	$[\text{L-LA}]_0/[\text{M}^+]_0/[ \text{ROH}]_0$	$T^\text{e}, ^\circ\text{C}$	$t, \text{h}$	Yield, % <sup>b</sup>	TOF, $\text{mol/mol}_{\text{Ae}} \text{ h}$	$M_{n,\text{theo}}, \text{g/mol}^c$	$M_{n,\text{SEC}}, \text{g/mol}^d$	$M_w/M_n^d$
<b>17</b>	BnOH	1000 : 1 : 10	60	8	72	90	10,500	10,700	1.06
<b>17</b>	BnOH	3000 : 1 : 10	60	24	96	120	41,600	30,000 <sup>e</sup>	1.06
<b>17</b>	BnOH	1000 : 1 : 50	60	8	83	104	2,500	2,400	1.12
<b>18</b>	<i>i</i> PrOH	1000 : 1 : 10	30	1	48	480	7,000	14,000	1.20
<b>19</b>	<i>i</i> PrOH	1000 : 1 : 10	100	0.05	30	6000	4,400	11,000	1.21
<b>20</b>	BnOH	1000 : 1 : 10	100	3	47	157	6,900	6,700	1.12
<b>21</b>	BnOH	1000 : 1 : 10	100	3	74	247	10,800	9,900	1.17
<b>22</b>	BnOH	1000 : 1 : 10	100	3	50	167	7,300	6,800	1.16
<b>21</b>	BnOH	1000 : 1 : 5	100	1.5	34	227	9,900	9,300	1.09
<b>21</b>	BnOH	1000 : 1 : 10	100	1.5	52	347	7,600	7,500	1.10
<b>21</b>	BnOH	1000 : 1 : 20	100	1.5	57	380	4,200	4,100	1.10
<b>21</b>	BnOH	1000 : 1 : 50	100	1.5	75	500	2,300	2,400	1.10
<b>21</b>	BnOH	2000 : 1 : 5	100	24	85	71	49,100	35,000 <sup>e</sup>	1.41

<sup>a</sup>Polymerizations carried out in toluene with  $[\text{L-LA}]_0 = 2.0 \text{ M}$ .

<sup>b</sup>Isolated yield after precipitation.

<sup>c</sup>Calculated from  $M_{n,\text{theo}} = [\text{L-LA}]_0/[\text{ROH}]_0 \times \text{yield} \times 144.13 + M_{\text{ROH}}$ , with  $M_{\text{BnOH}} = 108 \text{ g/mol}$  and  $M_{\text{iPrOH}} = 60 \text{ g/mol}$ .

<sup>d</sup>Determined by size-exclusion chromatography calibrated versus polystyrene standards, and corrected by a factor of 0.58.

<sup>e</sup>Note that the 0.58 factor applied to the correction of PLLA molecular weights determined versus polystyrene standards is inadequate at high molecular weights; higher factors should be utilized.

The *i*ROP of L-LA was promoted by **17–19** at 30–60 °C upon addition of an excess of *i*PrOH. The controlled character of the *i*ROP was established by NMR spectroscopy and MALDI-TOF mass spectrometry; no epimerization of the optically active centers was detected. The Sr and Ba complexes **18** and **19** afforded highly active binary catalysts, allowing rapid conversion of the monomer at the remarkably mild temperature of 30 °C (TOF up to 6000 mol<sub>L-LA</sub>/mol<sub>Ae</sub> h). However, rapid broadening of the molecular weight distributions was observed at high conversion. The Ca derivative **17** offered the best compromise in terms of activity and control, providing a very efficient binary catalyst for well-controlled *i*ROP upon

addition of 5–50 equiv *i*PrOH or BnOH at 60 °C. Full conversion of 3000 equiv of L-LA was achieved within 24 h with excellent control ( $M_{n,\text{theo}} \sim M_{n,\text{SEC}}$ ;  $M_w/M_n = 1.06\text{--}1.12$ ). The TOFs were in the range 80–100 mol<sub>L-LA</sub>/mol<sub>Ca</sub> h. There was no influence of the contents in BnOH on the catalytic activity in the concentration range examined (5–50 equiv vs **17**), but the molecular weights decreased linearly with increasing BnOH contents.

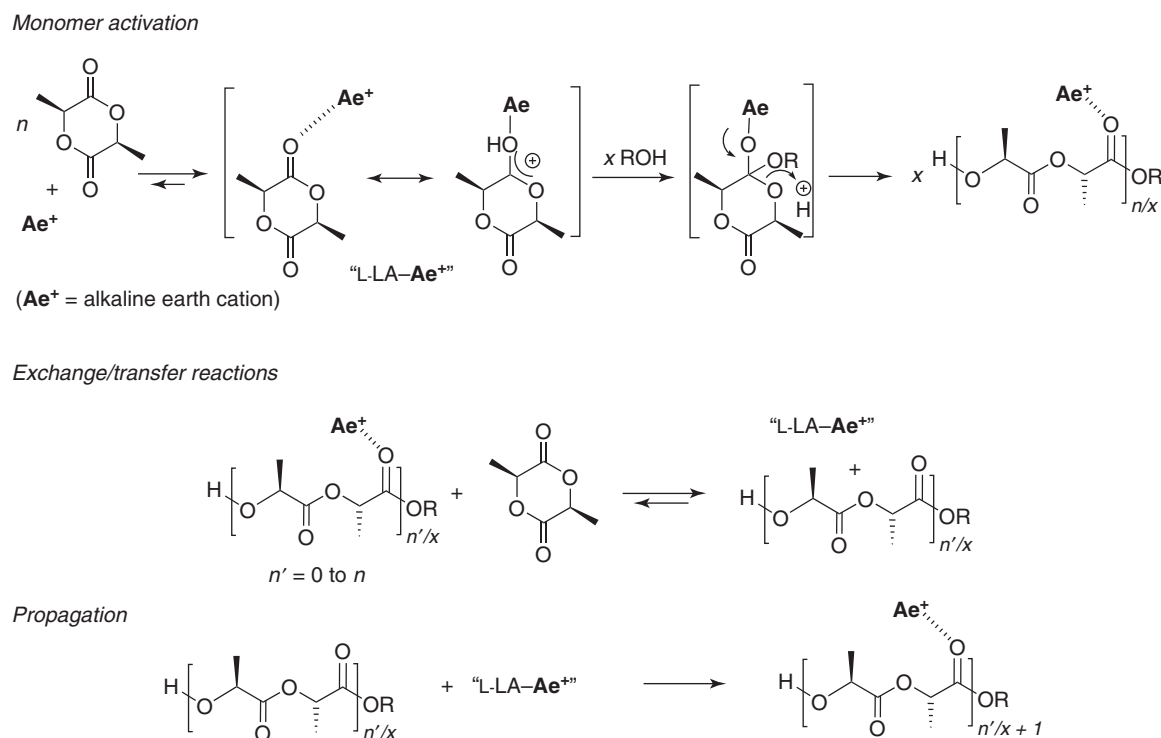
Effective catalytic systems were also generated upon addition of excess BnOH to the fluorinated complexes **20–22**. Partial conversion of 1000 equiv of L-LA was observed at 100 °C with  $[\text{L-LA}]_0/[\text{Ae}^+]_0/[\text{ROH}]_0 = 1000 : 1 : 10$ , with the Sr and Ba derivatives being the most active. General features of the systems **20–22**/BnOH included (i) relatively lower catalytic activity than their phenolate counterparts **17–19**, requiring higher polymerization temperature (80–100 °C) with TOFs in the range 100–500 mol<sub>L-LA</sub>/mol<sub>Ae</sub> h, (ii) very good agreement between  $M_{n,\text{theo}}$  and  $M_{n,\text{SEC}}$ , and generally narrow distributions ( $M_w/M_n \sim 1.10\text{--}1.20$ ), (iii) the trend Ca < Sr ∼ Ba, (iv) end-group reliability, and (v) absence of epimerization of the chiral centers. The Sr-based **21**/BnOH binary catalyst polymerized 2000 equiv of L-LA and withstood 50 equiv of BnOH.

Kinetic studies were conducted by NMR spectroscopy in toluene-*d*<sub>8</sub>. In the *i*ROP of L-LA (100 °C,  $[\text{L-LA}]_0 = 2.0$  M,  $[\text{L-LA}]_0/[\text{M}]_0/[\text{BnOH}]_0 = 136 : 1 : 6.6$ ) catalyzed by BnOH/**20–22**, apparent rate constants of 0.0004, 0.0013, and 0.0014 s<sup>-1</sup> were calculated for **20**, **21**, and **22**, respectively. The catalytic activity increased with the ionic radius of the metal. This was in line with the trend observed with complexes **17–19** supported by the phenolate ligand {LO<sup>3</sup>}<sup>-</sup>. The binary catalyst **21**/BnOH was selected for further NMR kinetics performed at 100 °C in toluene-*d*<sub>8</sub>. Partial first orders in monomer, catalyst, and initiator concentrations were determined, which gave the rate law

$$-\frac{d[\text{L-LA}]}{dt} = k_p \cdot [\text{L-LA}]^{1.0} \cdot [\text{BnOH}]^{1.0}$$

Eyring analyses (85–100 °C) confirmed first-order kinetics in monomer concentration, and the activation parameters  $\Delta H^\ddagger = 14.8(5)$  kcal/mol and  $\Delta S^\ddagger = -7.6(2.0)$  cal/K mol were determined. A commonly accepted activated monomer mechanism for *i*ROP, applicable to these binary catalyst systems Ae<sup>+</sup>/ROH, is depicted in Scheme 28.7.

The performances of the {BDI<sup>i</sup>Pr}<sup>-</sup>-supported cationic complexes **28** and **29** in the *i*ROP of L-LA (1000 equiv) were assessed in the presence of BnOH (10 equiv) [21]. Both binary catalytic systems exhibited high activities at 30 °C, with



**Scheme 28.7** Traditional activated monomer mechanism for the immortal ROP of L-LA catalyzed by a binary catalyst Ae<sup>+</sup>/ROH.

satisfactory control of all parameters. With the more active **29**, 82% conversion was already reached after 10 min, and the macromolecular features of the resulting polymer were well controlled ( $M_{n,\text{theo}} = 11,900 \text{ g/mol}$ ,  $M_{n,\text{SEC}} = 10,400 \text{ g/mol}$ ,  $M_w/M_n = 1.19$ ). In terms of activity, the **29/BnOH** Sr-based binary catalyst (TOF = 4920 mol<sub>L-LA</sub>/mol<sub>Sr</sub> h) outclassed all related cationic systems reported so far. The high activity unveiled by **29/BnOH** could be credited to the extreme electrophilicity and large accessibility of the metal center in this cationic Sr complex of relatively low coordination number associated to a poorly coordinating anion.

#### 28.3.4 Well-Defined Charge-Neutral and Cationic Complexes of the Large Alkaline Earths for ROP Catalysis: Outcome and Perspectives

Significant efforts were devoted by our group in the past 3 years to the conception, preparation, and implementation of ROP catalysts based on the large alkaline earth metals. The main outcomes can be summarized as follows:

- We have developed the first families of stable Ae-based ROP catalysts, both heteroleptic charge-neutral and cationic ones.
- Specific strategies were introduced to overcome the synthetic difficulties associated with these electropositive metals.
- The first discrete, solvent-free cations of the large Ae metals have been synthesized.
- Highly electrophilic Ae complexes can be stabilized by intramolecular secondary Ae···H–Si and Ae···F interactions.
- These Ae-based complexes mediate very efficiently the ROP of cyclic esters, and are among the most active catalysts known to date.
- Charge-neutral catalysts (operating according to a coordination-insertion mechanism) were much more active, but less controlled than their cationic derivatives (operating according to an activated monomer mechanism).

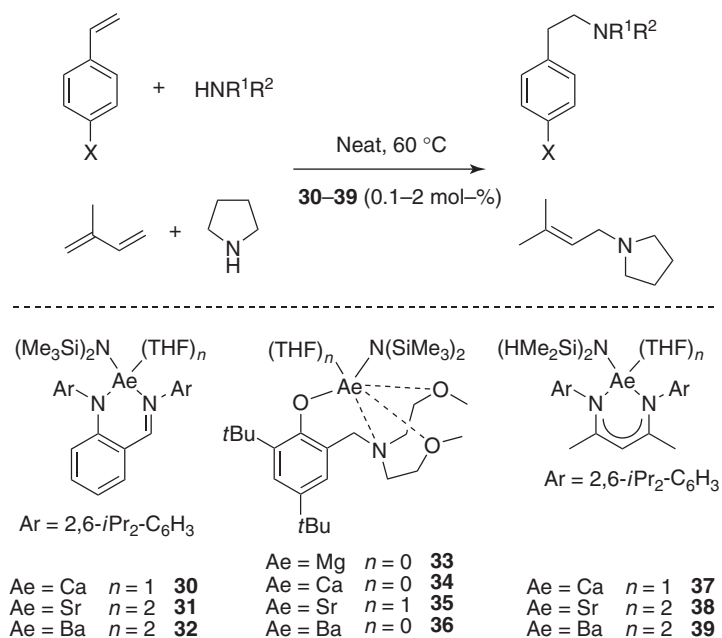
#### 28.4 INTERMOLECULAR HYDROAMINATION OF ACTIVATED ALKENES CATALYZED BY CHARGE-NEUTRAL HETEROLEPTIC COMPLEXES OF LARGE ALKALINE EARTHS

Hydroaminations of unsaturated substrates are of upmost interest in bulk and fine chemicals synthesis, notably because of their atom efficiency. Various metals, including late-transition ones, can catalyze this reaction, but  $d^0$  complexes of the rare earths [23] and alkaline earths have shown particularly good abilities, in particular for achieving stereoselective reactions [24]. Most examples that rely on catalysts based on the large alkaline earth metals, typically Ca and, in more seldom cases, Sr, are concerned with *intramolecular* cyclohydroamination of amino-alkenes [25]. Fewer examples of *intermolecular* hydroamination reactions of activated alkenes (vinyl aromatics, conjugated dienes) catalyzed by Ae complexes are known. Hill and coworkers [26] showed that in such reactions catalyzed by homoleptic complexes  $\{\text{Ae}[\text{N}(\text{SiMe}_3)_2]_2\}_2$  (Ae = Mg, Ca, Sr, Ba) and  $\{\text{Ae}[\text{CH}(\text{SiMe}_3)_2]_2(\text{THF})_2\}$  (Ae = Ca, Sr), the activity of Ae catalysts does not increase linearly with the size of the metal ( $\text{Mg}^{2+}(6)$ , 0.72 Å;  $\text{Ba}^{2+}(6)$ , 1.35 Å): the Sr complex was indeed superior to the Ca one, while the Mg and Ba derivatives displayed very poor activities. However, no such experimental data were available for *heteroleptic* complexes.

To get a better insight into this reactivity trend and to eventually determine the real abilities of large Ae elements, our group has developed three families of heteroleptic complexes supported by various monoanionic ancillary ligands—anilido-imino,  $\{\text{LN}^1\}$  (**30–32**), phenolate-amino-alkoxy  $\{\text{LO}^5\}$  (**33–36**), and  $\beta$ -diketiminate  $\{\text{BDI}^{\text{Pr}}\}$  (**37–39**)—and used them for the intermolecular hydroamination of styrene derivatives and isoprene (Scheme 28.8, Table 28.5) [27].

All these heteroleptic complexes proved able to promote fully regioselective (i.e., *anti*-Markovnikov) addition reactions at a moderate catalyst loading of at most 2 mol% in neat substrates at 60 °C. A clear superiority of these heteroleptic compounds, notably that of Ba complex **32** over the usual bis(amides)  $\text{Ae}[\text{N}(\text{SiMe}_3)_2]_2(\text{THF})_2$  (Ae = Ca, Sr) was demonstrated as, under identical conditions, the latter displayed much lower reaction rates. Contrary to expectations based on Hill's results [26], irrespective of the identity of the ligand, the catalytic activity increased with the size of the metal ( $\text{Mg} \ll \text{Ca} < \text{Sr} < \text{Ba}$ , as evidenced with anilido-imino-Ae complexes **30–32**, phenolate-amino-methoxy complexes **33–36**, and  $\beta$ -diketiminate complexes **37–39**). For any given metal, the maximal activity was achieved with the  $\{\text{BDI}^{\text{Pr}}\}^-$  ligand, the anilido-amino one displaying only slightly lower efficiency, whereas the lowest activity was recorded with the phenolate ligand. It must be noted, however, that complexes **30–32** are more readily synthesized than **37–39**, which constitutes a key advantage for catalytic applications.

The scope of the barium complex **32** was therefore briefly explored. The fastest reaction rates were achieved with pyrrolidine, with turnover frequencies up to 290 h<sup>-1</sup> at 0.1 mol% catalyst loading. These values exceed by 1 to 2 orders of



**Scheme 28.8** Intermolecular hydroamination of styrene derivatives and isoprene with amines catalyzed by heteroleptic Ae complexes **30–39** [27].

**TABLE 28.5** Intermolecular Hydroamination of Styrene and Isoprene with Amines Catalyzed by Heteroleptic Ae Complexes [27]<sup>a</sup>

Complex		Amine	<i>t</i> , h	Conv., % <sup>b</sup>
{LN <sup>1</sup> }CaN(SiMe <sub>3</sub> ) <sub>2</sub> (THF)	(30)	BnNH <sub>2</sub>	18.5	34
{LN <sup>1</sup> }SrN(SiMe <sub>3</sub> ) <sub>2</sub> (THF) <sub>2</sub>	(31)	BnNH <sub>2</sub>	18.5	71
{LN <sup>1</sup> }BaN(SiMe <sub>3</sub> ) <sub>2</sub> (THF) <sub>2</sub>	(32)	BnNH <sub>2</sub>	18.5	86
{LO <sup>5</sup> }MgN(SiMe <sub>3</sub> ) <sub>2</sub>	(33)	BnNH <sub>2</sub>	18.5	1
{LO <sup>5</sup> }CaN(SiMe <sub>3</sub> ) <sub>2</sub>	(34)	BnNH <sub>2</sub>	18.5	6
{LO <sup>5</sup> }SrN(SiMe <sub>3</sub> ) <sub>2</sub> (THF)	(35)	BnNH <sub>2</sub>	18.5	24
{LO <sup>5</sup> }BaN(SiMe <sub>3</sub> ) <sub>2</sub>	(36)	BnNH <sub>2</sub>	18.5	37
{BDI <sup>i</sup> Pr}CaN(SiHMe <sub>2</sub> ) <sub>2</sub> (THF)	(37)	BnNH <sub>2</sub>	2	29
{BDI <sup>i</sup> Pr}SrN(SiHMe <sub>2</sub> ) <sub>2</sub> (THF) <sub>2</sub>	(38)	BnNH <sub>2</sub>	2	42
{BDI <sup>i</sup> Pr}BaN(SiHMe <sub>2</sub> ) <sub>2</sub> (THF) <sub>2</sub>	(39)	BnNH <sub>2</sub>	2	64
{LN <sup>1</sup> }BaN(SiMe <sub>3</sub> ) <sub>2</sub> (THF) <sub>2</sub>	(32)	(CH <sub>2</sub> ) <sub>4</sub> NH	1	99
{LN <sup>1</sup> }BaN(SiMe <sub>3</sub> ) <sub>2</sub> (THF) <sub>2</sub> <sup>c</sup>	(32)	(CH <sub>2</sub> ) <sub>4</sub> NH	2	85
Ca[N(SiMe <sub>3</sub> ) <sub>2</sub> ] <sub>2</sub> (THF) <sub>2</sub> <sup>c</sup>		(CH <sub>2</sub> ) <sub>4</sub> NH	2	<1
Sr[N(SiMe <sub>3</sub> ) <sub>2</sub> ] <sub>2</sub> (THF) <sub>2</sub> <sup>c</sup>		(CH <sub>2</sub> ) <sub>4</sub> NH	2	10
{LN <sup>1</sup> }BaN(SiMe <sub>3</sub> ) <sub>2</sub> (THF) <sub>2</sub> <sup>d</sup>	(32)	(CH <sub>2</sub> ) <sub>4</sub> NH	1	99 <sup>e</sup>
{LN <sup>1</sup> }BaN(SiMe <sub>3</sub> ) <sub>2</sub> (THF) <sub>2</sub>	(32)	nHexNH <sub>2</sub>	18.5	55
{LN <sup>1</sup> }BaN(SiMe <sub>3</sub> ) <sub>2</sub> (THF) <sub>2</sub>	(32)	iPr <sub>2</sub> NH	18.5	0

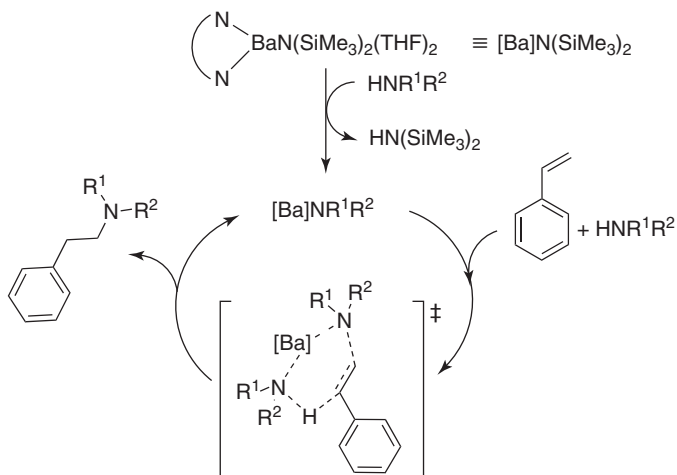
<sup>a</sup>Reaction conditions unless otherwise specified: [styrene]/[amine]/[catalyst] = 50:50:1, 10.5 μmol of catalyst, no solvent, *T* = 60 °C.

<sup>b</sup>Determined by <sup>1</sup>H NMR spectroscopy.

<sup>c</sup>[styrene]/[pyrrolidine]/[3] = 500:500:1.

<sup>d</sup>Reaction performed with isoprene instead of styrene, with [isoprene]/[pyrrolidine]/[3] = 220:50:1.

<sup>e</sup>Based on amine conversion.



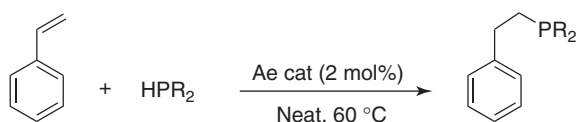
**Scheme 28.9** Possible six-centered concerted mechanistic pathway for styrene/amine intermolecular hydroamination catalyzed by **32** [27].

magnitude those reported to date for intermolecular hydroamination reactions catalyzed by rare-earth [23], Ae [25, 26] or even late-transition metal [28] complexes. The hydroamination of styrene with *n*-hexylamine also occurred fairly rapidly, in contrast to that with isopropylamine, obviously reflecting the sensitivity to steric factors. Consistent with earlier results with rare-earth [23] and Ae [25, 26] metals, the presence of an electron-donating methoxy substituent group on the aromatic ring in vinyl arenes led to a marked decrease in catalyst activity (5.5 equiv converted after 18.5 h), while the presence of a chlorine atom did not affect much the activity. The reaction of isoprene and pyrrolidine proceeded in the presence of as little as 0.1 mol% of **32** (TOF = 295 h<sup>-1</sup>), with 1,4-regioselective *anti*-Markovnikov addition.

Kinetic studies of the hydroamination of styrene with pyrrolidine catalyzed by **32** revealed an empirical rate law  $v = k[\text{styrene}]^{1.0}[\text{pyrrolidine}]^{1.0}[\mathbf{32}]^{1.0}$ . A strong kinetic isotope effect was observed in the reaction of styrene with *N*-deuterated pyrrolidine catalyzed by **32** ( $k_{\text{H}}/k_{\text{D}} = 6.8$  and 7.3 at 40 and 60 °C respectively). These results were conciliated in a mechanism, different from that proposed for rare-earth systems [23a], that involves a one-step, noninsertive route with a six-centered transition state via concerted proton transfer onto the unsaturation activated toward the attack of the nucleophile (Scheme 28.9) [25, 26].

## 28.5 INTERMOLECULAR HYDROPHOSPHINATION OF STYRENE CATALYZED BY CHARGE-NEUTRAL HETEROLEPTIC COMPLEXES OF LARGE ALKALINE EARTHS

Intermolecular hydrophosphination of activated alkenes and alkynes is another hydroelementation process of great interest. Yet, in contrast to hydroamination, rare-earth complexes are not known to catalyze this reaction. Our recent studies have revealed that heteroleptic alkaline earth complexes **30–32**, **33–36**, and **37–39** (Scheme 28.8) all catalyze the intermolecular *anti*-Markovnikov hydrophosphination of styrene with secondary phosphines such as HPCy<sub>2</sub> or HPPh<sub>2</sub> (Scheme 28.10; Table 28.6) [27]. As for hydroamination, the activity trend varied according to Ca < Sr < Ba, that is, it increases monotonously with the size of the metal center. However, a different dependence of the performances on the ligand was observed: {BDI<sup>iPr</sup>}<sup>−</sup> < {LN<sup>1</sup>}<sup>−</sup> ≈ {LO<sup>5</sup>}<sup>−</sup>. Complex **32** was thus the most active catalyst for this transformation, with TOF values (192 h<sup>-1</sup> with HPPh<sub>2</sub> at 60 °C) that outclass those reported with {BDI<sup>iPr</sup>}CaN(SiMe<sub>3</sub>)<sub>2</sub>(THF) (circa = ca 0.5 h<sup>-1</sup> at 75 °C) [29]. The reactions with the less basic HPPh<sub>2</sub> were considerably faster than with HPCy<sub>2</sub>.



**Scheme 28.10** Intermolecular hydrophosphination of styrene catalyzed by heteroleptic Ae complexes [27].

**TABLE 28.6** Intermolecular Hydrophosphination of Styrene Catalyzed by Heteroleptic Ae Complexes [27]<sup>a</sup>

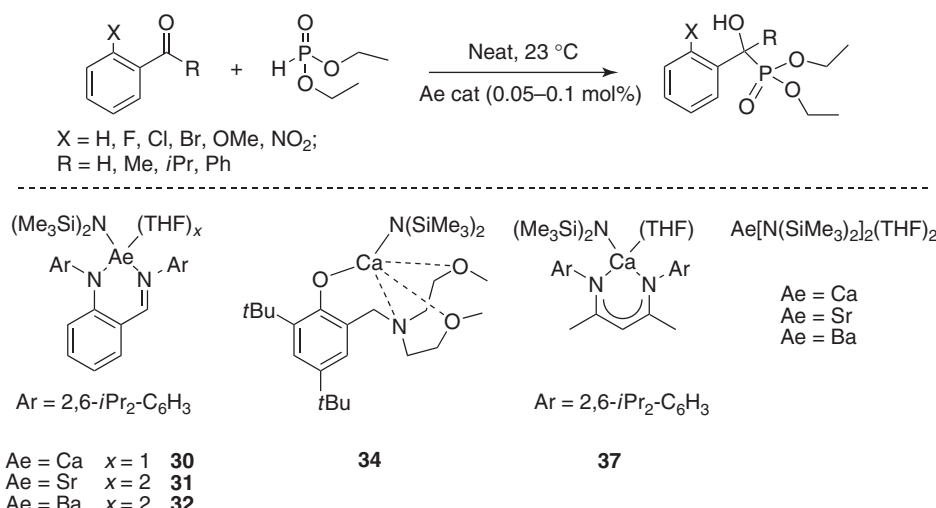
Complex		Phosphine	<i>t</i> , h	Conv., % <sup>b</sup>
{LN <sup>1</sup> }CaN(SiMe <sub>3</sub> ) <sub>2</sub> (THF)	(30)	HPCy <sub>2</sub>	18.5	31
{LN <sup>1</sup> }SrN(SiMe <sub>3</sub> ) <sub>2</sub> (THF) <sub>2</sub>	(31)	HPCy <sub>2</sub>	18.5	41
{LN <sup>1</sup> }BaN(SiMe <sub>3</sub> ) <sub>2</sub> (THF) <sub>2</sub>	(32)	HPCy <sub>2</sub>	18.5	42
{LO <sup>5</sup> }CaN(SiMe <sub>3</sub> ) <sub>2</sub>	(34)	HPCy <sub>2</sub>	18.5	12
{LO <sup>5</sup> }SrN(SiMe <sub>3</sub> ) <sub>2</sub> (THF)	(35)	HPCy <sub>2</sub>	18.5	26
{LO <sup>5</sup> }BaN(SiMe <sub>3</sub> ) <sub>2</sub>	(36)	HPCy <sub>2</sub>	18.5	46
{BDI <sup>iPr</sup> }CaN(SiHMe <sub>2</sub> ) <sub>2</sub> (THF)	(37)	HPCy <sub>2</sub>	18.5	4
{BDI <sup>iPr</sup> }SrN(SiHMe <sub>2</sub> ) <sub>2</sub> (THF) <sub>2</sub>	(38)	HPCy <sub>2</sub>	18.5	9
{BDI <sup>iPr</sup> }BaN(SiHMe <sub>2</sub> ) <sub>2</sub> (THF) <sub>2</sub>	(39)	HPCy <sub>2</sub>	18.5	18
{LN <sup>1</sup> }CaN(SiMe <sub>3</sub> ) <sub>2</sub> (THF)	(30)	HPPh <sub>2</sub>	0.25	42
{LN <sup>1</sup> }SrN(SiMe <sub>3</sub> ) <sub>2</sub> (THF) <sub>2</sub>	(31)	HPPh <sub>2</sub>	0.25	92
{LN <sup>1</sup> }BaN(SiMe <sub>3</sub> ) <sub>2</sub> (THF) <sub>2</sub>	(32)	HPPh <sub>2</sub>	0.25	>96

<sup>a</sup>Reaction conditions: [styrene]/[phosphine]/[catalyst] = 50 : 50 : 1, 10.5 μmol of catalyst, no additional solvent, *T* = 60 °C.<sup>b</sup>Determined by <sup>1</sup>H NMR spectroscopy.

## 28.6 HYDROPHOSPHONYLATION OF ALDEHYDES AND NONACTIVATED KETONES BY CHARGE-NEUTRAL HOMOLEPTIC AND HETEROLEPTIC COMPLEXES OF LARGE ALKALINE EARTHS

Ternary and quaternary α-hydroxy-phosphonates, an important class of biologically active compounds, are commonly obtained by addition of dialkylphosphites onto aldehydes or ketones [30]. Well-defined mono- or bimetallic complexes of rare-earth metals, titanium, or aluminum have emerged over the past two decades as effective catalysts for this so-called hydrophosphonylation of aldehydes [31] and, with more difficulty, that of ketones [31c,d, 32], which are far less reactive because of their lower electrophilicity. In some cases, good enantioselectivities could be achieved thanks to the use of chiral metal-based precatalysts [31, 32]. Despite their several similarities with rare-earth elements, we were surprised to see that discrete complexes of the large Ae metals had never been utilized to catalyze hydrophosphonylation reactions.

In fact, we found that hydrophosphonylation of aldehydes and nonactivated ketones could be achieved selectively and rapidly at room temperature using very low catalytic loadings (as low as 0.02 mol%) of the simple Ae[N(SiMe<sub>3</sub>)<sub>2</sub>]<sub>2</sub>(THF)<sub>2</sub> complexes (Ae = Ca, Sr, Ba) (Scheme 28.11, Table 28.7) [33]. Indeed these homoleptic Ae precatalysts turned out as

**Scheme 28.11** Ae heteroleptic and homoleptic complexes screened for the hydrophosphonylation of aldehydes and ketones [33].

**TABLE 28.7** Hydrophosphonylation of Benzaldehyde, Acetophenone, and Related Derivatives with Diethylphosphite Catalyzed by Homoleptic and Heteroleptic Ae Complexes [33]<sup>a</sup>

X	R	Complex	Cat., mol%	Time	Conv., <sup>b</sup> %	TOF <sup>c</sup> , min <sup>-1</sup>
H	H	{BDI <sup>iPr</sup> }CaN(SiMe <sub>3</sub> ) <sub>2</sub>	(37)	0.05	0.3 min	>99.9
H	H	Ca[N(SiMe <sub>3</sub> ) <sub>2</sub> ] <sub>2</sub> (THF) <sub>2</sub>		0.05	0.3 min	>99.9
H	Me	{LN <sup>1</sup> }Ca[N(SiMe <sub>3</sub> ) <sub>2</sub> ](THF)	(30)	0.05	1 min	61
H	Me	{LN <sup>1</sup> }Sr[N(SiMe <sub>3</sub> ) <sub>2</sub> ](THF) <sub>2</sub>	(31)	0.05	1 min	65
H	Me	{LN <sup>1</sup> }Ba[N(SiMe <sub>3</sub> ) <sub>2</sub> ](THF) <sub>2</sub>	(32)	0.05	1 min	71
H	Me	{LO <sup>5</sup> }Ca[N(SiMe <sub>3</sub> ) <sub>2</sub> ](THF)	(34)	0.05	60	59
H	Me	{BDI <sup>iPr</sup> }CaN(SiMe <sub>3</sub> ) <sub>2</sub>	(37)	0.05	1 min	55
H	Me	Ca[N(SiMe <sub>2</sub> H) <sub>2</sub> ] <sub>2</sub> (THF)		0.05	1 min	60
H	Me	Ca[N(SiMe <sub>3</sub> ) <sub>2</sub> ] <sub>2</sub>		0.05	1 min	58
H	Me	Ca[N(SiMe <sub>3</sub> ) <sub>2</sub> ] <sub>2</sub> (THF) <sub>2</sub>		0.05	1 min	60
H	Me	Sr[N(SiMe <sub>3</sub> ) <sub>2</sub> ] <sub>2</sub> (THF) <sub>2</sub>		0.05	1 min	70
H	Me	Ba[N(SiMe <sub>3</sub> ) <sub>2</sub> ] <sub>2</sub> (THF) <sub>2</sub>		0.05	1 min	74
H	Me	Ca[N(SiMe <sub>3</sub> ) <sub>2</sub> ] <sub>2</sub> (THF) <sub>2</sub>		0.1	10 min	93
H	<i>i</i> Pr	Ca[N(SiMe <sub>3</sub> ) <sub>2</sub> ] <sub>2</sub> (THF) <sub>2</sub>		0.1	10 min	10
F	Me	Ca[N(SiMe <sub>3</sub> ) <sub>2</sub> ] <sub>2</sub> (THF) <sub>2</sub>		0.1	10 min	85
Cl	Me	Ca[N(SiMe <sub>3</sub> ) <sub>2</sub> ] <sub>2</sub> (THF) <sub>2</sub>		0.1	10 min	55
Br	Me	Ca[N(SiMe <sub>3</sub> ) <sub>2</sub> ] <sub>2</sub> (THF) <sub>2</sub>		0.1	20 h	38
NO <sub>2</sub>	Me	Ca[N(SiMe <sub>3</sub> ) <sub>2</sub> ] <sub>2</sub> (THF) <sub>2</sub>		0.1	48 h	Traces
Me	Me	Ca[N(SiMe <sub>3</sub> ) <sub>2</sub> ] <sub>2</sub> (THF) <sub>2</sub>		0.1	48 h	Traces
OMe	Me	Ca[N(SiMe <sub>3</sub> ) <sub>2</sub> ] <sub>2</sub> (THF) <sub>2</sub>		0.1	4 h	33

<sup>a</sup>Reaction conditions: neat substrates in 1:1 ratio (10–20 mmol) at room temperature.<sup>b</sup>Conversion determined by <sup>1</sup>H NMR spectroscopy.<sup>c</sup>Nonoptimized catalyst turnover frequencies.

effective as and sometimes more effective than the more sophisticated heteroleptic complexes **30–39** that we used in hydroelementation reactions [27].

The reactions were performed in neat reagents with low catalyst loadings to optimize the overall atom efficiency of the reaction and reduce both organic and metallic wastes. With 0.05 mol% of the calcium heteroleptic complexes **30**, **34**, or **37** or the simple Ca[N(SiMe<sub>3</sub>)<sub>2</sub>]<sub>2</sub>(THF)<sub>2</sub>, quantitative addition of HP(O)(OEt)<sub>2</sub> to an equimolar amount of benzaldehyde was achieved within 20 s. The reactions were too fast to discriminate between these complexes, and full conversion was still obtained over the same short time period when 0.02 mol% of **30** was used. The addition of diethylphosphite to acetophenone also proceeded rapidly, equally using 0.05 mol% of heteroleptic or homoleptic complexes, although, in this case, only partial conversion was obtained after 1 min at room temperature. This evidenced that the catalytic activity increased slightly with the size and electropositive nature of the metal, Ca < Sr < Ba, although the influence of the metal and that of the ligand framework appeared at best moderate. Also, no difference was noted between Ca[N(SiMe<sub>3</sub>)<sub>2</sub>]<sub>2</sub>(THF)<sub>2</sub>, Ca[N(SiMe<sub>2</sub>H)<sub>2</sub>]<sub>2</sub>(THF), and Ca[N(SiMe<sub>3</sub>)<sub>2</sub>]<sub>2</sub>. Although the less active in the series of homoleptic Ae precatalysts, Ca[N(SiMe<sub>3</sub>)<sub>2</sub>]<sub>2</sub>(THF)<sub>2</sub> was prioritized ahead of its heavier congeners on account of the fully biocompatible and nontoxic nature of calcium, to determine the scope of the reaction.

Other ketones substituted by groups of varying steric bulk and electronic properties were investigated. The reaction proved obviously quite sensitive to steric considerations. First, the rate was an order of magnitude lower for isobutyrophenone than for acetophenone. Secondly, introduction of an *ortho*-aryl substituent in acetophenone derivatives affected the conversion very mildly on the basis of electronic factors, but preponderantly on steric grounds (note for instance the similar low reactivity of *o*-Me and *o*-NO<sub>2</sub> substrates).

Hence, the readily prepared Ae[N(SiMe<sub>3</sub>)<sub>2</sub>]<sub>2</sub>(THF)<sub>2</sub> provided efficient and easy access to catalyzed hydrophosphonylation reactions not only with benzaldehydes but also for less reactive, nonactivated ketones, for which turnover frequencies as high as 1200–1500 min<sup>-1</sup> were achieved; these values outclass those reported to date by a considerable margin.

## ACKNOWLEDGMENTS

This research was gratefully supported by the European Research Council (grant FP7-People-2010-IIF, *ChemCatSusDe*).

## REFERENCES

- (a) Uhrich, K. E.; Cannizzaro, S. M.; Langer, R. S.; Shakesheff, K. M. *Chem. Rev.* **1999**, *99*, 3181; (b) Drumright, R. E.; Gruber, P. R.; Henton, D. E. *Adv. Mater.* **2000**, *12*, 1841; (c) Albertsson, A.-C.; Varma, I. K. *Biomacromolecules* **2003**, *4*, 1466; (d) Auras, R.; Lim, L.-T.; Selke, S. E. M.; Tsuji, H. *Poly(Lactic Acid): Synthesis, Structures, Properties, Processing and Applications*; John Wiley & Sons: Hoboken, New Jersey, **2010**.
- For leading reviews, see: (a) Dechy-Cabaret, O.; Martin-Vaca, B.; Bourissou, D. *Chem. Rev.* **2004**, *104*, 6147; (b) Wheaton, C. A.; Hayes, P. G.; Ireland, B. J. *Dalton Trans.* **2009**, 4832; (c) Stanford, M. J.; Dove, A. P. *Chem. Soc. Rev.* **2010**, *39*, 486; (d) Dijkstra, P. J.; Du, H.; Feijen, J. *Polym. Chem.* **2011**, *2*, 520.
- For reviews, see: (a) Kamber, N. E.; Jeong, W.; Waymouth, R. M.; Pratt, R. C.; Lohmeijer, B. G. G.; Hedrick, J. L. *Chem. Rev.* **2007**, *107*, 5813; (b) Kiesewetter, M. K.; Shin, E. J.; Hedrick, J. L.; Waymouth, R. M. *Macromolecules* **2010**, *43*, 2093.
- Shannon, R. D. *Acta Cryst.* **1976**, *A32*, 751.
- Ajellal, N.; Carpentier, J.-F.; Guillaume, C.; Guillaume, S. M.; Hérou, M.; Poirier, V.; Sarazin, Y.; Trifonov, A. *Dalton Trans.* **2010**, *39*, 8363.
- (a) Chisholm, M. H.; Gallucci, J.; Phomphrai, K. *Chem. Commun.* **2003**, 48; (b) Chisholm, M. H.; Gallucci, J. C.; Phomphrai, K. *Inorg. Chem.* **2004**, *43*, 6717.
- (a) Dahrensborg, D. J.; Choi, W.; Richers, C. P. *Macromolecules* **2007**, *40*, 3521; (b) Dahrensborg, D. J.; Choi, W.; Karroonirun, O.; Bhuvanesh, N. *Macromolecules* **2008**, *41*, 3493.
- (a) Zhong, Z.; Dijkstra, P. J.; Birg, C.; Westerhausen, M.; Feijen, J. *Macromolecules* **2001**, *34*, 3863; (b) Westerhausen, M.; Schneiderbauer, S.; Kneifel, A. N.; Söltl, Y.; Mayer, P.; Nöth, H.; Zhong, Z.; Dijkstra, P. J.; Feijen, J. *Eur. J. Inorg. Chem.* **2003**, 3432; (c) Dahrensborg, D. J.; Choi, W.; Ganguly, P.; Richers, C. P. *Macromolecules* **2006**, *39*, 4374; (d) Sarazin, Y.; Howard, R. H.; Hughes, D. L.; Humphrey, S. M.; Bochmann, M. *Dalton Trans.* **2006**, 340; (e) Davidson, M. G.; O'Hara, C. T.; Jones, M. D.; Keir, C. G.; Mahon, M. F.; Kociok-Köhn, G. *Inorg. Chem.* **2007**, *46*, 7686.
- Poirier, V.; Roisnel, T.; Carpentier, J.-F.; Sarazin, Y. *Dalton Trans.* **2009**, 9820.
- (a) Herrmann, W. A.; Eppinger, J.; Spiegler, M.; Runte, O.; Anwander, R. *Organometallics* **1997**, *16*, 1813; (b) Anwander, R.; Runte, O.; Eppinger, J.; Gerstberger, G.; Herdtweck, E.; Spiegler, M. *J. Chem. Soc. Dalton Trans.* **1998**, 847; (c) Hieringer, W.; Eppinger, J.; Anwander, R.; Herrmann, W. A. *J. Am. Chem. Soc.* **2000**, *122*, 11983.
- Sarazin, Y.; Roșca, D.; Poirier, V.; Roisnel, T.; Silvestru, A.; Maron, L.; Carpentier, J.-F. *Organometallics* **2010**, *29*, 6569.
- Liu, B.; Roisnel, T.; Guégan, J.-P.; Carpentier, J.-F.; Sarazin, Y. *Chem. Eur. J.* **2012**, *18*, 6289.
- Itoh, S.; Kumei, H.; Nagatomo, S.; Kitagawa, T.; Fukuzumi, S. *J. Am. Chem. Soc.* **2001**, *123*, 2165.
- (a) Hanusa, T. P. *Chem. Rev.* **1993**, *93*, 1023; (b) Tesh, K. F.; Burkey, D. J.; Hanusa, T. P. *J. Am. Chem. Soc.* **1994**, *116*, 2409; (c) Chi, Y.; Ranjan, S.; Chou, T.-Y.; Liu, C.-S.; Peng, S.-M.; Lee, G.-H. *J. Chem. Soc., Dalton Trans.* **2001**, 2462.
- (a) Caulton, K. G.; Chisholm, M. H.; Drake, S. R.; Folting, K. *J. Chem. Soc., Chem. Commun.* **1990**, 1349; (b) Goel, S. C.; Matchett, M. A.; Chiang, M. Y.; Buhro, W. E. *J. Am. Chem. Soc.* **1991**, *113*, 1844; (c) Caulton, K. G.; Chisholm, M. H.; Drake, S. R.; Folting, K.; Huffman, J. C. *Inorg. Chem.* **1993**, *32*, 816.
- Carpentier, J.-F. *Dalton Trans.* **2010**, *39*, 37.
- (a) Sarazin, Y.; Poirier, V.; Roisnel, T.; Carpentier, J.-F. *Eur. J. Inorg. Chem.* **2010**, 3423; (b) Sarazin, Y.; Liu, B.; Roisnel, T.; Maron, L.; Carpentier, J.-F. *J. Am. Chem. Soc.* **2011**, *133*, 9069; (c) Liu, B.; Roisnel, T.; Sarazin, Y. *Inorg. Chim. Acta* **2012**, *380*, 2.
- (a) Lancaster, S. J.; Rodriguez, A.; Lara-Sánchez, A.; Hannant, M. D.; Walker, D. A.; Hughes, D. L.; Bochmann, M. *Organometallics* **2002**, *21*, 451; (b) Sarazin, Y.; Hughes, D. L.; Kaltsoyannis, N.; Wright, J. A.; Bochmann, M. *J. Am. Chem. Soc.* **2007**, *129*, 881; (c) Bochmann, M. *Coord. Chem. Rev.* **2009**, 253, 2000.
- (a) Buchanan, W. D.; Allis, D. G.; Ruhlandt-Senge, K. *Chem. Commun.* **2010**, *46*, 4449; (b) Torvisco, A.; O'Brien, A. Y.; Ruhlandt-Senge, K. *Coord. Chem. Rev.* **2011**, *255*, 1268.
- (a) Harder, S. *Chem. Rev.* **2010**, *110*, 3852; (b) Barrett, A. G. M.; Crimmin, M. R.; Hill, M. S.; Procopiou, P. A. *Proc. R. Soc. London Ser. A* **2010**, *466*, 927.
- Liu, B.; Dorcet, V.; Maron, L.; Carpentier, J.-F.; Sarazin, Y. *Eur. J. Inorg. Chem.* **2012**, 3023.
- (a) Asano, S.; Aida, T.; Inoue, S. *J. Chem. Soc., Chem. Commun.* **1985**, 1148; (b) Inoue, S. *J. Polym. Sci., Part A: Polym. Chem.* **2000**, *38*, 2861.
- (a) Hong, S.; Marks, T. J. *Acc. Chem. Res.* **2004**, *37*, 673; (b) Hultsch, K. C. *Adv. Synth. Catal.* **2005**, *347*, 367; (c) Müller, T. E.; Hultsch, K. C.; Yus, M.; Foubelo, F.; Tada, M. *Chem. Rev.* **2008**, *108*, 3795.
- For a recent example of enantioselective intra- and intermolecular hydroaminations of terminal amino-alkenes and styrene derivatives with heteroleptic chiral magnesium-phenolate complexes, see: Emge, T. J.; Hultsch, K. C. *Angew. Chem. Int. Ed.* **2012**, *51*, 394.
- For leading references, see: (a) Crimmin, M. R.; Casely, I. J.; Hill, M. S. *J. Am. Chem. Soc.* **2005**, *127*, 2042; (b) Crimmin, M. R.; Arrowsmith, M.; Barrett, A. G. M.; Casely, I. J.; Hill, M. S.; Procopiou, P. A. *J. Am. Chem. Soc.* **2009**, *131*, 9670; (c) Arrowsmith, M.;

- Crimmin, M. R.; Barrett, A. G. M.; Hill, M. S.; Kociok-Köhn, G.; Procopiou, P. A. *Organometallics* **2011**, *30*, 1493 and references cited therein; (d) Wixey, J. S.; Ward, B. D. *Chem. Commun.* **2011**, *47*, 5449; (e) Jenter, J.; Köppe, R.; Roesky, P. W. *Organometallics* **2011**, *30*, 1404 and references cited therein.
26. (a) Barrett, A. G. M.; Brinkmann, C.; Crimmin, M. R.; Hill, M. S.; Hunt, P.; Procopiou, P. A. *J. Am. Chem. Soc.* **2009**, *131*, 12906; (b) Brinkmann, C.; Barrett, A. G. M.; Hill, M. S.; Procopiou, P. A. *J. Am. Chem. Soc.* **2012**, *134*, 2193.
27. Liu, B.; Roisnel, T.; Carpentier, J.-F.; Sarazin, Y. *Angew. Chem. Int. Ed.* **2012**, *59*, 4943.
28. Hesp, K. D.; Stradiotto, M. *ChemCatChem* **2010**, *2*, 1192.
29. Crimmin, M. R.; Barrett, A. G. M.; Hill, M. S.; Hitchcock, P. B.; Procopiou, P. A. *Organometallics* **2007**, *26*, 2953.
30. Demmer, C. S.; Krogsgaard-Larsen, N.; Bunch, L. *Chem. Rev.* **2011**, *111*, 7981.
31. For leading references with lanthanide catalysts, see: (a) Yokomatsu, T.; Yamgishi, T.; Shibuya, S. *Tetrahedron Asymmetry* **1993**, *4*, 1783; (b) Sasai, H.; Bougauchi, M.; Arai, T.; Shibusaki, M. *Tetrahedron Lett.* **1997**, *38*, 2717; (c) Zhou, S.; Wang, H.; Ping, J.; Wang, S.; Zhang, L.; Zhu, X.; Wei, Y.; Wang, F.; Feng, Z.; Gu, X.; Yang, S.; Miao, H. *Organometallics* **2012**, *31*, 1696; (d) Zhou, S.; Wu, Z.; Rong, J.; Wang, S.; Yang, G.; Zhu, X.; Zhang, L. *Chem. Eur. J.* **2012**, *18*, 2653. For leading references with titanium catalysts, see: (a) Yokomatsu, T.; Yamgishi, T.; Shibuya, S. *Tetrahedron Asymmetry* **1993**, *4*, 1779; (b) Yang, F.; Zhao, D.; Lan, J.; Xi, P.; Yang, L.; Xiang, S.; You, J. *Angew. Chem. Int. Ed.* **2008**, *47*, 5646. For leading references with aluminum catalysts, see: (a) Arai, T.; Bougauchi, M.; Sasai, H.; Shibusaki, M. *J. Org. Chem.* **1996**, *61*, 2926; (b) Suyama, K.; Sakai, Y.; Matsumoto, K.; Saito, B.; Katsuki, T. *Angew. Chem. Int. Ed.* **2010**, *49*, 797 and references cited therein.
32. (a) Zhou, X.; Liu, Y.; Chang, L.; Zhao, J.; Shang, D.; Liu, X.; Lin, L.; Feng, X. *Adv. Synth. Catal.* **2009**, *351*, 2567; (b) Zhou, X.; Zhang, Q.; Hui, Y.; Chen, W.; Jiang, J.; Lin, L.; Liu, X.; Feng, X. *Org. Lett.* **2010**, *12*, 4296.
33. Liu, B.; Carpentier, J.-F.; Sarazin, Y. *Chem. Eur. J.* **2012**, *18*, 13259.

## **PART IV**

---

### **ORGANOMETALLIC POLYMERS AND MATERIALS**



## ORGANOMETALLIC POLYMERS

MANUEL SERRANO-RUIZ, FRANCO SCALAMBRA, AND ANTONIO ROMEROSA\*

Área de Química Inorgánica-CIESOL, University of Almería, Almería, Spain

### 29.1 INTRODUCTION

In a broad sense, an organometallic polymer is any macromolecule that contains both organic and metallic moieties linked by a carbon–metal bond. In 1955 F. S. Arimoto and A. C. Haven, which were working for DuPont, presented the first example of organometallic polymers with the successful synthesis of polyvinylferrocene by free radical polymerization of vinyl ferrocene [1]. Since that initial discovery, there have been tremendous efforts to grow, diversify, and apply this exciting area of macromolecular chemistry [2–5]. The vast majority of commercially available polymers feature an organic composition with C, N, and O as integral structural components. Nevertheless, benefits can be gained when metals are incorporated within an organic-polymeric framework, such as new luminescent and electronic-active materials, extensive flame resistance, high flexibility, redox activity, chemical sensing, and electrochromic behavior [6–12]. Irrespective of the application, the utility and performance of metal-containing polymers can, in varying degrees, be ascribed to the ability of the transition metal centers to change oxidation states and/or facilitate the electron flow in ways that organic materials simply cannot [13]. Nowadays, organometallic polymers are employed in a multitude of design concepts and their breadth of applications is as varied as their structures.

The dramatic increase in research in the area of metal-containing macromolecules has provided original articles and a number of excellent reviews and books that discuss developments in this exciting field and properties of new compounds [4, 14–20]. The isoelectronic diatomics, carbon monoxide and cyanide, have rich histories as ligands for transition metals and both ligands inevitably bond metal centers primarily through carbon, placing them among the simplest and most robust carbon-bound ligands. However, despite the clear analogy between CO and CN<sup>−</sup>, carbonyl is regarded as one of the quintessential ligands in organometallic chemistry whereas cyanide has traditionally been regarded a strictly inorganic ligand. The reasons for this designation include the analogy between CN<sup>−</sup> and the halides, its stability as an aqueous anion, and its ability to form simple metal salts. Cyanide complexes have a long history in inorganic chemistry that is summed up in some good recent reviews and books [21–27] and therefore cyano complexes will not be covered by the present chapter. In addition, recent findings on dendrimers and solid-supported organometallic polymers will be not discussed. For updating and extensive discussion regarding the use of metal dendrimers and solid-supported organometallic polymers see recent reviews and books [28–38].

The large number, variety, and diversity of properties of organometallic polymers can be classified in a large number of different ways depending on the polymer characteristic to be stressed. One of the simplest groupings for organometallic polymers is based in the position of the metal in the molecular structure of the polymer. From this point of view, the organometallic polymers could be classified into (i) main-chain or metal-backbone organometallic polymers (MBOP) and (ii) side-group or metallic-side organometallic polymers (MSOP). The MBOP need the formation of metal–ligand bonds in order to exist. The ligand must link the metals constituting the polymer, simultaneously enabling the coordinated transition

*Advances in Organometallic Chemistry and Catalysis: The Silver/Gold Jubilee International Conference on Organometallic Chemistry Celebratory Book*, First Edition. Edited by Armando J. L. Pombeiro.

© 2014 John Wiley & Sons, Inc. Published 2014 by John Wiley & Sons, Inc.

metal to exhibit a desired property and maintaining control over physical attributes of the overall material. MSOP are characterized by an organic polymer backbone substituted by organometallic groups. In these compounds, the polymeric structure exists regardless of the presence of metal atoms. The organic main-chain polymer disposes of metal binding sites. The characteristics of the metal center as well as the polymer backbone can generally be designed independently. The MSOP can be obtained by addition of a transition metal to the organic polymer and alternatively, a monomer containing a pendant metal-complex can often be polymerized directly. The first procedure used is complicated but provides an accurate control of the resulting polymer, while the second one is more convenient from a synthetic point of view but the accurate determination of metal content in the obtained material is very difficult.

Polymer chains of different chemical composition can be attached at a common junction constituting a block copolymer. Much of the current interest in block copolymer self-assembly is directed to the formation of more complex structures with broad and growing range of different structures and properties [39–41]. When the block copolymer is constituted by combination of an MBOP and an MSOP its classification becomes complicated. Some interesting examples of organometallic block copolymers have been included in any of the two proposed types of organometallic polymers depending on their most significant character as MBOP or MSOP.

In addition, a dual terminology is proposed for coordination polymers (CPs) and metal–organic frameworks (MOFs), compounds generated in interdisciplinary research fields with their origins in solid-state, inorganic, and coordination chemistry [42, 43]. A survey on organometallic polymers indicates that 1D, 2D, or 3D CPs cover all possible cases and for the classification of the organometallic polymers the MOF concept is a superfluous term and therefore is not used in this chapter. Nevertheless, the net influence of the metal on the properties of the organometallic polymers made convenient to classify both kind of organometallic polymers, MBOP and MSOP, depending on their metal composition in homo- and heterometallic polymers. Finally, emphasis is placed on the synthesis, characterization, physical properties, and possible applications of the organometallic polymers presented in this chapter, providing an overview of the actual state of the field.

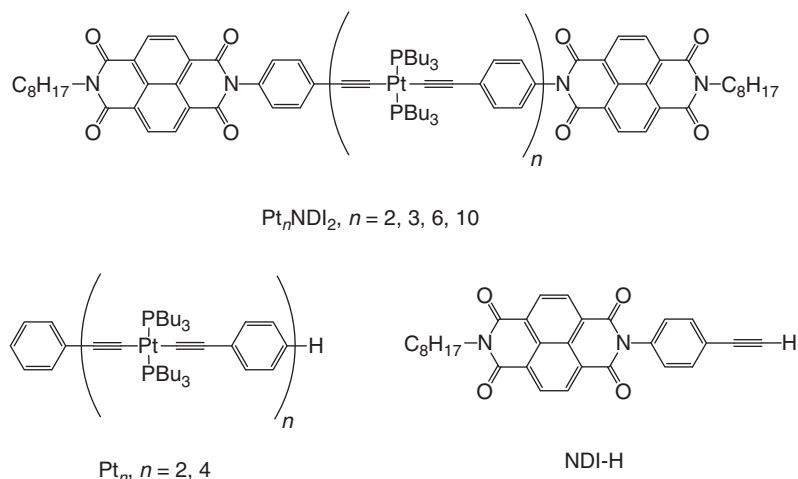
## 29.2 METAL-BACKBONE ORGANOMETALLIC POLYMERS

MBOP involve transition metals bonded by a carbon–metal bond as ligand linkers. Therefore both components of the backbone, the transition metal and the organic ligand, are essential for the continuation of the polymer. Metallic polymers that employ non-C-dative-type interactions between the metal atoms and the bridging ligands are sometimes called *coordination polymers* (non-C-CPs). The MBOP need the presence of metal–ligand bonds to exist. To synthesize an organometallic polymer the linker must be a ligand with two opposing points of contact capable of binding two metals. The adequate design of the organic moieties linking metal centers along the polymer backbone must be considered as well as the metal coordination number. Ligands that show high affinities toward selected transition metals must be employed in order to have sufficient thermodynamic driving force to facilitate polymerization and affording polymeric materials with high molecular weights. Ligand–metal bonds could be weak and under thermodynamic control the MBOP could depolymerize. This possibility introduces additional challenges regarding the synthesis and longevity in solid state, solution, and polymer storage. For an in-depth analysis of non-C-CPs literature, we recommend the excellent review by Dobrawa and Würthner [44].

### 29.2.1 Homo-Metal-Backbone Organometallic Polymers

The 1D-Pt-backbone organometallic polymers are among those with more interesting electronic properties. Electron and energy transfer are two of the most significant and fundamental processes in chemistry and biology, gaining interest for application in bulk heterojunction solar cells [45, 46]. Platinum acetylide oligomers and polymers with  $\pi$ -conjugated arylene units are a versatile platform for fundamental studies directed at understanding the effect of heavy metal centers on exciton structure and charge transport in  $\pi$ -conjugated systems [47–52]. These organometallic polymers are characterized by excited state properties, which are dominated by long-lived triplet excitons. These particular properties make Pt-acetylidy organometallic polymers also potentially useful for optoelectronic applications including polymer light-emitting diodes (PLEDs) [53, 54] and bulk heterojunction solar cells [55]. Although the monodisperse oligomers ( $\text{Pt}_n\text{NDI}_2$ , where  $n = 2, 3, 6$ , and 10) (Scheme 29.1) end capped with naphthalene diimide units are not extended polymers, they are long enough to exemplify how in larger polymers a similar combination serves as traps for triplet excitons via charge separation and negative polarons by charge shift from the chain to the end group [56].

Using fast time-resolved pulse radiolysis and laser flash photolysis methods, the authors have been able to directly probe the dynamics of electron and triplet exciton transport along the conjugated segments. The results show that transport of both carriers along these organometallic “molecular wires” is relatively rapid, occurring on timescales less than 200 ps over a



**Scheme 29.1** Structural formulas for Pt–acetylide-backbone organometallic oligomers containing naphthalene diimide units.

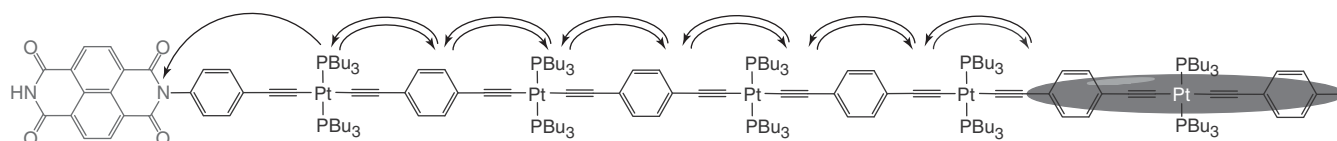
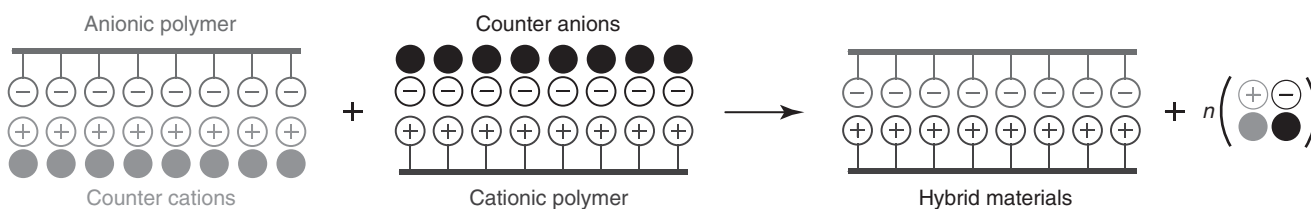


**Figure 29.1** Five units of a  $\text{Pt}_{10}(\text{naphthalene diimide})_2$  molecule showing the polaron or exciton diffusion via a random hopping mechanism.

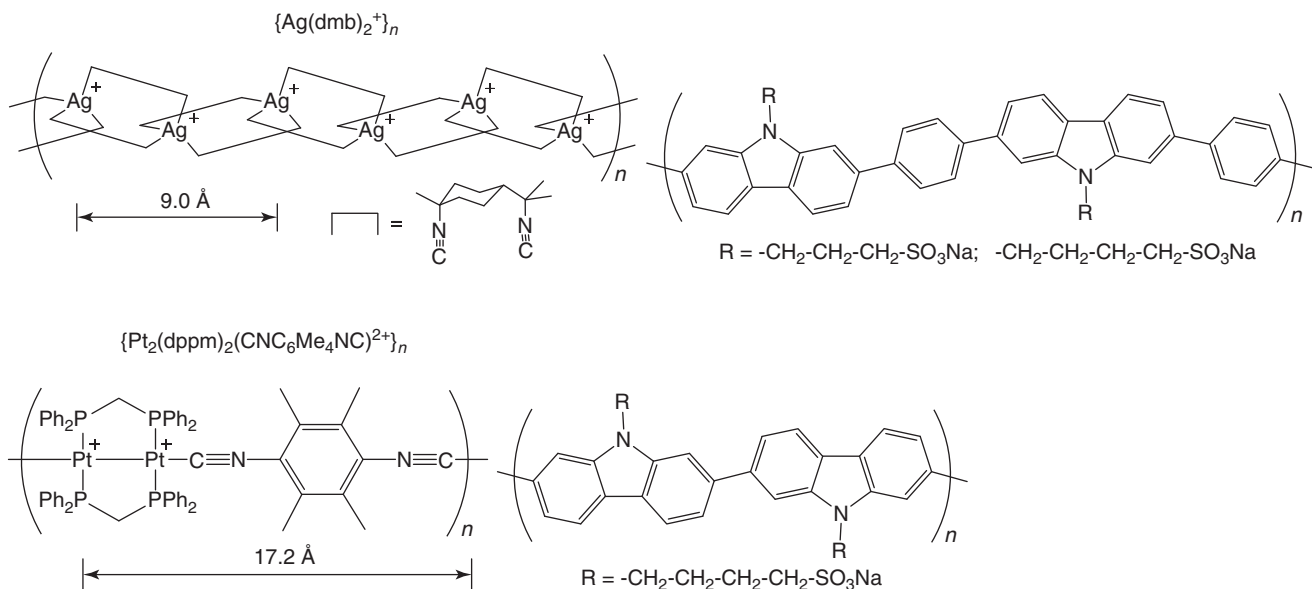


**Scheme 29.2** Possible combinations of ionic polymers to constitute a hybrid polymer.

distance of 3–5 nm. Analysis of the dynamics of charge and exciton transport suggests that the carriers move along the chain by an incoherent, site-to-site hopping mechanism. The triplet hopping process may be gated by changes in the conformation of the monomers, with a tentative assignment to large-amplitude torsional motion of phenylene units. Taken together, the results provide insight into the mechanism of transport of carriers in organometallic, conjugated electronic systems. Therefore, in the Pt-acetylide-backbone organometallic polymers containing naphthalene diimide units, the localized triplet excitons and negative polarons initially on the Pt-acetylide chain rapidly transport to the end chains and become trapped by charge separation or charge shift to the naphthalene diimide moieties (Fig. 29.1) [57].

One of the most interesting recent examples of Pt-MBOP are those containing polycarbazoles that have shown numerous applications in the area of photovoltaic cells [58–60] and PLEDs [61–69]. On combining two ionic polymers together (Scheme 29.2), their mutual effects on each other should modify the properties of the separate polymers, including optical and luminescence characteristics.

An interesting property that could provide the combination of two different polymers is the so-called the *antenna effect* [70]: the heavy atom constituting one of the polymers promotes the population of the triplet state and the resulting accentuated phosphorescence is transferred by a nonradiative process that allows the harvested light energy to flow through a material from one site to another. Interesting examples of this kind of hybrid polycarbazole polymers were presented by Leclerc et al. [71]; these are constituted by the organometallic polymers {as in Scheme 29.3 [ $\text{Ag}(\text{dmb})_2\text{BF}_4$ ]<sub>n</sub>}



**Scheme 29.3** Structures of  $\{[Ag(dmb)_2]BF_4\}_n$  and  $\{[Pt_2(dppm)_2(CNC_6Me_4NC)](BF_4)_2\}_n$  ( $dmb = 1,8$ -diisocyano-p-menthane;  $dppm = (Ph_2P)_2CH_2$ ) and the organic polymers of the class  $(-carbazone)_n$  and  $(-carbazone-C_6H_4)_n$ . The distance between repetitive units containing two positive charges are included.

and  $\{[Pt_2(dppm)_2(CNC_6Me_4NC)](BF_4)_2\}_n$  ( $dmb = 1,8$ -diisocyano-p-menthane;  $dppm = (Ph_2P)_2CH_2$ ;  $CNC_6Me_4NC = 1,4$ -diisocyano-tetramethylbenzene) and conjugated organic polymers of the type  $(-Cz-C_6H_4)_n$  and  $(-Cz)_n$ , where  $Cz$  is a 2,7-linked carbazole unit substituted by  $(CH_2)_3SO_3Na$  or  $(CH_2)_4SO_3Na$  pendant groups at the N-position (Scheme 29.3).

In 2005, Bielawski et al. [72–86] presented a variety of novel N-heterocyclic carbenes metal-backbone organometallic polymers (NHC-MBOP), which exhibit high thermal stability and versatile electronic properties. Following this finding, a number of similar compounds have been synthesized, which are useful for the preparation of self-assembled materials [87], and phosphorescent [88] and luminescent polymeric complexes [89–93]. Remarkably, these polymers have showed also to be active, efficient, and recyclable self-supported catalysts for the Suzuki–Miyaura catalytic coupling of a variety of aryl halides in water [94]. Metal-Backbone Organometallic Polymers could be assembled into capsular structures that provide a nanoenvironment with specific chemical behavior, different from the exterior surroundings [95–99]. These container-like structures can act as catalytic reaction chambers, thus affording a highly concentrated reaction site that lowers the energy barrier for chemical reactions.

The Ag(I)-NHC are very interesting and useful owing to their potential applications in various fields such as luminescent materials, host–guest chemistry, medicine, and catalysis [100, 101]. These polymers also show fascinating photophysical properties that can be strongly affected by the nature of the ligand. The  $d^{10}$  configuration of the silver ion is able to be combined with the  $\pi^*$  ligand orbitals to produce metal-to-ligand charge-transfer and/or intraligand transitions, which result in the luminescence of these systems [102, 103]. The vast majority of Ag(I) complexes are known to emit at low temperatures, while only a few monomeric and polymeric Ag complexes display intense photoluminescence at room temperature [104–106]. Reaction of a bis-bipyridyl-substituted imidazolium ligand ( $LX$ ,  $X = Br^-$ ,  $PF_6^-$ ,  $BPh_4^-$ ) linked through  $CH_2$  groups with  $Ag_2O$  afforded the silver(I)–NHC–MBOP complexes  $[AgL_2]Br$ ,  $[Ag_2L_2]X_2$  and the  $\{[Ag_3L_2](PF_6)_3 \cdot 4CH_3CN\}_n$  ( $X = Br$ ,  $PF_6$ ,  $BPh_4$ ) that is constituted by two alternate Ag(I) atoms with different coordination modes (Fig. 29.2). These compounds display interesting luminescent properties in solid state at room temperature [107].

Another interesting example of Ag(I)-backbone organometallic polymers are those based on diallylmelamine and poly-carboxylates. Silver–vinyl bonding represents a versatile synthon for the construction of polymeric metallosupramolecular architectures. The particular structural motifs result from the introduction of different auxiliary polycarboxylates into the silver/diallylmelamine system and the diverse coordination modes and conformations of diallylmelamine (Fig. 29.3) [108]. Remarkably, apparent silver–vinyl interactions with a  $\eta^2$  mode were commonly observed in the solid-state structures of these complexes ( $Ag-C = 2.311(4) - 2.467(5)\text{\AA}$ ). In addition, they display solid-state photoluminescence and moderate thermal stabilities at room temperature.

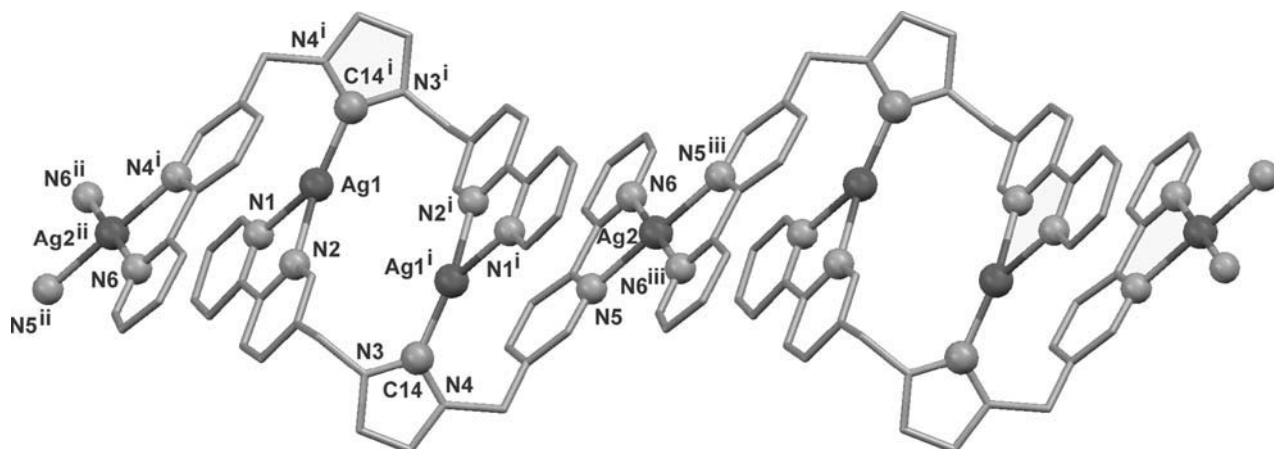


**Figure 29.2** Polymeric structure of  $\{[Ag_3L_2](PF_6)_3 \cdot 4CH_3CN\}_n$ . Hydrogen atoms, counter-ions, and solvent molecules are omitted for the sake of clarity.

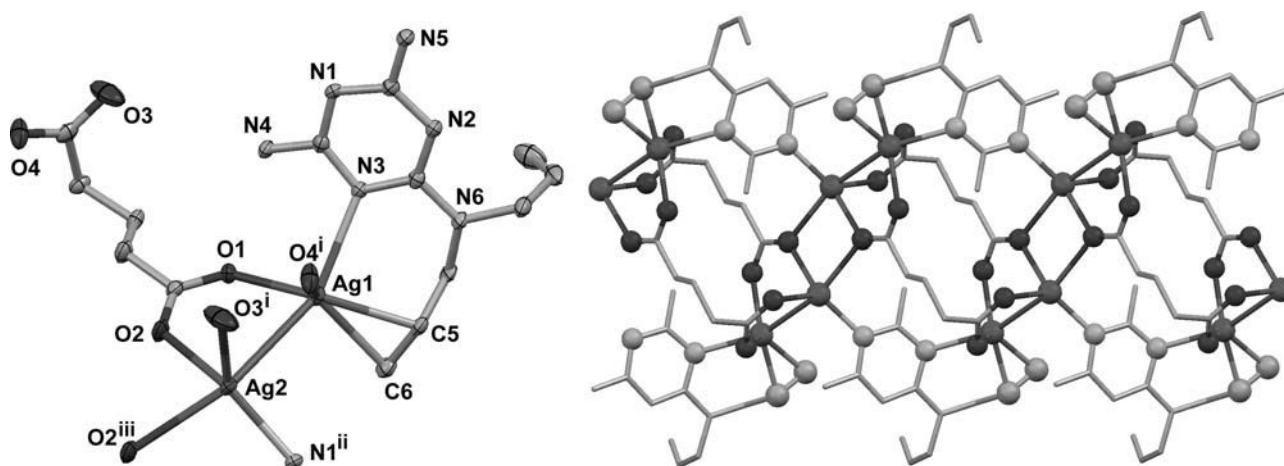
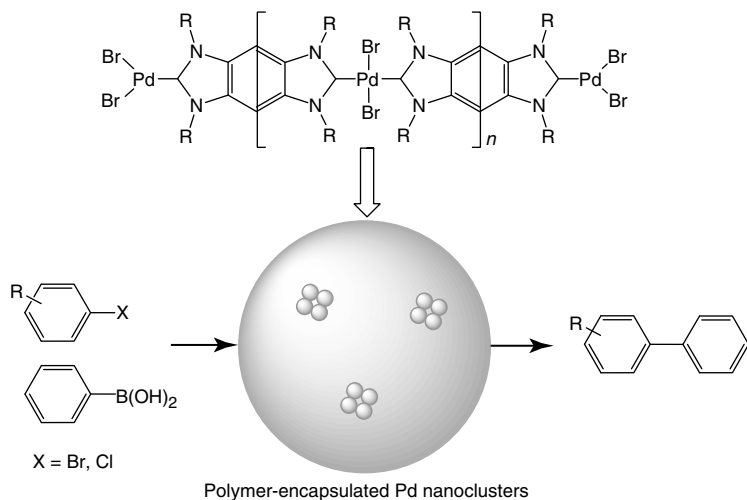


**Figure 29.3** Crystal structure of  $[Ag_2(\text{diallylmelamine})_2(\text{glutaric})]_n$  and a packing perspective. Hydrogen atoms are omitted for clarity.

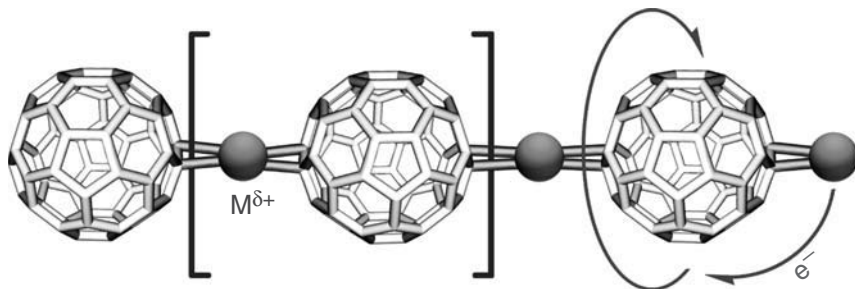
Actual and significant examples of NHC-MBOP were presented by Karimi and Akhavan [109] that described the preparation and characterization of a variety of Pd–NHC–MBOP materials with different N-alkyl functionalities. These compounds are active catalysts for the Suzuki–Miyaura coupling of chloroarenes in water (Scheme 29.4), the Pd-organopolymer with the N-dodecyl group being the most active catalyst. This reaction is characterized by the deactivated and hindered substrates under aqueous conditions without the need of any co-organic solvent. The catalysts seem to be highly recyclable and are the source of production of active soluble Pd species in the form of either Pd nanoparticles or fragmented Pd–NHC complexes.

The described organometallic polymers are not only a possible source of trace amounts of Pd nanoparticles but also the capsular structures of these polymers in water provide a way of entrapment of nanoclusters in the hydrophobic region. The authors suggest that the highest activity observed for the N-dodecyl-substituted palladium polymer for the Suzuki coupling is probably owing to a combination of lipophilic character of capsular chambers and the hydrophobic effect of water, which results in an increased concentration of coupling partners inside the capsular structures where the Pd species are located. Therefore, the observed reactivity might also be due, to some extent, to the faster production of active Pd species that could be entrapped in Pd nanoclusters.

Since the first discovery of fullerenes [110] and availability of synthetically useful amount of  $C_{60}$  and higher fullerenes ( $C_{70}$ ,  $C_{76}$ ,  $C_{78}$ , and  $C_{84}$ ) [111], much work has been done to investigate the physical properties and the reactivity of these stable molecules. The highly interesting electronic properties of fullerenes have lead to the possibility of using units of fullerenes in the formation of polymers. Transition metal–fullerene compounds are generally classified into two categories:



**Scheme 29.4** Suzuki–Miyaura coupling of chloroarenes in water catalyzed by the NHC-Pd organometallic polymers.

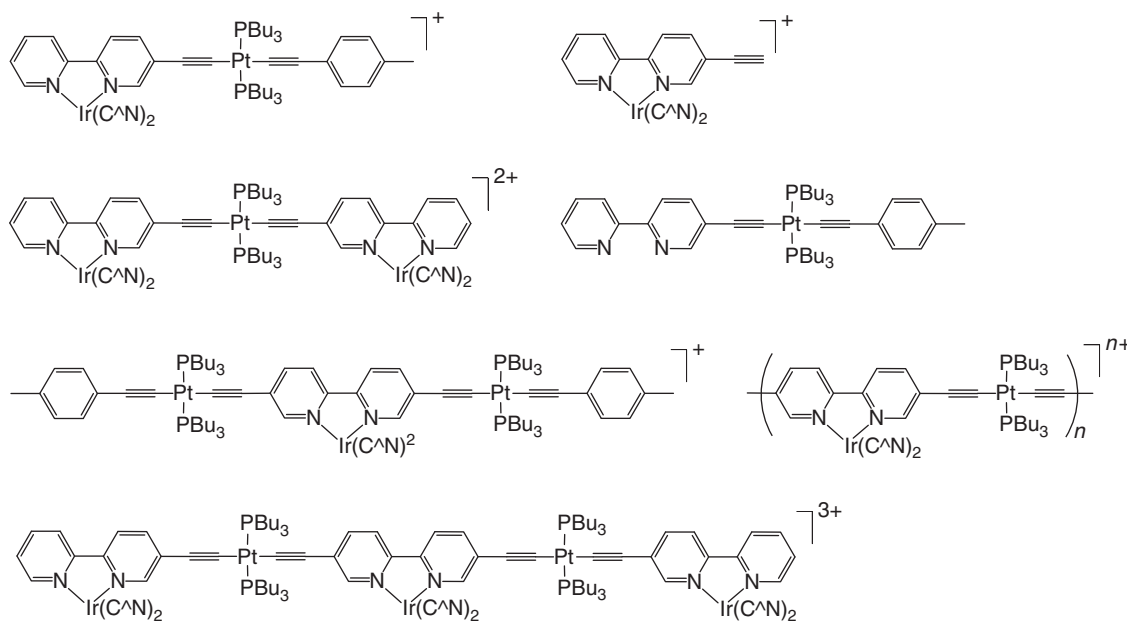


**Scheme 29.5** Probable disposition for  $[C_{60}M]_n$  ( $M = Pd, Pt, Ir, Rh, Au, Ag$ ) and proposed electronic pathway into the organometallic polymer.

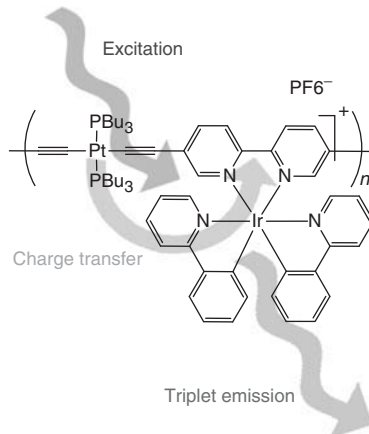
those involving metal encapsulation in which there is charge transfer from the metal to the fullerene cage [112] and the covalent  $\eta^2$ -transition metal complexes [113], which serve to relieve the strain in the fullerene structure [114]. However, exohedral metal complexes of higher hapticity are disfavored by fullerene curvature and it is difficult for  $C_{60}$  to function as a ligand in  $\eta^5$ - and  $\eta^6$ -complexation reactions because the fullerene  $\pi$ -orbitals are directed away from the metal as a result of the rehybridization of the ring carbon atoms. In  $C_{60}$ , the  $\pi$ -orbital axis vectors are directed away from the center of the respective rings hindering  $\eta^6$ -coordination that is even more strongly disfavored than  $\eta^5$ -complexation [115].  $C_{60}$  can be polymerized into directly linked fullerenes by light, high pressure, or high temperature [116–119]. Fullerenes may be attached regularly to a polymeric backbone chain through the Friedel–Crafts type reactions of fullerenating polystyrenes [120]. Moreover, indirectly linked fullerenes involving a spacer group are known. The polymers  $[C_{60}Pd]_n$  (Scheme 29.5) or  $[C_{60}Pt]_n$  are formed from  $C_{60}$  and  $[Pd_2(dba)_3] \cdot CHCl_3$  or  $[Pt(dba)_2]$ , respectively ( $dba =$  dibenzylideneacetone) [121–124], and others metals such as Ir, Rh, Au, and Ag [125–127]. These polymers have possible applications in catalysis, electronic devices [128, 129] and absorbent materials [130].

### 29.2.2 Heterometal-Backbone Organometallic Polymers

The photophysical properties of the heterometal-backbone organometallic polymers  $\{\text{Ir}\}-\{\text{Pt}\}-\{\text{Ir}\}-\{\text{Pt}\}-\{\text{Ir}\}$  ( $\{\text{Ir}\} = [\text{Ir}(\text{ppy})_2(\text{bpy}^*)]^+$  ( $[\text{Pt}] = \text{trans-}[\text{Pt}(\text{PBu}_3)_2(\text{C}\equiv\text{C}_2]$ ;  $\text{ppy} =$  phenyl-2-yl-pyridine,  $\text{bpy}^* =$  bipyridyl) (Scheme 29.6) reveal an unprecedented triplet energy transfer from the terminal iridium to the central iridium subunit [131] that is a new example of emission mechanism that arises from the distinct Ir subunits to conjugated systems [132]. This kind of emission is suggestive of the concept of localized triplet exciton for platinum-acetylidyne-containing oligomers introduced by Schanze and coworkers (commented previously) [50]. Consequently, localized triplet excited states are bound to exist and energy



**Scheme 29.6** Structures of polymers  $\{\text{Ir}\}-\{\text{Pt}\}-\{\text{Ir}\}-\{\text{Pt}\}-\{\text{Ir}\}$  ( $\{\text{Ir}\} = [\text{Ir}(\text{ppy})_2(\text{bpy}^*)]^+$  ( $[\text{Pt}] = \text{trans-}[\text{Pt}(\text{PBu}_3)_2(\text{C}\equiv\text{C})_2]$ ; ppy =  $\text{C}^\wedge\text{N} = \text{phenyl-2-yl-pyridine}$ ,  $\text{bpy}^* = \text{bipyridyl}$ ).



**Scheme 29.7** Hybrid excited states including excitation, charge transfer, and triplet emission from Pt to Ir chromophores in conjugated Pt-Ir polymer containing poly[*trans*-[(5,5'-ethynyl-2,2'-bipyridine) bis(phenyl-2-yl-pyridine)-iridium(III)]].

transfer should also be possible. The energy transfer is thus consistent with the Dexter mechanism (double-electron exchange) [133] in the triplet state that indicates that rate of energy transfer depends on the donor–acceptor orbital overlaps. This work stresses a very unusual excited state behavior whereby the terminal Ir unit emits as a discrete luminophore, despite conjugation, and also undergoes triplet energy transfer to the central Ir unit, for a second, lower energy emission.

Another type of interesting heterometal-backbone organometallic polymers are those obtained by reaction of *trans*-dichlorobis(tri-*n*-butylphosphine)platinum(II) with bis(2-phenylpyridinato)-(5,5'-diethynyl-2,2'-bipyridine)iridium(III) hexafluorophosphate. The resulting conjugated Pt–Ir polymers containing 5,5'-ethynyl-2,2'-bipyridine, 2-phenylpyridinato and tri-*n*-butylphosphine are luminescent (Scheme 29.7) [134]. Comparison of the absorption and emission band positions and their temperature dependence, emission quantum yields, and lifetimes with those for models containing only the {Pt} or the {Ir} units, indicates hybrid excited states including features from both chromophores [135] with charge transfer between the metals units. The presence of a hybrid excited state was also supported by density functional theory (DFT) and time-dependent density functional theory (TDDFT) calculations. Their photophysical parameters ( $\Phi$ ,  $\tau$ ) do not decrease

significantly compared with similar complexes including a fewer number of atoms [136, 137], and therefore the processability of these materials can be retain without loss in emission quantum yields, making them useful for the design of photonic materials such as PLEDs and light-emitting electrochemical cells [18, 138–140].

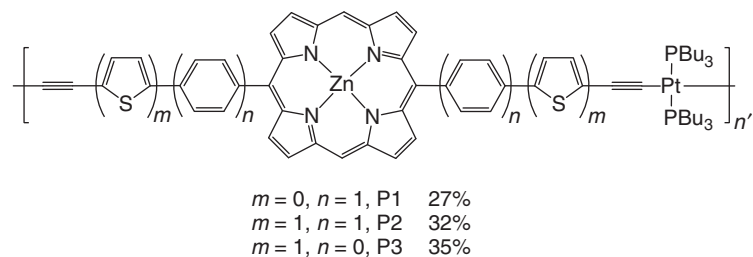
The presented approach to synthesize new p-type photovoltaic active materials serves as a good illustration of the recent trend in designing structures useful for obtaining solution-processable functional polymers [141–145]. By using metallocporphyrins as the building block in combination with linear conjugated systems of transition metal-alkyne polymers, a series of soluble platinum metallocpolyyne containing Zn-(porphyrin) chromophores and electron-rich aromatic rings (benzene and/or thiophene) (Scheme 29.8) were synthesized [146]. The introduction of a thiophene unit into the porphyrin-based polymer main chain extended the  $\pi$ -conjugation and covered the missing absorption region (430–530 nm) or enhanced the absorption of the weaker Q-bands (the region from 530 to 540 nm). This work represents the first example of porphyrin-containing polymetallaynes used for harvesting solar energy in solution-processed photovoltaic devices. These deeply colored absorbing polymers are thus attractive candidates as a new class of functional material toward organometallic photovoltaic technology. A continuous optimization of the chemical structures of porphyrin and polymer main chain by incorporating some special functional chromophores would improve the absorption properties and hence enhance the photovoltaic efficiency of porphyrin-containing polymers [147].

The structurally remarkable silver–tin clusters with stannylene stanna-*closo*-dodecaborate and coligands such as pyridine, bipyridine, and isonitriles that was published recently present different but also very interesting properties [148]. These complexes were synthesized from the salt  $[\text{Et}_4\text{N}]_8[\text{Ag}_4(\text{SnB}_{11}\text{H}_{11})_6]$  that served as a versatile starting material. From the reaction of the silver salt  $[\text{Et}_4\text{N}]_8[\text{Ag}_4(\text{SnB}_{11}\text{H}_{11})_6]$  with the bridging ligand 1,4-diisocyanobenzene (DIB), a linear polymeric coordination compound was formed, and a three-dimensional network structure was the product from the reaction of DIB with the silver salt  $[\text{Me}_4\text{N}][\text{Ag}(\text{SnB}_{11}\text{H}_{11})]$ . With the dianionic stannylene stanna-*closo*-dodecaborate  $[\text{SnB}_{11}\text{H}_{11}]^{2-}$ , silver–tin aggregation with coligands such as pyridines and isonitriles results in the formation of dimers, tetramers, polymers, and network-structured materials (Fig. 29.4). The tin-bridged silver–silver contacts show a very short interatomic Ag–Ag distances (Å) ( $\text{Ag1} - \text{Ag2} = 3.0549(9)$ ,  $\text{Ag1} - \text{Ag3} = 3.2512(12)$ ,  $\text{Ag2} - \text{Ag2}' = 2.8388(11)$ ,  $\text{Ag2} - \text{Ag3} = 2.7408(9)$ ).

The interesting heterometallic-organometallic complex  $\{[\text{Me}_4\text{N}]_4[\text{Ag}_4(\text{SnB}_{11}\text{H}_{11})_4(\text{DIB})_{6/2}]\}_n$  (Fig. 29.5) in dichloromethane exchange the acetonitrile and benzonitrile molecules in the inside channels with dichloromethane molecules, which was confirmed by the single-crystal structure determination. However the reported silver–tin network structure is not stable in the absence of solvent and repeated solvent exchange is not possible. Nevertheless, this complex is a good example of new porous materials built with organometallic reagents, which is of great interest as a possible new material that combines and changes properties depending on the inclusion molecules [149, 150].

Most of the heterometallic-backbone organometallic polymers are insoluble solids or only soluble in organic solvents. Very few examples of organometallic polymers that are soluble in water or are water compatible have been described. Water is the universal solvent, most of the natural systems contain water, and it is also an excellent solvent for chemical synthesis. In 2005, the first example of water-soluble organometallic polymeric complex in which two different metal-complex moieties built the backbone-polymeric chain  $\{[(\text{PTA})_2\text{CpRuDMSO}]-\mu-\text{AgCl}_2\}_n$  (Fig. 29.6) [151] was presented. The Ru–Ag-backbone organometallic polymer displays a 1D structure including PTA (3,5,7-triaza-phosphaadamantane) as metal-coordinating spacers between the monometallic  $\{\text{CpRu}(\text{DMSO})\}$  and  $\{\text{AgCl}_2\}$  units that are respectively bonded to the P and N-PTA atoms. This Ru–Ag organometallic polymer also retains its polymeric structure in water at high temperature as showed by light-scattering measurements.

This initial finding triggered research activity on the synthesis of polymers containing PTA and PTA-derivatives [152–155]. Recently, a new and interesting example of water-soluble Ru–Ru–Au organo-heterometallic polymer  $\{[(\text{PTA})_2\text{CpRu}-\mu-\text{CN-RuCp}(\text{PTA})_2]-\mu-\text{Au}(\text{CN})_4\}_n$  (Fig. 29.7) was presented. This water-soluble MBOP is constituted by



**Scheme 29.8** Platinum metallocpolyyne containing  $Z_n$ –C Porphyrin chromophores and electron-rich aromatic rings (benzene and/or thiophene).

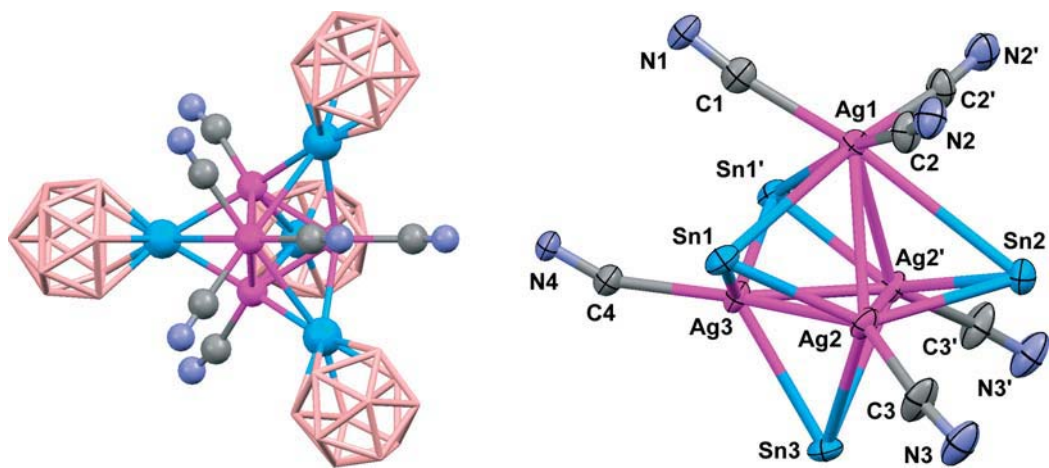


**Figure 29.4** Crystal structure of metal organization group of  $\{[\text{Me}_4\text{N}]_4[\text{Ag}_4(\text{SnB}_{11}\text{H}_{11})_4(\text{DIB})_{6/2}]\}_n$ . The cations, the hydrogen atoms, and the connecting phenyl rings (left) and the boron atoms (right) have been omitted for clarity.

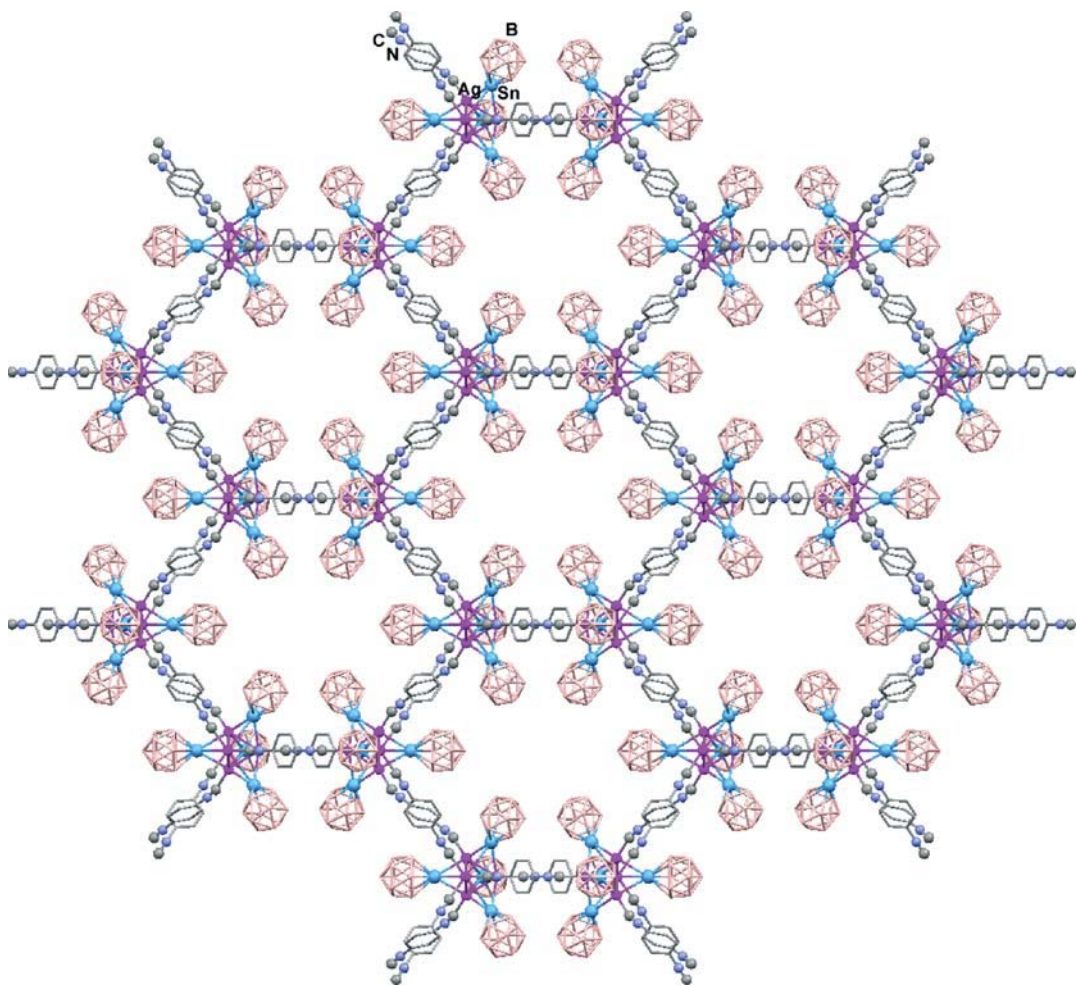


**Figure 29.5** View along the plane  $a-b$  of  $\{[\text{Me}_4\text{N}]_4[\text{Ag}_4(\text{SnB}_{11}\text{H}_{11})_4(\text{DIB})_{6/2}]\}_n$ . The solvents, the cations and the hydrogen atoms into the material porous were not represented for the sake of clarity. (See insert for color representation of the figure.)

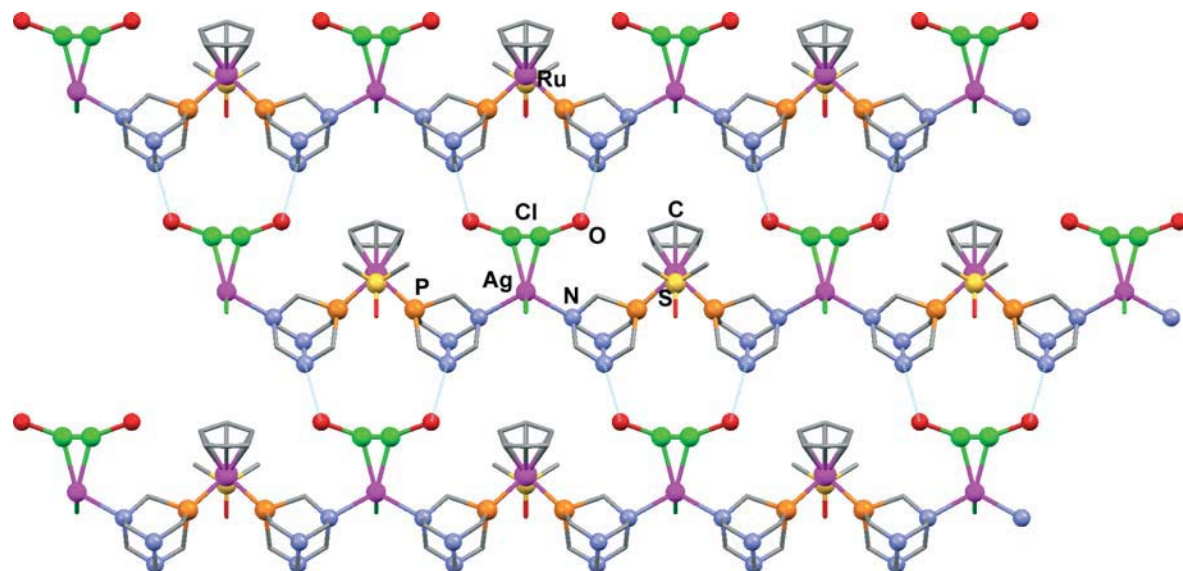


**Figure 29.6** Crystal structure and packing of water-soluble Ru–Ag-backbone organometallic polymer. (See insert for color representation of the figure.)

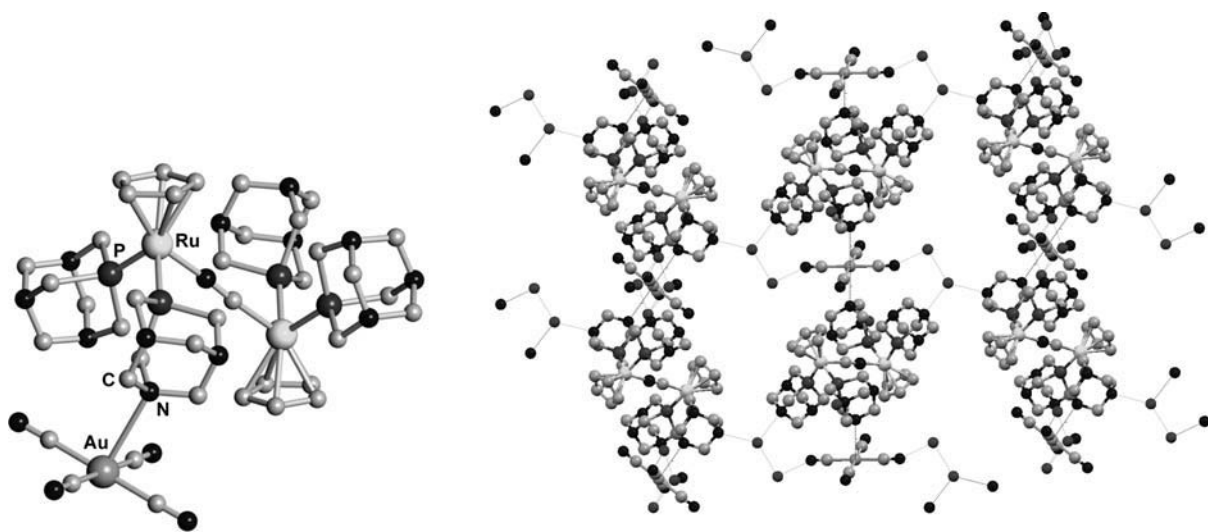


**Figure 29.7** Crystal structure and packing of the water-soluble Ru–Ru–Au polymer  $\{[(\text{PTA})_2\text{CpRu}-\mu\text{-CN-RuCp}(\text{PTA})_2]-\mu\text{-Au}(\text{CN})_4\}_n$ .

a dimeric  $\{\text{CpRu}(\text{PTA}-\kappa P)_2-\mu\text{-CN}-(\text{PTA}-\kappa P)_2\text{RuCp}\}^+$  moiety bonded to a  $\{\text{Au}(\text{CN})_4\}^-$  complex unit by a  $N$ -PTA atom. This organometallic polymer exhibits a thermo-gel behavior and is the first and unique example until now of a thermo-gel-hetero-organometallic polymer in water [156].

### 29.3 METALLIC-SIDE ORGANOMETALLIC POLYMERS

The organometallic polymers with metallic-side chain (MSOP) are constituted by an all-organic polymer backbone substituted by metal-complex groups and, therefore, the polymeric structure exists regardless of the presence of metal atoms coordinated to the ligand groups bonded to the main organic chain. The characteristics of the metal center as well as the polymer backbone can generally be independently adjusted. The side-chain organometallic polymers could be starting compounds

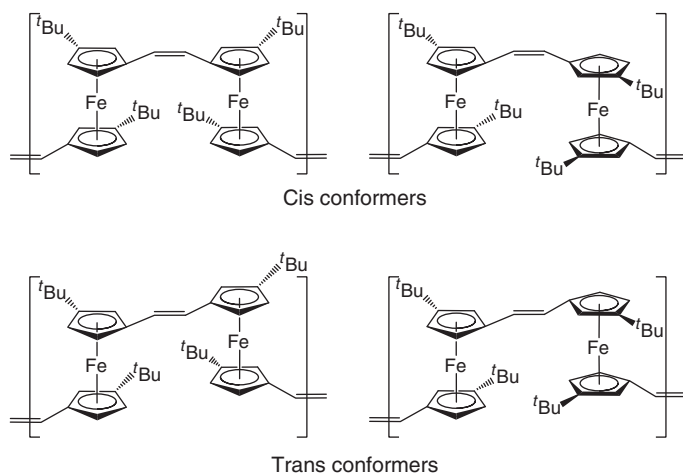
for providing hybrid materials by using known traditional polymerization reactions (standard addition such as ionic or radical polymerization, ring-opening polymerization (ROP) and condensation polymerization reactions) [157]. The synthesis of the MSOP can be accomplished by reaction of metals with the previously synthesized organic polymer with pendant ligand groups and by direct polymerization of a monomer containing a pendant metal-complex alone or with copolymers. The synthesis of MSOP is certainly advantageous, providing a large variety of possible structures with an elevated control and reproducibility. Nevertheless, the structural independence of the organic and inorganic components can complicate an accurate characterization of both the composition of the organic skeleton as well as the metal content.

### 29.3.1 Homo-Metallic-Side Organometallic Polymers

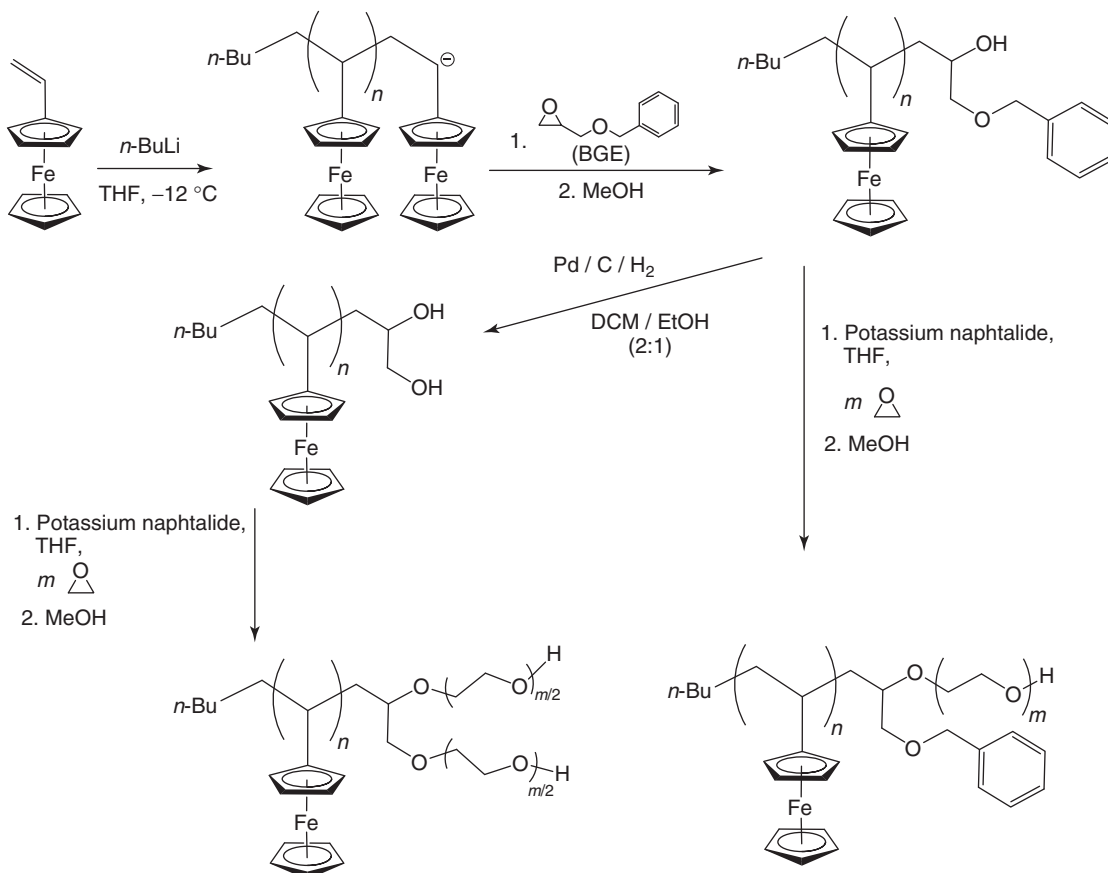
The first synthesized organometallic polymer was a homo-metallic-side organometallic polymer (HMSOP), prepared by Arimoto and Haven in 1955. Since this initial finding, the number of HMSOP has increased exponentially. One of the most interesting HMSOP are the metallocene-containing polymers, in particular the ferrocene polymers. They have attracted significant attention because of their great potential in catalytic, optical, magnetic, and biological applications owing to the unique geometries and physicochemical properties [2, 158–160].

Recently, Manners et al. have presented the synthesis and characterization of an analogous soluble electron-rich poly(ferrocenylenevinylene), addressing the solubility limitations of the poly(ferrocenylenevinylene) by introducing *t*-butyl groups on the Cp ligands of *ansa*-(vinylene)ferrocene followed by ring-opening metathesis polymerization (ROMP) [161]. UV-vis analysis of the synthesized compounds showed a bathochromic shift accompanied by a hyperchromic effect for the highest occupied molecular orbital (HOMO)–lowest unoccupied molecular orbital (LUMO) transition upon polymerization consistent with a moderate degree of conjugation in the synthesized polymer. The number of possible primary structures are four (Scheme 29.9), which are similar to those for the polymers obtained by ROMP of the 2,3-difunctional norbornadiene [162]. The NMR spectroscopy data indicate that none of the investigated polymerizations was stereoselective. This fact evidences the difficulty in obtaining selective side-chain organometallic polymers despite the efforts targeted to obtain them and the use of actual synthetic procedures.

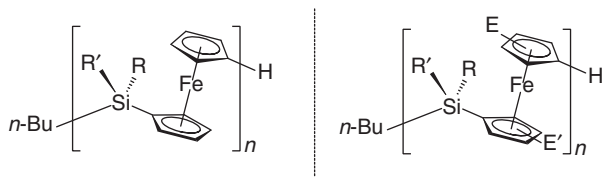
Another interesting water-soluble side-chain organometallic polymer containing poly(vinylferrocene) (PVFc) and poly(ethylene oxide) (PEO) blocks was presented by Gallei et al. [163]. The general synthetic described provides a facile route to a large variety of macromolecular architectures containing PVFc blocks combined with polyether chains. For the first time, utilizing a protected epoxide derivative as end-capping reagent, the combination of carb- and oxyanionic polymerization has been implemented for obtaining PVFcs. Two different glycidyl ethers [benzyl glycidyl ether (BGE) and ethoxy ethyl glycidyl ether (EEGE)] were employed for the functional end-capping of the PVFc block (Scheme 29.10). Molecular weights of the end-functionalized PVFcs range between 1000 and 3600 g/mol and block copolymers with 10,000–50,000 g/mol overall molar masses were obtained. These metal-containing amphiphilic block copolymers exhibit good solubility in water and the synthetic pathway provides an efficient approach to water-soluble and redox-active complex polymeric architectures.



**Scheme 29.9** Four possible primary structures for the monomer repeating units in side-chain organometallic polymer derive from poly(ferrocenylenevinylene).



**Scheme 29.10** Synthetic strategy to synthesizing amphiphilic ferrocene-containing block copolymers (PVFc-BGE-PEO) and AB<sub>2</sub> miktoarm star polymers (PVFc-(PEO)<sub>2</sub>).



**Scheme 29.11** Polyferrocenyldimethylsilanes.

In water, these polymers generate micelles and multicompartiment micellar structures, which are promising materials for bioorganometallic applications [164, 165].

Another interesting contribution to this field from Manners et al. [166] was the synthesis, characterization, and behavior study of new polyferrocenyldimethylsilanes that were obtained by metalation of the cyclopentadienyl groups of polyferrocenyldimethylsilane (Scheme 29.11), which was performed by reaction with the base pair 'BuLi/KO'Bu in tetrahydrofuran (THF). Subsequent treatment with a series of electrophiles affords a range of Cp-substituted polymers with up to an average of 1.8 new substituents per repeating unit with selective metalation at the  $\beta$ -carbon. Polymers with high degrees of substitution (up to nearly one per Cp) were prepared when a greater excess of bases was used. The loss of crystallinity, solubility in alkanes and the dramatic rise in glass-transition temperatures of the silylated polyferrocenyldimethylsilanes illustrate how substitution of the Cp ring can lead to materials with properties that greatly differ from those of the original polymer.

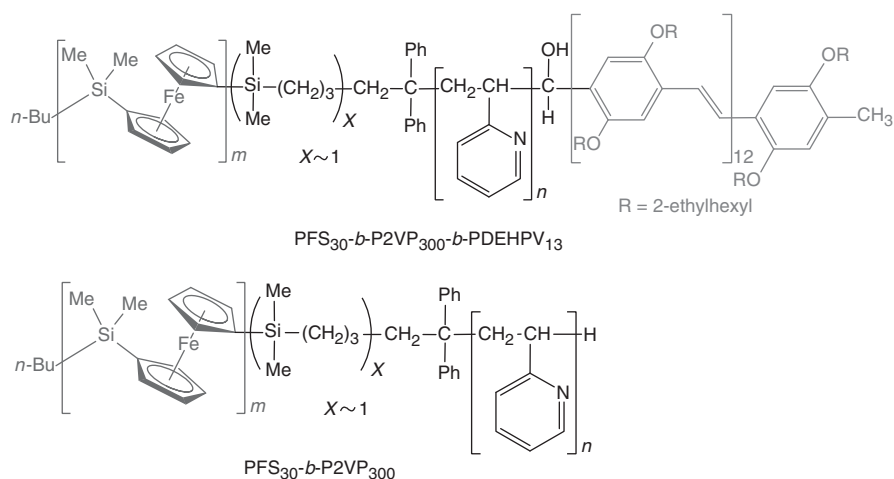
The controlled bottom-up fabrication of nanomaterials with well-defined but complex architectures [167–173] can be achieved by preparing the samples as colloidal stable entities. Cylindrical micelles [174, 175] obtained from the solution self-assembly of block copolymers have found use as additives for the enhancement of the toughness of epoxy resins [176], as templates for the mineralization of hydroxyapatite [177], the formation of metal nanoparticles [178–181], as

materials for flow-intensive drug delivery [182, 183], etc. A further important challenge is to extend living self-assembly to other semicrystalline polymers, especially  $\pi$ -conjugated polymers, in order to access colloidal suspensions of nanowires of controlled length [184, 185]. Such materials would possess useful electronic or optical properties. These types of colloidal nanowires might be patterned by spin-coating on substrates structured using electron beam resists and may prove useful as active components in the fabrication of devices [186]. The segmented nanowires show many of the features of the multicolored luminescent nanowire barcodes reported recently by Park et al. [187]. These authors carried out sequential electrochemical polymerization of 3-butylthiophene, 3-methylthiophene, and ethylenedioxythiophene using an anionic alumina oxide nanoporous template. In this way, they obtained uniform elongated structures of diameter ca. 200 nm and length 10 micrometers in which bar-like segments of the individual polymers could be detected by laser confocal fluorescence microscopy (LCFM) through their characteristic fluorescence. The multiblock co-micelles are significantly thinner (ca. 40 nm) and represent an interesting and novel example of barcoded nanowires that might provide a useful platform for sensing applications. The incorporation of transition metals and main group elements into one of the blocks provides an attractive method for expanding the range of properties present in the resulting self-assembled materials [17, 159, 188–198].

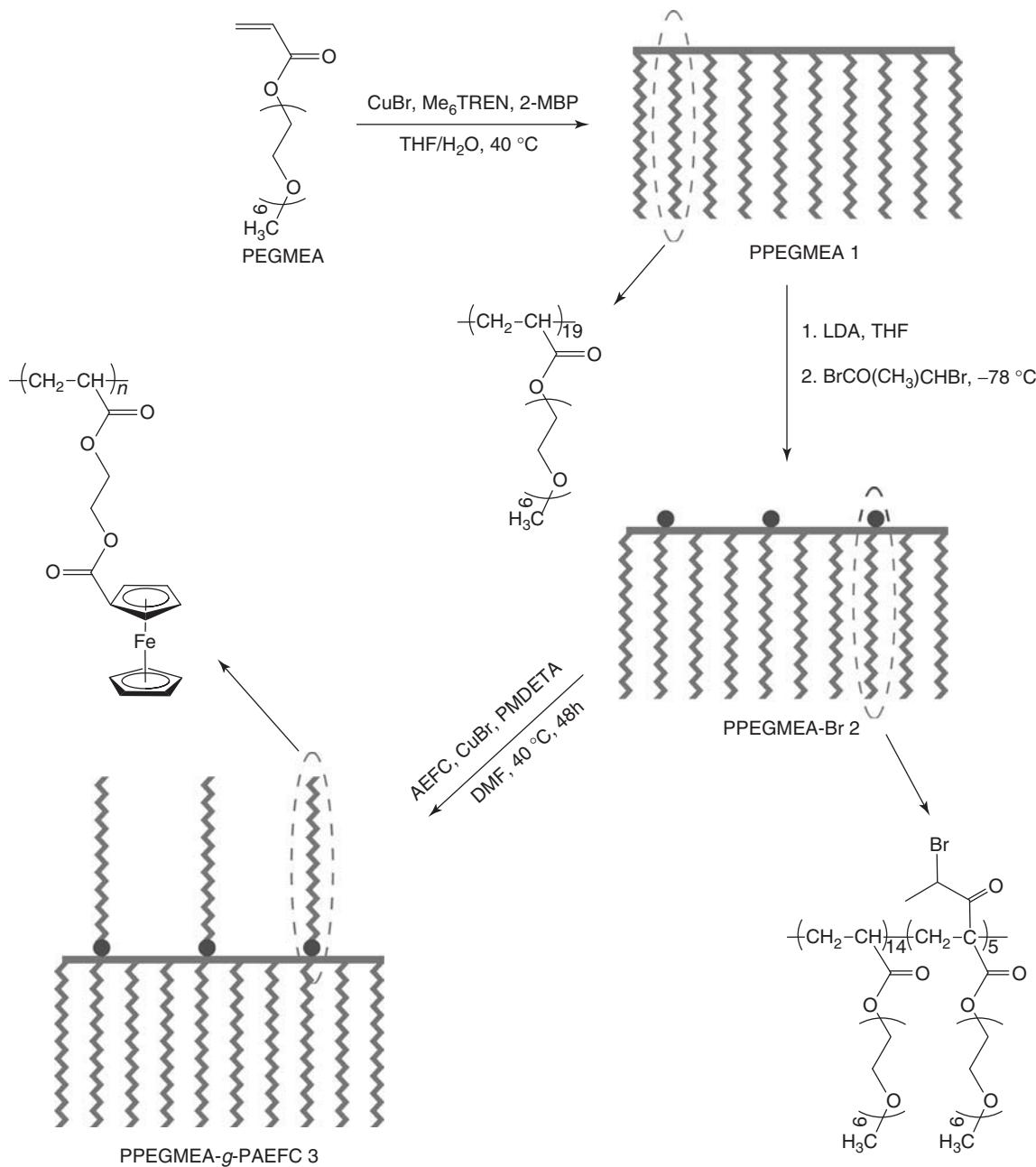
Another interesting example of multiblock polymer useful for obtaining colloids was synthesized by self-assembly of the triblock copolymer, poly(ferrocenyldimethylsilane-*b*-2-vinylpyridine-*b*-2,5-di(2'-ethylhexyloxy)-1,4-phenylvinylene) ( $\text{PFS}_{30}\text{-}b\text{-P2VP}_{300}\text{-}b\text{-PDEHPV}_{13}$ , the subscripts refer to the degree of polymerization) in 2-propanol (2-PrOH) (Scheme 29.12). The resulting polymers provide a useful structure for obtaining complex architectures with particular properties that, in solution, provide colloidally stable entities [199].

These flower-like aggregates that are obtained can be completely disassembled into well-dispersed cylindrical micelles of uniform length upon mild warming of the solutions in 2-PrOH. Using the micelle fragments obtained by sonication and sequentially adding aliquots of  $\text{PFS}_{30}\text{-}b\text{-P2VP}_{300}$  diblock copolymer and  $\text{PFS}_{30}\text{-}b\text{-P2VP}_{300}\text{-}b\text{-PDEHPV}_{13}$  fluorescent triblock copolymer, each as a solution in THF, long uniform cylindrical structures can be obtained, with alternating compartments containing nonfluorescent and fluorescent polymer, with light-emitting segments of a single color. A clever combination of blocks should probably provide multicolor polymers.

The research efforts in this field provided a new series of ferrocene-based, well-defined amphiphilic graft copolymers with interesting properties. The obtained HMSOP consists of hydrophilic poly[poly(ethylene glycol)-methyl-ether-acrylate] (PPEGMEA) backbone and hydrophobic poly(2-acryloyloxyethyl-ferrocenecarboxylate) (PAEFC) side chains, which were synthesized by successive single-electron-transfer living radical polymerization (SET-LRP) and atom transfer radical polymerization (ATRP). The backbone was prepared by SET-LRP of poly(ethylene glycol)-methyl-ether-acrylate (PEGMEA) macromonomer, and it was then treated with lithium di-isopropylamide and 2-bromopropionyl bromide at  $-78^\circ\text{C}$  to give PPEGMEA-Br macroinitiator [200]. The targeted well-defined graft copolymers with narrow molecular weight distributions ( $M_w/M_n \leq 1.32$ ) were synthesized via ATRP of 2-Acryloyloxyethyl-Ferrocenecarboxylate (AEFC) initiated by PPEGMEA-Br macroinitiator, and, remarkably, the molecular weights of the backbone and side chains were both controllable. The preparation method, the length of PAEFC segment, and the initial water content apparently affected the self-assembly behavior of PPEGMEA-*g*-PAEFC amphiphilic graft copolymers in aqueous solution (Scheme 29.13). The observed morphologies of



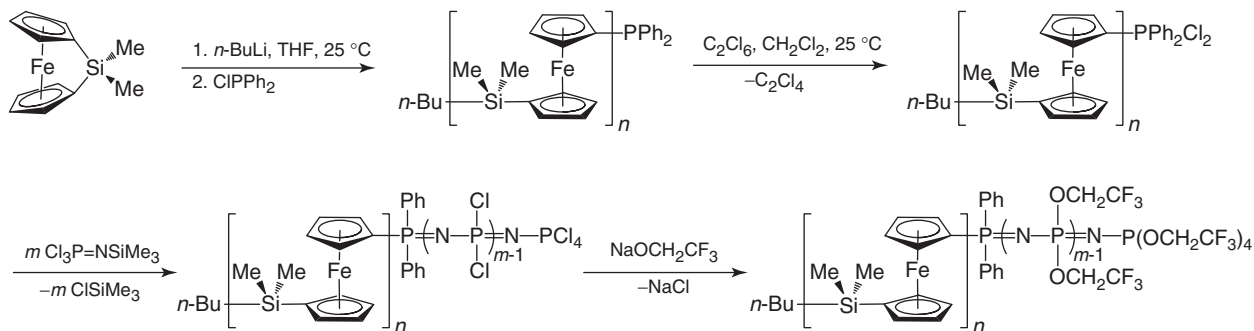
**Scheme 29.12** Structure of  $\text{PFS}_{30}\text{-}b\text{-P2VP}_{300}\text{-}b\text{-PDEHPV}_{13}$  and  $\text{PFS}_{30}\text{-}b\text{-P2VP}_{300}$ .



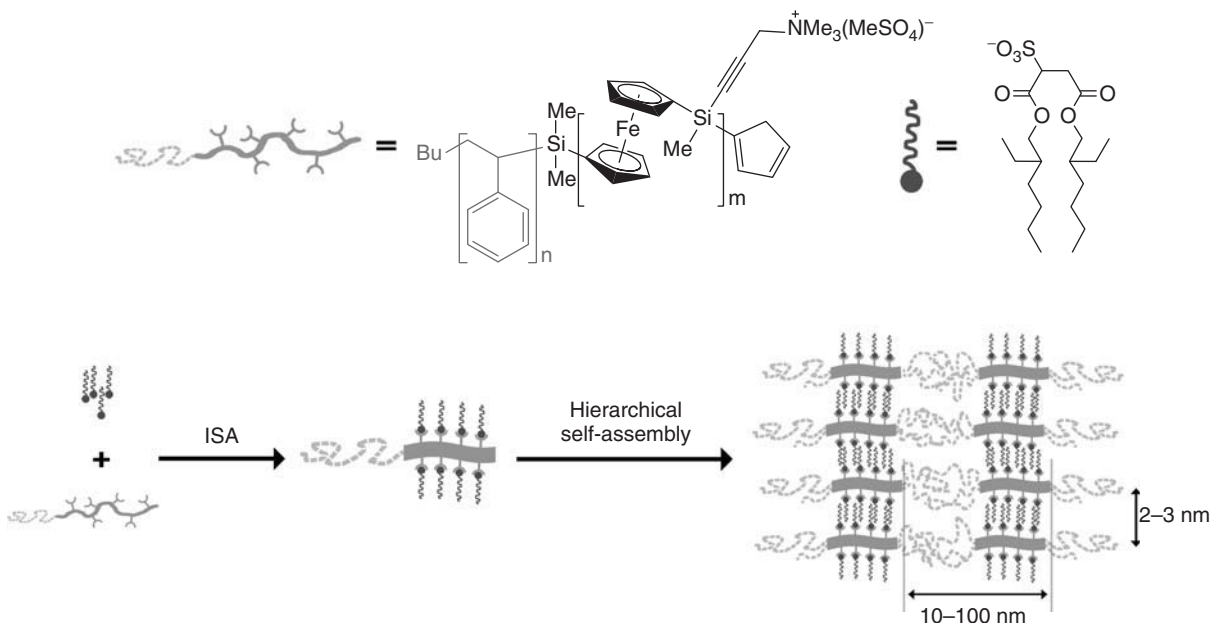
**Scheme 29.13** Synthesis of PPEGMEA-g-PAEFC amphiphilic graft copolymer.

micelles in water could transform from cylinders to spheres or rods on changing the preparation condition and the length of the side chains. The resulting micelles should be particularly interesting for a variety of potential applications such as amperometric biosensors and redox drug controlled-release carriers.

In addition, the self-assembly of block copolymers with immiscible segments is known to generate a variety of different morphologies because of phase separation in the solid state and selective solvation in block-selective solvents and provides an attractive route to different nanostructures [201–203]. Using the living anionic and the photocontrolled living anionic protocols and combining the obtained polyferrocenylsilane block with a second readily tuned block was possible the rational design of nanostructures such as block co-micelles, which are available via crystallization-directed living supramolecular polymerization processes. Finally, the rare organometallic-inorganic diblock copolymer polyferrocenylsilane-*b*-polyphosphazene was obtained (Scheme 29.14).



**Scheme 29.14** Synthesis of end-functionalized poly(ferrocenylsilane) homopolymer and poly(ferrocenylsilane)-*b*-polyphosphazene diblock copolymers.



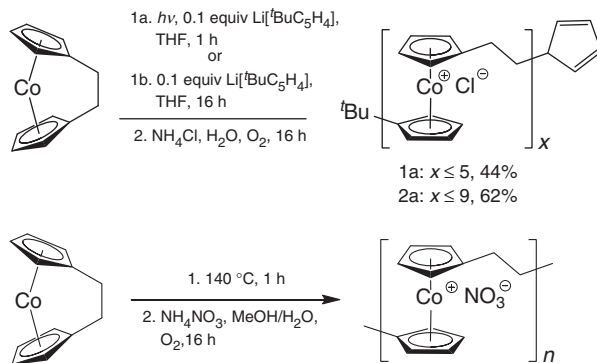
**Scheme 29.15** Schematic representation of the formation of hierarchically self-assembled architectures, illustrating the concept of structure-within-structure formation.

Newly, Manners et al. [204] have synthesized and characterized the first example of an organic–organometallic hierarchically organized nanostructure from the ionic complexation of polyferrocenylmethyl-dimethylaminopropylsilane diblock copolymer with low molecular weight amphiphilic molecules. A fine structural tuning can be achieved by careful selection of the amphiphile for complexation. In addition, the method can provide a simple route to achieve hierarchical organization at different length scales, the generation of nanostructured materials, and inducing certain functionality by careful selection of starting materials. Self-assembly of block copolymer–surfactant complexes was also studied in bulk and thin films and produced materials with structural hierarchy over multiple length scales (Scheme 29.15).

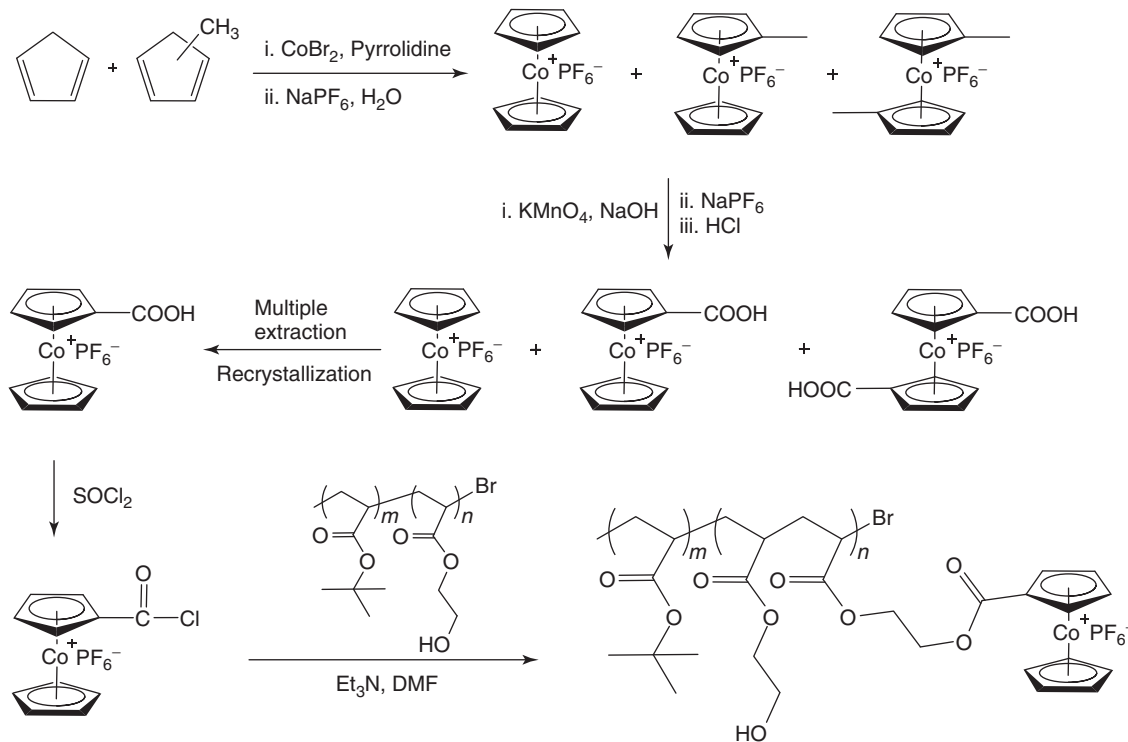
Compared to widely studied ferrocene and ferrocene polymers, cobaltocene has received far less attention, partly because of the greater difficulty in preparing substituted derivatives [205–210]. Cobaltocene (19-e) has one more valence electron than ferrocene (18-e) but it can lose an electron readily to form the cobaltocenium cation (18-e), isoelectronic with ferrocene [211]. Given the ease oxidation of cobaltocene and the great inertness of cobaltocenium salts, it is extremely difficult to prepare substituted derivatives from cobaltocene or cobaltocenium. A few main-chain cobaltocenium polymers were synthesized via condensation or ROP [212–214]. Owing to their cationic nature, side-chain cobaltocenium polymers exhibit interesting solubility behaviors in solvents such as water and acetone, in which solvents the polymer may present interesting self-assembly in solution and provide new materials with possible useful catalytic, magnetic, and redox properties.

Manners et al. [214] described the synthesis of the high molecular weight, water-soluble polycobaltocenium polyelectrolytes by ROP of dicarba[2]cobaltocenophanes (19-e). Anionic polymerization of the cobaltocenophane (19-e) and dicarba[2]cobaltocenophane using  $\text{Li}[t\text{-BuC}_5\text{H}_4]$  as initiator resulted in the formation of oligomers with up to nine repeat units. The observation that this process occurs in the absence of light, in contrast to the case for corresponding [1]ferrocenophanes, indicates that the M–Cp bond in the 19-electron dicarba[2]cobaltocenophane is intrinsically weaker, presumably because the unpaired electron occupies an antibonding orbital. Thermal ROP of the dicarba[2]cobaltocenophane followed by oxidation resulted in an interesting high molecular weight, water-soluble, redox-active polycobaltocenium (Scheme 29.16).

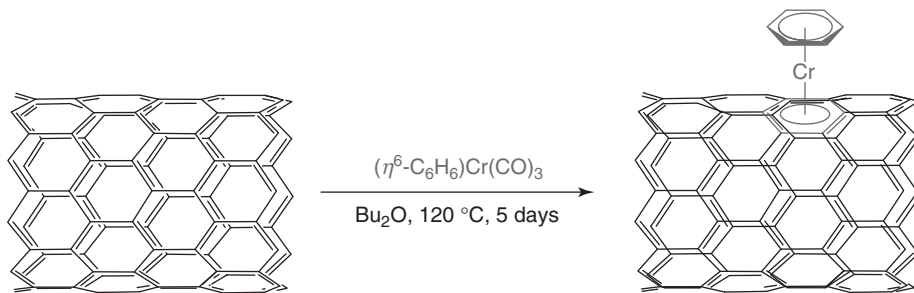
Soon after, Tang et al. synthesized highly pure monosubstituted carboxycobaltocenium and subsequently prepared side-chain cobaltocenium-containing block copolymers. These block copolymers exhibited self-assembled vesicle and nanotube structures depending on the solvent used (Scheme 29.17) [215]. Transmission electron microscopy (TEM) images showed that these micellar aggregates exhibited nonuniform vesicle morphology with diameter ranging from 50 to 300 nm.



**Scheme 29.16** Syntheses of water-soluble polymer derived from the dicarba[2]cobaltocenophane.



**Scheme 29.17** Synthesis of monocarboxycobaltocenium and side-chain cobaltocenium-containing block copolymers.



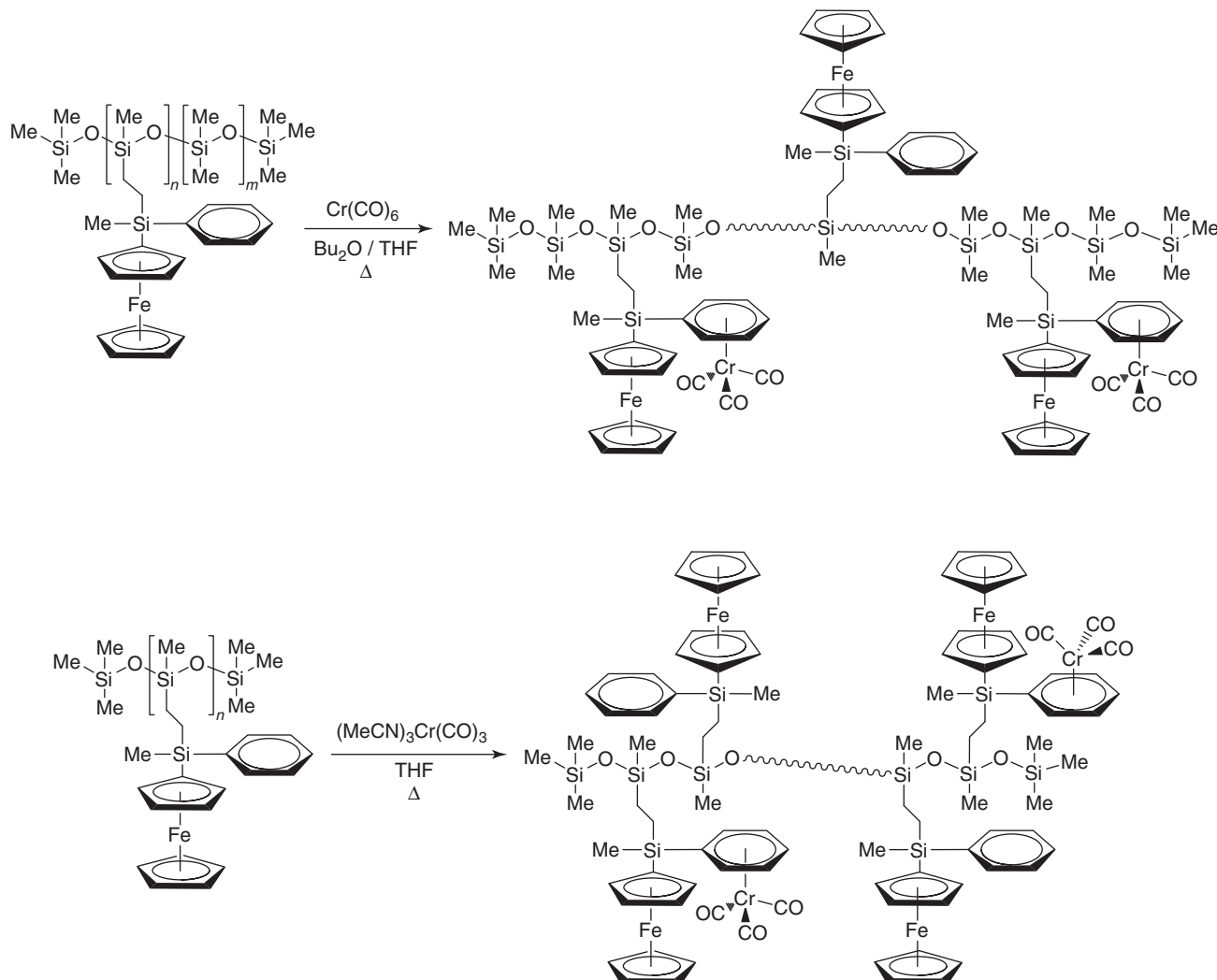
**Scheme 29.18** Reactions of single-walled carbon nanotubes with  $(\eta^6\text{-benzene})\text{chromium tricarbonyl}$ .

Probably one of the most exciting new research lines on side-chain organometallic polymers is the functionalization of carbon derivatives such as nanotubes and, more recently, graphene [216]. Nonetheless, research toward the wider application of side-chain graphene organometallic polymers is still in its infancy and much work remains to be done in facilitating the practical applications of graphene-based materials and broadening the scope of their electrochemical applications in the future. Apart from the electronic structure, the chemical reactivity of carbon nanotubes is governed by the curvature-induced pyramidalization and the misalignment of the  $\pi$ -orbitals, which renders carbon nanotubes a distinct class of materials between the usually more reactive fullerenes (commented previously) and graphene. The end-group functionalization and side-wall chemical addition reactions of carbon nanotubes have received a great deal of attention [217, 218]. Also, the endohedral filling of the nanotubes with various molecules, atoms, and complexes has been extensively investigated for fabrication of nanowires and in energy storage and drug delivery applications. The inner carbon nanotube cavities have been filled with fullerenes, metals [219–221], metal oxides [222, 223] and (noncovalently encapsulated) transition metal complexes [224]. The first reported [225] side-chain covalent organometallic complexation of carbon nanotubes was synthesized by reaction of purified single-walled carbon nanotubes with  $[\text{Cr}(\text{CO})_6]$  and  $[\text{Cr}(\eta^6\text{-benzene})(\text{CO})_3]$  (Scheme 29.18). The bonding of the  $\{\text{Cr}(\text{CO})_3\}$  and  $\{\text{Cr}(\eta^6\text{-benzene})\}$  moieties on the single-walled carbon nanotubes is primarily covalent in nature, with slight charge-transfer character in the case of  $\{\text{Cr}(\text{CO})_3\}$ . The side-chain carbon nanotube organometallic complexes obtained showed electronic conductivity different to that of the starting nanotube.

### 29.3.2 Heterometallic-Side Organometallic Polymers

There are not too many examples of side-chain hetero-organometallic polymers, which indicates the difficulty in synthesizing this kind of polymers. The first examples of ferrocenyl-containing dendronized polysiloxanes were prepared some years ago from polysiloxanes containing small pendant electroactive wedges possessing electronically communicated ferrocenyl moieties [226]. The synthesis via hydrosilylation chemistry of a series of new polysiloxanes functionalized with small appended dendritic wedges containing both electron-donor ferrocenyl units and electron-acceptor ( $\eta^6\text{-aryl}$ )tricarbonylchromium fragments were presented by Cuadrado et al. (Scheme 29.19) [227]. The novel ferrocenyl-polysiloxanes are stable under air and moisture, and soluble in common organic solvents. The TGA analysis showed that the thermal stability of the novel ferrocenyl-polysiloxanes strongly depends on the size of the ferrocenyl dendritic fragment appended to the siloxane backbones, some of them at temperature higher than  $250^\circ\text{C}$ , yielding ceramic residues in relatively high amounts. Electrochemical studies in dissolution showed that all the ferrocenyl redox units present in the ferrocenyl dendronized polysiloxanes are electrochemically independent. In addition, the authors have demonstrated the feasibility of modifying electrode surfaces with stable electroactive films of these siloxane-based polyferrocenyl dendronized molecules.

A very interesting heterometal polymer that can be considered as a combination of MSOP and MBOP were synthesized by living photocontrolled ROP of block copolymers based on ferrocene and cobaltocenium repeat units. This synthetic procedure, which had never been used before (Scheme 29.20), constituted a very interesting approach to obtaining new heterometallic materials [228]. The self-assembly procedure allows access to new heterobimetallic block co-micelle architectures through living self-assembly. The presented Fe–Co block copolymers display interesting redox properties owing to the electroactive ferrocene and cobaltocenium centers that yield oxidation and reduction waves separated by around 1.5 V. As a result, the Fe–Co block copolymers may have utility as three-stage switches in polymer-based functional materials.

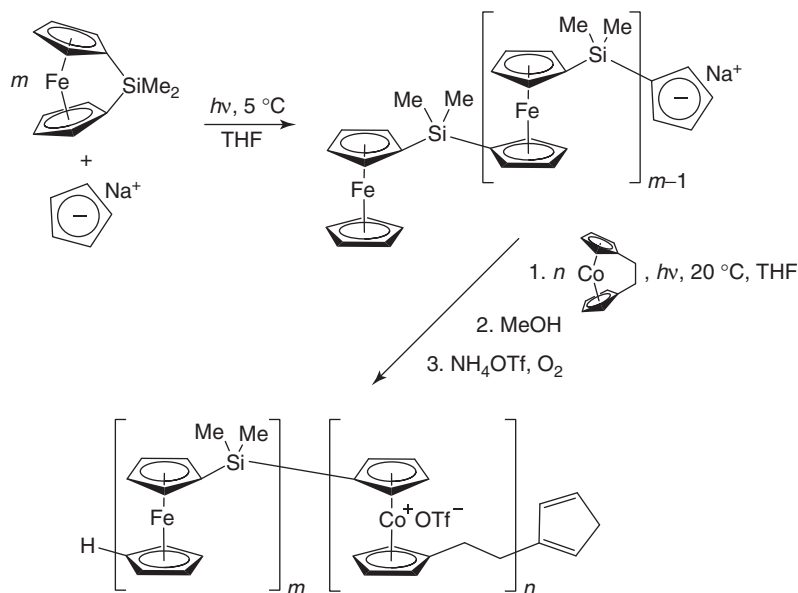


**Scheme 29.19** Synthesis of polysiloxanes with pendant silicon-bridged  $\{(\eta^5\text{-C}_5\text{H}_4)\text{Fe}(\eta^5\text{-C}_5\text{H}_5)\}$  and  $\{(\eta^6\text{-C}_6\text{H}_5)\text{Cr}(\text{CO})_3\}$  units.

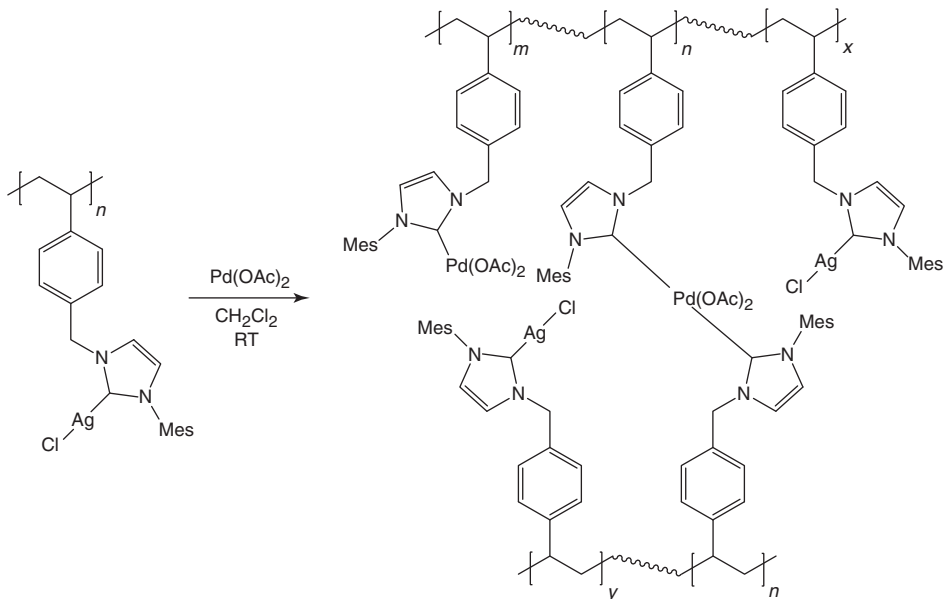
Luo et al. made a very interesting contribution to the synthesis of heterometallic-side organometallic polymers (HeteroMSOP). They envisioned that if a soluble Ag(I)-NHC-based side-chain polymer could be synthesized, then it could be further utilized as a carbene transfer agent to prepare a functional *N*-heterocyclic-based organometallic polymer with higher metal loading [229]. They describe the synthesis of a novel soluble and interesting Ag(I)-NHC-based side-chain heterometallic-organometallic polymer by postpolymerization modification of polychloromethylstyrene and its application in the synthesis of the Pd–NHC-containing polymer by the transmetalation reaction of the Ag(I)-NHC moieties (Scheme 29.21). This development offers a new methodology for constructing novel functional NHC-based organometallic polymers by a simple three-step synthesis under mild conditions. The resulting Pd–NHC-containing polymer showed high catalytic activity and reusability in the Suzuki reactions of the challenging, relatively inactive aryl chlorides and aryl boronic acids. Remarkably, even ortho-substituted and electronically deactivated 2-chloroanisole can be coupled with aryl boronic acids in good yields. In addition, the less reactive aryl boronic acids containing nitrile groups undergo the Suzuki reactions smoothly with this procedure, although the yield decreases.

#### 29.4 SUMMARY AND CONCLUSIONS

Organometallic polymers, pioneered in 1955, have been developed in a variety of ways that involve molecular engineering in order to target precise functions and applications. The nature of the structure of organometallic polymers governs the



**Scheme 29.20** Synthesis of Fe–Co-bimetallic block copolymers through photocontrolled ring-opening polymerization (ROP).



**Scheme 29.21** Preparation of functional palladium-NHC-containing polymer by transmetalation from a  $\text{Ag}(\text{I})$ –NHC-based side-chain heterometal-organometallic polymer.

solubility and properties in applications such as catalysis, molecular electronics, photonics, sensing, and nanomedicine. Actually, the most studied properties and possible application of organometallic polymers include light harvesting with the antenna effect to funnel energy from many photosensitive branch termini toward the focal group of the dendron, organic light-emitting diodes (OLEDs), organic field effect transistors (OFETs), and photovoltaic devices. The photophysical properties are a powerful source of sensors, as are the redox properties using, for instance, the ferrocenyl groups. Catalysis is another important application of organometallic polymers. Encapsulation and micellar structures play a key role, because small catalytically active transition metal nanoparticles can be embedded in the nanometric structures. The supramolecular properties of organometallic polymers could govern their functions. Recent breakthroughs in recyclable catalysts have

involved the development of metal-containing polymers whose metal centers are specifically designed to facilitate organic transformations. The supramolecular properties of organometallic polymers are thus involved in their applications. Last but not least, the importance of organometallic polymers synthesis should be emphasized because molecular engineering requires more and more sophisticated design and synthetic skill. Incorporation of metals as an integral component of a polymer backbone remains a synthetic challenge that will undoubtedly be met with the development of new methodologies in polymer, inorganic, and organometallic chemistry. Use of a combination of covalent bonds and supramolecular interactions has increased the span of the field and allowed researchers to develop unique structures with useful properties. The rapid expansion of the field shows that it is moving beyond mere refinement of synthetic technique and exploration of physical properties. The emphasis now must be on rational design and synthesis of new organometallic polymers with practical applications.

## ACKNOWLEDGEMENTS

Financial support cofinanced by the EU FEDER: the Spanish MINECO (CTQ2010-20952) and Junta de Andalucía through PAI (research teams FQM-317) and Excellence Projects P07-FQM-03092 and P09-FQM-5402. Thanks are also given to COST Action CM0802 (WG2, WG3, WG4). M. Serrano-Ruiz is grateful to Excellence project P09-FQM-5402 for a postdoctoral contract and F. Scalambra to the U. Almería for a PhD grant. Our thanks to Professor Antonio Barbero for language corrections.

## REFERENCES

1. Arimoto, F. S.; Haven, A. C. *J. Am. Chem. Soc.* **1955**, *77*, 6295.
2. Nguyen, P.; Gómez-Elipe, P.; Manners, I. *Chem. Rev.* **1999**, *99*, 1515.
3. Abd-El-Aziz, A. S. *Macromol. Rapid Commun.* **2002**, *23*, 995.
4. Swager, T. M.; Kingsborough, R. P. *Progress in Inorganic Chemistry*; John Wiley & Sons, Inc.: New York, **1999**, p 123; Vol. 48.
5. Manners, I. *Synthetic Metal-Containing Polymers*; Wiley-VHC Verlag GmbH: Weinheim, **2004**.
6. Abd-El-Aziz A. S.; Carraher Jr. C. E.; Pittman Jr. C. U.; Zeldin M.; Vol.1 to Vol. 10; *Macromolecules Containing Metal and Metal-Like Elements*; John Wiley & Sons, Inc.: New York; **2003–2010**.
7. Manners, I. *J. Polym. Sci. Part A: Polym. Chem.* **2002**, *40*, 179.
8. Whittell, G. R.; Manners, I. *Adv. Mater.* **2007**, *19*, 3439.
9. Puddephatt, R. J. *J. Inorg. Organomet. Polym. Mater.* **2005**, *15*, 371.
10. Chan, W. K. *Coord. Chem. Rev.* **2007**, *251*, 2104.
11. Wong, W-Y.; Ho, C-L. *Coord. Chem. Rev.* **2006**, *250*, 2627.
12. Zhou, G-J.; Wong W-Y. *Chem. Soc. Rev.* **2011**, *40*, 2541.
13. Whittell, G. R.; Hager, M. D.; Schubert, U. S.; Manners, I. *Nat. Mater.* **2011**, *10*, 176.
14. Schacher, F. H.; Rupar, P. A.; Manners, I. *Angew. Chem. Int. Ed.* **2012**, *51*, 7898.
15. Williams, K. A.; Boydston, A. J.; Bielawski, C. W. *J. R. Soc. Interface* **2007**, *4*, 359.
16. Spokoyny, A. M.; Kim, D.; Sumrein, A.; Mirkin, C. A. *Chem. Soc. Rev.* **2009**, *38*, 1218.
17. Bellas, V.; Rehahn, M. *Angew. Chem. Int. Ed.* **2007**, *46*, 5082.
18. Ulbricht, C.; Beyer, B.; Friebel, C.; Winter, A.; Schubert, U. S. *Adv. Mater.* **2009**, *21*, 4418.
19. Lu, J.; Toy, P. H. *Chem. Rev.* **2009**, *109*, 815.
20. Rivard, E. *Annu. Rep. Prog. Chem., Sect. A Inorg. Chem.* **2012**, *108*, 315.
21. Miller, J. S. *Inorg. Chem.* **2000**, *39*, 4392.
22. Ward, M. D. *Coord. Chem. Rev.* **2006**, *250*, 3128.
23. Lee, E.; Seo, J.; Lee, S. S.; Park, K-M. *Cryst. Growth Des.* **2012**, *12*, 3834.
24. Berenguer, J. R.; Fernández, J.; Lalinde, E.; Sánchez, S. *Chem. Commun.* **2012**, *48*, 6384.
25. Toma, L. M.; Ruiz-Pérez, C.; Lloret, F.; Julve, M. *Inorg. Chem.* **2012**, *51*, 1216.
26. Etaiw, S. E. H.; El-Zaria, M. E.; Fayed, T. A.; Abdou, S. N. *J. Inorg. Organomet. Polym. Mater.* **2011**, *21*, 465.
27. Ovens, J. S.; Leznoff, D. B. *Dalton Trans.* **2011**, *40*, 4140.
28. Campagna, S.; Ceroni, P.; Puntoriero, F. Eds. *Designing Dendrimers*; Wiley-VCH Verlag GmbH: Weinheim, **2012**.

29. Vögtle, F.; Richart, G.; Werner, N. *Dendrimer Chemistry. Concepts, Syntheses, Properties, Applications*; Wiley-VCH Verlag GmbH: Weinheim, Germany, **2009**.
30. Astruc, D.; Boisselier, E.; Ornelas, C. *Chem. Rev.* **2010**, *110*, 1857.
31. Newkome, G. R.; Shreiner, C. *Chem. Rev.* **2010**, *110*, 6338.
32. Tomalia, D. A.; Christensen, J. B.; Boas, U. *Dendrimer, Dendrons and Dendritic Polymers*; Cambridge University Press: UK, **2012**.
33. Kann, N. *Molecules* **2010**, *15*, 6306.
34. Buchmeiser, M. R. *Chem. Rev.* **2009**, *109*, 303.
35. Polshettiwar, V.; Len, C.; Fihri, A. *Coord. Chem. Rev.* **2009**, *253*, 2599.
36. Anwander, R. *Chem. Mater.* **2001**, *13*, 4419.
37. Green, K. A.; Cifuentes, M. P.; Samoc, M.; Humphrey, M. G. *Coord. Chem. Rev.* **2011**, *255*, 2025.
38. Newkome, G. R.; He, E.; Moorefield, C. N. *Chem. Rev.* **1999**, *99*, 1689.
39. Jenekhe, S. A.; Chen, X. L. *Science* **1999**, *283*, 372.
40. Matsen, M. W.; Bates, F. S. *Macromolecules* **1996**, *29*, 7641.
41. Raez, J.; Manners, I.; Winnik, M. A. *J. Am. Chem. Soc.* **2002**, *124*, 10381.
42. Abd-El-Aziz, A. S.; Shipman, P. O.; Boden, B. N.; McNeil, W. S. *Progr. Polymer Sci.* **2010**, *35*, 714.
43. Batten, S. R.; Champness, N. R.; Chen, X-M.; García-Martínez, J.; Kitagawa, S.; Öhrström, L.; O'Keeffe, M.; Suh, M. P.; Reedijk, J. *Cryst. Eng. Comm.* **2012**, *14*, 3001.
44. Dobrawa, R.; Würthner, F. *J. Polym. Sci. A Polym. Chem.* **2005**, *43*, 4981.
45. Guo, F. Q.; Kim, Y. G.; Reynolds, J. R.; Schanze, K. S. *Chem. Commun.* **2006**, 1887.
46. Mei, J.; Ogawa, K.; Kim, Y. G.; Heston, N. C.; Arenas, D. J.; Nasrollahi, Z.; McCarley, T. D.; Tanner, D. B.; Reynolds, J. R.; Schanze, K. S. *ACS Appl. Mater. Interfaces* **2009**, *1*, 150.
47. Chawdhury, N.; Köhler, A.; Friend, R. H.; Younus, M.; Long, N. J.; Raithby, P. R.; Lewis, J. *Macromolecules* **1998**, *31*, 722.
48. Haskins-Glusac, K.; Ghiviriga, I.; Abboud, K. A.; Schanze, K. S. *J. Phys. Chem. B* **2004**, *108*, 4969.
49. Silverman, E. E.; Cardolaccia, T.; Zhao, X. M.; Kim, K. Y.; Haskins-Glusac, K.; Schanze, K. S. *Coord. Chem. Rev.* **2005**, *249*, 1491.
50. Glusac, K.; Köse, M. E.; Jiang, H.; Schanze, K. S. *J. Phys. Chem. B* **2007**, *111*, 929.
51. Wong, W.-Y. *Dalton Trans.* **2007**, 4495.
52. Rogers, J. E.; Cooper, T. M.; Fleitz, P. A.; Glass, D. J.; McLean, D. G. *J. Phys. Chem. A* **2002**, *106*, 10108.
53. Wilson, J. S.; Dhoot, A. S.; Seeley, A.; Khan, M. S.; Köhler, A.; Friend, R. H. *Nature* **2001**, *413*, 828.
54. Zhou, G.; He, Y.; Yao, B.; Dang, J. S.; Wong, W.-Y.; Xie, Z.; Zhao, X.; Wang, L. *Chem. Asian J.* **2010**, *5*, 2405.
55. Wong, W. Y.; Ho, C. L. *Acc. Chem. Res.* **2010**, *43*, 1246.
56. Keller, J. M.; Schanze, K. S. *Organometallics* **2009**, *28*, 4210.
57. Keller, J. M.; Glusac, K. D.; Danilov, E. O.; McIlroy, S.; Sreearuothai, P.; Cook, A. R.; Jiang, H.; Miller, J. R.; Schanze, K. S. *J. Am. Chem. Soc.* **2011**, *133*, 11289.
58. Blouin, N.; Michaud, A.; Leclerc, M. *Adv. Mater.* **2007**, *19*, 2295.
59. Leclerc, N.; Michaud, A.; Sirois, K.; Morin, J.-F.; Leclerc, M. *Adv. Funct. Mater.* **2006**, *16*, 1694.
60. Li, J.; Dierschke, F.; Wu, J.; Grimsdale, A. C.; Müllen, K. *J. Mater. Chem.* **2006**, *16*, 96.
61. Fu, Y.; Sun, M.; Wu, Y.; Bo, Z.; Ma, D. *J. Polym. Sci. A Polym. Chem.* **2008**, *46*, 1349.
62. Wei, Z.; Xu, J.; Zeng, L.; Le, Z.; Shen, L.; Pu, S. *J. Mater. Sci.* **2008**, *43*, 1008.
63. Liu, R.; Xiong, Y.; Zeng, W.; Wu, Z.; Du, B.; Yang, W.; Sun, M.; Cao, Y. *Macromol. Chem. Phys.* **2007**, *208*, 1503.
64. Wang, H.; Ryu, J.-T.; Han, Y. S.; Kim, D.-H.; Choi, B. D.; Kwon, Y. *Mol. Cryst. Liq. Cryst.* **2007**, *463*, 285.
65. Baba, A.; Onishi, K.; Knoll, W.; Advincula, R. C. *J. Phys. Chem. B* **2004**, *108*, 18949.
66. Hameurlaine, A.; Dehaen, W.; Peng, H.; Xie, Z.; Tang, B. Z. *J. Macromol. Sci. Pure Appl. Chem.* **2004**, *41*, 295.
67. Huang, J.; Niu, Y.; Xu, Y.; Hou, Q.; Yang, W.; Mo, Y.; Yuan, M.; Cao, Y. *Synth. Met.* **2003**, *135–136*, 181.
68. Chen, X.; Liao, J.-L.; Liang, Y.; Ahmed, M. O.; Tseng, H. E.; Chen, S. A. *J. Am. Chem. Soc.* **2003**, *125*, 636.
69. Yavuz, O.; Ram, M. K. *Supramolecular Engineering of Conducting Materials*; Fractal System Inc.: Safety Harbor, FL, **2005**; p 303.
70. Harvey, P. D. In *The Porphyrin Handbook*; Kadish, K. M.; Smith, K. M.; Guilard, R., Eds. Academic Press: San Diego, CA, **2003**; Vol. 18, p 63.
71. Bellows, D.; Gingras, E.; Aly, S. M.; Abd-El-Aziz, A. S.; Leclerc, M.; Harvey, P. D. *Inorg. Chem.* **2008**, *47*, 11720.
72. Boydston, A. J.; Williams, K. A.; Bielawski, C. W. *J. Am. Chem. Soc.* **2005**, *127*, 12496.
73. Khoramov, D. M.; Boydston, A. J.; Bielawski, C. W. *Angew. Chem. Int. Ed.* **2006**, *45*, 6186.

74. Boydston, A. J.; Khoramov, D. M.; Bielawski, C. W. *Tetrahedron Lett.* **2006**, *47*, 5123.
75. Khoramov, D. M.; Boydston, A. J.; Bielawski, C. W. *Org. Lett.* **2006**, *8*, 1831.
76. Boydston, A. J.; Rice, J. D.; Sanderson, M. D.; Dykhno, O. L.; Bielawski, C. W. *Organometallics* **2006**, *25*, 6087.
77. Boydston, A. J.; Bielawski, C. W. *Dalton Trans.* **2006**, *35*, 4073.
78. Williams, K. A.; Boydston, A. J.; Bielawski, C. W. *Chem. Soc. Rev.* **2007**, *36*, 729.
79. Tennyson, A. G.; Norris, B.; Bielawski, C. W. *Macromolecules* **2010**, *43*, 6923.
80. Williams, K. A.; Bielawski, C. W. *Chem. Commun.* **2010**, *46*, 5166.
81. Tennyson, A. G.; Khramov, D. M.; Varnado, C. D., Jr.; Creswell, P. T.; Kamplain, J. W.; Lynch, V. M.; Bielawski, C. W. *Organometallics* **2009**, *28*, 5142.
82. Varnado, Jr, C. D.; Lynch, V. M.; Bielawski, C. W. *Dalton Trans.* **2009**, *38*, 7253.
83. Powell, A. B.; Bielawski, C. W.; Cowley, A. H. *J. Am. Chem. Soc.* **2009**, *131*, 18232.
84. Kamplain, J. W.; Bielawski, C. W. *Chem. Commun.* **2006**, *42*, 1727.
85. Powell, A. B.; Bielawski, C. W.; Cowley, A. H. *J. Am. Chem. Soc.* **2010**, *132*, 10184.
86. Norris, B. C.; Bielawski, C. W. *Macromolecules* **2010**, *43*, 3591.
87. Hahn, F. E.; Radloff, C.; Pape, T.; Hepp, A. *Organometallics* **2008**, *27*, 6408.
88. Tennyson, A. G.; Rosen, E. L.; Collins, M. S.; Lynch, V. M.; Bielawski, C. W. *Inorg. Chem.* **2009**, *48*, 6924.
89. Coady, D. J.; Norris, B. C.; Khramov, D. M.; Tennyson, A. G.; Bielawski, C. W. *Angew. Chem. Int. Ed.* **2009**, *48*, 5187.
90. Tennyson, A. G.; Kamplain, J. W.; Bielawski, C. W. *Chem. Commun.* **2009**, *45*, 2124.
91. Er, J. A. V.; Tennyson, A. G.; Kamplain, J. W.; Lynch, V. M.; Bielawski, C. W. *Eur. J. Inorg. Chem.* **2009**, 1729.
92. Boydston, A. J.; Vu, P. D.; Dykhno, O. L.; Chang, V.; Wyatt, A. R.; Stockett, A. S.; Ritschdorff, E. T.; Shear, J. B.; Bielawski, C. W. *J. Am. Chem. Soc.* **2008**, *130*, 3143.
93. Boydston, A. J.; Pecinovsky, C. S.; Chao, S. T.; Bielawski, C. W. *J. Am. Chem. Soc.* **2007**, *129*, 14550.
94. Hallberg, A.; Westfelt, L. *J. Chem. Soc. Perkin Trans. I* **1984**, 933.
95. Conn, M. M.; Rebek, J. Jr. *Chem. Rev.* **1997**, *97*, 1647.
96. Friedler, D.; Bergman, R. G.; Raymond, K. N. *Angew. Chem. Int. Ed.* **2004**, *43*, 6748.
97. Lee, M.; Jang, C.-J.; Ryu, J.-H. *J. Am. Chem. Soc.* **2004**, *126*, 8082.
98. Pluth, M. D.; Bergman, R. G.; Raymond, K. N. *Angew. Chem. Int. Ed.* **2007**, *46*, 8587.
99. Ryu, J.-H.; Hong, D.-J.; Lee, M. *Chem. Commun.* **2008**, *44*, 1043.
100. Steel, P. J. *Acc. Chem. Res.* **2005**, *38*, 243.
101. Seidel, S. R.; Stang, P. J. *Acc. Chem. Res.* **2002**, *35*, 972.
102. Bu, X.-H.; Liu, H.; Du, M.; Wong, K. M.-C.; Yam, V. W.-W.; Shionoya, M.; *Inorg. Chem.* **2001**, *40*, 4143.
103. Catalano, V. J.; Kar, H.; Garnas, J. *Angew. Chem. Int. Ed.* **1999**, *38*, 1979.
104. Wang, C.-C.; Yang, C.-H.; Tseng, S.-M.; Lin, S.-Y.; Wu, T.-Y.; Fuh, M.-R.; Lee, G.-H.; Wong, K.-T.; Chen, R.-T.; Cheng, Y.-M.; Chou, P.-T. *Inorg. Chem.* **2004**, *43*, 4781.
105. Ghosh, A. K.; Catalano, V. J. *Eur. J. Inorg. Chem.* **2009**, *48*, 1832.
106. Tong, M.-L.; Chen, X.-M.; Ye, B.-H.; Ji, L.-N. *Angew. Chem., Int. Ed.* **1999**, *38*, 2237.
107. Cui, F.; Yang, P.; Huang, X.; Yang, X.-J.; Wu, B. *Organometallics* **2012**, *31*, 3512.
108. Li, Y.-H.; Sun, D.; Hao, H.-J.; Zhao, Y.; Huang, R.-B.; Zheng, L.-S. *Dalton Trans.*, **2012**, 2289.
109. Karimi, B.; Akhavan, P. F. *Inorg. Chem.* **2011**, *50*, 6063.
110. Kroto, H. W.; Heath, J. R.; O'Brien, S. C.; Curl, R. F.; Smalley, R. E. *Nature* **1985**, *318*, 162.
111. Kratschmer, W.; Lamb, L. D.; Fostiropoulos, K.; Huffman, D. R. *Nature* **1990**, *347*, 354.
112. Lu, X.; Akasaka, T.; Nagase, S. *Chem. Commun.* **2011**, *47*, 5942.
113. Balch, A. L.; Olmstead, M. M. *Chem. Rev.* **1998**, *98*, 2123.
114. Haddon, R. C. *Science* **1993**, *261*, 1545.
115. Haddon, R. C. *J. Comp. Chem.* **1998**, *19*, 139.
116. Rao, A. M.; Zhou, Ping.; Wang, Kai-An.; Hager, G. T.; Holden, J. M.; Wang, Ying; Lee, W.-T.; Bi, Xiang-Xin; Ecklund, P. C.; Cornett, D. S.; Duncan, M. A.; Amster, I. J. *Science* **1993**, *259*, 955.
117. Iwasa, Y.; Arima, T.; Fleming, R. M.; Siegrist, T.; Zhou, O.; Haddon, R. C.; Rothberg, L. J.; Lyons, K. B.; Carter, H. L.; Hebard, A. F.; Tycko, R.; Dabbagh, G.; Krajewski, J. J.; Thomas, G. A.; Yagi, T. *Science* **1994**, *264*, 1570.
118. Wang, G. W.; Komatsu, K.; Murata, Y.; Shiro, M. *Nature* **1997**, *387*, 583.
119. Komatsu, K.; Wang, G. W.; Murata, Y.; Tanaka, T.; Fujiwara, K.; Yamamoto, K.; Saunders, M. J. *Org. Chem.* **1998**, *63*, 9358.

120. Liu, B.; Bunker C. E.; Sun, Y. P. *Chem. Commun.* **1996**, *10*, 1241.
121. Nagashima, H.; Nakaoka, A.; Saito, Y.; Kato, M.; Kawanishi, T.; Itoh, K. *J. Chem. Soc., Chem. Commun.* **1992**, 377.
122. Nagashima, H.; Yamaguchi, H.; Kato, Y.; Saito, Y.; Haga, M.; Itoh, K. *Chem. Lett.* **1993**, *23*, 2153.
123. Nagashima, H.; Kato, Y.; Yamaguchi, H.; Kimura, E.; Kawanishi, T.; Kato, M.; Saito, Y.; Haga, M.; Itoh, K. *Chem. Lett.* **1994**, *23*, 1207.
124. Van Wijnkoop, M.; Meidine, M. F.; Avent, A. G.; Darwish, A. D.; Kroto, H. W.; Taylor R.; Walton, D. R. M. *J. Chem. Soc., Dalton Trans.* **1997**, 675.
125. Balch, A. L.; Costa, D. A.; Winkler, K. *J. Am. Chem. Soc.* **1998**, *120*, 9614–9620.
126. Winkler, K.; Noworyta, K.; Kutner, W.; Balch, A. L. *J. Electrochem. Soc.* **2000**, *147*, 2597.
127. Hayashi, A.; De Bettencourt-Dias A.; Winkler K.; Balch, A. L. *J. Mater. Chem.* **2002**, *12*, 2116.
128. Pieta, P.; Grodzka, E.; Winkler, K.; Warczak, M.; Sadkowski, A.; Zukowska, G. Z.; Venukadasula, G. M.; D’Souza, F.; Kutner, W. *J. Phys. Chem. B* **2009**, *113*, 6682.
129. Grodzka, E.; Pieta, P.; Dłużewski, P.; Kutner, W.; Winkler, K. *Electrochimica Acta* **2009**, *54*, 5621.
130. Hayashi, A.; Yamamoto, S.; Suzuki, K.; Matsuoka, T. *J. Mater. Chem.* **2004**, *14*, 2633.
131. Soliman, A. M.; Fortin, D.; Zysman-Colman, E.; Harvey, P. D. *Chem. Commun.* **2012**, *48*, 6271.
132. Wong, W.-Y.; Harvey, P. D. *Macromol. Rapid Commun.* **2010**, *31*, 671.
133. Dexter, D. L.; *J. Chem. Phys.* **1953**, *21*, 836.
134. Soliman, A. M.; Fortin, D.; Zysman-Colman, E.; Harvey, P. D. *Macromol. Rapid Commun.* **2012**, *33*, 522.
135. Clément, S.; Goudreault, T.; Bellows, D.; Fortin, D.; Guyard, L.; Knorr, M.; Harvey, P. D. *Chem. Commun.* **2012**, *48*, 8640.
136. Liu, L.; Fortin, D.; Harvey, P. D. *Inorg. Chem.* **2009**, *48*, 5891.
137. Jiang, F.-L.; Fortin, D.; Harvey, P. D.. *Inorg. Chem.* **2010**, *49*, 2614.
138. Marin, V.; Holder, E.; Hoogenboom, R.; Schubert, U. S. *Chem. Soc. Rev.* **2007**, *36*, 618.
139. Kappaun, S.; Slugovc, C.; List, E. J. W. *Int. J. Mol. Sci.* **2008**, *9*, 1527.
140. Zhao, Q.; Liu, S.-J.; Huang, W. *Macromol. Rapid. Commun.* **2010**, *31*, 794.
141. Sariciftci, N. S.; Smilowitz, L.; Heeger, A. J.; Wudl, F. *Science* **1992**, *258*, 1474.
142. Guo, F.; Kim, Y.-G.; Reynolds, J. R.; Schanze, K. S. *Chem. Commun.* **2006**, *18*, 1887.
143. Wong, W.-Y.; Wang, X. Z.; He, Z.; Chan, K. K.; Djurišić, A. B.; Cheung, K. Y.; Yip, C. T.; Ng, A. M. C.; Xi, Y. Y.; Mak, C. S. K.; Chan, W. K. *J. Am. Chem. Soc.* **2007**, *129*, 14372.
144. Wong, W.-Y.; Wang, X. Z.; He, Z.; Djurišić, A. B.; Yip, C. T.; Cheung, K. Y.; Wang, H.; Mak, C. S. K.; Chan, W. K. *Nat. Mater.* **2007**, *6*, 521.
145. Baek, N. S.; Hau, S. K.; Yip, H.-L.; Acton, O.; Chen, K.-S.; Jen, A. K.-Y. *Chem. Mater.* **2008**, *20*, 5734.
146. Zhan, H.; Lamare, S.; Ng, A.; Kenny, T.; Guernon, H.; Chan, W.-K.; Djurišić, A. B.; Harvey, P. D.; Wong W.-Y. *Macromolecules* **2011**, *44*, 5155.
147. Goudreault, T.; He, Z.; Guo, Y. H.; Ho, C.-L.; Wang, Q.; Zhan, H.; Wang, Q.; Ho, Y.-F. K.; Wong, K.-L.; Fortin, D.; Yao, B.; Xie, Z.; Wang, L.; Kwok, W.-M.; Wong, W.-Y.; Harvey, P. D.; Wong, W.-Y. *Macromolecules* **2010**, *43*, 7936.
148. Schubert, H.; Wesemann L. *Organometallics* **2010**, *29*, 4906.
149. Deiters, E.; Bulach, V.; Hosseini, M. W. *Chem. Commun.* **2005**, *31*, 3906.
150. Braga, D. *Chem. Commun.* **2003**, *22*, 2751.
151. Ladrissi, C.; Romerosa, A.; Saoud, M.; Serrano-Ruiz, M.; Gonsalvi, L.; Peruzzini, M. *Angew. Chem. Int. Ed.* **2005**, *44*, 2568.
152. Mohr, F.; Falvello, L. R.; Laguna, M. *Eur. J. Inorg. Chem.* **2006**, *16*, 3152.
153. Frost, B. J.; Bautista, C. M.; Huang, R.; Shearer, J. *Inorg. Chem.* **2006**, *45*, 3481.
154. Kirillov, A. M.; Wieczorek, S. W.; Lis, A.; Guedes da Silva, M. F. C.; Florek, M.; Król, J.; Staroniewicz, Z.; Smoleński, P.; Pombeiro, A. J. L. *Cryst. Growth Des.* **2011**, *11*, 2711.
155. Kirillov, A. M.; Filipowicz, M.; Guedes da Silva, M. F. C.; Kłak, J.; Smoleński, P.; Pombeiro, A. J. L. *Organometallics* **2012**, *31*, 7921.
156. Serrano-Ruiz, M.; Romerosa, A.; Sierra-Martin, B.; Fernandez-Barbero, A. *Angew. Chem. Int. Ed.* **2008**, *47*, 8665.
157. Odian, G. *Principles of Polymerization*; John Wiley & Sons, Inc.: New York: **2004**.
158. Manners, I. *Synthetic Metal-Containing Polymers*; Wiley-VCH Verlag GmbH: Weinheim, **2004**.
159. Korczagin, I.; Lammertink, R. G. H.; Hempenius, M. A.; Golze, S.; Vancso, G. J. *Adv. Polym. Sci.* **2006**, *200*, 91.
160. Hudson, R. D. A. *J. Organomet. Chem.* **2001**, *637*–639, 47.
161. Masson, G.; Lough, A. J.; Ian Manners, I. *Macromolecules*, **2008**, *41*, 539.

162. Bazan, G. C.; Khosravi, E.; Schrock, R. R.; Feast, W. J.; Gibson, V. C.; Oregan, M. B.; Thomas, J. K.; Davis, W. M. *J. Am. Chem. Soc.* **1990**, *112*, 8378.
163. Tonhauser, C.; Mazurowski, M.; Rehahn, M.; Gallei, M.; Frey, H. *Macromolecules* **2012**, *45*, 3409.
164. Van Staveren, D. R.; Metzler-Nolte, N. *Chem. Rev.* **2004**, *104*, 5931.
165. Top, S.; Vessirés, A.; Leclercq, G.; Quivy, J.; Tang, J.; Vaissermann, J.; Huché, M.; Jaouen, G. *Chem. Eur. J.* **2003**, *9*, 5223.
166. Presa Soto, A.; Chabanne, L.; Zhou, J.; Gilroy, J. B.; Manners, I. *Macromol. Rapid Commun.* **2012**, *33*, 592.
167. Discher, D. E.; Eisenberg, A. *Science* **2002**, *297*, 967.
168. Gohy, J. F. *Advances in Polymer Science*; Springer-Verlag Berlin: Berlin, Vol. 190, **2005**, p 65.
169. Huang, Y.; Duan, X.; Cui, Y.; Lauhon, L. J.; Kim, K. H.; Lieber, C. M. *Science* **2001**, *294*, 1313.
170. Hecht, S. *Angew. Chem., Int. Ed.* **2003**, *42*, 24.
171. Jain, S.; Bates, F. S. *Science* **2003**, *300*, 460.
172. Hu, J.; Liu, G.; Nijkang, G. *J. Am. Chem. Soc.* **2008**, *130*, 3236.
173. Cao, L.; Massey, J. A.; Winnik, M. A.; Manners, I.; Riethmüller, S.; Banhart, F.; Spatz, J. P.; Möller, M. *Adv. Funct. Mater.* **2003**, *13*, 271.
174. Zhulina, E. B.; Adam, M.; LaRue, I.; Sheiko, S. S.; Rubinstein, M. *Macromolecules* **2005**, *38*, 5330.
175. LaRue, I.; Adam, M.; Pitsikalis, M.; Hadjichristidis, N.; Rubinstein, M.; Sheiko, S. S. *Macromolecules* **2006**, *39*, 309.
176. Dean, J. M.; Verghese, N. E.; Pham, H. Q.; Bates, F. S. *Macromolecules* **2003**, *36*, 9267.
177. Hartgerink, J. D.; Beniash, E.; Stupp, S. I. *Science* **2001**, *294*, 1684.
178. Li, Z.; Liu, G. *Langmuir* **2003**, *19*, 10480.
179. Yan, X.; Liu, G.; Haeussler, M.; Tang, B. Z. *Chem. Mater.* **2005**, *17*, 6053.
180. Wang, X.-S.; Wang, H.; Coombs, N.; Winnik, M. A.; Manners, I. *J. Am. Chem. Soc.* **2005**, *127*, 8924.
181. Wang, H.; Wang, X.; Winnik, M. A.; Manners, I. *J. Am. Chem. Soc.* **2008**, *130*, 12921.
182. Dalheimer, P.; Engler, A. J.; Parthasarathy, R.; Discher, D. E. *Biomacromolecules* **2004**, *5*, 1714.
183. Geng, Y.; Dalheimer, P.; Cai, S.; Tsai, R.; Tewari, M.; Minko, T.; Discher, D. E. *Nat. Nanotechnol.* **2007**, *2*, 249.
184. Chen, C.-K.; Lin, S.-C.; Ho, R.-M.; Chiang, Y.-W.; Lotz, B. *Macromolecules* **2010**, *43*, 7752.
185. Mihut, A. M.; Drechsler, M.; Möller, M.; Ballauff, M. *Macromol. Rapid Commun.* **2010**, *31*, 449.
186. Massey, J. A.; Winnik, M. A.; Manners, I.; Chan, V. Z. H.; Ostermann, J. M.; Enchelmaier, R.; Spatz, J. P.; Möller, M. *J. Am. Chem. Soc.* **2001**, *123*, 3147.
187. Park, D. H.; Hong, Y. K.; Cho, E. H.; Kim, M. S.; Kim, D.-C.; Bang, J.; Kim, J.; Joo, J. *ACS Nano* **2010**, *4*, 5155.
188. Manners, I. *Angew. Chem. Int. Ed.* **2007**, *46*, 1565.
189. Metera, K. L.; Sleiman, H. *Macromolecules* **2007**, *40*, 3733.
190. Miinea, L. A.; Sessions, L. B.; Ericson, K. D.; Glueck, D. S.; Grubbs, R. B. *Macromolecules* **2004**, *37*, 8967.
191. Bignozzi, C. A.; Ferri, V.; Scoponi, M. *Macromol. Chem. Phys.* **2003**, *204*, 1851.
192. Cheng, K. W.; Chan, W. K. *Langmuir* **2005**, *21*, 5247.
193. Qin, Y.; Cui, C.; Jäkle, F. *Macromolecules* **2008**, *41*, 2972.
194. Peckham, T. J.; Massey, J. A.; Honeyman, C. H.; Manners, I. *Macromolecules* **1999**, *32*, 2830.
195. Noonan, K. J. T.; Gates, D. P. *Angew. Chem. Int. Ed.* **2006**, *45*, 7271.
196. Qin, Y.; Sukul, V.; Pagakos, D.; Cui, C.; Jäkle, F. *Macromolecules* **2005**, *38*, 8987.
197. Rider, D. A.; Cavicchi, K. A.; Power-Billard, K. N.; Russell, T. P.; Manners, I. *Macromolecules* **2005**, *38*, 6931.
198. Chen, T.; Wang, L.; Jiang, G.; Wang, J.; Wang, X. J.; Zhou, J.; Wang, W.; Gao, H. *Polymer* **2005**, *46*, 7585.
199. He, F.; Gädt, T.; Manners, I.; Winnik, M. A. *J. Am. Chem. Soc.* **2011**, *133*, 9095.
200. Zhai, S.; Shang, J.; Yang, D.; Wang, S.; Hu, J.; Lu, G.; Huang, X. *J. Pol. Sci. A Polym. Chem.* **2012**, *50*, 811.
201. Hamley, I. W. *Angew. Chem. Int. Ed.* **2003**, *42*, 1692.
202. Lazzari, M.; Lopez-Quintela, M. A. *Adv. Mater.* **2003**, *15*, 1583.
203. Zhang, J.; Wang, Z.-L.; Liu, J.; Chen, S.; Liu, G.-Y. *Self-Assembled Nanostructures*; Kluwer Academic/Plenum Publishers: New York, **2003**.
204. Ahmed, R.; Patra, S. K.; Chabanne, L.; Faul, C. F. J.; Manners, I. *Macromolecules*, **2011**, *44*, 9324.
205. Sheats, J. E.; Rausch, M. D. *J. Org. Chem.* **1970**, *35*, 3245.
206. Sheats, J. E.; Carraher, J. C. E.; Pittman, J. C. P.; Zeldin, M.; Currell, B. *Inorganic and Metal-Containing Polymeric Materials*; Plenum: New York, **1985**.

207. Peckham, T. J.; Gómez-Elipe, P.; Manners, I. In *Metallocenes. Synthesis, Reactivity, Applications*; Togni, A.; Halterman, R. L. Eds. Wiley-VCH Verlag GmbH: Weinheim, **1998**; p. 723.
208. Astruc, D.; Ornelas, C.; Ruiz, J. *Acc. Chem. Res.* **2008**, *41*, 841.
209. Ornelas, C.; Ruiz, J.; Astruc, D. *Organometallics* **2009**, *28*, 2716.
210. Casado, C. M.; Gonzalez, B.; Cuadrado, I.; Alonso, B.; Moran, M.; Losada, J. *Angew. Chem., Int. Ed.* **2000**, *39*, 2135.
211. Bunz, U. H. F. *Top. Curr. Chem.* **1999**, *201*, 131.
212. Carraher, C. E. Jr.; Sheats, J. E. *Makromol. Chem.* **1973**, *166*, 23.
213. Pittman, C. U. Jr.; Ayers, O. E.; Suryanarayanan, B.; McManus, S. P.; Sheats, J. E. *Makromol. Chem.* **1974**, *175*, 1427.
214. Mayer, U. F. J.; Gilroy, J. B.; O'Hare, D.; Manners, I. *J. Am. Chem. Soc.* **2009**, *131*, 10382.
215. Ren, L.; Hardy, C. G.; Tang, C. *J. Am. Chem. Soc.* **2010**, *132*, 8874.
216. Chen, D.; Feng, H.; and Li, J. *Chem. Rev.* **2012**, *112*, 6027.
217. Niyogi, S.; Hamon, M. A.; Hu, H.; Zhao, B.; Bhowmik, P.; Sen, R.; Itkis, M. E.; Haddon, R. C. *Acc. Chem. Res.* **2002**, *35*, 1105.
218. Tasis, D.; Tagmatarchis, N.; Bianco, A.; Prato, M. *Chem. Rev.* **2006**, *106*, 1105.
219. Kiang, C.-H.; Choi, J.-S.; Tran, T. T.; Bacher, A. D. *J. Phys. Chem. B* **1999**, *103*, 7449.
220. Govindaraj, A.; Satishkumar, B. C.; Nath, M.; Rao, C. N. R. *Chem. Mater.* **2000**, *12*, 202.
221. Liu, S.; Zhu, J.; Mastai, Y.; Felner, I.; Gedanken A. *Chem. Mater.* **2000**, *12*, 2205.
222. Mittal, J.; Monthoux, M.; Allouche, H.; Stephan, O. *Chem. Phys. Lett.* **2001**, *339*, 311.
223. Thamavaranukup , N.; Hoppe, H. A.; Ruiz-Gonzalez, L.; Costa, P. M. F. J.; Sloan, J.; Kirkland, A.; Green, M. L. H. *Chem. Commun.* **2004**, 1686.
224. Li, L.-J.; Khlobystov, A. N.; Wiltshire, J. G.; Briggs, G. A. D.; Nicholas, R. J. *Nat. Mater.* **2005**, *4*, 481.
225. Kalinina I.; Bekyarova, E.; Sarkar, S.; Wang, F.; Itkis, M. E.; Tian, X.; Niyogi, S.; Jha, N.; Haddon, R. C. *Macromol. Chem. Phys.* **2012**, *213*, 1001.
226. Alonso, B.; González, B.; García, B.; Ramírez-Oliva, E.; Zamora, M.; Casado, C. M.; Cuadrado, I. *J. Organomet. Chem.* **2001**, *637–639*, 642.
227. Zamora, M.; Bruña, S.; Alonso, B.; Cuadrado, I. *Macromolecules* **2011**, *44*, 7994.
228. Gilroy, J. B.; Patra, S. K.; Mitchels, J. M.; Winnik, M. A.; Manners, I. *Angew. Chem. Int. Ed.* **2011**, *50*, 5851.
229. Zeng, X.; Zhang, T.; Qin, Y.; Wei, Z.; Luo, M.; *Dalton Trans.*, **2009**, 8341.



---

# 30

---

## FROM SERENDIPITY TO POROSITY: SYNTHESIS AND REACTIVITY OF COORDINATION POLYMERS BASED ON COPPER TRINUCLEAR TRIANGULAR MOTIFS

LUCIANO PANDOLFO

*Department of Chemical Sciences, University of Padova, Padova, Italy*

### 30.1 INTRODUCTION

In the word “serendipity,” some kind of magic is contained, as it approximately indicates the obtaining of an unexpected result, different from what we were searching for, that is more important with respect to the original target.

Even though in serendipity the concept of the unexpected is implicit, this does not mean *a priori* unforeseeable. If something happened, often it should be foreseeable, provided that we had considered different data instead of those we had taken into account. Obviously, our previous experiences, information, and knowledge drive us to prefer some data as the most important while, due to laziness, fossilized habits, etc., we disregard other data. Not complete information, in some cases unconsciously assembled in a not suitable way, may lead to expect some specific results that, instead, are not obtained.

The concept of serendipity, meaning a “happy accident” may be applied to every good result achieved without one’s looking for it. The discovery of a new continent, America, by Columbus, which happened while searching for a new route for Asia, is certainly one of the greatest cases of serendipity, even though Columbus was not aware of this unexpected result. Moreover, this discovery was serendipitous twice, because if America had not existed, it would have been almost certainly impossible for Columbus’s ships to have reached Asia.

Serendipity is particularly important in scientific research, because it is through the development of unexpected results that relevant advances in science can be pursued, as the discovery of the properties of penicillin clearly evidences. Carrying the concept to the extreme, if researchers knew exactly what is going to happen from their experiments, they would not need to research but only to verify, with very different approaches and results, according to Albert Einstein, “*If we knew what it was we were doing, it would not be called research, would it?*” A new discovery is substantially different from the experimental validation of a theory.

Obviously, new serendipitous discoveries then need further experimental validations to become a general theory and to be universally useful. The first time a new result is obtained is very often by chance, but any unexpected, interesting result must be deeply studied and exploited. Serendipity is thus a very important issue but it is not enough if the results that it produces are not developed and utilized at the best. As stated by Louis Pasteur, “*Dans les champs de l’observation le hasard ne favorise que les esprits préparés*” [1].

The words “unexpected,” “surprising,” or “unusual” can be found in numerous scientific articles (mainly in the titles), conference lectures, or poster presentations and they are normally employed to emphasize the novelty of the reported

data. Nevertheless, numerous researchers are ashamed to declare that the results they are reporting have been obtained serendipitously and not by following a specifically designed procedure, because this seems to suggest the absence of a serious study that should have been carried out before the experiment. Here the author would like to reappraise the relevance of the results obtained serendipitously. In particular, the author reports how serendipity was a relevant issue and, to some extent, drove his specific researches in the last years in the field of coordination polymers (CPs). For the inspiration of this note, the author is largely indebted to R.E.P. Winpenny [2] for his article where he highlights some advantages of the serendipitous assembly of polynuclear cage compounds with respect to the “designed assembly.”

### 30.2 COORDINATION POLYMERS

CPs, sometimes referred to as *metal–organic frameworks* (MOFs) [3], represent one of the most interesting class of hybrid (organic–inorganic) materials [4]. These crystalline compounds are characterized by peculiar polymeric structures that can be envisaged as the product of a rigorously regular copolymerization, where metal ions (or small assemblies of metal ions)—*nodes*—are joined through polytopic organic ligands—*linkers*. Depending both on the coordination geometries of the metals and the ligands structural features, CPs in 1-, 2-, or 3-dimensional scale can be obtained (Fig. 30.1).

Polytopic ligands mainly contribute to define the connectivity between the nodes, generating repetitive entities also referred to as *secondary building units* (SBUs) [5] that form the extended structures of CPs.

CPs can have interesting properties connected to their structures, such as porosity (with regular pores sizes), that may produce high surface area, sorption–desorption behavior of energetically or environmentally important gases, heterogeneous catalysis ability, etc. The porosity of CPs is mainly related to the rigidity of the linkers and to their specific structures [6], particularly to the structural characteristics of the spacer, that is, the fragment connecting the specific donor groups joining the metal centers. In Fig. 30.2, one possible structure of a 3D CP is sketched, where donor groups (D) and the spacer (S) are evidenced in the linkers, and the nodes M adopt an octahedral coordination geometry.

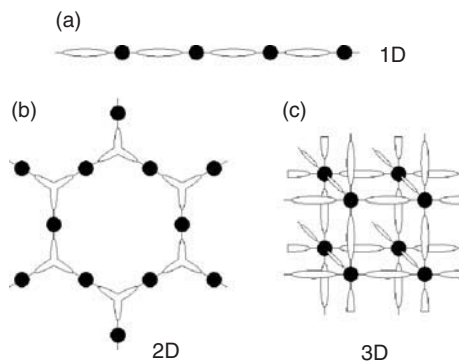


**Figure 30.1** Schematic examples of possible (a) 1D, (b) 2D, and (c) 3D CP architectures. Nodes are indicated as black spheres, while linkers are in white.

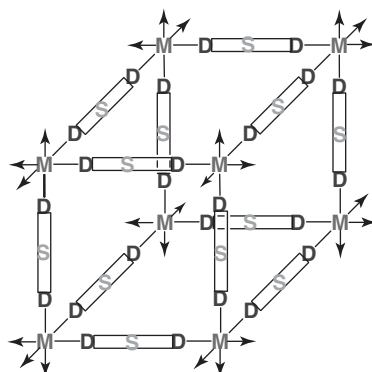


**Figure 30.2** Scheme of a 3D CP architecture where the octahedral metal nodes (M) are joined by ditopic linkers. The specific donor groups (D) and the spacer fragment (S) are evidenced.

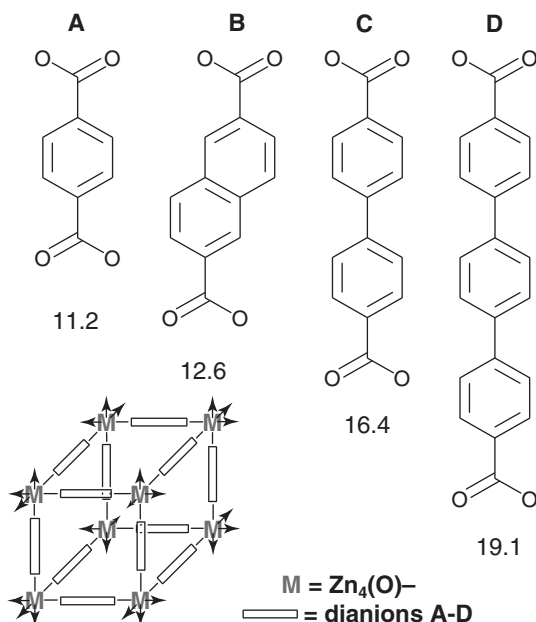


**Figure 30.3** Schematization of the IRMOFs obtained by Yaghi group [7] by connecting Zn<sub>4</sub>(O) with rigid dianions A–D. The number below each dianion indicates the size of the cubic structure sketched in the left, calculated as the diameter (in angstrom) of a sphere that can fit in it.

In numerous works on CPs that appeared in the last years, the so-called designed synthesis has been often claimed to be employed in order to obtain interesting derivatives, even though the author thinks that in some cases the word “serendipitous” should be more appropriate and not shameful. On the other hand, a very elegant example of a “true” designed synthesis was pursued by Yaghi and coworkers [7], which obtained a series of iso-reticular metal–organic frameworks (IRMOFs). Actually, the Yaghi group, exploiting the octahedral geometry of basic copper acetate, [Zn<sub>4</sub>(O)(MeCOO)<sub>6</sub>], connected the Zn<sub>4</sub>(O) moieties (M) through different bicarboxylates OOC-(S)-COO where (S) is a rigid spacer group, synthesizing a series of porous IRMOF, which differ only in the dimensions of the spacers placed between the two carboxylates groups.

The IRMOFs [Zn<sub>4</sub>O(OOC-(S)-COO)<sub>3</sub>] thus obtained all have the same primitive cubic structure sketched in Fig. 30.3, with three series of identical perpendicular channels whose free diameters are directly related to the dimensions of the spacers, provided that no interpenetration occurred [7]. This was certainly one of the best results in the designed synthesis of MOFs, evidencing the value of the researcher’s imagination, pursued with the aim to obtain a series of derivatives having structural properties directly related to the dimensions of the spacers used.

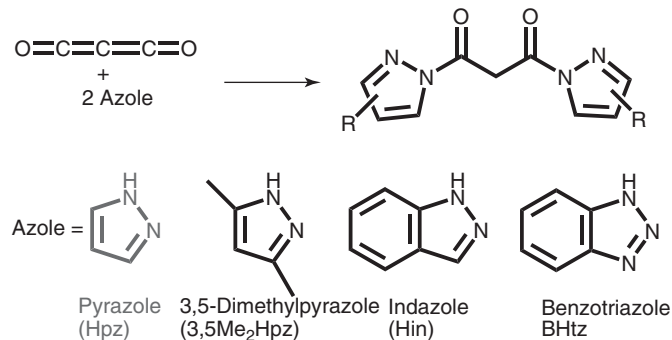
On the other hand, it is often useful to overcome also the researcher’s imagination and, according to Winpenny, “... design assembly approach (...) relies on a limited range of experience and on the imagination of the scientists involved.” [2], rely also on serendipity.

### 30.3 TRINUCLEAR TRIANGULAR Cu<sup>II</sup> MOIETIES TO BUILD CPS

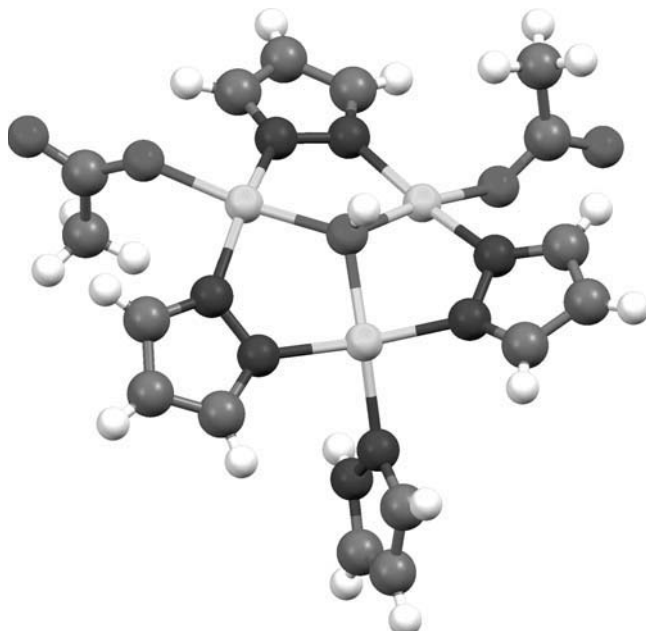
#### 30.3.1 Serendipitous Synthesis and Reactivity

As far as the author’s specific work in the CPs field is concerned, it certainly started from a serendipitous event, when, working with carbon suboxide, C<sub>3</sub>O<sub>2</sub>, he easily synthesized a series of diamidic derivatives, all having the malonate core and some azolate as the amidic moieties (Scheme 30.1), with the aim to use them as ligands, analogously to other extensively used azolate derivatives [8].

The malonyl diamides, easily obtained in good yields, are quite stable and, in some cases, it was possible to obtain their single-crystal (SC) X-ray diffraction (XRD) characterizations that were afterward reported [9]. To quickly check the possibility of these derivatives to act as ligands, the author treated an ethanol solution of the just-isolated Hpz-based diamide



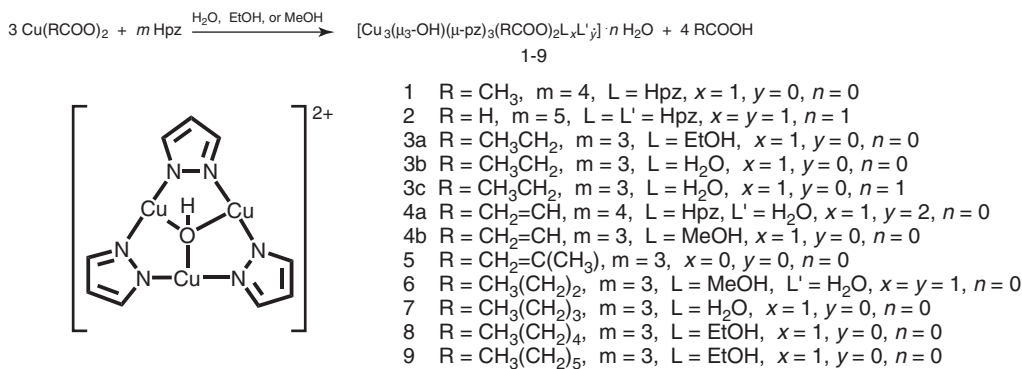
Scheme 30.1



**Figure 30.4** Ball-and-stick representation of the asymmetric unit of **1**. Color codes: light gray (Cu), dark gray (O), black (N), gray (C), and white (H).

with a water solution of copper(II) acetate that he happened to have on his work bench. The solution immediately turned deep blue, indicating that the coordination of some kind of nitrogen to copper(II) had occurred and, after some days, a few deep-blue hexagonal platelets formed. Owing to the scarcity of the obtained product, only an SC-XRD determination was carried out on the crystals, yielding a completely unexpected result. Instead of some kind of copper derivative of the malonyl diamide, the structure of the trinuclear triangular assembly  $[\text{Cu}_3(\mu_3\text{-OH})(\mu\text{-pz})_3(\text{MeCOO})_2(\text{Hpz})]$ , **1**, shown in Fig. 30.4, was found.

This synthesis was certainly serendipitous. In the presence of water,  $\text{Cu}^{\text{II}}$ , and acetate ions, the quite stable diamide underwent hydrolysis forming Hpz that generated the observed trinuclear triangular derivative through a series of nontrivial processes. First of all, we ascertained that it was possible to obtain compound **1** in a quantitative yield by directly reacting a water solution of copper acetate with Hpz [10]. Moreover, continuing the studies, we realized that serendipity worked hard in this reaction. As a matter of fact, the trinuclear triangular assembly was obtained thanks to the fact that copper(II) acetate instead of copper chloride, nitrate, or sulfate had on hand. Actually, the basicity of the acetate ions is needed to favor the deprotonation of pyrazole and water to form pyrazolates and the capping  $\mu_3\text{-OH}$ , respectively. This point was further confirmed by the obtaining of analogous trinuclear triangular derivatives by employing copper formate, propionate, and butyrate [11], while the reaction failed when copper trifluoroacetate was used [10], the basicity of the  $\text{CF}_3\text{COO}^-$  anion

**Scheme 30.2**

being too low. In this case, only the mononuclear  $[\text{Cu}(\text{CF}_3\text{COO})_2(\text{Hpz})_2]$  complex was produced, which self-assembled into a 1D CP. Another serendipitous event was the use of Hpz-derived amide, instead of any other, because it was found that the trinuclear assembly forms only with pyrazole, while, in absence of an exogenous base, the other azoles yield exclusively mono or dinuclear azole (not azolate) derivatives.

In any case, by treating a large number of Cu<sup>II</sup> carboxylates with Hpz in water or wet alcohols, the dicationic trinuclear triangular Cu<sup>II</sup> moiety,  $[\text{Cu}_3(\mu_3-\text{OH})(\mu-\text{pz})_3]^{2+}$ , whose charge is balanced by two carboxylate ions, was obtained quite easily, according to the reaction Scheme 30.2 [10–14]. Moreover, owing to the large number of coordination modes of COO<sup>-</sup> groups (monodentate, chelate, bridging *syn-syn* or *syn-anti*, etc.), the carboxylates are responsible for the further self-assembly of the trinuclear fragments (SBUs), leading to the formation of a series of structurally different CPs [11, 12, 14], two of which are sketched in Fig. 30.5.

As far as compounds **3a**–**3c** are concerned, again serendipity, or simply accidental events, led to the obtaining of three derivatives having slightly different formulations (and slightly different molecular structures too), as shown in Fig. 30.6. Compounds  $[\text{Cu}_3(\mu_3-\text{OH})(\mu-\text{pz})_3(\text{EtCOO})_2(\text{EtOH})]$ , **3a** [11],  $[\text{Cu}_3(\mu_3-\text{OH})(\mu-\text{pz})_3(\text{EtCOO})_2(\text{H}_2\text{O})]$ , **3b** [12], and  $[\text{Cu}_3(\mu_3-\text{OH})(\mu-\text{pz})_3(\text{EtCOO})_2(\text{H}_2\text{O})]\cdot\text{H}_2\text{O}$ , **3c** [12], were obtained by using almost identical synthetic protocols. The only difference was the use of EtOH as solvent for **3a**, while water was employed for **3b** and **3c**. Moreover, the crystallization of **3a** and **3b** was performed at circa 20 °C, while **3c** crystallized around 12 °C.

In spite of these small structural differences, shown in Fig. 30.6, and generated by slightly different reaction conditions, the three derivatives self-assemble in very different networks, as sketched in Fig. 30.7.

Compound **3a** [11] forms a 1D CP through two different carboxylate bridges, while **3b** and **3c** [12] generate different supramolecular networks thanks to H-bonds involving carboxylate oxygen, capping OH, and water. Particularly, in the case of **3c**, the crystallization water molecules are involved in a series of H-bonds that generate two spiraliform chains with

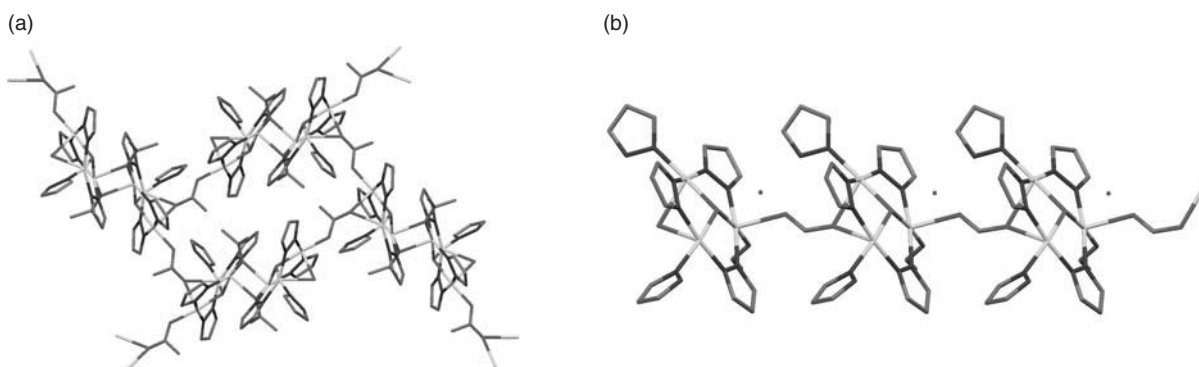


**Figure 30.5** Two CPs based on the trinuclear triangular  $[\text{Cu}_3(\mu_3-\text{OH})(\mu-\text{pz})_3]$  SBU. The 2D CP assembly of compound **1** (a) and the 1D CP from the assembly of  $[\text{Cu}_3(\mu_3-\text{OH})(\mu-\text{pz})_3(\text{HCOO})_2(\text{Hpz})_2]\cdot\text{H}_2\text{O}$ , **2** (b).

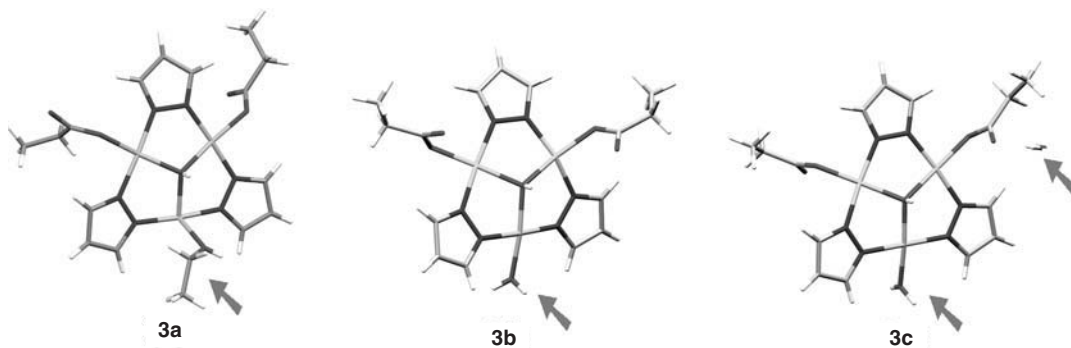


**Figure 30.6** Arbitrary views of the molecular structures of compounds **3a**–**3c**. The arrows evidence the slight differences among these compounds, that is, the coordination of EtOH in **3a**, while H<sub>2</sub>O coordinates in **3b** and **3c**. In **3c**, a molecule of crystallization water is also present.

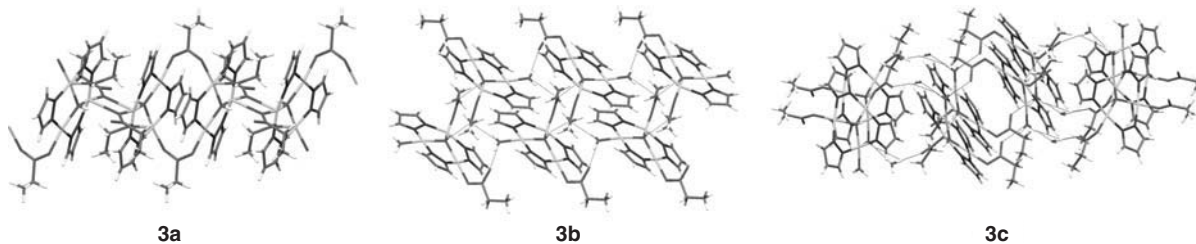


**Figure 30.7** Different self-assembling of compounds **3a**–**3c** generating, from left to right, a 1D CP and two different supramolecular assemblies.

opposite chiralities. These data highlight the difficulty to forecast, at least in the field of CPs, the results of the self-assembly of only slightly different SBUs.

On the other hand, the trinuclear [Cu<sub>3</sub>(μ<sub>3</sub>-OH)(μ-pz)<sub>3</sub>]<sup>2+</sup> assembly appears to be quite stable, remaining intact (in moderate to good entity) even when the above mentioned CPs were treated with strong acids, giving rise, in some cases, to CPs where the trinuclear fragments act as SBUs joined together by inorganic anions such as Cl<sup>−</sup> [15], SO<sub>4</sub><sup>2−</sup>, NO<sub>3</sub><sup>−</sup>, or weakly basic organic anions such as triflate or trifluoroacetate [16]. In particular, in the reaction of **1** with aqueous HCl, it was possible to isolate a CP, **10**, with permanent, star-shaped channels, as shown in Fig. 30.8, having an effective free pore diameter of circa 4.2 Å and accounting for circa 9% of free volume.

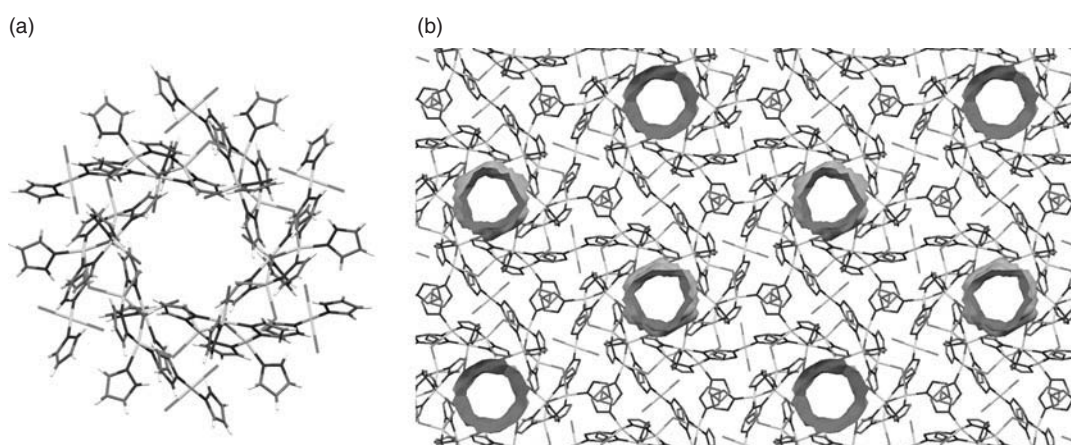


**Figure 30.8** Capped-stick view of one star-shaped pore formed by self-assembling of [{Cu<sub>3</sub>(μ<sub>3</sub>-OH)(μ-pz)<sub>3</sub>(Cl)<sub>2</sub>(Hpz)<sub>2</sub>(H<sub>2</sub>O)}<sub>2</sub>{CuCl<sub>2</sub>(Hpz)<sub>2</sub>}], **10**, (a) and its crystal packing (b) where the inner surfaces of channels are evidenced in black.

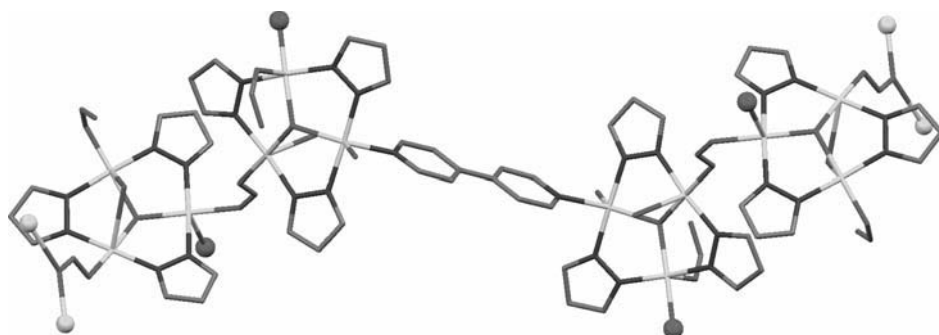


**Figure 30.9** Capped-stick representation of CP **11**. H atoms and crystallization water molecules have been omitted for sake of clarity. Balls indicate the connections leading to a 3D CP.

The stability of the trinuclear assembly was further exploited in the reaction of compound **2** with 4,4'-bipyridine (bpy), to exchange co-ordinate pyrazole with this ditopic ligand, with the aim to obtain porous coordination polymers (PCPs) thanks to the length and the rigidity of bpy, possibly bridging different trinuclear units. Once again we get one unexpected result. Actually, by treating compound **2** with bpy in MeOH in an almost equimolecular ratio, it was possible to crystallize the CP **11**,  $\{[\{\text{Cu}_3(\mu_3\text{-OH})(\mu\text{-pz})_3(\text{HCOO})_2(\text{H}_2\text{O})\} \cdot [\text{Cu}_3(\mu_3\text{-OH})(\mu\text{-pz})_3(\text{HCOO})_2(\text{H}_2\text{O})_2]\}_2 \cdot (\mu\text{-bpy})\} \cdot 6\text{H}_2\text{O}$ , which is schematically drawn in Fig. 30.9 [17]. Owing to the large number of formate connections, a 3D CP was obtained.

When compound **2** was instead treated with a large excess of bpy, besides Hpz molecules, one formate ion was also removed and exchanged with an OH<sup>-</sup> ion, likely coming from adventitious water. Two bpy molecules join two trinuclear fragments yielding the hexanuclear complex  $\{[\{\text{Cu}_3(\mu_3\text{-OH})(\mu\text{-pz})_3(\text{HCOO})(\text{H}_2\text{O})(\mu\text{-bpy})\} \cdot (\text{bpy})_2\} \cdot (\text{OH})_2\} \cdot (\text{bpy})$ , **12**, and a crystallization bpy molecule is also present [17].

The latter bpy molecule, evidenced in Fig. 30.10, plays a particular role in the crystal packing of **12**. Actually, the hexanuclear compound self-assembles, generating the supramolecular structure shown in Fig. 30.11.

Compound **12** does not generate a CP, nevertheless it packs, forming a porous supramolecular network sustained only by noncovalent interactions. The excess of bpy employed in the synthesis very likely plays a templating role in the crystal

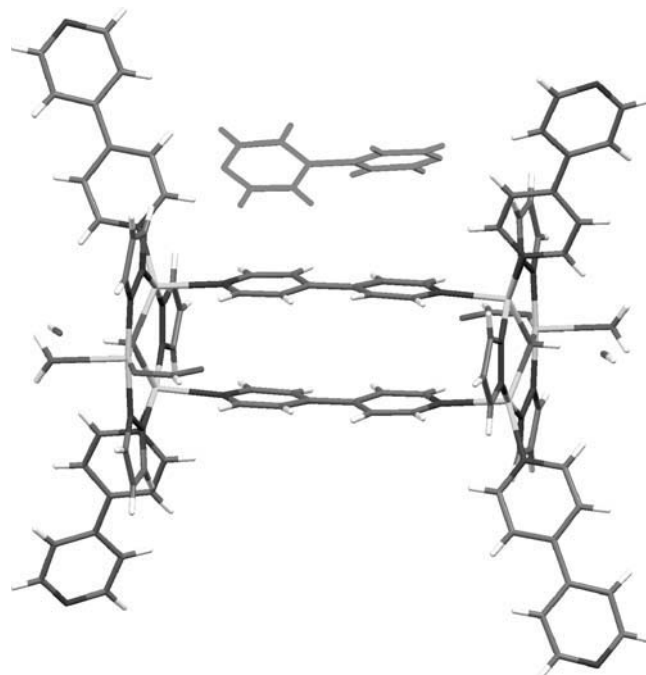


**Figure 30.10** Arbitrary capped-stick view of compound **12**. The crystallization bpy molecule is evidenced in light gray.

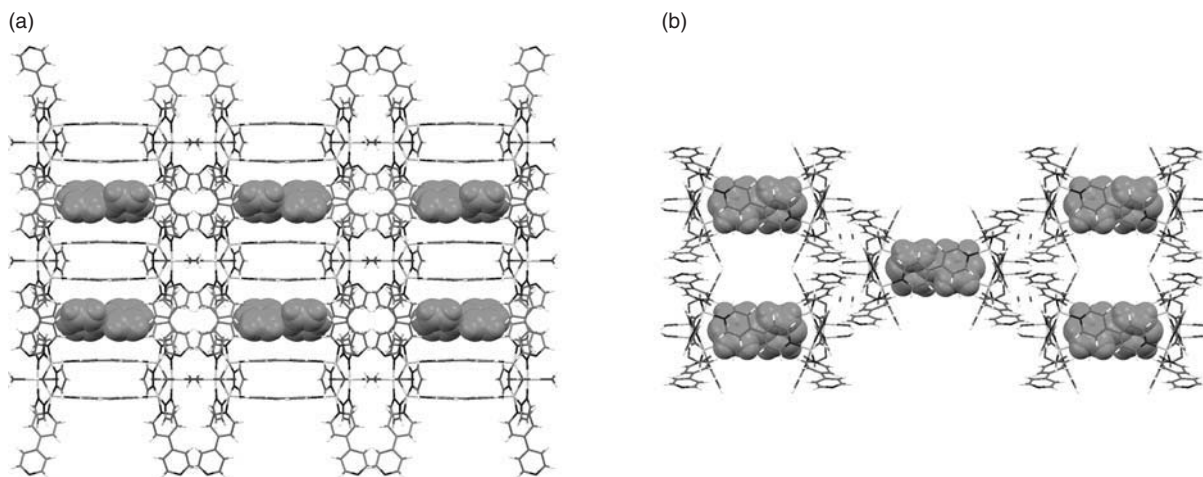


**Figure 30.11** View down the crystallographic *b*- (a) and *c*- (b) axes of the crystal packing of **12**. Crystallization bpy molecules are evidenced by a space-fill representation.

packing, particularly in the formation of one of the two kinds of channels present in the structure and contributes to the stability of the supramolecular network. Guest bpy molecules almost completely occupy the channels running parallel to the crystallographic *b*-axis (Fig. 30.11a), while the channels parallel to the *c*-axis (Fig. 30.11b) are empty, accounting for circa 23% of free volume. Unfortunately, attempts to eliminate guest bpy molecules by heating compound **12** under vacuum lead to the destruction of the crystal structure, thus indicating the importance of bpy in the sustainment of the structure itself. Analogous results were obtained when **12** was dissolved in MeOH and only different, nonporous derivatives crystallized from the solution. On the contrary, if crystals of **12** are soaked in benzene, toluene, or *c*-hexane, in which they are insoluble, guest bpy molecules pass into solution and some disordered solvent(s) molecules occupy the intersection of the two different channels. In this SC-to-SC process, the structures and cell parameters of soaked crystals remain almost identical to those of **12** [17], as shown in Fig. 30.12, in which the different localizations of the solvent with respect to the previously present guest bpy are evidenced.

Interestingly, by treating compound **1**,  $[\text{Cu}_3(\mu_3\text{-OH})(\mu\text{-pz})_3(\text{MeCOO})_2(\text{Hpz})]$ , which, besides having acetate instead of formate ions, differs from **2** by ancillary ligands, crystallization water, and by a very different self-assembled CP structure, with a large excess of bpy, a porous compound very similar to **12** was obtained. This compound, containing guest bpy

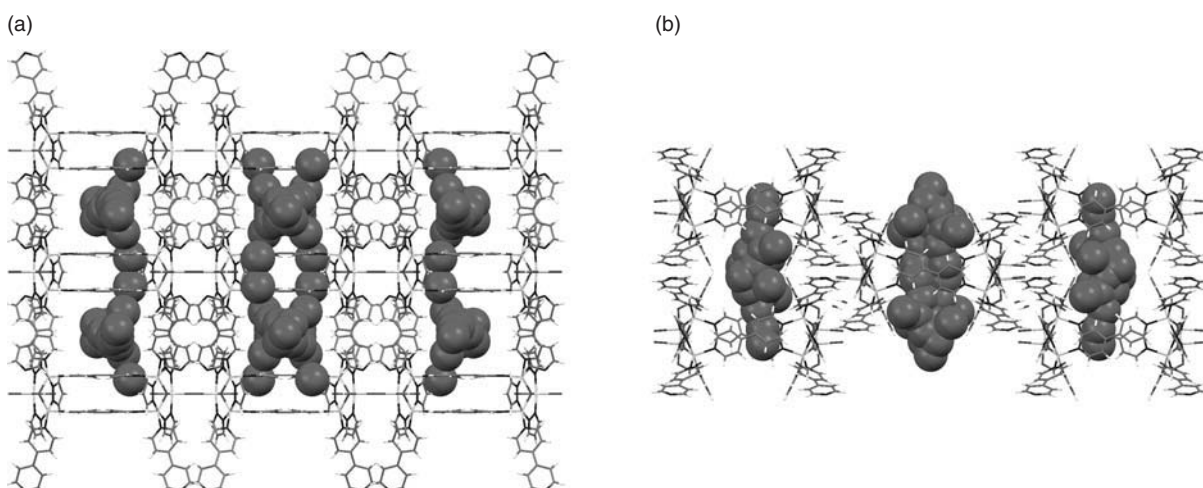


**Figure 30.12** View down the crystallographic *b*- (a) and *c*- (b) axes of the crystal packing of **12** after soaking in benzene. Disordered benzene molecules are evidenced by a space-fill representation.

and having the crystal structure, packing and cell dimensions almost identical to those of **12** [18], is a good example of “designed assembly,” but only after serendipity has done its work.

On the basis of the relevant stability of the trinuclear triangular  $[\text{Cu}_3(\mu_3\text{-OH})(\mu\text{-pz})_3]$  moiety, we decided to test the behavior of copper(II) bicarboxylates in the reaction with pyrazole, by employing fthalate, fumarate, 2-methylfumarate, and succinate ions. Numerous reactions were carried out, in different conditions (room temperature, reflux, solvothermal), with different solvents (water, MeOH, EtOH, DCM), and starting from different reagents (copper bicarboxylates and Hpz or Napz, copper nitrate and bicarboxylic acid and Hpz, copper nitrate and sodium bicarboxylate and Hpz, etc.). From these reactions, the only result that can be confidently stated is that the trinuclear triangular copper pyrazolate assembly is almost always preferred, if the geometry of the bicarboxylate allows it, with respect to the mononuclear copper pyrazole systems. In fact, when the ortho geometry of the fthalate ion hampers the possibility to generate trinuclear triangular pyrazolate assemblies, only 1D or 2D CPs based on the  $\text{Cu}(\text{phthalate})(\text{Hpz})_x$  SBUs have been obtained [19]. On the contrary, by using the other aforementioned rigid and flexible carboxylates, the trinuclear  $[\text{Cu}_3(\mu_3\text{-OH})(\mu\text{-pz})_3]$  moieties were instead obtained. Nevertheless, their strongly different (self)-assemblies resulted being largely dependent not only on the bicarboxylate employed but also mainly on the reaction conditions, even though some analogies were found.

As an example, by reacting copper fumarate and copper 2-methylfumarate with pyrazole in solvothermal conditions, two isomorphous derivatives based on the  $[\text{Cu}_3(\mu_3\text{-OH})(\mu\text{-pz})_3]$  moiety (see Fig. 30.13) were isolated. Moreover, both compounds self-assemble forming 1D waved CPs that further interconnect, generating almost identical 2D sheets [20].

On the other hand, when the reaction of copper 2-methylfumarate was carried out at room temperature, the most abundant product was the mononuclear complex  $[\text{Cu}(\text{MeFum})(\text{Hpz})_2(\text{H}_2\text{O})]\cdot(\text{H}_2\text{O})$  (MeFum = 2-methylfumarate dianion), which self-assembles to yield a 1D CP; we were unable to obtain any crystalline derivative by using copper fumarate in the same conditions [20].

In the reaction involving succinate ions, owing to the very scarce solubility of copper succinate, numerous different procedures were tried, giving different results. Actually, five different derivatives were obtained and we were unable to satisfactorily characterize some other compounds [21]. As a matter of fact, we obtained three different 3D CPs, all based on the  $[\text{Cu}_3(\mu_3\text{-OH})(\mu\text{-pz})_3(\text{Suc})]$  (Suc = succinate dianion) and differing for some small molecules (as water and Hpz) coordinated and/or present in the lattice. On the other hand, these very small differences produce largely different self-assemblies, almost impossible to forecast on the basis of the different reaction conditions, with a behavior analogous to that observed with compounds **3a–3c**. Particularly, in one case, a PCP, with channels accounting for a 31% of vacuum space was obtained [21]. Moreover, a 1D CP based on the  $[\text{Cu}(\text{Suc})(\text{Hpz})_2]$  SBU and the mononuclear  $[\text{Cu}(\text{HSuc})_2(\text{Hpz})_4]$  complex were also obtained [21].

It is noteworthy that most of the obtained trinuclear derivatives are active as catalysts (or catalyst precursors) in the mild peroxidative oxidation of cycloalkanes with  $\text{H}_2\text{O}_2$  in MeCN/water [12–14, 17]. Particularly, the compounds reported in Scheme 30.2, as well as compounds **11** and **12**, convert cyclohexane to cyclohexanol and cyclohexanone [22] with total yields ranging from 25% to 35%, values quite relevant for this kind of reaction and comparable to those found by using other valuable catalysts [23].

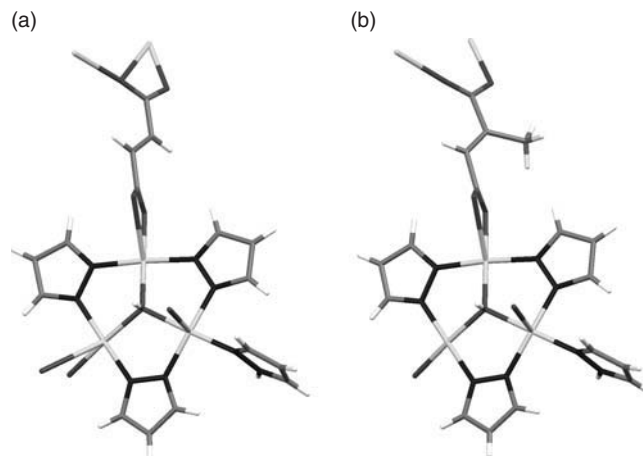


**Figure 30.13** Trinuclear triangular derivatives  $[\text{Cu}_3(\mu_3\text{-OH})(\mu\text{-pz})_3(\text{Fum})(\text{Hpz})]$  (a) and  $[\text{Cu}_3(\mu_3\text{-OH})(\mu\text{-pz})_3(\text{MeFum})(\text{Hpz})]$  (b) (Fum and MeFum = fumarate and 2-methylfumarate dianions, respectively).

### 30.4 Cu(pz)<sub>2</sub>-BASED COORDINATION POLYMERS. A CASE OF “POROSITY WITHOUT PORES”

A further relevant serendipitous event that the author encountered during his researches in the Cu<sup>II</sup> CPs field, happened when the reaction between Cu(MeCOO)<sub>2</sub>·(H<sub>2</sub>O) and Hpz (Cu : Hpz = 1 : 2) was performed in MeCN, instead of using protic solvents as water or alcohols. The stirred solution immediately became deep blue, followed, in a few seconds, by the formation of a pale-pink solid, while the solution became colorless. The solid analyzed well for [Cu(pz)<sub>2</sub>]·H<sub>2</sub>O, **13**, and acetic acid was the sole compound present in the mother liquors. Even though only microcrystalline powder formed, it was possible to obtain a molecular structure of this compound by an XRPD determination coupled with *ab initio* calculations [24].

As shown in Fig. 30.14, a 1D CP is formed, where copper(II) ions are bridged by pz<sup>-</sup> ions, according to a square planar coordination. Crystallization water molecules are quite far from the square plane (circa 2.9 Å), forming a very elongated octahedron. The compound crystallizes in the *Cmcm* space group and the crystal packing reveals that no porosity is present. As usual, we tried to eliminate crystallization water from **13** with the aim to obtain a porous solid and we succeeded in the obtaining the beige anhydrous species [Cu(pz)<sub>2</sub>], **14**, by heating **13** at circa 90 °C under moderate vacuum. Analogously to **13**, the structure was determined from the XRPD data [24], revealing that compound **14** is also a linear CP, where Cu<sup>II</sup> ions maintain the square planar coordination. Its molecular structure is almost identical to that of compound **13**, excluding crystallization water, as shown in Fig. 30.15 [25], but it crystallizes in the space group *P21/m*.

Furthermore, compound **14** is not porous but it quickly adsorbs water, even from the air, transforming into **13**, and the sorption–desorption process can be repeated indefinitely without any decomposition, in a reversible crystal-to-crystal process.

Taking a look at the space-fill models in Fig. 30.16, it is possible to find that, in compound **13**, water is accommodated in cavities that are not present in **14** and which are formed contextually to the water adsorption. This is likely a dynamic process involving the host (**14**) and the guest (water), whereby both cooperate to create holes where guest molecules can be hosted, that is, a case of “porosity without pores,” as defined by Barbour [26], where the formation of previously absent pores is achieved through the cooperation of **14** with H<sub>2</sub>O to give **13**. Moreover, an analogous process is likely effective when **14** is treated with gaseous NH<sub>3</sub> to form the blue species **15**, which crystallizes in the same *Cmcm* space group of **13**, with very similar cell parameters. Even though the structure of **15** was not obtained, due to its instability under X-rays [24], in this case also NH<sub>3</sub> can be easily removed by gentle heating under vacuum, yielding **14** quantitatively.

The obtaining of **13** is obviously due to the use of MeCN as solvent. It is likely that MeCN is not a suitable solvent to allow or favor the deprotonation of water to OH<sup>-</sup>, and/or the co-ordinating ability of MeCN, in some way, may hamper the capping μ<sub>3</sub>-OH coordination to Cu ions, which is necessary to generate the trinuclear triangular assembly. On the other hand,

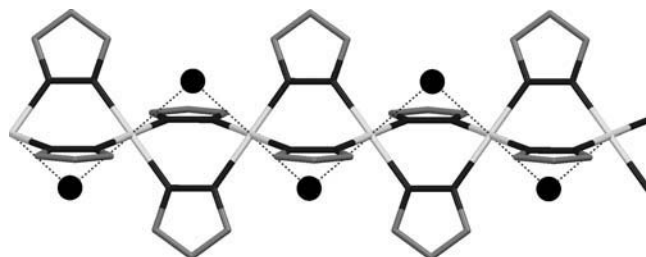


**Figure 30.14** Arbitrary capped-stick view of the 1D CP **13** showing the square planar coordination of Cu<sup>II</sup> and the crystallized water (black balls).



**Figure 30.15** Arbitrary capped-stick view of the 1D CP **14** showing the square planar coordination of Cu<sup>II</sup>.

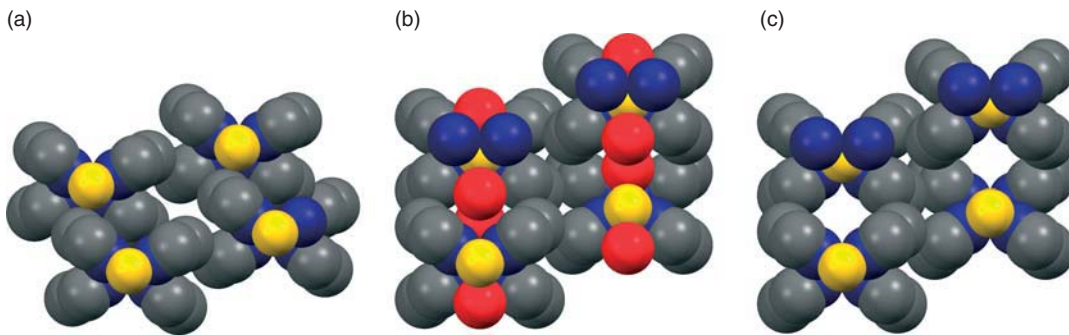


**Figure 30.16** Space-fill representation of **14** (a) and **13** (b). H atoms are not indicated and crystallized water molecules are indicated as red balls. In (c), the water molecules have been fictionally removed, evidencing the space they occupy in **13**. (See insert for color representation of the figure.)

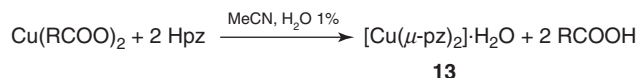
Hpz is instead deprotonated and pz<sup>-</sup> ions bridges Cu<sup>II</sup> ions, allowing the formation of the 1D CP based on the [Cu(pz)<sub>2</sub>] SBU.

In these events, serendipity seems not to play a relevant role, as it is expected that by changing the solvent, something different can happen. In this case, the role of serendipity was in the use of a “new,” just-opened bottle of MeCN. In fact, when, after some weeks, we tried to repeat the reaction we were unable to observe the quantitative precipitation of the pale-pink compound **13**, obtaining instead a blue-gray solid in which acetate ions were present in variable extent and a pale-blue solution. After several attempts, we realized that, in that time, MeCN had adsorbed atmospheric water, and we ascertained that if the water is more than 1%, it promotes the partial formation of the known trinuclear assembly, together with variable quantities of **13**. It is noteworthy, that the water present in Cu(MeCOO)<sub>2</sub>·(H<sub>2</sub>O) is completely employed in the formation of **13**. This is just what is needed! In conclusion, if the author had used an “old” MeCN bottle, containing more than 1% of water (which is quite possible, as we normally work in air, often using hydrated salts—such as copper acetate—thus, we do not take any particular care about the dryness of the solvents) very likely, we would not have been able to synthesize and characterize compounds **13–15**, whose samples are shown in Fig. 30.17.

Also the formation of **13** is quite general in these conditions and it was obtained in MeCN by starting from copper formate, copper propionate, or copper butyrate [27], provided that no more than 1% of water is present, according to Scheme 30.3.



**Figure 30.17** Samples of compounds **13–15**. (See insert for color representation of the figure.)



**Scheme 30.3**

Incidentally, compound **13** was afterward serendipitously (once again) obtained, through a completely different solvothermal procedure, as well-formed crystals [28], whose SC-XRD determination confirmed and improved the XRPD-based structure. Moreover, despite its ascertained stability, compound **2** transforms into compound **13** when treated in air with a large excess of Hpz by stirring it in a toluene suspension or, alternatively, by milling with a pestle in a mortar [28].

### 30.5 CONCLUDING REMARKS

In the CPs research field, the so-called solvothermal synthetic approach is largely used for some important reasons. As a matter of fact, numerous important CPs are insoluble in most solvents (due to their polymeric structure), and this fact makes it difficult to obtain them in the form of crystals of suitable size and quality for an SC-XRD structural determination. In order to try to overcome this problem (the products precipitate quickly as microcrystalline powders or, when dissolved for recrystallization, very often they lose, at least partly, the polymeric character) the solvothermal technique is employed. The reagents and the solvent are introduced into a sealed container (normally a Teflon-lined Parr digestor) and heated above the solvent boiling point. In these conditions, owing to the overheating, the high pressure, the low viscosity, the increased solubility, and other not always well-defined reasons, it is possible that well-formed crystals are obtained. On the other hand, these reactors are like “black boxes” and one will discover what happened only when the cooled reactor is opened. If serendipity has worked, everything would be all right, otherwise one would try again, with different conditions. In the last years, some research groups have implemented the so-called “high throughput synthetic methods” in a sort of combinatorial syntheses, by using, as an example, a series of mini-autoclaves that are differently charged and heated at the same temperature. The resulting compounds are screened by means of automatic or semiautomatic devices in order to detect the “good products” that will then be studied in depth. This method can save a lot of time, but requires the investment of a lot of money, mainly for the apparatus. Yet, in any case, this is again not a designed synthesis, but a just a way to force serendipity to work more rapidly.

In conclusion, in the author’s opinion there is still a lot of work to be done before it will be possible to forecast the structure or even the properties of CPs on the simple bases of the structure of the ligands, the kind of metal, and the reaction conditions employed. Besides, the author is not sure that this will be possible in every situation. So, let serendipity work and let us take advantage of it!

### ACKNOWLEDGMENTS

The University of Padova (Italy) (PRAT 2009 CPDA099411) and the MURST (Italy) (PRIN 2006038447\_003) are acknowledged for funding. Prof. Claudio Pettinari (University of Camerino, Italy), Prof. Magda Monari (University of Bologna, Italy), Prof. Norberto Masciocchi (University of Insubria, Italy), Prof. Armando J.L. Pombeiro (Instituto Superior Técnico, Lisbon, Portugal), Prof. Maurizio Casarin, Dr. Federica Garau, Dr. Arianna Lanza (University of Padova, Italy) have been largely engaged in the above described researches and are greatly acknowledged not only for their work, but mainly for their friendship, that made working with them a true pleasure.

### DEDICATION

I would like to dedicate this work to the memory of my late wife, Guia (1954–2010).

### REFERENCES

1. In the fields of observation chance favors only the prepared mind. Pasteur L. Lecture at the University of Lille (Dec 7, 1854).
2. Winpenny, R. E. P. *J. Chem. Soc. Dalton Trans.* **2002**, 1.
3. Yaghi et al. recently proposed to distinguish MOFs from CPs in terms of the bond strength between nodes and linkers. See Tranchemontagne, D. J.; Mendoza-Cortès, J. L.; O’Keeffe, M.; Yaghi, O. M. *Chem. Soc. Rev.* **2009**, 38, 1257.
4. For recent accounts on CPs see: (a) the Special Issue of *Chem. Soc. Rev.* **2009**, 38, 1201; (b) the Thematic Issue on Metal-Organic Frameworks of *Chem. Rev.* **2012**, 112, 673.
5. Eddaudi, M.; Moler, D. B.; Li, H.; Chen, B.; Reineke, T. M.; O’Keeffe, M.; Yaghi, O. M. *Acc. Chem. Res.* **2001**, 34, 319.

6. (a) Kitagawa, S.; Kondo, M. *Bull. Chem. Soc. Jpn.* **1998**, *71*, 1739. (b) Kitagawa, S.; Uemura, K. *Chem. Soc. Rev.* **2005**, *34*, 109.
7. Eddaudi, M.; Kim, J.; Rosi, M.; Vodak, D.; Watcher, J.; O'Keeffe, M.; Yaghi, O. M. *Science* **2002**, *295*, 469.
8. (a) Pettinari, C.; Pettinari, R. *Coord. Chem. Rev.* **2005**, *249*, 525; (b) Pettinari, C.; Pettinari, R. *Coord. Chem. Rev.* **2005**, *249*, 663; (c) Pettinari, C. *Scorpionates II: Chelating Borate Ligands*; Imperial College Press: London, **2008**.
9. Garau, F.; Monari, M.; Pandolfo, L.; Pettinari, C.; Venzo, A. *CrystEngCom*, **2010**, *12*, 1217.
10. Casarin, M.; Corvaja, C.; Di Nicola, C.; Falcomer, D.; Franco, L.; Monari, M.; Pandolfo, L.; Pettinari, C.; Piccinelli, F.; Tagliatesta, P. *Inorg. Chem.* **2004**, *43*, 5865.
11. Casarin, M.; Corvaja, C.; Di Nicola, C.; Falcomer, D.; Franco, L.; Monari, M.; Pandolfo, L.; Pettinari, C.; Piccinelli, F. *Inorg. Chem.* **2005**, *44*, 6265.
12. Di Nicola, C.; Karabach, Y. Y.; Kirillov, A. M.; Monari, M.; Pandolfo, L.; Pettinari, C.; Pombeiro, A. J. L. *Inorg. Chem.* **2007**, *46*, 221.
13. Di Nicola, C.; Garau, F.; Karabach, Y. Y.; Martins, L. M. D. R. S.; Monari, M.; Pandolfo, L.; Pettinari, C.; Pombeiro, A. J. L. *Eur. J. Inorg. Chem.* **2009**, *48*, 666.
14. Di Nicola, C.; Garau, F.; Karabach, Y. Y.; Martins, L. M. D. R. S.; Monari, M.; Pandolfo, L.; Pettinari, C.; Pombeiro, A. J. L. *Dalton Trans.* **2009**, 4928.
15. Casarin, M.; Cingolani, A.; Di Nicola, C.; Falcomer, D.; Monari, M.; Pandolfo, L.; Pettinari, C. *Cryst. Growth Des.* **2007**, *4*, 676.
16. Di Nicola, C.; Garau, F.; Gazzano, M.; Monari, M.; Pandolfo, L.; Pettinari, C.; Pettinari, R. *Cryst. Growth Des.* **2010**, *10*, 3120.
17. Di Nicola, C.; Garau, F.; Gazzano, M.; Guedes da Silva, M. F. C.; Lanza, A.; Monari, M.; Nestola, F.; Pandolfo, L.; Pettinari, C.; Pombeiro, A. J. L. *Cryst. Growth Des.* **2012**, *12*, 2890.
18. Monari, M.; Pandolfo, L.; Pettinari, C. Unpublished results.
19. Garau, F.; Lanza, A.; Pandolfo, L.; Monari, M.; Pettinari, C.; Zorzi, A. XL Congresso Associazione Italiana di cristallografia (AIC) Siena, Italy, Sept 19–22, 2011; pp 134; P13.
20. Di Nicola, C.; Forlin, E.; Garau, F.; Lanza, A.; Natile, M. M.; Nestola, F.; Pandolfo, L.; Pettinari, C. *J. Organomet. Chem.* **2012**, *714*, 74.
21. Di Nicola, C.; Forlin, E.; Garau, F.; Gazzano, M.; Lanza, A.; Monari, M.; Nestola, F.; Pandolfo, L.; Pettinari, C.; Zorzi, A.; Zorzi, F. *Cryst. Growth Des.* **2013**, *13*, 126.
22. In some cases cyclopentane was also tested, with analogous results.
23. (a) Kirillov, A. M.; Kopylovich, M. N.; Kirillova, M. V.; Haukka, M.; Guedes da Silva, M. F. C.; Pombeiro, A. J. L. *Angew. Chem. Int. Ed.* **2005**, *44*, 4345; (b) Kirillov, A. M.; Kopylovich, M. N.; Kirillova, M. V.; Karabach, E. Y.; Haukka, M.; Guedes da Silva, M. F. C.; Pombeiro, A. J. L. *Adv. Synth. Catal.* **2006**, *348*, 159; (c) Trettenhahn, G.; Nagl, M.; Neuwirth, N.; Arion, V. B.; Jary, W.; Pochlauer, P.; Schmid, W. *Angew. Chem. Int. Ed.* **2006**, *45*, 2794; (d) Velusamy, S.; Punniyamurthy, T. *Tetrahedron Lett.* **2003**, *44*, 8955. (e) Shul'pin, G. B.; Gradinaru, J.; Kozlov, Y. N. *Org. Biomol. Chem.* **2003**, *1*, 3611; (f) Raja, R.; Ratnasamy, P. *Catal. Lett.* **1997**, *48*, 1.
24. Cingolani, A.; Galli, S.; Masciocchi, N.; Pandolfo, L.; Pettinari, C.; Sironi, A. *J. Am. Chem. Soc.* **2005**, *127*, 6144.
25. Interestingly, compound **13** is a polymorphous species of a previously synthesized, green colored, 1D CP Cu(pz)<sub>2</sub>, obtained through a completely different procedure, where the coordination geometry of copper(II) is tetrahedral. See: Elhert, M. K.; Rettig, S. J.; Storr, A.; Trotter, J. *Can. J. Chem.* **1991**, *69*, 432.
26. Barbour, L. J. *Chem. Commun.* **2006**, 1163.
27. Pandolfo, L. Unpublished results.
28. Lanza, A. Unpublished results.



## ORGANOMETALLIC NANOPARTICLES

PATRICIA LARA AND KARINE PHILIPPOT

CNRS, LCC (*Laboratoire de Chimie de Coordination*), Toulouse, France; Université de Toulouse, Toulouse, France

LISE-MARIE LACROIX, SÉBASTIEN LACHAIZE, NIKOS LIAKAKOS, KATERINA SOULANTICA, AND BRUNO CHAUDRET\*

*Laboratoire de physique et Chimie des Nano-Objets, Institut National des Sciences Appliquées-CNRS-Université Paul Sabatier, Université de Toulouse, Toulouse, France*

### 31.1 INTRODUCTION

Metal nanoparticles (MNPs) are widely developed in view of their applications in various areas, such as optoelectronics, sensors, medicine, and catalysis [1]. This interest in metal nanoparticles stems mainly from their small size, which confers on them electronic properties at the frontier between the molecular and metallic states. In catalysis, metal nanoparticles are highly interesting systems because of their high proportion of surface atoms giving rise to numerous active sites [2]. Nanocatalysis has therefore emerged as a domain at the border between homogeneous and heterogeneous catalysis [3, 4], with the anticipation that precisely designed nanoparticles (NPs) in terms of size, shape and surface ligands should be able to combine the benefits of both homogenous and heterogeneous catalysts, namely high efficiency and selectivity. In another scientific area, the development of quantum dots has given a strong impetus to the field of conversion of solar energy as well as to the studies of interaction mechanisms in biology. MNPs appear also of interest in the field of magnetism for the production of permanent magnets as well as for the transport properties of their assemblies and for nanoelectronics. In all these cases, the organometallic approach, by judicious choice of the precursors and of the reactions conditions that avoid the incorporation of heteroatoms, potentially detrimental to the final properties of the resulting nano-objects, can bring solutions for producing NPs displaying reproducible properties, whether catalytic, electrical, photophysical, or magnetic. It is beyond the scope of this short chapter to give a comprehensive overview of this rapidly growing field. We will, however, describe three examples that highlight the importance of organometallic chemistry in the synthesis of nano-objects, and more generally in nanoscience.

Our group initiated, over 20 years ago, a new approach for the synthesis of metal nanoparticles starting from organometallic precursors. It followed (*inter alia*) the pioneering works of Chini et al. [5] on very large organometallic clusters, Basset et al. [6] on the use of organometallic complexes to prepare heterogeneous catalysts, Schmid et al. [7] on the preparation of Gold 55 clusters through borane reduction of  $\text{AuCl}(\text{PPh}_3)$ , and Bradley et al. [8] who decomposed carbonyl clusters to produce NPs in solution. Our approach has taken advantage of the method we had developed in the early 1980s to prepare hydrogen-rich complexes, the most popular being  $[\text{RuH}_2(\text{H}_2)_2(\text{PCy}_3)_2]$  [9]. This was first reported in 1982 as a hexahydride, and recognized to be a bis(dihydrogen) complex at the end of the 1980s. We could obtain a crystal structure at the end of the 1990s and a neutron structure for the analogous tricyclopentylphosphine complex  $[\text{RuH}_2(\text{H}_2)_2(\text{PCp}_3)_2]$  in 2005 [10]. This complex was originally prepared at room temperature by bubbling dihydrogen into a solution containing a ruthenium precursor  $[\text{Ru}(\text{COD})(\text{COT})]$  ( $\text{COD} = 1,5\text{-cyclooctadiene}$ ,  $\text{COT} = 1,3,5\text{-cyclooctatriene}$ ) and 2 equiv of a bulky

---

*Advances in Organometallic Chemistry and Catalysis: The Silver/Gold Jubilee International Conference on Organometallic Chemistry Celebratory Book*, First Edition. Edited by Armando J. L. Pombeiro.

© 2014 John Wiley & Sons, Inc. Published 2014 by John Wiley & Sons, Inc.

phosphine. With some ligands, the solution turned black, and in the absence of any ligand a black deposit of pyrophoric ruthenium powder precipitated. Fascinated by the works of Schmid and of Bradley, and in order to prepare a hydride containing large clusters, we attempted at the very end of the 1980s the controlled decomposition of [Ru(COD)(COT)] and used various stabilizers, initially polymers. Following this technique, we obtained various polymer-stabilized ruthenium nanoparticles (RuNPs) and extended the approach both to different stabilizers (ligands) and to different metals [11]. Thus besides noble metals, this approach could, through the judicious choice of precursors, be extended to copper for applications in microelectronics and to magnetic metals (Fe, Co, Ni, and their alloys) that display interesting magnetic properties and find applications as hard magnets, for tunnel magnetoresistance or hyperthermia, as well as for catalysis [12]. In those cases, a precursor similar to [Ru(COD)(COT)] (namely, [Co(COE)(COD)], [Ni(COD)<sub>2</sub>]; COE = cyclooctenyl) was used or, when such precursors did not exist, an aryl complex (Cu(Mes)<sub>4</sub>; Mes = mesityl) or an amido derivative (M[N(SiMe<sub>3</sub>)<sub>2</sub>]<sub>2</sub>; M = Fe, Co) since the resulting amine could be easily displaced from the NP surface. Finally, we also extended this approach to main group elements, quantum dots, and semiconducting oxides [13].

In the following, we will describe three representative cases: ruthenium, iron, and cobalt NPs with some small incursions toward platinum and bimetallics. Ruthenium is a metal displaying very good catalytic properties (hydrogenation or oxidation), and it can easily accommodate ligands and therefore allow studies on the influence of ligands on the growth of NPs. Furthermore, it hardly displays any Knight shift, which makes it a metal of choice to study ligand coordination by nuclear magnetic resonance (NMR), whether in solution or in the solid state. In addition, [Ru(COD)(COT)] is an “ideal” precursor because it decomposes easily below room temperature under dihydrogen and only produces cyclooctane which does not interact with the growing NPs. This is hence a source of “naked” Ru atoms in very mild conditions in solution. The resulting particles are, however, not naked since, as we will see, they are covered with hydrides and will interact with the added stabilizers present in solution [14]. Cobalt, like ruthenium, displays a hexagonal close-packed (hcp) structure, and [Co(COE)(COD)] can be decomposed under mild conditions to give rise to small NPs displaying superparamagnetic properties and an enhancement of magnetization compared to bulk cobalt. Furthermore, taking advantage of the “clean” nature of their surface, these particles can be grown into ferromagnetic nanorods which are monodisperse both in diameter and length. Finally, iron is an important metal from the point of view of its catalytic properties and numerous studies are presently devoted to this field. Iron is also magnetic, very abundant, and biocompatible, which makes it an interesting candidate for, for example, nanoelectronics or nanomedicine. In contrast to the preceding examples, there is no suitable alkene precursor. Iron bis(cyclooctatriene) is, for example, very difficult to decompose as are the ferrocene derivatives. However, as in the case of cobalt, by using the bis-amido derivative Fe[N(SiMe<sub>3</sub>)<sub>2</sub>]<sub>2</sub>, it was possible to obtain first very small superparamagnetic and catalytically active Fe NPs and to grow them further into iron nanocubes which organize into large superstructures.

## 31.2 RUTHENIUM

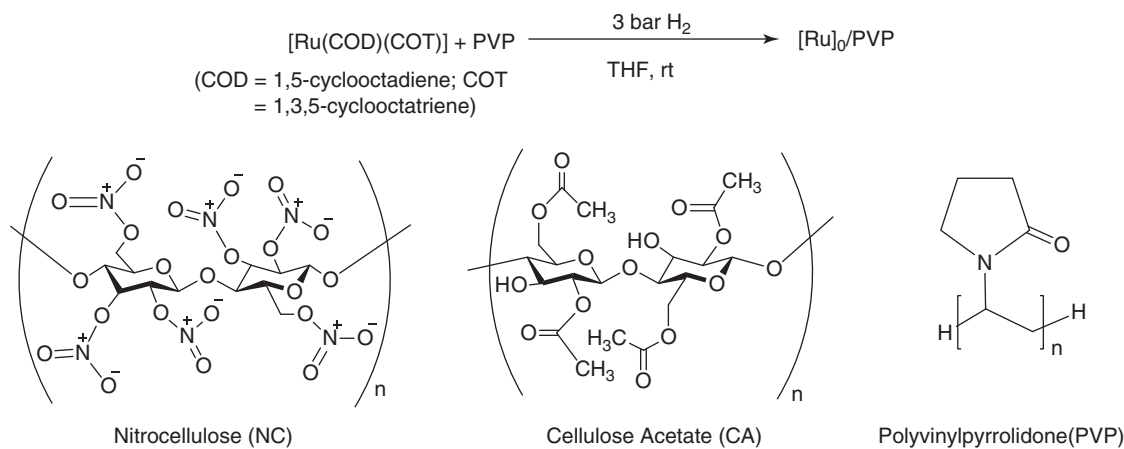
### 31.2.1 Steric Stabilization (Polymer-, Ionic Liquid-, and Alcohol-Stabilized Ruthenium Nanoparticles)

Polymers have long been used to stabilize metal nanoparticles [15]. In this case, the protection is steric: an organic polymer may display a structure containing voids, thus forming “nanoreactors” inside which the NPs can grow using the amount of precursor present. The size of the particles is therefore controlled by the concentration of the solution and the size and monodispersity of these “nanoreactors”. The NPs display little or no chemical interaction with the polymer and are free from ligands outside the solvent and hydrogen. It is therefore ideal for catalysis and surface studies.

The synthesis procedure (Scheme 31.1) was developed originally using as precursor [Ru(COD)(COT)] as precursor and dihydrogen as reducing agent in the presence of a polymer, namely, nitrocellulose (NC), cellulose acetate (CA), or poly(vinylpyrrolidone) (PVP) under mild conditions (3 bar H<sub>2</sub>, room temperature). The hydrogen treatment allows the reduction of the olefin ligands into cyclooctane, which is inert toward the metal surface. These NPs are stable and can be used for surface reactivity studies. With PVP, very small (1.1 nm) NPs were obtained (Fig. 31.1) [16].

Characterization by wide-angle X-ray scattering (WAXS) evidenced crystalline NPs displaying the expected hcp structure of bulk ruthenium. Reactivity studies were carried out in particular with CO [17]. It has been observed that there is an influence of the reaction time on the coordination mode of CO on the surface of the NPs and that CO is mobile. Short reaction times give rise to CO adsorption in the bridging mode, while longer reaction times allow adsorption of more CO molecules only in the linear or multicarbonyl modes.

Our initial results, as well as numerous literature data, showed that NPs could be stabilized in a polymer while interacting chemically only very weakly. The next question was how weak a stabilizer can be? For this purpose, the organometallic precursor [Ru(COD)(COT)] was dissolved in various solvents and reacted under a H<sub>2</sub> atmosphere. While in neat pentane, dichloromethane, or tetrahydrofuran (THF), only a black ruthenium precipitate was obtained, stabilization was observed in some neat alcohols and THF/alcohol mixtures in the absence of any further stabilizer [18, 19].



**Scheme 31.1** Organometallic synthesis of polymer-stabilized RuNPs.

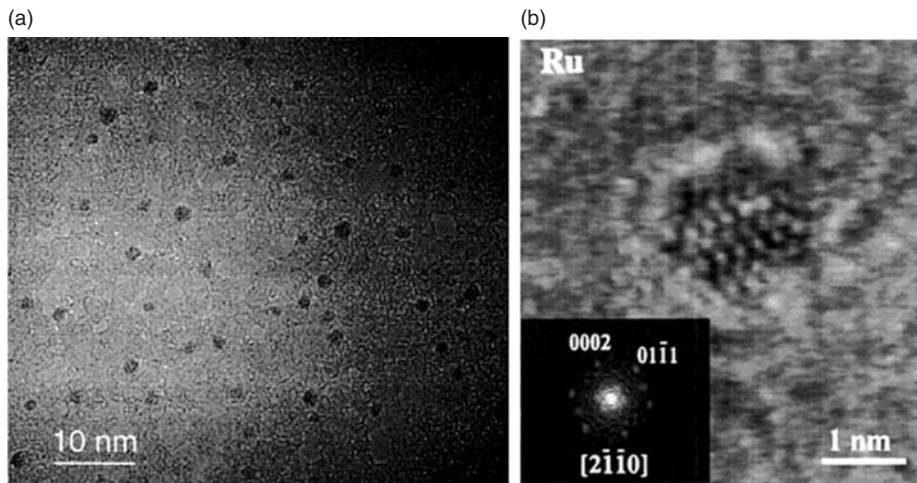


**Figure 31.1** (a) TEM and (b) HRTEM images of Ru nanoparticles in PVP.

Transmission electron microscopy (TEM) images and X-ray analyses revealed the presence of hcp NPs, in general polycrystalline and sponge-like and displaying a regular spherical envelope and a homogeneous size or, in some cases, the presence of isolated and well-dispersed monocrystalline particles, depending upon the solvent mixture and the alcohol alkyl chain (from C1 for methanol to C7 for heptanol, see Fig. 31.2). In all cases, the size distributions is relatively narrow. The size of the particles could be controlled by adjusting the reaction temperature or the composition of the solvent mixtures. For MeOH/THF mixtures, a surprising linear correlation was established between the solvent composition and the size of the particles in the range 4–85 nm. The size and morphology variations were related to the increase in polarity of the solution upon adding MeOH in THF and, consequently, led us to suspect a segregation of cyclooctane, resulting from the reduction of the precursor, from the rest of the solvent. In this respect, larger droplets are expected in the most polar solvent systems and hence the most segregated medium. Complementary experiments, carried out upon adding excess cyclooctane to a MeOH/THF 10:90 solution while keeping other parameters equal, allowed us to confirm this hypothesis. Upon addition of 2 or 20 equiv cyclooctane per mole of ruthenium, an increase of the particle size of a factor 1.5 or 2, respectively, was observed. These results were consistent with an increase in size of the cyclooctane droplets (nanoreactors) present in the reaction medium, inside which the ruthenium particles were formed. Thus the stabilization of the RuNPs in these systems derives from a segregation phenomenon in the reaction mixture. It is interesting to note that this result implies that the NPs are more soluble in cyclooctane than in alcohols. Although at that time the origin of this phenomenon was not clear, we have since then demonstrated that the surface of the particles prepared under H<sub>2</sub> accommodate between one and two hydrides per surface Ru [14]. Since the polarity of the Ru–H bond is comparable

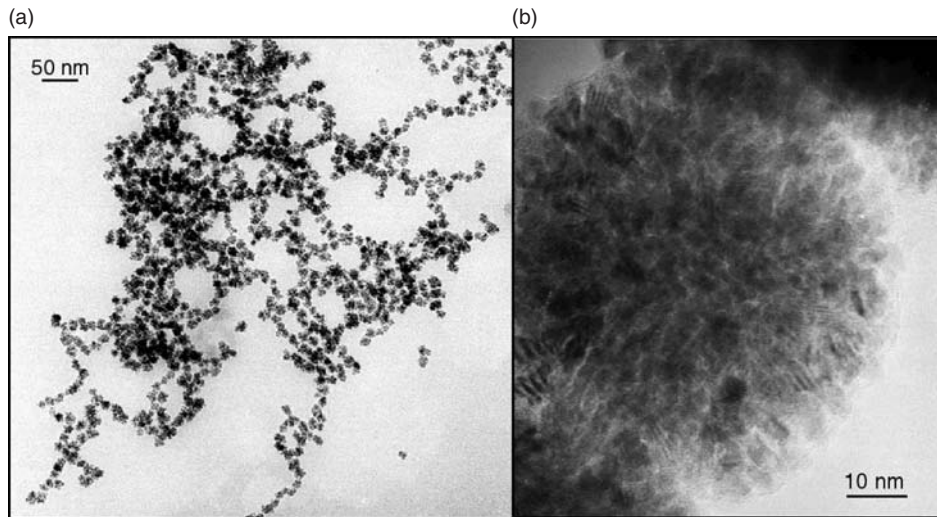


**Figure 31.2** Polycrystalline “sponge-like” Ru nanoparticles obtained (a) in pure methanol and (b) in a 10 : 90 mixture of methanol and THF.

to that of a C–H bond, these RuNPs will behave, in terms of solubility, like large, saturated organic molecules which is counterintuitive.

Since ionic liquids (ILs) are known in catalysis for providing more environmentally friendly conditions than usual solvents, their use is emerging as an alternative for the synthesis and stabilization of MNPs of interest in nanocatalysis [20]. ILs play a double role, acting as both the solvent and the stabilizer. The segregation between polar and nonpolar domains in imidazolium-based ILs has a strong influence on their solvation and ability to interact with different species [21]. After the work of Dupont et al. [22] we investigated in collaboration with Santini et al. [23–27], the synthesis of RuNPs to gain further knowledge on the way ionic liquids stabilize MNPs. The synthesis of RuNPs was first performed in 1-butyl-3-methylimidazolium bis(trifluoromethanesulfonyl)imide ( $\text{BMImNTf}_2$  or  $[\text{RMIm}][\text{NTf}_2]$  with  $\text{R} = \text{C}_4\text{H}_9$ ) to study the influence of temperature and stirring on the NPs formed [23]. The NPs were prepared by the decomposition of  $[\text{Ru}(\text{COD})(\text{COT})]$  under 4 bar of  $\text{H}_2$  at various reaction temperature (0 and 25 °C), leading to a mean size of  $2.4 \pm 0.3$  nm at 25 °C and  $1.1 \pm 0.2$  nm at 0 °C in the absence of stirring. As an explanation for this size difference, it was proposed that the size of RuNPs is governed by the size of the nonpolar domains. This hypothesis was further confirmed by using as reaction medium a series of various imidazolium-derived ionic liquids, namely:  $[\text{RMIm}][\text{NTf}_2]$  ( $\text{R} = \text{C}_n\text{H}_{2n+1}$  with  $n = 2, 4, 6, 8, 10$ ) and  $[\text{R}_2\text{Im}][\text{NTf}_2]$  ( $\text{R} = \text{Bu}$ ) to perform the synthesis of RuNPs, under 4 bar of  $\text{H}_2$  at 25 or 0 °C with or without stirring [24]. For the IL  $[\text{RMIm}][\text{NTf}_2]$  ( $\text{R} = \text{C}_n\text{H}_{2n+1}$  with  $n = 4, 6, 8$ ), a linear correlation between the size of RuNPs generated *in situ* and the length of the alkyl chain of the IL was established. The use of spectroscopic methods and labeling experiments developed in another context [14, 28] with RuNPs prepared in IL allowed confirming the presence of hydrides on the surface of the NPs [25].

### 31.3 LIGAND-STABILIZED RUTHENIUM NANOPARTICLES

Ligand coordination on NPs is similar to that in molecular complexes, in particular for the order of bond energy as a function of the nature of the binding function. The presence of these ligands prevents the particles from aggregation and allows their solubilization.

#### 31.3.1 Nitrogen-Donor Ligands

**31.3.1.1 Long Alkyl Chain Amines** Amines can act both as reducing agents and as stabilizers thanks to a  $\sigma$ -type coordination mode to the metallic surface [29]. When hexadecyl- and dodecylamine are employed as stabilizers, elongated NPs are obtained, the size of which is dependent upon the molar ratio  $\text{Ru:L}$  (in all cases the sizes are found between 1.8 and 2.6 nm with a broad size distribution) and which show a tendency to agglomerate when higher amounts of ligands are employed and when the concentration of the solution is increased (Fig. 31.3) [16].

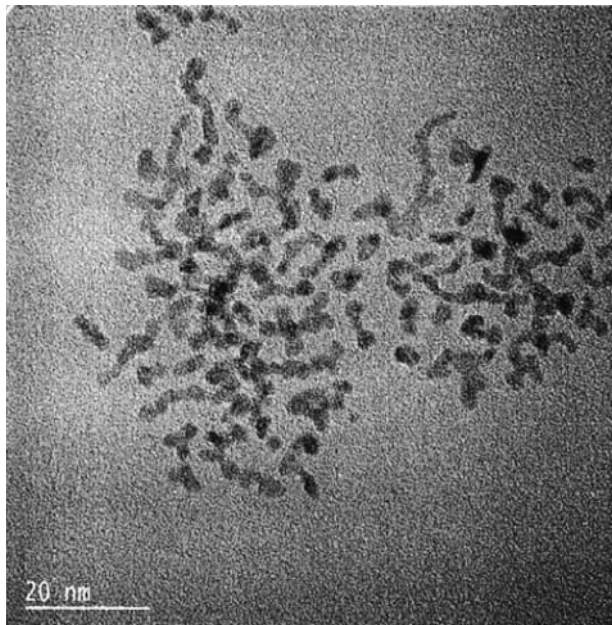


**Figure 31.3** RuNPs stabilized with 0.2 equiv of hexadecylamine.

This lack of control results from a weak coordination of the ligand as evidenced by liquid  $^1\text{H}$  and  $^{13}\text{C}$  NMR, which demonstrates the presence of a fast equilibrium between the free ligand and the ligand coordinated to the surface of the NPs at the NMR timescale. The wormlike shape observed may then result from an oriented attachment process of the initial NPs. Interestingly, on the NMR spectra registered for the NPs stabilized with hexadecylamine (0.2 equiv), the signals corresponding to the carbons located in the  $\alpha$ ,  $\beta$ , and  $\gamma$  positions relative to the amino group are not visible because of a very short  $T_2$  resulting from the slow tumbling of the particles in solution due to their large size.

**31.3.1.2 Phenyl Pyridine** The unusual 4-(3-phenylpropenyl)pyridine ligand was chosen for its simple structure containing a pyridine group, which, upon  $\sigma$ -coordination, can favor the flat phenyl approach to the metallic surface [30]. Homogeneously dispersed NPs showing a very narrow size distribution around a mean diameter of  $1.3 \pm 0.3$  nm were obtained using the standard procedure. This result contrasted with the formation of large and agglomerated particles that were observed otherwise using simple pyridines as stabilizers, in agreement with previous reports concerning gold particles containing pyridine [31].  $^{13}\text{C}$  CP-MAS (cross-polarization magic angle spinning) NMR and D MAS NMR experiments on RuNPs after treatment under deuterium atmosphere and substitution by stronger ligands (dodecanethiol) confirmed the  $\pi$ -coordination of both the phenyl and the pyridyl rings as a novel type of bidentate ligand.

### 31.3.2 Phosphorus-Containing Ligands

**31.3.2.1 Simple Mono- and Diphosphines** RuNPs were prepared from  $[\text{Ru}(\text{COD})(\text{COT})]$  and 0.1 equiv of the corresponding diphosphine (1,4-bis(diphenylphosphino)butane (dppb) and 1,10-bis(diphenylphosphino)decane (dppd)) [28], in THF under 3 bar of dihydrogen at room temperature. Stable, crystalline, and monodispersed hcp NPs of mean size 1.5 (dppb) and 1.9 nm (dppd) were obtained. The presence of the ligand at the surface of the NPs was confirmed by solution  $^{31}\text{P}$  NMR after releasing the oxidized phosphine upon addition of  $\text{H}_2\text{O}_2$  to the NPs and by MAS  $^{31}\text{P}$  NMR. A quantification of the hydrides present at the surface of the Ru/dppd particles was performed by titration with an olefin, leading to a reproducible value of 1.1 hydrides by surface ruthenium atom against 1.3 for both Ru/hexadecylamine (HDA) and Ru/PVP. The surface state of the dppb-stabilized RuNPs was investigated using  $^{13}\text{CO}$  as probe molecule, and IR and MAS NMR techniques [17]. These studies have demonstrated that, in contrast to the case of  $^{13}\text{CO}$  adsorbed on Ru/PVP NPs, the CO ligands are not fluxional and this is obviously related to the presence of the ancillary phosphine ligands at the surface of the RuNPs. The presence of a bridging terminal and multicarbonyl group is hence evidenced.

Similar studies carried out with labeled ethylene have demonstrated, quite unexpectedly, the breaking of the C–C bond to produce methyl groups firmly attached to the surface [28]. These results demonstrate the interest in spectroscopic methods for monitoring the reactivity of metal nanoparticles.

An important issue of this chemistry is to determine whether these ancillary phosphine ligands may influence the reactivity of the resulting NPs and how. In this respect, in a collaborative work with the group of van Leeuwen [32], the design of new roof-shaped phosphine ligands for the stabilization of RuNPs and their application as catalysts in hydrogenation of aromatics have been investigated (Fig. 31.4).

Different  $M/L$  ( $M = \text{Ru}$  and  $L = \text{phosphine}$ ) ratios were explored and in all cases, RuNPs of mean size between 1.1 and 2.1 nm were formed.  $^{31}\text{P}$ -HRMAS NMR confirmed the coordination of the triarylphosphines, dialkylphosphines, or trialkylphosphines at the surface of the particles, but also indicated the partial or total hydrogenation of the substituents resulting from the NP synthesis. This phenomenon had previously been observed with simple diphosphine ligands [28]. The resulting NPs are active in the hydrogenation of *o*-methylanisole, with a clear influence of the nature of the ligands on the catalytic performances. It was found that colloids containing triarylphosphines are not or only very poorly active, while colloids containing dialkylarylphosphines lead to the full hydrogenation of the substrate. This work points out the interest of designing appropriate ligands to tune the catalytic properties of the particles.

**31.3.2.2 Diphosphites** The question of the possibility of asymmetric catalysis led us to search for ligands specific to NPs. Following previous studies concerning diphosphite-stabilized PdNPs which gave rise to interesting and intriguing results in Heck-coupling reactions [33] in collaboration with the groups of Castillon, Claver, and Roucoux, we carried out the synthesis of RuNPs using carbohydrate-based diphosphites for their application as catalysts in the hydrogenation of anisole derivatives [34]. The NPs were prepared as usual from  $[\text{Ru}(\text{COD})(\text{COD})]$  and a ligand/Ru ratio of 1 : 0.1 as for diphosphines. Different diphosphite ligands (Fig. 31.5) were employed with the objective to analyze the influence of their structure on the characteristics of the NPs as well as on their catalytic activity.

TEM analysis of the obtained colloids showed the formation of RuNPs of mean size between 1 and 4 nm, depending on the diphosphite used. These particles were tested as nanocatalysts in the hydrogenation of *o*- and *m*-methyl anisoles. In pentane, the particles' activity was found to be ligand dependent. Thus the more flexible ligand containing one carbon

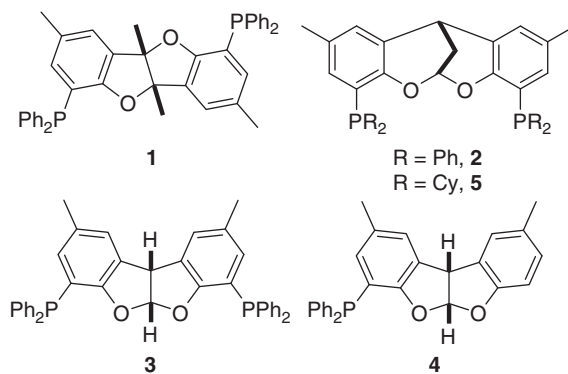


Figure 31.4 Ligands used as stabilizers for the Ru nanoparticles.

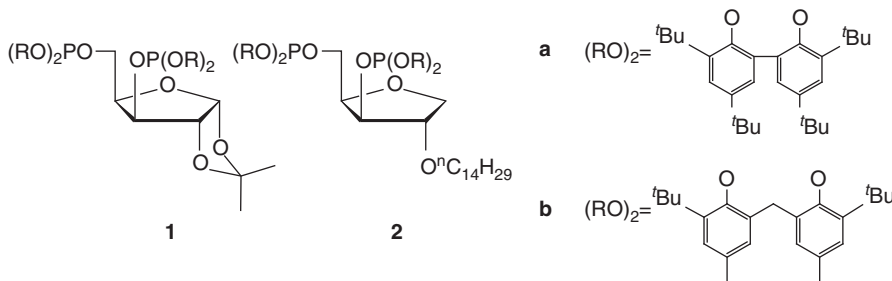


Figure 31.5 Carbohydrate-based diphosphites used as ligands for the synthesis of the ruthenium nanoparticles.

between the aromatic rings displays a better activity. The introduction of a long lipophilic chain in the ligand increased further the activity of the particles as a result of several factors including smaller mean particle size and higher solubility in pentane. In all cases, the cis product was formed, in contrast to the results obtained when oxazoline-stabilized RuNPs were investigated in the same catalytic reaction.

### 31.3.3 N-Heterocyclic Carbene ligands

N-Heterocyclic carbene ligands (NHCs) are, in molecular chemistry, strongly associated with ruthenium since the work of Grubbs on metathesis. However, these ligands had not been used for the stabilization of NPs. It was, therefore, of interest, after a comprehensive study of phosphine coordination on NPs, to study the interaction between RuNPs and NHCs [35]. The RuNPs were prepared by the decomposition of  $[\text{Ru}(\text{COD})(\text{COT})]$  in pentane, under dihydrogen atmosphere (3 bar) at room temperature, and in the presence of two different carbenes as stabilizing agents, namely, 1,3-bis(2,6-diisopropylphenyl)imidazol-2-ylidene (IPr) and *N,N*-di(*tert*-butyl)imidazol-2-ylidene (I<sup>t</sup>Bu), shown in Fig. 31.6.

Different colloids have been obtained depending on the amount and the type of the carbene. RuNPs of mean size 1.7 nm were formed by employing 0.2 equiv of IPr (Fig. 31.7) or 0.5 equiv of I<sup>t</sup>Bu and of 1.5 nm mean size in the presence of 0.5 equiv of IPr. In all cases, these NPs were homogeneous in size and shape and presented the expected hcp structure, as demonstrated by WAXS analysis. To study the coordination of the carbenes to the surface of the RuNPs by infrared (IR) and NMR spectroscopies, the synthesis of the Ru NPs was performed using NHCs  $^{13}\text{C}$ -labeled in the carbene position. The characterization of these particles by MAS NMR allowed the detection of the signals of the carbene bonded to the surface of the NPs, which resonates in the region between 195 and 205 ppm (depending on the type and amount of stabilizer employed). To probe the free sites at their surface, NHC-stabilized RuNPs were reacted with CO. In the case of the NPs prepared using 0.5 equiv of I<sup>t</sup>Bu, CO is present predominantly in the bridging mode. The same coordination mode is observed when the CO is added to the colloid prepared using 0.2 equiv of IPr. In contrast, no bridging CO is detected when the addition of this probe molecule is performed on the colloid prepared using 0.5 equiv of IPr. In this case, CO is present in linear and multicarbonyl modes. From these results, the location of the different carbene ligands on the surface of the NPs

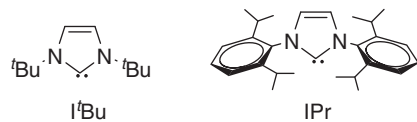


**Figure 31.6** NHCs employed as stabilizers for the RuNPs.

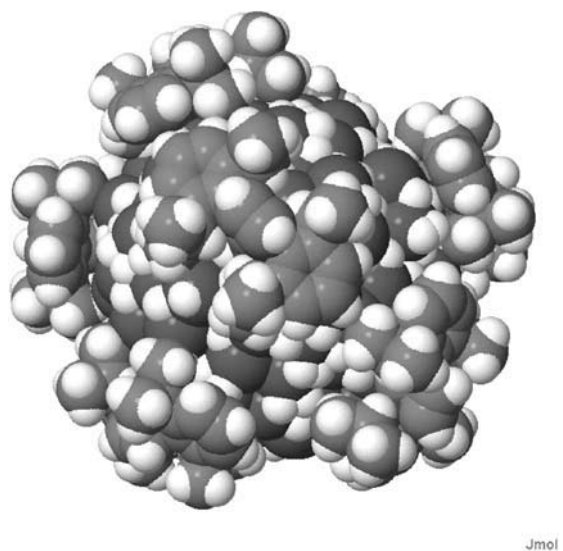


**Figure 31.7** Space-filling model of a 1.8 nm hcp Ru nanoparticle stabilized by 8 IPr NHC ligands and accommodating 1.5 hydrides per surface Ru. Adapted from Reference 6e.

could be proposed. In the case of the NPs prepared using 0.5 equiv of  $\text{I}^{\prime}\text{Bu}$  or 0.2 equiv of  $\text{IPr}$ , CO is located on the faces, indicating that the ligand is located on edges and apexes. In contrast, for NPs prepared with 0.5 equiv of  $\text{IPr}$ , the absence of bridging CO is in agreement with the presence of ligand all over the particles. These carbene-stabilized RuNPs have also been tested as catalysts in the hydrogenation of styrene under mild conditions. This study evidenced a moderate activity, and, as expected with RuNPs, a full hydrogenation of the vinyl bond is first observed followed by the hydrogenation of the aromatic ring.

### 31.4 IRON

Iron NPs are promising candidates for a wide range of applications, from magnetic data storage to chemical or biomedical uses such as contrast agents for sensitive magnetic resonance imaging (MRI) or efficient heater media for magnetic fluid hyperthermia (MFH) [36, 37]. Iron indeed combines a high saturation magnetization ( $M_S$ ) at room temperature ( $212 \text{ A}/(\text{m}^2 \cdot \text{kg})$ ) and a presumably low toxicity. Nevertheless, to achieve optimum operation conditions, these NPs should have well-controlled magnetic properties and biological functionalities, which are strongly dependent on the surface states, sizes and shapes of the NPs. Thus, a strict control of the NP synthesis is required.

A widely used approach to Fe NP preparation consists in thermal decomposition of  $\text{Fe}(\text{CO})_5$  in the presence of long-chain surfactants [38]. The NP size can be tuned from 4 to 20 nm by controlling the reaction parameters (time, temperature, surfactant concentration [39]) or by using a seed-mediated growth [40]. However, the magnetic properties of these NPs are usually degraded compared to bulk values because of the presence of an oxide shell around the NP surface [41]. Iron salts were also proposed to produce high-moment Fe NPs, although this implies harsh reaction conditions such as strong reducing agents or high temperatures.  $\text{FeCl}_2$  can be reduced with sodium borohydride, but boron contamination has been found to decrease the NP magnetic moment [42].

In order to avoid such surface contaminations and their drastic effects on magnetic properties, an organometallic approach could be advantageous since controlled decomposition under mild conditions can be achieved. Through intensive prospective work, we determined that amido precursors such as  $\text{Fe}[\text{N}(\text{SiMe}_3)_2]_2(\text{THF})$  ( $\text{Me} = \text{CH}_3$ , THF = tetrahydrofuran) [43] or the dimer  $\{\text{Fe}[\text{N}(\text{SiMe}_3)_2]_2\}_2$  [44] can yield unoxidized iron metal nanoparticles (MNPs) under mild conditions. These precursors exhibit a good compromise between stability (to be stored once prepared) and reactivity (to be decomposed under mild and reductive conditions).

To demonstrate the relevance of the precursor choice, ultrasmall Fe NPs (<2 nm) have been prepared by solely decomposing the dimer in mesitylene solvent under 3 bars of  $\text{H}_2$  at  $150^\circ\text{C}$  [45]. This demonstrates that  $\text{HN}[\text{Si}(\text{CH}_3)_3]_2$  or some of its derivatives released during the synthesis are able to stabilize the NP surface. Furthermore, these NPs exhibit a magnetization close to the bulk value, or even enhanced, compared to that in the presence of the polymer PPO (poly(2,6-dimethyl-1,4-phenyleneoxide)) [46]. The magnetic properties of ultrasmall NPs being drastically affected by pollutants, one can conclude that the by-products of the precursor reduction do not alter the surface states. In addition, these NPs were tested as catalysts and found active *inter alia* for alkene hydrogenation.

In order to grow larger NPs, displaying a higher potential for further applications, mixtures of long-chain surfactants—amine/acid or amine/ammonium—were added to the reaction. Iron nanocubes of 7 nm were prepared in this way by decomposing  $\text{Fe}[\text{N}(\text{SiMe}_3)_2]_2(\text{THF})$  under  $\text{H}_2$  at  $150^\circ\text{C}$  in mesitylene in the presence of a mixture of HDA and oleic acid or hexadecylammonium chloride. These objects exhibited bulk magnetization and self-organized into cubic superlattices, as shown in Fig. 31.8 [47]. These unoxidized Fe NPs and their tendency to form superlattices were an unprecedented result, which opened new perspectives for unique transport measurement on macroscopic but nanotextured objects [48, 49].

In order to understand and, possibly, propose a model for the size and shape control of iron NPs prepared in the presence of such surfactant mixtures, a systematic study was performed on the decomposition of  $\{\text{Fe}[\text{N}(\text{SiMe}_3)_2]_2\}_2$  in the presence of HDA and palmitic acid (PA) under mild conditions [50].

Acid concentration is a key parameter to tune the final mean size of the Fe NPs between 1.5 and 21 nm (Fig. 31.9a). This size increase is concomitant with the modification of the NPs shapes (Fig. 31.9b,c): spherical below 1.4 equiv acid per mol of iron atoms (equiv) and cubic above this value.

Such shape control can be understood in the framework of an environmentally dependent growth process. We observed the presence of organic superstructures filled with iron(II) species, containing carboxylates, at the very beginning of the reaction for large acid concentration (above 1.4 equiv), fairly similar to the superstructure of the cubes finally obtained (Fig. 31.10a–d). Based on a combined morphologic, magnetic and spectroscopic study of the reaction advancement, we proposed that the nucleation and growth can occur either outside these organic soft templates, i.e., in an isotropic environment, or inside them,

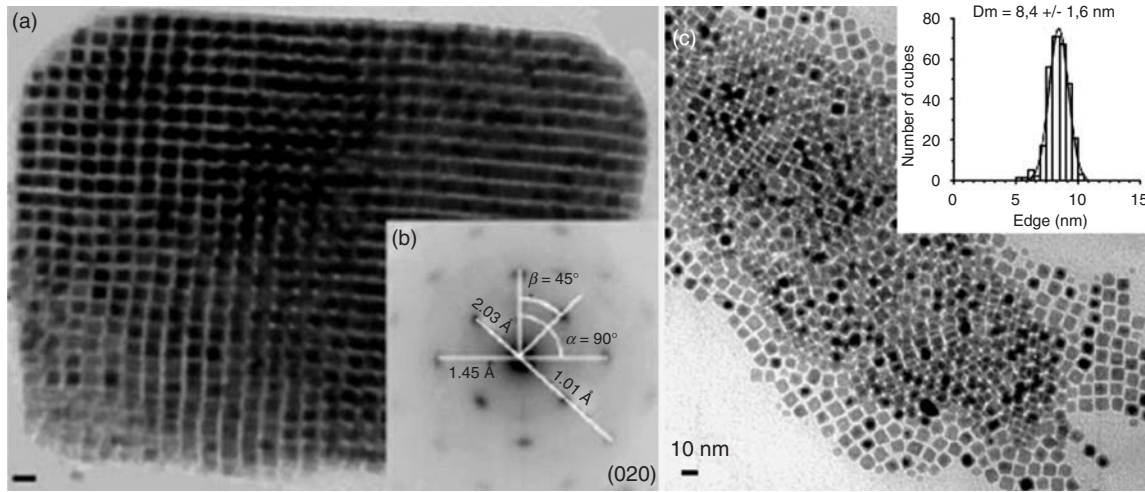


**Figure 31.8** (a) Transmission electron microscopy images of 7 nm nanocubes self-organized into cubic superlattices. (b) Electron diffraction pattern revealing base-centered cubic (bcc) structure of Fe(0) and the selective orientation of the nanocubes. (c) 2D assemblies obtained after dissolution of the super lattices.

that is, in an anisotropic environment (Fig. 31.10e). In the first case, we obtain spherical polycrystalline NPs of mean sizes increasing with the carboxylic acid concentration, as expected. In the second case, the reaction monitoring reveals several steps: (i) nucleation (ii) growth and coalescence favored by an amine-rich environment followed by (iii) growth and repair mechanisms in an acid-rich environment. These three main steps lead to cubic NPs organized into superstructures. The evolution of the environment from amine- to acid-rich is directly related to the decomposition of the iron(II) species that releases carboxylic acid in the medium.

Tuning the growth/coalescence steps by decreasing the reaction temperature (down to 120 °C) or by changing the mixture of surfactant used (dodecylamine/lauric acid) yielded NPs with unique features such as anisotropic stars [50] (Fig. 31.11a) or porous nanocubes, as revealed by electron tomography [51] (Fig. 31.11b–d).

In addition to their unique control of size and shapes, Fe NPs synthesized by this organometallic approach exhibit excellent magnetic properties. Magnetic vortex, a peculiar state which that at the transition between monodomain and multidomain configurations, has been for the first time evidenced in 30 nm Fe nanocubes by electron holography [52]. Magnetic interaction between self-assembled nanocubes usually leads to the disappearance of such vortices because of strong coupling. However, the presence of pores embedded within cubes could stabilize the vortices in assemblies of a few cubes [51], opening new a perspective toward spintronic applications (Fig. 31.12).

The drawback of the use of iron NPs is their air sensitivity. In an effort to combine good magnetic properties with air stability, we considered iron carbides. These phases form readily when iron is in the presence of a carbon source at high temperature, or at lower temperature under the conditions of the Fischer–Tropsch syntheses, namely in the presence of CO and H<sub>2</sub> at temperatures between 200 and 300 °C. Prior to our work no synthesis of monodisperse iron carbide NPs had been described. Addition of Fe(CO)<sub>5</sub> to preformed monodisperse iron NPs leads, depending on the gas atmosphere to iron carbide or core–shell iron/iron carbide NPs [53]. These particles were found to display excellent magnetic properties and to be stable in air after an initial period presumably corresponding to some surface oxidation.

## 31.5 COBALT

### 31.5.1 Cobalt Nanoparticles and Nanorods

Cobalt nanocrystals are also good candidates for many applications aiming at exploiting their magnetic properties [54]. This is due to their high magnetic moment and to their effective anisotropy which is much higher than that of iron. Furthermore, the possibility of cobalt in adopting different crystal phases facilitates a modulation of its magnetic properties through shape control.

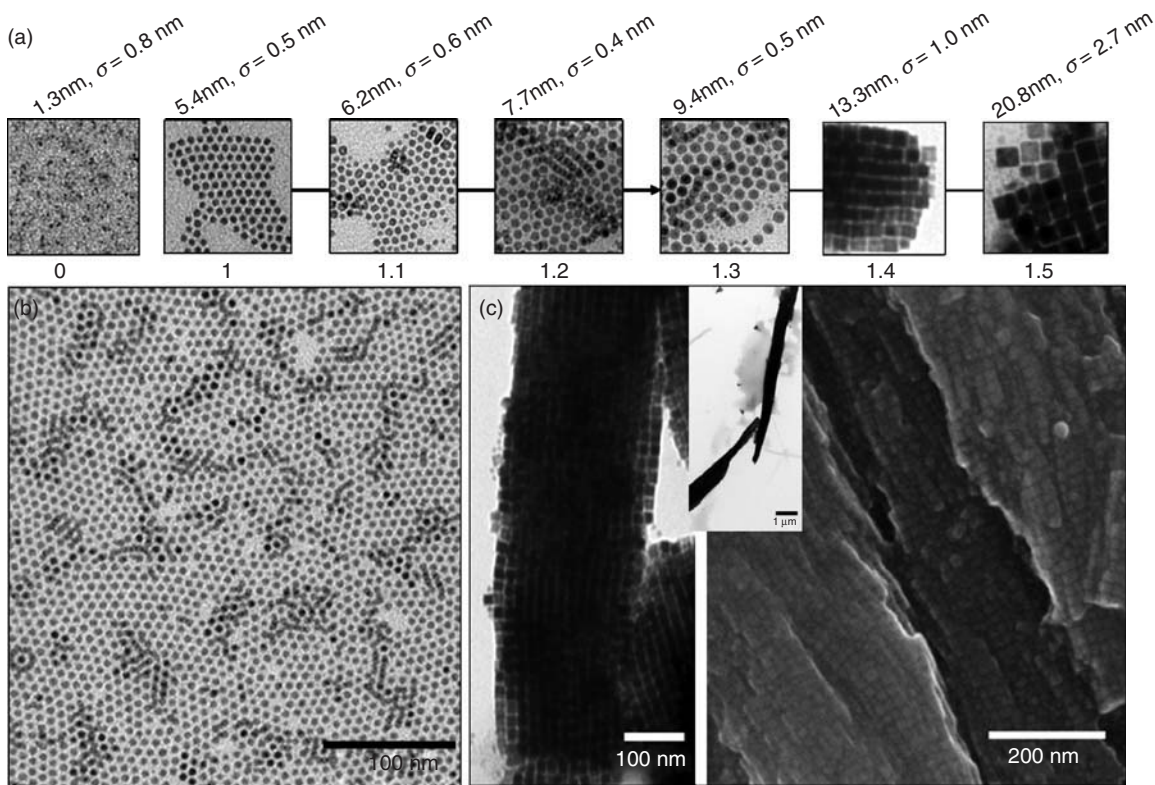


**Figure 31.9** TEM images of Fe NPs. (a) Size evolution as a function of the acid concentration between 0 and 1.5 equiv. (b) 5.5 nm nanospheres and (c) 13.3 nm nanocubes obtained with 1 and 1.4 equiv of acid, respectively. Nanocubes self-organized into micrometric wires [67].

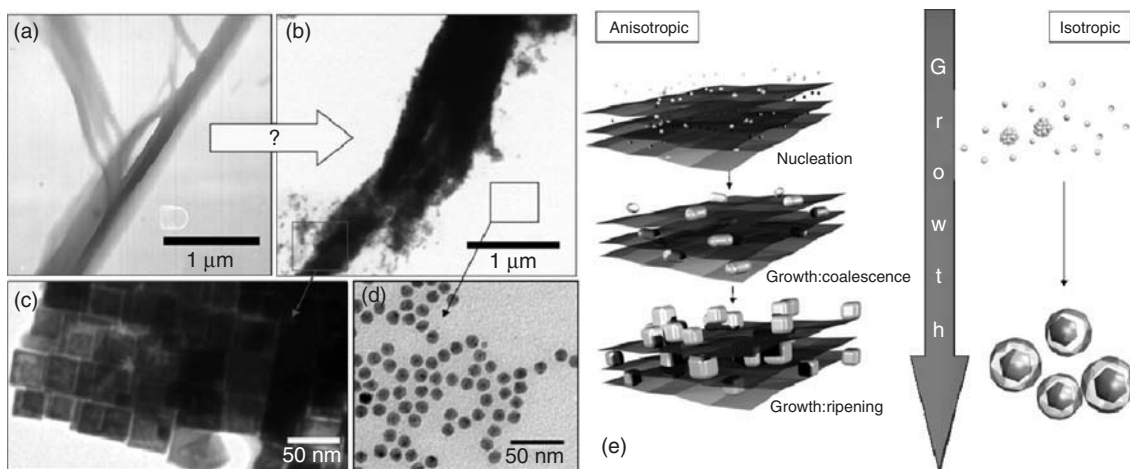


**Figure 31.10** TEM images of (a) organic super structure before decomposition and (b) self-assemblies obtained after 48 h; they are filled with (c) nanocubes while (d) nanospheres are found outside of these micrometric organizations. (e) Schematic view of the environment-dependent growth mechanism proposed.

The “organometallic” approach has greatly contributed to the enrichment of the arsenal of Co nanocrystals available by chemical routes, affording highly crystalline, oxide-free nanocrystals of various sizes and shapes. The first precursor used by our group was the  $\text{Co}^{\text{I}}$  organometallic complex  $[\text{Co}(\eta^3\text{-C}_8\text{H}_{13})(\eta^4\text{-C}_8\text{H}_{12})]$ . This compound in THF and in the presence of PVP affords, upon reaction with  $\text{H}_2$ , NPs of very small size (1.6–2 nm) even at temperatures as low as  $0^\circ\text{C}$  [55]. An important characteristic of these objects was the enhanced magnetic moment per cobalt atom ( $\mu_{\text{Co}} = 1.94 \pm 0.04 \text{ } \mu\text{B}$ )

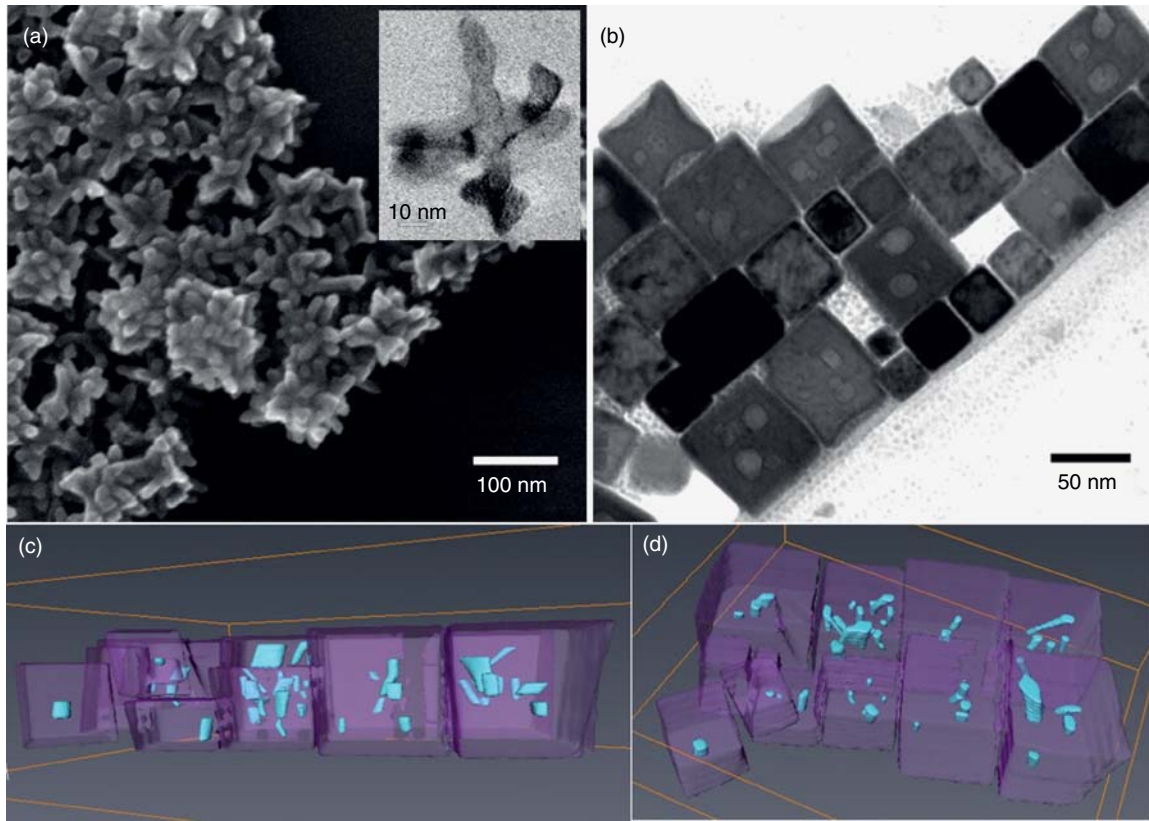


**Figure 31.11** (a) SEM image of nanostars. (Inset), TEM image of a single star. (b) TEM image of porous nanocubes, obtained with dodecylamine/lauric acid surfactants. (c), (d) 3D reconstruction of the nanocubes obtained from electron tomography study, the defects embedded within the objects are represented in blue, and the outer surface of the cubes are in light violet. (*See insert for color representation of the figure.*)

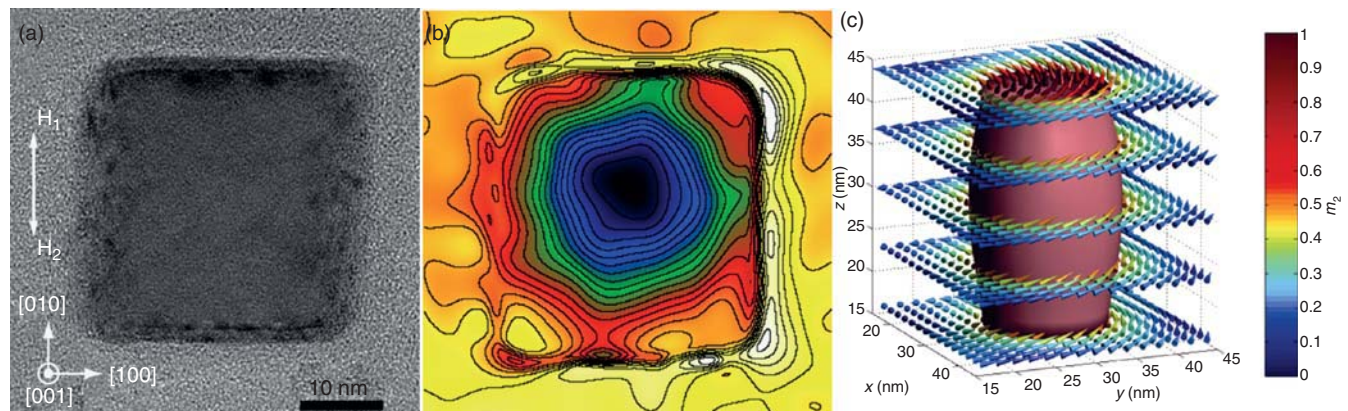


**Figure 31.12** (a) TEM image of a 30 nm nanocube. (b) Mapping of the induction field obtained from electronic holography. (c) 3D visualization of the magnetic moment simulated within the nanocube. (*See insert for color representation of the figure.*)

compared to the bulk value. This finding is attributed the high surface to volume ratio of the NPs. This enhancement, observed for the first time in NPs prepared by chemical methods, was found to cancel when CO was coordinated to the surface of the objects. A more detailed study of the magnetic properties of these particles and the effect of the high surface to volume ratio has shown that the influence of the surface atoms on the anisotropy is increased by decreasing the size and also that the magnetization enhancement increases with the applied magnetic field [56].

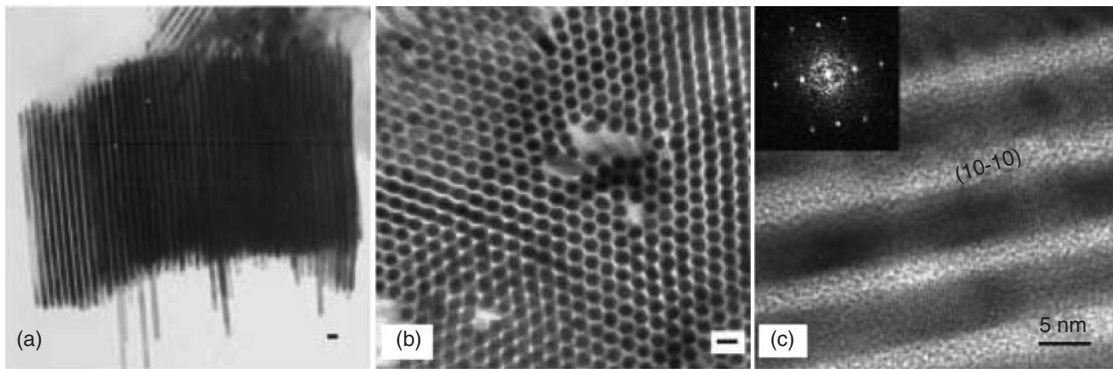


**Figure 31.13** (a,b) TEM images of self-organized nanorods (scale bar: 10 nm). (c) HRM image and electron diffraction pattern of some aligned rods.

The use of the binary ligand system long-chain amine/long-chain acid with the same compound has permitted the synthesis of anisotropic Co nano-objects by the reduction of the above mentioned precursor in anisole at 150 °C [12e, 57]. The role of dihydrogen was examined and found to be crucial for the formation of nanorods, since in its absence the formation of anisotropic nanorods is inhibited. The resulting objects varied from spherical NPs to long nanowires. The concentration in carboxylic acid had a strong influence on the shape of the final objects. For low acid concentrations (0.3 equiv), the resulting objects were spherical NPs, and for high concentrations long nanowires. Moreover, the length of the alkyl chain of the amine was shown to be critical for the dimensions of the objects obtained. Nano-objects with an aspect ratio between 1.7 and 22 could be formed by simply varying the nature of the amine. The nanorods obtained were found to be single crystalline with hcp structure and nonoxidized as revealed by high resolution electron microscopy (HREM) and WAXS studies. The impact of the shape anisotropy on the magnetic properties was evidenced by SQUID measurement (superconducting quantum interference device) of the hysteresis loops. The nanorods exhibited high coercive field (0.89 T) at 2 K. At the same time, the magnetic moment per atom was found to be identical to that of bulk cobalt (1.71  $\mu$ B). These nanorods self-assemble in solution, forming superlattices in which the rods are arranged with their long axes next to each other [58]. The mechanism invoked for their formation is an oriented attachment of the initially spherical NPs in a template formed by the organic ligands. TEM micrographs of these superlattices and an HREM images are shown in Fig. 31.13.

Cobalt nanodisks have also been prepared by the same method and the same precursor in the presence of rhodamine (RhB) and HDA. The bulkiness of RhB, which hinders its adsorption on the Co surface in the early growth stages as well as the specific adsorption of HDA at the {0001} facets, is responsible for this peculiar growth mode. An out-of-plane magnetization was observed. These nano-objects self-assemble into 1D chains with high magnetic anisotropy [59].

The  $\text{Co}^{\text{II}}$  coordination compound  $[\text{Co}\{\text{N}(\text{SiMe}_3)_2\}_2]$  is a precursor employed in more recent works. Being thermally more stable than  $[\text{Co}(\eta^3\text{-C}_8\text{H}_{13})(\eta^4\text{-C}_8\text{H}_{12})]$ , it has a longer “shelf-life”. Nevertheless, it is also readily reduced under  $\text{H}_2$ , giving rise to a great variety of cobalt nanocrystals. Similar reaction conditions give rise to qualitatively similar nanocrystals either when using  $[\text{Co}(\eta^3\text{-C}_8\text{H}_{13})(\eta^4\text{-C}_8\text{H}_{12})]$  or  $[\text{Co}\{\text{N}(\text{SiMe}_3)_2\}_2]$ . Indeed, when an HDA/lauric acid (LA) mixture is used with  $[\text{Co}\{\text{N}(\text{SiMe}_3)_2\}_2]$ , organized superlattices of several layers of arrays of vertically aligned nanorods are obtained in solution. The 3D arrays, the SEM (scanning electron microscopy) images of which are shown in Fig. 31.14, are larger than the ones obtained by  $[\text{Co}(\eta^3\text{-C}_8\text{H}_{13})(\eta^4\text{-C}_8\text{H}_{12})]$ . The nanorods are assembled in several layers of arrays in which the nanorods are arranged along their long axes [60].

Upon alignment under an external magnetic field in an organic matrix and after purification, these nanorods present increased coercive field values at room temperature (0.6 T), as well as a remnant magnetization value of about 0.90 Ms [61]. These characteristics make them good candidates for applications as permanent magnets or components for high-density magnetic recording devices.

### 31.5.2 Heterostructured Co Anisotropic Nanocrystals

An emerging direction in nanomaterials research concerns the synthesis of multifunctional nanocrystals [62]. “Seeded growth” [63] of a second material on already preformed nanocrystals has given access to nano-objects associating discrete, nonconcentric, and chemically different domains. Anisotropic nanocrystals due to their distinct reactivity along different facets offer the possibility to position the second domain on a specific facet [64]. Using as seeds cobalt nanorods we have

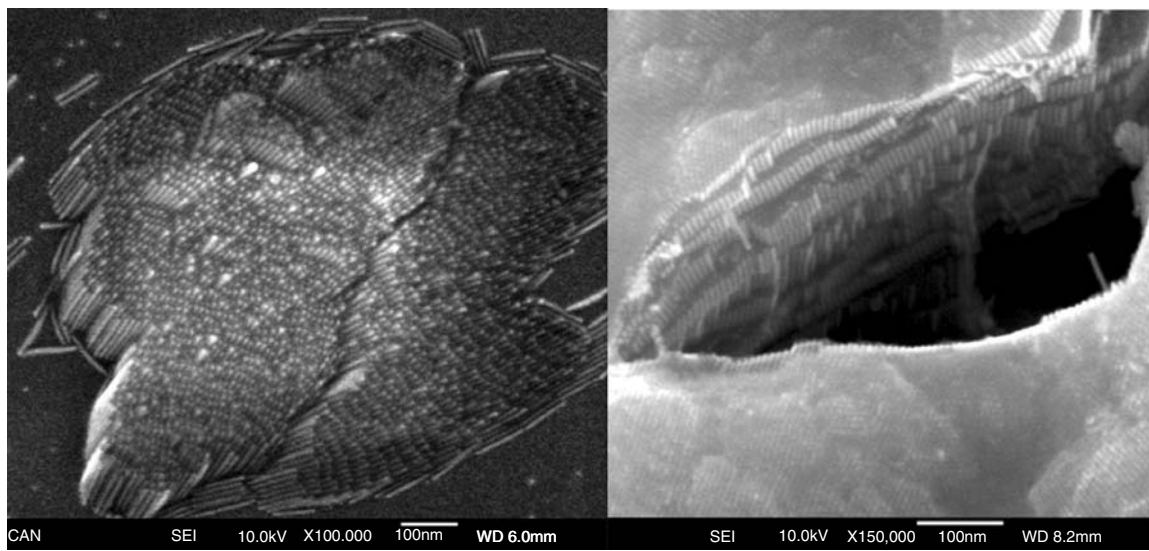


**Figure 31.14** SEM images of superlattices of Co nanorods prepared by  $[\text{Co}\{\text{N}(\text{SiMe}_3)_2\}_2]$ , in a mixture of HDA/LA.

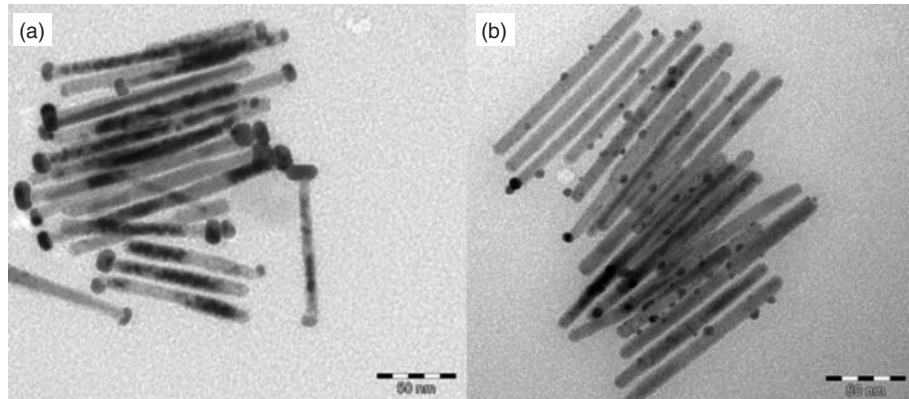


**Figure 31.15** (a) Au-tipped Co nanorods and (b) Au-decorated Co nanorods (scale bars 50 nm).

performed a secondary growth of gold toward Co–Au hybrid nano-objects. Control of the surface chemistry of the nanorods permits the control of the gold nucleation in a topologically selective way and growth of either gold-tipped or decorated nanorods, as shown in Fig. 31.15. The NPs on the lateral sides grow epitaxially, whereas the tips are strained because of lattice mismatch between the two metals across the (111) and (0002) planes of Au and Co, respectively [65].

Alternatively, we have used CdSe nanorods on which we have grown Co by reducing  $[\text{Co}(\eta^3\text{-C}_8\text{H}_{13})(\eta^4\text{-C}_8\text{H}_{12})]$  or  $[\text{Co}\{\text{N}(\text{SiMe}_3)_2\}_2]$  under conditions milder than usual in order to avoid any homogeneous nucleation of Co not associated to CdSe [66]. Cobalt tips initially growing as spheres finally adopt an anisotropic growth mode as shown in Fig. 31.16. Interestingly four growth modes have been identified by HREM, characterized by different angles between the long axes of CdSe and Co. These angles are dictated by the need to minimize of the lattice mismatch between the two materials along the various crystallographic directions. In heterostructured objects, the magnetic properties of Co are unaffected by the presence of CdSe, whereas the luminescence properties of CdSe are affected compared to pure CdSe but not completely quenched.

### 31.6 CONCLUSION

To conclude, the techniques and concepts of organometallic chemistry can be fruitfully adopted to the synthesis of NPs of various metals and of various size and shapes. Bimetallic nano-objects can also be easily produced, whether alloys, core–shell systems or heterostructures. Many different stabilizers can be used, whose choice is guided by the similarity

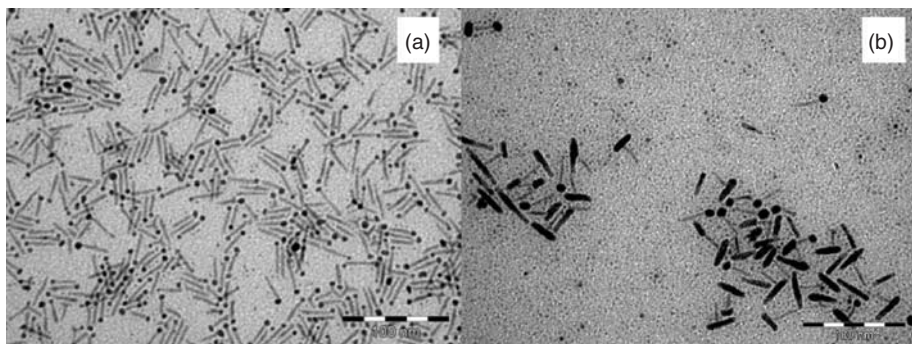


**Figure 31.16** CdSe nanorods with (a) spherical Co tips and (b) Co nanorods at the tips (scale bar 100 nm).

between the behavior of ligands on the molecular complexes and on NPs. Thus, hydrides and CO coordinate on the surface of these NPs, as well as olefins and methyl groups. The hydrides are always fluxional as determined by static D NMR whereas CO appears fluxional only when the surface of the particles is free. Amines are also fluxional but do not stabilize the particles unless they are added in excess. However, what is a drawback in molecular chemistry can be used here as an advantage since amines allow the growth of NPs and may lead to shape-controlled nano-objects. Phosphines and especially diphosphines are, as in molecular chemistry, the ligands of choice since their steric and electronic properties can be modulated. *N*-heterocyclic carbene ligands are definitely extremely well adapted to ruthenium and, if we want to look at complex ligands for, for example, asymmetric catalysis, we will have to consider them carefully.

Ligands are also involved in the growth of the NPs, and the choice of acid/amine mixtures allows the dissociation of a nucleation reservoir form a growth reservoir and, therefore, with the help of a dihydrogen atmosphere, the growth of large monodisperse nano-objects, iron nanocubes, and cobalt nanorods, the monodispersity of which results from thermodynamic control [67].

The need in surface chemistry will be the development of complex systems accommodating a combination of ligands some of which are specific for NPs to achieve selective catalytic transformations as well as cascade reactions. Similarly, complex nano-objects combining different functionalities (magnetic, optic, catalytic, electric) will be required in fields as different as energy conversion or nanomedicine. In all cases, the precise control of the nature and positioning of the different species and ligands will be required, which means that all these different aspects are new challenges for organometallic chemists who are likely to become more and more involved in the field.

## ACKNOWLEDGMENTS

The authors wish to acknowledge the financial support from CNRS, from the European Community's Seventh Framework Programme (FP7/2007–2013) under grant agreement no. 226716 and the ANR project Batmag.

## REFERENCES

1. (a) *Clusters and Colloids. From Theory to Applications*; Schmid,G., Ed.; Wiley-VCH Verlag GmbH: Weinheim, **1994**. (b) *Nanoparticles. From Theory to Application*; Schmid, G., Ed.; Wiley-VCH Verlag GmbH, Weinheim, **2004**.
2. (a) Zhou, B.; Han, S.; Raja R.; Somorjai G. *Nanotechnology in Catalysis*; Editors In Kluwer Academic/Plenum Publisher, New York, **2003**; (b) Ulrich, H.; Uzi L., Eds., *Nanocatalysis*; Nanoscience and Technology; Springer: Heidelberg, **2007**; (c) Roucoux, A.; Philippot, K. In *Handbook of Homogeneous Hydrogenations*; de Vries, J. G.; Elsevier, C. J.; Eds., Wiley-VCH Verlag GmbH: Weinheim, vol. 9, **2007**; p 217; (d) *Nanoparticles and Catalysis*; Astruc, D.; Ed., John Wiley & Sons, Inc.: New York, **2008**.
3. (a) Somorjai, G. A.; Frei, H.; Park, J. Y. *J. Am. Chem. Soc.* **2009**, *131*, 16589; (b) Somorjai, G. A.; Aliaga, C. *Langmuir* **2010**, *26*, 16190; (c) Somorjai, G. A.; Park, J. Y. *Surf. Sci.* **2009**, *603*, 1293; (d) Somorjai, G. A.; Li, Y. *Top. Catal.* **2010**, *53*, 311; (e) Zhang, Y.; Grass, M. E.; Kuhn, J. N.; Tao, F.; Habas, S. E.; Huang, W.; Yang, P.; Somorjai, G. A. *J. Am. Chem. Soc.* **2008**, *130*, 5868.
4. (a) Feng, L.; Hoang, D. T.; Tsung, C.; Huang, W.; Lo, S.; Wood, J. B.; Wang, H.; Tang, J.; Yang, P. *Nano Res.* **2011**, *4*, 61; (b) Tsung, C.; Kuhn, J. N.; Huang, W.; Aliaga, C.; Somorjai, G. A.; Yang, P. *J. Am. Chem. Soc.* **2009**, *131*, 5816.

5. See for example: (a) Vranka, R. G.; Dahl, L. F.; Chini, P.; Chatt, J. *J. Am. Chem. Soc.* **1969**, *91*, 1574; (b) Fumagalli, A.; Martinengo, S.; Chini, P.; Albinati, A.; Bruckner, S.; Heaton, B. T. *J. Chem. Soc. Chem. Comm.* **1978**, 195; (c) Washecheck, D. M.; Wucherer, E. J.; Dahl, L. F.; Ceriotti, A.; Longoni, G.; Manassero, M.; Sansoni, P. *J. Am. Chem. Soc.* **1979**, *101*, 6110.
6. Scott, S. L.; Bassett, J. M. *J. Mol. Catal.* **1994**, *86*, 5.
7. See for example: (a) Schmid, G.; Boese, R.; Pfeil, R.; Bandermann, F.; Meyer, S.; Calis, G. H. M.; van der Velden, J. W. A. *Chem. Ber.* **1981**, *114*, 3634; (b) Wallenberg, L. R.; Bovin, J. O.; Schmid, G. *Surf. Sci.* **1985**, *156*, 256; (c) Van Staveren, M. P. J.; Brom, H. B.; De Jongh, L. J.; Schmid, G. *Solid State Commun.* **1986**, *60*, 319; (d) Benfield, R. E.; Creighton, J. A.; Eadon, D. G.; Schmid, G. *Z. Phys. D Atom Mol. Cl.* **1989**, *12*, 533; (e) Schmid, G. *Inorg. Synth.* **1990**, *7*, 214.
8. Bradley, J. S.; Hill, E. H.; Leonowicz, M. E.; Wirzke, H. *J. Mol. Catal.* **1987**, *41*, 59.
9. Chaudret, B.; Commenges, G.; Poilblanc, R. *J. Chem. Soc. Chem. Comm.* **1982**, 1388.
10. Grellier, M.; Vendier, L.; Chaudret, B.; Albinati, A.; Rizzato, S.; Mason, S.; Sabo-Etienne, S. *J. Am. Chem. Soc.* **2005**, *127*, 17592.
11. Philippot K.; Chaudret, B. In Comprehensive Organometallic Chemistry III, Crabtree, R. H.; Mingos, M. P.; O'Hare, D.; Eds., Applications III: Functional Materials, Environmental and Biological Applications, Vol. 12; Elsevier: Oxford , **2007**; p 71, Chapter 03.
12. See for example: (a) Mehdaoui, B.; Carrey, J.; Stadler, M.; Cornejo, A.; Nayral, C.; Delpech, F.; Chaudret, B.; Respaud, M. *App. Phys. Lett.* **2012**, *100*, 052403; (b) Barriere, C.; Piettre, K.; Latour, V.; Margeat, O.; Turrin, C.-O.; Chaudret, B.; Fau, P. *J. Mater. Chem.* **2012**, *22*, 2279; (c) Meffre, A.; Lachaize, S.; Gatel, C.; Respaud, M.; Chaudret, B. *J. Mater. Chem.* **2011**, *21*, 13464; (d) Zadoina, L.; Soulantica, K.; Ferrere, S.; Lonetti, B.; Respaud, M.; Mingotaud, A.-F.; Falqui, A.; Genovese, A.; Chaudret, B.; Mauzac, M. *J. Mater. Chem.* **2011**, *21*, 6988; (e) Ciuculescu, D.; Dumestre, F.; Comesana-Hermo, M.; Chaudret, B.; Spasova, M.; Farle, M.; Amiens, C. *Chem. Mater.* **2009**, *21*, 3987; (f) Margeat, O.; Ciuculescu, D.; Lecante, P.; Respaud, M.; Amiens, C.; Chaudret, B. *Small* **2007**, *3*, 451.
13. See for example: (a) Coppel, Y.; Spataro, G.; Pages, C.; Chaudret, B.; Maisonnat, M.; Kahn, M. L. *Chem. Eur. J.* **2012**, *18*, 5384; (b) Cros-Gagneux, A.; Delpech, F.; Nayral, C.; Cornejo, A.; Coppel, Y.; Chaudret, B. *J. Am. Chem. Soc.* **2010**, *132*, 18147; (c) Kahn, M. L.; Glaria, A.; Pages, C.; Monge, M.; Saint Macary, L.; Maisonnat, M.; Chaudret, B. *J. Mater. Chem.* **2009**, *19*, 4044.
14. (a) Pery, T.; Pelzer, K.; Buntkowsky, G.; Philippot, K.; Limbach, H.-H.; Chaudret B. *Chemphyschem* **2005**, *6*, 605; (b) Schröder, F.; Esken, D.; Cokoja, M.; van den Berg, M. W. E.; Lebedev, O.; Van Tendeloo, G.; Walaszek, B.; Buntkowsky, G.; Limbach, H.-H.; Chaudret, B.; Fischer, R. A. *J. Am. Chem. Soc.* **2008**, *130*, 6119; (c) del Rosal, I.; Gutmann, T.; Maron, L.; Jolibois, F.; Chaudret, B.; Walaszek, B. *Limbach, H.-H.*; Poteau, R.; Buntkowsky, G. *Phys. Chem. Chem. Phys.* **2009**, *11*, 5657; (d) Gutmann, T.; Walaszek, B.; Yeping, X.; Wächtler, M.; del Rosal, I.; Grünberg, A.; Poteau, R.; Axet, R.; Lavigne, G.; Chaudret, B.; Limbach H.-H.; Buntkowsky, G. *J. Am. Chem. Soc.* **2010**, *132*, 11759.
15. Schmid G. in *Nanoparticles From Theory to Applications*, 2nd ed., Completely Revised and Updated Edition; G. Schmid, Ed.; Wiley-VCH Verlag GmbH: Weinheim, **2010**; p 217.
16. Pan, C.; Pelzer, K.; Philippot, K.; Chaudret, B.; Dassenoy, F.; Lecante, P.; Casanove, M.-J. *J. Am. Chem. Soc.* **2001**, *123*, 7584.
17. Novio, F.; Philippot, K.; Chaudret, B. *Catal. Lett.* **2010**, *140*, 1.
18. Vidoni, O.; Philippot, K.; Amiens, C.; Chaudret, B.; Balmes, O.; Malm, J.-O.; Bovin, J.-O.; Senocq, F.; Casanove, M.-J. *Angew. Chem. Int. Ed.* **1999**, *38*, 3736.
19. Pelzer, K.; Vidoni, O.; Philippot, K.; Chaudret, B.; Collière, V. *Adv. Funct. Mater.* **2003**, *13*, 118.
20. (a) Hallet, J. P.; Welton, T. *Chem. Rev.* **2011**, *111*, 3508; (b) Yan, N.; Xiao, C.; Kou, Y. *Coord. Chem. Rev.* **2010**, *254*, 1179; (c) Parvulescu, V. I.; Hardacre, C. *Chem. Rev.* **2007**, *107*, 2615.
21. (a) Padua, A. A. H.; Costa Gomes, M. F.; Canongia Lopes, J. N. A. *Acc. Chem. Res.* **2007**, *40*, 1087; (b) Pensado, A. S.; Padua, A. A. H. *Angew. Chem. Int. Ed.* **2011**, *50*, 8683.
22. (a) Prechtl, M. H. G.; Scariot, M.; Scholten, J. D.; Machado, G.; Teixeira, S. R.; Dupont, J. *Inorg. Chem.* **2008**, *47*, 8995; (b) Prechtl, M. H. G.; Scholten, J. D.; Dupont, J. *J. Mol. Chem.* **2009**, *313*, 74; (c) Scholten, J. D.; Leal, B. C.; Dupont, J. *ACS Catal.* **2012**, *2*, 184.
23. Gutel, T.; Garcia-Antón, J.; Pelzer, K.; Philippot, K.; Santini, C. C.; Chauvin, Y.; Chaudret, B.; Bassett, J. M. *J. Mater. Chem.* **2007**, *17*, 3290.
24. Gutel, T.; Santini, C. C.; Philippot, K.; Padua, A.; Pelzer, K.; Chaudret, B.; Chauvin, Y.; Bassett, J.-M. *J. Mat. Chem.* **2009**, *19*, 3624.
25. Campbell P. S.; Santini, C. C.; Bouchu, D.; Fenet, B.; Philippot, K.; Chaudret, B.; Padua, A. A. H.; Chauvin, Y. *Phys. Chem. Chem. Phys.* **2010**, *12*, 4217.
26. Salas, G.; Santini, C. C.; Philippot, K.; Colliere, V.; Chaudret, B.; Fenet, B.; Fazzini, P. F. *Dalton Trans.* **2011**, *40*, 4660.
27. Salas, G.; Podgorsek, A.; Campbell, P. S.; Santini, C. C.; Padua, A. A. H.; Gomes, M. F. C.; Philippot, K.; Chaudret, B.; Turmine, B. *Phys. Chem. Chem. Phys.* **2011**, *13*, 13527.
28. García-Antón, J.; Axet, M. R.; Jansat, S.; Philippot, K.; Chaudret, B.; Pery, T.; Buntkowsky, G.; Limbach, H. H. *Angew. Chem. Int. Ed.* **2008**, *47*, 2074.

29. See for example: (a) Sun, S.; Fullerton, E. E.; Weller, D.; Murray, C. B. *IEEE Trans. Magn.* **2001**, *37*, 1239; (b) Metin, O.; Mazumder, V.; Ozkar, S.; Sun, S. *J. Am. Chem. Soc.* **2010**, *132*, 1468; (c) Liu, Y.; Wang, C.; Wei, Y.; Zhu, L.; Li, D.; Jiang, J. S.; Markovic, N. M.; Stamenkovic, V. R.; Sun, S. *Nano Lett.* **2011**, *11*, 1614.
30. Favier, I.; Massou, S.; Teuma, E.; Philippot, K.; Chaudret, B.; Gomez, M. *Chem. Commun.* **2008**, 3296.
31. Weitz, D. A.; Huang, J. S.; Lin M. Y.; Sung, J. *Phys. Rev. Lett.* **1985**, *54*, 1416.
32. Gonzalez-Galvez, D.; Nolis, P.; Philippot, K.; Chaudret, B.; van Leeuwen, P. W. N. M. *ACS Catal.* **2012**, *2*, 317.
33. (a) Jansat, S.; Gomez, M.; Philippot, K.; Muller, G.; Guiu, E.; Claver, C.; Castillon, S.; Chaudret, B. *J. Am. Chem. Soc.* **2004**, *126*, 1592; (b) Favier, I.; Gomez, M.; Muller, G.; Axet, M. R.; Castillon, S.; Claver, C.; Jansat, S.; Chaudret, B.; Philippot K. *Adv. Synth. Catal.* **2007**, *349*, 2459.
34. Gual, A.; Axet, M. R.; Philippot, K.; Chaudret, B.; Denicourt-Nowicki, N.; Roucoux, A.; Castillón, S.; Claver, C. *Chem. Commun.* **2008**, 2759.
35. Lara, P.; Rivada-Wheelaghan, O.; Conejero, S.; Poteau, R.; Philippot, K.; Chaudret, B. *Angew. Chem. Int. Ed.* **2011**, *50*, 12080.
36. Mornet, S.; Vasseur, S.; Grasset, F.; Duguet, E. *J. Mater. Chem.* **2004**, *14*, 2161.
37. Lacroix, L.-M.; Ho, D.; Sun, S. *Curr. Top. Med. Chem.* **2010**, *10*, 1184.
38. Huber, D. *Small* **2005**, *1*, 482.
39. Yang, H.; Ito, F.; Hasegawa, D.; Ogawa, T.; Takahashi, M. *J. Appl. Phys.* **2007**, *101*, 09J112.
40. Farrell, D.; Majetich, S. A.; Wilcoxon, J. P. *J. Phys. Chem. B* **2003**, *107*, 11022.
41. Peng, S.; Wang, C.; Xie, J.; Sun, S. *J. Am. Chem. Soc.* **2006**, *128*, 10676.
42. Hadjipanayis, C. G.; Bonder, M. J.; Balakrishnan, S.; Wang, X.; Mao, H.; Hadjipanayis, G. C. *Small* **2008**, *4*, 1925.
43. Andersen, R. A.; Faegri, K.; Green, J. C.; Haaland, A.; Lappert, M. F.; Leung, W.-P.; Rydpal, K. *Inorg. Chem.* **1988**, *27*, 1782.
44. Olmstead M. M.; Power, P. P.; Shoner, S. C. *Inorg. Chem.* **1991**, *30*, 2547.
45. Lacroix, L.-M.; Lachaize, S.; Falqui, A.; Blon, T.; Carrey, J.; Respaud, M.; Dumestre, F.; Amiens, C.; Margeat, O.; Chaudret, B.; Lecante, P.; Snoeck, E. *J. Appl. Phys.* **2008**, *103*, 07D521.
46. Margeat, O.; Dumestre, F.; Amiens, C.; Chaudret, B.; Lecante, P.; Respaud, M. *Prog. Solid State Chem.* **2005**, *33*, 71.
47. Dumestre, F.; Chaudret, B.; Amiens, C.; Renaud, P.; Fejes, P. *Science* **2004**, *303*, 821.
48. Desvaux, C.; Amiens, C.; Fejes, P.; Renaud, P.; Respaud, M.; Lecante, P.; Snoeck, E.; Chaudret, B. *Nature Mater.* **2005**, *4*, 750.
49. Tan, R. P.; Carrey, J.; Desvaux, C.; Lacroix, L.-M.; Renaud, P.; Chaudret, B.; Respaud, M. *Phys. Rev. B Condens. Matter* **2009**, *79*, 174428.
50. Lacroix, L.-M.; Lachaize, S.; Falqui, A.; Respaud, M.; Chaudret, B. *J. Am. Chem. Soc.* **2009**, *131*, 549.
51. Lacroix, L.-M.; Lachaize, S.; Hüe, F.; Gatel, C.; Blon, T.; Tan, R. P.; Carrey, J.; Warot-Fonrose, B.; Chaudret, B. *Nano Lett.* **2012**, *12*, 3245.
52. Snoeck, E.; Gatel, C.; Lacroix, L.-M.; Blon, T.; Lachaize, S.; Carrey, J.; Respaud, M.; Chaudret, B. *Nano Lett.* **2008**, *8*, 4293.
53. Meffre, A.; Mehdaoui, B.; Kelsen, V.; Fazzini, P. F.; Carrey, J.; Lachaize, S.; Respaud, M.; Chaudret B. *Nano Lett.* **2012**, *12*, 4722.
54. (a) Weller, D.; Moser, A. *IEEE Trans. Magn.* **1999**, *35*, 4423; (b) Gutfleisch, O. *J. Phys. D Appl. Phys.* **2000**, *33*, R157.
55. Osuna, J.; de Caro, D.; Amiens, C.; Chaudret, B.; Snoeck, E.; Respaud, M.; Broto, J.-M.; Fert, A. *J. Phys. Chem.* **1996**, *100*, 14571.
56. Respaud, M. Broto, J. M.; Rakoto, H.; Fert, A. R.; Thomas, L.; Barbara, B.; Vereilst, M.; Snoeck, E.; Lecante, P.; Mosset, A.; Osuna, J.; Ould Ely, T.; Amiens, C.; Chaudret, B. *Phys. Rev. B Condens. Matter* **1998**, *57*, 2925
57. Dumestre, F.; Chaudret, B.; Amiens, C.; Fromen, M. C.; Casanove, M. J.; Renaud, P.; Zurcher, P. *Angew. Chem. Int. Ed.* **2002**, *41*, 4286.
58. Dumestre, F.; Chaudret, B.; Amiens, C.; Respaud, M.; Fejes, P.; Renaud, P.; Zurcher, P. *Angew. Chem. Int. Ed.* **2003**, *42*, 5213.
59. Comesana-Hermo, M.; Ciuculescu, D.; Li, Z-A.; Stienens, S.; Spasova, M.; Farle, M.; Amiens, C. *J. Mater. Chem.* **2012**, *22*, 8043
60. Wetz, F.; Soulantica, K.; Respaud, M.; Falqui, A.; Chaudret, B. *Mater. Sci. Eng. C* **2007**, *27*, 1162
61. Soulantica, K.; Wetz, F.; Maynadié, J.; Falqui, A.; Tan, R. P.; Blon, T.; Chaudret, B.; Respaud, M. *Appl. Phys. Lett.* **2009**, *95*, 152504.
62. Cozzoli, P. D.; Pellegrino, T.; Manna, L. *Chem. Soc. Rev.* **2006**, *35*, 1195.
63. (a) Yu, H.; Gibbons, P. C.; Kelton, K. F.; Buhro, W. E. *J. Am. Chem. Soc.* **2001**, *123*, 9198; (b) Wilcoxon, J. P.; Provencio, P. P. *J. Am. Chem. Soc.* **2004**, *126*, 6402.
64. (a) Mokari, T.; Rothenberg, E.; Popov, I.; Costi, R.; Banin, U. *Science* **2004**, *304*, 1787; (b) Costi, R.; Saunders E.; Banin, U. *Angew. Chem. Int. Ed.* **2010**, *49*, 4878.
65. Wetz, F.; Soulantica, K.; Falqui, A.; Respaud, M.; Snoeck, E.; Chaudret B. *Angew. Chem. Int. Ed.* **2007**, *46*, 7079.
66. Maynadié, J.; Salant, A.; Falqui, A.; Respaud, M.; Shaviv, E.; Banin, U.; Soulantica, K.; Chaudret, B. *Angew. Chem. Int. Ed.* **2009**, *48*, 1814.
67. Lacroix, L.-M.; Lachaize, S.; Carrey, J.; Respaud, M.; Chaudret, B. *Actualité chimique* **2011**, *351*, 28–35.

## ORGANOMETALLIC COMPOUNDS IN THE SYNTHESIS OF NEW MATERIALS: OLD LIGANDS, NEW TRICKS

PIOTR SOBOTA\* AND ŁUKASZ JOHN

*Faculty of Chemistry, University of Wrocław, Wrocław, Poland*

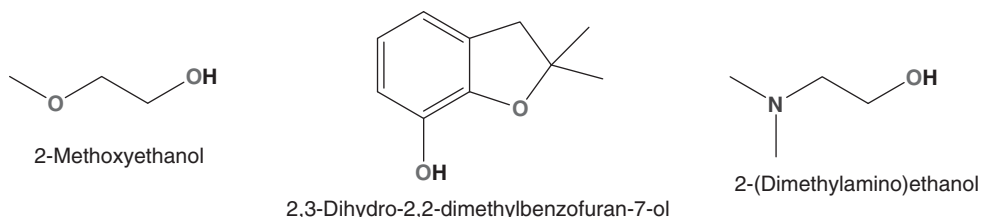
### 32.1 INTRODUCTION

Organometallic compounds and their derivatives, especially those containing alkoxide and aryloxide ligands, represent an enormous family of species featuring broad structural diversities and their chemistry has significantly expanded recently [1]. The development of modern technologies and synthetic approaches has allowed desired products to be produced under mild conditions and has provided more versatility over the stoichiometry, composition, structure, and morphology of the produced inorganic materials than can be obtained using conventional methods such as solid-state reactions [2]. For instance, these compounds are perfect candidates for sol–gel synthesis and various chemical vapor deposition techniques to produce highly phase-pure oxide products [3].

Interest in the field of mixed-metal alkoxo-organometallic and alkoxide chemistry has significantly expanded, largely because of their attractive structural chemistry, catalytic properties, and potential for industrial applications. The applicability of such compounds is related to the cooperation of two different metals in a single complex, which can result in interesting properties that are not the simple sum of the individual metal ions, and are often crucial to achieve the desired activity from a system. In this chapter we present three relatively unexplored synthetic methods for obtaining functional materials using organometallic-derived compounds aimed at producing heterometallic precursors for a wide range of oxide materials. First, stopping the common tendency toward oligomerization of metal alkoxides by the addition of organometallic Lewis acids to reaction systems, the so-called deoligomerization by cocomplexation strategy will be discussed [4]. Second, it will be shown that coordinated alcohol molecules that possess a hydroxyl group at the metal site are a perfect anchor for organometallic moieties [5]. Third, a simple and unique synthetic method comprising the elimination of a cyclopentadienyl ( $Cp$ ) ring from group 4 metallocenes to produce  $CpH$  using group 2 alkoxides and alcohol as a source of protons to produce heterometallic species will be highlighted [6]. Finally, the use of mixed-metal complexes as precursors to oxide materials will be highlighted.

### 32.2 FUNCTIONALIZED ALCOHOLS AS LIGANDS

Functionalized by O- and N-donor atoms, alcohols are now ubiquitous ligands in coordination chemistry because of their unique properties. Being relatively strong  $\sigma$ -donors and generally weak  $\pi$ -acceptors,  $O,O'$ - and  $O,N$ -ligands generally form bonds with various metal centers, resulting in heterometallic complexes with organometallic moieties, for example,  $MR_2^+$

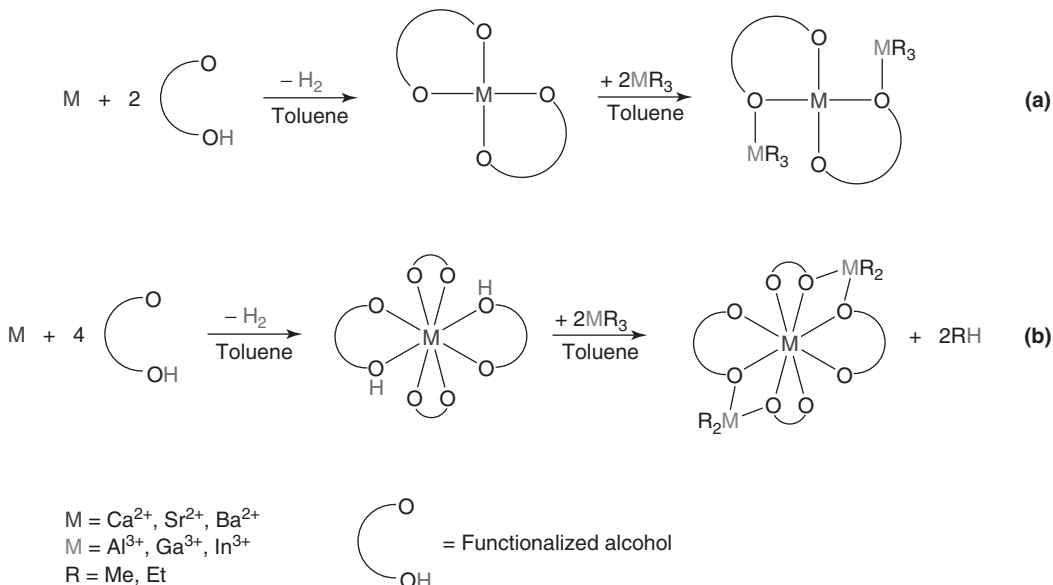
**Figure 32.1** Functionalized alcohols.

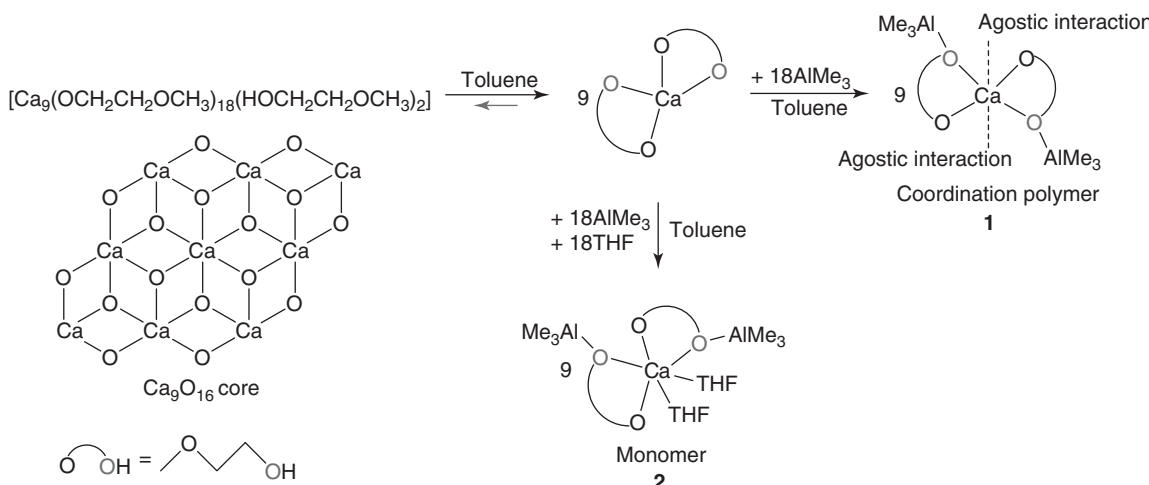
(M = group 13 metal; R = Me, Et, etc.). Donor-functionalized alcohols (Fig. 32.1) are potentially polydentate ligands, which can give rise to compounds with enhanced stability through ligand chelation. The choice of functionalized alcohols is generally dictated by how well their metal complexes crystallize from common hydrocarbon solutions.

### 32.3 ORGANOMETALLICS IN THE SYNTHESIS OF HETEROMETALLIC COMPLEXES

Heterometallic alkoxide complexes and their derivatives play key roles in many fields of chemistry. For example, they are an attractive group of molecular precursors to binary metal oxides such as perovskites  $\text{ABO}_3$  (A = group 2 cation, B = group 4 cation) and spinels  $\text{AB}_2\text{O}_4$  (B = group 13 cation). Coordinated alkoxo groups and alcohol molecules attached to the metal of a group 2 alkoxide result in excellent anchors for organometallic moieties. Such a connection can be created in two ways depending on the metal-to-alcohol ratio (Scheme 32.1). For instance, a group 2 alkoxide organometallic compound  $\text{M}'\text{R}_3$  (where M' = group 13 cation, R = alkyl group) can be bound directly to an alkoxide oxygen atom (Scheme 32.1, Eq. (a)).

Conversely, when a metal alkoxide also possesses coordinated alcohol molecules (Scheme 32.1, Eq. (b)), the driving force for the reaction is the evolution of a hydrocarbon RH, and the resulting  $\text{M}'\text{R}_2^+$  moiety becomes coordinated to a  $[\text{M}(\text{OR})_4]^{2-}$  core (M = group 2 cation, ROH = functionalized alcohol). It is worth noting that M-to-M' (1:2) is defined on the molecular level and exactly matches spinel-like double oxides.

**Scheme 32.1** Synthetic strategies for the cooperation of group 13 organometallic moieties with group 2 alkoxides.



**Scheme 32.2** General scheme for the addition of  $AlMe_3$  molecules to alkoxo oxygen atoms and the saturation of the calcium coordination sphere by THF.

### 32.3.1 Deoligomerization by Cocomplexation using Organometallics

A numbers of calcium alkoxides have been synthesized to date [7]. Because their derivatives possess groups such as  $MeO^-$ ,  $EtO^-$ , and  $^iPrO^-$ , they often form insoluble, large aggregates that have a tendency to continuously equilibrate in solution [8]. Because of this, the synthesis of calcium alkoxides of low nuclearity is cumbersome and usually requires the use of sterically large chelating ligands [9] or Lewis acids to prevent aggregation.

We have developed an efficient deoligomerization approach using organometallic compounds [4] (Scheme 32.2). For example, calcium 2-methoxyethoxide ( $[Ca_9(OCH_2CH_2OCH_3)_{18}(HOCH_2CH_2OCH_3)_2]$ ) [10], which contains nine calcium atoms, partially dissociates in toluene and then reacts with an excess of  $AlMe_3$  to produce a crystalline coordination polymer  $[Ca\{(\mu\text{-OCH}_2CH_2OCH}_3)(\mu\text{-Me})AlMe_2\}_2]_n$ , in which every monomer unit has a 1:2 calcium/aluminum ratio (Fig. 32.2, complex **1**) in the solid state. The polymeric structure is created by the presence of weak  $\gamma$ -agostic interactions of the methyl groups of trimethylaluminum with calcium atoms. Each unit possesses two bridging  $(\mu\text{-Me})AlMe_2$  groups that allow it to form a tetrametallaoctacyclic ring. A similar ring was found in the calcium-aluminum dimer reported by Hanusa et al. [11].  $AlMe_3$  acts as both a Lewis acid and as a neutral base, interacting through a methyl group. Such a coordination mode shows the carbanionic character of the alkyl group.

The analogous reaction using tetrahydrofuran (THF) leads to the saturation of calcium sites via the addition of two solvent molecules to form a six-coordinate monomeric  $[Ca\{(\mu\text{-OCH}_2CH_2OCH}_3)AlMe_3\}_2(THF)_2]$  complex causing the rupture of the agostic interactions that maintain the polymeric architecture (Fig. 32.2, complex **2**) [4].

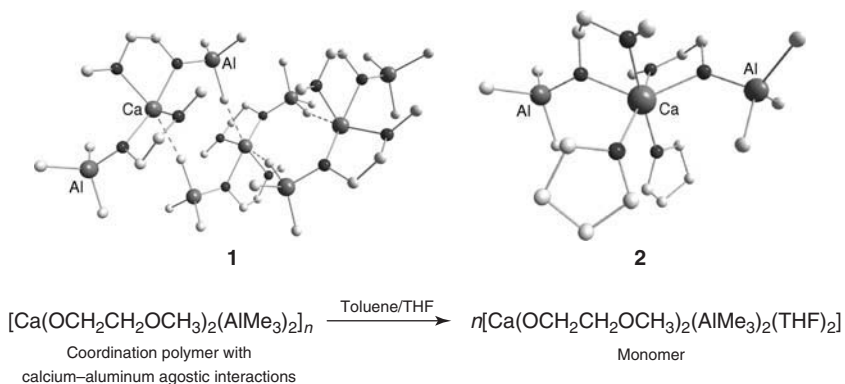


**Figure 32.2** Molecular structures of  $[Ca\{(\mu\text{-OCH}_2CH_2OCH}_3)(\mu\text{-Me})AlMe_2\}_2]$  (**1**) and  $[Ca\{(\mu\text{-OCH}_2CH_2OCH}_3)AlMe_3\}_2(THF)_2]$  (**2**) (the H atoms are omitted for clarity).

These examples clearly demonstrate that the oligomerization process can be easily shifted by organometallic species anchoring on alkoxo oxygens or by the introduction of weak donors such as THF to the reaction (Scheme 32.2). These two synthetic pathways effectively prevent agglomeration and allow the production of well-defined calcium–aluminum species that possess metal-to-metal ratios equivalent to those for spinels.

### 32.3.2 Coordinated Alcohol Molecules as a Perfect Anchor for Organometallics

Among the synthetic methods to obtain heterobimetallic alkoxo-organometallic compounds, one of the least explored reactions involves organometallic complexes with aryloxides that feature coordinated alcohols at the metal site [5]. Our laboratory has prepared group 2 aryloxide complexes  $[M(\text{ddbfO})_2(\text{ddbfOH})_2]$  ( $M = \text{Ba}^{2+}$  [5],  $\text{Sr}^{2+}$  [12];  $\text{ddbfOH} = 2,3\text{-dihydro-2,2-dimethylbenzofuran-7-ol}$ ) that possess protonated hydroxyl groups coordinated to the metal which could be used as supports for other organometallic fragments (Scheme 32.3) [13]. The driving force for these reactions, carried out in toluene, is the removal of the hydroxyl protons from the coordinated  $\text{ddbfOH}$  molecules [14] and the liberation of alkanes, resulting in the coordination of aryloxo oxygen atoms with an appropriate  $\text{MR}_x^+$  moiety to form  $[M\{(\mu\text{-ddbfO})_2\text{M}'\text{R}_x\}]_2$  ( $M = \text{Ba}^{2+}, \text{Sr}^{2+}; M' = \text{Zn}^{2+}, \text{Al}^{3+}, \text{Ga}^{3+}, \text{In}^{3+}; R = \text{Me, Et}; x = 1, 2$ ) (see examples in Fig. 32.3).

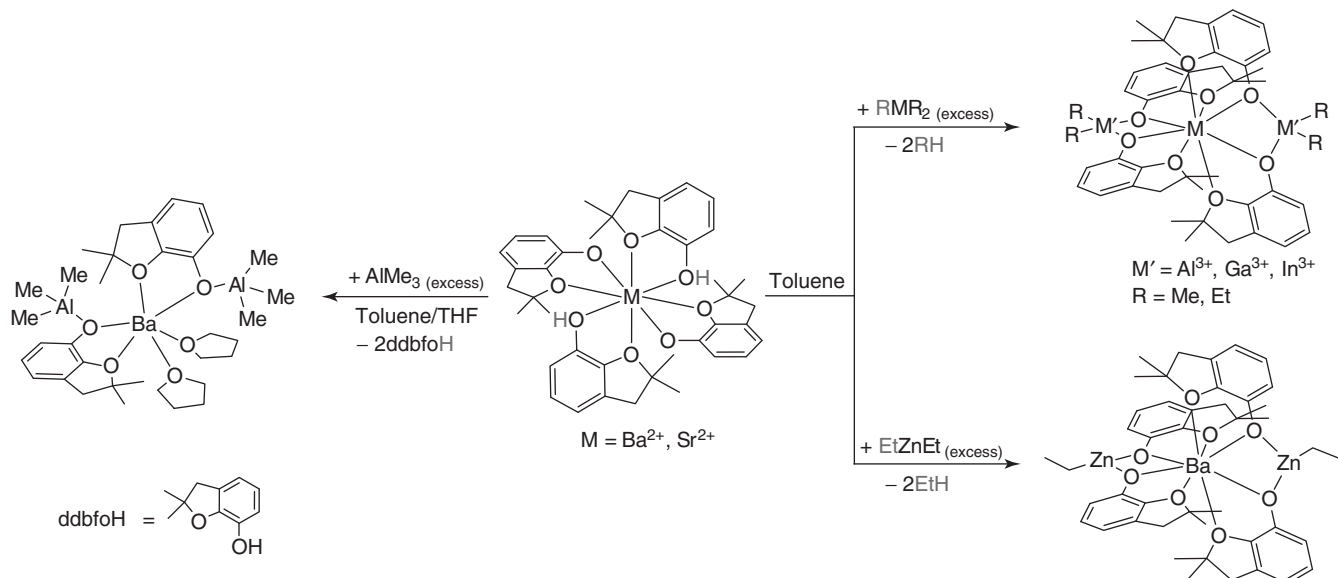
The reaction of barium 7-benzofuranoxide with an excess of  $\text{AlMe}_3$  in a toluene/THF mixture resulted in a six-coordinate  $[\text{Ba}\{(\mu\text{-ddbfO})_2\text{AlMe}_2\}_2(\text{THF})_2]$  compound.

In this case, the substitution of two  $\text{ddbfOH}$  molecules by THF is observed and trimethylaluminum simply coordinates to the aryloxo oxygen atoms [5] (Scheme 32.3).

Depending on these complexes compositions, the obtained compounds constitute well-defined molecular precursors to highly phase-pure perovskite-like (e.g.,  $\text{BaZn}_2\text{O}_3$ ) and spinel-like (e.g.,  $\text{BaAl}_2\text{O}_4$ ,  $\text{BaGa}_2\text{O}_4$ ,  $\text{BaIn}_2\text{O}_4$ ) binary oxides. For example, the thermolysis of  $[\text{Ba}\{(\mu\text{-ddbfO})_2\text{AlMe}_2\}_2]$  at  $1300^\circ\text{C}$  leads to a  $\text{BaAl}_2\text{O}_4$  double oxide. The diffraction pattern in Fig. 32.4 shows that the obtained barium–aluminum oxide matches the  $\text{BaAl}_2\text{O}_4$  spinel [11].

### 32.3.3 Promoting Effect of Group 2 Alkoxides on the Protonation of Metallocenes

Heterometallic complexes, especially those containing transition and main group metals, are of great interest [15]. Interest in these compounds stems from their applications in stoichiometric and catalytic reactions [16]. Furthermore, polymetallic clusters of paramagnetic metal ions have attracted much interest since the discovery that these molecules can display single-molecule magnetism [17]. They also constitute an interesting group of single-source precursors for mixed-metal oxides [3].



**Scheme 32.3** Synthesis of group 2/group 12 and 13 aryloxo-organometallic complexes.

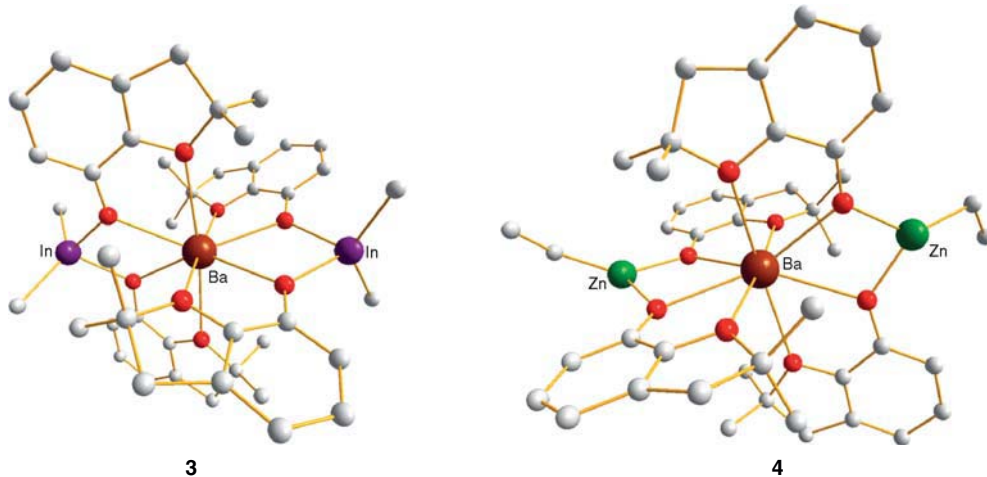


**Figure 32.3** Molecular structure of  $[\text{Ba}\{(\mu\text{-ddbfo})_2\text{InMe}_2\}_2]$  (**3**) and  $[\text{Ba}\{(\mu\text{-ddbfo})_2\text{ZnEt}\}_2]$  (**4**) (the H atoms are omitted for clarity). (See insert for color representation of the figure.)

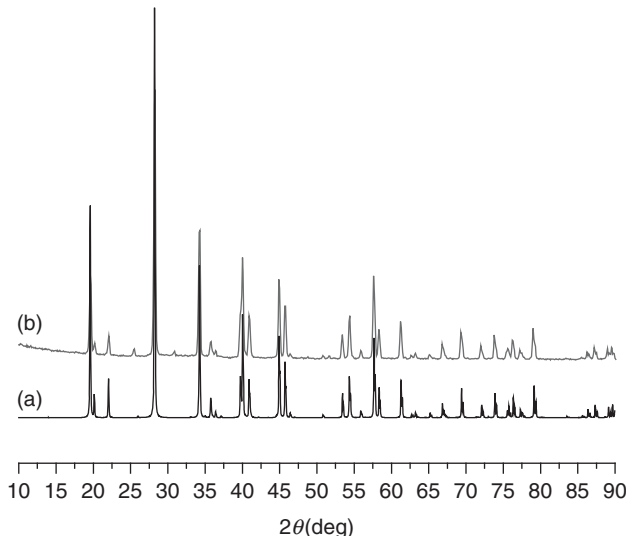


**Figure 32.4** Powder XRD patterns of (a)  $\text{BaAl}_2\text{O}_4$  (ICSD 10036) and (b)  $[\text{Ba}\{(\mu\text{-ddbfo})_2\text{AlMe}_2\}_2]$  decomposed at  $1300^\circ\text{C}$ .

Our recent studies on relatively cheap and air-stable group 4 metallocenes showed that  $\text{Cp}_2\text{MCl}_2$  ( $\text{M} = \text{Ti}^{4+}, \text{Zr}^{4+}, \text{Hf}^{4+}$ ) species are attractive precursors to an extensive range of novel polymeric molecular and supramolecular materials [3, 6, 15, 18, 19]. For example, the reaction of  $\text{Cp}_2\text{TiCl}_2$  with 2 equiv of  $\text{Ca}(\text{OCH}_2\text{CH}_2\text{OCH}_3)_2$  and an excess of  $\text{CH}_3\text{OCH}_2\text{CH}_2\text{OH}$  in toluene at room temperature produced the colorless,  $\text{Cp}$ -free, heterometallic  $[\text{Ca}_4\text{Ti}_2(\mu_6\text{-O})(\mu_3,\eta^2\text{-OCH}_2\text{CH}_2\text{OCH}_3)_8(\eta\text{-OCH}_2\text{CH}_2\text{OCH}_3)_2\text{Cl}_4]$  complex (Fig. 32.5). This synthetic approach comprised the elimination of a  $\text{Cp}$  ring from  $\text{Cp}_2\text{TiCl}_2$  as  $\text{CpH}$  and was promoted by calcium 2-methoxyethanoxide and alcohol as a source of protons. The same synthetic approach led us to obtain various heterometallic complexes, with a general formula presented in Scheme 32.4.

Whether only one or both  $\text{Cp}$  ligands are exchanged, or whether both processes take place side by side, strongly depends upon the reactants involved, their stoichiometric ratios, and the nature of alcohol [15, 19]. These guarantee practical control over the composition of the final product. Thus, on the basis of a metal's ratio at the molecular level, we can easily predict the composition of the oxide products after thermolysis (Scheme 32.5) [15].

Generally, halide-derived compounds are considered as unattractive precursors for metal oxides because their decomposition leads to by-products that are corrosive and they create multiphase systems. There are, however, some examples

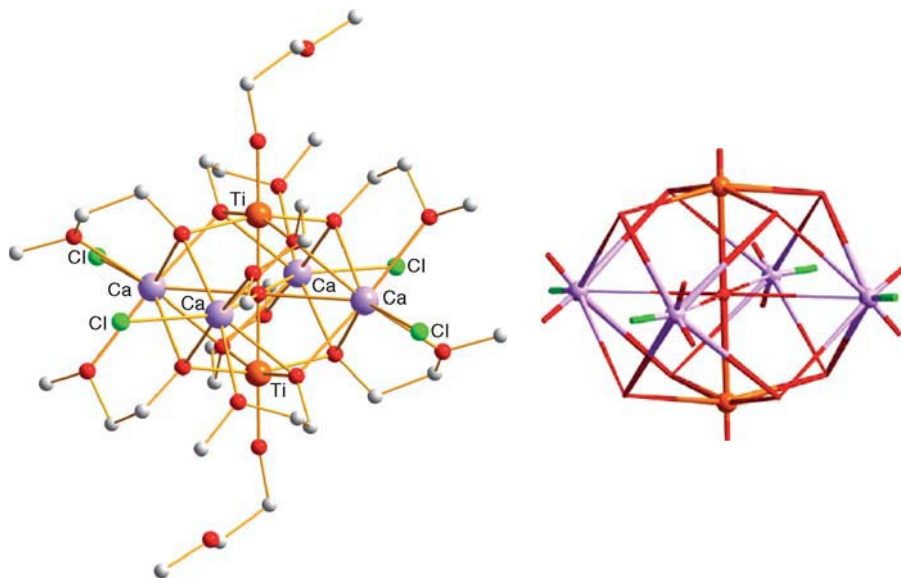
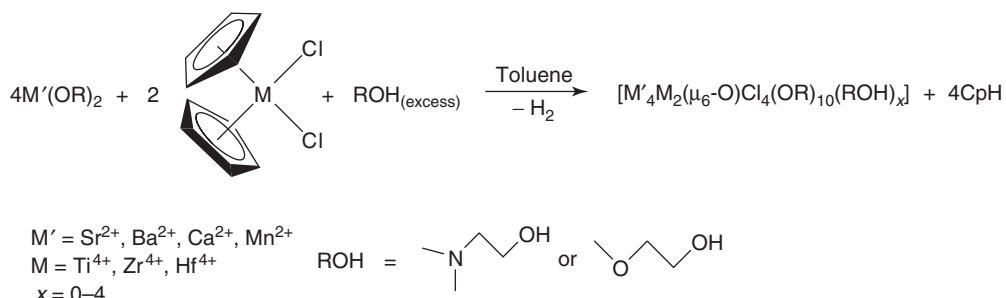
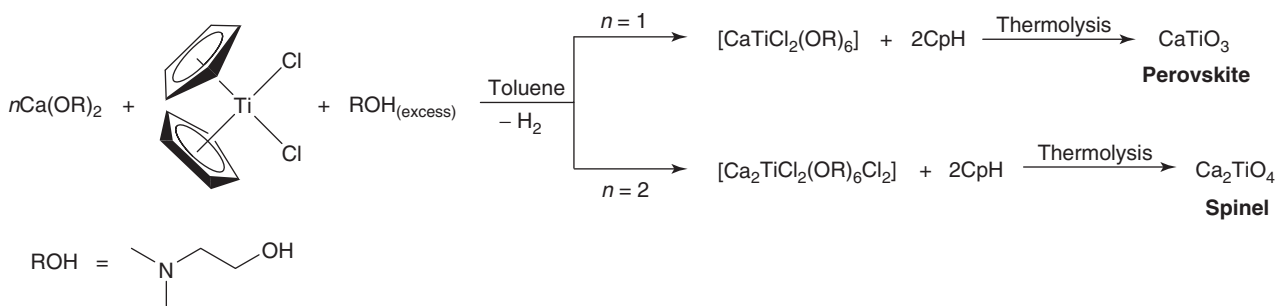


**Figure 32.5** Molecular structure of  $[\text{Ca}_4\text{Ti}_2(\mu_6\text{-O})(\mu_3,\eta^2\text{-OCH}_2\text{CH}_2\text{OCH}_3)_8(\eta\text{-OCH}_2\text{CH}_2\text{OCH}_3)_2\text{Cl}_4]$  (the H atoms are omitted for clarity) and its  $\text{Ca}_4\text{Ti}_2(\mu_6\text{-O})\text{O}_8\text{Cl}_4$  core. (See insert for color representation of the figure.)



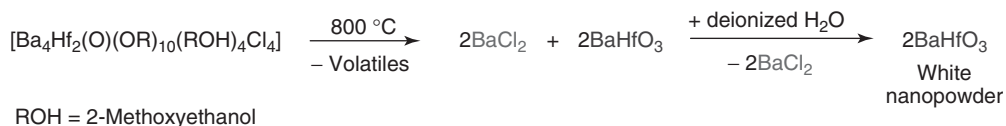
**Scheme 32.4** Synthesis of heterobimetallic complexes derived from  $\text{M}'(\text{OR})_2$  alkoxides and group 4 metallocenes.



**Scheme 32.5** Synthesis of heterometallic compounds with different  $\text{Ca}(\text{OR})_2/\text{Cp}_2\text{TiCl}_2$  ratios.

to the contrary. For instance,  $[\text{Zn}_7(\text{OAc})_{10}(\mu\text{-OH})_6\text{Cu}_5(\text{dmae})_4\text{Cl}_4]$  (dmae = 2-(dimethylamino)ethanolate) has been used in chemical vapor deposition to give highly phase-pure  $\text{Cu}_5\text{Zn}_7\text{O}_{12}$  [20].

Our recent studies have also confirmed such a phenomenon. For example, the barium–hafnium complex  $[\text{Ba}_4\text{Hf}_2(\mu_6\text{-O})(\mu_3,\eta^2\text{-OCH}_2\text{CH}_2\text{OCH}_3)_8(\eta\text{-OCH}_2\text{CH}_2\text{OCH}_3)_2(\eta\text{-HOCH}_2\text{CH}_2\text{OCH}_3)_4\text{Cl}_4]$  was obtained from the reaction of  $\text{Cp}_2\text{HfCl}_2$  and an appropriate group 2 barium alkoxide [18]. The key factor was to choose the appropriate thermolysis



**Scheme 32.6** Producing  $\text{BaHfO}_3$  nanoparticles from the barium–hafnium complex.

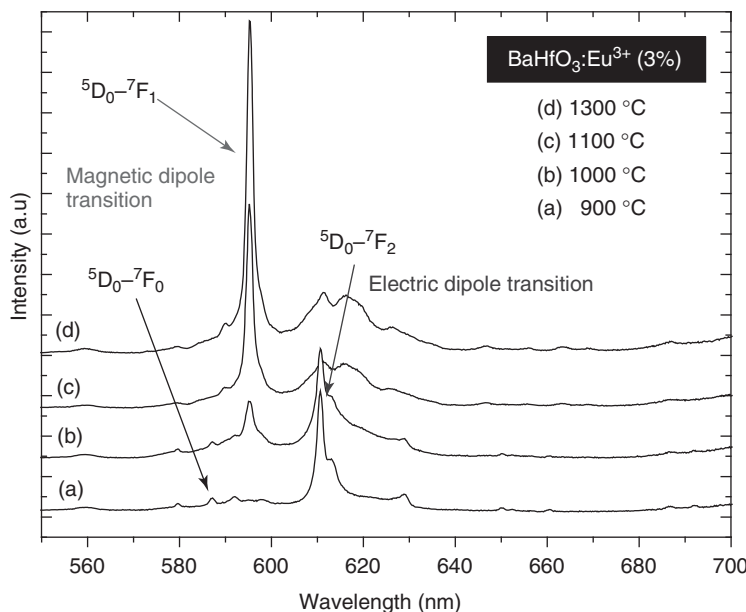


**Figure 32.6** Emission spectra of  $\text{BaHfO}_3:\text{Eu}^{3+}$  sintered at various temperatures.

conditions. This complex undergoes thermal decomposition at  $800^\circ\text{C}$  to a  $\text{BaCl}_2/\text{BaHfO}_3$  mixture in a 1:1 molar ratio. After barium dichloride has been leached from the raw powder using deionized water (Scheme 32.6), the resulting particles are in the size range of 30–50 nm.

We have also shown that the barium hafnate derived from this molecular precursor could be an attractive host lattice for Eu-doped phosphors. A strong emission, derived from the  ${}^5\text{D}_0-{}^7\text{F}_2$  transition in the  $\text{BaHfO}_3$  matrix, has been observed for the first time as a dominant line and could be particularly useful as a red-light-emitting phosphor (Fig. 32.6).

The oxidation number of the europium ion and, consequently, the photoluminescence properties of Eu-doped oxide materials depend strictly on the heating atmosphere. Sintering in air produces materials containing trivalent europium, which emits in the red wavelength region, while sintering in a  $\text{N}_2/\text{H}_2$  mixture produces europium dopant as a divalent ion with emissions in the green wavelength region [12]. Our investigations along these lines are currently underway and we intend to expand our studies to other technologically important elements [18].

### 32.4 CONCLUSIONS

Organometallic chemistry plays a crucial role in the development of new functional materials, both from a conceptual point of view and via the ability to tune microstructures. This chapter has shown efficient synthetic routes to access well-defined heterometallic complexes derived from organometallic species. The presented approaches are easily generalized, and other heterobimetallic and heteropolymetallic compounds can be obtained. The resulting compounds are excellent molecular precursors to double oxides. Our investigations have indeed shown that they produce highly phase-pure materials and the temperatures used for their preparation are significantly lower than in other conventional solid-state reactions. The obtained double oxides also constitute attractive matrices for lanthanide-doped phosphors.

## ACKNOWLEDGMENTS

The authors would like to express their gratitude to the National Science Centre (grant number: 2011/03/B/ST5/01040) for financial support.

## REFERENCES

1. Bradley, D. C.; Mehrotra, R. C.; Rothwell, I. P.; Singh, A. *Alkoxo and Aryloxo Derivatives of Metals*; Academic Press: London, **2001**.
2. Kessler, V. G. *Chem. Commun.* **2003**, 1213.
3. Szafert, S.; John, Ł.; Sobota, P. *Dalton Trans.* **2008**, 6509.
4. Utko, J.; Ejfler, J.; Szafert, S.; John, Ł.; Jerzykiewicz, L. B.; Sobota, P. *Inorg. Chem.* **2006**, *45*, 5302.
5. Utko, J.; Szafert, S.; Jerzykiewicz, L. B.; Sobota, P. *Inorg. Chem.* **2005**, *44*, 5194.
6. Sobota, P.; Utko, J.; John, Ł.; Jerzykiewicz, L. B.; Drąg-Jarząbek, A. *Inorg. Chem.* **2008**, *47*, 7939.
7. (a) Tesh, K. F.; Burkey, D. J.; Hanusa, T. P. *J. Am. Chem. Soc.* **1994**, *116*, 2409; (b) Hitchcock, P. B.; Lappert, M. F.; Lowless, G. A.; Royo, B. *J. Chem. Soc. Chem. Commun.* **1990**, 1141.
8. (a) Turova, N. Ya.; Turevskaya, E. P.; Kessler, V. G. Yanovsky, A. I.; Struchkov, Y. T. *J. Chem. Soc. Chem. Commun.* **1993**, *21*; (b) Turova, N. Ya.; Turevskaya, E. P.; Kessler, V. G.; Yanovskaya, M. I. *The Chemistry of Metal Alkoxides*; Kluwer Academic Publisher: Boston, **2002**.
9. Decon, G. B.; Forsyth, C. M.; Junk, P. C. *J. Organomet. Chem.* **2000**, *607*, 112.
10. Goel, S. C.; Matchett, M. A.; Chiang, M. Y.; Buhro, W. E. *J. Am. Chem. Soc.* **1991**, *113*, 1844.
11. Tomaszewski, P. *Phase Transit.* **1992**, *38*, 127.
12. John, Ł.; Kosińska-Klähn, M.; Jerzykiewicz, L. B.; Kępiński, L.; Sobota, P. *Inorg. Chem.* **2012**, *51*, 9820.
13. John, Ł.; Utko, J.; Szafert, S.; Jerzykiewicz, L. B.; Kępiński, L.; Sobota, P. *Chem. Mater.* **2008**, *20*, 4231.
14. John, Ł.; Sobota, P. Alkoxide Molecular Precursors for Nanomaterials: A One Step Strategy for Oxide Ceramics, *in Ceramic Materials*; Wunderlich, W.; Ed. Scivo: Croatia, **2010**.
15. Sobota, P.; Drąg-Jarząbek, A.; John, Ł.; Utko, J.; Jerzykiewicz, L. B.; Duczmal, M. *Inorg. Chem.* **2009**, *48*, 6584.
16. (a) Alt, H. G.; Köppl, A. *Chem. Rev.* **2000**, *100*, 1205–1222; (b) Coates, G. W. *Chem. Rev.* **2000**, *100*, 1223.
17. Sessoli, R.; Gatteschi, D.; Caneschi, A.; Novak, M. A. *Nature* **1993**, *365*, 141.
18. Drąg-Jarząbek, A.; Kosińska, M.; John, Ł.; Jerzykiewicz, L. B.; Sobota, P. *Chem. Mater.* **2011**, *23*, 4212.
19. Sobota, P.; Drąg-Jarząbek, A.; Utko, J.; Jerzykiewicz, L. B. *Organometallics* **2011**, *30*, 1741.
20. Hamid, M.; Tahir, A. A.; Mazhar, M.; Zeller, M.; Hunter, A. D. *Inorg. Chem.* **2007**, *46*, 4120.
21. Tanner, P. S.; Williams, R. A.; Hanusa, T. P. *Inorg. Chem.* **1993**, *32*, 2234.

## THE ROLE OF ORGANOMETALLIC COMPLEXES IN THE SYNTHESIS OF SHAPED CARBON MATERIALS

NEIL J. COVILLE\*

*DST/NRF Centre of Excellence in Strong Materials and Molecular Sciences Institute, School of Chemistry, University of the Witwatersrand, Johannesburg, South Africa*

EDWARD N. NXUMALO

*Department of Applied Chemistry, University of Johannesburg, Johannesburg, South Africa*

### 33.1 INTRODUCTION

The emergence of the field of nanotechnology is closely associated with discoveries and studies carried out in the field of carbon chemistry. The discovery of fullerene [1], followed by simple strategies to make fullerenes [2]; the seminal studies on carbon nanotubes (CNTs) [3], following extensive studies on carbon fibers [4]; and the recent simple synthesis of single layer graphene [5] have all furthered developments in the “nano” arena. A key feature in these new carbon structures is that carbon atoms bond together to lead to carbon-rich structures in which the presence of non-carbon atoms is limited. Typically, non-carbon atoms satisfy the carbon valences at the edges of the “all” carbon structures, although non-carbon atoms can also be substituted into the carbon structures purposefully to yield doped materials [6].

The wide range of carbon structures that have been made reveals that carbon atoms readily knit together to form the new 3D structures. The rules by which this happens are the same as those used to make the classical 1D and 2D structures commonly synthesized in chemical laboratories. However, synthetic strategies to make long-chain polymers (polyacetylene, for example) or to make the building blocks of graphene (e.g., naphthalene and anthracene) are well understood, whereas the same is not true for the 3D structures made of carbon.

The structural motifs that are formed are determined by (i) the hybridization state of the carbon, (ii) the carbon source, (iii) the energy supplied to the carbon reactants, and (iv) the template or catalyst used to make/break carbon bonds [7].

The focus of this mini-review is on the later factor, namely, the role of the catalyst in making a carbon material that has shape. In particular, the focus will be on the role of organometallic complexes in assisting this process.

Reviews of the literature on the role of organometallic complexes in the synthesis of CNTs [8] and nitrogen-doped carbon nanotubes (NCNTs) [6] have been written. However, to date, little has been discussed about the role of these catalysts in affecting the shape of the carbons produced.

### 33.2 GENERAL COMMENTS

A consideration of studies in which organometallic catalysts have been used to make shaped carbon materials (SCMs) reveals that studies are dominated by the use of ferrocene ( $\text{FeH}$ ) and  $\text{Fe}(\text{CO})_5$ , with many, many studies being reported

---

*Advances in Organometallic Chemistry and Catalysis: The Silver/Gold Jubilee International Conference on Organometallic Chemistry Celebratory Book*, First Edition. Edited by Armando J. L. Pombeiro.

© 2014 John Wiley & Sons, Inc. Published 2014 by John Wiley & Sons, Inc.

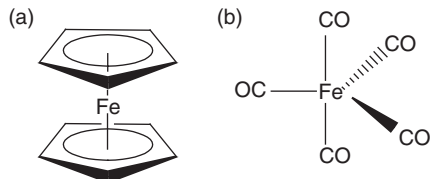


**Figure 33.1** (a) Ferrocene, (b)  $\text{Fe}(\text{CO})_5$ .

on the use of  $\text{FeH}$  (Fig. 33.1). Both are used because they are cheap and reasonably air-stable materials that are readily available and have excellent physical properties. These properties allow for simple synthetic methodologies to be used to make the SCMs.

Fe is a well-known catalyst that is used to make SCMs. A typical catalyst is made from a high-oxidation-state Fe precursor (typically placed on a support) that is reduced to  $\text{Fe}(0)$  before reaction with carbon-containing reactants. These reactants, when passed over the catalyst under appropriate conditions, decompose on the Fe to form carbon atoms that either dissolve in the Fe and reprecipitate or recombine on the Fe surface to give the product [9]. The diameter of the carbon structure is determined by the diameter of the Fe catalyst particle.

In contrast, the use of volatile organometallic catalysts provides an alternate route to the above process. In this type of reaction, the catalyst, together with the carbon reactants, is introduced into a reactor in the gas phase where they decompose to give metal atoms/clusters and carbon atoms/radicals. The process is referred to as a *floating catalyst* process since a volatile catalyst is used. An advantage is that CNTs made using this type of approach can be produced in a continuous manner, compared to the typical batch process using a conventional chemical vapor deposition (CVD) method. Indeed, the HiPco process is a commercial *continuous* process used to make single-walled carbon nanotubes (SWCNTs) and multiwalled carbon nanotubes (MWCNTs) using  $\text{Fe}(\text{CO})_5$  as a catalyst [10].

### 33.3 THE SHAPES TAKEN BY CARBON

Carbon atoms can be  $\text{sp}^1$ ,  $\text{sp}^2$ , or  $\text{sp}^3$  hybridized and this will impact on the way carbon–carbon bonds will link together. Linear structures will be generated by  $\text{sp}^1$  hybridized carbon atoms, while  $\text{sp}^2$  hybridized carbons will lead to 2D structures that may or may not show curvature (fullerene vs graphene sheet). In contrast, 3D structures are generated by  $\text{sp}^3$  hybridized carbon atoms, as found in diamond. Not unexpectedly, many of the new carbons that have been synthesized can contain a mixture of  $\text{sp}^2$  or  $\text{sp}^3$  hybridized carbon atoms and this allows for a diverse range of shapes. Carbons formed with mixed hybridized carbons will generally be amorphous with little long-range order as typically found in soot. However, even these mixed carbons can be structured to generate SCMs (see below).

Given that carbon can bond in different ways, a wide range of structures can be made. The well-known shapes include tubes and fibers. These structures are built up of  $\text{sp}^2$  carbon atoms arranged with graphene layers arranged perpendicular or at an angle to the tube/fiber axis. The ends of the carbon layers will be bonded to non-carbon atoms (typically O and H atoms) but may also be bonded to  $\text{sp}^3$  hybridized carbon atoms. The fibers may or may not have a hollow core (Fig. 33.2). While CNTs and carbon nanofibers (CNFs) are generally shown in cartoon form as being straight, this is rarely found in practice. Most CNTs and CNFs are twisted and can coil along their length. Figure 33.3 indicates the twisting that can occur, eventually leading to coil formation, while Fig. 33.4 indicates the TEM image of a real sample showing this phenomenon.

The carbon atoms can also arrange to give spherical structures as found in fullerenes. This type of structure is also found in carbon spheres (CSs): spherical carbons with a multilayer structure that can be hollow or filled (Fig. 33.5) [11]. Here the carbon atoms are found in domains that pack together to give the final structure.

The shapes generated as the carbon–carbon bonds form can also include horns [12], cages [12], coils, and spirals [13]. A wide range of coiled and spiral-shaped carbons can be formed that vary in terms of tube diameters and the coiling dimensions (see Reference 13, p. 196, for examples).

In the sections below, spherical carbon structures (including fullerenes) will not be discussed in any detail; in many instances their synthesis does not require a catalyst [11].

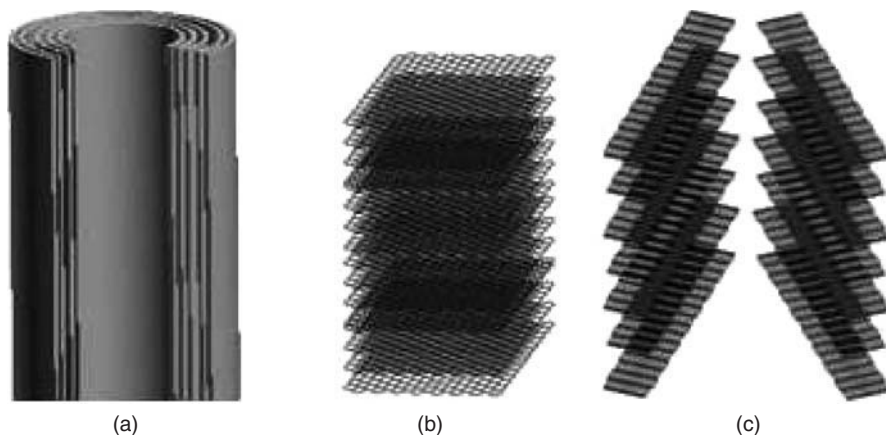


**Figure 33.2** Cartoon showing (a) multiwalled carbon nanotube, (b) solid plate-like carbon nanofiber, and (c) hollow herringbone carbon.

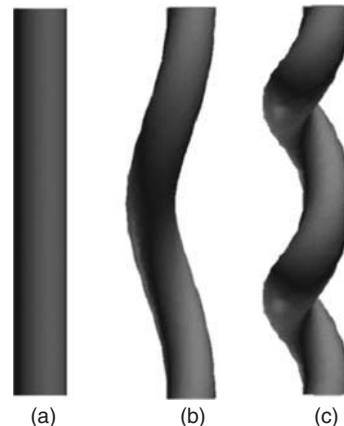


**Figure 33.3** Cartoon showing (a) a straight fiber, (b) a twisted fiber, and (c) a coiled fiber.



**Figure 33.4** TEM images of CNTs obtained from the pyrolysis of toluene and ferrocene in the presence of 4% aniline (Letsoala, P. Unpublished data, MSc thesis).

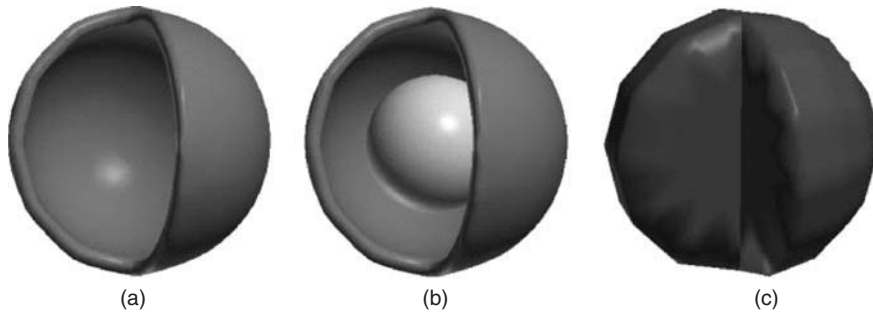


**Figure 33.5** Cartoon of (a) hollow, (b) core–shell, and (c) filled spheres [11]. Reprinted from Reference 11b. Copyright 2011, with permission from ScholarOne Manuscripts.

### 33.4 THE CATALYST–CARBON INTERACTION

Superimposed on the effect of carbon hybridization in affecting carbon shape is that of the catalyst particle. The catalyst particle influences the shape of the resultant carbon structure by (i) its size, (ii) its interaction with a support or template (when used), and (iii) its shape as reflected by the crystal faces exposed to the reactants. Control of the catalyst particle's morphology thus becomes a key determinant in generating the morphology of SCMs [14].

This would suggest that, if particles with controlled morphology could be made, then control of the SCM morphology would follow. There are a number of issues that complicate this relationship. The first is that at high temperatures the catalyst may be in the liquid phase; indeed, the melting point of a metal decreases with size, and metals in the nano regime will melt at much lower temperatures than those of bulk metal. Impurity atoms may also lead to the formation of eutectics, which may also lower the melting point of a metal (sulfur is believed to do this to Fe [15]) leading to liquid metals. Finally, it has been observed that the carbon reactant can modify the surface of the catalyst particle to generate new particle shapes during a reaction [7]. This process is driven by energy minimization issues through the formation of metal–carbon bonds. Thus, as a result of this *in situ* modification of a catalyst by the reactant, making supported or unsupported catalysts with a known shape does not always lead to the expected SCM.

The use of organometallic complexes may provide a means of making gas-phase clusters with some control over catalyst morphology (size/shape) that will lead to the controlled shape of the nano carbon material produced. As yet, this issue has not been evaluated.

### 33.5 MECHANISM OF CARBON GROWTH FROM A METAL PARTICLE

Most mechanistic information on carbon growth has been derived for solid or liquid metal particles, generated at  $T > 500^\circ\text{C}$ . In these mechanisms, a metal particle interacts with gas-phase carbon-containing reactants. These reactants (as molecules/ions/fragments) interact with the metal surface and decompose into carbon atoms. It is generally believed that the carbon then dissolves into the metal, and after supersaturation within the metal, carbon crystallization and formation of carbon tubes or fibers then takes place. This can occur via a base growth or tip growth process, as shown in Fig. 33.6. Simultaneously, the dissolved carbon can cause catalyst breakdown, leading to the phenomenon of “dusting” [16]. An alternative to the above involves breakdown of the carbon reactants on the surface of the metal particle (or near surface; first one to two layers) without dissolution into the metal. The mobile carbon atoms then form C–C bonds, which leads to the formation of tubes/fibers [17]. The various studies reported to date suggest that both mechanisms are operative and are metal–reactant–reaction parameter dependent. This metal–reactant–reaction parameter relationship is significant in a gas-phase reaction, as it helps control the resulting carbon shapes.

At  $T < 400^\circ\text{C}$ , alternative pathways could occur and these may involve a more typical mechanism based on organometallic principles. Our own studies using Cu or Ni as catalyst and using nontraditional carbon reactants have suggested that the carbon materials formed are dependent on the carbon reactant used. Thus, different alkene (or alkyne) isomers that would be expected to give the same carbon structures, if the carbon reactant decomposed completely on the catalyst, are found to give carbons with different morphologies [7]. A mechanism involving complete breakdown of the carbon reactant to C atoms is not consistent with the results. This suggests that the reactant (or fragments) interacts with the metal surface and creates new C–C bonds that generate the carbon materials produced.

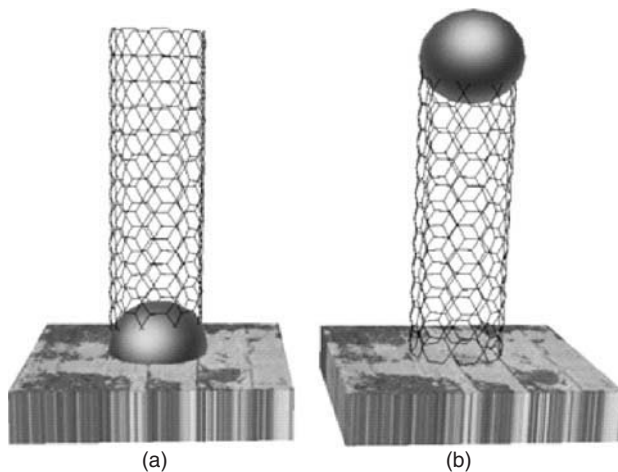


**Figure 33.6** CNT (or CNF) growth from a catalyst (gold sphere) particle initially deposited on a support showing (a) base growth and (b) tip growth [11]. Reprinted from Reference 11b. Copyright 2011, with permission from ScholarOne Manuscripts.

The different carbon sources also readily facilitate catalyst reconstruction, again suggesting reactant–metal complex formation. If different faces on the catalyst are generated from the different carbon sources, then different SCMs can be formed.

In low temperature studies (circa 450 °C) over a Ni catalyst, carbon fibers that formed varied with the alkene or alkyne reactant used. The carbon fiber formed was highly amorphous, suggesting the presence of substantial amounts of  $sp^3$  carbons. Thus, the C–C bond-forming reactions occurring on the surface generate a 3D structure. This is different to polymerization reactions that generate 1D strands of carbon atoms [18]. A proposed mechanism, in cartoon form, to indicate the steps required to make carbon tubes/fibers is shown in Fig. 33.7 [7].

This mechanism highlights (i) the possibility of reactant breakdown in the gas phase, (ii) the interaction of either the reactant (pathway i) or reactant fragments (pathway ii) with the catalyst particle, and (iii) the C–C bond-forming steps on the catalyst surface. However, little is known about (iii) above. An understanding of these processes of C–C bond formation on the metal catalyst will allow eventual control of the morphology (shape/size) of the carbon materials produced.

The implication in a mechanism of this type is that the interaction of the metal with carbon species should involve typical organometallic carbon–metal interactions, leading to the 3D carbon structures formed in the reaction.

### 33.6 ORGANOMETALLIC CATALYSTS AND CARBON SYNTHESIS

Organometallic complexes can create the catalysts for making carbons by two generic routes. One is to use the organometallic complex to generate a solid nonvolatile material, which is an alternative to the traditional means of making solid catalysts from metal salts.

The second method is to use a volatile metal complex that will make metal particles in the gas phase (as mentioned above). In this process, the organometallic complex will decompose in the gas phase, and the metal atoms then nucleate and react with the carbon source to make the carbon material. These metal atoms/clusters can deposit on the reactor walls before reaction with carbon and then a traditional carbon growth pattern will occur. Little is known as to the ratio of carbon products produced by these two competing pathways (i.e., from metal atoms in the gas phase or from metal atoms on the reactor wall) when “floating” organometallic catalysts are used. As in most studies MWCNTs are produced, typically with internal diameters greater than 5 nm, it appears that most growth (after any initial reaction in the gas phase) occurs on the reactor walls. The production of SWCNTs with smaller diameters (1–2 nm), by contrast, could result from metal particles spending more time in the gas phase before deposition on a reactor surface. From an organometallic perspective, the key issue will be the control of the growth of the metal particle (size, shape, content), irrespective of the pathway, to produce a carbon material with shape. The deposited metal clusters on the reactor walls should be different from the metal atoms/clusters produced from metal salts by reduction and hence could lead to novel structures.

It has been proposed that floating catalysts could add to the tips of growing CNTs (Fig. 33.8) [19]. This could provide an alternative mechanism to explain the presence of metal particles that appear inside a growing tube. However, the sizes

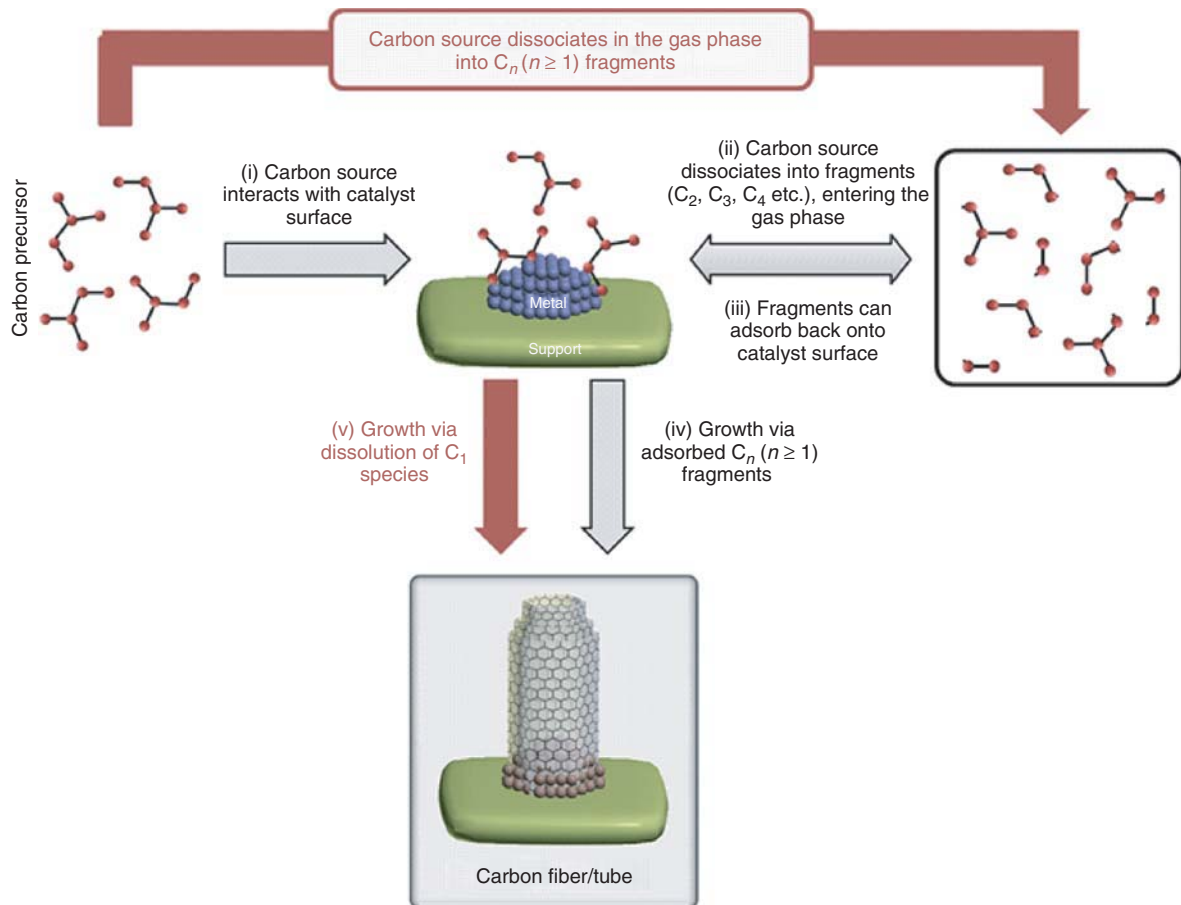


**Figure 33.7** Proposed mechanism for CNT/F growth via carbon fragments. (i) Carbon source adsorbs onto the surface of the catalyst particle. (ii) Carbon source fragments on the catalyst and is released into the gas phase, or (iii) gas-phase fragments are readSORBED onto the catalyst surface. (iv) Growth of CNT/F from adsorbed carbon fragments. (v) Base growth mechanism as proposed by Baker [7]. Reprinted from Reference 7b. Copyright 2012, with permission from Elsevier.

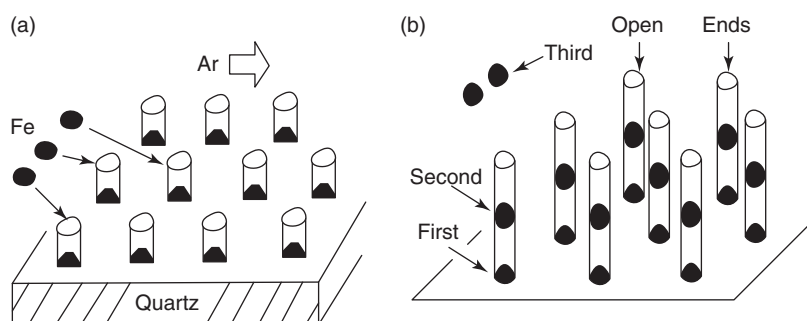


**Figure 33.8** A schematic model of the formation of uniformly distributed catalyst lines during the growth of nanotubes arrays [18]. Reprinted from Reference 19. Copyright 2001, with permission from American Chemical Society.

of the particles found seem inconsistent with the concentration of gas-phase metals used in the reaction, suggesting that this mechanism does not occur.

A range of studies, in which organometallic complexes have been used to make SCMs, are listed below. The types of structures produced have been divided up into sections as follows: (i) CNTs and CNFs, (ii) aligned and nonaligned carbons, (iii) branched structures, (iv) bamboo carbons, (v) coiled carbons, (vi) amorphous carbons, (vii) spherical carbons, and (viii)

**TABLE 33.1** Different Carbon Shapes Made from Ferrocene and Fe(CO)<sub>5</sub>

Carbon Shape	Catalyst	T, °C	Gases	Other Reactants	Methods	References
Tubular	FcH	400–650	Ar	Toluene	CVD	20d
Tubular	FcH	580–700	H <sub>2</sub>	Anthracene/dibromoanthracene	CVD	21b
Bamboo	FcH	850	Ar/H <sub>2</sub>	Toluene/benzylamine	Aerosol	22a
Bamboo	FcH	720–840	Ar	PPh <sub>3</sub> /benzylamine	Aerosol	23c,d
Bamboo	FcH	900	Ar/H <sub>2</sub>	Toluene/aniline/ferrocenylaniline	CVD	22c
CNFs	FcH	1150	H <sub>2</sub>	Thiophene, benzene	Aerosol	24b
Aligned CNTs	FcH	400–900	C <sub>2</sub> H <sub>2</sub>	Xylene	CVD	21g
Aligned CNTs	FcH	<600		Benzene	CVD	21h
aC and CSs	FcH	700–900		Anthracene	CVD	21a
HCSs	FcH	700	N <sub>2</sub>		autoclave	25c
HCSs	FcH	900–1000	N <sub>2</sub>	Benzene	CVD	25a
CSs	FcH	580–700	H <sub>2</sub>	Anthracene	CVD	21b
CSs	Fe(CO) <sub>5</sub>	700–1000	N <sub>2</sub>	Pentane	Pyrolysis	26
Filled CSs	FcH	1000	Ar	Camphor	CVD	25b
a-CNTs and nanobags	FcH	200	Cl <sub>2</sub>		CVD	27c
Y- or T-Junctions	FcH	1000	Ar/H <sub>2</sub>	Thiophene	CVD	28
Nano-onions	FcH or Fe <sub>3</sub> (CO) <sub>12</sub>	900	Ar		CVD	29c
Nanocoils	FcH	700	C <sub>2</sub> H <sub>2</sub>	Xylene, indium isopropoxide	Double-stage CVD	30b
Nanocoils	Fe(CO) <sub>5</sub>	700–800	Pyridine	Toluene	CVD	21b
Helical	FcH	700		Polyethylene glycol	Autoclave	30c
Helical	FcH	700	C <sub>2</sub> H <sub>2</sub>	Xylene–indium isopropoxide	Double-stage CVD	30d
SWCNTs	FcH or Fe(CO) <sub>5</sub>	1100	N <sub>2</sub> or CO	CO	Laminar flow reactor	31a
MWCNTs	FcH	850	Ar	Castor oil	CVD	32
MWCNTs	Fe(CO) <sub>5</sub>	1050–1150	N <sub>2</sub>	CH <sub>4</sub>	CVD	33b
MWCNTs	Fe(CO) <sub>5</sub>	2600	Ar	C <sub>2</sub> H <sub>2</sub>	CVD	33c
	C <sub>8</sub> H <sub>8</sub> Fe(CO) <sub>3</sub> ,					
MWCNTs	[(C <sub>5</sub> H <sub>5</sub> )Fe(CO) <sub>2</sub> ] <sub>2</sub>		Ar	Toluene	Injection CVD	33d
MWCNTs	Fe(CO) <sub>5</sub> , Fe <sub>3</sub> (CO) <sub>12</sub>		Ar	C <sub>2</sub> H <sub>2</sub>	Aerosol	33e
Fe/Fe carbide core/ carbon shell NPs	Fe(CO) <sub>5</sub>	<710 mbar	Ar	C <sub>2</sub> H <sub>2</sub> , C <sub>2</sub> H <sub>4</sub>	Laser pyrolysis	34a
Carbon-coated Fe NPs	Fe(CO) <sub>5</sub>	<710 mbar	Ar	C <sub>2</sub> H <sub>2</sub> , C <sub>2</sub> H <sub>4</sub>	CVD	34b

Abbreviations: aC, amorphous carbon; CNTs, carbon nanotubes; CNFs, carbon nanofibers; CVD, chemical vapor deposition; CSs, carbon spheres; FcH, ferrocene; HCSs, hollow carbon spheres; NPs, nanoparticles.

other shapes. The information in Table 33.1 provides a few examples from the literature relating to these different shapes. The examples, by no means covering all studies or carbon shapes produced, indicates the range of control possible using organometallic complexes. Further, the role of doping has not been treated separately, and examples of the effect of doping have been integrated into the sections listed above.

### 33.6.1 CNTs and CNFs

Carbons that grow with a linear or near-linear shape from a catalyst particle are referred to as CNTs or CNFs. The CNTs can be SWCNTs or MWCNTs, and these grow with their carbon layers parallel to the tube axis. CNFs, by contrast, have carbon layers perpendicular (or near perpendicular) to the fiber axis and can be hollow or solid. CNTs and CNFs have diameters ranging from 2 nm to greater than 100 nm and lengths varying from 20 nm to several centimeters. These tubes can be further classified as aligned or “cooked spaghetti” shaped (Fig. 33.9). The various morphologies taken by the carbons are determined during the synthesis process. This is affected by the type of organometallic catalyst used.

There is an extensive literature that reports on the production of tubes and fibers using different routes, synthetic conditions, carbon sources, and catalysts. Tibbetts and Gorkiewicz [20a] appear to have been the first researchers to use an organometallic complex, FcH, to produce CNFs and CNTs. Thermal decomposition of FcH alone resulted in the formation of SWCNTs [20]. Also, Barreiro et al. [20] used FcH as the sole source of both catalytic Fe particles and C feedstock which nucleated from the C species to form SWCNTs. As highlighted earlier, most tubular nanocarbons made in the gas phase are produced

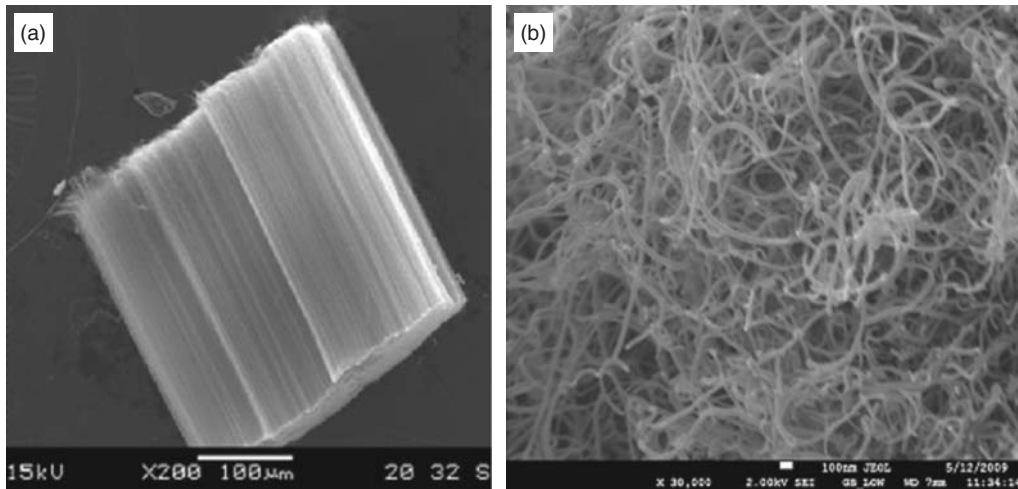


**Figure 33.9** SEM images showing (a) aligned CNFs and (b) “cooked spaghetti type” CNFs [7]. Reprinted from Reference 11b. Copyright 2011, with permission from ScholarOne Manuscripts.

by the conventional catalytic CVD method from a carbon feedstock (aliphatic, aromatic hydrocarbon, CO, etc.) using a volatile metallic species [20]. Some examples are given in Table 33.1 to give an indication of the carbon materials produced, and we describe some specific examples below.

SWCNTs, MWCNTs, and CNFs have been synthesized by a floating catalyst method with different tube diameters achieved by controlling the FcH/benzene mole ratio. It is evident that small FcH/C ratios yield SWCNTs, and higher ratios CNFs [35]. SWCNTs were synthesized by the CO disproportionation reaction on Fe catalyst particles formed by FcH vapor decomposition in a laminar flow aerosol (floating catalyst) reactor [31]. A mixture of CH<sub>4</sub>/H<sub>2</sub>/Ar with added Fe(CO)<sub>5</sub> was reacted in the presence of a microwave plasma torch for the synthesis of MWCNTs covered by iron oxide nanoparticles (NPs) [33].

Horvath and coworkers [36] have studied the efficiency of bimetallic catalyst particles by investigating FcH–cobaltocene and FcH–nickelocene mixtures against a FcH standard. Their findings show that FcH–cobaltocene and FcH–nickelocene mixtures increased CNT production compared to a standard FcH catalyst. The highest yields were obtained using the FcH–nickelocene mixture. The samples containing mainly straight nanotubes and negligible amounts of amorphous carbon imply that these bimetallic catalysts also improved the quality and purity of the nanotube samples.

Mohlala et al. [36] utilized a bimetallic catalyst system [FcH/W(CO)<sub>5</sub>(*t*-BuNC) and FcH/W(CO)<sub>5</sub>(*t*-BuNC)] to synthesize MWCNTs in 5% H<sub>2</sub> in Ar in the temperature range 700–900 °C. TEM analysis revealed the formation of large metal particles of Mo/Fe alloys rich in Fe. Under similar reaction conditions, FcH yielded MWCNTs and spheres while the W(CO)<sub>5</sub>(*t*-BuNC) complex yielded little carbonaceous material. It was observed that the diameters of the CNTs formed in the presence of FcH are smaller, while the diameters of CSs are larger relative to the diameters of CNTs and spheres produced by the bimetallic catalyst systems.

CNTs can also be made using natural precursors. For example, castor oil was the carbon source used in the spray pyrolysis synthesis of CNTs from a castor oil–FcH solution at 850 °C under an Ar atmosphere [32].

Fibers with diameters of 10–100 nm were produced by the floating catalyst method, using S additives. The temperature of the feedstock and the hydrogen flow had the expected effects on the growth of CNFs [24]. Thinner and straighter nanofibers were produced at low temperature. In the production of vapor-grown carbon fibers, ultrafine iron catalyst particles played an important role in the elongation process of the fibers. The activity of the catalyst particles were found to depend strongly on their size. This helped in the prediction of the size distribution of particles produced under various reaction conditions [24].

### 33.6.2 Aligned and Nonaligned Carbons

As highlighted earlier during the discussion on the synthesis of CNTs and CNFs, it is possible to generate both aligned and “cooked spaghetti” type materials (Fig. 33.9). For device manufacture, the former geometry will be required. It is likely that the aligned CNTs/CNFs are formed through the deposition of the metal from a floating catalyst on the reactor walls.

Well-aligned SWCNTs and MWCNTs can be obtained via the pyrolysis of a FeH/anthracene powered mixture, while both SWCNTs and spherical carbon-coated iron NPs can be obtained from powdered mixtures of FeH and dibromoanthracene [21]. A benzene/FeH mixture was used to obtain vertically aligned CNTs when the preheating temperature was set at 400 °C and the growth temperature was set at 900 °C [21]. High purity aligned MWCNTs that grow perpendicular to the quartz substrates were also synthesized through the catalytic decomposition of a FeH–xylene mixture [21]. Vertically oriented and thin nanotubes were grown by plasma- and filament-assisted CVD [21].

### 33.6.3 Branched Carbons

Branched structures are typically composed of several arms of tubes and fibers that form when non-hexagonal carbon rings are incorporated into the tube framework of the graphene sheet that builds the carbon nanostructure. Branched nanostructures formed from FeH can be either Y-branched (Fig. 33.10) or T-branched. Different growth techniques have been used for their fabrication in the temperature range of 650–1000 °C [28] using a range of reactors, namely, CVD, double-stage furnace CVD, a closed environment (e.g., an autoclave or sealed quartz container reactors), etc.

The addition of sulfur compounds to the floating catalyst appears to enhance Y-junction growth. Y-Junctions or Y-branches have been made at high temperatures using FeH with thiophene as an additive in an Ar/H<sub>2</sub> mixture [37]. Y-Junctions have also been produced in large quantities by the gas-phase decomposition of a FeH/thiophene mixture in a hydrogen atmosphere [37]. Further decomposition of Fe(CO)<sub>5</sub> with thiophene yields multiple Y-junction structures [38]. Y-Junctions that are bamboo shaped have been observed and are produced through the pyrolysis of FeH/monoethanolamine mixture over a GaAs substrate at 950 °C [8, 37].

### 33.6.4 Bamboo Structures

The incorporation of heteroatoms or other foreign atoms into a CNT modifies the tube characteristics. TEM and SEM studies reveal that nitrogen-containing CNTs are hollow inside and typically have bamboo compartments. Doping of the CNT lattice (particularly with N) has been found to give these bamboo structures. This is partly due to the formation of pentagons and heptagons, which increases the reactivity of the neighboring carbon atoms resulting in the formation of a highly disordered structure. Bamboo shapes are also referred to as having a “bell” shape, as the shape resembles a series of bells connected to each other (Fig. 33.11).

This unique morphology can also be due to the addition of nitrogen, for example, NH<sub>3</sub> in the presence of FeH. The N found in N-doped CNTs can be present as a pyridinic or pyrrolic N, readily differentiated by X-ray photoelectron spectroscopy

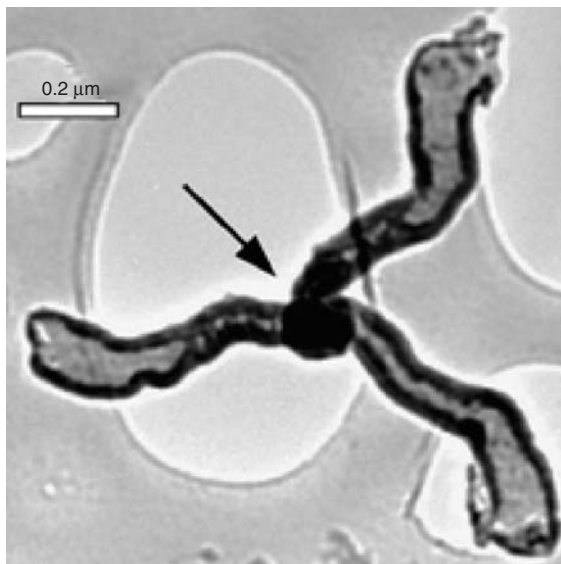


**Figure 33.10** Multibranched amorphous carbon nanostructure showing a spherical core with darker contrast (marked by an arrow), from where the lobes emerge. Reprinted from Reference 27c. Copyright 2005, with permission from Elsevier.

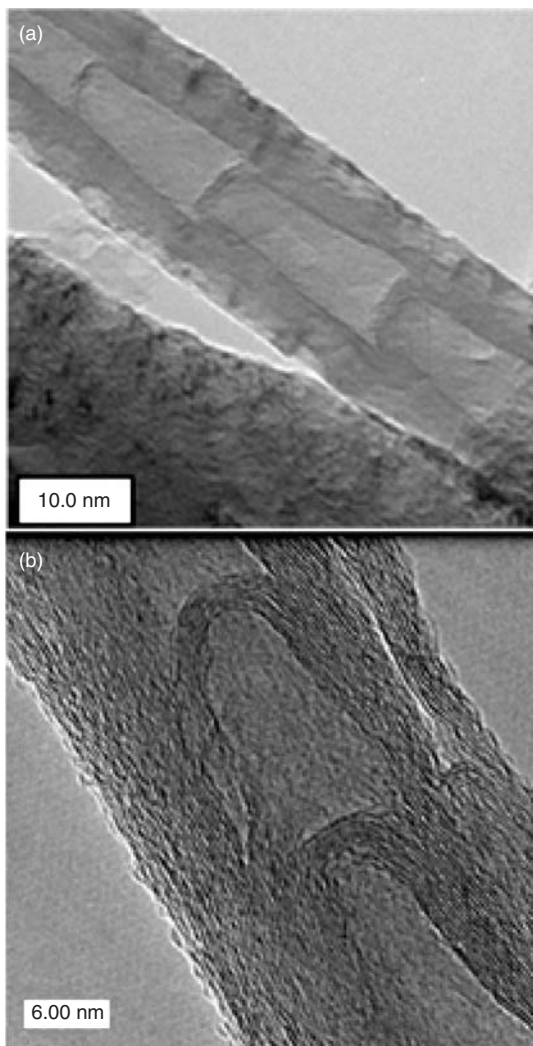


**Figure 33.11** Bamboo structures of CNTs obtained from the pyrolysis of toluene and ferrocene in the presence of 8% diethylamine [22]. Reprinted from Reference 22a. Copyright 2010, with permission from Elsevier.

(XPS). The presence of nitrogen also leads to the modified chemical behavior of the SCMs. Typically, nitrogen addition can also be achieved by using a N atom which is part of a ligand attached to the catalyst. The synthesis of bamboo-shaped tubular structures is usually performed using the CVD method. The synthesis can also be achieved by using a volatile C source that contains N (e.g., acetonitrile) [23]. Other common N sources include pyridine, melamine, benzylamine, etc. [6, 23].

Bamboo shapes were recently produced by a nebulized floating catalyst method using a mixture of toluene and nitrogen-containing reagents (e.g., aniline, benzylamine) by changing the ratio of the reactants [22]. This is a suitable method for controlling the bamboo compartments inside the tube axis as well as their lengths and diameters. Vertically aligned bamboo structures were recently grown on iron NPs deposited on silicon substrates by thermal decomposition of methane/ammonia and acetylene/ammonia mixtures at 900–1100 °C [39]. CNTs doped with a range of N concentrations of 0–10 at% were prepared via a floating catalyst CVD method using FcH, NH<sub>3</sub>, or pyridine and xylene [39]. The pyridinic-like fraction selectively increased from 0.0 to 4.5 at% as the N content in the reaction increased [39]. At higher N contents, the tubes are highly constricted.

A recent study reported the formation of bamboo nanostructures with different morphologies from turpentine oil by the aerosol route at 1000 °C. FcH was used as a catalyst source and sulfur as a promoter [40]. These structures have sharp tips, bamboo shapes, open ends, hemispherical caps, pipe-like morphology, and metal particles trapped inside the wide hollow cores.

### 33.6.5 Coiled Carbons

A beautiful example of the synthesis of coiled carbons made by using  $\text{Fe}(\text{CO})_5$  has been reported by Hou et al. [30]. In that study, the authors found that coiling was influenced by the carbon source (toluene, pyridine). Surprisingly no N-doped coils were observed when pyridine was used as reactant. Many types of helical carbons are known and are formed by the floating catalyst route either by the catalytic pyrolysis of polyethylene or through the use of tin and indium catalysts [30].

### 33.6.6 Amorphous Carbons

Recent studies on the crystallization behavior of amorphous CNTs annealed at high temperatures demonstrated that the microstructure of the CNTs (prepared by the floating catalyst route) have an amorphous character [27]. The tubes have finite dimensions and tube-like shapes, and their crystallization behavior is found to be completely different from bulk amorphous carbons. This unique type of SCM can also be made in a confined space at autogenic pressure and at a low temperature using FcH as a catalyst, benzene as carbon source, thiophene as additive, and  $\text{H}_2$  as the atmosphere [27]. The self-catalyzed decomposition of FcH/benzene at a low temperature ( $<210^\circ\text{C}$ ) gave long, amorphous CNT bundles and nanoribbons. This is the first paper to report nanotube bundles and nanoribbons composed of pure amorphous carbon.

### 33.6.7 Spherical Carbons

CSs (Fig. 33.5) are often observed when attempts to make CNTs are performed at high temperatures. It is not clear whether the catalyst plays any role in their synthesis [26] (Fig. 33.12). However, hollow carbon spheres (HCSs) do require the interaction of a catalyst as a template.

HCSs with smooth single shells, deformed single shells, double shells, and N-doped shells have been prepared using silica templates and FcH/benzene mixtures via the CVD process. The morphology of the HCSs was found to depend on the CVD reaction time and temperature. Results showed that relatively large silica spheres favored the formation of HCSs with a very smooth surface. However, a short CVD time led to a thin carbon shell and deformed HCSs [25]. Spherical carbons (solid and hollow) with a spongy appearance and controlled sizes were produced by CVD from camphor and FcH. The spheres were seen to be fused and interconnected [25].

Core–shell carbons can also be produced by floating catalysts. For example, a picric-acid-detonation-induced pyrolysis of FcH or  $\text{Fe}(\text{CO})_5$  gave carbon-encapsulated Fe NPs (5–20 nm) [29]. The reaction is characterized by a self-heating and extremely fast process. Tubular structures are formed at a high C/Fe ratio in this reaction. The pyrolysis of metallocenes such as FcH, cobaltocene, or nickelocene is known to yield CNTs and metal-filled onion-like structures [21]. The wall thickness (diameter) is controlled by the FcH content. Carbon onions have been synthesized in a CVD reactor at a temperature of  $900^\circ\text{C}$  using  $\text{Fe}_3(\text{CO})_{12}$  as the catalyst under an  $\text{Ar}/\text{O}_2$  atmosphere [29].

### 33.6.8 Other Shapes

Leaf-like carbon sheets were obtained by the pyrolysis of dichloromethane and FcH in an autoclave at  $300$ – $600^\circ\text{C}$  [41]. The formation process was studied by observing the product evolution utilizing the real-time imaging capabilities of emission SEM. The study also reported the synthesis of different carbon nanostructures by the chlorination of FcH at different temperature conditions; the products included amorphous CNTs, open-ended branches, and carbon nanobags [41] (Fig. 33.13).

A straightforward method for the preparation of novel CNTs/iron nanoparticle hybrids, amorphous carbon, T- or Y-junctions with some degree of shape control was reported [42, 43]. This was done by either the thermolysis CTP/FcH mixtures in a CVD reactor [42] or FcH/thiophene mixtures in a closed steel vessel [43].

In summary, FcH and  $\text{Fe}(\text{CO})_5$  have been shown to produce a wide range of carbons with different structures. In addition to the reaction temperatures and gas flow rates, which play important roles in the formation of different carbon nanostructures, the Fe/carbon ratios, the amount of Fe used, and even the use of additives and metal cocatalysts are also important synthesis parameters.

## 33.7 CONCLUSION

The objective of this chapter was not to give a comprehensive review of organometallic catalysts that had been used to make structured carbon materials or a discussion of the range of structured carbon materials that have been formed from

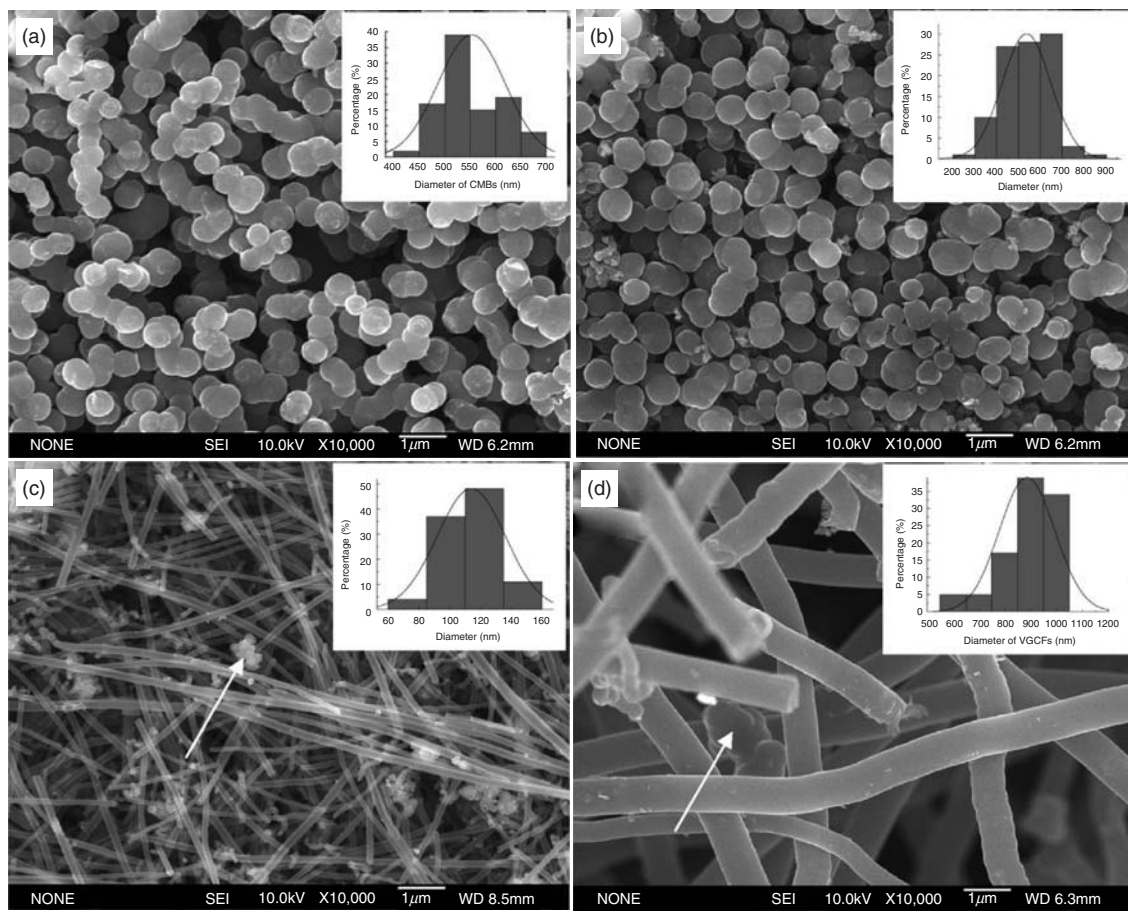


**Figure 33.12** FE-SEM images of the products of the pyrolysis of CTP–ferrocene mixtures with ferrocene (a) 0, (b) 5, (c) 10, and (d) 20 wt% in the reaction zone. Reprinted from Reference 42. Copyright 2007, with permission from Elsevier.

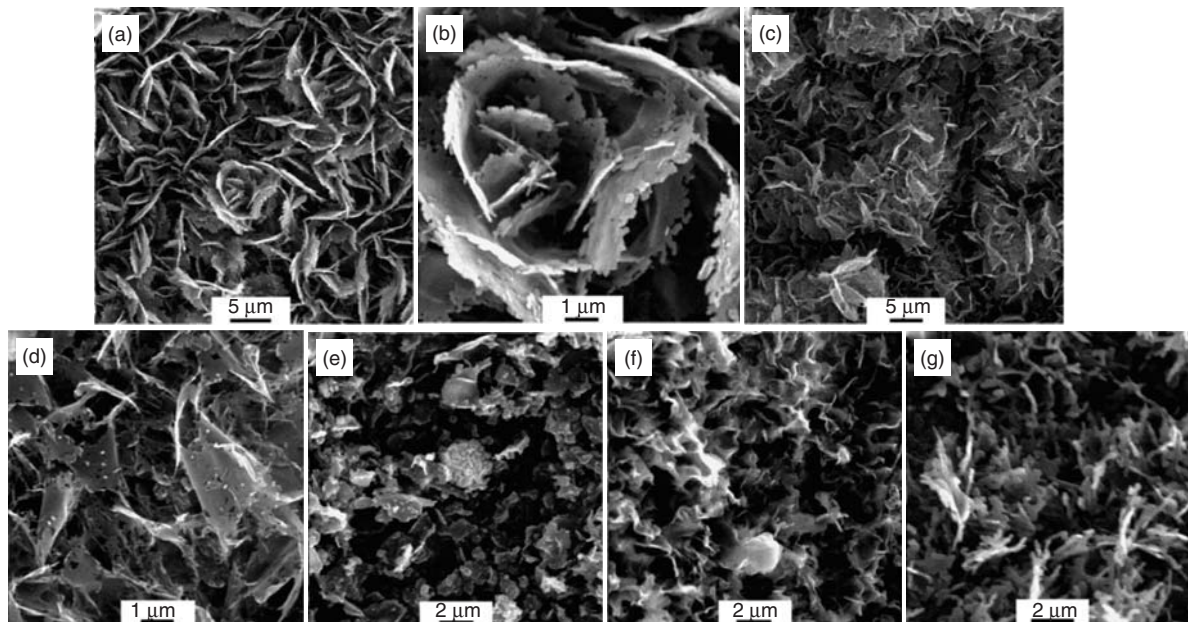


**Figure 33.13** FSEM images of leaf structures grown from FcH at different temperatures. Reprinted from Reference 40. Copyright 2010, with permission from Elsevier.

organometallic catalysts. Rather, the objective was to indicate the role that organometallic complexes can play and have played in making “carbon materials with shape”. This type of study is still in its infancy. Much effort will be required in future to generate appropriate catalysts from metal organometallic precursors that will lead to an understanding of the mode of C–C growth on the metal particles.

## ACKNOWLEDGMENTS

The authors wish to thank the University of the Witwatersrand, the DST/NRF Centre of Excellence in Strong Materials, and the NRF for financial support. They also wish to acknowledge the many postgraduate and postdoctoral fellows in the group who have assisted in the studies that have led to this paper.

## REFERENCES

- Kroto, H. W.; Heath, J. R.; O'Brien, S. C.; Curl, R. F.; Smalley, R. E. *Nature* **1985**, *318*, 162.
- Krätschmer, W.; Fostiropoulos, K.; Huffman, D. R. *Chem. Phys. Lett.* **1990**, *170*, 167.
- Iijima, S. *Nature* **1991**, *354*, 56.
- Davis, W. R.; Slawson, R. J.; Rigby, G. R. *Nature* **1953**, *171*, 756.
- Geim, A. K.; Novoselov, K. S. *Nat. Mater.* **2007**, *6*, 183.
- (a) Ewels, C. P.; Glerup, M. J. *Nanosci. Nanotechnol.* **2005**, *5*, 1345 (b) Nxumalo, E. N.; Coville, N. J. *Materials* **2010**, *3*, 2141; (c) Ayala, P.; Arenal, R.; Rummeli, M.; Rubio, A.; Pichler, T. *Carbon* **2010**, *48*(3), 575.
- (a) Shaikjee, A.; Coville, N. J. *Carbon* **2012**, *50*, 1099–1110; (b) Shaikjee, A.; Coville, N. J. *Carbon* **2012**, *50*, 3376.
- (a) Nyamori, V. O.; Mhlanga, S. D.; Coville, N. J. *J. Organomet. Chem.*, **2008**, *693*, 2205; (b) Govindaraj, A.; Rao, C. N. R., *Pure Appl. Chem.* **2002**, *74*, 1571; (c) A. Huczko, *Appl. Phys. A Mater. Sci. Process.* **2002**, *74*, 617; (d) Mondal, K.; Coville, N. J. *Encyclopedia of Nanoscience and Nanotechnology*; Nalwa H. S., ed., **2011**, Vol. 14; p 161, American Scientific Publishers, USA.
- Tessonier, J. P.; Su, D. S. *ChemSusChem*. **2011**, *4*, 824.
- Nikolaev, P. J. *Nanosci. Nanotechnol.* **2004**, *4*, 307.
- (a) Deshmukh, A. A.; Mhlanga, S. D.; Coville, N. J. *Mater. Sci. Eng.* **2010**, *70*, 1; (b) Coville, N. J.; Mhlanga, S. D.; Nxumalo, E. N.; Shaikjee, A. S. *Afr. J. Sci.* **2011**, *107*, 44.
- (a) Ajima, K.; Yudasaka, M.; Murakami, T.; Maigne, A.; Shiba, K.; Iijima, S. *Mol. Pharm.* **2005**, *2*, 475; (b) Ma, Y.; Hu, Z.; Huo, K.; Lu, Y.; Hu, Y.; Liu, Y.; Hu, J.; Chen, Y. *Carbon* **2005**, *43*, 1667.
- (a) Kawaguchi, M.; Nozaki, K.; Motojima, S.; Iwanaga, H. *J. Cryst. Growth*. **1992**, *118*, 309; (b) Fejes, D.; Hernadi, K. *Materials* **2010**, *3*, 2618; (c) Shaikjee, A.; Coville, N. J. *J. Adv. Res.* **2012**, *3*, 195.
- Hanson, P. L.; Wagner, J. B.; Helveg, S.; Rostrup-Nielsen, J. R.; Clausen, B. S.; Topsøe, H. *Science* **2002**, *295*, 2053.
- Tibbetts, G. G.; Bernardo, C. A.; Gorkiewicz, D. W.; Alig, R. L. *Carbon* **1994**, *32*, 569.
- Young, D. J.; Zhang, J.; Geers, C.; Schutze, M. *Mater. Corros.* **2011**, *62*, 7.
- Helveg, S.; Sehested, J.; Rostrup-Nielsen, J. R. *Catal. Today* **2011**, *178*, 42.
- (a) Liu, J.; Lam, J. W. Y.; Tang, B. Z. *Chem. Rev.* **2009**, *109*, 5799; (b) Plata, D. L.; Meshot, E. R.; Reddy, C. M.; Hart, A. J.; Gschwend, P. M. *ACS Nano* **2010**, *4*, 7185.
- Cao, A. Y.; Zhang, X. F.; Wei, J. Q.; Li, Y. H.; Xu, C. L.; Liang, J.; Wu, D. H.; Wei, B. Q. *J. Phys. Chem. B* **2001**, *105*, 11937.
- (a) Tibbetts, G. G.; Gorkiewicz, D. W. *Carbon* **2009**, *31*, 809; (b) Barreiro, A.; Kramberger, C.; Rummeli, M. H.; Gruneis, A.; Grimm, D.; Hampel, S.; Gemming, T.; Buchner, B.; Bachtold, A.; Pichler, T. *Carbon* **2007**, *45*, 55; (c) Barreiro, A.; Hampel, S.; Rummeli, M. H.; Kramberger, C.; Gruneis, A.; Biedermann, K.; Leonhardt, A.; Gemming, T.; Buchner, B.; Bachtold, A.; Pichler, T. *J. Phys. Chem. B* **2006**, *110*, 20973; (d) Lee D. C.; Mikule, F. V.; Korgel, B. A. *J. Am. Chem. Soc.* **2004**, *126*, 4951.
- (a) Nyamori, V. O.; Coville, N. J. *Organomet. Chem.* **2007**, *26*, 4083; (b) Hou, H.; Schaper, A. K.; Weller, F.; Greiner, A. *Chem. Mater.* **2002**, *14*, 3990; (c) Liu, H.; Cheng, G.; Zheng, R.; Liang, C. *Diamond Relat. Mat.* **2008**, *17*, 313; (d) Andrews, R.; Jacques, D.; Rao, A. M.; Derbyshire, F.; Qian, D.; Fan, X.; Dickey, E. C.; Chen, J. *Chem. Phys. Lett.* **1999**, *303*, 467; (e) Mohlala, M. S.; Liu, X.-Y.; Coville, N. J. *J. Organomet. Chem.* **2006**, *691*, 4768; (f) Merchan-Merchan, W.; Saveliev, A. V.; Kennedy, L.; Jimenez, W. C. *Prog. Energy Combust. Sci.* **2010**, *36*, 696; (g) Dichiara, A.; Bai, J. *Diamond Relat. Mater.* **2012**, *29*, 52; (h) Atiyah, M. R.; Awang Biak, D. R.; Ahmadun, F.; Ahamad, I. S.; Mohd Yasin, F.; Mohamed Yusoff, H. *J. Mater. Sci. Technol.*, **2011**, *27*, 296.
- (a) Nxumalo, E. N.; Letsoala, P. G.; Cele, L. M.; Coville, N. J. *J. Organomet. Chem.* **2010**, *695*, 2596; (b) Han, W.; Kohler-Redlich, P.; Seeger, T.; Ernst, F.; Ruhle, M.; Grobert, N.; Hsu, W.-K.; Chang, B.-H.; Zhu, Y.-Q.; Kroto, H. W.; Walton, D. R. M.; Terrones, M.; Terrones, H. *Appl. Phys. Lett.* **2000**, *77*, 1807; (c) Nxumalo, E. N.; Nyamori, V. O.; Coville N. J. *J. Organomet. Chem.* **2008**, *693*, 2942.

23. (a) Yadav, R. M.; Dabal, P. S.; Shripathi, T.; Katiyar, R. S.; Srivastava, O. N.; *Nanoscale Res. Lett.* **2009**, *4*, 197; (b) Villalpando-Paez, F.; Zamudio, A.; Elias, A. L.; Son, H.; Barros, E. B.; Chou, S. G.; Kim, Y. A.; Muramatsu, H.; Hayashi, T.; Kong, J.; Terrones, H.; Dresselhaus, G.; Endo, M.; Terrones, M.; Dresselhaus, M. S. *Chem. Phys. Lett.* **2006**, *424*, 345; (c) Terrones, M.; Grobert, N.; Terrones, H. *Carbon* **2002**, *40*, 1665; (d) Cruz-Silva, E.; Cullen, D. A.; Gu, L.; Romo-Herrera, J. M.; Muñoz-Sandoval, E.; López-Urías, F.; Sumpter, B. G.; Meunier, V.; Charlier, J.-C.; Smith, D. J.; Terrones, H.; Terrones, M. *ACS Nano* **2008**, *2*, 441.
24. (a) Ci, L.; Li, Y.; Wei, B.; Liang, J.; Xu, C.; Wu, D. *Carbon* **2000**, *38*, 1933; (b) Kato, T.; Kusakabe, K.; Morooka, S. J. *Mat. Sci. Lett.* **1992**, *11*, 674.
25. (a) Su, F.; Zhao, X. S.; Wang, Y.; Wang, L.; Lee, J. Y. *J. Mater. Chem.* **2006**, *16*, 44139; (b) Sharon, M.; Mukhopadhyay, K.; Yase, K.; Iijima, S.; Ando, Y.; Zhao, X. *Carbon* **1998**, *36*, 507; (c) Zou, G.; Yu, D.; Lu, J.; Wang, D.; Jiang, C.; Qian, Y. *Solid State Commun.* **2004**, *131*, 749.
26. Liu, X.-Y.; Huang, B.-C.; Coville, N. J. *Carbon* **2002**, *40*, 2791.
27. (a) Ci, L.; Wei, B.; Xu, C.; Liang, J.; Wu, D.; Xie, S.; Zhou, W.; Li, Y.; Liu, Z.; Tang, D. *J. Cryst. Growth* **2001**, *233*, 823; (b) Luo, T.; Chen, L.; Bao, K.; Yu, W.; Qian, Y. *Carbon* **2006**, *44*, 2844; (c) Urones-Garrote, E.; Ávila-Brande, D.; Katcho, N. A.; Gómez-Herrero, A.; Landa-Cánovas, A. R.; Otero-Díaz, L. C. *Carbon* **2005**, *43*, 978.
28. Deepak, F. L.; Govindaraj, A.; Rao, C. N. R. *Chem. Phys. Lett.* **2001**, *345*, 5.
29. (a) Lu, Y.; Zhu, Z.; Liu, Z. *Carbon* **2005**, *43*, 369; (b) Schnitzler, M. C.; Oliveira, M. M.; Ugarte, D.; Zarbin, A. J. G. *Chem. Phys. Lett.* **2003**, *381*, 541; (c) Sano, N.; Akazawa, H.; Kikuchi, T.; Kanki, T. *Carbon* **2003**, *41*, 2159.
30. (a) Hou, H.; Jun, Z.; Weller, F.; Greiner, A. *Chem. Mater.* **2003**, *15*, 3170; (b) Daraio, C.; Nesterenko, V. F.; Jin, S. J. *Appl. Phys.* **2006**, *100*, 0643091; (c) Kong, Q.; Zhang, J. *Polym. Degrad. Stab.* **2007**, *92*, 2005; (d) Wang, W.; Yang, K.; Gaillard, J.; Bandaru, P. R.; Rao, A. M. *Adv. Mater.* **2008**, *20*, 179.
31. (a) Moisala, A.; Nasibulin, A. G.; Brown, D. P.; Jiang, H.; Khriachtchev, L.; Kauppinen, E. I. *Chem. Eng. Sci.* **2006**, *61*, 4393. (b) Anisimov, A. S.; Nasibulin, A. G.; Jiang, H.; Launois, P.; Cambedouzou, J.; Shandakov, S. D.; Kauppinen, E. I. *Carbon* **2010**, *48*, 380.
32. Awasthi, K.; Kumar, R.; Raghubanshi, H.; Awasthi, S.; Pandey, R.; Singh, D.; Yadav, T. P.; Srivastava, O. N. *Bull. Mat. Sci.* **2011**, *34*, 607.
33. (a) Zajíčková, L.; Jašek, O.; Synek, P.; Eliáš, M.; Kudrle, V.; Kadlecíková, M.; Breza, J.; Hanzlíková, R. *Appl. Surf. Sci.* **2009**, *255*, 5421; (b) Kuo, C.-S.; Bai, A.; Huang, C.-M.; Li, Y.-Y.; Hu, C.-C.; Chen, C.-C. *Carbon* **2005**, *43*, 2760; (c) Castillejos E.; Bachiller-Baez, B.; Pérez-Cadenas, M.; Gallegos-Suarez, E.; Rodríguez-Ramos, I.; Guerrero-Ruiz, A.; Tamargo-Martinez, K.; Martínez-Alonso, A.; Tascón, J. M. D. *J. Alloys Comp.* **2012**, *536S*, S460; (d) Harris, J. D.; Raffaelle, R. P.; Gennett, T.; Landie, B. J.; Hepp, A. F. *J. Mater. Sci. Eng. B* **2005**, *116*, 369; (e) Edgar, K., Spencer, J. L. *Curr. Appl. Phys.* **2004**, *4*, 121.
34. (a) Dumitache, F.; Morjan, I.; Alexandrescu, R.; Ciupina, V.; Prodan, G.; Voicu, I.; Fleaca, C.; Albu, L.; Savoiu, M.; Sandu, I.; Popovici, E.; Soare, I. *Appl. Surf. Sci.* **2005**, *247*, 25; (b) Dumitache, F.; Morjan, I.; Alexandrescu, R.; Morjan, R. E.; Voicu, I.; Sandu, I.; Soare, I.; Ploscaru, M.; Fleaca, C.; Ciupina, V.; Prodan, G.; Rand, B.; Brydson, R.; Westwood, A. *Diamond Relat. Mater.* **2004**, *13*, 362.
35. Bai, S.; Li, F.; Yang, Q. H.; Cheng, H. M.; Bai, J. B. *Chem. Phys. Lett.* **2003**, *376*, 83.
36. (a) Horvath, Z. E.; Kertesz, K.; Petho, L.; Koos, A. A.; Tapaszto, L.; Vertes, Z.; Osvath, Z.; Darabont, A.; Nemes-Incze, P.; Sarkozi, Z.; Biro, L. P. *Curr. Appl. Phys.* **2006**, *6*, 135; (b) Mohlala, M. S.; Liu, X.-Y.; Robinson, J. M.; Coville, N. J. *Organomet. Chem.* **2005**, *24*, 972.
37. Satishkumar, B. C.; Thomas, P. J.; Govindaraj, A.; Rao, C. N. R. *Appl. Phys. Lett.* **2000**, *77*, 2530.
38. Rao, C. N. R.; Govindaraj, A. *Acc. Chem. Res.* **2002**, *35*, 998.
39. (a) Jang, J. W.; Lee, C. E.; Lyu, S. C.; Lee, T. J.; Lee, C. J. *Appl. Phys. Lett.* **2004**, *84*, 2877; (b) Maldonado, S.; Morin, S.; Stevenson, K. J. *Carbon* **2006**, *44*, 1429.
40. Ghosh, P.; Soga, T.; Ghosh, K.; Afre R.A.; Jimbo, T.; Ando, Y. *J. Non-Crys. Solids* **2008**, *354*, 4101.
41. Ju, Z.; Wang, T.; Wang, L.; Xing, Z.; Xu, L.; Qian, Y. *Carbon* **2010**, *48*, 3420.
42. Liu, X.; Yang, Y.; Ji, W.; Liu, H.; Zhang, C.; Xu, B. *Mater. Chem. Phys.* **2007**, *104*, 320.
43. Liu, S.; Wehmschulte, R. J. *Carbon* **2005**, *43*, 1550.

## METAL CATALYSIS IN FULLERENE CHEMISTRY

SALVATORE FILIPPONE, ENRIQUE E. MAROTO, AND ÁNGEL MARTÍN-DOMENECH

*Departamento de Química Orgánica I, Universidad Complutense, Madrid, Spain*

NAZARIO MARTÍN\*

*Departamento de Química Orgánica I, Universidad Complutense, Madrid, Spain; IMDEA Nanoscience, Madrid, Spain*

### 34.1 INTRODUCTION TO FULLERENES

The discovery of the soccer-ball-shaped  $C_{60}$  molecule as the third allotrope of carbon by Robert F. Curl, Sir Harold W. Kroto, and the late Richard E. Smalley in 1985 brought a new and unprecedented nanoform of molecular carbon, unlike the reticular diamond and graphite allotropes, and emerged as a new material exhibiting unique properties [1]. Soon afterwards, a major breakthrough in fullerene science occurred in 1990, when Wolfgang Krätschmer and Donald Huffman, two astrophysicists, prepared fullerene  $C_{60}$  from a carbon arc in multigram amounts, thus paving the way to the chemical functionalization of fullerenes and, therefore, to the synthesis of new and sophisticated fullerene architectures. It was in 1991 that Iijima achieved another major development in fullerene science with the discovery of multiwalled [2] and single-walled [3, 4] carbon nanotubes. More recently, another intriguing carbon-based material, named *graphene* [5], the thinnest and strongest material reported so far and formed by one-atom-thick flat sheet of carbon, has provoked great excitement in the scientific community due to the singular properties they exhibit (Fig. 34.1). Important landmarks in carbon nanostructure science occurred in 1996 when fullerenes' discoverers were awarded the Nobel Prize in Chemistry and in 2010 when André K. Geim and Konstantin S. Novoselov received the Nobel Prize in Physics for the discovery of graphenes.

However, the figure of carbon nanoforms is significantly larger than mentioned above, and other less explored nanoforms such as nanohorns, nanoonions, nanotorus, nanobuds, nanocups, and peapods. are only some of the possible presentations of carbon whose properties and chemical reactivity are quite unknown so far [6]. Furthermore, fullerenes have been skillfully combined with other elements in their inner space, affording the large and fruitful family of endohedral fullerenes or endofullerenes, which contain an atom, molecule, or cluster in their inner cavity [7].

An intriguing question, however, is, why among the many possible cages that can be formed with carbon atoms, that containing 60 atoms is the favored one? Furthermore, since all fullerenes  $C_n$  are constituted by hexagons ( $n \geq 20$  with the exception of  $n = 22$ ) and pentagons (12 for all fullerene cages, which are responsible for the curved geometry), why, among the 1812 possible isomers for 60 carbon atoms, was only the icosahedral symmetry  $I_h$   $C_{60}$  molecule (soccer-ball shape) formed?

These intriguing questions were answered by Kroto, who proposed that the local strain increases with the number of bonds shared by two pentagons (pentalene unit), thus affording less stable molecules. This rule was coined as the “isolated pentagon rule” (IPR), which states that all pentagons must be surrounded by hexagons, thus forming the corannulene moiety [8].

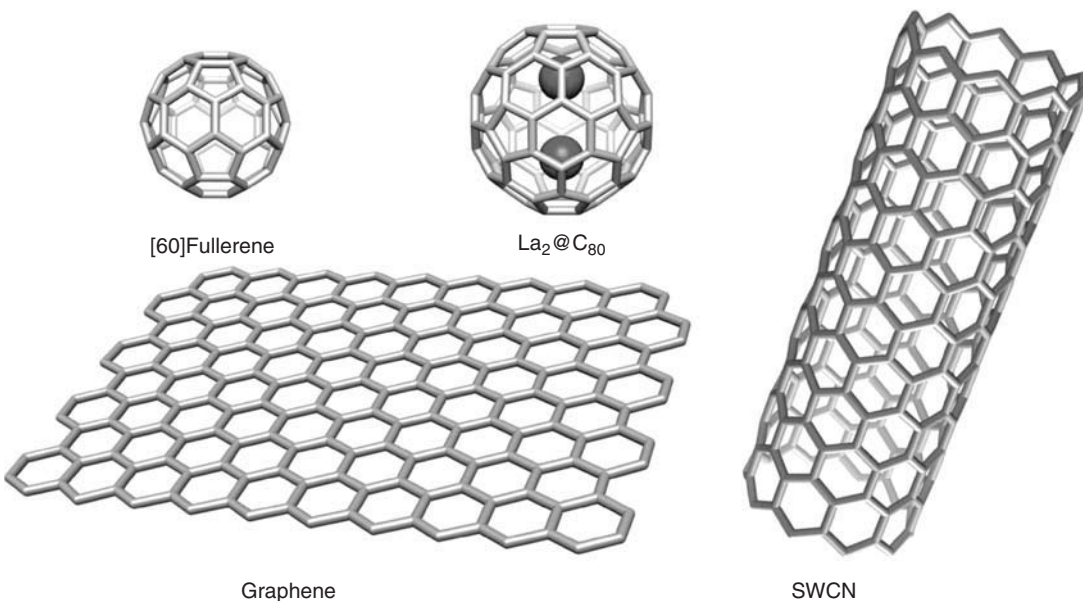


**Figure 34.1** Representative examples of [60]fullerene, endohedral fullerene, graphene and a single-walled carbon nanotube.

The resonance destabilization that results from the adjacent pentagons ( $8\pi$  electrons which do not satisfy the Hückel rule) and reduction of the  $\pi$ -orbital overlap due to the cage curvature explain the lower stability of those so-called non-IPR fullerenes [9–11].

## 34.2 GENERAL REMARKS ON THE CHEMICAL REACTIVITY OF FULLERENES

Fullerenes as molecular allotropes of carbon are soluble in some organic solvents such as carbon disulfide, toluene, *o*-dichlorobenzene (*o*-DCB), or chlorobenzene. Therefore, they undergo a variety of chemical reactions in solution to afford a huge number of fullerene derivatives which, in general, preserve the chemical and physical properties of pristine fullerenes. The singular 3D geometry of fullerenes showing a singular  $\text{sp}^{2,3}$  hybridization [12] and containing 30 (for  $\text{C}_{60}$ ) or more (for higher fullerenes such as  $\text{C}_{70}$  and  $\text{C}_{80}$ ) highly reactive double bonds constitutes a new scenario where a variety of different chemical reactions can be tested.

The calculated bond distances in the C–C bonds in [60]fullerene reveal significant differences between the [5,6]- and [6,6]-bonds with values of 1.45 and 1.38 Å, respectively. Because of the mixed character of 1,3,5-cyclohexatrienes and [5]radialenes,  $\text{C}_{60}$  behaves as a highly strained electron-deficient olefin whose chemical reactivity is mainly driven by strain relief. Therefore, addition reactions have been widely used [13]. Interestingly, although similar reactivity patterns have also been observed for higher fullerenes, the chemical reactivity tends to decrease significantly with their size [14–16].

Addition reactions, electron transfer reactions, and reactions involving the opening of the fullerene cage (chemical surgery) have been thoroughly studied on fullerenes. Other reactions such as nucleophilic additions, cycloaddition reactions, free-radical additions, halogenations, hydroxylation, redox reactions, and metal transition complexations have been reported for  $\text{C}_{60}$  as well. Furthermore, fullerenes are easily reduced by electron-rich chemical reagents as well as electrochemically. Their oxidation, however, is considerably more difficult to achieve [17]. Thus, electrochemical measurements showed the formation from the monoanion to the hexaanion [18].

For a more comprehensive and detailed study of the properties and reactivity of fullerenes, the reader is referred to the monographs that comprehensively cover the properties and chemical reactivity of  $\text{C}_{60}$  and higher fullerenes [13–16].

## 34.3 METAL-MEDIATED REACTIONS IN FULLERENE CHEMISTRY

The high electrophilicity of fullerenes has resulted in one of the first natural approaches in their chemical modification based on the nucleophilic addition of organometallic reagents, such as organolithium [19] or Grignard salts [20].

Although, it has become one of the classical methods for fullerene functionalization [21–23], the use of organometallic reagents presents important limitations, namely, the control of the reaction to the monoaddition product or the compatibility with some functional groups. More recently, however, fullerene chemistry has attracted an increasing interest in expanding its classical methodology to new reactions based on the use of transition metals. In this regard, the first example was the use of Fisher's carbene for the preparation of methanofullerenes [24] by thermal reaction of C<sub>60</sub> with [methyl(methoxymethylene)]pentacarbonylchromium. Nickel(0) has also been used for the construction of a fused cyclohexadiene ring to C<sub>60</sub> based on a [2+2+2] cycloaddition of 1,6-diynes to [60]fullerene [25].

Fulleropyrrolidines bearing one or two alkyne units on the pyrrolidine ring have been synthesized as building blocks analogous to 1,6-enynes, which have previously been used for the construction of a wide variety of carbo- and heterocyclic systems mostly through transition-metal-catalyzed processes. As a matter of fact, these so-called fuller-1,6-enynes (the term emphasizes the singularity of this highly strained double bond component, belonging to a curved surface molecule) gave rise to a series of chemical transformations affording novel structures on the fullerene sphere [26, 27].

Above all, fullerynes have also proved to be suitable substrates for the cobalt-mediated Pauson–Khand (PK) reaction [28]. Indeed, despite its electron-poor character, [60]fullerene has a spherical surface with 30 reactive double bonds; in addition, the typical competing  $\beta$ -hydride elimination reaction has been overcome through the absence of hydrogen atoms in its structure. Therefore, when a 1,6-fullerene (1) is treated with Co<sub>2</sub>(CO)<sub>8</sub> at room temperature, a cobalt–fullerene complex 2 could be isolated and characterized. This complex at 60 °C undergoes an intramolecular PK reaction that leads regioselectively to the formation of a *cis*-1 bis-cycloadduct (3) featuring a highly rigid system containing three fused pentagonal rings. Fullerenes 4, suitably functionalized with two propargyl groups, also underwent the PK reaction affording *cis*-1-bis-cycloadduct 5 resulting from only one [2+2+1] cycloaddition reaction as main product. The tris-cycloadduct 6 formed from a twofold PK reaction was also obtained, although in a poor yield (5%) due, probably, to the high strain of the resulting geometry, presenting the unprecedented structure with five fused pentagonal rings on the fullerene surface [29].

All attempts to carry out the intermolecular PK reaction with C<sub>60</sub> and alkynes using Co<sub>2</sub>(CO)<sub>8</sub> were unsuccessful. However, the reactivity of the fullerene double bond has proved to be as reactive as a conventional olefin. Indeed, fullerene 7 endowed simultaneously with an alkynyl and allyl systems affords both PK cycloadducts (8 and 9) in the same yields (Scheme 34.1) [28].

A further step has been the use of transition-metal catalysis in fullerene chemistry as a smart alternative to avoid high loading of organometallic reagent and to achieve remarkable levels of reactivity and selectivity. An interesting example of this approach has been the arylation and alkenylation of fullerenes, catalyzed by a rhodium complex, as reported by Itami [30]. Similar to the reaction of organoboron compounds with electron-deficient alkenes and alkynes, rhodium(I) complexes catalyze the hydroarylation of C<sub>60</sub> (or C<sub>70</sub>) with arylboronic acid in aqueous solution. The reaction proceeds in a monoaddition-selective manner with a high regioselectivity when [70]fullerene is used, affording products 10 and 11, respectively (Scheme 34.2).

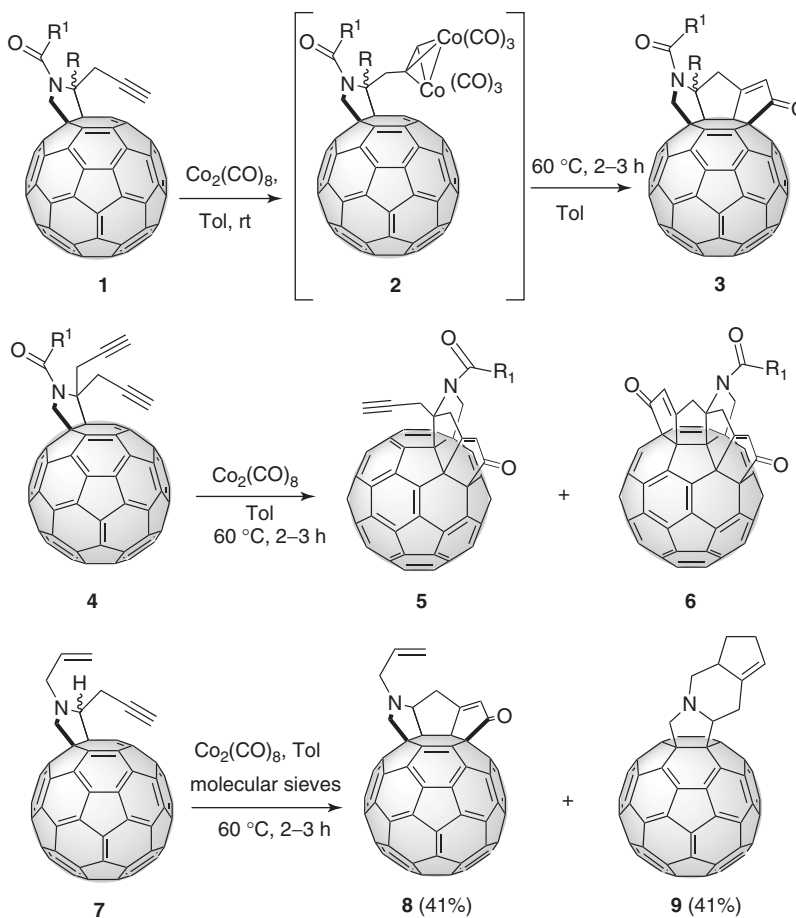
The use of [Rh(cod)(MeCN)<sub>2</sub>]BF<sub>4</sub> gave rise to an optimal combination of good yield (61%) and excellent selectivity (>95%), showing an important effect of the counteranion of the rhodium complexes in sharp contrast to the reported example of conventional olefins. The authors claimed a catalytic cycle reaction where the cationic Rh complex and water produce the Rh–OH species. After transmetalation with RB(OH)<sub>2</sub>, the Rh–R species undergoes addition on the C<sub>60</sub> double bond. Finally, protonolysis of the formed fulleranyl Rh species affords the product R–fullerene–H (10, 11) with the regeneration of the cationic Rh complex.

Shortly afterward, the same authors also developed a palladium(II) catalyst [Pd(2-PyCH= NPh)(OCOC<sub>6</sub>F<sub>5</sub>)<sub>2</sub>] for the hydroarylation of fullerene with boronic acids, which presents good catalytic activity (reaction generally occurring at room temperature), bench stability in the solid state, and efficiency under air conditions. Single-crystal X-ray diffraction analysis confirmed unequivocally the addition of the aryl moiety and hydrogen in a 1,2-fashion at the  $\alpha$  double bond of C<sub>70</sub>, with the phenyl group attached at the position close to the pole of the C<sub>70</sub> unit [31].

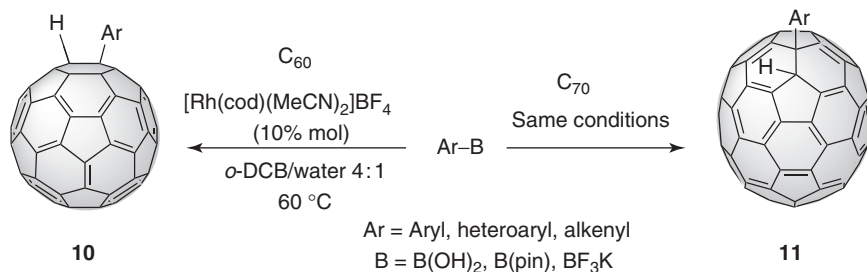
Analogously, Co-catalyzed hydroalkylation of C<sub>60</sub> with reactive alkyl bromides in the presence of Mn reductant and H<sub>2</sub>O at room temperature gave the monoalkylated C<sub>60</sub> (12) in good to high yields (Scheme 34.3). The reaction probably occurs through a reduced Co(0 or I) complex that promotes generation of a radical (R') and the addition to C<sub>60</sub> [32].

Single-bonded fullerene dimers RC<sub>60</sub>–C<sub>60</sub>R, featuring a direct covalent bond between the two C<sub>60</sub> cages, are unusual structures with potentially interesting properties due to the interaction of two adjacent fullerene cages. These dimers are formed as a mixture of racemic and meso isomers because of the lack of symmetry of their 1,4 addition pattern, which are in equilibrium with the monomer radical (RC<sub>60</sub>C $\bullet$ ) in solution [33].

A straightforward preparation was reported by Yamamoto et al. [34] by the dimerization of monosubstituted hydrofullerenes using catalytic amounts of copper(II) acetate in the presence of air to yield dimers 13 (Scheme 34.4).



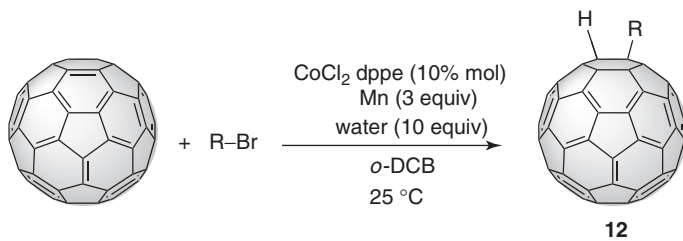
**Scheme 34.1** Fulleropyrrolidines endowed with one (**1**) or two (**4**) propargyl groups efficiently and regioselectively undergoing the PK reaction with  $[\text{Co}_2(\text{CO})_8]$  to afford *cis*-1 bis-cycloadduct and tris-cycloadduct fullerene structures with three or five pentagonal rings fused onto the fullerene surface, respectively.



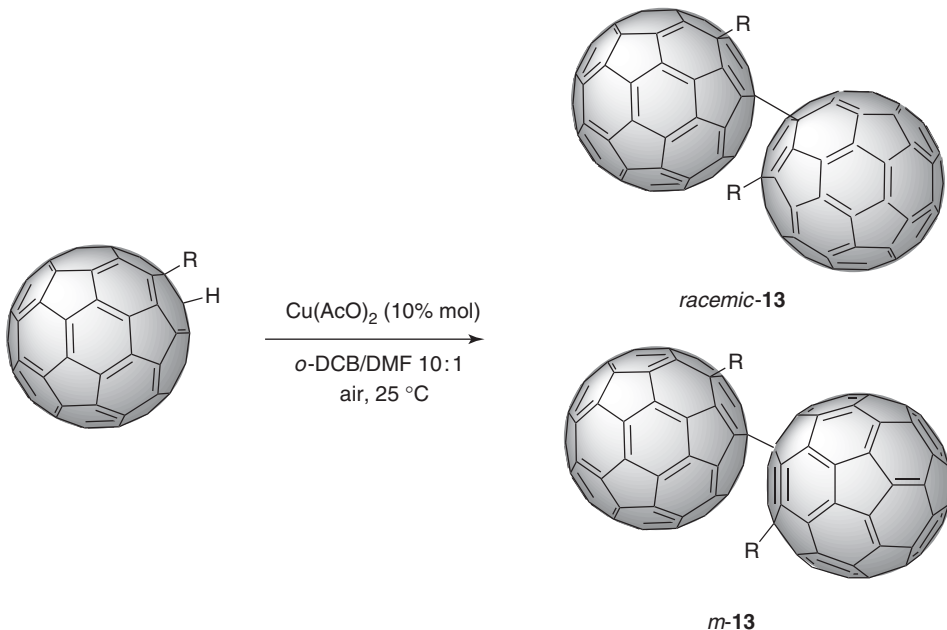
**Scheme 34.2** The addition of organoboron reagents onto fullerenes with good efficiency and selectivity by using catalytic amounts of Rh or Pd (*o*-DCB, *ortho*-dichlorobenzene).

A wide range of functional groups are tolerated: fullerene-bound dendritic homodimers and various cross-dimers, which are otherwise difficult to obtain, were thus synthesized in good to high yields.

An intriguing copper-catalyzed radical reaction that involves a formal C–H bond activation has been reported by Nakamura. The reaction efficiently couples an arylacetylene or enyne to a penta(aryl)[60]fullerene bromide in a formal [4 + 2] fashion to form a dihydronaphthalene ring fused to a fullerene sphere [35].



**Scheme 34.3** The reaction of alkyl bromides to fullerenes yielding monoalkylated addition products by using catalytic amounts of Co in the presence of Mn.

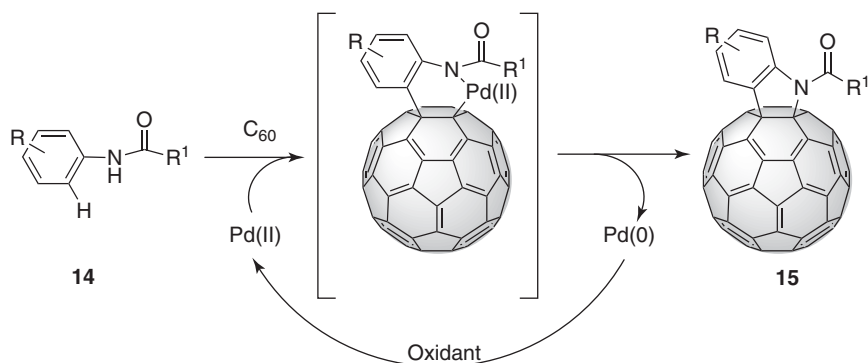


**Scheme 34.4** Copper(II)-mediated synthesis of [60]fullerene dimers.

Palladium acetate catalyzes cycloaddition onto C<sub>60</sub> of a variety of anilides (**14**) through a C–H bond activation, affording fulleroindolines (**15**) in a highly regioselective manner (Scheme 34.5) [36].

### 34.3.1 Metal-Mediated Retro-Cycloadditions

In parallel to the development of exohedral functionalization of the fullerene sphere, many efforts have been devoted to the search for efficient retro-functionalization methodologies for the most important fullerene cycloadduct derivatives.



**Scheme 34.5** Fulleroindolines prepared by Pd(II) catalysis from anilides and C<sub>60</sub>.

The sequences of cycloaddition–retro-cycloaddition could indeed be used as a smart strategy to carry out protection–deprotection protocols that could selectively add or remove addends from fullerenes while leaving others unperturbed. Therefore, retro-cycloaddition protocols have been reported by the use of thermal treatment [37], microwave irradiation [38], chemical reduction [39], electrochemical reduction [40], or electrochemical oxidation [41].

Important classes of fullerene derivatives have been successfully deprotected by transition-metal-mediated or catalyzed processes.

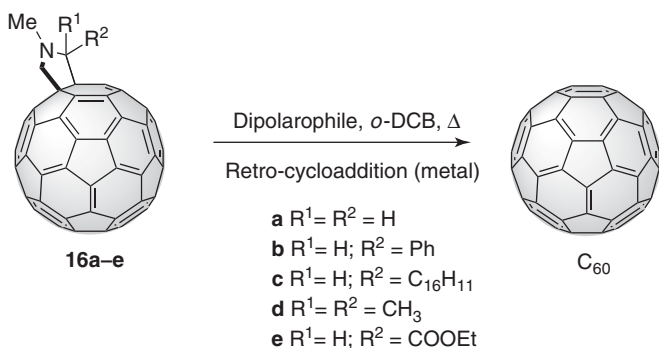
The 1,3-dipolar cycloaddition reaction of azomethine ylides onto fullerenes is considered one of the most straightforward procedures for their chemical functionalization. The resulting fulleropyrrolidines (pyrrolidino[3,4:1,2][60]fullerenes) are among the most frequently studied fullerene derivatives as a consequence of their easy synthetic preparation and their stability. Therefore, this functionalization procedure was frequently chosen as a suitable route for the preparation of a wide variety of stable modified fullerenes with interest in biology and materials science. Nevertheless, the use of transition metals, such as copper(II) or rhodium(I), promotes a highly efficient retro-cycloaddition from differently substituted pyrrolidino[60]fullerenes, affording quantitatively pristine [60]fullerene, with the recovery of the typical magenta color of the [60]fullerene solution [42].

The 1,3-dipolar retro-cycloaddition reaction turned out to be quite general and occurs in the presence of an excess of a highly efficient dipolarophile (30 equiv), such as maleic anhydride, which traps the corresponding ylide resulting from the thermal retro-cycloaddition. In the absence of the metal salts, the reaction yields depend on the refluxing temperature, the pyrrolidine substitution pattern [unsubstituted (**16a**), monosubstituted (**16b, c, e**), and disubstituted (**16d**)] (Scheme 34.6), and the nature of the substituents on the pyrrolidine ring, which influence the stability of the thermally generated 1,3-dipole.

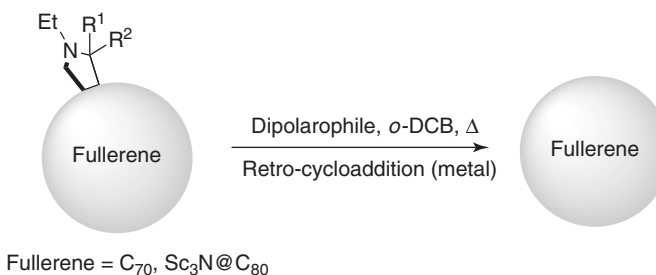
Thus, when compounds **16a–e** were refluxed in *o*-DCB for different times (8–18 h) in the presence of maleic anhydride (30 equiv) and 1 equiv of copper(II) triflate ( $\text{CuTf}_2$ ), the reaction led, in all cases, to the quantitative formation of the parent unsubstituted  $\text{C}_{60}$  (determined by HPLC), with the solutions showing the typical magenta color of  $\text{C}_{60}$ .

Interestingly, the reaction also proved to be highly efficient with the monoadduct mixture of the three isomers of [70]pyrrolidinofullerene and with the *N*-ethyl pyrrolidino- $\text{Sc}_3\text{N}@\text{C}_{80}$ , giving rise to pristine  $\text{C}_{70}$  and  $\text{Sc}_3\text{N}@\text{C}_{80}$  almost quantitatively, respectively (Scheme 34.7).

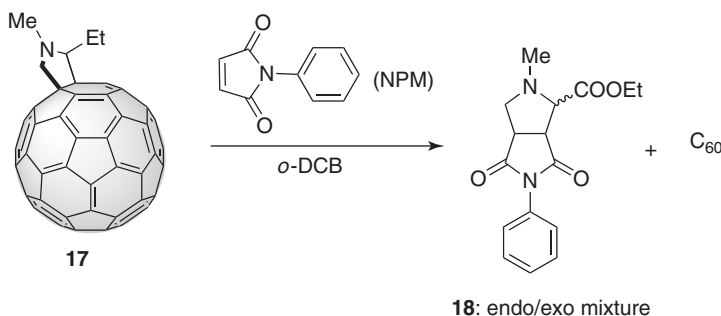
The formation of the azomethyne ylide as an intermediate resulting from the retro-cycloaddition process was proved by carrying out trapping experiments by using *N*-phenylmaleimide (NPM). Thus, compound **17** was refluxed in *o*-DCB in the presence of an excess of NPM (10 equiv). In addition to the obtained  $\text{C}_{60}$  (70%), the cycloadduct (**18**) resulting from the



Scheme 34.6 Retro-cycloaddition reaction of pyrrolidino[3,4:1,2][60]fullerenes (**16a–e**).



Scheme 34.7 Retro-cycloaddition reaction of higher and endohedral pyrrolidinofullerenes.



**Scheme 34.8** Trapping experiment using NPM as dipolarophile.

1,3-dipolar cycloaddition of the *in situ* generated azomethyne ylide to the NPM was obtained in 19% yield as an endo/exo mixture 66:33 (Scheme 34.8). However, it remains unclear whether the metal acts only as a Lewis acid activating the lowest occupied molecular orbital (LUMO) of the dipolarophile or whether it also triggers the azomethine ylide formation by complexation to the pyrrolidine [43].

This protocol of retro-cycloaddition reaction of azomethine ylides has proved to be so versatile that it can also be applied for the retro-functionalization of carbon nanotubes. Thus, a solution of functionalized multiwalled carbon nanotubes was heated to 150 °C in *o*-DCB for 48 h, with copper triflate as catalyst, in an excess of C<sub>60</sub> in order to trap the resulting ylide. As a result, pristine nanotubes were separated from the residue by filtration, and in the filtrate the presence of fullerene monoadduct was proven by thin-layer chromatography (TLC) and high performance liquid chromatography (HPLC) [44].

Other fullerene derivatives prepared by 1,3-dipolar cycloaddition reaction have undergone the same thermal treatment in the presence of an excess of a dienophile and Cu(II) catalysis. Isoxazolino[4.5:1.2][60] and [70]fullerenes underwent an efficient retro-cycloaddition reaction to pristine fullerene [45]. Pyrazolino[60]fullerenes proved to be more stable under these conditions with respect of the previously described fullerene derivatives prepared by 1,3-dipolar cycloaddition reaction. While C-aryl-N-aryl-2-pyrazolino[60]fullerenes do not undergo an efficient retro-cycloaddition process under a variety of experimental conditions, alkyl-substituted carbon atom of the pyrazole ring undergoes a partial cleavage of the 1,3-dipole, leading to pristine C<sub>60</sub> in good yields (72%) [46].

#### 34.4 ASYMMETRIC CATALYSIS IN FULLERENE CHEMISTRY

Only one year after fullerenes C<sub>60</sub> and C<sub>70</sub> became available in multigram amounts, the first chiral carbon cage C<sub>76</sub>-D<sub>2</sub> was chromatographically isolated from fullerene soot extract [47]. Since then, a large number of chiral fullerene derivatives have been obtained [48] and classified on the base of their chirality as follows:

- Derivatives of achiral parent fullerenes in which the derivatization creates a chiral functionalization pattern on the fullerene skeleton irrespective of the addends being identical or different—they have an *inherently chiral functionalization pattern*;
- Derivatives of achiral parent fullerenes in which a chiral functionalization pattern is due, exclusively, to nonidentities among addends—they have a *noninherently chiral functionalization pattern*;
- Derivatives of achiral parent fullerenes in which the addition of chiral residues does not create a chiral addition pattern on the fullerene surface—they have their chiral elements located exclusively in the addends [49].

Also, chiral fullerene derivatives have found use in biological applications [50] and in polymer science as helicity inducers [51]. Recently, fullerene chirality has demonstrated to be critical in generating a supramolecular architecture of donor–acceptor dyads (based in a chiral pyrrolidino[60]fullerene) giving rise to photoconductive nanofibers displaying very high ambipolar charge-carrier mobility ( $\sim 10^{-1}$  cm<sup>2</sup>/(V s)), which was higher than that obtained from racemic dyads in spherical assembly [52].

However, while the importance of chiral derivatives is increasing (especially in the field of organic electronics, where fullerenes present the more promising applications), the preparation of pure enantiomers has been based on the HPLC racemate resolution or on the use of chiral starting materials. The noncoordinating character of fullerene double bonds has indeed hampered the use of most part of the available chiral methodologies based on the activation of electron-deficient olefins.

A major breakthrough in this respect has been the introduction of asymmetric metal catalysis for the preparation pyrrolidino[3,4:1,2][60]fullerenes with a complete control on the absolute configuration [53].

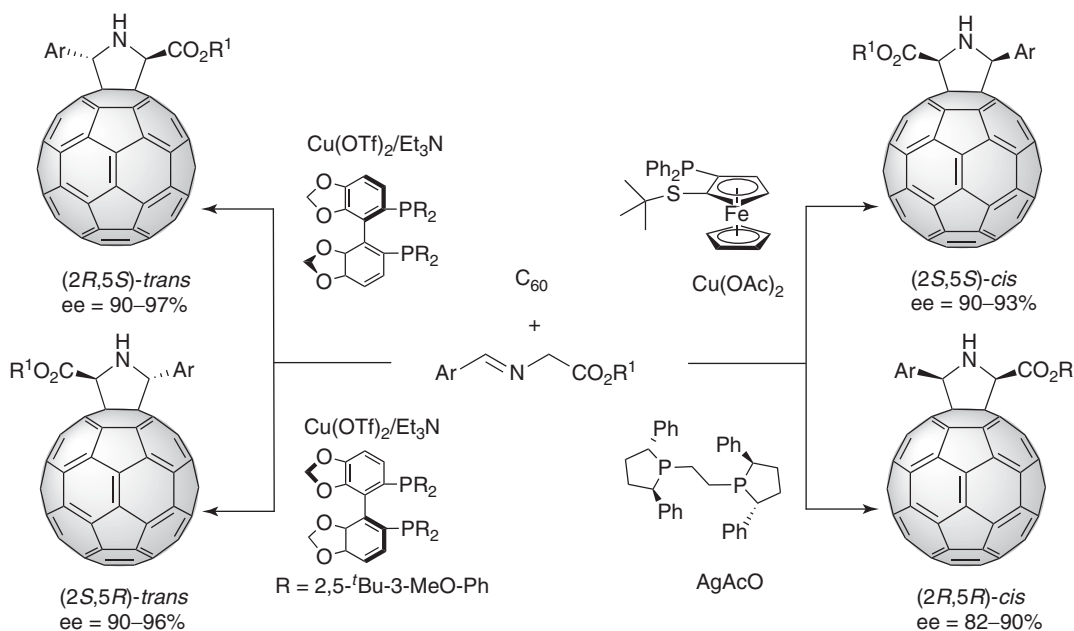
Pyrrolidinofullerenes are probably the most widely used fullerene derivatives because of their stability, versatility, and the availability of reactants. Their synthesis is based on the 1,3-dipolar cycloaddition of azomethine ylides formed by thermal treatment from aldehydes and amino acids [54, 55] or from iminoesters [56, 57]. The latter lacks selectivity since it affords a diastereomeric mixture (cis and trans) of 2,5-disubstituted pyrrolidinofullerenes.

On the other hand, the use of the suitable combination of a metal salt, chiral ligand, and base promotes at low temperature the formation *in situ* of chiral *N*-metalated azomethine ylides from the corresponding iminoester and the subsequent selective cycloaddition onto the fullerene cage. Thus, the P,S chiral ligand Fesulphos along with copper(II) acetate directs the addition toward the formation of the stereoisomer (2*S*,5*S*)-2-alkoxycarbonyl-5-arylpyrrolidino[3,4:1,2][60]fullerene with complete cis diastereoselectivity and enantiomeric excesses up to 93% (Scheme 34.9).

A complete cis diastereoselectivity was displayed also by the silver acetate/(-)BPE {(-)-1,2-Bis[(2*R*,5*R*)-2,5-diphenylphospholano]ethane} complex but with an inverted enantioselectivity affording the (2*R*,5*R*) compound with ee up to 90% [53]. The synthesis of these pyrrolidines was demonstrated to be completely stereodivergent by the use of copper(II) complexes with both atropoisomers of the ligand DTBM (3,5-di-*t*-butyl-4-methoxyphenyl) Segphos. The corresponding chiral *N*-copper azomethine ylides formed using triethyl amine as base underwent a stepwise cycloaddition affording the trans diasteromers, with both enantiomers in high optical purity [58].

The presence of two new chiral carbon atoms linked to the fullerene cage perturbs asymmetrically the symmetric  $\pi$ -system of pristine [60]fullerene chromophore, giving rise to circular dichroism (CD) spectra whose shape and intensity depend on the absolute configuration of the new formed pyrrolidine ring. Enantiomers obtained from the same catalytic complex give rise to CD spectra with the same sign and behavior at 430 nm. This peak corresponds to a UV-vis band considered to be the fingerprint for all fullerene monoadducts at 6,6 junctions (between two fused hexagons) regardless of the nature of the organic addend saturating the double bond and, therefore, has been used to assign the absolute configuration of the chiral [60]fullerene derivatives [59]. A sector rule has been proposed that consists in drawing a plane tangent to the  $C_{60}$  sphere at the attacked 6–6 single bond. This plane is, in turn, divided into four sectors by two other planes: one that goes through the 6–6 bond and the other that bisects the 6–6 single bond (Fig. 34.2).

Accordingly, all the compounds featuring a positive peak at 430 nm region are consistent with the presence of the bulkier substituent in the upper right quadrant (or, but it is the same, in the lower left quadrant) and vice versa. Therefore, since all the pyrrolidinofullerenes formed from the Cu(II)/Fesulphos catalytic complex showed in their CD spectra a positive peak at 430 nm, a (2*S*,5*S*) stereochemistry has been assigned considering that the phenyl group is bulkier than the alkoxycarboxyl group (Fig. 34.3).



**Scheme 34.9** Stereodivergent synthesis of [60]fulleropyrrolidines by asymmetric catalysis.

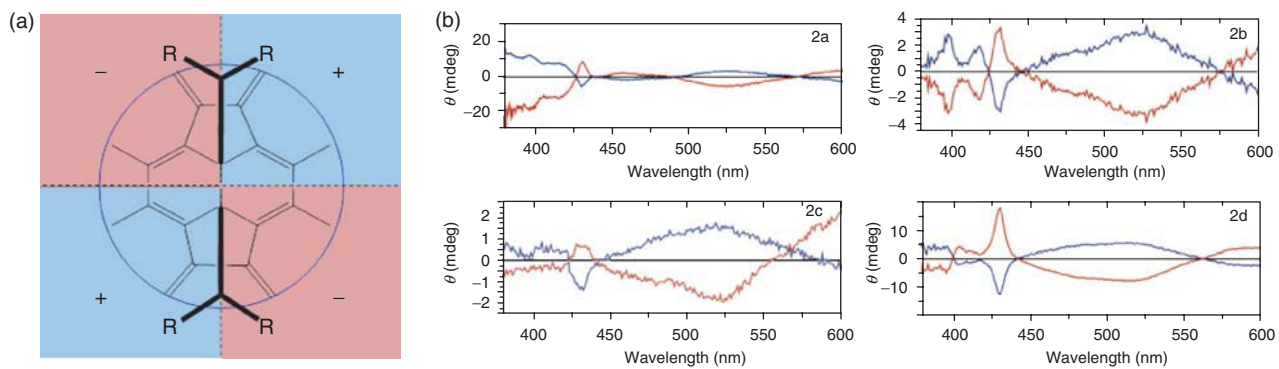


**Figure 34.2** (a) Schematic top view of the four sectors of the plane tangent to the attacked double bond with the respective sign. (b) CD spectra of both enantiomers of several *cis*-[60]fulleropyrrolidines (see Scheme 34.9): blue line represents (2*R*,5*R*) enantiomers obtained from Ag(I)/(-)-BPE and the red line (2*S*,5*S*) enantiomers synthesized using Cu(II)/Fesulphos. (See insert for color representation of the figure.)

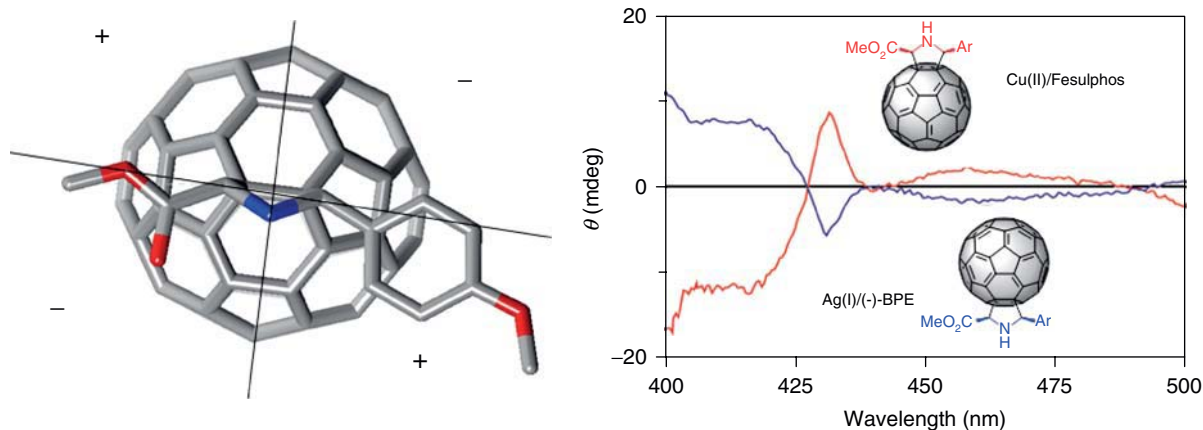


**Figure 34.3** Absolute configuration assigned for both *cis*-2-carboximethyl-5-(*p*-methoxyphenyl)pyrrolidino[3,4:1,2][60]fullerene enantiomers using the sector rule. (See insert for color representation of the figure.)

Similarly, when Cu(II)/(*R*)-DTBM segphos complexes are used, the *trans* pyrrolidino[60]fullerene features a (2*R*,5*S*) configuration. Moreover, chiral complexes affording the *trans* adduct present a higher intensity at the 430 nm peak, as both substituents lay above the sectors with the same sign, thereby resulting in an additive effect (Fig. 34.4).

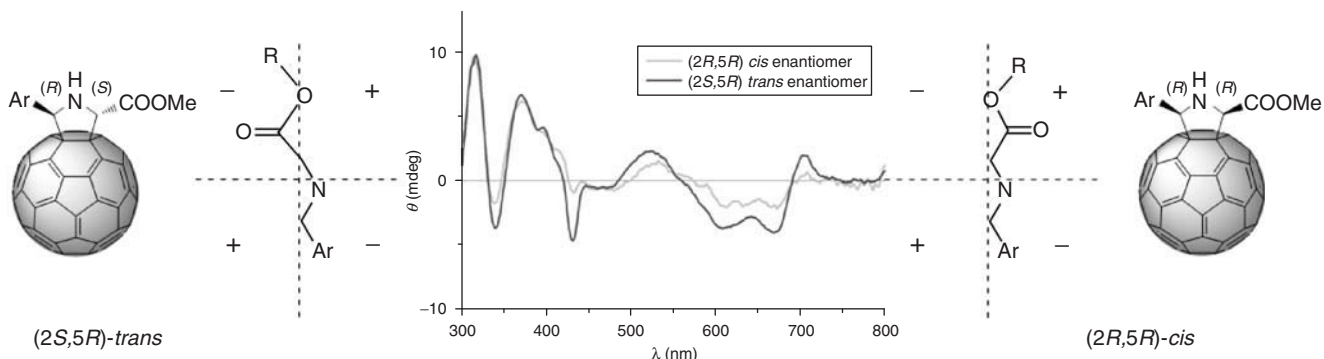


**Figure 34.4** *Trans* configuration in the pyrrolidine substituents giving rise to an additive effect in the CD peak at 425–430 nm. On the other hand, *cis* isomers present less pronounced peaks in that region, the effect of the heavier aromatic moiety being predominant with respect to the ester group.

Asymmetric functionalization of higher fullerenes has to face even more complicated selectivity issues. Indeed, just considering the next higher homolog of  $C_{60}$ , namely,  $C_{70}$ , different types of double bonds are accessible as a result of the lossing of the spherical symmetry of  $C_{60}$ . The most common additions to [70]fullerene take place at the more curved and reactive polar zone, namely, at the  $\alpha$  double bond ( $C(8)-C(25)$ ) (according to IUPAC nomenclature) followed by  $\beta$ ,  $C(7)-C(22)$ , then  $\gamma$  ( $C(1)-C(2)$ ) sites and only rarely to the  $\delta$  site, located in the equatorial region, the site selectivity being driven by the release of strain of the relevant double bond. All the chiral complexes described above catalyzed the  $N$ -metalated azomethine ylides cycloaddition with a high site selectivity, obtaining almost exclusively the  $\alpha$  site isomer. Furthermore, good levels of regioselectivity were also achieved, as the reaction afforded the regiosomer with the alkoxy carboxyl group on the polar region in 80% yield (Fig. 34.5) [60].

Analogous to the example in the addition to [60]fullerene, the use of Cu(II) triflate with (*R*)- or (*S*)-Segphos affords both enantiomers of trans diastereomer, whereas the use of Cu(II) acetate/Fesulphos or Ag(I) acetate/(-)BPE gives rise to (*S,S*) or (*R,R*) enantiomers, respectively, of the cis diastereoisomer [57, 59].

Density functional theory (DFT) calculations (at the B3LYP/LANL2DZ level of theory) account completely for the regio- and stereochemical result of the silver-catalyzed azomethine ylides cycloaddition onto  $C_{70}$  (Fig. 34.6). A stepwise mechanism indicates that the origins of the observed selectivity are determined by the first step of the cycloaddition at the site, regio, and enantio levels.

As far as the enantioselectivity of the reaction is concerned, the (*si,re*) attack requires a larger departure of the catalyst from its optimal conformation shown in Fig. 34.6, thus favoring the (*re,si*) attack, in good agreement with the experimentally observed enantioselectivity [59].

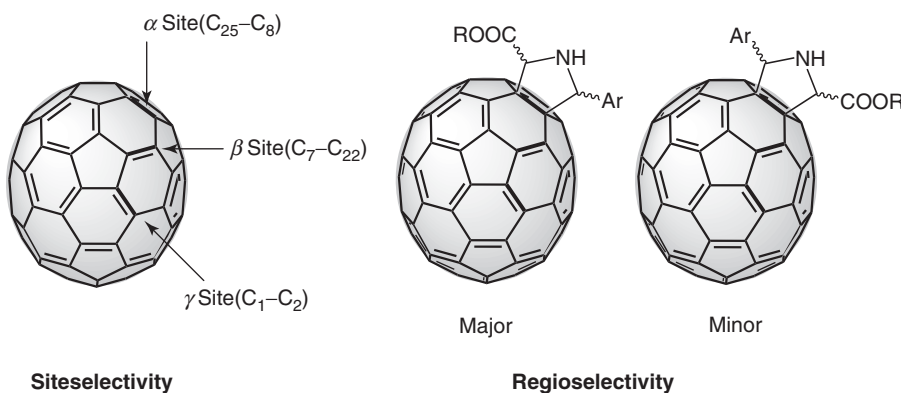


**Figure 34.5** Site- and regioselectivity in  $C_{70}$  1,3-dipolar cycloaddition of  $N$ -metalated azomethine ylides.

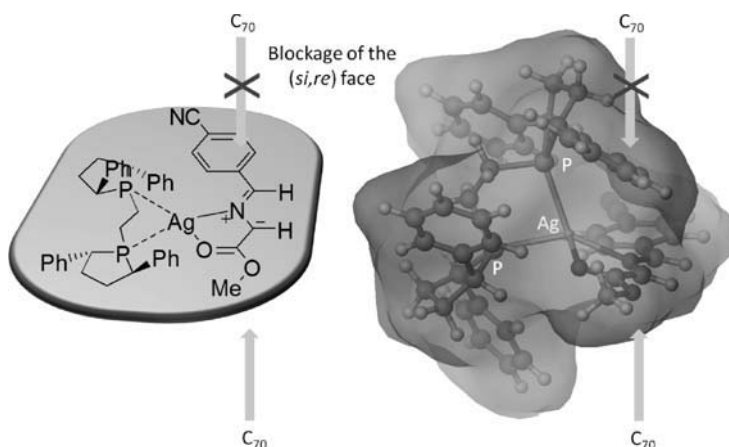


**Figure 34.6** Blockage of the (*si,re*) face of the 1,3-dipole in the silver-catalyzed azomethine ylides cycloaddition onto  $C_{70}$ , accounted by DFT calculations.

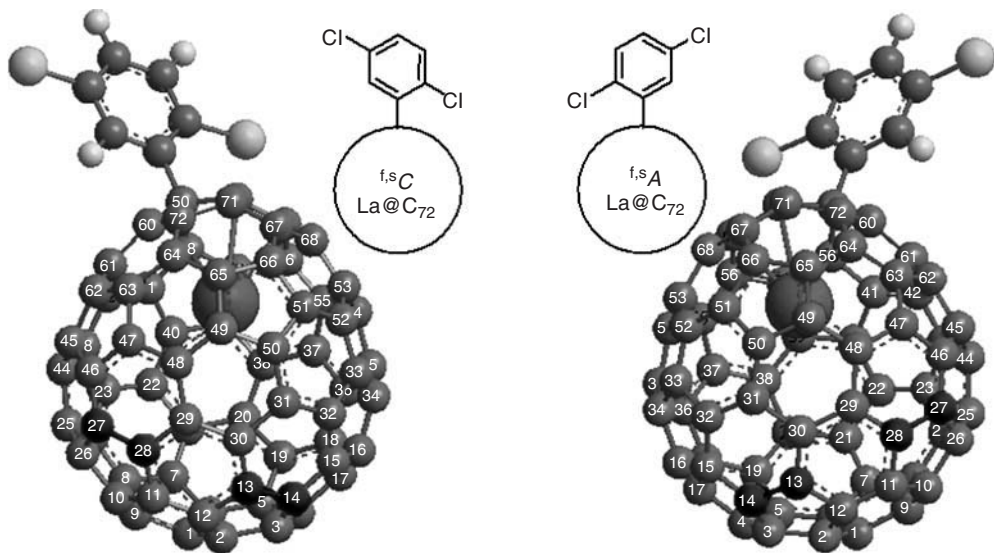


**Figure 34.7** Enantiomers of  $C_6H_4Cl_2La@C_{72}$ .

Endohedral metallofullerenes, which encapsulate one or more metal atoms, a molecule, or a cluster inside the fullerene cage, are promising molecules in biomedical and materials science, because they can radically enhance the molecular properties of fullerenes by changing the nature and composition of the encapsulated species [7, 61]. In particular, they are of interest as agents for magnetic resonance imaging (MRI) [62], photovoltaic devices [63], and semimetallic components [64]. The synthesis of chiral endofullerenes represents one step further in the potential use of these carbon allotropes. However, all attempts to extend this methodology to a series of pristine endofullerenes (namely,  $Sc_3N@C_{80}$ ,  $La@C_{82}$ , and  $La_2@C_{80}$ ) were unsuccessful, probably due to the energy mismatch between the HOMO of the 1,3-dipole and the lowest unoccupied molecular orbital (LUMO) energy of the endohedrals, which is considerably higher than that of  $C_{60}$  and  $C_{70}$ . In order to address this issue, a functionalized endohedral  $La@C_{72}$ , endowed with a strong electron-withdrawing substituent such as the dichlorophenyl radical was used. Furthermore, the intrinsic structure of this endohedral significantly modified the LUMO level (close to those of  $C_{60}$  and  $C_{70}$ ), thus allowing its further reactivity with *N*-metalated 1,3-dipoles [65]. On the other hand, the chosen endohedral starting material is inherently chiral and, therefore, it was used as a racemic mixture.

Nonetheless, and despite the high number of possible addition sites, the chiral metal complex proved to be able to afford only eight optically pure isomers. As resulted from UV analysis, the addition occurred site-selectively onto only two double bonds, identified as C(13)–C(14) and C(27)–C(28) by theoretical calculations (see atoms marked in black in Fig. 34.7). For each double bond, two possible regioisomers are formed and, finally, the racemic nature of the endohedral starting material leads to eight optically active isomeric compounds since all of them present a cis stereochemistry.

All the eight isomers are formed in high enantiomeric excesses and feature the pyrrolidine moiety with an absolute configuration (2*S*,5*S*) as a result of the employment of the Cu(II)acetate/Fesulphos pair (Fig. 34.8). However, the apparent mirror image of the registered CD spectra of the eight compounds demonstrates the dominant effect of the chiral cage over the effect of the chiral pyrrolidine ring.

### 34.5 CONCLUSIONS

The above examples describing the use of metals as catalysts for a variety of reactions in fullerene chemistry reveal the potential they have to afford new and unprecedented fullerene derivatives in an efficient and straightforward manner. The former chemical modification of pristine fullerenes was directed to the preparation of fullerene derivatives suitably functionalized to be tested in the search for properties and practical applications. In this regard, most of the classical reactions available in the arsenal of the organic chemistry were tested. However, important issues in fullerene chemistry such as selectivity and chirality had not been previously addressed in the appropriate way till the advent of metals in chemical reactions involving fullerenes. In this regard, in addition to the ease of preparation of some fullerene derivatives by metal-catalyzed reactions such as carbene insertions, arylations, and PK reaction, other important aspects such as the site,

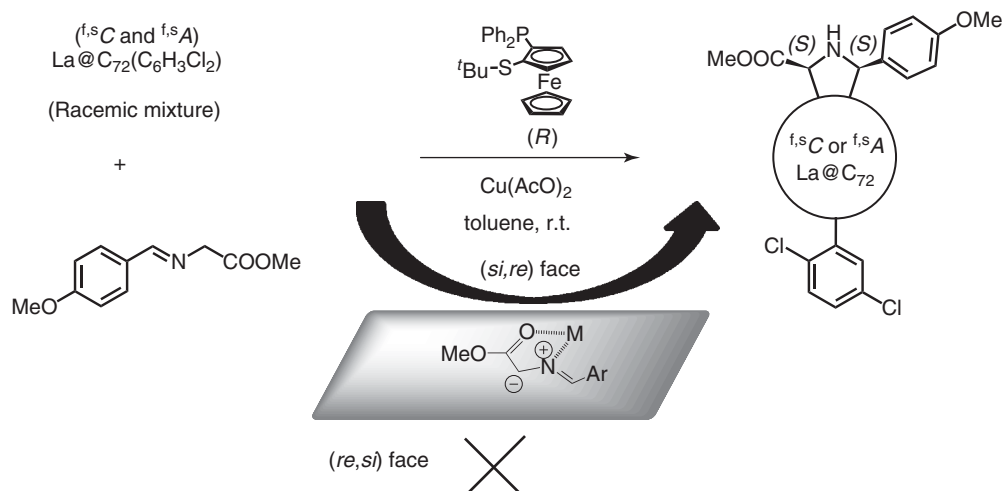


**Figure 34.8** The use of copper(II) acetate/Fesulphos directs the cycloaddition to the (*si*, *re*) face of the dipole affording eight pyrrolidino-functionalized endohedrals featuring the same (2*S*,5*S*) configuration. Four of these isomers are the result of the addition onto the clockwise enantiomeric starting material, and the others are formed by the addition onto the anticlockwise material.

regio, diastereo, and enantioselectivity of higher fullerenes have been successfully accomplished by means of metal catalysis. Furthermore, the most difficult stereocontrol in fullerene derivatives has also been recently achieved, and enantiomerically pure fullerenes of important derivatives such as pyrrolidinofullerenes can now be prepared at will.

The great advance in the chemical control of fullerene derivatives by means of metals can also be considered as a benchmark for the further development of the less known chemistry of the most-difficult-to-handle carbon nanotubes and graphenes. No doubt, the use of metals will enhance the possibilities of these new carbon-based materials in the search for practical applications.

## REFERENCES

- Kroto, H. W.; Heath, J. R.; O'Brien, S. C.; Curl, R. F.; Smalley, R. E. *Nature* **1985**, *318*, 162.
- Iijima, S. *Nature* **1991**, *354*, 56.
- Iijima, S.; Ichihashi, T. *Nature* **1993**, *363*, 603.
- Bethune, D. S.; Klang, C. H.; de Vries, M. S.; Gorman, G.; Savoy, R.; Vasquez, J.; Beyers, R. *Nature* **1993**, *363*, 605.
- Novoselov, K. S.; Geim, A. K.; Morozov, S. V.; Jiang, D.; Zhang, Y.; Dubonos, S. V.; Grigorieva, I. V.; Firsov, A. A. *Science* **2004**, *306*, 666.
- Delgado, J. L.; Herranz, M. A.; Martin, N. *J. Mater. Chem.* **2008**, *18*, 1417.
- (a) Akasaka, T.; Nagase, S., Eds., *Endofullerenes: A New Family of Carbon Cluster*; Kluwer Academic Publisher: Dordrecht, **2002**; (b) Yamada, M.; Akasaka, T.; Nagase, S. *Acc. Chem. Res.* **2010**, *43*, 92.
- Kroto, H. W. *Nature* **1987**, *329*, 529.
- Schmalz, T. G.; Seitz, W. A.; Klein, D. J.; Hite, G. E.; *Chem. Phys. Lett.* **1986**, *130*, 203.
- Martín, N. *Angew. Chem. Int. Ed.* **2011**, *50*, 5431.
- Tan, Y. Z.; Xie, S. Y.; Huang, R. B.; Zheng, L. S. *Nat. Chem.* **2009**, *1*, 450.
- Haddon, R. C., *Acc. Chem. Res.* **1992**, *25*, 127.
- Hirsch, A.; Brettreich, M. *Fullerenes: Chemistry and Reactions*; Wiley-VCH Verlag GmbH: Weinheim, Germany, **2005**.
- Guldi, D. M., Martín, N., Eds. *Fullerenes: From Synthesis to Optoelectronic Properties*; Kluwer Academic Publishers: Dordrecht, **2002**.
- Martín, N.; Nierengarten, J. F. *Supramolecular Chemistry of Fullerenes and Carbon Nanotubes*; Wiley-VCH Verlag GmbH: Weinheim, **2012**.
- Langa, F.; Nierengarten, J.-F., Eds. *Fullerenes. Principles and Applications*; RSC: Cambridge, **2011**.
- Haddon, R. C.; Brus, L. E.; Raghavachari, K. *Chem. Phys. Lett.* **1986**, *125*, 459.

18. Xie, Q.; Perez-Cordero, E.; Echegoyen, L. *J. Am. Chem. Soc.* **1992**, *114*, 3978.
19. Komatsu, K.; Murata, Y.; Takimoto, N.; Mori, S.; Sugita, N.; Wan, T. S. M. *J. Org. Chem.* **1994**, *59*, 6101.
20. Nagashima, H.; Terasaki, H.; Kimura, E.; Nakajima, K.; Itoh, K. *J. Org. Chem.* **1994**, *59*, 1246.
21. Hirsch, A.; Soi, A.; Karfunhel, H. R. *Angew. Chem. Int. Ed.* **1992**, *31*, 766.
22. Sawamura, M.; Iikura, H.; Nakamura, E. *J. Am. Chem. Soc.* **1996**, *118*, 12850.
23. Matsuo, Y.; Nakamura, E. *Chem. Rev.* **2008**, *108*, 3016.
24. Merlic, C. A.; Bendorf, H. D. *Tetrahedron Lett.* **1994**, *35*, 9529.
25. Hsiao, T.-Y.; Santhosh, K. C.; Liou, K.-F.; Cheng, C.-H. *J. Am. Chem. Soc.* **1998**, *120*, 12232.
26. Martin, N.; Altable, M.; Filippone, S.; Martin-Domenech, A.; Güell, M.; Sola, M. *Angew. Chem. Int. Ed.* **2006**, *45*, 1439.
27. Altable, M.; Filippone, S.; Martin-Domenech, A.; Güell, M.; Sola, M.; Martin, N. *Org. Lett.* **2006**, *8*, 5959.
28. Martin, N.; Altable, M.; Filippone, S.; Martin-Domenech, A. *Chem. Commun.* **2004**, *40*, 1338.
29. Martin, N.; Altable, M.; Filippone, S.; Martin-Domenech, A.; Poater, A.; Sola, M. *Chem. Eur. J.* **2005**, *11*, 2716.
30. Nambo, M.; Noyori, R.; Itami, K. *J. Am. Chem. Soc.* **2007**, *129*, 8080.
31. Nambo, M.; Segawa, Y.; Wakamiya, A.; Itami, K. *Chem. Asian J.* **2011**, *6*, 590.
32. Lu, S.; Jin, T.; Bao, M.; Yamamoto, Y. *J. Am. Chem. Soc.* **2011**, *133*, 12842.
33. Cheng, F.; Murata, Y.; Komatsu, K. *Org. Lett.* **2002**, *4*, 2541.
34. Lu, S.; Jin, T.; Kwon, E.; Bao, M.; Yamamoto, Y. *Angew. Chem. Int. Ed.* **2012**, *51*, 802
35. Xiao, Z.; Matsuo, Y.; Nakamura, E. *J. Am. Chem. Soc.* **2010**, *132*, 12234
36. Zhu, B.; Wang, G.-W. *Org. Lett.* **2009**, *11*, 4334.
37. Herranz, M. A.; Martin, N.; Ramey, J.; Guldi, D. M. *Chem. Commun.* **2002**, 2968
38. Guryanov, I.; Montellano Lopez, A.; Carraro, M.; Da Ros, T.; Scorrano, G.; Maggini, M.; Prato, M.; Bonchio, M. *Chem. Commun.* **2009**, *45*, 3940
39. Moonen, N. N. P.; Thilgen, C.; Echegoyen, L.; Diederich, F. *Chem. Commun.* **2000**, *36*, 335
40. Kessinger, R.; Crassous, J.; Herrmann, A.; Rüttimann, M.; Echegoyen, L.; Diederich, F. *Angew. Chem. Int. Ed.* **1998**, *37*, 1919.
41. Lukyanova, O.; Cardona, C. M.; Altable, M.; Filippone, S.; Domenech, A. M.; Martin, N.; Echegoyen, L. *Angew. Chem. Int. Ed.* **2006**, *45*, 7430.
42. Martín, N.; Altable, M.; Filippone, S.; Martín-Domenech, A.; Echegoyen, L.; Cardona, C. M. *Angew. Chem. Int. Ed.* **2006**, *45*, 110.
43. Filippone, S.; Barroso, M. I.; Martin-Domenech, A.; Osuna, S.; Sola, M.; Martin, N. *Chem. Eur. J.* **2008**, *14*, 5198.
44. Brunetti, F. G.; Herrero, M. A.; De, M. J.; Giordani, S.; Diaz-Ortiz, A.; Filippone, S.; Ruaro, G.; Meneghetti, M.; Prato, M.; Vazquez, E. *J. Am. Chem. Soc.* **2007**, *129*, 14580.
45. Martin, N.; Altable, M.; Filippone, S.; Martin-Domenech, A.; Martinez-Alvarez, R.; Suarez, M.; Plonska-Brzezinska, M. E.; Lukyanova, O.; Echegoyen, L. *J. Org. Chem.* **2007**, *72*, 3840.
46. Delgado, J. L.; Oswald, F.; Cardinali, F.; Langa, F.; Martin, N. *J. Org. Chem.* **2008**, *73*, 3184.
47. Ettl, R.; Chao, I.; Diederich, F.; Whetten, R. L. *Nature*, **1991**, *353*, 149.
48. Thilgen, C.; Gosse, I.; Diederich, F. *Top. Stereochem.* **2003**, *23*, 1.
49. C. Thilgen, F. Diederich, *Chem. Rev.* **2006**, *106*, 5049–5135.
50. (a) Friedman, S. H.; Ganapathi, P. S.; Rubin, Y.; Kenyon, G. L. *J. Med. Chem.* **1998**, *41*, 2424; (b) Zhu, Z.; Schuster, D. I.; Tuckerman, M. E. *Biochemistry* **2003**, *42*, 1326.
51. Nishimura, T.; Tsuchiya, K.; Ohsawa, S.; Maeda, K.; Yashima, E.; Nakamura, Y.; Nishimura, J. *J. Am. Chem. Soc.* **2004**, *126*, 11711.
52. Hizume, Y.; Tashiro, K.; Charvet, R.; Yamamoto, Y.; Saeki, A.; Seki, S.; Aida, T. *J. Am. Chem. Soc.* **2010**, *132*, 6628.
53. Filippone, S.; Maroto, E. E.; Martín-Domenech, Á.; Suarez, M.; Martín, N. *Nat. Chem.* **2009**, *1*, 578.
54. Maggini, M.; Scorrano, G.; Prato, M. *J. Am. Chem. Soc.* **1993**, *115*, 9798
55. Prato, M.; Maggini, M. *Acc. Chem. Res.* **1998**, *31*, 519.
56. Lian-He, S.; Guan-Wu, W.; Shi-Hui, W.; Hou-Ming, W.; Xia-Fei, L. *Tetrahedron Lett.* **1995**, *36*, 3871.
57. Wu, S.-H.; Sun, W.-Q.; Zhang, D.-W.; Shu, L.-H.; Wu, H.-M.; Xu, J.-F.; Lao, X.-F. *J. Chem. Soc. Perkin Trans. 1*, **1998**, *1*, 1733.
58. Maroto, E. E.; Filippone, S.; Martin-Domenech, A.; Suarez, M.; Martín, N. *J. Am. Chem. Soc.* **2012**, *134*, 12936.
59. Wilson, S. R.; Lu, Q.; Cao, J.; Wu, Y.; Welch, C. J.; Schuster, D. I. *Tetrahedron* **1996**, *52*, 5131.
60. Maroto, E. E.; de Cázar, A.; Filippone, S.; Martín-Domenech, Á.; Suarez, M.; Cossío, F. P.; Martín, N. *Angew. Chem. Int. Ed.* **2011**, *50*, 6060.
61. (a) Akasaka, T.; Wudl, F.; Nagase, S. *Chemistry of Nanocarbons*; John Wiley & Sons, Ltd.: Chichester, UK, **2010**; (b) Chaur, M. N.; Melin, F.; Ortiz, A. L.; Echegoyen, L. *Angew. Chem. Int. Ed.* **2009**, *48*, 7514.

62. Zhang, J.; Fatouros, P. P.; Shu, C.; Reid, J.; Owens, L. S.; Cai, T.; Gibson, H. W.; Long, G. L.; Corwin, F. D.; Chen, Z.-J.; Dorn, H. C. *Bioconjugate Chem.* **2010**, *21*, 610.
63. Ross, R. B.; Cardona, C. M.; Guldi, D. M.; Sankaranarayanan, S. G.; Reese, M. O.; Kopidakis, N.; Peet, J.; Walker, B.; Bazan, G. C.; Van Keuren, E.; Holloway, B. C.; Drees, M. *Nat. Mater.* **2009**, *8*, 208.
64. Sato, S.; Seki, S.; Honsho, Y.; Wang, L.; Nikawa, H.; Luo, G.; Lu, J.; Haranaka, M.; Tsuchiya, T.; Nagase, S.; Akasaka, T. *J. Am. Chem. Soc.* **2011**, *133*, 2766.
65. Sawai, K.; Takano, Y.; Izquierdo, M.; Filippone, S.; Martín, N.; Slanina, Z.; Mizorogi, N.; Waelchli, M.; Tsuchiya, T.; Akasaka, T.; Nagase, S. *J. Am. Chem. Soc.* **2011**, *133*, 17746.

## ORGANOMETALLIC COMPLEXES OF SUMANENE

TORU AMAYA AND TOSHIKAZU HIRAO\*

*Department of Applied Chemistry, Graduate School of Engineering, Osaka University, Osaka, Japan*

### 35.1 INTRODUCTION

Complexation of metals to curved carbon  $\pi$  surfaces has attracted continuous interest since the discovery of fullerenes. So far, fullerenes have been found to act as an  $\eta^2$ -coordination ligand to various transition metals from its *exo*- $\pi$ -surface [1, 2]. Other coordination modes in *exo* complexes were reported in the modified fullerene  $\pi$  systems [3], such as “buckyferrocene” [4]  $\text{Fe}(\text{C}_{60}\text{Me}_5)\text{Cp}$  ( $\text{Cp}$  = cyclopentadienyl). Fullerenes are also known to form the endohedral metal complexes to provide potential materials in carbon chemistry [5, 6]. On the other hand, fullerene fragments, termed as  $\pi$  bowls (we use this term in the present chapter, whereas they have been also called *open geodesic polyarenes* [7] or *buckybowls* [8]), also possess curved carbon  $\pi$  surfaces.  $\pi$  Bowls have attracted interest in the science of nonplanar  $\pi$ -conjugated carbon systems [9–14]. From the viewpoint of coordination chemistry, such molecules are quite unique because they can provide not only a convex surface but also an open concave surface for binding (a schematic illustration is shown in Fig. 35.1), which was first addressed by the computational study of hemifullerene ( $\text{C}_{30}\text{H}_{12}$ ) in 1993 [15].

As polar end-cap structural motifs of fullerene or carbon nanotube, there are two representative key subunits for  $\pi$  bowls. One is a  $C_{5v}$  symmetric “corannulene” (**2**,  $\text{C}_{20}\text{H}_{10}$ ) and the other is a  $C_{3v}$  symmetric “sumanene” (**1**,  $\text{C}_{21}\text{H}_{12}$ ) (Fig. 35.2). Corannulene (**2**) was first synthesized in 1966 [16]. More practical synthetic methods of **2** have been developed since then [17–19], which made a breakthrough in the coordination chemistry of the  $\pi$  bowl. On the other hand, research based on sumanene (**1**) started with our first synthesis in 2003 [20], besides some earlier synthetic and theoretical studies [21, 22]. The characteristic structural feature of **1** is three  $\text{sp}^3$ -hybridized carbon atoms at the benzylic positions. It is in sharp contrast to the structure of **2**, the rim of which is covered with five aromatic rings. The bowl depth of **1** (1.11 Å) [23] is larger than that of **2** (0.89 Å) [24] which may cause the effect attributed to the bowl structure in metal coordination. In this chapter, we describe the synthesis of organometallic complexes of **1**, including organolithium and  $\eta^6$ -coordination complexes with  $\text{RCpM}^+$  ( $\text{M} = \text{Fe}$  and  $\text{Ru}$ ).

### 35.2 ORGANOLITHIUM COMPLEXES OF SUMANENE

Organolithium compounds are one of the widely used reagents in organic synthesis. Another use of organolithium reagents is in the preparation of various organometallic compounds, usually by reaction with metal halides. Therefore, the preparation of organolithium is important even in  $\pi$ -bowl chemistry.

The study on the coordination chemistry of  $\pi$  bowls started from the lithiation of corannulene in 1992 [25]. Treatment of **2** with excess lithium can afford the corresponding tetralithiated complex **3** based on aromatization as a driving force (Fig. 35.3). More specifically, the doubly degenerate lowest unoccupied molecular orbital (LUMO) levels of **2** allow it to accept

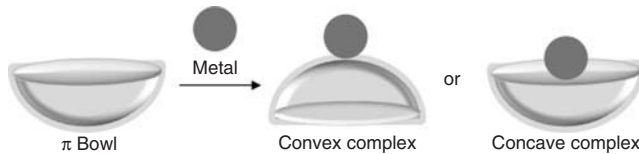


**Figure 35.1** Schematic illustration of convex and concave bindings of a metal to a  $\pi$  bowl.

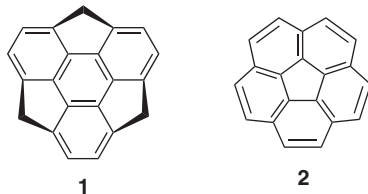


**Figure 35.2** Sumanene (**1**) and corannulene (**2**).

up to four electrons to form an aromatic Cp anion (6e/5C) suspended by five radial bonds within the hole of an aromatic 18e/15C annulenyl trianion. Interestingly, such a tetraanion **3** assembles to form the sandwich dimer complex with some lithium cations inside [26]. Recently, the supercharged dimer structure was confirmed using X-ray crystallographic analysis and  $^7\text{Li}$  NMR spectroscopy [27] as a sandwich **4**, consisting of five lithium cations jammed between two corannulene tetraanions (Fig. 35.3).

### 35.2.1 Stepwise Anion Generation at Benzylic Positions of Sumanene

In contrast to corannulene (**2**), sumanene (**1**) has three methylene carbons at the benzylic positions, which enables facile formation of organolithium species. The stepwise generation of the mono-, di-, and trianions was observed by NMR experiments (Fig. 35.4) [23]. Benzylic protons are kinetically deprotonated by the treatment of *t*-BuLi. Careful control of the amount of *t*-BuLi selectively led to the formation of the monoanion **5**. In the  $^1\text{H}$  NMR spectrum, the signals of **1** disappeared with the appearance of the signals for **5**. In addition, a singlet peak around 6.0 ppm, assignable to the benzyl anion species, was observed. Additional treatment with *t*-BuLi provided another set of the signals assigned to the dianion **6**. The difference in chemical shifts between the *exo/endo*-benzylic protons increased in the order of the number of anions (dianion **6** > monoanion **5** > **1**). Further addition of *t*-BuLi afforded only two singlets in the  $^1\text{H}$  NMR, assignable to the protons at the anion-generated carbons and aromatic rings. Such a simple spectrum is consistent with the symmetrical trianion **7**. Because of charge localization, trapping the anion with an electrophile leads to selective substitution at the desired benzylic positions. The reaction of **7** with  $\text{Me}_3\text{SiCl}$  gave the *exo*-introduced tris(trimethylsilyl) derivative **8** as a sole isomer quantitatively (Scheme 35.1). The observed stereoselectivity is probably due to the steric demand. Synthetic approaches via the benzylic anions can be applied for the facile preparation of various sumanene derivatives [28–30].

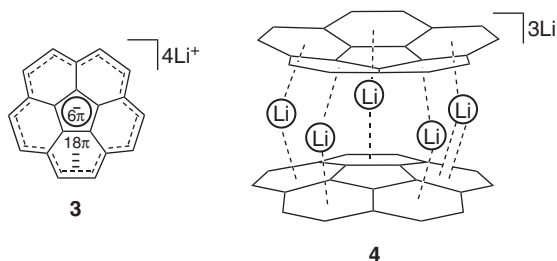


**Figure 35.3** Corannulene tetraanion **3** and sandwich **4** consisting of five lithium cations jammed between two corannulene tetraanions.

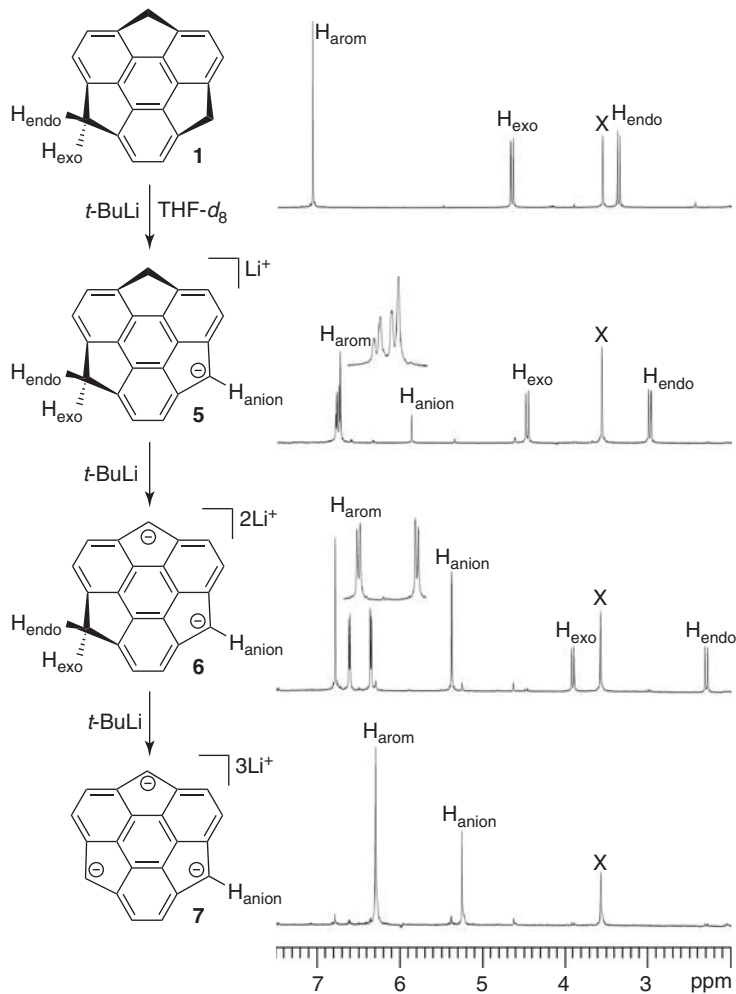
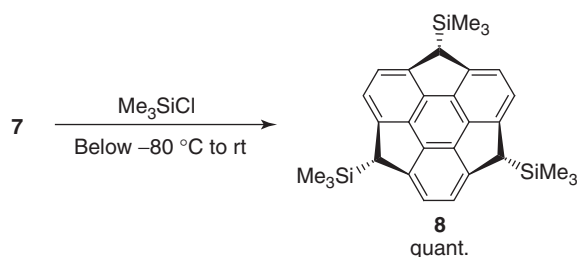


**Figure 35.4** Stepwise generation of mono-, di-, and trianions **5–7** from **1** and their  $^1\text{H}$  NMR spectra.



**Scheme 35.1** Synthesis of tris(trimethylsilyl)sumanene **8**.

### 35.2.2 Bowl-to-bowl Inversion of Sumanene's Benzylic Anion Species

Bowl-to-bowl inversion is one of the characteristic behaviors for some flexible  $\pi$  bowls such as corannulene (**2**) and sumanene (**1**) (Fig. 35.5). The bowl-to-bowl inversion of the corannulene derivative **9** (Fig. 35.6) occurs rapidly with an activation barrier of 10–11 kcal/mol [31]. The close relationship between the inversion energy barrier and the bowl depth was investigated using corannulene derivatives [32]. An equation between the bowl depth  $x$  and the energy barrier  $E_a$  ( $E_a = Cx^4$ ) has been suggested [32]. A relatively deep bowl sumanene, as compared to **2**, exhibits much slower inversion. The inversion barrier of **1** was estimated by a variable-temperature NMR study [20]. More detailed investigation was carried out by 2D

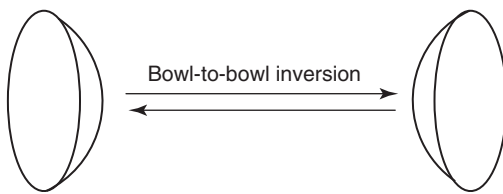


**Figure 35.5** Schematic representation of bowl-to-bowl inversion of  $\pi$  bowl.

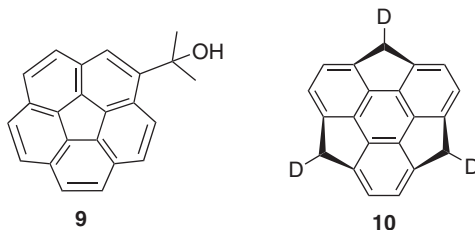


**Figure 35.6** Corannulene derivative **9** and trideuteriosumanene **10**.

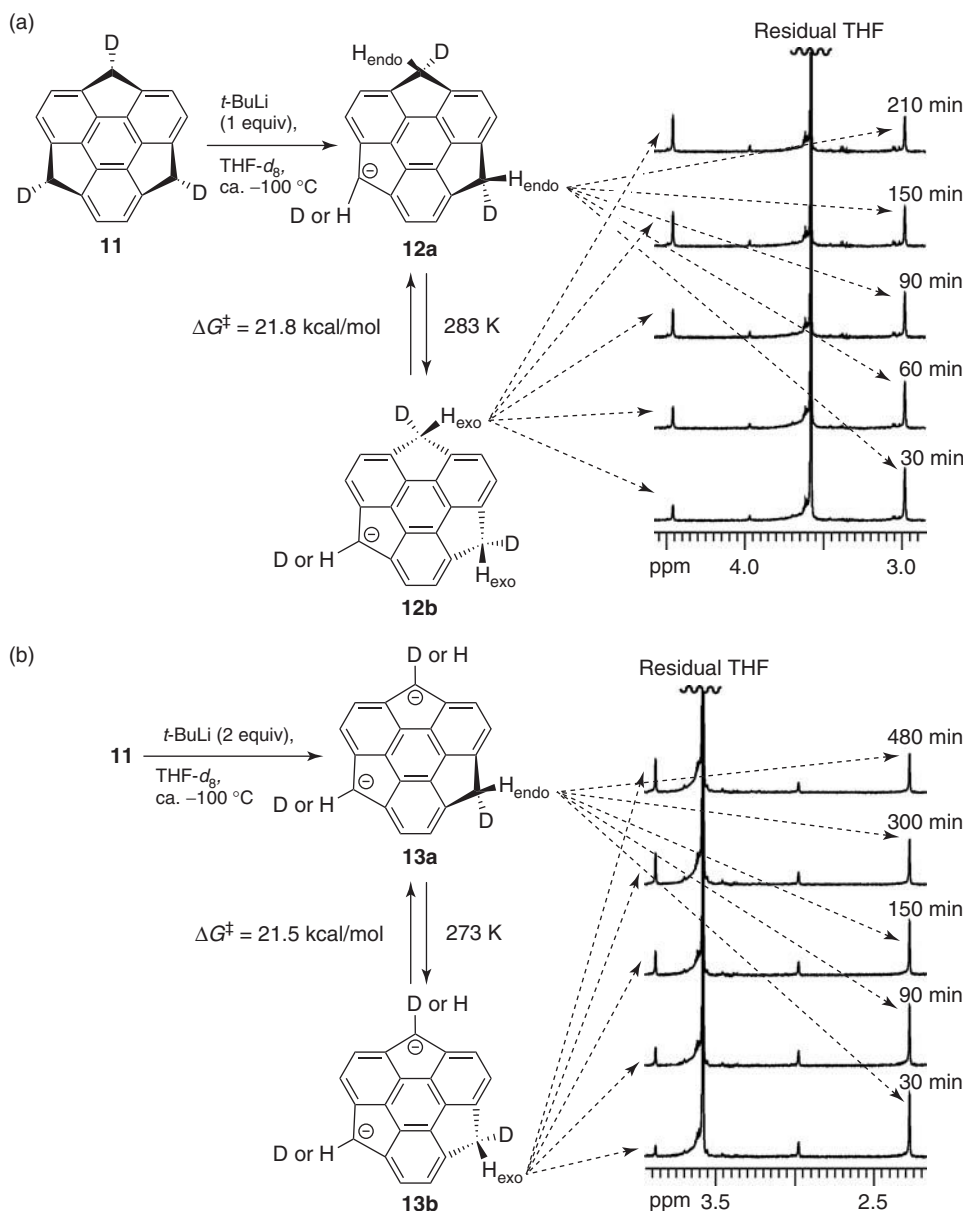
exchange spectroscopy (EXSY) NMR experiments using trideuteriosumanene **10** (Fig. 35.6), showing an inversion barrier of approximately 20 kcal/mol [29, 33]. In this molecule, the bowl-to-bowl inversion is equivalent to the isomerization between the diastereomers. Accordingly, estimation of the isomerization rate quantified by the cross peaks in a 2D EXSY NMR spectrum gives the inversion rate.

The dynamic behaviors of the mono- and dianion were investigated using trideuteriosumanene **10** as a starting material. Treatment of **10** with the requisite amount of *t*-BuLi generated **12** and **13**. The inversion behavior was first studied using 2D EXSY NMR experiments in THF-*d*<sub>8</sub>. However, no cross peak was observed in either of them. It suggests that the anions **12** and **13** maintain a relatively rigid bowl shape in this timescale [29]. So, we planned to monitor the equilibration of *exo*-deuterated **12a** and **13a** by simple <sup>1</sup>H NMR measurement to investigate such a slow inversion. Selective deuteration of the trianion **7** was achieved to give **11** (Fig. 35.7) by precipitation with CH<sub>3</sub>OD at approximately –100 °C. Keeping **11** as a solid at room temperature did not induce the bowl-to-bowl inversion. To generate monoanion **12a** and dianion **13a**, **11a** was treated with the requisite amount of *t*-BuLi at approximately –100 °C in THF-*d*<sub>8</sub> (Fig. 35.7); then the equilibration was monitored. The <sup>1</sup>H NMR spectra are shown in Fig. 35.7a and b. Growth of the *exo*-benzylic protons (4.46 and 3.88 ppm for **12b** and **13b**, respectively) was observed in both spectra (Fig. 35.7a and b) [29]. The half-life times were 2755 s for **12a** at 283 K and 7580 s for **13a** at 273 K. The rate constants (*k*'s) for the reversible equilibration of **12** and **13** were  $9.10 \times 10^{-5}$  s<sup>–1</sup> at 283 K and  $3.40 \times 10^{-5}$  s<sup>–1</sup> at 273 K, respectively, determined by regression analysis using the equation  $2kt = \ln[a/(a-x)]$ , where *a* is the initial concentration of **12a** (or **13a**) and *x* is the concentration of **12b** (or **13b**) at time *t*. Correlation coefficients of the linear regressions were 0.999 and 0.978.  $\Delta G^\ddagger$ 's were 21.8 and 21.5 kcal/mol for **12** and **13**, respectively, calculated from the Eyling equation. Monoanion **12** and dianion **13** possess 1.5 and 1.2 kcal/mol higher barrier than **10**, respectively.

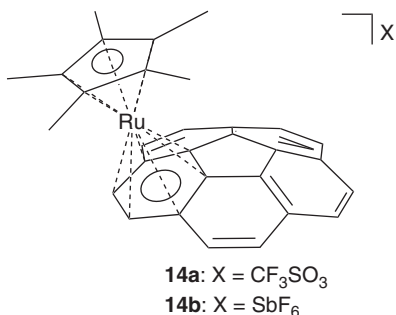
### 35.3 $\eta^6$ -COORDINATION COMPLEXES OF SUMANENE

Transition-metal complex of  $\pi$  bowls have attracted much attention [12, 34, 35]. Controlled positioning of metal centers inside the bowls is expected to provide a direct route to the inclusion complexes of fullerenes and nanotubes. On the other hand, the coordination of metal centers to the outside of the bowls should permit applications in the field of surface activation and functionalization of fullerenes and nanotubes. To date, some  $\pi$  bowl (mainly corannulene or its derivatives) complexes with several coordination modes have been synthesized [12, 34, 35]. In addition to the conventional liquid phase synthesis, a microscale gas-phase coordination method was introduced [36] to prepare  $\eta^1$ - and/or  $\eta^2$ -binding complexes, which is based on co-deposition of volatile complementary building units such as Rh<sub>2</sub>(O<sub>2</sub>CCF<sub>3</sub>)<sub>4</sub>, Ru<sub>2</sub>(O<sub>2</sub>C(3,5-CF<sub>3</sub>)<sub>2</sub>C<sub>6</sub>H<sub>3</sub>)<sub>2</sub>(CO)<sub>5</sub>, and Ru<sub>2</sub>(O<sub>2</sub>CCF<sub>3</sub>)<sub>2</sub>(CO)<sub>4</sub> under reduced pressure.

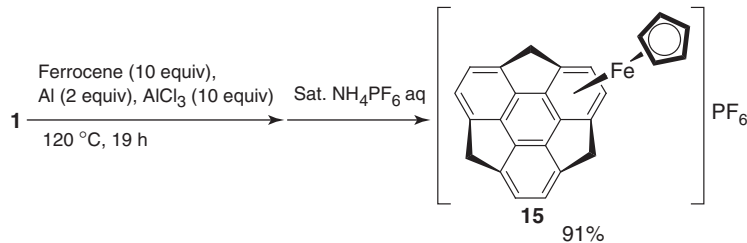
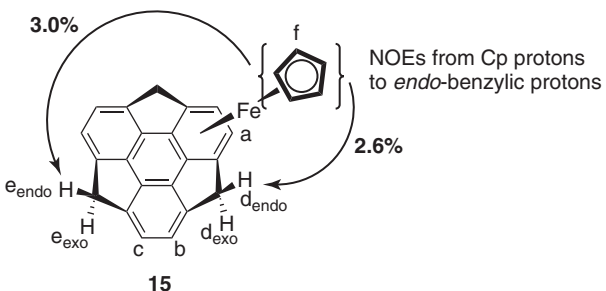
Among several coordination modes, some  $\eta^6$ -arene complexes have been prepared and characterized. In 1997, the first  $\eta^6$ -arene complex of **2**, [Cp<sup>\*</sup>Ru(corannulene)]CF<sub>3</sub>SO<sub>3</sub> (**14a**) (Cp<sup>\*</sup> = pentamethylcyclopentadienyl) (Fig. 35.8), was



**Figure 35.7** (a) Generation of monoanion **12a** and selected  $^1\text{H}$  NMR spectra for the equilibration at  $283\text{ K}$ . (b) Generation of dianion **13a** and selected  $^1\text{H}$  NMR spectra for the equilibration at  $273\text{ K}$ .



**Figure 35.8**  $[(\text{C}_5\text{Me}_5)\text{Ru}(\text{corannulene})]\text{X}$  ( $\text{X} = \text{CF}_3\text{SO}_3$ ; **14a**,  $\text{X} = \text{SbF}_6$ ; **14b**).

Scheme 35.2 Synthesis of  $[\text{CpFe}(\text{sumanene})]\text{PF}_6$  (**15**).Figure 35.9 NOEs from Cp protons to *endo*-benzylic protons in **15**.

synthesized; however, the face selectivity of the coordination was not confirmed at that time [37]. Eight years later, the convex binding of  $[\text{Cp}^*\text{Ru}(\text{corannulene})]\text{SbF}_6$  (**14b**) (Fig. 35.8) was finally revealed by X-ray crystallographic analysis [38]. Both convex and concave binding complexes  $[(\text{Cp}^*\text{Ru})_2(\mu_2\text{-}\eta^6\text{-corannulene})][\text{X}]_2$  ( $\text{X} = \text{PF}_6$  or  $\text{SbF}_6$ ) were also reported, where significant flattening of the bowl structure is induced [38, 39]. In addition to  $\text{Cp}^*\text{Ru}$ , some  $\eta^6$ -corannulene complexes bearing  $\text{Cp}^*\text{Ir}^{2+}$  [40],  $(\text{COE})_2\text{Ir}^+$  ( $\text{COE} = \text{cyclooctene}$ ) [41],  $(\text{COE})_2\text{Rh}^+$  [41],  $(\text{C}_6\text{Me}_6)\text{Ru}^{2+}$  [42], and (cymene) $\text{Os}^{2+}$  [42] were prepared, and all of them showed the convex coordination. Theoretical studies of corannulene complexes using DFT calculation were also carried out, which indicated the preferential convex binding to transition metals [43–45].

### 35.3.1 Concave- $\eta^6$ -Bound Cyclopentadienyl Iron Cation Complex of Sumanene

Coordination chemistry of sumanene (**1**) has been limited to the computational study. For example, the coordination of  $\text{M}(\text{PH}_3)_2$  ( $\text{M} = \text{Pd}$  or  $\text{Pt}$ ) was investigated to compare sumanene (**1**) with fullerene and corannulene (**2**) [46]. In this context, we started from the coordination of  $\text{CpFe}^+$  by taking stability into consideration.

The complexation of **1** with  $\text{CpFe}^+$  was performed by ligand exchange with a Cp group of ferrocene [47]. The reaction proceeded in the presence of aluminum powder and aluminum chloride without a solvent under argon at  $120^\circ\text{C}$  for 19 h. The counteranion of the crude complex was replaced by hexafluorophosphate, giving  $[\text{CpFe}(\text{sumanene})]\text{PF}_6$  (**15**) as an orange solid. The use of excess ferrocene and aluminum chloride selectively afforded the desired monometallated complex in 91% yield (Scheme 35.2). However, the reaction in decahydronaphthalene as a solvent did not yield **15** [47]. The complex **15** was fully characterized by fast atom bombardment (FAB) mass spectrometry,  $^1\text{H}$  and  $^{13}\text{C}$  NMR spectroscopy, and X-ray crystallography.

In the NMR study, the symmetry of a series of protons showed the coordination of  $\text{CpFe}^+$  at a flank benzene ring rather than the central (hub) benzene ring [47]. The benzylic protons appeared as two pairs of doublets in a 2 : 1 ratio ( $J = 19.1$  Hz, 4H,  $\text{H}_d$ ;  $J = 20.1$  Hz, 2H,  $\text{H}_e$ ). The high field *endo*-benzylic protons (4.96 and 3.92 ppm,  $\text{H}_{d,\text{endo}}$  and  $\text{H}_{e,\text{endo}}$ ) and low field *exo*-benzylic protons (5.21 and 4.94 ppm,  $\text{H}_{d,\text{exo}}$  and  $\text{H}_{e,\text{exo}}$ ) support the bowl-shaped structure, as observed for **1**. The signal of the Cp protons  $\text{H}_f$  at 3.26 ppm was shifted approximately by  $\Delta\delta = 1.3$  ppm to a higher field than the corresponding protons of  $[\text{CpFe}(\eta^6\text{-fluorene})]\text{PF}_6$  and  $[\text{CpFe}(\eta^6\text{-triphenylene})]\text{PF}_6$ . This strong ring-current effect also supports the concave binding. Furthermore, the concave binding structure of **15** was confirmed by nuclear Overhauser effect (NOE) experiments (Fig. 35.9) [47]. Irradiation of the Cp protons resulted in NOE signals at the *endo*-benzylic protons (2.6% for each  $\text{H}_{d,\text{endo}}$  and 3.0% for  $\text{H}_{e,\text{endo}}$ ), whereas no NOE signals were observed for the corresponding *exo*-benzylic protons.

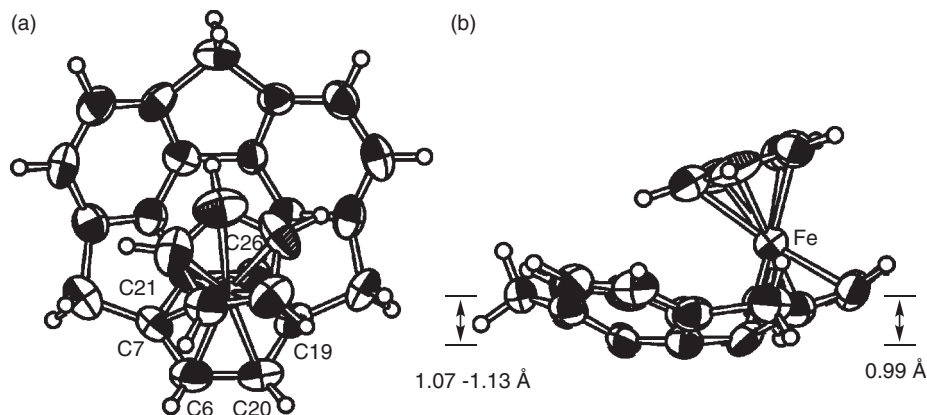


**Figure 35.10** ORTEP drawings of **15** with thermal ellipsoids set at 50% probability: (a) top and (b) side views.  $\text{PF}_6^-$  anion is omitted for clarity.

X-ray crystallographic analysis clearly showed the concave binding of the  $\text{CpFe}^+$  moiety to a flank benzene ring of **15** (Fig. 35.10) [47]. The Fe–C bonds from the iron center to the six-membered ring (C6, C7, C19, and C20) range from 2.01 to 2.07 Å. Although the distances to the hub carbon atoms (C21 and C26) are a little longer (2.136 and 2.135 Å, respectively), the coordination can be considered almost as  $\eta^6$ . Such a selective concave  $\eta^6$  coordination was thus achieved for the first time in the curved  $\pi$ -conjugated carbon system. The Cp ring is tilted 6° to the iron-bound benzene ring, perhaps because of steric repulsion with the sumanene skeleton. A small amount of bowl flattening was observed around the coordinated side (0.99 Å); in contrast, the bowl depth at the other side (1.07–1.13 Å) was almost the same as found for **1** (1.11 Å). Columnar stacking was observed in the crystal packing (Fig. 35.11). Partial  $\pi-\pi$  orbital overlap is probably present between the Cp and hub benzene rings of adjacent molecules.

The redox properties of **15** were investigated through electrochemical study. The complex **15** exhibited the  $\text{Fe(II)/Fe(I)}$  reduction, which displayed features of partial chemical reversibility [48].

Furthermore, the methyl-substituted complex  $[\text{MeCpFe}(\eta^6\text{-sumanene})]\text{PF}_6^-$  was synthesized.  $^1\text{H}$  NMR experiments suggested that the methyl group is directed out of the bowl with a restricted rotation [49].

Coordination to such curved  $\pi$  orbitals in a  $\pi$  bowl may give rise to unique reactivities in the catalysis of the transition-metal complexes.

### 35.3.2 Concave- $\eta^6$ -Bound Chiral *s*-Butyleclopentadienyl Iron Cation Complex of Sumanene

Chiral  $\pi$ -bowl complexes are desirable model structures for chiral endohedral metallofullerenes, asymmetric organometallic catalysts, as well as molecular recognition units. Synthesis of an  $\text{Fe(II)}^+$  complex of **1** having a Cp ligand with a chiral *s*-butyl group attached was performed in a manner similar to the preparation of **15**. The complex **16** also exhibited a concave-face-selective coordination at a flank benzene ring in solution (Fig. 35.12), in which the rotation of the Cp ring is restricted. Magnetic and optical desymmetrization in the sumanene ligand could be shown with the complex **16** [49]. Chirality on sumanene bowl is induced through the asymmetric center on *s*-butyl group in Cp ligand. This is the first optically active complex with a  $\pi$ -bowl ligand. Recently, an enantiometrically pure corannulene–Rh(II) complex with chiral norbornadiene ligand was reported [50].

### 35.3.3 Bowl-to-bowl Inversion of $\eta^6$ -Bound Cyclopentadienyl Ruthenium Cation Complex of Sumanene

The selectivity for *endo* complexation might reflect kinetic and/or thermodynamic control in the complexation, thermodynamic control in “bowl-to-bowl inversion,” or both. Corannulene and sumanene ligands themselves are known to exhibit the bowl-to-bowl inversion as described above [20, 31]. Concerning the dynamic behavior of  $\pi$ -bowl transition-metal complexes, the ring-to-ring migration of such as  $\eta^6$ -binding  $\text{Cp}^*\text{Ir}^{2+}$ ,  $\text{Cp}^*\text{Ru}^+$ ,  $(\text{COE})_2\text{Ir}^+$ , and  $(\text{COE})_2\text{Rh}^+$  is found on the corannulene ligands [40, 41, 44, 50]. However, the bowl-to-bowl inversion has not been elucidated with  $\pi$ -bowl transition-metal complexes.

The  $\text{CpRu}^+$  sumanene complex **17** (Fig. 35.13) was synthesized similarly to **15** and **16** [51]. Unlike them, a pair of two species was observed in the  $^1\text{H}$  NMR spectra of  $[\text{CpRu}(\text{sumanene})]\text{PF}_6^-$  (**17**). The major and minor species were assigned to

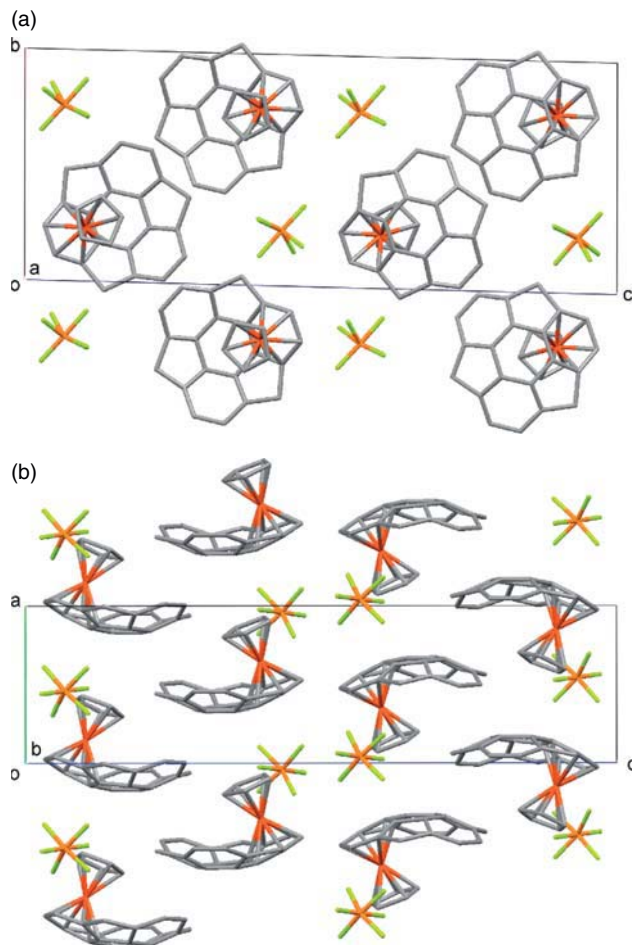


**Figure 35.11** Crystal cell and packing structure of **15**: (a) top and (b) side views. H atom is omitted for clarity. (See insert for color representation of the figure.)

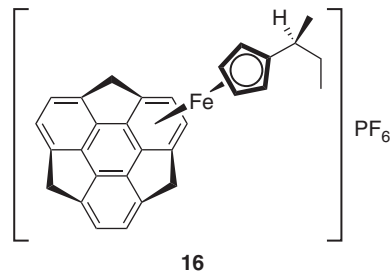


**Figure 35.12** Chiral  $\pi$ -bowl complex **16**.

the concave-bound complex **17<sub>concave</sub>** and the convex-bound isomer **17<sub>convex</sub>**, respectively, by NOE experiments. The ratio of the concave and convex complexes depends to some degree on the solvent. In CD<sub>2</sub>Cl<sub>2</sub>, the occupancy in the equilibrium is 75:25 for **17<sub>concave</sub>**/**17<sub>convex</sub>**. In more polar solvents, the equilibrium tends to the major isomer **17<sub>concave</sub>** (up to 90% in CD<sub>3</sub>CN and CD<sub>3</sub>NO<sub>2</sub>). Two-dimensional EXSY NMR experiment of **17** in CD<sub>2</sub>Cl<sub>2</sub> clearly showed negative cross peaks for the chemical exchange between H<sub>a-f</sub> and H<sub>a'-f'</sub> in one-to-one correspondence, as exemplified by a-a' (Fig. 35.13) [51]. The *endo*-benzylic protons H<sub>d,endo</sub> and H<sub>e,endo</sub> of **17<sub>concave</sub>** show correlations with the *exo*-benzylic peaks H<sub>d',exo</sub> and H<sub>e',exo</sub> of **17<sub>convex</sub>** (cross peaks: d<sub>endo</sub>-d'<sub>exo</sub> and e<sub>endo</sub>-e'<sub>exo</sub>, respectively), which are in a common region for *exo*-benzylic protons. Conversely, the *exo*-benzylic protons H<sub>d,exo</sub> and H<sub>e,exo</sub> of **17<sub>concave</sub>** show correlations with the *endo*-benzylic peaks H<sub>d',endo</sub>

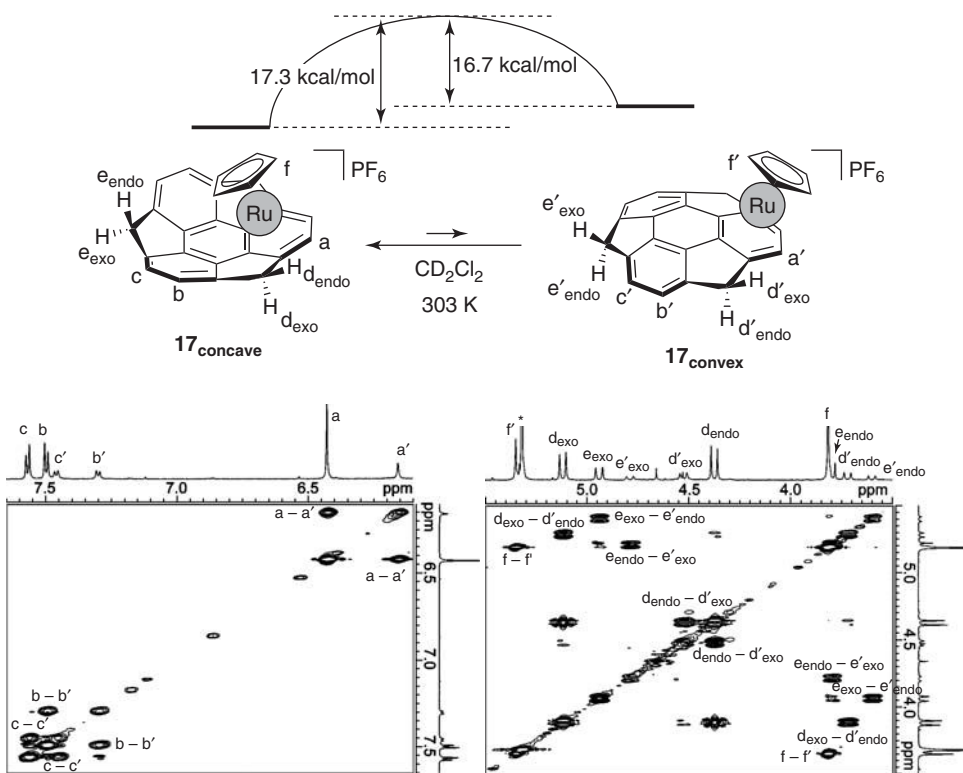


**Figure 35.13** (a) Bowl-to-bowl inversion of  $[CpRu(\text{sumanene})]PF_6$  (**17**). (b) 2D EXSY NMR spectra of **17** in  $CD_2Cl_2$ .

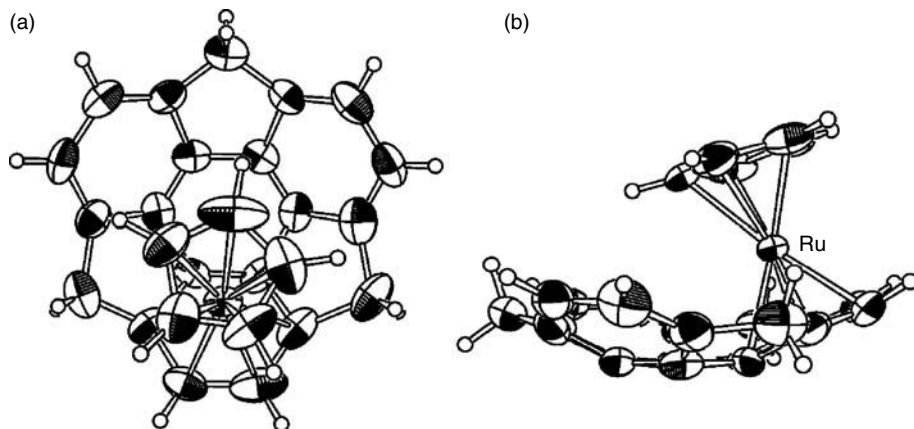


**Figure 35.14** ORTEP drawings of **17<sub>concave</sub>** with thermal ellipsoids set at 40% probability: (a) top and (b) side views. PF<sub>6</sub> anion is omitted for clarity.

and H<sub>e',endo</sub> of **17<sub>convex</sub>** (cross peaks: d<sub>exo</sub>–d'<sub>endo</sub> and e<sub>exo</sub>–e'<sub>endo</sub>, respectively), which are in a typical region for *endo*-benzylic protons. The bowl-to-bowl inversion can account for the phenomenon without inconsistency. The quantification of the cross peaks gives an inversion barrier of 16.7 and 17.3 kcal/mol at 303 K for **17<sub>convex</sub>** to **17<sub>concave</sub>** and the reverse inversion, respectively (Fig. 35.13). Linear van't Hoff plots give a positive  $\Delta H$  and a negative  $\Delta S$ .

From a mixture of the diastereomers, a single crystal of **17<sub>concave</sub>**, which is the major species, was obtained. In the X-ray crystallographic analysis, ORTEP diagrams clearly showed the concave coordination (Fig. 35.14) [51]. Once the crystal of **17<sub>concave</sub>** was dissolved, both isomers of **17** appeared again. These results indicate that the preference of the concave or convex isomers depends on the solvent and temperature under thermodynamic control.

### 35.4 CONCLUDING REMARKS AND FUTURE PROSPECTS

The coordination chemistry of sumanene (**1**) reported to date was reviewed here. Stepwise selective benzylic lithiation of **1** was presented. The benzylic anion species exhibits the bowl-to-bowl inversion. Recent study on **1** revealed that the single crystal of **1** shows high electron transport ability with anisotropy [52]. In the prospective view, trapping of such anion is considered to enable various substitutions at the benzylic positions stereoselectively, which is one of the promising approaches to create the functional materials based on **1**. Complexation with CpFe<sup>+</sup> demonstrated selective formation of the first concave-bound complex, which is expected to lead to the inclusion complexes of  $\pi$  bowls. The inversion behavior observed in the CpRu<sup>+</sup> complex may provide the idea of a dynamic catalytic system. Thus, some characteristic features of sumanene complexes are becoming apparent. In the future,  $\pi$  bowls such as **1** are expected to provide novel electrical materials, organometallic catalysts, etc.

### ACKNOWLEDGEMENTS

The authors wish to thank all their talented coworkers for their great contributions reported here. Financial support by Grants-in-Aid for Scientific Research (A), Young Scientists (A), and Challenging Exploratory Research from Japan Society for the Promotion of Science is gratefully appreciated. Financial support from JST, ACT-C is also acknowledged.

### REFERENCES

1. Fagan, P. J.; Calabrese, J. C.; Malone, B. *Science* **1991**, *252*, 1160.
2. Balch, A. L.; Olmstead, M. M. *Chem. Rev.* **1998**, *98*, 2123.
3. Nakamura, E. *J. Organomet. Chem.* **2004**, *689*, 4630.
4. Sawamura, M.; Kuninobu, Y.; Togano, M.; Matsuo, Y.; Yamanaka, M.; Nakamura, E. *J. Am. Chem. Soc.* **2002**, *124*, 9354.
5. Chai, Y.; Guo, T.; Jin, C.; Haufler, R. E.; Chibante, L. P. F.; Fure, J.; Wang, L.; Alford, J. M.; Smalley, R. E. *J. Phys. Chem.* **1991**, *95*, 7564.
6. Shinohara, H. *Rep. Prog. Phys.* **2000**, *63*, 843.
7. Scott, L. T.; Bronstein, H. E.; Preda, D. V.; Ansems, R. B. M.; Bratcher, M. S.; Hagen, S. *Pure Appl. Chem.* **1999**, *71*, 209.
8. Rabideau, P. W.; Abdourazak, A. H.; Folsom, H. E.; Marcinow, Z.; Sygula, A.; Sygula, R. *J. Am. Chem. Soc.* **1994**, *116*, 7891.
9. Rabideau, P. W.; Sygula, A. *Acc. Chem. Res.* **1996**, *29*, 235.
10. Wu, Y.-T.; Siegel, J. S. *Chem. Rev.* **2006**, *106*, 4843.
11. Tsefrikas, V. M.; Scott, L. T. *Chem. Rev.* **2006**, *106*, 4868.
12. Scott, L. T.; Petrukhina M. *Fragments of Fullerenes and Carbon Nanotubes: Designed Synthesis, Unusual Reactions, and Coordination Chemistry*; John Wiley & Sons, Inc.: Hoboken, NJ, **2011**.
13. Higashibayashi, S.; Sakurai, H. *Chem. Lett.* **2011**, *40*, 122.
14. Amaya, T.; Hirao, T. *Chem. Commun.* **2011**, *47*, 10524.
15. Faust, R.; Vollhardt, K. P. C. *J. Chem. Soc., Chem. Commun.* **1993**, 1471.
16. Barth, W. E.; Lawton, R. G. *J. Am. Chem. Soc.* **1966**, *88*, 380.
17. Scott, L. T.; Hashemi, M. M.; Meyer, D. T.; Warren, H. B. *J. Am. Chem. Soc.* **1991**, *113*, 7082.
18. Seiders, T. J.; Elliott, E. L.; Grube, G. H.; Siegel, J. S. *J. Am. Chem. Soc.* **1999**, *121*, 7804.
19. Sygula, A.; Rabideau, P. W. *J. Am. Chem. Soc.* **2000**, *122*, 6323.
20. Sakurai, H.; Daiko, T.; Hirao, T. *Science* **2003**, *301*, 1878.
21. Mehta, G.; Shah, S. R.; Ravikumar, K. *J. Chem. Soc., Chem. Commun.* **1993**, 1006.
22. Priyakumar, U. D.; Sastry, G. N. *J. Phys. Chem. A* **2001**, *105*, 4488.
23. Sakurai, H.; Daiko, T.; Sakane, H.; Amaya, T.; Hirao, T. *J. Am. Chem. Soc.* **2005**, *127*, 11580.
24. Hanson, J. C.; Nordman, C. E. *Acta Crystallogr. B* **1976**, *32*, 1147.
25. Ayalon, A.; Rabinovitz, M.; Cheng, P.-C.; Scott, L. T. *Angew. Chem. Int. Ed. Engl.* **1992**, *31*, 1636.
26. Ayalon, A.; Sygula, A.; Cheng, P.-C.; Rabinovitz, M.; Rabideau, P. W.; Scott, L. T. *Science* **1994**, *265*, 1065.
27. Zabula, A. V.; Filatov, A. S.; Spisak, S. N.; Rogachev, A. Y.; Petrukhina, M. A. *Science* **2011**, *333*, 1008.
28. Amaya, T.; Mori, K.; Wu, H.-L.; Ishida, S.; Nakamura, J.; Murata, K.; Hirao T. *Chem. Commun.* **2007**, 1902.

29. Amaya, T.; Sakane, H.; Muneishi, T.; Hirao, T. *Chem. Commun.* **2008**, 765.
30. Amaya, T.; Nakata, T.; Hirao, T. *J. Am. Chem. Soc.* **2009**, 131, 10810.
31. Scott, L. T.; Hashemi, M. M.; Bratcher, M. S. *J. Am. Chem. Soc.* **1992**, 114, 1920.
32. Seiders, T. J.; Baldridge, K. K.; Grube, G. H.; Siegel, J. S. *J. Am. Chem. Soc.* **2001**, 123, 517.
33. Amaya, T.; Hirao, T. *Pure Appl. Chem.* **2010**, 82, 969.
34. Petrukhina, M. A.; Scott, L. T. *Dalton Trans.* **2005**, 2969.
35. Petrukhina, M. A. *Angew. Chem. Int. Ed.* **2008**, 47, 1550.
36. Filatov, A. S.; Petrukhina, M. A. *Coord. Chem. Rev.* **2010**, 254, 2234.
37. Seiders, T. J.; Baldridge, K. K.; O'Connor, J. M.; Siegel, J. S. *J. Am. Chem. Soc.* **1997**, 119, 4781.
38. Vecchi, P. A.; Alvarez, C. M.; Ellern, A.; Angelici, R. J.; Sygula, A.; Sygula, R.; Rabideau, P. W. *Organometallics* **2005**, 24, 4543.
39. Vecchi, P. A.; Alvarez, C. M.; Ellern, A.; Angelici, R. J.; Sygula, A.; Sygula, R.; Rabideau, P. W. *Angew. Chem. Int. Ed.* **2004**, 43, 4497.
40. Alvarez, C. M.; Angelici, R. J.; Sygula, A.; Sygula, R.; Rabideau, P. W. *Organometallics* **2003**, 22, 624.
41. Siegel, J. S.; Baldridge, K. K.; Linden, A.; Dorta, R. *J. Am. Chem. Soc.* **2006**, 128, 10644.
42. Zhu, B.; Ellern, A.; Sygula, A.; Sygula, R.; Angelici, R. J. *Organometallics* **2007**, 26, 1721.
43. Dunbar, R. C. *J. Phys. Chem. A* **2002**, 106, 9809.
44. Seiders, T. J.; Baldridge, K. K.; O'Connor, J. M.; Siegel, J. S. *Chem. Commun.* **2004**, 950.
45. Kandalam, A. K.; Rao, B. K.; Jena, P. *J. Phys. Chem. A* **2005**, 109, 9220.
46. Kameno, Y.; Ikeda, A.; Nakao, Y.; Sato, H.; Sakaki, S. *J. Phys. Chem. A* **2005**, 109, 8055.
47. Amaya, T.; Sakane, H.; Hirao, T. *Angew. Chem. Int. Ed.* **2007**, 46, 8376.
48. Zanello, P.; Fedi, S.; de Biani, F. F.; Giorgi, G.; Amaya, T.; Sakane, H.; Hirao, T. *Dalton Trans.* **2009**, 9192.
49. Sakane, H.; Amaya, T.; Moriuchi, T.; Hirao, T. *Angew. Chem. Int. Ed.* **2009**, 48, 1640.
50. Bandera, D.; Baldridge, K. K.; Linden, A.; Dorta, R.; Siegel, J. S. *Angew. Chem. Int. Ed.* **2011**, 50, 865.
51. Amaya, T.; Wang, W.-Z.; Sakane, H.; Moriuchi, T.; Hirao, T. *Angew. Chem. Int. Ed.* **2010**, 49, 403.
52. Amaya, T.; Seki, S.; Moriuchi, T.; Nakamoto, K.; Nakata, T.; Sakane, H.; Saeki, A.; Tagawa, S.; Hirao, T. *J. Am. Chem. Soc.* **2009**, 131, 408.



# 36

## ADVANCES IN LUMINESCENT TETRACOORDINATE ORGANOBORON COMPOUNDS

D. SURESH AND PEDRO T. GOMES\*

*Centro de Química Estrutural, Instituto Superior Técnico, Universidade de Lisboa, Lisboa, Portugal*

### 36.1 INTRODUCTION

The design and synthesis of luminescent tri- and tetracoordinate organoboron compounds have received considerable attention in the past two decades [1]. The four-coordinate organoboron compounds are in general more stable compared to three-coordinate ones, which require bulky substituents to stabilize them. Consequently, the four-coordinate boron compounds have emerged as very attractive materials for various optoelectronic applications, sensory and biological imaging, and as photoresponsive materials [2]. Several luminescent tetracoordinate organoboron compounds of the type  $(L^{\cap}L')BR_2$  ( $R =$  alkyl, aryl;  $L^{\cap}L'$  = chelating ligands) containing a variety of conjugated anionic chelating ligands have been synthesized and reported [2a, 3]. The Lewis-acidic boron atom stabilizes negative anionic chelating ligands by forming covalent bonds and dissipating the negative charges of the ligand, thus reinforcing  $\pi$ -conjugation in the chelate. The lowest unoccupied molecular orbital (LUMO) of boron compounds is usually localized on the  $\pi$ -conjugated chelating ligand, while the highest occupied molecular orbital (HOMO) is localized either at the chelating ligand or the R group, depending on the nature of the latter. The  $\pi \rightarrow \pi^*$  electronic transitions of the chelate or charge-transfer transition from the R group to the chelate are usually responsible for their luminescent properties. Hence, variations on the chelating ligand or R group of the molecule would influence the HOMO–LUMO levels and thereby the color of emission. The boron dipyrromethene (BODIPY) family of tetracoordinate organic boron–fluoride complexes [4] and the four-coordinate boron-functionalized polymers [5] have been reviewed recently and will not be covered here. Thus, this chapter focuses on the recent advances in the synthesis of new tetracoordinate organoboron compounds and their applications.

### 36.2 LUMINESCENT TETRACOORDINATE ORGANOBORON COMPOUNDS

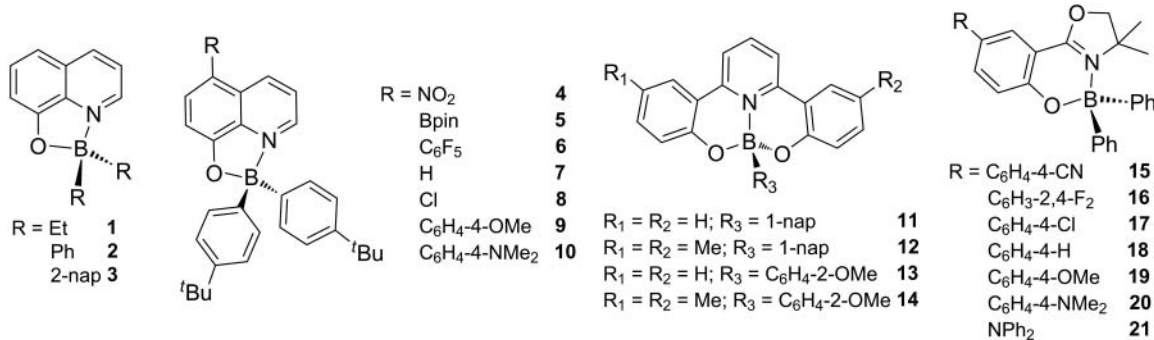
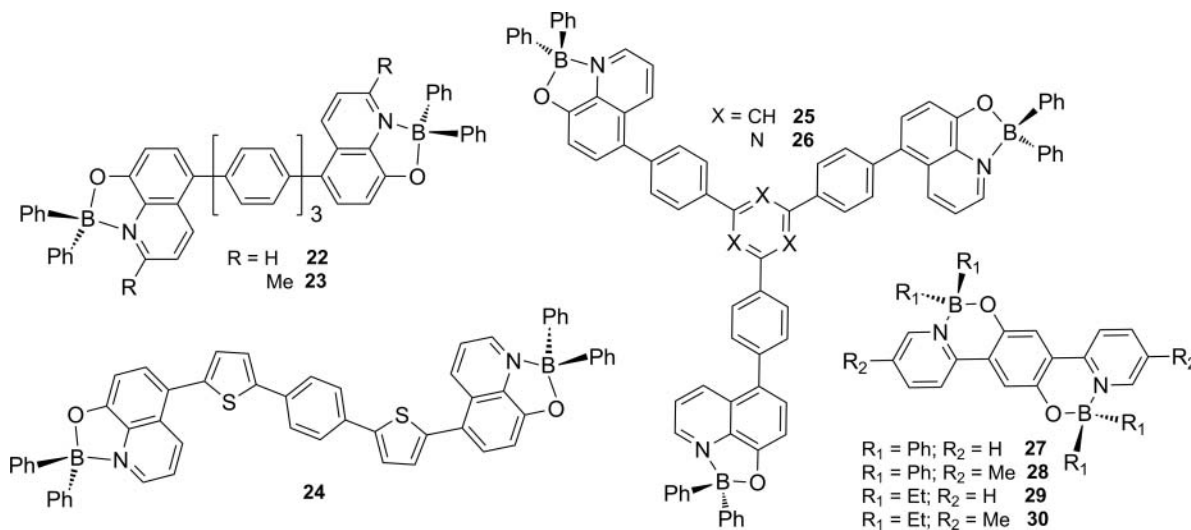
The luminescent tetracoordinate organoboron compounds can be broadly classified into four different types based on the nature of chelating ligands, namely, (i)  $N,O$ -chelate compounds, (ii)  $N,N'$ -chelate compounds, (iii)  $N,C$ -chelate compounds, and (iv) other chelate compounds.

#### 36.2.1 $N,O$ -Chelate Compounds

S. Wang and coworkers [6] first reported tetracoordinate organoboron compounds containing 8-hydroxyquinolate, a  $N,O$ -chelating ligand. Luminescent organoboron compounds of the type  $(N^{\cap}O)BR_2$  (Fig. 36.1, 1–3), where  $N^{\cap}O$  is the 8-hydroxyquinolate moiety and R can be ethyl, phenyl, or 2-naphthyl groups, show bright green-blue luminescence with

*Advances in Organometallic Chemistry and Catalysis: The Silver/Gold Jubilee International Conference on Organometallic Chemistry Celebratory Book*, First Edition. Edited by Armando J. L. Pombeiro.

© 2014 John Wiley & Sons, Inc. Published 2014 by John Wiley & Sons, Inc.

Figure 36.1 Luminescent organoboron compounds containing *N,O*-chelating ligands.Figure 36.2 Polynuclear organoboron compounds containing *N,O*-chelating ligands.

emission wavelengths of 495–500 nm [6a]. Later, Jäkle's group reported several luminescent organoboron compounds of the type (*N*<sup>o</sup>*O*)BPh<sub>2</sub> (Fig. 36.1, **4–10**) containing modified quinolate ligands [7]. The experimental observations showed that the emission wavelength is blue-shifted for the derivatives containing electron-withdrawing groups (**4–6**) relative to the unsubstituted compound (**7**), while electron-donating groups (**9** and **10**) lead to a strong red-shifted emission in the photoluminescence (PL) spectrum. The team of Y. Wang [8] reported a new type of stable blue luminescent compounds (*N*<sup>o</sup>*O*)BR<sub>2</sub> (Fig. 36.1, **11–14**) containing pyridyl phenoxylate ligands. These compounds emit in the blue region with emission maxima at 461, 478, 459, and 479 nm, with moderate quantum yields of 0.30, 0.21, 0.16, and 0.14, respectively. The organoboron compounds **15–21** (Fig. 36.1) containing oxazolyl phenolate ligands were reported by Kang and coworkers [9]. The photophysical properties of these complexes are modulated by the electron-push and electron-pull substituents at position 4 of the chelate's aryl group. The emission wavelengths are fine-tuned from 422 to 520 nm with relatively low quantum yields of 0.04–0.34.

To examine the impact of extended  $\pi$ -conjugation and the mutual influence of multiple boron centers, S. Wang and coworkers [6b] reported several linear (Fig. 36.2, **22–24**) and star-shaped (Fig. 36.2, **25–26**) polynuclear organoboron compounds with different  $\pi$ -conjugation lengths containing quinolate ligands. It was found that the inclusion of polychromophores or polyboron centers has a significant impact on the HOMO level of the molecule and the emission maxima are in the range 528–542 nm in the PL spectrum. Y. Wang et al. [10] reported binuclear ladder-type  $\pi$ -conjugated organoboron compounds (Fig. 36.2, **27–30**) with emission maxima in the range 584–604 nm, in THF, which were red-shifted by more than 100 nm in relation to the corresponding mononuclear compounds, because of a greater  $\pi$ -conjugation.

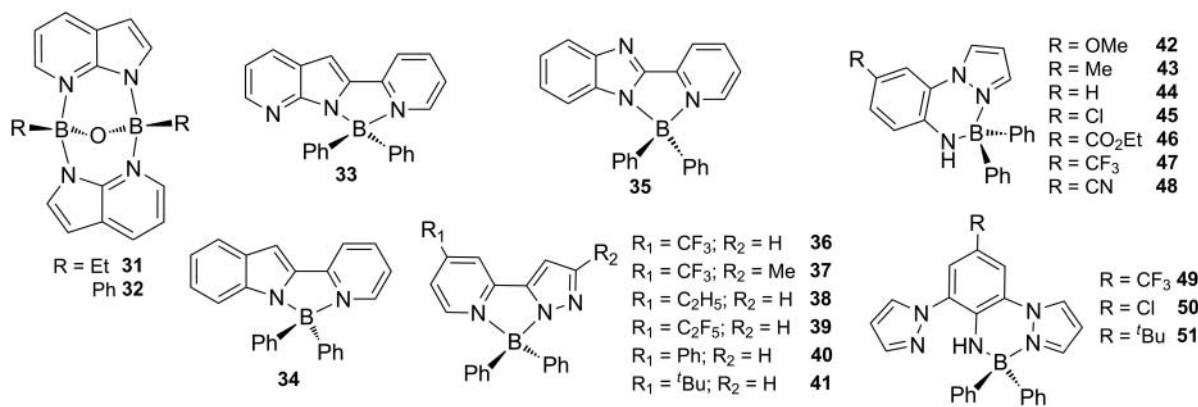


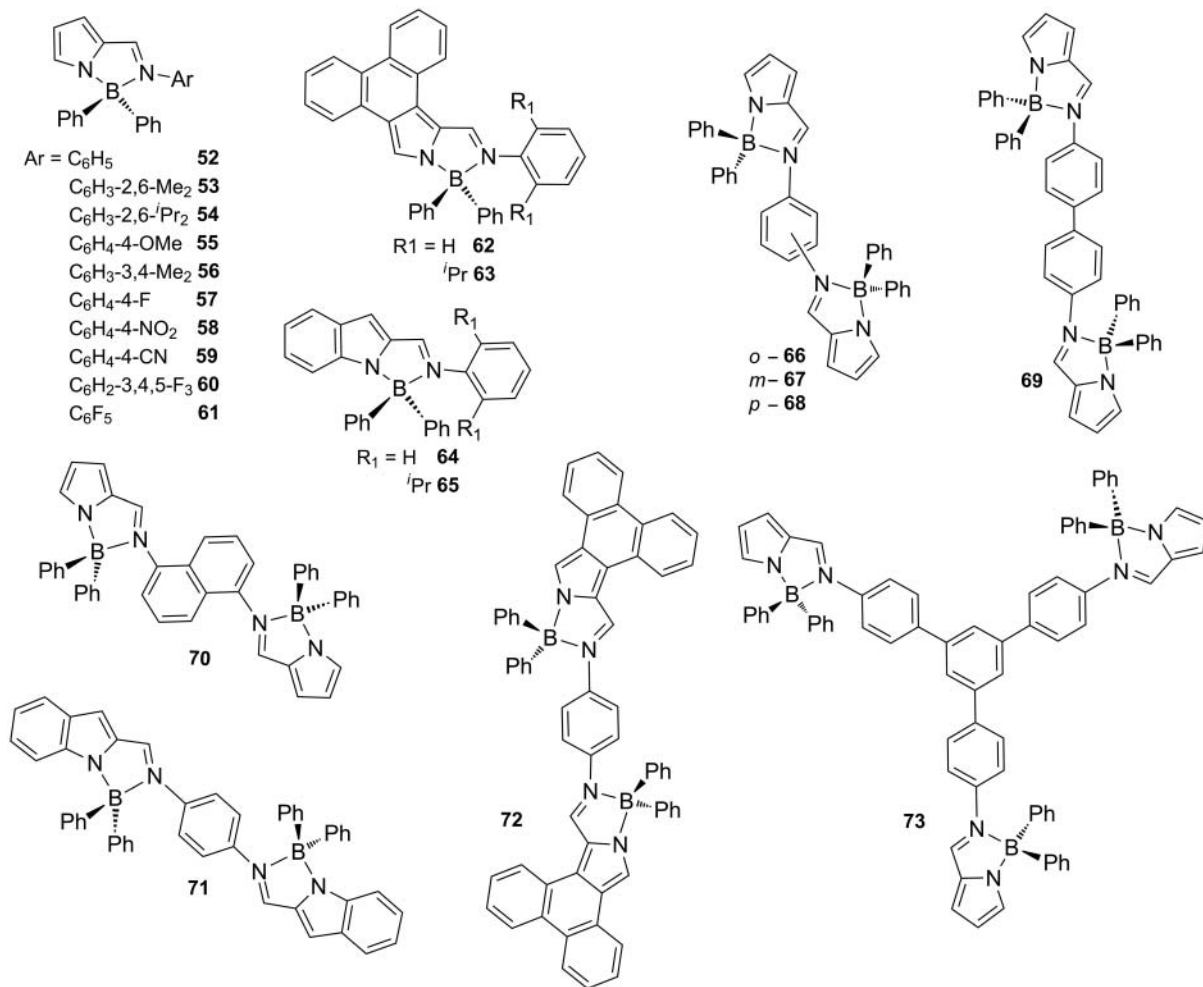
Figure 36.3 Luminescent organoboron compounds containing *N,N'*-chelating ligands.

### 36.2.2 *N,N*'-Chelate Compounds

The first example of tetracoordinate organoboron compounds containing a *N,N'*-chelating ligand  $[(\mu\text{-7-azain})\text{BR}]_2(\mu\text{-O})$ , reported by S. Wang's team, was found to be blue luminescent ( $\lambda_{\text{em}} = 419$  nm, R = Et, **31**;  $\lambda_{\text{em}} = 422$  nm, R = Ph, **32**; Fig. 36.3) [6c,d]. Later, this group extended their studies to organoboron compounds of the type  $(\text{N}^{\cap}\text{N}')\text{BPh}_2$  (Fig. 36.3, **33–35**) with different *N,N'*-donor ligands [6e]. The PL spectra of these complexes show emission maxima at 475 nm for 7-azaindolyl (**33**), 516 nm for indolyl (**34**), and 445 nm for benzimidazolyl (**35**) derivatives, showing that the location of the *N*-heteroatom in the chelating ligand plays an important role in the emission color.

Chi and coworkers [11] reported a series of tetracoordinate organoboron compounds  $(\text{N}^{\cap}\text{N}')\text{BPh}_2$  (Fig. 36.3, **36–41**) containing pyrazolyl pyridine chelating ligands. The boron complexes with electron-withdrawing groups show temperature-dependent dual fluorescence emission consisting of normal emission bands around 374–365 nm and an abnormally large Stokes-shifted emission around 488–512 nm in solution. Gardinier et al. [12] reported a series of tunable fluorophores based on 2-(pyrazolyl)anilide ligands (pzAn-X)BPh<sub>2</sub> (Fig. 36.3, **42–51**) [12a]. In their study, they found that the electron-withdrawing substituents of compounds **45–48** increase the chemical stability and show intense higher energy (blue) fluorescent emission, while the electron-donating groups of compounds **42** and **43** shift the emission to green and destabilize the compound toward hydrolysis. Improving upon their previous work, they modified the pyrazolyl anilide ligand by introducing an additional pyrazolyl ring at position 6 of the anilide moiety [12b]. These new compounds (pz<sub>2</sub>An-X)BPh<sub>2</sub> (Fig. 36.3, **49–51**) exhibit a number of advantageous properties compared to (pzAn-X)BPh<sub>2</sub> including high luminescence quantum yields and stability toward solvolysis.

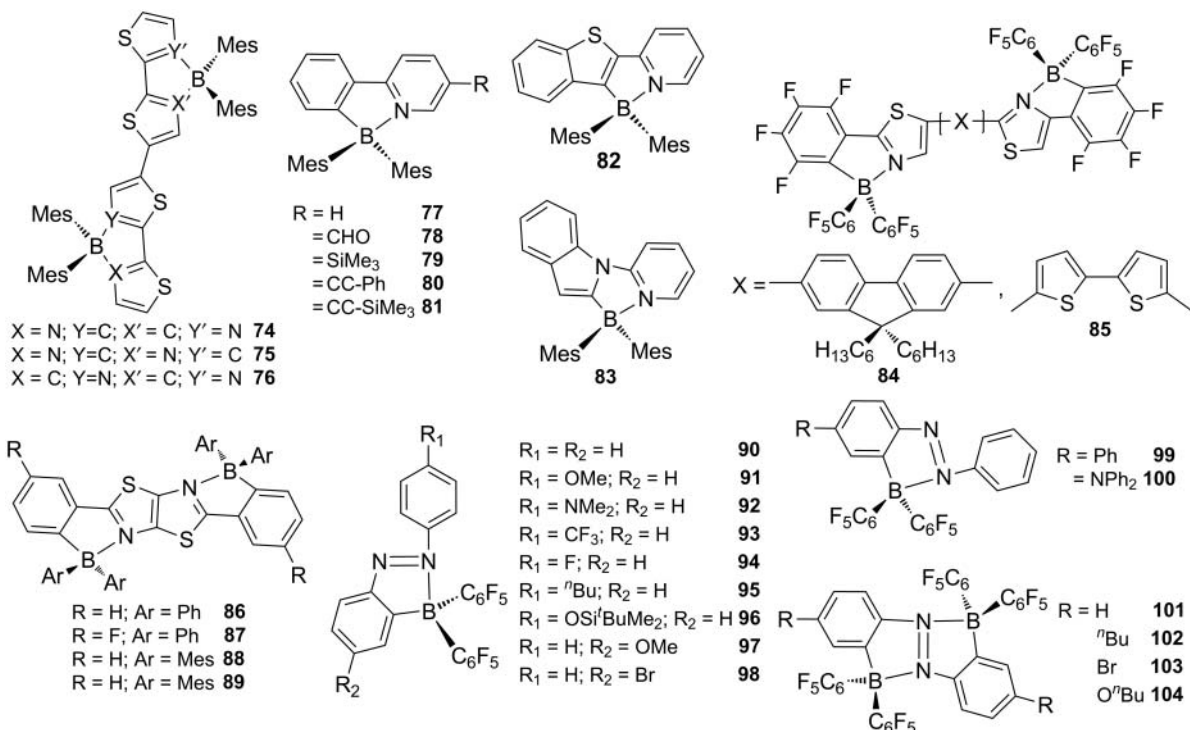
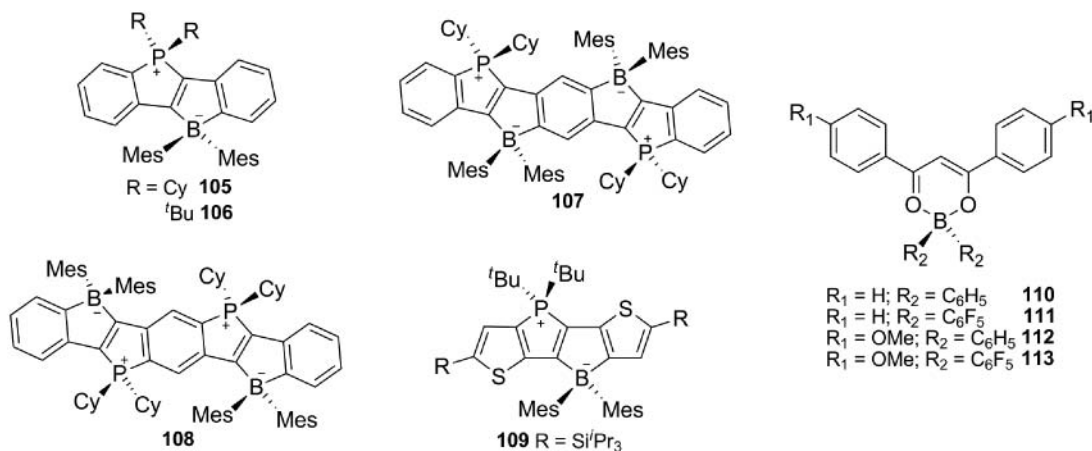
Gomes and coworkers [13] synthesized several organoboron complexes (Fig. 36.4, **52–73**) containing 2-(*N*-aryl)formiminopyrrolyl ligands. The mononuclear *N,N'*-2-formiminopyrrolyl organoboron compounds **52–61** have *N*-aryl rings of different electronic and steric natures [13a,b,e]. These compounds emit in violet, blue, or green regions of the spectrum, depending on the nature of the substituents of the *N*-aryl group, generally with high efficiencies. It was observed that the presence of bulkier groups at positions 2 and 6 of the *N*-aryl group (**53** and **54**) highly restricts its rotation about the C<sub>ipso</sub>–N bond, inducing an emission in the violet region (412 nm). The emission maxima are gradually blue-shifted from 478 to 465 nm depending on the number of fluorine substituents in the *N*-aryl ring (–C<sub>6</sub>H<sub>4</sub>F **57**, –C<sub>6</sub>H<sub>2</sub>F<sub>3</sub> **60**, and –C<sub>6</sub>F<sub>5</sub> **61**). Further, they synthesized new boron complexes **62–65** containing 2-(*N*-aryl)formiminophenanthro[9,10-*c*]pyrrolyl and 2-*N*-arylformiminoindolyl moieties, containing extended  $\pi$ -conjugation over the pyrrole moiety, in order to study the effects of the length of  $\pi$ -conjugation of the iminopyrrolyl ligand on the photophysical properties of these tetracoordinate organoboron complexes [13a,b,f]. The PL spectra of these complexes show emission maxima in blue to yellow regions with greater enhancement in the emission efficiencies attributed to their highly resonant  $\pi$ -conjugation. Extending their work from mononuclear to polynuclear tetracoordinate boron complexes, they prepared several bi- (**66–72**) and tri- (**73**) nuclear organoboron compounds having different lengths of  $\pi$ -conjugation [13a–d,g]. These polynuclear boron complexes were found to be highly fluorescent, their emission colors varied from blue to orange-red depending on the  $\pi$ -conjugation length, and they showed stable redox properties, indicating that they are possible candidates for emitters and charge-transporting materials.



**Figure 36.4** Luminescent organoboron compounds containing *N,N'*-2-iminopyrrolyl ligands.

### 36.2.3 *N,C*-Chelate Compounds

The first tetracoordinate boron compounds of the type  $(\text{N}^{\cap}\text{C})\text{BPh}_2$  (Fig. 36.5, **74–76**) containing nitrogen and carbon as donor atoms were reported by Yamaguchi's team for thiénylthiazole ligands [14]. These molecules have high electron mobility due to the extended  $\pi$ -conjugation and the boron chelation, but their quantum efficiencies are very low ( $<0.10$ ). S. Wang et al. [6f] reported a series of luminescent organoboron compounds containing substituted 2-phenylpyridyl (Fig. 36.5, **77–81**), benzo[*b*]thiophenylpyridine (**82**), and indolylpyridine (**83**) *N,C*-chelating ligands. Most of the compounds show bright fluorescence with emission maxima ranging from 360 to 527 nm and modest quantum yields. Recently, Wakamiya and coworkers demonstrated that the  $\text{B}(\text{C}_6\text{F}_5)_3$  coordination/cyclization protocol is an effective way for tuning the electronic nature of thiazoyl-capped  $\pi$ -conjugated compounds. The cyclized tetracoordinate compounds **84** and **85** (Fig. 36.5) show blue (476 nm) and yellow (548 nm) emissions with quantum efficiencies of 0.40 and 0.15, respectively, with an increase of the molar absorptivity in relation to the noncyclized derivatives [15]. Zhang's team reported a series of ladder-type  $\pi$ -conjugated diboron compounds (Fig. 36.5, **86–89**) containing *N,C*-chelating ligands [16]. These complexes possess high thermal stability ( $T_d \sim 343$ –400 °C) and intense fluorescence (435–520 nm;  $\phi_f = 0.18$ –0.39). Azobenzene derivatives as *N,C*-chelating ligands for the organoboron compounds **90–100** (Fig. 36.5) were reported by Kawashima and coworkers [17]. These compounds emit intense green, yellow, and orange fluorescence; in particular, compound **96** show the highest emission efficiency of 0.90 [17a]. The binuclear derivatives (Fig. 36.5, **101–104**) reported by the same group [17b] emit orange and red colors upon irradiation showing red shifts in both the absorption and emission maxima compared to their mononuclear analogs.

Figure 36.5 Luminescent organoboron compounds of the type  $(\text{N}^{\cap}\text{C})\text{BPh}_2$ .Figure 36.6 Luminescent organoboron compounds containing  $C,C'$ - or  $O,O$ -chelating ligands.

### 36.2.4 Other Chelate Compounds

Yamaguchi and coworkers reported significantly different tetracoordinate organoboron complexes **105–109** (Fig. 36.6) containing  $C,C'$ -chelating ligands [18]. The positively charged phosphonium chelating unit(s) balance the negatively charged borane unit(s), leading to a zwitterionic ladder-type structure and emissions in orange-red region with quantum yields of circa 0.40. Chujo's team reported 1,3-diketonato ligands ( $O,O$ -chelating ligands) derived organoboron compounds **110–113** (Fig. 36.6), which are structurally analogs to BODIPY. The PL spectra of these complexes show emission maxima around 430 nm, and the fluorescence quantum yields are in the range of 0.27–0.86 [19].

### 36.3 APPLICATIONS

Four-coordinate organoboron compounds with a  $\pi$ -conjugated chelate backbone have emerged recently as highly attractive materials for a number of applications including their use as emitters and charge-transport materials for organic light-emitting diodes (OLEDs) or photoresponsive materials and sensors.

#### 36.3.1 In OLEDs

OLEDs are simple devices that emit light in response to an electric current, and usually consist of an emitter layer of a luminescent molecule, a hole-transport layer (HTL), an electron-transport layer (ETL), the anode, and the cathode. The first boron-based OLEDs were fabricated by S. Wang's group using compound **32**. The corresponding electroluminescent (EL) device emits a bright-blue light with a turn-on voltage of circa 7 V and a luminance of 1024 cd/m<sup>2</sup> at 14 V [6c]. A bright orange electroluminescence (maximum brightness >8000 cd/m<sup>2</sup>) and efficient OLEDs (maximum efficiency >2.0 cd/A) were reported by Y. Wang [10] using the diboron compounds **27–30** as emitter layers. Very recently, Gomes and coworkers first fabricated efficient single-layer undoped OLEDs from the diboron compounds **68** and **69** [13c]. Green luminescences with luminance maxima in the order of 1000 cd/m<sup>2</sup> at less than 10 V and EL efficiency maxima of circa 0.3 cd/A were reported.

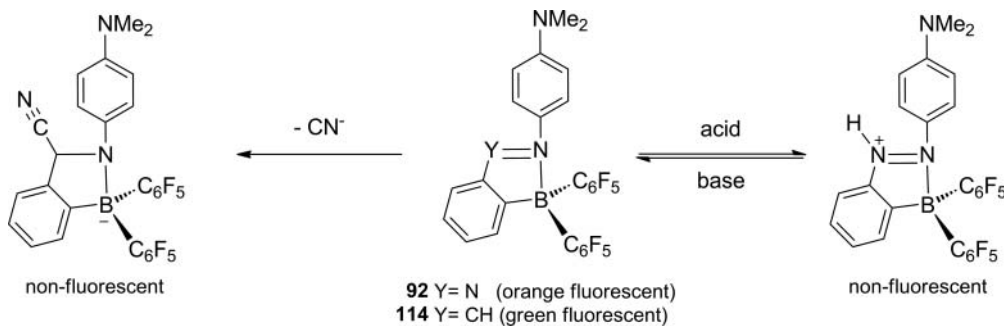
#### 36.3.2 In Sensors

Very few examples of tetracoordinate organoboron compounds were reported as potentially useful sensing systems when compared to the triaryl boron compounds. Kawashima and coworkers demonstrated the tetracoordinate organoboron compounds **92** and **114** as sensors [20]. The green fluorescence of **92** was quenched upon addition of an acid and could be restored by adding an amine and thus act as a fluorescence chemosensor (Scheme 36.1) [20a]. Compound **114** in presence of cyanide ion gave the corresponding cyanide adduct and quenched the fluorescence as a result of the disturbance of the  $\pi$ -conjugation in the backbone, thus acting as a cyanide ion sensor [20b].

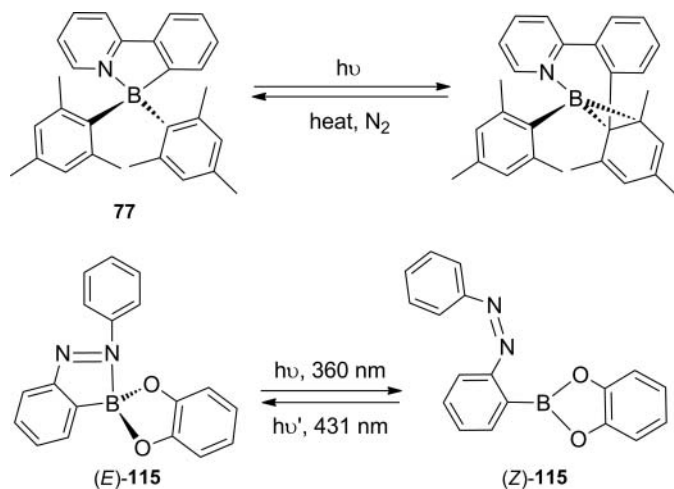
#### 36.3.3 As Photochromic Materials and Molecular Switches

Photochromic compounds are defined as molecules that are capable of undergoing a reversible transformation between two structural forms with a distinct color change when excited at least in one pathway by light. Many of the *N,C*-chelate organoboron compounds based on phenylpyridyl and other derivatives were found to undergo an unusual photoisomerization with a distinctive color change. The four-coordinate *N,C*-chelate organoboron compound (ppy)BMes<sub>2</sub> **77** was found to undergo reversible photochromic switching through the formation/breaking of a C–C bond, accompanied by a dramatic color change from colorless to dark blue (Scheme 36.2) [6f]. The corresponding dimer, containing two (ppy)BMes<sub>2</sub> units linked by a dimethylsilyl bridge, was found to undergo photochromic switching involving a single boryl unit only [6g].

The azobenzene organoboron derivative **115** undergoes photoisomerization from trans (*E*) to cis (*Z*) upon irradiation at 360 nm via dissociation of the B–N bond. The *Z* isomer can be reverted back to the *E* isomer by irradiation at 431 nm, enabling the photoswitching of the coordination number of boron between 3 and 4, which regulates the Lewis acidity of the boron center and the coordination of a base such as pyridine [21].



**Scheme 36.1** Tetracoordinate organoboron compounds as sensors.



**Scheme 36.2** Tetracoordinate organoboron compounds as photochromic materials and molecular switches.

### 36.4 CONCLUSIONS

In conclusion, the field of luminescent tetracoordinate organoboron compounds possessing a chelate  $\pi$ -conjugated backbone has greatly expanded over the past two decades. By exploiting the electronic and steric effects of the chelating ligands, the fluorescence emission of the organoboron complexes can be varied in a predictable manner. The presence of an electron-withdrawing group causes a blue shift of the emission energy, while an electron-donating group causes a red shift in the PL spectrum. Highly efficient organoboron fluorophores are effectively utilized as emitters and charge-transport materials in fabricating single or multilayer doped or undoped OLEDs. The *N,C*-chelate organoboron compounds were explored in a new arena for the development of photochromic materials and molecular switches, providing the organoboron compounds with new functionalities such as a sensing ability.

### ACKNOWLEDGMENT

The authors wish to thank the Fundação para a Ciência e Tecnologia for financial support (Project PTDC/QUI/65474/2006, cofinanced by FEDER) and a postdoctoral fellowship to S.D. (SFRH/BPD/47853/2008).

### REFERENCES

- Wong, T. K. S. In *Handbook of Organic Electronics and Photonics*; Nalwa, H. S., Ed.; American Scientific Publishers: Stevenson Ranch, CA, **2008**, Vol. 2; p 413.
- (a) Rao, Y.-L.; Wang, S. *Inorg. Chem.* **2011**, *50*, 12263; (b) Rao, Y.-L.; Amarne, H.; Wang, S. *Coord. Chem. Rev.* **2012**, *256*, 759.
- (a) Chen, C. H.; Shi, J. *Coord. Chem. Rev.* **1998**, *171*, 161; (b) Wang, S. *Coord. Chem. Rev.* **2001**, *215*, 79.
- Loudet, A.; Burgess, K. *Chem. Rev.* **2007**, *107*, 4891.
- (a) Jäkle, F. *Chem. Rev.* **2010**, *110*, 3985; (b) Nagai, A.; Chujo, Y. *Chem. Lett.* **2010**, *39*, 430.
- (a) Wu, Q.; Esteghamatian, M.; Hu, N.-X.; Popovic, Z.; Enright, G.; Tao, Y.; D'Iorio, M.; Wang, S. *Chem. Mater.* **2000**, *12*, 79; (b) Cui, Y.; Wang, S. *J. Org. Chem.* **2006**, *71*, 6485; (c) Wu, Q.; Esteghamatian, M.; Hu, N.-X.; Popovic, Z.; Enright, G.; Breeze, S. R.; Wang, S. *Angew. Chem. Int. Ed.* **1999**, *38*, 985; (d) Hassan, A.; Wang, S. *Chem. Commun.* **1998**, *211*; (e) Liu, Q.; Mudadu, M. S.; Schmider, H.; Thummel, R.; Tao, Y.; Wang, S. *Organometallics* **2002**, *21*, 4743; (f) Amarne, H.; Baik, C.; Murphy, S. K.; Wang, S. *Chem. Eur. J.* **2010**, *16*, 4750; (g) Murphy, S. K.; Baik, C.; Lu, J.-S.; Wang, S. *Org. Lett.* **2010**, *12*, 5266.
- Qin, Y.; Kiburu, I.; Shah, S.; Jäkle, F. *Org. Lett.* **2006**, *8*, 5227.
- Zhang, H.; Huo, C.; Ye, K.; Zhang, P.; Tian, W.; Wang, Y. *Inorg. Chem.* **2006**, *45*, 2788.
- Son, H.-J.; Han, W.-S.; Wee, K.-R.; Chun, J.-Y.; Choi, K.-B.; Han, S. J.; Kwon, S.-N.; Ko, J.; Lee, C.; Kang, S. O. *Eur. J. Inorg. Chem.* **2009**, 1503.

10. Zhang, Z.; Bi, H.; Zhang, Y.; Yao, D.; Gao, H.; Fan, Y.; Zhang, H.; Wang, Y.; Wang, Y.; Chen, Z.; Ma, D. *Inorg. Chem.* **2009**, *48*, 7230.
11. Cheng, C.-C.; Yu, W.-S.; Chou, P.-T.; Peng, S.-M.; Lee, G.-H.; Wu, P.-C.; Song, Y.-H.; Chi, Y. *Chem. Commun.* **2003**, 2628.
12. (a) Liddle, B. J.; Silva, R. M.; Morin, T. J.; Macedo, F. P.; Shukla, R.; Lindeman, S. V.; Gardinier, J. R. *J. Org. Chem.* **2007**, *72*, 5637; (b) Morin, T. J.; Linderman, S. V.; Gardinier, J. R. *Eur. J. Inorg. Chem.* **2009**, 104.
13. (a) Gomes, P. T.; Suresh, D.; Gomes, C. S. B.; Lopes, P. S.; Figueira, C. A. *Portuguese Patent PT 105885*, 13 Mar. 2013; priority date: 13 Sep. 2011; (b) Gomes, P. T.; Suresh, D.; Gomes, C. S. B.; Lopes, P. S.; Figueira, C. A. *World Patent WO2013039413*, 21 Mar. 2013; priority date: 13 Sep. 2011; (c) Suresh, D.; Gomes, C. S. B.; Gomes, P. T.; Di Paolo, R. E.; Maçanita, A. L.; Calhorda, M. J.; Charas, A.; Morgado, J.; Duarte, M. T. *Dalton Trans.* **2012**, *41*, 8502; (d) Calhorda, M. J.; Suresh, D.; Gomes, P. T.; Di Paolo, R. E.; Maçanita, A. L. *Dalton Trans.* **2012**, *41*, 13210; (e) Suresh, D.; Lopes, P. S.; Ferreira, B.; Figueira, C. A.; Gomes, C. S. B.; Gomes, P. T.; Di Paolo, R. E.; Maçanita, A. L.; Duarte, M. T.; Charas, A.; Morgado, J.; Calhorda, M. J. Submitted for publication; (f) Suresh, D.; Lopes, P. S.; Figueira, C. A.; Gomes, C. S. B.; Gomes, P. T.; Ferreira, B.; Di Paolo, R. E.; Maçanita, A. L.; Duarte, M. T.; Charas, A.; Morgado, J.; Calhorda, M. J. In preparation; (g) Suresh, D.; Gomes, C. S. B.; Lopes, P. S.; Figueira, C. A.; Gomes, P. T.; Ferreira, B.; Di Paolo, R. E.; Maçanita, A. L.; Duarte, M. T.; Charas, A.; Morgado, J.; Calhorda, M. J. In preparation.
14. Wakamiya, A.; Taniguchi, T.; Yamaguchi, S. *Angew. Chem. Int. Ed.* **2006**, *45*, 3170.
15. Job, A.; Wakamiya, A.; Kehr, G.; Erker, G.; Yamaguchi, S. *Org. Lett.* **2010**, *12*, 5470–5473.
16. Li, D.; Zhang, Z.; Zhao, S.; Wang, Y.; Zhang, H. *Dalton Trans.* **2011**, *40*, 1279.
17. (a) Yoshino, J.; Furuta, A.; Kambe, T.; Itoi, H.; Kano, N.; Kawashima, T.; Ito, Y.; Asashima, M.; *Chem. Eur. J.* **2010**, *16*, 5026; (b) Kano, N.; Furuta, A.; Kambe, T.; Yoshino, J.; Shibata, Y.; Kawashima, T.; Mizorogi, N.; Nagase, S. *Eur. J. Inorg. Chem.* **2012**, 1584.
18. Fukazawa, A.; Yamada, H.; Yamaguchi, S. *Angew. Chem. Int. Ed.* **2008**, *47*, 5582.
19. Nagai, A.; Kokado, K.; Nagata, Y.; Arita, M.; Chujo, Y. *J. Org. Chem.* **2008**, *73*, 8605.
20. (a) Yoshino, J.; Kano, N.; Kawashima, T. *Chem. Lett.* **2008**, *37*, 960; (b) Yoshino, J.; Kano, N.; Kawashima, T. *J. Org. Chem.* **2009**, *74*, 7496.
21. (a) Kano, N.; Yoshino, J.; Kawashima, T. *Org. Lett.* **2005**, *7*, 3909; (b) Yoshino, J.; Kano, N.; Kawashima, T. *Tetrahedron* **2008**, *64*, 7774.

## MECHANOCHEMISTRY: A TOOL IN THE SYNTHESIS OF CATALYSTS, METALLODRUGS, AND METALLOPHARMACEUTICALS

VÂNIA ANDRÉ, CLARA S. B. GOMES, AND M. TERESA DUARTE\*

*Departamento de Engenharia Química Centro de Química Estrutural, Instituto Superior Técnico, Universidade de Lisboa, Lisboa, Portugal*

### 37.1 INTRODUCTION

*Mechanochemistry* refers to reactions, usually of solids, induced by the input of mechanical energy. Within the diversity of reaction types, reaction conditions and reactive materials, metals, metal oxides and molecular crystals, in this chapter we will use a simple approach called *mechanochemical synthesis* (or mechanosynthesis) that corresponds to chemical reactivity achieved by grinding manually, using a mortar and a pestle, bulk solid reactants [1]. In recent years, mechanosynthesis became more widely used as it has proved to promote, promptly and quantitatively, reactions between solids, with either no added solvent (neat grinding) or only using very small amounts (liquid-assisted grinding, LAG). LAG, also known as *solvent drop grinding*, uses catalytic amounts of a liquid phase to accelerate mechanochemical reactions [2]. The liquid phase is thought to promote mobility in reaction components and thus stimulate reactivity in systems that are inactive on neat grinding, as well as push a reaction toward the formation of a particular product [3]. The amount of solvent used is always sufficiently small to avoid the effects of relative solubilities of reactants and products [4]. Nowadays, it is also well known that in order to obtain reproducibility and a better control on reaction conditions, the use of electrical mills is becoming mandatory.

The scope of this chapter is not to present an overview of what is the state of the art in this research field nor to address all the different reaction types covered by this technique; for that we recommend the recent review paper by James et al. [5]. Here, we intend to give some examples of what is being done and present some of our own work using this “new”<sup>1</sup> synthetic technique.

### 37.2 MECHANOCHEMISTRY IN SUPRAMOLECULAR SYNTHESIS

The application of mechanochemistry in supramolecular synthesis has been extensively used in the past 10 years for obtaining multicomponent molecular crystals in particular in the pharmaceutical field [5, 7]. The production of new solid forms, especially cocrystals is of utmost importance as it provides a way to derivatize active pharmaceutical ingredients (APIs), by modifying their solid-state arrangements rather than their internal molecular structures. Modification of the crystal

<sup>1</sup>The earliest documented mechanochemical reaction may have been grinding cinnabar with acetic acid in a copper vessel to give elemental mercury (fourth century BC) [6].

structure by cocrystallization can improve pharmaceutically relevant properties such as dissolution rate, solubility, thermal and hydration stability, or compressibility [8].

Pharmaceutical cocrystals generally consist of an API and one or more pharmaceutically acceptable molecules, known as the *cocrystal formers* or *coformers*. The coformers are typically compounds “generally regarded as safe” (GRAS compounds). The first examples were reported in 1993 by Caira and Etter, with the drug sulfadimidine and a variety of carboxylic acids such as acetylsalicylic acid (aspirin) [9]. A recent example is the use of cocrystals to enhance the hydration stability of a solid API, as in caffeine and theophylline by forming cocrystals with dicarboxylic acids [8c].

Cocrystal formation has been used intensively to enhance the solubility of low and high soluble APIs as demonstrated for theobromine [4] and as reported by us for gabapentin-lactam [10].

### 37.3 MECHANOCHEMISTRY IN ORGANIC AND COORDINATION SYNTHESIS

The sustainability of chemical reactions has gained relevance lately. In this context, the use of ball mills in solvent-free organic synthesis started to attract a considerable attention [5, 11]. In fact, until recently, all the methods employed in organic synthesis were restricted to reactions in solution because of the restricted conformational and translational degrees of freedom of molecules in solids [12]. However, in mechanochemical synthesis, ball milling modifies the conditions under which a chemical reaction commonly takes place, and various applications including C–C bond formations [11c], amine condensations, and syntheses of heterocycles [1c] were found.

In 2003, Kaupp et al. reported solvent-free Knoevenagel condensations carried out in a ball mill [13]. Domino oxa-Michael–aldol reaction, Morita–Baylis–Hillman reaction and Wittig reactions are other examples for which the ball-mill methodology was employed successfully [5]. Metal-catalyzed organic reactions, such as Suzuki, Heck, and Sonogashira coupling reactions, are very important in solution-state organic synthesis. These reactions can also be performed in ball mills, although, until now, they are limited to Pd-catalyzed cross-coupling reactions [11b]. In most cases, the reaction times are significantly shorter compared to reactions carried out in solution.

Recently, several reports suggest the effectiveness of mechanochemical synthesis in a wide range of metal complexation reactions. Examples of coordination compounds prepared by this method include  $[\text{Ni}(\text{phen})_3](\text{NO}_3)_2$ ,  $[\text{Fe}(\text{phen})_3]\text{Cl}_2$ ,  $\text{PtCl}_2(\text{PPh}_3)_2$ ,  $\text{MCl}_2(\text{imidazole})_2$  ( $\text{M} = \text{Co}, \text{Cu}, \text{Zn}$ ),  $\text{MCl}_2\text{L}_2$  ( $\text{M} = \text{Co}, \text{Ni}, \text{Cu}; \text{L} = \text{PPh}_3, \text{OPPh}_3, \text{OAsPh}_3$ , or toluidine), and  $\text{Pt}(\text{CO}_3)(\text{PPh}_3)_2$ . Mechanochemical syntheses of air-sensitive metal complexes have also been performed successfully [5]. Therefore, the preparation of metal complexes using solid-state techniques appears to be a powerful alternative to the commonly used solution-based methods.

The application of mechanochemistry for the construction of metal–ligand bonds can significantly improve the synthesis of porous MOFs, a class of materials with increasing technological importance. Different materials have been synthesized such as (HKUST-1) obtained by neat grinding or LAG of copper(II) acetate monohydrate with benzene-1,3,5-tricarboxylic acid that has shown comparable BET surface area to that of samples obtained by conventional solution-based routes [14]. Another example concerns a porous interpenetrated mixed ligand MOF  $\text{Zn}_2(\text{fma})_2(\text{bipy})$ , prepared mechanochemically from  $\text{Zn}(\text{OAc})_2 \bullet 2\text{H}_2\text{O}$ , fumaric acid, and 4,4-bipyridine [15].

### 37.4 MECHANOCHEMISTRY IN METALLOPHARMACEUTICALS AND METALLODRUGS

Coordination complexes with active pharmacological molecules, which comprise metallodrugs and metallopharmaceuticals, are a much less explored class of reactions. Metallodrugs, in which the metal ion is also the biologically active component, and metallopharmaceuticals, in which the metal ion plays the role of a carrier for the API molecule, similar to the counterion in a pharmaceutical salt or the coformer in a pharmaceutical cocrystal, have been successfully prepared by mechanochemistry [16].

Potential design for metallopharmaceuticals has been proposed by Moulton and Ma [17] who used the copper(II) carboxylate paddlewheel motif to enhance the lipophilicity of carboxylate APIs. In 2008, two derivatives of the neuroleptic drug gabapentin with zinc and copper(II) chlorides obtained by LAG were the first API metal complexes prepared by mechanochemistry [18]. This technique had already proven to significantly improve not only solid-state cocrystal synthesis but also the formation of coordination frameworks [19]. Since then, several other similar systems have been reported [20]. Worth mentioning are the silver nitrate and nickel chloride metal–organic derivatives with the antibiotic 4-aminosalicylic acid (4ASA) and the nootropic piracetam prepared by us [21]. The syntheses of complexes of silver nitrate and 4ASA are particularly interesting in terms of possible pharmaceutical applications because of the synergistic effect that can result from the combination of an antibiotic with a known antimicrobial agent ( $\text{Ag}^+$ ), demonstrating the potential of coordination



**Figure 37.1** Mechanochemistry reaction of 4ASA yielding an anhydrous network (top) and its recrystallization yielding an one-dimensional hydrate polymer (bottom).

chemistry in generating new solid forms of APIs. Complexation of  $\text{AgNO}_3$  and 4ASA by mechanosynthesis yielded an anhydrous network based on two-dimensional sheets held by Ag–O and Ag–N coordination bonds and O–H $\bullet\bullet\bullet$ O hydrogen bonds, whereas solution techniques resulted in a one-dimensional hydrated polymer based on O–H $\bullet\bullet\bullet$ O hydrogen bonds and Ag–O coordination bonds (Fig. 37.1).

The mechanosynthesis of API coordination complexes involving biologically benevolent magnesium ions directly from magnesium oxide [20, 22] is a good choice and several derivatives of the nonsteroidal anti-inflammatory drugs (NSAIDs), such as *S*- and *RS*-ibuprofen, salicylic acid, and *S*-naproxen, are obtained. The activity of ibuprofen was enhanced when formulated with MgO, because of the formation of a metal–organic material exhibiting a higher solubility than the neutral NSAID [20]. The variation of water activity in mechanochemical reactions of MgO and naproxen lead to the formation of three complexes with different hydration contents [23].

Widely known examples of metallodrugs are platinum complexes such as cisplatin, carboplatin, or oxaliplatin used in the treatment of cancer [24] and bismuth subsalicylate marketed as Pepto-Bismol [25]. In 2011, the rapid, efficient, and selective synthesis by ion- and liquid-assisted grinding (ILAG) [26] of bismuth subsalicylate, as well as of two other bismuth salicylates, directly from  $\text{Bi}_2\text{O}_3$  was reported by us revealing the first crystal structure of a bismuth salicylate without auxiliary ligands (Fig. 37.2) [27]. This structure was a particularly relevant addition to our understanding of the

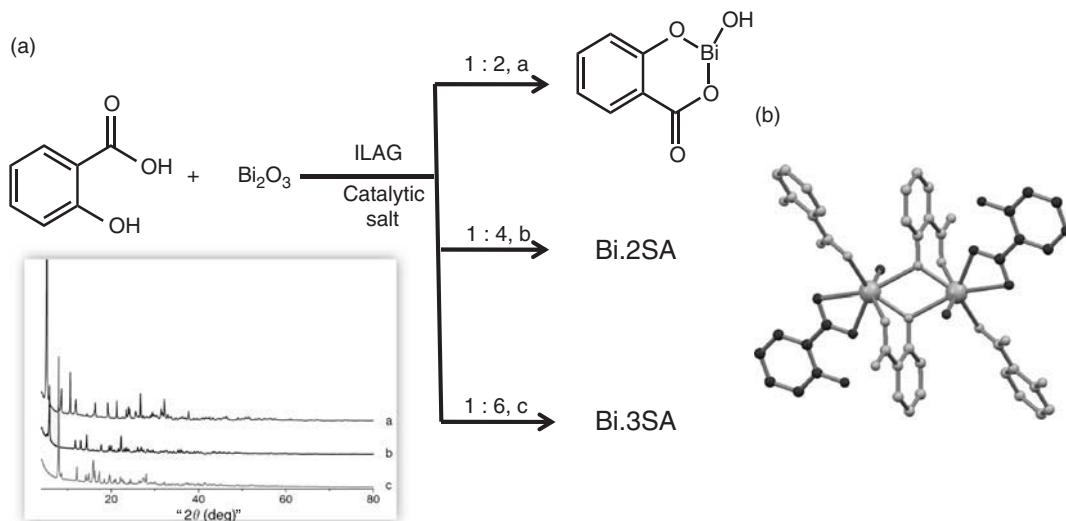


**Figure 37.2** (a) Mechanochemistry reaction of salicylic acid with  $\text{Bi}_2\text{O}_3$  yielding bismuth mono-, di-, and trisalicylate, depending on the starting conditions; (b) crystal structure of a bismuth disalicylate determined by XRPD data.

chemistry of bismuth salicylates as: (i) it complements the existing model compounds based on discrete oligonuclear clusters involving auxiliary organic ligands; (ii) it confirms the tendency of bismuth salicylate to adopt extended structures in the absence of organic auxiliaries; (iii) it demonstrates the absence of basic hydroxide or oxide species in bismuth disalicylate. The synthesis of bismuth salicylates from solution is complicated, requiring harsh conditions to which the product is sensitive, and the wide application of the solid-state synthetic methodologies previously proposed [28] is limited by issues of environmental nature and reactant toxicity. Thus, mechanochemistry presents major advantages in the preparation of bismuth subsalicylate.

### 37.5 MECHANO CHEMISTRY IN CATALYSIS AND CATALYSTS

Supramolecular catalysts can be compared to enzymes, giving rise to highly stereoselective, environmentally friendly, and cost-effective transformations. Very recently, MacGillivray et al. [12] reported an important development by coupling mechanochemical and covalent synthesis, to perform a catalytic [2+2] photodimerization reaction of a bis(pyridine)-substituted olefin (Fig. 37.3). The employed methodology consisted in alternating grinding periods with exposure to UV light in the presence of a substoichiometric amount of a resorcinol-based template. The UV light is responsible for the photochemical cyclization, and the catalytic resorcinol-based template is able to dissociate from the reaction product, allowing it to be redistributed by grinding to complex to further reactant and so enabling catalytic turnover [5, 12, 16].

Nickel(II) coordination compounds stabilized by  $\alpha$ -diimine ligands, generally known as *Brookhart type catalysts*, are olefin polymerization precatalysts, as these derivatives give rise to active catalytic species when activated with alkyl aluminum compounds, such as methylaluminoxane or diethyl aluminum chloride [29]. The simplest catalyst precursors are the metal dihalides. Although a number of routes have been developed, the easiest involves the addition of the appropriate ligand to a starting material containing a labile ligand, such as  $[\text{NiBr}_2(\text{DME})]$  (Scheme 37.1), being carried out in solution during 24 h.

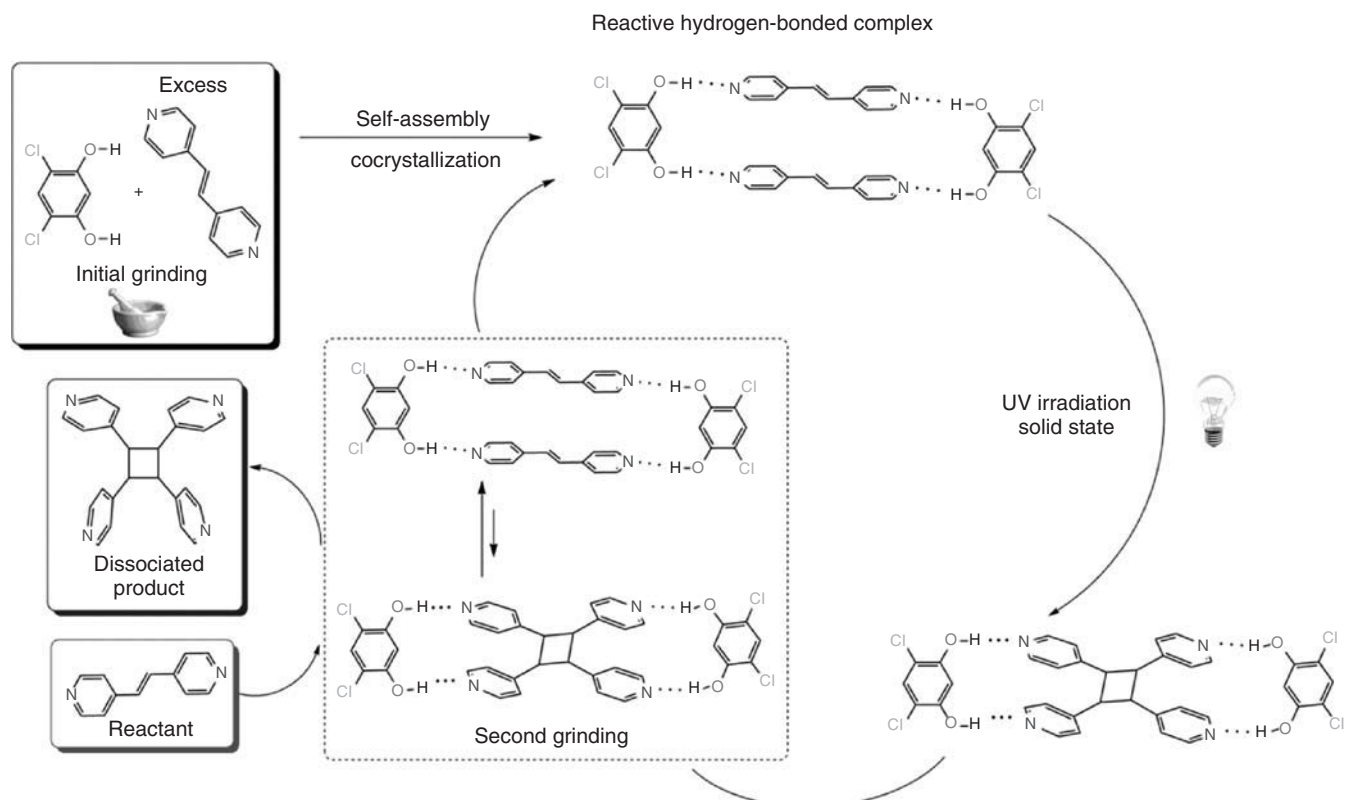
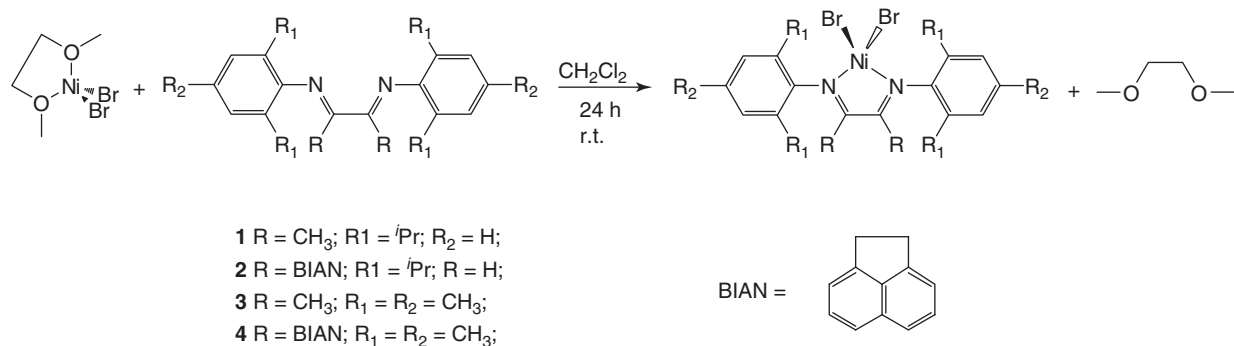


**Figure 37.3** Supramolecular catalytic [2+2] photodimerization, which involves alternating grinding periods and irradiation with UV light.



Scheme 37.1 Synthesis of nickel(II) compounds stabilized by alpha-diimine ligands.

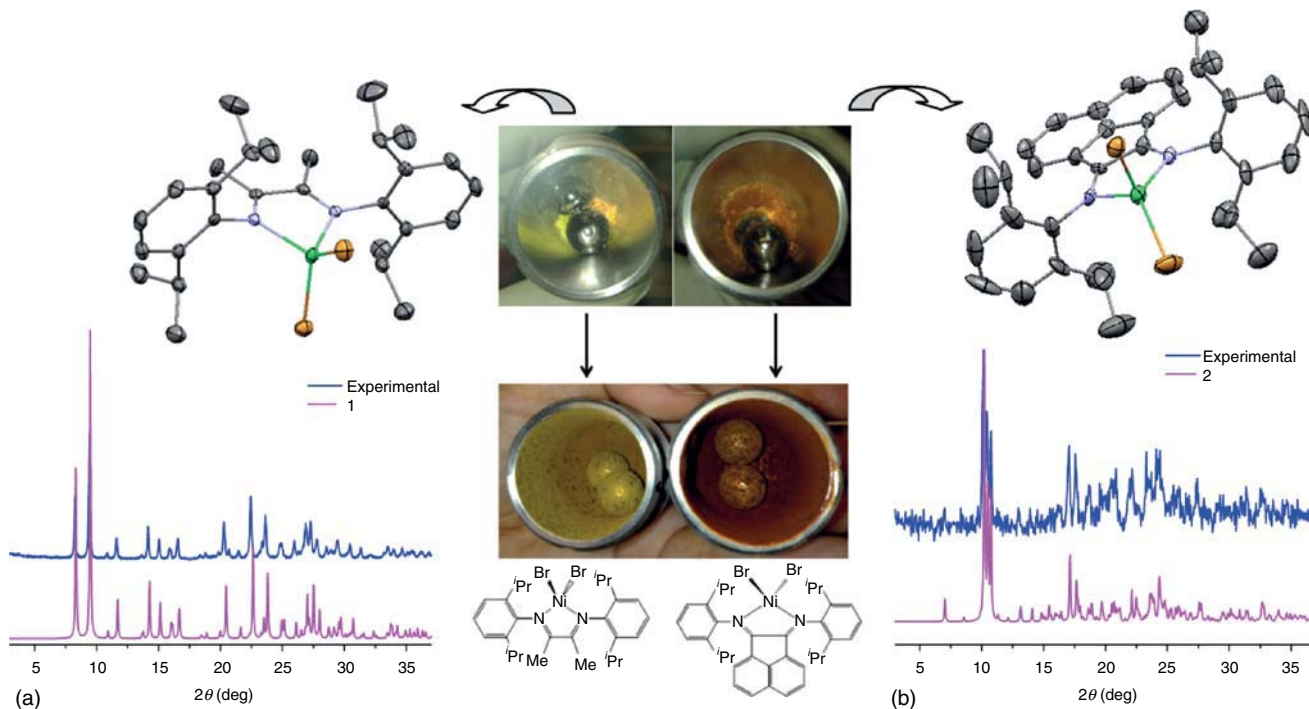


Figure 37.4 Syntheses and characterization of complexes derived from (a) **1** and (b) **2**. (See insert for color representation of the figure.)

Recently, we have prepared some of these Ni(II) and Co(II) complexes using solvent-free mechanochemical synthesis in a ball mill [30]. The first tests were performed with nickel, using [NiBr<sub>2</sub>(DME)] as the starting material. The reaction of [NiBr<sub>2</sub>(DME)] with one equivalent of the appropriate ligand, in the absence of any solvent, afforded quantitatively the coordination complexes derived from **1** and **2**, in 20 minutes. These compounds were characterized by single-crystal X-ray diffraction (SCXRD) and X-ray powder diffraction (XRPD) (Fig. 37.4). Experiments using anhydrous NiBr<sub>2</sub> instead of [NiBr<sub>2</sub>(DME)] gave rise to the formation of the same coordination compounds, as proven by SCXRD.

The solution preparation of Co(II) coordination compounds containing ligands **1–4** was already reported in the literature [31]. Nevertheless, we have been able to prepare the same compounds using solvent-free mechanochemical synthesis, quantitatively and only in 20 minutes. These complexes were characterized by XRPD and SCXRD, when possible. Interestingly, the Co(II) compound containing ligand **2** was proven to be isostructural with the corresponding Ni(II) compound.

### 37.6 CONCLUSIONS

Mechanochemistry has indeed proven its great potential in all the applications referred earlier. It was a major breakthrough in our work on supramolecular synthesis and also in the synthesis of metallodrugs, metallopharmaceuticals, and olefin polymerization precatalysts.

### REFERENCES

- (a) Braga, D.; Giaffreda, S. L.; Curzi, M.; Maini, L.; Polito, M.; Grepioni, F. *J. Therm. Anal. Calorim.* **2007**, *90*, 115; (b) Tanaka, K.; Toda, F. *Chem. Rev.* **2000**, *100*, 1025–1074; (c) Kaupp, G. *CrystEngComm.* **2006**, *8*, 794.
- (a) Friščić, T.; Trask, A. V.; Jones, W.; Motherwell, W. D. S. *Angew. Chem. Int. Ed.* **2006**, *45*, 7546; (b) Bowmaker, G. A.; Chaichit, N.; Pakawatchai, C.; Skelton, B. W.; White, A. H. *Dalton Trans.* **2008**, 2926; (c) Nguyen, K. L.; Friščić, T.; Day, G. M.; Gladden, L. F.; Jones, W. *Nat. Mater.* **2007**, *6*, 206; (d) Trask, A. V.; Motherwell, W. D. S.; Jones, W.; Feng, S. H.; Tan, R. B. H.; Carpenter, K. J. *Chem. Commun.* **2005**, 880.
- (a) Adams, C. J.; Colquhoun, H. M.; Crawford, P. C.; Lusi, M.; Orpen, A. G. *Angew. Chem. Int. Ed.* **2007**, *46*, 1124; (b) Trask, A. V.; Motherwell, W. D. S.; Jones, W. *Chem. Commun.* **2004**, *7*, 890.
- Karki, S.; Fabian, L.; Friščić, T.; Jones, W. *Org. Lett.* **2007**, *9*, 3133.
- James, S. L.; Adams, C. J.; Bolm, C.; Braga, D.; Collier, P.; Friščić, T.; Grepioni, F.; Harris, K. D. M.; Hyett, G.; Jones, W.; Krebs, A.; Mack, J.; Maini, L.; Orpen, A. G.; Parkin, I. P.; Shearouse, W. C.; Steedk, J. W.; Waddelli, D. C. *Chem. Soc. Rev.* **2012**, *41*, 413.
- Takacs, L. *JOM* **2000**, *52*(1), 12.
- Friščić, T. *J. Mater. Chem.* **2010**, *20*, 7599 and references therein.
- (a) McNamara, D. P.; Childs, S. L.; Giordano, J.; Iarricco, A.; Cassidy, J.; Shet, M. S.; Mannion, R.; O'Donnell, E.; Park, A. *Pharm. Res.* **2006**, *23*, 1888; (b) Good, D. J.; Rodríguez-Hornedo, N. *Cryst. Growth Des.* **2009**, *9*, 2252; (c) Trask, A. V.; Motherwell, W. D. S.; Jones, W. *Int. J. Pharm.* **2006**, *320*, 114; (d) Trask, A. V.; Motherwell, W. D. S.; Jones, W. *Cryst. Growth Des.* **2005**, *5*, 1013; (e) Karki, S.; Friščić, T.; Fabian, L.; Laity, P. R.; Day, G. M.; Jones, W. *Adv. Mater.* **2009**, *21*, 3905.
- (a) Caira, M. R.; Nassimbeni, L. R.; Wildervanck, A. F. *J. Chem. Soc. Perkin Trans. 2*, **1995**, 2213; (b) Etter, M. C.; Reutzel, S. M.; Choo, C. G. *J. Am. Chem. Soc.* **1993**, *115*, 4411.
- (a) Childs, S. L.; Rodríguez-Hornedo, N.; Reddy, L. S.; Jayasankar, A.; Maheshwari, C.; McCausland, L.; Shipplett, R.; Stahly, B. C. *CrystEngComm.* **2008**, *10*, 856; (b) Maheshwari, C.; André, V.; Reddy, S.; Roy, L.; Duarte, T.; Rodríguez-Hornedo, N. *CrystEngComm.* **2012**, *14*, 4801.
- For example: (a) Bruckmann, A.; Krebs, A.; Bolm, C. *Green Chem.* **2008**, *10*, 1131; (b) Stolle, A.; Szuppa, T.; Leonhardt, S. E. S.; Ondruschka, B. *Chem. Soc. Rev.* **2011**, *40*, 2317; (c) Rodriguez, B.; Bruckmann, A.; Rantanen, T.; Bolm, C. *Adv. Synth. Catal.* **2007**, *349*, 2213.
- Sokolov, A. N.; Bučar, D.-K.; Baltrusaitis, J.; Gu, S. X.; MacGillivray, L. R. *Angew. Chem. Int. Ed.* **2010**, *49*, 4273.
- Kaupp, G.; Naimi-Jamal, M. R.; Schmeyers, J. *Tetrahedron* **2003**, *59*, 3753.
- (a) Yuan, W.; Lazuen-Garay, A.; Pichon, A.; Clowes, R.; Wood, C. D.; Cooper, A. I.; James, S. L. *CrystEngComm.* **2010**, *12*, 4063; (b) Chui, S. S.-Y.; Lo, S. M.-F.; Charmant, J. P. H.; Orpen, A. G.; Williams, I. D. *Science* **1999**, *283*, 1148; (c) Schlesinger, M.; Schulze, S.; Hietschold, M.; Mehring, M. *Microporous Mesoporous Mater.* **2010**, *132*, 121.
- Fujii, K.; Lazuen Garay, A.; Hill, J.; Sbircea, E.; Pan, Z.; Xu, M.; Apperley, D. C.; James, S. L.; Harris, K. D. M. *Chem. Commun.* **2010**, *46*, 7572.
- Delori, A.; Friščić, T.; Jones, W. *CrystEngComm.* **2012**, *14*, 2350.
- (a) Ma, Z.; Moulton, B. *Cryst. Growth Des.* **2007**, *7*, 196–198; (b) Ma, Z.; Moulton, B. *Mol. Pharm.* **2007**, *4*, 373.
- Braga, D.; Grepioni, F.; Maini, L.; Brescello, R.; Cotarca, L. *CrystEngComm.* **2008**, *10*, 469.
- (a) Braga, D.; Curzi, M.; Johansson, A.; Polito, M.; Rubini, K.; Grepioni, F. *Angew. Chem. Int. Ed.* **2006**, *45*, 142; (b) Yuan, W.; Friščić, T.; Apperley, D.; James, S. L. *Angew. Chem. Int. Ed.* **2010**, *49*, 3916; (c) Bowmaker, G. A.; Hanna, J. V.; Hart, R. D.; Skelton, B. W.; White, A. H. *Dalton Trans.* **2008**, 5290; (d) Belcher, W. J.; Longstaff, C. A.; Neckenig, M. R.; Steed, J. W. *Chem. Commun.* **2002**, 1602; (e) Braga, D.; Grepioni, F. *Angew. Chem. Int. Ed.* **2004**, *43*, 4002.
- (a) Chow, E. H. H.; Strobridge, F. C.; Friščić, T. *Chem. Commun.* **2010**, *46*, 6368–6370; (b) Friščić, T. *J. Mater. Chem.* **2010**, *20*, 7599.
- Braga, D.; Grepioni, F.; André, V.; Duarte, M. *CrystEngComm.* **2009**, *11*, 2618.
- (a) Byrn, S. R.; Xu, W.; Newman, A. W. *Adv. Drug Deliv. Rev.* **2001**, *48*, 115; (b) Strobridge, F. C.; Judas, N.; Friščić, T. *CrystEngComm.* **2010**, *12*, 2409.
- Friščić, T.; Halasz, I.; Strobridge, F. C.; Dinnebier, R. E.; Stein, R. S.; Fabian, L.; Curfs, C. *CrystEngComm.* **2011**, *13*, 3125.

24. Guo, Z. J.; Sadler, P. J. *Angew. Chem. Int. Ed.* **1999**, *38*, 1513.
25. Ge, R. G.; Sun, H. Z. *Acc. Chem. Res.* **2007**, *40*, 267.
26. Friščić, T.; Reid, D. G.; Halasz, I.; Stein, R. S.; Dinnebier, R. E.; Duer, M. J. *Angew. Chem. Int. Ed.* **2010**, *49*, 712.
27. André, V.; Hardeman, A.; Halasz, I.; Stein, R. S.; Jackson, G. J.; Reid, D. G.; Duer, M. J.; Curfs, C.; Duarte, M. T.; Friščić, T. *Angew. Chem. Int. Ed.* **2011**, *50*, 7858.
28. Andrews, P. C.; Deacon, G. B.; Forsyth, C. M.; Junk, P. C.; Kumar, I.; Maguire, M.; *Angew. Chem. Int. Ed.* **2006**, *45*, 5638.
29. Ittel, S. D.; Johnson, L. K.; Brookhart, M. *Chem. Rev.* **2000**, *100*, 1169.
30. Gomes, C. S. B.; Gomes, P. T.; Duarte, M. T. *Inorg. Chem.*, submitted for publication.
31. Rosa, V.; Gonzalez, P. J.; Avilés, T.; Gomes, P. T.; Welter, R.; Rizzi, A. C.; Passeggi, M. C. G.; Brondino, C. D. *Eur. J. Inorg. Chem.* **2006**, 4761.



## **PART V**

---

### **ORGANOMETALLIC CHEMISTRY AND SUSTAINABLE ENERGY**



## ORGANOMETALLIC COMPOUNDS FOR DYE-SENSITIZED SOLAR CELLS (DSSC)

DELELE W. AYELE

*Department of Chemical Engineering, National Taiwan University of Science and Technology, Taipei, Taiwan, Republic of China*

WEI-NEIN SU

*Graduate Institute of Applied Science and Technology, National Taiwan University of Science and Technology, Taipei, Taiwan, Republic of China*

JOHN RICK, HUNG-MING CHEN, CHUN-JERN PAN, AND NIBRET G. AKALEWORK

*Department of Chemical Engineering, National Taiwan University of Science and Technology, Taipei, Taiwan, Republic of China*

BING-JOE HWANG\*

*Department of Chemical Engineering, National Taiwan University of Science and Technology, Taipei, Taiwan, Republic of China; National Synchrotron Radiation Research Center, Hsinchu, Taiwan*

### 38.1 INTRODUCTION

The demand for energy is one of the most important factors shaping human life in the twenty-first century [1]. The vast majority of the world's energy is generated from nonrenewable sources, specifically oil, coal and gas [2]. Just over 13% of global energy is derived from renewable sources, only a small percentage of which comes from hydrothermal, geothermal, solar, wind, tidal, and wave sources [2]. The increasing consumption of fossil fuels that has led to global warming and environmental pollution has now created an awareness of the need for renewable energy sources and sustainable development. The need to move toward a low carbon consumption economy has led to an unprecedented interest in renewable energy sources, including solar power. Depending on the device, the harvesting of light energy from the sun (i.e., solar energy) can generate power for conversion to either electricity [3] or chemical energy [4].

One type of solar-powered device, which is at the center of an ongoing research effort to utilize clean and renewable energy, is the dye-sensitized solar cell (DSSC) [5] containing ruthenium complexes in the photoanode and platinum in the counterelectrode (Fig. 38.1) first reported in 1991 by Michael Grätzel and coworkers at the Ecole Polytechnique Fédérale de Lausanne[6]. Thus, platinum group metals and organometallic complexes of ruthenium and its analogs appear to have a pivotal role in sustainable energy technology. More recently, metal complexes, and ruthenium complexes in particular, have been investigated intensively for DSSC applications [7]. DSSC technology has been seen as an inexpensive and promising alternative to the proven solid-state photovoltaic cells [8].

#### 38.1.1 The Working Principles of Dye-Sensitized Solar Cells (DSSCs)

So far, different metal complexes [9, 10] have been used as light-harvesting dyes in DSSC applications (see the working principle in Fig. 38.1). The DSSC components include a semiconductor (usually a TiO<sub>2</sub> film on conducting glass), the

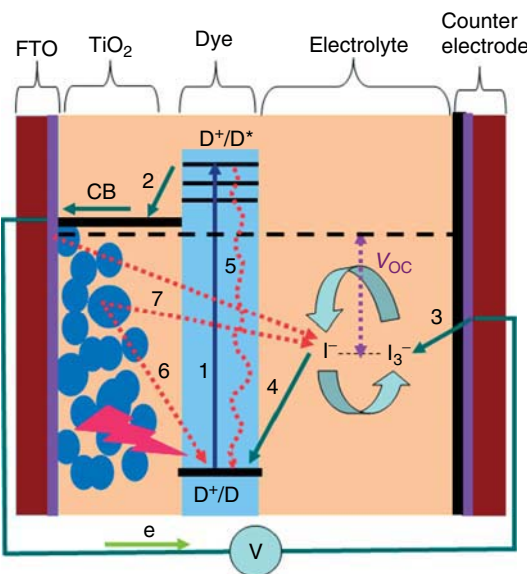


**Figure 38.1** The construction of a dye-sensitized solar cell (DSSC) and its operating principle. D, Dye; CB, conduction band of  $\text{TiO}_2$ ;  $V_{\max}$ , maximum voltage. (See insert for color representation of the figure.)

**TABLE 38.1** The Absorption Spectra and Conversion Efficiencies of Various Metal Complexes for DSSC Application

Dye	IPCE, %	Absorption (nm) $\varepsilon$ ( $10^3 \text{ m}^2/\text{mol}$ )	Short-Circuit Current, $J_{sc}$ , mA/cm $^2$	Fill Factor (FF)	Open-Circuit Voltage, $V_{oc}$ , mV	Efficiency, $\eta$ , %
N3	83	534 (1.42)	18.20	0.730	720	10.00 [15, 16]
N719	85	532 (1.40)	17.73	0.750	846	11.18 [10, 17]
N749	80		20.90	0.722	736	11.10 [18, 19]
Z907	72	526 (1.22)	13.60	0.692	721	6.80 [20]
Z907	72	526 (1.22)	14.60	0.693	722	7.30 [20]
K8	77	555 (1.80)	18.00	0.750	640	8.64 [21]
K19	70	543 (1.82)	14.61	0.671	711	7.00 [22]
N945	80	550 (1.89)	16.50	0.720	790	9.60 [23]
Z910	80	543 (1.70)	17.20	0.764	777	10.20 [24]
K73	80	545 (1.80)	17.22	0.694	748	9.00 [25]
K51	70	530 (1.23)	15.40	0.685	738	7.80 [26]
HRs-1	80	542 (1.87)	20.00	0.690	680	9.50 [27]
Z955	80	519 (0.83)	16.37	0.693	707	8.00 [28]

sensitizer (dye) absorbed on a semiconductor film, an electrolyte containing a redox mediator, and a counterelectrode capable of regenerating the redox mediator. At present, state-of-the-art DSSCs based on metal complexes (such as Ru and Zn) as the active materials have overall power conversion efficiencies over 11% under standard (Global Air Mass 1.5) illumination [9, 11]. Table 38.1 indicates the conversion efficiencies of various metal complexes for DSSC applications. More specifically, the high efficiencies of the ruthenium(II)-polypyridyl DSSCs [11] can be attributed to their wide absorption ranges from the visible to the near infrared (NIR). In addition, the carboxylate groups attached to the bipyridyl moiety lower the energy of the ligand  $\pi^*$  orbital. The absorption spectra of ruthenium polypyridyl systems can be tuned by careful consideration of the highest occupied molecular orbital (HOMO) and lowest unoccupied molecular orbital (LUMO) energy levels. Thus, research on metal complexes as dyes for DSSC applications remains an active topic specifically with regard to the molecular engineering of panchromatic dyes able to absorb visible light of all colors [11] and the stabilities of dyes with redox mediators [12]. Additionally, dyes binding modes with semiconductor films [13, 14] are being investigated to improve the performance of metal complex-based DSSCs.

The basic operating principle for DSSCs consists of light absorption, charge separation, and charge collection. These parameters are optimized by different cell types to attain greater efficiencies. The detailed working principles of DSSC based on Fig. 38.1 can be described by the following steps [7, 29]:

1.  $D + h\nu \rightarrow D^*$ , photoexcitation of the dye via absorption of light.
2.  $D^* \rightarrow D^+ + e^-$  (CB, conduction band), electron injection into  $TiO_2$ , resulting in the oxidation of the photosensitizer followed by electron transport:  $e^-$  (CB)  $\rightarrow e^-$  (FTO)  $\rightarrow e^-$  (CE, counterelectrode).
3.  $e^-(CE) + I_3^- \rightarrow I^-$ , the oxidized redox mediator,  $I_3^-$ , diffuses toward the counter electrode and is reduced to  $I^-$  ions (reduction of triiodide).
4.  $D^+ + I^- \rightarrow D + I_3^-$ , the oxidized dye ( $D^+$ ) accepts electrons from the  $I^-$  ion redox mediator, regenerating the ground state (D), and  $I^-$  is oxidized to the oxidized state ( $I_3^-$ ).
5. The photoexcited electron may also recombine directly with the oxidized dye ( $D^+$ ) before injection.
6.  $D^+ + e^-$  (CB)  $\rightarrow D$ , recombination of the injected electrons with the oxidized dye at the interface between the dyes and  $TiO_2$ .
7.  $I_3^- + e^-$  (CB) or  $e^-$  (FTO)  $\rightarrow I^-$ , recombination of the injected electrons with triiodide at the interface between  $TiO_2$  or FTO and the electrolyte.

The performance of a DSSC is predominantly based on four energy levels of the components: the excited state (approximately LUMO) and the ground state (HOMO) of the photosensitizer, the Fermi level of the  $TiO_2$  electrode, which is located near the conduction band level, and the redox potential of the mediator ( $I^-/I_3^-$ ) in the electrolyte [7, 29, 30]. The photocurrent obtained from a DSSC is determined by the energy difference between the HOMO and the LUMO of the photosensitizer (the gap between  $D^*/D$  and  $D^+/D$  shown by “1” in Fig. 38.1), analogous to the band gap, for example, for inorganic semiconductor materials. The smaller the HOMO–LUMO energy gap, the larger the photocurrent will be because of the utilization of the long-wavelength region in the solar spectrum. The energy gap between the LUMO level and the conduction band level of  $TiO_2$  (shown by “2” in Fig. 38.1),  $\Delta E_1$ , is important and the energy level of the LUMO must be sufficiently negative with respect to the conduction band of  $TiO_2$  to inject electrons effectively. In addition, substantial electronic coupling between the LUMO and the conduction band of  $TiO_2$  also leads to effective electron injection. The HOMO level of the complex must be sufficiently more positive than the redox potential of the  $I^-/I_3^-$  redox mediator to accept electrons effectively ( $\Delta E_2$ , shown by “4” in Fig. 38.1). The energy gaps,  $\Delta E_1$  and  $\Delta E_2$ , must be larger than approximately 200 mV to provide an effective driving force for each of the electron-transfer reactions to take place with optimal efficiency [31].

## 38.2 RUTHENIUM COMPLEXES FOR DSSC

Ruthenium complexes [32] have received particular interest as photosensitizers in DSSC applications because of their favorable photoelectrochemical properties and high stability in the oxidized state, making practical applications feasible [5]. Among the ruthenium complexes, the polypyridyl complexes of ruthenium dyes are the most efficient [33]. They can be categorized as carboxylate polypyridyl ruthenium dyes, phosphonate ruthenium dyes, polynuclear bipyridyl ruthenium dyes, and so on [34]. Polypyridinic complexes of  $d^6$  metal ions show intense metal-to-ligand charge transfer (MLCT) bands in the visible region and thus offer the potential to promote charge injection processes into the conduction bands of wide bandgap semiconductors, such as  $TiO_2$ ,  $SnO_2$ , and  $ZnO$  [10]. The energies of the MLCT states can be altered systematically by modifying the anchoring ligands as well as by changing the ancillary ligands or their substituents. The absorption of incident light can be improved by manipulating the dye’s molecular structure to either increase the degree of absorption of photons in the functional wavelength range (as measured by the molar extinction coefficient,  $\epsilon$ ), or to extend the functional range—ideally, to within the NIR [35, 36]. The structure in Fig. 38.2 has been altered by replacing one or both of the COOH groups on at least one of the bipyridyl ligands with a range of more highly  $\pi$ -conjugated moieties [35]. The presence of the electron-withdrawing nature of the carboxylic groups, which lowers the energy of the  $\pi^*$  orbital, can improve the photophysical and redox properties of metal complexes [37].

Figure 38.2 shows, the most well-known Ru complexes, that is, ruthenium polypyridyl complexes, for DSSCs such as N3, N719, and N749 (black dye) [11, 22, 38]. Ruthenium polypyridyl complexes are synthesized by the reaction of the polypyridyl ligand with ruthenium trichloride [10, 39]. The synthesis of polypyridyl ligands is well reported in the literature [40]. As an example, N3 has two bipyridine and two thiocyanato (NCS) ligands [35]; the latter of which, being loosely

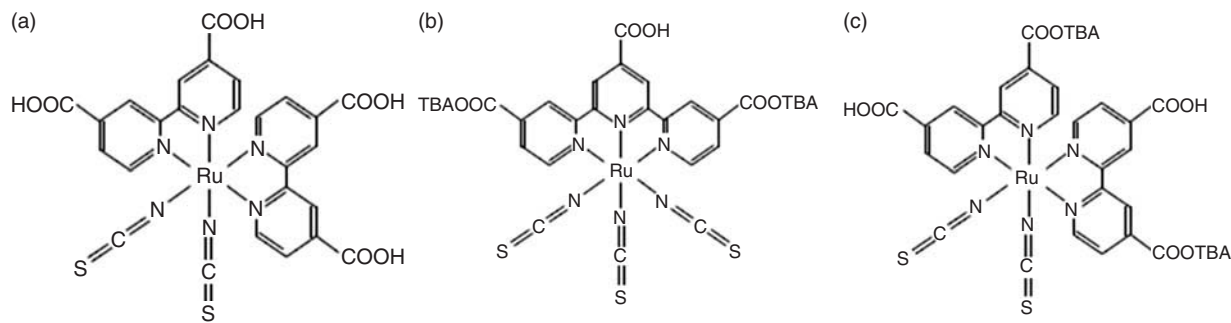


**Figure 38.2** Structures of some representative ruthenium-based complexes used as photosensitizers N3 (a), N719 (b), and black dyes (N749) (c), respectively. TBA, tetrabutylammonium cation.

attached, account for its ability to absorb radiation up to 800 nm. Although the N3 dye provides high  $J_{sc}$  (short-circuit current), it does not give a high  $V_{oc}$  (open-circuit voltage) as seen in Table 38.1 [15]. The N719 dye has the same structure as the N3 dye but has  $TBA^+$  (tetrabutylammonium) instead of  $H^+$  at two carboxyl groups [17, 41]. The difference in  $V_{oc}$  in these two dyes can be rationalized as being due to the difference in proton concentrations at the surfaces of  $TiO_2$  films. Since the N3 dye can provide up to four protons per dye, it can adsorb at the basic sites of the  $TiO_2$  surface and shift the  $E_{cb}$  (conduction-band-edge energy level) to positive [15]. As a result, the conversion efficiency of DSSC for these two dyes is different (Table 38.1). The N749 dye, which is called *black dye*, has achieved the maximum absorption up to 860 nm and showed performance similar to the N3 and N719 dyes [15, 41, 18, 42]. However, the absorption coefficient of N749 is lower than that of the N3 and N719 dyes. These low absorption coefficients require thicker  $TiO_2$  electrodes to adsorb more dye molecules on  $TiO_2$ . The increase in the thickness has disadvantages in terms of electron transport and the open-circuit voltage, that is,  $J_{sc}$  and  $V_{oc}$  may decrease. The  $V_{oc}$  of DSSC using N749 is lower than that of N719, which cannot be explained by a proton effect. As a result, N749 has shown a lower efficiency than N719 [42].

The N3 and N719 dyes (Table 38.1) show the highest incident photon-to-current conversion efficiency (IPCE) as compared with other dyes. When the optical properties of the dyes are taking into consideration, there are two quantum efficiencies (QEs), that is, an external quantum efficiency (EQE) and an internal quantum efficiency (IQE) [43]. EQE includes the effect of optical losses by transmission and reflection, while IQE refers to the efficiency of the photons that are not reflected or transmitted out of the cell [43]. From the reflection and transmission of a solar cell, the EQE curve can be corrected to obtain the internal quantum efficiency curve [43]. IPCE is related to EQE and therefore IPCE depends on the absorption of light as well as the collection of charges.

### 38.3 NON-RUTHENIUM METAL COMPLEXES FOR DSSC

Most of the work in DSSCs has focused on Ru(II) polypyridine complexes, mainly because of their intense charge transfer absorption across the whole visible range and the ease of tunability of their redox properties. However, research has also been extended to other metal complexes such as Fe(II), Re(I), Os(II), Cu(I), Pt(II), and Ir(II) [10].

#### 38.3.1 Complexes of Osmium

Complexes of osmium, platinum, rhenium, copper, iron, and iridium able to be used as sensitizers have been reported [33, 34]. The osmium complex (Fig. 38.3a) [26, 27] was synthesized and characterized and it was found that its IPCE values were lower than those of the Ru complexes [26]. Osmium complexes (Fig. 38.2a) used as sensitizers were found to be 50% less efficient than Ru complexes. However, osmium complexes have greater photochemical stability compared to the black dye [27, 34]. The osmium complex in  $CH_3OH$  showed a reversible  $Os^{II} \rightarrow Os^{III}$  oxidation process that extended the spectral response of  $TiO_2$  photoanodes [26, 27, 34].

#### 38.3.2 Complexes of Platinum

Square-planar platinum(II)-based dyes, see Fig. 38.3b [28], efficiently sensitize nanocrystalline  $TiO_2$  solar cells over a wide visible range, generating a short-circuit photocurrent of  $6.14\text{ mA/cm}^2$  and an open-circuit potential of  $600\text{ mV}$  with a solar energy conversion efficiency of approximately 2.6% under simulated AM 1.5 solar irradiation [28].

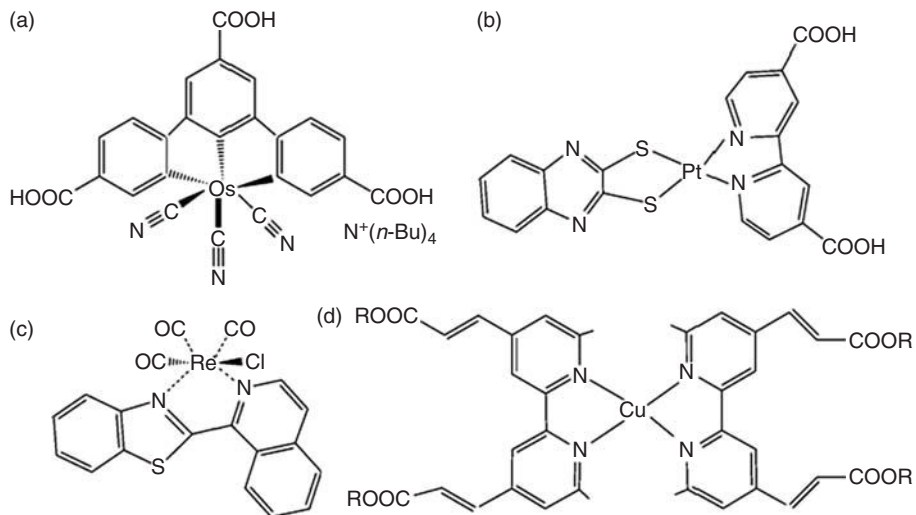


**Figure 38.3** Complexes of osmium (a), platinum (b), rhenium (c), and copper (d).

### 38.3.3 Complexes of Rhenium

A series of chlorotricarbonyl rhenium(I) complexes based on benzothiadiazole derivatives have been reported [34]. One of the chlorotricarbonyl rhenium(I) complexes, shown in Fig. 38.3c, exhibits a solar energy efficiency of around 1.43–1.76% [44]. Compared to other rhenium(I) 2,2'-bipyridine complexes, these were found to have a redshifted absorption because the heterocyclic ligands have lower  $\pi$ -to- $\pi^*$  energy levels [44].

### 38.3.4 Complexes of Copper

Copper(I) complexes, based on 6,6'-disubstituted-2,2'-bipyridines, have been reported to be effective sensitizers for  $TiO_2$  [18]. These dyes showed surprisingly high IPCE for DSSCs (above 50%) [18]. The current–voltage characteristics of dyes of copper(I) complexes, shown in Fig. 38.3d [18], were compared with that of N719 and were found to have a solar conversion efficiency of 2.3% [18].

### 38.3.5 Complexes of Iridium

A novel type of efficient iridium(III) sensitizer with carboxyl pyridine ligands was synthesized, yielding a maximum IPCE of 66% and a 2.16% power conversion efficiency under simulated AM 1.5 sunlight [45]. Cyclometalated Ir(III) complexes have two potential advantages: first, their high stability conferred by the chelate ring systems of cyclometalated Ir(III) complexes; second, because the excited-state lifetime of cyclometalated Ir(III) complex is longer than that of N3, a higher overall solar energy conversion efficiency may be anticipated [45]. Other metal complexes such as iron have been researched. Iron(II) ligands, for example, have shown higher stabilities toward photochemical degradation with solar energy efficiencies equal to 0.29% [18, 19].

## 38.4 STRUCTURE OF METAL COMPLEX SENSITIZERS

The proven, and thus preferred, general structure for sensitizers is  $ML_2(X)_2$ , where M can be Ru or Os, L is 2,2'-bipyridyl-4,4'-dicarboxylic acid, and X represents a halide, cyanide, thiocyanate, acetyl acetonate, thiocarbamate, or water subsistent group [29]. The structures of metal complexes used as sensitizers can also be mononuclear metal complexes (Figs. 38.2, 38.3, and 38.4a) [6, 41, 18], binuclear metal complexes [Ru–Ru (Fig. 38.4b) [30], and Ru–Os (Fig. 38.4c)] complexes [30]. Polynuclear complexes have been employed in order to increase absorption coefficients. However, these bulky sensitizers require more space on the  $TiO_2$  surface and penetrate less easily in the small cavities of the nanocrystalline  $TiO_2$  than the mononuclear complexes [34]. Hence, for polynuclear complexes, the increased absorption coefficients in solution do not necessarily lead to enhanced light absorption on the  $TiO_2$  electrode because of the reduced surface concentration of the bulkier sensitizer molecules on the nanoporous  $TiO_2$ .

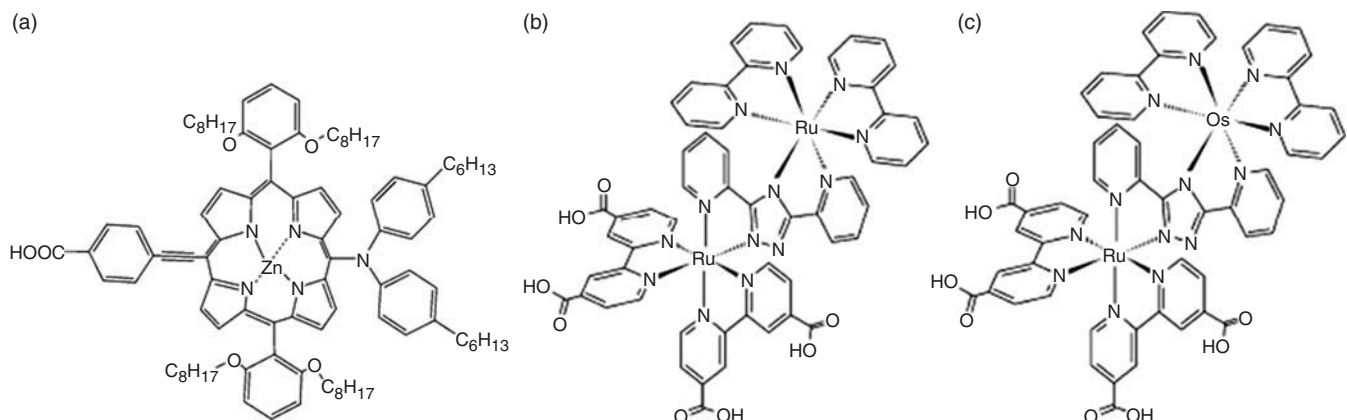


**Figure 38.4** The molecular structures of mononuclear zinc porphyrin dyes (a), Ru–Ru (b), and Ru–Os (c) binuclear complexes containing the bridging ligand 3,5-bis-(pyridin-2-yl)-1,2,4-triazole.

Metal complex dyes have given better results than organic dyes because of their excellent stability toward photodegradation. As the first DSSC was made 20 years ago [6], a lot of research has been carried out to find alternative transition-metal complexes, as well as natural or organic dyes, but none has been found that is able to match the performance of the ruthenium complexes with respect to conversion yield, durability, or long-term stability [46]. However, recently, using cosensitization of zinc porphyrin dye (Fig. 38.4a) [9] with another organic dye as sensitizer, an overall DSSC conversion efficiency greater than 12.3% has been obtained [9].

### 38.5 PERFORMANCE EVALUATION OF DYE-SENSITIZED SOLAR CELLS

The photovoltaic performance of DSSC can be analyzed in terms of conversion yield and long-term stability. For metal complex-based DSSCs, the polypyridyl complexes of ruthenium and osmium are known to fulfill both criteria [29]. After the solar cell has been fabricated, it has to be evaluated for a number of parameters such as IPCE (or quantum efficiency),  $I_{sc}$  (short-circuit current),  $V_{oc}$  (open-circuit voltage), FF (fill factor), and  $\eta$  (power conversion efficiency), which provide performance information for real-world applications. These DSSC parameters can be determined using a solar light simulator. The fill factor can assume values between 0 and less than 1 and is defined by the ratio of the maximum power ( $P_{max}$ ) of the solar cell per unit area divided by the  $V_{oc}$  and  $I_{sc}$  according to [7]

$$FF = \frac{P_{max}}{I_{sc} V_{oc}}.$$

Once these parameters are determined, the overall solar-to-electrical energy conversion efficiency,  $\eta$ , for a solar cell is given by the photocurrent density measured at short circuit ( $J_{sc}$ ), the open-circuit photovoltage ( $V_{oc}$ ), the fill factor of the cell (FF), and the intensity of the incident light ( $P_{in}$ ) [7].

$$\eta = \frac{I_{sc} V_{oc} FF}{P_{in}}.$$

The maximum power is obtained as the product of the photocurrent and photovoltage at the voltage where the power output of the cell is maximal.

### 38.6 RESEARCH DEVELOPMENT ON METAL COMPLEXES FOR DYE-SENSITIZED SOLAR CELLS

Current DSSC research focuses on performance by considering different component issues such as metal complexes, redox mediators, counter electrodes, and semiconductor films. The most important issues relate to stability, improving dye regeneration times using dyes by redox mediators, and the design of new dyes with wide range of absorption spectrum.

The choice of metal complex dyes as sensitizers must meet certain requirements: (i) they must be firmly grafted to the semiconductor oxide surface and inject electrons into the conduction band with a quantum yield of unity, (ii) their redox potential should be sufficiently high so that it can be regenerated rapidly via electron donation from the electrolyte or a hole conductor, and (iii) they should be stable enough to sustain at least 10<sup>8</sup> redox turnovers under illumination corresponding to about 20 years of exposure to natural sunlight, and so on [10, 11, 29, 34]. In addition, the optimal sensitizer for the DSSC should be panchromatic with all photons below a threshold wavelength of about 920 nm being harvested and converted to electric current [29].

Although several requirements have to be fulfilled by the dye, the molecular engineering of ruthenium complexes that can act as panchromatic charge transfer sensitizers for TiO<sub>2</sub>-based solar cells presents a series of challenges that are very difficult to address simultaneously. The LUMO and HOMO positions of the dye have to be maintained at levels where photoexcited electron transfer in the TiO<sub>2</sub> conduction band and regeneration of the dye by iodide can take place to give a near 100% yield [11]. This restricts greatly the options available to accomplish the desired redshift of the MLCT transitions to about 900 nm. Therefore, the existing research in dye chemistry is devoted to the identification and synthesis of dyes matching these requirements, while retaining stability in the photoelectrochemical environment [32, 47]. The molecular design of new sensitizers for nanocrystalline TiO<sub>2</sub> solar cells that can absorb all solar radiation thus remains a challenging task. Moreover, whether iodine regenerates the dye practically at 100% yield is another challenge [48]. The synthesis of a series of ruthenium polypyridyl complexes allowing the systematic tuning of the LUMO sensitizer for easy injection of the excited electrons to the semiconductor oxide and HOMO energy level of the sensitizer for efficient dye regeneration has been reported in the literature [49]. The possibility of tuning the MLCT energy has led to the preparation of many different organocompounds that have been investigated for semiconductor sensitization.

### 38.7 THE INTERACTION AND THE BINDING MODE OF DYES ON TiO<sub>2</sub> SURFACE

Metal complexes used as sensitizers for DSSC have two ligands specifically: ancillary and anchoring. Ancillary ligands are important for tuning the complexes' overall properties, whereas anchoring ligands are required for complex adsorption on the semiconductor's surface. Most of the dyes employed in DSSCs have either carboxylic acid or phosphonate groups to anchor them on the surface of semiconductor film electrode to enable electron injection into the conduction band of the semiconductor [7, 34]. When the sensitizer is chemically bound to TiO<sub>2</sub> by esterification, the protons of the anchoring group (carboxylic acid, phosphonic acid) are partly transferred to the surface of TiO<sub>2</sub>. The attachment group of the dye ensures that it spontaneously assembles as a molecular layer upon immersing the oxide film to a dye solution. It is now known that an electron passes from the dye molecule through the bridging carboxylate group to the semiconductor substrate within picoseconds, that is, faster than competing recombination processes. The surface composition, the coordination geometry, the type and number of functional groups, as well as the orientation of the dye on the surface of the TiO<sub>2</sub> electrode surface, directly influence the adsorption behavior, electron injection efficiency, and performance of the cell [50, 51].

The influence of the attaching group and the substitution position on the resulting photosensitization behavior of Ru polypyridyl complexes has been reported [52]. The report showed that the steric factor is very important as an influential parameter on the excited-state energy level of the sensitizers and the photoelectrochemical properties of the DSSC [52]. The interaction between two porphyrin ligands with different numbers of carboxyl groups and TiO<sub>2</sub> has been determined by UV-vis and IR spectra [50]. From the IR result, both of the porphyrin ligands adsorb by bridging or bidentate chelate coordination on the TiO<sub>2</sub> surface. Although, there is no difference in the luminescence spectra of the two porphyrins, the variation in the number of carboxyl groups has an influence on the fluorescence spectra of the adsorbed TiO<sub>2</sub> electrode and UV-vis adsorption behavior on the TiO<sub>2</sub> electrode's surface [50]. The photoelectrochemical properties of the cell such as the IPCE and the light-to-electrical conversion efficiency of the porphyrin-sensitized solar cell are influenced by the number of functional groups [50].

In another study, the binding states between the dye and TiO<sub>2</sub> surface were compared with the energy conversion efficiency in a DSSC and indicated that the binding state and the amount of adsorbed dye are important factors affecting the performance of DSSCs [51]. The relationship between the charge transfer from Ru–metal complexes to TiO<sub>2</sub> films with different synthesis temperatures of the TiO<sub>2</sub> films has been studied by Raman spectroscopy and the results correlated with the conversion efficiency of DSSC [14]. At a synthesis temperature of 190 °C for the TiO<sub>2</sub> nanoparticles, the surface of the TiO<sub>2</sub> films has shown a strong electronic coupling by chemical adsorption, indicating the overlapping of conduction bands and efficient charge transfer between the N3 dye and the TiO<sub>2</sub> substrate, resulting in the highest efficiency of DSSC [14].

### 38.8 METAL COMPLEXES AS REDOX MEDIATORS FOR DSSC

Recently, metal complexes, for example, cobalt-based complexes have been used as redox couples for DSSCs [53]. Cobalt complexes have negligible absorption in the visible region of the solar spectrum, while their redox properties can be tuned in a controlled fashion by selecting suitable donor/acceptor substituents on the ligand [53]. This approach offers an attractive alternate to the traditional  $I_3^-/I^-$  redox shuttle used in DSSCs. A cobalt complex using tridendate ligands  $[Co(bpy-pz)_2]^{3+/2+}$  ( $PF_6$ )<sub>3/2</sub> as redox mediator in combination with a cyclopentadithiophene-bridged donor–acceptor dye (Y123), adsorbed on  $TiO_2$ , yielded an open-circuit voltage of over 1000 mV and a power conversion efficiency of over 10% at 100 mW/cm<sup>2</sup> [53].

### 38.9 CONCLUSION

DSSCs will remain at the center of ongoing research effort to utilize clean and renewable solar energy, because the technology is an inexpensive and promising alternative to the proven solid-state photovoltaic cells. Among the various metal complexes, ruthenium complexes continue to receive particular interest as photosensitizers in DSSC application because of their favorable photoelectrochemical properties and high stability in the oxidized state, making practical applications feasible. Other metal complexes such Re, Pt, Cu, Os, and others have been proved to be useful as sensitizers for DSSCs. Ru and Zn metal-based complexes, used as dyes for DSSCs, can give conversion efficiencies over 11% [9, 10]. The absorption of incident light by metal complexes can be improved by manipulating their molecular structures. Current research related to metal complexes as dyes focuses on issues such as stability and the design of new dyes with wide absorption spectra, the fast regeneration of dyes by redox mediators, and the interaction of dyes with semiconductor films. Several studies report that dye/surface interactions influence the injection of excited electrons, thus opening another route to enhancing the performance of DSSCs.

## REFERENCES

1. Lior, N. *Energy* **2008**, *33*, 842.
2. U.S. Department of Energy, Energy Information Administration (2007), International Energy Outlook. <http://www.eia.doe.gov/iea/ieo/index.htm> (accessed Jun 2013).
3. Robertson, N. *Angew. Chem. Int. Ed Engl.* **2006**, *45*, 2338.
4. Nocera, D. G. *Acc. Chem. Res.* **2012**, *45*, 767.
5. Kohle, O.; Grätzel, M.; Meyer, A. F.; Meyer, T. B. *Adv. Mater.* **1997**, *9*, 904.
6. O'Regan, B.; Grätzel, M. *Nature* **1991**, *353*, 737.
7. Hagfeldt, A.; Boschloo, G.; Sun, L.; Kloo, L.; Pettersson, H. *Chem. Rev.* **2010**, *110*, 6595.
8. McConnell, R. D. E. *Future Generation Photovoltaic Technologies; American Institute of Physics Conference Proceedings*, Denver, **1997**, 404.
9. Yella, A.; Lee, H.-W.; Tsao, H. N.; Yi, C.; Chandiran, A. K.; Nazeeruddin, M. K.; Diau, E. W.-G.; Yeh, C.-Y.; Zakeeruddin, S. M.; Grätzel, M. *Science* **2011**, *334*, 629.
10. Polo, A. S.; Itokazu, M. K.; Iha, N. Y. M. *Coord. Chem. Rev.* **2004**, *248*, 1343.
11. Nazeeruddin, M. K.; Péchy, P.; Renouard, T.; Zakeeruddin, S. M.; Humphry-Baker, R.; Comte, P.; Liska, P.; Cevey, L.; Costa, E.; Shklover, V.; Spiccia, L.; Deacon, G. B.; Bignozzi, C. A.; Grätzel, M. *J. Am. Chem. Soc.* **2001**, *123*, 1613.
12. Hardin, B. E.; Snaith, H. J.; McGehee, M. D. *Nat. Photonics* **2012**, *6*, 162.
13. Labat, F.; Ciofini, I.; Adamo, C. *J. Mater. Chem.* **2012**, *22*, 12205.
14. Wang, H.-F.; Chen, L.-Y.; Su, W.-N.; Chung, J.-C.; Hwang, B.-J. *J. Phys. Chem. C* **2010**, *114*, 3185.
15. Kohle, O.; Ruile, S.; Grätzel, M. *Inorg. Chem.* **1996**, *35*, 4779.
16. Nazeeruddin, M. K.; Kay, A.; Rodicio, I.; Humphry-Baker, R.; Miiller, E.; Liska, P.; Vlachopoulos, N.; Grätzel, M. *J. Am. Chem. Soc.* **1993**, *115*, 6382.
17. Funaki, T.; Yanagida, M.; Onozawa-Komatsuzaki, N.; Kasuga, K.; Kawanishi, Y.; Sugihara, H. *Inorg. Chim. Acta* **2009**, *362*, 2519.
18. Bessho, T.; Constable, E. C.; Grätzel, M.; Redondo, A. H.; Housecroft, C. E.; Kylberg, W.; Nazeeruddin, M. K.; Neuburger, M.; Schaffner, S. *Chem. Commun.* **2008**, *32*, 3717.
19. Jayaweera, P. M.; Palayangoda, S. S.; Tennakone, K. *J. Photochem. Photobiol. A Chem.* **2001**, *140*, 173.
20. Onozawa-Komatsuzaki, N.; Yanagida, M.; Funaki, T.; Kasuga, K.; Sayama, K.; Sugihara, H. *Sol. Ene. Mater. Sol. Cells* **2011**, *95*, 310.

21. Onozawa-Komatsuzaki, N.; Yanagida, M.; Funaki, T.; Kasuga, K.; Sayama, K.; Sugihara, H. *Inorg. Chem. Commun.* **2009**, *12*, 1212.
22. White, R. C.; Benedetti, J. E.; Gon, A. D.; Alvesa, W. R.; Vaz, B. G.; Eberlin, M. N.; Correia, C. R. D.; Paoli, M. A. D.; Nogueira, A. F. *J. Photochem. Photobiol. A Chem.* **2011**, *222*, 185.
23. Sivakumar, R.; Marcelis, A. T. M.; Anandan, S. *J. Photochem. Photobiol. A Chem.* **2009**, *208*, 154.
24. Kuang, D.; Ito, S.; Wenger, B.; Klein, C.; Moser, J.-E.; Humphry-Baker, R.; Zakeeruddin, S. M.; Grätzel, M. *J. Am. Chem. Soc.* **2006**, *128*, 4146.
25. Sahin, C.; Ulusoy, M.; Zafer, C.; Ozsoy, C.; Varlikli, C.; Dittrich, T.; Cetinkaya, B.; Icli, S. *Dyes Pigm.* **2010**, *841*, 88.
26. Argazzi, R.; Larramona, G.; Contado, C.; Bignozzi, C. A. *J. Photochem. Photobiol. A Chem.* **2003**, *164*, 15.
27. Zabri, H.; Odobel, F.; Altobello, S.; Caramori, S.; Bignozzi, C. A. *J. Photochem. Photobiol. A Chem.* **2004**, *166*, 99.
28. Islam, A.; Sugihara, H.; Hara, K.; Singh, L. P.; Katoh, R.; Yanagida, M.; Takahashi, Y.; Murata, S.; Arakawa, H. *New J. Chem.* **2000**, *24*, 343.
29. Grätzel, M. *J. Photochem. Photobiol. C Photochem. Rev.* **2003**, *4*, 145.
30. Argazzi, R.; Iha, N. Y. M.; Zabri, H.; Odobel, F.; Bignozzi, C. A. *Coord. Chem. Rev.* **2004**, *248*, 1299.
31. Kalyanasundaram, K.; Grätzel, M. *Coord. Chem. Rev.* **1998**, *77*, 347.
32. Huang, W.-K.; Wu, H.-P.; Lin, P.-L.; Lee, Y.-P.; Diau, E. W.-G. *J. Phys. Chem. Lett.* **2012**, *3*, 1830–1835.
33. Karmakar, A. S.; Ruparelia, J. P. International Conference on Current Trends in Technology, NUICONE-2011, Ahmedabad, India; **2011**; 1.
34. Sekar, N.; Gehlot, V. Y. *Resonance* **2010**, *15*, 819.
35. Ryan, M. *Platinum Met. Rev.* **2009**, *53*, 216.
36. Liu, Y.; Shen, H.; Deng, Y. *Front. Mater. Sci. China* **2007**, *1*, 293.
37. Adeloye, A. O.; Olomola, T. O.; Adebayo, A. I.; Ajibade, P. A. *Int. J. Mol. Sci.* **2012**, *13*, 3511.
38. Nazeeruddin, M. K.; Zakeeruddin, S. M.; Humphry-Baker, R.; Jirousek, M.; Liska, P.; Vlachopoulos, N.; Shklover, V.; Fischer, C.-H.; Grätzel, M. *Inorg. Chem.* **1999**, *38*, 6298.
39. Weldon, F. M.; Vos, J. G. *Inorg. Chim. Acta* **2000**, *307*, 13.
40. Pechy, P.; Rotzinger, F. P.; Nazeeruddin, M. K.; Kohle, O.; Zakeeruddin, S. M.; Humphry-Baker, R.; Gratzel, M. *J. Chem. Soc.* **1995**, *1*, 65.
41. Jin, Z.; Masuda, H.; Yamanaka, N.; Minami, M.; Nakamura, T.; Nishikitani, Y. *J. Phys. Chem. C* **2009**, *113*, 2618.
42. Zhao, W.; Hou, Y. J.; Wang, X. S.; Zhang, B. W.; Cao, Y.; Yang, R.; Wang, W. B.; Xiao, X. R. *Sol. Energy Mater. Sol. Cells* **1999**, *58*, 173.
43. Park, N.-G. *Korean J. Chem. Eng.* **2010**, *27*, 375.
44. Wong, H. L.; Mak, C. S. K.; Chan, W. K.; Djurišić, A. B. *App. Phys. Lett.* **2007**, *90*, 081107.
45. Shinpuku, Y.; Inui, F.; Nakai, M.; Nakabayashi, Y. *J. Photochem. Photobiol. A Chem.* **2011**, *222*, 203.
46. Chiba, Y.; Islam, A.; Watanabe, Y.; Komiya, R.; Koide, N.; Han, L. *Jpn. J. Appl. Phys.* **2006**, *45*, L638.
47. Robson, K. C. D.; Koivisto, B. D.; Yella, A.; Sporinova, B.; Nazeeruddin, M. K.; Baumgartner, T.; Grätzel, M.; Berlinguette, C. P. *Inorg. Chem.* **2011**, *50*, 5494.
48. Islam, A.; Sugihara, H.; Arakawa, H. *J. Photochem. Photobiol. A Chem.* **2003**, *158*, 131.
49. Islam, A.; Singh, S. P.; Han, L. *Int. J. Photoenergy* **2011**, *204639*, 1.
50. Maa, T.; Inoue, K.; Yao, K.; Noma, H.; Shuji, T.; Abe, E.; Yu, J.; Wang, X.; Zhang, B. *J. Electroanal. Chem.* **2002**, *537*, 31.
51. Ma, T.; Inoue, K.; Noma, H.; Yao, K.; Abe, E. *J. Photochem. Photobiol. A Chem.* **2002**, *152*, 207.
52. Hou, Y. J.; Xie, P. H.; Zhang, B. W.; Cao, Y.; Xiao, X. R.; Wang, W. B. *Inorg. Chem.* **1999**, *38*, 6320.
53. Yum, J.-H.; Baranoff, E.; Kessler, F.; Moehl, T.; Ahmad, S.; Bessho, T.; Marchioro, A.; Ghadiri, E.; Moser, J.-E.; Yi, C.; Nazeeruddin, M. K.; Grätzel, M. C. *Nature Commun.* **2012**, DOI: 10.1038/ncomm1655.



# SYNTHETIC PHOTOSYNTHESIS FOR THE CONVERSION OF LARGE VOLUMES OF CARBON DIOXIDE INTO ENERGY-RICH MOLECULES: SAVING FOSSIL FUELS BY RECYCLING CARBON

MICHELE ARESTA\*

*Department of Chemistry, University of Bari, Bari, Italy*

ANGELA DIBENEDETTO

*CIRCC, University of Bari, Bari, Italy; Department of Chemistry, University of Bari, Bari, Italy*

## 39.1 INTRODUCTION

Nature is not able to buffer anthropogenic carbon dioxide (30 Gt/y), although it amounts to only a small percentage of the total carbon dioxide (circa 750 Gt/y) involved in the natural cycle. The parallel trend existing for the “*growth of population-increase of energy consumption-atmospheric concentration of CO<sub>2</sub>*” [1], is raising serious concerns about the future of our planet with regard to the potential effects of climate change that may generate the occurrence of extreme events that are out of human control. Scientists and technologists are much involved in identifying remedies that may stabilize the actual concentration of CO<sub>2</sub> in the *atmosphere or even reduce it to lower values* [2].

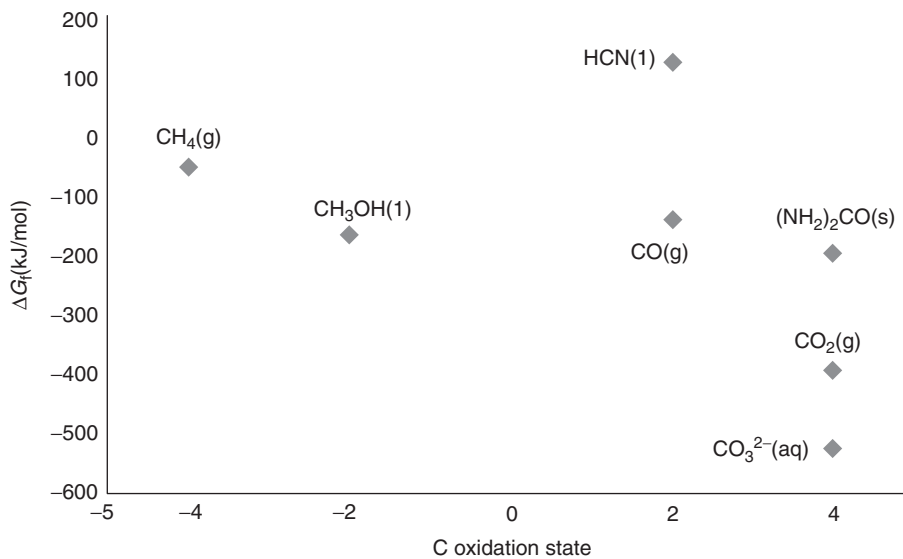
The capture of CO<sub>2</sub> from point sources (industry and power plants) or from the atmosphere has attracted much attention. Captured CO<sub>2</sub> can either be disposed in natural sites (capture of CO<sub>2</sub> and storage, CCS) or used in technological applications (Table 39.1, right side) or in chemical processes (Table 39.1 left side) (carbon dioxide capture and utilization, CCU), or else used in enhanced (industrial conditions) biological fixation (microalgae). Actually, the conversion of CO<sub>2</sub> into other chemicals (170 Mt/year) is the major application of CO<sub>2</sub>, much larger than CCS (only a few megatons in four experimental fields).

CCU has a distinct advantage over CCS, because it produces added value products and thus has economic benefits. From the energy point of view, the conversion of CO<sub>2</sub> will require an amount of energy that depends on how far down we can push the oxidation state of carbon from the value it has in CO<sub>2</sub>, that is, 4 (Scheme 39.1).

Conversely, CCS will anyway require energy and the amount will depend on the distance of the storage site from the source and the depth of the storage site. In this article, we wish discuss what has been possible in the past and the future expectations for CO<sub>2</sub> conversion, also touching upon the short-term possibilities we have of maximizing the conversion of “*exhaust carbon*” into “*working carbon*.”

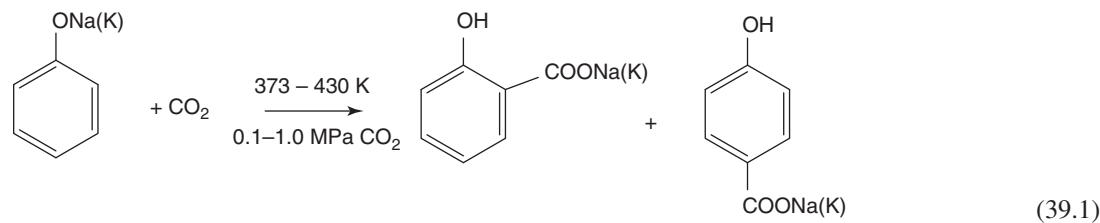
**TABLE 39.1** Carbon Dioxide Utilization

Chemical Processes (circa 170 Mt/y)	Technological Utilization (circa 28 Mt/y)
Urea	Mechanical industry (molding)
Salicylic acid	Fire extinguishers
Methanol (with syngas)	Air conditioning
Inorganic carbonates	Additive to beverages
Organic carbonates (cyclic)	Water treatment
	Cereal preservation ( <i>bactericide</i> )
	Food packaging/conservation
	Dry washing
	Extraction (fragrances and EOR)

**Scheme 39.1** Free energy of formation of C1 species versus oxidation state of carbon.

## 39.2 THE PAST

Syntheses based on the use of  $\text{CO}_2$  have been known for over 150 years, the oldest being the Solvay process (1861) for the production of  $\text{NaHCO}_3$  and  $\text{Na}_2\text{CO}_3$ . This was followed by the synthesis of salicylic acid (1869) [2] (Eq. 39.1). Soon after came the actual largest application of



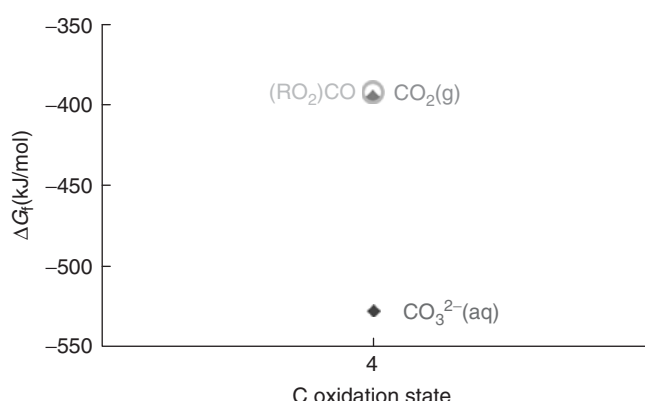
$\text{CO}_2$ , namely, the synthesis of urea (Eq. 39.2), which was discovered in 1870 [3].



The above three applications represent the quasi totality of the  $\text{CO}_2$  used in the chemical industry till today. As Table 39.2 shows, additional amounts of  $\text{CO}_2$  are used in the synthesis of methanol and some organic carbonates and polymers.

**TABLE 39.2** Present and Short-Term Use of CO<sub>2</sub>

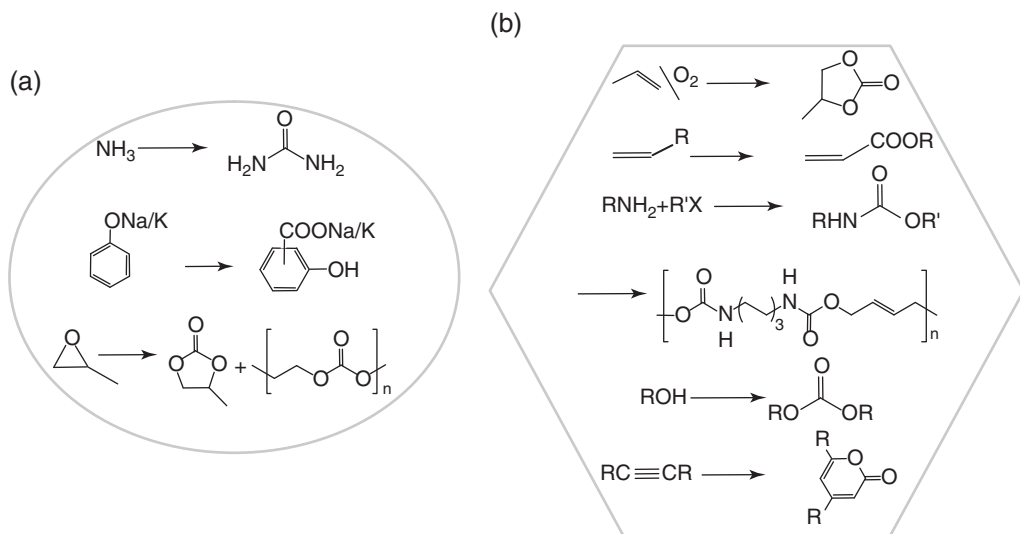
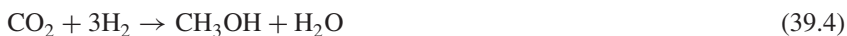
Compound	Actual Production	CO <sub>2</sub> Used	2016 Forecast	CO <sub>2</sub> Needed	2020 Forecast	CO <sub>2</sub> Used
Urea	155	114	180	132	210	154
Methanol	50	8	60	10	80	28
DME	11.4	3	>20	>5	>30	>7
TBME	30	1.5	40	3	>40	>3
CH <sub>2</sub> O	21	3.5	25	5	30	6
Other fuels					10	20
Higher alcohols						
Hydrocarbons						
Methane						
Carbonates	0.2	0.005	>2	0.5	>10	5
Polycarbonates	4	0.01	5	1	9–10	2–3
Carbamates	5.3	0	>6	1	11	Circa 4
Polyurethans	>8	0	10	0.5	15	5–10
Acrylates	2.5	0	3.0	1.5	8	5
Polyacrylates						
Formic acid	0.6	0	1	0.9	>10	>9
Inorganic carbonates						
CaCO <sub>3</sub> ,	200	Circa 50	250	70	400	100
Soda Solvay	113.9					
Pigments	50					
Total		172		207		332
Technological		28		80		200
Algae for the production of biodiesel	0.005	0.010	1	2	290	522
		200		299		1054

**Scheme 39.2** Free energy of CO<sub>2</sub>, inorganic and organic carbonates.

It is evident that, in the industrial applications discussed above, CO<sub>2</sub> maintains its +4 oxidation state (or goes to +3), thus requiring only minor, or zero, energy input for its conversion. As a matter of fact, the synthesis of inorganic carbonates is highly exergonic (Scheme 39.2), while the synthesis of organic carbonates has a Gibbs free energy that is either slightly negative or positive, depending on the R group (circle around CO<sub>2</sub> in Scheme 39.2).

The conversion into methanol (in such synthesis, CO<sub>2</sub> is used in mixture with CO) is an energy-requiring process and H<sub>2</sub> is the “energy carrier.” The higher consumption of H<sub>2</sub> required by CO<sub>2</sub> (Eq. 39.4) with respect to the use of CO alone (Eq. 39.3) is compensated by a better use of hydrogen and lower overall energy balance per mol of methanol produced [5].



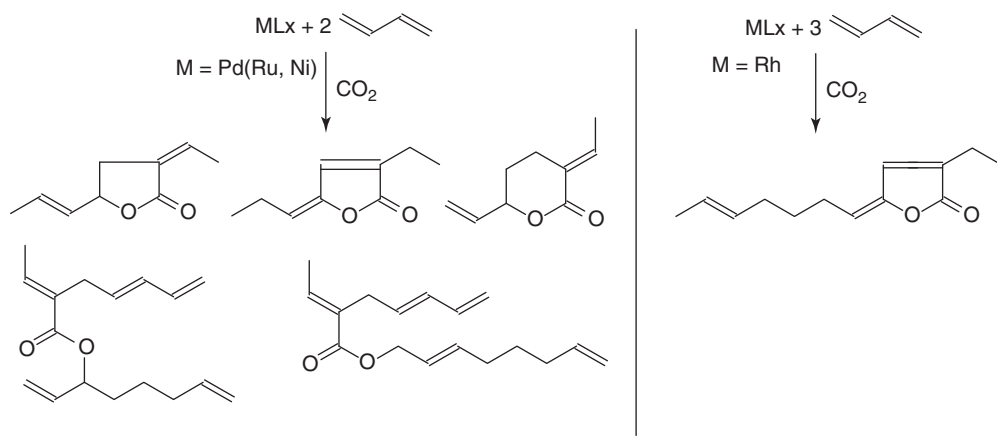
**Scheme 39.3** Low energy processes on stream (a) and under study (b).

Other high energy processes for the conversion of  $\text{CO}_2$  have not been developed so far. The simple reason for this is that it does not make sense to use fossil fuels to convert  $\text{CO}_2$ , as the process will finally emit more  $\text{CO}_2$  than it stores! Therefore, the chemistry developed in the past was based on the reaction of  $\text{CO}_2$  with “energy-rich” molecules, such as “electron-rich” species: amines, olefins, dienes, alkynes, and O-compounds. Scheme 39.3 shows the processes on stream (Scheme 39.3a) and those under development in which the co-reagent is the energy carrier (Scheme 39.3b).

None of the latter is on stream yet, except the copolymerization of  $\text{CO}_2$  and epoxides [6, 7].

The exploitation of the new synthetic methodologies has not attracted the interest of industry so far for the lack of convenience and incentives to invest in building new plants or converting existing ones. As a matter of fact, only the reaction of  $\text{CO}_2$  with butadiene (Scheme 39.4) has been investigated for long: it was discovered in the late 1970s [8] and studied until the 2000s [9–11] as it bears to fragrances that have a high added value.

In this case the up-scale of the process reached only a pilot scale, although it had been demonstrated that the reaction can be addressed with high conversion yield (>90%) and selectivity (98%) toward a six-membered lactone that may find large applications [12].

**Scheme 39.4** Conversion of butadiene into lactones and linear esters.

A reaction that is attracting much attention now is the production of acrylic acid from ethene and CO<sub>2</sub>. This type of reaction has been studied for years [13–15] without success, and it is only recently that alkyl acrylates [16] or acrylic acid sodium salts [17] have been produced in a quasi-catalytic way.

It is worth noting that the recent interest in the utilization of CO<sub>2</sub> picked up the mid-1970s (originated by the oil crisis of 1973), in the 1990s (oil crisis), and 2010s (increase of the price of oil and “carbon tax”). After each “oil or energy crisis” the price of oil went down to figures that did not encourage any new investment in innovative processes: the interest in CO<sub>2</sub> was like a mild morning breeze that passed by when the sun was shining.

In these days, we experience a quite different situation: the high price of oil (90–100 US\$/barrel compared to the old 20–30 US\$/barrel), but essentially the “carbon tax” and environmental legislation that require reduction in the emission of CO<sub>2</sub> and its immission into the atmosphere, are changing the frame: the interest in CO<sub>2</sub> conversion into useful chemicals is growing within industries that see in such technology a way to “pay less and cash more.” As a matter of fact, all the products that can be derived from CO<sub>2</sub> have a high added value. In principle, CO<sub>2</sub> may be a very cheap source of carbon: it is ubiquitous in the atmosphere (393 ppm) or in carbonate rocks. Its real cost is that of “separation” from the matrix in which it is contained. Recovering it from the atmosphere requires a “antientropy” work owing to its low concentration and for getting it from carbonate rocks, the latter must be heated to a temperature higher than 900 °C, depending on the metal cation.

It is noteworthy that natural deposits of CO<sub>2</sub> are available, which have been used so far for the extraction of very pure CO<sub>2</sub> used in the food industry, but also for less noble purposes such as enhanced oil recovery. The cost of such CO<sub>2</sub> is around 13–15 US\$/t. Some industrial processes also produce CO<sub>2</sub> that is quite pure (Table 39.3) that can be recovered at low cost and used as it is for many purposes.

CO<sub>2</sub> recovered from fermentation units is very pure and can find several applications. The most expensive “pure” anthropogenic CO<sub>2</sub> is that recovered from power plants flue gases in which it is contained at a concentration often lower than 14% in conjunction with SO<sub>x</sub> and NO<sub>y</sub> that must be separated for most uses of CO<sub>2</sub>. Table 39.1 (right) shows the nonchemical uses of CO<sub>2</sub> exploited so far. In such applications, some 28 Mt/year of CO<sub>2</sub> are used. Such use is fast expanding in sectors such as Enhanced Oil Recovery (EOR), dry washing, and refrigerators: the market will jump to over 200 Mt/year by 2020.

### 39.3 THE PRESENT

The limited amount of CO<sub>2</sub> used has increased the common belief that the conversion of CO<sub>2</sub> cannot provide any significant contribution to the reduction of the atmospheric level of spent carbon. As a matter of fact, if one considers the potential expansion in the short term of the uses listed in Table 39.2, one can foresee that in the next five years or so, the amount of used CO<sub>2</sub> may grow from circa 200 to 240 Mt, a substantial increase in terms of percentage (20%) but still a drop in the ocean if one considers that the increasing use of energy will expand the amount of emitted CO<sub>2</sub> to higher levels from the actual level of circa 30,000 Mt/year. Is there no hope then? Do we have to conclude that CCU has no role in the mitigation of the atmospheric level of CO<sub>2</sub>?

Hopefully, this is not so. In fact, the correct management of electric energy as produced today and the exploitation of perennial primary sources such as solar, wind, and geothermal energy may significantly contribute toward modifying the situation and to sensibly increase the conversion of CO<sub>2</sub>.

Today, we have several new options that make possible the conversion of *exhaust carbon* into *working carbon*. Some options are the use of excess electric energy produced today, wind energy, PV-cell energy, and geothermal energy. Such

**TABLE 39.3 Industrial Sources of CO<sub>2</sub> (Other than Power Generation)**

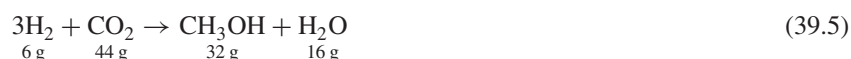
Source	Amount, Mt/y
Oil refineries	850–900
LNG sweetening	20–25
Ammonia	160
Ethene and other petrochemical processes	155
Ethene oxide	10
Fermentation (bioethanol, breweries, etc.)	>100
Cement production	>1000
Iron and steel	870

options can be exploited for the conversion of large volumes of CO<sub>2</sub> into fuels. The immediate benefit would be to recycle carbon, making fuels that can be used in existing transport or energy-generation facilities without any appreciable change and at affordable costs. Moreover, the conversion of CO<sub>2</sub> can be considered as a strategy for storing both hydrogen and electricity in a liquid form at room temperature, solving the problems connected to hydrogen storage and transport and electricity storage. The integration of the hydrogen economy with the utilization of CO<sub>2</sub> may represent the solution to two problems, opening a new era in the production of safe and easily “*transportable energy*.”

The most suited CO<sub>2</sub> sources are either the continuous point sources (electricity generation based on fossil fuels combustion) or the atmosphere (the best option for the future, when new technologies will lower the cost of capture). Both these routes have high economic (30–90 US\$/t) and energy costs. But if we consider the industrial point sources of CO<sub>2</sub> as different from power generation, we find that the petrochemical, chemical, fermentation, and cement industry produce large volumes of CO<sub>2</sub> that have a degree of purity that make it immediately usable in other industrial applications with a very low cost of capture (Table 39.3).

Such sources may represent, in the short term, an interesting reservoir of CO<sub>2</sub> ready for the conversion. Obviously, the conversion of CO<sub>2</sub> into fuels (alcohols or hydrocarbons) will require hydrogen that must be produced from water. The technology that is immediately ready is the electrolysis of water, already exploited on a significant scale. Obviously, such technology produces hydrogen at a cost that is higher than that produced by reforming. A cost analysis is made in the following to understand the barriers that need to be overcome for economic conversion of large volumes of CO<sub>2</sub> and foresee the expected level of application in the short term. Table 39.4 shows the cost of hydrogen produced using different technologies.

One kilogram of hydrogen will allow to convert 7.3 kg of CO<sub>2</sub> into methanol according to reaction 39.5, producing 5.3 kg of methanol



The production cost of methanol is today 0.08 €/kg, in the best case considering the capex and opex, methanol can be produced from electrolytic hydrogen at a cost of 0.3 €/kg, that is circa four times higher than current price. What may make the balance positive for industry is the fact that if CO<sub>2</sub> is converted into other products the C-tax (where it exists) does not need to be paid: at the moment such tax varies over a considerable: 30–100 €/t, that means 0.03–0.1 €/kg. With this benefit the cost of production of methanol would be equal to ca. 0.16–0.2 €/kg or 160–200 €/t, getting closer the price of production of methanol from electrolytic hydrogen to the price of production using H<sub>2</sub> from gas reforming.

*Excess energy produced at peak output* could, thus, advantageously be used for water electrolysis and CO<sub>2</sub> conversion into methanol, without influencing the electricity availability to day-to-day users. The real potential of such technology will depend on the up-scale of electrolyzers and the consequent cost of hydrogen.

The use of wind towers dedicated to produce electricity for water and CO<sub>2</sub> co-electrolysis to afford products (Fig. 39.1) is an interesting alternative.

In this case, the electricity is almost carbon-free and, in principle, water and CO<sub>2</sub> could be both recovered from the atmosphere. The use of wind as primary source of energy gives rise to the problem of intermittency. Indeed, this aspect has not been accorded a great importance in the application we are discussing; besides, a discontinued conversion of CO<sub>2</sub> caught from the atmosphere is also highly acceptable.

In all such applications, there is the need of optimizing the engineering and the integration of processes so to minimize the need of storage of both H<sub>2</sub> and CO<sub>2</sub>.

One could point out that if hydrogen is produced then it could be used directly. The advantages of coprocessing it with CO<sub>2</sub> are multiple. On the one hand, gasoline or diesel have a higher energy density by volume or mass (Figure 39.2) than H<sub>2</sub> and even batteries and would require less space for storage, while on the other hand, the storage of H<sub>2</sub> would be really minimized as H<sub>2</sub> would be used *in situ* and in a short time.

**TABLE 39.4 Cost of Production of Hydrogen (1 kg) using Various Technologies**

Technology	Gas reforming	Electrolysis with Nuclear	Electrolysis with Electricity from Oil-Powered Station	Electrolysis with PV	Electrolysis with wind	Electrolysis with SPC
Cost, €	1.10–1.15	1.45–1.50	3.50–2.20	2.8–4.0	3.8–5.20	3.50

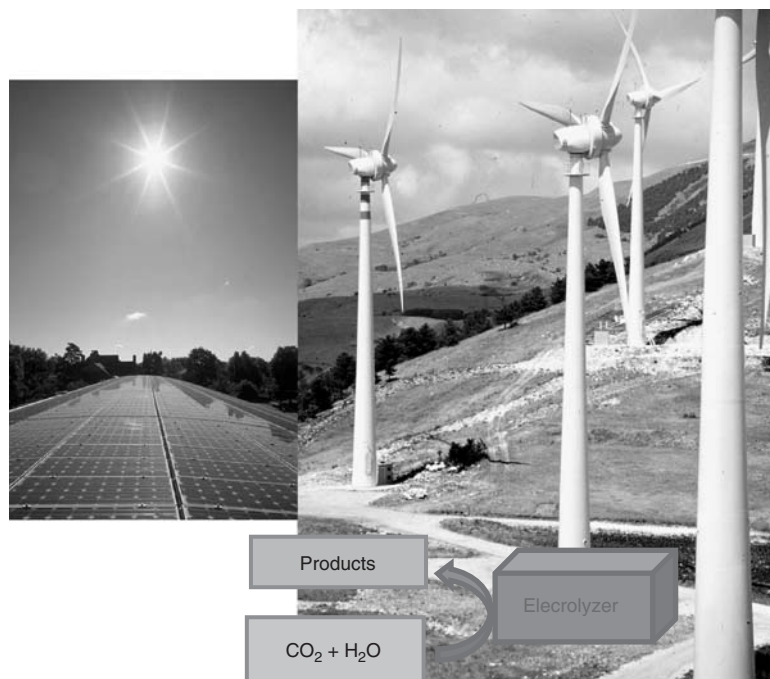


**Figure 39.1** The use of wind towers dedicated to produce electricity for water and  $\text{CO}_2$  co-electrolysis to afford products.

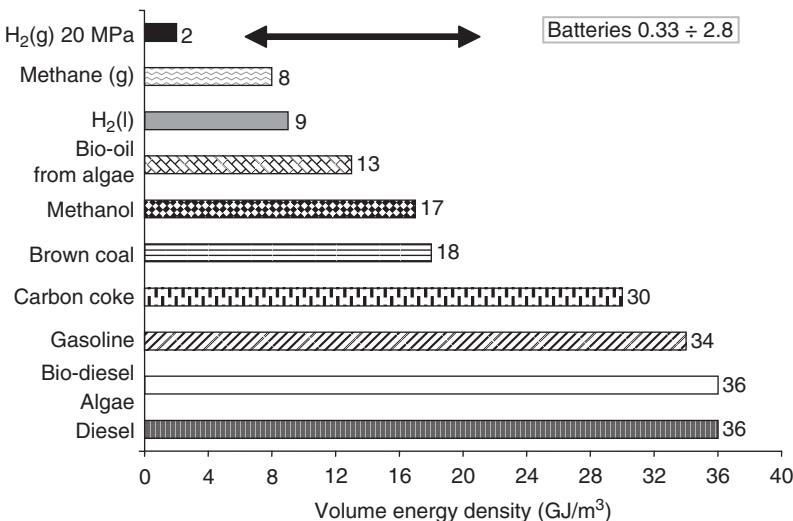


**Figure 39.2** Volume energy density of several liquid fuels,  $\text{H}_2$ , methane, and batteries.

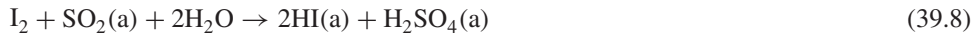
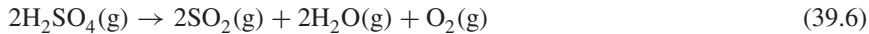
However, primarily, making liquid fuels that are already in use would not change the existing infrastructures with large economic benefits and higher safety compared with respect to the use of  $\text{H}_2$ .

An alternative to wind energy is the use of solar energy as photovoltaic (PV) energy for the production of  $\text{H}_2$  from water or for the co-electrolysis of  $\text{CO}_2$  and water. The cost of  $\text{H}_2$  produced from water using PV is still too high today (2.8–4 €/kg) and this would prevent large-scale exploitation. But the electricity cost produced via PV is estimated to decrease, in the near future, to quite acceptable levels for exploitation in electrolytic processes on a large scale.

Both the above technologies raise the problem of space: how much space is necessary for the conversion of 1 t of  $\text{CO}_2$  or the production of 1 t of  $\text{H}_2$ ? The reduction in space depends on the advancement of the technology and the increase in the W : m<sup>2</sup> ratio that is continuously increasing with new devices, making the exploitation of the use of PV or wind for the reduction of  $\text{CO}_2$  more attractive.

Also CSP (concentrators of solar power) can be used for CO<sub>2</sub> reduction or water splitting. CSP produce high temperature (up to 1300 °C) that can drive high energy processes such as those mentioned above. Metal-assisted dissociation of CO<sub>2</sub> to CO using CPS is an interesting area of investigation. Syngas (H<sub>2</sub> + CO) could be produced by applying the CSP technology and used in existing infrastructures.

The use of thermochemical cycles (Eqs. 39.6–39.8) may also be a way to produce H<sub>2</sub> from water.



What is important is that the production of H<sub>2</sub> and the reduction of CO<sub>2</sub> are carried out in close environments in order to avoid the problems of H<sub>2</sub> storage and transport. From this point of view, the co-electrolysis of CO<sub>2</sub> and water is the best solution.

The production of hydrogen for the conversion of CO<sub>2</sub> is a short-term option as it would make use of existing technologies that could be immediately implemented: it is a “*transition technology*” and not the technology of the future.

The co-electrolysis of CO<sub>2</sub> and water is a technology that has been under investigation for some time. The nature of the products formed depends on the electrodes used (Table 39.5).

Cu electrodes are of particular interest as they can afford ethene with quite a high selectivity [18]. However, there are problems, such as life of electrodes, selectivity, current density, and intensity, that need to be solved among others, but such technological issues can find a solution as these are not *a priori* constraints (the way negative thermodynamics can be). Looking at the products formed, the generation of ethene is an interesting option as ethene is not soluble in water and would spontaneously separate, avoiding separation costs that one would have in case alcohols such as methanol or ethanol are formed. In addition, the production of higher alcohols is of interest as they would have scarce solubility in water and so are easy to separate, resulting in a low production price. The production of a mixture of CO–H<sub>2</sub> is of interest as this mixture could be used as Syngas, eventually complemented with either species to reach the optimal molar ratio for application in methanol or Fischer–Tropsch (FT) syntheses. Summarizing, in the electrolysis of CO<sub>2</sub> in water, the target products would be CH<sub>4</sub> or CO/H<sub>2</sub>, as well as ethene or C<sub>n</sub>-alcohols and C<sub>n</sub>-hydrocarbons.

The co-electrolysis of CO<sub>2</sub> and water avoids the need to store or transport hydrogen and can be performed close to any source of CO<sub>2</sub>. Such processes could be integrated into existing ones that produce CO<sub>2</sub> that is quite pure (see Table 39.3) and convert it.

The co-electrolysis of CO<sub>2</sub> and water recovered from air has the further advantage that it can be carried out everywhere and, if the correct electrocatalytic process is found, the products of electrolysis can be insoluble in water (as stated above) and, so, easy to separate.

The implementation of such reduction technologies will expand the use of CO<sub>2</sub> to unprecedented levels, but not yet to such levels as to represent a substantial part of the CO<sub>2</sub> emitted today and substantially contribute to CO<sub>2</sub> mitigation.

#### 39.4 THE FUTURE: SYNTHETIC PHOTOSYNTHESIS

The real breakthrough in cycling CO<sub>2</sub> or recycling C will be represented by the development of synthetic photochemical processes based on the use of solar energy for converting CO<sub>2</sub> and water into chemicals, fuels, and O<sub>2</sub>. (Eq. 39.9)

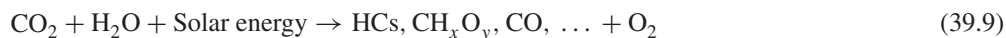


**TABLE 39.5** Electrodes and Products of Reduction of CO<sub>2</sub> in Water

Electrodes	Products
Cu	C <sub>2</sub> H <sub>4</sub> (32–80%)
Zn, Au, Ag, p-InP, p-GaAs,	C <sub>n</sub> H <sub>2n+2</sub>
Pt-Pd-Rh	CO
RuO <sub>x</sub> on conductive diamond, B-doped-C	CO + HCOOH MeOH, EtOH, C <sub>n</sub> H <sub>2n+1</sub> OH

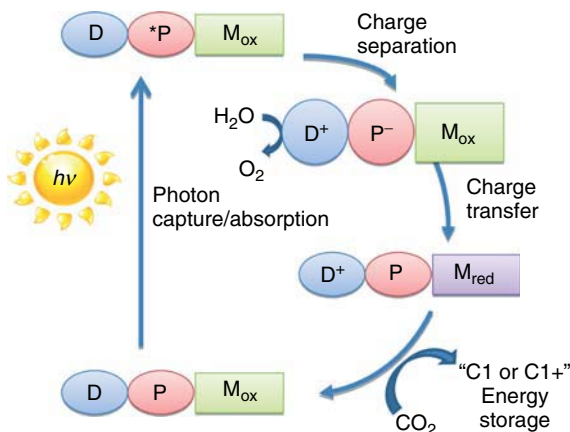


**Figure 39.3** Constitutional elements of a device for the photochemical reduction of  $\text{CO}_2$  in water under solar light irradiation. (See insert for color representation of the figure.)

This process has an unlimited capacity for  $\text{CO}_2$  conversion. With respect to the use of PV or wind, it should guarantee lower space occupancy and a higher capacity of conversion per unit surface. Several different systems have been used to this end: homogeneous-, heterogenized-, and heterogeneous-metal systems, or colloids.

The building elements of the device necessary for the conversion of solar light into chemical energy are well known: systems for photon capture, photosensitizers, charge separation (hole + electrons), electron transfer, reduction of  $\text{CO}_2$ , and oxidation of water (Fig. 39.3).

The mode of action of such systems is the following: the photosensitizer ( $\text{P}$ ) absorbs radiation (UV-vis) and generates an excited state ( $\text{P}^*$ ) that is quenched by an electron donor ( $\text{D}$ ) (amines are used in model systems,  $\text{H}_2\text{O}$  has to be used in applications) generating a mononegative photosensitizer ( $\text{P}^-$ ) and the oxidized donor ( $\text{D}^+$ ) (water will produce oxygen).  $\text{P}^-$  must now be able to transfer an electron efficiently to the catalyst in an oxidized state ( $\text{M}_{\text{ox}}$ ) and generate its reduced form ( $\text{M}_{\text{red}}$ ). If the catalyst is able to strongly absorb solar light, it will not be necessary to use a photosensitizer: the catalyst will play both roles— $[\text{Ru}(\text{dipy})_3]^{2+}$  is an example [19]. Commonly, Ni and Co stabilized by polydentate N-ligands, and Ru, Fe, or Re stabilized by di- or polypyridine, corrins, porphyrines, and phtalocyanines ligands are used in homogeneous systems [20–22].  $\text{M}_{\text{red}}$  binds  $\text{CO}_2$  that is converted into the products, the nature of which depends on the catalyst used.  $\text{M}_{\text{ox}}$  is regenerated and the cycle starts again. In the natural system (that synthetic photosynthesis must repeat), the net reaction is the transfer of electrons and protons from water to  $\text{CO}_2$  with production of reduced forms of the latter and oxygen. In model studies, amines are converted into their oxidized forms that have no practical application: the use of such sacrificial donors represents an economic loss as amines have a higher value than any of the reduced forms of  $\text{CO}_2$  that can be obtained using photochemical processes. Using water, oxygen is formed that can be collected and put on the market, substituting that recovered from the atmosphere by air distillation, the latter being an energy-intensive process.

How close is such system to a natural photosynthetic process? As often “artificial photosynthesis” and “artificial leaf” are used as synonyms, a question may be asked: will synthetic systems fully mimic what happens in a “leaf”? To answer such question, let us make a brief incursion into the biological world.

Four major pathways are used in nature for the conversion of  $\text{CO}_2$ , namely [23],

1. the Calvin cycle,
2. the acetyl-CoA pathway,
3. the 3-hydroxypropionate pathway,
4. the reductive tricarboxylic acid cycle.

Autotrophic organisms (that use  $\text{CO}_2$  trapped from the atmosphere as the source of carbon) can be divided into two categories according to the source of energy they use. *Chemoautotrophs*, in the reduction of  $\text{CO}_2$ , use electrons generally derived from inorganic (mineral) sources, such as hydrogen,  $\text{H}_2\text{S}$ , elemental sulfur, metal ions ( $\text{Fe}^{2+}$ ,  $\text{Mn}^{2+}$ ), ammonia, or nitrite, often (but not always) involving oxidation with  $\text{O}_2$ . Most of these organisms live in dark, extreme environments. Such fixation of  $\text{CO}_2$  is often reported as *chemosynthesis*.

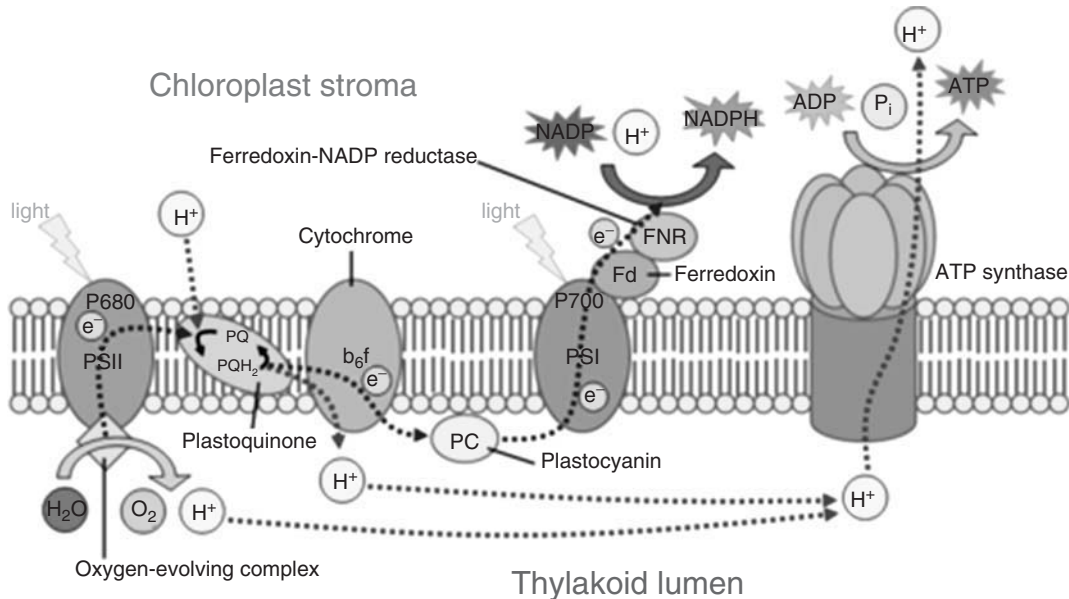


**Figure 39.4** Light-driven processes occurring in a leaf: water is split into 2H<sup>+</sup>, 1/2O<sub>2</sub>, and 2e<sup>-</sup>.

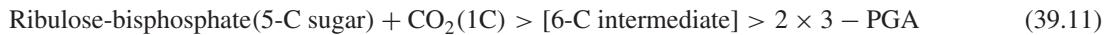
*Photoautotrophs* use light from the sun as source of energy and water as electron donor with formation of dioxygen. In terrestrial environments, plants and microorganisms are the predominant variety of photoautotrophs, while in aquatic systems, algae and (cyano)bacteria depend on this pathway. The process that occurs in a leaf is shown in Fig. 39.4 and highlighted in the follow-up of this section.

The fixation of CO<sub>2</sub> in a leaf takes place with the implication of two processes:

a light-driven process (Fig. 39.4) that brings to the formation of O<sub>2</sub> and 2 H<sup>+</sup> (Eq. 39.10)



a light-independent process in which CO<sub>2</sub> is converted (Eq. 39.11),



The 6-C intermediate in Eq. 39.11 is the highly unstable 3-keto-2-carboxyarabinitol-1,5-bisphosphate that fast converts into two phosphoglyceraldehyde (PGAL) units. Each 3-PGA is then reduced to 3-PGA<sub>yde</sub> (phosphoglyceraldehyde), which is finally converted into a C-6. This type of complex process is reported in many textbooks as shown in Eq. 39.12:



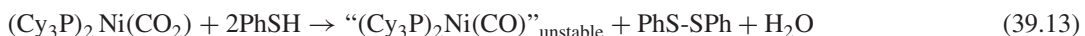
The process based on polyols, found in the leaves of the so-called C-3 plants, does not precisely correspond to what is depicted in Fig. 39.3. Therefore, while the label “artificial,” “man-made,” or “synthetic photosynthesis” is correct for the photochemical reduction of CO<sub>2</sub>, to speak in terms of “artificial leaf” or “artificial tree” does not at all correspond to the reality.

Synthetic photosynthesis, as shown above, will use solar light and photons for generating a charge separation in photoactive materials that may be used to oxidize water and reduce CO<sub>2</sub> to C1, C2, or else C2+ species. It is worth recalling that, as mentioned above, in Nature, the reduction of CO<sub>2</sub> may occur in many different ways, according to the organism in which it takes place. In organisms different from leaves, for example, in some bacteria, the following C1 species are formed as reduction products: HCOOH, CO, H<sub>2</sub>CO, CH<sub>3</sub>OH, CH<sub>4</sub>. Cn species are formed following complex reaction pathways.

The conversion of CO<sub>2</sub> into HCOOH is promoted by formatedehydrogenase (F<sub>ate</sub>DH) enzymes; formaldehydedehydrogenase (F<sub>ald</sub>DH) enzymes convert HCOOH into H<sub>2</sub>CO, while alcoholdehydrogenase (ADH) converts H<sub>2</sub>CO into CH<sub>3</sub>OH.

These enzymes equally act on more complex molecules bearing the same functionalities ( $\text{RCOOH} \rightarrow \text{RCHO} \rightarrow \text{RCH}_2\text{OH}$ ).  $\text{CO}_2$  is converted into CO by the enzyme carbonmonoxide dehydrogenase (CODH) and the tetrahydrofolate (THF) enzyme converts  $\text{CO}_2$  into  $\text{CH}_4$  through a multistep process. Such pathways are active in bacteria that convert biomass into biogas in nature or in bioreactors [24].

Chemical systems have been shown to mimic nature. For example, the complex  $(\text{Cy}_3\text{P})_2\text{Ni}(\text{CO}_2)$  when reacted with PhSH (thiophenol) affords “ $(\text{Cy}_3\text{P})_2\text{Ni}(\text{CO})$ ” very selectively and instantaneously, according to reaction 39.13 that mimics natural systems: two electrons, given by PhSH that is oxidized to diphenydisulphide, are used in the step.



This type of system is not recyclable as it further reacts with an oxidative addition of PhS-SPh to Ni(0) that is eventually oxidized to Ni(II), becoming the real end e-donor.

Recently, the conversion of  $\text{CO}_2$  into methanol in water at 300 K has been achieved using the enzymes  $\text{F}_{\text{ate}}\text{DH} + \text{F}_{\text{ald}}\text{DH} + \text{ADH}$  (Fig. 39.5).

As Fig. 39.5 shows, the conversion takes place in three steps, each requiring two electrons. In each step, 1 mol of NADH is oxidized to  $\text{NAD}^+$ : making the exploitation of such “dream” reaction absolutely not convenient from the economic point of view, unless  $\text{NAD}^+$  is converted back to NADH using cheap means; and the word “cheap” once again means to mimic nature and use solar light. An interesting result was recently obtained by us using modified semiconductors (Fig. 39.6), namely, by using Ru-modified ZnS irradiated at 400nm for reducing  $\text{NAD}^+$  back into NADH. This process coupled with the use of enzymes has completely changed the capacity of use of NADH, making it possible to produce 100 mol of  $\text{CH}_3\text{OH}$  per mol of NADH as against 1/3 mol of  $\text{CH}_3\text{OH}$  per mol NADH earlier [25].

In the experiment, aqueous bioglycerol was used as H-donor or reducing agent: glycerol is converted into oxidized forms that may find utilization. This type of hybrid system is quite interesting as it couples the high rate and selectivity of enzymes to the use of inorganic materials for closing the cycle and regenerating the reducing species, namely NADH.

The reduction of  $\text{CO}_2$  therefore requires  $2e^-$  per step. If one uses a semiconductor as a means for converting photons into electrons, one finds that one photon will generate a “hole +  $e^-$ ,” that is, a single photon will be able to transfer a single electron to  $\text{CO}_2$  with formation of the radical anion “ $\text{CO}_2^-$ ”. As Table 39.6 shows, the “one-electron” transfer is a high energy process with respect to “ $2e^-$ ” or “multiple  $e^-$ ” transfer. It is worthwhile to note that the values given in Table 39.6 are relevant to an aqueous medium. In general, the reduction potential depends on the medium in which the reduction of

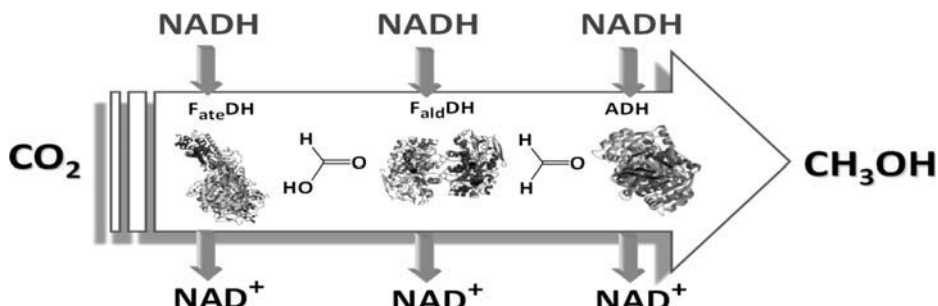


**Figure 39.5** Reduction of  $\text{CO}_2$  to  $\text{CH}_3\text{OH}$  with the use of the enzymes  $\text{F}_{\text{ate}}\text{DH}$ ,  $\text{F}_{\text{ald}}\text{DH}$ , and  $\text{ADH}$  at room temperature in water.

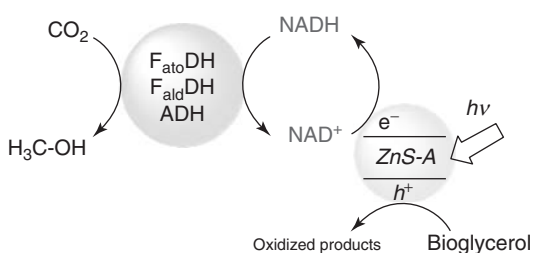


**Figure 39.6** Photochemical conversion of  $\text{NAD}^+$  into NADH using Ru-modified ZnS.

**TABLE 39.6** Energetics of Reduction of CO<sub>2</sub>

Process	Potential, V
CO <sub>2</sub> + e <sup>-</sup> → CO <sub>2</sub> <sup>·-</sup>	E° = -1.90 (-2.10 V in anhydrous media)
CO <sub>2</sub> + 2H <sup>+</sup> + 2e <sup>-</sup> → CO + H <sub>2</sub> O	E° = -0.53
CO <sub>2</sub> + 2H <sup>+</sup> + 2e <sup>-</sup> → HCO <sub>2</sub> H	E° = -0.61
CO <sub>2</sub> + 6H <sup>+</sup> + 6e <sup>-</sup> → CH <sub>3</sub> OH + H <sub>2</sub> O	E° = -0.38
CO <sub>2</sub> + 8H <sup>+</sup> + 8e <sup>-</sup> → CH <sub>4</sub> + 2H <sub>2</sub> O	E° = -0.24

CO<sub>2</sub> occurs—in aqueous media the reduction potential is lower than in anhydrous media, as shown for the single-electron reduction of CO<sub>2</sub> in Table 39.6. Aspects of paramount importance in the photocatalytic reduction of CO<sub>2</sub> to fuels are the kinetics of reaction and the electron transfer, processes in which the catalyst is implied; this requires that the catalyst must have energy levels that match the reduction potential of CO<sub>2</sub> to that of the wanted species [26].

Homogeneous catalysts are particularly suitable for an adaptation to the different potentials required as the properties of the metal system can be quite finely tuned through the ligands. A key point is, thus, to design metal catalysts that may work as close as possible to the thermodynamic conditions, avoiding the high overpotential that often is generated when a direct reduction of CO<sub>2</sub> occurs at an electrode surface. What is also of great importance is the fact that the metal centers may drive the reaction toward a specific product, as discussed above (Table 39.5).

Among the products shown, methanol has an important role as it sits on the border for chemicals and fuels, and may have very large markets. Formic acid is an interesting species because in addition to its chemical uses it can perform as a H<sub>2</sub>-vector. In fact, formic acid can be easily converted back to H<sub>2</sub> and CO<sub>2</sub>. Mixtures of H<sub>2</sub> and CO can be used for the synthesis of methanol using existing technologies or as Syngas in the synthesis of gasoline and diesel. Eventually, one of the gases can be added to achieve the best molar ratio. Ethene is very important as it can be used as bulk chemical or monomer for polymers. Not only poly(ethylene terephthalate) (PET) but also polystyrene (PS) as styrene is made from benzene by alkylation with ethene. Interestingly, ethene, CO, and H<sub>2</sub> are not soluble in water and will spontaneously separate from water, keeping the separation costs low.

Therefore, the photochemical reduction of CO<sub>2</sub> requires a careful design and engineering of the device so that the following issues have the correct solution:

- systems for the capture of photons;
- photosensitizers;
- photochemical systems able to produce a “hole + e<sup>-</sup>;”
- use of two photons for the production of two electrons;
- fast electron transfer for avoiding the backflow of electrons that may cancel the charge separation with generation of heat (the photons would be then converted into heat instead of generating electrical charges);
- correct number of junctions that may prevent the backflow of electrons;
- correct catalytic sites that may produce the reduced forms of CO<sub>2</sub> and dioxygen working close as possible to the thermodynamic potentials;
- separation of reduced carbon from dioxygen for preventing back oxidation of the former.

The photochemical reduction of CO<sub>2</sub> is also approached using inorganic materials such as the system developed at the Berkeley Laboratory on Natural and Artificial Photosynthesis that is quite intriguing because it represents a simple system that might have interesting applications (Fig. 39.7).

This is not yet the solution, but indicates a way to go. Such systems are tunable, changing the metals implied in the photons uptake and charge transfer, and may allow loading the right catalysts for the reduction–oxidation processes.

### 39.4.1 Photoelectrochemical Reduction of CO<sub>2</sub>

An alternative to the photochemical reduction is the photoelectrochemical reduction. p-Type semiconductor/liquid junctions are extensively studied as PV devices. The p-type semiconducting electrodes can act as photocathodes for photoassisted

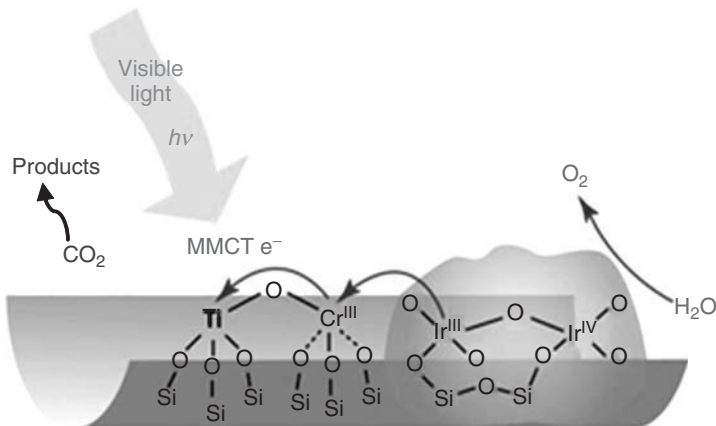


**Figure 39.7** Inorganic device for  $\text{CO}_2$  and water coprocessing using solar light.

$\text{CO}_2$  reduction. Four different schemes of photoassisted reduction of  $\text{CO}_2$  using a semiconducting photocathode have been approached: (i) direct heterogeneous  $\text{CO}_2$  reduction by a biased semiconductor photocathode [27–35], (ii) heterogeneous  $\text{CO}_2$  reduction by metal particles on a biased semiconductor photocathode [36–40], (iii) homogeneous  $\text{CO}_2$  reduction by a molecular catalyst through a semiconductor/molecular catalyst junction [41–45], and (iv) heterogeneous  $\text{CO}_2$  reduction by a molecular catalyst attached to the semiconductor photocathode [46–48].

These have recently been extensively reviewed by Kubiak [49].

While commercial PV electrolyzers have been used for  $\text{H}_2$  production [50], only few examples are applied to the conversion of  $\text{CO}_2$  [51–53].

In addition, in this case, the systems described in the literature often use a sacrificial donor of the electrons used in the reduction process. For the exploitation of such technology, water should be the source of both the electrons and hydrogen atoms for  $\text{CO}_2$  reduction.

### 39.5 CONCLUDING REMARKS

“Synthetic photosynthesis” is a process that may play a key role in the reduction of  $\text{CO}_2$  into energy-rich species, either C1 or C2+. Several approaches are possible to the exploitation of such a concept:

- the use of natural photosynthetic microorganisms for an enhanced  $\text{CO}_2$  fixation (microalgae or microorganisms grown under non-natural conditions, namely, high  $\text{CO}_2$  concentration);
- the use of hybrid systems that combine enzymes and synthetic systems for an accelerated  $\text{CO}_2$  fixation;
- the use of synthetic systems that may mimic nature and reduce  $\text{CO}_2$  in water, namely, photochemical and photoelectrochemical systems.

The elements that constitute a man-made system for driving such reactions are well identified. In order that they may be exploited at the industrial level, several key issues have to be resolved, namely, the discovery of efficient systems for solar energy capture, two-photon use for two-electron transfer to  $\text{CO}_2$  for an efficient and fast reduction, efficient charge separation systems (multijunctions that prevent the backflow of electrons), efficient catalysts for water oxidation and selective  $\text{CO}_2$  reduction, selection of catalysts for a preferable production of non-water-soluble organics from  $\text{CO}_2$  for reducing the processing cost for the recovery of energy rich species, use of cheap and naturally abundant compounds for catalyst making, use of recyclable catalytic materials, space separation of oxidation, and reduction processes on the catalysts.

The solution of such problems will require time, but all targets may be reached as there is no real (e.g., negative thermodynamics) barrier to doing so. If the development of such devices have the same investments that have been placed on the development of PV cells, it is foreseeable that in 20–30 years from now, the dream “solar-driven conversion of  $\text{CO}_2$  into fuels” will come true.

## REFERENCES

1. EPA-US. <http://www.epa.gov> (accessed Jun 2013).
2. Wikipedia.org/wiki/Copenhagen Agreement.
3. (a) Kolbe, H.; Lautemann, E. *Ann.* **1869**, *113*, 125; (b) Schmitt, R.; Burkard, E. *Ber.* **1877**, *20*, 2699.
4. The first report was by Bassarov in 1870, see Fromm, D.; Lutzov, D. *Chem. Unserer Zeit* **1979**, *13*, 78.
5. ICI process on stream since the 1970s.
6. Inoue, S.; Koinuma, H.; Tsuruta, T. *J. Polym. Sci. B* **1969**, *7*, 287.
7. Inoue, S.; Koinuma, H.; Tsuruta, T. *Makromol. Chem.* **1969**, *130*, 210.
8. Musco, A.; Perego, C.; Tartiari, V. *Inorg. Claim. Acta* **1978**, *28*, L147.
9. Gassner, F.; Haack, V.; Janssen, A.; Elsagir, A.; Dinjus, E. EP Appl 10329720000218, **2000**.
10. Behr, A.; Herdtweck, E.; Herrmann, W. A.; Keim, W.; Kipshagen, W. *J. Chem. Soc. Chem. Commun.* **1986**, *16*, 1262–1263.
11. Aresta, M.; Quaranta, E.; Tommasi, I. *New J. Chem.* **1994**, *18*, 133–142.
12. Behr, A.; Henze, G. *Green Chem.* **2011**, *13*, 25–39.
13. Hoberg, H.; Peres, Y.; Krüger, C.; Tsay, Y.-H. *Angew. Chem. Int. Ed.* **1987**, *26*, 771–773.
14. Alvarez, R.; Carmona, E.; Cole-Hamilton, D. J.; Galindo, A.; Gutiérrez-Puebla, E.; Monge, A.; Poveda, M. L.; Ruiz, C. *J. Am. Chem. Soc.* **1985**, *107*, 5529.
15. Fisher, R.; Langer, J.; Malassa, A.; Walther, D.; Gorls, H.; Vaughan, G. *Chem. Commun.* **2006**, 2510–2512.
16. Aresta, M.; Pastore, C.; Giannoccaro, P.; Kovács, G.; Dibenedetto, A.; Pápai, I. *Chem. Eur. J.* **2007**, *13*, 9028–9034.
17. Lejkowski, M. L.; Lindner, R.; Kageyama, T.; Bódizs, G. É.; Plessow, P. N.; Müller, I. B.; Schäfer, A.; Rominger, F.; Hofmann, P.; Futter, C.; Schunk, S. A.; Limbach, V. *Chem. Eur. J.* **2012**, DOI: 10.1002/chem.201201757.
18. Gattrell, M.; Gupta, N.; Co, A. *J. Electroanal. Chem.* **2006**, *594*, 1–19.
19. Durham, B.; Caspar, J. V.; Nagle, J. K.; Meyer, T. J. *J. Am. Chem. Soc.* **1982**, *104*, 4803–4810.
20. Doherty, M. D.; Grills, D. C.; Muckerman, J. T.; Polyansky, D.E.; Fujita, E. *Coord. Chem. Rev.* **2010**, *254*, 2472–2482.
21. Takeda, H.; Ishitani, O. *Coord. Chem. Rev.* **2010**, *254*, 346–354.
22. Grodkowski, J.; Neta, P.; Fujita, E.; Mohammed, A.; Simkhovich, L.; Gross, Z. *J. Phys. Chem. A* **2002**, *106*, 4772–4778.
23. Aresta, M.; Quaranta, E.; Tommasi, I.; Giannoccaro, P.; Ciccarese, A. *Gazz. Chim. Ital.* **1995**, *125*, 509.
24. *Biorefinery: from Biomass to Chemicals and Fuels*; Aresta, M.; Dibenedetto, A.; Dumeignil, F. Eds.; De Gruyter Publications: Berlin, Germany, **2012**; Chapter 17.
25. Dibenedetto, A.; Stufano, P.; Macyk, W.; Baran, T.; Fragale, C.; Costa, M.; Aresta, M.; *ChemSusChem* **2012**, *5*, 373–378.
26. Schneider, J.; Jia, H.; Muckerman, J. T., Fujita, E. *Chem. Soc. Rev.* **2012**, *41*, 2036–2051.
27. Taniguchi, Y.; Yoneyama, H.; Tamura, H. *Bull. Chem. Soc. Jpn.* **1982**, *55*, 2034–2039.
28. Taniguchi, I.; Aurian-Blajeni, B.; Bockris, J. O. M. *Electrochim. Acta* **1984**, *29*, 923–932.
29. Bockris, J. O. M.; Wass, J. C. *J. Electrochem. Soc.* **1989**, *136*, 2521–2528.
30. Noda, H.; Yamamoto, A.; Ikeda, S.; Maeda, M.; Ito, K. *Chem. Lett.* **1990**, *19*, 1757–1760.
31. Ikeda, S.; Yamamoto, A.; Noda, H.; Maeda, M.; Ito, K. *Bull. Chem. Soc. Jpn.* **1993**, *66*, 2473–2477.
32. Hirota, K.; Tryk, D. A.; Hashimoto, K.; Okawa, M.; Fujishima, A. *J. Electrochem. Soc.* **1998**, *145*, L82–L84.
33. Kaneko, S.; Katsumata, H.; Suzuki, T.; Ohta, K. *Chem. Eng. J.* **2006**, *116*, 227–231.
34. Ono, H.; Yokosuka, A.; Tasiro, T.; Morisaki, H.; Yugo S. *New Diamond Front. Carbon Technol.* **2002**, *12*, 141–144.
35. Halmann, M.; Aurian-Blajeni, B. *J. Electroanal. Chem.* **1994**, *375*, 379–382
36. Hinogami, R.; Nakamura, Y.; Yae, S.; Nakato, Y. *J. Phys. Chem. B* **1998**, *102*, 974–980.
37. Flaischer, H.; Tenne, R.; Halmann M. *J. Electroanal. Chem.* **1996**, *402*, 97–105.
38. Ikeda, S.; Saito, Y.; Yoshida, M.; Noda, H.; Maeda, M.; Ito, K. *J. Electroanal. Chem. Interfacial Electrochem.* **1989**, *260*, 335–345.
39. Kaneko, S.; Ueno, Y.; Katsumata, H.; Suzuki, T.; Ohta, K. *Chem. Eng. J.* **2009**, *148*, 57–62.
40. Cottineau, T.; Morin, M.; Belanger, D. *ECS Trans.* **2009**, *19*, 1–7.
41. Barton, E. E.; Rampulla, D. M.; Bocarsly, A. B. *J. Am. Chem. Soc.* **2008**, *130*, 6342–6344.
42. Kumar, B.; Smieja, J. M.; Kubiak, C. P. *J. Phys. Chem. C* **2010**, *114*, 14220–14223.
43. Petit, J. P.; Chartier, P.; Beley, M.; Sauvage, J. P. *Nouv. J. Chim.* **1987**, *11*, 751.
44. Parkinson, B. A.; Weaver, P. F. *Nature* **1984**, *309*, 148–149.
45. Zafrir, M.; Ulman, M.; Zuckerman, Y.; Halmann, M. *J. Electroanal. Chem.* **1983**, *159*, 373–389.
46. Cabrera, C. R.; Abruna, H. D. *J. Electroanal. Chem.* **1986**, *209*, 101–107.

47. Arai, T.; Sato, S.; Uemura, K.; Morikawa, T.; Kajino, T.; Motohiro, T. *Chem. Commun.* **2010**, *46*, 6944–6946.
48. Aurian-Blajeni, B.; Taniguchi, I.; Bockris, J. O. M. *J. Electroanal. Chem. Interfacial Electrochem.* **1983**, *149*, 291–293.
49. Kumar, B.; Llorente, M.; Froelhich, J.; Dang, T.; Sathrum, A.; Kubiak, C. *Annu. Rev. Phys. Chem.* **2012**, *63*, 541–569.
50. Atlam, O.; Barbir, F.; Bezmalinovic, D. *Int. J. Hydrogen Energy* **2011**, *36*, 7012–7018.
51. Ogura, K.; Yoshida, I. *Electrochim. Acta* **1987**, *32*, 1191–1195.
52. Ogura, K.; Yoshida, I. *J. Mol. Catal.* **1986**, *34*, 309–311.
53. Halmann, M.; Ulman, M.; Aurian-Blajeni, B. *Solar Energy* **1983**, *31*, 429–431.



## IONIC LIQUIDS FOR HYDROGEN STORAGE: OPPORTUNITIES FOR ORGANOMETALLIC CHEMISTRY

MARTIN H. G. PRECHTL\* AND SEBASTIAN SAHLER

*Institute of Inorganic Chemistry, Department of Chemistry, University of Cologne, Cologne, Germany*

### 40.1 INTRODUCTION

Even today, terrestrial, nautical, and aeronautic transportation strongly depends on petrol as energy carrier. Therefore, to maintain the current modern transportation systems running in the future, novel, advanced, hence sustainable and environmental, benign energy carrier systems have to be found and further developed. One interesting and highly energetic material that may help to overcome this problem is hydrogen gas [1, 2]. It is advantageous in terms of (i) very low weight, which means high energy density per kilogram; (ii) abundance in the form of water; and (iii) environmental friendly nature as the hydrogen gas is converted again into water during combustion. However, one has to keep in mind the drawbacks of this material while storing it “physically” in the molecular dihydrogen form: (i) low density in the gaseous state, (ii) the need for portable heavy pressure tanks to carry compressed gas in a reasonable small volume, and (iii) cryogenic storage of denser liquid hydrogen requiring efficient cooling systems [1, 3–6]. An alternative pathway to store hydrogen is the “chemical storage” of reactive protons and hydrides in organic and inorganic materials, which are accessible for catalytic bond activation, hence dehydrogenation. Thus the hydrogen is stored under ambient conditions in liquid or solid form with still reasonable high density, and molecular dihydrogen gas is released on demand. To be competitive to physical storage, chemical methods are restricted to low weight materials that contain high amounts of chemically bound protic and hydridic hydrogen.

One of the most interesting materials, in terms of weight efficiency (weight percent, wt%), is the Lewis pair ammonia borane (AB) (>19 wt%). Here, the reactive protons are carried on a nitrogen moiety and the hydridic counterparts on a boron entity. Besides, also some low weight derivatives of AB are investigated for hydrogen storage. Moreover, carbon dioxide as proton and hydride acceptor in the form of formic acid (FA) is considered as it is abundant on earth. The drawback of FA is the low hydrogen content of only 4.4 wt% [7–10].

In terms of energy density (weight-to-volume ratio), AB is quite competitive and even more efficient than molecular dihydrogen gas. However, the drawback of this compound is related to the difficult regeneration of the dehydrogenated residual products after hydrogen release and some aspects in transportation for mobile application. Today’s infrastructure for the carriage and handling of energetic materials is designed for liquid fuels, therefore, solid AB for example is at a disadvantage in competition with fossil or renewable liquid fuels. Additionally, liquid fuels are superior in terms of handling during the application in engines or fuel cells.

Therefore, it remains a challenge to find a liquid hydrogen storage material with accessible high hydrogen content. In this regard, ionic liquids (ILs) are quite promising because of their tunable physicochemical properties [11]. Currently, the main targets are catalytic dehydrogenation of hydrogen-enriched inorganic or organic molecules and the hydrogenation of used

materials for recycling purposes [12–16]. ILs revealed interesting behaviors in combination with hydrogen storage materials: (i) ILs promote hydrogen release even in the absence of catalysts, (ii) some are capable of dissolving hydrogen carriers, (iii) they help dissolve spent fuel products for regeneration purposes, and (iv) they play a role in the immobilization of catalysts for dehydrogenation and hydrogenation [16, 17]. Interestingly, all these properties can be combined, which makes the application of ILs in hydrogen storage systems as single additive especially attractive [16]. This is especially evident in combination with a transition metal catalyst, which further improves the efficiency of the hydrogen storage system in terms of fast hydrogen release and hydrogenation of the spent hydrogen carrier.

## 40.2 IONIC LIQUIDS

In the past two decades, ILs, often also called *molten salts*, revealed their high potential for application in various fields of natural science and technology, and all fields of chemistry [18–24]. Some general examples for applications are electrolytes, lubricants, surfactants, solvents, extractants, and catalyst stabilizers/immobilizers. The variety of applications of ILs is related to some thermodynamic and other physicochemical properties: (i) noninflammability, (ii) low vapor pressure, (iii) high solvation, (iv) often weakly coordinating nature, (v) tunable polarity/miscibility/viscosity, (vi) tunable acidity/basicity/functionality, (vii) good thermal stability, and, last but not the least, (viii) low melting point, defined as salts with melting points below 100 °C [11, 24–27]. The latter property is based on the reduced lattice energy due to large ion pairs and low symmetry of cations (Fig. 40.1) [11, 25, 28]. Although ILs were discovered about 100 years ago, in 1913, it was only the middle of the century that saw the first applications in electrochemistry and only at the end of the millennium that the potential for widespread application in other fields began to develop rapidly [29].

Modification of the backbone and side chains of the ion structures is a common way to tune their physical and chemical properties [30–34]. In this manner, task-specific ILs can be designed with tailored hydrophilicity or hydrophobicity, variable viscosity, and incorporating functional coordinating groups. In the particular case of imidazolium-based ILs, the acidity/basicity of the reaction system might play an important role because of the acidic proton in the C2-position [22, 24, 27, 35]. Dissolved metal species form carbene complexes [36]. The complex formation can be hindered by protection of the C2-position. In homogeneous as well as in heterogeneous catalysis, ILs are suitable agents for the stabilization and immobilization of the catalyst species, preventing decomposition and agglomeration [22]. One important parameter to obtain high yields is the solubility of the substrates, reactants, intermediates, and products. In case of hydrogen generation, the driving force is the extrusion of hydrogen gas from the IL mixture, as its solubility is rather low, and therefore the equilibrium can be forced to the product side [37, 38]. Interestingly, there are some examples where ILs have been employed as hydrogen storage materials and not as simple solvents.

## 40.3 HYDROGEN STORAGE MATERIALS: HYDROGEN-RICH MOLECULES

Since molecular dihydrogen is storable as pressurized gas or as liquid at low temperature, novel hydrogen storage materials must compromise some significant advantages. The storage of molecular hydrogen as compressed gas or as liquid requires the application of heavy pressure tanks or highly isolated cryogenic tanks, which make the application less effective and very

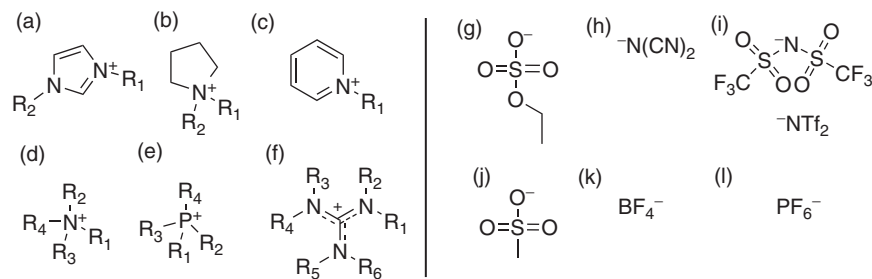


**Figure 40.1** Selected examples for IL-cations (left) and anions (right): (a) imidazolium, (b) pyrrolidinium, (c) pyridinium, (d) ammonium, (e) phosphonium and (f) guanidinium. The side chains R<sup>1–6</sup> are alkyl groups, which can also carry functionalities such as alcohols, ethers, and nitriles. Usually weakly coordinating anions are used as counterparts (g–l): ethyl sulfate, dicyanamide, bis(trifluoromethanesulfonylimide) (NTf<sub>2</sub><sup>-</sup>), methyl sulfonate, BF<sub>4</sub><sup>-</sup>, PF<sub>6</sub><sup>-</sup>, etc.

expensive. To visualize the drawback, we consider a short example: a car powered with hydrogen would consume 6 kg of H<sub>2</sub> for a 500 km trip, the volume occupied by it being approximately 67 m<sup>3</sup> at ambient pressure; therefore, the hydrogen is stored in a 260-l tank at 700 bar, resulting in a total tank weight of 125 kg [4]. As a consequence, the gravimetric efficiency of high pressure storage is rather low at 4.8 wt%. Even lower gravimetric efficiencies are reached with cryogenic methods, as this method suffers from easy evaporation of the gas; moreover, thermal isolation requires the application of further materials, which means further increase in weight. In summary, these disadvantages, resulting in gravimetric inefficiency, make the application of inorganic and organic materials, carrying protic and hydridic hydrogen, quite an attractive approach. Thus, the target is to achieve higher volumetric and gravimetric hydrogen density with a superior gravimetric efficiency in the condensed phase.

#### 40.3.1 Ammonia Borane and Derivatives

AB is a lightweight, hydrogen-rich Lewis pair, therefore an interesting material for this research area [6, 10, 17, 39–41]. It consists in total of 19.6 wt% hydrogen, with equal amounts of hydrides and protons. Simple thermal treatment (130 °C) of this air- and water-stable solid material results in a hydrogen release of 14 wt% [4]. The dehydrogenation of AB might be accompanied by the formation of ammonia, diborane, and borazine. This is problematic because these volatile compounds contaminate the gas stream and decrease the efficiency owing to incomplete dehydrogenation of the substrate. Moreover, fuel cells are sensitive against ammonia. The complete dehydrogenation of AB would need elevated temperatures greater than 500 °C. Under these conditions, the major by-products are solid materials such as insoluble polyborazylene as well as boron nitride (Fig. 40.2). The latter is highly stable in terms of its mechanical, thermodynamical, and chemical properties. Therefore, complete dehydrogenation of AB is not the major focus due to the high process temperature of the hydrogen generation and the stability of boron nitride. The desired aim is the selective partial dehydrogenation of AB that results in a competitive hydrogen storage capacity of approximately 14 wt%. The major drawback and challenge is related to the formation of the discussed by-products, as the AB-based “spent fuel” products are difficult to regenerate, hence their reconversion into the starting material, AB. One attempt for the regeneration of the dissolved spent fuels is their reduction with hydrazine in liquid ammonia, where the complete/selective reformation of AB has been observed, accompanied by nitrogen extrusion [42].

Besides AB, some of its derivatives have also been investigated for hydrogen storage, especially to overcome the previously mentioned problems. The derivatives hydrazine borane (HB) [13], guanidinium borohydride (GBH) [12], ethylenediamine bisborane (EDB) [43], methylguanidinium borohydride (Me-GBH) [44], and different alkyl amine boranes are the most interesting (Fig. 40.3) [45, 14]. Another compound class between molecular and metal hydride storage materials is that of metal amido boranes, which is not discussed in this chapter [46].

HB provides comparable weight efficiency as AB, and most of the hydrogen is thermally accessible [13]. The capacity of this material can be improved by blending it with a hydride donor, as pure HB contains four protons and three hydrides, therefore, the excess proton in HB should be combined with an external hydride donor. By blending HB with the lowest weighing metal hydride, lithium hydride, hydrogen production is significantly improved when applying a molar ratio of 1 : 1

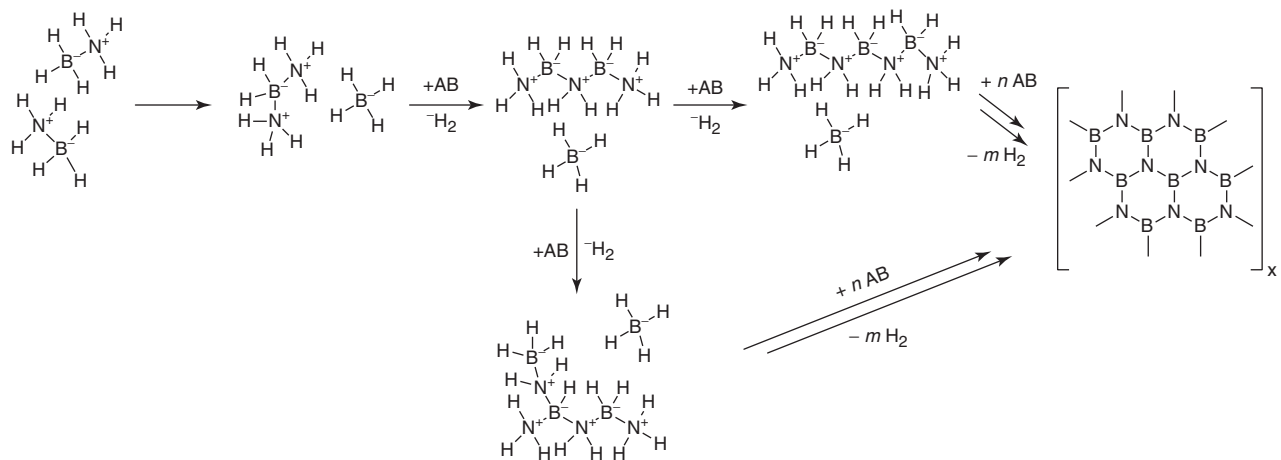


**Figure 40.2** Decomposition pathways of ammonia borane.

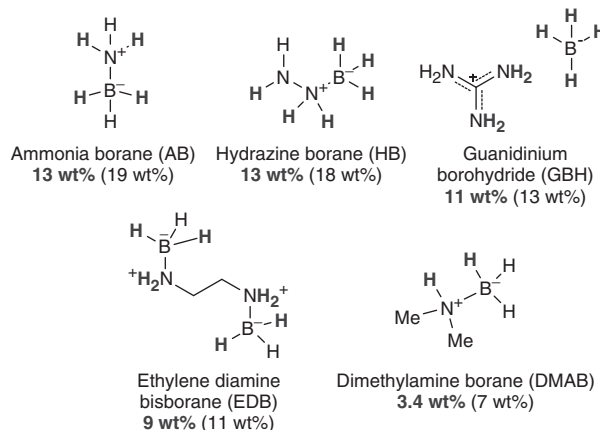


**Figure 40.3** Selected AB-related hydrogen storage materials (in gray: protons and hydrides that are initially capable for dehydrogenation).

of HB and LiH, giving a blend containing 14.8 wt% of hydrogen, while neat HB contains only slightly more hydrogen (15.4 wt%). This blended HB was capable of releasing approximately 12 wt% of hydrogen at 150 °C in 4.5 h, where the hydrogen produced contained ammonia as the single impurity in concentrations below 1%. The solid residual spent fuel shows reactivity in the presence of water and remains insoluble in organic solvents. The analog hydrazine bisborane adduct contains slightly more hydrogen than HB, but it is not quite suitable as hydrogen storage material, as it revealed to be quite unstable at elevated temperatures (>160 °C) or under rapid heating, when explosive decomposition occurred.

Another interesting material is GBH and its blends [12]. The protic moieties are carried by the cation, and the counterion contains the hydrides, resulting in a content of 10.8 wt% of hydrogen gas, theoretically, and 10.6 wt%, experimentally. Interestingly, the thermal decomposition is exothermic, therefore above a certain temperature, the hydrogen generation is accompanied by heat formation, and consequently it remains self-sustaining after initial heating. The dehydrogenation of GBH showed almost complete hydrogen release with ammonia as impurity of approximately 5 mol%. Similar to the discussed HB, GBH contains two excess protons, therefore blending this material with external hydrides is an elegant way for optimization. EDB is a suitable material, carrying two excess hydrides, thus blending GBH in an efficient manner. The GBH–EDB blend in an equimolar ratio is suitable for release of hydrogen in high yields with a low concentration of ammonia as impurity (Fig. 40.4). A blend in wt% ratio of 40:60 yields 10.1 wt% of hydrogen and ammonia impurity as low as 0.026 mol%. Similar to the previously mentioned AB derivatives, the major drawback of this blend is the solid state and the related problems in terms of regeneration of the spent fuel. Neat EDB is also suitable for fast hydrogen generation with high yields and high purities at process temperatures below 200 °C, showing no significant amounts of impurities [43]. The reaction rates of the hydrogen release from EDB are in the same range as the ones for AB-based systems.

#### 40.3.2 Formic Acid and Carbon Dioxide as Cheap Hydrogen Storage Materials

The research on the catalytic dehydrogenation of FA resulting in dihydrogen and carbon dioxide has undergone a renaissance in recent years (Fig. 40.5) [3, 7–9, 47–62]. Although FA contains only 4.4 wt% hydrogen, less than that in the previous mentioned AB derivatives, a great advantage is the relatively easy availability owing to the enormous natural feedstock of carbon dioxide; therefore, this represents a very cheap and environmentally benign hydrogen storage material. Interestingly, FA has been used as hydrogen source for hydrogen transfer reactions for several decades [63–74].

### 40.4 HYDROGEN STORAGE SYSTEMS INVOLVING IONIC LIQUIDS

The physicochemical properties of ILs make this solvent class highly interesting for application in hydrogen storage systems. In general, ILs are known to be highly solvating, and, owing to their tunable polarity, they are capable of solubilizing polar as well as apolar substances, hence molecular hydrogen storage materials. Moreover, owing to the negligible vapor pressure of ILs, the purity of the hydrogen gas stream can be enhanced; on the contrary, volatile solvents and impurities would contaminate the generated hydrogen gas. Besides, as later discussed herein, ILs may promote the dehydrogenation of certain

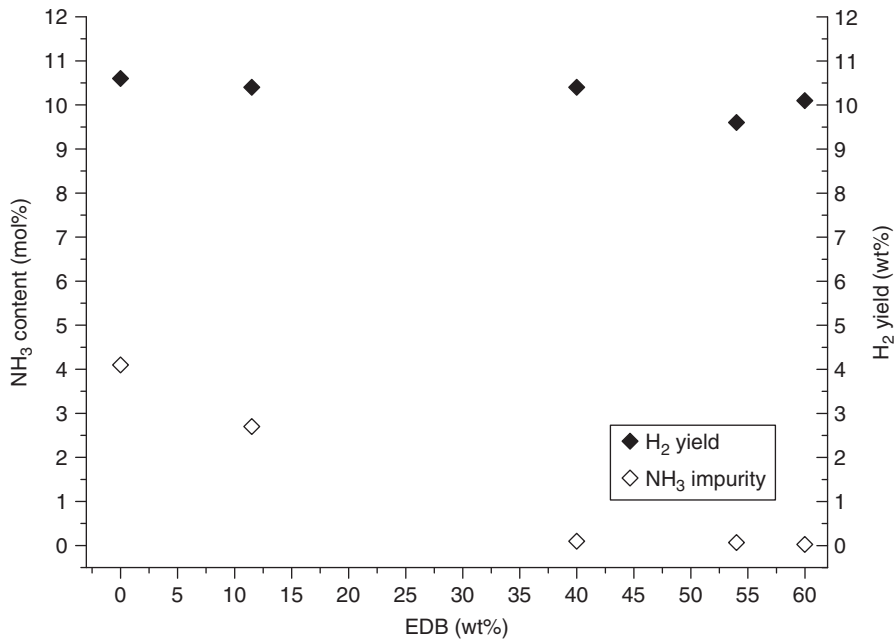


**Figure 40.4** GBH–EDB self-sustaining thermal decomposition. A mixture containing 60 wt% EDB is not self-sustaining [12].

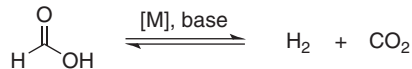


**Figure 40.5** Reversible splitting of formic acid in presence of metal catalysts.

hydrogen storage materials [17, 75]. ILs are also known to be suitable in stabilizing metal complexes and metal nanoparticle catalysts [9, 18, 22, 24, 76]. Furthermore, basic or acidic cocatalysts can be anchored in a side chain of the IL cation [9]. Most interestingly, lightweight, hydrogen-rich ILs can be directly used as hydrogen storage material, combining the previously mentioned properties [12, 44].

#### 40.4.1 ILs as Promoting Media for the Dehydrogenation of Ammonia Borane

It has been shown that certain ILs themselves are suitable for promoting the dehydrogenation of AB (Figs. 40.6 and 40.7) [17, 75]. IL-promoted thermal dehydrogenation of AB containing 50 wt% of AB in ionic liquid shows that some ILs are suitable for generating at least 2 equiv. of hydrogen gas per AB from the protic and hydridic entities (Fig. 40.7, a–c). The majority of the tested ILs significantly support the dehydrogenation; however, the initial rates of the  $\text{H}_2$ -generation are not fully related to the overall amount of released hydrogen. A tendency for the capability to promote dehydrogenation might be tentatively assigned to (i) an anion effect, (ii) coordinating or noncoordinating properties of the anion (and basicity), (iii) the volume of the anion, and (iv) the polarity of the ILs [77–79, 25, 11, 80, 81]. The tendency fits quite well with tested ILs from Entry A to J, where, with the largest anion (Entry J), most likely no promoting effect has been observed. The efficiency for dehydrogenation allows only the generation of 1 equiv of hydrogen gas, which is similar to the thermal decomposition of neat AB (Fig. 40.7).

The best results for the IL-promoted  $\text{H}_2$ -generation from AB has been obtained with [BMIM][Cl]; therefore, it has been studied in more detail [75]. The studies showed that the reaction rates and the hydrogen yield can be improved (Fig. 40.8). At a temperature as low as 85 °C, the hydrogen yield and reaction rate in the presence of 50 wt% [BMIM][Cl] is significantly higher than in the absence of IL, as also the weight efficiency of both systems, in comparison with that of neat AB (Fig. 40.8A (b)).

Moreover, the analysis of the gaseous phase clearly showed that only traces of borazine are detectable. This might be due to the suppression of the borazine formation or the dissolution in the liquid phase. As depicted in the reaction profile (Fig. 40.8A (a)), the influence of the IL [BMIM][Cl] during the dehydrogenation is drastic, as the reaction starts immediately,

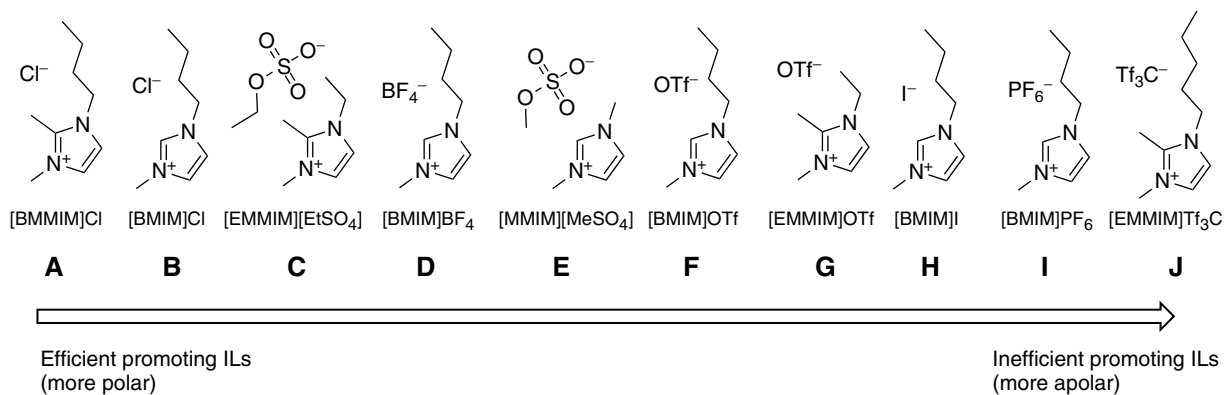


**Figure 40.6** Structures of promoting ILs for AB dehydrogenation; from A to J (left–right) with decreasing efficiency for promoting the dehydrogenation of AB [75].

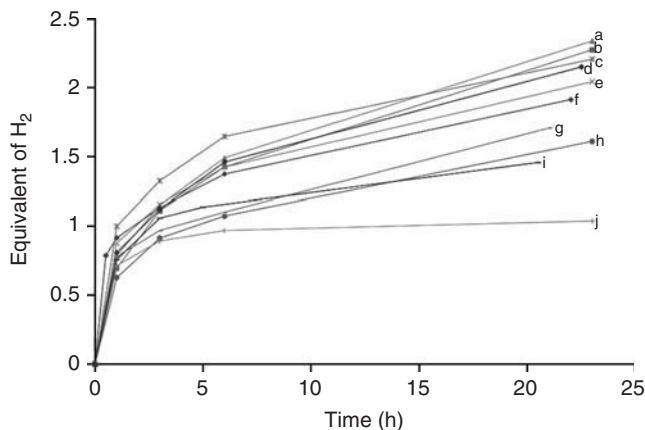


**Figure 40.7** H<sub>2</sub>-release measurements of 50 wt% AB (250 mg) at 85 °C in 250 mg of (a) [BMMIM]Cl, (b) [BMIM]Cl, (c) [EMMIM][EtSO<sub>4</sub>], (d) [BMIM]BF<sub>4</sub>, (e) [MMIM][MeSO<sub>4</sub>], (f) [BMIM]OTf, (g) [EMMIM]OTf, (h) [BMIM]I, (i) [BMIM]PF<sub>6</sub>, and (j) [PMMIM]Tf<sub>3</sub>C. Reprinted with permission from Reference 75. Copyright (2009) American Chemical Society.

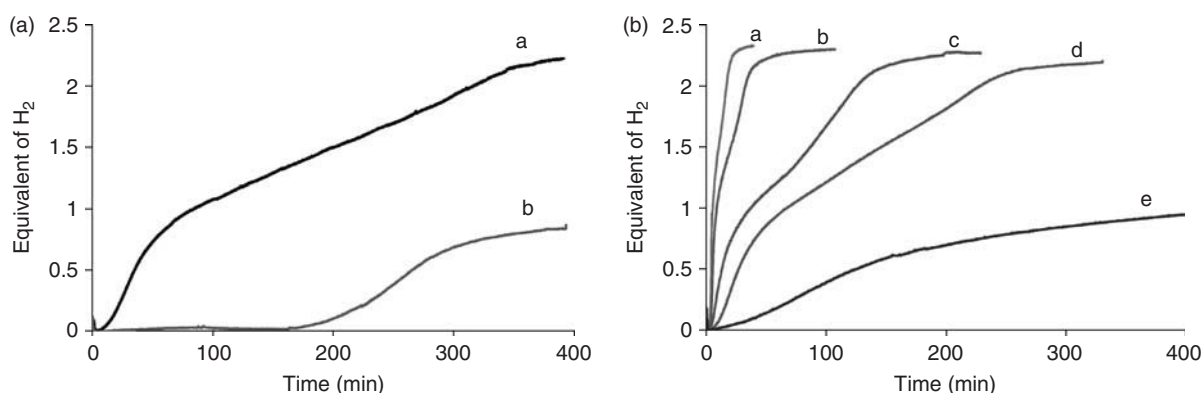


**Figure 40.8** (A) H<sub>2</sub>-release measurements at 85 °C of (a) IL-promoted generation with 50 wt% AB in [BMIM]Cl and (b) neat AB. (B) H<sub>2</sub>-release measurements of 50 wt% AB in [BMIM]Cl at (a) 110, (b) 105, (c) 95, (d) 85, and (e) 75 °C. Reprinted with permission from Reference 75. Copyright (2009) American Chemical Society.

no induction period is necessary, and the total yield is much higher. Interestingly, this effect remains even with lower IL loadings (20 wt%). The total hydrogen release at 75 °C is comparable to the one at 85 °C of *neat* AB, but the IL-based system has a higher reaction rate and no induction period; resulting in a more efficient system. The reaction rate of the AB/IL-system is sensitive toward the reaction temperature, where the maximum of the total yield is almost reached at only 85 °C (2.1 equiv. H<sub>2</sub>) after circa 4 h. Temperatures above 85 °C do not significantly improve total yield, but the reaction time is much shorter, for example at 110 °C, 2.3 equiv. of hydrogen are generated in less than 30 min.

#### 40.4.2 Ionic Liquid Stabilizers for Nanoscale Catalysts in Dehydrogenation Reactions

For the evaluation of the catalytic activity of molecular and nanoscale catalysts for the dehydrogenation of AB, an ideal model system is dimethyl amino borane (DMAB). In contrast to AB, DMAB does not tend to oligomerize as the two methyl groups completely suppress further dehydrogenation as a result of the absence of additional protons, hence only 1 equiv. of hydrogen gas is generated and oligomers do not form. Instead, DMAB derivatives are selectively dehydrogenated, forming only cyclic dimers or trimers [15]. DMAB-based systems are quite interesting for mechanistic studies, but the lower content of accessible hydrogen make them unattractive for application as hydrogen storage materials. DMAB is converted into its cyclic dimer under hydrogen extrusion via diammoniate of diborane as intermediate [82]. Obviously, DMAB can also act as reducing agent, for example, an excess of DMAB reduces dimeric Rh(II) hexanoate resulting in the formation of rhodium nanoparticles and the IL dimethyl ammonium hexanoate (Fig. 40.9). The small-sized (2 nm) nanoparticles exhibit high activity for the dehydrogenation of DMAB at low temperatures with high conversions (Fig. 40.9). The IL dimethyl ammonium hexanoate formed *in situ* showed that it can act as a stabilizer for the nanocatalysts to prevent agglomeration or deactivation.

#### 40.4.3 ILs Act as Catalyst Stabilizer and (Promoting) Solvent

Metal complexes are capable of catalytic dehydrogenation of AB and its derivatives. In this manner, reaction rates and applied temperatures can be optimized towards a continuous hydrogen release in portable hydrogen storage tanks [15, 83]. Combining the promoting properties of ILs for dehydrogenation of AB derivatives with those of metal catalysts for dehydrogenation, the catalytic activity, reaction rates, and total hydrogen yield should further improve. It has been shown that the addition of 5 mol% transition metal-based precatalysts (Rh, Ru, Pd, Ni) to a 1 : 1 mixture of [BMIM][Cl] and AB resulted in significantly lower reaction temperatures (45–85 °C), than in the absence of metals. Moreover, hydrogen generation is also improved (Fig. 40.10) [16].

The metal precursors depicted in Fig. 40.10 have not been studied in detail, therefore the active species remain unclear; however, these metal salts and complexes are well known to form metal nanoparticles under reductive conditions, for example, hydrogen atmosphere, and at higher temperatures, some even undergo thermal decomposition in ionic liquid media [23]. Therefore, in some cases at least, metal(0) nanoparticles might play an important role in the dehydrogenation of AB, where, in the case of Rh(0) nanoparticles and DMAB, isolated particles have been proven to be active for the dehydrogenation (see Section 40.3.2) [82]. The time-resolved reaction monitoring showed that most metal compounds improved the reaction rates and total hydrogen yields.

Another approach to optimize the selectivity, reaction rates, and total yields, is the formation of AB derivative blends. For example, the blend of AB with *sec*-butyl amine borane (SBAB) is successfully dehydrogenated in IL with higher selectivity, which means suppression of oligomerization [14]. Instead, it has been observed that this blend in [EMIM][EtSO<sub>4</sub>] results in the single formation of a cyclic trimer, a substituted monomolecular borazine derivative. On the contrary, oligomeric by-products and insoluble polyaminoboranes are not formed; however, the formation of volatile borazine (from AB dehydrogenation) or contamination by ammonia and diborane in the gas stream has not been reported in detail (Fig. 40.11). The alkyl chain in SBAB results in a loss of efficiency and the active hydrogen content drops to 5 wt%. The metal-catalyzed

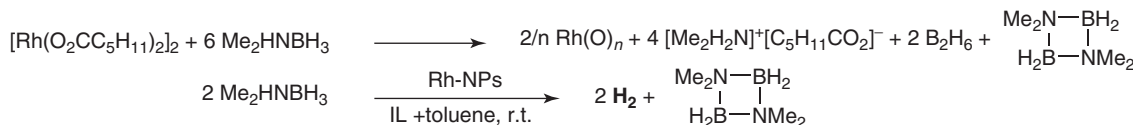


**Figure 40.9** Rhodium nanoparticle formation in presence of DMAB and subsequent catalytic dehydrogenation of DMAB. Adapted from Reference 82.

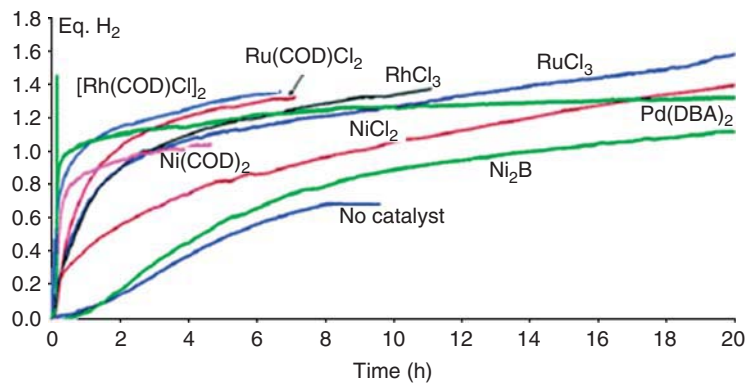


**Figure 40.10** Hydrogen evolution from AB-decomposition at 65 °C catalyzed by different metal-catalyst precursors in [BMIM][Cl]. Reproduced from Reference 16 with permission of The Royal Society of Chemistry. (See insert for color representation of the figure.)

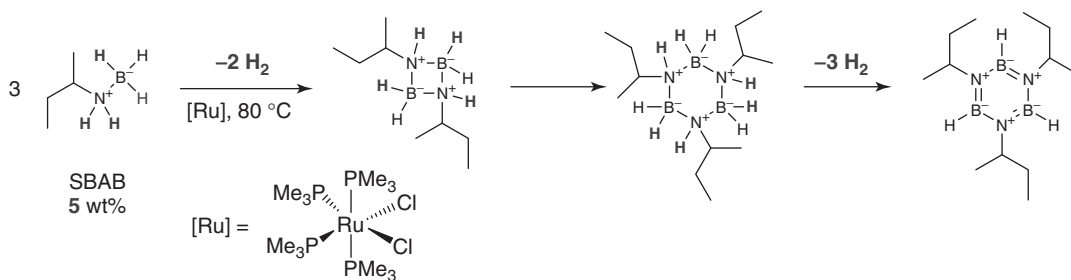


**Figure 40.11** Trimerization of SBAB to the corresponding borazine derivative during hydrogen production and the secondary products of SBAB decomposition [14].

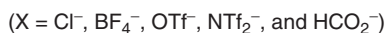
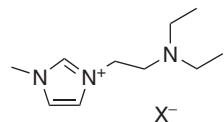


**Figure 40.12** Structure of the amino-functionalized IL [Et₂NC₂MIM][X] basic cocatalyst [9, 84].

dehydrogenation used 1 mol% of the ruthenium complex  $[\text{RuCl}_2(\text{PMe}_4)_3]$  at 80 °C; the active complex species or any intermediates have not been reported.

#### 40.4.4 Functionalized ILs as Cocatalyst for the Decomposition of Formic Acid

In the dehydrogenation of FA, the presence of catalytic amounts of a Lewis or Brønsted base as cocatalyst facilitates the dehydrogenation process. Indeed, FA is converted into the corresponding formate, which is then converted into hydrogen gas and carbon dioxide. Instead of adding an external base, an elegant approach is the incorporation of a Lewis base into the side chain of the IL cation, for example, there are the imidazolium-based ILs  $[\text{Et}_2\text{NC}_2\text{MIM}][\text{X}]$  ( $\text{X} = \text{Cl}^-$ ,  $\text{BF}_4^-$ ,  $\text{OTf}^-$ ,  $\text{NTf}_2^-$ , and  $\text{HCO}_2^-$ ). This type of IL acts as (i) solvent for the catalyst; (ii) the anchored amine simultaneously acts as a basic cocatalyst to convert the FA into the formate, which is subsequently dehydrogenated by a metal complex, and (iii) the IL is miscible with FA, which guarantees efficient contact between the catalyst and substrate (Fig. 40.12) [9, 84, 85].

The  $[\text{Et}_2\text{NC}_2\text{MIM}]$  cation has been tested with several anions, such as  $\text{Cl}^-$ ,  $\text{BF}_4^-$ ,  $\text{OTf}^-$ ,  $\text{NTf}_2^-$ , and  $\text{HCO}_2^-$  as cocatalyst for the FA dehydrogenation in the presence of the metal precursor, the dimeric ruthenium precatalyst  $[(p\text{-cymene})\text{RuCl}_2]_2$

[9, 85]. The total hydrogen yield and reaction rates strongly depend on (i) the reaction conditions in general, (ii) temperature, (iii) type of IL, and (iv) addition or absence of external base. The strongest influence is related to the external base; in the absence of the base, the obtained turnover frequency (TOF) was  $36\text{ h}^{-1}$  and in presence of the external base, the TOF rose to  $627\text{ h}^{-1}$ , suggesting but not proving that the active ruthenium species is monomeric [85]. Further studies revealed that the ruthenium dimer  $[(p\text{-cymene})\text{RuCl}_2]_2$  undergoes ligand exchange in the presence of FA, and is converted into the corresponding formate/chloro-bridged  $[(p\text{-cymene})\text{RuCl}(\text{HCO}_2^-)]_2$  and formate/hydride-bridged  $[(p\text{-cymene})\text{RuH}(\text{HCO}_2^-)]_2$  dimeric complexes [9]. Therefore, it is plausible that these ruthenium dimers play a role in the catalytic cycle (Fig. 40.13). Consequently, the reported TOFs of up to  $1684\text{ h}^{-1}$  without additional base suggest the role of dimeric ruthenium complexes; notably, no monomeric ruthenium species have been detected.

Furthermore, the concentration of ionic liquid, respectively base, plays an important role and is contrary to the expectations from systems based on organic solvents. It has been shown that lower IL (base) concentrations result in a more efficient system, than high cocatalyst loadings (basic IL). It is assumable that this is due to the much higher viscosity of the IL in comparison to that of organic solvents, because of the high conversions, resulting in a low FA concentration in the monophasic IL/FA mixture. Consequently, the mixture becomes highly viscous as well, which hinders the hydrogen extrusion and stirring becomes more difficult. Therefore, this homogeneous catalytic system is more efficient at low IL concentrations, with high FA loadings. The robustness of this catalyst/IL/hydrogen fuel triple has been shown in (i) recycling experiments (six runs) and (ii) can be performed without any precautions against moisture or air. The reaction monitoring showed that after the initial high activity in the first run, similar reaction slopes were obtained in the next runs, except in the fifth (Fig. 40.14). Monomeric ruthenium species have been detected.

The same catalyst precursor  $[(p\text{-cymene})\text{RuCl}_2]_2$  has also been applied for the dehydrogenative conversion of biomass in IL, that is, cellulose derivatives. Certain strongly solvating polar ILs are capable to solubilize these (in common solvents) hardly soluble materials; thus, in these media, biomass-based materials become accessible for homogeneous dehydrogenation

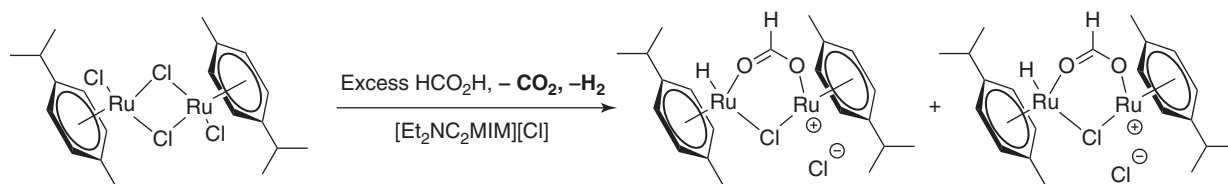


**Figure 40.13** Conversion of the  $[(p\text{-cymene})\text{RuCl}_2]_2$  with formic acid in IL  $[\text{Et}_2\text{NC}_2\text{MIM}][\text{Cl}]$ .

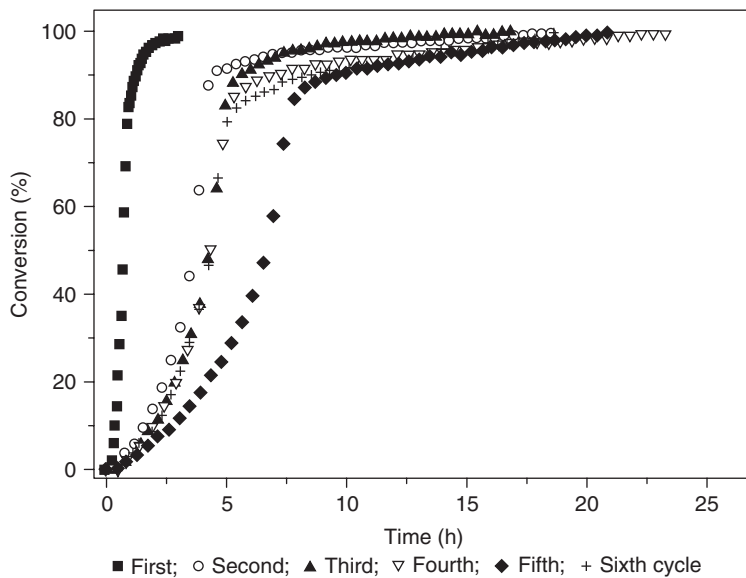


**Figure 40.14** Reaction profiles for FA decomposition in presence of  $[(p\text{-cymene})\text{RuCl}_2]$  in IL  $[\text{Et}_2\text{NC}_2\text{MIM}][\text{Cl}]$  at  $80^\circ\text{C}$  for six cycles. Reprinted with permission from Reference 9. Copyright (2010) John Wiley & Sons.

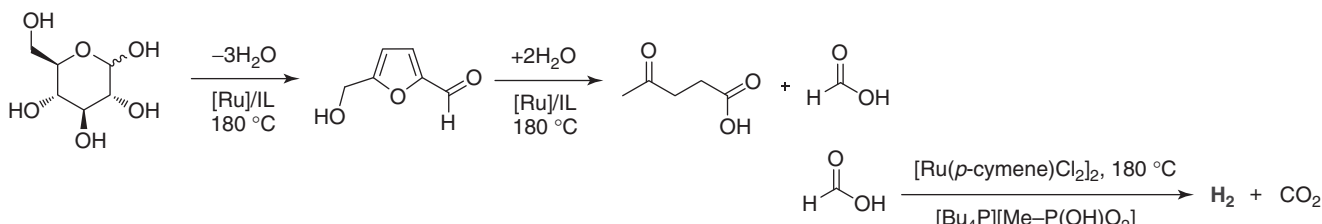


**Figure 40.15** Thermal conversion of glucose followed by catalytic dehydrogenation of formic acid in IL [86].

[86]. The studies about dehydrogenation of carbohydrates showed, for example, that glucose does not undergo conversion into the corresponding dehydrogenated product, but thermal decomposition occurred resulting in FA, which is subsequently converted into CO<sub>2</sub> and H<sub>2</sub> (Fig. 40.15). The high process temperatures make it crucial to apply ILs with high thermal stability.

#### 40.4.5 Ionic Liquids as Hydrogen Storage Materials

The GBH derivative Me-GBH is mono-methylated at one nitrogen of the guanidinium cation. This simple modification has a massive effect on the physical properties of this salt; in particular, the melting point is depressed resulting in a room temperature ionic liquid with high hydrogen content that is suitable as hydrogen storage material (Fig. 40.16) [44].

Me-GBH contains less hydrogen accessible for dehydrogenation in comparison to GBH (11 wt%). The methyl group results in distortion of the cation symmetry, which is responsible for the lower melting point of this salt [87]. Me-GBH represents the first room temperature IL with a melting point of -5 °C which is suitable as hydrogen storage material. It is easily dehydrogenated and has a hydrogen content of 9.0 wt%. Unfortunately, probably owing to high viscosity of the material, kinetic studies revealed that the simple thermal dehydrogenation at 75 °C is rather slow and still not satisfactory for application (2.3 equiv H<sub>2</sub>). The addition of Wilkinson's catalyst [Rh(PPh<sub>3</sub>)<sub>3</sub>Cl] improved the yield to 2.9 equiv. of hydrogen. Interestingly, the studies showed that the decomposition of the guanidinium salts also results in mass loss that exceed the theoretical capacity. Thus, this cannot be assigned to hydrogen generation. At temperatures higher than 120 °C, the gas stream is contaminated with ammonia, which indicates decomposition of the material. The quantification of the total hydrogen yield was assigned to 9.0 wt% on the basis of thermogravimetric analysis (TGA) and volumetric measurements. The dehydrogenation product of Me-GBH is solid and insoluble in the IL.

A different approach focused on anchoring a cyclohexyl ring into a side chain of an imidazolium cation [76]. The imidazolium salts were mixed with palladium on carbon and heated to greater than 230 °C, then with dehydrogenation, an aromatic ring started to form. Hydrogenation was then performed between 70 and 90 °C, demonstrating the reversibility (Fig. 40.17). Although the hydrogen content is too low for application and the process temperature is quite high (230–300 °C), this work represents the first in which an ionic liquid itself functioned as hydrogen storage material. The thermal stability of some of the employed ILs is remarkable.

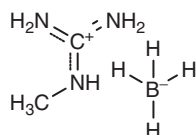


**Figure 40.16** Methyl guanidinium borohydride (Me-GBH).

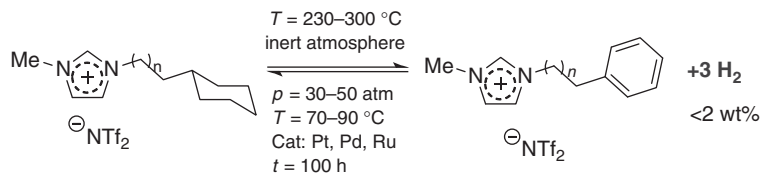


**Figure 40.17** Cyclohexyl-ILs for hydrogen storage [76].

## 40.5 CONCLUSION AND OUTLOOK

In summary, the number of publications in the research field of molecular hydrogen storage materials is still quite limited. Some results are promising, but still provide some challenges to be overcome. ILs have some physicochemical properties that might be helpful in resolving some aspects. ILs support hydrogen generation in several ways: (i) they are highly thermally-stable solvents with low vapor pressure, which allows elevated temperatures without contamination of the gas stream, (ii) ILs promote the dehydrogenation of AB derivatives, (iii) a cocatalyst can be anchored into side chains (i.e., Lewis bases), and (iv) highly solvating ILs are promising in the search for liquid hydrogen storage materials that remain in liquid state after hydrogen release. The latter aspect is also helpful for the regeneration of the material by hydrogenation with molecular or nanoscale catalysts. The single drawback of ionic liquids as additives to neat or blended hydrogen-rich materials is the additional weight, decreasing the gravimetric efficiency. Nevertheless, in certain cases, this drawback can be fully compensated, as IL-based systems give much higher total hydrogen yields and higher reaction rates than neat materials. In addition, for sure, the development of novel hydrogen-rich ILs for the application as hydrogen storage material is another interesting challenge to be resolved.

## REFERENCES

1. Hamilton, C. W.; Baker, R. T.; Staubitz, A.; Manners, I. *Chem. Soc. Rev.* **2009**, *38*, 279.
2. Schlapbach, L.; Zuttel, A. *Nature* **2001**, *414*, 353.
3. Felderhoff, M.; Weidenthaler, C.; von Helmolt, R.; Eberle, U. *Phys. Chem. Chem. Phys.* **2007**, *9*, 2643.
4. Eberle, U.; Felderhoff, M.; Schuth, F. *Angew. Chem. Int. Ed.* **2009**, *48*, 6608.
5. Marder, T. B. *Angew. Chem. Int. Ed.* **2007**, *46*, 8116.
6. Staubitz, A.; Robertson, A. P. M.; Manners, I. *Chem. Rev.* **2010**, *110*, 4079.
7. Fellay, C.; Dyson, P. J.; Laurenczy, G. *Angew. Chem. Int. Ed.* **2008**, *47*, 3966.
8. Loges, B.; Boddien, A.; Junge, H.; Beller, M. *Angew. Chem. Int. Ed.* **2008**, *47*, 3962.
9. Scholten, J. D.; Prechtl, M. H. G.; Dupont, J. *Chemcatchem* **2010**, *2*, 1265.
10. Stephens, F. H.; Pons, V.; Baker, R. T. *Dalton Trans.* **2007**, 2613.
11. Dupont, J.; Suarez, P. A. Z. *Phys. Chem. Chem. Phys.* **2006**, *8*, 2441.
12. Groshens, T. J.; Hollins, R. A. *Chem. Commun.* **2009**, 3089.
13. Hugle, T.; Kuhnel, M. F.; Lentz, D. *J. Am. Chem. Soc.* **2009**, *131*, 7444.
14. Mal, S. S.; Stephens, F. H.; Baker, R. T. *Chem. Commun.* **2011**, *47*, 2922.
15. Jaska, C. A.; Temple, K.; Lough, A. J.; Manners, I. *J. Am. Chem. Soc.* **2003**, *125*, 9424.
16. Wright, W. R. H.; Berkeley, E. R.; Alden, L. R.; Baker, R. T.; Sneddon, L. G. *Chem. Commun.* **2011**, *47*, 3177.
17. Bluhm, M. E.; Bradley, M. G.; Butterick, R.; Kusari, U.; Sneddon, L. G. *J. Am. Chem. Soc.* **2006**, *128*, 7748.
18. Scholten, J. D.; Leal, B. C.; Dupont, J. *ACS Catal.* **2012**, *2*, 184.
19. Prechtl, M. H. G.; Scholten, J. D.; Dupont, J. In *Ionic Liquids: Applications and Perspectives*; Kokorin, A., Ed.; InTech: Vienna, **2011**; p 393.
20. Scholten, J. D.; Prechtl, M. H. G.; Dupont, J. In *Handbook of Green Chemistry*; Anastas, P. T., Ed.; Wiley Interscience: Weinheim, **2011**; Vol. 8.
21. Dupont, J.; Scholten, J. D. *Chem. Soc. Rev.* **2010**, *39*, 1780.
22. Prechtl, M. H. G.; Scholten, J. D.; Dupont, J. *Molecules* **2010**, *15*, 3441.
23. Migowski, P.; Dupont, J. *Chem. Eur. J.* **2007**, *13*, 32.
24. Dupont, J.; de Souza, R. F.; Suarez, P. A. Z. *Chem. Rev.* **2002**, *102*, 3667.
25. Dupont, J. *J. Braz. Chem. Soc.* **2004**, *15*, 341.
26. Hallett, J. P.; Welton, T. *Chem. Rev.* **2011**, *111*, 3508.
27. Welton, T. *Chem. Rev.* **1999**, *99*, 2071.
28. Krossing, I.; Slattery, J. M.; Daguenet, C.; Dyson, P. J.; Oleinikova, A.; Weingartner, H. *J. Am. Chem. Soc.* **2006**, *128*, 13427.
29. Wilkes, J. S. *Green Chem.* **2002**, *4*, 73.
30. Cui, Y. G.; Biondi, I.; Chaubey, M.; Yang, X.; Fei, Z. F.; Scopelliti, R.; Hartinger, C. G.; Li, Y. D.; Chiappe, C.; Dyson, P. J. *Phys. Chem. Chem. Phys.* **2010**, *12*, 1834.
31. Yang, X.; Fei, Z. F.; Geldbach, T. J.; Phillips, A. D.; Hartinger, C. G.; Li, Y. D.; Dyson, P. J. *Organometallics* **2008**, *27*, 3971.

32. Fei, Z. F.; Zhao, D. B.; Pieraccini, D.; Ang, W. H.; Geldbach, T. J.; Scopelliti, R.; Chiappe, C.; Dyson, P. J. *Organometallics* **2007**, *26*, 1588.
33. Chiappe, C.; Pieraccini, D.; Zhao, D. B.; Fei, Z. F.; Dyson, P. J. *Adv. Synth. Catal.* **2006**, *348*, 68.
34. Zhao, D. B.; Fei, Z. F.; Geldbach, T. J.; Scopelliti, R.; Dyson, P. J. *J. Am. Chem. Soc.* **2004**, *126*, 15876.
35. Dupont, J. *Acc. Chem. Res.* **2011**, *44*, 1223.
36. Xu, L.; Chen, W.; Xiao, J. *Organometallics* **2000**, *19*, 1123.
37. Anthony, J. L.; Maginn, E. J.; Brennecke, J. F. *J. Phys. Chem. B* **2002**, *106*, 7315.
38. Jacquemin, J.; Gomes, M. F. C.; Husson, P.; Majer, V. *J. Chem. Thermodyn.* **2006**, *38*, 490.
39. Basu, S.; Zheng, Y.; Gore, J. P. *J. Power. Sources* **2011**, *196*, 734.
40. Al-Kukhun, A.; Hwang, H. T.; Varma, A. *Ind. Eng. Chem. Res.* **2011**, *50*, 8824.
41. Ahluwalia, R. K.; Peng, J. K.; Hua, T. Q. *Int. J. Hydrogen Energy* **2011**, *36*, 15689.
42. Sutton, A. D.; Burrell, A. K.; Dixon, D. A.; Garner, E. B.; Gordon, J. C.; Nakagawa, T.; Ott, K. C.; Robinson, P.; Vasiliu, M. *Science* **2011**, *331*, 1426.
43. Neiner, D.; Karkamkar, A.; Bowden, M.; Choi, Y. J.; Luedtke, A.; Holladay, J.; Fisher, A.; Szymczak, N.; Autrey, T. *Energy Environ. Sci.* **2011**, *4*, 4187.
44. Doroodian, A.; Dengler, J. E.; Genest, A.; Rosch, N.; Rieger, B. *Angew. Chem. Int. Ed.* **2010**, *49*, 1871.
45. Bowden, M. E.; Brown, I. W. M.; Gainsford, G. J.; Wong, H. *Inorg. Chim. Acta* **2008**, *361*, 2147.
46. Chua, Y. S.; Chen, P.; Wu, G. T.; Xiong, Z. T. *Chem. Commun.* **2011**, *47*, 5116.
47. Zhao, Y.; Deng, L.; Tang, S.-Y.; Lai, D.-M.; Liao, B.; Fu, Y.; Guo, Q.-X. *Energy Fuel* **2011**, *25*, 3693.
48. Boddien, A.; Mellmann, D.; Gartner, F.; Jackstell, R.; Junge, H.; Dyson, P. J.; Laurenczy, G.; Ludwig, R.; Beller, M. *Science* **2011**, *333*, 1733.
49. Tederee, K.; Li, T.; Jones, S.; Chan, C. W. A.; Yu, K. M. K.; Bagot, P. A. J.; Marquis, E. A.; Smith, G. D. W.; Tsang, S. C. E. *Nat. Nanotechnol.* **2011**, *6*, 302.
50. Yasaka, Y.; Wakai, C.; Matubayasi, N.; Nakahara, M. *J. Phys. Chem. A* **2010**, *114*, 3510.
51. Johnson, T. C.; Morris, D. J.; Wills, M. *Chem. Soc. Rev.* **2010**, *39*, 81.
52. Enthalier, S.; von Langermann, J.; Schmidt, T. *Energy Environ. Sci.* **2010**, *3*, 1207.
53. Boddien, A.; Loges, B.; Junge, H.; Gartner, F.; Noyes, J. R.; Beller, M. *Adv. Synth. Catal.* **2009**, *351*, 2517.
54. Junge, H.; Boddien, A.; Capitta, F.; Loges, B.; Noyes, J. R.; Gladiali, S.; Beller, M. *Tetrahedron Lett.* **2009**, *50*, 1603.
55. Loges, B.; Boddien, A.; Gartner, F.; Junge, H.; Beller, M. *Top. Catal.* **2010**, *53*, 902.
56. Boddien, A.; Loges, B.; Gartner, F.; Torborg, C.; Fumino, K.; Junge, H.; Ludwig, R.; Beller, M. *J. Am. Chem. Soc.* **2010**, *132*, 8924.
57. Boddien, A.; Gartner, F.; Jackstell, R.; Junge, H.; Spannenberg, A.; Baumann, W.; Ludwig, R.; Beller, M. *Angew. Chem. Int. Ed.* **2010**, *49*, 8993.
58. Boddien, A.; Gartner, F.; Mellmann, D.; Sponholz, P.; Junge, H.; Laurenczy, G.; Beller, M. *Chimia* **2011**, *65*, 214.
59. Gan, W. J.; Dyson, P. J.; Laurenczy, G. *React. Kinet. Catal. Lett.* **2009**, *98*, 205.
60. Fellay, C.; Yan, N.; Dyson, P. J.; Laurenczy, G. *Chem. Eur. J.* **2009**, *15*, 3752.
61. Gan, W.; Fellay, C.; Dyson, P. J.; Laurenczy, G. *J. Coord. Chem.* **2010**, *63*, 2685.
62. Laurenczy, G. *Chimia* **2011**, *65*, 663.
63. Bulushev, D. A.; Ross, J. R. H. *Catal. Today* **2011**, *163*, 42.
64. Kawasaki, I.; Tsunoda, K.; Tsuji, T.; Yamaguchi, T.; Shibuta, H.; Uchida, N.; Yamashita, M.; Ohta, S. *Chem. Commun.* **2005**, 2134.
65. Blum, J.; Sasson, Y.; Iflah, S. *Tetrahedron Lett.* **1972**, *13*, 1015.
66. Graf, E.; Leitner, W. *J. Chem. Soc. Chem. Commun.* **1992**, 623.
67. Leitner, W. *Angew. Chem. Int. Ed.* **1995**, *34*, 2207.
68. Hutschka, F.; Dedieu, A.; Eichberger, M.; Fornika, R.; Leitner, W. *J. Am. Chem. Soc.* **1997**, *119*, 4432.
69. Lange, S.; Leitner, W. *J. Chem. Soc. Dalton Trans.* **2002**, 752.
70. Brunner, H.; Leitner, W. *Angew. Chem. Int. Ed.* **1988**, *27*, 1180.
71. Brunner, H.; Graf, E.; Leitner, W.; Wutz, K. *Synthesis-Stuttgart* **1989**, 743.
72. Brunner, H.; Leitner, W. *J. Organomet. Chem.* **1990**, *387*, 209.
73. Brown, J. M.; Brunner, H.; Leitner, W.; Rose, M. *Tetrahedron Asymmetry* **1991**, *2*, 331.
74. Leitner, W.; Brown, J. M.; Brunner, H. *J. Am. Chem. Soc.* **1993**, *115*, 152.
75. Himmelberger, D. W.; Alden, L. R.; Bluhm, M. E.; Sneddon, L. G. *Inorg. Chem.* **2009**, *48*, 9883.
76. Stracke, M. P.; Ebeling, G.; Cataluna, R.; Dupont, J. *Energy Fuel* **2007**, *21*, 1695.

77. Zhang, S. J.; Sun, N.; He, X. Z.; Lu, X. M.; Zhang, X. P. *J. Phys. Chem. Ref. Data* **2006**, *35*, 1475.
78. Redel, E.; Thomann, R.; Janiak, C. *Chem. Commun.* **2008**, 1789.
79. Redel, E.; Thomann, R.; Janiak, C. *Inorg. Chem.* **2008**, *47*, 14.
80. Suarez, P. A. Z.; Einloft, S.; Dullius, J. E. L.; de Souza, R. F.; Dupont, J. *J. Chim. Phys. Phys. Chim. Biol.* **1998**, *95*, 1626.
81. Consorti, C. S.; de Souza, R. F.; Dupont, J.; Suarez, P. A. Z. *Quim. Nova* **2001**, *24*, 830.
82. Zahmakiran, M.; Ozkar, S. *Inorg. Chem.* **2009**, *48*, 8955.
83. Alcaraz, G.; Sabo-Etienne, S. *Angew. Chem. Int. Ed.* **2010**, *49*, 7170.
84. Olivier-Bourbigou, H.; Magna, L.; Morvan, D. *Appl. Catal. A* **2010**, *373*, 1.
85. Li, X. L.; Ma, X. Y.; Shi, F.; Deng, Y. Q. *ChemSusChem* **2010**, *3*, 71.
86. Taccardi, N.; Assenbaum, D.; Berger, M. E. M.; Bosmann, A.; Enzenberger, F.; Wolfel, R.; Neuendorf, S.; Goeke, V.; Schodel, N.; Maass, H. J.; Kistenmacher, H.; Wasserscheid, P. *Green Chem.* **2010**, *12*, 1150.
87. Mateus, N. M. M.; Branco, L. C.; Lourenco, N. M. T.; Afonso, C. A. M. *Green Chem.* **2003**, *5*, 347.



## **PART VI**

---

### **BIOORGANOMETALLIC CHEMISTRY**



## METAL CARBONYLS FOR CO-BASED THERAPIES: CHALLENGES AND SUCCESSES

CARLOS C. ROMÃO\*

*Instituto de Tecnologia Química e Biológica António Xavier (ITQB), Universidade Nova de Lisboa, Oeiras, Portugal; Alfama Limitida, Instituto de Biologia Experimental e Tecnológica (IBET), Oeiras, Portugal*

HELENA L. A. VIEIRA

*Instituto de Biologia Experimental e Tecnológica (IBET), Oeiras, Portugal; Chronic Diseases Research Center (CEDOC), Faculdade de Ciências Médicas, Universidade Nova de Lisboa, Lisboa, Portugal*

### 41.1 INTRODUCTION

Metals carbonyls, one of the most important families of complexes in organometallic chemistry, are already approaching their one hundred and twenty-fifth anniversary [1]. From their peculiar M–CO bonds, to their extraordinary role as starting materials for synthesis and catalysis, passing through the wondrous metal clusters they sustain, metal carbonyl complexes (MCC) enabled gigantic strides in chemistry, from theory to industrial applications. All this rich development took place in an artificial world essentially devoid of oxygen and water in which the low oxidation states of the metal, which stabilizes the M–CO bonds, are protected from oxidation. Sure enough, there existed metal carbonyls remarkably stable to air and water, but they were always regarded as highly dangerous materials that never escaped the spell of the original species, the really highly toxic  $\text{Ni}(\text{CO})_4$  [2]. The fact that they were obvious carriers of toxic CO did not help their reputation either. Altogether, these reasons kept metal carbonyls away from living organisms, biology, and life sciences. There seemed to exist no reason to change that situation until Sjöstrand [3] discovered that CO was endogenously produced in the human body and exhaled through respiration. It took 20 years until the human source of CO (the enzyme heme oxygenase, HO) was found [4], and another 20 to realize that it could have a biological role as a mediator, very much like NO [5]. At the time, the coordination of CO to heme proteins was already under intense study, but it took the power of protein crystallography to unveil the first biologically active MCC in living organisms, namely, in the hydrogenase enzymes of *Desulfovibrio gigas* [6] and *Clostridium pasteurianum* [7]. Clearly, the role of CO in biology was starting to emerge. The turn of the twenty-first century witnessed Otterbein and colleagues reporting the anti-inflammatory properties of CO gas in a mouse model of inflammation [1] at a time when MCCs were already patented for the therapeutic delivery of CO [8]. In the past 12 years, increasing interest has been given to the development of the biology and the pharmacological use of CO, and MCCs as versatile carriers of this active principle have played a central role in this research. In the remaining of this chapter, we describe the challenges met along this R&D process and the achievements that already brought MCCs close to clinical applications.

## 41.2 CO IN BIOLOGY AND IN THERAPY—ORIGIN, TARGETS, AND THERAPEUTIC POTENTIAL

### 41.2.1 Origin

The main source of endogenous formation of CO is the catabolism of heme, carried out by HO, an enzyme that is encoded by HMOX genes, ubiquitously expressed in living organisms. Indeed, this enzyme performs the oxidative cleavage of heme (Fe-protoporphyrin IX), which is opened and broken up into three products: CO, Fe<sup>2+</sup>, and biliverdin [4]. Fe<sup>2+</sup> is rapidly recycled through ferritin and biliverdin is enzymatically reduced to bilirubin, a potent antioxidant [9]. There are three described isoforms of HO. HO-1 is rapidly induced by cellular stress or injury [10]. HO-2 is constitutive, highly expressed mainly in the brain and cerebral vessels, and is rapidly activated in response to stress, maintaining brain homeostasis by increasing cerebral blood flow [11, 12]. The function of the putative HO-3 is still unclear [9].

The induction of HO-1 expression is very sensitive to any disruption of the balance of the intracellular redox state and/or to the presence of free heme, resulting from red blood cells senescence or other hemeproteins turnover [10]. Free heme is a powerful source of oxidative damage by its ability to catalyze the formation of hydroxyl radicals through the Fenton reaction, thus it must be rapidly destroyed by HO-1 [10, 13]. The resulting free CO is scavenged by hemoglobin and exhaled through the lungs. The average rate of CO excretion in a healthy individual is 0.4 ml/h [14], a value that increases in pathological conditions when HO-1 is activated in response to several distinct stimuli, namely, oxidative stress, ischemia–reperfusion, endotoxins, UVA radiation, or heat shock [9].

Therefore, owing to this cytoprotective and homeostatic function, HO-1 is a crucial enzyme. Deletion of *HMOX1* gene strongly compromises the survival of mammals, which become extremely sensitive to several pathologies: endotoxic shock, atherosclerosis, malaria, ischemia–reperfusion, or severe sepsis [10].

The salutary role of HO-1 activity is not limited to heme clearance or to antioxidant action of bilirubin, because its by-product CO emerges as a powerful gasotransmitter involved in tissue homeostasis, as well as modulation of inflammation and of cell death; for reviews, see [15, 16]. Stimulation of endogenously generated CO and/or its exogenous administration exerts remarkable beneficial biological effects in many tissues, namely, anti-inflammatory [17, 18], antiapoptotic [19–21], antiproliferative [22], antiatherogenic [23, 24], and more recently as bactericidal agent [25]. Three main areas of potential therapeutic applications have been extensively studied: cardiovascular diseases, inflammatory disorders, and organ transplantation, including several patent applications [15, 26]. Thus, these and several other observations created a very clear notion that CO could become a useful therapeutic principle. The perspective of therapeutic delivery of CO under the wider umbrella of the potent HO protective system is very interesting and provides a rationale for the breadth of indications potentially covered by CO administration.

### 41.2.2 Targets for CO Action

Several pathways have been described in the literature to explain the cytoprotective and therapeutic actions of CO. Nevertheless, those biochemical pathways and the actual physiological target(s) of CO are still a matter of great discussion.

CO is a rather chemically inert molecule and, in biological systems, it can only bind to transition metals present in several proteins. Of course, this binding modulates the activity of such proteins [27]. In mammals, iron-containing hemeproteins are the most studied and documented targets for CO. Importantly, CO can only bind to reduced Fe<sup>2+</sup>, limiting the potential target proteins, in contrast to NO, which binds both Fe<sup>2+</sup> and Fe<sup>3+</sup> [27].

The high affinity of CO for hemoglobin (from erythrocytes) and myoglobin (Mb, from myocytes) is implicated in CO toxicity as it hampers O<sub>2</sub> delivery into tissues by those hemeproteins.

The mediation of CO-induced cytoprotection by reactive oxygen species (ROS) generation and signaling is increasingly accepted in several cell models: macrophages [28], neurons [21], astrocytes [20], endothelial cells [27], or cardiomyocytes [29]. At least two proteins are recognized to be directly implicated in cell redox signaling by CO: cytochrome *c* oxidase (COX, mitochondrial respiratory complex IV) and NAD(P)H oxidase (plasmatic membrane). In addition, CO also controls ions channels and activates soluble guanylate cyclase, although their direct interaction with CO is a matter of debate.

### 41.2.3 CO and Cytochrome *c* Oxidase

Mitochondria are key organelles in cellular functioning. They are the cell's main energy source, being responsible for most of cellular ATP production via oxidative phosphorylation and modulation of cell death pathways through mitochondrial membrane permeabilization [29]. As COX is the final electron acceptor of the mitochondrial electron transport chain, its interaction with CO can modulate cell metabolism and survival [30].

In 1970, it was proposed that CO toxicity at cellular level can be due to its inhibition of COX activity [31]. Indeed, 20 years later, it was demonstrated that the binding of CO to cytochrome *a* and *a3* of COX is highly dependent on oxygen levels [32, 33]. In macrophage cells, CO limits inflammation by partially preventing COX activity [28, 34]. It is claimed that such decrease in COX activity facilitates electron leakage and reduction of O<sub>2</sub> into superoxide (O<sub>2</sub><sup>-</sup>), which is enzymatically converted into H<sub>2</sub>O<sub>2</sub> and other ROS that act as signaling factors. Indeed, CO cytoprotection is prevented by the addition of antioxidants in isolated mitochondria [20]. Therefore, salutary effects of CO are highly dependent on mitochondrial ROS generation. It is worth noting that modulation of COX activity is highly dependent on (i) CO concentration (low and signaling levels induce a transitory COX activity inhibition, while high concentrations of CO induce permanent inhibition [35, 36]) and (ii) oxygen levels.

#### 41.2.4 CO and NADPH Oxidase

NADPH oxidase is a plasmatic membrane complex containing heme proteins, whose function is ROS generation. Although it is present in almost all tissues, this enzymatic complex has been mostly studied in phagocytes such as neutrophils, monocytes, and macrophages, because these cells are involved in host defense. While the CO–COX interaction generates ROS that function as signaling factors, CO modulates NADPH oxidase activity by decreasing ROS production and limiting oxidative stress. For instance, in lung endothelial cells, low concentrations of CO prevented hyperoxia-induced cell death by attenuating hyperoxia-induced ROS production [37]. Many other examples have been reported. See, for instance, references [38, 39].

#### 41.2.5 CO and Ion channels

CO regulates the function of several ion channels but the molecular mechanisms by which this regulation takes place are still uncertain. The direct interaction of CO with ion channels is controversial because there is no transition metal present in the structure of these molecules. However, calcium-activated potassium (KCa) channels can bind covalently to heme [40]. Regardless of this debate, members of several ion channel families, both natively and heterologously expressed, are recognized molecular targets for the action of CO. Indeed, CO increases the opening probability of the large-conductance, voltage-activated K<sup>+</sup> channel, and Ca<sup>2+</sup>-activated K<sup>+</sup> channels, modulating vasomotor responses in smooth muscle cells [41], regulating oxygen sensing in glomus cells of carotid body [42], and controlling cerebral microvasculature [43, 44]. In the L-type voltage-activated Ca<sup>2+</sup> channel, CO appears with two opposite functions: inhibits the cardiac tissue of such channels [45] and activates them in intestinal smooth muscle via a NO-dependent mechanism [46]. The purinergic P2X receptors are the only ligand-gated ion channels described, which are modulated by CO [47]; however, it is not clear if CO directly binds to P2X receptors or if its effect is due to soluble guanylate cyclase (sGC) activity, ROS, or NO-dependent signaling.

#### 41.2.6 CO and Soluble Guanylate Cyclase, Nitric Oxide Synthase, and Mitogen-Activated Protein Kinases

Under physiological conditions, the capacity of CO to bind sGC and nitric oxide synthase (NOS) is still controversial. Although CO signaling pathways can involve cGMP and NO generation, high concentrations of CO are required for activating sGC and NOS.

Many effects mediated by CO-induced activation of sGC/cGMP have been described: inhibition of platelet activation and aggregation, smooth muscle relaxation, vasoactive effects, inhibition of cellular proliferation, prevention of apoptosis, and effects on neurotransmission [5, 21, 23, 48].

Generation of nitric oxide (NO) via activation and/or expression of NOS also appear as another process involved in CO biological activity, such as in the control of inflammation [49, 50] and inhibition of apoptosis in liver [51] and in neurons [21], for a review, see [52]. Yet, it is not clear whether CO activates sGC directly or indirectly via NO production. In any case, it is clear that CO and NO signaling can cross talk in several pathways.

Still, evidence suggests an important role of CO as a signaling molecule in modulating mitogen-activated protein kinases (MAPKs), especially p38 MAPK. CO-mediated activation of p38 MAPK has been shown to exert anti-inflammatory [17, 53], antiapoptotic [19, 54], and antiproliferative effects [55].

#### 41.2.7 CO and HO-1 Amplification Loop

In most of studies, exogenous CO biological effects were assessed in wild-type (Hmox1<sup>+/+</sup>) cells that can express HO-1. It is claimed that CO mimics the cytoprotective effects of HO-1, acting independently of HO-1 to exert its cytoprotection.

However, one should not exclude the possibility that the cytoprotective effects of CO might be mediated, at least in some cases, via induction of HO-1, participating in a positive forward feedback loop.

#### 41.2.8 Summary

Although different mechanisms explaining the cellular effects and biochemical pathways of CO have been described, the exact underlying signaling mechanisms and precise molecular targets of CO are only partially elucidated. However, such targets immediately disclose the very large setting of therapeutic applications of CO. Figure 41.1 summarizes the facts described in this section and points to some of the most important medical indications that can be treated with CO therapy.

### 41.3 THERAPEUTIC DELIVERY OF CO

The therapeutic use of CO should have several advantages. The first, and probably foremost, is the fact that CO is an endogenous molecule to which the organism is fully adapted. Secondly, CO does not react indiscriminately with intracellular targets as the other gasotransmitters NO and H<sub>2</sub>S do. CO reacts exclusively with transition metals [27], limiting its biological targets. Finally, from a pharmacological point of view, CO gas-based therapies have the major advantage of reducing metabolite-associated toxicity because, in this case, drug extraction occurs by exhalation. Beyond acute and chronic diseases, CO can also be used to prevent complications resulting from treatments or surgical interventions such as postoperative intestinal paralysis (in human clinical trials) or arteriosclerotic lesions associated with transplant and angioplasty [23]. In the following, we discuss how this therapeutic potential can be harnessed to make useful drugs.

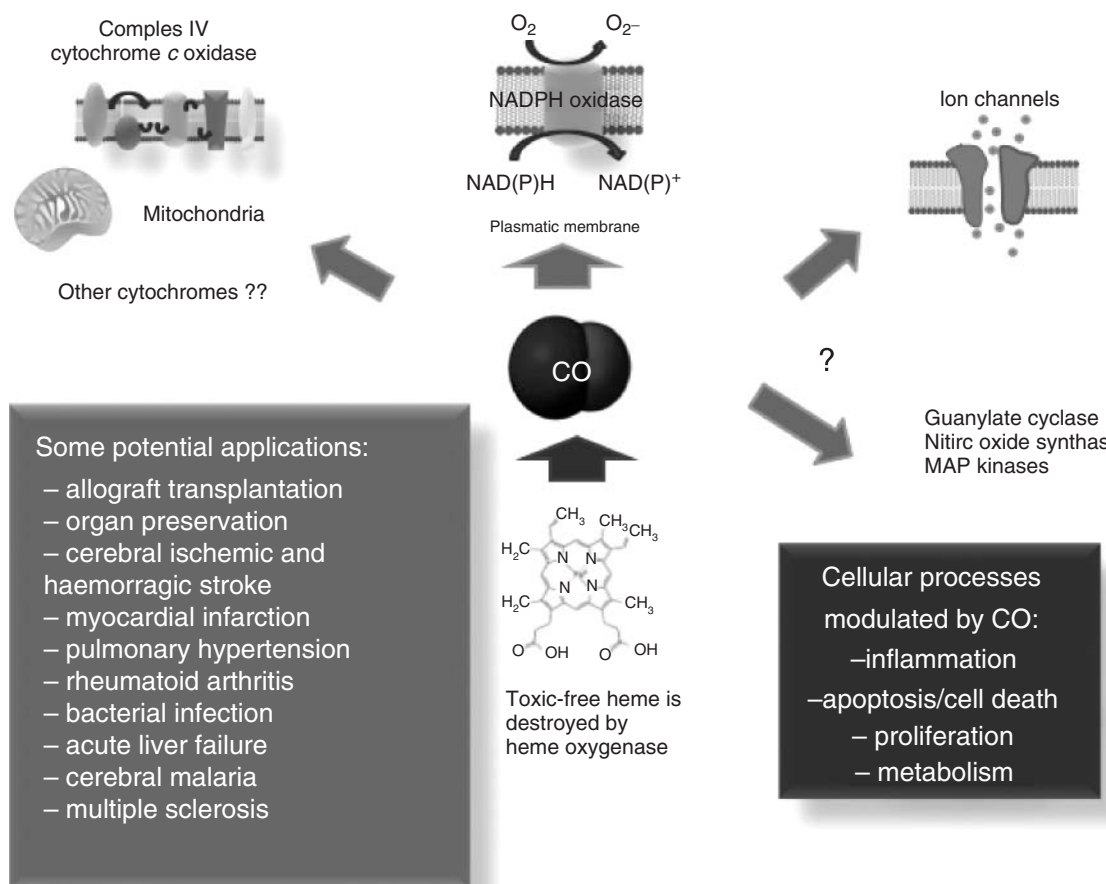


**Figure 41.1** Biological generation of CO, its targets, its signaling processes, and disease indications.

### 41.3.1 CO Gas and Inhalation Therapy

Inhalation, the simplest way of applying therapeutic CO, has been used *in vitro* and *in vivo*. The objects of treatment (cells, tissues, or rodents) are placed inside chambers into which controlled amounts of CO are admitted to maintain a suitable concentration for a given time, for example, 250 ppm CO and 1 h exposure. Crucial proofs-of-concept for the therapeutic use of CO have been obtained in this way [15, 26].

However, some shortcomings of this methodology are easy to identify: (i) toxicity confines this technology to hospital settings with specialized equipment [15]; (ii) even if carefully controlled, the effects of CO toxicity are not completely correlated to the amount of COHb in systemic circulation [56]; and (iii) the equilibrium of the competitive binding of O<sub>2</sub> and CO to Hb is such that it facilitates the transfer of CO from the tissues with low amounts of O<sub>2</sub> to blood and the lungs where the high partial pressure of O<sub>2</sub> readily displaces CO and reoxygenates Hb. Therefore, inhaled CO transported by Hb (COHb) is not likely to migrate from the red blood cells to the surrounding tissues. Dogs transfused with CO-saturated blood up to circa 80% COHb in circulation survive without intoxication [57]! This barrier against the natural thermodynamics of gas transport by Hb can only be overcome by administration of high amounts of inhaled CO, a constraint that limits the therapy in humans where the maximum COHb levels allowed are circa 13%. Furthermore, CO inhalation lacks tissue specificity: CO will be equally distributed to healthy and diseased tissues. While not preventing the launching of three clinical human trials, these observations led to the early proposal that CO therapy should be mediated by prodrugs that could deliver CO *in vivo*.

### 41.3.2 Prodrugs for Therapeutic Delivery of CO: CORMs

Ideally, such prodrugs should remain intact during their transit through the organism and, like HO-1, deliver small amounts of CO in the site of disease in response to some local stimulus. This process avoids the use of large amounts of CO in circulation and minimizes the dose of prodrug to be used.

A broad experimentation program at Alfama Inc. found that all the organic compounds such as tertiary aldehydes [58], haloalkanes [59], and organic oxalates were either too weak CO releasers or had a too high systemic toxicity. Sodium boranocarbonate, Na<sub>2</sub>[H<sub>3</sub>BCO<sub>2</sub>] (CORM-A1) and its ester and amide derivatives [60] showed very good results in many disease models [18, 61, 62], but had a rather narrow therapeutic window for most applications tried. So, transition MCC emerged as the more versatile source of CO prodrugs, now designated as CORM (CO-releasing molecule).

### 41.3.3 Metal Carbonyl Complexes (MCC) as CO-Releasing Molecules (CORM)

The release of CO through decomposition of MCCs may be initiated by different processes, namely, light irradiation, ligand substitution (dissociative or associative), pH variation, oxidatively induced ligand dissociation, enzymatic, and/or metabolic decomposition of the ligand sphere. With the exception of the enzymatic and metabolic processes, these reactions were widely studied in organometallic chemistry but most examples are largely irrelevant for biology and pharmacology owing to the anhydrous, anaerobic, thermal, and illumination conditions under which they were carried out. The only exception can be found for the metal carbonyl complexes [M<sup>I</sup>(CO)<sub>3</sub>L<sub>3</sub>]<sup>Z</sup> and [CpR]M(CO)<sub>3</sub>] (M = <sup>99m</sup>Tc, Re) used for radiopharmaceutical purposes [63, 64]. These water-soluble complexes based on d<sup>6</sup> metal ions are inert to substitution and oxidation reactions and are able to make their way through the body unchanged as required for the rapid elimination of radioactive metabolites [65]. On the contrary, CORMs will have to be decomposed making the formation of metabolites unavoidable, and the control over all the variables involved in their chemistry and biology much more complex.

So, the search for the controlled decomposition of MCCs under biologically relevant conditions and the validation of the biological outcome and therapeutic efficacy that they produced initiated a new chapter in the young field of bioorganometallic chemistry.

**41.3.3.1 The First-Generation or Experimental CORMs** The first examples of metal-based CORMs appeared in companies, which used them to prove the concept of therapeutic efficacy with CO prodrugs. The two groups of CORMs discussed in this section were, until 2012, the only ones reported to be tested in animal models of disease. Since these first-generation CORMs provided ground-breaking and invaluable information for the advancement of CORMs and CO therapy but still lack pharmacologically acceptable properties, we call them experimental CORMs.

*The Ru<sup>II</sup>(CO)<sub>3</sub> Derivatives CORM-2 and CORM-3* The first MCCs used as CORMs were reported by Motterlini and Mann (Fig. 41.2). As described in a recent personal overview [66], the DMSO-soluble [Ru(CO)<sub>3</sub>Cl<sub>2</sub>]<sub>2</sub> (CORM-2) was chosen on

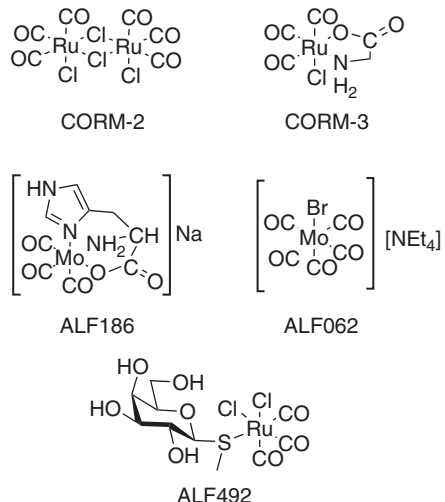


**Figure 41.2** Experimental CORMs tested in animal models of disease.

the basis of an educated guess and produced very encouraging results [67]. CORM-2 is a vasodilator of rat aortic rings *ex vivo*, and decreases the blood pressure of rats when administered *in vivo*. This last property was assigned to CO activity because it was not elicited by the CO-free control  $[\text{RuCl}_2(\text{DMSO})_4]$ . Although it has become the most popular CORM in the literature [62, 66], the pharmacology of CORM-2 remains uncharacterized. It breaks its dimeric structure in DMSO to form a mixture of *fac*- $[\text{Ru}(\text{CO})_3\text{Cl}_2(\text{OSMe}_2)]$  and *cis-cis-trans*- $[\text{Ru}(\text{CO})_2\text{Cl}_2(\text{SOMe}_2)_2]$ , none of which was studied separately. Notwithstanding, the coordination of the successful  $[\text{Ru}^{\text{II}}(\text{CO})_3]$  fragment to biological ligands that favor water solubility led to the very important glycinate derivative *fac*- $[\text{Ru}(\text{CO})_3\text{Cl}_2(\kappa^2-\text{O}_2\text{CCH}_2\text{NH}_2)]$  (CORM-3) [68].

During this initial discovery process, Motterlini and coworkers [67] searched for a simple methodology to quantify the ability of a given MCC to release CO and act as a potentially useful CORM. Their choice fell on the so-called Mb assay. The method comprises the addition of the candidate MCC to a solution of deoxy-Mb generated *in situ* from Mb and excess dithionite. The reaction medium remains anoxic for circa 2 h in which time CO may be transferred from the CORM to the hemeprotein. The amount of carboxymyoglobin (COMb) formed is quantified by UV-vis spectroscopy following the replacement of the absorption of deoxy-Mb at  $555 \text{ cm}^{-1}$  by the new absorptions of COHb at  $541$  and  $578 \text{ cm}^{-1}$ . The characterization and ranking of the CO-releasing activity of different CORMs can be made through the comparison of the value of their half-life,  $t_{(1/2)}$ , the time taken to form 0.5 equiv of COMb. This definition allows the comparison of CORMs that deliver different numbers of CO ligands per mole.

According to the Mb assay, CORM-3 was described as a fast CO releaser because it formed 1 equiv of COMb within minutes ( $t_{(1/2)} = 2.3 \text{ min}$ ) [68, 69]. Solutions of CORM-3 left aging for circa 18–24 h fail to carbonylate deoxy-Mb and are considered to contain an inactive decomposition product of CORM-3, named iCORM-3, which still contains *cis*- $[\text{Ru}(\text{CO})_2]$  fragments (IR evidence). CORM-3 became a reference CORM [66] producing impressive biological results *in vitro*, *ex vivo*, and *in vivo* with remarkable therapeutic efficacy in several major indications such as transplant [70, 71], organ preservation [72], myocardial infarct [73], and rheumatoid arthritis [74, 75]. The therapeutic action of CORM-3 was always assigned to CO in view of the inefficacy of the negative control iCORM-3. So, a small  $t_{(1/2)}$  in the Mb assay became the hallmark of an active CORM and made the Mb assay an almost mandatory test for the identification of CORMs. However, in spite of recent improvements [76], the interpretation and use of this assay has to be seriously revised because it was found that the fast transfer of CO from CORM-3 to deoxy-Mb results from the reaction of CORM-3 with dithionite and sulfite ions present in the test, which displace CO from the Ru center. In fact, both CORM-2 and CORM-3 are unable to carbonylate purified, dithionite-free deoxy-Mb or Hb [77]. Therefore, the early classification of CORM-3 as a fast CO releaser has to be abandoned since it is actually a no-releaser in this Mb assay. If we further consider that no CO gas can be detected in the headspace of aqueous solutions of CORM-3 and its analogs [78, 79], and the fact that an organometallic fluorescent scavenger detects CO in cells treated with CORM-3 [80], we realize that its chemistry is not straightforward. However, its therapeutic activity remains undisputed and its mode of action deserves to be explained. To this end, the first step is to consider its aqueous solution chemistry [81]. CORM-3, and indeed all other  $[\text{Ru}^{\text{II}}(\text{CO})_3\text{L}_3]$  type CORMs studied so far [79, 82], react with water at  $\text{pH} > 4$  to release  $\text{H}^+$  and form species such as  $[\text{Ru}(\text{CO})_2(\text{COOH})\text{L}_3]^-$  (water-gas shift reaction). At

physiological pH (7.4), these metallacarboxylates release CO<sub>2</sub> (GC detection; eventually H<sub>2</sub> also) [78] and form many other species, depending on the nature of the ancillary ligands L [high performance liquid chromatography mass spectrometry (HPLC-MS) evidence] [78, 79]. This chemical lability is also mirrored in the wide variation of the *t*<sub>1/2</sub> of CORM-3, which is highest in saline (0.9% aqueous NaCl) and shortest in plasma [69]. This chemistry explains that CO<sub>2</sub> is released during the preparation of iCORM-3 instead of CO [78], and explains the very rapid formation of adducts of CORM-3 and other related complexes with proteins (serum albumin, transferrin, Hb, Mb, and lysozyme) which bear the *cis*-[Ru(CO)<sub>2</sub>(H<sub>2</sub>O)<sub>3</sub>]<sup>2+</sup> or [Ru(CO)(H<sub>2</sub>O)<sub>4</sub>]<sup>2+</sup> fragments as ascertained by electrospray ionization mass spectrometry (ESI-MS), Fourier transform infrared spectroscopy (FTIR), and X-ray crystallography [78, 79].

The interaction with proteins such as serum albumin and transferrin also explains why CORM-3 does not raise the values of COHb in systemic circulation at therapeutic doses, which is one of the most welcome characteristics of the *in vivo* therapy with CORM-3 [73, 83]. In fact, after the loss of one CO as CO<sub>2</sub>, the resulting *cis*-Ru<sup>II</sup>(CO)<sub>2</sub> fragments are very slow CO releasers, similar to iCORM-3, which is an unidentified mixture containing such species [78].

These results suggest that CORM-3 is transported in circulation as a serum albumin or transferrin adduct that slowly decomposes to release CO without sudden bursts. This kind of mechanism is supported by the observation of steady, low levels of CO in the treatment of mice with CORM-3 in a cardiovascular model [83]. One important consequence of this mechanism is that it lacks tissue specificity. Actually, CORM-3 is active in a broad variety of indications affecting different tissues and organs [62, 66]. Interestingly, the methylthiogalactose ligand was able to convey a reasonable liver specificity to complex ALF492 (Fig. 41.2), which became much more efficacious than CORM-3 in the protection of mice in a model of cerebral malaria [82].

CO gas protection in this model had been reported but at the cost of very high levels of systemic COHb. Most importantly, though, this work showed that ALF492 also targets the pharmacological expression of HO-1. Such induction of HO-1 had already been shown for CORM-2 and CORM-3 [84], and may be a component of the therapeutic efficacy of these and many other CORMs through the already mentioned CO/HO-1 forward–feedback loop. To complicate things further, both CORM-2 and CORM-3 (and the Mo(0) complexes described next) have been shown to produce ROS species in aqueous solution, thereby raising the difficulty in the interpretation of their biological action [25, 85].

*The Mo<sup>0</sup>(CO)<sub>n</sub> Derivatives ALF062, ALF186* At Alfama, the initial search for metal-based CORMs was supported by quantification of the release of CO to the headspace of the solutions of the compounds in biological media, such as RPMI-1640 (Roswell Park Memorial Institute-1640), PBS (Phosphate Buffer Saline), HEPES (2-[4-(2-hydroxyethyl)piperazin-1-yl]ethanesulfonic acid), saline, or plasma. The Mb assay was not used because it was thought important to check the profile of the complexes in aerobic conditions, which are absent in the Mb assay. This search revealed that the overwhelming majority of the 18-electron metal carbonyl complexes tested (>500) had a reasonable stability to air and water, opening many windows for their use as CORMs. This meant that many MCCs when incubated in biological media under normoxic conditions released CO at reasonably controlled rates. Lack of aqueous solubility was found to be the main barrier to their development but this can be overcome through the use of appropriately functionalized ligands.

In order to capitalize on the existing data on CO gas therapy, Alfama's initial choice of experimental CORMs fell on compounds that delivered physically detectable amounts of free CO to the biological subject, either *in vitro* or *in vivo*. For *in vitro* applications, CO release was quantified in the headspace of samples by the gas chromatography-reducing compound photometer (GC-RCP) by using a technique implemented by Vreman [86]. For *in vivo* applications, CO release was controlled by %COHb in circulation, measured by oximetry, or by CO in tissues, measured through GC-RCP [86]. The benchmarking compound in this strategy was the water-soluble *fac*-[Mo(CO)<sub>3</sub>(histidinate)]Na (ALF186; Fig. 41.2).

ALF186 is stable in air as a solid and in anaerobic aqueous solution, but releases CO in aerobic solutions. When dissolved in whole sheep blood *in vitro*, it almost instantaneously releases its full load of CO (3 equiv), which can be easily measured by the value of %COHb read in a standard oximeter. Analysis of the same blood by GC-RCP confirmed this quantitative release of CO. When administered to mice, the total load of CO is rapidly released producing a peak of systemic %COHb at circa 10 min post injection, which is dose dependent and highly reproducible. When this peak is attained, the mean arterial blood pressure (MABP) of the animals has a significant drop. After circa 2–3 h, the mice have exhaled all CO in circulation and returned their %COHb and MABP close to the original basal levels (Alfama, unpublished work). This kind of CO delivery partially mimics CO inhalation replacing the gas by a bolus of “solid CO,” which results in a much faster increase of systemic %COHb. The dose of ALF186 needed to deliver a desired amount of CO to the organism can be accurately calculated, and the time evolution of CO in circulation known beforehand. Oral administration leads to a CO peak at circa 1 h post administration, and higher doses are needed to reach a targeted %COHb value in comparison to the intraperitoneal (ip) or intravenous (iv) administration. This compound proved to be a very powerful experimental tool and showed dose-dependent therapeutic efficacy for CO in a variety of animal models of disease. Interestingly, in several cases, the efficacy

of CORM-3 and ALF186 were mutually exclusive. For instance, ALF186 inhibits indomethacin-induced stomach ulcers, while CORM-3 does not in the same model [87]. ALF186 rescues the liver in a mouse model of acetaminophen-induced acute liver failure, yet CORM-3 is ineffective (Alfama, unpublished work). The opposite is observed in the prevention of myocardial infarction injuries, where CORM-3 is very effective [73] and ALF186 is not. Examples were found where both CORM-3 and ALF186 work and where none of them works.

ALF062, our code number for one of the oldest known Mo<sup>0</sup> carbonyl complexes,  $[\text{Mo}(\text{CO})_5\text{Br}][\text{NEt}_4]$  [88], is a rather lipophilic CORM that can be administered orally in olive oil and gave very good results in the treatment of adjuvant-induced arthritis [89] in a rat model or as bactericide [90]. In both cases, CORM-3 is also effective [74, 90].

**Summary** This historical overview shows that the chemical space of organometallic carbonyls is a suitable source of therapeutically effective CORMs. However, the criteria that inform the search for useful CORMs have to be broad and carefully checked to avoid instances of compounds such as CORM-3 being excluded in GC or Mb assays or of spontaneous O<sub>2</sub>-activated CO releasers being excluded at the start. Ultimately, *in vivo* (or surrogate) experiments are decisive owing to their prodrug characteristics.

Most importantly, it may be remarked that in spite of their therapeutic efficacy, none of the compounds in Fig. 41.2 can be considered a drug because of their lack of pharmacological profile and druglike properties.

**41.3.3.2 The Search for Other Potential CORMs** The very intense and fruitful research effort supported by the experimental CORMs attracted other research groups to the field and new molecules emerged. These new CORMs can be divided according to the type of trigger that initiates CO release: chemical reactions (substitution, pH changes, oxidation), photochemical reactions, and enzymatic reactions.

**Chemically Triggered CO Release and CORMs** Most compounds described in this section are summarized in the structures depicted in Figs. 41.3 and 41.4. The former belong to well-known structural motifs of organometallic chemistry such as the  $[\text{Fe}^0(\text{CO})_3(\eta^4\text{-diene})]$ ,  $[(\text{CpR})\text{Fe}(\text{CO})_2\text{L}]^{0/+}$ ,  $[(\text{CpR})\text{Mo}(\text{CO})_3\text{L}]^{0/+}$  ( $\text{CpR}$  = substituted Cp, indenyl; L = 2e neutral or negative ligand),  $[\text{M}(\text{CO})_5\text{L}]^{0/-}$  (M = Cr, Mo, W; L = 2e neutral or negative ligand or Fischer carbene),  $[\mu_2\text{-}(\text{RC}\equiv\text{CR}')\text{Co}_2(\text{CO})_6]$ , and  $[\text{Mn}(\text{CO})_4\text{L}_2]^{0/+}$ . Compounds in Fig. 41.4 belong to a family of octahedral complexes stabilized by pentadentate N5 ligands.

In order to characterize the compounds and rank their potential as CORMs, most authors carried on the *in vitro* “standard set” of tests (SST) inaugurated with the development of CORM-2 and CORM-3. None of these compounds was tested *in vivo* in any animal model of disease. The SST comprises the analysis of the CO-release profile through the Mb assay ( $t_{1/2}$ ), the determination of the cytotoxicity (generally on RAW264.7 macrophages) through the LDH (lactate dehydrogenase) assay, the determination of the cell viability through the Alamar blue test, and the determination of the iNOS inhibition by measuring the amount of inhibition of NO induced by the CORM in a cell culture of RAW246.7 macrophages stimulated with the proinflammatory lipopolysaccharide (LPS). Inhibition of NO production in the latter test is considered a sign of the anti-inflammatory activity of the CORM. The SST was often accompanied by the determination of the vasodilatory properties of the CORM through its effect on the relaxation of isolated aortic rings precontracted with ephedrine [67]. The two last types of activities are typical for CO gas and are expected to be replicated by a CORM. In this context, the comparison of the CO-releasing profiles is given by the value of the CO-release half-life ( $t_{1/2}$ ) of the CORM.

In the family of  $[\text{Fe}^0(\text{CO})_3(\eta^4\text{-2-pyrone})]$  complexes, the least cytotoxic compound, CORM-F3, was also the one that showed the more favorable CO-release  $t_{1/2}$ , anti-inflammatory, and vasodilatory properties. The trigger of this CO release is not ascertained and the substitution pattern at the 2-pyrone ring controls the rate of CO release [91, 92].

The substitution at the Cp ring in the  $[(\text{CpR})\text{Fe}(\text{CO})_2\text{L}]^{0/+}$  family of complexes controls both the slow CO-release  $t_{1/2}$  and solubility [93]. The related  $[\text{Fe}(\eta^5\text{-C}_9\text{H}_7)(\text{CO})_2\text{L}]^{0/+}$  complexes are very slow CO releasers, clearly more toxic, and do not show any improvement of the CO release rate, which could be expected through the action of the “indenyl effect” [94].

The  $[\text{CpFe}(\text{CO})_2(\kappa^1\text{-2-pyrone})]^+$  complex behaved as a nonreleaser in the Mb assay but the Mo analog behaved as the a very rapid CO releaser, with tolerable cytotoxicity and a strong vasodilatory activity. However, the difference of CO release rates between both compounds remained unexplained [95]. The cobalt alkyne-bridged carbonyl complexes  $[\mu_2\text{-}(\text{RC}\equiv\text{CR}')\text{Co}_2(\text{CO})_6]$  are too lipophilic to enable extracting safe conclusions as to their real value as CORMs [96], and spurred the mechanistic studies conducted with several  $\text{M}(\text{CO})_5(\text{amino ester})$  and  $\text{Mo}(\text{CO})_5(=\text{CRR}')$  (examples in Fig. 41.3) in aqueous PBS solutions [97] and  $[\text{M}(\text{CO})_5\text{X}]^-$  (M = Cr, Mo, W; X = Cl, Br, I) [98], which brought forward some specificities of the behavior of MCCs in water.

The complex  $[\text{Mn}(\text{CO})_4\{\text{S}_2\text{CNMe}(\text{CH}_2\text{CO}_2\text{H})\}]$  was studied in some depth. The complex releases only 0.33 equiv of CO after 4 h at 37 °C in PBS [99]. Kinetic studies, including substitution by <sup>13</sup>CO, and computational calculations consider that

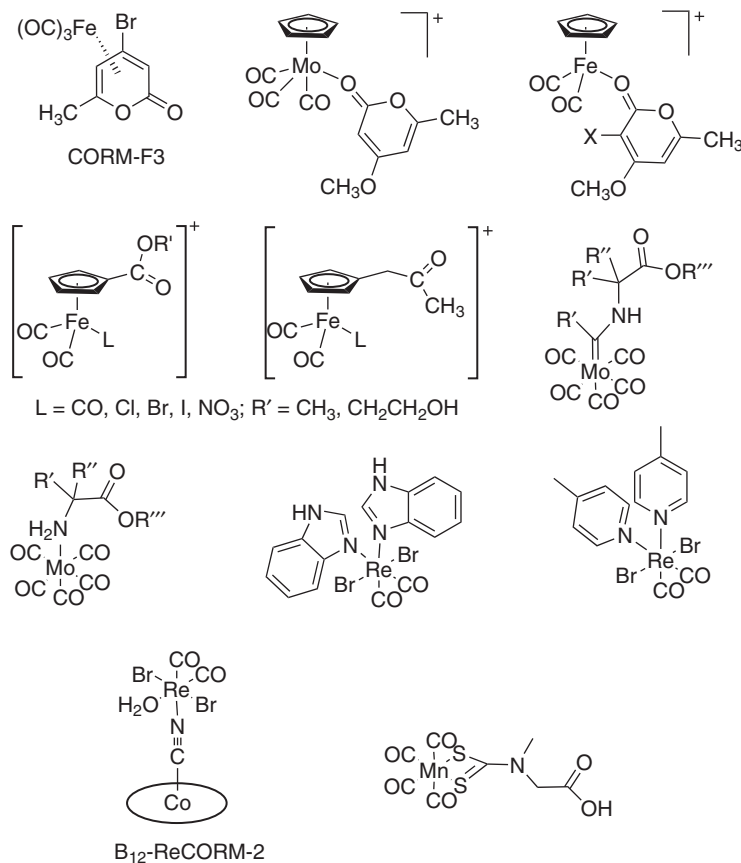


**Figure 41.3** Organometallic CORM candidates chemically triggered for CO release.

the loss of CO is dissociative and that the unsaturated 16-electron intermediate  $[\text{Mn}(\text{CO})_3\{\text{S}_2\text{CNMe}(\text{CH}_2\text{CO}_2\text{H})\}]$  efficiently recaptures CO in the absence of competing nucleophiles or CO scavengers. The fact that this release is dramatically extended to 3.2 equiv of CO in the Mb assay is interpreted by the authors as the result of the capture of CO by deoxy-Mb. However, use of dithionite-free deoxy-Mb decreases this CO release to circa 1.8 equiv [77]. DFT calculations support the dissociative mechanism proposed for a series of  $\text{Mn}(\text{CO})_4(\text{S},\text{S})$  type complexes, including the one above [100]. Thus, this CORM is a potential prodrug activated by a well-defined thermally induced CO dissociation. Although it has not been tested *in vivo*, the above characteristics suggest that it will have a CO-release profile similar to that of ALF186 in terms of the rate of systemic COHb formation. Thermally induced CO release can be a very useful tool for biological studies, namely, those made *in vitro* and *ex vivo* in the absence of the scavenging power of blood. A very well characterized family of such CO donors has been developed on the basis of pentadentate poly(pyridine) ligands such as those in Fig. 41.4 [101].

The lability of the CO is controlled by the type of N-donor function that occupies its trans position (this N-donor is circled in the scheme). The design can place CO trans to a negative carboxamido-N ( $\text{PaPy}3^-$ ; strong  $\sigma$ -donor), an imine-N ( $\text{SBPy}3$ ; moderately  $\pi$ -accepting), and a tertiary amine-N ( $\text{Tpmen}$ ; weak  $\sigma$ -donor) center, respectively. The SBPy3 and Tpmen complexes spontaneously release CO for  $\text{H}_2\text{O}$  in aqueous buffer, independently of the presence of  $\text{O}_2$  and effectively relax mouse aortic muscle rings in a dose-dependent manner. These very clean tests show that sGC is not involved in the relaxation mechanism but the  $\text{BK}_{\text{Ca}^{2+}}$  channels are. This contrasts with the  $[\text{Mn}(\text{CO})_4\{\text{S}_2\text{CNMe}(\text{CH}_2\text{CO}_2\text{H})\}]$  complex where sGC is considered to be implied in the vasodilation process [99]. However, both studies exclude the participation of the ATP-dependent  $\text{K}^+$  channels in the vasodilation. These  $[\text{Fe}(\text{N}5)(\text{CO})]^{2+}$  compounds ( $\text{N}5 = \text{SBPy}3$ ,  $\text{Tpmen}$ ) are the first ones with a really stable negative CORM control molecule. So, comparing the results obtained with  $[\text{Fe}(\text{N}5)(\text{CO})]^{2+}$  and  $[\text{Fe}(\text{N}5)(\text{H}_2\text{O})]^{2+}$  will be a very useful way of determining the genuine effects of CO delivery in the presence of CORMs and their genuine iCORM counterparts, in the absence of other physical (light, heat) or chemical difference. In all other compounds reported, namely, the experimental CORMs, the control complexes are undefined mixtures of metal-containing species, such as iCORM-3, and may produce rather strange results and dose-dependent outcomes [85]. Mo(0) complexes

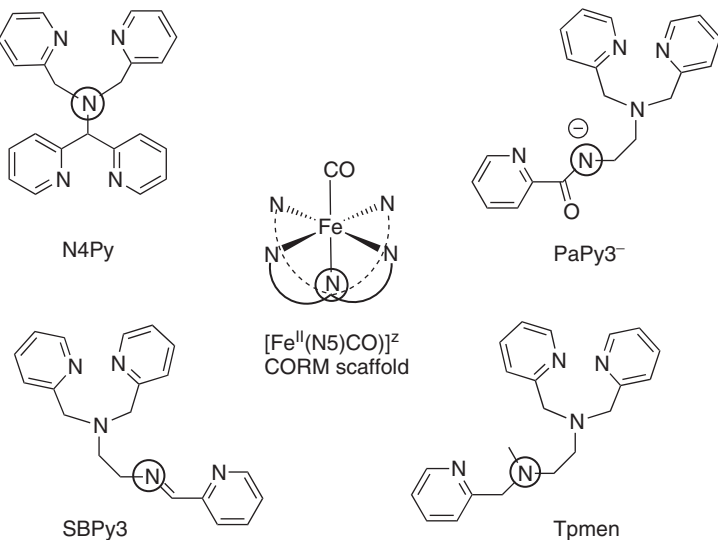


**Figure 41.4** Monocarbonyl complexes of the  $[\text{Fe}^{\text{II}}(\text{CO})(\text{N5})]^{z+}$  type.

are problematic in this respect, because once the CO is lost and the complex starts to oxidize, its chemistry becomes totally different from that of the original species and its scaffold is also rather different. Even the  $[\text{RuCl}_2(\text{DMSO})_4]$  complex is a false negative control for CORM-2 because the chemistry of the  $\text{Ru}(\text{CO})_3\text{Cl}_2(\text{DMSO})$  (the active component of CORM-2; Eq.1) is started by its water–gas shift reaction with water at the physiological pH.

The oldest example (1933) of a reversible CO carrier,  $[\text{Fe}(\text{l}-\text{cysteinate})_2(\text{CO})_2]^{2-}$ , was reexamined and the complex mixture of isomers reinterpreted in favor of the predominance of the *cis*- $\text{Fe}(\text{CO})_2$  species [102]. Since it is easily assembled from  $\text{Fe}^{2+}$ , CO, and cysteine, it could be formed close to sites of HO activity. Its toxicity is very low, yet it is totally inactive in the NO inhibition anti-inflammatory tests.

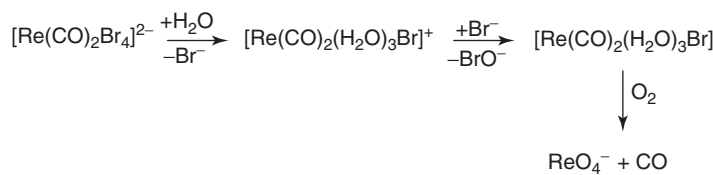
Breaking the usual dominance of 18-electron complexes in middle group transition metal organometallic chemistry, Zobi and coworkers [103] developed a remarkable series of 17-electron *cis-trans*- $[\text{Re}^{\text{II}}(\text{CO})_2\text{Br}_2\text{L}_2]$  complexes that are very efficient and competent CORMs and protect neonatal rat ventricular cardiomyocytes in an ischemia/reperfusion model *in vitro*. Only monodentate pyridine and imidazole-type ligands elicit the carbonylation of deoxy-Mb. The  $t_{1/2}$  value is sensitive to ligand substitution and pH, the pH being below the physiologic pH value (e.g., at pH 5.8). The ischemia-reperfusion tests cleanly reveal two crucial findings: (i) the rate of CO release in the Mb assay ( $t_{1/2}$ ) does not determine the cytoprotective effect and (ii) the compounds that offer best protection are those that do not permeate cell membranes. In this way, the most effective compound was the one with  $\text{L} = \text{benzimidazole}$  (Fig. 41.3), which is also the slowest releaser in the Mb assay. The compound with  $\text{L} = 4\text{-picoline}$  (Fig. 41.3) is a faster releaser but enters the cells and kills them.

The next big step from here was the synthesis of  $\text{B}_{12}\text{-ReCORM-2}$  (Fig. 41.3), which is the adduct of cyanocobalamin (vitamin B12) with the 17-electron fragment  $[\text{Re}(\text{CO})_2(\text{H}_2\text{O})\text{Br}_2]$  [104].

When administered at the “onset of reperfusion,”  $\text{B}_{12}\text{-ReCORM-2}$  is strongly cytoprotective in the ischemia-reperfusion of neonatal rat cardiomyocytes (NRC) in culture. The introduction of the biological ligand improved not only the solubility but also the activity and stability of the original  $[\text{Re}^{\text{II}}(\text{CO})_2]$  fragment.  $\text{B}_{12}\text{-ReCORM-2}$  does not penetrate cells. It does not impair the oxygen consumption of the NRC under the conditions of cytoprotection but shows acute antioxidant properties at the “onset of reperfusion,” which is attributed to the oxidation of the low valent Re(II) to the final  $\text{ReO}_4^-$ .

This system represents a major advance toward pharmaceutically acceptable CORMs because it provides important insights into the relationship between the CORM and the cell, which are necessary for the appearance of therapeutic activity, and also because it shows how the presence of biocompatible coordination spheres can improve the activity of CORMs.  $\text{B}_{12}\text{-ReCORM-2}$  undergoes rapid hydrolysis losing the two  $\text{Br}^-$  ligands before releasing CO. A  $\text{Re}^{\text{I}}(\text{CO})$  species was identified by ESI-MS, showing that a reduction of the Re(II) takes place in the process. A study on the mechanism of the decomposition of the parent  $[\text{Re}^{\text{II}}(\text{CO})_2\text{Br}_4]^{2-}$  proposes that such reduction is carried out by  $\text{Br}^-$  as summarized in Scheme 41.1.

Interestingly, the CO seems to be released from the stable Re(I) species upon oxidation, forming perrhenate. This oxidation parallels the formation of polyoxomolybdates from the oxidation of the Mo(0) complexes such as ALF186.

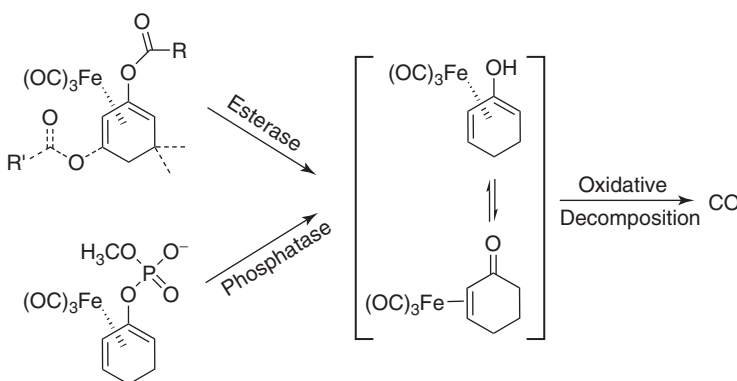


**Scheme 41.1** Decomposition of the 17-electron  $[\text{Re}(\text{CO})_2\text{Br}_4]^{2-}$  in aqueous medium.

**Enzyme-Triggered CO Release: ET-CORMs** In 2011, the first example of enzymatically triggered CO releasing molecules (ET-CORM) was published [105]. These acyloxy cyclohexadiene–iron tricarbonyl complexes are activated by esterase cleavage, producing the unstable diene-alcohol intermediate, which isomerizes to the ene-one complex (Scheme 41.2). Loss of this labile ligand allows rapid access of  $\text{O}_2$  to the coordination sphere of the  $\text{Fe}(\text{CO})_3$  fragment, which irreversibly decomposes to release CO, the ene-one ligand, and  $\text{Fe}^{n+}$  ions. This trigger mechanism was substantiated by CO-release experiments (Mb assay) and by the inhibition of NO production in the LPS-induced RAW246.7 macrophage cellular assay. Complexes such as  $\text{ET}_{\text{ac}}\text{-CORM-1}$  only released CO to deoxy-Mb and only inhibited NO production in the LPS-induced macrophage assay in the presence of an esterase. The best complex studied,  $\text{ET}_{\text{ac}}\text{-CORM-1}$  (Fig. 41.5), is a very potent inhibitor of iNOS in this macrophage test (30% NO inhibition at  $5 \mu\text{M}$ ), although it still has some toxicity. The (acyloxydiene) $\text{Fe}(\text{CO})_3$  complexes prepared do not respond equally to all esterases or lipases. Instead, each one of them seems to have a preference for a given type of esterase unless they are not very pure. This characteristic is very important because it brings an additional level of selectivity to the activation process. An extended variation of the substituents at the acyloxydiene ligand enabled the first structure–activity relationships: (i) high biological activity requires the acyl group to lie outside the diene system (dashed acyl in Scheme 41.2); (ii) increasing bulk of the acyl group decreases both NO inhibition activity and toxicity; (iii) introduction of a second acyloxy ester increases both NO inhibition activity and toxicity; and (iv) methylation of the ring (dashed methyl substituents in Scheme 41.2) strongly decreases toxicity only at the cost of a small decrease in activity. This led to the selection of the two complexes  $\text{ET}_{\text{ac}}\text{-CORM-1}$  and  $\text{ET}_{\text{ac}}\text{-CORM-2}$  (Fig. 41.5) as the best compounds, although the higher toxicity of  $\text{ET}_{\text{ac}}\text{-CORM-2}$  makes  $\text{ET}_{\text{ac}}\text{-CORM-1}$  the overall best choice of the compounds studied.

The possibility to control biological activity through the ligand sphere had been mentioned by several authors before, but this study was the first to be published with a rational framework for equipping CORMs with tissue or cell-specific active targeting. This approach has now been extended to a phosphatase-triggered CORM by decorating the diene ligand with phosphoryloxy groups as depicted in Scheme 41.2 [106].

Although the screening of phosphatases is still limited and unsatisfactory, the proof-of-concept was obtained based on the same platform of tests, that is CO release and iNOS inhibition promoted by the (phosphoryloxydiene) $\text{Fe}(\text{CO})_3$  CORMs in the presence of phosphatases. Interestingly, the more favored position of the phosphoryloxy substituent is now in the “inner” position ( $\text{ET}_{\text{P}}\text{-CORM-1}$ ) (Fig. 41.5) of the diene ligand instead of the “outer” position ( $\text{ET}_{\text{P}}\text{-CORM-2}$ ) that was favored for the esterase-triggered acyloxy complexes ( $\text{ET}_{\text{ac}}\text{-CORM-1}$ ).



**Scheme 41.2** Reaction pathways of enzyme-triggered CORMs.

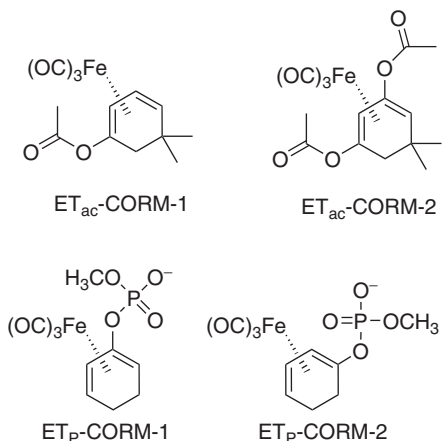


**Figure 41.5** Enzyme-triggered CORMs.

**Light-Triggered CO Release: PhotoCORMs** Cleavage of the M–CO bonds by light is a general property of MCCs and its first application to CO release used  $\text{Mn}_2(\text{CO})_{10}$  irradiation to deliver CO to the mice kidneys *in vivo* [107]. In 2008, Schatzschneider [108] reported that the photolysis of  $[(\text{tpm})\text{Mn}(\text{CO})_3]^+$  (tpm = tris(pyrazolyl)methane) releases 2 equiv of CO and results in a potent cytotoxic agent toward HT29 human colon cancer cells comparable to 5-fluorouracil (5-FU), an established anticancer drug. The biological action remains to be definitely assigned to CO, the decarbonylated metal fragment, or both. Importantly, Raman microscopy revealed that  $[(\text{tpm})\text{Mn}(\text{CO})_3]^+$  accumulates preferably at the cell wall and nucleus [109]. Active targeting of  $[(\text{tpm})\text{Mn}(\text{CO})_3]^+$  to the tumor tissue was approached by appending specific peptides to the tpm ligand [110]. Passive targeting through the enhanced permeability and retention effect of tumoral tissues was approached by grafting the  $[\text{Mn}^I(\text{CO})_3]^+$  motif on the surface of  $\text{SiO}_2$  nanoparticles [111] or polymeric methacrylate-based backbones [112].

The complex  $[\text{Fe}^{II}(\text{CO})(\text{N}4\text{Py})]^2+$  (Fig. 41.4) provides a similar platform for photodynamic therapy of cancer [113]. More in tune with the usual biological activity of CO, photoCORMs based on the  $[\text{Mn}^I(\text{CO})_3]^+$  fragment and tripodal polypyridine amine ligands effectively relax isolated aortic rings [114], whereas *cis*- $[\text{Fe}(\text{CO})_2(\text{SCH}_2\text{CH}_2\text{NH}_2)_2]$  activates  $\text{BK}_{\text{Ca}^{2+}}$  channels [115].

The photoCORM field was recently reviewed and attention called to the need to define the therapeutic targets to treat with CO or the decarbonylated metal fragment [116, 117]. PhotoCORMs have the great advantage that they have a “clean” triggering mode where an “onset” of therapy can be accurately defined and literally “switched on” by the use of a light source. However, their use will certainly remain limited to administration within hospital settings under strict medical/surgical control. In this way, photoCORMs share common limitations with CO inhalation.

#### 41.3.4 Making Pharmaceutically Acceptable or Druglike CORMs

At Alfama the ultimate goal is to develop CORMs that can be taken by any patient in the absence of direct medical assistance, that is, in ambulatory regimen. Therefore, CORMs must be pharmaceutically acceptable and behave like other regular drugs or prodrugs. They must be stable to air, water and blood, soluble in water, toxicologically safe, therapeutically effective and potent, and exhibit a recognizable and acceptable pharmacokinetic profile. Ideally, each one of them must be equipped to target a specific tissue where it decomposes and delivers the CO. Although producing many arguments in favor of CORM therapy, the experimental CORMs lacked such druglike properties. ALF062 and CORM-2 are not water soluble, whereas CORM-3 and ALF186 are decomposed by aqueous, aerobic, biologically compatible solutions at physiological pH, as well as by plasma or blood, thereby losing any kind of controllable pharmacokinetic profile or tissue specificity.

In early 2009, Alfama put together a methodology to produce druglike CORMs by selecting and assembling the building units of the model CORM depicted below (Fig. 41.6) in order to enable the final prodrug to target and specifically release therapeutic CO at the disease site [118].

This model CORM has three layers: the central metal ion, the first coordination sphere (inner sphere) formed by the ligands directly attached to the metal including the active principle CO, and an outer sphere (drug sphere) formed by the distal functional groups appended to the ligands, which largely control the solubility, biocompatibility, targeting,

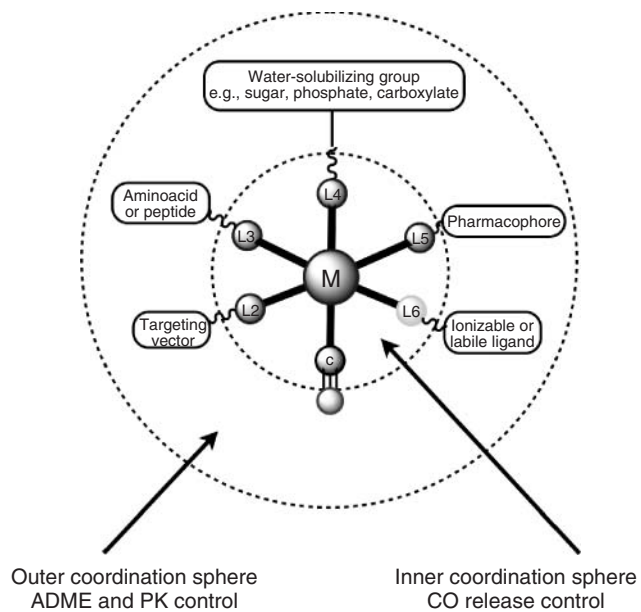


**Figure 41.6** Conceptual model of a druglike CORM. The number of CO ligands can be greater than 1 and the other ancillary ligands (L<sub>2</sub>–L<sub>6</sub>) can be the same or different. Distal substituents are just given as possible examples. ADME, administration, distribution, metabolism, and excretion; PK, pharmacokinetics.

pharmacological [absorption, distribution, metabolism, and excretion (ADME), pharmacokinetics (PK)], and toxicological properties of the prodrug. A wealth of data obtained from the broad screening of several hundred MCCs helped defining the inner sphere, whereas available tools of medicinal chemistry, metal-based drugs [119, 120], and radiopharmaceutical carbonyls,  $[M^I(CO)_3L_3]^{z\pm}$  ( $M = {}^{99m}Tc$  and Re) [64, 121], provide much of the information necessary to build the drug sphere.

Most importantly, the process requires the *a priori* identification of the disease to be treated by CO. The nature of the tissue, the specificities of the disease, and even of the type of drug administration are fundamental to define the types of functions of the outer sphere that guarantee adequate targeting of the drug. We have already mentioned the liver targeting obtained with ALF492 (Fig. 41.2) [82]. The choice of the tissues to treat helps in selecting the best local triggers that promote the cleavage of the inner sphere and initiate the release of CO. Among other factors, this chemistry is dependent on the metal, the choice of which is of paramount importance. The toxicity of a complex does not depend solely on the metal, rather on the whole molecule. However, CORMs decompose, generating new metal fragments that may accumulate and/or become toxic. Our contention is that the choices are reduced to Mn(I), Re(I–II), Fe(0), Fe(II), Ru(II), and Mo(0–IV) [118]. If one accounts for nonchemical arguments and prejudice against metals often met even in the drug-development industry, this choice may be even narrower. In general, inner spheres should obey the 18-electron rule although the paramagnetic, 17-electron Re(II) CORMs developed by Zobi et al. [104] really shattered this paradigm. Any ancillary ligand is allowed, in principle, unless open toxicity forbids. The combination of such ligands in the inner sphere dictates CORM stability, trigger type, and CO-release profile. Here is where the organometallic chemist has the most exciting playground because the number of options is very large, not necessarily obvious, and eventually redundant.

At Alfama, the medical indication chosen was the treatment (rescue) of acute liver failure induced by acetaminophen (Tylenol®, paracetamol), where the activity of CO gas had already been demonstrated in animal models (Fig. 41.7) [51]. The treatment is restricted to the critical care room where injectable drugs are preferred [122]. The goal was to obtain a CORM providing total liver rescue within a wide time window, enabling later onset of treatment after intoxication challenge, thus outperforming the present treatment with *N*-acetylcysteine.

The metal chosen was Mo(0), the ligand sphere was tested for a very large variety of combinations of CO with C, N, O, S, and P ligands in the  $Mo(CO)_5L$ ,  $Mo(CO)_4L_2$ , and  $Mo(CO)_3L_3$  stoichiometries. The ligands were decorated with functions that provide for enhanced solubility in water at physiological pH but had also tunable lipophilicity to gain liver specificity and avoid rapid excretion.

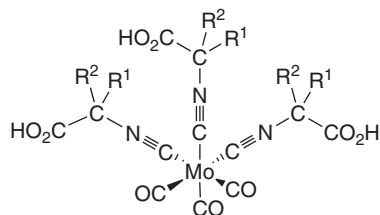


**Figure 41.7** General structure of the family of CORMs selected for treatment of acute liver failure, induced by acetaminophen (Tylenol<sup>®</sup>, paracetamol) poisoning. The lead compound, ALF794, corresponds to R<sup>1</sup>, R<sup>2</sup> = CH<sub>3</sub> [123].

New compounds were pushed along a pass/fail multistep testing protocol that followed the order: water solubility; stability in water, plasma, and whole blood; and hemolysis. Each failure resulted in the compound being discarded. Those passing the hemolysis test entered cytotoxicity tests in several cell lines, and, when positively cleared, entered the *in vivo* animal model test. The best readouts of acute liver failure rescue were obtained for the family of isocyanide derivatives Mo(CO)<sub>3</sub>(CNCR<sup>1</sup>R<sup>2</sup>COOH)<sub>3</sub>.

Such readouts include the inhibition of liver cell death measured by the dose-dependent reduction of the levels of the transaminase (ALT) and confirmed by liver histology, and total survival in a lethal model of acetaminophen poisoning [123]. Variation of the R<sup>1</sup> and R<sup>2</sup> substituents allowed the fine tuning of the biological activity and ADME properties. None of these compounds carbonylated whole blood *in vitro*. However, *in vivo*, low, sustained levels of COHb appeared in circulation, suggesting metabolic activation. Indeed, both rat and human liver microsomes accelerate the release of CO from the best compounds, relative to release in buffer. The distribution of CO in the tissues revealed a very high level of liver specificity that correlated directly with the biological activity *in vivo*. The PK profile of the more active compound Mo(CO)<sub>3</sub>(CNCMe<sub>2</sub>COOH)<sub>3</sub> (ALF794) was very much like that of a regular drug and straightforward to determine by standard HPLC methods. Last, but not least, *in vivo* acute toxicity is unusually low [maximum tolerated dose (MTD) > 1000 mg/kg]. ALF794 has, therefore, a full pharmacologically acceptable, druglike profile and its development is being pursued.

#### 41.4 FINAL REMARKS AND PERSPECTIVES

The biology and chemistry that was described in the sections above shows that CO is a very powerful therapeutic principle and that metal carbonyls can mediate the delivery of CO in a pharmacologically useful manner. However, to meet this goal, the design of CORMs requires inputs beyond simple CO-release kinetics and cell toxicity assays. The pharmaceutical CORMs of the future must have properties that are similar to those common to any other drug or prodrug in terms of physical–chemical and biocompatibility properties, toxicological safety, efficacy, potency, and general pharmacological ADME and PK properties. If we can prepare CORMs that specifically reach the disease targets and release CO there, we will certainly make many useful drugs. Moreover, the production of CORMs should be much more cost effective than that of most modern therapeutic approaches—such as recombinant proteins, antibodies, gene therapy, or, more recently, cell therapy. However, in order to achieve this end, it is necessary that the organometallic chemists learn to speak beyond their usual jargon and collaborate with other specialists, namely, pharmacologists, drug developers, physiologists, and medical doctors who can show them the profiles and properties of the drugs that are needed. These 11 years of CORM development have taken us over a number of barriers and it is now clear that making metal carbonyl complexes with real pharmacological application is not only possible but will be part of the future of organometallic chemistry.

#### REFERENCES

1. Herrmann, W. A. *J. Organomet. Chem.* **1990**, *383*, 21.
2. Trout, W. E. *J. Chem. Educ.* **1938**, *15*, 77.
3. Sjöstrand, T. *Nature* **1949**, *164*, 580.
4. Tenhunen, R.; Marver, H. S.; Schmid, R. *Proc. Natl. Acad. Sci. U.S.A.* **1968**, *61*, 748.
5. Verma, A.; Hirsch, D. J.; Glatt, C. E.; Ronnett, G. V.; Snyder, S. H. *Science* **1993**, *259*, 381.

6. Volbeda, A.; Charon, M.; Piras, C.; Hatchikian, E.; Frey, M.; Fontecillacamps, J. *Nature* **1995**, *373*, 580.
7. Peters, J.; Lanzilotta, W.; Lemon, B.; Seefeldt, L. *Science* **1998**, *282*, 1853.
8. Herrmann, F.; List, H. Patent WO 0,035,105, **1995**.
9. Ryter, S. W.; Alam, J.; Choi, A. M. *Physiol. Rev.* **2006**, *86*, 583.
10. Gozzelino, R.; Jeney, V.; Soares, M. P. *Annu. Rev. Pharmacol.* **2010**, *50*, 323.
11. Parfenova, H.; Leffler, C. W. *Curr. Pharm. Des.* **2008**, *14*, 443.
12. Schipper, H. M. *Free Radic. Biol. Med.* **2004**, *37*, 1995.
13. Vesely, M. J.; Exon, D. J.; Clark, J. E.; Foresti, R.; Green, C. J.; Motterlini, R. *Am. J. Physiol.* **1998**, *275*, C1087.
14. Roberts, G.; Youn, H.; Kerby, R. *Microbiol. Mol. Biol. Rev.* **2004**, *68*, 453.
15. Motterlini, R.; Otterbein, L. E. *Nat. Rev. Drug Discov.* **2010**, *9*, 728.
16. Soares, M. P.; Bach, F. H. *Trends Mol. Med.* **2009**, *15*, 50.
17. Otterbein, L.; Bach, F.; Alam, J.; Soares, M.; Lu, H.; Wysk, M.; Davis, R.; Flavell, R.; Choi, A. *Nat. Med.* **2000**, *6*, 422.
18. Fagone, P.; Mangano, K.; Quattrocchi, C.; Motterlini, R.; Di Marco, R.; Magro, G.; Penacho, N.; Romão, C. C.; Nicoletti, F. *Clin. Exp. Immunol.* **2011**, *163*, 368.
19. Brouard, S.; Otterbein, L. E.; Anrather, J.; Tobiasch, E.; Bach, F. H.; Choi, A. M.; Soares, M. P. *J. Exp. Med.* **2000**, *192*, 1015.
20. Queiroga, C. S. F.; Almeida, A. S.; Martel, C.; Brenner, C.; Alves, P. M.; Vieira, H. L. A. *J. Biol. Chem.* **2010**, *285*, 17077.
21. Vieira, H. L.; Queiroga, C. S.; Alves, P. M. *J. Neurochem.* **2008**, *107*, 375.
22. Song, R.; Mahidhara, R. S.; Zhou, Z.; Hoffman, R. A.; Seol, D. W.; Flavell, R. A.; Billiar, T. R.; Otterbein, L. E.; Choi, A. M. *J. Immunol.* **2004**, *172*, 1220.
23. Otterbein, L. E.; Zuckerbraun, B. S.; Haga, M.; Liu, F.; Song, R.; Usheva, A.; Stachulak, C.; Bodyak, N.; Smith, R. N.; Csizmadia, E.; Tyagi, S.; Akamatsu, Y.; Flavell, R. J.; Billiar, T. R.; Tzeng, E.; Bach, F. H.; Choi, A. M. K.; Soares, M. P. *Nat. Med.* **2003**, *9*, 183.
24. Taille, C.; El-Benna, J.; Lanone, S.; Boczkowski, J.; Motterlini, R. *J. Biol. Chem.* **2005**, *280*, 25350.
25. Tavares, A. F. N.; Teixeira, M.; Romão, C. C.; Seixas, J. D.; Nobre, L. S.; Saraiva, L. M. *J. Biol. Chem.* **2011**, *286*, 26708.
26. Bannenberg, G. L.; Vieira, H. L. *Expert Opin. Ther. Pat.* **2009**, *19*, 663.
27. Boczkowski, J.; Poderoso, J. J.; Motterlini, R. *Trends Biochem. Sci.* **2006**, *31*, 614.
28. Zuckerbraun, B. S.; Chin, B. Y.; Bilban, M.; de Costa d'Avila, J.; Rao, J.; Billiar, T. R.; Otterbein, L. E. *FASEB J.* **2007**, *21*, 1099.
29. Suliman, H. B.; Carraway, M. S.; Tatro, L. G.; Piantadosi, C. A. *J. Cell Sci.* **2007**, *120*, 299.
30. Queiroga, C. S. F.; Almeida, A. S.; Vieira, H. L. A. *Biochem. Res. Int.* **2012**, *2012*, 749845.
31. Chance, B.; Erecinska, M.; Wagner, M. *Ann. N. Y. Acad. Sci.* **1970**, *174*, 193.
32. Brown, S. D.; Piantadosi, C. A. *J. Appl. Physiol.* **1990**, *68*, 604.
33. Brown, S. D.; Piantadosi, C. A. *J. Clin. Invest.* **1992**, *89*, 666.
34. D'Amico, G.; Lam, F.; Hagen, T.; Moncada, S. *J. Cell Sci.* **2006**, *119*, 2291.
35. Queiroga, C. S. F.; Almeida, A. S.; Alves, P. M.; Brenner, C.; Vieira, H. L. A. *BMC Cell Biol.* **2011**, *12*: 10.
36. Almeida, A. S.; Queiroga, C. S.; Sousa, M. F.; Alves, P. M.; Vieira, H. L. A. *J. Biol. Chem.* **2012**, *287*, 10761.
37. Wang, X.; Wang, Y.; Kim, H. P.; Nakahira, K.; Ryter, S. W.; Choi, A. M. *J. Biol. Chem.* **2007**, *282*, 1718.
38. Basuroy, S.; Tcheranova, D.; Bhattacharya, S.; Leffler, C. W.; Parfenova, H. *Am. J. Physiol. Cell Physiol.* **2011**, *300*, C256.
39. Rodriguez, A. I.; Gangopadhyay, A.; Kelley, E. E.; Pagano, P. J.; Zuckerbraun, B. S.; Bauer, P. M. *Arterioscler. Thromb. Vasc. Biol.* **2010**, *30*, 98.
40. Tang, X. D.; Xu, R.; Reynolds, M. F.; Garcia, M. L.; Heinemann, S. H.; Hoshi, T. *Nature* **2003**, *425*, 531.
41. Wang, R.; Wu, L. *J. Biochem.* **1997**, *272*, 8222.
42. Riesco-Fagundo, A. M.; Perez-Garcia, M. T.; Gonzalez, C.; Lopez-Lopez, J. R. *Circ. Res.* **2001**, *89*, 430.
43. Jaggar, J. H.; Li, A.; Parfenova, H.; Liu, J.; Umstot, E. S.; Dopico, A. M.; Leffler, C. W. *Circ. Res.* **2005**, *97*, 805.
44. Williams, S. E.; Wootton, P.; Mason, H. S.; Bould, J.; Iles, D. E.; Riccardi, D.; Peers, C.; Kemp, P. J. *Science* **2004**, *306*, 2093.
45. Scragg, J. L.; Dallas, M. L.; Wilkinson, J. A.; Varadi, G.; Peers, C. *J. Biol. Chem.* **2008**, *283*, 24412.
46. Lim, I.; Gibbons, S. J.; Lyford, G. L.; Miller, S. M.; Stregel, P. R.; Sarr, M. G.; Chatterjee, S.; Szurszewski, J. H.; Shah, V. H.; Farrugia, G. *Am. J. Physiol. Gastrointest. Liver Physiol.* **2005**, *288*, G7.
47. Wilkinson, W. J.; Kemp, P. J. *J. Physiol.* **2011**, *589*, 3055.
48. Brune, B.; Ullrich, V. *Mol. Pharmacol.* **1987**, *32*, 497.
49. Sarady, J. K.; Zuckerbraun, B. S.; Bilban, M.; Wagner, O.; Usheva, A.; Liu, F.; Ifedigbo, E.; Zamora, R.; Choi, A. M. K.; Otterbein, L. E. *FASEB J.* **2004**, *18*, 854.
50. Sun, B.; Zou, X.; Chen, Y.; Zhang, P.; Shi, G. *Int. J. Biol. Sci.* **2008**, *4*, 270.

51. Zuckerbraun, B.; Billiar, T.; Otterbein, S.; Kim, P.; Liu, F.; Choi, A.; Bach, F.; Otterbein, L. *J. Exp. Med.* **2003**, *198*, 1707.
52. Mann, B. E.; Motterlini, R. *Chem. Commun.* **2007**, 4197.
53. Wang, X. M.; Kim, H. P.; Song, R.; Choi, A. M. *Am. J. Respir. Cell Mol. Biol.* **2006**, *34*, 434.
54. Kim, H. P.; Wang, X.; Zhang, J. L.; Suh, G. Y.; Benjamin, I. J.; Ryter, S. W.; Choi, A. M. K. *J. Immunol.* **2005**, *175*, 2622.
55. Kim, H. P.; Wang, X.; Nakao, A.; Kim, S. I.; Murase, N.; Choi, M. E.; Ryter, S. W.; Choi, A. M. K. *Proc. Natl. Acad. Sci. U.S.A.* **2005**, *102*, 11319.
56. Hampson, N. B.; Hauff, N. M. *Am. J. Emerg. Med.* **2008**, *26*, 665.
57. Goldbaum, L.; Ramirez, R.; Absalon, K. *Aviat. Space Environ. Med.* **1975**, *46*, 1289.
58. De Matos, M. N.; Romão, C. C. U.S. Patent 7, 968, 605, **2011**.
59. Buelow, R.; Woo, J. Patent WO 0,078,684, **2002**.
60. Pitchumony, T. S.; Spangler, B.; Motterlini, R.; Alberto, R. *Org. Biomol. Chem.* **2010**, *8*, 4849.
61. Alberto, R.; Motterlini, R. *Dalton Trans.* **2007**, 1651.
62. Mann, B. E. In *Medicinal Organometallic Chemistry*; Jaouen, G.; Metzler-Nolte, N., Eds.; Topics in Organometallic Chemistry, Vol. 32; Springer-Verlag: Berlin, Heidelberg, **2010**.
63. Santos, I.; Paulo, A.; Correia, J. *Top. Curr. Chem.* **2005**, *252*, 45.
64. Alberto, R. *Eur. J. Inorg. Chem.* **2009**, 21.
65. Uehara, T.; Uemura, T.; Hirabayashi, S.; Adachi, S.; Odaka, K.; Akizawa, H.; Magata, Y.; Irie, T.; Arano, Y. *J. Med. Chem.* **2007**, *50*, 543.
66. Mann, B. *Organometallics* **2012**, *31*, 5728.
67. Motterlini, R.; Clark, J.; Foresti, R.; Sarathchandra, P.; Mann, B.; Green, C. *Circ. Res.* **2002**, *90*, E17.
68. Clark, J.; Naughton, P.; Shurey, S.; Green, C.; Johnson, T.; Mann, B.; Foresti, R.; Motterlini, R. *Circ. Res.* **2003**, *93*, E2.
69. Motterlini, R.; Mann, B. E.; Johnson, T. R.; Clark, J. E.; Foresti, R.; Green, C. *J. Curr. Pharm. Des.* **2003**, *9*, 2525.
70. Bagul, A.; Hosgood, S. A.; Kaushik, M.; Nicholson, M. L. *Transplantation* **2008**, *85*, 576.
71. Pizarro, M. D.; Rodriguez, J. V.; Mamprin, M. E.; Fuller, B. J.; Mann, B. E.; Motterlini, R.; Guibert, E. E. *Cryobiology* **2009**, *58*, 248.
72. Musameh, M.; Green, C.; Mann, B.; Fuller, B.; Motterlini, R. *J. Heart Lung Transplant.* **2007**, *26*, 1192.
73. Guo, Y.; Stein, A. B.; Wu, W.-J.; Tan, W.; Zhu, X.; Li, Q.-H.; Dawn, B.; Motterlini, R.; Bolli, R. *Am. J. Physiol. Heart Circ. Physiol.* **2004**, *286*, H1649.
74. Ferrandiz, M. L.; Maicas, N.; Garcia-Arnandis, I.; Terencio, M. C.; Motterlini, R.; Devesa, I.; Joosten, L. A. B.; van den Berg, W. B.; Alcaraz, M. J. *Ann. Rheum. Dis.* **2008**, *67*, 1211.
75. Maicas, N.; Ferrández, M. L.; Devesa, I.; Motterlini, R.; Koenders, M. I.; van den Berg, W. B.; Alcaraz, M. J. *Eur. J. Pharmacol.* **2010**, *634*, 184.
76. Atkin, A. J.; Lynam, J. M.; Moulton, B. E.; Sawle, P.; Motterlini, R.; Boyle, N. M.; Pryce, M. T.; Fairlamb, I. J. S. *Dalton Trans.* **2011**, *40*, 5755.
77. McLean, S.; Mann, B. E.; Poole, R. K. *Anal. Biochem.* **2012**, *427*, 36.
78. Santos-Silva, T.; Mukhopadhyay, A.; Seixas, J.; Bernardes, G.; Romão, C.; Romão, M. *J. Am. Chem. Soc.* **2011**, *133*, 1192.
79. Santos, M. F. A.; Seixas, J. D.; Coelho, A. C.; Mukhopadhyay, A.; Reis, P. M.; Romão, M. J.; Romão, C. C.; Santos-Silva, T. J. *Inorg. Biochem.* **2012**, *117*, 285.
80. Michel, B. W.; Lippert, A. R.; Chang, C. J. *J. Am. Chem. Soc.* **2012**, *134*, 15668.
81. Johnson, T. R.; Mann, B. E.; Teasdale, I. P.; Adams, H.; Foresti, R.; Green, C. J.; Motterlini, R. *Dalton Trans.* **2007**, 1500.
82. Pena, A. C.; Penacho, N.; Mancio-Silva, L.; Neres, R.; Seixas, J. D.; Fernandes, A. C.; Romão, C. C.; Mota, M. M.; Bernardes, G. J. L.; Pamplona, A. *Antimicrob. Agents Chemother.* **2012**, *56*, 1281.
83. Wang, G.; Hamid, T.; Keith, R. J.; Zhou, G.; Partridge, C. R.; Xiang, X.; Kingery, J. R.; Lewis, R. K.; Li, Q.; Rokosh, D. G.; Ford, R.; Spinale, F. G.; Riggs, D. W.; Srivastava, S.; Bhatnagar, A.; Bolli, R.; Prabhu, S. D. *Circulation* **2010**, *121*, 1912.
84. Sawle, P.; Foresti, R.; Mann, B. E.; Johnson, T. R.; Green, C. J.; Motterlini, R. *Br. J. Pharmacol.* **2005**, *145*, 800.
85. Marazioti, A.; Bucci, M.; Coletta, C.; Vellecco, V.; Baskaran, P.; Szabó, C.; Cirino, G.; Marques, A. R.; Guerreiro, B.; Gonçalves, A. M. L.; Seixas, J. D.; Beuve, A.; Romão, C. C.; Papapetropoulos, A. *Arterioscler. Thromb. Vasc. Biol.* **2011**, *31*, 2570.
86. Vreman, H.; Wong, R.; Kadotani, T.; Stevenson, D. *Anal. Biochem.* **2005**, *341*, 280.
87. Rodrigues, S. S.; Seixas, J. D.; Guerreiro, B.; Pereira, N. M. P.; Romão, C. C.; Haas, W. E.; Gonçalves, I. U.S. patent 0,038,955, **2011**.
88. Abel, E. W.; Reid, J. G.; Butler, I. S. *J. Chem. Soc.* 1963, **2068**.
89. Haas, W. E.; Romão, C. C.; Royo, B.; Fernandes, A. C.; Gonçalves, I. U.S. patent 0,233,890, **2006**.

90. Nobre, L. S.; Seixas, J. D.; Romão, C. C.; Saraiva, L. M. *Antimicrob. Agents Chemother.* **2007**, *51*, 4303.
91. Sawle, P.; Hammad, J.; Fairlamb, I.; Moulton, B.; O'Brien, C.; Lynam, J.; Duhme-Klair, A.; Foresti, R.; Motterlini, R. *J. Pharm. Exp. Ther.* **2006**, *318*, 403.
92. Fairlamb, I.; Duhme-Klair, A.; Lynam, J.; Moulton, B.; O'Brien, C.; Sawle, P.; Hammad, J.; Motterlini, R. *Bioorg. Med. Chem. Lett.* **2006**, *16*, 995.
93. Scapens, D.; Adams, H.; Johnson, T. R.; Mann, B. E.; Sawle, P.; Aqil, R.; Perrior, T.; Motterlini, R. *Dalton Trans.* **2007**, 4962.
94. Hewison, L.; Crook, S. H.; Johnson, T. R.; Mann, B. E.; Adams, H.; Plant, S. E.; Sawle, P.; Motterlini, R. *Dalton Trans.* **2010**, *39*, 8967.
95. Fairlamb, I. J. S.; Lynam, J. M.; Moulton, B. E.; Taylor, I. E.; Duhme-Klair, A. K.; Sawle, P.; Motterlini, R. *Dalton Trans.* **2007**, 3603.
96. Atkin, A. J.; Williams, S.; Sawle, P.; Motterlini, R.; Lynam, J. M.; Fairlamb, I. J. S. *Dalton Trans.* **2009**, 3653.
97. Zhang, W.-Q.; Whitwood, A. C.; Fairlamb, I. J. S.; Lynam, J. M. *Inorg. Chem.* **2010**, *49*, 8941.
98. Zhang, W.-Q.; Atkin, A. J.; Thatcher, R. J.; Whitwood, A. C.; Fairlamb, I. J. S.; Lynam, J. M. *Dalton Trans.* **2009**, 4351.
99. Crook, S. H.; Mann, B. E.; Meijer, A. J. H. M.; Adams, H.; Sawle, P.; Scapens, D.; Motterlini, R. *Dalton Trans.* **2011**, *40*, 4230.
100. Vummaleti, S. V. C.; Branduardi, D.; Masetti, M.; De Vivo, M.; Motterlini, R.; Cavalli, A. *Chem. Eur. J.* **2012**, *18*, 9267.
101. Gonzalez, M. A.; Fry, N. L.; Burt, R.; Davda, R.; Hobbs, A.; Mascharak, P. K. *Inorg. Chem.* **2011**, *50*, 3127.
102. Hewison, L.; Johnson, T. R.; Mann, B. E.; Meijer, A. J. H. M.; Sawle, P.; Motterlini, R. *Dalton Trans.* **2011**, *40*, 8328.
103. Zobi, F.; Degonda, A.; Schaub, M. C.; Bogdanova, A. Y. *Inorg. Chem.* **2010**, *49*, 7313.
104. Zobi, F.; Blacque, O.; Jacobs, R. A.; Schaub, M. C.; Bogdanova, A. Y. *Dalton Trans.* **2012**, *41*, 370.
105. Romanski, S.; Kraus, B.; Schatzschneider, U.; Neudörfl, J.-M.; Amslinger, S.; Schmalz, H.-G. *Angew. Chem. Int. Ed.* **2011**, *50*, 2392.
106. Romanski, S.; Rücker, H.; Stamellou, E.; Guttentag, M.; Neudörfl, J.-M.; Alberto, R.; Amslinger, S.; Yard, B.; Schmalz, H.-G. *Organometallics* **2012**, *31*, 5800.
107. Arregui, B.; López, B.; García Salom, M.; Valero, F.; Navarro, C.; Fenoy, F. J. *Kidney Int.* **2004**, *65*, 564.
108. Niesel, J.; Pinto, A.; Peindy N'Dongo, H. W.; Merz, K.; Ott, I.; Gust, R.; Schatzschneider, U. *Chem. Commun.* **2008**, 1798.
109. Meister, K.; Niesel, J.; Schatzschneider, U.; Metzler-Nolte, N.; Schmidt, D. A.; Havenith, M. *Angew. Chem. Int. Ed.* **2010**, *49*, 3310.
110. Pfeiffer, H.; Rojas, A.; Niesel, J.; Schatzschneider, U. *Dalton Trans.* **2009**, 4292.
111. Dördelmann, G.; Pfeiffer, H.; Birkner, A.; Schatzschneider, U. *Inorg. Chem.* **2011**, *50*, 4362.
112. Brückmann, N. E.; Wahl, M.; Reiß, G. J.; Kohns, M.; Wätjen, W.; Kunz, P. C. *Eur. J. Inorg. Chem.* **2011**, 4571.
113. Jackson, C. S.; Schmitt, S.; Dou, Q. P.; Kodanko, J. J. *Inorg. Chem.* **2011**, *50*, 5336.
114. Gonzalez, M. A.; Yim, M. A.; Cheng, S.; Moyes, A.; Hobbs, A. J.; Mascharak, P. K. *Inorg. Chem.* **2012**, *51*, 601.
115. Kretschmer, R.; Gessner, G.; Görls, H.; Heinemann, S. H.; Westerhausen, M. *J. Inorg. Biochem.* **2011**, *105*, 6.
116. Schatzschneider, U. *Inorg. Chim. Acta* **2011**, *374*, 19.
117. Rimmer, R. D.; Pierri, A. E.; Ford, P. C. *Coord. Chem. Rev.* **2012**, *256*, 1509.
118. Romão, C. C.; Blättler, W. A.; Seixas, J. D.; Bernardes, G. J. L. *Chem. Soc. Rev.* **2012**, *41*, 3571.
119. Scott, L. E.; Orvig, C. *Chem. Rev.* **2009**, *109*, 4885.
120. Thompson, K.; Orvig, C. *Dalton Trans.* **2006**, 761.
121. Liu, Y.; Pak, J.; Schmutz, P.; Bauwens, M.; Mertens, J.; Knight, H.; Alberto, R. *J. Am. Chem. Soc.* **2006**, *128*, 15996.
122. Lee, W.; Squires, R., Jr.; Nyberg, S.; Doo, E.; Hoofnagle, J. *Hepatology* **2008**, *47*, 1401.
123. Marques, A. R.; Kromer, L.; Gallo, D. J.; Penacho, N.; Rodrigues, S. S.; Seixas, J. D.; Bernardes, G. J. L.; Reis, P. M.; Otterbein, S. L.; Ruggieri, R. A.; Gonçalves, A. S. G.; Gonçalves, A. M. L.; Matos, M. N. D.; Bento, I.; Otterbein, L. E.; Blättler, W. A.; Romão, C. C. *Organometallics* **2012**, *31*, 5810.



## THE FERROCIFEN FAMILY AS POTENT AND SELECTIVE ANTITUMOR COMPOUNDS: MECHANISMS OF ACTION

GÉRARD JAOUEN\* AND SIDEN TOP

*Chimie ParisTech (Ecole Nationale Supérieure de Chimie de Paris), Laboratoire Charles Friedel, Paris, France*

### 42.1 INTRODUCTION

Chemical Biology, a discipline that links chemical engineering and biology, differs from biochemistry by positioning itself as a broad chemical domain that makes available to biology the tools and techniques of chemistry, and thus allows biological entities to be controlled, manipulated, redirected or even transformed [1–3]. It has proved over the past number of years to be a scientific goldmine for molecular chemistry. We became involved via the biological aspect of the transition metal organometallics, a domain we helped to create under the title of *Bioorganometallic Chemistry*, and which made its first appearance in 1985 [4–6].

This field of research encompasses organometallics in biology and medicine, and indeed could be seen as an organometallic component of chemical biology.

At the beginning of the 1980s, the domain of organometallic catalysis held the high ground and its domination left little space for other fields of exploration. One important discovery, in the vitamin B12 series, the B12 coenzyme, methylcobalamin, was made by Dorothy Hodgkin whose determination of the structure of vitamin B12 by X-ray diffraction in 1956 earned her the Nobel Prize in 1964 [7]. However, this discovery of a proven role for organometallics in biology remained for some time an isolated example among the metalloenzymes of coordination complexes. The first structures of organometallic hydrogenases, for instance, date from 1995 [8, 9]. A few chemists however did take an interest in models of the vitamin B12 family as, in terms of their reactivity, their behavior was sometimes reminiscent of that of Grignard and Meerwein's reagents, and they could be sources of radicals for 1,2 rearrangements (e.g., of glutamic acid). This provided a conceptual basis that was reasonably familiar thanks to the connection with complexes with  $\sigma$ -type M–C bonds. This line of research however remained marginal. In fact one of the core beliefs prevalent at that time was that organometallics were unstable in the presence of oxygen and unusable in aqueous media. This doctrine made any large-scale application in biology prohibitive. Subsequently, this conviction was shown to be misplaced for myriads of organometallic complexes, thanks to the work of a few pioneers [10].

These early breakthroughs gradually lifted the taboos, liberated earlier restricted thinking, and overturned a number of unfounded assumptions. The viability of organometallics in biology has been the norm now for some years [11] and has allowed a new research community to develop. It is clear now that the flexibility of these species, the breadth of their applications, and their novel functionality provide a powerful stimulus to innovate. Their distinctive properties are finding ever wider applications within this new conceptual framework [10–16].

Organometallic chemical biology may be seen as a subset [17] of Inorganic Chemical Biology [18, 19] recently defined as referring to metal complexes of all kinds, without specifying the type of ligand–metal bonds involved. An organometallic

complex, for its part, is defined by the presence of at least one direct metal–carbon covalent bond (or a similar bond, e.g., M–H, M–P), and this bond frequently comes into play with metals in low oxidation states.

As for bioorganometallic chemistry (or its equivalent, organometallic chemical biology, *vide supra*), one can say that the discipline is concerned [20] *inter alia* with research on control of new sources of energy [21–23], for example, the study of hydrogenase models [24] and artificial photosynthesis [22, 23, 25], research into new enzyme inhibitors [26, 27], into vehicles for controlled release of CO and NO [28, 29], in the creation of innovative radiopharmaceuticals such as Alberto's reagent [30] [31], artificial metalloenzymes [32], new bioprobes (e.g., the carbonyl metalloimmunoassay, CMIA [33–36]), luminescent and fluorescent imaging agents [37–40], or the development of new therapeutic principles [15], to mention just a few of the lines being pursued.

One of the difficulties inherent in mechanistic studies of metal complexes for medicinal purposes is the extreme complexity of the possible events that can take place within affected cells [20, 41]. One discovery with significant and novel mechanistic implications in this context is that of the organometallic complexes of Ru with antitumoral potential involving catalytic properties [42]. This example is typical of the unusual approaches possible with these entities and of the contribution they can make to innovative medicinal chemistry.

At the present time, exploration, innovation, and indeed discovery and development, of new therapeutic principles are among the chief centers of activity, based on the entirety of effort expended [15]. For example, ferroquine, a novel antimalarial, was in phase II clinical trials at Sanofi-Aventis [43, 44] although it has been halted this year probably for economic reasons.

We provide here a rapid overview of the major representatives of the ferrocifen family and its associates, along with their prospective contributions in medicine. Their richness allows us to glimpse a number of mechanistic curiosities that are not yet completely elucidated. But first we will place these entities in the more general context.

## 42.2 CONTEXT AND BACKGROUND

In the arsenal of anticancer metallodrugs, the coordination complexes of platinum are currently the most commonly used antineoplastic agents as, alone or in association, they are involved in more than 70% of treatments [45–47]. The coordination complexes shown in Fig. 42.1 represent some of the most widely used species.

Worldwide, hospitals that do not use these species can no longer be found [48] and their usefulness continues to grow. *cis*-Platin **1** is routinely used for treatment of testicular, ovarian, and non-small-cell lung cancers, and its use is increasing in the treatment of head and neck tumors and those of the bladder [45]. Besides *cis*-platin, the less aggressive carboplatin **2** and oxaliplatin **3** were later introduced, the latter specifically for treatment of colorectal cancers. At the present time, a dozen other Pt complexes are in advanced clinical trials, and three derivatives (nedaplatin, loboplatin, and heptaplatin) are in clinical use although less universally so [48].

A key element in the mechanism of action of *cis*-platin **1** is the coordination of platinum to the N7 site of two adjacent guanines, causing a distortion of the DNA structure at the level of the cell nucleus and probably also that of the mitochondria [48]. It may perhaps be useful to mention here that, compared to the other group 10 metals (Ni, Pd), Pt shows higher activity linked to the kinetic exchange rate of this metal.

Despite their usefulness, these Pt compounds have a number of drawbacks including a high level of toxicity, susceptibility to resistance, a tendency to cause renal problems, and a still limited effective range [45]. These shortcomings led to development of the antitumoral chemistry of Ti and Ru, in which the first results, obtained by Dwyer et al. [49, 50] and now largely forgotten, date from the 1950s, 10 years before Rosenberg's serendipitous discovery of the properties of *cis*-platin [51].

Studies on the medicinal applications of Ru compounds [52–54] have been facilitated by the great diversity in the coordination and organometallic chemistry of Ru, both from a fundamental perspective [55] [56] as well as in relation to its use in catalysis [57] and photochemistry [58]. It is expected that this metal of the iron group may possess lower toxicity than

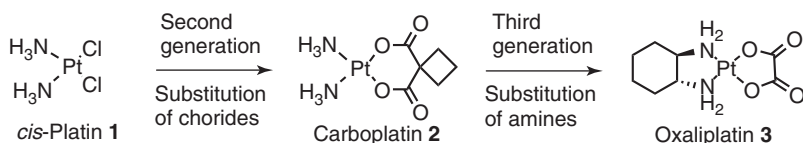


**Figure 42.1** The most widely used coordination complexes of Pt.

Pt. In addition, even though Ru(III) is the predominant oxidation state in physiological conditions, the oxidation states Ru(II) and Ru(IV) are easily accessible in the presence of either biological reducing agents (such as ascorbate or glutathione) or oxidizing agents ( $O_2$  or  $H_2O_2$ ) [59–61]. The three oxidation states of Ru form octahedral coordination complexes (usually with ligands bearing relatively soft nitrogen- or sulphur-containing groups). In contrast, typical organometallic complexes of Ru(II) are tetrahedral (pseudo-octahedral piano-stool geometry), often with a  $\pi$ -bond to an arene ligand. The history of the development of the anticancer drugs of Ru has been abundantly reported [59] [62–68]. We note only a characteristic of the evolution of this research. The first anticancer compounds of Ru, suggested by Clarke in the 1980s, for example, complex **4**, were clearly inspired by *cis*-platin [69] [70]. A gradual evolution has taken place toward complexes such as NAMI-A **5** reported by Sava and Alessio [55, 64, 65, 71] and KP1019 **6** by Keppler [72–76] that are fairly stable in terms of aquation and hydrolysis, and which are already in phase I or II clinical trials. Promising organometallics [77] include Ru(II) arenes such as RAPTA **8** reported by Dyson [67, 78], complexes of type **7** by Sadler [66, 79], and compound **9** by Pfeffer [80, 81] (Fig. 42.2). These latter complexes **7**, **8**, and **9** belong to the organometallic family.

With the exponential explosion of research into anticancer metallodrugs some original entities of Ru act via a structural role for the metal, which would give its shape to the compound and would favor noncovalent interactions with the target, as for example the organometallic **10** (Fig. 42.3), an excellent inhibitor of certain protein kinases developed by Meggers [27, 82].

The success of the anticancer drugs based on Pt and an understanding of their mechanism of action has weighed heavily on a large part of the research into other metallodrugs, and even on the search for other metal-based systems where, more or less implicitly, similarities with Pt have tended to be sought. In a sense, as underlined appositely by Keppler, Jakijec et al. [68], this presumption has tended to act as a brake on the development of new systems of anticancer metallodrugs. It is clear that several initiatives, thanks to some imaginative thinking, have succeeded in moving away from the initial classification scheme. These include antimetastatic entities such as NAMI-A or RAPTA [71, 78], which open up new approaches at the mechanistic level. The discovery of mechanisms of action beyond those that lead to apoptosis of cancer cells by alkylation of DNA by platinum is in fact an important challenge to address [78, 83, 84]. This may allow us to find new metallodrugs able to treat apoptosis-resistant cancers via alternative mechanisms (e.g., senescence). This can be envisioned for the ferrocene derivatives [85].

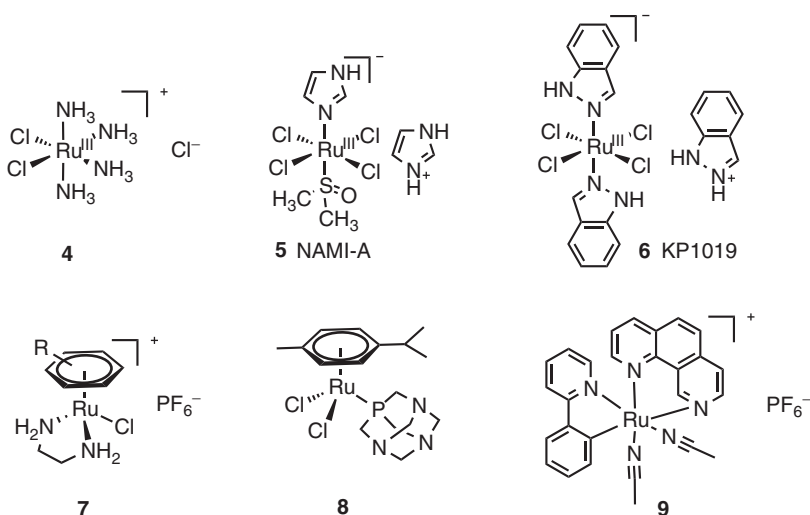


**Figure 42.2** Some promising anticancer Ru complexes.

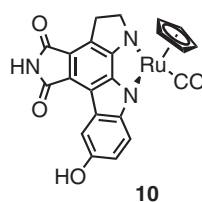


**Figure 42.3** Example of an inhibitor of certain protein kinases.

### 42.3 FERROCENE AND MEDICINAL CHEMISTRY

The synthesis of ferrocene in 1951 by Pauson [86] followed by the elucidation of its structure by Wilkinson et al. [87] and Fischer and Pfäb [88] constitutes a significant advance in modern chemistry. Indeed this time period, 1951–1952, marks the beginning of the explosion in transition metal organometallic chemistry. Ferrocene possesses an external structure that resembles that of an aromatic nucleus, it can be easily functionalized, is stable in a nonoxidizing environment, and is consequently well adapted to play the role of substituent in medicinal chemistry [89]. Besides this, it is also lipophilic and compact, and does not fundamentally modify the pharmacological properties of the molecule when it replaces a phenyl unless there are important bioisosteric considerations. In addition, it is not particularly toxic, with oral and LD<sub>50</sub> values of 1320 and 500 mg/kg for rat and 832 and 335 mg/kg for mouse [90].

Ferrocene was used very early on to replace functional groups, in particular phenyl moieties, in existing drugs to obtain novel species, with mixed results [91, 92].

Three typical examples are shown in Fig. 42.4.

Ferrocenyl derivatives of amphetamine and phenytoin have activity well below that of the parent organic compounds [93].

Those of penicillin and cephalosporin (Fig. 42.5) show activity against drug-resistant bacteria and low toxicity *in vivo* [94, 95]. Among the undeniable successes can be numbered ferroquine (FQ) synthesized in 1997 by Brocard et al. [96] and presently at the end of phase II clinical trials with Sanofi-Aventis, and the ferrocifen family reported in studies published by us since 1996 [97, 98]. The two products, FQ and OH-Fc (Fig. 42.6), share the characteristic of improving and even revolutionizing an older medication; in the former case, chloroquine, which had become resistant to certain strains of malaria, and in the latter tamoxifen, which can only be used against hormone-dependent breast cancers. It is this latter family of products, effective also on hormone-independent breast cancers, and for which we possess fairly rich data concerning the redox function of ferrocene and its chemical consequences on the local organic framework, that will be discussed in the following [85].

### 42.4 SYNTHESIS AND BEHAVIOR OF FERROCIFEN DERIVATIVES

The project began with the synthesis of Fc-OH-Tam, **14** (Fig. 42.6), corresponding to the replacement of the  $\beta$ -arene of OH-TAM **12**, with a ferrocenyl group and an adjustment of the length of the amino-alkyl chain. These syntheses can be carried out in various ways [97] but the McMurry coupling proved to be the most suitable [98–102]. Ferrocene itself gives

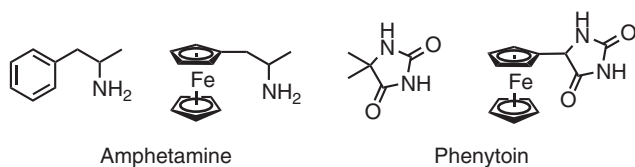


**Figure 42.4** Early examples of ferrocenyl modification of drugs.

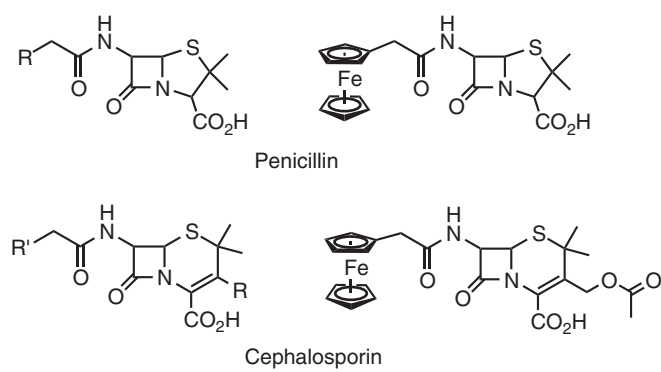


**Figure 42.5** Other examples of ferrocenyl modification of drugs.

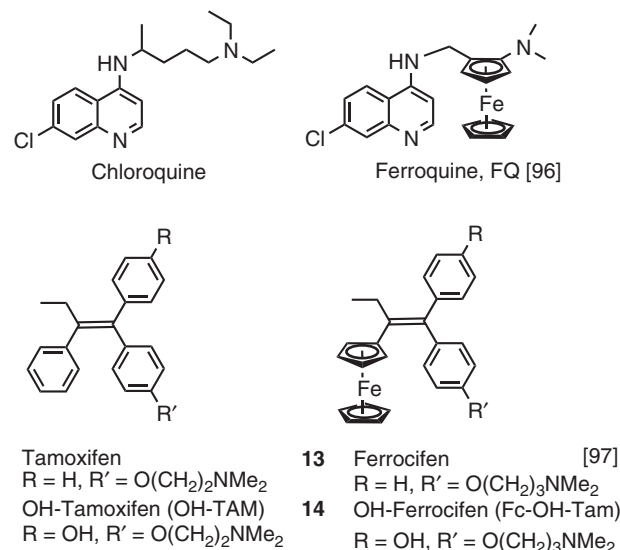


**Figure 42.6** Example of successful ferrocenyl modification of drugs.

an  $IC_{50}$  value of  $160 \mu\text{M}$  on hormone-independent breast cancer cells (MDA-MB-231) [103], and so hydroxytamoxifen **12** and ferrocene are not viable against hormone-independent breast cancer cells ( $\text{ER}\alpha^-$ ) (Table 42.1). However when the  $\beta$ -aryl group in OH-TAM **12** ( $IC_{50} = 30 \mu\text{M}$ ) is simply replaced by a ferrocenyl entity, inactive in itself, the species **14** is produced with an  $IC_{50}$  value of  $0.5 \mu\text{M}$ . This immediately changes the paradigm. The optimal length of the carbon chain can be 3 or 4 carbon atoms [100, 101] in Fc-OH-Tam **14**. On hormone-dependent ( $\text{ER}\alpha^+$ ) MCF-7 breast cancer cells, meanwhile, the  $IC_{50}$  values for **12** or **14** remain comparable [103]. Everything occurs as if the presence of the ferrocene preserved the initial properties of **12** while gaining an additional function in **14** that is absent from **12** and only becomes apparent on the cancerous cell.

It was quickly discovered that the presence of a basic chain was not absolutely essential for this new property, and this led to **15** with an  $IC_{50}$  on MDA-MB-231 of  $0.6 \mu\text{M}$  [104] (Table 42.1). The antiestrogenic effect present in **12** is lost but the cytotoxic component linked to the ferrocenyl group is maintained.

The  $IC_{50}$  value obtained with **16**, where a single paraphenol group is present, is  $1.13 \mu\text{M}$ , twice that of **15** which bears two paraphenols. Molecule **17**, where the second phenol is in the meta-position and thus cannot form a conjugated bond with the skeleton, gives an  $IC_{50}$  comparable ( $1.03 \mu\text{M}$ ) to that of **16** [105]. This is even clearer with **18** where the  $IC_{50}$  is  $3.5 \mu\text{M}$  [104]. The position and number of OH groups is thus an important element in the cytotoxic effect.

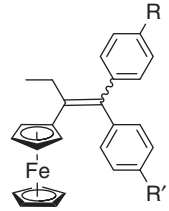
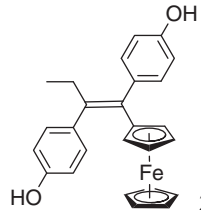
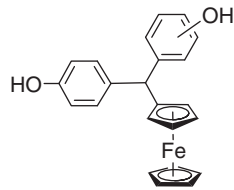
If OH is replaced by  $\text{NH}_2$  **18**, **19** (which can lead via oxidation to conjugated imines) or by  $\text{NHAc}$  **20**, also leading to oxidation after hydrolysis,  $IC_{50}$  values of  $0.47$  and  $0.65 \mu\text{M}$  are obtained, slightly better than the value for the corresponding phenol [106, 107]. Product **21**, differing from **15** in the position of the ferrocenyl entity, which prevents conjugated binding with the organic framework, gives an  $IC_{50}$  value of  $6.0 \mu\text{M}$  [104]. This demonstrates the importance of both the choice and the positioning of the substituents.

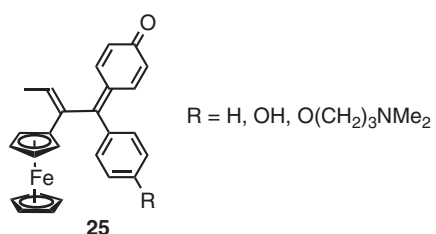
The series of compounds **22**, **23**, and **24** reveals the influence of disrupting the conjugation of the system by incorporating a central  $\text{sp}^3$  carbon ( $IC_{50}$  between  $2.8$  and  $4.1 \mu\text{M}$ ) [108]. The data given above illustrate the importance of the conservation in these series of the [ferrocenyl-conjugate spacer-paraphenol] motif [103]. Electrochemical and electron spin resonance (ESR) studies of species related to **14**, **15** and **16** have shown that one of the active metabolites could be an electrophilic quinone methide (QM) such as **25** [109–111] (Fig. 42.7) whose chemical reactivity is currently being elucidated although it is already known that organometallic QMs form 1,8 Michael adducts with various thiols.

Table 42.2 summarizes selected biological effects observed in the presence of  $1 \mu\text{M}$  of OH-TAM **12** or Fc-OH-TAM **14** [85].

The open series above produces reactive oxygen species (ROS) on cancerous cells [85, 112, 113] but this is not universally the case as this is not observed with metastatic melanoma cells, yet the cytotoxic effect is still in evidence [114]. The case of melanoma may be an exceptional one as these very exposed cells possess a sophisticated antioxidant system [114]. It should be noted that the presence of antioxidants added into the medium, such as *N*-acetyl cysteine or vitamin E with

**TABLE 42.1** Various Effects (Electronic, Substituent, Regiochemical) on IC<sub>50</sub> Values in the Ferrocifen Family

Compound	Cell Line. IC <sub>50</sub> , μM	References
<b>12</b>	30	103
Ferrocene	>160	103
		
<b>14</b> R = OH, R' = O(CH <sub>2</sub> ) <sub>3</sub> NMe <sub>2</sub>	0.5	101
<b>15</b> R = OH, R' = OH	0.6	104
<b>16</b> R = OH, R' = H	1.13	105
<b>17</b> R = OH, R' = m-OH	1.03	105
<b>18</b> R = H, R' = m-OH	3.5	105
<b>19</b> R = NH <sub>2</sub> , R' = H	0.47	106
<b>20</b> R = NHAc, R' = H	0.65	106
	6.0	104
	2.8	108
<b>23</b> <i>m</i> -OH	4.1	108
<b>24</b> <i>p</i> -OH	3.5	108



**Figure 42.7** Quinone methides (QM).

**TABLE 42.2 Biological Effects Observed in the Presence of 1  $\mu$ M of OH-TAM 12 or Fc-OH-TAM 14**

Biological Effect	Cell Line	OH-TAM 12	Fc-OH-TAM 14
Growth inhibitory effect after 4 days	MCF-7 ( $ER\alpha^+$ )	++	++
	MDA-MB-231 ( $ER\alpha^-$ )	No effect	++
Effect on cell cycle after 48 h	MCF-7	Cells accumulate in G0/G1 phase	Cells accumulate in G0/G1 phase
	MDA-MB-231	No effect	Cells accumulate in S phase
Induction of senescence after 5 days	MCF-7	+	++
	MDA-MB-231	No effect	++
ROS production ( $H_2O_2$ ) after 10 min	MCF-7	--	++
	MDA-MB-231	--	++

On  $ER\alpha^+$  breast cancer cells, Fc-OH-TAM displays an antihormone effect analogous to that of OH-TAM, together with a cytostatic effect.

On  $ER\alpha^-$  breast cancer cells, the cytostatic behavior is the only one expressed. This mechanism is distinct from the nongenomic pathway observed with high dose of OH-TAM.

**14** and **15**, inhibits the antiproliferative effect [85, 115]. DNA is not the primary target of these compounds [116, 117]. However, the possibility of a partial interaction is observed between the oxidized form of **15** and DNA [116]. Experiments with organometallics other than ferrocene (Ti, Ru, Re) attached to the organic framework below have shown the superiority of the Fc group due no doubt to the good redox capacity of this probe with reversible  $Fe^{II}/Fe^{III}$  oxidation [118–122]. We have also shown that although phenolic products such as **14** and **15** are very active at low concentrations on cancerous cells, antiproliferative activity on healthy cells such as astrocytes [123] or melanocytes [114] can only be obtained using concentrations of ferrocifens in the order of 100–200 times higher (>100–200  $\mu$ M) [114] [123]. This was recently confirmed by another laboratory [124]. There is thus a difference, probably in emission of ROS and/or presence of a target protein redox function, within cancer cells that is revealed by the ferrocifens, which have sensitivity to oxidation via the reduced  $Fe^{II}$  and good protection via two cyclopentadienyl ligands that form a sandwich and control the selectivity. This illustrates a fundamental difference between Pt complexes and the ferrocifens.

Another series of compounds, characterized by an inversion of the position between the ethyl and one of the aryl groups, was synthesized [125] (Fig. 42.8).

Of the compounds in this series, **31** is the most active (Table 42.3). It is the only one that can be oxidized by  $Ag_2O$ , while the others are inactive in these conditions. They also show little activity against MDA-MB-231 cells. This result reinforces the hypothesis of a mechanism of action for the ferrocenyl complexes via formation of QM. In addition, the methoxylated compounds **28**, **30**, and **31** are less active than the phenolic analogs **27**, **29**, and **31**. This confirms the importance of the phenol function, which is indispensable for the generation of QM.

It has been shown that tamoxifen and hydroxytamoxifen metabolize to 3,4-dihydroxytamoxifen [126]. This catechol can be oxidized by enzymes into ortho-quinone, which can react with DNA and proteins. A number of ferrocenyl catchols have been synthesized [127] (Fig. 42.9).

The additional presence of the phenolic function improves the antiproliferative activity of the compounds and for certain products such as **37** and **38**, their catechol analogs, **34** and **35**, are four times more active. All the catechols in Table 42.4, except **38** and **39**, are chemically oxidizable to QMs or *ortho*-quinones. It is also confirmed that the compounds unable to generate quinones, such as **38** and **39**, have little activity.

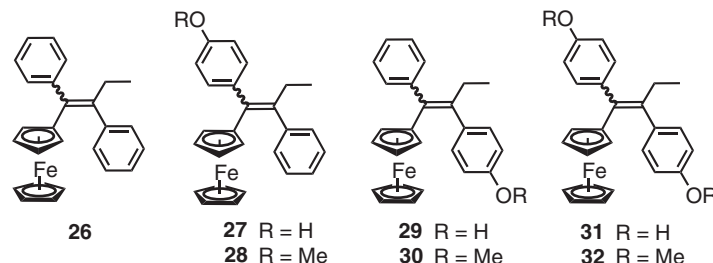


**Figure 42.8** Another series of compounds in which **31** is the most active.

**TABLE 42.3** Effect of Compounds 26–32 on Growth of Hormone-Independent Breast Cancer Cells

Compound	<b>26</b>	<b>27</b>	<b>28</b>	<b>29</b>	<b>30</b>	<b>31</b>	<b>32</b>
Formation of QM	No	No	No	No	No	Yes	No
Growth of cells, % <sup>a</sup>	53	40	53	49	93	16	90

<sup>a</sup>Effect on growth of cells of MDA-MB-231 at 10 µM. Control = cells without added compounds after 5 days of culture, set at 100%.

**TABLE 42.4** Effect of Compounds 33–39 on Growth of Hormone-Independent Breast Cancer Cells

Compound	<b>33</b>	<b>34</b>	<b>35</b>	<b>36</b>	<b>37</b>	<b>38</b>	<b>39</b>
Formation of QM or OQ	OQ	OQ	OQ	OQ	QM	No	No
$IC_{50}$ , $\mu M^a$	$1.10 \pm 0.07$	$1.21 \pm 0.07$	$2.4 \pm 0.2$	$0.48 \pm 0.04$	$5.3 \pm 0.9$	$9.0 \pm 1.0$	$12.7 \pm 1.6$

<sup>a</sup>Mean of two experiments  $\pm$  range.

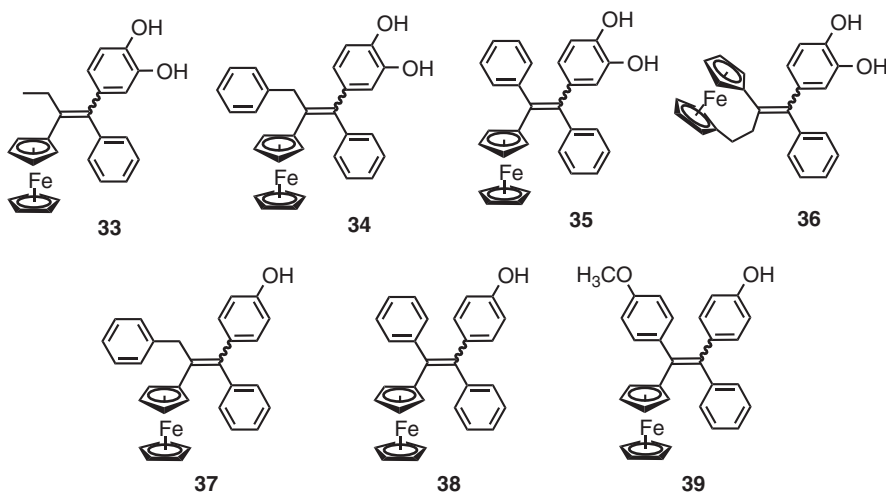


**Figure 42.9** Example of ferrocenyl cathecols.

## 42.5 SYNTHESIS AND BEHAVIOR OF FERROCENOPHANE DERIVATIVES

The results obtained in the open series showed that the position of the ferrocenyl group and the nature of the substituents present on the molecule have a significant impact on the antiproliferative activity of the compounds. Another possible structural modification is to alter the nature of the ferrocenyl group. For example, the creation of a bond between the last carbon of the ethyl and the second cyclopentadiene ring immobilizes the ferrocenyl group in a fixed position relative to the rest of the molecule. This bond generates a new ferrocenyl derivative of the ansa-ferrocene or ferrocenophane type. The first derivative of ferrocenophane was synthesized by Plazuk et al. [128] in the form of a diphenol compound, **40** (Fig. 42.10). It was obtained by a McMurry coupling reaction between ferrocenophanone and dihydroxybenzophenone.

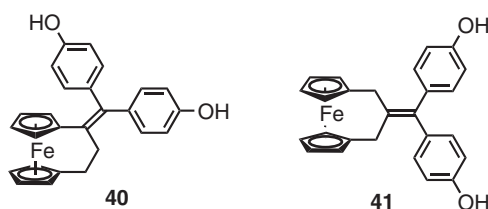


**Figure 42.10** Ansa-ferrocene diphenols.

**TABLE 42.5** RBA, Log  $P_{o/w}$ , and the Effect on Cancer Cell Growth of **40** and **41**

	RBA (%) for ER $\alpha$	$\log P_{o/w}$	IC <sub>50</sub> , $\mu\text{M}$	
			MDA-MB-231	PC3
<b>40</b>	7.2 ± 0.7	4.6	0.09 ± 0.01	0.094 ± 0.0067
<b>41</b>	7.6 ± 0.6	4.8	0.96 ± 0.03	1.08 ± 0.02

**TABLE 42.6** Cytotoxicity of Compounds **42–57** against Hormone-Independent MDA-MB-231 Breast Cancer Cells<sup>a</sup>

Compound	R	R'	IC <sub>50</sub> values, $\mu\text{M}$	Cytotoxicity Ratio <sup>b</sup>
<b>42</b>	H	H	0.92 ± 0.11	8.2
(E+Z)- <b>43</b>	OH	H	0.47 ± 0.06	3.3
(E+Z)- <b>50</b>	OAc	H	0.26 ± 0.004	7.6
(E+Z)- <b>44</b>	NH <sub>2</sub>	H	0.21 ± 0.03	4.1
(E+Z)- <b>53</b>	NHAc	H	0.47 ± 0.04	1.4
<b>40</b>	OH	OH	0.089 ± 0.006	7.2
(E+Z)- <b>48</b>	NH <sub>2</sub>	OH	0.061 ± 0.005	9.0
(E+Z)- <b>54</b>	NHAc	OH	0.092 ± 0.019	6.1
<b>49</b>	NH <sub>2</sub>	NH <sub>2</sub>	0.047 ± 0.01	
<b>45</b>	NHAc	NHAc	5.64 ± 1.13	
(E+Z)- <b>51</b>	OAc	OH	0.049 ± 0.003	8.6
<b>52</b>	OAc	OAc	0.044 ± 0.001	14.5
(E+Z)- <b>46</b>	Br	H	2.93 ± 0.62	>3.4
<b>47</b>	Br	Br	>10	
<b>55</b>	CN	H	0.85 ± 0.07 (E+Z)	12.8
<b>56</b>	CN	CN	7.98 ± 1.2	

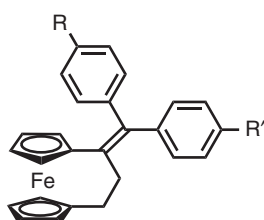
<sup>a</sup>From Reference 130.<sup>b</sup>IC<sub>50</sub> (ferrocifen)/IC<sub>50</sub> (ferrocenophane).

Compound **40** shows an IC<sub>50</sub> value of 0.09 ± 0.01  $\mu\text{M}$  against MDA-MB-231 cells (Table 42.5), making it six times more active than ferrocidiphenol **15** (IC<sub>50</sub> = 0.6  $\mu\text{M}$ ). Another type of ansa compound is represented by **41**. Its IC<sub>50</sub> value is 0.96 ± 0.03  $\mu\text{M}$ , showing that **41** is less active than hydroxyferrocifen **14** of the open series.

Excellent levels of antiproliferative activity for the ferrocenophanes as compared to classic ferrocenes were seen again in other compounds of this series. The antitumoral activity of these new compounds is listed in Table 42.6.

The result obtained clearly shows that the series of the closed ferrocenophanes is more active than the series of the open ferrocifens. The ratio of IC<sub>50</sub> (ferrocifen)/IC<sub>50</sub> (ferrocenophane) is greater than 7 for compounds **40**, **42**, **48**, **50**, **51**, **52**, and **55**. Acetamide **53** is the only compound that produces a fairly low ratio (1.4), perhaps because of a difficulty in hydrolyzing the amide. A similar effect of the substituents on antitumoral activity is found for both the ansa and open series. The hydroxylated and aminated derivatives are the most active. The electron-withdrawing groups, such as Br or CN, inhibit the activity of the compounds [106, 107].

Therefore, in the ansa series, the most promising products appear to be similar to those of the ferrocifen series, in terms of substituents. The most active molecules retain the [Fc-conjugated spacer—phenol (or aniline)] motif previously identified as essential. The organometallic ferrocenophane-type framework bears a short, three-carbon chain, bridging the two cyclopentadienyls. Despite the ring strain, the synthesis is viable but the two Cp rings are no longer parallel as in the ferrocifens, showing instead a dihedral angle of 11° [129, 130]. An IC<sub>50</sub> value of 89 nM on MDA-MB-231 is obtained with **40**.



This represents a general trend. With all the substituents studied in Table 42.6, the IC<sub>50</sub> values for the ferrocenophanes are always substantially lower. However, with these species, we have not been able to clearly identify the putative QM with a three-carbon bridge. If the ring strain is released with a bridge of four or five carbons, the results revert to those of the ferrocifens. This series of the ansa type has been less studied to date than the earlier series. However, the data obtained from the NCI for the ferrocenophanol **40** and the ferrocidiphenol **15** on 60 cancer cell lines show higher activity for the cyclic series [117]. The two lead compounds **15** and **40** reveal new mechanisms compared to those already listed by the NIH and also are probably not identical with each other. This is based on the absence of identifiable QMs in the ansa series and on the different shapes of the antiproliferative curves showing a plateau with the ansa molecule [117]. Nevertheless, the first part of the mechanism of action, involving oxidation of the elemental iron, may be similar between the two series, since both sets generate ROS in cancer cells.

#### 42.6 FERROCENOPHANE TRANSPOSITION PRODUCTS AND PINACOLS

The McMurry coupling reaction generally leads to three alkenes, two symmetrical products and one asymmetrical. However, depending on the reaction conditions, especially changes in temperature and medium, other secondary compounds are also formed, in particular, the transposition product and pinacol [129]. These two new species were synthesized and studied by orienting the reaction more specifically in their favor. The IC<sub>50</sub> values of these compounds are collected in Table 42.7.

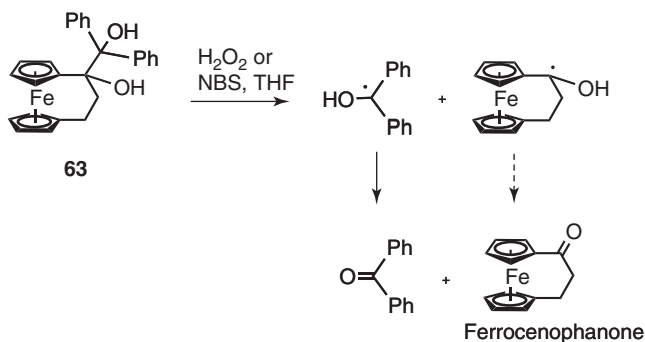
With the exception of compound **58** (IC<sub>50</sub> = 1.45 ± 0.49 μM), the transposition products, **52**, **59**, **60**, and **61**, have very little activity. Conversely, the pinacols **62** and **63** are particularly active.

It has been found that several metals, O<sub>2</sub>, H<sub>2</sub>O<sub>2</sub>, and *N*-iodosuccinimide can oxidize pinacols to radicals that undergo cleavage to ketones. The addition of H<sub>2</sub>O<sub>2</sub> or *N*-bromosuccinimide to a tetrahydrofuran (THF) solution of **63** led to the formation of benzophenone and ferrocenophanone although only small amounts of this compound were detected (Scheme 42.1). The antiproliferative activity of pinacols may be linked to the production of an intermediate ferrocenyl radical [129].

TABLE 42.7 IC<sub>50</sub> Values (μM) of Compounds on Breast Cancer Cells (MDA-MB-231)<sup>a</sup>

	R	R'	IC <sub>50</sub>
	<b>52</b>	OH	12.5 ± 0.3
	<b>58</b>	H	1.45 ± 0.49
	<b>59</b>	H	20.1 ± 5.4
	<b>61</b>	NH <sub>2</sub>	15.4 ± 0.2
	<b>60</b>	NHAc	9.38 ± 1.82
	<b>63</b>	H	0.17 ± 0.01
	<b>62a</b>	OH	0.06 ± 0.01
	<b>62b</b>	OH	0.14 ± 0.01
	<b>64</b>		3.48 ± 0.83

<sup>a</sup>From Reference 129.



Scheme 42.1 Tentative reactivity of pinacols.

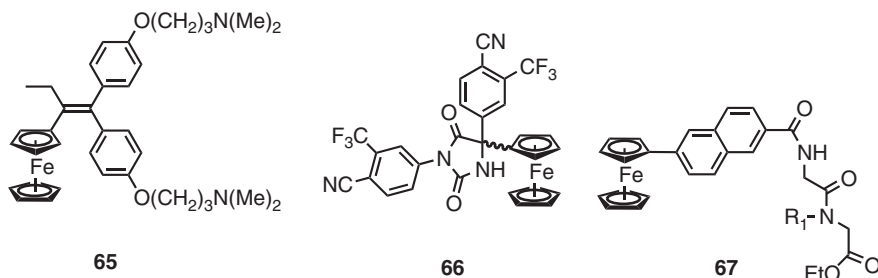


Figure 42.11 Examples of other ferrocenyl antimarial species.

Other ferrocenyl antitumorals have been described that involve mechanisms of action different from those in play in the ferrocifen-type species mentioned above. These include, for example, compounds **65**, **66**, **67** shown below (Fig. 42.11):

In compounds related to **65** [131] ( $IC_{50} = 0.4 \mu M$  with MDA-MB-231 cell lines), the lipophilic organometallic moiety does not produce a major effect (with the occasional exception of strong steric hindrance [132]) as compared to a pure organic aromatic group. The presence within the molecule of two vicinal amino alkyl chains, potentially allowing pincer complexation, could perhaps be the key to the antiproliferative efficacy of this series, which operates via a mechanism masking phenol functions. In addition, these species possess the distinctive feature of combining a strong antiproliferative effect with antibacterial and antifungal activity [133, 134].

The introduction of the ferrocenyl moiety at C-5 of a hydantoin ring gives rise to **66**. This complex displays an antiproliferative effect ( $IC_{50} = 5.4 \mu M$ ) on hormone-independent (PC3) prostate cancer cells. This cytotoxic effect is probably steric and non-androgen receptor-mediated [135, 136].

In the *N*-(6-ferrocenyl-2-naphthoyl) dipeptide ethyl ester **67**, a potent activity in the H1299 NSCLC cell line has been found ( $IC_{50} = 0.13 \mu M$  with  $R_1 = H$ , and  $IC_{50} = 0.14 \mu M$  with  $R_1 = CH_3$ ) [137].

For more examples showing the antitumor activity of ferrocenyl compounds, see a recent review by Ornelas [138].

## 42.7 FORMULATION: RESEARCH INTO NANOCAPSULES BEST SUITED FOR IN VIVO TESTING OF FERROCIFENS

The most active ferrocifens *in vitro* are generally lipophilic phenol species, for example, **14**, **15**, **40**, and **48**, and they present a double challenge, both chemical and physicochemical, to their successful delivery as potential medication. The effects of their organometallic character are not yet well known beyond an observed increased in lipophilicity. In common with many of the molecules currently under study in pharmaceutical research, the most promising complexes so far are insoluble in water. They thus require a formulation stage to make them suitable for administration [139–145]. The bioavailability of organic polyphenols is another major challenge [146] because in their free form these entities are rapidly eliminated from the body. In fact, polyphenols rarely occur naturally in the free form, being normally conjugated with sugars and fatty acid esters [146].

This question of the bioavailability of the polyphenols has been addressed by the pharmaceutical industry (Sanofi-Aventis with Endotelon), agrifood (Nestlé), and the cosmetic industry (Caudalie and antiaging skin care) [147–152]. Benoit et al have developed lipid nanocapsules (LNC), between 20 and 100 nm in size, perfectly stable from a physical standpoint, based on a phenomenon of phase inversion of a microemulsion [153]. The aim is to use this new product as a delivery system for anticancer agents [115, 123, 154] particularly in the treatment of glioma and breast cancer. In fact, the size and structure of the nanoparticle would potentially allow the vector to reach the dispersed cells that are the cause of recurrences frequently observed with this kind of cancer. Two types of treatment have been envisaged that could be combined: local injection into the brain by convection-enhanced delivery (CED), allowing distribution into large tissue volume; and/or intravenous injection by active targeting of the blood–brain barrier and the tumor cells, with the aid of particular polyethylene glycols (PEGs) or antibodies attached to the surface of the LNC. This second route would also provide access to other types of tumors such as melanomas, liver, breast, and ovarian cancers.

Preparation of LNC containing ferrocidiphenol **15** was performed [115, 123]. During this work, it was shown that after encapsulation in the LNC, organometallic agents have good efficacy and specificity *in vitro* on breast cancer and glioma 9L cells, and also *in vivo* in the model of subcutaneous glioma, by intratumoral action of the anticancer vectors that cause a significant reduction in tumor mass and volume [155]. Interestingly, activity is much reduced on the melanocytes and astrocytes, healthy cells with almost no potential for division. This selectivity of ferrocifens between cancer and normal cells is different from *cis*-platin.

In the same model of subcutaneous glioma, there has been recent work to inject, this time intravenously, LNC loaded with ferrocidiphenol **15** and coated with long PEG chains. The coating of the nanocapsules allows the LNC to remain longer in the bloodstream than conventional LNC, and thus to enhance accumulation in tumors through the EPR (enhanced permeability and retention) effect. Indeed, tumoral progression curves show a marked reduction in the size of tumors in treated rats. After several days, the tumor volume diminishes significantly to the point of disappearance at the end of the experimental period [156].

Classical LNC and long-circulating nanoparticles called *stealth nanoparticles* (DSPE-m-PEG2000-LNC) loaded with FcdiOH **15** have been used with 9L gliosarcoma in rats. A single intravenous injection of FcdiOH-LNC (400 µL, 2.4 mg/rat) considerably inhibited tumor growth when compared to the control. DSPE-mPEG2000-FcdiOH LNC exhibited a strong antitumor effect by nearly eradicating the tumor by the end of the study with this ectopic model (Fig. 42.12) [156].

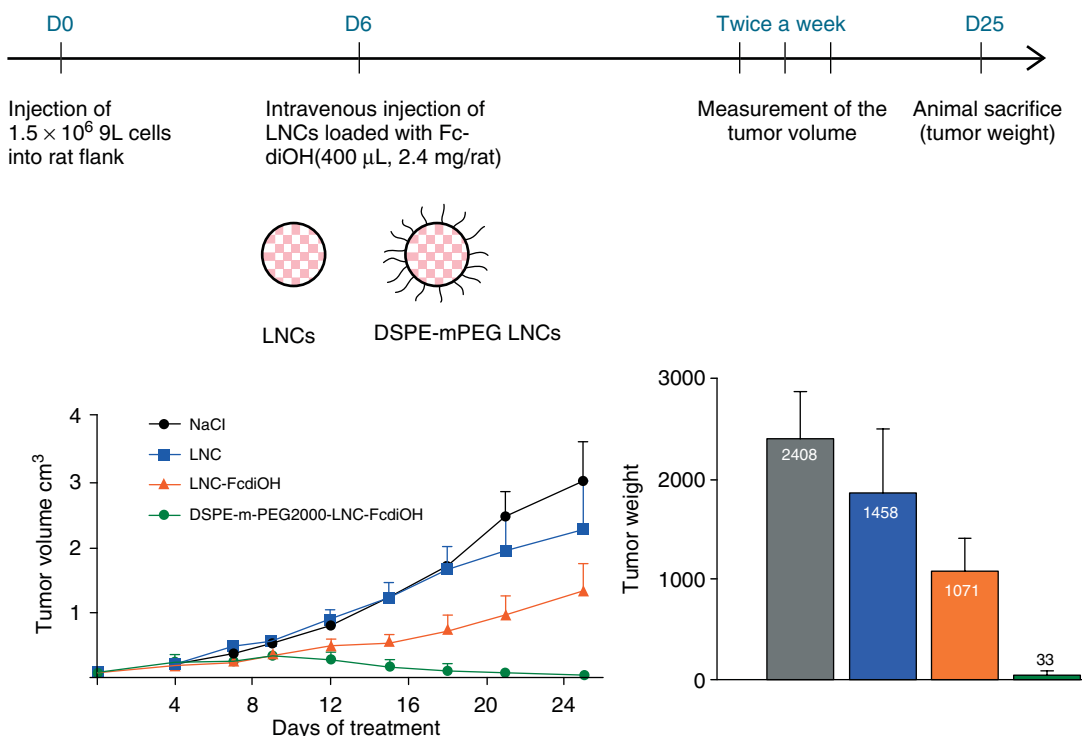


**Figure 42.12** Intravenous injection of two different sorts of LNC in ectopic tumors. (See insert for color representation of the figure.)

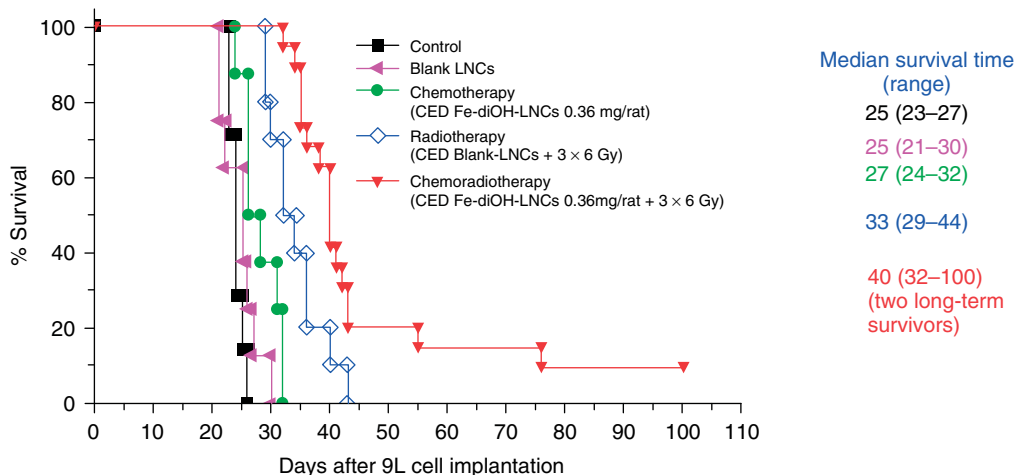


**Figure 42.13** Kaplan–Meier survival plots. (See insert for color representation of the figure.)

With this new formulation, DSPE-mPEG2000-LNC-FcdiOH, the tumor has almost totally disappeared [156].

In addition, it was shown that the association between **15** and X-photons is a synergistic one, conferring the properties of a radiosensitizing molecule [157].

Figure 42.13 below shows the Kaplan–Meier survival curves for 9L glioma-bearing rats. The best result appears so far with CED of Fc-diOH-LNC and external radiotherapy of  $3 \times 6$  Gy. In this group of interest, two rats were long-term survivors, as they survived up to 100 days, which certainly involves a total eradication of the tumor. The ionizing radiation can help trigger the generation of ferricinium in compound **15** and favor the occurrence of cytostatic species [157], even in a reducing organ like the brain.

The question of finding a good formulation is key for the development of ferrocifens.

The above results are very encouraging in this context.

Survival rate is significantly improved by the combination of chemo- and radiotherapy.

## 42.8 CONCLUSION

There is at present a notorious mismatch in oncology between therapeutic demands and the existing pharmacopeia. Currently available drugs consist of mostly (80%) proapoptotic compounds, for example alkylants of DNA such as *cis*-platin, and we are still relatively undersupplied in treatments against apoptosis-resistant primary cancers, acquired drug resistance, and spreading metastases. We are at a stage where metastatic cancers prove fatal in 90% of cases. The annual death rate for these pathologies is of the order of 13.5 million patients and is predicted to increase more quickly than the population since the projections show, at the current rate of change, 35 million deaths per year on the horizon for 2050. It is imperative to prevent this gloomy prediction from coming true.

For this reason, novel molecules are being sought that do not operate exclusively via an apoptotic mechanism, but instead are able to induce cytostatic properties by other routes such as senescence [158].

In this context, brain cancers (e.g., glioblastoma), esophageal cancers, melanomas, pancreatic cancers, ovarian cancers, and non-small-cell lung cancers (NSCLCs) are, among others, the cancers associated with the worst outcomes because of their ability to resist most of the standard therapies.

From this viewpoint, the ferrocifen family and associated compounds present dizzyingly broad perspectives, both for the richness of the effective structures they offer and for the variety of mechanisms they bring into play.

In the open series, of which **14** and **15** are the most studied representatives, a number of distinctive traits can be seen. It has been possible to change the paradigm, thanks to a ferrocenyl redox antenna that distinguishes them from their purely organic relatives. A 60- to 150-fold increase in efficacy has been shown in their IC<sub>50</sub> values on MDA-MB-231 cells, while healthy cells are not affected at the concentrations used. The [ferrocene-alkene spacer-paraphenol] motif appears to be essential for the compounds to become effective. These species do not operate via an alkylation of DNA, unlike *cis*-platin and its relatives. Several considerations militate in favor of a novel biological mechanism. These include the production

of ROS, the halting of the S/G2/M cell cycle, a modest apoptosis, the evidence of senescence, and the vacuolization of cells. In addition, the observed effect is ER $\alpha$  independent, ER $\beta$  is inoperative as is GPR30 [85]. QM metabolites have been identified and characterized [109–111]. At first sight, the ansa series **40** appears similar to the open series except for a stronger antiproliferative effect and a different mechanism. The two series have been tested by the National Cancer Institute (NCI) on 60 cancer cell lines. The mechanisms are different from any found in the National Institutes of Health (NIH) database, and also different from each other [130]. In particular, the generation of QM has not been observed in the ansa series with three-carbon bridges. Despite the similarities in the antiproliferative effects, it is possible that the target proteins or intermediaries are different between the two series, which both start with oxidation of the ferrocene to a ferricinium ion.

Steric hindrance of the phenol function of **15** and **40** by  $-\text{O}-(\text{CH}_2)_3\text{N}(\text{CH}_3)_2$  chains leads to different antiproliferative compounds that presumably operate via a pincer complexation of the basic substituents. These entities also reveal antibacterial and antifungal properties [131, 133, 134]. They thus open other horizons.

Finally, organometallic pinacols of the ansa series show powerful antiproliferative effects [129] probably via a free-radical mechanism.

The formulation of ferrocifens by LNC allows certain active species to be delivered *in vivo*. This is an essential step toward future development. The success of this step augurs well as the obstacles are gradually lifted [115, 123, 155–157]. The stakes, both scientific and social, are considerable. At present, these species, with their very rich potential, are an illustration of what we can look forward to in medical organometallic chemistry.

## ACKNOWLEDGEMENTS

We wish to thank all those who contributed to this research, and whose names appear in the references. We thank B. McGlinchey for linguistic assistance. The ANRs Mecaferrol and FerVect have allowed fruitful collaborations between our group and those of C. Amatore, D. Mansuy, C. Passirani, A. Vessières, R. A. Toillon, M. J. M. McGlinchey.

## REFERENCES

1. Schreiber, S. L.; Kapoor, T. M.; Wess, G. *Chemical Biology From Small Molecules to Systems Biology and Drug Design*; Wiley-VCH Verlag GmbH: Weinheim, **2007**, Vol. 1.
2. Waldmann, H.; Janning, P. *Chemical Biology: Learning through Case Studies*; Wiley-VCH Verlag GmbH: Weinheim, **2009**.
3. Lippard, S. J. *Nat. Chem. Biol.* **2006**, *2*, 504.
4. Top, S.; Jaouen, G.; Vessières, A.; Abjean, J. P.; Davoust, D.; Rodger, C. A.; Sayer, B. G.; McGlinchey, M. J. *Organometallics* **1985**, *4*, 2143.
5. Jaouen, G.; Vessières, A.; Top, S.; Ismail, A. A.; Butler, I. S. *J. Am. Chem. Soc.* **1985**, *107*, 4778.
6. Jaouen, G.; Vessières, A. *Pure Appl. Chem.* **1985**, *57*, 1865.
7. Hodgkin, D. C.; Kamper, J.; Mackay, M.; Pickworth, J.; Trueblood, K. N.; White, J. G. *Nature* **1956**, *178*, 64.
8. Volbeda, A.; Charon, M. H.; Piras, C.; Hatchikian, E. C.; Frey, M.; Fontecilla Camps, J. C. *Nature* **1995**, *373*, 580.
9. Peters, J. W.; Lanzilotta, W. N.; Lemon, B. J.; Seefeldt, L. C. *Science* **1998**, *282*, 1853.
10. *Bioorganometallics*; Jaouen, G., Ed.; Wiley-VCH Verlag GmbH: Weinheim, **2006**.
11. Jaouen, G.; Beck, W.; McGlinchey, M. J. In *Bioorganometallics: Biomolecules, Labeling, Medicine*; Jaouen, G., Ed.; Wiley-VCH Verlag GmbH: Weinheim, **2006**; p 1.
12. Hartinger, C. G.; Dyson, P. J. *Chem. Soc. Rev.* **2009**, *38*, 391.
13. Hillard, E. A.; Jaouen, G. *Organometallics* **2011**, *30*, 20.
14. Jaouen, G.; Dyson, P. J. In *Comprehensive Organometallic Chemistry III*; Crabtree, R. H.; Mingos, D. M. P., Eds.; Elsevier: Oxford, **2007**; Vol. 12, p 445.
15. Jaouen, G.; Metzler-Nolte, N. In *Medicinal Organometallic Chemistry*, 1st ed.; Topics in Organometallic Chemistry, Vol. 32; Springer-Verlag: Heidelberg, **2010**.
16. *Bioinorganic Medicinal Chemistry*; Alessio E., Ed.; Wiley-VCH Verlag GmbH: Weinheim, **2011**.
17. Patra, M.; Gasser, G. *Chembiochem* **2012**, *13*, 1232.
18. David, S. S.; Meggers, E. *Curr. Opin. Chem. Biol.* **2008**, *12*, 194.
19. Haas, K. L.; Franz, K. J. *Chem. Rev.* **2009**, *109*, 4921.
20. Coogan, M. P.; Dyson, P. J.; Bochmann, M. *Organometallics* **2012**, *31*, 5671.

21. Crabtree, R. H. *Organometallics* **2011**, *30*, 17.
22. Artero, V.; Chavarot-Kerlidou, M.; Fontecave, M. *Angew. Chem. Int. Ed.* **2011**, *50*, 7238.
23. Piers, W. E. *Organometallics* **2011**, *30*, 13.
24. Le Goff, A.; Artero, V.; Jousselme, B.; Tran, P. D.; Guillet, N.; Metaye, R.; Fihri, A.; Palacin, S.; Fontecave, M. *Science* **2009**, *326*, 1384.
25. Sasmal, P. K.; Carregal-Romero, S.; Parak, W. J.; Meggers, E. *Organometallics* **2012**, *31*, 5968.
26. Mulcahy, S. P.; Meggers, E. In *Medicinal Organometallic Chemistry*; Jaouen, G.; Metzler-Nolte, N., Eds.; Springer: Berlin, **2010**; Vol. 32, p 141.
27. Meggers, E. *Curr. Opin. Chem. Biol.* **2007**, *11*, 287.
28. Mann, B. E. In *Medicinal Organometallic Chemistry*; Jaouen, G.; Metzler-Nolte, N., Eds.; Springer: Berlin, **2010**; Vol. 32, p 247.
29. Marques, A. R.; Kromer, L.; Gallo, D. J.; Penacho, N.; Rodrigues, S. S.; Seixas, J. D.; Bernardes, G. J. L.; Reis, P. M.; Otterbein, S. L.; Ruggieri, R. A.; Gonçalves, A. S. G.; Gonçalves, A. M. L.; Matos, M. N. D.; Bento, I.; Otterbein, L. E.; Blättler, W. A.; Romao, C. C. *Organometallics* **2012**, *31*, 5810.
30. Alberto, R. In *Bioinorganic Medicinal Chemistry*; Alessio, E., Ed.; Wiley-VCH Verlag GmbH: Weinheim, **2011**; p 235.
31. Morais, G. R.; Paulo, A.; Santos, I. *Organometallics* **2012**, *31*, 5693.
32. Salmain, M. In *Bioorganometallics: Biomolecules, Labeling, Medecine*; Jaouen, G., Ed.; Wiley-VCH Verlag GmbH: Weinheim, **2006**; p 181.
33. Salmain, M.; Vessières, A. In *Bioorganometallics: Biomolecules, Labeling, Medecine*; Jaouen, G., Ed. Wiley-VCH Verlag GmbH: Weinheim, **2006**; p 263.
34. Salmain, M.; Vessières, A.; Varenne, A.; Brossier, P.; Jaouen, G. *J. Organomet. Chem.* **1999**, *589*, 92.
35. Vessières, A.; Salmain, M.; Brossier, P.; Jaouen, G. *J. Pharm. Biomed. Anal.* **1999**, *21*, 625.
36. Philomin, V.; Vessières, A.; Jaouen, G. *J. Immunol. Methods* **1994**, *171*, 201.
37. Akita, M. *Organometallics* **2011**, *30*, 43.
38. Thorp-Greenwood, F. L. *Organometallics* **2012**, *31*, 5686.
39. Mari, C.; Panigati, M.; D'Alfonso, L.; Zanoni, I.; Donghi, D.; Sironi, L.; Collini, M.; Maiorana, S.; Baldoli, C.; D'Alfonso, G.; Licandro, E. *Organometallics* **2012**, *31*, 5918.
40. (a) Policar, C.; Waern, J. B.; Plamont, M. A.; Clede, S.; Mayet, C.; Prazeres, R.; Ortega, J. M.; Vessières, A.; Dazzi, A. *Angew. Chem. Int. Ed.* **2011**, *50*, 860; (b) Kong, K. V.; Lam, Z.; Goh, W. D.; Leong, W. K.; Olivo, M. *Angew. Chem. Int. Ed.* **2012**, *51*, 9796.
41. Gasser, G.; Ott, I.; Metzler-Nolte, N. *J. Med. Chem.* **2011**, *54*, 3.
42. Pizarro, A. N.; Habtemariam, A.; Sadler, P. J. In *Medicinal Organometallic Chemistry*; Jaouen, G.; Metzler-Nolte, N., Eds.; Springer: Berlin, **2010**; p 21.
43. Botté, C. Y.; Dubar, F.; McFadden, G. I.; Maréchal, E.; Biot, C. *Chem. Rev.* **2012**, *112*, 1269.
44. Navarro, M.; Castro, W.; Biot, C. *Organometallics* **2012**, *31*, 5715.
45. Kelland, L. *Nat. Rev. Cancer* **2007**, *7*, 573.
46. Lippert, B. *Cisplatin: Chemistry and Biochemistry of a Leading Anticancer Drug*; Wiley-VCH Verlag GmbH: Weinheim, **1999**.
47. Reedijk, J. *Proc. Natl. Acad. Sci. U.S.A.* **2003**, *100*, 3611.
48. Reedijk, J. *Eur. J. Inorg. Chem.* **2009**, 1303.
49. Dwyer, F. P.; Gyarfus, E. C.; Rogers, W. P.; Koch, J. H. *Nature* **1952**, *170*, 190.
50. Dwyer, F. P.; Mayhew, E.; Roe, E. M. F.; Shulman, A. *Br. J. Cancer* **1965**, *19*, 195.
51. Rosenberg, B.; Vancamp, L.; Krigas, T. *Nature* **1965**, *205*, 698.
52. Fricker, S. P. *Dalton Trans.* **2007**, 4903.
53. Bruijnincx, P. C. A.; Sadler, P. J. *Curr. Opin. Chem. Biol.* **2008**, *12*, 197.
54. Hannon, M. J. *Pure Appl. Chem.* **2007**, *79*, 2243.
55. Schröder, M.; Stephenson, T. A. In *Comprehensive Coordination Chemistry*; Wilkinson, G.; Gillard, R. D.; McCleverty, J. A., Eds.; Pergamon: Oxford, **1987**; Vol. 4, p 277.
56. Housecroft, C. E. In *Comprehensive Coordination Chemistry II*; McCleverty, J. A.; Meyer, T. J., Eds.; Elsevier: Oxford, **2003**; p 555.
57. Wang, M.; Li, C. J. *Top. Organomet. Chem.* **2004**, *11*, 321.
58. Vos, J. G.; Kelly, J. M. *Dalton Trans.* **2006**, 4869.
59. Ang, W. H.; Dyson, P. J. *Eur. J. Inorg. Chem.* **2006**, 4003.
60. Chatterjee, D.; Mitra, A.; De, G. S.; *Platin. Met. Rev.* **2006**, *50*, 2.

61. Reisner, E.; Arion, V. B.; Keppler, B. K.; Pombeiro, A. J. L. *Inorg. Chim. Acta* **2008**, *361*, 1569.
62. Bratsos, L.; Jedner, S.; Gianferrara, T.; Alessio, E. *Chimia* **2007**, *61*, 692.
63. Clarke, M. J. *Coord. Chem. Rev.* **2003**, *236*, 209.
64. Alessio, E.; Mestroni, G.; Bergamo, A.; Sava, G. *Met. Ions Biol. Syst.* **2004**, *4*, 323.
65. Bergamo, A.; Sava, G. *Dalton Trans.* **2007**, 1267.
66. Dougan, S. J.; Sadler, P. J. *Chimia* **2007**, *61*, 704.
67. Dyson, P. J. *Chimia* **2007**, *61*, 698.
68. Heffeter, P.; Jungwirth, U.; Jakupc, M.; Hartinger, C.; Galanski, M.; Elbling, L.; Micksche, M.; Keppler, B.; Berger, W. *Drug Resist. Updat.* **2008**, *11*, 1.
69. Clarke, M. J. *Met. Ions Biol. Syst.* **1980**, *10*, 231.
70. Clarke, M. J. *Coord. Chem. Rev.* **2002**, *232*, 69.
71. Sava, G.; Capozzi, I.; Clerici, K.; Gagliardi, G.; Alessio, E.; Mestroni, G. *Clin. Exp. Metastasis* **1998**, *16*, 371.
72. Groessl, M.; Reisner, E.; Hartinger, C. G.; Eichinger, R.; Semenova, O.; Timerbaev, A. R.; Jakupc, M. A.; Arion, V. B.; Keppler, B. K. *J. Med. Chem.* **2007**, *50*, 2185.
73. Cebrian-Losantos, B.; Krokkin, A. A.; Stepanenko, I. N.; Eichinger, R.; Jakupc, M. A.; Arion, V. B.; Keppler, B. K. *Inorg. Chem.* **2007**, *46*, 5023.
74. Kapitza, S.; Pongratz, M.; Jakupc, M. A.; Heffeter, P.; Berger, W.; Lackinger, L.; Keppler, B. K.; Marian, B. *J. Cancer Res. Clin. Oncol.* **2005**, *131*, 101.
75. Hartinger, C. G.; Jakupc, M. A.; Zorbas-Seifried, S.; Groessl, M.; Egger, A.; Berger, W.; Zorbas, H.; Dyson, P. J.; Keppler, B. K. *Chem. Biodivers.* **2008**, *5*, 2140.
76. Lentz, F.; Drescher, A.; Lindauer, A.; Henke, M.; Hilger, R. A.; Hartinger, C. G.; Scheulen, M. E.; Dittrich, C.; Keppler, B. K.; Jaehde, U. *Anticancer Drugs* **2009**, *20*, 97.
77. Levina, A.; Mitra, A.; Lay, P. A. *Metallomics* **2009**, *1*, 458.
78. Casini, A.; Gabbiani, C.; Sorrentino, F.; Rigobello, M. P.; Bindoli, A.; Geldbach, T. J.; Marrone, A.; Re, N.; Hartinger, C. G.; Dyson, P. J.; Messori, L. *J. Med. Chem.* **2008**, *51*, 6773.
79. Dougan, S. J.; Habtemariam, A.; McHale, S. E.; Parsons, S.; Sadler, P. J. *Proc. Natl. Acad. Sci. U.S.A.* **2008**, *105*, 11628.
80. Meng, X. J.; Leyva, M. L.; Jenny, M.; Gross, I.; Benosman, S.; Fricker, B.; Harlepp, S.; Hebraud, P.; Boos, A.; Wlosik, P.; Bischoff, P.; Sirlin, C.; Pfeffer, M.; Loeffler, J. P.; Gaiddon, C. *Cancer Res.* **2009**, *69*, 5458.
81. Gaiddon, C.; Jeannequin, P.; Bischoff, P.; Pfeffer, M.; Sirlin, C.; Loeffler, J. P. *J. Pharmacol. Exp. Ther.* **2005**, *315*, 1403.
82. Smalley, K. S. M.; Contractor, R.; Haass, N. K.; Kulp, A. N.; Atilla-Gokcumen, G. E.; Williams, D. S.; Bregman, H.; Flaherty, K. T.; Soengas, M. S.; Meggers, E.; Herlyn, M. *Cancer Res.* **2007**, *67*, 209.
83. Bratsos, I.; Gianferrara, T.; Alessio, E.; Hartinger, C. G.; Jakupc, M. A.; Keppler, B. K. In *Bioinorganic Medicinal Chemistry*; Alessio, E., Ed.; Wiley-VCH Verlag GmbH: Weinheim, **2011**; p 151.
84. Sava, G.; Jaouen, G.; Hillard, E. A.; Bergamo, A. *Dalton Trans.* **2012**, *41*, 8226.
85. Vessières, A.; Corbet, C.; Heldt, J. M.; Lories, N.; Jouy, N.; Laios, I.; Leclercq, G.; Jaouen, G.; Toillon, R. A. *J. Inorg. Biochem.* **2010**, *104*, 503.
86. Pauson, P. L. *J. Organomet. Chem.* **2001**, *637*, 3.
87. Wilkinson, G.; Rosenblum, M.; Whiting, M. C.; Woodward, R. B. *J. Am. Chem. Soc.* **1952**, *74*, 2125.
88. Fischer, E. O.; Pfab, W. *Z. Naturforsch. B* **1952**, *7*, 377.
89. Dombrowski, K. E.; Baldwin, W.; Sheats, J. E. *J. Organomet. Chem.* **1986**, *302*, 281.
90. Yeary, R. A. *Toxicol. Appl. Pharmacol.* **1969**, *15*, 666.
91. Jaouen, G.; Top, S.; Vessières, A. In *Bioorganometallics: Biomolecules, Labeling, Medicine*; Jaouen, G., Ed.; Wiley-VCH Verlag GmbH: Weinheim, **2006**; p 65.
92. Hillard, E. A.; Vessières, A.; Jaouen, G. In *Medicinal Organometallic Chemistry*; Jaouen, G.; Metzler-Nolte, N., Eds.; Topics in Organometallic Chemistry, Vol. 32; Springer-Verlag: Heidelberg, **2010**; p 81.
93. Loev, B.; Flores, M. *J. Org. Chem.* **1961**, *26*, 3595.
94. Edwards, E. I.; Epton, R.; Marr, G. *J. Organomet. Chem.* **1975**, *85*, C23.
95. Edwards, E. I.; Epton, R.; Marr, G. *J. Organomet. Chem.* **1976**, *122*, C49.
96. Biot, C.; Glorian, G.; Maciejewski, L. A.; Brocard, J. S.; Domarle, O.; Blampain, G.; Millet, P.; Georges, A. J.; Abessolo, H.; Dive, D.; Lebib, J. *J. Med. Chem.* **1997**, *40*, 3715.
97. Top, S.; Tang, J.; Vessières, A.; Carrez, D.; Provot, C.; Jaouen, G. *Chem. Commun.* **1996**, 955.
98. Top, S.; Dauer, B.; Vaissermann, J.; Jaouen, G. *J. Organomet. Chem.* **1997**, *541*, 355.

99. Jaouen, G.; Top, S.; Vessières, A.; Leclercq, G.; Quivy, J.; Jin, L.; Croisy, A. *C.R. Acad. Sci., Série IIc* **2000**, 89.
100. Top, S.; Vessières, A.; Cabestaing, C.; Laios, I.; Leclercq, G.; Provot, C.; Jaouen, G. *J. Organomet. Chem.* **2001**, 637, 500.
101. Top, S.; Vessières, A.; Leclercq, G.; Quivy, J.; Tang, J.; Vaissermann, J.; Huche, M.; Jaouen, G. *Chem. Eur. J.* **2003**, 9, 5223.
102. Zanellato, I.; Heldt, J.-M.; Vessières, A.; Jaouen, G.; Osella, D. *Inorg. Chim. Acta* **2009**, 362, 4037.
103. Nguyen, A.; Vessières, A.; Hillard, E. A.; Top, S.; Pigeon, P.; Jaouen, G. *Chimia* **2007**, 61, 716.
104. Vessières, A.; Top, S.; Pigeon, P.; Hillard, E.; Boubeker, L.; Spera, D.; Jaouen, G. *J. Med. Chem.* **2005**, 48, 3937.
105. Hillard, E. A.; Pigeon, P.; Vessières, A.; Amatore, C.; Jaouen, G. *Dalton Trans.* **2007**, 5073.
106. Pigeon, P.; Top, S.; Zekri, O.; Hillard, E.; Vessières, A.; Plumont, M. A.; Labbé, E.; Buriez, O.; Huché, M.; Boutamine, S.; Amatore, C.; Jaouen, G. *J. Organomet. Chem.* **2009**, 694, 895.
107. Zekri, O.; Hillard, E.; Top, S.; Vessières, A.; Pigeon, P.; Plumont, M. A.; Huché, M.; Boutamine, S.; McGlinchey, M. J.; Müller-Bunz, H.; Jaouen, G. *Dalton Trans.* **2009**, 22, 4318.
108. Hillard, E.; Vessières, A.; Le Bideau, F.; Plazuk, D.; Spera, D.; Huche, M.; Jaouen, G. *ChemMedChem* **2006**, 1, 551.
109. Messina, P.; Labbé, E.; Buriez, O.; Hillard, E. A.; Vessières, A.; Hamels, D.; Top, S.; Jaouen, G.; Frapart, Y. M.; Mansuy, D.; Amatore, C. *Chem. Eur. J.* **2012**, 18, 6581.
110. Hillard, E.; Vessières, A.; Thouin, L.; Jaouen, G.; Amatore, C. *Angew. Chem. Int. Ed.* **2006**, 45, 285.
111. Hamels, D.; Dansette, P. M.; Hillard, E. A.; Top, S.; Vessières, A.; Herson, P.; Jaouen, G.; Mansuy, D. *Angew. Chem. Int. Ed.* **2009**, 48, 9124.
112. Wlassoff, W. A.; Albright, C. D.; Sivashinski, M. S.; Lvanova, A.; Appelbaum, J. G.; Salganik, R. I. *J. Pharm. Pharmacol.* **2007**, 59, 1549.
113. de Oliveira, A. C.; Hillard, E. A.; Pigeon, P.; Rocha, D. D.; Rodrigues, F. A. R.; Montenegro, R. C.; Costa-Lotufo, L. V.; Goulart, M. O. F.; Jaouen, G. *Eur. J. Inorg. Chem.* **2011**, 46, 3778.
114. Michard, Q.; Jaouen, G.; Vessières, A.; Bernard, B. A. *J. Inorg. Biochem.* **2008**, 102, 1980.
115. Nguyen, A.; Marsaud, V.; Bouclier, C.; Top, S.; Vessières, A.; Pigeon, P.; Gref, R.; Legrand, P.; Jaouen, G.; Renoir, J. M. *Int. J. Pharm.* **2008**, 347, 128.
116. Osella, D.; Mahboobi, H.; Colangelo, D.; Cavigiolio, G.; Vessières, A.; Jaouen, G. *Inorg. Chim. Acta* **2005**, 358, 1993.
117. Gormen, M.; Pigeon, P.; Top, S.; Hillard, E. A.; Huche, M.; Hartinger, C. G.; de Montigny, F.; Plumont, M. A.; Vessières, A.; Jaouen, G. *ChemMedChem* **2010**, 5, 2039.
118. Jaouen, G.; Top, S.; Vessières, A.; Pigeon, P.; Leclercq, G.; Laios, I. *Chem. Commun.* **2001**, 383.
119. Top, S.; Kaloun, E. B.; Vessières, A.; Laios, I.; Leclercq, G.; Jaouen, G. *J. Organomet. Chem.* **2002**, 643, 350.
120. Top, S.; Vessières, A.; Pigeon, P.; Rager, M. N.; Huché, M.; Salomon, E.; Cabestaing, C.; Vaissermann, J.; Jaouen, G. *Chembiochem* **2004**, 5, 1104.
121. Pigeon, P.; Top, S.; Vessières, A.; Huché, M.; Hillard, E. A.; Salomon, E.; Jaouen, G. *J. Med. Chem.* **2005**, 48, 2814.
122. Hillard, E. A.; Vessières, A.; Top, S.; Pigeon, P.; Kowalski, K.; Huché, M.; Jaouen, G. *J. Organomet. Chem.* **2007**, 692, 1315.
123. Allard, E.; Passirani, C.; Garcion, E.; Pigeon, P.; Vessières, A.; Jaouen, G.; Benoit, J. P. *J. Control. Release* **2008**, 130, 146.
124. Hagen, H.; Marzenell, P.; Jentzsch, E.; Wenz, F.; Veldwijk, M. R.; Mokhir, A. *J. Med. Chem.* **2012**, 55, 924.
125. Tan, Y. L. K.; Pigeon, P.; Hillard, E. A.; Top, S.; Plumont, M. A.; Vessières, A.; McGlinchey, M. J.; Muller-Bunz, H.; Jaouen, G. *Dalton Trans.* **2009**, 10871.
126. Poon, G. K.; Walter, B.; Lonning, P. E.; Horton, M. N.; McCague, R. *Drug Metab. Dispos.* **1995**, 23, 377.
127. Tan, Y. L. K.; Pigeon, P.; Top, S.; Labbé, E.; Buriez, O.; Hillard, E. A.; Vessières, A.; Amatore, C.; Leong, W. K.; Jaouen, G. *Dalton Trans.* **2012**, 41, 7537.
128. Plazuk, D.; Vessières, A.; Hillard, E. A.; Buriez, O.; Labbé, E.; Pigeon, P.; Plumont, M. A.; Amatore, C.; Zakrzewski, J.; Jaouen, G. *J. Med. Chem.* **2009**, 52, 4964.
129. Gormen, M.; Pigeon, P.; Hillard, E.; Vessières, A.; Huche, M.; Richard, M.; McGlinchey, M. J.; Top, S.; Jaouen, G. *Organometallics* **2012**, 31, 5856.
130. Gormen, M.; Pigeon, P.; Top, S.; Vessières, A.; Plumont, M. A.; Hillard, E. A.; Jaouen, G. *Medchemcomm* **2010**, 1, 149.
131. Pigeon, P.; Top, S.; Vessières, A.; Huche, M.; Gormen, M.; El Arbi, M.; Plumont, M. A.; McGlinchey, M. J.; Jaouen, G. *New J. Chem.* **2011**, 35, 2212.
132. Nikitin, K.; Ortin, Y.; Muller-Bunz, H.; Plumont, M. A.; Jaouen, G.; Vessières, A.; McGlinchey, M. J. *J. Organomet. Chem.* **2010**, 695, 595.
133. El Arbi, M.; Pigeon, P.; Rkhis, A. C.; Top, S.; Rhouma, A.; Rebai, A.; Jaouen, G.; Aifa, S. *J. Plant Pathol.* **2011**, 93, 651.
134. El Arbi, M.; Pigeon, P.; Top, S.; Rhouma, A.; Aifa, S.; Rebai, A.; Vessières, A.; Plumont, M. A.; Jaouen, G. *J. Organomet. Chem.* **2011**, 696, 1038.

135. Payen, O.; Top, S.; Vessières, A.; Brulé, E.; Plumont, M. A.; McGlinchey, M. J.; Muller-Bunz, H.; Jaouen, G. *J. Med. Chem.* **2008**, *51*, 1791.
136. Payen, O.; Top, S.; Vessières, A.; Brulé, E.; Lauzier, A.; Plumont, M. A.; McGlinchey, M. J.; Muller-Bunz, H.; Jaouen, G. *J. Organomet. Chem.* **2011**, *696*, 1049.
137. Mooney, A.; Tiedt, R.; Maghoub, T.; O'Donovan, N.; Crown, J.; White, B.; Kenny, P. T. M. *J. Med. Chem.* **2012**, *55*, 5455.
138. Ornelas, C. *New J. Chem.* **2011**, *35*, 1973.
139. Ornelas, C.; Pennell, R.; Liebes, L. F.; Weck, M. *Org. Lett.* **2011**, *13*, 976.
140. Buriez, O.; Heldt, J. M.; Labbé, E.; Vessières, A.; Jaouen, G.; Amatore, C. *Chem. Eur.J.* **2008**, *14*, 8195.
141. Petrovski, Z.; de Matos, M.; Braga, S. S.; Pereira, C. C. L.; Matos, M. L.; Goncalves, I. S.; Pillinger, M.; Alves, P. M.; Romao, C. C. *J. Organomet. Chem.* **2008**, *693*, 675.
142. Caldwell, G.; Meirim, M. G.; Neuse, E. W.; van Rensburg, C. E. *J. Appl. Organomet. Chem.* **1998**, *12*, 793.
143. Neuse, E. W. *Polym. Adv. Technol.* **1998**, *9*, 786.
144. Neuse, E. W. *Macromol. Symp.* **2001**, *172*, 127.
145. Johnson, M. T.; Kreft, E.; N'Da, D. D.; Neuse, E. W.; van Rensburg, C. E. *J. J. Inorg. Organomet. Polym. Mater.* **2003**, *13*, 255.
146. Hu, M. *Mol. Pharm.* **2007**, *4*, 803.
147. Vercauteran, J. (Caudalie). *WO 2009063439*, 2007.
148. Vercauteran, J. In *Brevet Français, Vol. Fr 1997–8964* (Ed.: Caudalie), 1997.
149. Manach, C.; Scalbert, A.; Morand, C.; Remesy, C.; Jumenez, L. *Am. J. Clin. Nutr.* **2004**, *79*, 727.
150. Scalbert, A.; Williamson, G. *J. Nutr.* **2000**, *130*, 2073S.
151. Kahkonen, M. P.; Hopia, A. I.; Vuorela, H. J.; Rauha, J. P.; Pihlaja, K.; Kujala, T. S.; Heinonen, M. *J. Agric. Food Chem.* **1999**, *47*, 3954.
152. Tapiero, H.; Tew, K. D.; Nguyen-Ba, G.; Mathé, G. *Biomed. Pharmacother.* **2009**, *56*, 200.
153. Heurtault, B.; Saulnier, P.; Pech, B.; Proust, J. E.; Benoit, J. P. *Pharm. Res.* **2002**, *19*, 875.
154. Allard, E.; Passirani, C.; Benoit, J. P. *Biomaterials* **2009**, *30*, 2302.
155. Allard, E.; Huynh, N. T.; Vessières, A.; Pigeon, P.; Jaouen, G.; Benoit, J. P.; Passirani, C. *Int. J. Pharm.* **2009**, *379*, 317.
156. Huynh, N. T.; Morille, M.; Bejaud, J.; Legras, P.; Vessières, A.; Jaouen, G.; Benoit, J. P.; Passirani, C. *Pharm. Res.* **2011**, *28*, 3189.
157. Allard, E.; Jarnet, D.; Vessières, A.; Vinchon-Petit, S.; Jaouen, G.; Benoit, J. P.; Passirani, C. *Pharm. Res.* **2010**, *27*, 56.
158. Frederick, R.; Bruyère, C.; Vancraeynest, C.; Reniers, J.; Meinguet, C.; Pochet, L.; Backlund, A.; Masereel, B.; Kiss, R.; Wouters, J. *J. Med. Chem.* **2012**, *55*, 6489.

## ON THE TRACK TO CANCER THERAPY: PAVING NEW WAYS WITH RUTHENIUM ORGANOMETALLICS

TÂNIA S. MORAIS AND M. HELENA GARCIA\*

*Centro de Ciências Moleculares e Materiais, Faculdade de Ciências da Universidade de Lisboa, Lisboa, Portugal*

### 43.1 INTRODUCTION

In the field of search for metallodrugs as anticancer agents, ruthenium chemistry has been an attracting field because of the promising results obtained for some families of the inorganic octahedral Ru(III) compounds. In this frame, NAMI-A [1] and KP1019 [2] appeared as the most representative examples being already in clinical evaluation. Although the original appeal for ruthenium drugs have circumvented the noxious effects of the highly toxic chemotherapy based on cisplatin drugs, the success in the treatment of metastases by some ruthenium compounds pointed out the important potential of these drugs in the field of innovative chemotherapies. At present, there is no drug capable of controlling metastases growth, thus making the fight against metastases one of the main problems in the battle against cancer that urge to be solved.

The strategy of synthesis for metallodrugs has been following the platinum models envisaging the cell death by interaction with DNA, preferentially by a different mechanism from that of cisplatin, to overcome tumor cell resistance. In this scenario, a variety of ruthenium(II) organometallic complexes have been designed viewing the classical target, the DNA.

Two main families of organometallic ruthenium(II)-arene complexes (see Fig. 43.1) were developed and studied by Sadler [3, 4] (RM complexes) and Dyson [5, 6] (RAPTA complexes), in which the basic structures present the piano-stool geometry and their reactivity toward biological targets is based on the leaving chloride ligands, as happens with cisplatin. Nevertheless, these two families of compounds besides the similarity of their structure present different characteristics.

While RM complexes reveal quite good cytotoxicity *in vitro*, RAPTA complexes show low cytotoxicity but are very efficient against invasion and metastasis effects. A third family of organometallic compounds was studied by Meggers [7, 8] (DW-complexes) and involves pyridocarbazole ligands (to mimic staurosporine) as organic moiety coordinated to the ruthenium(II)-cyclopentadienyl ligand fragment (see Fig. 43.1), which revealed strong and selective inhibitors of protein kinases GSK-3 and Pim-1, thus showing their potentiality as anticancer agents.

In spite of the development of ruthenium drugs and all the studies in some large classes of compounds, essentially typified in Fig. 43.1, there is not yet any direction concerning structure–activity relationship to serve as a guide line for future research in the field. However, all results gathered up now certainly point out for an added value of the ruthenium ion on the overall interaction in spite of the nonexistence of any plausible direct interaction with the target.

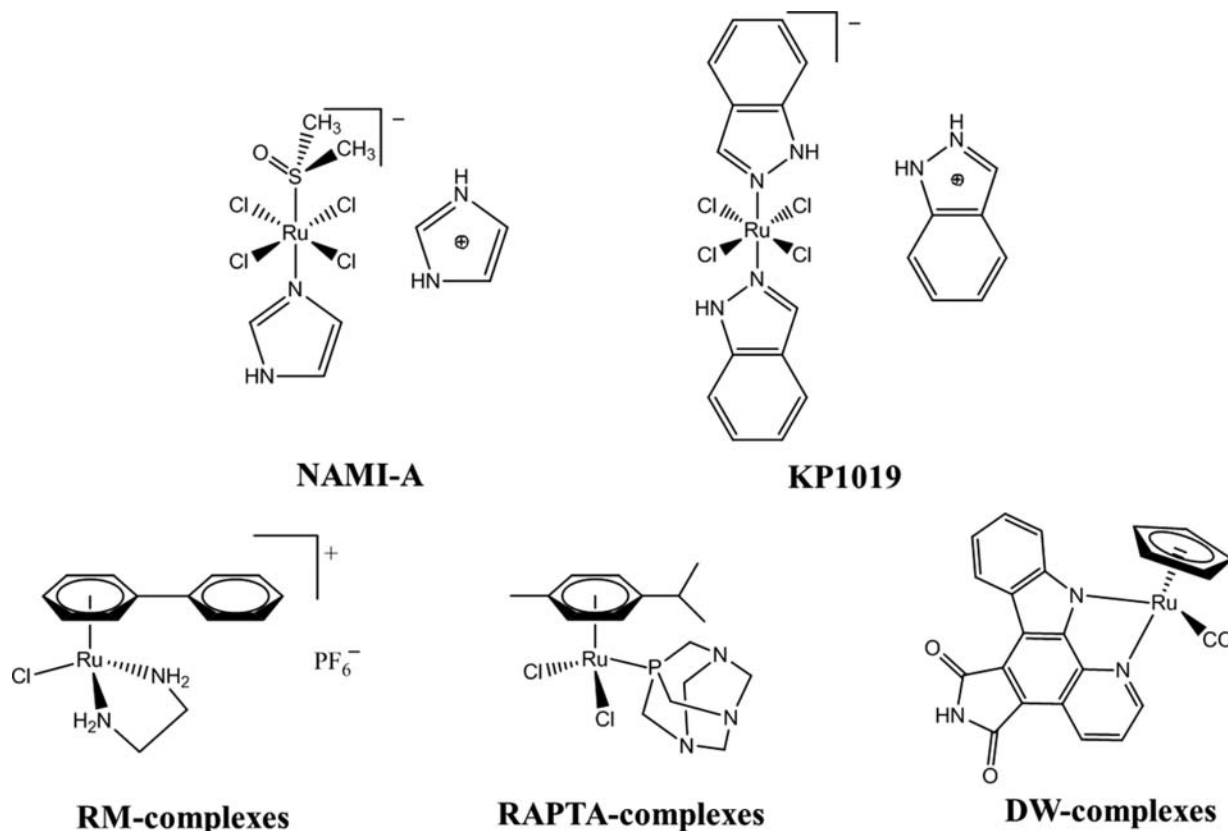


Figure 43.1 Chemical structures of some ruthenium compounds.

### 43.2 OUR STRATEGY IN BIOORGANOMETALLIC CHEMISTRY

In the frame of organometallic ruthenium drugs, our research group started to develop a new family of compounds based on the so-called *piano-stool* geometry, in which the reactivity mechanism is expected to be different from the complexes presented earlier because of the absence of any chloride leaving groups. The ruthenium–carbon bond of the “piano” is built with a cyclopentadienyl group (Cp), in which the negative charge gives additional electrostatic stability to the “Ru(II)Cp” fragment, compared to the equivalent “Ru(II)-arene” “piano” structure (see Fig. 43.2). Stability of the fragment “RuCp” was corroborated by our studies in gas phase by electrospray ionization mass spectrometry (ESI-MS), carried out with several complexes of the family  $[\text{RuCp}(\text{PP})_n\text{L}][\text{CF}_3\text{SO}_3]$  (where PP = phosphane, L = heteroaromatic ligand, and  $n = 1$  or 2), which in all the cases originate “RuCp” as final species, impossible to dissociate even at very high values of energy [9].

This general piano-stool structure allows us to play with the nonleaving groups on the legs of the piano, which were chosen to be phosphane ligands (mono or bidentate) and heteroaromatic ligands coordinated by N, O, S, etc. where the coordination can be by one or two atoms. The design of these compounds can lead to a significant structural diversity as we can play with each part of the molecule, such as functionalization on the Cp ring, coordination number, and nature of the coligands, and also with the counter-ion itself (Fig. 43.3). Several of these features can constitute an important advantage to control the solubility of the compounds, this being the most important to optimize the biological activity.



Figure 43.2 Building of piano-stool structures based on cyclopentadienyl and arene groups.

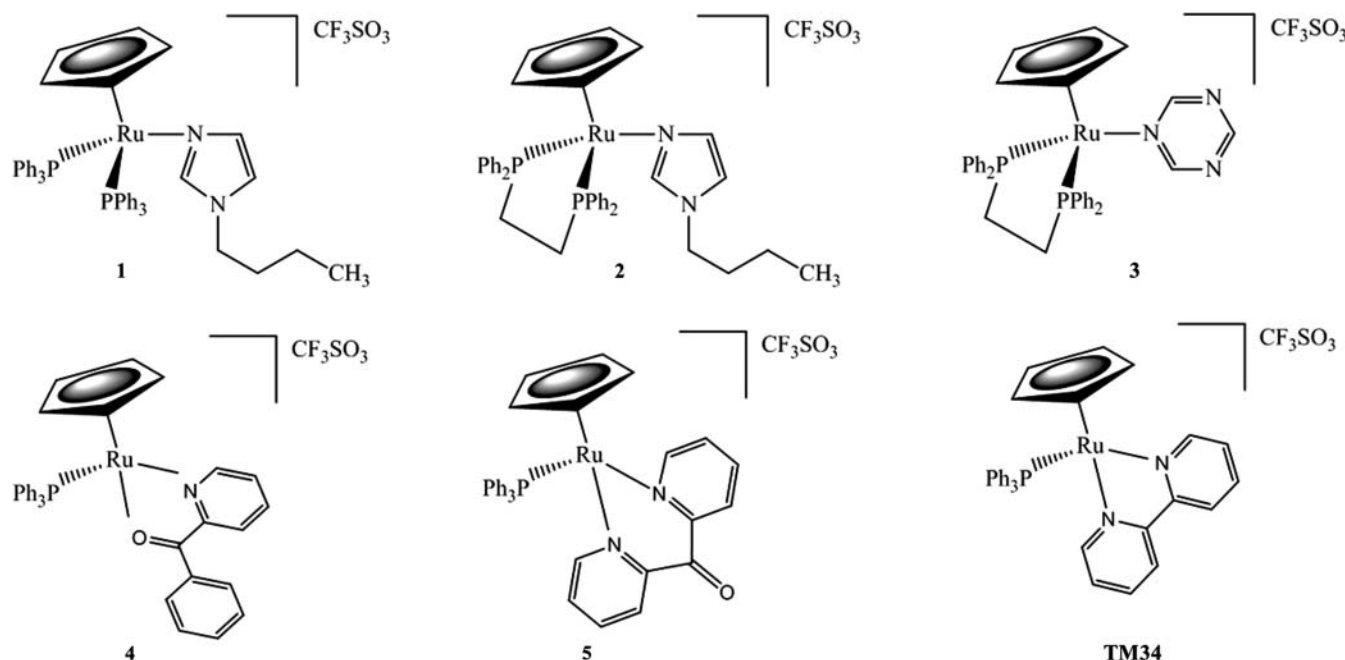


**Figure 43.3** Examples of several structures of “RuCp” compounds showing different coordination for the ligands.

**TABLE 43.1** IC<sub>50</sub> Values for Some “RuCp” Based Compounds for Several Human Cancer Cell Lines (72 h, 37 °C) [10, 11]

Compound	Tumor Cell Lines IC <sub>50</sub> , μM					
	A2780	A2780CisR	MCF7	MDAMDB231	HT29	PC3
<b>4</b>	0.19 ± 0.03	0.21 ± 0.04	0.05 ± 0.01	0.03 ± 0.01	0.08 ± 0.01	0.41 ± 0.08
<b>5</b>	0.46 ± 0.11	0.47 ± 0.16	0.41 ± 0.09	0.23 ± 0.07	0.53 ± 0.14	1.9 ± 0.3
<b>TM34</b>	0.14 ± 0.01	0.07 ± 0.02	0.29 ± 0.01	0.72 ± 0.25	0.41 ± 0.07	0.54 ± 0.10
Cisplatin	2.00 ± 0.10	17 ± 3.0	28 ± 6.0	39 ± 5.0	7.0 ± 2.0	51 ± 7.0

### 43.3 BIOLOGICAL ACTIVITY

Cytotoxicity studies for these “RuCp” compounds, carried out *in vitro* with several human cancer cell lines, namely, A2780 (ovarian carcinoma), A2780CisR (ovarian carcinoma, cisplatin resistant), HT29 (colon adenocarcinoma), MCF7 (breast adenocarcinoma—hormone dependent, ERα+), MDAMB231 (breast adenocarcinoma—hormone independent), and PC3 (prostate cancer) revealed excellent antitumor activities with IC<sub>50</sub> values much lower than those found for cisplatin [10, 11] (Table 43.1). Noteworthy, the excellent activity found for cisplatin-resistant cancer cells suggests that a mechanism of action different from cisplatin might be involved in the present case. It is important to mention the excellent values obtained with MDAMB231 cancer cells that have highly metastatic properties.

### 43.4 DISTRIBUTION IN THE BLOOD

Protein-drug binding greatly influences the distribution and pharmacological properties of a drug [12]. Human serum albumin (HSA) is the principal and most abundant protein of the circulatory system [12, 13]. The main function of albumin is to transport fatty acids and a broad range of drug molecules to its targets [14, 15]. HSA often increases the solubility of hydrophobic drugs in plasma [16]. As HSA serves as a drug transport carrier, the knowledge of the kind of interaction between drugs and plasma proteins is of major importance to understand the drug pharmacokinetics and pharmacodynamics.

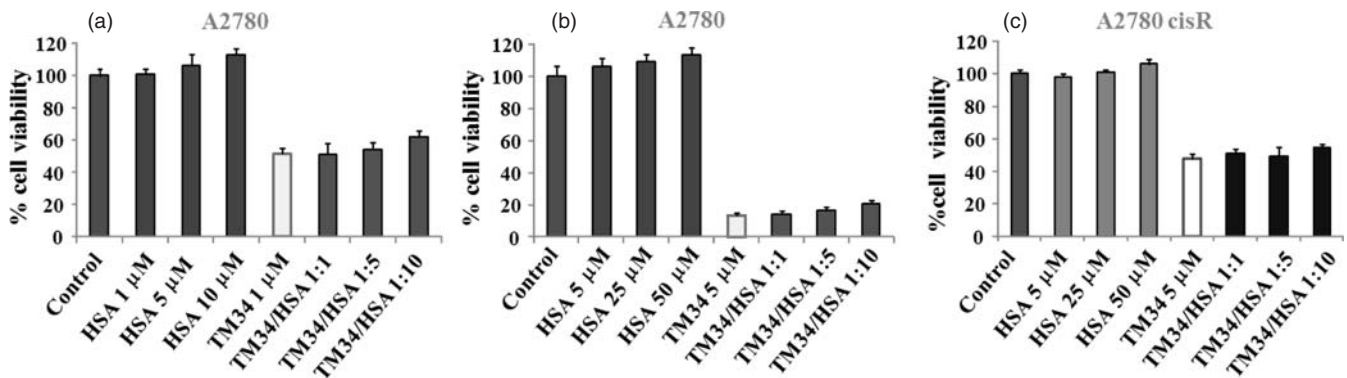


**Figure 43.4** Effect of HSA on the cytotoxicity of TM34 on A2780 (a) and A2780CisR cells (c) after a 24-h challenge. A2780 cells were treated with TM34 at 1  $\mu$ M (a and c) and 5  $\mu$ M (b) preincubated with HSA at 1 : 1, 1 : 5, and 1 : 10 complex-to-protein molar ratios. Data shown are the mean values ( $\pm$ SD) of two independent experiments, each performed with at least six replicates. *Control* indicates cells with no treatment (negative control), HSA (5, 25, and 50  $\mu$ M) indicates cells treated with HSA alone in the concentrations indicated, TM34 (1 and 5  $\mu$ M) are positive controls (cell treated with the complex in the absence of albumin). Adapted from Reference 11.

The binding of several “RuCp” compounds to HSA was studied as a first approach to outline its pharmacokinetics and had been investigated by spectroscopic methods (absorption and fluorescence) and ultrafiltration-UV-vis. as well. It was found that TM34 binds to HSA forming a 1 : 1 adduct; the stability constant calculated for this {HSA–TM34} adduct was  $\log K_b' = 4$ . This value is similar to that found for KP1019 and shows that the complex can be transported in the blood by HSA [11].

As the binding to HSA can affect the drug biological activity and toxicity, it was important to check the cytotoxicity in the presence of albumin. Our experiments carried out with the {HSA–TM34} adduct did not significantly affect the activity of TM34 in the A2780 ovarian adenocarcinoma cells even in the sensitivity or resistance to cisplatin [11] (see Fig. 43.4).

### 43.5 INTRACELLULAR DISTRIBUTION

Information concerning drug distribution and concentration in the tumor cells is of primordial importance for understanding the drug mechanism of action. Drugs must not only enter into the cell but also concentrate in the cell compartments where the target is localized. For many traditional and new anticancer agents, these targets are localized either in the cell membrane and cytosol or in the nucleus.

Studies carried out for some of our “RuCp” complexes by inductively coupled plasma mass spectrometry (ICP-MS) to quantify the amount of ruthenium ion in the several cell fragments, after incubation with different cancer cell lines, showed that ruthenium preferentially accumulates in the cell membrane. Nevertheless, a significant amount of this metal is also found in cytosol and nucleus. Comparison with results obtained for cisplatin reference, used in our studies in the same experimental conditions, reveals that Pt barely reaches these three compartments.

### 43.6 MECHANISMS OF ACTION

The study of metallodrugs has been inspired in the “cisplatin model” that is until now the only metallodrugs available for chemotherapy treatments. The ruthenium(III) complexes (NAMI-A [1] and KP1019 [2]) that are currently in clinical trials were synthesized having in view DNA as the main target. However, some evidences have been found for the involvement of other biomolecule targets such as proteins and enzymes besides DNA. In this frame, our studies were thought to envisage both classical and nonclassical targets thus being focused on the interaction studies with DNA, PARP-1 enzyme, and some cell proteins.

#### 43.6.1 DNA: The Classical Target

Our first approach in the interaction studies with DNA involved comparison of atomic force microscopy (AFM) images of the plasmid pBR322 DNA incubated with our “RuCp” compounds [17–20], which revealed several types of strong

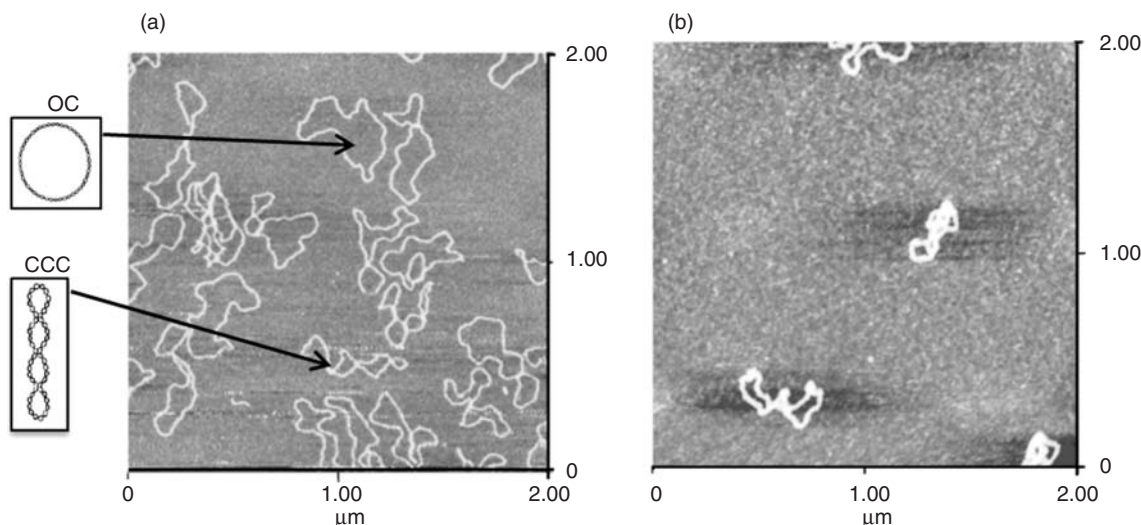


**Figure 43.5** AFM image of the (a) free plasmid pBR322 DNA and (b) plasmid pBR322 DNA incubated with the complex TM34 ( $[\text{RuCp}(\text{PPh}_3)(2,2'\text{-bipy})][\text{CF}_3\text{SO}_3]$ ) after 1 h, showing supercoiled forms (b). Adapted from Reference 20.

interactions when compared with the free plasmid. In fact, the images of TM34 displayed several supercoiled forms of plasmid DNA [20] (see Fig. 43.5) and were similar to the images previously observed for typical intercalating molecules such as 9-aminoacridine [21, 22] showing that TM34 was able to modify the DNA structure. Moreover, also a strong interaction was observed when compounds of this family were incubated with calf thymus DNA, which solutions presented visible aggregates slightly colored by the compound. This feature did not allow us to pursue further studies by other techniques, such as viscosity, fluorescence, and UV-vis spectroscopies, to collect experimental data concerning the type of interaction of “RuCp” with DNA. The observed formation of colored DNA aggregates is certainly a clear evidence of a strong interaction. Therefore, it might be concluded that DNA is a possible target of this family of compounds.

### 43.6.2 Nonclassical Targets: Proteins and Enzymes

The increasing evidence in the literature concerning the importance of enzymes and proteins as relevant targets for the mode of action of nonplatinum anticancer metallodrugs (for which multiple biological pathways have been proposed) [23, 24] led us to explore the role of proteins and enzymes in the antitumor activity of “RuCp” compounds [11]. PARP (poly-(adenosinediphosphate(ADP)-ribose)polymerases) enzymes play a key role in DNA repair mechanisms by detecting and initiating repair after DNA strand breaks [25]. PARP inhibitors have been evaluated as drugs for use in combinatorial therapies with DNA-damaging agents [26] and to sensitize cancer cells to subsequent treatment with cisplatin and carboplatin [27]. Phases I and II clinic trials evaluating the use of PARP inhibitors in combination therapies with platinum drug are currently underway [28]. It is known that PARP-1, the most studied member of the PARP family, is activated by mild DNA damage and is involved in DNA repair process, so that the cell survives. Moreover, PARP-1 may cause cellular death via necrosis or apoptosis, depending on the type, strength, and duration of genotoxic stimuli and the cell type. The ruthenium complex TM34 presents an  $\text{IC}_{50}$  value for PARP-1 inhibition of  $1 \mu\text{M}$  [11] (see Fig. 43.6), considerably lower than  $33 \mu\text{M}$  found for the classical inhibitor 3-aminobenzamide [29], for the ruthenium complexes RAPTA and NAMI-A (28 and  $18,9 \mu\text{M}$ , respectively) and cisplatin ( $12.3 \mu\text{M}$ ) [30]. Comparing these metallodrugs, TM34 is the strongest ruthenium inhibitor of PARP-1, its effect clearly surpassing those of RAPTA-T and NAMI-A and that of cisplatin as well (these being circa 30–10 times less effective) [11].

Apoptosis (programmed cell death) is involved in the development and elimination of the damaged cells. Deregulation of apoptosis can cause diseases such as cancers. Ubiquitin and cytochrome c are important in the mechanism of cell death being involved in the first steps of apoptosis. Apoptosis is executed by a subfamily of cysteine proteases known as *caspases*. In mammalian cells, a major caspase activation is the cytochrome c initiated pathway [31]. On the other hand, ubiquitin is used by cells as a covalent modifier of other proteins both to activate their function and to target them for degradation [32].

Our most recent studies by ESI-MS of “RuCp” complexes with these proteins show significant interaction and importantly reveal that ruthenium compounds preserve their initial structure.

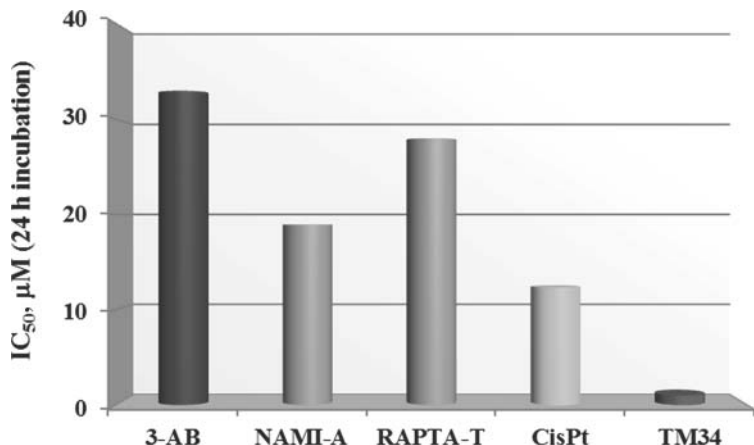


**Figure 43.6**  $IC_{50}$  value for TM34 inhibition compared to the reference benchmark PARP-1 inhibitor 3-aminobenzamide (3-AB) [29], cisplatin, and ruthenium complexes that exhibit antimetastatic activity *in vivo* NAMI-A and RAPTA-T (data for comparison taken from [30]). Adapted from Reference 11.

### 43.7 FINAL REMARKS

Organometallic compounds offer much potential for the search of anticancer drugs in particular with relevance for the treatment of metastases and thus for an innovative chemotherapy. Results published in the literature involving ruthenium complexes show that inorganic (e.g., NAMI-A and KP1019) and organometallic compounds (e.g., RM and RAPTA complexes) can be considered promising metallodrugs to circumvent the noxious effects of platin drugs and therefore present some potentialities to be used in chemotherapy.

In this context, our “RuCp” compounds appear exhibiting excellent anticancer activity *in vitro* and their kinetic stability gives them a vital advantage for a possible therapeutic formulation. The framework of this family of compounds provides considerable scope for optimizing the design of new molecules, by the introduction of substituent groups in Cp ring, using different hapticity of the coligands and varying the counter-ion. Albumin (HSA) revealed to be a good carrier without influencing significantly the cytotoxicity of the compounds. Our most recent studies showed that “RuCp” compounds can reach the nucleus and cytosol besides their preferential accumulation in the cell membrane. The excellent values obtained for some of the studied compounds with MDAMB231 cancer cells, which have highly metastatic properties, can pave the way for the potentiality of these compounds in metastasis treatments. Notably, TM34 was found to be the most efficient PARP-1 inhibitor compared with the published ruthenium and cisplatin compounds.

All the results gathered so far may possibly foresee a promising role of “RuCp” compounds as metallodrugs in innovative chemotherapies.

### ACKNOWLEDGMENTS

We thank Fundação para a Ciência e Tecnologia for financial support (PTDC/QUI-QUI/101187/2008, PTDC/QUI-QUI/118077/2010, PEst-OE/QUI/UI0536/2011). Tânia S. Morais thanks FCT for her Ph.D. Grant (SFRH/BD/45871/2008). The ruthenium(II) cyclopentadienyl compounds from our laboratory described in this review are the subject of a patent application PCT/IB2012/054914.

### REFERENCES

- Alessio, E.; Mestroni, G.; Bergamo, A.; Sava, G. *Curr. Top. Med. Chem.* **2004**, *4*, 1525.
- Hartinger, C. G.; Jakupc, M. A.; Zorbas-Seifried, S.; Groessl, M.; Egger, A.; Berger, W.; Zorbas, H.; Dyson, P. J.; Keppler, B. K. *Chem. Biodivers.* **2008**, *5*, 2140.
- Melchart, M.; Habtemariam, A.; Parsons, S.; Sadler, P. J. *J. Inorg. Biochem.* **2007**, *101*, 1903.
- Bergamo, A.; Masi, A.; Peacock, A. F.; Habtemariam, A.; Sadler, P. J.; Sava, G. *J. Inorg. Biochem.* **2010**, *104*, 79.

5. Morris, R. E.; Aird, R. E.; Murdoch, P. D.; Chen, H. M.; Cummings, J.; Hughes, N. D.; Parsons, S.; Parkin, A.; Boyd, G.; Jodrell, D. I.; Sadler, P. *J. J. Med. Chem.* **2001**, *44*, 3616.
6. Vock, C. A.; Ang, W. H.; Scolaro, C.; Phillips, A. D.; Lagopoulos, L.; Juillerat-Jeanneret, L.; Sava, G.; Scopelliti, R.; Dyson, P. J. *J. Med. Chem.* **2007**, *50*, 2166.
7. Maksimoska, J.; Feng, L.; Harms, K.; Yi, C. L.; Kissil, J.; Marmorstein, R.; Meggers, E. *J. Am. Chem. Soc.* **2008**, *130*, 15764.
8. Anand, R.; Maksimoska, J.; Pagano, N.; Wong, E. Y.; Gimotty, P. A.; Diamond, S. L.; Meggers, E.; Marmorstein, R. *J. Med. Chem.* **2009**, *52*, 1602.
9. Madeira, P. J. A.; Morais, T. S.; Silva, T. J. L.; Florindo, P.; Garcia, M. H. *Rapid Comm. Mass Spectrom.* **2012**, *26*, 1675.
10. Morais, T. S.; Silva, T. J. L.; Marques, F.; Robalo, M. P.; Avecilla, F.; Madeira, P. J. A.; Mendes, P. J. G.; Santos, I.; Garcia, M. H. *J. Inorg. Biochem.* **2012**, *114*, 65.
11. Tomaz, A. I.; Jakusch, T.; Morais, T. S.; Marques, F.; de Almeida, R. F.; Mendes, F.; Enyedy, E. A.; Santos, I.; Pessoa, J. C.; Kiss, T.; Garcia, M. H. *J. Inorg. Biochem.* **2012**, *117*, 261.
12. Fanali, G.; di Masi, A.; Trezza, V.; Marino, M.; Fasano, M.; Ascenzi, P. *Mol. Aspects Med.* **2012**, *33*, 209.
13. Kratz, F. *J. Control. Release* **2008**, *132*, 171.
14. Sudlow, G.; Birkett, D. J.; Wade, D. N. *Molec. Pharmacol.* **1975**, *11*, 824.
15. Curry, S.; Mandelkow, H.; Brick, P.; Franks, N. *Nat. Struct. Mol. Biol.* **1998**, *5*, 827.
16. Beckford, F. A. *Int. J. Inorg. Chem.* **2010**, *2010*, 1.
17. Garcia, M. H.; Morais, T. S.; Florindo, P.; Piedade, M. F.; Moreno, V.; Ciudad, C.; Noe, V. *J. Inorg. Biochem.* **2009**, *103*, 354.
18. Moreno, V.; Lorenzo, J.; Aviles, F. X.; Garcia, M. H.; Ribeiro, J. P.; Morais, T. S.; Florindo, P.; Robalo, M. P. *Bioinorg. Chem. Appl.* **2010**.
19. Garcia, M. H.; Valente, A.; Florindo, P.; Morais, T. S.; Piedade, M. F. M.; Duarte, M. T.; Moreno, V.; Avilés, F. X.; Loreno, J. *Inorg. Chim. Acta* **2010**, *363*, 3765.
20. Moreno, V.; Font-Bardia, M.; Calvet, T.; Lorenzo, J.; Aviles, F. X.; Garcia, M. H.; Morais, T. S.; Valente, A.; Robalo, M. P. *J. Inorg. Biochem.* **2011**, *105*, 241.
21. Riera, X.; Moreno, V.; Ciudad, C. J.; Noe, V.; Font-Bardia, M.; Solans, X. *Bioinorg. Chem. Appl.* **2007**, 98732.
22. Ruiz, J.; Lorenzo, J.; Vicente, C.; López, G.; López-de-Luzuriaga, J. M.; Monge, M.; Avilés, F. X.; Bautista, D.; Moreno, V.; Laguna, A. *Inorg. Chem.* **2008**, *47*, 6990.
23. Casini, A.; Gabbiani, C.; Sorrentino, F.; Rigobello, M. P.; Bindoli, A.; Gelbach, T. J.; Marrone, A.; Re, N.; Hartinger, C. G.; Dyson, P. J.; Messori, L. *J. Med. Chem.* **2008**, *51*, 6773.
24. Bergamo, A.; Sava, G. *Dalton Trans.* **2007**, 1267.
25. Schreiber, V.; Dantzer, F.; Ame, J.-C.; de Murcia, G. *Nat. Rev. Mol. Cell Biol.* **2006**, *7*, 517.
26. Lord, C. J.; Ashworth, A. *Curr. Opini. Pharmacol.* **2008**, *8*, 363.
27. Miknyoczki, S. J.; Jones-Bolin, S.; Pritchard, S.; Hunter, K.; Zhao, H.; Wan, W.; Ator, M.; Bihovsky, R.; Hudkins, R.; Chatterjee, S.; Klein-Szanto, A.; Dionne, C.; Ruggeri, B. *Mol. Cancer Ther.* **2003**, *2*, 371.
28. Donawho, C. K.; Luo, Y.; Penning, T. D.; Bauch, J. L.; Bouska, J. J.; Bontcheva-Diaz, V. D.; Cox, B. F.; DeWeese, T. L.; Dillehay, L. E.; Ferguson, D. C.; Ghoreishi-Haack, N. S.; Grimm, D. R.; Guan, R.; Han, E. K.; Holley-Shanks, R. R.; Hristov, B.; Idler, K. B.; Jarvis, K.; Johnson, E. F.; Kleinberg, L. R.; Klinghofer, V.; Lasko, L. M.; Liu, X.; Marsh, K. C.; McGonigal, T. P.; Meulbroek, J. A.; Olson, A. M.; Palma, J. P.; Rodriguez, L. E.; Shi, Y.; Stavropoulos, J. A.; Tsurutani, A. C.; Zhu, G.-D.; Rosenberg, S. H.; Giranda, V. L.; Frost, D. J. *Clin. Cancer Res.* **2007**, *13*, 2728.
29. Curtin, N. J. *Expert Rev. Mol. Med.* **2005**, *7*, 1.
30. Mendes, F.; Groessl, M.; Nazarov, A. A.; Tsypkin, Y. O.; Sava, G.; Santos, I.; Dyson, P. J.; Casini, A. *J. Med. Chem.* **2011**, *54*, 2196.
31. Jiang, X.; Wang, X. *Ann. Rev. Biochem.* **2004**, *73*, 87.
32. Mani, A.; Gelmann, E. P. *J. Clin. Oncol.* **2005**, *23*, 4776.



## ORGANOMETALLIC CHEMISTRY OF RHENIUM AND TECHNETIUM FUELED BY BIOMEDICAL APPLICATIONS

ANTÓNIO PAULO, GORETI RIBEIRO MORAIS, AND ISABEL SANTOS\*

*Unidade de Ciências Químicas e Radiofarmacêuticas, Campus Tecnológico e Nuclear, Instituto Superior Técnico, Universidade de Lisboa, Lisboa, Portugal*

### 44.1 INTRODUCTION

Metal-based compounds play an important role in the design of drugs for diagnostic or therapeutic applications, namely, anticancer agents, radiopharmaceuticals for nuclear imaging or radionuclide therapy, and contrast agents for magnetic resonance imaging (MRI). Compared to purely organic molecules, metals offer several advantages as a result of their structural diversity, varied reactivity pattern, and unique photo- and electrochemical properties. In this field, organometallic complexes play an emerging role, mainly because of the encouraging results obtained with ferrocene-tamoxifen derivatives for breast cancer therapy [1]. Since then, a variety of cyclopentadienyls or arenes of Fe, Ru, or Ti have been synthesized and their therapeutic effect explored [2]. Radiopharmaceutical chemistry is another important field in which organometallic compounds have a large potential, mainly after the introduction of the precursors *fac*-[M(CO)<sub>3</sub>(H<sub>2</sub>O)<sub>3</sub>]<sup>+</sup> (M= Re, Tc) by Alberto et al. [3–5]. These compounds can be obtained in aqueous solution starting from the respective permatalates, [MO<sub>4</sub>]<sup>−</sup>, which are the starting materials available to synthesize radiopharmaceuticals of <sup>99m</sup>Tc or <sup>186/188</sup>Re. Since their introduction, a plethora of M(I) tricarbonyl complexes with a large variety of ligands have been synthesized and evaluated by many research groups, aiming the design of new diagnostic or therapy radiopharmaceuticals. This chapter reviews some of the results obtained in the area, giving particular attention to the more promising results for biomedical applications. This chapter will start with some basic concepts on radiopharmaceuticals, nuclear medicine imaging modalities, and radionuclide therapy. Then the research efforts of the authors' group in the field will be presented and discussed in context with the major achievements reported by other groups worldwide.

### 44.2 BASIC CONCEPTS ON NUCLEAR MEDICINE AND RADIOPHARMACEUTICALS

Nuclear Medicine uses radioactive compounds for *in vivo* imaging and therapeutic purposes. Such compounds, named *radiopharmaceuticals*, are used in very low concentration ( $10^{-8}$ – $10^{-12}$  M), having no pharmacological effect. Depending on the intrinsic physical characteristics of the radionuclide, the radiopharmaceuticals are used for *in vivo* imaging or targeted radionuclide therapy (TRT).

**TABLE 44.1 Relevant Radionuclides for Medical Applications**

Nuclide	Physical Half-Life	Mode of Decay, %	Application
<sup>99m</sup> Tc	6.0 h	IT (100)	SPECT
<sup>186</sup> Re	3.72 d	$\beta^-$ (92) EC (8)	Therapy
<sup>188</sup> Re	17 h	$\beta^-$ (100)	Therapy
<sup>123</sup> I	13.2 h	EC (100)	SPECT
<sup>131</sup> I	8.02 d	$\beta^-$ (100)	Therapy
<sup>18</sup> F	1.83 h	$\beta^+$ (97) EC (3)	PET
<sup>11</sup> C	20.3 min	$\beta^+$ (100)	PET
<sup>86</sup> Y	14.7 h	$\beta^+$ (33) EC (66)	PET
<sup>90</sup> Y	2.67 d	$\beta^-$ (100)	Therapy
<sup>111</sup> In	2.80 d	EC (100)	SPECT
<sup>67</sup> Ga	3.26 d	EC (100)	SPECT
<sup>68</sup> Ga	1.13 h	$\beta^+$ (90) EC (10)	PET
<sup>60</sup> Cu	23.7 min	$\beta^+$ (93) EC (7)	PET
<sup>61</sup> Cu	3.3 h	$\beta^+$ (62) EC (38)	PET
<sup>62</sup> Cu	9.67 min	$\beta^+$ (98) EC (2)	PET
<sup>64</sup> Cu	12.7 h	$\beta^-$ (40), $\beta^+$ (19) EC (41)	PET/therapy
<sup>67</sup> Cu	2.58 d	$\beta^-$ (100)	Therapy
<sup>89</sup> Zr	3.27 d	$\beta^+$ (22.7) EC (77)	PET
<sup>153</sup> Sm	46.3 d	$\beta^-$ (100)	Therapy
<sup>166</sup> Ho	26.8 d	$\beta^-$ (100)	Therapy
<sup>177</sup> Lu	6.73 d	$\beta^-$ (100)	Therapy

For *in vivo* imaging there are two nuclear modalities: single photon emission computed tomography (SPECT) and positron emission tomography (PET), which use  $\gamma$ - or  $\beta^+$ -emitting radionuclides, respectively (Table 44.1). In the case of SPECT, the radionuclides decay by electron capture (EC) or isomeric transition (IT) with the emission of penetrating  $\gamma$  photons having energies in the range of 100–250 KeV. In PET, the  $\beta^+$  particles emitted by the radionuclide react with the electrons from the medium releasing two photons of 511 KeV as a result of annihilation reactions. In both cases, the resulting photons (100–250 or 511 KeV) are efficiently detected outside the body leading to clinically useful medical images (Fig. 44.1).

For therapy, the radiopharmaceuticals must contain radionuclides emitting ionizing particles (Auger electrons,  $\beta^-$  or  $\alpha$  particles). These particles have a high linear energy transfer (LET) inducing damage to targeted tumor tissues. However, their range in tissues is variable, following the order  $\beta^- > \alpha >$  Auger electrons. Therefore, unlike  $\beta^-$ - or  $\alpha$ -emitters, Auger-emitting radionuclides need to be accumulated by the nucleus of tumor cells in order to elicit significant DNA damage and therapeutic effect.

The biodistribution of radiopharmaceuticals can be determined by their chemical and physical properties, *perfusion radiopharmaceuticals*, or by their biological interactions, *target-specific radiopharmaceuticals* (Fig. 44.2). The biological distribution of *perfusion agents* is determined by blood flow and these agents target high capacity systems, such as phagocytosis, hepatocyte clearance, and glomerular filtration. The *target-specific radiopharmaceuticals* target low capacity systems, and their biodistribution is determined by specific protein interactions, for example, antigen, enzymatic, or receptor-binding interactions.

Based on the use of target-specific radiopharmaceuticals, SPECT and PET can determine the concentration of biomarkers in the human body in a noninvasive way, and these techniques are sensitive enough to visualize interactions between physiological targets and ligands, enabling a variety of molecular imaging applications. For molecular imaging, SPECT and PET present the advantage of high intrinsic sensitivity and unlimited depth penetration of the  $\gamma$ -radiation, if compared

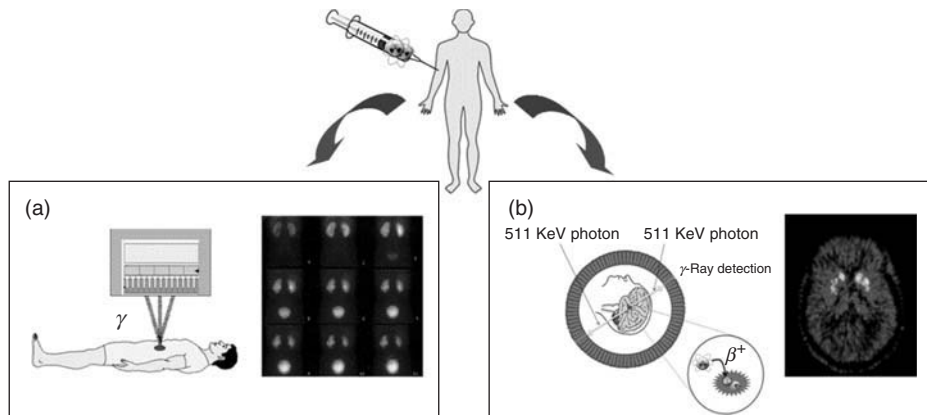


**Figure 44.1** Examples of SPECT (a) and PET (b) images obtained after injection of a  $\gamma$ - or  $\beta^+$ -emitting radiopharmaceutical.



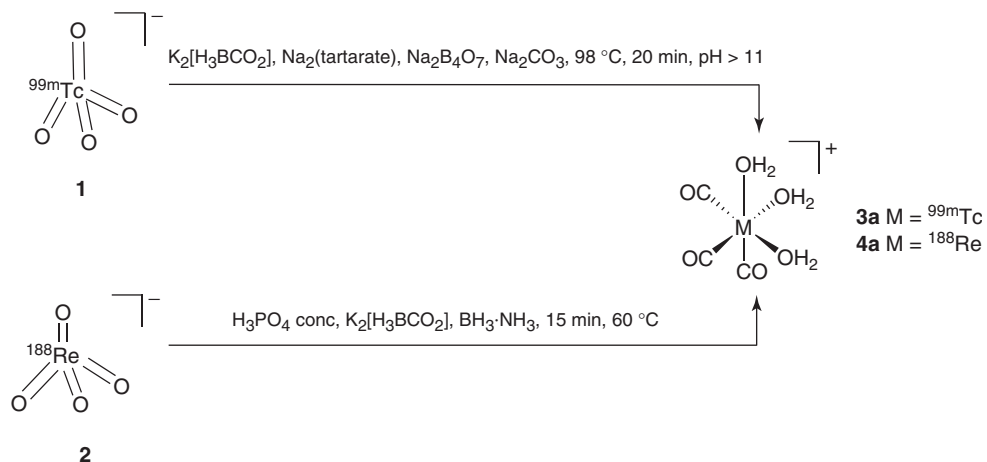
**Figure 44.2** Schematic representation of (a) perfusion and (b) target-specific metal-based radiopharmaceuticals.

with other imaging modalities, such as MRI, computed tomography (CT), ultrasound (US), bioluminescence imaging, and fluorescence imaging. PET has the additional advantage of being fully quantitative providing higher spatial resolution than SPECT.

As shown in Table 44.1, of all the radionuclides relevant for medical applications, radiometals play an important role either for imaging or therapy. In particular for SPECT imaging, the overwhelming majority of radiopharmaceuticals in clinical use correspond to complexes of  $^{99m}\text{Tc}$ , which remains the workhorse of nuclear medicine as a result of its ideal nuclear properties, low cost, and convenient availability from commercial generators. Rhenium, the group 7 congener of technetium, has two  $\beta$ -emitting isotopes,  $^{186}\text{Re}$  and  $^{188}\text{Re}$  (Table 44.1), with nuclear properties suitable for the development of therapeutic radiopharmaceuticals. In addition, Re complexes are commonly used as surrogates for  $^{99m}\text{Tc}$  congeners. This approach benefits from the physicochemical similarities of these two elements and avoids the use of the long-lived  $\beta$ -emitter  $^{99}\text{Tc}$  for the characterization of the  $^{99m}\text{Tc}$  complexes. Despite their differences in the kinetics of ligand exchange reactions and redox chemistry, Tc and Re can also be considered a *matched pair* suitable to obtain radiolabeled compounds for nuclear imaging ( $^{99m}\text{Tc}$ ) or radionuclide therapy ( $^{186/188}\text{Re}$ ). On the basis of isostructural Re and Tc compounds, *theranostic agents* can be achieved, which can deliver ionizing particles ( $^{186}\text{Re}/^{188}\text{Re}$ ) to treat a tumor or provide images ( $^{99m}\text{Tc}$ ) for diagnosis. Such possibility overcomes undesirable differences in biodistribution and selectivity, which currently exist between distinct imaging and therapeutic tools.

#### 44.3 Re(I) AND Tc(I) TRICARBONYL PRECURSORS

For the majority of metals studied in radiopharmaceutical chemistry, for example, lanthanides, gallium, indium, or copper, the most relevant compounds are coordination complexes [6–9]. However, for Tc and Re, as a result of their rich chemistry, organometallic complexes have recently assumed a growing importance through the possibility of preparing the precursors *fac*- $[\text{M}(\text{CO})_3(\text{H}_2\text{O})_3]^+$  ( $\text{M} = \text{Re}, \text{Tc}$ ) in aqueous solution, as already mentioned in the introductory part [3–5]. The availability of these precursors brought renewed interest on the design of Tc(I) organometallic radiopharmaceuticals as an alternative to classical strategies based on the  $[^{99m}\text{Tc}(\text{O})]^{3+}$ , *trans*- $[^{99m}\text{TcO}_2]^+$ ,  $[^{99m}\text{Tc}(\text{N})]^{2+}$ , or  $[^{99m}\text{Tc}-\text{HYNIC}]$  (HYNIC = 6-hydrazinonicotinic acid) cores [10–12].



**Scheme 44.1** Aqueous synthesis of *fac*-[M(CO)<sub>3</sub>(H<sub>2</sub>O)<sub>3</sub>]<sup>+</sup> (M = <sup>99m</sup>Tc (**3a**), <sup>188</sup>Re (**4a**))).

As referred earlier, for <sup>99m</sup>Tc and <sup>188</sup>Re, the synthesis of the compounds starts always from pertechnetate or perrhenate in saline, obtained by elution of <sup>99</sup>Mo/<sup>99m</sup>Tc and <sup>188</sup>W/<sup>188</sup>Re generators, respectively. Initially, Alberto et al. showed that the halide (NEt<sub>4</sub>)<sub>2</sub>[<sup>99</sup>TcCl<sub>3</sub>(CO)<sub>3</sub>] could be obtained directly from [<sup>99</sup>TcO<sub>4</sub>]<sup>-</sup> by reduction with BH<sub>3</sub> in refluxing tetrahydrofuran (THF) saturated with CO [3]. It was also shown that the halides in (NEt<sub>4</sub>)<sub>2</sub>[MCl<sub>3</sub>(CO)<sub>3</sub>] are readily replaceable by water, affording the corresponding aquo-tricarbonyl precursors *fac*-[M(CO)<sub>3</sub>(H<sub>2</sub>O)<sub>3</sub>]<sup>+</sup> (M = <sup>99</sup>Tc (**3**), Re (**4**)). Later, it was also shown that *fac*-[<sup>99m</sup>Tc(CO)<sub>3</sub>(H<sub>2</sub>O)<sub>3</sub>]<sup>+</sup> (**3a**) could be obtained by treating [<sup>99m</sup>TcO<sub>4</sub>]<sup>-</sup> (**1**) with NaBH<sub>4</sub> in the presence of CO [4]. However, CO is a toxic gas, unsuitable for use in hospitals and in commercial radiopharmaceutical kits, a problem that was overcome by the use of boranocarbonate, K<sub>2</sub>[H<sub>3</sub>BCO<sub>2</sub>]. This compound reduces the Tc(VII) and acts as a CO source, through mechanisms not yet fully understood (Scheme 44.1) [13]. As shown in Scheme 44.1, the synthesis of *fac*-[<sup>188</sup>Re(CO)<sub>3</sub>(H<sub>2</sub>O)<sub>3</sub>]<sup>+</sup> (**4a**) is only possible by reducing **2** with a combination of K<sub>2</sub>[H<sub>3</sub>BCO<sub>2</sub>] and amine borane (BH<sub>3</sub>·NH<sub>3</sub>), reflecting the different redox chemistry of Tc and Re [5].

#### 44.4 ORGANOMETALLIC BUILDING BLOCKS FOR THE DESIGN OF RADIOPHARMACEUTICALS

Using the precursors *fac*-[M(CO)<sub>3</sub>(H<sub>2</sub>O)<sub>3</sub>]<sup>+</sup> (M = <sup>99</sup>Tc (**3**), <sup>99m</sup>Tc (**3a**), Re (**4**), <sup>188</sup>Re(**4a**))), a multitude of building blocks bearing the *fac*-[M(CO)<sub>3</sub>]<sup>+</sup> unit have been synthesized in the last few years. The d<sup>6</sup> low spin electronic configuration of the metal in **3/3a** and **4/4a** leads to highly stable M–C bonds and to weakly bound water molecules, easily replaceable by chelators with different donor atoms sets and denticity. Under physiological conditions, a variety of *classical* bi- or tridentate chelators have been studied with these metal moieties [14–26]. From all the studies undertaken, it has been shown that, in general, the complexes based on tridentate chelators presented a more favorable biodistribution profile and pharmacokinetics to be further used as building blocks in the design of radiopharmaceuticals. Some examples of stable buildings blocks containing the tricarbonyl core and tridentate chelators are shown in Fig. 44.3.

Other typically organometallic ligands explored in this area were cyclopentadienyls, carboranes, and bridging hydrides [27–29]. All these ligands allowed the synthesis in aqueous medium of Re and Tc tricarbonyl complexes (Fig. 44.4).

Alberto et al. have shown that complexes of the type *fac*-[<sup>99m</sup>Tc(η<sup>5</sup>-Cp-R)(CO)<sub>3</sub>] can be synthesized in aqueous conditions starting from *fac*-[<sup>99m</sup>Tc(CO)<sub>3</sub>(H<sub>2</sub>O)<sub>3</sub>]<sup>+</sup> (**3a**) and using carboxylic and amide derivatives of cyclopentadienyls with a keto group in α position. They further extended the scope of the aqueous chemistry of cyclopentadienyls, showing that Diels–Alder dimerized CpH derivatives also react directly with **3a** affording the same type of half-sandwich complexes [27, 30, 31]. Valliant et al. [32–34] studied the aqueous chemistry of carborane <sup>99m</sup>Tc tricarbonyl complexes and confirmed their relevance for the design of target-specific radiopharmaceuticals, despite the initial difficulties that have been found in the synthesis of this type of complexes using **3a** as the starting material.

The first examples of Re(I) and Tc(I) complexes containing coordinated hydrides stable in aqueous medium have been reported by our group. These complexes were obtained by reacting dihydrobis(2-mercaptopimidazolyl)borates and trihydro(2-mercaptopimidazolyl)borates with *fac*-[M(CO)<sub>3</sub>(H<sub>2</sub>O)<sub>3</sub>]<sup>+</sup> (M = Re, <sup>99</sup>Tc, <sup>99m</sup>Tc), as for example complexes **5** and **6** (Schemes

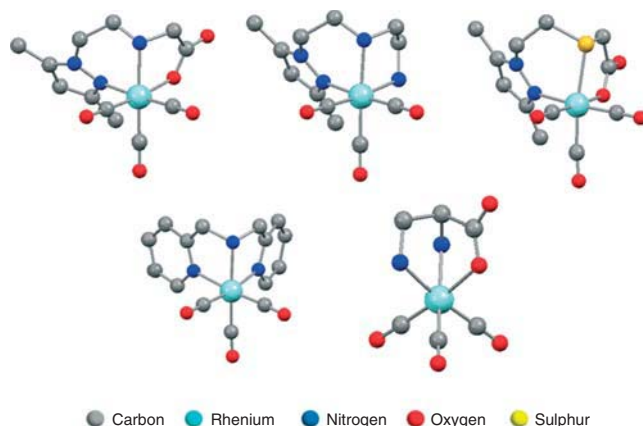


**Figure 44.3** Selected examples of Re(I) tricarbonyl complexes with tridentate Werner-type ligands [14–18]. (See insert for color representation of the figure.)

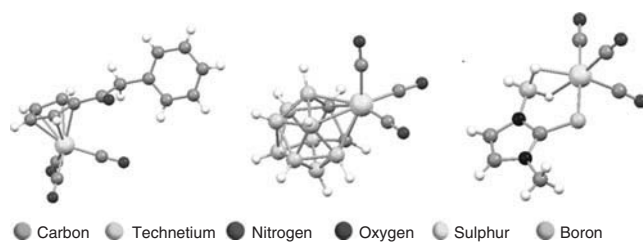


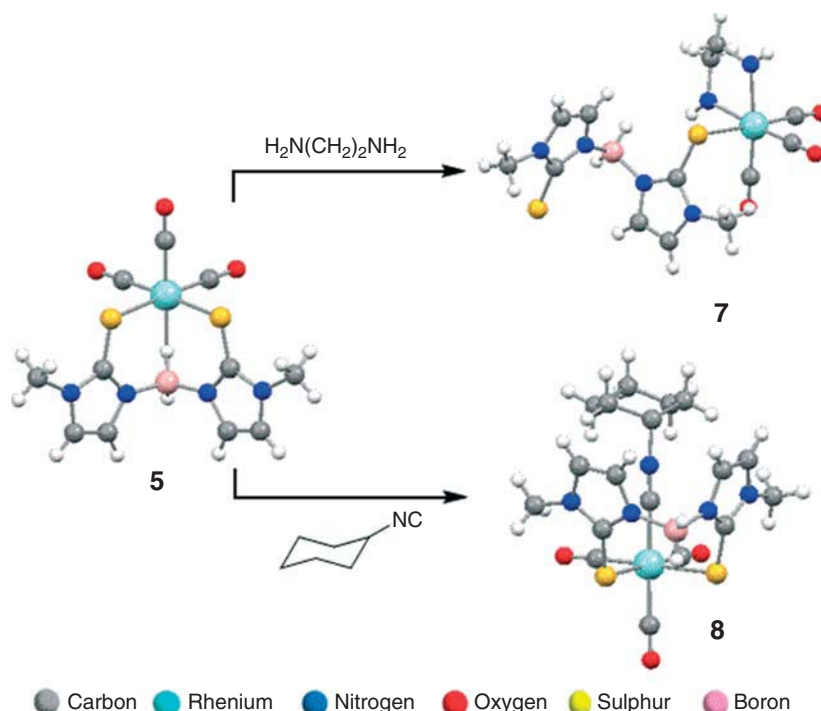
**Figure 44.4** Selected examples of  $^{99}\text{mTc}$ (I) tricarbonyl complexes stabilized by a cyclopentadienyl, a carborane, and a dihydro-bis(mercaptoimidazolyl)borate [27–29].

44.2 and 44.3). The coordination mode of the respective boron-containing ligands ( $\kappa^3\text{-S},\text{S},\text{H}$  or  $\kappa^3\text{-S},\text{H},\text{H}$ ) was assessed by X-ray structural analysis, multinuclear NMR and IR spectroscopy of the  $^{99}\text{Tc}$  and Re complexes [29, 35, 36]. At tracer level ( $^{99}\text{mTc}$ ), the complexes are formed at room temperature with low ligand concentrations, and are remarkably stable under physiologic conditions. The water and the  $\sim 10^5$  fold excess of  $\text{Cl}^-$  present in solution does not compete with the bridging hydrides. Biodistribution in mice of the  $^{99}\text{mTc}$  congener of **5** has shown that this class of complexes cross the blood–brain barrier (BBB). Such *in vivo* behavior motivated their use as building blocks to design target-specific complexes for imaging of brain receptors [37].

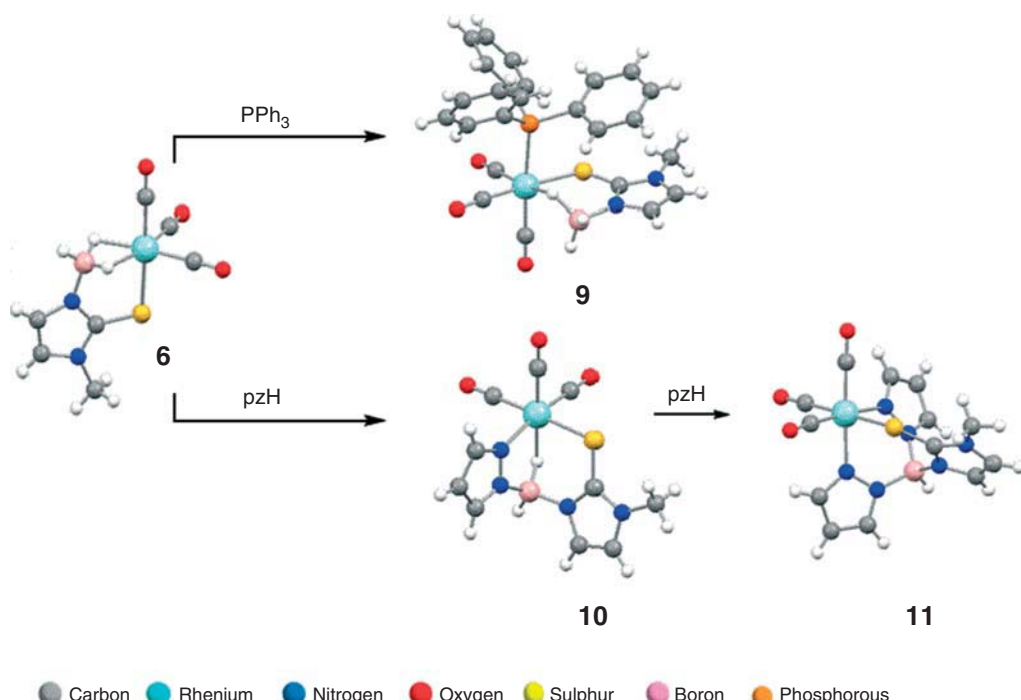
The B–H $\cdots$ M bonds in complexes **5** and **6** (Schemes 44.2 and 44.3) resist to physiologic conditions, but are cleaved by neutral and unidentate substrates (L), such as pyridine, isonitriles, and phosphines, yielding monomeric mixed-ligand complexes (e.g., **8** and **9**) of the type *fac*-[Re{ $\kappa^2$ -(R)H<sub>2</sub>B(tim<sup>Me</sup>)}(CO)<sub>3</sub>(L)] (R = H, tim<sup>Me</sup>) (Schemes 44.2 and 44.3) [38–40]. The reaction of **5** with 1,2-ethylenediamine (en) led to the replacement of both B–H $\cdots$ Re bonds with the formation of complex **7**, stabilized by a  $\kappa^1\text{-S}$ -scorpionate [38]. Reactions of **6** with different azoles, such as mercaptimidazoles, mercaptobenzothiazoles, and pyrazoles, were also studied (Scheme 44.3). These reactions gave complexes anchored by tridentate poly(azolyl)borates generated *in situ* most probably by metal-assisted processes [41]. For pyrazoles, these reactivity studies allowed the synthesis of complexes anchored by unprecedented hybrid poly(azolyl)borates (**10** and **11**). The  $^{99}\text{mTc}$  congeners with hybrid scorpionates could not be obtained using this approach but their synthesis was achieved in high yield by reacting precursor **3a** with the sodium salt of the corresponding dihydrosobis(azolyl)borate [42].

#### 44.5 PERFUSION AGENTS

To replace some established  $^{99}\text{mTc}$ -perfusion agents in clinical use, several research groups worldwide have recently investigated  $^{99}\text{mTc}$  tricarbonyl complexes as perfusion agents for kidney or myocardium imaging, with encouraging *in vivo* results [43–52]. For myocardial imaging, several research groups have searched for lipophilic and cationic  $^{99}\text{mTc}$  complexes of greater efficiency than those in clinical use [ $^{99}\text{mTc}$ -Sestamibi and  $^{99}\text{mTc}$ -Tetrofosmin (Fig. 44.5)] [47–52].



**Scheme 44.2** Reactions of *fac*-[ $\text{Re}(\kappa^3-\text{H}_2\text{B}(\text{tim}^{\text{Me}})_2)(\text{CO})_3$ ] (**5**) with ethylenediamine and cyclohexyl isonitrile ( $\text{tim}^{\text{Me}} = 2\text{-mercapto-1-methylimidazolyl}$ ) [38, 39]. (See insert for color representation of the figure.)



**Scheme 44.3** Reactions of *fac*-[ $\text{Re}(\kappa^3-\text{H}_3\text{B}(\text{tim}^{\text{Me}}))(\text{CO})_3$ ] (**6**) with triphenylphosphine and pyrazole ( $\text{tim}^{\text{Me}} = 2\text{-mercapto-1-methylimidazolyl}$ ) [40, 41]. (See insert for color representation of the figure.)

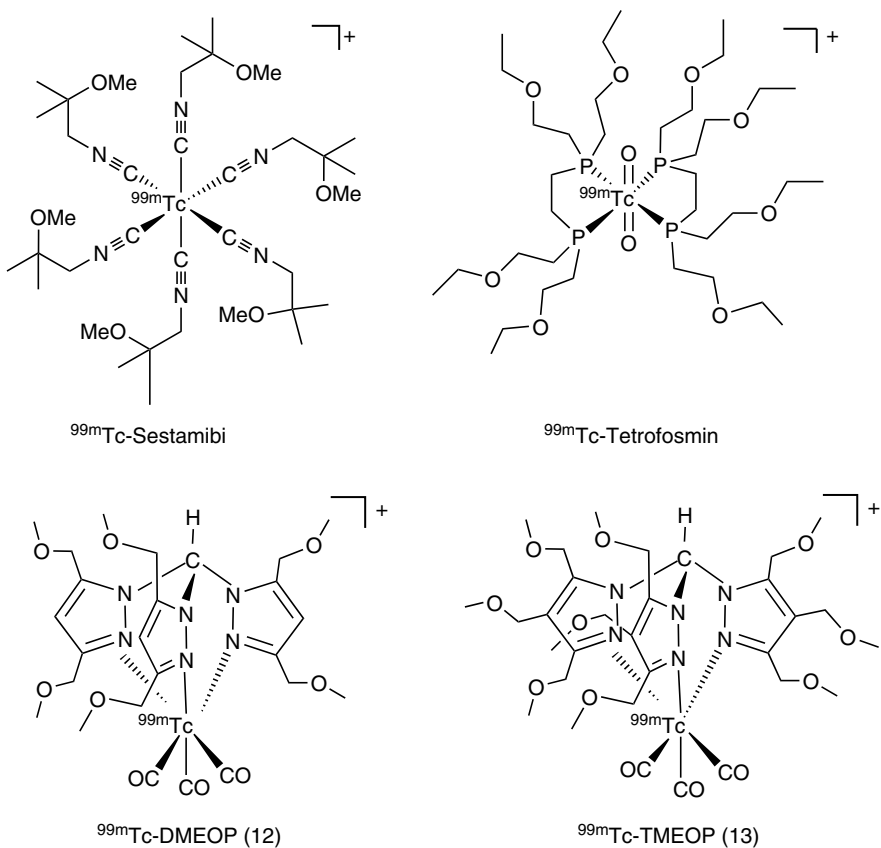


**Figure 44.5** Structures of  $^{99\text{m}}\text{Tc}(\text{I})$  tricarbonyl complexes with potential as myocardial imaging agents.

Our group studied cationic tris(pyrazolyl)methane technetium tricarbonyl complexes bearing a variety of ether functional groups at the pyrazolyl rings and/or at the central carbon atom [49–52]. We expected to improve their biodistribution profile, namely, the heart/liver and heart/lung uptake ratios, as the activity retained in adjacent nontarget organs may hamper the clinical analysis of the heart images. These studies allowed the identification of the lead complexes **12** and **13** (Fig. 44.5), which are anchored by the tris(pyrazolyl)methane ligands  $\text{HC}[3,5-(\text{MeOCH}_2)_2\text{pz}]_3$  (DMEOP) and  $\text{HC}[3,4,5-(\text{MeOCH}_2)_3\text{pz}]_3$  (TMEOP), respectively.

Owing to the relatively low water solubility of these ligands, we prepared the respective sodium complexes  $[\text{Na}\{\text{HC}[3,5-(\text{MeOCH}_2)_2\text{pz}]_3\}_2]\text{I}$  and  $[\text{Na}\{\text{HC}[3,4,5-(\text{MeOCH}_2)_3\text{pz}]_3\}_2]\text{I}$  (Fig. 44.6). These salts are completely soluble in aqueous medium and react quantitatively with *fac*- $[^{99\text{m}}\text{Tc}(\text{CO})_3(\text{H}_2\text{O})_3]^+$  affording the desired compounds (**12** and **13**) under aqueous conditions [49].

Complexes **12** and **13** exhibited a significant fast and stable heart uptake, as well as a fast blood and liver clearance. Within the tricarbonyl approach, only another  $^{99\text{m}}\text{Tc}(\text{I})$  complex stabilized by a tridentate PNP ligand bearing a pendant crown ether has shown a biological behavior comparable to that of **12** and **13** [48]. Our preclinical results were particularly encouraging for *fac*- $[^{99\text{m}}\text{Tc}(\text{CO})_3\{\text{HC}[3,4,5-(\text{CH}_3\text{OCH}_2)_3\text{pz}]_3\}]^+$  (**13**) that exhibited an extremely fast liver clearance compared to  $^{99\text{m}}\text{Tc}$ -Sestamibi and  $^{99\text{m}}\text{Tc}$ -Tetrofosmin (Fig. 44.7) [49, 50]. *In vivo* data indicated that this  $^{99\text{m}}\text{Tc}(\text{I})$  tricarbonyl complex improves the diagnostic accuracy of coronary artery disease, and so deserve to be further evaluated in larger animals and humans as a myocardial perfusion agent. As described earlier for  $^{99\text{m}}\text{Tc}$ -sestamibi, the authors have also shown that complex **13** has potential for early detection of cancer and noninvasive monitoring of tumor multidrug resistance (MDR) [52].

#### 44.6 TARGET-SPECIFIC COMPLEXES

Advances in proteomics and genomics have significantly improved the understanding of molecular alterations underlying different diseases, such as changes in expression and functionality of different genes and/or proteins. The noninvasive

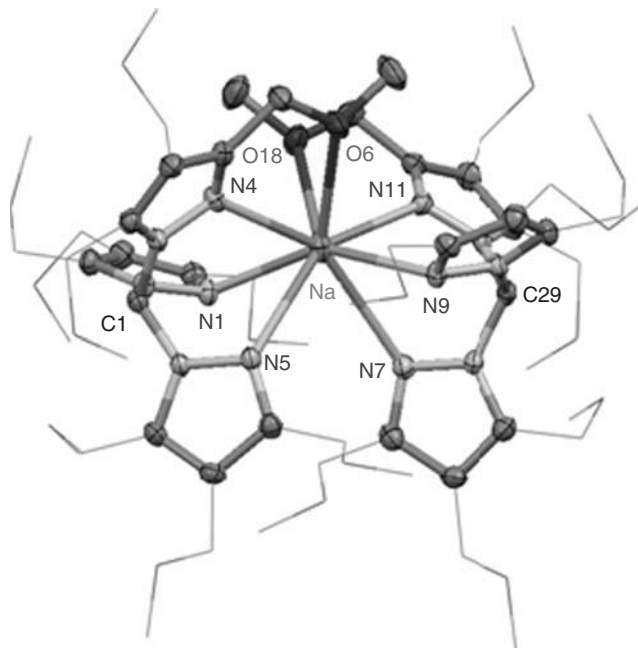


**Figure 44.6** Molecular structure of the cation of compound  $[\text{Na}\{\text{HC}[3,4,5-(\text{MeOCH}_2)_3\text{pz}]\}_3]^2\text{I}$ .

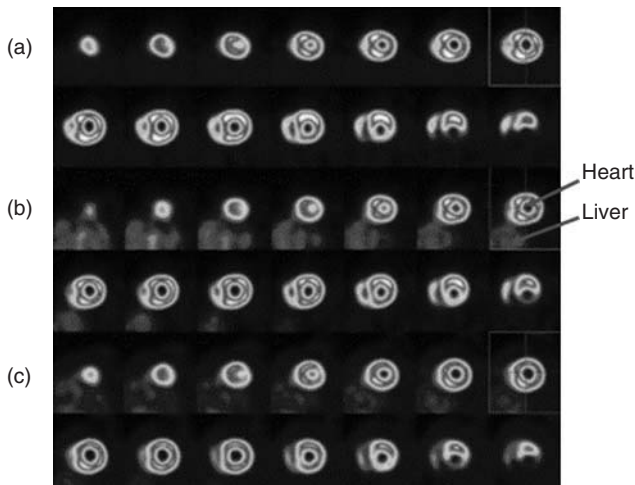


**Figure 44.7** Representative SPECT image analysis at 40 min after administration of (a)  $^{99\text{m}}\text{Tc}$ -TMEOP (**13**), (b)  $^{99\text{m}}\text{Tc}$ -Sestamibi, and (c)  $^{99\text{m}}\text{Tc}$ -Tetrofosmin. Reproduced with permission from John Wiley & Sons.

imaging of such alterations with target-specific radiopharmaceuticals can contribute to the monitoring of disease onset and progression, follow-up of innovative therapies in patients, or preclinical models and dosage optimization of novel drugs. In the past few years, the tricarbonyl technology has been abundantly explored on the design of target-specific radiopharmaceuticals, based on protein-like molecules (e.g., peptides, peptide nucleic acids, antibodies, nanobodies, or affibodies) or on small nonpeptidic organic molecules (e.g., amino acids, carbohydrates, folic acid, vitamin B12 derivatives, phosphonates, and enzyme substrates/inhibitors) [11, 12, 53–59]. For bioactive peptides, important achievements have been already obtained, based on, for example, the single amino acids chelate technology (SAAC) that allows a highly flexible functionalization of peptides using solid-phase peptide synthesis (SPPS) [53]. For small nonpeptidic biomolecules, the progresses can be considered more mitigated despite the significant efforts developed worldwide, namely, on steroid derivatives, amino acids, and sugars. Several  $^{99\text{m}}\text{Tc}(\text{CO})_3$ -labeled small biomolecules with encouraging *in vitro* properties have been obtained but,

so far, none of them have shown sufficiently good biological profile for further clinical evaluation in humans. The present contribution will not cover all the reported work on the field, to avoid overlap with other comprehensive reviews recently published [11, 12, 53–60].

We have used the tricarbonyl technology for labeling different bioactive peptides, for example, bombesin analogs, RGD (Arg-Gly-Asp)-containing peptides, and melanocortin analogs [61–72]. Concerning melanocortin analogs, it is worth highlighting the achievements obtained on the modulation of their pharmacokinetics, profiting from the versatility of the pyrazolyl-diamine bifunctional chelators (BFCAs). Following initial studies with linear analogs that have shown moderate tumor-targeting capability, a lactam bridge-cyclized  $\alpha$ -melanocyte-stimulating hormone ( $\alpha$ -MSH) derivative,  $\beta$ AlaNleCycMSH<sub>hex</sub>, was synthesized and labeled with the *fac*-[<sup>99m</sup>Tc(CO)<sub>3</sub>]<sup>+</sup> core using a pyrazolyl-diamine BFCAs with Me substituents at the 3- and 5-positions of the azolyl ring. The resulting radiolabeled cyclic peptide exhibited a very high tumor uptake in B16F1 melanoma tumor-bearing mice (among the highest values reported in the literature), but showed an undesirable accumulation of activity in the liver and intestine [66]. Thereafter, the effect of different azolyl-ring substitution patterns (free carboxylate at the 4-position and/or methyl groups at the 3- and 5-positions) (Fig. 44.8) on the pharmacokinetic profile of the <sup>99m</sup>Tc(CO)<sub>3</sub>-labeled cyclic  $\alpha$ -MSH derivative was studied.

The different radiopeptides (**14–16**) displayed subnanomolar binding affinity for the melanocortin type 1 receptor (MC1R) with high and comparable melanoma uptake in B16F1 melanoma-bearing C57BL/6 mice at 1 h p.i. (between 9.90 ± 1.10 %IA/g and 11.82 ± 3.91 %IA/g). The presence of carboxylate substituents at the 4-position of the pyrazolyl ring caused a significant reduction in kidney (circa 90% and 96%) and liver (circa 92% and 88%) uptake, particularly for complex **16** without Me substituents at the 3- and 5-positions, as can be clearly seen in the scintigraphic images presented in Fig. 44.9. Furthermore, the radiopeptide **16** presented the highest tumor-to-kidney ratio (7.1 at 4 h p.i.) among all the evaluated  $\alpha$ -MSH lactam-based cyclic radiopeptides [72]. Altogether, these results showed that the versatility and favorable coordination capability of pyrazolyl-diamine chelators allowed the tuning of the pharmacokinetic properties of <sup>99m</sup>Tc(CO)<sub>3</sub>-labeled bioactive peptides, without compromising their *in vitro* and *in vivo* targeting ability.

Owing to their compact and lipophilic character, the *fac*-[<sup>99m</sup>Tc(CO)<sub>3</sub>]<sup>+</sup> core has also been studied for the labeling of central nervous system (CNS) receptor ligands, aiming to find radioactive probes for *in vivo* monitoring of the density of these receptors. In particular, several research groups have studied <sup>99m</sup>Tc-labeled aryl-piperazine derivatives looking for radioactive probes for specific targeting of 5-hydroxytryptamine (5-HT<sub>1A</sub>) receptors, implicated in major neuropsychiatric disorders such as schizophrenia, anxiety, and depression. Several BFCAs, such as cyclopentadielyls [27], carboranes [73], and dihydrobis(mercaptoimidazolyl)borates [37, 74], have been explored to achieve this goal. Our group focused on dihydrobis(mercaptoimidazolyl)borates, which stabilize neutral and lipophilic <sup>99m</sup>Tc-tricarbonyl complexes easily functionalized with arylpiperazine pharmacophores, through the mercaptoimidazolyl rings. Complexes containing one or two pharmacophores (Fig. 44.10) were synthesized and biologically evaluated. Most of the complexes presented excellent

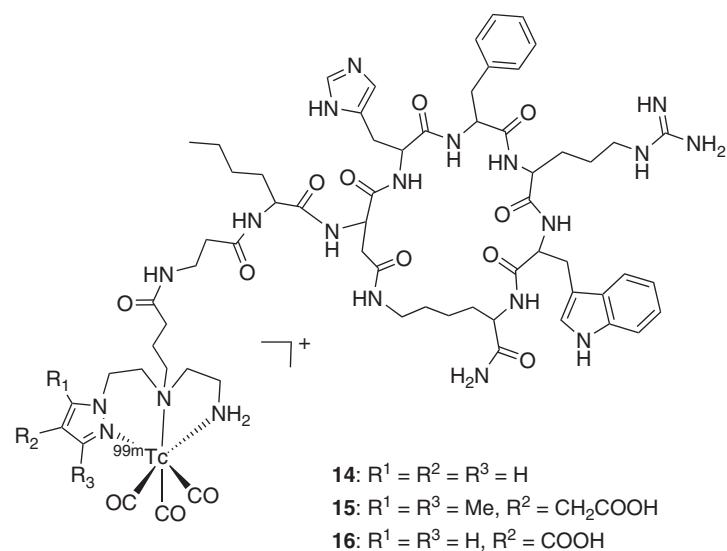


**Figure 44.8** Structures of <sup>99m</sup>Tc(CO)<sub>3</sub>-labeled lactam bridge-cyclized  $\alpha$ -MSH derivatives obtained using different pyrazolyl-diamine BFCAs.

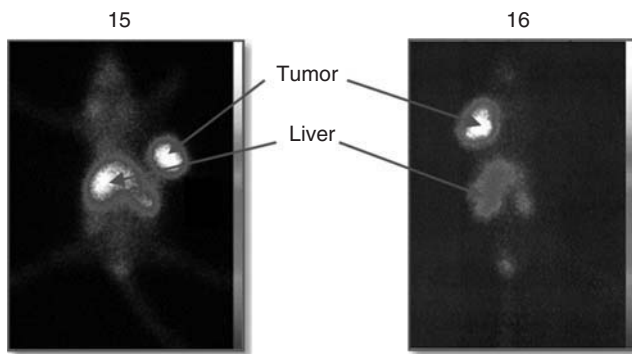


**Figure 44.9** Scintigraphic images of a melanoma-bearing mouse injected with  $^{99\text{m}}\text{T}(\text{CO})_3$ -labeled melanocortin analogs **15** and **16**. [72].

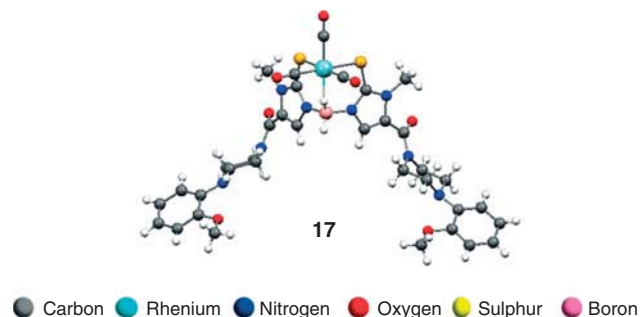


**Figure 44.10** Molecular structure of a dihydrobis(mercaptoimidazolyl)borate Re(I) tricarbonyl complex containing two arylpiperazine pharmacophores [74] (See insert for color representation of the figure.)

nanomolar or subnanomolar affinity ( $\text{IC}_{50}$  values) toward the  $5\text{-HT}_{1\text{A}}$  receptors, when linkers of appropriate length were used to attach the pharmacophore to the metal moiety. However, all the complexes have shown a relatively poor brain uptake in mice.

The targeting of enzymes with radioactive probes is considered of great importance in the diagnosis and follow-up of different oncological pathologies and cardiovascular diseases. Several groups investigated the labeling of enzyme inhibitors or substrates using the tricarbonyl approach (e.g., carbonic anhydrase [75], histone deacetylase [76], epidermal growth factor receptor tyrosine kinase (EGFR-TK) [16], and human thymidine kinase (hTK)[77–81]). In our group, we studied pyrazolyl-diamine Re(I) and  $^{99\text{m}}\text{Tc(I)}$  complexes bearing L-arginine derivatives for *in vivo* nitric oxide synthase (NOS) targeting (Fig. 44.11) [82–84]. NOS is the eukaryotic enzyme responsible for the endogenous catalytic oxidation of L-arginine to L-citrulline that generates nitric oxide (NO), a key mammalian signaling mediator in several physiological processes. Overproduction of NO by iNOS has been linked to many diseases, particularly cancer. *In vitro* studies with Re

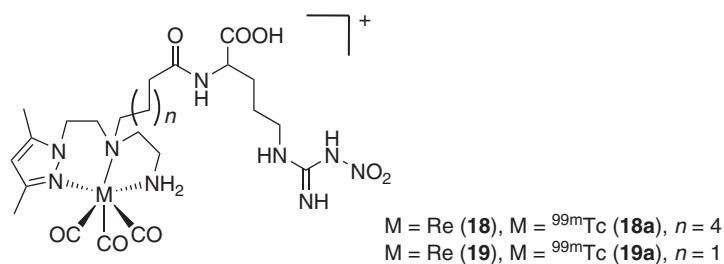


**Figure 44.11** Examples of L-arginine-containing M(I) tricarbonyl complexes.

complexes have shown that the affinity of inhibitor-containing conjugates to iNOS is less affected on metallation than the substrate-containing conjugates. The Re complexes bearing guanidino-substituted analogs of L-arginine retained considerable inhibitory action, and are the first examples of organometallic complexes inhibiting the iNOS [82, 83]. Remarkably, a nitro-arginine-containing Re complex (**18**) (Fig. 44.11) showed a  $K_i$  value of 6  $\mu\text{M}$ , comparable to that of the organic inhibitor  $N^{\omega}\text{-nitro-L-arginine}$ . Complex **18** also suppressed NO biosynthesis in lipopolysaccharide (LPS)-treated macrophages, but the  $^{99\text{m}}\text{Tc}$  congener (**18a**) did not show any significant uptake in most tissues of LPS-treated mice compared to a control group. However, the related complex **19a** (Fig. 44.11) showed an enhanced uptake in the LPS-treated animal model, due most probably to iNOS upregulation [83]. These results indicate that this family of complexes may hold promise for the design of SPECT probes for *in vivo* targeting of iNOS.

Bisphosphonates (BPs) are a class of small molecules highly important in the treatment of osteoporosis as they inhibit osteoclastic bone resorption. Owing to their osteotropic properties, the labeling of BPs with  $^{99\text{m}}\text{Tc}$  and  $^{186/188}\text{Re}$  can provide radioactive tools useful for bone scintigraphy and therapy, respectively. Taking this into consideration, the authors' group has studied the labeling of pamidronate (PAM) and alendronate (ALN) with the *fac*-[ $^{99\text{m}}\text{Tc}(\text{CO})_3$ ]<sup>+</sup> core using pyrazolyldiamine chelators (Fig. 44.12) [85, 86].

The resulting  $^{99\text{m}}\text{Tc}$  complexes were chemically identified by high performance liquid chromatography (HPLC) comparison with their corresponding Re surrogates, which were fully characterized. The biological evaluation of the PAM derivatives (complexes **20a** and **21a**) in mice has shown a bone uptake comparable to that of a radiopharmaceutical in clinical use ( $^{99\text{m}}\text{Tc-MDP}$ ) with a favorable and fast clearance from most soft tissues (Fig. 44.13). Other authors have also labeled the same BPs with *fac*-[ $^{188}\text{Re}(\text{CO})_3$ ]<sup>+</sup> using dipyradyl amine (dpa) BFCAs. Most relevantly, preclinical studies of one of these complexes, *fac*-[ $^{188}\text{Re}(\text{CO})_3(\text{dpa-ALN})$ ], indicated that it is superior to  $^{188}\text{Re-HEDP}$ , presenting greater accumulation in regions of high metabolic activity and displaying an enhanced resistance toward *in vivo* oxidation to perrhenate [87].

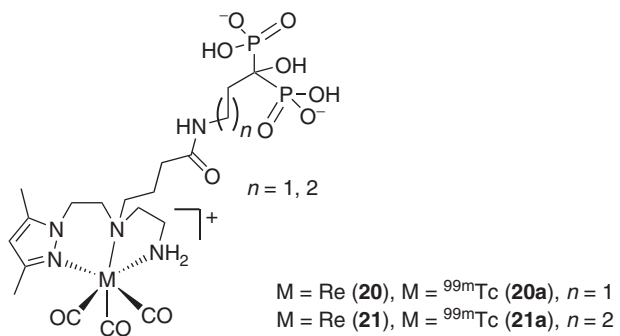


**Figure 44.12** BP-containing pyrazolyldiamine M(I) tricarbonyl complexes for bone targeting.

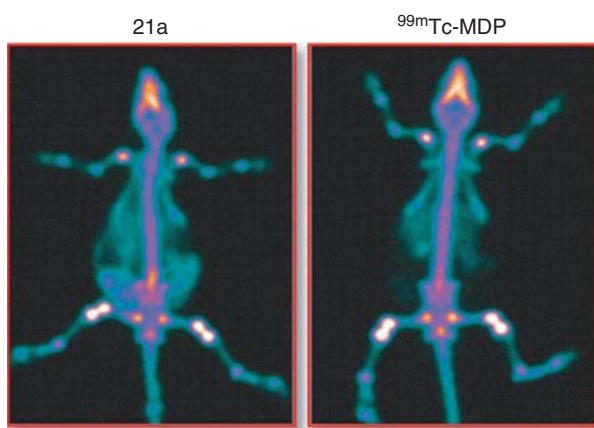


**Figure 44.13** Planar whole-body gamma camera images of rats injected with complex **21a** and  $^{99\text{m}}\text{Tc-MDP}$  at 2 h p.i. Reproduced with permission from The Royal Society of Chemistry. (See insert for color representation of the figure.)

Altogether, these results clearly indicate that these Tc(I)/Re(I) tricarbonyl complexes are a class of complexes with great potential as bone targeting radiopharmaceuticals for diagnostic or therapeutic applications in nuclear medicine.

Multifunctional  $^{99m}\text{Tc}$  compounds displaying cell-specific uptake and ability to target the nucleus might have potential for targeted therapy as  $^{99m}\text{Tc}$  is also an Auger electron-emitting radiometal. The design of this type of complexes has been pioneered by Alberto et al., who have shown that a trifunctional  $^{99m}\text{Tc}(\text{I})$  tricarbonyl complex, containing a pyrene intercalator and an nuclear localisation signal (NLS) peptide, reaches the nucleus of B16-F1 mouse melanoma cells and induces much stronger radiotoxic effects than  $^{99m}\text{TcO}_4^-$  [88]. Alberto et al. also demonstrated that a [2+1] Re(I) tricarbonyl complex bearing acridine orange (AO) as a DNA-binding group can target the nucleus of murine B16F1 cells without needing a carrier NLS sequence [89]. For this type of application, we have also evaluated pyrazolyl-diamine Re(I) $^{99m}\text{Tc}(\text{I})$  tricarbonyl complexes bearing anthracene (**22/22a**) and AO groups (**23/23a**) (Fig. 44.14) [90–92]. We have shown that this type of complexes rapidly entered the cells and accumulated inside the nucleus. Complex **22a**, having the anthracenyl substituent at the 4-position of the pyrazolyl ring, exhibited pronounced radiotoxicity and induced an apoptotic cellular outcome [91].

These encouraging results prompted the synthesis of pyrazolyldiamine  $^{99m}\text{Tc}(\text{I})/\text{Re}(\text{I})$  tricarbonyl complexes bearing Bombesin (BBN) analogs and AO intercalators. We have shown that complex **24a**, containing the GGG-BBN Bombesin [7–14] peptide (Fig. 44.14), presented a high cellular internalization in PC3 cells and a remarkably high nuclear uptake in the same cell line. Live cell confocal imaging microscopy studies (Fig. 44.15) with the Re congener (**24**) have shown a considerable accumulation of fluorescence into the nucleus with uptake kinetics similar to that exhibited by **24a**. These compounds are the first examples of  $^{99m}\text{Tc}$  bioconjugates that combine specific cell targeting with nuclear internalization, a crucial issue for the exploitation of  $^{99m}\text{Tc}$  in Auger therapy [93].

The design of nanoplatforms for *in vivo* molecular imaging applications and/or drug delivery is a growing field. We and other groups have explored the tricarbonyl technology to label mannosylated dextran derivatives, aiming the design of specific nanostructures for sentinel lymph node detection (SLND). To achieve this goal, dextran was functionalized with pyrazolyldiamine or cysteine chelators to stabilize the *fac*- $[\text{M}(\text{CO})_3]^+$  ( $\text{M} = {^{99m}\text{Tc}}$ , Re) core and with mannose to provide

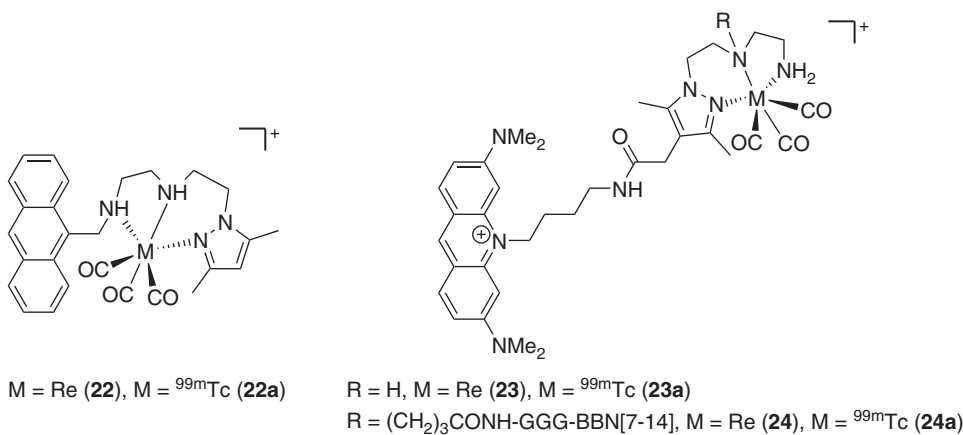


**Figure 44.14** M(I) tricarbonyl complexes functionalized with polyaromatic DNA intercalators and BBN analogs.

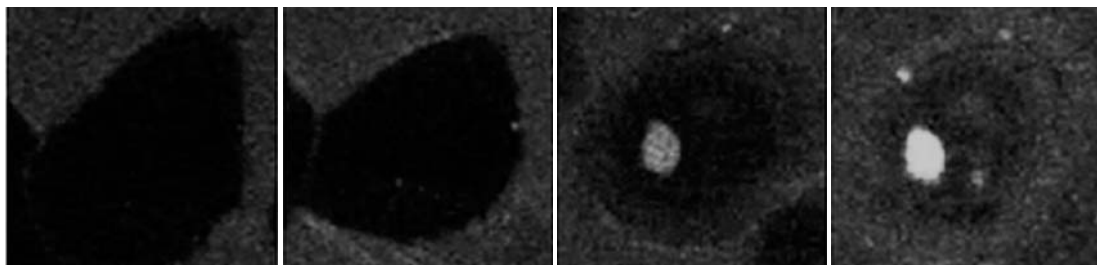
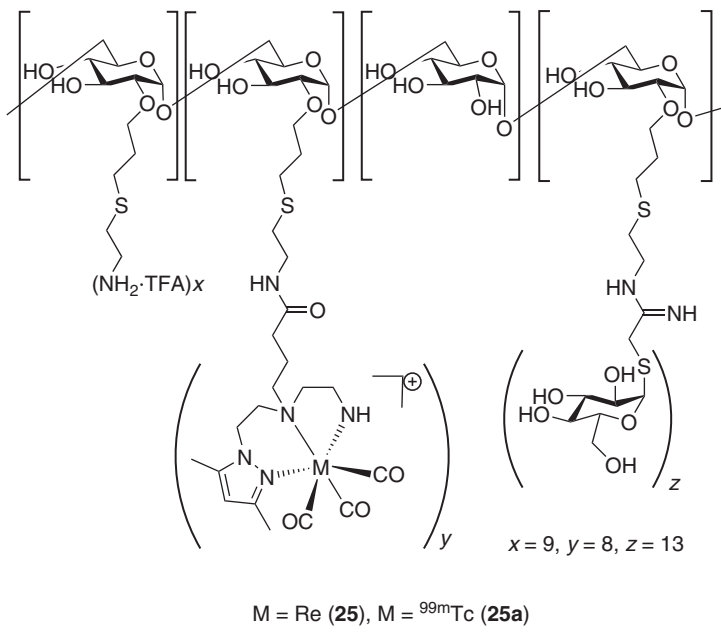


**Figure 44.15** Live cell uptake of complex **24** in PC3 cells, visualized by time-lapse confocal microscopy imaging [93].



$\text{M} = \text{Re } (25), \text{M} = {}^{99\text{m}}\text{Tc } (25\text{a})$

**Figure 44.16** Schematic representation of mannosylated dextran derivatives functionalized with pyrazolyldiamine  ${}^{99\text{m}}\text{Tc(I)}/\text{Re(I)}$  tricarbonyl complexes.

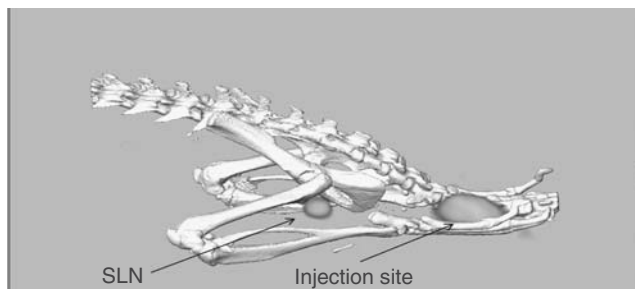


**Figure 44.17** SPECT/CT image in mice after subcutaneous injection of the  ${}^{99\text{m}}\text{Tc}$ -labeled dextran derivative 25a (see Fig. 44.16) [96].

specificity (Fig. 44.16) [94–96]. The chemical and physical characterization of the  ${}^{99\text{m}}\text{Tc}$  nanostructures was based on the rhenium congeners. The hydrodynamic diameter of the nanopolymers increases with the polymer backbone functionalization (dextran 4.3 nm and final polymeric compounds 6.5–7 nm) and the overall charge was positive for the pyrazolyldiamine-dextran and negative for the cysteine-dextran derivatives. SPECT/CT studies in mice confirmed that the corresponding  ${}^{99\text{m}}\text{Tc}$ -labeled dextran nanopolymers accumulate in the popliteal lymph node, allowing their clear visualization (Fig. 44.17). Therefore, these nanocompounds hold promising as radiopharmaceuticals for SLND and deserve further clinical evaluation.

#### 44.7 CONCLUDING REMARKS

The introduction of the precursors  $\text{fac-}[M(\text{CO})_3(\text{H}_2\text{O})_3]^+$  ( $M = \text{Re}, \text{Tc}$ ) opened new avenues in radiopharmaceutical chemistry. On the basis of these starting materials, we and other groups have introduced a variety of organometallic building blocks stable in water and with biological features favorable to design perfusion or target-specific tools for molecular imaging applications and TRT. For kidney and myocardium imaging, some complexes have shown biological properties superior to those of radiopharmaceuticals in clinical use, deserving further evaluation in larger animals or in humans. The labeling of peptidic biomolecules for imaging of receptors has also given encouraging results. Despite the hydrophobicity of the  $\text{fac-}[M(\text{CO})_3]^+$  ( $M = \text{Tc}, \text{Re}$ ) core, it has been shown that it is possible to modulate the pharmacokinetics of peptide-based

complexes using BFCAs with substituents of different polarity. By an appropriate choice of such substituents, the abdominal and hepatobiliar accumulation can be improved without compromising the tumor uptake. However, the labeling of small biomolecules with this core still remains very challenging and the corresponding bioconjugates with clinical potential are scarce. This reflects the difficulties encountered by several authors to avoid the interference of the organometallic fragments with the biological performance of small biomolecules, such as, for example, amino acids or sugar derivatives [97–112]. To overcome these drawbacks and fully profit from the unique features of Re(I)/Tc(I) tricarbonyl complexes, it is necessary to pursue with the innovative design of chelators that can mimic structural motifs of small biomolecules to minimize the probability of inducing changes on their biological behavior.

## REFERENCES

1. Top, S.; Dauer, B.; Vaissermann, J.; Jaouen, G. *J. Organomet. Chem.* **1997**, *541*, 355.
2. Strohfeldt, K.; Tacke, M. *Chem. Soc. Rev.* **2008**, *37*, 1174.
3. Alberto, R.; Schibli, R.; Egli, A.; Schubiger, P. A.; Herrmann, W. A.; Artus, G.; Abram, U.; Kaden, T. A. *J. Organomet. Chem.* **1995**, *493*, 119.
4. Alberto, R.; Schibli, R.; Egli, A.; Schubiger, A. P.; Abram, U.; Kaden, T. A. *J. Am. Chem. Soc.* **1998**, *120*, 7987.
5. Schibli, R.; Schwarzbach, R.; Alberto, R.; Ortner, K.; Schmalle, H.; Dumas, C.; Egli, A.; Schubiger, P. A. *Bioconjug. Chem.* **2002**, *13*, 750.
6. Liu, S.; Edwards, D. S. *Bioconjug. Chem.* **2001**, *12*, 7.
7. Shokeen, M.; Anderson, C. J. *Acc. Chem. Res.* **2009**, *42*, 832.
8. Mewis, R. E.; Archibald, S. J. *Coord. Chem. Rev.* **2010**, *254*, 1686.
9. Wadas, T. J.; Wong, E. H.; Weisman, G. R.; Anderson, C. J. *Chem. Rev.* **2010**, *110*, 2858.
10. Liu, S. *Chem. Soc. Rev.* **2004**, *33*, 445.
11. Abram, U.; Alberto, R. *J. Braz. Chem. Soc.* **2006**, *17*, 1486.
12. Correia, J. D. G.; Paulo, A.; Raposinho, P. D.; Santos, I. *Dalton Trans.* **2011**, *40*, 6144.
13. Alberto, R.; Ortner, K.; Wheatley, N.; Schibli, R.; Schubiger, A. P. *J. Am. Chem. Soc.* **2001**, *123*, 3135.
14. Moura, C.; Fernandes, C.; Gano, L.; Paulo, A.; Santos, I. C.; Santos, I.; Calhorda, M. J. *J. Organomet. Chem.* **2009**, *694*, 950.
15. Alves, S.; Paulo, A.; Correia, J. D. G.; Domingos, A.; Santos, I. *J. Chem. Soc. Dalton Trans.* **2002**, 4714.
16. Fernandes, C.; Santos, I. C.; Santos, I.; Pietzsch, H. J.; Kunstler, J. U.; Kraus, W.; Rey, A.; Margaritis, N.; Bourkoula, A.; Chiotellis, A.; Paravatou-Pestotis, M.; Pirmettis, I. *Dalton Trans.* **2008**, 3215.
17. Banerjee, S. R.; Levadala, M. K.; Lazarova, N.; Wei, L. H.; Valliant, J. F.; Stephenson, K. A.; Babich, J. W.; Maresca, K. P.; Zubietta, J. *Inorg. Chem.* **2002**, *41*, 6417.
18. Liu, Y.; Pak, J. K.; Schmutz, P.; Bauwens, M.; Mertens, J.; Knight, H.; Alberto, R. *J. Am. Chem. Soc.* **2006**, *128*, 15996.
19. Schibli, R.; La Bella, R.; Alberto, R.; Garcia-Garayoa, E.; Ortner, K.; Abram, U.; Schubiger, P. A. *Bioconjug. Chem.* **2000**, *11*, 345.
20. Alberto, R.; Pak, J. K.; van Staveren, D.; Mundwiler, S.; Benny, P. *Biopolymers* **2004**, *76*, 324.
21. Hafliger, P.; Mundwiler, S.; Ortner, K.; Spingler, B.; Alberto, R.; Andocs, G.; Balogh, L.; Bodo, K. *Synth. React. Inorg. Met.-Org. Nano-Met. Chem.* **2005**, *35*, 27.
22. van Staveren, D. R.; Benny, P. D.; Waibel, R.; Kurz, P.; Pak, J. K.; Alberto, R. *Helv. Chim. Acta* **2005**, *88*, 447.
23. Liu, Y.; Oliveira, B. L.; Correia, J. D. G.; Santos, I. C.; Santos, I.; Spingler, B.; Alberto, R. *Org. Biomol. Chem.* **2010**, *8*, 2829.
24. Mindt, T. L.; Struthers, H.; Spingler, B.; Brans, L.; Tourwe, D.; Garcia-Garayoa, E.; Schibli, R. *ChemMedChem* **2010**, *5*, 2026.
25. Mindt, T. L.; Schweinsberg, C.; Brans, L.; Hagenbach, A.; Abram, U.; Tourwe, D.; Garcia-Garayoa, E.; Schibli, R. *ChemMedChem* **2009**, *4*, 529.
26. Pak, J. K.; Benny, P.; Spingler, B.; Ortner, K.; Alberto, R. *Chem. Eur. J.* **2003**, *9*, 2053.
27. Bernard, J.; Ortner, K.; Spingler, B.; Pietzsch, H. J.; Alberto, R. *Inorg. Chem.* **2003**, *42*, 1014.
28. Valliant, J. F.; Morel, P.; Schaffer, P.; Kaldis, J. H. *Inorg. Chem.* **2002**, *41*, 628.
29. Maria, L.; Paulo, A.; Santos, I. C.; Santos, I.; Kurz, P.; Spingler, B.; Alberto, R. *J. Am. Chem. Soc.* **2006**, *128*, 14590.
30. Wald, J.; Alberto, R.; Ortner, K.; Candreia, L. *Angew. Chem. Int. Ed.* **2001**, *40*, 3062.
31. Liu, Y.; Spingler, B.; Schmutz, P.; Alberto, R. *J. Am. Chem. Soc.* **2008**, *130*, 1554.
32. Sogbein, O. O.; Merdy, P.; Morel, P.; Valliant, J. F. *Inorg. Chem.* **2004**, *43*, 3032.
33. Sogbein, O. O.; Green, A. E. C.; Valliant, J. F. *Inorg. Chem.* **2005**, *44*, 9585.
34. Green, A. E. C.; Causey, P. W.; Louie, A. S.; Armstrong, A. F.; Harrington, L. E.; Valliant, J. F. *Inorg. Chem.* **2006**, *45*, 5727.

35. Garcia, R.; Paulo, A.; Domingos, A.; Santos, I.; Ortner, K.; Alberto, R. *J. Am. Chem. Soc.* **2000**, *122*, 11240.
36. Garcia, R.; Paulo, A.; Domingos, K.; Santos, I. *J. Organomet. Chem.* **2001**, *632*, 41.
37. Garcia, R.; Gano, L.; Maria, L.; Paulo, A.; Santos, I.; Spies, H. *J. Biol. Inorg. Chem.* **2006**, *11*, 769.
38. Garcia, R.; Domingos, A.; Paulo, A.; Santos, I.; Alberto, R. *Inorg. Chem.* **2002**, *41*, 2422.
39. Garcia, R.; Paulo, A.; Domingos, A.; Santos, I.; Pietzsch, H. J. *Synth. React. Inorg. Met.-Org. Nano-Met. Chem.* **2005**, *35*, 35.
40. Videira, M.; Maria, L.; Paulo, A.; Santos, I. C.; Santos, I.; Vaz, P. D.; Calhorda, M. J. *Organometallics* **2008**, *27*, 1334.
41. Videira, M.; Moura, C.; Datta, A.; Paulo, A.; Santos, I. C.; Santos, I. *Inorg. Chem.* **2009**, *48*, 4251.
42. Moura, C.; Gano, L.; Santos, C. I.; Paulo, A.; Santos, I. *Curr. Radiopharm.* **2012**, *5*, 150.
43. He, H. Y.; Lipowska, M.; Christoforou, A. M.; Marzilli, L. G.; Taylor, A. T. *Nucl. Med. Biol.* **2007**, *34*, 709.
44. He, H. Y.; Lipowska, M.; Xu, X. L.; Taylor, A. T.; Marzilli, L. G. *Inorg. Chem.* **2007**, *46*, 3385.
45. Lipowska, M.; He, H. Y.; Malveaux, E.; Xu, X. L.; Marzilli, L. G.; Taylor, A. T. *J. Nucl. Med.* **2006**, *47*, 1032.
46. Lipowska, M.; Marzilli, L. G.; Taylor, A. T. *J. Nucl. Med.* **2009**, *50*, 454.
47. Liu, S. *Dalton Trans.* **2007**, 1183.
48. Liu, Z. L.; Chen, L. Y.; Liu, S. A.; Barber, C.; Stevenson, G. D.; Furenlid, L. R.; Barrett, H. H.; Woolfenden, J. M. *J. Nucl. Cardiol.* **2010**, *17*, 858.
49. Maria, L.; Fernandes, C.; Garcia, R.; Gano, L.; Paulo, A.; Santos, I. C.; Santos, I. *Dalton Trans.* **2009**, 603.
50. Goethals, L. R.; Santos, I.; Caveliers, V.; Paulo, A.; De Geeter, F.; Lurdes, P. G.; Fernandes, C.; Lahoutte, T. *Contrast Media Mol. Imaging* **2011**, *6*, 178.
51. Maria, L.; Cunha, S.; Videira, M.; Gano, L.; Paulo, A.; Santos, I. C.; Santos, I. *Dalton Trans.* **2007**, 3010.
52. Mendes, F.; Gano, L.; Fernandes, C.; Paulo, A.; Santos, I. *Nucl. Med. Biol.* **2012**, *39*, 207.
53. Bartholoma, M.; Valliant, J.; Maresca, K. P.; Babich, J.; Zubietta, J. *Chem. Commun.* **2009**, 493.
54. Alberto, R. *Eur. J. Inorg. Chem.* **2009**, *2013*, 21.
55. Alberto, R. *Top. Organomet. Chem.* **2010**, *32*, 219.
56. Alberto, R. *J. Organomet. Chem.* **2007**, *692*, 1179.
57. Santos, I.; Paulo, A.; Correia, J. D. G. *Top. Curr. Chem.* **2005**, *252*, 45.
58. Garcia, R.; Paulo, A.; Santos, I. *Inorg. Chim. Acta* **2009**, *362*, 4315.
59. Correia, J. D. G.; Paulo, A.; Santos, I. *Curr. Radiopharm.* **2009**, *2*, 277.
60. Mendes, F.; Paulo, A.; Santos, I. *Dalton Trans.* **2011**, *40*, 5377.
61. Alves, S.; Paulo, A.; Correia, J. D. G.; Gano, L.; Smith, C. J.; Hoffman, T. J.; Santos, I. *Bioconjug. Chem.* **2005**, *16*, 438.
62. Alves, S.; Correia, J. D.; Santos, I.; Veerendra, B.; Sieckman, G. L.; Hoffman, T. J.; Rold, T. L.; Figueroa, S. D.; Retzloff, L.; McCrate, J.; Prasanphanich, A.; Smith, C. J. *Nucl. Med. Biol.* **2006**, *33*, 625.
63. Retzloff, L. B.; Heinzke, L.; Figueroa, S. D.; Sublett, S. V.; Ma, L.; Sieckman, G. L.; Rold, T. L.; Santos, I.; Hoffman, T. J.; Smith, C. J. *Anticancer Res.* **2010**, *30*, 19.
64. Decristoforo, C.; Santos, I.; Pietzsch, H. J.; Kuenstler, J. U.; Duatti, A.; Smith, C. J.; Rey, A.; Alberto, R.; Von Guggenberg, E.; Haubner, R. *Q. J. Nucl. Med. Mol. Imaging* **2007**, *51*, 33.
65. Alves, S.; Correia, J. D.; Gano, L.; Rold, T. L.; Prasanphanich, A.; Haubner, R.; Rupprich, M.; Alberto, R.; Decristoforo, C.; Santos, I.; Smith, C. J. *Bioconjug. Chem.* **2007**, *18*, 530.
66. Raposinho, P. D.; Correia, J. D. G.; Alves, S.; Botelho, M. F.; Santos, A. C.; Santos, I. *Nucl. Med. Biol.* **2008**, *35*, 91.
67. Raposinho, P. D.; Xavier, C.; Correia, J. D. G.; Falcao, S.; Gomes, P.; Santos, I. *J. Biol. Inorg. Chem.* **2008**, *13*, 449.
68. Valldosera, M.; Monso, M.; Xavier, C.; Raposinho, P.; Correia, J. D. G.; Santos, I.; Gomes, P. *Int. J. Pept. Res. Ther.* **2008**, *14*, 273.
69. Morais, M. M.; Raposinho, P. D.; Correia, J. D. G.; Santos, I. *J. Pept. Sci.* **2010**, *16*, 186.
70. Correia, J. D. G.; Morais, M.; Raposinho, P. D.; Oliveira, M. C.; Santos, I. *Biopolymers* **2011**, *96*, 504.
71. Morais, M.; Raposinho, P. D.; Oliveira, M. C.; Correia, J. D. G.; Santos, I. *J. Biol. Inorg. Chem.* **2012**, *17*, 491.
72. Morais, M.; Raposinho, P. D.; Correia, J. D. G.; Santos, I. *J. Med. Chem.* **2013**, *56*(5), 1961.
73. Louie, A. S.; Vasdev, N.; Valliant, J. F. *J. Med. Chem.* **2011**, *54*, 3360.
74. Garcia, R.; Xing, Y. H.; Paulo, A.; Domingos, A.; Santos, I. *J. Chem. Soc. Dalton Trans.* **2002**, 4236.
75. Can, D.; Spangler, B.; Schmutz, P.; Mendes, F.; Raposinho, P. D.; Fernandes, C.; Carta, F.; Innocenti, A.; Santos, I.; Supuran, C.; Alberto, R. *Angew. Chem. Int. Ed. Engl.* **2012**, *51*, 3354–3357.
76. Can, D.; Schmutz, P.; Raposinho, P. D.; Santos, I.; Alberto, R. *Chem. Biodivers.* **2012**, *9*(9), 1849.
77. Schibli, R.; Netter, M.; Scapozza, L.; Birringer, M.; Schelling, P.; Dumas, C.; Schoch, J.; Schubiger, P. A. *J. Organomet. Chem.* **2003**, *668*, 67.

78. Desbouis, D.; Schubiger, P. A.; Schibli, R. *J. Organomet. Chem.* **2007**, *692*, 1340.
79. Stichelberger, M.; Desbouis, D.; Spiwok, V.; Scapozza, L.; Schubiger, P. A.; Schibli, R. *J. Organomet. Chem.* **2007**, *692*, 1255.
80. Desbouis, D.; Struthers, H.; Spiwok, V.; Kuster, T.; Schibli, R. *J. Med. Chem.* **2008**, *51*, 6689.
81. Struthers, H.; Viertl, D.; Kosinski, M.; Spingler, B.; Buchegger, F.; Schibli, R. *Bioconjug. Chem.* **2010**, *21*, 622.
82. Oliveira, B. L.; Correia, J. D. G.; Raposo, P. D.; Santos, I.; Ferreira, A.; Cordeiro, C.; Freire, A. P. *Dalton Trans.* **2009**, *152*.
83. Oliveira, B. L.; Raposo, P. D.; Mendes, F.; Figueira, F.; Santos, I.; Ferreira, A.; Cordeiro, C.; Freire, A. P.; Correia, J. D. G. *Bioconjug. Chem.* **2010**, *21*, 2168.
84. Oliveira, B. L.; Raposo, P. D.; Mendes, F.; Santos, I. C.; Santos, I.; Ferreira, A.; Cordeiro, C.; Freire, A. P.; Correia, J. D. G. *J. Organomet. Chem.* **2011**, *696*, 1057.
85. Palma, E.; Oliveira, B. L.; Correia, J. D. G.; Gano, L.; Maria, L.; Santos, I. C.; Santos, I. *J. Biol. Inorg. Chem.* **2007**, *12*, 667.
86. Palma, E.; Correia, J. D. G.; Oliveira, B. L.; Gano, L.; Santos, I. C.; Santos, I. *Dalton Trans.* **2011**, *40*, 2787.
87. de Rosales, R. T. M.; Finucane, C.; Foster, J.; Mather, S. J.; Blower, P. J. *Bioconjug. Chem.* **2010**, *21*, 811.
88. Haefliger, P.; Agorastos, N.; Renard, A.; Giambonini-Brugnoli, G.; Marty, C.; Alberto, R. *Bioconjug. Chem.* **2005**, *16*, 582.
89. Agorastos, N.; Borsig, L.; Renard, A.; Antoni, P.; Viola, G.; Spingler, B.; Kurz, P.; Alberto, R. *Chem. Eur. J.* **2007**, *13*, 3842.
90. Vitor, R. F.; Correia, I.; Videira, M.; Marques, F.; Paulo, A.; Pessoa, J. C.; Viola, G.; Martins, G. G.; Santos, I. *ChemBioChem* **2008**, *9*, 131.
91. Vitor, R. F.; Esteves, T.; Marques, F.; Raposo, P.; Paulo, A.; Rodrigues, S.; Rueff, J.; Casimiro, S.; Costa, L.; Santos, I. *Cancer Biother. Radiopharm.* **2009**, *24*, 551.
92. Esteves, T.; Xavier, C.; Gama, S.; Mendes, F.; Raposo, P. D.; Marques, F.; Paulo, A.; Pessoa, J. C.; Rino, J.; Viola, G.; Santos, I. *Org. Biomol. Chem.* **2010**, *8*, 4104.
93. Esteves, T.; Marques, F.; Paulo, A.; Rino, J.; Nanda, P.; Smith, C. J.; Santos, I. *J. Biol. Inorg. Chem.* **2011**, *16*, 1141.
94. Morais, M.; Subramanian, S.; Pandey, U.; Samuel, G.; Venkatesh, M.; Martins, M.; Pereira, S.; Correia, J. D. G.; Santos, I. *Mol. Pharm.* **2011**, *8*, 609.
95. Pirmettis, I.; Arano, Y.; Tsotakos, K.; Okada, K.; Yamaguchi, A.; Uehara, T.; Morais, M.; Correia, H. D. G.; Santos, I.; Martins, M.; Pereira, S.; Triantis, C.; Kyriyanidou, P.; Pelecanou, M.; Papadopoulos, M. *Mol. Pharm.* **2012**, *9*, 1681.
96. Arano, Y.; Yamaguchi, A.; Uehara, T.; Morais, M.; Correia, J. D. G.; Santos, I. Unpublished results.
97. Bowen, M. L.; Orvig, C. *Chem. Commun.* **2008**, 5077.
98. Petrig, J.; Schibli, R.; Dumas, C.; Alberto, R.; Schubiger, P. A. *Chem. Eur. J.* **2001**, *7*, 1868.
99. Dumas, C.; Petrig, J.; Frei, L.; Spingler, B.; Schibli, R. *Bioconjug. Chem.* **2005**, *16*, 421.
100. Bayly, S. R.; Fisher, C. L.; Storr, T.; Adam, M. J.; Orvig, C. *Bioconjug. Chem.* **2004**, *15*, 923.
101. Storr, T.; Fisher, C. L.; Mikata, Y.; Yano, S.; Adam, M. J.; Orvig, C. *Dalton Trans.* **2005**, 654.
102. Storr, T.; Sugai, Y.; Barta, C. A.; Mikata, Y.; Adam, M. J.; Yano, S.; Orvig, C. *Inorg. Chem.* **2005**, *44*, 2698.
103. Storr, T.; Obata, M.; Fisher, C. L.; Bayly, S. R.; Green, D. E.; Brudzinska, I.; Mikata, Y.; Patrick, B. O.; Adam, M. J.; Yano, S.; Orvig, C. *Chem. Eur. J.* **2005**, *11*, 195.
104. Ferreira, C. L.; Bayly, S. R.; Green, D. E.; Storr, T.; Barta, C. A.; Steele, J.; Adam, M. J.; Orvig, C. *Bioconjug. Chem.* **2006**, *17*, 1321.
105. Ferreira, C. L.; Ewart, C. B.; Bayly, S. R.; Patrick, B. O.; Steele, J.; Adam, M. J.; Orvig, C. *Inorg. Chem.* **2006**, *45*, 6979.
106. Bowen, M. L.; Chen, Z. F.; Roos, A. M.; Misri, R.; Hafeli, U.; Adam, M. J.; Orvig, C. *Dalton Trans.* **2009**, 9228.
107. Bowen, M. L.; Lim, N. C.; Ewart, C. B.; Misri, R.; Ferreira, C. L.; Hafeli, U.; Adam, M. J.; Orvig, C. *Dalton Trans.* **2009**, 9216.
108. Ferreira, C. L.; Marques, F. L. N.; Okamoto, M. R. Y.; Otake, A. H.; Sugai, Y.; Mikata, Y.; Storr, T.; Bowen, M.; Yano, S.; Adam, M. J.; Chammas, R.; Orvig, C. *Appl. Radiat. Isot.* **2010**, *68*, 1087.
109. Gottschaldt, M.; Koth, D.; Muller, D.; Klette, I.; Rau, S.; Gorls, H.; Schafer, B.; Baum, R. P.; Yano, S. *Chem. Eur. J.* **2007**, *13*, 10273.
110. Banerjee, S. R.; Babich, J. W.; Zubietta, J. *Inorg. Chim. Acta* **2006**, *359*, 1603.
111. Dapueto, R.; Castelli, R.; Fernandez, M.; Chabalgoity, J. A.; Moreno, M.; Gambini, J. P.; Cabral, P.; Porcal, W. *Bioorg. Med. Chem. Lett.* **2011**, *21*, 7102.
112. Schibli, R.; Dumas, C.; Petrig, J.; Spadola, L.; Scapozza, L.; Garcia-Garayoa, E.; Schubiger, P. A. *Bioconjug. Chem.* **2005**, *16*, 105.

---

# METAL-BASED INDOLOBENZAZEPINES AND INDOLOQUINOLINES: FROM MODERATE cdk INHIBITORS TO POTENTIAL ANTITUMOR DRUGS

MICHAEL F. PRIMIK, LUKAS K. FILAK, AND VLADIMIR B. ARION\*

*Institute of Inorganic Chemistry, University of Vienna, Vienna, Austria*

## 45.1 INTRODUCTION

The first metal complexes synthesized for medical purposes can be dated back to the dawn of the last century, when Paul Ehrlich (1854–1915, 1908 Nobel Prize winner in physiology or medicine) and coworkers synthesized and systematically screened more than 600 compounds in order to assess their biological activity. This ultimately led to the discovery of the organoarsenic arsphenamine, also referred to as *Salvarsan*, the first medicine providing efficient treatment for syphilis [1]. Although *Salvarsan* is no longer in clinical use, as it was replaced by “modern” antibiotics, such as penicillin derivatives, Ehrlich’s approach is still widely used in biochemical research. The second very important concept introduced by Ehrlich has been termed *magic bullet* and describes the goal of targeted chemotherapy. In Ehrlich’s words, chemotherapeutics should be substances “that fly in search of the enemy after the manner of the bewitched bullets” [2]. More than a century later, the hunt for those “magic bullets” is still a hot topic of medicinal research. Scientists attempt to develop substances that would enable physicians to provide chemotherapy without any side effects. Although the meaning of the words changed over the years, the principle has remained the same: gaining selectivity for cancerous cells over normal tissue.

The next tremendous impact on medicine made by metal-based drugs was the introduction of square-planar platinum(II) complexes in clinical cancer therapy. Approved in the late 1970s, *cis*-platin (*cis*-diamminedichloroplatinum(II)) and its second- and third-generation derivatives carboplatin and oxaliplatin, are administered in 80% of all chemotherapies. The results speak for themselves, as before the clinical use of cisplatin, testicular cancer manifested a mortality rate of 90%, which was literally inverted by a platinum drug-based combination therapy regimen. This leaves 10% of the diseases incurable, mainly owing to late diagnosis accompanied by already strong metastasis [3]. The well-recognized target of anticancer platinum drugs is DNA. As tumor cells tend to divide more frequently than healthy ones, it is possible to obtain certain selectivity for cancer over normal tissue [4]. However, as nearly all benign cells also replicate themselves from time to time, the general toxicity of the drug is high and side effects, such as nausea, hair loss, nephrotoxicity, and neuropathy, are frequent. Furthermore, certain types of cancer are intrinsically resistant or acquire resistance against platinum-containing drugs throughout consecutive chemotherapy cycles [5]. All these findings prompted researchers to gain insight into the interactions between the platinum drugs and biomolecules such as nucleic acids, proteins, and carbohydrates, ultimately leading to a better understanding of the mode of action of these drugs and building the foundation for rational metal-based drug design.

Soon it became clear that DNA alone is possibly neither the only nor the best target for platinum (and possibly other) anticancer drugs. This becomes evident when one takes a closer look at DNA lesions caused by cisplatin and carboplatin. Although the platinum core after activation by hydrolysis in the cells and the application area are the same for both drugs, the ratio and the nature of DNA adducts formed is different. While cisplatin predominantly cross-links neighboring guanine bases present on the same DNA strand (~65%), carboplatin generates by far more fragments that are believed to originate from two guanines that have another base in between (~36%) [6]. As a consequence, carboplatin-caused DNA damages are processed differently by DNA repair enzymes than cisplatin-induced lesions, resulting in different active concentrations and (dose-limiting) side effects of the two closely related drugs. Moreover, focusing on DNA damage as the only mode of action does not entirely explain the varying sensitivity and resistance patterns of different cancer cell types.

On the basis of those findings, scientists expanded their field of research. On the one hand, much effort was put into the development of platinum(II) complexes with different ligands [7], allowing for the fine-tuning of physicochemical properties and thereby affecting the biological distribution of the drugs in the organism. This led to the development of the third-generation platinum drug, oxaliplatin [8], which is approved worldwide against colon cancer. The next generation of platinum anticancer agents will presumably consist of octahedral platinum(IV) complexes, which are considered inert prodrugs in the healthy tissues and get activated in, or in the surroundings of, the tumors [9]. On the other hand, chemists remembered Ehrlich's "magic bullet" concept and restarted the search for more selective chemotherapeutics. Nowadays, targeted chemotherapy is believed to be one of the most promising ways to fight cancer [10–12]. A variety of rewarding targets, mostly enzymes or proteins, have been identified. Among them are

*Ribonucleotide Reductases.* This class of enzymes catalyzes the reduction of ribonucleotides to deoxyribonucleotides, the building blocks of DNA. Interference with this process leads to a depletion of the dNTP pool, slowing down DNA synthesis and reparation, two mechanisms affected in many types of cancer [13]. Thus inhibition of the enzyme can be regarded as a therapeutic option that can be achieved by using organic molecules [14] or gallium compounds [15, 16].

*Tyrosine Kinases.* They are enzymes that transfer a phosphate group from ATP to a tyrosine amino acid side chain of a protein. (De)phosphorylation is a major on/off-switch for a vast array of proteins and particularly interesting regarding cancer, as tyrosine kinases were found to be overexpressed in many solid tumors. Chemotherapeutics that target these enzymes are erlotinib, an epidermal growth factor receptor (EGFR) inhibitor, and imatinib, which is also approved by the FDA (US Food and Drug Administration) as an anticancer agent [17].

*Topoisomerases.* DNA topoisomerase II is an enzyme that is able to cleave, unwind, and ligate DNA strands, providing an opportunity for correction of irregularly twisted DNA [18]. This enzyme is overexpressed in various cancer types, making it a major target for therapy, either by poisoning the DNA topoisomerase complex or by catalytic inhibition of the enzyme [19, 20]. Three drugs of this class are widely used in combination anticancer therapy, namely, doxorubicin, etoposide, and mitoxantrone [21, 22]. Within the past years, several organometallic complexes have been found to exhibit topoisomerase-inhibiting properties [23–25].

*Hormone Receptors.* Certain types of cancer, mainly breast cancer, endometrial cancer, and prostate cancer, show a growth dependency on sexual hormones such as estradiol and testosterone [26]. As those cells overexpress hormone receptors, down-regulation of the hormone concentration is a powerful tool in the fight against those cancer types. Among the chemotherapeutics approved for treatment is tamoxifen [27, 28]. In recent years, also related complexes, that is, the ferrocifenes [29] were developed for that purpose. For detailed information on this class of molecules, please see Chapter 42.

*Cyclin-Dependent Kinases (cdks).* These enzymes play a crucial role in cell cycle progression. They facilitate the transfer of a phosphate group to threonine and serine residues of their respective target, strictly regulated by activators (cyclins) and different inhibitors. Activated or inhibited at certain cell cycle checkpoints, cdks trigger the cell to proceed with or cease the cycle, respectively [30]. There are various cdk/cyclin combinations known today, of which some appear to be essential for all cells, while others seem to regulate the cell cycle of highly specialized cells. In many human cancers, overactivity of cdks has been identified as one of the mechanisms underlying the pathological hyperproliferation. Therefore, inhibition of cdk activity may offer a therapeutic option for fighting cancer [31]. Flavopiridol (**1**, Fig. 45.1), a semisynthetic flavonoid, was the first cdk inhibitor that entered clinical trials as an anticancer drug [32].

This review is an account of the investigation of a class of compounds, namely, indolobenzazepines, which attracted our attention as likely cdk inhibitors.

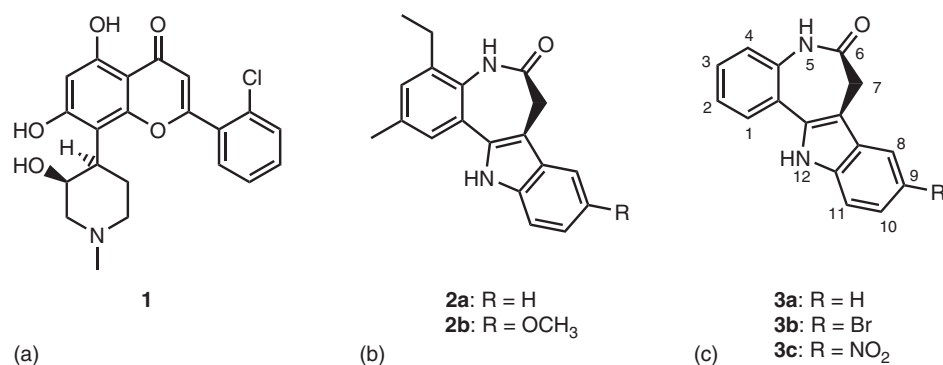


**Figure 45.1** Flavopiridol (a); indolobenzazepinones described by MacPhillamy et al. (b); paullone core structure (**3a**), kenpaullone (**3b**) and alsterpaullone (**3c**) with atom numbering scheme (c).

## 45.2 INDOLOBENZAZEPINES AS MODERATE cdk INHIBITORS

Substituted 7,12-dihydroindolo[3,2-*d*][1]benzazepin-6(5*H*)ones **2a** and **2b** were first reported in 1958 by MacPhillamy et al. [33] as the last intermediate in an 11-step synthesis of 4-ethyl-5,6,7,12-tetrahydro-2-methylindolo[3,2-*d*][1]benzazepine. In 1992, Kunick reported the preparation of six indolo[3,2-*d*][1]benzazepin-6(5*H*)ones [34] in a three-step procedure. The crucial step was the decarboxylation reaction of 2,3-dihydro-5-hydroxy-2-oxo-1*H*-benz[*b*]azepin-4-carboxylic acid ethyl ester into 3,4-dihydro-1*H*-benz[*b*]azepin-2,5-dione, which made possible the subsequent Fischer indole synthesis, with formation of the desired 7,12-dihydroindolo[3,2-*d*][1]benzazepin-6(5*H*)ones.

Kenpaullone<sup>1</sup> **3b** (Fig. 45.1) was identified as a potential cdk inhibitor in a program search performed at the National Cancer Institute (NCI; NCI60 screen) with an antiproliferative activity profile similar to that of Flavopiridol [35].

Subsequent inhibitory experiments revealed that kenpaullone **3b** is indeed a moderate ATP-competitive inhibitor of cdk1/cyclin B, cdk2/cyclin A and cdk5/p35 [36], with the lactam moiety as an important binding motif [37, 38]. Therefore, **3b** is a good candidate for further structural optimization. Structure–activity relationship studies have shown that electron-withdrawing substituents in position 9 are favorable for the cdk inhibitory activity, provided that the lactam moiety remains underivatized. Alsterpaullone, the 9-nitro-derivative, was found to be the best inhibitor of the paullone family [39]. At the same time, a number of paullones prepared by modification of the lactam unit have shown high antiproliferative activity, which does not parallel their cdk inhibitory profile [40]. Therefore, other intracellular targets have been suggested for this class of compounds. In a screen on 28 commercially available kinases, kenpaullone and alsterpaullone selectively inhibited cdks, gsk-3 and Lck, the latter being a member of the Src family of tyrosine kinases (abbreviation derived from sarcoma) [40]. Gsk-3 enzymes belong to the family of serine/threonine kinases as well, with structural similarity to cdks. In screens for the gsk-3 inhibitory potential of paullones, alsterpaullone was again found to be the best performing derivative [40].

## 45.3 TOWARD METAL-BASED INDOLOBENZAZEPINES AS POTENTIAL ANTICANCER DRUGS

One of the limitations encountered in the development of paullones as antitumor drugs was, and still is, their low aqueous solubility and bioavailability. Given the experience of our group in the development of metal-based anticancer agents [41–45], we expected that coordination to metal ions can mitigate the imposed limitations, leading to improved pharmacokinetics and, maybe by synergistic effects with metal ions, to more favorable pharmacodynamic properties. Coordination to metal ions can result in (i) stabilization of certain, sometimes unusual, ligand geometries, (ii) redox activity, (iii) increased solubility, (iv) enhanced lipophilicity, (v) improved cellular uptake, (vi) different modes of action, and (vii) synergistic effects from metal and ligand(s) [46–48]. Biological effects exhibited by metal complexes, but unobserved for free ligands were also reported [49, 50]. Certain long-term side effects can be diminished or even avoided as metal complexes can break down and the metal ion can then interact with the organism [51–53]. Although the library of paullone derivatives prepared by Kunick et al. was large, metal-based derivatives were not known. This is primarily because the original paullones do not contain binding sites able to chelate metal ions. The only possibility is the binding via the lactam or thiolactam unit with

<sup>1</sup>Named in honor of Dr. Kenneth Paull, contributor to the NCI60 screen.

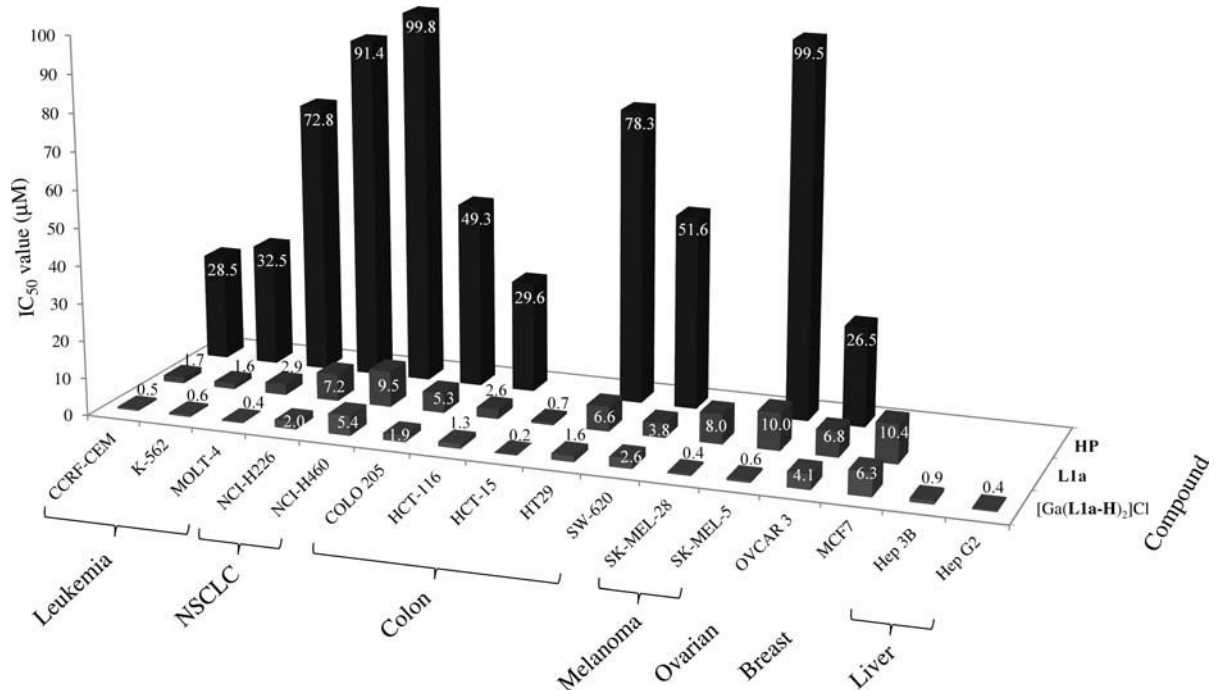


**Figure 45.2**  $IC_{50}$  (50% cell proliferation inhibition concentrations) of the hydrazino-paullone (**HP**), ligand **L1a**, and its gallium complex  $[Ga(L1a-H)_2]Cl$  on different cancer cell lines [54].

formation of thermodynamically nonstable four-membered metallocycles. Therefore, our primary aims were the design and synthesis of paullones, which contain binding sites able to accommodate specific metal ions and the study of the effect of metal coordination on the antiproliferative activity, cdk inhibitory activity, and cell cycle progression.

The first indolobenzazepine ligand was designed for coordination to gallium(III). By reacting the methyl thioimidate [54] with hydrazine hydrate, the corresponding hydrazino-paullone (**HP**) was obtained, which was further converted into potentially tridentate ligands (**L1a** and **L1b**, Fig. 45.3) by condensation reaction with 2-hydroxybenzaldehyde [54] or 2-acetylpyridine [55], respectively. Given our experience with complexes of  $\alpha$ -N-heterocyclic thio- and semicarbazones, gallium(III) complexes with paullone ligands, having  $N_2O$  (**L1a**) [54] and  $N_3$  (**L1b**) [55] donor sets, were prepared. Hydrazino-paullone **HP**, ligand **L1a** and its gallium(III) complex  $[Ga(L1a-H)_2]Cl$ , were tested for antiproliferative activity in a panel of 14 human cancer cell lines. The results, summarized in Fig. 45.2, clearly show a significantly improved cytotoxicity of **L1a** over its precursor **HP** by factors of 4–25. Upon complexation, activity against cancer cells could be further improved by a factor of 1.5–18, depending on the cell line (Fig. 45.2).

However, the low aqueous solubility and hydrolytic instability of the positively charged cationic complex prompted us to search for other derivatives and, in particular, those able to coordinate to ruthenium(II). We expected that  $d^6$  low spin ruthenium(II) species would be kinetically more resistant to hydrolysis. As a binding unit to be attached to the original paullone,  $\alpha$ -picolylamine, an excellent bidentate chelator for ruthenium(II), was chosen. As we were interested in the elucidation of the influence of electron-withdrawing substituents in position 9 of the paullone scaffold on the antiproliferative activity, ligands with bromo (**L2b**) and nitro (**L2c**) substituents, as well as the unsubstituted ligand (**L2a**), were prepared by reaction of thiolactam derivatives with  $\alpha$ -picolylamine in tetrahydrofuran (THF) (Fig. 45.3) in excellent yields and high purity without using mercury salts to promote the reaction or activation via thiolactam methylation. In addition, the location of the binding site was changed to position 9 by reducing the nitro group to the amino function, which was further reacted with 2-formylpyridine, to yield a paullone ligand with an intact lactam moiety (**L3**) [56]. Our attempts to develop a paullone ligand bearing a stable 2,2,6,6-tetramethylpiperidin-1-yl)oxyl (TEMPO) free-radical unit (**L2d**) were also successful [57].

Other potentially tridentate ligands were prepared by using pyridoxal (**L1c**) [58] and 2-formylpyridine (**L1d**) [59] instead of 2-hydroxybenzaldehyde or 2-acetylpyridine, respectively.

The first ruthenium(II) complexes with paullone ligands were prepared by reaction of *cis*- $[RuCl_2(DMSO)_4]$  with **L2a** and **L2b**, respectively. Depending on the reaction conditions, complexes with metal-to-ligand ratio 1 : 1 and 1 : 2 were isolated. Bis-ligand complexes  $[Ru^{II}Cl(DMSO)(L2a)_2]Cl$  and  $[Ru^{II}Cl(DMSO)(L2b)_2]Cl$  were tested for antiproliferative activity and

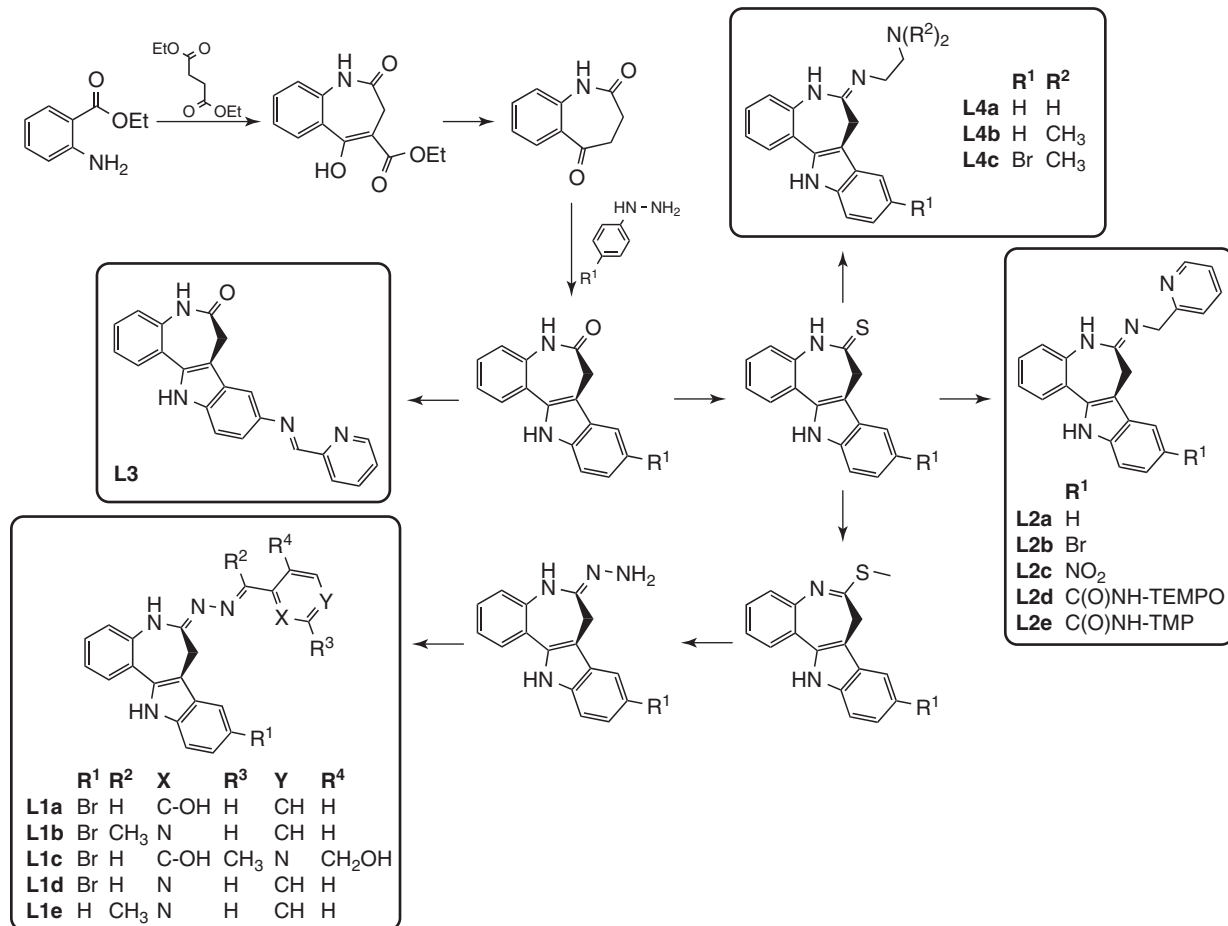


**Figure 45.3** Synthesis of paullone ligands with different location of their binding sites. TEMPO = (2,2,6,6-tetramethylpiperidine-1-yl)-oxyl. TMP, 2,2,6,6-tetramethyl-piperidine.

showed IC<sub>50</sub> values in the low micromolar concentration range [46]. Electrophoretic mass titration studies revealed both compounds to alter the cDNA secondary structure, leading to relaxation of the supercoiled form of the plasmid. UV-vis and NMR investigations of ruthenium(II) bis-ligand complexes did not show any evidence for binding to 5'-GMP, a model system for nucleotide binding. In addition, ethidium bromide was displaced with increasing amounts of the complexes. Thus, intercalation rather than monofunctional binding to nucleotides was assumed to be responsible for the alteration of DNA secondary structure.

Another paullone metal coordination approach was based on using metal-arene compounds as an ideal metal scaffold to deliver biologically active compounds into the cell, as they combine proper lipophilicity to cross the cell membrane with sufficient aqueous solubility. In addition, binding to the arene stabilizes ruthenium and osmium in oxidation state 2+ [56]. As ligands to be attached to the metal-arene fragment, **L2a–L2c** and **L3** with similar but differently placed binding sites (Fig. 45.3) were chosen. By exploiting the  $\mu$ -chlorido bridge-splitting reaction of  $[M^{II}(p\text{-cymene})(\mu\text{-Cl})Cl]_2$  ( $M = Ru, Os$ ) with **L2a–L2c** and **L3** complexes  $[M^{II}(p\text{-cymene})(L2a–L2c)Cl]Cl$  and  $[M^{II}(p\text{-cymene})(L3)Cl]Cl$  were prepared. Interestingly, two types of differently shaped crystals were discovered by inspection of the product,  $[Ru^{II}(p\text{-cymene})(L2c)Cl]Cl$ , under the microscope. They were large enough to be separated mechanically and studied by NMR spectroscopy. In addition, the crystals were suitable for X-ray diffraction analysis, which revealed the presence of two different isomers: E (block-shaped crystals) and Z (stick-shaped crystals). The structures of both isomers are shown in Fig. 45.4. The E/Z isomerization occurs at the exocyclic C<sup>6</sup>=N<sup>13</sup> double bond. This isomerization was found to be solvent and concentration dependent. By investigation of the process at different temperatures and usage of the Eyring plot, activation parameters were determined [56].

Cell culture experiments showed IC<sub>50</sub> values in the micromolar concentration range, whereas binding to 5'-GMP remained rather poor (10%). Ruthenium(II)- and osmium(II)-arene complexes with **L2a**, a ligand modified at the lactam unit, were

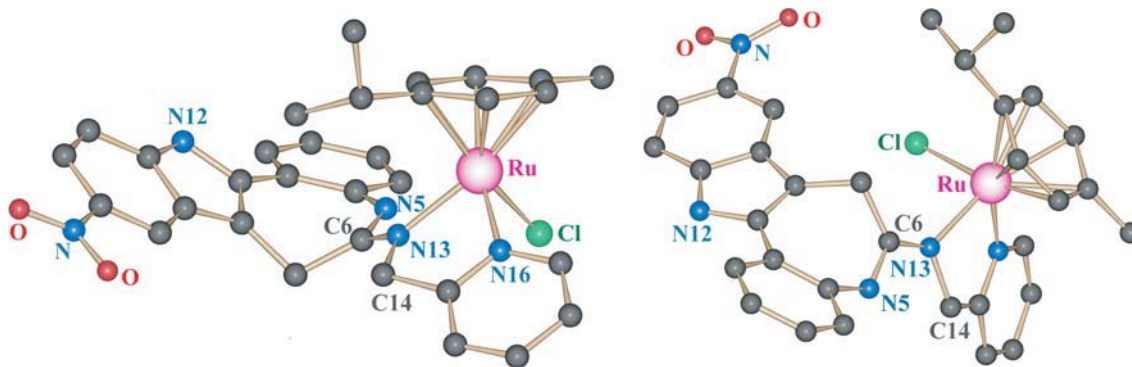


**Figure 45.4** Structures of the cationic *E*- (a) and *Z*-isomers (b) of  $[\text{Ru}^{\text{II}}(\text{p-cymene})(\text{L2c})\text{Cl}]^+$ . Non-labeled atoms represent carbons. Hydrogen atoms were omitted for clarity. (See insert for color representation of the figure.)

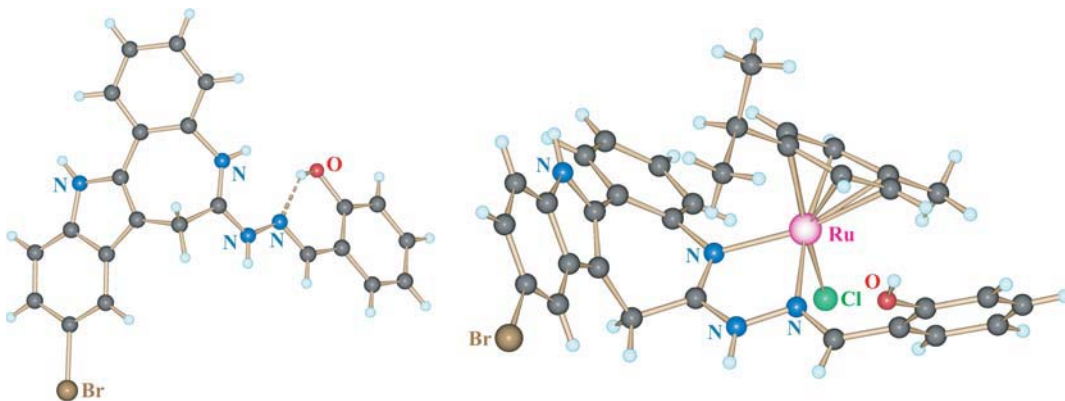


**Figure 45.5** Structures of the protonated paullone ligand  $\text{HL1a}^+$  with an intramolecular hydrogen bond  $\text{O}-\text{H}\cdots\text{N}$  (a) and ruthenium-arene complex cation  $[\text{Ru}(\text{p-cymene})(\text{L1a})\text{Cl}]^+$  (b). Non-labeled atoms represent carbon atoms. (See insert for color representation of the figure.)

found to reduce the rate of DNA synthesis more efficiently than the corresponding complexes with **L3**, the ligand modified in position 9 of the original paullone. In addition, cell cycle perturbations were more pronounced in the case of the **L2a**-based complexes. These results indicate that other intracellular targets might be responsible for the observed cytotoxicity [56].

The next type of complex  $[\text{M}^{\text{II}}(\text{p-cymene})(\text{L1a,c})\text{Cl}]\text{Cl}$  was synthesized by reacting  $[\text{M}^{\text{II}}(\text{p-cymene})(\mu-\text{Cl})\text{Cl}]_2$  ( $\text{M} = \text{Ru}, \text{Os}$ ) with potentially tridentate ligands **L1a** and **L1c**, originally designed for coordination to gallium(III). Both compounds act as bidentate ligands in  $[\text{M}^{\text{II}}(\text{p-cymene})(\text{L1a,c})\text{Cl}]\text{Cl}$  with the phenolic oxygen not involved in the coordination to the central metal ion, as shown in Fig. 45.5.

All four complexes exhibited similar cytotoxicity in the low micromolar concentration range. Both ruthenium complexes showed 5'-GMP binding behavior remarkably different from that for the previously described ruthenium-arene complexes with **L2a** and **L3** ligands, forming several adducts, with the most abundant reaching 47%. Osmium(II)-arene complexes with **L1a** and **L1c** ligands did not react with 5'-GMP [58]. Biological studies have shown that the complexes are able to induce apoptosis and, to a lower extent, also necrosis. In addition, inhibition of cdk2/cyclin E was found in a cell-free assay, but this is rather unlikely to be decisive for the antiproliferative activity of the complexes, given weak effects on cell cycle progression [60]. Thus, it appears that induction of apoptosis constitutes a new mode of action for paullone-based metal complexes.

Attachment of a TEMPO free-radical unit to a paullone ligand with a carboxylic acid group in position 9, by using a well-developed active ester coupling protocol from peptide synthesis, afforded ligand **L2d**, with enhanced aqueous solubility [57]. Its molecular structure is shown in Fig. 45.6. The TEMPO-bearing ligand showed high cytotoxicity, with  $\text{IC}_{50}$  values in either the nanomolar concentration range in A549 (non-small-cell lung carcinoma), CH1 (ovarian carcinoma), SW480 (colon carcinoma), N87 (gastric cancer), and SK-Mel-28 (skin melanoma) cell lines, or in the low micromolar concentration range

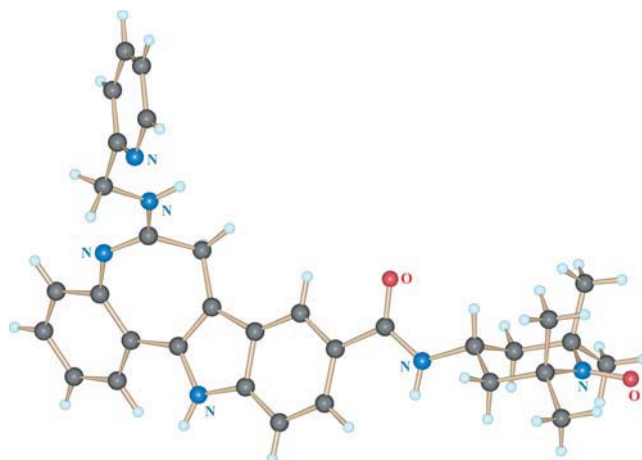


**Figure 45.6** X-ray structure of the paullone ligand **L2d**, bearing a TEMPO free-radical unit. Non-labeled atoms represent carbon atoms. (See insert for color representation of the figure.)

in T47D (ductal breast epithelial tumor) cells. Binding of the ligand to the ruthenium- or osmium-arene fragment resulted in significant reduction of antiproliferative activity, exhibited in the micromolar concentration range. **L2d** was found to be from 30 to more than 200 times more cytotoxic than **L2e**, the closely related compound that does not contain the oxyl radical, indicating the important role of the free radical for cytotoxicity. The impact of the compounds with a TEMPO radical unit on DNA secondary structure was studied to determine whether DNA is a possible intracellular target. Partial untwisting of the supercoiled form of the plasmid but no DNA fragmentation was found for the ruthenium and osmium complexes. The metal-free ligand **L2d** has no effect on DNA. Moreover, the untwisting of DNA required higher concentrations than those necessary for inhibition of cancer cell growth. These results indicate that DNA is not the crucial target of these compounds [57].

As a natural extension to our work, complexation reactions with biologically abundant metal ions, namely, copper(II), have also been performed. The ligands chosen were either bidentate, bearing an *N,N*-dimethylethylenediamine binding site (**L4b** and **L4c**) or tridentate, incorporating pyridine-2-carboxaldazine/hydrazone (**L1d**) and 2-acetylpyridine ketazine/hydrazone (**L1b** and **L1e**) binding motifs [59]. The complexes were prepared by reacting equimolar amounts of ligand and copper(II) chloride in methanol at reflux. The aqueous solubility of bidentate ligands **L4b** and **L4c**, and copper(II) complexes thereof, was sufficient for performing MTT assays. The IC<sub>50</sub> values measured in A549, CH1, SW480, A2780 (ovarian carcinoma), and A2780cisR (cisplatin resistant) human cancer cells were between 1.6 and 44 μM, depending on the cell line and the compound. With one exception, the activity of the complexes was comparable to the corresponding ligands. This is due to the copper(II) complexes dissociating easily in aqueous solution with liberation of the free ligands, as confirmed by UV-vis measurements and ESI mass spectra.

To increase the thermodynamic stability of copper(II) complexes, sp<sup>2</sup>-hybridized nitrogen atoms were introduced and tridentate ligands (**L1b**, **L1d**, and **L1e**) were used for complexation reactions with copper(II) chloride in refluxing methanol, yielding five-coordinate complexes (Fig. 45.3). These are highly cytotoxic in A549, CH1, SW480, A2780, and A2780cisR cells, with IC<sub>50</sub> values in the nanomolar concentration range.

Further efforts by us were focused on the replacement of the seven-membered folded azepine ring by a six-membered flat pyridine ring. This structural modification was realized in a straightforward manner via a two-step procedure leading to a new class of biologically active compounds, namely, indolo[3,2-*c*]quinolines.

#### 45.4 INDOLO[3,2-*c*]QUINOLINES AND THEIR METAL COMPLEXES

Indoloquinolines are alkaloids naturally occurring in the West African climbing shrub *Cryptolepis sanguinolenta*. Extracts made of the roots of these plants have been used for ages by the local people against several severe diseases including malaria, hepatitis, and bacterial infections. The healing effect was mainly due to the indolo[3,2-*b*]quinoline cryptolepine and, to a lesser extent, caused by an indolo[3,2-*c*]quinoline. Indoloquinolines exhibit a broad spectrum of biological properties, for example, antibacterial, antifungal, antiprotozoal, antitumor, antihyperglycemic, as well as anti-inflammatory activity

[61]. Several mechanisms for the antitumor activity were suggested for these compounds, among them DNA intercalation, topoisomerase inhibition, and G-quadruplex DNA binding, leading to telomerase inactivation [62]. Indoloquinolines are chemically related to indolobenzazepines. Nevertheless, the structural difference has substantial consequences, as the whole ligand system of indoloquinolines is conjugated (heteroaromatic) and therefore planar. This difference between the two ligand backbones is shown in Fig. 45.7. The dihedral angle between the pyridine ring and indole moiety amounts  $101.4^\circ$  in the copper(II) complex with paullone ligand **L1d**, whereas the planarity of the related indoloquinoline ligand **L6l** is preserved in the complex.

The first indoloquinolines used as ligands for binding to metal ions were **L5a** and **L5b**, which have shown activity against several human cancer cell lines [63–66]. Synthesis of the indoloquinoline backbone was achieved using a one-step reaction of 2-aminobenzylamine and isatin in glacial acetic acid [67]. The indolo[3,2-*c*]quinoline-6-ones can be further activated by chlorination with  $\text{POCl}_3$ , yielding the corresponding 6-chloro derivatives. By condensation reaction with amines, chelating moieties could be attached, allowing for the binding to metal scaffolds [63, 68]. Figure 45.8 shows the synthesis route to these ligands.

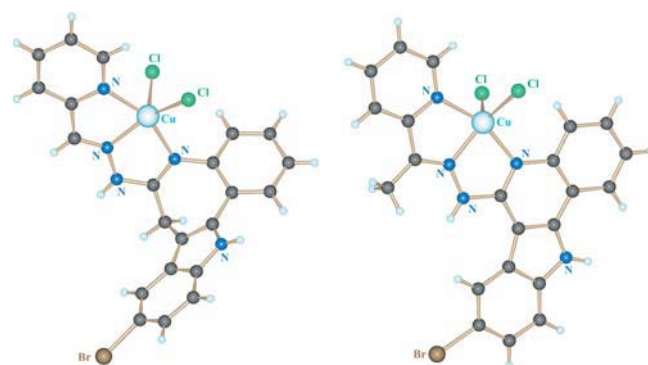


**Figure 45.7** Structures of the Cu(II) complexes of the paullone ligand **L1d** (a) and the related indoloquinoline-based ligand **L6l** (b). While the paullone backbone is considerably folded, the indoloquinoline backbone is planar. Non-labeled atoms represent carbon atoms. (See insert for color representation of the figure.)

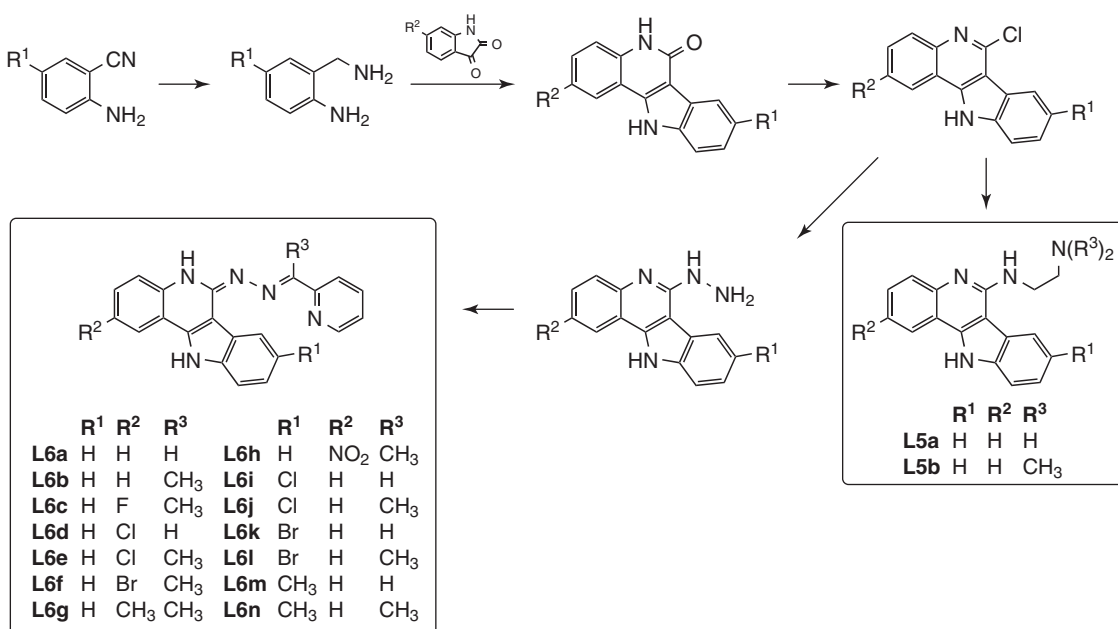


**Figure 45.8** Synthesis scheme for the indoloquinoline-based ligands **L5a,b** and **L6a–L6n**.

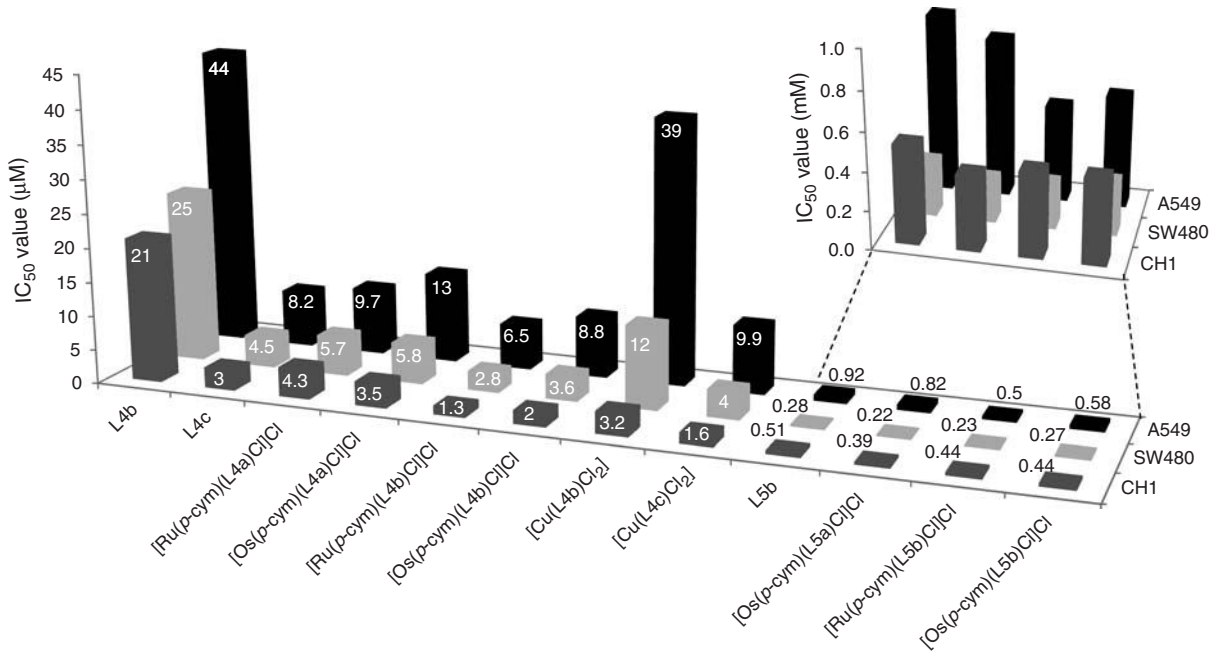


**Figure 45.9** IC<sub>50</sub> values of ethylenediamine-based paullone ligands (**L4b**, **L4c**), their Cu(II), Ru(II), and Os(II) complexes, and of the corresponding indoloquinoline derivatives, as obtained by the MTT assay (96 h incubation time). Antiproliferative activity was determined in three human cancer cell lines, namely, CH1 (ovarian carcinoma, dark gray bars), SW480 (colon carcinoma, light gray bars), and A549 (non-small-cell lung carcinoma, black bars). The inset shows the expanded diagram for the indoloquinolines.

Although ruthenium- and osmium *p*-cymene complexes of **L5a** or **L5b** were highly active in three human cancer cell lines (A549, non-small-cell lung carcinoma; CH1 ovarian cancer; SW480, colon carcinoma) with IC<sub>50</sub> values in the low micromolar range, they dissociated readily with liberation of the indoloquinoline ligand [68]. The results of the MTT tests are summarized in Fig. 45.9.

One of the complexes, [Ru(*p*-cymene)(**L5b**)Cl]Cl, as well as the metal-free ligand **L5b**, have shown high DNA intercalation potential in a cell-free methyl green displacement assay, strong and concentration-dependent cell cycle perturbations, as well as a weak, concentration-dependent, cdk2/cyclin E inhibition in a cell-free kinase assay. Interestingly, cdk1/cyclin B was not inhibited even at concentrations more than 100-fold higher than the IC<sub>50</sub> value for A549 chemoresistant non-small-cell lung cancer cells. To increase the thermodynamic stability of ruthenium(II) and osmium(II) complexes we introduced into the potential indoloquinoline ligands sp<sup>2</sup>-hybridized donor atoms, affording **L6a** [69]. As expected, the complexes prepared were more resistant to hydrolysis and remained intact in aqueous solution over 24 h. MTT tests of ruthenium- and osmium-cymene complexes with **L6a** revealed that the cytotoxic activity was preserved, as depicted in Fig. 45.10. Therefore, further derivatizations were performed to achieve extended chemical diversity and to establish novel structure–activity relationships. Substitutions in positions 2 and 8 were realized [69–71], the latter position being comparable with the corresponding position 9 of the paullone backbone. We used both electron-withdrawing (F, **L6c**; Cl, **L6d,e,i,j**; Br, **L6f,k,l**) and electron-donating (CH<sub>3</sub>, **L6g,m,n**) groups. Ruthenium and osmium complexes of ligand **L6h**, with a strongly electron-withdrawing NO<sub>2</sub>-group in position 2 were not assayed for cytotoxicity because of very low aqueous solubility. The third position for fine-tuning the biological properties was R<sup>3</sup>, being either a hydrogen atom (**L6a,d,i,k,m**) or a methyl group.

MTT results (Fig. 45.10) indicate that SARs are not clear cut. Obviously, electron-withdrawing substituents in position 2 lead to a slight decrease in cytotoxicity, whereas substitution in position 8 has no effect essentially. The picture is a bit different when comparing the ruthenium complexes with their osmium congeners. In most of the cases, the osmium analogs exhibit similar or slightly higher activity, but there are also cases (**L6a**) where the osmium complex is more than one order of magnitude more cytotoxic than its ruthenium counterpart. The difference between the formyl- and the acetylpyridine azine-based ligands (R<sup>3</sup> = H or CH<sub>3</sub>, correspondingly) is by far not as clear as for the copper(II) complexes, strongly dependent on the cell line and the substituent R<sup>2</sup>. Interestingly, variation of substituents R<sup>3</sup> had no pronounced effect on cytotoxic activity. Copper(II) complexes with ligands **L6a,b** and **L6i–n** were by far the most active of the whole series,

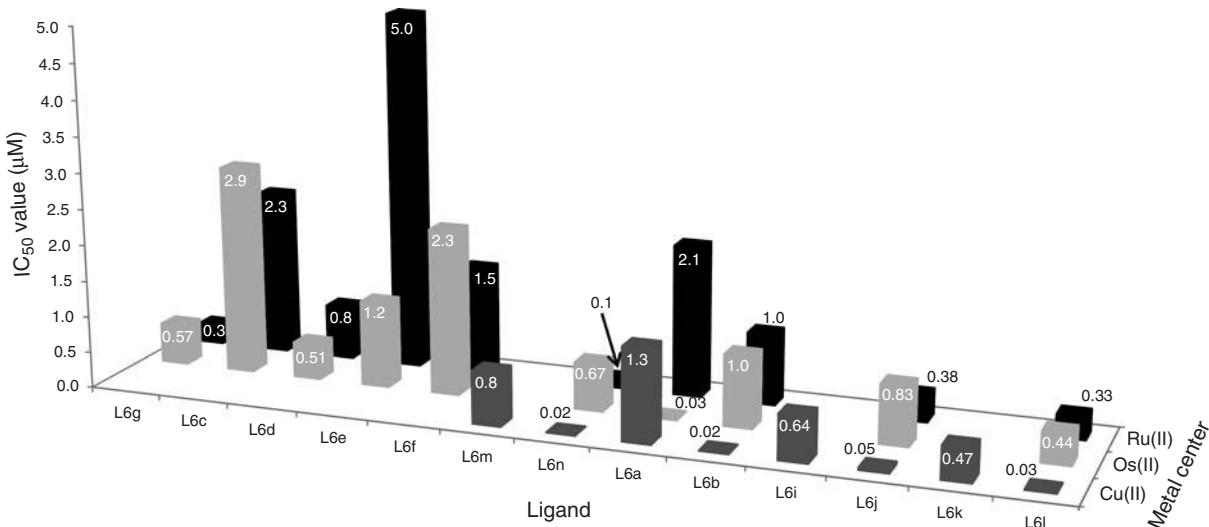


**Figure 45.10** IC<sub>50</sub> values of indoloquinoline-based complexes [Cu(L6)Cl<sub>2</sub>] (Cu(II), dark gray bars), [Ru(p-cymene)(L6)Cl]Cl (Ru(II), light gray bars), and [Os(p-cymene)(L6)Cl]Cl (Os(II), black bars), on the human colon carcinoma cell line SW480, as obtained by the MTT assay after 96 h incubation time.

with IC<sub>50</sub> values as low as 30 nM in CH1 cells. While in the case of paullone-based copper(II) complexes, the methyl group of the 2-acetylpyridine moiety caused a fivefold increase in cytotoxicity [59], this effect is even more evident in the indoloquinoline-based complexes. Differences of one order of magnitude were detected in A549 and CH1 human cancer cell lines, while a 50-fold increase in SW480 colon carcinoma cell line was outstanding [71], as can be seen in Fig. 45.10. These findings clearly show that a careful selection of the (i) metal center, (ii) the ligands, and (iii) exploring the metal–ligand interactions are essential for biological utility of the resulting complexes.

## 45.5 OUTLOOK

Novel strategies have been developed for the effective delivery of the anticancer drugs to the desired tumor tissue to improve their selectivity and, consequently, to reduce their side effects [72–76]. By exploration of these targeting strategies, cancer nanotherapeutics based on polymers (polymeric nanoparticles, micelles, or dendrimers), lipids (liposomes, nanocapsules), viruses (viral nanoparticles), or carbon nanotubes, an enhancement of the intracellular concentration of drugs in cancer cells can be easily achieved, usually without being blocked by P-glycoprotein, a plasma membrane protein responsible for drug efflux from cells and involved in multidrug resistance (MDR) [74]. These emerging approaches have been mainly applied to organic anticancer drugs (e.g., doxorubicin, paclitaxel) [72] and clinically used inorganic platinum drugs [76], although examples of conjugation of organoruthenium compounds to recombinant human serum albumin (rHSA), an effective drug delivery system [77], with a marked increase in cytotoxicity have also been recently reported [78–80].

Targeted delivery of anticancer drugs will continue to be an important research field for cancer therapy in the future [81]. A large number of homing peptides (HPs) and cell-penetrating homing peptides (CPHPs) targeting specific cells via molecular recognition events have been discovered by using phage-display technology, by exploring synthetic peptide libraries (SPLs) or by applying a direct targeting approach [82–84]. Some of the discovered peptides have entered clinical trials, as for example, the tumor HP asparagine-glycine-arginine (NGR) which recognizes and binds an aminopeptidase that is overexpressed on tumor blood vessels, or cyclo[Arg-Gly-Asp-D-Phe-(NMeVal)], also referred to as *cRGD* or *Cilengitide*, an antiangiogenic agent showing affinity to  $\alpha_v\beta_3$  and  $\alpha_v\beta_5$  integrins, and have been used for selective delivery of clinically used organic drugs, while others, for example, F3, a 31-aa CPHP that targets nuclei of tumor cells [85] or BMHP1 (PFSSTKT) showing affinity to neural stem cells have not yet been linked to any druglike compound [82, 86, 87]. Arg<sub>5</sub> and Arg<sub>8</sub> conjugates of the organosmium(II) complex [ $(\eta^6$ -biphenyl)Os(picolinate)Cl] have been shown to increase osmium uptake into human ovarian cancer cells A2780, by a factor of 2 and 10, respectively [88], while a cobaltocenium-SV4-40T antigen nuclear localization signal (NLS) peptide conjugate has shown a significant accumulation in the nucleus of HepG2 cells [89]. Conjugation of biological targeting peptides, for example, bombesin derivatives, to copper(II) bis(thiosemicarbazones)

[90] or copper(II) complexes with hexaaminemacrocyclic cage ligands [91, 92], also known as *sarcophagines*, which are remarkably thermodynamically stable, proved to be very promising in terms of their potential application as targeted PET tracers for noninvasive diagnostic imaging. We expect the exploration of similar approaches in cancer chemotherapy for targeted delivery of coordination and organometallic compounds with biologically active ligands such as indolobenzazepines and indoloquinolines to diseased tissues in the nearest future. The carboxylate group in position 9 and 8, respectively, of indolobenzazepines and indoloquinolines is well suited as site of attachment for cancer-targeting peptides. Advances in synthetic coordination and organometallic chemistry, as well as in peptide-coupling methodologies in conjunction with modern analytical separation techniques will continue to play the pivotal role in realization of these challenging tasks.

The large heterogeneity of tumor cells, even of the same type, emerging on tumor development due to additional mutations, is the basis for the implementation of personalized therapy [10]. Rapid screening and identification of patient- and tumor-specific CPHPs, which is becoming reality with the development of novel peptide screening technologies in conjunction with next-generation peptide sequencing techniques, makes the implementation of personalized approach feasible [82]. Development of multifunctional nanoparticles or “heterofunctional conjugates” for simultaneous real-time *in vivo* imaging and targeted delivery of drugs for cancer treatment will contribute to this exciting future direction as well [74].

Experimental evidence has just been reported by three different groups of researchers that cancer stem cells (CSC) exist [93–95]. The published data indicate that a small population of stem cells sustains tumor growth and that by killing the right type of cell the cancer disease can, in principle, be cured. This CSC hypothesis can conceptually change the evaluation of the efficacy of chemotherapy and the way of development of antitumor agents [96]. Taking this paradigm shift into account [94], much effort focused on cancer stem cells investigation and potential drug candidates capable to kill them is expected in the nearest future.

## ACKNOWLEDGMENTS

We are indebted to the Austrian Science fund (FWF) for financial support of the projects P20897-N19 and P22339-N19.

## REFERENCES

1. Ehrlich, P.; Bertheim, A. *Ber. Dtsch. Chem. Ges.* **1912**, *45*, 756.
2. Ehrlich, P. *Br. Med. J.* **1913**, *2*, 353.
3. Feldman, D. R.; Bosl, G. J.; Sheinfeld, J.; Motzer, R. J. *J. Am. Med. Assoc.* **2008**, *299*, 672.
4. Moucheron, C. *New J. Chem.* **2009**, *33*, 235.
5. Heffeter, P.; Jungwirth, U.; Jakupcak, M.; Hartinger, C.; Galanski, M.; Elbling, L.; Micksche, M.; Keppler, B.; Berger, W. *Drug Resist. Updat.* **2008**, *11*, 1.
6. Todd, R. C.; Lippard, S. J. *Metallomics* **2009**, *1*, 280.
7. Jakupcak, M. A.; Galanski, M.; Keppler, B. K. *Rev. Physiol. Biochem. Pharmacol.* **2003**, *146*, 1.
8. Kidani, Y.; Noji, M.; Tashiro, T. *Gann* **1980**, *71*, 637.
9. Wheate, N. J.; Walker, S.; Craig, G.; Oun, R. *Dalton Trans.* **2010**, *39*, 8113.
10. Sava, G.; Jaouen, G.; Hillard, E. A.; Bergamo, A. *Dalton Trans.* **2012**, *41*, 8226.
11. Hait, W. N. *Cancer Res.* **2009**, *69*, 1263.
12. Gasser, G.; Ott, I.; Metzler-Nolte, N. *J. Med. Chem.* **2011**, *54*, 3.
13. Kolberg, M.; Strand, K. R.; Graff, P.; Andersson, K. K. *Biochim. Biophys. Acta* **2004**, *1699*, 1.
14. Shao, J.; Zhou, B.; Chu, B.; Yen, Y. *Curr. Cancer Drug Targets* **2006**, *6*, 409.
15. Jakupcak, M. A.; Keppler, B. K. *Curr. Top. Med. Chem.* **2004**, *4*, 1575.
16. Timerbaev, A. R. *Metallomics* **2009**, *1*, 193.
17. Barf, T.; Kaptein, A. *J. Med. Chem.* **2012**, *55*, 6243.
18. Berger, J. M.; Gamblin, S. J.; Harrison, S. C.; Wang, J. C. *Nature* **1996**, *379*, 225.
19. Larsen, A. K.; Escargueil, A. E.; Sklandanowski, A. *Pharmacol. Ther.* **2003**, *99*, 167.
20. Bailly, C. *Chem. Rev.* **2012**, *112*, 3611.
21. Holden, J. A. *Curr. Med. Chem. Anticancer Agents* **2001**, *1*, 1.
22. Hande, K. R. *Eur. J. Cancer* **1998**, *34*, 1514.

23. Vashisht Gopal, Y. N.; Konuru, N.; Kondapi, A. K. *Arch. Biochem. Biophys.* **2002**, *401*, 53.
24. Zeglis, B. M.; Divilov, V.; Lewis, J. S. *J. Med. Chem.* **2011**, *54*, 2391.
25. Kurzwernhart, A.; Kandioller, W.; Bartel, C.; Bächler, S.; Trondl, R.; Mühlgassner, G.; Jakupec, M. A.; Arion, V. B.; Marko, D.; Keppler, B. K.; Hartinger, C. G. *Chem. Commun.* **2012**, *48*, 4839.
26. Shang, Y. *Nat. Rev. Cancer* **2006**, *6*, 360.
27. Kasiotis, K. M.; Haroutounian, S. A. *Curr. Org. Chem.* **2012**, *16*, 335.
28. Polyak, K.; Vogt, P. K. *Proc. Natl. Acad. Sci. U.S.A.* **2012**, *109*, 2715.
29. Nguyen, A.; Vessières, A.; Hillard, E. A.; Top, S.; Pigeon, P.; Jaouen, G. *Chimia* **2007**, *61*, 716.
30. Malumbres, M.; Barbacid, M. *Nat. Rev. Cancer* **2001**, *1*, 222.
31. Malumbres, M.; Barbacid, M. *Nat. Rev. Cancer* **2009**, *9*, 153.
32. Kelland, L. R. *Expert Opin. Investig. Drugs* **2000**, *9*, 2903.
33. MacPhillamy, H. B.; Dziemian, R. L.; Lucas, R. A.; Kuehne, M. E. *J. Am. Chem. Soc.* **1958**, *80*, 2172.
34. Kunick, C. *Arch. Pharm. (Weinheim)* **1992**, *325*, 297.
35. Sausville, E. A.; Zaharevitz, D.; Gussio, R.; Meijer, L.; Louarn-Leost, M.; Kunick, C.; Schultz, R.; Lahusen, T.; Headlee, D.; Stinson, S.; Arbuck, S. G.; Senderowicz, A. *Pharmacol. Ther.* **1999**, *82*, 285.
36. Zaharevitz, D. W.; Gussio, R.; Leost, M.; Senderowicz, A.; Lahusen, T.; Kunick, C.; Meijer, L.; Sausville, E. A. *Cancer Res.* **1999**, *59*, 2566.
37. Gussio, R.; Zaharevitz, D. W.; McGrath, C. F.; Pattabiraman, N.; Kellogg, G. E.; Schultz, C.; Link, A.; Kunick, C.; Leost, M.; Meijer, L.; Sausville, E. A. *Anticancer Drug Des.* **2000**, *15*, 53.
38. McGrath, C. F.; Pattabiraman, N.; Kellogg, G. E.; Lemcke, T.; Kunick, C.; Sausville, E. A.; Zaharevitz, D. W.; Gussio, R. *J. Biomol. Struct. Dyn.* **2005**, *22*, 493.
39. Schultz, C.; Link, A.; Leost, M.; Zaharevitz, D. W.; Gussio, R.; Sausville, E. A.; Meijer, L.; Kunick, C. *J. Med. Chem.* **1999**, *42*, 2909.
40. Leost, M.; Schultz, C.; Link, A.; Wu, Y.-Z.; Biernat, J.; Mandelkow, E.-M.; Bibb, J. A.; Snyder, G. L.; Greengard, P.; Zaharevitz, D. W.; Gussio, R.; Senderowicz, A. M.; Sausville, E. A.; Kunick, C.; Meijer, L. *Eur. J. Biochem.* **2000**, *267*, 5983.
41. Hartinger, C. G.; Zorbas-Seifried, S.; Jakupec, M. A.; Kynast, B.; Zorbas, H.; Keppler, B. K. *J. Inorg. Biochem.* **2006**, *100*, 891.
42. Jakupec, M. A.; Galanski, M.; Arion, V. B.; Hartinger, C. G.; Keppler, B. K. *Dalton Trans.* **2008**, *37*, 183.
43. Reisner, E.; Arion, V. B.; Keppler, B. K.; Pombeiro, A. J. L. *Inorg. Chim. Acta* **2008**, *361*, 1569.
44. Kandioller, W.; Kurzwernhart, A.; Hanif, M.; Meier, S. M.; Henke, H.; Keppler, B. K.; Hartinger, C. G. *J. Organomet. Chem.* **2011**, *696*, 999.
45. Jungwirth, U.; Kowol, C. R.; Keppler, B. K.; Hartinger, C. G.; Berger, W.; Heffeter, P. *Antioxid. Redox Signal.* **2011**, *15*, 1085.
46. Schmid, W. F.; Zorbas-Seifried, S.; John, R. O.; Arion, V. B.; Jakupec, M. A.; Roller, A.; Galanski, M.; Chiorescu, I.; Zorbas, H.; Keppler, B. K. *Inorg. Chem.* **2007**, *46*, 3645.
47. Milunovic, M. N. M.; Enyedy, E. A.; Nagy, N. V.; Kiss, T.; Trondl, R.; Jakupec, M. A.; Keppler, B. K.; Krachler, R.; Novitchi, G.; Arion, V. B. *Inorg. Chem.* **2012**, *51*, 9309.
48. Smith, G. S.; Therrien, B. *Dalton Trans.* **2011**, *40*, 10793.
49. Chellan, P.; Land, K. M.; Shokar, A.; Au, A.; An, S. H.; Clavel, C. M.; Dyson, P. J.; de Kock, C.; Smith, P. J.; Chibale, K.; Smith, G. S. *Organometallics* **2012**, *31*, 5791.
50. West, D. X.; Padhye, S. B.; Sonawane, P. B. *Structure and Bonding* **1991**, *76*, 1.
51. Farrel, N. *Coord. Chem. Rev.* **2002**, *232*, 1.
52. Beraldo, H.; Gambino, D. *Mini Rev. Med. Chem.* **2004**, *4*, 31.
53. Hughes, M. N. *The Inorganic Chemistry of Biological Processes*; John Wiley & Sons, Ltd: Chichester, **1981**.
54. Dobrov, A.; Arion, V. B.; Kandler, N.; Ginzinger, W.; Jakupec, M. A.; Rufińska, A.; Graf von Keyserlingk, N.; Galanski, M.; Kowol, C.; Keppler, B. K. *Inorg. Chem.* **2006**, *45*, 1945.
55. Ginzinger, W.; Arion, V. B.; Giester, G.; Galanski, M.; Keppler, B. K. *Cent. Eur. J. Chem.* **2008**, *6*, 340.
56. Schmid, W. F.; John, R. O.; Mühlgassner, G.; Heffeter, P.; Jakupec, M. A.; Galanski, M.; Berger, W.; Arion, V. B.; Keppler, B. K. *J. Med. Chem.* **2007**, *50*, 6343.
57. Arion, V. B.; Dobrov, A.; Göschl, S.; Jakupec, M. A.; Keppler, B. K.; Rapta, P. *Chem. Commun.* **2012**, *48*, 8559.
58. Schmid, W. F.; John, R. O.; Arion, V. B.; Jakupec, M. A.; Keppler, B. K. *Organometallics* **2007**, *26*, 6643.
59. Primik, M. F.; Mühlgassner, G.; Jakupec, M. A.; Zava, O.; Dyson, P. J.; Arion, V. B.; Keppler, B. K. *Inorg. Chem.* **2010**, *49*, 302.
60. Mühlgassner, G.; Bartel, C.; Schmid, W. F.; Jakupec, M. A.; Arion, V. B.; Keppler, B. K. *J. Inorg. Biochem.* **2012**, *116*, 180.
61. Lavrado, J.; Moreira, R.; Paulo, A. *Curr. Med. Chem.* **2010**, *17*, 2348.

62. Zhou, J.-L.; Lu, Y.-J.; Ou, T.-M.; Zhou, J.-M.; Huang, Z.-S.; Zhu, X.-F.; Du, C.-J.; Bu, X.-Z.; Ma, L.; Gu, L.-Q.; Li, Y.-M.; Chan, A. S.-C. *J. Med. Chem.* **2005**, *48*, 7315.
63. Hu, X.-W.; Chien, C.-M.; Yang, S.-H.; Lin, Y.-H.; Lu, C.-M.; Chen, Y.-L.; Lin, S.-R. *Cell Biol. Toxicol.* **2006**, *22*, 417.
64. Yang, S.-H.; Chien, C.-M.; Lu, C.-M.; Chen, Y.-L.; Chang, L.-S.; Lin, S.-R. *Leuk. Res.* **2007**, *31*, 1413.
65. Chien, C.-M.; Yang, S.-H.; Lin, K.-L.; Chen, Y.-L.; Chang, L.-S.; Lin, S.-R. *Chem. Biol. Interact.* **2008**, *176*, 40.
66. Tzeng, C.-C.; Chen, Y.-L.; Lin, J.-J.; Lu, C.-M.; U.S. Patent Appl. U.S. 0,298,846, **2009**.
67. Bergman, J.; Engqvist, R.; Stålhandske, C.; Wallberg, H. *Tetrahedron* **2003**, *59*, 1033.
68. Filak, L. K.; Mühlgassner, G.; Jakupc, M. A.; Heffeter, P.; Berger, W.; Arion, V. B.; Keppler, B. K. *J. Biol. Inorg. Chem.* **2010**, *15*, 903.
69. Filak, L. K.; Mühlgassner, G.; Bacher, F.; Roller, A.; Galanski, M.; Jakupc, M. A.; Keppler, B. K.; Arion, V. B. *Organometallics* **2011**, *30*, 273.
70. Filak, L. K.; Göschl, S.; Hackl, S.; Jakupc, M. A.; Arion, V. B. *Inorg. Chim. Acta* **2012**, *393*, 252.
71. Primik, M. F.; Göschl, S.; Jakupc, M. A.; Roller, A.; Keppler, B. K.; Arion, V. B. *Inorg. Chem.* **2010**, *49*, 11084.
72. Haley, B.; Frenkel, E. *Urol. Oncol.* **2008**, *26*, 57.
73. Hawkins, M. J.; Soon-Shiong, P.; Desai, N. *Adv. Drug Deliv. Rev.* **2008**, *60*, 876.
74. Cho, K.; Wang, X.; Nie, S.; Chen Z.; Shin, D. M. *Clin. Cancer Res.* **2008**, *14*, 1310.
75. Haag, R.; Kratz, F. *Angew. Chem. Int. Ed.* **2006**, *45*, 1198.
76. Sanchez-Cano, C.; Hannon, M. J. *Dalton Trans.* **2009**, 10702.
77. Kratz, F. *J. Control. Release* **2008**, *132*, 171.
78. Ang, W. H.; Daldini, E.; Juillerat-Jeanneret, L.; Dyson, P. J. *Inorg. Chem.* **2007**, *46*, 9048.
79. Ang W. H.; Casini, A.; Sava, G.; Dyson, P. J. *J. Organomet. Chem.* **2011**, 989.
80. Stepanenko, I. N.; Casini, A.; Edafe, F.; Novak, M. S.; Arion, V. B.; Dyson, P. J.; Jakupc, M. A.; Keppler, B. K. *Inorg. Chem.* **2011**, *50*, 12669.
81. Meunier, B. *Angew. Chem. Int. Ed.* **2012**, *51*, 8702.
82. Swensen, N.; Walton, J. G. A.; Bradley, M. *Trends Pharmacol. Sci.* **2012**, *33*, 186.
83. Laakkonen, P.; Vuorinen, K. *Integr. Biol.* **2010**, *2*, 326.
84. Sugahara, K. N.; Teesalu, T.; Karmali, P. P.; Kotamraju, V. R.; Agemy, L.; Greenwald, D. R.; Ruoslahti, E. *Science* **2010**, *328*, 1031.
85. Porkka, K.; Laakkonen, P.; Hoffman, J. A.; Bernasconi, M.; Ruoslahti, E. *Proc. Natl. Acad. Sci. U.S.A.* **2002**, *99*, 7444.
86. Christian, S.; Pilch, J.; Akerman, M. E.; Porkka, K.; Laakkonen, P.; Ruoslahti, E. *J. Cell Biol.* **2003**, *163*, 871.
87. Gelain, F.; Silva, D.; Caprini, A.; Taraballi, F.; Natalello, A.; Villa, O.; Nam, K. T.; Zuckermann, R. N.; Diglia, S. M.; Vescovi, A. *ACS Nano* **2011**, *5*, 1845.
88. Van Rijt, S. H.; Kostrhunova, H.; Brabec, V.; Sadler, P. J. *Bioconjug. Chem.* **2011**, 218.
89. Noor, F.; Wustholz, A.; Kinscherf, R.; Metzler-Nolte, N. *Angew. Chem. Int. Ed.* **2005**, *44*, 2429.
90. Paterson, B. M.; Karas, J. A.; Scanlon, D. B.; White, J. M.; Donnelly, P. S. *Inorg. Chem.* **2010**, *49*, 1884.
91. Ma, M. T.; Karas, J. A.; White, J. M.; Scanlon, D.; Donnelly, P. S. *Chem. Commun.* **2009**, 3237.
92. Ma, M. T.; Cooper, M. S.; Paul, R. L.; Shaw, K. P.; Karas, J. A.; Scanlon, D.; White, J. M.; Blower, P. J.; Donnelly, P. S. *Inorg. Chem.* **2011**, *50*, 6701.
93. Driessens, G.; Beck, B.; Caauwe, A.; Simons, B. D.; Blanpain, C. *Nature* **2012**, *488*, 527.
94. Chen, J.; Li, Y.; Yu, T.-S.; McKay, R. M.; Burns, D. K.; Kernie, S. G.; Parada, L. F. *Nature* **2012**, *488*, 522.
95. Schepers, A. G. *Science* **2012**, *337*, 730.
96. Baker, M. *Nature* **2012**, *488*, 13.



## METAL-BASED CHELATES AND NANOSYSTEMS AS MRI CONTRAST AGENTS

SARA FIGUEIREDO

*Department of Life Sciences, University of Coimbra, Coimbra, Portugal*

CARLOS F. G. C. GERALDES\*

*Department of Life Sciences, University of Coimbra, Coimbra, Portugal; Center of Neurosciences and Cell Biology, University of Coimbra, Coimbra, Portugal; Coimbra Chemistry Center, University of Coimbra, Coimbra, Portugal*

### 46.1 INTRODUCTION

Molecular imaging deals with all the noninvasive imaging techniques that are able to detect and characterize biological processes, at the cellular and/or molecular level, thus allowing higher insights to be achieved from them. It is based on the single or combined use of different imaging techniques, such as optical imaging (OI; bioluminescence and fluorescence), ultrasounds, photoacoustic imaging (PAI), magnetic resonance imaging (MRI), magnetic resonance spectroscopy (MRS), nuclear medicine positron-emission tomography (PET), or single photon-emission computed tomography (SPECT) [1–3].

PET and SPECT are the most sensitive imaging techniques and use a number of radioactive tracers that are already available for experimental and clinical applications. However, patient exposure to ionizing radiation is a major drawback that, together with its inherent low spatial resolution, makes it less favorable than other imaging tools such as MRI. Unfortunately, the gain in resolution associated with an MRI is accompanied by a loss in sensitivity, which is a problem that has been tackled with the use of contrast agents (CAs), endowed with very high relaxivity, or resorting to nanotechnological tools [4].

A recent improvement in imaging modalities is the development of hybrid systems, in which the use of multimodality probes exploits the best characteristics of each system. Nowadays, imaging scanners tend to house different modalities, combining PET/CT (computed tomography) and even PET/MRI. Together with the design of new purposely tailored imaging probes, the hybrid scanners overcome the drawbacks and limitations of a single technique, thus considerably improving the overall diagnostic potential of the procedure.

Over the past 10 years, models derived from nanotechnology have been used to overcome the limitations of conventional modalities, thus improving the sensitivity and accuracy of the diagnosis. Moreover, advances in nanoparticle (NP) technology have given rise to theragnostics platforms, defined as the combination of therapeutic and diagnostic agents in a single particle. These techniques unite early diagnosis and possible higher efficiency treatment methods. Typical platforms include liposomes, polymeric micelles, and dendrimers that generally accommodate surface functionalization with hydrophilic polymers and targeting ligands. Despite success in evaluating the expression of molecular markers, the imaging of the same with an MRI

remains a challenge mainly because of the technique's low sensitivity. Considerable endeavor has been made in order to overcome this drawback and the encapsulation of MRI CAs in nanocarriers emerges as a strategy of great potential.

This review emphasizes the importance of MRI as an imaging tool through the use of probes for enhanced MR imaging via particles as carriers for conventional CAs.

## 46.2 MAGNETIC RESONANCE IMAGING

MRI is an outstanding noninvasive technology that allows the acquisition of anatomic images with exceptional spatial resolution. The acquisition of images uses the properties of nuclear magnetic resonance (NMR) and among all the NMR active nuclei (such as  $^{13}\text{C}$ ,  $^{19}\text{F}$ ,  $^{31}\text{P}$ ,  $^{15}\text{N}$ , and  $^{29}\text{Si}$ )  $^1\text{H}$  is the most commonly used nucleus in routine MRI because of its high abundance in the human body, essentially as hydrogen atoms in water molecules.

The intensity of the NMR signal is proportional to the energy difference between the two energy states of the nucleus in the external magnetic field  $B_0$ , and therefore, the strength of  $B_0$  strongly affects the MR image. Its increase causes an enhancement in the signal-to-noise ratio (SNR), and consequently, a higher signal per voxel allows the achievement of better spatial resolution, which leads to the final outcome of high-quality images. MR signal intensity is affected by three major parameters, namely, the proton density (PD) in a given region, the longitudinal relaxation time  $T_1$ , and the transverse relaxation time  $T_2$ . PD concerns the concentration of protons in a given region and  $T_1$  and  $T_2$  relaxation times are the time constants of the processes by which the longitudinal and transverse magnetization components, respectively, return to their equilibrium values as protons revert to their resting state, after a stimulatory radio frequency (RF) pulse. These proton characteristics reflect the local mobility of water molecules, which may change according to the tissue nature and can be different in healthy or pathological regions [5]. The differences in those parameters can be used to create image contrast in the region of interest (ROI) [6].

## 46.3 CONTRAST ENHANCEMENT

Although PD,  $T_1$ , and  $T_2$  are primary determinants of the contrast, it can be enhanced by means of applying proper pulse sequences [7–11]. Manipulating certain operational parameters (such as the repetition time  $T_R$  and the echo time  $T_E$ ), it is possible to acquire three main types of MR images, namely, PD,  $T_1$ -weighted, and  $T_2$ -weighted images. In a  $T_1$ -weighted image, the contrast is mainly because of differences in the  $T_1$  values of tissues. To create this effect, both short  $T_E$  and  $T_R$  are necessary. When long  $T_R$  is used, the tissues in a given region (e.g., water vs fat) would have already totally recovered their magnetization over the period, and so no contrast would be observed. Thus, when using short values of  $T_R$ , the signal in regions with short  $T_1$  is more intense (brighter image) than in regions with long  $T_1$  (darker image). On the other hand, in a  $T_2$ -weighted image,  $T_E$  controls the contrast. Consequently, to perceive contrast, which depends on the transverse relaxation mechanism, a long  $T_E$  must be employed thus allowing the different  $T_2$  decays of the spins to be discriminated. If a short  $T_E$  is used, almost no decay takes place and consequently no differences are detected. Thus, when short values of  $T_E$  are used, the signal coming from regions with short  $T_2$  is less intense (darker image) than that in regions with long  $T_2$  (brighter image). Finally, in a PD image, the effects of  $T_1$  and  $T_2$  are minimized and the contrast is solely dependent on the number of protons in the ROI. Therefore, a sequence with long  $T_R$  (minimizing the  $T_1$ -weighting) and short  $T_E$  (reducing the  $T_2$  effect) is used. In this case, almost all the regions of a brain are colored the same way, with the exception of the skull that presents lower PD. However, sometimes, the inherent contrast in the MR image is insufficient for the proper characterization of the tissue, even after applying the proper pulse sequences. Therefore, in these cases, the application of CAs is required in order to amplify the contrast differences between healthy and pathological regions, with the final achievement of improved diagnosis and, consequently, the outcome for the patient health.

## 46.4 CONTRAST AGENTS

MRI CAs are paramagnetic substances that are able to modify signal intensity by altering the relaxation times of water protons in the area where they distribute. CAs are in general referred as  $T_1$  or  $T_2$  agents according to whether they predominantly affect the longitudinal or the transverse relaxation time.

The concept of molecules that are able to change water relaxation times comes from the early times of MRI, when Bloch showed that  $\text{Fe}(\text{NO}_3)_3$  had the ability to decrease water proton  $T_1$  and  $T_2$  [12]. Later in 1978, Paul Lauterbur considered

paramagnetic ions as CAs, showing the potential of manganese chloride in myocardial infarction imaging, in rats and dogs [13]. However, by this time, the toxic effect of free metal ions was already known and therefore the use of stable chelate complexes was indicated as the way to reduce this effect. Actually, in the mid-1980s, [Gd(DTPA)]<sup>2-</sup> (H<sub>5</sub>DTPA = diethylenetriaminepentaacetic acid) was proposed as a CA in clinical studies [14].

The efficiency of a particular CA is expressed by its relaxivity,  $r_i$ , which corresponds to its capacity to shorten the relaxation rates  $R_i = 1/T_i$  of the water protons and is usually normalized to 1 μM CA concentration [CA] (Eq. 46.1) [15]

$$R_i = R_{\text{dia}} + r_i[\text{CA}] \quad (i = 1, 2). \quad (46.1)$$

where  $R_{\text{dia}}$  is the contribution measured for the system containing the same medium and a diamagnetic analog of the CA.

## 46.5 T<sub>1</sub> CONTRAST AGENTS

CAs that affect  $T_1$  are also called positive CAs, because of their ability to virtually increase the signal intensity in the  $T_1$ -weighted images. After Lauterbur's *in vivo* experiments [13], it has become clear that free Mn<sup>2+</sup> was highly toxic to living beings and so other paramagnetic metal ions, since then, have been considered for MR imaging. Other paramagnetic ions such as Gd<sup>3+</sup> and Fe<sup>3+</sup>, among others, are still being continuously studied. Gadolinium(III) (Gd<sup>3+</sup>) is one of the most frequently used lanthanides because of its particularly favorable characteristics. With seven unpaired electrons and long electron spin relaxation, it has a high effect on nuclei  $T_1$  relaxation times. Nevertheless, as is the case of all other lanthanides, the use of this metal ion in its free form is not compatible with *in vivo* use, as it is extremely toxic, even in low doses.

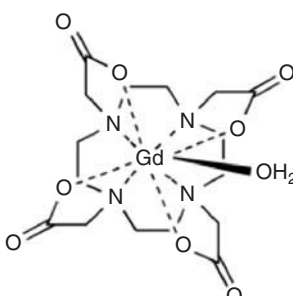
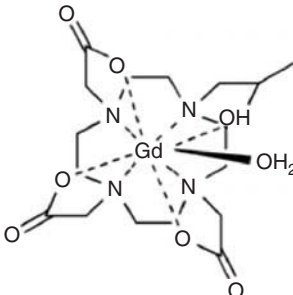
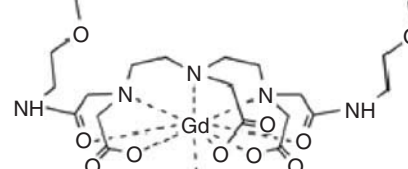
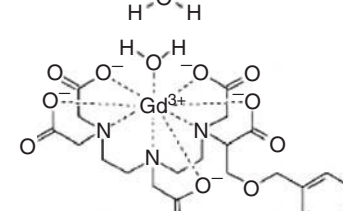
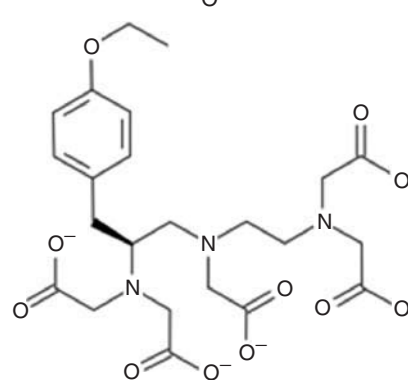
In 1984, Laniado et al. [16] reported the first *in vivo* use of a Gd<sup>3+</sup> complex, [Gd(DTPA)]<sup>2-</sup>, a CA that was approved for clinical application in 1988. Nowadays, complexes containing gadolinium are among the most popular CAs used regularly in Medicine, and the ligands that complex the metal ion are mainly DTPA or DOTA (1,4,7,10-tetraazacyclododecane-1,4,7,10-tetraacetic acid) derivatives. In Table 46.1, the major characteristics of several clinically approved CAs are represented.

**TABLE 46.1 Characteristics of Some Clinically Approved Extracellular Fluid and Hepatobiliary Contrast Agents<sup>a</sup>**

Generic Name	Registered Name	Abbreviation	Manufacturer	$T_1$ -Relaxivity in Plasma, $\text{s}^{-1} \cdot \text{mM}^{-1}$ , 1.5 T	Schematic Representation
Gadobutrol	Gadovist	Gd-BT-DO3A	Bayer	5.2	
Gadodiamide	Omniscan	Gd-DTPA-BMA	GE Healthcare	4.3	
Gadopentate dimeglumine	Magnevist	Gd-DTPA	Bayer	4.1	

(continued)

**TABLE 46.1 (Continued)**

Generic Name	Registered Name	Abbreviation	Manufacturer	$T_1$ -Relaxivity in Plasma, $\text{s}^{-1} \cdot \text{mM}^{-1}$ , 1.5 T	Schematic Representation
Gadoterate meglumine	Dotarem	Gd-DOTA	Guerbet	3.6	
Gadoteridol	ProHance	Gd-HPDO3A	Bracco	4.1	
Gadoversetamine	Optimark	Gd-DTPA-BMEA	Mallinckrodt	4.7	
Gadobenate dimeglumine	MultiHance	Gd-BOPTA	Bracco	6.3	
Gadoxetate disodium	Eovist	Gd-EOB-DTPA	Bayer	6.9	

<sup>a</sup>Adapted from Reference 17.

As mentioned earlier, the efficiency of a particular CA is expressed by its relaxivity,  $r_i$  ( $i = 1,2$ ) and commercially available Gd<sup>3+</sup> CAs have relaxivities of circa  $4\text{--}5 \text{ s}^{-1}\text{mM}^{-1}$  at typical clinical magnetic field strengths (e.g., 1.5 T, Table 46.1), consequently inducing poor enhancement in an MR image. Thus, the main challenge presented to chemists in the field has been to design CAs with higher relaxivities that are able to concentrate in specific regions of the body or to respond to certain physiological stimuli. A good CA should be highly stable and have the capacity to enhance the relaxation rate of the solvent protons to their potential maxima. The total relaxivity of a Gd<sup>3+</sup> complex consists of the additive contributions from its inner-sphere, outer-sphere, and, sometimes, second-sphere water molecules. CA relaxivity optimization can be achieved by increasing the efficiency of several of the molecular parameters that determine the relaxivity of its inner-sphere contribution. These include the number of water molecules coordinated to the metal ion ( $q$ ), the exchange lifetime of those water molecules ( $\tau_M$ ), and the reorientational correlation time ( $\tau_R$ ) of the complex [15].

The number of water molecules in the first coordination sphere ( $q$ ) is typically equal to one because of the octadentate of the ligands normally used and the fact that the Gd<sup>3+</sup> ion generally hosts nine donor atoms in its coordination sphere. This type of coordination scheme allows the formation of highly stable complexes that prevent the leakage of the metal ion [18]. Several groups have been extensively working on the preparation of coordination cages leading to Gd<sup>3+</sup> complexes with a higher  $q$  number and, consequently, improved relaxivity. Examples of these highly sensitive CAs have been prepared by Raymond's group using the hexadentate HOPO (tripodal hydroxypyridinone ligand) or related ligands (e.g., HOPO-TAM), with six oxygen donor atoms, thus allowing the coordination of two (and even three) water molecules. Other solutions are represented by the use of ligands such as PCTA-[12] (3,6,9,15-tetraazabicyclo[9.3.1]pentadeca-1(15),11,13-triene-3,6,9-triacetate), DO3A (1,4,7,10-tetraazacyclododecane-tris acetic acid), or AAZTA (6-amino-6-methylperhydro-1,4-diazepinetetraacetic acid), as shown in the Fig. 46.1 [15, 18–22].

The molecular rotational correlation time,  $\tau_R$ , mainly depends on the molecular radius of the complex and thus (if extensive internal flexibility is not present) higher molecular weight induces a lengthening of the  $\tau_R$  and consequently the relaxivity is higher at magnetic fields of 0.5–1.5 T.

A great deal of effort has been made in order to increase the  $\tau_R$  parameter, for instance, by covalently or noncovalently binding the complexes to macromolecules. Vasovist® (Bayer Schering Pharma AG, Berlin/Germany, code name MS-325) was the first clinically approved CA, which can boast this characteristic. This probe consists of a [Gd(DTPA)] cage functionalized with a diphenylcyclohexylphosphate group that confers a strong affinity to human serum albumin (HSA). Hence, after intravenous injection, Vasovist strongly and noncovalently binds to the serum protein, resulting in a significant increase in the relaxivity (Table 46.2) [23, 24].

Finally, the exchange lifetime of the water molecules,  $\tau_M$ , is also a crucial parameter that affects the observed relaxivity. An excessively slow  $\tau_M$  has a detrimental effect on  $r_1$  (essentially because the effect of the paramagnetism is inefficiently passed to the bulk water), whereas a fast water exchange has the same effect on  $r_1$ , as the water molecules are not in contact to the lanthanide ion long enough to efficiently experience its paramagnetic effect [15, 19, 25].

The water exchange lifetime is strongly affected by several factors that influence the water exchange mechanism. These include the nature of the coordination arms (e.g., carboxoamide vs carboxylate), the overall charge of the complex, and the presence of bulky substituents, which destabilize the complex structure relative to its transition state and thus promote a water dissociative mechanism [15, 26]. The  $\tau_M$  value can be calculated from the fitting of the temperature dependence profiles of the transverse relaxation rate of the <sup>17</sup>O nucleus of labeled water.

Nowadays, some of the most sensitive CAs are substituted Gd-calix[4]arenes, whose  $r_1$  relaxivity of around  $70 \text{ s}^{-1}\text{mM}^{-1}$  increases up to  $100 \text{ s}^{-1}\text{mM}^{-1}$  when conjugated to HSA [27]. Despite their high relaxivity, it is necessary to inject several grams of CA into the blood stream to obtain satisfactory contrast, and nonspecific CAs are systematically and rapidly cleared through the kidneys. An ideal CA should also be specific to a certain body region so that the amount of probe injected into the patient could be significantly decreased. A way to overcome this problem is by using systems that are able to

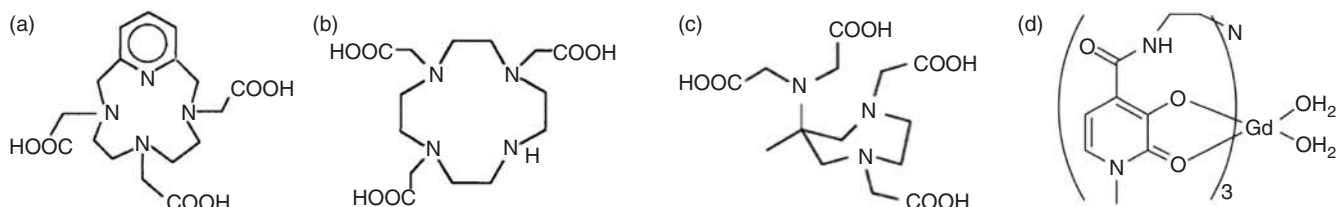


**Figure 46.1** Schematic structure of some ligand cages used to prepare highly sensitive gadolinium-based contrast agent with  $q = 2$ . (a) PCTA-[12], (b) DO3A, (c) AAZTA, and (d) TREN-1-Me-3,2-HOPO.

**TABLE 46.2 Comparison of Gd-DTPA and Vasovist Relaxivity Values<sup>a</sup>**

		Field Strength		
		0.47 T	1.5 T	3.0 T
Gd-DTPA		3.8	4.1	3.7
Vasovist		28–47	19–28	10–19

<sup>a</sup> Adapted from Reference 24.

work as carriers for the CAs. Currently, different types of carriers are reported in the literature as ways of increasing the concentration of the probe in the area of diagnostic interest. This aspect will be further discussed.

#### 46.6 $T_2$ CONTRAST AGENTS

A successful way of decreasing  $T_2$  is the use of iron-oxide-based CAs that, besides their ability to decrease the transverse relaxation time, are also able to cause local field inhomogeneities, thus leading to even faster NMR signal decay [28]. Consequently, in a  $T_2$ -weighted image, the region in which the probe is accumulated becomes darker. However, it has recently been demonstrated that, using the proper sequence, iron-oxide-based CAs can also enhance the  $T_1$  contrast in an MR image [29, 30]. In this way, it is still possible to observe the effect of superparamagnetic iron oxide NPs (SPIO), in regions without any signal, thus overcoming one of the major drawbacks of negative CAs. SPIOs usually consist of a magnetite ( $\text{Fe}_3\text{O}_4$ ) or maghemite ( $\gamma\text{Fe}_2\text{O}_3$ ) core, coated with a natural or synthetic polymer. They can be characterized according to their mean size and are divided into three main categories, oral SPIO, standard superparamagnetic iron oxide (SSPIO), and ultrasmall superparamagnetic iron oxide (USPIO), as shown in Table 46.3.

The low toxicity of SPIOs allows their application in imaging procedures, such as macrophage infiltration in inflammatory regions, cancer diagnosis, and the early detection of cardiovascular diseases. Nevertheless, the most promising application of this type of CAs concerns the detection of the fate of cells *in vivo*, after their previous labeling [31, 32].

**TABLE 46.3 Name and Characteristics of Commercial Superparamagnetic Iron Oxide Nanoparticles**

Classification	Trade Name	Coating Material	Hydrodynamic Diameter
Oral SPIO	Lumirem	Silicon	300 nm
	Abdoscan	Sulphonated styrene	3.5 $\mu\text{m}$
SSPIO	Endorem®	Dextran	80–180 nm
	Resovist®	Carboxydextran	60 nm
USPIO	Clariscan	Pegylated starch	20 nm
	Supravist®	Carboxydextran	30 nm
	Sinerem®	Dextran	15–40 nm

**TABLE 46.4 Classification of Contrast Agents<sup>a</sup>**

Classification	Characteristics	Examples
Nonspecific extracellular agents	After intravenous injection, leak from the blood pool into the interstitial space because of their small molecular weight These agents do not have the ability to cross an intact blood–brain barrier. They provide visualization of regions with abnormally high permeability, such as tumors or lesions	Magnevist®, Dotarem®, Omniscan®, ProHance®, Gadovist®, MultiHance®, and OptiMARK®
Blood pool agents	Agents in this class have higher molecular weight than those in the previous class, a fact that prevents their release into the interstitial space and so they remain for longer periods in the blood stream This characteristic allows for the imaging of the vasculature	Vasovist®, Vistarem®, Sinerem®, Combidex®, and Supravist®
Organ-specific agents	Some existing contrast agents have a natural tendency to be internalized by a specific cell type Several subclasses could be considered but one could take, for instance, some derivatives of Gd-DTPA that are already in clinical use as a tool for the diagnostic of hepatic lesions, after it was demonstrated that they are entrapped by the hepatocytes	Primovist®, Eovist®, Tealascan®, Feridex®, Endorem®, and Resovist®
Targeting agents	These agents are able to recognize specific moieties on the cell surface Although this is a rather elegant methodology, it suffers from low target area concentration, making it difficult to achieve sufficient contrast. Nevertheless, targeted nanoparticles seem to be a way of overcoming this major drawback	Liposomes associated with RGD moiety, for neovasculature targeting. Liposomes functionalized with folate [47, 48]
Responsive agents	These so-called <i>smart agents</i> are sensitive to certain stimuli that include pH, enzymatic activity, and redox potential, allowing the characterization of the microenvironment of the region of interest to be achieved A typical example of this type of CAs is Egad, a Gd-DOTA derivative. In this molecule, a sugar moiety blocks the access of the water molecule to its coordination site. On enzyme activation, the sugar is released and allows the coordination of H <sub>2</sub> O to the paramagnetic center. In this case, the increase in the water relaxivity is directly correlated to the activity of b-galactosidase (the enzyme studied), a commonly used gene marker	Egad and Gd-DOTA-serotonin

<sup>a</sup> Adapted from References 35 and 36.

Paramagnetic liposomes can also be included in the class of *T*<sub>2</sub> agents and their effect mainly depends on the magnetic moment of the paramagnetic complexes, the amount of agent entrapped in the vesicle, and its dimensions and the magnetic field. Still, few reports are available in the literature on such systems [33, 34].

## 46.7 CLASSIFICATION OF CONTRAST AGENTS

The search for the ideal CA has led to the appearance of a massive number of potential candidates and led to the need for a proper classification based on their chemical properties, mechanism of action, or biological distribution. For instance, most typical Gd<sup>3+</sup>-based CAs (Magnevist, Dotarem, and others) distribute in the extracellular compartment. On the other hand, hepatobiliary system agents tend to accumulate in the hepatocytes, as represented in Table 46.4.

## 46.8 NANOCARRIERS

The interest in nanosystems arose from the need to enhance the *in vivo* efficiency of many drugs once it was proven that the optimal concentration of the therapeutic agents in cell cultures needs to be increased to higher concentrations *in vivo*, resulting in more intense side effects. Actually, several pharmaceuticals display poor solubility, instability, or short half-life

in blood, resulting in inefficient treatment and higher toxicity risks. Indeed, nanocarriers offer several advantages when working as drug delivery vehicles and an extensive number of NPs have been reported in the literature of which liposomes are one of the most cited types. Nowadays, more than 20 nanosystems are in clinical use and several more under clinical trials or preclinical development [37].

More recently, the ability of NPs to work as carriers for a variety of molecules has come into play, in a new strategy in which therapeutics and diagnostics are combined in a single particle, giving rise to new theragnostic agents. The word theragnostics is derived from the Greek words *therapeia* (to treat) and *gnosis* (knowledge) referring to the monitorization of the response to a specific treatment and, for this reason, molecular imaging is providing new opportunities in the preclinical and clinical development of new and improved therapies.

Several types of NPs have been constructed to generate MRI contrast, such as lipid-based systems including micelles, liposomes, and lipoproteins; polymer-based systems including dendrimers, nanospheres, nanocapsules, perfluorocarbon emulsions, inorganic NPs based on iron oxide particles, lanthanide(III), and manganese(II) oxides; nanozeolites; nanoMOFs (MOF, metal-organic frameworks); quantum dots (QDs); silica NPs; carbon nanotubes; and nanocomposites [18, 39, 40]. Some of these systems are schematically illustrated in Fig. 46.2 [40, 41]. All these types of particles can be passively targeted or functionalized by the association of targeting ligands to the outer surface of the NP, as, for example, VCAM (an inflammatory marker), annexin-5 (to detect apoptosis), or even RGD (Arg-Gly-Asp) peptides (for  $\alpha$ -v- $\beta$ -3-integrin).

Lipid-based NPs are among the most intensively studied groups of NPs and liposomes are the vehicles most frequently used. The diversity present within this type of systems is illustrated in Table 46.5.

Bangham first referred to liposomes in 1964, while he was studying red blood cell membranes, and often these particles are “affectionately” called *Bangasomes*. Liposomes can be described as nanosized artificial unilamellar vesicles of a commonly spherical shape, prepared with either natural or chemically modified lipids, which can be loaded with a variety of water-soluble or water-insoluble drugs [44]. The entrapment of the chosen drug can be achieved through several different processes, including (i) the incorporation of the drug in the aqueous solution, (ii) the use of lipophilic drugs, (iii) active entrapment methods such as pH gradient protocols, and (iv) electrostatic interactions between drug and the liposome membrane.

The characteristics of the liposome membrane can be tuned by changing the lipid composition, thus achieving certain physicochemical properties, as size, surface charge (defined by the zeta potential), stability, bilayer rigidity, and permeability. In this way, liposomes can be classified according to their structural properties, that is, size and number of lamellae or charge.

The MRI CA can be either incorporated in the lipidic membrane, either through the use of lipophilic chelates, or entrapped in the core of the particle. The bigger the particle, the higher the amplification of the MR signal; thus several micrometer-sized particles have also been considered, as will be further discussed.

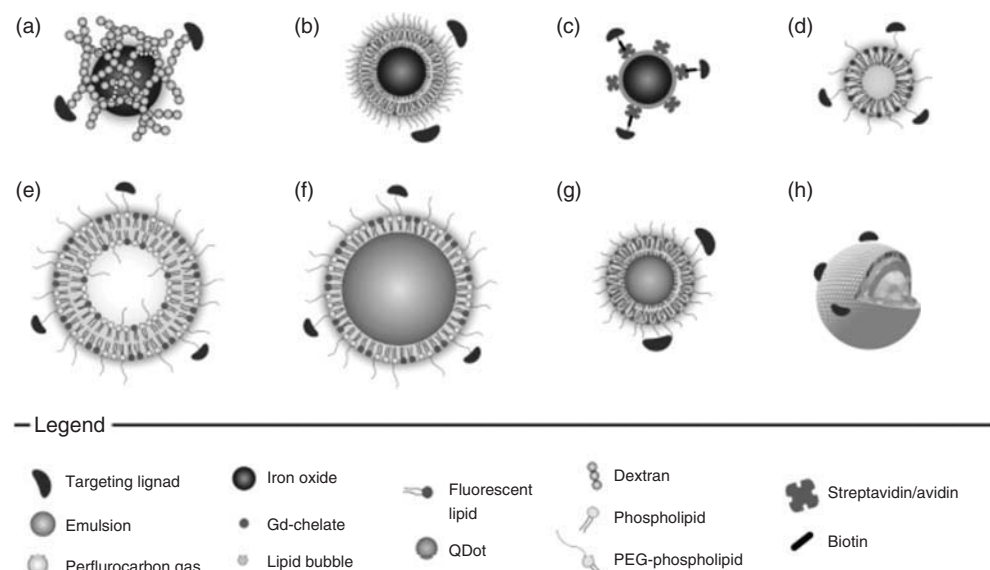


**Figure 46.2** Schematic representation of various types of targeted nanoparticle platforms proposed for multimodal molecular imaging applications. (a) CLIO, (b) MCIO, (c) SPIO, (d) micelle, (e) liposome, (f) emulsion, (g) Qdot micelle, and (h) microbubble. Reproduced from Reference 40 with permission from the publisher.

**TABLE 46.5 Characteristics of Lipid-Based Nanoparticles<sup>a</sup>**

Carrier	Size Range	Composition	Common Preparation Technique
Liposomes	25 nm to few micrometers	Natural or synthetic phospholipids	Passive and active loading
Solid lipid nanoparticles	50–1000 nm	Fats with high melting points of natural origin	High pressure homogenization, microemulsion, and precipitation
Oily suspensions	10 nm to few micrometers	Natural or synthetic oils	Dispersion technique
Lipid microbubbles	Few micrometers	Lipids, phospholipids polymers, and proteins	Sonication
Lipid microspheres	0.2–100 $\mu\text{m}$	Lipids or phospholipids with high melting points	Melt method, multiple microemulsions, and preincorporation into lipophilic carriers

<sup>a</sup> Adapted from References 42 and 43.

The fate of liposomes after their intravenous injection is determined by a subset of properties. Shortly after they were proposed as drug carriers, it became apparent that liposomes were rapidly recognized and removed from the circulation by the reticuloendothelial system (RES). To avoid detection by the immune system, “stealth liposomes” were purposed. These are functionalized with a hydrophilic coating on the outside of the liposome membrane, which enables longer blood half-life. The first approach consisted in preparing liposomes with characteristics similar to red blood cells by adding monosialoganglioside (GM1) to the liposome surface. Later, liposomes coated with a synthetic lipid derivative of poly(ethylene glycol) (PEG) were also proposed and this is nowadays the most widely used method of increasing the circulation time of liposomes [45–47]. However, although PEG is able to decrease the extent of liposomal uptake by the RES, recent reports have shown evidence that, after a second dose, PEG-coated liposomes were rapidly cleared from the blood [48].

The use of positive ( $T_1$ ) CAs appears promising [38] but it requires the entrapment of  $10^7$ – $10^8$  complexes per cell, to achieve a sufficient imaging response for the visualization of the labeled cells. Thus, the search for a labeling procedure for which one particle is sufficient for a single cell led to the use of carriers that can be loaded with large payloads of  $\text{Gd}^{3+}$  complexes. This consideration led to the exploitation of yeast cell-wall particles (YCWPs) as carriers of imaging reporters (Fig. 46.3) [49]. Attempts to include hydrophilic molecules in the particle core failed because of the high porosity of the wall but the peculiar chemical stability of yeast walls could undertake a loading procedure in which the inner cavity of the particle acts as a microreactor, allowing the formation of large emulsions that remain entrapped in the particle.

Paramagnetic liposomes also appear to have a good potential for being considered. These systems are able to dephase the magnetization of water protons around them. As this aspect depends on the paramagnetism of the CA,  $\text{Dy}^{3+}$ -containing complexes appear to be the most efficient agents to be used in liposomes [19].

Recently, Eric Ahrens and coworkers were able to label *in vivo* immune cells with the commercially available perfluoro-15-crown-5-ether (PCE), and track them by means of  $^{19}\text{F}$  MRI to organs experiencing rejection. Although  $^{19}\text{F}$  MRI is able to provide unambiguous detection of fluorine because of the complete absence of background signal,  $^{19}\text{F}$  MR images may take up to 60 min per scan and the detection of low levels of inflammation remains a challenge. Moreover, the proposed *in vivo* cell labeling does not allow the identification of the cell type involved in the inflammatory process, as it is a nonspecific labeling procedure and it is time consuming, as the animals are imaged 24–48 h post injection [50, 51].

Inorganic NPs are another important class of CAs, such as the iron-oxide-based SPIOs, previously presented, which represent by far the most commonly used  $T_2$  agents [39]. They have been functionalized at the surface to be made multimodal by covalent conjugation to additional probes, such as for MRI/ OI by coupling to fluorophores such as rhodamine and Cy5.5, and eventually targeting moieties such as RGD peptides and annexin V. By far, the largest body of work in the literature is for cross-linked iron oxide (CLIO)–Cy5.5 conjugates from the group of Weissleder [52]. Before the conjugation, the iron oxide NPs can be coated with a layer of amphiphilic polymers or PEG. In addition to adding an optical functionality, iron oxides can also be modified for PET or SPECT. NPs have been radiolabeled with, for example,  $^{64}\text{Cu}^{2+}$ ,  $^{111}\text{In}^{3+}$ , or  $^{18}\text{F}$ . DOTA or DTPA chelates have been introduced for the cationic radioisotopic species.

Iron oxide NPs can be enclosed in a shell (core–shell NPs), such as dextran, lipids, or silica. The porosity of silica allows noncovalent entrapment of many other kinds of probes, such as rhodamine dyes and inorganic complexes, or covalently conjugating probes and/or targeting functions. They can also be doped with other ions, such as luminescent  $\text{Tb}^{3+}$  or  $\text{Co}^{2+}$  in ferrite NPs.

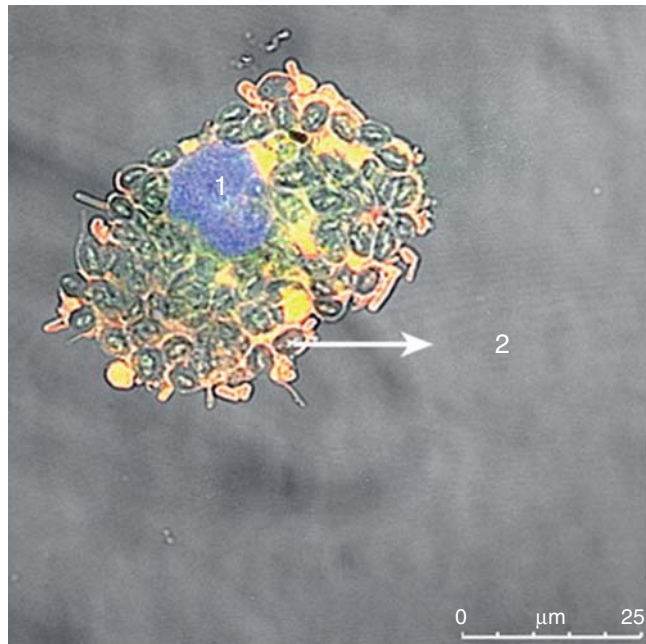


**Figure 46.3** Confocal image of macrophage (J777A.1) showing nucleus (1) with yeast cell-wall particles (2). (See insert for color representation of the figure.)

QDs are another important platform for bimodal MRI/OI [18]. QDs are nanoparticulate clusters of semiconductor material, for example, CdSe (smaller than the Bohr exciton radius), that show quantum confinement effects, meaning that their optical properties are controlled by their size rather than their composition, which makes them useful OI agents. They have bright fluorescence, photostability and a narrow and size-tunable emission spectrum [53]. The surface of the QD can be coated with micellar pegylated phospholipids (PEG-DSPE) and derivatized with paramagnetic chelates (Gd-DTPA-bis(stearylamide)), giving high relaxivity agents for MRI/OI. The QDs have also been bioconjugated, for example, with cyclic RGD [54].

Rigid inorganic nanostructures have been applied as matrices of paramagnetic ions (e.g., Gd<sup>3+</sup>), for example, nanoMOFs, silica NPs, and nanoporous silicas [55]. Zeolites can include Gd<sup>3+</sup> ions in their cavities with high relaxivities [56], and carbon nanotubes may act as a framework to hold Gd<sup>3+</sup> ions, either in the structural defect sites or on their surface [57]. Other examples are nanosized particles of gadolinium salts, such as oxide, fluoride, or phosphate, useful as  $T_1$  MRI CAs [38]. Gold NPs have also been derivatized in their surface with Gd<sup>3+</sup> chelates, leading to high relaxivities [58]. Many other examples can be found in the literature, in particular in specialized reviews [18, 39].

In summary, nanotechnology plays an extraordinary role in the development of imaging, diagnosis, and drug delivery tools. Newly developed systems offer the possibility of achieving an improved knowledge of their interaction with biological systems. Moreover, there is the hope that the increasing research in this field will contribute to the translation of the technology to the clinics.

## REFERENCES

1. Cai, W.; Chen, X. *Small* **2007**, *3*, 1840.
2. Frullano, L.; Meade, T. J. *J. Biol. Inorg. Chem.* **2007**, *12*, 939.
3. Wang, X.; Fowlkes, J. B.; Cannata, J. M.; Hu, C.; Carson, P. L. *Ultrasound Med. Biol.* **2011**, *37*, 484.
4. Massoud, T. F.; Gambhir, S. S. *Genes Dev.* **2003**, *17*, 545.
5. Damadian, R. *Science* **1971**, *171*, 1151.
6. Lauterbur, P. C. *Nature* **1973**, *242*, 190.
7. Brown, M. A.; Semelka, R. C. *MRI: Basic Principles and Applications*; **2010**, Wiley-Blackwell: Oxford.
8. Westbrook, C.; Roth, C. K.; Talbot, J. *MRI in Practice*, 3rd ed.; Wiley-Blackwell: Oxford, **2007**.
9. Hashemi, R. H.; Bradley, W. G. *MRI—The Basics*; Lippincott Williams & Wilkins: Baltimore, **1997**.

10. Rinck, P. A., *Magnetic Resonance in Medicine*, 4th ed.; Wiley-Blackwell: Oxford, **2001**.
11. McRobbie, D. W.; Moore, E. A.; Graves, M. J.; Prince, M. R. *MRI from Picture to Proton*; Cambridge University Press: Cambridge, **2007**.
12. Bloch, F. *Phys. Rev.* **1946**, *70*, 460.
13. Mendonça-Dias, M. H.; Gaggelli, E.; Lauterbur, P. C. *Semin. Nucl. Med.* **1983**, *13*, 364.
14. Carr, D. H. *J. Thorac. Imaging* **1985**, *1*, 74.
15. Aime, S.; Botta, M.; Terreno, E. *Adv. Inorg. Chem.* **2005**, *57*, 173.
16. Laniado, M.; Weinmann, H. J.; Schörner, W.; Felix, R.; Speck, U. *Physiol. Chem. Phys. Med. NMR* **1984**, *16*, 157.
17. Aime, S.; Caravan, P. *J. Magn. Reson. Imaging* **2009**, *30*, 1259.
18. Bottrill, M.; Kwok, L.; Long, N. *J. Chem. Soc. Rev.* **2006**, *35*, 557.
19. Terreno, E.; Castelli, D. D.; Viale, A.; Aime, S. *Chem. Rev.* **2010**, *110*, 3019.
20. Aime, S.; Botta, M.; Geninatti C. S.; Giovenzana, G.; Pagliarin, R.; Sisti, M.; Terreno, E. *Magn. Reson. Chem.* **1998**, *36*, S200.
21. Aime, S.; Calabi, L.; Cavallotti, C.; Gianolio, E.; Giovenzana, G. B.; Losi, P.; Maiocchi, A.; Palmisano, G.; Sisti, M. *Inorg. Chem.* **2004**, *43*, 7588.
22. Pierre, V. C.; Botta, M.; Aime, S.; Raymond, K. N. *Inorg. Chem.* **2006**, *45*, 8355.
23. Fink, C.; Goyen, M.; Lotz, J. *Eur. Radiol.* **2007**, *17* (Suppl 2), B38.
24. Goyen, M. *Vasc. Health Risk Manag.* **2008**, *4*, 1.
25. Caravan, P. *Chem. Soc. Rev.* **2006**, *35*, 512.
26. Merbach, A. E.; Tóth, É. *The Chemistry of Contrast Agents in Medical Magnetic Resonance Imaging*; John Wiley & Sons, Inc.: New York, **2001**.
27. Schühle, D. T.; Schatz, J.; Laurent, S.; Vander, E. L.; Muller, R. N.; Stuart, M. C.; Peters, J. A. *Chem. Eur. J.* **2009**, *15*, 3290.
28. Makowski, M. R.; Wiethoff, A. J.; Jansen, C. H.; Botnar, R. M. *Top. Magn. Reson. Imaging* **2009**, *20*, 247.
29. Saleh, A.; Schroeter, M.; Jonkmanns, C.; Hartung, H. P.; Mödder, U.; Jander, S. *Brain* **2004**, *127*, 1670.
30. Bjornerud, A.; Johansson, L. *NMR Biomed.* **2004**, *17*, 465.
31. Mahmoudi, M.; Hosseinkhani, H.; Hosseinkhani, M.; Boutry, S.; Simchi, A.; Journeay, W. S.; Subramani, K.; Laurent, S. *Chem. Rev.* **2011**, *111*, 253.
32. Huang, C.; Neoh, K. G.; Wang, L.; Kang, E. T.; Shuter, B. *Contrast Media Mol. Imaging* **2011**, *6*, 298.
33. Castelli, D. D.; Terreno, E.; Cabella, C.; Chaabane, L.; Lanzardo, S.; Tei, L.; Visigalli, M.; Aime, S. *NMR Biomed.* **2009**, *22*, 1084.
34. Castelli, D. D.; Dastrù, W.; Terreno, E.; Cittadino, E.; Mainini, F.; Torres, E.; Spadaro, M.; Aime, S. *J. Control. Release* **2010**, *144* (3), 271.
35. Bellin, M. F. *Eur. J. Radiol.* **2006**, *60*, 314.
36. Geraldès, C. F. G. C.; Laurent, S. *Contrast Media Mol. Imaging* **2009**, *4*, 1.
37. Zhang, L.; Gu, F. X.; Chan, J. M.; Wang, A. Z.; Langer, R. S.; Farokhzad, O. C. *Clin. Pharmacol. Ther.* **2008**, *83*, 761.
38. Na, H. B.; Hyeon, T. *J. Mater. Chem.* **2009**, *19*, 6267.
39. Louie, A. *Chem. Rev.* **2010**, *110*, 3146.
40. Agrawal, P.; Strijkers, G. J.; Nicolay, K. *Adv. Drug Deliv. Rev.* **2010**, *62*, 42.
41. Strijkers, G. J.; van Tilborg, G. A. F.; Geelen, T.; Reutelingsperger, C. P. M.; Nicolay, K. *Cancer Nanotechnol.* **2010**, *10*, 325.
42. Mulder, W. J.; Strijkers, G. J.; van Tilborg, G. A.; Griffioen, A. W.; Nicolay, K. *NMR Biomed.* **2006**, *19*, 142.
43. Rawat, M.; Singh, D.; Saraf, S. *J. Pharm. Soc. Jpn.* **2008**, *128*, 269.
44. Lasic, D. D., *Liposomes in Gene Delivery*, 1st ed.; CRC-Press: London, **1997**.
45. Drulis-Kawa, Z.; Dorotkiewicz-Jach, A.; Gubernator, J.; Gula, G.; Bocer, T.; Doroszkiewicz, W. A. *Int. J. Pharm.* **2009**, *387*, 187.
46. Gabizon, G.; Papahadjopoulos, D. *Proc. Natl. Acad. Sci. U.S.A.* **1988**, *85*, 6949.
47. Allen, T. M.; Hansen, C.; Martin, F.; Redemann, C.; Yau-Young, A. *Biochim. Biophys. Acta* **1991**, *1066*, 29.
48. Ishida, T.; Harada, M.; Wang, X. Y.; Ichihara, M.; Irimura, K.; Kiwada, H. *J. Control. Release* **2005**, *105*, 305.
49. Figueiredo, S.; Moreira, J. N.; Geraldès, C. F. G. C.; Rizzitelli, S.; Aime, S.; Terreno, E. *Chem. Commun.* **2011**, *47*, 10635.
50. Hitchens, T. K.; Ye, Q.; Eytan, D. F.; Janjic, J. M.; Ahrens, E. T.; Ho, C., *Magn. Reson. Med.* **2011**, *65*, 1144.
51. Ahrens, E. T.; Young, W. B.; Xu, H.; Pusateri, L. K., *Biotechniques* **2011**, *50*, 229.
52. Pittet, M. J.; Swirski, F. K.; Reynolds, F.; Josephson, L.; Weissleder, R., *Nat. Protoc.* **2006**, *1*, 73.
53. Sutherland, A. J. *Curr. Opin. Solid State Mater. Sci.* **2002**, *6*, 365.
54. Mulder, W. J. M.; Koole, R.; Brandwijk, R. J.; Storm, G.; Chin, P. T. K.; Strijkers, G. J. and Donega, C. M.; Nicolay, K.; Griffioen, A. W., *Nano Lett.* **2006**, *6*, 1.

55. Rocca, J. D.; Lin, W. *Eur. J. Inorg. Chem.* **2010**, 3725.
56. Platas-Iglesias, C.; Elst L. V.; Zhou, W.; Muller, R. N.; Geraldes, C. F.; Maschmeyer, T.; Peters, J. A. *Chem. Eur. J.* **2002**, 8, 5121.
57. Sitharaman, B.; Kissell, K. R.; Hartman, K. B.; Tran, L. A.; Baikalov, A.; Rusakova, I.; Sun, Y.; Khant, H. A.; Ludtke, S. J.; Chiu, W.; Laus, S.; Tóth, E.; Helm, L.; Merbach, A. E.; Wilson, L. J. *Chem. Commun.* **2005**, 3915.
58. Ferreira, M. F.; Mousavi, B.; Ferreira, P. M.; Martins, C. I. O.; Helm, L.; Martins, J. A.; Geraldes, C. F. G. C. *Dalton Trans.* **2012**, 41, 5472.

## **PART VII**

---

### **ORGANOMETALLIC ELECTROCHEMISTRY**



# ELECTROCHEMISTRY AND SUPRAMOLECULAR INTERACTIONS OF “FERROCIFEN” ANTICANCER DRUGS WITH CYCLODEXTRINS AND LIPID BILAYERS: AN ELECTROCHEMICAL OVERVIEW

OLIVIER BURIEZ\*, ERIC LABBÉ, AND CHRISTIAN AMATORE

Département de Chimie, Ecole Normale Supérieure, Paris, France

## 47.1 INTRODUCTION

Breast cancer is a predominant form of cancer among western women, with an incidence of one case per eight women [1]. The standard reference for endocrine therapy related to this disease is tamoxifen, a selective estrogen receptor modulator (SERM), which was introduced in cancer therapy during the early 1970s, although it had originally been envisioned as a potent contraceptive drug (Fig. 47.1).

Tamoxifen is widely prescribed for patients diagnosed with hormone-dependent breast cancers, namely, those targeting cells in which the estrogen receptor (ER) is present (ER(+)) (Scheme 47.1). The antiproliferative action of the hydroxylated form of tamoxifen (**2** in Fig. 47.1) arises primarily from its competitive binding to the ER, which represses estradiol-mediated DNA transcription [2]. Unfortunately, some breast cancer cells are resistant to tamoxifen because they either do not express ER (classified as ER(–)) or have developed resistance following prolonged exposure to the drug. Hence, tamoxifen remains ineffective against 40% of breast cancers and several negative effects have been identified, such as a higher risk for endometrial cancer as well as a risk of developing blood clots in the lung [3]. The search for drugs combining antiestrogenicity and cytotoxicity to fight both ER(+) and ER(–) breast cancers is therefore of high relevance [4, 5].

Cisplatin, the pioneer metal-containing antitumoral drug, has recently proved to be an alternative in the treatment of a subgroup of hard-to-treat breast cancers [6]. However, it is inefficient against platinum-resistant tumors and has severe side effects such as nephrotoxicity. From the chemical point of view, the Pt–N coordination bond in cisplatin and its derivatives is too weak and it appeared that the metal is not always stable to reach its target because it hydrolyzes too quickly and is too bulky in size [7].

In this context, organometallic compounds, which are defined as metal complexes containing at least one direct covalent metal–carbon bond have recently been reconsidered as potent anticancer drug candidates [8]. Accordingly, Jaouen and coworkers [9–11] proposed a new class of molecules possessing both a ferrocenyl unit and a tamoxifen-like diphenyl methylene skeleton (see, for instance, compound **3** in Fig. 47.1). The antiproliferative activity of a variety of these compounds has been established in both hormone-dependent and hormone-independent breast cancer cell lines [12–15]. Importantly, the replacement of the phenyl by a ferrocene group in complex **2** exalted the cytotoxicity of the latter [11, 16]. Ferrocene by itself is not particularly toxic nor does it play a significant biological role. Conversely, the ferricinium cation, obtained by the one-electron oxidation of ferrocene, was the first iron compound for which an antiproliferative effect was demonstrated on certain types of cancer cells [17]. On the other hand, it is known that the quinone methide (QM) obtained by oxidation

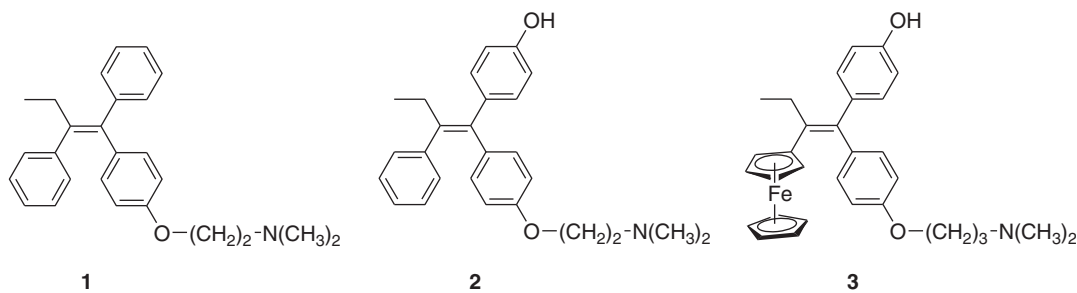
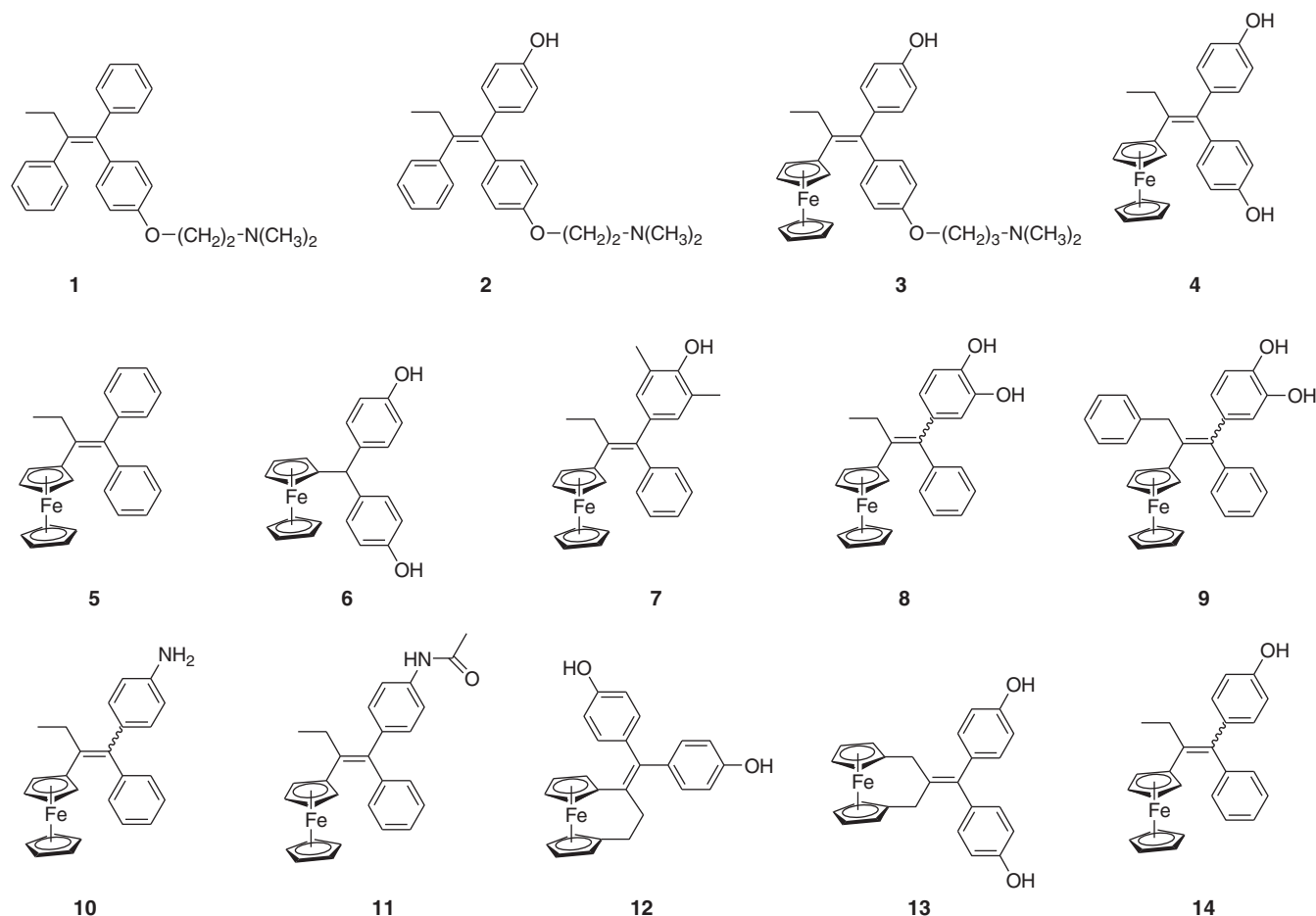


**Figure 47.1** Structures of tamoxifen **1**, its active metabolite (4-hydroxytamoxifen, **2**), and the corresponding ferrocifen **3**.



**Scheme 47.1** Chemical structures of complexes **1–14**.

of the 4-hydroxytamoxifen (**2** in Fig. 47.1) may damage cancer cells by adduct formation with glutathione or nucleobases [18]. In this context, the redox properties of ferrocifens, possessing both a ferrocene group and a  $\pi$ -conjugated tamoxifen skeleton, appeared as a key issue in the understanding of their oxidative metabolism. To reach this goal, a series of ferrocifens was synthetized and electrochemically investigated to characterize not only their reactivity but also the conditions related to their administration, that is, their solubilization/vectorization in the presence of cyclodextrins (CDs), as well as their ability to incorporate into or cross lipid bilayers, an issue which has been first addressed using planar lipid bilayer-modified electrodes.

## 47.2 DECIPHERING THE ACTIVATION SEQUENCE OF FERROCIFENS

### 47.2.1 Ferrociphenols

Ferrocifens possessing at least one phenol group are called *ferrociphenols*. These compounds have been the most investigated *in vitro* and *in vivo* because they exhibit both endocrine and cytotoxic strong activities. *In vitro* studies established that the cytotoxicity of ferrociphenols arises from the presence of both a tamoxifen backbone and a ferrocenyl unit [19]. For instance, the antiproliferative effect of compound **3** (Fig. 47.1) against a hormone-independent breast cancer cell line (MDA-MB231) was found 60 times higher than for the active metabolite of tamoxifen (**2** in Fig. 47.1) evidencing the dramatic effect cytotoxicity associated to the presence of the ferrocene group linked to a tamoxifen-like structure. In summary, the motif [Fc]-[conjugated spacer]-*p*-[phenol] was considered crucial for strong cytotoxic effects.

In order to connect the cytotoxicity to a coherent physicochemical frame, a series of ferrocifens, not possessing the dimethylamino chain (which is assumed to only allow the antiestrogenic effect), was investigated. Considering that the oxidation sequence of ferrocifens most likely involved the oxidizable ferrocene and phenol functions, electrochemical methods appeared appropriate to monitor the evolution of these compounds. Electrochemical studies were performed in model environments where pyridine or imidazole were used as base models, as their  $pK_a$  values are similar to those of peptide, or DNA nitrogen intracellular bases. Under these conditions, a correlation between the cytotoxic activity of ferrocifens and their electrochemical behavior was observed [20]. Figure 47.2 compares the typical electrochemical behaviors obtained for representative cytotoxic and noncytotoxic compounds.

In the absence of any added base, both compounds exhibited voltammograms characteristic of the ferrocene/ferricinium ( $\text{Fc}/\text{Fc}^+$ ) redox couple. This evidenced that even when potentially  $\pi$ -conjugated with phenol moieties, the  $\text{Fc}/\text{Fc}^+$  redox potential was not affected. This indicated that the degree of intramolecular cross-talk was minimal presumably because of the too large separation between the standard redox potentials of the two redox moieties. However, two distinct evolutions were observed when pyridine was added. Very little change was observed in the cyclic voltammograms upon the addition of pyridine for compounds that showed slight or no cytotoxic effects *in vitro* (Fig. 47.2a). Conversely, the addition of pyridine caused two major changes to the voltammograms of the biologically active compounds (Fig. 47.2b). First, the  $\text{Fc}/\text{Fc}^+$  system became irreversible at low scan rates, indicating that the ferricinium cation engaged in a chemical sequence prior to the reverse sweep. The loss of reversibility was accompanied by an increase of the  $\text{Fc}$  oxidation wave peak current, featuring the passage from a monoelectronic to a multielectronic oxidation process upon addition of a base. A new wave appeared simultaneously at a more positive potential value (wave  $\text{O}_2$ ). The multielectronic sequence triggered upon addition of the

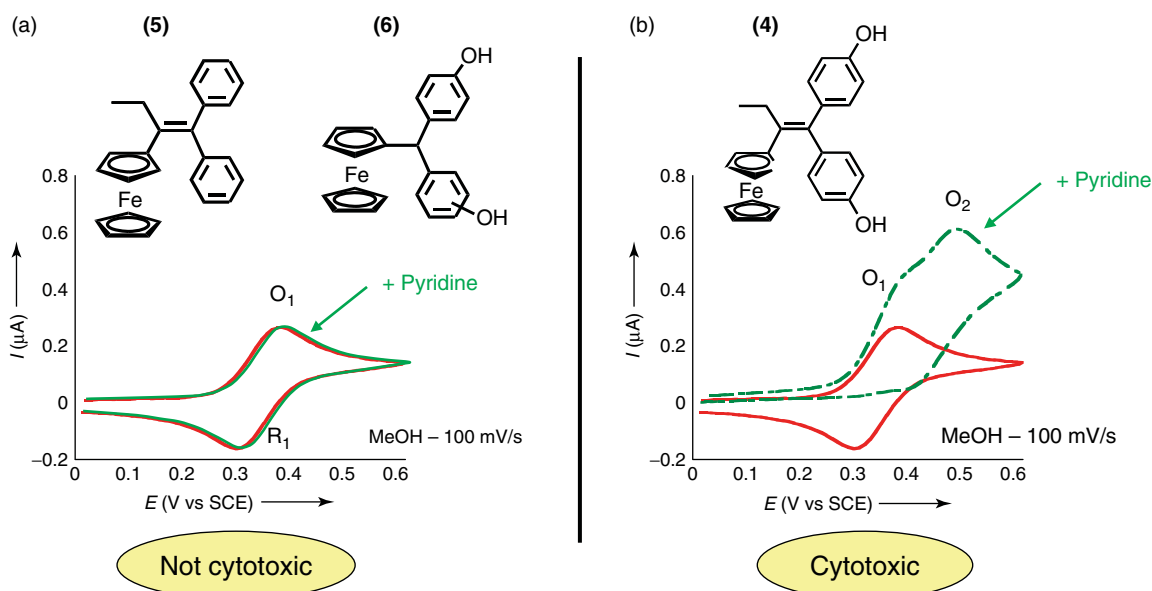


**Figure 47.2** Typical cyclic voltammograms of cytotoxic (b) and noncytotoxic (a) ferrocifens (2 mM in 0.1 M  $\text{Bu}_4\text{NBF}_4$ /MeOH) obtained in the absence and the presence of pyridine used as a base model. Electrode: Pt, 0.5 mm diameter; scan rate 0.5 V/s. (See insert for color representation of the figure.)

base appeared to involve both the ferricenium cation and the phenol function, considering the inertness of the nonphenolic compound **5** to pyridine (Fig. 47.2a). Since the unconjugated compound **6** was also unaffected by the presence of pyridine, the oxidation sequence of biologically and electrochemically “active” ferrociphenols such as (**4**) undoubtedly featured an intramolecular electron transfer between the phenol (donor) and the ferricenium center (acceptor), made possible through a slight coupling in the conjugated  $\pi$ -system. A further electrochemical experiment to support this interpretation was performed using a mixture of ferrocene and 1,1-di-*p*-hydroxyphenyl-2-phenylbut-1-ene in pyridine/MeOH. Under these conditions, the  $\text{Fc}/\text{Fc}^+$  couple remained reversible, and a wave was observed at a more positive potential (circa 1 V/SCE), typical of the direct electrochemical oxidation of phenols. This evidenced the important role of the intramolecular  $\pi$ -conjugation in the oxidation of **4** and related species. We proposed the following proton-coupled intramolecular electron-transfer mechanism to explain the origin of the cytotoxicity of the ferrociphenol compounds (Fig. 47.3) [20]. This is written for sake of simplicity as an EC sequence although one may envision that pyridine coordination to the phenol precedes the oxidation [chemical–electrochemical (CE) sequence] or that the electron and proton transfers are concerted. Anyway, beyond these mechanistic subtleties, it is important that in the presence of a base, oxidation of **4** gives rise to a phenoxy radical coupled electronically to the ferrocene.

In summary, the oxidation sequence starts with the oxidation of the ferrocene, the charge of the resulting ferricenium being only very slightly delocalized over the  $\pi$ -system of the molecule, which *in fine* makes the hydroxy group more acidic, prone to react with a pyridine base [21]. The resulting phenoxy radical shows many mesomeric structures, one of the most stable being the quinoid in which the radical is positioned on the  $\alpha$ -carbon with respect to the ferrocene moiety. This species is prone to be readily oxidized at the potential value of the starting compound in agreement with a peak current increase of the first oxidation wave according to a second proton-coupled electron transfer located on the ethyl group, resulting in a QM formation. The latter was found to be oxidizable at wave  $\text{O}_2$  as verified with an authentic QM.

The ferrocifen cytotoxicity must then certainly proceed through the production of a QM, a strong electrophile known to damage cells by adduct formation with DNA, GSH (glutathione), or proteins [18]. From the electrochemical point of view,

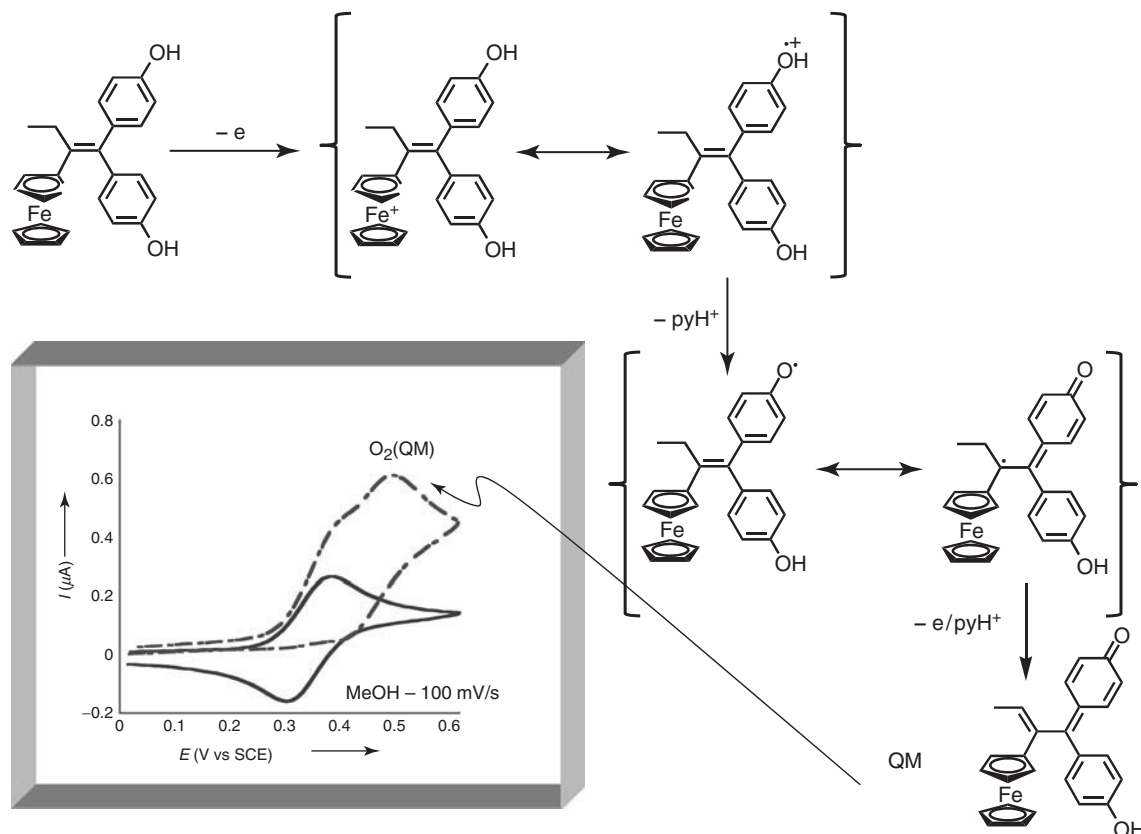


**Figure 47.3** Proposed mechanism for transformation of a ferrociphenol to the corresponding quinone methide species in the presence of pyridine.

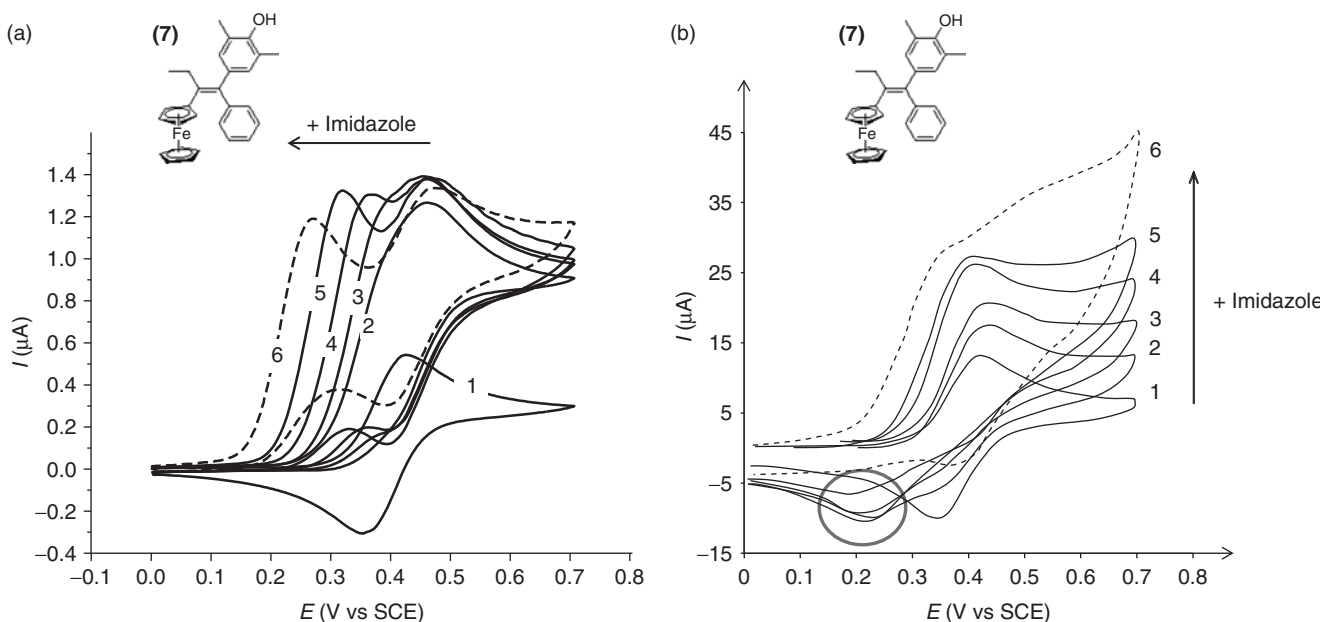


**Figure 47.4** (a) Cyclic Voltammograms of **7** (0.9 mM) in acetonitrile/TBABF<sub>4</sub> (0.1 M) with increasing concentration of imidazole: (1) 0, (2) 0.9, (3) 4.5, (4) 18, (5) 90, and (6) 560 mM (dashed curve). Electrode: Pt, 0.5 mm diameter; scan rate 100 mV/s. (b) Cyclic voltammograms of compound **7** (0.9 mM) in acetonitrile/TBABF<sub>4</sub> (0.1 M) with increasing concentration of imidazole: (1) 0, (2) 0.9, (3) 4.5, (4) 18, (5) 90, and (6) 720 mM (dashed curve). Electrode: Pt, 0.5 mm diameter; scan rate: 75 V/s.

we showed that the presence of the ferrocene unit allows the facile oxidation of the phenol group, which proceeds at less positive potential values than for the tamoxifen analog. In other words, the ferrocene acts as an intramolecular oxidation “antenna” and may oxidize the phenol group through an intramolecular pathway [22], thus producing the biologically active QM in milder oxidizing conditions.

In order to strengthen the proposed mechanism, the electrochemical behavior of ferrocifen **7**, substituted with two methyl groups on each side of the hydroxyl group, was investigated (Fig. 47.4) [23]. With this compound it was indeed expected that the inductive effect of the *ortho*-methyl substituents would stabilize the radical intermediates, facilitate their detection, and incidentally create a protective effect against condensation reactions. In this respect, it is worth recalling that radical cations of cresols and resorcinols are more easily formed and more acidic than their phenol analogs [24]. Similarly, a recent calorimetric study established that the enthalpy of formation of *o*-methylphenoxy radicals has a value that is circa 40 kJ/mol more negative than that of phenoxy radicals [25].

At low scan rate, in the absence of a base, and as observed for compound **4**, the voltammogram of **7** exhibited a reversible oxidation wave corresponding to the ferrocene/ferricinium redox couple. Upon addition of increasing amounts of imidazole, used as the base model, the intensity of the oxidation wave dramatically increased and progressively split, leading ultimately to two distinct peaks at large imidazole excesses (Fig. 47.4a). The determination of the absolute number of electrons involved at the second oxidation wave was circa 3, which was consistent with the bielectronic formation of the QM followed by a one-electron oxidation of its ferrocene group.

More importantly, a new reduction wave could be evidenced during the backward scans by repeating the same experiment at higher scan rates (Fig. 47.4b). This new wave located at 0.2 V could not be ascribed to any reversibility of the oxidation waves and exhibited a peculiar behavior with the base concentration. For example, at 75 V/s, this new species was only observed between 5 and 100 M equiv of base. This behavior is characteristic of a transient intermediate whose concentration was both time and base dependent. This result suggested that the new reduction wave corresponded to the reduction of the carbocation obtained after the one-electron oxidation of this radical. At large base excesses and/or moderate timescales (low scan rates range), this cation is fully deprotonated to afford the QM and its reduction may not be observed any longer. Similarly, at extremely fast scan rates and/or low base concentration range it is not produced in sufficient amounts. Conversely, at intermediate base concentrations and/or time windows, the carbocation is still produced and has a sufficient lifetime for its reduction to be observable during the backward voltammetric scan (Fig. 47.5).

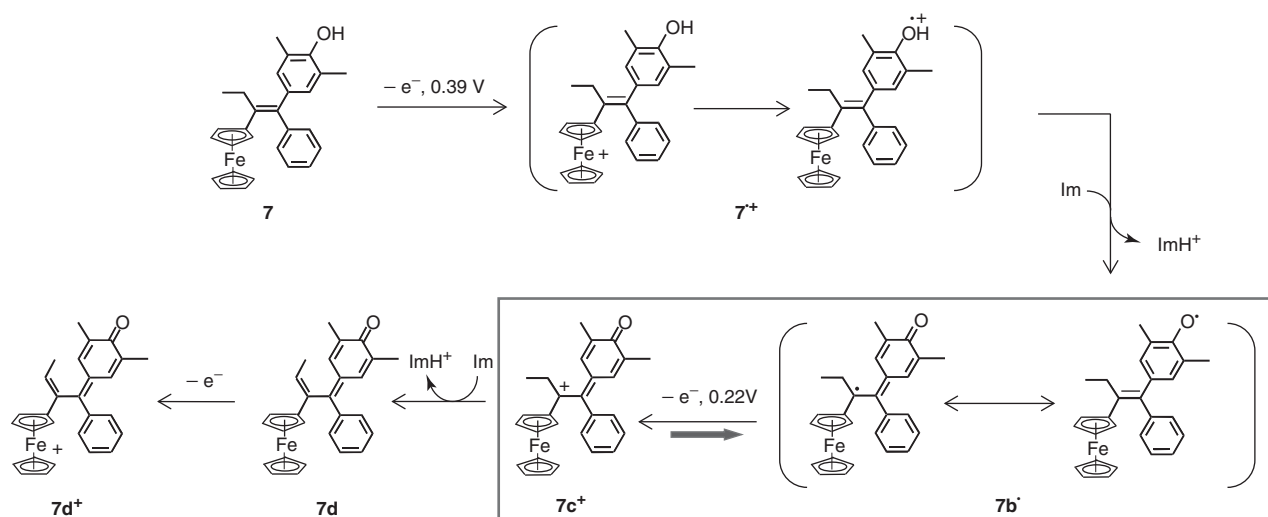


**Figure 47.5** Detailed oxidation sequence of ferrociphenol 7.

To further characterize the transient species successively formed during the two-electron oxidation of the ferrociphenol to its QM, EPR was used to monitor the fate of the paramagnetic species generated upon addition of imidazole to the electrogenerated ferricenium. This study performed in collaboration with D. Mansuy's group revealed the passage between the electrogenerated Fe<sup>III</sup> (ferricenium) to a carbon-centered radical upon addition of imidazole; the corresponding radical was then observed to decay, being oxidized to yield QM, the biologically active species [23].

Finally, and of importance, the formation of the QM has been confirmed under biological conditions. Indeed, this QM was formed upon metabolism of the ferrocifen by rat liver microsomes. Furthermore, the corresponding freshly synthesized QM was found to be toxic against MDA-MB-231 cells. This strongly suggests that QMs are the actual active drug obtained along the oxidation sequence of ferrociphenols, being formed inside the cells whenever oxidation of the ferrocifen phenolic prodrug can be oxidized. Since the threshold for such oxidation is imposed by the Fc/Fc<sup>+</sup> couple, this appears a facile process in cells with a high oxidation state such as many cancer cells [26]. Thus the oxidative sequence in Fig. 47.5 is certainly playing a major role in the anticancer properties of ferrocenyl phenols [27].

#### 47.2.2 Ferrocenyl Catechols

Ferrocenyl catechols **8** and **9** also exhibited interesting cytotoxic activities. On MDA-MB-231 breast cancer cell lines, the catechol compounds displayed a similar or greater antiproliferative potency (IC<sub>50</sub> values ranging from 0.48 to 1.21 μM) than their corresponding phenolic analogs (0.57–12.7 μM) in complete agreement with their easiest oxidation [28].

The electrochemical behavior of **8** and **9** was explored by cyclic voltammetry in acetonitrile (Fig. 47.6). In the absence of a base, the one-electron oxidation of **8** occurred at 0.42 V. In agreement with the behavior of the corresponding phenolic analogs, this electrochemical step featured the reversible oxidation of the ferrocene group (Fc) to ferricenium (Fc<sup>+</sup>). In the presence of an imidazole excess, two oxidation steps were observed. A nearly two-electron irreversible oxidation peak appeared, the potential of which shifted toward less positive values as the imidazole concentration increased. Another peak located at 0.52 V featured a one-electron reversible oxidation process, its potential being independent of base concentration. The cyclic voltammograms obtained with **9** under the same conditions were akin to those for **8** (Fig. 47.6b). Except for the fact that no reduction wave featuring the reduction of a transient α-cation, the behavior was extremely similar to that described above for the mono-phenol.

Hence, by analogy to what was observed with ferrociphenols, the oxidation sequence most likely yielded an *o*-quinone (OQ) instead of the QM due to the easy oxidation of the second hydroxyl, as featured in Fig. 47.7 [28].

In the absence of imidazole, only the reversible one-electron oxidation of **8** and **9** (step (A) in Fig. 47.7) is observed. In the presence of excess imidazole, a fast two-electron oxidation sequence occurred according to steps (A) + (B) + (C). At low scan rates (Fig. 47.6), the potential dependence of this bielectronic wave with excess imidazole featured the thermodynamically and kinetically favored passage from a monoelectronic Fc oxidation to a proton-coupled bielectronic

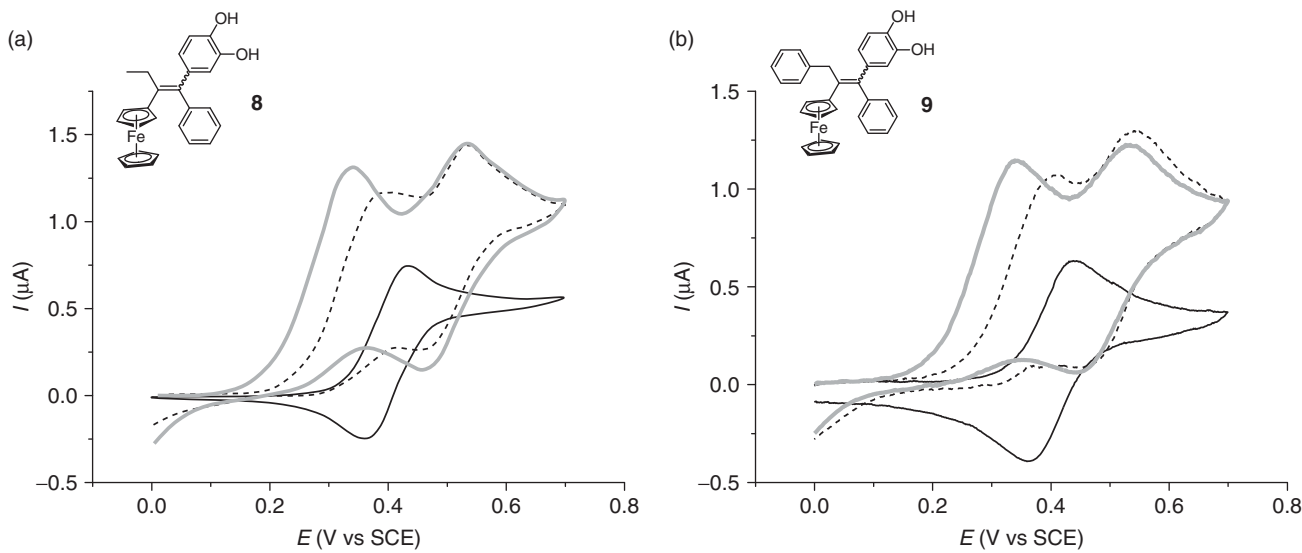


**Figure 47.6** Cyclic voltammograms of **8** (a) and **9** (b) 1 mM in acetonitrile/ $\text{Bu}_4\text{NBF}_4$  (0.1 M). Platinum electrode (0.5 mm diameter), scan rate 0.2 V/s. Cyclic voltammograms recorded in the absence (black solid line) and in the presence of 1 M equiv (black dashed line) and 10 M equiv (gray solid line) of imidazole.

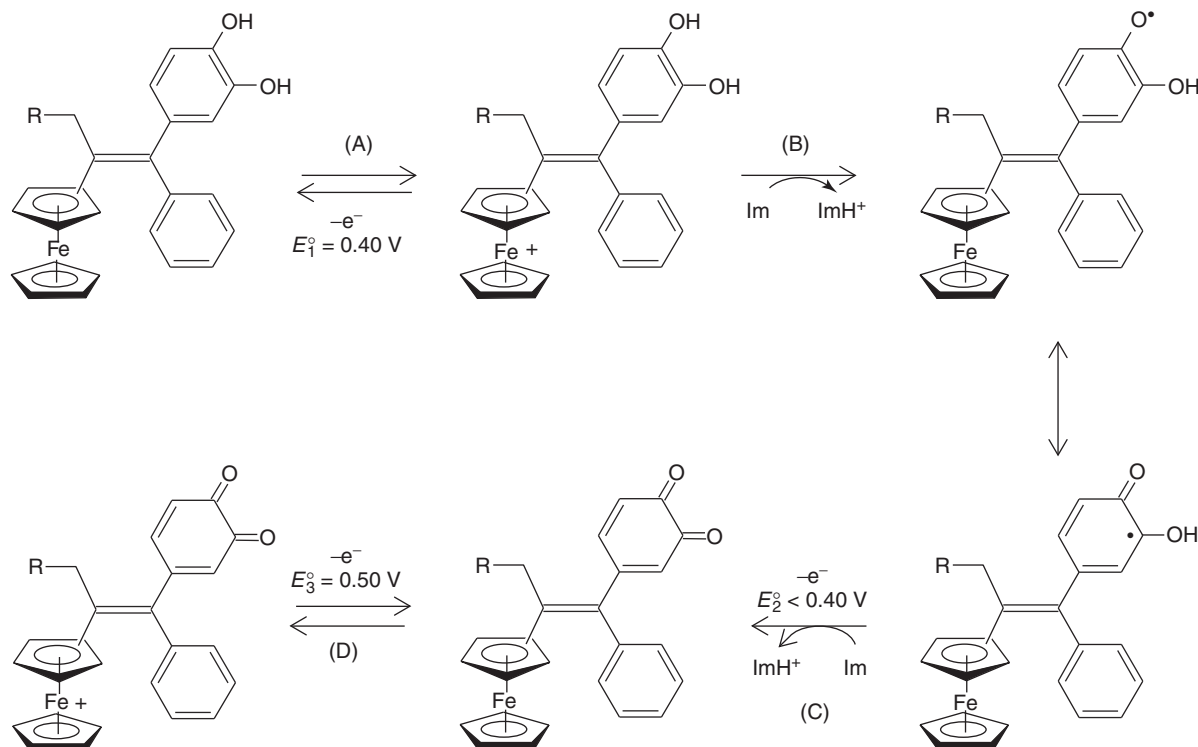


**Figure 47.7** Base-promoted oxidation sequence of catechols **8** ( $\text{R} = \text{CH}_3$ ) and **9** ( $\text{R} = \text{Ph}$ ).

oxidation of the catechol. Note that the deprotonations may be concerted with the electron transfers but such discussion is beyond the scope of this chapter. The second wave (one-electron process) corresponded to the reversible oxidation of the *ortho*-quinone into its ferricenium analog (step (D)). Moreover, the (A) + (B) + (C) sequence was fast enough to be observed within the same scan in the presence of imidazole. In order to confirm this oxidation mechanism, preparative electrolyses of catechols **8** and **9** were performed in the presence of imidazole at 0.48 V/SCE, that is, the potential value

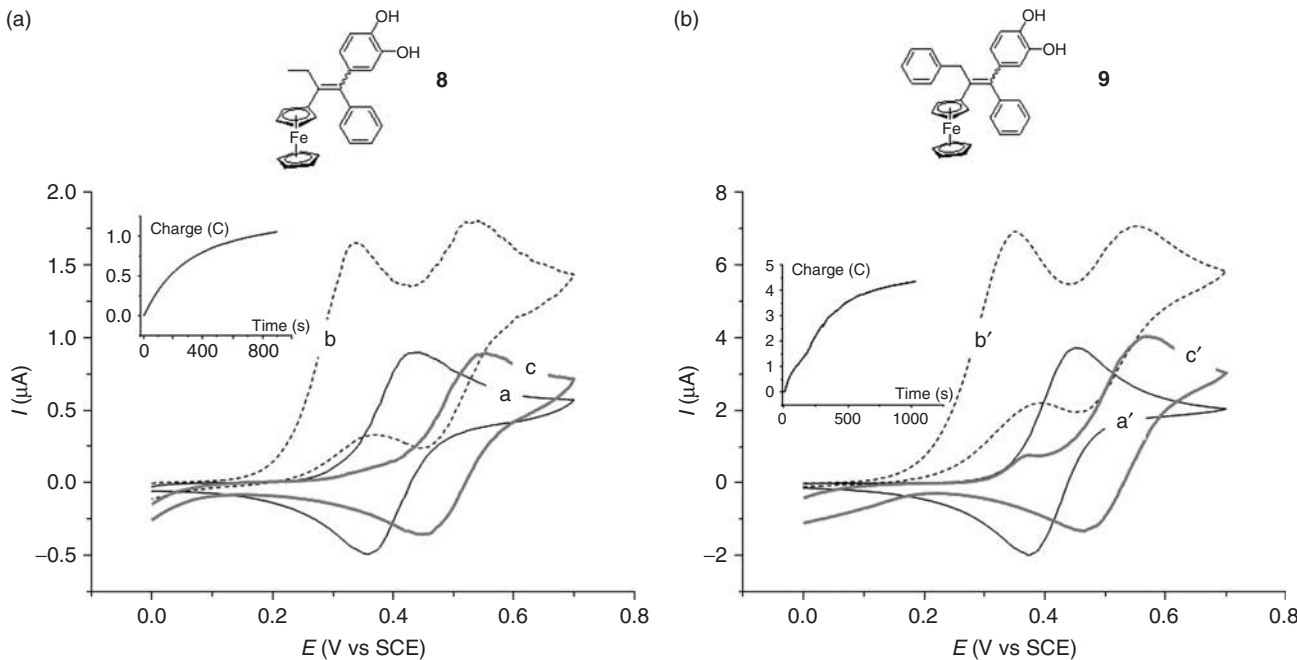


**Figure 47.8** Cyclic voltammograms of acetonitrile/ $\text{Bu}_4\text{NBF}_4$  (0.2 M) solutions (Pt electrode of 0.5 mm diameter, scan rate 0.1 V/s) at various electrolysis stages. (a) Compound **8** (1.2 mM) (curve a); compound **8** (1.2 mM)+ imidazole (15 mM) (curve b); and compound **8** (1.2 mM) + imidazole (15 mM) + 1.95 F/mol electrolysis at 0.48 V/SCE (curve c). (b) compound **9** (6 mM) (curve a'); compound **9** (6 mM) + imidazole (75 mM) (curve b'); and compound **9** (6 mM) + imidazole (75 mM) + 1.8 F/mol electrolysis at 0.48 V/SCE (curve c'). Insets = evolution of the charge versus time during electrolysis.

corresponding to the diffusion tail of the first bielectronic wave and to the foot of the second monoelectronic wave. The concentration of the species was monitored by cyclic voltammetry, as reported in Fig. 47.8.

For both compounds, a complete electrolysis at 0.48 V/SCE in the presence of imidazole corresponded to a total charge circa 2 F/mol. Curves c and c', recorded after the electrolyses, no longer displayed the first two-electron oxidation wave (as seen in curves b and b' recorded before the electrolyses) but only the more anodic reversible one-electron oxidation ascribed to the OQ. Finally, the bielectronic nature of the first wave was quantitatively confirmed at the timescale of preparative electrolyses.

The electrochemical oxidation of catechols **8** and **9** was dramatically affected by the presence of imidazole. In the absence of this base, both catechols only oxidized according to a reversible one-electron process centered on the ferrocene group. In the presence of imidazole, the cyclic voltammograms displayed two distinct processes, the first one corresponding to the bielectronic oxidation of the catechol to the OQ, the second one being the ferrocene-centered one-electron reversible oxidation of the OQ formed at the first wave. The oxidation sequence, although leading to OQs instead of QM, displayed kinetic and thermodynamic features very similar to those encountered in the electrochemical oxidation of ferrociphenols to QMs. Since orthoquinones are also potent anticancer drugs (through the involvement of their easily generated cation radicals [29]) formation of OQ may be an important issue.

#### 47.2.3 Ferrocenyl Aniline and Acetanilide

Interestingly, the cytotoxic activity of ferrocifen compounds is not restricted to phenolic substituents. For instance, the substitution of the hydroxyl group by another protic and oxidizable functionality such as aniline or acetanilide (compounds **10** and **11**, respectively) also provides strong cytotoxic action against hormone-dependent MCF-7 and hormone-independent MDA-MB-231 breast cancer cell lines [30].

Yet, the electrochemical behavior changes of both **10** and **11** observed in the presence of a base were less dramatic than those obtained with the phenolic ferrocifen derivatives. Accordingly, the cyclic voltammograms of **10** and **11** obtained in DMF and DMF/imidazole showed a weaker base dependence, that is, a lower increase of the first oxidation wave coupled to a smaller decrease of its reversibility, especially for the acetanilide derivative (Fig. 47.9).

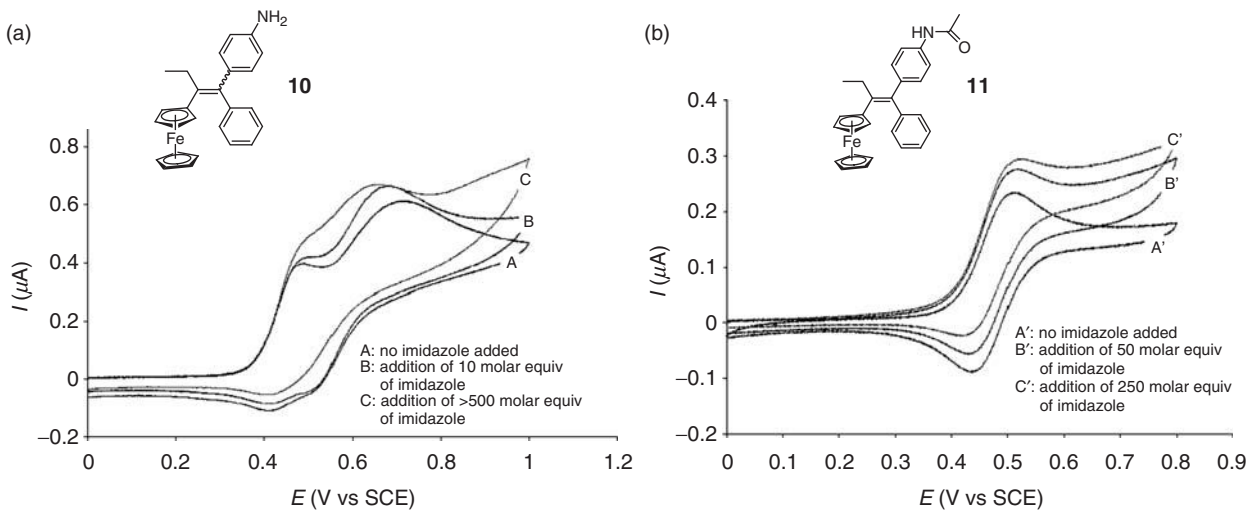


**Figure 47.9** Cyclic voltammograms for **10** (a) and **11** (b), in DMF. Pt (0.5 mm diameter) working electrode, platinum mesh counter-electrode, SCE reference electrode, scan rate 0.1 V/s. For **10**, the first wave corresponds to the ferrocene oxidation, while the second corresponds to the amine oxidation.

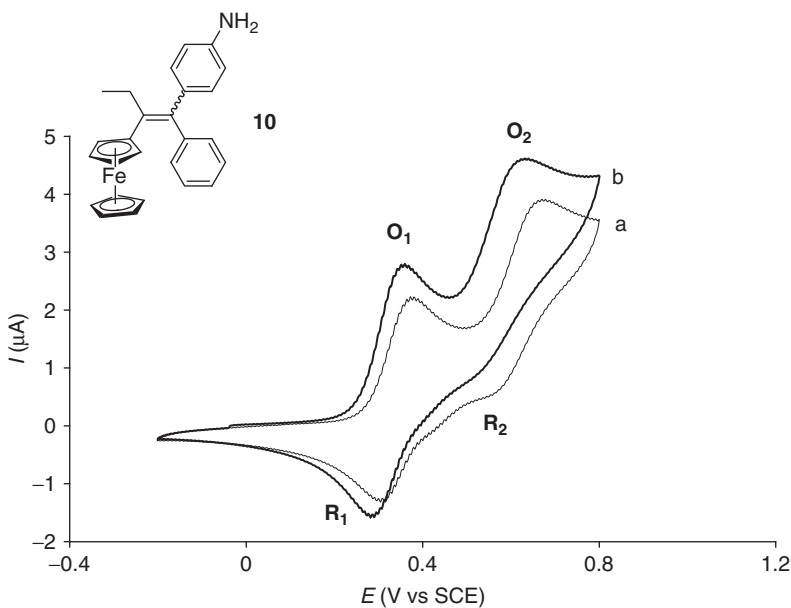


**Figure 47.10** Cyclic voltammograms of **10** (1 mM) in  $\text{MeOH} + \text{LiClO}_4$  (0.1 M) recorded at a bare glassy carbon electrode (1 mm diameter) at 100 mV/s in the absence (a), and the presence (b) of collidine (50 equiv).

Similar results were obtained in methanol in the presence of 2,4,6-trimethylpyridine (collidine,  $\text{p}K_a = 7.4$ ) used as the base [31]. In fact, in DMF, the cyclic voltammogram of complex **10** exhibited a superimposition of the two successive oxidation waves corresponding to the respective oxidations of the ferrocene and the amino centers without any evidence of interactions. In the presence of added collidine, the  $\text{Fc}/\text{Fc}^+$  system was slightly shifted toward more positive potential values, but remained reversible suggesting that the intramolecular electron transfer was too slow to be observed at the cyclic voltammetry timescale (Fig. 47.10). The second oxidation wave experienced an increase of its current peak associated to a partial loss of its reversibility showing that the dication presented some acidity.

Importantly, it was shown that the oxidation wave corresponding to the oxidation of the amino group gradually decreased upon repeated scans, suggesting the formation of a coating on the electrode surface. Electrolysis performed at the potential

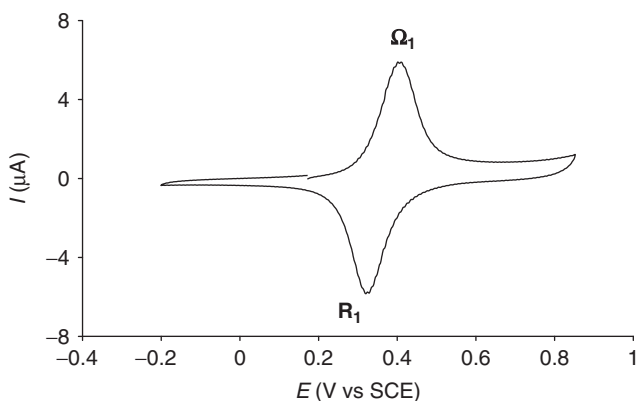


**Figure 47.11** Cyclic voltammogram performed in  $\text{MeOH} + \text{LiClO}_4$  (0.1 M) with the modified working glassy carbon electrode (1 mm diameter) obtained after the controlled-potential electrolysis ( $E = +0.70$  V). Sweep rate is 500 mV/s.

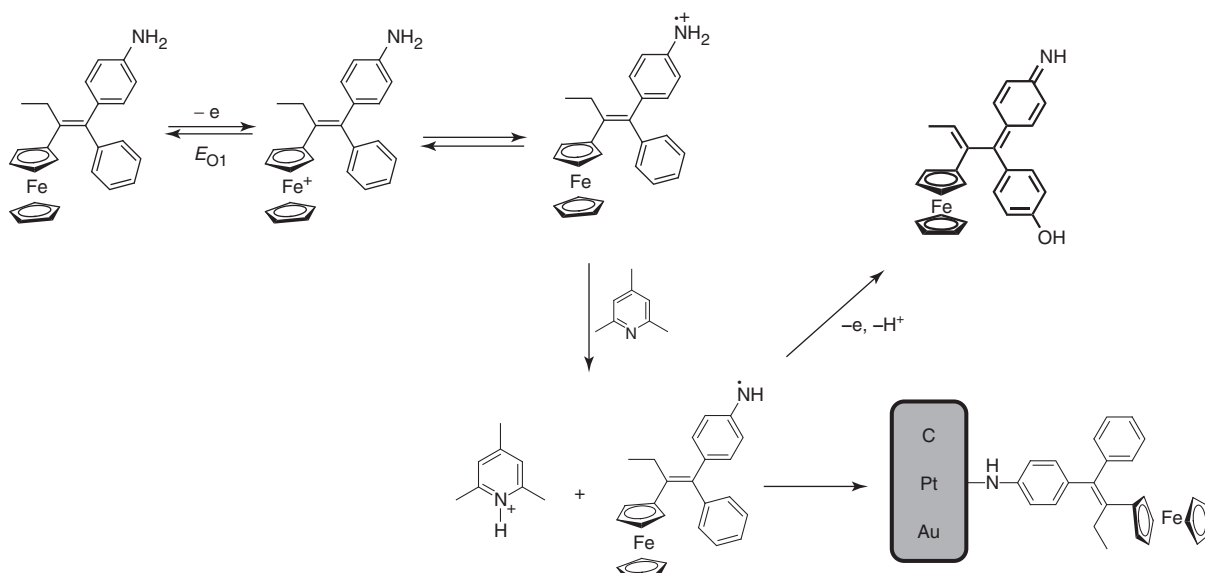


**Figure 47.12** Proposed mechanism for the covalent attachment of the amino-ferrocifen complex **10** via the oxidation of the ferrocenyl group.

value at which the amino moiety was oxidized (i.e., wave  $O_2$ ) confirmed the covalent grafting of the ferrocenyl aniline onto the electrode surface. A characteristic cyclic voltammogram of the modified electrode is shown in Fig. 47.11.

As already reported with other amino derivatives, the oxidation of the amino group produces a cation radical which, upon deprotonation, yields an aminal radical that reacts with the electrode surface [32–34]. More importantly, the grafting of complex **10** could be also achieved by oxidation at the potential value of the first wave  $O_1$  (at which the ferrocene group is oxidized). This demonstrated that, given a much longer reaction time than voltammetric ones, the amine function could be indirectly oxidized through an intramolecular electron transfer from the amino group to the ferrocenyl center along the conjugated  $\pi$ -system (Fig. 47.12) and confirmed the mechanism proposed for the oxidation of ferrociphenols. It is noteworthy that the grafting of compound **10** was achieved not only on glassy carbon but also on metallic surfaces such as gold and platinum.

By analogy to the results obtained with the phenol ferrocifen derivatives, the cytotoxicity of compounds **10** and **11** may be ascribed to the intermediate formation of imino methides (Fig. 47.12). Actually, imino methides have been implicated in cytotoxic processes [35–40]. However, while acetylated quinone imines are important toxic compounds, namely, identified in the metabolism of Parkinson's disease drug tolcapone [41] and the analgesic acetaminophen [42], acetylated imine methides

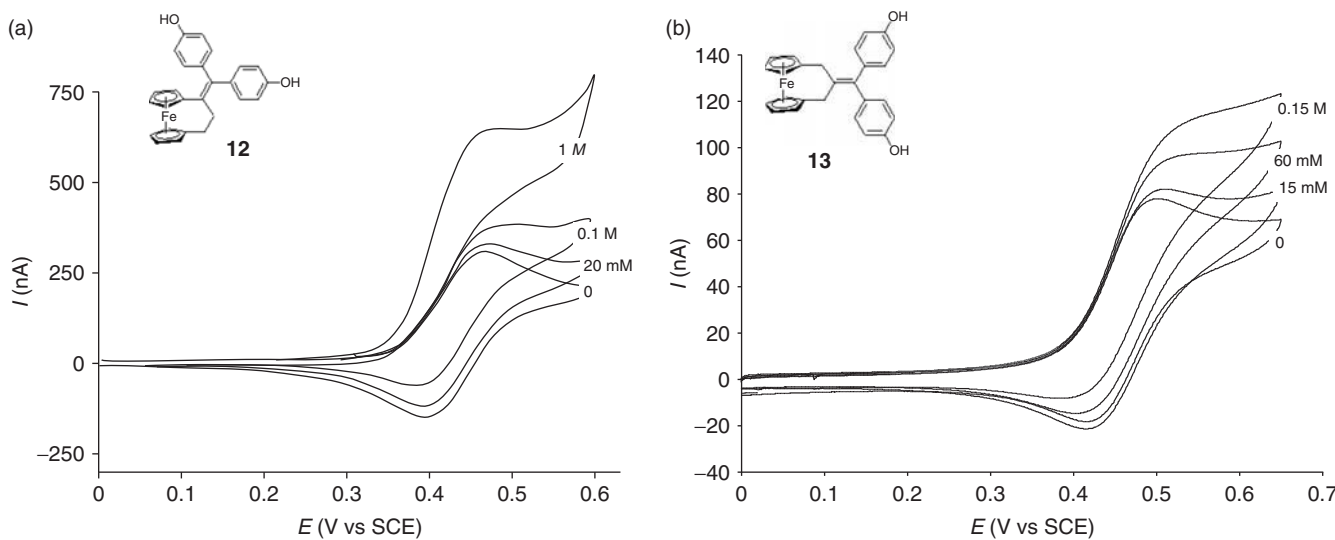


**Figure 47.13** Cyclic voltammograms of **12** (1 mM, scan rate 100 mV/s, a) and **13** (0.3 mM, scan rate 50 mV/s, b) in the presence of varying concentrations of imidazole.

are rare. Actually, the only evidence of an acetylated *p*-imine methide was a short-lived species (1 ms) generated from laser flash photolysis of 4-acetylaminostilbene [43]. These compounds are probably unstable owing to the effect of the electron-withdrawing acetyl group, and delocalization of the nitrogen atom *p*-electrons over the ring favors the quinoid form over the aromatic form [44].

From a mechanistic point of view, the overall oxidation sequence of ferrocifens is thermodynamically and kinetically controlled by the acidity of either the phenol or the amino group of the original species. Such an energetic hurdle has been overcome upon oxidation of ferrocene into ferricenium, which dramatically enhanced the acidity of these groups through intramolecular electron transfer, allowing deprotonation and concerted or consecutive electron transfer from the phenol or amine to the ferricenium. Actually, the “reactivity” of a given ferrocifen toward oxidation depends on the relative  $pK_a$  values of its functional group (hydroxyl or amino) and of the base used, as well as the  $pK_a$  values of the formal hydroxy or amino radical cations that can be envisioned as limit forms of the electrogenerated ferricenium (e.g.,  $\text{Fc}^+ - \text{OH}$  and  $\text{Fc} - (\text{OH})^+$ ).

#### 47.2.4 Ferrocenophanes

The quest for more active (cytotoxic) ferrocifen compounds led to the design of new molecules based on the [3] ferrocenophane molecular structure. These new structures, which preserve the key ferrocenyl-phenol core, appeared more cytotoxic than their noncyclic analogs. This could be ascribed to the rigidity of the molecules, which can bind more strongly to a receptor. In this context, two ferrocenophanes (**12** and **13**) were prepared and electrochemically investigated [45].

In the absence of imidazole, compounds **12** and **13** exhibited a monoelectronic oxidation process at 0.46 (**12**) and 0.48 V (**13**), ascribed to the ferrocenyl oxidation (Fig. 47.13). Upon addition of excesses of imidazole, the intensities of the oxidation waves of both compounds increased, a fact that supports the occurrence of the “classical” oxidation sequence of ferrociphenols, depicted above for compounds **4** and **7**.

However, the voltammograms were affected only at high imidazole excesses, suggesting that oxidation sequence is harder to trigger for compounds **12** and **13** than for **4** and, *a fortiori*, **7**. For compound **12**, the intramolecular proton/electron transfer from the phenol to the ferricenium can be rationalized by the delocalized structure. For the unconjugated **13**, one must consider that the electron transfer proceeds either “through space,” or via the formation of an intermediate  $\alpha$ -methylene radical (such  $\alpha$ -methylene ferricenium molecules possess acidic protons) [46], which can delocalize over the  $\pi$ -system and undergo an additional oxidation step to yield the QM. Despite a kinetically and thermodynamically less-favored intramolecular electron transfer, compound **13** exhibited an  $\text{IC}_{50}$  of 0.96  $\mu\text{M}$ , a value in the same range as the ferrociphenol **4**. Surprisingly, compound **12** possessed an outstanding  $\text{IC}_{50}$  value of 0.09  $\mu\text{M}$  [45]. Actually, the biological activity of **13** and, even more, that of **12**, could not be derived nor anticipated from the electrochemical behavior of these compounds. In short, if the biological activity of a ferrocifen molecule appears to require an oxidizable hydroxy or amino function on the phenyl ring,

the energetics and kinetics associated to its initial cation radical conversion to QMs or imines may not directly correlate with their cytotoxicity.

### 47.3 SUPRAMOLECULAR INTERACTIONS OF FERROCIFENS WITH CYCLODEXTRINS AND LIPID BILAYERS

#### 47.3.1 Solubilization

In order to anticipate the use of ferrocifens in clinical studies, several formulation strategies have been envisioned, for example, using nanoparticles, lipid nanocapsules, or CDs [15, 47–49]. In this context, an interesting entry to the general topic related to the vectorization of ferrocifen drugs consisted in the electrochemical monitoring of (i) the electroactive species formed along the oxidative metabolism of ferrocifens in the presence of CDs or lipid bilayers and (ii) the possible modifications of the oxidation sequence in the presence of supramolecular interactions between ferrocifens and their host. The questions that first arose focused on the inclusion or noninclusion of the ferrocifens and their ferricinium metabolites in the CD cavity, and the reactivity of the latter species toward bases if encapsulated in the CD.

The cyclic voltammetric experiments performed in MeOH/H<sub>2</sub>O (1 : 1) clearly demonstrated the effective inclusion of ferrocifens **4** in the cavity of Me- $\beta$ -CD, most likely via the apolar ferrocene moiety (Fig. 47.14).

The potential shift observed in Fig. 47.14 when Me- $\beta$ -CD was added is due to the stabilization of **4** by the CD, which then becomes harder to oxidize as the cation radical is *a priori* less stabilized. On the other hand, the decrease in the peak current of wave O<sub>1</sub> could not be ascribed only to a bulkier (then more slowly diffusing) **4**-CD complex compared to **4**, as the shape of the voltammetric wave also evolved. We discuss that point in the next paragraph.

As expected, the inclusion of **4** in the CD cavity was favored as the solvent polarity increased, and also depended on the nature of the CD. Fig. 47.14B compares the cyclic voltammograms obtained for the same concentration of **4** in MeOH/H<sub>2</sub>O (1 : 1) in the absence of and presence of 10 M equiv of either Me- $\beta$ -CD or native  $\beta$ -CD. This figure clearly shows that both the decrease in I<sub>O<sub>1</sub></sub> and the shift in E<sub>O<sub>1</sub></sub> are greater in the presence of Me- $\beta$ -CD than of  $\beta$ -CD, featuring a stronger complexation effect in the former case. This can be ascribed to strongest hydrophobic interactions between the cyclopentadienyl and/or the aromatic rings and the methoxy groups of the partially methylated CD.

As mentioned above, an interesting point is the trend of wave O<sub>1</sub> to adopt a sigmoidal shape, which features the involvement of a consecutive chemical–electrochemical (CE) mechanism. In short, if an electroactive species forms a stable

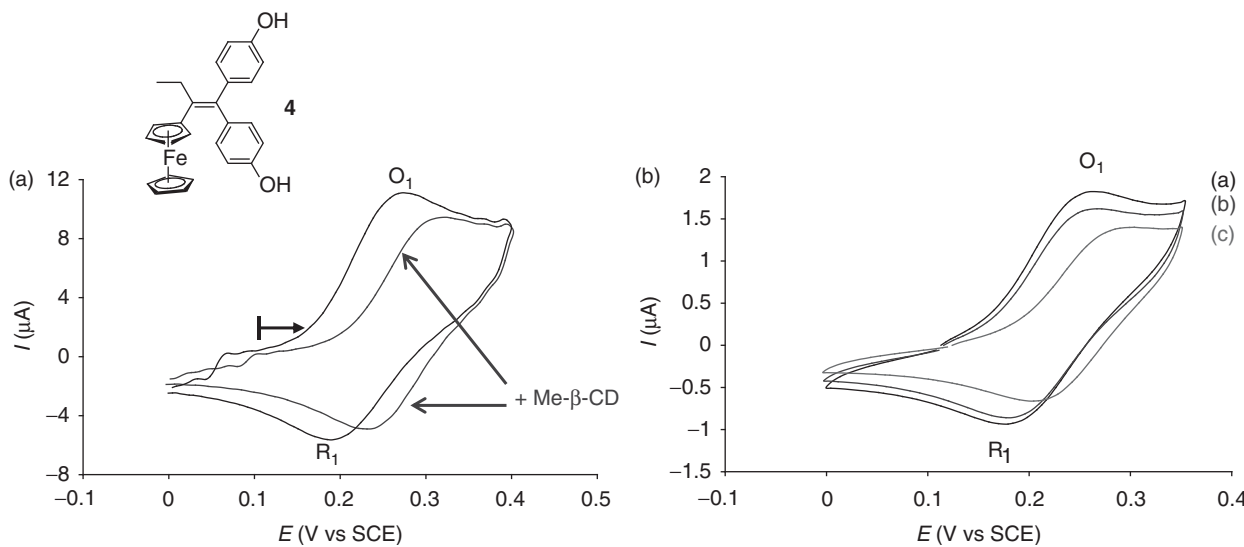


**Figure 47.14** (a) Cyclic voltammograms of **4** (1 mM) in MeOH/H<sub>2</sub>O (1 : 1) with TBABF<sub>4</sub> (0.1 M) as the supporting electrolyte, recorded at a glassy carbon electrode (3 mm diameter) at a scan rate of 200 mV/s, in the absence and presence of Me- $\beta$ -CD (5 equiv). (b) Cyclic voltammograms of **4** (1 mM) in MeOH/H<sub>2</sub>O (1 : 1) with TBABF<sub>4</sub> (0.1 M) as the supporting electrolyte, recorded at a glassy carbon electrode (3 mm diameter) at a scan rate of 50 mV/s, (a) in the absence of CD or (b), (c) in the presence of 10 equiv of  $\beta$ -CD and Me- $\beta$ -CD, respectively.

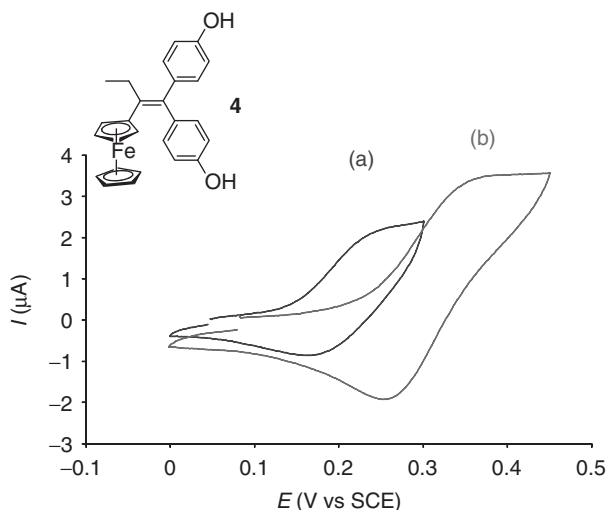


**Figure 47.15** Cyclic voltammograms of **4** (1 mM) in H<sub>2</sub>O with Na<sub>2</sub>SO<sub>4</sub> (0.1 M) as the supporting electrolyte, recorded at a glassy carbon electrode (3 mm diameter) at a scan rate of 50 mV/s and in the presence (a) of β-CD or (b) Me-β-CD (20 equiv).

host–guest inclusion complex with a CD, the resulting complex generally will not undergo any direct electrochemical reaction [50–52]. Indeed, the complex must dissociate and release its electroactive moiety, which depicts a classical CE process. The inclusion constant of the **4**•Me- $\beta$ -CD complex, evaluated in MeOH and MeOH/H<sub>2</sub>O (1 : 1), was found equal to 80 and 825 M<sup>-1</sup>, respectively, in agreement with the polarity medium [49].

Importantly, CDs allowed the solubilization of ferrocifens in pure water, that is, in the absence of any organic solvent. Typical cyclic voltammograms obtained after complete solubilization of ferrocifen **4** in the presence of either  $\beta$ -CD or Me- $\beta$ -CD are shown in Fig. 47.15.

As expected, the oxidation of **4** occurred at a more positive potential, with respect to the studies performed in less polar media such as MeOH and MeOH/H<sub>2</sub>O evidencing a stronger complexation of **4** by the CD. The oxidation wave showed a more pronounced plateau shape, thus featuring a fully developed CE process proceeding under pure kinetic control. On the contrary, the current on the reverse scan exhibited a peak shape rather than a plateau, confirming that the electrogenerated, electrically charged, polar ferricinium species was not complexed by the CD. Interestingly, when the same experiment was performed with  $\beta$ -CD instead of Me- $\beta$ -CD the oxidation peak of O<sub>1</sub> appeared at a less positive potential value and its intensity was smaller, suggesting that **4** was more strongly complexed by the former randomly methylated CD (Fig. 47.15). Accordingly, the peak current of O<sub>1</sub> was smaller in the presence of  $\beta$ -CD, a lower amount of **4** being solubilized in that case. Interestingly, the cyclic voltammogram obtained for an unsubstituted ferrocene (Cp<sub>2</sub>Fe) in the presence of  $\beta$ -CD, under conditions identical to those mentioned in Fig. 47.15, gave no significant electrochemical response (the Cp<sub>2</sub>Fe/CD complex was not soluble in water). This suggested that, in the case of ferrocifens, the presence of the phenol groups, which presumably extrude from the cavity, provides a higher solubility of the inclusion complex. In line with this view, the replacement of  $\beta$ -CD by Me- $\beta$ -CD made the complex Cp<sub>2</sub>Fe/Me- $\beta$ -CD sufficiently soluble in water to be observed by cyclic voltammetry, which appears related to the higher solubility of Me- $\beta$ -CD compared to  $\beta$ -CD [53]. As expected, the intrinsic solubility of the CD determines the solubility of the corresponding host-guest complexes.

Other ferrocenyl compounds were investigated under the conditions favoring the best complexation, that is, in the presence of Me- $\beta$ -CD (Fig. 47.16) [49].

Qualitatively, the time required to partially or totally dissolve the four complexes decreased in the order **5** > **14** > **4** > **6**. Here again, comparison of the cyclic voltammograms of compounds **5**, **14**, and **4** showed that the presence of phenol groups was of great importance for solubilizing the ferrocene-CD adducts. Indeed, compounds **4** and **14** were totally solubilized after 1 day, whereas **5** was only partially dissolved after 2 days. This also explains the much lower oxidation current of **5** compared to those of **14** and **4**. The smaller peak current at O<sub>1</sub> observed with **4** compared to **14** was likely due to a stronger complexation for the former compound in agreement with a more pronounced trend to adopt a plateau shape for **4** [thus indicating a kinetically disfavored decomplexation before the electron transfer (CE mechanism) than for **14**]. As expected, the absence of the apolar ethyl–vinyl fragment increased the solubility of the complex in water (compare **4** and **6**). However, the cyclic voltammogram shape indicated that the complexation dynamics were faster for **6** than for **4**.

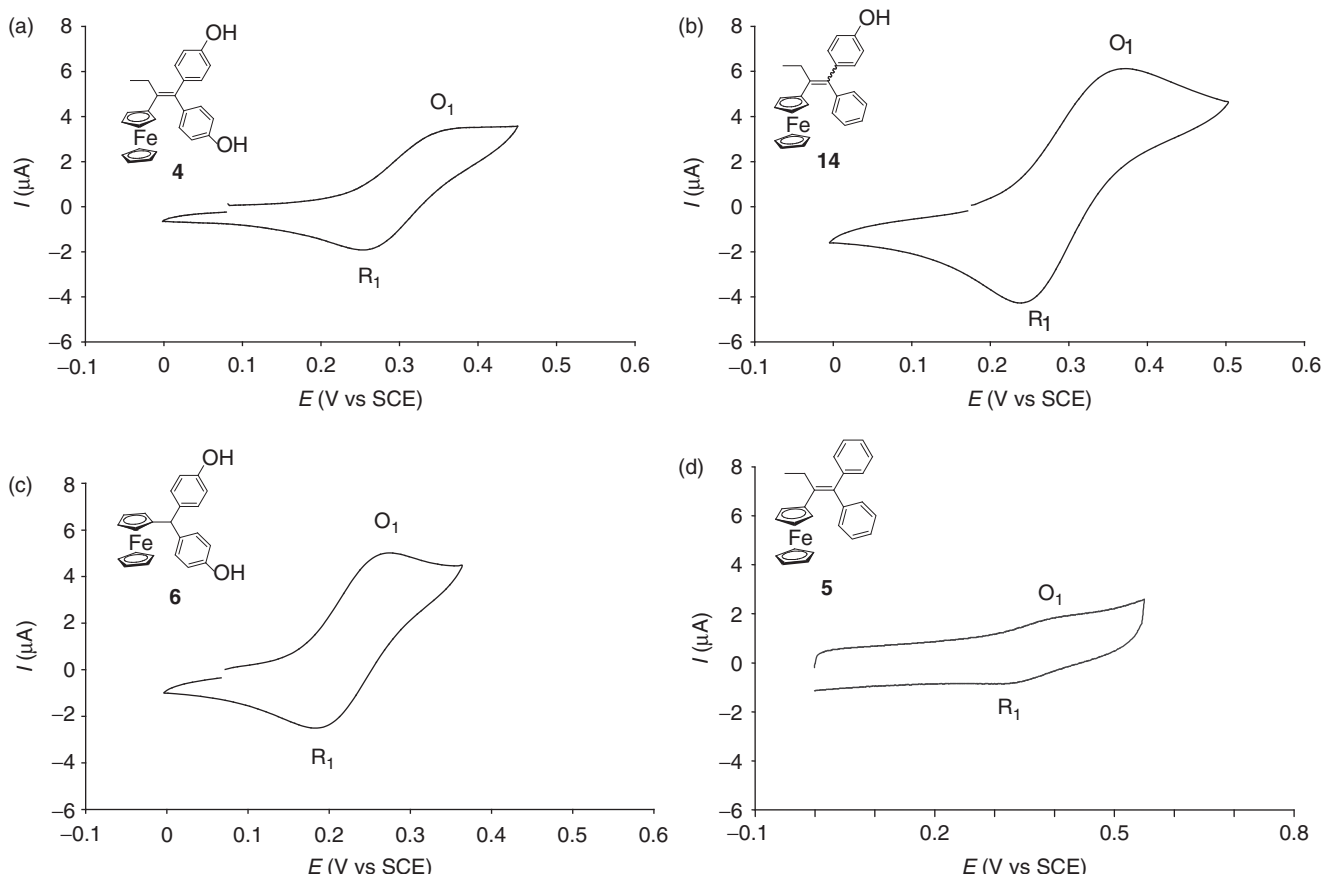


**Figure 47.16** Cyclic voltammograms of ferrocifen-type molecules **4** (a), **14** (b), **6** (c), and **5** (d) (1 mM) in  $\text{H}_2\text{O}$  with  $\text{Na}_2\text{SO}_4$  (0.1 M) as the supporting electrolyte, recorded at a glassy carbon electrode (3 mm diameter) at a scan rate of 50 mV/s in the presence of Me- $\beta$ -CD (20 equiv).

Cyclic voltammetry was used above to rationalize the relationship between the oxidizability and the biological activity of the ferrocifen compounds in a model environment. Since we just showed that using CD/ferrocifens complexes constituted a valuable alternative to the poor water-solubility of ferrocifens, it was then important to ensure if their oxidation mechanism was retained or not after complexation by CDs. As shown in Fig. 47.17, the addition of an excess of pyridine to a **4**/Me- $\beta$ -CD solution led to a circa threefold increase of the peak current of  $O_1$  together with a pronounced change in the wave shape, with a loss of reversibility suggesting an EC sequence.

Considering the initial sluggish one-electron CE process current, it was inferred that the maximum current value obtained in the presence of pyridine corresponded roughly to a three-electron process. This evolution of the CVs showed that the presence of pyridine kinetically favored the dissociation of the complex **4**/CD and opens a subsequent two-electron pathway after the initial formation of the ferricinium derivative. This appeared fully consistent with the former investigation of pyridine-induced effects on the voltammetry of **4** in apolar medium [20]. This strongly suggests that the overall mechanism previously depicted for oxidation of **4** in the presence of a base (see Fig. 47.3) still prevails when **4** is initially complexed by a CD; note that this implies that oxidation of [**4**, CD] produces an uncomplexed **4** $^{\bullet+}$  (EC) or that **4** is oxidized after decomplexation (CEC). So, a three-electron oxidation sequence is most likely triggered in the presence of pyridine, irrespective of the fact that **4** is borne initially by a CD. The corresponding mechanism is summarized in Fig. 47.18.

Note that the third electron transfer most likely corresponds to a further oxidation of the ferrocene moiety of the QM structure. In addition, the passage from a one-electron plateau shape to a three-electron peak shape for wave  $O_1$  in the presence of both CD and pyridine (Fig. 47.17) suggests that pyridine interacts with the phenolic group of the adduct [**4**, CD], allowing a faster decomplexation of **4** along the EC-initiated sequence in Fig. 47.18 (if pyridine reacted only with uncomplexed compound **4** (namely, as in the CEC sequence of Fig. 47.18), a plateau shape would still be observed with a circa threefold current intensity). Similarly, although not indicated in Fig. 47.18 for simplicity, the neutral species (phenoxy

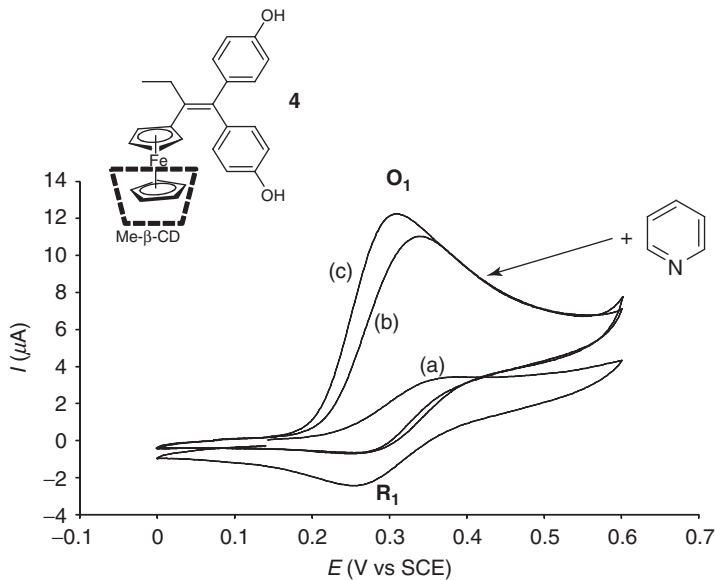


**Figure 47.17** Cyclic voltammograms of **4** (1 mM) in  $\text{H}_2\text{O}$  with  $\text{Na}_2\text{SO}_4$  (0.1 M) as the supporting electrolyte, recorded at a glassy carbon electrode (3 mm diameter) at a scan rate of 50 mV/s, in the presence of Me- $\beta$ -CD (20 equiv) and (a) in the absence of pyridine or in the presence of (b) 0.1 and (c) 0.2 M, respectively, of pyridine.

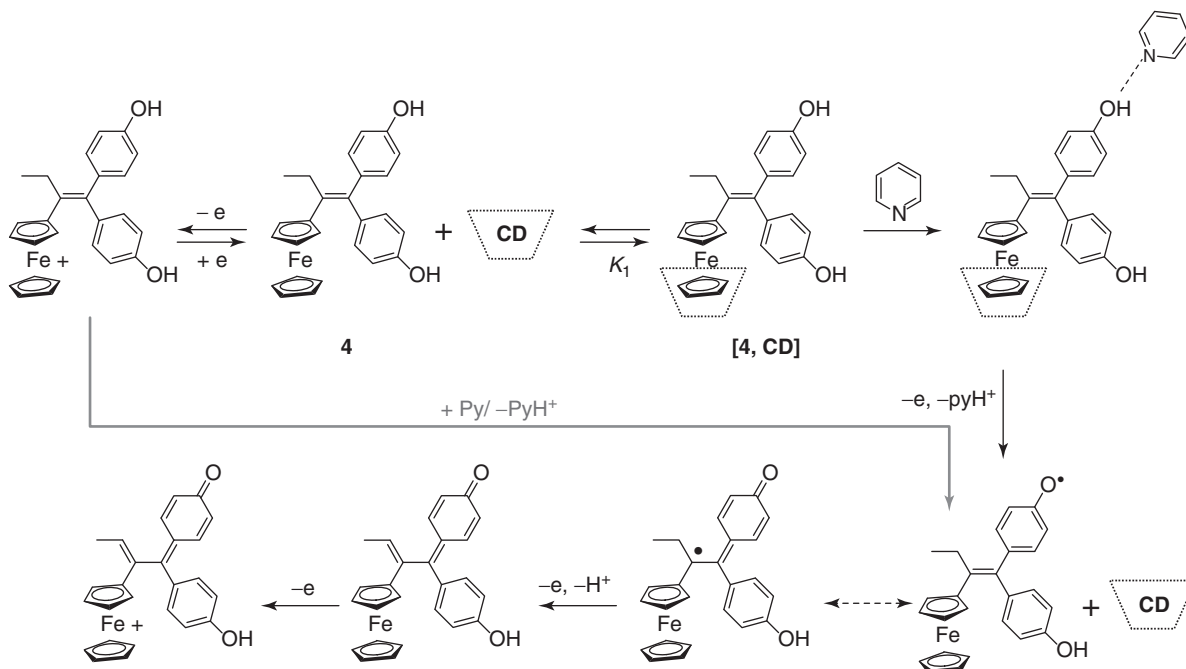


**Figure 47.18** Electrooxidation of **4** in the presence of CD in the absence and the presence of pyridine.

radical, and QM) formed along the oxidation sequence may also exist as inclusion complexes. One may also consider a competitive complexation between pyridine and the ferrocene moiety with the CD host, leading thus to a decrease in the value of the association constant.

The *in vitro* effect of the organometallic complexes alone or encapsulated in Me- $\beta$ -CD was investigated using the hormone-independent breast cancer cell lines MDA-MB-231 after 4 days of culture to assess whether or not the inclusion of **4** or **6** into the CD affected their bioavailability. The corresponding results are reported in Fig. 47.19 [49].

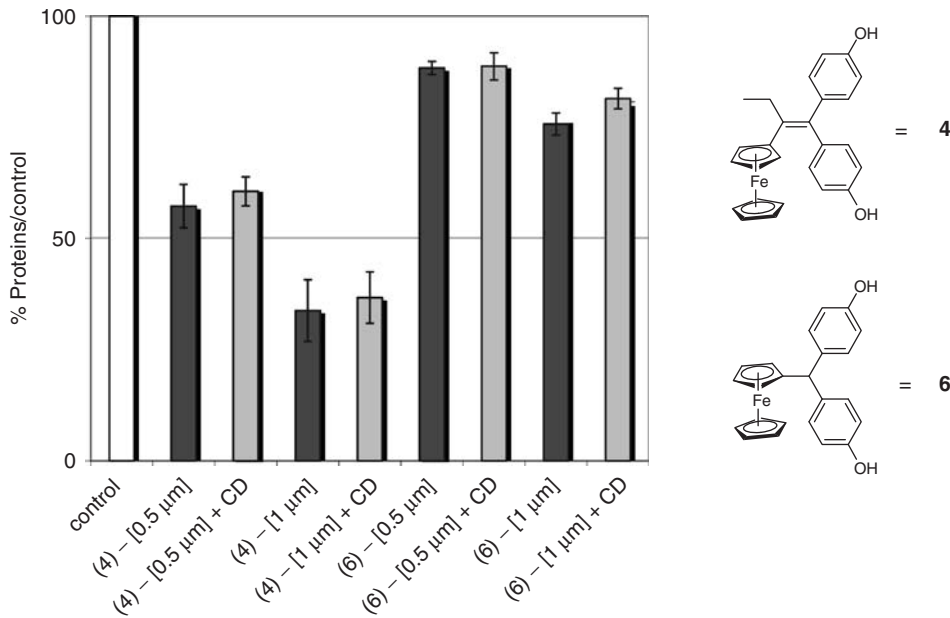


**Figure 47.19** Comparison of the antiproliferative effect of ferrocenyl complexes **4** and **6** (0.5 or 1  $\mu$ M) alone or encapsulated in Me- $\beta$ -CD (20  $\mu$ M) on hormono-independent breast cancer cell lines (MDA-MB231) after culturing for 96 h. Results are the average value of two independent experiments.

Clearly, no statistically significant difference could be observed between the free and CD-complexed ferocifens, their antiproliferative activities being identical within the precision of their determinations [19, 54]. A similar result was also observed with tamoxifen citrate  $\beta$ -CD nanoparticles [55]. With respect to the association constant determined in MeOH/H<sub>2</sub>O, one may also consider that complexes are most likely dissociated at such low concentrations although the polarity (and therefore the association constant) is much higher in pure water. Nevertheless, as **4** and **6** may be delivered intravenously at much more significant doses thanks to the higher solubilities of their inclusion complexes compared to the uncomplexed compounds, this opens encouraging routes for more effective formulations of ferrocifens for anticarcinogenic therapies.

### 47.3.2 Interaction with Lipid Bilayers

We have shown above that ferrocifens delivery to cells could be improved by CD complexation. However, it is clear that whether ferrocifens are delivered free or encapsulated, they must cross the bilipidic cellular membranes. The purpose of this section is to investigate their interactions with such bilayers.

Electrochemistry may also be used to probe the interactions between ferrocifens and nonpolar molecular architectures, with respect to the hydrophobic architectures/barriers that compose cell membranes as well as lipidic cargoes/vectors (e.g., liposomes) using model systems consisting of glassy carbon electrodes modified with a planar bilayer of 1,2-dimyristoyl-sn-glycero-3-phosphocholine (DMPC) (Fig. 47.20) [56].

Such model systems established that the affinity of neutral ferrocifen derivatives toward the lipid bilayer depended on both their size and their polarity. Conversely, the electrogenerated ferricinium derivatives were expelled reversibly from the bilayer owing to their positive charge. This led to unsymmetrical redox processes reflecting a different partition of the species between the lipid film and the solution. Fig. 47.21a illustrates this typical behavior for compound **7** and shows the accumulation of the parent ferrocifen in the DMPC-modified glassy carbon electrode (GCE) as a function of time. The corresponding apparent coverage of the electrode was investigated by monitoring the oxidation peak growth. As depicted in Fig. 47.21b, distinct kinetic features were obtained for compounds **7** and **5**. Presumably, favorable interactions between the phenolic hydroxy group in compound **7** and the polar extremities of the lipid molecules sustain the observed faster incorporation of **7** with respect to **5**.

On the other hand, considering the  $5 \times 10^{-10}$  mol/cm<sup>2</sup> coverage of a surface as a reference for a close-packed layer of comparable ferrocene molecules in SAMs [57], the saturation observed at circa  $3 \times 10^{-10}$  mol/cm<sup>2</sup> for compound **7** shows that the loading of **7** in the bilipid film is considerable, being enough to drastically disorganize the original bilayer

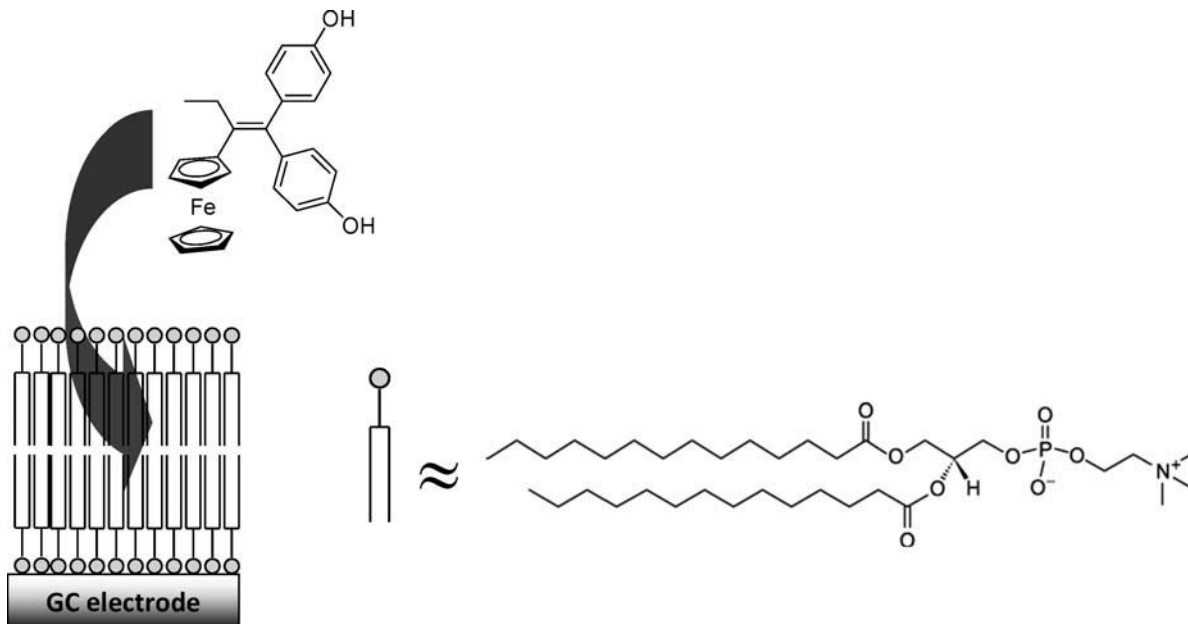


**Figure 47.20** Schematic representation of the glassy carbon electrode (GCE) modified with DMPC film (1,2-dimyristoyl-*sn*-glycero-3-phosphocholine) used to investigate the interactions between ferrocifens with a model membrane.

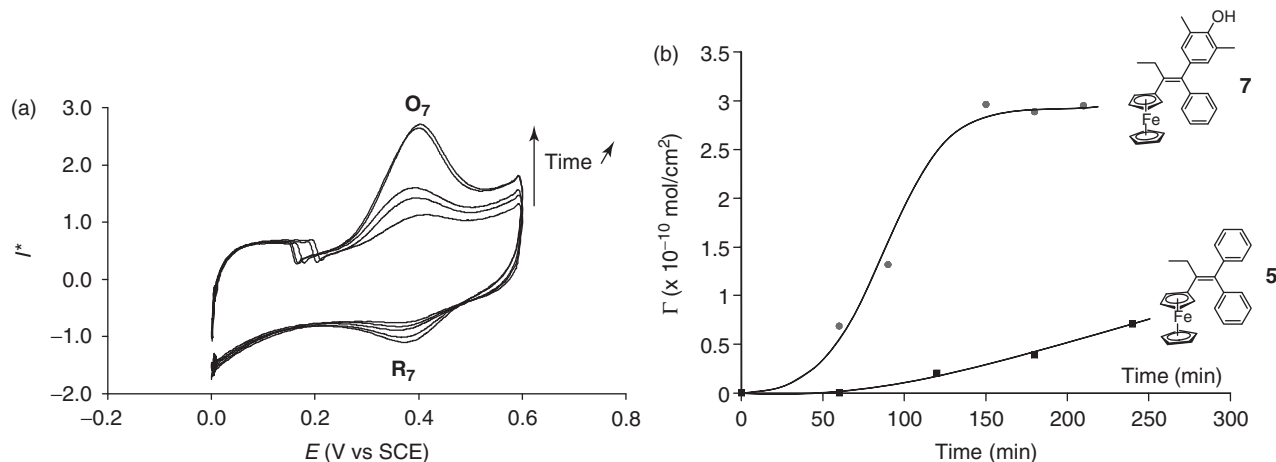


**Figure 47.21** (a) Cyclic voltammograms of **7** (0.2 mM) recorded at a glassy carbon electrode (3 mm diameter) modified with a DMPC film as a function of the equilibration time (0, 45, 90, 150, and 210 min) in  $\text{H}_2\text{O} + \text{EtOH}$  (20%) + KCl (0.1 M) and at  $v = 100 \text{ mV/s}$ . (b) Evolution of the apparent coverage of the DMPC-modified GCE electrode for **5** and **7** (0.2 mM each in EtOH (8/2) + KCl (0.1 M)) as a function of the time of incubation in the corresponding ferrocifen solution.  $I^*$  is the normalized current,  $I^* = I (\mu\text{A})/C (\text{mM})$ .

structure. The presence of small molecules such as anesthetics (chloroform for instance) is well known to induce a strong reorganization, typically, swelling of membranes [58]. This swelling is, in fact, at the origin of the anesthetic effect through the increased pressure created onto ion-channels crossing the outer membrane of the nerves; so, one cannot exclude similar behavior for ferrocifens.

Interestingly, these results established that within the limit that a DMPC is a sufficiently correct model of a cell membrane, large delivery fluxes of ferrocifens are expected to disrupt cell membranes. This may be an important factor to consider in view of side toxicity of these species at sufficiently high concentration. In other words, if their delivery to cell membranes is highly desirable it should not be excessive unless the delivery is properly targeted to tumor cells. Then ferrocifens may act both as biochemical agents (i.e., via the QM generated by their oxidation) and as a kind of detergent disrupting the cell membranes. This should lead to noncommon cell death processes in agreement with experimental observations still under the way.

#### 47.4 CONCLUSION

Cyclic voltammetry has proved to be very useful in investigating not only the reactivity, but also the solubilization and interaction with lipidic bilayers of organometallic ferrocene-based anticancer drugs. It was notably established that ferrocifens cytotoxicity relies on a proton transfer coupled sequentially or not with an intramolecular electron transfer between a protic and oxidizable functionality (phenol, aniline, catechol, etc.) and the ferrocenyl moiety. This process in which the ferricenium group acts as an intramolecular “antenna” leads ultimately to the formation of extremely cytotoxic species (QM, quinone imines, *ortho*-quinone) even under moderate oxidizing conditions. On the other hand, we established that CDs may be an excellent alternative to increase their solubility in water and their bioavailability as the ferrocifens complexation by CDs did not affect the ultimate production of the cytotoxic species following their oxidation. Cyclic voltammetry also provided valuable information on the interactions and on the reactivity of ferrocifens in the presence of lipid bilayers used as simple models of cell membranes.

In conclusion, this chapter illustrates how electrochemical techniques allow the elucidation of the mechanisms involved in the metabolism of a drug, as well as characterizing the interactions of these molecules with supramolecular structures, such topics being essential for the development of more active drugs and the establishment of coherent reaction frames related to their vectorization and administration.

#### ACKNOWLEDGMENTS

The authors thank Prof. Gérard Jaouen, Prof. Anne Vessières, and Dr. Elizabeth Hillard (UMR CNRS 7223, Paris) for supplying the ferrocifens complexes synthesized in their laboratory and for this fruitful collaboration. This work was supported in part by the Centre National de la Recherche Scientifique (UMRs 8640 and 7223), the Ministère de la Recherche (MESR), the Ecole Normale Supérieure, Université P. et M. Curie, and the Agence Nationale de la Recherche (No. ANR-06-BLAN-0384-01, “FerVect”).

#### REFERENCES

1. Siegel, R.; Naishadham, D.; Jemal, A. *CA Cancer J. Clin.* **2012**, *62*, 10.
2. (a) Bardon, S.; Vignon, F.; Derocq, D.; Rochefort, H. *Mol. Cell. Endocrinol.* **1984**, *35*, 89; (b) for recent reviews on the biological mechanisms of SERMs, see: Jordan, V. C. *J. Med. Chem.* **2003**, *46*, 883, 1081.
3. Marshall, E. *Science* **1998**, *280*, 196.
4. Jakupc, M. A.; Galanski, M.; Arion, V. B.; Hartinger, C. G.; Keppler, B. K. *Dalton Trans.* **2008**, *2*, 183.
5. Dyson, P. J.; Sava, G. *Dalton Trans.* **2006**, 1929 and references therein.
6. Leong, C.-O.; Vidnovic, N.; DeYoung, M.; Sgroi, D.; Ellisen, L. *J. Clin. Invest.* **2007**, *117*, 1370.
7. Top, S.; Vessières, A.; Leclercq, G.; Quivy, J.; Tang, J.; Vaissermann, J.; Huché, M.; Jaouen, G. *Chem. Eur. J.* **2003**, *9*, 5223.
8. Gasser, G.; Ott, I.; Metzler-Nolte, N. *J. Med. Chem.* **2011**, *54*, 3.
9. (a) Top, S.; Tang, J.; Vessières, A.; Carrez, D.; Provot, C.; Jaouen, G. *Chem. Commun.* **1996**, 955–956; (b) Top, S.; Vessières, A.; Cabestaing, C.; Laios, I.; Leclercq, G.; Provot, C.; Jaouen, G. *J. Organomet. Chem.* **2001**, *637*, 500.
10. Jaouen, G.; Top, S.; Vessières, A.; Leclercq, G.; Quivy, J.; Jin, L.; Croisy, A. *C. R. Acad. Sci. Ser. IIc* **2000**, *3*, 89.
11. Jaouen, G.; Top, S.; Vessières, A.; Leclercq, G.; McGlinchey, M. J. *Curr. Med. Chem.* **2004**, *11*, 2505.
12. Zanellato, I.; Heldt, J. M.; Vessières, A.; Jaouen, G.; Osella, D. *Inorg. Chim. Acta* **2009**, *362*, 4037.
13. Michard, Q.; Jaouen, G.; Vessières, A.; Bernard, B.A. *J. Inorg. Biochem.* **2008**, *102*, 1980.
14. Heilmann, J. B.; Hillard, E. A.; Plumont, M.-A.; Pigeon, P.; Bolte, M.; Jaouen, G.; Vessières, A. *J. Organomet. Chem.* **2008**, *693*, 1716.
15. (a) Nguyen, A.; Vessières, A.; Hillard, E. A.; Top, S.; Pigeon, P.; Jaouen, G. *Chimia* **2007**, *61*, 716; (b) Nguyen, A.; Top, S.; Pigeon, P.; Vessières, A.; Hillard, E. A.; Plumont, M.-A.; Huché, M.; Rigamonti, C.; Jaouen, G. *Chem. Eur. J.* **2009**, *15*, 684; (c) Nguyen, A.; Marsaud, V.; Bouclier, C.; Top, S.; Vessières, A.; Pigeon, P.; Gref, R.; Legrand, P.; Jaouen, G.; Renoir, J. M. *Int. J. Pharm.* **2008**, *347*, 128.
16. Yao, D.; Zhang, F. G.; Yu, L. N.; Yang, Y. N.; van Breemen, R. B.; Bolton, J. L. *Chem. Res. Toxicol.* **2001**, *14*, 1643.
17. Köpf-Maier, P.; Köpf, H.; Neuse, E. W. *Angew. Chem. Int. Ed. Engl.* **1984**, *23*, 456.

18. (a) Fan, P. W.; Zhang, F.; Bolton, J. L.; *Chem. Res. Toxicol.* **2000**, *13*, 45; (b) Zhang, F.; Fan, P. W.; Liu, X.; Shen, L.; van Breeman, R. B.; Bolton, J. L. *Chem. Res. Toxicol.* **2000**, *13*, 53; (c) Dehal, S. S.; Kupfer, D. *Cancer Res.* **1995**, *55*, 1283; (d) Hardcastle, I. R.; Horton, M. N.; Osborne, M. R.; Hewer, A.; Jarman, M.; Phillips, D. H.; *Chem. Res. Toxicol.* **1998**, *11*, 369; (e) Shibutani, S.; Dsaradhi, L.; Terashima, I.; Banoglu, E.; Duffel, M. W. *Cancer Res.* **1998**, *58*, 647; (f) Dasaradhi, L.; Shibutani, S. *Chem. Res. Toxicol.* **1997**, *10*, 189.
19. Vessières, A.; Top, S.; Pigeon, P.; Hillard, E. A.; Boubeker, L.; Spera, D.; Jaouen, G. *J. Med. Chem.* **2005**, *48*, 3937.
20. Hillard, E. A.; Vessières, A.; Thouin, L.; Jaouen, G.; Amatore, C. *Angew. Chem. Int. Ed.* **2006**, *45*, 285.
21. Schlesener, C. J.; Amatore, C.; Kochi, J.K. *J. Am. Chem. Soc.* **1984**, *106*, 7472.
22. Amatore, C.; Bayachou, M.; Boutejengout, F.; Verpeaux, J. N. *Bull. Soc. Chim. Fr.* **1993**, *130*, 371.
23. Messina, P.; Labbé, E.; Buriez, O.; Hillard, E. A.; Vessières, A.; Hamels, D.; Top, S.; Jaouen, G.; Frapart, Y. M.; Mansuy, D.; Amatore, C. *Chem. Eur. J.* **2012**, *18*, 6581.
24. Dixon, W. T.; Murphy, D. *J. Chem. Soc. Faraday Trans. 2* **1976**, *72*, 1221.
25. Richard, L. S.; Bernardes, C. E. S.; Diogo, H. P.; Leal, J. P.; da Piedade, M. E. M. *J. Phys. Chem. A* **2007**, *111*, 8741.
26. Amatore, C.; Arbault, S.; Guille, M.; Lemaitre, F. *Chem. Rev.* **2008**, *108*, 2585.
27. Hamels, D.; Dansette, P. M.; Hillard, E. A.; Top, S.; Vessières, A.; Herson, P.; Jaouen, G.; Mansuy, D. *Angew. Chem. Int. Ed.* **2009**, *48*, 9124.
28. Tan, Y. L. K.; Pigeon, P.; Top, S.; Labbé, E.; Buriez, O.; Hillard, E.A.; Vessières, A.; Amatore, C.; Leone, W. K.; Jaouen, G. *Dalton Trans.* **2012**, *41*, 7537.
29. Ferreira, D. C. M.; Tapsoba, I.; Arbault, S.; Bouret, Y.; Moreira, M. S. A.; Pinto, A. V.; Goulart, M. O. F.; Amatore, C. *Chembiochem* **2009**, *10*, 528.
30. Pigeon, P.; Top, S.; Zekri, O.; Hillard, E. A.; Vessières, A.; Plumont, M.-A.; Buriez, O.; Labbé, E.; Huché, M.; Boutamine, S.; Amatore, C.; Jaouen, G. *J. Organomet. Chem.* **2009**, *694*, 895.
31. Buriez, O.; Labbé, E.; Pigeon, P.; Jaouen, G.; Amatore, C. *J. Electroanal. Chem.* **2008**, *619–620*, 169.
32. Barbier, B.; Pinson, J.; Désarmot, G.; Sanchez, M. *J. Electrochem. Soc.* **1990**, *137*, 1757.
33. Holm, A. H.; Vase, K. H.; Winther-Jensen, B.; Pedersen, S. U.; Daasbjerg, K. *Electrochim. Acta*, **2007**, *53*, 1680.
34. Liu, J.; Cheng, L.; Liu, B.; Dong, S. *Langmuir* **2000**, *16*, 7471.
35. Huijzer, J. C.; James, J.; Adams, D.; Yost, G. S. *Toxicol. Appl. Pharmacol.* **1987**, *90*, 60.
36. Nocerini, M. R.; Yost, G. S.; Carlson, J. R.; Liberato, D. J.; Breeze, R. G.; *Drug Metab. Dispos.* **1985**, *13*, 690.
37. Charmantry, F.; Duflos, A.; Lhommea, J.; Demeunynck, M. *J. Chem. Soc. Perkin Trans. I* **2001**, 2962.
38. Powers, J. C.; Oleksyszyn, J.; Narasimhan, S. L.; Kam, C.-M.; Radhakrishnan, R.; Meyer, J. E. F. *Biochemistry* **1990**, *29*, 3108.
39. Chow, M. M.; Edgar, J.; Meyer, F.; Bode, W.; Kam, C.-M.; Radhakrishnan, R.; Vijayalakshmi, J.; Powers, J. C. *J. Am. Chem. Soc.* **1990**, *112*, 7183.
40. Powers, J. C.; Kam, C.-M.; Narasimhan, L.; Oleksyszyn, J.; Hernandez, M. A.; Ueda, T. *J. Cell. Biochem.* **2004**, *39*, 33.
41. Smith, K. S.; Smith, P. L.; Heady, T. N.; Trugman, J. M.; Harman, W. D.; Macdonald, T. L. *Chem. Res. Toxicol.* **2003**, *16*, 123.
42. Hinson, J. A.; Reid, A. B.; McCullough, S. S.; James, L. P. *Drug Metab. Rev.* **2004**, *36*, 805 and references therein.
43. Bose, R.; Ahmad, A. R.; Dicks, A. P.; Novak, M.; Kayser, K. J.; McClelland, R. A. *J. Chem. Soc. Perkin Trans. I* **1999**, *2*, 1591.
44. Morao, I. A.; Hillier, I. H.; *Tetrahedron Lett.* **2001**, *42*, 4429.
45. Plazuk, D.; Vessières, A.; Hillard, E. A.; Buriez, O.; Labbé, E.; Pigeon, P.; Plumont, M.-A.; Amatore, C.; Zakrzewski, J.; Jaouen, G. *J. Med. Chem.* **2009**, *52*, 4964.
46. Hisatome, M.; Watanabe, J.; Yamakawa, K. *Bull. Chem. Soc. Jpn.* **1994**, *67*, 280.
47. Allard, E.; Huynh, N. T.; Vessières, A.; Pigeon, P.; Jaouen, G.; Benoit, J. P.; Passirani, C. *Int. J. Pharm.* **2009**, *379*, 317.
48. Allard, E.; Passirani, C.; Garcion, E.; Pigeon, P.; Vessières, A.; Jaouen, G.; Benoit, J.-P. *J. Control. Release* **2008**, *130*, 146.
49. Buriez, O.; Heldt, J. M.; Labbé, E.; Vessières, A.; Jaouen, G.; Amatore, C. *Chem.;Eur. J.* **2008**, *14*, 8195.
50. Matsue, T.; Evans, D.H.; Osa, T.; Kobayashi, N. *J. Am. Chem. Soc.* **1985**, *107*, 3411.
51. Lewis, E. A.; Hansen, L. D. *J. Chem. Soc. Perkin Trans. 2* **1973**, *2*, 2081.
52. Cardona, C. M.; Mendoza, S.; Kaifer, A. E. *Chem. Soc. Rev.* **2000**, *29*, 37 and references cited therein.
53. Szejtli, J. *Chem. Rev.* **1998**, *98*, 1743.
54. Hillard, E.A.; Vessières, A.; Le Bideau, F.; Plazuk, D.; Spera, D.; Huché, M.; Jaouen, G. *ChemMedChem* **2006**, *1*, 551.
55. Memisoglu-Bilensoy, E.; Vural, I.; Bochot, A.; Renoir, J. M.; Duchene, D.; Hincal, A. A. *J. Control. Release* **2005**, *104*, 489.
56. Mertins, O.; Messina, P.; Labbé, E.; Vivier, V.; Arbault, S.; Lemaitre, F.; Buriez, O.; Amatore, C. *Inorg. Chim. Acta* **2011**, *374*, 59.
57. Kondo, T.; Kanai, T.; Uosaki, K. *Langmuir* **2001**, *17*, 6317.
58. Inoue, T.; Kamaya, H.; Ueda, I. *Biochim. Biophys. Acta* **1985**, *812*, 393.



---

# 48

---

## ELECTROCHEMISTRY OF FISCHER AMINOCARBENE COMPLEXES: EFFECTS OF STRUCTURE ON REDOX PROPERTIES, ELECTRON DISTRIBUTION, AND REACTION MECHANISMS

JIŘÍ LUDVÍK\*

*J. Heyrovský Institute of Physical Chemistry, Academy of Science of the Czech Republic, Prague, Czech Republic*

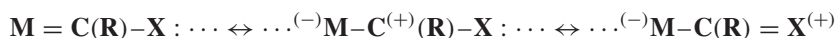
IRENA HOSKOVCOVÁ

*Department of Inorganic Chemistry, Institute of Chemical Technology Prague, Prague, Czech Republic*

### 48.1 INTRODUCTION

Carbene complexes are characterized by the presence of a formal double bond between a central metal atom and a carbene ligand,  $M = CR_2$ . Generally, these compounds are divided into three groups according to the nature of the metal–carbon bond: nucleophilic Schrock carbenes, where the carbon center has a nucleophilic character,  $M(\delta^+) = C(\delta^-)$ ; and electrophilic Fischer carbenes with the metal–carbon bond polarized in the opposite sense  $M(\delta^-) = C(\delta^+)$  (the fifteenth annual survey describing their chemistry was recently published [1]). The third group includes transition-metal complexes with *N*-heterocyclic carbene ligands (e.g., the Hoveyda–Grubbs catalyst), in which the multiple character of metal–carbon bond is negligible [2]. This chapter is devoted to carbenes of the Fischer type, that is, to aminocarbene complexes.

A typical Fischer carbene molecule is composed of a central metal atom in its low oxidation state, coordinated to  $\pi$ -electron acceptor ligands (CO). The metal–carbene carbon bond (formally a double bond) is polarized  $M(\delta^-) = C(\delta^+)$  giving electrophilic character to the carbon atom. The complex is then stabilized by the presence of a  $\pi$ -donor substituent  $X = -OR'$  or  $-NR'_2$  (Fig. 48.1).



Fischer carbene complexes are useful starting materials in organic synthesis [3–5] and promising catalysts [6, 7]. Their molecules offer high structural as well as substitution variability, therefore a fine modification (“tuning”) of their reduction and/or oxidation abilities, structure, and stability of their redox intermediates (often of radicalic nature) and thus their specific reactivity is of high interest. A detailed insight into the structure–reactivity relationship enables better understanding of mechanism of synthetic or catalytic reactions and facilitates design and aimed syntheses of the next generation of compounds with required specific properties.

### 48.2 VALUE OF ELECTROCHEMISTRY

Electrochemical approach is a very powerful tool for fundamental chemical characterization of molecules that are able to be oxidized or reduced (organic substances, complexes, as well as organometallic compounds), that is, for the research

*Advances in Organometallic Chemistry and Catalysis: The Silver/Gold Jubilee International Conference on Organometallic Chemistry Celebratory Book*, First Edition. Edited by Armando J. L. Pombeiro.

© 2014 John Wiley & Sons, Inc. Published 2014 by John Wiley & Sons, Inc.

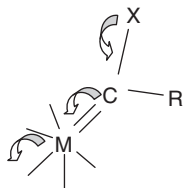


**Figure 48.1** Electron shifts in Fischer carbene complexes.

of structure–reactivity relationship. The possibility of a precise setting of any required working potential can guarantee a maximal selectivity and reproducibility of the redox process. The continuous change of the working potential, starting in real time up to microsecond scale, its cycling or keeping constant, enables not only determination of the respective oxidation or reduction potentials but also revelation of reversibility of the redox processes, nature, kinetics, and equilibrium constants of follow-up reactions, stability and structure of intermediates, type and yield of products, etc. In addition to this, a combination of electrochemical methods with various *in situ* spectroscopic measurements [UV–vis, near infrared (NIR), infrared (IR), Raman, electron paramagnetic resonance (EPR), mass spectrometry (MS), nuclear magnetic resonance (NMR)] and separation techniques tandem high performance liquid chromatography (HPLC) represents a substantial broadening of the scientific benefit of the electrochemical approach.

Interpretation of electrochemical data is usually based on comparison of experimental values acquired from systematic research of similar molecules. The best situation occurs if the studied compounds form homologous series, where only one substituent is systematically changed. Then the group of substances can be treated using the linear free-energy relationship (LFER) approach [8] to analyze the role of substitution and the influence of structural modifications on redox properties [9, 10]. According to the LFER approach, reduction (oxidation) potentials of compounds belonging to the mentioned series are proportional to the experimentally determined Hammett-type constant  $\sigma$ , which is characteristic for each substituent (special tables are available [8, 9, 11]). Recently, a theoretical treatment of substituent constants was published [12]. For characterization of coordination compounds, special electrochemical parameters were introduced [13].

The  $\sigma$ -constants were originally derived for substituents on a benzene ring and reflect their “pushing” or “withdrawing” electronic influence on the rest of the molecule (for more details consult the references). Nevertheless, this concept has rather general significance and  $\sigma$ -constants often fit even for nonaromatic systems. The most used is  $\sigma_p$ , originally for substituents in the para position toward the reaction center on the benzene ring, reflecting both induction and mesomeric effects, and  $\sigma_i$ , reflecting the inductive effect (e.g., in saturated, nonaromatic systems). In this work, both the sigma constants were used according to Eq. 48.1 and the better fit was taken into account for evaluation of inductive and/or mesomeric effects.

$$E_{\text{ox(red)}} = \rho \cdot \sigma + c. \quad (48.1)$$

In Eq. 48.1, the value of the reaction constant  $\rho$  reflects the extent of interaction (electronic communication) between the substituent and the reaction center, that is, how much the measured potential depends on electron pushing/withdrawing ability of the substituent. In this way, a level of  $\pi$ -delocalization along the molecule or displacement of oxidation and reduction centers, respectively, can be experimentally followed and correlated with quantum chemical calculations. Since the energy (potential) needed for oxidation or reduction of the studied molecule is proportional to the energy of the respective frontier molecular orbitals (and can be determined experimentally as  $E_{\text{ox}}$  and  $E_{\text{red}}$  by an appropriate electrochemical method), their difference ( $E_{\text{ox}} - E_{\text{red}}$ ) correlates well with the HOMO–LUMO gap obtained spectrophotometrically or using calculations.

When a linear correlation of the measured potentials  $E_{\text{red}}$  (or  $E_{\text{ox}}$ ) of all involved derivatives versus the corresponding  $\sigma_p$  ( $\sigma_i$ ) values (Eq. 48.1) is observed, it follows that, in the frame of the studied series, the reduction (oxidation) centers remain unchanged, the structure of all starting derivatives as well as intermediates is analogous and thus the same reduction (oxidation) mechanism occurs. Any potential value not fitting the linear dependence points to an anomalous behavior of the respective molecule in the frame of the studied series. The anomaly may be caused by a different electron displacement (i.e., different shape of HOMO (LUMO) and different localization of redox centers), hence by a different reaction mechanism yielding thus different intermediates and products. (An example will be given below.)

The  $\rho$ -values reflect also the distance between the substitution site and the reaction center of the molecule and simultaneously the electronic “conductivity” of the molecular structure (bridge) connecting the substituent and redox center. Investigating several series of compounds, the obtained  $\rho$ -values are compared and every difference in their values requires explanation on the basis of the structure and electron delocalization.

The additive constant  $c$  in Eq. 48.1 is significant when several analogous substitution series with different reduction (oxidation) centers are studied and compared. Then the constant  $c$  (in V) speaks about their energetic difference, that is, it compares the reduction (oxidation) abilities of the redox centers involved.

The application of electrochemistry to the investigation of new organometallic molecules is illustrated in this contribution on two groups of recently synthesized Fischer-type aminocarbene complexes of chromium, tungsten, and iron involving about 40 derivatives. All of them represent molecules with two separated redox-active centers where the extent of their interaction (mutual influence) is given by the electron delocalization of the bridging unit, by the distance between the centers and/or by sterical effects.

### 48.3 FUNDAMENTAL ELECTROCHEMICAL BEHAVIOR OF AMINOCARBENE COMPLEXES

All synthesized aminocarbene derivatives underwent systematic electrochemical investigation in aprotic media [nonaqueous dimethylformamide (DMF) with 0.1 M tetrabutylammonium tetrafluoroborate (TBATFB) as an electrolyte] in order to determine their potentials of reduction and oxidation, to find out the eventual reversibility of the redox process, to elucidate the fate of intermediates, to reveal products of such electrochemically initiated redox reactions, and to discuss the possible reaction pathway or mechanism.

From the experimental point of view, for reductions, DC-polarography at the dropping mercury electrode (DME) or cyclic voltammetry (CV) at the hanging mercury drop electrode (HMDE) were used; and for controlled-potential electrolyses at negative potentials, a mercury pool electrode was employed. For both oxidative and reductive experiments, voltammetry at the platinum rotating disk electrode (RDE) and CV at the stationary platinum electrode were applied. All experiments were performed in a three-electrode system with a platinum counter electrode. For measurements in analytical scale (a standard aminocarbene concentration was  $3 \times 10^{-4}$  mol/l), an undivided cell for 5–10 ml was used; and for preparative electrolyses a two-compartment cell of the H-type was employed [14]. The potentials were referred to the saturated calomel electrode (SCE), which was separated from the investigated solution by a double-frit bridge.

In addition to the purely electrochemical methods, some *on-line* as well as *off-line* combined techniques were used (electrochemistry + UV/vis, IR, NMR, EPR, MS, HPLC), for detection and identification of intermediates and products.

The most important data for our study are the first reduction and the first oxidation potentials. The general electrochemical pattern is presented in Fig. 48.2.

The first oxidation process is quasi reversible, involving one electron. The quasi-reversibility means that the primary one-electron intermediate is not fully stable and undergoes a follow-up reaction. Therefore, the cathodic counterpeak appears often only at higher scan rates (this is different for individual compounds). The oxidation potential is then determined as a

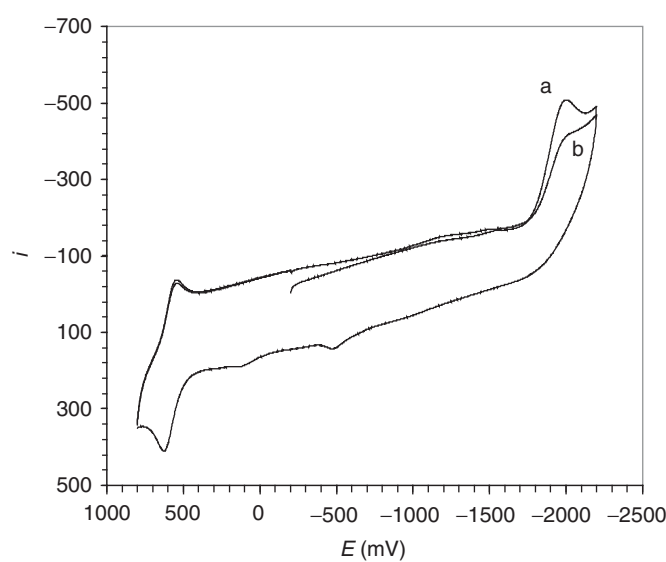


**Figure 48.2** Cyclic voltammetry of **II f**; a, first scan; b, second scan.

medium value between the anodic peak potential ( $E_{\text{pa}}$ ) and cathodic peak potential ( $E_{\text{pc}}$ ):

$$E_{\text{ox}} = \frac{1}{2}(E_{\text{pa}} + E_{\text{pc}}). \quad (48.2)$$

The first reduction step is a two-electron irreversible process accompanied by adsorption or a surface film formation partly blocking the electrode, as evident from the difference between the first and second scan on CV. As reduction potentials, polarographic half-wave potentials ( $E_{1/2}$ ) were taken for further correlations as cathodic peak potentials ( $E_{\text{pc}}$ ) taken from cyclic voltammetry are always more negative and depend on the scan rate and other factors. It is necessary to point out that the oxidation as well as reduction potentials taken from various methods and measured on different electrodes were consistent.

When the whole available potential range is scanned (approximately from +2 to -3 V vs SCE in aprotic media), the first reduction, as well as oxidation step, is followed by one or two other processes at more negative (more positive) potentials representing stepwise reduction (oxidation) of intermediates and products. Since various follow-up reactions occur after the first electron transfer, the interpretation of such voltammograms is very complicated, if at all possible, and would deserve special investigation that is beyond the scope of this study.

#### 48.4 BASIC GROUP OF AMINOCARBENES

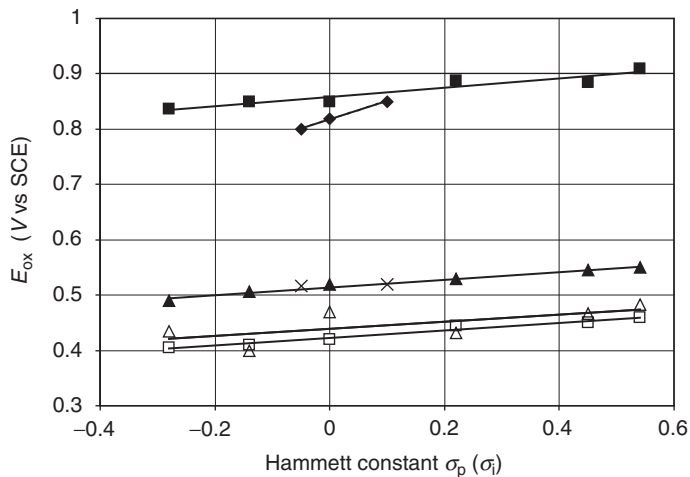
In the first group of aminocarbene complexes (Table 48.1) *p*-substituted aryl substituents, methyl, or hydrogen were attached to the carbene carbon. Several structural features were electrochemically followed in order to elucidate and formulate how the structural/substituent changes can influence the oxidation and/or reduction potentials. For this reason, several homologous series of compounds were created (**I–VIII**) and mutually compared.

TABLE 48.1 Overview of the Basic Group of Aminocarbene Complexes

non-chelates			Chelates		
No.	M	R	No.	M	R
<b>I a</b>	Cr	<i>p</i> -OCH <sub>3</sub> -phenyl	<b>II a</b>	Cr	<i>p</i> -OCH <sub>3</sub> -phenyl
<b>I b</b>	Cr	<i>p</i> -CH <sub>3</sub> -phenyl	<b>II b</b>	Cr	<i>p</i> -CH <sub>3</sub> -phenyl
<b>I c</b>	Cr	<i>p</i> -H-phenyl	<b>II c</b>	Cr	<i>p</i> -H-phenyl
<b>I d</b>	Cr	<i>p</i> -Cl-phenyl	<b>II d</b>	Cr	<i>p</i> -Cl-phenyl
<b>I e</b>	Cr	<i>p</i> -COOCH <sub>3</sub> -phenyl	<b>II e</b>	Cr	<i>p</i> -COOCH <sub>3</sub> -phenyl
<b>I f</b>	Cr	<i>p</i> -CF <sub>3</sub> -phenyl	<b>II f</b>	Cr	<i>p</i> -CF <sub>3</sub> -phenyl
<b>III c</b>	W	<i>p</i> -H-phenyl	<b>IV c</b>	W	<i>p</i> -H-phenyl
<b>V a</b>	Fe <sup>a</sup>	<i>p</i> -OCH <sub>3</sub> -phenyl	<b>VI a</b>	Fe <sup>b</sup>	<i>p</i> -OCH <sub>3</sub> -phenyl
<b>V b</b>	Fe <sup>a</sup>	<i>p</i> -CH <sub>3</sub> -phenyl	<b>VI b</b>	Fe <sup>b</sup>	<i>p</i> -CH <sub>3</sub> -phenyl
<b>V c</b>	Fe <sup>a</sup>	<i>p</i> -H-phenyl	<b>VI c</b>	Fe <sup>b</sup>	<i>p</i> -H-phenyl
<b>V d</b>	Fe <sup>a</sup>	<i>p</i> -Cl-phenyl	<b>VI d</b>	Fe <sup>b</sup>	<i>p</i> -Cl-phenyl
<b>V e</b>	Fe <sup>a</sup>	<i>p</i> -COOCH <sub>3</sub> -phenyl	<b>VI e</b>	Fe <sup>b</sup>	<i>p</i> -COOCH <sub>3</sub> -phenyl
<b>V f</b>	Fe <sup>a</sup>	<i>p</i> -CF <sub>3</sub> -phenyl	<b>VI f</b>	Fe <sup>b</sup>	<i>p</i> -CF <sub>3</sub> -phenyl
<b>VII b</b>	Cr	CH <sub>3</sub>	<b>VIII b</b>	Cr	CH <sub>3</sub>
<b>VII c</b>	Cr	H			
<b>VII g</b>	Cr	<i>p</i> -H-phenyl (= <b>I c</b> )	<b>VIII g</b>	Cr	<i>p</i> -H-phenyl (= <b>II c</b> )
<b>IX a</b>	Cr	<i>o</i> -CH <sub>3</sub> - <i>p</i> -OCH <sub>3</sub> -phenyl			
<b>IX c</b>	Cr	<i>o</i> -CH <sub>3</sub> - <i>p</i> -H-phenyl			
<b>IX f</b>	Cr	<i>o</i> -CH <sub>3</sub> - <i>p</i> -CF <sub>3</sub> -phenyl			

<sup>a</sup>(CO)<sub>4</sub>.

<sup>b</sup>(CO)<sub>3</sub>.



**Figure 48.3** Electrochemical oxidation of aminocarbene complexes—fluence of substituents. Symbol code: ■ Series I, Cr nonchelates; ▲ Series II, Cr chelates; □ Series V, Fe nonchelates; △ Series VI, Fe chelates; ♦ Series VII, Cr nonchelates substituted directly on the carbene C (values against  $\sigma_i$ ); × Series VIII, Cr chelates substituted directly on the carbene C (values against  $\sigma_i$ ).

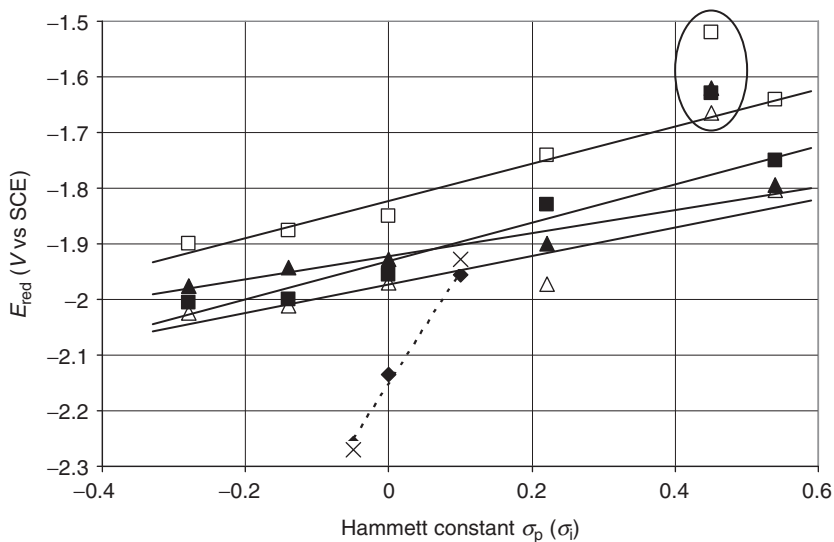


**Figure 48.4** Electrochemical reduction of aminocarbene complexes—fluence of substituents. Symbol code: ■ Series I, Cr nonchelates; ▲ Series II, Cr chelates; □ Series V, Fe nonchelates; △ Series VI, Fe chelates; ♦ Series VII, Cr nonchelates substituted directly on the carbene C (values against  $\sigma_i$ ); × Series VIII, Cr chelates substituted directly on the carbene C (values against  $\sigma_i$ ). Encircled: molecules bearing  $p$ -COOCH<sub>3</sub>-phenyl substituent.

The first oxidation and first reduction potentials of aminocarbene complexes presented above were plotted against the  $\sigma$  values belonging to the individual substituents—Fig. 48.3 for oxidation and Fig. 48.4 for reduction (for the  $\sigma_p$  and  $\sigma_i$  values see Table 48.2). The corresponding  $\rho$ -values, that is, slopes of the linear dependencies are quoted in Table 48.3.

This group of aminocarbene complexes represents, in fact, a multidimensional set of relative compounds, where comparison of potentials and slopes of various series of derivatives enables to elucidate individual properties, influences, and structural features:

1. The comparison between the slopes ( $\rho$ -values) of oxidation and reduction dependencies point to the localization of the oxidation and/or reduction center (i.e., HOMO and LUMO orbitals).
2. The comparison of potentials as well as the  $\rho$ -values between the nonchelates **I**, **V**, and **VII b** on one side, and the corresponding chelates **II**, **VI**, and **VIIIb** enables to explain the role of presence/absence of the chelate ring.

**TABLE 48.2** Selected  $\sigma_p$  and  $\sigma_i$  Values of Substituents Involved in this Contribution<sup>a</sup>

Substituent	$-\text{OCH}_3$	$-\text{CH}_3$	$-\text{H}$	$-\text{Cl}$	$-\text{COOCH}_3$	$-\text{CF}_3$	$-\text{phenyl}$
$\sigma_p$ value	-0.28	-0.14	0	0.22	0.45	0.54	
$\sigma_i$ value		-0.05	0				0.10

<sup>a</sup>Ref. 8.**TABLE 48.3** Slopes of the Linear Free Energy Relationship (LFER) Dependencies  $E_{\text{ox}}$  ( $R_{\text{red}}$ ) Versus  $\sigma_p$  (Without the Data for the Compounds with—COOCH<sub>3</sub> Substituent)

Series	$\rho_{\text{oxidation}}$	$\rho_{\text{reduction}}$
<b>I</b>	0.082; $R^2 = 0.908$	0.344; $R^2 = 0.957$
<b>II</b>	0.070; $R^2 = 0.981$	0.224; $R^2 = 0.925$
<b>V</b>	0.069; $R^2 = 0.968$	0.334; $R^2 = 0.976$
<b>VI</b>	0.065; $R^2 = 0.450$	0.255; $R^2 = 0.857$
<b>VII</b> <sup>a</sup>	0.330; $R^2 = 0.997$	2.00; $R^2 = 0.993$

<sup>a</sup>Values against  $\sigma_i$ .

- The comparison of the derivatives **I c** and **II c** with the tungsten analogs **III c** and **IV c** evaluates the differences within the Group 6 metals.
- The comparison of the series **I** and **II** against **V** and **VI** reflects not only different central metal atom, but also its different coordination number.
- The comparison of compounds **IX** with the analogous derivatives from the group **I** and **II** reflects the sterical hindrances affecting the electron delocalization.
- The comparison of the slopes ( $\rho$ -values) of compounds **VII** and **VIII** against the corresponding derivatives from the groups **I** and **II** illustrates the role of the phenylene unit on the ligand.

#### 48.4.1 Localization of Oxidation and Reduction Center: Role of the Ligand Substitution and the Central Metal Atom

One of the rules mentioned above and following from the LFER treatment is that the higher slope (higher  $\rho$ -value) indicates either a shorter distance between the substituent and the reaction center, or, in the case of the same distance, a higher level of electron communication–delocalization.

From a comparison of Figs. 48.3 and 48.4, it is evident that in all the presented series, the substituents in the *p*-position of the phenyl ring have negligible influence on the oxidation potential of the whole molecule ( $\rho$ -values are between 0.06 and 0.08), whereas the reduction potential is significantly affected by the substituents ( $\rho$ -values are between 0.22 and 0.34).

In addition to this, when the phenyl ring is let out and the substituents are bound directly to the carbene carbon (compounds **VII**, **VIII**), the influence of the slope of the substitution on oxidation potential is significantly higher than that of the compounds **I** and **II** (Fig. 48.3), but still much lower than the slope for reduction potentials (Fig. 48.4, Table 48.3). This enormous dependence of the reduction potential reflects the direct connection of the substituent with the reduction center. Since only the inductive effect acts in the case of series **VII** and **VIII**, the constants  $\sigma_i$  fit much better to the LFER treatment than the  $\sigma_p$  constants, where a mesomeric effect is also included.

On the other hand, the exchange of Cr by W (Group 6 metals) shifts the oxidation potential significantly (by 200–300 mV) to more positive potentials, reflecting the stabilizing effect of the more diffuse nature of tungsten *d*-orbitals, whereas the difference in reduction potential is around 50 mV [10]. The comparison of the Cr and Fe complexes is more complicated, because, besides their different intrinsic electronic properties, the different number of CO ligands also plays a role. Owing to the fact that iron is more electron rich than chromium and has one carbonyl ligand less, the oxidation of iron complexes proceeds more easily than that of chromium and tungsten (Fig. 48.3).

As an experimental result, the oxidation center in aminocarbene complexes (and thus the HOMO) is localized on the central metal atom and the reduction center (LUMO) is on the carbene carbon.

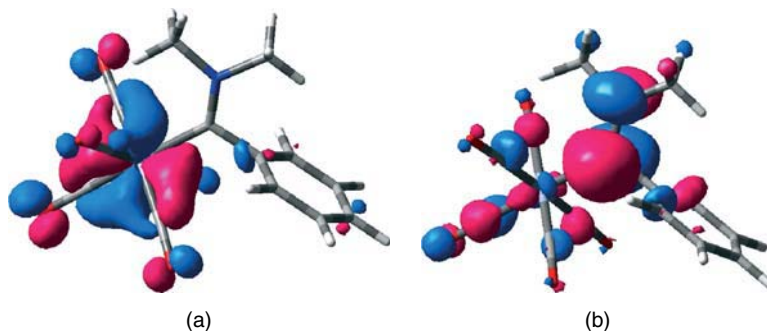


**Figure 48.5** HOMO (a) and LUMO (b) of the compound **I c**. (See insert for color representation of the figure.)

This was confirmed by quantum chemical calculations of displacement of HOMO and LUMO (Fig. 48.5). The calculated shape of the LUMO revealed that the reduction center involves not only the carbene carbon but also the nitrogen and the interconnecting bond. This is consistent with one of the mesomeric structures:  ${}^{\text{O}}\text{M}-\text{C}(\text{R})=\text{X}^{(+)}$ .

This shape of the frontier orbitals leads to a specific feature of their UV-vis spectra: the lowest energy absorption band exhibits a metal-to-ligand charge transfer (MLCT) character. This type of behavior was confirmed by comparing experimental UV-vis spectra with their theoretical models [15].

The above results show that carbene ligands are redox active and behave as so-called “non-innocent ligands.” This type of redox behavior is of great importance in electron-transfer processes taking place in nature [16]. In Fischer-type carbenes, an intramolecular electron transfer from a d<sup>7</sup>-metal center to the carbene ligand has been described, resulting in a d<sup>6</sup>-metal and carbene radical [17].

#### 48.4.2 Chelating Versus Nonchelating Structures in Cr and W Complexes

A remarkable feature presented in Fig. 48.3 is that the oxidation potential of nonchelated complexes of Cr and W is by 250–350 mV more positive than that of the corresponding chelates, hence, the chelates are oxidized much more easily. This difference is caused by the fact that the number of electron-withdrawing carbonyl ligands directly connected to the metal (oxidation center) is lower by one in chelates. Another example of electrochemical oxidation of molecules differing in Cr/W center can be found in [18].

In the case of reduction (Fig. 48.4), the situation is different: the chromium (as well as tungsten) complexes exhibit very similar reduction potentials. This fact is consistent with the previous finding that the distant carbonyl ligands do not influence the reduction properties.

However, a question arose as to why the reduction potentials of nonchelates are more dependent on the substitution than those of chelates; in other words, why the two linear dependencies have different  $\rho$ -values and are crossing at  $\sigma_{\text{p}} = 0$ . On the basis of the above consideration about LFER, the higher slope reflects the higher level of electron communication between the substituted phenyl ring and the aminocarbene center. From the structure analysis [19], it is known that the aryl ring attached to the carbene carbon is in its most stable position oriented orthogonally to the metal–carbon–nitrogen plane in solid state as well as in solution [20]. One can expect that the efficient overlap of the two  $\pi$ -systems will depend on the ease of phenyl ring rotation [9].

The hindered rotation is a result of steric interactions between the N-alkyl substituent and *o*-hydrogen atoms of an aromatic ring. It was experimentally proved that the flexible N-methyl substituent in the nonchelated complexes **I** enables easier rotation of the phenyl ring than the more rigid noncoordinated N-allyl substituent in chelated complexes **II** (Fig. 48.6a and b). The corresponding values of  $\Delta G^\ddagger_{298}$  are 62.5 kJ/mol for chelated N-allyl derivative (**II c**) and 54.5 kJ/mol for the corresponding N-methyl derivative [21]. Moreover, introduction of the *o*-methyl substituent (series **IX**) prevents the rotation even more: the  $\rho$ -values for nonchelates, chelates, and *o*-methyl nonchelates are 0.344, 0.224, and 0.137, respectively.

In support of the above statement, it has been observed [20] that in the series of chelated complexes **II**, the height of the rotation barrier depends also on the electronic nature of a p-substituent on the phenyl ring: Electron donors make the *o*-CH bond shorter and thus lower the rotational barrier, while electron withdrawing p-substituents have the opposite effect (Fig. 48.5c).

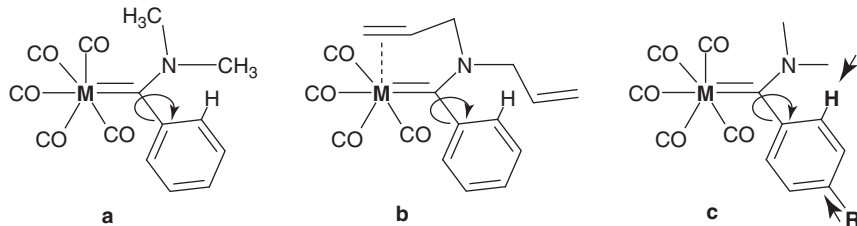


**Figure 48.6** Relationship between the structure and ease of rotation.

#### 48.4.3 Chelating Versus Nonchelating Structures in Cr and Fe Complexes

The interpretation of the different manifestation of chelates and nonchelates in Cr and Fe complexes (series **I** and **II** vs **V** and **VI**) is more complicated. From the LFER treatment (Fig. 48.3 and Fig. 48.4), it follows that, in Cr complexes, chelates are more easily oxidized by about 350 mV than nonchelates, on the other hand, reduction of nonchelates proceeds in the same region of potentials as the reduction of chelates (both findings were discussed above).

In the case of Fe complexes, however, the situation is reversed: whereas the oxidation of chelates as well as nonchelates occurs at similar potentials, the reduction of chelates is more difficult than reduction of nonchelates by about 100 mV. The question is, why (in contradiction to the Cr derivatives), in iron complexes  $E_{\text{ox}}(\text{chel}) = E_{\text{ox}}(\text{nonchelate})$ , whereas  $|E_{\text{red}}|(\text{chel}) > |E_{\text{red}}|(\text{nonchelate})$ .

The most reasonable explanation is based on the difference in the coordination number. Chromium has the coordination number 6 (octahedral), thus the allylic ligand is pushed out by the remaining four CO ligands and therefore the distances Cr–allyl and Cr–C are relatively long. As a result, the coordination of the allyl is weak and back donation Cr → C is negligible. Reduction potential (LUMO) is not influenced by substitution of allyl for methyl and oxidation potential (HOMO) is strongly influenced (by 350 mV) by the substitution of the electron-withdrawing ligand CO by an electron-donating allylic π-system.

Iron, as a more electron-rich metal than chromium, has the coordination number 5 (trigonal bipyramidal) and enables shorter length Fe–allyl and Fe–C bonds. As a consequence, stronger allyl coordination and thus stronger back donation Fe → C occurs, and owing to the back donation, the reduction potential of chelates is slightly more negative (by 100 mV) than that of nonchelates. In the case of oxidation, the stronger back donation in chelates aimed to both carbene and allyl ligands compensates the effect of the lower number of the CO ligand.

The experimental values of  $E_{\text{red}}$  and  $E_{\text{ox}}$  can be used for deriving values of  $\Delta E = E_{\text{red}} - E_{\text{ox}}$  that can be taken as an experimental value relative to the HOMO–LUMO gap or  $d$ - $d$  splitting. Mean values of  $\Delta E$  for the structural series discussed above are  $\Delta E(\mathbf{I}, \text{Cr nonchelates}) = 2.79 \text{ V}$ ;  $\Delta E(\mathbf{II}, \text{Cr chelates}) = 2.44 \text{ V}$ ;  $\Delta E(\mathbf{V}, \text{Fe nonchelates}) = 2.25 \text{ V}$ ;  $\Delta E(\mathbf{VI}, \text{Fe chelates}) = 2.43 \text{ V}$ . The data reflects higher stability of chromium complexes **I** compared with **II**, which may be attributed to a different number of CO groups, and a reverse situation in their iron analogs:  $\Delta E$  of **VI** (chelates) is higher than that of **V** (nonchelates). This fact gives the reason for the higher tendency of iron to form chelated carbene complexes compared to chromium, as described in [22].

#### 48.4.4 Anomalous Behavior of the *p*-Carbonyl Substituent

Taking advantage of the LFER treatment of the electrochemical data, we have found an irregularity in reduction of all compounds where the phenyl ring is substituted in *p*-position by methyl ester function [23] (**I e**, **II e**, **V e**, **VI e**). While all other substituents follow the linear Hammett relationship, the derivatives substituted by the *p*-carbonyl group are always reduced more easily and the observed values of  $E_{\text{red}}$  are always shifted by 150 mV toward less negative potentials (cf., anomalous values in Fig. 48.4). This observation points to a different reduction mechanism, caused by a different, more-delocalized system where the carbonyl is involved.

The situation resembles the unusual reduction mechanism of *p*-dicarbonyl benzenes [24] published in 1960s, where, in aqueous solutions, a two-electron reversible process was found. The explanation was based on the assumption that the two equal carbonyls provide the planar shape of the molecule where an extended quinoid mesomeric structure takes place involving both carbonyls. In our case, however, the experiments proceed in aprotic media, only one carbonyl is present, and the substitution in *p*-positions is nonsymmetric and complicated by the carbene function. Nevertheless, the second carbonyl can be mimicked either by the formal Cr=C double bond or by the hypothetical C=N double bond and the observed anomalous reduction potentials can be explained by the model of *p*-dicarbonyl benzene.

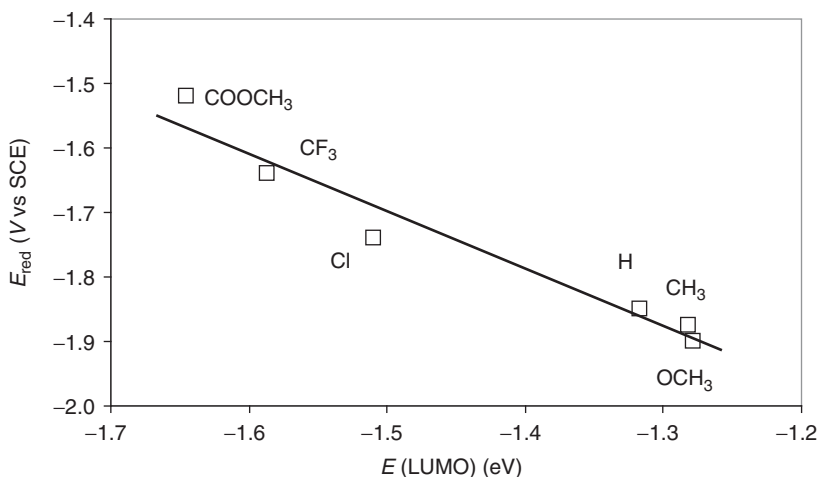


**Figure 48.7** Correlation of the measured reduction potentials and the calculated energies of LUMO of the series V.

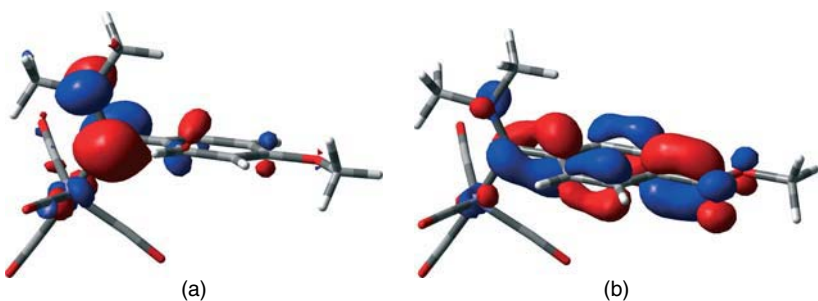


**Figure 48.8** LUMOs of the methoxy derivative **V a** (a) and the methylester derivative **V e** (b). (See insert for color representation of the figure.)

Theoretical treatment proved this analogy, which has not been reported up to now. Density functional theory (DFT) calculations show that the energy of the LUMO decreases as the shape of the orbital spreads across the whole phenyl group of the carbene moiety. In contrast to the Hammett dependence, the calculated LUMO energies of the whole series correlate well with the measured reduction potentials (Fig. 48.7).

The difference in the shape of the LUMO of the methoxy-substituent and methyl ester (Fig. 48.8) is a good illustration. Even from the picture, a different participation of the Ph-OMe and Ph-COOMe on the LUMO is evident. The calculated LUMO composition is

**Va:** C<sub>carbene</sub> 51%, NMe<sub>2</sub> 22%, Ph-R' 13%

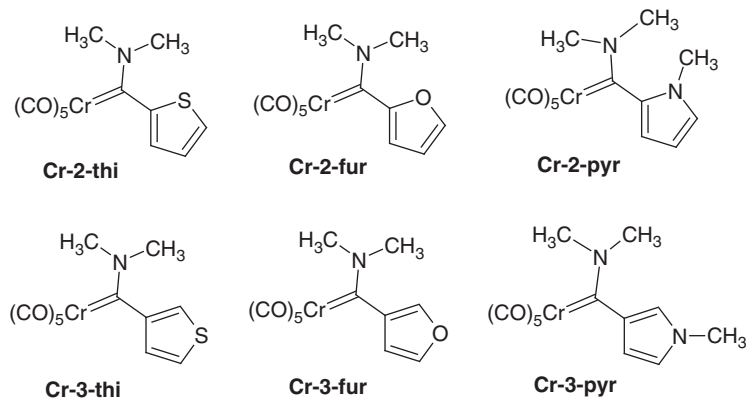
**Ve:** C<sub>carbene</sub> 11%, NMe<sub>2</sub> 6%, Ph-R' 76%

In addition to this, the calculated shape of the LUMO of *p*-diacetylbenzene is practically identical to that in Fig. 48.8b.

The above-mentioned example shows, how a “small” change in a remote substituent can cause an unexpected and total rearrangement of the LUMO displacement accompanied by different redox properties of these potential catalysts.

## 48.5 HETARYL CHROMIUM(0) AMINOCARBENES

In Section 48.4.4, it was shown that the attached phenyl ring with its *p*- and *o*-substituents significantly influences the reduction potential, which is closely connected with the shape and distribution of the LUMO, in other words, with the extent

**Figure 48.9** Structures of studied hetaryl chromium(0) aminocarbene complexes.**TABLE 48.4** Oxidation and Reduction Potentials of Investigated Hetaryl Chromium(0) Aminocarbene

Heterocycle	Compound	Binding Site 2		Binding Site 3		
		$E_{\text{ox}}$	$E_{\text{red}}$	Compound	$E_{\text{ox}}$	$E_{\text{red}}$
Furan	Cr-2-fur	0.897	-1.591	Cr-3-fur	0.874	-1.909
Thiophene	Cr-2-thi	0.856	-1.601	Cr-3-thi	0.832	-1.915
1-Methylpyrrol	Cr-2-pyr	0.826	-1.894	Cr-3-pyr	0.823 <sup>a</sup>	-2.036

$E_{\text{ox}}$  represents the medium value between oxidation and reduction peak potential of the reversible couple, taken at 0 °C using cyclic voltammetry.

$E_{\text{red}}$  is a polarographic half-wave potential  $E_{1/2}$ .

<sup>a</sup>Owing to absence of reversibility, potential of the anodic peak is presented.

of electron delocalization and intramolecular communication between the aryl and carbene moieties. In the next series of compounds [25], instead of a para-substituted phenyl ring (cf., Table 48.1), three five-membered heteroaromatic cycles were attached to the carbene carbon by their positions 2 and 3, respectively (Fig. 48.9). Analyzing their electrochemical oxidation and reduction behavior, the role of the nature of the aromatic system and the influence of the binding position were followed (Table 48.4) and the interpretation was correlated with quantum chemical calculations.

The first reduction represents a two-electron irreversible process similar to that in the previous series. The oxidation pattern of these compounds is analogous to that of **I c**, however, the reversibility at room temperature is partially lost and the cathodic counterpeak is clearly observable only at decreased temperature and higher potential scan rate.

From the Table 48.4 one can follow and distinguish the inductive and the mesomeric effects.

Comparing the influence of the heterocycle itself, the oxidation potentials differ only slightly and follow the sequence of increasing donor ability:  $E_{\text{ox}}$  (fur) >  $E_{\text{ox}}$  (thi) >  $E_{\text{ox}}$  (pyr). The reduction potentials of furane and thiophene derivatives follow the same principle. The situation is different in both methylpyrrol derivatives, where the additional electron-donating effect of the methyl group shifts the potential to significantly more negative values, for example, in the case of **Cr-2-pyr**. (In the latter case, mesomeric effect also plays a role—see below). These results illustrate the inductive effects caused by electron-withdrawing or electron-pushing nature of the studied groups. In this series, however, the difference in inductive effects is rather small.

Comparing the influence of the binding site,  $E_{\text{ox}}$  of the 2- and 3-derivatives of the same heterocycle differ only very slightly (<25 mV). This is in accordance with the above general conclusion that the structural changes in the ligand have a negligible effect on oxidation potential. A significant mesomeric effect, however, manifests itself when comparing the reduction potentials. The 2-hetaryl derivatives are reduced at much less negative potentials than the 3-hetaryl analogs. The difference is caused by the fact that the heterocycle attached in the position 2 can be involved in full conjugation with the carbene double bond, making this part of the molecule planar. Therefore, formation of an enlarged  $\pi$ -system is possible, which makes the reduction much easier by stabilizing the reduction intermediate. The mesomeric effect plays a significant role here as the delocalized system is extended to the heterocycle. A similar effect of an extended  $\pi$ -system on the reduction potential was mentioned above in the case of *p*-carbonyl substituted derivatives.

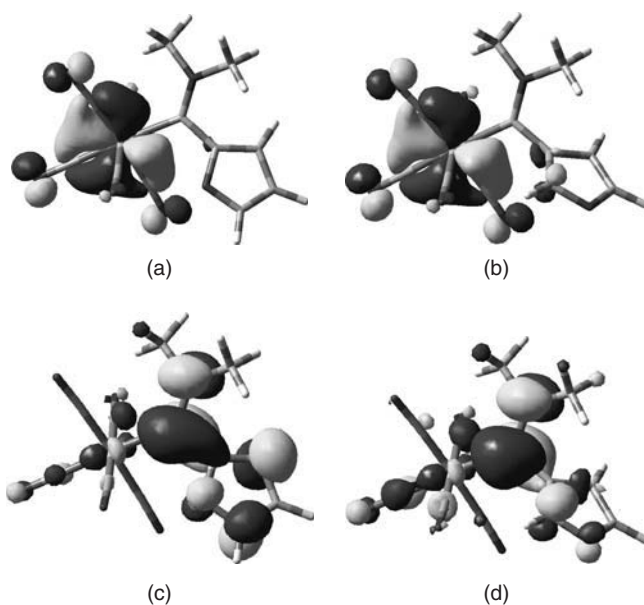


**Figure 48.10** Visualization of HOMO Cr-2-thi (a), HOMO Cr-3-thi (b), LUMO Cr-2-thi (c), and LUMO Cr-3-thi (d).

This conclusion is consistent with the generally known ability of thiophene and pyrrol to form large, linear, delocalized systems (conducting polymers) where the heterocycles are interconnected through the positions 2 and 5.

The correlation of these results with quantum chemical calculations confirms the presented interpretation. As an example, thiophene derivatives were selected, nevertheless, the other heterocycles exhibit a similar behavior. While the HOMOs of **Cr-2-thi** and of **Cr-3-thi** are very similar and are totally localized at the chromium atom and CO ligands (Fig. 48.10a and b), the shapes of their LUMOs differ substantially: The thiophene ring attached to the rest of the molecule **Cr-2-thi** through its position 2 (Fig. 48.10c) forms a nearly planar delocalized system with the carbene grouping, where the heterocycle participates in LUMO substantially (by about 40%). In contrast to this, the LUMO of **Cr-3-thi** (Fig. 48.10d) is localized prevalently on the C–N moiety with only small participation (about 15%) of the heterocycle.

## 48.6 MECHANISTIC INVESTIGATIONS

Generally, during electrochemical oxidation of aminocarbene complexes the central metal atom is oxidized by one electron. The limited CV reversibility of the oxidation process, for example, of hetaryl-substituted aminocarbenes, however, points to a relatively slow follow-up reaction occurring after the primary oxidative electron transfer. During preparative electrolysis at potentials of oxidative limiting current, small bubbles were observed at the surface of the platinum electrode. The IR spectroelectrochemical experiment showed that in the course of electrochemical oxidation, the bands at  $\approx 1930\text{ cm}^{-1}$  belonging to the CO vibration disappear (Fig. 48.11). The electrochemical oxidation is thus followed by a decomposition, which is accompanied by release of CO gas. The process is faster in heterocyclic derivatives.

The electrochemical reduction proceeds at the carbene ligand as a two-electron irreversible process. Since a single reduction wave is observed, the first reduction step must be followed by a very fast chemical reaction yielding the intermediate (probably of radicalic nature), which is reduced even more easily than the starting compound to a final product (the so-called electron transfer, chemical reaction, electron transfer (ECE) mechanism). To understand the mechanism more deeply, the products of electrochemical reduction were separated during the preparative electrolysis from the solution using a continuous extraction to hexane, isolated, and analyzed.

The mass spectra of the **Cr-2-thi** reduction products revealed the presence of *N,N*-dimethyl(thiophen-2-yl)methanamine. The most probable interpretation begins with the reductive splitting of the carbene bond ( $\text{Cr} = \text{C}$ ). The organic intermediate is then protonated by traces of protons from the solvent and reduced to the hydrogenated product. As for the fate of the split-off metal part, the simultaneous IR spectroelectrochemical experiment during the electrolysis confirmed that the vibration bands of the CO groups were present even after the electrolysis, but their energy and number were changed. The chromium carbonyl complexes were thus preserved, but rearranged to lower

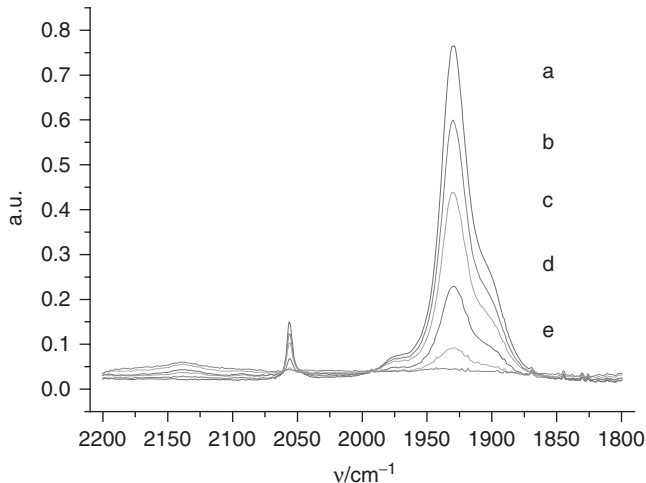


**Figure 48.11** Oxidative electrolysis of **Cr-2-fur**, followed by IR spectra. Time of electrolysis: 0 min—before electrolysis (curve a); 3 min (curve b); 6 min (curve c); 9 min (curve d); 12 min (curve e).

symmetry, yielding most probably dimeric products. This mechanism is consistent with the synthetic use of Fischer aminocarbenes.

#### 48.7 COMPARISON OF AMINOCARBENE AND ALKOXYCARBENE COMPLEXES

Electrochemical measurements permit also a quantitative comparison of two types of Fischer carbene complexes with different stabilizing heteroatom: the aminocarbene complexes of Cr and W (data from Fig. 48.1; Table 48.1) and some analogous alkoxy carbene complexes of Cr and W (data published in Reference 26), whose reduction potentials were measured by cyclic voltammetry under similar conditions (in nonaqueous acetonitrile vs SCE).

Replacement of the dimethylamino group by the methoxy group facilitates reduction of the compounds very strongly—the reduction potentials are shifted positively by about 600 mV as the carbene carbon atom becomes more positively charged when bonded to a more electronegative atom of oxygen. This difference is the most important one. Coming from chromium methoxycarbene to tungsten ones, reduction becomes easier by several tens of millivolts, as in the case of aminocarbenes.

Similarly, the influence of the substituent in para-position of the phenyl ring attached to the carbene carbon on reduction potentials is comparable: For  $[(CO)_5Cr=C(OCH_3)(C_6H_5)]$  complex **I\*c** (analogous to **I c**),  $E_{1/2} = -1.34$  V was found, for  $[(CO)_5Cr=C(OCH_3)(C_6H_4-p-CH_3)]$  complex **I\*b** (analogous to **I b**),  $E_{1/2} = -1.37$  V. This difference of 30 mV corresponds well with the 45 mV difference between **I c** and **I b** reduction potentials.

Oxidation potentials of chromium alkoxy carbene complexes, published in [27], are shifted by about 150 mV toward higher  $E_{ox}$  values comparing with their aminocarbene analogs. The sense of the shift reflects electronegativity of the oxygen heteroatom and its small size (comparing with the shift of  $E_{red}$  mentioned above) gives evidence that oxidation is less sensitive to changes in the carbene ligand structure.

#### 48.8 SUMMARY

An overview of systematic fundamental electrochemical investigation of about 40 compounds was presented and discussed. The interpretation of experimental data offered a more detailed insight into electronic and redox properties of the title compounds, their reactivity, and reaction mechanisms. As a result, important structural parameters influencing reduction and/or oxidation potentials and stability of intermediates were described and discussed.

The electrochemically acquired  $E_{ox}$  and  $E_{red}$  values were treated by the LFER approach in order to find the extent of electron intramolecular communication, to localize redox centers and to reveal and explain eventual abnormalities. Simultaneously, the role of sterical hindrance and molecular geometry in intramolecular electronic communication was evaluated.

Potential of oxidation depends on the central metal nature and on the presence of  $\pi$ -accepting ligands.  $E_{\text{ox}}$  of the Cr complexes reflects only the number of CO ligands. Behavior of the Fe compounds, with lower coordination number and shorter M–L bonds, shows that the  $\eta^2$ -bonded allyl group and the carbene double bond also act as important  $\pi$ -acceptors.

Owing to the fact that aminocarbene are “non-innocent” ligands,  $E_{\text{red}}$  is governed mainly by substitution of the carbene carbon atom and it is sensitive to the presence of a  $\pi$ -conjugated electron system. The conclusions have been supported by other experimental and theoretical methods (NMR, IR, and UV-vis spectrometry; mass spectra; MO calculations). The presented conclusions can be used in targeted design of next “generations” of aminocarbene complexes with specific redox requirements for application as, for example, catalysts.

Electrochemistry is a strong experimental tool for fundamental investigation and understanding of electronic properties of molecules (intramolecular interactions, extent of delocalization, relationship between structure and redox properties). Suitable electrochemical treatment reveals even very subtle features and “irregularities,” provokes questions, and suggests the answers. For their proof, combination with spectrometry and correlation with quantum chemistry is necessary.

## REFERENCES

1. Herndon, J. W. *Coord. Chem. Rev.* **2012**, *256*, 1281.
2. Green, J. C.; Herbert, B. J. *Dalton Trans.* **2005**, 1214.
3. Hegedus, L. S. *Transition Metals in the Synthesis of Complex Organic Molecules*; University Science Books: Sausalito, **1994**.
4. Dotz, K. H.; Stendel, J. *J. Chem. Rev.* **2009**, *109*, 3227.
5. Santamaría, J. *J. Curr. Org. Chem.* **2009**, *13*, 31.
6. Watanuki, S.; Ochiai, N.; Mori, M. *Organometallics* **1995**, *14*, 4129.
7. Fernández-Rodrígues, M. A.; García-Carcía, P.; Aguillar, E. *Chem. Commun.* **2010**, *64*, 7670.
8. Zuman, P. *Substituent Effects in Organic Polarography*; Plenum Press: New York, **1967**.
9. Hoskova, I.; Roháčová, J.; Meca, L.; Tobrman, T.; Dvořák, D.; Ludvík, J. *Electrochim. Acta* **2005**, *50*, 4911.
10. Hoskova, I.; Roháčová, J.; Dvořák, D.; Tobrman, T.; Záliš, S.; Zvěřinová, R.; Ludvík, J. *Electrochim. Acta* **2010**, *55*, 8341.
11. Exner, O. In Correlation Analysis in Chemistry, Recent Advances; Chapman, N.B., Shorter, J., Eds., Plenum Press, New York-London, **1978**; Chapter 10.
12. Klein, E.; Lukeš, V.; *J. Mol. Struct. (THEOCHEM)* **2006**, *767*, 43; **2007**, *805*, 153.
13. Pombeiro, A. J. L. *Eur. J. Inorg. Chem.* **2007**, 1473. (review) and references therein.
14. Sawyer, D. T.; Sobkowiak, A.; Roberts, J. L. *Electrochemistry for Chemists*; John Wiley & Sons, Ltd: Chichester, **1995**.
15. Kvapilová, H.; Domingo Tor, A.; Kayanuma, M.; Daniel, Ch.; Záliš, S., submitted.
16. Kaim, W.; Schwederski, B. *Coord. Chem. Rev.* **2010**, *254*, 1580.
17. Dzik, W. I.; Zhang, X. P.; de Bruin, B. *Inorg. Chem.* **2011**, *50*, 9896.
18. Baldoli, C.; Cerea, P.; Falciai, L.; Ginnini, C.; Licandro, E.; Maiorana, S.; Mussini, P.; Perdicchia, D. *J. Organomet. Chem.* **2005**, *690*, 5777.
19. Schubert, U. *Coord. Chem. Rev.* **1984**, *55*, 261.
20. Amin, S. R.; Jayaprakash, K. N.; Nandi, M.; Sathe, K. M.; Sarkar, A. *Organometallics* **1996**, *15*, 3528.
21. Tobrman, T.; Meca, L.; Dvořák, H.; Černý, J.; Dvořák, D. *Organometallics* **2006**, *25*, 5540.
22. Vyklický, I.; Dvořáková, H.; Dvořák, D. *Organometallics* **2001**, *20*, 5419.
23. Hoskova, I.; Zvěřinová, R.; Roháčová, J.; Dvořák, D.; Záliš, S.; Ludvík, J. *Electrochim. Acta* **2011**, *56*, 6853.
24. Zuman, P.; Manoušek, O.; Vig, S. K. *J. Electroanal. Chem.* **1968**, *19*, 147.
25. Metelková, R.; Tobrman, T.; Kvapilová, H.; Hoskova, I.; Ludvík, J. *Electrochim. Acta* **2012**, *82*, 470.
26. Casey, C. P.; Albin, L. D.; Saeman, M. C.; Evans, D. H. *J. Organomet. Chem.* **1978**, *155*, C37.
27. Lloyd, M. K.; McCleverty, J. A.; Orchard, D. G.; Connor, J. A.; Hall, M. B.; Hillier, I. H.; Jones, E. M.; McEwen, G. K. *J. Chem. Soc. Dalton Trans.* **1973**, *17*, 1743.
28. Exner, O. Correlation Analysis of Chemical Data; Plenum Press: New York, **1988**.



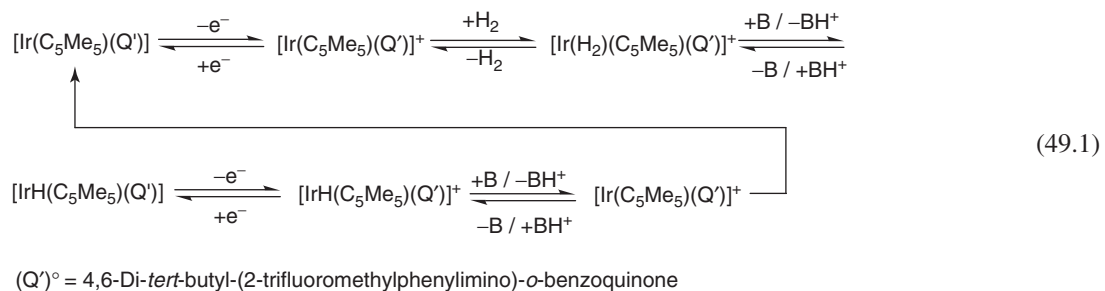
# ELECTRON TRANSFER-INDUCED COORDINATION CHANGES IN ORGANOMETALLIC COMPLEXES WITH NONINNOCENT HEMILABILE LIGANDS

WOLFGANG KAIM\*, MARTINA BUBRIN, AND RALPH HÜBNER

*Institut für Anorganische Chemie, Universität Stuttgart, Stuttgart, Germany*

## 49.1 INTRODUCTION

The recognition of “noninnocent” ligand behavior of redox-active molecules bound to transition metals has become a popular exercise in electron transfer research [1]. While the emphasis has long been on the establishing of appropriate oxidation states by various physical methods such as structure determination, magnetic analysis, or spectroscopy [2, 3], there is an increasing tendency to use this concept for understanding, inducing, and controlling the chemical reactivity. Recently highlighted examples include unexpected oxidative addition processes [4], the activation of coordinated olefins [5], the creation of useful radicals from organometallics [6], or the mimicking of hydrogenase behavior ( $H_2/2H^+$  conversion) [7]. Especially the latter example (Eq. 49.1) has received considerable attention [8] because the relatively inert prototypical “small molecule” dihydrogen could be oxidized by reversibly converting a dianionic *o*-amidophenolate “noninnocent” ligand into an anion radical containing reactive intermediate complex (“redox-switched  $H_2$  oxidation”) [7a].



Unconnected to the recent developments [1–7] around noninnocent ligand behavior, it has long been recognized that hemilabile ligands (Eq. 49.2) [9, 10] in coordination compounds can be valuable constituents of active homogeneous catalysts through the reversible creation of vacant coordination sites for substrates [11]. The control of hemilability has

been competently discussed; however, the involvement of redox-active ligands capable of influencing hemilability through fractional charge transfer remained an area essentially unexplored.

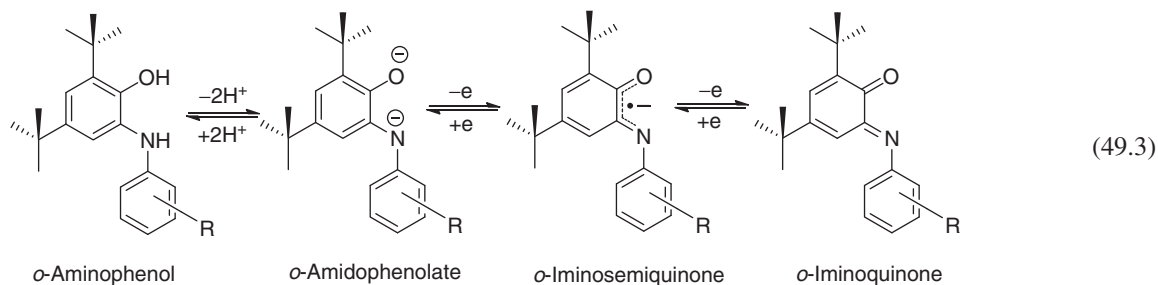


Within the reviewed research field of noninnocent ligand chemistry [3, 12, 13], our own attempts have focused on the scope and consequences of electron transfer. An additional aspect is the recognition of noninnocent ligands in the bioinorganic context [13] where the metal-ligand interplay often facilitates the catalysis of multielectron processes [13, 14].

Among the noninnocent ligands, the 1,2-dioxolene (*o*-quinone/catecholate) redox system has been favored because of its stability (via chelate binding) and variability (via substitution of O by NR functions and of H by substituents). While the aromatic catecholate forms are  $\sigma$ - and  $\pi$ -electron rich, the semiquinones and especially the quinones are  $\pi$ -electron accepting.

Equation 49.3 shows the redox system that is based on modified *o*-quinones, propagated by Wieghardt, Chaudhuri, Neese and coworkers [2, 15], reviewed in 2009 [16], and structurally categorized by Brown [17] in 2012. It combines

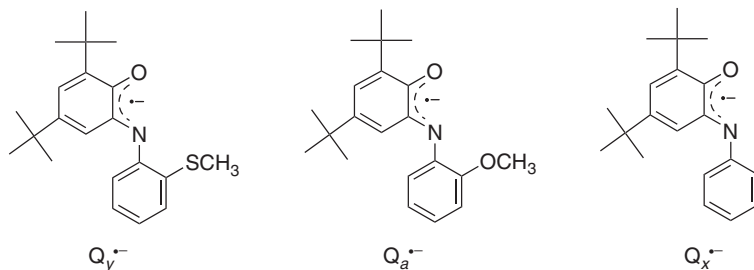
1. steric protection of the sensitive O donor atom,
2. good basicity through the N function,
3. widely variable tuning potential through the N substituent.



The N-aryl groups in (Eq. 49.3) can include

- R = H (the parent system without additional coordination function and steric hindrance),
- R = *o*-CF<sub>3</sub> (the Ringenberg/Rauchfuss example [7] without additional coordination function but steric bulk),
- R = *o*-OMe (containing a weakly coordinating ether function in strategic ortho position for potential coordination),
- R = *o*-SMe (having a potentially coordinating [18, 19] thioether group in strategic ortho position),
- R = *m*-SMe (having the electronic effect of the thioether in meta position without the chelate coordination capability).

The potentially coordinating neutral O or S functions constitute the labile part (2: Y) of the hemilabile chelate ligands, which can thus adopt either a bidentate or a meridional tridentate function (see Q<sub>y</sub><sup>•-</sup> and Fig. 49.1 [20]).



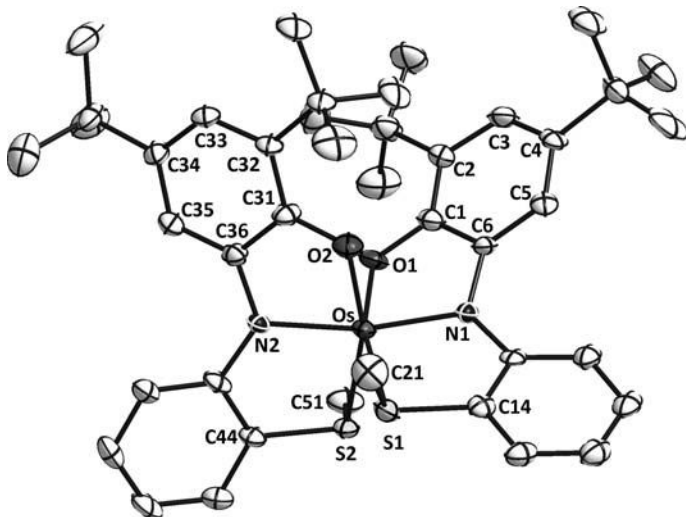
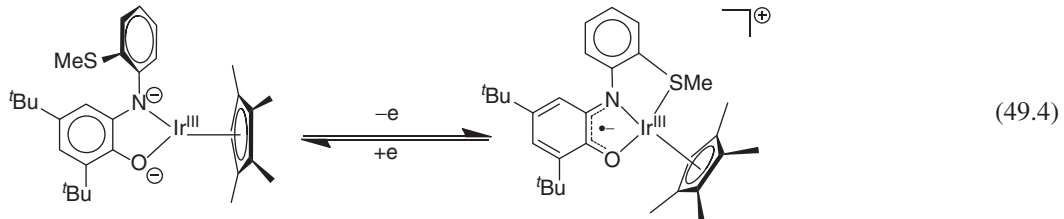


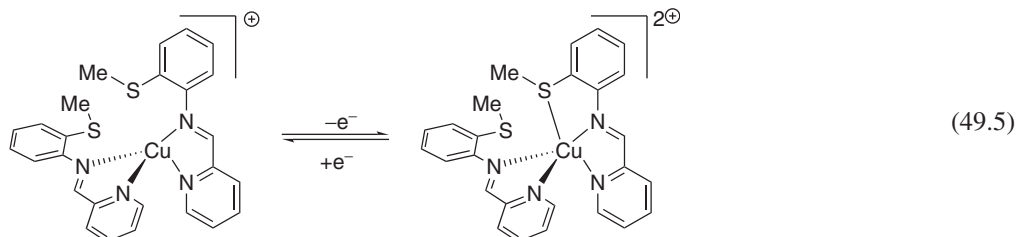
**Figure 49.1** Molecular structure of  $[\text{Os}(\text{Q}_y)_2]$  ( $\text{R} = \text{o-SMe}$ ) [20].

## 49.2 DISCUSSION OF RESULTS

Using the hemilabile noninnocent ligand 4,6-di-*tert*-butyl-(2-methylthiophenylimino)-*o*-benzosemiquinone  $\text{Q}_y^{\bullet-}$  (which was developed during efforts to modify a radical/metal/radical three-spin interaction) [18], we could obtain and investigate a system (Eq. 49.4) to prove a predominantly *ligand-based* electron transfer during the reversible coordination of a thioether sulfur donor [19].



Electron-transfer-dependent reversible coordination changes are known from systems with mostly metal-based electron transfer, for example, for  $\text{Cu}^{\text{I}}/\text{Cu}^{\text{II}}$  couples such as (Eq. 49.5) [21],

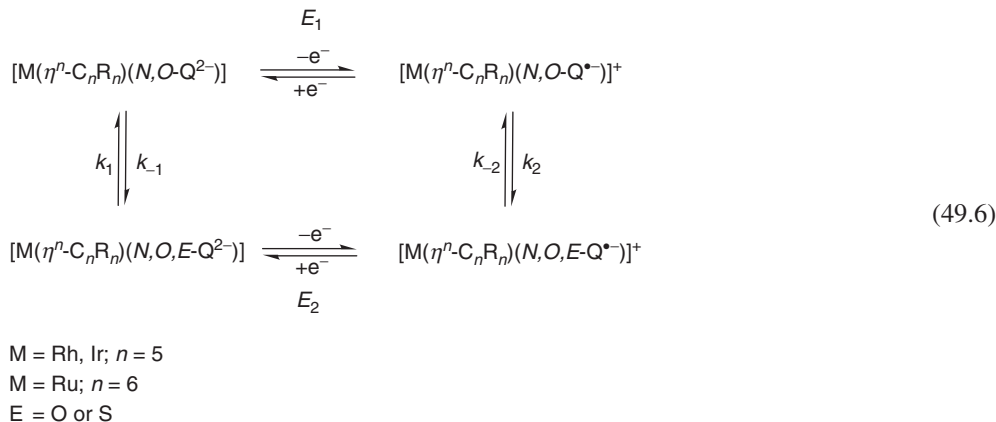


however, the electron paramagnetic resonance (EPR) and computational analysis of the system (Eq. 49.4) reveals only a fractional spin amount  $\delta$  of about 8%, delocalized from the iminosemiquinone ligand to the 5d transition metal in the reactive oxidized form. The potentially  $\text{H}_2$  activating metal [7] thus adopts an  $18 + \delta$  valence electron configuration, in agreement with previous concepts of organometallic electron transfer activation involving fractional oxidation states [22].

Separately prepared and characterized  $[\text{Ir}(\text{C}_5\text{Me}_5)(\text{Q}_y)]$  and its oxidized form  $[\text{Ir}(\text{C}_5\text{Me}_5)(\text{Q}_y)](\text{PF}_6)$  were found to be connected via Eq. 49.4 before a fully reversible second oxidation for the couple  $[\text{Ir}(\text{C}_5\text{Me}_5)(\text{Q}_y)]^{2+/+}$  takes place.

Structural evidence, supported by DFT calculations, was available to clarify this reactivity: The neutral  $[\text{Ir}(\text{C}_5\text{Me}_5)(\text{Q}_y)]$  exhibits coordinative unsaturation because the electron deficit at the trivalent metal is mitigated by strong  $\sigma$ - and  $\pi$ -electron donation from an *o*-amidophenolate ligand with averaged and little variable C–C distances of about 1.39 Å in the aromatic ring. Such coordinative unsaturation for  $d^6$  systems has also been found for related  $[\text{Ir}(\text{C}_5\text{Me}_5)(\text{Q}')]$  [7] and  $[\text{Ir}(\text{C}_5\text{Me}_5)(\text{RNCHCHNR})]$  [23] systems as well as for  $[\text{Rh}(\text{C}_5\text{Me}_5)(\text{cat})]$ ,  $[\text{Cr}(\text{CO})_3(\text{cat})]^{2-}$  and  $[\text{Mn}(\text{CO})_3(\text{cat})]^-$ , cat = catecholate [24]. Consequently, there is no bonding interaction between Ir and S ( $d > 4.0$  Å), and the further structure parameters of the ligand reveal not only an aromatic ring but also C–O and C–N single bonds.

On one-electron oxidation, the structure rearranges characteristically Eq. 49.4: Iridium–sulfur coordination occurs with a standard [25] bond length of 2.35 Å, leading to coordinative saturation, a piano-stool arrangement. The metric parameters of the noninnocent ligand reveal bond alternance compatible with a benzosemiquinone ring as well as shortened C–O and C–N bonds. In addition to UV–vis–NIR spectroelectrochemical analysis [19], electron spin resonance (ESR) spectroscopy shows DFT-supported  $g$  tensor components at  $g_1 = 1.996$ ,  $g_2 = 1.985$ , and  $g_3 = 1.951$ ,  $A_3(^{14}\text{N}) = 1.7$  mT. This observation illustrates nonnegligible metal contributions [about 8% according to density functional theory (DFT)] from a 5d element with a high spin-orbit coupling constant. The cation is essentially an anion radical complex [26], corresponding to a semiquinone/Ir<sup>III</sup> formulation [23]. Apparently, the one-electron oxidation of the *o*-amidophenolate to the *o*-iminobenzosemiquinonate is sufficient to remove the tolerance of coordinative unsaturation, resulting in binding of either weakly donating thioether-S [19], dihydrogen [7], or halogen species [23]. Square schemes (Eq. 49.6), similar to those derived for electron transfer-induced isomerizations [27], involving calculated structures and energy differences can illustrate and confirm that the *indirect* oxidative addition [28] *at the metal* involving one-electron exchange [29] *on the ligand* is made possible through the participation of a noninnocently behaving ligand while maintaining a formally invariant metal oxidation state.



This variant differs from the classical oxidative addition—reductive elimination sequence, one of the most useful and most frequently applied reaction patterns in transition metal chemistry [28]. Metal-based electron configuration changes such as the  $d^8/d^6$  two-electron interchange have been employed to provide very different coordination situations for substrate binding, conversion, and release, and the special one-electron variant may also prove useful.

The different (electro)chemical reversibility patterns of two-step oxidation processes involving  $[\text{Ir}(\text{C}_5\text{Me}_5)]^{2+}$  are remarkable: While the  $[\text{Ir}(\text{C}_5\text{Me}_5)(\text{Q}')]^n$  system exhibits two conventional waves in the cyclic voltammogram [7], the  $[\text{Ir}(\text{C}_5\text{Me}_5)(\text{RNCHCHNR})]^n$  redox system with R = 2,6-dimethylphenyl showed a reversible first but irreversible second oxidation in propylene carbonate [23]. In yet another variant, the example  $[\text{Ir}(\text{C}_5\text{Me}_5)\text{Q}_y]^{0/+2+}$  described here (Eq. 49.4) is distinguished by a first oxidation process of the N,O-coordinated species involving intramolecular thioether coordination after initial electron transfer. The return wave in the cyclic voltammogram is due to the reduction of N,O,S-coordinated  $[\text{Ir}(\text{C}_5\text{Me}_5)\text{Q}_y]^+$  at considerably shifted potential [19].

The above example has shown in a prototypical way the relationship between a reactive (here even catalytically active) metal complex redox system and an intramolecular model exhibiting a hysteresis-type structure change as a response to electron transfer. To generalize this behavior, we have recently explored [30] the following modifications:

1. using an O-ether ( $\text{Q}_a$ ) instead of an S-ether function ( $\text{Q}_y$ ) in the ligand;
2. removing  $n$ -donor functions from the ortho-positions of the ligand ( $\text{Q}_x$ );

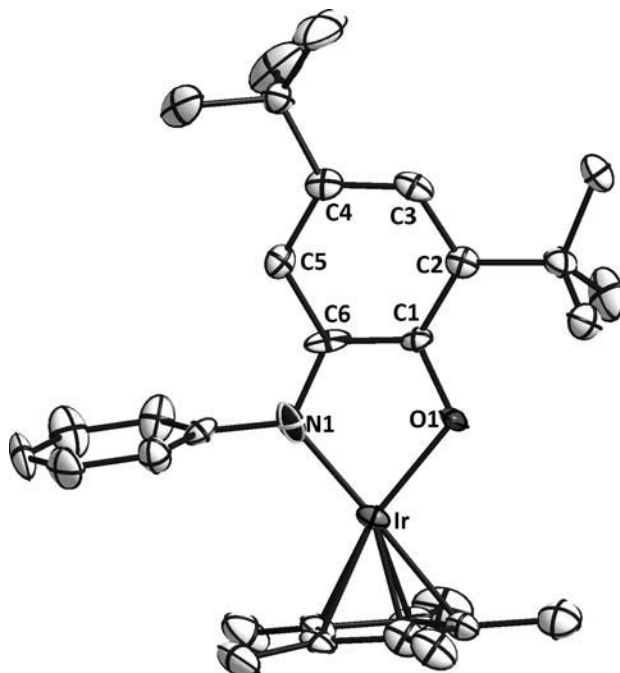


**Figure 49.2** Molecular structure of  $[(C_5Me_5)Ir(Q_x)]$ .

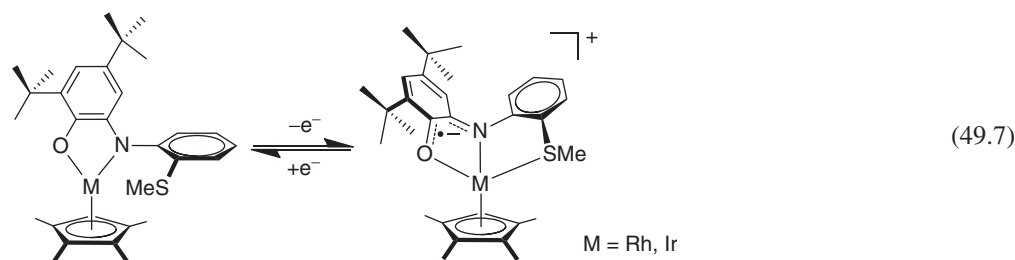
3. replacing Ir by the lighter homolog Rh;
4. replacing the  $M(\eta^5-C_5R_5)$  organometallic fragment ( $M = Rh, Ir$ ) by  $Ru(\eta^6-C_6R_6)$ ,  $C_6R_6 = p$ -cymene = 1-iso-propyl-4-methyl-benzene = Cym.

To start with, all neutral precursor complexes exhibit the previously mentioned coordinative unsaturation at the metal (see Fig. 49.2) [30] caused by the highly electron-rich  $o$ -amidophenolate ligands such as  $Q_y^{2-}$ ,  $Q_a^{2-}$ , or  $Q_x^{2-}$ .

The first oxidation of the iridium complexes  $[Ir(C_5Me_5)(Q)]^{0/+}$  shows different manifestations of the ECEC process (Eq. 49.6). A large splitting is noted between anodic and cathodic peak potentials,  $E_{pa}$  and  $E_{pc}$ , at  $-0.15$  and  $0.60$  V versus  $Fe^{+/-}$  in  $CH_2Cl_2/0.1$  M  $Bu_4NPF_6$  (250 mV/s) for the structurally characterized thioether example ( $Q = Q_y$ ) [19]. By comparison, the corresponding values at  $-0.10/-0.26$  V ( $Q = Q_a$ ) and  $-0.03/-0.12$  V ( $Q = Q_x$ ) illustrated in Figure 49.3 show much smaller effects [30]. The  $O$ -ether donor function is expected to coordinate in a much more labile bond than the thioether analog, and with absent intramolecular donors the  $E_{pa}/E_{pc}$  difference becomes rather normal, approaching 60 mV. It has to be noted that the not completely “noncoordinating” anions in the excess of electrolyte can albeit weakly bind to the oxidized compounds in order to remove coordinative unsaturation. In contrast, the second oxidation  $[Ir(C_5Me_5)(Q)]^{+/2+}$  is generally well behaved ( $E_{pa} - E_{pc} < 0.07$  V; Fig. 49.3), reflecting negligible structural change [19, 30].

The replacement of iridium by rhodium in the redox systems  $[M(C_5Me_5)(Q)]^{n/n+1}$  is illustrated in Figure 49.4.

The data analysis [30] reveals less pronounced wave distortion for the first oxidations: The peak potentials  $E_{pa}$  and  $E_{pc}$ , at  $-0.26$  and  $0.40$  V versus  $Fe^{+/-}$  in  $CH_2Cl_2/0.1$  M  $Bu_4NPF_6$  (250 mV/s) for  $Q = Q_y$  and  $-0.12/-0.20$  V ( $Q = Q_a$ ) show less splitting than in the iridium system. However, the behavior of the first oxidation wave (Fig. 49.4) still signifies a structural change according to Eq. 49.7.



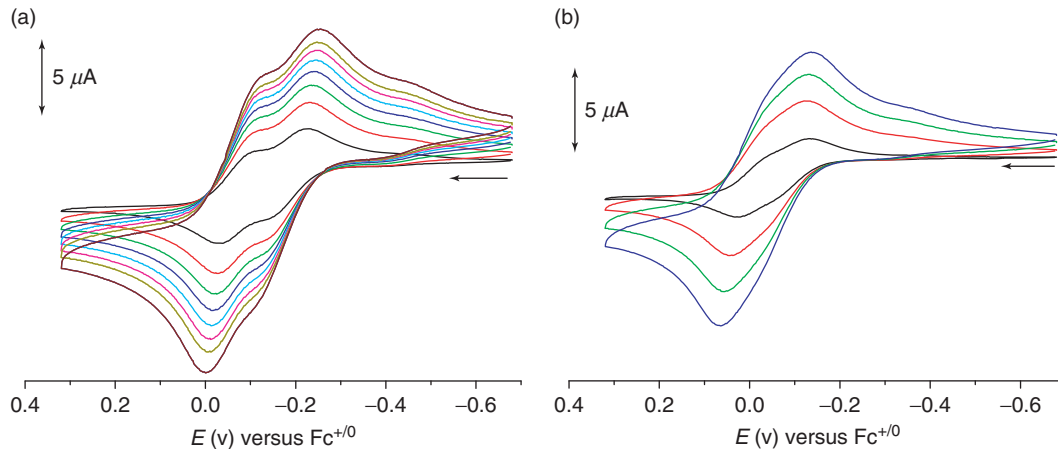


**Figure 49.3** Cyclic voltammograms of (a)  $[(C_5Me_5)Ir(Q_a)]$  and (b)  $[(C_5Me_5)Ir(Q_x)]$  in  $CH_2Cl_2/0.1\text{ M }Bu_4NPF_6$  at different scan rates. (See insert for color representation of the figure.)

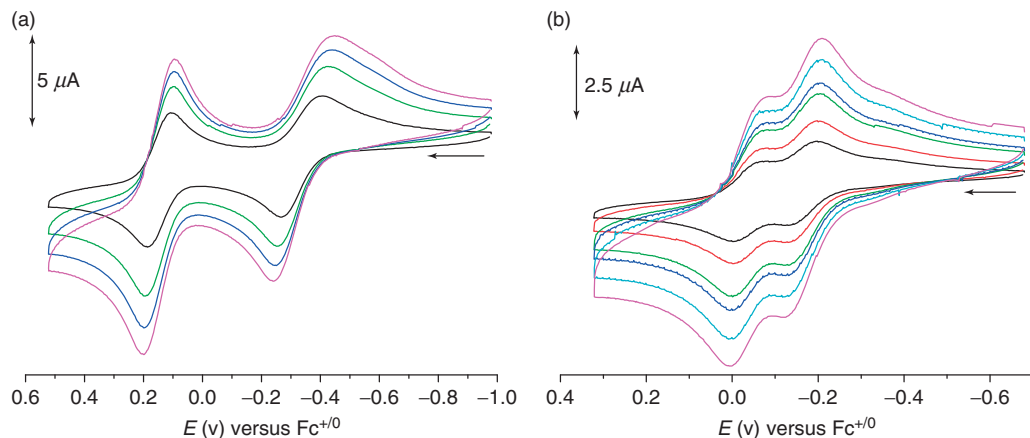
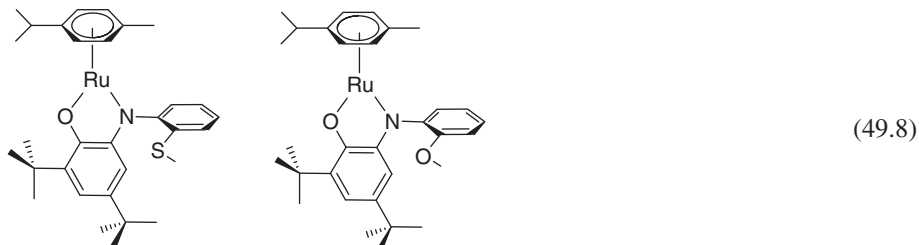


**Figure 49.4** Cyclic voltammograms of (a)  $[(C_5Me_5)Rh(Q_y)]$  and (b)  $[(C_5Me_5)Rh(Q_a)]$  in  $CH_2Cl_2/0.1\text{ M }Bu_4NPF_6$  at different scan rates. (See insert for color representation of the figure.)

A notable feature is the small difference between the potentials for first and second oxidation in the case of  $Q = Q_a$  or  $Q_x$ . A careful analysis of the whole set in terms of kinetics and equilibrium constants will be required to rationalize this effect.

An important kind of information regarding the electronic structure comes from EPR spectroscopy of the paramagnetic intermediates [19], which are also crucial for the small molecule activation reactivity [7]. Figure 49.5 shows the spectrum for  $[Rh(C_5Me_5)(Q_a)]^+$  at 110 K, which, like that of  $[Ir(C_5Me_5)(Q_y)]^+$  [19], illustrates largely semiquinoneimine ligand-based spin and no  $Rh^{II}$  or  $Rh^{IV}$  configuration.

Employing the correspondence [31, 32] of complexes  $[(\eta^n-C_nR_n)M(Q)]^x$ ,  $M = Ir$  or  $Rh$  and  $n = 5$  with organometallic “half-sandwich” analog involving  $M = Ru$  and  $n = 6$ , we have recently obtained the ruthenium compounds (Eq. 49.8) with  $C_6R_6 = p$ -cymene = Cym, and characterized them electrochemically.



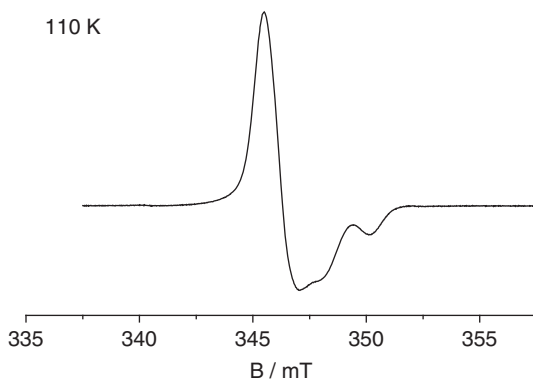
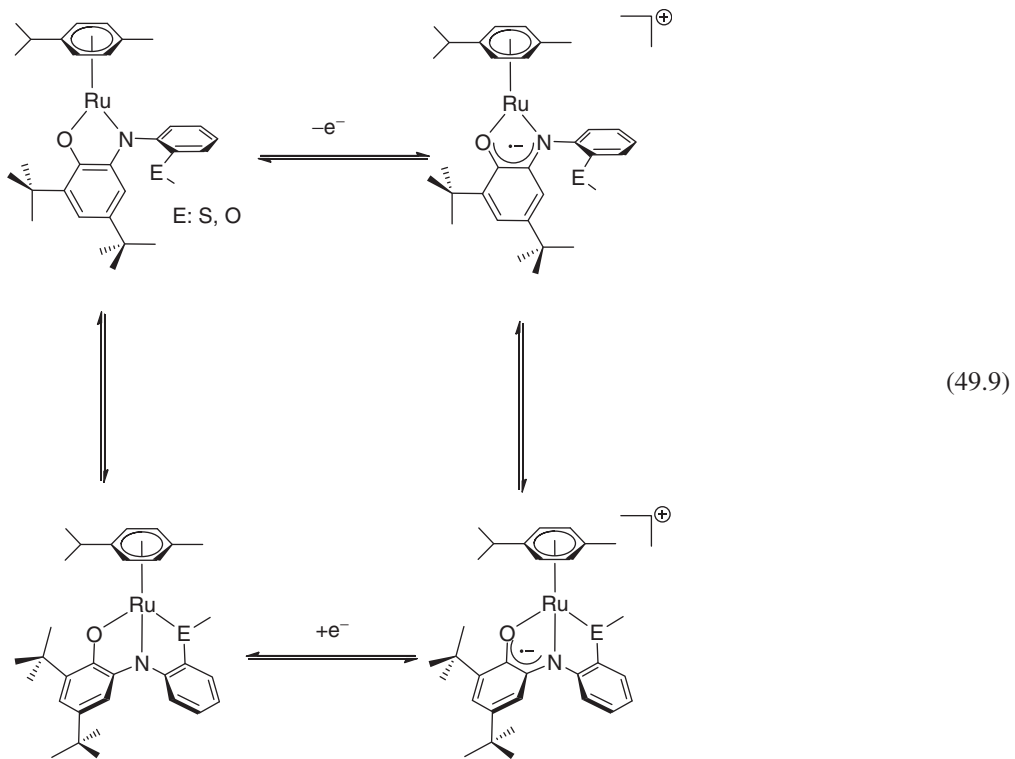


**Figure 49.5** X-Band EPR spectrum of  $[(\text{C}_5\text{Me}_5)\text{Rh}(\text{Q}_a)]^+$  at 110 K, generated *in situ* in  $\text{CH}_2\text{Cl}_2/0.1 \text{ M } \text{Bu}_4\text{NPF}_6$ .

Areneruthenium compounds are popular organometallic complex fragments in areas such as catalysis [33] and inorganic drug development [34]. Figure 49.6 shows that the systems  $[\text{Ru}(\text{Cym})(\text{Q})]^n$  behave similarly to the  $\text{M}(\text{C}_5\text{Me}_5)$  examples described earlier, suggesting an ECEC mechanism (Eq. 49.9) for the first oxidation. Differences between the thioether ( $\text{Q} = \text{Q}_y$ ) and *O*-ether analogs ( $\text{Q} = \text{Q}_a$ ) will have to be analyzed quantitatively with the help of digital simulation and DFT-supported spectroelectrochemistry [35, 36].



### 49.3 CONCLUDING REMARKS

Using a series of new coordination compounds of some platinum group metals with potentially hemilabile redox-active chelate ligands based on the *o*-benzosemiquinoneimine intermediate, the extent of noninnocent behavior has been established experimentally, via structure determination and EPR, UV-vis-NIR spectroelectrochemistry [35, 36], and computationally

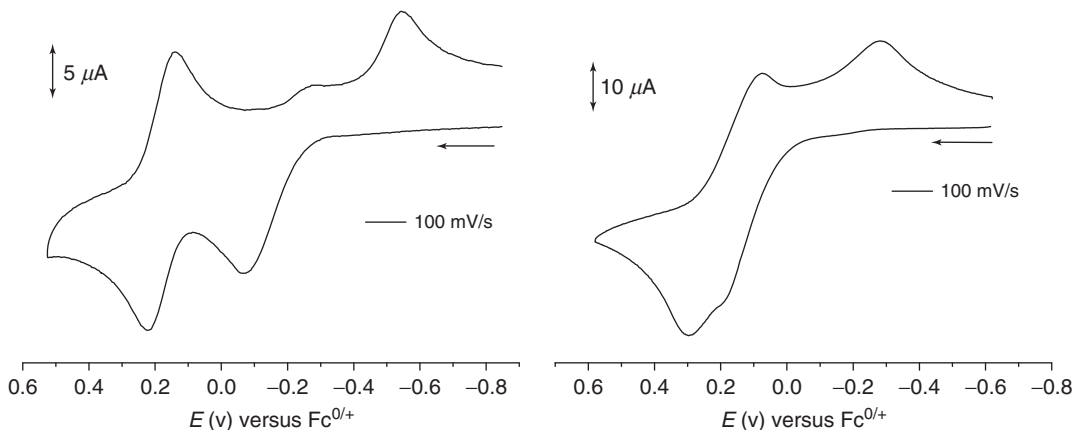


**Figure 49.6** Cyclic voltammograms of (a)  $[\text{Ru}(\text{Cym})(\text{Q}_y)]$  and (b)  $[\text{Ru}(\text{Cym})(\text{Q}_a)]$  in  $\text{CH}_2\text{Cl}_2/0.1 \text{ M } \text{Bu}_4\text{NPF}_6$ .

(DFT). As a consequence of the fractional oxidation-state situation corresponding to an  $18 + \delta$  valence electron count, we can expect a potential to adopt unusual metal configurations through electron-transfer-dependent intramolecular coordination, accompanied by intermolecular reactivity enhancement toward small molecule activation.

One possible function of complexes with noninnocent hemilabile ligands is their role as intramolecular models for intermolecular reactivity, involving weak donor substrates such as dihydrogen. Like for the spin-shift example  $[\text{Cu}(\text{Q}_y)_2]$  described previously [18], it is remarkable that a rather small change in metal/ligand interaction can bring about a qualitatively altered behavior, for example, in terms of coordination number and substrate activation.

## ACKNOWLEDGMENTS

Support from the Land Baden-Württemberg and from the COST program is gratefully acknowledged. Special thanks are due to Angela Winkelmann for her contributions to the preparation of this article and to Drs. Jan Fiedler and Stanislav Záliš (J. Heyrovský Institute, Prague, Czech Republic) for continued cooperation.

## REFERENCES

1. (a) Chirik, P. J. *Inorg. Chem.* **2011**, *50*, 9737; (b) Special Issue: Cooperative & Redox Non-Innocent Ligands in Directing Organometallic Reactivity, *Eur. J. Inorg. Chem.* **2012**, 340.
2. Chaudhuri, P.; Verdani, C.N.; Bill, E.; Bothe, E.; Weyhermüller, T.; Wieghardt, K. *J. Am. Chem. Soc.* **2001**, *123*, 2213.
3. Kaim, W. *Inorg. Chem.* **2011**, *50*, 9752.
4. Haneline, M. R.; Heyduk, A. F. *J. Am. Chem. Soc.* **2006**, *128*, 8410.
5. Boyer, J. L.; Cundari, T. R.; DeYonker, N. J.; Rauchfuss, T. B.; Wilson, S. R. *Inorg. Chem.* **2009**, *48*, 638.
6. (a) Dzik, W. I.; Zhang, X. P.; de Bruin, B. *Inorg. Chem.* **2011**, *50*, 9896; (b) Hetterscheid, D. G. H.; Grützmacher, H.; Koekoek, A. J. J.; de Bruin, B. *Progr. Inorg. Chem.* **2007**, *55*, 247.
7. (a) Ringenberg, M. R.; Kokatam, S. L.; Heiden, Z. M.; Rauchfuss, T. B. *J. Am. Chem. Soc.* **2008**, *130*, 788; (b) Ringenberg, M. R.; Nilges, M. J.; Rauchfuss, T. B.; Wilson, S. R. *Organometallics* **2010**, *29*, 1956; (c) Ringenberg, M. R.; Rauchfuss, T. B. *Eur. J. Inorg. Chem.* **2012**, 490.
8. (a) Geiger, W. E. *Organometallics* **2011**, *30*, 28; (b) Lyaskovskyy, V.; de Bruin, B. *ACS Catal.* **2012**, *2*, 270.
9. Jeffrey, J. C.; Rauchfuss, T. B. *Inorg. Chem.* **1979**, *18*, 2658.
10. Braunstein, P.; Naud, F. *Angew. Chem.* **2001**, *113*, 702; *Angew. Chem. Int. Ed.* **2001**, *40*, 680.
11. Steinborn, D. *Fundamentals of Organometallic Catalysis*; Wiley-VCH Verlag GmbH, Weinheim, **2012**; p 155.
12. Kaim, W. *Eur. J. Inorg. Chem.* **2012**, 343.
13. Kaim, W.; Schwederski, B. *Coord. Chem. Rev.* **2010**, *254*, 1580.
14. Praneeth, V. K. K.; Ringenberg, M. R.; Ward, T. R. *Angew. Chem. Int. Ed.* **2012**, DOI: 10.1002/anie.201204100.

15. Herebian, D.; Bothe, E.; Neese, F.; Weyhermüller, T.; Wieghardt, K. *J. Am. Chem. Soc.* **2003**, *125*, 9116.
16. Poddel'sky, A. I.; Cherkasov, V. K.; Abakumov, G. A. *Coord. Chem. Rev.* **2009**, *253*, 291.
17. Brown, S. N. *Inorg. Chem.* **2012**, *51*, 1251.
18. Ye, S.; Sarkar, B.; Lissner, F.; Schleid, Th.; van Slageren, J.; Fiedler, J.; Kaim, W. *Angew. Chem.* **2005**, *117*, 2140; *Angew. Chem. Int. Ed.* **2005**, *44*, 2103.
19. Hübner, R.; Weber, S.; Strobel, S.; Sarkar, B.; Záliš, S.; Kaim, W. *Organometallics* **2011**, *30*, 1414.
20. Hübner, R.; Sarkar, B.; Záliš, S.; Kaim, W. *Eur. J. Inorg. Chem.* **2012**, 3569.
21. Schnödt, J.; Manzur, J.; Garcia, A.-M.; Hartenbach, I.; Su, C.-Y.; Fiedler, J.; Kaim, W. *Eur. J. Inorg. Chem.* **2011**, 1436.
22. Klein, A.; Vogler, C.; Kaim, W. *Organometallics* **1996**, *15*, 236.
23. Kaim, W.; Sieger, M.; Greulich, S.; Sarkar, B.; Fiedler, J.; Záliš, S. J. *Organomet. Chem.* **2010**, *695*, 1052.
24. (a) Espinet, P.; Bailey, P. M.; Maitlis, P. M. *J. Chem. Soc. Dalton Trans.* **1979**, 1542; (b) Dahrenbourg, D. J.; Klausmeyer, K. K.; Reibenspies, J. H. *Inorg. Chem.* **1995**, *34*, 4676; (c) Hartl, F.; Vlček, Jr., A.; deLearie, L. A.; Pierpont, C. G. *Inorg. Chem.* **1990**, *29*, 1073; (d) Hartl, F.; Stufkens, D. J.; Vlček, A. *Inorg. Chem.* **1992**, *31*, 1687.
25. (a) Albrecht, M.; Scheiring, T.; Sixt, T.; Kaim, W. *J. Organomet. Chem.* **2000**, *596*, 84; (b) Ye, S.; Kaim, W.; Albrecht, M.; Lissner, F.; Schleid, T. *Inorg. Chim. Acta* **2004**, *357*, 3325.
26. Kaim, W. *Coord. Chem. Rev.* **1987**, *76*, 187.
27. Pombeiro, A. J. L.; Guedes da Silva, M. F. C.; Lemos, M. A. N. D. A. *Coord. Chem. Rev.* **2001**, *219–221*, 53.
28. Crabtree, R. H. *The Organometallic Chemistry of the Transition Metals*, 5th ed.; Wiley-VCH Verlag GmbH: Weinheim, **2009**, Chapter 6.
29. Tejel, C.; Ciriano, M. A.; López, J. A.; Jiménez, S.; Bordonaba, M.; Oro, L. A. *Chem. Eur. J.* **2007**, *13*, 2044.
30. Hübner, R. Dissertation, Universität Stuttgart, **2011**.
31. Kaim, W.; Reinhardt, R.; Sieger, M. *Inorg. Chem.* **1994**, *33*, 4453.
32. Kaim, W. In *New Trends in Molecular Electrochemistry*; Pombeiro, A. J. L., Ed., Fontis Media: Lausanne, **2004**, p 127.
33. Therrien, B. *Coord. Chem. Rev.* **2009**, *253*, 493.
34. Kilpin, K. J.; Clavel, C. M.; Edafe, F.; Dyson, P. J. *Organometallics* **2012**, *31*, 7031.
35. Kaim, W.; Klein, A., Eds. *Spectroelectrochemistry*; Royal Society of Chemistry: Cambridge, **2008**.
36. Kaim, W.; Fiedler, J. *Chem. Soc. Rev.* **2009**, *38*, 3373.



# REDOX POTENTIAL–STRUCTURE RELATIONSHIPS AND PARAMETERIZATION IN CHARACTERIZATION AND IDENTIFICATION OF ORGANOMETALLIC COMPOUNDS

M. FÁTIMA C. GUEDES DA SILVA\*

*Centro de Química Estrutural, Instituto Superior Técnico, Universidade de Lisboa, Lisboa, Portugal; Universidade Lusófona de Humanidades Tecnologias, ULHT, Lisboa, Portugal*

ARMANDO J. L. POMBEIRO\*

*Centro de Química Estrutural, Instituto Superior Técnico, Universidade de Lisboa, Lisboa, Portugal*

## 50.1 INTRODUCTION

The properties of coordination compounds in general, and organometallic ones in particular, depend on the metal, ligands, and coordination geometry, features that influence, for example, their electrochemical behavior, catalytic performances, and biological activity. The redox potential of metal complexes has been correlated [1–17] with a number of their properties, for instance, IR stretching frequencies, charge-transfer bands energy, ligand field stabilization energy, and Hammett's  $\sigma$  and related constants, nuclear magnetic resonance (NMR) spectroscopy parameters, macrocyclic ligand structural parameters, gas-phase ionization potential, or the highest energy occupied molecular orbital (HOMO) energy. Since these properties, which correlate with the redox potential, are dependent on the electron-donor/acceptor abilities of the ligands and metal center, the redox potential would be expected to provide a tool to quantify the latter features and to be used as an important characterization parameter. Following preliminary recognition of ligand additivity effects on the redox potential [1, 2] in a series of closely related octahedral-type 18-electron first-row transition metal complexes of the general type  $[M(CO)_{6-x}L_x]^{y+}$  undergoing a one-electron reversible metal-centered oxidation, Pickett [18–20], Lever [21–24], and Bursten [25–27] have proposed systematic approaches for redox potential–structure relationships (or redox potential parameterization). The Bursten proposal is not as easy to apply as the others, has been much less explored, and is not discussed here. Further strategies have been oriented, namely, by the present authors, toward the extension of the proposed models to other geometries and electron counts, and to a wider variety of ligands and metal centers, as illustrated below.

However, parameterization of the redox potentials of organometallic complexes other than those of carbonyl or isocyanide ones has seldom been attempted, regardless of the great development of their chemistry. Gathering of electrochemical parameters for these and other metal-ligating species relevant in organometallic chemistry has been presented [21–32], but the topic still requires further expansion.

## 50.2 PARAMETERIZATION OF LIGANDS AND METAL CENTERS

### 50.2.1 Octahedral-Type Complexes

According to Pickett's model [18], an electrochemical ligand parameter,  $P_L$ , is defined as the difference between the oxidation potentials ( $E_{1/2}^{\text{ox}}$ ) of the complexes  $[\text{Cr}(\text{CO})_5\text{L}]$  and  $[\text{Cr}(\text{CO})_6]$  (Eq. 50.1). Consequently,  $P_L$  is a measure of the effect of the change of a ligand CO (for which  $P_L = 0$ ) by a ligand L on the redox potential, and the more negative value it adopts, the stronger is the electron-donor ability of L. It is noteworthy to mention that the  $P_L$  ligand parameter (similar to the parameter  $E_S$  for the metal centers—see below) reflects the overall (net)  $\pi$ -electron-acceptor minus  $\sigma$ -donor character of the ligand and not the differentiated electron acceptance and electron-donor abilities. The stronger the net electron-acceptor character, the higher the  $P_L$ . For simplicity, the “net” or “overall” feature is commonly omitted in the discussion.

The  $P_L$  ligand parameter is linearly dependent on the redox potential, within series of closely related 18-electron  $[\text{M}_S\text{L}]$  metal complexes—therefore possessing a common 16-electron square pyramidal metal center,  $\{\text{M}_S\}$ —as expressed by the simple Eq. 50.2 involving two other parameters,  $E_S$  and  $\beta$ .  $E_S$  represents the value of  $E_{1/2}^{\text{ox}}$  of the carbonyl complex  $[\text{M}_S(\text{CO})]$  and is termed the *electron richness* of the metal center  $\{\text{M}_S\}$ , adopting the lowest (more negative) values for the richest  $\{\text{M}_S\}$  sites. The parameter  $\beta$  (slope of the linear relationship of Eq. 50.2) concerns the sensitivity of the redox orbital energy (commonly based on the metal center) to a changing of the ligand L. It is called the *polarizability* of the metal site.

$$P_L = E_{1/2}^{\text{ox}}[\text{Cr}(\text{CO})_5\text{L}] - E_{1/2}^{\text{ox}}[\text{Cr}(\text{CO})_6] \quad (50.1)$$

$$E_{1/2}^{\text{ox}}[\text{M}_S\text{L}] = E_S + \beta P_L \quad (50.2)$$

The parameter  $P_L$  can be derived either directly by definition from Eq. 50.1 when the  $[\text{Cr}(\text{CO})_5\text{L}]$  complex and its oxidation potential are known, or from Eq. 50.2 if the oxidation potential of the complex  $[\text{M}_S\text{L}]$  and the parameters  $E_S$  and  $\beta$  for the  $\{\text{M}_S\}$  metal site are known. Examples of ligands with proposed  $P_L$  value [9, 18, 33–66] are given in Table 50.1.  $E_S$  and  $\beta$  values have also been reported [18, 33, 36–39, 41, 53, 66–70] for a number of metal centers  $\{\text{M}_S\}$ .

Pickett's parameterization method was quite useful in several cases, such as (just to mention a few) (i) in the identification of unstable complexes in solution, for example,  $[\text{Mo}(\text{N}_2)(\text{NH}_3)(\text{dppe})_2]$  [18], formed *in situ* upon reaction of the dinitrogen

**TABLE 50.1** Values of the  $P_L$  Ligand Parameter for Selected Ligands<sup>a</sup>

L	$P_L$ , V	References
$\text{NO}^+$	1.40	18
Carbynes	0.24–0.21	40
$\eta^2$ -Vinyl ( $\eta^2-\text{C}(\text{CH}_2)\text{CH}_2\text{Ph}$ )	0.22	44
Aminocarbene ( $\text{CNH}_2^+$ )	0.09	44
CO	0	21
Isocyanides (bent) <sup>b</sup>	−0.07 to −0.18	33, 34, 36, 47
Vinylidines	0 to −0.6	28, 40
$\eta^2$ -Allene	−0.21	44
Ferricinium isocyanides	−0.22 to −0.28	49, 50
Allenylidenes ( $=\text{C}=\text{C=CR}_2$ )	0 to −0.8	28, 52
Isocyanides (linear) <sup>c</sup>	−0.33 to −0.44	33, 34, 36, 53
$\text{CN-BPh}_3^-$	−0.51	56
Oxocarbenes [ $=\text{C}(\text{OR})\text{Y}$ ]	−0.51 to −0.64	28
Thiocarbenes [ $=\text{C}(\text{SR})\text{Y}$ ]	−0.66 to −0.68	28
Aminocarbenes [ $=\text{C}(\text{NRR}')\text{Y}$ ]	−0.69 to −0.80	28, 85
Fc-oxocarbenes	−0.70 to −0.9	28
$\text{C}\equiv\text{N}^-$ <sup>c</sup>	−1.00	18
Alkynyls( $-\text{C}\equiv\text{CR}^-$ )	−0.9 to −1.7	28, 48, 62, 63, 85
Aryl, alkyl, $\text{NO}^-$	−1.7 to −1.9	28

<sup>a</sup>Ordered generally from higher to lower  $P_L$  values; for multidentate ligands the values refer to each ligating arm.

<sup>b</sup>At an electron-rich metal center such as *trans*-{MX(dppe)<sub>2</sub>} (M = Re, Tc; X = Cl, H).

<sup>c</sup>At an electron-poor metal center such as {Cr(CO)<sub>5</sub>}.

analog  $[\text{Mo}(\text{N}_2)_2(\text{dppe})_2]$  with ammonia; (ii) for discriminating the geometry (linear or bent) of an isocyanide ligand, as in  $[\text{ReCl}(\text{CNR})(\text{dppe})_2]$  and  $[\text{Re}(\text{CNR})_2(\text{dppe})_2]$  [33–36] with  $P_L$  values dependent on the geometry of CNR; (iii) in the mathematical expressions for the prediction of  $E_{1/2}^{\text{ox}}$  values for 18-electron octahedral compounds of the types  $[\text{M}_S\text{L}_2]$  or  $[\text{M}_S\text{LL}']$  with a square-planar 14-electron  $\{\text{M}_S\}$  metal site or for compounds  $[\text{M}_S'\text{L}_3]$  with a 12-electron  $\{\text{M}_S'\}$  metal center [35–37]. We have also extended the model to open-shell 17- and 16-electron octahedral-type complexes [38, 39].

The Pickett and other derived models are only partially additive, as the effects on the redox potential of the complex  $[\text{M}_S\text{L}_n]$  are assumed to concern only the  $\{\text{M}_S\}$  metal site and the particular  $n\text{L}$  ligand(s). The Pickett model itself ( $n = 1$ , Eq. 50.2) corresponds to the minimum additivity requirement. Since additivity of the ligand effects can fail in some cases, for example, owing to ligand synergisms, the model can be more appropriate than any other, with more extensive additivity requirements, but it presents a relatively limited scope, being valid only for rather closely related complexes of a series with a common  $\{\text{M}_S\}$  center that includes not only the metal itself but all the other co-ligands distinct from L. Therefore, in accord with the limited number of  $\{\text{M}_S\}$  centers with available values of  $E_S$  and  $\beta$ , Pickett's model has not found a wide application.

In contrast, a full additivity model has been proposed by Lever [21–24] where additivity has been extended to all the ligands. For such a purpose, he selected the  $\text{Ru}^{\text{III}}/\text{Ru}^{\text{II}}$  redox pair, for which a wide number of complexes are known, as the standard one, and defined a novel, fully additive ligand parameter,  $E_L$ , normally obtained through a statistical analysis of the known redox potentials of the complexes with such redox couple ( $E_L$  values can also be estimated from Hammett's relationships [24, 34–37, 71, 72]). From the thus determined  $E_L$  values, he proposes that for each particular  $\text{M}^n/\text{M}^{n-1}$  redox pair, its complexes with a certain stereochemistry and spin state satisfy the linear relationship given by Eq. 50.3.

$$E = S_M(\Sigma E_L) + I_M \quad (50.3)$$

in which the potentials ( $E$ ) are in V versus the normal hydrogen electrode (NHE), and  $S_M$  (slope) and  $I_M$  (intercept) are parameters characteristic of the  $\text{M}^n/\text{M}^{n-1}$  redox couple, assuming values of 1 and 0, respectively, for the ruthenium standard. A slope ( $S_M$ ) greater than unity concerns a greater sensitivity, relative to the  $\text{Ru}^{\text{III}}/\text{Ru}^{\text{II}}$  standard, of the redox potential of the complexes bearing the  $\text{M}^n/\text{M}^{n-1}$  redox pair on the ligands contributions. The intercept ( $I_M$ , also in V vs NHE) depends on the gas-phase ionization energy, the electronic repulsion energy both in the ligand and in the metal, and also on the difference in solvation energies for  $\text{M}^n$  and  $\text{M}^{n-1}$ .

Lever's model has been applied to numerous ligands with wide ranges of electron-donor and  $\pi$ -electron-acceptor characters and binding various types of metal centers; extensions thereof have also been achieved. Table 50.2 lists the values of  $S_M$  and  $I_M$  for a variety of metal redox couples, whereas  $E_L$  values for a diversity of ligands with relevance in organometallic chemistry are presented in the subsequent tables, some of them were obtained from the literature but others were estimated through application of Eq. 50.4 (see below) from the already known parameter  $P_L$ .

Lever's approach became the most popular one in view of its wide scope of application, simple use, and availability of data. Nevertheless, its full additivity character confers a higher risk of failure than a more limited model (such as Pickett's) based on a lower additivity.

The  $P_L$  and  $E_L$  parameters are a measure of the net (overall) electron-donor ability of the ligands and are expected to follow parallel trends in accord with the empirical Eq. 50.4 [21] but exceptions were found for strong  $\pi$ -acceptor ligands, namely, CO [21, 69], carbynes [40], and isocyanides [21, 41], which present relevant  $\pi$ -stabilization effects on the HOMO. For these cases, apart from corrections to the  $E_L$  parameters, improvements to the general expression 50.3 have been required; for a complex with two very strong  $\pi$ -acceptor ligands (e.g., CO and CNR), the novel expression 50.5 was proposed [21, 24] in which  $c$  and  $c'$  are empirical corrections and  $x$  and  $x'$  are the number of  $\pi^*$  orbitals from such ligands that interact with the HOMO. Depending on the presence of other different  $\pi$ -acceptors, additional positive corrections could be added to Eq. 50.5. Such corrections to the potential values can reach values as high as 0.3 V per ligand [21, 24, 41].

$$P_L = 1.17 E_L - 0.86 \quad (50.4)$$

$$E = S_M(\Sigma E_L) + I_M + cx + c'x' \quad (50.5)$$

Other limitations of the model have been recognized, in particular due to failure of ligand additivity [42], to isomeric effects [21, 22] and to deviations from the linearity expressed by Eq. 50.3 for a wide range of  $\Sigma E_L$  [22, 38, 40], eventually suggesting the need for specific  $S_M$  and  $I_M$  values for a particular metal center or even the consideration of a curved relationship between the redox potential and  $\Sigma E_L$  or of different expressions along the  $\Sigma E_L$  scale. The possible dependence of the  $E_L$  ligand parameter on the metal center is also a difficulty which was recognized in the cases of isocyanides [33, 34, 36, 37, 47], cyanide [43], nitriles [38], cyanamides [37, 57, 59], vinylidines [28], allenylidenes [28], and alkynyls [28].

**TABLE 50.2** Values of the  $S_M$  and  $I_M$  Parameters for Selected Metal Redox Pairs, in Organic Medium<sup>a</sup>

Redox Pair	$S_M$	$I_M$ (V) versus NHE	References
Cr <sup>III</sup> /Cr <sup>II</sup> (LS)	1.18	-1.72	21
Cr <sup>III</sup> /Cr <sup>II</sup> (HS)	0.84	-1.18	21
Cr <sup>I</sup> /Cr <sup>0</sup>	0.5	-1.75	21
Fe <sup>IV</sup> /Fe <sup>III</sup> (specific) <sup>b</sup>	1.49	-0.18	47
Fe <sup>III</sup> /Fe <sup>II</sup> (LS)	1.10	-0.43	21
Fe <sup>III</sup> /Fe <sup>II</sup> (specific) <sup>c</sup>	1.07	-0.3	37
Fe <sup>III</sup> /Fe <sup>II</sup> (specific) <sup>d</sup>	1.32	-0.57	47
Fe <sup>III</sup> /Fe <sup>II</sup> (HS)	0.89	-0.25	21
Mn <sup>II</sup> /Mn <sup>I</sup>	0.81	-1.76	21
Mo <sup>I</sup> /Mo <sup>0</sup>	0.74	-2.25	21
Mo <sup>II</sup> /Mo <sup>I</sup>	0.81	-1.76	21
Nb <sup>V</sup> /Nb <sup>IV</sup>	0.76	-1.24	21
Nb <sup>IV</sup> /Nb <sup>III</sup>	0.75	-0.12	21
Os <sup>III</sup> /Os <sup>II</sup>	1.01	-0.40	21
Re <sup>IV</sup> /Re <sup>III</sup>	0.86	0.51	22
Re <sup>III</sup> /Re <sup>II</sup>	1.17	-0.88	22
Re <sup>II</sup> /Re <sup>I</sup> (upper)	0.76	-0.95	22
Re <sup>II</sup> /Re <sup>I</sup> (lower)	0.27	-1.43	22
Ru <sup>IV</sup> /Ru <sup>III</sup>	1.03	1.68	73
Ru <sup>III</sup> /Ru <sup>II</sup>	0.97	0.04	21
Ta <sup>V</sup> /Ta <sup>IV</sup>	0.79	0.66	21
Tc <sup>IV</sup> /Tc <sup>III</sup>	1.00	0.65	22
Tc <sup>III</sup> /Tc <sup>II</sup>	1.28	-0.89	22
Tc <sup>II</sup> /Tc <sup>I</sup>	1.42	-2.09	22
Rh <sup>II</sup> /Rh <sup>Ie</sup>	1.68	-0.87	39
Rh <sup>II</sup> /Rh <sup>If</sup>	0.80	-0.95	76

Abbreviations: HS, high spin; LS, low spin.

<sup>a</sup>Six-coordinate metal center, except when stated otherwise.

<sup>b</sup>Established for the series *trans*-[FeBrL(depe)<sub>2</sub>]<sup>2+/3+</sup> (L = CO, aryl and alkyl N≡CR).

<sup>c</sup>Established for the series *trans*-[FeL<sub>2</sub>(depe)<sub>2</sub>]<sup>2+/3+</sup> (L = CO, aryl and alkyl N≡CR, N≡C-NR<sub>2</sub>).

<sup>d</sup>Established for the series *trans*-[FeBrL(depe)<sub>2</sub>]<sup>+/-2+</sup> (L = CO, aryl and alkyl N≡CR, Br<sup>-</sup>).

<sup>e</sup>Four-coordinate metal center.

<sup>f</sup>Five-coordinate metal center.

The estimate of the  $E_L$  value of a particular ligand (L) can be achieved provided one knows (i) the redox potential of a complex with that ligand L bound to a M<sup>n+1/n</sup> metal redox couple with known  $I_M$  and  $S_M$  parameters and (ii) the  $E_L$  values of the other ligands. Following this procedure, the  $E_L$  data set has been greatly enlarged to a wide variety of ligands and further extensions are expected as more metal complexes are being synthesized and their redox potentials measured. The availability of various complexes with the same ligand should also allow the refinement of its  $E_L$  value and checking of its nondependence on the metal center.  $E_L$  can also be obtained from Hammett's relationships [24, 34–37, 71, 72].

Once the  $E_L$ ,  $I_M$ , and  $S_M$  electrochemical parameters are established, they can be used to predict the redox potential of a species and enable the *in situ* identification of an (un)known complex, product, or intermediate, thus avoiding its isolation and eventual decomposition. Examples include some chloro/azole-ruthenium [73, 74] or chloro-osmium [75] complexes derived upon ligand replacement induced by electron transfer. The identification of such species, generated *in situ*, has allowed the establishment of the detailed mechanisms of the reactions by digital simulation of cyclic voltammetry.

The Lever model has typically been applied to octahedral-type six-coordinate complexes, with metal-centered redox processes, but extensions to other types of complexes have also been proposed, namely, to square-planar four-coordinate and five-coordinate Rh<sup>II</sup>/Rh<sup>I</sup> complexes [39, 76, 77], to sandwich complexes [23, 24, 31, 32], to Ru clusters [78–80], and also to complexes with ligand-centered reduction processes [24]. Relevant or representative cases are discussed in the following sections.

### 50.2.2 Tetra- and Pentacoordinate Rh<sup>II/I</sup> Complexes

The  $S_M$  and  $I_M$  values (1.83 and  $-1.22$  V vs NHE, respectively) for the square-planar Rh<sup>II/Rh<sup>I</sup></sup> couple were firstly estimated [77] through the knowledge of the  $E_{1/2}^{\text{ox}}$  of the complexes  $[\text{RhCl}(\text{L})(\text{P}^i\text{Pr}_3)_2]$  [ $\text{L}$  = ethylene ( $0.94$  V), CO ( $1.36$  V)] and the known [21]  $E_L$  values for Cl<sup>-</sup>, ethylene, CO, and trimethylphosphine instead of the unknown triisopropylphosphine ( $E_L = -0.24$ ,  $0.76$ ,  $0.99$ , and  $0.33$  V vs NHE, respectively [21]) by applying Eq. 50.3. These values were further refined [39, 76] through the application of the same method to a broader series of rhodium(I) complexes and the values of  $S_M = 1.68$  and  $I_M = -0.87$  V were those lastly achieved (Table 50.2). The value of  $1.68$  for the  $S_M$  (slope) parameter is higher than those reported for the hexacoordinate redox pairs (Table 50.2) and suggests a higher susceptibility of the square-planar Rh<sup>II/Rh<sup>I</sup> metal center to a change of the ligands. However, the generalization of this observation would need an even broader number of Rh<sup>I</sup> square-planar complexes. The subsequent application of Eq. 50.3 with the novel values of  $S_M$  and  $I_M$  parameters enabled the estimate of the  $E_L$  values for a set of unsaturated organic ligands of the type  $=\text{C}(=\text{C})_n\text{Ph}_2$  ( $n = 0, 1, 2$ ; Tables 50.3–50.5).</sup>

Expectedly, distinct  $S_M$  and  $I_M$  parameters were found for the pentacoordinated Rh<sup>I</sup> compounds  $[\text{RhH}(\text{CO})\text{L}_3]$  and  $[\text{RhHL}'_4]$  [ $\text{L} = \text{P}(\text{NC}_4\text{H}_4)_3$ , PPh<sub>3</sub>, P(OPh)<sub>3</sub> or P(OC<sub>6</sub>H<sub>4</sub>Me-4)<sub>3</sub>;  $\text{L}' = \text{PPh}_3$  or P(OC<sub>6</sub>H<sub>4</sub>Me-3)<sub>3</sub>]:  $0.80$  and  $-0.95$  V, respectively [76] (Table 50.2), but these values should be considered with great care in view of the limited number of compounds used in their estimate.

### 50.2.3 Sandwich and Half-Sandwich Complexes

The low spin Fe<sup>III/II</sup> redox couple was initially proposed by Lever et al. [23, 24, 31] as the most appropriate standard for sandwich complexes bearing two cyclopentadienyl (Cp) or derived ligands, as such compounds are known in a large number and exhibit metal-based reversible or quasi-reversible redox processes that are fairly independent of the solvent/electrolyte system. For homoleptic complexes the value for the  $E_L$  parameter would be given by Eq. 50.6 and for mixed sandwich species,  $[\text{FeLL}']$ , Eq. 50.7 should be applied [31]. For the Cp ligand itself, an  $E_L$  value of  $0.33$  V was thus proposed [31].

$$E_L = \frac{E_{1/2}^{\text{ox}}(\text{Fe}^{\text{III}/\text{II}})}{2} \quad (50.6)$$

$$E_L(L) + E_L(L') = E_{1/2}^{\text{ox}}(\text{Fe}^{\text{III}/\text{II}}) \quad (50.7)$$

For  $\pi$ -complexes with  $\eta^6$ -benzene-type ligands, as there are no Fe<sup>III/II</sup> complexes available, other redox pairs [Fe<sup>II/Fe<sup>I</sup></sup>, Co<sup>III/Co<sup>II</sup></sup>, Co<sup>II/Co<sup>I</sup></sup>, Cr<sup>II/Cr<sup>I</sup></sup> or Cr<sup>I/Cr<sup>0</sup></sup>] were used as standards [31]. For benzene itself, for example, this method leads to an  $E_L$  value of  $1.86$  V [31].

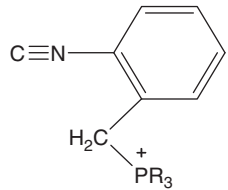
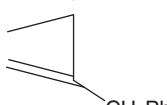
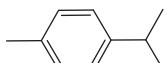
However, such a type of parameterization approach is based on expressions that are quite different from the original one (Eq. 50.3) and thus generate  $E_L$  values that fall in distinct scales and are not directly comparable with those concerning Eq. 50.3. It would be much more convenient to preserve the initial Lever approach based on the standard Ru<sup>III/Ru<sup>II</sup></sup> redox couple and on Eq. 50.3. This is the approach we have proposed and described in the following section.

### 50.2.4 $\eta^6$ -Arene and Other $\pi$ -Ligands

The application of the initial Lever model to  $\pi$ -sandwich or  $\pi$ -half-sandwich complexes requires the assumption of the validity of Eq. 50.3 to such types of complexes and of the  $S_M$  and  $I_M$  values quoted for the metal redox couples in octahedral-type complexes. Although full confirmation of this hypothesis requires the consideration of wider series of complexes, it has been applied by us [32] to half (or full)-sandwich complexes bearing  $\pi$ -aromatic (benzene or *p*-cymene) ligands or polydentate boron-based or carbon-based scorpionate-type ligands. For the estimate of the corresponding  $E_L$  values for such polytopal ligands (based on Eq. 50.3), the  $E_L$  values of the co-ligands in their complexes should be known, as well as the  $S_M$  and  $I_M$  values of their metal redox couples.

The application of this method to the series of half-sandwich *p*-cymene Ru<sup>II</sup> complexes  $[\text{RuCl}_2(\eta^6\text{-L})\text{L}']$  ( $\text{L}' = \text{PPh}_3$ , PTol<sub>3</sub>, SMe<sub>2</sub>), and  $[\text{RuCl}(\eta^6\text{-L})(\text{SMe}_2)_2]^+$  leads to an average overall  $E_L$  value of  $1.63$  V versus NHE for  $\eta^6$ -*p*-cymene ( $\eta^6\text{-L}$ ) (i.e.,  $0.54$  V per each C=C two-electron-donor moiety of the aromatic ring) (Table 50.3) [32]. In addition, the average overall  $E_L$  value of  $1.77$  V ( $0.59$  V per each C=C moiety) was estimated [32] for  $\eta^6$ -benzene by the same method applied to  $[\text{RuCl}_2(\eta^6\text{-L})(\text{PPh}_3)]$ ,  $[\text{Cr}(\eta^6\text{-L})(\text{CO})_3]$ ,  $[\text{Cr}(\eta^6\text{-L})(\text{CO})_2]_2(\mu\text{-dppm})$  and  $[\text{Cr}(\eta^6\text{-L})_2]$  ( $\eta^6\text{-L} = \eta^6$ -benzene). Expectedly, in view of the electron-donor substituents (methyl and isopropyl) in the aromatic ring, *p*-cymene presents a slightly lower  $E_L$  value than benzene.

**TABLE 50.3** Values for the  $E_L$  Ligand Parameter for Selected L Ligands

L	Metal Center	$E_L$ (V) versus NHE, from Eq. 50.3	Reference	$E_L$ (V) versus NHE, from Eq. 50.4
$\text{NO}^+$	$\{\text{Mo}(\text{NO})(\text{dppe})_2\}^+$	>1.5	21, 24	1.85
Carbynes ( $\equiv \text{CR}$ ) $\text{R} = \text{CH}_2\text{CO}_2\text{R}'$ ( $\text{R}' = \text{Me, Et}$ ), $\{\text{ReF}(\text{dppe})_2\}^+$ $\text{CH}_2\text{R}''$ ( $\text{R}'' = \text{Ph, C}_6\text{H}_4\text{Me-4, H, }'\text{Bu}$ )		circa 1.2	40	0.94–0.91
Aminocarbyne ( $\equiv \text{CNH}_2$ )	$\{\text{ReCl}(\text{dppe})_2\}^+$	circa 1.1	28	0.81
CO	$\{\text{Ru}(\text{bpy})_2\}^{+2}$	0.99	21	0.74
Vinylidenes ( $=\text{C}=\text{CRR}'$ )	See Table 50.4	0.83–0.24	28	0.74–0.24
Allenylidenes ( $=\text{C}=\text{C=CR}_2$ )	See Table 50.5	0.8–0	28	0.74–0.05
Bent isocyanides (bent $\text{C}\equiv\text{NR}$ ) $\text{R} = \text{aryl, alkyl}$	$\{\text{TcH}(\text{dppe})_2\}$ , $\{\text{ReX}(\text{dppe})_2\}$ ( $\text{X} = \text{Cl or H}$ )	0.68–0.58	32–34, 87	0.68–0.58
Benzoyl isocyanide [ $\text{C}\equiv\text{NC(O)Ph}$ ]	$\{\text{FeH}(\text{dppe})_2\}^+$	0.60	43	0.91
Carbenes	See Table 50.6	0.5 to –0.7	28	
Ferricinium isocyanides		0.55–0.50	49	
Linear isocyanides (linear $\text{C}\equiv\text{N-R}$ )	$\{\text{ReX}(\text{dppe})_2\}^+$ ( $\text{X} = \text{CO, NCR, CNR}$ ) $\{\text{M}(\text{CO})_5\}$ ( $\text{M} = \text{Cr, Mo or W}$ )	0.56–0.32	32–34	
Phosphines ( $\text{PR}_3$ ) and diphosphines <sup>a</sup>		0.43–0.28	21, 28	
$\text{C}\equiv\text{N}-\text{BF}_3^-$	$\{\text{FeH}(\text{dppe})_2\}^+$	0.20	43	0.53
$\text{C}\equiv\text{N}-\text{NiCl}_2(\text{PCy}_3)^-$	$\{\text{FeH}(\text{dppe})_2\}^+$	0.19	51	0.52
Phosphonium isocyanides	$\{\text{M}(\text{CO})_5\}$ ( $\text{M} = \text{Cr, Mo or W}$ )		31	0.50–0.43
				
$\text{PR}_3 = \text{PPh}_3, \text{PPh}_2(\text{CH}_2\text{Ph}), \text{PMMe}_3$				
$\text{NH}_3$	$\{\text{Ru}(\text{bpy})_2\}^{+2}$	0.07	21	0.07
$\text{C}\equiv\text{N}-\text{VCl}_3(\text{thf})_2^-$	$\{\text{FeH}(\text{dppe})_2\}^+$	0.03	43	0.38
$\text{C}\equiv\text{N}-\text{BPh}_3^-$	$\{\text{FeH}(\text{dppe})_2\}^+$	–0.05	43	
$\text{C}\equiv\text{N}-\text{ReOCl}_3(\mu-\text{CN})\text{FeH}(\text{dppe})_2^-$	$\{\text{FeH}(\text{dppe})_2\}^+$	–0.09	51	
$\text{C}\equiv\text{N}-\text{PdCl}_2(\text{PPh}_3)^-$	$\{\text{FeH}(\text{dppe})_2\}^+$	–0.14	51	
$\text{C}\equiv\text{N}^-$	$\{\text{Ru}(\text{bpy})_2\}^{2+}$	0.02	21	
Alkynyls ( $-\text{C}\equiv\text{CR}^-$ )	See Table 50.7	–0.1 to –0.7	28	
Aryl, alkyl, $\text{NO}^-$		–0.70 to –0.90	24	
<i>π-Ligands</i>				
$\eta^2$ -Vinyl	$\{\text{ReCl}(\text{dppe})_2\}$	circa 1.2	44, 28	0.92
				
$\eta^2$ -C <sub>2</sub> H <sub>4</sub>	$\{\text{Ru}(\text{bpy})_2\}^{2+}$	0.76	21	
$\eta^6$ -Benzene	$\{\text{RuCl}_2(\text{PPh}_3)\}, \{\text{Cr}(\text{CO})_3\}$ , among others	0.59 <sup>b</sup> (1.77) <sup>c</sup>	32	
$\eta^2$ -Allene ( $\text{CH}_2=\text{C=CHPh}$ )	$\{\text{ReCl}(\text{dppe})_2\}$	0.56	28	
$\eta^6$ - <i>p</i> -Cymene	$\{\text{RuCl}_x\text{L}'_z\}_n$ ( $n = 0, x = 2, z = 1$ ; $n = 1, x = 1, z = 2$ ; $\text{L}' = \text{PPh}_3, \text{PTol}_3$ or $\text{SMe}_2$ )	0.54 <sup>b</sup> (1.63) <sup>c</sup>	32	
				

<sup>a</sup>For chelating diphosphines, the  $E_L$  value concerns each two-electron-donor coordinating arm.<sup>b</sup>Value for each  $\text{C}=\text{C}$  moiety (two-electron donor) of the aromatic ring.<sup>c</sup>Overall value (for the overall six-electron-donor ligand).

**TABLE 50.4** Values for the  $E_L$  Ligand Parameter for Selected Vinylidene Ligands,  $=\text{C}=\text{R}$  (L)

R	Metal Center	$E_L$ (V) versus NHE <sup>a</sup>	References
CPh <sub>2</sub>	{RhCl(P <i>i</i> Pr <sub>3</sub> ) <sub>2</sub> }	0.73, 0.83	28, 77
C(Me) <sup>t</sup> Bu	{Mo( $\eta^7$ -C <sub>7</sub> H <sub>7</sub> )(dppe)} <sup>+</sup>	0.64	28
CHCO <sub>2</sub> R' (R' = Me, Et)	{ReCl(dppe) <sub>2</sub> }	0.62	40
CH <sub>2</sub>	{ReCl(dppe) <sub>2</sub> }	0.56	40
CHX (X = Ph, C <sub>6</sub> H <sub>4</sub> Me-4, <sup>t</sup> Bu)	{ReCl(dppe) <sub>2</sub> }	0.52–0.50	40
CHCHPh <sub>2</sub>	{RuCl(dppe) <sub>2</sub> } <sup>+</sup>	0.70	28
CHC <sub>6</sub> H <sub>4</sub> NO <sub>2</sub> -4	{RuCl(dppe) <sub>2</sub> } <sup>+</sup>	0.62, 0.59	28
CHC <sub>6</sub> F <sub>4</sub> OMe-4	{RuCl(dppe) <sub>2</sub> } <sup>+</sup>	0.58	28
CHC <sub>6</sub> H <sub>4</sub> CHO-4	{RuCl(dppe) <sub>2</sub> } <sup>+</sup>	0.56	28
CHC <sub>6</sub> H <sub>4</sub> C≡CC <sub>6</sub> H <sub>4</sub> NO <sub>2</sub> -4,4'	{RuCl(dppe) <sub>2</sub> } <sup>+</sup>	0.54	28
CHC <sub>6</sub> H <sub>4</sub> CHO(CH <sub>2</sub> ) <sub>3</sub> O-4	{RuCl(dppe) <sub>2</sub> } <sup>+</sup>	0.50	28
CHPh	{RuCl(dppe) <sub>2</sub> } <sup>+</sup>	0.48	28
CHC <sub>6</sub> H <sub>4</sub> CH=CHPh-4	{RuCl(dppe) <sub>2</sub> } <sup>+</sup>	0.44, 0.38	28
CHC <sub>6</sub> H <sub>4</sub> CHO-3	{RuCl(dppe) <sub>2</sub> } <sup>+</sup>	0.44	28
CHC <sub>6</sub> H <sub>4</sub> C≡CPh-4	{RuCl(dppe) <sub>2</sub> } <sup>+</sup>	0.40	28
CHC <sub>6</sub> H <sub>4</sub> CH=CHC <sub>6</sub> H <sub>4</sub> NO <sub>2</sub> -4,4'	{RuCl(dppe) <sub>2</sub> } <sup>+</sup>	0.29, 0.24	28
CHC <sub>6</sub> H <sub>4</sub> CHO-2	{RuCl(dppe) <sub>2</sub> } <sup>+</sup>	0.28	28
CHPh	{ReCl(Me <sub>2</sub> bpy)(PPh <sub>3</sub> ) <sub>2</sub> } <sup>+</sup>	0.44, 0.55	28, 92
CHC <sub>6</sub> H <sub>4</sub> Me-4	{ReCl(Me <sub>2</sub> bpy)(PPh <sub>3</sub> ) <sub>2</sub> } <sup>+</sup>	0.36, 0.47	28, 92

<sup>a</sup>From Eq. 50.3.

In comparison with  $\eta^2$ -allene ( $E_L = 0.56$  V for CH<sub>2</sub>=C=CHPh [28]), each C=C (two-electron-donor) moiety ( $E_L = 0.59$  V) of the  $\eta^6$ -benzene ligand exhibits a similar electron-donor character, being a significantly stronger electron donor than  $\eta^2$ -ethylene ( $E_L = 0.76$  V [21]), and much stronger than the  $\eta^2$ -vinyl =C(CH<sub>2</sub>)CH<sub>2</sub>Ph ligand ( $E_L$  circa 1.2 V [28, 44]) (Table 50.3).

However, each C=C moiety of benzene is a weaker electron donor (stronger electron acceptor) than, for example, organophosphines ( $E_L$  in the 0.43–0.28 V range) or each coordinating arm of C-based scorpionates (e.g., tris(pyrazolyl)methane,  $E_L = 0.20$  V) [32] or B-based ones (e.g., tris(pyrazolyl)borate,  $E_L = 0.17$  V) [32].

### 50.2.5 Carbyne Ligands

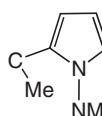
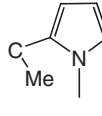
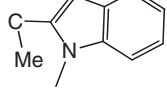
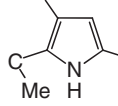
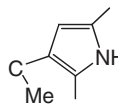
The Pickett  $P_L$  ligand parameter was estimated for carbyne (C–CH<sub>2</sub>R) and aminocarbyne (CNH<sub>2</sub>) ligands (L) at *trans*-[ReX(L)(dppe)<sub>2</sub>]<sup>+</sup> (X = F or Cl) complexes, and the corresponding  $E_L$  values (circa 1.2 and circa 1.1 V, respectively, Table 50.3) were obtained by using Eq. 50.4 [28, 36]. Such values are even higher than that of CO ( $E_L = 0.99$  V [21]), being exceeded only by that of NO<sup>+</sup>, accounting for the strong  $\pi$ -electron acceptance of the carbyne and aminocarbyne CNH<sub>2</sub> ligands, in accord with molecular orbital (MO) calculations [53]. As indicated by X-ray data [81, 82], the aminocarbyne presents a considerable carbene character (carbene ligands display  $E_L$  values over a very wide range, as shown in the following).

### 50.2.6 Isocyanide Ligands

As shown in Table 50.3, bent isocyanides and benzoyl isocyanide are strong  $\pi$ -electron acceptors and exhibit high  $E_L$  values (0.68–0.58 V range) [32–34, 43]. Linear isocyanides, as well as ferricinium isocyanides, with  $E_L$  values in the 0.55–0.32 V range, are weaker  $\pi$ -acceptors. Cyano adducts, constructed at the *trans*-{FeH(dppe)<sub>2</sub>}<sup>+</sup> metal center, are quite sensitive to the Lewis acid but are always stronger net electron acceptors (weaker net electron donors) than cyanide: CNBF<sub>3</sub><sup>−</sup> ≥ CN–NiCl<sub>2</sub>(PCy<sub>3</sub>)<sup>−</sup> > CN–VCl<sub>3</sub>(thf)<sub>2</sub><sup>−</sup> > CN–BPh<sub>3</sub><sup>−</sup> > C≡N–ReOCl<sub>3</sub>( $\mu$ -CN)FeH(dppe)<sub>2</sub><sup>−</sup> > CN–PdCl<sub>2</sub>(PPh<sub>3</sub>)<sup>−</sup> > CN<sup>−</sup> ( $E_L = -0.26$  V) [43, 51].

The bending of coordinated isocyanides occurs at electron-rich metal centers and was attributed [64, 83–86] to electronic effects. At the electron-rich {ReY(dppe)<sub>2</sub>} (Y = Cl or H) metal sites, a strong bending was observed for methyl isocyanide [64, 87] (139.4(10) $^{\circ}$  or 147.7(7) $^{\circ}$ , respectively) which, consequently, may be considered with a carbene character. The weaker bending that occurs for *trans*-[Mo(CNMe)<sub>2</sub>(dppe)<sub>2</sub>] (156(1) $^{\circ}$ ) [86] and, even lesser, for *trans*-[Re(CNMe)<sub>2</sub>(dppe)<sub>2</sub>] (168.2(4) $^{\circ}$ ) [88], can result from the weaker  $\pi$ -electron release of the metal centers, the competition of the two isocyanides for the

**TABLE 50.5** Values for the  $E_L$  Ligand Parameter for Selected Allenylidene Ligands,  $=\text{C}=\text{C}=\text{R}$  ( $\text{L}$ )

R	$E_L$ (V) versus NHE <sup>a</sup>
$\text{C}(\text{C}_6\text{H}_4\text{Cl}-4)_2$	0.80 <sup>b</sup>
$\text{CPh}_2$	0.74 <sup>b</sup> , 0.71 <sup>c</sup> , 0.58 <sup>c</sup> , 0.45 <sup>d</sup>
$\text{C}(\text{C}_6\text{H}_4\text{Me}-4)_2$	0.67 <sup>b</sup>
$\text{C}(\text{C}_6\text{H}_4\text{X}-4)_2$ X = Cl, H, Me	0.61–0.47
$\text{C}(\text{Me})\text{Ph}$	0.58
$\text{C}(\text{SeR})(\text{alkyl})$	0.55–0.51
$\text{C}(\text{SR})(\text{alkyl})$	0.51–0.47
$\text{C}(\text{Me})\text{Ph}$	0.42 <sup>d</sup>
$\text{CEt}_2$	0.40 <sup>d</sup>
	0.28 N,N-dimethyl-2-pyrrolylamine
	0.27 N-methyl-2-pyrrolylamine
	0.26 N-methyl-2-indolyl
	0.23 3,5-dimethyl-2-pyrrolyl
	0.18 2,5-dimethyl-3-pyrrolyl
$\text{C}(\text{NMe}_2)\text{X}$ $\text{X} = \text{CH}_2\text{CH}(\text{CH}=\text{CH}_2)(\text{CH}_2\text{NMe}_2),$ $\text{CH}_2\text{C}(\text{Et})(=\text{C}=\text{CH}_2), (\text{CH}_2\text{CH}_2\text{CH}=\text{CH}_2)$	0.27–0.17
$\text{C}(\text{CH}_2\text{CH}_2\text{CH}=\text{CH}_2)(\text{piperidin-1-yl})$	0.17, 0.24, 0.27
$\text{C}(\text{Me})\text{X}$	0.18–0.02
$\text{X} = \text{NEt}_2, \text{N}(\text{Me})(\text{CH}_2\text{Ph}), \text{N}(\text{Me})(^{\prime}\text{Bu}),$ $\text{N}(\text{Me})(9\text{-anthracenylCH}_2)$	
$\text{C}(\text{Me})\text{X}$	–0.39 or –0.41
$\text{X} = \text{dibenzazepin-5-yl or phenothiazin-10-yl}$	

<sup>a</sup>From Reference 28 and at the  $\{\text{RuCl}(\text{dppm})_2\}^+$  center, unless stated otherwise. Equation 50.3 was applied.

<sup>b</sup>At the  $\{\text{OsCl}(\text{dppm})_2\}^+$  center.

<sup>c</sup>At the  $\{\text{RhCl}(\text{P}^{\prime}\text{Pr}_3)_2\}^+$  center, from Reference 77.

<sup>d</sup>At the  $\{\text{FeBr}(\text{depe})_2\}^+$  center, from Reference 41.

metal  $\pi$ -backbonding, and/or steric influences. It is concomitant with the longer Re–C bond lengths at the diisocyanide compounds, as compared with the monoisocyanide ones in which there occurs an extensive  $\pi$ -backbonding.

### 50.2.7 Vinylidene and Allenylidene Ligands

Vinylidenes usually behave as stronger  $\pi$ -electron acceptors than carbenes, their  $E_L$  values (Table 50.4) [28, 40] falling in the range of 0.83 to 0.24 V versus NHE. Diphenylvinylidene,  $=\text{C}=\text{CPh}_2$ , presents the highest  $\pi$ -acceptance character of this group of ligands. Expectedly, for the  $=\text{C}=\text{CHR}$  series, the order of electron acceptance parallels that of the R group:  $\text{C}_6\text{H}_4\text{NO}_2\text{-}4 > \text{CO}_2\text{R} > \text{C}_6\text{F}_4\text{OMe}\text{-}4, \text{C}_6\text{H}_4\text{COH}\text{-}4 > \text{Ph} > \text{C}_6\text{H}_4\text{Me}\text{-}4 > \text{'Bu}$ . A conjugated phenyl substituent of the yne- or ene-type appears to lead to an increase of the net electron-donor character of the vinylidene.

Allenylidenes (Table 50.5) appear to behave as weaker net electron acceptors. The order of net electron acceptance reflects the electronic effects of the group at the  $\text{C}_\gamma$  carbon: arylallenylidenes  $=\text{C}=\text{C}=\text{CRR}' >$  selenoallenylidenes  $=\text{C}=\text{C}=\text{C}(\text{SeR})\text{R}' >$  thioallenylidenes  $=\text{C}=\text{C}=\text{C}(\text{SR})(\text{alkyl}) >$  aminoallenylidenes [28]. Therefore, allenylidenes can behave as considerable net electron donors [as in  $=\text{C}=\text{C}=\text{C}(\text{NET}_2)\text{Me}$  with an  $E_L$  value of 0.02 V, comparable to that of ammonia] or as strong  $\pi$ -acceptors (e.g., in  $=\text{C}=\text{C}=\text{CPh}_2$ ) [28]. A possible dependence of the  $E_L$  ligand parameter on the nature of the binding metal center has been recognized in some cases, for both vinylidenes and allenylidenes [28].

### 50.2.8 Carbene Ligands

$E_L$  parameter values for carbenes span a very wide range (0.5 to –0.7 V vs NHE), as shown in Table 50.6, where they are commonly ordered from the strongest to the weakest  $\pi$ -electron-acceptor character: diphenylcarbene  $=\text{CPh}_2$ , bithiophene-carbenes  $\geq$  oxocarbenes  $=\text{C}(\text{OR})\text{Y} >$  thiocarbenes  $=\text{C}(\text{SR})\text{Y} >$  aminocarbenes  $=\text{C}(\text{NRR}')\text{Y} \geq$  phosphoylide-aminocarbenes  $>$  anionic oxocarbene  $=\text{C}(\text{O}^-)\text{Y}$ . The most effective  $\pi$ -acceptors present extended conjugated  $\pi$ -systems and this order reflects the increase in the electron-donor ability (to the carbene carbon) of the group with the heteroatom [28].

As regards hydroxocarbenes  $=\text{C}(\text{OH})\text{R}$ , in view of their tendency for hydrogen bonding, their net electron-donor character depends on the experimental conditions, but is still lower than those of the parent benzoyl  $\text{COPh}^-$  ligand and of the oxocarbene  $=\text{C}(\text{O}^-)\text{Y}$  ligands. On account of their anionic character, the oxocarbene  $=\text{C}(\text{O}^-)\text{Y}$  are the strongest electron donors (even stronger than halides). Aminocarbenes are more effective  $\pi$ -electron acceptors than phosphoylide-aminocarbenes, in accord with the electron donation from the ylide moiety to the carbene carbon [28].

### 50.2.9 Alkynyl Ligands

Alkynyls (Table 50.7) are anionic strong electron donors, presenting  $E_L$  values between –0.06 and –0.74 V versus NHE. Phosphonium or ammonium-containing alkynyls, for example,  $-\text{C}\equiv\text{C}-\text{CPh}_2(\text{PMe}_3^+)$  or  $-\text{C}\equiv\text{C}-\text{C}(\text{=CH}_2)(\text{NR}_3^+)$ , are overall neutral ligands and the weakest net electron donors of the series ( $E_L$  in the –0.06 to –0.28 V range). Alkynyls with electron-acceptor substituents in the aromatic ring (such as  $\text{NO}_2$ ,  $\text{CHO}$ ,  $\text{CN}$ ,  $\text{F}$ , or azo group,  $-\text{N}=\text{N}-$ ) ( $E_L$  from –0.24 to –0.37 V) appear next. Moreover, an yne- or ene-type conjugated phenyl substituent appears to promote the net electron-donor character of the alkynyl [28]. Substituent effects can be transmitted along quite extended conjugated systems, which can be of significance for the design of species with nonlinear optical (NLO) properties [89–91]. With regard to the butenyls of the type  $-\text{C}\equiv\text{C}-\text{C}(\text{=CH}_2)\text{X}^-$ , the following order of net electron release to the metal is observed:  $\text{NR}_3^+ < \text{PR}_3^+ < \text{aromatic} < \text{alkyl}$  [28]. Despite the two phenyl groups and due to the electron donation by resonance of the amino group, the aminoalkynyls  $-\text{C}\equiv\text{C}-\text{CPh}_2(\text{NR}_2)$  ( $\text{R}_2 = \text{H}/\text{Me}, \text{Me}_2$ ) are among the strongest electron donors ( $E_L$  values of circa –0.5 V [52]). The most effective electron donors are the alkyl-alkynyls  $-\text{C}\equiv\text{C}-\text{R}$  ( $E_L$  in the range from –0.5 to –0.7 V).

Alkynyl ligands illustrate a difficulty concerning the possible localization of the HOMO at the ligand instead of the metal, thus leading to anomalous  $E_L$  values [28].

## 50.3 FINAL COMMENTS

The redox potential of a coordination or an organometallic compound reflects its structural and electronic features, and the establishment of redox potential–structure relationships enables methods for the quantification of the net electron-donor/acceptor character of ligands and of the electronic properties of the binding metal centers.

Systematic studies on relevant ligands in organometallic chemistry have already been reported, but usually still concern a limited number of metal complexes, and thus the proposed values of the electrochemical parameters should be taken

**TABLE 50.6** Values for the  $E_L$  Ligand Parameters for Selected Carbene Ligands (L)

L	$E_L$ (V) versus NHE <sup>a</sup>
Diphenylcarbene ( $=\text{CPh}_2$ )	0.51 <sup>b</sup> , 0.39
Bithiophene-carbenes	0.41–0.21
$=\text{C}(\text{OR})\text{Y}$ R = Me, Et or Ph; Y = 2-methyl-furyl or -thiophenyl, Ph, 4-methylthiazol-2-yl, $\text{C}_6\text{H}_4\text{Cl}-4$ , or $\text{C}_6\text{H}_4\text{OMe}-4$	0.30–0.19
	0.27
Hydroxocarbenes (H-bonded), $=\text{C}(\text{OH}\cdots\text{X}^-)\text{Ph}$ X=HSO <sub>4</sub> , ClO <sub>4</sub> , CF <sub>3</sub> CO <sub>2</sub>	0.19 to –0.12
$=\text{C}(\text{SR})(2\text{-methylfuryl})$ R = alkyl, Ph	0.17–0.15
$=\text{C}(\text{OR})Fc$ R = alkyl	0.14 to –0.04
$=\text{C}(\text{R}-1\text{-yl})\text{Ph}$ R = aziridin, azetidin, pyrrolidin, or piperidin	0.15–0.09
Aminocarbenes, $=\text{C}(\text{NRR}')\text{Y}$ R = R' = Me or Et; Y = Ph or Me R = R' = H; Y = 2-methyl-furyl or -thiophenyl. R = H, R' = Cy or Me; Y = Et or Me	0.09–0.05
Aminocarbenes, $=\text{C}(\text{pyrrolidin-1-yl})\text{Y}$ Y = 2-methylfuryl, 2-methylthiophenyl	0.06, 0.05
Phosphoylide-aminocarbene, 	0.06 to –0.01 <sup>c</sup>
$Fc$ -aminocarbenes $=\text{C}(\text{O}^-)\text{R}(\text{NMe}_4^+)$ R = 4-methylthiazol-2-yl, 2-methylfuryl, $\text{CH}_2\text{SiMe}_3$ , or Fc	–0.11 to –0.21 –0.16 to –0.73

<sup>a</sup>Estimated from  $P_L$  values by using Eq. 50.4; metal centers of the type {M(CO)<sub>5</sub>} (M = Cr, W, Mo) were commonly used; from Reference 28, unless stated otherwise.

<sup>b</sup>From Reference 77.

<sup>c</sup>From Reference 41.

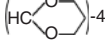
cautiously. Nevertheless, common C-ligands can be ordered as follows, according to their net electron  $\pi$ -acceptor minus  $\sigma$ -donor character, as expressed by their  $E_L$  values: carbynes > aminocarbyne > CO > vinylidenes > allenylidenes > carbenes > alkynyls [28].

The proposed models bear some limitations, namely, those concerning the possible failure of the additivity hypothesis. The risk is higher for the Lever's model, with maximum additivity, and lower for the Pickett's approach, with minimum additivity. However, the former model has a wider scope and has been much more applied, although it is less sensitive to subtle structure or composition changes and, in the initial form, insensitive to isomeric affects.

The eventual dependence of the ligand parameters on the properties of the binding metal sites and the (de)localization of the redox orbital at the ligand (instead of being localized at the metal) also constitute difficulties that usually are not easy to overcome and can lead to anomalous parameter values.

Extensions from octahedral-type geometries and 18-electron complexes to others have already been achieved, and of particular significance in organometallic chemistry are those concerning sandwich and half-sandwich  $\pi$ -complexes. Different

**TABLE 50.7** Values for the  $E_L$  Ligand Parameter for Alkynyl Ligands,  $-C\equiv C-R$  ( $L$ )

R		Metal Center	$E_L$ (V) versus NHE <sup>a</sup>
$C_6H_3(C\equiv CX)_2$ -1,3,5	X = H or Fc	$\{OsCl(dppm)_2\}^+$	-0.20
$C_6H_4C\equiv CPh$ -4		$\{OsCl(dppm)_2\}^+$	-0.21
Ph		$\{OsCl(dppm)_2\}^+$	-0.24
$CPh_2(PMe_3)^+$		$\{Fe(NCMe)(depe)_2\}^+$	-0.28 <sup>b</sup>
$CPh_2(C\equiv N)$		$\{FeBr(depe)_2\}^+$	-0.27 <sup>b</sup>
$C(=CH_2)Ph$		$\{FeBr(depe)_2\}^+$	-0.33 <sup>b</sup>
$CHPh_2$		$\{FeBr(depe)_2\}^+$	-0.38 <sup>b</sup>
$C(=CHMe)Et$		$\{FeBr(depe)_2\}^+$	-0.4 <sup>b</sup>
$CPh_2(NHMe)$		$\{FeBr(depe)_2\}^+$	-0.47 <sup>b</sup>
$CPh_2(NMe_2)$		$\{FeBr(depe)_2\}^+$	-0.49 <sup>b</sup>
Ph		$\{WH_2(dppe)_2\}^+$	-0.30 <sup>c</sup>
$C(=CH_2)X$		$\{RuCl(dppm)_2\}^+$	-0.06 to -0.19
	X = $NMe_2CH_2C\equiv CEt^+$ , $NMe_3CH_2Ph^+$ , $NEt_3^+$ , $NEt(C_2H_4)_2O^+$ ,		
			
	$NMe_2CH_2C_6H_4OMe$ -3 <sup>+</sup> , $NPr_3^+$ , $N(CH_2CH_2)_3CH^+$ , $NC_5H_4NMe_2^+$		
$C_6H_4X$	X = $CH=CHPh$ , $NO_2$ -4, $CHO$ -4, $OME$ -4, $N=NC_6H_4NO_2$ -4,4', $CHO$ -3, $C\equiv CPh$ -4, $C\equiv CC_6H_4NO_2$ -4,4', $CH=CHC_6H_4NO_2$ -4,4', $C\equiv CC_6H_4C\equiv CC_6H_4NO_2$ -4,4',4'',	$\{RuCl(dppm)_2\}^+$	-0.51 to -0.24
			
$C_6H_3(C\equiv CX)_2$ -1,3,5		$\{RuCl(dppm)_2\}^+$	-0.39
Ph		$\{RuCl(dppm)_2\}^+$	-0.41, -0.46
$CHPh_2$		$\{RuCl(dppm)_2\}^+$	-0.42
Me or $iPr$		$\{RuCl(dppm)_2\}^+$	-0.51
Ph		$\{RuCl(Me_2bpy)(PPh_3)_2\}^+$	-0.62, -0.48 <sup>d</sup>
$C_6H_4Me$ -4		$\{RuCl(Me_2bpy)(PPh_3)_2\}^+$	-0.65, -0.51 <sup>d</sup>
$tBu$		$\{RuCl(Me_2bpy)(PPh_3)_2\}^+$	-0.74, -0.60 <sup>d</sup>

<sup>a</sup>From Eq. 50.3 and Reference 28, unless stated otherwise.<sup>b</sup>From Reference 52.<sup>c</sup>From Reference 63.<sup>d</sup>From Reference 92.

metal redox standards have been considered, leading to distinct scales of ligand parameters, but a proposal to maintain the initial model and overcome this limitation has been presented. Nevertheless, the generality has to be further tested.

Another perspective that deserves to be further explored concerns the application of the redox potential parameterization models to the prediction (estimate) of the redox potential of complexes. This can be of a relevant identification significance of unknown compounds, by comparing the predicted and the measured values of the redox potential. Important cases of application can include the identification *in situ* of reaction intermediates or products without requiring their isolation.

Hence, a broader application of redox potential parameterization methods in organometallic chemistry, for both characterization and identification purposes, is expected.

## ACKNOWLEDGMENTS

This work has been partially supported by the Fundação para a Ciência e a Tecnologia (FCT), Portugal (project PEst-OE/QUI/UI0100/2013).

## ABBREVIATIONS

$\beta$	Polarizability parameter
bpy	2,2'-Bipyridine
depe	1,2-Bis(diethylphosphino)ethane
dppe	1,2-Bis(diphenylphosphino)ethane
dppm	1,2-Bis(diphenylphosphino)methane
$E_L$	Lever electrochemical ligand parameter
$E_S$	Electron-richness parameter
Et	Ethyl
Fc	Ferrocenyl
HOMO	Highest occupied molecular orbital
HS	High spin
$i\text{Pr}$	Isopropyl
IR	Infrared
LS	Low spin
Me	Methyl
MO	Molecular orbital
NHE	Normal hydrogen electrode
NLO	Nonlinear optical
NMR	Nuclear magnetic resonance
Ph	Phenyl
Pr	Propyl
$t\text{Bu}$	<i>tert</i> -Butyl
THF	Tetrahydrofuran
Tol	Tolyl

## REFERENCES

1. Sarapu, A. C.; Fenske, R. F. *Inorg. Chem.* **1975**, *14*, 247–253.
2. Pickett, C. J.; Pletcher, D. J. *Organomet. Chem.* **1975**, *102*, 327–333.
3. Pombeiro, A. J. L. *Port. Electrochim. Acta* **1983**, *1*, 19–143.
4. Silva, M. E. N. P. R. A.; Pombeiro, A. J. L.; Fraústo da Silva, J. J. R.; Herrmann, R.; Deus, N.; Castilho, T. J.; Guedes da Silva, M. F. C. J. *Organomet. Chem.* **1991**, *421*, 75–90.
5. *Molecular Electrochemistry of Inorganic, Bioinorganic and Organometallic Compounds*; Pombeiro, A. J. L.; McCleverty, J., Eds.; NATO ASI Series; Kluwer Academic Publishers: Dordrecht, **1993**.
6. Vlcèk, A. *Chemtracts Inorg. Chem.* **1993**, *5*, 1–35.
7. Silva, M. E. N. P. R. A.; Pombeiro, A. J. L.; Fraústo da Silva, J. J. R.; Herrmann, R.; Deus, M.; Bozak, R. E. J. *Organomet. Chem.* **1994**, *480*, 81–90.
8. Astruc, D. *Electron Transfer and Radical Processes in Transition Metal Chemistry*; John Wiley & Sons, Inc.: New York, **1995**.
9. Pombeiro, A. J. L. *New J. Chem.* **1997**, *21*, 649–660.
10. Dahrenbourg, M. Y.; Lyon, E. J.; Smee, J. J. *Coord. Chem. Rev.* **2000**, *206–207*, 533–561.
11. Konarev, D. V.; Lyubovskaya, R. N.; Drichko, N. V.; Yudanova, E. I.; Shul'ga, Y. M.; Litvinov, A. L.; Semkin, V. N.; Tarasov, B. P. *J. Mater. Chem.* **2000**, *10*, 803–818.
12. Zanello, P. *Inorganic Electrochemistry: Theory, Practice and Application*; Royal Society of Chemistry: Cambridge, **2003**.
13. Trujillo, A.; Fuentealba, M.; Manzur, C.; Carrillo, D.; Hamon, J.-R. *J. Organomet. Chem.* **2003**, *681*, 150–157.
14. Ackermann, M. N.; Moore, K. B.; Colligan, A. S.; Thomas-Wohlever, J. A.; Warren K. J. *J. Organomet. Chem.* **2003**, *667*, 81–89.
15. *Trends in Molecular Electrochemistry*; Pombeiro, A. J. L.; Amatore, C., Eds.; Marcel Dekker/FontisMedia: New York/Lausanne, **2004**.
16. Bhaumik, C.; Das, S.; Saha, D.; Dutta, S.; Baitalik, S. *Inorg. Chem.* **2010**, *49*, 5049–5062.
17. Costuas, K.; Rigaut, S. *Dalton Trans.* **2011**, *40*, 5643–5658.
18. Chatt, J.; Kan, C. T.; Leigh, G. J.; Pickett, C. J.; Stanley, D. R. *J. Chem. Soc. Dalton Trans.*, **1980**, 2032–2038.

19. Chatt, J. *Coord. Chem. Rev.* **1982**, *43*, 337–347.
20. Pickett, C. J. In *Comprehensive Coordination Chemistry*; Wilkinson, G.; Gillard, R. D.; McCleverty, J. A., Eds.; Pergamon Press: Oxford, **1987**, Vol. 1; p 493, Chapter 8.3.
21. Lever, A. B. P. *Inorg. Chem.* **1990**, *29*, 1271–1285.
22. Lever, A. B. P. *Inorg. Chem.* **1991**, *30*, 1980–1985.
23. Lever, A. B. P.; Dodsworth, E. S. *Inorganic Electronic Structure and Spectroscopy*; John Wiley & Sons, Inc.: New York, **1999**; Vol. 2.
24. Lever, A. B. P. In *Comprehensive Coordination Chemistry II*; Lever, A. B. P., Ed.; Elsevier: Oxford, **2004**, Vol. 2; p 251, Chapter 2.19.
25. Bursten, B. E. *J. Am. Chem. Soc.* **1982**, *104*, 1299–1304.
26. Bursten, B. E.; Green, M. R. *Prog. Inorg. Chem.* **1988**, *36*, 393–485.
27. Bursten, B. E.; Green, M. R.; Katovic, V.; Lightner Jr., D. *Inorg. Chem.* **1986**, *25*, 831–834.
28. Pombeiro, A. J. L. *J. Organomet. Chem.* **2005**, *690*, 6021–6040.
29. Pombeiro, A. J. L. *Eur. J. Inorg. Chem.* **2007**, 1473–1482.
30. Pombeiro, A. J. L.; Guedes da Silva, M. F. C.; Lemos, M. A. N. D. A. *Coord. Chem. Rev.* **2001**, *219–221*, 53–80.
31. Lu, S.; Strelets, V. V.; Ryan, M. F.; Pietro, W. J.; Lever, A. B. P. *Inorg. Chem.* **1996**, *35*, 1013–1023.
32. Guedes da Silva, M. F. C.; Pombeiro, A. J. L. *Electrochim. Acta* **2012**, *82*, 478–483.
33. Pombeiro, A. J. L.; Pickett, C. J.; Richards, R. L. *J. Organomet. Chem.* **1982**, *224*, 285–294.
34. Pombeiro, A. J. L. *Inorg. Chim. Acta* **1985**, *103*, 95–103.
35. Pombeiro, A. J. L. *Port. Electrochim. Acta* **1985**, *3*, 41–65.
36. Carvalho, M. F. N. N.; Pombeiro, A. J. L. *J. Chem. Soc. Dalton Trans.* **1989**, 1209–1216.
37. Martins, L. M. D. R. S.; Pombeiro, A. J. L. *Port. Electrochim. Acta* **1996**, *14*, 151–155.
38. Guedes da Silva, M. F. C.; Martins, L. M. D. R. S.; Fraústo da Silva, J. J. R.; Pombeiro, A. J. L. *Coll. Czech. Chem. Commun.* **2001**, *66*, 139–154.
39. Guedes da Silva, M. F. C.; Trzeciak, A. M.; Ziolkowski, J. J.; Pombeiro, A. J. L. *J. Organomet. Chem.* **2001**, *620*, 174–181.
40. Almeida, S. S. P. R.; Pombeiro, A. J. L. *Organometallics* **1997**, *16*, 4469–4478.
41. Facchin, G.; Mozzon, M.; Michelin, R. A.; Ribeiro, M. T. A.; Pombeiro, A. J. L. *J. Chem. Soc. Dalton Trans.* **1992**, 2827–2835.
42. Heath, G. A.; Humphrey, D. G. *J. Chem. Soc. Chem. Comm.* **1991**, 1668–1671.
43. Almeida, S. S. P. R.; Guedes da Silva, M. F. C.; Fraústo da Silva, J. J. R.; Pombeiro, A. J. L. *Port. Electrochim. Acta* **2001**, *19*, 371–376.
44. Lemos, M. A. N. D. A.; Pombeiro, A. J. L. *J. Organomet. Chem.* **1988**, *356*, C79–C82.
45. Pickett, C. J. In: *Electrochemistry*; Pletcher, D., Ed.; Royal Society of Chemistry: Cambridge, **1983**, Vol. 8; p 81.
46. Meidine, M. F.; Lemos, M. A. N. D. A.; Pombeiro, A. J. L.; Nixon, J. F.; Hitchcock, P. B. *J. Chem. Soc. Dalton Trans.* **1998**, 3319–3323.
47. Wang, Y.; Pombeiro, A. J. L.; Kaden, L.; Wahren, M. In: *Molecular Electrochemistry of Inorganic, Bioinorganic and Organometallic Compounds*; Pombeiro, A. J. L.; McCleverty, J., Eds.; NATO ASI Series; Kluwer Academic Publishers: Dordrecht, **1993**, p 63.
48. Venâncio, A. I. F.; Kuznetsov, M. L.; Guedes da Silva, M. F. C.; Martins, L. M. D. R. S.; Fraústo da Silva, J. J. R.; Pombeiro, A. J. L. *Inorg. Chem.* **2002**, *41*, 6456–6467.
49. El-Shihi, T.; Siglmüller, F.; Herrman, R.; Carvalho, M. F. N. N.; Pombeiro, A. J. L. *J. Organomet. Chem.* **1987**, *335*, 239–247.
50. El-Shihi, T.; Siglmüller, F.; Herrman, R.; Carvalho, M. F. N. N.; Pombeiro, A. J. L. *Port. Electrochim. Acta* **1987**, *5*, 179–185.
51. Almeida, S. S. P. R.; Guedes da Silva, M. F. C.; Pombeiro, A. J. L. *Collect. Czech. Chem. Commun.* **2003**, *68*, 1663–1676.
52. Venâncio, A. I. F.; Guedes da Silva, M. F. C.; Martins, L. M. D. R. S.; Fraústo da Silva, J. J. R. *Organometallics* **2005**, *24*, 4654–4665.
53. Zhang, L.; Guedes da Silva, M. F. C.; Kuznetsov, M. L.; Gamasa, M. P.; Gimeno, J.; Fraústo da Silva, J. J. R.; Pombeiro, A. J. L. *Organometallics* **2001**, *20*, 2782–2793.
54. Limberg, A.; Lemos, M. A. N. D. A.; Pombeiro, A. J. L.; Maiorana, S.; Papagni, A.; Licandro, E. *Port. Electrochim. Acta* **1995**, *13*, 319–323.
55. Pombeiro, A. J. L.; Costa, M. T. A. R. S.; Wang, Y.; Nixon, J. F. *J. Chem. Soc. Dalton Trans.* **1999**, 3755–3758.
56. Almeida, S. S. P. R.; Guedes da Silva, M. F. C.; Fraústo da Silva, J. J. R.; Pombeiro, A. J. L. *J. Chem. Soc. Dalton Trans.* **1999**, 467–472.
57. Cunha, S. M. P. R. M.; Guedes da Silva, M. F. C.; Pombeiro, A. J. L. *Port. Electrochim. Acta* **1999**, *17*, 221–224.
58. Ribeiro, L. M. D.; Pombeiro, A. J. L. *Port. Electrochim. Acta* **1995**, *13*, 329–333.
59. Carvalho, M. F. N. N.; Pombeiro, A. J. L. *Organomet. Chem.* **1991**, *410*, 347–355.

60. Carvalho, M. F. N. N.; Pombeiro, A. J. L.; Hills, A.; Hughes, D. L.; Richards, R. L. *J. Organomet. Chem.* **1993**, *469*, 179–187.
61. Alegria, E. C. B. A.; Cunha, S. M. P. R. M.; Martins, L. M. D. R. S.; Guedes da Silva, M. F. C.; Pombeiro, A. J. L. *Port. Electrochim. Acta* **2004**, *22*, 19–23.
62. Venâncio, A. I. F.; Martins, L. M. D. R. S.; Pombeiro, A. J. L. *Port. Electrochim. Acta* **2003**, *21*, 85–90.
63. Hills, A.; Hughes, D. L.; Kashef, N.; Lemos, M. A. N. D. A.; Pombeiro, A. J. L.; Richards, R. L. *J. Chem. Soc. Dalton Trans.* **1992**, 1775–1782.
64. Carvalho, M. F. N. N.; Duarte, M. T.; Galvão, A. M.; Pombeiro, A. J. L. *J. Organomet. Chem.* **1994**, *469*, 79–87.
65. Zhang, L.; Gamasa, M. P.; Gimeno, J.; Guedes da Silva, M. F. C.; Pombeiro, A. J. L.; Graiff, C.; Lanfranchi, M.; Tiripicchio, A. *Eur. J. Inorg. Chem.* **2000**, 1707–1715.
66. Pombeiro, A. J. L. In: *Inorganic Electrochemistry*; Scholz, F.; Pickett, C. J., Eds.; Encyclopedia of Electrochemistry, Vol. 7; Wiley-VCH Verlag GmbH: Weinheim, **2006**; p 77.
67. Carriedo, G. A.; Riera, V.; Connelly, N. G.; Raven, S. J. *J. Chem. Soc. Dalton Trans.* **1987**, 1769–1773.
68. Guedes da Silva, M. F. C.; Fraústo da Silva, J. J. R.; Pombeiro, A. J. L.; Pellinghelli, M. A.; Tiripicchio, A. *J. Chem. Soc. Dalton Trans.* **1996**, 2763–2772.
69. Wang, Y.; Pombeiro, A. J. L. *Port. Electrochim. Acta* **1993**, *11*, 111–115.
70. Disley, S. P. M.; Grime, R. W.; McInnes, E. J. L.; Spencer, D. M.; Swainston, N.; Whiteley, M. W. *J. Organomet. Chem.* **1998**, *566*, 151–158.
71. Masui, M.; Lever, A. B. P. *Inorg. Chem.* **1993**, *32*, 2199–2201.
72. Perrin, L.; Clot, E.; Eisenstein, O.; Loch, J.; Crabtree, R. H. *Inorg. Chem.* **2001**, *40*, 5806–5811.
73. Reisner, E.; Arion, V. B.; Guedes da Silva, M. F. C.; Lichtenecker, R.; Eichinger, A.; Keppler, B. K.; Kukushkin, V. Y.; Pombeiro, A. J. L. *Inorg. Chem.* **2004**, *43*, 7083–7093.
74. Reisner, E.; Arion, V. B.; Eichinger, A.; Kandler, N.; Geister, G.; Pombeiro, A. J. L.; Keppler, B. K. *Inorg. Chem.* **2005**, *44*, 6704–6716.
75. Guedes da Silva, M. F. C.; Pombeiro, A. J. L.; Geremia, S.; Zangrandi, E.; Calligaris, M.; Zinchenko, A. V.; Kukushkin, V. Y. *J. Chem. Soc. Dalton Trans.* **2000**, 1363–1371.
76. Trzeciak, A. M.; Borak, B.; Ciunik, Z.; Ziolkowski, J. J.; Guedes da Silva, M. F. C.; Pombeiro, A. J. L. *Eur. J. Inorg. Chem.* **2004**, 1411–1419.
77. Kovacik, I.; Gevert, O.; Werner, H.; Schmittel, M.; Söllner, R. *Inorg. Chim. Acta* **1998**, *275*–*276*, 435–439.
78. Toma, H. E.; Araki, K.; Alexiou, A. D. P.; Nikolaou, S.; Dovidauskas, S. *Coord. Chem. Rev.* **2001**, *219*–*221*, 187–234.
79. Bierdeman, D. J.; Keister, J. B.; Jelski, D. A. *J. Organomet. Chem.* **2001**, *633*, 51–65.
80. Feighery, W. G.; Yao, H.; Hollenkamp, A. F.; Allendoerfer, R. D.; Keister, J. B. *Organometallics* **1998**, *17*, 872–886.
81. Pombeiro, A. J. L.; Guedes da Silva, M. F. C. *J. Organomet. Chem.* **2001**, *617*–*618*, 65–69.
82. Guedes da Silva, M. F. C.; Lemos, M. A. N. D. A.; Fraústo da Silva, J. J. R.; Pombeiro, A. J. L.; Pellinghelli, M. A.; Tiripicchio, A. *J. Chem. Soc. Dalton Trans.* **2000**, 373–380.
83. Pombeiro, A. J. L. In: *Transition Metal Carbyne Complexes*; Kreissl, F. R., Ed.; NATO ASI Series; Kluwer Academic Publishers: Dordrecht, The Netherlands, **1993**, pp. 105–121.
84. (a) Pombeiro, A. J. L. In: *Molecular Electrochemistry of Inorganic, Bioinorganic and Organometallic Compounds*; Pombeiro, A. J. L.; McCleverty, J. Eds.; NATO ASI Series; Kluwer Academic Publishers: Dordrecht, The Netherlands, **1993**, pp. 331–344; (b) Pombeiro, A. J. L.; Richards, R. L. *Coord. Chem. Rev.* **1990**, *104*, 13–38.
85. Pombeiro, A. J. L. *New J. Chem.* **1994**, *18*, 163–174.
86. Chatt, J.; Pombeiro, A. J. L.; Richards, R. L.; Royston, G.; Muir, K.; Walker, R. *J. Chem. Soc. Chem. Comm.* **1975**, 708–709.
87. Carrondo, M. A. A. F. C. T.; Domingos, A. M. T. S.; Jeffrey, G. A. *J. Organomet. Chem.* **1985**, *289*, 377–383.
88. Carvalho, M. F. N. N.; Duarte, M. T.; Galvão, A. M.; Pombeiro, A. J. L. *J. Organomet. Chem.* **1996**, *511*, 163–169.
89. Hurst, S. K.; Cifuentes, M. P.; Morrall, J. P. L.; Lucas, N. T.; Whittall, I. R.; Humphrey, M. G.; Asselberghs, I.; Persoons, A.; Samoc, M.; Luther-Davies, B.; Willis, A. C. *Organometallics* **2001**, *20*, 4664–4675.
90. Hurst, S. K.; Lucas, N. T.; Humphrey, M. G.; Isoshima, T.; Wostyn, K.; Asselberghs, I.; Clays, K.; Persoons, A.; Samoc, M.; Luther-Davies, B. *Inorg. Chim. Acta* **2003**, *350*, 62–76.
91. Powell, C. E.; Cifuentes, M. P.; Morrall, J. P.; Stranger, R.; Humphrey, M. G.; Samoc, M.; Luther-Davies, B.; Heath, G. A. *J. Am. Chem. Soc.* **2003**, *125*, 602–610.
92. Adams, C. J.; Pope, S. J. A. *Inorg. Chem.* **2004**, *43*, 3492–3499.

---

# 51

---

## ENDOHEDRAL METALLOFULLERENES TODAY: MORE AND MORE VERSATILE SHIPS IN MULTIFORM BOTTLES—ELECTROCHEMISTRY OF X-RAY CHARACTERIZED MONOMETALLOFULLERENES

FABRIZIA FABRIZI DE BIANI AND PIERO ZANELLO\*

*Dipartimento di Chimica, dell'Università di Siena, Siena, Italy*

### 51.1 INTRODUCTION

Endohedral metallofullerenes (EMFs) constitute a rapidly expanding topic in the scientific background, as proved by the substantially linear increase in the number of papers devoted to such nanoderivatives with respect to their detection in the late 1980s (by the buckminsterfullerene discoverers themselves [1]) (Fig. 51.1).

In confirmation of the interest in EMFs, the state of art of their different properties are periodically and intensively reviewed [2]. In fact, starting from the elucidation of their physicochemical fundamentals [2d, g], they have progressively expanded their applications in many areas of chemistry and physics, ranging from advanced materials to medicinal science and from molecular electronics to photovoltaics [3].

As one of the most characteristic features of endohedral fullerenes is the charge transfer from the encaged species to the fullerene cage, it is well conceivable that electrochemistry can experimentally look at the redox properties of EMFs with respect to the corresponding free fullerenes. In this light, we will deal with the electrochemical behavior of those EMFs that have been characterized by single-crystal X-ray diffraction (which is the most reliable technique able to solve definitely the molecular structure of any type of molecules), neglecting, if unnecessary, the different isomers of the metal cages. We point out that tutorial approaches to the electrochemistry of EMFs [4] and descriptions of the X-ray resolved EMFs [2l, p, q] have recently appeared.

Finally, it is useful to remind that there exist three types of EMFs as a function of their inner metal content: mono-EMFs, di-EMFs, and cluster-EMFs.

In this picture, we will deal here with monometal endohedral metallofullerenes (MEMFs), which, because of their relative structural simplicity, better help in understanding the physicochemical properties of such new molecules.

### 51.2 C<sub>60</sub>-MONOMETAL ENDOHEDRAL METALLOFULLERENES

In order of increasing dimensions of fullerene cages, the first EMF to be considered is the single-crystal-resolved [Li@C<sub>60</sub>]<sup>+</sup> [5a]. As illustrated in Fig. 51.2, it undergoes a sequence of one-electron reductions reminiscent to those of the C<sub>60</sub> parent [5c], even if they are almost rigidly anodically shifted by 0.5–0.7 V.

The pertinent redox potentials are compiled in Table 51.1.

*Advances in Organometallic Chemistry and Catalysis: The Silver/Gold Jubilee International Conference on Organometallic Chemistry Celebratory Book*, First Edition. Edited by Armando J. L. Pombeiro.

© 2014 John Wiley & Sons, Inc. Published 2014 by John Wiley & Sons, Inc.

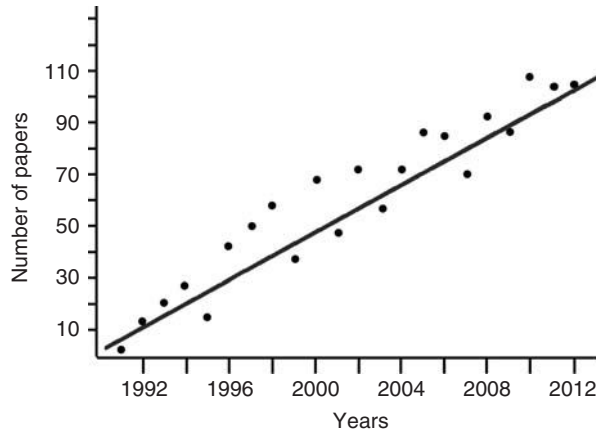


**Figure 51.1** An overall picture of the number of papers annually devoted to EMFs since their discovery (from a personal recognition in the web pages. Conferences proceedings, patents, and dissertations are excluded).  $\circ \bullet$  Updated to September 2012.

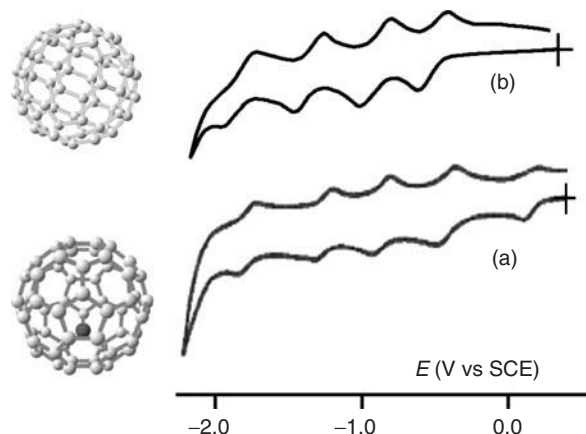


**Figure 51.2** Cyclic voltammetric responses recorded at a platinum electrode in 1,2-dichlorobenzene solution of (a)  $[\text{Li}@\text{C}_{60}](\text{PF}_6)$  and (b)  $\text{C}_{60}$ . Scan rate: 0.1 V/s. Adapted from Reference 5b.

**TABLE 51.1 Formal Electrode Potentials (V vs SCE) of the Redox Processes of the  $[\text{C}_{60}]$  Cage of  $[\text{Li}@\text{C}_{60}]^+$  in 1,2-Dichlorobenzene Solution**

Complex	$[\text{C}_{60}]^{+/0}$	$[\text{C}_{60}]^{0/-}$	$[\text{C}_{60}]^{-2/-}$	$[\text{C}_{60}]^{2/-3/-}$	$[\text{C}_{60}]^{3/-4/-}$	$[\text{C}_{60}]^{4/-5/-}$	References
$[\text{Li}@\text{C}_{60}](\text{SbCl}_6)$		+0.18	-0.41	-0.87	-1.26	-1.79	5a
$[\text{Li}@\text{C}_{60}](\text{PF}_6)$		+0.19	-0.38	-0.84	-1.22	-1.75	5c
$\text{C}_{60}$	+1.72	-0.52	-0.91	-1.35	-1.81		5c

The  $\text{C}_{60}^{+/0}$  oxidation process observed at +1.72 V for free  $\text{C}_{60}$  is absent for  $[\text{Li}@\text{C}_{60}]^+$ , being most likely anodically shifted up to be driven out of the accessible experimental window. In fact, UV-vis spectra suggest that the energy differences between the frontier orbitals is almost unchanged by encapsulation of  $\text{Li}^+$  in the  $\text{C}_{60}$  cage [5b], so that both the lowest unoccupied molecular orbital (LUMO) and the highest occupied molecular orbital (HOMO) of  $[\text{Li}@\text{C}_{60}]^+$  are expected to be stabilized to almost the same extent in comparison with those of  $\text{C}_{60}$ . Interestingly, a similar result has also been obtained by *ab initio* calculations, which shows that the interaction between the  $\text{Li}^+$  ion and  $\text{C}_{60}$  in the endohedral complex results in a pronounced stabilization of the orbital energy levels without their splitting. This is indicative of the absence of chemical bonding between the lithium ion and the fullerene cage and confirms that the interaction between them is primarily

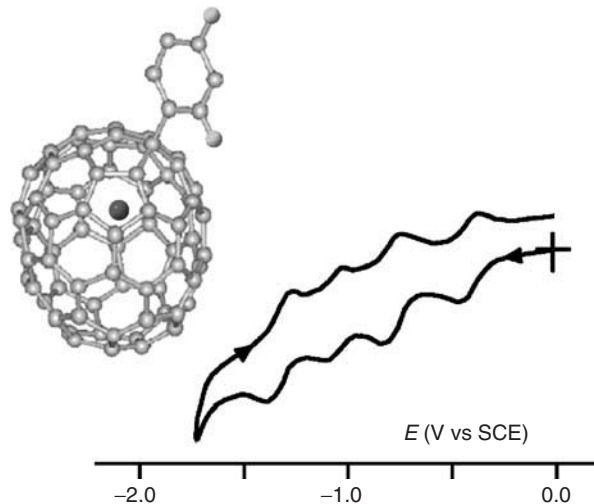


**Figure 51.3** Cyclic voltammetric response recorded at a platinum electrode in 1,2-dichlorobenzene solution of La@C<sub>72</sub>(C<sub>6</sub>H<sub>3</sub>Cl<sub>2</sub>) (X-ray characterized isomer). Scan rate: 0.02 V/s. Adapted from Reference 7.

electrostatic [6]. Thus, the Coulombic effects played by the positive charge inside the C<sub>60</sub> cage in [Li@C<sub>60</sub>]<sup>+</sup> make easier the reduction processes with respect to free C<sub>60</sub> [5a,c] and is nicely evocative of the periodical behavior of the electron affinity, which generally increases across a period in the Periodic Table of Elements.

### 51.3 C<sub>72</sub>-MONOMETAL ENDOHEDRAL METALLOFULLERENES

Let us consider La@C<sub>72</sub>. Given the insolubility of La@C<sub>72</sub> in the common organic solvents, it was extracted from the soot by treatment with 1,2,4-trichlorobenzene affording the dichlorophenyl adduct La@C<sub>72</sub>(C<sub>6</sub>H<sub>3</sub>Cl<sub>2</sub>). The complex is described as [La]<sup>3+</sup>[C<sub>72</sub>(C<sub>6</sub>H<sub>3</sub>Cl<sub>2</sub>)]<sup>3-</sup> [7]. Of the three isolated isomeric forms, one has been X-ray characterized. As Fig. 51.3 shows, the pertinent cyclic voltammetric response displays four sequential reductions with features of chemical reversibility, which are formally assigned to the sequence [C<sub>72</sub>]<sup>3-/4-</sup> ( $E^\circ = -0.43$  V vs SCE (saturated calomel electrode)), [C<sub>72</sub>]<sup>4-/5-</sup> ( $E^\circ = -0.76$  V), [C<sub>72</sub>]<sup>5-/6-</sup> ( $E^\circ = -1.07$  V), and [C<sub>72</sub>]<sup>6-/7-</sup> ( $E^\circ = -1.33$  V) [7]. Not shown in the figure, a couple of irreversible oxidations are present, which are naively assigned to the passage [C<sub>72</sub>]<sup>3-/2-/1-</sup>.

Unfortunately, neither structural nor electrochemical data exist for the pristine La@C<sub>72</sub>.

### 51.4 C<sub>74</sub>-MONOMETAL ENDOHEDRAL METALLOFULLERENES

La@C<sub>74</sub> was X-ray characterized as La@C<sub>74</sub>(C<sub>6</sub>H<sub>3</sub>Cl<sub>2</sub>) too [8]. Also in this case, it exists in different isomeric forms, two of which have been X-ray solved. All the derivatives, however, afford poorly defined cyclic and differential pulse voltammetric profiles [8b].

### 51.5 C<sub>80</sub>-MONOMETAL ENDOHEDRAL METALLOFULLERENES

A number of M@C<sub>80</sub> lanthanides have been crystallographically characterized (M = La [9], Sm [10], and Yb [11]). Let us start with La@C<sub>80</sub>, which was isolated and X-ray characterized as La@C<sub>80</sub>(C<sub>6</sub>H<sub>3</sub>Cl<sub>2</sub>). As illustrated in Fig. 51.4, it exhibits three reductions and two oxidations with features of more or less defined chemical reversibility. The reduction processes are assigned to the passages [C<sub>80</sub>]<sup>3-/4-</sup> ( $E^\circ = -0.58$  V vs SCE), [C<sub>80</sub>]<sup>4-/5-</sup> ( $E^\circ = -0.98$  V), and [C<sub>80</sub>]<sup>5-/6-</sup> ( $E^\circ = -1.15$  V). The oxidation processes are assigned to [C<sub>80</sub>]<sup>3-/2-</sup> ( $E^\circ = +1.02$  V), and [C<sub>80</sub>]<sup>2-/1-</sup> ( $E^\circ = +1.52$  V) [9].

Concerned with Sm@C<sub>80</sub> and Yb@C<sub>80</sub>, Fig. 51.5 shows that they afford three well-defined reductions and one oxidation [10, 12].

Premitted that such EMFs are considered as [M]<sup>2+</sup>[C<sub>80</sub>]<sup>2-</sup>, the formal electrode potentials of such redox changes are summarized in Table 51.2.

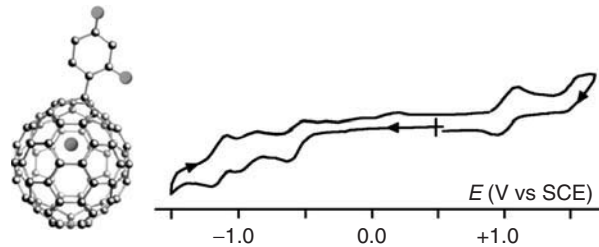


**Figure 51.4** Cyclic voltammetric response recorded at a platinum electrode in 1,2-dichlorobenzene solution of  $\text{La}@\text{C}_{80}(\text{C}_6\text{H}_3\text{Cl}_2)$ . Scan rate: 0.02 V/s. Adapted from Reference 9.

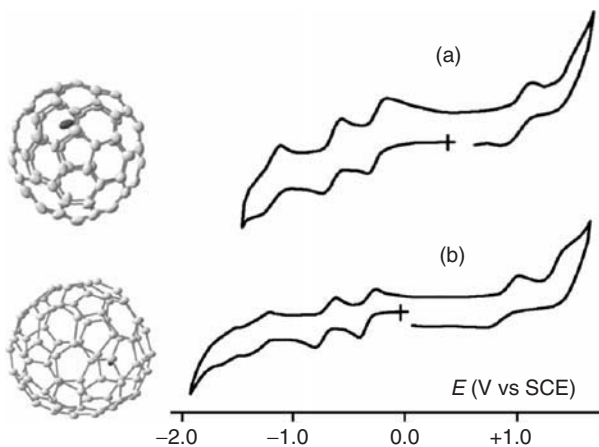


**Figure 51.5** Cyclic voltammetric responses recorded at a platinum electrode in 1,2-dichlorobenzene solution of (a)  $\text{Sm}@\text{C}_{80}$  and (b)  $\text{Yb}@\text{C}_{80}$ . Scan rate: (a) 0.1 V/s and (b) 0.02 V/s. (a) Adapted from Reference 10; (b) adapted from Reference 12.

**TABLE 51.2 Formal Electrode Potentials (V vs SCE) of the Redox Processes of the  $[\text{C}_{80}]^{2-}$  Cage of  $\text{Sm}@\text{C}_{80}$  and  $\text{Yb}@\text{C}_{80}$  in 1,2-Dichlorobenzene Solution**

Complex	$[\text{C}_{80}]^{2-/-}$	$[\text{C}_{80}]^{2-/3-}$	$[\text{C}_{80}]^{3-/4-}$	$[\text{C}_{80}]^{4-/5-}$	References
$\text{Sm}@\text{C}_{80}$	+1.00	-0.28	-0.66	-1.19	10
$\text{Yb}@\text{C}_{80}$	+0.91	-0.32	-0.70	-1.30	12

## 51.6 $\text{C}_{82}$ -MONOMETAL ENDOHEDRAL METALLOFULLERENES

A rich series of  $\text{M}@\text{C}_{82}$  EMFs has been X-ray characterized ( $\text{M} = \text{Sc}$  [13],  $\text{Y}$  [14],  $\text{La}$  [15a–g],  $\text{Ce}$  [16],  $\text{Sm}$  [17],  $\text{Gd}$  [18], and  $\text{Dy}$  [19]). We will limit our discussion to those derivatives that display well-defined electrochemical responses. It must be premitted that the oxidation state of the encaged metal in EMFs of  $\text{Y}$ ,  $\text{La}$ ,  $\text{Ce}$ ,  $\text{Gd}$ , and  $\text{Dy}$  is commonly assumed as +3, whereas in EMFs of  $\text{Sm}$  is +2. In reality, as we will note briefly, in some cases such assumption are controversial.

Let us therefore start with EMFs having the inner metal ion in the +3 oxidation state.

Crystal structure and electrochemistry of  $\text{Sc}@\text{C}_{82}(\text{Ad})$  ( $\text{Ad} = \text{adamantylidene}$ ) (in the  $C_{2v}(9)$  isomeric form) have been reported [13]. We report in Table 51.3 the redox potentials of its electron transfer processes together with those of the precursor  $\text{Sc}@\text{C}_{2v}(9)\text{C}_{82}$ . In both derivatives, the authors assigned the oxidation state +3 to the incarcerated metal ion. We note that, in previous studies, the oxidation state +2 has been assigned to  $\text{Sc}@\text{C}_{82}$  [20].

The HOMO–LUMO separation for each species, as measured in first approximation by the difference in potential values between the first oxidation and the first reduction, is reported in Table 51.4.

**TABLE 51.3 Formal Electrode Potentials (V vs SCE) of the Redox Processes of the [C<sub>82</sub>]<sup>3-</sup> Cage of the X-Ray Characterized M@C<sub>82</sub> Derivatives (with Respect to the Corresponding Passages of Free C<sub>82</sub>) in 1,2-Dichlorobenzene Solution**

Complex	[C <sub>82</sub> ] <sup>2-/</sup>	[C <sub>82</sub> ] <sup>3-/2-</sup>	[C <sub>82</sub> ] <sup>3-/4-</sup>	[C <sub>82</sub> ] <sup>4-/5-</sup>	[C <sub>82</sub> ] <sup>5-/6-</sup>	[C <sub>82</sub> ] <sup>6-/7-</sup>	[C <sub>82</sub> ] <sup>7-/8-</sup>	References
Sc@C <sub>82</sub>		+1.07 <sup>a</sup>	+0.22	-0.72				13
Sc@C <sub>82</sub> (Ad)		+0.66	+0.18	-0.86				13
Y@C <sub>82</sub>	+1.64 <sup>a</sup>	+0.67	+0.23	-0.77	-0.77	-1.65	-1.90	21b,c
Y@C <sub>82</sub> (Ad)		+0.55	+0.03	-0.94	-1.27			14b
Ce@C <sub>82</sub>	+1.65 <sup>a</sup>	+0.65	+0.16	-0.84	-0.96	-1.22	-1.68	21c
Ce@C <sub>82</sub> (Ad)		+0.59	+0.15	-0.78	-1.17			16
La@C <sub>82</sub>	+1.64 <sup>a</sup>	+0.64	+0.15	-0.80	-0.96	-1.69	-1.89	21a,c
La@C <sub>82</sub> (C <sub>6</sub> H <sub>3</sub> Cl <sub>2</sub> )		+1.22 <sup>a</sup>	-0.55	-0.85	-1.37			15e
La@C <sub>82</sub> {C <sub>5</sub> (CH <sub>3</sub> ) <sub>5</sub> }		+0.59	+0.12	-1.14	-1.65			15d
Gd@C <sub>82</sub>		+0.66	+0.18	-0.81	-0.81			21c
Gd@C <sub>82</sub> (Ad)		+0.63	+0.05	-0.91	-1.19			18c
C <sub>82</sub>	-1.04	-1.01	-1.37					21a,c,d

Ad, adamantylidene carbene.

<sup>a</sup>Peak potential for irreversible processes.**TABLE 51.4 Differences between the Electrode Potentials of the First Oxidation and the First Reduction of M@C<sub>82</sub> Derivatives (in eV) in 1,2-Dichlorobenzene Solution**

Complex	0/+	0/-	ΔE°'
Sc@C <sub>82</sub>	+1.07 <sup>a</sup>	+0.22	≈0.75
Sc@C <sub>82</sub> (Ad) <sup>b</sup>	+0.66	+0.18	0.48
Y@C <sub>82</sub>	+0.67	+0.23	0.44
Y@C <sub>82</sub> (Ad)	+0.55	+0.03	0.52
Ce@C <sub>82</sub>	+0.65	+0.16	0.49
Ce@C <sub>82</sub> (Ad)	+0.59	+0.15	0.44
La@C <sub>82</sub>	+0.64	+0.15	0.49
La@C <sub>82</sub> (C <sub>6</sub> H <sub>3</sub> Cl <sub>2</sub> )	+1.22 <sup>a</sup>	-0.55	≈1.8
La@C <sub>82</sub> {C <sub>5</sub> (CH <sub>3</sub> ) <sub>5</sub> }	+0.59	+0.12	0.47
Gd@C <sub>82</sub>	+0.66	+0.18	0.48
Gd@C <sub>82</sub> (Ad)	+0.63	+0.05	0.58
C <sub>82</sub> <sup>a</sup>	+1.29	-1.12	1.41

Ad, adamantylidene carbene.

<sup>a</sup>From Reference 21a,c,d.

Going on, Fig. 51.6 shows the different redox changes exhibited by Y@C<sub>82</sub>(Ad) (Ad = adamantylidene) [14b] with respect to the pristine precursor. Also, in this case, the oxidation state +3 is assigned to the incarcerated metal ion in both the adamantylidene adduct [14b] and the pristine derivative [21b]. Also in this case, previous studies assigned the oxidation state +2 to Y@C<sub>82</sub> [20a].

The pertinent redox potentials are compiled in Tables 51.3 and 51.4.

In turn, Fig. 51.7 gives an overall picture of the redox activity of different La@C<sub>82</sub> EMFs.

From Table 51.3, it is evident that the inductive effects of the different exohedral substituents affect appreciably the redox potentials.

Passing to the Ce derivatives, it has to be premitted that assignation of the oxidation state of cerium ion in Ce@C<sub>82</sub> has been debated. In fact, preliminary theoretical calculations assigned +2 [23a], whereas experimental studies and more recent theoretical calculations assigned +3 [23b, c]. Figure 51.8 illustrates the cyclic voltammetric behavior of the Ce<sup>3+</sup> adduct Ce@C<sub>82</sub>(Ad) (Ad = adamantylidene) (isomer 2b in Reference 16).

The difference in redox potentials between the pristine derivative and the adamantylidene adduct, Table 51.3, is even more attenuated with respect to the couple Y@C<sub>82</sub>/Y@C<sub>82</sub>(Ad).

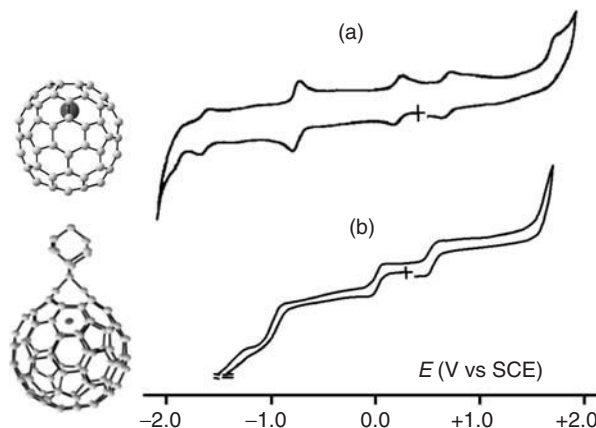


**Figure 51.6** Comparison between the cyclic voltammetric responses of (a) Y@C<sub>82</sub> and (b) Y@C<sub>82</sub>(Ad). Platinum working electrode. 1,2-Dichlorobenzene solution. Scan rate: (a) 0.02 V/s and (b) not specified. (a) Adapted from Reference 21b,c; (b) adapted from Reference 14b. The optimized structure of Y@C<sub>82</sub> is adapted from Reference 22.

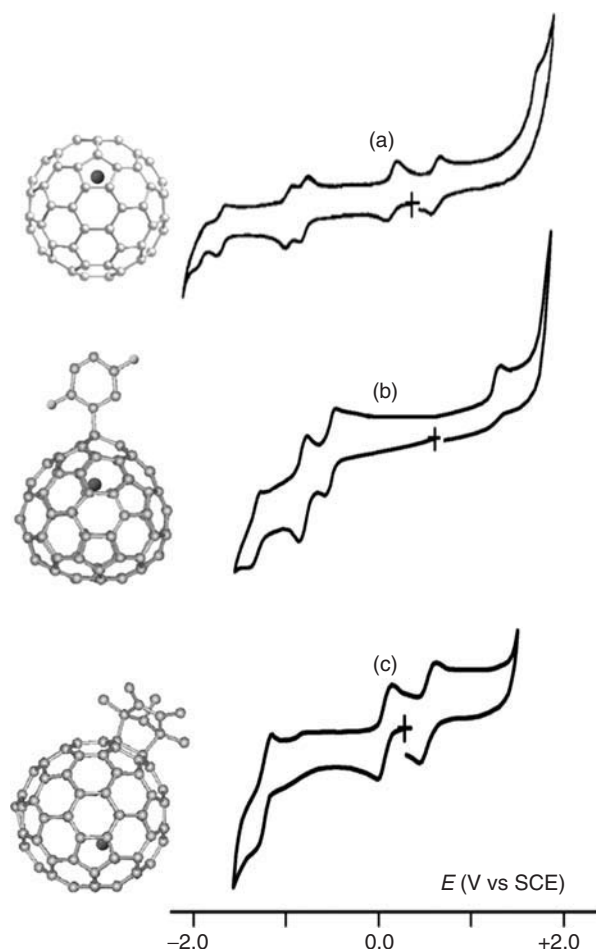


**Figure 51.7** Cyclic voltammetric responses recorded at a platinum electrode in 1,2-dichlorobenzene solution of (a) La@C<sub>82</sub>; (b) La@C<sub>82</sub>(C<sub>6</sub>H<sub>5</sub>Cl<sub>2</sub>); and (c) La@C<sub>82</sub>C<sub>5</sub>(CH<sub>3</sub>)<sub>5</sub>. Scan rate: (a) 0.1 V/s; (b) 0.02 V/s; and (c) 0.05 V/s. (a) Adapted from Reference 21c; (b) adapted from Reference 15e; (c) adapted from Reference 15d.

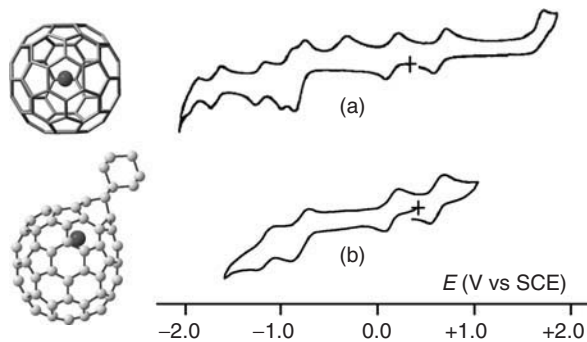


**Figure 51.8** Cyclic voltammetric responses recorded at a platinum electrode in 1,2-dichlorobenzene solution of (a) Ce@C<sub>82</sub> and (b) Ce@C<sub>82</sub>(Ad). Scan rate 0.02 V/s. (a) Adapted from Reference 21c; (b) adapted from Reference 16. The optimized structure of Ce@C<sub>82</sub> is adapted from Reference 23c.

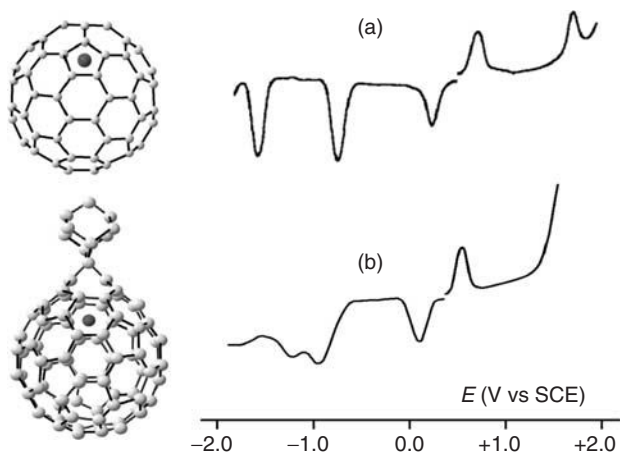


**Figure 51.9** Differential pulse voltammetric profiles recorded at a platinum electrode in 1,2-dichlorobenzene solutions of (a) Gd@C<sub>82</sub> and (b) Gd@C<sub>82</sub>(Ad). Scan rate: 0.02 V/s. (a) Adapted from Reference 21c; (b) adapted from Reference 18a.

In confirmation of the chemical reversibility of the first reduction [Ce@C<sub>82</sub>(Ad)]<sup>0/-</sup>, the crystal structure of the monoanion has been solved [16].

Concerned with Gd@C<sub>82</sub>, Fig. 51.9 compares the differential pulse voltammetric profiles of Gd@C<sub>82</sub> and Gd@C<sub>82</sub>(Ad) (both as C<sub>2v</sub> isomers) [18]. The pertinent redox potentials are compiled in Table 51.3.

As happens for the related Y@C<sub>82</sub> and Y@C<sub>82</sub>(Ad), also in the case of Gd@C<sub>82</sub> and Gd@C<sub>82</sub>(Ad), the coordination of the exohedral adamantlylidene results in an increase in the HOMO-LUMO separation with respect to the pristine derivative.

It is noted that in spite of the formally negative charge of the C<sub>82</sub> cage (namely, 3-) induced by the incarcerated M<sup>3+</sup> ion, the oxidation processes of the EMFs are more difficult and the reduction processes are easier with respect to the corresponding processes of free C<sub>82</sub><sup>3-</sup>. Excluding obviously Coulombic effects, this means that the intramolecular metal ion/fullerene electron exchange modifies appreciably the nature of both the HOMO and LUMO levels with respect to those of free C<sub>82</sub>, as on the other hand theoretically proved [21c, 24].

As seen, in general, the presence of exohedral groups do not afford great variations in the HOMO-LUMO gap, but for the C<sub>6</sub>H<sub>3</sub>Cl<sub>2</sub> substituent, which highly stabilizes the [C<sub>82</sub>]<sup>3-</sup> oxidation state.

Figure 51.10 shows the electrochemical behavior of Dy@C<sub>82</sub> derivatives. In particular, it compares the cyclic voltammetric profiles of Dy@C<sub>82</sub>[CCN(COOMe)<sub>2</sub>PPh<sub>3</sub>] [19] and Dy@C<sub>82</sub>. The pertinent redox potentials are compiled in Table 51.5.

Also in this case, the HOMO-LUMO gap of the pristine derivative is not affected by the presence of the exohedral group.

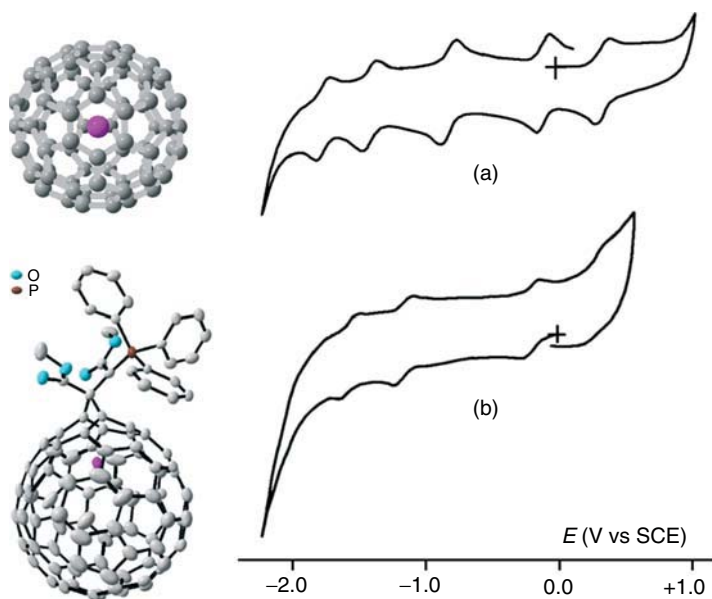


**Figure 51.10** Cyclic voltammetric profiles recorded at a platinum electrode in toluene-acetonitrile (4:1) solution of (a) Dy@C<sub>82</sub> and (b) Dy@C<sub>82</sub>[CCH(COOMe)<sub>2</sub>PPh<sub>3</sub>]. Scan rate: 0.05 V/s. (a) Adapted from Reference 25; (b) adapted from Reference 19. The optimized structure of Dy@C<sub>82</sub> is adapted from Reference 26. (See insert for color representation of the figure.)

**TABLE 51.5 Formal Electrode Potentials (V vs SCE) of the Redox Processes of the [C<sub>82</sub>]<sup>3-</sup> Cage of the Dy@C<sub>82</sub> EMFs and Separation of the First Oxidation and First Reduction (in eV) in Toluene–Acetonitrile (4 : 1) Solution**

Complex	[C <sub>82</sub> ] <sup>3-/2-</sup>	[C <sub>82</sub> ] <sup>3-/4-</sup>	[C <sub>82</sub> ] <sup>4-/5-</sup>	[C <sub>82</sub> ] <sup>5-/6-</sup>	[C <sub>82</sub> ] <sup>6-/7-</sup>	$\Delta E^{\circ'}$	References
Dy@C <sub>82</sub> [CCH(COOMe) <sub>2</sub> PPh <sub>3</sub> ]	+0.23	-0.23	-1.20	-1.61		0.46	19
Dy@C <sub>82</sub>	+0.34	-0.11	-0.82	-1.43	-1.78	0.45	25

**TABLE 51.6 Formal Electrode Potentials (V vs SCE) of the Redox Processes of the [C<sub>82</sub>]<sup>2-</sup> Cage of Sm@C<sub>82</sub> and Separation of the First Oxidation and First Reduction (in eV) in 1,2-Dichlorobenzene Solution**

Complex	[C <sub>82</sub> ] <sup>0/+</sup>	[C <sub>82</sub> ] <sup>-/0</sup>	[C <sub>82</sub> ] <sup>2-/1-</sup>	[C <sub>82</sub> ] <sup>2-/3-</sup>	[C <sub>82</sub> ] <sup>3-/4-</sup>	[C <sub>82</sub> ] <sup>4-/5-</sup>	[C <sub>82</sub> ] <sup>5-/6-</sup>	$\Delta E^{\circ'}$	Reference
Sm@C <sub>82</sub>			+0.99 <sup>a</sup>	-0.27	-0.44	-0.94	-1.33	1.26	17b
C <sub>82</sub>	+1.29	-0.12	-0.47	-1.01	-1.37			1.41	21c

<sup>a</sup>Better defined in DPV.

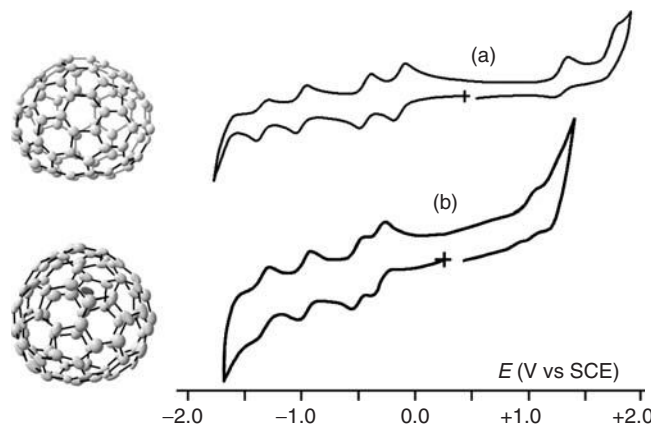
Let us finally examine the electrochemical behavior of Sm@C<sub>82</sub> derivatives, in which the inner metal ion has oxidation state +2.

Figure 51.11 compares the cyclic voltammetric profile of the isomer Sm@C<sub>2</sub>(5)-C<sub>82</sub> [17b] with that of C<sub>82</sub> [21c]. On passing, we point out that the crystal structure of C<sub>82</sub> is known [27].

As deduced by Table 51.6, once again the redox processes of M@C<sub>82</sub> follow the previously discussed trend M@C<sub>82</sub> with respect to free fullerene, even if the HOMO–LUMO gap looks like to be unaffected.

## 51.7 C<sub>84</sub>-MONOMETAL ENDOHEDRAL METALLOFULLERENES

Concerned with C<sub>84</sub> EMFs, the only X-ray characterized monometal derivative is Sm@C<sub>84</sub> in its D<sub>3d</sub> and C<sub>2</sub> isomeric forms [28]. The electrochemistry of the C<sub>2</sub> isomer has been investigated in MeCN-C<sub>6</sub>H<sub>5</sub>Me solution [29], but the voltammetric profiles are not well resolved, probably because of the low solubility of the derivative.



**Figure 51.11** Cyclic voltammetric responses recorded at a platinum electrode in 1,2-dichlorobenzene solution of (a) C<sub>82</sub> and (b) Sm@C<sub>82</sub> ( $C_2(5)$  isomer). Scan rate 0.1 V/s. (a) Adapted from Reference 21d; (b) adapted from Reference 17b.

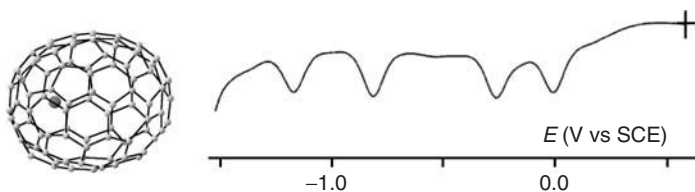


**Figure 51.12** Differential pulse voltammetric profile recorded at a platinum electrode in toluene–acetonitrile (4 : 1) solution of Sm@C<sub>90</sub>. Scan rate 0.01 V/s. Adapted from References 30 and 31.

### 51.8 C<sub>90</sub>-MONOMETAL ENDOHEDRAL METALLOFULLERENES

The crystal structure of Sm@C<sub>90</sub> in the  $C_2(40)$  isomeric form is known [30]. As shown in Fig. 51.12, in MeCN-C<sub>6</sub>H<sub>5</sub>Me solution, it affords four well-resolved reduction processes in differential pulse voltammetry (DPV) [29], the assignment of which is reported in Table 51.7, together with that of Sm@C<sub>94</sub> discussed in the following.

### 51.9 C<sub>92</sub>-MONOMETAL ENDOHEDRAL METALLOFULLERENES

The molecular structure of the two isomeric forms Sm@C<sub>1</sub>(42)-C<sub>92</sub> and Sm@C<sub>s</sub>(24)-C<sub>92</sub> have been X-ray characterized [31], but the electrochemical behavior of Sm@C<sub>1</sub>(42)-C<sub>92</sub> (in MeCN-C<sub>6</sub>H<sub>5</sub>Me solution) does not afford sufficiently resolved voltammetric profiles [29].

### 51.10 C<sub>94</sub>-MONOMETAL ENDOHEDRAL METALLOFULLERENES

The last mono-EMF we discuss is the X-ray characterized Sm@C<sub>3v</sub>(134)-C<sub>94</sub> [31], which gives rise to a well-defined voltammetric profile, Fig. 51.13 [29].

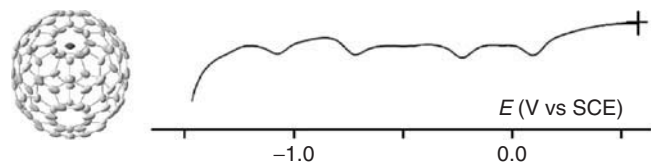


**Figure 51.13** Differential pulse voltammetric profile recorded at a platinum electrode in toluene–acetonitrile (4 : 1) solution of Sm@C<sub>94</sub>. Scan rate 0.01 V/s. Adapted from References 29 and 31.

**TABLE 51.7 Formal Electrode Potentials (V vs SCE) of the Redox Processes of the  $[C_n]^{2-}$  Cage of  $\text{Sm}@\text{C}_{90}$  and  $\text{Sm}@\text{C}_{94}$  in MeCN- $\text{C}_6\text{H}_5\text{Me}$  Solution<sup>a</sup>**

	$[C_n]^{2-/-3-}$	$[C_n]^{3-/4-}$	$[C_n]^{4-/5-}$	$[C_n]^{5-/6-}$
$\text{Sm}@\text{C}_{90}$	-0.01	-0.26	-0.81	-1.17
$\text{Sm}@\text{C}_{94}$	+0.10	-0.23	-0.72	-1.08

<sup>a</sup>Reference 29.

The pertinent formal electrode potentials are compiled in Table 51.7.

As seen,  $\text{Sm}@\text{C}_{94}$  results slightly easier to reduce than  $\text{Sm}@\text{C}_{90}$ .

## 51.11 CONCLUSION

Endohedral monometallofullerenes are the “sine qua non” key to understand nature and physicochemical properties of the widest class of EMFs, a field that had extraordinarily grown in the last years and that will become more and more important in the following years, also in view of the multiple technological applications of such innovative molecules. In this light, we have given an updated survey of the electron transfer ability of those monometallic endohedral fullerenes, the molecular structure of which has been unequivocally stated by single-crystal X-ray diffraction. Given the high electron transfer activity of EMFs, which often gives rise to sequences of chemically reversible redox steps, it sounds surprising that no crystal structure of such molecules in different oxidation states is available, which would allow to judge if and at which extent the location of the incarcerated metal(s) might be conditioned by electron addition/removal processes. In fact, there are a number of electrochemical and spectral evidences that monometallofullerenes are stable in oxidized and reduced forms [32], but attempts to crystallize such ionic species seem to have not been carried out or to have failed.

## AKNOWLEDGMENT

The University of Siena is gratefully acknowledged for making available the on-line facilities.

## REFERENCES

- (a) Heath, J. R.; O'Brien, S. C.; Zhang, Q.; Liu, Y.; Curl, R. F.; Kroto, H. W.; Tittel, F. K.; Smalley, R. E. *J. Am. Chem. Soc.* **1985**, *107*, 7779; (b) Chai, Y.; Guo, T.; Jin, C. M.; Haufler, R. E.; Chibante, L. P. F.; Fure, J.; Wang, L. H.; Alford, J. M.; Smalley, R. E. *J. Phys. Chem.* **1991**, *95*, 7564.
- A few representative examples: (a) Bethune, D. S.; Johnson, R. D.; Salem, J. R.; de Vries, M. S.; Yannoni, C. S. *Nature* **1993**, *366*, 123; (b) Shinohara, H. *Rep. Prog. Phys.* **1998**, *63*, 843; (c) Liu, S.; Sun, S. *J. Organomet. Chem.* **2000**, *599*, 74; (d) Nagase, S.; Kobayashi, K.; Akasaka, T.; Wakahara, T. *Fullerenes: Chemistry, Physics, and Technology*; John Wiley & Sons, Inc.: New York, **2000**; p 95; (e) Sidorov, L. N.; Boltalina, O. V. *Russ. Chem. Rev.* **2002**, *71*, 535; (f) Guha, S.; Nakamoto, K. *Coord. Chem. Rev.* **2005**, *249*, 1111; (g) Dunsch, L.; Yang S. *Small* **2007**, *3*, 1298; (h) Chaur, M. N.; Melin, F.; Ortiz, A. L.; Echegoyen, L. *Angew. Chem. Int. Ed.* **2009**, *48*, 7514; (i) Yamada, M.; Akasaka, T.; Nagase, S. *Acc. Chem. Res.* **2010**, *43*, 92; (j) Meng, J.; Wang, D.; Wang, P. C.; Jia, L.; Chen, C.; Liang, X.-J. *J. Nanosci. Nanotech.* **2010**, *10*, 1; (k) Dorn, H. C.; Fatouros, P. P. *Nanosc. Nanotech. Lett.* **2010**, *2*, 65; (l) Feng, L.; Akasaka, T.; Nagase, S. *Carbon Nanotubes and Related Structures: Synthesis, Characterization, Functionalization, and Applications*; Wiley-VCH Verlag GmbH; Weinheim: **2010**, 455; (m) Yang, S.; Liu, F.; Chen, C.; Wei, T. *Chem. Comm.* **2010**, *47*, 11822; (n) Rodríguez-Fortea, A.; Balch, A. L.; Poblet, J. M. *Chem. Soc. Rev.* **2011**, *40*, 3551; (o) Yan, L.; Zhao, F.; Li, S.; Hu, Z.; Zhao Y. *Nanoscience* **2011**, *3*, 362; (p) Akasaka, T.; Lu X. *Chem. Rec.* **2012**, *12*, 256; (q) Lu, X.; Feng, L.; Akasaka, T.; Nagase, S. *Chem. Soc. Rev.*, in press, **2012**, *41*.
- (a) Pinzón, J. R.; Plonska-Brzezinska, M. E.; Cardona, C. M.; Athans, A. J.; Gayathri, S. S.; Guldi, D. M.; Herranz, M. Á.; Martín, N.; Torres, T.; Echegoyen, L. *Angew. Chem. Int. Ed.* **2008**, *47*, 4173; (b) Jorn, R.; Zhao, J.; Petek, H.; Seideman, T. *ACS Nano* **2011**, *5*, 7858.
- (a) Echegoyen, L.; Palkar, A.; Melin, F. *Electrochemistry of Functional Supramolecular Systems*; John Wiley and Sons, Inc.: Hoboken, NJ, **2010**; p 201; (b) Zanello, P.; Nervi, C.; Fabrizi de Biani, F. *Inorganic Electrochemistry. Theory, Practice and Application*, 2nd ed.; RSC Cambridge: UK, **2011**; p 355.

5. (a) Aoyagi, S.; Nishibori, E.; Sawa, H.; Sugimoto, K.; Takata, M.; Miyata, Y.; Kitaura, R.; Shinohara, H.; Sakai, T.; Ono, Y.; Kawachi, K.; Yokoo, K.; Ono, S.; Omote, K.; Kasama, Y.; Ishikawa, S.; Komuro, T.; Tobita, H. *Nat. Chem.* **2010**, *2*, 678; (b) Aoyagi, S.; Nishibori, E.; Sawa, H. *Spring-8 Research Frontiers*; **2010**, p 92; (c) Okada, H.; Komuro, T.; Sakai, T.; Matsuo, Y.; Ono, Y.; Omote, K.; Yokoo, K.; Kawachi, K.; Kasama, Y.; Ono, S.; Hatakeyama, R.; Kaneko, T.; Tobita, H. *RSC Adv.* **2012**, *2*, 10624.
6. Varganov, S. A.; Avramov, P. V.; Ovchinnikov, S. G. *Phys. Sol. State* **2000**, *42*, 388.
7. Wakahara, T.; Nikawa, H.; Kikuchi, T.; Nakahodo, T.; Rahman, G. M. A.; Tsuchiya, T.; Maeda, Y.; Akasaka, T.; Yoza, K.; Horn, E.; Yamamoto, K.; Mizorogi, N.; Slanina, Z.; Nagase, S. *J. Am. Chem. Soc.* **2006**, *128*, 14228.
8. (a) Nikawa, H.; Kikuchi, T.; Wakahara, T.; Nakahodo, T.; Tsuchiya, T.; Rahman, G. M. A.; Akasaka, T.; Maeda, Y.; Yoza, K.; Horn, E.; Yamamoto, K.; Mizorogi, N.; Nagase, S. *J. Am. Chem. Soc.* **2005**, *127*, 9684; (b) Lu, X.; Nikawa, H.; Kikuchi, T.; Mizorogi, N.; Slanina, Z.; Tsuchiya, T.; Nagase, S.; Akasaka, T. *Angew. Chem. Int. Ed.* **2011**, *50*, 6356.
9. Nikawa, H.; Yamada, T.; Cao, B.; Mizorogi, N.; Slanina, Z.; Tsuchiya, T.; Akasaka, T.; Yoza, K.; Nagase, S. *J. Am. Chem. Soc.* **2009**, *131*, 10950.
10. Xu, W.; Niu, B.; Shi, Z.; Lian, Y.; Feng, L. *Nanoscale* **2012**, *4*, 6876.
11. Nikawa, H.; Yamada, T.; Cao, B.; Mizorogi, N.; Slanina, Z.; Tsuchiya, T.; Akasaka, T.; Yoza, K.; Nagase, S. *J. Am. Chem. Soc.* **2011**, *133*, 10772.
12. Lu, X.; Slanina, Z.; Akasaka, T.; Tsuchiya, T.; Mizorogi, N.; Nagase, S. *J. Am. Chem. Soc.* **2010**, *132*, 5896.
13. Hachiya, M.; Nikawa, H.; Mizorogi, N.; Tsuchiya, T.; Lu, X.; Akasaka, T. *J. Am. Chem. Soc.* **2012**, *134*, 15550.
14. (a) Takata, M.; Umeda, B.; Nishibori, E.; Sakata, M.; Saito, Y.; Ohno, M.; Shinohara, H. *Nature* **1995**, *377*, 46; (b) Lu, X.; Nikawa, H.; Feng, L.; Tsuchiya, T.; Maeda, Y.; Akasaka, T.; Mizorogi, N.; Slanina, Z.; Nagase, S. *J. Am. Chem. Soc.* **2009**, *131*, 12066.
15. (a) Maeda, Y.; Matsunaga, Y.; Wakahara, T.; Takahashi, S.; Tsuchiya, T.; Ishitsuka, M. O.; Hasegawa, T.; Akasaka, T.; Liu, M. T. H.; Kokura, K.; Horn, E.; Yoza, K.; Kato, K.; Okubo, S.; Kobayashi, K.; Nagase, S.; Yamamoto, K. *J. Am. Chem. Soc.* **2004**, *126*, 6858; (b) Feng, L.; Nakahodo, T.; Wakahara, T.; Tsuchiya, T.; Maeda, Y.; Akasaka, T.; Kato, T.; Horn, E.; Yoza, K.; Mizorogi, N.; Nagase, S. *J. Am. Chem. Soc.* **2005**, *127*, 17136; (c) Takano, Y.; Yomogida, A.; Nikawa, H.; Yamada, M.; Wakahara, T.; Tsuchiya, T.; Ishitsuka, M. O.; Maeda, Y.; Akasaka, T.; Kato, T.; Slanina, Z.; Mizorogi, N.; Nagase, S. *J. Am. Chem. Soc.* **2008**, *130*, 16224; (d) Maeda, Y.; Sato, S.; Inada, K.; Nikawa, H.; Yamada, M.; Mizorogi, N.; Hasegawa, T.; Tsuchiya, T.; Akasaka, T.; Kato, T.; Slanina, Z.; Nagase, S. *Chem. Eur. J.* **2008**, *16*, 2193; (e) Akasaka, T.; Lu, K.; Kuga, H.; Hidefumi, H.; Mizorogi, N.; Slanina, Z.; Tsuchiya, T.; Yoza, K.; Nagase, S. *Angew. Chem. Int. Ed.* **2010**, *49*, 9715; (f) Lu, X.; Nikawa, H.; Takahiro Tsuchiya, T.; Akasaka, T.; Makoto Toki, M.; Sawa, H.; Mizorogi, N.; Nagase, S. *Angew. Chem. Int. Ed.* **2010**, *41*, 594; (g) Sato, S.; Nikawa, H.; Seki, S.; Wang, L.; Luo, G.; Lu, J.; Haranaka, M.; Tsuchiya, T.; Nagase, S.; Akasaka, T. *Angew. Chem. Int. Ed.* **2012**, *51*, 1581.
16. Takano, Y.; Aoyagi, M.; Yamada, M.; Nikawa, H.; Slanina, Z.; Mizorogi, N.; Ishitsuka, M. O.; Tsuchiya, T.; Maeda, Y.; Akasaka, T.; Kato, T.; Nagase, S. *J. Am. Chem. Soc.* **2009**, *131*, 9340.
17. (a) Yang, H.; Jin, H.; Wang, X.; Liu, Z.; Yu, M.; Zhao, F.; Mercado, B. Q.; Olmstead, M. M.; Balch, A. L. *J. Am. Chem. Soc.* **2012**, *134*, 14127; (b) Xu, W.; Niu, B.; Feng, L.; Shi, Z.; Lian, Y. *Chem. Eur. J.* **2012**, *18*, 14246.
18. (a) Akasaka, T.; Kono, T.; Takematsu, Y.; Nikawa, H.; Nakahodo, T.; Wakahara, T.; Ishitsuka, M. O.; Tsuchiya, T.; Maeda, Y.; Liu, M. T. H.; Yoza, K.; Kato, T.; Yamamoto, K.; Mizorogi, N.; Slanina, Z.; Nagase, S. *J. Am. Chem. Soc.* **2008**, *130*, 12840; (b) Suzuki, M.; Lu, X.; Sato, S.; Nikawa, H.; Mizorogi, N.; Slanina, Z.; Tsuchiya, T.; Nagase, S.; Akasaka, T. *Inorg. Chem.* **2012**, *51*, 5270.
19. Li, X.; Fan, L.; Liu, D.; Sung, H. H. Y.; Williams, I. D.; Yang, S.; Tan, K.; Lu, X. *J. Am. Chem. Soc.* **2007**, *129*, 10636.
20. (a) Nagase, S.; Kobayashi, K. *Chem. Phys. Lett.* **1993**, *214*, 57; (b) Nishibori, E.; Takata, M.; Sakata, M.; Inakuma, M.; Shinohara, H. *Chem. Phys. Lett.* **1998**, *298*, 79.
21. (a) Suzuki, T.; Maruyama, Y.; Kato, T.; Kikuchi, K.; Achiba, Y. *J. Am. Chem. Soc.* **1993**, *115*, 11006; (b) Kikuchi, K.; Nakao, Y.; Suzuki, S.; Achiba, Y. *J. Am. Chem. Soc.* **1994**, *116*, 9367; (c) Suzuki, T.; Kikuchi, K.; Oguri, F.; Nakao, Y.; Suzuki, S.; Achiba, Y. *Tetrahedron* **1996**, *52*, 4973; (d) Zalibera, M.; Raptis, P.; Dunsch, L. *Electrochem. Comm.* **2007**, *9*, 2843.
22. Feng, L.; Wakahara, T.; Tsuchiya, T.; Maeda, Y.; Lian, Y.; Akasaka, T.; Mizorogi, N.; Kobayashi, K.; Nagase, S.; Kadish, K. M. *Chem. Phys. Lett.* **2005**, *405*, 274.
23. (a) Nagase, S.; Kobayashi, K. *Chem. Phys. Lett.* **1994**, *228*, 106; (b) Ding, J.; Weng, L.-T.; Yang, S. *J. Phys. Chem.* **1996**, *100*, 11120; (c) Muthukumar, K.; Larsson, J. A. *J. Phys. Chem. A* **2008**, *112*, 1071.
24. Ton-That, C.; Shard, A. G.; Egger, S.; Tanimaka, A.; Shinohara, H.; Welland, M. E. *Surf. Sci.* **2003**, *522*, L15.
25. Fan, L.; Yang, S.; Yang, S. *Chem. Eur. J.* **2003**, *9*, 5610.
26. Iida, S.; Kubozono, Y.; Slovokhotov, Y.; Takabayashi, Y.; Kanbara, T.; Fukunaga, T.; Fujiki, S.; Emura, S.; Kashino, S. *Chem. Phys. Lett.* **2001**, *338*, 21.
27. (a) Kawada, H.; Fujii, Y.; Nakao, H.; Murakami, Y.; Watanuki, T.; Suematsu, H.; Kikuchi, K.; Achiba, Y.; Ikemoto, I. *Phys. Rev. B* **1995**, *51*, 8723; (b) Ziegler, K.; Amsharov, K. Y.; Halasz, I.; Jansen, M. Z. *Anorg. Allg. Chem.* **2011**, *637*, 1463.
28. Yang, H.; Yu, M.; Jin, H.; Liu, Z.; Yao, M.; Liu, B.; Olmstead, M. M.; Balch, A. L. *J. Am. Chem. Soc.* **2012**, *134*, 5331.
29. Liu, J.; Shi, Z.; Gu, Z. *Chem. Asian J.* **2009**, *4*, 1703.

30. Yang, H.; Jin, H.; Zhen, H.; Wang, Z.; Liu, Z.; Beavers, C. M.; Brandon, Q; Mercado, B. Q.; Olmstead, M. M.; Balch, A. L. *J. Am. Chem. Soc.* **2011**, *133*, 6299.
31. Jin, H.; Yang, H.; Yu, M.; Liu, Z.; Beavers, C. M.; Olmstead, M. M.; Balch, A. L. *J. Am. Chem. Soc.* **2012**, *134*, 10933.
32. (a) Akasaka, T.; Wakahara, T.; Nagase, S.; Kobayashi, K.; Waelchli, M.; Yamamoto, K.; Kondo, M.; Shirakura, S.; Okubo, S.; Maeda, Y.; Kato, T.; Kako, M.; Nakadaira, Y.; Nagahata, R.; Gao, X.; Van Caemelbecke, E.; Kadish, K. M. *J. Am. Chem. Soc.* **2000**, *122*, 9316; (b) Akasaka, T.; Wakahara, T.; Nagase, S.; Kobayashi, K.; Waelchli, M.; Yamamoto, K.; Kondo, M.; Shirakura, S.; Maeda, Y.; Kato, T.; Kako, M.; Nakadaira, Y.; Gao, X.; Van Caemelbecke, E.; Kadish, K. M. *J. Phys. Chem. B* **2001**, *105*, 2971; (c) Sun, B.; Li, M.; Luo, H.; Shi, Z.; Gu, Z. *Electrochim. Acta* **2002**, *47*, 3545; (d) Wakahara, T.; Okubo, S.; Kondo, M.; Maeda, Y.; Akasaka, T.; Waelchli, M.; Kako, M.; Kobayashi, K.; Nagase, S.; Kato, T.; Yamamoto, K.; Gao, X.; Van Caemelbecke, E.; Kadish, K. M. *Chem. Phys. Lett.* **2002**, *360*, 235; (e) Tsuchiya, T.; Wakahara, T.; Shirakura, S.; Maeda, Y.; Akasaka, T.; Kobayashi, K.; Nagase, S.; Kato, T.; Kadish, K. M. *Chem. Mat.* **2004**, *16*, 4343; (f) Maeda, Y.; Miyashita, J.; Hasegawa, T.; Wakahara, T.; Tsuchiya, T.; Feng, L.; Lian, Y.; Akasaka, T.; Kobayashi, K.; Nagase, S.; Kako, M.; Yamamoto, K.; Kadish, K. M. *J. Am. Chem. Soc.* **2005**, *127*, 2143.

# POSTSCRIPT: A SHORT HISTORY OF THE ICOMC CONFERENCES

F. EKKEHARDT HAHN

*Institut für Anorganische und Analytische Chemie, Westfälische Wilhelms-Universität Münster, Münster, Germany*

## 1 INTRODUCTION

The XXVth International Conference on Organometallic Chemistry (ICOMC-XXV) was held in Lisbon, Portugal, from September 2 to 7, 2012. Professor Armando J. L. Pombeiro (Centro de Quimica Estrutural, Instituto Superior Tecnico, Lisboa) acted as conference chairman. The Lisbon conference, being the silver edition (the 25th ICOMC conference held) and organized in the gold year (50th year after the first ICOMC conference was held in Cincinnati in 1963), attracted over 1200 participants from 54 countries all over the world (circa 1100 were foreigners) making it one of the most successful ICOMC conferences ever held, in spite of the on-going general economical crises. ICOMC-XXV featured 5 plenary, 17 keynote lectures, and 88 invited special satellite lectures in addition to 195 contributed oral presentations. A total of 794 posters were presented in two poster sessions, and 165 flash oral presentations were delivered mainly by young researchers (a possibility that was introduced for the first time in this series of conferences). About 38% of the participants were students. While many younger scientists have so far only participated in a few ICOMC conferences, ICOMC-XXV featured one participant, Professor Bruce King from Athens, Georgia, who managed to attend all 25 ICOMC meetings over the past 50 years.

To celebrate the success of the ICOMC conferences in general and the ICOMC-XXV in particular, Professor A. J. L. Pombeiro acts as editor of the book entitled “Recent Advances in Organometallic Chemistry and Catalysis.” As you hold it in your hands, you will notice that eminent scientists from diverse areas have provided chapters dealing with hot topics of current interest thereby illustrating the diversity, richness, and potential of modern organometallic chemistry. The success of ICOMC-XXV and of the preceding 24 ICOMC conferences provide evidence that international meetings of organometallic chemists are very useful and attractive. I am, therefore, sure that the organometallic community worldwide can look forward to the next 50 years of ICOMC conferences. The ICOMC conferences will continue to serve as forum for the exchange of ideas and for the presentation of new and exciting findings in the field of organometallic chemistry.

## 2 HISTORICAL DEVELOPMENT OF THE ICOMC CONFERENCES

The rapid development of organometallic chemistry starting around 1951 when the discovery of ferrocene led to a significant increase in the number of research groups active in this evolving field of research. Early on, it became apparent that a forum for the exchange of results and ideas for chemists working in the field would be helpful in the development of organometallic chemistry. A first meeting of organometallic chemists named “Symposium in Organometallic Compounds” was held at the University of British Columbia. This symposium attracted a total of 79 attendees (78 from the United States and Canada and one from the United Kingdom). The symposium, however, was not considered to have been the first ICOMC, probably because of the limited number of attendees from only three countries.

The first ICOMC, then named “Current Trends in Organometallic Chemistry” was held at the University of Cincinnati, Cincinnati, Ohio, from June 12 to 15, 1963. The meeting, organized by Professor R. E. Dessy, attracted 119 participants with 21 foreign participants representing eight countries. The successor to this meeting, the “Second International Symposium on Organometallic Chemistry” held during August 30–September 3 in Madison, Wisconsin, is considered as ICOMC-II. This meeting already attracted 238 participants. Among them were 55 foreign participants from 15 countries. The “Third Symposium on Organometallic Chemistry,” designated as ICOMC-III, was organized by Professor E. O. Fischer in Munich from August 1–September 1, 1967. The number of participants again increased significantly to 395 with 340 foreign participants representing 24 countries. A subsequent meeting in Bristol was held during July 27–August 1, 1969, and was termed the “Fourth International Conference on Organometallic Chemistry” (Fig. 1). The title “International Conference on Organometallic Chemistry” has been applied ever since. For the Bristol and all subsequent meetings, a sketch of the metallocene was adopted as the logo for the ICOMC conferences (Fig. 1).

Even though the chairmen of the first ICOMC conferences are no longer engaged with organometallic chemistry, their vision and foresight have been clearly major factors in the development of the “International Conferences on Organometallic Chemistry.” Since the first meeting in 1963, conferences were held in many countries across four continents, including the

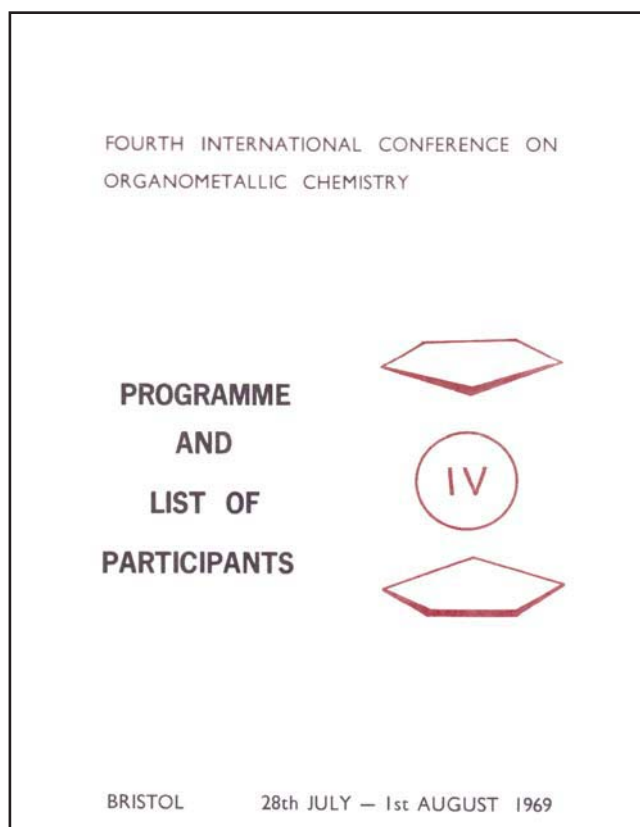


Figure 1 Cover of the program for ICOMC-IV.

**TABLE 1** Selected Statistics for the ICOMC Conferences

Chairman	Year	No.	Venue	Total Number of Participants	Foreign Participants	Countries Represented
R. E. Dessy	1963	I	Cincinnati	119	21	9
R. C. West	1965	II	Madison	238	55	16
E. O. Fischer	1967	III	Munich	395	340	24
F. G. A. Stone	1969	IV	Bristol	600	450	25
A. N. Nesmeyanov	1971	V	Moscow	965	455	26
M. D. Rausch	1973	VI	Amherst	550	155	26
U. Croatto	1975	VII	Venice	440	380	27
Y. Ishii	1979	VIII	Kyoto	642	212	24
J. Tirouflet	1981	IX	Dijon	950	687	37
H. C. Clark	1983	X	Toronto	494	399	29
E. G. Ashby	1985	XI	Atlanta	289	109	21
K. Schlägl	1985	XII	Vienna	750	721	40
F. Calderazzo	1988	XIII	Turin	597	425	34
J. P. Oliver	1990	XIV	Detroit	283	159	29
S. Pasynkiewicz	1992	XV	Warsaw	202	155	29
M. F. Lappert	1994	XVI	Brighton	750	540	39
C. Raston	1996	XVII	Brisbane	427	282	34
H. Schmidbaur	1998	XVIII	Munich	916	375	43
C. T. Qian and L. X. Dai	2000	XIX	Shanghai	481	234	29
C. G. Screttas	2002	XX	Corfu	680	662	42
M. D. Fryzuk	2004	XXI	Vancouver	397	286	31
L. A. Oro	2006	XXII	Zaragoza	1154	810	50
P. H. Dixneuf and C. Bruneau	2008	XXIII	Rennes	1281	1056	50
J.-T. Chen and Y. Chi	2010	XXIV	Taipei	749	496	35
A. J. L. Pombeiro	2012	XXV	Lisbon	1218	1102	54

United States, Germany, England, France, Canada, Italy, Russia, Greece, Poland, Australia, Austria, Japan, Spain, China, and Taiwan (for a full listing see Table 1).

Immediately after the first ICOMC conferences, it became apparent that international meetings involving organometallic chemists were both useful and successful. It was also clear that some coordination between groups of organometallic chemists was becoming necessary. The rapid growth and expansion of the organometallic community was discussed by colleagues attending the ICOMC-VI held in Amherst in 1973. After considerable discussions, Professor Eddie Abel of the University of Exeter was invited to serve as coordinator for the ICOMC conferences. He accepted this request and chose the title of Permanent Secretary of the ICOMC.

Professor Abel was a very successful and organized organometallic chemist. His organizational abilities were also recognized and appreciated by his university, the University of Exeter. In 1988, he was selected as president of that prestigious institution. Owing to his many administrative duties as president of the University of Exeter, it became necessary for him to give up his active research programs, and his position as Permanent Secretary of the ICOMC.

At the ICOMC-XXIII, which was held in Turin in 1988, Professor Fausto Calderazzo discussed this matter with several members of the ICOMC's International Advisory Board. Professor Marvin Rausch, chairman of ICOMC-VI in 1973, was at this time heavily involved with ICOMC business and had served on the International Advisory Boards of various ICOMC conferences. Professor Calderazzo and other colleagues invited Marvin Rausch to take over the position of Eddie Abel as Permanent Secretary, and he accepted.

Marvin Rausch told me later that it became a gratifying experience to be associated with a prestigious series of international conferences such as the ICOMC. He served for 16 years as Permanent Secretary (1988–2004) and found it very enjoyable to interact and collaborate with colleagues all over the world. He also established a collection of pictures, programs, correspondence, and reports for all ICOMCs between 1963 and 2004. This valuable collection was later given to the current Permanent Secretary. Owing to health problems, Professor Rausch suggested in 2004 to initiate a search for a new Permanent Secretary to replace him in the near future.

During the ICOMC-XXI 2004 in Vancouver, the International Advisory Board selected Professors M. Fryzuk, P. Dixneuf, and L. Oro to seek out any persons who might be interested in the position of Permanent Secretary to take over from Professor

Marvin Rausch. At the time, these three colleagues were either chairperson of the current ICOMC or were elected to be chairpersons of upcoming ICOMCs. This committee decided to offer the position of Permanent Secretary to Professor F. Ekkehardt Hahn from the University of Münster who gladly accepted it.

Professor Hahn studied chemistry at the Technische Universität Berlin (Dipl.-Chem. and Dr. rer. nat. with H. Schumann) and the University of Oklahoma (M.S. with J. J. Zuckerman). He was a postdoctoral associate at the University of California, Berkeley (with K. N. Raymond). After the Habilitation at the Technische Universität Berlin and an appointment as Associate Professor at the Freie Universität Berlin (1992–1996), he accepted the position as Chair of Inorganic Chemistry at the University of Münster, a position which he still holds.

My tenure as Permanent Secretary of ICOMC started in the fall of 2004. From the beginning on, I have found this job in fact very enjoyable. I attended the first ICOMC in 1990 (ICOMC-XIV in Detroit) and have participated in all subsequent ICOMCs. As my predecessor Marvin Rausch did, I have enjoyed working with organometallic chemists throughout the world. It is particularly satisfying to note the increased participation in the ICOMCs over the past couple of years. An attendance in excess of 1000 active participants (the record stands at 1282 for ICOMC-XXIII in Rennes 2008, or, for foreign participants, at 1102 for the ICOMC-XXV in Lisbon) representing 50 or even more countries (the record stands at 54 countries for the ICOMC-XXV in Lisbon) has become nowadays a reality. This is particularly pleasing when looking back at the humble beginnings of the ICOMC in the 1960s. The ICOMC conferences have indeed become thriving scientific events.

In the future, the ICOMC conferences should focus to further increase the participation of doctoral students in the scientific program. While the ICOMC conferences have been held in many countries, there are still white spots on the map. Among these are the whole of Africa and India. With the rapid development of organometallic chemistry in these countries, I am sure ICOMC will move there in the future. Today, we are looking back to an extremely successful series of 25 ICOMC conferences held over the past 50 years. I am sure, this legacy will continue.

## ACKNOWLEDGMENTS

The author thanks Professor Marvin D. Rausch (deceased May 2, 2008) for his valuable collection of ICOMC memorabilia and Professor Jane Rausch for sending these to the author.

# INDEX

- absorption coefficient, 506, 507  
absorption of light, 505, 510  
acquired drug resistance, 576  
acute liver failure, 548, 552, 557, 558  
acyclic diaminocarbenes, 145–153  
acylpyrazolones, 280–281  
additive electrochemical ligand parameter, 677, 679, 686  
aerobic oxidation, 239–242  
aerobic photooxygenation, 5  
agostic interaction, 360–362  
alcoholdehydrogenase, 522  
alcohols oxidations, 233–244  
alkaline-earths, 359, 364–368, 371–376, 439, 442  
alkane functionalization,  
    carboxylation to carboxylic acids, 9, 20–22, 286, 288, 290–291  
    C–H activation, 3–12, 16, 19–22, 33–35, 39, 41–55, 60–68, 73–76  
    dual-role catalyst, 17, 23  
    hydrocarboxylation to carboxylic acids, 9, 20–22, 29, 33–36  
    metal-free, 20, 21  
    multinuclear catalysts, 17, 18  
    nontransition metal catalyst, 19  
    oxidation of cyclohexane, 5–11, 16, 30–32, 286, 288–291  
    oxidation to alcohols and ketones, 5–11, 15–20, 31, 32, 60, 63, 66,  
        286–290  
    oxidation to alkyl hydroperoxides, 5–11, 19  
    radical mechanism, 6–11, 19, 21, 22, 32–35, 286, 290, 291  
        water role, 18–21  
alkenylation, 82–84, 89, 90  
alkoxycarbene complexes, 678, 682, 685, 686  
alkyl hydroperoxides, 5, 8  
alkyl aromatics, 62  
alkylbenzenes, 60, 62  
alkynes functionalization, 207, 209–211, 214, 221  
    alkynyls, 678, 679, 682, 685  
allenes functionalization, 207, 209–210, 214, 216, 220  
allenylidenes, 678, 679, 682, 684, 685  
alsterpaullone, 607  
amavadin, 21, 22  
amidophenolate, 667, 668, 670, 671  
aminocarbene complexes, 114–129, 134–141, 146–153, 238, 653, 656,  
    678, 682, 685, 686  
aminopolyalcohols, 16, 18  
ammonia borane, 529, 531–533  
anaerobic oxidation, 236–237, 239–240  
anchoring ligands, 505, 509  
ancillary ligands, 505–509  
anionic chelating ligands, 485  
anisotropy, 482  
*ansa*-ferrocenes, 161, 570  
*ansa*-metallocenes, 157  
*ansa*-nickelocene, 163  
*ansa*-ruthenocenes, 161  
*ansa*-zirconocene dichloride, 167, 168  
anthracene, 65  
anti-apoptotic, 546, 547  
antibacterial and antifungal activity, 573  
anti-cancer drugs, 556, 564, 565, 574, 605–615, 633, 638, 640, 642, 644,  
    650  
        mechanism of action, 563–575  
anti-inflammatory, 545–547, 552, 554  
anti-oxidants, 547  
anti-proliferative, 546–547  
anti-proliferative activity, 569–572  
anti-tumor (*see* anti-cancer),  
apoptosis, 547, 565, 575, 576  
apoptosis-resistant primary cancers, 575  
aqueous medium reactions, 15, 17–25, 27, 28, 30, 35, 199–204  
arene ( $\eta^6$ ) complex, 476, 609–611, 613, 614  
artificial leaf, 521, 522  
artificial photosynthesis, 521, 524  
arylhydrazones of  $\beta$ -diketone (AHBD) complexes, 16–18  
astrocytes, 546  
asymmetric synthesis, 366–376, 465–468  
autotrophic organisms, 521

- axial chirality, 164  
azoderivatives of  $\beta$ -diketone (ADB) complexes, 17  
azonium cations, 114, 122, 125
- Baeyer-Villiger reaction, 291–293  
bamboo structures, 453, 454  
barium, 359–376  
base,  
  pyridine, 101, 102, 635, 636, 646, 647  
  imidazole, 635, 636, 638–641, 643  
  collidine, 641  
bent metallocene, 165, 169  
benzene ligand, 681–683  
benzene oxidation, 11, 12  
benzenopolycarboxylic acids, 16, 18, 29–32  
benzoxazolin-2-ylidene ligands, 120  
biliverdin, 546  
binary oxide materials,  
  matrices for luminescence materials, 443  
  perovskites, 438, 440, 442  
  phosphors, 443  
  spinels, 438, 440, 442  
binuclear metal complexes, 17, 28–30, 507, 508, 537  
bioavailability of polyphenols, 574  
bioconjugative desulfurative catalysis, 295–302  
biology,  
  chemical biology, 563, 564  
  organometallic chemical biology, 563, 564  
  inorganic chemical biology, 563  
biomimetic, 23, 68  
bioorganometallic chemistry, 543, 549, 563–575, 582–586, 589–601, 608–615, 621–628  
bis(pyrazolyl)azine, 277–278  
black dye, 505, 506  
blue-shift, 486, 487  
bond activation,  
  B–H, 308, 310, 311  
  C–F, 39, 51  
  C–H (*see* alkane functionalization),  
  C–O, 41, 42  
  C–X, 73–78  
  M–H, 97–108  
  O–H, 97–108, 306, 307  
 $\pi$ -bowl complexes, 473–476, 479, 480  
  concave complex, 474, 478, 479–482  
  convex complex, 474, 478, 480, 481  
bowl-to-bowl inversion, 475, 476, 479, 481, 482  
breast cancer,  
  hormone-dependent, 566, 567, 633  
  hormone-independent, 566, 567, 570, 571, 573, 633, 635, 647  
Buchwald–Hartwig amination, 153  
buckybowl, 473
- cacodyl oxide, xi  
calcium, 360–376  
cancer stem cells, 615  
cancer therapy, 581–586  
carbenes (*see* aminocarbenes),  
carbon chemistry, 445, 459–470  
carbon dioxide, 15, 513–525, 529, 532, 536  
carbon fibers, 445, 449, 450, 452  
carbon nanotubes, 445–447, 451–455, 473, 476  
carbon spheres, 446, 451, 455  
carbon-based scorpionates, 15–17, 285–293, 683
- carbon materials, 445–456  
carbon monoxide dehydrogenase, 523  
carbon recycling, 513, 520–524  
carbon tax, 517  
carboplatin, 605, 606  
carbonyl metalloimmunoassay (CMIA), 564  
carbonylation 3, 259–268 (*see also* alkane functionalization),  
carborane functionalization, 81–94  
carbonyne, 81–94  
carboxyhemoglobin (COHb), 549–551, 553, 558  
carboxylic acids, 16, 17, 20–22, 29–32, 102, 259, 260, 262, 264, 266, 507–509  
carboxymyoglobin (COMb), 550  
carbynes, 678, 679, 682, 685  
cardiomyocytes, 546, 554  
(+)-3-carene, 64, 65  
catalysis,  
  alcohol oxidation, 234–244  
  alkane carboxylation and hydrocarboxylation (*see* alkane functionalization),  
  alkane oxidation (*see* alkane functionalization),  
  aqueous media, 15–21, 27–36, 199–204, 285–293  
  Baeyer–Villiger oxidation of ketones, 291–293  
  click, 199–204  
  cooperative, 325–334, 338  
  cross coupling, 145, 147–153  
  glycerol oxidation, 247–255  
  homogeneous, 3–12, 15–22, 27–36, 39–55, 59–68, 139–141, 199–204, 207–223, 227–231, 233–239, 247–255, 259–268, 285–293, 305–314, 315–322  
  heterogeneous, 66, 239–244  
  hydroamination, 319  
  metal-organo, 295–297, 325–339  
  methanol carbonylation, 259–268  
  multicatalysis, 325–339  
  olefin epoxidation, 19  
  oxidation, 3–11, 15–22, 32, 60–64, 305–308  
  polymerization, 157–160, 321, 345–357, 359–376, 391, 395–397, 399  
  relay, 326, 338  
  sequential, 326, 334, 335  
  sulfides oxidation, 305–308  
  sulfone formation, 305–314  
  sulfoxidations, 227–231  
  sulfoxide oxidation and reduction, 305–314  
  supported, 227–231, 240, 242, 289  
catalyst–carbon interaction, 448  
catalysts (*see* metal catalysts and complexes),  
catalytic dipolar cycloadditions,  
  azides and alkynes: synthesis of substituted triazoles, 200, 202–203  
  aqueous media reactions, 199–204  
  N-metallated azomethine ylides, 465–470  
catechol, 569  
catecholborane,  
  B–H activation, 308  
  sulfoxide reduction, catalysed by Mo complexes, 310  
cdk (cyclin-dependent kinase) inhibitors, 605–615  
cell membrane, 584, 586  
C–F bond activation (*see* bond activation),  
C–F bond cleavage, 51–53  
  to form difluorocarbene complexes, 53  
C–H bond activation (*see* alkane functionalization),  
charge collection, 505  
charge separation, 505, 521, 522, 524, 525  
Chatt–Dewar–Duncanson model, xii  
chelate ring size, 185–186, 189, 192

- chemical biology, 563, 564  
 chemoautotrophs, 521  
 chemosensor, 490  
 chiral fullerenes, 465  
 chlorins, 66–67  
 chlorotricarbonyl rhenium(I), 507  
 circular dichroism, 466, 467, 469  
*cis*-cyclooctene, 65–66  
 cisplatin, 564, 565, 574, 575  
 C–O bond activation (*see* bond activation),  
 C–O bond cleavage, 40, 44, 51  
 CO based therapies, 545–558  
 CO targets, 546–548, 551  
 cobalt bis(dicarbollide),  
   derivatives, 73–74, 76  
 coiled carbon, 450, 455  
 commercial PV electrolyzers, 525  
 competition experiment, 43, 45  
   between methyl and ethyl aryl ethers, 45  
 composite organometallic materials, 386, 394, 397  
 concentrators of solar power (CSP), 520  
 conduction-band level, 506  
 $\pi$ -conjugated moieties, 505  
 $\pi$ -conjugation length, 486, 487  
 contrast agents,  
   blood pool agents, 625  
   exchange lifetime of water molecules, 623  
   first coordination sphere, 623  
   gadolinium chelates, 621, 623  
   iron oxide-based contrast agents, 624  
   non-specific extracellular agents, 625  
   number of coordinated water molecules, 623  
   organ-specific agents, 625  
   relaxivity, 623  
   re-orientational correlation time, 623  
   responsive agents, 625  
   targeting agents, 625  
   T<sub>1</sub> contrast agents, 621  
   T<sub>2</sub> contrast agents, 624  
   T<sub>1</sub>-weighted image, 620  
   T<sub>2</sub>-weighted image, 620  
 controlled-potential electrolysis, 655  
 convection enhanced delivery (CED), 574, 575  
 cooperative (or synergistic) catalysis, 325–334, 338  
 coordination polymers (CPs), 17, 18, 27–35, 407–418  
 coordinative chain transfer polymerization,  
   conjugated dienes (isoprene, butadiene, myrcene) 347, 349–353, 356  
   ethylene, 346–349, 351–355  
   polymer chain shuttling, 345–346, 353, 355  
   sequenced copolymers, 353  
   statistical copolymers, 347, 352–353, 357  
   styrene, 347, 350–354  
 copper(II) azolate CPs,  
   mono and trinuclear Secondary Building Units (SBU), 408, 411–412,  
   415, 417  
 copper carboxylates, 296–298, 411, 415  
 copper catalysts,  
   alkane hydrocarboxylation, 21, 29, 30, 33  
   alkane oxidation, 15–23, 30, 32, 33, 35, 286–289, 415  
   alcohol oxidation, 23, 234–235, 237–238  
   aqueous media reactions, 17, 18, 27–36, 199–204  
   click chemistry reactions, 199–204  
   fullerene synthesis, 463–466  
   glycerol oxidation, 252, 254  
   copper complexes, 17, 18, 21, 27–36, 234–235, 286–289, 408, 411–412,  
   415, 417  
   corannulene, 473–479  
   CORM (CO Releasing Molecule),  
   CORM-A1, 549  
   drug like CORMs, 556  
   enzyme triggered CORMs, 555, 556  
   esterase, 555  
   experimental CORMs, 549–553, 556  
   iCORM-3, 550, 551, 553  
   inactivated CORMs, 550  
   Mo(0)-based CORMs, 551  
   organic CORMs, 549  
   phosphatase, 555  
   photoCORMs, 556  
   Ru(II)-based CORMs, 549  
   counter electrode, 504, 505, 508  
   coupling reactions, 209, 217, 220, 222  
   covalent grafting, 642  
   cross-coupling catalysis, 145, 147–153  
   crystal structure, 694, 697–699  
   C-scorpionates, 285–293, 683  
   Cu-catalyzed desulfurative coupling, 298–299  
   Cu-desulfurative catalysis, 298–299  
   cumene, 62, 64  
   current–voltage features, 507  
   curved carbon  $\pi$  surface, 473  
   cyanamides, 679  
   cyclam based liands, 315–322  
   cyclam functionalization, 321  
   cyclic GMP (cGMP, cyclic guanosine monophosphate), 547  
   cyclic voltammetry, 635–651, 655, 670, 672, 674, 692–699  
   cyclin dependent kinases, 606  
   cycloadditions,  
   azide-alkyne, 199–204  
   [2+2+2], 81–87, 91–93  
   [2+3] dipolar, 171–176, 178, 465–470  
   cycloalkanes, 3–10, 15–18, 27–36, 60, 63, 286–291  
   cycloalkenes, 62, 65–66  
   cyclodextrins, 633, 634, 644–649  
   cyclododecane, 60, 61  
   cyclohexane, 3–10, 15–18, 27–36, 60, 286–291  
   cyclohexane oxidation, 3–10, 15–18, 27–36, 60, 289–290, 415  
   cyclohexanol, 3–10, 15–18, 27–36, 60, 286–291, 415  
   cyclohexanone, 3–10, 15–18, 27–36, 60, 286–291, 415  
   cyclohexene, 65  
   cyclohexyl hydroperoxide, 5–7, 31  
   cyclooctane, 3, 8, 10, 11, 60, 66  
   cyclopentadienyl, 133–141, 158–169, 681, 682  
   cyclopentadienyl metal complexes, 136–141, 158–169, 581–586  
   p-cymene, 62, 537, 681, 682  
   cytochrome c oxidase, 546, 548  
   cytoprotection, 546, 547, 548, 554  
   cytostatic properties, 575  
   cytotoxic effect, 567, 573  
   cytotoxic species,  
   imino methide, 642  
   orthoquinone, 640  
   quinone methide, 633, 636–638, 643, 644, 646, 647, 649, 650  
   cytotoxicity, 552, 558, 581, 583, 584, 586  
   DC-polarography, 655  
   decamethylosmocene, 8

- dehydroaryloxylation (*see* dehydroxygenation),  
 dehydrofluorination,  
   of alkyl fluorides, 55  
 dehydrogenation, 3, 529–539  
 dehydroxygenation,  
   of ethyl acetate, 49, 50  
   of ethyl aryl ethers, 45  
   of ethyl tosylate, 50  
 desulfitative catalysis, 295–302  
 desulfitative cross-coupling, 295–298  
 desulfitative transformations, 295–296, 300–301  
 DFT calculations,  
   [2+2] additions, 308–309, 311  
   [3+2] additions, 308–309, 311  
   electronic energy, 312  
   energy profile, 45–50, 54, 309, 310  
   functionalization of alkanes, 18–23  
   intermediates, 19–22, 307, 308, 310  
   reaction mechanisms, 18–23, 178, 306–311  
   redox chemistry of sulfides, sulfoxides and sulfones catalysed by Mo complexes, 305–314  
   transition states, 20, 308, 310  
   Wiberg indices, 308, 312  
 diaminocarbenes, 143–153  
*diansa*-ferrocene, 163, 165  
*diansa*-nickelocene, 163  
 differential pulse voltammetry, 699  
 dihydrogen complexes,  
   dihydrogen bonding, 98, 100, 106  
   heterolytic cleavage, 106, 107  
   homolytic cleavage, 106, 107  
 1,2-dihydronaphthalene, 65  
 dinickelocene, 163  
(2,3- $\eta$ -1,4-diphenylbut-2-en-1,4-dione)undecacarbonyl triangulotriosmium, 11  
 diphosphites, 426  
 dipolar cycloaddition, 171–176, 178, 199–204, 459–470  
 direct self-assembly, 18  
 donor/acceptor substituent, 510  
 drug resistance, 575  
 dye regeneration times, 508  
 dye sensitized solar cells, 503, 504, 508, 510  
 EIE (*see* equilibrium isotope effect),  
 $E_L$  Lever ligand parameter, 679–688  
 electrochemical and ESR studies, 567  
 electrochemical oxidation, 657, 669–674  
 electrochemical reduction, 657  
 electrochemistry, 631–700  
 electrodes, 655  
 electroluminescence, 490  
 electrolysis, 640, 642  
 electrolysis of water, 518  
 electrolyte, 504, 505, 509  
 electron-donating groups, 486, 487  
 electron donor ability, 678, 679, 685  
 electron injection, 505, 509  
 electron recombination, 505, 509  
 electron transfer, 505, 509, 521, 523–525, 656, 667–674, 694  
 electron transport ability, 482  
 electron-richness, 678  
 electron-transport layer, 490  
 electron-withdrawing group, 486, 487  
 enantioselectivity, 230–231, 459–470  
 encaged metal, 694  
 encapsulation, 574  
 endohedral fullerenes, 459, 460  
 endothelial cells, 546, 547  
 endotoxic shock, 546  
 energy,  
   renewable energy sources, 503  
   sustainable energy technology, 503  
 energy gaps, 505  
 energy levels, 504, 505, 507, 509  
 epoxidation, 3  
 EPR (Electron Paramagnetic Resonance) spectroscopy, 229–230, 669, 672, 673  
 equilibrium isotope effect, 43  
 esterification, 509  
 ethylbenzene, 62  
 ethylnaphthalene, 64  
 exhaust carbon, 513, 517  
 external quantum efficiency (EQE), 506  
 Fe<sup>II</sup>/Fe<sup>III</sup> oxidation, 569  
 Fermi level, 505  
 ferricinium cation, 633, 635, 636  
 ferrocene, 5, 8, 9, 157–158, 160–163, 165–169, 445–447, 451, 454, 456, 566–571, 575, 576, 633–650  
 ferrocenium (*see* ferricinium),  
 ferrocenophane, 159–160  
   transposition, 572  
   ferrocenophanyl group, 570, 571  
   ferrocenophanol, 572  
 ferrocenyl,  
   catechols, 569, 570  
   redox antenna, 575  
   redox products, 569  
 ferrocidiphenol, 571, 572, 574  
 ferrocifen drugs, 563–576, 633–650  
 ferrocifen complexes,  
   ferrocenophanes, 643  
   ferrocenyl acetanilide, 640  
   ferrocenyl aniline, 640  
   ferrocenyl catechols, 569, 570, 638–640  
   ferrociphenol, 635, 636, 638, 640  
 ferroquine, 566, 567  
 fill-factor (FF), 504, 508  
 fine chemicals, 359, 372  
 Fischer aminocarbene complexes, 653–665  
 flank benzene ring, 478, 479  
 flavopiridol, 606, 607  
 floating catalyst, 446, 449, 452–455  
 fluorescence, 487–491  
 $\alpha$ -fluoride elimination, 53  
 $\beta$ -fluoride elimination, 54, 55  
 formaldehyde dehydrogenase, 522  
 formate dehydrogenase, 522  
 formic acid, 529, 532, 533, 536–538  
 fullerenes, 459–470, 473, 474, 476, 478, 479, 691–700  
 functional groups, 509  
 $\beta$ -functionalized isocyanides, 118–119, 121  
 functionalised N-heterocyclic carbenes, 133–141  
 functional phosphines, 189–194  
 functionalization of alkanes (*see* alkane functionalization),  
 functionalization of carboranes (*see* carborane functionalization),  
 functionalization of sp<sup>2</sup> carbon, 64, 66  
 functionalization of sp<sup>3</sup> carbon, 60, 61, 66  
 functionalized alcohols,  
   2,3-dihydro-2,2-dimethylbenzofuran-7-ol, 438, 440

- 2-(dimethylamino)ethanol, 438, 442  
 2-methoxyethanol, 438, 443
- gaseotransmitter,  
 signaling, 546–548
- geraniol, 64–67
- glioma, 574, 575
- gliosarcoma in rats, 574
- glycerol oxidation,  
 catalysts, 248–254  
 with H<sub>2</sub>O<sub>2</sub>, 248–254  
 with tert-butyl hydroperoxide, 252–254
- gold catalysis, 207–222
- gold catalysts, 207, 210–213, 222, 242–244
- green oxidant, 3–10, 15–18, 22, 27–36, 286–291
- Grubbs' catalysts, 157, 161
- H/D exchange, 3
- half-sandwich complexes, 16, 17, 134, 136–141, 269–282, 609–611, 613, 614, 681
- Hammett's constant, 654
- H-donor, 523
- healthy cells, 569, 574, 575
- Heck reaction, 150–152
- heme,  
 free heme, 546, 548  
 heme oxygenase (HO), 545–549  
 amplification loop, 547
- hemilabile ligand, 667–669, 673, 674
- hemilability, 185
- hemoproteins, 546, 547, 550
- heterocyclic ligands, 507–509
- heterogeneous systems, 66, 239–244
- heterometallic, 18
- heterometallic alkoxide derivatives, synthesis,  
 coordinated alcohols as anchors for organometallics, 438, 440  
 deoligomerization by cocomplexation, 439  
 protonation of metallocenes, 440
- heteropolyanions, 60
- hexanuclear rhodium carbonyl cluster, 11
- hole-transport layer, 490
- homing peptides, 614
- homogeneous catalysis (*see* catalysis, homogeneous)
- homogeneous systems, 66
- HOMO and LUMO, 98, 653, 654, 659, 662, 692, 694, 697, 698
- hormone receptors, 606
- hybrid ligands, 185–186
- hybrid systems, 525
- hydroamination, 372–374
- hydrocarboxylation,  
 of alkanes, 20–22, 29, 33–36  
 metal-free alkane hydrocarboxylation, 20, 21
- hydrogen, 422, 425, 426, 432
- hydrogen bond,  
 non-classical, 97, 100, 105  
 formation enthalpy, 101
- hydrogen peroxide, 8, 10, 11, 15, 17, 19–23, 59–65, 247–255, 286–293, 307–309
- hydrogen storage, 529–539
- hydrogen transfer, 139
- hydrogenation, 529, 530, 532, 538, 539
- hydrosilylation, 139–141
- hydrogen-transfer type oxidations of alcohols, 237, 240–241
- hydrophosphonylation, 375–376
- hydrosoluble complexes, 15–17, 19–23, 27–31, 286–289, 291
- hydrosoluble ligands, 15–17, 286, 287
- hydroxyalkylisocyanides, 118
- hydroxylating agent, 20–21
- hydroxyl radical, 6, 8, 10, 11, 19–20, 23
- hydroxytamoxifen, 567, 569
- IC<sub>50</sub>, 608–610, 613, 614
- ICOMC (International Conferences on Organometallic Chemistry), xii, xiii, 703–706
- silver/gold jubilee book, xii
- silver/gold jubilee medal, xii
- I*<sub>M</sub> electrochemical parameter, 679–681
- imidazolin-2-ylidene, 115, 117, 125
- in vivo* testing, 573
- incident photon to current conversion efficiency (IPCE), 504, 506–509
- indane, 61
- 1*H*-indene, 61–62, 65
- indolo[3,2-*c*]quinolines complexes,  
 copper, 612–614  
 osmium-arene, 610, 611, 613, 614  
 ruthenium-arene, 609–611, 613, 614
- indolo[3,2-*d*]benzazepines complexes,  
 copper, 612–614  
 gallium, 608, 610  
 osmium-arene, 610, 611, 613, 614  
 ruthenium-arene, 609–611, 613, 614
- inflammation, 545–548
- inhalation, 549, 551, 556
- inorganic chemical biology, 563
- ischemia-reperfusion, 546, 554
- insertion reaction, 91
- intensity of the incident light, 508
- intermolecular oxidative addition, 40–42
- internal quantum efficiency (IQE), 506
- intramolecular electron transfer, 636, 641–643, 650, 662
- intramolecular hydroamination, 317, 319
- intravenous injection, 551, 574
- inversion barrier, 475, 476, 481
- ion channels, 546, 547, 548, 553, 556
- ionic liquids, 424, 529–539
- iridium sensitizer, 507
- iridium-pincer complexes, 39, 40, 54
- iron catalysts, 133–136, 139–140, 234–235, 240, 242
- iron complexes, 136–139, 234–236, 286–289, 546, 555
- iron N-heterocyclic carbenes, 136–139
- iron pentacarbonyl, 446, 451, 453, 455
- IR-spectroelectrochemistry, 664
- isocyanides, 117–119, 121, 123, 145–153, 171–173, 176–177, 181, 677–679, 682, 683
- isomers, 187, 194–195
- isotope effects, 43, 53
- Kaplan-Meier survival curves, 575
- kenpaullone, 607
- KIE (*see* kinetic isotope effect),
- kinetic isotope effect, 43, 44, 50–52  
 of alkyl fluoride C–F oxidative addition, 52  
 of ether C–O oxidative addition, 43, 50  
 of tosylate C–O oxidative addition, 50
- KP1019, 565
- labeling studies, 43

- lactide, 359, 370  
 lactide ring opening polymerization, 317, 321  
 Lever electrochemical model, 680, 681  
 ligand design,  
     amido ligands, 316  
     macrocyclic systems, 316–320  
     tetraazamacrocycles, 319  
 light alkanes, 17, 21, 22, 29, 33, 34, 290, 291  
 light-driven process, 522  
 light-independent process, 522  
 Linear Free Energy Relationship (LFER), 654, 658, 660  
 lipid bilayers, 633, 634, 644, 648  
 lipid nanocapsules (LNC), 574–576  
 long-circulating nanoparticles, 574  
 long-term survivors, 575  
 luminescent organoboron compounds, 485–489
- macrocyclic functionalization, 321  
 manganese catalysts,  
     glycerol oxidation, 248–249  
 materials, organometallic, 379  
 maximum power, 508  
 MCF-7 cell lines, 567, 569  
 McMurry coupling, 566, 572  
 MDA-MB-231 cell lines, 567–572, 575  
 mechanisms,  
     alkane carboxylation, 21, 22  
     alkane hydrocarboxylation, 20, 21  
     alkane oxygenation, 3–12, 18–20  
     1,2-dehydroaryloxylation of ethyl aryl ethers, 45  
     1,2-dehydrofluorination of alkyl C–F bonds, 53  
     1,2-dehydroxygenation of ethyl acetate, 49  
     electron transfer induced reactions, 655, 663, 667–670, 673  
     methanol carboxylation, 260, 262–267  
     methyl acetate C–O oxidative addition, 43, 47, 48  
     methyl tosylate C–O oxidative addition, 50, 51  
     net oxidative addition of alkyl fluoride C–F bonds, 53  
     net oxidative addition of methyl aryl ether C–O bonds, 43  
     oxidation of sulfides, 305–314  
     oxidation and reduction of sulfoxides, 305–314  
 mechanochemistry, 493–498  
 medicinal chemistry, 557, 566  
*meta*-chloroperoxybenzoic acid, 11  
 metal catalysis (*see* catalysis)  
 metal catalysts and complexes,  
     alkaline earths (*see* alkaline earths)  
     aluminium 20, 440  
     barium 441  
     bismuth 495  
     boron 74–78, 81–94  
     carbonyls for CO based therapies (*see* CO based therapies)  
     chromium 122, 656  
     cobalt 18, 73–78, 510  
     copper (*see* copper catalysts, copper complexes)  
     gallium 608  
     gold 118, 121, 207–223  
     indium 441  
     iridium 5, 39–55, 118, 121, 126, 274, 278–280, 387, 506, 507, 671  
     iron 5–7, 16–18, 124, 136–140, 235–238, 288, 506, 507, 656 (*see also* ferrocene)  
     manganese 61, 62, 64–67, 116, 119, 249  
     molybdenum 7, 102–106, 122, 124, 158, 305–312, 551, 553, 558  
     nickel 81–89, 92–93, 100, 104, 136–141, 163, 167, 187, 188, 190  
     organometallic 445–451, 454  
     osmium 10, 248–250, 506–508, 669  
     palladium 86–88, 119, 128, 145–152, 176, 193, 236, 238, 386, 463  
     platinum 4, 123, 128, 173–175, 188, 189, 195, 384, 387, 506, 507  
     polyoxometalates 59, 60, 62, 63  
     rare earths 345–357, 621, 624  
     rhodium 11, 12, 127, 237, 239, 241, 259–268, 260–266, 274, 278, 280, 462  
     ruthenium 106, 116, 117, 125–127, 158, 237, 241, 270–282, 447, 503, 505, 506, 508–510, 536–538, 564, 565, 582, 583, 609–611, 613, 614, 672  
     scorpionates 15–17, 272–277, 285–293, 683  
     silver 384–386, 389, 390, 466, 495  
     technetium 549, 589–602  
     titanium 442  
     tungsten 102–106, 121–124, 656  
     vanadium 12, 17–22, 227–231, 286, 289, 291  
     zinc 441, 508  
     zirconium 88–94, 315–322  
 metal complex redox mediators 508  
 metal to ligand charge transfer (MLCT), 505, 509  
 metal nanoparticles, 533, 535  
 metal oxides, 239, 241  
 $\alpha$ -metallation, 118  
 metallocenes, 88–94, 157–169 (*see also* ferrocene)  
 metallocene dichlorides, 165, 169  
 metallodrugs, 493–496, 498, 564, 565, 581, 584–586  
 metalloenzymes, 563, 564  
 metallofullerenes, 691–700  
 metal-organo catalysis (*see* catalysis),  
 metallopharmaceuticals, 493–498  
 metalloporphyrins, 59, 60, 64–66, 68  
 metallothionein mimic, 300  
 Metal Organic Frameworks (MOFs), 382, 408–409  
 metastases, 575  
 metathesis, 157–169 (*see also* ring opening metathesis)  
 methanol carbonylation, 259–268  
 methyldiene formation, 45, 48, 53  
 M–H bond,  
     activation, 97, 102  
     heterolytic splitting, 100, 103  
     polarization, 98, 100, 103  
 micro-emulsion, 574  
 microwave assisted oxidations, 233–244  
 migration,  
     acetate, 48–50  
     aryloxide, 43  
     hydride, 48, 50, 53  
 mitogen-activated protein kinases (MAPKs), 547  
 mixed sandwich complexes, 681  
 modified semiconductors, 523  
 molecular engineering, 504, 509  
 molecular imaging,  
     contrast enhancement, 620  
     magnetic resonance imaging, 619, 620  
 molecules with two redox centers, 655  
 molybdenum catalysis,  
     CpMo(CO)<sub>3</sub>X, 306–307  
     hydride complexes, 308, 311  
     MoO<sub>2</sub>Cl<sub>2</sub>, 306–311  
 monoterpenes, 64, 65  
 MRI contrast agents, 619–628  
 MTT assay, 611, 613, 614  
 multicopper complexes and coordination polymers,  
     aminoalcohols, 28,

- N,O-ligands, 29, 30, 36  
 self-assembly synthesis, 17, 27, 28, 30, 410–418  
 water-soluble compounds, 15–19, 27–30, 33, 286–289  
 multicatalysis, 325–339  
 multinuclear assemblies, 17, 27–31  
 myocardial infarct, 548, 550, 552
- N<sub>3</sub> dye, 506, 509  
 N-alkylimidazoles, 115  
 NAMI-A, 565  
 nanocapsules, 573, 574  
 nanoparticles,  
   cobalt, 422, 429–433  
   drug delivery vehicles, 626  
   iron, 428  
   iron oxide, 624, 626, 627  
   lipid-based, 626, 627  
   lipid microbubbles, 627  
   lipid microspheres, 627  
   liposomes, 626, 627  
   magnetic, 422, 428–433  
   metal, 421, 422, 426  
   oily suspensions, 627  
   organometallic, 421–434  
   quantum dots, 626, 628  
   ruthenium, 422–428  
   solid lipid nanoparticles, 627  
   yeast cell wall particles (YCWPs), 627  
 nanoreactors, 422–423  
 nanotechnology, 619, 628  
 naphthalene, 62, 65  
 nerol, 64  
 N-heterocyclic carbenes, 113–129, 133–141, 145–153, 238, 330–333, 336–337, 339  
 N-heterocyclic carbene palladium catalysts, 145–153, 236–239  
 nickel, 81–89, 92–93, 136–141  
 nickel alkoxides, 140  
 nickel catalysts, 139–141  
 nickel N-heterocyclic carbenes, 138–141  
 nickelocene, 163, 167  
 nitric oxide synthase (NOS), 547, 552, 555  
 nitriles, 172–181, 679  
 Nobel prizes, xi  
 non-innocent ligand, 667–670, 673, 674  
 non-planar  $\pi$ -conjugated carbon system, 473, 479  
 nuclear imaging, 589, 591  
 nuclear medicine, 589, 591, 600
- octahedral-type complexes, 677, 678, 681  
 OLEDs, 490, 491  
 olefin metathesis,  
   acyclic diene (ADMET), 157–158, 160, 165  
   alkyne cross metathesis, 168  
   cross metathesis (CM), 160, 165–167  
   enantioselective RCM, 162  
   ring-closing (RCM), 161–163  
     ring opening polymerization (ROMP), 157–160, 391  
 open circuit voltage, 504, 506, 508, 510  
 open geodesic polyarene, 473  
 organic light-emitting diodes (*see* OLEDs)  
 organoboron compounds, 485–491  
 organometallic,  
   anti-cancer agents (*see* anti-cancer drugs)  
   catalysis (*see* catalysis)
- chemical biology 563, 564  
 complexes (*see* metal catalysts and complexes)  
 hydrogenases 563  
 polymer properties  
   biological 391  
   catalytic 391, 395, 398, 400  
   electronic 382–393, 397–399  
   photovoltaic 383  
   quinone methides 568  
 othometalation 319  
 over-potential, 524  
 oxaliplatin, 605, 606  
 oxazoline based ligands, 185–189, 191–194  
 oxidant, 59–67  
 oxidation catalysis,  
   alcohols, 233–244  
   alkanes to alcohols and ketones, 5–11, 15–20, 31, 32, 60, 63, 66, 286–290, 415  
   alkanes to carboxylic acids, 20–22, 286, 288, 290–291  
   glycerol to carbonyl compounds, 248–253  
   glycerol to dihydroxyacetone (DHA), glycolic acid and hydroxypyruvic acid, 249–254  
   ketones (*see* Baeyer–Villiger reaction)  
   sulfides to sulfoxides and sulfones 305–314  
   sulfoxides to sulfones 305–314  
 oxidation potential 654  
 oxidation state, 667, 669, 670, 674, 694, 695, 697, 698, 700  
 oxidation with hydrogen peroxide, 234, 236, 240, 242–244, 305–314, 415  
 oxidation with *tert*-butyl hydroperoxide, 3, 5, 8, 11, 67, 234, 305–314  
 oxidative addition,  
   of azoles, 124–125, 127  
   of alkyl fluoride C–F bonds, 51–53  
   of ether C–O bonds, 40, 42, 44  
   of ester C–O bonds, 45, 50  
   of tosylate C–O bonds, 50
- (PCP)Ir (*see* iridium-pincer complexes)  
 P,N chelating ligands, 185–194  
 palladium, 85–87  
 palladium catalysts, 145–153, 236, 238  
 palladium(II) complexes, 145–153, 236  
 palladium-catalyzed desulfitative coupling, 295–299  
 PARP-1 inhibitor, 585, 586  
 PEG (polyethylene glycol) chains, 574, 575  
 perfusion agents, 590, 593  
 Periana system, 3, 4  
 peroxydative halogenations, 22  
 peroxydative oxidation, 286, 289–291, 293, 305–314, 415 (*see also* hydrogen peroxide)  
 peroxydisulfate,  
   for alkane carboxylation, 8, 9, 20–22, 35  
 phenanthrene, 65  
 phenol functions, 569, 573, 576  
 phenylazo-pyrazoles, 277–278  
 phosphines, 187, 189–194  
 phosphonate groups, 509  
 photoactive materials, 522  
 photoautotrophs, 522  
 photocatalysis, 329  
 photocathode surface, 525  
 photochemical stability, 506  
 photochemical systems, 524  
 photoelectrochemical reduction, 524  
 photoelectrochemical systems, 525

- photoexcitation of dye, 505  
 photoisomerization, 490  
 photoluminescence, 486  
 photoresponsive materials, 485, 490  
 photosensitizer, 505, 506, 510, 521, 524  
 photosynthesis, synthetic, 513–525  
 photovoltaic (PV), 519  
 piano stool structures, 582  
 Pickett electrochemical model, 677–679, 683, 686  
 pinacol, 572, 573, 576  
 pincer complexes, 39  
 $P_L$  electrochemical ligand parameter, 677–679  
 planar chirality, 168  
 platinum drug,  
     carboplatin, 564, 605, 606  
     cisplatin, 564, 565, 574, 575, 605, 606  
     oxaliplatin, 564  
 polarizability, 678, 687  
 poly(pyrazolyl)alkanes, 276, 286–289, 291  
 poly(pyrazolyl)borates, 270, 272–277, 280  
 polycyclic aromatic hydrocarbons, 62, 64  
 polyfunctional ligands, 185  
 polymers,  
     coordination, 17, 18, 28–31, 382, 407–417  
     metal fullerene, 385–386  
     metal graphene, 397  
     metal-backbone organometallic, 382  
     metal-side organometallic, 390–397  
     organometallic, 381–400  
     properties (*see* organometallic polymer properties)  
     tailor made 345  
 polymerization  
     coordinative chain transfer, 345–357  
     copolymerizations, 345–357  
     ring opening metathesis (ROMP), 157–160, 391  
     ring opening (ROP), 359–376, 391, 395–397, 399  
 poly-nuclear boron complexes, 487  
 polyoxometalates (*see* metal catalysts and complexes)  
 polyphenols, 573, 574  
 poly(vinylpyrrolidone) (PVP), 422, 423, 425, 430  
 porosity,  
     without pores, 416–417  
     sorption, 408, 416  
 porphyrins, 59–67,  
 Positron Emission Tomography (PET), 590, 591  
 power conversion efficiencies, 504, 507, 508, 510  
 proapoptotic compounds, 575  
 protic NHCs, 115, 117  
 proton transfer,  
     activation free energy, 101  
     energy profile, 103, 106  
     enthalpy, 101  
     entropy, 101  
     solvent effect, 104–105  
 p-type semiconductor, 524  
 pyrazine-2-carboxylic acid (PCA or HpcA), 5, 19, 20  
 pyrazole based ligands, 269–270, 277–278  
 quantum yield, 486–489  
 quasi-borinium cation,  
     C–H bond activation, 74–75  
     C–X bond activation, 76  
     Lewis acidity, 77  
 quasi-reversibility, 655  
 quinone, 667–673  
 quinone methide, 567–572, 576  
 radical, 6, 7, 10–12, 19–22, 32–35, 667, 669, 670  
 radical mechanism, 19, 21, 22, 32–35, 286, 290–291  
 radionuclide therapy, 589, 591  
 radiopharmaceuticals, 564, 589–592, 596, 600, 601  
 rare earths catalysts, 345–348, 351, 354  
 rate-determining-step, 260–262  
 reactive oxygen species (ROS), 546, 547  
 redox, 305–314, 566, 569, 575  
 redox inactive, 19–20  
 redox mediator, 504, 505, 508, 510  
 redox potential, 691, 694, 695, 697  
 redox potential-structure relationships, 677–688  
 redox potential parameterization, 677, 687  
 redox properties and processes, 633–650, 653, 657, 658, 660, 662, 664, 667–674, 692, 694, 695, 698, 699  
 red-shift, 486  
 reduction, 670–674  
 reduction of sulfoxides, 140, 305–314  
 reduction potential, 654  
 reduction reactions, 139–141  
 reductive elimination, 43, 51, 259–268  
 reductive elimination mechanism, 264–266  
 relay catalysis, 326, 338  
 relay and sequential, 326, 334–335  
 retro-cycloadditions, 463–465  
 rhodium catalysts (*see* metal catalysts and complexes)  
 ribonucleotide reductases, 606  
 ring-opening polymerization, 359–360, 363, 365–372  
 ROS (Reactive Oxygen Species), 567, 569, 572, 576  
 Ru albumin, 584  
 ruthenium,  
     anticancer compounds, 581–586  
     catalysts (*see* metal catalysts and complexes)  
     complexes (*see* metal catalysts and complexes)  
     CO-Releasing Molecules (CORMs) 549–551  
 sacrificial donors, 521  
 Salvarsan, 605  
 sandwich complexes, 15, 680, 681  
 sec-butylbenzene, 62  
 Secondary Building Unit (SBU), 408, 411–412, 415, 417  
 Schrock catalyst, 166–167  
 scorpionate complexes (*see* metal catalysts and complexes)  
 self-assembly synthesis, 17, 27, 28, 30  
 semiconductor,  
     SnO<sub>2</sub>, 505  
     TiO<sub>2</sub>, 505  
     ZnO, 504–507, 509  
     sensitization, 509  
 semiquinone, 668–670, 672, 673  
 senescence, 565, 569, 575, 576  
 sensitizers, 506–510  
 sensory materials, 485  
 sequential catalysis, 326, 334–335  
 serendipity, 407–418  
 shaped carbon materials, 445, 446, 448, 449, 454  
 Shilov chemistry, 3  
 short circuit current, 504, 506, 508  
 silica nanoparticles, 67  
 Single Photon Emission Computed Tomography (SPECT), 590, 591, 596, 599, 601

- single-pot synthesis, 15, 22–23  
 skeletal rearrangements, 207–221  
 small molecules, functionalization (*see* alkane functionalization)  
 $S_M$  electrochemical parameter, 679–681  
 solar energy, 519, 520, 525  
 solar light simulator, 508  
 soluble guanylate cyclase (sGC), 547, 553  
 solvent-free peroxidative oxidations, 234, 237, 239  
 Sonogashira coupling, 152  
 spectroelectrochemistry, 673  
 square planar complexes, 506, 681  
 stealth nanoparticles, 574  
 structure-reactivity relationship, 653  
 structure-redox properties relationships (*see* redox potential-structure relationships)  
 styrene, 65  
 subcutaneous glioma, 574  
 sulfides,  
   oxidation, with Mo catalysts, 306–307  
 sulfones,  
   formation, with Mo catalysts, 306  
 sulfoxides,  
   formation, with Mo catalysts, 305–306  
   reduction, with Mo catalysts, 308  
   oxidation, with Mo catalysts, 306  
 sumanene complex, 473–482  
 supported catalysts,  
   metal composite, 240, 242  
   polystyrene supported, 227–231, 289  
   preparation, 228–229  
 sustainable energy, 494, 501  
 Suzuki-Miyaura coupling, 149  
 syngas conversion, 3  
 synthetic photochemical processes, 520  
 tamoxifen, 566, 567, 569, 633–635  
 target proteins, 576  
 targeted chemotherapy, 605, 606  
 target-specific complexes, 593–599  
 tautomers, 194–195  
 TBHP (*tert*-butylhydroperoxide),  
   O–H activation (*see* bond activation)  
   sulfides and sulfoxides oxidation, catalysed by Mo complexes  
     306–308  
     alcohols oxidation 234, 236–238  
 technetium 549, 589–602  
 template synthesis, 117  
 TEMPO radical, 233, 608–611  
 tetracarbene complex, 117, 122  
 tetrahydrofolate, 523  
 tetralin, 61  
 theragnostics, 619, 626  
 thermal decomposition, 451, 454  
 thermodynamic potentials, 524  
 thiazoline based ligands, 185–194  
 thioether, 668–671, 673  
 thioorganics, 295–296, 299  
 three-component reaction, 84, 92–93, 203  
 toluene, 62  
 topoisomerases, 606  
 transfer hydrogenation, 3  
 transition metal hydrides,  
   acidity, 101  
   basicity, 105  
   proton accepting ability, 101  
   proton donor, 105, 107  
 transition state, 43, 49  
 transportable energy, 518  
 tricarbonyl complexes, 589, 592, 593, 595, 597–602  
 trifluoroacetic acid (TFA), 21–23, 102  
 trinuclear assembly, 411, 413, 417  
 trinuclear triangular Cu(II), 409–416  
 triosmium dodecacarbonyl, 8  
 tris(pyrazolyl)borate, 15  
 tris(pyrazolyl)methanes, 15, 286–293  
 tris(pyrazolyl)methane sulfonate, 15, 289  
 turnover number (TON), 5, 8, 11, 17, 18, 21, 32, 236–239, 286, 288–292  
 tyrosine derivatives, 227–230  
 tyrosine kinases, 606, 607  
 unsaturated substrates, 81, 93, 172–181  
 valence electron, 669, 674  
 vanadium catalysts (*see* metal catalysts and complexes)  
   alkane carboxylation, 17–22  
   alkane oxidation, 12, 17–22, 286, 287, 289–291  
   sulfoxidations, 227, 230–231  
 vinylidene, 682, 683, 685  
 vitamin B12, 563  
 water gas shift reaction, 3, 550, 554  
 water soluble complexes, 15, 17–25, 27, 28, 30, 35, 199–204, 549, 557  
 wavelength, 486  
 WAXS (Wide Angle X-ray Scattering) analysis, 427  
 wind tower, 518, 519  
 working carbon, 513, 517  
 zirconium, 89–94, 316–321  
 Zeise's salt, xi





**Figure 1** ICOMC Silver/Gold Jubilee medal.

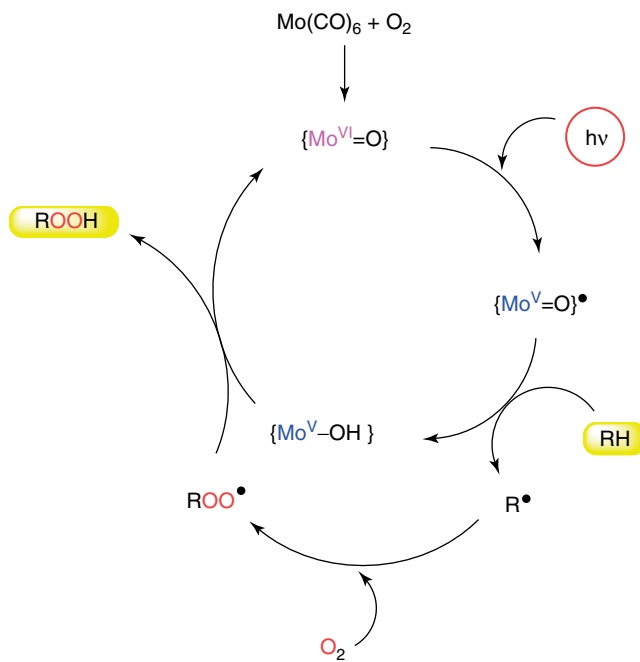
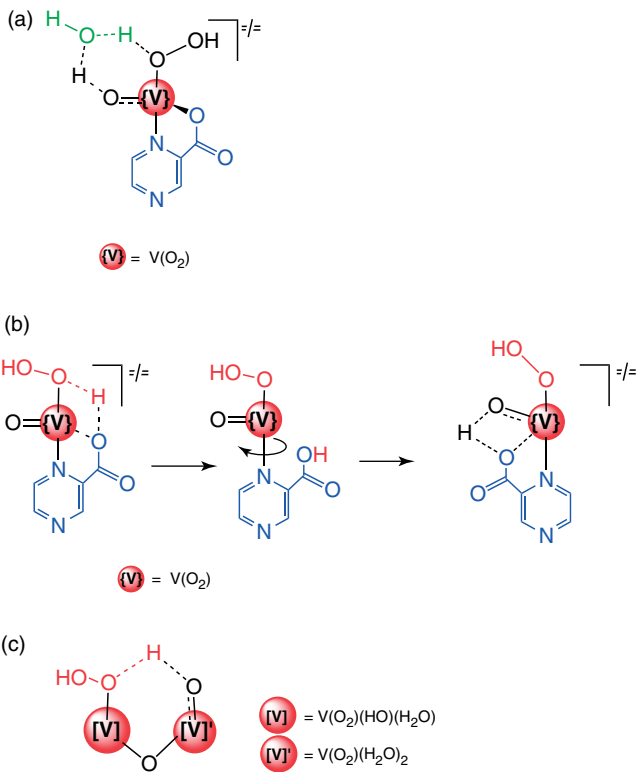
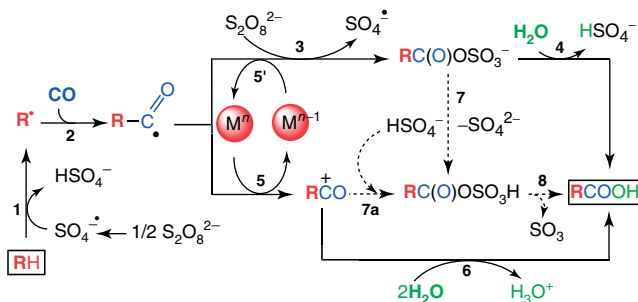


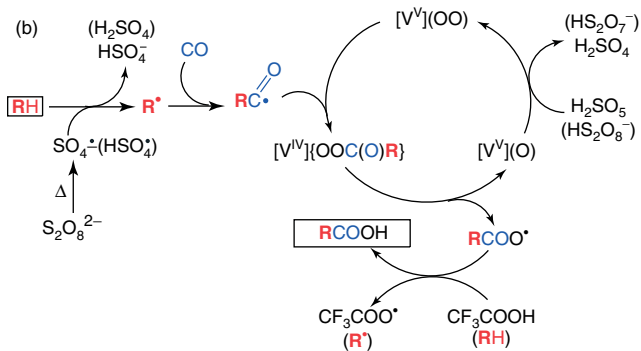
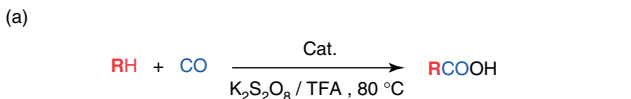
**Figure 1.5** Mechanism proposed for the photooxygenation of alkanes, RH, in the presence of Mo or W carbonyls.



**Scheme 2.6** Examples of transition states (TSs) involved in a proton-transfer step from a ligated  $H_2O_2$  to an oxo ligand on the way to generate the hydroxyl radical: (a) six-membered TS (water-assisted  $H^+$ -transfer) at a PCA-V catalyst (PCA=pyrazine carboxylate) [40]; (b) five- or four-membered TSs (PCA-assisted  $H^+$ -transfer, “robot’s arm” mechanism) at a PCA-V catalyst [43–45]; and (c) six-membered oxo-divanadium TS at a divanadate-type model [42].



**Scheme 2.8** Main radical mechanism of the hydrocarboxylation of alkanes with peroxydisulfate,  $CO$ , and water, in aqueous ( $H_2O/MeCN$ ) medium [53]. The minor 7 (or 7a) to 8 alternative pathway does not concern water as the hydroxylating agent.



**Scheme 2.9** Alkane carboxylation with CO and  $\text{K}_2\text{S}_2\text{O}_8$ , in TFA: (a) General reaction [13, 17, 54–62] and (b) proposed mechanism for an oxo-vanadium catalyst [54, 55].

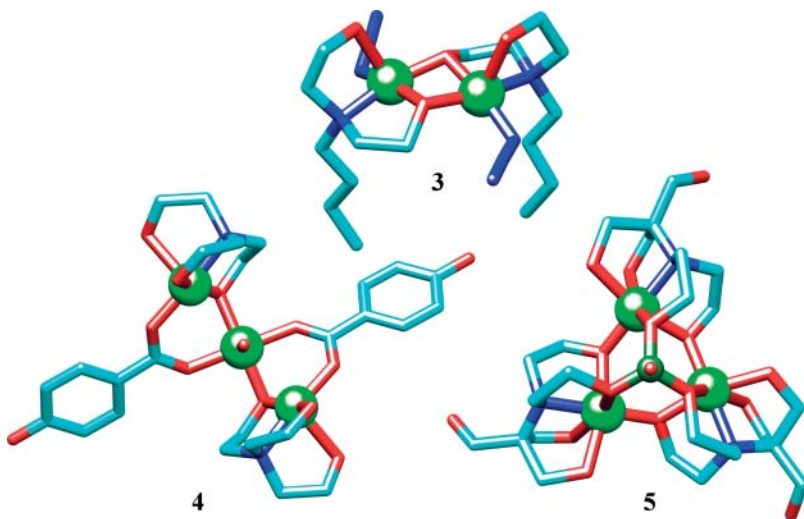


**Figure 3.1** X-ray crystal structures of complexes  $[\text{Cu}_2(\mu-\text{Hbdea})_2(\text{N}_3)_2]$  (**3**),  $[\text{Cu}_3(\mu-\text{H}_2\text{tea})_2(\mu-\text{poba})_2\text{H}_2\text{O}] \cdot 4\text{H}_2\text{O}$  (**4**), and  $[\text{Cu}_3(\mu_3-\text{BO})(\mu-\text{H}_3\text{bts})_3][\text{BF}_4]2\text{H}_2\text{O}$  (**5**). All H atoms,  $[\text{BF}_4]^-$  anion (in **5**), and crystallization  $\text{H}_2\text{O}$  molecules (in **4**, **5**) are omitted for clarity. Color codes: Cu, green balls; O, red; N, blue; C, cyan; B, dark green ball. Adapted from References 6, 11, and 13.

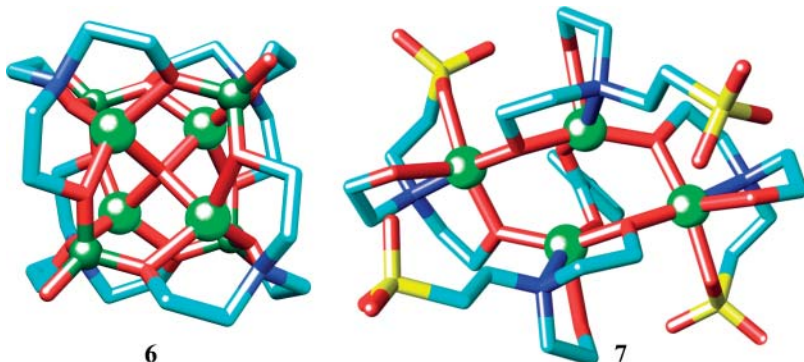


**Figure 3.2** X-ray crystal structures of complexes  $[\text{Cu}_4(\mu_4-\text{O})(\mu_3-\text{tea})_4(\mu_3-\text{BOH})_4][\text{BF}_4]_2$  (**6**)  $[\text{Li}(\text{H}_2\text{O})_4][\text{Cu}_4\mu-\text{Hbes})_4(\mu-\text{ba})] \cdot \text{H}_2\text{O}$  and (**7**). All H atoms,  $[\text{BF}_4]^-$  anions (in **6**),  $[\text{Li}(\text{H}_2\text{O})_4]^+$  cations, and crystallization  $\text{H}_2\text{O}$  molecules (in **7**) are omitted for clarity. Color codes: Cu, green balls; O, red; N, blue; C, cyan; B, dark green balls. Adapted from References 6 and 14.

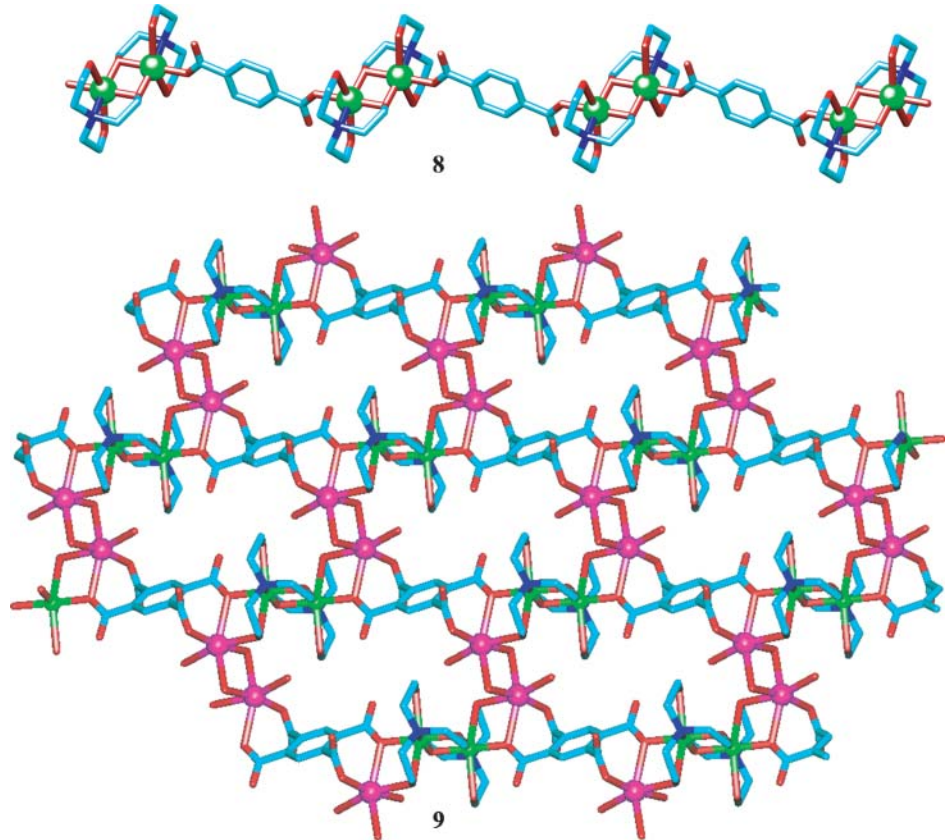


**Figure 3.3** X-ray crystal structures of 1D and 2D polymers  $[\text{Cu}_2(\mu-\text{H}_2\text{tea})_2(\mu_2-\text{tpa})]_n \cdot 2n\text{H}_2\text{O}$  (**8**) and  $[\text{Cu}_2(\mu_3-\text{H}_2\text{tea})_2(\mu_4-\text{pma}) \{\text{Na}_2(\text{H}_2\text{O}_4\}_n \cdot 10n\text{H}_2\text{O}$  (**9**), respectively. All H atoms and crystallization  $\text{H}_2\text{O}$  molecules are omitted for clarity. Color codes: Cu, green balls; O, red; N, blue; C, cyan; Na, magenta. Adapted from References 6 and 8.

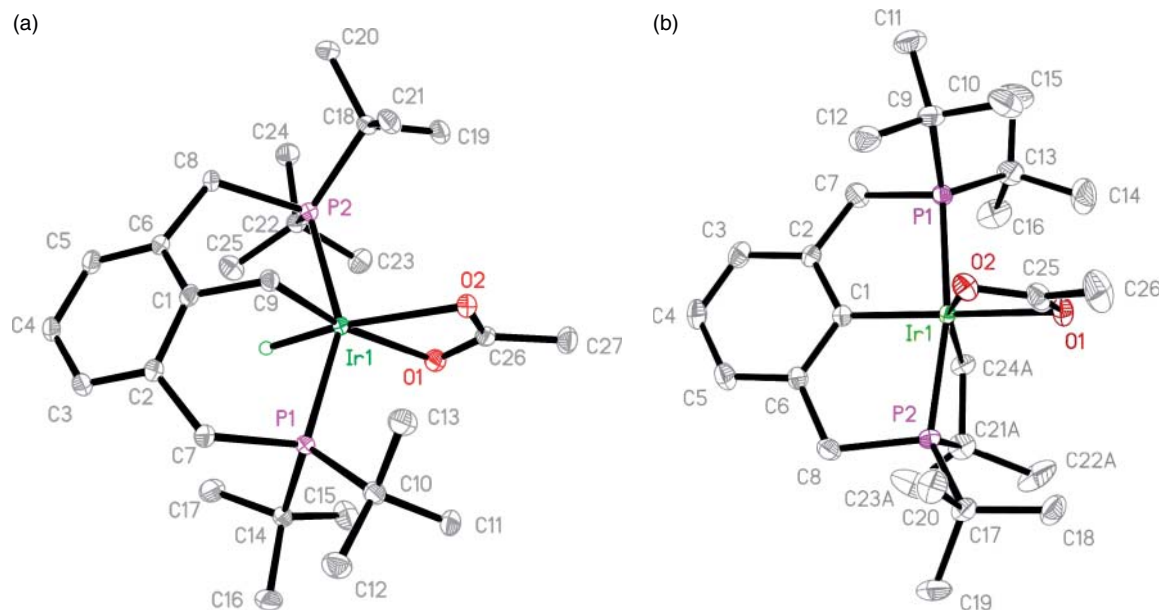


**Figure 4.6** X-ray structures of (a)  $(\text{PCP}-\text{CH}_2)\text{Ir}(\text{H})(\kappa^2-\text{O}_2\text{CMe})$  and (b) cyclometalated  $(\text{PCP})\text{Ir}(\text{acetate}), [\kappa^4-\text{C}_6\text{H}_3-2-(\text{CH}_2\text{P}'\text{Bu}_2)-6-(\text{CH}_2\text{P}'\text{Bu}(\text{CMe}_2\text{CH}_2))]\text{Ir}(\kappa^2-\text{O}_2\text{CMe})$ .

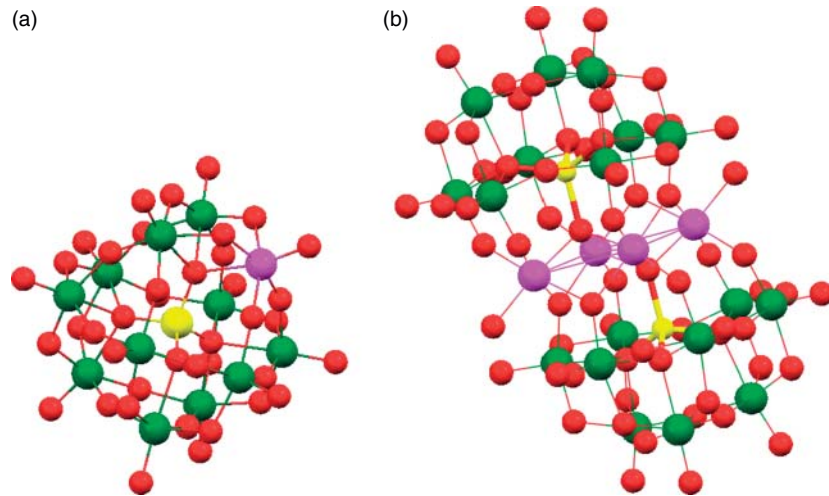


**Figure 5.1** General structure of the Keggin-type (a) and sandwich-type (b) transition metal substituted polyoxometalates (TMSPs) used in catalysis; W (green); O (red); heteroatom X (yellow); transition metal M (pink).

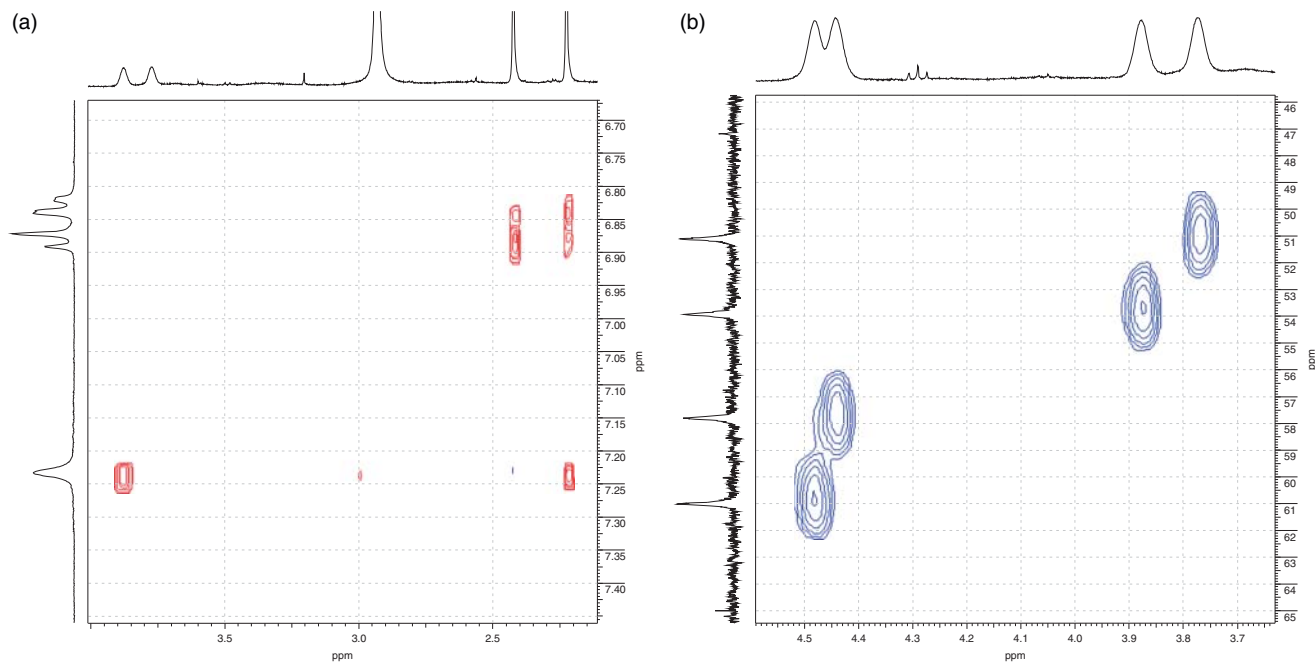


**Figure 6.1**  $^1\text{H}$ - $^1\text{H}$  NOESY (a) and  $^1\text{H}$ - $^{13}\text{C}$  HSQC (b) spectra of  $[8\text{-I-}8'\text{-(2,5-}\text{Me}_2\text{C}_6\text{H}_3\text{)-}3,3'\text{-Co(1,2-}\text{C}_2\text{B}_9\text{H}_{10}\text{)}_2]^-$ .

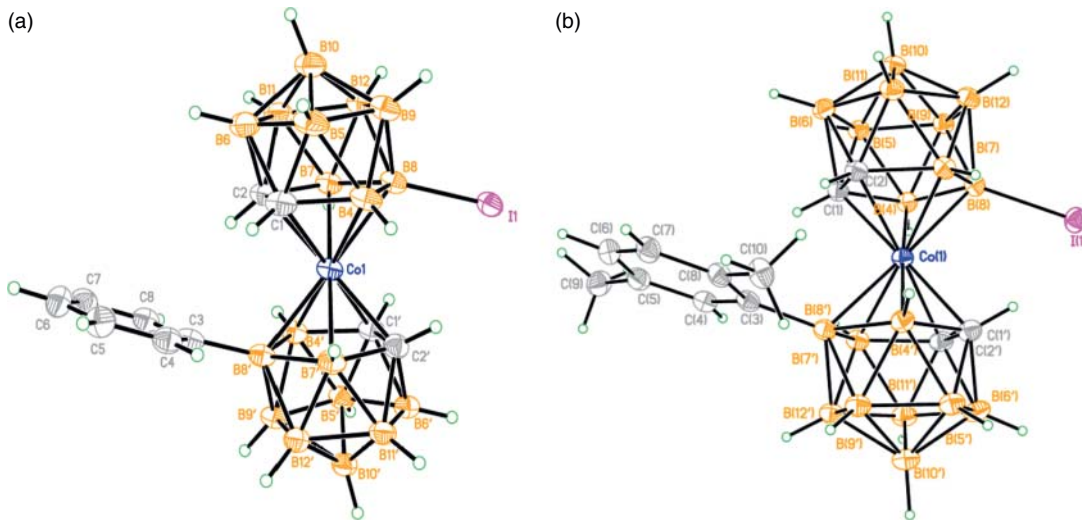
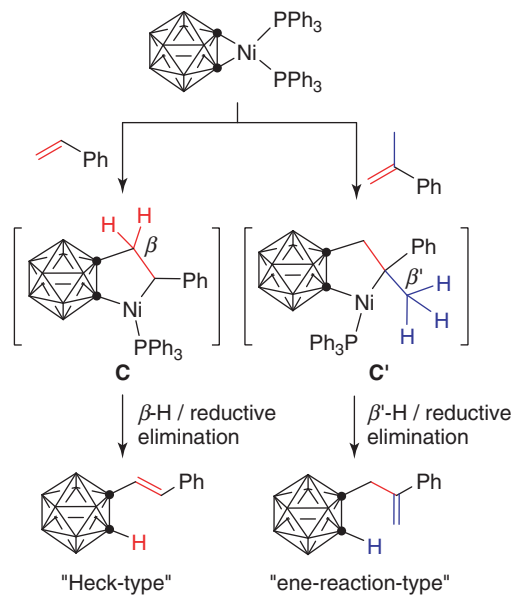


**Figure 6.2** Molecular structures of  $[8\text{-I}\text{-}8'\text{-Ph}\text{-}3,3'\text{-Co}(1,2\text{-}_2\text{B}_9\text{H}_{10})_2]^-$  (a) and  $[8\text{-I}\text{-}8'\text{-(2,5-Me}_2\text{C}_6\text{H}_3)\text{-}3,3'\text{-Co}(1,2\text{-C}_2\text{B}_9\text{H}_{10})_2]^-$  (b) anions. Adapted with permission from Reference 21. Copyright (2010) American Chemical Society.



**Scheme 7.3** Proposed mechanism for reaction of Ni–carbonyne with alkenes.

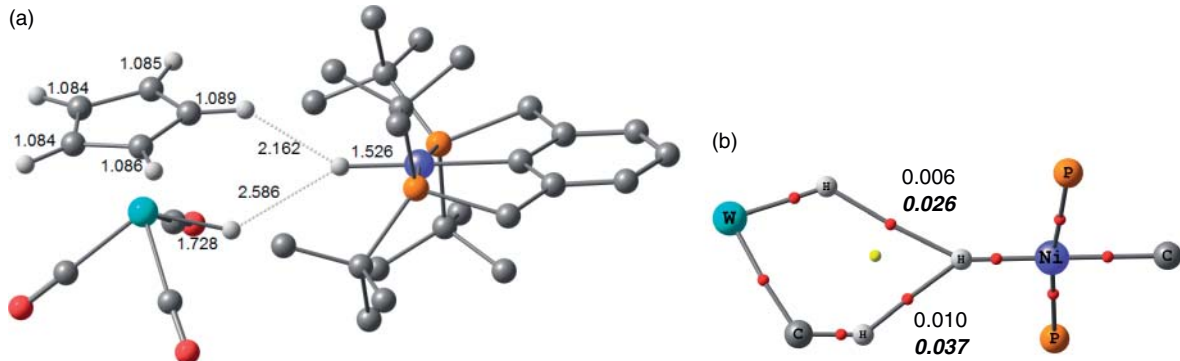


**Figure 8.3** (a) Optimized structure of dihydrogen-bonded adduct between  $(^{\text{t}\text{Bu}}\text{PCP})\text{Ni}(\text{H})$  and  $\text{CpW}\text{H}(\text{CO})_3$  with selected bond lengths (Å). Hydrogen atoms of the  ${}^{\text{t}\text{Bu}}\text{PCP}$  ligand are omitted for clarity. (b) Fragment of molecular graph of the system. Electron density at the (3,-1) bond critical point and bond order (as a delocalization index [21], in bold italic) are reported for W–H ··· H–Ni and C–H ··· H–Ni contacts. Color codes: ●-bond critical points, ●-ring critical points.

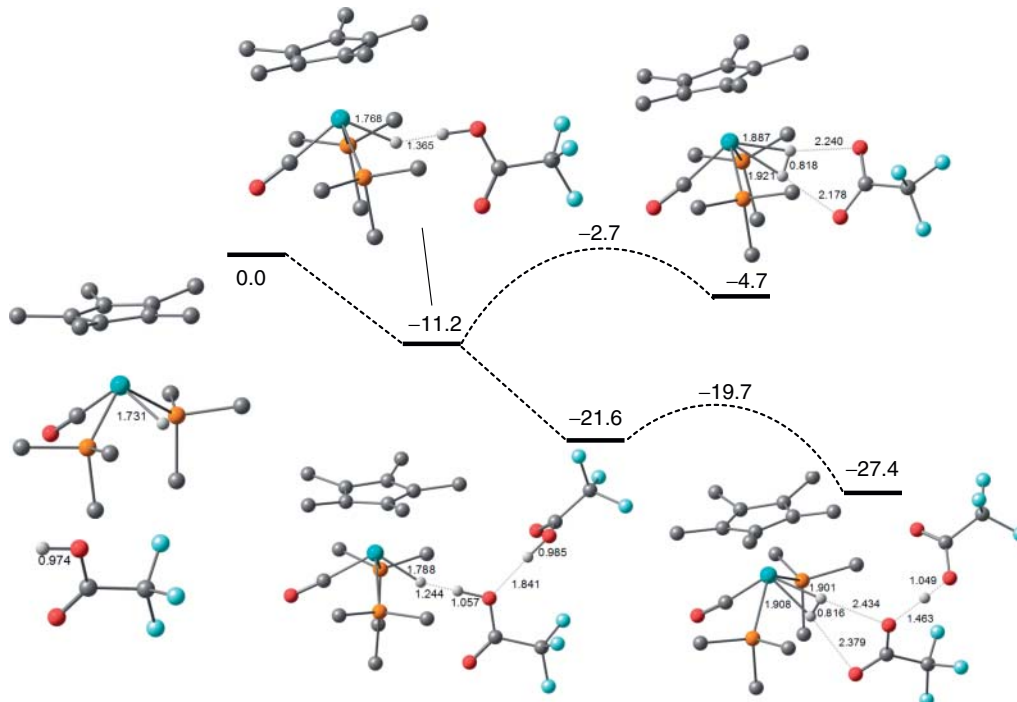


**Figure 8.6** Optimized (DFT M05) geometries and energy profile ( $\Delta E$ , kcal/mol) calculated for protonation of  $\text{Cp}^*\text{MoH}(\text{CO})(\text{PMe}_3)_2$  by  $\text{CF}_3\text{COOH}$  (one and two molecules) in gas phase. Selected bond lengths are reported (Å). Hydrogen atoms of  $\text{CH}_3$  groups are removed for transparency. Data from Reference 43.

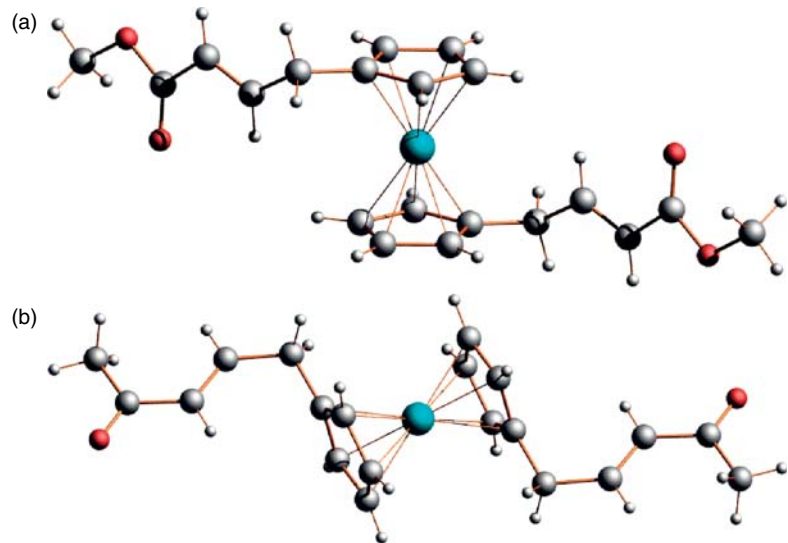
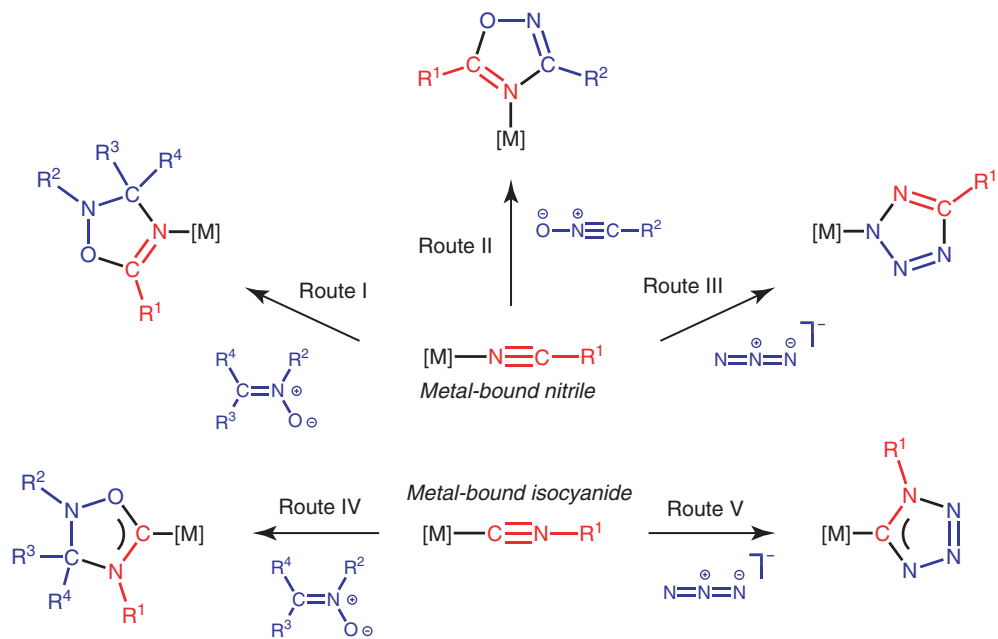
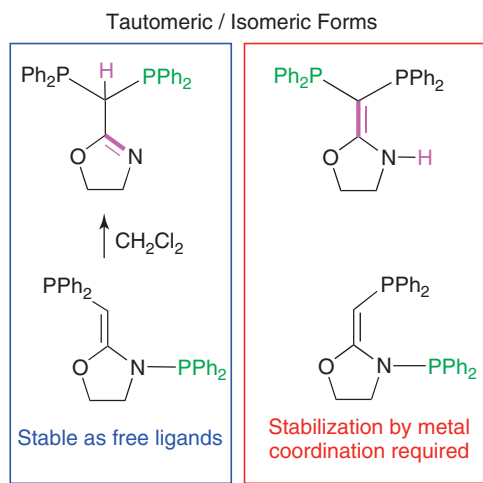


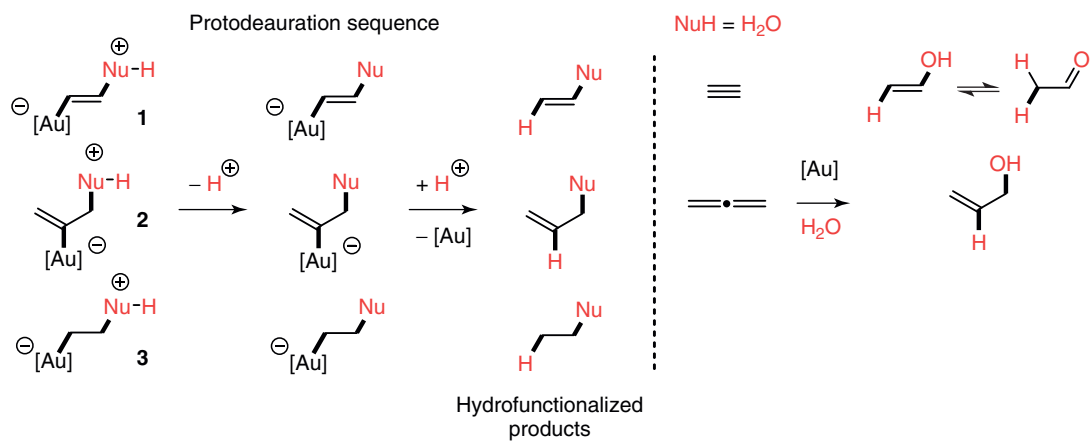
**Figure 12.6** The molecular structures of **4-2**; (a)  $Z = \text{CO}_2\text{Me}$  and (b)  $Z = \text{COMe}$ .



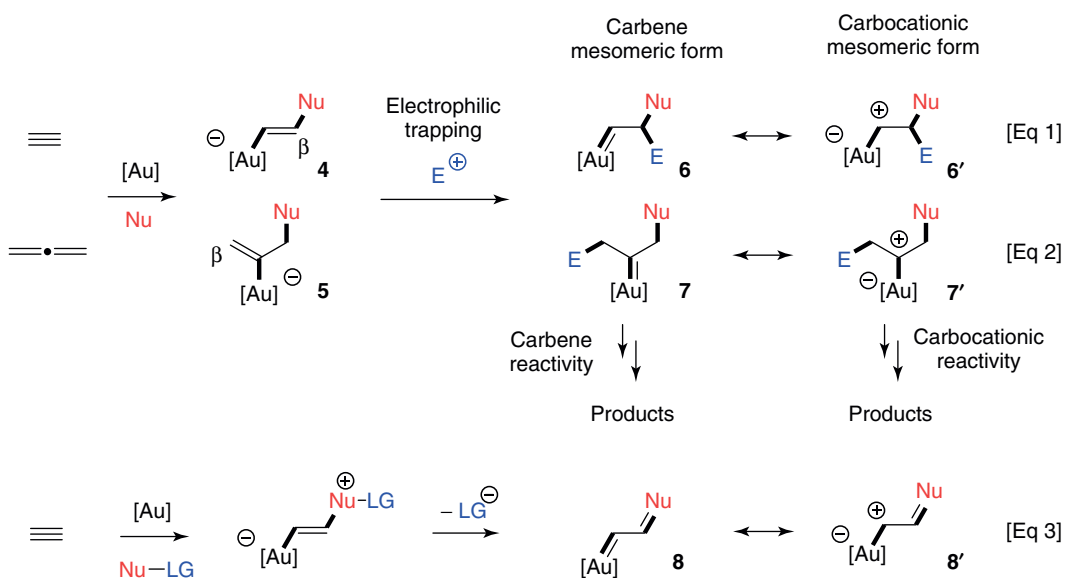
**Scheme 13.1** Metal-mediated dipolar cycloaddition to nitriles and isocyanides and dipoles employed.



Scheme 14.27



Scheme 16.5



Scheme 16.6

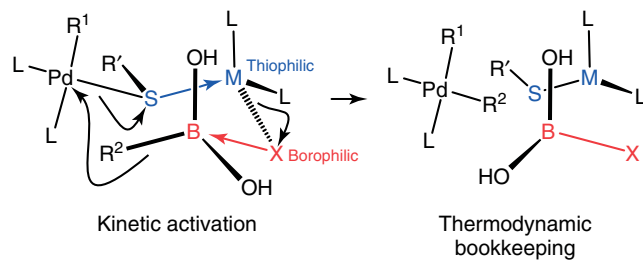
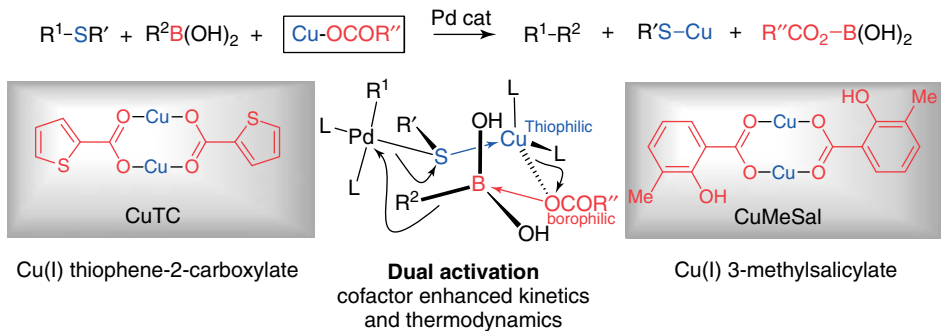
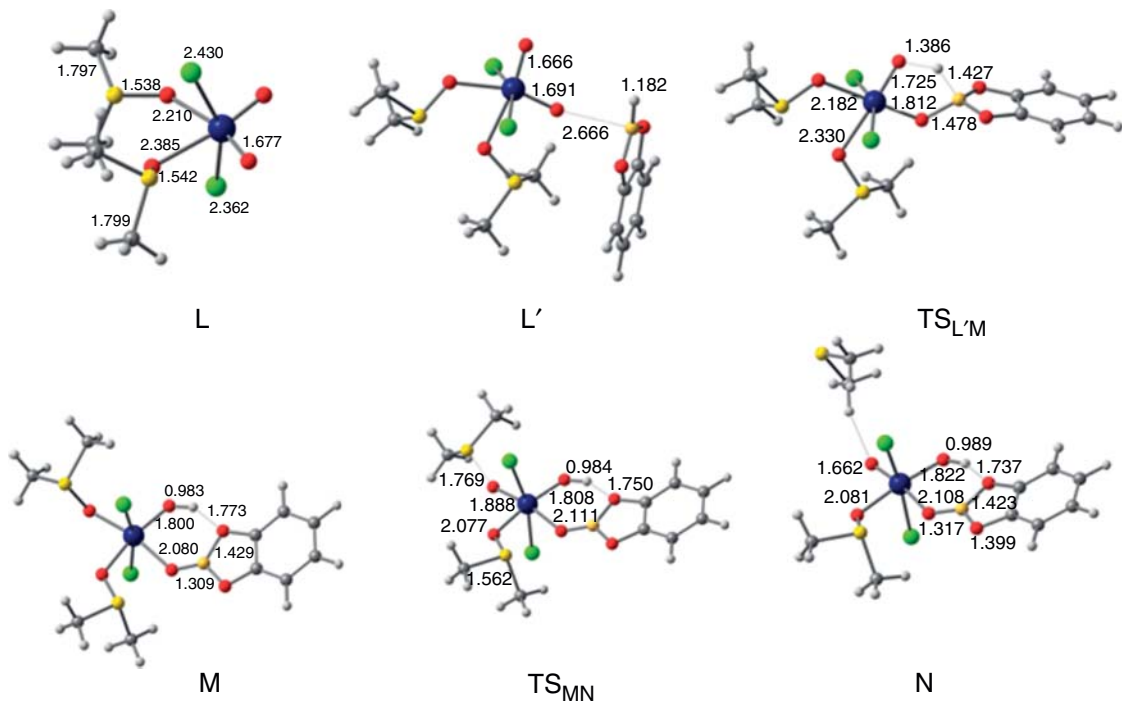


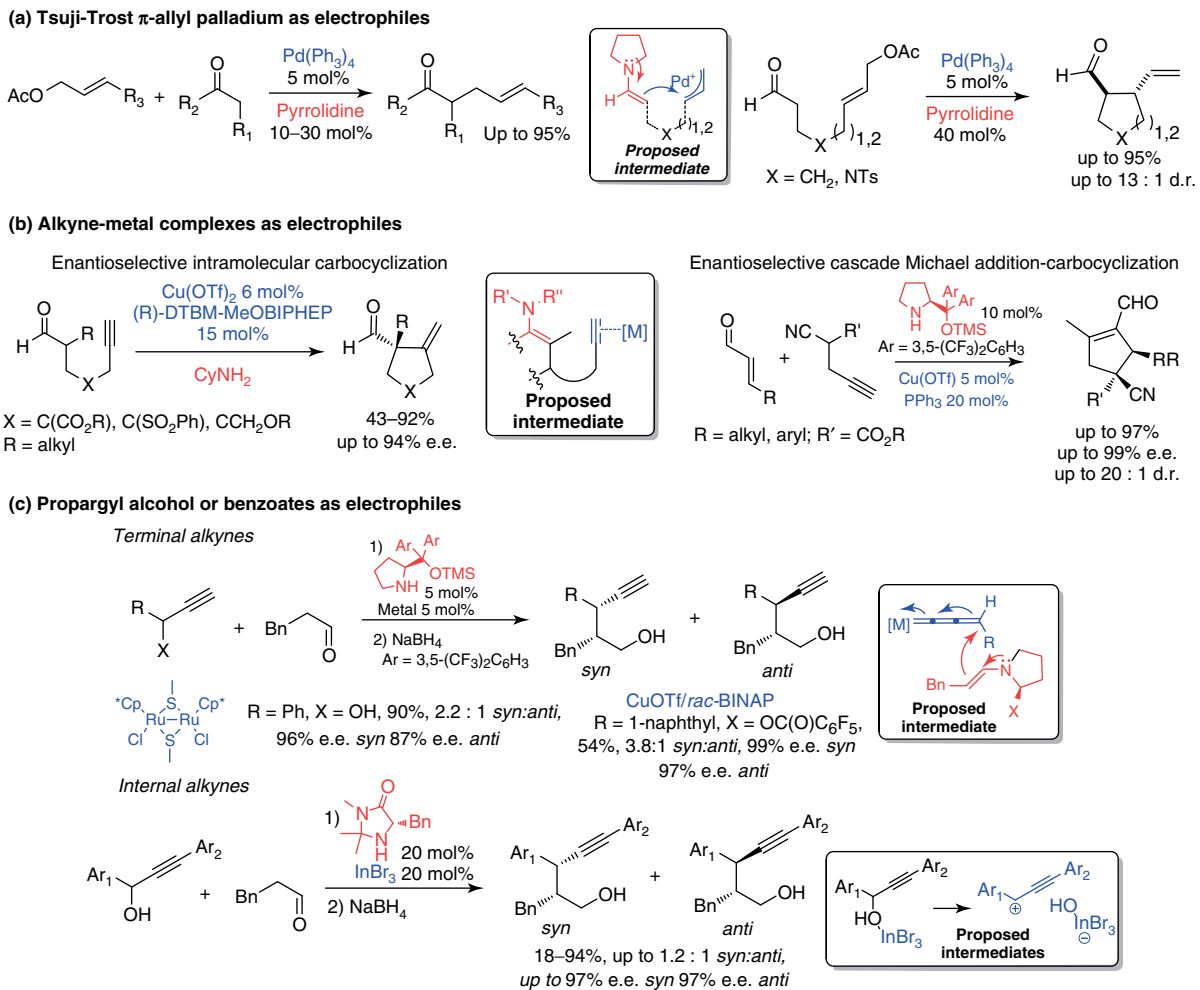
Figure 23.2 Dual thiophilic–borophilic activation of transmetalation.



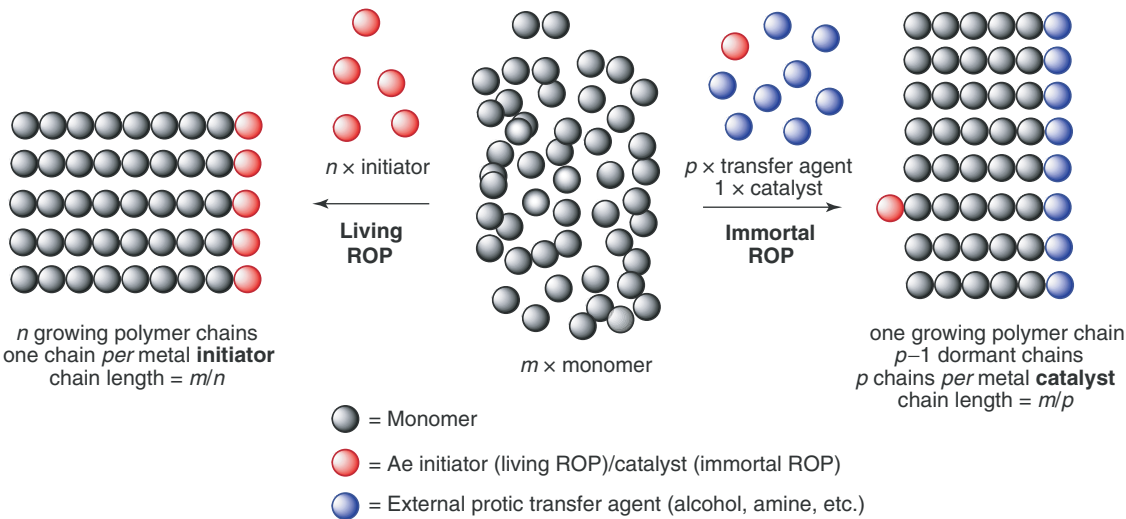
**Figure 23.3** Pd-catalyzed, Cu(I) carboxylate-mediated desulfitative catalysis.



**Figure 24.9** Intermediates and transition states in the sulfoxide reduction catalyzed by  $\text{MoO}_2\text{Cl}_2(\text{H}_2\text{O})_2$  (**L**) with relevant distances (Å).



**Scheme 26.4** (a–c) Selected examples of cooperative enamine addition into metal-activated electrophiles.



Scheme 28.5 Illustrative comparison of the living and immortal ROP processes.

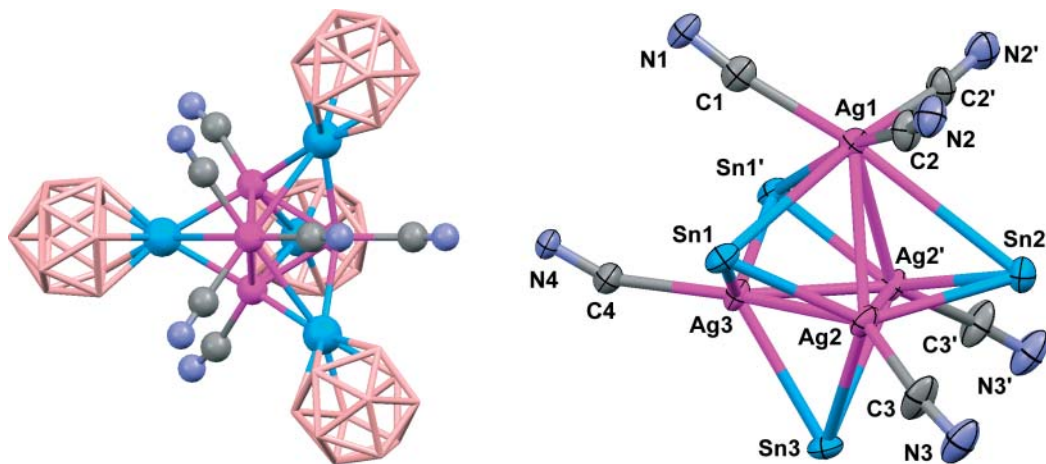
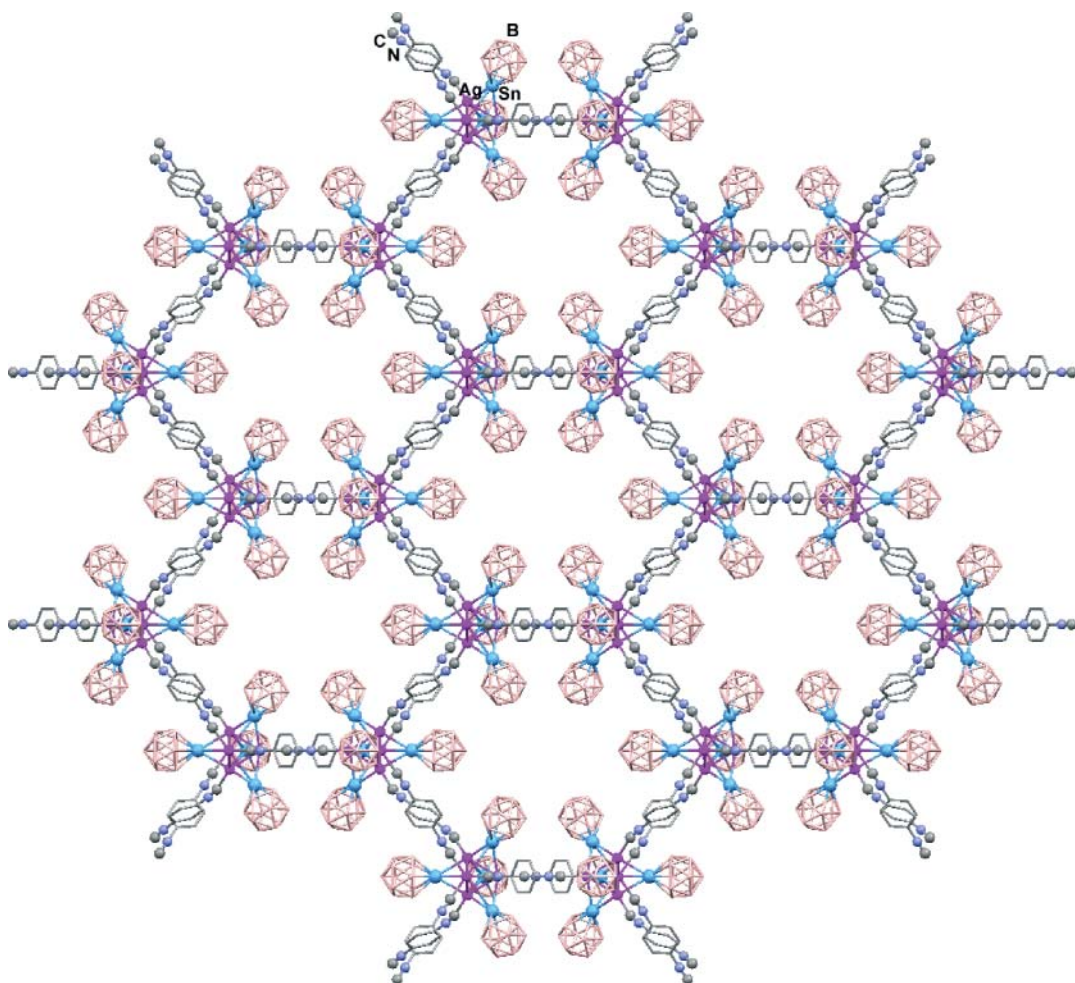
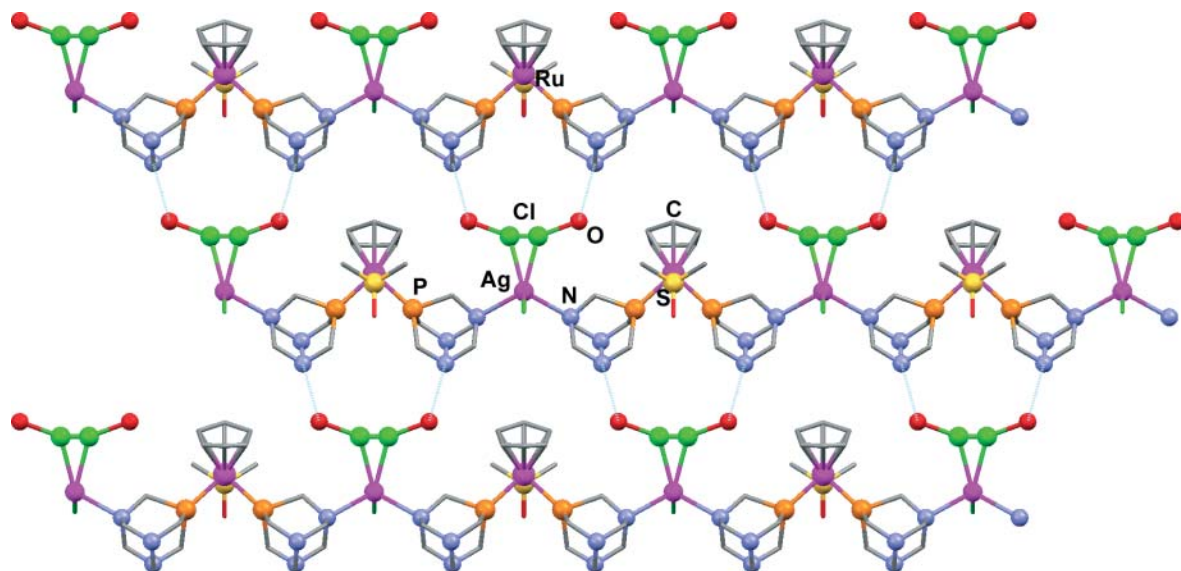


Figure 29.4 Crystal structure of  $[Me_4N][Ag(SnB_{11}H_{11})]$  and its metal organization group.



**Figure 29.5** View along the plane  $a-b$  of  $\{[\text{Me}_4\text{N}]_4[\text{Ag}_4(\text{SnB}_{11}\text{H}_{11})_4(\text{DIB})_{6/2}]\}_n$ . The solvents into the material porous were not represented for the sake of clarity.



**Figure 29.6** Crystal structure and packing of water-soluble Ru–Ag-backbone organometallic polymer.

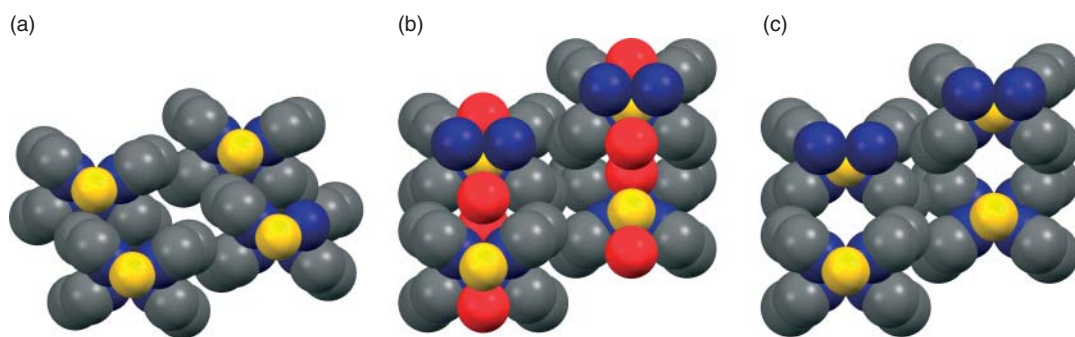


**Figure 30.16** Space-fill representation of **14** (b) and **13** (c). H atoms are not indicated and crystallized water molecules are indicated as red balls. In (a), the water molecules have been fictionally removed, evidencing the space they occupy in **13**.



**Figure 30.17** Samples of compounds **13–15**.

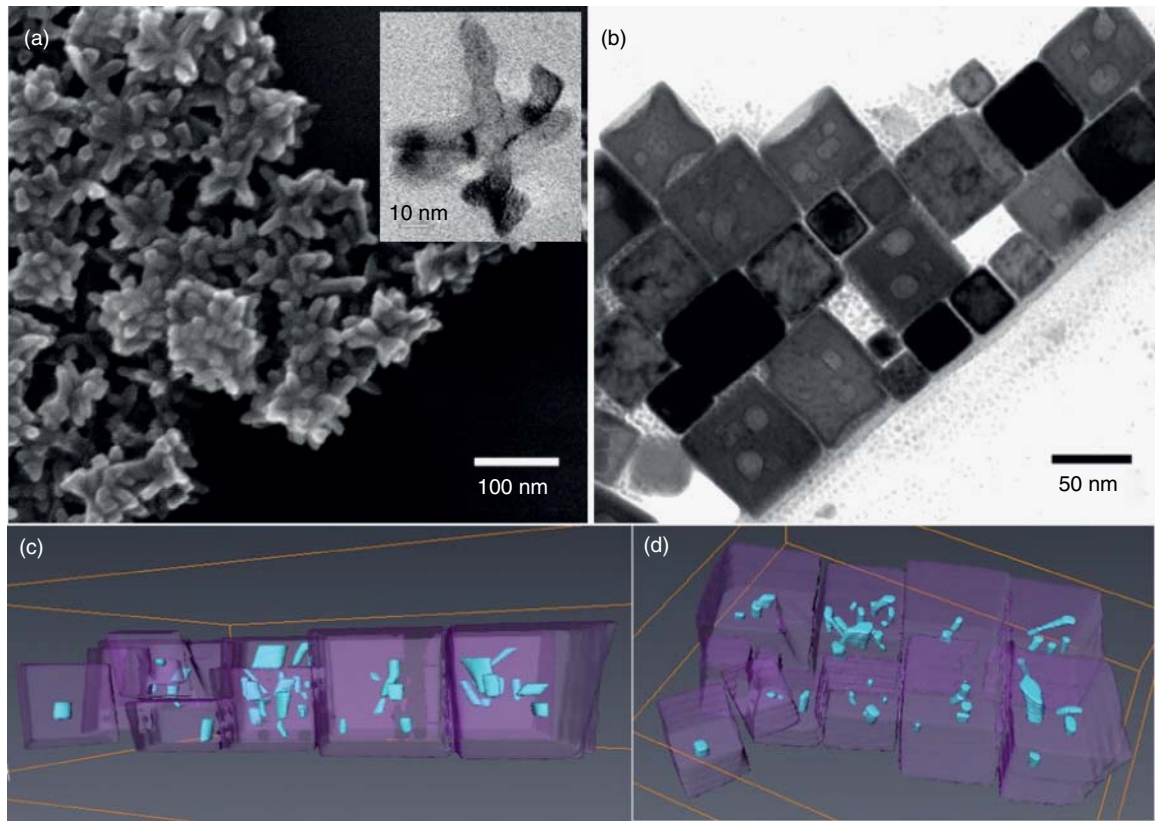


**Figure 31.11** (a) SEM image of nanostars. (Inset), TEM image of a single star. (b) TEM image of porous nanocubes, obtained with dodecylamine/lauric acid surfactants. (c), (d) 3D reconstruction of the nanocubes obtained from electron tomography study, the defects embedded within the objects are represented in blue, and the outer surface of the cubes are in light violet.

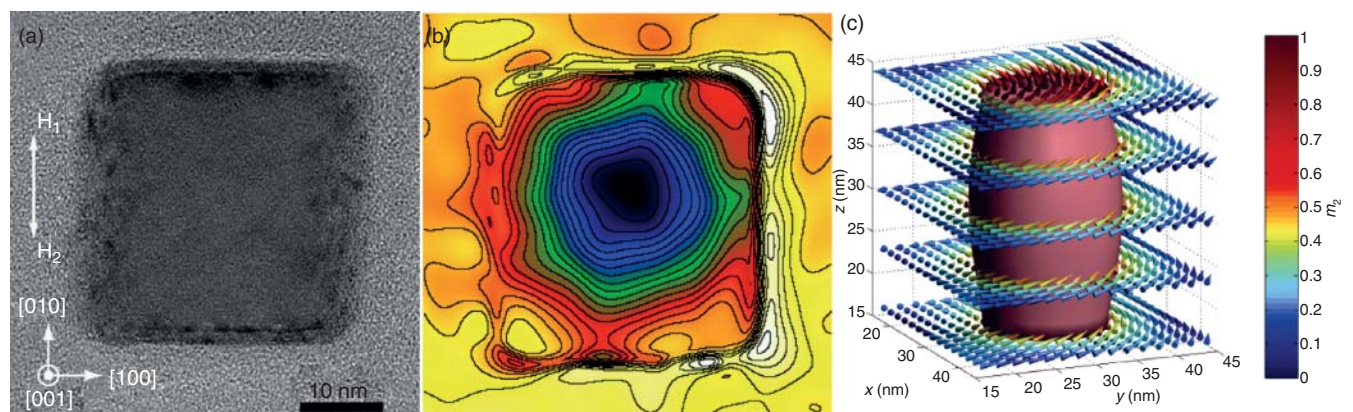


**Figure 31.12** (a) TEM image of a 30 nm nanocube. (b) Mapping of the induction field obtained from electronic holography. (c) 3D visualization of the magnetic moment simulated within the nanocube.

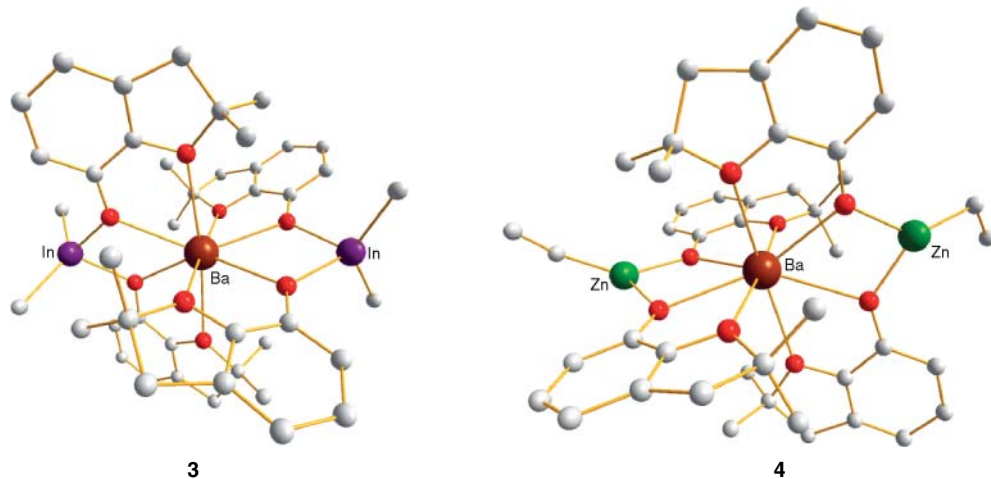


**Figure 32.3** Molecular structure of  $[\text{Ba}\{(\mu\text{-ddbfo})_2\text{InMe}_2\}]$  (**3**) and  $[\text{Ba}\{(\mu\text{-ddbfo})_2\text{ZnEt}\}]$  (**4**) (the H atoms are omitted for clarity).

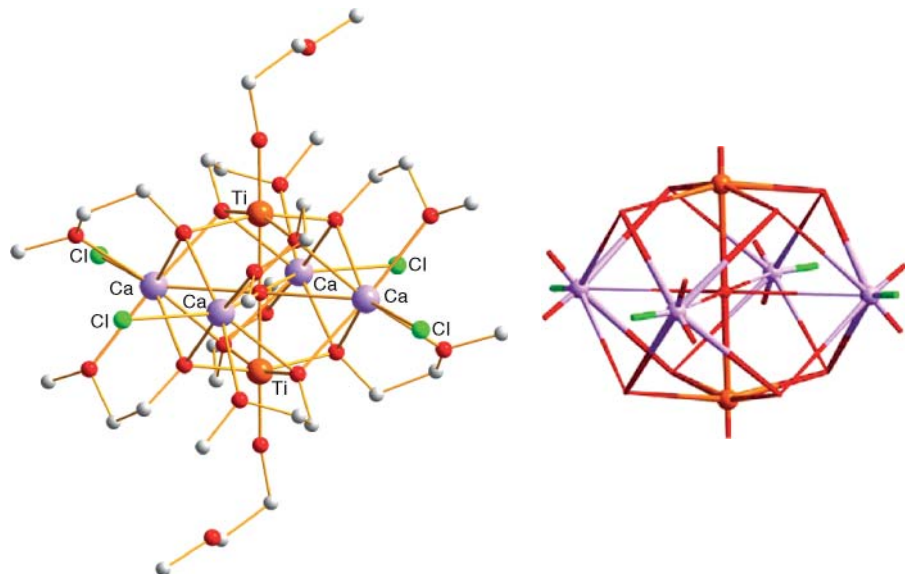


**Figure 32.5** Molecular structure of  $[\text{Ca}_4\text{Ti}_2(\mu_6\text{-O})(\mu_3, \eta^2\text{-OCH}_2\text{CH}_2\text{OCH}_3)_8(\eta\text{-OCH}_2\text{CH}_2\text{OCH}_3)_2\text{Cl}_{14}]$  (the H atoms are omitted for clarity) and its  $\text{Ca}_4\text{Ti}_2(\mu_6\text{-O})\text{O}_8\text{Cl}_{14}$  core.

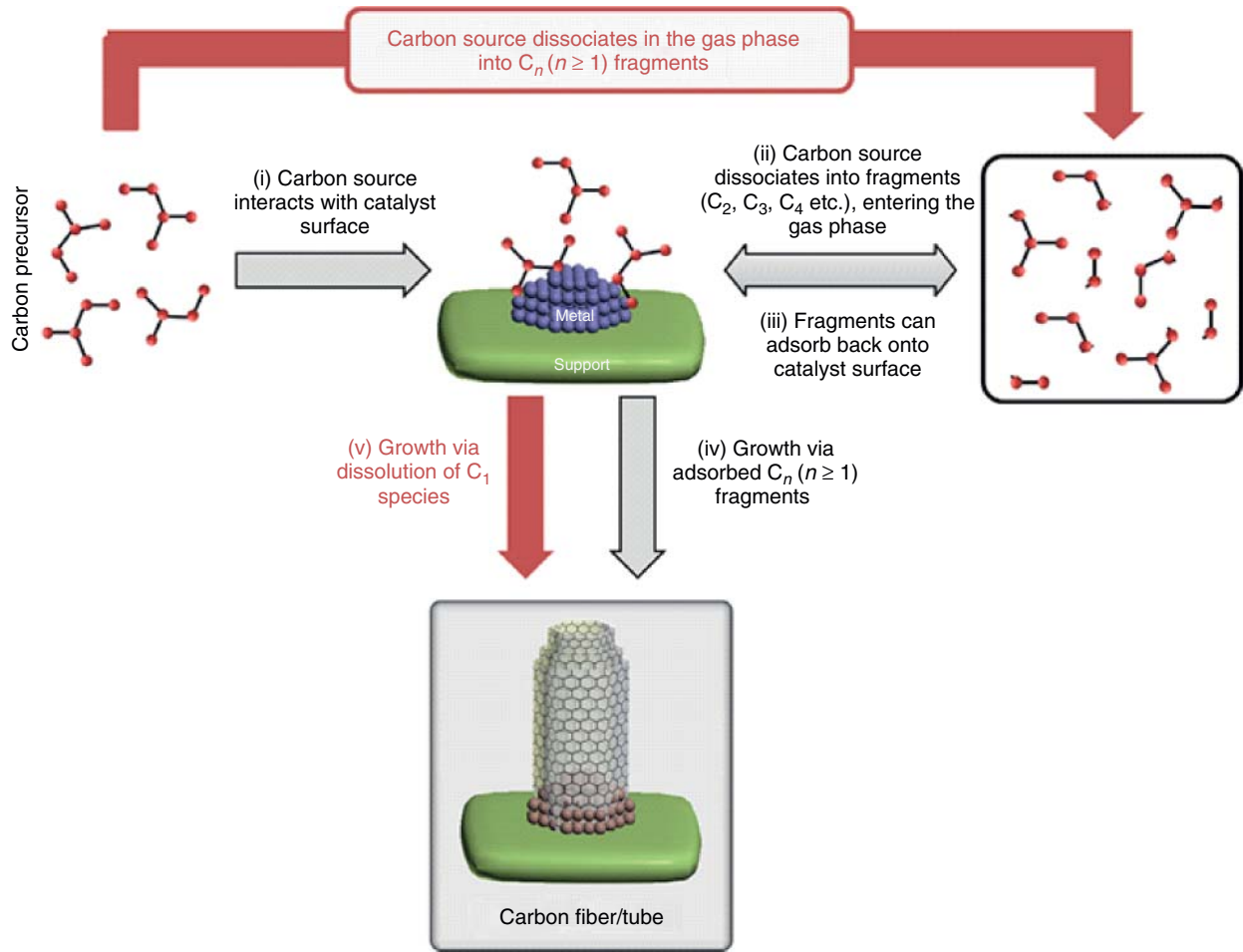


**Figure 33.7** Proposed mechanism for CNT/F growth via carbon fragments. (i) Carbon source adsorbs onto the surface of the catalyst particle. (ii) Carbon source fragments on the catalyst and is released into the gas phase, or (iii) gas-phase fragments are readsorbed onto the catalyst surface. (iv) Growth of CNT/F from adsorbed carbon fragments. (v) Base growth mechanism as proposed by Baker [7]. Reprinted from Reference 7b. Copyright 2012, with permission from Elsevier.

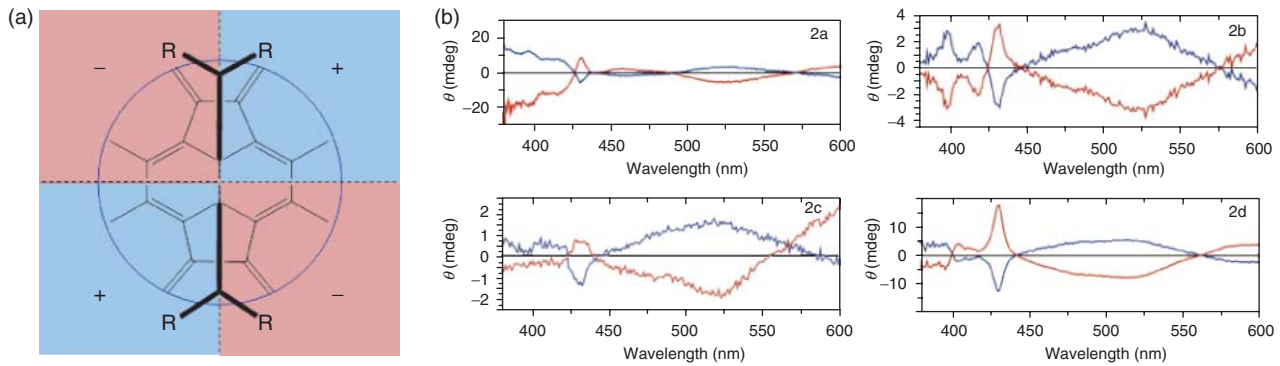


**Figure 34.2** (a) Schematic top view of the four sectors of the plane tangent to the attacked double bond with the respective sign. (b) CD spectra of both enantiomers of several *cis*-[60]fulleropyrrolidines (see Scheme 34.9): blue line represents (2*R*,5*R*) enantiomers obtained from Ag(I)/(-)-BPE and the red line (2*S*,5*S*) enantiomers synthesized using Cu(II)/Fesulphos.

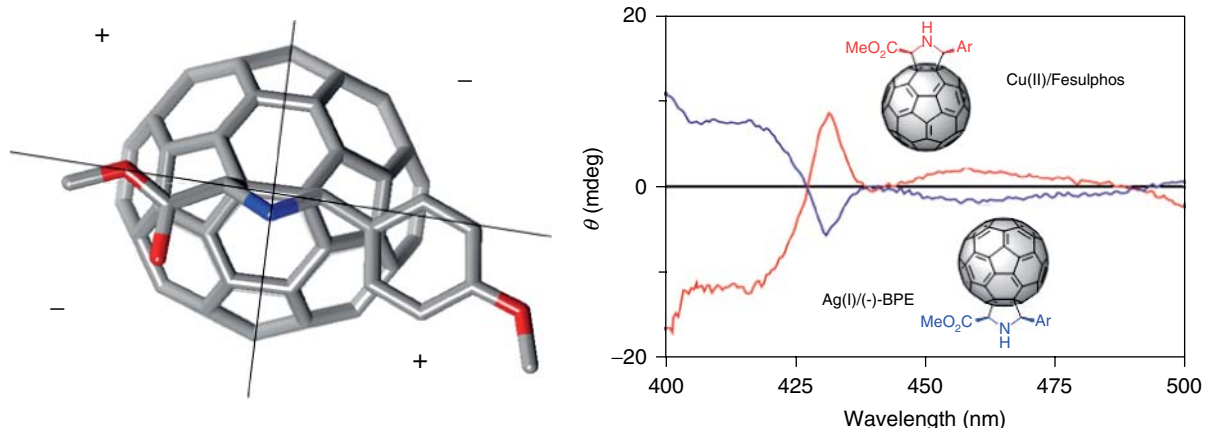


**Figure 34.3** Absolute configuration assigned for both *cis*-2-carboximethyl-5-(*p*-methoxyphenyl)pyrrolidino[3,4:1,2][60]fullerene enantiomers using the sector rule.

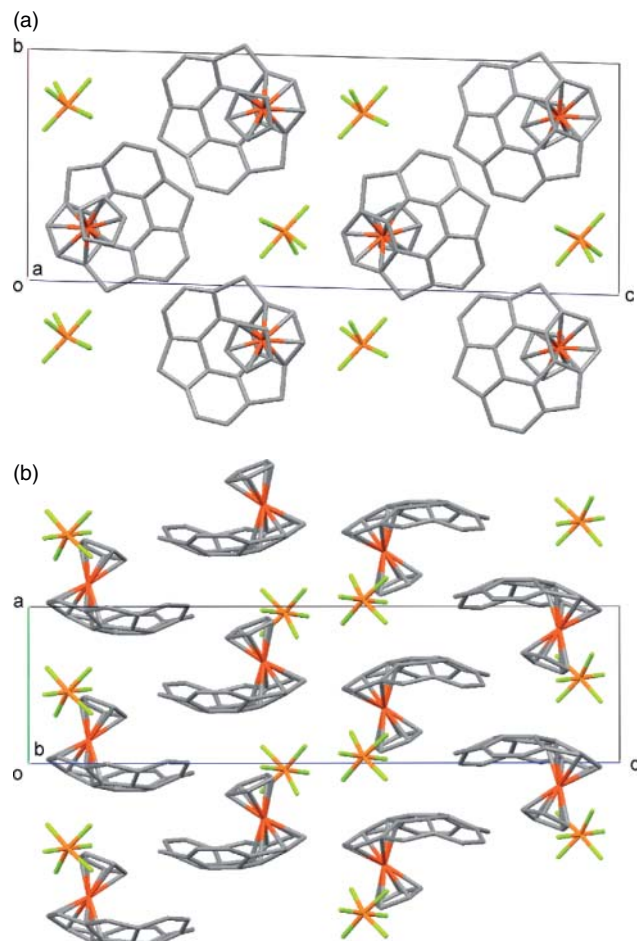


**Figure 35.11** Crystal cell and packing structure of **15**: (a) top and (b) side views. H atom is omitted for clarity.

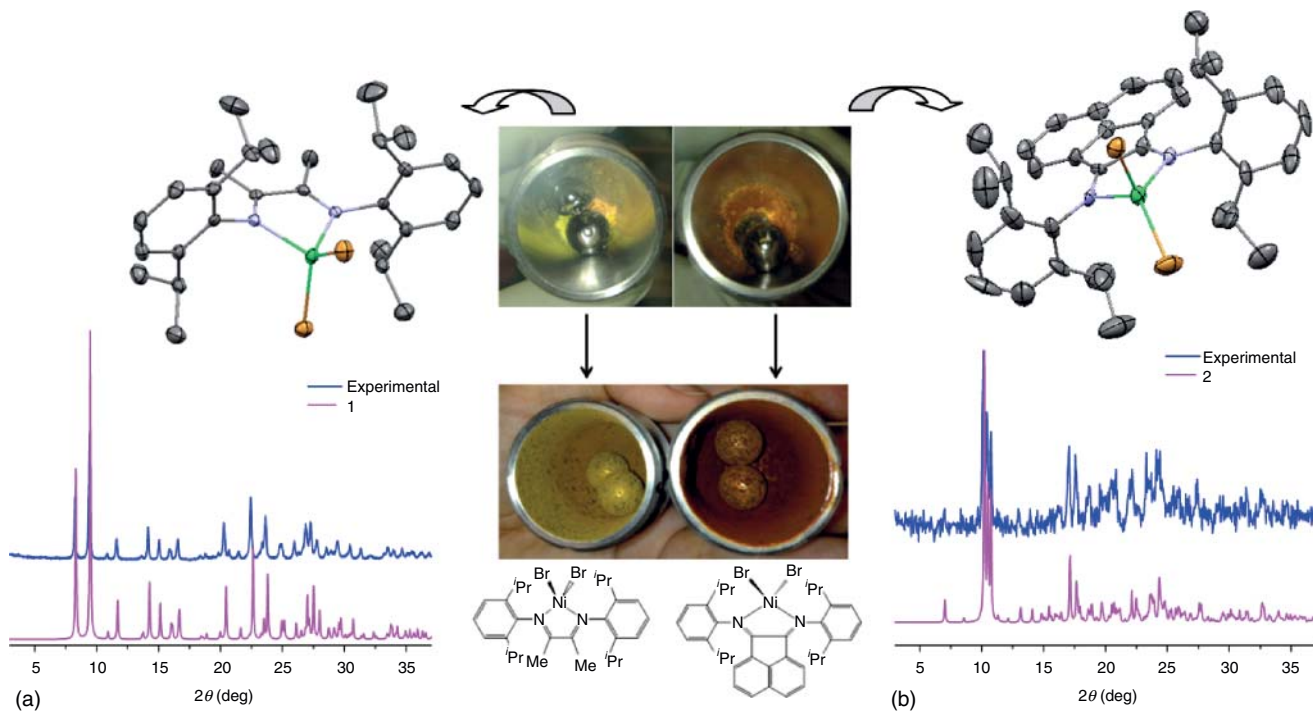


**Figure 37.4** Syntheses and characterization of complexes derived from (a) **1** and (b) **2**.

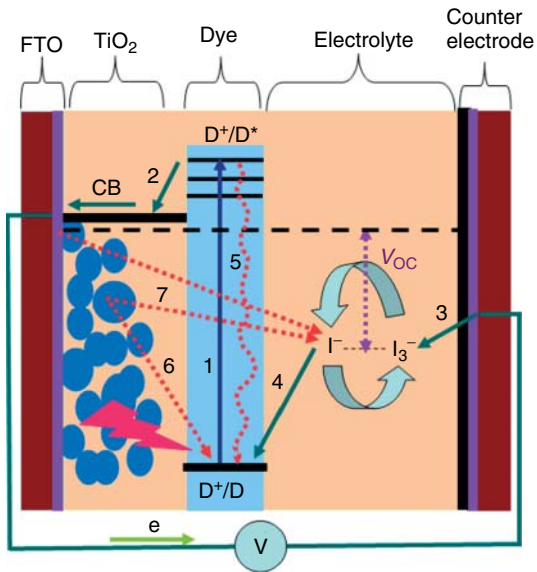


**Figure 38.1** The construction of a dye-sensitized solar cell (DSSC) and its operating principle. D, Dye; CB, conduction band of TiO<sub>2</sub>;  $V_{max}$ , maximum voltage.

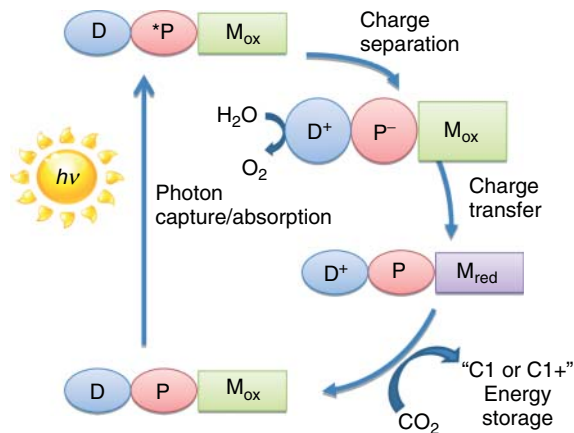


**Figure 39.3** Constitutional elements of a device for the photochemical reduction of  $\text{CO}_2$  in water under solar light irradiation.

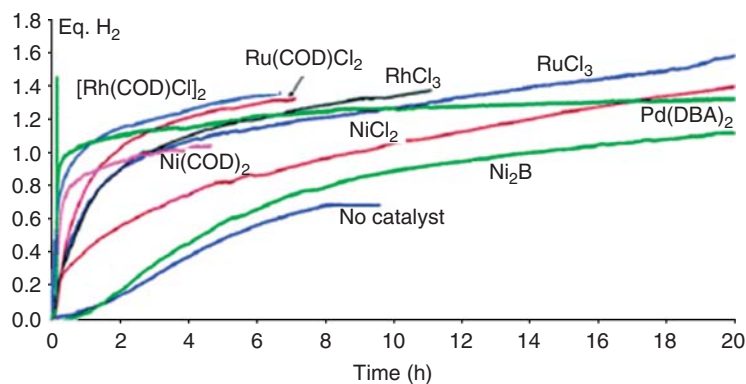


**Figure 40.10** Hydrogen evolution from AB-decomposition at  $65^\circ\text{C}$  catalyzed by different metal-catalyst precursors in  $[\text{BMIM}][\text{Cl}]$ . Reproduced from Reference 16 with permission of The Royal Society of Chemistry.

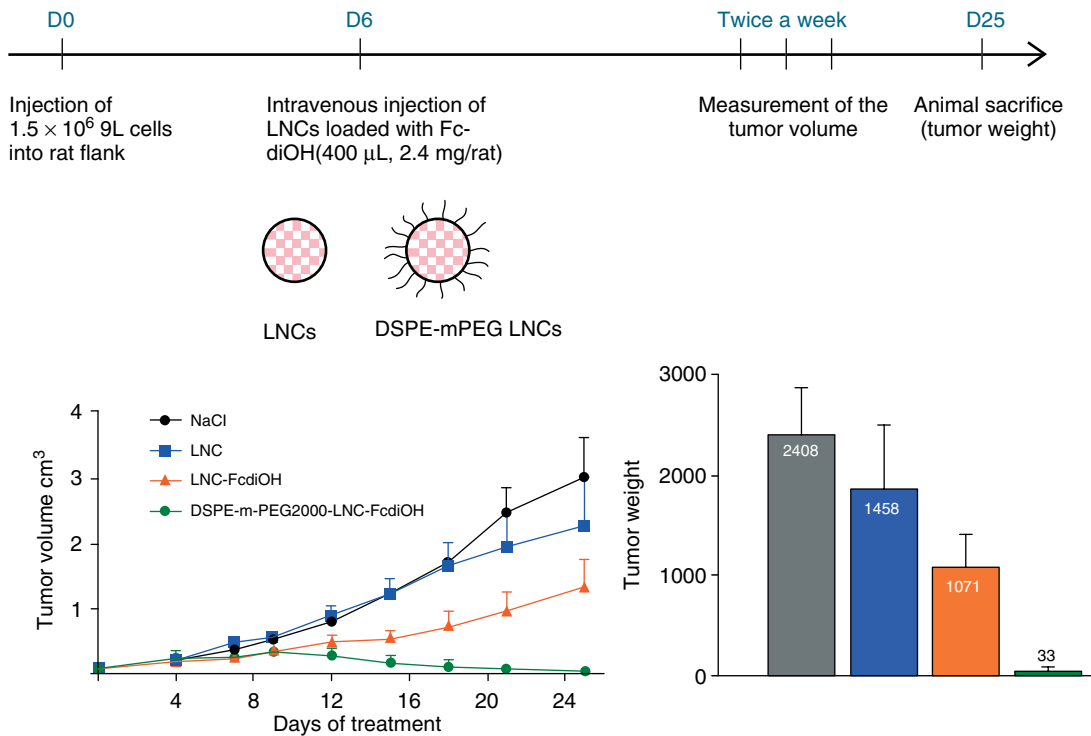


**Figure 42.12** Intravenous injection of two different sorts of LNC in ectopic tumors.

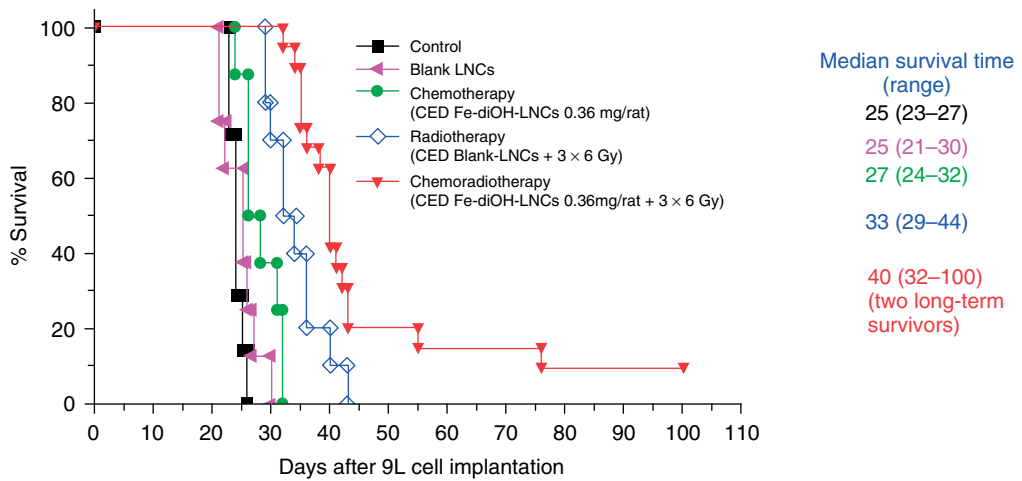
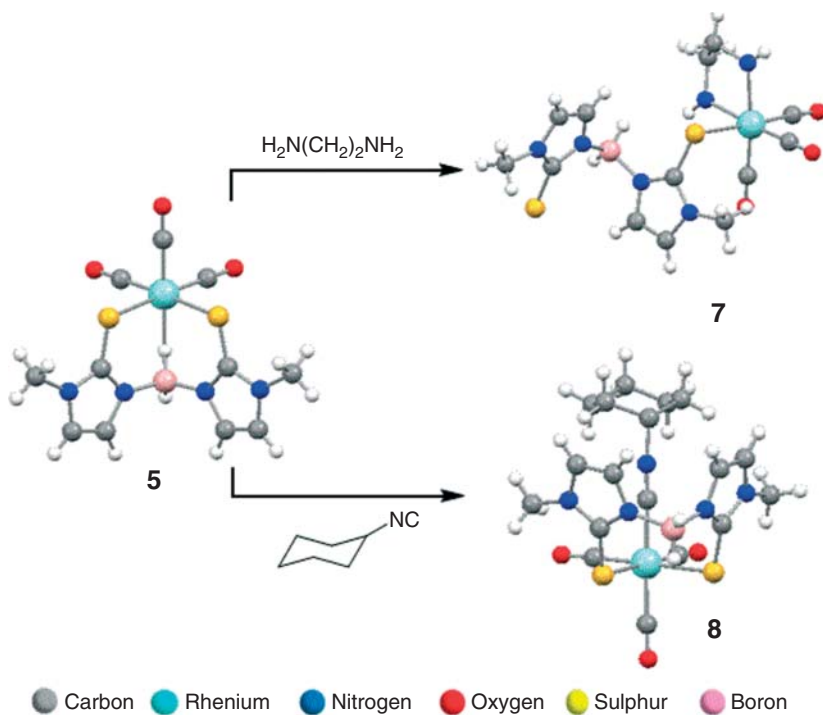
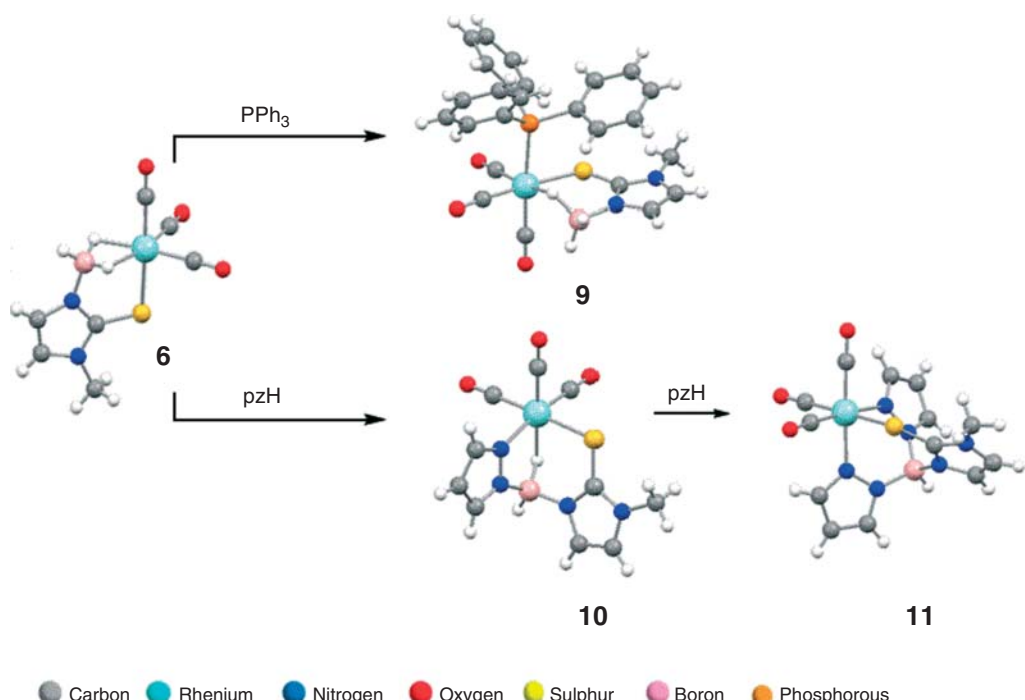


**Figure 42.13** Kaplan–Meier survival plots.



**Scheme 44.2** Reactions of *fac*-[Re{ $\kappa^3$ -H<sub>2</sub>B(tim<sup>Me</sup>)<sub>2</sub>}(CO)<sub>3</sub>]. (**5**) with ethylenediamine and cyclohexyl isonitrile (tim<sup>Me</sup> = 2-mercaptop-1-methylimidazolyl) [38, 39].



**Scheme 44.3** Reactions of *fac*-[Re{ $\kappa^3$ -H<sub>3</sub>B(tim<sup>Me</sup>)}(CO)<sub>3</sub>]. (**6**) with triphenylphosphine and pyrazole (tim<sup>Me</sup> = 2-mercaptop-1-methylimidazolyl) [40, 41].

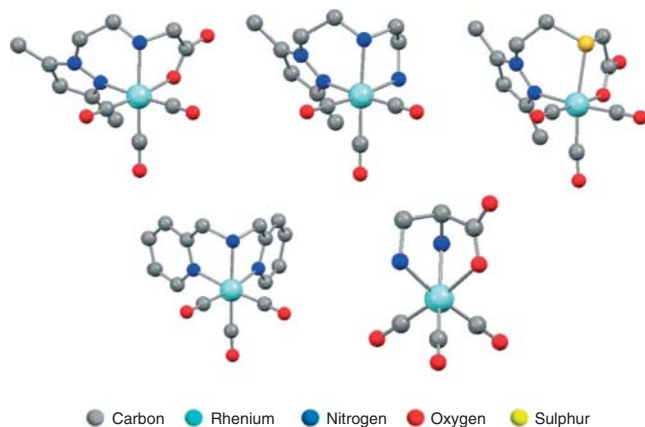


**Figure 44.3** Selected examples of Re(I) tricarbonyl complexes with tridentate Werner-type ligands [14–18].

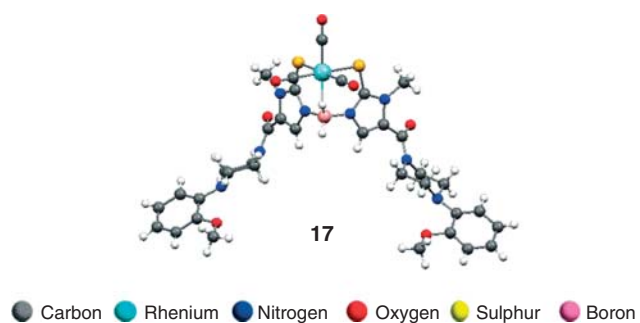


**Figure 44.10** Molecular structure of a dihydrobis(mercaptoimidazolyl)borate Re(I) tricarbonyl complex containing two arylpiperazine pharmacophores [74]

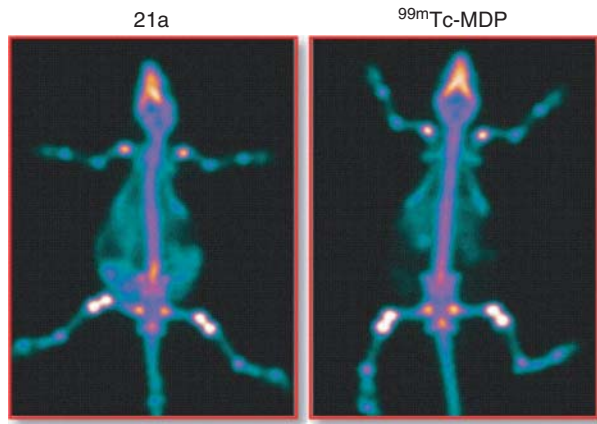


**Figure 44.13** Planar whole-body gamma camera images of rats injected with complex **21a** and  $^{99\text{m}}\text{Tc}$ -MDP at 2 h p.i. Reproduced with permission from The Royal Society of Chemistry.

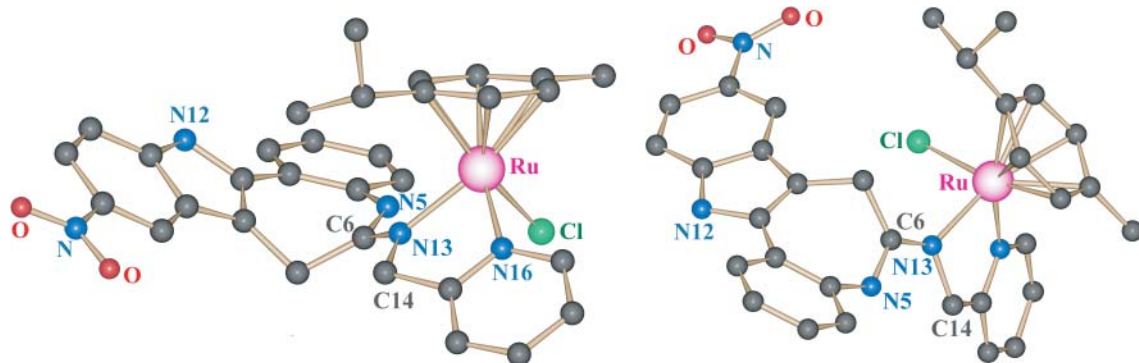


**Figure 45.4** Structures of the cationic *E*- (a) and *Z*-isomers (b) of  $[\text{Ru}^{\text{II}}(\text{p-cymene})(\text{L2c})\text{Cl}]^+$ . Atoms are depicted in black (carbon), blue (nitrogen), red (oxygen), green (chlorine), magenta (ruthenium). Hydrogens and the anion ( $\text{Cl}^-$ ) were omitted for clarity.

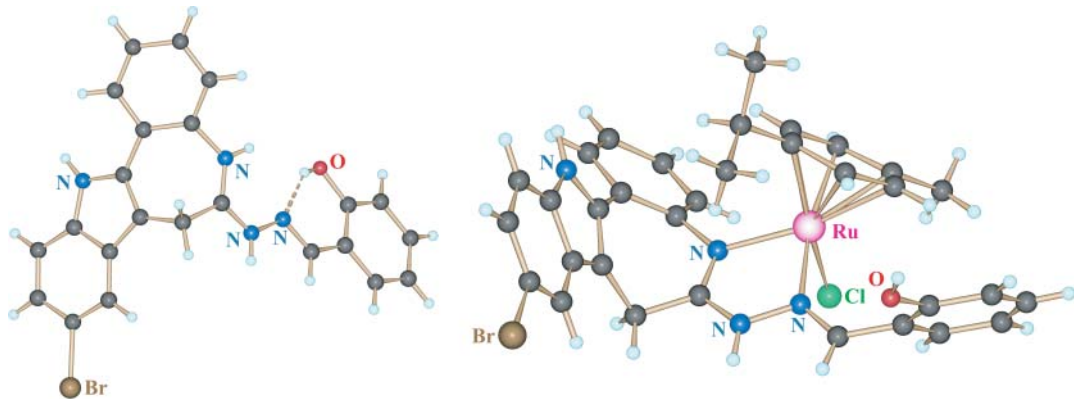


**Figure 45.5** Structures of the protonated paullone ligand  $\text{HL1a}^+$  with an intramolecular hydrogen bond  $\text{O}-\text{H}\cdots\text{N}$  (a) and ruthenium-arene complex cation  $[\text{Ru}(p\text{-cymene})(\text{L1a})\text{Cl}]^+$  (b). Atoms are depicted in black (carbon), cyan (hydrogen), blue (nitrogen), red (oxygen), green (chlorine), magenta (ruthenium), and brown (bromine).

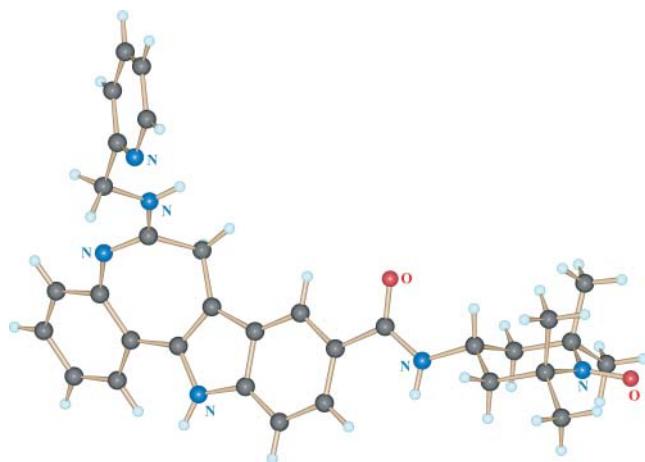


**Figure 45.6** X-ray structure of the paullone ligand  $\text{L2d}$ , bearing a TEMPO free-radical unit. Atoms are depicted in black (carbon), cyan (hydrogen), blue (nitrogen), red (oxygen).

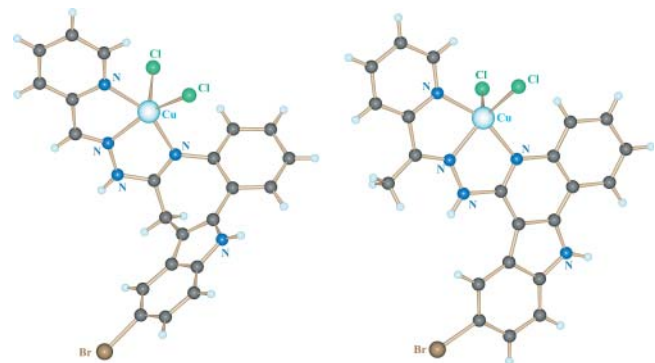


**Figure 45.7** Structures of the Cu(II) complexes of the paullone ligand **L1d** (a) and the related indoloquinoline-based ligand **L6l** (b). While the paullone backbone is considerably folded, the indoloquinoline backbone is planar. Non-labeled atoms represent carbon atoms.

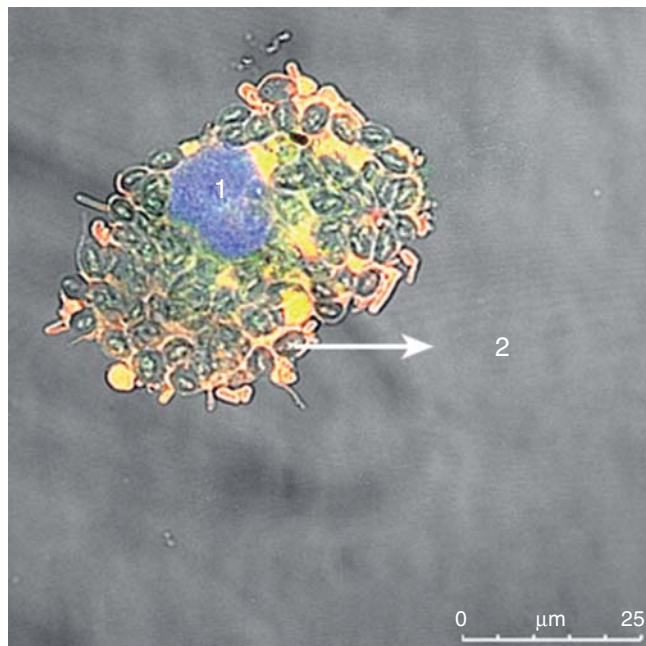


**Figure 46.3** Confocal image of macrophage (J777A.1) showing nucleus (1) with yeast cell-wall particles (2).

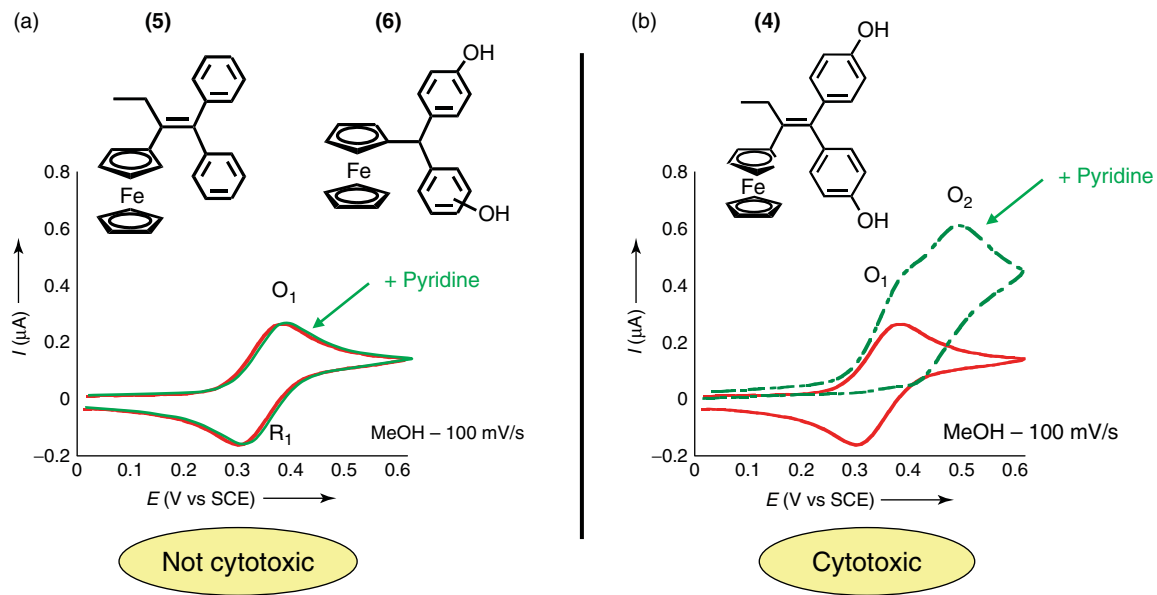


**Figure 47.2** Typical cyclic voltammograms of cytotoxic (b) and noncytotoxic (a) ferrocenfens (2 mM in 0.1 M  $\text{Bu}_4\text{NBF}_4$ /MeOH) obtained in the absence and the presence of pyridine used as a base model. Electrode: Pt, 0.5 mm diameter; scan rate 0.5 V/s.

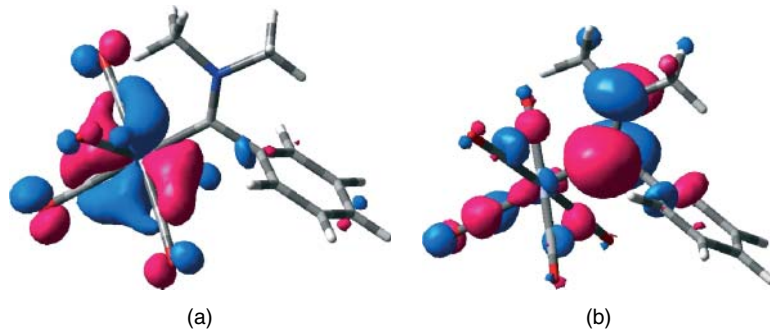


**Figure 48.5** HOMO (a) and LUMO (b) of the compound I c.

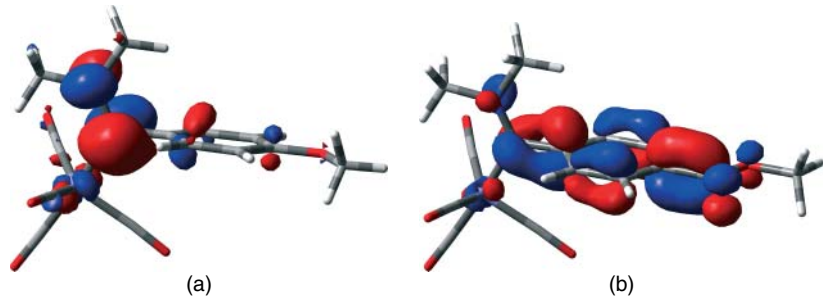


**Figure 48.8** LUMOs of the methoxy derivative **V a** (a) and the methylester derivative **V e** (b).

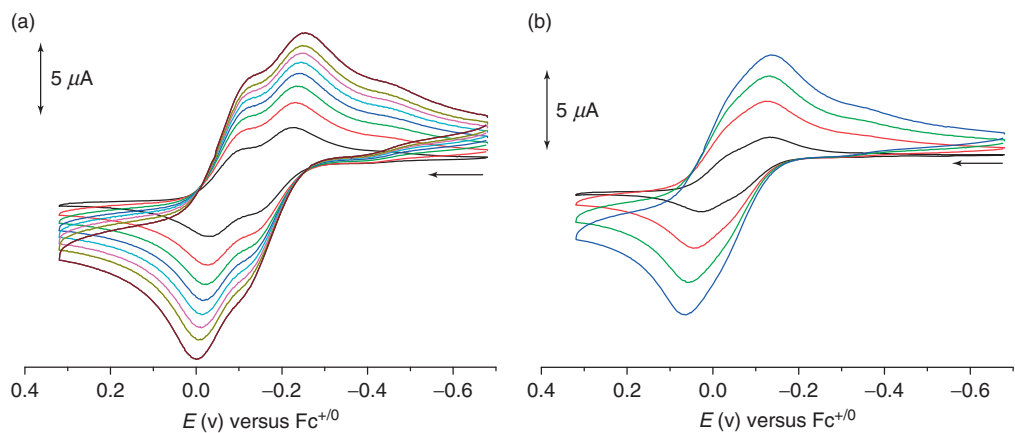


**Figure 49.3** Cyclic voltammograms of (a)  $[(C_5Me_5)Ir(Qa)]$  and (b)  $[(C_5Me_5)Ir(Qx)]$  in  $CH_2Cl_2/0.1\text{ M }Bu_4NPF_6$  at different scan rates.

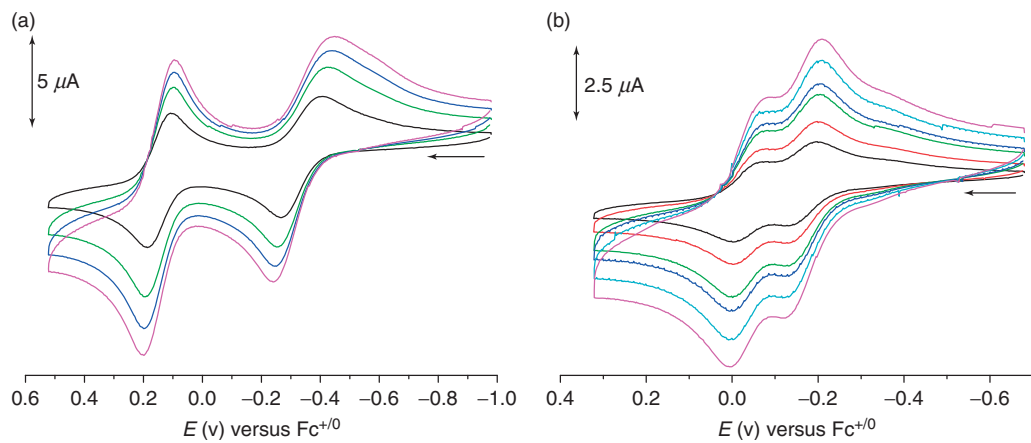


**Figure 49.4** Cyclic voltammograms of (a)  $[(\text{C}_5\text{Me}_5)\text{Rh}(\text{Qy})]$  and (b)  $[(\text{C}_5\text{Me}_5)\text{Rh}(\text{Qa})]$  in  $\text{CH}_2\text{Cl}_2/0.1 \text{ M } \text{Bu}_4\text{NPF}_6$  at different scan rates.

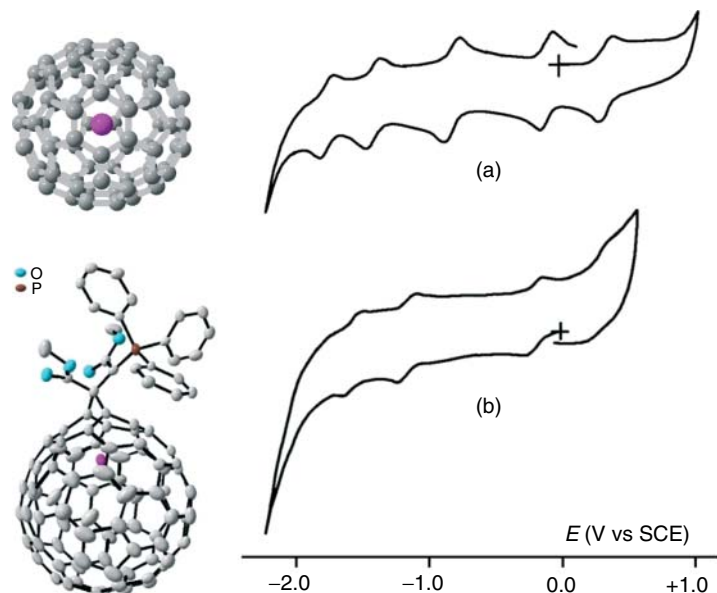
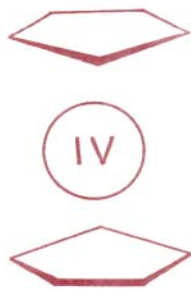


**Figure 51.10** Cyclic voltammetric profiles recorded at a platinum electrode in toluene-acetonitrile (4:1) solution of (a) Dy@C<sub>82</sub> and (b) Dy@C<sub>82</sub>[CCH(COOMe)<sub>2</sub>PPh<sub>3</sub>]. Scan rate: 0.05 V/s. (a) Adapted from Reference 25; (b) adapted from Reference 19. The optimized structure of Dy@C<sub>82</sub> is adapted from Reference 26.

FOURTH INTERNATIONAL CONFERENCE ON  
ORGANOMETALLIC CHEMISTRY

PROGRAMME  
AND  
LIST OF  
PARTICIPANTS



BRISTOL      28th JULY — 1st AUGUST 1969

Figure 1